NUCLEAR FUSION
FUSION NUCLEAIRE
ЯДЕРНЫЙ СИНТЕЗ
FUSION NUCLEAR

1962 SUPPLEMENT

PART 1

PROCEEDINGS OF THE CONFERENCE ON PLASMA PHYSICS AND CONTROLLED NUCLEAR FUSION RESEARCH, 4—9 SEPTEMBER 1961, SALZBURG, AUSTRIA

LES ACTES DE LA CONFERENCE SUR LA PHYSIQUE DES PLASMAS ET LA RECHERCHE CONCERNANT LA FUSION NUCLEAIRE CONTROLEE, 4—9 SEPTEMBRE 1961, SALZBOURG, AUTRICHE

ТРУДЫ КОНФЕРЕНЦИИ ПО ИССЛЕДОВАНИЯМ В ОБЛАСТИ ФИЗИКИ ПЛАЗМЫ И УПРАВЛЯЕМОГО ЯДЕРНОГО СИНТЕЗА, 4—9 СЕНТЯБРЯ 1961 г., ЗАЛЬЦБУРГ, АВСТРИЯ

LAS ACTAS DE LA CONFERENCIA SOBRE LAS INVESTIGACIONES EN MATERIA DE FISICA DEL PLASMA Y FUSION NUCLEAR CONTROLADA, 4 AL 9 DE SEPTIEMBRE DE 1961, SALZBURGO, AUSTRIA

INTERNATIONAL ATOMIC ENERGY AGENCY • AGENCE INTERNATIONALE DE L'ENERGIE ATOMIQUE • МЕЖДУНАРОДНОЕ АГЕНТСТВО ПО АТОМНОЙ ЭНЕРГИИ • ORGANISMO INTERNACIONAL DE ENERGIA ATOMICA

Selection and Program Committee — Comité de sélection et d'établissement du programme — Комитет по отбору докладов и разработке программы — Comité de Selección y del Programa

P. HUBERT ..... Chef du Service de recherches sur la fusion contrôlée, Commissariat à l'énergie atomique, France

K. V. ROBERTS ..... Theoretical Physics Division, Culham Laboratory, United Kingdom Atomic Energy Authority, United Kingdom

C. VAN ATTA ..... Associate Director, Lawrence Radiation Laboratory, University of California, United States of America

Scientific Secretariat — Secrétariat scientifique — Научный секретариат — Secretaría Científica

B. BURAS ..... *(Co-ordinating Scientific Secretary)* Division of Research and Laboratories, International Atomic Energy Agency

P. A. DAVENPORT .... *(Scientific Secretary)* Culham Laboratory, United Kingdom

C. ETIEVANT ..... *(Secrétaire scientifique)* Association Euratom — CEA, Service de recherches sur la fusion contrôlée, Fontenay-aux-Roses, France

W. F. GAUSTER ..... *(Scientific Secretary)* Oak Ridge National Laboratory, United States of America

Е. В. ПИСКАРЕВ..... *(Ученый секретарь)* Институт атомной энергии им. И. В. Курчатова, Москва, СССР (E. V. PISKAREV)

B. TORKI ..... *(Assistant Scientific Secretary)* Division of Research and Laboratories, International Atomic Energy Agency

I. DRUTMAN ..... *(Technical Secretary)* Division of Research and Laboratories, International Atomic Energy Agency

Editor of "Nuclear Fusion" — Rédacteur de la revue «Fusion Nucléaire»—Редактор журнала «Ядерный синтез» — Redacteur de "Fusión Nuclear"

J. G. BECKERLEY .... Division of Scientific and Technical Information, International Atomic Energy Agency

Executive Secretary — Secrétaire exécutif — Исполнительный секретарь — Secretario Ejecutivo

W. LISOWSKI ..... Division of Scientific and Technical Information, International Atomic Energy Agency

Conference Services — Services linguistiques — Обслуживание конференции — Servicios de la Conferencia

A. BERNSTEIN ..... *(Chief Interpreter)* International Atomic Energy Agency

L. S. LIEBERMAN ..... *(Records Officer)* International Atomic Energy Agency

Public Information — Information — Общественная информация — Información pública

P. FENT ..... *(Press Officer)* International Atomic Energy Agency

MISS M. NAPIER ..... *(Special Media Officer)* International Atomic Energy Agency

FOREWORD — AVANT-PROPOS — ПРЕДИСЛОВИЕ — PREFACIO

In 1958, at the Second United Nations Conference on the Peaceful Uses of Atomic Energy, the results of research on controlled nuclear fusion obtained in a few technically advanced countries were first disclosed to the world at large. Since then, it has become more and more evident that a better understanding of fundamental phenomena is needed before the goal of energy extraction from nuclear fusion may be reached. Consequently, the intensive research undertaken in recent years has been primarily basic research in plasma physics.

The fact that such research is most complex and costly has enhanced the desirability of co-operation and exchange of information and experience between all those engaged in this field of nuclear science and technology. It has become obvious that the International Atomic Energy Agency can play an important part in promoting such co-operation on a world-wide scale.

After consultation with a number of leading scientists, the Agency convened an international conference on Plasma Physics and Controlled Nuclear Fusion Research. The extent of the interest shown by Member States did not merely confirm that such a conference was actually needed at the present time, but greatly exceeded expectations. The quality and volume of the papers submitted, the number of participants and of countries represented, all bore witness to this interest.

Today, plasma physics and controlled thermonuclear fusion research is a more-or-less academic study. All that can be said at this stage is that it should eventually lead to a practical energy source. The day may come when the energy from nuclear fusion will be needed and when the well-being of mankind may depend on the ability to draw on this almost limitless reservoir.

The publication of the conference proceedings is intended to promote international co-operation and accelerate progress in this most important field of scientific endeavor.

INTRODUCTION – ВВЕДЕНИЕ – INTRODUCCIÓN

The Conference on Plasma Physics and Controlled Nuclear Fusion Research was held in Salzburg, Austria, on 4—9 September 1961. More than 500 scientists, representing 29 nations and 6 international organizations, participated in the Conference. The Proceedings are published in three parts as a 1962 supplement to this journal.

Because of the many interconnections between the various problems of plasma physics, it was decided to have no parallel plenary sessions. Accordingly, nine sessions were held during the six days of the Conference. During these sessions, 111 papers were presented. The "free" afternoons and evenings were devoted to at least fourteen informal discussions of topics of special interest to the participants. The present Proceedings do not include the records of these informal discussions (the discussions would have ceased to be "informal" if recorded), although it seems certain that new ideas generated in these discussions will lead to publication of papers elsewhere.

"Part 1" contains the texts (in original language only) of all papers delivered in Sessions I, II and IV of the Conference, the records (in English) of the discussions of these papers, as well as the texts (in English and Russian) of the two concluding speeches by Prof. Artsimovich and Dr. Rosenbluth summarizing the Conference. Translations of the abstracts of each paper (Sessions I, II, IV) are given at the end of this part of the Proceedings. In addition there is an author index.

The remainder of the Proceedings is published in "Part 2" (Sessions III, V, VI, VIII) and in "Part 3" (Sessions VII, IX). The abstracts of those papers accepted but not presented to the Conference, a list of participants, subject and author indexes for the entire Proceedings are included in the third part.

In preparing the Proceedings the Editor gratefully acknowledges the substantial help of B. Buras, P. A. Davenport, C. Etievant, W. F. Gauster, W. A. Newcomb and E. V. Piskarev.

CONTENTS — SOMMAIRE — СОДЕРЖАНИЕ — INDICE

SUMMING UP SESSION

SYNTHÈSE DE LA CONFÉRENCE

ИТОГОВОЕ ЗАСЕДАНИЕ

RECAPITULACIÓN DE LA CONFERENCIA

9 SEPTEMBER 1961 — 9 SEPTEMBRE 1961

9 СЕНТЯБРЯ 1961 Г — 9 DE SEPTIEMBRE DE 1961

Chairman — Le président — Председатель — El Presidente

G. Vendryès *(France)*

Scientific Secretary — Secrétaire scientifique — Ученый секретарь — Secretario Científico

B. Buras *(International Atomic Energy Agency)*

СОСТОЯНИЕ ИССЛЕДОВАНИЙ ПО УПРАВЛЯЕМОМУ ЯДЕРНОМУ СИНТЕЗУ НА СЕНТЯБРЬ 1961г. ОБЗОР РЕЗУЛЬТАТОВ ЭКСПЕРИМЕНТАЛЬНЫХ РАБОТ*

Л. А. АРЦИМОВИЧ

АКАДЕМИЯ НАУК СССР,

МОСКВА, СОЮЗ СОВЕТСКИХ СОЦИАЛИСТИЧЕСКИХ РЕСПУБЛИК

Г-н Председатель,

Закончившаяся сегодня Конференция продемонстрировала широкий размах исследований, связанных с проблемой управляемого термоядерного синтеза. Более 250-ти экспериментальных и теоретических работ было представлено в качестве материалов для Конференции и более 30-ти часов стремительный поток новой научной информации низвергался с этой кафедры на головы многочисленных слушателей. Обмен мнениями и результатами как в рамках официальных заседаний, так и во время так называемых «неформальных» дискуссий и отдельных бесед был очень интенсивным и обсуждение научных вопросов носило плодотворный, хотя иногда, быть может, и очень горячий характер.

И все же, подводя итоги работы Конференции, мы вынуждены признать, что за много лет интенсивного труда пройден лишь первый, сравнительно небольшой этап на пути к поставленной великой цели и мы еще только приближаемся к главному барьеру, преграждающему вход в область сверхвысоких температур.

Нагретая до высокой температуры плазма очень легко освобождается от накопленной тепловой энергии посредством различных механизмов неустойчивости. В экспериментах, осуществленных до сих пор, плотную плазму удавалось удерживать при относительно высокой температуре в течение промежутков времени по порядку величины, не превышающих сотни микросекунд. До сих пор интенсивность так называемых настоящих термоядерных реакций в плазме оказывается настолько малой, что они могут быть полностью замаскированы различными ускорительными процессами. Пока еще не установлен достаточно тесный контакт между результатами экспериментальных исследований и теоретического анализа. В особенности это относится к важнейшему вопросу об устойчивости плазмы. Вследствие этого пока еще слабо продвинута разработка методов стабилизации плазменных неустойчивостей. Ответственность за такое положение вещей ложится, конечно, прежде всего на экспериментаторов. Однако у них есть все же серьезное оправдание. Оно следует из специфических свойств изучаемого объекта, которые крайне осложняют постановку и проведение экспериментов.

Получение достаточно чистой водородной или дейтериевой плазмы само по себе представляет нелегкую задачу, т. к. из-за взаимодействия со стенками вакуумной камеры сгустки горячей плазмы очень быстро загрязняются атомами и ионами примесей тех веществ, которые адсорбированы на поверхности стенок, вследствие чего возникают очень большие радиационные потери. В качестве примера заметим, что в опытах с тороидальными плазменными шнурами, даже после длительной вакуумной тренировки, при каждом разряде вспыхивает интенсивное излучение примесей. Это один из основных факторов, мешающих подъему температуры плазмы в опытах подобного рода. Очень большие трудности возникают при самой попытке исследования свойств плазмы в таких кольцевых шнурах, так как здесь проявляется своеобразный принцип неопределенности, состоящий в том, что чистота условий опыта находится в непримиримом противоречии с использованием диагностической методики.

Спрятанный за металлическими оболочками и сложными обмотками, плазменный шнур, оказывается, вследствие своей недоступности и крайней чувствительности к любому прикосновению, исключительно неудобным объектом для исследования. В установках, принцип действия которых основан на инжекции быстрых частиц в магнитное поле, нас встречает другая трудность: из-за малой эффективности источников потоки частиц имеют сравнительно небольшую интенсивность и поэтому для заполнения ловушек требуется длительное время. За это время даже сравнительно слабые неустойчивости или же такие явления, как перезарядка на остаточном газе, успевают увести частицы из объема и поэтому не удается получать плазму с заметной концентрацией.

Если же мы пытаемся инжектировать в ловушку струю плазмы, то возникает сразу три до сих пор не решенные проблемы: 1) как добиться, чтобы произошел захват плазмы, 2) как превратить направленный поток частиц струи в сгустки с более или менее изотропным распределением скоростей, и 3) как избавиться от нейтрального газа, который вместе с плазменной струей выходит из инжектора.

После этих общих замечаний, которые в какой-то степени оправдывают сравнительно медленное

* Речь проф. д-ра Арцимовича на заключительной сессии. Зальцбург, 9 сентября 1961 г.

продвижение вперед интересующей нас области науки, я перехожу к очень краткому и естественно также очень поверхностному обзору основных результатов, установленных в работах последних лет.

В целом в состоянии проблемы несомненно произошел очень большой сдвиг по сравнению с тем уровнем, который был продемонстрирован на Женевской конференции в 1958 году. Тогда основной объем научной информации по существу представлял собой нечто такое, что можно назвать выставкой идей. Эти идеи в большинстве своем были лишь слегка задрапированы грубыми и плохо проверенными экспериментальными данными, имевшими рекогносцировочный характер. В противоположность этому, сейчас почти по каждому разделу общей термоядерной программы можно назвать большое число тщательно выполненных экспериментальных работ и очень ценных результатов, образующих в своей совокупности достаточно надежный фундамент, опираясь на который можно будет в дальнейшем значительно ускорить темп исследований.

Знаменательно, что при этом запас основных физических идей практически остался неизменным — за последние три года не было предложено ни одного существенно нового метода получения высокотемпературной плазмы. Вместе с тем произошло заметное перемещение центра тяжести в усилиях, направленных на разработку отдельных направлений общей программы. В начальной стадии разработки проблемы управляемых термоядерных реакций большое внимание уделялось исследованию простейшего способа получения высоких температур, в основе которого лежит использование линейных импульсных разрядов очень большой мощности и очень малой длительности (это так называемый быстрый линейный пинч). Усилия, направленные на исследование быстрого пинч-эффекта позволили еще до Женевской конференции получить ясную картину явлений, происходящих при разрядах такого типа, и найти механизм, лежащий в основе динамики плазменного шнура. Как известно, этот механизм заключается в ускорении плазмы под действием электродинамических сил. Одной из наиболее интересных черт, характерных для процессов указанного рода, является возникновение жестких излучений: нейтронов (в дейтериевой плазме) и гамма-лучей. В настоящее время мы знаем, что в типичных условиях эксперимента жесткие излучения обусловлены ускорительными процессами, причиной которых являются определенные формы неустойчивости, свойственные плазменным шнурам с большой силой тока. Повидимому, главную роль в возникновении быстрых положительных ионов, (а следовательно и нейтронов), играют неустойчивости типа перетяжек, а за возникновение быстрых нейтронов ответственна винтовая неустойчивость, связанная с тенденцией плазменного шнура к образованию так называемых «бессиловых конфигураций».

Хотя в опытах с линейными пинчами удалось получить в плазме температуры, превышающие 1 млн. градусов, однако вскоре выяснилось, что вряд ли может быть серьезная надежда на практическое использование такого метода для получения интенсивных термоядерных реакций в масштабе, представляющем техническое значение. Поэтому интересы естественным образом переместились в сторону изучения систем несколько иного типа, в которых быстрое сжатие плазмы происходит под действием нарастающего внешнего поля. Речь идет о процессах, получивших название тета-пинч.

При тета-пинч-эффекте достигается максимальная концентрация магнитной энергии в малых объемах. Поэтому сжатие плазмы внешним полем представляет значительно более эффективный метод создания высоких температур, чем линейный разряд. Сравнительная простота экспериментальной аппаратуры и заманчивые перспективы исследований в этой области привели к тому, что изучение свойств тета-пинч стало за последние годы одной из наиболее популярных тем в репертуаре исследований по управляемому синтезу. Об интересе к этому направлению говорит с достаточной ясностью большое количество докладов, представленных на конференцию, — 20 по сравнению с 2—3 в Женеве. Если дело так пойдет и дальше, то мы скоро приблизимся к осуществлению лозунга: «каждая домашняя хозяйка должна иметь свой собственный тета-пинч». Основные факты, установленные при исследовании устройств, в которых образуется тета-пинч, сводятся к следующему: обычно в таких процессах внутри плотного цилиндрического слоя сжимающейся плазмы сохраняется захваченное магнитное поле, по направлению противоположное тому, которое давит на внешнюю поверхность плазмы. Работа сил магнитного сжатия расходуется в начальной стадии процесса главным образом на ускорение ионов, а релаксация захваченного внутреннего магнитного поля может вносить существенный вклад в нагревание электронной компоненты. Тета-пинч не является устойчивым плазменным образованием. Это обнаруживается особенно отчетливо на фотографиях свечения плазмы, полученных с помощью СФР.

В плоскости, перпендикулярной силовым линиям поля, сжимающийся комок плазмы напоминает чернильную кляксу или отдыхающего осминога с дырой посредине. Мы имеем здесь дело с типичным случаем магнитогидродинамической неустойчивости, так называемого желобкового типа. Она обусловлена, во-первых, тем, что в процессе быстрого сжатия и последующих радиальных пульсаций плазма испытывает сильное ускорение и, во-вторых, тем, что линии поля имеют неблагоприятную форму (выпуклостью наружу). Несмотря на недостаточную согласованность данных, которые приводятся различными авторами, можно все же принять, что на установках с предельными параметрами, построенных в Вашингтоне и Лос-Аламосе, удается на время порядка нескольких

микросекунд получать сгустки плазмы концентрации 10^{16} и температурой порядка 10^3 эв. Я не хочу здесь затрагивать вопрос о природе нейтронного излучения, наблюдаемого в некоторых случаях быстрого сжатия дейтериевой плазмы, так как этот вопрос имеет чисто спортивный интерес.

Заметим, что если бы кто-либо из счастливых наблюдателей этого эффекта привез с собой в Зальцбург горсточку чистых нейтронов, образующихся в среднем за один разряд, то ее вряд ли хватило бы для того, чтобы подарить в качестве сувенира всего по одному нейтрону каждому гражданину гостеприимной Австрии.

Следует признать, что несмотря на многочисленные ценные исследования свойств тета-пинч, выполненные в Англии, СССР, США и других странах, природа этих процессов остается в достаточной степени темной во многих отношениях (сюда относится вопрос о механизме релаксации захваченного поля, о причинах вращения плазменного сгустка, об утечке частиц и т. д.). Неизвестно также, можно ли рассчитывать на то, что с помощью быстрого сжатия удастся в дальнейшем без существенных изменений формы магнитного поля получить достаточно устойчивый комок горячей плазмы. Анализируя вопрос о дальнейшей судьбе этого направления исследований, мы должны принять во внимание, что в настоящее время нет способов, которые позволяли бы создавать более плотные сгустки горячей плазмы, чем те, которые получаются в устройстве типа тета-пинч. Поэтому можно предположить, что на протяжении ближайших лет экспериментальные исследования сверхбыстрого сжатия плазмы нарастающим полем будут продолжаться, хотя, по-видимому, мало вероятно, чтобы они имели самостоятельные практические перспективы в рамках термоядерной программы.

Традиционным разделом термоядерной программы является исследование так называемых квазистационарных или медленных разрядов в тороидальных камерах. В этом разделе до сих пор было два основных направления. Первое из них происходит от идеи создания парамагнитного плазменного шнура с током, впитывающего в себя продольное магнитное поле сравнительно небольшой напряженности. Эта идея, как известно, реализована в установке «Зета», в установках «Альфа» и «Скептр». Второе направление основано на идее стабилизации тороидального разряда продольным полем, во много раз превышающим магнитное поле тока. Установки, принадлежащие к семейству «Токамак», являются материальным воплощением этого принципа. По существу, к тому же типу можно отнести стелларатор, если он работает в режиме омического нагрева.

Рассмотрим сначала ту ситуацию, которая сложилась на первом из указанных здесь основных направлений. Уже из доклада работников Харуэлла и Олдермастона на Женевской конференции выяснилось, что парамагнитный плазменный шнур становится жертвой неустойчивости. Последующие работы, выполненные как в Англии, так и в СССР на установке «Альфа», подтвердили эти первоначальные заключения. Однако это не должно было привести, и в действительности не привело к прекращению работ. Эксперименты продолжались и дали ряд ценных сведений о поведении парамагнитных шнуров и свойствах образующей их плазмы. Мы укажем здесь только наиболее значительные результаты этих исследований.

Из-за малой величины газокинетического давления в плазменном шнуре создается бессиловая геометрия магнитного поля, т.е. ток везде течет почти точно вдоль линии результирующего магнитного поля. Заметим, между прочим, что в квазистационарном режиме такая конфигурация поля и тока формально эквивалентна состоянию с предельной анизоторопией электропроводности. Энергия, вводимая в плазму от источника электрического питания, в режимах с относительно небольшой мощностью уходит в виде излучения примесей, а в более напряженных режимах выбрасывается на стенку потоками частиц.

Спектроскопические измерения, выполненные на всех трех перечисленных выше установках, обнаруживают полное согласие в одном пункте. Из них следует, что средняя энергия ионов в разряде значительно выше, чем тепловая энергия электронов. По поводу зависимости энергии ионов от заряда Z и массы M единого мнения, по-видимому, не существует. Из измерений, выполненных в Харуэлле, как будто бы следует, что энергия ионов растет линейно с M и практически не зависит от заряда. Опыты на «Альфе» дают существенно иной результат, указывая на то, что энергия многозарядных ионов приблизительно пропорциональна Z и не очень сильно зависит от массы. Происхождение быстрых ионов пока еще не выяснено. Очень интересным эффектом является обнаруженное на «Зете» аномальное сопротивление плазмы, которое играет существенную роль в общем ходе процесса при низком начальном давлении газа в камере. Априори ответственность за резкое увеличение сопротивления плазмы можно возлагать на самые различные формы неустойчивости. Однако от этого еще очень далеко до настоящего объяснения. Несмотря на большое количество важной и интересной научной информации, представленной на конференцию различными лабораториями, в которых ведутся исследования парамагнитных плазменных шнуров, все же складывается впечатление, что это направление приближается к тому моменту, когда источник свежих данных будет исчерпан.

Говоря о результатах работ, выполненных на установках типа «Зета», нельзя не отметить, что эти работы стимулировали развитие целого ряда новых методов диагностики плазмы. Одним из самых блестящих методических достижений последнего времени является разработанный в Харуэлле способ измерения излучения плазмы на длинах волн субмиллиметрового диапазона. Несомненным методическим достижением является

также тонкая техника измерения энергетического спектра частиц плазмы, разработанная в Ленинграде и использованная на установке «Альфа».

Изучение процессов омического нагревания плазмы, находящейся в сильном магнитном поле, пока прошло только начальную стадию. Установлено, что при достаточно большой величине отношения $H_Z H_\varphi$ (H_Z — напряженность продольного поля, а H_φ — напряженность поля тока) внешние признаки грубой нестабильности как будто бы исчезают. Вместе с тем обнаружено, что диффузия плазмы поперек силовых линий в таких системах имеет аномальный характер. Коэффициент диффузии на много порядков превышает значение, вытекающее из классической теории и приближается к той предельной величине, которую дает эвристическая формула Бома. Аномальная диффузия приводит к очень быстрому уходу частиц из плазменного шнура и в существующих установках ограничивает время его существования в лучшем случае несколькими сотнями микросекунд. Однако имеются некоторые экспериментальные факты, указывающие, что измерение скорости ухода частиц характеризует только поведение периферических областей плазменного кольца в тороидальной камере, в то время как внутри этого кольца существует более плотный ствол, в котором концентрация частиц удерживается на довольно высоком уровне (10^{12}—10^{13}) в течение длительных промежутков времени. Истинный механизм процессов, являющихся причиной аномальной диффузии, в системах типа «Токамак» и «Стелларатор» в настоящее время является предметом обсуждения.

Теория может предложить несколько возможных объяснений этого явления — магнитогидродинамические неустойчивости высших мод, неустойчивость, характерная для плазмы с неоднородным распределением температуры, генерация ионного звука и т. д., однако имеющихся экспериментальных данных пока еще недостаточно для того, чтобы произвести окончательный выбор между этими возможностями. Пуск в ход «Стелларатора С», с которым мы все должны поздравить ученых и инженеров, работающих в Принстоне, вероятно, позволит значительно ускорить получение информации, необходимой для окончательного разъяснения механизма аномальной диффузии при омическом нагреве плазмы.

Вряд ли могут существовать какие-либо надежды на то, что с помощью одного лишь омического нагрева плазму в системах «Токамак» или в «Стеллараторах» удастся довести до термоядерных температур, однако не исключено, что этот метод создания горячей плазмы может быть очень полезен на первой стадии, когда температура поднимается до нескольких сотен электронвольт.

Исследования квазистационарных разрядов в сильном магнитном поле представляют несомненную ценность также с точки зрения физики плазмы. В таких разрядах плазма с высокой концентрацией заряженных частиц впервые предстает перед нами как объект с достаточно хорошо очерченной геометрической формой, освобожденный от тех катастрофических деформаций, которые за несколько микросекунд меняют все параметры в мощных разрядах малой длительности.

Наиболее широкий размах за последние годы приобрела разработка широкого класса систем, которые можно объединить под общим названием магнитных ловушек. Сюда относятся различные типы так называемых «зеркальных» машин, магнитные системы с остроконечной геометрией, «Астрон» и системы, в которых плазма должна удерживаться высокочастотным полем. К этой же категории следует отнести и стелларатор, так как по основному принципу действия он не связан с квазистационарными разрядами. В магнитных ловушках функции удержания плазмы возлагаются на внешние поля, и величина P, может быть в принципе сколь угодно мала по сравнению с $H^2/8\pi$. При малой величине $8\pi P/H^2$ плазма не оказывает существенного влияния на сильное внешнее поле, и это облегчает задачу стабилизации некоторых опасных форм плазменной неустойчивости.

Рассмотрим сначала состояние экспериментальных исследований «по зеркальным» машинам. Системы, в которых плазма образуется путем инжекции и последующего захвата быстрых частиц, представлены в настоящее время «Огрой» и DCX (я говорю только о действующих установках). На Огре в течение последних лет изучался метод образования плазмы, основанный на инжекции молекулярных ионов, которые затем диссоциируют при столкновении с молекулами остаточного газа в камере. Обнаружено, что получающаяся таким путем плазма с низкой концентрацией подвержена действию характерной неустойчивости, которую, по-видимому, можно рассматривать как предельный случай желобковой неустойчивости магнитогидродинамического типа. Эту неустойчивость можно резко ослабить с помощью электрического поля. Однако даже при наличии такой стабилизации и при большой величине инжектируемого ионного тока концентрацию быстрых ионов пока удалось поднять только до уровня порядка 10^7 см^3. На установке DCX, в которой диссоциация молекулярных ионов происходит на дуге, также наблюдаются явления, свидетельствующие о наличии неустойчивости (изменение энергетического спектра и распухание области, занятой плазмой). Однако в этом случае механизм процессов, приводящих к потере устойчивости, может носить совершенно иной характер, чем в других магнитных ловушках, так как в DCX мы имеем дело с совершенно своеобразным коллективом частиц (большая ионная карусель в атмосфере привязанного к ней электронного газа).

У тех, кто в настоящее время изучает свойство ловушек рассматриваемого типа, заботы связаны не только с поисками методов подавления неустойчивости, но еще в большей степени с разработкой новых методов инжекции и захвата частиц, так как метод инжекции, основанный на диссоциа-

ции молекулярных ионов, не представляется особенно эффективным. В связи с этим полезную роль могут сыграть интересные опыты, сделанные в Олдермастоне. Речь идет об образовании атомов с высшими возбужденными уровнями в процессе диссоциации молекулярных ионов водорода.

Ионизация потока таких возбужденных атомов магнитным полем дает новый механизм захвата заряженных частиц в ловушку. Однако условия для того, чтобы такой метод захвата был достаточно эффективным, очень критические, так как вероятность ионизации должна экспоненциально зависеть от величины $\mathbf{V} \times \mathbf{H}$.

Существенное значение для выяснения важнейшего вопроса об устойчивости плазмы в зеркальных ловушках имеют тщательные исследования свойств плазмы, которые в течение ряда лет проводились в Институте атомной энергии Академии наук СССР на установке, получившей название ионного магнетрона. Плазма с концентрацией быстрых ионов порядка 10^9—10^{10}, заполняющая камеру ионного магнетрона, обнаруживает характерную неустойчивость, которая ограничивает длительность удержания частиц в магнитном поле промежутками времени порядка ста микросекунд. Анализ спектра и геометрического распределения высокочастотных колебаний плазмы показывает, что в данном случае имеет место типичный случай развития желобковой неустойчивости. Вместе с тем этот результат интересен еще в одном отношении — он демонстрирует, что грубая оценка времени распада неустойчивой плазменной конфигурации, в которой не учитывается стабилизирующее действие стенки и скорость развития деформации определяется в линейном приближении, может давать результат, на два порядка отличающийся от полученного на опыте. Это означает, что к интерпретации измерений времени удержания плазмы нужно подходить с очень большой осторожностью — благодаря действию целого ряда стабилизирующих факторов бурная неустойчивость, разбрызгивающая сгустки плазмы за время, измеряемое долями микросекунды, может превратиться в медленное рассасывание плазмы, продолжающееся десятые доли миллисекунды.

Несомненный интерес представляют исследования магнитных ловушек с динамическими полями, которые уже в течение многих лет проводятся в Ливерморской лаборатории. В этой лаборатории разработана остроумная техника обращения с плазмой, с помощью которой сгусток плазмы в несколько этапов передвигается из одного участка ловушки в другой, постепенно сжимаясь и нагреваясь. Таким путем, повидимому, удается получать плазму с энергией ионов в несколько киловольт и концентрацией частиц порядка 10^{12}—10^{13}, существующую в течение нескольких десятков микросекунд. Это, безусловно, очень ценный результат.

Вопрос об устойчивости плазмы в этих опытах пока остается открытым.

За последние годы появился ряд экспериментальных работ, посвященных исследованию удержания плазмы в ловушках с так называемой остроконечной геометрией. Магнитная система такой ловушки создает поле с силовыми линиями, имеющими гиперболическую форму. Напряженность этого поля возрастает во все стороны от центральной области, в некоторой точке, в которой $H=0$. Согласно предсказаниям теории, плазма, наполняющая такую ловушку, должна быть магнитогидродинамически устойчивой. Однако это преимущество по сравнению с системами типа обычных зеркальных машин покупается дорогой ценой. Простые соображения показывают, что заряженные частицы могут ускользать из ловушки, подходя достаточно близко к боковому краю области, занятой плазмой (она имеет форму детского волчка). Подсчет числа частиц, уходящих из плазмы таким путем (через кольцевую щель), очень сильно зависит от конкретных предположений, которые делаются при теоретическом анализе. Поэтому оценка времени удержания плазмы в ловушке с остроконечной геометрией поля может быть получена только из прямых экспериментов.

Имеющиеся до сих пор в СССР, в Англии и США экспериментальные данные по ловушкам с гиперболическим полем носят лишь предварительный характер. Метод заполнения ловушки плазмой в большинстве экспериментов один и тот же. Струя плазмы из инжектора проходит ловушку и частично захватывается в ней под действием процессов, механизм которых еще не очень ясен. В согласии с предположениями простейших теорий, оказывается, что частицы уходят из магнитной системы в радиальном направлении через кольцевую «щель». Время удержания плазмы в таких установках составляет несколько десятков микросекунд. Большинство опытов до сих пор было проделано со сравнительно холодной плазмой $T_E \sim 10$ эв, и поэтому в механизме ухода частиц могли играть определенную роль кулоновские столкновения. Следует отметить, что поведение плазмы в ловушке должно существенно зависеть от характера ее распределения в пространстве. Механизм ухода частиц может иметь совершенно различный характер в случае, когда плазма сосредоточена в объеме, из которого поле вытеснено, и в случае, когда плазма и поле перемешаны друг с другом. В проделанных до сих пор экспериментах имел место второй из указанных случаев.

Первые опыты, в которых плазменный сгусток, впущенный в ловушку рассматриваемого типа, подвергается быстрому сжатию в нарастающем магнитном поле, пока еще не дали достаточно определенных результатов, но зато продемонстрировали хорошую экспериментальную технику.

В связи с тем, что как «зеркальные машины», так и ловушки с встречными магнитными полями обладают (по крайней мере, теоретически) крупными дефектами и, вероятно, не могут служить для длительного удержания высокотемпературной плазмы, естественно возникает мысль о создании

магнитной ловушки с полями комбинированного типа, в которой должны объединиться достоинства простых систем и исчезнуть их недостатки. Простым примером такой ловушки может служить устройство, в котором к полю магнитных зеркал добавляются поля токов, текущих по металлическим проводникам, расположенным вдоль линий магнитного поля зеркальной системы симметрично относительно ее оси. Первые же опыты с этой комбинацией полей, выполненные в Институте атомной энергии, позволили обнаружить интересные факты. Оказалось, что с помощью проводников с таким расположением можно повысить время жизни быстрых частиц, примерно на порядок величины.

Одновременно с увеличением длительности удержания ионов наблюдается резкое снижение амплитуды высокочастотных колебаний в плазме. Если этот, сугубо предварительный, результат получит дальнейшее развитие, то это будет означать, что имеется эффективное средство борьбы с той формой магнитогидродинамической неустойчивости, которая представляет главную опасность для системы с магнитными пробками.

Наиболее совершенной ловушкой с комбинированными полями, очевидно, является стелларатор. Однако он представляет собой настолько сложную установку, что проведение экспериментальных работ на нем является очень нелегкой задачей. Поэтому необходимо искать также другие пути создания полей, обеспечивающих устойчивость плазменных конфигураций.

Следует сказать несколько слов о так называемой проблеме «универсальной аномальной» диффузии, которая время от времени появляется на горизонте в качестве мрачного предвестника грядущих бедствий. В настоящее время мы вряд ли можем согласиться с тем, что аномальная диффузия является неизбежным пороком плазмы, запертой в магнитном поле. Гораздо вероятнее, что она связана с характерными свойствами магнитных ловушек и зависит от тех манипуляций, которые проводятся с плазмой. Так, например, создается впечатление, что при омическом нагреве аномальная диффузия трудно устранима. Если же плазма не подвергается воздействию тока, текущего вдоль линий магнитного поля, то аномальная диффузия может полностью отсутствовать или же проявляться в сильно ослабленной форме.

Разрешите мне перейти к заключению. Проблема управляемого термоядерного синтеза по своей трудности оставляет позади все другие научно-технические проблемы, порожденные успехами естествознания в 20 веке. Эти трудности особенно резко заметны по контрасту с простотой тех физических идей, на которых основаны конкретные методы удержания и нагревания плазмы.

При оценке дальнейших перспектив наибольшую неопределенность представляет вопрос о том, какая опасность связана с различными формами неустойчивости плазмы. И вместе с тем именно этот вопрос и есть единственное по-настоящему больное место всей проблемы. Мы видим, что теоретические исследования все время обнаруживают новые механизмы возникновения неустойчивости. Вместе с тем они отнюдь не идут в сторону доказательства универсальной нестабильности плазмы. Нужно также иметь в виду, что степень убедительности всех прогнозов на устойчивость не очень велика, и поэтому практическое применение теории устойчивости дает скорее осторожные рекомендации, чем строгие правила. Хотя это и невозможно доказать, но все же создается убеждение, что при дальнейшем развитии способов нагревания и термоизоляции плазмы, известных в настоящее время, удастся, используя достаточно сильные магнитные поля, создать высокотемпературную плазму с довольно высокой плотностью, устойчивую, в первом приближении, и способную генерировать интенсивные термоядерные реакции. При этом, вероятно, величина $\beta = 8\pi P/H^2$ будет не велика. Это удастся выполнить, если разрабатываемые в настоящее время методы устранения наиболее опасной магнитогидродинамической формы неустойчивости дадут успешные результаты. Такой ход событий не будет, однако, означать достижения окончательной практической цели, а лишь преодоление первого большого барьера на пути к ней. За этим барьером нас могут поджидать другие неприятности, роль которых станет вырастать по мере того, как мы будем шагать в сторону более высоких температур. Заметим, что если в плазме существует флюктуация электрического поля, с частотой порядка 1 мегагерц при напряженности всего лишь порядка 10 вольт/см, то и этого может оказаться достаточным, чтобы свести время жизни быстрых частиц до нескольких миллисекунд.

Сейчас всем ясно, что первоначальные предположения о том, что двери в желанную область сверхвысоких температур откроются без скрипа при первом же мощном импульсе творческой энергии физиков, оказались столь же необоснованными, как и надежда грешника войти в царство небесное, минуя чистилище.

И все же вряд ли могут быть какие-нибудь сомнения в том, что в конечном счете проблема управляемого синтеза будет решена. Неизвестно только, насколько затянется наше пребывание в чистилище. Из него мы должны будем выйти с идеальной вакуумной технологией, отработанными магнитными конфигурациями с точно заданной геометрией силовых линий, с программированными режимами электрических контуров, неся в руках спокойную, устойчивую высокотемпературным плазму, чистую как мысль физика-теоретика, когда она еще не запятнана соприкосновением с экспериментальными фактами.

От имени советской делегации я хочу выразить искреннюю признательность бургомистру города Зальцбург, г-ну Беку за гостеприимство и Секретариату МАГАТЭ за хорошую организацию конференции.

CONTROLLED NUCLEAR FUSION RESEARCH, SEPTEMBER 1961: REVIEW OF EXPERIMENTAL RESULTS*

L. A. ARTSIMOVICH

ACADEMY OF SCIENCES OF THE UNION OF SOVIET SOCIALIST REPUBLICS

MOSCOW, UNION OF SOVIET SOCIALIST REPUBLICS

Mr. Chairman,

The Conference ending today has demonstrated the wide scope of research connected with the problem of controlled thermonuclear fusion. Over 250 experimental and theoretical papers have been presented as material for the Conference and for more than 30 hours a mighty stream of new scientific information has poured from this platform. The exchange of views and of data on results obtained, both in the official sessions and during the informal discussions and private conversations, has been highly intensive and the debates on scientific questions have borne a fruitful, although at times perhaps, a very forceful, character. And yet, when we assess the work of the Conference, we are forced to admit that, after many years of intensive work, all that emerges is a first, initial step towards the great goal we have set ourselves, and that as yet we are only making an approach to the main barrier blocking our entry into the desired region of ultrahigh temperatures.

Plasma heated to a high temperature very readily rids itself of accumulated heat energy by means of various instability mechanisms. In the experiments done thus far, dense plasma has been successfully contained, at relatively high temperature, for time intervals of an order of magnitude not exceeding hundreds of microseconds. Thus far, the so-called true thermonuclear reactions in plasma are still of such low intensity that they can be completely masked by various accelerating processes. As yet, there has not been sufficiently close correlation between the results of experimental research and theoretical analysis. This is especially true with respect to the extremely important subject of plasma stability. Consequently, there has been very little progress in the development of methods to overcome plasma instabilities. The responsibility for this state of affairs naturally lies primarily with the experimenters, but there are serious arguments in their defense. These are connected with the specific characteristics of the subject under study, which involves major complications in setting up and performing experiments.

The production of a sufficiently pure hydrogen or deuterium plasma is itself a difficult task since, due to interaction with the walls of the vacuum chamber, the bunches of hot plasma very rapidly become contaminated with impurity atoms and ions which are adsorbed on the surface of the walls—resulting in very high radiation losses. For example, in experiments with toroidal plasma rings, there are intense flashes of radiation from impurities, even after prolonged vacuum conditioning. This is one of the basic factors preventing a rise in plasma temperature in experiments of this kind. Very serious difficulties arise merely in the attempt to study the properties of the plasma in such annular columns, since in this case we are confronted with a characteristic uncertainty principle, by which the purity of the experimental conditions is in irreconcilable opposition to the use of diagnostic methods.

A column of plasma concealed behind metal sheaths and complex windings is, by reason of its inaccessibility and extreme sensitivity to any contact, an extremely inconvenient subject for investigation. In apparatus where the principle of operation is based on the injection of fast particles into a magnetic field, we encounter another difficulty: due to the low efficiency of the sources, the streams of particles are of relatively low intensity and therefore a very long time is required for filling the traps. During this time even comparatively weak instabilities or such phenomena as capture and loss charge-exchange in the residual gas can carry off particles from the body of the plasma, and for this reason a plasma of appreciable concentration cannot be obtained. If, however, we attempt to inject a stream of plasma into a trap, we are confronted with three problems which are as yet unresolved. Firstly, how do we ensure that trapping of the plasma takes place? Secondly, how do we transform a directed beam of particles into bunches with more or less isotropic distribution of velocities? Thirdly, how do we eliminate the neutral gas which emerges from the injector together with the plasma stream?

After these general observations, which afford some justification for the comparatively slow progress in the branch of science with which we are concerned, I shall turn to a brief and, naturally, very superficial survey of the main results achieved in the work of the last years. On the whole, with respect to the status of the problem, there can be no doubt that very great progress has been made, by comparison with the situation which was revealed at the 1958 Geneva Conference. At that time the main body of scientific information was, essentially, something that might be called a display of ideas. Most of these ideas were only thinly draped with rough

* Address (translated from Russian) given by Dr. Artsimovich at the Concluding Session, 9 September 1961.

and insufficiently verified experimental data, exploratory in character. By contrast, we can now point in nearly every part of the general thermonuclear program to a large number of carefully executed experimental studies and to valuable and reliable results which, in the aggregate, constitute a sufficiently reliable foundation for a substantial acceleration in the rate of research in the future.

It is significant in this connection that the stock of fundamental physical conceptions has remained practically unchanged. During the past three years not one essentially new method for obtaining a high-temperature plasma has been proposed. At the same time there has been a noteworthy shift of emphasis in the efforts to develop the various trends within the overall program. In the initial stage of work on the problem of controlled thermonuclear reactions, much attention was paid to experimental investigation of the simplest method of obtaining high temperatures. The basis of this method is the use of linear impulse discharges of very great magnitude and very short duration. This is what is known as the fast linear pinch. The efforts devoted to investigating the fast pinch enabled all concerned even before the Geneva Conference, to get a clear picture of the phenomena taking place in discharges of this type and to discover the basic mechanism underlying the dynamics of a plasma column. As is known, this mechanism consists in the acceleration of the plasma under the action of electrodynamic forces. One of the most interesting features characteristic of processes of this type is the appearance of hard radiation, consisting of neutrons in a deuterium plasma, and of gamma rays. At present, we know that in typical experimental conditions the hard radiation is due to accelerating processes caused by a particular form of instability characteristic for high intensity plasma columns. The main role in the appearance of fast positive ions, and therefore of neutrons as well, is apparently played by instabilities of the "sausage" type, whereas a helical instability, connected with the tendency of a plasma column to form so-called force-free configurations, is responsible for the appearance of fast neutrons. Although plasma temperatures of over one million degrees were obtained in experiments with linear pinches, it soon became clear that serious consideration could hardly be given to this method as a practical means of obtaining intensive thermonuclear reactions on a scale which was of technological interest. For this reason, interest naturally shifted to the study of systems of a somewhat different type, in which a rapid compression of plasma takes place under the action of a rising external field. The processes in question have been named theta pinch processes.

In the theta pinch effect, a maximum concentration of magnetic energy is obtained in small volumes. For this reason, the compression of the plasma by an external field is a considerably more efficient method than linear discharge for producing high temperatures. In view of the comparative simplicity of the experimental apparatus involved and the alluring prospects of research in this field, investigation of the properties of the theta pinch effect has, during recent years, become one of the most popular subjects in the whole range of controlled fusion research. Sufficient evidence of the interest in this trend is provided by the number of papers presented at the present Conference: i.e. twenty, as compared with two or three at Geneva. If things go on this way, we shall soon come nearer to the realization of the slogan: "Every housewife should have her own theta pinch".

The basic facts established by research on theta pinches can be summarized as follows. In processes of this kind within a dense cylindrical layer of plasma under compression, the trapped magnetic field is generally maintained in a direction opposite to that of the forces pressing against the external surface of the plasma. The work of the forces of magnetic compression is spent, in the initial stage of the process, mainly in accelerating the ions, and relaxation of the trapped internal magnetic field can make a substantial contribution to the heating of the electron component, although this is not entirely clear to me personally. The theta pinch is not a stable plasma process. This is especially clear from photographs of plasma luminescence, obtained by means of high-speed streak cameras. In a plane perpendicular to the lines of force, the lump of plasma undergoing compression resembles an ink blot or a resting octopus with a hole in the middle. We are dealing here with a typical case of a magneto-hydrodynamic instability of the so-called flute type. It is due, in the first place, to the fact that in the processes of rapid compression and of subsequent radial pulsations, the plasma undergoes strong acceleration; and in the second place, to the fact that, the lines of the field have an unfavorable form which is convex. Despite the inadequate agreement between the data cited by various authors, it can nevertheless be assumed that, in the installations with maximum parameters built at Washington, D.C., and Los Alamos, plasma bunches having a concentration of about 10^{16} cm^{-3} and a temperature in the region of 1000 eV can be obtained for periods of the order of a few microseconds. I do not wish to deal here with the question of the nature of the neutron radiation observed in some cases of fast compression of a deuterium plasma because this problem is of interest only as a sport. I would point out that if any of the fortunate persons who have observed this effect have brought with them to Salzburg a small handful of pure neutrons formed, on the average, during one discharge, there would hardly be enough of them to give one neutron apiece as a souvenir to the inhabitants of hospitable Austria.

It must be recognized that in spite of the many valuable studies on the properties of the theta pinch which have been done in the United Kingdom, the Soviet Union, the United States and elsewhere, the nature of these processes continues to be rather obscure in many respects. This applies to the

mechanism of relaxation of the internal trapped field, to the causes for the rotation of the plasma bunch, to the escape of particles, and so forth. Nor do we know whether we can count on being able in the future, by means of fast compression and without substantial changes in the form of the magnetic field, to obtain a sufficiently stable lump of hot plasma. When we analyze the prospects of this line of investigation, we must bear in mind that at present there are available no methods permitting the creation of denser bunches of hot plasma than those obtained in devices of the theta pinch type. It may be assumed that during the next few years experimental research on ultrahigh-speed compression of plasma by a rising field will be continued, although there seems to be little probability that there are any independent practical prospects for it under the thermonuclear program.

A traditional part of the thermonuclear program is research on the so-called quasi-stationary discharges or slow discharges in toroidal chambers. There have thus far been two main trends in this connection. The first proceeds from the idea of creating a paramagnetic plasma column with a current which incorporates within itself a longitudinal magnetic field of comparatively low intensity. As you know, this idea has been realized in the "Zeta", "Alpha" and "Sceptre" installations. The second trend is based on the idea of stabilization of a toroidal discharge by a longitudinal field many times greater than the magnetic field of the current. Installations belonging to the "Tokamak" family are material embodiments of this principle. Essentially, the Stellarator can also be included in the same category, if it operates under ohmic heating conditions.

Let us consider the situation which has developed with respect to the first of the above-mentioned trends. Even from the papers which the people from Harwell and Aldermaston read at the Geneva Conference it was clear that a paramagnetic plasma column falls victim to instability. Subsequent work done both in the United Kingdom and in the USSR on the "Alpha" assembly has confirmed these initial conclusions. However, this should not lead—and in fact has not led—to abandonment of the work. The experiments have been continued and have yielded valuable data concerning the behavior of paramagnetic columns and the properties of the plasma forming them. We shall refer here to the most significant results. Owing to the low value of kinetic pressure in a plasma column, a force-free magnetic field geometry is formed, i.e. the current everywhere flows almost exactly along the line of the resulting magnetic field. Let us note, *inter alia*, that under a quasi-stationary condition such a field and current configuration is equivalent, formally, to a state of maximum anisotropy of electrical conductivity. Under comparatively low power conditions, the energy introduced into the plasma from the electrical supply escapes in the form of impurity radiation, but under higher voltage systems it is ejected onto the wall as streams of particles.

Spectroscopic measurements made on all three of the above-mentioned assemblies are in complete agreement on one point: they show that the average ion energy in the discharge is considerably higher than the thermal energy of the electrons. As regards the dependence of the ion energy on charge Z and mass m, there appears to be no unanimity of views. The measurements done at Harwell, as far as I can understand them, would appear to show that the ion energy increases in proportion to mass and is practically independent of charge. The experiments with "Alpha" yield a substantially different result, indicating that the energy of multiply-charged ions is approximately proportional to Z and not very strongly dependent on mass. The origin of the fast ions has not yet been clarified. A very interesting effect is the anomalous resistance which is found in "Zeta" and which apparently plays an important part in the general course of the process at low starting pressure of gas in the chamber. The responsibility for the sharp increase in the resistance of the plasma can be assigned, *a priori*, to the most varied forms of instability. However, it is very far from this to a real explanation. In spite of the large volume of important and interesting scientific information presented to the Conference by the various laboratories conducting research on paramagnetic plasma columns, there is a growing impression that this trend is approaching a point at which the source of fresh data will be exhausted.

In discussing the results of the work done on assemblies of the "Zeta" type, we must not fail to point out that it has inspired the development of a number of new methods of plasma diagnostics. One of the most brilliant achievements in this field during recent years has been the method developed at Harwell for the measurement of plasma radiation for wavelengths in the sub-millimeter range. Another undoubted diagnostic achievement is also the delicate technique for measuring the energy spectrum of plasma particles which was developed at Leningrad and used with "Alpha".

Thus far, only the initial stage has been reached in the study of the processes of ohmic heating of a plasma in a strong magnetic field. It has been established that where the ratio H_z/H_φ (H_z-intensity of the longitudinal field, H_φ-intensity of the field of the current) is sufficiently high, the indications of gross instability disappear. At the same time it has been found that the diffusion of a plasma across the lines of force in such systems is anomalous in character, the coefficient of diffusion exceeding by many orders the value according to classical theory and approaching the terminal value given by the heuristic formula of Bohm. The anomalous diffusion results in a very rapid escape of particles from the plasma column and, in existing installations, limits the period of its existence, at best, to a few hundred microseconds. However, there are some experimental facts which indicate that measurement of the speed of particle escape describes the behavior only of the peripherical regions of a plasma ring

in a toroidal chamber, while inside this ring there exists a denser core in which the concentration of particles is maintained at a fairly high level, $10^{12}-10^{13}$ cm^{-3}, over extended periods of time. The true mechanism of the process which is the cause of anomalous diffusion in systems of the Tokamak and Stellarator type is a subject for discussion at present. Theory can offer a number of possible explanations for this phenomenon: magnetohydrodynamic instability of higher modes; the instability characteristic of plasmas with inhomogeneous temperature distribution, generation of ionic sound waves, etc. However, the available experimental data are still insufficient to justify a final choice between these possibilities. The entry into operation of the C-Stellarator—an event for which the congratulations of us all are due to the scientists and engineers working at Princeton—will probably speed up considerably the output of information necessary for finally elucidating the mechanism behind anomalous diffusion which occurs during the ohmic heating of a plasma.

It is unlikely that there are any grounds for hoping that it will be possible, merely by ohmic heating in Stellarator-type systems, to raise a plasma to thermonuclear temperatures. However, it is not out of the question that this method of creating a hot plasma may be very useful in the first stage, when the temperature is rising to the few hundred electron volt level. Research on quasi-stationary discharges in a strong magnetic field is undoubtedly of value also from the point of view of plasma physics. In discharges of this kind, the plasma with a high concentration of charged particles appears to us for the first time as an object of sufficiently well-defined geometrical form, free of the catastrophic deformations which, within a few microseconds, modify all the parameters in powerful discharges of short duration.

During recent years there has been a very great increase in the development of a broad range of systems which can be classified under the general heading of magnetic traps. This designation applies to various types of so-called mirror machines, magnetic systems with a cusped geometry, the "Astron" device, and systems in which the plasma must be contained by a high-frequency field. The Stellarator must be assigned to the same category, since according to the basic principle of action it is not connected with a quasi-stationary discharge. In magnetic traps, the functions of containing the plasma are transferred to the external fields and the value of p can in principle be as low as desired compared with $H^2/8\pi$. At a low value of $8\pi p/H^2$, the plasma does not exert an appreciable effect on a powerful external field, and this facilitates the task of stabilizing some dangerous forms of plasma instability.

Let us first consider the status of experimental research on mirror machines. Systems in which the plasma is formed by injection and subsequent trapping of fast particles are represented at present by "Ogra" and "DCX". (I am referring here only to assemblies actually in operation). During recent years, studies have been made on "Ogra" of a method of plasma formation on the basis of injecting molecular ions which then dissociate upon collision with the molecules of residual gas in the chamber. It has been found that the low-concentration plasma thus formed is subject to the action of a characteristic instability which can be considered as an extreme case of a flute instability of the magnetohydrodynamic type. This instability can be sharply attenuated by means of an electric field. However, even with such stabilization and with a high value of injected ion current, it has not been possible thus far to raise the concentration of fast ions above a level of the order of 10^7 cm^{-3}. In the "DCX" installation, where the dissociation of the ions takes place in an arc, we also observe a phenomenon testifying to the presence of an instability, i.e. a change in the energy spectrum and expansion of the region occupied by the plasma. In this case, however, the mechanism of the process leading to the loss of stability can be entirely different in nature from that in other magnetic traps, since in "DCX" we are dealing with a quite unique collection of particles: a large ion whirligig in an attached atmosphere of electron gas.

Those who are at present studying the properties of traps of this kind are concerned not only with research on methods of suppressing instability but even more with the development of new methods of injection and trapping of particles, since the injection method based on the dissociation of molecular ions is not especially effective. An important part may be played in this connection by the interesting experiments made at Aldermaston. These have to do with the formation, in a process of dissociation of molecular hydrogen ions, of atoms having higher excited levels. The ionization of a stream of such excited atoms by a magnetic field affords a new mechanism for the capture of charged particles in a trap. However, the conditions necessary for such a method of capture to be sufficiently effective are very critical, since the probability of ionization is exponentially dependent on the vector product of the speed of the particles and the intensity of the magnetic field.

A factor of considerable importance in the further clarification of the extremely important question of plasma stability in mirror traps would appear to be the careful research on the properties of plasma which has been carried on for a number of years at the Atomic Energy Institute of the USSR Academy of Sciences, using an apparatus which has been called the ion magnetron. A plasma having a fast ion concentration of the order of 10^9–10^{10} cm^{-3}, when it fills the chamber of the ion magnetron, displays a characteristic instability which limits the length of the containment time of the particles by the magnetic field to a duration of the order of 100 μs. Analysis of the spectrum and geometrical distribution of the high-frequency oscillations of the plasma show that what takes place is a typical case of the development of a flute instability. This result is also interesting in another respect. It shows that a rough estimate of the decay time of an unstable plasma configuration, in which

no account is taken of the stabilizing effect of the walls and in which the speed of development of the deformation is determined in linear approximation, can yield a result which differs by two orders of magnitude from that obtained experimentally. This means that very great caution must be exercised in interpreting measurements of plasma containment time. Because of a number of stabilizing factors, a violent instability, ejecting bunches of plasma during a period of fractions of a microsecond, can be transformed into a slow decay of plasma lasting tenths of a millisecond and even longer.

A matter of undoubted interest is the research on magnetic traps with dynamic fields, which has been going on at the Livermore laboratory for many years. A very elaborate technique for handling plasma has been developed there. By means of this method, a bunch of plasma is moved in a number of stages from one part of the trap to another, being gradually compressed and heated. In this way it is possible to obtain a plasma having an ion energy of a few kilovolts and a particle concentration in the order of 10^{12}–10^{13} cm^{-3}, which exists for a duration of a few decades of microseconds. Of course, the question of the stability of the plasma in these experiments still remains open.

In the last few years a number of experimental papers have appeared, devoted to research on the confinement of plasma in traps of so-called cusped geometries. The magnetic system of this type of trap creates a field with lines of force which have hyperbolic shape. The magnetic field strength increases with distance from the central zero field region ($H=0$) in all directions. According to the predictions of theory the plasma filling the trap must be magnetohydrodynamically stable. This advantage over the usual mirror machines, however, is purchased at heavy cost. Simple considerations indicate that charged particles may slip out of the trap and approach fairly close to the lateral edge of the area taken up by the plasma—it is the shape of a child's top. An estimate of the number of particles leaving the plasma through the ring cusp in this way depends very considerably on the specific assumptions made during theoretical analysis. An estimate of the time the plasma is confined in a trap with a field of cusped geometry can therefore be obtained only by direct experiment.

As regards traps with hyperbolic fields such experimental data as have so far been obtained in the USSR, USA and United Kingdom are provisional in character. The method of filling the trap with plasma is the same in the majority of experiments. The stream of plasma from the injector passes into the trap and is partly captured in it in consequence of processes the mechanism of which is not yet quire clear. According to the assumptions made in the simplest theories, it appears that particles from the magnetic system leave in a radial direction through the ring cusp. The time the plasma is confined in such devices is some tens of microseconds. It is characteristic that confinement time apparently increases with an increase in the size of the trap. Until now, the majority of experiments have been carried out with comparatively cold plasma with an electron temperature of approximately 10 eV, so that Coulomb collisions could also play an important part in the process of particle loss. It should be remarked that the behavior of the plasma in the trap must very substantially depend on the nature of its distribution in space. The mechanism of particle loss may be entirely different, depending on whether the plasma is concentrated in a volume from which the field has been expelled or whether the plasma and the field are mixed up together. In the experiments which have so far been performed. the latter case has occured. The first experiments, in which a plasma bunch let into a trap of this type was subjected to swift compression in an expanding magnetic field, have not so far yielded conclusive results, though they have demonstrated a good experimental technique.

The fact that both mirror machines and traps with opposing magnetic fields possess, at least theoretically, considerable defects and probably cannot be used for the prolonged confinement of high-temperature plasma leads us naturally to the idea of creating a magnetic trap with fields of composite type, in which the merits of the simple systems would be brought together and their defects disappear. A simple example of such a trap might be a device in which fields formed by metallic conductors, symmetrically disposed along the lines of the magnetic field of the mirror system itself, are added to the magnetic mirror field. The first experiments with such composite fields, which were carried out in the Institute for Atomic Energy, have revealed a number of interesting facts. It was found that by using conductors arranged in this way, the life of fast particles could be increased, by approximately one order of magnitude. Simultaneously with the increase in duration of confinement of the ions an abrupt decrease in amplitude of the high-frequency oscillations was observed. If this strictly provisional result is confirmed in further work, it will imply that an effective method exists for dealing with the form of magnetohydrodynamic instability, which represents the main danger for systems with magnetic mirrors.

The stellarator is obviously the most perfected trap with composite fields. It does however represent so complicated a piece of apparatus that it is by no means simple to carry out experimental work in a stellarator. It is therefore necessary to look for other ways of creating fields which will ensure the stability of plasma configurations.

A few words should be said on the so-called problem of universal anomalous diffusion as a whole, or turbulent diffusion, which every now and then appears on the horizon as a harbinger of disaster. At the present time we can hardly agree that anomalous diffusion constitutes an inevitable defect in plasma enclosed within a magnetic field. It is much more probable that it is connected

with the characteristic properties of magnetic traps and that it depends on the way in which the plasma is handled. It seems, for instance, that in ohmic heating anomalous diffusion is difficult to eliminate, whilst for plasma not subject to the influence of a current produced by an external field, it may not appear at all. If the plasma is not subjected to the effect of a current flowing along the lines of the magnetic field, then the anomalous diffusion may be completely absent or manifest itself in a weakened form.

Allow me to conclude. By reason of its difficulty, the problem of controlled thermonuclear fusion takes precedence over all other scientific and technical problems raised by the successes of natural science in the twentieth century. These difficulties are particularly noticeable in contrast with the simplicity of the physical ideas upon which the specific techniques of confining and heating plasma are based.

In evaluating future prospects the point that gives rise to the greatest uncertainty is the nature of the danger connected with various forms of plasma instability. And, indeed, it is this question which at present is the only sore spot in the whole problem. We see how those engaged in theoretical research are continually discovering new processes by which instability can arise. Yet that does not by any means mean that they have proved the universal instability of plasma. It must also be borne in mind that the degree of conviction inherent in all instability prognoses is not very great and the practical application of the theory of stability therefore involves cautious recommendations rather than strict rules. Although it is impossible to prove this, the conviction is ever growing that, once the existing techniques for the heating and thermal isolation of plasma are further developed, it will be possible, using sufficiently strong magnetic fields, to create a high-temperature plasma with a sufficiently high density—stable in the first approximation and capable of generating intense thermonuclear reactions. Probably in this case the β-value equals $8\pi p/H^2$. Achievement of this aim will depend on bringing to a successful conclusion the work that is at present being done on methods of eliminating the most dangerous magnetohydrodynamic instability. This will not mean, however, that the final goal has been reached in practice but only that the first great obstacle in the way to it has been overcome. Other unpleasant surprises may be lying in wait for us beyond that obstacle, and their importance may increase as we progress towards higher and higher temperatures. It should be borne in mind that if fluctuations of the electric field exist in the plasma with a frequency, let us say, of the order of 1 MHz, and a strength of the order of only 10 V/cm, this may prove sufficient to bring the lifetime of the fast particles down to some milliseconds.

It is now clear to all that our original beliefs that the doors into the desired region of ultra-high temperatures would open smoothly at the first powerful pressure exerted by the creative energy of physicists, have proved as unfounded as the sinner's hope of entering Paradise without passing through Purgatory. And yet there can be scarcely any doubt that the problem of controlled fusion will eventually be solved. Only we do not know how long we shall have to remain in Purgatory. We shall have to leave it with an ideal vacuum technology, with the magnetic configurations worked out, with an accurate geometry for the lines of force and with programmed conditions for the electrical contours, bearing in our hands the high temperature plasma, stable and in repose, pure as a concept in theoretical physics when it is still unsullied by contact with experimental fact.

On behalf of the Soviet delegation, I thank the Authorities of the Province and City of Salzburg, and also the Secretariat of the International Atomic Energy Agency for the excellent organization of this Conference.

CONTROLLED NUCLEAR FUSION RESEARCH, SEPTEMBER 1961: REVIEW OF THEORETICAL RESULTS*

M. N. ROSENBLUTH

GENERAL ATOMIC DIVISION OF GENERAL DYNAMICS CORPORATION

SAN DIEGO, CALIFORNIA, UNITED STATES OF AMERICA

Mr. Chairman, Delegates:

The only thing remaining to be understood after Professor Artsimovich's clear and incisive summary is whether or not we theoreticians are to be left behind in Purgatory. In any event, I hope it will not be too much of an anticlimax for you to now spend a few minutes in the pleasant Eldorado of plasma mathematics in which we theorists usually live, being only occasionally brought face to face with the harsh world of the experimentalist.

Before beginning, however, I would like to take the opportunity to thank those responsible for the wonderful atmosphere of this Conference. To Director General Cole and to Dr. Buras and the Secretariat I can only say that we have not only been made to feel welcome and comfortable but have to some extent been reinfused with a sense of the importance of our work on peaceful nuclear fusion. We know that organizing such a meeting is a difficult task and we thank you for your efforts.

As for our local hosts in this fairyland city of Salzburg it is sufficient to say that the charm and beauty of your town has been well matched by the cheer and helpfulness your citizens have displayed towards us and by these most excellent Congress facilities.

Finally it is impossible not to notice the violent contrast between the grim headlines we have been reading all week and the atmosphere of almost complete cordiality and co-operation which has existed here. It is certainly true that information has been exchanged freely and in a spirit of friendship and helpfulness by the workers of all the many nations here. In fact, as will unfortunately become apparent in my talk, my difficulty is in quite the opposite direction, namely, that the brief time span has made it impossible to digest the great mass of interesting work which has been presented here. In particular, I must apologize in advance for the fact that I am obviously most familiar with the work of my American colleagues, especially in the experimental area, and probably will weight it more heavily than it deserves.

Since any one of the theoretical papers here has, of course, been overflowing with long equations, it is obviously impossible to discuss all this diverse work in any great detail. I am afraid you will have to be content with a fairly platitudinous discussion of the broad trends which I have detected in the thinking here. To make what I am afraid is an untranslatable joke, I must again resort to "the random phrase approximation".

If we begin on the most fundamental level—the plasma as a many-body problem—, it is perhaps worth noting that there now appears to be almost universal acceptance of the Boltzmann equation as an adequate description of a plasma. Many workers have shown how it may be derived by a modification of the Boguliubov, Born, Green, Kirkwood and Yvon techniques so that, in the limit as one passes to a completely fluidized plasma (i.e., one in which $n\to\infty$, $e\to 0$, $m\to 0$, and ne, nm, v are constant) one obtains, as the basic working equation, the collisionless Boltzmann, or Vlasov equation, with the Fokker-Planck correction needed for estimating thermalization, transport, radiation, etc.

Another fundamental subject which appears to have been given a good foundation in the past few years is that of single particle motion, at least for slowly varying electromagnetic fields. Here the remarkable theorems of Kruskal and others concerning the constancy to all orders of the adiabatic invariants of particle motion allow us at least to show the existence of confined plasma—equilibrium states in the collisionless approximation.

And it is, of course, at this point that the real difficulties of the subject begin. It must always be kept in mind that what we are attempting in controlled fusion work is to keep a plasma for a long time in a state of non-thermodynamic equilibrium. To begin with, of course, the plasma is out of equilibrium with the radiation field, the latter having a completely intolerable specific heat at thermonuclear temperatures. Fortunately, there appears to be no reason to expect any surprises in the frequency region well above the plasma frequency—except for the question of impurities, which I think will eventually prove to be the greatest difficulty in the entire thermonuclear business, but fortunately is not for the theoretician to worry about. In the region of lower frequencies, where one expects black body radiation, it appears that we can tolerate at least in a DT reactor the levels, the equilibrium levels that is, of cyclotron radiation to be expected.

Next we turn to what Dr. Artsimovich has said is the fundamental question and certainly the much more difficult question of the stability, within the

* Address given by Dr. Rosenbluth at the Concluding Session, 9 September 1961.

framework of the Vlasov equation, of possible quiescent plasma states. Most work here has been based on the study of rather drastically simplified cases —either an infinite homogeneous plasma, or a perturbation covered by the adiabatic conditions R_L/L, ω/Ω, $\omega/\omega_p \ll 1$ (R_L = Larmor radius, L = characteristic distance in the plasma, ω = frequency, Ω = cyclotron frequency, ω_p = plasma frequency) for which the hydrodynamic approximation is valid.

It is perhaps worthwhile to digress at this point and mention a formal theorem, suggested by Krall and myself and proven by Francis Low, concerning the validity of such approximate calculations. The question is the following: Suppose we find that our approximate plasma is indeed stable so that, to lowest order in the approximation, there are various modes of oscillation characterized by real frequencies ω_0. How do we know that in a more exact calculation with $\omega = \omega_0 + \varepsilon\omega_1 + \ldots$, the various higher terms $\varepsilon\omega_1$, etc., might not be complex, yielding possible instability? Since the parameters $\varepsilon = R_L/L$ etc. are in fact not very small in cases of practical interest, such overstable growth would be catastrophic. Low, in fact, demonstrates that all higher terms are real in the following way. The system of Maxwell equations and particle equations is evidently Lagrangian in character, so that the equations of plasma motion can be derived variationally from a Lagrangian $\mathcal{L}$, as we have heard earlier from Dr. Newcomb and Dr. Cotsaftis:

$$\mathcal{L} = \int d^3\mathbf{x}\, d^3\mathbf{v}\, \{\dot{\xi} O_1 \dot{\xi} + \dot{\xi} O_2 \xi + \xi O_3 \xi\},$$

where ξ is the displacement in phase space due to the perturbation, and where the various operators O are, for steady-state equilibria, functions only of the phase-space variables $\mathbf{x}$ and $\mathbf{v}$, and not explicitly of the time. This being the form of the Lagrangian, it is easy to see that, if we write the equations of motion by performing the variation with respect to ξ, assume $\xi \sim \exp(i\omega t)$, multiply by ξ^* and integrate over phase space, we can then derive an expression for the frequency of the following type:

$$\omega = \frac{-\beta \pm \sqrt{\beta^2 - 4\alpha\gamma}}{2\alpha},$$

which comes directly from solving a quadratic equation. The coefficients α, β, γ are positive-definite, quadratic, real functionals of the displacement ξ. This being the case, we see that if we pass from our original approximate calculation to the more exact calculation, what we will have done is make small changes in the parameters α, β, γ. Therefore we will not change the reality properties of the eigenfrequency ω. If our approximate calculation showed stability, then the more exact calculation, at least in a small neighborhood of the approximate calculation, will also indicate stability. In fact, it can easily be seen that if we exclude the unexpandable resonance terms of the Landau type, then the frequency is real to all orders in ε, where ε is the small parameter describing the effects, for example the finite Larmor radius effects, neglected in the approximate calculation.

An example of this theorem is provided by the study of non-Maxwellian infinite homogeneous plasmas. As is well known, there is a vast array of the so-called micro-instabilities which occur in this case. However, they are all characterized by one of two mitigating features. Either, first, the anisotropy must reach a certain definite critical value before instability sets in, as in the mirror instability; or, second, for small anisotropy the instability is of the Landau resonance type with extremely small growth rate, as in the Alfvén-wave instability. I believe it follows from Low's theorem that one would expect this type of behavior.

This leads one to hope that in the neighborhood of true thermodynamic equilibrium there must indeed exist a finite region of effective stability, in which we can hope to put our plasma devices. Needless to say, as we have heard from Dr. Artsimovich, this region may be rather difficult to reach when we consider the difficulties of plasma injection and stability. But that's not my problem.

One must recognize, of course, that all such expansion procedures are fraught with some dangers. For example, as I have discussed in my paper, the expansion on which hydromagnetics is based assumes that R_L/L and ω/Ω are of the same order of smallness. If we consider cases for which $\omega/\Omega \sim (R_L/L)^2$, cases which are often of practical interest, then new phenomena may occur. For example, the separation of ions and electrons may give improved stability to the flutes. On the other hand, there now arises the possibility of completely new types of waves. For example, we have heard at this conference of the possible existence of drift waves in inhomogeneous magnetic fields, for which the phase velocity of the wave, ω/k, is of order v_D, the drift velocity characterizing the magnetic field. This sort of drift velocity, of course, does not occur in the homogeneous case at all, so that what we have to expect here is a totally new type of wave. These have been investigated by various workers and are characterized by the fact that, under these conditions of resonance between the drift velocity and the phase velocity, particles are no longer tied to the magnetic field lines, as they are in the hydromagnetic approximation, but are able to drift across the field lines under the influence of this resonance. Various instabilities of this type have been studied and discussed at the micro-instability session. While this study is still in its infancy, I think the following statement can be made: almost all of these instabilities are very slowly growing, the growth rate depending, for example, on m_e/m_i, the ratio of electron mass to ion mass, except for the convective thermal instabilities, first discussed by Tserkovnikov and further elaborated by Velikhov at this conference, which are somewhat analogous to the familiar stellar gravitational instabilities. Fortunately, these convective instabilities seem to be unstable only for relatively large temperature gradients and may perhaps be possible to avoid.

Needless to say, we would indeed be happy if our present laboratory plasmas were well enough confined to study such subtle effects.

To pass now to the more usual theory based on the hydromagnetic equations and the energy principle, I think we can now say that this field is fairly well understood. It has certainly been verified in many cases, such as the pinch, that violation of these stability requirements quickly leads to disaster. Moreover, we have heard at this conference the excellent agreement with experiment which has been obtained in the numerical calculations of Hain and others using the hydromagnetic model with simple transport coefficients, indicating again that these are valid equations for studying a wide range of conditions.

Another formal point which perhaps should be made is that in the last few years many people have demonstrated theoretically that confined stable, that is stable in the hydromagnetic approximation, systems can indeed be found. Of these systems I believe that only the linear hard-core pinch (which is not really well confined because of end losses) has been thoroughly experimented with. I will return to this later. It will be quite interesting to see the developments of the next few years with cusps, levitrons and modified mirror machines of the sort reported on by Dr. Ioffe. Certainly the few preliminary indications we have are encouraging.

The rest of the points which I would like to discuss may perhaps best be considered in relation to three major experimental paradoxes which appear to exist today and which are as yet only incompletely understood:

(1) Why are hard-core pinches unstable? According to hydromagnetic theory they should be totally stable, but as we have heard from Dr. Bickerton and Dr. Colgate, in fact they are not.

(2) How do we explain stellarator pumpout and its apparent agreement with Bohm's old conjecture about diffusion? You recall the famous Bohm diffusion coefficient, which, like Fermat's last theorem, written down but never explained: $D = ckT/eB$.

(3) How do we explain the fact that flute instabilities apparently are sometimes effectively suppressed in mirror machines and perhaps in theta pinches?

The hard-core instability is almost certainly a finite-conductivity effect. From the example of hydrodynamic flow instability we must be prepared for the possibility that the introduction of dissipative terms may lead to new types of instability. Moreover, the fact that these difficulties do not apparently show up in the theta pinches suggests strongly that they are connected with electric fields parallel to the magnetic field. We have heard two theories about this here. First is the Kadomtsev theory, which has had such striking success in explaining the positive-column results. Second is the Bickerton theory based on the conventional fluid equations with finite conductivity. One point which evidently needs further investigation is the relationship, if any, between these two theories. At first sight they appear quite different in the important respect that, in the limit of high conductivity σ, Kadomtsev's growth rate goes like $1/\sigma$, in other words very small, and Bickerton's like $1/\sqrt{\sigma}$. Under thermonuclear conditions Kadomtsev would be tolerable and Bickerton would not. I believe that in situations where the magnetic field is not greatly disturbed by the plasma then the behavior $\sim 1/\sigma$ prevails. On the other hand if there is a large reservoir of magnetic energy due to a sheared field which is produced by plasma currents parallel to **B** then one should expect the more dangerous $1/\sqrt{\sigma}$ dependence.

Passing on now to the stellarator question, there are again two hypotheses which have been made to explain the initial instability leading to pumpout. The first and probably correct one is again the Kadomtsev positive-column theory. The second is the excitation of microinstabilities, such as unstable ion-acoustic waves. These instabilities no doubt exist and are present in stellarator devices, but the quasilinear theories of Velikhov and Drummond lead us now to expect that they would not cause large diffusion. I now plot the particle distribution functions for the ion-acoustic waves, see Fig. 1. The electron distribution f_e is very broad (I am not drawing it to scale) and displaced slightly to one side of the ion distri-

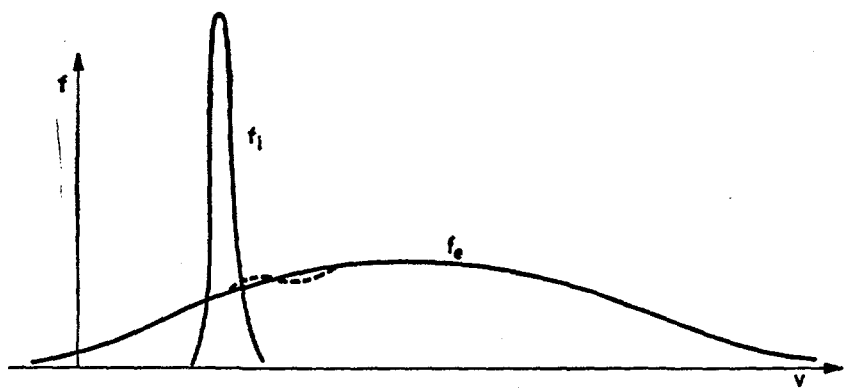

Fig. 1

bution f_i, since it is carrying a current. Now, what the quasilinear theory tells us is that the only effect of the instability is a little flattening of the electron distribution in the neighborhood of the ion sound speed (*see broken line on figure*). Therefore the small amount of kinetic energy removed from these electrons is converted into fluctuating electrostatic energy. If one then makes the relatively trivial calculation of how much diffusion one would expect from the fluctuating field at this frequency, it is easy to see that it is much too small to explain the existence of pumpout. In fact, in general I think we can infer from those quasilinear theories that many of these resonance instabilities will be much less troublesome than we had feared.

How do we explain the apparent agreement with Bohm diffusion? I would say that only one really serious attempt has been described here to understand the turbulent plasma—the remarkable work of Kadomtsev—which however does not yield the Bohm diffusion, although order-of-magnitude agreement has been obtained in many other situations. Frankly, the Kadomtsev theory is much too subtle and difficult for me to understand on such short acquaintance. I hope, however, that I may be excused for remarking that even the hydrodynamic turbulence theory contains within it many heuristic elements such as the concept of mixing length, which can only be justified by incorporating many empirical results. In view of the incomplete analogy between plasma physics and hydrodynamics, I am afraid that a completely successful theory of plasma turbulence is more than we can expect in the next few years. Nonetheless, even such an approximate theory provides a most invaluable link between theory and present day experiment. For example, as you have heard, the work of Kadomtsev has provided a very useful interpretation of Dr. Ioffe's experiments.

It is easy, of course, to make rough arguments leading to the Bohm diffusion. For example, Dr. Taylor has pointed out that if we assume the turbulent waves are of such a character that their time of coherent interaction with the ions is less than an ion cyclotron period, then we recover the well known diffusion coefficient: $D \sim (v^2 \tau)/[1 + (\Omega \tau)^2]$, where τ is now the effective collision time for an ion with the waves. The maximum value as a function of τ is just the Bohm diffusion coefficient. Another simple dimensional argument may easily be given for a low-β plasma. In a low-β plasma the magnetic field must remain unperturbed in any motion which takes place, so the perturbation is described by an electrostatic potential φ; and we can say that φ is limited in amplitude by the following relationship: $e\varphi < k T_e$. This must be so because of the possibility of electrons moving freely along the magnetic lines of force. If such a potential exists, then it leads to a drift across the magnetic field given by the usual formula $v = cE/B$, which becomes, when we substitute our maximum value for the electrostatic potential, $v \approx c\,(k T_e)/(e B \lambda)$, where λ is the wavelength of the perturbation. Now, if we take over from hydrodynamics the concept that the mean free path of an eddy is essentially the same as the eddy size λ (remember that λ is the wavelength perpendicular to the magnetic field), then we recover for the diffusion coefficient $D = \langle \lambda v \rangle = D_{\text{Bohm}}$. So perhaps some such argument as this could explain the Bohm diffusion. Needless to say, this type of reasoning is only dimensional analysis, which we would not consider seriously were it not for the stellarator evidence which is forcing us to think about such problems. Again, however, I must reiterate that the fundamental task for fusion is not to understand turbulence but to prevent it—which may be even more difficult.

Finally we come to the question of the mirror machine. Even though Dr. Coensgen's new results are most discouraging, we cannot overlook the fact that in the old Table Top experiments of Post, in the case of hot electrons, neither the flute instability nor the Bohm anomalous diffusion were observed over long periods of time. Further encouragement may perhaps be taken from the considerable stabilization accruing from the application of end potentials on the Ogra device, and also from the good behavior of theta pinches, which in at least some cases apparently remain stable for anomalously long times. To what do we attribute this pleasant deviation from theory? Perhaps finite Larmor radius effects, finite gradient effects and rotation effects play a role, as well as some properties of the as yet not understood sheath which must exist toward the outside of such a confined plasma. Nonetheless, I believe the bulk of evidence still supports the idea that the principal stability arises from electrical contact provided by cold plasma in the exterior region between the trapped plasma and the conducting walls, thereby shorting out and preventing the interchange. Strong support for this idea comes from the natural radiation belts around the earth, where the ionosphere of course plays the role of external conductor. Perhaps if we learn to imitate Nature here we will also be able to duplicate her success with fusion devices, though of course she has a few principles like gravitation at her control which are beyond our means.

Let me close by saying that while it is unfortunately true that theorists have not told the experimentalists how to build a thermonuclear machine, it is also true that we have been looking hard for very many years for a fundamental reason why a plasma fusion reactor should be impossible and we have not found any such reason. Indeed, the evidence strongly suggests that when the experimentalist is able to produce by not-too-violent means a hot plasma which satisfies the hydromagnetic stability requirement, and which does not have excessive electric fields parallel to the magnetic field—then we will have a relatively quiescent plasma, at least by present standards. If I may make a statement from the heart, I believe the chances are very good that in twenty years or so mankind will have solved the problem of controlled fusion if only he has not lost in the meantime the far more difficult struggle against uncontrolled fusion. Thank you.

СОСТОЯНИЕ ИССЛЕДОВАНИЙ ПО УПРАВЛЯЕМОМУ ЯДЕРНОМУ СИНТЕЗУ НА СЕНТЯБРЬ 1961г. ОБЗОР РЕЗУЛЬТАТОВ ТЕОРЕТИЧЕСКИХ РАБОТ*

М. Н. РОЗЕНБЛЮТ

ДЖЕНЕРАЛ АТОМИК, ДЖЕНЕРАЛ ДАЙНАМИКС КОРПОРЕЙШН

САН-ДИЕГО, КАЛИФОРНИЯ, СОЕДИНЕННЫЕ ШТАТЫ АМЕРИКИ

Г-н Председатель, г-да делегаты,

После ясного и проницательного обзора, сделанного профессором Арцимовичем, неразрешенным остается лишь вопрос о том, не останемся ли мы, теоретики, в чистилище. Однако я надеюсь, что вам не покажется слишком резким переход на несколько минут в Эльдорадо математики плазмы, в котором мы, теоретики, обычно пребываем, лишь изредка сталкиваясь с суровым миром экспериментаторов. Однако, прежде чем начать, я хотел бы воспользоваться случаем поблагодарить тех, кто создал прекрасную атмосферу на этой конференции. Генеральному директору Коулу и д-ру Бурасу, а также секретариату я мог лишь сказать, что благодаря их радушному приему мы не только чувствовали себя здесь хорошо, но в нас укрепилось убеждение в важности нашей работы по использованию ядерного синтеза в мирных целях. Мы знаем, что организация такой конференции является трудной задачей и благодарим вас за ваши усилия. Что же касается наших хозяев в этом сказочном городе Зальцбурге то достаточно сказать, что красоте вашего города вполне соответствуют отзывчивость и гостеприимство ваших сограждан, которое мы испытали на себе, и прекрасное здание конгресса. Наконец, нельзя не отметить резкий контраст между мрачными заголовками газет, которые мы читали в течение всей недели с атмосферой почти полной сердечности и сотрудничества, которая царила здесь. Несомненно то, что обмен информацией проводился свободно, в духе дружбы и сотрудничества среди ученых многочисленных наций, собравшихся здесь. В самом деле, как это выяснится из моей речи, я встретился с затруднениями совершенно иного порядка, так как оказалось невозможным переварить в такой короткий срок огромное количество представленных здесь интересных работ. В частности, я прошу заранее извинить меня за то, что я, естественно, лучше всего знаком с работами моих американских коллег, в особенности экспериментаторов и, вероятно, буду уделять этим работам больше внимания, чем они этого заслуживают.

Учитывая то, что теоретические доклады были насыщены громадным количеством длиннейших уравнений, невозможно обсудить сколько-нибудь подробно все представленные здесь самые разнообразные работы. Вам, к сожалению, придется примириться с довольно поверхностным обсуждением того широкого диапазона взглядов, с которым я встретился на конференции. Поэтому я снова воспользуюсь приближением с помощью « случайных фраз », что, боюсь, окажется непереводимой шуткой.

Начиная с самой основы, а именно с плазмы, как проблемы многих тел, пожалуй стоит отметить, что в настоящее время все, по-видимому, считают, что уравнение Больцмана достаточно хорошо описывает плазму. Многие ученые показали, как это уравнение можно вывести путем модификации методов Боголюбова, Борна, Грина, Керквуда и Ивона таким образом, что в пределе происходит переход к полностью гидродинамической плазме (т.е. к такой, в которой $n\to\infty$, $e\to 0$, $m\to 0$ и — ne, nm, v являются постоянными величинами). В качестве основного рабочего уравнения получается бесстолкновительное уравнение Больцмана, или уравнение Власова, с поправкой Фоккера-Планка, которая нужна для оценки термализации, переноса, излучения и т.д.

Другой фундаментальной темой, по-видимому, получившей хорошую основу за последние несколько лет, является движение отдельных частиц, по крайней мере, в медленно меняющихся электромагнитных полях. Связанные с этой проблемой замечательные теоремы Крускала и других, касающиеся постоянства во всех порядках адиабатических инвариантов движения частиц, дают нам возможность, по крайней мере, показать существование удерживаемой плазмы — т.е. существование равновесия в бесстолкновительном приближении.

Именно в этом пункте и начинаются настоящие затруднения. Надо всегда иметь в виду, что то, к чему мы стремимся в работе по управляемому синтезу — это удержать плазму в состоянии нетермодинамического равновесия в течение длительного периода времени. Во-первых, плазма, конечно, выходит из равновесия с полем излучения, так как при термоядерных температурах удельная теплоемкость этого поля имеет совершенно недопустимую величину. К счастью, по-видимому, нет причин ожидать каких-либо сюрпризов в области частот, значительно превосходящих плазменную частоту — за исключением вопроса о примесях,

* Речь Д-ра Розенблюта на заключительной сессии. Зальцбург, 9 сентября 1961 г.

который, по-моему, в конечном итоге, окажется самым трудным во всей термоядерной проблеме. Однако, к счастью, не теоретикам приходится ломать себе над этим голову. В области более низких частот, где ожидается излучение черного тела, по-видимому, можно примириться с существованием уровней (равновесных уровней) циклотронного излучения, по крайней мере, в реакторе типа DT.

Обратимся теперь к тому, что профессор Арцимович назвал основным вопросом — к несомненно гораздо более трудному вопросу об устойчивости (в рамках уравнения Власова) возможных состояний покоющейся плазмы. Большая часть работ, представленных здесь, основывается на изучении очень сильно упрощенных случаев — либо бесконечной однородной плазмы, либо возмущения, удовлетворяющего адиабатическим условиям R_L/L, ω/Ω, $\omega/\omega_p \ll 1$ (R_L — ларморовский радиус, L — характеристическое расстояние в плазме; ω — частота, Ω — циклотронная частота и ω_p — плазменная частота), при которых действительно гидродинамическое приближение.

Пожалуй здесь стоит уклониться в сторону и упомянуть о формальной теореме, предложенной Краллом и мною, и доказанной Франсисом Лоу, касающейся строгости таких приближенных вычислений. Вопрос заключается в следующем: Предположим, что наша приближенная плазма действительно устойчива, так что вплоть до самого низкого порядка приближения существуют разные моды колебаний, характеризуемые действительными частотами ω_0. Откуда мы можем знать, что при более точном вычислении с

$$\omega = \omega_0 + \varepsilon\omega_1 + \ldots .$$

различные более высокого порядка члены $\varepsilon\omega_1$ и т.д. не окажутся комплексными и, возможно, приводящими к неустойчивости? Учитывая, что параметры $\varepsilon = R_L/L$ и т.д. действительно не слишком малы в случаях, представляющих практический интерес, такое сверхустойчивое нарастание было бы катастрофическим. Лоу доказал, что все высшие члены имеют действительную величину следующим образом: Система уравнений Максвелла и уравнений частиц по своему характеру, очевидно, является лагранжевой, так как уравнения движения плазмы можно вывести вариационными методами из лагранжиана $\mathcal{L}$, как мы слышали от д-ра Ньюкомба и д-ра Котсафтиса

$$\mathcal{L} = \int \mathrm{d}^3\mathbf{x}\,\mathrm{d}^3\mathbf{v}\,\{\dot{\xi}\,O_1\,\dot{\xi} + \dot{\xi}\,O_2\,\xi + \xi\,O_3\,\xi\},$$

— где ξ является смещением в фазовом пространстве, вызванном возмущением и где разные операторы O для стационарных равновесных состояний являются функциями только переменных фазового пространства $\mathbf{x}$ и $\mathbf{v}$ и не явно времени. Учитывая, что это выражение является формой лагранжиана, легко понять, что если мы напишем уравнение движения варьируя по ξ, предполагая $\xi \sim \exp(\mathrm{i}\omega t)$, умножая на ξ^* и интегрируя по фазовому пространству, сможем вывести выражение для частоты следующего типа,

$$\omega = \frac{-\beta \pm \sqrt{\beta^2 - 4\alpha\gamma}}{2\alpha}$$

которое следует непосредственно из решения квадратичного уравнения. Коэффициенты α, β, γ, — являются положительно-определенными, квадратичными, действительными функциями смещения ξ. В этом случае видно, что если перейти от первоначальных приближенных вычислений к более точным, то результатом этих вычислений окажутся небольшие изменения в параметрах α, β, γ. Поэтому свойства действительности собственной частоты ω не изменяются. Если бы наши приближенные вычисления привели к устойчивости, тогда более точные вычисления — по крайней мере при небольших отступлениях от области приближенных вычислений — тоже приведут к устойчивости. Действительно, легко видеть, что если мы исключим неразложимые в ряд резонансные члены типа Ландау, тогда частота является действительной величиной во всех порядках по ε, где ε — малый параметр, описывающий влияние, например, конечности ларморовского радиуса и другие эффекты, которыми пренебрегают в приближенных вычислениях.

Примером, относящимся к этой теореме, является изучение немаксвеллевской бесконечной однородной плазмы. Хорошо известно, что имеется огромное число так называемых микронеустойчивостей, которые появляются в этом случае. Однако все эти неустойчивости характеризуются какой-нибудь из двух благоприятных особенностей, либо анизотропия должна достичь некоторого определенного критического значения до возникновения неустойчивости, как в случае пробочной неустойчивости, либо в случае малой анизотропии неустойчивость является резонансной неустойчивостью типа Ландау с чрезвычайно малой скоростью нарастания, как, например, неустойчивость, связанная с альфвеновской волной. По-моему, все это следует из теоремы Лоу. Это позволяет думать, что вблизи истинного термодинамического равновесия действительно должна существовать конечная область устойчивости, которую, возможно, удастся достигнуть в наших плазменных устройствах. Излишне говорить, что, как это нам сказал д-р Арцимович, эта область может оказаться довольно трудно досягаемой, если учесть трудности, связанные с инжектированием и устойчивостью плазмы. Но это — не моя задача.

Следует, конечно, признать, что все такие действия по разложению в ряд несколько рискованы. Например, как я говорил в своем докладе, то разложение в ряд, на котором основывается магнитная гидродинамика, предполагает, что R_L/L и ω/Ω одного порядка малости. Если учесть случаи, для которых $\omega/\Omega \sim (R_L/L)^2$ т.е. случаи, которые часто представляют практический интерес, тогда могут обнаружиться новые явления. Например, разделение ионов и электронов может

улучшить устойчивость желобков. С другой стороны, теперь возможно появление волн совершенно нового типа. Например, мы слышали на этой конференции о возможности существования волн дрейфа в неоднородных магнитных полях, для которых фазовая скорость волны ω/k, имеет порядок величины v_D скорости дрейфа, характеризующей магнитное поле. Конечно, скорость дрейфа такого рода вовсе не имеет места в случае однородного поля, так что здесь следует ожидать появления волны совершенно нового типа. Такие волны были исследованы многими учеными; они характеризуются тем, что в условиях резонанса между скоростью дрейфа и фазовой скоростью частицы более не привязаны к силовым линиям магнитного поля, как это бывает в гидромагнитном приближении, но под влиянием этого резонанса могут дрейфовать поперек поля. Различные виды неустойчивостей такого типа были изучены и обсуждены на заседании, посвященном микронеустойчивостям. Хотя это исследование все еще находится в начальной стадии, я думаю, что можно утверждать следующее: почти все эти неустойчивости растут очень медленно, причем скорость их роста зависит, например, от отношения массы электронов к массе ионов m_e/m_i, за исключением конвективных тепловых неустойчивостей, впервые изученных Церковниковым и разработанных далее на настоящей конференции Велиховым; они несколько сходны с хорошо известными звездными гравитационными неустойчивостями. К счастью, эти конвективные неустойчивости, по-видимому, существенны лишь при относительно больших градиентах температуры и, может быть, их удастся избежать. Излишне говорить, что мы были бы чрезвычайно рады, если бы получаемая в настоящее время в лаборатории плазма удерживалась достаточно долго, чтобы можно было изучить такие тонкие эффекты.

Переходя теперь к обычной теории, основанной на магнито-гидродинамических уравнениях и энергетическом принципе, мне кажется, сейчас можно сказать, что она достаточно хорошо изучена. Во многих случаях, как, например, в пинче, было установлено, что нарушение критериев устойчивости быстро ведет к катастрофическим последствиям. Более того, на этой конференции мы заслушали сообщение о хорошем согласии с экспериментом численных расчетов Хайна и других, использовавших магнитогидродинамическую модель с простыми коэффициентами переноса, что опять-таки указывает на применимость этих уравнений для изучения явлений в широком диапазоне условий.

Может быть следует отметить еще один факт, а именно, что за последние несколько лет многим исследователям удалось доказать теоретически, что действительно можно найти устойчивые (т.е. устойчивые в магнитогидродинамическом приближении) системы удержания плазмы. Я думаю, что из этих систем только линейный пинч с твердым сердечником (в котором плазма в действительности не очень хорошо удерживается из-за потерь через торцы) был подвергнут тщательному экспериментальному изучению. Я вернусь к этому позже. Было бы чрезвычайно интересно в течение ближайших нескольких лет проследить за дальнейшим ходом развития исследований гиперболической геометрии, на левитронах и видоизмененных магнитных ловушках, о которых сообщал д-р Йоффе. Несомненно, некоторые полученные предварительные результаты представляются обнадеживающими.

Остальные вопросы, которые мне хотелось бы обсудить, может быть, было бы предпочтительно рассмотреть в связи с тремя основными экспериментальными парадоксами, которые существуют в настоящее время и еще недостаточно понятны:

1. Почему неустойчивы пинчи с твердым сердечником? Согласно магнитогидродинамической теории они должны быть совершенно устойчивыми, но, как мы узнали от д-ра Биккертона и д-ра Колгейта, фактически это не так.
2. Как объяснить потери частиц в стеллараторе и их очевидное соответствие со старым предположением Бома относительно диффузии? Вы помните знаменитый бомовский коэффициент дифф узии, который, как и последняя теорема Ферма, был написан, но так и остался без объяснения:

$$D = ckT/eB.$$

3. Как объяснить то обстоятельство, что желобковые неустойчивости, по-видимому, иногда успешно подавляются в установках с пробками, а, может быть, и в тета пинчах?

Неустойчивость пинча с твердым сердечником является почти несомненно следствием конечной проводимости. Пример гидродинамической конвективной неустойчивости должен подготовить нас к возможности появления новых типов неустойчивости, обязанных введению диссипативных членов. Более того, то обстоятельство, что эти трудности, по-видимому, не обнаруживаются в тета пинчах, наводит на мысль об их связи с электрическими полями, параллельными магнитному полю. Здесь мы заслушали две теории таких процессов. Первая — это теория Кадомцева, которая так блестяще объяснила поведение положительного столба плазмы. Вторая — это теория Бикертона — основанная на обычных уравнениях жидкости с конечной проводимостью. Один вопрос очевидно требует дальнейшего исследования, это — вопрос о связи, если таковая вообще имеется, между этими двумя теориями. С первого взгляда они кажутся совершенно различными по той существенной причине, что в пределе при высокой проводимости σ скорость нарастания по Кадомцеву следует закону $1/\sigma$ иными словами очень мала, а по Бикертону — выражению $1/\sqrt{\sigma}$. Теория Кадомцева позволяет создать термоядерные условия, а теория Бикертона — нет. Я считаю, что поведение $\sim 1/\sigma$ преобладает в таких положениях, при которых магнитное поле не очень сильно

нарушается плазмой. С другой стороны, если имеется большой запас магнитной энергии благодаря сдвигу поля, созданному плазменными, потоками параллельнымн **B**, то следует ожидать более опасной зависимости $1/\sqrt{\sigma}$.

Переходя теперь к вопросу о стеллараторе, мы опять-таки встречаем две гипотезы, предложенные для объяснения неустойчивости в начальный период, приводящих к потерям частиц. Первой и, вероятно, правильной является опять-таки теория Кадомцева, касающаяся положительного столба. Вторая — это теория возбуждения микроустойчивостей, таких как неустойчивые ионные звуковые волны. Эти неустойчивости, несомненно, существуют и встречаются в стеллараторных установках, но квази-линейные теории Велихова и Дримонда заставляют нас теперь предполагать, что они не приведут к большой диффузии. Построим график функции распределения частиц для ионно-звуковых волн (рис. 1). Электронное распределение f_e очень широкое (я рисую не в масштабе) и несколько смещено в сторону от распределения ионов f_i, так как оно служит носителем тока. Квазилинейная теория говорит, что единственным следствием неустойчивости явится небольшое уплощение распределения электронов вблизи скорости ионного звука. Поэтому небольшое количество кинетической энергии, полученной от этих электронов, превращается в энергию электростатических колебаний. Если проделать сравнительно простой подсчет того, какую диффузию следует ожидать в результате воздействия таких колебаний, легко убедиться, что она слишком мала, чтобы объяснить существование потерь плазмы («pump-out»). И действительно я думаю, что вообще на основании этих квазилинейных теорий мы можем заключить, что многие из этих резонансных неустойчивостей создадут нам гораздо меньше хлопот, чем мы опасались.

Как можно объяснить кажущееся согласие с диффузией Бома? Я бы сказал, что мы слышали только об одной действительно серьезной попытке понять турбулентную плазму — о замечательной работе Кадомцева, которая, однако, не приводит к диффузии Бома, хотя во многих других случаях дает правильные по порядку величины результаты. Откровенно говоря, в теории Кадомцева слишком много тонкостей, и мне трудно ее понять при таком беглом ознакомлении с ней. Однако я надеюсь, что меня извинят, если я замечу, что даже теория гидродинамической турбулентности содержит в себе много эвристических элементов, таких, как например, понятие о длине перемешивания, которое можно оправдать только с помощью многочисленных эмпирических результатов. Ввиду неполной аналогии между физикой плазмы и гидродинамикой, я боюсь, что вряд ли мы можем рассчитывать на создание успешной теории турбулентности плазмы в ближайшие годы. Все же, даже такая приблизительная теория является неоценимым звеном между теорией и современными экспериментами. Например, как вы слышали, работа Кадомцева позволила истолковать опыты Иоффе.

Конечно, легко дать грубое обоснование диффузии Бома. Например, д-р Тэйлор отметил, что если предположить турбулентные волны такими, чтобы время их когерентного взаимодействия с ионами было меньше ионно-циклотронного периода, тогда мы вновь получим хорошо известный коэффициент диффузии:

$$D = \frac{v^2 \tau}{1 + (\Omega \tau)^2}$$

где τ теперь эффективное время столкновения иона с волнами. Максимальное значение в функции от τ является как раз коэффициентом диффузии Бома. Другое простое рассуждение, основанное на соображениях размерности можно провести для случая плазмы с малым значением β. В плазме с малым β магнитное поле должно оставаться невозмущенным при любом движении. Поэтому возмущение описывается электростатическим потенциалом φ и можно сказать, что φ ограничено по амплитуде следующим соотношением:

$$e\varphi < \mathrm{k}T_e .$$

Это является следствием возможности свободы движения электронов вдоль магнитных силовых линий. Если такой потенциал существует, то он вызывает дрейф поперек магнитного поля, описываемый обычной формулой $v = cE/B$, которая

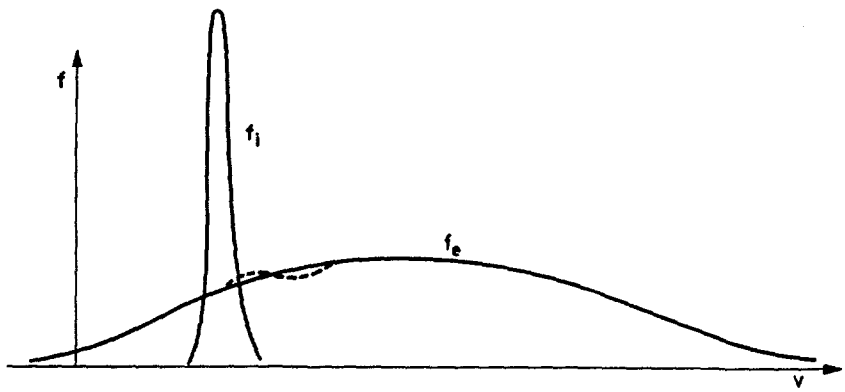

Рис. 1

после подстановки максимального значения электростатического потенциала переходит в

$$v \approx c \frac{\mathrm{k}\, T_e}{e B \lambda}$$

где λ является длиной волны возмущения. Теперь, если мы позаимствуем из гидродинамики концепцию, что средний свободный пробег вихревого движения практически равен размеру вихря λ (напомним, что λ является длиной волны перпендикулярной к магнитному полю), тогда мы получаем для коэффициента диффузии $D = \langle \lambda v \rangle = D_{\text{Бома}}$. Поэтому, может быть, какое-нибудь рассуждение вроде этого сможет объяснить бомовскую диффузию. Излишне говорить, что такого рода рассуждения, основанные лишь на анализе размерностей, не могли бы рассматриваться сколько-нибудь серьезно, не будь полученных на стеллараторах результатов, заставляющих нас думать над этими проблемами. Однако я должен опять-таки повторить, что основной задачей термоядерной программы является не объяснение турбулентности, а ее преодоление, что может оказаться еще более трудным.

Наконец, мы приходим к вопросу о магнитных ловушках. Хотя новейшие результаты, полученные д-ром Кензгенсом весьма пессимистичны, мы не можем не обратить внимания на то обстоятельство, что в старых опытах Поста на установке «Тейбл Топ» с горячими электронами не наблюдалось в течение длительных промежутков времени ни желобковой неустойчивости, ни аномальной диффузии Бома. Другими обнадеживающими факторами являются получение значительной стабилизации при приложении потенциалов на торцах установки Огра и поведение тета пинчей, которые, по крайней мере в некоторых случаях, по-видимому, остаются устойчивыми в течение необычно долгого времени. Чем можно объяснить такое приятное отклонение от теории? Может быть известную роль играют эффекты конечности ларморовского радиуса, конечности градиентов и другие эффекты вращения, а также некоторые свойства до сих пор еще непонятного поверхностного слоя, который должен существовать вблизи наружной границы удерживаемой плазмы. Тем не менее я думаю, что основная масса результатов все еще подтверждает мысль о том, что устойчивость возникает, главным образом, вследствие электрического контакта, создаваемого холодной плазмой во внешней области между захваченной в ловушку плазмой и проводящими стенками, которая тем самым служит замораживающим проводником, предотвращающим обмен со стенками. В пользу этого соображения говорит наличие природных поясов радиации вокруг Земли, для которых ионосфера играет роль внешнего проводника. Может быть, если мы научимся подражать природе, то также будем в состоянии повторить ее успех в получении реакции синтеза, хотя, конечно, природа имеет в своем распоряжении некоторые принципы, вроде гравитации, которые выходят за пределы наших возможностей.

Позвольте мне в заключение сказать, что, хотя к сожалению верно то, что теоретики не смогли подсказать экспериментаторам, как построить термоядерную машину, точно так же справедливо и то, что в течение долгих лет мы пытались найти главные причины для обоснования невозможности осуществления реактора на принципе синтеза плазмы, и до сих пор таких причин не нашли. В самом деле, имеются все основания думать, что, когда экспериментатор сможет создавать не слишком резкими способами горячую плазму, которая удовлетворяла бы условиям гидромагнитной устойчивости и в которой не было бы слишком сильных электрических полей, параллельных магнитному полю, тогда мы будем иметь относительно спокойную плазму, по крайней мере по существующим нормам. Позвольте мне высказать от души: я верю, что человечество имеет весьма большие шансы через каких-нибудь 20 лет разрешить проблему управляемого ядерного синтеза, если до этого оно не потерпит поражения в еще более трудной борьбе с неуправляемым синтезом. Благодарю вас.

SESSION I — SÉANCE I

ЗАСЕДАНИЕ I — SESIÓN I

4 SEPTEMBER 1961 — 4 SEPTEMBRE 1961

4 СЕНТЯБРЯ 1961 Г. — 4 DE SEPTIEMBRE DE 1961

Chairman — Le président — Председатель — El Presidente

B. Lehnert *(Sweden)*

Scientific Secretary — Secrétaire scientifique — Ученый секретарь — Secretario Científico

P. A. Davenport *(United Kingdom)*

[Papers presented: CN-10/23, 24, 34, 65, 69, 154, 172, 202, 204]

GAS INSULATION OF A HOT PLASMA: THEORY AND EXPERIMENT*

H. ALFVÉN, C.-G. FÄLTHAMMAR, R. B. JOHANSSON, E. A. SMÅRS, B. WILNER, E. WITALIS

ROYAL INSTITUTE OF TECHNOLOGY, STOCKHOLM, SWEDEN

The attempts to heat a plasma to thermonuclear temperatures have started from the idea of having the plasma separated from the walls of the vessel by magnetic fields in vacuum. In this paper another possibility is discussed, namely, to insulate the plasma from the walls by means of gas at high pressure in a strong magnetic field. The power lost from a plasma column by heat conduction through a surrounding gas has been studied in two different models. In the first one, heat is assumed to be produced, e.g. by thermonuclear reactions, within a central core of the column. In the second model, ohmic heating is assumed to take place by a constant homogeneous electric field applied parallel to the column. With reasonable values of the magnetic field the losses by heat conduction are small.

A toroidal high current discharge at initial gas pressures up to 600 torr is being studied experimentally. It has been shown that it is possible to create an electrodeless circular arc discharge which starts in a narrow channel and is surrounded by cool gas. Streak photographs indicate an increasing stability of the plasma ring with increasing gas pressure. Spectra taken from this high-pressure discharge are compared with those taken from the same apparatus under low-pressure conditions, when an ordinary fast pinch discharge takes place. The observations give clear evidence that the plasma is much more free from wall impurities in the high-pressure discharge than in the low-pressure case. Estimates of temperature, ion densities, and energy input are made.

1. Introduction

In plasma experiments performed to study the possibilities of reaching thermonuclear temperatures the principle has been to confine a hot plasma in a region which is surrounded by vacuum. There is then no power loss by thermal conduction to the chamber walls. However, it has been suggested by ALFVÉN and SMÅRS [1] that there may be some advantages in insulating the plasma from the walls not by vacuum but by gas of high density. This may be done in a gas of high pressure by starting a discharge as a spark and letting it develop into a high-current arc. As shown below, the power loss by heat conduction in the surrounding gas can be kept small by a strong magnetic field perpendicular to the temperature gradient.

The stability of a plasma surrounded by dense gas is different from that of one surrounded by vacuum. In a theoretical model MURTY [2] has studied the influence of a surrounding non-conducting medium on the stability of a current-carrying plasma cylinder. It is found that the growth rate of hydromagnetic instabilities is decreased by the medium. Similar results have been reported recently by WILHELM [13]. Experimental results to be described later give some indication that the stability of a high current toroidal arc column increases with increasing gas pressure.

As already at the start the hot plasma is concentrated to the central region and hence surrounded by pure gas of high density, impurities are kept out of the plasma. This is in striking contrast to the ordinary pinch where the discharge current starts at the walls, from which impurities are brought into the plasma during the compression.

High-current arc discharges have been studied, among others, by BURHORN, MAECKER, and PETERS [3], who report a temperature of 50000 °K in a continuously operated arc at a current of 1450 A. ALLEN and CRAGGS [4] describe an investigation of high current spark channels with current peaks up to 265 kA and estimated temperatures of 72000 to 160000 °K. HÖCKER and KLUGE [5] have also reported experiments with pulsed arcs in the 100 kA-range.

2. Theoretical models

The thermal conductivity $\varkappa$ perpendicular to a magnetic field of a hydrogen or deuterium gas is a complicated function of temperature, pressure and magnetic field. Figure 1 shows qualitatively the

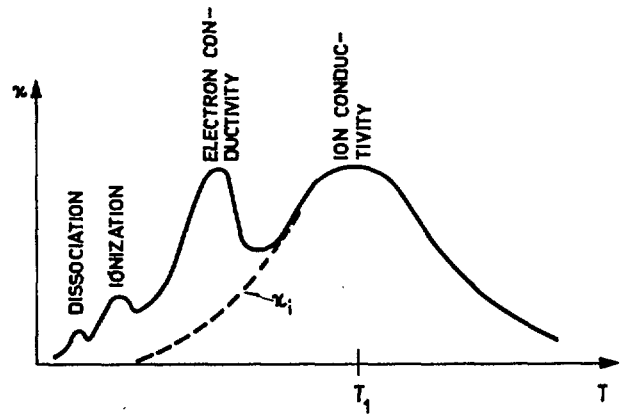

Fig. 1 Qualitative representation of the temperature variation of the thermal conductivity perpendicular to a strong magnetic field when the pressure and the magnetic field are constant.

* Conference paper CN-10/23, presented by E. A. Smårs. Discussion of this paper is given on page 93. Translations of the abstract are at the end of this volume of the Conference Proceedings.

temperature variation when the pressure and the magnetic field are both constant [1]. The first maximum is due to the dissociation and the second to ionization [6], whereas the third is produced by the electron conductivity and the fourth by the ion conductivity. At high temperature the ion conductivity dominates and, as we shall see, its asymptotic temperature variation is as $T^{-5/2}$.

2.1. Simple model

We shall first investigate a simple model [1]. The power losses by heat conduction are studied in a plasma column within a cylindrical vessel with wall radius r_w and wall temperature zero. A constant magnetic field is applied in axial direction and the pressure $p=nkT$ is assumed to be constant. A central core with radius r_c is heated, e.g. by thermonuclear reactions to the temperature T_c. Neglecting radiation losses from the region outside the central core the power lost by heat conduction per unit length is $Q=-2\pi r \varkappa \, dT/dr$ or

$$Q = \frac{2\pi}{\log (r_w/r_c)} \int_0^{T_c} \varkappa \, dT . \tag{1}$$

Because for high values of T_c the largest part of the integral is due to the ion-gas contribution to $\varkappa$, in an approximate calculation we can use the thermal conductivity of the ion gas. According to Braginsky [7] this is

$$\varkappa = \frac{3}{4\sqrt{\pi}} \frac{k\,(kT)^{\frac{5}{2}}}{\sqrt{m_i}\, e^4 \lambda} \frac{2.645 + 2\,(\omega_i \tau_i)^2}{0.677 + 2.70\,(\omega_i \tau_i)^2 + (\omega_i \tau_i)^4}, \tag{2}$$

where

$$\omega_i \tau_i = \frac{eH}{m_i c} \frac{3\sqrt{m_i}\,(kT)^{\frac{3}{2}}}{4\sqrt{\pi}\, e^4 n_i \lambda} \tag{3}$$

is the product of the gyro-frequency and the collision time of the ions. λ is the Coulomb logarithm. If the pressure is constant the ion density n_i varies as T^{-1} and $\omega_i \tau_i$ is then proportional to $T^{5/2}$. This means that, as easily seen from Eq. (2), $\varkappa$ decreases as $T^{-5/2}$ for high temperatures in the presence of a magnetic field.

Introducing Eqs. (2) and (3) into Eq. (1) we can write

$$Q = bK\, T_1^{\frac{7}{2}}, \tag{4}$$

where $T_1 = 4.0 \cdot 10^4 \; (p/H)^{2/5}$ is approximately the temperature that corresponds to maximum ion conductivity $(\omega_i \tau_i \approx 1)$, $K = 0.53 \cdot 10^{-14}$ W cm^{-1} deg$^{-7/2}$ and

$$b = \frac{2\pi}{\log (r_w/r_c)} \int_0^{\infty} \frac{x^{\frac{5}{2}}\,(1 + 0.756\, x^5)}{1 + 3.99\, x^5 + 1.48\, x^{10}} \, dx . \tag{5}$$

It is presumed that $T_c/T_1 \gg 1$. If the ratio r_w/r_c is of the order of 10, the constant b is approximately 3. Then we get $Q = 200\,(p/H)^{1.4}$ W cm^{-1}. If the temperature of the central core is $T_c = 2 \cdot 10^8$ degrees and $n = 10^{14}$ cm^{-3}, the pressure is $p = nkT \approx 3 \cdot 10^6$ dynes cm^{-2} and we get (for two values of the magnetic field):

Magnetic field:

$H = 10^4$ G $\qquad$ $H = 10^5$ G

Temperature for maximum thermal conductivity:

$T_1 \approx 4 \cdot 10^5$ degrees $\qquad$ $T_1 \approx 1.6 \cdot 10^5$ degrees

Power loss by heat conduction:

$Q \approx 600$ kW cm^{-1} $\qquad$ $Q \approx 24$ kW cm^{-1}

2.2. More refined model

Another theoretical model has been studied by Fälthammar [8]. In this model a fully ionized plasma column is heated by ohmic losses associated with a distributed axial current $i(r)$ driven by a homogeneous axial electric field E. A stationary state with local thermal equilibrium is considered but the stability of the configuration is not investigated. The only magnetic field present is the azimuthal field $H_\varphi(r)$ produced by the axial current $i(r)$. The four quantities $H_\varphi(r)$, $p(r)$, $i(r)$, and $T(r)$ satisfy the four differential equations (electrostatic cgs-units)

$$\frac{1}{r} \frac{d}{dr} (r H_\varphi) = \frac{4\pi i}{c} \tag{6}$$

$$\frac{dp}{dr} = -\frac{1}{c} i H_\varphi \tag{7}$$

$$i = E/\eta \tag{8}$$

$$-2\pi r \varkappa \frac{dT}{dr} = \int_0^r E\, i\, 2\pi r \, dr - \int_0^r \beta\, n^2\, T^{\frac{1}{2}}\, 2\pi r \, dr \tag{9}$$

The second equation is the condition of pressure balance, the third is Ohm's law in the case where the Hall current is inhibited and the fourth describes the balance of heat. The last term in Eq. (9) represents the power radiated as bremsstrahlung (no reabsorption). In Eqs. (8) and (9) any coupling terms between the electric current density and the heat flux density have been neglected.

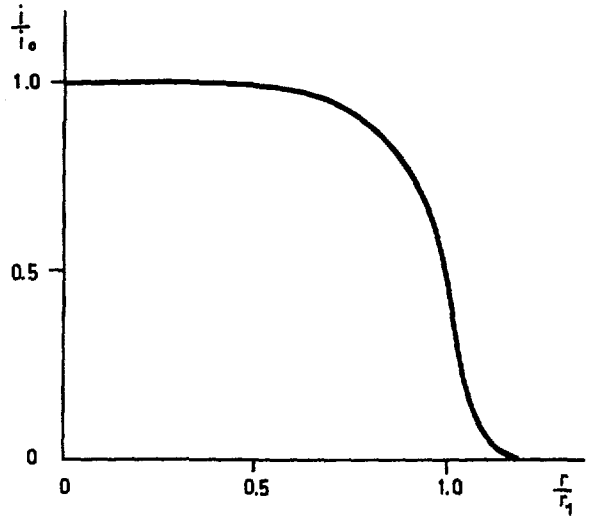

Fig. 2 Radial variation of the normalized current density.

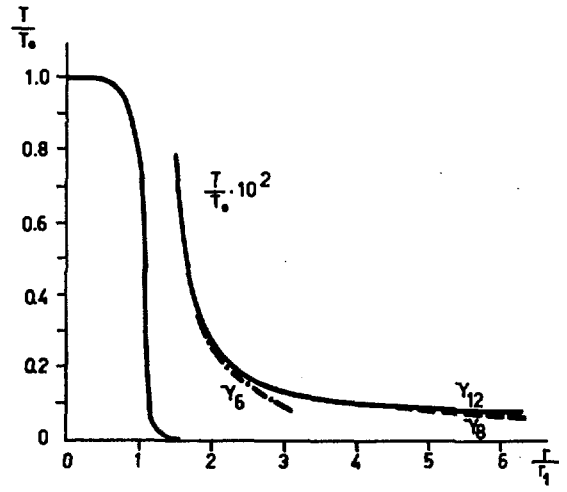

Fig. 3 Radial variation of the normalized temperature ($\gamma = \gamma_n$ corresponds to $10^{22}\, p_0/T_0^5 = 10^{-n}$), see reference [8].

For η and β the values given by SPITZER [9] have been used and for $\varkappa$ the expression Eq. (2) above, which is an adequate approximation at high temperatures.

Eqs. (6)—(9) have been solved numerically for the case where heat conduction is the dominating loss mechanism so that the bremsstrahlung term in Eq. (9) can be neglected. This case corresponds to total currents small compared to 10^6 A. Some results of the integrations as given in [8] are reproduced in Figs. 2—4, where i_0, T_0, and n_0 are values of current density, temperature and particle density at the center ($r=0$) and

$$r_1 = 2.8 \cdot 10^{-5}\, n_0^{\frac{1}{2}} / (E T_0)\,. \qquad (10)$$

It is seen from Fig. 2 that the current is concentrated within the radius r_1. In the same region the temperature (Fig. 3) is almost constant but drops abruptly

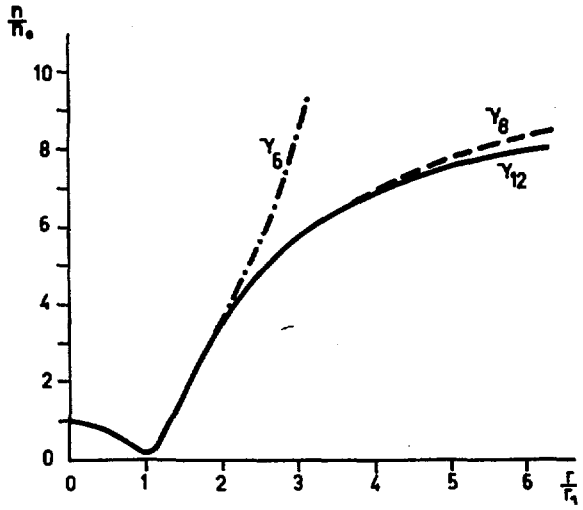

Fig. 4 Radial variation of the normalized density ($\gamma = \gamma_n$ corresponds to $10^{22}\, p_0/T_0^5 = 10^{-n}$), see reference [8].

near the radius r_1. The density (Fig. 4) is many times higher outside the current channel than inside it, which is of great importance in this connection.

The magnetic field is strong near the radius r_1 and in this region cyclotron radiation is emitted. However, the total power loss by cyclotron radiation is estimated to be less than the bremsstrahlung power as long as the central temperature does not exceed $2 \cdot 10^8$ degrees.

Because of the sharply bounded current channel, reasonably constant temperature inside the channel, and much lower pressure outside than inside, the pinch relation

$$(I/c)^2 = 2\, N \mathrm{k}\, T_0 \qquad (11)$$

is applicable with good approximation. Because of the nearly parabolic density distribution within the channel (Fig. 4) relation (11) can also be approximately written as

$$(I/c)^2 = \pi\, r_1^2\, p_0 \qquad (12)$$

Thus this model of a gas-insulated plasma has several properties in common with the ordinary pinch, the most interesting difference being the density distribution with large density outside the current channel.

The calculations verify that, assuming stability, the presence of dense ionized gas around a very hot plasma column need not cause large power loss, because the thermal conduction can be very efficiently reduced by a magnetic field. However, the analyses rest on simplifying assumptions and great care must be taken in applying the results to present experimental situations where the assumptions made are only partially appropriate.

3. Experimental studies

3.1. EARLIER STUDY

A preliminary experimental study of a high current toroidal discharge in helium gas at high pressure has been performed [10]. The toroidal configuration with a ring shaped circulating discharge current was chosen to avoid effects of processes at electrode surfaces and to avoid electrode impurities in the plasma. The discharge vessel was a glass torus with a 10 cm major diameter and a 3 cm bore. On each side of the glass torus there was a one-turn disc-shaped loop, the two loops connected in series and carrying the primary current (Fig. 5). They were connected through a triggered low-pressure spark gap switch [11] to a 2.2 μF condenser bank charged to a voltage of 30 kV. The oscillation period of the circuit was 4.5 μs and the peak current in the primary was 85 kA. The induced voltage in the torus before breakdown was 10 kV per turn, corresponding to an electric field strength of 310 V cm^{-1} at the torus centerline. At gas pressures higher than 50 torr it was necessary to preionize the gas by discharging a separate condenser through the gas between a number of internal tungsten electrodes according to Fig. 6. The predischarge current started 50 to 100 μs before the main discharge

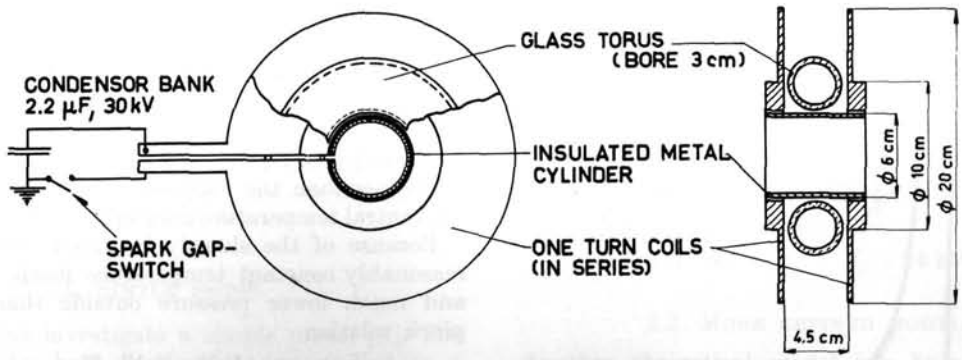

Fig. 5 Simplified sketch of the toroidal discharge circuit.

and it was kept as low as about 250 A. The peak value of the plasma current was 16 kA at a pressure of 400 torr and 25 kA at 50 torr.

The voltage across the primary coil was measured with a capacitive voltage divider, the primary current with a magnetic pick-up coil in the feed line to the coil, and the circulating plasma current with a Rogowsky coil around the glass torus.

The discharge was photographed using a Kerr-cell shutter with an exposure time of about 0.03 μs. Fig. 7 shows a series of such pictures taken at a small

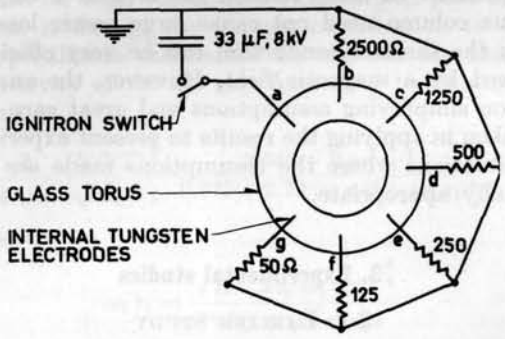

Fig. 6 Predischarge arrangement with internal electrodes.

angle to the symmetry plane of the torus. The oscillograms in Fig. 7 show the plasma current (upper) and the primary voltage (lower) with a time scale of 2 μs per large division. The moments of photographic exposure are indicated by arrows. The initial He gas pressure was 400 torr and the predischarge between the internal electrodes started 50 μs before the main discharge. The pictures show that the current starts in a concentrated channel and develops into an arc-like discharge separated from the walls at least during the first period of oscillation.

The discharge was also examined with a streak camera. Fig. 8 shows streak photographs taken at different pressures. The first one (a) was taken at 1 torr. In this case we have an ordinary low pressure discharge of the pinch type. The gas over the whole cross-section is ionized and the main part of the current starts to flow along the wall surface and contracts to a pinch followed by an expansion. This is repeated several times in approximate synchronism with the

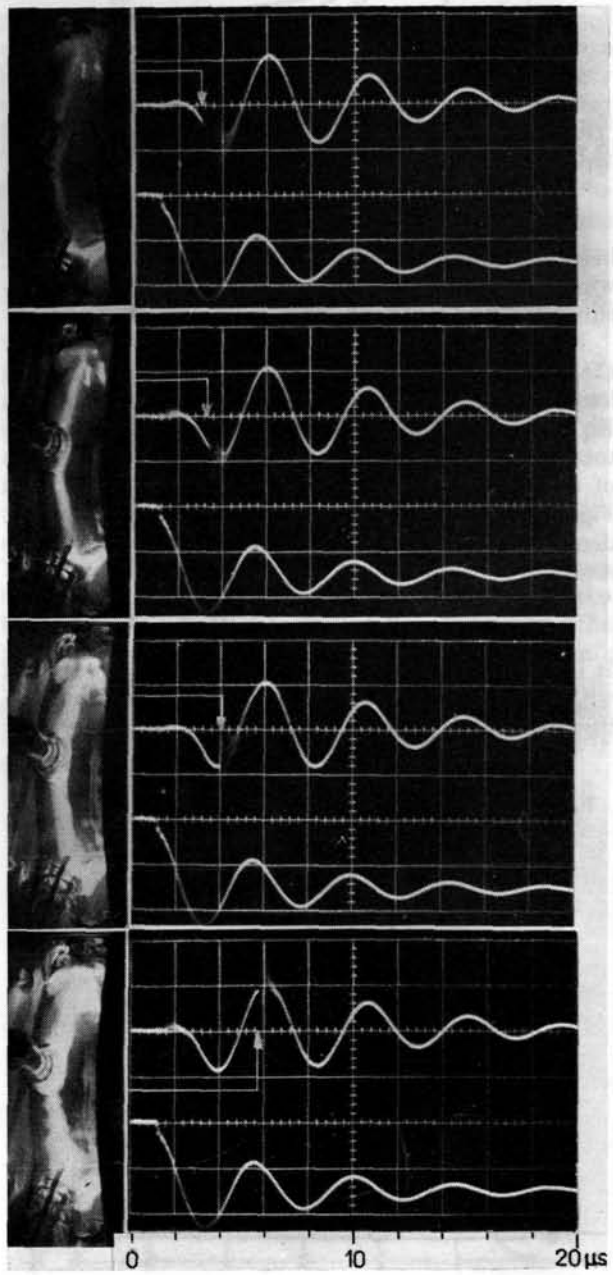

Fig. 7 Kerr-cell photographs of toroidal discharge in He gas at 400 torr initial pressure. Arrows on oscillograms indicate time of exposure. Upper trace: plasma current. Lower trace: primary voltage.

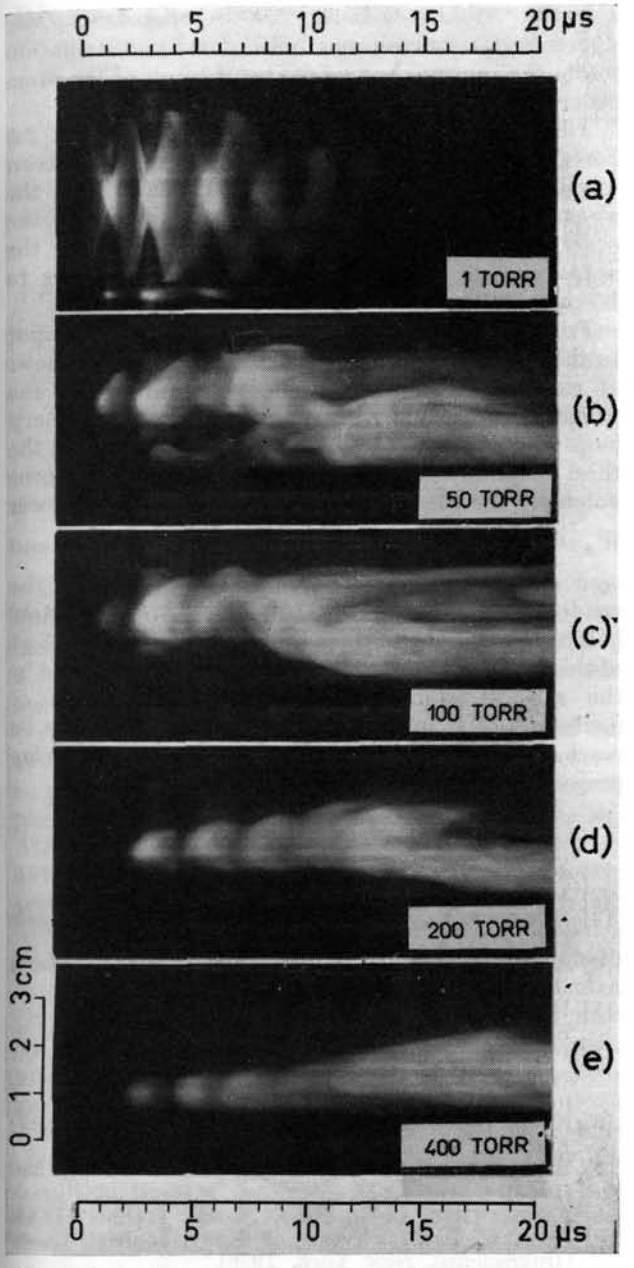

Fig. 8 Streak photographs at different initial gas pressures: (a) 1 torr, (b) 50 torr, (c) 100 torr, (d) 200 torr, and (e) 400 torr.

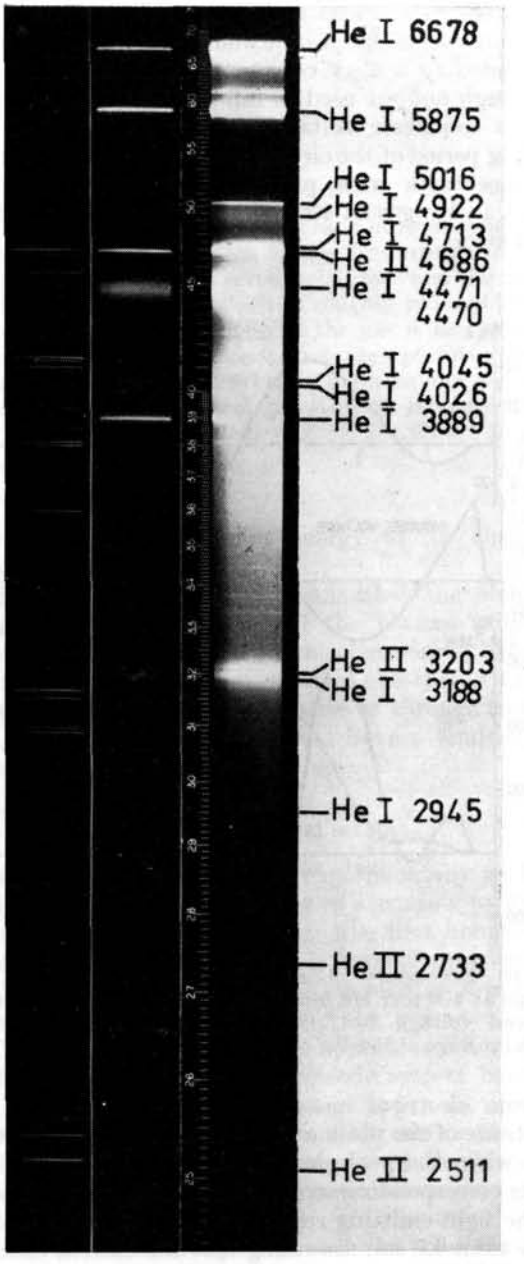

Fig. 9 Time-integrated optical spectra. Left: 1 torr, 1 discharge; Middle: 400 torr, 1 discharge; Right: 400 torr, 10 discharges superposed.

oscillating discharge current. At higher pressures, 50 torr (b), 100 torr (c), 200 torr (d), and 400 torr (e) the behaviour is quite different. It is seen that the current starts in a narrow channel and expands but remains rather concentrated for some time. Moreover, these pictures, (b)—(e), indicate that the stability of the plasma increases with increasing initial gas pressure which may be an effect of the surrounding gas.

The purity of the plasma has been examined qualitatively. Optical spectra from the discharge were taken at different gas pressures. A couple of these are reproduced in Fig. 9. At 1 torr pressure a very large number of strong impurity lines, mainly from Si but also from C and O, appear besides the comparatively weak He lines. With increasing gas pressure the He lines become much stronger and the impurity lines decrease very fast in intensity, so that at 400 torr all lines from wall material are absent. This observation shows that the high pressure discharge gives a much cleaner plasma than the low pressure type. The absence of impurities must be due to the isolating effect of the surrounding dense gas.

3.2 More recent results

Finally, some preliminary results from a new discharge apparatus will be given. The size of the torus is about the same, 10 cm major diameter and 2 cm

bore. The primary loop is a metal torus more or less enclosing the discharge tube which is made of quartz. It is connected to a 5 μF condenser bank rated at 50 kV (although not yet used at full voltage). Sixty percent of the condenser voltage appears on the load. The ringing period of the circuit is 4 μs. A few observations on discharges with plasma currents up to about 60 kA in He gas at 400 torr initial gas pressure have been made.

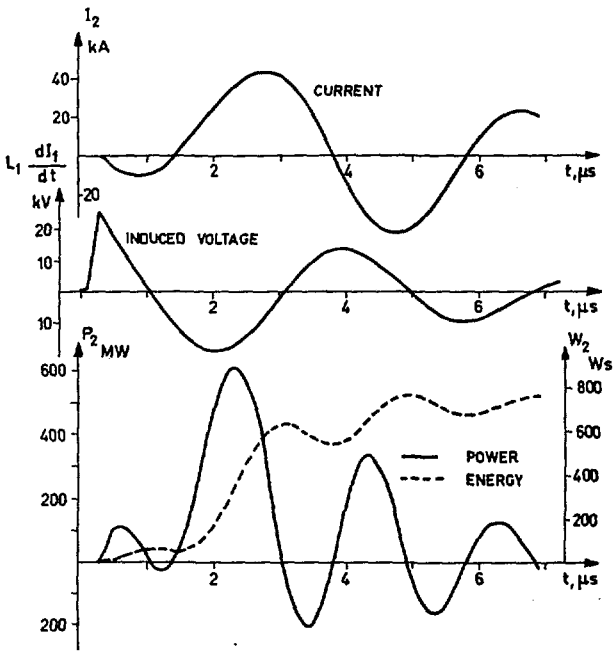

Fig. 10 Secondary characteristics for a toroidal discharge at 400 torr He initial pressure: plasma current I_2, induced voltage $L_1 dI_1/dt$, power P_2, and energy W_2. Bank voltage = 25 kV.

From electrical measurements on the circuit the resistance of the plasma ring was calculated to be 0.18 ohm when the peak current was 43 kA (see Fig. 10). From corresponding streak photographs the diameter of the light-emitting region was estimated to be not more than 0.5 cm. Assuming that the current channel occupied the same region a value of 10^{-3} ohm-cm on the plasma resistivity was deduced. SPITZER's relation [9] between temperature T and resistivity perpendicular to a strong magnetic field gives $T \geq 4 \cdot 10^5$ degrees.

The electron density has been estimated. The Inglis-Teller relation used on two He I series and one He II series studied on time-resolved spectra gave a value of $n_e \approx 5 \cdot 10^{18}$ cm^{-3}. By using the pinch relation, Eq. (11), and the value of the temperature given above and assuming parabolic density distribution inside the current channel, we get a result of the same order of magnitude.

Time resolved spectra from discharges when 2.5 percent CO_2 was added to the He gas have been examined. The appearance of O IV lines and the absence of O V lines indicates a temperature of the order $1—2 \cdot 10^5$ degrees. The relaxation times for the appearance of ionized states of oxygen according to KNORR [12] have been taken into account.

From the electrical measurements the power input to the torus volume has been calculated. Fig. 10 shows an example of this. I_2 is the plasma current, I_1 the primary current and L_1 the inductance of the primary loop. The product $P_2 = I_2 \cdot L_1 \cdot dI_1/dt$ (solid line in the third diagram) is then the power fed into the torus volume. The dashed line is the integrated power $W_2 = \int P_2 \, dt$, which is used to ionize, excite, heat, and magnetize the plasma. The total stored energy in the condensers in this case was 1500 joules. Approximately half of the stored energy is thus fed into the gas. Most of this seems to be lost as line radiation. This may not be the case if helium is substituted by hydrogen or deuterium so that much higher temperatures may be reached. Experiments with these gases are being prepared.

References

[1] ALFVÉN, H., SMÅRS, E. A., *Nature* **188** (1960) 801.
[2] MURTY, G. S., *Arkiv Fysik* **19** (1961) 511.
[3] BURHORN, F., MAECKER, H., PETERS, TH., *Z. Physik* **131** (1951) 28.
[4] ALLEN, J. E., CRAGGS, J. D., *Brit. J. Appl. Phys.* **5** (1954) 446.
[5] HÖCKER, K. H., KLUGE, W., Proceedings of the Fourth International Conference on Ionization Phenomena in Gases, Uppsala, 1959 (North-Holland Pub. Co., Amsterdam, 1960), Vol. II, p. 904.
[6] KING, L. A., *Appl. Sci. Research* **5B** (1955) 189; *E.R.A. Tech. Report* G/XT 155 (1957).
[7] BRAGINSKY, S. I., *Sov. Phys. JETP* **6** (33), 358 (1958).
[8] FÄLTHAMMAR, C.-G., *Phys. Fluids* **4** (1961) 1145.
[9] SPITZER, L. S., Physics of Fully Ionized Gases (Interscience, New York, 1956).
[10] SMÅRS, E. A., JOHANSSON, R. B., *Phys. Fluids* **4** (1961) 1151.
[11] JOHANSSON, R. B., SMÅRS, E. A., Proceedings of the Fifth International Conference on Ionization Phenomena in Gases, Munich, 1961 (North-Holland Pub. Co., Amsterdam).
[12] KNORR, G., *Z. Naturf.* **13a** (1958) 944.
[13] WILHELM, H. E., Proceedings of the Fifth International Conference on Ionization Phenomena in Gases, Munich, 1961 (North-Holland Pub. Co., Amsterdam).

EXPERIMENTS WITH PARTLY IONIZED ROTATING PLASMAS*

Bo Angerth, Lars Block, Ulf Fahleson, Karl Soop

Royal Institute of Technology

Stockholm, Sweden

The interaction between a neutral gas and plasma moving relative to each other has been investigated by means of rotating plasmas where the current has been limited by resistors in order to prevent complete ionization. The measurements have included seven light gases and the results show that the voltage across the discharge is fixed at a level which is roughly independent of current and pressure, and proportional to the magnetic field as long as the gas is incompletely ionized. For all seven gases investigated so far this voltage corresponds to a mean plasma velocity $\bar{v}$ given by $m_i\bar{v}^2/2 = eV_i$ where V_i is the ionization potential of the gas in question and m_i is the ion mass. Apparently the interaction between plasma and neutral gas is much stronger above this velocity than below it.

1. Introduction

In an earlier publication one of us has given a preliminary report on some experiments with plasma moving through neutral gas [1]. The present paper is a continuation of that report and the same apparatus has been used for more extended investigations.

As pointed out by Alfvén [2] the interaction between a plasma and a neutral gas moving with respect to each other is of great importance both in general plasma physics and in astrophysics. A long time ago Alfvén [3, 4, 5, 6] suggested that this effect may have played an important role when the planetary system was formed. He assumed that neutral gas falls in towards a central body, e.g. the sun or a planet, and becomes ionized and stopped in the magnetic field of the sun. The situation is thus, that neutral gas moves through plasma and is accelerated by gravity as it approaches the central body. The main problem is then to find out where and how the neutral gas is ionized.

Energetically this can only occur if the neutral gas velocity v_n relative to the plasma at least fulfills the condition that

$$\frac{1}{2} m_n v_n^2 > \frac{1}{2} m_n v_c^2 \equiv e V_i \qquad (1)$$

where m_n is the neutral particle mass and V_i the ionization potential of the neutral atoms. Eq. (1) serves as a definition of the velocity v_c.

Alfvén has shown that the orbits of the planets and satellites in the solar system can be explained if the neutral gas is ionized when $v_n \approx v_c$ so that Eq. (1) is not only a necessary but also a sufficient condition.

It is well known that the probability for ionization by ions is extremely small unless the relative velocity between the atoms and ions exceeds v_c by more than a factor 10. Hence, ionization cannot take place by direct collision. Instead, if we should accept Alfvén's assumption that ionization takes place as soon as v_c is exceeded we must assume that the neutrals in some way rapidly transfer their energy to the electrons which can then ionize.

If that is true then it means that the coupling between the neutral gas and the plasma suddenly increases very much when the relative velocity between the two media exceeds v_c. Hence, one should expect that, if a plasma is forced to move through neutral gas, the relative velocity should have a tendency to stabilize at a value close to v_c.

2. Experimental setup

In order to investigate this experimentally we have designed a rotating plasma device according to Fig. 1. This device is rather similar to the first homopolars described by Anderson *et al.* [7] except that we here deliberately limit the current by a resistor R in order to avoid complete ionization of the gas.

The fundamental part of the apparatus is a vacuum tank containing a coaxial electrode system bounded by pyrex-glass end insulators. Copper is used as electrode material. The inner electrode is provided with a sharp edge in the central plane to facilitate the ignition of the discharge. The basic dimensions of the apparatus are given in Fig. 1.

The vacuum tank is put between the poles of a large electromagnet capable of giving up to 10^4 G. The magnet was designed many years ago to give a homogeneous field. However, since it is desirable to use a mirror configuration, a pair of iron pieces, visible in Fig. 1, have been introduced. This arrangement gives a mirror ratio of about 1.2. The field configuration is very nearly the same for all field strengths. In experiments without these iron pieces the end insulators become severely burned, but the mirror field practically eliminates this type of damage.

A base vacuum of $2—4 \cdot 10^{-6}$ mm Hg has been used. Immediately prior to a discharge the pump baffle is closed and gas is let in to the desired pressure. After the discharge, pumping is resumed. One minute's pumping then yields about 10^{-5} mm. The lowest gas

* Conference paper CN-10/24, presented by L. Block. Discussion of this paper is given on page 93. Translations of the abstract are at the end of this volume of the Conference Proceedings.

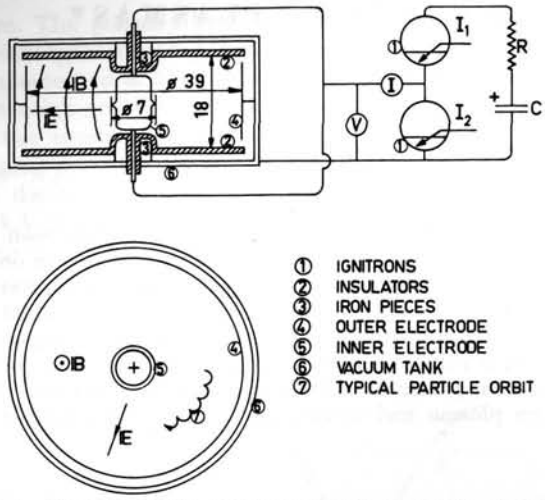

Fig. 1 Sketch of the apparatus with a circuit diagram.

pressure used, 5 microns, lies about a factor 1000 above base vacuum and a factor 500 above "between-firings" vacuum. During discharges with the highest currents increases in pressure of about 3—4 microns have always had to be accepted. This may of course be quite serious when working with low initial pressures.

The discharge circuit is shown in Fig. 1. Energy stored in the capacitor bank C is discharged via a series resistor R, and the main ignitron I_1 serves as a switch. After a certain time, often about 80 μs, the discharge is short-circuited by the crowbar ignitron I_2.

The various parameters used for the experiments are listed in Table I.

TABLE I. Basic parameters

Gases used:	H_2, D_2, He, N_2, O_2, Ne, A
Pressure:	$p = 5$—200 microns
Magnetic field:	$B_0 = 1000$—10 000 G at inner electrode
	$B_1 = 450$—4500 G at outer electrode
Mirror ratio:	1.2
Condenser battery:	$C = 20$—150 μF
	$V_A = 5$—15 kV
	$W = 1$—11.7 kJ
Series resistor:	$R = 1$—200 ohms
Maximum current during a discharge:	
	$I = 10^2$—10^4 A
Inner electrode:	
radius	$r_0 = 3.5$ cm (1.7 cm a few times)
height	$h = 10$ cm (2.5 cm a few times)
Outer electrode:	
radius	$r_1 = 19.5$ cm (5.7 cm a few times)
height	$h = 15$ cm always

The experiments which have been performed are the following:

(1) Current and voltage measurements.
(2) Short-circuit experiments.
(3) Time integrated Doppler-shift measurements along chords through the discharge in order to obtain the plasma velocity.
(4) Photomultiplier measurements of the light as a function of time and distance from the central plane.
(5) Time integrated spectrograms.
(6) Time resolved photomultiplier measurements of certain spectral lines.
(7) Magnetic probe measurements.

3. Operation of the discharge

In most experiments the larger electrodes have been used with inner electrode diameter = 7 cm and outer electrode diameter = 39 cm (see Table I). Unless otherwise specified the results in the following always refer to experiments with these electrodes.

Fig. 2 shows some typical oscilloscope traces of discharge voltage and current versus time in hydrogen, nitrogen and argon discharges. Idealized voltage curves of these types of discharges are shown in Fig. 3. Fig. 3a refers to hydrogen discharges and Fig. 3b to nitrogen and argon discharges. The points where the voltage and current are measured are indicated in the circuit diagram of Fig. 1. An analysis of the voltage and current reveals that the current is determined mainly by the resistance and that the inductance of the circuit plays a minor role. If the resistance is made

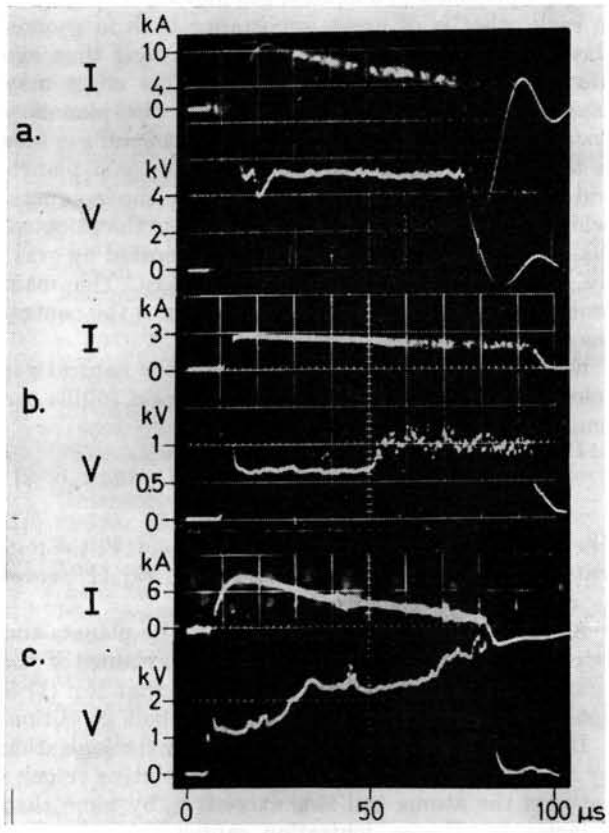

Fig. 2 Typical voltage and current traces for
(a) Hydrogen: $p = 30$ μ Hg, $B_0 = 8000$ G, $R = 1$ Ω, $V_A = 12.5$ kV;
(b) Nitrogen: $p = 40$ μ Hg, $B_0 = 2000$ G, $R = 4$ Ω, $V_A = 12.5$ kV;
(c) Argon: $p = 60$ μ Hg, $B_0 = 8000$ G, $R = 1$ Ω, $V_A = 12.5$ kV.

very small, the current maximum reaches about 50 kA at $C=66$ μF and $V_A=15$ kV. The total inductance of the circuit is about 3 μH.

According to Fig. 3a the hydrogen discharges may be described as follows. At $t=t_0$ the ignitron I_1 is triggered and the capacitor bank voltage V_A appears between the electrodes. After a certain waiting time (a few μs in typical cases) breakdown occurs at $t=t_1$ and the voltage begins to fall. The gas is ionized and put into rotation by the $\mathbf{I}\times\mathbf{B}$ tangential force. We may denote this "the ignition phase". This lasts 5—10 μs and after this time $t=t_2$ the voltage stabilizes on a remarkably constant value. The time of this voltage plateau will be called "the burning phase". At the pre-determined time $t=t_3$ ignitron I_2 is triggered and the discharge is short-circuited. The voltage then drops to zero and the current reverses so that the

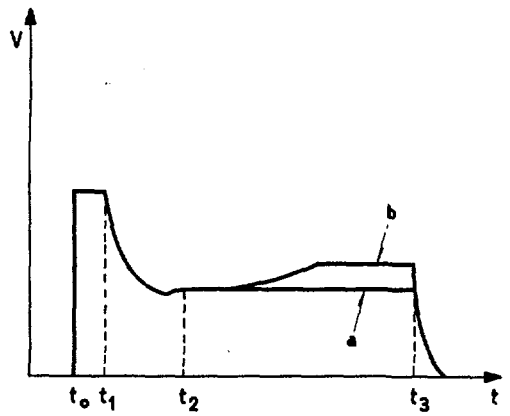

Fig. 3 Idealized voltage curves for discharges with unbaked electrodes (a) in hydrogen and (b) in nitrogen and argon.

rotation of the plasma is braked. This means that the kinetic energy of the plasma mass motion is transformed into electrical energy.

The argon type of discharge shown in Fig. 3b differs from the hydrogen discharge mainly in one respect, viz. that there are two voltage plateaus during the burning phase, one lower first and then a higher one. This is true for all gases other than hydrogen but it is more pronounced the heavier the gas is.

4. The voltage plateau

We shall here focus our interest on the burning phase, which is characterized by the voltage plateau. This exhibits some remarkable properties.

In Figs. 4, 5 and 6 the voltage plateau is given as a function of pressure p, current I and magnetic field B for some of the gases used. In case there are two plateaus we have here taken only the first (lower) one. The second (higher) plateau will be discussed later.

It is seen from these figures that each gas gives a characteristic burning voltage independent of pressure and current within wide limits and about proportional to the magnetic field. The ratio V_p/B_0 is roughly a constant, characteristic of each gas.

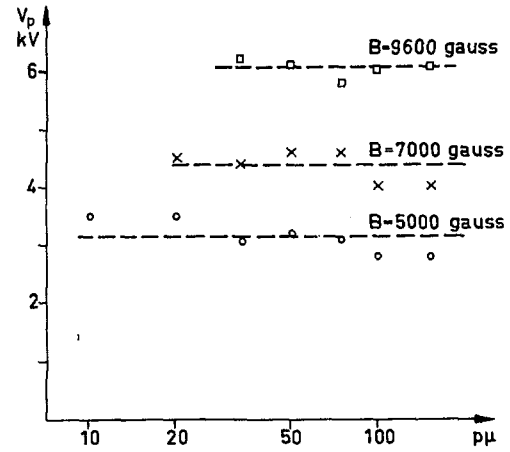

Fig. 4 Burning phase voltage V_p as a function of pressure in μ Hg for hydrogen discharges with $V_A=10$ kV, $R=2$ Ω.

It seems reasonable to assume that the burning voltage is largely due to the back e.m.f. produced by the polarization field $\mathbf{v}\times\mathbf{B}$. According to the theory of rotating plasmas we have for each ion of mass m_i and charge Ze

$$Ze\,E+\frac{m_i v_\theta^2}{r}=Ze\,v_\theta B_z \tag{2}$$

which means that the voltage across the plasma between the radii r_0 and r_1 is

$$V=\int_{r_0}^{r_1}E\,\mathrm{d}r=\int_{r_0}^{r_1}v_\theta B_z\,\mathrm{d}r-\int_{r_0}^{r_1}\frac{m_i v_\theta^2}{Ze\,r}\,\mathrm{d}r\,. \tag{3}$$

If r_0 and r_1 are equal to the electrode radii, we obtain the burning voltage V_p minus the voltage V_s across possible electrode sheaths. Hence,

$$V_p=V_s+\int_{r_0}^{r_1}v_\theta B_z\,\mathrm{d}r-\int_{r_0}^{r_1}\frac{m_i v_\theta^2}{Ze\,r}\,\mathrm{d}r\,. \tag{4}$$

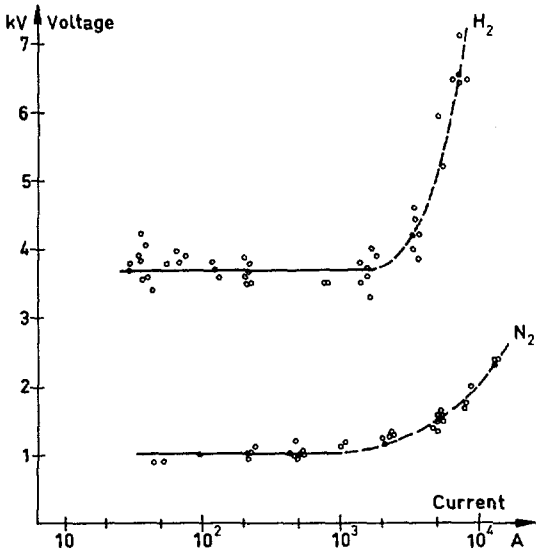

Fig. 5 Burning phase voltage versus current for hydrogen and nitrogen discharges. $B_0=6000$ G, $p=30$ μ Hg.

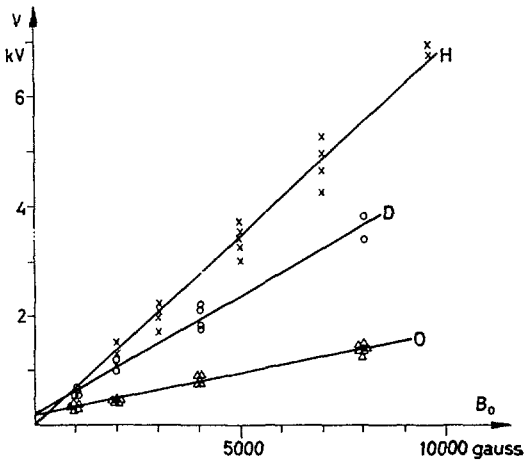

Fig. 6 Burning phase voltage versus magnetic field. Upper curve—H_2: $V_A = 15$ kV, $R = 1\,\Omega$, $p = 10$—$150\,\mu$ Hg. Middle curve—D_2: $V_A = 12.5$ kV, $R = 16\,\Omega$, $p = 20$—$40\,\mu$ Hg. Lower curve—O_2: $V_A = 12.5$ kV, $R = 16$—$52\,\Omega$, $p = 5$—$80\,\mu$ Hg.

The results according to Fig. 6 suggest that the second term is dominating.

Alfvén's hypothesis, that the neutral gas is ionized as soon as the relative velocity between the plasma and the neutral gas exceeds the value given by Eq. (1), implies that the coupling between the two media increases very much at this critical velocity. Hence, if the neutral gas in the discharge vessel is in sufficiently good contact with the walls so that it is moving very slowly, the plasma velocity v_θ should have a tendency to settle at a value about equal to v_c given by Eq. (1). This should then occur in the discharge wherever there is neutral gas which is moving sufficiently slowly. It may be expected that at sufficiently low currents this should be the case at every value of the radius r, at least near the end walls. Then $v_\theta = v_c$ independent of r so that v_θ can be taken outside the integrals of Eq. (4). Assuming that V_s is small we may then for every ion compute the value of v_θ from V_p and B_0.

In order to test Alfvén's hypothesis we have analysed the burning voltages corresponding to all discharges in this way. Some typical results are shown in Figs. 7 and 8. In Fig. 7 the velocities v_θ for hydrogen are given in km/s as a function of p and I. It is seen that few values differ by more than 20% from the value $v_c = 54$ km/s computed from Eq. (1). At low pressures and currents, where the velocities have been labelled "high", Alfvén's hypothesis probably does not apply because these values correspond to a glow discharge. At high pressures the velocities are just a little lower than 54 km/s. At very high currents (> 10 kA), not indicated in the figure, the velocities are increasing rather much above v_c and this may either be due to complete ionization or to very strong $\mathbf{I} \times \mathbf{B}$-forces which may put even the neutral gas into rotation by elastic collisions between ions and atoms. However, in these cases there are usually no voltage plateaus but rather a damped oscillating voltage.

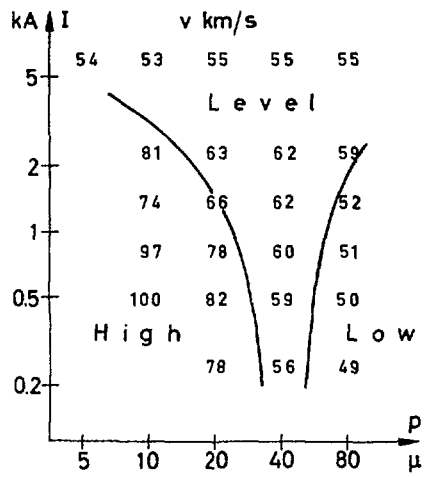

Fig. 7 Hydrogen plasma velocities versus pressure and current calculated from the burning phase voltage according to Eq. (3). $B_0 = 2000$ G.

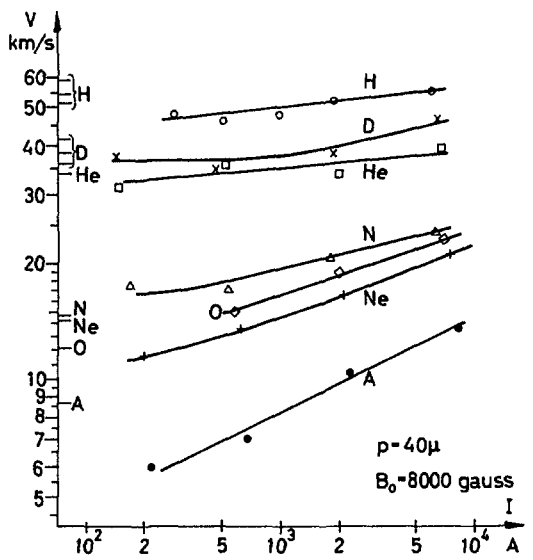

Fig. 8 Plasma velocities versus current for seven gases calculated from first voltage plateau.

Fig. 8 gives v_θ versus I for all the seven gases investigated so far at $p = 40\,\mu$ and $B_0 = 8000$ G. On the ordinates are indicated the critical velocities v_c according to (1) for all gases used. For hydrogen and deuterium three values have been indicated corresponding to the ionization potential for the reactions $H \rightarrow H^+ + e$, $H_2 \rightarrow H_2^+ + e$ and $H_2 \rightarrow H + H^+ + e$. For m_n we have always used the atomic mass.

It is seen from Fig. 8 that the burning voltages in all cases very nearly correspond to the critical velocities. All gases come in the right order except O and Ne which are exchanged but they are so close that this may be due to the experimental errors.

For other pressures and magnetic fields we may construct diagrams similar to the one shown in Fig. 8. The gases then all come in the same order but the velo-

cities may differ somewhat. This may have the following possible explanations:

(*a*) Alfvén's hypothesis may be incorrect;
(*b*) Alfvén's hypothesis is correct but the neutral gas is dragged with the plasma;
(*c*) The gas is almost fully ionized so the influence of the neutral gas is negligible;
(*d*) Impurities may enter the discharge region to such an extent that they change the conditions appreciably.

In order to investigate this more in detail we have made the following experiments.

5. Influence of electrode diameter

According to Alfvén's hypothesis the velocity in the discharge region would not depend very much on position in the discharge. If this is true, the burning voltage would be approximately proportional to $\int_{r_0}^{r_1} B_z \, dr$ according to Eq. (4), if the first and the last terms are small. This would hold if we change not only B_z but also the electrode radii. To test this we made some experiments with considerably reduced electrode radii according to Table I. In these experiments hydrogen was used. The result was that for weak magnetic fields the burning voltage was somewhat larger than it should be according to Alfvén's hypothesis, but not at all as large as it would be if a velocity distribution corresponding to the $1/r$ vacuum electric field between the large electrodes would also hold in the case of small electrodes. This is shown in Table II.

TABLE II. Comparison between corresponding experiments with small ($r_0 = 1.7$ cm, $r_1 = 5.7$ cm) *and large* ($r_0 = 3.5$ cm, $r_1 = 19.5$ cm) *electrodes*

B_0 (gauss)	p (μ Hg)	I_{max} (kA)	V_{ps}/V_{pl}		
			Experiment	$v = v_c$	$v \sim 1/r$
8000	15	8.1	0.21—0.31	0.26	0.66
8000	60	2.4	0.21—0.26	0.26	0.66
4000	15	2.5	0.22—0.26	0.25	0.60
4000	60	8.8	0.26—0.38	0.25	0.60
2000	15	2.8	0.28—0.33	0.25	0.49

(V_{ps} = voltage plateau with small electrodes, V_{pl} = voltage plateau with large electrodes.)

It is natural that the experimental values of the ratio of voltage plateau with small electrodes to that with large electrodes, V_{ps}/V_{pl}, should be somewhat larger than the theoretical values with $v = \text{constant}$ because the sheath voltage V_s would influence the results more at smaller radii than at larger.

6. The second higher voltage plateau for heavier gases

As mentioned before, the burning voltage for gases heavier than hydrogen increases after some time so that the burning phase gives two voltage plateaus.

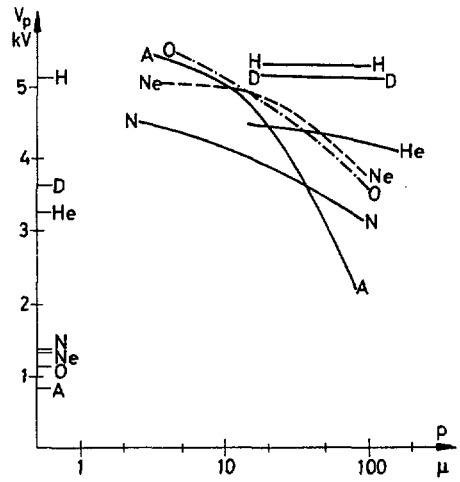

Fig. 9 Second higher voltage plateau V_p as a function of pressure for various gases. $B_0 = 8000$ G, $R = 1$ Ω.

What has been reported above refers to the first lower plateau.

The second higher plateau is somewhere between the lower and the hydrogen plateau. The exact value of the voltage depends mainly on the pressure. Its variation with pressure is shown in Fig. 9. It is seen that lower pressures give higher second plateaus and at $p \lesssim 10$ μ it is very near the hydrogen level.

The duration of the first plateau has also been investigated as a function of pressure and current. This is shown in Fig. 10. It is seen that the duration of the first plateau and hence also the elapsed time until the second plateau appears is longer for high pressures, and small currents, i.e. high series resistance R.

It is suggested that the second plateau is due to hydrogen impurities which enter the discharge after some time. The discharge then runs on a gas mixture which gives a higher velocity so that the heavier gas

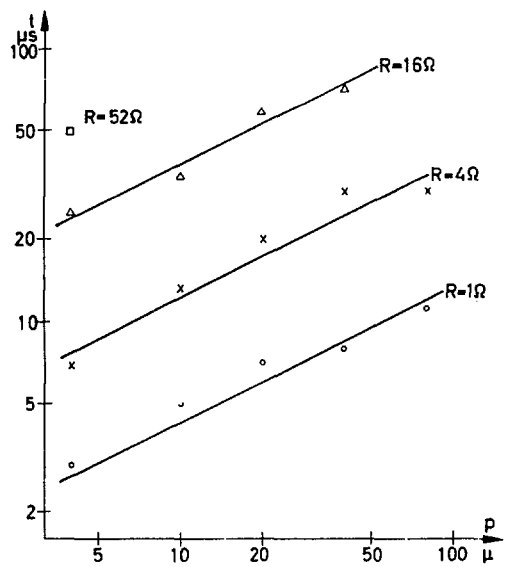

Fig. 10 Duration of the first voltage plateau as a function of pressure and series resistor value for argon discharges. $B_0 = 4000$ G.

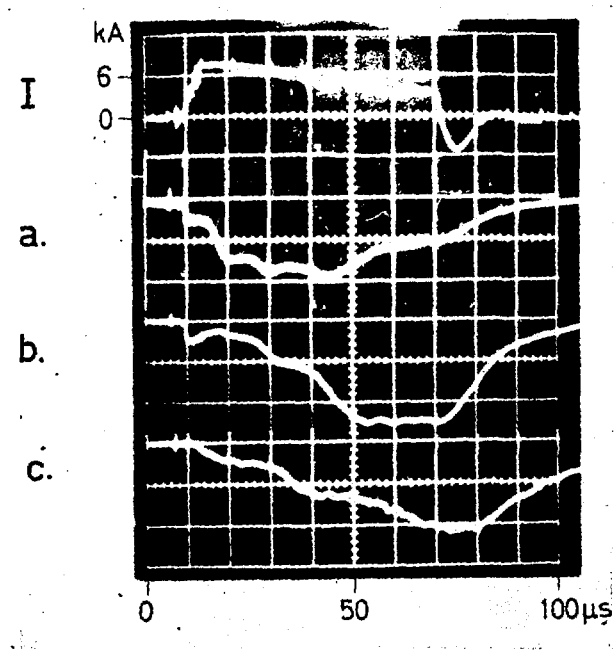

Fig. 11 Oscilloscope traces of current and light from a nitrogen discharge as seen by a photomultiplier through a monochromator, with $p = 8$ μ Hg, $B_0 = 7000$ G, $R = 1$ Ω and $V_A = 12.5$ kV. (a) N II (3994 Å), (b) C II (4267 Å), and (c) Hβ (4860 Å).

is centrifuged out. This idea agrees with the results indicated in Figs. 9 and 10 that the second plateau occurs earlier and is closer to the hydrogen level at low pressures and high currents. To test this suggestion we made two different kinds of experiments. Firstly, we investigated the light of certain spectral lines of the main gas and of impurities as a function of time in several discharges by means of monochromators and photomultipliers. Three oscilloscope traces of this are shown in Fig. 11 for a nitrogen discharge. The light of the main gas follows the current fairly well but the impurity light, both C and H increases with time practically throughout the discharge. Whenever we looked for hydrogen in discharges with two plateaus we found it. Apparently the electrodes and walls of

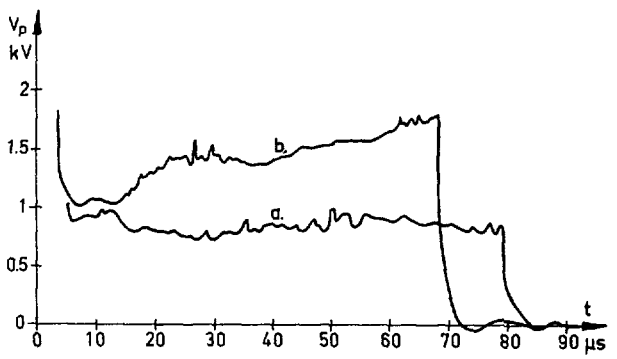

Fig. 12 Comparison between nitrogen discharges with baked and unbaked electrodes.
(a) Baked electrodes: $p = 10$ μ Hg, $B_0 = 8000$ G, $V_A = 12.5$ kV and $R = 4$ Ω.
(b) Unbaked electrodes: $p = 15$ μ Hg, $B_0 = 8000$ G, $V_A = 12.5$ kV and $R = 4$ Ω.

the apparatus were saturated with hydrogen from previous discharges. After all, hydrogen has been used much more frequently than any other gas.

These facts encouraged us to make a second kind of experiment in order to get rid of the hydrogen. The apparatus was not bakeable. However, a new set of electrodes were baked in a vacuum tank and inserted in the apparatus. Then a number of nitrogen and neon discharges were run. The result is seen in Fig. 12. There was no increase in voltage in the particular discharge shown here when the electrodes were baked, but the corresponding earlier discharge showed an increase in burning voltage almost all the time. Even the lower plateau was a little too high earlier, if we compare it with the plateau corresponding to $v = v_c$ for nitrogen. However, with baked electrodes we get very nearly the voltage level corresponding to Alfvén's hypothesis.

It was quite apparent that the nitrogen and neon burning voltages were reduced towards the $v = v_c$ voltage with baked electrodes in all cases where it was previously higher, for the first 15—20 discharges after the baked electrodes were installed. Later on the electrodes were apparently again contaminated by hydrogen in spite of the fact that no hydrogen discharges were run. The hydrogen must then have come from the glass insulators and walls of the vessel which were not baked.

It was observed that the current and voltage traces quite often were much less hashy with baked electrodes than with unbaked. The hash is usually in the form of voltage spikes upwards from the ordinary burning voltage. It looks as if the discharge is partly extinguished.

From these experiments we may draw the conclusion that the cleaner the discharge, the better is the agreement with the assumption that $v = v_0$ everywhere in the discharge. The deviations from this were therefore probably to a large extent due to impurities.

7. Doppler effect measurements

Doppler effect measurements on some spectral lines have been made along four chords through the discharge. The minimum distances of the chords from the axis of the apparatus were 5, 10, 14 and 18 cm. With the spectrograph aligned along one of the chords, discharges were run with the magnetic field first up and then down, say, so that spectra for both plasma velocity directions were recorded on the same photographic plate. Since the light intensity in most cases was insufficient to obtain good spectra in one shot, we had to superimpose several shots. Hence, the most reliable data were obtained at the highest currents, which gave most light so that only 2—4 shots had to be superimposed.

Because of the small light intensity we did not make any time resolved spectra. Instead we put a monochromator and photomultiplier at the other end of the chord and measured the intensity versus time of the spectral lines which were used for the Doppler effect measurements. Since the spectrograph had the

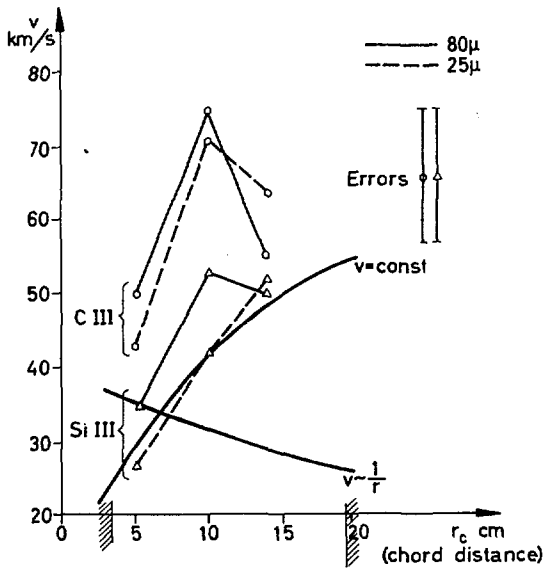

Fig. 13 Proton velocities in hydrogen discharges calculated from observed Doppler shifts of C III and Si III lines. Theoretical curves assuming $v = v_c = \text{constant}$ and $v \sim 1/r$. $B_0 = 8000$ G, $R = 1\ \Omega$.

best dispersion in the ultraviolet the lines C III (2296 Å) and Si III (2542 Å) were used.

Figs. 13 and 14 give the results for the most reliable measurements. The measured velocities must be corrected to proton velocities because according to Eq. (2) particles with different masses and charges move with different velocities due to the difference in the centrifugal force. The corrected velocities are given in Fig. 13. The differences of the curves calculated from the carbon and silicon Doppler shifts are within the experimental errors, but there may also be some discrepancies due to differences in the density distribution versus radius in the discharge. A closer examination of the experimental data shows that in these particular discharges the intensity of the C III line had a peak at an early stage when the voltage was high before it had gone down to the plateau. The Si III light was strongest later during the burning phase. This explains why the C III shows such large Doppler shifts.

Since we only measure the velocity components along the line of sight, we must compare the average of this velocity along each chord with the experimental values. This average must be weighted according to light intensity distribution. This is not very well known but according to Fig. 14 we get most light from the chord 10 cm from the axis. The intensity diminishes towards both electrodes. A uniform intensity distribution would give the theoretical curves in Fig. 13 for the two cases $v = \text{constant}$ and $v \sim 1/r$, so that the experimentally observed Doppler shifts agree best with $v = \text{constant}$. Inhomogeneous intenrity distributions may change the curves considerably, but it is impossible to construct any intensity distribution which would fit the observed Doppler shifts with a $1/r$-velocity distribution.

It would be extremely tedious to make a complete determination of the velocity distribution by means of Doppler shift measurements. However, the results so far have not been in conflict with the idea of a roughly constant velocity. We have never observed any Doppler shifts corresponding to higher velocities than v_c outside the experimental errors for discharges with voltage plateaus corresponding to $v = v_c$.

The line profiles indicate random velocities of the same order as the ordered velocities if there is only Doppler broadening present.

The neutral gas spectra have not been very extensively studied but in most cases no Doppler shifts have been observed in agreement with the assumption that the neutral gas is at rest.

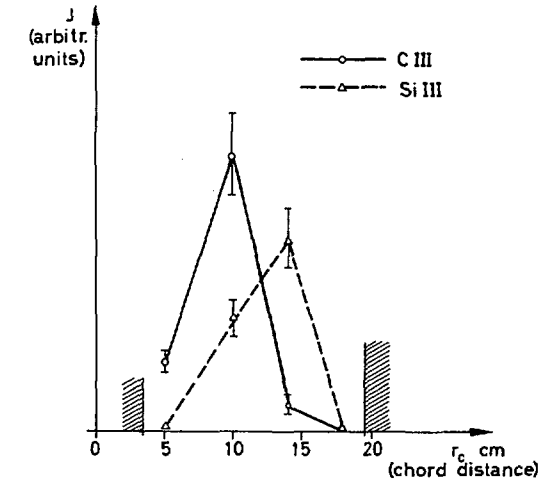

Fig. 14 Observed average intensities of C III (2297 Å) and Si III (2542 Å) lines in hydrogen discharges during the burning phase. $B_0 = 8000$ G, $R = 1\ \Omega$.

8. Short-circuit experiments

As has been mentioned above, there is a back pulse of current through the discharge when the ignitron I_2 (Fig. 1) is triggered so that the discharge is short-circuited. This back pulse corresponds to an energy which has been stored in the plasma. The kinetic energy of the plasma rotation therefore at least partly appears as electrical energy at the short-circuiting. Hence, we may in this way calculate a lower limit of the plasma kinetic energy. If we also assume that the velocity $v = \text{constant}$, we may obtain a lower limit of the number of ions participating in the rotation. How this calculation is done has been shown by FAHLESON [1]. In this way it is found that, when the burning voltage is higher than the value corresponding to $v = v_c$, the ionization degree is high, often nearly 100%. For hydrogen this has been true in all cases so far investigated. According to Fig. 5 this is the case when the current exceeds about 10 kA. For other gases we have earlier seen that higher voltages may be caused by impurities.

9. Interaction between plasma and neutral gas

Theoretical calculations of the conditions in our discharges have been made and the details will be published elsewhere. However, a brief report will be given here.

It is mentioned above that the neutral gas spectra show no Doppler shifts, indicating that the neutral gas is nearly at rest. However, this does not exclude that the neutral gas is centrifuged out from the central parts of the plasma so there is only a thin sheath of neutral gas near the electrodes and walls of the discharge chamber. The light then comes from this sheath which is approximately at rest. To investigate this one may assume that the force $\mathbf{i}_r \times \mathbf{B}_z$ which drives the plasma is transferred to the neutral gas by elastic and charge exchange collisions. In the case of an infinitely long cylindrical discharge the momentum balance of the neutral gas in the azimuthal direction is then determined by

$$i_r B_z = \varkappa \left[r \frac{\partial^2 \omega_n}{\partial r^2} + 3 \frac{\partial \omega_n}{\partial r} \right] \qquad (5)$$

where $\varkappa$ is the coefficient of viscosity of the neutral gas and ω_n is the angular velocity of the neutral gas. In the radial direction the centrifugal force is taken up by a pressure gradient. It can then easily be shown that less than 100 A in our discharge suffices to create a sheath of neutral gas 1 cm thick at the outer electrode provided the neutral gas is at room temperature.

In the actual apparatus a neutral gas sheath may be created also near the end walls as shown in Fig. 15.

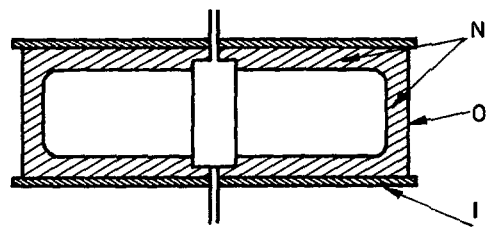

Fig. 15 Probable distribution of neutron gas in the discharge region at $p \gtrsim 20$ μ Hg. N—Neutral gas regions, O—Outer electrode, I—Insulating end wall.

If this is the case, one should expect that the interaction between the neutral gas and the plasma takes place in thin layers near the walls. It is also possible that the discharge occurs in the form of rotating spokes, but this is unlikely since neither magnetic probe nor light measurements show any large variations in azimuth.

If the mean free path of the neutral particles is of the same order as the dimensions of the apparatus, the above theory according to Eq. (5) is not valid. This occurs at the lowest pressures (~ 10 μ) and then the neutral gas fills the whole volume.

The mean free path for a hydrogen molecule before it is ionized in a plasma with 6 eV electron temperature and 10^{14} ion pairs/cm^3 is about 6 cm. In our discharges the densities and temperatures may be both higher and lower than these values.

Considerations of the energy balance for the electrons including collisions with ions and neutral particles, ionization and excitation processes lead to electron temperatures between 5 and 10 eV in most of our hydrogen discharges, provided there exists an electron temperature, and if the ion thermal energy is equal to the kinetic energy due to the drift motion of the ions. The relaxation time for the electrons to obtain a Maxwellian velocity distribution is extremely short, about 1 μs even if the electron density is only 10^{12} cm^{-3}. Thus, since the discharges last much more than 10μs it is probable that the electrons are thermal.

The critical velocity may be explained if the electrons are heated to temperatures of the same order as the kinetic energy of the ions, so that they can ionize. Hence, the heating time for the electrons should be shorter than the time it takes for the plasma to settle at the critical velocity. If the heating is due to binary collisions only, it may be rapid enough in most cases when the experiments indicate that the plasma moves with the velocity v_c. However, at the lowest pressures this is not true. In these cases we must probably look for an explanation in terms of thin sheaths across which there is an electric potential equal to the ionization potential, perhaps as proposed by COLGATE [8].

A theoretical examination of dissociation and ionization processes shows that already when the ionization degree has reached a value of the order of one per cent, most of the gas is dissociated. Hence it is reasonable to use the atomic mass in Eqs. (1)—(4).

Acknowledgements

The authors wish to thank Professor H. Alfvén for his advice and constant interest in the present work.

Dr. G. A. Sawyer from Los Alamos has visited us for some time and his help during many of the experiments was invaluable. Mr. Stefan Lundgren, Mr. Bengt Nilsson and Mr. Sune Malmgren have also collaborated during the experiments.

The work has been financed by the Swedish State Council of Atomic Research and the Swedish Atomic Energy Company.

References

[1] FAHLESON, U. V., *Phys. Fluids*, 4 (1961) 123.
[2] ALFVÉN, H., *Rev. Mod. Phys.* 32 (1960) 710.
[3, 4, 5] ALFVÉN, H., *Stockholms Observatoriums Annaler* (Stockholm, 1942, 1943, 1946).
[6] ALFVÉN, H., On the Origin of the Solar System (Oxford University Press, New York, 1954).
[7] ANDERSON, O. A., BAKER, W. R., BRATENAHL, A., FURTH, H. P., ISE, J., Jr., KUNKEL, W. B., STONE, J. M., Proceedings of Second U.N. International Conference on Peaceful Uses of Atomic Energy, Geneva, 32 (1958) 155.
[8] COLGATE, S. A., U. S. Atomic Energy Commission Report UCRL—6176 (1961).

ON THE DIFFUSION IN THE POSITIVE COLUMN IN A LONGITUDINAL MAGNETIC FIELD*

G. v. GIERKE AND K. H. WÖHLER

MAX-PLANCK-INSTITUT FÜR PHYSIK UND ASTROPHYSIK, MUNICH, AND

INSTITUT FÜR PLASMAPHYSIK G.M.B.H., GARCHING NEAR MUNICH,

FEDERAL REPUBLIC OF GERMANY

Several theories and hypotheses have been proposed by different authors for the explanation of the anomalous diffusion in the positive column in a longitudinal magnetic field which was first observed by Lehnert. More detailed measurements on this subject have been done in a similar discharge. The dependence of the diffusion on the magnetic field (by measurement of the longitudinal electric field) has been recorded simultaneously with radial potential distributions, with the electron temperatures and with the influence of additional radiofrequency ionization. All these measurements are compatible with the theory of Kadomtsev *et al.* but do not exclude completely other explanations.

Application of an additional multipolar helical or azimuthal magnetic field changes the dependence of the longitudinal electric field on the longitudinal magnetic field. In both cases the direction of the current is shown to be significant. The stabilizing and destabilizing action of the additional field and its dependence on the main magnetic field strength, the gas pressure, and the current direction will be discussed. In the case of the multipolar field, effects of enhanced diffusion have been found which are not easy to explain. In the case of the additional azimuthal field there was a distinct dependence of the magnitude and sign of the azimuthal field on the critical magnetic field which seems to be a strong support for the theory of Kadomtsev *et al.*

1. Introduction

The particle and energy losses from a long positive column of a helium glow discharge, were shown first by LEHNERT [1] and afterwards by other authors [2, 3, 4, 5, 6, 7, 8] to decrease with increasing longitudinal magnetic field, as predicted by ambipolar diffusion theory, but only for fields less than a critical field B_c. Above B_c the losses increase. Several theories and hypotheses have been proposed by different authors for the explanation of the origin of this anomalous diffusion. HOH [9] in his theory made use of BOHM's [10] criterion for the existence of a stable wall sheath. By combination of that criterion with the plasma balance equation for the positive column he calculated a critical value of the magnetic field B_c above which the condition for the existence of a stable sheath is no longer satisfied. This theory has been criticized [7, 11] because it is not clear how the discharge can be affected if the sheath criterion is not satisfied. On the other hand this theory as a possible explanation of the instability cannot yet distinctly be excluded by the experimental results.

Measurements of T. K. ALLEN *et al.* [5] and MÜLLER [17] have shown that in the positive column with longitudinal magnetic field, the ambipolar diffusion of the charged particles perpendicular to the magnetic field can be changed, in some cases, in such a way that above a critical value of the magnetic field, the transverse diffusion of the ions exceeds that of the electrons and the wall which first was negative with respect to the discharge now becomes positive. One can ask if there is any connection between direction and strength of the radial field and the critical magnetic field.

Another interpretation of the observed enhanced diffusion is by the two-stream-instability. BERNSTEIN *et al.* [12] gave a criterion for the appearance of the two-stream instability:

$$u_d \geq v_{et} (m_e/m_i)^{\frac{1}{2}} \cdot A ,$$

where u_d is the mean drift velocity of the electrons parallel to the magnetic field; v_{et} the electron thermal velocity and m_e/m_i the mass ratio of electrons and ions, and the factor A is of the order of unity. The fluctuating electrical fields induced by this instability can probably produce an enhanced diffusion as pointed out by SPITZER [13].

The theory mostly discussed is that of KADOMTSEV *et al.* [14]. They show that a helical perturbation of the discharge column has to grow when diffusion to the walls can no longer overcome the effects of $\mathbf{j} \times \mathbf{B}$ forces that tend to increase the perturbation. This theory predicts, by a dispersion relation, a critical value B_c, frequency, wavelength, and growth rate of the oscillation which can be partly compared with the experimental results. More detailed experiments have been done with regard to these theories.

2. Experimental investigation

2.1. EXPERIMENTAL ARRANGEMENT

The experimental arrangement is shown in Figure 1. The discharge tube of 6 cm diameter and 260 cm length was placed on the axis of a solenoid 170 cm

* Conference paper CN-10/34, presented by K. H. Wöhler. Discussion of this paper is given on page 93. Translations of the abstract are at the end of this volume of the Conference Proceedings.

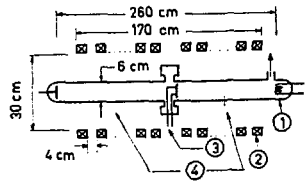

Fig. 1 Apparatus for anomalous diffusion experiment (not to scale). 1—hot cathode, 2—coils, 3—radial movable electrostatic probes, 4—electrostatic probes.

long. The discharge was run at constant current of 100 mA. In all cases the gas was helium. The criterion of SIMON [15] for the lack of end effects is

$$\frac{L}{R} > \frac{2\,(\omega_e \tau_e)^2\, e E_z R}{k T_e\,(2.4)^2}\,.$$

In our experiments this condition is satisfied at gas pressure higher than 10^{-1} torr. When the pressure is less than 10^{-1} torr the short circuit of the ends can

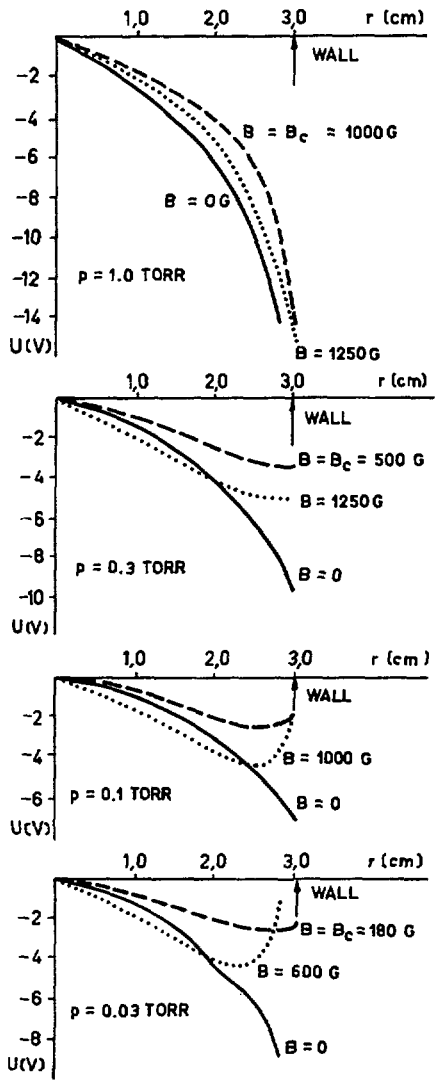

Fig. 2 Radial potential distribution for different longitudinal magnetic field strengths and different gas pressures.

already cause some effects. The particle losses to the walls were measured by measuring the longitudinal electric field between two identical floating cylindrical probes 100 cm apart.

2.2. Radial potential distribution

The radial potential distribution was measured with two plane molybdenum probes of 2 mm diameter which were moveable in the radial direction and which had a fixed separation of 1 cm. The planes were directed perpendicularly to the longitudinal magnetic field. The result of these measurements is shown in Figure 2. The radial potential distribution with respect to the potential on the axis is plotted for different magnetic field strengths and different gas pressures. For gas pressures higher than $p = 0.3$ torr there was no reversal of the radial electric field to be found. For pressures less than 0.3 torr there was a field reversal for values of the magnetic field near the critical magnetic field B_c. The region in which a reversed electric field is to be observed is that right near the wall and had the thickness of some ion mean free paths, i.e. the region of the wall sheath. In that range the validity of the measurement is dubious because of the interaction with the sheath of the probe. But anyhow the fact remains that at pressures of about 1 torr, where the instability is very distinctive, there is no radial field reversal. Therefore one may conclude that there is no causal connection between radial field reversal and the observed sharp onset of the instability.

2.3. Two-stream instability

Single-probe and double-probe measurements have been made to determine the dependence of the electron temperature T_e on the magnetic field. The distribution of the electron velocity, which was found by measuring the second derivative of the probe characteristic, showed that there is no essential deviation of the velocity distribution from a Maxwellian distribution, especially that there is no fast velocity component of electrons. This distribution is not changed very much by the increasing magnetic field. In Figure 3 the ratio

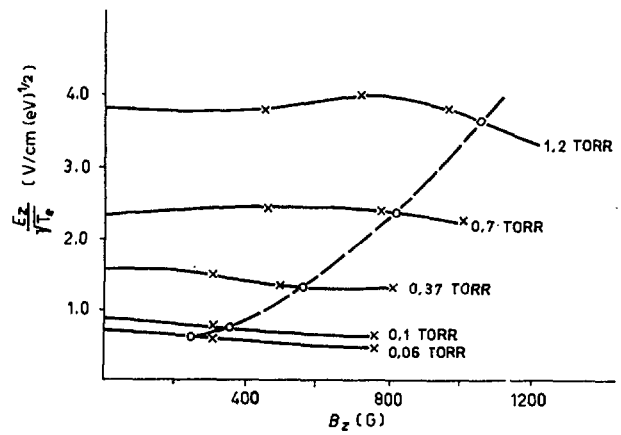

Fig. 3 Dependence of the ratio $E_z/\sqrt{T_e}$ (which equals electron mean drift velocity/electron thermal velocity) on the longitudinal magnetic field B_z. Encircled points are critical points.

$E_z/\sqrt{T_e}$ of the measured values of E_z and $\sqrt{T_e}$ is plotted against the magnetic field B. This ratio is proportional to the ratio u_d/v_{et} which is decisive for the existence of the two-stream-instability. If one calculates the ratio u_d/v_{et} for $p=1$ torr, $T_e=3$ eV, $E_z=4$ V/cm taking the electron mobility from S. C. BROWN [18], one finds that two-stream instability might be possible. Figure 3, however, shows that $E_z/\sqrt{T_e}$ is rather independent of the magnetic field and thus the interpretation of the observed instability as a two-stream instability seems rather difficult because it is not clear how to explain the critical dependence of the observed instability on the magnetic field. One has to say, however, that the probe measurement of the electron temperature in a magnetic field is rather dubious. On the other hand the measured relative values of T_e in connection with the measured B_c fit a smooth curve nicely (Fig. 3), showing that the results are not quite unreasonable.

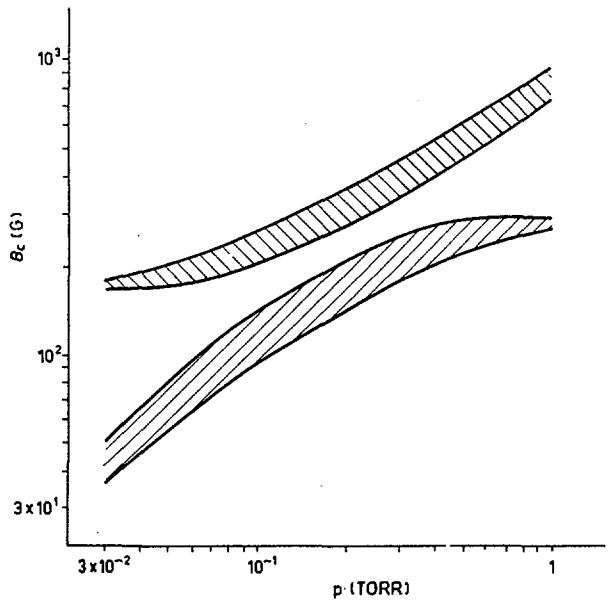

Fig. 4 Critical magnetic field B_c vs gas pressure. Upper shaded region corresponds to measured values for $R=6$ cm. Lower shaded region corresponds to values calculated from the theory of Kadomtsev, *et al.*

2.4. DIFFUSION WITH ADDITIONAL RF-IONIZATION

For the experimental proof of the theory of KADOMTSEV *et al.* [14], first the observed dependence of the critical magnetic field B_c on the gas pressure has been compared with B_c (theory), calculated from the measured values E_z, T_e and the theoretical stability criterion. The pressure range was $3\cdot10^{-2}$ to 1 torr. The results are (Fig. 4) in fair agreement as already shown by ALLEN *et al.* [7]. Unfortunately the range of our measurements does not permit a decision between the theories of HOH and KADOMTSEV *et al.*

A graphical representation of the stability criterion of the Kadomtsev theory (Fig. 5) shows that a decrease

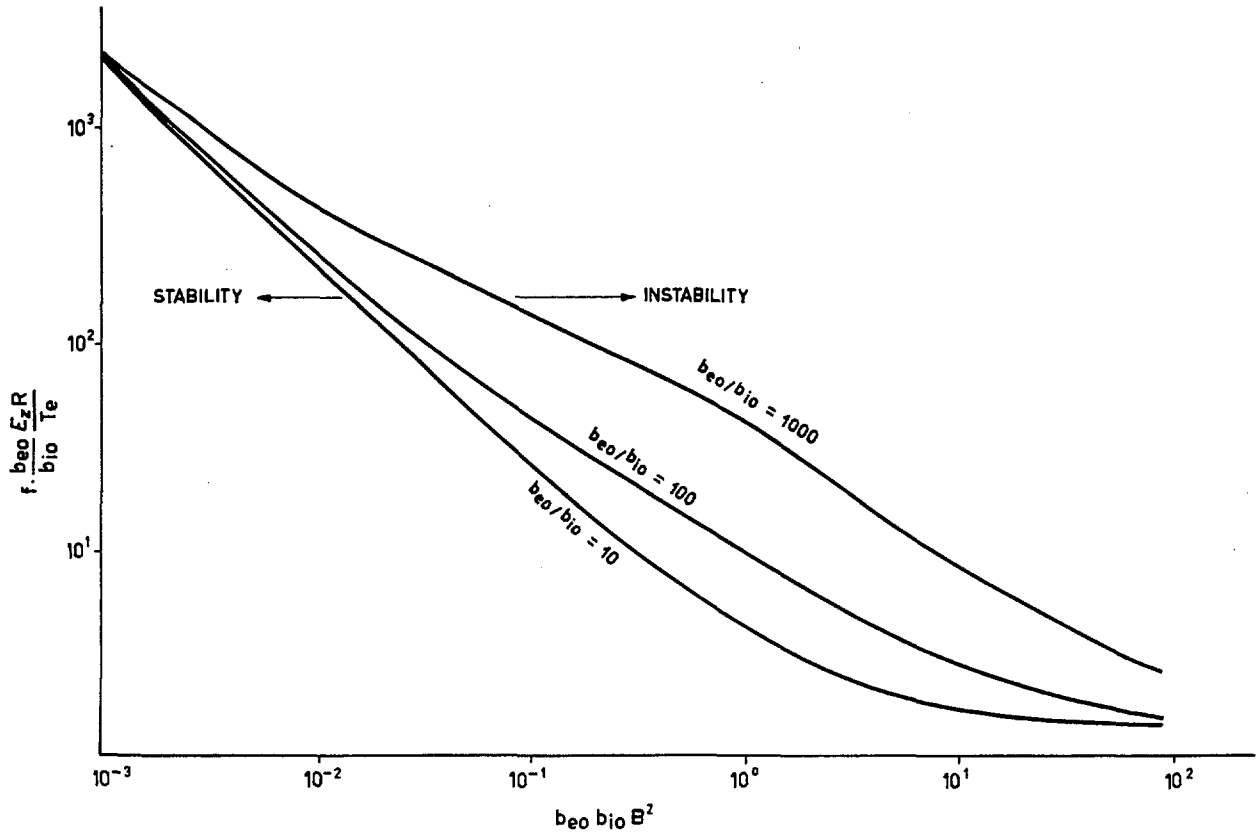

Fig. 5 Representation of the stability criterion of the theory of Kadomtsev *et al.* $f=0.15\cdot e/2.4\cdot k$, E_z = longitudinal electric field, T_e = electron temperature, R = tube radius, b_{e0}, b_{i0} = mobility of electrons and ions, respectively, in the z-direction and B_z = magnetic field.

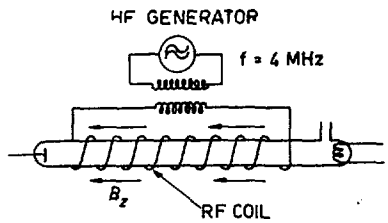

Fig. 6 Apparatus for diffusion experiment with additional RF ionization.

of the longitudinal electric field, leaving constant the remaining parameters of the discharge leads to an increase of the critical magnetic field strength. To verify this fact the whole discharge tube was placed in a long radiofrequency solenoid which was inductively coupled with an RF-generator of 4 MHz frequency (Fig. 6). The RF-energy input was variable in a wide range. By this additional RF-ionization with the discharge current left constant, the longitudinal electric field could be decreased. Figure 7 shows the dependence of the critical magnetic field on the longitudinal electric field for different gas pressures. To compare these results with the theory, knowledge of the electron temperature T_e at the critical point is necessary. An attempt to measure the electron temperature in the discharge with magnetic field and RF-ionization by the double-probe method was made. Electron temperatures of about 20 eV have been measured. The calculated theoretical values for B_c using this temperature are much higher than the measured values of B_c (Fig. 8). The reason may be that the electron temperature used in the calculation is too high and that the right temperature is much smaller. It is possible that the electron velocity distribution which now, because of the RF, could not be measured in the above described way, is no longer a Maxwellian distribution, but that there is a group of fast electrons in the 20 eV range. Similar results were also found in other RF-excited plasmas [19]. Indeed, the analysis of the double-probe measurements makes use only of that part of the probe characteristic which comes from the fastest electrons.

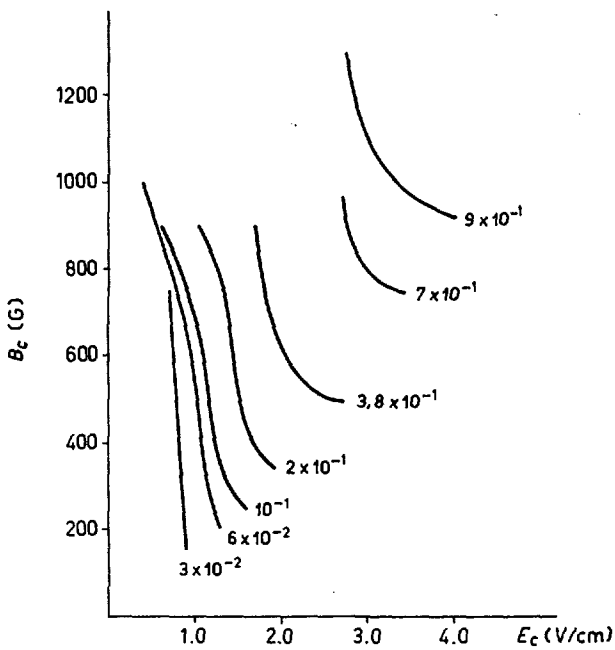

Fig. 7 Stability with additional RF ionization. Critical magnetic field B_c vs longitudinal electric field at the critical point for different pressures (in torr).

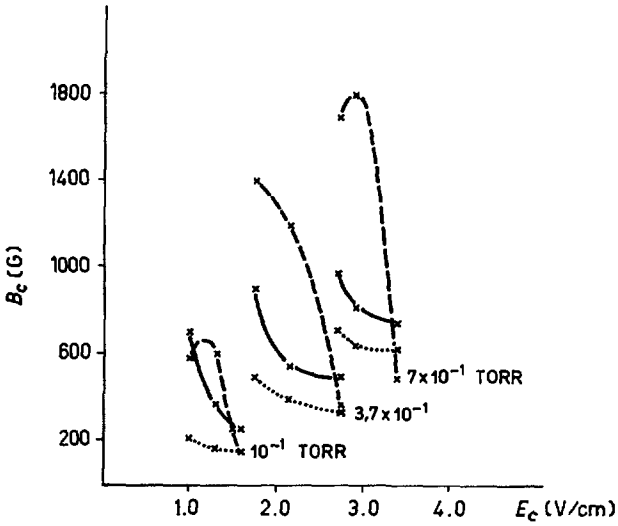

Fig. 8 Stability with additional RF ionization. Comparison between experimental results and theory. Critical magnetic field vs longitudinal electric field. Solid lines show measured values, dashed lines are values calculated from Kadomtsev's theory with T_e measured and dotted lines are values calculated with $T_e = 5$ eV.

If one recalculates the critical magnetic field with the original electron temperature of about 5 eV, one finds values of B_c less than the measured values (Fig. 8). With the very plausible assumption that the real temperature lies between the two values 5 eV and 20 eV, the agreement between the theory of Kadomtsev and the experimental results seems to be very good. A comparison between those results and the theory of Hoh seems to be difficult because n'/n_0, the ratio of the charged particle density at the sheath boundary to that at the discharge axis, enters the stability criterion and it is difficult to state how the RF-ionization influences this ratio.

2.5. Diffusion in an additional helical magnetic field

The vacuum magnetic field in a cylindrical tube with multipolar helical windings and a longitudinal magnetic field is in rough approximation a helical winding of the magnetic field lines; i.e. we have the B_z component and an additional azimuthal component B_θ. At the first we do not consider the influence of the additional radial component B_r of the magnetic field which is of the same order of magnitude as the B_θ component [16]. One would expect that the azimuthal magnetic field in the positive column of the discharge together with the electric longitudinal field E_z, yields

a drift velocity $\mathbf{E} \times \mathbf{B}$ of the charged particles, the direction of which is dependent on the direction of E_z and the direction of the helix. In the sense of the theory of KADOMTSEV *et al.* an additional drift to the wall may be interpreted as an additional diffusion mechanism which acts as a damping mechanism for the instability, and vice versa when the drift is directed to the axis. There is, however, an additional effect of the helical field. The effects of the $\mathbf{j} \times \mathbf{B}$ forces resulting from the perturbation of the discharge channel are also changed by the helical magnetic field. When the B_z field is in the direction of the current $\mathbf{j}$, the influence of a right-hand helical winding should be stabilizing for the right-hand helical perturbation of the current channel. (These two influences, diffusion stabilizing and current stabilizing, are opposite each other but one can suppose that the influence of the changed $\mathbf{j} \times \mathbf{B}$ forces is rather small as the wavelength of the magnetic helix is long, whereas the wavelength of the current perturbation can take nearly all values.)

We made experiments with systems of multipolar windings of $l=2$ (4 windings) and $l=3$ (6 windings) on the discharge tube. The results with $l=2$ windings are very similar to, but not quite as confusing as, the results with the $l=3$ windings. For this reason we only discuss the case $l=2$. The dimension of the tube was the same as described above. The period of the windings was $L=100$ cm (Fig. 9). The maximum current through the helical windings was 400 A, which yields a maximum of the magnetic field at the wall of the discharge tube of about 150 G. We measured the dependence of the longitudinal electric field on the longitudinal magnetic field for different pressures and different currents in the helical windings. The measurements show the losses of the discharge to be dependent on the direction of the current with respect to the direction of the longitudinal magnetic field. In all cases, the losses with helical field are higher than without helical field and the losses are higher for E_z in the direction of B_z than for E_z in the direction opposite to B_z. The critical magnetic field could in some cases be determined only by the rise of the noise because the curve of E_z versus B_z showed different bends caused probably by the different effects mentioned above. In Figure 10 the dependence of the longitudinal electric field on the longitudinal magnetic field is plotted for different pressures and for the cases: (a) without helical field, (b) with maximum helical field and E_z in direction opposite to B_z and (c) with

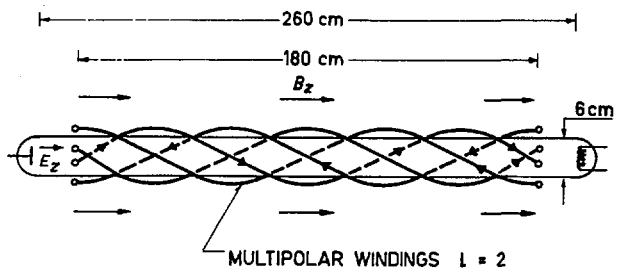

Fig. 9 Apparatus for diffusion experiment with additional helical magnetic field of $l=2$.

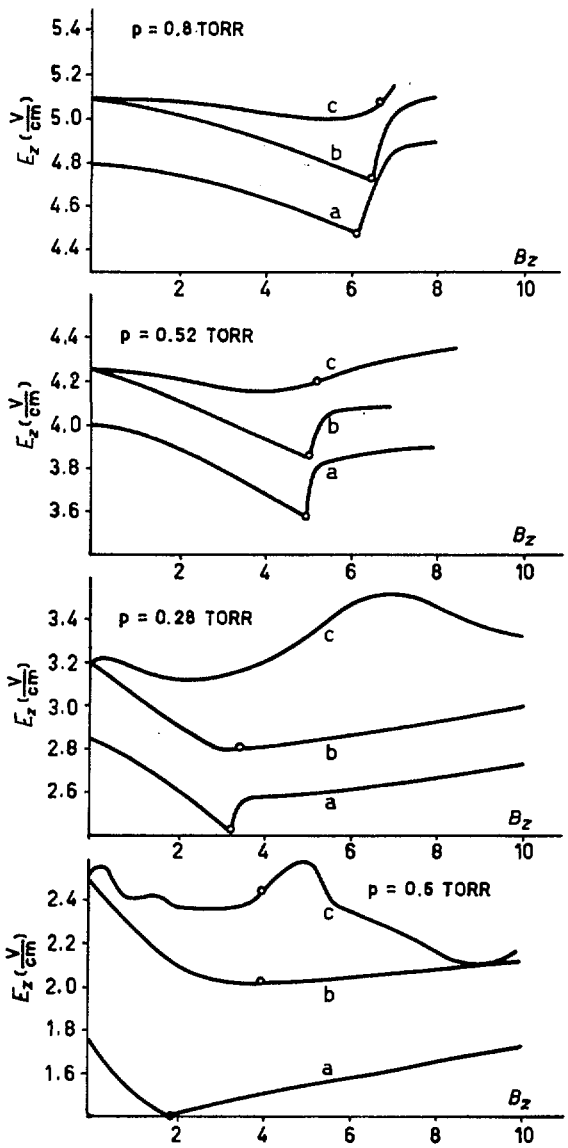

Fig. 10 Diffusion effects with additional helical magnetic field. The dependence of longitudinal electric field on the longitudinal magnetic field is plotted for different pressures for the following cases: (a) without helical field, (b) with helical field and E_z in direction opposite to B_z, (c) with helical field and E_z in the same direction as B_z. Encircled points indicate rising point of the noise from a probe in the central position marking B_0. The maximum current through the helical windings was 400 A, producing a magnetic field at the wall of the discharge tube with a maximum of about 150 G.

maximum helical field and E_z in direction of B_z. The critical magnetic field was shifted in both cases to higher values, more in the low pressure than in the high pressure range. These results show that the main influence on the diffusion cannot be explained by the $E_z \times B_0$ contribution, for this does not yield the enhanced losses in both cases of E_z direction. Moreover, the fact that losses for the case of E_z in the direction of B_z are higher than for the opposite direction of E_z is in contradiction to this assumption. The fact that the discharge itself shows higher stability in

both cases can be explained by the higher losses which were induced by the helical field in both cases. A possible interpretation for these higher losses in both cases is the influence of the B_r-component of the helical field which causes field lines to penetrate the wall. These penetrations force the charged particles to reach the wall moving along the field lines. At higher longitudinal magnetic fields this effect contributes less to the diffusion but higher order terms become more effective for the drift to the wall.

This experiment shows that the helical field produces a very complicated situation inside the discharge by perturbation of the ordinary cylindrical symmetry and it seems difficult to estimate the influence of the additional forces on the stability. Nevertheless this experiment shows higher particle losses to have a stabilizing action.

2.6. Diffusion in an additional azimuthal magnetic field

To investigate the influence of an additional drift velocity of the charged particles on the stability in a more simple case, an isolated copper wire was placed in the axis of a similar discharge tube in our next experiment. A pure azimuthal magnetic field was produced inside the discharge in this way (Fig. 11). The azimuthal field together with the main field again yields a helical magnetic field which in this case has no B_r components. The maximum field strength at the tube wall was 30 G. This azimuthal field together with E_z produces a drift to the wall or to the axis according to the polarity of the current through the axial wire. This should cause a stabilizing or destabilizing action on the observed instability according to the theory of Kadomtsev *et al.* Again the dependence of the longitudinal electric field on the longitudinal magnetic field was measured as a hint for the particle losses to the wall. Measurements without excitation of the azimuthal field showed the perturbation of the discharge by the axial wire to be not essential at pressures higher than 0.4 torr. The measurements with the azimuthal magnetic field (Fig. 12) show obviously a stabilizing action for the field direction causing a drift to the wall and a destabilizing action in the opposite case. In this experiment, too, it is found that the losses are increased by the azimuthal field only, the reason for which may be the decreased mobility of the electrons in the z-direction produced by the azimuthal field. From Schottky's theory it follows that there is an increasing electric field when the mobility is decreasing and the electron temperature is left constant. A quantitative comparison of the results with the theories of Kadomtsev *et al.* and Hoh is not possible because these theories do not include the influence of an azimuthal magnetic field component.

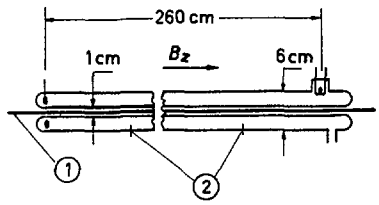

Fig. 11 Apparatus for diffusion experiment with additional azimuthal magnetic field. 1—conductor for the production of the azimuthal field, 2—electrostatic probe.

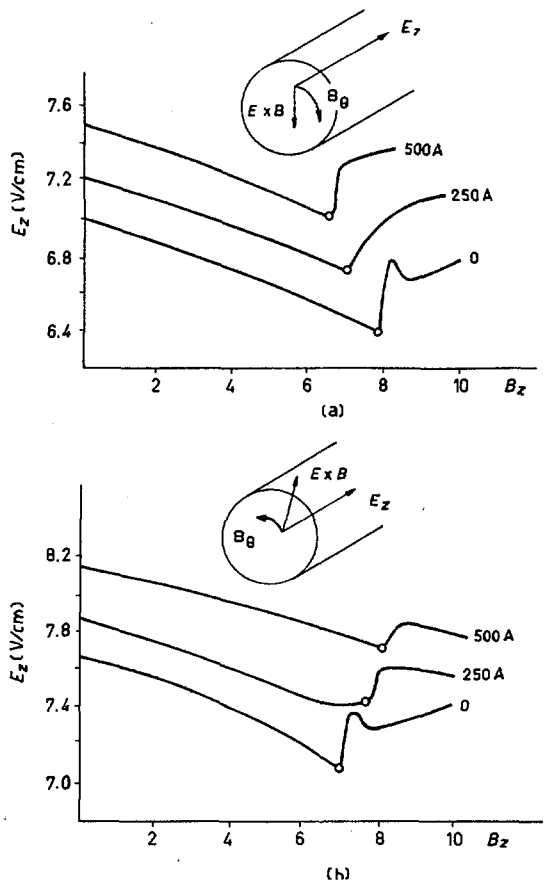

Fig. 12 Particle losses in the positive column with (a) azimuthal magnetic field clockwise (drift $\mathbf{E} \times \mathbf{B}$ inward) and (b) azimuthal magnetic field counterclockwise (drift $\mathbf{E} \times \mathbf{B}$ outward). The maximum of the magnetic field produced at the wall of the discharge tube by the helical winding was about 150 G. Encircled points indicate onset of noise.

3. Conclusion

The measurements of the radial potential distribution in the range of high gas pressure (0.3 torr to 1 torr) showed no radial electric field reversal at high magnetic field strength. A causal connection between radial field reversal and the observed instability seems therefore to be rather unlikely. The ratio u_d/v_{et} of the electron drift velocity in the electric field direction to the electron thermal velocity is shown to be independent of the longitudinal magnetic field which seems to be good reason against interpreting the observed instability as a two-stream instability.

An additional RF-ionization with the discharge current left constant results in a decrease of the longi-

tudinal electric field and in an increase of the critical magnetic field, which can be explained by the theory of KADOMTSEV, *et al.* Reasonable agreement was found between the measured dependence of B_c on the electric field and the values calculated by KADOMTSEV's theory. Superposition of a helical multipolar magnetic field gives effects of enhanced diffusion which are dependent on the direction of the discharge current with respect to the direction of the longitudinal magnetic field. The application of the helical multipolar field has a small stabilizing action for the onset of the instability but it is not quite clear which forces cause this stabilizing influence.

Application of a pure azimuthal magnetic field, produced by an isolated axial conductor, on the discharge shows a stabilizing action when the drift velocity is directed to the wall and a destabilizing action in the opposite case. This fact can be explained by the theory of KADOMTSEV, *et al.*, if one assumes a drift velocity acting similarly to the ordinary diffusion mechanism. To compare these results qualitatively with the theories of HOH and of KADOMTSEV, *et al.*, theoretical investigations on a discharge with additional azimuthal magnetic field are in progress.

Acknowledgements

We have to thank G. Müller for the measurements of the electron velocity distribution and G. Müller, D. Pfirsch and F. Schwirzke for many discussions.

References

[1] LEHNERT, B., Proceedings of Second International Conference on Peaceful Uses of Atomic Energy, Geneva, **32** (1958) 349.

[2] LEHNERT, B., HOH, F. C., Proceedings of the Fourth International Conference on Ionization Phenomena in Gases, Uppsala 1959 (North Holland, Pub. Co., Amsterdam, 1960) Vol. II p. 604.

[3] LEHNERT, B., HOH, F. C., *Phys. Fluids* **3** (1960) 600.

[4] ALLEN, T. K., HORTON, M. C., PANLIKAS, G. A., PYLE, R. V., VOELKER, F. *Bull. Am. Phys. Soc.* **5** (1960) 314.

[5] ALLEN, T. K., HORTON, M. C., PANLIKAS, G. A., PYLE, R. V., VOELKER, F. Universityof California Radiation Laboratory Report No. UCRL-8887 (1959) p. 92.

[6] ALLEN, T. K., HORTON, M. C., PANLIKAS, F. A., PYLE, R. V., RUGGE, H. F., STEARNS, J. W., VOELKER, F. University of California Radiation Laboratory Report No. UCRL-9002 (1959) p. 90.

[7] ALLEN, T. K., PAULIKAS, G. A., PYLE, R. V., *Physical Review Letters* **5** (1960) 409.

[8] EKMAN, C., HOH, F. C., LEHNERT, B. *Phys. Fluids* **3** (1960) 833.

[9] HOH, F. C., *Physical Review Letters* **4** (1960) 559.

[10] BOHM, D., The Characteristics of Electrical Discharges in Magnetic Fields (Guthrie and Wakerling, Ed.) McGraw Hill, New York, 1949, Chapters I, II.

[11] HALL, L. S., *Phys. Fluids* **4** (1961) 388.

[12] BERNSTEIN, I. B., *Phys. Fluids* **3** (1960) 136.

[13] SPITZER, L. Jr., Princeton University, Matterhorn Project Report MATT-40 (1960).

[14] KADOMTSEV, B. B., NEDOSPASOV, A. V., *J. Nuclear Energy* **C1** (1960) 230.

[15] SIMON, A., Oak Ridge National Laboratory Report ORNL-1960 (1958).

[16] JOHNSON, J. L., U.S. Atomic Energy Commission Report NYO-8051 (1958).

[17] MÜLLER, G., Unpublished.

[18] BROWN, S. C., Basic Data of Plasma Physics (John Wiley, New York, 1959).

[19] SCHLÜTER, H., Thesis München 1961; Proceedings of the Fifth International Conference on Ionization Phenomena in Gases, Munich, 1961 (North-Holland, Amsterdam).

PLASMA CONFINEMENT USING AN ALTERNATING MAGNETIC FIELD*

H. A. BLEVIN, P. C. THONEMANN

CULHAM LABORATORY

ABINGDON, BERKSHIRE, UNITED KINGDOM

It is shown theoretically and experimentally that magnetic fields of megacycle frequencies can penetrate a dense plasma if the conductivity is sufficiently high. In the presence of an external axial magnetic field certain configurations of alternating magnetic fields lead to the diffusion of plasma either towards the walls or towards the axis. In the latter case confined plasmas have been produced in which an external axial field of about 1,000 gauss is reduced to zero at the axis. Examples of radial electron density profiles are presented.

1. Introduction

If the electrical conductivity is sufficiently high, a plasma behaves as though it were "frozen" to lines of magnetic force. In order that the plasma closely follows the "motion" of a periodically varying magnetic field both the electron and ion cyclotron frequencies must be much greater than the frequency at which the magnetic field changes. If the frequency of magnetic field variation exceeds the ion cyclotron frequency but is much less than the electron cyclotron frequency, electrons tend to be "frozen" to the lines of force whereas the ions are not. In most circumstances differential motion of electrons and ions resulting from a perturbation of the magnetic field is prevented by space-charge electric fields. However, if the lines of force "move" in a direction parallel to a surface of constant electron density, no charge separation takes place and the magnetic field carries the electrons with it.

It is possible, therefore, to produce steady electrical currents in a plasma by using "moving" magnetic fields. This phenomena was demonstrated experimentally in 1952 by THONEMANN, COWHIG and DAVENPORT [1, 2]. Conversely, if a cylindrical plasma rotates sufficiently rapidly in a steady magnetic field normal to the axis of rotation, steady electric currents and an associated axial magnetic field are produced in the plasma. The electrons are "tied" to the lines of force whilst the ions continue their rotation unhindered. If the plasma is completely isolated, collisions between electrons and ions will eventually bring both charges to the same velocity and the currents vanish. In laboratory plasmas momentum transfer to the walls of the vessel either by charge-exchange or by the direct impact of ions ensures the maintenance of such currents.

In the experiments to be described a magnetic field "rotates" about the axis of a cylindrical plasma in a manner similar to the fields in an induction motor. If the conductivity is sufficiently high the electrons are "frozen" to the rotating lines of force and circulating currents up to 750 amperes per centimeter length have been observed. In the presence of an externally produced steady axial magnetic field the plasma can be driven towards the walls or collapsed toward the axis until the radial component of the force $\mathbf{J} \times \mathbf{B}$ is balanced by the plasma pressure gradient.

2. Theory

Consider a plasma, bounded by a cylindrical insulating wall to which is applied a magnetic field rotating about the axis of the cylinder with an angular frequency ω, much greater than the ion cyclotron frequency ω_i but much less than the electron cyclotron frequency.

The following assumptions are made.

(*a*) The positive ions are so massive that their motion in the alternating fields can be neglected.
(*b*) The density gradient of the ions in the radial direction is arbitrary.
(*c*) All quantities are independent of position in the axial direction.
(*d*) The electron temperature is constant in space and time.
(*e*) The frequency of the applied field is much less than the electron gyrofrequency in that field so that electron inertia may be neglected.
(*f*) The plasma is sufficiently highly ionised so that the electrical resistance is determined by electron ion collisions.
(*g*) The currents in the plasma are sufficiently small so that the distortion of the applied field may be neglected.

The equation of electron motion

$$\mathbf{E} - \frac{\mathbf{J} \times \mathbf{B}}{n e} + \frac{\nabla (\varrho_e)}{n e} - \eta \mathbf{J} = 0 \,, \qquad (1)$$

together with an applied field of the form

$$B_r = B_0 \cos(\omega t - \theta),$$
$$B_\theta = B_0 \sin(\omega t - \theta),$$
$$B_z = B_a$$

are to be solved for the steady component of electron current J_0.

* Conference Paper CN-10/65, presented by H. Blevin. Discussion of this paper is given on page 94. Translations of the abstract are at the end of this volume of the Conference Proceedings.

The θ and z components of Eq. (1) are

$$E_\theta - \frac{1}{ne}[J_z B_r - J_r B_z] - \eta J_\theta = 0\,, \qquad (2)$$

$$E_z - \frac{1}{ne}[J_r B_\theta - J_\theta B_r] - \eta J_z = 0\,. \qquad (3)$$

Multiplying Eq. (3) by B_r and solving for J_θ yields

$$J_\theta\left(1+\frac{B_r^2}{(ne\eta)^2}\right) = -\frac{\omega r B_r^2}{ne\eta^2} + \frac{Ee}{\eta} + \frac{J_r B_z}{ne\eta} + \frac{J_r B_\theta B_r}{(ne\eta)^2}\,. \qquad (4)$$

where E_z has been replaced by $\omega r B_r$.

Assuming that $J_r=0$, $\nabla\cdot\mathbf{J}=0$ and $\partial\mathbf{J}/\partial z=0$, it follows that J_θ is independent of θ and the line integral of Eq. (4) in the θ direction taken between the limits $(0, 2\pi)$ yields

$$J_\theta' = \frac{-ne\omega r}{1+2\,(ne\eta/B_0)^2}\,. \qquad (5)$$

For the two cases

$$\eta = 0\,,\ \frac{\partial n}{\partial r} \neq 0\,,$$

$$\eta \neq 0\,,\ \frac{\partial n}{\partial r} = 0\,,$$

it can be shown that there is no solution for J_r which satisfies the condition $J_r=0$ at the plasma boundary, and the assumption $J_r=0$ is valid for these two cases. If $J_r\neq 0$ in the general case, then there will be components of J_θ and J_r which are θ dependent. Thus a contribution to the component of J_θ independent of θ can arise from the last two terms of Eq. (4). Provided that $ne\eta/B_0 \ll 1$ then $J_\theta' = -ne\omega r$ and the electrons are "tied" to the rotating magnetic lines of force. From Eq. (3) it follows that $J_z=0$ and the applied field remains uniform throughout the plasma.

3. Ion motion

If the frequency of the rotating field lies well above the gyrofrequency of the ions, the induced ion currents are very much smaller than the electron currents and the ions are set into rotation principally by electron ion collision. If the plasma is completely isolated, both ions and electrons must ultimately rotate synchronously with the field. The characteristic time constant for this rotation is $B_0/ne\eta\omega_i$. In practice, loss of momentum, by ions striking the tube walls or by charge exchange, will ensure a net electron current even in the steady state. A heavy gas was chosen for the experiments so that the time for the ions to gain appreciable velocity in the θ direction due to electron collision was much longer than the observation time.

4. Equilibrium radial density distribution

The electrons circulating in the θ direction produce an axial magnetic field which decreases with increasing radius. The plasma is therefore driven radially outwards. If an externally produced axial magnetic field of sufficient strength is superimposed in a direction opposite to the self field, the plasma is driven towards the axis until the plasma pressure gradient balances the inward Lorentz force. The equilibrium density distribution in this latter case will now be calculated.

Assuming that the sum of the electron and ion temperature is independent of radius and the condition $ne\eta/B_0 \ll 1$ is fulfilled the equations

$$-\frac{\partial B_z}{\partial r} = \mu_0 J_0' = -\mu_0 ne\omega r$$

$$J_\theta' B_z = \mathrm{k}T\frac{\partial n}{\partial r}\,,$$

lead to

$$\frac{\partial}{\partial r}\left(\frac{1}{nr}\frac{\partial n}{\partial r}\right) = -\frac{\mu_0^2 e^2\omega^2}{\mathrm{k}T} nr\,. \qquad (6)$$

The solution of Eq. (6) is (MKS units):

$$n\mathrm{k}T = \frac{\frac{2B_a^2}{\mu_0}\left(\frac{4\pi B_a}{\mu_0 N_0 e\omega}-1\right)\exp\left(\frac{B_a e\omega r^2}{2\,\mathrm{k}T}\right)}{\left[1+\left(\frac{4\pi B_a}{\mu_0 N_0 e\omega}-1\right)\exp\left(\frac{B_a e\omega r^2}{2\,\mathrm{k}T}\right)\right]^2}\,, \qquad (7)$$

where T is the sum of the electron and ion temperatures, N_0 is the number of electrons per unit axial length and B_a is the intensity of the applied axial magnetic field. Eq. (7) is valid for an unbounded axisymetric plasma. Provided n(wall) $\ll n$(axis) it may be used without significant error for a bounded plasma.

There are three special cases of interest,

(1) If $\frac{4\pi}{\mu_0}\frac{B_a}{N_0 e\omega} > 2$, n decreases monotonically with increasing radius and the axial field is everywhere in the same direction.

(2) If $1 < \frac{4\pi}{\mu_0}\frac{B_a}{N_0 e\omega} < 2$, n is a maximum and $B_z=0$ when $\frac{B_a e\omega r^2}{2\,\mathrm{k}T} = \ln\left(\frac{\mu_0 N_0 e\omega}{4\pi B_a - \mu_0 N_0 e\omega}\right)$. At smaller values of radius the axial field is reversed.

(3) If $\frac{4\pi B_a}{\mu_0 N_0 e\omega} < 1$, the reverse field is greater than B_a and the plasma cannot be confined.

Examples of these distributions are given in Section 6.

The object of the experiments was threefold:

(*a*) To show that a steady circulating electron current and an associated magnetic field could be produced by rotating a magnetic field about the axis of a cylindrical plasma;

(*b*) To show that the electrons were tied to the rotating lines of force provided $ne\eta/B_0<1$; and

(*c*) To verify Eq. (7) for the particle, density distribution.

5. Apparatus

The experimental conditions were determined by the plasma resistivity η, the gas pressure at which a well ionised plasma can be produced readily and the requirement that the frequency of the alternating magnetic field should lie between the electron and ion gyrofrequency in this field. Assuming an electron temperature of 40,000 °K, a singly ionised gas and an initial gas pressure of 10^{-2} mm. of mercury, the condition $ne\eta/B_0<1$ requires $B_0 > 10^{-2}$ webers/m^2

(100 gauss). The gyrofrequency of a singly charged helium ion in a field 100 gauss is about 4×10^4 cycles/second so that frequencies in the range 1—10 MHz are suitable. In most cases argon or xenon were used.

The production of magnetic fields of 100 G in the megahertz frequency range is a matter of some difficulty if continuous operation is envisaged. However, it is a simple matter to produce such fields by the transient discharge of a condenser in an oscillatory circuit and this latter method was adopted.

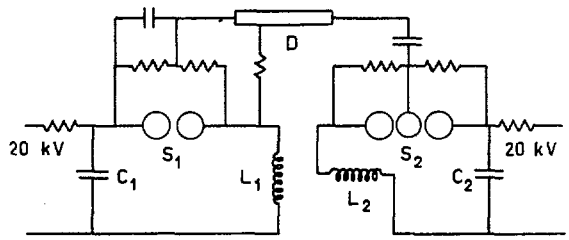

Fig. 1a Schematic diagram of the electrical circuit showing 0.04 μF mica capacitors C_1 and C_2, spark gaps S_1 and S_2, delay line D and inductors L_1 and L_2 adjusted to minimize mutual inductance.

The electrical circuit and the arrangement of the apparatus is shown in Figure 1. Two mica capacitors C_1 and C_2 (0.04 μF) were charged to 15—20 kV and discharged $\pi/2$ out of phase through conductors which passed parallel to the axis of a pyrex discharge tube about 3 cm in diameter and 20 cm long. The spark gap S_1 was adjusted to break down when the condensers were charged to a predetermined voltage, and the spark gap S_2 then triggered half a period later by means of the delay cable D. The two inductances L_1 and L_2 were adjusted to minimize the mutual inductance.

The frequencies used were in the range 1—1.5 MHz and in the absence of a discharge the circuit current decayed almost linearly to zero in about 30 cycles. The Q of the resonant circuit without spark gaps was several hundred so that the rapid decrement was due to the spark gap losses.

A re-entrant tube T, 3 mm in diameter and placed diametrically across the discharge tube permitted a variety of probes to be inserted to measure the local magnetic fields. Flux coils F encircled the discharge tube and together with a suitable integrating circuit served to determine the change in the total axial magnetic flux at different positions along the tube. A continuous flow of gas was maintained through the tube and the gas pressure measured by a Pirani gauge.

The probe coils inevitably gave a signal at the frequency of the rotating magnetic field due to misalignment and electrostatic interference, so that low pass filters with a cut-off frequency of 1.0 MHz were used to eliminate this interference.

6. Measurements

Figure 2 shows typical oscillograph records of the axial magnetic field taken with a probe on the plasma axis. The oscillatory traces are the applied rotating field. Trace b was obtained with an external field sufficient to confine the plasma and trace d with the same field reversed in direction. The gas was not pre-ionised so that the time delay between the start of the growth of the axial and the rotating field (1—2 μs) is due to both the growth of ionisation, and to the rate at which energy is supplied to build up the B_z field. The decay of the axial magnetic field in trace d is attributed to the expansion of the plasma to the walls followed by wall recombination and a drop in electron temperature. The time scale of the decrease is consistent with acceleration of positive ions to the walls by the "magnetic pressure". Trace b shows the axial magnetic field remaining constant for about 2.5 microseconds, when a confining axial field is used. The decay of the circulating currents in this case is due to the decrease in the rotating field to a value where it is screened from the interior of the plasma. Figure 3 shows a comparison of the alternating magnetic field amplitude at the axis and at the tube walls. A noticeable feature is the phase lag of the internal field when the amplitude is small. Such a phase shift is to be expected as $ne\eta/B_0$ approaches unity and increases further.

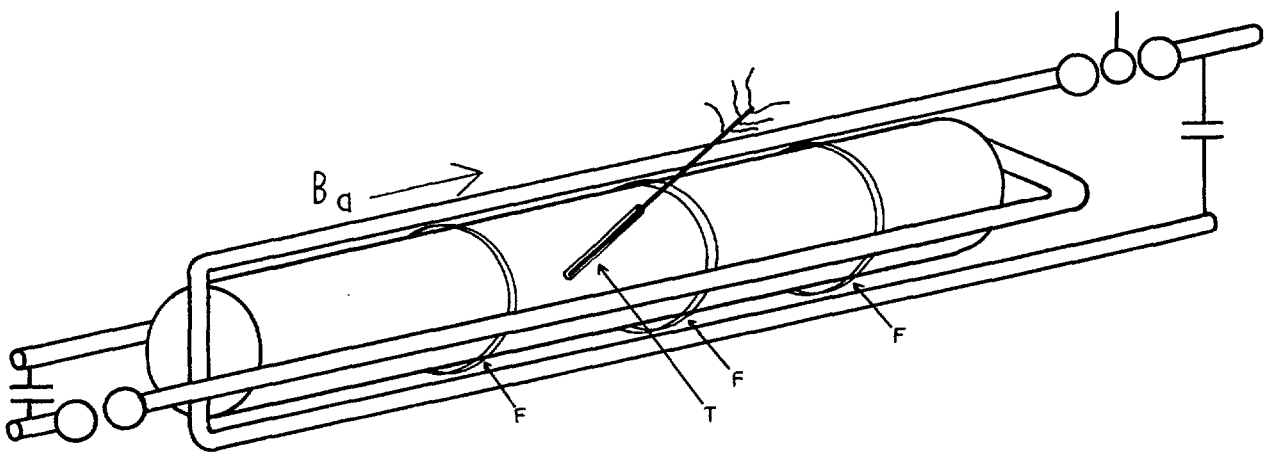

Fig. 1b Arrangement of the apparatus showing the discharge tube with flux coils F and re-entrant tube T.

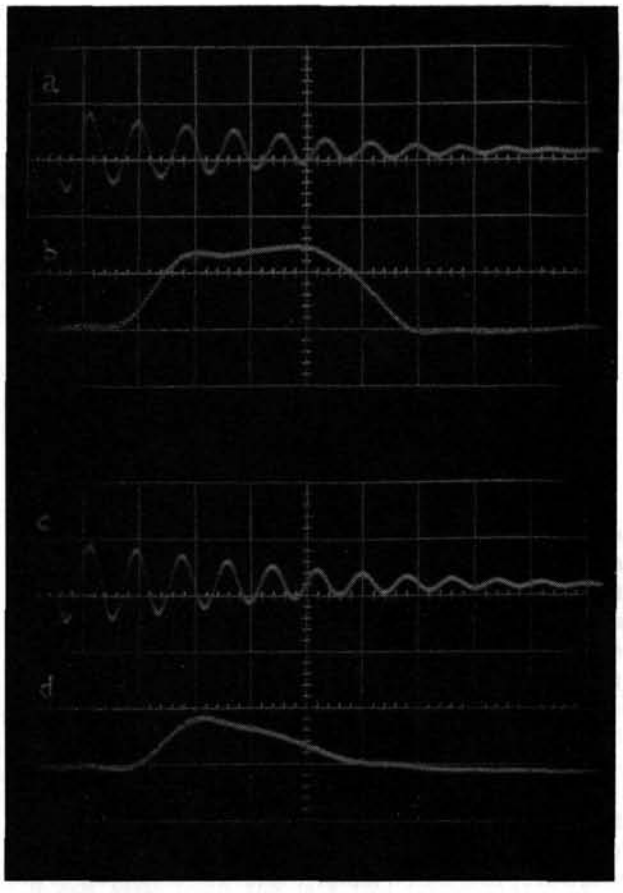

Fig. 2 Oscillograph traces of the change in the axial magnetic field. (a) and (c) are the applied rotating fields measured at the tube walls. (b) shows the change in the axial field when the applied voltage gave confinement and (d) the change in axial field when the applied field was reversed. The time scale is 1 μs per division. The experimental conditions were: gas—Xe, $N_0 = 3 \times 10^{15}$ cm^{-1}, $f = 1.18$ MHz, $N_g = 2.2 \times 10^{15}$ cm^{-1}, $B_a = +660$ G in (b), $B_a = -660$ G in (d).

When the electrons are rotating with synchronous velocity the z component of current vanishes so that the rotating magnetic field is neither attenuated nor distorted within the plasma. The amplitude or the phase of the rotating magnetic field at the axis compared to the same quantities at the walls is thus an indication of the degree of slip. When the rotating field was intense, little phase shift was found, whereas towards the end of the oscillatory period the phase shift became pronounced. Phase shifts of 180° were observed when the rotating magnetic field decayed to a small amplitude.

If $N(r)$ is defined as the number of electrons per unit length which lie outside a cylinder of radius r so that

$$N = 2\pi \int_r^\infty nr \, \mathrm{d}r \,,$$

then the difference between the external and internal axial fields is given by

$$B_a - B_z = \frac{\mu_0}{2\pi} N e \omega \,. \qquad (8)$$

Values of N_0 calculated from the observed fields are compared to the initial number of gas atoms in Table I.

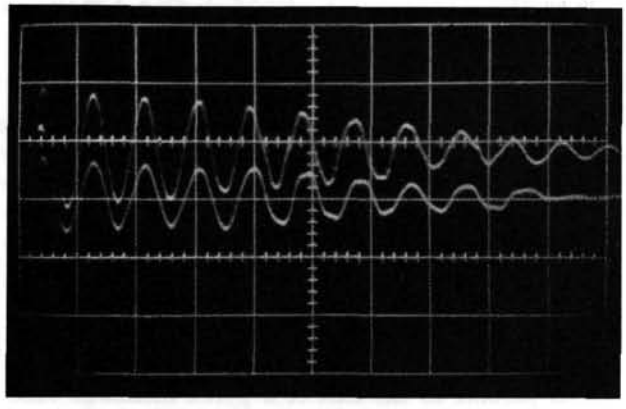

Fig. 3 Comparison of rotating field amplitude at walls and on plasma axis showing phase shift towards end of pulse. Scale is 1 μs per division.

The results quoted were obtained under conditions of negligible slip.

In some cases the calculated value of N_0 is greater than the number of gas atoms and sometimes less, depending on the initial currents in the conductors producing the rotating field and initial gas pressures. The number of electrons will be less than the number of gas atoms if the ionisation is incomplete, and greater if the gas is multiply ionised. This fact accounts for the difference between the two values of N. When hydrogen was used, the rotating field decayed to a small value before appreciable ionisation had time to build up, and to make measurements with this gas intense pre-ionisation is required.

TABLE I

Gas	Gas pressure (microns)	Tube diameter (cm)	ω	B_a (Gauss)	Initial rotating field on axis (Gauss)	$B_a - B_z$ on axis	Gas atoms per cm N_g	Electrons per cm N_e
Xenon	5	4.9	7.9×10^6	730	460	970	4.1×10^{15}	3.9×10^{15}
Xenon	12	3.3	7.9×10^6	650	600	333	3.7×10^{15}	1.3×10^{15}
Argon	14	3.3	7.9×10^6	0	600	870	4.4×10^{15}	3.5×10^{15}
Xenon	3.1	3.3	5.5×10^6	550	420	370	0.94×10^{15}	2.1×10^{15}

The electron density as a function of radius was found using the equation

$$\frac{dB_z}{d(r^2)} = \frac{1}{2}\mu_0 ne\omega , \qquad (9)$$

obtained by differentiating Eq. (8). B_z was determined from probe records at various radii.

Two examples of density profiles are shown. In Fig. 4 the solid lines are the density distributions calculated using Eq. (7) assuming electron temperatures which give the best fit. The circles are the experimental points. The curves correspond to the case when $4\pi B_a/(\mu_0 N_0 e\omega) > 2$ and the electron density has its maximum value on the axis. Fig. 5 corresponds

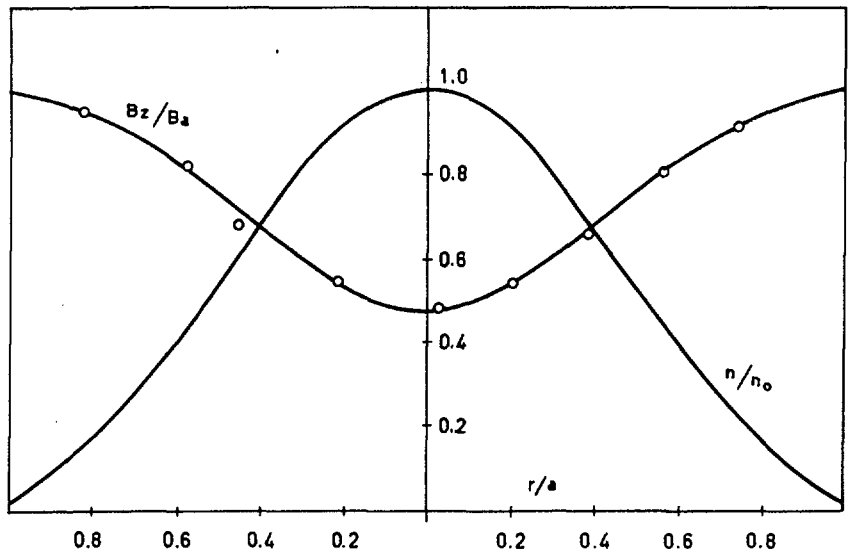

Fig. 4 Measured magnetic field profile. The solid curve is drawn according to Eqs. (7) and (9) choosing temperatures to give the best fit for the experimental results. Encircled points are at 6 μs. Experimental conditions: gas—Xe, $p = 1.2 \times 10^{-2}$ mm Hg, $B_a = 650$ G, $n_0 = 4.4 \times 10^{14}$ cm^{-3}, $N_0 = 1.3 \times 10^{15}$ cm^{-1}, $T_i + T_e = 2.1 \times 10^5$ °K.

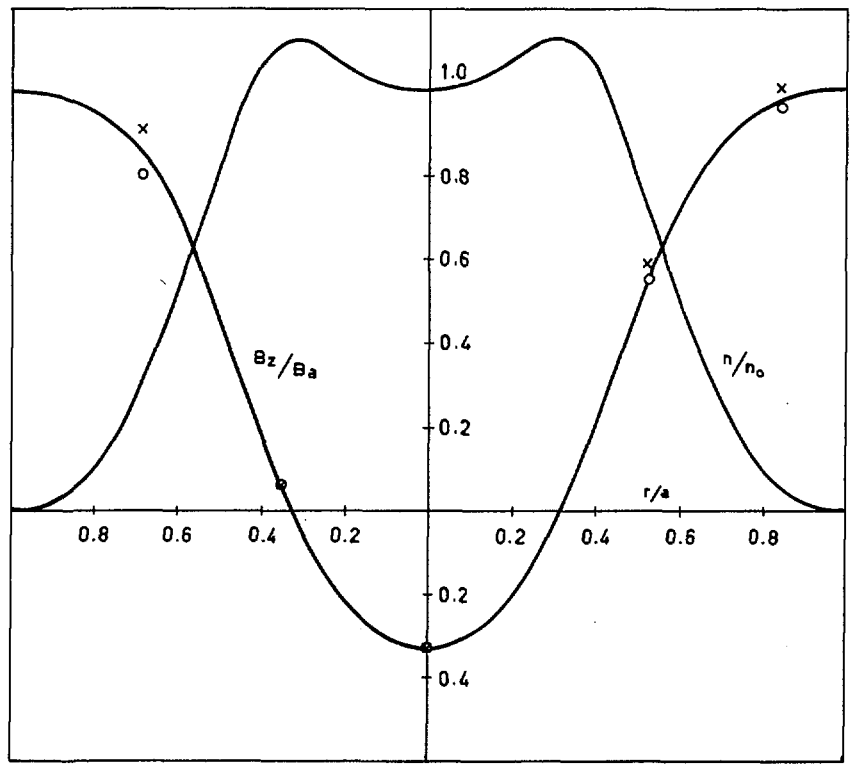

Fig. 5 Measured magnetic field profile. The solid curve is drawn according to Eqs. (7) and (9) choosing temperatures to give the best fit for the experimental results. Encircled experimental points are at 3 μs, those marked with × are at 2.5 and 4 μs. In this example, the axial magnetic field is reversed at radii less than 0.78 cm. Experimental conditions: gas—Xe, $p = 5 \times 10^{-3}$ mm Hg, $B_a = 730$ G, $n_0 = 4.1 \times 10^{14}$ cm^{-3}, $N_0 = 3.8 \times 10^{15}$ cm^{-1}, $T_i + T_e = 2.8 \times 10^5$ °K.

to the case for which $1 < 4\pi B_a/(\mu_0 N_0 e\omega) < 2$. The axial magnetic field is reversed at the axis whilst the maximum electron density occurs at a radius of 0.78 cm. It is possible therefore to produce a cylindrical shell of plasma with an axial field in different directions on each side of the shell.

7. Discussion

For a more precise comparison of theory and experiment independent measurements of electron density and temperature are required. Langmuir double probes were tried, but in the presence of the strong alternating field arcing at the probes took place. Probe measurements taken after the decay of the alternating field gave electron temperatures considerably less than those required for the best-fit density distribution. However the electron densities found were of the same order as those calculated from gradients of the B_z field.

In the absence of a plasma the amplitude of the rotating field at the axis was about twice that at the walls due to the non-uniformity of the applied field. In the pressure of the plasma the amplitude of the rotating field at the axis was often five times that at the walls. The magnetic "pressure" resulting from this excess was comparable with the plasma pressure. No allowance was made for this enhanced rotating field in the calculation of the plasma pressure balance, and the unexpectedly high value of the plasma temperature can be accounted for by this omission. Such an amplification could arise from end effects in the following manner. Radial currents at the tube ends interact with the axial B_z field and produce a J_z current in such a phase as to enhance the rotating field at the axis and decrease it near the walls. Estimates of resistivity, based on the observed phase shift between the alternating field at the walls and the axis and the rate of decay of the B_z field indicated electron temperatures less than 10^5 °K. Because of these uncertainties the results presented cannot be considered more than a qualitative confirmation of theory.

Table I shows that the secondary axial field can be considerably stronger than the applied rotating field. No special attempt was made to increase this ratio in these experiments. By choosing a suitably large dimension for a plasma, the secondary axial field could exceed the transverse field by orders of magnitude. Conversely, a plasma rotating in a constant magnetic field directed normal to the axis of rotation develops a dipole-like magnetic field directed along the axis of rotation which could greatly exceed the primary field. Such an arrangement is a magnetic field amplifier, the energy required being derived from energy of rotation. By combining the magnetic field of plasmas rotating about axes which are not parallel, a variety of self-excited dynamos can be imagined.

Acknowledgement

The authors would like to thank the Director of A.E.R.E. Harwell for his support for this work.

References

[1] THONEMANN, P. C., COWHIG, W. T., DAVENPORT, P. A., *Nature* **169** (1952) 34.
[2] DAVENPORT, P. A., D. Phil. Thesis, Oxford University, 1954.

NON-ADIABATIC ORBITS IN A CUSPED MAGNETIC FIELD*

HAROLD GRAD, ROGER VAN NORTON

INSTITUTE OF MATHEMATICAL SCIENCES

NEW YORK UNIVERSITY, NEW YORK, UNITED STATES OF AMERICA

It is found that the possible orbits in a magnetic field which has a low field region can be conveniently classified into three distinct categories: (1) highly adiabatic orbits which would be contained indefinitely were it not for diffusion into a loss cone by encounters with other particles; (2) highly non-adiabatic orbits which undergo substantial and apparently random changes of magnetic moment passing near the zero field region; (3) an intermediate class of orbits for which the changes in adiabatic invariant on successive passes are relatively small but are found to be uncorrelated. The separation into classes (1) and (2) has been used elsewhere as the basis of a theory of containment valid for general cusped field configurations.

In this paper we consider the third group of particles. The long term behavior can be treated as a diffusion process in velocity space. The diffusion coefficient is given (within a numerical factor) by $D \sim \langle(\delta\mu/\mu)^2\rangle\ V^2/\tau$ when τ is the mean transit time and $\delta\mu/\mu$ is the proportional change in magnetic moment in one pass (obtained numerically in representative cases). This is to be compared with the standard (Coulomb encounter) diffusion coefficient $D_c \sim V^2/\tau_0$ when τ_0 is the mean collision time. In estimating $\delta\mu/\mu$ great care must be taken not to confuse actual non-adiabatic variations with fluctuations which are due to the magnetic moment being only an approximation to the true adiabatic invariant.

1. Introduction

The analysis of nonadiabatic particle orbits is a very difficult problem. There is a theory available only in a few very special cases as a result of fortuitous analytical simplifications [1, 2]. In a certain sense, the adiabatic theory is too good! Although the statement can be made that an orbit is adiabatic to arbitrarily high order in the appropriate expansion parameter ε (roughly, the ratio of a Larmor radius to a distance over which the field changes appreciably) [3, 4], the adiabatic theory itself offers no useful error estimates. The significance of this theory can only be appreciated by noting that the adiabatic expansion in ε is asymptotic rather than convergent [5]. Thus the higher order adiabatic theory may give very great accuracy when the first term is already quite good, but it usually makes matters worse when the first term is mediocre.

The uncertain range of validity of the adiabatic theory may also impose difficulties in recognizing legitimate nonadiabatic effects obtained numerically. Since the adiabatic invariant can only be estimated asymptotically, one may be hard put to distinguish true nonadiabatic changes in the value of the invariant from uncertainties in its definition or lack of higher order corrections.

We wish to investigate, in this paper, certain properties of slightly nonadiabatic orbits in a magnetic field of the cusped geometry type [6]. The conditions were chosen to allow a relatively complete description of such orbits by a suitable combination of mathematical analysis and numerical experiment. Moreover, it seems likely that the general behavior which is observed will not be strongly dependent on the precise magnetic field considered and may therefore allow extrapolation to other problems.

A more complete description of the nature of the orbits will be found elsewhere [7]. One feature, viz., the existence of a relatively quick transition between very adiabatic and very nonadiabatic orbits [8, 9] has been used to obtain a theory of containment in cusped geometries [10]. Another feature, the very complex behavior of the transitional class of slightly non-adiabatic orbits [11], is used to advantage in this paper to describe a stochastic model of the orbits. The present results make it possible to improve the above-mentioned cusped geometry containment theory. They also have some application to the containment problem in a mirror device, especially one with a large mirror ratio. But the major conclusion may lie in the conjecture that nonadiabatic effects can be properly analyzed only by statistical means.

2. The magnetic configuration

We consider an axially symmetric magnetic field which is described by the stream function (magnetic flux)

$$\psi = r^2 z. \tag{1}$$

This represents a (vacuum) cusped geometry in which the field coils have been moved to infinity and in which the magnitude of the magnetic field increases linearly with radius,

$$\begin{aligned} B_z &= 2z \\ B_r &= -r \\ B^2 &= 4z^2 + r^2 . \end{aligned} \tag{2}$$

* Conference paper CN-10/172, presented by H. Grad. Discussion of this paper is given on page 94. Translations of the abstract are given at the end of this volume of the Conference Proceedings.

On a given magnetic line, B has a minimum value, $B_0^2=3\psi^{2/3}$, which is attained at the point $Z_0=\psi^{1/3}/2$. The variation of B along the line is given by

$$(B/B_0)^2=\frac{1}{3}(\zeta^2+2/\zeta) \tag{3}$$

where $\zeta=|z/Z_0|$. All particles are contained, but we may apply the results to a finite problem by considering a particle to be lost when it temporarily emerges from a specified finite region.

From the nature of the results, we shall see that they are not likely to be strongly dependent on the particular magnetic field we have chosen.

3. Qualitative description of the orbits

We consider only orbits which are slightly nonadiabatic and which have distant turning points. More precisely, the latter criterion is that the value of B at a turning point is very large compared to the minimum value of B attained near the origin on the given guiding magnetic line. For purposes of discussion, let us assume that the values have been chosen to yield a change in magnetic moment in one transit which is the order of 20% or smaller.

The fact of the large mirror ratio allows a very simple qualitative description of the orbit. First, we note that the orbit is composed of sections which are very adiabatic (near the turning points) joined by successive nonadiabatic passes through the central region (Fig. 1). It is this fact which allows us to identify

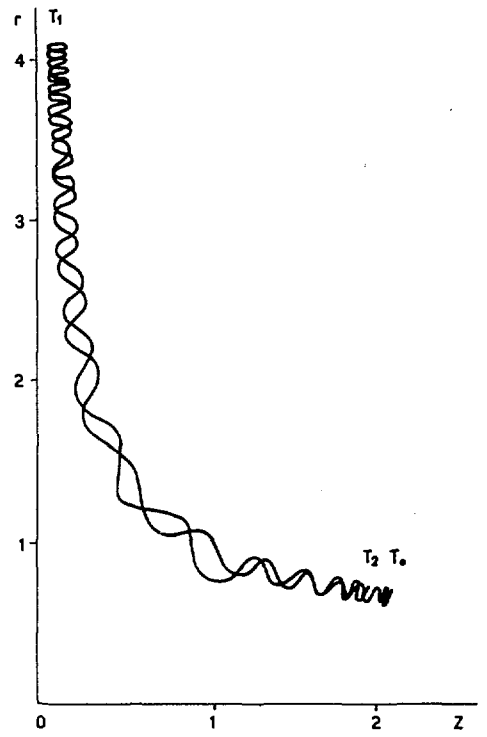

Fig. 1 Slightly nonadiabatic orbits which have distant turning points. The orbits are composed of very adiabatic sections near the turning points joined by successive nonadiabatic passes through the central region.

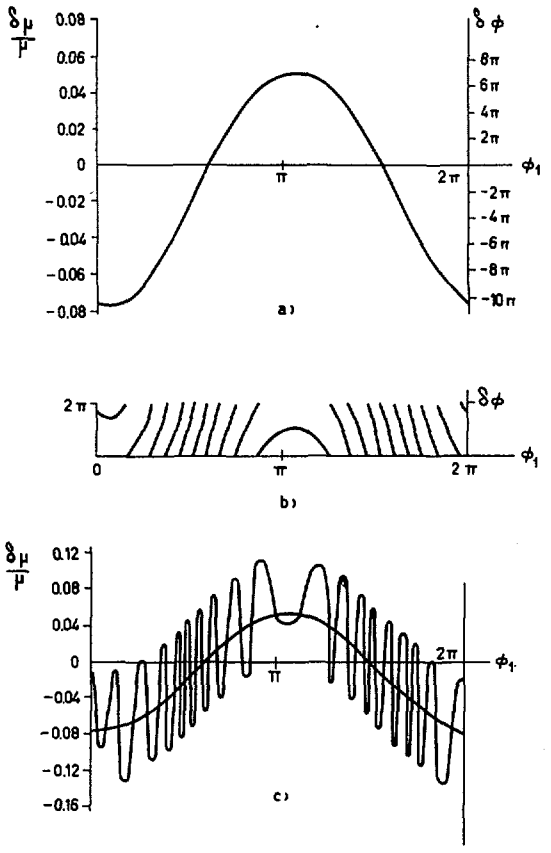

Fig. 2 (a) The changes in magnetic moment $\delta\mu/\mu$ and phase $\delta\Phi$ are plotted as functions of the initial phase Φ_1 at a given turning point. (b) $\delta\Phi$ replotted as a function of Φ_1, but reflected back to its principal value $(0<\delta\Phi<2\pi)$. (c) $\delta\mu/\mu$ plotted as a function of Φ_1, on the second traverse through the central region.

observed changes in the value of the magnetic moment, μ, as being definitely nonadiabatic rather than only fluctuations resulting from use of an approximation to the true adiabatic invariant. Also we may rely on theoretical analysis for the "ends" of the orbits (which are numerically tedious) and need numerical computation only for the central portion (which is theoretically inaccessible).

Next we observe that the motion is almost parallel to the magnetic field in the central, low field, region. In particular, the measure of nonadiabaticity must be made with respect to a Larmor radius, $\lambda=mV/eB$, which is composed of the total particle speed, V, not its perpendicular component. Nonadiabaticity is a consequence of the change in field observed as the particle moves forward a distance $2\pi\lambda$ in one Larmor period.

Since the motion is almost parallel to B in the central region, the turning point will be very sensitive to any slight perturbation of the velocity in this region. In particular, a small range of velocities near the magnetic field direction covers all turning points from the given one to infinity. The total change in phase from one passage through the center to the next (i.e., the number of Larmor cycles) will be even more

sensitive to a slight perturbation. To be definite, consider two initial states at the same turning point and the same guiding center, but with slightly different Larmor phases. In passing through the central region, a slightly different nonadiabatic change in μ will be experienced by the two particles. A relatively large difference in the location of the second turning point will ensue followed by a large difference in phase by the time the central region is next approached. Thus the second nonadiabatic increments in μ will be essentially uncorrelated with the original phases.

This description is the classical one of a process which can be considered to be random. Just as in a roulette wheel or the toss of a coin, a small change in initial state produces a large discrepancy some time later.

Quantitatively, we plot in Fig. 2a the change in μ as a function of initial phase, Φ_1, at a given turning point. The change in phase, $\delta\Phi = \Phi_2 - \Phi_1$, in passing to the opposite turning point and back to the center follows the change in μ, but on an exaggerated scale. The same quantity, $\delta\Phi$, is replotted as a function of Φ_1 in Fig. 2b, but reflected back to its principal value, $0 < \delta\Phi < 2\pi$. On the second traverse through the central region, μ changes again as a smooth function of the phase Φ_2 after passing the center, but this is a very rapidly varying function, Fig. 2c, when considered as a function of Φ_1. It is clear that after two or three passes, it is impossible to even attempt to follow the precise changes in μ.

Numerical computation of orbits which depend so sensitively on initial data is quite difficult. Fortunately, it is only the smooth function, $\delta\mu$ as a function of Φ_1, which must be obtained numerically. The ensuing rapid fluctuations arise from the adiabatic portion of the orbit and can be computed analytically.

4. Phase plane mapping

A complete catalogue of all orbits is provided by a description of the image of an arbitrary initial state after a complete transit. Let us fix the speed V and the guiding magnetic line ψ; (the latter is more precisely described as the value of the ignorable azimuthal momentum). Then we choose a sequence of turning point co-ordinates (these may be quite arbitrarily defined, e.g., by the orthogonal trajectories of the magnetic lines), all safely within the adiabatic regions, $a, b, c, \ldots$ on one side and $a', b', c', \ldots$ on the other (Fig. 3a). At the station a, we plot the two transverse velocity components for any particle which happens to be passing by. Initial states with turning points at a itself lie on a circle of radius V (Fig. 3b). A particle coming from a more distant turning point b will correspond to an interior point of this circle; (it must have a parallel component of velocity when it reaches a). Insofar as the orbits beyond a can be considered adiabatic, the images of the initial conditions with turning points at $b, c, \ldots$ will be circles concentric with the original circle V. An exact orbit computation would yield a family of simple closed curves, approximately circles, for the mapping of each of the more

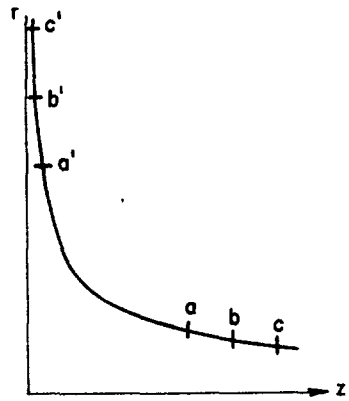

Fig. 3a Choosing turning point co-ordinates (see text).

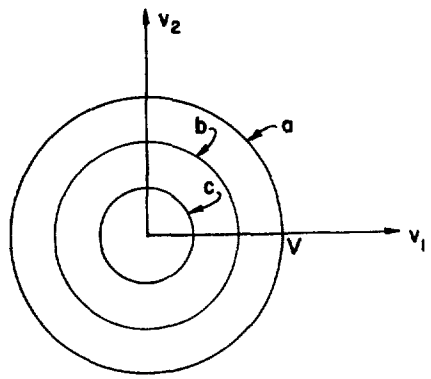

Fig. 3b Transverse velocity components for particles from various turning points (see text).

distant turning points. These curves will converge upon a point which represents the single orbit extending to infinity.

Keeping the adiabatic approximation of concentric circles, let us consider the orbits traced by particles which lie on the circle b as they pass through station a headed for the turning point b and then return again to a. The circle b is mapped onto itself and is rotated through a definite angle, viz., the total Larmor phase rotation over the entire orbit. Thus each of the circles is mapped into itself, with a fixed angle of rotation assigned to it ranging from the value zero for the outermost circle a to infinity as one approaches the center. In particular, for distant turning points, the angle of rotation varies very rapidly with the radius of the circle.

Exactly the same description can be made for the adiabatic orbits beyond a' at the other turning point. All that remains is to describe the mapping from a to a' across the central region. By our choice of the value of V and of the guiding magnetic line, the mapping from a to a' is a not very large perturbation of the identity, cf. Fig. 4 (this is merely schematic). This figure can be used to follow an orbit for an indefinite period of time (depending on the accuracy with which the map is known). For example, take the infinite turning point corresponding to the center of the circle

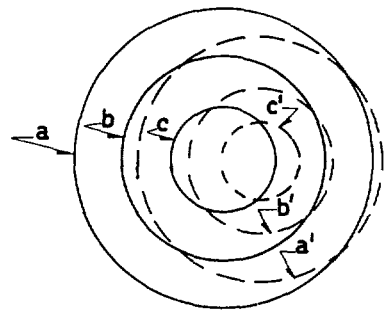

Fig. 4 Orbit mapping (see text).

a; this is an orbit with $\mu=0$. On crossing the central region to the station a', this maps onto a point of the circle c' which corresponds to a finite turning point. The trip to this turning point and back is described by a certain rotation of the circle c'. We may then map back across the central region, rotate the appropriate circle, etc.

All the very distant turning points undergo approximately the same nonadiabatic change in μ, viz., the value assigned to the point at infinity. This can be taken as a rough measure of the maximum nonadiabaticity on the given guiding magnetic line, since there will be a tendency for the change in μ to be smaller for orbits with closer turning points and tighter spirals near the center. Although the complete phase plane mapping involves an inordinate amount of calculation, a complete description of the displacement $\delta\mu_\infty$ of the point at infinity is given by the expression

$$\delta\mu_\infty/\mu_0 \sim 0.018\left[1+\frac{1.0}{\psi}+\frac{1.7}{\psi^2}\right]\psi^{\frac{1}{3}}\,e^{-4\psi} \qquad (4)$$

where μ_0 is the magnetic moment composed of the full velocity V and the minimum value B_0 on the given magnetic line (cf. Eq. (3)). Whether this is merely an empirical formula (valid for $\frac{1}{4}<\psi<4$) or a numerical approximation to a strict asymptotic formula (valid for all sufficiently large ψ) has yet to be determined.

The basic measure of nonadiabaticity can be taken as the ratio of the maximum Larmor radius $\lambda=mV/eB_0$ to the scale length Z_0 in Eq. (3),

$$\lambda_0/Z_0=0.305\,\psi^{-\frac{2}{3}}. \qquad (5)$$

In a given physical problem one would compute the dimensionless flux parameter ψ from a given value of λ_0/Z_0 using Eq. (5) and then employ Eq. (4) to estimate the degree of nonadiabaticity.

5. Stochastic approximation

Let us now take the family of initial states represented by the small circular segment in Fig. 5a. On crossing the central region from station a to a', this is slightly distorted, Fig. 5b. In particular, the distorted segment straddles several circles which rotate at different rates in describing the following adiabatic motion to the next turning point and back. If this next turning point is distant, the segment then appears after returning to station a', as in Fig. 5c, wrapped entirely around a circle. If the family of initial states were taken as a small domain instead of a segment (Fig. 6a), the mapped domain would fill the interior of a ring (Fig. 6b). It would seem quite appropriate to describe this process as randomization of phase or diffusion.

A complete description of this situation as a stochastic process requires evaluation of the mean value $\langle\delta\mu\rangle$ and the mean square value $\langle\delta\mu^2\rangle$ taken from the curve giving $\delta\mu$ as a function of Φ_1 (see Fig. 2a). Furthermore, these coefficients must be evaluated as functions of μ (i.e., of turning point). One would obtain a diffusion equation in the variable μ. This

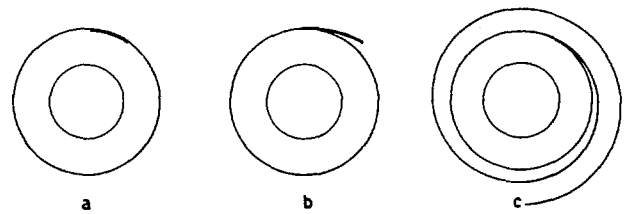

Fig. 5 (a) Family of initial states (heavy arc). (b) Distortion on crossing central region from a to a'. (c) Distorted segment after returning to a'.

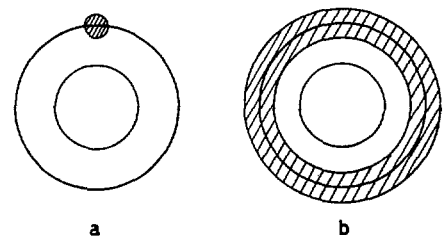

Fig. 6 (a) Family of initial states (shaded area). (b) Mapped domain filling interior of ring ("randomization of phase").

has yet to be done. But, as a semi-quantitative description, one can estimate the value of $\langle\delta\mu^2\rangle^{1/2}$ by the displacement $\delta\mu_\infty=\Delta$ of the point at infinity and construct a diffusion coefficient

$$D_\mu=\langle(\delta\mu)^2\rangle/\tau\sim\Delta^2/\tau \qquad (6)$$

where τ is the transit time between successive turning points. This is the diffusion coefficient in μ-space; in velocity space the equivalent diffusion coefficient is

$$D_V=\langle(\delta\mu/\mu)^2\rangle\,V^2/\tau\sim(\Delta^2/\mu^2)(V^2/\tau). \qquad (7)$$

One must remember that this coefficient represents a diffusion in direction only; the magnitude V remains fixed. From Eq. (4) we see that for very large turning points D_V becomes infinite although D_μ does not.

6. Conclusions

It has been seen that when there is only a small degree of nonadiabaticity coupled with a large mirror ratio, the long-time behavior of a particle can be accurately described in stochastic terms. The particular

simplicity results from the separation of nonadiabatic changes and phase mixing in two distinct parts of the orbit. One application of this theory would be to improve the theory of containment in cusped geometries. In particular, one could refine the position of the "cutoff" which separates definitely adiabatic particles which are subject to Coulomb mirror losses from definitely nonadiabatic particles which are subject to cusp losses [10].

But there is also information to be obtained about mirror devices. The arguments would carry over quite precisely in a mirror machine with very large mirror ratio. There is even a certain amount of information to be gleaned when the mirror ratio is moderate. Consider, specifically, a problem in which containment is desired for very many transits. The Coulomb diffusion coefficient has the order of magnitude

$$D_c \sim V^2/\tau_c \tag{8}$$

where τ_c is the mean collision time. The nonadiabatic diffusion effects can be neglected compared to Coulomb encounters if $D_V < D_c$ or

$$\langle(\delta\mu/\mu)^2\rangle < \tau/\tau_c\,. \tag{9}$$

But, for long containment, τ_c must be much larger than the transit time τ. For example, in a device in which a containment time of 10^6 transits is desired, one must be sure to have the mean value of $\delta\mu/\mu$ in one transit smaller than 10^{-3}.

With a moderate value of the mirror ratio it becomes very difficult, in interpreting numerical data, to distinguish a small nonadiabatic change in μ from a roughly periodic reversible variation which results from higher order terms in the adiabatic theory. Of course, computation of an orbit for very many transits will improve the signal to noise ratio. But a simpler expedient, which might not be inaccurate, would be to extrapolate to smaller mirror ratios the exponential dependence for $\delta\mu$, Eq. (4), which is relatively easily computed.

Acknowledgment

The work presented in this paper is supported by the Institute of Mathematical Sciences, New York University, under Contract AT(30-1)-1480 with the United States Atomic Energy Commission.

References

[1] HERTWECH, F., SCHLÜTER, A., *Z. Naturforsch.* **12A** (1957) 844.
[2] CHANDRASEKHAR, S., "Adiabatic Invariants in the Motions of Charged Particles", in The Plasma in a Magnetic Field, ed. R. Landshoff (Stanford University Press, 1958).
[3] KRUSKAL, M. D., "The Gyration of a Charged Particle", Project Matterhorn Report PM-S-33, U.S. Atomic Energy Commission Report NYO-7903 (March 1958).
[4] GARDNER, C. S., *Phys. Rev.* **115** (1959) 791.
[5] BERKOWITZ, J., GARDNER, C. S., *Comm. Pure and Appl. Math.* **12** (1959) 501.
[6] BERKOWITZ, J., FRIEDRICHS, K. O., GOERTZEL, H., GRAD, H., KILLEEN, J., RUBIN, E., Proceedings of the Second International Conf. on the Peaceful Uses of Atomic Energy, Geneva, **31** (1958) 171.
[7] VAN NORTON, R., "The Motion of a Charged Particle Near the Zero Field Point", Institute of Mathematical Sciences, U.S. Atomic Energy Commission Report NYO-9495 (May 1961).
[8] GRAD, H., "Thermonuclear Plasma Containment in Open-Ended Systems", Institute of Mathematical Sciences, U.S. Atomic Energy Commission Report NYO-9355 (August 1960).
[9] VAN NORTON, R., *Bull. Am. Phys. Soc., Ser. II*, **6** (1961) 201.
[10] GRAD, H., "Containment in Cusped Plasma Systems", to appear in Progress in Nuclear Energy, Series XI, (Pergamon Press, 1961).
[11] VAN NORTON, R., "Motion of a Charged Particle near the Zero Field Point of a Counter Helmholtz Field", talk presented at Sherwood Theoretical Meeting, Princeton, April 29, 1961.

EXPERIMENTS ON CUSP COMPRESSION*

T. K. ALLEN, R. W. P. McWHIRTER, I. J. SPALDING

ATOMIC ENERGY RESEARCH ESTABLISHMENT

HARWELL, BERKSHIRE, UNITED KINGDOM

A fast compression experiment in spindle cusp geometry is performed on plasma pre-ionized and pre-heated to above 10^5 °K by colliding shock waves. Two 22 cm diameter coils are used with a 1 MJ capacitor bank to give peak magnetic fields of 100 kilogauss or more rising in 18 μs and, in clamped circuit, decaying with a time constant of 250—400 μs.

Two forms of instability associated with acceleration during the compression phase are observed at high initial densities in hydrogen or with heavy gases. At lower pressures in hydrogen the expected stable compression occurs.

A comparison between the experimental results and existing theories of cusp systems is described.

1. Introduction

The confinement of plasma by a magnetic field having a cusped shape has been discussed by several writers [1—5]. The main advantages of this configuration are that it has unusually favourable stability properties and that cyclotron radiation losses can be avoided by having plasma contained in a region of low or zero magnetic field. The main disadvantages are that magnetic energy is used uneconomically, and that there is a continuous loss of particles through the cusps.

The most optimistic considerations [3] show that the virtual "hole", through which particles are lost, has a minimum size of several electron Larmor radii. However, this size is increased by diffusion of the particles into the magnetic field and the consequent flow along adjacent field lines in which there is some reflection due to the mirror effect.

In order to establish the cusped configuration it is necessary to inject plasma into an existing vacuum field [6—10] or to compress a plasma into a cusped shape by an increasing magnetic field [11]. In either case plasma has to be accelerated and this must be done sufficiently slowly to avoid Rayleigh-Taylor instabilities.

Many varieties of cusped configuration have been discussed [3, 12]. The experiments discussed here are based on the simplest spindle-cusp geometry, in which currents flowing in opposition in two single-turn coils produce a magnetic field which compresses a plasma previously created by shock waves. Particle losses can occur at the line and point cusps. The object of the experiment is to study the adiabatic heating, the stability, and the containment of a plasma of high density and moderate temperature confined by very strong magnetic fields.

2. Apparatus

The discharge vessels shown in Fig. 1 are made of pyrex with quartz liners to protect the glass from excessive thermal shock in the region of the line cusp. For Tube I the cusp field coils were 22 cm in diameter with separation variable between 6 and 16 cm. The wedge-shaped cross-section was chosen to reduce the forces between the coils at very close spacing and to give the maximum bearing area on the mechanical support structure. For Tube II profiled copper inserts were fitted inside the coils to ensure that the magnetic field lines had a uniform and maximum curvature convex to the plasma at the wall of the tube. As far as possible the tube was shaped to follow the field profile in the cusp region and the centre section was made with a diameter large enough to have the position of maximum field inside the tube. The coil separation

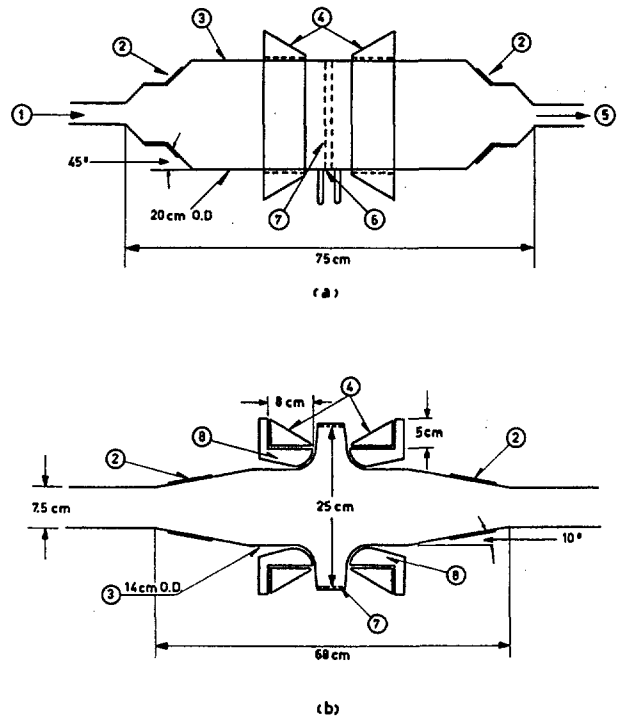

Fig. 1 The pyrex discharge vessels: (a) Tube I, (b) Tube II. 1 — gas inlet, 2 — shock coils, 3 — pyrex vessel, 4 — cusp coils, 5 — pumps, 6 — quartz window, 7 — quartz liner, 8 — inserts.

* Conference paper CN-10/69, presented by T. K. Allen. Discussion of this paper is given on page 95. Translations of the abstract are at the end of this volume of the Conference Proceedings.

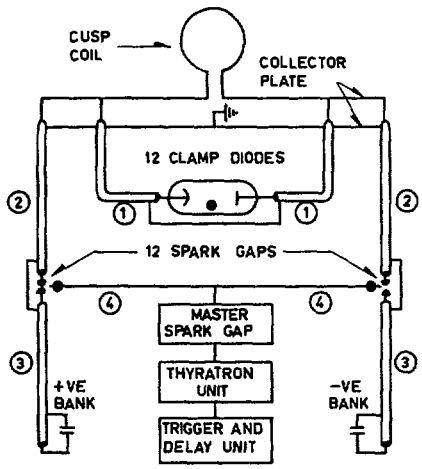

Fig. 2 Basic circuitry for one cusp coil. (1) 60 cables: 4×10^{-9} H, 0.12×10^{-3} Ω; (2) 60 cables: 6.6×10^{-9} H, 0.8×10^{-3} Ω; (3) 120 cables: 8.3×10^{-9} H, 1×10^{-3} Ω; (4) 12 trigger cables. 12 clamp diodes: 8.4×10^{-9} H, 0.25×10^{-3} Ω; 12 spark gaps: 5×10^{-9} H, 0.5×10^{-3} Ω; collector plate: 16×10^{-9} H, 0.2×10^{-3} Ω; +VE and —VE Bank: 1200 μF, 2.1×10^{-9} H, 0.2×10^{-3} Ω. Cusp coil: with insert (5 cm spacing) initially 120×10^{-9} H and 1.2×10^{-3} Ω, no insert (8 cm spacing) initially 200×10^{-9} H and 0.6×10^{-3} Ω. Full bank, no insert 8 cm coil spacing, rise time 18 μs. Full bank, with insert 5 cm coil spacing, rise time 15 μs. Half bank, no insert 8 cm coil spacing, rise time 13.5 μs.

in this case was not variable and was chosen to be 5 cm so that the magnetic field was approximately equal at the spindle and line cusps.

Each coil was connected to a positively charged and a negatively charged capacitor bank by means of low inductance co-axial cables, spark gaps, and collector plate as shown in Fig. 2. The circuit parameters given are design estimates only, although experimental results confirm the values deduced for the complete circuit to be reasonably accurate. When operating at capacitor voltages of + and — 17.5 kV, permissible only under clamped conditions, peak coil currents of about 1.5 MA can be obtained. In these conditions the total energy storage is approximately $\frac{3}{4}$ MJ.

The capacitor banks each consist of 120, 10 μF units, with co-axial terminations, ten such units being connected to one swinging cascade spark gap (operated at a pressure between $\frac{1}{3}$ and $\frac{2}{3}$ atmosphere). Thus two groups of 12 parallel spark gaps form the starting switches for each coil and these 24 switches are fired from one master gap and thyratron unit as shown.

The collector plate terminates both starting and clamp switch cables and forms the series connection between capacitor banks. It is made from brass sheet reinforced with insulated bolts and steel beams to withstand the large electromagnetic forces of hundreds of tons. The cusp coils are of precipitation-hardened beryllium copper to give adequate strength and conductivity.

Each circuit is clamped by 12 mercury diodes which become conducting as the voltage across them reverses at approximately peak current. They have continuously conducting auxiliary anodes, supplied from a D.C. generator insulated for 20 kV, and are equipped with an automatic ignition circuit which functions if an auxiliary anode is extinguished between shots. When clamped the current decays to 1/e of its peak value in about 300 μs without inserts and 160 μs with inserts fitted. Fig. 3 shows clamped and unclamped current-time curves for different conditions.

The magnitude of the magnetic field increases approximately linearly in the axial and radial directions from the centre of the cusp region. The measured values of maximum field with the full capacitor bank charged to ±10 kV are 39 kG for the 8 cm separation without inserts and 56 kG for the 5 cm separation with inserts.

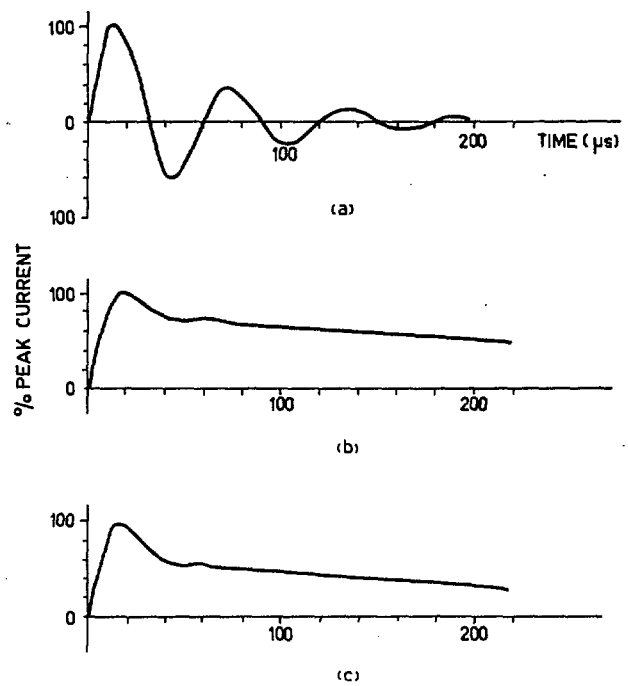

Fig. 3 Cusp coil current-time curves. (a) half capacitor bank, unclamped, no inserts, 8 cm spacing; (b) full capacitor bank, clamped, no inserts, 8 cm spacing; (c) full capacitor bank, clamped, with inserts, 5 cm spacing.

The shock waves which ionize and pre-heat the initially neutral gas are produced by the simultaneous discharge of two auxiliary condenser banks, 4 μF rated at 40 kV, into the shock coils. The ringing current in these coils rises to about 200 kiloamps in 1.5 μs. The gas does not break down until the second half-cycle, or even later at very low pressure, so that the shocks do not move down the tube until 4—5 μs after initiating the current.

3. Experiments in Tube I

Tube I was used primarily for photographic observations and for these only half of the cusp capacitor

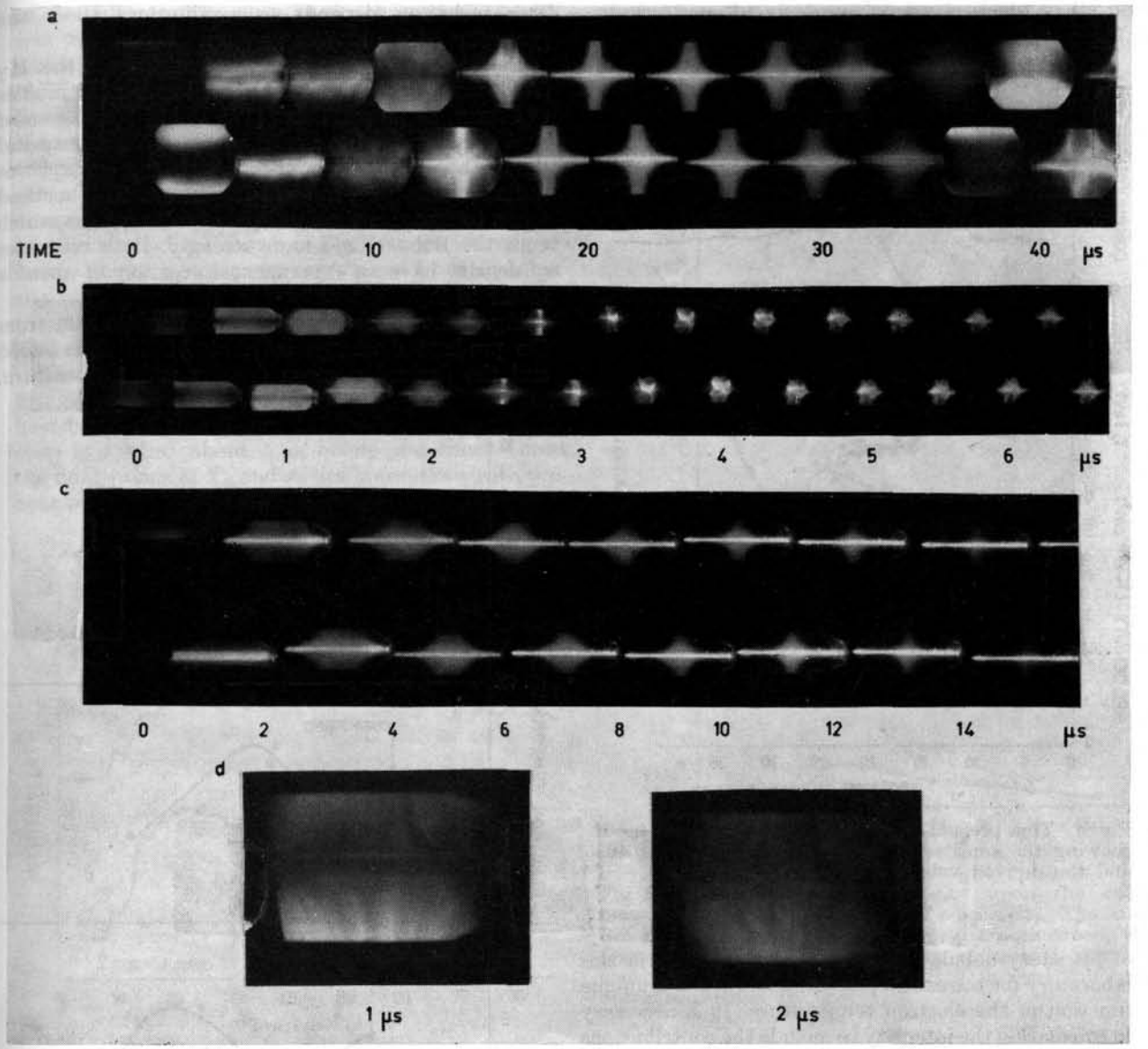

Fig. 4 Framing camera photographs of plasma in the rising cusp field. In (a), (b), (c) time zero is on the left and successive shots alternate between the top and bottom traces. The entire region between the cusp coils has been photographed in each case. (a) 20 millitorr of H_2 (5% Ar), exposure time 2 μs; (b) 5 millitorr of Ar; exposure time $^1/_4$ μs; (c) 35 millitorr of H_2; exposure time 1 μs; (d) 10 millitorr of He; exposure time 1 and 2 μs.

bank was used; the circuit was not clamped so that the bank voltage was limited to 13 kV and maximum magnetic field to 32 kG. Some examples of high-speed framing camera photographs of the effect of the rising cusp field are shown in Fig. 4. Fig. 4a shows the shocks approaching and meeting followed by the first half-cycle and part of the second half-cycle of the cusp field. Fig. 4b shows the growth of an instability after 2—3 μs in a typical discharge where the speed of contraction exceeded the estimated speed of sound in the plasma. Fig. 4c shows a condition in hydrogen in which no gross instability is observed and the full course of adiabatic compression can be seen. Fig. 4d shows an example of flute-type instability in helium in the very early stage of compression.

4. Experiments in Tube II

4.1. Spectroscopic measurements

Spectroscopic studies have included examination of the Balmer continuum, the Stark-broadened Hγ line, and the impurity spectrum. Two monochromators, with photomultipliers having a time resolution better than 1 μs, have been used. Quartz windows allowed radial viewing at the centre of the cusp region.

Measurements of the continuum in the Balmer region have yielded estimates of the electron temperature and density. The method of measuring the intensity ratio across the Balmer step, based on an astrophysical method of determining the temperature

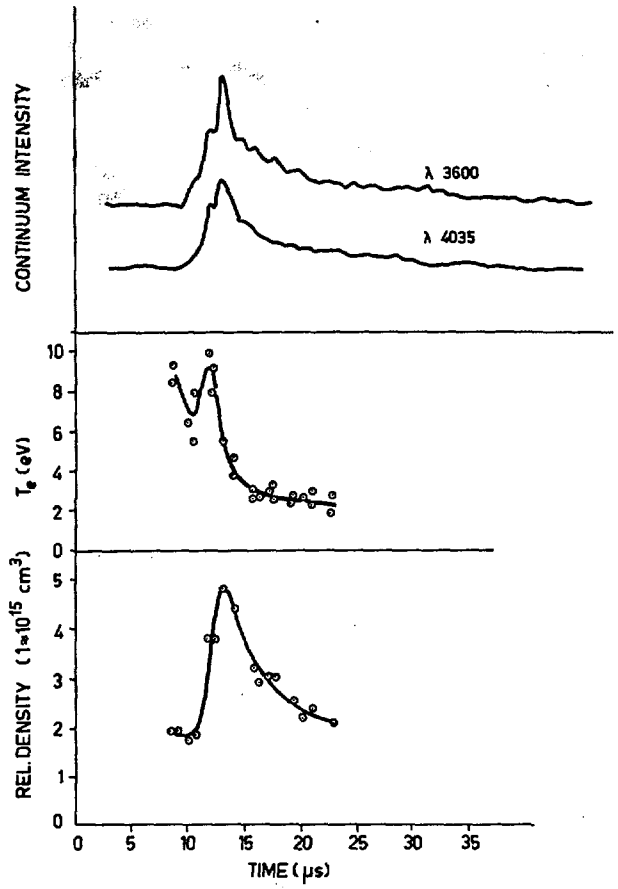

Fig. 5 The preheat discharge at 30 millitorr in H_2, showing the continuum intensity at λ 3600 and 4035, and the derived values of N_e and T_e.

of planetary nebulae [13], has been developed in this laboratory for terrestrial plasma. This ratio is a unique function of the electron temperature. It is necessary in calculating the intensity to include the contributions from both bremsstrahlung and recombination continua with the respective Kramers-Gaunt correction factors. The usable limits of the method are shown by the following estimate of uncertainty in our measurements. The errors in the measured ratio were about $\pm 12\%$ and for this value the table shows the range of uncertainty in the derived electron temperature.

Mean electron temperature (kT_e)	Range of uncertainty
17 eV	8.6—∞ eV
9.6	6.7—15.5
6.7	5.2— 8.6
3.6	3.0— 4.3
2.0	1.9— 2.2
1.5	1.4— 1.6

The absolute intensity of the continuum, which gives a measure of the number of ions in the line of sight, has been used to measure the plasma density. This technique depends on assumptions about the geometry of the emitting region.

Densities have also been measured from the Hγ Stark width using the method and computed profiles of GRIEM, KOLB and SHEN [17]. It has been assumed that the lines are broadened by Stark effect only and that other broadening effects, due for example to radiation trapping, are not important. This method tends to measure the density in cooler regions which emit the Balmer lines more strongly. Both estimates of density have an experimental accuracy of about a factor of 2.

Fig. 5 shows the intensity of the continuum, from the pre-heat discharge only, at λ 3600 and λ 4035 and the derived electron density and temperature.

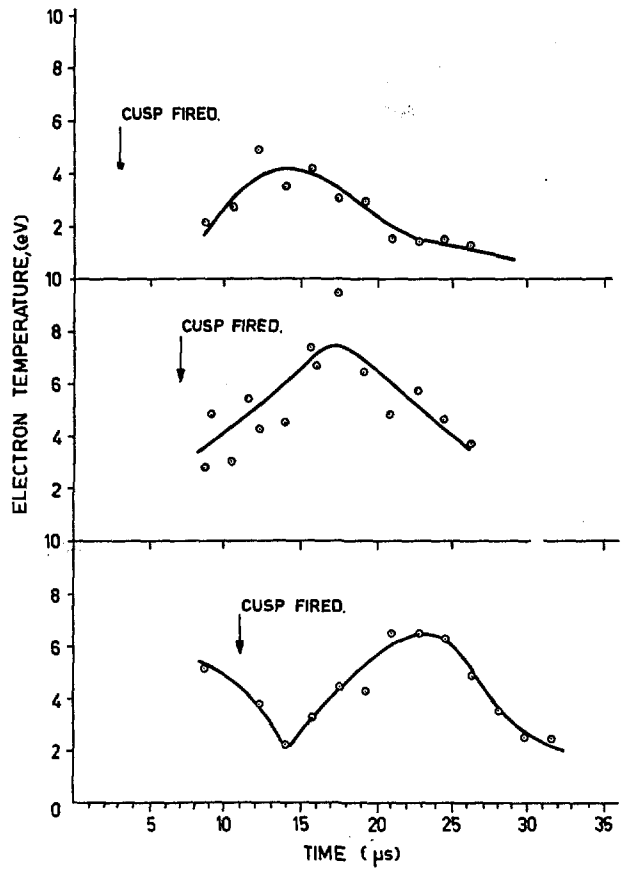

Fig. 6 The dependence of T_e upon the delay between firing the preheat and cusp coils. The cusp firing time is indicated on each trace; the pressure was 30 millitorr of H_2.

Some of the structure in the early part of the continuum intensity pulse is due to the pre-cursor and "fast-front" effects which have velocities faster than the shock waves. For the conditions used in the present experiments the shock velocities have been measured and are higher than 5×10^6 cm/s at the centre of the cusp region.

Figs. 6, 7 and 8 refer to conditions when both preheat and cusp bank are fired in hydrogen at a pressure

of 30 millitorr. The cusp bank, charged to ± 7 kV, was fired at different intervals after the pre-heat which was fired at zero time on the traces.

Fig. 7 shows typical Hγ time profiles as used in the Stark-broadening measurements. In the lower trace, the exit slit of one monochromator was wide enough to accept the whole of the line; in the upper trace, the slit of the second monochromator was adjusted to accept only the core of the line. Densities obtained by this method are shown in Fig. 8 where for comparison is shown a similar curve obtained from the intensity of the continuum. The latter is not corrected for the geometrical factor mentioned above, so that it is probably a low value.

The effect on electron temperature and density of firing the cusp bank at different times after the pre-heat banks can be seen in Figs. 6, 7 and 8. When the cusp is applied about 5 μs before the shocks meet the final values of T_e and n_e are lower than with pre-heat only. When it is applied just before the shocks

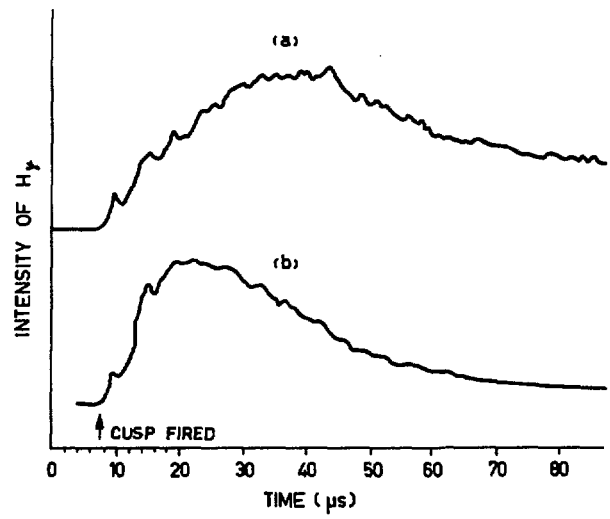

Fig. 7 Hγ time profiles for 30 millitorr of H_2. (a) Narrow slits to pass only the core of Hγ, (b) slits set to pass whole width of Hγ.

meet, T_e and n_e reach higher maximum values of 8 eV and 10^{16} cm^{-3} respectively, in about 11 μs and they then decrease with an e-folding time of 11 to 12 μs. If the cusp is not applied until several microseconds after the shocks have met, T_e and n_e rise to somewhat lower values but they decrease at approximately the same rate. In these circumstances the temperature of the pre-heated gas falls to a low value before being heated again by the cusp compression.

Only a few measurements have been made at other pressures and bank voltages but results seem to be generally similar.

The time dependence of carbon impurity lines is shown in Fig. 9. The C III λ 2297 line, which is the strongest impurity line in the quartz region of the spectrum, rises sharply at 14—15 μs; i.e. at the time when the electron density is rising to its peak value. The C I λ 2479 line rises to a maximum 7 μs later than C III.

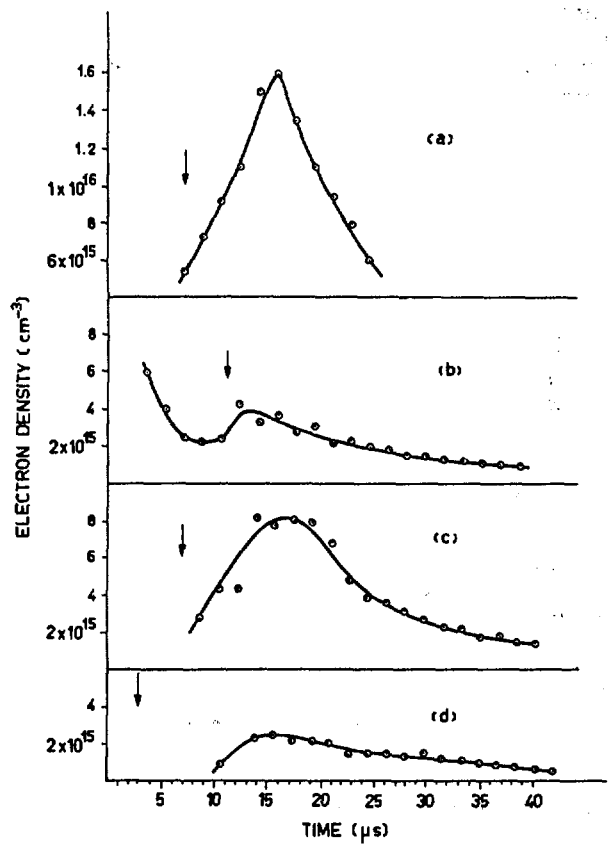

Fig. 8 The dependence of density upon the delay between firing the preheat and cusp coils. The cusp firing time is indicated by arrows on each trace; the pressure was 30 millitorr of H_2. (a) n deduced from the continuum intensity, (b), (c), (d) n derived from the Stark broadened Hγ line.

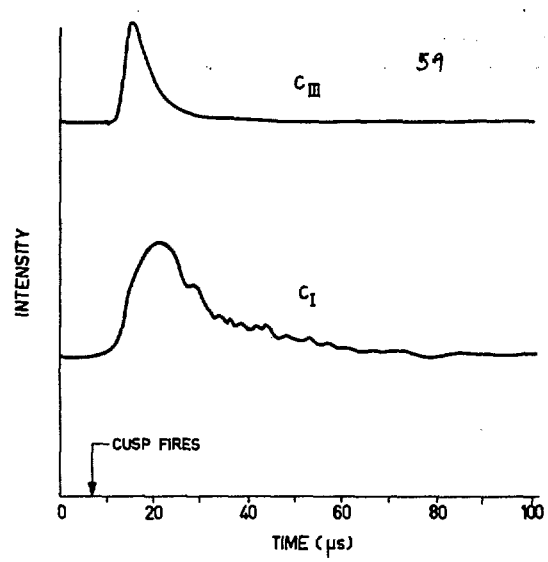

Fig. 9 Time dependence of carbon impurity lines.

4.2. Piezo-electric probe measurements

The temporal and spatial distribution of particle losses in the region of the line cusp has been measured with an acoustic line pressure gauge of a type discussed by Edwards [14]. The device consists of a fused quartz rod 2 mm in diameter and 60 cm long with a thin piezo-electric disc of lead zirconate

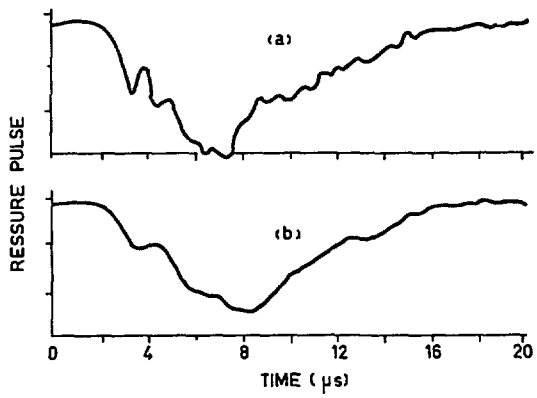

Fig. 10 Plasma pressure pulse detected by the piezo-electric probe at the line cusp: (a) no filter, (b) with 1 MHz filter.

connected into the line 25 cm from one end; the tip of the probe is shielded from lateral shocks by a concentric quartz tube, c.f. de Silva [15]. Critically damped magnetic impulses of variable duration were applied to the probe to estimate its frequency response and pressure sensitivity, c.f. Stern and Dacus [16]. The probe was inserted radially through a side arm on the centre section of the tube, and was scanned across the line cusp, i.e. moved parallel to the axis of symmetry, at a distance of 14 cm from it. The maximum field in the plane of the line cusp is at 10.2 cm from this axis, so that the field at the pressure probe was actually somewhat less than that at the cusp "hole". For this reason the effective width of the 2 mm probe was only 1.3 mm and all our measurements have been scaled by this factor.

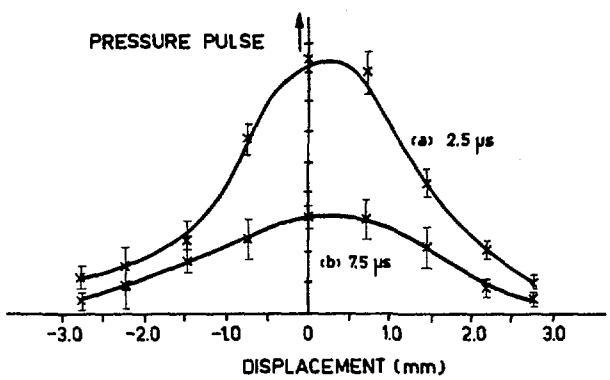

Fig. 11 The variation of the plasma pressure pulse with piezo-electric probe position in the line cusp region. (a) 2.5 μs after the cusp bank has fired, (b) 7.5 μs after the cusp bank has fired.

Typical signals produced by the plasma are shown in Fig. 10; the lower trace was filtered at 1 MHz to remove a $1\frac{1}{4}$ MHz mechanical "ring" in the probe, which is due to the finite breadth of the acoustic line. Time-resolved signals of this nature were used to plot profiles of the spatial distribution of the plasma over a wide range of operating conditions. Preliminary results (for a pressure of 30 mT of H_2) indicate cusp widths of order 2.2 ± 0.3 mm and 1.6 ± 0.3 mm at maximum fields of 39 kG and 55 kG respectively, when the main bank is fired 7 μs after the pre-heat. The pressure-pulse, which is proportional to the product of density and temperature, has an e-folding decay time of about 5.5 μs, which is consistent with the spectroscopic values of 11—12 μs for T_e and n_e. Fig. 11 shows the pressure profile across the line cusp about 2.5 μs and 7.5 μs after the cusp bank has fired; in this experiment the bank was deliberately fired 13 μs after the pre-heat so that the plasma should have a low temperature. The half-width is clearly wider at the later time.

5. Discussion

It is suggested that the instabilities observed in the Tube I experiment are of the Rayleigh-Taylor type [18], i.e. resulting from the acceleration of the plasma by the magnetic field. Such acceleration occurs during the initial stages of the compression, Fig. 4d, and additionally, on the reflection of complex strong shock patterns at the boundary in those cases where the contraction velocity exceeds the sound speed in the pre-heated plasma, Fig. 4b. The criterion for stability in the relevant case of a plasma accelerated by a curved magnetic field is [2]

$$\frac{B^2}{4\pi R} > nMf$$

where R is the radius of curvature of the magnetic field lines, (taken positive for lines convex to the plasma), f is the plasma acceleration, (positive for acceleration directed from the plasma towards the magnetic field) and nM is the plasma density. The observations are qualitatively consistent with this criterion in that (1) the system is more unstable in heavier gases, (2) instabilities appear to start in regions where R is large, and (3) there is evidence of considerable stabilisation during the later stages of compression when the sign of f changes. It should be emphasized that the instabilities discussed here are associated with the establishment of an equilibrium state, and no comprehensive results concerning the stability of such an equilibrium have been obtained in these preliminary experiments.

It is possible that the shape of the coils contributed to the instabilities since accelerations are highest in the initial stage of compression when the plasma is near the tube wall and the coils tend to behave like 8 cm long θ-pinch coils in which there is little or no stabilising curvature of the field lines. Tube II was designed to give maximum possible curvature of the field lines at the walls but as yet there is no experi-

mental evidence to show whether or not this is beneficial to the stability properties.

When the operating conditions in Tube I were such that the initial instabilities were not present, the cusp boundary appeared to remain quite sharp during the first quarter cycle. Analysis of framing camera pictures for some of the most stable and reproducible conditions, viz. 22 millitorr of hydrogen, gives a volume compression ratio of about 20.

The construction of Tube II makes it difficult to photograph the plasma; hence, the volume compression cannot be found by this technique, but it may be assumed comparable with that in Tube I. Estimates of temperature and density from spectroscopic measurements show that they do not increase, as would be expected from an adiabatic compression of this magnitude acting on an initially uniform plasma. However, the pre-heat conditions have been measured only over a 1 cm wide strip in the centre region, whereas the cusp field compresses plasma from an appreciably larger volume. In view of the limited range of measurements so far made, and their experimental uncertainties, no firm conclusion can yet be drawn about the behaviour of these plasmas during compression.

The simplest collision-free model in which the hole size is several electron Larmor radii, viz. about .001 cm, gives a containment time of the order of 1 ms for the measured experimental conditions. The measured hole size, 2—3 mm, for these conditions, assuming the plasma volume to be 50 cm^3 and neglecting mirror effects, should give a containment time of a few microseconds although this value may be improved by the mirror effects. However, we have insufficient information to account properly for the measured containment times of 11—12 μs.

The hole size, measured by the pressure probe, is probably consistent with diffusion processes. The exact model is complex and can only be tackled by computation but a crude estimate of diffusion effects can be made using the Spitzer formula. A plasma with an electron temperature of 5 eV will after 5 μs have diffused 1.5 cm so that the skin depth at the plasma boundary should be about this thickness. The plasma is contained chiefly near the centre of the cusp region where the field at the boundary is perhaps 15% of the maximum value at the cusps. Plasma diffusing at the centre region and flowing out along adjacent lines of force thus emerges through a hole of one-sixth of the skin depth, i.e. about a few millimetres wide.

Acknowledgements

We wish to thank Dr. R. J. Bickerton and Mr. R. S. Pease for their interest and helpful discussion, Mr. P. A. Worsnop, Mr. T. E. James, and Mr. J. Allen for engineering support, Mr. J. N. Burcham for much of the experimental work, and Mr. T. J. L. Jones for assistance with the spectroscopic measurements.

References

[1] Tuck, J. L., U.S. Atomic Energy Commission Report WASH-184 (1954) 77.
[2] Grad, H., U.S. Atomic Energy Commission Reports: WASH-289 (1955) 115, and NYO-7969 (1957).
[3] Berkowitz, J., *et al.*, Proc. Second United Nations Conf. on Peaceful Uses of Atomic Energy, **31** (1958) 171.
[4] Kadomtsev, B. B., Braginsky, S. I., Proc. Second United Nations Conf. on Peaceful Uses of Atomic Energy, **32** (1958) 233.
[5] Firsov, O. B., Plasma Physics and the Problem of Controlled Thermonuclear Reactions (Pergamon Press, Oxford, 1959) Vol. 3, p. 386.
[6] Tuck, J. L., *Phys. Rev. Letters* **3** (1959) 313.
[7] Grad, H., *Phys. Rev. Letters* **4** (1960) 222.
[8] Coensgen, F. H., *et al.*, *Phys. Fluids* **3** (1960) 764.
[9] Lukyanov, S. Yu., Podgorny, I. M., *J.E.T.P.* **36** (1960) 18.
[10] Scott, F. R., Voorhies, H. G., *Phys. Fluids* **4** (1961) 600.
[11] Watteau, J. H., *Phys. Fluids* **4** (1961) 607.
[12] Tuck, J. L., *Nature*, No. 4740 (1960) 863.
[13] Seaton, M. J., *Mon. Not. R. Astr. Soc.* **115** (1955) 279.
[14] Edwards, D. H., *J. Sci. Instr.* **35** (1958) 346.
[15] De Silva, A. W., United States Atomic Energy Commission Report UCRL-8887 (1959) 81.
[16] Stern, M. O., Dacus, E. N., *Rev. Sci. Instr.*, **32** (1961) 140.
[17] Griem, H. R., Kolb, A. C., Shen, K. Y., *Phys. Rev.* **116** (1959) 4.
[18] Taylor, G. I., *Proc. Roy. Soc.* **A 201** (1950) 192.

SOME EXPERIMENTAL STUDIES OF PLASMA INJECTED INTO A CUSPED MAGNETIC FIELD*

D. C. HAGERMAN

LOS ALAMOS SCIENTIFIC LABORATORY, UNIVERSITY OF CALIFORNIA

LOS ALAMOS, NEW MEXICO, UNITED STATES OF AMERICA

A hydromagnetic gun is used to inject an 8 μs high β jet of helium plasma axially into a picket fence magnetic field. The field (generated by external dc coils) has a distance between axial cusps of 80 cm and a maximum field strength of 430 G. Magnetic probe studies show a high β disturbance near the center lasting for 30—40 μs; this is followed by a long-lived low β perturbation in the field. These disturbances are asymmetric about the medium plane, their configurations being consistent with a reflection of particles between the axial cusp furthest from the gun and radial cusp. Measurements of the He II 4686 Å line profile indicate an average ion energy of 100 eV 50—80 μs after injection; this is observed perpendicular to the initial jet direction. This energy is consistent with the average ion injection energy of between 100 and 160 eV. Insertion of a magnetic probe decreases this observed ion energy by one-half; apparently a region of cold gas (≈ 10 cm typical dimension) surrounds a probe in this plasma which makes quantitative probe results unreliable. The electron temperature is measured in the interval between 50 and 140 μs by a comparison of the intensities of the He I lines 4921 and 4713; it shows a slight decrease with time (6 eV/100 μs) and has an average value of 17 eV. With this electron temperature plasma field intermixing occurs in ≈ 20 μs. Since the electron temperature is constant the ion lifetime may be estimated from the decay of the intensity of the He II line which gives exponential ion lifetimes of 200 μs. This time is approximately equal to charge-exchange times between the injected ions and the background of neutral helium released by the gun.

1. Introduction

The goal of our experimental work on cusped magnetic fields is to produce a high-β plasma confined by such a field and study its properties [1, 2, 3]. Theoretically [4], such a plasma would be stable for all values of $\beta < 1$ (where β is the ratio of the internal plasma pressure to the confining field pressure); the cusped geometries are the only ones in which this is true. The advantage in keeping β high comes from the increasing favorable power balance in any thermonuclear reactor as β is increased; for example, typical values for mirror machines are given by POST [5].

The experimental procedure has been to produce the plasma external to the confining field with a hydromagnetic plasma gun [6, 7, 1] and inject into the confining field. The hydromagnetic gun is adjusted to inject a high-β plasma in which the average ion energy is $\approx$ 100—160 eV. The plasma remaining in the field for relatively long times (50—100μ s) was studied by optical methods and magnetic probes. TUCK [8] proposed a scheme of trapping such a jet of plasma, in which the jet enters the field and is trapped around the zero in the magnetic field remaining a high-β plasma during the entire process. Experimentally, the injection and trapping of the plasma is more complicated than in his original scheme.

2. Experimental apparatus

A schematic view of the apparatus is given in Fig. 1. The aluminum vacuum vessel is 75 cm in diameter and 150 cm long; this large a chamber should reduce interaction of the plasma with the walls. The magnetic field is produced by external dc coils; the graph (Fig. 1) shows the spatial distribution of the z component of the vacuum field along the tank axis (the z axis is defined to lie along the tank axis with its center in the median plane). The vacuum system maintains the vessel at a pressure $\leq 10^{-5}$ mm of Hg before the gun is pulsed. Windows are provided in the median plane and in the end of the tank for optical and magnetic probe measurements.

The plasma gun consists of coaxial electrodes connected to a 2 μF condenser bank. In the center electrode a fast valve admits a gas pulse (≈ 0.3 atm cm^3) into the annular region between the electrodes. Breakdown of the gas is initiated by a sparkplug. The resulting discharge accelerates the plasma along the electrode structure. The collimating baffles reduce the amount of plasma injected at large angles; these baffles are necessary since the plasma gun emits plasma in a cone whose half-angle is large ($\approx 30°$). The gun is operated in the field-free region provided by the iron shielding.

The gun is adjusted so that it emits a helium plasma jet containing an average total energy of ≈ 8 J as measured by the temperature rise of a copper foil placed at $z = -45$ cm. The injection pulse lasted ≈ 8 μs. The input ion energy was determined by a time of flight measurement from the diamagnetic signal generated by the plasma during injection. It was assumed that all ions started in the gun when the gun current started; this introduces an error causing an underestimate of the ion energy but it is small

* Conference paper CN-10/154, presented by D. C. Hagerman. Discussion of this paper is given on page 95. Translations of the abstract are at the end of this volume of the Conference Proceedings.

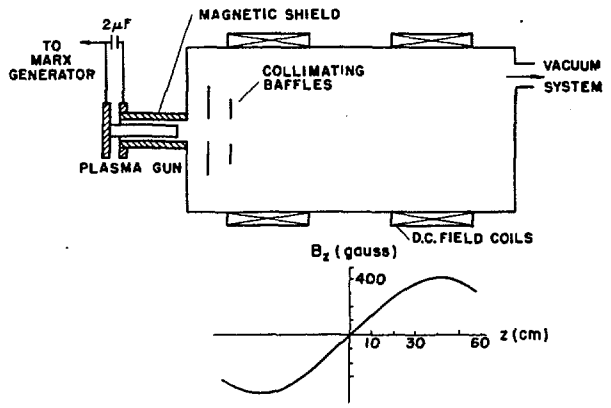

Fig. 1 Schematic drawing of the apparatus. The graph shows the z component of the magnetic field along the axis of the vacuum vessel.

since most of the plasma is ejected during the first quarter-cycle of the gun current (0.5 μs) and typical flight times are 6 μs. Fig. 2 shows the average β seen as a function of ion velocity ($\beta = 1 - B^2/B_0^2$). The errors shown in Fig. 2 represent the rms variation in the data; these serve to emphasize that the gun output is non-reproducible. These data show that the most probable velocity is 9 cm/μs (160 eV for helium ions). The average ion energy may be estimated by integrating over this distribution. If one assumes $W_\perp \propto W_\parallel$ (note that $W_\perp$ creates the field disturbance and $W_\parallel$ is what is measured by time of flight) as a weighting function, the average energy is 166 eV; if one assumes $W_\perp$ is constant, the average is 96 eV. Hence 130 eV is a reasonable average ion energy. The gun also emits an appreciable amount of neutral He before firing since there is a finite delay between opening the gun valve and firing the gun. At the center of the tank this neutral helium background (as measured with a fast ion gauge) at the time the gun fires amounts to 6×10^{11} He atoms/cc and doubles in 90 μs. These measurements were made when the gun valve alone was operated and give a lower limit on the neutral helium background.

3. Experimental results

Magnetic probes [9] were used in the early stages of the experiment to determine the spatial distribution of the β produced by the plasma. As shown below, the probe results for long-time phenomena underestimate the plasma densities due to the interaction of the probe with the plasma. In the region of trapped plasma the probe signals typically show a relatively large pulse ($\beta \approx 1$ depending on position in space) of ≈ 30 μs full width at half maximum followed by a relatively slowly decaying tail. A typical z-axis run is shown in Fig. 3 which shows the average z-field distribution 50 μs after the gun fires. The most striking feature of this distribution is the decided asymmetry about $z=0$; as expected the field is decreased for $z>0$ but surprisingly the field is *increased* for $z<0$. This anomalous behavior of the field perturbation is caused by a preferential trapping of the plasma in the low field region furthest from the gun. The individual particle orbits are equivalent to reflections between the mirror at the positive z point cusp and the mirror at the ring cusp. Probe measurements about the median plane of the radial field component confirm this asymmetry. This asymmetry is also seen in the high-β portion of the magnetic signal which implies that the high-β plasma never reaches its equilibrium configuration in the time available. The reason for this asymmetrical trapping is not understood. One conjecture is that the plasma undergoes some unstable configuration during injection in the field decreasing region and is preferentially lost there.

Fig. 4 shows the radial extent of the B_z perturbation 50 μs after injection at $z=15$ cm. It is interesting that this seems to be a moderately (≈ 10 cm radius) localized disturbance about the axis with a "sheath" width of ≈ 5 cm. From such a graph the z component of the flux change may be computed; this has also been measured with a loop (radius 18 cm) which gives a flux change of roughly twice that obtained from the probe data. This result is an indication that the loop interferes with the plasma to a lesser extent than the probes; presumably, because the probe is in closer

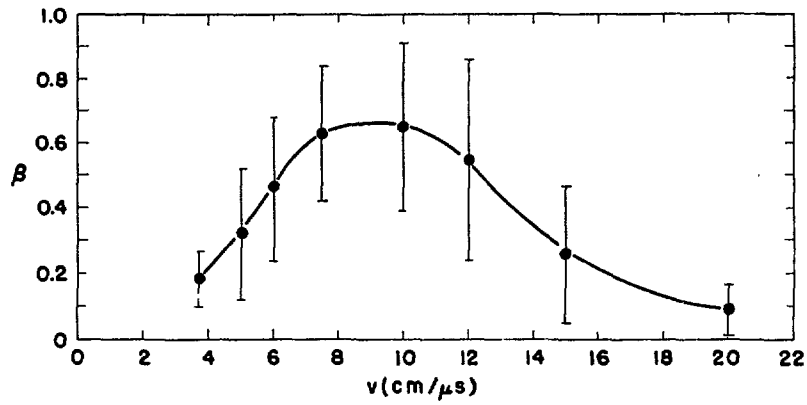

Fig. 2 The average β of the injection pulse (at the input cusp) as a function of the ion velocity. The cusp field was 430 G, the errors show the r.m.s. deviation in the data.

proximity to the plasma than the loop. From the loop signal an average plasma energy density over the loop may be obtained which is 1.2×10^{14} eV/cm^3. This number will be used later to set a lower bound on the density (cusp field = 430 G).

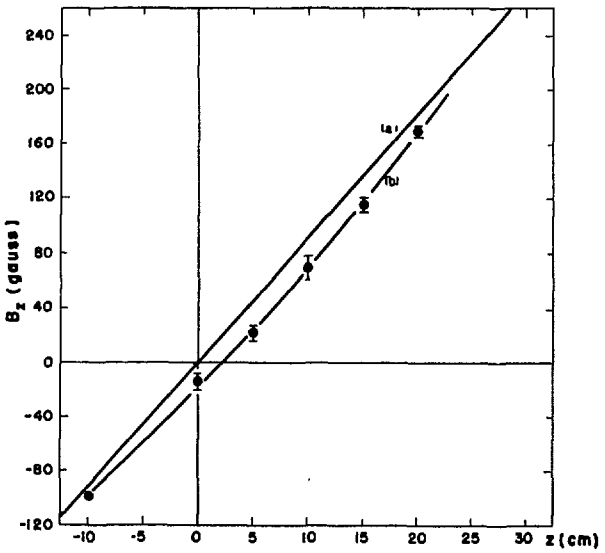

Fig. 3 The z components of (a) the vacuum magnetic field and (b) the field 50 μs after plasma injection as a function of distance along the vacuum vessel axis. The cusp field was 270 G. The gun fired from the left.

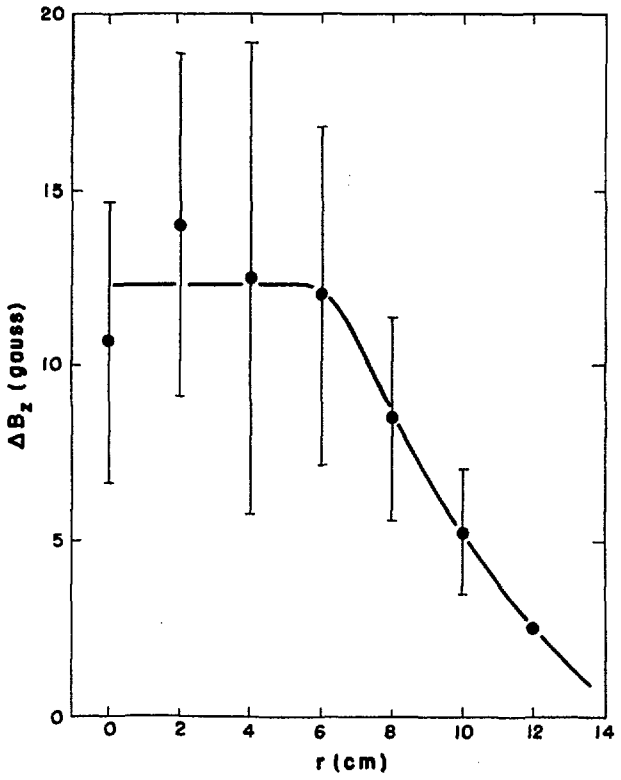

Fig. 4 The perturbation in the z component of the vacuum field 50 μs after injection as a function of radius. The perturbation reduced the total field. These data were taken in a plane 15 cm beyond the median plane of the vacuum vessel.

The electron temperature may be estimated from a measurement of the relative intensities of the neutral helium lines at 4921 Å and 4713 Å [10]. These intensities were measured looking in the radial direction at the median plane with a monochromator whose slit system was adjusted so that the full width at half-maximum of a narrow line is 1.65 Å. The intensity ratios are averages of several shots and include an average subtracted background. The results are shown in Fig. 5 as a function of time. The straight line is the linear least-square fit to the experimental points. It shows that the temperature is decreasing at ≈ 6 eV/100 μs. The reproducibility of the data does not permit a more accurate measurement of the electron energies.

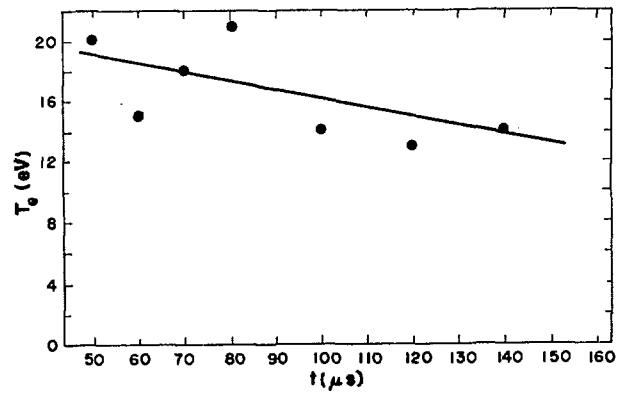

Fig. 5 The electron temperature as a function of time as deduced from the intensity ratios of the neutral He lines at 4921 Å and 4713 Å.

The ion energies may be estimated from the width of the singly ionized He line at 4686 Å [11]. This width was measured in the radial direction at the median plane; since the depth of focus of the optical system was large, no region of plasma preferentially contributed to the light intensity. The monochromator permitted measurement of only one component of the line at a time. The procedure was to take 3 shots per wavelength, change wavelengths in such a manner as to cover the entire line at 0.25 Å intervals in several successive sweeps and then repeat the entire profile (the monochromator resolution is 0.82 Å). This averages out systematic drifts of the apparatus. A rather involved procedure was adopted to determine the line width from the data; the purpose of this being to remove any "artistic" tendencies of the experimenter in drawing line profiles. Briefly, the procedure is: An average background intensity determined from measurements outside the line was subtracted; typically this was a 15—20% correction. The resulting profile was plotted on probability paper which always gave a reasonably straight line. (This does not imply that the line profiles are strictly Gaussian since any bell-shaped curve gives a fairly straight line when plotted on probability paper.) The full width at half-maximum was determined from the appropriate points on the straight line; this width is a result of a combination of the actual line profile and the mono-

chromator resolution. The latter was removed by taking the theoretical line profiles for various ion energies, folding in the measured monochromator resolution and finding a total width via probability paper for a particular ion energy. It should be noted that the theoretical profiles assume a Maxwellian distribution of energies; this is not actually true since insufficient time for thermalization (discussed below) exists; however, the data are nowhere sufficiently precise to distinguish whether or not the distribution is Maxwellian.

TABLE I. Average ion energies as deduced from the width of the singly ionized helium at line 4686 Å. In all cases the cusp field is 430 G.

Conditions	Time (μs)	Average Ion Energy (eV)
Base pressure $3—6\cdot10^{-6}$ mm Hg	50	80
	60	115
	70	105
	80	90
Base pressure $3—6\cdot10^{-6}$ mm Hg Probe inserted to $z=0$	50	50
	60	65
	70	50
	80	35
Base pressure $3—6\cdot10^{-6}$ mm Hg Probe inserted to $z=10$ (out of direct view of monochromator	50	60
	60	40
	70	35
	80	35
He admitted to system to raise base pressure to $8\cdot10^{-5}$ mm Hg	50	50
	60	35
	70	55
	80	45

The results of this procedure are shown in Table I. The ion energies of the unperturbed plasma between 50 and 80 μs are within reasonable agreement with average injected energy. The insertion of a probe (along the z axis) causes a marked decrease in the ion energy—even when the probe itself is out of view of the monochromator. This decrease in energy may come from a cooling of the entire plasma by the probe or by an averaging effect caused by a very low temperature region around the probe and energetic ions at large distances from the probe. This latter interpretation is supported to some extent by the halation which appears around the probe. Line profile measurements at greater times could not be made because of insufficient intensity.

A very approximate measurement of ion lifetime may be made by observing the total intensity of this ionic line as a function of time. Since the electron temperature (15—20 eV) is well below the excitation energy (≈ 50 eV) of this line and is falling with time, the probability of excitation does not increase with time. Then, assuming the plasma remains the same size and the excitation probability remains constant, the intensity is proportional to the product of the electron density and ion density. This product is proportional to the square of the ion density. Hence, the square root of the intensity is proportional to the ion density. This quantity is an exponential out to 200 μs with an e-folding time of ≈ 200 μs; insufficient intensity prevented measurements for longer times.

Other atomic species were observed such as nickel (from the stainless steel electrodes in the gun), oxygen, silicon. The only conclusion drawn from this is that we are definitely not dealing with a clean plasma, the source of the contaminants being the plasma gun.

4. Discussion

That the high-β magnetic disturbance lasts for a short time (≈ 30 μs) is not surprising when one considers the rate of field penetration into a plasma whose electron temperature is low. For example, consider a long cylinder of radius r which carries a current in a sheath of thickness δ whose resistivity is ϱ. The e-folding time for current decay is

$$\tau = \frac{\mu_0 r\delta}{2\varrho}.$$

For an order of magnitude result, let $r=0.1$ m, $\delta=0.03$ m and ϱ the resistivity [12] of a fully ionized helium gas at an electron temperature of 15 eV. The result is $\tau=25$ μs. Whether such a simple picture is true cannot be ascertained without much more data but such effects must be important at these low electron temperatures. After the field mixing takes place the electrons should be at a higher temperature (approximately the ion energy times the ratio of the ion density to electron density) than that observed; some loss process, such as exchange with "cold" electrons from the walls, must be keeping the average electron energy down. Since this field mixing is an irreversible process it may be playing an important part in the trapping process.

The effect of the probe on the ion energies is not unexpected; indeed, similar effects [3] have been seen previously where it was shown that any probe in contact with the plasma perturbs other probe signals. This merely points out the obvious, that any material touching a high temperature plasma cools it drastically. The best that one can do with the probe results is to use them to set lower limits on the size of the trapped plasma and its density. A lower limit on the density then is 1.2×10^{12} cm^{-3} using the average ion energy of 100 eV and the observed energy density of 1.2×10^{14} eV/cm^3 (*since this energy density is averaged* over the loop area it represents an underestimate even if there were no cooling effects). The volume of the trapped plasma is then approximately 10 liters so the lower limit on the ratio of the amount of trapped plasma at 50 μs to that injected is 1%.

Using this density one can calculate thermalization times [12, page 76] with the following results:

$$t_{ce} = 0.7 \ \mu s$$

$$t_{ii} = 150 \ \mu s$$

$$t_{ei} = 700 \ \mu s.$$

We see that it is proper to speak of an electron temperature but not of an ion temperature for this plasma.

Within experimental error the ion energy determined from the line width measurement agrees with the injected ion energy. The last set of conditions in Table I in which the base pressure was increased by the addition of helium provides a reassuring check on this method of ion energy measurement. For this base pressure the e-folding time for charge exchange [13] is (including transient pressure from gun at 50 μs) 40 μs; hence, the average ion energy at 50 μs should be much lower than the injected energy. Nor is it surprising that no systematic decrease in the ion energy is observed between 50 and 80 μs in this case, since the line width is now comparable to the instrumental width and errors in measurement must be large. Charge-exchange time on the transient pressure alone is 150 μs which is approximately the decay time observed for the ion density. Since the ion density is of the same order as the neutral density, this process, in reality, is not a simple exponential decay. With this short charge-exchange time it was not possible to observe any systematic effect of varying the field on the lifetime. The lifetime however is long enough so that the ions must undergo on the order of 50 reflections in the field which is an order of magnitude longer than that seen (experimentally and theoretically) when single ions are injected into a cusped geometry [14].

5. Conclusion

In conclusion we summarize what we believe that this experiment has shown: Plasma injected in a high-β manner into a picket fence field is trapped (this is not what is observed for low-β injection). The ion energy of the trapped plasma (≈ 100 eV), within experimental error, is not different from that of the injected plasma. The lifetime (≈ 200 μs) of the plasma is governed by loss processes associated with the background pressure and impurities. The electron temperature of this plasma is low (≈ 20 eV) which allows field mixing in fairly short times. Insertion of a probe into the plasma seriously degrades the average ion energy; nevertheless, there is apparently a real asymmetry in the distribution of the trapped plasma about the equatorial plane.

Acknowledgments

The writer gratefully acknowledges the help and encouragement of the other members of this laboratory. J. L. Tuck originally suggested this experimental problem. J. E. Osher and J. A. Phillips have been most helpful in discussing methods and results. R. Dike, R. Holm, A. Schofield, and J. Sherwood assisted in the design, construction and operation of the experiment.

The work was performed under the auspices of the United States Atomic Energy Commission.

References

[1] Hagerman, D. C., Osher, J. E., *Bull. Am. Phys. Soc., Series II*, **5** (1960) 350.
[2] Osher, J. E., Hagerman, D. C., *Bull. Am. Phys. Soc., Series II*, **6** (1961) 195.
[3] Hagerman, D. C., Osher, J. E., *Phys. Fluids* **4** (1961) 905.
[4] Berkowitz, J., *et al.* Proceedings of the Second United Nations International Conference on the Peaceful Uses of Atomic Energy, Geneva, **31** (1958) 171.
[5] Post, R. F., "Some Aspects of the Economics of Fusion Reactors" UCRL-6077, Controlled Thermonuclear Processes UC-20, U.S. Atomic Energy Commission Report TID-4500 (August, 1960).
[6] Marshall, J., *Phys. Fluids* **3** (1960) 134.
[7] Marshall, J., "Hydromagnetic Plasma Gun", Proceedings of the Fourth Lockheed Symposium on Magnetohydrodynamics (S. W. Kash, Ed., Stanford Univ., 1960) 60.
[8] Tuck, J. L., *Phys. Rev. Letters* **3** (1959) 313.
[9] Lovberg, R. H., *Ann. Phys. (New York)* 8 (1959) 311.
[10] Glasstone, S., Lovberg, R. H., Controlled Thermonuclear Reactions (D. Van Nostrand Company, Inc., Princeton, New Jersey, 1960) 189.
[11] Weimer, K. E., "Doppler Broadening of the He^+ 4686 Line in Ion Temperature Measurements," U.S. Atomic Energy Commission Report NYO-7885 (1957).
[12] Spitzer, L., Jr., Physics of Fully Ionized Gases (Interscience Publishers, Inc., New York, 1956) 83.
[13] Massey, H. S. W., Burhop, E. H. S., Electronic and Ionic Impact Phenomena (Oxford, Clarendon Press, 1956) 519.
[14] Knapp, E. A., Private communication, 1961.

ИССЛЕДОВАНИЕ ПОВЕДЕНИЯ ПЛАЗМЫ В МАГНИТНОЙ ЛОВУШКЕ «ОРЕХ»*

Н. Г. Ковальский, С. Ю. Лукьянов, И. М. Подгорный

Институт Атомной Энергии им. И. В. Курчатова

Академии Наук СССР, Москва,

Союз Советских Социалистических Республик

Система «Орех» является аксиально-симметричной магнитной ловушкой с полем сложной формы нарастающим к периферии. Максимальный диаметр вакуумной камеры 1000 мм, высота 900 мм. Максимальное значение магнитного поля в магнитных щелях составляет 4,5 кэ. Эксперименты проводились при давлении остаточного газа в камере $2-4.10^{-7}$ мм. рт.ст. Плазма инжектировалась вдоль оси системы из электродинамического инжектора коаксиального типа. Полупериод тока в цепи инжектора составляет 3 мксек. Скорости плазменных сгустков, инжектируемых в ловушку, измерялись различными методами и составляют, приблизительно, 10^7 см/сек.

Применялись следующие методы исследования плазмы: электрические и магнитные зонды, калориметрическая фотоэлектрическая и спектроскопичесая методики.

В ходе исследований было показано, что около 70% инжектированной в ловушку плазмы выходит через кольцевую магнитную щель. Моменты прохождения сгустков через аксиальные магнитные щели регистрировались по вытеснению магнитного поля из области, занимаемой сгустком. Определена зависимость плотности плазмы в центральной зоне от величины напряженности магнитного поля при различных условиях работы электродинамического инжектора. Произведена оценка электронной температуры плазмы. Измерено время жизни плазмы в ловушке и подтверждена независимость этого времени от магнитного поля в широком интервале значений поля. Время жизни плазмы в ловушке при плотностях $10^{13}-10^{14}$ 1/см^3 составляет, примерно, 60 мксек.

Полученные результаты согласуются с качественной картиной поведения плазмы в системах подобного рода.

1. Введение

После установления основных фактов, относящихся к поведению плазмы в магнитных ловушках с полем, нарастающим к периферии, целесообразно было перейти к систематическим исследованиям в более определенных условиях эксперимента.

В предыдущих работах длительность процесса заполнения ловушки плазмой была соизмерима со временем жизни плазмы. Не уделялось должного внимания чистоте инжектируемой плазмы. Отсутствовали данные о балансе энергии. Не изучалась с необходимой подробностью связь между плотностью плазмы в ловушке и напряженностью магнитного поля.

В настоящей работе сделана попытка заполнить, до некоторой степени, эти пробелы.

2. Установка и методы исследования

Система «Орех» является аксиально-симметричной магнитной ловушкой с полем сложной формы, нарастающим к периферии (рис. I) Магнитное поле создается двумя основными и двумя дополнительными катушками, питаемыми постоянным током. Максимальное значение магнитного поля в магнитных щелях составляет 4500 эрс. Вакуумная камера, изготовленная из нержавеющей стали, по форме напоминает грецкий орех и в центральной плоскости имеет диаметр 1000 мм. Откачка установки осуществлялась паромасляным насосом производительностью 5000л/сек. Пары масла вымораживались ловушкой, охлаждаемой жидким азотом. Давление остаточного газа в камере составляло $2-4\cdot10^{-7}$ мм рт.ст.

Плазма инжектируется в ловушку, вдоль оси, из электродинамического инжектора коаксиального типа, расположенного над ловушкой. Конденсаторная батарея разрядного контура имеет ёмкость 12 мкф; рабочее напряжение составляет 10 кв. Конденсаторная батарея присоединяется к инжектору через вакуумный разрядник. В инжектор с помощью быстродействующего клапана вводится 1 см^3 водорода при нормальных условиях. Момент старта разряда задается электронной схемой. Оптимальное время запаздывания старта относительно момента срабатывания клапана подбиралось экспериментально и составляет 200 мксек. Для сокращения длительности процесса инжекции, в ряде случаев, использовался дополнительный вакуумный разрядник, закорачивающий конденсаторную батарею через 3,1 мксек после старта разряда. (Период колебания разрядного тока в инжекторе — 6,2 мксек).

Моменты прохождения плазменного сгустка через верхнюю и нижнюю магнитные щели регистрировались по вытеснению магнитного поля из витков, размещенных в двух плоскостях, перпенди-

* Доклад CN-10/202 представленный на Конференцию. Докладчик: Ю. Ф. Наседкин. Дискуссия (на английском языке) по этому докладу дана на стр. 95. Переводы аннотаций находятся в конце этого тома Трудов Конференции.

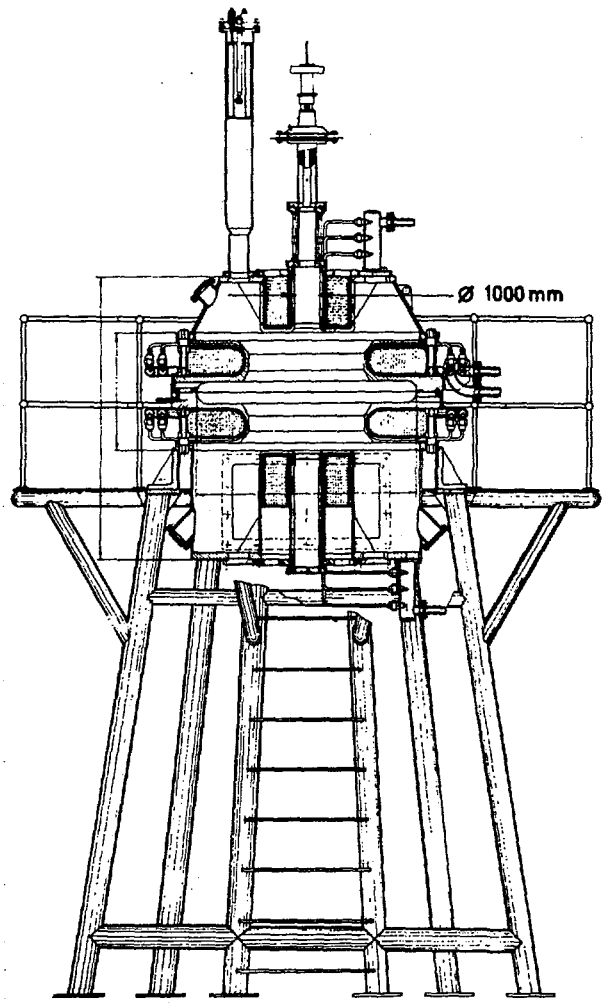

Рис. 1 Схема установки « Орех ».

кулярных к оси установки. Измеряя временной интервал между импульсами от витков, можно было определить направленную скорость сгустков плазмы. Для контроля, направленная скорость измерялась также с помощью фотоэлектрической методики.

При выполнении спектроскопических измерений использовались спектрографы типа ИСП-51 и ИСП-28. Излучение плазмы из центральной зоны ловушки направлялось на входную щель оптического инструмента через окно с кварцевым стеклом. Ход спектральных линий во времени регистрировался с помощью монохроматора с фотоумножителем.

Для определения времени жизни плазмы и ее плотности, а также для оценки электронной температуры, использовался зонд Ленгмюра, который помещался в области минимального магнитного поля, подобно тому как это делалось в предыдущих работах.

Количество энергии, вносимой плазмой в ловушку, измерялось с помощью подвижного калориметра, имеющего форму полого цилиндра с перегородками. Такая конструкция, как известно, позволяет исключить эффект отражения плазмы от твердой поверхности. Для измерения энергии, вытекающей через нижнюю щель, калориметр помещался за этой щелью. Измерение энергии, уходящей через боковую щель, производилось с помощью плоского калориметра.

Временной ход поступления энергии на стенку камеры определялся при помощи методики, разработанной Л. Л. Гореликом, описание которой содержится в работе [1]. Все конструкторские работы по сооружению установки были выполнены Э. Н. БРАВЕРМАНОМ.

3. Результаты

В течение последних лет в ряде работ по физике горячей плазмы особое внимание уделялось вопросу чистоты плазмы. Наличие даже небольшого количества примесей приводит к интенсивному охлаждению плазмы за счет излучения. В ловушках со встречными полями, где времена жизни измеряются десятками микросекунд, проблема примесей имеет меньшее значение, чем в процессах большой длительности (стелларатор, адиабатические магнитные ловушки). Тем не менее улучшение вакуумных условий оказывается полезным и в этом случае, так как упрощается толкование наблюдаемых явлений.

Рис. 2 Спектры излучения плазмы в ловушке. Нижняя часть — вакуумный разрядник закорочен. Верхняя часть — оптимальный режим работы инжектора (задержка 200 μсек). Рисунок основывается на фотографии, сделанной при экспозиции в 10 разрядов.

На рис. 2 представлены спектры, полученные при наполнении ловушки плазмой из инжектора, работающего в двух различных режимах. Спектр, приведенный в нижней части рисунка, получен при закороченном основном вакуумном разряднике. В этом случае на электродах инжектора «дежурит» высокое напряжение и разряд начинается, когда давление водорода в инжекторе становится достаточным для пробоя. Второй снимок получен при оптимальной задержке между моментом открытия клапана и стартом разряда. Остальные условия опыта при снятии спектров совпадали. На первом снимке, помимо водородного спектра, отчетливо видны линии ионизованных атомов углерода и кальция. Сопоставление снимков явно

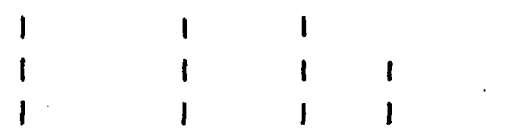

Рис. 3 Спектры излучения плазмы в ловушке при напряжениях на инжекторе 5 кв, 7 кв, 9 кв.
Рисунок основывается на фотографии, сделанной при экспозиции в 10 разрядов.

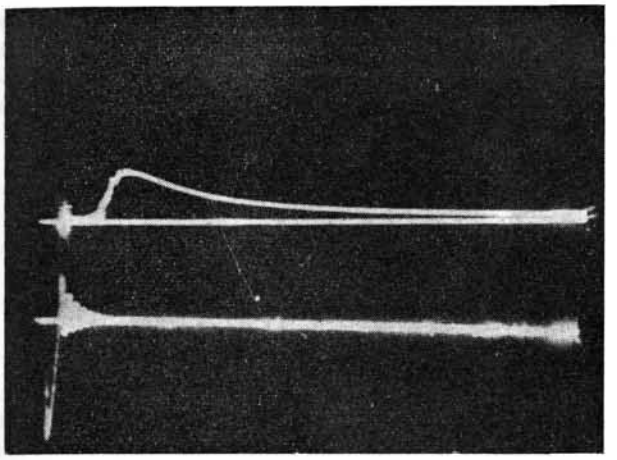

Рис. 4 Осцилограммы ионного тока насыщения на зонд и разрядного тока в цепи инжектора. Длительность развертки 170 μсек.

показывает преимущества второго режима работы. Для установления «порога» появления спектральных линий примесей в видимой области были сняты спектры при различных начальных напряжениях на инжекторе. На рис. 3 видно постепенное изменение вида спектра при повышении напряжения. В дальнейшем, за исключением специально оговоренных случаев, измерения производились при напряжении 7 кв, когда в видимой области спектра линии примесей не обнаруживались. Разумеется, это не означает, что плазма в этих условиях оказывается совершенно свободной от примесей. При больших экспозициях (около ста разрядов) в ультрафиолетовой области обнаруживаются резонансные линии Ca II (3968 Å; 3934 Å) и Cu I (3274 Å; 3248 Å). Интенсивности этих линий много меньше интенсивностей первых линий бальмеровской серии. Появление атомов кальция и меди в плазме не удивительно, если учесть, что электроды инжектора изготовлены из меди и укреплены на переходном изоляторе из фарфора.

Скорость плазмы, определенная, как указано выше, по измерению пролетных времен сгустка, составляла около $0.7 \cdot 10^7$ см/сек при стандартном значении напряжения -7 кв.

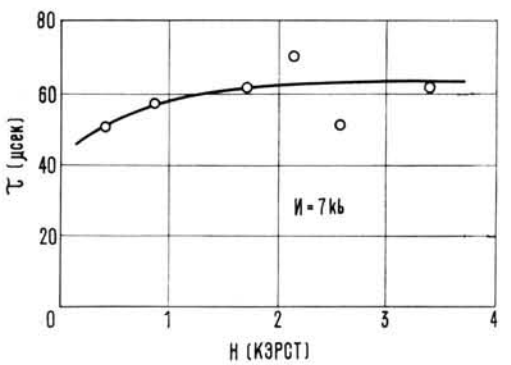

Рис. 5 Зависимость времени жизни плазмы в ловушке от напряженности магнитного поля в щелях.

Обратимся теперь к рассмотрению временных характеристик плазмы в ловушке. Ионный ток насыщения на зонд, как функция времени, представлен на рис. 4. Если температура плазмы в ловушке существенно не меняется со временем, то ионный ток насыщения пропорционален плотности плазмы. Спадание плотности плазмы укладывается в зависимость $n = n_0 \exp(-t/\tau)$. За время жизни плазмы в ловушке, принималась постоянная τ. К сожалению электронная часть зондовой характеристики, как известно, оказывается сильно

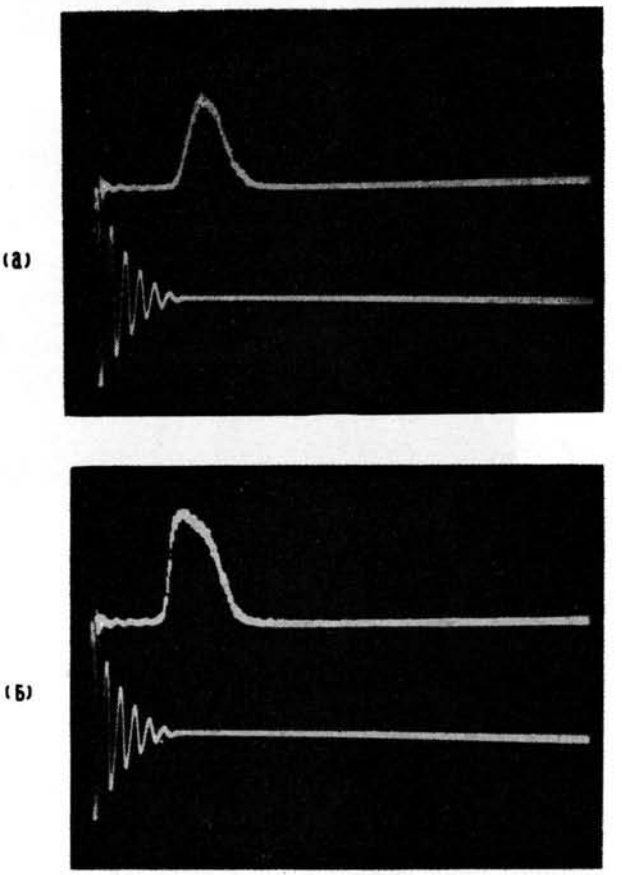

Рис. 6 Осцилограммы интенсивности линии Hβ ($\Delta\lambda - 10$Å, длительность развертки 170 μсек): (а) $H = 0$, (б) $H = 4000$ эрст

искаженной даже в слабых магнитных полях. Поэтому к оценке температуры сделанной зондовым методом нужно подходить с достаточной осторожностью. В качестве наиболее достоверного значения в настоящей работе принимается $T_e = 15$ эв.

Отмеченное ранее [2] постоянство времени жизни плазмы при разных значениях напряженности магнитного поля было изучено более детально. На рис. 5 представлена зависимость времени жизни плазмы от магнитного поля в интервале от 500 эрс до 4500 эрс. В пределах разброса точек, время жизни, в исследованных условиях, оказывается практически не зависящим от магнитного поля. Величина τ составляет приблизительно 60 мксек.

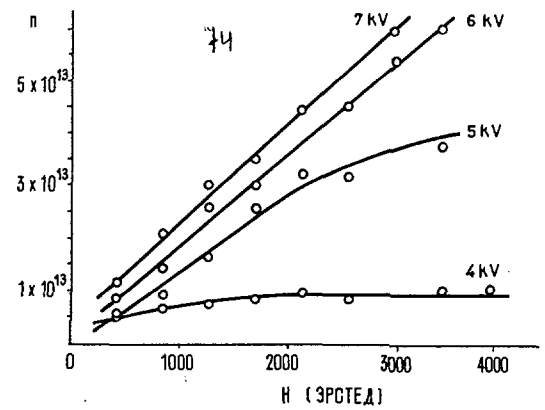

Рис. 8 Зависимсеть плотности плазмы в ловушке от напряженности магнитного поля при разных напряжениях на инжекторе.

При подстановке экспериментальных значений, входящих в формулу величин легко убедиться, что Q и $Q_{бок.}$ согласуются между собой с точностью до множителя 2—3.

На рис. 8 представлена зависимость плотности плазмы в ловушке от напряженности магнитного *поля при разных режимах работы инжектора. При* относительно небольших напряжениях на инжекторе плотность плазмы вначале быстро возрастает с магнитным полем, а затем, начиная с полей порядка 1000 эрс, быстрый рост сменяется насыщением. С увеличением напряжения на инжекторе, в исследованной области магнитных полей, наблюдается непрерывное возрастание плотности.

Совокупность всех полученных экспериментальных данных согласуется с предварительными результатами болометрических измерений, выполненных Л. Л. Гореликом и В. В. Синицыным. Время ухода тепла из ловушки через нижнюю магнитную щель, определенное при помощи болометра с постоянной времени в несколько микросекунд, указывает на эффект захвата плазменного сгустка в центральной области ловушки. Дальнейшие работы в этом направлении вероятно позволят получить количественные данные.

4. Заключение

Изложенные экспериментальные результаты приводят к следующей картине физических процессов, происходящих в ловушке с магнитным полем, нарастающим к периферии. Плазма, поступающая из инжектора в ловушку, обладает небольшой проводимостью и время ее прохождения через магнитный барьер достаточно велико. Поэтому, плазма, захваченная в ловушку, оказывается перемешанной с магнитным полем. Экспериментальным подтверждением этого факта являются недавно выполненные опыты на малой ловушке со встречными полями [3]. В этих опытах миниатюрный магнитный зонд, помещенный в центре ловушки, обнаруживал появление магнитного поля, захваченного плазмой при прохождении через магнитный барьер.

Другое подтверждение рассматриваемой картины можно видеть в постоянстве времени жизни плазмы в ловушке в широком интервале значений напряженности магнитного поля. В модели с вытесненным полем [4, 5] время жизни должно было бы убывать с ростом магнитного поля [3].

Наконец, в модели с вытесненным магнитным полем плотность плазмы должна обращаться в нуль через конечное время, а не убывать экспоненциально.

Параметры плазмы, полученные к настоящему времени на магнитной ловушке «Орех», разумеется, еще, далеки от тех, которые необходимы для осуществления физической управляемой термоядерной реакции. Возможности системы, однако, не могут считаться исчерпанными. Если мы научимся инжектировать в ловушку более быстрые сгустки более плотной плазмы, то оптимизм, которым руководствовались авторы при сооружении этой установки окажется оправданным.

Литература

[1] Горелик Л. Л., Лобиков Е. А., *Журнал технической физики* **31** (1961) 125.
[2] Подгорный И. М., Сумароков В. Н., *J. Nuclear Energy* **C 1** (1960) 236.
[3] Подгорный И. М., Сумароков, В. Н., «Захват плазмы в ловушку с магнитным полем, нарастающим к периферии» (Доклад на настоящей конференции).
[4] Фирсов О. Б., «Физика плазмы и проблема управляемых термоядерных реакций», Москва (1958), том III, 327.
[5] Беркович Я., Фридрикс К. О., Герцель Г., Град Киллин Ж., Рубин Е., Доклад № 1538 на конференции в Женеве 1958 г.
(Proceedings of Second Conference on Peaceful Uses of Atomic Energy, Geneva **31** (1958) 171).

ЗАХВАТ ПЛАЗМЫ В ЛОВУШКУ С МАГНИТНЫМ ПОЛЕМ, ВОЗРАСТАЮЩИМ К ПЕРИФЕРИИ*

И. М. ПОДГОРНЫЙ, В. Н. СУМАРОКОВ

ИНСТИТУТ АТОМНОЙ ЭНЕРГИИ ИМ. И. В. КУРЧАТОВА

АКАДЕМИИ НАУК СССР, МОСКВА,

СОЮЗ СОВЕТСКИХ СОЦИАЛИСТИЧЕСКИХ РЕСПУБЛИК

В выполненных ранее исследованиях было показано, что время жизни плазмы в ловушках с магнитным полем, нарастающим к периферии, составляет десятки микросекунд. Полагая, что сгусток плазмы, инжектированный в ловушку, полностью вытеснил магнитное поле из некоторой области вблизи центра и учитывая линейный ход напряженности поля, получим следующее выражение для времени жизни плазмы:

$$\underset{(\text{мксек})}{\tau} = 0{,}7\, \underset{(\text{эв})}{T^{\frac{1}{6}}}\, \underset{(\text{эрг см}^2/\text{эрс}^2)}{(WR^2/H^2)^{\frac{4}{15}}}$$

где W — энергия сгустка, R — радиус ловушки. Подставляя экспериментально полученные значения, нетрудно убедиться, что τ составляет несколько десятков микросекунд и слабо зависит от напряженности магнитного поля, что согласуется с экспериментальными данными.

В работе описаны эксперименты, предпринятые с целью проверки применимости предпосылок, использованных при выводе формулы, в условиях изложенных ранее опытов. Для исследования процесса захвата плазмы использовались калориметрическая методика, магнитные зонды и сверхскоростная киносъемка.

Диаметр вакуумной камеры ловушки, изготовленной из стекла, составлял 20 см. Магнитное поле ловушки создавалось двумя катушками, включенными навстречу друг другу. Катушки располагались на расстоянии 7 см друг от друга. Напряженность магнитного поля в зазоре между катушками достигала 6000 эрстед. Для инжекции плазмы использовался коаксиальный электродинамический инжектор обычного типа.

Было показано, что распределение потоков тепла на стенки камеры сильно зависит от напряженности магнитного поля. При больших магнитных полях потоки тепла на стенку как в направлении инжекции плазмы, так и в направлении противоположном инжекции становятся одинаковыми. При этом основная часть энергии уходит через магнитные щели.

Магнитными зондами измерялись распределения магнитного поля вдоль оси симметрии ловушки, отвечающие различным моментам времени. При вхождении сгустка в магнитный барьер наблюдается диамагнитный сигнал. Показания зондов, расположенных внутри ловушки, свидетельствуют о захвате магнитного поля сгустком и затягивании его в центральную область ловушки. Из этих данных следует, что предположение о вытеснении магнитного поля из центральной части ловушки в начальной стадии процесса не является верным. Таким образом совпадение экспериментально полученного времени жизни плазмы с величиной, полученной из приведенной формулы, оказывается случайным.

Данные магнитных зондов хорошо согласуются с данными, полученными при помощи сверхскоростной киносъемки.

1. Введение

По мере углубления и расширения наших представлений о высокотемпературной плазме непрерывно выясняются недостатки ранее выбранных направлений осуществления управляемых термоядерных реакций. Одновременно возрастает относительная роль некоторых других методов решения этой проблемы, которые ранее считались менее перспективными. Неудачи, связанные с получением термоядерных реакций в адиабатических ловушках, повысили роль исследований поведения плазмы в ловушках с полем, нарастающим к периферии. В системах такого типа, повидимому, должны отсутствовать наиболее опасные формы гидромагнитных неустойчивостей.

На протяжении последних лет появилось несколько экспериментальных исследований [1, 2, 3, 4, 5], посвященных инжекции и удержанию плазмы в ловушках с магнитным полем, нарастающим к периферии. Результаты этих работ свидетельствуют о том, что время жизни плазмы в интервале плотностей 10^{12}—10^{14} см$^{-3}$ слабо зависит от напряженности магнитного поля и составляет десятки микросекунд.

Полагая, что сгусток плазмы, инжектированной в ловушку, полностью вытесняет магнитное поле

* Доклад CN-10/204 представленный на Конференцию. Докладчик: Ю. Ф. Наседкин. Дискуссия (на английском языке) по этому докладу дана на стр. 95. Переводы аннотации находятся в конце этого тома Трудов Конференции.

из некоторой области вблизи центра и учитывая линейное возрастание напряженности магнитного поля от центра к периферии, получим следующее выражение для времени жизни водородной плазмы:

$$\underset{\text{мксек}}{\tau} = 0{,}7\ \underset{\text{эв}}{T^{\frac{1}{6}}}\ (\underset{\text{эрг}}{W}\ \underset{\text{см}^2/\text{эрс}^2}{R^2/H^2})^{\frac{4}{15}}.$$

где W — энергия сгустка, R — радиус ловушки.

При выводе формулы считалось, что уход частиц из ловушки происходит через диффузионно расширяющуюся кольцевую магнитную щель [6]. Дополнительное нагревание плазмы, вызванное сжатием плазмы по мере ее вытекания через щель, не учитывалось. Подставляя в формулу значения параметров, взятые из указанных выше работ, нетрудно убедиться, что τ составляет несколько десятков микросекунд и слабо зависит от магнитного поля, что согласуется с экспериментальными данными. Для определения правильности предпосылок, использованных при выводе формулы, были предприняты описанные здесь эксперименты.

2. Аппаратура

Магнитное поле ловушки создавалось двумя катушками, включенными навстречу друг другу. Максимальная напряженность поля в кольцевой магнитной щели составляла 6000 эрс. Вакуумная камера ловушки была изготовлена из стекла, что сделало возможным использование сверхскоростной киносъемки. Установка откачивалась паромасляным насосом с ловушкой, охлаждаемой жидким азотом. Инжекция плазмы в ловушку производилась с помощью электродинамического инжектора коаксиального типа, обеспечивающего плотность плазмы в ловушке, превышающую 10^{14} см$^{-3}$. Для питания инжектора использовалась конденсаторная батарея емкостью 3,6 мкф, которая могла заряжаться до напряжения 18 кв. Индуктивность контура составляла 70 см. Порция водорода ~0,3 см^3 при нормальных условиях вводилась в инжектор через быстродействующий клапан.

Для измерения потоков тепла на стенку применялись теплоприемники, расположенные как на фланцах, так и в районе магнитной щели. Теплоприемник представлял из себя медную пластинку толщиной 50 μ, к которой была припаяна медно-константановая термопара, подключенная к прибору постоянного тока. Расположение приемников тепла показано на рис. 1.

Распределение магнитного поля измерялось с помощью магнитного зонда диаметром 2 мм, перемещающегося вдоль оси ловушки. Сигналы с магнитного зонда подавались на импульсный осциллограф ОК-17 М. Для сверхскоростной киносъемки применялась камера СФР.

3. Результаты измерений

Калориметрические измерения, проведенные при фиксированном режиме работы инжектора и различных значениях напряженности магнитного

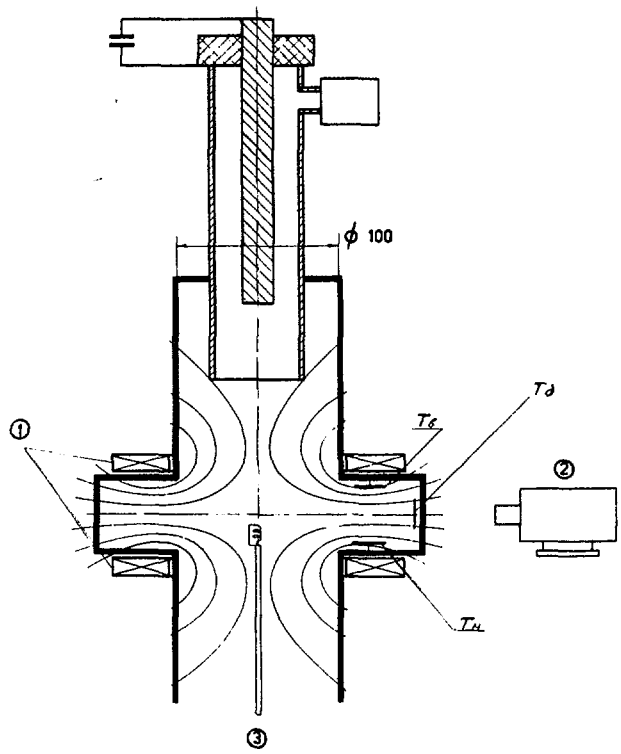

Рис. 1 Схема установки. 1 — катушки, создающие магнитное поле, 2 — камера СФР, 3 — магнитный зонд.

поля показали, что распределение потоков тепла на стенку камеры сильно зависит от величины магнитного поля. Зависимость отношения потоков тепла на фланцы $q_б/q_н$ (смысл обозначений понятен из рис. 1) от напряженности поля в щели приведена на рис. 2б. При малых значениях поля основной поток тепла направлен на фланец, находящийся в поле зрения инжектора $q_н$ и лишь небольшая часть энергии, введенной в ловушку, по-видимому, обусловленная рассеянием, попадает на поверхность другого фланца. По мере увеличения магнитного поля потоки выравниваются и при напряженности в щели ~3000 эрс отношение становится близким к единице.

Отношение плотности потока тепла на фланец к плотности потока тепла в районе кольцевой щели в зависимости от напряженности магнитного поля представлено на рис. 2а (верхняя кривая). По мере увеличения напряженности поля до значения ~3000 эрс доля энергии, попадающая на стенку защищенную магнитным барьером уменьшается. При больших значениях напряженности поля отношение $q_ф/q_б$ практически не меняется. При этом через магнитную щель выделяется примерно столько же энергии, сколько уходит на остальную часть внутренней поверхности камеры. Одним из механизмов такого ухода, в принципе, может быть перезарядка на нейтральных атомах, поступающих вместе с плазмой из инжектора. Для уменьшения концентрации нейтрального газа инжектор был отодвинут на расстояние 120 см от ловушки. Между инжектором и ловушкой располагался

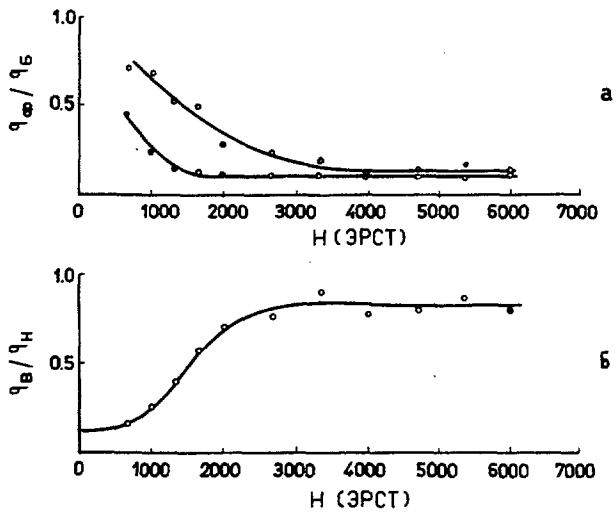

Рис. 2 Зависимость потоков тепла на стенки камеры от напряженности магнитного поля.

специальный плазмопровод, состоящий из системы диафрагм, расположенных в продольном магнитном поле напряженностью около 300 эрс. Снятая в таких условиях кривая (нижняя кривая рис. 2а) указывает на некоторое снижение доли тепла, попадающего на фланец. Тем не менее и даже в этом случае несколько десятков процентов энергии выделяется на стенке, защищенной магнитным барьером. Для объяснения этого результата достаточно предположить, что перезарядка происходит на атомах, образованных при нейтрализации ионов, уходящих через магнитную щель.

Для определения конфигурации магнитного поля, отвечающей различным моментам времени, осциллографировались сигналы с магнитного зонда при различных его положениях. На протяжении всего цикла измерений режим инжектора и ток в катушках создающих магнитное поле оставались неизменными. Работа инжектора контролировалась измерением потока тепла через кольцевую щель. При обработке исключались осциллограммы, при снятии которых потоки тепла составляли меньше 50% от среднего значения.

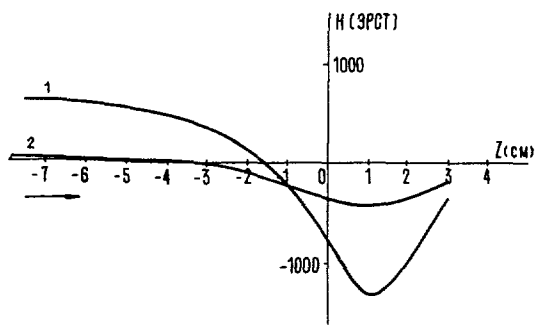

Рис. 3 Величина сигнала от магнитного зонда как функция расстояния вдоль оси ловушки для моментов времени 6 μсек [кривая (1)] и 18 μсек [кривая (2)] после начала инжекции. Направление инжекции с лева на право на рисунке.

Измеряя на отобранных таким образом кадрах величину изменения магнитного поля для фиксированного момента времени, нетрудно определить искажение магнитного поля, обусловленное присутствием в ловушке плазмы и отвечающее выбранному моменту времени. На рис. 3 изображена кривая возмущения магнитного поля для моментов времени 6 и 18 мксек после начала инжекции.

Положительный сигнал соответствует вытеснению магнитного поля плазмой. Из рис. 3 видно, что вхождение плазменной струи в магнитное поле

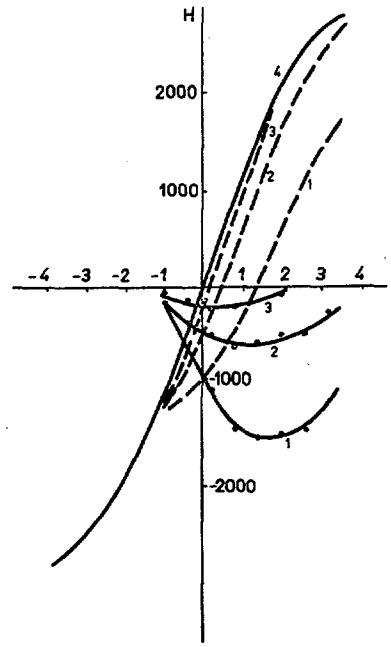

Рис. 4 Распределение составляющей H_z магнитного поля в присутствии плазмы в ловушке. Кривая (4) соответствует распределению магнитого поля в отсутствие плазмы. Направление инжекции с лева на право на рисунке.

сопровождается частичным вытеснением поля из области, занимаемой плазмой. На выходе из магнитного барьера сигнал на зонд обращается в нуль, а затем (внутри ловушки) становится отрицательным. На рис. 4 изображены кривые возмущения (кривые 1, 2, 3) составляющей напряженности магнитного поля H_z внутри ловушки для трех моментов времени (5,5;1 0,5; 15,5 мксек). Пунктирными линиями нанесены кривые напряженности, соответствующие указанным моментам времени. Кривая 4, изображенная сплошной линией представляет зависимость $H_z=f(z)$ в отсутствие плазмы в ловушке.

Фотографирование процессов инжекции и удержания плазмы в ловушке производилось со скоростью 5.10^5 кадров в секунду. В первой строке рис. 5 приведены отдельные кадры сверхскоростной съемки. Временные интервалы между ними указаны на рисунке. Из соображений экономии места промежуточные кадры опущены.

Из рассмотрения приведенных фотографий следует, что плазма, проникая через верхнюю осевую щель, заполняет объем ловушки и удерживается в

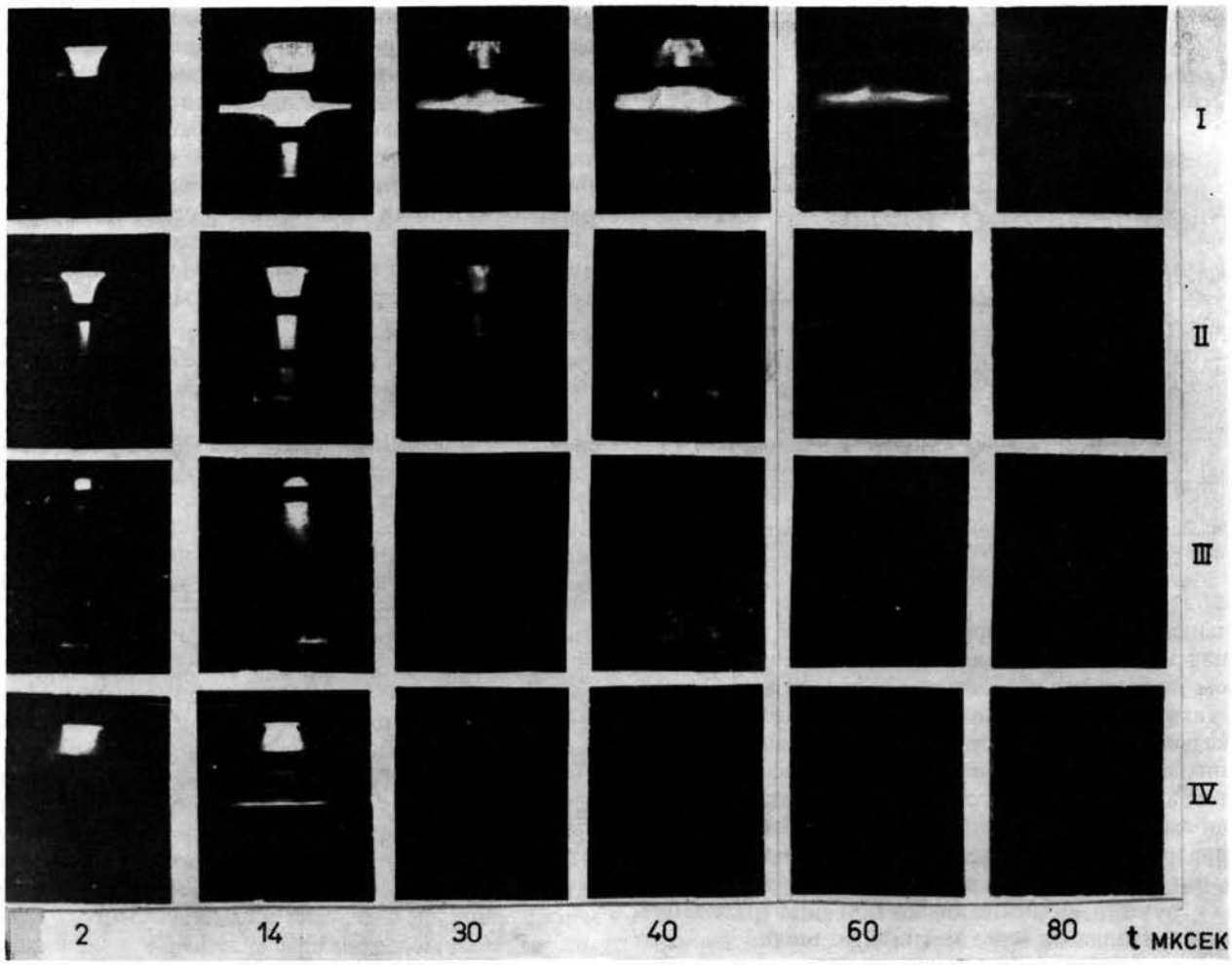

Рис. 5 Кадры сверхскоростной съемки процесса инжекции в магнитные поля различной конфигурации. Кадры I, II, III строк получены при зазоре между катушками 5 см. Для образования конфигурации адиабатической ловушки при снятии кадров IV строки зазор был увеличен до 15 см.

ней десятки микросекунд после окончания процесса инжекции. Некоторая часть плазмы в процессе инжекции прорывается через нижнюю щель. Для сравнения в четвертой строке представлены кадры, снятые при выключенном магнитном поле. Эти кадры характеризуют длительность работы инжектора. Во второй строке помещены снимки, сделанные при включении катушек в одном направлении. Кадры третьей строки получены для конфигурации поля адиабатической ловушки. В обоих этих случаях не наблюдается захват плазмы постоянным магнитным полем, поэтому делать какие-либо заключения о ее удержании в этих полях на основании приведенных данных невозможно.

4. Обсуждение результатов

Из результатов калориметрических измерений следует, что при инжекции в ловушку с полем нарастающим к периферии, плазма вытекает в основном через магнитные щели. При этом, доля энергии, вытекающая через кольцевую щель, по мере роста напряженности магнитного поля сначала возрастает, а затем в интервале значений напряженности 3000—6000 эрс в пределах ошибок измерений остается неизменной. Этот результат не противоречит предположению о наличии в ловушке области, в которой имеется плазма полностью вытеснившая магнитное поле. Действительно в этом случае ширина магнитной щели должна быть пропорциональна H^{-1}, следовательно при наличии других, не зависящих от магнитного поля механизмов ухода плазмы, нагрев теплоприемника, расположенного в районе щели вначале будет расти с увеличением H, а затем, когда ширина щели станет меньше размеров теплоприемника — падать. Отсутствие роста приведенной на рис. 2б кривой при больших значениях H, в принципе может быть объяснено недостаточной величиной магнитного поля в описанных здесь экспериментах.

Кадры сверхскоростной съемки, помещенные в первой строке рис. 5 свидетельствуют о том, что по мере проникновения в магнитный барьер происходит уменьшение поперечных размеров плазменной струи. После прохождения через магнит-

ный барьер, образованный верхней катушкой, и отражения от значительно более крутого барьера, образованного нижней катушкой, плазма оказывается захваченной в ловушку.

Следует иметь в виду, что в случае инжекции вдоль оси симметрии системы сгусток плазмы, при прочих равных условиях, должен легче проникнуть через магнитный барьер с медленно меняющимся в пространстве магнитным полем, чем через барьер с резкими границами. Если τ — объем, занимаемый плазмой в области максимального поля, то условие прохождения через барьер записывается следующим образом:

$$\alpha \cdot \frac{H^2_{\text{макс.}}}{8\pi} \tau < W_{\text{к}}$$

где $W_{\text{к}}$ — кинетическая энергия сгустка, α — коэффициент, больший 1, зависящий от формы плазменного сгустка. Это соотношение, строго говоря, справедливо лишь для идеально проводящего сгустка, полностью вытеснившего поле из занимаемого объема. При взаимодействии сгустков с полем, давление которого превосходит газокинетическое давление плазмы, будет происходить сжатие плазмы. Если магнитное поле барьера нарастает достаточно плавно, чтобы в каждый момент времени имело место равновесие между газокинетическим давлением внутри плазменного сгустка и магнитным давлением, то, по мере проникновения в магнитный барьер, объем сгустка будет непрерывно уменьшаться и при максимальном значении магнитного поля станет минимальным. При резких границах барьера сгусток не успеет достаточно сильно сжаться при вхождении в барьер. В результате, может оказаться, что для двух барьеров с различной крутизной при одинаковых $H_{\text{макс.}}$ и $W_{\text{к}}$ сгусток проникнет через барьер с плавно нарастающим магнитным полем, но отразится от крутого магнитного барьера. Таким образом сгусток, прошедший через барьер, образованный верхней катушкой, может отразиться от барьера, образованного нижней катушкой, даже в отсутствие необратимых потерь.

Измерения, выполненные с магнитными зондами, показали, что в условиях описанных здесь экспериментов процесс взаимодействия плазмы с магнитным полем происходит значительно сложнее. Плазма, проникая в магнитный барьер, не полностью вытесняет поле из занимаемого ею объема. Из-за конечной проводимости плазмы электронная температура которой составляет несколько электронвольт, при скорости движения струи $\sim 5.10^6$ см/сек магнитное поле успевает частично проникнуть в плазму. Это приводит к тому, что после прохождения через магнитный барьер в плазме появятся замкнутые азимутальные токи [1]. т.е. плазма оказывается намагниченной. При этом постоянная времени вытекания поля из плазмы будет больше, чем постоянная времени проникновения поля в плазму, т.к. перемешивание поля и плазмы сопровождается повышением температуры плазмы. В результате магнитный момент плазмы, прошедшей через верхний барьер, оказывается не равным нулю, чем облегчаются условия ее отражения от нижнего магнитного барьера. Конфигурация силовых линий, обусловленная наличием магнитного момента плазмы, показана на рис. 6. На кадрах киносъемки, отвечающих начальной стадии процесса наполнения ловушки, плазма принимает форму силовых линий магнитного поля. На рис. 7 приведен в увеличенном масштабе типичный снимок, отвечающий моменту времени 5 мксек после начала инжекции.

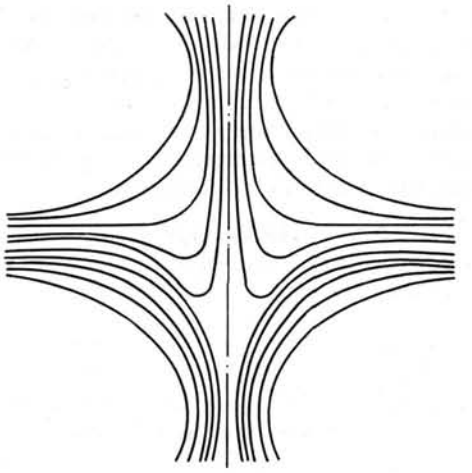

Рис. 6 Конфигурация магнитных силовых линий, обусловленная магнитным моментом плазмы.

Из совокупности приведенных выше результатов вытекает, что в условиях этих экспериментов пред-

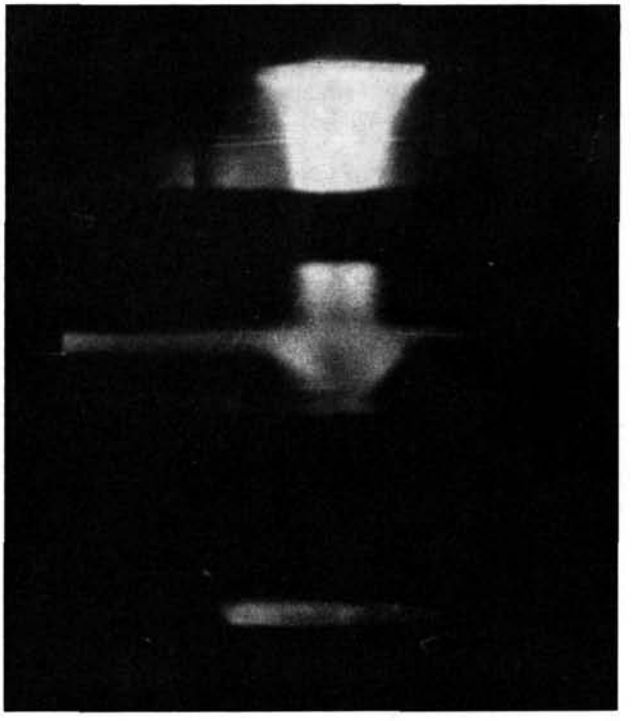

Рис. 7 Начальная стадия процесса инжекции.

положение о наличии в начальной стадии области внутри ловушки, в которой плазма полностью вытесняет магнитное поле, не соответствует действительности, и совпадение вычисленного и измеренного значений времени жизни плазмы в ловушке с полем, нарастающим к периферии, повидимому, является случайным.

Литература

[1] Подгорный, И.М., Сумароков, В.Н., *J. Nuclear Energy* **C 1** (1960) 236.

[2] Scott, F. P., Wenzel, R. F., *Phys. Rev.* **119** (1960) 1187.

[3] Tuck, J., Доклад в Институте Атомной Энергии, 1960.

[4] Лукьянов, С.Ю., Подгорный, И.М., Сумароков, В.Н., *Журнал экспериментальной и теоретической физики*, **40** (1961) 448.

[5] Ковальский, Н. Г., Лукьянов, С. Ю., Подгорный, И. М., «Исследование плазмы в магнитной ловушке ‚Орех'» (Доклад на настоящей конференции).

[6] Фирсов, О. Б., «Физика плазмы и проблема управляемых термоядерных реакций», Москва (1958), том III, 327.

DISCUSSIONS (SESSION I) — DISCUSSIONS (SÉANCE I) — ДИСКУССИИ (ЗАСЕДАНИЕ I) — DEBATES (SESIÓN I)

Paper CN-10/23 *was presented by E. A. Smårs* (Sweden). *The text of the paper is on pages 33 to 38 inclusive. The following discussion took place:*

S. A. Colgate *(United States of America):* Regarding the thermonuclear application of this principle, have you considered the radiation rate due to optical emission arising from free-bound and bound-bound transitions in the cold region near the walls, where the temperature is probably between 3 and 5 eV? I believe this region would behave as a black body, leading to an insupportable radiation loss.

E. A. Smårs *(Sweden):* We have not yet looked into this problem in any detail.

P. Hubert *(France):* Using the principle you have described, one can calculate the critical dimensions for a thermonuclear reactor. The result is quite discouraging. What is your opinion on this matter?

E. A. Smårs: No, we have not yet made any calculations concerning the possibility of using this principle in a thermonuclear reactor.

U. Grossmann-Doerth *(Federal Republic of Germany):* When calculating the power loss from the plasma, did you take charge-exchange collisions into account?

E. A. Smårs: Charge-exchange collisions occur only in the region where there are both neutral and ionized particles, that is, in the comparatively low temperature region. This process will contribute to the heat conductivity curve, but we have not yet included it in our calculations. However, we realize it is a very important question.

F. Yenicay *(Turkey):* Firstly, although you use the normal pinch relationships between current and temperature, you do not say how far you are from pinch conditions.

Secondly, I think that from the point of view of cleanliness of the plasma it would be better to use inductive coupling rather than tungsten electrodes for pre-ionization.

E. A. Smårs: Since the particle density is low at the boundary of the hot, current-carrying region, we feel justified in applying pinch relationships.

Concerning pre-ionization, at these high pressures we have been unable to get breakdown by inductive methods. I would be very pleased to receive suggestions as to how we can avoid using electrodes.

L. Artsimovich *(Union of Soviet Socialist Republics):* The only advantage this system seems to offer is that it may give greater stability. However, this is neither evident from *a priori* considerations, nor is it demonstrated in the paper.

E. A. Smårs: I agree that the stability of the system has yet to be demonstrated experimentally. However, the possibility of greater stability, coupled with the promise of a high degree of purity, seem to be important enough to justify further studies of such systems.

Paper CN-10/24 *was presented by L. Block* (Sweden). *The text of the paper is on pages 39 to 46 inclusive. The following discussion took place:*

F. Ribe *(United States of America):* I should like to refer to abstract number 115, which describes experiments on a somewhat similar rotating plasma device, the Ixion experiment. In this case the plasma is fully ionized—there is no current limiting resistor—and a limiting velocity is also observed, but a few times higher. Spectroscopic studies indicate that the velocity is radiation limited, and the energy loss is accounted for (within a factor of two) by emitted ultraviolet impurity radiation. A similar energy limitation has been observed in toroidal pinches in both USA and USSR.

L. Block *(Sweden):* The velocity limit I have described is caused by the interaction between plasma and neutral gas, and is thus of a different nature from that in fully ionized gases.

Paper CN-10/34 *was presented by K. H. Wöhler* (Federal Republic of Germany). *The text of the paper is on pages 47 to 53 inclusive. The following discussion took place:*

B. Kadomtsev *(Union of Soviet Socialist Republics):* I have a minor comment to make. One of the mechanisms of enhanced diffusion which might explain the Lehnert effect is ionic sound as suggested by Bernstein and others to explain the escape of particles from the stellarator. In the paper we have just heard it was shown that this effect is not likely to operate in the positive column. A similar result is given by Nedospasov in paper 217. Although ionic sound oscillations were sharply excited when the drift velocity of the electrons exceeded the speed of sound, in the presence of a longitudinal magnetic field of the order of 500 G and at a pressure of 0.2 mm Hg, it did not lead to any appreciable enhancement of particle diffusion across the magnetic field. Hence we may conclude that, at least in the positive column, ionic sound turns out to be a much weaker mechanism of particle escape than the current convective instability examined in the paper of Nedospasov and myself.

K. H. Wöhler *(Federal Republic of Germany):* As I have not yet studied the paper, perhaps we could have a private discussion on this subject.

O. Buneman *(United States of America):* The numerous explanations of enhanced crossed field diffusion seem to have one thing in common, instabilities with azimuthal variation. Has an azimuthal phase-dependence of the radiofrequency output been observed in this experiment?

K. H. Wöhler: No. We have measured the radiofrequency noise output but have not yet looked for directional effects.

B. Lehnert *(Sweden):* So far there have been suggested several mechanisms for the abnormal behavior of the positive column above the critical magnetic field. For one of the mechanisms, by Kadomtsev and Nedospasov, Dr. Hoh and I have recently tried to give a physical explanation [*Phys. Rev. Letters* 7 (1961) 75]. According to this interpretation the situation is as indicated in Fig. 1, where a density perturbation of screw type is assumed to be superimposed on the unperturbed steady state distribution. With the directions given in the figure the axial electric field $\mathbf{E}_{0z}$ tends to "lift up" the electron screw relative to the ion screw. This is equivalent to a rotation of the electron screw in the positive ψ-direction and gives a charge separation and an azimuthal electric field $\mathbf{E}_{\psi}'$. The latter then tends to drive the particles radially outwards with a speed $\mathbf{E}_{\psi}' \times \mathbf{B}_z/B_z^2$ across the magnetic field B_z and to destabilize the plasma. The critical magnetic field is reached when this effect just balances the azimuthal drift $\mathbf{E}_{0r} \times \mathbf{B}_z/B_z^2$ of the electrons in the unperturbed ambipolar field $\mathbf{E}_{0r}$.

A mechanism of this type is not limited by the ionization degree and it is quite likely that it occurs in all situations where there is a sufficiently strong electric field component in the direction of the magnetic field.

A. Kuckes *(United States of America):* Although I agree that the instability is related to the separation of the ion and electron helices, as Dr. Lehnert suggests, I do not think the separation in the fully ionized case is as strong as he implies, since the plasma resistance is only weakly dependent on electron density. However, I believe that, in spite of the small coupling between the applied electric field and the helical separation, the effect may still be important in a fully ionized plasma.

E. L. Oleson *(United States of America):* I would like to ask if moving striations were observed, since the experimental conditions were favorable for their existence. If so, there could be some doubt about the longitudinal electric field measurements and, more important, a question could be raised as to the validity of the general theory when moving striations are present.

K. H. Wöhler: On occasion we observed both moving and stationary striations, but since our measurements of the longitudinal electric field were made with probes spaced one meter apart, we were able to eliminate their effects and measured the mean electric field.

Paper CN-10/65 *was presented by H. A. Blevin* (United Kingdom). *The text of the paper is on pages 55 to 60 inclusive. The following discussion took place:*

T. Consoli *(France):* Have you done the experiment both above and below the ion-cyclotron frequency, by varying either the strength of the applied axial magnetic field or the frequency of the rotating field? If so, did you observe a sign-reversal of the escape flux?

H. A. Blevin *(United Kingdom):* All our experiments were done at frequencies considerably higher than the ion-cyclotron frequency. Hence ion motion did not contribute to the current distribution in the plasma and could be neglected in the analysis of our experiment.

R. Demirkhanov *(Union of Soviet Socialist Republics):* I should like to ask two questions:

1. How uniform was the initial axial magnetic field?
2. Was a measurement made of the radial variation of the rotating field?

H. A. Blevin:

1. The externally applied magnetic field was slightly mirror-shaped, having a mirror ratio of about 1.1 in the absence of plasma.
2. The amplitude of the rotating field was measured as a function of radius, and no attenuation was observed provided $ne\eta/B_0 \ll 1$. In fact, an amplification is observed at the axis, and we attribute this to end effects.

When $ne\eta/B_0 \gg 1$, as occurs towards the end of the pulse, the rotating field becomes attenuated at the axis, and only under these conditions does it exert any radial confining pressure. We have observed complete penetration of the rotating field when $B_0/B_a \simeq 0.1$ and have no evidence that penetration of the rotating field into the plasma is in any way affected by the axial applied field B_a.

A. Dattner *(Sweden):* Did you have an independent method of measuring the electron density apart from magnetic probes?

H. A. Blevin: We also measured the electron density in the afterglow period with double Langmuir probes. The results agreed with the magnetic probe determinations to within a factor of two.

Paper CN-10/172 *was presented by H. Grad* (United States of America). *The text of the paper is on pages 61 to 65 inclusive. The following discussion took place:*

G. Schmidt *(United States of America):* There are two comments I would like to make.

It is of interest to look at the particle motion in a cusp geometry in the opposite limiting case, where the orbits are far from adiabatic. Since it is easy to find two strict constants of motion, the energy and the canonical angular momentum P_θ, there are a number of general results one may obtain. It can be seen, for instance, that a particle moving close to a flux surface on one half of the cusp will not do so when it passes the central plane. Furthermore, if a particle encircles the axis in one cusp-half, it will not do so in the other half, and vice versa.

In the second comment, I simply would like to stress the importance of investigating particle orbits when a plasma is injected into the cusp on the axis and it moves over to the other cusp-half. In the moving (plasma) co-ordinate system this problem is closely related to the problem of field reversal in a θ-pinch since the particles experience in both cases a reversal of the magnetic field.

H. Motz *(United Kingdom):* Changes in the action integral can be estimated if discontinuities of a known order occur along the path. I wonder whether one could obtain an estimate of the effect of passage through the center by treating the change of turning point as a discontinuity.

H. Grad *(United States of America):* The essential difficulty in estimating nonadiabatic effects is exactly that one can *not* replace a smooth field with a discontinuous approximation without grave risk. Although one knows that the physical result cannot greatly be altered by such a change, the mathematics is very sensitive to any change in analytical properties. For example, a discontinuity in the seventh derivative will give a nonadiabatic effect of order ε^7 etc. If the field has all derivatives continuous, the nonadiabatic effect is of transcendental order. More precisely, if one looks at the orbits for arbitrarily long times, the results depend on *exact* mathematical knowledge. Practically, one needs to know the answer for some finite time, even though this may be very long. Thus the validity of a discontinuous approximation to the magnetic field depends in a very complex way on exactly how long one needs to follow the orbit.

J. L. Tuck *(United States of America):* Could we not treat the anadiabaticity as due to the presence in the cusp system of an imaginary scattering gas whose density has some reciprocal relation to the magnetic field? By obtaining the scattering coefficient of this gas we could proceed to calculate the behavior of cusp systems as simply as that of mirror machines.

H. Grad: The application of this orbit theory to containment was omitted from this talk since it will appear elsewhere. The complex behavior of nonadiabatic particles can be treated as if they collide with some randomizing agent—actually the magnetic field—possibly, as you suggest, with a fictitious gas; but this "gas" would have have to very strange properties.

Paper CN-10/69 *was presented by T. K. Allen* (United Kingdom). *The text of the paper is on pages 67 to 73 inclusive. The following discussion took place:*

N. J. Phillips *(United Kingdom):* Are wall effects playing any part in short-circuiting the radial space charge in your apparatus?

T. K. Allen *(United Kingdom):* We have no information on this point.

J. L. Tuck *(United States of America):* The measured width of the line-cusp escape channel is encouragingly narrow. This suggests that diffusion across field lines is occurring at the slow rate appropriate to a quiescent plasma.

T. K. Allen: Yes, we think this is probably true.

A. Berezin *(Union of Soviet Socialist Republics):* Have measurements been made of the Doppler broadening of impurity lines?

T. K. Allen: Not yet, but we intend to make such measurements in the very near future.

A. S. Kaufman *(Israel):* In your paper you refer to the measurements of electron temperature. Would it not be better to measure the ion temperature in this type of experiment?

T. K. Allen: The equipartition time is very short, about one microsecond, so ion and electron temperatures will be more or less equal.

Paper CN-10/154 *was presented by D. C. Hagerman* (United States of America). *The text of the paper is on pages 75 to 79 inclusive. The following discussion took place:*

L. Artsimovich *(Union of Soviet Socialist Republics):* I have a comment to make, namely, that there is a simple explanation for the shift of the field towards the second coil. It is connected with the trapping of magnetic field during the passage of the plasma through the first coil.

D. C. Hagerman *(United States of America):* This is not a satisfactory explanation of the observed fields since the resistivity of the plasma is high enough for trapped fields to diffuse out of the plasma in a relatively short time.

Papers CN-10/202 *and* CN-10/204 *were presented by Yu. F. Nasedkin* (Union of Soviet Socialist Republics). *The text of the papers is on pages 81 to 92 inclusive. The following discussion took place:*

D. C. Hagerman *(United States of America):* Have you observed any effect on lifetime, temperature or density when your probe is inserted into the plasma?

Yu. Nasedkin *(Union of Soviet Socialist Republics):* In our opinion the insertion of the probe does not have a decisive effect.

J. L. Tuck *(United States of America):* It seems to me that there is an alternative and quite straightforward explanation for the shift of the neutral point observed by both Hagerman and the Russian workers which is easier than the hypothesis of fields entrained from the left-hand side (injection from the left) and displaced toward the center proposed by Dr. Artsimovich.

We agree that the position of the neutral point is somewhat sensitive to field weakening on either side, since it is located at the point of zero algebraic sum of two comparatively large magnetic fields. We also know that there can be two types of orbits. Those which pass near the center are highly anadiabatic and escape rapidly and orbits more deeply embedded in the field are nearly adiabatic and can live long.

The method of plasma trapping used in both experiments (entropy trapping) depends on deformation of the field by the plasma pressure. It is most unlikely that the field deformations, which occur both at the entry cusp, and at the right-hand inside of the trap (which receives the full blast of the plasma jet at nearly normal incidence), are always stable configurations. Probably the plasma produces unstable dents in the field, resulting in rapid and deep mixing. Hence we have a mechanism for the generation of deep-lying, long-lived, adiabatic orbits, on both sides of the neutral point. According to this hypothesis, since the neutral point is displaced to the right, more of such orbits are apparently trapped on right-hand inside than on the left-hand inside. There is no difficulty in accounting for the long life (>50 μs) of the displacement this way. But the entrained field hypothesis could hardly produce displacements lasting more than a few microseconds. It seems more likely to me that plasma containing entrained field in the manner proposed by Artsimovich is responsible for the rapid side-to-side surging reported by Hagerman and Osher (*Phys. Fluids* **7** (1961) 905) during the first few microseconds after injection.

L. Artsimovich *(Union of Soviet Socialist Republics):* I still think that the most natural explanation for the displacement of the field is purely electrodynamic and lies in the trapping of the field by the plasma current. For the time being I feel that the status of theory and experiment are such that comparisons are premature.

J. L. Tuck: I must agree with Dr. Artsimovich's remarks concerning the preliminary nature of the discussions. However, I think his displacement hypothesis seems to give an answer of the wrong sign, since the plasma happens to be denser on the side away from the gun.

H. Grad *(United States of America):* It is an easy matter to explain how an asymmetry (in either direction!) can maintain itself for times long compared with the collisional diffusion time. Those particles which diffuse from one side to the other do so as they pass near the zero field point. They are therefore very nonadiabatic and have a good probability of being lost out of the cusps before they have a chance to penetrate more deeply into the second region. The apparent independence of the containment time with respect to the magnitude of B is not surprising in view of the containment theory for low-β plasmas, which predicts a logarithmic dependence on B.

M. B. Gottlieb *(United States of America):* One factor which could be responsible for the asymmetry is trapping between the mirrors at the point and line cusps.

I would like to ask Dr. Artsimovich if he agrees that it has not been shown that the cusp geometry gives stable confinement. Rather it might be proper to say that no instability effects have yet been observed.

L. Artsimovich: So far no instabilities have been observed in cusped geometries which are theoretically stable. In Allen's experiment there are competing processes. The acceleration of plasma can cause instability, but the fast-rising fields have a stabilizing effect. In the work described by Nasedkin, the plasma ball may exhibit flute instabilities at the moment of injection, but these should disappear once the plasma is inside the steady cusped fields.

SESSION II — SÉANCE II

ЗАСЕДАНИЕ II — SESIÓN II

5 SEPTEMBER 1961 — 5 SEPTEMBRE 1961

5 СЕНТЯБРЯ 1961 Г. — 5 DE SEPTIEMBRE DE 1961

Chairman — Le président — Председатель — El Presidente

A. E. Ruark *(United States of America)*

Scientific Secretary — Secrétaire scientifique — Ученый секретарь — Secretario Científico

W. F. Gauster *(United States of America)*

[Papers presented: CN-10/3, 131, 148, 149, 151, 153, 167, 170, 174, 175, 216, 261]

CRITICAL CONDITIONS FOR SELF-SUSTAINING REACTIONS IN THE MIRROR MACHINE*

RICHARD F. POST

LAWRENCE RADIATION LABORATORY, UNIVERSITY OF CALIFORNIA

LIVERMORE, CALIFORNIA, UNITED STATES OF AMERICA

Some fundamental aspects of obtaining a self-sustaining fusion reaction in a simple mirror machine are considered. The combined effects of inefficiencies associated with plasma injection, heating, and energy recovery, as well as the losses expected from escape of unreacted particles and radiation are calculated and compared with the nuclear energy released. It is shown that there exist, in theory, accessible plasma regimes which should permit a positive power balance against all known losses, provided losses arising from co-operative effects can be reduced to negligible levels. This latter requirement, which is especially restrictive for the mirror machine, is expressed in terms of critical confinement conditions. These conditions serve to define the maximum allowable disparity between *achievable* and classical *theoretical* plasma transport and loss rates. The theoretical importance and practical value of utilizing low β (low plasma pressure compared to magnetic pressure) regimes are shown. The essential importance of developing cryogenic or superconducting magnet coils in order to achieve this end with systems of reasonable size is discussed. The relative merits of several possible fuel cycles and injection methods are considered, especially in the light of the requirement of maintaining stability during plasma build-up and confinement. The results of the study are used to define a series of critical experiments which would establish (or reject) the possibility of obtaining self-sustaining reactions in a simple mirror machine.

1. Introduction

This study is concerned with calculations of critical conditions for achieving self-sustaining reactions in a simple mirror machine [1, 2]. One of the most difficult aspects of planning experimental studies around a particular approach to controlled fusion research is the selection of the plasma regime which is to be studied. Plasma density, temperature, and volume, as well as time scales and other parameters must be chosen. No single research team can hope to investigate effectively the whole range of these parameters. Nevertheless, the choice of the regime to study should be made on an objective basis. One possible criterion to apply in planning experiments is that they should aim toward achieving the "critical" plasma conditions, i.e., those which approximate the calculated *minimum* conditions required to achieve a self-sustaining fusion reaction in the simplest visualizable reactor employing the confinement scheme under study. On the basis of a hoped-for "economic" use, one can therefore narrow the range of plasma conditions to be studied to a definite list.

Essential to the validity of the calculation of such critical conditions is, of course, the as yet unproved assumption that an adequately stably confined plasma can be achieved. However, the calculations presented here will themselves, as is to be shown, shed considerable light on the nature of the plasma stability problems in the mirror machine. This is because they show that the minimum plasma pressure conditions required for a self-sustaining reaction are much less demanding than previously suspected. Generally speaking, it is clear from first principles that the smaller the value of β (plasma pressure relative to magnetic pressure) which can be utilized, the less likely it is that instabilities will be encountered. The studies show that in the mirror machine the minimum required values of β are determined primarily by magnet coil losses. This being the case, the incipient technological revolution in the efficient generation of large volumes of high magnetic fields by cryogenically cooled magnets [3], or by the use of new superconducting materials [4], has a great influence on the whole stability question. It now seems entirely possible to consider mirror machines in which the β values are only a few per cent. This augurs well for the possibility of achieving stability. In a field of endeavor which is at the same time so exceedingly difficult and of such great importance for the future of mankind, it is reassuring to see some sunlight in the distance, even though the immediate future is clouded in uncertainty.

2. Energy production and energy losses—general

To discuss the critical conditions for self-sustaining reactions we must be precise in our definition of "self-sustaining". In this discussion we shall confine ourselves to mirror machines where the *over-all system* is energetically self-sustaining; that is, the total electrically recovered energy exceeds the total electrical energy input. This is not the same thing as requiring the plasma itself to maintain its temperature and

* Conference paper CN-10/153, presented by R. F. Post. Translations of the abstract are at the end of this volume of the Conference Proceedings.

its reactivity by the energy directly derived from captured reaction products. In the mode of operation we here consider, the plasma temperature is to be maintained by injection or heating processes exterior to the plasma, not by the plasma itself.

To calculate the conditions for self-sustaining reactions according to the definition we have given, one must obviously calculate the total recoverable nuclear power from the fusion reaction and compare this with the totality of the energy losses. We consider first some general aspects of the question of energy losses.

Two kinds of losses compete against the nuclear energy released in a fusion reactor: direct and indirect losses. Direct losses are those associated either with the escape of bremsstrahlung (x-radiation) or other radiation from the plasma, or with the escape of charged particles out of the magnetic bottle. Indirect losses are those chargeable to any energy losses which arise necessarily in the operation of the reactor.

Direct losses are crucial in determining whether a power balance is possible at all. Although part of the energy escaping as direct particle losses or radiation could be recovered through, for example, a thermal cycle, nevertheless, some unrecoverable loss of energy will always be associated with these processes. One can therefore assign to each volume element of the plasma an intrinsic unrecoverable direct energy-loss rate. It is obvious that the reactor cannot possibly produce a positive power balance if this direct loss rate exceeds the recoverable nuclear power.

Power balance against direct particle losses, being primarily a question of the rates of energy gain and loss for each unit volume of the reacting plasma, is determined in the mirror machine by factors which are essentially independent of plasma volume. By contrast, indirect losses have a direct bearing on the minimum plasma volume.

In a net power-producing mirror machine reactor, the coil power loss per unit length would have to be supplied by using a portion of the nuclear power developed by the reactor in the plasma volume contained in that same unit length. We will later see that the key to achieving power balance in a simple mirror machine of practical size resides in the development of cryogenic and superconducting magnets in order to reduce indirect losses.

A question equal in importance to that of reducing indirect losses in considering the problem of the minimum reactor size is that of the achievable maximum energy release from the nuclear reactions employed. This has a critical bearing on the possibility of achieving a power balance against direct losses, as well as being of obvious importance to the over-all power balance.

The nuclear fusion reactions that are of main interest are the following:

1. $D + D \rightarrow He^3 + n + 3.25$ MeV;
2. $D + D \rightarrow T + p + 4.0$ MeV;
3. $T + D \rightarrow He^4 + n + 17.6$ MeV;
4. $He^3 + D \rightarrow He^4 + p + 18.3$ MeV.

In addition to these reactions, other reactions, such as neutron capture reactions (for example, the capture reaction in lithium) will also be of interest because of their contribution to the energy balance. In this discussion, reaction fuel cycles that utilize the DT, DD, and DHe^3 reactions will be considered. The calculations are in many ways similar to the excellent reaction-cycle studies performed by the Risö group [5] which should be referred to for additional insight into more general problems than the ones considered here.

In the DT cycle, tritium would normally be generated in a breeding cycle, using, for example, neutron capture in lithium. The tritium would then be separated and subsequently remixed with the primary deuterium fuel to sustain the reaction. The advantage of such a cycle is the large reaction cross-section exhibited by DT and the large energy release of the reaction. The disadvantages are the problems of chemical separation of the tritium from lithium, the relatively low abundance of lithium (probably not a problem for a long time to come), and the more serious problem of the large radioactive tritium "inventory" which would have to be accumulated to start and maintain the reaction. These are certainly not overwhelming difficulties, but they do detract from the ultimate desirability of the DT cycle.

To calculate the power release in a proposed fuel cycle, we need to establish the basic rate equations. Let us consider the general case, a plasma into which is being injected a mixture of various fuel particles. Deuterons will be designated by (1), tritons by (2), and He^3 nuclei by (3). Then, since the DD reaction goes with nearly equal probability to either of the two reactions listed, if we disregard changes in the branching ratio we have for the total reaction energy yield per unit volume:

$$p_{\mathrm{nuc}} = \frac{1}{4} n_1^2 \langle \sigma v \rangle_{11} W_{11\mathrm{p}} + \frac{1}{4} n_1^2 \langle \sigma v \rangle_{11} (W_{11\mathrm{n}} + W_{\mathrm{c}}) + n_1 n_2 \langle \sigma v \rangle_{12} (W_{12} + W_{\mathrm{c}}) + n_1 n_3 \langle \sigma v \rangle_{13} W_{13} . \quad (1)$$

The corresponding equation for the total rate of reactions is:

$$r_{\mathrm{nuc}} = \frac{1}{2} n_1^2 \langle \sigma v \rangle_{11} + n_1 n_2 \langle \sigma v \rangle_{12} + n_1 n_3 \langle \sigma v \rangle_{13} . \quad (2)$$

In Eq. (1), $W_{11\mathrm{p}}$, etc., are the various reaction energies, and W_{c} is the neutron capture energy. We will be visualizing a reactor where a steady-state fuel cycle is set up, i.e., where unburned fuel particles, burnable reaction products, and regenerated tritium are cycled so that the composition of the reacting fuel remains constant. Let us first consider the case of the DT cycle, where tritium is regenerated in a lithium cycle.* In this case, the tritium fraction of the fuel can be set

* The discussion of the DT reaction cycle in this report is derived in part from the report, UCRL-6077, "Some Aspects of the Economics of Fusion Reactors", August, 1960, also reproduced in Risö Report No. 18, lecture material from the 1960 International Plasma Physics Summer School. See these reports for additional discussion of the DT cycle.

at will, so long as it does not exceed the capabilities of the regeneration cycle. The balance of the mixture will then be composed of either pure deuterium or an equilibrium of deuterons and recovered He^3 nuclei. In the latter case, we can readily calculate the equilibrium concentration of He^3, since approximately one-half of the DD reactions give birth to a He^3 nucleus. Thus in steady-state we have

$$\frac{1}{4} n_1^2 \langle \sigma v \rangle_{11} = n_1 n_3 \langle \sigma v \rangle_{13} , \tag{3}$$

so that

$$n_3 = \frac{1}{4} n_1 \frac{\langle \sigma v \rangle_{11}}{\langle \sigma v \rangle_{13}} . \tag{4}$$

Consider a fuel mixture in which the concentration of D is kept at 50% and the balance consists of T and the equilibrium amount of He^3. Then if n is the total ion density ($n = n_1 + n_2 + n_3$), the nuclear energy released at equilibrium fuel concentration is given by

$$p_{DT} = \frac{1}{4} n^2 \langle \sigma v \rangle_{12} \left\{ 1 + \frac{1}{4} \left[\frac{\langle \sigma v \rangle_{11}}{\langle \sigma v \rangle_{12}} \left(\frac{W_{11\,p} + W_{11\,n} + W_c + W_{13}}{W_{12} + W_c} \right) - \frac{\langle \sigma v \rangle_{11}}{\langle \sigma v \rangle_{13}} \right] \right\} \cdot \{ W_{12} + W_c \} . \tag{5}$$

Putting in the energy values from the reactions, and inserting 4.6 MeV for W_c (the neutron capture energy released in lithium), we have the result:

$$p_{DT} = \frac{1}{4} \langle \sigma v \rangle_{12} \left\{ 1 + \frac{1}{4} \left[1.34 \frac{\langle \sigma v \rangle_{11}}{\langle \sigma v \rangle_{12}} - \frac{\langle \sigma v \rangle_{11}}{\langle \sigma v \rangle_{13}} \right] \right\} \cdot \{ 22.4\,\text{MeV} \}$$
$$= \frac{1}{4} n^2 \overline{\langle \sigma v \rangle}_{DT} \cdot [22.4\,\text{MeV}] . \tag{6}$$

The term in brackets is responsible for a small but appreciable positive contribution at high temperatures. Of more importance is its effect on the breeding cycle. In steady-state, the required tritium breeding ratio, from Eqs. (2) and (4), is given by

$$K = \frac{1 - \frac{1}{4} \left[\frac{\langle \sigma v \rangle_{11}}{\langle \sigma v \rangle_{13}} + \frac{\langle \sigma v \rangle_{11}}{\langle \sigma v \rangle_{12}} \right]}{1 - \frac{1}{4} \left[\frac{\langle \sigma v \rangle_{11}}{\langle \sigma v \rangle_{13}} \right]} , \tag{7}$$

where K will be found to be appreciably less than 1.0 at high temperatures. By choosing larger relative proportions of deuterium, smaller K values can clearly be allowed, though at a sacrifice in specific nuclear power.

The nuclear power given by Eq. (6) represents the total achievable thermal energy release that is available to be recovered from the DT reaction, with a tritium breeding cycle, using neutron capture in lithium. This figure will be used in the power-balance calculations of subsequent sections.

We may in similar manner calculate the available specific nuclear power from a DD fuel cycle. We will here assume that the neutrons from the primary DD reaction and those from the secondary DT reactions (resulting from recycling of the tritium produced by the T,p branch of the primary reaction) are captured in sodium, with the release (in steady-state) of the capture energy of 12.6 MeV. We obtain, therefore,

$$p_{DD} = \frac{1}{4} n^2 \langle \sigma v \rangle_{11} \left\{ 1 - \frac{1}{4} \left[\frac{\langle \sigma v \rangle_{11}}{\langle \sigma v \rangle_{12}} + \frac{\langle \sigma v \rangle_{11}}{\langle \sigma v \rangle_{13}} \right] \right\}^2 \{ W_{11\,p} + W_{11\,n} + W_{12} + W_{13} + 2\,W_c \}$$
$$= \frac{1}{4} n^2 \overline{\langle \sigma v \rangle}_{11} \{ 68.4\ \text{MeV} \} . \tag{8}$$

It is noted that, when written in the same form as Eq. (6), the power density per reaction for the complete DD cycle is much larger than that for DT. This difference will partially compensate for the lower reaction cross-section of the primary reactions. The end result will be that, except for operating temperature, the DD cycle is nearly as favorable as the DT reaction in achieving a positive power balance against direct losses.

To evaluate the reaction power yields it is necessary to obtain values for $\langle \sigma v \rangle$, the mean reaction-rate parameters. While it is customary to utilize Maxwellian average values for those parameters taken at a single temperature, this is not necessarily a reliable procedure in the present case. In using values of $\langle \sigma v \rangle$ to compute the power rates in a mirror machine, it is important to notice a fundamental difference between it and other proposed fusion reactors, such as the stellarator. In the mirror machine, the various types of charged particles, deuterons, tritons, electrons, etc., are too weakly coupled by collisions ever to reach temperature equilibrium with each other during their confinement time. In principle, it should therefore be possible to arrange matters so that different types of particles are injected and confined at different mean energies, chosen to maximize some particular parameter. It will also turn out that the electrons may have a relatively small mean energy compared with that of the confined ions. This reduces some of the losses. At the same time, it would be possible to control the mean energies of the various ion types so as to optimize their reactivity or their confinement time.

In the results to be presented, we will use $\langle \sigma v \rangle$ values as calculated by ROBERTS [6] from particle distributions appropriate to ions confined in diffusion equilibrium in a mirror machine.

3. Direct losses

To compute the actual recoverable nuclear power, and to examine the problem of obtaining a power balance against these losses, the direct losses must be calculated explicitly. Here, of course, we will assume that stable confinement is achievable.

Since it will turn out that, in the mirror machine, plasma mean ion energies much above the so-called "ideal ignition temperature" for DT or DD will be required, and since the electron temperature will be substantially smaller than the ion mean energies, energy loss by bremsstrahlung will be small compared with the nuclear power and need only be introduced as a correction. Also, for the DT reaction in the mirror machine, it appears that the so-called plasma "syn-

chrotron radiation" as discussed by TRUBNIKOV [7] will be relatively unimportant in the over-all power balance. For the DD reaction this is less obviously so, but it will be shown to follow for the plasma conditions which are considered. Of much greater importance are the "end losses" associated with scattering of particles into the escape cone of the mirrors. These would represent the dominant direct-loss process in a simple mirror machine. Provided some reasonable scaling and other requirements are met, and provided plasma turbulence is not present, all other particle-loss mechanisms, such as particle transport across the magnetic field or losses by nonadiabatic effects, should be negligible compared with the end loss. This process is one that does not depend appreciably on the spatial distribution of the particles, and acts to remove any particle, upon its next encounter with the mirror, as soon as it is deflected into the loss-cone angle. End losses, therefore, arise solely from "velocity space" diffusion effects, and not from diffusing across the field. This means that in a machine the length of which is great compared with its diameter, each cubic centimeter of the plasma can be thought of as contributing essentially equally to the loss rate, making the assignment of direct losses an exceedingly straightforward matter.

The rate of end losses then depends on the density of the plasma, the mean collisional cross-section between the charged particles, and upon their mean relative velocity. Since collisional cross-sections are reduced at high energies, whereas nuclear reaction cross-sections generally increase, there is a real premium on reaching high ion energies—higher in the mirror machine than in any other proposed magnetic bottle.

End losses arise from binary collisions between the ions of the plasma, and therefore depend on the square of the plasma density (as does the nuclear power density) and on the mean scattering rate of the ions. The scattering rate in turn is dominated by the Coulomb scattering cross-section, the magnitude of which varies inversely with the square of the relative ion energies. The end loss rate per unit volume can thus be represented by an equation of the form:

$$\frac{dn}{dt} = -n^2 \langle \sigma v \rangle_s f(R), \tag{9}$$

where $\langle \sigma v \rangle_s$ is a mean scattering-rate parameter (Coulomb cross-section multiplied by mean relative velocity) appropriate to the energy distribution of the ion population, and $f(R)$ is a function expressing the influence of the mirror ratio, $R = B_M/B_0$, in controlling the losses. For $R \to \infty$, $f(R) \to 0$.

Eq. (9) can be employed in either of two ways. The first applies if the proposed reactor is to be used in a cyclic way. In this case the fusion fuel would be injected, either at the operating temperature or at some lower temperature from which it would be heated to the operating value. The plasma would then react while its density decayed through end losses. The total energy released would be given by the integral of the reaction rate during the decay period.

For this (transient) case, Eq. (9) can be integrated if we assume that $\langle \sigma v \rangle_s$ does not change with time. There is obtained

$$n(t) = n_0 \left(\frac{1}{1 + t/\tau_{1/2}} \right), \tag{10}$$

$$\tau_{1/2} = \frac{1}{n_0 \langle \sigma v \rangle_s f(R)}. \tag{11}$$

Using this expression we can obtain the total number of nuclear reactions occurring per unit volume by integrating again over time.

The second way in which Eq. (9) can be used is to apply it to a steady-state case. Here one must include a source or injection terms to compensate for the loss rate. Eq. (9) then becomes:

$$\frac{dn}{dt} = 0 = -n_0^2 \langle \sigma v \rangle_s f(R) + S_0. \tag{12}$$

Here, $\langle \sigma v \rangle_s f(R)$ is to be evaluated for the steady-state velocity distribution functions, and S_0 is the mean steady-state injection current required per unit volume.

Since S_0 is equal to n_0/τ_L, S_0 can be written in terms of the mean life of an ion against loss, τ_L. Thus we find from Eq. (12)

$$\tau_L = \frac{1}{n_0 \langle \sigma v \rangle_s f(R)}. \tag{13}$$

In general, τ_L is not the same as $\tau_{1/2}$, but may be appreciably longer because it represents the steady-state mean life for a particle which has been injected at a given energy and angle, whereas $\tau_{1/2}$ represents the mean lifetime of ions that have already diffused in angle and energy to the form of the decaying distribution.

To determine the competition between the nuclear energy released and the end losses in steady-state, it is necessary to calculate the probability that a reaction will occur during the lifetime of the ion. The number of reactions per second is given by

$$\begin{aligned} q_{DT} &= \frac{1}{4} n_0^2 \langle \sigma v \rangle_{DT} \\ q_{DD} &= \frac{1}{2} n_0^2 \langle \sigma v \rangle_{DD}. \end{aligned} \tag{14}$$

It will be useful to introduce a fractional reaction coefficient, φ, which is here defined as the ratio of the mean number of reactions per second and per unit volume, q, and the steady-state injection rate per unit volume and second, S_0:

$$\begin{aligned} \varphi = \frac{q}{S_0} &= \frac{1}{4} \left[\frac{\langle \sigma v \rangle_{DT}}{\langle \sigma v \rangle_s f(R)} \right] \quad DT, \\ &= \frac{1}{2} \left[\frac{\langle \sigma v \rangle_{DD}}{\langle \sigma v \rangle_s f(R)} \right] \quad DD. \end{aligned} \tag{15}$$

Note that φ is independent of the ion density and the plasma volume.

We may use Eq. (15) to evaluate the important ratio of nuclear power released to particle energy escaping, per unit volume. This is

$$Q = \frac{p_n}{p_L} = \varphi \cdot \frac{\sum W_{nuc}}{\overline{W}_i}, \tag{16}$$

where $\overline{W}_i$ is the mean injection energy.

It is clear that the requirement for a positive power balance is closely related to the value of Q. The exact relationship between Q and power balance will be derived later.

As has been noted, it is not possible to calculate accurate values of $\langle\sigma v\rangle_s \cdot f(R)$ without a detailed knowledge of the ion energy distribution. Also, although it is relatively easy to obtain approximate values of the scattering lifetimes from relaxation time considerations [8], these values cannot be trusted for accurate power-balance calculations. In attempting to perform more precise calculations of the end losses, JUDD, MACDONALD, and ROSENBLUTH have applied the Fokker-Planck equation to the problem and have obtained, under certain simplifying assumptions, an integro-differential equation which can be used to predict the loss rates. BING [9] and ROBERTS [6] have used a digital computer to evaluate solutions to the J-M-R equation by numerical methods, under various approximations. Bing's calculations apply to a steady-state problem, but under some rather restrictive assumptions which lead to over-estimation of the theoretical loss rates. Roberts' calculations have been performed subject to fewer approximations than Bing's, but have thus far been concerned only with transient cases. It is possible, however, to use Roberts' results to improve the accuracy of Bing's calculational code by renormalization. This has been done in deriving the results presented here.

The numerical results, corrected in the manner indicated above, can be used to obtain values of Q for two different mirror ratios. These results are, with $T_i = (2/3)\overline{W}_i$ (in kilovolts), and $\overline{W}_i$ = mean injection energy of ions:

$$\begin{aligned} Q_{DT} &= 6.1 \times 10^{14} \langle\sigma v\rangle_{DT} T_i^{1/2} \quad R = 3.3 \\ Q_{DT} &= 12.1 \times 10^{14} \langle\sigma v\rangle_{DT} T_i^{1/2} \quad R = 10 \end{aligned} \tag{17}$$

$$\begin{aligned} Q_{DD} &= 16.7 \times 10^{14} \langle\overline{\sigma v}\rangle_{DD} T_i^{1/2} \quad R = 3.3 \\ Q_{DD} &= 33.4 \times 10^{14} \langle\overline{\sigma v}\rangle_{DD} T_i^{1/2} \quad R = 10. \end{aligned} \tag{18}$$

Some values of Q_{DT} and Q_{DD} are given in Table I, for various temperatures.

The apparently casual manner in which these critical numbers are presented is perhaps misleading. The numbers which are given here have been checked by comparison with several independent calculations. The most recent and most comprehensive of these, by BENDANIEL [10], have been carried out with the inclusion of spatial effects which would arise for machines of small aspect ratio (length comparable to diameter). However, in the limit of long machines, which we here consider, BenDaniel's results agree reasonably well with the values used here. It is clear from the comparison of all valid calculations of the end losses that the differences in assumptions made or computational methods used do not lead to large discrepancies between the results. Putting the question another way, if the Q values here assumed are adopted, the value of mirror ratio to which they apply may turn out to be somewhat higher or lower when the "exact" calculation is finally made. However, none of the corrections, as yet only approximately calculated, arising from "classical" effects (such as spatial effects or ambipolar potentials) appear to be important enough to make more than about a factor of 2 change in the Q values which are used here. The main concern is that co-operative effects could cause much larger departures.

TABLE I. Q_{DT} and Q_{DD} as a function of ion temperature and mirror ratio.

R	T_i (keV)	Q_{DT}	$\langle\sigma v\rangle_{DT}$ (normal mode) (cm^3 sec^{-1})
3.3	60	4.5	9.5×10^{-16}
	80	5.2	9.5
	100	5.5	9.0
	120	5.6	8.4
	140	5.6	7.8
10.0	60	8.9	
	80	10.3	
	100	10.9	
	120	11.1	
	140	11.2	
R	T_i (keV)	Q_{DD}	$\langle\overline{\sigma v}\rangle_{DD}$ (cm^3 sec^{-1})
3.3	150	1.21	0.59×10^{-16}
	200	1.76	0.74
	250	2.28	0.86
	300	2.74	0.99
	350	3.18	1.02
	400	3.54	1.06
10	150	2.43	
	200	3.52	
	250	4.55	
	300	5.49	
	350	6.35	
	400	7.08	

Values of Q can also be computed for the transient case. In general, although Q values greater than 1 can also be obtained in this case, the ratios are not quite so favorable as for the steady-state case.

Although in typical cases they are appreciably greater than 1, the Q values that have been calculated are not large enough to allow one to be complacent, either about the accuracy of the theoretical calculations themselves, or the need for agreement between the actual diffusion rates and the theoretical result. The only sure check will be that provided by experiment itself.

We may calculate, from the Q values and Eq. (15), the fraction of primary ions that will react in steady-state. These fractions are:

$$\begin{aligned}\varphi_{DT} &= 4.1\times10^{10}\langle\sigma v\rangle_{DT}T_i^{3/2} \quad R=3.3\\ &= 8.2\times10^{10}\langle\sigma v\rangle_{DT}T_i^{3/2} \quad R=10\end{aligned} \tag{19}$$

$$\begin{aligned}\varphi_{DD} &= 7.3\times10^{10}\overline{\langle\sigma v\rangle}_{DD}T_i^{3/2} \quad R=3.3\\ &= 14.6\times10^{10}\overline{\langle\sigma v\rangle}_{DD}T_i^{3/2} \quad R=10\,.\end{aligned} \tag{20}$$

As an example, values of φ_{DT} are tabulated in Table II for various temperatures. It will be noted

TABLE II. Values of φ_{DT} at various temperatures.

R	T_i (keV)	φ_{DT}
3.3	60	0.018
	80	0.028
	100	0.037
	120	0.045
	140	0.053
10.0	60	0.036
	80	0.056
	100	0.074
	120	0.091
	140	0.106

that they are relatively small. This means that there probably is little need to consider the effect of accumulation of inert reaction products in the plasma in considering its reactivity, since it is possible to insure that their steady-state concentration is kept low. The reason that the fractional burn-up can be so small and yet permit a Q value greater than 1 is of course due to the fact that the mean energy released by the nuclear reactions is very large compared with the mean kinetic energy of the reacting particles.

If the mean fractional burn-up is φ, and the over-all efficiency of converting the nuclear power to electrical power is η_e, then the steady-state total nuclear power yield in electrical form is simply given by

$$P_n = I_0\varphi\eta_e W_n, \tag{21}$$

where I_0 is the total injected current in ions per second, and W_n is the average nuclear energy released per reaction. For the DT cycle this is, therefore (in watts/ampere injected):

$$\frac{P_n(DT)}{I_0} = 2.2\times10^7\,\eta_e\,\varphi_{DT}\,. \tag{22}$$

For the DD cycle (in watts/ampere injected):

$$\frac{P_n(DD)}{I_0} = 3.3\times10^7\,\eta_e\,\varphi_{DD}\,. \tag{23}$$

Note that these expressions are independent of plasma density.

4. Energy recovery

Disregarding some corrections for the moment, in the previous section we showed, in theory, that a favorable power balance against direct losses can be established, but only in the following sense: the intrinsic total nuclear power generation rate per unit volume can, in principle, be made to exceed the rate of escape of kinetic energy through end losses from the same unit volume. To show the possibility of an actual positive power balance in terms of useful net electrical or mechanical power generated, it is necessary to study the problem in more detail.

Consider the power-balance relationship that must apply, on the average, to each volume element of the reacting plasma. This is illustrated in Fig. 1, which

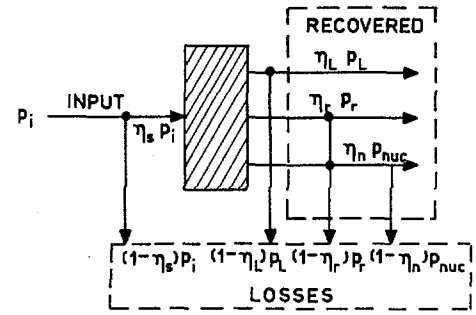

Fig. 1 Power-balance relationships in terms of *electrical* power input and outputs.

shows the power-balance relationships in terms of *electrical* power input and outputs.

As shown schematically, the injected and heated fuel supplies a power input (in the form of energetic particles) of $\eta_s p_i$, corresponding to an amount of electrical power p_i expended in the injection and heating operations, here assumed to be carried out with an efficiency η_s. Escaping is the nuclear power p_{nuc} in the form of fast neutrons or charged reaction products. Also escaping are the power fluxes p_L resulting from the escape of unburned fuel particles, and that associated with the radiation losses, p_r. Some fraction of these latter losses is assumed to be recoverable, in electrical form with efficiencies η_L and η_r, respectively. Therefore, if we write down the power-balance requirement in terms of electrical power recovered and expended (including only direct losses), we must require that:

$$[\eta_n\,p_{nuc}+\eta_L\,p_L+\eta_r\,p_r]-p_i>0\,. \tag{24}$$

On the other hand, the power flow balance of the plasma volume element itself requires that

$$\eta_s\,p_i = p_L + p_r\,, \tag{25}$$

i.e., the energy input must balance with energy escape, not including the energy produced within the volume.*

* Note that in the operation of the mirror machine, as here visualized, there is no need to assume that the plasma temperature is maintained by the charged reaction products. In fact, in steady-state the primary means for maintaining the plasma temperature is the injection process itself. This is because the mean containment time is always of the order of, or less than, the collisional relaxation time of the reaction products.

Therefore, the condition for a power balance against direct losses becomes

$$\eta_n p_{nuc} - \left[\left(\frac{1}{\eta_s} - \eta_L\right) p_L + \left(\frac{1}{\eta_s} - \eta_r\right) p_r\right] > 0 . \quad (26)$$

At the temperatures, plasma densities, and plasma volumes that will be considered, p_r is substantially less than p_L, and will therefore, for the time being, be ignored in the expressions to be derived below. Thus, the condition for power balance against direct losses becomes:

$$Q_r = \left[\frac{\eta_s \eta_n}{1-\eta_s \eta_L}\right] \frac{p_{nuc}}{p_L} = \left[\frac{\eta_s \eta_n}{1-\eta_s \eta_L}\right] Q > 1 . \quad (27)$$

Note that this expression is independent of the plasma density.

The net electrical power recoverable per unit volume is then given by

$$p_n = (1 - 1/Q_r)\, \eta_n\, p_{nuc} \equiv \eta_e\, p_{nuc} , \quad (28)$$

where η_e is the over-all efficiency factor for conversion of nuclear power to electrical form, including all direct losses. The total power produced in electrical form is simply p_n times the total plasma volume, i.e., $P_n = \eta_e\, p_{nuc}\, V$.

It follows that the complete condition for achieving a net electrical power from the reactor is simply

$$P = P_n - P_{indirect} > 0 , \quad (29)$$

where P is the net electrical power produced by the reactor, and $P_{indirect}$ is the summation of the electrical power required to sustain all the indirect losses. The net nuclear power depends on the square of the plasma density, and directly on the plasma volume, whereas indirect losses depend much more weakly on the reactor volume, and not at all on the plasma density. Therefore, even in those cases where Q_r is not much larger than 1, it is always possible, in principle, to achieve a positive power balance against indirect losses simply by employing a sufficiently large reactor volume. Power balance against indirect losses is therefore primarily a practical question rather than a fundamental one.

Returning to the question of the value of Q_r, let us consider first a purely thermal recovery cycle with efficiency η_t. In this case, $\eta_n = \eta_L = \eta_t$. It is clear that in this case it is irrelevant whether the charged reaction products are temporarily confined or escape immediately since this would not appreciably affect the over-all energy recovery. In this case, we have

$$Q_r = \left(\frac{\eta_s \eta_t}{1 - \eta_s \eta_t}\right) \cdot Q . \quad (30)$$

It is evident from the form of Eq. (30) that much is to be gained in maximizing the values of η_s and η_t. The role of η_s, the injection efficiency, is clearly important, and the achievement of large values of this parameter will be dependent on developing injection methods to a high degree of perfection. Although in some proposed injection methods values of η_s approaching 1 might be achieved, this is yet to be demonstrated.

The larger the values of η_s which can be reached, the greater will be the premium placed on achieving a high value of η_t. To see what might actually be accomplished, it is necessary to examine information on existing or projected thermal plants and their efficiencies:

(1) There is now in operation a steam-turbine plant with an over-all plant efficiency, when operated with a conventional boiler, of $\eta_t = 0.44$ (Eddystone Plant, Philadelphia Electrical Company). It can be estimated that if this plant were to be operated in a closed cycle, as it would be if used with fusion reactors as the heat source, its efficiency should rise to nearly 0.50.

(2) It can be estimated on the basis of cycle analysis that, even without substantial improvements in metallurgy, large closed-cycle gas turbine plants could be developed to achieve an efficiency $\eta_t = 0.6$.*

(3) If there were compelling economic reasons to achieve yet higher thermal efficiencies, it is conceivable that thermal conversion efficiencies higher than 0.6 could be achieved by straightforward, albeit expensive, development.

The effect of these considerations in determining the values of Q_r obtainable can be assessed from a tabulation of the value of Q_r/Q resulting from various assumptions as to the values of η_s and η_t.

Q_r/Q

η_t	$\eta_s = 0.5$	$\eta_s = 0.7$	$\eta_s = 0.9$	$\eta_s = 0.95$
0.4	0.25	0.39	0.56	0.61
0.5	0.33	0.54	0.82	0.91
0.6	0.43	0.72	1.18	1.32

This table shows the importance of achieving both high source and thermal recovery efficiencies, since Q_r/Q varies by a factor of over 5 between the extreme cases of the assumed efficiencies, while η_t and η_s vary by only 50% and a factor of 1.9, respectively. Furthermore, at the highest values of η_s and η_t, Q_r/Q actually becomes larger than 1. The effect of this on the problem of achieving a net power balance can readily be seen from Eq. (28). If Q_r/Q is greater than 1, even those situations where the plasma end losses are such that Q is less than 1 could conceivably be made to yield a net power. On the other hand, the same equation shows that there is little to be gained in trying to achieve Q_r values much greater than 3; even a "perfect" magnetic bottle ($Q_r = \infty$) would have an efficiency only 33% higher than one with Q_r equal to 3.

To summarize the results of these calculations, and also those of the previous sections, the values of Q_r obtainable by thermal power recovery for certain

* James Hodge, Cycles and Performance Estimation, Gas Turbine Services (Butterworth Scientific Publications, London, 1955), Vol. 1, p. 169.

TABLE III. Values of Q_r obtainable by thermal power recovery.

Cycle	R	T_i (keV)	Q_r ($\eta_t = 0.5$)			Q_r ($\eta_t = 0.6$)		
			$\eta_s = 0.5$	0.7	0.9	$\eta_s = 0.5$	0.7	0.9
DT	3.3	60	1.5	2.4	3.7	1.9	3.2	5.3
		80	1.7	2.8	4.3	2.2	3.7	6.1
		100	1.8	3.0	4.5	2.4	4.0	6.5
		120	1.8	3.0	4.6	2.4	4.0	6.6
		140	1.9	3.0	4.6	2.4	4.0	6.6
	10.0	60	2.9	4.8	7.3	3.8	6.4	10.5
		80	3.4	5.6	8.4	4.4	7.4	12.1
		100	3.6	5.9	8.9	4.7	7.8	12.9
		120	3.7	6.0	9.1	4.8	8.0	13.1
		140	3.7	6.0	9.2	4.8	8.0	13.2
DD	3.3	150	<1	<1	<1	<1	<1	1.4
		200	<1	<1	1.5	<1	1.3	2.1
		250	<1	1.2	1.9	<1	1.6	2.7
		300	<1	1.5	2.2	1.2	2.0	3.2
		350	1.1	1.7	2.6	1.4	2.3	3.7
		400	1.2	1.9	2.9	1.5	2.5	4.2
	10	150	<1	1.3	2.0	1.0	1.8	2.9
		200	1.2	1.9	2.9	1.5	2.5	4.1
		250	1.5	2.5	3.7	2.0	3.3	5.4
		300	1.8	3.0	4.5	2.4	4.0	6.5
		350	2.1	3.4	5.2	2.7	4.6	7.5
		400	2.4	3.8	5.8	3.0	5.1	8.3

assumed plasma temperatures, mirror ratios, and η_e and η_s values are shown in Table III. A net power balance is, of course, only possible where Q_r is greater than 1. Even when this is the case, however, too small a value of Q_r would aggravate the problem of achieving a net power balance against indirect losses, as shown by Eq. (29).

The table shows that there is a reasonably wide range of plasma temperatures and source and conversion efficiencies for which a net power balance against all direct losses ($Q_r > 1$) is theoretically possible. It is furthermore clear that, provided large mirror ratios ($R \approx 10$) can be utilized, there is an appreciable margin for error in the theoretical conditions or for the influence of co-operative effects before all hope of obtaining a power balance by the simple methods assumed here is lost. The question of the practicality of large mirror ratios hinges on the successful development of cryogenic or superconducting coils.

At this juncture, it is relevant to point out that the theoretical or "ideal" margins for power balance in the mirror machine are much smaller than for other magnetic bottles, such as the stellarator. It only requires one or two effective collisions to scatter an ion into the mirror loss cone in a mirror machine, whereas in the stellarator many collisions would be expected to be required to transport the average ion to the chamber wall. Thus, the actual plasma confinement time in the stellarator can apparently be as much as two orders of magnitude shorter than the theoretical times without seriously compromising the possibility of obtaining a power balance against direct losses.

Q_r represents the most important of the "critical numbers" which determine the required conditions for achieving self-sustaining fusion reactions in a simple mirror machine. It is determined primarily by the plasma temperature, mirror ratio, injection method, and the fuel cycle chosen. It is, however, intrinsically independent of total plasma volume and of plasma density or β. Thus, the remaining critical constants are those which will relate the required values of β (as dictated by considerations of indirect losses, radiation losses, and stability) to the physical size and configuration of the plasma.

5. Optimum operating temperature

The considerations of the previous sections still leave unanswered the question of the optimum operating ion "temperature." If the only criterion for this was to achieve the highest possible value of Q, i.e., the most favorable ratio of intrinsic nuclear power generation to end leakage losses, then it is clear from the expressions given for Q that very high temperatures would be indicated; for example, more than 100 keV for the DT reaction. On the other hand, the criterion which emerges from stability considerations is that one should achieve the smallest possible value of the relative plasma pressure, $\bar{\beta}_i$, consistent with obtaining a positive power balance in a reactor of practical size. Therefore, if we assume that the theoretical Q_r values given earlier are realizable, and express the net electrically recovered nuclear power in terms of $\bar{\beta}_i$, an entirely different criterion will emerge, indicating substantially lower temperatures. Because of omitted or unforeseen corrections to Q_r, it may not be possible to operate exactly at these theoretical optimum temperatures, but they will serve as a guide.

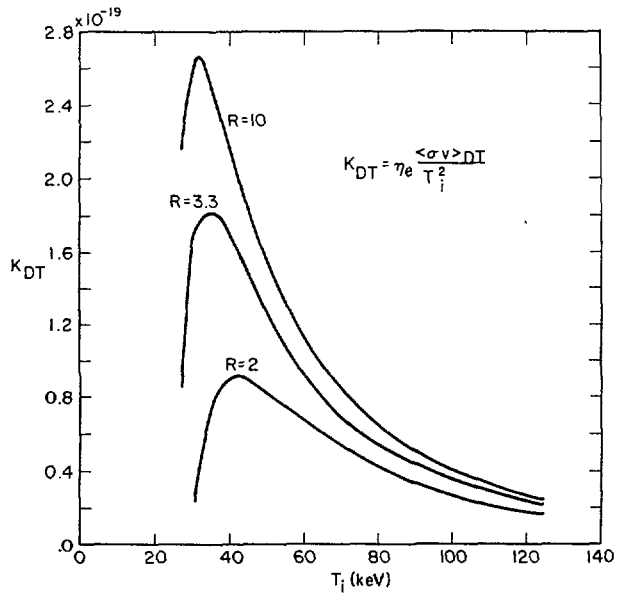

Fig. 2 Reaction parameter, K_{DT}, as a function of R and T_i.

It is easily shown that the net recoverable electrical power per unit volume of the plasma is given by an expression of the form

$$p_n = \eta_e\, p_{nuc} = K_B\, \bar{\beta}_i^2\, B_0^4\,, \tag{31}$$

where $\beta_i = nkT_i/(B_0^2/8\pi)$, with B_0 being the strength of the external confining field.

Putting in the appropriate units for energy release in the DT cycle, we have

$$K_B\,(\mathrm{DT}) = 5.5\times 10^2\,[\eta_e\,\langle\sigma v\rangle_{DT}/T_i^2]\ \mathrm{watts/cm^3}$$
$$= 0.55\times 10^3\,K_T\,(\mathrm{DT})\,. \tag{32}$$

Similarly, for the DD cycle

$$K_B\,(\mathrm{DD}) = 1.7\times 10^3\,K_T\,(\mathrm{DD})\,. \tag{33}$$

Thus, for given values of β_i and B_0, the maximum electrically recovered nuclear power will be obtained at the temperature at which K_T is a maximum. From the definition of η_e this can be written as

$$K_T = \eta_e \frac{\langle\sigma v\rangle}{T_i^2} = \eta_n\left[1-\frac{1}{Q_r}\right]\frac{\langle\sigma v\rangle}{T_i^2}\,. \tag{34}$$

Since Q_r as well as $\langle\sigma v\rangle$ depends on T_i, the value of T_i at which this function reaches a maximum will be determined by the competition between the term $\langle\sigma v\rangle/T_i^2$, which favors somewhat low temperatures, and the term $(1-1/Q_r)$, which decreases monotonically as the temperature is reduced.

In Figures 2 and 3 the values of $\eta_e\,\langle\sigma v\rangle/T_i^2$ for the DT and the DD cycles are plotted as a function of T_i. They have been computed by assuming the values $\eta_s = 0.9$ and 0.5 for the source and thermal-plant efficiencies, respectively. They are thus clearly optimistic, since these values, particularly that for η_s, would seem to represent about the limit of what can be hoped for with presently foreseeable technology. If the actual achievable values of Q or η_s fall below the theoretical values used, the indicated optimum temperatures will rise accordingly. Take the case where $R=2$, for example. If the actual Q value turned out to be one-half of the theoretical value, then the optimum DT temperature would rise from 43 keV to 85 keV. At the same time, the value of K_{DT} would drop to 12% of its former peak value, showing the loss in p_n that would result. Therefore, to make the final results somewhat less sensitive to departures from the theoretical Q_r values, in the numerical cases

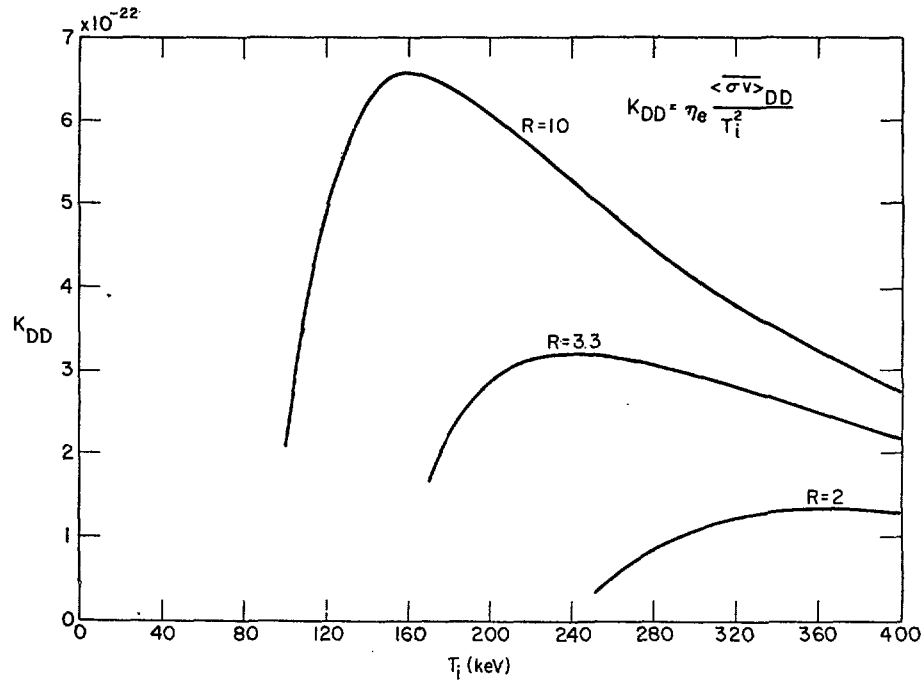

Fig. 3 Reaction parameter, K_{DD}, as a function of R and T_i.

to be given below only examples for high mirror ratios will be considered ($R=10$ and $R=3.3$), and operating temperatures somewhat higher than the theoretical optimum values will be assumed.

6. Over-all power balance—magnet losses

The total nuclear power output is directly proportional to the volume of the reacting plasma. Indirect losses, being dominated by the power required to generate and sustain the magnetic field, depend much more weakly on reactor chamber volume. Thus, provided certain scaling conditions relating to stability and radiation losses are satisfied, power balance against indirect losses can always be achieved simply by scaling the reactor size. However, if one assumes that the magnetic fields are to be generated by conventional coils, he soon discovers that the required reactor sizes and minimum self-sustaining power become very large, even if the β values (which determine the nuclear power density) are increased to uncomfortably high values. If there were no way to avoid this circumstance, it would certainly color one's attitude about the eventual feasibility of mirror machines for thermonuclear power. However, there appear to be two methods, previously alluded to, by which this problem can be greatly alleviated and thus lead to the possibility of achieving self-sustaining reactions in systems of modest size, at very low values of β. These are: (1) The use of coils made with ultra-pure metal conductors, refrigerated to very low temperatures—the so-called "cryogenic coil" [3]; and (2) The fabrication of coils from newly-discovered superconducting alloys [4] which maintain their electrical properties at very high current densities and in the presence of intense fields.

In the case of the cryogenic coil, theoretical and experimental work has progressed far enough to say that practical coils with predictable characteristics and costs are essentially assured. The practical problems and economic costs of superconducting coils are not as well foreseen at this time, but their promise is great. For the mirror machine, it appears that both techniques could be of use; for example, cryogenic coils for the large diameter, long solenoid which provides the main confining field, and superconducting coils for auxiliary conductors and for the compact, high field coils required to produce the mirror fields. In this case, the central solenoid which provides the confining field will account for essentially all of the indirect losses. It is important to note that, under the plasma and field conditions we shall consider, the electrical power required to maintain the central field in many cases would not be greatly reduced even if superconductors were substituted for the "normal" conductors. This is because of the fact that, at fields below about 30 kilogauss for large diameter coils, heat leakage through the magnet coil container walls at superconductor temperatures is comparable to the total calculated volume joule-heating losses in the conventional cryogenic coil. The choice between the two approaches is therefore, in this case, to be made also on grounds of cost and practicality, rather than on power loss alone.

Assuming the magnet losses have been specifically evaluated, the over-all power balance for the complete reactor system can be calculated. Formally, the basic relationship for the total electrical power from the reactor can be written:

$$P=P_{\mathrm{n}}\,(1-1/Q_{\mathrm{m}})-P_{\mathrm{aux}}\,, \tag{35}$$

where P_{n}, the total electrically recovered nuclear power, is given by

$$P_{\mathrm{n}}=\eta_{\mathrm{e}}\,p_{\mathrm{n}}\,V\,, \tag{36}$$

where η_{e} is equal to $\eta_{\mathrm{t}}\,(1-1/Q_{\mathrm{r}})$. P_{aux} represents any power demands of auxiliary equipment, such as vacuum pumps, and should usually be negligible. Q_{m} is the ratio of total electrically recovered nuclear power to the power required to generate the magnetic field. Q_{m} is thus the second of the "critical numbers" which we must determine in order to define the conditions for achieving a self-sustaining reaction.

The expression for P might alternatively be written (disregarding P_{aux}) as,

$$P=\eta_0 p_{\mathrm{nuc}} V \tag{37}$$

where

$$\eta_0=\eta_{\mathrm{t}}\,(1-1/Q_{\mathrm{r}})\,(1-1/Q_{\mathrm{m}})\,. \tag{38}$$

Thus, η_0 is the over-all efficiency of the entire reactor-energy recovery plant-coil refrigerator system in converting nuclear fusion energy into electrical form. Written in this way, it is easy to discern the role of the two critical numbers, Q_{r} and Q_{m}, in determining the possibility of obtaining a self-sustaining reaction.

All three possibilities mentioned, i.e., (1) cryogenic coils for all magnets, (2) superconductors for all magnets, and (3) superconducting mirror coils and cryogenic central solenoid, have been considered. We shall first discuss (3) above, by way of illustration. In this case, the power required to generate the mirror fields is negligible, and we need only consider the long central solenoid.

As shown in [3], the power per unit length of a long solenoid is independent of its diameter and depends only on the ratio of its inner to outer diameter and on the effective resistivity of its conductors. Thus, in a formulation similar to that first employed by Fabry one can write the magnet electrical power per unit length in terms of the energy density of the field and a "figure of merit," F_{m}

$$p_{\mathrm{m}}=\frac{B_0^2}{8\pi}\left(\frac{1}{F_{\mathrm{m}}}\right)\text{watts/cm}. \tag{39}$$

As an example, for a solenoid with a uniform current distribution,

$$F_{\mathrm{m}}=\frac{1}{50}\left(\frac{\alpha-1}{\alpha+1}\right)\frac{1}{\bar{\varrho}}\,, \tag{40}$$

where $\alpha=r_2/r_{\mathrm{i}}$, the ratio of outer to inner radius, and $\bar{\varrho}$ is the mean "effective" resistivity of the coil conductors.

TABLE IV. Minimum value of $(\bar{\beta}_i B_0 a)$ as a function of T_i and mirror ratio.

Cycle	R	T_i (keV)	$(\bar{\beta}_i B_0 a)_{min}$ (gauss-cm)	$(Q/2)$	$\eta_s=0.5$	$\eta_s=0.5$ $(Q/2)$
DT	3.3	35	3.6×10^4	$(6.2)\times10^4$	$(\infty)\times10^4$	$(\infty)\times10^4$
		67	5.5	(6.9)	(7.8)	(∞)
		100	8.5	(10)	(11)	(∞)
	10	32	3.0	(3.6)	(4.1)	(∞)
		67	5.0	(5.5)	(5.7)	(7.8)
		100	7.6	(8.2)	(8.5)	(11)
DD	3.3	200	4.9×10^5	$(\infty)\times10^5$	$(\infty)\times10^5$	
		250	4.9	(∞)	(∞)	
		300	5.2	(12)	(∞)	
		350	5.5	(9)	(10.4)	
	10	150	3.4	(∞)	(∞)	
		200	3.5	(5)	(4.7)	
		250	3.9	(5)	(5.8)	
		300	4.3	(5)	(5.7)	

On the other hand, from the discussion of the previous sections, the electrically recovered nuclear power per centimeter of the reactor is

$$p_n = K_B \bar{\beta}_i^2 B_0^4 \pi a^2 \text{ watts/cm}, \tag{41}$$

where $\bar{\beta}_i$ is the root mean square value of β_i, a is the reactor chamber radius, and K_B is a previously defined function of the plasma parameters.

Thus, in this case, Q_m is determined through the expression

$$Q_m = \frac{p_n}{p_m} = 8\pi^2 K_B F_m (\bar{\beta}_i B_0 a)^2 . \tag{42}$$

Since F_m can be determined from the properties of the coil conductors, and K_B is determined by Q_r and the plasma temperature, see Eq. (34), the critical condition $Q_m > 1$ serves to determine the minimum value of the product $(\bar{\beta}_i B_0 a)$. In Table IV, values of this critical product are given for the DT and DD reaction cycles under the conditions indicated. The values of F_m are computed from [3] for Na conductors operated at 10 °K, but assuming magneto-resistance values appropriate to 100 kilogauss. Since the values of Q_r used in computing the table may turn out to be optimistic, values of $(\beta_i B_0 a)_{min}$ are shown (in parentheses) which would be required if the actual values of Q turned out to be one-half of the theoretical values used, and if the attainable values of the injection efficiency should turn out to be only 0.5 instead of 0.9 as assumed in the table for DT. Values are also shown for the case where *both* η_s and Q have the above diminished values.

Since the achievement of a value of Q_m greater than 1 necessarily implies also that Q_r is greater than 1, it is clear from Table IV that, theoretically, it should be possible to achieve an over-all power balance for reasonable values of $(\bar{\beta}_i B_0 a)$, even under somewhat pessimistic assumptions with respect to Q values and injection efficiency. Thus, there appears to be an appreciable, if not large, margin for unforeseen corrections, particularly for the DT cycle.

Considering for a moment the hoped-for eventual practical application of these calculations, it should be recognized that the $(\bar{\beta}_i B_0 a)$ values presented in Table IV represent break-even values, so that somewhat larger values would actually have to be used in practice. To take a numerical example for the DT reaction, if $T_i = 100$ keV and $R = 3.3$, then $(\bar{\beta}_i B_0 a)_{min}$ has the value 8.5×10^4 gauss-cm. Therefore, if $\beta_i = 0.1$ and $a = 100$ cm, for example, a value of B_0 of about 8.5 kilogauss would be sufficient to make Q_m equal 1. At $B = 15$ kilogauss, $Q_m = 3$, a reasonable operating point. By contrast, if ordinary copper coils were to be used, B_0 would have to be raised to about 100 kilogauss to achieve a comparable value of Q_m. This would require the mirror fields to be more than 300 kilogauss.

For the DD cycle, the values of $(\bar{\beta}_i B_0 a)$ are seen to be about a factor of 8 or more larger than the DT figures. This could, for example, be satisfied by increasing each parameter by about a factor 2, as compared with a typical DT case. The size and operating β value of DD reactors would therefore be substantially larger than for DT, but still seemingly within the bounds of practicality.

The calculations to this point allow the determination of the critical numbers, Q_r and Q_m, for the cases considered. Q_r is determined by the fuel cycle used, the operating temperature, and the mirror ratio. Q_m can be specified in terms of the product $(\bar{\beta}_i B_0 a)$. Except for the restriction that the mirror field $B_m = R B_0$ shall not exceed practical limits, the choice of each individual variable is as yet left open.

If it is assumed that all magnet coils are fabricated with superconductors, a somewhat different scaling law emerges. In this case, the dominant indirect loss is the power required to overcome the heat leaks of the thermal insulation of the coils. Again the central solenoid dominates, but the losses are now proportional to the coil surface area. If the reactor chamber radius is a cm and the combined thickness of the capture and shielding blanket and inner coil heat insulation

is t cm, then if the radial thickness of the coil is small,

$$p_m = 4\pi K(a+t) \text{ watts/cm}, \tag{43}$$

where K is the effective heat leakage of the coil in watts/cm², i.e., the actual heat conduction multiplied by the refrigeration factor which relates the heat pumped at the operating temperature to the total refrigerator power. Taking an operating temperature of 4.2 °K (liquid helium), an average heat leak value of 100 microwatts/cm² at 4.2 °K and a refrigeration factor of 250 gives $K = 2.5 \times 10^{-2}$ watts/cm². For this case, therefore,

$$Q_m = \frac{p_n}{p_{\text{magnetic}}} = 10 K_B \frac{\bar{\beta}_i^2 B_0^4 a^2}{(a+t)}. \tag{44}$$

Since the minimum value for t in order to provide sufficient shielding and heat insulation is about 100 cm, we may write

$$Q_m = 10 K_B \bar{\beta}_i^2 B_0^4 \left[\frac{a}{1+100/a}\right]. \tag{45}$$

Values of the product $\bar{\beta}_i B_0^2 a$ which make $Q_m = 1$ are tabulated in Table V for the DT cycle for various

TABLE V. Values of $(\bar{\beta}_i B_0^2 a)$ for the DT cycle using superconducting coils.

R	T_i (keV)	$(\bar{\beta}_i B_0^2 a)$	
		$a = 50$ cm	$a = 100$ cm
3.3	35	3.9×10^8	4.5×10^8
	67	6.1	7.1
	100	8.7	11
10	32	3.1	4.1
	67	5.5	7.1
	100	6.0	7.4

temperatures and for $a = 50$ and 100 cm. Comparison with the data of Table IV shows that, for $a = 100$ cm and $B_0 \approx 10^4$ gauss, the values of $(\bar{\beta}_i B_0 a)$ are comparable. For higher fields, the superconducting solenoid coil begins to show an appreciable advantage, one which increases linearly with B_0 (for constant Q_m). But since B_0 is eventually limited by the value of the mirror field which can be reached (perhaps 300 kilogauss), at high mirror ratios no order of magnitude advantage can be expected, as compared with the use of ordinary cryogenic coils for the main solenoid. The choice between the two will be likely to be, therefore, largely a question of relative cost.

At this point, relationships which establish the critical conditions for power balance against direct losses ($Q_r > 1$) and against indirect losses ($Q_m > 1$) have been given. As yet undetermined are the limitations on the allowable range of β values. The effects of plasma synchrotron radiation and some theoretical limitations imposed by plasma stability will enable something to be said about the limits on β. However, much more experimental evidence on both of these will be required before values can be specified with certainty.

7. Synchrotron radiation

TRUBNIKOV and co-workers [7, 11, 12] have calculated the fundamental rates of radiation losses from a hot plasma caused by synchrotron radiation from the plasma electrons. They have used these rates to calculate, under special circumstances, the "critical dimensions" which a thermonuclear plasma must have in order to permit achieving a self-sustaining reaction. DRUMMOND and ROSENBLUTH [13, 14, 15] have also considered the problem, finding about the same results for the basic-radiation rates as Trubnikov, but extending the calculations to somewhat higher approximation [14, 15] and specifically considering the role of metallic reflecting walls. While there is general agreement as to the magnitude of the radiation losses, the effect of these losses on power balance depends sensitively on the nuclear aspects of the problem. We shall use the basic radiation rates derived by these authors to calculate critical parameters for the mirror machine which apply under steady-state conditions. Less restrictive conditions than in the case considered by Trubnikov are found. This result agrees generally with the conclusions reached by Drummond and Rosenbluth [15].

The reason that synchrotron radiation imposes limitations on minimum values of plasma radius and plasma β is that the nuclear power and the radiation processes depend in different ways on these parameters. The basic synchrotron radiation process varies linearly with electron density, and the total radiation is determined by considerations of self-absorption of the radiation, which scale differently from the nuclear power.

In order to calculate properly the role of synchrotron radiation in the mirror machine, the calculations should be performed with realistic particle distribution functions. These, for the electrons, would include the actual energy transfer rates from ions to electrons, the transfer of energy within the distribution, and the truncation of the high energy "tail" of the distribution by ambipolar effects. These effects would tend to reduce somewhat the radiation rates relative to the values calculated by Trubnikov or by Drummond and Rosenbluth, particularly at small values of β. Their values in some sense stand therefore as upper limits in a determination of the critical values of plasma dimensions and β.

At the ion temperatures required to insure power balance against end losses ($Q_r > 1$), the radiation losses by bremsstrahlung are negligible compared to the nuclear energy yield (provided the impurity content is low). We need, therefore, only consider the synchrotron radiation losses in calculating the effect of plasma radiation. Since these losses vary less rapidly with plasma radius than does the total nuclear power, they can always be overcome, in principle, by scaling up to a sufficient size. We shall see that synchrotron radiation poses no problem for the DT cycle in the mirror machine. For the DD cycle, these losses will impose a lower limit on the β value which can be used for practical plasma radii.

As pointed out by Trubnikov, in calculating the flux of synchrotron radiation emitted from a hot plasma, one must take into account the emission and reabsorption of high harmonics of the fundamental or cyclotron frequency of the plasma electrons. The crux of the radiation calculation then consists in finding the highest harmonic which is self-absorbed, i.e., for which the mean free path of the emitted photons is equal to the plasma radius. Above this harmonic, the absorption (and thus the emission) falls off rapidly. Thus, to a close approximation, the total radiation emitted as synchrotron radiation will be given by the integral of the Rayleigh-Jeans or black-surface spectral emission, up to the frequency $m^* \omega_c$, where m^* is the "critical" harmonic number. We call on the calculations cited to provide the value of m^*. The rest of the calculation follows from the energy balance relationships which we have earlier defined for the mirror machine. Note that we are here considering a somewhat different problem from that posed by Trubnikov. He considered the problem of achieving self-sustaining DD reactions supported solely by the charged-particles reaction products of the primary DD reactions. We are considering the over-all electrical power balance, and are considering all reaction products, including the energy recoverable from the ensuing DT and DHe^3 and neutron capture reactions.

A convenient and succinct approximate representation for m^* which has been shown to follow from the analyses of DRUMMOND and ROSENBLUTH [15] is

$$(m^*)^3 = K\,(\bar{\beta}_e B_0 a)^{1/2}, \tag{46}$$

where K is a relatively slowly varying function of the electron temperature, and $\bar{\beta}_e$ is the rms value of β attributable to the electrons. Table VI presents some values of K, calculated from TRUBNIKOV'S [11] results for m^*, and as calculated by Drummond and Rosenbluth. For comparison, some values of K deduced from the calculations of HIRSHFIELD, BALDWIN, and BROWN [16], performed under somewhat different assumptions, are included.

TABLE VI. Values of radiation parameter K

T_e	T-B[a]	D-R[b]	H-B-B[a]
10 keV	0.37	—	0.28
25	0.39	0.34	—
40	—	0.52	—
50	0.69	0.54	0.43

(a) For case $A = 10^3$ (slab geometry).
(b) Cylindrical geometry, mean values.

To determine the critical constants which apply to the mirror machine, we rewrite the condition for a net electrically recovered nuclear power in the presence of synchrotron radiation losses. For over-all balance, we have, in terms of electrical power quantities,

$$\eta_0 p_{nuc} - \left(\frac{1}{\eta_s} - \eta_r\right) p_s > 0\,, \tag{47}$$

where η_0 (defined earlier) $= \eta_n\,(1-1/Q_r)\,(1-1/Q_m)$, and p_{nuc} and p_s represent, respectively, the nuclear and synchrotron radiation powers per unit length of the plasma. We therefore define a critical Q number for power balance against synchrotron radiation through

$$\eta_0 p_{nuc} = Q_s \left(\frac{1}{\eta_s} - \eta_r\right) p_s\,. \tag{48}$$

For a self-sustaining reaction, $Q_s > 1$. In this case, the over-all efficiency of conversion of the reaction energy is

$$\eta = \eta_n\,(1-1/Q_r)\,(1-1/Q_m)\,(1-1/Q_s)\,. \tag{49}$$

From the Rayleigh-Jeans law we can find the radiation loss per unit length of the plasma. We consider first the case in which no reflectors are used. In this case

$$p_s = \frac{1}{6\pi}\left(\frac{e}{mc}\right)^3 \frac{1}{c^2}\,(m^*)^3\,(kT_e)\,B_0{}^3 a \text{ ergs sec}^{-1}\text{cm}^{-1}. \tag{50}$$

The recovered nuclear power per unit length of the plasma is given by

$$p_n = \frac{1}{4}\,\bar{n}^2 \langle\sigma v\rangle\,\eta_0 W_n \cdot \pi a^2\,, \tag{51}$$

where, when written in this form, the W_n are the reaction energy yields as given earlier, 22.4 MeV and 68.4 MeV, for DT and DD cycles respectively. p_n has also been written in the form

$$p_n = K_n \bar{\beta}_i{}^2 B_0{}^4 \cdot \pi a^2\,, \tag{52}$$

so that in this case

$$K_n = \frac{1}{4\,(8\pi)^2}\,\frac{\langle\sigma v\rangle}{(kT_i)^2} \cdot \eta_0 W_n\,. \tag{53}$$

From Eqs. (48), (50) and (53) we therefore find the value of the critical product $\bar{\beta}_e{}^3 B_0 a$ as

$$\bar{\beta}_e{}^3 B_0\, a = \left[\frac{4\times 32}{3}\right]^2 \left(\frac{e}{mc}\right)^6 \frac{1}{c^4} \left[\left(\frac{1-\eta_s\eta_r}{\eta_s\eta_0}\right) \frac{Q_s\,(kT_e)^3\,K}{\langle\sigma v\rangle\,W_n}\right]^2. \tag{54}$$

With T_e in kilovolts and W_n in MeV, this becomes

$$\bar{\beta}_e{}^3 B_0\, a = 4.4\times 10^{-37} \left[\left(\frac{1-\eta_s\eta_r}{\eta_s\eta_0}\right) \frac{Q_s\,T_e{}^3\,K}{\langle\sigma v\rangle\,W_n}\right]^2. \tag{55}$$

As shown by DRUMMOND and ROSENBLUTH [13], if the plasma chamber wall reflects the microwave frequencies emitted by the plasma with an average reflectivity r, the effect is to reduce the critical radius by a factor $(1-r)$ so that in Eq. (55) above the factor a is to be replaced by $a/(1-r)$. Since r can readily be as high as 0.98 to 0.99, this can ostensibly make a substantial difference in the critical size.

All the factors in Eq. (55) are determined except T_e. In the mirror machine, it is possible to exercise some degree of control over T_e. This will be discussed in a later section. In any event, T_e will always remain substantially smaller than T_i and cannot exceed the upper limit value at which there exists a balance between energy transfer from the plasma ions (which decreases with increasing T_e) and radiation losses

(which increase with increasing T_e). Under the operating conditions contemplated for the mirror machine, energy transfer to the plasma electrons from charged reaction products can be rendered unimportant, and need not be considered here. We may, therefore, obtain an upper limit to the radiation critical conditions by considering the steady-state balance between plasma ion-electron energy transfer and the synchrotron radiation. We calculate the transfer rate from the equipartition time of a Maxwellian group of "hot" ions as given by SPITZER [8], corrected for the effect of distortion of the distribution function as calculated by HECKROTTE and KILLEEN [17]. Thus, the total transfer power per cm of plasma is

$$p_t = \frac{\alpha}{2}\left[\frac{8(2\pi)^{1/2}}{3}\left(\frac{m}{M}\right)\frac{e^4 \log \Lambda}{m^{1/2}}\right]\cdot\frac{3}{2}\frac{\bar{\eta}_e^2 (kT_i)}{(kT_e)^{3/2}}\left[1-\frac{T_e}{T_i}\right]\pi a^2 . \tag{56}$$

For low enough electron temperature, $\alpha \approx 1$.

If this is equated to the expression for plasma radiation loss, Eq. (50), an equation for T_e results. Taking $\alpha \approx 1$, we find for a deuterium plasma, with reflectors:

$$T_e = 11.0\left[\frac{\bar{\beta}_i}{K}\left(1-\frac{T_e}{T_i}\right)\right]^{\frac{2}{7}}\left(\frac{\bar{\beta}_e B_0 a}{1-r}\right)^{\frac{1}{7}} . \tag{57}$$

This expression is seen to depend only weakly on the plasma and radiation parameters. The effect of synchrotron radiation is therefore to tend to "clamp" the electron temperature, at a value substantially smaller than the ion temperature.

Calculation of the critical dimensions requires self-consistent evaluation of Eqs. (55) and (57) above. Let us consider an example for the DD cycle. We choose $R=10$, $T_i = 200$ keV, $B_0 = 10^4$ gauss, and $a = 200$ cm. From the discussion of power balance, the factor $(1-\eta_s\eta_r)/(\eta_s\eta_0) \cong 2.6$. We insert $T_e = 41$ keV, anticipating the solution to Eq. (57), and $\overline{\langle\sigma v\rangle}_{DD} = 0.9\times 10^{-16}$. There results, for $Q_s = 1$,

$$\bar{\beta}_e^3 B_0 a = 180\,(1-r) . \tag{58}$$

If we take $r = 0.98$, $\bar{\beta}_e^3 B_0 a = 3.6$.

The minimum, or critical condition, ($Q_s = 1$) is therefore, for this case, $\bar{\beta}_e = 0.012$ so that $\bar{\beta}_i$ (min) $= 0.059$.

If we insert into Eq. (55) the conditions considered by TRUBNIKOV [11] (DD primary reactions, charged particle components only, and no reflecting walls), the plasma diameters calculated agree reasonably well with his numerical results (calculated for a slab).

It should be noted that the results we obtain for $\bar{\beta}_i$ (min) are not particularly sensitive to the value of the reflectivity of the chamber walls. This is because this quantity appears in nearly the same way in both the radiation critical condition and the transfer-limited electron temperature expression. Thus, if we take $r = 0.90$, for example, a factor 5 lower, $\bar{\beta}_i$ (min) in the example above rises only to about 0.10. In this case, therefore, the critical conditions are controlled largely by the transfer rate. This also implies that small errors in the calculated theoretical coefficients for the radiation (such as the value of m^*) will not lead to substantial errors in calculating $\bar{\beta}_i$ (min). This does not follow for the insertion of the constants for the nuclear energy released, since the expressions for the critical constants depend sensitively on these parameters.

We may obtain a clearer idea of the sensitivity of $\bar{\beta}_i$ to the various parameters of the system by eliminating T_e and β_e between Eqs. (55) and (57). If we ignore the term $(1-T_e/T_i)$ in the transfer equation, the following approximate scaling relationship for the parameters $\bar{\beta}_i$, B_0 and a is found:

$$\bar{\beta}_i^3 B_0 a \sim K^2 (1-r)\, T_i^5 \left[\left(\frac{1-\eta_s\eta_r}{\eta_s\eta_0}\right)\frac{Q_s}{\langle\sigma v\rangle W_n}\right]^4 . \tag{59}$$

$\bar{\beta}_i$ is seen to be the controlling parameter, varying only very slowly with B_0 and a (if the other parameters are held fixed). Conversely, a given percentage reduction in B_0 or a can be compensated for by a much smaller percentage increase in $\bar{\beta}_i$. The sensitivity to the nuclear and power conversion constants is also clearly shown.

In summary, it appears that if the classical radiation and ion-electron transfer rates hold in plasmas confined by a mirror machine, synchrotron radiation poses no severe restriction on the critical constants, provided a minimum $\bar{\beta}_i$ can be exceeded. In the DD example given, with $Q_s = 2$, $\bar{\beta}_i \approx 0.14$, the product $\bar{\beta}_i B_0 a$ is about 2.8×10^5. This value is comparable, for this example, to the critical value of this constant imposed by considerations of the indirect losses (Table IV). It is, therefore, not surprising that if the DT cycle is considered, where the reaction rates are greater, the critical numbers are even smaller, so that except at very small values of $\bar{\beta}_i$, synchrotron radiation may be ignored in this case.

Whether the limitations on the minimum value of $\bar{\beta}_i$ for the DD cycle implied by synchrotron radiation are also consistent with plasma stability is yet to be shown. We shall consider both this problem and the problem of reducing the critical $\bar{\beta}_i$ in subsequent sections.

8. The role of plasma instabilities

Essential to all of the calculations of the critical constants is the assumption that the plasma is stably confined. This implies much more than merely that the plasma does not escape immediately to the walls. The presence of enhanced fluctuations or "micro-instabilities" which might modify the rate of transport or radiation processes would also be of serious concern.

The fundamental instability to which the mirror machine is predicted to be vulnerable is the hydromagnetic interchange or "flute" instability [18, 19]. To date, we have apparently not observed this instability experimentally*. Our explanations [20] for this

* For discussion of some effects which may be related to the flute instability in our work, see the paper following this.

fact are tentative, but share one factor in common: the probability of stability is greater if $\beta \ll 1$. Our experimental evidence and tentative theoretical calculations by others [21] indicate that critical β values of 0.10 or more may be expected, but there is no firm assurance that this is the case. We must still, therefore, label the elucidation of the "flute" instability as unfinished business, and only note that our theoretical understanding and evidence to date is not incompatible with the possibility of achieving stability in plasmas at $\beta \approx 0.1$, i.e., at values comparable to the values considered in the previous discussions.

A note on one of the possible explanations of why the flute instability may be inhibited in the simple mirror machine is in order. "Tying" of the field lines by electrical conduction along the field lines to external conducting surfaces or media has been suggested to be important. In the "particle" picture of the flute instability, such as that given by ROSENBLUTH and LONGMIRE [19], the flutes are shown to be driven by azimuthally varying charge accumulations, these in turn being fed by particle drifts in the regions of negative curvature (lines concave inward) of the magnetic field*. Any mechanism which preferentially drains off such charge would inhibit or slow the development of a flute. If slowed sufficiently, other effects, such as the smoothing effect of the precessional drifts of the particles, could stabilize the plasma. One charge drain mechanism, noted first by KAUFMAN [22] and being re-examined by Rosenbluth** is the following:

In the long-time confinement of plasmas in a mirror machine, plasma potentials must develop because of the intrinsically different rate of diffusion in velocity-space of the electrons and the ions. In such a case it will always turn out that there are some electrons (or ions) which are "hanging on by their eyebrows" and will escape if the potential on any given line of force changes by a small amount. This amounts to the preferential charge drain mechanism for which we are looking. Note that it would be presumably most effective in plasmas which have approached diffusion equilibrium with the end losses, and less effective in highly anisotropic plasmas.

It is not possible to be quantitative about this stabilizing mechanism until detailed calculations are made. However, some general features of the mechanism, which indicate how it will scale with the plasma parameters, can be indicated. Being dependent on scattering rates, other things being equal, this mechanism would be expected to be more effective at low electron temperatures. Being dependent on the total diffusion flux, its effectiveness should increase if the length of the central (uniform field) region of the plasma is increased. This region contributes to the scattering, but does not contribute to the charge separation which drives the instability (which arises, in a long machine, only in those regions near the mirrors where the field curvature is unfavorable). If important, this mechanism therefore favors low electron temperatures and large aspect ratio machines (i.e., long compared to their diameter).

It seems important in one's thinking to keep the question of hydromagnetic interchange instabilities in the mirror machine in proper perspective. It, among all of the classes of instabilities, is the one which should be entirely controllable (if it appears) by many different methods. For example, the same general type of "shear" stabilization (by use of additional stabilizing magnetic fields), superimposed on the main confinement fields, as proposed by the Princeton theoretical group and others, could be employed. There are many possible variations of this idea, and one might use either external current-carrying conductors or currents carried along the central axis of the magnetic field.

Beside the use of dc stabilizing fields, one would expect from first principles that time-varying fields, such as rf fields, or currents controlled in accordance with the plasma motion might be used.

One might summarize our present attitude toward the interchange instabilities as one of respect, but with confidence that they can either be avoided or controlled in ways which would not seriously compromise the basic principles of operation of the mirror machine, nor require a substantial change in the general picture presented in this paper.

While we do not yet sufficiently understand the role which flute instabilities may play, the situation is clearer with respect to the "micro-instabilities." These are the highly localized "unstable wave" or wave-particle "resonance" instabilities that are predicted to arise from the presence of plasma gradients—particularly gradients in velocity-space (i.e., anisotropic plasma particle distribution functions). Confinement of a plasma in a mirror machine necessarily requires some anisotropy in the plasma pressure. Injection and heating processes can lead to additional degrees of anisotropy. We must, therefore, carefully consider the critical conditions for the onset of these instabilities to discover the limitations which they may impose on the plasma parameters.

Before discussing the specific instabilities which might be encountered, some general remarks about plasma confinement in a mirror machine must be made. We recognize two different "states" of the confined plasma which must be considered. The first, and most important state, which might be called the "ground state" of the system, we shall call "State A." This is the state reached after the plasma has achieved a state of quasi-equilibrium with the end losses and the energy transfer between ions and electrons. This state then possesses the lowest degree of order compatible with confinement, and is *a priori* the least likely to be subject to instabilities. "State B" then includes any state which is not in diffusion equilibrium and thus is of lower entropy than State A. The importance of B states is that they must be passed through to

* Rosenbluth, Krall and Rostoker (Paper CN-10/170) have discussed at this Conference a stabilizing mechanism which functions through higher order drifts of this kind, arising from the difference in orbit size of the electrons and ions of the plasma, This mechanism would appear to be an important one for many situations of practical interest in the mirror machine.

** Private communication.

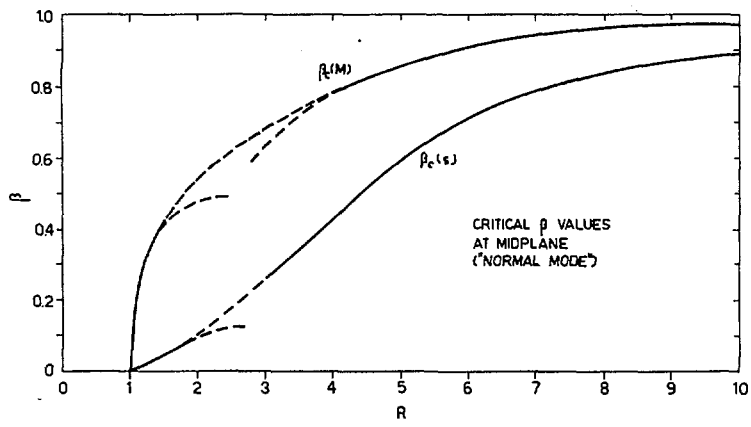

Fig. 4 Dependence of critical parameters for "mirror" and "slow" Alfvén wave as a function of mirror ratio R.

reach A. Clearly, from a practical standpoint, the plasma must remain adequately stable during the entire course of buildup and approach to State A. This imposes restrictions on the injection and heating methods which can be used.

In the category of micro-instabilities which feed on gradients in velocity-space, there are three which we here consider. These are:

(1) The "mirror" hydromagnetic instability.
(2) The electrostatic "resonance" instability.
(3) The "slow" Alfvén wave instability.

All three of these instabilities owe their origin to departures from isotropy of the plasma pressure. The critical conditions for each of these has been calculated, and can be represented in terms of the temperature anisotropy factor $t = T_{\|}/T_{\perp}$, where $T_{\|}$ and $T_{\perp}$ are the component temperatures of the plasma distribution function, expressed at the midplane as a "two-temperature Maxwellian," or as a superposition of such functions;

$$f = \exp\left\{-\frac{1}{2}m\left(\frac{v_{\perp}^2}{T_{\perp}} + \frac{v_{\|}^2}{T_{\|}}\right)\right\}. \qquad (60)$$

(1) The "mirror" instability, first discussed by Rosenbluth [23], has been treated by several authors [24, 25, 26] and may have been observed by Perkins and Post [27]. If present, it would presumably manifest itself through a greatly enhanced rate of transport processes. It exhibits a critical value of β, $\beta_0 \approx t$. Since $1 - t \ll 1$ in State A, this instability is only likely to be present in States B.

(2) The electrostatic "resonance" instability, first considered by Harris [28], can be loosely described as a resonance between longitudinal electrostatic plasma oscillations and the ion cyclotron motion. This instability requires a substantial anisotropy, which is a function of T_e/T_i, in order to occur. If this critical anisotropy is exceeded, the instability will presumably grow whenever the particle density exceeds about 10^7 to 10^8 cm^{-3}, and give rise to enhanced transport effects.

(3) The "slow" Alfvén wave instability, first considered by Rosenbluth and Wilson [29], and also discussed by Sagdeev and Shafranov [30], is a wave-particle type of instability involving a Doppler-shifted resonance between an Alfvén wave propagating along the field lines and ions in the high-energy tail of the Maxwellian. In principle, this instability may occur for arbitrarily small deviations from isotropy, except that its growth rate becomes exponentially long in the limit $t \to 1$ or $\beta \to 0$. The critical β condition for this instability then must be stated in terms of a given buildup rate. But, because the growth rate varies as exp $[-f(t)/\beta]$, this means of defining the critical β will not lead to appreciable ambiguity, but note that the presence or absence of a Maxwellian tail may have a significant effect on this instability.

If we consider the situation for States A of the plasma, we see that the anisotropy of the plasma should be a known function of the mirror ratio, so that the critical conditions (in the central region of the plasma between the mirrors) for the microinstabilities which we are considering can be specified as a function of the mirror ratio. Fig. 4 shows the dependence of the critical parameters for the "mirror" and the "slow" Alfvén wave instability as a function of the mirror ratio R. In the case of the "slow" Alfvén wave instability, the critical β cannot be precisely defined, owing to the exponentially varying nature of the growth rate. In the figure, the exponent has been arbitrarily set equal to unity, so that these curves may somewhat overestimate the "practical" critical β, where the instability is sufficiently slowly growing to be unimportant.

Examination of Fig. 4 shows that, particularly at large mirror ratios, the values of critical β are adequately high* apparently to permit stability under the conditions which we consider in this report. However, in the mirror machine, the anisotropy of the plasma is not independent of position, but must increase in the regions near the peak of the mirror fields. But since β also decreases, the question is rather whether the local critical β decreases faster, so that the plasma would become more unstable as the

* We here define β as $(p_{\perp})/(p_{\perp} + B^2/8\pi)$, which has the limit 1 and reduces to the usual definition in a field with straight field lines.

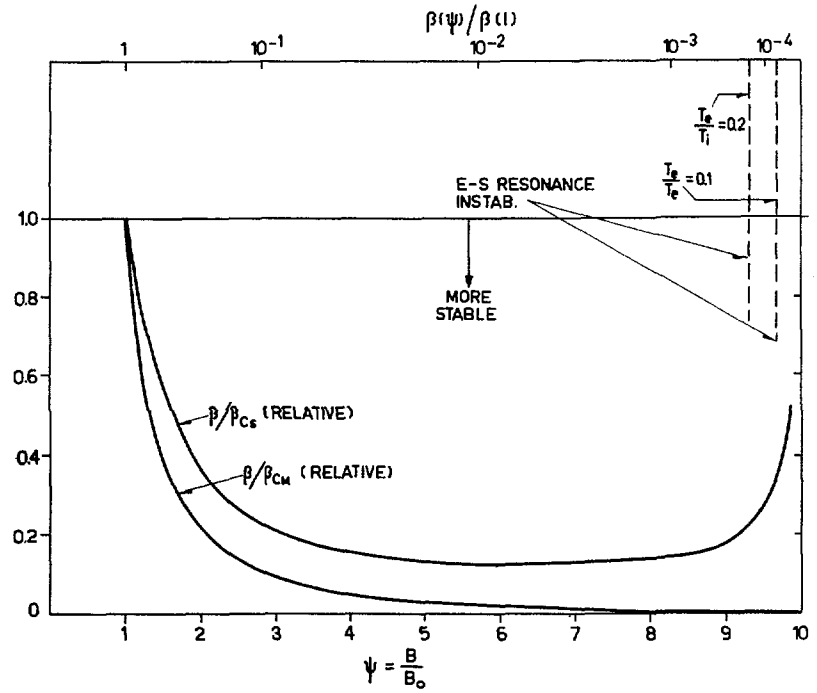

Fig. 5 Critical β, calculated results, for $R = 10$. Critical boundaries for Harris instability.

mirrors are approached. We have calculated these effects, using approximate "normal mode" distribution functions for the plasma. The results of these calculations are shown in Fig. 5 for the case $R=10$. It is seen that the "mirror" instability rapidly becomes less likely as the mirrors are approached ($\Psi \to 10$) and except for a region very close to the peak of the mirror ($10 - \Psi \approx 10^{-3}$ to 10^{-4}) the slow Alfvén instability is also less likely. Recognizing that at the mirror peak β is very low and the medium is very dispersive at the unstable frequency of this instability, we see that

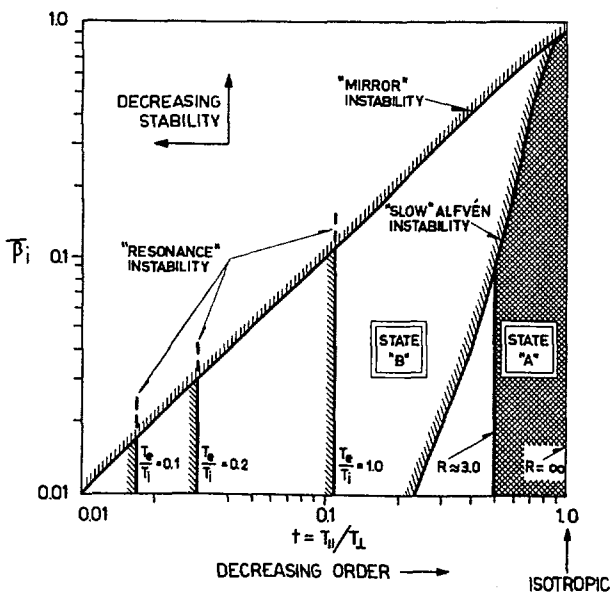

Fig. 6 Critical boundaries for velocity-space instabilities in the mirror machine.

it should nowhere be of importance. Also shown in Fig. 5 are the calculated critical boundaries for the Harris instability. In this case it is not so clear that some instability might not be encountered. Again, however, β at these boundaries is very low, the wave is dispersive (ion cyclotron frequency and density vary rapidly with position) and the instability may not occur. Theory also shows that the presence of a small amount of cold plasma in the regions near the mirrors would have a strongly stabilizing effect on the Harris instability.

Fig. 6 shows a composite plot of the midplane critical conditions for the three instabilities which have been discussed. The curve for the "mirror" instability is given for the case $R=2$, and is taken from calculations by POST [31]. The critical anisotropies for the "Harris" instability are those computed by DRUMMOND, ROSENBLUTH, and JOHNSON [32]. The critical β for the "slow" Alfvén instability is taken from the work of ROSENBLUTH and WILSON [33]. Also shown are the approximate boundaries of States A in the mirror machine for values of $R > 3.0$.

Inspection of the plot shows that the "slow" Alfvén instability is apparently the most restrictive of the instabilities, but there is a substantial regime for which β values below 0.1 (at $R \approx 3.0$) up to several times this value (at $R \approx 10$) should be stable against all of these instabilities. To be sure, substantial difficulties may be encountered in attempting to reach this region via the more anisotropic regions to the left of the bounding line.

We conclude that none of the micro-instabilities here considered should introduce a serious limitation on the value of β, provided that the method of creating

and "feeding" the reacting plasma does not introduce a degree of anisotropy which is substantially greater than regimes in which a state of diffusion equilibrium has been reached. This requirement may not be easy to satisfy in practical cases, however.

9. Streaming instabilities arising from transverse drifts

In the presence of pressure and field gradients, relative drift motions of the ions and electrons of a confined plasma will occur. In the mirror machine, these drifts are axially symmetric, leading to no net charge separation. However, the counter-streaming motion between ions and electrons implied by the presence of these drifts might become a source of instability. ROSENBLUTH and KRALL [34] have considered instabilities of this type, finding slow growing, but very short wave-length modes. In fact, the wavelengths were found to be small even compared to ion gyromagnetic radii.

While there is some doubt that these instabilities will play a significant role in the plasma behavior, owing to their singular nature, one can state, from the results given by Rosenbluth and Krall, conditions under which the plasma would certainly be stable against the instability which they have considered. The instability is presumed to occur for those plasma wave modes which have a phase velocity equal to the drift velocity, and a frequency about equal to the ion cyclotron frequency: $v_{\text{phase}} \approx \omega_{ce}/k = v_d$. Thus $\lambda \approx (v_d/v_\perp) a_i$ where a_i is the ion gyromagnetic radius. But $(v_d/v_\perp) = a_i(\nabla_\perp B/B) \ll 1$, under adiabatic, low β, conditions. Therefore, $\lambda \approx a_i^2 (\nabla B/B) \ll a_i$, so that the wavelengths are very short.

Rosenbluth and Krall have considered cases where $T_e \approx T_i$. For this case, they state that a sufficient condition for the instability *not* to grow is that $\lambda < \beta^{1/2} \lambda_D$. This is equivalent to the condition

$$B^2 \lambda_B^2 > \frac{1}{2}\left(\frac{e^2}{Mc^2}\right)^{-1} Mc^2, \text{ stable}, \qquad (61)$$

where $\lambda_B = [\nabla_\perp B/B]^{-1}$, the characteristic distance associated with the radial field gradient and $[e^2/Mc^2] = 0.76 \times 10^{-16}$ cm, the "classical radius" of the ion (if it is a deuteron). For a deuterium plasma (61) becomes

$$B^2 \lambda_B^2 > 2 \times 10^{13}, \text{ stable}. \qquad (62)$$

In the case of straight field lines (as in the middle of a long mirror machine), the field gradient arises solely from the presence of a plasma pressure, so that $\lambda_B \approx 2\bar{r}/\bar{\beta}_i$, where $\bar{r}$ is the mean plasma radius. In this case (62) becomes

$$\bar{\beta}_i (B_0)^{-1} (\bar{r})^{-1} < 4.5 \times 10^{-7}. \qquad (63)$$

To take an example, $\bar{r} = 10$ cm and $B = 10^4$ gauss, (63) gives the condition $\bar{\beta}_i < 0.04$. Thus, although this instability might appear and become a problem in small-diameter plasmas at modest fields, its scaling with field and plasma radius is such that it should always be possible to avoid it in the central regions of a long machine, simply by appropriate scaling.

Transverse drift instabilites might also occur when the drifts arise from gradients in the vacuum field. Although not specifically treated by Rosenbluth and Krall, in such cases one might expect that a condition such as (62) would then apply, independent of β (for $\beta \ll 1$). This condition again shows that physical scale and magnetic field are the important parameters. In this case, (62) shows that the product $B\lambda_B$ must exceed about 5×10^6.

We conclude that transverse drift instabilites might appear in small scale, low field experiments, but that they can be overcome, in principle, by scaling.

A summary of the types of instabilities considered in the previous discussion, and of some of the possible means of controlling them is given in Table VII.

10. Ion-electron energy transfer

We have already referred to some aspects of the problem of ion-electron energy transfer in connection with the discussion of synchrotron radiation. To see the conditions under which it is necessary to correct the simple assumption of fixed ion energies used in the reaction calculations, we shall consider the transfer problem in somewhat more detail.

We shall consider the time history of the plasma ions and the electrons, as influenced by energy transfer between them. We shall use the Spitzer energy transfer calculation, as corrected by HECKROTTE and KILLEEN [17].

The corrected deuteron-electron transfer equation is, approximately,

$$\frac{1}{W}\frac{dW}{dt} = -0.45 \times 10^{-12} \frac{\alpha n_e}{T_e^{3/2}}, \qquad (64)$$

where W is the mean ion energy in keV, T_e is the electron temperature in keV, and $\alpha \approx 1$ in cases of interest

TABLE VII. Instability types

Instability	Type[a]	Stabilization
Interchange	HM	End conductors, shear, $\beta \ll 1$, scale, etc.
"Mirror"	HM	Control $p_\perp/p_\parallel$, $\beta \ll 1$, $R \gg 1$
"Slow" resonance	W-P (HM)	$p_\perp/p_\parallel$, $\beta \ll 1$, $R \gg 1$, scale
Electrostatic resonance (Harris)	W-P (ES)	$p_\perp/p_\parallel$, $R \gg 1$, scale, cold plasma
Transverse drift	W-P (ES)	Scale, $\beta \ll 1$

[a] HM means "hydromagnetic", W-P is "wave-particle" and ES is "electrostatic".

(low electron temperature). Also, from the previous equations, taking $R=3.3$ as an example, we have for the mean confinement time:

$$\tau_L = 16.4\times 10^{10} T_i^{3/2}/n_i = 8.9\times 10^{10}\overline{W}^{3/2}/n_i\,. \qquad (65)$$

Let us set n_i equal to n_e, $\alpha=1$, and dt equal to $\tau_L\,d\tau$; then we have

$$\frac{1}{W}\frac{dW}{d\tau} = -7.4\times 10^{-2}\left(\frac{T_i}{T_e}\right)^{\frac{3}{2}} = -4.0\times 10^{-2}\left(\frac{\overline{W}}{T_e}\right)^{\frac{3}{2}}. \qquad (66)$$

Eq. (66) may be utilized in two ways. First, if it is assumed that the electron temperature is held at a fixed value, integration of the equation yields

$$\frac{W(\tau)}{W_0} = \frac{1}{[1+6\times 10^{-2}(W_0/T_e)^{3/2}\cdot\tau]^{2/3}}\,. \qquad (67)$$

To take an example, if W_0 is 100 keV ($T_i=67$ keV) and T_e is 25 keV, then in one mean confinement time ($\tau=1$), $W(1)/W(0)$ is equal to 0.77, i.e., the energy of ions of the mean energy will have fallen about 23%, so that its time-averaged value would be about 87% of W_0. This does not appear to imply the need for a large correction to the simple results that have been calculated. Roughly speaking, in this example the time-averaged mean ion energy could be restored to its nominal (100 keV) value by increasing the initial energy of the injected ions by about 18%. This implies, in effect, a downward correction in the value of Q_r of about the same amount.

If the mean ion energy is assumed fixed and the electron temperature is allowed to climb from zero as a result of the energy transfer, then, since in this case

$$\frac{3}{2}\frac{dT_e}{d\tau} \approx -\frac{dW}{d\tau}\,, \qquad (68)$$

integration of the approximate transfer equation, assuming no electron losses, yields

$$\left(\frac{T_e}{W}\right) \approx 0.34\,\tau^{\frac{2}{5}}\,. \qquad (69)$$

Thus when τ is equal to 1, if there had been no electron exchange with electrons coming in from outside the mirrors and no energy loss from the electrons, the electron temperature would rise to about 34% of the ion mean energy, thus having a time-averaged value of about 24% of W during a mean confinement time. This result could only apply if T_e remained below the value where synchrotron radiation becomes important. We have already seen, however, that in the case of the DD reaction this effect tends to "clamp" the electron temperature to a value of about 40 keV under typical plasma conditions. For the DT cycle, T_e is characteristically even lower.

The correction to the Q_r values implied by ion-electron energy transfer clearly depends on the mode of operation envisaged, but unless these transfer rates are somehow increased by co-operative effects, it does not appear from the examples given that the corrections are unduly large.

11. Injection methods

In the mode of operation of the mirror machine which we have here considered, the plasma temperature is determined and maintained by the injection and trapping of energetic fuel ions. The nature and the efficiency of this process is therefore crucial to the achievement of a self-sustaining reaction. In principle, several different schemes, such as energetic plasma injection, magnetic, collisional, or radio-frequency heating of low-temperature plasma, and the injection of energetic ions or neutral particles (atoms or molecules), offer the possibility of solving the injection problem.

We shall here discuss, briefly, only one of these schemes, which possesses some considerable advantages from the standpoint of simplicity and predictability. This is the process of neutral atom or molecule injection. Recently, DAMM and POST and co-workers have been examining this technique in connection with the ALICE experiment at Livermore [35, 36, 37]. In this experiment, an intense beam of 20-keV neutral atoms is passed diametrically through a confinement chamber immersed in a dc magnetic mirror field. Provided some very stringent vacuum and stability conditions can be satisfied, buildup and maintenance of a steady-state plasma by ionization of the neutral beam is predicted. The neutral beam is produced by charge-exchange conversion of a parallel beam of ions in a gas cell. The inefficiencies associated with such an injection scheme can be divided into four categories: (1) the efficiency of the original ion source, which can apparently be made rather high; (2) the efficiency of conversion of the ion beam to neutrals; in the ALICE experiment this is about 70%, but is a decreasing function of energy; (3) the efficiency of trapping the beam upon passage through the plasma; and (4) the efficiency of recovery of energy from the portion of the beam which passes completely through the chamber without being trapped. Processes (1), (2), and (4) are independent of scale, but are functions of the injected particle energy. It appears upon preliminary analysis that the over-all inefficiencies associated with these might be made reasonably small. The efficiency of (3) depends on scale effects, i.e., on the particle density and diameter of the confined plasma, which determine the probability that an injected particle is captured. We may use this fact to derive another approximate "critical number" for the mirror machine, applicable if steady-state neutral injection is used.

We adopt the criterion that the plasma is to be scaled so that the mean free path for ionization of the injected neutral beam is n times the radius of the plasma. The optimum value of n will presumably turn out to be about 2. Since ionization rates in the plasma are dominated by the electrons, we have for the mean free path for ionization

$$\lambda = \frac{v_0}{n_e\langle\sigma v\rangle_i}\,, \qquad (70)$$

where $\langle\sigma v\rangle_i$ is the ionization rate parameter for the electrons, and v_0 is the velocity of the injected neutral

particles. If we set $\lambda = na$, and express the resulting criterion in terms of ion "temperature" ($T_i = 2/3\ \overline{W}$), and $\bar{\beta}_i$ and B_0 (which can be related to the plasma density), we find

$$\bar{\beta}_i B_0^2 a = 1.53 \frac{T_i^{3/2}}{n \langle \sigma v \rangle_i}, \tag{71}$$

with T_i in kilovolts.

The ionization rate parameter is a slowly varying function of electron temperature at the temperatures of interest, and is equal to about 2×10^{-8} cm^2 sec^{-1}. If we take this value, the final condition is, approximately,

$$\bar{\beta}_i B_0^2 a \approx 7.7 \times 10^7 \frac{T_i^{3/2}}{n}. \tag{72}$$

For the DD cycle, for $n=1$, this is a somewhat more restrictive scaling condition than either the condition for balance against indirect losses or the condition imposed on the system by synchrotron radiation.

It is clear that, in order to achieve high capture efficiency, the fields must be rather high or the system relatively large in diameter. This can be helped somewhat by injection at oblique angles, provided the limitations imposed by plasma stability and by the mirror loss cone are taken into account.

If we put $(R+1)/2 = (\cos\theta)^{-2}$, i.e., inject at angles which are "halfway" up the mirror, the efficiency of capture in this case is

$$\varepsilon_t \approx 0.93 \frac{(R+1)^{\frac{1}{2}} \langle \sigma v \rangle_i (\bar{\beta}_i B_0^2 a)}{T_i^{3/2}}, \tag{73}$$

and the critical condition becomes

$$\bar{\beta}_i B_0^2 a = \frac{1.1\ T_i^{3/2}}{n\ (R+1)^{\frac{1}{2}} \langle \sigma v \rangle_i}. \tag{74}$$

To take an example, if $T_i = 200$ keV, $\bar{\beta}_i = 0.1$, $a = 2 \times 10^2$ cm and $R = 3.3$, for $n=1$, the condition is satisfied for $B_0 \geq 60$ kilogauss.

12. Alternative cycles

The importance of the efficiency of injection and energy recovery leads to the consideration of alternative modes of operation or fuel cycles from the ones which have been discussed. A complete discussion of these alternatives is not possible, pending more theoretical and experimental work, but some avenues which seem to show promise can be mentioned.

Up to this point, we have been tacitly assuming that the injection-confinement-energy recovery systems would be operated in steady-state. There are many advantages to this mode of operation, particularly in that it does not require the magnetic field to vary in time. There are reasons, however, for considering a "modified steady-state" mode which would function as follows: The confining magnetic field would be maintained constant, but the injection, reaction, and energy recovery processes would be made cyclic. Some time after the plasma had been built up to reacting density and temperature (for example, by fast neutral injection), a relatively high-density burst of cold, but highly ionized plasma would be injected into the plasma through one of the mirrors. During the time that it took for this burst to pass through the confinement chamber and dissipate itself, the trapped hot ions would have a high probability of making a collision with the ions of the cold plasma. The reaction rate per unit volume during this time would be given very nearly by

$$r = n n_0 \sigma \bar{v}(t) \tag{75}$$

where $n_0 \gg n$ is the density of the cold plasma ions, and $\bar{v}$ the mean velocity of the hot ions. Energy degradation of the hot ions by their heating of the cold electrons of the plasma would lead to their eventual loss, but an appreciable momentary reaction energy yield would result. The significance of this yield is, however, that it would occur without the expenditure of any additional injection energy, the energy required to inject the cold plasma burst being negligible. Thus, the total energy yield per cycle time would be expected to be larger than if the system had simply been allowed to run at steady-state.

In calculating this transient reaction effect, we need to take into account the fact that, after buildup to steady-state, the *contained* ions in a mirror machine have a substantially higher energy than the injected ions (more than a factor of 2 at $R=10$). It is then calculated that the probability that an ion will react during the transient phase is comparable to the probability it will react during its mean lifetime in the steady-state phase, provided the total effective number of particles injected in the plasma burst is not more than about a factor of ten larger than the number of confined ions.

In addition to the reaction yield "bonus" which may be possible if this transient mode of operation is used, there are other practical advantages of periodically injecting cold plasma. One of these is that it serves to control and to reduce the electron temperature below its normal value. This would reduce the time-averaged ambipolar and synchrotron radiation effects. Also, injection of such bursts would tend to "purge" the system of trapped charged reaction products. In connection with this latter point, it is to be noted that there would be a finite probability that these reaction products would themselves react with the ions of the plasma burst before being scattered out. For a very high energy (many MeV) particle, where the "distant" Coulomb collision cross-section is smaller than the large-angle nuclear scattering, the effectiveness, per scattering collision, of the mirrors is enhanced. In such a case, the mean number of "collisions", N, required to lose a particle approaches the reciprocal of the fractional loss cone solid angle, so that $N \approx 2R$, varying linearly rather than logarithmically with R.

Finally, the fact that the DHe^3 reaction leads to a 14.7-MeV proton reaction product suggests that an

interesting "breeding" cycle, not involving a neutron-capture blanket, might be accomplished. If the injected plasma burst contains some Li^6, there is an appreciable probability that a trapped 14.3-MeV proton will react with it before being lost. The pLi^6 reaction goes to $He^3 + He^4 + 4$ MeV. In this way one can hope to "breed" He^3. To close the breeding cycle, it appears that the He^3, the p, and the T (which decays to He^3) from the concurrent DD reactions would also have to be used. By calculation, He^3 concentrations in the vicinity of 30% seem to be consistent with a closed breeding cycle, assuming reasonable reaction probabilities. It is clear that the the neutron flux in such a cycle would be substantially smaller than in the DD or DT cycles.

The special injection and fuel cycles just discussed are illustrations of some of the ways in which the nuclear power balance might be improved. It is clear that none of these "tricks" is likely to lead to an order of magnitude improvement in the values of Q_r, but they could lead to improvements of a factor of 2 or more. However, because of the sensitivity of some of the scaling parameters to even a factor of 2 change, even "tricks" might become of some importance.

Another method of increasing the attainable values of Q_r is through improvements in the energy recovery cycle. It appears that, if the added difficulty warrants it, several different methods of direct conversion might be applicable to the mirror machine, ranging from electrical conversion directly from the escaping plasma particles to complicated expansion cycles. If the attainment of a positive power balance were to hinge on the use of direct conversion, it appears that some improvement in the over-all system efficiency might be possible. However, the fact that conventional thermal plants already have conversion efficiencies approaching 0.5 means that the direct conversion system would either have to be substantially more efficient than this, or substantially simpler and cheaper in order to justify its use.

13. Recapitulation of the critical numbers

Several critical numbers and critical parametric relationships have been derived. These serve to define our present understanding of the allowed plasma regimes for self-sustaining reactions in simple steady-state mirror machines. We divide the critical numbers into three categories:

1. Those independent of plasma scale and β:

$Q = F(R, T_i, \text{cycle})$

$Q_r = F_r(R, T_i, \eta_s, \eta_t, \text{cycle})$ — over-all power balance against end losses

2. Those which depend on scale, magnetic field, and $\bar{\beta}_i$:

$Q_m = F[(\bar{\beta}_i B_0 a), Q_r, \text{cycle}]$ — balance against coil power

$Q_s = F[(\bar{\beta}_i^3 B_0 a), T_i, (1-r)]$ — balance against synchrotron radiation

$\bar{\beta}_s = F[(T_{i\parallel}/T_\perp), R]$ — limitations imposed by the slow Alfvén instability

$\bar{\beta}_d = F[(B_0 a), (T_e/T_i)]$ — limitations possibly imposed by transverse drift instabilities

3. Those which relate to injection requirements:

$\varepsilon_i = F[(\bar{\beta}_i B_0^2 a), T_i, R]$ — efficiency of breakup of injected neutral beams.

Of the three categories, the first is the most fundamental and the most vulnerable to departures from "classical" behavior of the plasma. The second category defines our present understanding of the $\bar{\beta}_i B_0 a$ regime in which it is possible to hope for a self-sustaining reaction. The third category is not a fundamental one, but delineates some aspects of the problem of injection.

In order to make the requirements imposed by these limitations more apparent, we have chosen to illustrate them by three specific examples, one a DT cycle, and the other two, DD cycles. On the basis of the calculated Q_r values, we choose ion temperatures compatible with the assumed mirror ratios (3.3 and 10). The plasma radii are also fixed at values which appear to be reasonable for the cycle involved. The relevant parameters are listed in Table VIII.

Since it has been shown that all of the important "scalable" critical conditions can be described, at least approximately, by various powers of the parameters $\bar{\beta}_i$, B_0, and a, it is convenient to represent the available regions for self-sustaining reactions as a log-log plot of $\bar{\beta}_i$ vs B_0, with a as a parameter. Figures 7, 8, and 9 show such plots. The area cut out by the critical boundaries defines the regions in which there is reason to believe that stable confinement and energetically self-sustaining reactions (including all known losses) can be expected, provided unforeseen phenomena do not appear. Also shown by way of illustration are "practical" operating points which were picked to achieve a reasonable compromise between the mutually conflicting requirements of stability, balance against losses, and a reasonable minimum value of total power output.

The critical boundaries for stability do not include the "flute" instability, for which no adequate theory of stabilization is yet available. Shown, however, are the two micro-instabilities which are potentially important in State A, namely, the slow Alfvén instability and the transverse drift instability. In the case of the transverse drift instability, the characteristic distance has been arbitrarily set equal to $0.1\,a$, implying that the particle density gradient would all occur in the outer 10% of the plasma column. Although advantageous from the standpoint of efficiency, this requirement is clearly not essential, so that the indicated boundary is probably overly conservative.

Examination of the figures shows that there exist accessible regimes for self-sustaining reactions for both the DT and the DD cycle. However, the DD regime is much more limited in extent and more vulnerable to small departures from the theoretical calculations. Nevertheless, there is reason to hope that,

TABLE VIII. Examples of self-sustaining reactors (based on calculations only, not on experimental data).

	Q_r	$\bar{\beta}_i$	B_0[a] (kilo-gauss)	$\bar{n}_i$ (cm^{-3})	p_n[b] (W/cm^3)	P[c] [kW (electrical)]
EXAMPLE A						
DD cycle	1.9	0.15	60	2×10^{14}	7.5	120×10^3
$R = 3.3$						
$T_i = 250$ keV						
$a = 200$ cm						
$L = 100$ m						
EXAMPLE B						
DD cycle	2.9	0.15	30	5×10^{13}	0.4	12×10^3
$R = 10$						
$T_i = 200$ keV						
$a = 200$ cm						
$L = 100$ m						
EXAMPLE C						
DT cycle	4.0	0.05	30	1.7×10^{13}	0.20	25×10^3
$R = 3.3$		0.03	60	4.0	1.1	150×10^3
$T_i = 67$ keV		0.01[d]	60	1.4×10^{13}	0.12	15×10^3
$a = 100$ cm						
$L = 100$ m						

(a) Coil packing fractions (for cryogenic solenoids) are assumed to be 0.8. Coil dissipations are calculated with magneto-resistance as though at 100 kilogauss for conservatism. This, therefore, probably overestimates the magnet power at low fields.

(b) Nuclear power densities (p_n) include the total energy released by the plasma (including neutrons), but not the neutron capture energy, for the example values given.

(c) Total nuclear power, P, is the approximate net electrical power output under the plasma conditions indicated.

(d) Superconducting coils are assumed for all coils in Example C, $\bar{\beta}_i = 0.01$.

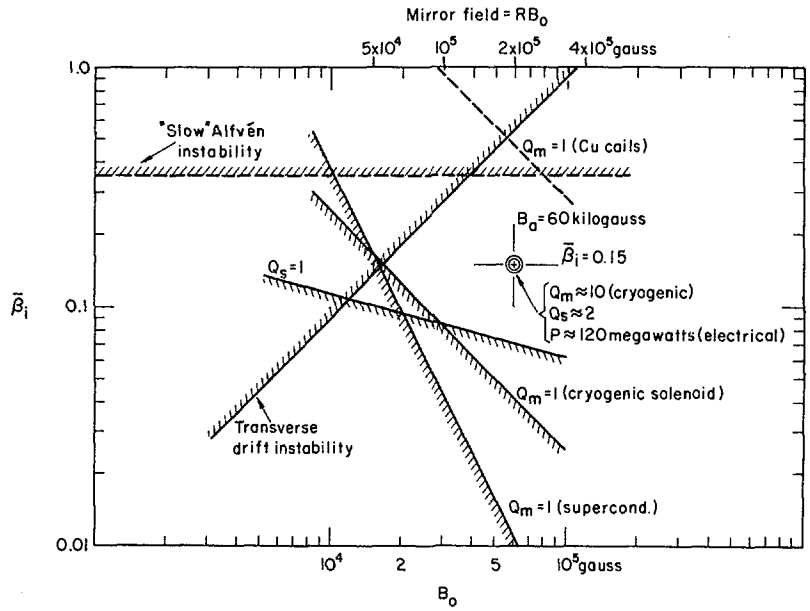

Fig. 7 Composite of critical boundaries for self-sustaining reactions — DD cycle, Example A. $T_i = 250$ keV, $R = 3.3$, $a = 200$ cm, $L = 100$ m.

even for the DD reaction, these required conditions might be achieved by attention to all details of the problem, possibly by taking advantage of "tricks" of the kind mentioned earlier.

From a long-range standpoint, the comparison between three possible methods of producing the confining fields (ordinary copper coils, cryogenic sodium conductor coils, and superconducting coils) is particularly important. The use of ordinary copper coils is seen to be practically ruled out, except possibly for the DT cycle, although even this case would involve very large total reactor power. The choice between systems using cryogenic central solenoids as opposed to ones using superconducting solenoids is

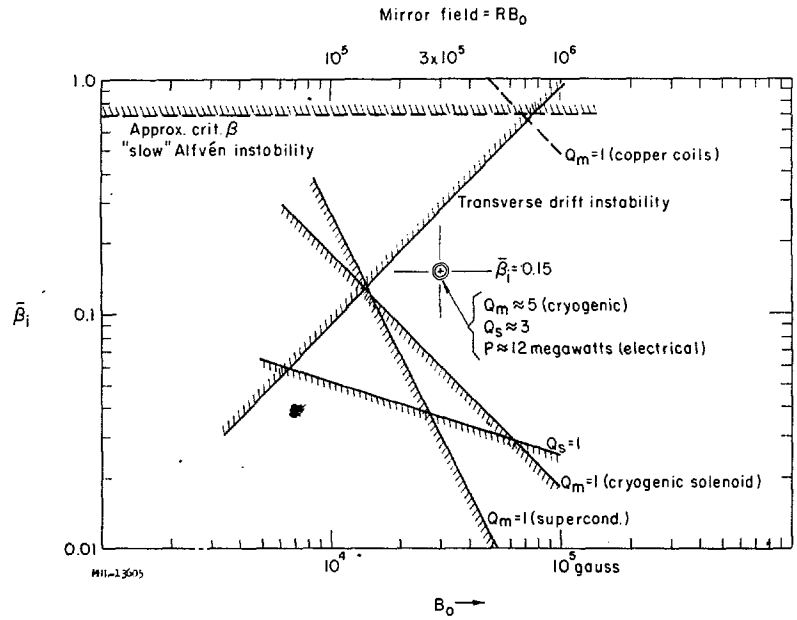

Fig. 8 Composite of critical boundaries for self-sustaining reactions — DD cycle, Example B. $T_i = 200$ keV, $R = 10$, $a = 200$ cm, $L = 100$ m.

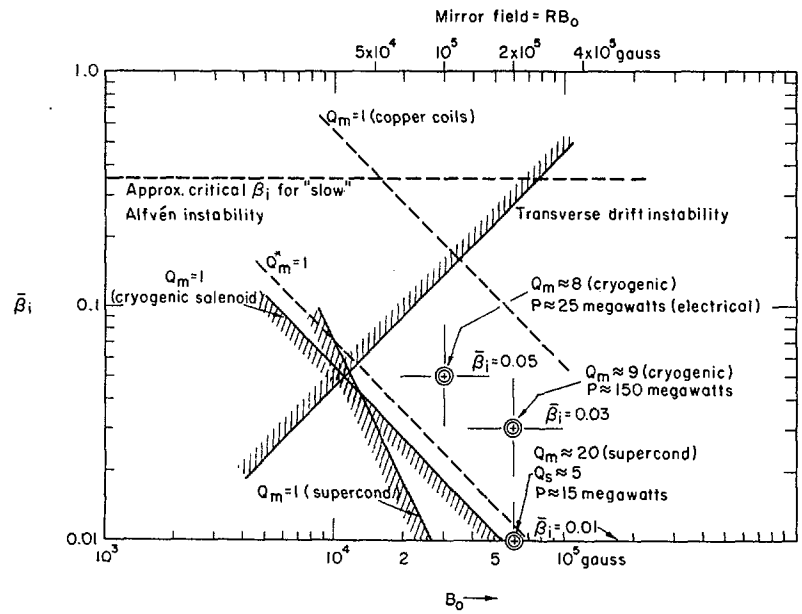

Fig. 9 Composite of critical boundaries for self-sustaining reactions — DT cycle, Example C. $T_i = 67$ keV, $R = 3.3$, $a = 100$ cm, $L = 100$ m.

not so easily made. In the DD cycle, it appears that the synchrotron radiation imposes a lower limit on $\bar{\beta}_i$ which is more restrictive than that imposed by magnet losses. In this case, therefore, it would appear that in the long-range view the relative capital and operating costs of the two types of coil represent a better criterion from which to make the choice. As of today, the picture is not clear enough to say which will be cheaper, except to note that the material and fabrication cost for large superconducting coils is likely to be much higher than for a "conventional" cryogenic coil. In the case of the DT reaction, the energetics clearly favor the superconducting magnet. However, if $\bar{\beta}_i$ is decreased too far, the power output per unit volume of the reactor may become too small to be practical. The operating points shown in Fig. 9 seem to represent reasonable compromises. In these cases, either type of coil could be used. With the exception of the dotted line marked $Q_m^* = 1$ in the DT case, the $Q_m = 1$ lines in all the figures have been drawn under the assumption that the mirror coils (which are small relative to the main solenoid) would be fabricated from superconductors. This seems to be the most likely place where superconductors should

show a real advantage. However, it is not essential that such coils be developed, as the line $Q_m^* = 1$ shows. This line is drawn to show the effect of constructing *all coils* (in this example) as "ordinary" cryogenic coils.

Another practical limitation, not discussed previously, is indicated in the figures. Along the top margin are indicated the values of mirror field which go with the indicated central field value. Mechanical and technological factors will impose limits on these fields. While it appears that mirror fields of 200 kilogauss should be entirely feasible, to attain fields higher than this would involve substantially more difficulty. Five hundred kilogauss seems about the upper limit of what could be achieved, in the light of what we know today. Clearly, the development of efficient high-field coils (perhaps based on "force-free" configurations) seems to be of great importance for the future practicality of the mirror machine.

14. Critical experiments

As indicated at the beginning of this report, the main present utility of studies of this kind is likely to be the insight they give into the planning of experiments rather than any expectation that they closely define the form an actual fusion reactor might take. Some of the questions suggest that it should be possible to define a series of "critical experiments" which would prove (or disprove) the validity of the calculations made.

Among the problems which the calculations show to be important to explore by critical experiments are the following:

1. The hydromagnetic stability, under adiabatic, steady-state conditions, of mirror systems of large aspect ratios (long and thin), with high mirror ratios (3 to 10) and with $\overline{\beta}_1$ values of 0.01 to about 0.1;
2. how to avoid the micro-instabilities which may be associated with buildup or injection processes, where substantial deviations from State A may occur;
3. the role of ambipolar potentials in plasma stability and particle loss rates;
4. the possible coupling between secondary phenomena, i.e., radiation, or trapped reaction products, and plasma stability and energy loss rates; and
5. precision values of the transport coefficients in a quiescent hot plasma (if one can be made!).

It is clear that to obtain satisfactory answers to all of these will require many years work, work which there is no guarantee will be rewarded with success. Nevertheless, the reward which could come with favorable answers to these questions would be the probable assurance that thermonuclear power could be generated in the mirror machine.

Acknowledgment

This research was performed under the auspices of the United States Atomic Energy Commission.

References

[1] Post, R. F., Sixteen lectures on Controlled Thermonuclear Reactions, U.S. Atomic Energy Commission Report UCRL-4231 (Feb. 1954); also summarized and extended in Post, R. F., Proceedings of Second U. N. International Conference on Peaceful Uses of Atomic Energy, Geneva **32**, (1958) 245.
[2] Budker, G. I., Plasma Physics and the Problem of Controlled Thermonuclear Reactions, Vol. III, (Moscow, 1958).
[3] Post, R. F., Taylor, C. E., Advances in Cryogenic Engineering, Vol. V (Plenum Press, New York, 1960) p. 13.
[4] Kunzler, J. E., *et al.*, *Phys. Rev. Letters* **6** (1961) 89.
[5] Hesselberg-Jensen, T., Kofoed-Hansen, O., Wandel, C. F., Proceedings of Second U. N. International Conference on Peaceful Uses of Atomic Energy, Geneva **32** (1958) 431.
[6] Roberts, J. E., Carr, M. L., U.S. Atomic Energy Commission Report UCRL-5651-T (unpublished) April 1960.
[7] Trubnikov, B. A., Kudryavtsev, V. S., Proceedings of Second U. N. International Conference on Peaceful Uses of Atomic Energy, Geneva **31** (1958) 93.
[8] Spitzer, L., Physics of Fully Ionized Gases (Interscience, New York, 1956).
[9] Garren, A., Riddell, R. J., Smith, L., Bing, G., Henrich, L. R., Northrop, T. G., Roberts, J. E., Proceedings of Second U. N. International Conference on Peaceful Uses of Atomic Energy, Geneva **31** (1958) 65.
[10] Ben Daniel, D., U.S. Atomic Energy Commission UCRL-6326 (unpublished) 1961.
[11] Trubnikov, B. A., Bazhanova, A. E., Plasma Physics and the Problem of Controlled Thermonuclear Reactions, Vol. III (Moscow 1958).
[12] Trubnikov, B. A., *Phys. Fluids* **4** (1961) 195.
[13] Drummond, W. E., Rosenbluth, M. N., *Phys. Fluids* **3** (1960) 45.
[14] Drummond, W. E., Rosenbluth, M. N., *Phys. Fluids* **4** (1961) 277.
[15] Drummond, W. E., Rosenbluth, M. N., Proceedings of Lockheed Magnetohydrodynamics Conference, Dec. 1960 (to be published); also, *Bull. Am. Phys. Soc.* II **6** (1961) 205.
[16] Hirshfield, J. L., Baldwin, D. E., Brown, S. C., *Phys. Fluids* **4** (1961) 198.
[17] Killeen, J., Heckrotte, W., *Bull. Am. Phys. Soc.* **5** (June 1960).
[18] Bernstein, I. B., Frieman, E. A., Kruskal, M. O., Kulsrud, R. M., *Proc. Roy. Soc.* (*London*) **A 244** (1958) 17.
[19] Rosenbluth, M. N., Longmire, C. L., *Ann. Phys.* (N. Y.) **1** (1957) 120.
[20] Post, R. F., Ellis, R. E., Ford, F. C., Rosenbluth, M. N., *Phys. Rev. Letters* **4** (1960) 166.
[21] Berkowitz, J., Grad, H., Rubin, H., Proceedings of Second U. N. International Conference on Peaceful Uses of Atomic Energy, Geneva **31** (1958) 65.
[22] Kaufman, A., "Conference on Controlled Thermonuclear Reactions, Gatlinburg, Tenn., 1956," U. S. Atomic Energy Commission Report TID-7520 (Pt.2).
[23] Rosenbluth, M. N., U. S. Atomic Energy Commission Report LA-2030 (1956) (unpublished).
[24] Chandrasekhar, S., Kaufman, A., Watson, K., *Proc. Roy. Soc.* (*London*) **A 245** (1958) 435.
[25] Rudakov, L. I., Sagdeev, R. F., Plasma Physics and the Problem of Controlled Thermonuclear Energy, Vol. III. (Moscow, 1958); also Vedenov, A. A., Sagdeev, R. F., *ibid.*
[26] Kutsenko, A. B., Stepanov, K. N., *J. Exptl. Theoret. Phys.* (*U.S.S.R.*) **38** (1960) 1840.
[27] Post, R. F., Perkins, W. E., *Phys. Rev. Letters* **6** (1961) 85.

[28] HARRIS, E., *Phys. Rev. Letters* **2** (1959) 34.

[29] ROSENBLUTH, M. N., Proceedings of Second U. N. International Conference on Peaceful Uses of Atomic Energy, Geneva **31** (1958) 90.

[30] SAGDEEV, R. F., SHAFRANOV, V. D., *J. Exptl. Theoret. Phys. (U.S.S.R.)* **39** (1960) 181.

[31] POST, R. F., International Summer Course in Plasma Physics, 1960, Risö, Denmark (Risö Report No. 18); also U.S. Atomic Energy Commission Report UCRL-6079 (unpublished).

[32] DRUMMOND, W. E., ROSENBLUTH, M. N., JOHNSON, M. L., *Bull. Am. Phys. Soc.* II **6** (1961) 185.

[33] ROSENBLUTH, M. N., WILSON, K., Dispersion Relations for Infinite Plasmas (unpublished, 1957).

[34] ROSENBLUTH, M. N., KRALL, N. A., *Bull. Am. Phys. Soc.* II **5** *(1960) 306.*

[35] DAMM, C. C., POST, R. F., *Bull. Am. Phys. Soc.* II **5** (1960) 233.

[36] POST, R. F., Proc. of Fourth International Conference on Ionization Phenomena in Gases, Uppsala, Sweden (1959) 987.

[37] POST, R. F., International Summer Course in Plasma Physics, 1960, Risö, Denmark (Risö Report No. 18); also U.S. Atomic Energy Commission Report UCRL-6078 (unpublished).

PRODUCTION AND CONTAINMENT OF HOT DEUTERIUM PLASMAS IN MULTISTAGE MAGNETIC COMPRESSION EXPERIMENTS*

F. H. COENSGEN, W. F. CUMMINS, W. E. NEXSEN, JR., A. E. SHERMAN

LAWRENCE RADIATION LABORATORY, UNIVERSITY OF CALIFORNIA

LIVERMORE, CALIFORNIA, UNITED STATES OF AMERICA

Deuterium plasmas of several keV mean ion energy have been produced using the multistage magnetic compression method for heating highly ionized plasma which is injected into an initially evacuated chamber. The heating of the plasma is found to agree within experimental accuracy with that predicted by the adiabatic theory. There is also evidence that the energy exchange between the electronic and ionic components does not exceed that expected from Coulomb collision. In the final magnetic compression stage the plasma has been found to drift to the walls of the chamber with a velocity of 2×10^5 cm/s, so that the total containment time is limited to 90 μs. The plasma drifts as a coherent column. It has been shown that the drift is associated with asymmetries in the second stage pulsed magnets. Whether or not this drift can be classed as a "flute" instability of the $m=1$ mode is not clear.

1. Introduction

It is the purpose of the multistage magnetic compression experiments to produce and confine a hot ion plasma so that the physical processes within the plasma as well as the interaction of the plasma and the confining magnetic field can be studied. In view of the large number of predicted instabilities and co-operative effects, many of which have been experimentally observed, the simple production of a hot plasma is in itself a significant accomplishment. Evidence [1] of the production and confinement of plasma in magnetic mirror fields was obtained earlier in single-stage adiabatic magnetic-compression experiments and the significance of these results has been discussed [2]. However, in these experiments the measured electron temperatures were in the range of 10 to 25 keV while the ion energies, although not measured, could not have exceeded 1 keV. The question remained whether or not the more interesting plasmas in which the ion energies exceed the electron temperature could also be stably confined. Significant differences could be expected due to the change of sign of the plasma potential, to altered ambipolar diffusion effects, and to the possibility of new types of plasma instabilities.

Recently, as briefly reported [3], the preliminary results of the present experiment indicate at least gross stability in magnetic mirror fields of hot ion plasmas. The evidence supports the conclusion that a deuterium plasma of a few keV mean ion energy and an electron temperature of the order of 100 eV has been contained for approximately 1 ms. This time interval is nearly 1000 times the growth time of hydromagnetic instabilities as predicted by simple theory.

2. Description of method and experiment

This experiment is quite similar to the multistage magnetic compression experiment described earlier [4] and, like previous adiabatic magnetic-compression experiments, is designed on the basis of the adiabatic theory of free particles [1, 5]. Most of the results can be easily obtained from the equation of motion of an ion and the two adiabatic invariants. One of these is that the magnetic moment of a charged particle is constant, i.e., $\mu = W_\perp/B = \text{const.}$, where $W_\perp$ is the ion's rotational energy about the direction of the magnetic field, and B is the magnitude of the field. The second adiabatic invariant is $\oint p_z \, dz = \text{const.}$, where $p_z = mv_z =$ the component of momentum parallel to the magnetic field. This condition applies to such cyclic motion as an ion which is reflected between two magnetic fields. Of course, these quantities are constants only in the absence of collisions. In order to approximate a collisionless plasma, any manipulation of the plasma must be accomplished in a time short compared to the relaxation time [6],

$$t_D = 1.8 \times 10^{10} \frac{A^{\frac{1}{2}} W^{\frac{3}{2}}}{Z^4 n}$$

where Z is the ionic charge and n the density in ions/cm^3. It is obvious that, as the particle density is increased, deviations from the single-particle predictions should occur. It is one of the aims of the present work to determine the maximum densities for which this theory is a useful approximation.

In these experiments, the energetic plasma is produced by injecting a cold but highly ionized plasma into an evacuated chamber which is located in and aligned with a weak magnetic field. The magnetic field is then increased to a high value in a time which is short compared to the ion-ion relaxation time, but which is long with respect to the ion cyclotron period. Under these conditions, the charged plasma particles gain energy in proportion to their initial rotational energy, $W_\perp$, and the ratio, α, of the final to initial field values. The diameter of the plasma decreases as $\alpha^{1/2}$. If the magnitude of the magnetic

* Conference paper CN-10/149, presented by F. H. Coensgen. Discussion of this paper is given on page 207. Translations of the abstract are at the end of this volume of the Conference Proceedings.

field is greater at the ends of a linear section than in the center, the final compressed plasma is located in a magnetic mirror containment region. As is well known, the containment condition for an ion in such a region is

$$\sin\theta_c > \left[\frac{B_c}{B_m}\right]^{\frac{1}{2}} = \frac{1}{\sqrt{R}}$$

where θ_c is the angle between the ion velocity vector and the magnetic field vector at the center of the containment region. B_c is the magnitude of the field at the center, and B_m is the maximum value of the field at the end of the region. Collisions scatter ions into the loss cone, which is defined by the minimum value of θ_c, leading to a continual particle loss through the ends of the system.

As discussed previously [4], a simple scaling of this single-stage experiment to high compression ratios, α, especially if high initial field values are required, is not feasible, either from economic or technical considerations. However, both of these factors can be overcome if the single-stage compression is replaced by a number of stages so that only a weak magnetic field is established over the largest volume. As the plasma is compressed, successively stronger fields are established over increasingly smaller volumes. If each radial compression is accompanied by a translation, some separation of the energetic plasma ions from the slower neutral and heavy ion impurities can be accomplished, as well as a physical separation of the compression region from the subsequent plasma position. This latter feature results in a considerable simplification in the instrumentation necessary for investigation of the plasma. In the present experiment, the fields are adjustable so that the plasma can be compressed and retained in a mirror confinement region; or, alternatively, the plasma can be compressed and transferred completely through the system into an analyzing chamber.

The multistage method is based on the fact that a plasma is approximately bound to a given tube of magnetic flux, so that a magnetic field can be used to guide plasma through a tapered vacuum chamber where the diameter decreases from the injection end to the final compression chamber. The vacuum chamber and magnet system of the present experiment are shown in the schematic drawing in Fig. 1. As is seen from the solid curve, A, in Fig. 1, the magnitude of the guide field increases by a factor of four in the region where the diameter of the chamber decreases from 18 to 9 inches. The diameter of the vacuum chamber could again be decreased in the region of higher fields at about the two-foot position. However, the 9-inch diameter of the chamber is maintained to facilitate the investigation of the plasma.

As a charged particle moves into a region of higher magnetic field it will be reflected at the point where the field is $B_z = B_1/\sin^2\theta$. B_1 is the value of the magnetic field at the injection point and θ is the angle at the injection point between the magnetic field vector and the particle velocity vector. Thus, the field change at each transition in the vacuum chamber appears as a barrier. In general, the plasma must be forced along the field lines through the barrier by means of pulsed magnetic fields. However, prior to the construction of this experiment the angular distribution of the injected plasma ions was measured as a function of ion energy. It was determined that most of the ions would penetrate a 4-to-1 magnetic barrier so that a transfer magnetic field from the 18- to 9-inch section was unnecessary.

In operation, immediately after the plasma generators are fired, plasma streams along the dc field. Those ions whose initial θ values are less than 30° follow the field lines into the 9-inch chamber. Of these ions, those whose initial θ value is greater than 10.5° are reflected from the high magnetic barrier at the 2-foot position. A fast (rise time = 6 μs) magnetic gate field at 6.5 ft is applied 10 μs after the plasma is injected. This field traps some of the ions which are reflected by the magnetic barrier in the 9-inch section of the vacuum chamber. In effect, part of the leading front of the plasma, which is known to be predominantly D^+ ions, is trapped in this section. The gate also serves to reject part of the latter plasma which contains a large fraction of heavy impurity ions.

Two other pulsed magnets, shown in Fig. 1 as transfer magnets, are used to provide the field to compress the trapped plasma. These magnets can be actuated independently in time and in magnitude. Their rise time is 50 μs. The total magnetic field pattern is shown as a function of time by the curves A through F in Fig. 1. In this operation, the firing sequence is: plasma injection at 0 time, gate field at 10 μs, first transfer magnet at 10 μs, and second transfer magnet at 16 μs. It is apparent that a trapped ion is compressed by the rising magnetic field and is located in a magnetic mirror containment region until it is forced over the magnetic barrier by longitudinal compression or until the mirror region is essentially destroyed as shown in curve F, Fig. 1. In an extension of this method, a vacuum chamber of smaller diameter would be used in the high dc field region and additional pulsed fields would be used to further compress the plasma. However, at this time, the final field pattern used for the containment experiments is shown by curve E, Fig. 1. Curve F represents the final field for measurements where it was necessary to transfer the entire plasma.

The completed experimental facility extends about 20 ft beyond that part shown by the drawing in Fig. 1. The 18-inch vacuum chamber and guide field extends about 10 ft, followed by a 3-ft expansion chamber (4.5 ft long), followed by an ion energy analyzer. By use of this rather long system, the magnetic field conditions at the analyzer are maintained independent of the field conditions in the compressed region.

The ion analyzer is essentially a tandem mass-spectrograph consisting of a magnetic analyzer followed by an electrostatic analyzer. At the analyzer position, the magnetic field has decreased to 10 gauss from several thousand gauss in the compression chamber. The plasma ions are essentially moving in straight-line paths at the analyzer, for the rotational energy

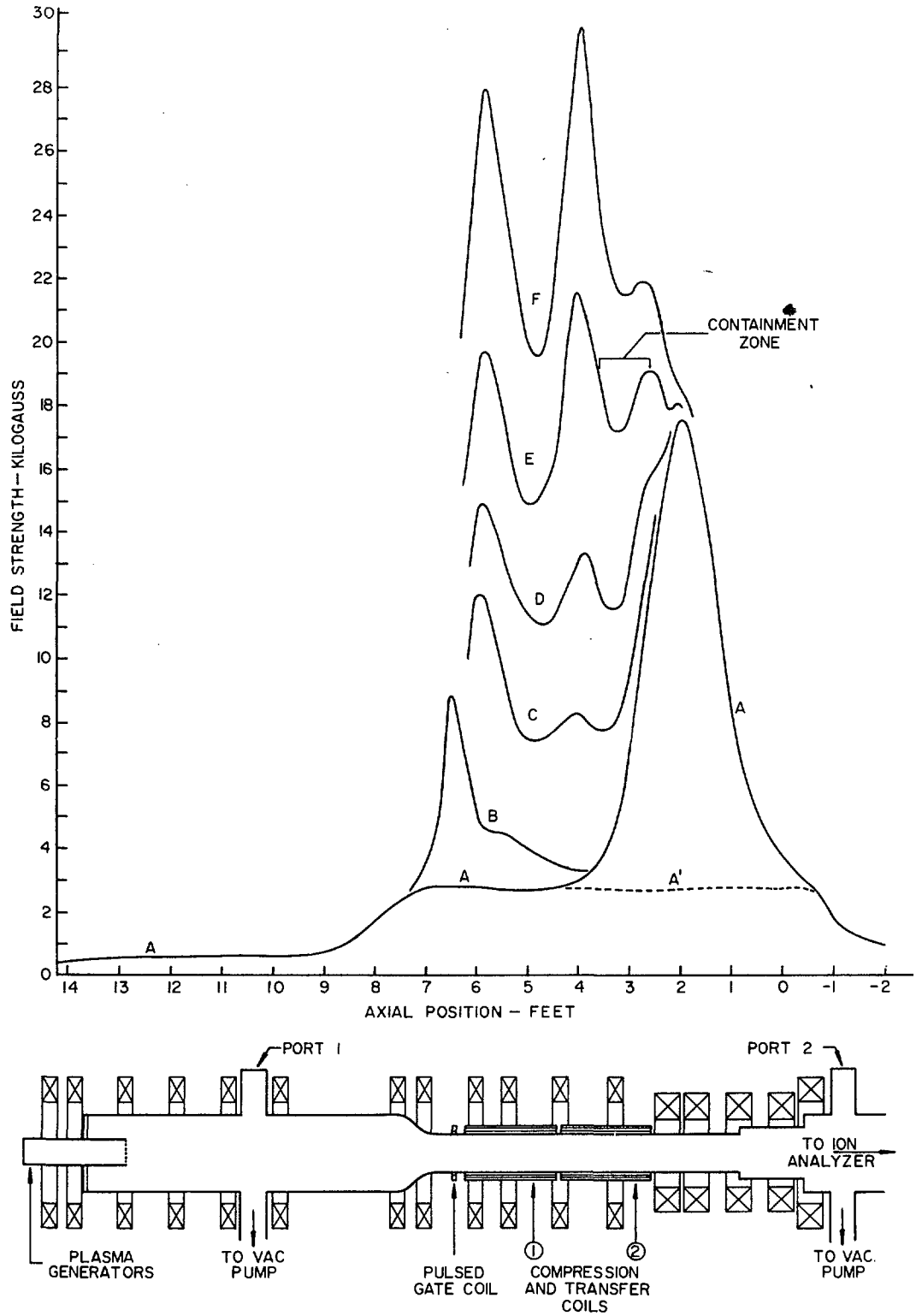

Fig. 1 Schematic diagram of experiment and graph of magnetic fields. Curve AA: dc guide field with maximum magnetic barrier; Curve AA′: dc guide field with zero magnetic barrier; Curves B, C, D, and E are total magnetic fields at 20, 30, 40, and 75 μs for the plasma containment; Curve F: final total field (75 μs) for complete plasma transfer.

of the ions about the field lines converts to longitudinal energy along the field lines as the ion proceeds to weaker fields. This instrument has been the most useful single tool for investigating the plasmas from the generators, as well as a constant monitor of the plasma ion energy in this experiment.

3. Plasma heating

An array of nine plasma generators, such as described earlier [4, 7], were used to inject plasma into the 18-inch chamber at the 12.8-foot point. It is known that each generator emits a burst of plasma which contains about 5×10^{17} ions. About half of these are D^+ ions and the remainder predominantly multiply-charged titanium ions.

The angular distribution of the injected D^+ ions was determined by varying the magnetic barrier field from zero, as shown by the curve AA′ of Fig. 1, to its maximum value of 18 000 gauss. Assuming that the plasma ions are reflected as single particles, the condition for reflection is

$$\sin^2 \theta_1 = \frac{B_1}{B_m} = \frac{W_\perp}{W}$$

where B_1 is the magnitude of the field at the injection point, B_m is the barrier field required for reflection, W is the total ion energy, and $W_\perp$ the rotational energy about the field lines. By measuring the energy distribution for a number of values of the barrier field, it was possible to determine the angular distribution as a function of ion energy and to compute the rotational energy distribution as a function of longitudinal energy or velocity. From this information, and the known time variation of the field, the energy distribution of the trapped D^+ ions was estimated and this distribution is shown as curve I, Fig. 2.

The density of the injected plasma was measured by inserting an electrostatic probe through port 1 (Fig. 1) and into the plasma stream. This probe is a small Faraday cup which is completely enclosed in a grounded shield. Plasma is admitted through a small hole in the front face of the shield, toward the injector. The ions are separated from the plasma by the potential difference between the cup and the shield. Secondary electron effects appear to be suppressed by the magnetic field as the collected charge reaches a constant value as the negative potential of the cup is increased. The density can be estimated from the observed rate of charge delivery to the cup; i.e., $dQ/dE = neAv$, where n is the density, e the electronic charge, A the area of the admitting hole, and v the longitudinal velocity of the plasma ions. The largest uncertainty is in the estimate of v.

From the measurements described above, the conditions in the initially trapped plasma (9-inch section) are estimated to be: density $= (8 \pm 4) \times 10^{12}$, average D^+ energy 1300 ± 200 eV, average rotational energy 360 ± 80 eV, and average electron temperature 7 ± 2 eV. The electron temperature was measured by means of a double probe [8].

The angular distributions as a function of energy, together with the known time variation of the fields, were used to estimate the energy distribution of the D^+ ions after they were trapped, heated, and transferred over the 18 000-gauss dc barrier. This estimated distribution is shown as curve II, Fig. 3. The measured energy distribution of the D^+ ions in the plasma which was transferred over the dc barrier is shown as curve III, Fig. 2. There remains at the end of the compression and transfer cycle a small mirror containment region with about a 2% mirror ratio, see curve F, Fig. 1. It was found in this experiment that such regions effectively trap a significant amount of the

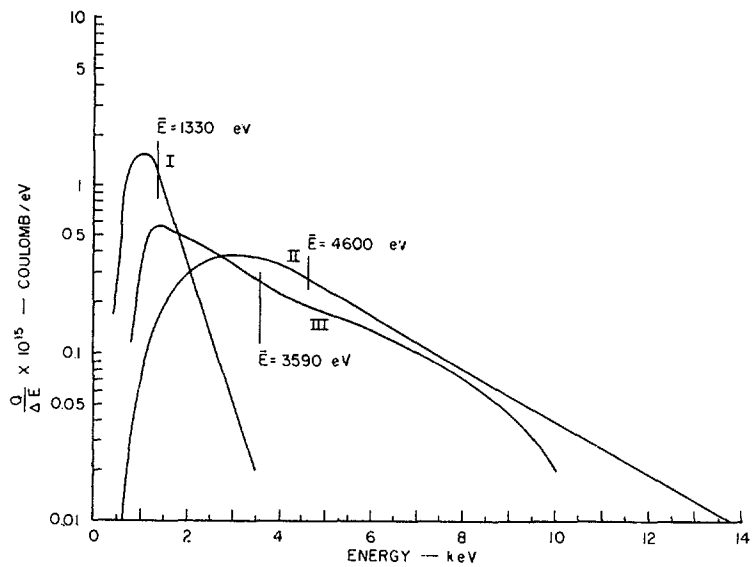

Fig. 2 Comparison of predicted and observed D^+ energy distributions. Curve I: Initial energy distribution of the plasma ions trapped in the 9-inch chamber; Curve II: energy distribution of ions in the compressed and transferred plasma as predicted on the basis of the adiabatic theory from the measured angular distribution of the ions in the injected plasma; Curve III: measured energy distribution of the ions in the compressed and transferred plasma.

heated plasma. It is quite possible that part of the discrepancy at high energies between curves II and III (Fig. 2) is due to this trapping.

The average energy of the injected plasma which penetrated the 4-to-1 barrier at the first transition was found to be 1330 eV. Also, the estimated initial average energy of the trapped plasma was 1330 eV. The predicted average energy after compression and transfer was 4600 eV compared to 3590 obtained from the measured distribution. If it is assumed that the high energy end has been trapped and that the experimental curve follows that predicted at high energies, an average energy of 3940 eV is obtained. The observed average value (3590) is 22% less than that predicted. This agreement is quite close considering that the accuracy of the points on both the predicted and observed distributions is estimated to be $\pm 10\%$.

The excess number of low-energy ions (compare curves II and III, Fig. 2) could, in part, be due to energy loss from the ions to the electrons during the heating cycle. Some energy exchange is expected. If for some reason the electrons were to remain cold, this exchange could seriously inhibit the ion heating. The fact that the ions gained energy nearly as predicted indicates that the plasma electrons also remained trapped and gained enough energy so the exchange rate was relatively slow.

Electron temperatures were determined after compression by observing the microwave noise [9], and were found to be in the range of 100 eV.

4. Containment observations

The total amount of plasma which passed through a transverse plane at the position of port 2 (Fig. 1) was measured by means of electrostatic probes such as described above. Time-integrated values of the positive charge delivered to the probe at various points in the plane were measured, and this function was integrated over the area to obtain the total charge. It was found that 30% of the plasma which was transmitted through the plane without the magnetic barrier (curve AA′, Fig. 1), but with all the pulsed magnets activated, was retained for the final field conditions shown by curve E, Fig. 1. This indicates that an appreciable amount of plasma is retained in the mirror containment region at 3 ft. The integrated energy distributions for the trapping condition and the transfer condition (curves E and F, Fig. 1) also indicate that 30% of the density was retained in the containment region. About 3.75×10^{-3} coulombs of positive charge was retained. If this is all D^+, it corresponds to 2.35×10^{16} ions. Making the assumption, which was verified in earlier experiments [1], that the plasma compresses as predicted by the adiabatic theory, i.e., that its diameter at any position, z, is

$$D_z = D_1 \left[\frac{B_1}{B_z}\right]^{\frac{1}{2}}$$

and the containment region is about 12 inches long (as indicated in curve E), the plasma is found to have

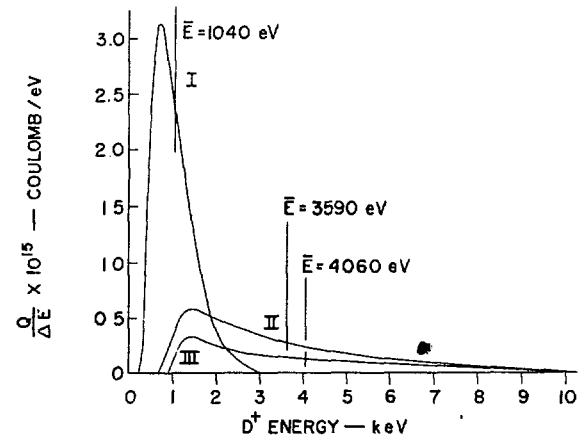

Fig. 3 Estimate of energy distribution of ions in compressed and contained plasma. Curve I: Energy distribution of ions in the plasma from a single injector; Curve II: Energy distribution of ions in compressed and transferred plasma (same as curve III, Fig. 2); Curve III: Estimated energy distribution of ions in the compressed and contained plasma.

a volume of about 2.00 liters. Thus, it appears that the average density of the trapped plasma is of the order of 10^{13} ions/cm^3.

An estimate of the energy distribution of the trapped plasma was obtained by subtracting the energy distribution of the transferred portion of the plasma under containment conditions from that of the totally transferred plasma. This distribution is shown as curve III, Fig. 3. The energy distributions of the D^+ ions from an injector and that of the totally transferred plasma (curves I and II, Fig. 3) are shown for comparison.

Thus, at the end of the compression cycle (70 μs after plasma injection) the conditions in the trapped plasma are estimated to be: total volume $= 2 \pm 0.4$ liters, average density $= (1 \pm 0.3) \times 10^{13}$ ions/cm^3, electron temperature $= 100 \pm 50$ eV, average ion energy $= 3.6 \pm 0.5$ keV, and the ratio of the energy density in the plasma to that in the magnetic field $= \beta = (0.5 \pm 0.25)\%$. The mirror ratio was 1.11 ± 0.03.

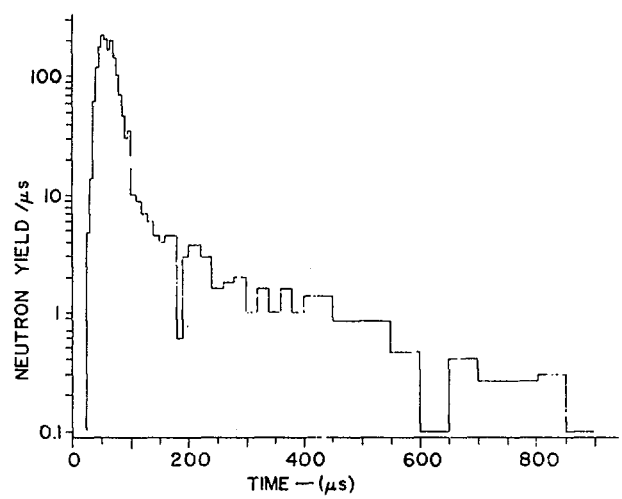

Fig. 4 Histogram of neutron production.

An appreciable DD reaction rate is expected for these conditions, and, indeed, about 10^4 neutrons were detected per operation. The initial identification of the neutrons was made through the characteristic light pulses produced in a LiI-crystal scintillator from the reaction Li^6 (n, H^3) He^4. A 2-inch by 2-inch NaI-crystal scintillator was used to search for large x-ray bursts and energetic x-rays which could have confused the neutron identification. However, as is consistent with the low compression ratio ($\alpha=30$), no x-rays were observed. Nuclear emulsions placed inside of the vacuum chamber were used to detect the protons from the reaction D (D, p) H^3. The detection of these protons provides the strongest corroborative evidence for neutron production through the reaction D (D, n) He^3.

The neutron production rate as a function of time was obtained through the use of lead-shielded plastic scintillators which detect neutrons through the detection of knock-on protons. Identification of the events as due to neutrons was made by measurement of their absorption length in lead. As seen from the histogram shown in Fig. 4, prompt neutrons were observed as late as 900 μs. The initial rapid decrease in the reaction rate after the peak at 60 μs is probably associated with the transfer of plasma past the dc barrier. At later times, the decrease in rate is consistent with the decay of the pulsed magnetic field ($L/R=700$ μs) which lowers both the plasma density and the average ion energy.

5. Conclusions

Containment and hence gross stability of the plasma during the compression and heating cycle is certainly demonstrated by the measured transferred plasma.

The close agreement of the measured energy distribution of the ions in the transferred plasmas and those predicted from adiabatic theory is also indicative of stable plasma confinement during the compression cycle, as well as an indication that the energy transport from the ions to electrons during this period does not greatly exceed the rates as calculated from Coulomb collision theory.

There appears to be little doubt that a deuterium plasma was trapped, contained, and compressed to a density of 10^{13} ions/cm^3, and that the mean ion energy of this plasma near the end of the compression at about 60 μs was of the order of 3600 eV. The observed rate of neutron production during this period is compatible with the observed plasma conditions.

After 60 μs, a large fraction of the plasma is transferred out of the containment zone. From the estimated ion energy distribution (curve III, Fig. 3), the mean ion energy of the remaining plasma is also of the order of 3600 eV. The neutron production rate after 60 μs is compatible with the estimated plasma conditions. However, as the ion density and energy distributions have not been measured at times later than 60 μs, the implications of alternative explanations of the observed neutron production rate should be examined. First, the question arises whether or not the production is due to a few high-energy ions bombarding a target of cold gas. This appears to be improbable; for, if the observed reaction rate is assumed to be due to a group of exceedingly energetic deuterons (e.g., 10^5 eV) bombarding a cold gas, the density of the cold gas required is such that the ions would be lost in less than one microsecond through charge exchange. Secondly, it is possible to explain the observed rates by postulating the containment of only energetic ions (i.e., between 30 and 100 keV). Such an assumption leads to densities greater than 10^{10} ions/cm^3, which is a significant plasma. A third possible explanation is the containment of a group of high-energy D^+ ions and a low-energy (a few hundred eV) plasma. For a rate of one neutron per μs and a group of 100-keV ions, the product of the densities of the two groups must be $n_1n_2=10^{20}$. Thus, for an energetic ion density of 10^7, the cold plasma density must be 10^{13} ions/cm^3. The conclusion is that any reasonable explanation of the late neutron production requires the assumption of plasma containment for the observed neutron production period of 1 ms.

There are at present two main goals in the continuation of this work. First is a more detailed investigation of the contained plasma; in particular, the investigation of energy and particle losses from the plasma. Second, the extension of the method to the production of more energetic plasmas in which the origin of the neutron flux will be unequivocally thermonuclear, and the reaction rate will serve as a reliable measure of plasma density.

6. More recent experiments

Through the addition of another stage of magnetic compression to the system described above, the compression ratio was increased by a factor of two and the decay time of the final magnetic compression field was extended from 700 μs to 8.6 ms. The dc guide field used in the modified system is shown as curve H in Fig. 5 (compare with curve AA′ in Fig. 1). The total magnetic field intensity is shown at 40, 150, and 300 μs, by curves I, J, and K. It is seen that the last compression in this system is relatively slow requiring 250 μs to increase the field from 18 kG to 40 kG; whereas the initial compression is completed in 50 μs.

Although the magnitude of the dc guide field in the final compression region would allow the use of a smaller vacuum chamber, the diameter of the vessel was maintained at 9 inches. Thus, if the plasma follows the field lines, there is a plasma-free region between the plasma and the walls where equipment may be introduced without interfering with the plasma.

As discussed above, the plasma behavior in the first 70 μs of the cycle closely follows the predictions of the adiabatic theory. On the basis of this theory the reaction rate in the modified system should have been increased by a factor of 10 to 100 over that previously observed and the period of neutron production should have been increased by a factor of 10.

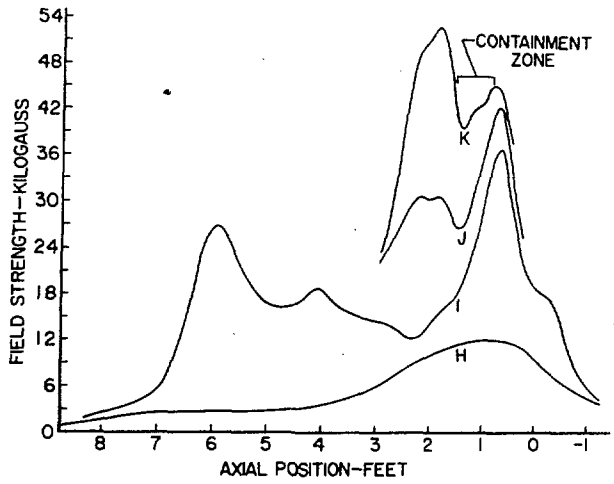

Fig. 5 Total magnetic field of 3-stage system at 0, 40, 150, and 300 μs.

Neither of these predicted effects was observed, Rather the shape of the neutron histogram, Fig. 4. was surprisingly insensitive to timing and field levels, although the total neutron production was quite dependent upon these parameters. A typical histogram obtained for the field conditions shown in Fig. 5 is shown by the dotted curve in Fig. 6. The rate has been normalized to unity at the time of its maximum value. For comparison, the data from Fig. 4, similarly normalized, is shown by the solid curve in Fig. 6. The similarity of the decay of the reaction rate in the two cases is true for all other conditions which have been investigated. Changes in the operating parameters produced some variation in the rate at times prior to its peak value and in the time of its maximum value as well as in the total neutron production.

Investigations of the light emission and plasma flow were also made. The light was observed transverse to the axis of the system, at the 1.5-ft position, by means of a photomultiplier. Electrostatic probes were used to measure the flux to the vacuum chamber walls.

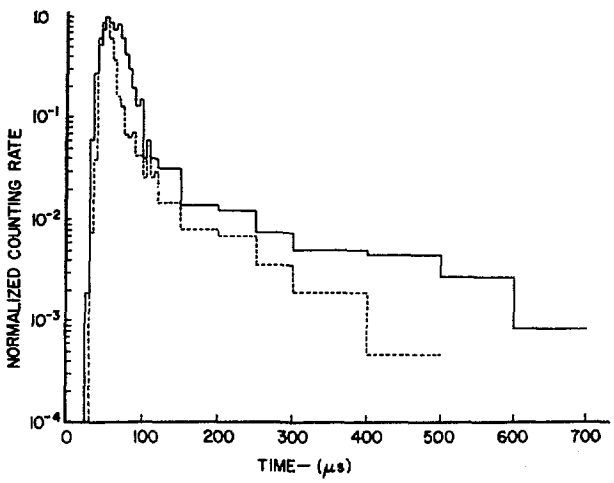

Fig. 6 Neutron histograms for 2-stage and 3-stage (dotted curve) systems.

Signals were detected as early as 50 μs by probes which were 3.8 cm from the wall. When the probe was positioned near the port through which light was observed, the two signals were quite similar and there was complete time correlation between them.

Multiple arrays of probes were placed along field lines and azimuthally around the vacuum chamber wall. These arrays could be moved along the chamber and rotated around its axis. It was found (1) that signals were received simultaneously along field lines, (2) that the azimuthal extent of the plasma was 2 to 3 inches at the position of the probes which were 3 inches from the center of the chamber, and (3) that the plasma bombardment of the wall was not uniform but rather it was greatest at certain azimuthal positions.

From the time lapse between the arrival of the plasma in the final chamber and the time at which the plasma was detected by the probes, the radial velocity of the plasma across the field was found to be 2×10^5 cm/sec. This value of drift velocity is consistent with the observation that the light signals were detected about 20 μs earlier when the probe was in the system near the observation port than when the probe was absent. This indicates that the plasma drifted 3.8 cm in 20 μs which, in turn, indicates that the velocity of the plasma is not a function of radial position. Additional evidence of this drift velocity is given by the fact that the 20 μs difference in the peak neutron production rate evident between the two curves in Fig. 6 was due to the presence of the probe in the system when the data for the dotted curve was obtained. Without the probe in the system the plasma reaches the wall between 70 and 80 μs as judged from the light signals. From the magnitude of the wall probe signals and the above value of drift velocity the maximum density of the plasma striking the wall was 10^{14} ions/cm^3. The quantity of plasma which reaches the wall along one set of magnetic lines in a coherent manner is consistent with a drift of the entire plasma to the wall at one azimuthal position. The 30 to 40 μs observed duration of the probe signals is also consistent with this hypothesis, for it is just the time necessary for a plasma column of the predicted diameter (6 to 8 cm) moving with velocity of 2×10^5 cm/s to pass the probe position.

The positions of maximum wall bombardment appeared to be associated with the operation of the two transfer magnets, see Fig. 1. To investigate this hypothesis the array of nine injectors was replaced by a single injector on axis and the flat dc field shown as curve AA′, Fig. 1, was used. With only a small magnetic barrier provided by a pulsed magnet at the—1-ft position, the wall bombardment was studied as a function of transfer magnet operation. If only the transfer magnet nearest the injection end was pulsed the intensity of the wall bombardment as a function of angular position was as shown by curve II, Fig. 7. If only the second transfer magnet was pulsed the wall bombardment was as shown by curve I, Fig. 7. These curves are obtained from a number of operations and thus show the average position of

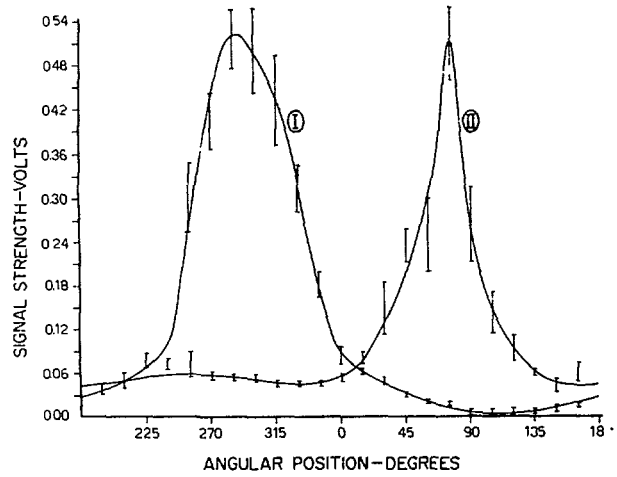

Fig. 7 Position of wall bombardment. Curve I, second transfer magnet and uniform dc field. Curve II, first transfer magnet and uniform dc field.

wall bombardment. The difference in the effect of the two magnets when operated individually is apparent from these curves. In each instance, the plasma has moved to the wall toward the position of the magnet leads and connecting links between magnet turns. The magnet leads were diametrically opposite for the two transfer magnets.

As the plasma is known to bombard the walls, the question arises whether or not the observed reactions are in the plasma or due to bombardment of the wall. Only 10^{10} fast (50 to 100 keV) D^+ ions/cm^3 in the plasma would produce, through wall bombardment, the total observed number of neutrons. The following observations are evidence that the reactions occur within the plasma. First, most of the neutrons as detected by the prompt counter are observed before the plasma is detected at the wall. This fact is illustrated in Fig. 8 where the histogram shown as the dotted curve in Fig. 6 is replotted on a linear scale, together with a composite of signals received by a probe at the position of maximum wall bombardment.

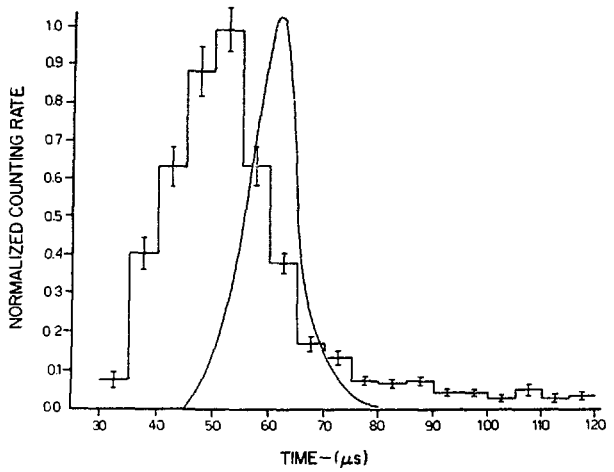

Fig. 8 Time dependence of neutron production and wall bombardment (smooth curve).

The probe signals were taken simultaneously with the neutron data. It is seen that the counting rate reached a maximum about the time that plasma was first detected by the probe. As the plasma continued to encounter the probe, the reaction rate declined sharply. Secondly, as the neutron production in the final compression region is of the order of 10^4 without the final compression fields, it is easy to determine whether or not a significant fraction of the neutrons is produced at the wall. Most of the plasma is transferred into the final chamber between 40 and 50 μs when the magnetic field distribution is similar to curve I, Fig. 5. The actual position of the minimum field value is somewhat to the right of that shown in curve I, and its value is about 18 kG. If a pyrex plate is put at this position every plasma ion will encounter the plate on its first transit into the final compression region. As the ions cannot gain energy in this region without the final compression they bombard such a target with the same energy as they have when the plasma drifts to the wall. If the reactions are due to wall bombardment, the neutron production should be the same whether or not the target is in the system. When a pyrex glass plate about 7 inches in diameter was introduced as described, no neutrons were observed. If the plate was moved slightly to the right so as to be in a slightly stronger magnetic field some of the ions could not reach it and some neutrons were again detected. As the plate was moved into stronger fields the number increased to its normal value. We conclude that at least 90% of the reactions take place in the contained plasma before it encounters the wall.

Even before it was known that the plasma drifted to the wall, the persistent similarity of the tail of the various neutron histograms cast doubt on the validity of identification of the counts observed at the late times with late DD reactions. Therefore, simultaneously with the probe investigations just described a complete duplicate of the final compression section was fabricated and installed in the Cockcroft-Walton target area. The 500 keV D^+ beam from this accelerator was allowed to bombard deuterated targets placed in the final containment region of this duplicate system. These targets were bombarded for 50 μs and the counting rate was measured using the same counters in the same relative positions as used to obtain the neutron histograms. The counting rate was greatest during the 50 μs bombardment, then it dropped almost discontinuously to a lower value from which it decayed with the same slope as the decay of the counting rate, after 100 μs, in the plasma experiments. This evidence indicates that the effect of the "slowing down" of neutrons in the scintillator itself is small and that the half life of such neutrons is no longer than 15 μs. We conclude that the reaction rate is essentially correctly depicted by the histograms during the first 80 μs to 100 μs. However, at times later than 100 μs the counting rate is due primarily to γ-rays from the capture of neutrons which have been slowed down and have been rattling around in the large mass of plastic and copper of the pulsed and demagnet systems. As mentioned in the earlier sections

of this report, the late counts were previously identified as neutrons by measuring their absorption length in lead. Because the counting rate is low, the detector could not be moved very far from the system so it was known that the counting geometry was "poor" and that the observed absorption length would be greater than the 2 cm value one would expect if "good counting geometry" could have been used. The absorption length obtained was 10 cm which was assumed to be sufficiently greater than 2 cm to indicate that the late counts were neutrons. For the extended γ-ray source represented by the magnet system and close position of the recoil counters this assumption is now believed incorrect.

It should be pointed out that for most of this work the glass vacuum chamber was not given a conducting coating. However, such a coating was provided recently by evaporating a metallic layer onto the 9-inch glass vessel and painting the remainder of the system with "aquadag" (a carbon suspension in water). The resistance from one end of the system to the other was 500 ohms. This conducting coating had no effect whatsoever on the observed phenomena.

As can be seen from the scale in Fig. 1, the system is quite long and it is doubtful that enough cold plasma exists outside of the containment region to provide conduction to the ends. The center three plasma injectors were fired at later times to provide such a plasma but there was no observable effect.

7. Summary

It now appears that the history of the plasma in this experiment is as follows: 1) at $t=0$ to $t=5$ μs the plasma is born at the injector; 2) from $t=0$ to $t=14$ μs plasma streams along the dc field, some of it flowing into the 9-inch chamber; 3) from $t=14$ μs to $t=50$ μs, the plasma in the region from 6.5 to 3 ft. is compressed and heated by the transfer magnets; 4) from 40 μs to 60 μs the plasma enters the final compression region between the 2.5 and 1-ft positions; and 5) from $t=40$ μs to $t=100$ μs the plasma drifts to the vacuum chamber wall.

Nothing in the recent experiments is in disagreement with the previous conclusions that ion heating during the compression proceeds adiabatically and that the energy transport to the electrons from the ions is not in excess of that expected on the basis of Coulomb collisions. It is concluded that the average ion energy in these experiments has been increased from approximately 1 keV to approximately 3.5 keV, that the ion density in the plasma column is in the range of 2×10^{13} ions/cm^3, and that the β-value of the plasma is of the order of one percent. The neutron production which has been shown to be due to DD reactions within the plasma is consistent with these values. It has been shown that the density of the high energy D^+ ions in the plasma is less than 10^9 per cm^3.

The life of the plasma and the neutron production are destroyed by a drift which carries the plasma to the walls. The evidence leads to the conclusion that this drift is initiated by asymmetries in the time-rising transfer fields. Whether or not the phenomena can be classed as a hydromagnetic "flute" instability is not clear. First the velocity is quite slow and unlike the situation observed by IOFFE, *et al.* [10, 11] the plasma does not approach metallic walls. Indeed, the evidence indicates that the velocity is independent of radial position. It should be pointed out that after the transfer fields start to rise the plasma is never free of the influence of this driving force. That is, the plasma strikes the wall about the same time that these fields reach their maximum value and before the final compression fields are effective. Thus, it has not been possible to study the drift under dc field conditions or under the influence of time-rising fields of greater symmetry.

It is of considerable interest to know if these drifts can be eliminated by improving the symmetry of the time-rising fields and whether or not very small drifts "damp out" rather than grow in time. At this time magnets are under construction to investigate these questions. If the plasma drifts persist, stabilizing mechanisms such as "magnetic shear" will be introduced.

Acknowledgments

We wish to thank Dr. C.M. Van Atta and Dr. R.F. Post for their continued support and encouragement. D.R. Branum of the laboratory's electrical engineering staff has had the complete responsibility for the design, construction, and operation of all the electrical systems. H.C. Saulter has been responsible for the construction and maintenance of the vacuum and magnet systems.

This work was performed under the auspices of the United States Atomic Energy Commission.

References

[1] COENSGEN, F. H., FORD, F. C., ELLIS, R. E., Proc. Second U.N. International Conference on Peaceful Uses of Atomic Energy, Geneva, **32** (1958) 266.

[2] POST, R. F., ELLIS, R. E., FORD, F. C., ROSENBLUTH, M. N., *Phys. Rev. Letters* **4** (1960) 166.

[3] COENSGEN, F. H., CUMMINS, W. F., NEXSEN, W. E., JR., SHERMAN, A. E., *Phys. Rev. Letters* **5** (1961) 520.

[4] COENSGEN, F. H., CUMMINS, W. F., SHERMAN, A. E., *Phys. Fluids* **2** (1959) 350.

[5] POST, R. F., Proc. Second U. N. International Conference on Peaceful Uses of Atomic Energy, Geneva, **32** (1958) 245.

[6] SPITZER, L., Physics of Fully Ionized Gases (Interscience Publishers, New York, 1956).

[7] CUMMINS, W. F., COENSGEN, F. H., SHERMAN, A. E., NEXSEN, W. E., JR., *Bull. Am. Phys. Soc.* **5** (1960) 318.

[8] JOHNSON, E. O., MALTER, L., *Phys. Rev.* **80** (1950) 58.

[9] WHARTON, C. B., HOWARD, J. C., HEINZ, O., Proc. Second U.N. International Conference on Peaceful Uses of Atomic Energy, Geneva **32** (1958) 388.

[10] IOFFE, M. S., SOBELEV, R. I., TELKOVSKII, V. G., YUSHMANOV, E. E., *JETP* **40** (1961) 40.

[11] KADOMTSEV, B. B., *JETP* **40** (1961) 328.

STABILITY OF AN INHOMOGENEOUS PLASMA IN A MAGNETIC FIELD*

B. LEHNERT

ROYAL INSTITUTE OF TECHNOLOGY

STOCKHOLM, SWEDEN

The stability of a plasma confined by a magnetic field has earlier been discussed by Rosenbluth and Longmire in terms of particle orbits. Their theory applies to a plasma separated from vacuum by a sharp boundary which is rippled by a sinusoidal perturbation. In the present paper the earlier theory is reconsidered and extended to include the effects of a continuous density distribution. The gradient drift in an inhomogeneous magnetic field is deduced from the macroscopic theory. Account is also taken of drift motions along the boundary which give rise to displacements comparable to and exceeding the wavelength of the perturbation. For small wavelengths the plasma is found to be stable against small "flute" deformations, not only for a magnetic field which is convex towards the plasma but also for a field which is concave towards the plasma. This occurs when the field gradient is strong enough and the density distribution is not too steep. For larger wavelengths steadily growing oscillations occur, but the growth rate is reduced considerably below that given by the earlier theory. Similar conclusions apply to the problem of gravitation instability. The result provides a possible explanation of the observed stability of the Van Allen radiation belts and of the absence of rapidly growing disturbances in experiments with magnetic mirrors and rotating plasma devices.

1. Introduction

The stability of a plasma boundary has earlier been investigated by ROSENBLUTH and LONGMIRE [1] in a theory based on particle orbits. They have assumed the plasma to be separated from a vacuum region by a sharp boundary which initially is rippled by a sinusoidal perturbation and where a magnetic field exists in the direction parallel with the boundary. Drift motions which make ions and electrons move in opposite directions will then produce a charge separation. This generates an electric field by which ions and electrons drift in a direction perpendicular to the boundary and produce a perturbation with increasing amplitude. The phenomenon is suggested to be important to the formation of an interchange (or flute-type) instability [1]. The mechanism of the instability does not depend upon the plasma density.

Recent experiments with mirror machines [2] and with rotating plasma devices [3, 4] as well as observations of the Van Allen radiation belts [5] have not confirmed the existence of the predicted instability. One possibility to remove this apparent contradiction is to assume that a short-circuit of the separated charges takes place at the ends of the configuration [1, 2]. Since non-conducting end plates have been used in some of the experiments with magnetic mirrors and with a rotating plasma, the charge removal should be provided by an extremely thin metallic coating on the walls of the discharge chamber [2]. For the Van Allen belts the short-circuit should be produced by the upper parts of the ionosphere. Even if these explanations do not seem to be quite unlikely they are complicated by a mirror effect which prevents part of the space charges to be removed along the field lines. Further, the short-circuit in the ionosphere has to take place across a magnetic field.

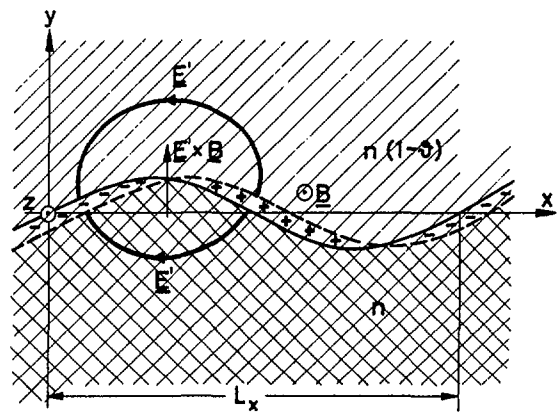

Fig. 1 Perturbed density distributions of ions and electrons drifting with different velocities in the x-direction. Density jump from n to $n(1-\theta)$ at perturbed boundary gives rise to an electric field $\mathbf{E}'$ and a drift motion $\mathbf{E}' \times \mathbf{B}/B^2$.

In a recent investigation [6] another possibility has been suggested according to which the contradiction can be removed by extending the earlier theory in two ways. Firstly, the boundary is assumed to separate two regions of plasma with slightly different densities, n and $n(1-\vartheta)$, where $\vartheta \ll 1$ as indicated in Fig. 1. This is a situation which corresponds more closely to that of a real plasma where the density does not drop abruptly to zero in a narrow boundary region. Secondly,

* Conference paper CN-10/3, presented by B. LEHNERT. Discussion of this paper is given on page 207. Translations of the abstract are at the end of this volume of the Conference Proceedings.

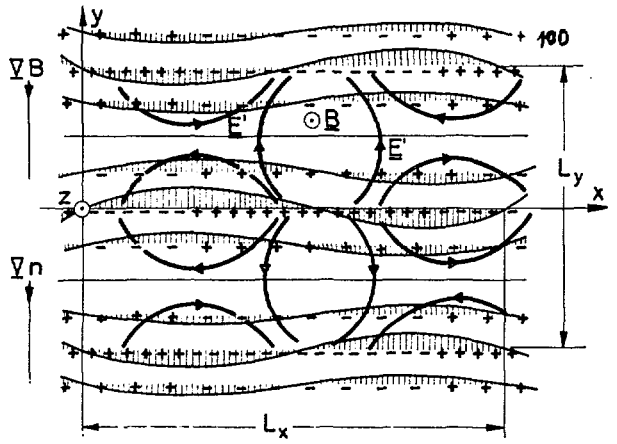

Fig. 2 Continuous density distribution. Continuous perturbation of density at initial stage symbolized by sinusoidal shaded areas for the case $s_i = s_e = 0$, $c_i = c_e$.

the amplitude growth has been studied in the modified theory [6] also for time intervals t during which the displacement $u_{ie}t$ by the relative drift velocity u_{ie} along the boundary is comparable to and even exceeds the wavelength L_x of the perturbation. As a consequence, the growth rate of the perturbation will be reduced considerably and the system may even become stable under certain circumstances.

In the present paper the discussion will be extended to include a plasma with a continuous density distribution and with density perturbations which are continuously distributed in the plasma as is outlined in Fig. 2. In this figure a mode of the perturbation is shown which is characterized by the two wavelengths L_x and L_y in the plane perpendicular to the magnetic field $\mathbf{B}$. Surfaces of constant density become perturbed as shown in the figure and determined by Eq. (1). It will be shown that the situations corresponding to Figs. 1 and 2 lead to results which are closely related to each other.

2. Assumptions and approximations

In the present paper we are interested in the situation given by Fig. 2, where the magnetic field is in the z-direction with a transverse gradient in the y-direction and a radius of curvature R pointing in the (positive or negative) y-direction. A constant acceleration g due to gravity in the same direction may also be taken into account. The unperturbed density distribution is assumed to be a function $n_0 = N(y)$ for both ions and electrons and the perturbed charge distributions of ions and electrons are given by

$$en_i = eN(y - a_i) \qquad en_e = eN(y - a_e), \tag{1}$$

where a_i and a_e are small perturbations. The initial condition is $a_i(x, y, 0) = a_e(x, y, 0)$. As will be seen later an electric polarization also has to be taken into account when the electric field is deduced from the perturbed charge distributions.

The radius of curvature R and the characteristic lengths $L_{cB} = B/|\nabla B|$ and $L_{cn} = n_0/|\nabla n_0|$ of the magnetic field and of the density distribution are assumed to be much larger than the wavelengths L_x and L_y of the perturbation. Therefore, it is stated that ∇B and ∇n_0 are approximately constant and that all quantities are independent of z. The radii of gyration ϱ_i and ϱ_e of ions and electrons are assumed to be much smaller than L_x and L_y.

The electric space charge which arises from a separation of the perturbed ion and electron distributions will then generate an electric field $\mathbf{E}'$ which is situated in the xy-plane. We restrict the discussion to situations where ions and electrons have temperatures T_i and T_e corresponding to isotropic pressures which are low enough for the induced magnetic field to be neglected.

Finally, the configuration is supposed to obey periodic boundary conditions in the x-direction, i.e., the situation at $x = +X_0$ is the same as at $x = -X_0$, where $2X_0$ is an integral number of wavelengths L_x. In the y-direction the configuration is assumed to be bounded by two electrically conducting walls at $y = \pm Y_0$, where $2Y_0$ is an integral number of L_y.

3. Basic considerations

3.1. Particle drift motions

According to the perturbation theory by Alfvén [7] a particle of charge q_ν and mass m_ν will gyrate around the magnetic field lines with a velocity $\mathbf{W}_\nu$ and drift along and across the field with the velocities $\mathbf{u}_{\parallel\nu}$ and $\mathbf{u}_{\perp\nu}$ at the same time. When the induced magnetic field is neglected the perpendicular drift velocity of the centre of gyration in an electric field $\mathbf{E}$ and a gravitation field $\mathbf{g}$ becomes approximately

$$\mathbf{u}_{\perp\nu} = \mathbf{u}_E + \mathbf{u}_{B\nu} + \mathbf{u}_{g\nu} = m_\nu \left[\left(\frac{\partial}{\partial t} + \mathbf{u}_\nu \cdot \nabla\right)\mathbf{u}_{\perp\nu}\right] \times \mathbf{B}/q_\nu B^2 \qquad (\nu = \mathrm{i},\ \mathrm{e}). \tag{2}$$

In Eq. (2) $\mathbf{u}_\nu = \mathbf{u}_{\parallel\nu} + \mathbf{u}_{\perp\nu}$, $M_\nu = m_\nu W_\nu^2/2B$ is the equivalent magnetic moment of the particle and

$$\mathbf{u}_E = \mathbf{E} \times \mathbf{B}/B^2, \tag{3}$$

$$\mathbf{u}_{B\nu} = -M_\nu (1 + 2\, u_{\parallel\nu}^2/W_\nu^2)\, \nabla B \times \mathbf{B}/q_\nu B^2, \tag{4}$$

$$\mathbf{u}_{g\nu} = m_\nu \mathbf{g} \times \mathbf{B}/q_\nu B^2 \tag{5}$$

are the electric, gradient and gravitation drifts, respectively. The centrifugal force due to the curvature $\mathbf{R}$ of the magnetic field gives rise to the second term within the bracket of Eq. (4).

A further analysis in terms of particle orbits will not be undertaken here. Eqs. (3)—(5) only serve as illustrations to the macroscopic theory presented in the following Sections.

3.2. Drift of density distributions

Consider the equation expressing conservation of momentum of a gas of mass velocity $\mathbf{v}_\nu$ with n_ν particles per unit volume;

$$m_\nu n_\nu \frac{\mathrm{d}_\nu \mathbf{v}_\nu}{\mathrm{d}t} = q_\nu n_\nu \mathbf{E} + q_\nu n_\nu \mathbf{v}_\nu \times \mathbf{B} + m_\nu n_\nu \mathbf{g} - \nabla(n_\nu \mathrm{k} T_\nu), \qquad (\nu = \mathrm{i},\ \mathrm{e}) \tag{6}$$

where $d_\nu/dt = \partial/\partial t + \mathbf{v}_\nu \cdot \nabla$. Eq. (6) can also be written as

$$n_\nu \mathbf{v}_\nu = n_\nu \mathbf{u}_E + n_\nu \mathbf{u}_{g\nu} - \nabla(n_\nu k T_\nu) \times \mathbf{B}/q_\nu B^2 - m_\nu n_\nu \frac{d_\nu \mathbf{v}_\nu}{dt} \times \mathbf{B}/q_\nu B^2 . \quad (7)$$

Conservation of mass requires that

$$-\frac{\partial n_\nu}{\partial t} = \operatorname{div}(n_\nu \mathbf{v}_\nu) = (\mathbf{u}_E + \mathbf{u}_{g\nu}) \cdot \nabla n_\nu - \frac{2}{q_\nu B^3} (\nabla B \times \mathbf{B}) \cdot \nabla(n_\nu k T_\nu) + n_\nu \operatorname{div}(\mathbf{u}_E + \mathbf{u}_{g\nu}) - \operatorname{div}\left(m_\nu n_\nu \frac{d_\nu \mathbf{v}_\nu}{dt} \times \mathbf{B}/q_\nu B^2\right) + (1/q_\nu B^2) \nabla(n_\nu k T_\nu) \cdot \operatorname{curl} \mathbf{b} , \quad (8)$$

where $\mathbf{b}$ is the induced magnetic field due to currents in the plasma.

Now, consider the situation specified in Section 2 where the electric field consists of a contribution $\mathbf{E}'$ and a constant part $\mathbf{E}_0$ present also in the stationary state. Both $\mathbf{E}_0$ and $\mathbf{g}$ have components only in the y-direction and are constant (see Section 3.3). In first order the acceleration term of Eq. (8) can be dropped provided that the gyro period of the charged particle is much shorter than the characteristic time changes. Further, assume the contributions from curl σ to be negligible. This is justified, both in the perturbed and unperturbed states, when $\mathbf{B}$ is strong enough for the Alfvén velocity to exceed the thermal velocity considerably. When T_ν is constant and L_{cB} exceeds the wavelengths L_x and L_y considerably it is easily shown by a number of vector operations that Eq. (8) reduces to

$$\frac{\partial n_\nu}{\partial t} + (\mathbf{u}_E + \mathbf{u}_{g\nu} + \mathbf{u}_{B\nu}) \cdot \nabla n_\nu = n_\nu \mathbf{E}' \cdot [\nabla(1/B^2) \times \mathbf{B}] . \quad (9)$$

Here the bracket of Eq. (4) has the value 2 and M_ν is replaced by kT_ν/B as expected when the pressures are assumed to be isotropic.

There are two cases which shall be distinguished here:

(*i*) When the total density varies considerably in space over dimensions which are small compared to L_{cB} the right hand member of Eq. (9) can be dropped. This implies that the whole density distribution moves, without being distorted, with a velocity equal to the total drift velocity $\mathbf{u}_{\perp\nu}$ given by the orbit theory in first approximation. Observe that the gradient drift $\mathbf{u}_{B\nu}$ displaces the distribution without giving rise to any mass motion, whereas the density gradient produces a mass motion without having any first-order effect on the displacement of the density distribution. This agrees with conclusions earlier drawn by SPITZER [8] in a different way. When the temperature varies in space the relation (9) does not hold and the particle cloud is distorted by the temperature gradient. This is also understandable from the orbit theory where a spatial variation of the equivalent magnetic moment M_ν gives rise to a dispersion in the gradient drift. There also exists a dispersion in this drift due to the thermal velocity distribution. This effect will be neglected here. It can be taken into account in a macroscopic approach by considering the drift of any group of particles with velocities in the range dW_ν separately.

(*ii*) When the density deviates only little from a constant value n_0 over distances L_x and L_y, as in the present problem on stability, the right hand member of Eq. (9) cannot necessarily be neglected. Observe the ion and electron clouds at a particular point in space in a co-ordinate system which moves with the local vertical velocity $u_{Ey} = -E_x'/B$. Then, the contribution to the increase in density from the right hand member of Eq. (9) will be the same for ions and electrons since $n_\nu \mathbf{E}' \approx n_0 \mathbf{E}'$ for small perturbations. Thus, no resulting electric space charge is generated by this effect (see also Section 5). We therefore treat the problem as if the density clouds were displaced in the y-direction by the velocity $\mathbf{u}_{Ey}$ and by the velocities $u_{\nu x} = u_{Ex} + u_{g\nu} + u_{B\nu}$ in the x-direction. The approximation implies that we neglect the compression of the particle clouds by div $\mathbf{u}_E$ compared to the displacement by $\mathbf{u}_E + \mathbf{u}_{g\nu} + \mathbf{u}_{B\nu}$.

3.3. The unperturbed state

Throughout the rest of this paper we assume the ion and electron temperatures to be constant. With the configuration discussed in Section 2 the unperturbed, stationary state is determined by

$$0 = q_\nu n_0 \mathbf{E}_0 + q_\nu n_0 \mathbf{v}_{0\nu} \times \mathbf{B} + m_\nu n_0 \mathbf{g} - k T_\nu \nabla n_0 . \quad (10)$$

Consider situations where the centre of mass of the unperturbed plasma is at rest, which implies that $\mathbf{v}_{0i} \approx 0$ since $m_i \gg m_e$. For a rotating plasma $\mathbf{g}$ then represents the centrifugal acceleration in a frame of reference following the rotation. Then, one also has to add a contribution from the Coriolis force, but this effect is negligible when the angular velocity of rotation is much smaller than the gyro-frequency of ions [9]. For the electrons we cannot assume $\mathbf{v}_{0e}$ to be negligible, because the gravitation force and the pressure gradient have to be balanced by the electrodynamic force $-en_0 \mathbf{v}_{0e} \times \mathbf{B}$ and an electric field $\mathbf{E}_0$ which couples ions and electrons. Both $\mathbf{E}_0$ and $\mathbf{g}$ have a component only in the y-direction.

4. The density perturbation

For the problem specified in Section 2 and illustrated by Fig. 2 the motion of the ion and electron clouds will be given by Eq. (9) in first order. Introduce $\mathbf{E} = \mathbf{E}_0 + \mathbf{E}'$, where $\mathbf{E}'$ is the electric field arising from the perturbation. According to the discussion in Section 3.2 both particle clouds can be considered to move with the velocity

$$u_{Ey} = -E_x'/B \quad (11)$$

in the y-direction. In the x-direction the ion cloud is propagated with the constant velocity

$$u_{ix} = \left(E_0 + \frac{m_i}{e} g_y - \frac{2kT_i}{eB} \cdot \frac{dB}{dy}\right)/B \qquad (12)$$

and the electron cloud with

$$u_{ex} = \left(E_0 - \frac{m_e}{e} g_y + \frac{2kT_e}{eB} \cdot \frac{dB}{dy}\right)/B \qquad (13)$$

for a small perturbation.

Now study a density perturbation given by the elementary mode (cf. Fig. 2 and Eq. (1))

$$a_\nu = [S_\nu(t) \sin(k_x x - \alpha_\nu t) + C_\nu(t) \cos(k_x x - \alpha_\nu t)] \cdot (s_\nu \sin k_y y + c_\nu \cos k_y y); \qquad (\nu = i, e), \quad (14)$$

where $k_x = 2\pi/L_x$, $k_y = 2\pi/L_y$ and $\alpha_\nu = k_x u_{\nu x}$. The initial conditions are $S_i(0) = S_e(0)$, $C_i(0) = C_e(0) = 0$ and $a_i(x, y, 0) = a_e(x, y, 0)$ for all values of x and y. This implies that we can put $s_i = s_e = s$ and $c_i = c_e = c$.

Eq. (11) immediately leads to the condition that the rates of change of the perturbation amplitudes should be equal for ions and electrons and become

$$-E_x'/B = \left[\frac{dS_\nu}{dt} \sin(k_x x - \alpha_\nu t) + \frac{dC_\nu}{dt} \cos(k_x x - \alpha_\nu t)\right] \cdot (s \sin k_y y + c \cos k_y y) \qquad (15)$$

for any value of x and y.

Eqs. (14) and (1) yield a corresponding electric space charge

$$\sigma = e(n_i - n_e) = eN(y - a_i) - eN(y - a_e)$$
$$\approx e(-a_i + a_e) N' = -eN'(s \sin k_y y + c \cos k_y y)$$
$$\times [S_i \sin(k_x x - \alpha_i t) + C_i \cos(k_x x - \alpha_i t)$$
$$- S_e \sin(k_x x - \alpha_e t) - C_e \cos(k_x x - \alpha_e t)], \qquad (16)$$

where $N' = dn_0/dy$ is approximately constant.

5. Electric polarization

The electric field $\mathbf{E}'$ now has to be connected with the space charge σ. From Eqs. (16), (15), (14) and (1) we obtain

$$\frac{\partial \sigma}{\partial t} = -u_{ix} \frac{\partial}{\partial x}(e n_i) + u_{ex} \frac{\partial}{\partial x}(e n_e), \qquad (17)$$

which is a direct consequence of the definition of a_ν and σ. The electric field in the plasma is not given solely by the charge σ generated by the density perturbations which arise from the drift motion in first order. There also arise displacements of the ion and electron clouds which produce an electric polarization. These displacements are much smaller than those of the density perturbations and do not appear in first order in Eq. (9). However, since the polarization is generated by displacements of the entire charge clouds, it still contributes appreciably to the electric field $\mathbf{E}'$.

To take the polarization into account we now have to reconsider Eq. (8) in a higher approximation where the inertia of ions produces small displacements of the entire ion cloud. The inertia of electrons is neglected since $m_e \ll m_i$. Start with Maxwell's equation

$$\operatorname{curl} \mathbf{B}/\mu_0 = \mathbf{i} + \varepsilon_0 \frac{\partial \mathbf{E}'}{\partial t}, \qquad (18)$$

where $\mathbf{i} = e(n_i \mathbf{v}_i - n_e \mathbf{v}_e)$ is the exact expression for the total convection current and ε_0 is the dielectric constant in vacuo. A divergence operation on Eq. (18) then gives when $b \ll B$ and L_x, $L_y \ll L_{cB}$

$$-\varepsilon_0 \frac{\partial}{\partial t} \operatorname{div} \mathbf{E}' = \operatorname{div} \mathbf{i} = -\frac{\partial \sigma}{\partial t} - \operatorname{div}\left(m_i n_0 \frac{\partial \mathbf{v}_i}{\partial t} \times \mathbf{B}/B^2\right), \qquad (19)$$

where use has been made of Eqs. (8) and (17) and $d_i \mathbf{v}_i/dt \approx \partial \mathbf{v}_i/\partial t$ since $\mathbf{v}_{i0} \approx 0$. In first order Eq. (7) yields

$$\frac{\partial \mathbf{v}_i}{\partial t} = \frac{\partial \mathbf{E}'}{\partial t} \times \mathbf{B}/B^2 + (kT_i/eB^2)\, \mathbf{B} \times \frac{\partial}{\partial t}\left(\frac{1}{n_i} \nabla n_i\right). \qquad (20)$$

In cases where the last term of Eq. (20) can be neglected Eq. (19) reduces to

$$\operatorname{div}\left(\varepsilon_{eq} \frac{\partial \mathbf{E}'}{\partial t}\right) = \frac{\partial \sigma}{\partial t}; \quad \varepsilon_{eq} = \varepsilon_0 + \varrho_0/B^2, \qquad (21)$$

where ϱ_0 is the unperturbed mass density of the plasma. An estimation of orders of magnitude shows that this occurs when $\varrho_i^2/(1/L_x^2 + 1/L_y^2) \ll 1$, where ϱ_i is the radius of gyration of an ion. It also occurs when T_i is small and the separation of the charge clouds in Eq. (17) is provided by the displacement of electrons ($T_e \gg T_i$), or by the influence of a gravitation field g. In the following sections we limit the discussion to disturbances where L_x and L_y definitely exceed ϱ_i. This is also a necessary restriction on the validity of the present theory.

6. Solution

The characteristic lengths L_{cB} and L_{cn} of the density distribution and the magnetic field are large and the spatial variation of the equivalent dielectric constant ε_{eq} in Eq. (21) is slow. Therefore, when the induced magnetic field is neglected

$$\operatorname{curl}(\varepsilon_{eq} \mathbf{E}') \approx \varepsilon_{eq} \operatorname{curl} \mathbf{E}' \approx 0 \qquad (22)$$

and we can put

$$\varepsilon_{eq} \mathbf{E}' = -\nabla \psi; \quad \nabla^2 \psi = -\sigma, \qquad (23)$$

since $\mathbf{E}'$ and σ start from zero.

With the substitution

$$\psi = \Phi + \sigma/(k_x^2 + k_y^2), \qquad (24)$$

Eq. (23) reduces to

$$\nabla^2 \Phi = 0. \qquad (25)$$

The general solution of Eq. (23) becomes

$$\psi = \sigma/(k_x^2 + k_y^2) + (\Phi_1 \sin px + \Phi_2 \cos px) \times (\Phi_3 \sinh py + \Phi_4 \cosh py), \qquad (26)$$

where Φ_1, Φ_2, Φ_3, Φ_4 and p are arbitrary functions of time. For symmetry reasons p must be real since the perturbation has to be periodic in the x-direction.

The boundary conditions in the y-direction are given by two conducting plates at $y = \pm Y_0$ where E_x' has to vanish and the electric potential has to be constant for all values of x and t. Since ε_{eq} varies slowly and only in the y-direction, the latter condition applies also to ψ with a high degree of approximation. This requires that the third bracket of Eq. (26) vanishes at $y = \pm Y_0$ which yields $\Phi_3 = \Phi_4 = 0$. It also implies that either $s = 0$ and $\cos k_y Y_0 = 0$ or $c = 0$ and $\sin k_y Y_0 = 0$ when the trivial solution $s = c = 0$ is excluded.

From Eqs. (23), (26) and (16) we now obtain

$$u_{Ey} = -E_x/B = -\frac{eN'k_x}{B\varepsilon_{eq}(k_x^2+k_y^2)}(s\sin k_y y + c\cos k_y y) \cdot [S_i(\cos k_x x - \alpha_i t) - C_i \sin(k_x x - \alpha_i t) - S_e \cos(k_x x - \alpha_e t) + C_e \sin(k_x x - \alpha_e t)] \quad (27)$$

Introduce

$$\gamma = -\omega \cdot \frac{dn_0}{dy}[n_0 u_{ie}(k_x^2+k_y^2)(1+\varepsilon_0 B^2/\varrho_0)]^{-1}; \quad \omega = eBn_0/\varrho_0 \quad (28)$$

and the parameters $u_{ie} = u_{ix} - u_{ex}$ and $\varphi = k_x u_{ie} t$. Combination of Eqs. (27) and (15) gives after the substitution $x' = x - \alpha_e t/k_x$ the result

$$\gamma[S_i\cos(k_x x' - \varphi) - C_i\sin(k_x x' - \varphi) - S_e\cos k_x x' + C_e \sin k_x x'] = \frac{dS_i}{d\varphi}\sin(k_x x' - \varphi) + \frac{dC_i}{d\varphi}\cos(k_x x' - \varphi) = \frac{dS_e}{d\varphi}\sin k_x x' + \frac{dC_e}{d\varphi}\cos k_x x' . \quad (29)$$

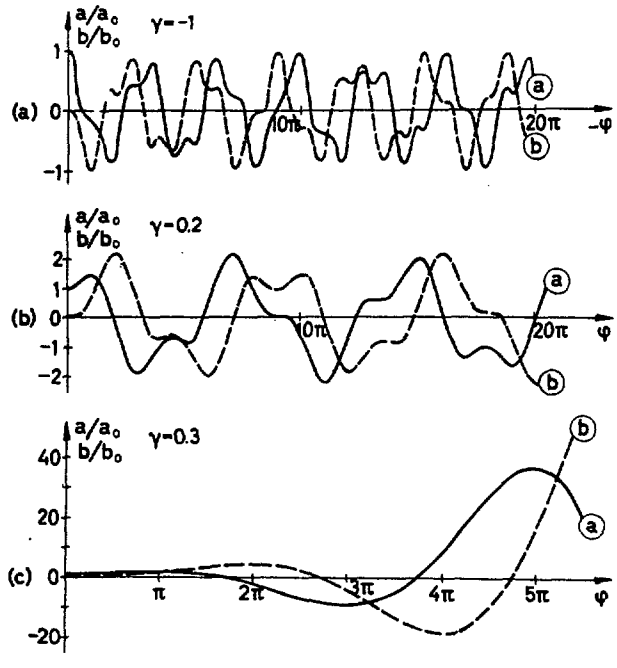

Fig. 3 The amplitudes a and b of the perturbation as a function of the phase angle φ and time t. (a) $\gamma = -1$, $u_{ie} < 0$; $\varphi = -2\pi|u_{ie}|t/L_x$. (b) $\gamma = 0.2$, $u_{ie} > 0$; $\varphi = 2\pi|u_{ie}|t/L_x$. (c) $\gamma = 0.3$, $u_{ie} > 0$; $\varphi = 2\pi|u_{ie}|t/L_x$.

This system of equations is identical with the system treated in an earlier paper [6] where the solution was found to be

$$a/a_0 = \cos\varphi' \cdot \cosh(\varkappa\varphi') + \varkappa^{-1}\sin\varphi' \cdot \sinh(\varkappa\varphi'); \quad \gamma > 1/4 \quad (30)$$

$$a/a_0 = \cos\varphi' \cdot \cos(|\varkappa|\varphi') + |\varkappa|^{-1}\sin\varphi' \cdot \sin(|\varkappa|\varphi'); \quad \gamma < 1/4, \quad (31)$$

with a_0 as the initial amplitude and

$$S_i = S_e = a;\ C_i = -C_e = b;\ \varphi' = \varphi/2;\ \varkappa^2 = 4\gamma - 1 . \quad (32)$$

For the amplitude b a differential equation is obtained which can be brought to the same form as that for a; the difference is represented only by a phase shift in φ and in the initial condition which is $b_0 = 0$.

Consequently, the result shows that unstable oscillations occur when $\gamma > 1/4$, whereas oscillations of limited amplitude arise when $\gamma < 1/4$, including negative values. Three examples are given in Figs. 3a, b and c corresponding to $\gamma = -1$, 0.2 and 0.3.

It should be observed that the special case where $b = 0$, $\varepsilon_0 B^2/\varrho_0 = 0$, $p = 0$, $(dn_0/dy)/k_x n_0 = 1$ and $k_x x - \varphi \approx k_x x$ (initial phase) gives relations which are formally identical with those earlier obtained by ROSENBLUTH and LONGMIRE [1] for a plasma separated from vacuum by a sharp boundary. Then, the amplitude is given by

$$a/a_0 = \cosh(k_x u_{ie}\,\omega t^2)^{\frac{1}{2}} = 1 + \frac{1}{2}k_x u_{ie}\,\omega t^2 + O(t^4) \quad (33)$$

in the initial phase, where the last term indicates contributions of fourth and higher orders, see also [6]. In the present linearized theory a number of modes with different wave numbers k_x and k_y can be superimposed where each mode obeys relations of the form of Eq. (29).

7. Discussion

The existence of an interchange instability has earlier been suggested by TELLER [10] for magnetic fields bending concavely towards a confined plasma. This has to be understood both from a macroscopic point of view and from considerations of particle orbits. For the instability it is necessary to show that an interchange of fluid elements gives rise to a lower state of potential energy. However, this is not a sufficient condition, as it has also to be shown that the particles actually are able to perform the required displacements.

According to the present theory, the boundary between unstable and stable solutions is given by $\gamma = 1/4$ and not by $\gamma = 0$ which, in the absence of gravitation, divides magnetic fields which bend concavely towards the plasma (∇B and ∇n_0 parallel) from those bending convexly towards the plasma (∇B and ∇n_0 antiparallel). There exist three different possibilities as illustrated by Figs. 3a, b and c:

(*i*) $\gamma < 0$. The drift u_{ie} is in the negative x-direction and ∇B points in the positive y-direction when $g = 0$. The main part of the plasma is in regions

where the magnetic field is weak. This is the situation for cusped geometry which should correspond to stable oscillations with finite amplitude according to the present theory. The amplitude of the perturbation decreases during the initial phase since $u_{ie}<0$.

(*ii*) $0<\gamma<\frac{1}{4}$. The drift u_{ie} is in the positive x-direction and ∇B in the negative y-direction when $g=0$. The main part of the plasma is in regions where the magnetic field is strong, such as in a mirror field which bends concavely towards the plasma. The amplitude increases during the initial phase as seen from Eq. (31) but the growth stops after some time when the separation φ becomes comparable with $k_x x'$ and the electric field drift is reversed in the y-direction. Thus, oscillations with finite amplitude occur also in this case. When the ion and electron temperatures do not differ too much, $\varepsilon_0 B^2/\varrho_0 \ll 1$ and account is taken of the acceleration $\mathbf{g}$, Eq. (28) can be written as

$$\gamma^{-1}=8\pi^2 L_{cn}(1/L_x^2+1/L_y^2)(\varrho_i^2/L_{cB}+g_y/2\omega^2);$$
$$\left(\frac{dB}{dy}<0;\ \frac{dn_0}{dy}<0,\ g_y>0\right), \tag{34}$$

where ϱ_i is the radius of gyration of an ion. Observe that γ depends on the ratio L_{cn}/L_{cB} when $g_y=0$. Thus, when the magnetic field has a strong gradient, the density distribution is not too steep and one of the wavelengths L_x and L_y does not exceed ϱ_i too much a rapid drift u_{ie} will provide a scrambling mechanism which reverses and smooths out the electric field drift and stabilizes the system. The drift u_{ie} is enhanced by an acceleration $\mathbf{g}$ which is antiparallel to ∇n_0 and ∇B.

(*iii*) $\gamma>\frac{1}{4}$. The directions of the drift u_{ie} and of ∇B and the growth of the perturbation in the initial phase are the same as in (*ii*) and still apply to a field which bends concavely towards the plasma. Now the mixing effects due to the scrambling mechanism are too weak to secure stability and the oscillations are steadily growing. However, Eqs. (30) and (33) show that the growth rate is reduced considerably according to the present theory compared with that earlier deduced by Rosenbluth and Longmire. The ratio between the arguments determining the growth rates is

$$\Theta=(\varkappa\varphi')/(ku_{ie}\omega t^2)^{\frac{1}{2}}=[ku_{ie}(\gamma-1/4)/\omega]^{\frac{1}{2}}$$
$$\approx\left[\frac{L_x L_y^2}{2\pi L_{cn}(L_x^2+L_y^2)}-\frac{\pi\varrho_i^2}{L_x L_{cB}}-\frac{\pi g_y}{2\omega^2 L_x}\right]^{\frac{1}{2}};\ \left(\gamma>\frac{1}{4}\right), \tag{35}$$

when the thermal motion is isotropic, T_i and T_e are of the same order of magnitude and $dB/dy<0$, $dn_0/dy<0$, $g/>0$. For the problem of a plasma supported against gravity by a magnetic field similar conclusions apply with the stability condition given by $\gamma<\frac{1}{4}$.

The present mechanism provides a possible explanation of the observed stability of the Van Allen belts as well as of the absence of the extremely rapid growth rates of flutes in mirror machines and rotating plasma devices as predicted by the earlier theory [1]. When L_{cB} and L_{cn} are of the same order of magnitude and *one* of the wavelengths L_x and L_y does not exceed the radius of gyration ϱ_i too much, the perturbation should be stable according to Eq. (34). At the same time, it should be kept in mind that the applicability of the present theory becomes somewhat doubtful when L_x and L_y approach ϱ_i. However, even for larger wavelengths where the perturbation is in the unstable region with $\gamma>\frac{1}{4}$ the growth rate is reduced considerably according to Eq. (35) as compared with earlier calculations [1].

Some examples are given in Table I to illustrate the results. The two last columns of the table show the relative increase of the perturbation amplitude after the drift u_{ie} has displaced the particle clouds one wavelength L_x relative to each other. The amplitude growth is very large in the case treated by Rosenbluth and Longmire, whereas the present theory gives a moderate increase even in the unstable situations of Table I. In the table are also included examples where a centrifugal acceleration g_y is produced in the positive y-direction in a rotating plasma with thermal and mass

TABLE I. *Stability conditions and growth rates of a density disturbance of wavelengths* $L_x=L_y$. The characteristic lengths of the magnetic field and the unperturbed distribution are L_{cB} and L_{cn} and the radius of gyration of an ion is ϱ_i. The two last columns give the relative increase of the perturbation amplitude after one period $\varphi=2\pi$ according to the theory by Rosenbluth and Longmire for a sharp boundary and to the present theory for a continuous density distribution.

$L_x=L_y$	L_{cB}	L_{cn}	$g_y/2\ \omega^2$	$\varkappa^2=4\gamma-1$	a/a_0 Eq. (33)	a/a_0 Eqs. (30), (31)
$10\ \varrho_i$	$200\ \varrho_i$	$400\ \varrho_i$	0	0.271 unstable	10^{34}	2.65
$10\ \varrho_i$	$200\ \varrho_i$	$600\ \varrho_i$	0	—0.155 stable	10^{34}	1.0
$10\ \varrho_i$	$200\ \varrho_i$	$400\ \varrho_i$	$\varrho_i/800$	0.020 unstable	3×10^{30}	1.1
$10\ \varrho_i$	$100\ \varrho_i$	$200\ \varrho_i$	0	0.271 unstable	10^{24}	2.65
$10\ \varrho_i$	$100\ \varrho_i$	$200\ \varrho_i$	$\varrho_i/400$	—0.155 stable	2.5×10^{21}	1.0
$20\ \varrho_i$	$200\ \varrho_i$	$600\ \varrho_i$	0	2.39 unstable	2×10^{48}	63.9
$20\ \varrho_i$	$200\ \varrho_i$	$600\ \varrho_i$	$\varrho_i/1200$	1.91 unstable	6×10^{44}	38.7

velocities of the same magnitude. This enhances the scrambling mechanism by u_{ie} and has a stabilizing effect, as long as the energy density of the plasma is small compared to the "magnetic pressure" of the imposed magnetic field.

Observe that the results obtained so far are limited to situations where the last term in Eq. (20) is negligible. Discussions of this point will be made in Section 8. Further restrictions which apply to the case of an inhomogeneous magnetic field, but not to the problem of gravitation instability, are due to the omission of the $div\, \mathbf{u}_E$ term in Eq. (8). This term represents a compression by an inhomogeneous electric field drift which for strong magnetic field inhomogeneities modifies the stability criterion and the results of Table I.

When the perturbation can last for some time without growing to excessively large values, it is not unimaginable that a dispersion in the drift velocity, differential motion, dissipation and other mixing and damping mechanisms may have time to make the system practically stable, even in cases where γ exceeds $\frac{1}{4}$ by limited amounts.

Large asymmetries in the density distribution will be of great disadvantage from the point of view of stability. It should therefore be stressed that smooth and well defined starting conditions may be as important to the stability of a plasma device as the design of the confining magnetic field.

It may be mentioned that the present mechanism provides a kind of "short circuit" of space charges by drift motion of ions across the magnetic field. In favourable situations with strong magnetic field gradients this is almost as effective as the short circuit provided by electrons along the magnetic field in the rotational transform of a stellarator [11].

Even if the plasma can become practically stable against phenomena of the kind discussed here, there are other effects such as the "mirror instability" and unstable ion and electron plasma oscillations which may complicate the problem [2].

8. Influence of separation current

Due to the finite ion Larmor radius the mean electric field acting on a gyrating ion will differ from that acting on an electron. This effect, which has been discovered by ROSENBLUTH, KRALL, ROSTOKER [12], gives rise to an additional current which separates ions and electrons.

Consider the mean force $\overline{\mathbf{F}}$ arising from any force field $\overline{\mathbf{F}}$ acting on a particle which has a Larmor radius given by the vector $\boldsymbol{\rho}_\nu$ which rotates at a frequency ω_ν. A Taylor expansion of $\overline{\mathbf{F}}$ around the centre of gyration yields for small values of ϱ_ν:

$$\overline{\mathbf{F}} = \mathbf{F} + \frac{1}{4}\varrho_\nu^2 \nabla_\perp^2 \mathbf{F} \quad (\nu = \mathrm{i},\ \mathrm{e}). \tag{36}$$

This is the force which has to be put into the equations of the perturbation theory describing the drift motion of a particle. The effect of the finite Larmor radius also comes out directly from the macroscopic equations in a higher approximation.

The separation current $\mathbf{i}_F$ arising from the difference between the mean forces $\overline{\mathbf{F}}_\mathrm{i}$ and $\overline{\mathbf{F}}_\mathrm{e}$ acting on individual ions and electrons is comparable with the polarization current $\mathbf{i}_\mathrm{p}$ given by the last term in Eq. (7) when

$$|\mathbf{i}_F/\mathbf{i}_\mathrm{p}| \approx (\varrho_\mathrm{i}/L)\cdot(W_\mathrm{i}/U_\mathrm{ph}) \tag{37}$$

becomes comparable to unity. This can occur even for characteristic lengths L of the phenomenon which are small compared to ϱ_i, provided that the phase velocity U_ph of the phenomenon is much smaller than the transverse "thermal velocity" W_i of ions.

We shall now treat the gravitation instability of an inhomogeneous plasma with less restricted approximations than in the earlier parts of the present paper. Thus, all terms of order $\varrho_\mathrm{i}^2\,(1/L_x^2 + 1/L_y^2)$ will be retained which implies that the second term of the right hand member of Eq. (20) will be taken into account. We still restrict ourselves to low ratios between particle pressure and "magnetic pressure". Since $m_\mathrm{i} \gg m_\mathrm{e}$ and $L_x,\ L_y \ll N/N'$ we obtain from Eqs. (8) and (1) with the condition (10) on the unperturbed state:

$$\frac{\partial a_\mathrm{i}}{\partial t} = \frac{1}{B}\frac{\partial}{\partial x}\Phi - \omega_\mathrm{i}\varrho_\mathrm{i}^2\frac{N'}{2N}\frac{\partial a_\mathrm{i}}{\partial x} - \frac{N}{N' a_\mathrm{i} B}\nabla^2\frac{\partial}{\partial t}\Phi + \tfrac{1}{2}\varrho_\mathrm{i}^2\nabla^2\frac{\partial a_\mathrm{i}}{\partial t}, \tag{38}$$

$$\frac{\partial a_\mathrm{e}}{\partial t} = \frac{1}{B}\frac{\partial}{\partial x}\Phi + \frac{g}{\omega_\mathrm{i}}\frac{\partial a_\mathrm{e}}{\partial x} - \omega_\mathrm{i}\varrho_\mathrm{i}^2\frac{N'}{2N}\frac{\partial a_\mathrm{e}}{\partial x}, \tag{39}$$

where Φ is the electric potential of the perturbed electric field $\mathbf{E}'$. A divergence operation on Eq. (18) yields

$$a_\mathrm{i} - a_\mathrm{e} = (\varepsilon_0/e\,N')\,\nabla^2\Phi, \tag{40}$$

where ε_0 is the dielectric constant in vacuo.

Assume all quantities to vary as $\exp[\mathrm{i}\,(k_x x + k_y y + \omega t)]$ and introduce the notations

$$f = k_x\omega_\mathrm{i}\varrho_\mathrm{i}^2(N'/2N);\quad \alpha = g\,k_x/\omega_\mathrm{i};\quad \lambda = \tfrac{1}{2}\varrho_\mathrm{i}^2(k_x^2 + k_y^2). \tag{41}$$

Eqs. (38), (39) and (40) then lead to a dispersion relation which has the solutions

$$\omega = -\tfrac{1}{2}(f - \alpha + \alpha\lambda\gamma) \pm \tfrac{1}{2}[(f - \alpha + \alpha\lambda\gamma)^2 - 4\alpha^2\gamma]^{\frac{1}{2}} \tag{42}$$

when $\varepsilon_0/\varepsilon_\mathrm{eq} \ll 1$ which is usually a very good approximation. The stability condition becomes

$$(f - \alpha + \alpha\lambda\gamma)^2 > 4\alpha^2\gamma, \tag{43}$$

The terms f and $\alpha\lambda\gamma$ are due to the refined approximations. The latter comes from the last term in Eq. (38) and is of the order $\varrho_\mathrm{i}^2\,(1/L_x^2 + 1/L_y^2)$ compared to the left hand member of the same equation.

If the terms including α in the left hand member of relation (43) are dropped the result would become

$$(k_x\varrho_\mathrm{i})\,(\varrho_\mathrm{i}N'/N) > 4\,\omega_\mathrm{H}/\omega_\mathrm{i} \tag{44}$$

where we have introduced the growth rate ω_H given by $\omega_H^2=\alpha^2\gamma$ and corresponding to the earlier theory by ROSENBLUTH and LONGMIRE [1]. Condition (44) is identical with that given by Rosenbluth *et al.* [12]. However, from the definitions of f, α, λ and γ given by Eqs. (41) and (28) we obtain $\alpha\lambda\gamma=-f$ which implies that an exact cancellation of the additional terms in relation (43) takes place and the stability condition remains the same as that given earlier in Section 6.

The cancellation is probably due to currents arising from the density gradients of the perturbed state. It remains to investigate whether a treatment on gravitation instability by direct application of the Boltzmann equation gives additional information beyond that obtained from the macroscopic equations. The latter arise from a mean value formation based on Boltzmann's equation.

Acknowledgement

The author wants to express his sincere thanks to Dr. Marshall N. Rosenbluth and his collaborators for sending a report of their investigations before publication.

References

[1] ROSENBLUTH, M. N., LONGMIRE, C. L., *Ann. Phys.* (*N. Y.*) **1** (1957).
[2] POST, R. F., ELLIS, R. E., FORD, F. C., ROSENBLUTH, M. N., *Phys. Rev. Letters* **4** (1960) 166.
[3] BOYER, K., HAMMEL, J. E., LONGMIRE, C. L., NAGLE, D., RIBE, F. L., RIESENFELD, W. B., Proc. Second U. N. International Conference on Peaceful Uses of Atomic Energy, Geneva, **31** (1958) 319.
[4] BERGSTRÖM, J., HOLMBERG, S., LEHNERT, B., *Phys. Rev. Letters* **6** (1961) 525 and paper submitted to this conference (second part of Proceedings).
[5] VAN ALLEN, J. A., *J. Geophys. Res.* **64** (1959) 1683.
[6] LEHNERT, B., *Phys. Fluids* **4** (1961) 847.
[7] ALFVÉN, H., Cosmical Electrodynamics, (Oxford Univ. Press, 1950).
[8] SPITZER, L., *Astrophys. J.* **116** (1952) 299.
[9] LEHNERT, B., Progress in Nuclear Energy: Series XI; Vol. 2, "Plasma Physics and Thermonuclear Research", Ed. by J. L. Tuck (Pergamon Press, Oxford, 1961).
[10] TELLER, E., Project Sherwood, Ed. by A. S. Bishop (Addison-Wesley, Reading, Mass., 1954).
[11] SPITZER, L., Proc. Second U.N. International Conference on the Peaceful Uses of Atomic Energy, Geneva, **31** (1958) 181.
[12] ROSENBLUTH, M. N., KRALL, N. A., ROSTOKER, N., Proceedings of this Conference, page 143.

FINITE LARMOR RADIUS STABILIZATION OF "WEAKLY" UNSTABLE CONFINED PLASMAS*

M. N. ROSENBLUTH**, N. A. KRALL, N. ROSTOKER

JOHN JAY HOPKINS LABORATORY FOR PURE AND APPLIED SCIENCE,

GENERAL ATOMIC DIVISION OF GENERAL DYNAMICS CORPORATION,

SAN DIEGO, CALIFORNIA, UNITED STATES OF AMERICA

It is well known that the "modified" magnetohydrodynamic equations of motion follow from the exact plasma kinetic theory in the limit of small Larmor radius and low frequency, so that a magnetohydrodynamic prediction of instability is usually valid. However, in weakly unstable systems such as mirror machines, slowly rotating plasmas, large aspect ratio torii, etc., the expansion is no longer correct since the growth rate is very small, i.e., $(ka_i)^2$ may become comparable to ω/Ω_i so that ω must also be considered a small quantity. Here Ω_i is the ion cyclotron frequency, a_i the ion gyro-radius and k the wave number of the perturbation. We have studied several such cases—a plasma under gravity, a mirror machine, and a slowly rotating plasma. In all these cases the characteristic flute type instability is effectively stabilized if $(ka_i)^2 > \omega_H/\Omega$ where ω_H is the growth rate predicted by the hydrodynamic theory. It should be noted that present mirror experiments and fast-compression experiments are operating in the region $(a_i/r)^2 \approx \omega_H/\Omega_i$ and some detailed discussion of these cases will be made.

The dominant physical effect is the breakdown of the condition that ions and electrons move together across the magnetic field with characteristic velocity $\mathbf{v} = c\delta\mathbf{E} \times \mathbf{B}/B^2$, where $\delta\mathbf{E}$ is the perturbed electric field. Due to the finite ion Larmor radius the mean electric field seen by the ions is slightly different from the electrons so that their velocity across the field is different. This builds up a charge separation out of phase with the characteristic charge separation due to particle drifts which drive the flute type instability. If the above inequality is satisfied, the result is a stable oscillation.

1. Introduction

It is well known that the "modified" magnetohydrodynamic equations [1] of motion follow from the exact plasma kinetic theory in the limit of small Larmor radius and low frequency, so that a magnetohydrodynamic prediction of instability is usually valid. However, in weakly unstable systems such as mirror machines, slowly rotating plasmas, large aspect ratio torii, etc., the expansion is no longer correct since the growth rate ω is very small, i.e., $(ka_i)^2$ may become comparable to ω/Ω_i so that ω must also be considered a small quantity and terms $(ka_i)^2\,\Omega_i/\omega$ must be retained. Here Ω_i is the ion cyclotron frequency, a_i the ion gyro-radius, and k the wave number of the perturbation. We have studied several such cases—a plasma under gravity, a mirror machine, and a slowly rotating plasma. In all these cases the characteristic flute type instability [2] is effectively stabilized if $(ka_i)^2 > \omega_H/\Omega_i$ where ω_H is the growth rate predicted by the hydrodynamic theory. It should be noted that present mirror experiments [3] and fast-compression experiments [4] are operating in the region $(a_i/r)^2 \approx \omega_H/\Omega_i$ and some detailed discussions of these cases will be made.

The dominant physical effect is the breakdown of the condition that ions and electrons move together across the magnetic field with characteristic velocity $\mathbf{v} = c\delta\mathbf{E} \times \mathbf{B}/B^2$, where $\delta\mathbf{E}$ is the perturbed electric field. Due to the finite ion Larmor radius the mean electric field seen by the ions is slightly different from the electrons so that their velocity across the field is different. This builds up a charge separation out of phase with the characteristic charge separation due to particle drifts [2] which drives the flute type instability. If the above inequality is satisfied, the result is a stable oscillation.

This may be estimated as follows. Particles move across the field with velocity $\mathbf{v} = c\delta\mathbf{E} \times \mathbf{B}/B^2$. However, the electric field which should be used here is the mean electric field seen by the particle in its gyration. In particular, there is a difference between ion and electron velocity. Thus there is a separation current given roughly by $\mathbf{j}_F = a_i^2\,(\nabla^2\delta\mathbf{E} \times \mathbf{B})\,n_0 ec)B^2$. This is to be compared with the current which drives the instability in the hydrodynamic theory [2]. This current is equal to $\mathbf{j}_H = \mathbf{v}_D e\delta n$ where $\mathbf{v}_D$ is the equilibrium drift due to the destabilizing force, e.g., the gravitational drift $g \times \mathbf{B}/\Omega B$; and δn is the perturbed number density due to the hydrodynamic motion $\delta n = -(c/i\omega)\,(\delta\mathbf{E} \times \mathbf{B}/B^2) \cdot \nabla n_0$. Recalling that $\omega_H = [g|\nabla n_0|/n_0]^{1/2}$ we see that $\mathbf{j}_F$ becomes comparable to $\mathbf{j}_H$ if $(ka_i)^2 \approx \omega_H/\Omega_i$.

In the following sections we study several situations of this kind. In all of these cases we treat the small amplitude stability problem by means of a self-

* Conference paper CN-10/170, presented by M. N. Rosenbluth. Discussion of this paper is given on page 208. Translations of the abstract are at the end of this volume of the Conference Proceedings.

** General Atomic and the University of California, La Jolla, California. United States of America.

consistent solution of Maxwell's equation and the collisionless Boltzmann (Vlasov) equation, making use of an expansion which assumes $(ka_i)<1$; $\omega/\Omega_i \approx (ka_i)^2$. These cases are further simplified by the assumption of low β (ratio of particle pressure to magnetic pressure); and by the fact that the equilibrium magnetic field is taken constant (to order β) with no shear or curvature. Other weakly unstable situations such as surface instabilities in pinches [5, 6] are not discussed in this paper although again important deviations from hydrodynamics will occur.

In Section 2 the gravitational instability problem is studied in detail. We discover that indeed the situation becomes almost stable for $(ka_i)^2 > \omega_H/\Omega_i$. There remains however a small residual instability of the Landau growth [7] type due to a resonant transfer with electrons drifting at the phase velocity of the wave.

In Section 3 the stability of a rotating cylindrical plasma is considered. Again the separation between ions and electrons is found to stabilize the motion. In this case the above condition leads to the stability requirement that the macroscopic rotation be not much greater than the rotation associated with the ion diamagnetic current. We also model the (unobserved!) flute instability caused by field line curvature by means of a radially outwards gravitational force. In this case we find the possibility of stabilizing all modes except one, a mode characterized by a constant electric field which it may be possible to stabilize by an external conductor.

2. Plasmas with plane geometry

The non-uniform plasma considered here is acted on by a magnetic field $\mathbf{B}=B_0\mathbf{i}_z(1+\varepsilon x)$, and a gravitational force $gm\mathbf{i}_x$. The equilibrium distribution function f_0 must satisfy the collisionless Boltzmann (Vlasov) equation and Maxwell's equations

$$\frac{\partial f}{\partial t}+\mathbf{v}\cdot\nabla f+\frac{e}{m}\left[\frac{\mathbf{v}\times\mathbf{B}}{c}+\frac{m}{e}g\,\mathbf{i}_x\right]\cdot\nabla_v f=0$$

$$\frac{\partial f_0}{\partial t}=0;\quad \nabla\times\mathbf{B}=\frac{4\pi}{c}\mathbf{j}=\frac{4\pi}{c}\sum_j e_j\int \mathbf{v} f_{0j}\,\mathrm{d}^3\mathbf{v} \qquad (2.1)$$

$$\varrho=\sum_j e_j\int f_{0j}\,\mathrm{d}^3 v=0.$$

Here j refers to particle species and is to be summed over values i and e for ions and electrons.

f_0 can be constructed from the constants of the motion: $\frac{1}{2}m_j v^2 - m_j g x$, $x+(v_y/\Omega_j)$. We choose a simple function

$$f_{0j}=\left(\frac{\alpha_j}{\pi}\right)^{3/2} n_{0j}\mathrm{e}^{-\alpha_j v^2}\left[1-\varepsilon_j'\left(x+\frac{v_y}{\Omega_j}\right)\right]\mathrm{e}^{2\alpha_j g x}, \qquad (2.2)$$

where we have defined $\Omega_j=e_jB/m_jc$. The parameter α_j is clearly $(v_{\text{thermal}})^{-2}$ and is related to a_j by $a_j=1/\Omega_j\sqrt{\alpha_j}$. The parameter ε_j' is related to the magnetic field gradient through the second and third of Eqs. (2.1), which give

$$-\frac{1}{n}\frac{\mathrm{d}n}{\mathrm{d}x}=\varepsilon_e'-2\alpha_e g=\varepsilon_i'-2\alpha_i g;\ \varepsilon\frac{B^2}{4\pi}=\sum_j n_j m_j\left[\frac{\varepsilon_j'}{2\alpha_j}-g\right]. \qquad (2.3)$$

Thus ε'/ε is related to β, the ratio of particle pressure to magnetic field pressure, and in the cases we shall consider here the condition $\varepsilon'>\varepsilon$ obtains. Equation (2.2) thus describes an equilibrium slightly non-uniform plasma. We now examine the stability of this equilibrium in the presence of small perturbations. In the magnetohydrodynamic limit this equilibrium is unstable with growth rate $\sqrt{g\varepsilon'}$.

We write $f=f_0+\delta f$, and use the Boltzmann Eq. (2.1) to obtain

$$\frac{\partial\delta f}{\partial t'}+\mathbf{v}\cdot\nabla\delta f+\frac{e}{m}\left[\frac{\mathbf{v}\times\mathbf{B}}{c}+\frac{m}{e}g\,\mathbf{i}_x\right]\cdot\nabla_v\delta f = -\frac{e}{m}\left[\delta\mathbf{E}+\frac{\mathbf{v}\times\delta\mathbf{B}}{c}\right]\cdot\nabla_v f_0, \qquad (2.4)$$

where we have neglected non-linear terms such as $\delta\mathbf{E}\cdot\nabla_v\delta f$. We can formally solve this equation by introducing the parameter t, and defining the transformation t', $\mathbf{x}$, $\mathbf{v}\to t$, $\mathbf{x}'(t)$, $\mathbf{v}'(t)$ by

$$t'=t,\quad \frac{\mathrm{d}\mathbf{x}'}{\mathrm{d}t}=\mathbf{v}'(t),\quad \frac{\mathrm{d}\mathbf{v}'}{\mathrm{d}t}=\Omega(\mathbf{v}\times\mathbf{i}_z)(1+\varepsilon x')+g\,\mathbf{i}_x. \qquad (2.5)$$

We observe that these equations describe orbits of charged particles moving in the unperturbed force fields $\mathbf{F}=(e/c)\,\mathbf{v}\times\mathbf{B}+mg\mathbf{i}_x$. In terms of the transformation (2.5), the Boltzmann equation becomes

$$\frac{\mathrm{d}}{\mathrm{d}t'}\delta f(x',v',t')=-\frac{e}{m}\left[\delta\mathbf{E}+\frac{\mathbf{v}'\times\delta\mathbf{B}}{c}\right]\cdot\nabla_{v'}f_0 \qquad (2.6)$$

and choosing the boundary conditions $\mathbf{x}'(t=0)=\mathbf{x}$, $\mathbf{v}'(t=0)=\mathbf{v}$ we have

$$\delta f(x,v,t=0)=-\frac{e}{m}\int_{-\infty}^{0}\mathrm{d}t\left[\delta\mathbf{E}+\frac{\mathbf{v}'\times\delta\mathbf{B}}{c}\right]\cdot\nabla_{v'}f_0. \qquad (2.7)$$

We now assume that all perturbed quantities have time-space dependence $\mathrm{e}^{i\omega t}g(\mathbf{x})$. This procedure will yield the same results as the rigorous procedure using Laplace transforms if we assume that ω has a small negative imaginary part, such that at $t=-\infty$, δf vanishes. Combining Eq. (2.7) with Maxwell's equation then gives a dispersion relation for ω. We assume that the perturbation is associated only with a longitudinal electrostatic field $\delta\mathbf{E}=-\nabla\Psi$. In fact, of course, the longitudinal waves are coupled to the transverse waves. The coupling can be shown to be small for small values of β=particle pressure/magnetic field pressure, and our approximation is valid only in that limit. This decoupling must occur for unstable waves, since a transverse electric field would lead to a modification of the magnetic field and an increase of field energy which in the low β limit would exceed the change in particle energy. In a separate paper we explicitly examine transverse modes and demonstrate

that the present results are indeed valid for small β. Our dispersion relation is then

$$\nabla^2 \Psi = -\frac{4\pi}{c}\sum e_j \int \delta f_j \, \mathrm{d}^3 \mathbf{v}$$
$$= -\frac{4\pi}{c}\sum \frac{e_j^2}{m_j}\int \mathrm{d}^3 \mathbf{v} \int_{-\infty}^{0} \mathrm{d}t \{\nabla \Psi(\mathbf{x}',t)\cdot \nabla_{v'} f_0(\mathbf{x}',t)\}. \quad (2.8)$$

The lowest order solutions to the orbit equations (2.5) are

$$\begin{aligned} v_y &= v_\perp \sin(\theta - \Omega t) + v_D \\ y &= \frac{v_\perp}{\Omega}\cos(\theta - \Omega t) - \frac{v_\perp}{\Omega}\cos\theta + v_D t \\ v_D &= \frac{1}{2}\frac{\varepsilon v_\perp^2}{\Omega} - \frac{g}{\Omega} \\ \frac{\mathrm{d}}{\mathrm{d}t}\left(x + \frac{v_y}{\Omega}\right) &= \frac{\mathrm{d}}{\mathrm{d}t}(v^2 - 2gx) = 0, \end{aligned} \quad (2.9)$$

with similar expressions for x, v_x, and v_z. We have explicitly indicated two constants of the motion allowed by the orbit equation, $x + (v_y/\Omega)$ and $(v^2 - 2gx)$. Thus $f_0(x', v') = f_0(x, v)$, and $\mathrm{e}^{-\alpha(v')^2}\,\mathrm{e}^{2\alpha g x'} = \mathrm{e}^{-\alpha v^2}\,\mathrm{e}^{2\alpha g x}$.

An interesting and important feature of these orbits is the drift velocity v_D, which has two parts, the $\varepsilon v^2/2\Omega$ field gradient drift, and the $-g/\Omega$ gravitational drift. Since $\nabla|B|$ and $\mathbf{g}$ are both vectors pointing in the x-direction and $\mathbf{B}$ is in the z-direction, both of those drifts are in the y-direction. These particle drifts represent a possible source of instability [2], causing a pile-up of space charge along the instability flutes. With this in mind we solve Eq. (2.8) for $\Psi \approx \mathrm{e}^{\mathrm{i}\omega t + \mathrm{i}ky}$. For $k > \varepsilon'$ the x dependence of the perturbation is weak and may be neglected [8]. In the next Section we retain the complete space dependence.

With the simplifications, using the explicit orbits of Eq. (2.9), the integrals in Eq. (2.8) can be evaluated. Thus

$$\nabla_v f_{0j} = -2\alpha_j \mathbf{v} f_{0j} - \frac{\varepsilon_j'}{\Omega_j}\left(\frac{\alpha_j}{\pi}\right)^{3/2} n_{0j}\mathrm{e}^{-\alpha_j[v^2 - 2gx]}\mathbf{i}_y .$$

We note that

$$\mathbf{v}\cdot\nabla\Psi = \frac{\mathrm{d}\Psi}{\mathrm{d}t} - \mathrm{i}\omega\Psi; \quad \mathbf{i}_y\cdot\nabla\Psi = \mathrm{i}k\Psi,$$

where $\mathrm{d}/\mathrm{d}t$ means total derivative along the particle orbit. Noting that f_0 and $v^2 - 2gx$ are constants of the motion, we may write the time integral in Eq. (2.8) in the form

$$\int_{-\infty}^{0} \mathrm{d}t \nabla\Psi\cdot\nabla_v f_0 = -2\alpha_j f_0 \Psi + \mathrm{i}\left\{2\alpha_j\omega - \frac{\varepsilon_j' k}{\Omega_j}\right\} f_0 \int_{-\infty}^{0} \mathrm{d}t\, \mathrm{e}^{\mathrm{i}k(y'-y)+\mathrm{i}\omega t}.$$

This expression neglects a small term of order ε'^2 which may easily be shown to vanish in a subsequent integration.

Using Eq. (2.9) we have

$$\mathrm{e}^{\mathrm{i}k(y'-y)} = \exp\left\{\mathrm{i}k\left[\frac{1}{2}\frac{\varepsilon v_\perp^2}{\Omega} - \frac{g}{\Omega}\right]t\right\} \sum_{l,m} J_l\left(\frac{kv_\perp}{\Omega}\right) J_m\left(\frac{kv_\perp}{\Omega}\right)\mathrm{e}^{\mathrm{i}(l-m)\pi/2}\mathrm{e}^{\mathrm{i}(l-m)\theta}\mathrm{e}^{-\mathrm{i}l\Omega t}.$$

The integration over the azimuthal velocity space angle, θ, t, and v_z is now easily done to give the dispersion relation:

$$-k^2 = 8\pi e^2 n\left(\frac{\alpha_i}{M} + \frac{\alpha_e}{m}\right) - 4\pi\sum_{j,l}\int \frac{\mathrm{e}^{-\alpha_j v_\perp^2} 2\alpha_j v_\perp \mathrm{d}v_\perp [2\alpha_j\omega - (k\varepsilon_j/\Omega_j)] J_l^2(kv_\perp/\Omega_j)}{(\omega + l\Omega_j + kv_D)}. \quad (2.10)$$

In obtaining Eq. (2.10) we have set $x = 0$ in expressions like $\mathrm{e}^{2\alpha g x}$, consistent with setting $\Psi = \mathrm{e}^{\mathrm{i}\omega t + \mathrm{i}ky}$. It is obvious that all the terms in the sum over Bessel functions may be ignored except the $l = 0$ terms, higher terms being smaller by a factor $(ka_i)^2(\omega/\Omega_i)^2 \ll 1$. We reiterate that our calculation assumes ka_i, $\varepsilon' a_i < 1$, as in the magnetohydrodynamic limit, and that the importance of higher orders in ka_i arises not from large values of ka_i but from extremely small values of the parameter ω/Ω for "weakly unstable" situations. In particular, in Eq. (2.10) we treat $k\varepsilon'/\Omega_j$ as of the same order as $2\alpha_j\omega$.

Expanding the Bessel function and neglecting the Debye length compared to Larmor radius, we have:

$$0 = F(\omega) = 2\sum_j \frac{\alpha_j}{m_j} - \sum_j\left(2\alpha_j\omega - \frac{k\varepsilon_j'}{\Omega_j}\right)\frac{1}{m_j}\int_0^\infty \frac{\mathrm{e}^{-x}[1 - (k^2 x/2\alpha_j\Omega_j^2])\,\mathrm{d}x}{\omega - (kg/\Omega_j) + (k\varepsilon x/2\alpha_j\Omega_j)}. \quad (2.11)$$

The singularities of the integral are to be interpreted in the usual way, passing to the limit as ω has a small negative imaginary part [7]. To study the stability of the system we must determine whether there exist solutions ω of Eq. (2.11) with negative imaginary part. This question can be systematically answered by studying the behavior of $F(\omega)$ in the complex plane as ω goes from $-\infty$ to $+\infty$ along the real axis, the number of unstable roots being given by the number of times the origin is encircled by the curve $F(\omega)$. We omit the details and give only the result—if the density decreases in the direction of gravity, i.e., $\varepsilon' > 2\alpha g > 0$, there is one unstable root. We will subsequently find this root by approximate means.

As we are primarily concerned with the case of low β, i.e., $\varepsilon'/\varepsilon \gg 1$, we disregard the last term in the denominator of Eq. (2.11) except for the imaginary part which arises from the singularity of the integral. This small term will eventually yield a slow Landau damping or growth of our solutions.

The integrals may now be performed to give

$$0=\sum_j\left\{\frac{\alpha_j}{m_j}-\left(\frac{\alpha_j\omega}{m_j}-\frac{k\varepsilon_j'}{2\Omega_j m_j}\right)\left[\frac{1-(k^2/2\alpha_j\Omega_j^2)}{\omega-(kg/\Omega_j)}+i\gamma_j\right]\right\}, \tag{2.12}$$

where

$$\gamma_j=\frac{\pi}{k\varepsilon/2\alpha_j|\Omega_j|}\exp\left[-\left(\omega-\frac{kg/\Omega_j}{k\varepsilon/2\alpha_j\Omega_j}\right)\right]$$

or $\gamma_j=0$ depending on whether the exponent is negative or positive. Equation (2.12) may now easily be reduced to a quadratic and solved. First we neglect the small terms γ_j, and terms of order m_e/m_i. Using Eq. (2.3) we find

$$\omega=\frac{1}{2}\left\{\left(\frac{k\varepsilon_i'}{2\alpha_i\Omega_i}\right)\pm\left[\left(\frac{k\varepsilon_i'}{2\alpha_i\Omega_i}\right)^2-4g\varepsilon_e'\right]^{\frac{1}{2}}\right\}. \tag{2.13}$$

This is to be compared with the hydrodynamic result $\omega_H=\pm i\sqrt{g\varepsilon'}$. We see that now the system is "stable" if

$$\frac{k\varepsilon'}{2\alpha_i\Omega_i}>2\omega_H$$

or

$$(ka_i)(\varepsilon' a_i)>\frac{4\omega_H}{\Omega_i}. \tag{2.14}$$

Thus we see that for weakly unstable systems the hydrodynamic approximation may break down even for $ka_i\ll 1$. It is interesting to note that the larger the density gradient, the more stable the systems. This may possibly be relevant in relation to the van Allen radiation belts. We also note that the condition (Eq. (2.14)) is considerably more favorable to stability than the requirement that the growth period be short compared to the time required to drift a wavelength.

Finally we return to Eq. (2.12) to examine the effect of the small imaginary terms in the dispersion relation. It is easily seen that only the electron terms contribute in the neighborhood of the roots (Eq. (2.13)) and that the negative sign in Eq. (2.13) yields the unstable root. In the "stable" limit $k\varepsilon'/2\alpha_i\Omega_i\gg 2\omega_H$ we have for the exponential dependence of the growth rate

$$\begin{aligned}\mathrm{Im}(\omega)&\propto e^{-4(g/\varepsilon k^2)\alpha_i\Omega_i\alpha_e|\Omega_e|}\\&\propto e^{-(8/\beta)(T_i/T_e)g\alpha_i/\varepsilon' k^2 a_i^2}.\end{aligned} \tag{2.15}$$

Thus at wavelengths comparable to the ion Larmor radius and for moderate β even this overstability may lead to sizable growth although it is not clear how seriously to take this in view of our assumptions β, $ka_i\ll 1$. For example, we might require for all wavelengths for which our calculation is valid, i.e., $1/a_i>k>\varepsilon'$, that the system be stable in the sense of satisfying Eq. (2.14) and having the exponent in Eq. (2.15) greater than 8. This effective stability condition is

$$\left(\frac{\varepsilon' a_i}{4}\right)^2>\frac{\alpha g}{\varepsilon'}>\beta\frac{T_e}{T_i}.$$

3. Confined plasma with cylindrical symmetry

In this Section we study the stability of a cylindrical plasma confined by a longitudinal magnetic field. Taking advantage of the results of the preceding Section, we are able to neglect the small drifts due to magnetic field gradients and expand the denominators which occur in the various integrals over the particle distribution function. On the other hand, in this Section we will do the calculation self-consistently, taking properly into account the radial dependence of the disturbances rather than assuming a localized perturbation.

The first problem we treat is that of a uniformly rotating plasma. It is easy to show in the magnetohydrodynamic approximation that such a plasma is unstable to long-wave length perturbations with a growth rate equal to $\sqrt{m-1}\,W$, where m is the azimuthal wave number and W the angular velocity. From the microscopic viewpoint the rotation of the plasma may be split into two parts, that associated with the diamagnetic current and that produced by a radial electric field. The diamagnetic current is carried by an azimuthal velocity of the particles equal to their mean velocity multiplied by the ratio of the Larmor radius to plasma radius. Hence $W_{\text{diamagnetic}}=(a_i/r)^2\Omega_i$. We see that the growth rate associated with the diamagnetic rotation is just such as to fall within our definition of weak instability. Thus the hydromagnetic approximation is inadequate for discussing the possible rotational instability associated with plasma diamagnetism. We proceed to calculate the stability of such a diamagnetic plasma allowing also for an electric field induced rotation of the same order as the diamagnetic rotation. In what follows we treat ω/Ω_i, $W/\Omega_i\approx O(a_i/r)^2$.

The plasma is assumed to be infinite in the z-direction. All perturbations are proportional to $\exp i(\omega t+kz+m\varphi)$; the present calculations will however be restricted to perturbations for which $k=0$. A further restriction to be imposed is that the plasma density is so low that the particles are unable to perturb the magnetic field. In addition to the usual expansion parameters of the modified magnetohydrodynamic approximation [1], $\beta=8\pi P/B^2$ where P is the plasma pressure will be considered to be a small quantity and calculations will be carried out to the lowest order in β; i.e., in the limit $\beta\to 0$. In this limit we can take the unperturbed magnetic field B to be constant and in the z-direction. Moreover, since the perturbed magnetic field $\delta\mathbf{B}=0$ in this limit, the perturbed electric field $\delta\mathbf{E}=\nabla\delta\Psi$ is the gradient of a potential.

3.1. Stationary state of the plasma

The initial distribution function $f_j(\mathbf{x},\mathbf{v})$ satisfies the Vlasov equation

$$\frac{\partial f_j}{\partial t}+\mathbf{v}\cdot\nabla f_j+\frac{e_j}{m_j}\left(\mathbf{E}+\frac{1}{c}\mathbf{v}\times\mathbf{B}\right)\cdot\frac{\partial f_j}{\partial\mathbf{v}}=0, \tag{3.1}$$

where $\mathbf{B}=[0,0,B]$ and B is constant. $\mathbf{E}=-(WB/c)[x,y,0]$ is a radial electric field; W is the constant angular velocity of guiding centers which is assumed to be a small quantity such that $W/\Omega_j=O(\bar{a}_j/r_0)^2$ where $\Omega_j=e_jB/m_jc$ is the Larmor frequency and $\bar{a}_j$

is the mean Larmor radius for particles of species j; r_0 is the radius of the plasma.

The unperturbed orbit equations are

$$\begin{aligned} \ddot{x} &= -\Omega_j [W x - \dot{y}] \\ \ddot{y} &= -\Omega_j [W y + \dot{x}] \\ \ddot{z} &= 0 , \end{aligned} \tag{3.2}$$

where $\dot{x} = \mathrm{d}x/\mathrm{d}t = v_x$ etc. The constants of the motion are the energy

$$\varepsilon_j = \frac{m_j}{2} (v^2 + \Omega_j W r^2) , \tag{3.3}$$

and the canonical angular momentum

$$L_j = m_j (x v_y - y v_x) + \frac{e_j}{c} r A_\varphi . \tag{3.4}$$

$A_\varphi = Br/2$ is the vector potential of the magnetic field and $r^2 = x^2 + y^2$.

The solution of Eq. (3.1) is an arbitrary function of the constants of the motion ε_j and L_j. A specific function will be assumed of the form

$$f_j(\mathbf{x}, \mathbf{v}) = \frac{A_j}{(2\pi v_j^2)^{3/2}} \exp\left(-\frac{\varepsilon_j + \omega_j L_j}{m_j v_j^2}\right). \tag{3.5}$$

The particle density $n_j(r) = \int f_j \mathrm{d}\mathbf{v}$ must be independent of species in the sense that $\delta n/n \ll (\bar{a}_j/r_0)^2$, since we are looking for effects of this order.

As it is also true that $\delta n/n \approx (L_\mathrm{D}/r_0)^2$ where L_D is the Debye length, we must require the Debye length to be much less than the ion Larmor radius or

$$1 \gg \beta > \frac{v_\mathrm{i}^2}{c^2} . \tag{3.6}$$

After integrating Eq. (3.5) over velocity space the following result is obtained for particle density

$$n(r) = \frac{N}{\pi r_0^2} \exp -\left(\frac{r}{r_0}\right)^2, \tag{3.7}$$

where $N = \pi r_0^2 A_j$ is the number of particles per unit length and A_j is independent of species. The radius of the plasma is r_0 where

$$\frac{1}{r_0^2} = \frac{1}{2 v_j^2} \{\Omega_j (W + \omega_j) - \omega_j^2\} .$$

This determines the parameter ω_j as

$$\begin{aligned} \omega_j &= \frac{\Omega_j}{2} \left\{1 - \sqrt{1 - \frac{4}{\Omega_j} (\overline{W}_\mathrm{i} - W)}\right\} \\ &= \overline{W}_j - W + \frac{1}{\Omega_j} (\overline{W}_j - W)^2 + \mathrm{O}\left(\frac{\bar{a}_j}{r_0}\right)^3 . \end{aligned} \tag{3.8}$$

In this equation $\bar{a}_j = v_j/\Omega_j$ and $\overline{W}_j = 2(\bar{a}_j/r_0)^2 \Omega_j$. Eq. (3.5) can be expressed as

$$\begin{aligned} f_j(\mathbf{x}, v) &= \frac{n(r)}{(2\pi v_j^2)^{3/2}} \\ &\exp\left\{-\left[\frac{v^2}{2 v_j^2} + \frac{\omega_j}{v_j^2} (x v_y - y v_x) + \frac{\omega_j^2 r^2}{2 v_j^2}\right]\right\}. \end{aligned} \tag{3.9}$$

This provides a complete description of the stationary state to be considered.

We note that $\overline{W}_j$ is the angular frequency associated with the motion of the particles carrying the plasma diamagnetic current. It provides a natural unit of angular frequency and we are interested in studying cases where $W/\overline{W} \approx 1$.

3.2. Solution of the unperturbed orbit equations

With the substitution $\xi = x + \mathrm{i}y$, Eqs. (3.2) simplify to

$$\begin{aligned} \ddot{\xi} + \mathrm{i}\Omega_j \dot{\xi} + \Omega_j W \xi &= 0 \\ \ddot{z} &= 0. \end{aligned} \tag{3.10}$$

The solution is

$$\begin{aligned} \xi(t) &= a\mathrm{e}^{\mathrm{i}\omega_a t} + b\mathrm{e}^{\mathrm{i}\omega_b t} \\ \dot{z} &= v_z , \end{aligned} \tag{3.11}$$

where

$$\omega_b = -\frac{\Omega_j + \sqrt{\Omega_j^2 + 4\Omega_j W}}{2} = W\left\{1 - \frac{W}{\Omega_j} \dots\right\}$$

$$\omega_a = -\Omega_j \left\{1 + \frac{W}{\Omega_j} - \left(\frac{W}{\Omega_j}\right)^2 \dots\right\}.$$

The complex constants a and b can be identified by the initial conditions

$$\begin{aligned} \xi(0) &= r\mathrm{e}^{\mathrm{i}\varphi} = a + b \\ \dot{\xi}(0) &= v_\perp \mathrm{e}^{\mathrm{i}\theta} = \mathrm{i}[\omega_a a + \omega_b b]. \end{aligned} \tag{3.12}$$

The solution may be expressed as

$$\xi \mathrm{e}^{-\mathrm{i}\omega_b t} = b + a\mathrm{e}^{\mathrm{i}(\omega_a - \omega_b)t} .$$

Since $b \cong r$, $a = v_\perp/\Omega_j$, $\omega_b \cong W$ and $\omega_a - \omega_b \cong -\Omega_j$ the unperturbed orbit consists approximately of a conventional Larmor orbit about a guiding center a distance $|b|$ from the origin which rotates with angular velocity W.

3.3. Linearized stability analysis

The linearized Vlasov equation is

$$\begin{aligned} &\frac{\partial}{\partial t} \delta f_j + \mathbf{v} \cdot \frac{\partial}{\partial \mathbf{x}} \delta f_j + \frac{e_j}{m_j} \left(\mathbf{E} + \frac{1}{c} \mathbf{v} \times \mathbf{B}\right) \cdot \frac{\partial}{\partial \mathbf{v}} \delta f_j \\ &\qquad = -\frac{e_j}{m_j} \left(\delta \mathbf{E} + \frac{1}{c} \mathbf{v} \times \delta \mathbf{B}\right) \cdot \frac{\partial f_j}{\partial \mathbf{v}} . \end{aligned} \tag{3.13}$$

We consider only the limit $\beta \to 0$ in which case $\delta \mathbf{B} \to 0$ and $\delta \mathbf{E} = \nabla \delta \Psi$. Perturbations will be considered of the form $\delta \Psi = \Psi(r) \exp \mathrm{i}(\omega t + m\varphi)$.

The first step is to integrate Eq. (3.13) along the unperturbed orbits:

$$\delta f_j = -\frac{e_j}{m_j} \int_{-\infty}^{t} \mathrm{d}t' \left(\delta \mathbf{E} \cdot \frac{\partial f_j}{\partial \mathbf{v}}\right)_{t'} .$$

Making use of Eq. (3.9) for f_j

$$\left(\delta \mathbf{E} \cdot \frac{\partial f_j}{\partial \mathbf{v}}\right) = -\frac{f_j}{v_j^2} \{\mathbf{v} \cdot \nabla \delta \Psi + \omega_j (x \delta E_y - y \delta E_x)\} .$$

f_j is a function of the constants of the motion of the unperturbed orbits and as such can be taken

outside the integral. $(\mathrm{d}/\mathrm{d}t)\ \delta\Psi = i\omega\delta\Psi + \mathbf{v}\cdot\nabla\delta\Psi$ and $x\delta E_y - y\delta E_x = im\,\delta\Psi$. It is assumed that ω has a small negative imaginary part* so that $\delta\Psi(-\infty)=0$. With these substitutions, and making use of Eq. (3.11) for $\xi(t)$, the following result obtains for δf_j,

$$\delta f_j = \frac{e_j f_j}{m_j v_j^2}\exp \mathrm{i}(\omega t + m\varphi)\left\{\Psi(r) - \mathrm{i}(\omega - m\omega_j)\int_{-\infty}^{0} \frac{\Psi(|\xi|)}{|\xi|^m}\xi^m \mathrm{e}^{\mathrm{i}\omega t}\,\mathrm{d}t\right\}. \quad (3.14)$$

In order to carry out the indicated time integration it is necessary to make an expansion in powers of $\lambda = \bar{a}_j/r_0$. It is assumed that ω/Ω_j, $W/\Omega_j = \mathrm{O}(\lambda^2)$ and we consider $v_\perp/r\Omega_j$ to be of order λ. A Taylor series is employed for $\Psi(|\xi|)$, i.e.,

$$|\xi(t)| = r + \delta r(t) \text{ and } \Psi(|\xi(t)|) = \Psi(r) + \delta r(t)\,\Psi'(r) + \frac{[\delta r(t)]^2}{2!}\Psi''(r)\ldots$$

$$= (\Psi - r\Psi' + \frac{r^2}{2}\Psi'') + \frac{|\xi(t)|}{r}(r\Psi' - r^2\Psi'') + \frac{|\xi(t)|^2}{2}\Psi''.$$

After some algebra we find the general term of the expansion is of the form

$$\xi^m \frac{|\xi|^{n-m}}{r^n} = \exp[im(\varphi + \omega_b t)]\left\{1 - n(W/\Omega_j) + \frac{(n^2-m^2)}{2}\left(\frac{v_\perp}{r\Omega_j}\right)^2 - \frac{im}{r^2\Omega_j}(xv_x + yv_y) + \frac{n}{r^2\Omega_j}(xv_y - yv_x)\right\}. \quad (3.15)$$

In deriving (3.15) we have of course only retained terms of the proper order; $(v/r\Omega_j)^2$, W/Ω_j. We have moreover dropped terms containing factors $\exp \mathrm{i}(\omega_a - \omega_b)t$ and $v_x^2 - v_y^2$ since they will become of higher order after subsequent integration.

After carrying out the time integration in Eq. (3.14) the result is

$$\delta f_j = \frac{e_j}{m_j v_j^2} f_j \exp[\mathrm{i}(\omega t + m\varphi)]\left\{\Psi(r) - \frac{(\omega - m\omega_j)}{(\omega + m\omega_b)} \times \left\{\Psi(r)\left[1 - \frac{im}{r^2\Omega_j}(xv_x + yv_y) - \frac{m^2}{2}\left(\frac{v_\perp}{r\Omega_j}\right)^2\right] + r\Psi'(r)\left[\frac{(xv_y - yv_x)}{r^2\Omega_j} - \frac{W}{\Omega_j} + \frac{1}{2}\left(\frac{v_\perp}{r\Omega_j}\right)^2\right] + \frac{r^2}{2}\Psi''(r)\left(\frac{v_\perp}{r\Omega_j}\right)^2\right\}. \quad (3.16)$$

It is now possible to calculate the perturbation of macroscopic variables. For example, the perturbation of charge density is

$$\delta\varrho_e = \sum_j e_j \int \delta f_j\,\mathrm{d}\mathbf{v} = \exp[\mathrm{i}(\omega t + m\varphi)]\sum_j \frac{n(r)e_j^2}{m_j v_j^2}\left(\Psi(r) - \frac{\omega - m\omega_j}{\omega + m\omega_b}\left\{\Psi(r)\left[1 - m^2\left(\frac{\bar{a}_j}{r}\right)^2\right] - r\Psi'(r)\left[\frac{\omega_j + W}{\Omega_j} - \left(\frac{\bar{a}_j}{r}\right)^2\right] + r^2\Psi''(r)\left(\frac{\bar{a}_j}{r}\right)^2\right\}\right). \quad (3.17)$$

* $\delta\psi = \lim_{\gamma\to 0}\psi(r)\exp \mathrm{i}m\varphi \exp(\mathrm{i}\omega + \gamma)t$ means that the perturbation is switched on adiabatically at $t=-\infty$. The same procedure obtains if we let $p = \mathrm{i}\omega + \gamma$ be the Laplace transform variable.

To complete the expansion procedure substitute ω_j from Eq. (3.8) and making use of Eq. (3.11)

$$\frac{1}{\omega + m\omega_b} = \frac{1}{\omega + mW}\left\{1 + \frac{mW^2/\Omega_j}{\omega + mW}\ldots\right\}$$

After carrying out the indicated multiplication

$$4\pi\delta\varrho_e = \exp[\mathrm{i}(\omega t + m\varphi)]\sum_j \frac{1}{L_j^2}\left\{\Psi\left[\frac{\overline{W}_j}{\bar{\omega}W} + \frac{\overline{W}_j(\overline{W}_j - 2W)}{W\Omega_j\bar{\omega}} - \frac{\overline{W}_j}{\Omega_j\bar{\omega}^2}\right] + \left[1 - \frac{\overline{W}_j}{\bar{\omega}W}\right]\left[\bar{a}_j^2\left(\frac{m^2}{r^2}\Psi - \frac{\Psi'}{r} - \Psi''\right) + r\Psi'\frac{\overline{W}_j}{\Omega_j}\right]\right\},$$

where $\bar{\omega} = (\omega + mW)/mW$, $\overline{W}_j = 2(\bar{a}_j/r_0)^2\Omega_j$ and $1/L_j^2 = 4\pi n(r)e_j^2/m_j v_j^2$. The first term gives zero after summing because $\overline{W}_j/L_j^2 = 8\pi cn(r)e_j/r_0^2 B$ which is equal and opposite for electrons and ions. In the remaining terms the contributions from the ions dominate so that we can omit the sum and finally obtain

$$4\pi\delta\varrho_e = \left(\frac{\bar{a}_i}{L_i}\right)^2\left[\frac{\overline{W}_i}{\bar{\omega}W} - 1\right]\exp[\mathrm{i}(\omega t + m\varphi)]\left[\Psi'' + \frac{\Psi'}{r} - \frac{m^2}{r^2}\Psi - \frac{2}{r_0^2}(r\Psi' - \nu\Psi)\right] \quad (3.18)$$

where

$$\nu = -\frac{(1/\bar{\omega}) + (\overline{W}_i/W) - 2}{\bar{\omega} - (\overline{W}_i/W)}.$$

$\delta\psi$ satisfies the differential equation $\nabla^2\delta\psi = +4\pi\delta\varrho_e$. It has already been assumed that $(L_i/\bar{a}_i)^2 \ll \lambda^2 \ll 1$ so that ψ must satisfy

$$\Psi'' + \frac{\Psi'}{r} - \frac{m^2}{r^2}\Psi - \frac{2}{r_0^2}(r\Psi' - \nu\Psi) = \mathrm{O}\left(\frac{L_i}{\bar{a}_i}\right)^2 \cong 0. \quad (3.19)$$

If the following substitutions are made

$$x = (r/r_0)^2,\ \mu = \frac{1+\nu}{2},\ s = \frac{m}{2},\ \Psi = \frac{y(x)}{\sqrt{x}}\exp\frac{x}{2},$$

this equation becomes

$$y'' + \left\{-\frac{1}{4} + \frac{\mu}{x} + \frac{1/4 - s^2}{x^2}\right\}y = 0, \quad (3.20)$$

which is Whittaker's equation [9]. The solutions are Whittaker functions $W_{\mu,s}(x)$ and $W_{-\mu,s}(-x)$. The asymptotic form for large $|x|$ is

$$\lim_{|x|\to\infty} W_{\mu s}(x) = x^\mu \mathrm{e}^{-\frac{x}{2}}\left\{1 + \sum_{l=1}^{\infty}\frac{1}{l!\,x^l}\prod_{l'=1}^{l}\left[s^2 - \left(\mu + \frac{1}{2} - l'\right)^2\right]\right\}. \quad (3.21)$$

If $\mu - \frac{1}{2} - s = n$ where n is an integer the sum terminates at $l = n + 2s$. The asymptotic form for ψ from this solution is $\lim \psi(r) = r^{m+2n}$ as $r\to\infty$. The second solution from $W_{-\mu,s}(-x)$ diverges like $\exp(r/r_0)^2$ so that boundary conditions at large r can be satisfied with the first solution dominating. This is an eigenvalue problem with the eigenvalues for ν or μ

$$\nu = 2\mu - 1 = m + 2n, \text{ and therefore}$$

$$\nu\bar{\omega} = \left\{ \frac{\overline{W}_i}{2\overline{W}} (\nu - 1) + 1 \pm \sqrt{\left[\frac{\overline{W}_i}{2\overline{W}} (\nu - 1) + 1 \right]^2 - \nu} \right\}, \tag{3.22}$$

where we have made use of Eq. (3.18). If $n=0$, $\omega = 2W - \overline{W}_i$ for $m=0$, and $\omega = 0$ for $m=1$. For $\nu > 1$ the condition for stability is

$$\left(\frac{\overline{W}_i}{2\overline{W}} (\nu - 1) + 1 \right)^2 > \nu, \text{ or } \frac{1+\sqrt{\nu}}{2} > \frac{W}{\overline{W}_i} > \frac{1-\sqrt{\nu}}{2}. \tag{3.23}$$

A symmetric form of this criterion is obtained by noting that the macroscopic velocity V_φ in the initial state is given by

$$\varrho_m V_\varphi = \sum_j \frac{m_j}{r} \int f_j (x v_y - y v_x) \, \mathrm{d}v$$

so that

$$V_\varphi = r(W - \overline{W}_i), \tag{3.24}$$

and the stability criterion for $m > 1$ is

$$\frac{\sqrt{\nu}}{2} > \frac{1}{2\overline{W}_i} \left(\frac{V_\varphi}{r} + W \right) > -\frac{\sqrt{\nu}}{2}. \tag{3.25}$$

Thus we see that the rotation associated with the plasma diamagnetic currents is not sufficient to induce instability by itself. However, if the rotation produced by a radial electric field exceeds this natural rotation by an appreciable factor, then the hydrodynamic instability occurs.

3.4. Application to the fast B_z-compression (Scylla)

It has been observed [4] that the plasma formed in a fast B_z-compression develops an $m=2$ instability after a quiescent period of about 5 μs. If the radial displacement is proportional to $\exp i[\omega t + m\varphi + kz]$ and only the $m=2$ mode grows, the plasma should appear to fission into two parts which have an apparent rotational frequency of $\mathrm{d}\varphi/\mathrm{d}t = -\mathrm{Re}\,\omega/2$. This is in fact observed and direct measurements from streak camera photographs give $\mathrm{Re}\,\omega/2 = 10^7 \mathrm{s}^{-1}$. The observed rotation is in the same sense as ion orbits in the external field.

On the basis of Kolb's measurements of ion temperature ($\Theta_i = 2$ keV), plasma radius ($r_0 = 0.8$ cm) and magnetic field (B = 50 kG) we can estimate $\overline{W}_i = 2(a_i/r_0)^2 \Omega_i \cong \frac{1}{4} \times 10^8 \mathrm{s}^{-1}$. For an $m=2$ instability, Eq. (3.22) gives

$$\mathrm{Re}\,\omega = -\left(W - \frac{\overline{W}_i}{2} \right) = 2 \times 10^7 \mathrm{s}^{-1},$$

from which we deduce that $W/\overline{W}_i = -0.3$. The stability predictions of the previous analysis are that $m=0$, 1 should be stable and from Eq. (3.23) the stability limits are

$$1.207 > \frac{W}{\overline{W}_i} > -0.207 \text{ for } m=2,$$

$$1.366 > \frac{W}{\overline{W}_i} > -0.366 \text{ for } m=3.$$

The experimental value of $W/\overline{W}_i = -0.3$ is in agreement with the observed fact that only the $m=2$ mode is unstable, although the quantitative agreement with theory is not to be taken seriously in view of the idealized theory and experimental inaccuracies. In another paper [4] it has been shown that the redistribution of currents associated with the decay of trapped magnetic field should produce rotations $W/W_i \approx 1$ and hence lead to $m=2$ instabilities.

3.5. Application to mirror machines

The geometry of a mirror machine makes an exact treatment of stability somewhat unpleasant. The present calculations for an infinite cylinder may be adapted to the mirror machine if we include the essential feature of the curvature of the field lines. It is well known [2] that the effect is similar to that of a gravitational field and produces flute instabilities with a growth rate of the order of $\sqrt{mg/r_0}$ where the effective gravitational constant is $g \sim v_i^2/R$, where R is the average radius of curvature of the field lines and v_i is the thermal speed of the ions. For sufficiently large

$$R \sim r_0^3/\bar{a}_i^2, \tag{3.26}$$

the instability is weak and $\sqrt{gk_0}/\Omega_i \sim (a_i/r_0)^2$ so that the magnetohydrodynamic approximation breaks down. This case is of some practical significance since in most experiments $\bar{a}_i/r_0$ is not very large and $r_0/R \ll 1$ and can be treated by a slight extension of the present calculations.

In order to take account of the fact that the curvature of the field lines increases with r we assume an equivalent gravitational force of the form

$$\left[\frac{m_i v_i^2}{R} \frac{x}{r_0}, \; \frac{m_i v_i^2}{R} \frac{y}{r_0}, \; 0 \right].$$

The unperturbed equations of motion are then the same as Eq. (3.2) if we simply replace W by $W_i = W - v_i^2/\Omega_i r_0 R$. The entire previous analysis can be carried through except that the final expansion produces an additional term. Eq. (3.14) is obtained with the new definition of ν:

$$\nu = -\frac{\left\{ \frac{1}{\bar{\omega}} \left(1 + \frac{v_i^2}{W^2 r_0 R} \right) + \frac{\overline{W}_i}{W} - 2 \right\}}{\bar{\omega} - \frac{\overline{W}_i}{W}}, \tag{3.27}$$

or

$$\nu\bar{\omega} = \frac{\overline{W}_i}{2\overline{W}} (\nu - 1) + 1 \pm \sqrt{\left[\frac{\overline{W}_i}{2\overline{W}} (\nu - 1) + 1 \right]^2 - \nu \left[1 + \frac{v_i^2}{W^2 r_0 R} \right]},$$

where the eigenvalues for ν are $\nu = m + 2n$ as before. The effects of rotation W are much the same here as in the previous section so we specialize to the case of no initial rotation, $W=0$, and find for the most unstable mode, $m=\nu$,

$$2\omega = -\overline{W}_i (1 - \nu) \pm \sqrt{\overline{W}_i^2 (1-\nu)^2 - 4\nu v_i^2/r_0 R}. \tag{3.28}$$

If finite Larmor radius effects had been omitted, i.e., $\overline{W}_i=0$, the result would have been

$$\omega^2=-\frac{\nu v_i^2}{r_0 R}.$$

Now, however, we can obtain stability if

$$\overline{W}_i^2(1-\nu)^2>4\nu v_i^2/r_0 R \text{ or if } \frac{\sqrt{\nu}}{\nu-1}\sqrt{\frac{r_0}{R}}<\frac{\bar{a}_i}{r_0}, \quad (3.29)$$

$$\text{and } \nu>1.$$

For $\nu=0$ $\omega=0, -\overline{W}_i$ which is stable, but for $\nu=1$ $\omega^2=-v_i^2/r_0 R$ so that this mode is still unstable.

The reason that the mode $\nu=m=1$ is unaffected by these finite Larmor radius corrections is easily understood in terms of the physical model given in Section 1. This mode corresponds to $\Psi=re^{i\varphi}$ so the electric field is a constant independent of position. The physical origin of the stabilizing effect is that the electric field, and hence the electric drift, are different for electrons and ions due to being averaged over the Larmor orbit. For a constant electric field this mechanism is obviously ineffective. However, this mode may perhaps be stabilized by an external conductor. For example, if the parameters are such that by Eq. (3.29) the mode $m=2$ is just stable, then the external conductor at radius $r/r_0=1.7$ will also stabilize $m=1$, as may be seen from the expansion of the Whittaker factors (Eq. 3.20). Since in practice one would of course have to place the conductor completely outside the plasma and as our theory does not apply within a Larmor radius of the surface, it is not clear whether this method of stabilization is feasible.

We have attempted to compare the stability criterion (Eq. 3.29) with the conditions in Coensgen's successful high temperature ion confinement experiment [3]. The data is not sufficiently accurate, nor the theory sufficiently refined to allow a comparison for low m [2, 3] but the stability criterion is certainly well satisfied for higher m values.

Work is in progress on another situation in which strong stabilizing effects are to be anticipated—the surface instabilities [5] such as are encountered in the pinch or stellarator configurations. These are characterized both by low growth rates and by very localized disturbances and may be strongly modified by finite Larmor radius effects.

Acknowledgment

This work was done under a joint General Atomic—Texas Atomic Energy Research Foundation program on controlled thermonuclear reactions.

References

[1] ROSENBLUTH, M. N., ROSTOKER, N., *Phys. Fluids* **2** (1959) 23.
[2] ROSENBLUTH, M. N., LONGMIRE, C., *Ann. Phys. (N.Y.)* **1** (1957) 120.
[3] COENSGEN, F. H., CUMMINGS, W. F., NEXSEN, W. E., JR., SHERMAN, A. E., *Phys. Rev. Letters* **5** (1960) 459.
[4] KOLB, A., ROSTOKER, N., American Physical Society, Division of Plasma Physics, Gatlinburg, Tennessee, Paper K-3, Nov. 2, 1960.
[5] ROSENBLUTH, M. N., Proceedings of Second U.N. International Conference on Peaceful Uses Atomic Energy, Geneva **31** (1958) 85.
[6] SUYDAM, B. R., Proceedings of Second U.N. International Conference on Peaceful Uses Atomic Energy, Geneva **31** (1958) 157.
[7] LANDAU, L., *J. Phys. U.S.S.R.* **10** (1946) 25.
[8] BERNSTEIN, I. B., FRIEMAN, E. A., KRUSKAL, M. D., KULSRUD, R. M., *Proc. Roy. Soc.* **A-244** (1958) 17.
[9] KAMKE, E., Differential Gleichungen (Chelsea Publishing Co., New York, 1948) 473.

CONTAINMENT OF POSITRONS IN AN ASYMMETRIC MIRROR GEOMETRY*

G. GIBSON**, W. C. JORDAN***, AND E. J. LAUER

LAWRENCE RADIATION LABORATORY, UNIVERSITY OF CALIFORNIA

LIVERMORE, CALIFORNIA, UNITED STATES OF AMERICA

The precessional surfaces on which charged particles move in an asymmetric mirror field have been investigated theoretically and experimentally. Two mirror coils (spaced $\simeq 2$ mean radii) have been tilted from their symmetric position to form a section of a "Bumpy Torus". Two-dimensional computations, similar to those reported elsewhere, of J (the action integral) as a function of the magnetic moment and starting position, ϱ, along the intersection of the I-plane (symmetry plane between the coils) and the S-plane (symmetry plane containing the axes of the coils) locate points on the adiabatic precessional surfaces. The character of the J versus ϱ curves is qualitatively the same as for the complete "Bumpy Torus". That is, the precessional surfaces are displaced toward the side of minimum separation of the coils. Experimentally these surfaces have been investigated by the technique of trapping positrons emitted from a gaseous radioactive source. The positrons are contained for many seconds. The effect of probes, inserted to some radial position in the I-plane, on the leakage of trapped particles at various radial positions through one of the mirrors is observed.

1. Introduction

The equations of motion of charged particles in a magnetic mirror geometry have not been solved analytically for the case of axial symmetry. The behavior of charged particles in an asymmetric mirror field, which is the subject of this paper, is even less tractable to an analytical treatment. It is necessary to resort to guiding-center approximations [1, 2, 3] and small deviations from symmetry [4] or numerical calculation of adiabatic invariants [5] in order to make any predictions of the motion in the asymmetric case. The latter approach has been used in the calculations reported below.

The geometry for which the precessional surfaces are calculated is one in which the coils are tilted equal amounts but in opposite directions from the symmetric case (i.e., one section of a "Bumpy Torus" which is described in [5]). Comparison of experiment with theory for this case would serve as a check on the validity of the longitudinal adiabatic invariant [6, 7]. Experimentally, the technique of trapping positrons emitted by a radioactive gas has been used. Information on the validity of the adiabatic theory for the symmetric case has already been obtained in this way [8]. Within certain limits the apparatus described in [8] is adaptable to the study of asymmetric cases. However, it is difficult to locate the individual surfaces experimentally because of a diffusion across the magnetic field which is predictable (see [5]) from the calculations. It is to be distinguished from the ordinary diffusion. The data to be presented confirm the existence of this "drift-surface diffusion" but do not establish the location of the individual surfaces. A comparison is made with the axially symmetric geometry where drift-surface diffusion does not occur. Experiments which make use of fast-moving probes are in progress at present in an attempt to locate the precessional surfaces for the asymmetric geometry.

2. Theory

Consider a static magnetic field of the mirror geometry such as that obtained from two coaxial coils. The precessional surface on which the guiding center of a charged particle of a given energy is constrained to move in the adiabatic theory can be specified for the symmetric case by the initial position and the transverse invariant ($\mu = p_\perp^2/B$) where $p_\perp$ is the momentum component transverse to the field B. Because of the axial symmetry there is a degeneracy with respect to the cross sections of the precessional surfaces normal to the axis, since for a particle starting at a given radial position the precessional surfaces enclose the same lines of force independent of $p_\perp$. However, the extension of a precessional surface along the lines of force does depend on $p_\perp$. When an asymmetry such as tilting the coils is introduced, the degeneracy is removed and the invariance of another parameter is necessary to specify the precessional surface. Here use is made of the longitudinal invariant $J = \oint p_\parallel \, dl$, where $p_\parallel$ is the component of momentum parallel to the field, dl is the element of path length parallel to the field, and the integral is carried out over a longitudinal period of the motion. For simplicity in calculating J and making comparisons with experiment, the asymmetric fields studied were those which result from

* Conference paper CN-10/175, presented by E. J. Lauer. Discussion of this paper is given on page 209. Translations of the abstract are at the end of this volume of the Conference Proceedings.

** Westinghouse Electric Corporation, Atomic Power Department, Pittsburgh, Pennsylvania.

*** The Bendix Corporation, Research Labs. Div., Southfield, Michigan.

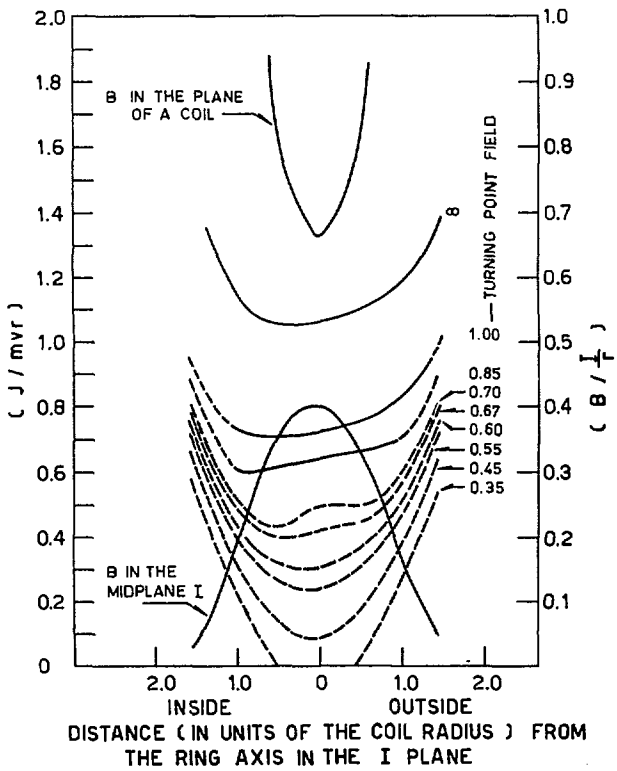

Fig. 1 Adiabatic invariants and field magnitude (B) for a tilt angle of 5.6° between coils and a coil spacing of 2.13 coil mean radii. For each of the curves of J versus distance from the ring axis in the I-plane, μ is a constant; mv = momentum, r = coil radius, I = amperes per coil.

two circular current loops tilted equal amounts but in opposite directions from their symmetric position. For this geometry there are two planes of symmetry, the S-plane containing the axes of the coils and the I-plane between the coils. The integral J is evaluated for various values of μ at points along the intersection of these two planes, the integration being along field lines which lie in the S-plane, as is done in [5] for the complete torus. In Fig. 1 the results of the calculation are plotted for an angle φ between the coils of $2\pi/64$ radian. The separation measured along the ring axis (the circle in the S-plane passing through the centers of the current loops and having its center at the intersection of the planes of the two current loops) is 2.13 times the radius of the current loops. As is to be expected the μ, J curves are similar to those calculated for the complete "Bumpy Torus" in which the coils are separated the same distance.

On each curve μ is a constant, therefore points of equal J on a given curve define the boundaries of the precessional surfaces in the I-plane. Compared with the symmetric case the surfaces are displaced toward the inside of the ring; and the smaller μ, the greater the displacement. Because the degeneracy has been removed, a diffusion across field lines is predicted which does not exist for the symmetric case. That is, when a scattering occurs, the transverse and longitudinal invariants change (a vertical transition in Fig. 1) so that the guiding center is constrained to move on a new precessional surface that has a different extension across field lines than did the original surface. (When the coils are moved sufficiently close together so that there is a region in which the field does not have a minimum at the I-plane with regard to motion along the flux lines, the μ, J curves exhibit two minima instead of the single minimum as in Fig. 1. This interesting case is not under consideration here.)

3. Experimental results and discussion

The motion of charged particles in the static asymmetric mirror geometry has been investigated experimentally by injecting energetic positrons (≤ 2.2 MeV) by means of a radioactive gas, Ne^{19}. The basic apparatus has been described in [8] and will be described only briefly here. Figure 2 shows the apparatus schematically with an angle of $2\pi/64$ (or 5.6°) between the coils. The flux lines are shown for the idealized case where the coils are replaced by circular current loops having radii equal to the mean radius of the coils. The vacuum chamber can be made a closed system with selective pumping provided by a surface which is kept at the temperature of liquid nitrogen and on which fresh titanium is intermittently deposited. The base pressure of the system under these conditions is in the range 10^{-8} to 10^{-7} mm Hg. However, there is no "pumping effect" on the Ne^{19} or the stable Ne which is added to serve as a known scattering gas. The partial pressure of the Ne^{19} is less than 10^{-12} mm Hg, which is negligible compared with the base pressure of the system. The positrons that escape along flux lines which intercept the scintillator pass through a thin aluminum window in the end of the vacuum tank and are counted if their energy is in a selected interval. The window is elongated so that the position of the detector can be varied within the range ± 15 cm from the axis of the vacuum tank along the line of intersection of the S-plane and a plane that is 71 cm from and parallel to the I-plane. Four probes, which can be inserted at right angles to each other in the I-plane, are used to investigate the motion of the trapped positrons. Two of the probes move parallel to the allowed motion of the counter. In all of the data to be reported the separation of the coils was 2.13 coil radii, the field at the ring axis in the midplane, I, was approximately 1300 gauss, and the detector was set at 0.50 ± 0.05 MeV which means that the maximum ratio of particle orbit diameter to coil mean diameter was of the order of 0.1.

Two different procedures are used in collecting data. The first is referred to as an equilibrium experiment, a typical one of which is described below. With the scattering gas density (for all of the equilibrium data presented, 10^{-4} mm Hg of Ne was added), counter position, probe position, and magnetic field set at the desired values the system is allowed to approach a steady state, i.e., the number of positrons emitted per unit time in the containment region is equal to the rate escaping, and the flow of Ne^{19} through a pipe-

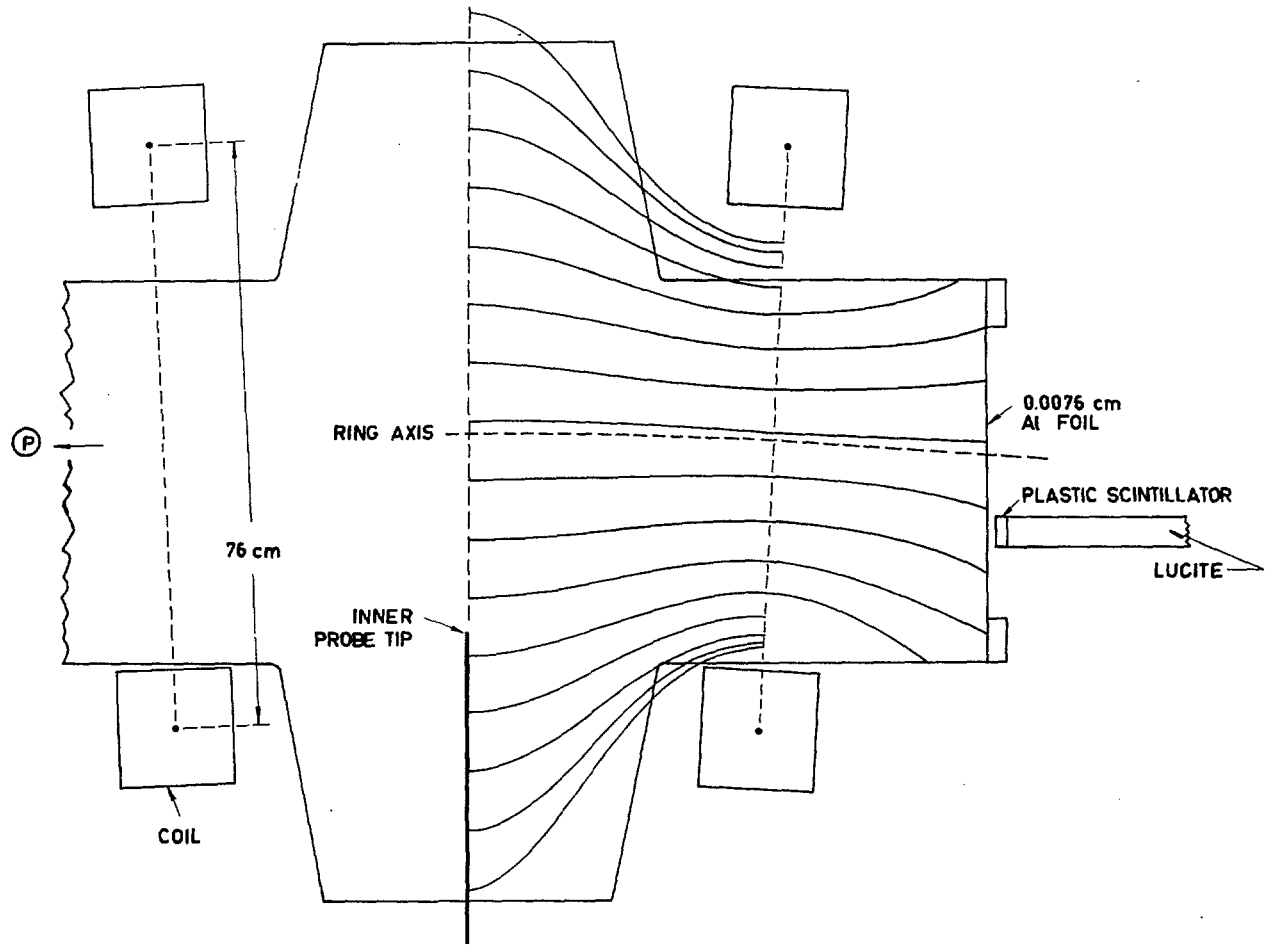

Fig. 2 Apparatus and magnetic flux lines, 5.6° angle between coils. P fast-opening valve and diffusion pump.

line into the vacuum chamber is held nearly constant. Then the flow of Ne^{19} is stopped by closing a valve, and the positrons in the energy interval 0.50 ± 0.05 MeV that strike the scintillator during a fixed time interval are counted and recorded. The magnetic field is turned off and a normalization count proportional to the Ne^{19} density is recorded during a time interval that occurs at a fixed time after the initial count. The probe position is then changed and the procedure repeated.

Of the positrons that are emitted between the mirrors while the field is on, some are born in the loss regions and promptly escape. Those that are born trapped will escape when, due to scattering, their velocity vector enters a loss cone—provided they behave according to adiabatic theory and are not intercepted by a wall or probe. If the current through the coil nearest the counter is less than the current through the far coil (positive bias by definition) most of the trapped particles which scatter into a loss cone will escape out of the counter end of the system. A bias of $+15\%$ with respect to the mean current was used for all of the equilibrium experiments. This value was selected as a compromise. It is sufficiently large to insure that most of the trapped particles escape at the counter end but not so large as to introduce a large perturbation in the mirror geometry to be studied. Examples of the data from such experiments are shown in Figs. 3 and 4 where the normalized counting rate is plotted as a function of probe position. (The probe positions and other linear dimensions are expressed in units of the mean radius of the coils, which is 38 cm.) Fig. 3 shows data obtained with the coils parallel and the counter 0.20 unit off axis while Fig. 4 shows similar data for the asymmetric geometry with $\varphi = 5.6°$ and the counter 0.11 unit inside the ring axis. As the probe is moved inward toward the ring axis it initially has no effect on the counting rate. Eventually it commences to remove the trapped particles which would normally be detected by the counter. If the probe is inserted far enough, it completely removes this component and any further travel produces no change in the counting rate. The prompt component of the counting rate is not appreciably affected by the probe. In Fig. 3 three of the curves are similar. The fourth curve differs only because the probe can intercept flux lines which pass through the scintillator. As the probe moves "in front" of the scintillator an extra component is added to the counting rate due to the trapped positrons which are scattered into the loss cone without annihilation in the probe. Hence a peak is observed on

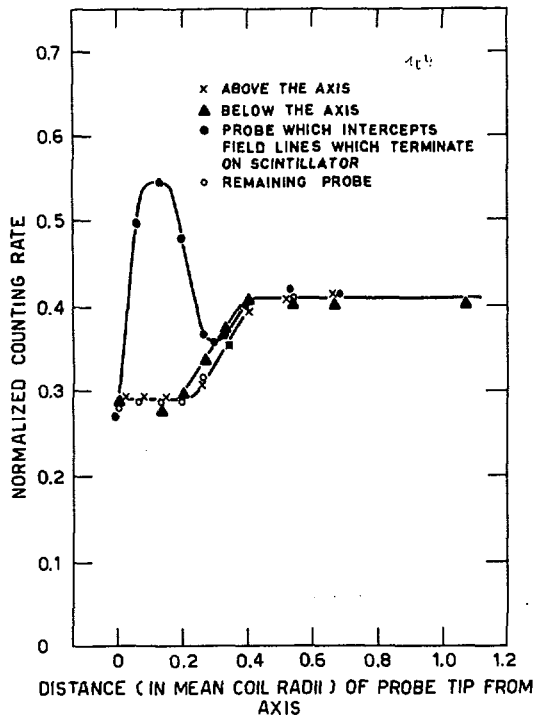

Fig. 3a Equilibrium counting rate normalized to source gas density as a function of the position of four probes which move at right angles to each other in the I-plane for symmetric mirror geometry and the counter 0.20 of a coil mean radius off axis.

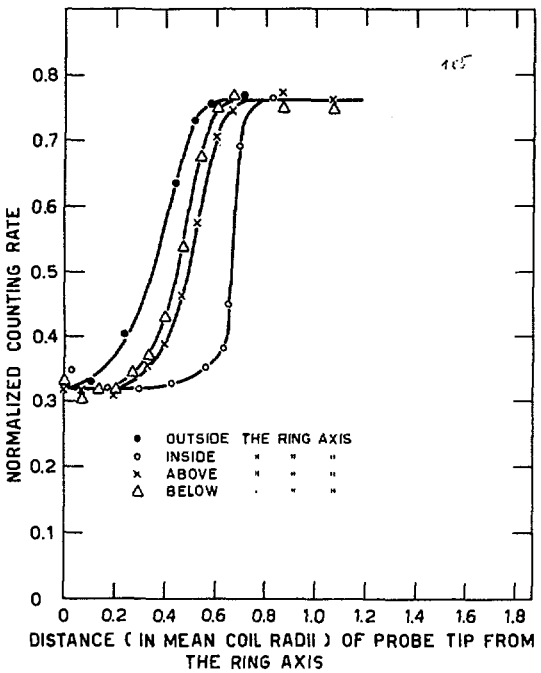

Fig. 3b Equilibrium counting rate normalized to source gas density as a function of the position of four probes which move at right angles to each other in the I-plane for a tilt angle of 5.6° between the planes of the coils and the counter 0.11 of a coil mean radius inside the ring axis.

this curve. A peak does not appear in Fig. 4 because in this instance the trapped positrons which the counter normally detects are intercepted at probe positions farther from the ring axis than those flux lines which intersect the scintillator.

Two positions (inner cutoff and outer cutoff) may be defined as the locations of the intersections of straight-line extrapolations of the transition parts of the curves with the horizontal lines through the minimum and maximum counting rates, respectively. These cutoff positions for each of the four probes for various counter positions and for various angles

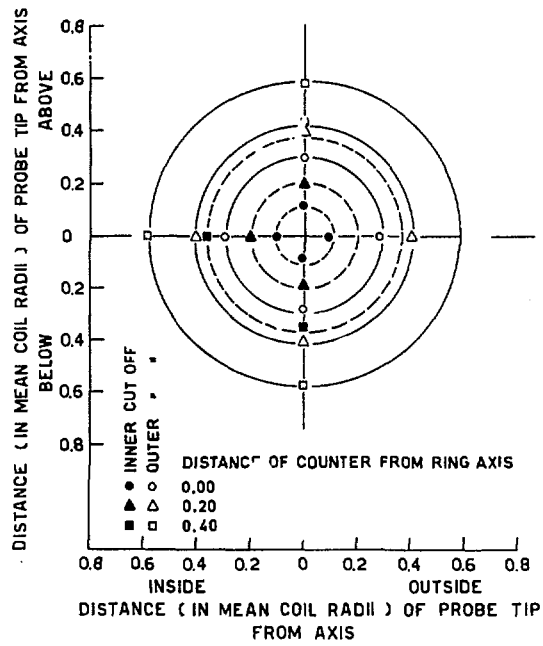

Fig. 4a Inner boundaries (dashed) are distance of a probe tip from the ring axis during an equilibrium experiment such that almost all (~90%) of the trapped positrons, which normally strike the scintillator with all probes withdrawn, are removed. Outer boundaries (solid) are the distance from the ring axis at which the probe removes ~10% of the trapped positrons. Symmetric geometry.

between the coils are summarized in Figs. 5, 6, 7 and 8.

For the symmetric case, Fig. 5, each probe has about the same effect for a given counter position, and the cutoff positions may be connected by circles. Solid lines are used for the outer cutoff and dashed lines for the inner cutoff. As the counter is moved farther from the axis the probes remove the trapped fraction at a greater distance from the axis. This is as predicted from the adiabatic theory which was described in Section 2; i.e., the intersection of the precessional surfaces with the I-plane are concentric circles, and particles can move radially only by the usual type of diffusion. During the time it takes for a particle to escape (time for the pitch angle of the velocity vector to change ~45° due to scattering), the particle may diffuse only a small distance (of the order of its orbit size) across the magnetic field. The

case of the counter on axis is special since the particles that pass through the axis are intercepted by the probes at a distance of an orbit diameter away from the axis. With the counter off axis, however, particles can be detected with guiding centers precessing on surfaces which lie both within and without the counter's radial position. Hence the probe must move "in front" of the counter to remove all of the trapped positrons which are normally detected. Therefore the circles drawn for the on-axis case, Fig. 5, would tend to be moved out radially with respect to the other two counter positions.

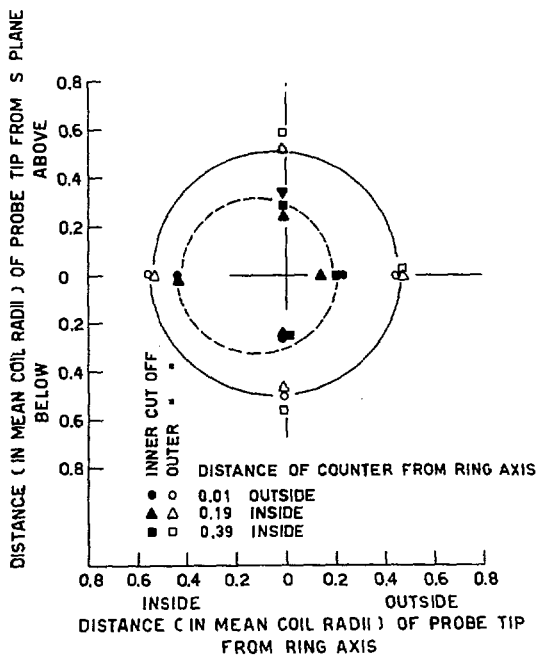

Fig. 4b Inner boundaries (dashed) are distance of a probe tip from the ring axis during an equilibrium experiment such that almost all (~90%) of the trapped positrons, which normally strike the scintillator with all probes withdrawn, are removed. Outer boundaries (solid) are the distance from the ring axis at which the probe removes ~10% of the trapped positrons. 1.4° angle between the planes of the coils.

Tilting the coils (see Figs. 6, 7 and 8) produces a marked difference in these results. The important observations are listed below:

(a) The trapped fraction which the counter normally detects is removed by a particular probe at a distance from the ring axis which is nearly independent of the counter position (observed for counter positions in the range approximately from the ring axis to 0.4 of a mean coil radius inside of the ring axis). This is observed even for very small tilt angles between the coils (~1°). This means that the particles move freely across flux lines within a well-defined boundary.* This

* It has been shown that this boundary is a real one associated with the field shape and is not a boundary set by the vacuum chamber wall. This was done by observing that the results are unchanged when the two coils and counter are shifted as a rigid unit relative to the vacuum chamber.

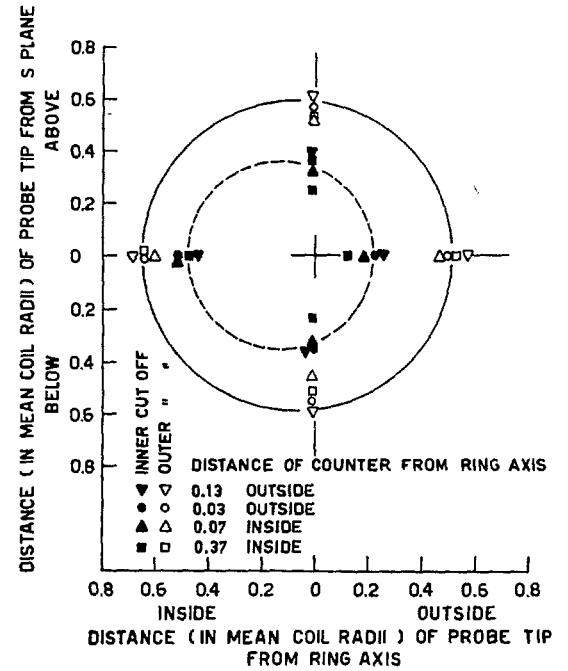

Fig. 4c Inner boundaries (dashed) are distance of a probe tip from the ring axis during an equilibrium experiment such that almost all (~90%) of the trapped positrons, which normally strike the scintillator with all probes withdrawn, are removed. Outer boundaries (solid) are the distance from the ring axis at which the probe removes ~10% of the trapped positrons. 2.8° angle between the planes of the coils.

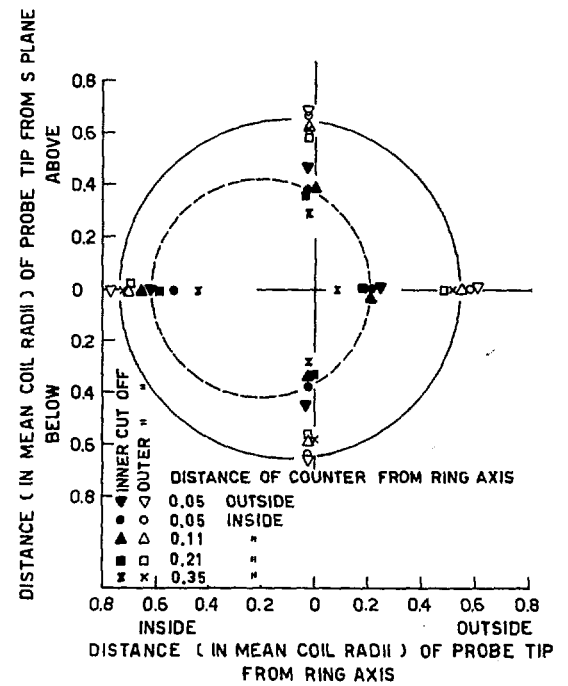

Fig. 4d Inner boundaries (dashed) are distance of a probe tip from the ring axis during an equilibrium experiment such that almost all (~90%) of the trapped positrons, which normally strike the scintillator with all probes withdrawn, are removed. Outer boundaries (solid) are the distance from the ring axis at which the probe removes ~10% of the trapped positrons. 5.6° angle between the planes of the coils.

motion could be caused by drift-surface diffusion or by a breakdown of the adiabatic invariants. The results are independent of scattering gas pressure (varied over the range 10^{-6} to 10^{-4} mm Hg of neon). This suggests that the motion is caused by drift-surface diffusion, since radial diffusion and end loss both vary linearly with pressure.

(*b*) The inner probe removes the trapped fraction at a much larger distance from the ring axis than the outer probe, and this inward shift increases with increasing tilt of the coils. The top and bottom probes have effects which are intermediate but similar to each other, as is expected because of the symmetry about the S-plane. The fact that the inner probe has an effect at a greater distance from the ring axis than the outer probe is consistent with the location of the precessional surfaces predicted from the results of the calculations, which are shown in Fig. 1. As the particle scatters and μ approaches a value such that the particle may escape (indicated by the solid portions of the curves), the precessional surfaces which enclose the minimum of the μ, J curves are shifted inward from the ring axis (~ 0.65 of a coil mean radius for a tilt angle of 5.6°). Furthermore, the theoretical results show that the shift of the minimum increases as the tilt angle increases.

Some data were obtained for a magnetic field strength 1.3 times that for the data presented. Also, the counter in some instances was set to detect positrons whose energy was in the range 1.00 $\pm$0.23 MeV. The conclusions are insensitive to these changes. The coils at various times were tilted in opposite directions. This did not affect the results.

Figure 9 shows the normalized trapped fraction observed as a function of the counter position for axial symmetry and for $\varphi = 5.6°$. For $\varphi = 5.6°$ few trapped particles escape at distances greater than 0.1 unit outside the ring axis. The maximum in the distribution is at approximately 0.18 coil mean radius inside the ring axis. If we follow the flux line from the scintillator to the I-plane this corresponds to about the same distance inside the ring axis. These results do not mean that trapped positrons do not exist farther outside the ring axis than this in the I-plane. In fact, with the counter at 0.33 coil mean radius outside the ring axis, trapped positrons were detected by moving a probe onto the flux lines terminating on the scintillator. These particles would escape near to or inside the ring axis if gas scattering dominated.

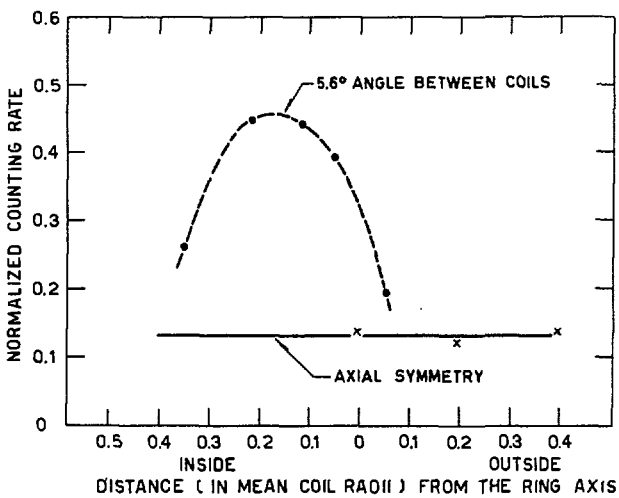

Fig. 5 The normalized trapped counting rate as a function of the counter position obtained from the equilibrium experiment. All probes withdrawn.

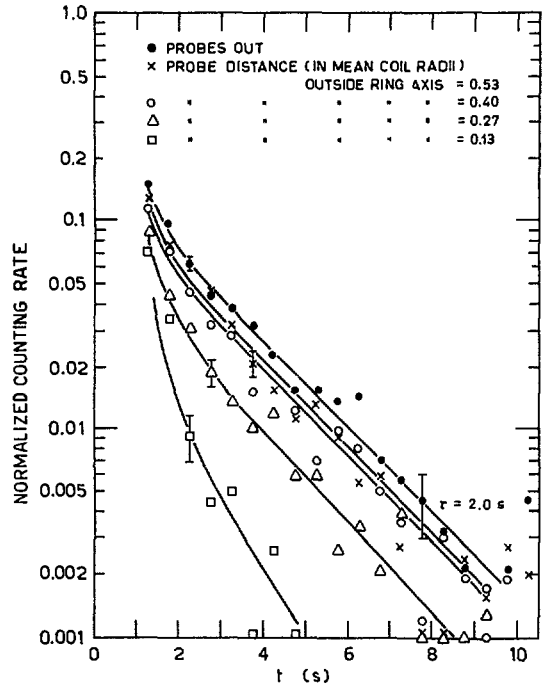

Fig. 6 Normalized counting rate as a function of time for a fast-empty experiment. 5.6° angle between the planes of the coils, 1.0×10^{-6} mm Hg stable neon added, counter 0.25 coil mean radius inside the ring axis.

The second procedure used in investigating the asymmetric mirror geometry is called the "fast-empty" experiment. In this experiment, after the flow of source gas, Ne^{19}, into the vacuum tank is stopped, a valve is opened suddenly (<0.05 sec) and the vacuum tank communicates with a large oil diffusion pump. The source gas is removed with an e-fold time of about 0.5 sec. The escape of the trapped particles in a particular energy interval is monitored as a function of time. In this way, the containment time and also a measure of the trapped fraction are obtained.

Figure 10 is an example of the decay of the counting rate as a function of time for various probe positions. The counter is located 0.25 coil mean radius inside the ring axis. Normalization is carried out by measuring the number of counts (both trapped and prompt) in a time interval just prior to opening the fast valve. The initial decay of the counting rate (e-fold time $\cong 0.5$ s) after opening the fast valve

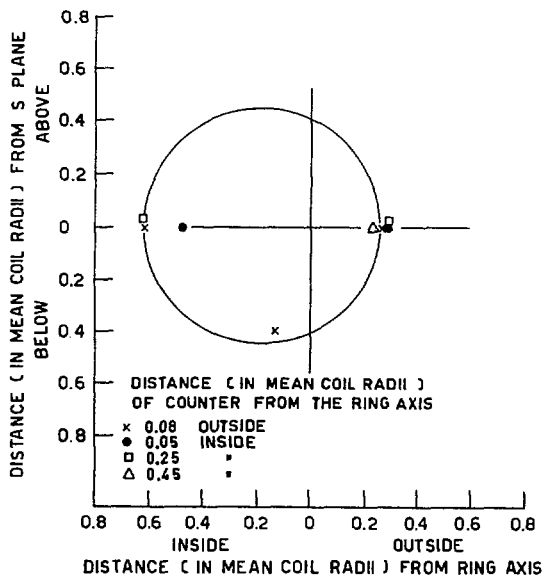

Fig. 7 Distance of a probe tip from the ring axis in the fast-empty experiment such that 50% of the trapped positrons, which normally strike the scintillator with all probes withdrawn, are intercepted. 5.6° angle between the planes of the coils.

is due to the removal of the prompt component. The counting rate due to the trapped particles persists with an exponential decay within our experimental uncertainty. For the asymmetric geometry where $\varphi = 5.6°$ and 1.0×10^{-6} mm Hg of Ne is added, a mean containment time of ~ 2 seconds is observed. Halving this pressure doubles the containment time, as is expected when multiple Coulomb scattering is the dominant loss mechanism. By projecting the straight line obtained on a semi-log plot (Fig. 10) back to zero time, one obtains the fraction of the total observed counting rate that is due to trapped positrons. By plotting these zero-time intercepts versus probe position, one obtains curves which may be compared with the equilibrium data of which Figs. 3 and 4 are examples. Since the containment time varies inversely as the pressure p and the energy loss rate is proportional to p, the energy degradation during a mean containment time is independent of p. Similarly, unless nonadiabatic effects are important, the effects of diffusion should be independent of the pressure. Hence the effects of probes on the trapped fraction may be compared for the two types of experiment. Of course the equilibrium experiments yield no information on the containment time. The probe position which can best be defined as a cutoff is the position at which half of the trapped component is removed, since the experimental uncertainties are rather large for the fast-empty experiment ($\sim \pm 0.1$). These data (Fig. 11) are in agreement with the corresponding equilibrium data.

Acknowledgement

The research work reported here was performed under the auspices of the United States Atomic Energy Commission.

References

[1] e.g., ALFVÉN, H., Cosmical Electrodynamics (Clarendon Press, Oxford, 1950), Chapter 2.
[2] SPITZER, L., *Astrophys. J.* **116** (1952) 299.
[3] NORTHROP, T. G. *Ann. Phys.* (*N. Y.*) **15** (1961) 79.
[4] MOROZOV, A. I., SOLOV'EV, L. S., *Zhurnal Tekhnicheskoi Fiziki* **30** (1960) 261.
[5] GIBSON, G., JORDAN, W. C., LAUER, E. J., *Phys. Rev. Letters* **4** (1960) 217.
[6] KADOMTSEV, B. B., Plasma Physics and the Problem of Controlled Thermonuclear Reactions (U.S.S.R. Academy of Sciences, Moscow, 1958) Vol. III, p. 285.
[7] NORTHROP, T. G., TELLER, E., *Phys. Rev.* **117** (1960) 215.
[8] GIBSON, G., JORDAN, W. C., LAUER, E. J., *Phys. Rev. Letters* **5** (1960) 141.

ENERGY BALANCE IN THE ASTRON DEVICE*

NICHOLAS C. CHRISTOFILOS

LAWRENCE RADIATION LABORATORY, UNIVERSITY OF CALIFORNIA

LIVERMORE, CALIFORNIA, UNITED STATES OF AMERICA

Most of the energy input in the Astron thermonuclear device is injected in the form of kinetic energy of relativistic electrons required to maintain the E-layer. The ratio of the thermonuclear energy, expected to be released in the device, to the input energy is of extreme interest in order to evaluate the device for practical applications. The life time of the electrons in the E-layer depends on the rate of energy loss by Coulomb collisions and Bremsstrahlung interaction with the plasma and by Schwinger radiation. The latter is proportional to (γ^4/R^2), whereas the others are lineraly proportional to the plasma density. The plasma pressure p_0 can be expressed as a function of the magnetic field at the surface of the E-layer, hence as a function of the electron energy (γV_0) and the E-layer radius, R, and the ratio (β) of the plasma pressure to the pressure of the external magnetic field at the surface of the plasma, namely, $p_0 = [\beta/(1-\beta)]\ (\gamma V_0)^2/8\pi R^2$.

As a consequence all three types of electron losses become proportional to $(1/R^2)$, whereas the rate of thermonuclear reactions per unit length of the plasma, along the axis of the E-layer, become proportional to (γ^4/R^2). Therefore, the ratio of the released thermonuclear energy to the input energy is only a function of the ratio β and the electron energy and is independent of the radius of the E-layer. This ratio has been calculated as a function of β, optimizing the E-layer electron energy. Results of these calculations will be presented. At a value of $\beta = 0.5$, approximately, the released thermonuclear energy is equal to the input energy required to maintain the E-layer. The electron energy however must satisfy two additional conditions, namely, it must be high enough to heat a plasma of a desired density up to the ignition temperature, and to permit the electrons to oscillate in and out of the plasma along the surface of the E-layer. The conditions required to achieve ignition temperature will be discussed. The parameters and the E-layer electron energy required for positive power gain will be presented.

1. Introduction

In the Astron device it is planned to trap the plasma within a pattern of magnetic lines which are closed onto themselves within a cylindrical vacuum vessel. This pattern is produced [1] by the combination of a vacuum axially symmetric field substantially parallel to the axis of symmetry with the field of a cylindrical layer of rotating electrons known as the E-layer. The rotating electrons are trapped irreversibly between two mirror fields by injection through an arrangement of resistors (Fig. 1). As the injected electrons move through the resistor region they lose most of the axial momentum acquired while falling in the mirror field, thus becoming trapped and oscillating between the two mirror coils. During the build-up of the E-layer the current in the mirror coils varies in such a way that both the vector potential and the axial component of the vacuum field remain constant at the injection point. As a result the total flux generated by the E-layer links all the newly injected electrons. When the number of electrons per unit length of the E-layer reaches the critical number (γ/r_e) required to reduce to zero the net magnetic field at the axis of symmetry, far from the ends, the self-mirror field is so strong that the azimuthal mechanical momentum of the electrons, far from the ends, is reduced to approximately one-half of the total momentum.

The thickness of the E-layer before the plasma is formed depends on the velocity distribution in the radial direction. After the E-layer is established the E-layer electrons lose energy by Schwinger radiation, as well as by bremsstrahlung and Coulomb collisions with the residual gas or plasma. Therefore they lose energy at a rate depending on the plasma density, as well as on their initial energy and Larmor radius. While losing energy they undergo scattering until the spatial momentum distribution is spread out to a very large solid angle as the electron energy approaches 1 MeV. Therefore, it can be assumed that the electrons are lost to the organized motion of the E-layer as soon as their energy becomes 1.5 MeV ($\gamma = 4$). Since the E-layer must be maintained in a steady state, continuous injection of electrons is required in order to replace the particles which have lost their energy. As a result, the E-layer electrons have a continuous energy spectrum. The upper limit is at the injection energy, while the lower limit is the assumed cutoff at $\gamma = 4$. The velocity distribution caused by scattering is Maxwellian. Therefore, we can define a mean thermal velocity as being equal to $\langle \Theta^2 c^2 \rangle^{1/2}$ where $\langle \Theta^2 \rangle^{1/2}$ is the probable scattering angle. Accordingly, a scalar pressure p can be assigned to the E-layer,

$$p = \frac{1}{2} \Theta^2 \gamma m c^2 \qquad (1)$$

* Conference paper CN-10/148, presented by N. C. Christofilos. Translations of the abstract are at the end of this volume of the Conference Proceedings.

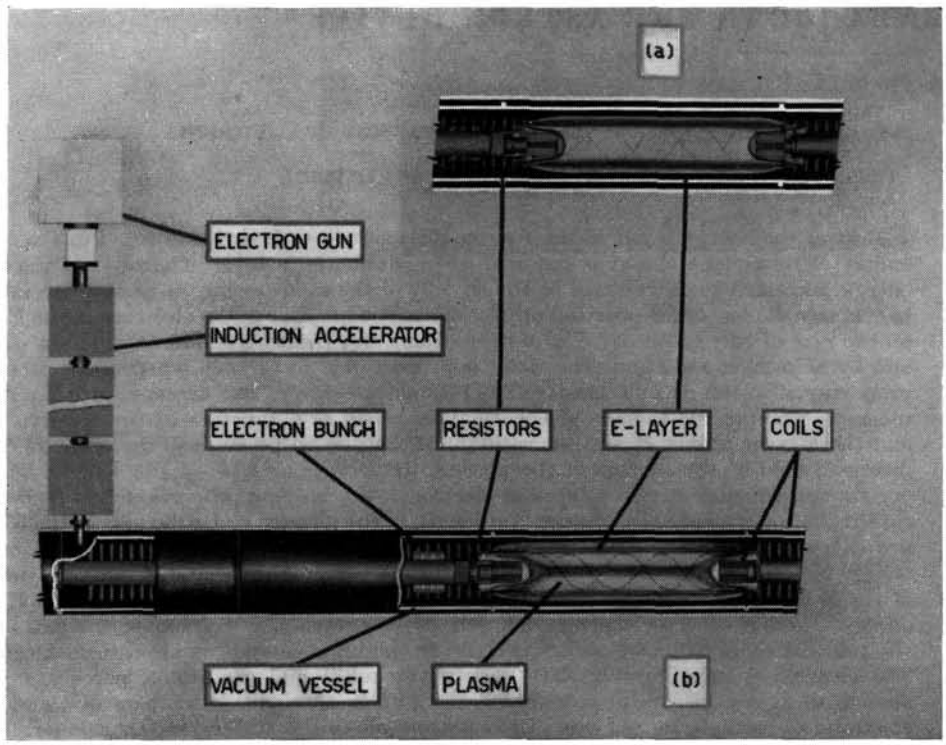

Fig. 1 E-layer and plasma configurations.

where $\Theta^2\gamma$ is averaged through the energy spectrum. An analytical expression does not exist for a self-consistent density distribution in the radial direction. By extrapolating from a solution for a planar E-layer we find that its thickness, before the plasma is formed, is equal approximately to the mean gyration radius (Fig. 1). However, after the plasma has been built up to a substantial pressure, the E-layer thickness is reduced considerably (Fig. 1a).

We have carried out a self-consistent equilibrium solution of the plasma pressure distribution, assuming that the E-layer is very thin [1]. This, however, is a simplified mathematical picture of the plasma pressure profile. Since the E-layer can never become very thin, the derived plasma pressure profile should be considered as being only approximate, but still very useful for certain calculations on the Astron, e.g., energy balance.

As soon as the closed magnetic field pattern is established, plasma can be trapped therein. Initially, a low temperature plasma is formed by ionization of neutrals through Coulomb collisions with the E-layer electrons. Thereafter, the continuing energy loss of the E-layer electrons by Coulomb collisions with the plasma electrons heats the plasma up to a temperature depending on the diffusion and other plasma losses as well as on the number of the E-layer electrons.

Since the energy loss of the E-layer electrons is a necessary price to pay in order to establish and maintain the closed pattern of magnetic lines, it would be very convenient if the plasma and E-layer parameters could be properly chosen so that the Coulomb collision energy loss is adequate to heat the plasma up to the so-called ignition temperature and maintain it at this temperature. In this way we will need no other heat sources, or any requirement for charged-particle injection or compression or ohmic heating of the plasma, etc. Furthermore, Coulomb collision heating of the plasma does not create any macroscopic electric fields or disturb the magnetic field at all. Preliminary calculations [1] have shown that the E-layer electron energy loss is sufficient to heat the plasma up to ignition temperature. In these calculations the diffusion losses were assumed to be almost equal to the theoretical value. However, it is quite possible that, due to microturbulences or other effects, that the actual diffusion loss can be much larger than the theoretical value predicted by classical diffusion theory. Therefore the selected parameters must be such as to allow a generous margin between actual and theoretical diffusion losses. It appears that the optimum parameters for the highest ratio between the thermonuclear power produced and the electrical power consumed do provide a large enough margin to allow a diffusion loss of more than ten times the theoretical value. In view of these results the parameters of the Astron device will be chosen on the basis of the optimum ratio of the produced to the consumed power. Thereafter, we shall calculate the ratio between the permissible and theoretical diffusion losses, as well as calculate the existing margin against other plasma losses, Schwinger radiation, bremsstrahlung, etc. In order to compare the produced thermonuclear power to the E-layer electron losses let us express

them in the same units. It appears that it is convenient to express both the energy release and the electron losses in units of the quantity ψ defined as

$$\psi = \left(\frac{\gamma^4}{\pi R^2 r_e}\right) \cdot (mc^2)\ \text{ergs/cm}^3, \tag{2}$$

where mc^2 is the electron rest energy, r_e is the classical electron radius, γ the E-layer electron energy in (mc^2) units, and R is the mean radius of the E-layer. The unit ψ is equal to the mean energy density of the E-layer multiplied by γ^2.

At this time it might appear somewhat premature to derive the parameters of a power reactor while there is not yet experimental evidence or proof of the basic concepts of the Astron device. However, only by knowing the parameters and the properties of an Astron power reactor can one possibly design a meaningful experiment to prove conclusively the Astron concept.

2. Rate of thermonuclear energy release in the Astron device

It is contemplated that, eventually, the Astron power reactor will operate on D-T reactions. The tritium will be regenerated in a blanket containing Li^6 and enclosing the reaction volume. Hence, the total energy released per reaction is 22 MeV or $(43\, mc^2)$. Under this condition the energy w_f released per unit volume of plasma is

$$w_f = 43\ (mc^2)\ (n^2/4)\ (\overline{\sigma v}_{DT})\ \text{ergs/cm}^3\,\text{sec}, \tag{3}$$

where n is the plasma ion density. The plasma pressure p is

$$p = 2\, n\, (eu/mc^2)\, mc^2, \tag{4}$$

where (eu/mc^2) is the mean kinetic energy of the plasma ions or electrons in units of mc^2. The energy released per unit length of the plasma is

$$W_f = \pi\, R^2 \cdot w_f \cdot \eta_0, \tag{5}$$

where

$$\eta_0 = \frac{2}{R^2 p_0^2} \int_0^{R_0} p^2\, r\, dr \tag{6}$$

and p_0 is the peak value of the pressure in the plasma. This occurs at $r = R$ where the magnetic field vanishes; R is the mean radius of the E-layer and R_0 the radius of the plasma volume. The value of η_0 depends on the particular equilibrium solution selected. The general expression for the pressure as a function of the magnetic field (B_w, B_i) at the outer and inner surfaces, respectively, of a thin E-layer is (see [1] p. 9):

(a) In the region enclosed by the E-layer $(0 < r < R)$,

$$p = \frac{B_i^2}{8\pi}\{\sinh(\lambda R^2) - \sinh[\lambda(r^2 - R^2)]\}; \tag{7}$$

(b) In the region outside of the E-layer $(R < r < R_0)$,

$$p = \frac{B_w^2}{8\pi}\{\sinh[\lambda(R_0^2 - R^2)] - \sinh[\lambda(r^2 - R^2)]\}, \tag{8}$$

where

$$\lambda R^2 = \sinh^{-1}\left(\frac{B_w}{B_i}\, y\right), \tag{9}$$

$$\lambda R_0^2 = \sinh^{-1}(y) + \sinh^{-1}\left(\frac{B_w}{B_i}\, y\right), \tag{10}$$

and

$$y = \sqrt{8\pi p_0}/B_w. \tag{11}$$

The maximum plasma pressure can be expressed as a function of the field B_w and the quantity β, which is defined usually as

$$\beta = 8\pi p_0/B_0^2, \tag{12}$$

where B_0 is the value of the magnetic field at the surface of the plasma. The maximum plasma pressure is

$$p_0 = (B_0^2 - B_w^2)/8\pi. \tag{13}$$

Equations (11), (12), and (13) yield

$$p_0 = \frac{B_w^2}{8\pi}\left(\frac{\beta}{1-\beta}\right), \tag{14}$$

$$y = [\beta/(1-\beta)]^{\frac{1}{2}}. \tag{15}$$

We observe that the pressure profile is a function of both β and the ratio (B_w/B_i). Thus the quantity η_0 is a function of β only for a given value of (B_w/B_i). The values of η_0 and R_0 as a function of β for $(B_w/B_i) = 10$ are listed in Table I.

TABLE I

β	η_0	R_0/R
0.50	0.93	1.14
0.60	0.96	1.15
0.70	0.99	1.16
0.80	1.04	1.18
0.90	1.11	1.20
0.95	1.17	1.22
0.97	1.21	1.23

The field, B_w, just outside the E-layer is (see [1] p. 10)

$$B_w = mc^2\, (\zeta + 1)\, (\gamma \cos\delta)/(eR), \tag{16}$$

where δ is the angle between the mechanical azimuthal to the total momentum of the electrons, and ζ is the "loading factor" of the E-layer defined as the ratio of the actual number of electrons of the E-layer per unit length to the critical number γ/r_e. The value of ζ is

$$\zeta = \frac{B_w + B_i}{B_w - B_i}. \tag{17}$$

The rate of energy release W_f per unit length can now be written in a more convenient form thus

$$W_f = 0.042\left[F(u)\, \eta_0\, (\zeta+1)^4 \cos^4\delta \left(\frac{\beta}{1-\beta}\right)^2\right]\psi\ \text{ergs/cm}, \tag{18}$$

where

$$F(u) = (\overline{\sigma v}_{DT}/r_e)\ (mc^2/eu)^2\ \text{cm}^2/\text{sec}. \tag{19}$$

We observe that the rate of energy release depends on the quantity β only if the plasma temperature and the E-layer parameters are fixed. For given β and plasma temperature the produced power is proportional to (γ^4/R^2), i.e., depends in the same way on the E-layer parameters as the Schwinger radiation.

3. E-layer electron losses

The E-layer electrons lose energy by Coulomb collisions, bremsstrahlung, and synchrotron radiation. respectively, at a rate

$$-\dot{\gamma}=a+(\xi a)\,\gamma+b\,\gamma^2 \text{ rest mass units/sec}, \quad (20)$$

where

$$a=n_0\,\sigma_0\,c, \quad (21)$$

$$\sigma_0=4\,\pi\,r_e^2\ln(\overline{\Lambda}). \quad (22)$$

The value of $\ln(\overline{\Lambda})\approx 20$, thus $\sigma_0=2\times10^{-23}$ cm^2; c is the velocity of light; $\xi\gamma$ is the ratio of bremsstrahlung loss to Coulomb collision loss, for hydrogen $\xi=1.5\times10^{-3}$; and the coefficient b is

$$b=2\times10^{-9}\,\overline{B}^2\cos^2\delta, \quad (23)$$

where $\overline{B}$ is the rms value of the field acting upon the E-layer electrons which oscillate about a mean value within the thickness of the layer. The highest energy electrons oscillate about a field $(B_w/2)$. The instantaneous value of the field acting upon these electrons is

$$B=(B_w/2)\cdot(1+\cos\omega t), \quad (24)$$

where ω is the betatron frequency. The average value of B^2 is

$$\overline{B^2}=\frac{3}{8}\,B_w^2. \quad (25)$$

The lower energy electrons oscillate about a smaller mean value of the field. However, since they are scattered to large angles, they travel part of the time in a field as high as B_w. The average value of B^2 is somewhat smaller for the lower energy electrons than the value given in Eq. (25). However, if we adopt for all the electrons the value of $\overline{B^2}$ as given in Eq. (25), the error will be unimportant, resulting in somewhat smaller lifetime. Of course, the mean value of the orbit radius is the same for all the electrons in the thin layer approximation.

The lifetime T_e of the E-layer electrons is obtained by integrating Eq. (20) namely,

$$T_e=2\,\varphi/q, \quad (26)$$

where

$$\varphi=\left[\tan^{-1}\left(\frac{2b\gamma_0+\xi a}{q}\right)-\tan^{-1}\left(\frac{2b\gamma_1+\xi a}{q}\right)\right] \quad (27)$$

$q^2=4\,ab-(\xi\,a)^2$,

γ_0 = the electron injection energy,

and

γ_1 = the cutoff energy, or, $\gamma_1=4$.

The power required to maintain the E-layer is

$$W_e=(\gamma\,mc^2)\,N_e/T_e \text{ ergs/cm sec}. \quad (28)$$

Since $N_e=\zeta\,\gamma/r_e$, Eq. (28) becomes

$$W_e=\zeta\,\frac{\gamma^2}{r_e}\,\frac{mc^2\,q}{2\varphi} \text{ ergs/cm}. \quad (29)$$

The quantity q can be written

$$q=\sigma_0 c n_0\left(4\frac{b}{a}-\xi^2\right)^{1/2}. \quad (30)$$

The coefficients b and a are proportional to B_w^2 and the plasma density, respectively. Since the plasma density is proportional to B_w^2 we observe that the ratio b/a is independent of the energy density ψ and depends only on the plasma temperature and on the value of cos δ. Substituting the plasma density and the other quantities from Eqs. (2), (14), (16), (29), and (30), we find:

$$W_e=\frac{0.0304}{\varphi}\left[\zeta(\zeta+1)^2\cos^3\delta\left(\frac{mc^2}{eu}\right)^{\frac{1}{2}}\left(\frac{\beta}{1-\beta}\right)^{\frac{1}{2}}\right]\psi \quad (31)$$

$$\varphi=\tan^{-1}\left[\frac{\lambda\gamma_0+(\xi/\lambda)}{\sqrt{2}}\right]-\tan^{-1}\left[\frac{4\lambda+(\xi/\lambda)}{\sqrt{2}}\right] \quad (32)$$

$$T_e=100\left(\frac{R}{\gamma}\right)^2\left(\frac{eu}{mc^2}\right)^2\left(\frac{1-\beta}{\beta}\right)^{\frac{1}{2}}\frac{\varphi}{(\zeta+1)^2\cos^3\delta}, \quad (33)$$

where T_e is in seconds and where

$$\lambda^2=2\,(b/a) \quad (34)$$

or

$$\lambda=0.32\,(\cos\delta)\left(\frac{eu}{mc^2}\right)^{\frac{1}{2}}\left(\frac{1-\beta}{\beta}\right)^{\frac{1}{2}}. \quad (34a)$$

The term ξ^2, in the quantity enclosed by parantheses in Eq. (30), is negligible in comparison with the term $4\,b/a$ in the region of parameters of interest. Thus, it has been omitted in the derivation of Eq. (32).

4. Selection of parameters optimizing the energy balance

We shall derive in this section the optimum conditions to achieve positive power gain. We define a new quantity Q, the quality of the reactor, as the ratio of the actual produced electric power to the total electric power required to operate the reactor, i.e., to maintain the E-layer and energize the external coils generating the vacuum field B_0. The quality Q of the reactor is

$$Q=\frac{\eta_e\,W_t}{[(1/\eta_a)-\eta_e]\,W_e+W_c}, \quad (35)$$

where η_e and η_a are the efficiency of the power plant and the electron accelerator, respectively. It is assumed that the E-layer electron energy loss is collected in the form of heat, thus producing electric power at a rate $\eta_e\,W_e$.

The quantity W_c is the power required per unit length of the reactor to energize the external coils generating the vacuum field:

$$W_c=2\cdot\left(\frac{D+1}{D-1}\right)\frac{B_w^2}{(1-\beta)}\,\frac{\varrho}{s} \text{ watts/cm}, \quad (36)$$

where D is the ratio of the outer to the inner radius of the coil, B_w and β are defined in Sections 2 and 3, ϱ and s are the specific resistivity and the space factor of the coil, respectively. Expressing the coil loss in units of ψ and substituting $\varrho = 1.8 \cdot 10^{-6}$ ohms cm, we find

$$W_c = 113 \left(\frac{D+1}{D-1}\right) \frac{(\zeta+1)^2 \cos^2\delta}{s\gamma^2(1-\beta)} \cdot \psi \text{ erg/cm sec} . \quad (37)$$

Equations (18), (31), (35), and (37) yield

$$Q = \frac{4.2\,[F(u)\,\eta_0\,(\zeta+1)^2\cos^2\delta]\left(\frac{\beta}{1-\beta}\right)^2 \eta_e}{\frac{3.04}{\varphi}\left(\frac{1-\eta_e\eta_a}{\eta_a}\right)\zeta\left(\frac{\beta}{1-\beta}\frac{mc^2}{eu}\right)^{\frac{1}{2}}\cos\delta + \frac{1.13}{s(1-\beta)}\left(\frac{D+1}{D-1}\right)\left(\frac{100}{\gamma}\right)^2} . \quad (38)$$

We observe that the quality of the reactor is independent of the radius of the E-layer. The magnetic coil losses are calculated for conventional conductors at room temperature. However, recent developments indicate that superconductive lossless coils are not beyond the realm of the technology a few years hence, while supercooled coils as proposed by R. F. Post will reduce the coil losses to a negligible amount in comparison to the E-layer losses. Therefore the quality Q_0 of the reactor for zero coil losses becomes

$$Q_0 = 1.38\,\varphi\left(\frac{eu}{mc^2}\right)^{\frac{1}{2}} F(u)\,\eta_0 \frac{(\zeta+1)^2}{\zeta}\cos\delta\left(\frac{\beta}{1-\beta}\right)^{\frac{3}{2}}\left(\frac{\eta_e\eta_a}{1-\eta_e\eta_a}\right) . \quad (39)$$

The quantity $F(u)\,(eu/mc^2)^{\frac{1}{2}}$ is maximized for a temperature of 20 keV.

Let us calculate the quantities Q and Q_0 for a plasma temperature of 20 keV assuming the following numerical values:

$$\eta_e = 0.45, \qquad \eta_a = 0.50;$$
$$\zeta = 1.22, \qquad \cos\delta = 0.5;$$
$$D = 2, \qquad s = 0.7.$$

The quantity $F(u) = 1$ for $eu = 20$ keV. After substitution of the numerical values, Eqs. (38) and (39) become

$$Q = \frac{[\beta/(1-\beta)]^2\,\eta_0}{\frac{6.25}{\varphi}\left(\frac{\beta}{1-\beta}\right)^{\frac{1}{2}} + \frac{2.09}{1-\beta}\left(\frac{100}{\gamma}\right)^2} \quad (40)$$

$$Q_0 = 0.160\,\eta_0\varphi\left(\frac{\beta}{1-\beta}\right)^{\frac{3}{2}} . \quad (41)$$

The pertinent quantities φ, Q and Q_0 are given in Tables II and III as functions of β and γ.

In Table II the values of a new quantity $\varkappa$ are given also. The quantity $\varkappa$ is unique to the Astron device; it can be defined as the ratio of the kinetic energy of the plasma to the kinetic energy of the electrons of the E-layer, namely,

$$\varkappa = \left[2\pi \int_0^{R_0} pr\,dr\right] \Big/ \left[\bar{\gamma} mc^2 (\zeta\gamma_0/r_e)\right] , \quad (42)$$

TABLE II

β	η_p	$\varkappa$	φ		
			$\gamma=10$	$\gamma=100$	$\gamma=200$
0.5	1.04	0.26	0.094	1.033	1.23
0.6	1.07	0.40	0.078	0.967	1.19
0.7	1.11	0.65	0.062	0.878	1.14
0.8	1.15	1.15	0.048	0.758	1.05
0.9	1.22	2.75	0.044	0.572	0.88
0.95	1.27	6.00	0.030	0.417	0.69
0.97	1.29	11.00	0.023	0.325	0.57

where $\bar{\gamma} = \gamma_0/2$ is the mean energy of the E-layer electrons. After substitution of the values of quantities according to the relations derived in Sections 2 and 3, Eq. (42) becomes

$$\varkappa = \frac{(\zeta+1)^2}{4\zeta}(\eta_p \cos^2\delta)\left(\frac{\beta}{1-\beta}\right) \quad (43)$$

where

$$\eta_p = \frac{2}{p_0 R^2}\int_0^{R_0} pr\,dr . \quad (44)$$

In the useful range of ζ (1 to 1.25) the expression $(\zeta+1)^2/4\zeta$ is approximately unity. Thus the quantity $\varkappa$ is a function only of β and $\cos\delta$. For $\cos\delta = 0.5$

$$\varkappa = (\eta_p\beta)/4(1-\beta). \quad (45)$$

The quantities $\varkappa$, Q_0, Q are plotted in Figs. 2 and 3 for $\gamma = 100$ and 200, respectively. We observe that

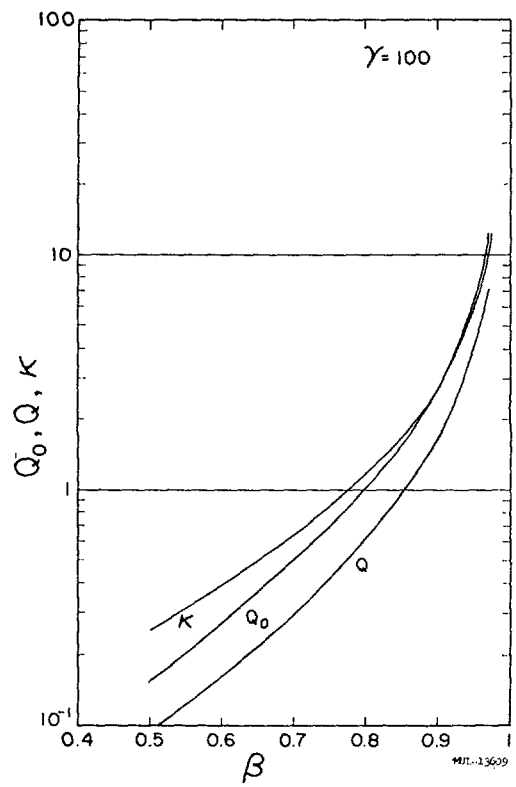

Fig. 2 Reactor quality for $\gamma = 100$.

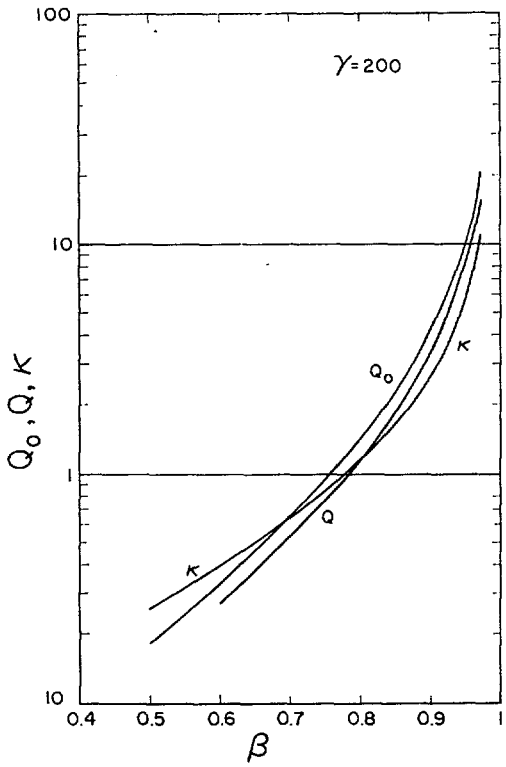

Fig. 3 Reactor quality for $\gamma = 200$.

the value of $\varkappa$ is approximately equal to the reactor quality Q. Therefore at the break-even point where the reactor is just self-sustained, the kinetic energy of the plasma does not exceed the total kinetic energy of the E-layer electrons. Since the magnetic field does not enclose only the plasma gas but the E-layer too, which is partially responsible for the closed pattern of magnetic lines, we might expect that if the E-layer is hydromagnetically stable it might be able to support a plasma of total kinetic energy not greatly exceeding its own kinetic energy. Thus it is considered useful to calculate the quantity $\varkappa$, since it appears that it might be significant as a criterion for stability of the Astron.

Some preliminary calculations indicate that an economical break-even might be achieved for values of $Q \geq 5$.

The values of Q given in Table III indicate that higher values can be obtained with higher energy

TABLE III

β	$\gamma=100$		$\gamma=200$	
	Q_0	Q	Q_0	Q
0.5	0.154	0.091	0.183	0.152
0.6	0.273	0.165	0.337	0.280
0.7	0.497	0.302	0.643	0.533
0.8	1.011	0.618	1.40	1.15
0.9	2.75	1.68	4.23	3.39
0.95	6.49	3.95	10.86	8.56
0.97	11.58	7.07	20.33	15.88

electrons. This advantage, however, might be offset by the higher cost of the electron accelerator. At this time it appears that the optimum value of the E-layer electron energy is somewhere between 30 and 100 MeV. The actual optimum value cannot be derived since it depends on detailed cost estimates which are considered premature at this time.

In the above calculations it is assumed that the plasma ion and electron temperatures are approximately equal. Since the ions are heated indirectly through Coulomb collisions with the plasma, electron temperature equality can be achieved only if the plasma density is high enough, approximately $10^{14}/\text{cm}^3$. This is not the case at $\gamma = 10$. Hence no Q values are given for $\gamma = 10$.

The radius of the E-layer is selected on the basis of technological and economical considerations. At a 50-MeV electron energy, the range of 30 to 40 cm appears to be suitable for the E-layer radius. After the selection of this value the quantity ψ can be derived, and thus all the other quantities.

4.1 Numerical example

$\gamma = 100, \quad R = 35$ cm, $\quad \zeta = 1.22, \quad \eta_e = 0.45.$

The other quantities are

$$\psi = 7.4 \cdot 10^{10} \text{ ergs/cm}^3$$
$$\beta = 0.97, \quad Q = 7.07, \quad \varkappa = 11.0$$
$$\eta_e W_t = 270\,000 \text{ watts/cm}$$
$$W_e = 15\,000 \text{ watts/cm}$$
$$B_0 = 31\,000 \text{ gauss}$$
$$n_0 = 6 \cdot 10^{14} \text{ ions/cm}^3$$
$$R_0 = 43 \text{ cm}.$$

The E-layer and plasma parameters derived in this section were optimized from the point of view of power economy. In the next section we shall examine whether or not these parameters are adequate to allow heating of the plasma up to the ignition temperature.

5. Plasma heating up to ignition temperature

After the initial plasma formation, through ionization of the residual neutral gas, the plasma electrons gain energy by Coulomb collisions with the E-layer electrons. The rate of energy gain per cm length of the plasma by this process is

$$W_p = \zeta(\gamma/r_e)\sigma_0 c n_0 (mc^2) \text{ ergs/cm sec}. \qquad (46)$$

The plasma loses energy by diffusion outwards. The energy loss by diffusion per cm length of the plasma [1] is

$$W_d = \frac{\sigma_0 c}{r_e} \mu (2\pi)^{\frac{1}{2}} (n_0 mc^2)^{\frac{3}{2}} \frac{F}{B_w} \text{ ergs/cm sec}, \qquad (47)$$

where μ is the ratio of the actual to the theoretical diffusion loss, and

$$F = \frac{\sinh^{-1} y + \sinh^{-1}(yB_w/B_1)}{(1+y^2)^{1/2}} \qquad (48)$$

and

$$y=[\beta/(1-\beta)]^{\frac{1}{2}}. \tag{48a}$$

The plasma temperature will continue to rise as long as

$$W_p + W_{fe} > W_d \tag{49}$$

where W_{fe} is the fusion energy released in the plasma in the form of trapped charged reaction products. If D-T reaction is employed,

$$W_{fe}=0.16\, W_f. \tag{50}$$

The quantities W_p, W_{fe} and W_d can be written in terms of the energy density ψ, namely,

$$W_p = 2.12 \cdot \frac{\zeta(\zeta+1)^2\cos^2\delta}{16\gamma}\left(\frac{mc^2}{eu}\right)\left(\frac{\beta}{1-\beta}\right)\psi \tag{51}$$

$$W_{fe} = 6.72 \cdot 10^{-3}\left[\eta_0 F(u)(\zeta+1)^4\cos^4\delta\left(\frac{\beta}{1-\beta}\right)^2\right]\psi \tag{52}$$

$$W_d = 0.75\,\mu F\left(\frac{mc^2}{eu}\right)^{\frac{3}{2}}\frac{(\zeta+1)^2}{16\gamma^2}(\cos^2\delta)\left(\frac{\beta}{1-\beta}\right)^{\frac{3}{2}}\psi. \tag{53}$$

Equations (45), (47), (48), (49) yield:

$$\frac{\mu}{\gamma} < \frac{\zeta}{F}\left(\frac{8\,eu}{mc^2}\right)^{\frac{1}{2}}\left(\frac{1-\beta}{\beta}\right)^{\frac{1}{2}} + 0.143\,\frac{\gamma}{F}\left(\frac{eu}{mc^2}\right)^{\frac{3}{2}}F(u)\,\eta_0(\zeta+1)^2(\cos^2\delta)\left(\frac{\beta}{1-\beta}\right)^{\frac{1}{2}}. \tag{54}$$

Substituting the numerical values $\cos\delta=0.5$, $\zeta=1.22$, $eu=20$ keV, we find

$$\frac{\mu}{\gamma} < \frac{0.672}{F}\left(\frac{1-\beta}{\beta}\right)^{\frac{1}{2}} + 1.34 \cdot 10^{-3}\,\frac{\gamma}{F}\left(\frac{\beta}{1-\beta}\right)^{\frac{1}{2}}. \tag{55}$$

The allowed maximum values of μ as a function of β (for $\beta>0.5$) are given in Table IV for $\gamma=100$ and 200, respectively.

TABLE IV

β	μ	
	$\gamma=100$	$\gamma=200$
0.5	29.1	67.4
0.6	26.3	64.5
0.7	25.3	66.6
0.8	26.7	78.0
0.9	35.8	119.0
0.935	47.2	167.0
0.970	84.0	316.0

We observe that there is a wide margin between heat input and theoretical losses. At $\gamma=100$ and a temperature of 20 keV the allowed loss rate is 25 times the theoretical diffusion losses.

It is of interest to calculate the temperature and density of the plasma as a function of μ and γ neglecting the contribution from fusion. Then, neglecting the second term on the right-hand side of Eq. (54) and solving for eu we find

$$\frac{eu}{mc^2} = \left(\frac{\mu}{\zeta\gamma}\right)^2\frac{F^2}{8}\left(\frac{\beta}{1-\beta}\right). \tag{56}$$

For values of $\beta \ll 0.01$, Eq. (52) becomes

$$\frac{eu}{mc^2} = \left(\frac{\mu}{\gamma}\right)^2\frac{\beta^2}{2(\zeta-1)^2}. \tag{57}$$

The plasma density is

$$n_0 = \frac{[\zeta(\zeta+1)\cos\delta]^2}{2\,\mu^2 F^2}\left(\frac{\gamma^4}{\pi R^2 r_e}\right)\text{ions/cm}^3. \tag{58}$$

The plasma parameters have been derived for a range of values of the parameters μ and γ. The values of the loading factor ζ and the E-layer radius R are assumed to be 1.22 and 35 cm, respectively.

The plasma temperature and density are plotted in Figs. 4, 5 and 6 as a function of β, for different values of μ and γ. The temperature ranges from 4 eV up to 100 keV and the ion density from 10^{10} up to 10^{16} depending on the values of μ and γ. The

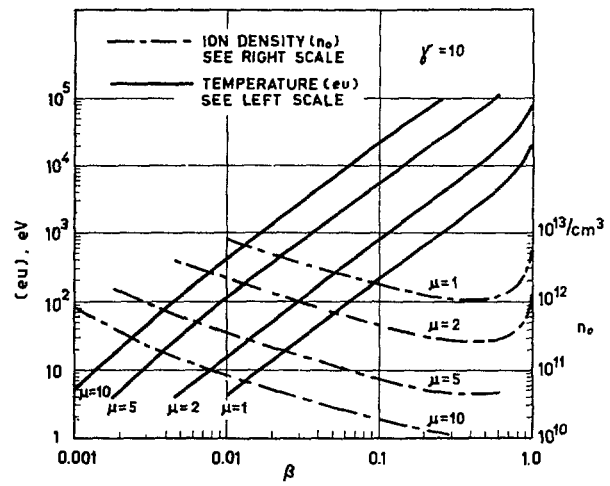

Fig. 4 Plasma parameters for $\gamma=10$.

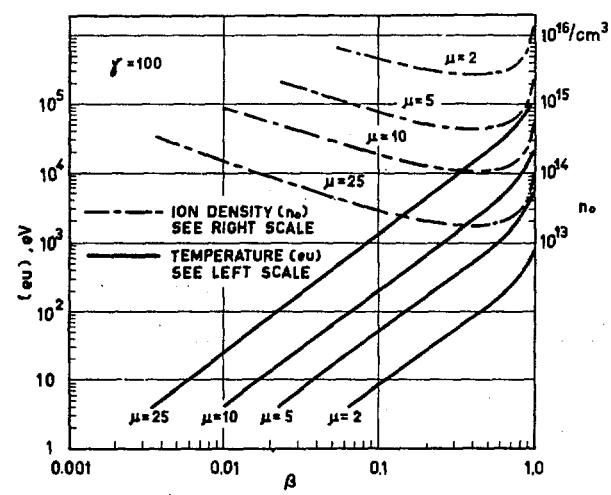

Fig. 5 Plasma parameters for $\gamma=100$.

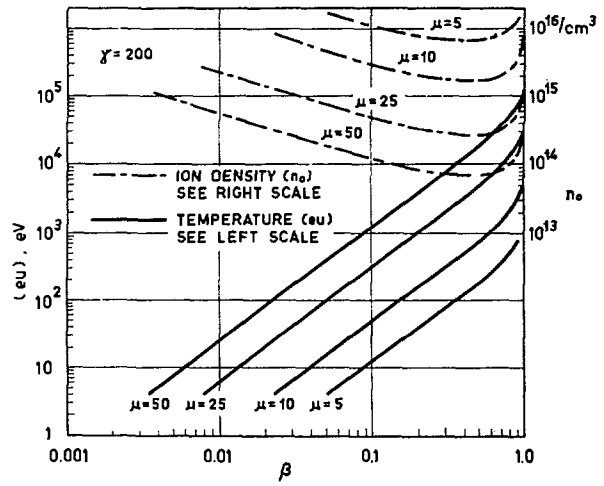

Fig. 6 Plasma parameters for $\gamma = 200$.

values of temperature and density shown in the figures are steady-state values. At each temperature point the steady state can be maintained by injecting the required number of neutrals which replace the diffused plasma. By changing the rate of injection of neutrals it is possible to move to a new temperature level and a new β. The external magnetic field B_0 is

$$B_0 = B_w/(1-\beta)^{\frac{1}{2}}. \tag{59}$$

Thus a change in the external magnetic field B_0 results in a new value of β. Therefore a change of β and temperature requires simultaneous change of the external magnetic field and the rate of injection of neutral gas. The rate of change however can be very slow, e.g., 10 eV per second, thus not requiring any specific programming either of the rate of rise of the external field or the injection of neutral gas.

We observe that at $\beta = 0.5$ the density goes through a minimum value as the diffusion losses are maximized at this value of β. At $\gamma = 10$ the plasma density is too small to allow equality of ion and electron temperature. At $\gamma = 100$, however, the ion plasma density can exceed 10^{14} ions/cm^3 at all temperatures even if the rate of diffusion loss is 10 times higher than the theoretical rate.

Other plasma losses are bremsstrahlung, synchrotron radiation and charge exchange. Let us calculate the plasma synchrotron radiation, neglecting any reflection from the walls, or reabsorption by the plasma, and compare this loss with the rate of fusion energy release in the plasma. The plasma synchrotron radiation [2], neglecting wall reflection, is

$$w_r = \frac{4e^2}{3c}\left(\frac{eu}{mc^2}\right)\left(\frac{eB}{mc^2}\right)^2 n \text{ erg/cm}^3\,\text{sec}. \tag{60}$$

The radiation loss per unit length of plasma is

$$W_r = \frac{4}{3}\left(\frac{eu}{mc^2}\right) r_e^2 c (B_0 R)^2 n_0 \eta_r, \tag{61}$$

where

$$\eta_r = \frac{2}{R^2 n_0 B_0^2}\int_0^{R_0} B^2 n r\, dr. \tag{61a}$$

The fusion energy trapped in the plasma is given by Eq. (52). After substitution of the quantities according to above relations, Eqs. (52) and (60) yield

$$\frac{W_r}{W_{fe}} = \frac{1}{3F(u)}\frac{\eta_r}{\beta\eta_0}. \tag{62}$$

The quantities η_r, $(\eta_r/\beta\eta_0)$ are given as a function of β in Table V.

TABLE V

β	η_r	$(\eta_r/\beta\eta_0)$
0.5	0.205	0.44
0.7	0.180	0.26
0.9	0.138	0.14
0.97	0.113	0.10

At 20 keV and $\beta = 0.5$

$$W_r/W_{fe} = 0.146.$$

It should be noted that at $\beta = 0.5$ and $\gamma = 100$ the contribution from fusion is only 20% of the total heat input to the plasma. Therefore, the plasma radiation loss is a small fraction either of the E-layer losses or of the fusion energy trapped in the plasma. It should be noted that in the above calculations of the radiation loss we neglected any wall reflection or reabsorption from the plasma. The bremsstrahlung loss is even smaller than the synchrotron radiation loss.

The charge-exchange loss is proportional to the diffusion loss, since the only available neutrals which can undergo charge exchange are the neutral atoms injected to replace the diffused plasma. If a fraction α of the injected neutrals that are charge-exchanged come out again as hot neutrals, the total loss by charge exchange is

$$\alpha + \alpha^2 + \alpha^3 \ldots = \frac{1}{1-\alpha} - 1. \tag{63}$$

Consequently the value of μ is effectively increased by a factor

$$\left(1 - \frac{\alpha}{2}\right)\Big/(1-\alpha).$$

Therefore the charge-exchange loss appears as an enhanced diffusion loss. At 20 keV the value of α is approximately one-half; hence the diffusion loss is enhanced by 50%.

From the above investigation one can conclude that the selected parameters which optimize the quality of the reactor are more than adequate to heat the plasma up to the ignition temperature.

6. Experimental program

The theoretical results derived in the previous sections are very encouraging but they can be accomplished only if both the E-layer by itself and in combination with plasma are hydromagnetically stable. Therefore, a sequence of experiments are

required to explore step by step the soundness of the Astron concept.

The most critical parameter in such an experiment is the energy of the E-layer electrons. It is obvious that the higher the electron energy, the more margin is available against unexpected plasma losses; thus easier to achieve ignition temperature. However, the cost of the electron accelerator and the time required for building it increase almost linearly with the electron energy. Therefore, after careful consideration an electron energy of 5 MeV has been selected. The accelerator is contemplated to operate at 200 amperes in short pulses of 0.3-microsecond duration. The repetition rate is 60 pulses per second. The objectives of the first experimental step are as follows:

(1) To establish the E-layer and study its stability as a function of the loading factor ζ. A value of ζ slightly larger than unity is required to establish the desired closed pattern of magnetic lines.
(2) To build up a plasma up to $\beta=0.5$ and study the stability of this plasma as a function of temperature with the parameter μ varying from the minimum actual value up to 15 to 20. The parameter μ can be enhanced by introducing atoms of high atomic number in the plasma.
(3) To reach an ion temperature of up to 10 keV and under these conditions study the plasma behavior.
(4) To measure the actual value of μ under a variety of conditions.
(5) Should instability set in at a certain critical β, to study the nature of the instability and possible cure. It might be noted that during transition from stability to instability the growth rate will be very slow, thus allowing a "slow motion" study of the plasma behavior.
(6) To determine the required value of γ, from the measured actual value of μ, to achieve positive power gain.

The 5-MeV accelerator and the other components of the Astron model are now under construction. The length of the assembly of the E-layer, injection, and resistor tanks is 90 ft. The electron gun and the accelerator consist of nine units, approximately 600 keV each. The length of the entire accelerator assembly itself is approximately 40 ft.

The inner radius of the E-layer tank is 50 cm. The mean radius R and the length of the E-layer are 27 and 600 cm, respectively. The plasma parameters shown in Fig. 4 are calculated for $R=35$ cm. Consequently, the calculated ion density in the Astron model as a function of μ and β is 70% more than the values shown in Fig. 4. Therefore, the maximum plasma density expected at $\mu=2$ and $eu=4$ eV is $7\cdot10^{12}$ ions/cm^3. The repetition rate and pulse length of the accelerator are calculated to maintain the E-layer at a loading factor $\zeta=1.22$ in the presence of a plasma of 10^{13} ions/cm^3. This is the maximum plasma density expected at a temperature of 20 keV even if $\mu\approx1$ and a $\beta=0.97$ could be achieved. (See Fig. 4.) At a plasma density of 10^{13} ions/cm^3, the lifetime of the E-layer electrons is approximately one second. The heat input to the plasma through Coulomb collisions with the E-layer electrons is 20 watts/cm. At $\beta=0.97$ the plasma energy is 190 joules/cm and the external magnetic field $B_0=4000$ gauss.

Any plans for future experiments cannot be formulated before completion of the first step as outlined above.

7. Discussion

There are two critical conditions which must be met by a controlled fusion device: plasma confinement, and heating of the plasma up to the so-called ignition temperature. Furthermore, a device will be useful only if the released thermonuclear power is several times larger than the electric power required to operate the device.

The theoretical results obtained in this paper indicate that there is no heating problem in the Astron device. The energy input to the plasma by Coulomb collisions with the E-layer electrons appears to be adequate to offset the plasma losses by a large margin, thus a plasma temperature of any desired value can be achieved within the range of interest for thermonuclear reactions. Furthermore, the above calculations indicate that it is possible to select such plasma and E-layer parameters that the electric power produced is several times greater than the power required to operate the reactor. An interesting result of this study is that the reactor quality is independent of the radius of the machine. Consequently the dimensions of the reactor can be selected on technological and other considerations, not restricted by conditions imposed by the plasma and the E-layer parameters.

The plasma synchrotron radiation loss which has been discussed so much during the last three years appears to be very small in the Astron even in the absence of reflecting walls.

Therefore the crucial question in the Astron is that of plasma confinement. The equilibrium solution permits a plasma of very high β. However, there is no rigorous proof either on the stability of the E-layer or the combination of the E-layer with the plasma. The problem is extremely difficult to treat theoretically inasmuch as there is not available an analytical self-consistent solution of the E-layer. Tonks' calculations [3] give solutions under certain assumptions and approximations which are not in analytical form. Certain attempts to calculate the marginal stability of the E-layer [4, 5, 6] indicate that the E-layer is stable provided that the mean square of the scattering angle $\langle\Theta^2\rangle$ is of the order of one half. However, the marginal stability approximation is valid only for perturbations of the form $\mathbf{k}\cdot\mathbf{v}=0$ (where $\mathbf{k}$ is the wave vector and $\mathbf{v}$ the organized motion of the E-layer). The only perturbation of this type is an axially symmetric perturbation. The E-layer is stable against such perturbation because of its very large axial pressure. The most dangerous perturbation appears to be a wave normal to one of the two crossed beams. However this perturbation satisfies the condition $\mathbf{k}\cdot\mathbf{v}=0$ for one of the beams but not for the other. If momentarily the presence of the second beam is ignored, then one

finds a criterion of marginal stability [4, 5], namely stability, is possible if the velocity spread is larger than a certain critical value. However, the presence of the other beam violates the condition $\mathbf{k}\cdot\mathbf{v}=0$; hence the validity of the marginal stability is questionable for this type of perturbation. Furthermore one cannot exclude the existence of a perturbation with complex ω, with growing amplitude, which cannot be discovered in a treatment where marginal stability has been assumed. Consequently, the stability of the E-layer either by itself or in combination with the plasma is from the theoretical point of view open to question.

One can reason intuitively that if the E-layer is stable by itself it will be able to support a plasma of total kinetic energy not greatly exceeding the kinetic energy of the E-layer. Since it appears theoretically difficult to treat the stability problem in the Astron device, the only way to find the stability conditions is by the experimental approach. For these reasons, any theoretical results, either favorable or unfavorable, can be considered to be only tentative but useful for interpretation of the experimental results. Therefore, it is expected that many years of work will be required to obtain satisfactory answers on stability of the E-layer and the confined plasma, as well as to prove the validity of the above energy-balance calculations.

Acknowledgment

The work reported here was performed under the auspices of the United States Atomic Energy Commission.

References

[1] CHRISTOFILOS, N. C., Proc. Second U.N. International Conference on Peaceful Uses of Atomic Energy, Geneva, **32** (1958) 279.

[2] TRUBNIKOV, B. A., KUDRYAVTSEV, V. S., Proc. Second U.N. International Conference on the Peaceful Uses of Atomic Energy, Geneva, **31** (1958) 93.

[3] TONKS, LEWI, "The Structure of the Astron E-Layer": see abstract CN-10/113 in final volume of these Proceedings.

[4] FURTH, H. P., IAEA Conference on Plasma Physics and Controlled Nuclear Fusion Research, Salzburg, 1961: paper CN-10/174, page 169 of this volume.

[5] CHRISTOFILOS, N. C., Note on the Stability of the E-Layer, UCID-4274, May 12, 1961.

[6] CHRISTOFILOS, N. C., Marginal Stability of an Infinite, Cylindrical E-Layer of Finite Thickness, UCID-4277, May 18, 1961.

THE "MIRROR INSTABILITY" FOR FINITE PARTICLE GYRO-RADIUS*

HAROLD P. FURTH

LAWRENCE RADIATION LABORATORY, UNIVERSITY OF CALIFORNIA

LIVERMORE, CALIFORNIA, UNITED STATES OF AMERICA

A plasma in an axial magnetic field is subject to the "mirror instability" when $p_\perp > p_\parallel$, and when $\beta = 8\pi p_\perp/B^2$ is sufficiently large. For stability of a plasma of infinite extent, the standard condition $\beta\,(p_\perp/p_\parallel - 1) < 1$ is obtained from the Vlasov equation in the limits $k_\parallel \ll k_\perp$ and $\varepsilon = (k_\perp r_g)^2 \ll 1$ (r_g being the thermal gyro-radius). For finite ε, the left side of the standard inequality must be multiplied by $e^{-\varepsilon}[I_0(\varepsilon) - I_1(\varepsilon)]$. Stability improves with growing ε, due to linkage of out-of-phase regions of the perturbation by the particle orbits.

For a nearly monoenergetic assembly of gyrating particles forming a single tubular layer, a sheet-pinch approximation is appropriate. A plane sheet pinch with density distribution $n = n_0 \operatorname{sech}^2(2z/\delta)$, with isotropic thermal velocity spread v^2, and with directed velocity $v_\perp$ has the stability condition $2\pi\,(v_\perp^2/v^2)\,(1 + k_\parallel\,\delta/2)^{-1}\,r_c\,n_0\,\delta/k_\parallel < 1$, where $r_c = e^2/mc^2$. The stabilizing effects of conducting walls and of cylindrical geometry have been calculated. In every case, stability is most difficult to obtain for $k_\parallel\delta \ll 1$. In this limit, and for $\delta \ll r_g$, the stability condition for cylindrical geometry is $2\pi\,(v_\perp^2/v^2)\,r_c\,n\delta\,r_g\,(1 - r_g^2/r_w^2) < 1$, where r_w is the radius of the outer conducting wall.

For application to high-energy-injection mirror machines, this condition may be rewritten as $(\beta/4)\,(p_\perp/p_\parallel - 1)\,(1 - r_g^2/r_w^2) < 1$. The stabilizing factor of $^1/_4$ relative to the standard stability condition reflects the absence of neighboring particle orbits, which in the infinite-medium case act co-operatively to promote instability.

The stability conditions obtained for sheet pinches are also applicable to configurations having a region of reverse axial field, such as Astron and certain theta-pinches. For the plane pinch without walls, the stability condition can be reduced conveniently to $k_\parallel\delta > 2$. Restrictive conditions on the minimum thickness of the E-layer and its maximum distance from a stabilizing shell have been derived. Reverse-field theta-pinches are generally unstable, which provides the basis for a plausible explanation of the observed neutron production.

1. Introduction

A thermally anisotropic collisionless plasma of infinite extent in a uniform magnetic field is known to be unstable [1, 2] for sufficiently high values of $\beta = 8\pi p_\perp/B^2$. For the case where the transverse pressure, $p_\perp$, exceeds the longitudinal pressure, $p_\parallel$, the instability consists in the growth of local constrictions or "mirrors" in the uniform magnetic field, hence the name "mirror instability."

Previous analyses have confined themselves to the limit where particle gyro-radii are small compared with the wavelengths of instabilities. The growth-rate of the "mirror instability" has, however, been found to be inversely proportional to its wavelength [2]. The analysis in the long-wavelength limit, therefore, has the peculiarity of being inapplicable to precisely those fast-growing modes that are actually expected to be seen in an experimental plasma. The present analysis covers the case of finite thermal gyro-radius, and is, therefore, able to describe the modes of maximum growth-rate and to obtain their wavelengths in terms of the thermal gyro-radius.

The approximation of small gyro-radius relative to *plasma size* is suited to describe some actual plasma experiments [3], but is quite unsuitable for an important class of thermally anisotropic plasmas, namely those obtained by high-energy ion injection into a mirror machine [4]. The extreme case where the "plasma" consists of a single tubular layer of gyrating particles is treated in the present paper, and stability conditions are found that are somewhat more easily satisfied than those for an infinite homogeneous plasma.

The conventional small-gyro-radius treatment is confined to initial configurations where magnetic-field gradients are either absent or at least involve characteristic lengths that are large compared with thermal gyro-radii [5]. This restriction excludes the extremely important case where the magnetic field actually reverses inside the plasma [6, 7]. The present paper examines the field-reversal case and finds instabilities that are similar to the "mirror instability."

In the treatment of all of these problems, the essential features of the instability can be obtained by assuming an "active" particle species, to which the analysis explicitly refers, and a "passive" species, of the opposite charge, which is assumed massless and of null temperature, and which serves only to provide charge neutrality. In many experimental cases, this is roughly the situation that actually prevails. In cases where the "passive" species is actually the heavier one, the marginal stability criterion is unaltered, but the growth rates reflect the presence of the greater mass. In cases where the temperature of the "passive" species is not negligible compared with

* Conference paper CN-10/174, presented by H. P. FURTH. Discussion of this paper is given on page 209. Translations of the abstract are at the end of this volume of the Conference Proceedings.

that of the "active" species, the marginal stability criterion is affected, greater stability being achieved if the thermal distribution of the "passive" species is such as to lower the total plasma-pressure anisotropy. For simplicity, the present treatment will omit these effects and confine itself throughout to consideration of the "active" particle species.

2. The "mirror instability" in an infinite plasma

A uniform magnetic field, B, and a plasma of distribution function

$$f_0 = \frac{n_0}{(2\pi)^{3/2} a v^3} \exp\left[-\frac{v^2}{2}\left(\frac{v_x^2}{a^2} + v_y^2 + v_z^2\right)\right] \quad (1)$$

are subjected to the perturbation

$$B_z = b e^{\omega t} \sin k_\parallel x \sin k_\perp z \quad (2)$$

$$B_x = B + (k_\perp/k_\parallel)\, b e^{\omega t} \cos k_\parallel x \cos k_\perp z \quad (3)$$

$$E_y = (\omega/c k_\parallel)\, b e^{\omega t} \cos k_\parallel x \sin k_\perp z \quad (4)$$

$$f = f_0 + f_1 e^{\omega t},$$

where b is a constant. From the linearized Vlasov equation, one obtains

$$\omega f_1 + v_x \frac{\partial f_1}{\partial x} + v_z \frac{\partial f_1}{\partial z} + \frac{e}{mc}\left[B\frac{\partial f_1}{\partial \varphi} + \frac{b v_y}{v^2} f_0 \sin k_\perp z \left\{\left(1 - \frac{1}{a^2}\right) v_x \sin k_\parallel x - \frac{\omega}{k_\parallel}\cos k_\parallel x\right\}\right] = 0, \quad (5)$$

where $\varphi = \tan^{-1}(v_y/v_z)$. The solution of Eq. (5) is used to derive a current density

$$i_y = \frac{e}{c} e^{\omega t} \int_{-\infty}^{\infty} dv_x\, dv_y\, dv_z\, f_1\, v_y \quad (6)$$

$$= -(b/4\pi k_\parallel)(k_\parallel^2 + k_\perp^2) \cos k_\parallel x \sin k_\perp z. \quad (7)$$

Eq. (7) is required for consistency with Eqs. (2) and (3). Combining Eqs. (6) and (7), one obtains the dispersion relation for ω. Here the displacement current is being neglected, which is appropriate if the plasma is non-relativistic.

In the limit $(k_\parallel r_g)^2$, $(k_\perp r_g)^2 \ll 1$, where $r_g = mvc/eB$, Eq. (5) is readily solved, and the dispersion relation for $\omega = 0$ yields the familiar marginal stability condition

$$[(1/a^2) - 1]\beta \frac{k_\perp^2 - (a^2/2) k_\parallel^2}{k_\parallel^2 + k_\perp^2} < 1, \quad (8)$$

where $\beta = 8\pi m n_0 v^2/B_{x0}^2$. For $a^2 < 1$, the "mirror instability" can occur, the required value of β being lowest when $k_\parallel^2 \ll k_\perp^2$, so that Eq. (8) reduces to

$$[(1/a^2) - 1]\beta < 1. \quad (9)$$

An alternative approach to Eq. (5) is to make the approximation $\alpha^2 = k_\parallel^2/k_\perp^2 \ll 1$, but refrain from imposing conditions on $k_\perp r_g$. In that case, it is convenient to write

$$f_1 = (1/\alpha) f_0 \{\psi_s \cos k_\parallel x + \psi_a \sin k_\parallel x\}, \quad (10)$$

so that Eq. (5) yields

$$\alpha\left\{\frac{v_x}{v}\psi_s - \Omega\psi_a + \frac{v_x v_y}{v^2}\left(\frac{1}{a^2} - 1\right)\frac{b}{B r_g k_\perp}\sin\zeta\right\} = \frac{v_z}{v}\frac{\partial\psi_a}{\partial\zeta} + \frac{1}{r_g k_\perp}\frac{\partial\psi_a}{\partial\varphi} \quad (11)$$

$$\alpha\left\{-\frac{v_x}{v}\psi_a - \Omega\psi_s + \Omega\frac{v_y}{v}\frac{b}{B r_g k_\perp}\sin\zeta\right\} = \frac{v_z}{v}\frac{\partial\psi_s}{\partial\zeta} + \frac{1}{r_g k_\perp}\frac{\partial\psi_s}{\partial\varphi}, \quad (12)$$

where $\Omega = \omega/k_\parallel v$, and $\zeta = k_\perp z$.

The solutions of Eqs. (11) and (12) have the form

$$\psi_s = \psi_{s0}(\zeta - g\sin\varphi) + \alpha\psi_{s1}(\zeta, \varphi) \quad (13)$$

$$\psi_a = \psi_{a0}(\zeta - g\sin\varphi) + \alpha\psi_{a1}(\zeta, \varphi), \quad (14)$$

where $v_y = (gv/r_g k_\perp)\sin\varphi$. The structure of the functions ψ_{s0} and ψ_{a0} is obtained from the consideration that they, as well as ψ_{s1} and ψ_{a1}, must be periodic in ζ and φ. A convenient technique is to multiply Eq. (11) by $\sin\zeta \sin(g\sin\varphi)$ and integrate over ζ and φ; repeat this step, multiplying by $(g\sin\varphi)$, and then add the two resultant equations. It follows that

$$\frac{v_x}{v}\psi_{s0} - \Omega\varphi_{a0} = -\frac{v_x}{v}\left(\frac{1}{a^2} - 1\right)\frac{b g J_1(g)}{B r_g k_\perp} \{\sin\zeta \sin(g\sin\varphi) + \cos\zeta\cos(g\sin\varphi)\}, \quad (15)$$

where J_1 is the Bessel function of first order. By the same procedure, Eq. (12) yields a similar expression, and this, together with Eq. (15), gives finally

$$\psi_{s0} = -\frac{b g J_1(g)}{B r_g k_\perp}\left[\left(\frac{1}{a^2} - 1\right)\frac{v_x^2}{v_x^2 + \Omega^2 v^2} - \frac{\Omega^2 v^2}{v_x^2 + \Omega^2 v^2}\right] [\sin\zeta \sin(g\sin\varphi) + \cos\zeta\cos(g\sin\varphi)]. \quad (16)$$

Since ψ_{a0} is odd in v_x, it drops out of the integral in Eq. (6), and we obtain the dispersion relation

$$\beta\left\{\frac{1}{a^2} - 1 - \frac{1}{a^2}F(\Lambda)\right\} G(\varepsilon) = 1, \quad (17)$$

where $\Lambda = \omega/\sqrt{2}\, k_\perp v a$, $\varepsilon = (k_\perp r_g)^2$, and

$$F(\Lambda) = \Lambda e^{\Lambda^2}\left\{\sqrt{\pi} - 2\int_0^\Lambda d\Lambda_1 e^{-\Lambda_1^2}\right\} \quad (18)$$

$$= \sqrt{\pi}\,\Lambda \text{ for } \Lambda^2 \ll 1 \quad (19)$$

$$G(\varepsilon) = e^{-\varepsilon}\{I_0(\varepsilon) - I_1(\varepsilon)\} \quad (20)$$

$$= 1 - (3/2)\,\varepsilon \text{ for } \varepsilon \ll 1 \quad (21)$$

$$= \frac{\varepsilon^{-\frac{3}{2}}}{2\sqrt{2\pi}} \text{ for } \varepsilon \gg 1. \quad (22)$$

I_0 and I_1 are imaginary Bessel functions.

For $\Lambda \ll 1$, $\varepsilon \ll 1$, the wavelength having the maximum growth-rate corresponds to

$$(k_\perp)_m = (\sqrt{2}/3\, r_g)\left\{\beta\left(\frac{1}{a^2} - 1\right) - 1\right\}^{\frac{1}{2}} \quad (23)$$

and the maximum growth-rate is

$$\omega_m = (4/9\sqrt{\pi})\,(a^3 v/\beta r_g)\left\{\beta\left(\frac{1}{a^2}-1\right)-1\right\}^{\frac{3}{2}}. \quad (24)$$

3. Stability of a plane sheet pinch

A nearly monoenergetic assembly of gyrating particles forming a single tubular layer (as in a high-energy-injection mirror machine) is better approximated as a tubular sheet pinch than as a continuous plasma. In this connection, it is useful to begin by considering a plane infinite sheet pinch.

A familiar self-consistent solution [8] of the zero-order Vlasov equation and Maxwell's equation is given by

$$f_0 = \frac{n_0}{(2\pi)^{3/2} v^3 \delta}\,\frac{\exp\{-[v_x^2+v_z^2+(v_y^2-v_\perp^2)]/2v^2\}}{\cosh^2(2z/\delta)} \quad (25)$$

$$B_{x0} = 2v\,(2\pi n_0 m)^{\frac{1}{2}}\tanh(2z/\delta), \quad (26)$$

where

$$\delta^2 = (2/\pi n_0 r_c)\,(v/v_\perp)^2 \quad (27)$$

$$r_c = e^2/mc^2. \quad (28)$$

In analogy to the "mirror instability," we consider the perturbation

$$B_z = b e^{\omega t}\sin k_\parallel x \quad (29)$$

$$B_x = B_{x0} + \frac{1}{k}\frac{db}{dz}e^{\omega t}\cos k_\parallel x \quad (30)$$

$$E_y = (\omega/ck)\,b e^{\omega t}\cos k_\parallel x, \quad (31)$$

so that the linearized Vlasov equation becomes

$$\omega f_1 + v_x\frac{\partial f_1}{\partial x} + v_z\frac{\partial f_1}{\partial z} + \frac{e}{mc}\left[B\frac{\partial f_1}{\partial \varphi} + \frac{1}{v^2}f_0\left\{-bv_x v_\perp \sin k_\parallel x + \frac{db}{dz}\frac{v_\perp v_z}{k_\parallel}\cos k_\parallel x - b\frac{\omega}{k_\parallel}(v_y - v_\perp)\cos k_\parallel x\right\}\right] = 0. \quad (32)$$

The current density derived from Eq. (32) must be consistent with

$$i_y = -\frac{k_\parallel}{4\pi}\left(b - \frac{1}{k_\parallel^2}\frac{d^2 b}{dz^2}\right)\cos k_\parallel x. \quad (33)$$

The solution, f_1, of Eq. (32) for $\omega = 0$ is simply

$$f_1 = -\frac{b v_\perp}{B r_g k_\parallel v} f_0 \cos k_\parallel x \quad (34)$$

and the marginal stability condition is

$$4\pi\,(v_\perp/v)^2 r_c n_0 \delta^2 < \lambda, \quad (35)$$

where the eigenvalue λ is to be determined from a differential equation in $\zeta = z/\delta$,

$$\frac{d^2 b}{d\zeta^2} = b\left\{(k_\parallel\delta)^2 - \frac{\lambda}{\cosh^2(2\zeta)}\right\}, \quad (36)$$

with the boundary conditions $b = 0$ at $\zeta = w$, $db/d\zeta = 0$ at $\zeta = 0$.

In the absence of conducting walls, we have $w = \infty$. The solution of Eq. (36) is then

$$b = b_0\,(\cosh 2\zeta)^{-k_\parallel\delta/2} \quad (37)$$

$$\lambda = k_\parallel\delta\,(2 + k_\parallel\delta) \quad (38)$$

and the marginal stability criterion becomes

$$2\pi\,(v_\perp/v)^2\,(1 + k_\parallel\delta/2)^{-1}\,r_c n_0 \delta/k_\parallel < 1. \quad (39)$$

By means of Eq. (27), one can transform Eq. (35) simply into $\lambda > 8$, and Eq. (39) into $k_\parallel\delta < 2$. For the purpose of deriving "mirror-instability" criteria in a form comparable with Eq. (9) (see next section), it is most convenient, however, to work with Eq. (35) as it stands.*

When there are conducting walls at $z = \pm\delta w$, the zero-order solution, Eq. (25), is no longer exact, but, as long as $w > 1$, the approximation is very good. It is helpful to recognize that Eq. (36) is a transformation of the associated Legendre equation**, where $\zeta = (1/2)\tanh^{-1}\mu$, $\lambda = 4n(n+1)$, $k_\parallel\delta = 2m$. Accordingly, λ is minimized for $k_\parallel = 0$ (the limit in which the stability condition of Eq. (8) is also most difficult to satisfy). For the marginally stable case $\lambda = 8$, we have

$$b = b_0 P_1^{k_\parallel\delta/2}(\tanh 2\zeta) + b_1 Q_1^{k_\parallel\delta/2}(\tanh 2\zeta) \quad (40)$$

where the constants b_0 and b_1 are chosen so as to make $b(\zeta)$ an even function. For $k_\parallel = 0$, one obtains

$$b = b_1\{2\zeta\tanh(2\zeta) - 1\} \quad (41)$$

and $w = 0.60$. For $k_\parallel\delta = 1.0, 1.9, 2.0$, the wall positions required for marginal stability are given by $w = 0.68$, 1.10, ∞. These results illustrate that the sheet pinch cannot be stabilized unless conducting walls are brought exceedingly close to the plasma. How close the walls must be brought is not rigorously determinable from the present analysis, since f_0 becomes inaccurate for $w < 1$.

Many of the preceding results can be conveniently approximated by treating the sheet pinch as an infinitely thin current layer, thus eliminating v_z and z from the Vlasov equation. This treatment becomes exact in the limits $k_\parallel\delta \to 0$, $w \to \infty$. For $\omega = 0$, the marginal stability condition is

$$2\pi\,(v_\perp^2/v^2)\,r_c n_0\,(\delta/k_\parallel)\tanh(k_\parallel\delta w) < 1. \quad (42)$$

The present analysis applies to relativistic pinches, provided $v_\perp^2 \approx c^2 \gg v^2$, and with m in Eq. (28) signifying the relativistic mass.

A dispersion relation for finite ω has been obtained in the thin-layer approximation by V. K. Neil [10]. Both relativistic and non-relativistic sheet pinches are treated rigorously, and the effect of the neutralizing particle species is included.

The thin-current-layer approximation of the sheet pinch is especially convenient when one passes from plane to cylindrical geometry. The marginal stability problem has been solved for the general case of helical current flow, neglecting the radial motion of the

* The similarity between Eq. (35) and the marginal condition for "mirror instability" was first pointed out to me by R. F. Post.

** This property is demonstrated for the same equation in a different context in [9].

layer. When the flow is not purely azimuthal, periodicity imposes a lower limit on $k_\parallel$. The resultant stabilizing effect is, however, offset by a geometrical destabilizing factor. A stability criterion first obtained by NEIL [10] (in somewhat more general form) for purely azimuthal flow and for $k_\parallel = 0$,

$$2\pi\,(v_\perp^2/v^2)\,r_c n_0 r_t \delta\,(1 - r_t^2/r_w^2) < 1 \qquad (43)$$

is found in the present analysis to apply also to the case of purely axial flow, and approximately to the case of equal axial and azimuthal flow, with $k_\parallel = 1/r_t$. The velocity, $v_\perp$, now signifies the mean velocity in the helical direction of flow. When the axial component of flow is smaller than the azimuthal component, but not zero, stability is greater than indicated by Eq. (43). A cylindrical conducting wall has been assumed at radius r_w, coaxial with the current-carrying tube at radius r_t.

Thus far, the analysis has concerned sheet pinches having regions of opposite magnetic field on either side of the sheet. In the thin-current-layer approximation, however, the structure of the zero-order field does not enter into the first-order Vlasov equation, and so Eq. (43) still applies when the field inside the current-carrying tube has the same direction as that outside.

One can thus apply Eq. (43) to a tubular layer of particles gyrating in a nearly homogeneous axial field B, where $r_t = r_g = m v_\perp c/eB$ and

$$\beta = (8\pi m n_0 v_\perp^2)/(r_g B^2) = 8\pi r_c n_0 r_g \delta. \qquad (44)$$

If, for the sake of form, we identify $p_\perp = m n_0 (v_\perp^2 + v^2)$, $p_\parallel = m n_0 v^2$, then the marginal stability condition becomes

$$\frac{\beta}{4}\left(\frac{p_\perp}{p_\parallel} - 1\right)(1 - r_g^2/r_w^2) < 1\,, \qquad (45)$$

which differs from Eq. (9) only by $(1 - r_g^2/r_w^2)/4$. The stabilizing factor due to the conducting wall is readily explained in terms of the "diamagnetic" effect of the wall on the return-flux of the perturbation field passing through the sheet pinch, and the consequent increase of the magnetic-field energy required to create the perturbation. The additional stabilizing factor of 1/4 relative to the standard stability condition comes from an analogous effect. In the infinite-medium case, plasma regions occupying neighboring half-wavelengths act co-operatively to promote the instability. Thus, there is no counterpart to the "vacuum" region surrounding the single tubular layer, where energy has to be stored in the return flux of the perturbation field. One might say that the homogeneous medium acts "paramagnetically" on the return flux, thus lowering the energy required for the growth of the perturbation.

4. Applications to experimental devices

4.1. High-energy-injection mirror machines

Mirror machines where a charged D_2 beam is injected [4, 11] with a view to break-up on an arc or on a dilute gas are preferentially designed so as to maximize the path traversed by the injected beam before its return to the source. Accordingly, the angle of injection with respect to the machine axis is kept as close to 90° as is consistent with keeping the beam from striking the source at the very outset. In this connection, beam spreading of less than a degree is found desirable and technically feasible. The stability condition of Eq. (45) then restricts operation to $\beta < 3 \times 10^{-4}$ (where r_g^2/r_w^2 has been neglected). Enhancement of the beam spread after injection, by collisions and co-operative effects, may help to ease the limitation on β.

The practical question arises as to whether the "mirror instability," even if it does occur, will prove seriously damaging to plasma containment. In experiments approximating a homogeneous medium [3], a catastrophic loss of containment appears to result when the conditions for "mirror instability" are violated. For a single tube of gyrating particles, the instability may simple take the form of "bunching" into local rings of current trapped in their own local mirror fields. Before such a stable secondary equilibrium can be reached, a non-linear oscillatory transient must take place. Whether such an oscillation can be damped without loss of particles is problematical.

4.2. Astron

For the purpose of making a qualitative judgment of stability, Eq. (43) can be rewritten in two alternative ways, reflecting the zero-order conditions for (1) a high degree of field reversal inside the tubular E-layer and (2) almost no field reversal.

For Case 1, the zero-order analysis for a plane E-layer can be adapted to give an approximate measure of the E-layer thickness. In general, the E-layer will consist of two electron populations in helical trajectories, crossing at an angle θ_c. The appropriate form of Eq. (27) is given by

$$\delta^2 = [2\,(v/v_\perp)^2]\,[\pi n_0 r_c \cos^2(\theta_c/2)]^{-1}, \qquad (46)$$

where $n_0/2$ is the density of each population, and $v_\perp$ is the directed velocity of each population. The stability condition of Eq. (43) then becomes

$$[2/\cos^2(\theta_c/2)]\,(r_t/\delta)\,(1 - r_t^2/r_w^2) < 1\,. \qquad (47)$$

(As will be recalled, Eq. (43) holds exactly for $\theta_c = 180°$, and approximately for $\theta > 90°$, which is the range of interest.) Assuming $\theta_c > 90°$ and $r_w^2 > 2\,r_t^2$, stability evidently cannot be obtained under the conditions where the present analysis applies, namely $\delta \ll r_t$. The mode that would be expected to grow is similar to the "cork-screw mode" of the stabilized pinch [12], except that a double rather than a single cork-screw develops, conforming with the pattern of the trajectories.

When the field reversal inside the tubular E-layer is only slight (Case 2), the zero-order regime must be derived from the balance of the electron centrifugal pressure against the outer magnetic field, instead of from the balance of electron "thermal" pressure

against the inner and outer fields. In that case, one can write in analogy to Eq. (44)

$$\varkappa = 2\,\pi r_c n_0 r_t \delta, \tag{48}$$

where $\varkappa$ is the "field-reversal parameter," which equals unity for zero inner field. (Note that $\varkappa = \beta/4$, because the effective field for the gyro-motion is now $B/2$ instead of B.) In Eq. (48), unlike Eq. (46), θ_c does not enter. Allowing for the fact that each of the crossing electron populations has density $n_0/2$, we can now write Eq. (43) as

$$\left(\frac{\varkappa}{2}\right)(v_\perp/v)^2\,(1 - r_t^2/r_w^2) < 1. \tag{49}$$

When $r_w^2 > 2\,r_t^2$, this condition cannot be satisfied for the thin-layer conditions where the analysis applies, since these imply $v^2 \ll v_\perp^2$.

Intuitively, one would expect that in a very diffuse E-layer, $v^2/v_t^2 \sim 1/4$) stability can be obtained for $\varkappa \approx 1$. This is also the result that follows from the stability condition of Eq. (49) if it is extended somewhat arbitrarily beyond the range where its derivation is rigorous.

The question of whether Astron is stable against the generalized form of the "mirror instability" can thus be summarized as follows: a thin-E-layer Astron, like that in the idealized representations given in [7], would be unstable; however, the actual parameters envisaged for the Astron Thermonuclear Reactor [13] are such as to justify a provisional expectation of stability, with the rigorous analysis remaining to be done. The problem of the stability of a diffuse E-layer in cylindrical geometry is currently being studied by N. C. CHRISTOFILOS [14].

Aside from the approximations that relate to E-layer thickness and velocity spread, a number of minor simplifications have been made in the present analysis, and these deserve some comment.

When two electron populations with intersecting helical trajectories are present, the effect of their interaction must be considered. For $\theta_c \sim 90°$, it is easy to show that the factor $v_\perp^2/v^2$ in the stability conditions is replaced by $(v_\perp^2/v^2 - 1)$, where $v_\perp$ is now meant to be taken in one of the two helical directions. (Only for $\theta_c \approx 180°$ is the interaction actually destabilizing.)

A second idealization that remains to be justified involves the spatial variation of the modes in the direction of particle motion. The present analysis assumes uniformity in the direction of motion, whereas in practice disturbances will arise locally and propagate in the direction of motion. CHRISTOFILOS [14] points out that, for a flat energy spectrum of the E-layer electrons and for a large turning-around distance at the ends of the E-layer, momentum dispersion at the ends will act to smooth out small transverse density modulations in the electron flow. How effective this mechanism is depends on how many e-foldings of the perturbation can take place over one length of the Astron Device. If the initial disturbance is *stationary*, one can readily show that the spatial e-folding rate for $\delta \ll r_t \sim 1/k_\parallel$ is given essentially by $k_e = (v/v_\perp) \times (2\,k_\parallel/\delta)^{1/2}$, so that, for a 45° helical beam, the number of e-foldings is roughly $N_e = k_e l = (v/v_\perp)\,(2\,l^2/\delta r_t)^{1/2}$ where l is the length of the E-layer. In this case, typical values of l, r_t, and δ for Astron suggest that the instability could not be suppressed by the end effect alone. For a transient initial disturbance, the analysis is more complex and has not yet been carried out.

4.3. THETA PINCHES WITH TRAPPED REVERSE FIELD

The hypothetical connection [15] between trapping of reverse axial field in a theta pinch and the production of neutrons has been verified by experiment [16] and is now generally accepted [17] on an empirical basis, as well as on a rudimentary theoretical basis. The rapid disappearance of the trapped reverse flux in typical experiments implies a high rate of conversion of magnetic-field energy into particle energy, as well as an induced betatron-type emf sufficient to accelerate particles into the low-keV region.

Two major questions remain unresolved: what is the nature of the anomalously high "resistivity" that permits disappearance of trapped reverse flux at the high rates observed; and what is the particle energy spectrum subsequent to "reverse-field heating"?

The present analysis appears directly relevant to the first of these questions. When ordinary collisional effects are not sufficient to account for observed resistivity, one thinks naturally in terms of an "enhanced resistivity" due to the occurrence of instabilities. Theta pinches, unlike Astron, have their tubular region of current flow far from any stabilizing shell, and so the instability governed by Eqs. (35) and (43) would definitely be anticipated.

In theta pinches having lengths comparable to their radii [18, 19], the initial current tube is found to collapse rapidly into a single current ring (i.e., an ordinary toroidal pinch), which then disintegrates via the usual short-wave hydromagnetic instabilities. In theta pinches where the length considerably exceeds the radius, and the time required for the entire current tube to collapse is correspondingly increased, break-up into a number of separate ring currents seems to be a fairly plausible occurrence. There are even some experimental magnetic probe data [20], that can be interpreted as providing direct evidence for the occurrence of this instability.

The break-up of the current tube into current rings does not in itself provide a mechanism for the escape of the trapped reverse axial field. The "velocity-space" instabilities considered in the present paper have as their energy source the kinetic energy of the plasma particles, and tend actually to increase the energy stored in magnetic field, rather than to help transform it into plasma energy. For the purpose of providing instability-enhanced plasma "resistivity," it is necessary to assume that the current rings resulting from the velocity-space instability develop secondary hydromagnetic instabilities of approximately the kind that have been seen when only a single current ring is present [18, 19].

In regard to the question of whether or not a thermal ion distribution results from the "reverse-field heating," neither the present analysis nor any experimental data published so far seem to afford a reliable clue. In view of the familiar experience with particle acceleration in dynamic pinches [21], there is no apparent reason to discount the possibility that some runaway component of the ion population is given considerable directed energy, while the rest of the population remains relatively "cold." The early disappearance of the trapped reverse field would force the runaway ions to assume regular gyro-orbits, and the subsequent adiabatic compression would energize them to the point of neutron production. The distinction between a thermal plasma at two or three keV and a plasma at, for example, 500 eV, with a tail suitably enlarged by runaway ions, is very slight in regard to effects measurable from fusion-reaction products. The best hope for resolving this question seems to lie with the eventual determination of bulk plasma parameters, such as β.

5. Relation to "finite-conductivity" instabilities

The instability of a hydromagnetic sheet-pinch of finite conductivity against the mode described by Eqs. (29) and (30) has been previously reported [22], When B_{x0} is taken to have the same z-dependence as in Eq. (26), the condition for hydromagnetic pressure balance with $\omega = 0$ yields the same eigenvalue problem (Eq. 36) as the present analysis.

In spite of this formal similarity, there is an essential difference between the velocity-space instability considered in the present analysis and the hydromagnetic "finite-conductivity" instability. In either case, a growing B_z component at $z=0$ is necessary for the growth of the instability. The associated electric field E_y, see Eq. (31), cannot be supported inside the plasma in the infinite-conductivity hydromagnetic approximation, hence the instability does not appear in this limit. For finite conductivity, the instability can take place, with a resultant transfer of magnetic-field energy into Joule heat and plasma kinetic energy. The collisionless-plasma limit, as treated by the Vlasov equation (the present analysis), is different from the infinite-conductivity hydromagnetic limit in that the inertia of the current-carriers is taken into account. Accordingly, a finite E_y can be supported inside the plasma, and the instability can develop. In this case, however, the energy transfer is from the kinetic energy of the current-carriers, which, on the average, are decelerated by the field, E_y into the magnetic-field energy of the perturbation.

In Astron and in high-energy-injection mirror machines, the directed kinetic energy of the current-carriers is larger than the thermal energy [i.e., $v_\perp > v^2$ in Eq. (25)]. Accordingly, the instability in the collisionless limit can draw on a non-trivial energy source, and, in this respect, is not precluded from attaining substantial magnitude in the non-linear phase of its growth.

In conventional pinches [12] on the other hand, the directed kinetic energy of the current-carriers tends to be negligible compared with their thermal energy. The only energy source that can drive instabilities to non-trivial magnitude is the potential energy stored in the magnetic field. Accordingly, the "finite-conductivity" treatment would be better suited than the collisionless treatment to explain the instabilities observed in some experimental pinch-current layers [23].

In high-powered theta-pinches, the situation is ambiguous. The kinetic energy that must be assumed for the electrons in order to account for the extremely high measured current density in the region of field reversal is at least as great as the electron thermal energy estimated from bremsstrahlung [24]. Accordingly, the presence of collisional effects is not a prerequisite for instability growth into the non-linear stage. The instability mode that actually grows may, however, turn out to be an expedient mixture of the "collisionless" and "finite-conductivity" modes.

Acknowledgement

The research work reported here was performed under the auspices of the United States Atomic Energy Commission.

References

[1] CHANDRASEKHAR, S., KAUFMAN, A. N., WATSON, K. M., *Proc. Roy. Soc. (London)* **A 245** (1958) 435.
[2] VEDENOV, A. A., SAGDEEV, R. Z., Plasma Physics and the Problem of Controlled Thermonuclear Reactions, (Pergamon Press, London, 1959) Vol. III, 332.
[3] POST, R. F., PERKINS, W. A., *Phys. Rev. Letters* **6** (1961) 85.
[4] BELL, P. R., KELLEY, H. G., MACKIN, R. J., Jr., IAEA Conference on Plasma Physics and Controlled Nuclear Fusion Research, Salzburg, 1961: Paper CN-10/191, page 251 of this Volume.
[5] NEWCOMB, W. A., *Ann. Phys. (N. Y.)* (to be published).
[6] KOLB, A. C., GRIEM, H. R., FAUST, W. R., Proceedings Fourth International Conference on Ionization Phenomena in Gases, Uppsala (North-Holland Pub. Co., Amsterdam, 1959), Vol. 2, 1037.
[7] CHRISTOFILOS, N. C., Proceedings Second U.N. International Conference on Peaceful Uses of Atomic Energy, Geneva **32** (1958) 279.
[8] HARRIS, E. G., U.S. Naval Research Laboratory Report NRL-4944 (1957).
[9] CHRISTOFILOS, N. C., "Interaction of Relativistic Electrons with a Quasi-Neutral Plasma", U.S. Atomic Energy Commission Report UCRL-5774-T (1959).
[10] NEIL, V. K., "Stability of Thin Electron Layers", U.S. Atomic Energy Commission Report UCRL-6463 (1961).
[11] GOLOVIN, I. N., ARTEMENKOV, L. I., BOGDANOV, G. F., PANOV, D. A., PISTUNOVICH, V. I., SEMASHKO, N. N., On the Work on the Thermonuclear Experimental Facility Ogra, to be published in *Uspekhi Fiz. Nauk.*
[12] COLGATE, S. A., FURTH, H. P., *Science* **128** (1958) 337. Other references are given.
[13] CHRISTOFILOS, N. C., IAEA Conference on Plasma Physics and Controlled Nuclear Fusion Research, Salzburg, 1961: Paper CN-10/148, page 159 of this Volume.
[14] CHRISTOFILOS, N. C., private communication.

[15] ANDERSON, O. A., FURTH, H. P., STONE, J. M., WRIGHT, R. E., *Phys. Fluids* **1** (1958) 489 (see especially p. 494).

[16] KOLB, A. C., DOBBIE, C. B., GRIEM, H. R., *Phys. Rev. Letters* **3** (1959) 5.

[17] LITTLE, E. M., QUINN, W. E., RIBE, F. L., IAEA Conference on Plasma Physics and Controlled Nuclear Fusion Research, Salzburg, 1961: Paper CN-10/155, see next Volume of these Proceedings.

[18] ALIDIERES, M., AYMOR, R., ETIEVANT, C., JOURDAN, P., SAMAIN, A., Proceedings Fourth International Conference on Ionization Phenomena in Gases, Uppsala (North-Holland Pub. Co., Amsterdam, 1959) Vol. 2, 1042.

[19] JOSEPHSON, V., DAZEY, M. H., WUERKER, R., *Phys. Rev. Letters* **5** (1960) 416.

[20] GOLDMAN, L. M., POLLOCK, H. C., "Internal Magnetic Field Measurements in a 14 cm diameter theta-pinch device": see abstract CN-10/135 in final volume of these Proceedings.

[21] ANDERSON, O. A., BAKER, W. R., COLGATE, S. A., ISE, J., JR., PYLE, R. V., *Phys. Rev.* **110** (1958) 1375.

[22] KILLEEN, J., FURTH, H. P., *Bull. Am. Phys. Soc. II* **6** (1961) 309.

[23] COLGATE, S. A., FURTH, H. P., *Phys. Fluids* **3** (1960) 982.

[24] SAWYER, G. A., BEARDEN, A. J., RIBE, F. L., STRATTON, T. F., *Bull. Am. Phys. Soc. II* **6** (1961) 310.

ЭКСПЕРИМЕНТАЛЬНОЕ ИССЛЕДОВАНИЕ НЕУСТОЙЧИВОСТИ ПЛАЗМЫ В ЛОВУШКЕ С МАГНИТНЫМИ ПРОБКАМИ*

М. С. ИОФФЕ, Е. Е. ЮШМАНОВ

АКАДЕМИЯ НАУК, СССР,

МОСКВА, СОЮЗ СОВЕТСКИХ СОЦИАЛИСТИЧЕСКИХ РЕСПУБЛИК

В опытах, описанных ранее, было установлено, что плазма, заполняющая ловушку, подвержена действию некоторого плазменного механизма, вызывающего перенос заряженных частиц поперек магнитного поля. Наблюдаемые времена удержания (порядка 100—1000 мксек) не могут быть однако объяснены простой теорией желобковой неустойчивости, т.к., согласно последней, они должны были быть меньше примерно на 2 порядка величины.

Б. Б. Кадомцев рассмотрел вопрос о потерях плазмы под влиянием желобковой неустойчивости, учитывая краевые условия на границе между плазмой и окружающими ее проводящими стенками. В частности, он указал на то, что азимутальные слагающие электрического поля, под действием которых плазма движется к стенке, должны обращаться в нуль в пристеночном слое толщиной порядка ϱ_i (ϱ_i — средний ларморовский радиус ионов), и это должно привести к значительному уменьшению скорости потерь.

Согласно развитой им теории турбулентной конвекции разреженной плазмы время удержания плазмы в ловушке τ определяется соотношением:

$$\tau \simeq Ca\left(\frac{\Omega_H^2 + \Omega_0^2}{\Omega_0^2} \cdot \frac{R_0 M}{\varrho_i T}\right)^{\frac{1}{2}}$$

где: C — множитель, зависящий от доли частиц, теряемых плазменной трубкой при ее соприкосновении со стенкой, a — радиус ловушки, Ω_H и Ω_0 ларморовская и плазменная частоты для ионов, R_0 — средний радиус кривизны силовых линий вблизи стенки, M и T масса и температура ионов.

Настоящая работа имела целью экспериментальную проверку теории Кадомцева. В работе изучались:

а) детальный характер колебаний плотности плазмы в пристеночной области и во внутренних областях ловушки,

б) радиальное распределение плотности плазмы,

с) зависимость времени удержания плазмы от ее плотности (в интервале плотностей 10^7—10^9 см$^{-3}$).

Совокупность полученных результатов по пунктам а) и б) качественно согласуется с физической моделью турбулентной конвекции, рассматриваемой теорией, а для зависимости времени удержания от плотности имеется и вполне удовлетворительное количественное согласие между теорией и экспериментом.

1. Введение

В опытах, описанных ранее [1, 2], было установлено, что плазма, заполняющая ловушку, подвержена действию некоторого плазменного механизма, вызывающего перенос заряженных частиц поперек магнитного поля и потерю их на боковой стенке ловушки. Наблюдаемые времена удержания (порядка 100—1000 мксек) не могут быть, однако, объяснены простой теорией желобковой неустойчивости [3], т.к., согласно последней, они должны были бы быть меньше примерно на два порядка величины.

Л. А. Арцимович обратил внимание на то, что такое несоответствие между теорией и экспериментом может быть связано с наличием вокруг плазмы проводящих стенок, расположенных по силовым линиям магнитного поля.

Азимутальные слагающие электрического поля E_φ, возникающие вследствие поляризации плазменных трубок в неоднородном магнитном поле и обусловливающие радиальное движение плазмы, должны ослабляться металлической стенкой, становясь в непосредственной близости от неё равными нулю (в силу непрерывности тангенциальной компоненты электрического поля на границе металл-плазма). Иными словами, согласно этой точке зрения, металлическая стенка оказывает тормозящее действие на плазму и способствует тем самым более длительному её удержанию.

Вопрос о влиянии проводящей стенки, окружающей плазму, на скорость потерь вследствие желобковой неустойчивости был рассмотрен более детально Б. Б. Кадомцевым [4]. Качественная схема, лежащая в основе этого рассмотрения, сводится к следующему. Отдельные плазменные трубки с повышенной плотностью частиц движутся наружу — к стенке — со скоростью $V_{др} = cE_\varphi/H$ Приблизившись к стенке на расстояние, близкое к ϱ_i (ϱ_i — средний ионный ларморовский радиус), трубки плазмы (или плазменные языки, как мы их будем также называть в дальнейшем) вступают с ней в электрический контакт, который осуществляется за счет быстрой потери избыточной

* Доклад CN-10/216, представленный на Конференцию. Докладчик: М. С. Иоффе. Дискуссия (на английском языке) по этому докладу дана на стр. 209. Переводы аннотаций находятся в конце этого тома Трудов Конференции.

части ионов на стенке и ухода соответствующего количества электронов вдоль силовых линий на торцевые части металлической камеры. Вследствие этого, пристеночный слой плазмы толщиной порядка ϱ_1 оказывается практически эквипотенциальным и скорость $V_{др}$ в нем падает до нуля. В последующем, как только плотность плазмы в языках, соприкасающихся со стенкой, становится несколько меньше плотности окружающей плазмы, направление E_φ в них изменяется на обратное, и возникает, соответственно, обратное движение этих областей внутрь. Т.о., в плазме, помещенной в неоднородное магнитное поле, убывающее к периферии, должно происходить интенсивное перемешивание внутренних и внешних областей, напоминающее конвекцию неоднородно нагретой жидкости в поле тяжести. Благодаря такому перемешиванию, плазма должна распределяться почти равномерно по всему поперечному сечению ловушки вплоть до пристеночного слоя толщиной порядка ϱ_1, в котором и сосредоточено практически все падение плотности. Т.к. при каждом соприкосновении со стенкой плазменный язык теряет не все содержащиеся в нем частицы, а лишь некоторую часть их, то средняя скорость потерь оказывается существенно меньшей по сравнению со случаем, когда проводящая стенка отсутствует. Теория турбулентной конвекции разреженной плазмы, развитая в [4] на основе изложенной качественной модели, приводит к следующему выражению для времени удержания плазмы в ловушке:

$$\tau \simeq Ca\left(\frac{\Omega_H^2 + \Omega_0^2}{\Omega_0^2} \cdot \frac{R_0 M}{\varrho_1 T}\right)^{\frac{1}{2}}, \qquad (1)$$

где C — множитель, зависящий от доли частиц, теряемых плазменной трубкой при её соприкосновении со стенкой, a — радиус ловушки, Ω_H и Ω_0 — ларморовская и ленгмюровская частоты для ионов, R_0 — средний радиус кривизны силовых линий вблизи стенки, M и T — масса и температура ионов.

Настоящая работа имела целью экспериментальную проверку теории Кадомцева. В работе изучались:

а) детальный характер пульсаций плотности плазмы в пристеночной области и во внутренних областях ловушки;

б) радиальное распределение плотности плазмы;

в) зависимость времени удержания плазмы от её плотности (в интервале плотностей 10^7 — 10^9 см$^{-3}$).

2. Исследование плазменных пульсаций

В предыдущих экспериментах [1, 2] было обнаружено, что ток ионов на отдельные элементы боковой стенки ловушки имеет характер нерегулярных выбросов, хорошо скоррелированных вдоль силовых линий магнитного поля. Из этого можно было заключить, что вблизи стенки в плазме имеются неоднородности, и их продольный размер соответствует длине ловушки.

Согласно модели турбулентной конвекции, следует ожидать, что поперечные размеры таких неоднородностей (плазменных языков) должны быть ограничены снизу величиной порядка ларморовского радиуса ионов, а сверху — поперечными размерами ловушки. Для качественной проверки этого положения, а также для выяснения характера движения плазменных неоднородностей, были предприняты наблюдения за локальными пульсациями плотности плазмы в поперечном сечении ловушки с помощью электрических зондов.

Зонд представлял собой металлический шарик диаметром 1,5 мм, укрепленный на тонкой подводящей проволочке. Проволочка изолировалась кварцевой трубкой, пропущенной в свою очередь через металлическую трубку диаметром 2 мм. Металлическая трубка находилась под потенциалом земли и выполняла роль экрана, устраняя емкостную связь подводящей проволочки с плазмой. Было установлено, что присутствие такого зонда в ловушке не влияет на плотность плазмы и её время жизни.

Изучение плазменных неоднородностей производилось на установке, описанной в [1], при магнитном поле 5000 эрст. и ускоряющем напряжении 30 кв, что соответствовало средней энергии ионов в плазме около 1,5 кэв. Плотность плазмы составляла величину $1 - 3 \cdot 10^9$ см$^{-3}$. Опыты проводились при давлении водорода в камере, равном $0{,}8 - 1{,}0 \cdot 10^{-6}$ мм Hg. Время перезарядки ионов на нейтральном газе составляло 1 — 0,8 мсек, а время добавочного ухода — около 0,13 мсек. По сравнению с опытами, описанными в [1, 2], имелось отличие, состоявшее в том, что внутрь вакуумной камеры помещался медный кожух такой формы, что его образующие совпадали с силовыми линиями магнитного поля. Диаметр ловушки в центральном сечении составлял 40 см.

Мгновенная плотность плазмы в той или иной точке ловушки регистрировалась по ионному току на зонд. Для запирания электронов из плазмы достаточно было подать на зонд отрицательный потенциал, равный 10 — 20 в. Дальнейшее увеличение отрицательного смещения (до 100 в и более) не изменяло величины и формы сигнала с зонда, что указывает на отсутствие значительного количества медленных ионов в ловушке.

Для измерения поперечных размеров плазменных языков зонды помещались вблизи стенки ловушки в разных точках по азимуту центрального сечения. Соприкосновение каждого плазменного языка со стенкой отмечается выбросом ионного тока на соответствующем зонде. Снимая одновременные осциллограммы токов на два зонда, отстоящие друг от друга на то или иное расстояние в азимутальном направлении, можно по степени корреляции выбросов судить о поперечных размерах плазменных языков вблизи стенки. Если расстояние между зондами меньше размеров плазменного языка, то соответствующие ему выбросы

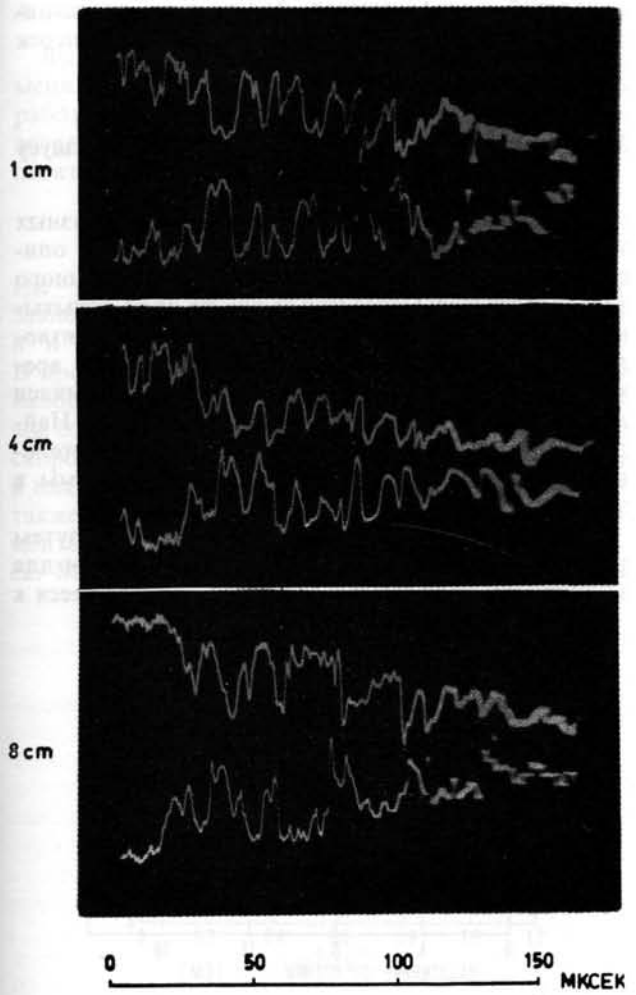

Рис. 1 Корреляция тока ионов на зонды, удаленные на различные расстояния по азимуту. Лучи осциллографа отклоняются в разные стороны.

должны присутствовать, очевидно, на обеих осциллограммах. Нарушение такой корреляции укажет на то, что расстояние между зондами превышает размер языка. Сигнал ионного тока на зонд, помещенный вблизи стенки, состоит из большого числа нерегулярных выборосов различной длительности и амплитуды. Максимальная длительность отдельных выбросов составляет 30—50 мксек; эти широкие пики промодулированы более высокочастотными пульсациями. Наименьшая длительность выбросов составляет 2—3 мксек.

На рис. 1 приведены парные осциллограммы токов на два зонда, отстоящие друг от друга на различные расстояния по азимуту. Видно, что при расстоянии между зондами в 1 см формы сигналов практически совпадают. При увеличении расстояния сначала происходит нарушение корреляции между наиболее кратковременными пиками, распространяясь затем на более низкочастотные составляющие спектра пульсаций. Одновременно наблюдается возрастающий временной сдвиг коррелирующих импульсов на одном зонде относительно другого. Анализ многих осциллограмм показывает, что при расстоянии между зондами в 4 см сильно нарушается корреляция выбросов длительностью в 2—3 мксек; при расстоянии в 8 см назрушается корреляция выбросов длительностью в 8—10 мксек; при расстоянии в 12 см остается корреляция только широких пиков длительностью в десятки мксек (рис. 2). При расстоянии между зондами, соответствующем азимутальному углу в 180°, отсутствует какая-либо корреляция сигналов на обоих зондах.

Из сказанного следует, что поперечные размеры плазменных языков имеют различную величину, которая тесно связана со временем существования языка. Наименьший размер имеют языки, живущие наиболее короткое время (2—3 мксек); ширина этих языков составляет 3—4 см, т.е. величину порядка среднего ларморовского диаметра ионов, который равен примерно 2,5 см. Языки длительностью до 10 мксек имеют размеры около 10 см; наконец, языки со временем жизни в десятки мксек имеют поперечные размеры, превышающие 12 см, т.е. уже сравнимые с поперечным размером ловушки.

Наличие сдвига по времени между выбросами тока на различных зондах и его увеличение с увеличением азимутального расстояния между зондами указывает на вращение плазменных языков в азимутальном направлении. Линейная скорость вращения, вычисленная по величине сдвига при известном расстоянии между зондами, составляет величину около $1 \cdot 10^6$ см/сек. Вращение свидетельствует о существовании в пристеночном слое плазмы электрического поля, направленного по радиусу. Величина этого поля, вычисленная по скорости вращения, составляет примерно 50 в/см. Согласно теории, положительный потенциал должен приобретаться плазмой вследствие развития желобковой неустойчивости (при наличии заземленных торцов, как это имеет место в описываемом опыте). Однако возможны и другие причины того, что плазма заряжается положительно, например более быстрый уход электронов по сравнению с ионами вдоль магнитного поля.

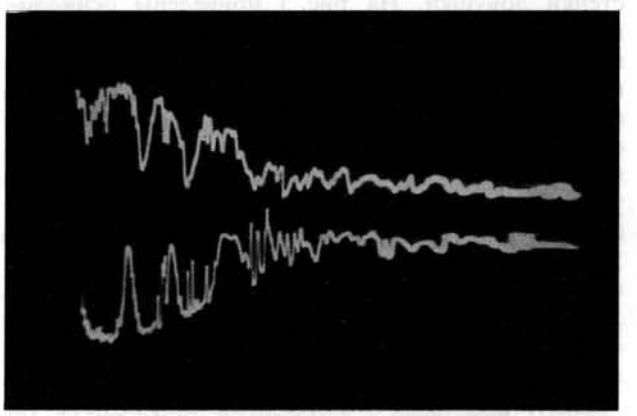

Рис. 2 Корреляция тока при расстоянии между зондами 12 см (длительность развертки 400 мксек).

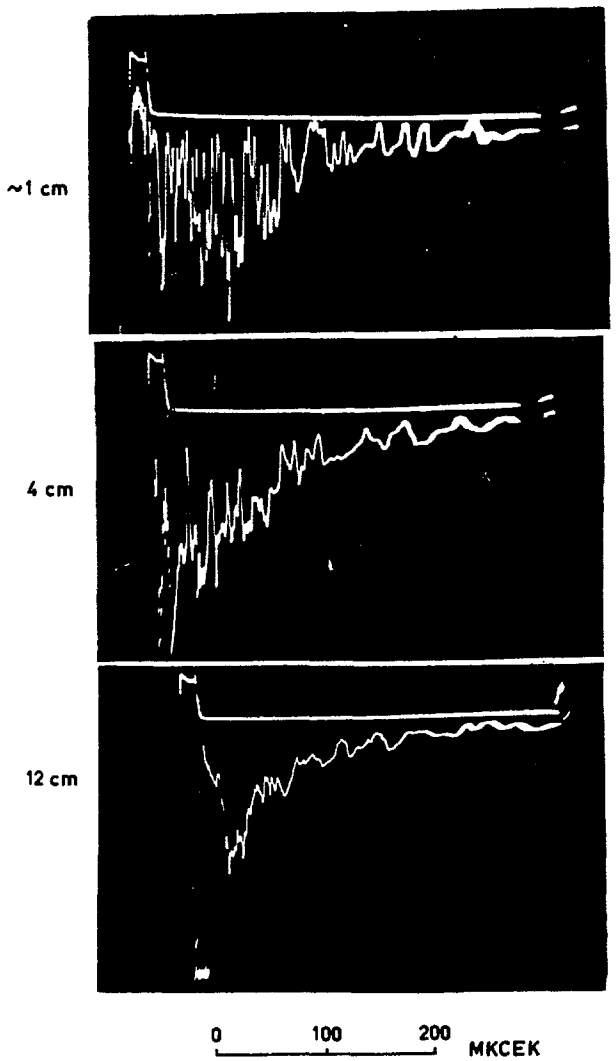

Рис. 3 Изменение формы сигнала ионного тока на зонд с увеличением расстояния от стенки (верхний луч — ускоряющий импульс, нижний луч — ионный ток, отклонение направлено вниз).

С помощью зондов исследовался также характер пульсаций плазмы на различных расстояниях от стенки ловушки. На рис. 3 приведены осциллограммы ионных токов на зонд, помещенный вблизи стенки, а также на расстоянии в 4 и в 12 см от стенки. Отчетливо видно, что в более глубоких слоях плазмы резко сокращается амплитуда высокочастотных выбросов, и ток на зонд носит более плавный характер, чем вблизи стенки. Это указывает на то, что мелкомасштабные пульсации (размером в несколько см и длительностью 2—3 мксек.) развиваются лишь в пристеночном слое толщиной 3—4 см. В центральных областях ловушки имеется более однородный плазменный фон, промодулированный крупномасштабными пульсациями.

Как видно из всех приведенных результатов, пространственная структура и временные характеристики наблюдающихся плазменных неоднородностей соответствуют физическим представлениям о конвективном переносе плазмы поперек магнитного поля к стенке.

3. Распределение плотности плазмы по радиусу ловушки

Относительные величины плотности в разных точках по радиусу определялись с помощью описанного ранее зонда, путем измерения ионного тока. Поскольку мгновенный ток на зонд испытывает сильные беспорядочные колебания, производилось интегрирование тока за промежуток времени в 40 мксек. Полученный результат усреднялся для большого числа отдельных измерений. Найденная величина рассматривалась как относительная характеристика средней плотности плазмы в заданной точке.

На рис. 4 приведено найденное таким путем распределение плотности по радиусу ловушки для магнитного поля в 5 и 8 тыс. эрст., относящееся к

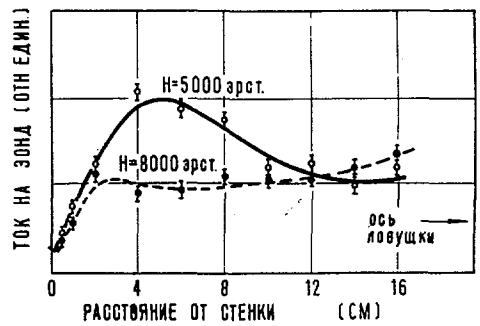

Рис. 4 Радиальное распределение плотности плазмы при магнитных полях в 5 и 8 тыс. эрст.

моменту времени спустя 60 мксек после окончания импульса ускоряющего напряжения. Прежде всего следует отметить тот факт, что хотя образование быстрых ионов во время ускоряющего импульса происходит в приосевой области ловушки (из центрального плазменного пучка), полученные кривые свидетельствуют, что к моменту измерения большая часть плазмы оказывается рассредоточенной по периферии. Это указывает на существование интенсивного механизма, перемещающего плазму поперек магнитного поля. Обращает на себя внимание также наличие максимума плотности в пристеночной области при магнитном поле 5000 эрст. Можно полагать, что это связано с различной скоростью радиального переноса плазмы внутри ловушки и в пристеночной области. Т.к. вблизи стенки плазма испытывает торможение, то это и должно соответственно приводить к увеличению плотности. С этой точки зрения, отсутствие подобного максимума при поле 8000 эрстед может указывать на то, что с ростом поля различие в скоростях переноса внутри ловушки и вблизи стенки сильно сокращается.

4. Зависимость скорости ухода плазмы от плотности

Выше было приведено выражение (1) для времени жизни плазмы в ловушке, вычисленное в работе [4]. Для заданных магнитного поля H и энергии ионов T соотношение (1) можно переписать в виде:

$$\tau_д \simeq \text{Const}\left(\frac{B}{n}+1\right)^{\frac{1}{2}}, \qquad (2)$$

где $B=H^2/4\pi Mc^2$. Соотношение (2) описывает зависимость скорости ухода плазмы от плотности n и может быть проверено экспериментально. В проводившихся с этой целью опытах использовалось естественное уменьшение плотности плазмы со временем в процессе её распада. Измерялась скорость уменьшения плотности быстрых ионов в плазме (т.е. полное время жизни τ, включающее также потери на перезарядку) в различные моменты времени после конца ускоряющего импульса. Максимальная плотность соответствовала ну-

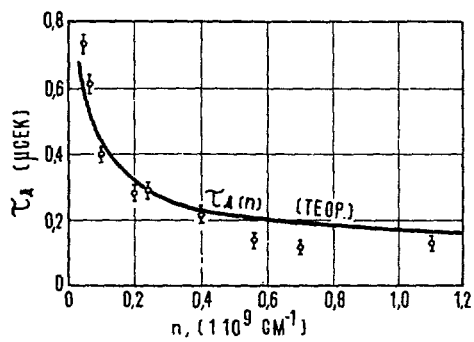

Рис. 5 Экспериментальная и теоретическая зависимость времени добавочного ухода от плотности плазмы.

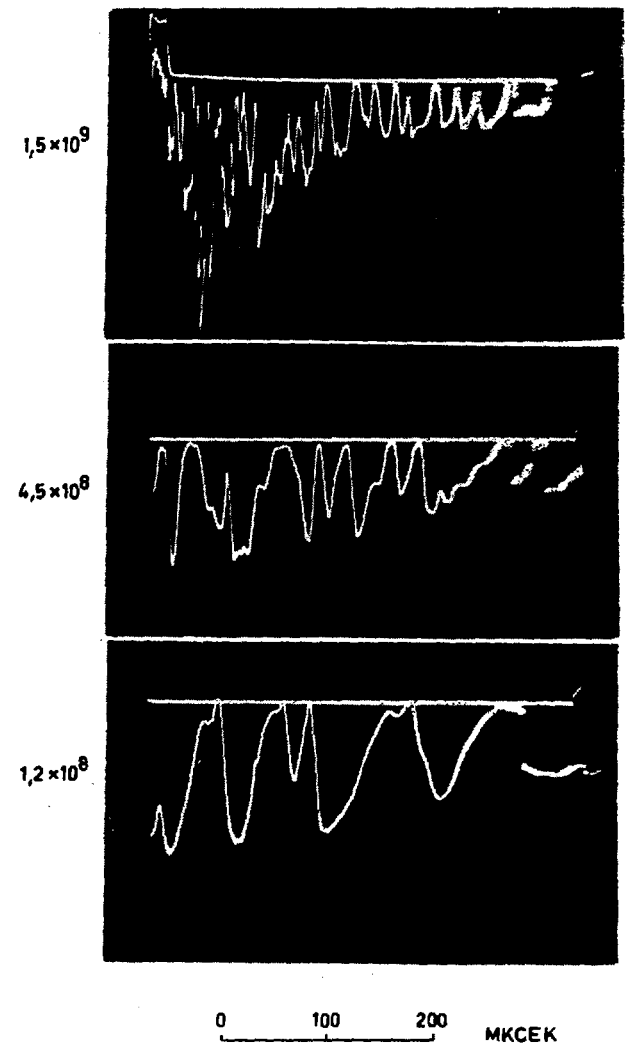

Рис. 6 Изменение частоты плазменных пульсаций с уменьшением плотности.

левой задержке, а минимальная — задержке 850 мксек. Величина плотности, средней по сечению ловушки, и время жизни определялись так же, как и в работе [1], по потоку быстрых атомов перезарядки. При вычислении плотности и времени перезарядки использовалось найденное ранее значение величины $\langle v\sigma\rangle_n$, равное $3{,}5\cdot10^{-8}$ см^3/сек. Измерения производились при магнитном поле 5000 эрст. и давлении $4\cdot10^{-7}$ мм Hg, что соответствует времени перезарядки $\tau_n=2$ мсек. Время добавочного ухода вычислялось из соотношения $1/\tau=1/\tau_n+1/\tau_д$. Предполагалось, что во все моменты времени энергия ионов в плазме остается постоянной. Это предположение основано на результатах работы [2], из которых следует, что за времена, меньшие одного времени перезарядки при данном давлении, величина $\langle v\sigma\rangle_n$ не меняется.

На рис. 5 приведены результаты измерений зависимости $\tau_д$ от плотности для интервала плотностей от $5\cdot10^7$ до $1{,}1\cdot10^9$ см$^{-3}$. На этом же рисунке приведена для сравнения теоретическая кривая согласно выражению (2); при этом константа выбрана так, чтобы вычисленная кривая проходила через одну из средних экспериментальных точек. Видно, что найденный в опыте закон изменения $\tau_д$ в зависимости от плотности находится в удовлетворительном согласии с ожидаемым согласно теории.

Уменьшение скорости ухода плазмы поперек магнитного поля по мере уменьшения плотности сопровождается также изменением и характера плазменных пульсаций. На рис. 6 приведены осциллограммы ионного тока на зонд вблизи стенки, снятые с различными задержками относительно заднего фронта ускоряющего импульса ($t=0$, 200 и 500 мксек), т.е. при различных плотностях (примерно $1{,}5\cdot10^9$, $4{,}5\cdot10^8$ и $1{,}2\cdot10^8$ см$^{-3}$ соответственно). Видно, что с уменьшением плотности плазмы среднее время пульсаций, а, следовательно, и их поперечный размер (в соответствии со сказанным ранее) увеличиваются. Такой результат качественно согласуется с выводами теории, согласно которой минимальный масштаб возможных пульсаций тем больше, чем ниже плотность.

5. Заключение

Настоящая работа явилась продолжением начатых ранее исследований поведения плазмы в ловушке с магнитными пробками.

В связи с экспериментальными данными об уходе плазмы из ловушки, которые были получены в работах [1, 2], Б. Кадомцевым был предложен механизм конвективной утечки плазмы. Такой механизм проявляется в условиях, когда плазма окружена проводящими стенками. Как было показано в [4], на основе представлений о конвективном характере потерь удается удовлетворительно объяснить наблюдаемые времена удержания.

В настоящей работе теория Кадомцева получила свое дальнейшее экспериментальное подтверждение. Установлено, что экспериментальная зависимость времени жизни от плотности находится в близком соответствии с теоретической. В хорошем согласии с моделью турбулентной конвекции, лежащей в основе теории, находятся также результаты детального исследования плазменных пульсаций в пристеночной и во внутренней областях ловушки и данные о радиальном распределении плотности плазмы. Таким образом, на основании проведенных исследований можно придти к выводу, что удерживающие свойства ловушки с магнитными пробками зависят существенным образом от проводимости ее стенок. Хорошо проводящие стенки заметно стабилизируют желобковую неустойчивость, и благодаря этому сокращается скорость утечки плазмы.

Однако, как следует из теории Кадомцева и как показывают результаты экспериментов, стабилизирующее действие стенок является далеко недостаточным, если иметь в виду конечную задачу термоизоляции плазмы полем пробочной конфигурации.

В заключение авторы выражают свою благодарность Л. А. Арцимовичу и Б. Б. Кадомцеву за их интерес к данной работе и полезные обсуждения.

Литература

[1] Иоффе М., Соболев Р., Тельковский В., Юшманов Е. *ЖЭТФ* **39** (1960) 1602.
[2] Иоффе М., Соболев Р., Тельковский В., Юшманов Е. *ЖЭТФ* **40** (1961) 40.
[3] Rosenbluth, M., Longmire, C., *Ann. of. Phys.*, (*N. Y.*) **1** (1957) 120.
[4] Кадомцев Б., *ЖЭТФ* **40** (1961) 328.

ENERGY TRANSFER FROM HOT IONS TO COLD ELECTRONS IN A PLASMA*

JOHN KILLEEN, WARREN HECKROTTE, GARRET BOER

LAWRENCE RADIATION LABORATORY, UNIVERSITY OF CALIFORNIA

LIVERMORE, CALIFORNIA, UNITED STATES OF AMERICA

It is of importance to know the details of the energy loss of the ions in any scheme for producing a hot plasma by high energy injection. Two approaches under way in this country are the injection of energetic neutral atoms and the breakup of high energy molecular ions using an arc. Plasma buildup in these schemes has been calculated, including spatial dependence and energy loss to the arc. In this paper the energy exchange rate between plasma ions and electrons is examined. The usual procedure is to use the Chandrasekhar result for a Maxwellian distribution of velocities. This is inadequate for our needs, because when the ions are much hotter than the electrons they exchange energy primarily with slow electrons, and it has been shown that this causes a significant perturbation of the electron distribution function which reduces the exchange rate. In addition, we need to include particle losses and sources, and an equilibrium theory is not justified. A theoretical description of the interaction of the ions and electrons among themselves is given by the inverse-square law Fokker-Planck equations for the particle distribution functions in velocity space. In studying energy transfer problems we can assume isotropic velocity distributions for the ions and electrons. In studying scattering losses from a mirror machine the angular dependence of the distribution function can be separated out and solved analytically using Legendre functions. We have, then, two coupled partial differential equations for the functions $f_+ (v, t)$ and $f_- (v, t)$, where v is the magnitude of velocity and t the time. The equations are solved by difference methods using an IBM 709 code. The equations are not linearized, i.e., the coefficients which involve moments of the distribution functions are computed at each time step. An implicit difference scheme is used which eliminates instabilities in the calculation. Cases of interest to the two experimental methods have been calculated and detailed results will be presented. We determine the regime of validity of the Spitzer formulae, and any corrections that should be made.

1. Introduction

In experiments in controlled fusion research it is desirable to produce a plasma in which the ions are at a higher temperature than the electrons. In those schemes for producing a hot plasma by the injection of energetic neutral atoms or molecular ions there will be hot ions in the presence of cold electrons. It is important to know the details of the energy transfer from ions to electrons in these cases. For example, in studies of plasma production by the injection of high energy molecular ions with subsequent dissociation by an arc, the inclusion of energy loss to the arc dominated the buildup calculations [2].

In this paper the energy exchange rate between plasma ions and electrons is examined. In studying such problems, the most suitable mathematical description is by means of the Fokker-Planck equations for the ion and electron distribution functions in velocity space. This is because the dominant mechanism for energy transfer among the particles is by long range Coulomb interactions. The Fokker-Planck equations for the distribution functions of several species of particle, where the two-body force is an inverse-square law, have been derived in the paper of ROSENBLUTH, MACDONALD, and JUDD [5]. With that result as a starting point, in Section 2 we derive the appropriate equations for the ions and electrons with the assumption that the velocity distributions are isotropic.

We have two coupled nonlinear partial differential equations for the functions $f_+ (v, t)$ and $f_- (v, t)$, where v is the magnitude of velocity and t the time. We are interested in the numerical solution of these equations by replacing them by a pair of difference equations. In Section 3 the difference equations are derived, and the method of solution of the difference equations is discussed. In the course of the solution the electron distribution function will cover a much larger range of the velocity variable than the ion distribution function. Consequently, an increasing increment in the velocity variable is used. In replacing partial differential equations by explicit difference equations a severe restriction is imposed on the size of the time step that can be taken [6]. To avoid this difficulty an implicit difference scheme is solved. Instabilities in the calculation are thus avoided, even with time steps several orders of magnitude greater than that imposed by the stability criterion of explicit methods. This advantage is an essential part of the calculations. In studying the heating of electrons by ions which are much hotter, the transfer rate decreases rapidly as the electron temperature increases. Consequently, the time step must be continually increased during the calculation in order to progress towards equilibrium in a sensible manner. An IBM 709 code has

* Conference paper CN-10/151, presented by J. KILLEEN. Discussion of this paper is given on page 210. Translations of the abstract are at the end of this volume of the Conference Proceedings.

been written for the solution of the difference equations.

Numerical results are presented in the following section. These cases have been selected to examine the energy transfer in some of the proposed high-energy injection schemes. Particular attention is given in this paper to a comparison of the numerical results of electron heating with those predicted by the transfer rates given by SPITZER [3]. These transfer rates are based on a quasi-equilibrium theory assuming that the electrons have Maxwellian velocity distributions. It had been conjectured [7, 8, 9] that the transfer rate would be less than the stated value in those cases where the ions are considerably hotter than the electrons. The ions exchange energy primarily with electrons whose velocities are lower than the mean ion velocity. Estimates were made that the slow electrons would be scattered by ions to higher velocities faster than they would diffuse downward in velocity to fill this hole in the distribution. This depletion of the small velocity end of the electron distribution is observed in the numerical results. The consequence in these cases is that the transfer rates are less than those usually stated [3]. A reduction of this kind is of importance in assessing the feasibility of the high energy injection schemes.

A modification to the Spitzer formula has been given by ROSENBLUTH [10], where the electron distribution is perturbed from the Maxwellian and the ion distribution is taken to be Maxwellian. This modification gives a reduction in the transfer rate. The numerical results are compared with this theory also in those cases for which it can be applied.

It is important to point out that the numerical solution of the Fokker-Planck equations is not carried out merely to check the usual transfer rates [3]. The distribution functions are obtained as a function of time and the numerical solution is the only way to follow the approach to equilibrium of several species of particles. With the code, more than two species can be considered without much difficulty. In addition, the code has been used to compute loss rates from mirror machines, in which case the equation for the ions only is solved with a loss term determined by the mirror ratio [11]. In studying scattering losses, the angular dependence of the distribution function can be separated out [11, 12] and solved analytically using Legendre functions. The speed distribution is then solved numerically using the code.

2. The Fokker-Planck equations for ions and electrons

In the paper of ROSENBLUTH, MACDONALD and JUDD, the Fokker-Planck equations for an inverse-square force are derived [5]. In Eq. (31) of that paper the result is given in spherical polar co-ordinates in velocity space, assuming azimuthal symmetry, i.e., no φ dependence. We further assume that the distribution functions are isotropic in velocity space, i.e., there is no θ dependence. The functions depend only on v, the magnitude of the velocity, and t, the time. Under this assumption the equation becomes

$$\Gamma_a^{-1}\frac{\partial f_a}{\partial t}=\frac{\partial^2 f_a}{\partial v^2}\left[\frac{1}{2}\frac{\partial^2 g}{\partial v^2}\right]+\frac{\partial f_a}{\partial v}\left[-\frac{\partial h_a}{\partial v}-\frac{1}{v^2}\frac{\partial g}{\partial v}+\frac{2}{v}\frac{\partial^2 g}{\partial v^2}+\frac{\partial^3 g}{\partial v^3}\right]+f_a\left[-\frac{2}{v}\frac{\partial h_a}{\partial v}-\frac{\partial^2 h_a}{\partial v^2}+\frac{2}{v}\frac{\partial^3 g}{\partial v^3}+\frac{1}{2}\frac{\partial^4 g}{\partial v^4}\right]. \quad (1)$$

The function $f_a(v, t)$ is the distribution function for particles of type a. The functions $h_a(v, t)$ and $g(v, t)$ are defined by the equations

$$h_a(v,t)=4\pi\sum_b\frac{m_a+m_b}{m_b}\left[\int_0^v f_b(v',t)\frac{v'^2}{v}\mathrm{d}v'+\int_v^\infty f_b(v',t)v'\,\mathrm{d}v'\right], \quad (2)$$

$$g(v,t)=4\pi\sum_b\left[\int_0^v f_b(v',t)\,v\left(1+\frac{1}{3}\frac{v'^2}{v^2}\right)v'^2\,\mathrm{d}v'+\int_v^\infty f_b(v',t)\left(1+\frac{1}{3}\frac{v^2}{v'^2}\right)v'^3\,\mathrm{d}v'\right]. \quad (3)$$

The summations are taken over all the species of particle being considered, including type a. The constant Γ_a is defined by the equation

$$\Gamma_a\equiv\frac{4\pi e^4}{m_a^2}\ln D.$$

The quantity D is the ratio of the Debye length to the classical distance of closest approach.

Using Eqs. (2) and (3), we can evaluate the coefficients of Eq. (1). We then have

$$(4\pi\Gamma_a)^{-1}\frac{\partial f_a}{\partial t}=\frac{\partial^2 f_a}{\partial v^2}\left[\sum_b\left\{\frac{1}{3v^3}\int_0^v f_b(v',t)\,v'^4\,\mathrm{d}v'+\frac{1}{3}\int_v^\infty f_b(v',t)\,v'\,\mathrm{d}v'\right\}\right]+\frac{\partial f_a}{\partial v}\left[\frac{1}{v}\sum_b\left\{\frac{m_a}{m_b}\frac{1}{v}\int_0^v f_b(v',t)v'^2\mathrm{d}v'-\frac{1}{3v^3}\int_0^v f_b(v',t)v'^4\mathrm{d}v'+\frac{2}{3}\int_v^\infty f_b(v',t)\,v'\,\mathrm{d}v'\right\}\right]+f_a\left[\sum_b\frac{m_a}{m_b}f_b\right]. \quad (4)$$

We introduce the dimensionless variable $x=v/v_0$, where v_0 is some characteristic velocity. Let $F_b=(4\pi v_0^3/K_b)f_b$, where K_b is a constant to be determined. The total number of particles of type b is given by

$$n_b(t)=4\pi\int_0^\infty f_b(v,t)\,v^2\,\mathrm{d}v=K_b\int_0^\infty F_b(x,t)\,x^2\,\mathrm{d}x.$$

Let

$$I_2{}^b(0)=\int_0^\infty F_b(x,0)\,x^2\,\mathrm{d}x;$$

then $K_b = n_b(0)/I_2{}^b(0)$, i.e., the constant is determined from the initial conditions.

Now consider two species, electrons and ions of $Z=1$. We determine the time scale by the electron equation, i.e., let

$$\tau = \frac{\Gamma_e}{2}\frac{K_e}{v_0{}^3}t\,.$$

We have $\Gamma_i = \mu^2\Gamma_e$, where $\mu = m_e/M_i$. For simplicity of notation let $F_e(x,\tau) \equiv f(x,\tau)$, $F_i(x,\tau) \equiv g(x,\tau)$, $K = K_i/K_e$. We introduce the functionals

$$M(f) = \int_x^\infty f(y,\tau)\,y\,dy\,, \tag{5}$$

$$N(f) = \int_0^x f(y,\tau)\,y^2\,dy\,, \tag{6}$$

$$E(f) = \int_0^x f(y,\tau)\,y^4\,dy\,. \tag{7}$$

The equation for the electron distribution function becomes

$$\frac{\partial f}{\partial \tau} = A\frac{\partial^2 f}{\partial x^2} + B\frac{\partial f}{\partial x} + Cf\,, \tag{8}$$

where

$$A = \frac{2}{3}\left\{\left[\frac{1}{x^3}E(f) + M(f)\right] + K\left[\frac{1}{x^3}E(g) + M(g)\right]\right\} \tag{9}$$

$$B = \frac{4}{3x}\left\{\left[\frac{3}{2x}N(f) - \frac{1}{2x^3}E(f) + M(f)\right] + K\left[\mu\frac{3}{2x}N(g) - \frac{1}{2x^3}E(g) + M(g)\right]\right\} \tag{10}$$

$$C = 2\{f + K\mu g\}\,. \tag{11}$$

The equation for the ion distribution function becomes

$$\frac{\partial g}{\partial \tau} = F\frac{\partial^2 g}{\partial x^2} + G\frac{\partial g}{\partial x} + Hg\,, \tag{12}$$

where

$$F = \frac{2}{3}\mu^2\left\{\left[\frac{1}{x^3}E(f) + M(f)\right] + K\left[\frac{1}{x^3}E(g) + M(g)\right]\right\} \tag{13}$$

$$G = \frac{4}{3x}\mu^2\left\{\left[\frac{1}{\mu}\frac{3}{2x}N(f) - \frac{1}{2x^3}E(f) + M(f)\right] + K\left[\frac{3}{2x}N(g) - \frac{1}{2x^3}E(g) + M(g)\right]\right\} \tag{14}$$

$$H = 2\mu^2\left\{\frac{1}{\mu}f + Kg\right\}. \tag{15}$$

In the next section we shall discuss the method of solution of Eqs. (8) and (12).

3. The difference equations and methods of solution

We wish to solve the two nonlinear differential equations

$$\frac{\partial f}{\partial \tau} = A(f,g,x,\tau)\frac{\partial^2 f}{\partial x^2} + B(f,g,x,\tau)\frac{\partial f}{\partial x} + C(f,g,x,\tau)f \tag{16}$$

$$\frac{\partial g}{\partial \tau} = F(f,g,x,\tau)\frac{\partial^2 g}{\partial x^2} + G(f,g,x,\tau)\frac{\partial g}{\partial x} + H(f,g,x,\tau)g \tag{17}$$

in the domain $0 \le x \le \infty$, $\tau \ge 0$, with the boundary conditions $f \to 0$, $g \to 0$ as $x \to \infty$, and $\partial f/\partial x = \partial g/\partial x = 0$ at $x = 0$ for $\tau > 0$. The initial distributions $f(x,0)$ and $g(x,0)$ are given.

For the numerical solution we choose a domain $0 \le x \le x_J$, where x_J is specified for each problem and is taken large enough to include the high velocity tail of the electron distribution. As the electrons increase in temperature, the distribution spreads out. Thus the choice of x_J determines when the calculation must be stopped in order to preserve accuracy. At $x = x_J$, we take the boundary condition $f = g = 0$.

In the domain $0 \le x \le x_J$, $\tau \ge 0$, consider the mesh defined by $x_j = j\Delta x$, $j = 0, 1, 2, \ldots, J$; $\tau^n = n\Delta\tau$, $n = 0, 1, 2, \ldots$. For simplicity, we are here taking the velocity increment, Δx, to be constant. In the actual calculations we take an increasing increment between points x_j as j increases. We use small values of Δx for small x to describe accurately the ion distribution function, and we use larger values of Δx as x increases to include the high velocity tail of the electron distribution function.

Let $f_j{}^n = f(x_j, \tau^n)$ and $g_j{}^n = g(x_j, \tau^n)$; $A_j{}^n = A(f_j{}^n, g_j{}^n, x_j, \tau^n)$, $B_j{}^n = B(f_j{}^n, g_j{}^n, x_j, \tau^n)$, etc. We introduce the first and second differences as

$$(\delta^2 f)_j{}^n = \frac{f_{j+1}{}^n - 2f_j{}^n + f_{j-1}{}^n}{(\Delta x)^2}\,,$$

$$(\delta f)_j{}^n = \frac{f_{j+1}{}^n - f_{j-1}{}^n}{2\Delta x}\,.$$

With this difference scheme we can now replace Eqs. (16) and (17) by the following pair of implicit difference equations:

$$f_j{}^{n+1} - f_j{}^n = \frac{1}{2}\Delta\tau\{A_j{}^{n+1}(\delta^2 f)_j{}^{n+1} + B_j{}^{n+1}(\delta f)_j{}^{n+1} + C_j{}^{n+1}f_j{}^{n+1} + A_j{}^n(\delta^2 f)_j{}^n + B_j{}^n(\delta f)_i{}^n + C_j{}^n f_j{}^n\}\,, \tag{18}$$

$$g_j{}^{n+1} - g_j{}^n = \frac{1}{2}\Delta\tau\{F_j{}^{n+1}(\delta^2 g)_j{}^{n+1} + G_j{}^{n+1}(\delta g)_j{}^{n+1} + H_j{}^{n+1}g_j{}^{n+1} + F_j{}^n(\delta^2 g)_j{}^n + G_j{}^n(\delta g)_j{}^n + H_j{}^n g_j{}^n\}\,. \tag{19}$$

We note that these equations are centered in space and time. We wish to consider a method of solving the above equations, i.e., if $f_j{}^n$, $g_j{}^n$, $j = 0, 1, 2, \ldots, J$ are known, we wish to solve for the unknowns $f_j{}^{n+1}$, $g_j{}^{n+1}$, $j = 0, 1, 2, \ldots, J$.

We can write the above difference equations as a set of simultaneous algebraic equations:

$$\alpha_j{}^{n+1} f_{j+1}^{n+1} - (1 + \beta_j{}^{n+1})f_j{}^{n+1} + \gamma_j{}^{n+1} f_{j-1}^{n+1} = \psi_j{}^n\,, \tag{20}$$

$$\zeta_j{}^{n+1} g_{j+1}^{n+1} - (1 + \eta_j{}^{n+1})g_j{}^{n+1} + \theta_j{}^{n+1} g_{j-1}^{n+1} = \varphi_j{}^n\,, \tag{21}$$

for $j = 1, 2, \ldots, J-1$. The coefficients are defined by

$$\alpha_j{}^n = \frac{1}{2}\frac{\Delta\tau}{\Delta x}\left[\frac{A_j{}^n}{\Delta x} + \frac{1}{2}B_j{}^n\right],$$

$$\beta_j{}^n = \frac{1}{2}\Delta\tau\left[\frac{2A_j{}^n}{(\Delta x)^2} - C_j{}^n\right],$$

$$\gamma_j{}^n = \frac{1}{2}\frac{\Delta\tau}{\Delta x}\left[\frac{A_j{}^n}{\Delta x} - \frac{1}{2}B_j{}^n\right],$$

$$\psi_j{}^n = -\alpha_j{}^n f_{j+1}{}^n - (1 - \beta_j{}^n)f_j{}^n - \gamma_j{}^n f_{j-1}{}^n\,;$$

$$\zeta_j^n = \frac{1}{2}\frac{\Delta\tau}{\Delta x}\left[\frac{F_j^n}{\Delta x} + \frac{1}{2}G_j^n\right],$$

$$\eta_j^n = \frac{1}{2}\Delta\tau\left[\frac{2F_j^n}{(\Delta x)^2} - H_j^n\right],$$

$$\theta_j^n = \frac{1}{2}\frac{\Delta\tau}{\Delta x}\left[\frac{F_j^n}{\Delta x} - \frac{1}{2}G_j^n\right],$$

$$\varphi_j^n = -\zeta_j^n g_{j+1}^n - (1-\eta_j^n) g_j^n - \theta_j^n g_{j-1}^n .$$

In the above coefficients we have

$$A_j^n = \frac{2}{3}\left\{\frac{1}{x_j^3}E_j(f^n+Kg^n) + M_j(f^n+Kg^n)\right\},$$

$$B_j^n = \frac{4}{3x_j}\left\{\frac{3}{2x_j}N_j(f^n+K\mu g^n) - \frac{1}{2x_j^3}E_j(f^n+Kg^n) + M_j(f^n+Kg^n)\right\},$$

$$C_j^n = 2\left\{f_j^n + K\mu g_j^n\right\},$$

$$F_j^n = \mu^2 A_j^n,$$

$$G_j^n = \frac{4}{3x_j}\mu^2\left\{\frac{1}{\mu}\frac{3}{2x_j}N_j(f^n+K\mu g^n) - \frac{1}{2x_j^3}E_j(f^n+Kg^n) + M_j(f^n+Kg^n)\right\},$$

$$H_j^n = 2\mu^2\left\{\frac{1}{\mu}f_j^n + Kg_j^n\right\}.$$

In the above expressions the moments of the distribution functions are given by the following:

$$M_j(f^n) = \Delta x\left\{\frac{1}{2}f_j^n x_j + \sum_{i=j+1}^{J} f_i^n x_i\right\},$$

$$N_j(f^n) = \Delta x\left\{\frac{1}{2}f_j^n x_j^2 + \sum_{i=1}^{j-1} f_i^n x_i^2\right\},$$

$$E_j(f^n) = \Delta x\left\{\frac{1}{2}f_j^n x_j^4 + \sum_{i=1}^{j-1} f_i^n x_i^4\right\}.$$

In Eqs. (20) and (21) we have the unknowns f_j^{n+1}, g_j^{n+1}, $j=1, 2, \ldots, J-1$ on the left-hand side of the equation, and the known quantities on the right-hand side. We are interested in solving these equations for the interior points, $j=1, 2, \ldots, J-1$, since the boundary conditions at $x=0$ and $x=x_J$ determine the solutions for $j=0$ and $j=J$. Consequently, we do not have to worry about singularities at $x=0$ in the coefficients. The system given by (20) and (21) is nonlinear in the unknowns f_j^{n+1}, g_j^{n+1}. If we extrapolate the coefficients, α_j^{n+1}, β_j^{n+1}, etc., from their values at the previous times τ^n, τ^{n-1}, then Eqs. (20) and (21) become a linear algebraic system in the unknowns f_j^{n+1}, g_j^{n+1}. The procedure is to extrapolate the coefficients and solve the linear system, then compute the coefficients α_j^{n+1}, β_j^{n+1}, etc., with the new values of f_j^{n+1}, g_j^{n+1}, and solve the linear system again to correct the values of f_j^{n+1}, g_j^{n+1}. This procedure works very well since the coefficients change in a very smooth manner with time.

We shall now give the method of solving the linearized equations. In Eq. (20) let

$$f_{j-1}^{n+1} = e_{j-1}^{n+1} f_j^{n+1} + d_{j-1}^{n+1}, \tag{22}$$

where e, d are to be determined. Then Eq. (20) becomes

$$\alpha_j^{n+1} f_{j+1}^{n+1} - (1+\beta_j^{n+1}) f_j^{n+1} + \gamma_j^{n+1} e_{j-1}^{n+1} f_j^{n+1} + \gamma_j^{n+1} d_{j-1}^{n+1} = \psi_j^n,$$

or

$$f_j^{n+1} = \frac{\alpha_j^{n+1} f_{j+1}^{n+1} + \gamma_j^{n+1} d_{j-1}^{n+1} - \psi_j^n}{1 + \beta_j^{n+1} - \gamma_j^{n+1} e_{j-1}^{n+1}}.$$

From Eq. (22) we can define

$$e_j^{n+1} = \frac{\alpha_j^{n+1}}{1 + \beta_j^{n+1} - \gamma_j^{n+1} e_{j-1}^{n+1}}$$

$$d_j^{n+1} = \frac{\gamma_j^{n+1} d_{j-1}^{n+1} - \psi_j^n}{1 + \beta_j^{n+1} - \gamma_j^{n+1} e_{j-1}^{n+1}} \tag{23}$$

$$j = 1, 2, \ldots, J-1.$$

In Eq. (21) let

$$g_{j-1}^{n+1} = a_{j-1}^{n+1} g_j^{n+1} + b_{j-1}^{n+1}, \tag{24}$$

then

$$a_j^{n+1} = \frac{\zeta_j^{n+1}}{1 + \eta_j^{n+1} - \theta_j^{n+1} a_{j-1}^{n+1}}$$

$$b_j^{n+1} = \frac{\theta_j^{n+1} b_{j-1}^{n+1} - \varphi_j^n}{1 + \eta_j^{n+1} - \theta_j^{n+1} a_{j-1}^{n+1}} \tag{25}$$

$$j = 1, 2, \ldots, J-1.$$

From the boundary conditions at $x=0$ we take $f_0^{n+1} = f_1^{n+1}$, $g_0^{n+1} = g_1^{n+1}$, so we have $e_0^{n+1} = 1$, $d_0^{n+1} = 0$, $a_0^{n+1} = 1$, $b_0^{n+1} = 0$ for all n. The computational procedure is to calculate e_j^{n+1}, d_j^{n+1}, a_j^{n+1}, b_j^{n+1}, $j=1, 2, \ldots, J-1$, from the recursion formulae (23) and (25); set $f_j^{n+1} = 0$, $g_j^{n+1} = 0$; and then calculate f_j^{n+1}, g_j^{n+1}, $j=0, 1, 2, \ldots, J-1$ from Eqs. (22) and (24).

4. Discussion of numerical results

From the calculations described in the preceding section we obtain the distribution functions, $f(x, \tau)$ and $g(x, \tau)$; we also tabulate their second and fourth moments, e.g.,

$$I_2^-(\tau) = \int_0^\infty f(x,\tau)\, x^2\, \mathrm{d}x,$$

$$I_4^-(\tau) = \int_0^\infty f(x,\tau)\, x^4\, \mathrm{d}x.$$

The second moment, I_2^-, is proportional to the number of electrons and should remain constant. It is calculated at each time step and provides a check on the numerical solution. If I_2^- begins to decrease rapidly, it usually means that the domain, $0 \leq x \leq x_J$, is not large enough to accommodate the tail of the electron distribution.

The mean electron energy is given by

$$E_- = \frac{3}{2} kT_- = \frac{1}{2} m v_0^2 \frac{I_4^-}{I_2^-},$$

and the mean ion energy by

$$E_+ = \frac{3}{2} kT_+ = \frac{1}{2} M v_0^2 \frac{I_4^+}{I_2^+}.$$

The quantity v_0 is some characteristic speed for the problem and is a constant. Since I_2 is a constant, we then have that the mean energy is proportional to the fourth moment, I_4.

We have selected several cases to present which are of interest to the experimental programs of high-energy molecular ion injection and intermediate-energy neutral atom injection. In order to make a comparison of the energy transfer obtained by the numerical solution of the Fokker-Planck equations and that obtained from the exchange rates given in SPITZER [3], we have kept the ion temperature fixed in six cases. In these cases the ion distribution function, $g(x, \tau)$, is kept constant in time, i.e., the equation for $g(x, \tau)$ is not solved. This function changes very slowly because of the factor μ^{-2} in the ion equation, so this assumption is quite valid over a limited time. In all cases, the ions are deuterons, so $\mu = (3671.3)^{-1}$. The equation for $f(x, \tau)$ is solved and we compare the mean electron energy, represented by $I_4^-(\tau)$, with that obtained from the Spitzer formulae. In these six cases we take an equal number of deuterons and electrons.

In the first three cases, we consider the situation where the ions are all of the same velocity, αv_0. The ion energy is then

$$E_+ = \frac{1}{2} M v_0^2 \alpha^2.$$

From page 79 of Spitzer [3] we have for the rate of energy gain of the electrons the following expression:

$$\frac{dE_-}{dt} = \frac{(4\pi e^4 n_- \ln \Lambda)}{\sqrt{2ME_+}} \left(1 + \frac{M}{m}\right) [\varphi(x) - x\varphi'(x)],$$

where

$$x = \left(\frac{3}{2} \frac{m}{M} \frac{E_+}{E_-}\right)^{\frac{1}{2}},$$

$$\varphi(x) = \frac{2}{\sqrt{\pi}} \int_0^x e^{-y^2} dy.$$

In the variables of this paper the above becomes

$$\frac{dI_4^-}{d\tau} = 4\alpha^{-1} (I_2^-)^2 (1 + \mu) [\varphi(x) - x\varphi'(x)] \qquad (26)$$

where

$$x = \alpha \left(\frac{3}{2} \frac{I_2^-}{I_4^-}\right)^{\frac{1}{2}}.$$

We can then calculate $I_4^-(\tau)$ by

$$\tau(I_4^-) = \int_{I_4^-(0)}^{I_4^-} \left(\frac{dI_4}{d\tau}\right)^{-1} dI_4.$$

In the first case we consider deuterons with an energy of 200 keV. We place the ion distribution function at $x=3$, i.e., $\alpha=3$ in the above formulae. This choice determines v_0 by the equation

$$\frac{1}{2} M (3v_0)^2 = 200 \text{ keV}.$$

This value of v_0 will be used to normalize all the cases presented in this paper. In the first case the initial electron distribution is a Maxwellian corresponding to an average electron energy of 7.5 eV. In Fig. 1 we show the solution, $f(x, \tau_1)$, at a time τ_1 when $I_4^-(\tau_1) = 100\, I_4^-(0)$, i.e., the average electron energy has increased to 750 eV. In Fig. 1 we also show the Maxwellian of the same average energy given by

$$f_{\text{Max}}(x, \tau_1) = 4\pi I_2^- \left(\frac{3}{2\pi} \frac{I_2^-}{I_4^-(\tau_1)}\right)^{\frac{3}{2}} \exp\left(-\frac{3}{2} \frac{I_2^-}{I_4^-(\tau_1)} x^2\right).$$

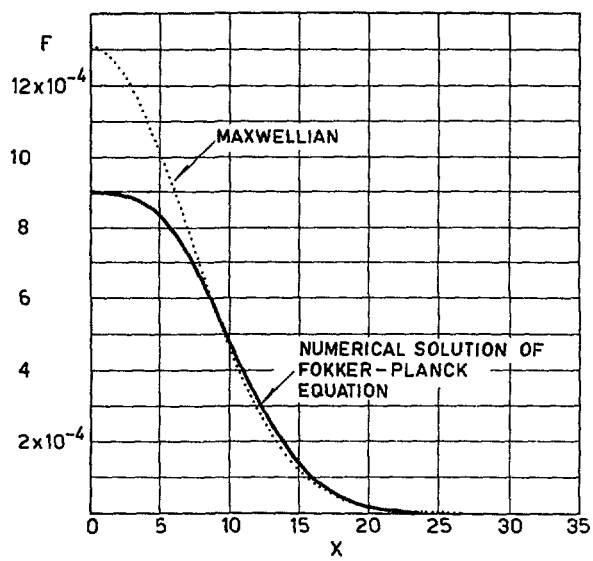

Fig. 1 Electron distribution function at a time corresponding to an energy gain from 7.5 eV to 750 eV, in the presence of an equal number of 200-keV deuterons.

The decrease in low velocity electrons from the Maxwellian is quite evident. In Fig. 2 the energy gain is compared. An I_4^- of 10^2 corresponds to an average electron energy of 1 keV. It is of interest to note that the time required for the electrons to reach 1 keV is about twice as long from the numerical solution as from the Spitzer calculation. This indicates that the energy transfer rate is less than the value predicted by the quasi-equilibrium theory.

In the second case we again keep the deuterons at 200 keV. The initial distribution is the Maxwellian shown in Fig. 1. We follow the electron heating to an average energy somewhat above 2 keV, and compare the energy gain in Fig. 3 with the Spitzer formula and a modification by Rosenbluth which will be described later. We find that the transfer rate is again reduced from the Spitzer formula, but the effect is less since the electrons are a factor of 10^2 hotter to begin with.

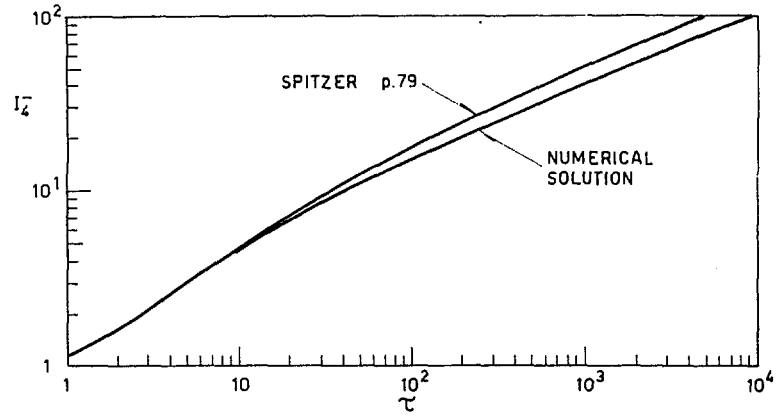

Fig. 2 Electron energy gain as a function of time, 7.5 eV to 1000 eV, 200-keV deuterons.

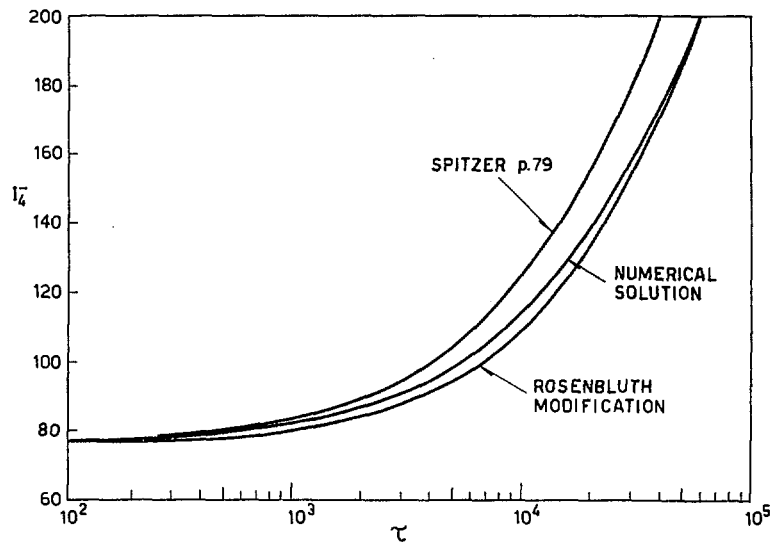

Fig. 3 Electron energy gain as a function of time, 750 eV to 2 keV, 200-keV deuterons.

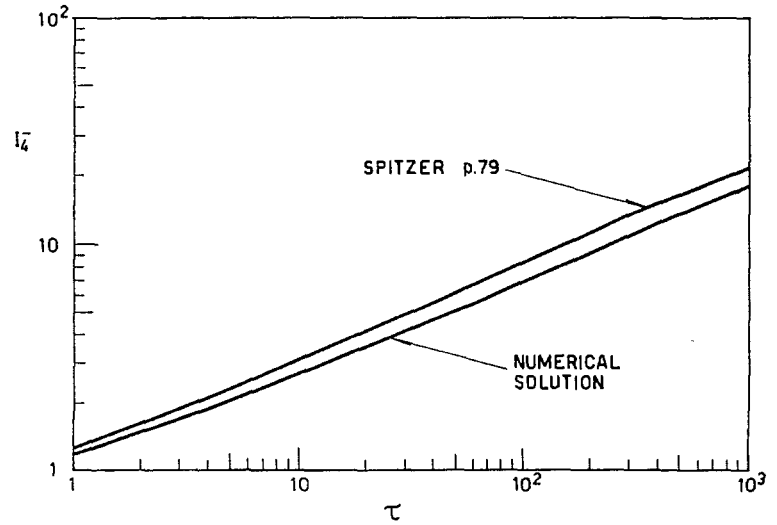

Fig. 4 Electron energy gain as a function of time, 7.5 eV to 150 eV, 22-keV deuterons.

In the third case the ion distribution function is kept at $x=1$, i.e., $\alpha=1$. This corresponds to deuterons at 22 keV. The initial electron distribution is the same as the first case, i.e., a Maxwellian corresponding to 7.5 eV. The energy gain from the two calculations is compared in Fig. 4.

In the next three cases the ion temperature is kept constant in time as before, but the ions are not all the same velocity. The ion distribution function is a Maxwellian corresponding to an average deuteron energy of 28 keV. The initial electron distributions are Maxwellians corresponding to average energies of 7.5 eV, 75 eV, and 750 eV, respectively.

In the expression for the energy transfer rate that we have been using for comparison, the electrons are assumed Maxwellian. If the ion distribution is taken to be Maxwellian also, then the transfer rate is given on page 80 of SPITZER [3] as follows:

$$\frac{dT_-}{dt} = \frac{8(2\pi)^{\frac{1}{2}} ne^4 \ln \Lambda}{3Mmk^{3/2}} (T_+ - T_-)\left(\frac{mT_+ + MT_-}{Mm}\right)^{-\frac{3}{2}}.$$

In terms of the variables of this paper, we have

$$\frac{dI_4^-}{d\tau} = 8\left(\frac{3}{2\pi}\right)^{\frac{1}{2}} (I_2^-)^2 (I_4^+ I_2^- - \mu I_4^- I_2^+) \\ (I_2^+ I_2^-)^{\frac{1}{2}} (I_4^+ I_2^- + I_4^- I_2^+)^{-\frac{3}{2}}.$$

The only variable on the right-hand side is I_4^-, so we can find the energy gain $I_4^-(\tau)$ as before. ROSENBLUTH [10] has derived a modification to the above formula under the assumptions that the ions are Maxwellian at one temperature and the electrons nearly Maxwellian at a different temperature:

$$\left(\frac{dT_-}{dt}\right)_R = \left(\frac{dT_-}{dt}\right)_s \left[1 - 3\left(\mu \frac{T_+}{T_-}\right)^{\frac{2}{3}}\right],$$

where $(dT/dt)_s$ is the expression given above from page 80 of SPITZER [3]. In the derivation [10] it is assumed that the average electron velocity is much greater than the average ion velocity. This is not true in some of our cases; e.g., in the case of deuterons with an average energy of 28 keV and electrons with an initial distribution corresponding to 7.5 eV, the Maxwellians are the same. We can express the above modification in the variables of this paper by

$$\left(\frac{dI_4^-}{d\tau}\right)_R = \left(\frac{dI_4^-}{d\tau}\right)_s \left[1 - 3\left(\frac{I_4^+ I_2^-}{I_2^+ I_4^-}\right)^{\frac{2}{3}}\right] = \left(\frac{dI_4^-}{d\tau}\right)_s R(I_4^-).$$

In the case just mentioned the factor in the bracket R is initially equal to -2, which is not reasonable, so the modification is not applied with this case. In Fig. 5 we have the energy gain compared to the energy gain calculated from the transfer rate for two Maxwellians. We can compare this case to the previous case, shown in Fig. 4, where the electrons are initially the same Maxwellian, but the deuterons are all at the same velocity equivalent to 22 keV. We see that the results are essentially identical, so it does not seem to make much difference whether the ions are taken to be monoenergetic or Maxwellian.

In the next case the electrons have an initial distribution which is a Maxwellian corresponding to an average energy of 75 keV. The deuteron distribution is the same as the previous case at 28 keV. The factor R is initially equal to 0.35, which is a substantial reduction in the transfer rate. From the results of the numerical solution, in Fig. 6, we see that this modification overestimates the reduction in transfer rate at this electron energy. As I_4^- increases, the factor $R(I_4^-)$ approaches one and the modified energy gain comes closer to the numerical solution. We note that the time to reach an I_4^- of 25, which corresponds to an electron energy of 250 eV, is the same for the numerical solution and the Rosenbluth modification.

In the next case the electrons have an initial distribution which is a Maxwellian corresponding to an average energy of 750 eV. The deuteron distribution is still the same at 28 keV. The factor R is initially equal to 0.86 and approaches 1 as I_4^- increases. The

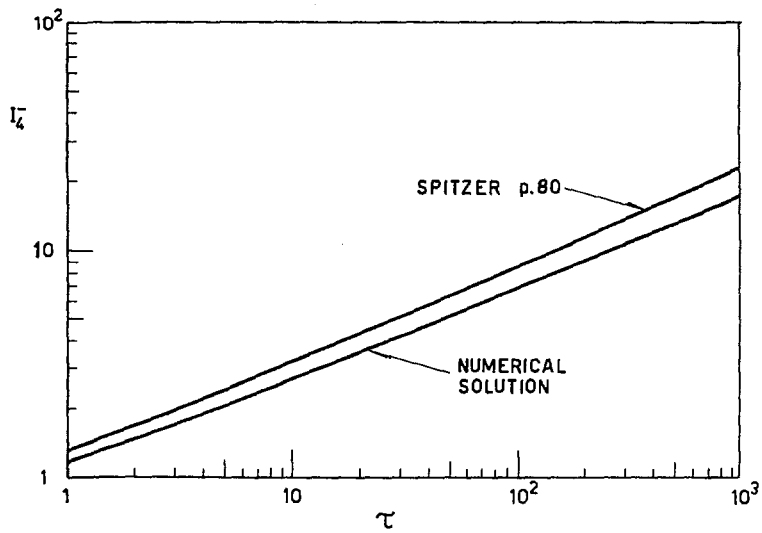

Fig. 5 Electron energy gain as a function of time, 7.5 eV to 150 eV, 28-keV deuterons.

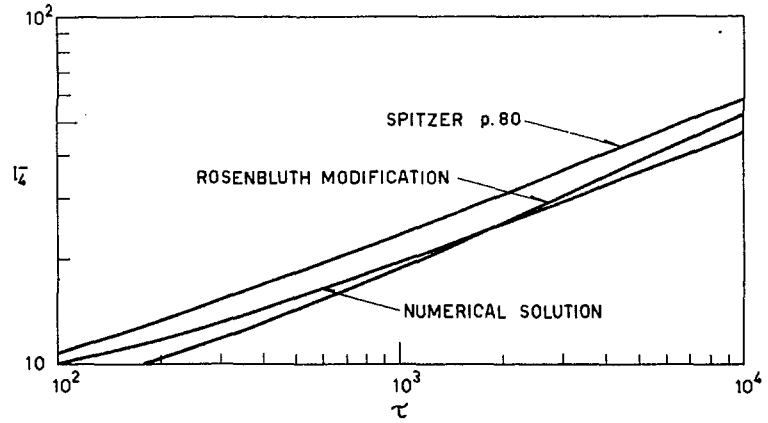

Fig. 6 Electron energy gain as a function of time, 75 eV to 300 eV, 28-keV deuterons.

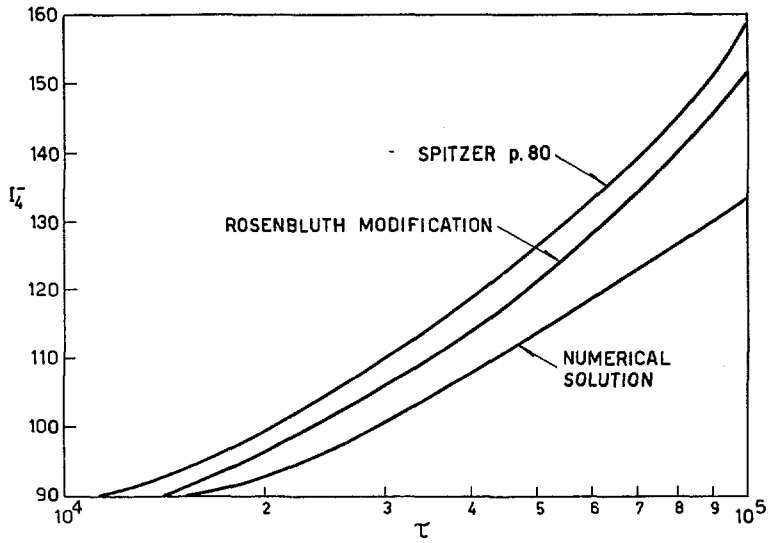

Fig. 7 Electron energy gain as a function of time, 750 eV to 1100 eV, 28-keV deuterons.

correction to the Spitzer energy gain is small in this case. From the results of the numerical solution, in Fig. 7, we see that the transfer rate is reduced somewhat more than the Rosenbluth estimate. We note that the time to reach an I_4^- of 100, which corresponds to an electron energy of 1 keV, is about 50% longer than the estimate from the Spitzer transfer rate.

In the derivation of the modification by ROSENBLUTH [10], the ions are assumed to be Maxwellian. We have found from the numerical results that there is very little difference in the energy gain of the electrons, whether we assume that the ions are monoenergetic or a Maxwellian distribution at the same average energy. It seems reasonable then to apply the modification to a case where the ions are monoenergetic. The transfer rate, $(dI_4^-/d\tau)_s$, for this situation is given in Eq. (26). The modification becomes

$$\left(\frac{dI_4^-}{d\tau}\right)_R = \left(\frac{dI_4^-}{d\tau}\right)_s \left[1 - 3\left(\frac{I_2^-}{I_4^-}\alpha^2\right)^{\frac{2}{3}}\right] = \left(\frac{dI_4^-}{d\tau}\right)_s R(I_4^-).$$

In the first case considered, where the deuterons are at 200 keV and the electrons are initially at 7.5 eV, the factor R is equal to -10, which is unreasonable. However, in the second case, where the electrons start at 750 eV, the factor R is initially equal to 0.53 and approaches 1 as I_4^- increases. From the numerical results, in Fig. 3, we see that this modification overestimates the reduction in transfer rate to begin with, but comes closer to the correct energy gain as I_4^- increases. The time taken to reach an I_4^- of 200 is the same in both calculations.

The conclusion that we have reached from the calculations described is that in those cases where the ion temperature is much higher than the electron temperature the transfer rates given in Spitzer must be modified. In some situations the modification of Rosenbluth gives a good estimate of the transfer rate. However, in many cases it does not apply, and we need to use the numerical solution. In any case, with the code available we can investigate a wide variety of energy exchange problems.

Acknowledgements

We wish to thank Mrs. Julia Kleinecke for valuable assistance with the calculations of the transfer rates.

The work reported here was performed under the auspices of the United States Atomic Energy Commission.

References

[1] FUTCH, A. H., DAMM, C. C., HECKROTTE, W., KILLEEN, J., MISH, L., *Bull. Am. Phys. Soc. II* **6** (1961) 201.
[2] GILBERT, F. C., HECKROTTE, W., HESTER, R. E., KILLEEN, J., VAN ATTA, C. M., U.S. Atomic Energy Commission Report UCRL-5827 (1960).
[3] SPITZER, L., Physics of Fully Ionized Gases (Interscience Pub. Inc., New York, 1956) 79.
[4] KILLEEN, J., HECKROTTE, W. *Bull. Am. Phys. Soc. II* **5** (1960) 372.
[5] ROSENBLUTH, M. N., MACDONALD, W. M., JUDD, D. L., *Phys. Rev.* **107** (1957) 1.
[6] RICHTMYER, R. D., Difference Methods for Initial-Value Problems (Interscience Publishers Inc., New York, 1957).
[7] POST, R. F., private communication.
[8] LINLOR, W. I., *Bull. Am. Phys. Soc. II* **4** (1959) 351.
[9] SHAW, C. B., *Bull. Am. Phys. Soc. II* **5** (1960) 311.
[10] ROSENBLUTH, M. N., General Atomic Report No. GAMD-1710 (San Diego, U.S., 1960).
[11] ROBERTS, J. E., CARR, M. L., U.S. Atomic Energy Commission Report UCRL-5651-T (1960).
[12] BENDANIEL, D. J., U.S. Atomic Energy Commission Report UCRL-6236 (1961).

LOSS OF CHARGED PARTICLES IN A STELLARATOR*

W. STODIEK**, R. A. ELLIS, JR., J. G. GORMAN***

PLASMA PHYSICS LABORATORY, PRINCETON UNIVERSITY

PRINCETON, NEW JERSEY, UNITED STATES OF AMERICA

The confinement of plasma in a stellarator during the ohmic heating process is not in accordance with classical collisional diffusion. Observations in the B-3 stellarator yield a diffusion coefficient $D = 2 \times 10^4\ T_e/B$ cm^2/s (T_e in electron-volts, B in kilogauss), about three times greater than estimated by Bohm. The rate of particle loss is found to be inversely proportional to the square of the plasma diameter and to be independent of the degree of ionization. The results are discussed in relation to theoretical models concerning instabilities that possibly exist under the conditions of the experiment.

1. Introduction

It has been observed that during ohmic heating of hydrogen plasmas in stellarators the charged particle density reaches a maximum and decreases rapidly during a time when the ohmic heating field is still applied (See Fig. 1). The loss rate was observed to be much faster than that predicted by classical collisional diffusion for a quiescent plasma [1, 2]. The dependence of the loss rate during ohmic heating on externally controlled parameters was first presented by BERSTEIN, HEALD and KRANZ [1] and more completely by ELLIS, GOLDBERG and GORMAN [2].

We cannot measure the outward flux of charged particles directly, therefore, in order to determine the intrinsic loss rate from the time behavior of the observed electron density, we must make some assumption about the simultaneous ionization rate. In [1] and [2] the loss rates were determined from the decay of the electron density only, where the ionization should be small. The observed loss rates showed a dependence on the initial pressure as well as the confining field and the pressure dependence was attributed to particles which left the discharge, and subsequently returned as neutrals (recycling). The intrinsic loss-rates reported in [2] were based on a model which took account of this recycling. According to this model the magnitude of the observed loss rate depends on the amount of recycling, but the magnetic field dependence of the loss rate does not. This paper is a continuation of the investigations reported in [2].

We will use a simple model for the variation of the electron density with time, neglecting all recycling, as a first approximation, which allows us to determine the loss rate during the density rise. We will show that the enhanced loss rate prevails during the initial increase of electron density, independent of the degree of ionization, and that the loss rate during the rise varies roughly as B^{-1} where B is the confining field.

At present we find that the loss rate during the decay of electron density is also more nearly proportional to B^{-1}, rather than to $B^{-1/2}$ as reported in [2], both for discharges produced with constant heating fields, as used in [2], and in discharges which have constant electron temperatures. We do not know the source of this discrepancy. The principal differences in the present operating conditions of the B-3 stellarator are that the working gas has fewer impurities and the influx of impurities in the later stages of the discharge is definitely reduced, so that higher heating fields can be applied without introducing an overpowering amount of impurity ions. A further difference is that we have a power amplifier which enables us to control the electron temperature during the ohmic heating process, especially during the decaying phase of the density.

2. The model

The electron density, after full ionization, has been observed to decrease nearly exponentially if the electron temperature, as determined from the plasma resistivity, is more or less constant. We therefore make the assumption that the loss of plasma can be described by a constant τ independent of density and time, in the following way:

$$\frac{\mathrm{d}n_e}{\mathrm{d}t} = -\frac{1}{\tau} n_e , \qquad (1)$$

where n_e is the electron density. We further assume that current-dependent hydromagnetic instabilities are unimportant in our discharges [2].

The ionization rate by electron collisions can be described in the usual way by

$$\frac{\mathrm{d}n_e}{\mathrm{d}t} = n_e\, n_0\, \sigma^* , \qquad (2)$$

where n_0 denotes the neutral particle density and σ^* is the ionization rate constant. Therefore the following

* Conference paper CN-10/131, presented by R. W. MOTLEY. Discussion of this paper is given on page 210. Translations of the abstract are at the end of this volume of the Conference Proceedings.

** On leave from Max-Planck-Institut für Physik und Astrophysik, Munich.

*** On loan from Westinghouse Electric Corporation.

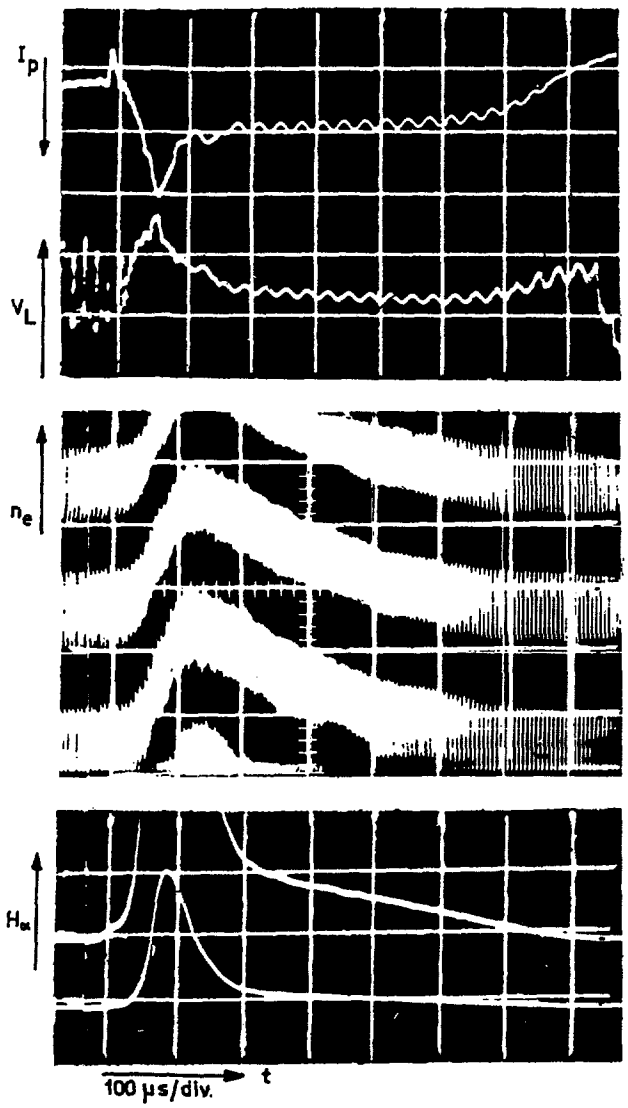

Fig. 1 The general behavior of a hydrogen discharge in the B-3 stellarator. The time scale is 100 μs/div. The middle trace shows the electron density; one fringe corresponds to about 1.1×10^{13} electrons/cm^3. The bottom pictures show H_α light at two gains, in the ratio 1:4; this is related in some way to the production of charged particles (See dotted curve in Fig. 2). In the top picture are shown loop voltage (50 V/div) and plasma current (200 A/div). The confining field is 30 kG and the initial hydrogen pressure is 0.25 μ Hg.

equation gives the net change of electron density with time:

$$\frac{dn_e}{dt} = n_e n_0 \sigma^* - \frac{1}{\tau} n_e . \qquad (3)$$

Because all of our discharges were in hydrogen gas we will restrict the analysis to this particular case. Collisions with electrons lead to the following processes for dissociation and ionization in hydrogen:

$$\begin{aligned} H_2 &\rightarrow H_2^+ \rightarrow H^+ + H^0 \\ &\rightarrow H_2^+ \rightarrow 2H^+ \\ &\rightarrow 2H^+ \\ &\rightarrow 2H^0 \end{aligned}$$

In the range of electron temperature from 5 to 10 eV and in the density range near 10^{13} particles/cc there are three simplifications possible if the tube diameter is less than 20 cm.

(1) We can neglect the process $H_2^+ \rightarrow 2H^+$ in comparison with $H_2^+ \rightarrow H^+ + H^0$, and the process $H_2 \rightarrow 2H^+$ in comparison with all other processes.

(2) Because the dissociation takes place from an excited state, the neutral atoms have a kinetic energy of approximately 4 eV and, consequently, escape from the discharge tube before they undergo an ionizing collision. We can therefore treat the whole ionization process as a one-step process for production of charged particles and atoms. We denote by β the ratio of electrons produced per hydrogen atom initially in the discharge, and β depends on the electron temperature only and not on the confinement of H_2^+ ions, nor on the tube dimensions.

(3) In hydrogen, the atoms as well as the ions which are lost from the discharge hit the tube wall and stick there to a great amount, i.e., the number of hydrogen atoms or molecules which re-enter the discharge is assumed negligible.

Thus we can write the neutral density at any given time as

$$n_0(t) = N_0 - \frac{1}{\beta}\left(n_e + \frac{1}{\tau}\int_0^t n_e(t')\,dt'\right), \qquad (4)$$

where N_0 is the initial density of hydrogen atoms (twice the initial density of hydrogen molecules). Substituting Eq. (4) into Eq. (3) we get

$$\frac{dn_e}{dt} = \left[\sigma^*\left\{N_0 - \frac{1}{\beta}\left(n_e + \frac{1}{\tau}\int_0^t n_e(t')\,dt'\right)\right\} - \frac{1}{\tau}\right] n_e . \qquad (5)$$

We will assume that the electron temperature and therefore τ, σ^* and β are constant during the discharge. The scaling law, nt = constant, allows us to reduce all solutions of Eq. (5) to one family with a parameter. $p = 1/\tau^*\sigma^* N_0^*$. Figure 2 shows some solutions obtained by means of an analogue computer. The dotted curve represents the rate of electron production for the case $p = 0.25$. When $\tau \ll 1/\sigma^* N_0$, the production is also important during the decaying part of the density, so that the apparent loss-rate is not the intrinsic loss-rate in such a case. We can express the effect of production of charged particles during the density decay by computing for each curve the quantity $p^* = 1/\tau\sigma^* N_0$ where τ^* is the effective time constant for decay determined at half peak density. In Fig. 2 we have plotted the value of p^* on each curve at the point where it was determined. The peak values of electron density are plotted as a function of $1/p$ in Fig. 3.

In principle it would be possible to obtain for any discharge the corresponding values of σ^*, τ and β by comparison with one of these curves, but our experimental data are too rough to allow this. We, therefore,

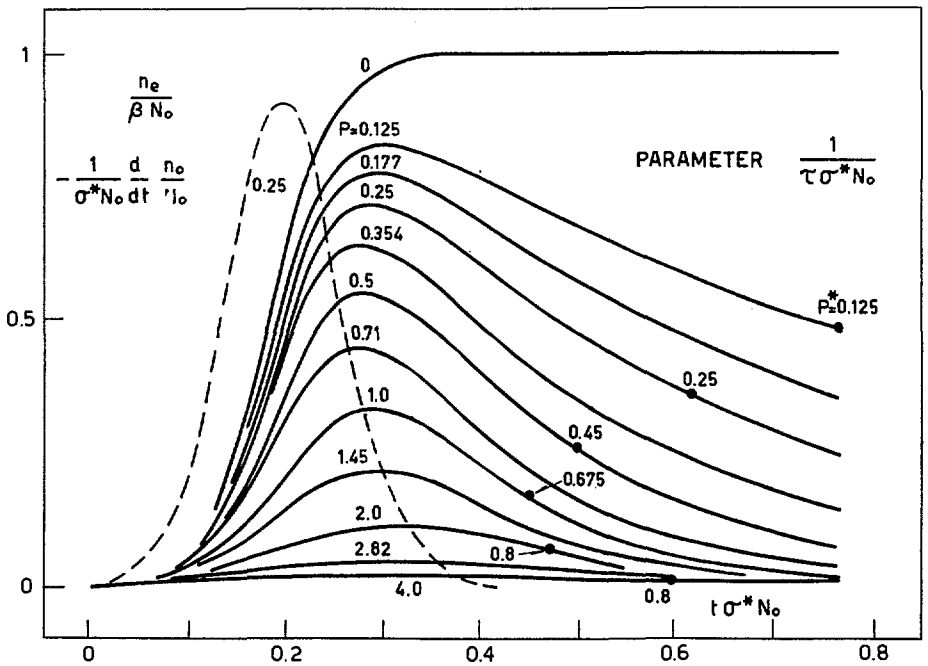

Fig. 2 The solid curves show the electron density as a function of time for different values of the parameter $1/p = \tau\,\sigma^*\,N_0$. The dotted curve shows the production of electrons for the case $p = 0.25$.

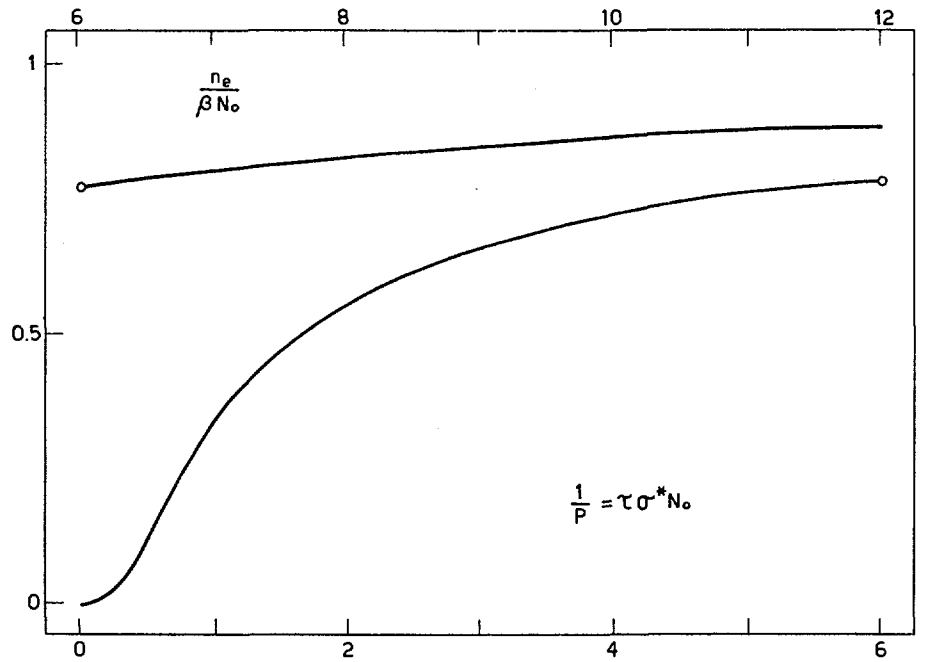

Fig. 3 The peak electron density as a function of $1/p = \tau\,\sigma^*\,N_0$. This curve was obtained from Fig. 2.

will rely on more insensitive characteristics of the electron density curves as, for example, the peak density, the time to reach the peak, and the time constant for the decay.

In the following we will apply this analysis mainly to determine the dependence of the confinement on the magnetic field, on the electron temperature, and on the diameter of the discharge channel, for the ionization phase of the discharge.

3. Determination of the loss rate during the ionization phase of the discharge

All data were obtained from hydrogen discharges in the B-3 stellarator. For a discussion of the methods of measurement see [2]. A programmed power amplifier was used to produce the discharges with nearly constant electron temperature. All other discharges were produced with constant ohmic heating fields [2].

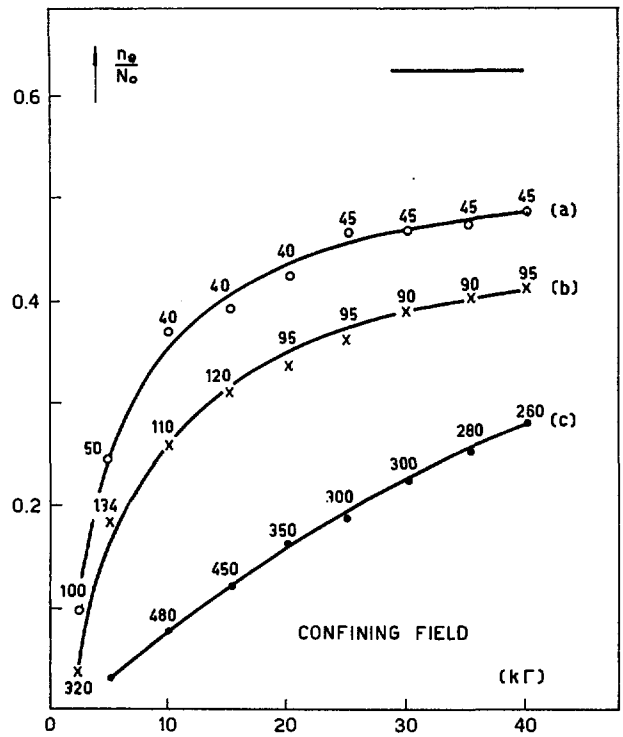

Fig. 4 The relative observed peak densities as a function of confining field are shown for different pressures but roughly the same E/P. $n_e/\beta N_0 = 1$. (a) $E = 0.31$ V/cm, $p = 58 \times 10^{-5}$ mm Hg, (b) $E = 0.10$ V/cm, $p = 30 \times 10^{-5}$ mm Hg, (c) $E = 0.06$ V/cm, $p = 11 \times 10^{-5}$ mm Hg. The numbers adjacent to each point are the rise times to peak density in μs. $n_e/\beta N_0 = 1$ (solid line, upper right of figure) indicates the peak density that would be obtained in the case of perfect confinement.

Figure 4 shows a plot of the observed relative peak density versus confining field for different ohmic heating fields and initial pressures. The significance of the quantities given in Fig. 4 is explained in the caption.

Consider a constant confining field in Fig. 4. The observed values of peak density are fitted to Fig. 3 in the following way. We assume that τ and σ^* are constants for discharges at the same confining field and the same E/p. Since the values of N_0 are different for the discharges, the ratios of the values of $1/p = \tau \sigma^* N_0$ are in the ratios of the N_0's. The ratios of the observed peak electron densities are computed and these two sets of ratios are used to fit the observed data to Figure 3. This procedure yields a value of $n_e/\beta N_0$, and a value of $1/p$ for each discharge. All of these data are consistent with a fairly constant value of β. The value of β given by this analysis, about 0.6, is higher than the maximum (0.5) which is permitted by the ionization processes taken into consideration. However this value is well within the uncertainties in the absolute pressure measurements and is of no importance in the determination of τ.

In order to determine τ, we make use of the fact that the rise time to peak density t_r is an observed quantity. The p values, determined from fitting the data to Fig. 3, are used to identify the appropriate curve in Fig. 2 and from these curves the value of τ/t_r is obtained; from the observed values of t_r, one then readily obtains τ.

This procedure was applied to each point for the discharges with a pressure of 58×10^{-5} mm of Hg and the time constants so obtained are plotted as circles lying near curve A of Fig. 5.

This method can also be applied to the data for the two lower pressures as long as their respective rise times do not change too much. The constancy of the rise time for different values of the magnetic field, i.e., for different values of τ and therefore p, is to be expected from the curves of Fig. 2. Thus for the higher magnetic field points the lower pressure data yield the crosses and dots near curve A of Fig. 5. It is reasonable to ignore the discharges with relatively longer rise times because, on closer examination, their electron temperatures are lower and the assumption of constant σ^* and τ is not valid. It is interesting to note if σ^* and τ are assumed to have thesa me values for the low-temperatures discharges as for those at higher temperatures, then the values of β obtained are also the same for both types of discharges. This result first led us to suspect that the confinement time must be longer for lower electron temperature in order to explain the observed peak density in the presence of the longer rise time. Note that the values of τ fit roughly a linear dependence on B.

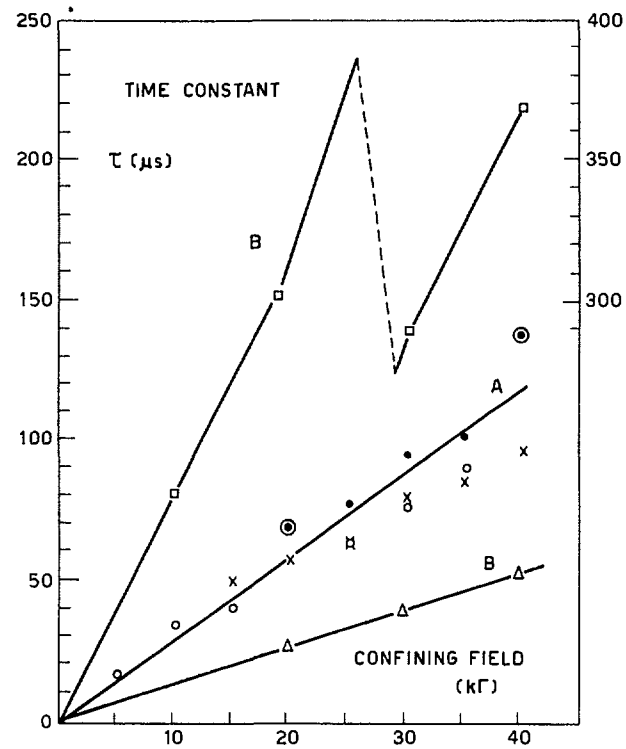

Fig. 5 The dependence of τ on the magnetic field. The points near A are derived from the curves of Fig. 4 for the ionization phase of the discharges. The points near the B curves were obtained from the decaying phase of discharges with different electron temperatures. (5 eV in the lower and 17 eV in the upper curve.)

4. Dependence of the loss rate during the decay of electron density on the confining field and on the electron temperature

The dependence of the loss rate on the confining field during the decay can be obtained in an almost direct manner from the microwave density measurements. Only for discharges with a very low confining field or slow rise, i.e., for larger values of p, would we have to use Fig. 2 to correct the data for the production, which is then still important during the density decay. Typical values of τ are shown on the B curves of Fig. 5 for different ohmic heating fields.

We are able to obtain nearly constant electron temperature throughout the decay by means of a programmed ohmic heating pulse. Figure 6 shows τ versus electron temperature for a confining field of 30 kilogauss, derived from the decaying part of the electron density.

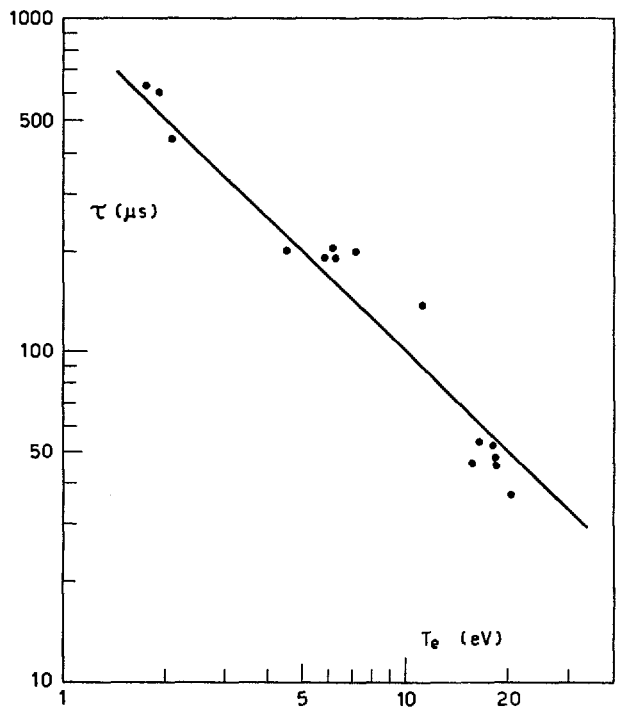

Fig. 6 The dependence of τ on electron temperature during the decaying phase of the discharge.
$D = 2 \times 10^4 \times T_e B^{-1}$, $p = 0.25\,\mu H_2$, $B = 30$ kG, $d = 40$ mm.

If we assume a zero order Bessel function dependence for the radial density distribution, the data of Fig. 6 are roughly consistent with a diffusion constant D of about $2 \times 10^4\, T_e B^{-1}$. This can be compared with the value $D = 0.6 \times 10^4\, T_e B^{-1}$ cm^2/s given by BOHM [3, 4].

The change with pressure of the confinement time determined from the density decay has not been found to be as large in the present data as in [2]. The reason for this change is not known and needs a further investigation together with the recycling model.

5. The dependence of the loss-rate on the discharge diameter

By inserting a sheet of stainless steel into the discharge we were able to limit the diameter of the current-carrying channel to smaller values. The rotational transform insures that this method acts almost as well as a circular diaphragm. We shall determine roughly the dependence of τ on the discharge diameter by assuming that the entire plasma is confined to the current-carrying channel. This assumption is difficult to justify, especially for the smallest diameters considered. Figure 7 shows a parabola fitted to values of τ determined from the data by applying the model described in Section 2. This result is in disagreement with the observations of the decaying part of the electron density where the confinement times first increase as the plasma diameter decreases and then decrease with a further decrease of plasma diameter. This effect was also reported in [2]. The explanation has not yet been determined, but it may be due to temperature changes. However, we should point out that our model should be modified to take into account the fact that the neutral particle density does not change, in the limiter case, in the simple way assumed in Eq. (4). To get some indication that all of the gas initially in the tube underwent the ionization or dissociation processes, we computed the total energy input from the observed current and voltage and found this value to be independent of the discharge diameter down to

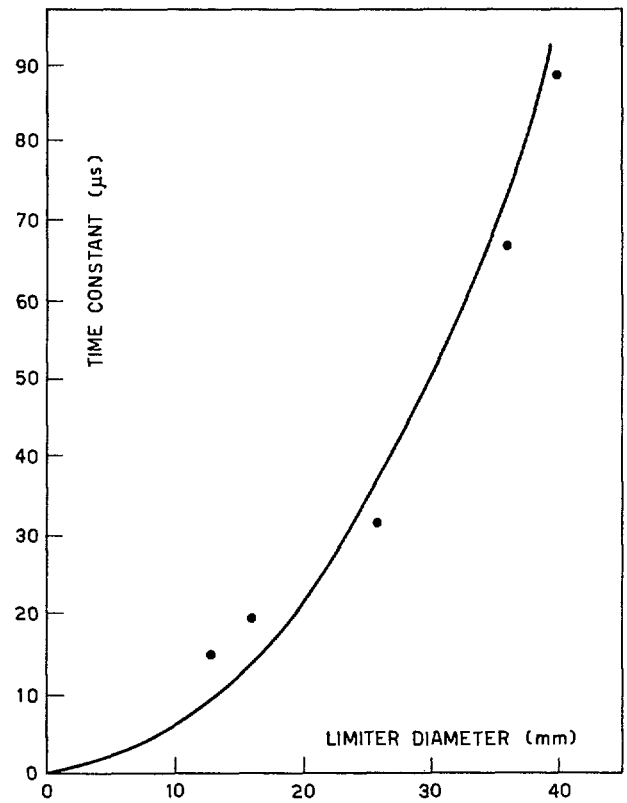

Fig. 7 Confinement time constant as a function of discharge diameter. Confining field is 30 kG, $p = 35 \times 10^{-5}$ mm Hg.

17 mm. Although we feel that this experiment would be improved if carried out in discharge tubes of different diameters, we believe that these measurements give some indication of the dependence of τ on the plasma diameter during the rise of the electron density, when the electron temperature is held relatively constant, controlled by the ionization and dissociation processes.

6. Dependence of the loss rate on the form of the ohmic heating pulse

In order to see the possible influence of runaway electrons on the particle loss-rate, we investigated discharges in which the production of runaway electrons was favored (unidirectional ohmic heating discharges), and discharges which were unfavorable to the production of runaway electrons (programmed ohmic heating pulses which could be varied in frequency, pulse width, amplitude, and which could be unidirectional or bidirectional). Although the expected amount of high energy runaways should be different, we could not find significant differences in the decay time constants, as long as the average input power was the same or, according to our present understanding, as long as the electron temperatures were roughly the same.

7. Dependence of the loss-rate on the magnitude of the heating current

The possibility that the rapid loss rate from stellarators during ohmic heating is caused by ion-wave instabilities is currently under detailed investigation [5]. Figure 8 shows a plot of the highest stable currents, according to the ion-wave instability model, for the B-3 stellarator for various ratios of electron to ion temperature as a function of electron temperature [6]. Also plotted in Fig. 8 are points taken from the discharges of Fig. 6. These data do not permit us to decide that an ion-wave instability is the operative mechanism. For all but the lowest two currents, the ion-wave instability situation is undetermined because we do not know the ion temperature. However, the lowest current point should be stable according to this theory for any ion temperature, but we observe that the τ's are shorter by two orders of magnitude than the classical collisional values. A definitive test of the ion-wave instability theory for enhanced loss may require a more complete knowledge of the *spatial* variation of the electron density, the current density, the electron and ion temperatures, and the damping mechanisms of the ion waves after the current is shut off completely.

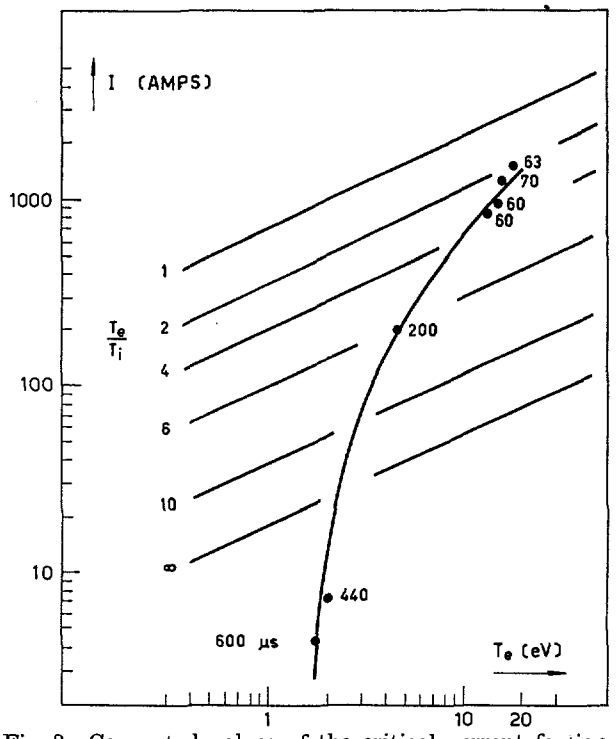

Fig. 8 Computed values of the critical current for ion-wave instability in the B-3 stellarator. Sloping lines indicate I critical for $n_e = 5 \times 10^{12}$ and T_e/T_i in hydrogen. Also shown are experimental points showing the discharge current and time constant plotted against electron temperature.

8. Conclusions

(1) A model has been presented which enabled us to determine for hydrogen discharges the dependence of the loss-rate of charged particles on magnetic field, and plasma diameter during the ionization phase.

(2) The analysis shows that the loss-rate has the same values during the ionization phase as well as the decaying phase and that it is roughly consistent with a diffusion constant $D = 2 \times 10^4\ T_e B^{-1}$ cm^2/s with T_e expressed in electron-volts and B in kilogauss. The data also indicate that the loss rate is inversely proportional to the square of the plasma diameter.

(3) The data do not permit us to conclude that runaway electrons or ion-wave instabilities are the underlying causes of the enhanced loss-rate.

Acknowledgements

We gratefully acknowledge the efforts of the B-3 operating crew and of the Power Electronics Section of the Plasma Physics Laboratory who designed the programmed ohmic heating device. The authors have greatly benefited from discussions with M.B. Gottlieb, L. Spitzer, Jr. and members of the Plasma Physics Laboratory, Experimental Physics Division.

This work was performed under the auspices of the United States Atomic Energy Commission.

References

[1] Berstein, W., Heald, M. A., Kranz, A. Z., United States Atomic Energy Commission Report NYO-7901 (1957).

[2] Ellis, R. A. Jr., Goldberg, L. P., Gorman, J. G., *Phys. Fluids* **3** (1960) 468.

[3] Bohm, D., The Characteristics of Electrical Discharges in Magnetic Fields (Edited by A. Guthrie and R. K. Wakerling: McGraw-Hill, New York, 1949), Chapter 2, Section 5.

[4] Spitzer, L., *Phys. Fluids* **3** (1960) 659.

[5] Motley, R. W., IAEA Conference on Plasma Physics and Controlled Nuclear Fusion Research, Salzburg, 1961: Paper CN-10/167, page 199 of this volume.

[6] Jackson, E. A., *Phys. Fluids* **3** (1960) 786.

DIFFUSION OF PLASMA FROM THE STELLARATOR*

ROBERT W. MOTLEY

PLASMA PHYSICS LABORATORY, PRINCETON UNIVERSITY

PRINCETON, NEW JERSEY, UNITED STATES OF AMERICA

We have measured the plasma currents during the onset of enhanced diffusion in cold recombining stellarator plasmas. The magnitudes of the currents are found to coincide with those predicted for the growth of ion wave instabilities, if one assumes an ion temperature much less than the electron temperature. However, when experimental conditions are adjusted to bring the electrons and ions more closely into thermal equilibrium, there is no observable increase in the magnitude of the critical currents, as one would expect from theory.

1. Introduction

It has recently been recognized [1, 2, 3, 4] that a plasma carrying a current may be unstable to the growth of low frequency fluctuations of electric potential and that these fluctuations may impair plasma confinement in a magnetic field.** The plasma in the stellarator has been found to be unstable when ohmic heating currents flow [7]. L. Spitzer has suggested that fluctuating electric fields may be responsible for the enhanced diffusion. Bernstein, Kulsrud, Frieman, and Rosenbluth then suggested that ion waves, which under some conditions can be amplified above thermal equilibrium levels, may be the mechanism for the generation of the fluctuating electric fields.

According to theory, the ion waves will not grow unless the electron drift velocity exceeds a certain critical level. If the electron and ion temperatures are comparable, this critical velocity is close to the electron thermal velocity; if the electron temperature greatly exceeds the ion temperature, the critical drift velocity is the ion thermal velocity (if the ions be at the electron temperature).

This paper reports measurements which show that enhanced diffusion in weakly ionized stellarator discharges occurs for electron drift velocities which are close to the theoretical critical velocities; however, in plasmas in which the electron and ion temperatures should be comparable, the measured critical velocities are more than an order of magnitude smaller than those predicted by theory.

2. The experiment

The experiment consisted of observing the effect of inducing a small current in a recombining B-1 stellarator plasma. This plasma, which is the afterglow of an ohmic discharge, and which has been described in previous papers [8], is cold ($\sim$0.1 eV), partially ionized, and is recombining with a time constant of order one millisecond. Previous work has shown that diffusion under these conditions causes a negligible fraction of the plasma loss and that there is no evidence of coherent oscillations or other indications of collective behavior.

A sinusoidal constant amplitude, 20 kHz electric field ($\sim$0.02 V/cm) is induced around the plasma loop in the manner previously described [8]. The resulting plasma current is detected by a pickup coil encircling the vacuum tube. The electron density is inferred from the phase shift of a 4.3 mm microwave beam sent across the tube diameter; a sensitive microwave bridge enabled measurement of electron densities to 10^{11} cm^{-3}.

3. Results

Fig. 1 shows the time variation of the electron density in a cold helium plasma with and without an applied electric field. In the absence of the electric field the density of the plasma falls smoothly as the plasma recombines with a time constant between 1 and 2 milliseconds. If a small electric field is induced in the plasma, however, the time behavior is different.

In Fig. 1 we note that the initial effect on the plasma loss rate is minor, but as the current increases and the electrons heat up the recombination proceeds more slowly. Finally, as the electron temperature and the current continue to increase, a rapid diffusion of plasma sets in, near $t=3$ ms. The time constant of the diffusion is 0.3 ms in helium if the magnetic field is 18 kG. As the electron density falls the plasma current continues to increase until the plasma resistivity is determined by electron-neutral collisions; then the current falls with the electron density.

The electron density at which the electron heating and the instability occur is determined by the magnitude of the applied electric field. In a series of discharges, identical except for the electric field strength, we have measured the currents and electron densities at the time of instability. In Fig. 2 are plotted the (peak) current density and the electron density at the point of instability, each data point representing one discharge. The electric field strength was varied from 0.009 V/cm to 0.027 V/cm. The data suggest that the

* Conference paper CN-10/167, presented by R. W. MOTLEY. Discussion of this paper is given on page 211. Translations of the abstract are at the end of this volume of the Conference Proceedings.

** Recent experimental evidence for the existence of ionic or sound waves in plasmas created by dc discharges has been reported [5, 6].

important parameter characterizing the onset of diffusion is the electron drift velocity rather than the magnitude of the current density. The critical drift velocity does not appear to be a function of the neutral pressure, at least between 0.25 and 4 microns. For helium pressures higher than 4 microns the recombination rate is more rapid and is comparable to the diffusion rate. Therefore there is no distinct separation between recombination and diffusion to be inferred from the time variation of the electron density.

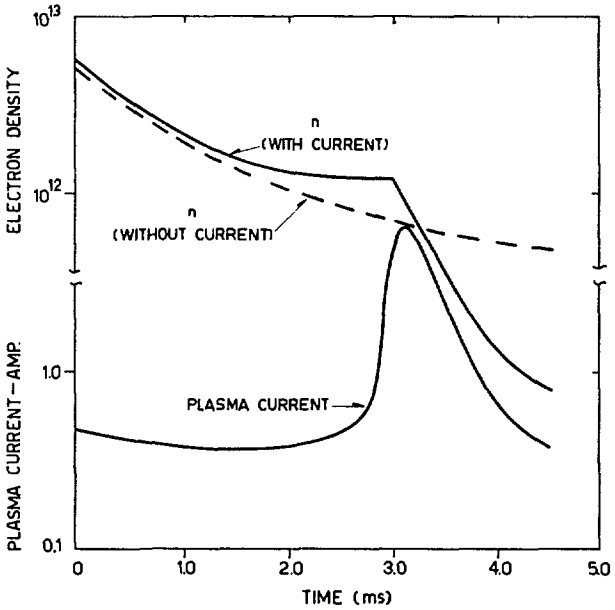

Fig. 1 Time variation of electron density in a cold stellarator discharge in helium (0.6 μ Hg) with and without a 0.02 V/cm electric field. The peak amplitude of the AC current is shown as a function of time. The magnetic confining field is 18 kG. Conditions existing at the onset of rapid diffusion are electron density 1.2×10^{12} electrons/cm^3 current density 0.4 A/cm^2, electric field 0.02 V/cm, average power input $3 \cdot 10^{-3}$ W/cm^3, electron temperature 1 V, and ion temperature 1/4 V.

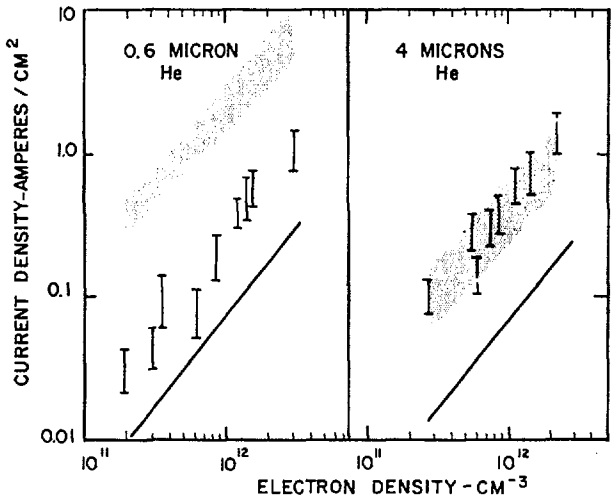

Fig. 2 Critical current densities for the onset of diffusion in helium discharges in the B1 stellarator. The bars represent the experimental data. The lower line is the predicted current for the growth of ion waves, if $T_e/T_i \gg 1$. The upper shaded area shows the predicted currents if the ion temperature is included. The magnetic confining field is 18 kG.

The lower line in Fig. 2 gives the predicted critical currents for the growth of ion waves if the electron temperature is much greater than the ion temperature, that is, if there are no ions traveling at the phase velocity of the waves. This critical current for a shifted Maxwellian velocity distribution [1] is

$$j_c = n_e e \left(\frac{kT_e}{m_i}\right)^{\frac{1}{2}}$$

where m_i is the ion mass. The electron temperature was calculated from the plasma resistivity under the assumption that the electron temperature was uniform across the discharge aperture (12 cm^2). The calculated temperatures range from 0.5 eV ($n = 2 \times 10^{11}$ cm^{-3}) to 1.7 eV ($n = 3 \times 10^{12}$ cm^{-3}).

Under the conditions of our experiment it is generally not a good approximation to neglect wave damping by ions traveling at the phase velocity of the wave. The influence of ion damping on the critical currents has been calculated by E. A. JACKSON [9] for the case in which the electron and ion distributions are Maxwellian. We have computed the ion temperatures from the percentage ionization and the electron temperatures, assuming a charge-exchange cross section of 3×10^{-15} cm^2 for helium [10]. For 0.6 microns of helium the ratio of electron to ion temperature varies from 2.8 (lowest densities) to 4.5 (highest densities). For 4 microns this ratio varies from 7 to 10. The computed critical current densities, taken from Jackson's tabulations, are shown in the shaded areas of Fig. 2, the vertical width of the areas corresponding to an uncertainty of 30% in the computed temperature ratios.

As shown in Fig. 2, the calculated critical currents depend on the gas pressure. If the helium pressure is low (< 1 micron), the ion and electron temperatures should be comparable. In this case the computed critical velocities lie near the electron thermal velocity. On the other hand, if a plentiful supply of neutral atoms is present (4 microns) the critical drift velocity should be closer to the ion thermal velocity. The experimental result is that there is no change in the critical velocities as the neutral pressure is varied. The 4 micron data show no real discrepancy between theory and experiment; the 0.6 micron data show critical drift currents which are an order of magnitude less than the theoretical value.

We have performed similar but not as extensive measurements in hydrogen and in argon. The results are shown in Figs. 3 and 4. In argon the results are similar to those in helium at 0.6 microns pressure. The electron temperatures range from 0.5 eV (lowest density) to 1.1 eV (highest density), and the electron-ion temperature ratios from 5 to 7. Theory predicts critical currents about ten times greater than are measured.

In hydrogen we have analyzed the data on the assumption that the ions present are H^+. Because

of the lack of H^+-H charge exchange and the short electron-ion equilibrium time the ions and electrons should be almost in thermal equilibrium. The electron temperatures range from 0.4 eV to 1.3 eV. The observed critical currents are two orders of magnitude less than those predicted theoretically. It is possible that the ions in the afterglow discharge are H_2^+ or H_3^+; these ions have been observed in low temperature discharges. If the ion species is H_2^+, the discrepancy between theory and experiment disappears.

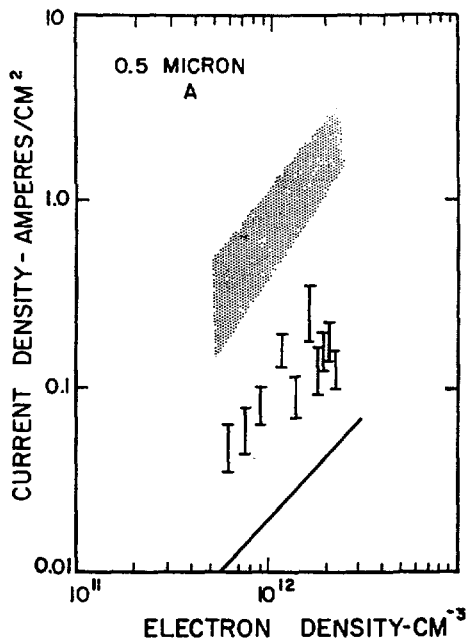

Fig. 3 Critical currents for the onset of instability in argon discharges in the B1 stellarator.

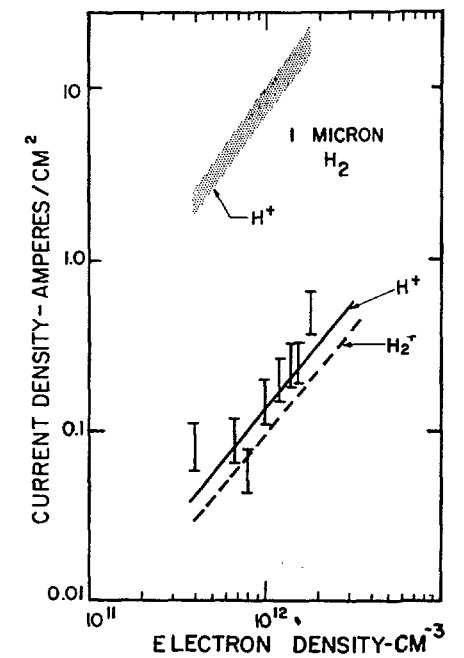

Fig. 4 Critical currents for the onset of instability in hydrogen discharges in the B1 stellarator.

4. Discussion

We have observed that enhanced diffusion in the stellarator sets in when the electron drift velocity reaches a critical level. The magnitude of this drift velocity is close to the critical velocity predicted for the spontaneous growth of ion wave fluctuations in a plasma, if the ion temperature is much less than the electron temperature. These measurements are consistent with the hypothesis that ion waves are responsible for enhanced diffusion in the stellarator. However, theory also predicts that the critical electron drift velocity should be greatly increased if the ion and electron temperatures are comparable. The experimental measurements, on the other hand, show no increase in critical currents if the conditions are chosen to provide comparable ion and electron temperatures.

There remains the possibility that for some reason the ion damping, which is responsible for the increased critical velocities for non-zero ion temperatures, is ineffective. Two possibilities have been investigated by BERNSTEIN and KULSRUD [11]. In considering the effect of non-Maxwellian electron and ion energy distributions on the critical currents they have found that the distortion of the electron distribution by the applied electric field *increases* the critical current by a factor of two. The depletion of the tail of the ion distribution by ion-neutral collisions is a minor effect under our conditions and should not lead to appreciably smaller critical currents.

Acknowledgement

This work was performed under the auspices of the United States Atomic Energy Commission.

References

[1] BUNEMAN, O., *Phys. Rev. Letters* **1** (1958) 8.
[2] SPITZER, L., *Phys. Fluids* **3** (1960) 659.
[3] BERNSTEIN, I. B., FRIEMAN, E. A., KULSRUD, R. M., ROSENBLUTH, M. N., *Phys. Fluids* **3** (1960) 136.
[4] BERNSTEIN, I. B., KULSRUD, R. M., *Phys. Fluids* **3** (1960) 937.
[5] ALEXEFF, I., NEIDIGH, R., *Bull. Am. Phys. Soc.* **6** (1961) 309.
[6] CRAWFORD, F. W., *Phys. Rev. Letters* **6** (1961) 663.
[7] ELLIS, R. A., GOLDBERG, L. P., GORMAN, J. G., *Phys. Fluids* **3** (1960) 468.
[8] MOTLEY, R. W., KUCKES, A. F., Proceedings of the Fifth International Conference on Ionization Phenomena in Gases, Munich (North-Holland Pub. Co., Amsterdam, 1961).
[9] JACKSON, E. A., *Phys. Fluids* **3** (1960) 786.
[10] MCDOWELL, M. R. C., *Proc. Phys. Soc. (London)* **72** (1958) 1087.
[11] BERNSTEIN, I. B., KULSRUD, R. M., private communication.

SOME PRELIMINARY RESULTS ON CONTAINMENT TIME IN THE MODEL C STELLARATOR*

D. J. GROVE**, R. M. SINCLAIR, W. STODIEK***, W. L. HARRIES, L. P. GOLDBERG

PLASMA PHYSICS LABORATORY, PRINCETON UNIVERSITY

PRINCETON, NEW JERSEY, UNITED STATES OF AMERICA

A brief description is given of the Model C stellarator and the results of the first experiments are presented for discussion. A comparison is made with the corresponding data from the B-3 stellarator.

Somewhat as we expected, a considerable number of people have asked about our progress with the Model C stellarator. We have, in fact, obtained some very preliminary information on containment time which has not been cross-checked nor otherwise carefully confirmed. However, we have no desire to withhold information of general interest, and with this understanding we are pleased to share with you our initial observations on Model C. I might emphasize the preliminary nature of this data by telling you that substantially all the data to be reported today was taken last week.

Let me begin by reminding you briefly of some of the important characteristics of the C stellarator. The vacuum vessel is 20 cm in diameter in the form of a plane oval race track measuring 1220 cm in axial length. There are external coils for producing a magnetic field up to 40 kG in a direction parallel to the vacuum vessel. We have so far used only ohmic heating and we do not yet have helical windings on the machine.

Fig. 1 shows schematically the important elements of the machine and the associated power inputs. The equipment indicated for magnetic pumping and ion cyclotron heating has not yet been installed.

Our experimental procedure was essentially that described by STODIEK, ELLIS, and GORMAN [1]. The ohmic heating voltage was programed to raise the electron temperature quickly to a predetermined value and to hold it reasonably constant during the peak and the decay of the electron density. In the paper by Stodiek *et al.*, it was shown that the containment time varies directly as the magnetic field and inversely as the electronic temperature, as long as current is flowing. With this in mind, a comparison can be made with the B-3 stellarator as shown in Fig. 2. In both cases, the initial gas pressure was 10^{-4} torr of hydrogen. It should be noted that the time scale for the Model C data is 500 μs/division, compared with 100 μs/division for B-3. Furthermore, the electron temperature in the case of Model C is approximately twice that for the data shown for B-3.

A more direct comparison with the B-3 results is shown in Fig. 3. Here we have plotted what is essentially the ratio of the apparent containment time for Model C to that of B-3. The value of the apparent containment time τ was taken directly from the decay in electron density and was measured for a number of values of magnetic field and plasma current. For each point the corresponding electron temperature was determined from the conductivity and the containment time normalized according to the prescription $\tau \sim B/T_e$. In the B-3 experiments the corresponding procedure gave a value which varied only slightly over the entire range, and therefore a single fixed value of $(\tau T_e B^{-1})_{B\text{-}3}$ was used to form the ratio. The dotted line is drawn at a value $(180/40)^2$ corresponding to the square of the ratio of the plasma diameters in Model C and B-3. We do not understand the reason for the relatively low values in the region of low current. They do correspond to cases where the electron temperature was perhaps somewhat less than 10 eV, whereas the remaining points correspond to temperatures 15 to 23 eV.

In a somewhat different set of experiments, the ohmic heating system was programed for constant plasma current, that is, a current which increased rapidly at first and then remained constant during the course of a discharge. From the data on these experiments we have extracted an interesting quantity shown in Fig. 4. Here we have plotted what we call the "energy replacement time", that is, the ratio of the total kinetic energy of the electrons in the plasma to the power input. This quantity has been plotted as a function of the magnetic field in kilogauss. For all of these points the plasma current was 3 kA and the pressure was 10^{-4} torr of hydrogen. The precise shape of this curve is not well known. The important point is that we generally observe an increase of this quantity with increasing magnetic field.

I would like to summarize, not our results, but our observations. This very preliminary data indicates an apparent particle containment time of about 1 ms at an electron temperature of 20 eV and with a con-

* Text of presentation by D. J. Grove at the Conference on Plasma Physics and Controlled Nuclear Fusion Research, Salzburg, Austria, on 5 September 1961. This paper has been designated as CN-10/261.

** On loan from Westinghouse Research Laboratories, Pittsburgh, Pennsylvania.

*** On leave from Max-Planck-Institut für Physik und Astrophysik, München.

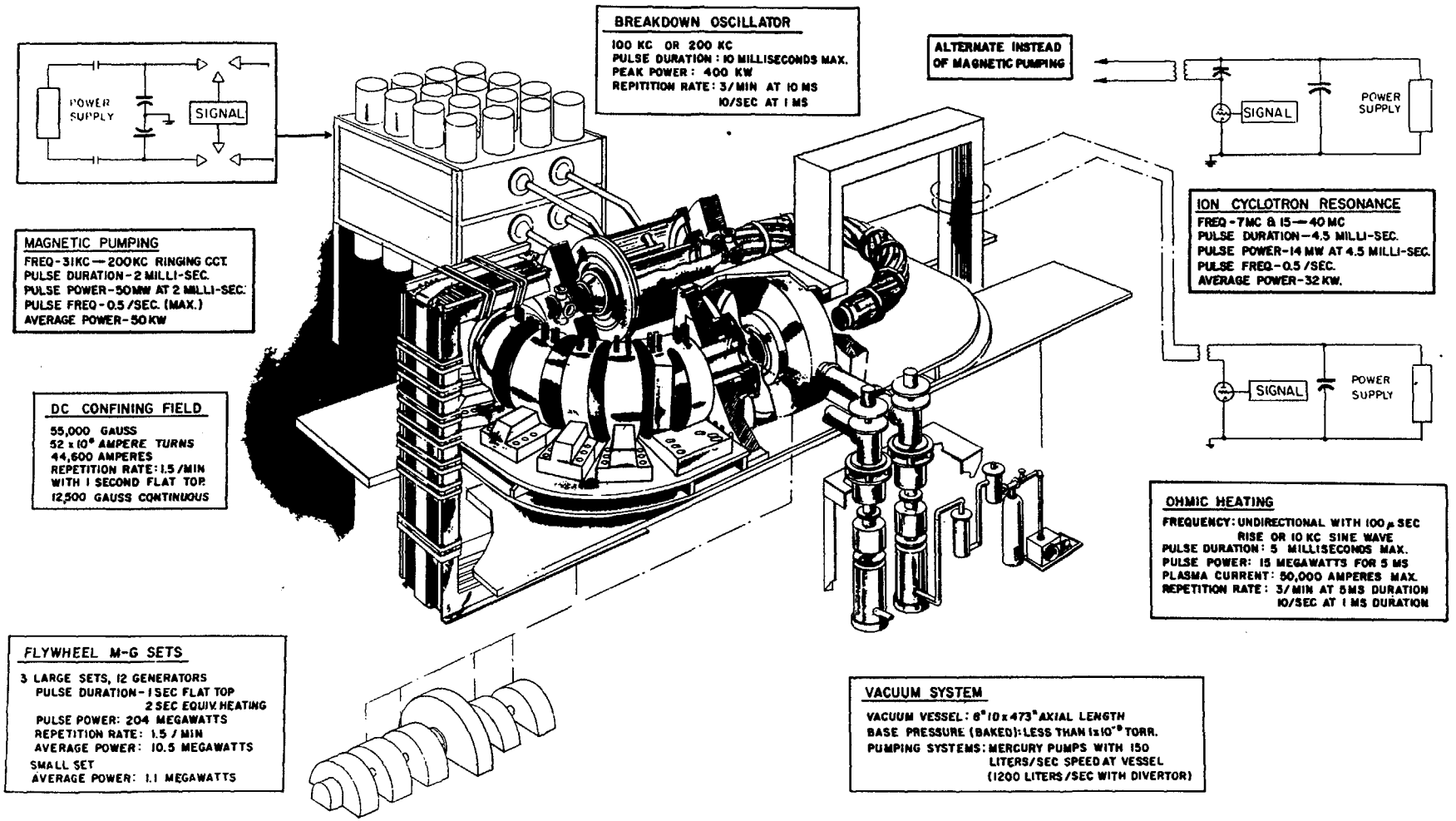

Fig. 1 Semischematic drawing of the Model C stellarator showing the arrangement of the various components and specifying the power inputs to the machine.

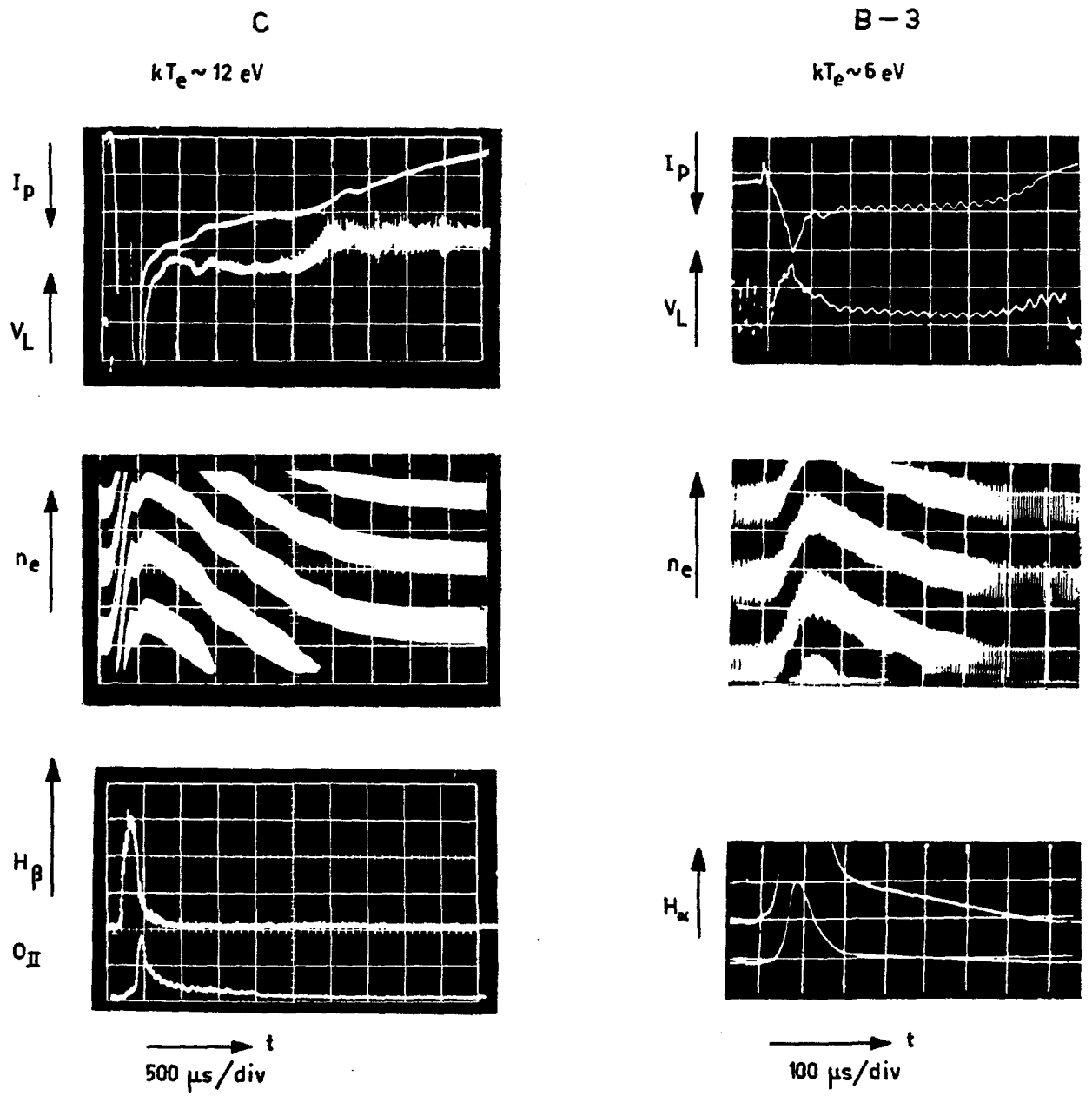

Fig. 2 Comparison of general plasma behavior of Model C with that of B-3. Note that the time scale for the Model C traces is 500 μs/div compared to 100 μs/div for the B-3 data. Note also that the electron temperature is a factor of two higher for C. The top pictures compare the plasma current and voltage for the two machines. The middle pictures compare the 4 mm microwave traces used for measuring the electron density with Model C having clearly a slower decay. The bottom traces show the hydrogen light signals H_β and H_α and there is also for Model C a trace of the impurity light from O II ($\lambda = 4416$ Å and 4418 Å).

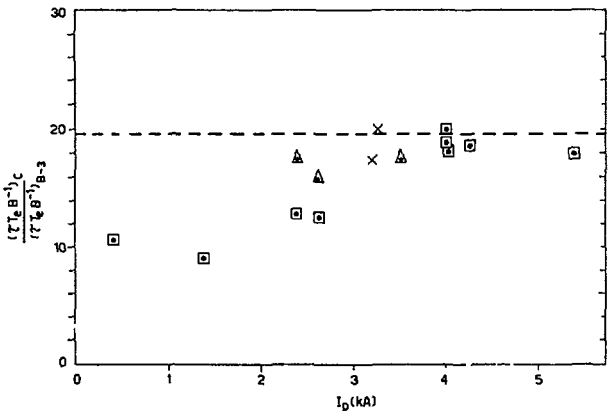

Fig. 3 The ratio of the apparent confinement time in Model C to that of B-3 as a function of the plasma current in Model C. As indicated by the ordinate of the curve, the times have been normalized according to the prescription $\tau \sim B/T_e$. Only a single value was used for B-3 since for this machine $\tau T_e B^{-1}$ remained constant over a wide range of field and temperature. The dotted line is the value expected of this ratio if the containment time varies as the square of the plasma diameter. Points in squares are for $B = 40$ kG, triangles for $B = 20$ kG and crosses for $B = 12.5$ kG.

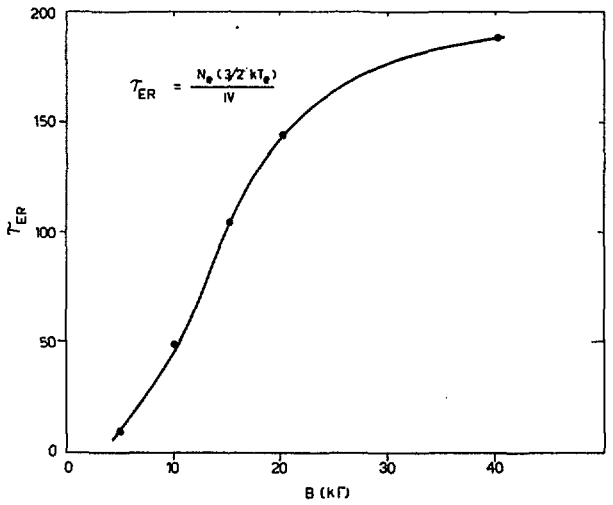

Fig. 4 The energy replacement time as a function of magnetic field in kilogauss. The pressure $p = 10^{-4}$ torr and $I_D = 3$ kA. The energy replacement time is defined as the ratio of the total kinetic energy of the electrons in the plasma to the power input. The exact shape of the curve is not well known as it is sensitive to plasma current and initial pressure among other things.

fining field of 40 kG. We have observed an energy replacement time in excess of 150 μs (at 40 kG and 10^{-4} torr hydrogen) and a scaling factor certainly greater than linear, possibly as large as the square of the plasma radius.

Acknowledgements

The authors wish to acknowledge the constant encouragement and help from M. B. Gottlieb and the many fruitful discussions of the data with Lyman Spitzer, Jr.

The work reported here was performed under the auspices of the U.S. Atomic Energy Commission.

Reference

[1] Stodiek, W., Ellis, R. A., Jr., Gorman, J. G., I.A.E.A. Conference on Plasma Physics and Controlled Nuclear Fusion Research, Salzburg, 1961: Paper CN-10/131, page 193 of this volume.

DISCUSSIONS (SESSION II) — DISCUSSIONS (SÉANCE II) — ДИСКУССИИ (ЗАСЕДАНИЕ II) — DEBATES (SESIÓN II)

Paper CN-10/153 *was presented by R. F. Post* (United States of America). *The text of the paper is on pages 99 to 123 inclusive. No discussion took place.*

Paper CN-10/149 *was presented by F. H. Coensgen* (United States of America). *The text of the paper is on pages 125 to 133 inclusive. The following discussion took place:*

M. B. Gottlieb *(United States of America):* What is your explanation of this motion or drift of the plasma across the field?

F. H. Coensgen *(United States of America):* We have done considerable work on this. We find that the plasma does not bombard the wall in a random fashion but rather is localized in one azimuthal position. To check this further we used only one pulsed magnet at a time and used a flat, or uniform, DC field with just a small barrier at the end (Fig. 1, Curve AA′). What happens is that the plasma always ends up in one position. There is a linear system of two transfer magnets shown as (1) and (2) in Fig. 2. The magnetic field is uniform with the bump at the —1 foot position. If the first transfer magnet is pulsed, the distribution shown as curve II in Fig. 7 is obtained — which indicates that the plasma has bombarded only one side of the chamber. If the other magnet is pulsed, curve I, Fig. 7, is obtained, which indicates that the plasma has bombarded the opposite side of the chamber. It is found that the plasma always moves toward the position where the current is brought into these low inductance coils. These are essentially single turn coils. The lead side has a low field, and we believe that there is a driving force that gives the plasma a shove or push across the magnetic field leading to the transverse drift. Now, of course, the question arises: can we get rid of it by symmetrizing the magnetic field? We are doing such experiments but we do not know the answer. The question also arises whether or not this is an instability. I can only say that if it is an instability it looks like an $m=1$ flute instability; other than that I will only say that we have to wait until we have done further experiments to see whether or not we can stabilize the plasma. If we can't, of course we will introduce magnetic shear into our system and see if we can then get rid of such drifts.

L. A. Artsimovich *(Union of Soviet Socialist Republics):* I have one question for Dr. Coensgen. In the curve showing the time dependence of the neutron yield, which has been demonstrated in your talk, it was indicated that the lifetime of the hot plasma is about 900 μs. Do you still think that this curve actually indicates such a long plasma containment time?

F. H. Coensgen: The answer is no; we now consider that the plasma is contained for approximately 90 to 100 μs and that the evidence for containment beyond that time was due to spurious or misinterpretation of the counting data.

L. A. Artsimovich: So you say 90 μs? Do you have any other proofs of such a containment time besides neutron yield?

F. H. Coensgen: Yes, the plasma is ejected at the end of this time, as we detect the plasma either at the walls or coming out the end after 90 μs. Does that answer your question? That is we take the probe; we trace or detect the plasma. It comes across the field hitting the walls at the end of the 90 μs time and actually, if we integrate this signal over the walls, it accounts for most of the plasma. A little can come out the end.

L. A. Artsimovich: I want to say a few words about your curve showing the time dependence of the yield of neutrons. It is evident that the tail on the graph is due to the neutrons that have been slowed down in the plastic scintillator and counted by the detector. Therefore the actual time of neutron emission after the maximum is probably of the order of 20—30 μs and the rest of the tail is due to neutrons moderated in the scintillator. This is not very surprising since anyone who has been using such counters knows well that there always is a background of slow neutrons. Now my second remark. All which has been said becomes particularly evident if the curve you demonstrated is drawn not in a logarithmic, but in the usual linear scale. Then it becomes clear that practically the total neutron pulse takes place during twenty to thirty microseconds after the maximum, and the remaining part of the curve represents a negligibly small background.

F. H. Coensgen: I believe that I have covered this point. I am aware that the counter itself acts as a thermalizing device. The decay time for the particular scintillator system which we used was 15 μs. The spurious counts which were misinterpreted as neutrons are due to slowing down of neutrons in the magnets, subsequent capture by hydrogen in the magnet and the detection of 2.2 MeV capture gamma rays. I tried to make this clear in my presentation.

Paper CN-10/3 *was presented by B. Lehnert* (Sweden). *The text of the paper is on pages 135 to 142 inclusive. The following discussion took place:*

G. Schmidt *(United States of America):* Is there really a contradiction between your paper and the energy principle? Obviously in the high β and sharp boundary case there is a possibility of lowering the energy of the system by perturbation. In the case of

a finite density gradient, however, this is not clear at all. It would be very surprising indeed if there existed a lower energy state in the vicinity of a steady state and the plasma were unable to reach it.

B. Lehnert *(Sweden):* If the energy principle is worked out by taking all constraints into consideration, there is no contradiction between it and the treatment of the present paper. I have only stated that one cannot make an arbitrary exchange of fluid elements and deduce a stability condition from the corresponding energy change of the system. Take, as an example, the situation of a low β and a sharp boundary dividing two plasma regions with different densities. By an arbitrary exchange of fluid elements a lower energy state can then be obtained in the case of a heavy fluid on top of a lighter one. However, a detailed description of the motion of the perturbed particle clouds shows that the system still remains stable under certain conditions for $\gamma < \frac{1}{4}$ with the notation of this paper. The perturbations will then grow at the start as expected from earlier hydrodynamic models, but the drift which causes this growth will soon be reversed and stable oscillations of limited amplitude will occur. In this case the system will never be able to reach a state of lower energy.

G. Schmidt: The scrambling mechanism, which is important as a stabilizing agent in your theory, supposes particle drifts. Therefore the zero order approximation, with no reaction of the particle currents on the magnetic field, is not justified for use in the energy principle.

B. Lehnert: The statement which I have made regarding the energy principle should be applied to the case of flutes, where the magnetic field is left unchanged, as well as the magnetic flux enclosed by the perturbed boundary (see also Rosenbluth & Longmire, *Ann. Phys. (N.Y.)* **1** (1957) 120. The flutes are characterized by not having any reaction on the magnetic field, in the situation of a low β.

G. S. Murty *(India):* In your calculations you assumed that the induced magnetic field is negligible. Can one, then, compare your results with those that are obtained on the basis of the energy principle, which is developed for a fluid of large, electrical conductivity? Is it right to say that your results are applicable only for the cases when the conductivity is very small?

B. Lehnert: I only neglect the induced field as far as the drifts due to the magnetic field gradient and to the electric field are concerned. This approximation is very good when the characteristic velocities of the phenomenon are much smaller than the Alfvén velocity, which is fulfilled in a strong magnetic field.

The conductivity does not enter into my problem. I have neglected the influence of collisions, and the situation is governed only by the drift motions in the magnetic, electric and gravitation fields.

Paper CN-10/170 *was presented by M. N. Rosenbluth* (United States of America). *The text of the paper is on pages 143 to 150 inclusive. The following discussion took place:*

A. A. Ware *(United Kingdom):* Dr. Rosenbluth and his colleagues have derived an extra drift velocity term to add to the $\mathbf{E}+\mathbf{v}\times\mathbf{B}=0$ equation. Dr. Lehnert in the previous paper has taken equations which correspond to adding to this equation not only the Rosenbluth *et al.*, term, but also the terms $(1/ne)\mathbf{j}\times\mathbf{B}$ and $-(1/ne)\nabla p_e$. Does this not mean that he has included the same effect twice?

M. N. Rosenbluth *(United States of America):* Perhaps Dr. Lehnert should answer this.

B. Lehnert *(Sweden):* If you just carry on your expansions one order further, you will get this term in your equation.*

A. A. Ware: If one goes to the first order in the ratio of Larmor radius to characteristic length, one includes terms such as the Hall effect and the gradient of electron pressure. You have added an extra term, the Rosenbluth term.

B. Lehnert: There is, of course, the restriction that the Larmor radius should be much smaller than the spatial dimensions of the disturbance. I think that this applies also to Dr. Rosenbluth's treatment. In my stability criterion the term f represents the effect discussed by Rosenbluth *et al.* It arises directly from the basic equations (6) of my paper when the second-order terms are retained. Dr. Rosenbluth's stability criterion comes out from my condition (43) when terms containing the parameter α in the left-hand member are dropped. If the latter are taken into account, however, the stability criterion becomes identical with that discussed earlier in my paper.

A. A. Ware: I think you get the same thing twice, but perhaps we could discuss this afterwards.

R. S. Pease *(United Kingdom):* Has your work been extended to the case when shear is present in the magnetic field, and in particular to the case of pinch containment?

M. N. Rosenbluth: I should point out that it is quite obvious that the same sort of correction will apply in that case, in particular to the case of the so-called surface instabilities of the pinch, that is, instabilities which take place within the narrow current layer at the surface of the pinch. In this case one meets the condition in both ways: the growth rates are very small, in proportion to the thickness of the surface layer, and of course also the gradients are very steep. So it is clear that the hydrodynamic theory does break down violently in this case. We are working on these calculations but they are not so easy.

* Dr. Lehnert amended his paper (CN-10/3, see page 135) after the Conference. The theory now retains some higher order terms.

W. Linlor *(United States of America):* Would the stabilization effect take place in machines like DCX and Ogra ?

M. N. Rosenbluth: This is a point I meant to make but did not. You will notice in this derivation at one point I assumed that the dielectric constant $4\pi nmc^2/B^2$ was very large compared with unity. Now it is a trivial change to not make this approximation, which I believe for Ogra and DCX is not a good approximation. All that happens in that case (if you remember the quadratic dispersion relation which I got) is that the coefficient of the term ω^2 becomes very large if the dielectric constant is not much greater than unity, and in this case the stabilizing effects are considerably reduced. So, in cases where the plasma dielectric constant is not large compared with unity, one does not get as much stabilization from the finite Larmor radius as was indicated by these results. Now unfortunately, I have not yet had the opportunity to compare this quantitatively with Dr. Golovin and Dr. Ioffe, so I don't know whether there is a quantitative comparison or not. These calculations were made with Dr. Post and Dr. Coensgen tenderly in mind, so I mostly used parameters appropriate to their situation.

Paper CN-10/175 *was presented by E. J. Lauer* (United States of America). *The text of the paper is on pages 151 to 157 inclusive. The following discussion took place:*

T. H. Stix *(United States of America):* Please sketch the "Japanese Lantern" surfaces and show the points of intersection.

E. J. Lauer *(United States of America)* shows a sketch (Fig. II-1).

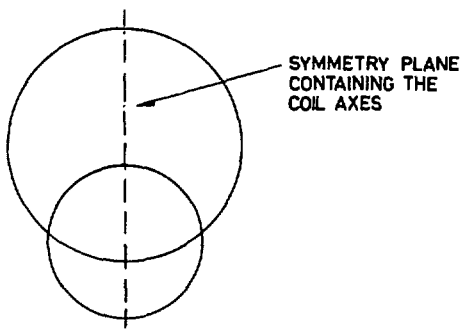

Cross section of two drift surfaces in the plane midway between the coils.

Paper CN-10/174 *was presented by H. P. Furth* (United States of America). *The text of the paper is on pages 169 to 175 inclusive. The following discussion took place:*

M. N. Rosenbluth *(United States of America):* Do you know of any experimental observations to date demonstrating your sheet-pinch instability ?

H. P. Furth *(United States of America):* I would say that what one has seen on reverse-field theta-pinches falls into this class. In the reverse-field pinches, if one treats the whole machine as one instability half wavelength, then one gets exactly the mode I'm talking about. Of course, that's really cheating. A proper demonstration of the instability would require a very long and uniform zero-order configuration, which could then break up randomly into a number of instability wavelengths. I am still waiting for people to build reverse-field pinches which are sufficiently long. I would say, however, that one of the papers submitted to this Conference on the theta-pinch, by the people at General Electric Co., exhibits some random magnetic probe signals which strongly suggest that they may have the effect that I am talking about.

W. H. Bostick *(United States of America):* At the Max-Planck-Institute the work of Remy and others employs a theta-pinch in which the coil is toroidal and thus is effectively infinitely long. The circumference of the torus is approximately one meter. Some of their Kerr cell pictures suggest the type of bunching which you indicated. I think, in this connection, that the work of Vernal Josephsen at Aerospace Labs should be mentioned. He has photographed, both axially and radially with an image converter camera, the break-up of the theta pinch. His photographs show a sausage instability which he says is due to collapsing of the sheet pinch into a circular linear pinch. This is perhaps a confirmation of the type of instability which you have talked about.

Paper CN-10/216 *was presented by M. S. Ioffe* (Union of Soviet Socialist Republics). *The text of the paper is on pages 177 to 182 inclusive. The following discussion took place:*

R. F. Post *(United States of America):* I have the following two questions: (1) Have you measured the anisotropy of the plasma ? (2) Does the mechanism of Kadomtsev require the flute instability or could it work with other instabilities as the driving mechanism ? I am particularly curious about the Harris instability.

M. S. Ioffe *(Union of Soviet Socialist Republics):* We have not made any special measurements on the anisotropy in the velocity distribution in our experiments, but it is certain that we could not have the "mirror instability" in such conditions since our β was very small (of the order of 10^{-5}) and the transverse energy of the ions was about 1000 eV. That would mean that for the mirror instability to appear the longitudinal ion energy must be less than 0.01 eV, which appears to be practically excluded in our experiments.

As for the second question, I think that the experimental results indicate that the instability we observe and which is responsible for the loss of plasma

is really the flute instability. It follows from the fact that, as I have already mentioned, the signal of the particle flux reaching the side wall of the trap is characterized by a very good correlation between the oscillations of current along the total length of lines of force in the trap, while in the azimuthal direction these correlation regions have different lengths up to the minimum Larmor radius which could not occur if this instability were of the mirror type.

R. F. Post: With respect to your first question I really had in mind other instabilities such as the Harris one for which there is no condition on β. Perhaps you can assure me that this one also will not occur due to the conditions of your experiment.

L. A. Artsimovich *(Union of Socialist Soviet Republics):* I want to say that Ioffe's results are in sharp contradiction with the attractive picture of a thermonuclear Eldorado which has just been drawn by Dr. Post. After the initial assertions of Dr. Coensgen that the plasma containment time was about 1 ms have proved erroneous, we now do not have a single experimental fact indicating long and stable confinement of plasma with hot ions within a simple magnetic mirror geometry. Therefore our hopes must rest on combined geometries.

E. J. Lauer *(United States of America):* Have you tried any changes in the geometry of the conducting wall to see if it affects the instability?

M. S. Ioffe: We have performed experiments with such a geometry of the walls in which magnetic lines of force are touching a conducting surface along their total length. I have not mentioned these experiments and we did not publish these results for the simple reason that they were essentially the same as the results obtained before. We noticed a small change in the dependence of lifetime on the magnetic field, but it is insufficient to attach any significance to it.

M. B. Gottlieb *(United States of America):* It is quite apparent that there is a serious misunderstanding of the measurements that have been made on mirror confinement. The question of mirror stability is a very serious one. I suggest a special session on this subject.*

Paper CN-10/151 *was presented by J. Killeen* (United States of America). *The text of the paper is on pages 183 to 191 inclusive. The following discussion took place:*

I. N. Golovin *(Union of Soviet Socialist Republics):* I have a question and a remark. The experiments we performed on the Ogra indicate that there apparently exists a much more powerful mechansim of the energy transfer from ions to electrons. While the calculations indicated an energy transfer of the order of 100 eV, the actual energy exceeds tens of keV. It would be interesting to include in the theory other transfer mechanisms connected with instabilities of plasma. Does the author intend to take these ways of energy transfer into account?

J. Killeen *(United States of America):* This of course is just a first stage in solving energy losses from mirror machines. We haven't incorporated yet into this formalism the idea of energy loss through instability since this is at this point strictly a velocity space calculation.

A. Rukhadze *(Union of Soviet Socialist Republics):* I want to make a remark and to ask a question. In the paper the rate of equalization of temperatures of electrons and ions is discussed with the help of the Fokker-Planck equation in the very trivial Landau form where excitation of waves is not taken into account. It would be interesting to determine equalization of temperatures and its rate taking into account excitation of waves. This can be done by using the Fokker-Planck equation as developed by Rostocker, Silin and others which considers wave excitation. This, perhaps, could give an answer to Golovin's question.

Now here is a question: The equation which has been numerically integrated contains a certain logarithmic function of temperature, the Coulomb logarithm. This function varies slowly with temperature but as temperature changes by a thousand eV, which actually takes place in the experiment, it cannot be thought of as a constant, as assumed in the paper. Therefore some doubts appear concerning the actual numerical results. What can the author say about that?

J. Killeen: The results presented in the paper showing the energy gain of the electrons as calculated by the two different methods are in the form I_4^- vs τ where I_4^- is directly proportional to the electron energy and τ is related to the real time t by the equation preceding Eq. (5) in the paper. It is seen that the relationship between τ and t involves the $\ln\Lambda$ which is the slowly varying function of temperature referred to in your question. It is true that in the results presented today $\ln\Lambda$ is taken to be constant; in fact, it doesn't appear in either calculation since we are using the variable τ. In order to check this effect we should compute I_4^- vs t, the real time, by putting the temperature dependence into our relationship between τ and t. This will be done.

Papers CN-10/131 *and* 167 *were presented by R. Motley* (United States of America). *The texts of the papers are on pages 193 to 201 inclusive. The following discussion took place:*

W. Linlor *(United States of America):* Does the current in Fig. 1 (of CN-10/167) have a frequency of 20 kilocycles per second?

* Editor's note: Angular momentum considerations regarding plasma stability in mirror machines were discussed at an informal Session on 7th September. A short paper by W. I. Linlor (Hughes Research Laboratories, Malibu, California) summarizing his discussion has been submitted to "Nuclear Fusion".

R. Motley *(United States of America):* That is correct.

W. Linlor: For this frequency, the E-B (Lehnert type) instability should not be important, because the time for plasma loss is much longer than the period of the current. Nevertheless, the plasma does disappear in correlation with the plasma current pulse. Thus, the observed enhanced loss due to current in this case cannot be of the Lehnert type (which was adduced from the Kadomtsev analysis).

R. Motley: That's true if the frequency is high. It probably means that the oscillations which are so readily defined in the case of positive columns will not be very well defined in this case. And we have looked with probes to determine whether there are any well-defined oscillations of frequencies higher than 20 kilohertz but have not seen anything outstanding.

B. Lehnert *(Sweden):* A frequency of 20 kHz is just in the range where oscillations have been observed due to the instability in the positive column. The time of plasma loss by such an instability seems to be of the same order as the period you have mentioned. Therefore, it may be somewhat difficult to decide whether the screw instability mechanism of Kadomtsev applies to the present experiments or not.

R. Motley: Of course the Kadomtsev theory does not apply directly to these discharges because of the high degree of ionization and the very strong magnetic field.

W. Linlor: I was just going to say, however, when this current is applied there is an increased loss and a loss mechanism results without the necessity for a unidirectional current.

R. Motley: The rate of diffusion is essentially independent of whether you vary the electric field sinusoidally or not. But the rate of diffusion is essentially independent of the exact shape of the electric field one applies.

T. H. Stix *(United States of America):* Please clarify the agreement of the H^+ experimental points with the solid and dotted lines in the last figure (Fig. 4 of CN-10/167).

R. Motley: The smooth line is for the cold-ion theory assuming that the ions present are H^+. The dotted line is the prediction if the ions present are H_2^+. At the time this paper was written we didn't really know just which ions were present. It appears from recent evidence that the plasma was overwhelmingly H^+.

SESSION IV — SÉANCE IV

ЗАСЕДАНИЕ IV — SESIÓN IV

6 SEPTEMBER 1961 — 6 SEPTEMBRE 1961

6 СЕНТЯБРЯ 1961 Г. — 6 DE SEPTIEMBRE DE 1961

Chairman — Le président — Председатель — El Presidente

G. von Gierke *(Federal Republic of Germany)*

Scientific Secretary — Secrétaire scientifique — Ученый секретарь — Secretario Científico

W. F. Gauster *(United States of America)*

[Papers presented: CN-10/74, 97, 100, 158, 160, 178, 190, 191, 210, 212, 225, 233, 254, 255]

СВОЙСТВА ПЛАЗМЫ, ОБРАЗУЮЩЕЙСЯ В ОГРЕ ПРИ ИНЖЕКЦИИ ПУЧКА МОЛЕКУЛЯРНЫХ ИОНОВ ВОДОРОДА*

Г. Ф. БОГДАНОВ, И. Н. ГОЛОВИН, Ю. А. КУЧЕРЯЕВ, Д. А. ПАНОВ

ИНСТИТУТ АТОМНОЙ ЭНЕРГИИ ИМ. И. В. КУРЧАТОВА

МОСКВА, СОЮЗ СОВЕТСКИХ СОЦИАЛИСТИЧЕСКИХ РЕСПУБЛИК

При инжекции в Огру пучка ионов H_2^+ с энергией до 160 кэв и с силой тока до 150 ма образуется запертая магнитными пробками плазма с концентрацией быстрых ионов около 10^7 см$^{-3}$. Давление остаточного газа при максимальных токах вводимого пучка не превышало $1{,}5 \cdot 10^{-7}$ мм рт.ст. Напряженность магнитного поля в центре ловушки равна 2000—2700 гаусс, пробочное отношение 2,5—3. Конфигурация магнитного поля такова, что ионы дрейфуют вокруг оси ловушки в направлении, совпадающем с направлением их ларморовского вращения.

Образующаяся в Огре плазма, если не приняты специальные меры, неустойчива относительно образования «языков», вытянутых в продольном направлении. В этих режимах время жизни быстрых ионов H_1^+ приблизительно в 20 раз меньше, чем время жизни относительно перезарядки на молекулах остаточного газа, равное $\sim$10 мсек при давлении газа 10^{-7} мм рт.ст. Имеют место существенные потери электронов, образующихся при ионизации остаточного газа, в результате чего положительный потенциал плазмы относительно стенок камеры достигает нескольких десятков киловольт при максимальном токе инжекции.

В концах камеры Огры, вне пространства, занятого быстрыми ионами, были установлены два одинаковых изолированных электрода, размер которых выбирался из условия, чтобы они захватывали весь поток магнитного поля, проходящий через среднее сечение камеры. Положительный потенциал около 10 кв, подаваемый на один из электродов или на два сразу, стабилизирует плазму. Плазма приобретает симметричную форму. Время жизни ионов возрастает, оставаясь, однако, в 2—3 раза меньше времени жизни из-за перезарядки. Механизм стабилизации плазмы в настоящее время исследуется.

Проведенные за последнее время исследования показали, что плазма с плотностью порядка 10^7 см$^{-3}$, образующаяся в Огре при инжекции ионного пучка с силой тока до 150 ма, неустойчива относительно образования «языков» и что время жизни быстрых атомарных ионов водорода гораздо меньше, чем время жизни до перезарядки при давлениях остаточного газа $\sim 10^{-7}$ мм рт.ст. Этот результат не противоречит предсказаниям теории о том, что плазма должна быть неустойчива в магнитном поле с положительной кривизной магнитных силовых линий.

Нам удалось стабилизировать плазму относительно этой неустойчивости, воздействуя на нее положительными электродами, установленными в торцах камеры, вне пространства, занятого быстрыми ионами. Не исключено, что стабилизирующий эффект связан с тем, что ларморовский радиус ионов в Огре сравним с диаметром плазмы и на несколько порядков превышает ларморовский радиус электронов.

В настоящее время математическими методами и на электронной модели Огры ведутся исследования различных конфигураций магнитного поля, в которых наблюдавшаяся неустойчивость не должна осуществляться и без воздействия внешними электрическими полями.

1. Условия экспериментов

В Огру инжектировался пучок молекулярных ионов водорода с энергией 160 кэв и с силой тока от долей миллиампера до 150 ма. При максимальном токе инжекции давление остаточного газа удавалось поддерживать на уровне $0{,}7—1{,}5 \cdot 10^{-7}$ мм рт.ст.

Молекулярные ионы вводились в ловушку через магнитный канал. При выходе из магнитного канала угол между вектором скорости ионов и направлением магнитных силовых линий был равен 70^0. Напряженность магнитного поля в средней части Огры подбиралась таким образом, чтобы орбиты молекулярных ионов проходили вблизи оси камеры (2800 гаусс при энергии молекулярных ионов 160 кэв). Напряженность магнитного поля в пробках от 6500 до 6900 гаусс. Четыре секции соленоида (рис. 1), расположенные перед пробочными катушками (по две обмотки с каждого конца), имели независимое питание. Это позволяло путем изменения величины и направления тока в этих секциях изменять крутизну нарастания магнитного поля в магнитных пробках, что, в свою очередь, влияло на скорость магнитного дрейфа ионов вокруг оси соленоида. Поэтому эти секции соленоида называются дальше «управляющей» обмоткой. Зависимость между углом дрейфа за

* Доклад CN-10/210, представленный на Конференцию. Докладчик: Г. Ф. Богданов. Дискуссия (на английском языке) по этому докладу дана на стр. 353. Переводы аннотаций находятся в конце этого тома Трудов Конференции.

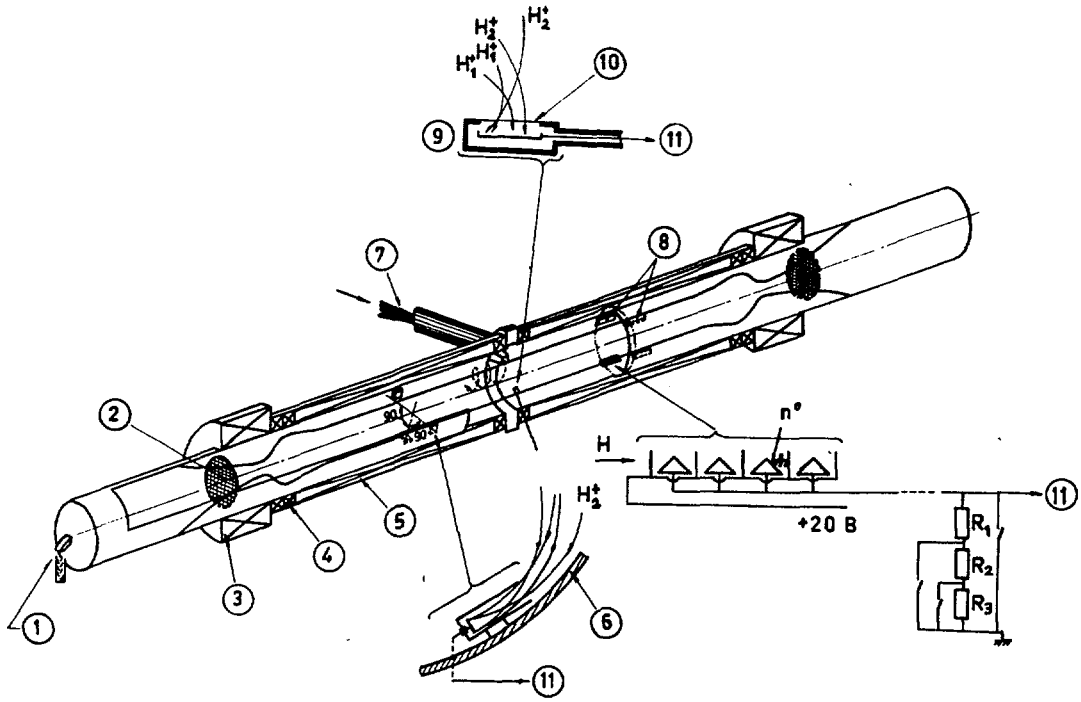

Рис. 1 Схема расположения регистрирующих устройств в камере Огры: 1 — электростатический анализатор ионов; 2 — торцевой электрод; 3 — пробочная обмотка; 4 — управляющая обмотка; 5 — основная обмотка; 6 — стенка камеры; 7 — пучок ионов H_2^+; 8 — детекторы нейтралов; 9 — радиальный зонд; 10 — фольга 2 = 0,12 мк; 11 — к усилителю.

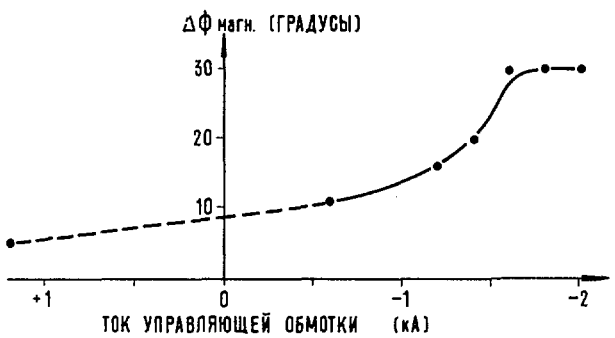

Рис. 2 Зависимость угла дрейфа ионов H_2^+ за одно отражение от тока «управляющей» обмотки.

одно отражение от магнитной пробки и током в «управляющей» обмотке показана на рис. 2. Направление магнитного дрейфа ионов совпадает с направлением их ларморовского вращения.

2. Измерительные устройства

На рис. 1 показано расположение измерительных устройств в камере Огры.

В правой половине камеры установлено четыре детектора быстрых нейтралов. Схематический рисунок устройства детектора полностью поясняет принцип его работы. Детектор регистрирует суммарный поток быстрых нейтралов, образующихся в процессах.

$$H_2^+ + A \begin{matrix} \nearrow H_2^0 + A^+ \\ \searrow H_1^0 + H_1^+ + A \end{matrix} \quad (1)$$

$$H_1^+ + A \rightarrow H_1^0 + A^+. \quad (2)$$

Можно показать, что если концентрация ионов H_1^+ находится в равновесии с концентрацией ионов H_2^+ и нет иных потерь ионов H_1^+, кроме перезарядки, то в полном потоке нейтралов вклад от процесса (2) не превышает 2/3. Если имеются дополнительные потери ионов H_1^+, то вклад нейтралов от процесса (2) в общем потоке нейтралов падает. Так как вклад ионов H_1^+ в общей концентрации быстрых ионов заранее не известен, то в оценках концентрации ионов H^+_2, сделанных по интенсивности потока быстрых нейтралов, будет заметная недостоверность. Однако можно показать, что вычисленная концентрация ионов H_2^+ будет завышена не более чем в три раза по сравнению с истинной, если считать, что весь поток нейтралов образуется в процессе (1). Далее во всех случаях, когда будет называться плотность молекулярных ионов в относительных или абсолютных единицах, будет иметься в виду величина, оцененная по полному потоку нейтралов в стационарном режиме в предположении, что идет только процесс (1).

Детекторы нейтралов позволяют наблюдать распад плазмы после быстрого выключения инжекции и, соответственно, измерять время жизни быстрых ионов в распадающейся плазме. Коллекторы детекторов присоединены к усилителю, имеющему входное сопротивление, состоящее из

трех отдельных сопротивлений, закороченных контактами реле. Примерно за 2 мсек до выключения пучка размыкается первое реле, в результате чего на входе и, соответственно, на выходе усилителя появляется сигнал, который подается на вход осциллографа. Управляющее устройство (на схеме не показанное) через заданные промежутки времени размыкает контакты второго и третьего реле. Таким образом, коэффициент усиления усилителя по току возрастает тремя ступенями, что позволяет на одной осциллограмме наблюдать ток, изменяющийся в 10^3 раз. В качестве иллюстрации на рис. 3 показана полученная описанным выше способом осциллограмма потока нейтралов распадающейся

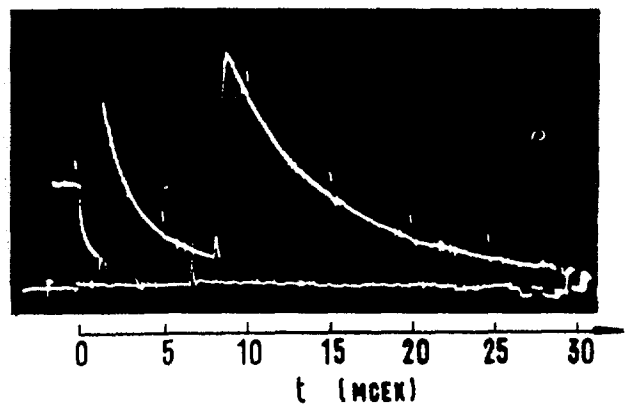

Рис. 3 Осциллограмма потока нейтралов из плазмы, распадающейся после быстрого выключения инжекции.

плазмы. Примерно через 1 мсек после выключения пучка практически все молекулярные ионы погибают на магнитном канале, и поток нейтралов становится пропорциональным концентрации ионов H_1^+, оставшихся к этому моменту в камере Огры.

В левой половине камеры установлены три зонда, измеряющие поток быстрых ионов в пристеночном слое. С помощью этих зондов исследовались искажения поверхности плазмы и вращение плазмы вокруг оси камеры.

В среднем сечении камеры расположен радиальный зонд, который можно вводить в плазму. Коллектор зонда закрыт двумя слоями алюминиевой фольги по 0,12 микрона каждый. Радиальным зондом изучались колебания плотности быстрых ионов на различных расстояниях от стенки камеры.

На торцовом фланце левой половины камеры установлен электростатический анализатор энергии ионов, образующихся в пространстве между магнитными пробками при ионизации остаточного газа быстрыми частицами и выходящих из плазмы вдоль магнитных силовых линий. Ионы, попадающие в анализатор, отклоняются на угол 90° и фокусируются в двух направлениях. В качестве детектора ионов в анализаторе используется электронный умножитель. Прибор позволяет получать спектры ионов в диапазоне от ~ 5 эв до 40 кэв при токе $\sim 10^{-12}$ а, проходящем через входную диафрагму размером 2×10 мм^2. Разрешающая способность анализатора, измеренная с помощью электронов из электронной пушки, равна 5%.

3. Потенциал плазмы. Вращение плазмы. Неустойчивость плазмы

Измерения, проведенные с помощью электростатического анализатора показали, что энергия вторичных ионов, выходящих через магнитные пробки вдоль оси камеры Огры, зависит от условий опытов и максимальное значение достигает нескольких десятков килоэлектронвольт.

На рисунках 4 и 5 приведены типичные результаты измерений с помощью электростатического анализатора. Графики изображают энергетический спектр вторичных ионов, полученный следующим образом: на пластины анализатора подается постоянное регулируемое напряжение и регистрируется ток электронного умножителя, который служит детектором ионов. Представленные на рисунках спектры можно интерпретировать двояко: либо как результат наличия в любой момент широкого набора энергий ионов, либо как усредненную во времени картину колебаний сравнительно узкого пика. Электростатический анализатор позволял, кроме того, получать спектр за времена порядка сотни микросекунд и повторять анализ через несколько миллисекунд. Для этого к

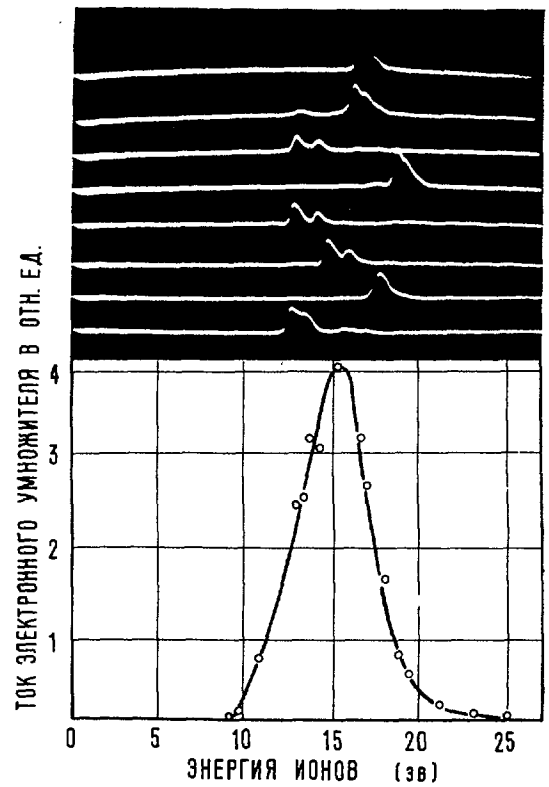

Рис. 4 Спектр ионов, выходящих через магнитные пробки вдоль оси камеры. Длительность развертки 400 мксек. Задержка между строчками растра 2,8 мсек. $I_{инж} = 0{,}5$ ма, $p = 5{,}5 \cdot 10^{-7}$ мм рт. ст., $I_{упр} = -1{,}5$ ка.

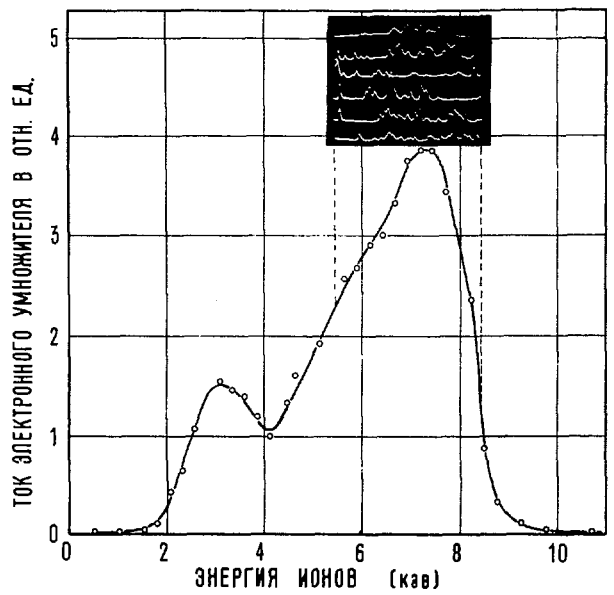

Рис. 5 Спектр ионов, выходящих через магнитные пробки вдоль оси камеры. Длительность развертки 400 мксек. Задержка между строчками растра 2,8 мсек. $I_{инж} = 100$ ма, $p = 3{,}7 \cdot 10^{-7}$ мм рт. ст., $I_{упр} = -0{,}15$ ка.

постоянному потенциалу, поданному на пластины (0 вольт на рис. 4 и 5,3 кв на рис. 5), добавлялась серия пилообразных импульсов с амплитудой, регулируемой от нескольких вольт до 2 кв. Управляющая схема одновременно с началом каждой пилы запускала развертку осциллографа и смещала луч по вертикали, чтобы различить последовательные во времени спектры. На вход вертикального усилителя подавался сигнал с электронного умножителя. Таким способом получены осциллограммы на рис. 4 и 5.

Сравнение графика и осциллограммы (рис. 4), зарегистрированных при малом токе инжекции, показывает, что спектр вторичных ионов довольно узок (относительная ширина не превышает 10%), но средняя энергия пика колеблется во времени.

Весьма вероятным кажется предположение, что плазма не полностью компенсирована и вторичные ионы ускоряются вне плазмы полем её пространственного заряда. Тогда энергия анализируемых ионов равна потенциалу относительно стенок камеры силовой трубки, входящей в анализатор.

Узкий спектр означает, что мала разность потенциалов вдоль трубки в области, где генерируются вторичные ионы. Колебания энергии ионов можно интерпретировать как изменение потенциала рассматриваемой трубки за счет изменения интегрального заряда и перемещения положения плазмы в Огре. В дальнейшем всюду предполагается, что средняя энергия спектра вторичных ионов равна среднему значению потенциала плазмы относительно стенок камеры.

Осциллограмма на рис. 5, снятая с тем же временем анализа (400 мксек), но при большем токе инжекции, отличается от осциллограммы на рис. 4 наличием нескольких пиков на каждой строке. Можно было бы предположить, что в данном случае зарегистрирован участок широкого энергетического распределения ионов, ток которых модулирован во времени на 100%. Для проверки этого предположения с помощью специального зонда (на рис. 1 не указан) были получены осциллограммы полного, т.е. не разрешенного по энергиям, потока вторичных ионов, выходящих из плазмы вдоль магнитного поля. На рис. 6 показана одна из таких осциллограмм, свидетельствующая, что за время, большее, чем время анализа, ток ни разу не падает до нуля. Таким образом, можно заключить, что и в данном случае спектр по-прежнему остается достаточно узким, но увеличение тока инжекции настолько увеличило частоту колебаний потенциала, что характерное время изменения последнего стало меньше, чем время анализа.

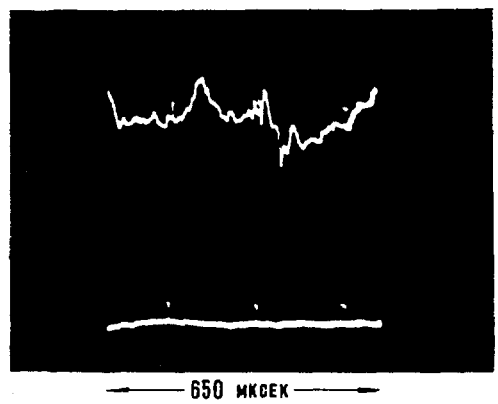

Рис. 6 Осциллограмма потока ионов, выходящих через магнитные пробки вдоль оси камеры. $I_{инж} = 100$ ма, $p = 5{,}5 \cdot 10^{-7}$ мм рт. ст., $I_{упр} = -0{,}15$ ка.

Поэтому потенциал успевает несколько раз «пересечься» с нарастающим напряжением на пластинах, и каждому «пересечению» соответствует импульс тока на детектирующей системе. Смысл усредненного во времени спектра, изображенного на графике под осциллограммой, остается тем же, что и в случае рис. 4. Для изучения детальной формы спектра вторичных ионов в режимах с большой частотой колебаний необходимо увеличить скорость анализа по крайней мере на порядок.

Потенциал плазмы возрастает с увеличением тока инжекции и уменьшением давления остаточного газа. На рис. 7 показана зависимость среднего значения энергии ионов (потенциала плазмы) от давления остаточного газа при трех значениях тока инжекции.

Если бы накапливающаяся в Огре плазма была спокойна, то потенциал плазмы, определяемый балансом рождения и потерь электронов и ионов, не превосходил бы нескольких электронных температур. Простые оценки скорости передачи энергии от быстрых ионов к электронам при парных соударениях показывают, что температура электронов в нашем случае не должна превышать 30—50 эв. Большая величина потенциала, обнару-

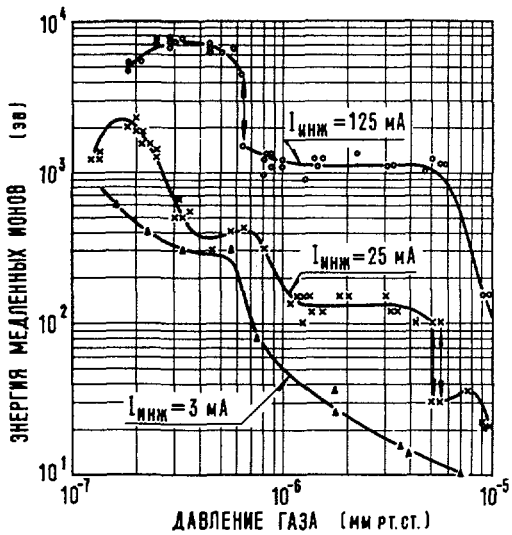

Рис. 7 Зависимость средней энергии вторичных ионов от давления газа в камере Огры. Давление газа изменялось напуском аргона. $I_{упр} = -1{,}8$ ка.

женная в экспериментах, говорит об увеличенных потерях электронов из плазмы. Имеется две возможности для ухода электронов — вдоль и поперек магнитного поля. В первом случае в плазме должны были бы происходить неизвестные нам процессы, приводящие к очень быстрому увеличению продольной кинетической энергии электронов. Во втором — существовать азимутальные электрические поля, создающие потоки электронов и ионов к периферии плазмы. В настоящее время у нас нет достаточных экспериментальных данных, чтобы доказать, какой из способов ухода электронов осуществляется, хотя, как будет видно из дальнейшего, имеются основания считать, что основную роль играет второй процесс.

Наличие положительного объемного заряда плазмы приводит к появлению радиального электрического поля, которое, в свою очередь, вызывает вращение плазмы вокруг продольной оси из-за дрейфа ионов в скрещенных магнитном и электрическом полях. Нетрудно сделать оценки, которые покажут, что скорость вращения плазмы вокруг оси камеры под действием радиального электрического поля при наблюдаемых на опыте потенциалах плазмы может более чем в 10 раз превышать скорость азимутального магнитного дрейфа ионов. Если потенциал плазмы на оси равен U, то, полагая, что скорость азимутального дрейфа дается обычным выражением cE/H, где E — среднее значение радиального электрического поля равное U/R (R — радиус плазмы), получим

$$f = \frac{c\,U}{\pi R^2 H} \qquad (3)$$

где f — число оборотов плазмы в секунду вокруг оси камеры. Если подставить численные значения $R=55$ см и $H=2800$ для Огры, то получим

$$f = 3{,}8\,U. \qquad (4)$$
герц вольт

Максимальный магнитный дрейф (см. рис. 2) обеспечивает скорость прецессии ионов вокруг оси системы, равную $8 \cdot 10^3$ оборотов в секунду. Такая же скорость электрического дрейфа должна получаться при потенциале 2,1 кэв.

Электрический дрейф, существенно влияя на траектории ионов, препятствует в исследованных режимах уменьшению длины пробега молекулярных ионов до гибели на корпусе магнитного канала при уменьшении величины магнитного дрейфа. На рис. 8 показана зависимость отношения плотности молекулярных ионов к току инжекции, которое мы будем именовать заполнением ловушки, от тока в «управляющей» обмотке при двух токах инжекции (2 и 30 ма) и прочих равных условиях. При малом токе инжекции уменьшение магнитного дрейфа приводит к уменьшению заполнения ловушки плазмой, так как молекулярным ионам необходимо совершить большее число колебаний между пробками, прежде чем их орбиты перестанут зацеплять корпус магнитного канала. При этом растет доля ионов, погибающих за первые пролеты между магнитными пробками. При токе 30 ма уменьшения заполнения при уменьшении магнитного дрейфа не происходит, так как в этом случае величина электрического дрейфа достаточно велика, чтобы независимо от магнитного дрейфа увести ионы из зацепления с каналом после первого отражения.

Ранее уже сообщалось [1], что в большинстве режимов работы установки сигналы всех детекторов, регистрирующих те или иные параметры плазмы, модулированы переменной составляющей, причем частота колебаний сигналов всех детекторов одинакова. С помощью двух детекторов нейтралов (на рис. 1 не указаны), коллимирован-

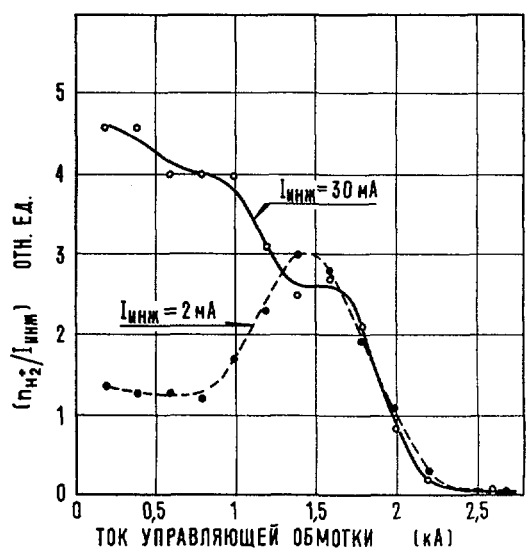

Рис. 8 Зависимость плотности молекулярных ионов, приведенной к току инжекции, от тока в управляющей обмотке при токах инжекции 2 ма и 30 ма. $p = (4-7) \cdot 10^{-7}$ мм рт. ст. Токи в «управляющих» и пробочных обмотках противоположны по направлению.

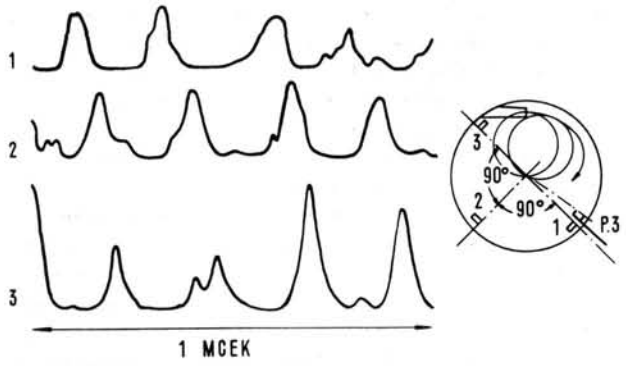

Рис. 9 Одновременно зафиксированные осциллограммы токов пристеночных зондов.

ных таким образом, что они видели по половине плазменного цилиндра, было установлено, что потоки нейтралов из двух полуцилиндров имеют переменные составляющие, колеблющиеся в противофазе. Это могло указывать на вращение плазменного цилиндра, форма которого азимутально несимметрична.

Для того, чтобы убедиться, что мы имеем дело с вращением плазмы, и измерить скорость её вращения, на стенке камеры были установлены три пристеночных зонда, упомянутых в п. 2.

На рис. 9 показаны одновременно зафиксированные осциллограммы токов всех трех зондов. Минимальный уровень сигнала каждого из зондов

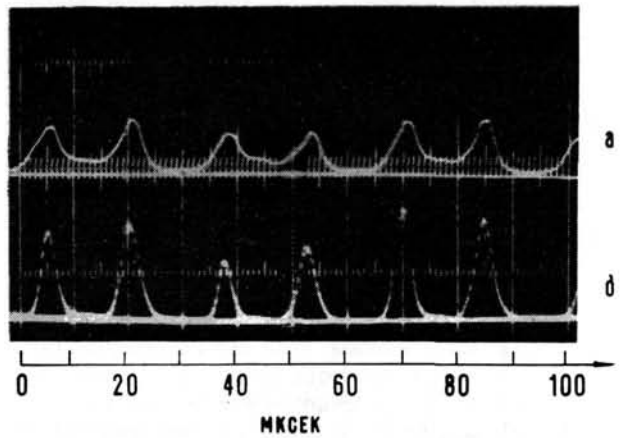

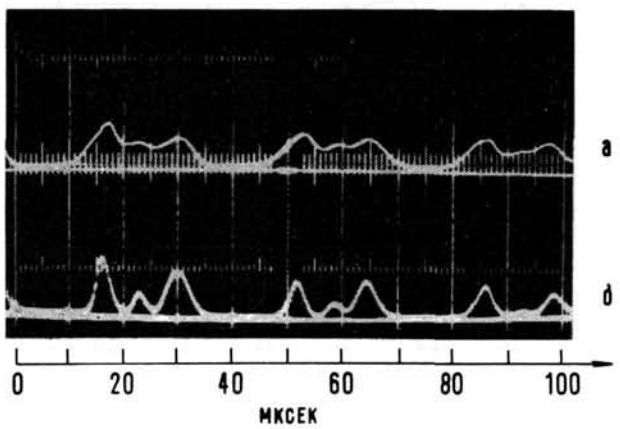

Рис. 10 Осциллограмма токов пристеночного зонда № 1 (ст. рис. 9) и радиального зонда. (а) — радиальный зонд, (б) — пристеночный зонд № 1.

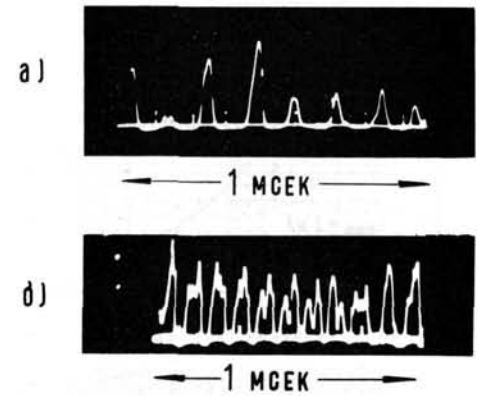

Рис. 11 Типичные осциллограммы потока быстрых ионов, регистрируемого пристеночными зондами (а) при первом моде искажения поверхности плазмы и (б) при искажении поверхности плазмы более высокими модами, наряду с первым модом.

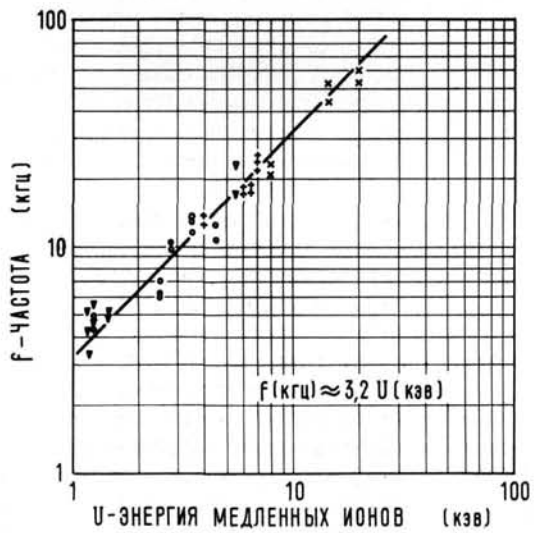

Рис. 12 Зависимость частоты колебания на пристеночных зондах, равной скорости вращения плазмы, от энергии медленных ионов (потенциала плазмы). $I_{упр} = -(0.2-1,5)$ ка. о — 25 ма, $(1,3-1,8)\cdot 10^{-7}$ мм рт. ст.; ∇ — 25 ма, $(0,8-1,0)\cdot 10^{-6}$ мм рт. ст.; х — 120 ма, $(1,9-3,3)\cdot 10^{-7}$ мм рт. ст.; + — 120 ма, $(0,8-1,3)\cdot 10^{-6}$ мм рт. ст.

соответствует нулю тока. Каждую из осциллограмм можно интерпретировать следующим образом. На поверхности плазмы имеется « язык » или несколько « языков », которые, вращаясь вместе с плазмой, по очереди проходят мимо пристеночных зондов, « состругиваясь » ими. Фазировка сигналов, показанная на рис. 9, соответствует первому моду возмущения поверхности, т.е. такому возмущению, когда плазменный столб представляет собой эксцентрик, вращающийся вокруг оси камеры. С помощью радиального зонда

и первого пристеночного зонда, расположенных примерно на одном азимуте на расстоянии примерно 3 м один от другого, показано, что во всех случаях «языки» на поверхности плазмы вытянуты в продольном направлении (рис. 10).

Во многих случаях по виду осциллограмм можно заключить, что наряду с первым модом возмущения поверхности имеют место и более высокие моды возмущения. Примеры таких осциллограмм показаны на рис. 11. По мере увеличения инжектируемого тока первый мод возмущения появляется всегда раньше, чем второй, третий и т.д., однако, подробно этот вопрос нами не исследовался.

В одной из серий экспериментов было зафиксировано большое количество осциллограмм колебаний токов пристеночных зондов при различных токах инжекции, давлениях остаточного газа, различных токах в управляющей обмотке. Из полученного набора данных удалось установить, что при инжектируемом токе, большем 20 ма, частота колебаний связана с потенциалом плазмы линейной зависимостью. Эта зависимость приведена на рис. 12, где на оси абсцисс отложен потенциал плазмы, а по оси ординат частота колебаний, характеризующая скорость вращения плазмы.

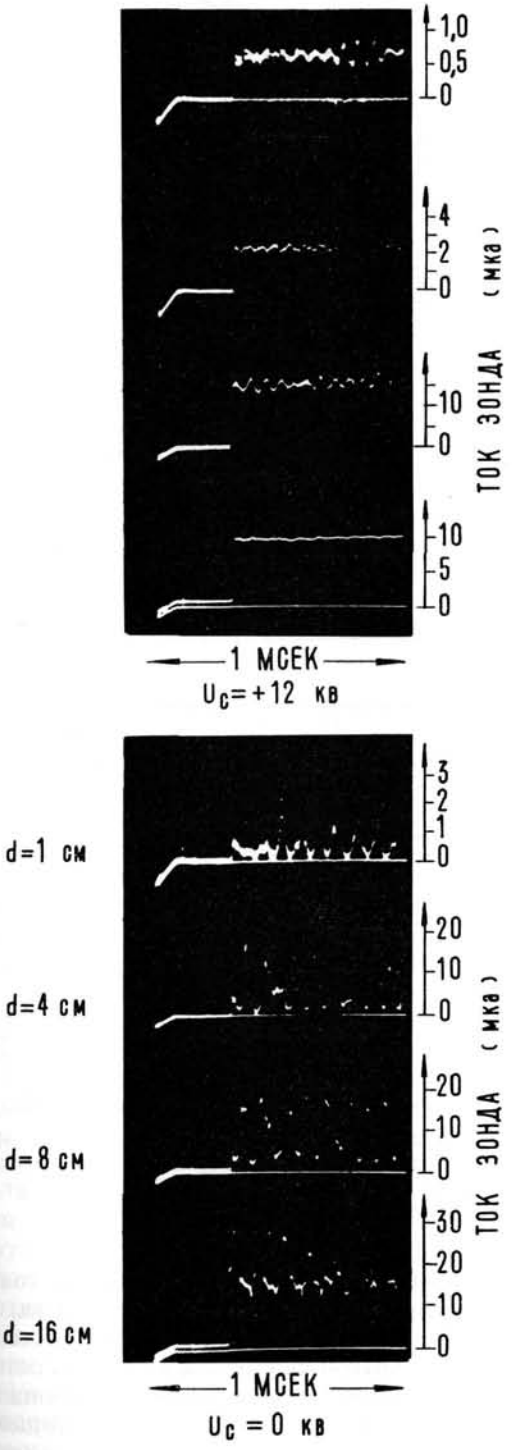

Рис. 13 Осциллограммы потока быстрых ионов на радиальный зонд. d — расстояние от стенки камеры, U_c — потенциал торцовых электродов. $I_{инж} = 20$ ма, $I_{упр} = -1{,}5$ ка, $p = 2 \cdot 10^{-7}$ мм. рт. ст.

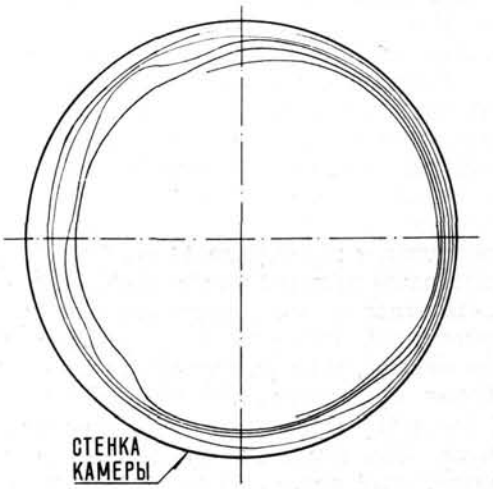

Рис. 14 Поверхность плазмы (линии равной плотности), построенная по осциллограммам, полученным с помощью радиального зонда. (Часть осциллограмм показана в левой колонке на рис. 12.)

Прямая, проведенная на том же графике, хорошо совпадает с рассчитанной по формуле (4) зависимостью частоты от потенциала, отличаясь от нее на 16 %. Поэтому можно считать, что возмущение перемещается по поверхности плазмы со скоростью дрейфа заряженных частиц в скрещенных электрическом и магнитном полях. Это означает, что быстрые ионы, скорость дрейфа которых имеет аддитивную добавку, равную скорости магнитного дрейфа, во время своего движения вокруг оси ловушки обгоняют вращение формы плазмы.

В левой колонке рис. 13 приведена часть серии осциллограмм потока молекулярных ионов, измеряемого радиальным зондом при постепенном его погружении в плазму. Зонд вводился на такую глубину, на которой еще не чувствовалось его воздействие на столб плазмы в целом, т.е. не изменялся поток нейтралов на детекторы нейтралов, сохранялся постоянным потенциал плазмы и не изменялась частота колебаний. По полному

набору этих осциллограмм сделана попытка построить линии одинаковой плотности плазмы. Полученная диаграмма показана на рис. 14.

Совокупность полученных результатов свидетельствует о том, что плазма, образующаяся в Огре, неустойчива относительно образования « языков ». Наиболее правдоподобное предположение сводится к тому, что неустойчивость возникает из-за разделения ионов и электронов при магнитном дрейфе [2].

4. Стабилизация неустойчивости внешними электродами

Вне объема, занятого быстрыми ионами, были установлены два электрода, изготовленные из сетки с размером ячейки 1 мм^2 (рис. 1). Размер электродов выбирался из условия, чтобы весь поток магнитного поля, пронизывающий плазму в среднем сечении ловушки, проходил через электроды. Нами исследовалось влияние подаваемого на электроды потенциала на поведение плазмы. Было обнаружено, что положительный потенциал в несколько киловольт на одном из электродов или на двух сразу стабилизировал плазму. В правой колонке на рис. 13 показаны осциллограммы, аналогичные осциллограммам слева, но полученные при поданном на один из электродов положительном потенциале 12 кв. Сопоставление осциллограмм из левой и правой колонок показывает, что относительная амплитуда колебаний при положительном потенциале на электроде значительно меньше, и на расстоянии 16 см от стенки колебания практически отсутствуют. Это означает, что деформация поверхности плазмы ликвидируется, или, иначе говоря, это означает, что положительный потенциал на торцовых электродах стабилизирует плазму относительно образования « языков ».

Стабилизация поверхности плазмы сопровождается уменьшением потока быстрых ионов на поверхность камеры. На рис. 15 показана зависимость суммарного тока трех пристеночных зондов

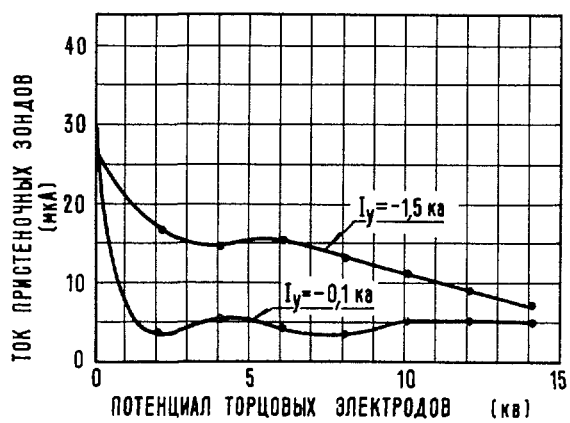

Рис. 15 Зависимость суммы токов на три пристеночных зонда от потенциала торцовых электродов. I_y — ток «управляющей» обмотки. $I_{инж} = 120$ ма, $p = 1{,}3 \cdot 10^{-7}$ мм рт. ст.

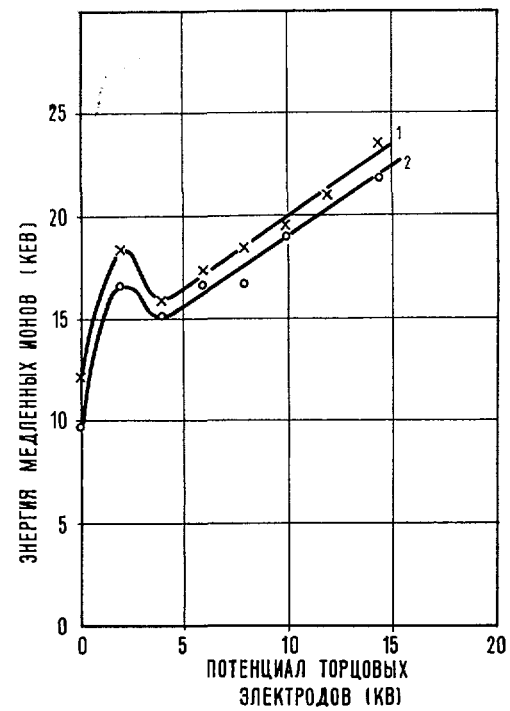

Рис. 16 Зависимость энергии медленных ионов (потенциала плазмы) от потенциала торцовых электродов при $I_{инж} = 120$ ма, $p = 1 \cdot 10^{-7}$ мм рт. ст., $I_{упр} = -1{,}5$ ка (кривая 1) и $I_{упр} = -0{,}1$ ка (кривая 2).

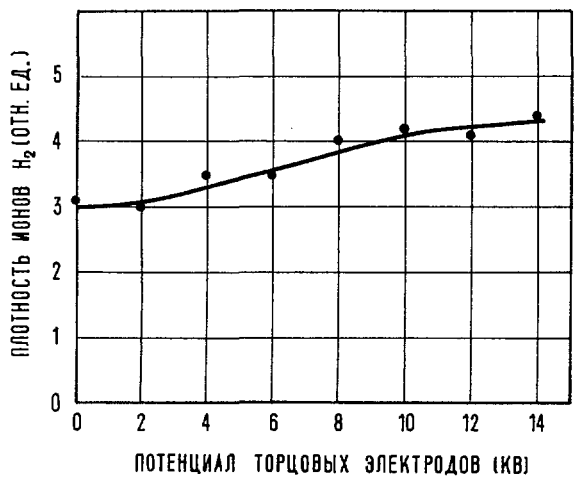

Рис. 17 Зависимость плотности быстрых ионов H_2^+ в относительных единицах от потенциала торцовых электродов. $I_{инж} = 120$ ма, $p = (1{,}2 - 1{,}5) \cdot 10^{-7}$ мм рт. ст., $I_{упр} = -1{,}5$ ка.

от потенциала торцовых электродов при токах в « управляющих » обмотках $-0{,}1$ и $-1{,}5$ ка.

Несмотря на стабилизацию неустойчивости, увеличенные потери электронов из плазмы остаются. Это следует из того, что разность потенциалов между плазмой и положительным торцовым электродом при токах инжекции около ста миллиампер не падает ниже нескольких киловольт (рис. 16). Возрастание потенциала плазмы вместе с увеличением напряжения на торцовых электродах

означает увеличение положительного объемного заряда. Измерения плотности электронов и интенсивностей электромагнитных излучений электронов, проведенные В. Т. Карпухиным, А. Н. Кархо-вым и В. И. Пистуновичем показали, что при подаче положительного потенциала на торцовые электроды плотность электронов падает, что находится в соответствии с кривой, приведенной на рис. 16.

Плотность молекулярных ионов, определяемая по величине потока быстрых нейтралов на детекторы нейтралов, мало зависит от напряжения на электродах (рис. 17).

5. Потери быстрых атомарных ионов

Влияние того или иного вида неустойчивости на накопление плазмы в ловушке определяется интенсивностью потерь быстрых ионов, которая вызывается данной неустойчивостью. Поскольку нас интересуют свойства образующейся в Огре плазмы в стационарном режиме, нам необходимо знать эти потери также в стационарном режиме. Концентрации молекулярных и атомарных ионов приближенно даются выражениями

$$n(H_2^+) = \frac{I}{\Omega\left[\frac{1}{\tau_п} + \frac{1}{\tau(H_2^+)}\right]} \qquad (5)$$

$$n(H_1^+) = \frac{n(H_2^+)}{\tau_д\left[\frac{1}{\tau'_п} + \frac{1}{\tau(H_1^+)}\right]} \qquad (6)$$

где I — ток инжекции, Ω — объем плазмы, $\tau_п$, $\tau_п'$ — время жизни ионов H_2^+ и H_1^+, которое было бы при потерях ионов из ловушки под воздействием только неустойчивости, $\tau(H_2^+)$, $\tau(H_1^+)$ — время жизни ионов H_2^+ и H_1^+ в устойчивой плазме и $\tau_д$ — время жизни ионов H_2^+ до их диссоциации. Следует ожидать, что дополнительные потери будут гораздо сильнее влиять на концентрацию атомарных ионов, чем на концентрацию молекулярных, так как время жизни $\tau(H_2^+)$, определяемое гибелью на корпусе магнитного канала, гораздо меньше, чем $\tau(H_1^+)$ — время жизни ионов H_1^+, обусловленное перезарядкой. По изменению концентрации ионов H_2^+ при переходе от одного режима ловушки к другому нельзя судить об изменении интенсивности потерь из-за неустойчивости, так как изменение $n(H_2^+)$ может быть вызвано изменением длины пробега до гибели на канале, которая зависит от скорости азимутального дрейфа. Наилучшей характеристикой потерь, вызываемых неустойчивостью, было бы отношение $n(H_1^+)/n(H_2^+)$ в стационарном режиме. К сожалению, мы не имеем возможности проводить измерения $n(H_1^+)$ или отношения $n(H_1^+)/n(H_2^+)$ в стационарном режиме, так как детекторы нейтралов не позволяют разделить нейтралы, родившиеся от ионов H_2^+ и от ионов H_1^+. Единственное, что мы можем делать, это изучать осциллограммы потока нейтралов из плазмы, распадающейся после быстрого выключения инжекции, и по ним судить о концентрации ионов H_1^+ и H_2^+ до момента выключения инжекции. В ранее проведенных измерениях [3] было установлено, что компонента потока нейтралов, связанная с молекулярными ионами, распадается с постоянной времени ~ 300 мксек. Поэтому через 1,5—2 мсек после прекращения инжекции компонента потока нейтралов, образующихся при диссоциации и перезарядке ионов H_2^+, падает приблизительно в 500 раз и измеряемый в это время и позже поток нейтралов определяется только перезарядкой атомарных ионов.

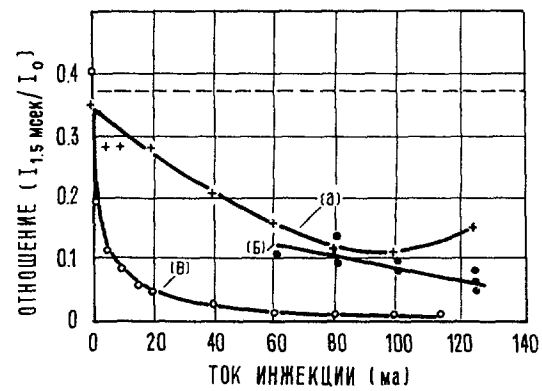

Рис. 18 Зависимость отношения токов на детекторы нейтралов через 1,5 мсек после обрыва инжекции к току на детектор до выключения пучка от величины инжектируемого тока. Пунктиром указан приблизительный уровень отношения токов при отсутствии негазовых потерь ионов. $p = (0{,}8 - 1{,}2) \cdot 10^{-7}$ мм рт. ст. (а) $I_у = -0{,}1$ ка, $U_с = +12$ кв; (б) $I_у = -1{,}5$ ка, $U_с = +12$ кв; (в) $I_у = -1{,}5$ ка, $U_с = 0$.

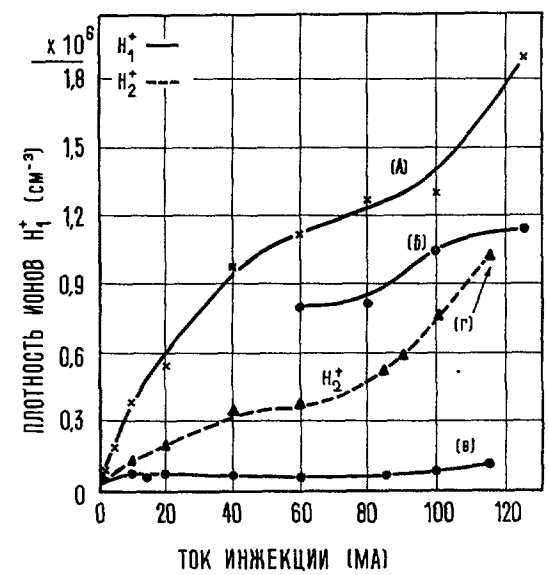

Рис. 19 Зависимость плотности ионов H_1^+, измеренной через 1,5 мсек после выключения пучка, от тока инжекции при потенциале $\div 12$ кв на торцовых электродах и заземленных электродах. Пунктиром показана плотность молекулярных ионов в относительных единицах $p' = (0{,}8 - 1{,}2) \cdot 10^{-7}$ мм рт. ст. (А) H_1^+, $I_у = -0{,}1$ ка, $U_с = 12$ кв; (Б) H_1^+, $I_у = -1{,}5$ ка, $U_с = 12$ кв; (В) H_1^+, $I_у = -1{,}5$ ка, $U_с = 0$; (Г) $n_{H_2^+} \approx (0{,}5 - 1{,}0) \cdot 10^7$ $см^{-3}$.

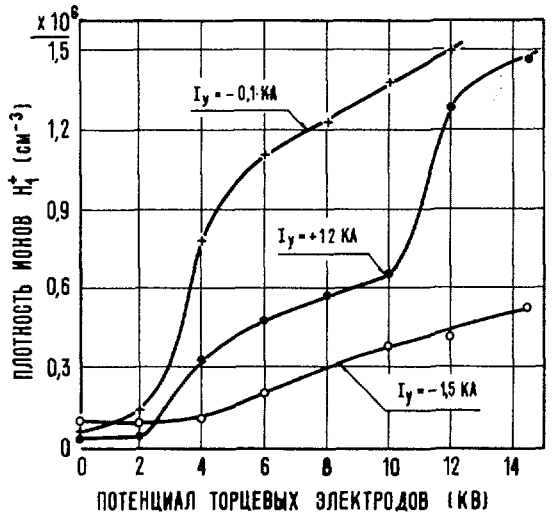

Рис. 20 Зависимость плотности ионов H_1^+, измеренной через 1,5 мсек после выключения инжекции, от потенциала торцовых электродов. $I_{инж} = 120$ ма, $p = (1 - 1{,}5) \cdot 10^{-7}$ мм рт. ст.

На рис. 18 показано как изменяется отношение тока, измеряемого детекторами нейтралов через 1,5 мсек после выключения пучка к току, измеряемому до выключения пучка, при изменении тока инжекции. Видно, что при заземленных торцовых электродах отношение падает примерно в 40 раз при переходе от тока инжекции 0,5 ма к току 115 ма. При потенциале +12 кв на обоих торцовых электродах концентрация протонов на порядок возрастает, но все же при токе инжекции 100 ма отношение в 3 раза меньше, чем при малом токе инжекции. На рис. 19 показано, как изменяется измеренная через 1,5 мсек после выключения инжекции концентрация атомарных ионов при увеличении тока инжекции. При заземленных электродах концентрация атомарных ионов достигает $7 \cdot 10^4$ см$^{-3}$ при инжектируемом токе 10 ма и при дальнейшем увеличении тока в 10 раз остается практически постоянной. При потенциале + 12 кв концентрация атомарных ионов с увеличением тока инжекции возрастает во всем интервале изменения тока инжекции, но возрастание плотности происходит медленнее увеличения тока вводимого пучка. На этом же графике в относительных единицах показана зависимость плотности молекулярных ионов от инжектируемого тока при заземленных сетках. Оценка абсолютной величины плотности молекулярных ионов, указанная на рис. 19, зависит от компонентного состава остаточного газа, поскольку им определяется эффективность диссоциации и перезарядки молекулярных ионов и, следовательно, интенсивность потока нейтралов, по которому вычисляется концентрация молекулярных ионов. Для вычисления абсолютной величины плотности атомарных ионов знание компонентного состава газа не нужно, так как эффективность перезарядки определяется по постоянной распада плотности атомарных ионов

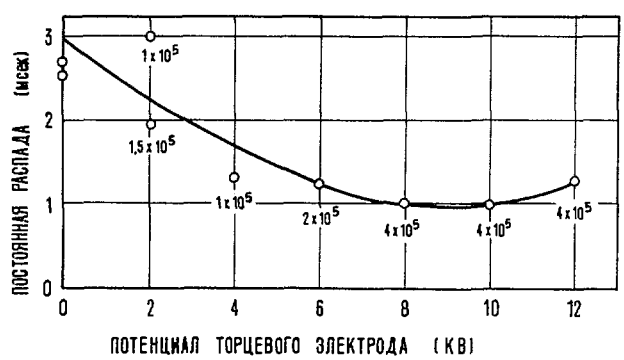

Рис. 21 Зависимость времени жизни плотности ионов H_1^+ через 1,5 мсек после выключения инжекции от потенциала торцовых электродов. $I_{инж} = 120$ ма, $p = (1 - 1{,}5) \cdot 10^{-7}$ мм рт. ст., $I_{упр} = -1{,}5$ ка. Цифры около точек означают плотности атомарных ионов.

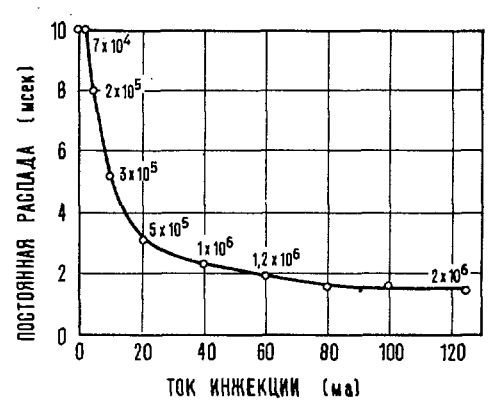

Рис. 22 Зависимость постоянной распада плотности ионов H_1^+ через 1,5 мсек после выключения пучка от тока инжекции при потенциале + 12 кв на торцовых электродах. $p = (0{,}8 - 1{,}2) \cdot 10^{-7}$ мм рт. ст.; $I_{упр} = -0{,}1$ ка. Цифры около точек означают плотности атомарных ионов.

через пятнадцать — двадцать миллисекунд после обрыва инжекции, когда перестают действовать коллективные взаимодействия, приводящие к дополнительным потерям.

На рис. 20 приведены графики, показывающие, как изменяется концентрация ионов H_1^+ при увеличении потенциала торцовых электродов и неизменном токе инжекции равном 120 ма.

На рис. 21 и 22 показано, как зависит от потенциала торцовых электродов и от тока вводимого пучка время жизни атомарных ионов через 1,5 мсек после выключения пучка. Обращает на себя внимание следующее обстоятельство. При увеличении потенциала на электродах время жизни падает. Имеет место кажущееся противоречие: плотность атомарных ионов растет, что свидетельствует об увеличении времени жизни ионов, а фактически измеряемое время жизни атомарных ионов через 1,5 мсек после выключения инжекции уменьшается. Повидимому, это связано с тем, что обрыв инжекции вызывает какой-то механизм дополнительных потерь ионов, усиливающийся по мере увеличения концентрации ионов.

Не исключено, что быстрое выключение инжекции (время обрыва пучка ~ 15 мксек), сопровождающееся прохождением по всему объему ловушки заднего фронта оборванного пучка, приводит к заметному возмущению плазмы и, соответственно, потерям ионов. Специально этот вопрос нами не изучался.

Из сказанного ясно, что мы, не обладая возможностью выделять из потока нейтралов компоненту, связанную с перезарядкой ионов H_1^+, не можем измерять время жизни атомарных ионов в стационарном режиме, изучая процесс распада плазмы после быстрого выключения инжекции.

6. Заключение

Общие выводы настоящей работы можно сформулировать следующим образом: (1) Показано, что в магнитном поле Огры с положительной кривизной магнитных силовых линий плазма с плотностью быстрых ионов 10^6-10^7 см$^{-3}$, образующаяся при инжекции ионного пучка, неустойчива относительно образования «языков». (2) Имеют место значительные потери электронов, образующихся в плазме при ионизации остаточного газа, что приводит к появлению большого положительного объемного заряда. (3) С помощью внешних электродов удается стабилизировать плазму. (4) В стабилизированной электродами плазме время жизни атомарных ионов на порядок больше, чем в нестабилизированной плазме.

Объем экспериментального материала недостаточен для того, чтобы можно было остановиться на каком-либо определенном механизме стабилизации плазмы. Наиболее простая возможность состоит в том, что при наличии вне плазмы положительного электрода из наружного слоя плазменного цилиндра уходят практически все электроны и отсутствуют условия для образования поляризованных «языков». На другую возможность объяснения стабилизации указал Б. Б. Кадомцев. Из проведенных им расчетов [4] следует, что вычисленная им в [5] критическая плотность, ниже которой плазма устойчива, зависит не только от температуры ионов, размера плазмы и радиуса кривизны магнитных силовых линий, но зависит еще и от отношения концентраций электронов и ионов, причем критическая плотность возрастает с уменьшением отношения. Не исключено, что этот эффект имеет место в нашем случае, так как в стабилизированной плазме плотность электронов ниже, чем в нестабилизированной. Имеется и третья возможность для объяснения стабилизации. Если при включенных электродах в наружном слое плазмы возникнет увеличенный объемный заряд, то перераспределение электрического поля может привести к тому, что угловая скорость дрейфа электронов превысит угловую скорость дрейфа ионов. Ввиду того, что диаметры их ларморовских окружностей различаются на несколько порядков, это создаст условия, затрудняющие развитие языков.

Неустойчивость такого типа обнаружена ранее М. С. Иоффе с сотрудниками [6], в магнитной ловушке с магнетронным ускорением ионов при значительно больших плотностях плазмы и другом распределении ионов по энергиям. Возможно, что механизмы развития неустойчивости в обоих случаях имеют существенные различия, несмотря на аналогичность внешних признаков, характеризующих неустойчивость.

Авторы пользуются возможностью выразить благодарность К. З. Тушабрамишвили, Ю. М. Пустовойту и А. В. Честному, операторам В. Ф. Богданову и М. В. Никифорову и всему обслуживающему персоналу, обеспечивающему бесперебойную работу установки. Плодотворные обсуждения опытов с Б. Б. Кадомцевым, Е. П. Велиховым и коллективом физиков, работающих на Огре, помогли выяснению физической природы явлений.

Литература.

[1] Головин И. Н., Артеменков Л. И., Богданов Г. Ф., Панов Д. А., Пистунович В. И., Семашко Н. Н., *УФН*, **73** (1961) 685.
[2] Rosenbluth, M. N., Longmire, C. L., *Ann. Phys. (N. Y.)* **1** (1957) 120.
[3] Bogdanov, G. F., Panov, D. A., Semashko, N. N., *J. Nucl. Energy* C **3** (1961) 106.
[4] Кадомцев Б. Б. В печати.
[5] Кадомцев Б. Б. *ЖЭТФ*, **40** (1961) 328.
[6] Иоффе М., Соболев Р., Тельковский В., Юшманов, Е. *ЖЭТФ* **39** (1960) 1602; **40** (1961) 40.

ЦИКЛОТРОННОЕ И ТЕПЛОВОЕ ИЗЛУЧЕНИЯ ПЛАЗМЫ В ОГРЕ*

А. Е. БАЖАНОВА, В. Т. КАРПУХИИ, А. Н. КАРХОВ, В. И. ПИСТУНОВИЧ

ИНСТИТУТ АТОМНОЙ ЭНЕРГИИ ИМ. И. В. КУРЧАТОВА

АКАДЕМИИ НАУК СССР, МОСКВА, СССР

Исследовалось излучение быстрых ионов, движущихся в магнитном поле Огры в условиях « вакуума » (плотность электронов $n_e \lesssim 10^7$ см$^{-3}$) и при наличии холодной плазмы ($n_e \gtrsim 10^8$ см$^{-3}$). Приводятся результаты измерений резонансных пиков напряженности электрического поля на циклотронных частотах ионов H_2^+ и H^+ и их обертонах. При плотности электронов $n_e \approx 10^7$ см$^{-3}$ наблюдаются два пика, которые соответствуют основным циклотронным частотам ионов H_2^+ и H^+. По мере увеличения плотности электронов появляются резонансные пики напряженности электрического поля на частотах, кратных циклотронным частотам ионов H_2^+ и H^+. С целью возможного качественного объяснения наблюдаемого эффекта была решена задача об излучении ионов, движущихся по спирали в холодной плазме. Результаты вычислений находятся в качественном согласии со смещением максимума наблюдаемых резонансных пиков напряженности электрического поля.

Измерялось излучение электронов в диапазоне длин волн $\lambda = 3{,}07$-4 см. Интенсивность излучения максимальна на электронной циклотронной частоте ($\lambda_B \approx 3{,}7$ см). Получена зависимость циклотронного излучения электронов ($\lambda = 3{,}68$ см) и теплового излучения ($\lambda = 3{,}1$ см) от давления остаточных газов в камере. Измерения показали, что происходит накопление излучения в камере Огры.

Приводится относительное изменение температуры электронов от давления.

1. Электрическое поле на циклотронной частоте ионов H_2^+ и H_1^+ и на обертонах

При движении в магнитном поле заряженная частица излучает энергию на циклотронной частоте и на обертонах. Если точка наблюдения расположена от излучающей частицы на расстоянии, малом по сравнению с длиной излучаемой волны ($r < \lambda$), то обычно говорят об электромагнитном поле движущегося заряда. Такой случай реализуется на Огре. Быстрые ионы водорода H_2^+ и H_1^+, движущиеся в магнитном поле Огры, создают электромагнитное поле на циклотронной частоте и на обертонах. Так как скорости ионов малы по сравнению со скоростью света ($v \ll c$) (энергия ионов H_2^+ менялась от опыта к опыту в пределах от 100 до 160 кэв), то, с одной стороны можно осуществить такие режимы, когда электрическое поле наблюдается только на циклотронных частотах f_1 и f_2 соответственно ионов H_2^+ и H_1^+. С другой стороны, возможны режимы, в которых присутствует электрическое поле на обертонах. Причем величина поля на обертонах, как будет видно ниже, может в несколько раз превосходить поле на циклотронной частоте. Эти два случая существенно отличаются друг от друга в постановке задачи и в способах их осуществления. В первом случае целью эксперимента является изучение зависимости величины электрического поля от плотности быстрых частиц в объеме. Во втором случае имеем задачу о поле, которое создают отдельные частицы (быстрые ионы H_2^+ и H_1^+) при движении в холодной плазме, находящейся в магнитном поле, и исследуется зависимость электрического поля от плотности холодной плазмы.

Первый режим достигается при наилучших вакуумных условиях ($p \leqslant 10^{-7}$ мм.рт.ст.), во втором — в камеру Огры специально напускается газ (например, аргон) до давления $p \lesssim 10^{-5}$ мм.рт.ст.

Сначала рассмотрим результаты измерений спектрального распределения электрического поля, создаваемого быстрыми ионами водорода при движении в холодной плазме.

Измерения электрического поля проводились с помощью анализатора спектра [1], который мог регистрировать сигналы величиной от 4 мкв. до нескольких сот милливольт в диапазоне частот от 1 до 18 Мгц. Сигнал принимался штыревой антенной, находившейся внутри камеры Огры на расстоянии одного метра от торцевого фланца.

При малом инжектируемом токе молекулярных ионов H_2^+ ($I_{инж} = 15$ ма) и давлении остаточных газов $P = 2.10^{-7}$ мм.рт.ст., т.е. когда плотность электронов в камере $n_e \lesssim 10^7$ см$^{-3}$ (плотность холодной плазмы), наблюдаются два резонансных пика напряженности электрического поля (рис. 1). Первый пик ($f_1 = 1{,}7$ Мгц) соответствует циклотронной частоте ионов H_2^+ в магнитном поле $H_0 = 2100$ эрст. Второй пик приходится на циклотронную частоту ионов H_1^+ ($f_2 = 3{,}4$ мгц). Магнитное поле, вычисленное по наблюдаемым частотам, с точностью до ошибок измерений соответствует основному полю Огры. При изменении магнитного поля происходит сдвиг наблюдаемых пиков в соответствии с формулой $f = eH/(2\pi Mc)$. Спектр качественно меняется, если увеличить давление газов в камере. Например, при давлении аргона $p = 2.10^{-6}$ мм.рт.ст. на осциллограмме отчетливо видны шесть пиков (рис. 2). Плотность электронов, измеренная интерферометром, работавшим на длине волны $\lambda = 10$ см (смотри [2]), в средней части ловушки составляет в этом режиме $n_e \approx 4.10^8$ см$^{-3}$. Максимальное число пиков, которое удавалось наблюдать, равно девяти. На рис. 3 показан пример

* Доклад СИ-10/212 представленный на Конференцию. Докладчик: В. И. Пистунович. Дискуссия (на английском языке) по этому докладу дана на стр. 353. Переводы аннотаций находятся в конце этого тома Трудов Конференции.

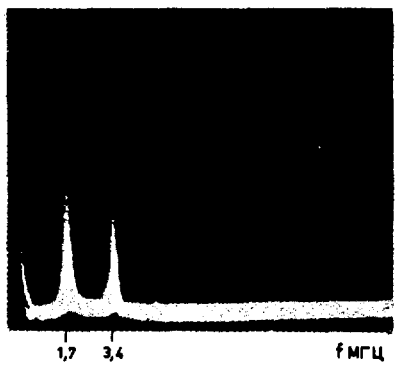

Рис. 1 Спектр электрического поля ионов H_2^+ и H_1^+ при плотности электронов $n_e \approx 10^7$ см$^{-3}$, $\varepsilon = 100$ кэв, $I_{инж} = 15$ ма.

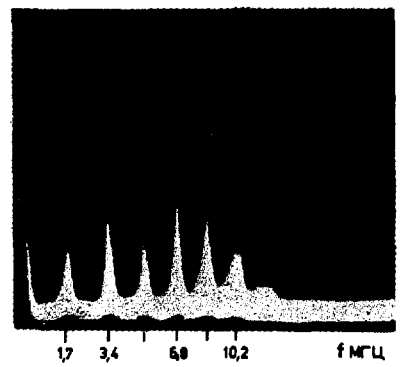

Рис. 2 Спектр электрического поля. $n_e \approx 4 \cdot 10^8$см$^{-3}$, $\varepsilon = 100$ кэв, $I_{инж} = 15$ ма.

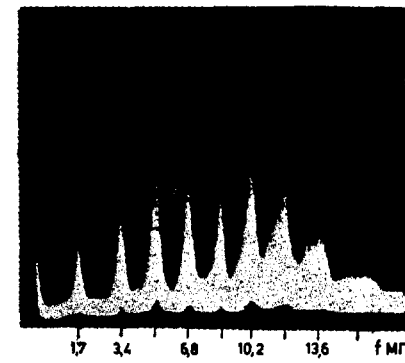

Рис. 3 Спектр электрического поля. $n_e \approx 2 \cdot 10^9$ см$^{-3}$, $\varepsilon = 100$ кэв, $I_{инж} = 15$ ма.

спектра, когда появляется девятый пик (давление аргона $p = 10^{-5}$ мм.рт.ст., $n_e \approx 2.10^9$ см$^{-3}$). Чтобы выяснить вопрос о том, при каких плотностях электронов (плотностях холодной плазмы) появляются обертоны основных частот и как величина электрического поля на обертонах изменяется с увеличением плотности электронов, для разных режимов были построены зависимости напряженности электрического поля на циклотронной частоте ионов H_2^+ и на обертонах от давления газов в камере. Для инжектируемого тока $I_{инж} = 5$ ма такая зависимость приведена на рис. 4; $I_{упр} = -1{,}8$ ка (о влиянии тока управляющей обмотки $I_{упр}$ на азимутальный дрейф быстрых частиц смотри [3]). Ниже шкалы давлений на рис. 4 даны значения плотности электронов. Видно, как при увеличении плотности электронов возрастает напряженность электрического поля на обертонах. При плотности электронов $n_e \approx 4.10^8$ см$^{-3}$ максимальное значение напряженности электрического поля приходится на частоту $f_4 = 4f_1$ ($f_1 = eH/(4\pi Mc)$, где M — масса протона).

При инжектированном токе более 10 ма была получена плотность электронов $n_e \approx 10^9$ см$^{-3}$, при которой максимальная напряженность электрического поля приходится на частоту $f = (5/6)\, f_1$. Напряженность электрического поля, суммарная по всем частотам, возрастает по мере увеличения плотности электронов. Таким образом, из измерений следует, что нерелятивистские ионы ($v \ll c$) могут создавать электрическое поле на обертонах, если они движутся в холодной плазме с показателем преломления $N(\omega) > 1$. Спектральное распределение электрического поля при постоянной скорости ионов зависит от плотности холодной плазмы, т.е. от величины показателя преломления $N(\omega)$.

Так как измерения производились не в волновой зоне, для объяснения эффекта необходимо рассчитать средний квадрат напряженности квазистационарной части флюктуационного электрического поля с учетом граничных условий. В качестве первого шага естественно решить более простую задачу определения интенсивности излучения. Такая задача с приближенным выражением для показателя преломления холодной плазмы, справедливым при плотностях $n_0 > 5.10^8$ см$^{-3}$, была решена в работе [4]. Результаты вычислений качественно подтверждают наблюдаемые эффекты, т.е. интенсивность излучения ионов растет с увеличением плотности холодной плазмы. Характер распределения интенсивности излучения по обертонам существенно зависит от величины показателя преломления холодной плазмы $N(\omega)$ и, следовательно, от фазовой скорости волны $v_ф = c/N(\omega)$. По мере приближения фазовой скорости волны к скорости иона максимум интенсивности смещается с циклотронной частоты на все более высокие обертоны $\omega = m\omega_н$.

Как уже отмечалось выше, другая постановка задачи заключается в изучении спектра электрического поля при отсутствии холодной плазмы ($n_e \lesssim 10^7$ см$^{-3}$), когда наблюдаются в основном два

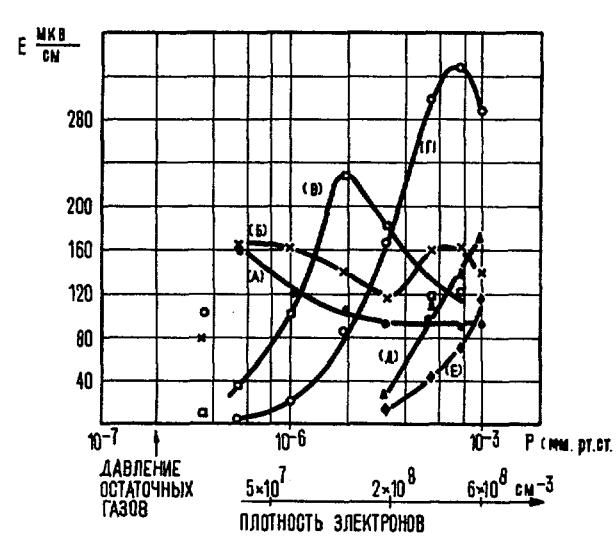

Рис. 4 Зависимость напряженности электрического поля на циклотронной частоте ионов $H_2^+(f_1)$ и H_1^+ ($f_2 = 2f_1$) и ее обертонах от давления аргона. $\varepsilon = 100$ кэв, $I_{инж} = 5$ ма, $I_{упр} = -1{,}8$ ка. Обозначения: (а) частота f_1, (б) частота $f_2 = 2f_1$, (в) частота $f_3 = 3f_1$, (г) частота $f_4 = 4f_1$, (д) частота $f_5 = 5f_1$, (е) частота $f_6 = 6f_1$.

резонансных пика. Из общих соображений следует (смотри, например [5]), что интенсивность некогерентного излучения пропорциональна плотности излучающих частиц N, а электрическое поле, следовательно, пропорционально $N^{1/2}$. В случае когерентного излучения интенсивность пропорциональна N^2, а поле — N. Поэтому естественно было ожидать, что измеряя величину электрического поля (при отсутствии обертонов) на циклотронной частоте ионов H_2^+ и H_1^+ (f_1 и f_2), можно получить сведения об общем числе быстрых ионов H_2^+ и H_1^+ в ловушке. С этой целью были поставлены опыты в тех режимах ($p \gtrsim 10^{-7}$ мм.рт.ст.), которые наиболее интересны с точки зрения поведения горячей плазмы в магнитном поле Огры. Электрическое поле на циклотронной частоте принималось штыревой антенной, ориентированной по радиусу в центральной части Огры на уровне стенок камеры. Одновременно регистрировался сигнал с детектора нейтралов (смотри [3]), величина которого, будучи приведена к единице давления, равна с некоторым коэффициентом $\varkappa$ плотности N быстрых ионов H_2^+. Коэффициент пропорциональности в зависимости от условий опыта мог меняться до полутора раз. Зависимость электрического поля на частоте f_1 от плотности быстрых ионов H_2^+ (N — в относительных единицах) показана на рис. 5. Множество приведенных экспериментальных точек есть результат большого числа измерений, сделанных в разное время при несколько отличных давлениях остаточных газов. Давление остаточных газов менялось в пределах от $0{,}7 \cdot 10^{-7}$ до $3{,}2 \cdot 10^{-7}$ мм.рт.ст. в зависимости от величины инжектируемого тока молекулярных ионов H^+_2 ($I_{инж}$ от 0,5 до 120 ма, $\varepsilon = 160$ кэв). Несмотря на сравнительно большой разброс экспериментальных точек (при некоторых значениях N электрическое поле менялось от опыта к опыту в два раза), кривая имеет область, где наклон ее к оси абсцисс резко меняется.

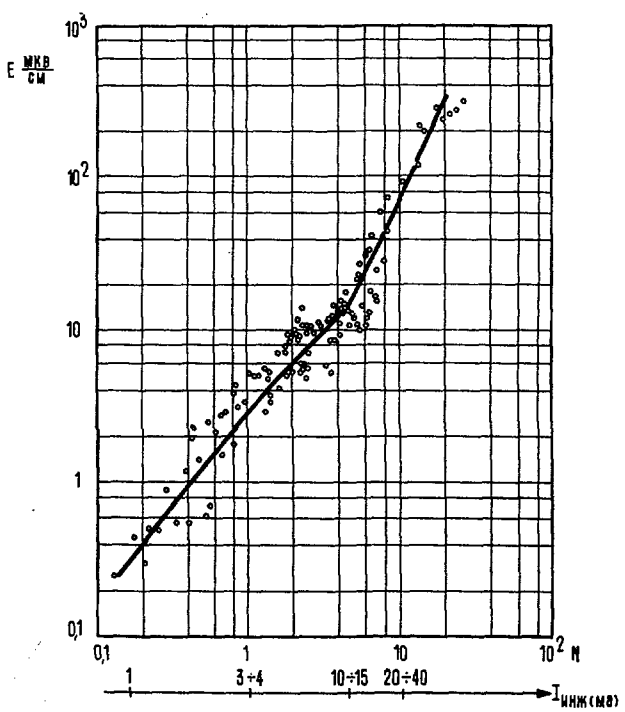

Рис. 5 Напряженность электрического поля на циклотронной частоте ионов H_2^+ ($f_1 = 2{,}2$ Мгц) в зависимости от плотности быстрых ионов H_2^+ (в относительных единицах). $\varepsilon = 160$ кэв, $I_{инж} = 0{,}5$ — 120 ма, $I_{упр} =$ — 1,5 ка, $U_c = 0$.

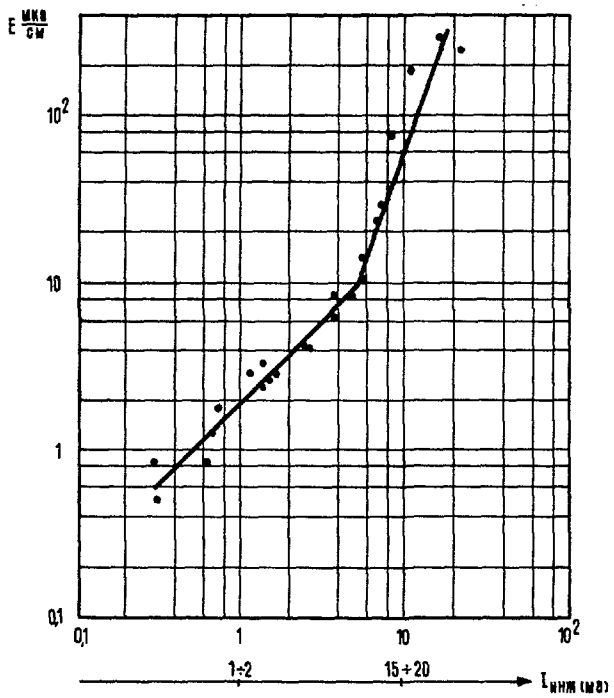

Рис. 6 Напряженность электрического поля на циклотронной частоте ионов H_2^+ ($f_1 = 1{,}7$ Мгц) в зависимости от плотности быстрых ионов H_2^+ (в относительных единицах). $\varepsilon = 100$ кэв, $I_{инж} = 0{,}5$—60 ма, $I_{упр} =$ — 1,5 ка, $U_c = 0$.

Величина изменения наклона кривой лежит вне ошибок измерений и разброса экспериментальных точек. Приблизительно при тех же значениях плотности быстрых молекулярных ионов N имеется излом в аналогичной зависимости, снятой при энергии инжектируемых ионов $\varepsilon = 100$ кэв. (смотри рис. 6). В обоих случаях область излома лежит в пределах изменения инжектируемого тока $I_{инж}$ от 10 до 15 ма. Сейчас трудно сказать, какие изменения происходят в плазме при увеличении инжектируемого тока свыше 10 ма, но было наблюдено, что в аналогичных режимах при этом прекращается рост плотности протонов [6], что можно приписать развитию неустойчивостей в плазме, и замедляется рост потенциала плазмы.

Из измерений следует, что напряженность электрического поля E на частоте f_1 может быть связана с плотностью ионов H_2^+ соотношением $E \sim N^\alpha$, где $\alpha \approx 1$ до точки излома и $\alpha \approx 2$ после точки излома.

Таким образом, связь напряженности электрического поля на циклотронной частоте с плотностью быстрых частиц N в условиях эксперимента на Огре носит нетривиальный характер и требует детального изучения.

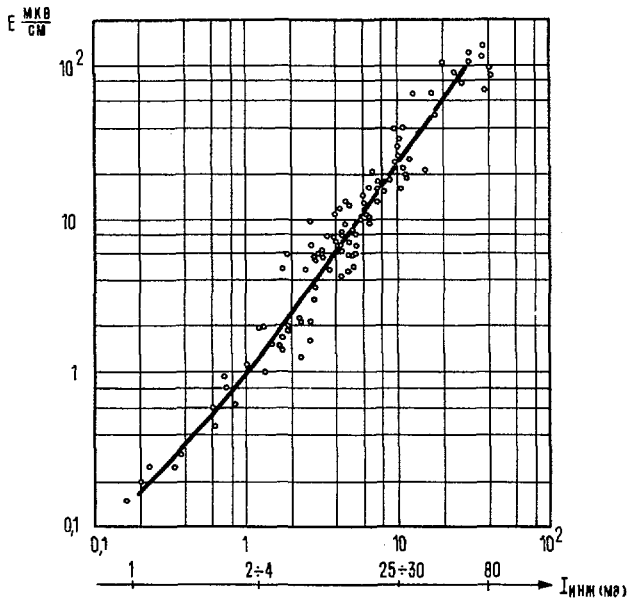

Рис. 7 Зависимость напряженности электрического поля на циклотронной частоте ионов H_2^+ ($f_1=2{,}2$ Мгц) от плотности быстрых ионов H_2^+ (в относительных единицах). $\varepsilon=160$ кэв, $I_{инж}=0{,}5-120$ ма, $I_{упр}=-1{,}5$ ка, $U_C=+12$ кв.

Характер изменения напряженности электрического поля от плотности быстрых частиц выглядит иначе, если на сетки, помещенные за магнитными пробками, подавать положительный потенциал относительно стенок камеры (о стабилизирующем действии сеток на плазму в Огре смотри работу [6]). На кривой, построенной при потенциале на сетках $U_C=+12$ кв (рис. 7), нельзя обнаружить столь резкого излома, какой есть при нулевом потенциале ($U_C=0$) (рис. 5,6). Значение показателя степени α лежит в пределах $1\leq\alpha\leq 1{,}4$. При сравнении этих двух случаев следует учитывать, что абсолютные значения плотности молекулярных ионов известны с точностью до 50%.

Итак, из измерений следует, что характер зависимости напряженности электрического поля (E) от плотности быстрых частиц (N) вероятно, во многом определяется устойчивостью самой плазмы. Величина напряженности электрического поля больше в тех режимах, когда наблюдаются интенсивные колебания плотности быстрых частиц у стенок камеры и есть большой уход частиц поперек магнитного поля ловушки. Наблюдаемое увеличение электрического поля на циклотронной частоте ионов может быть связано с тем, что происходит раскачка колебаний в плазме на этой частоте.

2. Излучение электронов.

Излучение электронов плазмы в Огре измерялось в диапазоне длин волн λ от 3,07 до 4 см в направлении, перпендикулярном к направлению магнитного поля, с помощью двух супергетеродинных приемников. Приемная антенна находилась внутри центральной части камеры Огры. Генератор шумов, расположенный в волноводном тракте, служил эталоном мощности при калибровке приемника и модулятором (с частотой модуляции 2 кгц) для высокочастотного сигнала, принимаемого из плазмы. Модулированный по амплитуде сигнал поступал на вход балансного смесительного моста. Чувствительность приемников была $\sim 10^{-13}$ вт. при отношении сигнала к шуму, равном единице.

Мощность излучения электронов плазмы в Огре была измерена в зависимости от длины, излучаемой волны λ. Пример такой зависимости приведен на рис. 8. Видно, что максимум мощности излучения приходится на длину волны $\lambda\approx 3{,}7$ см, что соответствует циклотронной частоте электронов в основном магнитном поле Огры $H_0=2900$ эрст. Ширина максимума в пределах ошибок измерений может быть объяснена неоднородностью магнитного поля ловушки. Циклотронное излучение электронов в Огре ($\lambda_H\approx\lambda=3{,}7$ см) в исследуемом режиме больше, чем на порядок, превышает тепловое излучение ($\lambda\approx 3{,}1$ см).

Как известно, в области электронной циклотронной частоты при $\omega_H>\omega_0$ ($\omega_H=eH/mc$, $\omega_0=\sqrt{4\pi e^2 n_e/m}$) показатель преломления плазмы $N(\omega)\approx 1$. Такой случай реализуется на Огре. Электроны, двигающиеся в магнитном поле ловушки, в основном излучают энергию на циклотронной частоте, так как в исследуемых режимах скорость электронов v_e значительно меньше скорости света ($v_e\ll c$). Мощность циклотронного излучения электронов, находящихся в объеме V с плотностью n_e, и имеющих одинаковые скорости в направлении, нормальном к направлению магнитного поля, в телесном угле $d\Omega$ равна:

$$P_ц=\frac{e^2}{8\pi c^3}\omega_H^2 v_\perp^2\left(1+\frac{v_z^2}{c^2}\right)n_e V\,d\Omega, \qquad (1)$$

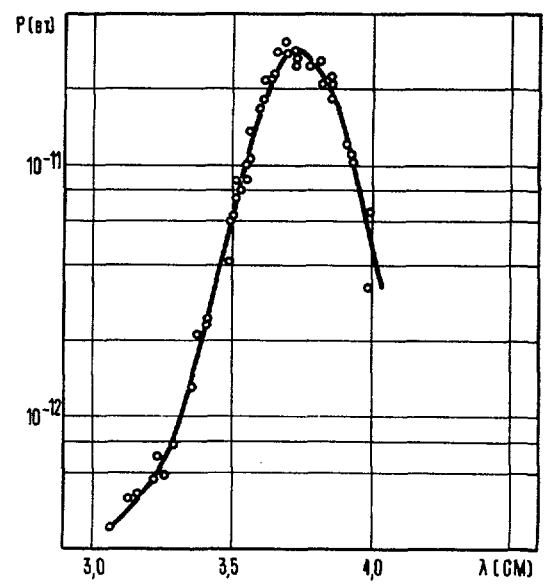

Рис. 8 Мощность излучения электронов в зависимости от длины волны. $\varepsilon=160$ кэв, $I_{инж}=100$ ма, $p=(1{,}5-2{,}5)\cdot 10^{-7}$ мм рт. ст., $I_{упр}=-1{,}5$ ка.

где $v_\perp$ и v_z — соответственно поперечная и продольная по отношению к направлению магнитного поля составляющие скорости электрона. В выражении (1) первый член соответствует излучению на необыкновенной волне (электрический вектор волны **E** перпендикулярен к направлению магнитного поля **H**, $\mathbf{E} \perp \mathbf{H}_0$), второй член — на обыкновенной волне ($\mathbf{E} \parallel \mathbf{H}_0$). Видно, что излучение во втором случае должно быть в v_z^2/c^2 раз меньше, чем в первом случае. Поэтому измерения проводились так, чтобы регистрировалось излучение волн с электрическим вектором **E**, перпендикулярным вектору магнитного поля $\mathbf{H}_0$ ($\mathbf{E} \perp \mathbf{H}_0$). Отношение мощности циклотронного излучения к плотности электронов ($P_ц/n_e$) характеризует величину поперечной скорости электронов ($v_{e\perp}$) или поперечную температуру. Мощность циклотронного излучения электронов ($P_ц$) измерялась при изменении давления газов в камере. Пример такой зависимости от давления аргона при энергии инжектируемых ионов H_2^+, $\varepsilon = 160$ кэв, приведен на рис. 9 для двух значений инжектируемого тока ($I_{инж} = 50$ ма и 100 ма). Пунктиром на рисунке построены зависимости величины $P_ц/n_e$ от давления аргона. Плотность электронов измерялась с помощью интерферометра, работавшего на длине волны $\lambda = 10$ см. При уменьшении давления газов в камере поперечная температура электронов возрастает и, например при давлении $p = 4.10^{-7}$ мм.рт. ст., инжектируемом токе $I_{инж} = 100$ ма из оценок получается величина порядка 100 эв.

Тепловое излучение электронов при энергии инжектируемых ионов $\varepsilon = 160$ кэв принималось на длине волны $\lambda = 3{,}1$ см. Чтобы убедиться в том, что мощность теплового излучения не зависит от длины излучаемой волны в рассматриваемом диапазоне, необходимо было изменить величину

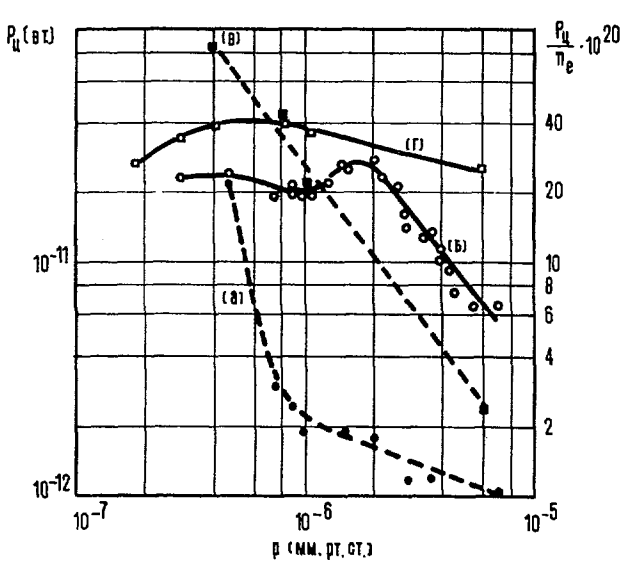

Рис. 9 Циклотронное излучение электронов ($\lambda = 3{,}7$ см) в зависимости от давления аргона. $\varepsilon = 160$ кэв, $I_{упр} = -1{,}5$ ка Обозначения (а), (б) $I_{инж} = 50$ ма, (в), (г) $I_{инж} = 100$ ма, сплошные кривые — значения $P_п$, пунктирные кривые — величина $P_ц/n_e$.

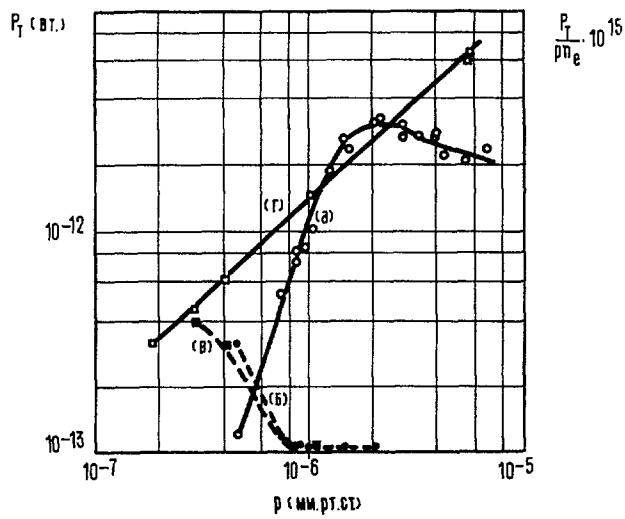

Рис. 10 Тепловое излучение электронов ($\lambda = 3{,}1$ см) в зависимости от давления аргона. $\varepsilon = 160$ кэв, $I_{упр} = -1{,}5$ ка. Обозначения (а), (б) $I_{инж} = 50$ ма, (в), (г) $I_{инж} = 100$ ма, сплошные кривые — значения $P_т$, пунктирные кривые — величина $P_т/p \cdot n_e$.

магнитного поля H_0 (следовательно, и энергию инжектируемых ионов H_2^+) так, чтобы циклотронная частота электронов лежала бы вне диапазона частот измерительных приемников. Такие измерения были проделаны при энергии инжектируемых ионов $\varepsilon = 100$ кэв ($H_0 = 2100$ эрст) и оказалось, что мощность теплового излучения практически не зависит от длины излучаемой волны и одинакова для обеих поляризаций ($\mathbf{E} \perp \mathbf{H}_0$ и $\mathbf{E} \parallel \mathbf{H}_0$).

При энергии инжектируемых ионов H_2^+ $\varepsilon = 160$ кэв была измерена зависимость мощности теплового излучения $P_т$ ($\lambda = 3{,}1$ см) от давления аргона в камере (смотри рис. 10).

Чтобы оценить температуру электронов, зная мощность теплового излучения и плотность электронов, в нашем случае анизотропной среды с $N(\omega) \approx 1$ можно воспользоваться законом Кирхгофа, предполагая, что электроны имеют максвелловское распределение по скоростям. Действительно, при давлении аргона $p = 10^{-6}$ мм.рт.ст. и плотности электронов $n_e \approx 10^9$ см$^{-3}$ ($P_т \approx 10^{-12}$ вт) преобладают соударения электронов с атомами газа, и поглощательная способность плазмы $\alpha_{\omega l}$ может быть вычислена. Проделав элементарные оценки, получим значение для излучательной способности такой плазмы $\eta_{\omega l}$ в виде

$$\eta_{\omega l} = \frac{1}{2} \cdot 8 \cdot 10^{-40} T_e \cdot p \cdot n_e \text{ (вт)} \qquad (2)$$

где $l = 1, 2$ — номер поляризации, T_e — температура электронов в электронвольтах, p — давление газов в единицах 10^{-6} мм.рт.ст. Полагая, что электроны излучают во всех направлениях равномерно, получим выражение для мощности теплового излучения из объема V

$$P'_т = 4\pi \eta_{\omega l} V \frac{S_{эфф}}{S} \Delta\omega \text{ (вт)} \qquad (3)$$

Здесь $S_{эфф}$ — эффективная поверхность приемной антенны,

S — полная поверхность камеры Огры,

$\Delta\omega$ — ширина полосы частот измерительного приемника.

В рассматриваемом случае ($p=10^{-6}$ мм.рт.ст., $n_e\approx 10^9$ см$^{-3}$)

$$P_T' \approx 10^{-17}\, T_e \text{ (вт)} \qquad (4)$$

Температура электронов в данном режиме не может быть оценена больше 100 эв, исходя из общих соображений об элементарных процессах, происходящих в такой плазме, и из оценок поперечной температуры, сделанных выше по измерениям мощности циклотронного излучения электронов. Подставляя $T_e=100$ эв. в формулу (4), получаем $P_T' \approx 10^{-15}$ вт, что на три порядка меньше мощности, наблюдаемой в опытах ($P_T\approx 10^{-12}$ вт). Это можно объяснить тем, что коэффициент поглощения плазмы в нашем случае на несколько порядков меньше коэффициента поглощения волн в металлических стенках камеры, сделанной из нержавеющей стали. Электромагнитные волны, излучаемые электронами претерпевают приблизительно 10^3 отражений от стенок камеры прежде, чем их интенсивность уменьшится в 5/10 раз. Следовательно, тепловое излучение электронов в Огре накапливается и достигает наблюдаемой на опыте интенсивности.

Из выражения (3) следует, что величина мощности теплового излучения P_T, отнесенная к давлению газов p и плотности электронов n_e, пропорциональна температуре электронов ($P_T/pn_e\sim T_e$). Пример зависимости величины P_T/pn_e от давления аргона в камере приведен на рис. 10.

Видно, что температура электронов возрастает при уменьшении давления газов в камере.

Таким образом, из измерений и сделанных оценок следует, что поперечная температура электронов, и температура электронов, полученная из измерений теплового излучения электронов, возрастают при уменьшении давления газов в камере.

Авторы выражают глубокую благодарность И. Н. Головину за полезные советы и ценные замечания, высказанные при обсуждении результатов работы, и В. Ф. Нефедову за помощь при проведении ряда измерений.

Литература

[1] Кархов А. Н. *Журнал Приборы и техника эксперимента* **5** (1961) 115.

[2] Головин И. Н., Артеменков Л. И., Богданов Г. Ф., Панов Д. А., Пистунович В. И., Семашко Н. Н., *УФН* **73** (1961) 685.

[3] Bogdanov, G. F., Panov, D. A., Semashko, N. N., *J. Nucl. Energy* **C 3** (1961) 106.

[4] Пистунович В. И., Шафранов В. Д., *Ядерный синтез* **1** (1961) 189.

[5] Иваненко Д., Соколов А. Классическая теория поля (ГИТТЛ г. Москва 1949 г.).

[6] Богданов Г. Ф., Головин И. Н., Кучеряев Ю. А., Панов Д. А. Доклад, представленный на Зальцбургскую конференцию. (Стр. 215 этого тома Трудов Конференции.)

RADIATION AND ION ENERGY DISTRIBUTIONS OF THE DCX-1 PLASMA*

J. L. DUNLAP, C. F. BARNETT, R. A. DANDL, H. POSTMA

OAK RIDGE NATIONAL LABORATORY

OAK RIDGE, TENNESSEE, UNITED STATES OF AMERICA

A high energy plasma has been created in the DCX mirror machine by injecting 600 keV diatomic hydrogen ions in the median plane. Dissociating collisions with residual gas molecules produce a plasma of atomic ions concentric with the magnetic axis, and having a density of about 10^6 fast ions per cm^3.

Electromagnetic radiation has been observed by inserting an electrostatically shielded dipole antenna in the median plane outside the ring of trapped particles. In addition, the optical radiation arising from excitation of the residual gas has been monitored. The frequency range of 150 kilohertz to 1000 megahertz was scanned by feeding the output of the antenna into a frequency analyzer. Some discrete frequencies were found throughout this range with no obvious correlation to any parameter except the presence of the plasma. In addition, a strong proton cyclotron frequency of 14.65 megahertz was observed, with multiples to the seventh harmonic. The envelope of the oscillations was observed by feeding the antenna output directly to an oscilloscope. The envelope was composed primarily of the cyclotron fundamental frequency, and its amplitude was directly proportional to the input H_2^+ current. Observation of the envelope as the plasma density increased from zero showed that the time for onset of the oscillations was inversely proportional to the magnitude of the H_2^+ current to the 0.8 power.

The energy distributions of the circulating protons, determined by recharging the energetic neutral particles formed by electron capture collisions and sending them through an electrostatic analyzer, were also investigated as a function of H_2^+ current. For input currents of 0.1 mA the energy distributions of the protons were sharp, with mean energies of 300 keV. For H_2^+ currents of 3.5 mA the energy distributions were broad, with a mean energy of 260 keV and maximum energies of 400 keV.

The observations suggest that particle bunching is taking place in the plasma, probably giving rise to circumferential electric fields.

Introduction

In the DCX-1 apparatus, a plasma is created by accelerating diatomic hydrogen ions to 600 keV and injecting them into the median plane of a magnetic mirror. Here a portion of the diatomic ions is dissociated by collisions either in an arc discharge or with residual gas molecules. The atomic hydrogen ions thus produced are trapped in the magnetic field. This approach to the attainment of a controlled thermonuclear reaction and general features of the machine have been described previously [1, 2].

Studies have recently been made of the energy distributions of the trapped circulating protons as functions of various operational parameters. A particle spectrometer was used to measure the energy distributions of neutral hydrogen atoms escaping from the 300 keV proton storage ring in DCX-1 as the result of electron capture collisions between trapped protons and background gas molecules. A portion of the atoms were converted to protons by passage through an argon filled gas cell, and the proton beam was then electrostatically analyzed. Energy distributions of the protons circulating within the plasma volume were obtained by transformations applied to the measured distributions. A report of the first series of these experiments is now in press [3]. The measurements showed that with either gas or carbon arc dissociation the rate at which the circulating protons lost energy increased as the injected H_2^+ current was increased. With arc breakup the additional energy loss had the consequence of decreasing the mean storage time of the circulating protons. With gas breakup the scatter in measurements of the storage time prevented conclusions as to its dependence on injected current. Also with either gas or arc dissociation, the response of the energy distributions to increases in injected H_2^+ current indicated the presence of a non-collisional dispersing mechanism, one which increased in importance with increases in injected current. The nature of the mechanisms associated with the increasing energy losses and dispersion was not clear.

Work was then undertaken to investigate the responses of other features of the DCX-1 plasma to increases in injected current. In the sections that follow we describe measurements of magnetic and optical radiation from the plasma. Since the experimental environment is greatly complicated by the presence of a dissociating arc discharge, this work was done with plasmas established by gas dissociation.

Description of DCX-1

Fig. 1 is a schematic diagram of the DCX-1 apparatus. The two innermost coils, which produce the magnetic mirror field used for particle confinement, have centers spaced 76 cm apart. The mirror ratio is 2:1 and the axial field strength in the median plane is

* Conference paper CN-10/160, presented by J. L. Dunlap. Discussion of this paper is given on page 354. Translations of the abstract are at the end of this volume of the Conference Proceedings.

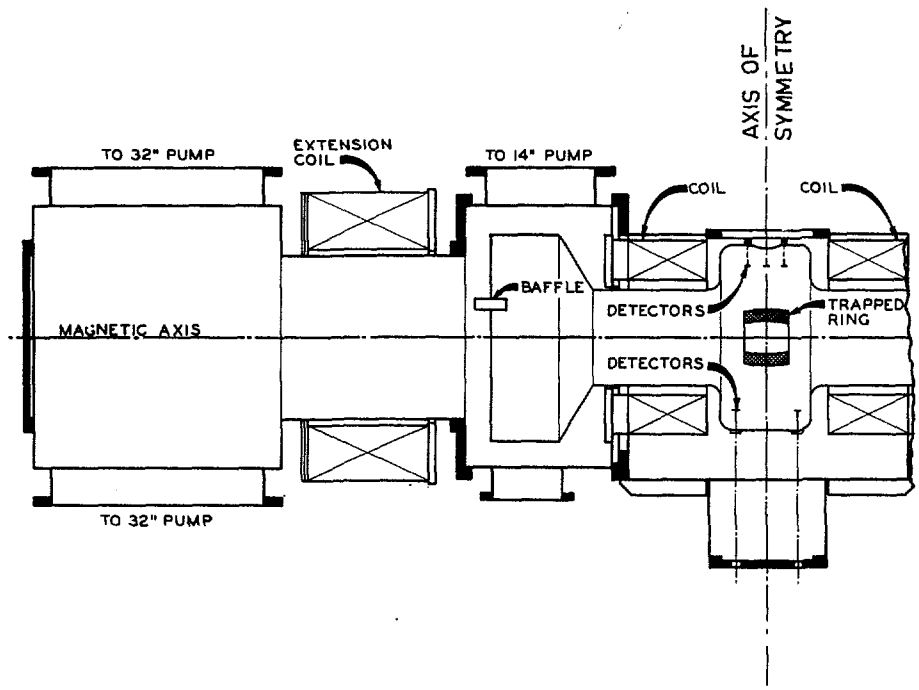

Fig. 1 A longitudinal section of the DCX-1 apparatus.

10 kG. The equilibrium radius for 300 keV protons is then 8.2 cm. The two outer coils increase the axial extent of the magnetic field for operation of long arcs and do not contribute materially to the midplane magnetic field in the plasma region.

A two region vacuum system was employed. The plasma volume is surrounded by a copper liner which can be baked either by operating the carbon arc or with superheated steam. Oil diffusion pumps operating in the outer vacuum region produce a base pressure in the plasma region of about 1×10^{-6} mm Hg without the arc in operation.

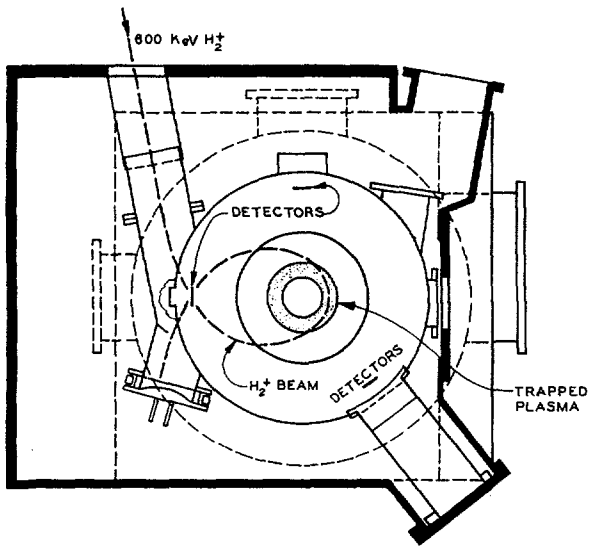

Fig. 2 A cross section of the median plane of the DCX-1 apparatus.

Fig. 2 shows the ion orbits in the median plane of the machine. The H_2^+ beam enters the magnetic volume through an unshielded tube, circles the magnetic axis, and passes through an aperture to the outer vacuum region. Dissociation collisions over a portion of this trajectory produce protons satisfying DCX-1 containment criteria [4] which are then trapped in the magnetic field. With an input beam of 1 mA H_2^+, fast-ion densities of 10^6 to 10^7 ions cm^{-3} are produced in a volume of approximately one liter.

Each of the detectors shown in Figs. 1 and 2 consists of a 2.5×10^{-5} cm thick Ni foil backed at a small distance by a Faraday cup. Energetic hydrogen neutrals, formed by electron capture collisions between the circulating protons and background gas molecules, impinge on the detector foils. Those with sufficient energy (the energy cut-off is 50 keV) penetrate the foils, emerge mostly charged, and constitute a current flowing from foil to collector. The current from each collector is amplified and displayed on an oscilloscope. The mean containment time τ of the plasma is defined as the time interval required for the current to decay to 1/e of the steady state value after interruption of the H_2^+ beam.

RF radiation measurements

An electrostatically shielded dipole antenna was installed in the median plane outside the trapped ring. The frequency spectrum was scanned from 150 kHz (kilocycles/second) to 1000 MHz (megacycles/second) with a radio-frequency noise analyzer. The strongest component was the 14.65 MHz proton cyclotron frequency. Harmonics of cyclotron radiation through the seventh were detected. In addition, a number of other

frequencies were found which required the presence of the trapped plasma but which were otherwise independent of the injected beam current and the magnetic field. Among these were 215, 295, 292, 460 and 960 MHz. It is believed that this radiation was due to cavity resonances excited by the beam.

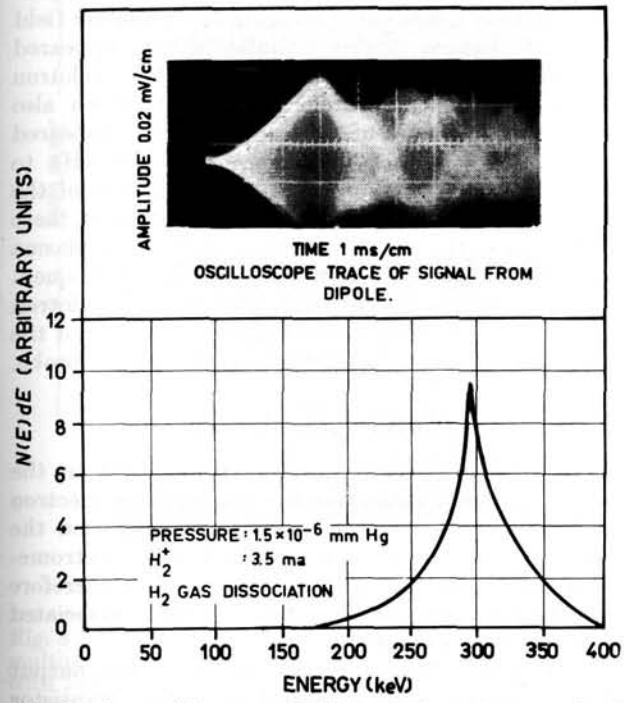

Fig. 3 An oscilloscope display of the antenna signal and an energy distribution of circulating protons measured under the same experimental conditions.

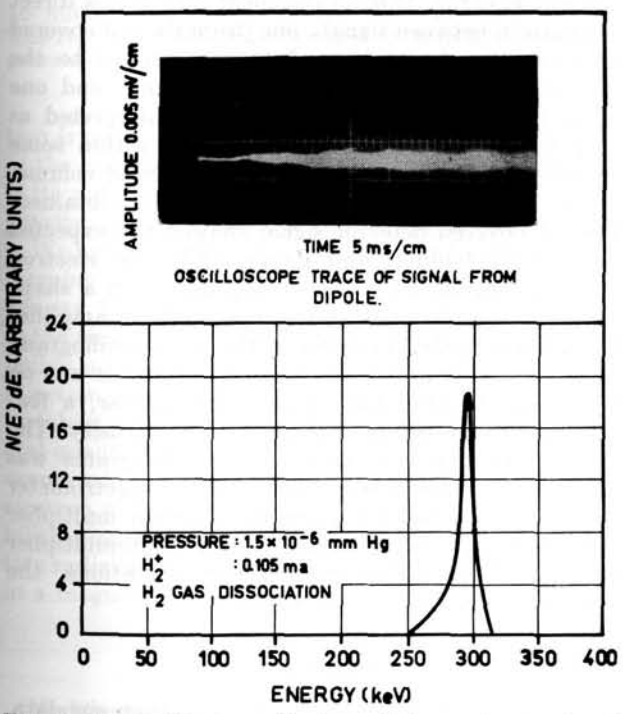

Fig. 4 An oscilloscope display of the antenna signal and an energy distribution of circulating protons measured under the same experimental conditions.

Fig. 3 shows an oscilloscope display of the antenna signal and an energy distribution of circulating protons, both measured under the same experimental conditions. The beginning of the oscilloscope trace corresponds to the time that the 3.5 mA H_2^+ beam was turned on. The indicated response of the radio-frequency probe signal was typical. At some time after the beam was turned on, in this instance 0.4 ms, the envelope of the oscillations gradually increased in amplitude and then disintegrated into chaotic modulation. Note the broad nature of the energy distribution. It does not appear that collisional diffusion can

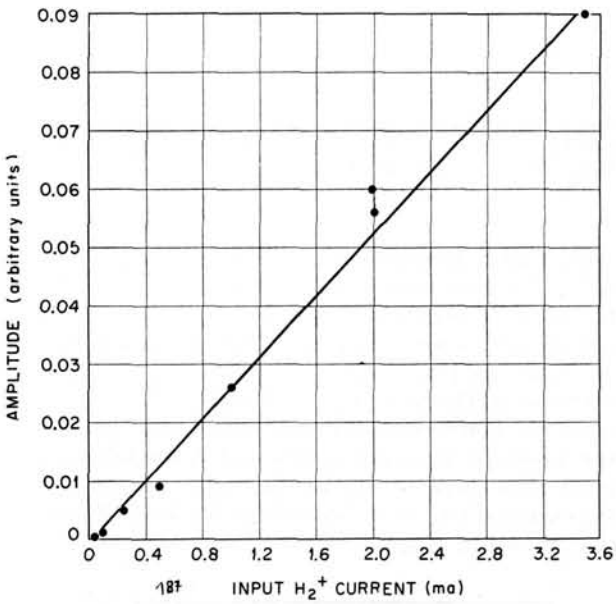

Fig. 5 Peak-to-peak amplitude of the radio-frequency envelope as a function of injected H_2^+ current. Measured with gas dissociation at a pressure of 1.5×10^{-6} mm Hg.

account for the presence of such large numbers of protons at energies significantly higher than 300 keV. Diffusion times calculated on the basis of coulomb collisions are orders of magnitude larger than the observed proton containment times, which, for the conditions of Fig. 3 were approximately 7 ms.

Fig. 4 presents similar data made at the same pressure but with the H_2^+ current reduced from 3.5 to 0.1 mA. The amplitude sensitivity of the oscillogram is greater by a factor of 40 and the time scale has been increased by a factor of 5. As compared with the previous figure, the onset occurs later, the amplitude of the envelope is greatly reduced, and the energy distribution is much less diffuse.

Repeated measurements of the peak-to-peak amplitude of the radio-frequency envelope as a function of input current indicated the linear dependence shown in Fig. 5. The time for onset of the oscillations after the H_2^+ beam was turned on is shown as a function of input current in Fig. 6.

Fig. 7 shows the radio-frequency envelope and energy distribution obtained with a 3.45 mA H_2^+ beam and with the liner pressure raised to 1.1×10^{-5} mm Hg by a hydrogen gas leak. The envelope reached a

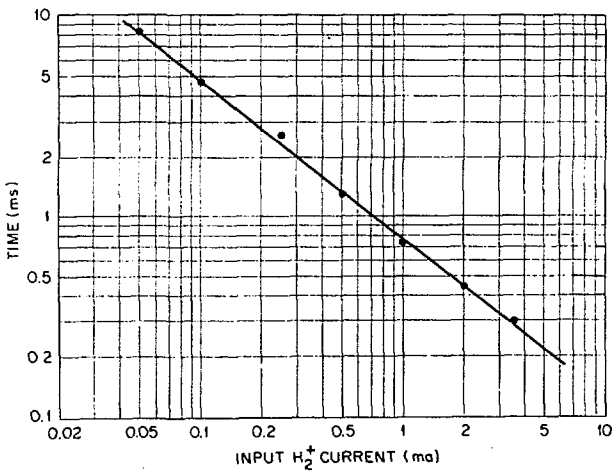

Fig. 6 The time for onset of the radio-frequency oscillations as a function of injected H_2^+ current. Measured with gas dissociation at a pressure of $1.5 \times \times 10^{-6}$ mm Hg. $T(\text{ms}) = 0.77/I^{0.785}$ (mA).

peak amplitude approximately the same as that shown in Fig. 3 for the same injected current at 1.5×10^{-6} mm Hg, but this time the subsequent radiation occurs with a considerably lower amplitude. The time for onset of the oscillations is shorter, approximately 0.1 ms, as compared with 0.4 ms. The time required for the proton density to reach the equilibrium value is also shorter because of the increased dissociation rate and decreased containment time characteristic of the higher pressure. Here the energy distribution is considerably less diffuse than that shown in Fig. 3.

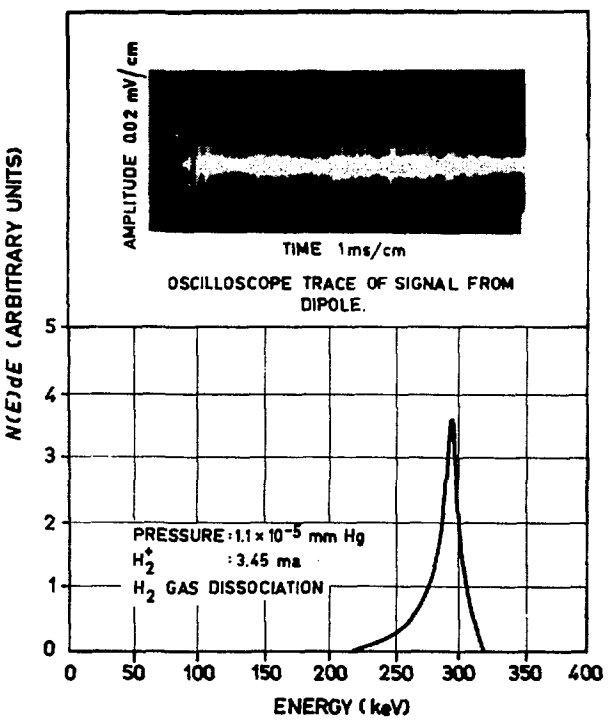

Fig. 7 An oscilloscope display of the antenna signal and an energy distribution of circulating protons measured under the same experimental conditions.

Optical radiation

A photomultiplier was mounted at one end of the apparatus to monitor light due to excitation of residual gas by a portion of the circulating plasma, and the radio-frequency spectrum of the output from this detector was scanned. The most prominent modulation occurred in a broad band centered about the proton cyclotron frequency. Changing the magnetic field produced changes in this modulation that appeared to correspond with changes in the proton cyclotron frequency. Weaker coherent modulation which also required the presence of the trapped plasma appeared at a number of other frequencies from 540 kHz to 200 MHz. Some of these were near multiples of the proton cyclotron frequency but the relation of these frequencies to the magnetic field strength in the plasma region was not definitely established. Those frequencies that were not near multiples of the cyclotron frequency did not appear to coincide with any of the frequencies measured with the radio-frequency probe.

Particle measurements

The neutral particle spectrometer utilized in the energy spectrum measurements employed an electron multiplier as the particle detector. In operation the output of this detector was amplified in an electrometer circuit. Rapid fluctuations in signal were therefore smoothed out by the long time constant associated with the electrometer.

To examine these rapid fluctuations, the output of the detector was amplified in a fast transistor circuit and then displayed on a dual beam oscilloscope along with the signal from a foil-covered neutral particle detector. This arrangement provided a direct comparison between signals, one (from the foil-covered detector) that is interpreted as proportional to the total density of trapped energetic protons, and one (from the electron multiplier) that is interpreted as proportional to the density of protons within some specific energy interval in a small element of volume.

Fig. 8 shows oscillograms of the results obtained. The foil-covered detector signal showed the expected exponential buildup and decay while the electron multiplier signal was a series of pulses with a shape that was the characteristic response of the amplifier to a current spike. As shown in the lower oscillogram, some time is required after the H_2^+ beam is cut on before the electron multiplier spikes appear, a feature that suggests some form of critical density. The general behavior indicated in the oscillograms was independent of the energy selection of the spectrometer and was also observed when the electron multiplier was replaced with a zinc sulfide photomultiplier detector. Even under steady state conditions, the pulses did not appear to be periodic.

Conclusions

Perhaps the most definite conclusion from our data, suggested by the sharp frequency definition of the observed radio-frequency radiation, is that the radia-

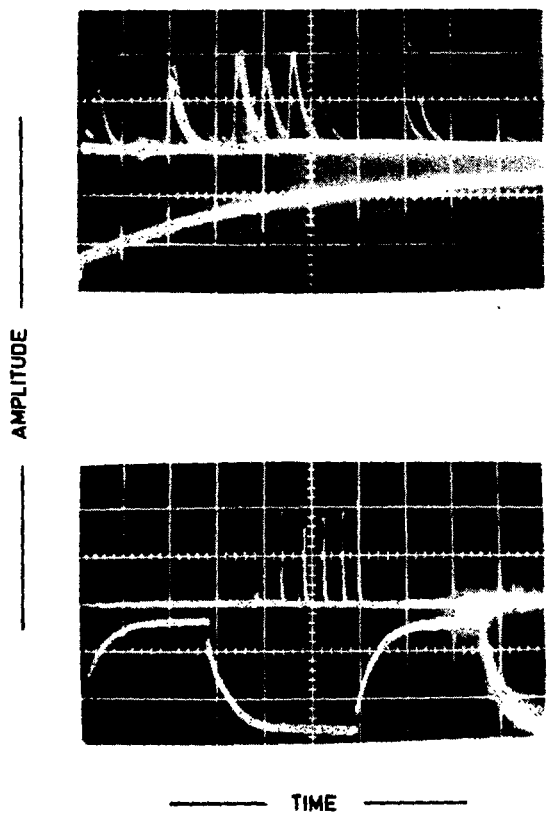

Fig. 8 The time variation of signals from the electron multiplier and the neutral particle detector, measured with gas dissociation at a pressure of 1.5×10^{-6} mm Hg. In each oscillogram the upper trace is the signal from the electron multiplier and the lower trace is that from the neutral particle detector. The time base is one millisecond per division in the upper oscillogram, and 10 milliseconds per division in the lower oscillogram. The H_2^+ beam was pulsed on and off with a square-wave generator, and at time $t = 0$, the H_2^+ beam was pulsed off.

tion is coherent cyclotron radiation of lumped charges in the circulating ring. Such a lump should radiate as if its net charge were concentrated at the center of gravity, which follows a circular orbit in the field.

We have already noted a second conclusion, that the lumping of charge results from an instability with a density threshold. This was suggested by the delay in the onset of radio-frequency radiation as the plasma builds up and the linear dependence of this delay on injection current. We are examining two possible instability mechanisms possessing the necessary general qualitative features. One, proposed by HARRIS [5], occurs when the ion cyclotron motion resonates with electron plasma oscillations. The other [6] is an instability observed in accelerators when there is a negative radial gradient in the magnetic field, as is the case in a magnetic mirror field.

Recent experiments

Modifications to the apparatus have permitted operation with gas dissociation at a few times 10^{-8} mm Hg with up to 10 mA of injected H_2^+ current.

Plasma potentials have been measured by accelerating lithium ions toward the plasma and noting the energy required for these ions to penetrate the plasma. At the lower pressures the potential varied linearly with the H_2^+ current at a rate of about 70 V/mA. When raising the pressure with a helium gas leak, this rate gradually decreased to about one-half its former value at 1×10^{-6} mm Hg. Although more work is required to make certain, present evidence indicates that the observed plasma potentials require heating of the electrons at faster rates than can be accomplished by coulomb collisions with hot ions. The additional heating mechanism is presumed to be the electric fields associated with uneven charge distributions in the circulating ring.

The most important question proposed by the evidence for instabilities was whether the phenomena would limit the proton containment time as the pressure in the plasma region was decreased or as the injected H_2^+ current was increased.

Recent experiments in the modified apparatus have investigated the proton containment time as functions of pressure and injected H_2^+ current. These have yielded mean containment times of at least 5 s. They have shown no indication that the proton lifetime is limited by anything other than charge exchange reactions and have shown no dependence of containment time on injected current in the range up to 10 mA.

These studies have then relieved some of our fears regarding the implications of the earlier experiments. Examinations of the energy spectra and radiation with the apparatus operating in the new regimes of pressure and injected current are planned and should provide interesting results.

Acknowledgments

The authors wish to acknowledge numerous helpful discussions with Drs. T.K. Fowler, H.S. Robertson, and A.H. Snell.

This work was performed at Oak Ridge National Laboratory, operated by Union Carbide Corporation for the United States Atomic Energy Commission.

References

[1] BARNETT, C. F., BELL, P. R., LUCE, J. S., SHIPLEY, E. D., SIMON, A. Proceedings of Second UN International Conference on the Peaceful Uses of Atomic Energy, Geneva **31** (1958) 298.

[2] SNELL, A. H., Proceedings of the Fourth International Conference on Ionization Phenomena in Gases (North-Holland Pub. Co., Amsterdam, 1959) Vol. II, 997.

[3] BARNETT, C. F., DUNLAP, J. L., EDWARDS, R. S., HVSTE, G. R., RAY, J. A., REINHARDT, R. G., SCHILL, W. J., WARNER, R. M., WELLS, E. R. *Nuclear Fusion* (in press).

[4] FOWLER, T. K., RANKIN, M., Oak Ridge National Laboratory Report ORNL-2802, sec. 7.1 (1959).

[5] HARRIS, E. G., *Phys. Rev. Letters* **2** (1959) 34; BURT, P., HARRIS, E. G., *Bulletin Amer. Phys. Soc.* **6** (1961) 300.

[6] NIELSEN, C. E., *et al.*, International Conference on High Energy Accelerators and Instrumentation, CERN (1959); *Rev. Sci. Instr.* **30** (1959) 80.

CALCULATION OF ION TRAJECTORIES AND MAGNETIC FIELDS FOR THE MAGNETIC TRAPPING OF HIGH ENERGY PARTICLES*

W. F. GAUSTER, G. G. KELLEY, R. J. MACKIN, JR., G. R. NORTH

OAK RIDGE NATIONAL LABORATORY

OAK RIDGE, TENNESSEE, UNITED STATES OF AMERICA

Several thermonuclear research devices generate a hot, dense plasma by the accumulation in a magnetic container of high-energy ions which are injected from outside and trapped there. A particle-trapping method whose prospects seem favorable is that of dissociating diatomic or triatomic molecular ions. In the course of several years of study on this concept, a great deal of practical work has been done on the synthesis of magnetic fields with certain desired properties and on the calculation of single-particle trajectories in them. Furthermore, consideration has been given to perturbations arising from collective ion effects such as space charge, plasma diamagnetism and the magnetic field of the input ion beam. This paper presents a summary of these studies.

The problem of injection in the plane of symmetry between a pair of magnetic mirror coils is solved by analytical and geometrical techniques. Other injection problems arise for machines with helical ion paths (for instance, DCX-2 where the aim is to minimize the helical pitch angle). Necessary concepts are developed to establish criteria of initial beam divergence and magnetic field homogeneity for maximizing path length. Ion movement in injection-duct fields and precession of the molecular-ion orbit upon reflection from a mirror are discussed.

Methods are shown which have been applied to synthesize magnetic fields with a central zone homogeneous to within less than 0.1% over a length of about half the distance between the mirrors. These fields are produced by means of spaced, lumped coils and mirror coils giving mirror ratios from 2 to 5. The scheme requires also a carefully controlled field dip of about 2% at the injection point located between the mirrors and the homogeneous central zone. Under these circumstances, it appears possible to achieve a total path length of at least 80 times the length of the homogeneous zone. The collective phenomenon which might most seriously affect these results is space charge. For its effect to be negligible, it is required that the variation of the electrostatic potential energy along the axis inside of the homogeneous zone be much less than 0.1% of the trapped ion energy.

A generally useful product of this program is a new code for the rapid and accurate computation of magnetic fields. It proves to be especially advantageous for determining ion trajectories over extended distances in magnetic fields from arbitrary coil assemblies.

1. Introduction

The concept of generating a plasma of thermonuclear temperature and density by the injection and trapping of energetic ions is now being studied in a variety of forms. This paper describes a series of calculations of ion trajectories and magnetic fields motivated by the design of the devices DCX-1 and DCX-2. The calculations form a basis for the DCX-2 design criteria given in the accompanying paper [1]. However, certain aspects of them are for more general interest and apply also to several of the other contemporary experimental devices. Some of these devices are listed in [1].

The present paper does not treat phase-space formalism for estimating potentially attainable path length. While this technique has not yet played an important role, it is apt to be valuable for generating more sophisticated injection concepts.

2. Ion movement in a plane

2.1. Analytical

In the DCX-1 machine diatomic hydrogen molecular ions are accelerated outside the magnetic mirror field, pass through a mass-separating magnet, enter the field along a path in the plane of symmetry between the two mirror magnet coils, pass through a dissociating arc, and re-emerge from the field (Fig. 1). Given an arc position and desired angle of passage through the arc, the requirements of the design are: determining the layout of the accelerator, magnet and arc; determining the conditions for focusing the beam at the arc; and locating the target for the undissociated beam.

Two procedures were followed, one analytical and the other graphical. The analytical procedure was based on the circular symmetry of the system and the

* Conference paper CN-10/190, presented by G. G. Kelley. Discussion of this paper is given on page 355. Translations of the abstract are at the end of this volume of the Conference Proceedings.

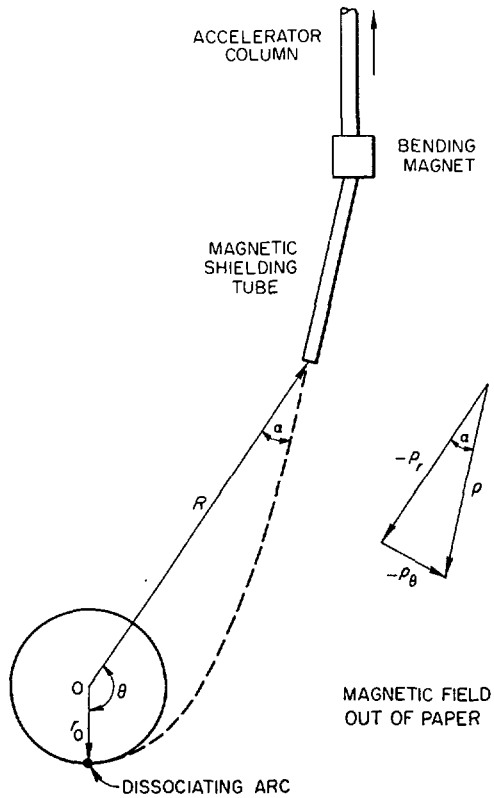

Fig. 1 DCX-1 configuration.

conservation [2] of canonical angular momentum P_θ. Particle motion in a rotationally symmetrical magnetic field (with $B_\theta = 0$) is described in cylindrical co-ordinates by a Hamiltonian:

$$H = \frac{1}{2M}\left[P_r^2 + P_z^2 + \left(\frac{Pe}{r} - \frac{e}{c}A\right)^2\right], \tag{1}$$

where M is the molecular-ion mass, P_r, and P_z are ordinary radial and axial momentum components, and $A \equiv A_\theta(r, z)$ magnetic vector potential which describes the field. The equation to be used is:

$$\frac{\partial H}{\partial P_\theta} = \dot{\theta}\,, \tag{2}$$

which gives:

$$\frac{P_\theta}{r} - \frac{e}{c}A = Mr\dot{\theta}\,. \tag{3a}$$

Alternatively:

$$\begin{aligned}\sin\alpha &= -r\dot{\theta}/v \\ &= \frac{P_\theta - (e/c)\,rA}{Mvr}\,,\end{aligned} \tag{3b}$$

where v is the particle velocity and α is the angle between the velocity vector and a vector from the particle to the axis (Fig. 1).

The vector potential is found by numerical integration using measured field values $B(r)$ in the plane of symmetry:

$$A(r) = \frac{1}{r}\int_0^r r'\,B(r')\,\mathrm{d}r'\,. \tag{4}$$

Two steps are involved in calculating the layout. First P_θ is evaluated by the required conditions at the arc. For instance, it is usually desired to produce a trapped proton orbit centered on the axis. Thus, the arc is located at a radius r_0, such that

$$\frac{e}{c}r_0\,B(r_0) = \frac{1}{2}Mv \tag{5}$$

and $\alpha(r_0) = \pi/2$. Accordingly,

$$P_\theta = \frac{e}{c}\left[A(r_0) - 2r_0\,B(r_0)\right]r_0\,. \tag{6}$$

At any other radius, for instance r_1 at which the ions emerge from the magnetic analyzer operations (3b), (5) and (6) give:

$$\sin\alpha(r_1) = \frac{r_0}{r_1} + \frac{r_1 A(r_1) - r_0 A(r_0)}{2r_1 r_0 B(r_0)}\,. \tag{7}$$

This expression is used to determine the position and orientation with respect to the magnetic axis of the accelerator-analyzer system. The second step is that of locating the arc on the circle at r_0, that is, determining $\Delta\theta(R_1, r_0)$, the difference in azimuth between the analyzer and the arc.

$$\Delta\theta(R, r_0) = \int \dot{\theta}\,\mathrm{d}t \tag{8a}$$

$$= \int_{r_0}^{R} \frac{\dot{\theta}}{\dot{r}}\,\mathrm{d}r \tag{8b}$$

$$= \int_{r_0}^{R} \frac{r\dot{\theta}}{[v^2 - r^2\dot{\theta}^2]^{\frac{1}{2}}}\,\frac{\mathrm{d}r}{r}\,, \tag{8c}$$

where the radial dependence of $r\dot{\theta}$ is given by Eq. (3a). Alternatively,

$$\Delta\theta(R_1, r_0) = \int_{r_0}^{R} \tan\alpha(r)\,\frac{\mathrm{d}r}{r} \tag{9}$$

and $\tan\alpha(r)$ is evaluated with the help of Eq. (7).

The integrand is infinite at $r = r_0$ and it is necessary to approximate the integral over a short range. Letting

$$n = -\frac{r_0}{B(r_0)}\,\frac{\mathrm{d}B(r_0)}{\mathrm{d}r}\,, \tag{10}$$

we find:

$$\begin{aligned}&\Delta\theta(r_0(1+\varepsilon), r_0) \\ &= 2\sqrt{\varepsilon}\left[1 - \frac{5+2n}{24}\varepsilon + \frac{369 - 124n + 36n^2}{1920}\varepsilon^2 + \ldots\right].\end{aligned} \tag{11}$$

The focusing conditions on the beam may be evaluated by the use of Eq. (3b). We consider two extreme rays of an initially parallel beam at r_1, separated by a distance d. For the two rays

$$\Delta P_\theta = -Mvd + \frac{e}{c}r_1\,B(r_1)\,d\cdot\sin\alpha\,. \tag{12}$$

For simplicity, let $B(r_1)=0$. Then, at r_0, assuming again (there is only a second order difference in α between the two rays),

$$\begin{aligned}\Delta P_\theta &= (-Mv + r_0 B(r_0))\,\Delta r \\ &= -\frac{1}{2} Mv\,\Delta r\end{aligned} \tag{13}$$

and the distance between the extreme rays at the arc is

$$\Delta r = 2d. \tag{14}$$

To calculate the convergence at r_1 necessary for a focus at r_0, we consider two orbits intersecting at r_0, one with $\alpha=\pi/2$ and the other rotated through an infinitesimal angle γ:

$$\begin{aligned}\Delta P_\theta &= Mvr_0(1-\cos\gamma) \\ &= O(\gamma^2).\end{aligned} \tag{15}$$

At r_1 the orbits will have a separation d and an angular separation δ. For $\Delta P_\theta=0$

$$\delta = \frac{d}{r_1 \cos\alpha}. \tag{16}$$

That is, the orbits should be directed so as to intersect at the projected distance of closest approach to the axis.

2.2. Graphical

An ion moving in a trajectory orthogonal to the magnetic field lines (as in the midplane of a mirror coil system) will be deflected according to the relation

$$\varrho = 4.567 \frac{\sqrt{A\mathcal{E}}}{nB}, \tag{17}$$

where A is the mass number, $\mathcal{E}$ the energy in keV, n the number of electron charges, B the magnetic field strength in kG, and ϱ the radius of curvature in cm. In a magnetic field without high gradients the ion trajectories can be approximated over short path lengths by circular arcs. Practically, in the case of DCX-1 it proved to be sufficient to divide the midplane of the rotationally symmetrical field in concentric rings each radially about 2 cm wide.

Instead of calculating for each of these ring zones the radius of curvature ϱ (corresponding to the average value of B in this zone), it is convenient to use a special device, the "Trajectory Compass" (Fig. 2), which has been developed by R.L. Brown [3]. Use of this device greatly simplifies the determination of ion trajectories. The accuracy depends of course on the path length and is sufficient if only a small number of revolutions are considered.

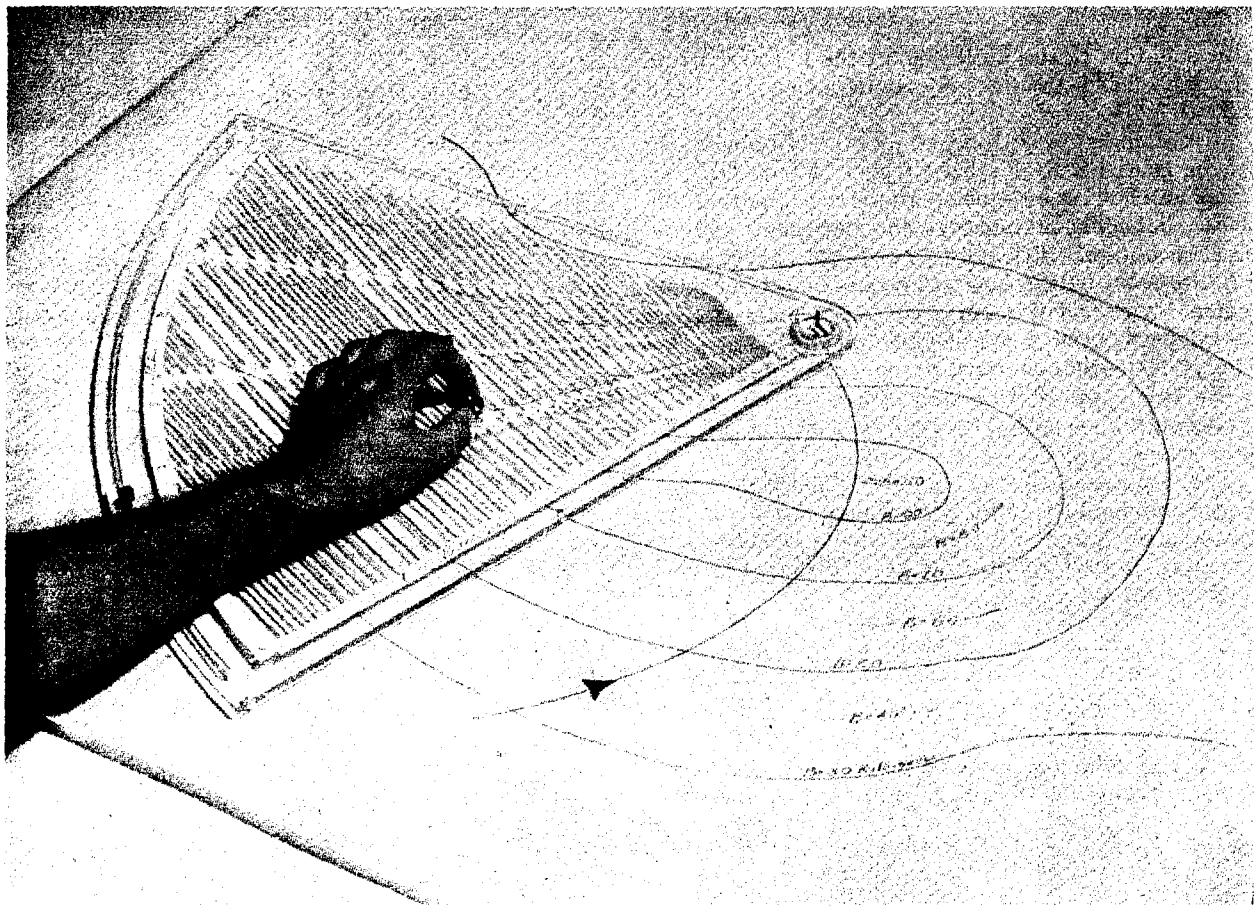

Fig. 2 Trajectory compass.

3. Ion movement in a helix: path length considerations

In DCX-2 extended molecular-ion path lengths will be achieved by injecting through a magnetically shielded duct at a small angle with respect to a plane perpendicular to the axis. The resultant trajectory is a helix whose pitch angle it is desired to minimize. The injection angle is chosen so that the ions just miss the duct after their first revolution in the field.

The analysis in this section will consider only the axial motion of the ions and neglect effects associated with radial field gradients.

A charged particle in a magnetic field moves in such a way that its magnetic moment remains constant so long as the percentage field change is small over one revolution. This relationship may be written

$$\cos^2\alpha = \mu\frac{B}{\mathcal{E}}, \tag{18}$$

where μ is the magnetic moment of the particle, α the angle between the particle's velocity vector and a plane perpendicular to the magnetic field, B the magnetic field intensity and $\mathcal{E}$ the kinetic energy of the particle.

For small α

$$\cos^2\alpha \cong 1-\alpha^2; \tag{19}$$

therefore, in this case

$$\alpha^2 = \alpha_i^2 - \frac{\delta B}{B_i}. \tag{20}$$

This equation relates at any point the injection angle α_i, the field at the injection point B_i, and $\delta B = B(z) - B_i$.

It is intended in DCX-2 to inject the beam near one mirror in a sharply localized region of reduced field. This "dip" will be adjusted to remove most of the axial component of velocity from the beam after the first revolution. Typically, $\alpha_i = 0.126$ radians and $\delta B(\text{dip})/B_i = 0.016$. Ions enter the central flat-field region with a small mean α chosen to maximize the path lengths. Too small an angle results in reflection of part of the beam in the dip, too large in an unnecessarily coarse pitch. This situation is investigated in more detail by considering separately the dip and flat-field regions.

The dip region influences only slightly the path length but modifies initially the angular distribution. For a given range of injection angles δ_i, the beam emerging from the dip will be distributed over a range given by

$$\delta = \sqrt{(\alpha_i+\delta_i)^2 - \frac{\delta B}{B_i}} - \sqrt{\alpha_i^2 - \frac{\delta B}{B_i}}$$
$$= \sqrt{\alpha_m^2 + 2\alpha_i\delta_i} - \alpha_m, \tag{21}$$

where α_m is the minimum angle at the second point.

If upon entering the flat field region $\alpha_m \approx 0$, then

$$\delta = \sqrt{2\alpha_i\delta_i}. \tag{22}$$

For the given value of α_i, an initial divergence of $\delta_i = 5\times10^{-3}$ radians gives an angular spread in the flat field region of $\delta = 3.5\times10^{-2}$ radians.

In general, if the initial distribution is denoted by $P(\alpha_i)\,d\alpha_i$, the distribution at an arbitrary point before any of the rays have been reflected will be $P(\sqrt{\alpha^2+(\Delta B/B)}\,\alpha\,d\alpha/\sqrt{\alpha^2+(\Delta B/B)})$. For example, in the case of a uniform cylindrical input beam, having a distribution denoted by

$$P(\alpha_i)\,d\alpha_i = \frac{\pi}{2\delta_i}\sin\left(\pi\,\frac{\alpha_i-\alpha_{i0}}{\delta_i}\right)d\alpha_i \tag{23}$$

(with full width at half maximum of $0.67\,\delta_i$), the modified distribution is

$$P'(\alpha_f)\,d\alpha_f = \frac{\pi}{\delta_f}\sin\left(\pi\,\frac{\alpha_f^2}{\delta_f^2}\right)\frac{\alpha_f}{\delta_f}\,d\alpha_f \tag{24}$$

(with full width at half maximum of $0.45\,\delta_f$) at the point where the ray of minimum α is reflected. Fig. 3 shows the two distributions.

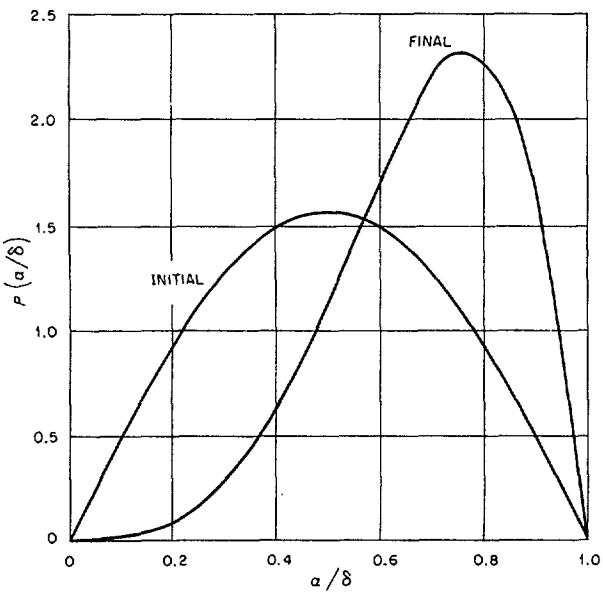

Fig. 3 A comparison of the distribution of axial components of ray angles in an ion beam between the point of injection and the flat-field region. The initial distribution is that of a uniform cylindrical beam.

Clearly, field irregularities in the flat region will have little effect on the average path length as long as $\Delta B/B \ll \delta_f^2$. For example, when $\alpha_i = 0.126$ and $\delta_i = 5\times10^{-3}$ as above, $\delta_f^2 = 1.2\times10^{-3}$.

An approximation to the path length, taking into account the very long paths of some particles, has been obtained by assuming that the field can be expressed as

$$B = B_0\left[1 - \frac{\delta B}{B_0}\left(\frac{z}{L}\right)^{2n}\right], \tag{25}$$

where z is measured from the center of the machine; the injector is taken to be at $z=-L$, and the opposite mirror at $+L$. The path length of a particle over the axial range $-L$ to $+L$ is

$$\mathcal{L}^* = \int_{-L}^{z^*}\frac{dz}{\alpha} = \int_{-L}^{z^*}\frac{dz}{\sqrt{\alpha_i^2 - \Delta B(z)/B_i}}, \tag{26}$$

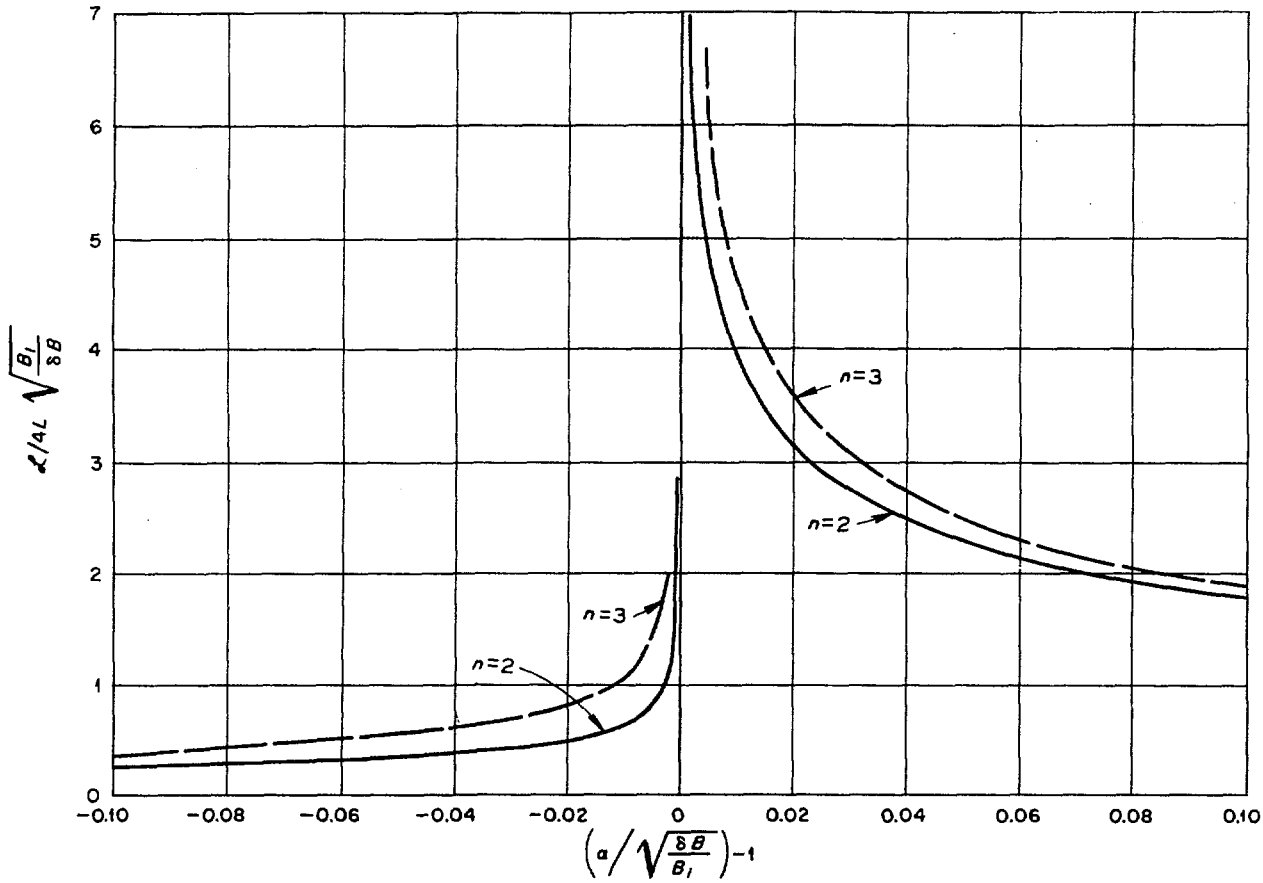

Fig. 4 Path length of beam injected at $-L$ for field $B=B_0\,[1-\delta B/B_0\,(z/L)^{2n}]$. Reflection at $z=+L$ is assumed for $\alpha_1>\sqrt{\Delta B/B_0}$.

where $z^*=+L$ for $[\alpha_i^2-(\Delta B/B_i)]^{\frac{1}{2}}\neq 0$ anywhere in the region; otherwise, $z^*=z\,(\alpha=0)$, the axial co-ordinate of the reflection point.

Substitution for $\Delta B/B_i$ yields after some manipulation

$$\mathcal{L}=2L\sqrt{\frac{B_i}{\delta B}}\int_{-1}^{x^*}\frac{dx}{\sqrt{x^{2n}-\gamma}}, \qquad (27)$$

where $\mathcal{L}$ is the path length including return from the reflection point and

$$x=Z/L,\ \gamma=1-(\alpha_i^2 B_i/\delta B)$$
$$x^*=+1 \qquad (\gamma<0)$$
$$x^*=-\gamma^{1/2n} \qquad (\gamma>0).$$

The integral was evaluated numerically for $n=2$ and 3. Fig. 4 shows the results.

It will be recognized that the abscissa is approximately the fractional angular deviation of a ray leaving the injector from the path which just results in reflection. Using the values assumed above for α_i and δ_i, the effective path is an average over an abscissa interval 0.04 units wide. The ordinate is the ratio of actual path length to that which would be obtained if the beam continued to the mirror and back at a constant pitch equal to $\sqrt{B_i/\delta B}$. For the parameters given above, a uniform distribution of injection angle gives $\mathcal{L}/[4\,L\sqrt{B_i/\Delta B}]=4.1$ (for $n=3$) and 3.5 (for $n=2$) for the best choice of α_i. This result suggests a path length of about 250 meters in DCX-2.

The insensitivity of path length to choice of exponent in the field shape characterized by Eq. (25) for the cases calculated indicates that the exact shape of the actual containing field should be unimportant. The curves provide an insight into the effects on path length of certain limiting parameters such as the magnitude of the field dip and the average injection angle.

4. Field optimization

An ideal magnetic field configuration for an experimental device like DCX-2 would consist of two magnetic mirrors and a central zone which is perfectly homogeneous, with the exception of a "field dip" which serves to change the injection angle (as determined by the injection duct) into the pitch angle of the helix. Because of the necessary accessibility (port holes for plasma diagnostics, space for injection duct), lumped magnet coils must be provided and it is therefore impossible to make the central zone perfectly homogeneous. Calculations for an infinite array of lumped

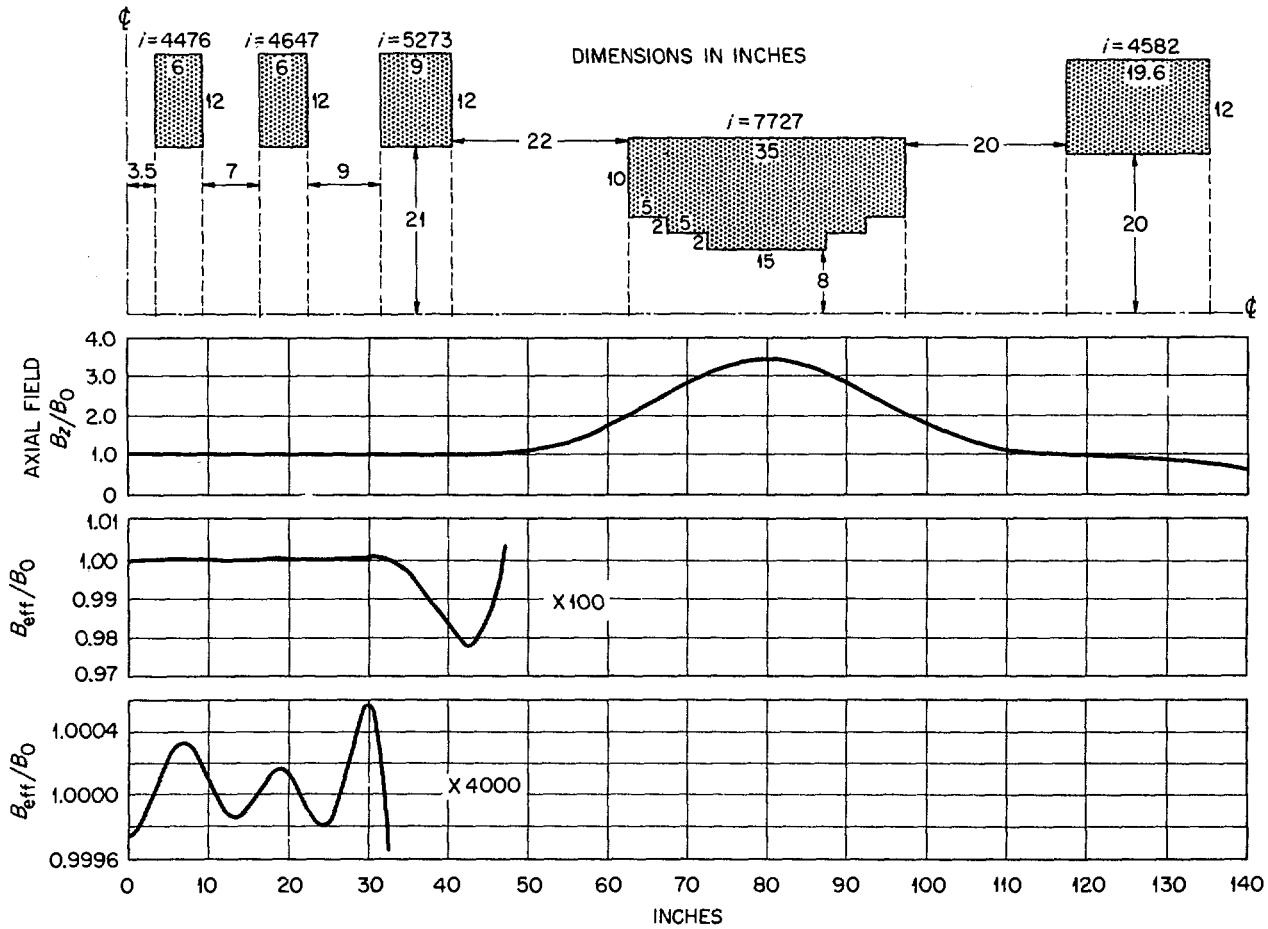

Fig. 5 DCX-2 coil arrangement with field plots.

solenoids [4] predict for similar coil dimensions a ripple amplitude in the order of several parts in 10^5. One cannot expect to produce the same extremely good homogeneity in the central magnetic field zone of a DCX device, since the magnetic field strength has to increase over a short distance to the full value under the mirror coils, for instance to 350%.

Fig. 5 shows a coil arrangement for DCX-2. For the field design the following procedure was used [5]. All geometrical coil dimensions, including distances between coils, have been assumed for a first trial calculation. Free variables are the current densities i_1, i_2, and i_3 in the three inside booster coil pairs, and the average flux density B_0 in the central zone. The power dissipated in one mirror coil is assumed to be 6 MW (for operation with deuterium), producing a magnetic flux density of 59 kG, and each outside booster coil is energized with 0.875 MW. The field deviation along the axis is

$$\Delta B = B_z(z) - B_0. \tag{28}$$

The optimization is performed by making

$$\int_0^{L_h} (\Delta B)^2 \, dz \rightarrow \text{minimum} \tag{29}$$

or

$$\frac{\partial}{\partial i_k} \int_0^{L_h} (\Delta B)^2 \, dz = 0 \tag{30}$$

$$\frac{\partial}{\partial B_0} \int_0^{L_h} (\Delta B)^2 \, dz = 0 . \tag{31}$$

The half-length of the central homogeneous zone is represented by L_h. From Eq. (31) the current densities i_k and the magnetic field strength B_0 can be obtained by solving four linear equations ("optimization with floating mirror ratio"). In order to achieve a desired B_0 value, the procedure has to be repeated with other distances between the mirror coils.

Up to now the optimization of $B_z(z)$, the flux density along the axis, has been considered. For orbit calculations, however, the quantity

$$B_{\text{eff}}(z) = \frac{5}{8} B_z(0, z) + \frac{3}{8} B_z(r = r_{\max}, z) \tag{32}$$

the "effective flux density", is of more importance (see Section 8). The optimization procedure described above can be applied here directly. Computer codes have been programmed [6] which permit performing this optimization procedure for any similar coil arrange-

ment in a very convenient way. In Fig. 5 the three plots represent the magnetic flux density component B_z, normalized to the value at the center of the coil system. The first plot shows B_z on axis. The homogeneous central zone extends on both sides of the center for a distance of more than 75 cm; the mirror ratio is approximately 3.5. On the second plot B_{eff} is drawn 100 times enlarged and a "field dip" is easily recognizable. The scale of the third plot is 4000 times enlarged. B_{eff} ripples of several parts in 10^4 can be seen; the ripples of B_z on axis are still appreciably smaller. From this fact, it follows that the ripples of the DCX-2 coil arrangement are only a few times larger than those of a corresponding infinite coil array. This result seems to be very satisfactory when the relatively large mirror ratio 3.5 is considered.

Besides this "optimization with floating mirror ratio" a somewhat simpler optimization procedure can be used when the value B_0 is specified. The only unknowns are now i_1, i_2 and i_3, and Eq. (30) yields the necessary three linear equations ("optimization with fixed mirror ratio"). Fields obtained in this way are not as homogeneous as those optimized with floating mirror ratio. However, if the specified B_0 is only a few percent different from the value found by means of this latter method, the homogeneity does not change significantly.

5. Synthesis of optimized fields by superposition

In order to form an appropriate "field dip" near the point of injection, it proved to be necessary to provide a special "dip coil" between the injection duct and the adjacent mirror coil. It is of course possible to assume shape and location of the dip coil and to find for each value i_D of its current density the current densities i_1, i_2 and i_3 of the booster coil pairs as described previously (Eq. (30)). Detailed studies demonstrated, however, that an appropriate field dip could not be obtained along with an optimized homogeneous central field merely by intelligently guessing the value i_D. It was only by applying the following superposition theorems that satisfactory results could be easily achieved [7]. Without giving a proof here, the essential concept can be set forth as follows:

(*a*) The mirror coils and the outside booster coils energized with known current densities, produce along the axis the flux density $B_a(z)$. Using Eq. (30) it is possible to find the current densities i_{ak} of the three inside booster coils so that the resulting field $B_a'(z)$ approaches as well as possible the value zero in the zone $-L_h \leqq z \leqq +L_h$, Fig. 6a.

(*b*) The dip coil pair energized with any arbitrarily assumed current density i_D^* produces along the axis a flux density $B_D^*(z)$. Again by means of Eq. (30) it is possible to determine current densities i_{bk} of the three inside booster coils so that the resulting field $B_b'(z)$ approaches as well as possible the value zero in the mid-zone, Fig. 6b.

(*c*) The inside booster coil pairs energized with the current densities i_{ck} produce on the axis a field $B_c'(z)$ which approaches as well as possible in the mid-zone an arbitrarily assumed constant value B_0^*, Fig. 6c.

With energized mirror and outside booster coils and with the inside booster coils energized with the current densities

$$i_k = i_{ak} + \frac{i_D}{i_D^*} i_{bk} + \frac{B_0}{B_0^*} i_{ck}, \qquad (k = 1, 2, 3) \qquad (33)$$

a resulting field is produced (Fig. 6a, dotted line) which deviates as little as possible from B_0 in the mid-zone. Finding the optimized field $B_z(z)$ by means of

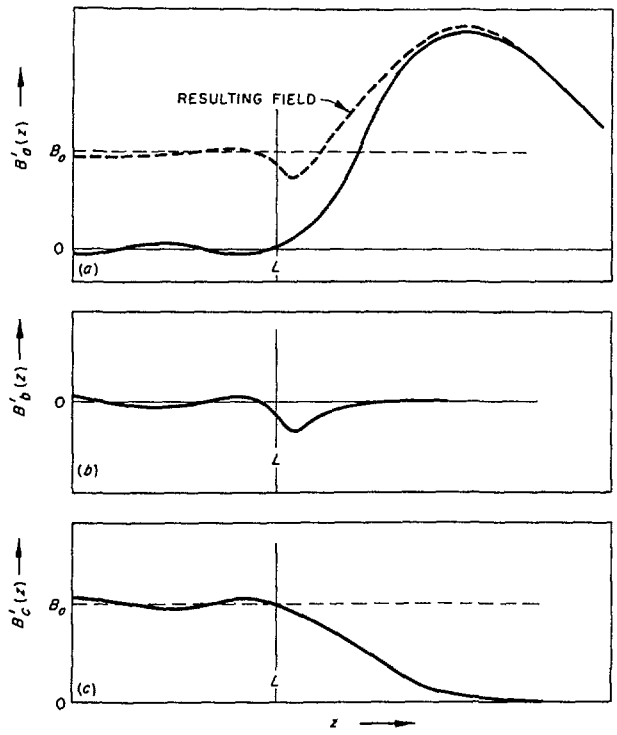

Fig. 6 Field synthesized by superposition of component fields (not drawn to scale to show more clearly the field deviations in the "homogeneous" zone and the dip region).

the described superposition of the three optimized component fields has the advantage that it is not necessary to re-optimize for each selected value of B_0 and i_D. Furthermore, the independent component fields permit rapid synthesis of a desired field shape. The same method can be used for optimizing $B_{\text{eff}}(z)$ instead of B_z along the axis. Finally a synthesis by superposition of optimized component fields is also possible if B_0 is not specified ("floating mirror ratio").

6. Some geometrical properties of ion trajectories [8]

The trajectory of a charged particle (rest mass m_0, charge q) moving with the velocity $\mathbf{v}$ (velocity of light $= c$) through an electromagnetic field (electric

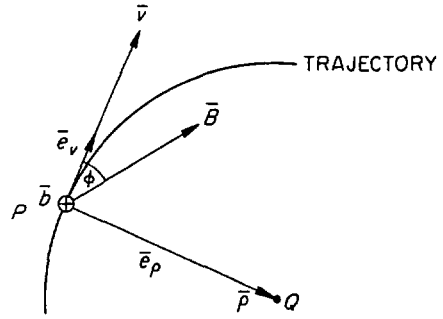

Fig. 7 Trajectory with principle unit vectors $\hat{\mathbf{e}}_v$, $\hat{\mathbf{e}}_\varrho$ and $\hat{\mathbf{b}}$, see Eq. (35).

field strength **E**, magnetic flux density **B**) is determined by Lorentz' equation

$$\frac{\mathrm{d}}{\mathrm{d}t}\frac{m_0\mathbf{v}}{\left(1-\frac{v^2}{c^2}\right)^{\frac{1}{2}}}=q(\mathbf{E}+\mathbf{v}\times\mathbf{B})\,. \tag{34}$$

The unit vectors in the directions of **v**, of the principal normal, and the binormal of the trajectory are

$$\begin{aligned}\hat{\mathbf{e}}_v&=\mathbf{v}/v\\ \hat{\mathbf{e}}_\varrho&=\boldsymbol{\rho}/\varrho\\ \hat{\mathbf{b}}&=\mathbf{e}_v\times\mathbf{e}_\varrho,\end{aligned} \tag{35}$$

where $\boldsymbol{\rho}$ is a vector pointing from the particle position P to the center of curvature Q of the trajectory, Fig. 7.

The vector

$$\mathbf{w}=\frac{q}{m_0}(\mathbf{E}+\mathbf{v}\times\mathbf{B}) \tag{36}$$

can be split into two perpendicular components

$$\mathbf{w}=\mathbf{w}_v+\mathbf{w}_\varrho, \tag{37}$$

where

$$\mathbf{w}_v=\left(\frac{\mathbf{w}\cdot\mathbf{v}}{v^2}\right)\mathbf{v}\,. \tag{38}$$

It can be shown [8] that

$$\boldsymbol{\rho}=\frac{v^2}{\left(1-\frac{v^2}{c^2}\right)^{\frac{1}{2}}}\frac{\mathbf{W}_\varrho}{W_\varrho{}^2}\,. \tag{39}$$

Knowledge of the curvature and of the direction of the principal normal, that is $\boldsymbol{\rho}$ as given by Eq. (39), at any point of the space curve is sufficient to determine the orbit step by step.

Several graphical methods use the projections of trajectories on a stationary plane. The radius of curvature of such a curve for the non-relativistic movement of charged particle in a rotationally symmetrical magnetic field (cylindrical co-ordinates r, θ, z) can be easily found [8]. If $\varrho_\perp$ is the radius of curvature of the trajectory-projection on a plane perpendicular to the z-axis, then

$$\frac{1}{\varrho_\perp}=-\frac{qB}{m\sqrt{v_r{}^2+v_\theta{}^2}}\left[1-\left(\frac{v_r v_z}{v_r{}^2+v_\theta{}^2}\right)\frac{B_r}{B_z}\right]. \tag{40}$$

This expression is useful for discussing the accuracy of graphical methods for determining ion orbits.

In the case of a rotationally symmetrical magnetic field and of $\mathbf{E}=0$ the Hamiltonian of Eq. (1) leads to a description of the r-z motion independent of the $\theta\,(t)$ motion. A trajectory of the r-z movement is of course not the projection of the actual trajectory (in space) on a given plane. The velocity vector of the r-z movement is

$$\mathbf{u}=\hat{\mathbf{e}}_z v_z+\hat{\mathbf{e}}_r v_r, \tag{41}$$

$$u^2=v^2-v_\theta{}^2.$$

The projection of the vector

$$\mathbf{B}_{rz}=\hat{\mathbf{e}}_z B_z+\hat{\mathbf{e}}_r B_r \tag{42}$$

on the direction of **u** is

$$B'=B_z\cos\alpha+B_r\sin\alpha, \tag{43}$$

as shown in Fig. 8. An auxiliary quantity ϱ' is introduced by

$$\varrho'=-\frac{m v_\theta}{q B'}\,, \tag{44}$$

which applies to a circular movement around the z axis. Then the radius of curvature ϱ of the trajectory of the r-z movement is given by

$$\frac{1}{\varrho}=-\frac{v_\theta{}^2}{v^2-v_\theta{}^2}\left(\frac{1}{\varrho'}-\frac{\cos\alpha}{r}\right). \tag{45}$$

This relation allows a simple graphical determination of the r-z movement trajectory. It must be noted,

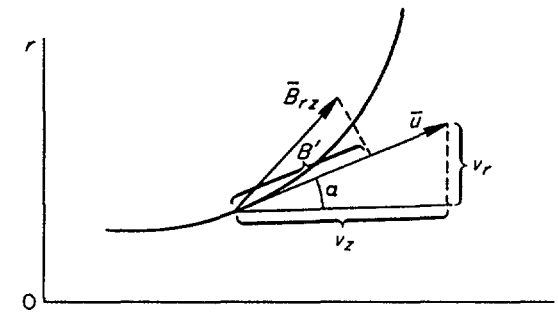

Fig. 8 Trajectory of the r-z movement.

however, that graphical methods directly connected with the actual movement in space should give in general better results. This follows from the fact that a spatial trajectory with little change in curvature corresponds to an r-z movement with rapidly changing ϱ if the trajectory passes near the z-axis.

7. Higher approximations to injected orbits

7.1. Effective magnetic field

The use of lumped coils to produce the homogeneous central field of DCX-2 leads to the presence of field ripples which grow with distance from the axis. It follows to ask what will be the effects of these ripples on the tightly pitched orbits and, more explicitly, what effective field to use in the orbit calculations based on the magnetic moment.

The approximate analysis consists of evaluating the axial impulse per turn imparted by radial magnetic field components and thus deriving an expression to compare with Eq. (20). The magnetic field components off-axis at given z are given in terms of the derivatives on-axis $B^{(n)}(z)$ by

$$B_z(r,z) = \sum_{n=0}^{\infty} B^{(n)}(z) P_n(0) \frac{r^n}{n!}, \tag{46}$$

$$B_r(r,z) = \sum_{n=0}^{\infty} B^{(n)}(z) P_{n+1}(0) \frac{r^n}{n!}, \tag{47}$$

where the $P_n(0)$ are Legendre Polynominals of argument zero.

The impulse per turn may be expressed by the resulting change in pitch angle $\Delta\alpha$.

$$\Delta\alpha = -\frac{e}{Mvc} \int_0^{2\pi/\omega} r\dot{\theta} B_r \, dt. \tag{48}$$

Using (47) and (3a) for an orbit which cuts the axis, integrating and dividing by the advance per turn $2\pi a \alpha$ leads to

$$2\alpha \frac{\Delta\alpha}{\Delta z} = \frac{1}{B} \frac{d}{dz} \left[B^{(0)}(z) - \frac{3}{8} B^{(2)}(z) a^2 + \frac{5}{48} B^{(4)}(z) a^4 - \cdots \right] \tag{49}$$

which is essentially the desired form.

The quantity in brackets represents the desired effective field B_{eff}. To a good approximation in the first three terms:

$$B_{\text{eff}} = \frac{5}{8} B_z(0) + \frac{3}{8} B_z(2a). \tag{50}$$

Use of this field is mainly of importance for estimating the size of the field dip.

7.2. Stepwise integration of helical orbits

The approximation of the previous paragraph was not found sufficient for following actual orbits in the dip region, both because it neglected the change in axial co-ordinate in evaluating B_r and because Eq. (50) did not adequately describe B_r in the dip. A second approximation consisted in integrating Eq. (48) over small arcs of a helix of constant radius and successively inserting appropriate values of z and r, and computer values for B_r. The equations used at each step were

$$\alpha_1 = \alpha_0 - \cos\beta \left(\frac{B_r(r_0)}{B_z(0)} \right) \Delta\theta, \tag{51}$$

where β is the angle between v and $r\dot{\theta}$, and

$$z_1 = z_0 + a\alpha_0 \Delta\theta. \tag{52}$$

This method was used for orbits which did not cut the axis, as well as for those which did. In fields varying less than 10% over a Larmor diameter, 30-degree increments $\Delta\theta$ were satisfactory for following a few revolutions.

In more strongly varying fields constant radius of curvature could not be assumed; it was necessary to supplement the above method by following the azimuthal motion with the graphical technique of Section 2.2. That is, for each step a new center of curvature was calculated and the azimuthal increment made graphically.

This combined technique was used for calculating the amount of precession resulting from passage through a dip and reflection from a mirror.

7.3. Field and orbit computer code

A major problem confronting the use of high-speed digital computers for calculating particle orbits in magnetic fields encountered in actual practice has always been the impracticality of storing a network of field values, then retrieving the appropriate values (and interpolating) at each point on the orbit. Most such calculations have thus employed synthetic fields which reproduced only roughly the features of actual fields. A code has been written in connection with the DCX-2 design which bypasses this limitation and which appears to make possible for the first time the calculation of extended ion orbits in fields produced by arbitrary co-axial assemblies.

The code makes use of an ingenious routine, written by M. W. Garrett assisted by C. E. Parker [9], for calculating the field in terms of Legendre polynomials. The coefficients, which can be expressed analytically for coils of rectangular cross section, must be recalculated each time the particle moves out of a zone of convergence of the series which describes the field. In the DCX-2 calculations this occurred one in several hundred integration steps along the orbit. Thus there are the following advantages: the field is described to an accuracy of a few parts in 10^7; in the input data the magnetic geometry is given solely in terms of coil co-ordinates and currents; and the computation is extremely fast. In writing the orbit code, a fourth-order Runge-Kutta method was used to integrate the equations of motion. Nyström [10] has developed a technique especially designed for second-order differential equations, which has the advantage that in each integration step the magnetic quantities need be evaluated only 3 times instead of the usual 4.

Accuracy of the code is dependent on the choice of a co-ordinate system because of the different forms taken by the equations of motion. Experience has shown that in cylindrical co-ordinates the error is a function of the initial conditions—the error increasing as the orbit approaches the co-ordinate axis. In Cartesian co-ordinates no such difficulty is encountered; with an integration step of 6% of the Larmor radius, the particle can be followed reliably in the DCX-2 field for at least 50 turns (requiring about 10 minutes on the IBM 7090).

8. Perturbations and collective effects

It is inherent in most schemes leading to extended molecular-ion trajectories that the attainable path

length is subject to drastic effects of small perturbations. This section contains estimates of such effects, some of which apply also to the trapped ions.

8.1. Orbit precession in a magnetic field gradient

The path length in the DCX-2 injection system will be increased by a large factor if the molecular-ion orbit on its first reflection from a magnetic mirror is caused to precess around the magnetic axis just far enough to miss the injection duct.

As a simple example which gives relationships adequate to estimate the magnitude of the effect one may consider the first-order precession of a planar orbit which cuts the axis in a parabolic field $B(r)$:

$$B(r) = B_0 (1 - \delta r^2). \tag{53}$$

The precession per revolution is given by a modification of Eq. (8c):

$$\Delta\theta = \pi - 2\int_0^{r_m} \frac{\dot{\theta}\, dr}{[v^2 - r^2\dot{\theta}^2]^{\frac{1}{2}}}. \tag{54}$$

Evaluating $\dot{\theta}$ by means of Eq. (3a) and Eq. (53):

$$\Delta\theta = \pi - \frac{1}{a}\int_0^{r_m} \frac{(1 - \delta r^2/2)\, dr}{[1 - (r^2/4a^2)(1 - \delta r^2/2)^2]^{\frac{1}{2}}}, \tag{55}$$

where $a = Mvc/eB_0$ and $r_m = 2a(1 + 2\delta a^2) + O(\delta^2 a^4)$ is the extreme value of r. Transforming to r/r_m as the variable of integration permits expanding the denominator in powers of δ and gives to first order

$$\Delta\theta = -2\pi\, \delta a^2$$
$$= -2\pi [1 - B(a)/B(0)]. \tag{56}$$

The negative sign indicates the direction of precession in a right-handed co-ordinate system with B directed along the positive z axis; $\dot{\theta}$ is also negative.

In DCX-2, molecular-ions experience the largest field gradient in the fraction of a turn during reflection from the mirror. For 25 cm diameter orbits (e.g. H_2^+) the precession angle is 12 degrees, about 25% of that required to miss the injection duct now contemplated.

8.2. Precession resulting from plasma diamagnetism

The difference in magnetic field between the exterior and interior of a uniform, slightly diamagnetic plasma is given by

$$\frac{\Delta B}{B} = \frac{1}{2}\beta, \tag{57}$$

where β is the ratio of plasma pressure to magnetic field pressure. Fig. 9 shows a cylindrical plasma column in a uniform field. The arc of the molecular-ion orbit inside the plasma column subtends an angle α. If the orbit center is located a distance r_0 from the plasma

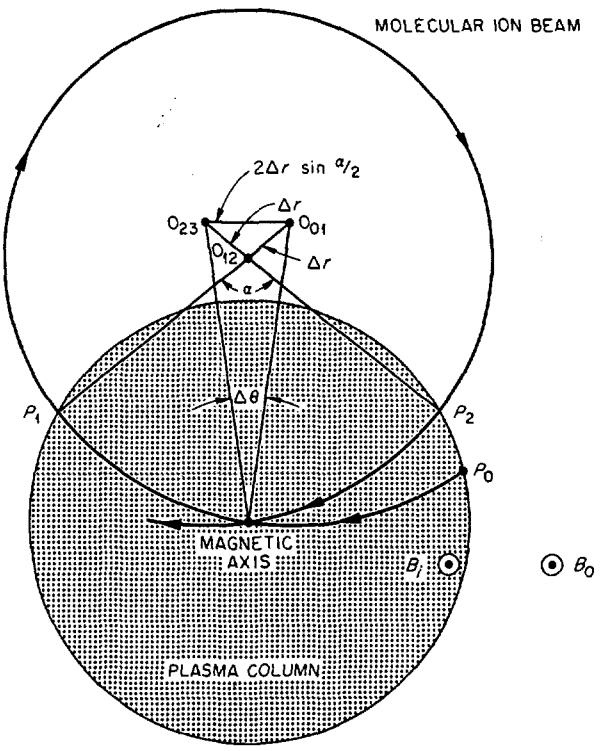

Fig. 9 Orbit precession in a diamagnetic plasma column.

axis, simple geometrical considerations (Fig. 9) show

$$\Delta\theta \cong 2\frac{\Delta r_0}{r_0}\sin\frac{\alpha}{2} \tag{58a}$$
$$= 2\frac{\Delta a}{a}\frac{a}{r_0}\sin\frac{\alpha}{2} \tag{58b}$$
$$= 2\frac{\Delta B}{B}\frac{a}{r_0}\sin\frac{\alpha}{2}, \tag{58c}$$

where a, as above, is the radius of curvature.

For H_2^+ in DCX-2, $r_0 \cong a$ and $\sin \alpha/2 \cong 1$. Since the region of reduced field is traversed about 100 times per reflection from a mirror, $\Delta B/B$ need be only 3% of the field drop cited in Eq. (56) in order to offset entirely the precession at the mirror. Alternatively, β need be only 1% to give a precession of about one radian. This β is expected to occur at roughly the critical density for burnout.

Eq. (58c) also describes the precession of the trapped protons in the magnetic field of non-precessing molecular ions ($\Delta B/B \lesssim 10^{-4}$). Precession around the center of the molecular ion orbit would result in particle loss from the machine even for the expected $\Delta B/B$, inasmuch as 10^6—10^8 revolutions of trapped protons are expected. However, proton precession around the magnetic axis will cancel the effect to first order.

8.3. Precession in the radial electric field resulting from a plasma potential

Under certain conditions a secondary cold plasma at wall potential may surround the main plasma, the electric field appearing in a well-localized sheath. For

near-normal passage through the sheath, the resulting precession may be calculated from Eq. (58c) of the preceding paragraph, using $\Delta a/a = -\frac{1}{2} eV/\mathcal{E}$ where eV is the plasma potential energy and $\mathcal{E}$ is the particle kinetic energy:

$$\Delta\theta = -\frac{eV}{\mathcal{E}} \frac{a}{r_0} \sin\frac{\alpha}{2}. \tag{59}$$

A plasma potential energy of the order of 1% of the kinetic energy would not be at all surprising in view of the OGRA results [11] even at densities far below the critical density. Thus a substantial precession of the molecular-ion orbit may be expected.

Eq. (59) also describes the precession resulting from the presence of an arc at a potential different from that of the surrounding plasma. In this case, α is small enough that the effect for molecular ions is ordinarily negligible. The effect for trapped protons may be comparable with the expected precession in the magnetic field gradient.

In the absence of the secondary plasma the electric field will extend to the chamber wall and will vary inversely as the radius. Approximating this by

$$E = E_0\left(2 - \frac{r}{r_0}\right) \tag{60}$$

(where E_0 is the field strength at r_0, the co-ordinate of the plasma surface) results in a linear equation of radial motion for an orbit which cuts the axis. The angular velocity about the axis ($-\omega/2$) is unaffected by the radial field. Integration of the radial equation gives the period of the motion T and thus:

$$\Delta\theta = -\frac{\omega}{2} T = -4\left[\cos^{-1}\gamma - 3\gamma(1-\gamma^2)^{\frac{1}{2}}\right] \frac{eE_0}{Mr_0\omega^2} \tag{61a}$$

$$= -\frac{1}{2\gamma^2}\left[\cos^{-1}\gamma - 3\gamma(1-\gamma^2)^{\frac{1}{2}}\right] \frac{eV}{\mathcal{E}\ln(r_2/r_0)}, \tag{61b}$$

where $\gamma = r_0/2a$ and r_2 is the chamber radius. The plasma potential energy necessary to give 0.01 radian precession per turn in DCX-2 is about 2.5% of the kinetic energy.

8.4. Effects of the injection duct

The magnetic field perturbation by the magnetically compensated injection duct [1] is expected to result mainly from imperfect compensation at the end. Measurements on a test model suggest that this perturbation may be represented by a magnetic dipole located at $R = 25$ cm whose field strength at the DCX-2 axis (B_1) is about 1 gauss, maximum. In the plane perpendicular to the axis and containing the effective dipole

$$B = B_0(r) + \frac{B_1 R^3}{[R^2 + r^2 - 2Rr\cos\theta]^{\frac{3}{2}}}, \tag{62}$$

where B_0 is the main field.

It is of interest to consider the problem of precession of the trapped protons around the perturbing dipole, which is potentially a loss mechanism. Neglecting the curvature of the path, the first-order drift velocity $\mathbf{u}$ in a field gradient in a plane [12]

$$\mathbf{u} = \frac{c}{2eB^3} Mv_\perp^2 \mathbf{B} \times \nabla_\perp B. \tag{63}$$

The drift path thus follows contours of equal $|\mathbf{B}|$. The main DCX-2 field in the plane under discussion drops about 1% over the diameter of a proton orbit, a field change an order of magnitude larger than that of the perturbing dipole. The equal $|\mathbf{B}|$ contours are thus distorted only very slightly and there is expected to be no net radial drift.

An asymmetrical electrostatic field between the plasma surface and the injector duct may be a source of greater concern. The drift, to first order, will follow contours of constant $|\mathcal{E}_\perp(\nabla_\perp B/B) + \nabla_\perp V|$. The two terms may be of comparable magnitude and thus may give contours that lead to the wall. Firsov, quoted by Golovin *et al.* [11], has considered this phenomenon and pointed out that the addition of helical magnet windings to OGRA would prevent it. If, however, the trapped protons are surrounded by a cold secondary plasma at wall potential, the asymmetric field will not exist.

8.5. Space charge effects on molecular-ion orbits

Complete space-charge neutralization was assumed in making the path-length estimates of Section 3. The extent to which this must be satisfied can be estimated as follows. As a particle moves along the field, its axial component of kinetic energy changes by an amount

$$\frac{1}{2} M\Delta(v_z)^2 = \frac{1}{2} Mv^2 \Delta(\alpha)^2 = \frac{1}{2} Mv^2 \frac{\Delta B}{B}, \tag{64}$$

where Eq. (20) has been used. For static space-charge forces to be considered negligible, the space-charge potential energy variations along the axis ($e\Delta V$) must be much less than the variations described in Eq. (64):

$$e\Delta V \ll \frac{1}{2} Mv^2 \frac{\Delta B}{B}. \tag{65}$$

Using the conservative field requirements, it thus is required that $(\Delta V) \ll 1.4$ kV. If $L \sim 1$ m, $dV/dz \ll 14$ V/cm; this would not appear to be too stringent a condition in steady state. Achieving it may require a gradual beam buildup in order to avoid oscillations.

8.6. Effect of the magnetic field of an arc

Each near-normal passage of an ion through the magnetic field of a dissociating arc will result in an axial displacement Δz of the orbit plane. For passage through the arc center this is given to first order by

$$\Delta z = \frac{0.2 I_a}{B_0}\left[\frac{\pi}{2}\ln 2 + r_a \ln(2a/r_a)\right], \tag{66}$$

where a is the orbit radius, r_a the arc radius, and I_a the arc current. In DCX-2, with a 300-A arc, $\Delta z = 0.1$ mm. No effect on containment is expected.

Acknowledgments

The authors wish to acknowledge the significant contributions of R. L. BROWN, D. L. COFFEY, C. E. PARKER, MOZELLE RANKIN and J. E. SIMPKINS, Jr.; the clarifying discussions with P. R. BELL, A. C. DOWNING, W. GAUTSCHI and N. H. LAZAR; and the most helpful editorial assistance of P. A. THOMPSON.

This work was performed at Oak Ridge National Laboratory, operated by Union Carbide Corporation for the United States Atomic Energy Commission.

References

[1] BELL, P. R., KELLEY, G. G., LAZAR, N. H., MACKIN, R. J., JR., IAEA Conference on Plasma Physics and Controlled Nuclear Fusion Research, Salzburg, 1961: Paper CN-10/191, page 251 of this volume.
[2] PANOFSKY, W. K. H., PHILLIPS, Melba, Classical Electricity and Magnetism (Addison-Wesley Pub. Co., Massachusetts, 1955) 351—63.
[3] BROWN, R. L., in U.S. Atomic Energy Commission Report ORNL-2926 (January 1960) 81.
[4] NORTH, G. R., U.S. Atomic Energy Commission Report, ORNL-2975 (Aug. 10, 1960).
[5] LAING, E. W., "A Note on Magnetic Field Shaping", UKAEA (AERE Harwell) Report M-522 (1959); COFFEY, A. B., GAUSTER, W. F., SIMPKINS, C. O., in U.S. Atomic Energy Commission Report ORNL-3011 (July 31, 1960) 80.
[6] NORTH, G. R., RANKIN, M., U.S. Atomic Energy Commission Report ORNL-3011 (July 31, 1960) 83.
[7] GAUSTER, W. F., U.S. Atomic Energy Commission Report ORNL-3104 (Jan. 31, 1961) 101.
[8] *Ibid.*, 106.
[9] GARRETT, M. W., PARKER, C. E., to be published.
[10] NYSTROM, E. J., *Acta Soc. Sci. Fennicae* **50** (13) (1925) 1.
[11] GOLOVIN, I. N., ARTEMENKOV, L.I., BOGDANOV, G. F., PANOV, D. A., PISTUNOVICH, V. I., SEMASHKO, N. N., *Uspekhi Fiz. Nauk* **73** (1961) 685.
[12] ALFVÉN, H., Cosmical Electrodynamics (Oxford Univ. Press, London, 1950) 13—36.

THE DCX-2 PROGRAM OF PLASMA ACCUMULATION BY HIGH ENERGY INJECTION*

P. R. BELL, G. G. KELLEY, N. H. LAZAR, R. J. MACKIN, JR.

OAK RIDGE NATIONAL LABORATORY

OAK RIDGE, TENNESSEE, UNITED STATES OF AMERICA

This paper describes the experimental program associated with a new device being assembled to exploit the DCX scheme of plasma accumulation by dissociation-trapping of high-energy molecular ions. The long particle-containment time obtained in DCX-1 and a consideration of the known instabilities indicate that a high temperature plasma limited in density by mirror losses will be obtained in the new device provided no new instabilities occur.

The apparatus provides for an extended trajectory of the injected beam in the plasma region, permitting the use of much more tenuous dissociation media. Advantage will be taken of the ion-pumping action of the plasma to secure pumping speeds of approximately 0.5 million liters per second. The shape and strength of the magnetic field will provide containment of the trapped atomic ions governed by the adiabatic approximation.

A brief summary is given of the theory of plasma accumulation in a machine of this type, and the requirements imposed upon the system parameters are evaluated.

Existing elements in this program, which are the main subject of the paper, are:

1. A 600-keV accelerator and ion source designed to obtain 400 mA of ions in a well-organized beam. This system has provided 215 mA at 610 keV. The source itself has produced a continuous beam of 340 mA at 80 keV.
2. Almost-fully-ionized lithium and deuterium arcs with temperatures in the range of 10 to 50 eV. In the deuterium arc a degree of ionization as large as 99% has been obtained. Lithium arcs of large Li^{++} content have been operated in gas pressures as low as 4×10^{-7} mm Hg. Means have been found to adjust the density of the breakup column of the arc from very low densities to as high as 10^{14} cm^{-3}.
3. A beam-injection channel, shielded against the 12-kG field and highly compensated to minimize perturbation of the surrounding field.

1. Introduction

The goal of the Oak Ridge National Laboratory's DCX program is the accumulation of a hot, dense plasma by means of the injection and trapping of high energy ions in a magnetic container. Trapped protons are to be attained by injecting hydrogen molecular ions and dissociating them within the magnetic container. This scheme is under study in a number of forms at various laboratories. The container in every case is a magnetic mirror machine.

In DCX-1, the dissociation was first accomplished [1] by means of an energetic carbon arc. The arc was found to have two strongly adverse effects on plasma accumulation. First it served as a source of charge exchange centers and limited the lifetime of trapped ions to about 10 milliseconds. Second, it was found to interact with the trapped plasma so as to produce an anomalously large spreading in the energy of the trapped particles [2]. This effect, not yet quantitatively understood, served further to limit the attainable plasma density. However, with no arc, using dissociation on the background gas, lifetimes up to 3 sec have been attained [3, 4] with an estimated plasma density of 10^7.

In OGRA [5] (Atomic Energy Institute, USSR Academy of Sciences, Moscow) dissociation is achieved by collisions in the background gas and subsequently in the trapped plasma itself. For this approach to be feasible in a practical range of parameters, it is necessary that the injected molecular ions have a long path length within the magnetic container. In OGRA, with 6 meters between the magnetic mirrors, path lengths in excess of 1.5 km have been achieved [6].

Another machine employing the dissociation of molecular ions is under study at Euratom-CEA, Fontenay-aux-Roses [7]. It will have a multiple-turn molecular-ion trajectory and a dissociating arc. In the Phoenix machine [8] (AWRE, Aldermaston) and Alice [9] (UCRL, Livermore) trapped ions will be produced by the ionization of energetic neutral atoms.

DCX-2 is designed with the aim of achieving long path lengths for the molecular ions by a scheme different from that of OGRA or the Fontenay machine. Either arc dissociation or background-gas dissociation may be employed. The design parameters are such that the achievement of a high density plasma by either means is theoretically within reach.

Analyses of plasma accumulation in a device fed by molecular-ion dissociation in the background gas have been given by SIMON [10], MACKIN [11], GILBERT *et al.* [12], PREVOT and GOURDON [13], and GOLOVIN *et al.* [6]. References [11] and [13] and a report by SIMON [14], include calculations on plasma accumula-

* Conference paper CN-10/191, presented by G. G. Kelley. Discussion of this paper is given on page 355. Translations of the abstract are at the end of this volume of the Conference Proceedings.

tion using arc dissociation to achieve a critical density for buildup on the trapped plasma alone. Reference [12] and reports by FOWLER [15] and PREVOT [16] extend the analysis to include energy degradation by Coulomb collisions. DAMM *et al.* [9] and GOURDON and PREVOT [17] have analyzed the energetic-neutral atom injection concept.

Section 2 gives a brief description of DCX-2, and the subsequent sections describe elements of the system which have reached an advanced stage of development.

Many members of the ORNL Thermonuclear Division have made significant contributions to the DCX-2 program. Their efforts are gratefully acknowledged.

2. Brief description of DCX-2

DCX-2 has a magnetic mirror configuration with mirror coils 4 m apart and a central chamber 1 m in diameter. With the present arrangement of supplementary coils, the central field will be 12 kG and the mirror ratio 3.3. In one experiment (Fig. 1) a long molecular-ion path length or, alternatively, a large number of passes through a dissociating arc will be achieved by injecting the ions into a helical orbit with a very fine pitch. The beam will be injected near one of the mirrors through a magnetically shielded duct. After travelling the length of the machine and reflecting from the opposite mirror, the undissociated

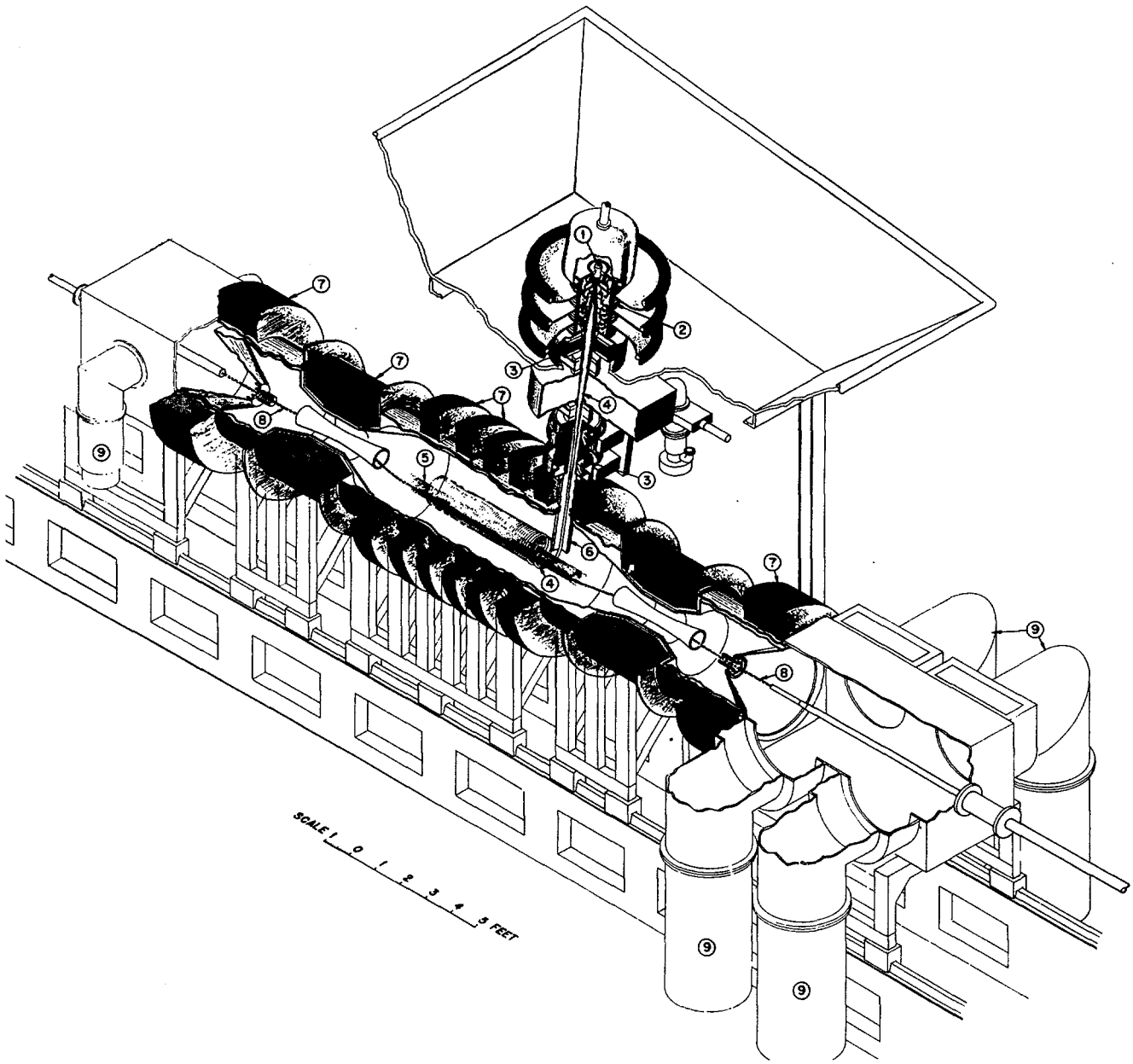

Fig. 1 Conceptual view of DCX-2 experiment for accumulation of thermonuclear plasma through the injection and trapping of high energy ions. 1—ion source, 2—accelerator tube, 3—magnetic lens, 4—molecular ion beam, 5—trapped plasma, 6—magnetically shielded injector, 7—magnetic field coils, 8—vacuum arc, 9—vacuum pumps.

particles will return and strike the duct. The injector will be inclined along the axis of the machine at such an angle that ions leaving it will just miss the duct after their first revolution in the magnetic field. The injection point will be in a region of slightly reduced field, and the molecular ions will sharpen up their pitch as they move into the uniform field region which extends over most of the length of the machine.

The stringent requirements imposed upon magnetic field homogeneity and on ion-beam divergence by this injection scheme are described in the companion paper [18]. Briefly, the axial magnetic field is designed to be uniform to within a few parts in 10^4 over a 1.5 m length. To exploit this field requires a beam divergence under 0.005 rad. It is expected that molecular ion path lengths in the plasma region in excess of 30 m can be attained, corresponding to about one hundred traversals of a dissociating arc.

The injection system is expected to be capable of producing 400 mA of 600-keV molecular ions in a continuous well-collimated beam. The magnetically-shielded duct is designed to produce minimal perturbation of the surrounding field.

The ion-pumping action of the trapped plasma will be used to maintain a high vacuum in the central region of the machine in the presence of the input beam. When the plasma density exceeds 10^{11} cm^{-3}, it is expected that the effective pumping speed will be greater than 500,000 l/s. Ions which drift through the magnetic mirrors will be pumped by evaporated titanium in a region beyond. The over-all pumping system will be such as to accommodate either condensable-vapor arcs or gas arcs.

The construction of the machine is such that a number of other injection concepts are feasible with only minor modifications.

3. The ion-injection system

The ion injection system is arranged as shown in Fig. 2. The source is described in [19]. Fig. 3 shows the details of the accelerator tube. Ions from the source are accelerated in four 150 kV gaps over a 30-cm path and are focused by a short magnetic solenoid lens whose center is 58 cm below the source. The resulting beam can be expected to fill the 15-cm lens aperture at about 500 mA.

Below the accelerator tube and lens will be a pumping chamber with a 25-cm diffusion pump and titanium evaporators. The desired mass component selected by the lens (either H_2^+ or H_3^+) will be directed through a magnetically shielded channel into the trapping region. The other mass components for the most part will strike the water-cooled walls of the system between the shielded channel and the pumping chamber. A second lens just above the shielded channel will be required under certain conditions.

The accelerator tube and upper lens are under test in the assembly shown in Fig. 4. The ion beam is projected through a pumping manifold into a large vacuum tank where its profile may be studied visually and by means of probes. The target, 315 cm below the

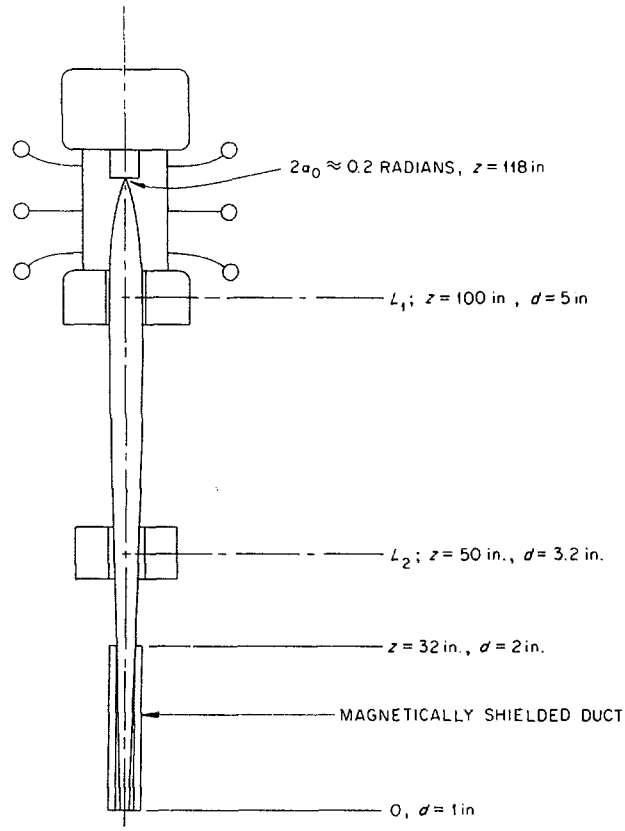

Fig. 2 Ion injection system for DCX-2 showing proposed un neutralized ion trajectory.

lens, is composed of a bank of parallel 0.9-cm diameter copper tubes set at an angle of 30° to the beam axis. Water flowing through each tube is caused to swirl by means of a spiral inconel ribbon. The ribbon which has a pitch of about 1/2 turn per centimeter is swaged into the tube. This target has operated at a power density of at least 3.5 kW/cm^2 and is expected to withstand more than twice this amount.

The accelerator tube has held 700 kV with no beam and 610 kV with a hydrogen ion beam of 215 mA. Cylindrical tungsten probes, 0.5 cm in diameter, may be swept through the beam at distances of 1.4, 1.9, and 2.4 m below the center of the lens. The probe current profiles permit a crude analysis of the beam. These measurements indicate that greater than 50% H_2^+ has been obtained at about 200 mA beam current.

Probe data also are used to determine the diameter of the ion beam in the lens. With an ion extraction geometry chosen to deliver 400 mA, this diameter is a minimum of 8.1 cm at 75 mA, increasing to 9.4 cm at 150 mA. Its rate of increase is much less than the one-half power of the current, probably because of changes in the shape of the ion emission surface in the source.

The use of magnetic focusing causes trapping of electrons released from the walls, the target and the background gas, and results in space-charge neutralization of the beam below the lens. A cross-over may be

formed and observed in the drift space. The beam shows no tendency to diverge above the cross-over but is dispersed so rapidly below that it seems to disappear.

Quantitative measurements in another test facility between 50 kV and 70 kV confirm the self-neutralization effect. They also show that the beam is no longer neutralized when an electric field is provided to drain the electrons from it. For example, a positive target

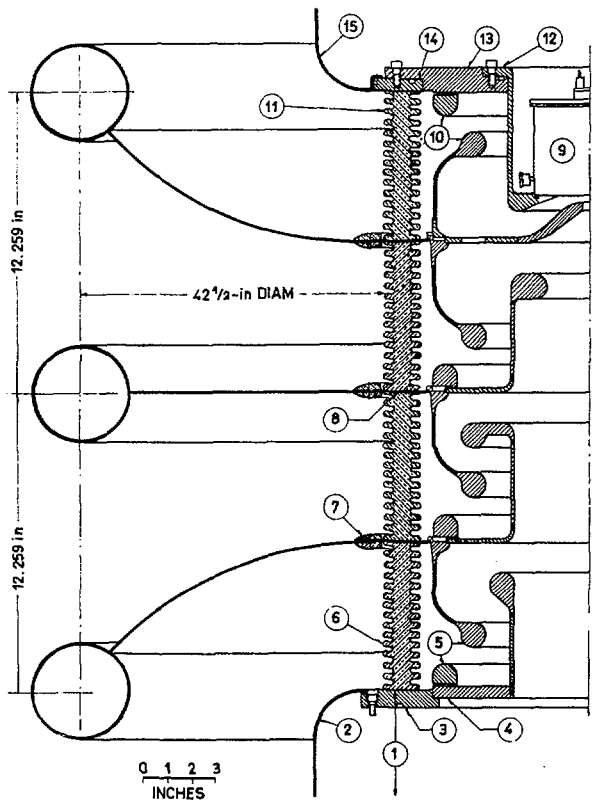

Fig. 3 Details of electrode configuration for 600 keV accelerator tube. The beam radius shown assuming 10° initial divergence. 1—exact static shield length to be determined in field installation, 2—bottom static shield, 3—bottom support flange, 4—bottom flange, 5—guard ring, 6—insulator tube, 7—clamping ring, 8—electrode support ring, 9—source assembly, 10—guard ring, 11—insulator tube, 12—source bucket, 13—top flange, 14—top support flange, 15—top static shield.

bias causes the beam to diverge to the extent expected in the absence of neutralization. A localized transverse magnetic field above the target prevents target bias from de-neutralizing the beam between the transverse field and the lens.

It is expected that the injector may be operated with either a neutralized or an unneutralized beam. An unneutralized beam profile is shown in Fig. 2. The beam is parallel entering the trapping volume. With neutralization only the upper lens will be used and will focus the beam to a cross-over at the channel exit.

These experiments were carried out in collaboration with O. B. Morgan and R. C. Davis.

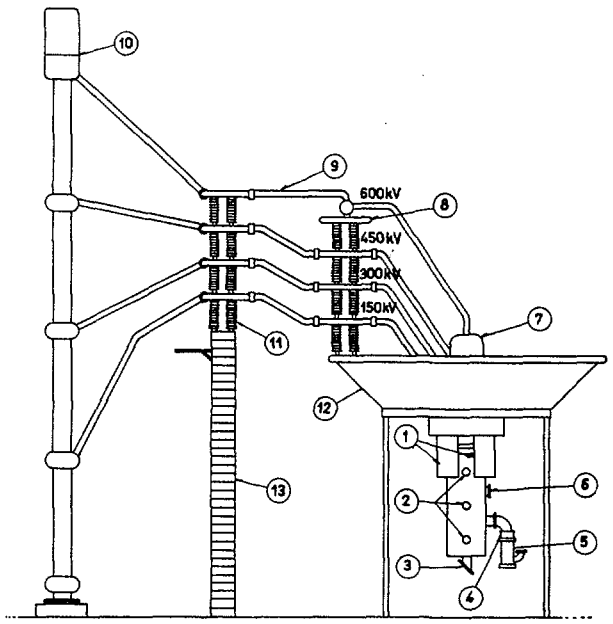

Fig. 4 General view of accelerator test facility. 1—pumps, 2—probe ports, 3—target plate, 4—liquid nitrogen cold trap, 5—10-inch diffusion pump, 6—view port, 7—corona shield atop accelerator tube, 8—corona shield, 9—4-inch Al tube conductors, 10—voltage divider stack, 11—ceramic insulators, 12—accelerator tube platform, 13—wall surrounding HV power supply.

4. Magnetically shielded injection duct

Magnetic shielding will be provided around the injection channel to reduce the beam's deflection to a small amount. For example, for H_2^+ injection at 600 keV, the field inside the injection channel must be less than 70 G if the beam is not to strike the channel wall. Further, the main field must not be greatly perturbed by the presence of the shielding in

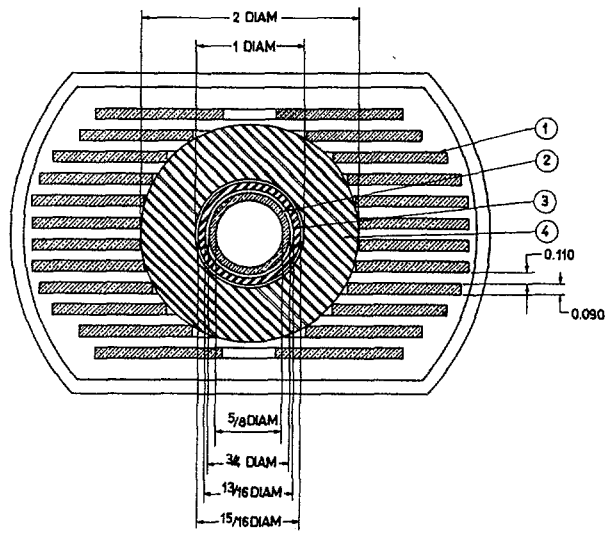

Fig. 5 Cross-sectional view of an early model test duct. All dimensions given in inches. 1—copper winding, 2—copper vacuum liner, 3—hipernik, 4—hiperco.

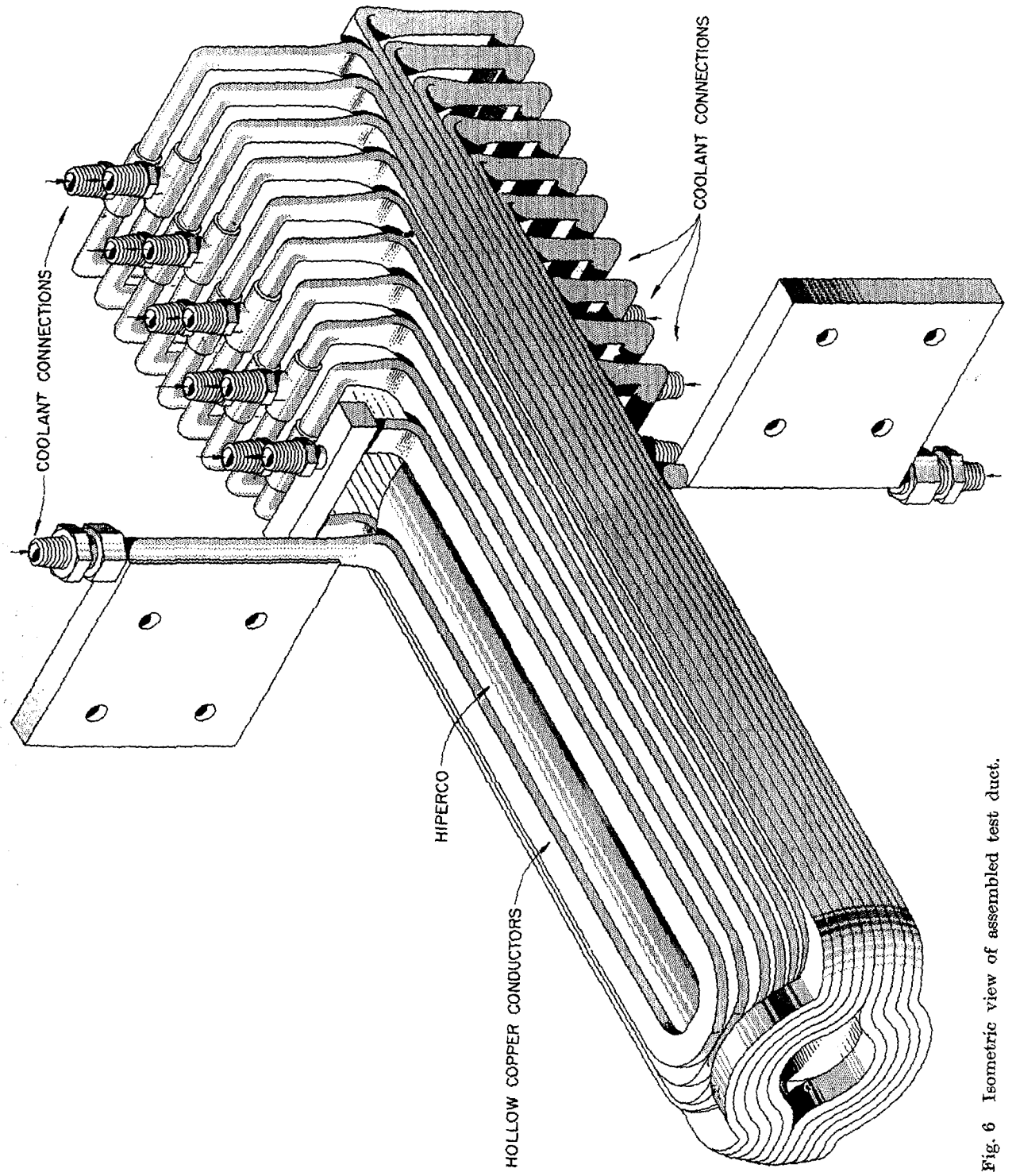

Fig. 6 Isometric view of assembled test duct.

order that there not be a rapid "walking out" of the trapped plasma onto the injection assembly.

In principle it is possible to shield completely against a transverse external field in a cylindrical region without introducing a perturbation to the field outside the shield. Consider a ferro-magnetic cylinder of elliptical cross-section immersed in a uniform magnetic field perpendicular to the cylinder axis and to one of the principle axes. When the permeability of the material is large compared with unity, the field inside the cylinder is aligned parallel to the applied field. It is clear, therefore, that a real current distribution, similar to the effective surface magnetization current, can likewise produce a uniform field in the same region. By arranging the magnitude and direction of the real current distribution so that the field in the material is equal to the external field, the external effects of the ferromagnetic material and the current will just cancel*. This presumes that the real currents and magnetization currents lie on the same surface area. An axial hole through the ferromagnetic material will have a negligible effect on the external fields so long as the permeability in the material remains high.

Fig. 5 shows a cross-sectional view through the center of an early model test duct with circular cross-section. The maximum field B in the "hiperco" tube** is given by

$$B = (B_0 - B_w)\frac{d_2}{d_2 - d_1}\frac{2\mu}{1+\mu}$$

where B_0 is the applied field and B_w is the field produced by the current carrying winding; d_2 and d_1 are the outer and inner diameters of the ferromagnetic cylinder of permeability μ. The purpose of the "hipernik"* is to ensure a high permeability, unsaturated layer inside the hiperco to reduce further the field in the channel. The winding is arranged to produce a $\cos\theta$ current distribution and the resulting uniform field inside the winding is given by

$$B_w = \frac{\pi n I}{r}$$

where nI is the number of ampere turns and r the mean radius of the distribution. Fig. 6 shows an isometric view of an assembled test coil which has been operated in magnetic fields up to 12 kG. This device was designed and constructed by R. L. Brown.

Experiments carried out without the inner hipernik layer showed effects of saturation of the hiperco at the maximum field. Nevertheless, the perturbation of the external field 8 cm from the end of the test model was less than 25 G. The field inside the beam channel was 125 G. At applied fields of ~7000 G, tests on another model produced fields in the channel of less than 10 G with only small external field perturbations.

* This concept has a long history. It has most recently been described and extended by F. C. GILBERT [20].

** Hiperco 35 is a registered trademark of Westinghouse Electric Corporation, Blairsville, Pennsylvania, for an alloy of 65% Fe, 35% Co.

* Hipernik is a registered trademark of Westinghouse Electric Corporation, Blairsville, Pennsylvania, for an alloy of 50% Ni, 50% Fe.

5. Deuterium arc

A fully-ionized gas discharge has been developed which operates between a tungsten cathode and the interior of a tubular, water-cooled copper anode. Gas is introduced into the anode where it is ionized with almost 100% efficiency by the arc column. The basic configuration is shown in Fig. 7. The ions drift along the arc column and recombine at the cathode. Most studies have been made with deuterium, although hydrogen, helium, nitrogen, and argon have also been run.

The electrodes are placed in chambers which are isolated from the central volume of the machine, and differential pumping is used to reduce the pressure in the central region. The ion-pumping action of the arc results in a pumping speed for deuterium of about 6000 l/s per meter length. The pressure around the arc column has been made as low as 10^{-5} mm Hg, limited by a source of gas other than influx from the ends. Despite a series of experiments aimed at elucidating this source, its nature is still unknown. The impurity ion level is found to be less than 0.1% without any special gas or chamber purification techniques being employed. An argon arc in this configuration has been successfully used for de-gassing the chamber walls.

Current-voltage characteristics for a series of gas flows are shown in Fig. 8. The characteristics do not vary significantly with magnetic field for fields above 5 kG.

Measurements were made of various plasma properties of a deuterium arc under a set of standard operating conditions: $B=7$ kG, $I=150$ A, $Q=5$ atmospheric cm^3/s, and $V=90$ V. Line shifts in spectra of introduced impurity ions (He II and C III) indicated an ion drift velocity of approximately 1.5×10^6 cm/s near the anode and 1.1×10^6 cm/s near the cathode. The density, estimated from 2-mm and 4-mm microwave attenuation results and from ion accountability calculations, is about 0.7×10^{14} cm^{-3}. Doppler-broadening of spectral lines from a number of different impurity ions indicates a unique ion temperature, 15 eV, at a point about 0.5 m from the anode. Other spectroscopic data suggest a somewhat higher electron temperature.

A more detailed description of the arc is given in [21]. R. A. Gibbons collaborated in these experiments.

6. Lithium arc

A fully-ionized lithium vapor arc has been developed which operates between a tantalum cathode and the interior of a tubular tantalum anode. A major problem which had to be solved in anode development was that of keeping the anode walls and end plate hot enough to prevent lithium deposition and yet below the melting point of tantalum. One of several successful configurations is shown in Fig. 9. By varying the amount of water cooling on the stainless steel pot containing the lithium, and thus the vapor feed, the ratio of Li^{++} to Li^{+} can be varied over a wide range. Anodes incorporating auxiliary resistance-heated lith-

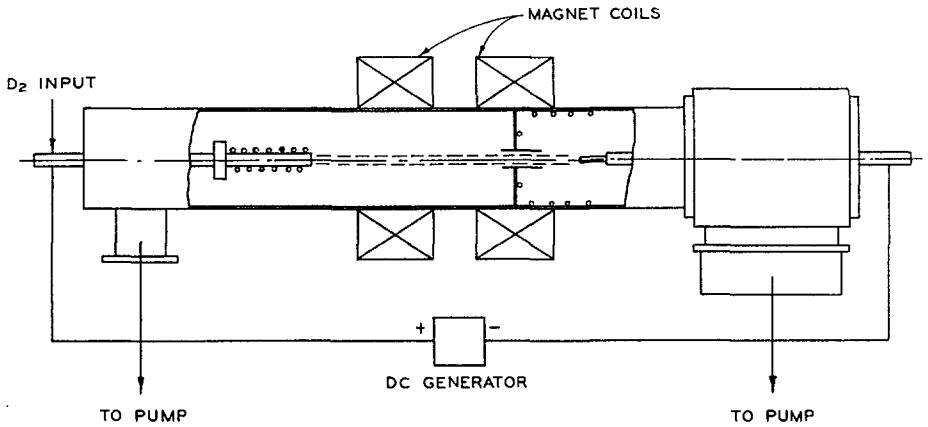

Fig. 7 Gas arc experimental configuration.

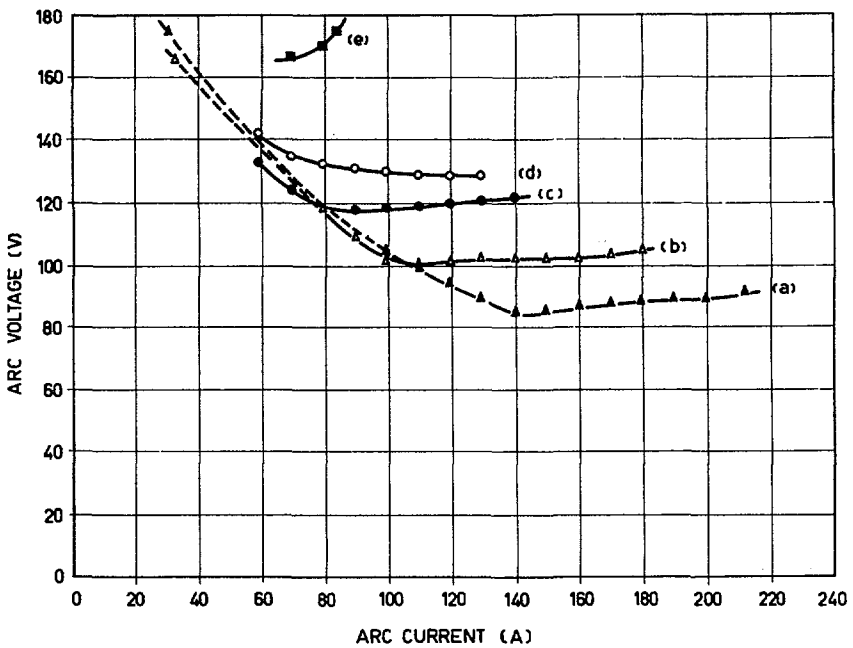

Fig. 8 Current-voltage characteristics for deuterium arc for various gas flow rates. $B_0 = 8.75$ kG. D_2 gas flow (atm-cc/sec): (a) 5.0, (b) 4.0, (c) 3.0, (d) 2.5, (e) 1.5.

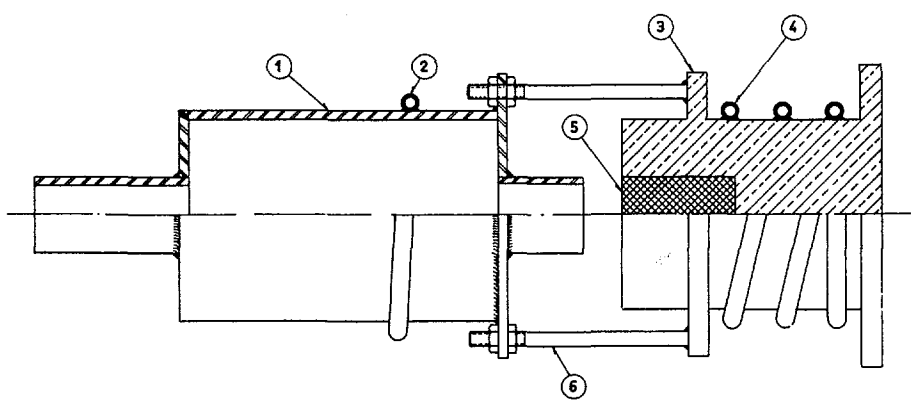

Fig. 9 Split anode used in Li arc. Li metal is placed in front section. 1—stainless steel, 2—cooling coil, 3—copper, 4—cooling coils, 5—tungsten, 6—$^1/_4$-inch stainless steel bolts.

ium chambers have also been used. The relative populations of the various charge states have been measured at the edge of the arc using an ion mass analyzer.

Lithium arcs have been operated in the range from 60 to 200 A. The voltage has been as low as 60 V and as high as 250 V, depending on the vapor feed. In appearance, the lithium arc usually has a bright green core equal in diameter to the diameter of the cathode, surrounded by a somewhat dimmer aureole approximately 4 to 5 cm in diameter. No spectral lines from neutral lithium are detected in the arc more than a few centimeters away from the anode.

The amount of ionized lithium transported along the arc was determined by measuring the weight of lithium deposited on cool surfaces near the cathode. Approximately 60% of the lithium lost from the anode during the run was found in these deposits. The amount of lithium thus transported corresponded to an ion current of $(19 \times Z)$ percent of the total current, where Z is the mean ionic charge.

Doppler-shift measurements of Li^+ lines indicated a drift velocity of 5×10^6 cm/s near the anode and 4×10^6 cm/s near the cathode. The apparent ion temperature was 15—20 eV, corresponding to a random velocity less than the drift velocity.

Acknowledgments

Portions of this work were carried out by the Laboratories for Applied Science of the University of Chicago and by J. E. Francis of Oak Ridge National Laboratory.

Oak Ridge National Laboratory is operated by Union Carbide Corporation for the United States Atomic Energy Commission.

References

[1] BARNETT, C. F., BELL, P. R., LUCE, J. S., SHIPLEY, E. D., SIMON, A., Proc. of Second U.N. International Conference on the Peaceful Uses of Atomic Energy, Geneva **31** (1958) 298.

[2] BARNETT, C. F., DUNLAP, J. L., EDWARDS, R. S., HASTE, G. R., RAY, J. A., REINHARDT, R. G., SCHILL, W. J., WARNER, R. M., WELLS, E. R., *Nuclear Fusion* **1** (1961) (in press).

[3] BARNETT, C. F., DUNLAP, J. L., EDWARDS, R. S., HASTE, G. R., POSTMA, H., RAY, J. A., REINHARDT, R. G., SCHILL, W. J., WARNER, R. M., WELLS, E. R., *Phys. Rev. Letters* **6** No. 4 (1961) 589.

[4] DUNLAP, J. L., BARNETT, C. F., DANDL, R. A., POSTMA, H., IAEA Conference on Plasma Physics and Controlled Nuclear Fusion Research, Salzburg, 1961: Paper CN-10/160, page 233 of this volume.

[5] KURCHATOV, I. V., *Atomnaya Energiya* **5** (1958) 105.

[6] GOLOVIN, I. N., ARTEMENKOV, L. I., BOGDANOV, G. F., PANOV, D. A., PISTUNOVICH, V. I., SEMASHKO, N. N., *Uspekhi Fiz. Nauk* **23** (1961) 685.

[7] PREVOT, F., HUBERT, P., GOURDON, C., *Comptes Rendus (Paris)* **249** (1959) 997.

[8] SWEETMAN, D. R., IAEA Conference on Plasma Physics and Controlled Nuclear Fusion Research, Salzburg, 1961: Paper CN-10/74, page 279 of this volume.

[9] DAMM, C. C., POST, R. F., FUTCH, A. H., Fourth International Conference on Ionization Phenomena in Gases, Uppsala (North-Holland Pub. Co., Amsterdam) **2** (1959) 988.

[10] SIMON, A., *J. Nucl. Energy*, **C 1** (1960) 215.

[11] MACKIN, R. J., JR., ORNL-Report CF 60—11—50 (1960); *Nuclear Fusion* **1** (1961) 131.

[12] GILBERT, F. C., HECKROTTE, W., HESTER, R. E., KILLEEN, J., VAN ATTA, C. M., U.S. Atomic Energy Commission Report UCRL-5827 (1960).

[13] PREVOT, F., GOURDON, C., Euratom-CEA Internal Report No. 80 (January, 1961).

[14] SIMON, A., U.S. Atomic Energy Commission Report ORNL-2831 (1959).

[15] FOWLER, T. K., U.S. Atomic Energy Commission Report ORNL-3037 (1960).

[16] PREVOT, F., Euratom-CEA Internal Report No. 27 (March, 1960).

[17] GOURDON, C., PREVOT, F., Euratom-CEA Internal Report No. 107 (May, 1961).

[18] GAUSTER, W. F., KELLEY, G. G., MACKIN, R. J. JR., NORTH, G. R., IAEA Conference on Plasma Physics and Controlled Nuclear Fusion Research, Salzburg, 1961: Paper CN-10/190, page 239 of this volume.

[19] KELLEY, G. G., LAZAR, N. H., MORGAN, O. B., *Nucl. Instr. and Methods* **10** (1961) 263.

[20] GILBERT, F. C., U.S. Atomic Energy Commission Report UCRL-5698 (1960).

[21] GIBBONS, R. A., MACKIN, R. J., JR., Fifth International Conference on Ionization Phenomena in Gases, Munich (North-Holland Pub. Co., Amsterdam, 1961).

ВЗАИМОДЕЙСТВИЕ ВЫСОКОЧАСТОТНОГО ЭЛЕКТРОМАГНИТНОГО ПОЛЯ С ПЛАЗМОЙ*

Р. А. ДЕМИРХАНОВ, Ю. С. ХОДЫРЕВ, Н. И. ЛЕОНТЬЕВ, Т. И. ГУТКИН

АКАДЕМИИ НАУК СССР, МОСКВА

СОЮЗ СОВЕТСКИХ СОЦИАЛИСТИЧЕСКИХ РЕСПУБЛИК

Настоящая работа посвящена изучению взаимодействия электромагнитных бегущей и стоячей волн в диапазоне частот от 600 килогерц до 6 мегагерц. На установках с разрядными трубками тороидальной и прямой конфигурации экспериментально исследовано: характер затухания высокочастотного поля в плазме в зависимости от параметров плазмы и поля. Изучено влияние высокочастотного поля на распределение заряженных частиц в плазме. Показано наличие радиальных сил, действующих на плазму в в/ч поле и вызывающих сжатие плазмы к оси трубки.

На установках с бегущей волной исследовались азимутальные постоянные токи, возникающие в результате увлечения электронов плазмы волной. Найдены зависимости этого тока от параметров плазмы и волны. Показано, что азимутальные токи при значениях, выше некоторых критических, вызывают в плазме тороида неустойчивости «пучкового» типа.

Настоящая работа посвящена экспериментальному изучению взаимодействия с плазмой мощных электромагнитных бегущей и стоячей волн в диапазоне частот от 0,6 до 6 мегагерц. В этих экспериментах плазма создавалась исследуемой волной и давление переменных полей ($H^2\infty/16\pi$) было сравнимо с газодинамическим давлением плазмы.

Основные параметры плазмы и высокочастотных полей варьировались в следующих пределах:

концентрация заряженных частиц $n=10^{12}$—2.10^{14} см$^{-3}$,

процент ионизации $\gamma=1-30\%$,

напряженность высокочастотного магнитного поля, H_z^2 20—1100 эрстед,

длительность высокочастотного импульса 1—4 мсек.

Исследования проводились с плазмой водорода и инертных газов. В этих условиях изучалось проникновение высокочастотных полей в плазму и распределение плотности заряженных частиц. Для бегущей магнитной волны в случае геометрически замкнутых разрядных камер (тороиды) исследовались также постоянные токи в плазме и вызываемые ими неустойчивости.

Проникновение высокочастотного поля в плазму

Проникновение высокочастотного поля в плазму исследовалось в диапазоне частот от 600 килогерц до 6 мегагерц для бегущей и стоячей (с $\lambda=\infty$) H—волны. Как известно, толщина скин-слоя в плазме определяется соотношением частоты соударения электрона с атомами и ионами ν и частоты внешней волны ω. В случае, когда $\nu/\omega>1$, толщина скин-слоя определяется так же, как для металлического проводника, т.е.

$$\delta \simeq (\omega\sigma)^{-\frac{1}{2}}$$

Как показали измерения, почти во всех случаях наблюдаемая толщина скин-слоя совпадает с толщиной скин-слоя, подсчитанной для случая металлического проводника [1]. Такое соответствие сохраняется вплоть до относительно высоких степеней ионизации газа. В качестве примера на рис. 1 приводится кривая распределения напряженности продольной компоненты высокочастотного поля

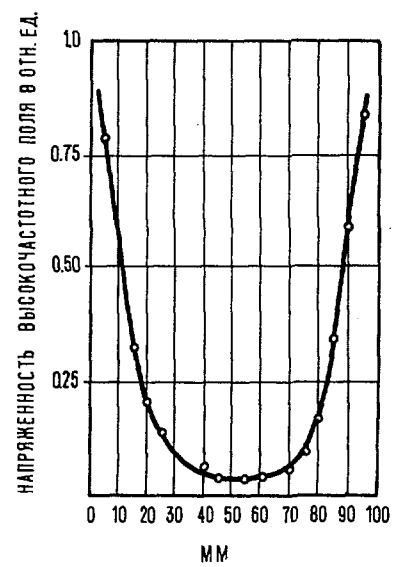

Рис. 1 Распределение напряженности высокочастотного магнитного поля по диаметру разрядной трубки. Диаметр трубки 10 см. Давление $p=3\cdot10^{-3}$ мм. рт. ст. Плотность заряженных частиц на оси трубки $3\cdot10^{13}$ см$^{-3}$. Частота волны 2,2 Мгц.

* Доклад CN-10/233 представленный на Конференцию. Докладчик: Р. А. Демирханов. Дискуссия (на английском языке) по этому докладу дана на стр. 355. Переводы аннотаций находятся в конце этого тома Трудов Конференции.

Рис. 2 Общий вид установки.

H-волны по диаметру разрядной камеры для момента времени 1 мсек от начала разряда. Кривая рис. 1 получена в кварцевой тороидальной камере с большим и малым диаметрами, соответственно 50 см и 10 см. Водородная плазма возбуждалась полем бегущей волны с частотой 2,2 мегагерца. Высокочастотная мощность питающего устройства равнялась 8 мгвт. На рис. 2 показан общий вид установки. Для плазмы с концентрацией $2\cdot10^{14}$ см$^{-3}$ при степени ионизации 10—30% измеренная толщина скин-слоя составила 0,6—0,8 см. В этом случае величина проводимости плазмы, определенная из измеренной толщины скин-слоя и вычисленная по значениям концентрации и температуры электронов, хорошо согласуются между собой ($\sigma=10^{14}$ $CGSE$). Кривая на рис. 3 иллюстрирует распределение напряженности продольного магнитного поля высокочастотной волны по диаметру разрядной трубки для случая $f=6.10^6$ герц. В пристеночной области затухание волны носит

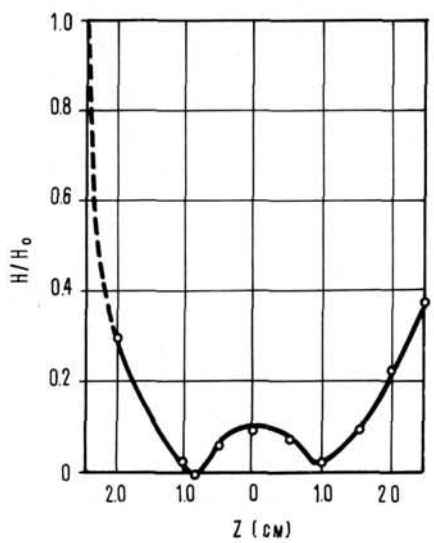

Рис. 3 Распределение напряженности высокочастотного магнитного поля по диаметру разрядной трубки. Диаметр трубки 4,5 см. Давление $1{,}3\cdot10^{-2}$ мм. рт. ст. Плотность заряженных частиц $4\cdot10^{12}$ см$^{-3}$. Частота волны 6 Мгц.

такой же характер, как и в рассмотренных выше случаях. В центральной части трубки при определенных условиях из-за пространственно-дисперсионных свойств плазмы наблюдаются отклонения от обычного хода кривой затухания волны. В этом случае фазовая скорость проникающей в плазму волны сравнима с тепловой скоростью электронов, а длина свободного пробега электронов сравнима с длиной электромагнитной волны в плазме [2, 3]. Следует ожидать, что этот эффект будет проявляться в более сильной степени с повышением температуры электронов.

Распределение плотности заряженных частиц в плазме.

На рис. 4 представлены кривые распределения плотности заряженных частиц по диаметру разрядной трубки, полученные для двух характерных

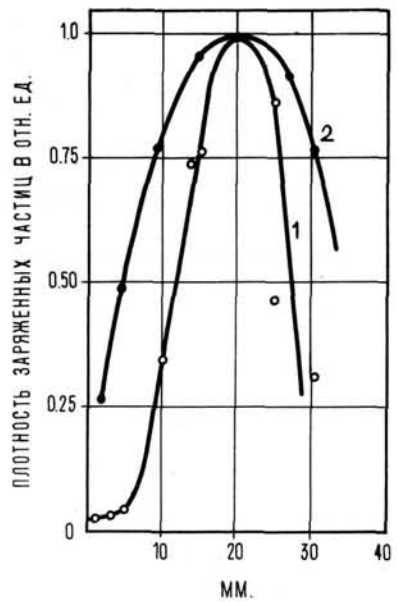

Рис. 4 Распределение плотности заряженных частиц по диаметру разрядной трубки для установки с напряженностью высокочастотного магнитного поля 1100 э (кривая 1) и 170 э (кривая 2).

режимов. Обе кривые получены для тороидальных разрядных камер с большим и малым диаметрами, соответственно 18 см и 4 см. В первом случае (кривая 1) разряд создавался бегущим полем частотой 1,5 мегагерца, фазовой скоростью $8\cdot10^6$ см/сек. и напряженностью высокочастотного поля 1100 эрстед. Вдоль тора укладывалось 8 длин волн. При этом глубина ямы продольной составляющей магнитного поля на оси трубки достигала 30%. Как известно, такая конфигурация магнитного поля позволяет существенно уменьшить тороидальную неоднородность. В нашем случае эта неоднородность не превышала 12%.

На рис. 5 представлена фотография этой установки, на рис. 6 — вид тороидальной камеры с высокочастотным контуром. Во втором случае

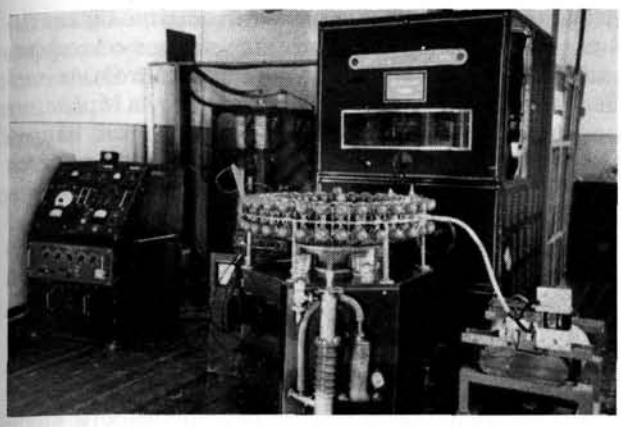

Рис. 5 Общий вид установки.

(кривая 2) разряд создавался бегущим полем с напряженностью 170 эрстед. Вдоль линии укладывалась одна волна с частотой один мегагерц. В этом случае тороидальная неоднородность не компенсировалась и составляла 45%.

Из сравнения кривых следует, что характер распределения плотности заряженных частиц по диаметру трубки существенно зависит от напряженности высокочастного поля и его конфигурации.

В первом случае давление высокочастотного поля оказывается достаточным для отжатия плазмы от стенок трубки, в то время как во втором случае примерно при том же газодинамическом давлении плазмы ($n\,k\,T \simeq 10^3$ дин/см^2) давление высокочастотного поля практически не влияет на характер распределения плотности заряженных частиц. Необходимо отметить, что во втором случае при отсутствии ямы для продольной составляющей высокочастотного поля тороидальная неоднородность приводит к относительно медленному переносу плазмы к внешней стенке разрядной трубки со скоростью $5 \cdot 10^2$ см/сек.

Отжатие плазмы бегущей магнитной волной было показано также на установке с прямолинейной разрядной трубкой (длина 50 см, диаметр 5 см), в которой плазма создавалась самостоятельным разрядом между двумя вспомогательными электродами.

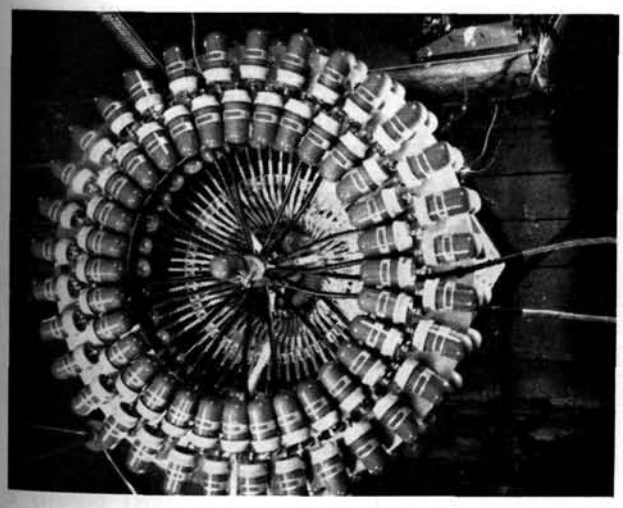

Рис. 6 Разрядная камера с высокочастотным контуром.

На длине трубки укладывалось 16 длин волн. Соответствующая глубина ямы продольной составляющей поля равнялась 80%. Наложение бегущей магнитной волны на плазму, как и в предыдущем случае, приводило к эффекту отжатия плазмы от стенок разрядной трубки. Высокочастотное полетой же конфигурации в случае стоячей волны приводило к эффекту отжатия плазмы от стенок только в пучностях напряженности магнитного поля.

Токи в плазме

П. Тонеманом и его сотрудниками [4] было показано, что при взаимодействии бегущей магнитной волны с плазмой тороидальной конфигурации в

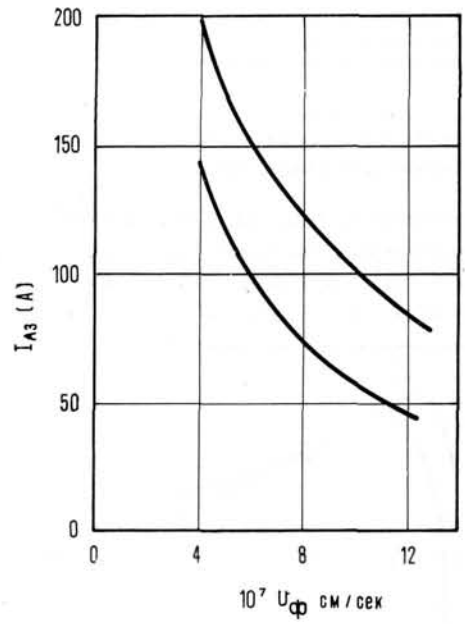

Рис. 7 Зависимость постоянного тока от фазовой скорости. Диаметр трубки 4.2 см. Давление $2 \cdot 10^{-3}$ мм. рт. ст. Плотность заряженных частиц $3 \cdot 10^{12}$ см$^{-3}$. Частота волны 1,6 Мгц.

плазме возникает постоянный электронный ток в направлении распространения волны.

Проведенные нами исследования показали, что эти токи в вышеописанных установках достигают нескольких килоампер. Величина постоянного тока существенно зависит от фазовой скорости волны, частоты и напряженности бегущего магнитного поля.

На рис. 7 представлена зависимость величины постоянного тока от фазовой скорости волны. На рис. 8 — зависимость от частоты. С уменьшением фазовой скорости и увеличением частоты величина тока возрастает.

Экспериментальная зависимость для величины постоянного тока от параметров волны и плазмы

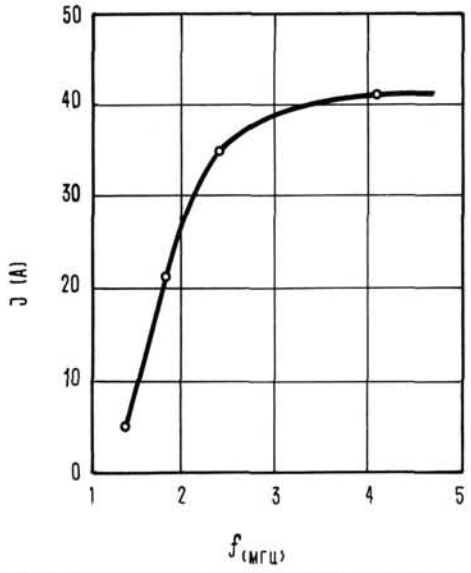

Рис. 8 Зависимость постоянного тока от частоты волны. Диаметр трубки 4,2 см. Давление $2 \cdot 10^{-2}$ мм. рт. ст. Плотность заряженных частиц 10^{12} см$^{-3}$.

хорошо согласуется с выражением для тока, полученного из рассмотрения движения электронов в дрейфовом приближении.

Неустойчивость плазмы в поле бегущей волны

В исследуемых системах тороидальной конфигурации с бегущей магнитной волной были обнаружены неустойчивости, регистрируемые как колебания амплитуды высокочастотного поля, светимости и плотности заряженных частиц с коэффициентом модуляции до единицы. Частоты колебаний всех этих величин совпадают в пределах точности измерений, растут с увеличением напряженности высокочастотного поля и находятся в диапазоне 3—50 килогерц. Наличие примесей в разряде приводит к гашению этих колебаний.

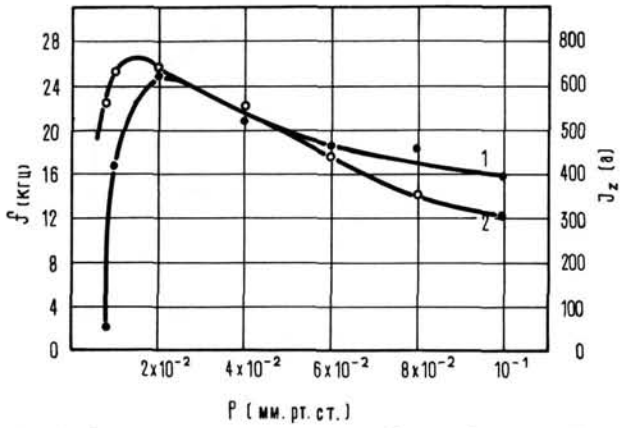

Рис. 9 Зависимость частоты колебаний (кривая 1) и постоянного тока (кривая 2) от давления газа. Диаметр трубки 4 см. Частота волны 1 Мгц.

В цилиндрических разрядных трубках с бегущей волной и в тороидальных камерах со стоячей волной, в которых постоянные токи отсутствуют, колебания такого рода не были обнаружены. Это дало основание предположить, что ответственными за возникновение колебаний являются постоянные токи, вызывающие в плазме неустойчивости «пучкового» типа. Характерно, что частоты колебаний по порядку величины совпадают с частотами магнитозвуковых волн в магнитном поле постоянного тока. Зависимость частоты колебаний от давлений газа аналогична зависимости постоянного тока от давления газа (рис. 9). На рис. 10 показаны фотографии тороидального разряда в режиме лупы времени, полученные с интервалом в 10 микросекунд. Верхний снимок соответствует режиму с колебаниями; нижний режиму без колебаний. Видно, что вдоль трубки тора возникает продольная волна светимости, движущейся по направлению бегущей волны со скоростью $7 \cdot 10^5$ см/сек. Период обращения волны светимости равен периоду колебаний плотности плазмы. Наблюдаемые колебания плазмы связаны с существованием в торе продольной волны плотности заряженных частиц.

Заключение

Результаты экспериментального исследования взаимодействия высокочастотных полей с плазмой в диапазоне частот 0,6—6 мегагерц показывают, что при достаточно высоких значениях напряженности магнитного поля может быть осуществлено отжатие плазмы от стенок разрядной камеры. Однако в тороидальных системах с бегущим магнитным полем возникают неустойчивости «пучкового» типа, обусловленные постоянными токами в плазме.

В работе принимали участие Ю. К. Удовиченко, И. Р. Ямпольский, И. А. Косый, В. В. Логвинов, Т. М. Филатова, Ю. Н. Губин, А. Н. Король, Р. Н. Кухарский, И. Я. Кадыш и И. С. Фурса.

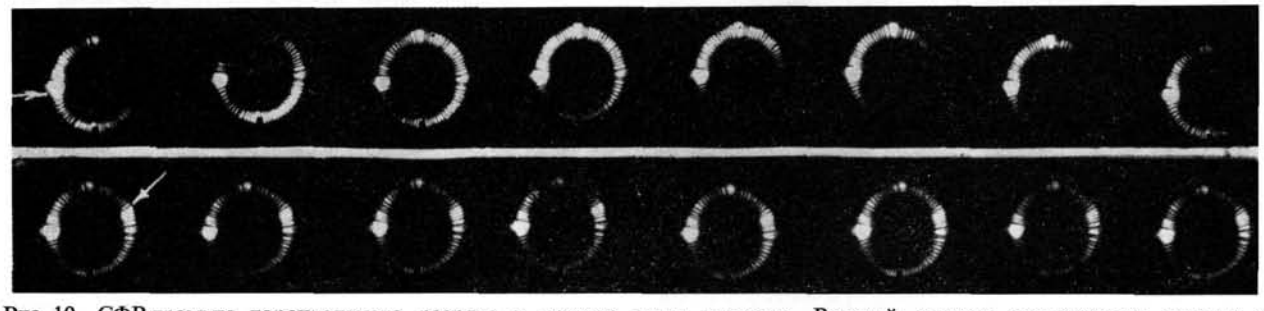

Рис. 10 СФР-граммы тороидального разряда в режиме лупы времени. Верхний снимок соответствует режиму с колебаниями. Нижний — без колебаний.

В разработке установок и решении различных инженерно-технических проблем принимали участие: А. С. Вознюк, С. Е. Гигиберия, А. З. Рахелькин, Ш. М. Арчвадзе, А. П. Пятницкий, В. Н. Рыбин, В. Лепехин, В. П. Волков, П. С. Бростюк.

Авторы благодарят С. Н. Лазовского за обсуждение некоторых результатов работы.

Литература

[1] Carruthers R., Appl. Sci. Res. B-5, 135, 1955.

[2] Шафранов В. Д., *ЖЭТФ* **34** (1958) 1475

[3] Гинзбург В. Л. Распространение электромагнитных волн в плазме, М., 1960.

[4] Thonemann P. C., Cowhig W. T., Davenport P. A., *Nature* **169** (1952) 34.

FORMATION D'UN PLASMA PAR INJECTION DE PARTICULES RAPIDES*

C. GOURDON, F. PRÉVOT

GROUPE DE RECHERCHES DE L'ASSOCIATION EURATOM-CEA SUR LA FUSION

FONTENAY-AUX-ROSES, SEINE, FRANCE

On étudie l'évolution et l'équilibre d'un plasma à très haute température ($T_i > 10^8$ °K) par injection d'ions moléculaires ou d'atomes neutres rapides. Un système d'équations différentielles couplées décrit les densités des diverses populations des ions et des molécules neutres à l'intérieur et à l'extérieur du plasma. Ce système représente le bilan de matière du plasma supposé stable.

Les solutions d'équilibre se traduisent en fonction du courant injecté par des courbes de formes caractéristiques, en S pour le plasma et en Z pour le gaz neutre. On calcule et on discute les valeurs des deux courants critiques.

On compare l'injection d'ions moléculaires avec l'injection d'atomes rapides. La première méthode tire un avantage important d'une bonne efficacité de capture provisoire (passage multiple). Le passage unique des atomes, par contre, permet une réduction importante des sources de gaz neutre, condition nécessaire et très critique pour le succès de la seconde méthode. Pour les conditions critiques, la densité de gaz neutre est alors toujours très supérieure dans le premier cas à ce qu'elle est dans le second cas. Il en résulte que l'on peut exploiter utilement l'effet de pompage ionique pour abaisser le courant critique dans le cas des ions moléculaires alors que cet effet est négligeable dans le cas des atomes rapides.

Si on utilise un plasma auxiliaire à basse température pour la capture, on définit un courant de transition au delà duquel le plasma chaud évolue favorablement si l'on supprime le plasma auxiliaire. En tenant compte de l'échange d'énergie entre le plasma chaud et le plasma froid, on démontre l'existence de conditions optima et on calcule la valeur du courant de transition optimum. L'utilisation du plasma auxiliaire ne peut présenter d'intérêt notable qu'associée à une capture provisoire des particules injectées.

Un certain nombre d'autres propriétés et l'influence détaillée de divers paramètres sont montrées sur des résultats numériques obtenus avec calculateur arithmétique.

En particulier, l'évolution au cours du temps des densités présente des changements caractéristiques au voisinage des conditions critiques.

1. Introduction

Les interactions d'un gaz ionisé avec un gaz neutre aux faibles densités peuvent être étudiées à partir des différents processus de collision entre particules, tels que l'ionisation, l'échange de charge, etc.

Ce genre d'interaction est particulièrement important dans le cas où l'on veut former une assemblée d'ions à haute température, par injection et capture de particules de haute énergie dans une configuration magnétique. En effet ces processus imposent des conditions nécessaires très sévères pour la formation du plasma. Ce problème a été étudié par différents auteurs dans un certain nombre de cas particuliers (références [1] à [9]). Nous étudions ici la formation d'un plasma par injection de particules rapides dans deux cas qui font l'objet d'un important effort expérimental dans plusieurs laboratoires: l'injection d'ions moléculaires et l'injection d'atomes rapides dans une configuration magnétique à miroirs.

2. Injection d'ions moléculaires

Un faisceau d'intensité I, d'ions moléculaires (masse $2M$), d'énergie $2V$, (vitesse v) est injecté entre des miroir magnétiques. Champ au centre $= B_0$ (gauss), rapport de miroir $= R$, distance entre miroirs $= L$ [10].

Par un procédé convenable, les ions moléculaires subissent une capture temporaire avec un parcours de longueur $\mathcal{L}$, correspondant à un nombre ν de révolutions.

Si 2ϱ est leur rayon de giration moyen,

$$\mathcal{L} = 4\pi\varrho\nu, \tag{1}$$

$$\varrho\,(\mathrm{cm}) = \frac{144\sqrt{M_1 V}}{B_0\,(1+R)/2}\,. \tag{2}$$

La dissociation se fait par collision, sur le gaz résiduel de densité moléculaire $\bar{n}_0$ sur le plasma préalablement formé de densité n, enfin éventuellement sur un plasma auxiliaire (arc) de densité n_1, rayon r_1, température électronique V_1 (eV).

Les ions atomiques sont formés dans un volume $\mathcal{V}$ défini en première approximation par l'enveloppe des trajectoires des ions moléculaires. Dans le cas particulier où les trajectoires des ions injectés passent au voisinage de l'axe du système, on peut écrire:

$$\mathcal{V} = \pi\,(4\varrho)^2 L\,. \tag{3}$$

Pour simplifier le problème, on admettra que la surface S délimitant ce volume forme une frontière pour les différentes sortes de particules dont les densités seront supposées uniformes, on aura donc dans $\mathcal{V}$ des ions chauds de densité n, des ions froids de densité n_f et des molécules neutres de densité $\bar{n}_0$.

* Mémoire CN-10/97, présenté par F. Prévot. La discussion concernant ce mémoire est donnée page 356. Les traductions du résumé se trouvent en fin de volume.

Autour de $\mathcal{V}$ et dans un volume $\mathcal{V}'$ on aura simplement une densité de molécules neutres n_0. Enfin, en communication avec $\mathcal{V}'$ par une conductance C, le volume $\mathcal{V}''$ de l'accélérateur contient une densité de neutres N_0.

Les molécules neutres qui pénètrent le volume $\mathcal{V}$ peuvent être ionisées, avec libération d'électrons (section efficace σ_i) ou par échange de charge avec les ions rapides (section efficace σ_e); on peut écrire entre $\bar{n}_0$ et n_0 la relation d'équilibre

$$(n_0 - \bar{n}_0)\frac{v_0 S}{4} = \bar{n}_0 \cdot n\,(2\sigma_i + \sigma_e)\,v\mathcal{V}, \qquad (4)$$

où v_0 est la vitesse d'agitation des molécules neutres

$$\bar{n}_0 = k n_0 = \frac{n_0}{1 + 8\varrho\, n\,(2\sigma_i + \sigma_e)\,(v/v_0)} \qquad (5)$$

le coefficient 2 appliqué à σ_i tient compte de l'ionisation par les électrons.

Une conséquence de ce couplage entre n_0 et $\bar{n}_0$ est que toute source ou perte Q de neutres dans $\mathcal{V}$ ou dans $\mathcal{V}'$ se répercute sur les densités n_0 et $\bar{n}_0$ en raison inverse des « volumes réduits »

$$\Delta n_0 = \frac{Q}{\mathcal{V}_r} \qquad \Delta \bar{n}_0 = \frac{Q}{\mathcal{V}_r}$$

$$\mathcal{V}_r = \frac{\mathcal{V}' - \mathcal{V}}{k} + \mathcal{V} \qquad \mathcal{V}_r' = (\mathcal{V}' - \mathcal{V}) + k\mathcal{V}. \qquad (6)$$

2.1 Equations d'évolution.

Au cours de son parcours $\mathcal{L}$ entre les miroirs, le faisceau d'ions moléculaires est affaibli d'un facteur η par dissociation et échange de charge. Nous appellerons σ_d la section efficace de dissociation qui produit un ou deux ions atomiques par particule cible. Nous prendrons la même valeur de σ_d pour les différentes espèces de cible, atome, ions ou électrons. De même nous appellerons σ_e la section efficace de neutralisation par échange de charge avec ou sans dissociation.

On a alors

$$\eta = 1 - \exp\left\{-\mathcal{L}\left[\sigma_d\left(2(\bar{n}_0 + n_f) + 2n + 2n_1\frac{r_1}{2\pi\varrho}\right) + \sigma_e \bar{n}_0\right]\right\}. \qquad (7)$$

La fraction du faisceau dissociée avec formation d'ions atomiques est alors

$$\eta_d = \eta \times \frac{2\sigma_d\left[(\bar{n}_0 + n_f) + n + n_1\frac{r_1}{2\pi\varrho}\right]}{2\sigma_d\left[(\bar{n}_0 + n_f) + n + n_1\frac{r_1}{2\pi\varrho}\right] + \sigma_e\,\bar{n}_0}. \qquad (8)$$

Si nous appelons $(1+\alpha)$ le nombre de protons produits par dissociation du type σ_d, le terme source des ions chauds s'écrira

$$\left(\frac{dn}{dt}\right)_d = \frac{I\,(1+\alpha)\,\eta_d}{\mathcal{V}}, \qquad (9)$$

I étant exprimé en nombre de particules par unité de temps.

Les pertes des ions atomiques se feront par échange de charge sur le gaz neutre $\bar{n}_0$, par diffusion coulombienne à travers les miroirs (section efficace σ_c et probabilité P liée au rapport de miroir) et enfin éventuellement par suite des interactions avec l'arc.

Ces pertes dues à l'arc peuvent être représentées par un temps caractéristique τ. Nous considérerons ici un arc complètement ionisé n'entraînant donc pas par lui-même de pertes par échange de charge. Il subsistera des pertes par suite du refroidissement des ions chauds sur les électrons de l'arc. Si l'énergie initiale $2\ V$ n'est pas trop élevée (<200 keV), seule la diffusion élastique sera augmentée. En utilisant les coefficients de diffusion donnés par Chandrasekhar et Spitzer, on évalue

$$\tau = \frac{V^{\frac{1}{2}} \cdot V_1^{\frac{3}{2}}}{1{,}8\cdot 10^{-11} n_1 r_1 B_0 \frac{1+R}{2}} \quad \text{(s, eV, cm}^{-3}\text{, cm, G)}. \qquad (10)$$

Nous négligerons ici toute autre cause possible de perte et en particulier tout effet collectif et instabilité. Finalement l'équation d'évolution de la densité du plasma chaud s'écrit

$$\frac{dn}{dt} = I\frac{1+\alpha}{\mathcal{V}}\eta_d - n\bar{n}_0\sigma_e v - \frac{n}{\tau} - n^2\langle\sigma_c v\rangle P. \qquad (11)$$

On pourrait écrire une équation d'évolution pour la densité n_f des ions froids (résultant par exemple d'un échange de charge entre un ion chaud et une molécule neutre). Pour simplifier le système d'équations on écrira plus simplement dans les expressions (7) et (8) $\bar{n}_0 + n_f \sim n_0$.

Soit q_0 le dégazage total des parois dans le volume $\mathcal{V}'$ et θ_0 la vitesse de pompage des pompes sur ce volume. La surface interne S' du volume $\mathcal{V}'$ peut être rendue absorbante pour les particules (neutres et ions) qui la frappent, à l'aide d'un dépôt actif. En admettant que cette activité ne varie pas beaucoup pendant le temps d'évolution du plasma, on peut appeler Γ la probabilité moyenne de réémission d'une particule frappant la paroi. Γ est compris entre 0 et 1 selon l'état de la surface. La vitesse de pompage totale des neutres n_0 dans le volume $\mathcal{V}'$ sera donc

$$\theta = \theta_0 + (1 - \Gamma)\frac{v_0 S'}{4}. \qquad (12)$$

Les ions lents et rapides du plasma, perdus par diffusion à travers les miroirs, vont se recombiner sur une paroi de l'appareil. On peut disposer en ce point un système de pompage tel que la molécule neutre formée ait la probabilité γ d'être pompée sur place et de ne pas retourner dans le volume $\mathcal{V}'$ ($0 \leqslant \gamma \leqslant 1$). Cet effet de pompage ionique peut être réalisé en pratique par le même équipement que celui nécessaire à l'arc.

On peut écrire alors l'équation d'évolution de la densité n_0 des molécules neutres dans $\mathcal{V}'$ sous la forme

$$\frac{\mathrm{d}n_0}{\mathrm{d}t} = \frac{\Gamma I}{\mathcal{V}_r'}\left(1 - \frac{1+\alpha}{2}\eta_d\right) + \frac{\Gamma}{2} n\,\bar{n}_0\,\sigma_e\,v\,\frac{\mathcal{V}}{\mathcal{V}_r'} + \frac{1-\gamma'}{2}\frac{n}{\tau}\frac{\mathcal{V}}{\mathcal{V}_r'} + \frac{1-\gamma}{2}\,n^2\langle\sigma_c v\rangle P\,\frac{\mathcal{V}}{\mathcal{V}_r'} + \frac{q_0}{\mathcal{V}_r'} + \left(\frac{N_0 - n_0}{\mathcal{V}_r'}\right)C - \frac{\theta n_0}{\mathcal{V}_r'} - \gamma\, n\,\bar{n}_0\,(\sigma_e + 2\sigma_i)\,v\,\frac{\mathcal{V}}{\mathcal{V}_r'} - \frac{\gamma I}{\mathcal{V}_r'}\eta_I. \quad (13)$$

Les différents termes de cette équation représentent successivement: la fraction non capturée du faisceau incident, l'échange de charge du plasma chaud, le retour des ions refroidis et perdus par les miroirs, le retour des ions chauds perdus par les miroirs, le dégazage des parois, le gaz provenant de la source d'ions, le pompage de v', le pompage ionique du gaz neutre ionisé par le plasma et enfin le pompage ionique du gaz neutre ionisé par le faisceau avec

$$\eta_I = \eta\,\frac{\bar{n}_0\,(\sigma_e + \sigma_i)}{2\,\sigma_d\,[n_0 + n + n_1\,(r_1/2\pi\varrho)] + \sigma_e \bar{n}_0}. \quad (14)$$

Remarquons que nous n'avons pas mis de source ou perte de n_0 dues à l'arc. Il nous semble préférable d'utiliser les solutions des équations pour déterminer les conditions de n_0 que doit remplir l'arc.

Enfin on complète le système par l'équation d'évolution des neutres N_0 du caisson de l'accélérateur, qui a un volume $\mathcal{V}''$, un dégazage Q_0, une vitesse de pompage Θ, et la source ayant un rendement en gaz g.

$$\frac{\mathrm{d}N_0}{\mathrm{d}t} = \frac{I}{\mathcal{V}''}\,\frac{1-g}{g} + \frac{Q_0}{\mathcal{V}''} - \frac{(N_0 - n_0)\,C}{\mathcal{V}''} - \frac{\Theta N_0}{\mathcal{V}''}. \quad (15)$$

Le système des trois équations différentielles couplées (11), (13) et (15) représente l'évolution du plasma et des neutres. Ce système est très complexe et aucune information, même qualitative, ne peut s'en déduire directement de façon simple.

2.2 Conséquences et applications des équations d'évolutions

L'exploitation des équations d'évolution peut se faire par deux méthodes différentes. On peut les intégrer numériquement à l'aide d'un calculateur électronique. On peut aussi effectuer des simplifications et déduire certaines propriétés des équations simplifiées. Nous présentons ici quelques résultats obtenus par chacune des deux méthodes.

Une première simplification résulte de l'élimination du temps. Le régime stationnaire est représenté par les équations (22) après élimination de $\dot{N}_0$:

$$0 = I(1+\alpha)\eta_d - \frac{n_0\,n\,\sigma_e\,v\,\mathcal{V}}{1 + 8\varrho\,n\,(\sigma_e + 2\sigma_i)\,(v/v_0)} - \frac{n\mathcal{V}}{\tau} - n^2\langle\sigma_c v\rangle P\mathcal{V}$$

$$0 = \left[\Gamma + \frac{C}{C+\Theta}\,\frac{1-g}{g}\right]I + \frac{1-\Gamma}{2}\left(\frac{n\mathcal{V}}{\tau} + n^2\langle\sigma_c v\rangle P\mathcal{V}\right) - \left[\theta_0 + \frac{1-\Gamma}{4}\,v_0 S' + \frac{C\Theta}{C+\Theta}\right]n_0 + q_0 - \frac{\gamma\,n\,n_0\,(\sigma_e + 2\sigma_i)\,v\mathcal{V}}{1 + 8\varrho\,n\,(\sigma_e + 2\sigma_i)\,(v/v_0)} - \frac{\gamma'}{2}\frac{n}{\tau}\mathcal{V} - \frac{\gamma}{2}\,n^2\langle\sigma_c v\rangle P\mathcal{V}. \quad (22)$$

Remarquons que dans tous les cas où la dissociation sur les neutres est négligeable devant la dissociation sur le plasma formé ou l'arc, η_d ne contient plus n_0 et le système peut se résoudre sous la forme $I = f(n)$. A. Simon [1, 2, 3] a montré que la courbe représentative de la variation de n en fonction de I présente dans certains cas une forme caractéristique en S, qui permet de définir deux valeurs importantes de I, le courant critique supérieur I_{cs} et le courant critique inférieur I_{ci}.

Une seconde simplification importante résulte de la considération de domaines limités des densités. Un cas particulièrement intéressant est celui où la dissociation est faible

$$\eta_d \approx \mathcal{L}\cdot 2\sigma_d\left(n_0 + n + n_1\frac{r_1}{2\pi\varrho}\right),$$

et le plasma transparent pour le gaz neutre

$$k \approx 1 \text{ ou } 8\varrho\,n\,(2\sigma_i + \sigma_e)\frac{v}{v_0} \ll 1,$$

ce qui entraîne $n^2\langle\sigma_c v\rangle P$ négligeable dans les équations.

Ce cas correspond à la branche inférieure de la courbe en S. Sans arc, sur cette branche, il existe une partie linéaire où n est proportionnel à I et ν et est indépendant de n_0, γ et Γ sauf au voisinage de I_{cs}. La valeur correspondante de n_0 (et $\bar{n}_0$) est proportionnelle à I, indépendante de γ et ν, mais diminue avec Γ.

On peut calculer dans cette approximation une expression approchée du courant critique supérieur sans arc

$$I_{cs} = \left[\frac{\sigma_e\cdot v\cdot\mathcal{V}}{(1+\alpha)\,2\sigma_d\cdot\mathcal{L}} - \frac{\frac{\theta_0 + (1-\Gamma)\,v_0 S'}{4} + \frac{C\Theta}{C+\Theta}}{\Gamma + \frac{C}{C+\Theta}\,\frac{1-g}{g}}\right]^2 \times \left[\frac{\Gamma + \frac{C}{C+\Theta}\,\frac{1-g}{g}}{4\gamma\,(\sigma_e + 2\sigma_i)\,v\mathcal{V}}\right], \quad (23)$$

pour $\Gamma = 1$ cette expression se simplifie et, certains termes étant négligeables, elle devient

$$\underset{(\gamma=1)}{I_{cs}} \sim \left[\left(1 + \frac{c+\Theta}{c}\,\frac{1-g}{g}\right)\Big/ 4\,(1+\alpha)^2\right] \times \left(\frac{\sigma_e}{2\sigma_d}\right)^2 \times \frac{1}{\sigma_e + 2\sigma_i} \times \frac{1}{\gamma} \times \frac{v\mathcal{V}}{\mathcal{L}^2}. \quad (24)$$

Le courant critique I_{cs} dépend de l'énergie V des particules par l'intermédiaire des σ, α et $\mathcal{V}$. Cette variation est peu marquée jusqu'à 2 $V = 200$ keV environ. Au delà de 200 keV, I_{cs} diminue fortement à cause de la variation rapide de σ_e; cependant la dégradation d'énergie des ions dans le plasma peut réduire considérablement cet effet. [11]

Les dimensions de l'appareil interviennent dans l'expression de I_{cs} par le terme $\mathcal{V}/\mathcal{L}^2$ qui avec nos notations varie comme L/ν^2, or ν dépend à la fois de L et du procédé d'injection. Une machine très longue est certainement intéressante car ν est alors proportionnel à L (c'est le cas de OGRA). Une

machine courte peut aussi présenter de l'intérêt car c'est au voisinage des miroirs que les trajectoires temporairement capturées sont les plus serrées.

Remarquons que pour $\Gamma=1$, I_{cs} est
indépendant de ϱ et par conséquent de la valeur du champ magnétique,
indépendant de θ_0, et
inversement proportionnel au facteur γ de pompage ionique (en particulier pour $\gamma=0$ il n'y a pas de courant critique et n tend vers une valeur limite peu élevée).

Enfin l'expression de I_{cs} contenant Γ montre une dépendance de l'absorption des parois qui sera précisée plus loin.

Dans l'approximation développée ci-dessus, on peut montrer que pour $I=I_{cs}$, $n=n_0$.

Un autre domaine dans lequel des simplifications importantes se produisent est obtenu lorsque le plasma est devenu opaque (ou absorbant) pour les molécules qui le pénètrent.

$$k \ll 1 \qquad 8\varrho\, n\,(2\sigma_i + \sigma_e)\,\frac{v}{v_0} \gg 1$$

Ce cas correspond à la branche supérieure de la courbe S.

Dans le régime sans arc n devient proportionnel à $I^{1/2}$ (pertes par les miroirs, prédominantes par rapport aux pertes par échange de charge) tandis que n_0 (autour du plasma) reste proportionnel à I. Ce domaine est limité par le courant critique inférieur I_{ci} dont on peut écrire une expression approchée:

$$I_{ci} = \frac{4\langle\sigma_c v\rangle P\mathcal{V}[\Gamma+(C/(c+\Theta))\,(1-g)/g]}{(1+\alpha)^2\mathcal{L}^2(2\sigma_d)^2\,\frac{\sigma_e+2\sigma_i}{\sigma_e}\left[\gamma+\frac{8\varrho}{v_0\mathcal{V}}\left(\theta_0+\frac{1-\Gamma}{4}v_0S'+\frac{C\Theta}{C+\Theta}\right)\right]} \times\left\{1-\frac{[(1-\Gamma)/2]+(\gamma/2)}{\frac{\sigma_e+2\sigma_i}{\sigma_e}\left[\gamma+\frac{8\varrho}{v_0\mathcal{V}}\left(\theta_0+\frac{1-\Gamma}{4}v_0S'+\frac{C\Theta}{C+\Theta}\right)\right]}\right\}. \tag{25}$$

Dans le cas où l'on utilise un arc (n_1 r_1, V_1) la discussion formelle des propriétés est plus compliquée. La courbe représentative de n (I) peut avoir une forme générale en S mais avec une structure complexe dans la branche inférieure, ou bien une pente toujours positive avec ou sans point d'inflexion.

Dans tous les cas, la branche inférieure (plasma transparent aux neutres) est toujours au-dessus de la branche correspondante de la courbe sans arc tandis que la branche supérieure (plasma opaque aux neutres) est toujours au-dessous de la courbe sans arc. Deux courbes avec et sans arc se coupent donc dans la région médiane en un point de transition T.

Sous réserve de ne pas provoquer d'autres pertes que celles prévues dans les hypothèses de notre calcul, l'emploi d'un arc peut donc permettre de passer sur la branche supérieure de la courbe avec un courant injecté plus faible que sans arc. Bien entendu, après la transition on aura tout intérêt à supprimer l'arc.

On peut démontrer que dans une famille de courbes avec arc, définie par le paramètre variable n_1 r_1, toutes celles qui ont la forme en S (et qui correspondent aux faibles valeurs de n_1 r_1,) passent par le même point T. Les autres ont un point de transition qui correspond à un courant d'autant plus grand que n_1 r_1 est plus grand. La courbe limite entre les deux cas a une tangente verticale en T et correspond à des caractéristiques d'arc permettant de passer sur la branche supérieure avec le courant minimum.

Il existe donc un arc optimum et un courant de transition correspondant I_{T_0}. La signification physique de cet optimum est la fin de la partie linéaire de η_d, ce qui correspond à la dissociation d'environ la moitié du faisceau injecté. On peut calculer une expression approchée de I_{T_0}, voir équation (26) en bas de page, avec

$$n_1 r_1 \tau = \frac{V^{\frac{1}{2}}\cdot V_1^{\frac{3}{2}}}{1{,}8\cdot 10^{-11} B_0\,(1+R)/2}, \quad \text{(référence [12])}$$

$$F_1 = \Gamma + \frac{C}{C+\Theta}\,\frac{1-g}{g},$$

$$F_2 = \Theta_0 + \frac{1-\Gamma}{4}v_0S' + \frac{C\Theta}{C+\Theta}, \quad G = \frac{1-\Gamma}{2}+\frac{\gamma'}{2}$$

qui se simplifie pour $\Gamma=1$ et $\nu<10^3$ et devient

$$I_{T_0} = \frac{\left(1+\frac{C}{C+\Theta}\,\frac{1-Q}{Q}\right)\sigma_e\,\mathcal{V}\,2\pi\varrho\left[\gamma(\sigma_e+2\sigma_i)-\frac{\gamma'}{2}\sigma_e\right]}{\gamma^2(1+\alpha)^2L^2(2\sigma_d)^2(\sigma_e+2\sigma_i)^2\,\frac{V^{\frac{1}{2}}\cdot V_1^{\frac{3}{2}}}{1{,}8\cdot 10^{-11}B_0\,(1+R)/2}} \tag{27}$$

De même que I_{cs}, I_{T_0} varie en ν^{-2}.

Le gain relatif en courant critique (I_{cs}/I_{T_0}) augmente avec la température électronique de l'arc $V_1^{\frac{3}{2}}$.

Il serait dangereux de pousser trop loin l'analyse formelle à partir des formules approchées données ci-dessus sans la vérifier et la compléter par des applications numériques plus exactes.

L'intégration directe du système différentiel constitué par les équations (11), (13), (15) a été réalisé sur calculateur électronique pour certaines valeurs particulières des paramètres. Ces valeurs ont été choisies pour l'étude du dispositif expérimental actuellement en cours de réalisation à Fontenay-aux-Roses.

$$I_{T_0} = \frac{F_2 + \frac{F_1\sigma_e v\mathcal{V}[\gamma(\sigma_e+2\sigma_i)-G\sigma_e]}{\gamma(1+\alpha)\mathcal{L}\,2\sigma_d(\sigma_e+2\sigma_i)}}{(1+\alpha)\mathcal{L}\,2\sigma_d\left[\frac{\gamma(\sigma_e+2\sigma_i)}{2\pi\varrho}\,v\,n_1 r_1\,\tau\left(1+\frac{(1+\alpha)\mathcal{L}\,2\sigma_d F_2}{F_1 v\mathcal{V}\sigma_c}-G\right)\right]} \tag{26}$$

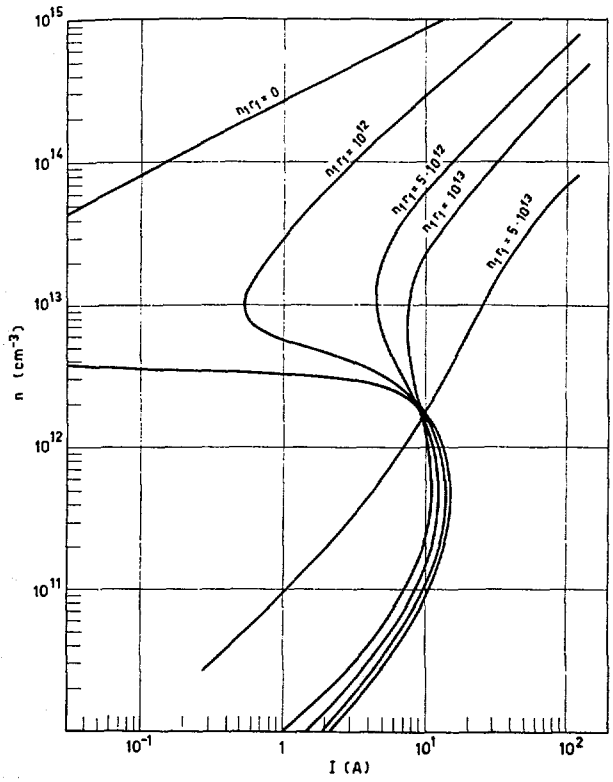

Figure 1 $n\,(I)$ du régime stationnaire pour $\Gamma = 1$, $\gamma = 0{,}5$, $\gamma' = 0{,}9$, $\nu = 10$ et H_2— 100 keV.

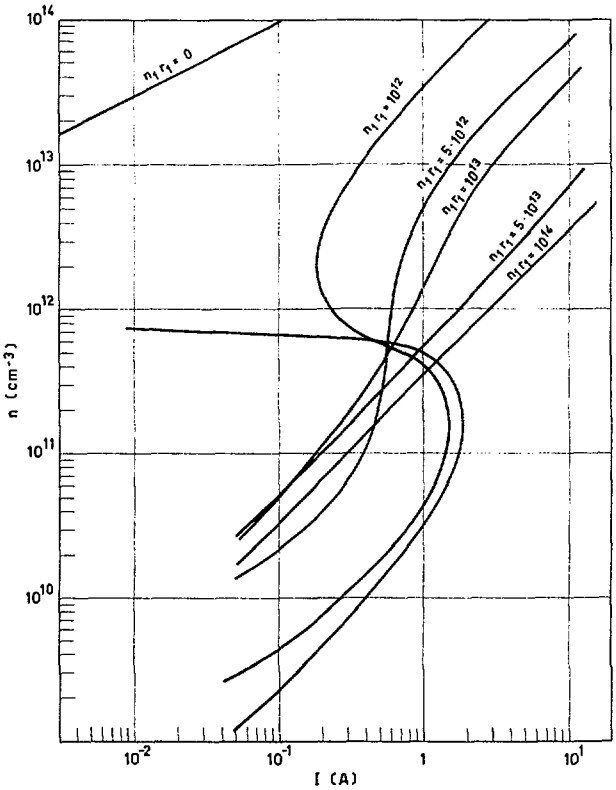

Figure 2 $n\,(I)$ du régime stationnaire pour $\Gamma = 1$, $\gamma = 0{,}5$, $\gamma' = 0{,}9$, $\nu = 50$ et H_2— 100 keV.

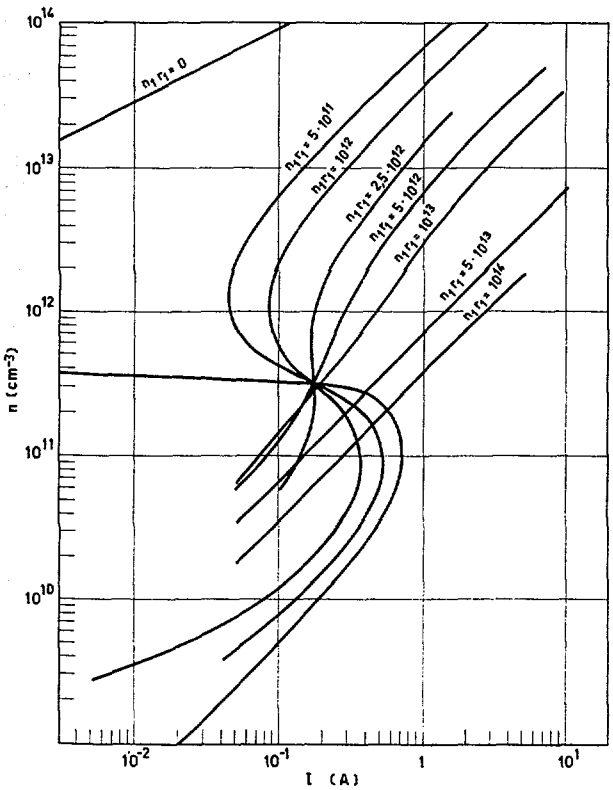

Figure 3 $n\,(I)$ du régime stationnaire pour $\Gamma = 1$, $\gamma = 0{,}5$, $\gamma' = 0{,}9$, $\nu = 100$ et H_2— 100 keV.

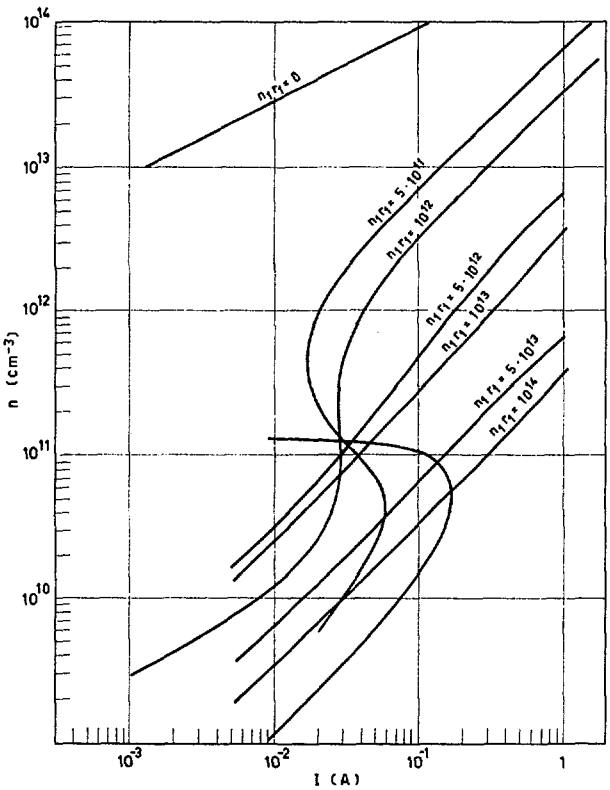

Figure 4 $n\,(I)$ du régime stationnaire pour $\Gamma = 1$, $\gamma = 0{,}5$. $\gamma' = 0{,}9$ $\nu = 250$ et H_2— 100 keV.

Soit:
$L=40$ cm; $B_0=1{,}5\cdot10^4$ G; $R=2$; $\mathcal{V}'=2\cdot10^4$ cm^3; $\mathcal{V}''=7\cdot10^5$ cm^3; $C=10^6$ cm^3/s; $\Theta=10^7$ cm^3/s; $\theta_0=2\cdot10^6$ cm^3/s; $\gamma=0{,}5$; $\gamma'=0{,}9$; $g=0{,}5$.

On a négligé les dégazages devant les autres sources de gaz

$$(q_0=0;\ Q_0=0).$$

Les grandeurs physiques qui correspondent au choix des particules injectées et de leur énergie sont

$M=1$; $2V=10^5$ eV; $2\sigma_d=3\cdot10^{-16}$ cm^2; $\sigma_e=8\cdot10^{-17}$ cm^2; $\sigma_i=3\cdot10^{-16}$ cm^2; $\sigma_c=2{,}4\cdot10^{-22}$ cm^2; $(1+\alpha)=1{,}4$; $v_0=2\cdot10^5$ cm/s; $V_1=10$ eV.

Nous avons conservé ν, Γ et n, r_1 comme paramètres.

Les figures 1 à 4 groupent les courbes $n(I)$ du régime stationnaire pour $\Gamma=1$, sans arc et avec arc, pour plusieurs valeurs de ν ($\nu=10$, 50, 100 et 250 révolutions). Leur comportement général est conforme à la description ci-dessus.

La figure 5 montre le courant critique et le courant de transition déduits des résultats précédents en fonction des caractéristiques d'arc (n_1 r_1).

La figure 6 donne en fonction de l'efficacité de la capture temporaire (ν) les valeurs du courant critique I_{cs} sans arc et du courant de transition optimum I_{T_0}.

On constate que le courant critique sans arc varie moins vite que ν^{-2} et que les valeurs prévues par la formule approchée (24) sont nettement pessimistes surtout pour les faibles efficacités de capture temporaire.

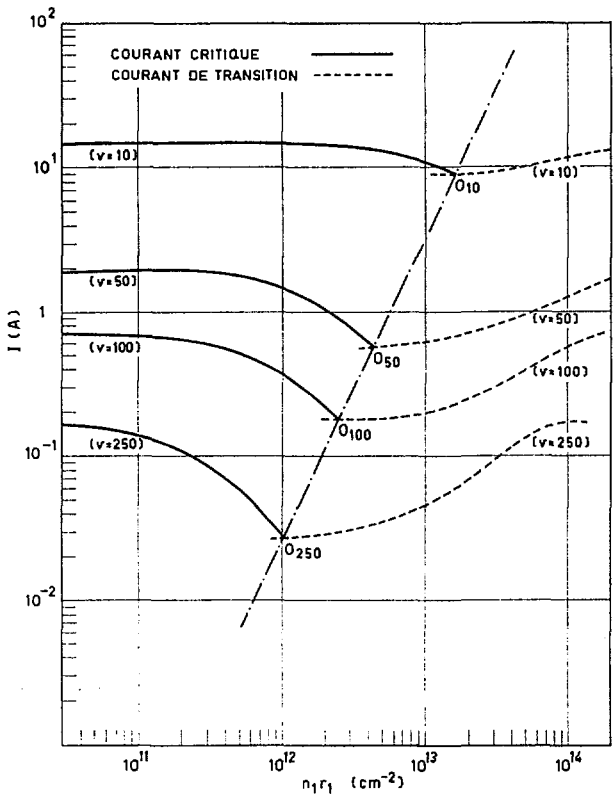

Figure 5 Le courant critique et le courant de transition déduits des résultats précédents en fonction des caractéristiques d'arc (n_1 r_1).

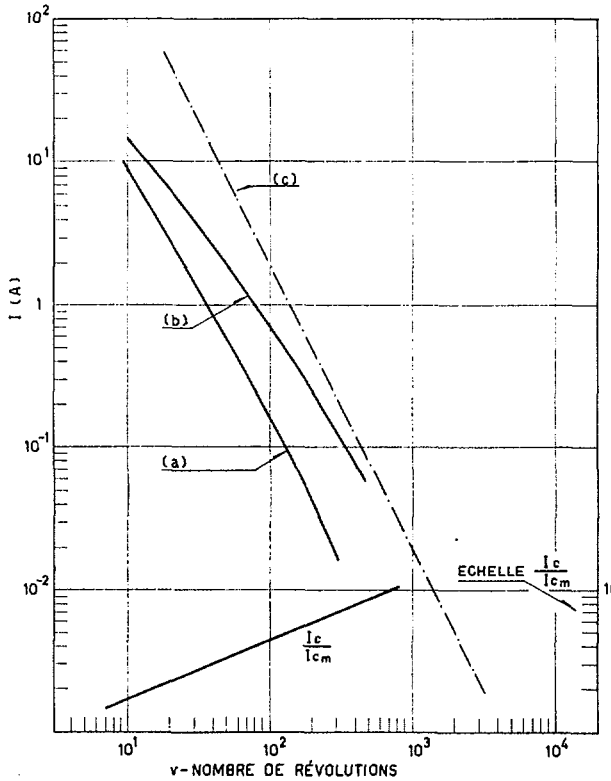

Figure 6 Valeurs du courant critique I_{cs} sans arc et du courant de transition optimum I_{T_0} en fonction de l'efficacité de la capture temporaire (ν). (a) I_{cm} — courant critique sur arc optimum. (b) I_c — courant critique sans arc (c) courant critique sans arc (formule approchée). H_2 — 100 keV, $\Gamma=1$, $\gamma=0{,}5$, $\gamma'=0{,}9$.

Par contre le courant de transition optimum varie presque comme ν^{-2}. Il en résulte que le gain relatif sur le courant critique I_{cs}/I_{T_0} apporté par la présence de l'arc optimum est d'autant plus important que ν est plus grand, à tel point que si la capture temporaire est peu efficace ($\nu<10$) l'arc n'apporte pratiquement plus aucun gain sur le courant critique minimum.

La figure 7 enfin donne en fonction de ν les caractéristiques de l'arc optimum (n_1 r_1) et la densité n des ions au point de transition.

Les caractéristiques de l'arc optimum varient pratiquement en $1/\nu$ ainsi que la densité des ions au point de transition. On note aussi que la dissociation sur les ions est équivalente à la dissociation sur l'arc, au passage au point de transition.

Sur les figures 8 à 13 nous avons repris certaines des courbes en S données sur les figures 1 à 4 en leur adjoignant les courbes donnant la densité moléculaire n_0 correspondante. On constate que la courbe $n_0(I)$ a une allure caractéristique en Z. Au voisinage du courant critique supérieur la densité des neutres est bien équivalente à la densité des ions. La valeur de cette densité est assez élevée (10^{11} à 10^{12} cm^{-3}); ceci permet l'emploi d'un arc à hydrogène (ou deuterium) qui a l'avantage de n'avoir qu'un électron lié par

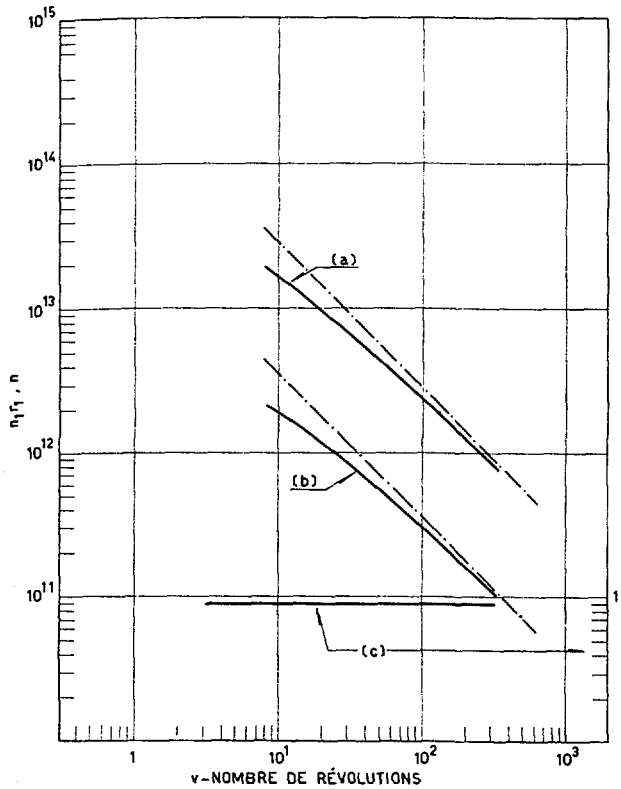

Figure 7 Caractéristiques de l'arc optimum ($n_1 r_1$) et densité n des ions au point de transition en fonction de ν. (a) $n_1 r_1$ de l'arc optimum. (b) n^* densité des ions au point de transition sur arc optimum, (c) dissociation sur l'arc/dissociation sur $n^* = (\nu \cdot \sigma_\alpha \cdot n_1 \cdot v_1 / \nu \cdot \sigma_\alpha \cdot n \cdot 2\pi\varrho) \sim 1$. H_2 — 100 keV, $\Gamma = 1$, $\gamma = 0{,}5$, $\gamma' = 0{,}9$.

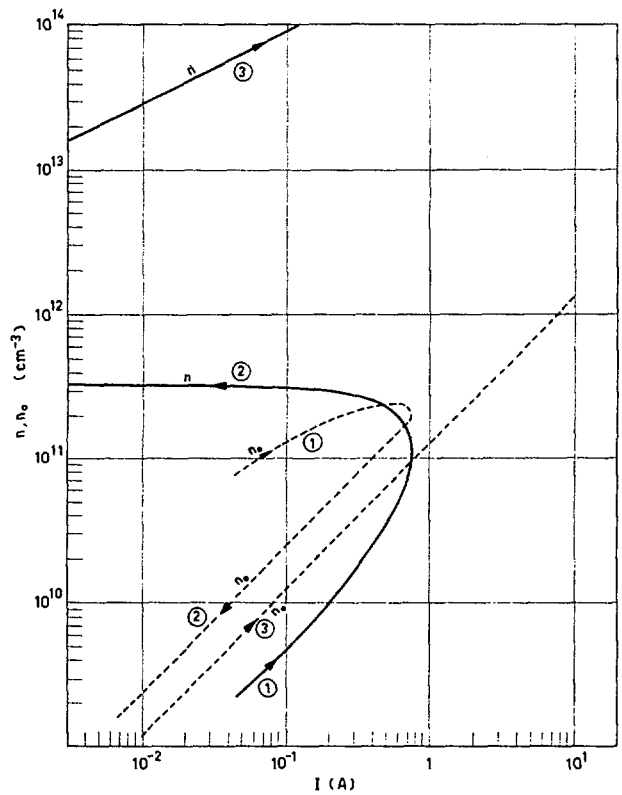

Figure 8 Certaines des courbes en S données sur les figures 1 à 4 en leur adjoignant les courbes donnant la densité moléculaire n_0 correspondante. Régime stationnaire. $n_1 r_1 = 0$ (sans arc), $\Gamma = 1$, $\gamma = 0{,}5$, $\gamma' = 0{,}9$, $\nu = 100$.

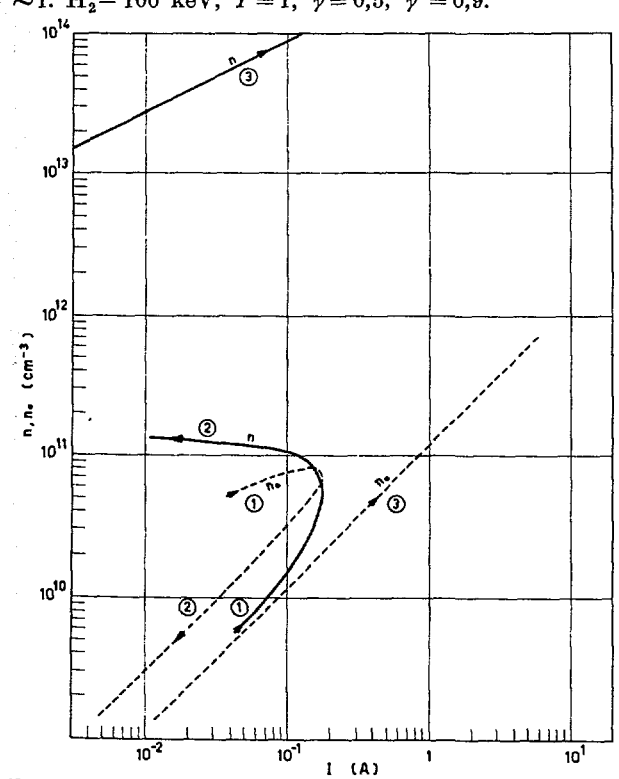

Figure 9 Certaines des courbes en S données sur les figures 1 à 4 en leur adjoignant les courbes donnant la densité moléculaire n_0 correspondante. Régime stationnaire. $n_1 r_1 = 0$, $\Gamma = 1$, $\gamma = 0{,}5$, $\nu = 250$.

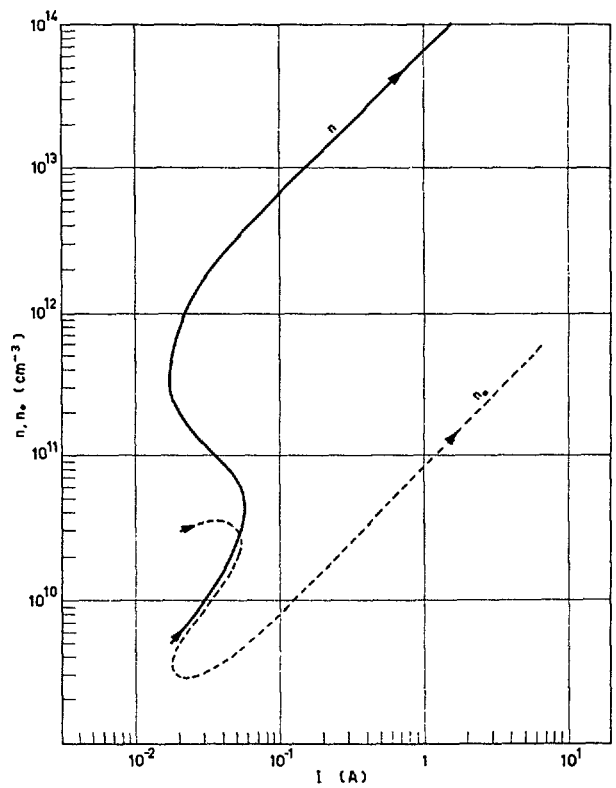

Figure 10 Certaines des courbes en S données sur les figures 1 à 4 en leur adjoignant les courbes donnant la densité moléculaire n_0 correspondantes. Régime stationnaire. $n_1 r_1 = 5 \cdot 10^{11} <$ arc optimum, $\Gamma = 1$, $\gamma = 5$, $\gamma' = 09$, $\nu = 250$.

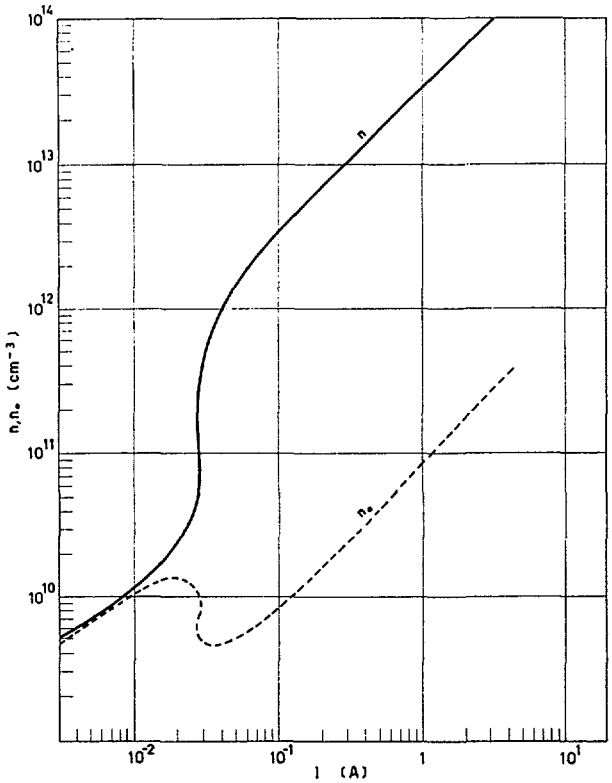

Figure 11 Certaines des courbes en S données sur les figures 1 à 4 en leur adjoignant les courbes donnant la densité moléculare n_0 correspondante. Régime stationnaire. $n_1 r_1 = 10^{12} \sim$ arc optimum. $\Gamma = 1$, $\gamma = 0{,}5$. $\gamma' = 0{,}9$, $\nu = 250$.

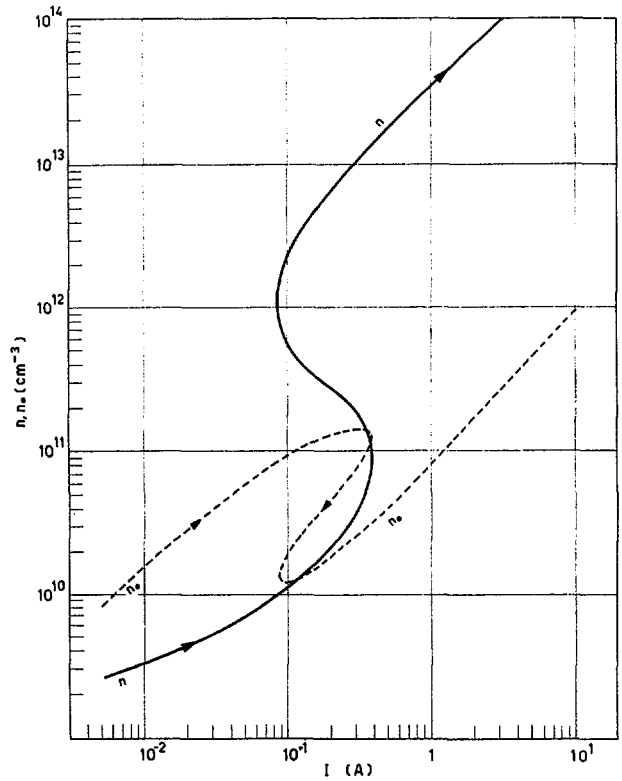

Figure 12 Certaines des courbes en S données sur les figures 1 à 4 en leur adjoignant les courbes donnant la densité moléculaire n_0 correspondante. Régime stationnaire. $n_1 r_1 = 10^{12} <$ arc optimum, $\Gamma = 1$, $\gamma = 0{,}5$, $\gamma' = 0{,}9$, $\nu = 100$.

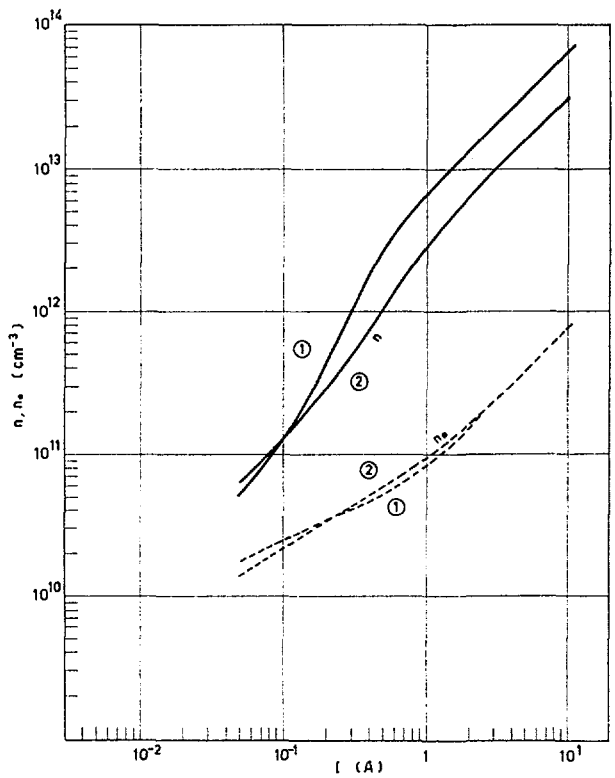

Figure 13 Certaines des courbes en S données sur les figures 1 à 4 en leur adjoignant les courbes donnant la densité moléculaire n_0 correspondante. Régimes stationnaires. $1 - n_1 r_1 = 5 \cdot 10^{12} >$ arc optimum, $2 - n_1 r_1 = 10^{13} >$ arc optimum, $\Gamma = 1$, $\gamma = 0{,}5$, $\gamma' = 0{,}9$, $\nu = 100$.

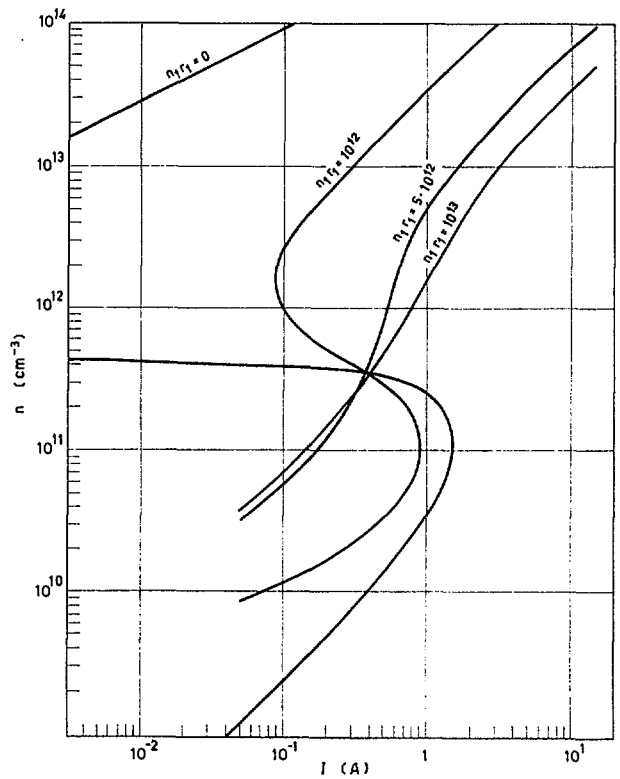

Figure 14 Quelques courbes en S calculées avec $\Gamma = 0{,}8$. Régime stationnaire. $H_2 - 100$ keV, $\nu = 100$, $\gamma = 0{,}5$, $\gamma' = 0{,}9$.

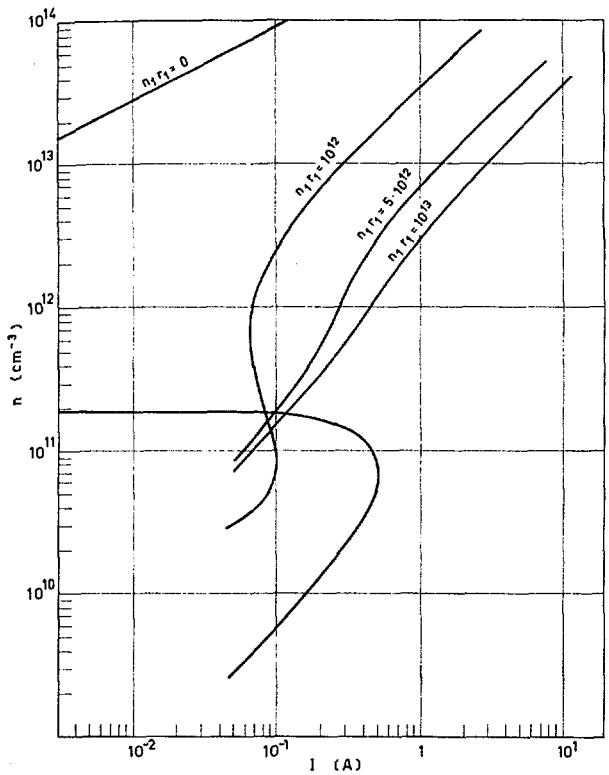

Figure 15 Quelques courbes en S calculées avec $\Gamma = 0{,}8$. Régime stationnaire. $H_2 - 100$ keV, $\nu = 100$, $\gamma = 0{,}5$, $\gamma' = 0{,}9$.

atome mais qui fonctionne difficilement à très basse pression.

Quelques courbes en S calculées avec $\Gamma = 0{,}8$ sont données sur les figures 14 et 15.

On peut tirer dans ce cas des conclusions analogues à celles de l'étude détaillée du cas $\Gamma = 1$.

On constate que le gain apporté par l'activation des parois apporte une réduction d'un facteur de l'ordre de 1,5 sur le courant critique sans arc et de l'ordre de 2 sur le courant de transition pour $\nu = 100$ et que ce gain semble croître avec la valeur de ν.

On remarque cette fois encore que la transition est possible lorsque la dissociation sur le plasma est égale à la dissociation sur l'arc.

Sur les figures 16 à 21 nous avons tracé, pour certains cas particuliers, l'évolution en fonction du temps des densités n et n_0, au cours de la formation du plasma.

Sur ces courbes on peut distinguer trois régions:

1. Dans une première phase les constantes de temps sont très rapides; cette phase correspond à un régime dominé par les pertes par échange de charge, sa durée est toujours inférieure à 10^{-2} s.
2. Un palier atteint au bout de 10^{-2} s environ.
3. Au delà du palier, 2 évolutions sont possibles.

Si $I < I_{cs}$, les densités restent peu modifiées et vont vers un état d'équilibre stationnaire qui est atteint en quelques dixièmes de seconde.

Si $I > I_{cs}$, n croît vers une valeur élevée correspondante à la branche supérieure de la courbe en S: n_0 décroît (le pompage ionique croît très vite) puis remonte vers un régime stationnaire. Cette dernière remontée se produit lorsque n atteint des valeurs élevées pour lesquelles les fuites par les miroirs sont dominantes (et par suite le retour de neutres par les miroirs $(1-\gamma)$ important). Les constantes de temps de cette dernière phase sont assez longues, de l'ordre de quelques dixièmes de seconde, les phénomènes étant alors dominés par la diffusion coulombienne.

On remarque que si $n_1 r_1$ devient supérieur aux valeurs correspondant à l'arc optimum le régime est complètement commandé par l'arc et les phénomènes évolutifs décrits ci-dessus sont écrasés par l'influence des pertes par refroidissement sur l'arc. Plusieurs conséquences importantes peuvent être déduites de cette étude du régime évolutif.

La densité de transition, lorsqu'elle est atteinte, l'est toujours très rapidement (quelques centièmes de seconde). De façon analogue, pour le régime sans arc avec $I > I_{cs}$ on atteint au bout d'un temps du même ordre des densités telles que l'on peut réduire le courant injecté sans retomber sur la branche inférieure de la courbe en S. Il en résulte qu'on pourra atteindre des points intéressants de fonctionnement sur la branche supérieure de la courbe en S, par deux voies: soit amorçage sur un arc avec coupure de celui-ci au bout d'un temps très court, soit contournement du courant critique supérieur par une impulsion courte (quelque 10^{-2} s) du courant injecté. Une telle

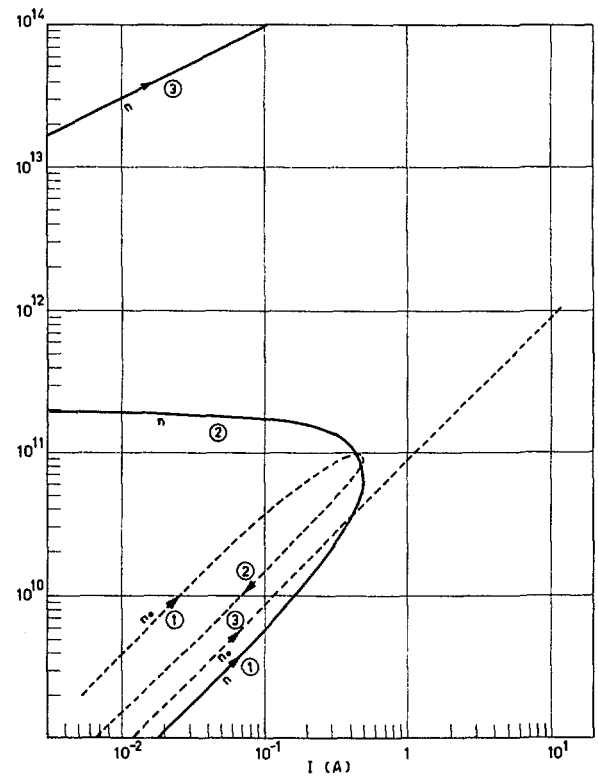

Figure 16 Evolution en fonction du temps des densités n et n_0, au cours de la formation du plasma pour certains cas particuliers. Régime stationnaire, $n_1 r_1 = 0$, H_2 $- 100$ keV, $\nu = 100$, $\Gamma = 0{,}8$, $\gamma = 0{,}5$, $\gamma' = 0{,}9$.

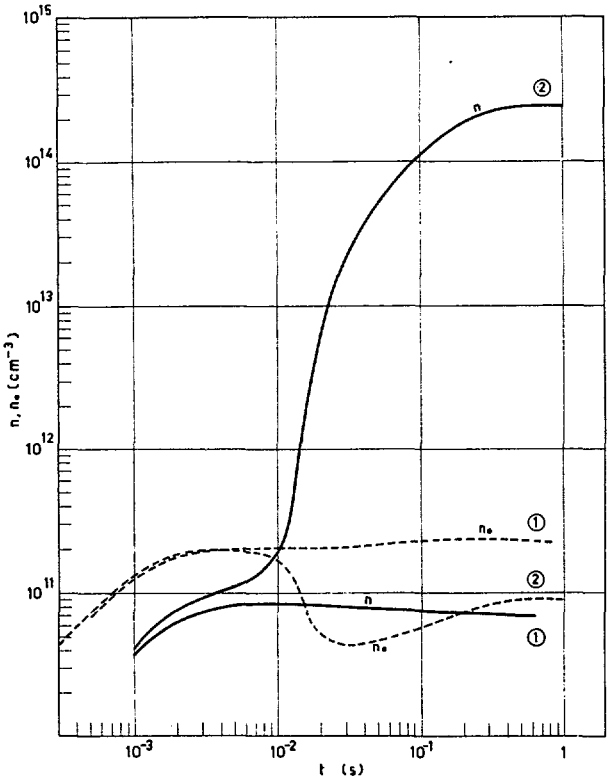

Figure 17 Evolution en fonction du temps des densités n et n_0, au cours de la formation du plasma pour certains cas particuliers. 1 — $I = 0{,}687$ A $= 0{,}97\ I_c$, 2 — $I = 0{,}734$ A $= 1{,}03\ I_c$, $n_1 r_1 = 0$ (sans arc), $\Gamma = 1$, $\gamma = 0{,}5$, $\gamma' = 0{,}9$, $\nu = 100$.

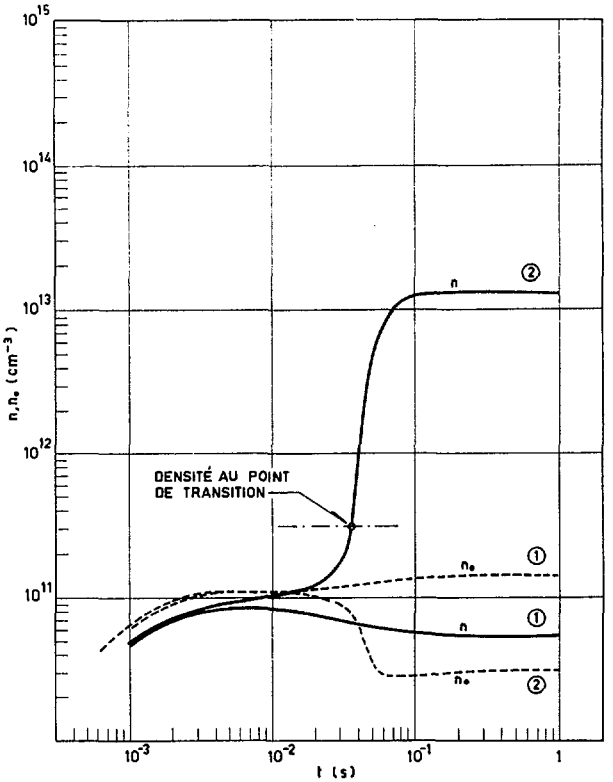

Figure 18 Evolution en fonction du temps des densités n et n_0, au cours de la formation du plasma pour certains cas particuliers. 1 — $I = 0{,}359$ A $= 0{,}97\ I_c$, 2 — $I = 0{,}375$ A $= 1{,}02\ I_c$, $n_1 r_1 = 10^{12}$ ($< n_1 r_1$ optimum), $\Gamma = 1$, $\gamma = 0{,}5$, $\gamma' = 0{,}9$, $\nu = 100$.

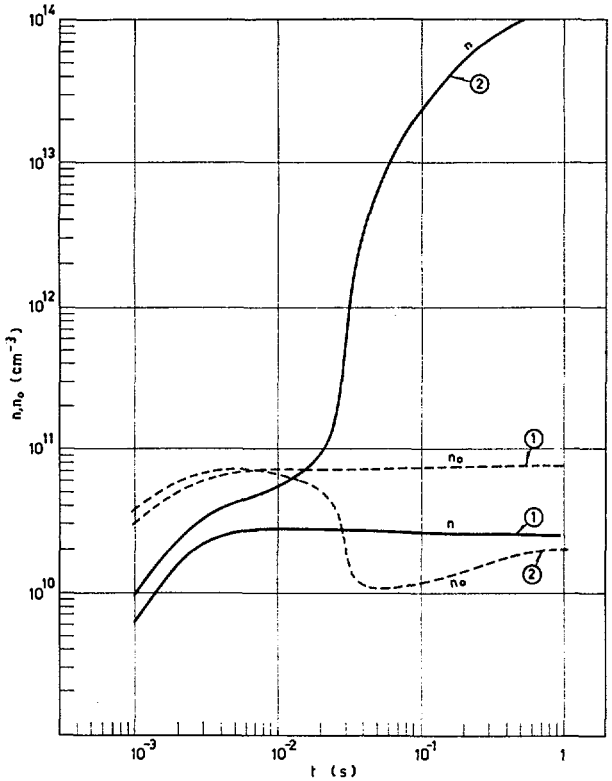

Figure 19 Evolution en fonction du temps des densités n et n_0, au cours de la formation du plasma pour certains cas particuliers. 1 — $I = 0{,}138$ A $= 0{,}8\ I_c$, 2 — $I = 0{,}175$ A $= 1{,}03\ I_c$, $n_1 r_1 = 0$ (sans arc), $\Gamma = 1$, $\gamma = 0{,}5$, $\gamma' = 0.9$, $\nu = 250$.

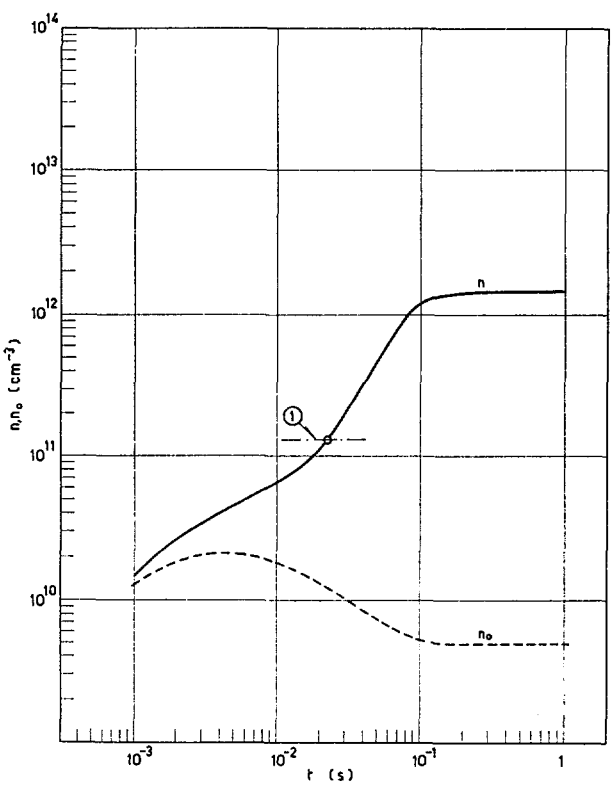

Figure 20 Evolution en fonction du temps des densités n et n_0, au cours de la formation du plasma pour certains cas particuliers. 1 — densité au point de transition. $I = 0{,}05$ A $= 1{,}7\ I_t$. $n_1 r_1 = 10^{12}$ (arc optimum), $\Gamma = 1$, $\gamma = 0{,}5$, $\gamma' = 0{,}9$, $\nu = 250$.

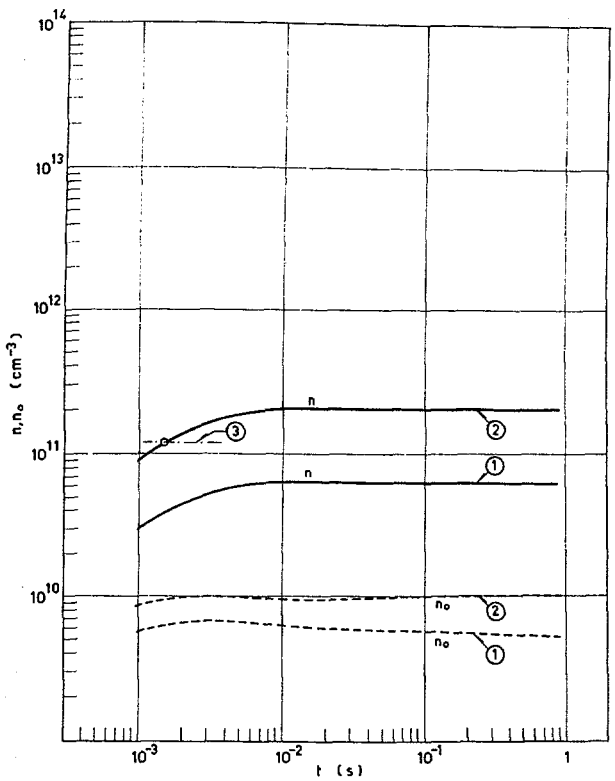

Figure 21 Evolution en fonction du temps des densités n et n_0, au cours de la formation du plasma pour certains cas particuliers. 1 — $I = 0{,}025$ A $= 0{,}5\ I_t$, 2 — $I = 0{,}075$ A $= 1{,}5\ I_t$, 3 — densité au point de transition. $n_1\ r_1 = 10^{13}$ (régime dominé par l'arc), $\Gamma = 1$, $\gamma = 0{,}5$, $\gamma' = 0{,}9$, $\nu = 250$.

impulsion de courant est possible en principe avec l'injection circulaire, qui n'est pas limitée par la charge d'espace dans le domaine de quelques ampères. Le fonctionnement sur la branche supérieure peut être conservé avec un courant d'injection du courant réduit à quelques dizaines de milliampères. Cette réduction du courant permet de travailler avec une pression cinétique du plasma (β) faible et variable pour l'étude de la stabilité.

Par ailleurs, dans le cas où le régime n'est pas dominé par la présence d'un arc dense, l'existence d'un minimum prononcé dans la densité n_0 au cours de l'évolution du plasma est caractéristique de l'obtention du courant critique. Les constantes de temps d'évolution de cette densité sont telles qu'elles pourraient être facilement suivies par une jauge d'ionisation ouverte placée immédiatement au voisinage du plasma. Le relevé sur oscillogramme de $n_0 = f(t)$ permettrait donc de remonter de façon simple à l'évolution de la densité des ions dans le plasma.

On notera aussi que la valeur élevée de n_0 au courant critique (10^{11} à 10^{12} mol./cm^3) ainsi que les valeurs des temps d'évolution permettent d'espérer que la neutralité du plasma sera facilement assurée par ionisation du gaz résiduel.

Remarquons enfin que, en fait, contrairement à l'hypothèse initiale, la densité du plasma n'est pas uniforme. Elle peut être notablement plus grande que celle calculée dans un volume inférieur à $\mathcal{V}$, par suite du mode d'injection (l'injection circulaire donne une concentration sur l'axe) ainsi que par l'emploi d'un arc. Dans ces conditions on devrait avoir un courant critique plus petit que celui qui a été calculé.

2.3. Injection d'ions atomiques incomplètement ionisés

A la méthode ci-dessus on peut rattacher l'injection d'ions atomiques incomplètement ionisés et capturés par arrachement d'un ou plusieurs électrons au cours de leur trajet dans la bouteille magnétique. En effet, en première approximation, les équations d'évolution ont la même forme que ci-dessus, et les courants critiques la même expression, en remplaçant la section efficace de dissociation par la section efficace d'ionisation correspondante. On bénéficie de la même façon du passage multiple. Un choix convenable de l'élément peut permettre une réduction appréciable du courant critique, et faciliter ainsi l'étude expérimentale des plasmas à très haute température. Certains éléments de Z élevé présentent certainement des sections efficaces d'ionisation favorables. Cependant, leur emploi doit conduire à des pertes par rayonnement considérables. L'emploi d'un faisceau de Li^+ nous semble le plus avantageux en raison de son numéro atomique ($Z = 3$) et de sa faible tension de vapeur qui permet d'écrire $\gamma = 1$ et $\Gamma = 0$ dans les équations.

3. Injection d'atomes neutres rapides

Dans ce type d'injection, la capture se fait par ionisation de l'atome incident, soit par échange de charge avec un ion (σ_e) soit par libération de l'électron (σ_i) par choc avec ion électron ou molécule neutre. Par ailleurs l'atome incident ne peut effectuer qu'un trajet très limité dans le volume du plasma ($\mathcal{L} = 2\,\mathcal{R}$), ce qui limite à des valeurs très faibles la probabilité de capture mais permet de recevoir le faisceau non capturé sur une cible disposée de manière à éviter autant que possible la réémission du gaz neutre vers le plasma [13].

3.1. Equations d'évolution

La capture étant toujours faible, on peut développer le terme exponentiel en le limitant au premier ordre

$$\eta_c \sim 2\,\mathcal{R}\left[2\,\sigma_i\left(n_0 + n + n_1\frac{r_1}{\mathcal{R}}\right) + \frac{n_1\,r_1}{\mathcal{R}}\,\sigma_e\right], \qquad (28)$$

en admettant que la section efficace d'ionisation est la même sur les atomes, ions et électrons.

Le terme correspondant à l'échange de charge faisceau plasma chaud est à la fois terme source et terme perte, il s'élimine donc de l'équation mais nous devrons le faire intervenir dans l'équation des neutres.

L'équation d'évolution des ions prend alors exactement la même forme que dans le cas des ions moléculaires

$$\frac{dn}{dt} = \frac{I\eta_c}{\mathcal{V}} - n\,\bar{n}_0\,\sigma_e\,v - \frac{n}{\tau} - n^2\,\langle\sigma_c\,v\rangle\,P, \qquad (29)$$

avec

$$\bar{n}_0 = \frac{n_0}{1 + 2\mathcal{R}(v/v_0)(\sigma_e + 2\sigma_i)n}.$$

Pour l'étude de l'évolution des neutres, nous remplacerons les termes sources dus au faisceau non dissocié et au gaz provenant du caisson accélérateur par un seul terme dans lequel KI représente la fraction du faisceau injecté qui finalement se retrouvera sous forme de neutres autour du plasma.

L'équation d'évolution s'écrit dans ce cas

$$\frac{dn_0}{dt} = \frac{KI}{2\mathcal{V}_r'} + \frac{\Gamma}{2} n \bar{n}_0 \sigma_e v \frac{\mathcal{V}}{\mathcal{V}_r'} + \frac{1-\gamma'}{2} \cdot \frac{n}{\tau} \cdot \frac{\mathcal{V}}{\mathcal{V}_r'} + \frac{1-\gamma}{2} n^2 \langle \sigma_c v \rangle \frac{P\mathcal{V}}{\mathcal{V}_r'} + \frac{q_0}{\mathcal{V}_r'} - \frac{\theta n_0}{\mathcal{V}_r'} - \gamma n \bar{n}_0 (\sigma_e + 2\sigma_i) v \frac{\mathcal{V}}{\mathcal{V}_r'} - \frac{\gamma I}{\mathcal{V}_r'} 2\mathcal{R}\bar{n}_0\sigma_i + \frac{\Gamma I}{2} \frac{2\mathcal{R}}{\mathcal{V}_r'} n \sigma_e + \frac{I}{2} \frac{2 n_1 r_1 \sigma_0}{\mathcal{V}_r'}. \quad (30)$$

Les deux derniers termes représentent respectivement l'échange de charge du faisceau avec les ions chauds et avec les ions de l'arc.

3.2. Conséquences et applications

Le système constitué par les équations (29) et (30) peut être exploité par intégration directe à l'aide d'un calculateur électronique. Nous nous contenterons ici d'exploiter les équations en régime stationnaire dans le cas où la capture se fait sans plasma auxiliaire et en nous limitant à des densités faibles, de telle façon que le terme $n^2 \langle \sigma_c v \rangle P$ soit négligeable.

Dans ce cas le système peut se mettre sous la forme d'une équation du second degré en n^2

$$an^2 + bn + c = 0, \quad (31)$$

dont les coefficients a, b, et c dépendent de I:

$$a = 4\sigma_i(2\sigma_i + \sigma_e)\mathcal{R} \cdot I \cdot v\mathcal{V} \times \left\{ \frac{2\mathcal{R}\theta}{v_0 \mathcal{V}} + \gamma - \Gamma \frac{\sigma_e}{2(\beta\sigma_i + \sigma_e)} \right\},$$

$$b = 8\mathcal{R}^2\sigma_i^2 \left[\gamma + \Gamma \frac{\sigma_e}{4\sigma_i} \right] I^2 + \left(4\mathcal{R}\sigma_i\theta - \frac{K}{2}\sigma_e \mathcal{V} v \right) I - q_0 \sigma_e v \mathcal{V},$$

$$c = 2\mathcal{R}\sigma_i I \left(q_0 + \frac{KI}{2} \right). \quad (32)$$

La densité des neutres est alors donnée par

$$\bar{n}_0 = \frac{4\mathcal{R}\sigma_i I n}{n\sigma_e v\mathcal{V} - 4\mathcal{R} I \sigma_i}.$$

On peut montrer que la possibilité d'obtention d'un courant critique pour une valeur physiquement acceptable de I_{cs} est subordonnée à deux conditions. Une condition nécessaire et suffisante d'existence d'un courant critique s'exprime par une inégalité faisant intervenir les divers paramètres de pompage θ, γ et Γ.

$$\left[\theta_0 + \frac{S' v_0}{4}(1 - \Gamma) \right] + \frac{v_0 \mathcal{V}}{2\mathcal{R}} \left[\gamma - \Gamma \frac{\sigma_e}{2(\beta\sigma_i + \sigma_e)} \right] > 0. \quad (34)$$

Cependant le courant critique ne prend de valeurs réalisables que si la valeur de K satisfait à l'inégalité

$$K < \frac{8\mathcal{R}\sigma_i}{\sigma_e v\mathcal{V}} \left[\theta_0 + \frac{S' v_0}{4}(1 - \Gamma) \right]. \quad (35)$$

Si ces deux conditions sont réalisées le courant critique supérieur peut s'exprimer par l'expression approchée

$$I_{cs} \simeq \frac{q_0 \cdot \sigma_e \cdot v \cdot \mathcal{V}}{4\mathcal{R}\sigma_i\theta - \frac{K}{2}\sigma_e v \mathcal{V}}, \quad (36)$$

expression valable tant qu'elle ne conduit pas à des valeurs du courant (équivalent) supérieures à quelques ampères.

Cette expression du courant critique diffère notablement de celle obtenue par l'injection d'ions moléculaires. I_{cs} ne dépend pas ici de γ, mais par contre il contient q_0 et θ. Ceci tient au fait (ainsi que nous le vérifions par les applications numériques) que les valeurs de n et n_0 pour le courant critique sont beaucoup plus basses que dans le cas de l'injection moléculaire et l'action du pompage ionique est peu sensible dans ce domaine.

I_{cs} dépend de l'énergie des particules par l'intermédiaire de σ_i, σ_e, v, $\mathcal{V}$ et $\mathcal{R}$. Le champ magnétique intervient également par $\mathcal{V}$ et $\mathcal{R}$; ces dernières grandeurs ne peuvent d'ailleurs pas être évaluées dans le cadre des hypothèses que nous avons faites.

En fait les conditions critiques seront réalisées avec un courant critique minimum dans le plus faible

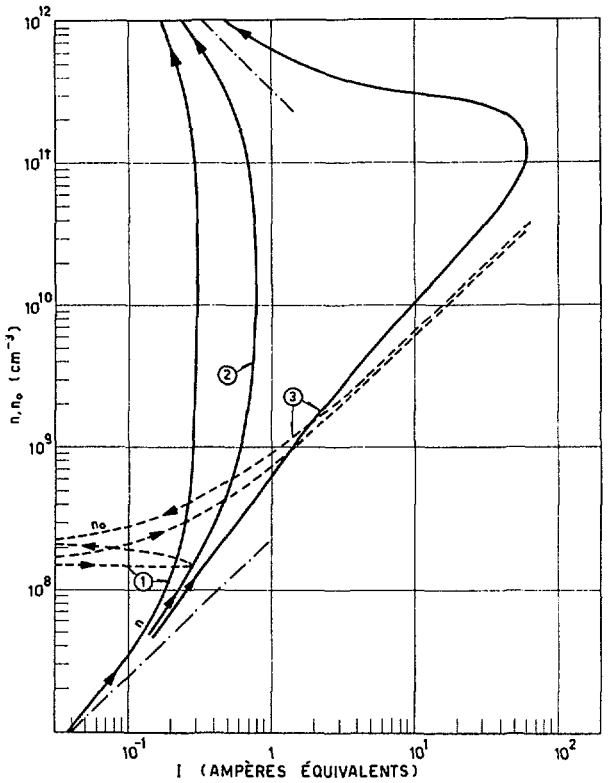

Figure 22 Injection de particules neutres rapides. Influence des sources de gaz extérieures. (Régime stationnaire.) $\Gamma = 1$, $\gamma = 0{,}3$ pas d'arc, $V = 20$ keV, $H = 50$ kG. 1 — $K = 0$, 2 — $K = 10^{-3}$, 3 — $K = 2 \times 10^{-3}$.

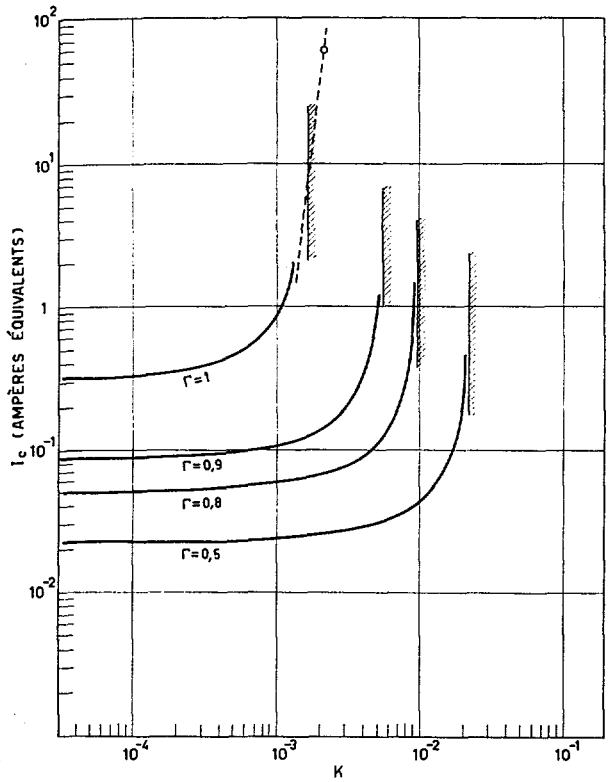

Figure 23 Injection de neutres rapides. Courant critique. Influences des sources de gaz extérieures et de l'état des parois. $V=20$ keV, $H=50$ kG.

volume qui pourra effectivement contenir un plasma de l'énergie considérée dans le champ magnétique de la configuration. Il semble logique d'admettre que ce volume diminue quand le champ magnétique augmente et quand l'énergie des atomes injectés diminue; ces conditions sont justement réalisées dans la machine ALICE à Livermore [5].

Une fois les conditions critiques réalisées dans le volume minimum, on peut penser que ce volume augmentera.

Nous présentons ici des applications numériques des équations (31) à (33) avec un choix de paramètres en accord avec ces considérations, soit:

$V=20$ keV, $\sigma_i=2\cdot10^{-16}$ cm², $\sigma_e=5\cdot10^{-16}$ cm²,

$H=5\cdot10^4$ G d'où $\varrho=0{,}408$ cm.

Nous prendons alors $\mathcal{V}=\pi\,\mathcal{R}^2\,L$ avec $\mathcal{R}=2\,\varrho$ et $L=40$ cm: $\mathcal{V}=84$ cm³.

Il nous semble que ce soit là une valeur très optimiste; ce volume est le plus petit que l'on puisse considérer, tant pour l'existence du plasma lui-même que par suite de la section finie du faisceau des atomes incidents.

Les résultats de cette application numérique sont rassemblés sur les figures 22 et 23. Le dégazage des parois a été évalué à $q_0=1{,}5\cdot10^{15}$ particules par seconde.

Nous avons en outre admis

$v_0=2\cdot10^5$ cm/s $\quad S'=5\cdot10^3$ cm³ $\quad \theta_0=10^7$ cm³/s.

La valeur choisie pour θ_0 satisfait la relation (34), même dans le cas $\Gamma=1$; $\gamma=0$ ($\theta_0>0{,}64\cdot10^7$). Il y aura donc toujours un courant critique.

a) Influence des sources de gaz extérieures (figure 22). En adoptant $\Gamma=1$; $\gamma=0{,}3$, nous avons tracé $n=f(I)$ en régime stationnaire pour $K=0$; $K=10^{-3}$ et $K=2\cdot10^{-3}$. Nous voyons que lorsque K passe de 10^{-3} à $2\cdot10^{-3}$, c'est-à-dire selon que la relation (35) est satisfaite ou non, le courant critique passe de 0,75 ampère à 60 ampères, ce qui montre bien l'extrême sensibilité du plasma à la valeur de K.

Remarquons ici les valeurs de n et n_0 pour le courant critique, beaucoup plus basses que pour l'injection d'ions moléculaires.

b) Nous avons ensuite supposé que l'on pouvait abaisser Γ à des valeurs inférieures à 1 par un dépôt actif sur les parois: la figure (23) donne le courant critique tiré de l'équation (36) en fonction de K pour diverses valeurs de Γ. On note que la diminution de Γ présente un intérêt double. D'une part la valeur du courant critique s'abaisse notablement, et d'autre part la valeur limite de K se relève, ce qui signifie que la nécessité de contrôler le faisceau devient sensiblement moins sévère pour $\Gamma<1$. Nous n'avons pas calculé de valeur sur la branche supérieure de la courbe de n, ni d'expression du courant critique inférieur dans le cas de l'injection des atomes rapides, faute d'une estimation du volume $\mathcal{V}$ et du rayon $\mathcal{R}$ du plasma formé.

Des applications numériques, faites dans l'approximation précédente en présence d'un arc, montrent l'existence possible d'un arc optimum. Cependant ce cas semble d'un intérêt pratique assez douteux, d'une part parce que le gain sur le courant critique reste faible et d'autre part que ces conditions optima semblent difficiles à réaliser (n_1 de l'ordre de 10^{10} ion/cm³, dans un vide $n_0=10^8$ à 10^9 molécules/cm³).

Remarquons enfin que si la condition de l'existence d'un courant critique n'est pas satisfaite, l'évolution de n en fonction de I manifeste cependant une montée linéaire suivie d'une montée brusque puis d'une saturation à basse valeur. Cette situation, qu'on peut qualifier de pseudocritique, montre l'extrême sensibilité de la méthode à la source de gaz neutre que constitue le plasma lui-même.

3.3. Injection d'ions moléculaires ou d'ions atomiques avec passage simple

L'injection d'ions moléculaires avec capture par dissociation ainsi que l'injection d'ions atomiques avec capture par ionisation supplémentaire, peuvent également être envisagées avec passage simple dans la bouteille magnétique. Les équations d'évolution sont alors très analogues à celles que l'on a utilisées pour l'injection d'atomes neutres, et les mêmes conclusions s'appliquent. Cependant, à cause de la très faible densité du gaz neutre, le problème de la neutralisation du plasma reste entier. L'emploi d'un faisceau de Li^+

permet de réaliser facilement la condition $K=0$; mais est évidemment moins favorable que dans le cas du passage multiple.

4. Conclusion

Par la seule considération des interactions binaires des diverses particules du plasma et du gaz neutre, on a pu obtenir des résultats assez détaillés sur l'évolution et l'équilibre d'un plasma formé par injection de particules accélérées.

Ces résultats peuvent être utilisés pour le choix d'une méthode d'injection, pour la conception d'un appareil d'étude et pour l'interprétation des résultats expérimentaux.

Jusqu'à présent, à notre connaissance, la quasi-totalité des résultats de ces calculs n'a pas encore reçu de vérification expérimentale. Plusieurs expériences de ce type en cours actuellement dans divers laboratoires devraient apporter prochainement des observations intéressantes à confronter avec les calculs.

Certes de nombreux et importants phénomènes ont été délibérément laissés de côté dans les hypothèses de départ. Les défauts les plus graves du calcul présenté ici peuvent être trouvés dans la répartition spatiale des particules, la répartition de l'énergie et les interactions collectives.

Des modifications adéquates pourraient sans doute être apportées aux équations en tenant compte des informations que les expériences amèneraient.

Nous remercions le Service de calcul électronique de Saclay, et particulièrement MM. F. ROCHE et J. LEBRISS pour la programmation et l'exécution des calculs sur machine.

Références

[1] SIMON, A., *Phys. Fluids* **1** (1958) 495.
[2] SIMON, A., *Phys. Fluids* **2** (1959) 336.
[3] SIMON, A., *J. Nucl. Energy* **C 1** (1960) 215.
[4] KURCHATOV, I. V., *Atomnaya Energiya* **5** (1958) 105.
[5] GIBSON, G., LAMB, W. A. S., LAUER, E. J., Proceedings of the Second UN International Conference on Peaceful Uses of Atomic Energy, Geneva, **32** (1958) 275.
[6] BINEAU, M., CONSOLI, T., MAISONNIER, CH., PRÉVOT, F., RICATEAU, P., *Nucl. Instr. & Methods* **4** (1959) 290.
[7] POST, R. F., Proceedings of the Fourth International Conference on Ionization Phenomena in Gases, Uppsala (North-Holland Pub. Co., 1959): Vol. 2, p. 987.
[8] GILBERT, F. C., HECKROTTE, W., HESTER, R. E., KILLEEN, J., VAN ATTA, C. M., U.S. Atomic Energy Commission Report UCRL-5827 (1960).
[9] MACKIN, R. J., JR., *Nuclear Fusion* **1** (1961) 131.
[10] PRÉVOT, F., GOURDON, C., Rapport interne n° 80 (Janvier, 1961).
[11] FOWLER, T. K., U. S. Atomic Energy Commission Report ORNL-3037 (1960).
[12] PRÉVOT, F., Rapport interne n° 27 (Mars, 1960).
[13] GOURDON, C., PRÉVOT, F., Rapport interne n° 107 (Mai, 1961).

Récapitulation des notations

σ_d section efficace de dissociation des ions
σ_e section efficace d'échange de charge des ions avec le gaz résiduel
σ_i section efficace d'ionisation des neutres
σ_0 section efficace de diffusion coulombienne (90°)
α probabilité relative de la réaction $H_2^+ \rightarrow H^+ + H^+ + e$
M nombre de masse des ions dissociés
V énergie des ions dissociés (eV)
V_1 énergie des électrons de l'arc (eV)
v_0 vitesse d'agitation du gaz neutre
v vitesse des ions dissociés
ϱ rayon de giration moyen des ions dissociés
L longueur de la machine entre miroirs
B_0 champ magnétique au centre
R rapport de miroirs
P probabilité de fuite par les miroirs (pour un choc)
$\mathcal{V}$ volume du plasma
$\mathcal{R}$ rayon du plasma
S aire de la surface limitant le plasma
$\mathcal{V}'$ volume du récipient matériel contenant le plasma
$\mathcal{V}''$ volume de l'enceinte contenant la source d'ions
C conductance entre $\mathcal{V}'$ et $\mathcal{V}''$
Θ vitesse de pompage mécanique dans $\mathcal{V}''$
θ_0 vitesse de pompage mécanique dans $\mathcal{V}'$
q_0 dégazage des parois entourant le plasma $\mathcal{V}''$
Q_0 dégazage des parois de l'enceinte contenant les sources
Γ coefficient de réémission des parois pour les particules rapides
γ efficacité de pompage ionique du plasma
γ' efficacité de pompage ionique au voisinage de l'arc
g rendement en gaz de la source d'ions
I courant injecté ($cm^{-3}\ s^{-1}$)
KI terme source de neutres dû au mécanisme d'injection
n_1 densité de l'arc
r_1 rayon géométrique de l'arc
ν nombre de révolutions du faisceau pendant la capture provisoire
$\mathcal{L}$ parcours total du faisceau pendant la capture provisoire
τ temps caractéristique de refroidissement des ions dissociés sur l'arc
n densité des ions chauds dans le plasma
n_f densité des ions froids dans le plasma
n_0 densité des neutres autour du plasma
$\bar{n}_0$ densité des neutres dans le plasma
N_0 densité des neutres dans l'enceinte contenant la source d'ions
k coefficient de couplage entre n_0 et $\bar{n}_0$
$\mathcal{V}_r$ volume réduit associé aux neutres dans le plasma
$\mathcal{V}_r'$ volume réduit associé aux neutres à l'extérieur du plasma
η fraction du faisceau qui disparaît pendant le parcours
η_d fraction du faisceau dissocié pendant le parcours
η_I fraction du faisceau qui correspond à une ionisation du gaz résiduel
I_{cs} courant critique supérieur
I_{ci} courant critique inférieur
I_T courant de transition pour le passage du régime avec arc au régime sans arc.

MIRROR MACHINE EXPERIMENTS AND RELATED ATOMIC CROSS-SECTION MEASUREMENTS AT A.W.R.E. ALDERMASTON*

D. R. SWEETMAN

ATOMIC WEAPONS RESEARCH ESTABLISHMENT

ALDERMASTON, BERKSHIRE, ENGLAND

An experiment (Phoenix) is described in which a beam of 30 keV neutral atoms is injected into a magnetic mirror field with 50 kG central value and 100 kG in the mirrors. The conditions for achieving exponential build-up of the plasma density are discussed and the significance of the initial trapping efficiency is brought out.

The magnetic field is required to last for several seconds, and this has been achieved using a very simple design of pancake wound coils cooled to liquid nitrogen temperature. The low gas pressure and high pumping speed required have been obtained by getter pumping using titanium evaporated on to surfaces cooled to liquid nitrogen temperature. Sticking probabilities for hydrogen of more than 0.5 have been obtained by such a technique.

At present the experiment is being operated with a low intensity neutral source (1 mA equivalent) and the neutral atoms emitted from the plasma by charge exchange are being observed. At high gas pressures the intensity of the emitted neutrals, and hence the trapping efficiency, is proportional to gas pressure, but at low pressure the trapping efficiency is independent of pressure. This constant trapping efficiency at low pressure is interpreted as due to ionization of highly excited beam atoms by the $\mathbf{v} \times \mathbf{B}$ equivalent electric field present while the atoms traverse the magnetic bottle.

The observed effect gives a trapping efficiency 400 times that due to gas trapping at 10^{-9} torr. Subsidiary experiments with electric fields applied directly to high energy H^0 atoms indicate that much higher trapping efficiencies are possible; approximately 1.0 per cent of the beam has been ionized by an electric field of only 220 kV/cm.

The significance for the achievement of a thermonuclear plasma of this very efficient new trapping mechanism is discussed. Also, a brief summary is given of recent unpublished atomic cross-section measurements relevant to the thermonuclear field, involving the dissociation of H_2^+ and H_3^+ by gases. The essential results of experiments on the dissociation of a range of molecular ions by electric fields are also given.

1. Introduction

In most attempts to produce plasma of density and temperature suitable for thermonuclear purposes, the energy is first put into the electron component of the plasma and is only later transferred to the ion component where it is required. Such methods result in a plasma with an electron temperature higher than the average ion energy and therefore the plasma has a much higher ratio of kinetic to magnetic pressure (β) than is desirable for stability considerations. Also the cyclotron radiation is excessively high. In our mirror machine work at A.W.R.E. we are interested in the production of a plasma with a high average ion energy and an electron energy sufficient only to prevent excessive energy loss from the ion component. We wish also to satisfy the conditions for effective trapping of the ions in the mirror field which suggest that the particle orbits should either encircle the axis [1] or should have a cyclotron radius very small compared with the radius of curvature of the magnetic field lines [2].

One of the most attractive methods of producing such a plasma is to separate the problems of heating and containment, by the injection of pre-accelerated particles. Of the various methods of high energy particle injection, we consider the method of neutral injection, originally suggested for very high injection energies by G. GIBSON *et al.* [3], to be very attractive for the following reasons:

(1) The criterion that the Larmor radius should be small compared with the mirror dimensions is easily satisfied.
(2) A plasma diameter of many Larmor diameters can be produced and the effects of radial diffusion, etc. studied under calculable conditions.
(3) The injection mechanism is independent of the detailed properties of the plasma. It is dependent only on the neutral gas and plasma densities and hardy at all on the plasma temperature. Axial variations of space charge and magnetic field which can so easily upset injection mechanisms which rely on multiple transits by molecular ions are unimportant in the case of neutral injection.
(4) Should initial experiments be successful, it is possible to envisage the scaling up of such a system to reactor dimensions without radical change in the injection mechanism.

* Conference paper CN-10/74 presented by D. R. Sweetman. Discussion of this paper is given on page 356. Translations of the abstract are at the end of this volume of the Conference Proceedings.

For these reasons we initiated in 1958 a programme of research which involved the building of a neutral injection mirror machine (called Phoenix) to study the problems involved in such an approach, and a more broadly based programme of atomic cross-section measurements to supply data essential for the proper assessment of the various possible approaches to high energy injection. The essential results of the cross-section measurements will be summarized in the final section of this paper, the major part being devoted to a discussion of the Phoenix experiment.

2. Discussion of build-up process

The coupled equations governing the density of charged and neutral particles in a neutral injection experiment may be written in the following form:

$$\frac{\mathrm{d}n_+}{\mathrm{d}t} = \frac{IL}{V}(n_0\sigma_t^0 + n_+\sigma_t^+ + X) - n_+ n_0 \sigma_x v - n_+^2 \sigma_m v$$

$$\frac{\mathrm{d}n_0}{\mathrm{d}t} = (N - n_0)\frac{v_0}{L} - n_+ n_0 \sigma_D v$$

$$\frac{\mathrm{d}N}{\mathrm{d}t} = (q_1 n_0 n_+ \sigma_+ v + q_2 n_+^2 \sigma_m v + q_3 I/V)\frac{V}{V_e} - \alpha(N - N_0) - \frac{v_0 V}{L V_e}(N - n_0)$$

where

n_+	density of high energy ions,
n_0, N	density of neutral molecules within plasma and outside plasma, respectively,
σ_t^+, σ_t^0	cross-section for ionization of beam atom by plasma ion and by gas molecule, respectively,
σ_x	cross-section for charge exchange of plasma ion with gas molecule,
σ_m	cross-section for scattering through mirrors,
σ_D	cross-section for destruction of a neutral molecule by a plasma ion,
v	velocity of fast neutral/ion,
v_0	velocity of slow neutral molecules,
V	effective volume of plasma,
V_E	volume of vacuum vessel,
L	effective trapping length,
I	intensity of neutral beam,
X	trapping efficiency for initiating plasma or other trapping mechanism, e.g. excited state trapping,
q_1, q_2, q_3	number of neutral molecules returning to central chamber for each (1) fast atom incident on wall, (2) fast ion scattered through mirrors, and (3) fast atom untrapped, respectively, and
α	pumping speed per unit volume.

The above equations have been solved both for the time-dependent and for the equilibrium solutions. It is instructive to look at the equilibrium solutions, in order to understand the behaviour in the various regimes of plasma build-up, and the time-dependent solutions, in order to determine the build-up time for specific cases. First of all let us consider the optimum parameters for a neutral injection experiment assuming that we wish to minimize the intensity of neutral atoms required. We may then calculate the solutions of the equations for such an optimized experiment.

In such an experiment the high energy plasma is trapped initially by ionization on the residual gas of the system, or by ionization on a subsidiary plasma or other means of trapping should it be present. With low injection intensities the high energy plasma density is given by a balance of trapped current and loss by charge exchange on the residual gas. In the gas build-up case the critical condition for exponential build-up occurs when the plasma density becomes comparable with the residual gas density and trapping by ionization on the already trapped plasma becomes important. Since the total intensity of neutral particles is restricted in a practical experiment and it is the current per unit area which is effective in building up the central density, it is essential to minimize the beam area. Moreover, to achieve the density predicted by the above equations, the Larmor radius must be small compared with the beam dimensions. It is therefore desirable to use a high magnetic field and a relatively low injection energy (the latter is not as critical as is the magnetic field requirement). The requirements of neutral beam production indicate that the most suitable injection energy for preliminary experiments using hydrogen is in the region of 20 to 80 keV, though higher energy neutral beams suitable for reactor injection can be produced economically by dissociation of molecular ions. With an energy of 30 keV a magnetic field of some 40 kG in the central region and 80 kG in the mirrors (for a mirror ratio of 2) is required to reduce the Larmor diameter to about 1 cm.

It may readily be seen from the above equations that the rate of build-up in the exponential region is given approximately by the equation

$$\frac{1}{n_+}\frac{\mathrm{d}n_+}{\mathrm{d}t} = \frac{IL\sigma_t^+}{V} - n_0\sigma_x v.$$

Thus the maximum exponentiation rate (at low gas pressure) is decided by the neutral beam intensity and this cannot be appreciably increased by further reduction of gas pressure. As the magnetic field and low gas pressure cannot conveniently be maintained for more than a few seconds, this sets a limit to the total build-up time and a minimum value to the beam intensity required. The gas pressure must then be reduced to a value appreciably below the critical value for this beam intensity so that the build-up time is not excessively increased by charge exchange loss. Time-dependent solutions of the above equations which illustrate the profound change of build-up time with pressure near the critical value and the relative independence at very low gas pressures are illustrated in Fig. 1. No initial trapping other than that due to the gas is present for these calculations. From this it is seen that a neutral intensity of 5 mA cm² equivalent over an area of at least 10 cm² with a hydrogen gas pressure of 10^{-9} Torr would give a build-up time of about 4 sec.

Plots of the equilibrium plasma density against neutral beam intensity are instructive. At high gas pressures the curves have the characteristic S shape. At low gas pressures the lower hump of the S curve flattens appreciably. Such a curve is shown in Fig. 2. For build-up to be maintained, the plasma must always remain to the right of the equilibrium curve. Thus it is necessary for the gas pressure to remain low until the curve has developed an appreciable negative slope; then the conditions become less stringent and build-up will be maintained even for a rising background pressure. The negative slope region corresponds to a significant "burn out", i.e. to a neutral density within the plasma region appreciably less than that outside. It is important to find a means of reducing the flat region of the curve so that the low gas pressures need be maintained for the minimum time.

The effect of an initial trapping mechanism other than gas trapping is to raise the linear portion of the equilibrium curve in the way indicated by the dashed line. Such a trapping mechanism, if it is sufficiently large, can have a profound effect on the build-up time, can considerably ease the vacuum conditions by reducing the flat portion of the curve and may even reduce the critical current required to achieve high plasma densities. In a later section it will be shown that we have such an initiation mechanism in the ionization

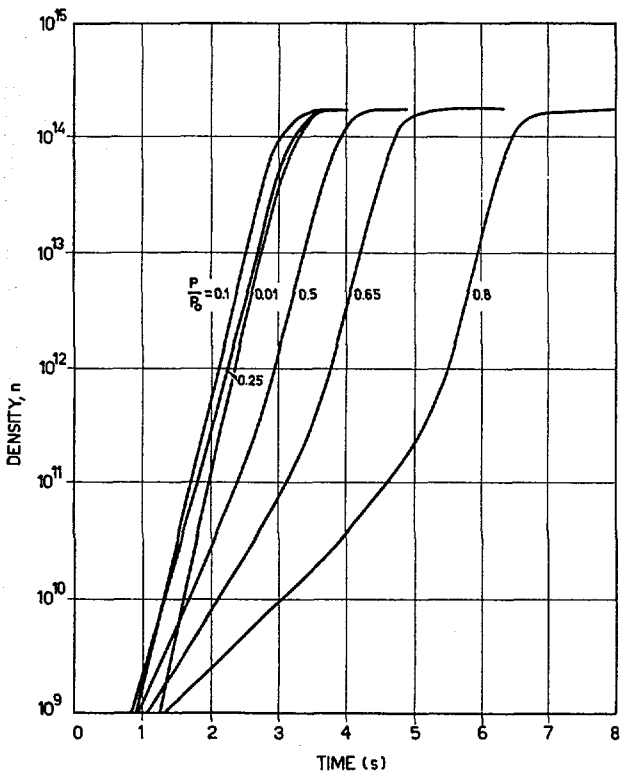

Fig. 1 Build up of particle density as a function of time for various ratios of pressure (P) to critical pressure (P_0).
Intensity of injected neutral beam = 50 mA equivalent n 10 cm² area. $P_0 = 2 \times 10^{-9}$ torr. No initial trapping s assumed.

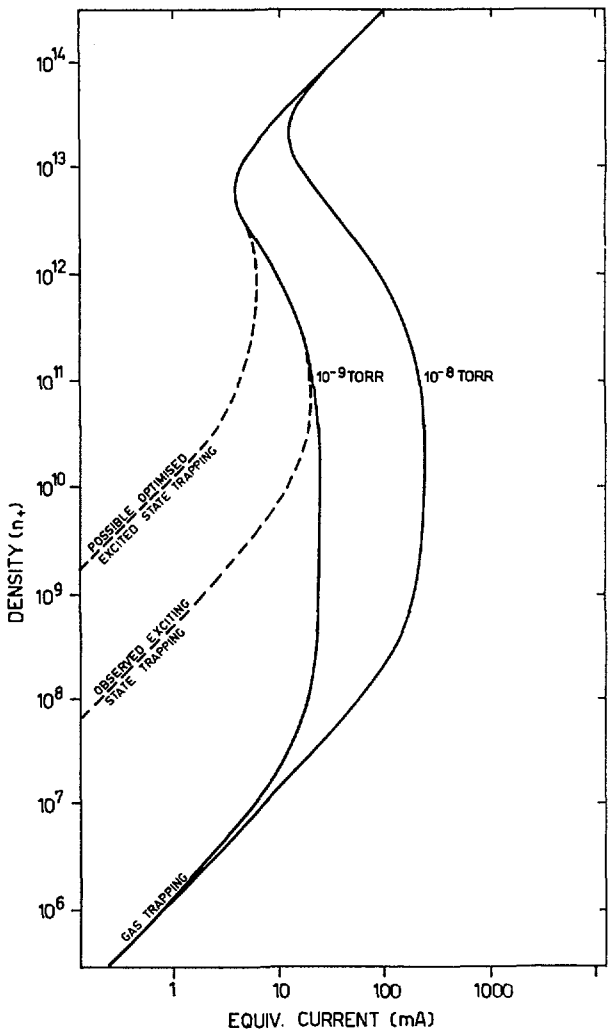

Fig. 2 Equilibrium density as a function of intensity of neutral beam (expressed as equivalent proton current). Beam area = 10 cm². Dashed curves show effect of excited state trapping.

of those beam atoms that are in a highly excited state.

In the above discussion the coefficients for emission of gas molecules from surfaces on bombardment by the high energy particles (q_1, q_2, q_3) are assumed to be zero. This is probably justified for the case of q_1 and q_2, the coefficients for "reflection" from the walls and from the mirrors, but is certainly not true for q_3, that for the untrapped neutral beam. However, for a given neutral beam this is a constant factor and it is simpler to consider the problem as one of achieving a given gas pressure in the presence of the beam. Many calculations have been carried out with the reflection coefficients non-zero and the results are in agreement with expectations.

3. Experimental apparatus

In the Phoenix apparatus the mirror magnetic field is obtained from two coils of inside diameter 15.4 cm, outside diameter 39.5 cm and thickness

12.0 cm, with their mid-planes mounted 32 cm apart. To reduce power consumption, the coils are cooled to liquid nitrogen temperatures and the supply current is applied for a few seconds, during which time the temperature rises several tens of degrees centigrade. The coils are cooled again to liquid nitrogen temperature between pulses. The coils are made from flat copper strip 0.203 cm × 1.70 cm wound in the form of pancakes of 56 turns each, the insulation between turns being 0.13 mm fibreglass. The pancakes are separated by 3.2 mm tufnol spacers with channels carved in them to allow contact between the liquid nitrogen and the pancakes. A whole coil assembly with the 6 pancakes connected in series is a tight fit into a stainless steel box which is kept filled with liquid nitrogen from a 2000 liter storage vessel. These coils have been tested up to a maximum of 120 kG at which field the forces are sufficient to cause some flow of the copper. The change of current, voltage and magnetic field with time during the pulse are shown in Fig. 3. The current is supplied by lead-acid accumulator cells, the total resistance of the bank being approximately matched to the coil at the maximum of the current pulse. The current rises slowly due to inductive effects and later falls due to the rise in the temperature, and hence resistance, of the coils.

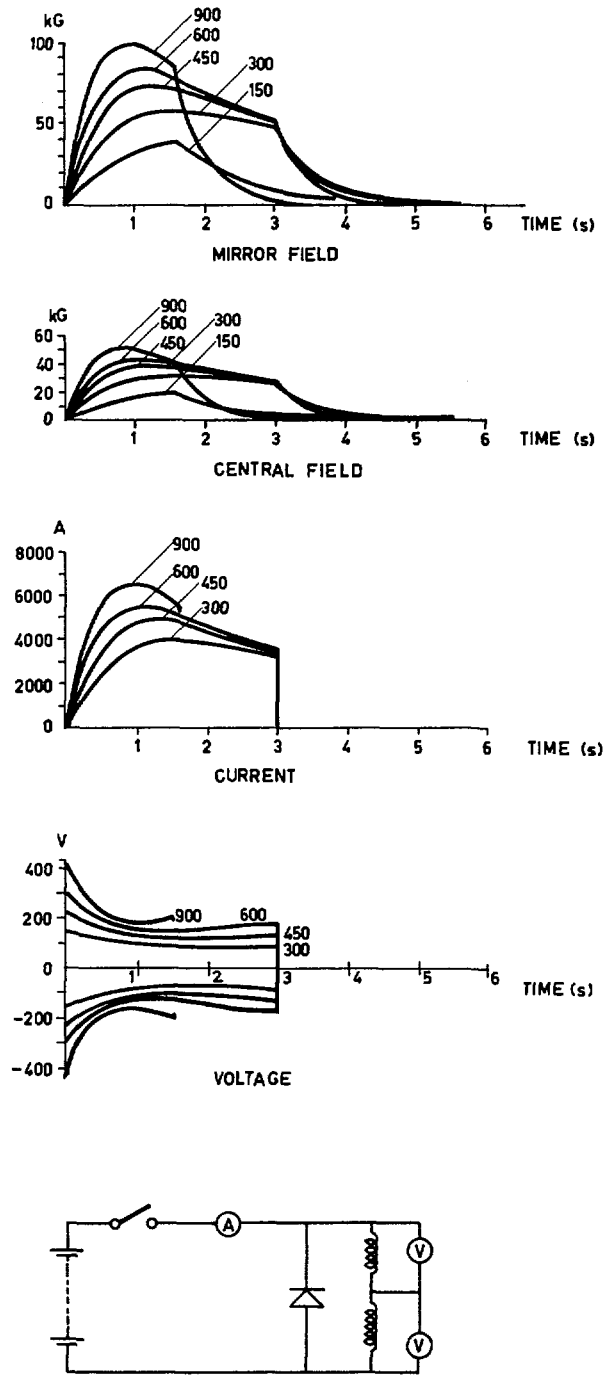

Fig. 3 Magnetic field, coil current and voltage as a function of time. Numbers on curves refer to open circuit capacitor bank voltage.

The 30 keV H^0 atoms are obtained by accelerating to 90 keV H_3^+ ions from a duoplasmatron source. The H_3^+ ions enter a dissociation chamber where they dissociate and charge exchange. Under equilibrium conditions a yield of 1.7 H^0 atoms per incident H_3^+ ions is obtained. Formation of the neutral beam from H_3^+ has the advantages over formation by charge exchange from H^+ of yielding three times the neutral intensity per charged particle accelerated and enabling a high extraction voltage to be used on the ion source, thus reducing the space charge problems. The slight extra spread in angle introduced by the dissociation process has been measured and is not serious.

The principal sources of gas influx into the centre chamber are from the dissociation chamber, which must be maintained at a pressure of some 2×10^{-2} torr; hydrogen from the ion source; and gas emitted in the region where the untrapped neutral beam is finally deposited. Influx from the dissociation chamber is minimized by use of water vapour as the dissociation medium. The injector line on each side of the dissociation chamber and the central chamber itself are cooled to liquid nitrogen temperature. The vapour pressure of water at this temperature is negligible, so that effectively all the water vapour which hits the cooled surfaces is trapped before reaching the plasma formation region. However, molecules which are streaming in the direction of the plasma and do not touch the walls are not eliminated by this technique; they represent a gas influx corresponding to a pressure of about 10^{-8} torr in the plasma region. To remove these molecules there has been developed for insertion in the injector line a velocity filter consisting of a paddle wheel rotating at sufficient speed to deflect the slow gas molecules, travelling at say 10^5 cm per second, while leaving undisturbed the fast neutral atoms, travelling at over 10^8 cm per second.

The gas influx from the ion source and beam deposit region consists largely of hydrogen. Experiments have been performed with the central chamber of the Phoenix experiment to determine the efficiency of titanium gettering for hydrogen removal and somewhat surprising results have been obtained [4]. Titanium is evaporated from titanium wire wrapped around a tungsten filament situated centrally in the

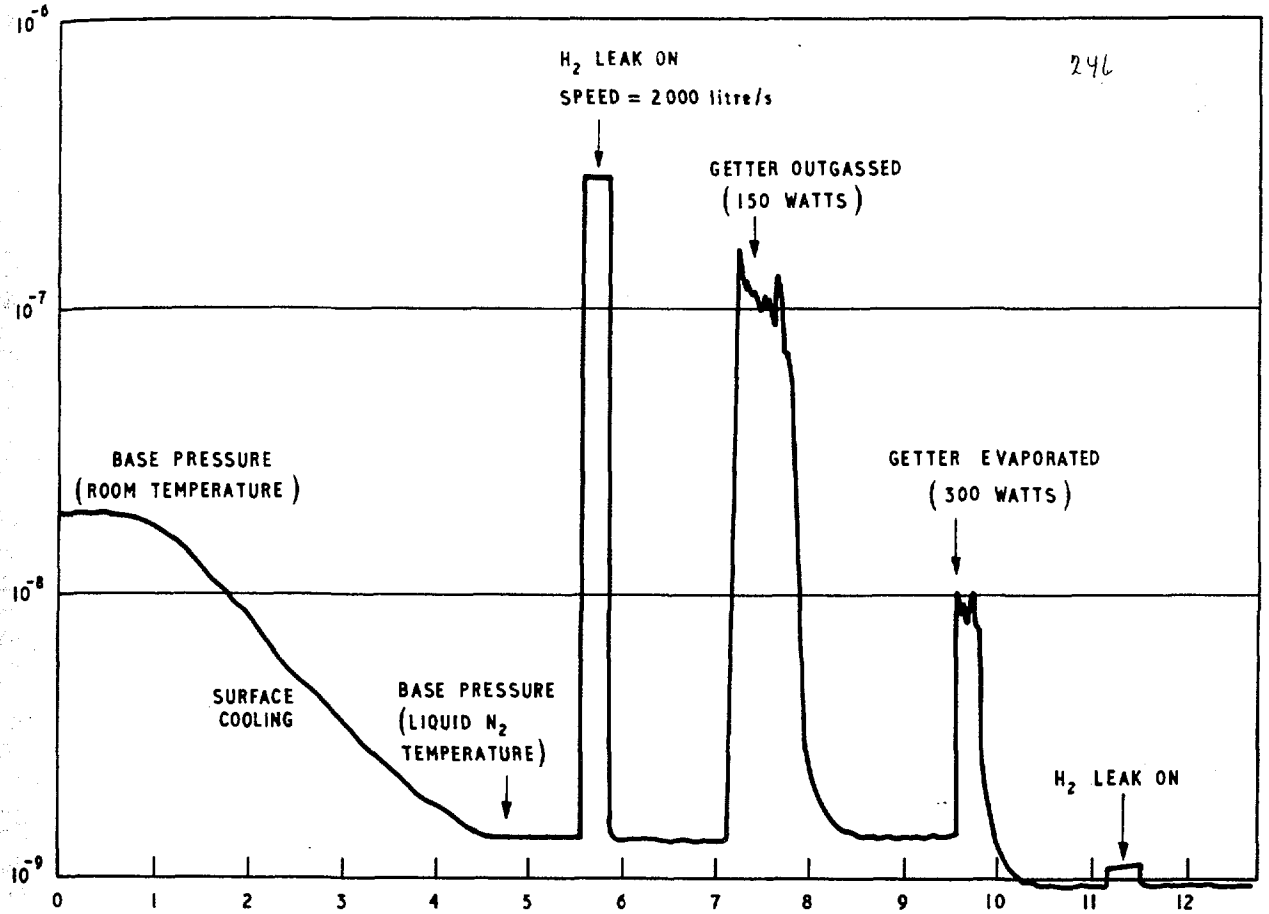

Fig. 4 Pressure as a function of time for a typical gettering run. Ordinate: pressure (torr). Abscissa: time (minutes).

chamber. A known leak of hydrogen may be switched on for short periods to determine the pumping speed. The pressure is measured by an Alpert ionization gauge situated on a side limb shielded from the getter by a baffle. When the getter was evaporated, the pressure rise due to the calibrated leak indicated the pumping speed of the diffusion pump, 2000 liters per second for hydrogen. After evaporation of the getter on to the chamber walls (maintained at room temperature) the pressure rise due to the leak indicated a speed of 30 000 liters per second, an estimated sticking probability of 0.13. Evaporation of the getter on to the walls maintained at liquid nitrogen temperature resulted in much higher sticking probabilities; the pressure rise was scarcely measurable even though the base pressure of the apparatus was below 10^{-9} torr. Pumping speeds obtained by dividing the leak rate by the pressure rise become meaningless under these conditions as apparent speeds of several million liters per second were obtained — many times the theoretical total absorption limit. However, when allowance is made for the effects of differential pumping, it is estimated that the sticking probability is certainly greater than 0.5 and is probably greater than 0.8. A run carried out at liquid nitrogen temperature is illustrated in Fig. 4. The dependence of sticking probability on the temperature of the surface is illustrated by experiments in which the titanium was evaporated at room temperature and the surface cooled. Also experiments were performed in which

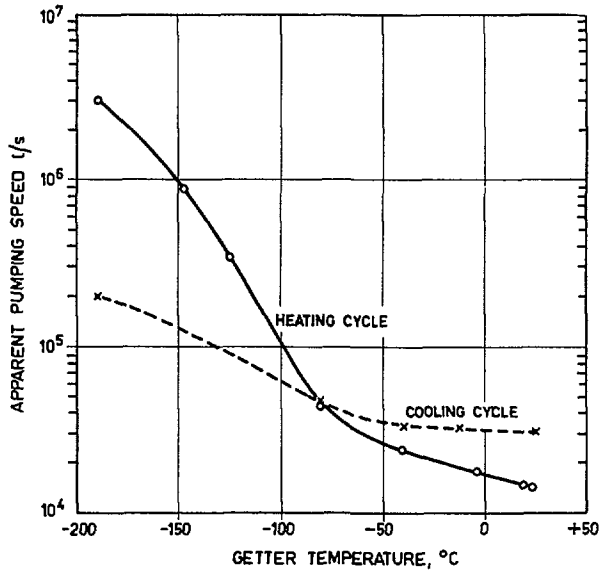

Fig. 5 Leak/pressure rise as a function of surface temperature for two evaporation temperatures. Note that no account is taken of differential pumping effects due to high sticking probability.

the getter was evaporated at liquid nitrogen temperature and the surface heated. The results of these experiments are shown in Fig. 5 where the "apparent pumping speed" plotted is simply the hydrogen leak rate divided by the pressure rise. It is apparent that both the surface temperature during the gettering and the surface temperature during evaporation is important. It should be noted that these high speeds are maintained only for sufficient time for a monolayer to form on the surface. However with a leak rate of 1 liter micron per second, typical of that from the sources of gas in the system, the high speed is maintained for many seconds, adequate for experimental purposes.

4. Results of initial experiments

At present the apparatus is set up with a low intensity, 1 mA equivalent, source of 30 keV neutral particles. This is being used to investigate the initial stages of plasma build-up, prior to the installation of a higher intensity source which should enable the region to be investigated when ionization by the already trapped plasma is dominant. The velocity filter (chopper) is not installed for these experiments.

Measurements have been made on the neutral atoms produced by charge exchange of the trapped ions and emitted at right angles to the axis in the median plane of the magnetic field. The neutral atoms were detected with a CsI crystal mounted on a photomultiplier. The current from this photomultiplier was monitored and simultaneously the pulses due to individual particles were displayed on an oscilloscope. It was possible to raise the gas pressure by letting in argon gas.

Fig. 6 shows the intensity of neutral atoms as a function of argon pressure. Assuming that charge

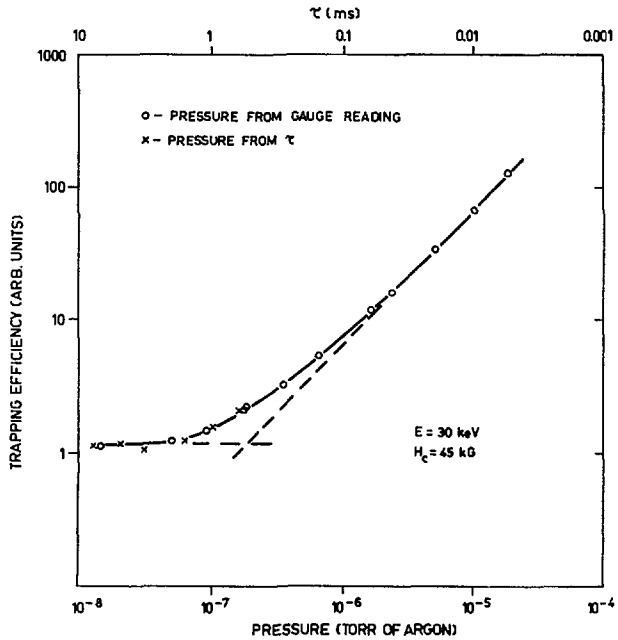

Fig. 6 Neutral particle emission as a function of pressure of argon.

exchange is the only loss mechanism, the intensity is a measure of the trapping efficiency. In the high pressure region the ionization gauge, mounted on a baffled side limb connected to the central chamber, gives a reliable account of the gas pressure in the plasma. In the low pressure region (below 10^{-7} torr) the presence of the various sources of residual gas makes such measurements unreliable and in this region the actual gas density was determined by measuring the time constant for decay of the plasma when the beam was switched off. The time constant is converted to an equivalent pressure of argon by use of the published charge exchange cross-section.

The results indicate a trapping efficiency proportional to gas pressure in the high pressure region but at low pressures the trapping efficiency becomes constant at a value equivalent to about 2×10^{-7} torr of argon.

We believe that the enhanced trapping at low pressures is due to the ionization of highly excited neutral atoms by the $\mathbf{v}\times\mathbf{B}$ field in the centre of Phoenix. In these experiments the central magnetic field reaches a value of 45 kG. With the neutral atom velocity of 2.4×10^{8} cm per second, the equivalent electric field is 108 kV/cm. The early experiments of Rausch von Traubenberg *et al.* [11] on the quenching of the Balmer series in the hydrogen spectrum indicate that excited states down to about $n=10$ may be ionized by such an electric field. Hiskes at U.C.R.L. [12] has shown that these states may have a lifetime of several microseconds, sufficiently long for them to travel from the charge exchange chamber to the region of high magnetic field. There is some doubt as to the efficiency for production of these high excited states but Hiskes has estimated that the $n=10$ state might contain 2×10^{-5} of the total population. On the assumption that excited-state trapping is the dominant effect at low pressures, our results would indicate that the trapping efficiency due to the process is about equal to that for argon gas at 2×10^{-7} torr. This would indicate an average trapping efficiency over the observed volume of about 10^{-5} per cm^3. An estimate based on the known magnetic field variation along the axis of the neutral beam suggests that a region from the magnetic field maximum (at the centre) to a field value 17 per cent lower contributes to the observed trapping. From this we estimate that about 50 per cent of the population of the $n=10$ level (say) might contribute to the observed trapping for a field value optimized for this particular level. As we shall show below, the above results do indeed correspond to about the peak of the $n=10$ state, indicating that the population of this level is about 2×10^{-5} of the total. It should be emphasized that these conclusions are only very approximate and more accurate results must await the elucidation of the various geometrical factors in the experiment. It is probable that this is a considerable understatement of the actual population and that this is much greater than that predicted by Hiskes.

The most convincing demonstration of the existence of this trapping mechanism is obtained from

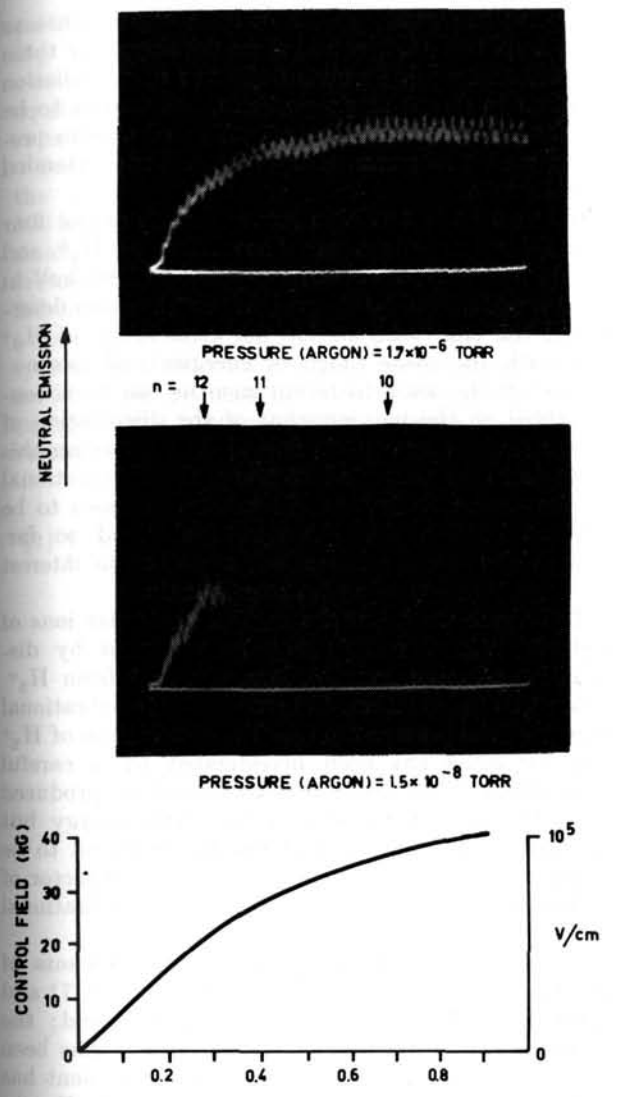

Fig. 7 Neutral particle emission as a function of magnetic field. Upper oscillogram — gas trapping region. Lower oscillogram — electric field ionization region. The ripple in the curves is due to 50 cps modulation of the beam intensity. The fine structure in the lower curve is due to the short integration time constant used for this experiment (0.06 ms).

the variation of trapping efficiency with magnetic field. Observations were made on the rising part of the magnetic field pulse. In the top curve of Fig. 7 the neutral emission (proportional to trapping efficiency) is shown for a typical high pressure pulse. The emission rises smoothly to a constant value at high field. The slight ripple is due to 50 cycle per second modulation on the beam intensity. At low pressures, however, the neutral emission intensity shows a series of peaks as in the middle curve of Fig. 7. The lower curve shows the central magnetic field as a function of time. The peaks we interpret as successive levels of the hydrogen atom ionizing in the rising magnetic field. The provisional level assignments, based on the Balmer series quenching experiments, are indicated.

5. Electric field ionization measurements

In order to obtain more accurate quantitative information on the ionization of highly excited hydrogen atoms, an experimental apparatus was set up to observe the effect directly. The apparatus was basically the same as that used for the dissociation of H_2^+ ions by electric fields [6, 7]. A beam of H^0 atoms was prepared by charge exchange on hydrogen gas of 200 keV protons from a Van de Graaff accelerator. They were then passed through a region of high electric field situated about 20 cms from the exchange region and the resulting mixture of protons and H^0 atoms was analysed using a magnetic field and detected with CsI scintillation crystals. The plot of the fraction ionized against applied electric field is shown in Fig. 8. It may be seen that as much as 1 per cent of the beam is ionized by a field of 220 kV/cm. Of direct interest for thermonuclear experiments is the differential coefficient of the above curve which indicates the fraction of particles that may be ionized for a given ratio of central equivalent electric field to that at the boundary of the trapping region. This is difficult to determine with sufficient accuracy by subtracting neighbouring points so a system was

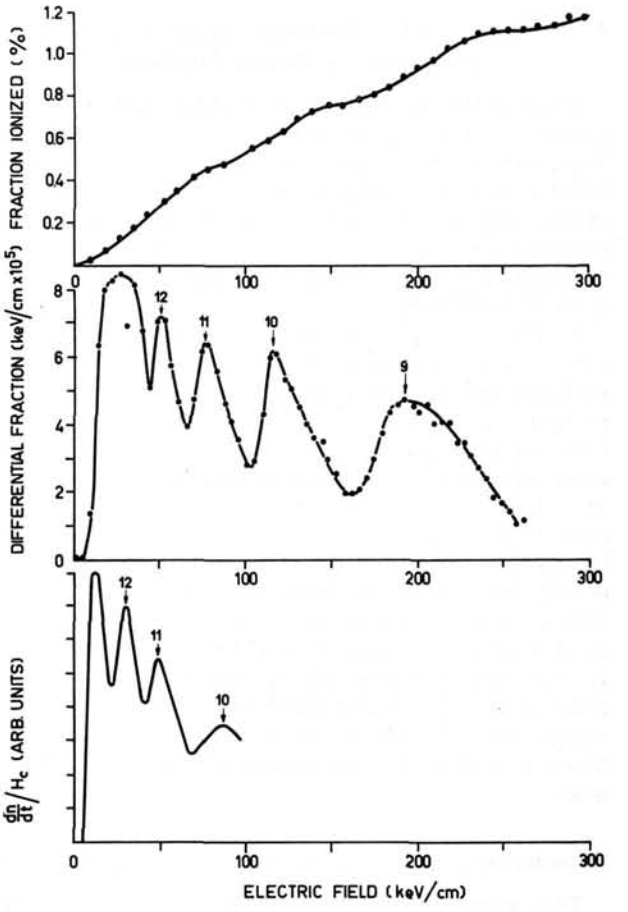

Fig. 8 Upper two curves: results of separate measurements with 200 keV H^0 particles. Bottom curve results from Phoenix. The displacement of the groups is due to the different time spent in the high field region ($\sim 10^{-10}$ seconds and $\sim 10^{-8}$ seconds respectively).

devised by which a small oscillating field was superimposed on the main electric field and the resulting modulated count rate from the crystal detecting the proton beam was fed to a phase sensitive detector and integrator system. The resulting differential curve is plotted in Fig. 8 together with the results from the Phoenix experiment. It is seen that they both show the hydrogen atom shapes very clearly. The difference in the positions of the levels is attributed to the very different times spent in the field in the two cases and is in agreement with the calculations of Hiskes.

It would seem that the populations observed in our electric field experiments (approximately 0.24 per cent in the $n=10$ state) are much higher that those observed in the Phoenix apparatus. This difference is probably accounted for in part by the drastic geometrical simplifications assumed in calculating the populations from the Phoenix results and in part by the several differences between the parameters of the two experiments.

We are at present investigating in detail the dependence of the excited state populations on the various parameters and the results will be published as soon as they are available.

6. Significance of excited-state trapping for plasma production by neutral injection

Some of the advantages of the high energy neutral injection scheme have been outlined in Section 1. The great disadvantage of a neutral injection method which relies on gas trapping is the relative inefficiency of the trapping in the initial stages of build up and the resulting long build-up time during which gas influx is critical. Excited-state trapping would seem to overcome the difficulty.

In Fig. 2 we have plotted the equilibrium density curve for a pressure of 10^{-9} torr both without and with excited-state trapping. Two dashed curves are plotted, one corresponding to the trapping actually observed in the present Phoenix and one corresponding to an optimized experiment in which the parameters are adjusted to utilize as much as is possible of the ionization observed in our electric field experiments. In the first case, the critical beam intensity required is not reduced appreciably but the build-up time during which the gas influx is critical is reduced from several seconds to several hundred milliseconds. In the optimized case the critical beam intensity is reduced also. The exact parameters for an optimized experiment will only be known when a more detailed investigation of the population mechanism has been made.

7. Summary of atomic cross-section measurements

This work was initiated in 1958 with the specific intention of making accurate measurements of the cross-section for the dissociation of H_2^+ ions by gases. The considerable disagreement amongst the various workers for these cross-sections has great significance regarding the practicability of such experiments as Ogra and DCX II. The technique developed for these measurements [5], involving the use of scintillation counters to detect single particles, has proved to be a valuable tool in the investigation of atomic processes and the measurements have been extended considerably.

We now have available measurements of the four possible cross-sections for dissociation of H_2^+ and D_2^+ ions over the range of energy 40 to 3000 keV in the gases H_2, H_e, N_2, O_2, and A. We have also determined the cross-sections for the dissociation of H_3^+ ions with the same range of energies and gases.

Most of the work in recent months has been concentrated on the measurement of the dissociation of molecular ions by electric fields [6]. A paper on this work is to be presented at the Fifth International Conference on Ionization Phenomena in Gases to be held at Munich [7]. The results obtained so far, though showing a small effect, are of some interest for molecular ion injection experiments.

The above work has shown that molecular ions of high vibrational energy may be produced by dissociation of more complex ions, e.g. H_2^+ from H_3^+. Using this information, the sensitivity to vibrational energy of the cross-section for the dissociation of H_2^+ ions by gases has been investigated by a careful comparison of the cross-sections using ions produced from H_3^+ and using ions of the same energy but accelerated directly [8]. The effects are found to be surprisingly small: less than 7 per cent for a factor of 5 change in the population of the upper vibrational states.

In addition to the above work, measurements of the He^- ions have been made both with [6, 7] and without [9] the presence of an electric field; the cross-section for the production of H^- ions has been determined at high energies; and an experiment has been performed to test the validity of the Frank-Condon principle for H_2^+ dissociation.

8. Neutral particle production cross-sections

In connection with neutral injection proposals, a number of experiments have been performed to determine the yield of neutral atoms as a function of gas pressure for the charge exchange of H^0 atoms by water vapour and hydrogen, and for the dissociation of H_2^+ and H_3^+ ions by these gases. The charge exchange results for hydrogen gas are in agreement with previous workers [10]. The, previously undetermined, equilibrium fractions of neutral atoms emerging from a water vapour target follow the same energy dependence as those for hydrogen but are about 18 per cent lower.

The neutral yield from the dissociation of H_2^+ ions shows an interesting variation with pressure of H_2 or H_2O. At high pressure the equilibrium fractions calculable, for the case of hydrogen, from the results of [10] are obtained. For H_2^+ energies above 170 keV, however, higher yields may be obtained by using lower pressures, due to the high yield of neutral

particles from the reaction $H_2^+ \rightarrow H^0 + H^+$. At 400 keV H_2^+ energy, for instance, a gain of a factor 5.5 is obtained by this process over that predicted from equilibrium cross-section measurements. Similar results are obtained for the dissociation of H_3^+ ions.

Such results indicate the possibility of extending the neutral injection method to energies above 100 keV. Although neutral yields per particle may be small, e.g. 20 per cent for a 200 keV D^0 energy, (obtained from D_2^+), a very large part of the energy fed into the charged particles can be recovered, in a convenient form for feeding back into the injector system, by deceleration of the charged ions. A similar method can be used to recover essentially all the energy in the untrapped neutral beam, it being converted to the charged state in a gas cell or a sheet arc.

References

[1] TAYLOR, J. B., U.S. Atomic Energy Commission Report TID-7582 (1959).

[2] DAMM, C. C., EBY, F. S., Proceedings of Second UN Conference on Peaceful Uses of Atomic Energy, Geneva **32** (1958) 273.

[3] GIBSON, G., LAMB, W. A. S., LAUER, E. J., Proceedings of Second UN Conference on Peaceful Uses of Atomic Energy, Geneva **32** (1958) 275.

[4] SWEETMAN, D. R., To be published in *Nuclear Instruments and Methods.*

[5] SWEETMAN, D. R., *Proc. Roy. Soc. Ser.* **A 256** (1960) 416.

[6] RIVIERE, A. C., SWEETMAN, D. R., *Phys. Rev. Letters* **5** (1960) 360.

[7] RIVIERE, A. C., SWEETMAN, D. R., Fifth International Conference on Ionization Phenomena in Gases, Munich (North-Holland Pub. Co., Amsterdam, 1961).

[8] RIVIERE, A. C., SWEETMAN, D. R., Submitted to *Proc. Phys. Soc.*

[9] SWEETMAN, D. R., *Proc. Phys. Soc. A* **76** (1960) 998.

[10] ALLISON, S. K., *Rev. Mod. Phys.* **30** (1958) 1137.

[11] RAUSCH v. TRAUBENBERG, H., GEBAUER, R., LEWIN, G., *Naturwissenschaften* **18** (1930) 417.

[12] HISKES, J. R., U.S. Atomic Energy Commission Report UCRL-6372 (1959).

ИССЛЕДОВАНИЕ ПЛАЗМЫ В АДИАБАТИЧЕСКОЙ ЛОВУШКЕ «ОГРЕНОК»*

Н. Н. Бревнов, М. К. Романовский, Ю. Ф. Томащук

Академия наук СССР, Москва,

Союз Советских Социалистических Республик

Описывается установка « Огренок », представляющая собой цилиндрическую вакуумную камеру из нержавеющей стали, длиной 2 м и диаметром $\varnothing = 0{,}5$ м, помещенную в аксиально-симметричное магнитное поле, напряженностью в центре до 3000 эрстед и до 4500 эрстед в магнитных пробках. В камеру, в ее центральной части, инжектируется атомарный пучек ионов водорода с энергией 10 кэв. Описываются два устройства для ввода пучка внутрь камеры: железно-токовый и электростатический каналы. Исследованы условия инжекции и поведение пучка ионов внутри системы при использовании обоих типов каналов.

Для изучения поведения пучка быстрых ионов в ловушке с магнитными пробками (движение и удержание ионов, компенсации объемного заряда, взаимодействия инжектируемого пучка с остаточным газом и холодной плазмой и т.д.) применен пучек атомарных, а не молекулярных ионов, так как система малых размеров не предназначена для перехода в режим « выгорания » остаточного газа (« достижения тока перевала »). Поэтому опыты велись с пучком атомарных ионов. Оценочная плотность быстрых ионов в ловушке менялась в зависимости от тока инжектируемого пучка от 10^5 до 10^7 ионов в $см^3$.

Экспериментально определены области отражений пучка от магнитных пробок, углы сдрейфовывания пучка при отражении, изучено распределение плотности быстрых ионов по радиусу, азимуту и длине системы. Определены пути, проходимые быстрыми ионами в ловушке. Показано, что быстрые ионы выходят в пробки раньше, чем это возможно за счет кулоновского рассеяния. Доказано, что одной из причин ухода быстрых ионов в пробки является наличие локальной неоднородности магнитного поля, создаваемой железнотоковым каналом. Показано, что местное возмущение магнитного поля приводит и к смещению быстрых ионов поперек магнитного поля, исследован уход медленных ионов и электронов, образующихся при перезарядке быстрых ионов на остаточном газе. Изучено распределение уходящих в пробки медленных ионов и электронов по радиусу и азимуту. Показано, что медленные ионы уходят вблизи оси системы.

Верхняя граница распределения выходящих в пробки медленных ионов, снятая методом диафрагм с задерживающим потенциалом, смещается в сторону меньших энергий с увеличением радиуса. Это свидетельствует о наличии и своеобразном распределении объемного заряда, а, следовательно, и неполной компенсации инжектируемого пучка. Показано, что отношение электронного тока к току медленных ионов вблизи оси системы, по крайней мере на порядок меньше отношения, соответствующего их рождению в объеме на данном радиусе. Форма кривой распределения плотности электронного тока, уходящего в пробки и аномально малый ток электронов на малых радиусах указывают на быстрый уход электронов поперек магнитного поля.

Характер распределения токов ионов и электронов, выходящих в пробки, практически не зависит от давления остаточного газа в интервале от $3 \cdot 10^{-8}$ до $8 \cdot 10^{-6}$ мм Hg.

Метод диафрагменных зондов с задерживающими потенциалами дает средние во времени значения токов электронов и медленных ионов. Осциллографическими измерениями установлено наличие колебаний распределения плотности заряженных частиц в объеме. Показано, что в системе имеются колебания холодной плазмы с частотой 10 кц и 100% модуляцией и частотами 100—120 кц и 1—1,2 мц с 10—15% модуляцией. Частоты 100 кц и выше обнаружены и в инжектируемом пучке быстрых ионов, но частота 10 кц в нем, по-видимому, отсутствует. Особенностью колебаний является синфазность их разных азимутах на данном радиусе и на разных z на данном азимуте. Это указывает на пульсацию всего объема, занятого медленными ионами и электронами.

1. Введение

Одним из способов создания условий, необходимых для получения управляемых термоядерных реакций, является накопление горячих ионов в системе с магнитными пробками. По этому пути ведутся исследования в СССР (ОГРА), США (ДСХ), Франция (установка ПРЕВО).

Во всех этих установках предполагается непрерывная инжекция пучка молекулярных ионов внутрь ловушки.

Однако заранее предсказать поведение пучка ионов, его взаимодействие со вторичной плазмой, степень компенсации, величину объемного заряда и т.д. — довольно трудно.

В настоящей работе исследованы инжекция пучка быстрых ионов в адиабатическую ловушку, распределение быстрых ионов по объему ловушки, их уход вдоль и поперек магнитного поля, а также создаваемый пучком объемный заряд, колебания плотности быстрых ионов и вторичной плазмы.

* Доклад CN-10/225 представленный на Конференцию. Докладчик: М. К. Романовский. Дискуссия (на английском языке) по этому докладу дана на стр. 357. Переводы аннотаций находятся в конце этого тома Трудов Конференции.

2. Описание установки и аппаратуры

Магнитная ловушка «Огренок» схематически изображена на рис. 1. Вакуумная камера ловушки представляет собой цилиндр из нержавеющей стали диаметром $\varnothing = 500$ мм и длиной $\approx L = 2000$ мм. Камера откачивается диффузионными парамасляными насосами, снабженными азотными ловушками. Перед работой производился прогрев камеры до температуры 400° С пропусканием по ней тока 5000 ампер. Давление остаточного газа после прогрева составляло $5 \cdot 10^{-7}$ мм рт.ст. В рабочем режиме разряжение не опускалось ниже $3 \cdot 10^{-6}$ мм рт.ст.

Магнитное поле создавалось двумя основными, двумя пробочными и двумя компенсационными катушками. Для получения необходимого азимутального дрейфа ионов магнитное поле было подкорректировано стальными кольцами, расположенными на стенке камеры. Максимальная напряженность магнитного поля в центральной плоскости ловушки составляла $(H_0) \simeq 3000$ эрстед, в максимуме пробки $(H_п) \simeq 4500$ эрстед. Пробочное отношение составляло 1,5. В экспериментах величина поля могла меняться. Изменение поля вдоль оси ловушки приведено на рис. 2.

В центральной плоскости ловушки на радиусе $R = 170$ мм производилась инжекция пучка быстрых ионов (рис. 1). Ионы водорода ускорялись в источнике циклотронного типа с осциллирующим разрядом. В магните источника ионы поворачивались на угол в 115° и попадали в камеру сепарирующего магнита. Здесь пучок разделялся на компоненты и фокусировался. Выбранная компонента пучка дополнительно фокусировалась тонкой магнитной линзой и вводилась в магнитный (или электростатический) канал. Магнитный канал имеет стальную оболочку, на которой расположены взаимоперпендикулярно две обмотки. Одна обмотка служит для частичной компенсации магнитного поля внутри канала, а вторая — для сообщения иону скорости вдоль оси ловушки. (В принципе конструкция магнитного канала аналогична примененному на установке «Огра».)

Несмотря на наличие компенсирующих обмоток, канал возмущает магнитное поле ловушки, нарушая азимутальную симметрию. Такое возмущение приводит к уменьшению эффективности удержания ионов, что более подробно показано ниже. В электростатическом канале нет экранировки магнитного поля, но с помощью пластин (типа плоского конденсатора) создается электрическое поле, перпендикулярное магнитному полю, так, что при движении иона в канале суммарная сила $\mathbf{F} = e\,\mathbf{E} + (e/c)\,[\mathbf{vH}]$ близка к нулю. В этом случае частица движется по траектории, близкой к прямой. Вводимый внутрь ловушки ионный ток составлял 2 *ma* в случае магнитного канала и 300 μa при применении электростатического канала. Непосредственными измерениями были определены угол инжекции ψ (угол между вектором скорости и силовой линей магнитного

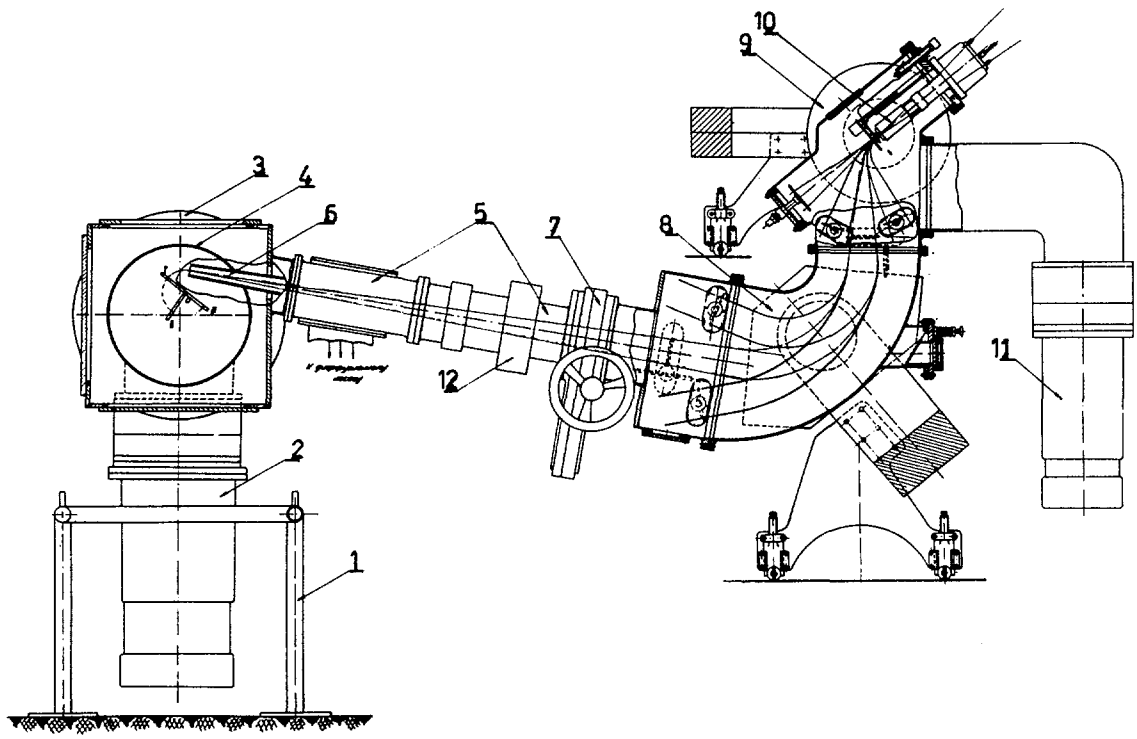

Рис. 1 Схема установки Огренок. 1 — подставка, 2 — диффузионный насос ВА-5, 3 — катушки, 4 — камера, 5 — ионовод, 6 — магнитный канал, 7 — шибер, 8 — сепарирующий магнит, 9 — магнит источника, 10 — источник, 11 — диффузионный насос ВА-2, 12 — магнитная линза.

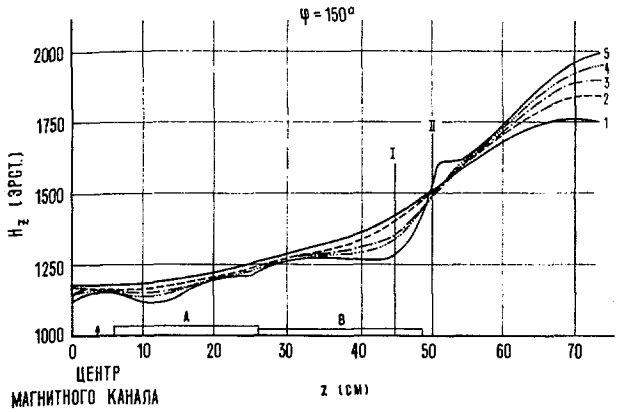

Рис. 2 Конфигурация магнитного поля. А — кольца толщиной 6 мм. В — кольца толщиной 4 мм. (1) $R=0$; (2) $R=12$ см; (3) $R=16$ см; (4) $R=18$ см; (5) $R=20$ см.

поля) и расходимость пучка $\Delta\psi$. В случае магнитного канала угол инжекции $\psi=66°$ и $\Delta\psi=3°$, в случае электростатического — $\psi=69°$.

Попав в ловушку, ионный пучок движется по винтовой траектории, смещающейся по азимуту. После дрейфа на угол 2σ ионный пучок улавливается оболочкой канала. При этом объем, занимаемый пучком, должен ограничиваться по радиусу большим радиусом инжекции [$R=(170+5)$ мм], а вдоль оси — областью отражения, определяемой для данной конфигурации магнитного поля углом инжекции.

Для изучения распределения плотности быстрых ионов в ловушке применялись специальные зонды. В зависимости от назначения конструкция зондов менялась, но всегда это были модификации «цилиндра Фарадея».

Для измерения тока быстрых ионов вдоль оси системы был применен цилиндрический зонд, передвигаемый с помощью штока вдоль оси. Конструкция зонда представлена на рис. 3. Быстрые ионы, движущиеся по винтовым линиям, попадают на внутренние или внешние токопринимающие кольца. Передняя диафрагма защищает токопринимающие кольца от холодных ионов и электронов, движущихся с малым ларморовским радиусом вдоль силовых линий. На каждом кольце имеется изолированная пластинка шириной в 15 мм (по хорде). Изменение тока на пластинке, при вращении зонда вокруг оси, дает азимутальную зависимость тока быстрых ионов. Нетрудно представить, что каждому положению пластинки по азимуту соответствует и определенный азимут расположения центра ларморовской окружности иона, попавшего на пластинку.

Для измерения распределения быстрых ионов по радиусу в центральной плоскости был применен зонд, изображенный на рис. 4. Зонд имеет два коллимированных токоприемника, один из которых закрыт тонкой серебряной фольгой (фольга пропускала ионы водорода с $E\geqq 5$ килоэлектронвольт), а другой — сетками с потенциалами. Коллимация зонда была выбрана таким образом, чтобы

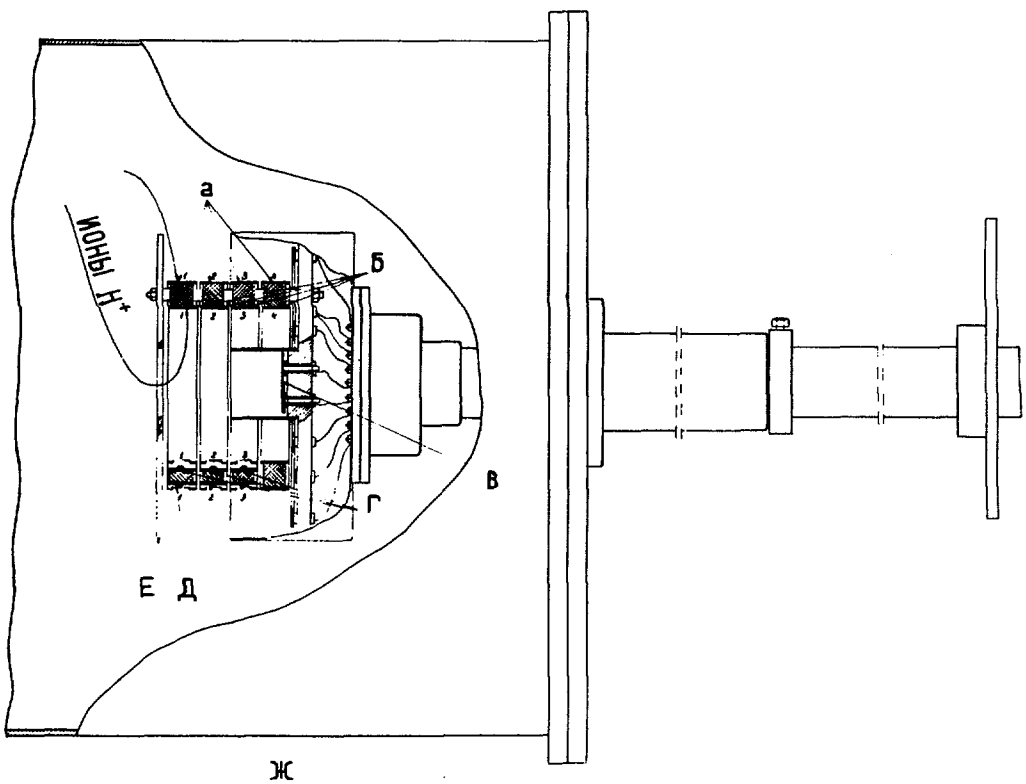

Рис. 3 Устройство цилиндрического зонда. (а) наружные кольца, (б) внутренние кольца, (в) диск, (г) внутренние ламели, (д) наружные ламели, (е) диафрагма, (ж) камера.

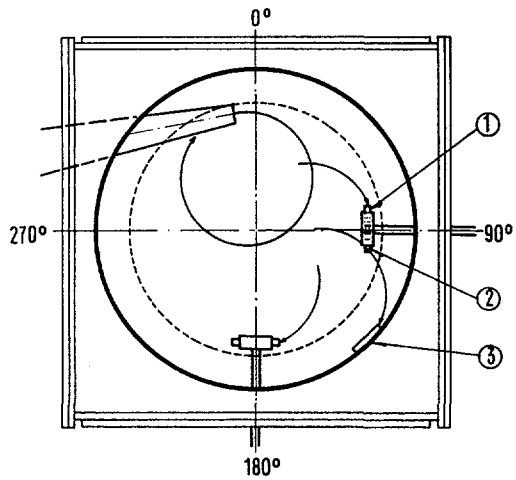

Рис. 4 Схема расположения зондов. (1) сеточный зонд, (2) фольговый зонд, (3) пристеночный зонд.

быстрые нейтральные частицы, образующиеся внутри ловушки, не попадали на токоприемник. (Размер входного окна 5×20 мм, глубина коллимации — 30 мм).

Для измерения распределения потока быстрых ионов около стенки камеры был использован аналогичный коллимированный токоприемник, закрытый серебряной фольгой (входное окно 5×50 мм, глубина коллимации — 40 мм). Токоприемник можно было перемещать по внутренней поверхности стенки камеры.

3. Распределение плотности быстрых ионов по оси и радиусу ловушки

Для определения области отражения пучка при первом заходе в магнитную пробку в плоскость симметрии камеры ($z=0$) вставлялся экран, на

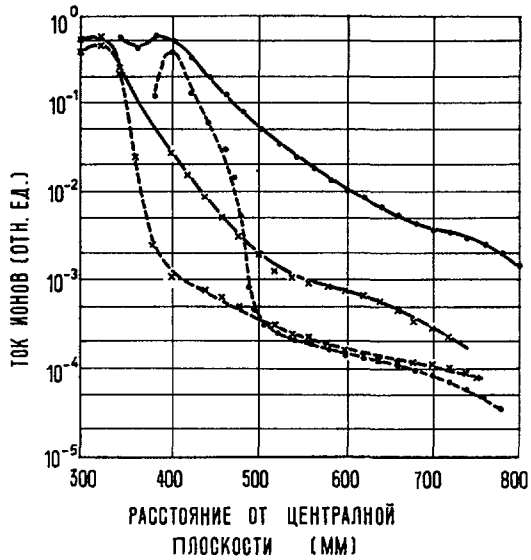

Рис. 5 Распределение плотности быстрых ионов по оси ловушки. Пунктирные кривые — при наличии экрана в центральной плоскости. Сплошные кривые — без экрана. Кресты — электростатический канал. Кружки — железно-токовый канал. $p=5\cdot10^{-6}$ мм рт. ст.

который улавливался пучок при возвращении его после первого отражения. Зонд передвигался по оси ловушки.

Измеренный при таких условиях ток на цилиндр в зависимости от положения зонда показан на рис. 5. Положительный ток весьма мал, как в области за пробками, так и в максимуме магнитного поля. Ток начинает резко возрастать при $z=50$ см, достигая наибольшего значения при $z=45$ см. Таким образом эти значения определяют границу отражения первичного пучка ионов.

Положение точек отражения соответствует ожидаемому из условия сохранения адиабатического инварианта:

$$\frac{H_0}{H_\text{п}} = \sin^2\psi$$

Для углов инжекции 66° и 63° при данной конфигурации поля (рис. 2) формула дает координаты точек отражения соответственно:

$$z=45 \text{ см и } z=50 \text{ см.}$$

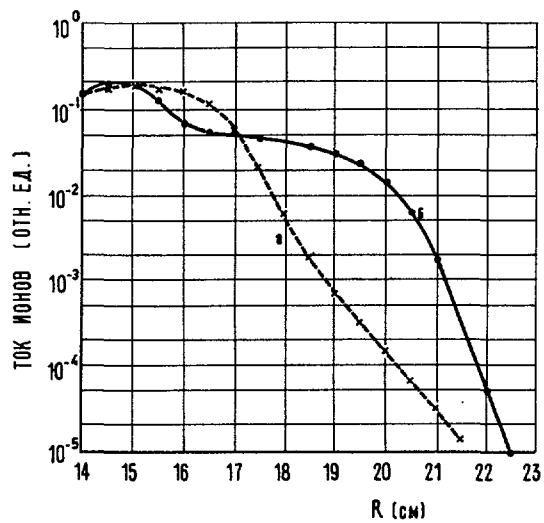

Рис. 6 Распределение плотности быстрых ионов по радиусу ловушки. (а) электростатический канал, (б) железно-токовый канал. $p=5\cdot10^{-6}$ мм рт.ст.

В случае электростатического канала область первого отражения несколько ближе к центральной плоскости, так как угол инжекции был несколько больше.

При удалении экрана из центральной плоскости область отражения размывается. Ток на зонд в максимуме пробки возрастает: в случае магнитного канала ~в 50 раз, а электростатического ~в 4 раза. Это указывает на наличие, в случае магнитного канала, дополнительного ухода быстрых ионов в пробки.

На рис. 6 представлено распределение быстрых ионов по радиусу в центральной плоскости. Видно, что в случае электростатического канала плотность быстрых ионов резко уменьшается (с увеличением радиуса) на радиусах, больших радиуса инжекции ($R=170$ мм). В случае магнитного канала плот-

ность быстрых ионов мало меняется до радиуса $R=200$ мм, и лишь затем быстро убывает. Это опять указывает на связанный с магнитным каналом механизм сильного рассеяния быстрых ионов.

4. Влияние локального возмущения магнитного поля на движение быстрых ионов

Из рис. 5 и 6 видно, что при применении магнитного канала уход быстрых ионов и через пробки и поперек поля относительно больше, чем при применении электростатического канала. Измерение распределения по азимуту тока уходящих в пробки быстрых ионов показало, что максимум ухода находится вблизи месторасположения канала, но смещен, ~на 60° относительно максимума, соответствующего первому отражению от магнитной пробки (рис. 7). Естественно предположить, что эти явления связаны с рассеянием на местном возмущении магнитного поля, вызванном ферромагнитной массой и собственным магнитным полем магнитного канала.

Для определения степени влияния возможных местных возмущений магнитного поля на поведение пучка, были проведены измерения распределения тока в пробках по азимуту, и тока на пристеночный зонд, в зависимости от положения вводимого в систему «магнитного диполя» — железного стержня диаметром 10 мм и длиной 50 мм. На рис. 7 (пунктир) отчетливо видно появление дополнительного максимума тока быстрых ионов, как раз в месте, соответствующем положению диполя.

Величина тока быстрых ионов в магнитной пробке или вблизи стенки камеры зависит от положения магнитного диполя. Например, на рис. 8 показано, как менялся ток на пристеночные зонды в зависимости от положения диполя. Видно, что уход быстрых ионов в радиальном направлении на стенку камеры возрастает при введении диполя, причем тем больше, чем ближе диполь к пучку. Так, на $R=15$ мм пучок пересекал диполь и возрастание ухода быстрых ионов максимальное. На этом же рисунке пунктиром показано изменение тока на пристеночные зонды в случае замены железного стержня на латунный. Видно, что в последнем случае ток на пристеночные зонды уменьшался, что объясняется гибелью части быстрых ионов на латунном стержне. Таким образом, на основании рис. 7 и 8 можно однозначно утверждать, что быстрые ионы рассеиваются на локальных неоднородностях магнитного поля, что вызывает ускоренный уход быстрых ионов из системы как через пробки, так и поперек магнитного поля.

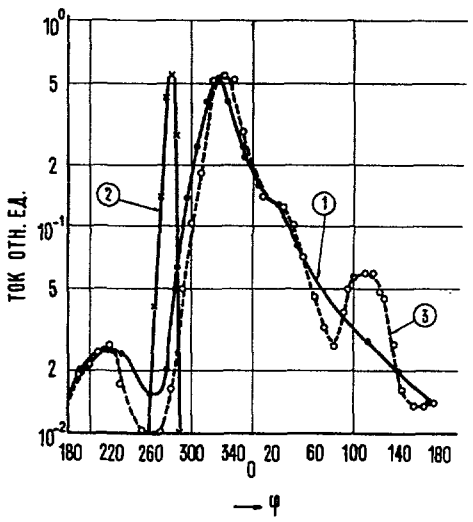

Рис. 7 Азимутальное распределение тока быстрых ионов в магнитной пробке. (1) $z=790$; $p=7{,}8\cdot10^{-6}$ мм рт.ст.; (2) $z=450$ (экран в плоскости симметрии); (3) $z=790$ (магнитный диполь на $R=20$ см); $p=9\cdot10^{-6}$ мм рт.ст.

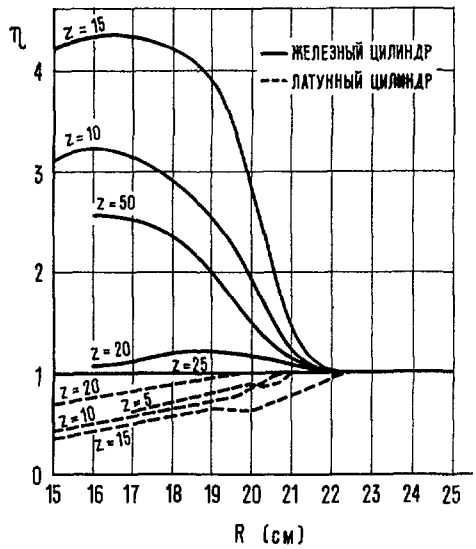

Рис. 8 Изменение тока быстрых ионов на стенку камеры в зависимости от положения магнитного диполя. $\eta=I_{\text{дип}}/I_0$, где I_0 — ток на пристеночный зонд в отсутствии металлического цилиндра. $I_{\text{дип}}$ — ток в присутствии металлического цилиндра.

5. Среднее время жизни и средняя плотность быстрых ионов

Так как в систему инжектируются атомарные ионы, то среднее время жизни основной части их принципиально ограничено временем возвращения на инжектор и в пробки может уходить лишь незначительная часть, — ионы изменившие свой импульс за это время. Интенсивность пучка убывает по мере удаления от инжектора вследствие перезарядки:

$$I=I_0\,e^{-n_0\sigma_{\text{п}}l}$$

где n_0 — концентрация нейтральных атомов;
$\sigma_{\text{п}}$ — сечение перезарядки;
l — путь, пройденный ионом.

Прежде чем уйти в пробки на азимуте φ, ион проходит в ловушке путь длиной l. Изменяя давление и регистрируя изменение тока на изолиро-

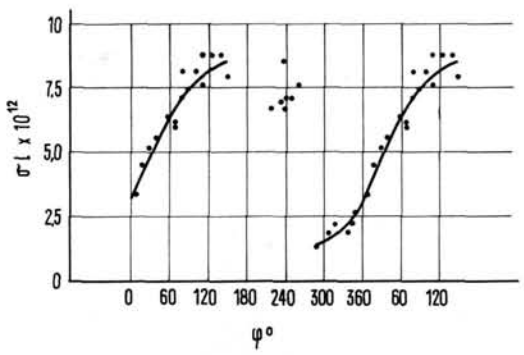

Рис. 9 Зависимость $\sigma_{\text{п}} l$ от азимута.

ванную пластинку, установленную на выбранном азимуте, можно определить $\sigma_{\text{п}} l$ из наклона кривых

$$\sigma_{\text{п}}\, l = 3{,}5 \cdot 10^{16} \frac{\Delta \ln I}{\Delta \varrho}$$

Возможная погрешность в определении наклона прямых, учитывая разброс точек, составляла $\sim 10\%$. Однако, плохое знание компонентного состава газа в системе и, следовательно, абсолютного значения ϱ (измеряемого ионизационным манометром), позволило определить $\sigma_{\text{п}} l$ с точностью до множителя 2.

Эта систематическая ошибка несущественна при относительном сравнении расстояний, проходимых быстрыми ионами до ухода в пробки. За масштаб такого сравнения естественно принять величину $\sigma_{\text{п}} l$ основного пучка, прошедшего путь от точки инжекции до области первого отражения. Это значение $\sigma_{\text{п}} l$, определенное со стоящим в плоскости симметрии ($z=0$) экраном, равно $1{,}3 \cdot 10^{-13}$ см^3.

Зависимость $\sigma_{\text{п}} l$ для ионов, выходящих в пробку, от азимута приведена на рис. 9. В областях малых токов, на $\varphi = 140° - 220°$ и $\varphi = 260° - 290°$, чувствительность аппаратуры была мала для измерений.

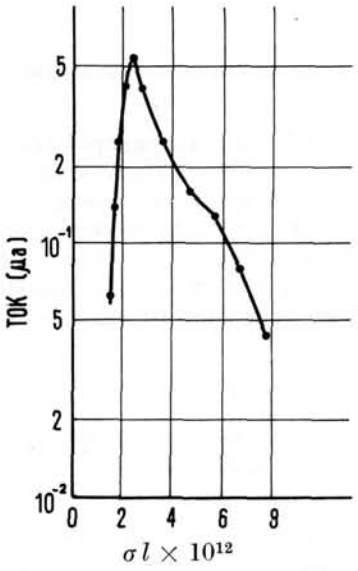

Рис. 10 Зависимость тока быстрых ионов от величины.

На рис. 10 приведена связь тока ионов, выходящих в пробки, с величиной $\sigma_{\text{п}} l$. Видно, что максимум находится при $\sigma l = 2 \cdot 10^{-12}$, что соответствует $l \approx 10^3$ см. Такой путь проходил пучок, сделав первые колебания между пробками.

Длину, проходимую пучком ионов в ловушке до гибели на оболочке канала, независимо можно определить из осциллограммы спада тока на оболочку при внезапном прекращении инжекции. Такие измерения были сделаны при работе с электростатическим каналом (рис. 11). Быстрый спад тока вначале соответствует гибели на канале части быстрых ионов после первых отражений от пробок. Затем следует ступенька, соответствующая времени дрейфа на 2π. Длина ступеньки, как и следовало ожидать, не зависит от давления и составляет $\tau = 40 - 50$ мсек (второй луч калибровка $f = 40$ кц), что дает значение $l = (5-6) \cdot 10^3$ см.

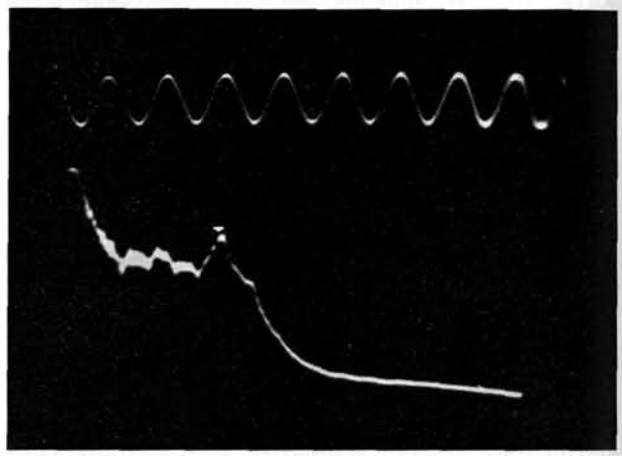

Рис. 11 Спад тока на оболочке инжектора.

Предположив, что быстрые ионы равномерно распределены по всему объему, можно оценить среднюю плотность их в ловушке:

$$n^+ = I\tau/\Omega = 3 \cdot 10^9 I$$

где n^+ — число быстрых ионов в единице объема;
I — инжектируемый ток (в амп.);
τ — среднее время жизни быстрого иона;
Ω — объем системы.

При электростатическом канале $I \sim 2{,}5 \cdot 10^{-4}$ а и $n^+ \approx 7 \cdot 10^5$ см$^{-3}$ при магнитном канале $I \sim 2 \cdot 10^{-3}$ а и $n^+ \approx 6 \cdot 10^6$ см^3.

Подчеркиваем, что это — средняя плотность, на самом деле, возможно, что полное размытие пучка не происходило и плотность быстрых ионов была различной в разных точках объема.

6. О компенсации объемного заряда

Кроме инжектируемых ионов с энергией $E = 10$ кэв, в системе имеются медленные ионы, образующиеся при перезарядке, и медленные ионы и электроны, образующиеся при ионизации остаточного газа. Обычно предполагается, что мед-

ленные ионы должны быстро выходить в пробки (из-за большого сечения рассеяния), а избыточные электроны компенсируют заряд инжектированных и удерживаемых в системе быстрых ионов. Поэтому в системе появится небольшой (масштаба электронной температуры) положительный объемный заряд.

В стационарных условиях должно установиться равновесие между токами покидающих систему электронов и ионов, так чтобы суммарный положительный ток был равен инжектируемому току.

Учитывая, что подвижности ионов и электронов вдоль поля значительно больше подвижностей поперек поля, естественно предположить, что должно существовать и более детальное равновесие: токи ионов и электронов, уходящих вдоль поля, должны приблизительно относиться как количества рождающихся на данной силовой трубке ионов и электронов. В наших условиях это отношение

$$\frac{\sigma_{\text{п}} + \sigma_{\text{н}}}{\sigma_{\text{п}}} \sim 5$$

Для проверки этих предположений были проведены измерения зависимости выходящих в пробку медленных ионов и электронов от запирающего потенциала и распределение их по радиусу и азимуту. Измерения проводились 3-сеточным зондом, а затем специальным диафрагменным зондом.

Конструкция диафрагменного зонда приведена на рис. 12. В кожухе 1 помещались 3 диафрагмы d, d_1, d_2 и коллектор К. В диафрагмах имелось по 12 соосных отверстий ⌀6 мм в диафрагме d, d_1 и ⌀4 мм в d_2. Диафрагма d находилась под потенциалом корпуса камеры, на диафрагмы d_1 и d_2 подавались соответствующие потенциалы. Соотношения диаметров отверстий и расстояний между диафрагмами обеспечивало отбор ионов и электронов коллектором с преимущественной продольной составляющей скорости. Зонд укреплялся на штоке в пробке так, чтобы его можно было перемещать по радиусу. Установленный в положение для измерений зонд был проверен с помощью пучка электронов. Проверка показала, что зонд правильно отюстирован по магнитному полю и что потенциал диафрагм, прекращающий

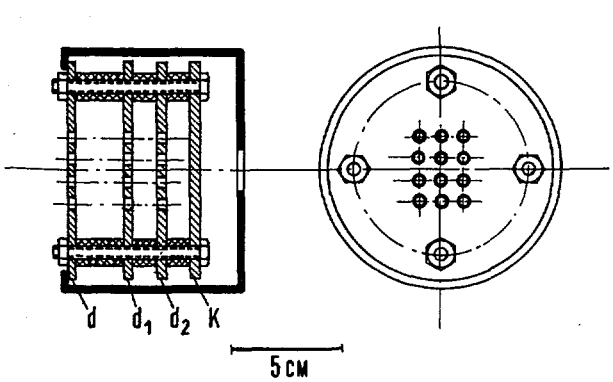

Рис. 12 Схема диафрагменного зонда.

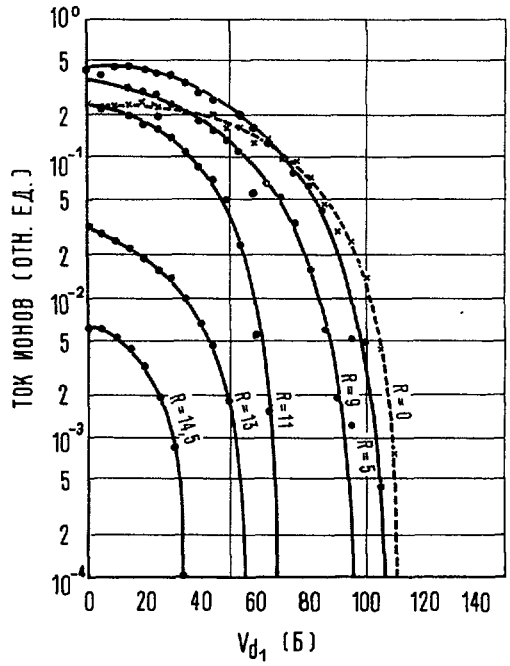

Рис. 13 Зависимость тока вторичных ионов в магнитной пробке от запирающего потенциала. $p=4\cdot10^{-6}$ мм рт.ст. $V_{d_2}=-150$ в.

попадание электронов на коллектор К, соответствует энергии электронов пучка. Была также проведена серия контрольных опытов по влиянию на результаты измерений возможной вторичной эмиссии с коллектора и диафрагм, подтвердивших преимущества (в наших условиях) диафрагменного зонда перед сеточным.

На рис. 13 приведена зависимость ионного тока на коллектор от потенциала на диафрагме d_1 (потенциал диафрагмы d_2 при этом $V(d_2)=-150$ в) на разных радиусах и на азимуте $\varphi=180°$. Аналогичные кривые получены и на $\varphi=90°$; 270°; 0°.

Видно, что потенциал, запирающий ионы (строго говоря, уменьшающий ток до пределов чувствительности прибора), уменьшается с увеличением радиуса. Это свидетельствует о наличии положительного объемного заряда, большего в центре и убывающего к периферии.

На рис. 14 приведены распределения ионного и электронного токов на коллектор в зависимости от радиуса (на $\varphi=0°$ и 180°). Из рисунка следует, что вблизи оси системы отношение ионного тока к электронному порядка $\sim10^2$, вместо ожидаемого 5 и убывает с увеличением радиуса. На радиусах $R=13$ см электронный ток быстро возрастает и достигает максимума на радиусе $R=15-16$ см. Подобные кривые были получены для различных φ и при разных давлениях нейтрального газа. При всех измерениях величина электронного тока вблизи оси системы была меньше предполагаемой, по крайней мере, на порядок, и возрастала к периферии. Само по себе то, что на периферии ($R\cong\cong15$ см) имеется большой электронный ток может

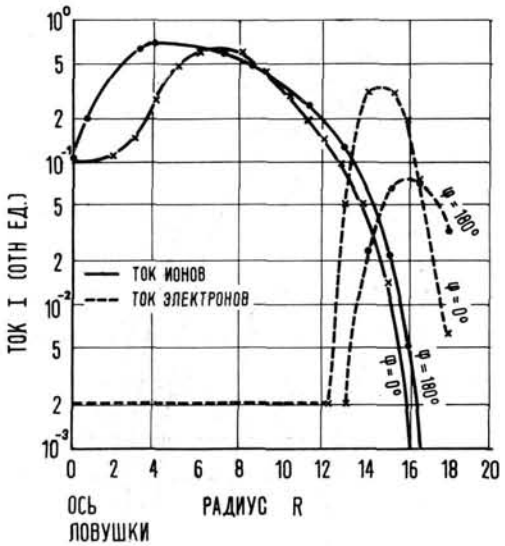

Рис. 14 Распределение токов вторичных ионов и электронов в магнитной пробке по радиусу. $p = 3{,}5 \cdot 10^{-6}$ мм рт.ст.

быть объяснено эмиссией электронов с инжектора под действием ионной бомбардировки и дрейфом этих электронов по азимуту. Труднее объяснить аномально малое количество электронов на $R \cong$ $\cong 12$ см. Рождение электронов должно быть максимальным на радиусах $R = 1{,}5-2$ см (область наибольшей плотности быстрых ионов), а наблюдаемый выход оказывается меньше, чем на радиусах $R = 12{,}5$ см. Остается предположить, что электроны быстрее дрейфуют поперек магнитного поля, чем выходят в пробки.

Сам факт выхода электронов в пробки на радиусах $R \cong 12-14$ см так же удивителен. При изучении энергетического распределения выходящих в пробки электронов было установлено, что они полностью запираются потенциалом 25—30 в, а из кривых рис. 14 следует, что энергия ионов, выходящих на этих радиусах, более 30 в.

Трудно объяснить вышеизложенное поведение электронов в системе, если не предположить, что в камере возникают колебания плотности электронной и ионной компонент плазмы.

7. Колебание плотности быстрых ионов

Для исследования характера колебаний плотности быстрых частиц в объеме, заполненном пучком быстрых ионов, было проведено осциллографирование тока быстрых частиц с радиальных зондов. Зонд представлял собой токоприемник размером $15 \times 15 \times 7$ мм, закрытый серебряной фольгой. Зонды установлены на $\varphi = 90°$ и $\varphi = 180°$ и могли передвигаться по радиусу (рис. 4). Ввиду малости токов быстрых частиц на радиусах, больших радиуса инжекции чувствительность аппаратуры была недостаточна для осциллографирования. Поэтому были сняты осциллограммы колебаний тока быстрых частиц, глубина модуляции и азимутальная корреляция колебаний только на радиусах, близких к радиусу инжекции. Проведенный анализ частот показал, что на обоих датчиках существуют близкие к регулярным колебаниям с частотами 10—20 кц, 100—200 кц и несколько мегагерц. Глубина модуляции низкой частоты значительно больше глубин модуляции высоких частот. Частоты 100—200 кгц и несколько мегагерц были найдены в пучке в инжекторе. Однако, низкая частота повидимому в инжекторе отсутствует и возникает (или очень усиливается) только при движении пучка в самой ловушке. На рис. 15 приведены осциллограммы с радиальных зондов, смещенных по азимуту на 90° и установленных на границе цилиндрического объема, занятого пучком быстрых ионов. На осциллограммах виден отчетливый фазовый сдвиг 90°. При движении зонда ($\varphi = 180°$) внутрь объема сдвиг уменьшается. Это естественно, так как в зонд начинают попадать частицы, сдрейфовавшие на азимуты меньше 180°, а, следовательно, как бы уменьшается азимутальный угол между зондами. В рассмотренном случае движение зонда по радиусу в некоторой степени равноценно движению по азимуту по цилиндрической поверхности объема. Глубина модуляции тока уменьшается с уменьшением радиуса.

Вся совокупность сведений, полученных с помощью радиальных зондов, позволяет предполагать, что «горячая плазма» (созданная пучком ионов), неустойчива относительно образования выпуклостей («языков»), вращающихся вокруг продольной оси ловушки. Причиной возникновения выпуклостей может быть поляризация

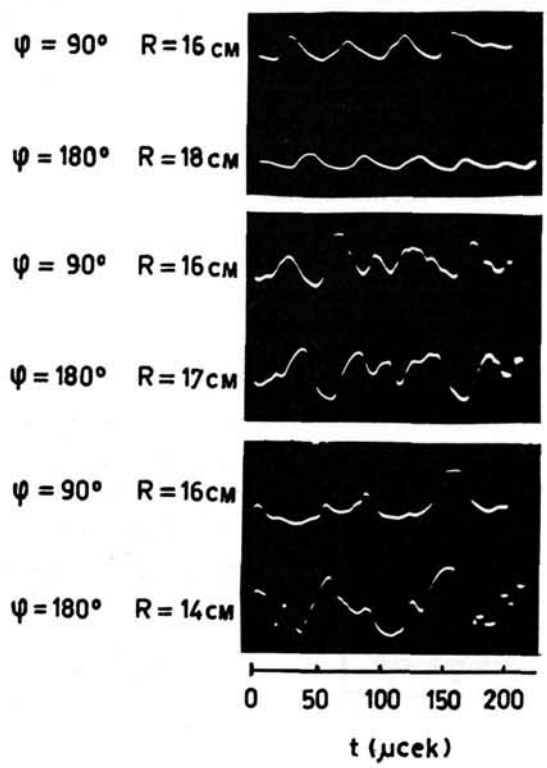

Рис. 15 Колебания плотности быстрых ионов на радиальных зондах.

плазмы вследствие различного магнитного дрейфа электронов и ионов. Поляризация приводит к созданию азимутальных электрических полей, которые, по-видимому, ответственны за уход электронов из внутренних областей поперек магнитного поля на периферию (рис. 14) и неполную компенсацию объема, занятого пучком.

Следует заметить, что характерная частота колебаний 10—20 кц меньше частоты азимутального магнитного дрейфа иона и близка к частоте вращения плазменного цилиндра, заряженного до потенциала близкого к 100 в, в магнитном поле нашей ловушки. Из рис. 13 видно, что выходящие в пробку вторичные ионы, имеют энергию как раз близкую к этой величине.

8. Колебания плотности вторичной плазмы.

Для выяснения колебаний плотности вторичной плазмы были сняты (с помощью открытых токовых датчиков) осциллограммы колебаний тока вблизи стенки камеры и в магнитной пробке.

На рис. 16 приведены характерные осциллограммы колебаний положительного тока частиц на пристеночных датчиках. На первом луче сигнал с неподвижного датчика, установленного на азимуте 90°. На втором — сигнал с подвижного датчика, вращающегося по азимуту в направлении дрейфа быстрых ионов. Характерно, что при любом азимутальном удалении подвижного датчика от неподвижного (разные $\Delta\varphi$) на обоих датчиках наблюдается полная корреляция сигналов, но без сдвига фаз, хотя характерная частота колебаний 10—20 кц соответствует частоте колебаний быстрых ионов. Кроме этой частоты, присутствуют собственные частоты пучка 100—200 кц и несколько мегагерц. (На приводимых осциллограммах амплитуда этих частот уменьшена фильтрами.) «Глубина модуляции» амплитуды колебаний по низкой частоте 100%.

Аналогичные осциллограммы тока ионов, выходящих из ловушки через магнитную пробку на радиусах $R \simeq 9-11$ см и тока электронов на

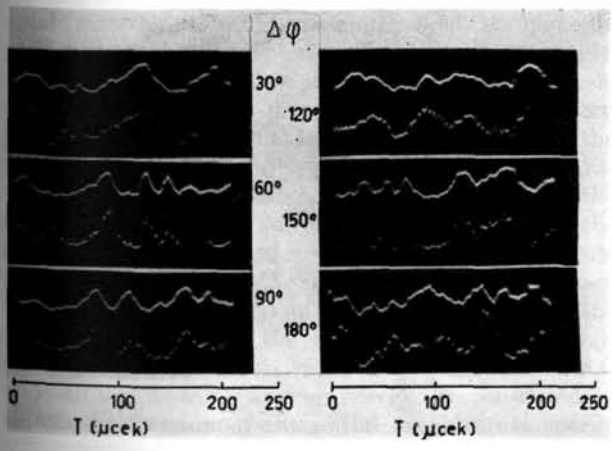

Рис. 16 Корреляция колебаний тока ионов вблизи стенки камеры.

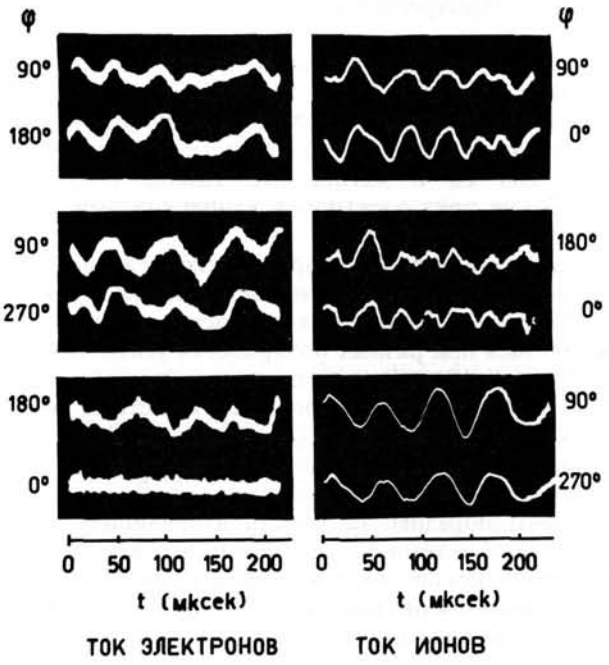

Рис. 17 Корреляция колебаний тока вторичных ионов и электронов в магнитной пробке.

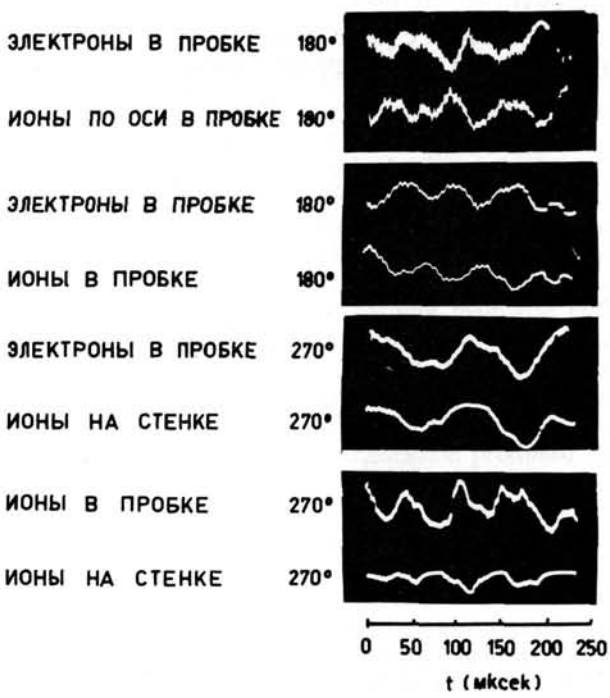

Рис. 18 Корреляция колебаний тока ионов и электронов вблизи стенки камеры и в магнитной пробке.

радиусах $R \simeq 12-16$ см приведены на рис. 17. Глубина модуляции тока на электронных датчиках (30—50%), ионных (10—20%). Токовые датчики были защищены от попадания быстрых ионов заземленным цилиндром (диаметром $\varnothing = 16$ см и длиной 10 см), установленным на оси камеры перед ними. Так же, как и в случае пристеночных датчиков наблюдается синфазность ион-ионных и

электрон-электронных колебаний на датчиках, установленных на различных азимутах. Особый вид имеет осциллограмма электронного тока на датчике, расположенном на азимуте канала ($\varphi = 0°$). Нет выраженной частоты в 10—20 кц, присутствуют в основном собственные частоты пучка (100—200 кц и мегагерцы). Повидимому, эти колебания тока электронов вторичной эмиссии с оболочки инжектора.

На рис. 18 приведены примеры корреляций колебаний токов на стенки и токов в магнитной пробке (осциллограммы ионных и электронных токов снимались при разных полярностях усилителя).

Из рис. 18 можно сделать вывод, что уменьшению выхода ионов в пробки соответствует увеличение выхода ионов на стенку камеры. Уход электронов в пробки происходит одновременно с уходом ионов на стенку камеры.

Таким образом, плотность вторичной плазмы колеблется с теми же частотами, что и плотность быстрых ионов. Однако, колебания плотности медленных ионов *синфазны по азимуту*, т.е. объем вторичной плазмы как бы пульсирует.

9. Заключение

Приведенные выше результаты указывают на то, что:

1) в системах с магнитными пробками, где энергичные ионы инжектируются извне и затем долго движутся в ловушке, весьма существенно отсутствие местных возмущений магнитного поля. Такие возмущения приводят к уходу быстрых частиц, как через пробки, так и поперек поля;

2) даже при весьма низких плотностях энергичных ионов ($n \sim 10^6$ см$^{-3}$) поведение плазмы в ловушке определяется не только бинарными взаимодействиями, но и сложными коллективными процессами;

3) не происходит полной компенсации объемного заряда извне инжектируемых ионов за счет ионизации остаточного газа. Так, в данной системе имеется объемный заряд положительного знака порядка 100 вольт;

4) среднее во времени радиальное распределение потенциала объемного заряда таково, что он максимален на оси и убывает по радиусу;

5) колебания плотности ионов, повидимому, ответственны за уход электронов поперек магнитного поля и неполную компенсацию объема;

6) плотность вторичной плазмы колеблется с теми же частотами, что и плотность быстрых частиц. Однако, в отличие от быстрых частиц плотность вторичных ионов и электронов колеблется синфазно по азимуту;

7) уход вторичных ионов поперек поля связан с одновременным уменьшением выхода их в пробки и с увеличением выхода в пробки электронов.

CYCLOTRON RESONANCE IN THE STATIC MAGNETIC FIELD OF A HELIX*

H. DREICER, H. J. KARR, E. A. KNAPP, J. A. PHILLIPS, E. J. STOVALL, JR., J. L. TUCK

LOS ALAMOS SCIENTIFIC LABORATORY, UNIVERSITY OF CALIFORNIA

LOS ALAMOS, NEW MEXICO, UNITED STATES OF AMERICA

An experimental and theoretical investigation of cyclotron resonant transfer of longitudinal to transverse energy in a static magnetic field is described. The field configuration consists of a uniform axial field superimposed upon a transverse perturbing field of variable pitch which rotates spatially in phase with a particle in resonance. The efficiency of this device as an injector and trapping mechanism inside of a magnetic mirror geometry has been studied by 1) tracing electron orbits with a scintillator, 2) detecting the leakage current out of the mirrors, and 3) measuring the diamagnetic effect due to the helical motion of trapped electrons. Numerical calculations carried out on a digital computer and analytic solutions to the equations of motion obtained for perturbing fields which closely approximate the experimental conditions are presented. These calculations as well as the experiments show that a resonant transfer of energy $> 70\%$ from the longitudinal to the transverse direction is easily achieved. Containment time in the mirror geometry has been shown to be limited by the inverse process which causes a return of energy into the longitudinal direction.

1. Introduction

There are several methods by which a low β hot plasma may be formed from the accumulation of fast ions injected into magnetic confinement geometries. The objective of these methods is to trap the ions in the confinement region for times comparable with the mean lifetime of the ions for the fusion reaction. Well-known methods include (1) the injection of molecular ion beams which are dissociated in arcs [1] or in the residual background gas [2], (2) injection of fast neutral atoms which are trapped when ionized as a result of encounters with the residual gas or accumulated plasma [3, 4], and (3) the scattering of two colliding neutral plasma beams [3, 5].

A fourth approach has been examined by FEDORCHENKO *et al.* [6] SINEL'NIKOV *et al.* [7, 8], and more recently by LAING and ROBSON [9]. Here a beam of charged particles is injected parallel to the axis of a conventional mirror geometry in which the magnetic field spatially modulated by a set of auxiliary perturbing coils spaced periodically with respect to the axial direction. Radial magnetic field components produced by these coils exist off-axis only. A charged particle injected off-axis encounters both the main axial field and a series of radially inward and outward perturbing magnetic fields. These fields deflect the particle and transfer energy into the direction transverse to the main axial field at the expense of the longitudinal energy. To optimize this transfer the auxiliary coils are spaced so that the radial components of the perturbing field change direction in phase with each half rotation of the Larmor orbit as the particle moves along the main axial field. Analysis shows that a cyclotron resonance condition exists; and although the particle energy is conserved, a significant fraction of the initial longitudinal energy is transformed into transverse energy. As a result, the particle may be reflected by a magnetic mirror.

On the single-particle model, the main defect of this method appears to be the occurrence of the inverse process, i.e., the conversion of transverse energy back into longitudinal energy on subsequent traversals of the perturbed fields, with the eventual escape of particles out through the mirrors. Electron beam experiments [8] have shown some accumulation of injected particles by this method.

This concept has been extended by R. C. WINGERSON [10], who designed and experimented with a helical magnetic configuration which attempts to keep the perturbing field oriented perpendicular to the trajectory of the particle. This perturbing magnetic field configuration rotates spatially in phase with a certain class of orbiting particles, and it possesses non-reciprocal properties with respect to the direction of traversal along the axis. Using electrons injected into such a magnetic field configuration produced by a ferromagnetic helix, he has demonstrated the transfer of longitudinal into transverse energy and the subsequent reflection of these particles from a magnetic mirror.

This paper reports on experiments with electrons injected into a similar field configuration produced by means of bifilar conductors wound helically with variable spacing and coaxial with the main field. These experiments also show that longitudinal energy is transferred into transverse energy, and a resonance condition for this transfer has been observed. Containment time for electrons in a magnetic mirror geometry perturbed by this field configuration has been measured.

In Section 2 we give a qualitative picture of the resonant properties and the non-reciprocal nature of the helical perturbing field when superimposed

* Conference paper CN-10/178, presented by J. A. Phillips. Discussion of this paper is given on page 357. Translations of the abstract are at the end of this volume of the Conference Proceedings.

on an axial magnetic field. A theoretical discussion based on the equations of motion is also presented. An experiment using electrons to study both the energy transfer and containment is described in Section 3. Finally, numerical orbit calculations carried out on a digital computer and a discussion on the inverse process of transferring transverse energy into the longitudinal direction are presented in Section 4.

2. Orbit properties and perturbing field design considerations

2.1. Cyclotron resonance in a static magnetic field

The role played by cyclotron resonance in the motion of an electron through a spatially periodic magnetic field has been displayed in the treatments mentioned above. For a certain range of particle velocities along the axial magnetic field an electron is subject to a periodic force which acts at right angles to the total magnetic field and remains in phase with one velocity component associated with the Larmor rotation. This results in a cyclotron resonant transfer of energy from the direction along the field into the Larmor rotation. The fraction of energy thus transferred in a uniformly periodic perturbing field is limited by the fact that the electron does not remain in resonance with the field when its longitudinal energy decreases. In such systems the periodic fields appear linearly polarized in the reference frame moving in the axial direction with the orbiting electrons.

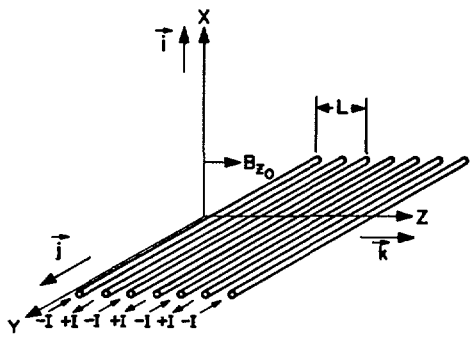

Fig. 1a Current configuration to produce a two-dimensional periodic perturbation field.

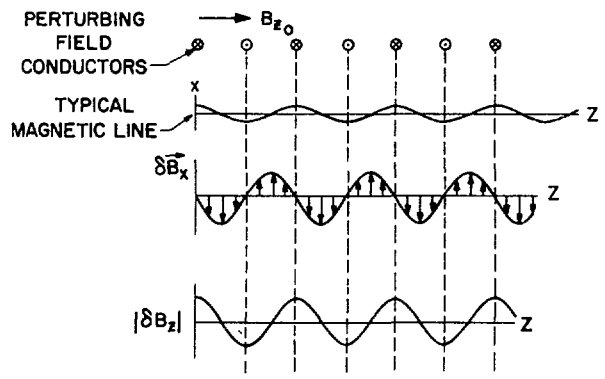

Fig. 1b Relative values of the x- and z-components of the perturbing field as a function of axial distance.

The principal extension to be discussed in this section concerns the effect of a perturbing field of circular polarization. To begin with we shall briefly review the periodic linearly polarized case. Consider the fixed co-ordinate system shown in Fig. 1a. A uniform magnetic field B_{z0} is applied along the z-direction, and an infinite set of parallel wires in which the current direction alternates lies in the y-z plane. It provides the perturbation field, and its spatial period, as shown, is L. A typical magnetic line is shown in Fig. 1b together with the δB_x and δB_z components due to the perturbing coils. These components are all static in the fixed co-ordinate system; however, to an electron moving along the z-direction with a velocity v_z there appear to first order in v_z/c the Lorentz transformed electric and magnetic fields

$$\delta \mathbf{B}_x' = \delta \mathbf{B}_x = \delta \mathbf{B}_{x0}\, e^{-i(2\pi/L)v_z t} \tag{1}$$

$$\delta \mathbf{E}_t' = \frac{1}{c}\mathbf{v} \times \delta \mathbf{B}_{x0}\, e^{-i(2\pi/L)v_z t}\,. \tag{2}$$

The time variation is made up of a single Fourier component provided δB_x varies sinusoidally, with the period L, in the z-direction. If v_z is chosen so that

$$\frac{2\pi}{L} v_z = \omega_B \tag{3}$$

where

$$\omega_B = \frac{e}{mc} B_{z0}\,,$$

then there is a resonant transfer of energy into the direction transverse to B_{z0}. This is cyclotron resonance in a static magnetic field, and the total energy must be conserved. To see how conservation comes about we examine the components of the force in the primed system

$$\mathbf{F}_t' = e\,\delta \mathbf{E}_t' + \frac{e}{c}\mathbf{v}_t' \times \delta \mathbf{B}_z + \frac{e}{c}\mathbf{v}_t' \times \mathbf{B}_{z0}'$$

$$F_z' = \frac{e}{c}\mathbf{v}_t' \times \delta \mathbf{B}_x' \tag{4}$$

where $\mathbf{v}_t'$ is the velocity transverse to $\mathbf{B}_{z0}$ in the primed system. Of these forces, only eE_t' can change the primed energy of the system, and it contributes only to the transverse energy. The rate at which work is done in the primed system is given by

$$\left(\frac{dW}{dt}\right)' = e\,\delta \mathbf{E}_t' \cdot \mathbf{v}_t' = \frac{e\,\mathbf{v}_t' \cdot \mathbf{v}_z \times \delta \mathbf{B}_{0x}}{c}\, e^{-i(2\pi/L)v_z t}\,. \tag{5}$$

To find the rate of energy change in the fixed (laboratory) frame, we use the fact that it is the time component of the force four-vector. This yields immediately

$$\frac{dW}{dt} = \left[\left(\frac{dW}{dt}\right)' + v_z F_z'\right]\sqrt{1 - \frac{v_t^2}{c^2}} \tag{6}$$

and substitution of Eqs. (4) and (5) into (6) yields

$$\frac{dW}{dt} = 0\,.$$

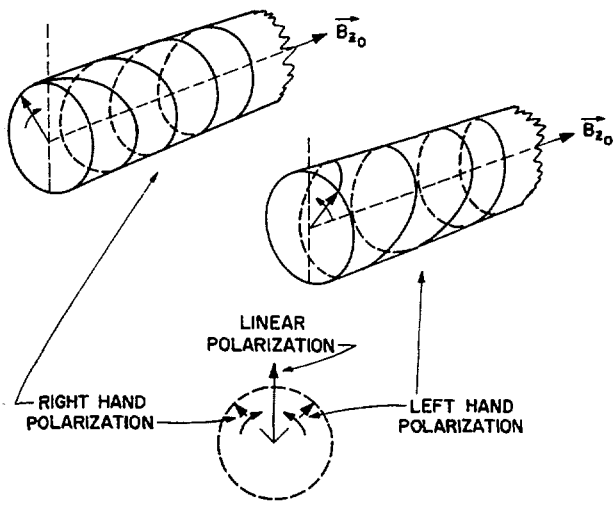

Fig. 2 Resolution of a linearly polarized vector into two circularly polarized vectors as seen from a coordinate system moving along the z-axis.

This shows that the force $(e/c)\mathbf{v}_t' \times \delta\mathbf{B}_x$ is responsible for removing energy from the longitudinal motion while the force $e\mathbf{E}_t'$ builds up the transverse energy.

In the primed system both the electric and transverse magnetic fields, given in Eqs. (1) and (2), appear linearly polarized. We may equally well regard them as a sum made up of right and left circularly polarized components E_r and E_l, i.e.,

$$\mathbf{E}_t' = \mathbf{E}_r + \mathbf{E}_l$$

$$\mathbf{E}_r = \frac{E_t'}{2}\left(\mathbf{i}\cos\frac{2\pi}{L}v_z t + \mathbf{j}\sin\frac{2\pi}{L}v_z t\right) \qquad (7)$$

$$\mathbf{E}_l = \frac{E_t'}{2}\left(\mathbf{i}\cos\frac{2\pi}{L}v_z t - \mathbf{j}\sin\frac{2\pi}{L}v_z t\right).$$

This is illustrated in Fig. 2. In the stationary (laboratory) frame these circularly polarized components are static fields whose azimuthal orientation about $\mathbf{B}_{z0}$ varies periodically with z, and, as shown in Fig. 2, they are distinguished by the sense of left- and right-handed screws. If the component of the electron velocity along $\mathbf{B}_{z0}$ satisfies the cyclotron condition given in Eq. (3), then it is in resonance with the right-hand circularly polarized component, and energy conversion to the transverse direction occurs. At the same time v_z decreases and the electron goes out of resonance. To increase the Q of the system the period L of the field must be decreased and matched to the electron motion so that Eq. (3) is satisfied everywhere [9, 10]. The design of such a system is discussed later in this section.

A spatially periodic magnetic field may be considered reciprocal with respect to the direction of transit along $\mathbf{B}_{z0}$ if cyclotron resonance can occur for both directions. This is a property of the linearly polarized fields previously studied [6, 7, 8, 9]. On the forward pass in the direction $\mathbf{B}_{z0}$, the resonant interaction can occur with the right-hand circularly polarized component only, whereas the left-hand component produces only small periodic perturbations which will nearly average to zero. In the reverse direction the left-hand circularly polarized component is responsible for the resonant interaction, and the effects due to the right-hand component nearly average to zero.

A non-reciprocal system can be constructed in which the perturbing field has only one circularly polarized component. If such a non-reciprocal system is placed between two magnetic mirrors, its behavior on repeated transits through the system must be considered. Suppose that the magnetic perturbation has been matched to the electron motion, which is initially purely longitudinal, and resonance occurs on the first transit. Upon reflection from the first mirror it re-enters the perturbation field in the reverse direction, but now the screw sense is incorrect, and the effects of the perturbing fields average very nearly to zero over each local period. After a second mirror reflection, it re-enters the perturbing field in the forward direction. Since its axial velocity is no longer matched to the entrance of the perturbing field, the electron receives only periodic perturbations which very nearly cancel until it reaches a section of the field where Eq. (3) is nearly satisfied. When this occurs E_t' and v_t rotate with nearly the same angular velocity. However, the angle subtended by these vectors in this third pass may differ greatly from zero. If $e\mathbf{E}_t' \cdot \mathbf{v}_t' > 0$ then absorption takes place, and the transverse energy increases. If $e\mathbf{E}_t' \cdot \mathbf{v}_t' < 0$ then energy is removed from the transverse direction and the electron may leave the perturbing field with an increase in longitudinal energy.

2.2 Helix design calculations

The equation of motion of a charged particle in a magnetic field is

$$\frac{d\mathbf{v}}{dt} = \frac{e}{mc}\mathbf{v}\times\mathbf{B}. \qquad (8)$$

In this treatment, the magnetic field near the axis of a real bifilar helical winding is approximated by neglecting off-axis variations and end effects. Then it follows that δB_t, the magnitude of the transverse perturbing field, and ψ, its azimuthal direction with respect to some fixed transverse directions, are functions of z only, and B_z, the axial component of the magnetic field, is constant. This approximation violates the condition curl $\mathbf{B}=0$ near the axis, but div $\mathbf{B}=0$ is satisfied. Let

θ = the angle subtended by $\mathbf{B}_z$ and $\mathbf{v}$,
ψ = the azimuthal angle of transverse field,
φ = the azimuthal angle of the velocity, and
v_0 = the constant magnitude of $\mathbf{v}$.

In terms of these variables, Eq. (8) can be resolved into component equations of motion

$$\frac{d}{dz}\sin\theta = \frac{e\,\delta B_t}{mcv_0}\sin(\varphi-\psi) \qquad (9)$$

$$\frac{d}{dz}(\varphi-\psi) = -\frac{d\psi}{dz} - \frac{eB_z}{mcv_0\cos\theta} + \frac{e\,\delta B_t\cos(\varphi-\psi)}{mcv_0\sin\theta}. \qquad (10)$$

Here

$$v_0 \cos\theta = v_z$$
$$v_0 \sin\theta = v_t.$$

If a particle orbit starts with pure axial motion and is always in exact resonance with the perturbing transverse field, δB_t, in accordance with Eq. (3), then the transverse velocity v_t is always at right angles to δB_t and the phase angle is

$$\varphi - \psi = 90°.$$

In this case, Eq. (9) can be integrated to give

$$v_t = v_0 \sin\theta = \frac{e}{mc}\int \delta B_t(z)\,dz\,. \qquad (11)$$

Equation (10) then becomes

$$\frac{d\psi}{dz} = -\omega_B \frac{1}{v_0 \cos\theta}$$

or

$$\frac{d\psi}{dz} = -\frac{\omega_B}{v_0}\left[1-\left(\frac{e}{mcv_0}\int \delta B_t(z)\,dz\right)^2\right]^{-\frac{1}{2}} \qquad (12)$$

which yields a relation between the magnitude of $\delta \mathbf{B}_t$ and the rate at which its orientation changes with z for the exact resonance conditions described above. A second relationship between δB_t and $d\psi/dz$ is required before both δB_t and $d\psi/dz$ can be determined, but once this is established, Eqs. (11) and (12) can form the basis for the design of the actual perturbing fields.

One choice of the second relationship is to require that δB_t be proportional to the local wavelength

$$|\delta B_t| \propto L(z) = 2\pi\left(\frac{d\psi}{dz}\right)^{-1}.$$

Substitution of this relation into Eqs. (11) and (12) yields

$$L(z) = L_0 \cos\frac{\pi z}{2h} \qquad (13)$$

$$|\delta B_t| = \delta B_{t0} \cos\frac{\pi z}{2h},$$

where

$$L_0 = \frac{2\pi v_0}{\omega_B}, \qquad \delta B_{t0} = \frac{\pi mcv_0}{2eh},$$

and h is the value of z at which v_z becomes zero. With this choice, particle orbits can be calculated completely, as described in Section 4. The design of Helix 1 in Section 3 was based on this choice.

A second possible choice is to require that the relationship between δB_t and $d\psi/dz$ be the same as for an infinitely long helix of constant spatial period, which has been calculated by SMYTHE [11] in terms of tabulated functions. This relationship was substituted in Eqs. (11) and (12) and the design of Helix 2 calculated by numerical integration.

3. Electron injection experiment

An electron injection experiment (Fig. 3) was set up to determine (a) the effectiveness of the helical field in transferring energy from the longitudinal to the transverse direction, and (b) the confinement time of particles trapped in magnetic mirror geometry which contains a resonant helix.

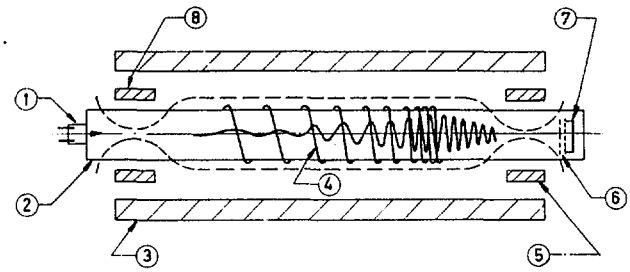

Fig. 3 Diagram of apparatus used in electron injection experiments. 1 — electron gun, 2 — pyrex tube, 3 — main solenoid coil, 4 — helix, 5 — far mirror coil, 6 — grid, 7 — current collector, 8 — near mirror coil.

An axial magnetic field of 90 G was produced by an air coil solenoid of ≈ 2 m length and inside diameter of 50 cm. The mirror fields separated by ≈ 150 cm provided mirror ratios up to 6. An electron gun located outside the first mirror injected a ≤ 1 mA, 2 keV electron beam of ≈ 3 mm diameter down the axis of the system. The vacuum chamber was a 10-cm outside diameter Pyrex tube lined with a grounded stainless steel wire mesh to avoid effects of charge accumulation on the walls. Normal operating pressure was 10^{-6} mm Hg.

The coil producing the perturbation field consisted of two bifilar helical windings (Fig. 4) wound around the vacuum chamber. The two windings are wound in the same sense around the tube but are displaced by 180°. The four conductors involved are equally spaced around the circumference. This produces a relatively uniform transverse field in the axial region. The axial distance between any two adjacent wires is equal to one-fourth of the local wavelength. The two helices used in these experiments were designed by using different approximations to the relationship between δB_t and $d\psi/dz$ ($=2\pi/L(z)$) which is necessary for solution to the design Eqs. (11) and (12).

Helix 1 was based upon the assumption that δB_t is proportional to the local wavelength $L(z)$ of the helix, as stated in Section 2.2. A short helix was wound in accordance with Eq. (13) with $B_{z0} = 90$ G, electron energy $W_0 = 2$ keV, and $h = 50$ cm. For these parameters $\delta B_{t0} \cong 4.7$ G and $L_0 = 10$ cm. The field measured in this helix is shown in Fig. 4, along with a drawing of the winding. Note that the magnitude of the field falls off more rapidly than the cosine dependence assumed, and its amplitude is negligible beyond 35 cm length. This is not a serious mismatch for a helix with only four to five turns, and the helix was quite effective in practice. Note also the slow variation of δB_t with r in Fig. 4. The helix satisfies fairly well the assumption made in Section 2 that δB_t is independent of r in the central region traversed by the electron orbits.

Helix 2 was based upon the assumption that for a long helix of variable period $d\psi/dz$ varies slowly enough with z so that the relation between δB_t and

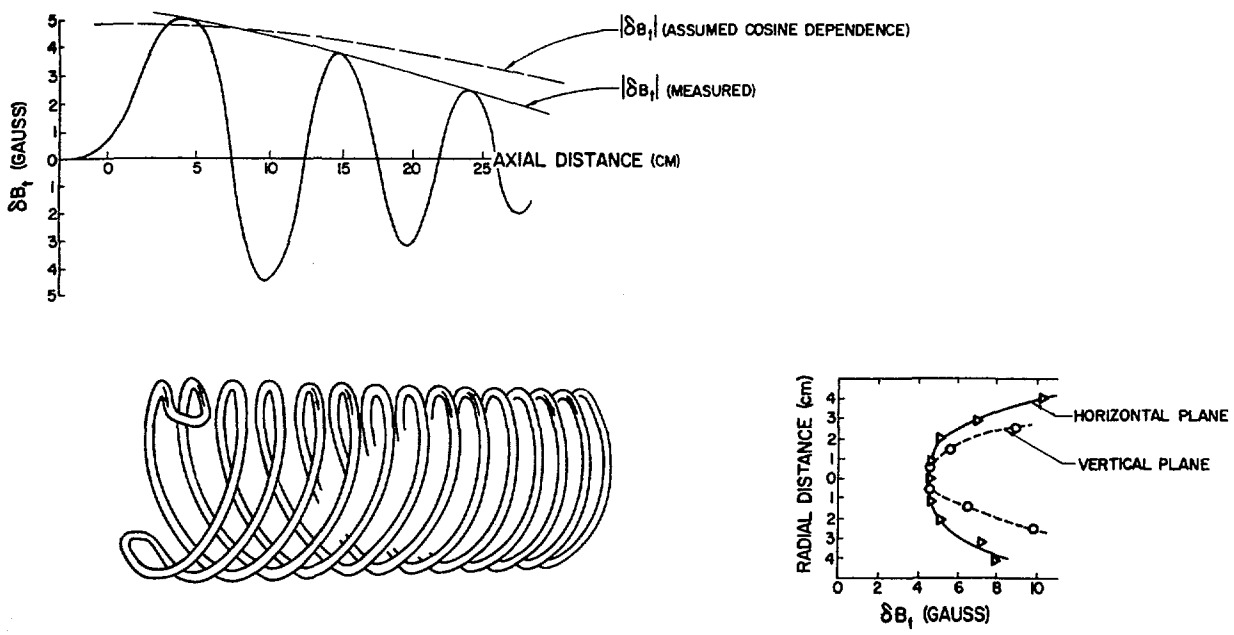

Fig. 4 Bifilar helical winding used to produce the perturbation field. The measured value of the vertical component of the transverse field on the axis for Helix 1 is shown at top of the figure, and its variation in amplitude across a diameter of the helix is shown at the right.

$d\psi/dz$ is the same as it would be if $d\psi/dz$ were constant. Using Smythe's equations, δB_t and ψ were calculated numerically as functions of z, as described in Section 2.2, and Helix 2 constructed to agree with this ψ. The same initial period L_0 and axial field were used in this helix as in Helix 1. The initial perturbing field, δB_{t0} was 1.6 G in this longer helix and its diameter was somewhat greater (13 cm). Comparison of the performance of these two helices is given later in this section.

3.1. Resonance observations

Observations on the performance of the resonant helix system were made by following the orbits of the injected electrons with a calcium tungstate scintillator coated on a glass plate which could be moved axially through the system. The scintillator surface was covered with a thin evaporated layer of aluminum which was grounded to prevent charge accumulation. As the scintillator disc was moved along the axis starting at the helix entrance, the beam trace was observed to rotate about the axis in a spiral of increasing radius in phase with the rotation of the transverse field. The diameter of the last orbit at the output of the helix was a maximum for the values of axial magnetic field, injected electron energy, and helix current satisfying the resonance conditions given earlier. The trace on the scintillator was a spot at the input of the helix but developed into an arc, or full Larmor circle in some cases, at the output. This spread in phase of the emerging electrons may be due to the beam divergence and velocity spread from the gun, but these effects have not been investigated fully.

The magnitude of the transverse velocity of the electrons at the helix output was determined both by measuring the diameter of the Larmor orbit traced by the arcs appearing on the scintillator, and measuring the axial displacement of the scintillator for one full rotation of the arc. The resonant behavior of Helix 1 is shown in Fig. 5 as a function of injected electron energy W_0. A rather broad maximum is shown with fine structure which is believed to be due to secondary effects resulting from the coil design. At resonance, >75% of the initial energy was transferred into transverse energy. Resonances were also observed with axial field and helix current as

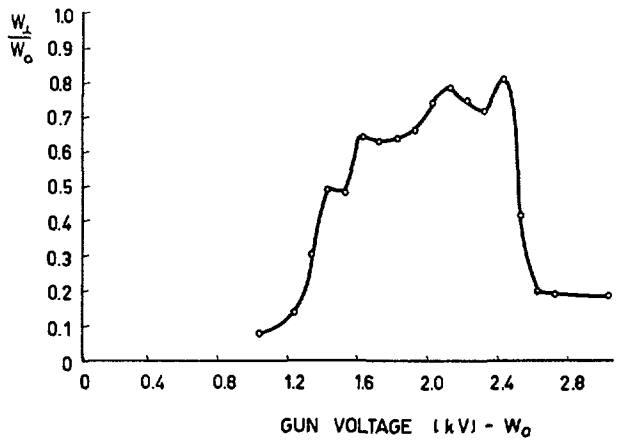

Fig. 5 Fraction of energy transferred into the transverse direction by Helix 1 for an electron beam injected axially with energy W_0. Helix current = 150 A, main field = 90 G.

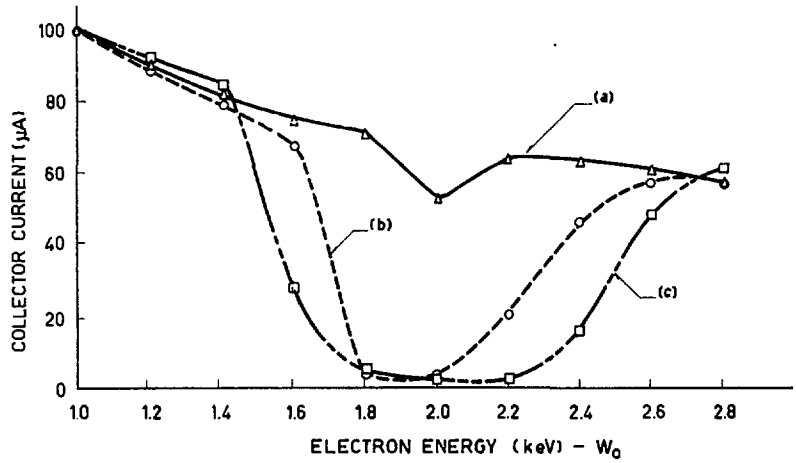

Fig. 6 Current transmitted through magnetic mirror at the output of Helix 1 vs electron energy and helix current. The magnetic mirror ratio $R_m = 2$. Helix current in (a) 120 A, (b) 130 A, (c) 140 A.

variables. The second helix exhibited a sharper response, probably due to its greater length, and the closer correspondence between the design calculations and the physically realized fields. As expected, with the B_z field reversed, all evidence of resonant behavior disappeared.

Observations of the resonance were also made using a Faraday collector cup located on the axis behind the far mirror coil, as shown in Fig. 3. The current transmitted to the collector cup was measured as a function of electron energy, helix current, and mirror ratio. Fig. 6 shows the amount of current transmitted through the far magnetic mirror (near mirror off) as a function of W_0, with helix current as a parameter. At 140-A helix current, a mirror ratio of 2 reflects nearly all electrons having initial energies between 1.6 and 2.4 keV. With 120-A helix current, the amount of transverse energy given to the beam is small and the electrons are not reflected by the magnetic mirror.

3.2. Visual observations

Figs. 7 and 8 show photographs of the electron beam made visible by raising the background gas pressure to $\approx 5 \times 10^{-5}$ mm Hg. With the helix current off, the electron current (≈ 1 mA) excited a pencil of light down the axis of the tube (Fig. 7b). With the mirrors and helix turned on, the luminous region occupied a cylinder (Fig. 7c) of diameter equal to the diameter of the Larmor orbit of an electron with ≈ 1.5 keV transverse energy in the 90-G axial field. The diameter and intensity of the glow reached a maximum at the resonance conditions. Photographs of the luminous trace of the electron beam taken without the magnetic mirrors on are shown in Fig. 8. The helical trajectory of the beam was observed both on and off resonance by varying the axial magnetic field. The spiral reached its maximum diameter at resonance ($B_z = 90$ G) and fell off rapidly as the field was either increased or decreased. A change of $\approx 5\%$ reduced the Larmor diameter by a factor of ≈ 3 as shown in the figure. Despite the increased background pressure, these observations are in agreement with the scintillator measurements.

3.3. Observations of the inverse process

The inverse process, i.e., the conversion of transverse back into longitudinal velocity, was examined experimentally by passing the electron beam through two identical helices placed in tandem. The first helix was used to control the ratio of transverse to longitudinal energy of 2-keV electrons entering the second helix, which was operated at resonance current. This simulated successive re-entry in the forward direction after reflection from the magnetic mirrors.

The electron beam emerging from the first helix was distributed in phase over part or all of a Larmor circle, as described earlier. To reduce this phase spread a notched glass disc was placed between the two helices. The disc was phosphor coated to permit observation of the trace of the particles emerging from the first helix and aluminized to avoid charge accumulation. The notch, which had a width of 6 mm, transmitted a narrow sector of the orbiting electrons which continued to rotate and advance along the axis toward the second helix. This motion was observed on an axially movable scintillator, and a travelling telescope was used to measure the Larmor diameter. The phase of the electrons at the input to the second helix was varied in 90° steps by moving the second helix in steps of $L/4$ where L is the axial distance the electron group moved in one Larmor rotation. The transverse energy at the input and at the output of the second helix was determined from the measured diameter of the Larmor orbit. In general, more than one transverse energy was observed at the output for each phase injected. In some cases a large transverse energy spread was indicated by a number of discrete Larmor orbits or a spiral of several turns on the scintillator. The amount of energy spread varied with both the phase and transverse energy at the input to the helix. The

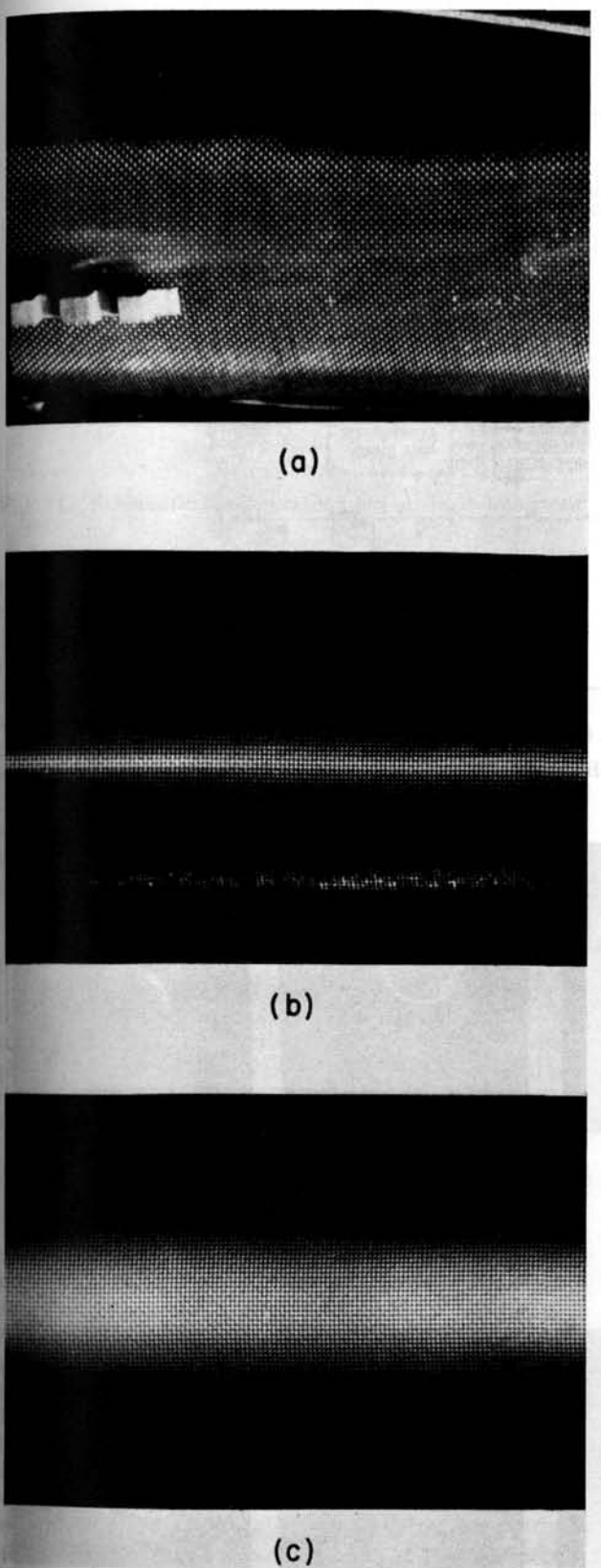

Fig. 7 Photographs of (a) Pyrex tube vacuum chamber and stainless steel wire mesh liner, (b) trace of electron beam with the helix turned off (high background gas pressure, exposure time = 6 min) and (c) luminous region excited by trapped electrons with mirrors turned on and helix on resonance (exposure time = 30 sec).

spread in energy was due to the strong dependence of the behavior of the helix on input energy and phase.

Results of these measurements are shown in Fig. 9. The energy of longitudinal motion at the input ($W_{\parallel, \text{in}}$) to the second helix is shown on the ordinate, and the ratio of the longitudinal energy at the output to that at the input is the abscissa. The points above each given value of $W_{\parallel}$ correspond to four phases at 90° intervals injected into the second helix. Points

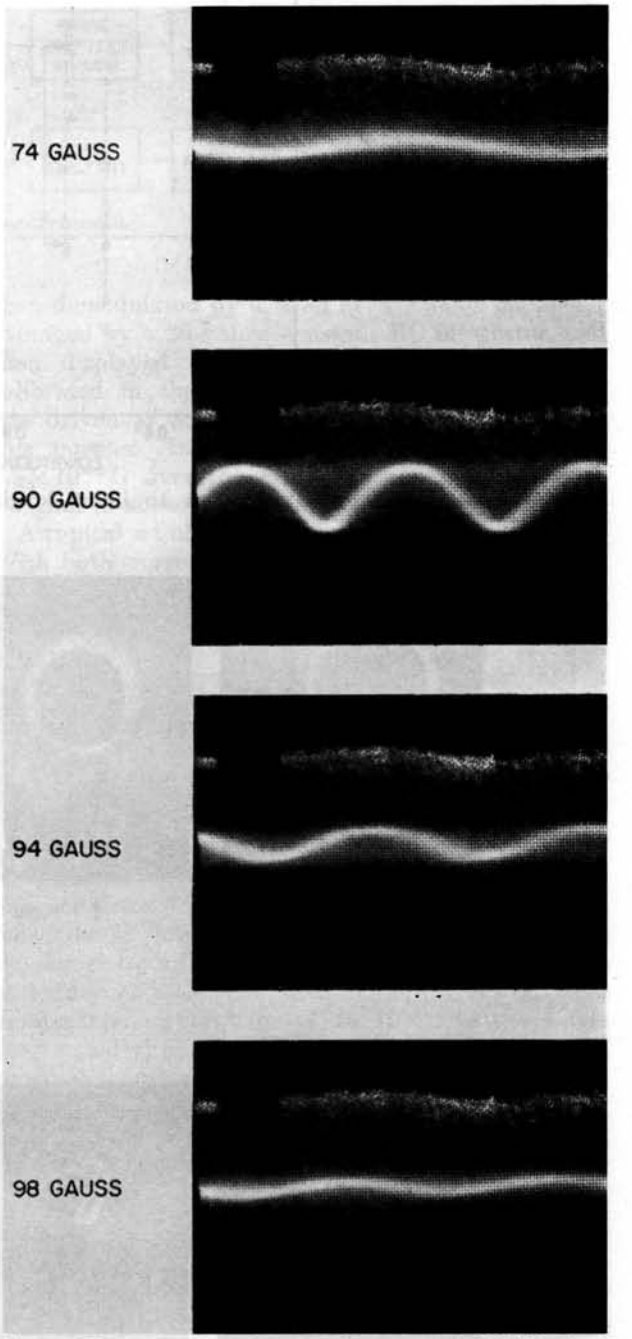

Fig. 8 Photographs taken at the output of Helix 2 of electron beam traces with high background gas pressure as a function of main longitudinal field. Note that the maximum transverse energy occurs at the resonant field of 90 G.

connected by arrows in Fig. 9 show extremes of the corresponding ratio ($W_{\parallel, \text{out}}/W_{\parallel, \text{in}}$) for cases in which this energy spread was observed for a single input phase.

These changes in the transverse velocity distribution are illustrated in Fig. 10 by photograph of scintillator traces obtained at the input (top row of traces) and at the output (bottom row of traces) of the second helix. For these observations the notched disc was removed so that a wide range of phases, as indicated in the upper row of traces, was admitted into the helix. The narrow band of transverse energies at

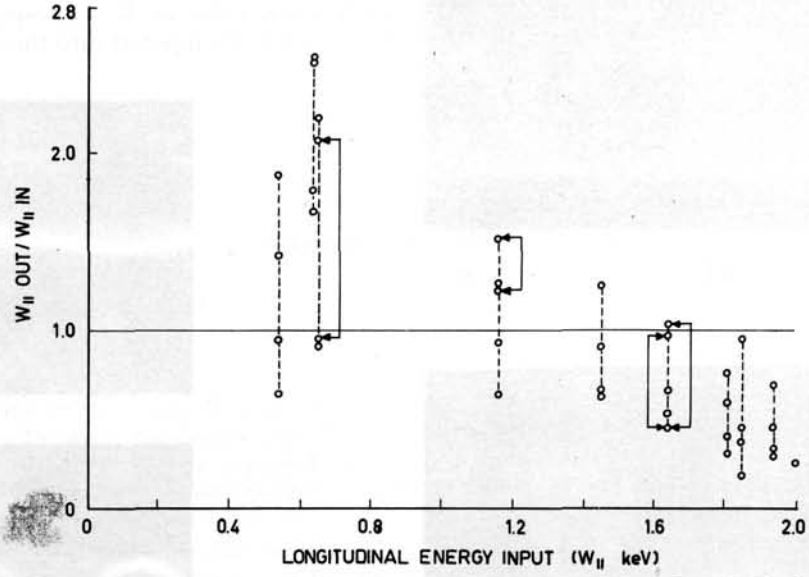

Fig. 9 Experimental ratio of output to input longitudinal energy vs input longitudinal energy with phase as a parameter.

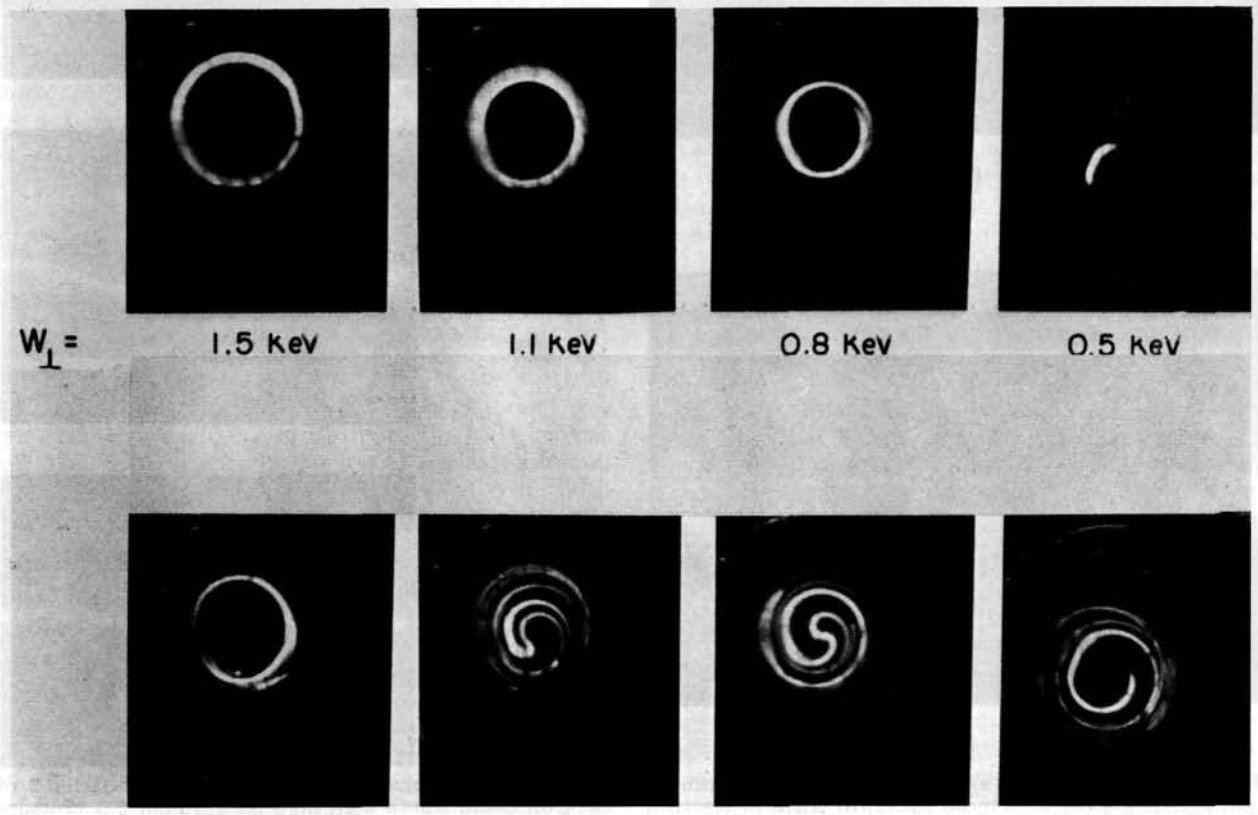

Fig. 10 Photographs of scintillator traces made by the electron beam. The top row shows the intersection of the beam with the scintillator at the output of the first helix. The computed transverse energy is indicated below each photograph. The bottom row shows the corresponding traces obtained at the output of the second helix.

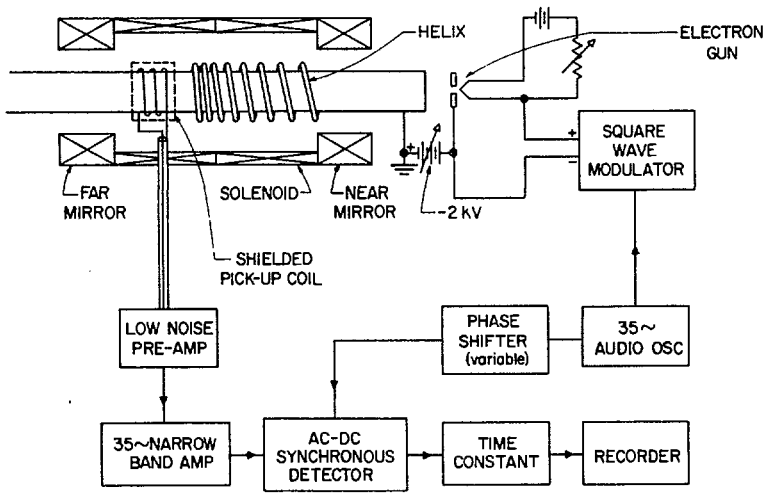

Fig. 11 Schematic of apparatus used in the diamagnetic measurements.

the entrance to the second helix obtained by varying the current in the first helix is indicated by the well-defined circle or arc in each case. It is apparent from the distorted multi-turn spiral traces that there is a wide spread in transverse energies generated in the second helix. Measurements made on these multi-turn spirals indicate Larmor radii both larger and smaller than the Larmor radius at the input. This demonstrates that the transverse energy may be either decreased or increased on successive traversals through the system, i.e., the inverse process mentioned earlier does take place.

3.4. Measurements of containment times

The containment times for 2-keV electrons trapped by the resonant helix were determined by two methods: (1) a measurement of the diamagnetic effect produced by the electron beam, and (2) the leakage rate of electrons out the far mirror when the electron beam is turned off.

3.4.1. Diamagnetic effect

The reduction in axial magnetic field due to the diamagnetism of the injected electron beam was measured. Sufficient sensitivity with a reasonable signal-to-noise ratio was achieved by modulating the injected beam and using a narrow bandwidth phase-sensitive detector connected to a multi-turn pickup coil. The experimental apparatus shown in Fig. 11 operated as follows: The 2-keV, 1-mA electron beam was modulated by an auxiliary gun electrode connected to a 35-cycle/s square wave generator which turned the beam off completely during half of the modulation period. A 3000-turn, 11-cm i.d. electrostatically shielded pickup coil was placed coaxially around the glass tube and centered between the end of the helix and the far magnetic mirror. Signals picked up by the coil were first fed to a low-noise preamplifier and then to a 35 cycle/s amplifier with a 1 cycle/s bandwidth. The amplified signal was then demodulated by a ≈ 35 cycle/s ac-dc chopper,* averaged by a 20-s time constant RC integrator, and then displayed on a recorder. The detector was calibrated in the main axial magnetic field which was driven at 35 cycle/s by an audio oscillator for this purpose. Its sensitivity was measured to be 2.8×10^{-6} G over the area of the pickup coil with a signal-to-noise ratio of 2.

A typical set of measurements was made as follows: With both mirrors and helix off and the main field on, the modulated electron beam was turned on, and the residual diamagnetism associated with the slight amount of transverse energy of the electron beam was measured. Typically, this signal had a signal-to-noise ratio of 5 to 10. The helix current was then turned on and increased in steps. The resulting "single pass" signal shown in Fig. 12 measured the diamagnetism due to a single traversal through the pickup coil. It exhibited a maximum in the neighborhood of 150-A helix current with a half width of 15 A. Operation of the far mirror with the helix adjusted for resonance caused the electrons to reflect back through the pickup coil, and increased the signal by a factor of 2, as expected. Subsequent operation at resonance with both mirrors on gave diamagnetic signals from 8 to 10 times the single pass signal (Fig. 12). The variation of diamagnetic signal with mirror current is shown in Fig. 13.

The diamagnetic signal due to the single pass is proportional to the magnetic flux, Φ, introduced by the hollow electron beam leaving the helix, where

$$\Phi = \frac{4\pi^2 I}{10\omega_B} \frac{v_t^2}{v_z}.$$

This shows that due to the redistribution of energy between the transverse and longitudinal directions on repeated traversals, the number of traversals is not simply given by the number of single pass signals

* This modulation frequency was chosen only because a phase-sensitive detector was available at this frequency.

but is probably larger. Measurements were made with beam currents varying from 0.05 to 1.0 mA, and the number of apparent passes through the pickup coil was nearly constant in this current range.

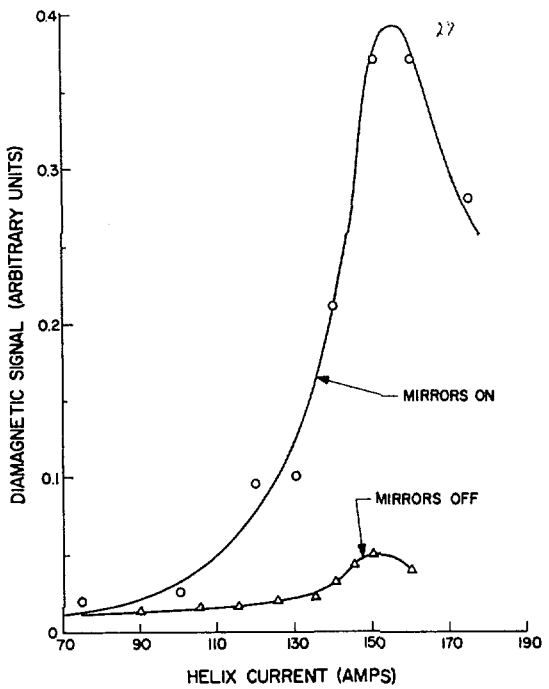

Fig. 12 Amplitude of the diamagnetic signal vs helix current. Two cases are shown, mirror ratios 1 and 6.

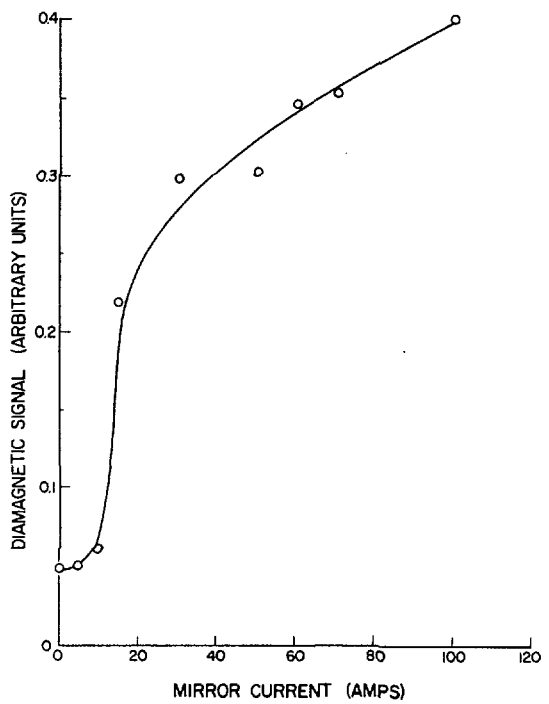

Fig. 13 Amplitude of diamagnetic signal vs mirror current obtained with Helix 1. The mirror ratio varies from 1 to 6 over the range of mirror currents shown.

3.4.2. Electron leakage rate

Measurements of the dc current collected by the Faraday cup showed that the steady state electron loss out of the far mirror was independent of the mirror and helix magnetic field and equal to the current emitted by the gun. This established that within the accuracy of measurement, all the electrons were lost

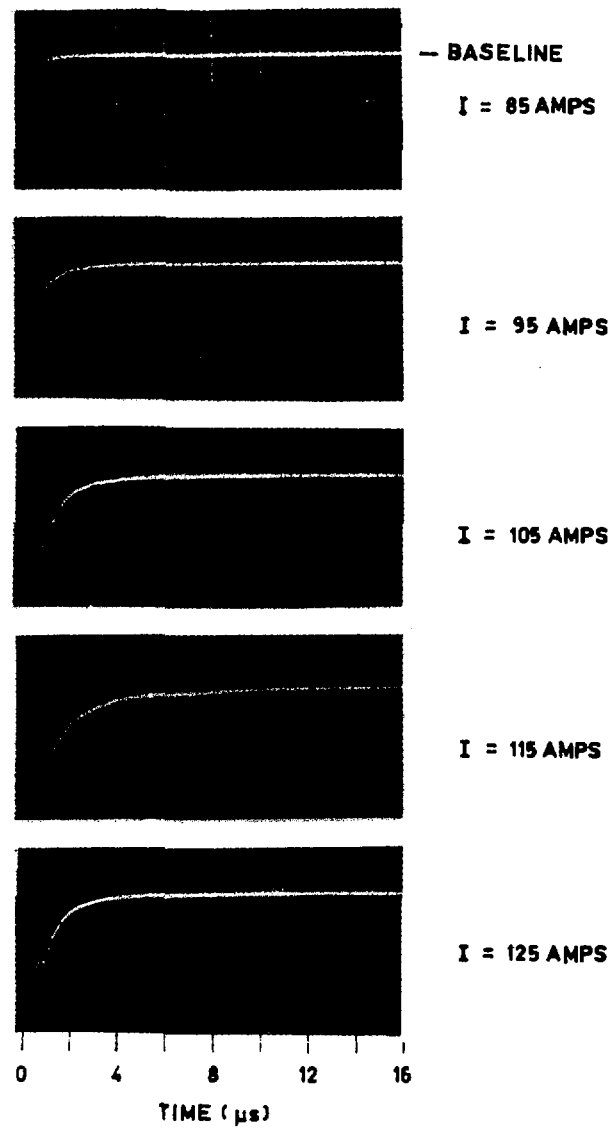

Fig. 14 Leakage current through magnetic mirror vs time after electron gun is cut off at $t = 0$, with helix current as a parameter (Helix 2). Decay period is a maximum at the resonance helix current of 115 A.

out of the far mirror due to the "inverse process," and that radial drifts to the walls and other losses were relatively insignificant. Energy analysis of the escaping electrons using a double grid assembly in front of the collector showed that only energetic electrons were being detected, and that charged particles produced in ionization of the residual gas were unimportant.

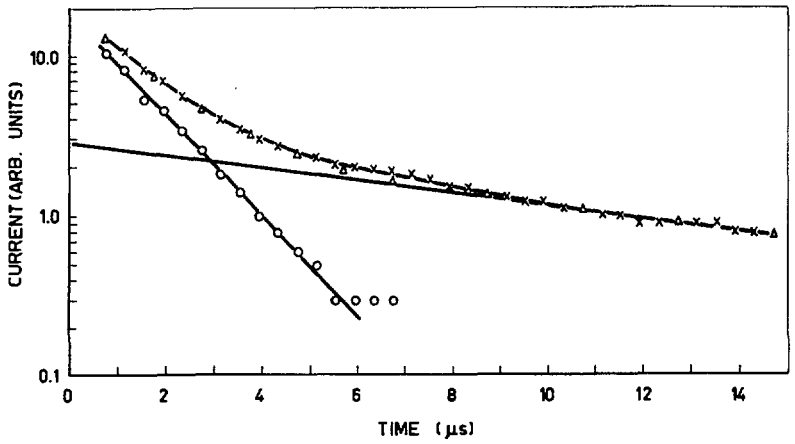

Fig. 15 Decay of the leakage current vs time through the magnetic mirror. The short period exponential (indicated by circles) is the difference between the experimental data and the extrapolated long period exponential. Triangular points show the agreement between the sum of the two exponentials and the experimental data.

Confinement times of electrons trapped in the system at resonance were determined by pulsing the electron beam off and measuring the decay time of the current to the collector. The intrinsic decay time of the gun and collector circuits was 0.2 μs. Measurements were made with both the Helix 1 and the Helix 2.

Fig. 14 shows photographs of oscilloscope traces of collector current versus time for various currents in Helix 2. The start of these traces is coincident with the time at which the beam is turned off. The figures show that charge continued to flow to the collector after the beam was turned off, indicating that confinement does occur for some time. The decay of the current tail was sensitive to helix current, axial magnetic field, and energy of injected electrons. From Fig. 14 it is seen that, as the resonance condition (helix current = 115 A) is approached, the current remains constant at the equilibrium level for the first 0.5 μs after the electron beam is turned off. For this period of time, equivalent to the three transit periods through the helix, the system behaves ideally and all particles are trapped. After this delay the confined electrons leak out of the mirror system with a lifetime apparently determined by the inverse process. The current decay at resonance can be fitted by the two exponential decay curves, as shown in Fig. 15. A summary of the data for the two helices is given in Table I. In this table the ratio of the initial currents associated with the long and short lifetime decay curves was determined from the intercepts of the two exponentials extrapolated back to that time ($t = 0.5$ μs) at which the currents begin to decrease. Also, the average number of traversals between the magnetic mirrors, spaced 150 cm apart, was calculated by assuming an average longitudinal velocity of 10^9 cm/s and adding three traversals. The ratios of the lifetimes for the helices are approximately equal to the ratio of their lengths. Although the analysis of the current tail indicates two lifetimes, two separate loss mechanisms have not been established.

TABLE I. Confinement results for Helix 1 and Helix 2.

	Helix 1	Helix 2
1) Short period	0.6 μs	1.4 μs
2) Long period	3.8 μs	11 μs
3) Fraction of initial decay current in long period	0.3	0.2
4) Average number of traversals between mirrors for		
Short period	7	12
Long period	28	78

4. Orbit computations

Numerical calculations of particle trajectories have been performed on an IBM-704 digital computer for magnetic fields which satisfy the Eqs. (11) and (12) and approximate those used in the electron experiment. If it is assumed that the magnitude of δB_t varied as

$$|\delta B_t| = \delta B_{t0} \cos \frac{\pi z}{2h},$$

where h is the length at which all the energy would be converted into the transverse direction, then there exists a specific relationship between δB_{t0} and h implied by Eq. (11). This permits analytic integration of Eq. (12). For $z = h$, $\sin\theta = 1$ and Eq. (11) becomes

$$\frac{e}{mcv_0}\int_0^h \delta B_t \, dz = 1, \quad h = \frac{\pi mcv_0}{2e\,\delta B_{t0}}$$

or

$$|\delta B_t| = \delta B_{t0} \cos\left(\frac{e\,\delta B_{t0}\, z}{mcv_0}\right).$$

Successive integrations of Eq. (12) yield

$$\frac{d\psi}{dz} = \frac{-eB_z}{mcv_0 \cos\left(\frac{e\delta B_{t0} z}{mcv_0}\right)}$$

and

$$\psi(z) = -\frac{B_z}{\delta B_{t0}} \log \tan\left(\frac{\pi}{4} + \frac{e\delta B_{t0} z}{2mcv_0}\right).$$

These equations give the magnitude and direction of the perturbing field used for trajectory studies.

Computations were carried out for two different field configurations. For these cases the energy was 2 keV, $B_z = 100$ G, $\delta B_{t0} = 2.5$ and 0.5 G. To approximate the experimental conditions the perturbing fields were cut off at 60 and 300 cm respectively, where approximately three-fourths of the initial longitudinal energy was expected to be transferred into the transverse direction. In both fields a 2-keV electron injected axially into the system monotonically transferred its energy into the transverse direction, following the expected behavior. The non-reciprocity of the field configuration was also demonstrated by reversing the sign of v_z after a resonance traversal and following the particle trajectory back to the entrance. In this case v_z changed less than 1% over the length of the helical field, in agreement with the experimental observations.

The occurrence of the inverse process on a forward traversal was investigated using the field configuration with δB_{t0} of 2.5 G and 60 cm length. In this case the trajectories of 2-keV electrons with initial axial velocities corresponding to 0.25, 0.50, 0.75, 1.00, 1.25, 1.50, and 1.75 keV were followed during transit through the helical field. The phase angles subtended by v_t and δB_t were taken to be 0°, 90°, 180°, and 270° at $z=0$. The ratio of the axial energy of the electrons at the exit to that at the entrance of the helix is plotted in Fig. 16 for these four phases versus axial energy at entrance. Comparison of these results with the experimental data given in Fig. 9 shows good agreement.

To gain further understanding of the resonant and non-resonant portions of the orbit and the inverse process, computations were made using the 0.5-G perturbing field. In stronger perturbing fields the resonant and non-resonant portions of the orbit cannot be clearly separated. Results for various initial conditions are shown in Fig. 17. In this figure the axial component of velocity v_z is plotted versus the axial distance along the perturbing field. The top curve corresponds to axial injection of electrons into the field and shows the axial velocity monotonically decreasing throughout the length of the helix. The other curves correspond to four different phases, 90° apart, for particles injected into the helical field with $v_{z0} = 1.87 \times 10^9$ cm/s, i.e., with 50% of their total energy in the transverse direction. The amplitude of the axial velocity oscillates as the perturbing field and the transverse particle velocity come in and out of phase. In some region of the system the axial period of the particle's motion and that of the rotating transverse magnetic field nearly coincide. In this region there is a resonant interchange of energy and the axial velocity may undergo a step, Δv_z. Amplitude of the non-resonant oscillations and the resonant step as a function of helix parameters have also been studied. In the case of the nonresonant oscillations their amplitude varies inversely as the length of the helix, if δB_{t0} is adjusted to maintain resonance. The average of the magnitude of the step due to resonance interaction varies as the inverse square root of h. This result can be demonstrated qualitatively as follows. If the magnitude of the step as a result of resonant interaction is Δv_z, then the time required for the interaction is

$$\tau = \frac{L}{\Delta v_z}$$

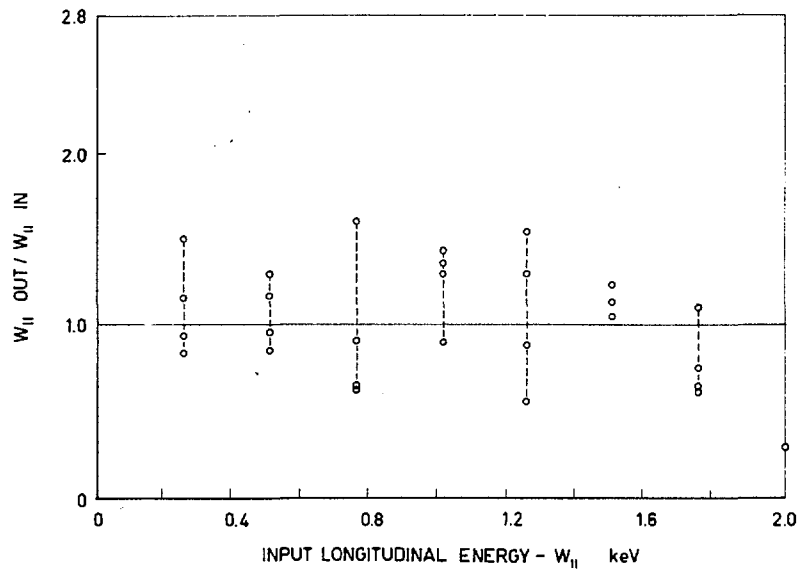

Fig. 16 Computed ratio of output to input longitudinal energy vs input longitudinal energy with phase as a parameter.

where L is the local period of the perturbing field. The step Δv_z is also given by the impulse due to the perturbing force δF, where

$$\delta F \tau \propto \frac{e}{c} v_z \delta B_t \tau \propto \Delta v_z .$$

When these relations are combined and δB_t is taken inversely proportional to h we find

$$\Delta v_z \propto \sqrt{\delta B_t} \propto 1/\sqrt{h}. \qquad (14)$$

If it is assumed that divergence of the beam and reflections from magnetic mirrors introduce sufficient spread in phase to justify the use of random walk approximation, then the number of reflections before loss as a function of length can be estimated. According to this approximation, the number of reflections before loss for a given mirror ratio is inversely proportional to the average mean square step size and, following Eq. (14), is proportional to the length. This dependence is supported by our experimental work. (See Table I.)

In an attempt to simulate a random distribution of phases, a calculation was made for 24 equally spaced initial phases. Fig. 18 shows the resulting v_z at the exit of the 300-cm helical field for $v_{z0}=1.87 \times 10^9$ cm/s. Several conclusions may be drawn from this curve. One of its striking features is the three sharp minima corresponding to those phases at which the particle returns into synchronism with the perturbing field and exits at the velocity corresponding to optimum transfer. The sharpness of these minima explains the large phase spreading observed in some of the photographs shown in Fig. 10. Also, the areas under this curve above and below the v_{z0} lines are approximately equal, indicating that the average change in axial velocity for a large number of particles distributed randomly in phase is zero. But it appears

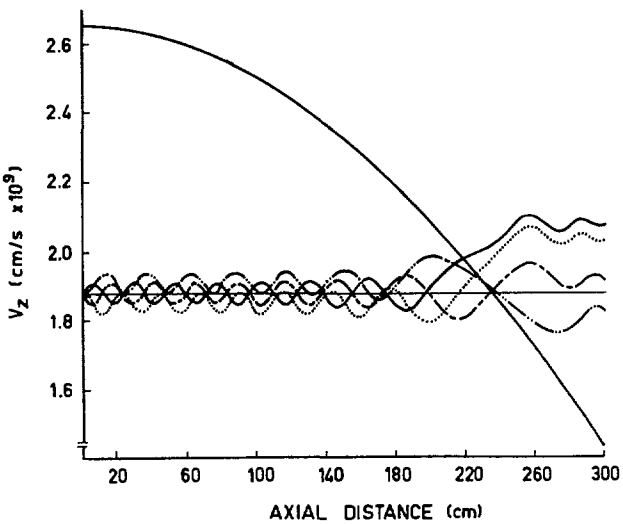

Fig. 17 Computed axial velocities vs axial distance for particles injected into 300 cm helical field. The top curve corresponds to a 2 keV electron injected axially. The four lower curves correspond to 2 keV electrons injected with an axial energy of 1 keV and four phases chosen 90° apart.

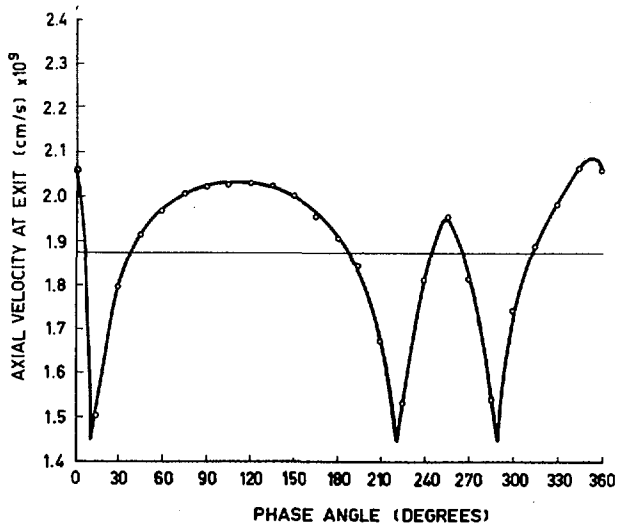

Fig. 18 Axial velocity of 2 keV electrons at exit of 300 cm helical field vs input phase. The axial velocity of electrons at entrance, indicated by horizontal line, was 1.87×10^9 cm/s.

from these results (Fig. 18) that, although the average axial velocity remains constant, a particle entering the helix has a higher probability of being stepped to higher than to lower v_z.

To simulate injection of H_2^+ ions which are subsequently dissociated [9], we have also investigated the orbits of particles with one-half the mass necessary for resonance. In the case when the perturbing field is cut off after 75% of the initial energy of the injected particle is transferred into the transverse direction, it is found that no resonance step exists. Then the non-resonant behavior dominates the interaction and the number of traversals between the mirrors should then vary as the length of the perturbing region squared.

5. Discussion

The experiments show that the resonant helix is highly successful in transferring energy from the longitudinal to the transverse direction and permits trapping of all axially injected particles in magnetic mirror geometries on the first pass. However, we have also shown that on subsequent traversals through the perturbing field the inverse process occurs and all particles eventually escape. In spite of this loss, if the behavior of these fields may be extrapolated to the injection of ions, this device has certain properties that make it attractive for the study of the accumulation of low β plasmas. These include (1) high efficiency for trapping, (2) ease of injection, and (3) a reduction in gas load within the confinement region over molecular dissociation schemes.

To estimate the maximum achievable density in an ideal magnetic bottle for a given injection rate we can make use of phase space arguments borrowed from accelerator theory.* Consider the steady state

* We are indebted to R. L. Garwin for this observation.

of such a magnetic bottle being supplied by an injector which also provides the only avenue of escape, due to the inverse of the injection process. The injector mechanism is characterized by a range of initial conditions of the particles at its input which are transformed into a distribution in velocities at the output for which confinement is possible (i.e., for mirror machines, the region outside the escape cone). This range of input conditions defines an acceptance volume or "bucket" in phase space. As the particles with these initial conditions enter the injector, this bucket moves into the phase space of the bottle. We shall assume that after injection sufficient randomization is present to redistribute the particles uniformly throughout the available phase space. Liouville's theorem requires that phase space in the bottle behave like an incompressible fluid. This means that the entrance of the bucket displaces an equal volume out of the phase space of the system and for a steady state the density in the bottle must equal the density in the bucket. Then

$$\frac{\mathrm{d}\varphi}{\mathrm{d}t} = \frac{\Phi}{\tau}$$

where the rate at which phase space volume is moved into the bottle by the injector is $\mathrm{d}\varphi/\mathrm{d}t$, Φ is the total available phase space in the bottle, and τ is the mean lifetime of all parts of phase space in the bottle. The lifetime τ becomes a maximum when $\mathrm{d}\varphi/\mathrm{d}t$ is a minimum for a given Φ. The maximum density will occur for a given source current when (a) the beam from the source has maximum density in phase space, i.e., minimum spread in energy and angle, and (b) the injector is made so sharply resonant that its acceptance volume in phase space matches that of the input beam.

It is clear, however, that the behavior of this helix must be reconsidered when plasma effects become important.

Acknowledgments

We wish to thank R. C. Wingerson for showing us his early results and discussing the problem with us. We wish to thank H. Hoyt and R. Gilmer, who made the orbit calculation. We gratefully acknowledge the aid given us by T. Putnam; and R. Dike, R. Holm, N. Salazar, A. Schofield, and F. Wittman were indispensable in setting up and operating the equipment.

The work reported was performed under the auspices of the U.S. Atomic Energy Commission.

References

[1] "The ORNL Thermonuclear Program," U.S. Atomic Energy Commission report ORNL-2457 (1958).
[2] ARTSIMOVICH, L. A., Proceedings of Second U.N. International Conference on Peaceful Uses of Atomic Energy, Geneva **31** (1958) 3.
[3] POST, R. F., Proceedings of Second International U.N. Conference on Peaceful Uses of Atomic Energy, Geneva **32** (1958) 245.
[4] GIBSON, G., LAMB, W. A. S., LAUER, E. J., Proceedings of Second U.N. International Conference on Peaceful Uses of Atomic Energy, Geneva **32** (1958) 275.
[5] MARSHALL, J., STRATTON, T. F., I.A.E.A. Conference on Plasma Physics and Controlled Nuclear Fusion Research, Salzburg: see next volume of these Proceedings.
[6] FEDORCHENKO, V. D., RUTKEVICH, B. N., CHERNI, B. M., *Zhur. Tek. Fiz.* **29** (1959) 1212.
[7] SINEL'NIKOV, K. D., RUTKEVICH, B. N., FEDORCHENKO, V. D., *Zhur. Tek.Fiz.* **30** (1960)249.
[8] SINEL'NIKOV, K. D., FEDORCHENKO, V. D., RUTKEVICH, B. N., CHERNY, B. M., SAFRONOV, B. G., *Zhur. Tek. Fiz.* **30** (1960) 256.
[9] LAING, E. W., ROBSON, A. E., *J. Nuclear Energy, Part C* **3** (1961) 146.
[10] WINGERSON, R. C., private communication, January, 1961; *Phys. Rev. Letters* **6** (1961) 446.
[11] SMYTHE, W. R., Static and Dynamic Electricity, 2nd ed. (MacGraw-Hill Book Co., 1950) 276.

ПОЛУЧЕНИЕ ЧИСТОЙ ВЫСОКОТЕМПЕРАТУРНОЙ ПЛАЗМЫ В КВАЗИСТАЦИОНАРНЫХ СИСТЕМАХ. ПРОЦЕССЫ, ПРИВОДЯЩИЕ К ПОСТУПЛЕНИЮ ПРИМЕСЕЙ В ПЛАЗМУ*

В. А. СИМОНОВ, Б. Н. ШВИЛКИН, Г. П. КУТУКОВ

АКАДЕМИЯ НАУК СССР, МОСКВА,

СОЮЗ СОВЕТСКИХ СОЦИАЛИСТИЧЕСКИХ РЕСПУБЛИК

Одна из трудностей в получении высокотемпературной плазмы в квазистационарных установках с самосжимающимися разрядами связана с поступлением примесей, приводящих к большим потерям энергии из плазмы. В докладе приводятся результаты исследования процессов взаимодействия плазмы со стенками, приводящих к поступлению примесей в плазму, и процессов газообмена между плазмой и стенками.

Исследование проводилось на тороидальных установках со стабилизацией сильным магнитным полем и на установках с прямым разрядом и тэта-пинчем. В исследовании использовалась специально разработанная импульсная масс-спектрометрическая аппаратура, а также обычная спектральная и микроволновая методика. Вакуумтехническая подготовка установок включала режимы, рассматриваемые в настоящее время как оптимальные.

С помощью изотопного метода исследован газообмен плазмы разряда в водороде и других газах со стенками. Определены количества газа, участвующие в обмене в течение каждого импульса; исследованы процессы сорбционного активирования стенок, осуществляющегося при разрядах, и процессы связывания газа на стенках (pump-out).

Выяснено, что для установок, прошедших аккуратную вакуумтехническую подготовку, поступление многоэлектронных примесей в водородную плазму происходит преимущественно за счет двух процессов: а) каталитические химические реакции на стенках, приводимых разрядом в сорбционно-активное состояние; б) микроразряды («униполярные дуги»), возникающие на участках стенок или диафрагм, соприкасающихся с плазмой, и имеющих отрицательный потенциал относительно плазмы. Исследованы основные каталитические реакции на стенках, состав и количество примесей, поступающих за их счет в плазму, зависимость от свойств материала стенок, режимов вакуумтехнической подготовки, режимов тренировки и разряда. Установлен механизм возникновения микроразрядов, зависимость от свойств материала стенок (от наличия диэлектрических включений и пленок); состав и скорость поступления примесей из катодных пятен микроразрядов; закономерности распространения поперек магнитного поля плазмы, несущей ионы примесей.

Поступление примесей в плазму существенно зависит от интенсивности ее взаимодействия со стенками (от степени неустойчивости). При одной и той же степени неустойчивости плазмы, повышение чистоты может быть достигнуто путем рационального выбора материалов стенок, конструкции и технологии подготовки разрядной камеры (локализации мест интенсивного взаимодействия плазмы со стенками; применение для участков стенок и диафрагм, на которые выходят ионы из плазмы, чистометаллических материалов, без поверхностных диэлектрических слоев и включений; применение для стенок материалов, не сорбирующих водород в атомарном и ионизованном состоянии; материалов с пониженным содержанием углерода и кислорода; в применении режимов вакуумтехнической подготовки и откачных средств, не приводящих к образованию на стенках слоев поверхностных загрязнений).

1. Введение

Одна из трудностей в получении высокотемпературной плазмы в квазистационарных установках с самосжимающимися разрядами связана с поступлением примесей, приводящих к большим потерям энергии из плазмы [1, 2]. Поступление примесей со стенок в определенной степени связано с неустойчивостями плазмы, усиливающими воздействие на стенки. Улучшение удержания плазмы будет одновременно способствовать и уменьшению примесей. С другой стороны, понижение примесей возможно путем рационального выбора материалов стенок, конструкции разрядной камеры, технологии вакуумной подготовки. Уменьшение примесей может позволить поднять температуру плазмы при той же степени ее неустойчивости, и быть может, способствовать улучшению удержания, за счет ослабления влияния неустойчивостей, специфических для начальных стадий нагрева плазмы.

За последние годы на ряде экспериментальных установок проведены технологические мероприятия, улучшившие вакуумные условия проведения опытов: использование металлических камер без изолирующих разрезов или с минимальным числом разрезов; прогрев стенок до температуры 400—500° С; начальная откачка до сверхвысокого вакуума; аккуратная очистка впускаемого газа; работа на протоке; длительная тренировка разрядами. Принятые меры привели к снижению примесей на один-два порядка величины, и к повы-

* Доклад CN-10/254 представленный на Конференцию. Докладчик: В. А. Симонов. Дискуссия (на английском языке) по этому докладу дана на стр. 358. Переводы аннотаций находятся в конце этого тома Трудов Конференции.

шению температуры плазмы, по сравнению с тем, что имеет место в установках без тщательной вакуумтехнической подготовки [3, 4]. Однако поступление примесей при этом не устраняется, и остается все еще много большим допустимого уровня [2].

По мере улучшения вакуумных условий и снижения общего уровня примесей, получает значение все большее число различных процессов взаимодействия плазмы со стенками, приводящих к поступлению примесей. Процессы, характерные для установок, не прошедших аккуратной вакуумтехнической подготовки — загрязнение рабочего газа остаточными газами, выделение при разряде сорбированных газов, испарение термически-нестойких (неметаллических) материалов, дуговые разряды на краях разрезов, перестают играть определяющую роль в загрязнении плазмы. Определяющими становятся такие процессы, как химические реакции на стенках, микроразряды. Можно ожидать, что по мере дальнейшего повышения температуры и плотности плазмы, длительности удержания, будут приобретать значимость и другие механизмы воздействия плазмы на стенки, такие, как фотодесорбция, катодное распыление. Специфические трудности в сохранении чистоты плазмы возникнут в случае больших энерговыделений на стенках. На каждом этапе работы, для повышения чистоты плазмы необходимо выяснение относительной роли различных процессов взаимодействия плазмы со стенками, приводящих к поступлению примесей в конкретных условиях определенного класса установок, и разработка технологических приемов, способствующих снижению интенсивности соответствующих процессов. В ряде случаев, для нахождения эффективных мер борьбы с загрязнениями плазмы, требуется детальное изучение механизма взаимодействия.

В докладе приводятся результаты исследования процессов взаимодействия со стенками плазмы квазистационарного разряда большой длительности, в установках, в которых предусмотрены упомянутые вакуумтехнологические меры предварительной очистки. Исследование проводилось на тороидальных установках типа Токамак (самосжимающийся разряд со стабилизацией сильным магнитным полем), в режимах, для которых удовлетворяется критерий гидромагнитной устойчивости плазмы. Стенки разрядной камеры в установках выполнены в виде сплошного тонкостенного лайнера из нержавеющей стали. Подробное описание установок, режимов вакуумной подготовки, характеристики плазмы приведены в работах [4, 5, 6]. Для более детального изучения отдельных процессов взаимодействия плазмы со стенками, в связи с малой доступностью тороидальных установок для размещения некоторых диагностических приборов, использовались модельные установки, с линейным разрядом и с тэта-пинчем. Материалы разрядных камер, режимы вакуумтехнологической подготовки, длительности разряда во всех установках аналогичны. Сопоставление экспериментальных данных показало, что при этих условиях состав примесей и пути их поступления в плазму в полномасштабных тороидальных установках и в модельных установках близки между собой.

Изучение процессов взаимодействия плазмы со стенками проводилось в работе путем компонентного анализа плазмы в течение разряда, и путем анализа нейтрального газа в разрядной камере в моменты времени перед разрядом и непосредственно по его окончании. Основная диагностическая аппаратура, использованная в работе — специального разработанные быстродействующие масс-спектрометры, с анализом по времени пролета и изображением спектра масс на экране осциллографа (конструктивные разновидности масс-спектрометра хронотрон). Масс-спектрометрический анализ заряженных компонент плазмы (потоков ионов, выходящих из плазмы на стенки) сопоставлялся со спектральным анализом излучения плазмы, и синхронно проводимой скоростной съемкой плазмы с помощью электронно-оптических преобразователей.

Экспериментальные данные, полученные в работе, показывают, что в установках с металлическими разрядными камерами, выполненными из обычных технических материалов и прошедшими аккуратную вакуумтехническую подготовку и тренировку, поступление примесей со стенок связано преимущественно с двумя процессами: а) каталитические химические реакции на стенках, приводимых разрядом в сорбционно-активное состояние; б) микроразряды («униполярные дуги»), возникающие на участках стенок или диафрагм, соприкасающихся с плазмой, и имеющих отрицательный потенциал относительно плазмы. Протекание каталитических реакций на стенках с выделением в объем многоэлектронных примесей тесно связано с сорбционным связыванием рабочего газа (водорода) на стенках и газообменом между плазмой и стенками во время разряда.

2. Поглощение рабочего газа и каталитические реакции на стенках при импульсных разрядах большой длительности

Неустойчивости плазмы, существующие в квазистационарных системах с импульсными разрядами большой длительности, приводят к тому, что среднее время жизни ионов в плазме, как правило, в несколько раз меньше полной длительности разряда. Так, по данным работы [7], для плазмы в стеллараторе В-3, получаемой путем омического нагрева, среднее время жизни ионов составляет 0,1 мсек, при длительности разряда около 0,5 мсек. Аналогичное соотношение между временем жизни ионов и длительностью разряда имеет место в установках, на которых проводилась настоящая работа. В течение длительности разряда, все ионы рабочего газа совершают в среднем по нескольку циклов ухода на стенку, нейтрализации, возврата нейтрального атома или моле-

кулы в плазму, ионизации. При работе на водороде, в начальной стадии разряда, до завершения полной ионизации, на стенки поступает также нейтральный газ в атомарном состоянии. Поступление ионов рабочего газа на стенки и нейтрализация сопровождаются рядом вторичных процессов, зависящих от химической природы газа, от материала и состояния поверхности стенки, распределения по поверхности стенок участков выхода ионов и временной зависимости тока на стенки. Для разрядных камер, не подвергнутых предварительной очистке и тренировке, стенки которых на участках выхода ионов содержат большие количества сорбированных газов, вторичные процессы идут преимущественно в направлении выделения газов со стенок и повышения давления газа в объеме. Для прогретых и оттренированных камер преобладают процессы связывания газа, в результате которых в ходе разряда происходит уменьшение количества газа, находящегося в объеме, и соответственно снижение плотности плазмы (pump-out). Давление газа после импульса, по сравнению с начальным, снижается. Регистрация плотности полностью ионизованной плазмы, снижающейся в течение импульса из-за связывания газа на стенках, в определенных условиях может быть использована для измерения или оценки времени жизни

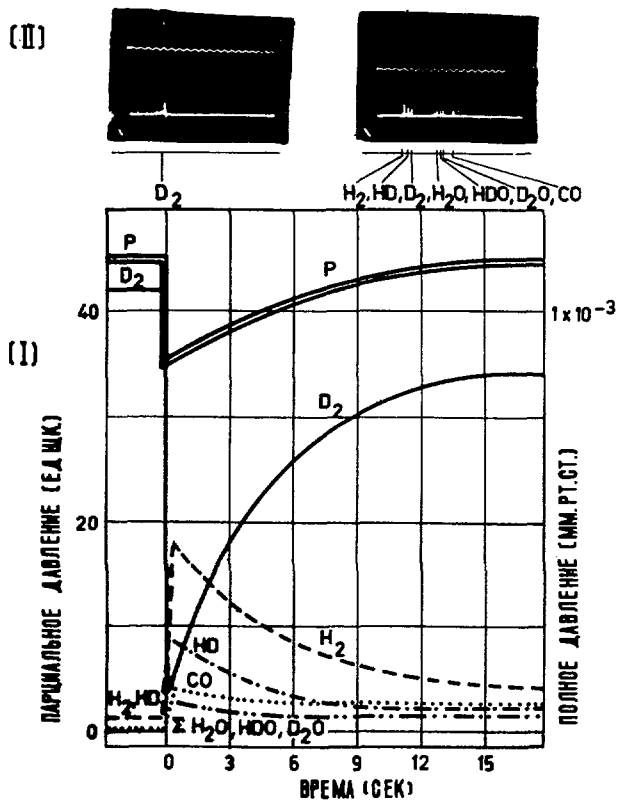

Рис. 1 а Поглощение рабочего газа; десорбция газа со стенок; поступление примесей к газу при разрядах в водороде (изотопный метод исследования). Разряд в дейтерии, после разрядов в водороде. I — графики изменения парциальных давлений при импульсе и в промежутке между импульсами; II — масс-спектрограммы состава газа.

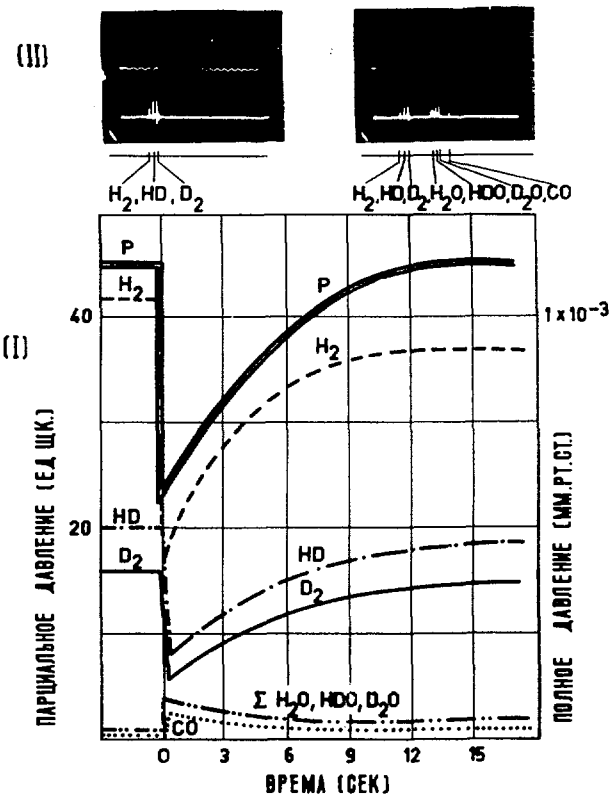

Рис. 1 б Поглощение рабочего газа; десорбция газа со стенок; поступление примесей к газу при разрядах в водороде (изотопный метод исследования). Разряд в смеси водорода и дейтерия. I — графики изменения парциальных давлений при импульсе и в промежутке между импульсами; II — масс-спектрограммы состава газа.

ионов в плазме [7]. Механизм связывания ионов на стенках может быть различным для ионов разной природы и энергии (хемосорбция медленных ионов, внедрение ионов средних энергий).

Исследование газообмена плазмы со стенками на установках Токамак и на модельных установках проводилось путем масс-спектрометрического анализа газа в разрядной камере — до импульса, в моменты времени, следующие за импульсами с интервалом 0,05 сек; и в промежутках между импульсами. В качестве рабочих газов использовались водород, гелий, аргон, кислород и смеси газов. Для изучения взаимодействия водородной плазмы со стенками применялся изотопный метод, с попеременной работой на водороде и дейтерии. На рисунках 1—4 приведены образцы масс-спектрограмм состава газа в камере, и графики парциальных давлений рабочего газа и образующихся при разрядах примесей, для разных моментов времени, при задании одиночных разрядов или серий импульсов (с работой на непрерывном протоке газа и постоянной откачкой). Все приводимые экспериментальные данные относятся к стандартному режиму подготовки стенок (прогрев, откачка до сверхвысокого вакуума, тренировка разрядами). Вакуумная откачная аппаратура использовалась двух типов: а) паромасляные насосы с ловушками,

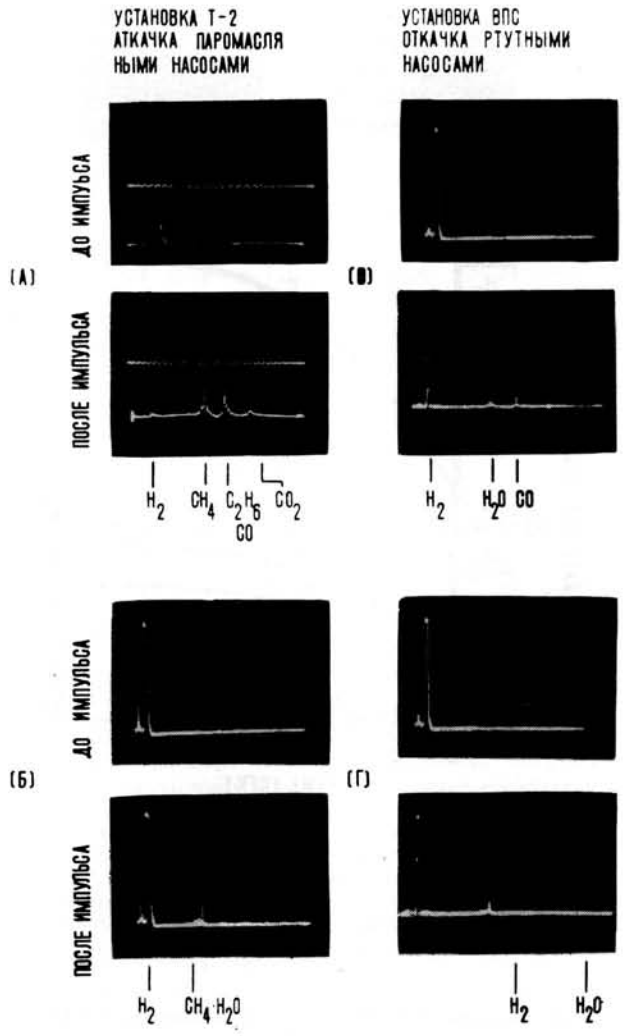

Рис. 2 Поглощение рабочего газа и поступление примесей при различном состоянии стенок разрядной камеры (масс-спектрограммы). а, б — установка с откачкой паромасляными насосами; в, г — установка с безмасляной откачкой; а, в — после тепловой обработки; б, г — после тренировки разрядами.

охлаждаемыми жидким азотом и ротационные масляные насосы; б) паро-ртутные насосы и водоструйные насосы предварительного разрежения. При одинаковом остаточном давлении в системе (ниже $1 \cdot 10^{-9}$ мм рт.ст.), состояние поверхности стенок (и, соответственно, поступление примесей) при использовании откачной аппаратуры двух указанных типов оказывается неодинаковым.

Основные закономерности газообмена плазмы со стенками следующие. При импульсном разряде в водороде и в кислороде происходит интенсивное связывание рабочего газа на стенках (жестчение); давление рабочего газа после импульса снижается в 3—20 раз по сравнению с начальным, в зависимости от режима (рис. 1, 2, 4). При импульсном разряде в гелии и аргоне, связывание рабочего газа на стенках во много раз слабее (рис. 3, 4). Парциальное давление инертных газов до и после разряда практически одинаково. Имеющееся все же слабое связывание инертных газов в разряде обнаруживается при переходе на работу с другим газом, по небольшому выделению инертного газа, поглощенного в предшествующих импульсах. При разряде в смеси инертного газа и химически активных газов (например, в смеси аргона, азота, кислорода), наблюдается поглощение активных газов, и неизменность парциального давления инертного газа (рис. 3в, 4в). Из приведенных данных вытекает, что связывание газа на стенках камеры при разрядах вызывается хемосорбцией ионов и возбужденных атомов, и не связано с внедрением энергичных ионов в толщу материала стенки (поскольку хемосорбция ионизованного водорода и кислорода происходит много эффективнее сорбции ионов инертных газов, внедрение же энергичных ионов инертных газов происходит не менее эффективно, чем ионов водорода, и вне-

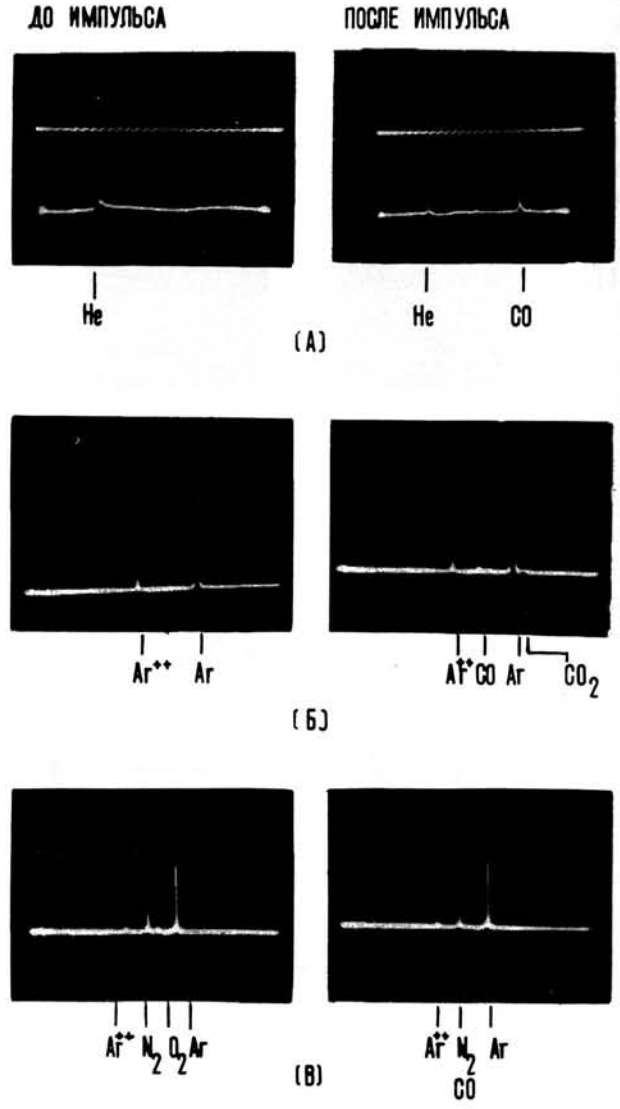

Рис. 3 Поглощение рабочего газа и поступление примесей при разрядах в инертных газах (масс-спектрограммы). (а) He, установка ВПС-1, (б) Ar, установка Т-2, (в) Ar (70%), N (25%), O (5%), установка Т-2.

дренные атомы инертных газов удерживаются прочнее).

Поглощение стенками водорода и кислорода при импульсах происходит не только в результате активации газа в разряде, но и в результате активации стенок. Это вытекает из того факта, что при напуске газа с неизменной скоростью (при постоянной откачке), давление газа в камере, восстанавливающееся после импульсов, в случае повторной подачи импульсов устанавливается на более низком значении, чем перед первым импульсом (рис. 4а, б). Эффективная быстрота откачки газа, впускаемого в установку, в промежутках между импульсами возрастает, за счет сорбции на стенках, активированных при разряде (со скоростью, небольшой по сравнению с сорбцией во время разряда). Активированное состояние стенок сохраняется в течение нескольких десятков секунд после импульса; оно сильнее выражено в случае кислорода, чем водорода. При подаче

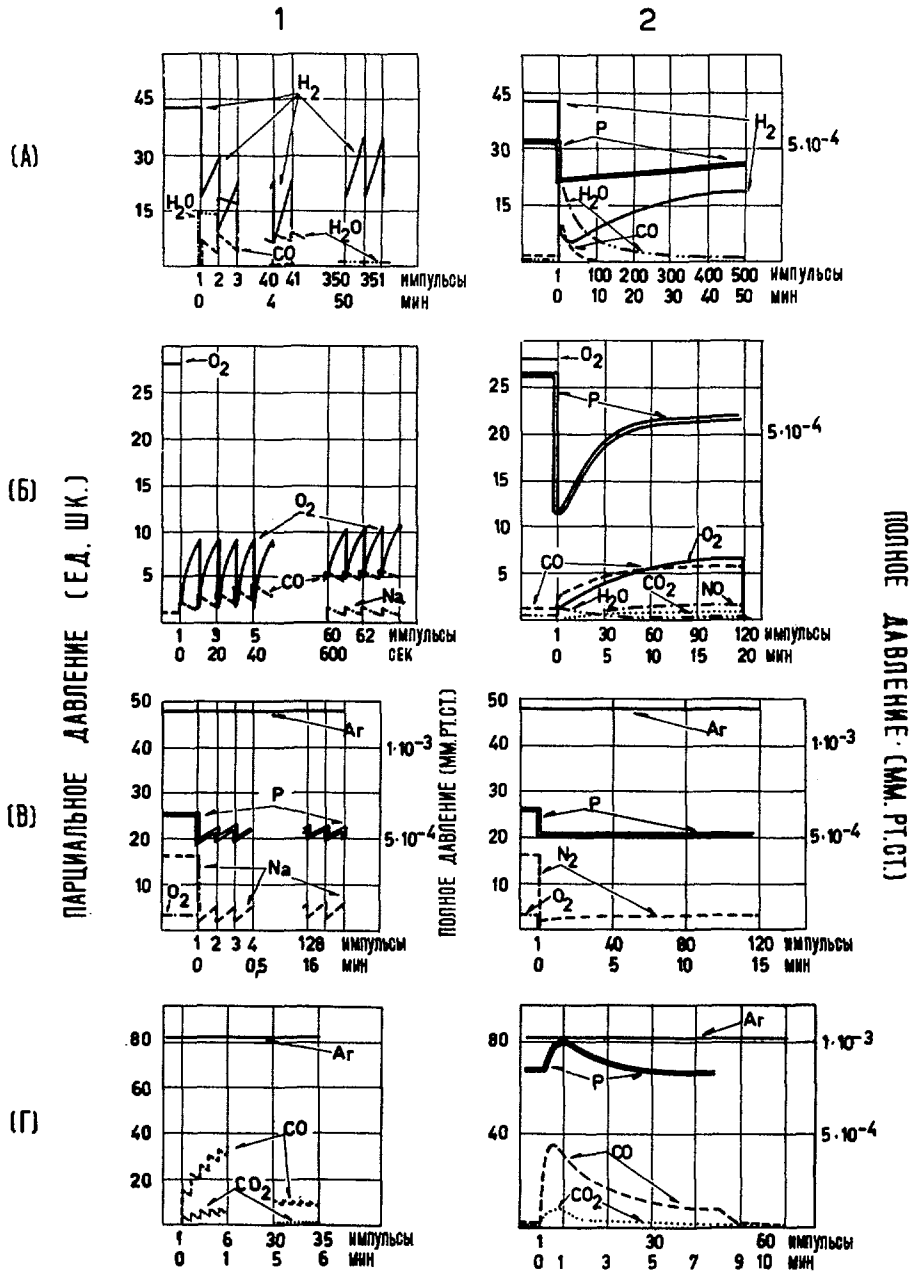

Рис. 4 Изменение парциальных давлений рабочего газа и примесей к газу при сериях разрядов в различных газах на установке Т-2. (а) — водород, (б) — кислород, (в) — смесь аргона с воздухом, (г) — аргон. Ряд 1 — изменение давлений при импульсах и в промежутке между импульсами. Ряд 2 — парциальные давления непосредственно после импульсов (огибающая кривых на графиках ряда 1).

большого числа импульсов, поглощение водорода стенками подчиняется следующим закономерностям. Сильное поглощение при первых импульсах серии, со снижением парциального давления водорода в 5—10 раз, по мере повторения импульсов ослабляется (устанавливается снижение давления в 2—3 раза), и далее сохраняется, без признаков насыщения, в течение большого числа импульсов. В одном из опытов на установке Токамак-2 отсутствие насыщения в поглощении водорода было прослежено в течение 10 тысяч импульсов (в тренировочном режиме). За время опыта стенки камеры поглотили 0,2 грамма водорода. В случае равномерного распределения сорбированного газа по поверхности разрядной камеры, средняя толщина слоя соответствует тысяче мономолекулярных слоев. Поглощение газа в таких количествах, без насыщения, показывает, что связывание газа при импульсных разрядах происходит не на неизменной поверхности стенок, а на возобновляющейся при разрядах, подобно тому, как происходит поглощение газов в сорбционных насосах, с поверхностью, возобновляемой путем периодического испарения металла. Осмотр камеры Токамак-2 показывает, что в ней имеются участки поверхности — края апертурных диафрагм, с которых распыляется металл (за счет микроразрядов, см. ниже). Конденсируясь на прилегающих участках боковых стенок, распыляемый металл может обусловливать значительную долю всего газопоглощения на стенках. Апертурные диафрагмы в камере Т-2 выполнены из того же материала, что и вся остальная камера — из хромоникелевой нержавеющей стали. Компоненты нержавеющей стали — железо, никель, хром, активно взаимодействуют с водородом. Пассивность нержавеющей стали по отношению к молекулярному водороду связана только с наличием защитной окисной пленки, целостность которой нарушается под воздействием плазмы и при испарении металла.

Изучение газообмена с помощью изотопной методики показывает, что он не сводится к поглощению на стенках некоторой доли поступающих атомов или ионов, и к нейтрализации и возвращению в плазму остального газа. При каждом разряде происходит десорбция газа, связанного на стенках при предыдущих импульсах. В опытах с заменой в сериях импульсов водорода на дейтерий и обратно, обнаруживается, что в течение значительного числа импульсов, изотопный состав газа в камере после разряда оказывается отличающимся от изотопного состава до разряда в результате десорбции ранее связанного газа (рис. 1а). На установке Токамак, в течение 30—40 импульсов после замены, в газах, остающихся в камере после разряда, содержание десорбированного газа больше, чем содержание рабочего газа. Это указывает на то, что в обмене со стенками при каждом импульсе участвует количество водорода, превышающее начальное содержание газа в объеме. В связи с упоминавшимся соотношением среднего времени жизни ионов в плазме и длительности разряда, такой результат естественен. Прекращение выделения газа, сорбированного в предшествующей серии импульсов, наблюдается после задания 100—150 разрядов. Отсюда следует, что в газообмене между плазмой и стенками участвует поверхностный слой, содержащий сорбированный газ в количестве, в 50—100 раз превышающем содержание газа в объеме камеры.

Интенсивность десорбции газа со стенок за время импульса на установке Токамак увеличивается, если при задании серии импульсов изменяется режим разряда (в частности, напряженность магнитного поля). Объяснить это можно тем, что в камере с апертурными диафрагмами, с плазмой, гидромагнитно устойчивой, участки интенсивного воздействия плазмы на стенки и участки связывания водорода пространственно разделены и сравнительно жестко локализованы. При изменении режима, воздействию плазмы подвергаются участки, на которых при предшествующих импульсах сорбировался водород. В модельной установке ВПС-2, плазма в которой неустойчива, наблюдаются мгновенные выделения больших количеств водорода, в моменты времени, когда плазма соприкасается с участками стенки, «пропитанными» хемосорбированным водородом. Аналогичные явления описаны для установки «Альфа», на которой наблюдались всплески потоков быстрых нейтральных атомов, образующихся путем перезарядки ионов на нейтральном газе, десорбирующемся со стенки при соприкосновении с нею плазмы [8].

Сорбированный на стенках водород находится в атомарном состоянии. При напуске в установку смеси водорода и дейтерия, происходит быстрый дейтерообмен, с образованием молекул дейтероводорода HD. Какой-либо разницы в поведении водорода и дейтерия в смеси не обнаруживается (рис. 1б).

Интенсивная хемосорбция водорода на стенках разрядной камеры, активирующихся при разрядах, сопровождается протеканием вторичных химических реакций, в результате которых образуются летучие продукты, поступающие в объем, и создающие примеси многоэлектронных атомов в плазме. Каталитические реакции сорбированных газов и компонент материала стенок, способных образовывать летучие соединения (углерод, кислород), весьма распространены в вакуумтехнической практике, и существенным образом определяют характеристики вакуумных материалов и систем. К числу наиболее распространенных реакций относятся образование и выделение из металлов окиси и двуокиси углерода, активируемое повышением температуры; каталитический синтез метана и этана, протекающий при хемосорбции водорода металлами, содержащими углерод; восстановление поверхностных окислов активным водородом. Перечисленные реакции характерны для технических материалов, содержащих углерод и кислород. Содержание этих элементов в конструкционных материалах, из которых изготавливают в настоя-

щее время вакуумные камеры, весьма высоко. Поверхность нержавеющих сталей всегда покрыта пассивирующей пленкой окислов, не удаляемой при прогреве в вакууме или водороде. Содержание углерода на поверхности стенок вакуумных камер может быть выше, чем в толще металла, за счет образования пленок углеводородов из откачной аппаратуры, и крекинга углеводородов при прогреве. Вакуумтехническая практика показывает, что интенсивность каталитических реакций при хемосорбции водорода на поверхностях значительна, даже при использовании наиболее чистых доступных в настоящее время материалов. Так, фактором, ограничивающим предельный вакуум сорбционных насосов, использующих в качестве сорбента иодидно-рафинированный титан, является синтез метана.

Проведенный в настоящей работе масс-спектрометрический анализ газа в установках с импульсными разрядами показал, что на стенках разрядных камер, одновременно с хемосорбцией водорода протекают все три вышеперечисленные каталитические реакции, летучие продукты которых выделяются в объем. В течение времени существования плазмы, продукты реакций диссоциируют и ионизуются в плазме, загрязняя ее ионами углерода и кислорода. Выделение продуктов реакций со стенок продолжается и в течение некоторого времени после окончания разряда, с быстро снижающейся скоростью. Не успевшие диссоциировать продукты поверхностных реакций регистрируются масс-спектрометром, как примеси к рабочему газу — окись углерода, метан, или пары воды.

Относительная роль каждой из каталитических реакций зависит от свойств материала стенок, состояния их поверхности и от природы рабочего газа. Соответствующие экспериментальные данные приведены на масс-спектрограммах и графиках рис. 2—4.

При применении для откачки разрядных камер паромасляных насосов, стенки покрываются в большей или меньшей степени пленкой тяжелых углеводородов — продуктов крекинга масел. При прогреве вакуумной камеры до температуры 400—450° С, происходит дальнейший крекинг, приводящий к образованию прочного налета труднолетучих смолообразных углеводородов, с большим относительным содержанием углерода. Получению сверхвысокого вакуума в камере пленка не мешает. При импульсных разрядах в водороде и хемосорбции водорода на стенках, преобладающей вторичной реакцией является синтез летучих углеводородов, метана и этана (масс-спектрограммы рис. 2а). Преобладающим загрязнением плазмы являются ионы углерода (спектрограмма рис. 5). При разрядах, производимых после тепловой обработки камеры, до тренировки импульсами, уровень загрязнения плазмы высок. Содержание метана после разряда может быть близким к содержанию водорода. После длительной тренировки разрядами, содержание примесей, по отношению к конечному давлению водорода, снижается на

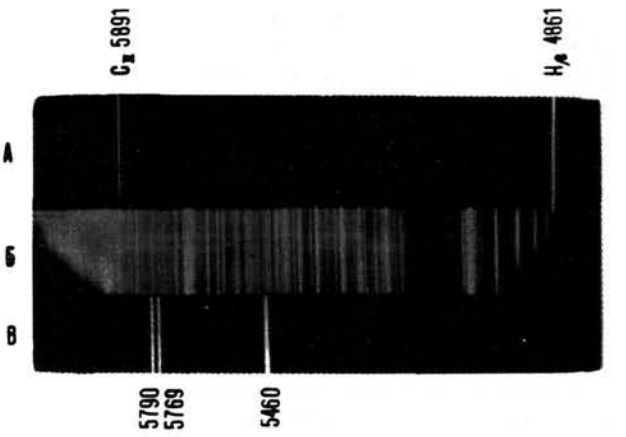

Рис. 5 Спектр излучения импульсного разряда в водороде (модельная установка ВПС). (а) — спектр разряда; (б) спектр железа; (в) спектр ртутной лампы.

порядок величины; качественный состав примесей к газу сохраняется (рис. 2б). Второй примесью к газу после разряда является окись углерода, образующаяся при реакции углерода с кислородом, содержащимся в пленке поверхностного окисла.

При безмасляной откачке разрядной камеры, каталитические реакции протекают в поверхностном слое нержавеющей стали. Основными реакциями в этом случае являются восстановление поверхностных окислов водородом, с образованием воды, и поверхностная реакция между кислородом и углеродом металла, с образованием окиси углерода (масс-спектрограммы рис. 2в). В плазму поступают ионы кислорода, и в меньшем количестве, углерода. Уровень примесей к газу непосредственно после тепловой обработки составляет несколько процентов к конечному давлению водорода (т.е. ниже, чем при откачке масляными насосами). Дальнейшая тренировка импульсными разрядами менее действенна, чем при наличии углеводородной пленки. При тренировке снижается выделение окиси углерода, и практически не снижается выделение воды (рис. 2г). То обстоятельство, что вода выделяется в объем не из-за неполного обезгаживания стенок, а в результате химической реакции, легко проверяется при работе на дейтерии. В этом случае в объем поступают пары тяжелой воды D_2O. При попеременной работе на водороде и дейтерии, со стенок поступают молекулы H_2O, HDO, D_2O (рис. 1а).

При импульсных разрядах на инертных газах (гелии, аргоне), химических реакций с образованием водородсодержащих продуктов (метана, воды) не происходит. Основной вторичной реакцией здесь является образование окиси углерода, в количествах, близких к тем, что имеет место при разряде в водороде (масс-спектрограммы рис. 3а, б). Механизм активации реакции углерода и кислорода при импульсных разрядах, в настоящее время неясен. Возможно, что активация имеет тепловую природу (локальный нагрев поверхностных слоев металла, в областях макроскопического или микроскопического масштабов).

На модельной установке ВПС-2 было установлено, что выполнение части поверхности стенок разрядной камеры из специальной нержавеющей стали с пониженным содержанием углерода (в виде обкладки листами), заметно снижает поступление окиси углерода при разрядах в водороде и гелии.

Скорость поступления примесей за счет каталических реакций наибольшая в период интенсивной хемосорбции водорода, во время разряда, и в течение нескольких миллисекунд после разряда. Далее скорость образования примесей снижается, но сохраняет конечное значение в течение довольно длительного промежутка времени после импульсов, порядка нескольких десятков секунд, пока сохраняется активированное состояние стенок. Поэтому, несмотря на непрерывное поступление чистого газа и постоянную откачку, уже при не очень значительной частоте следования импульсов, газ в камере не полностью освобождается от примесей к моменту каждого следующего разряда (рис. 4а). При тренировке разрядами, повышение частоты следования импульсов выше некоторой определенной (порядка 10 импульсов в минуту) не увеличивает полной скорости удаления углерода или кислорода из камеры, определяющейся скоростью образования летучих соединений при каталитических реакциях, и их откачкой из камеры. Если поставить задачу удаления со стенок камеры углеродных или окисных пленок путем тренировки разрядами, то она может быть решена лишь увеличением абсолютного времени тренировки, но не повышением частоты следования импульсов (сверх указанной выше). Максимальная скорость удаления углерода и кислорода из камеры при тренировке разрядами, на установке Токомак-2 была найдена равной 10^{-2} г/час. При начальной толщине поверхностного слоя порядка одного микрона, для его перевода в летучие соединения потребовалась бы тренировка с полной длительностью масштаба 1000 часов, что непрактично. Эффективность тренировки разрядами определяется не удалением поверхностных пленок со всей поверхности камеры, а очисткой отдельных участков, на которых происходит наиболее интенсивное взаимодействие плазмы со стенками. Для установки Токомак такими участками являются края апертурных диафрагм.

При задании импульсных разрядов в камерах со стенками, поддерживаемыми при повышенной температуре (200—400° С), уменьшается связывание водорода стенками. При одном и том же времени жизни ионов в плазме, скорость снижения плотности плазмы уменьшается, и время существования плазмы увеличивается (за счет большего возврата водорода со стенок). Интенсивность каталитических реакций на стенках и поступление примесей за их счет возрастают. Одновременно несколько снижается поступление примесей за счет микроразрядов (см. ниже). На установках, разрядные камеры в которых изготовлены из обычных технических конструкционных материалов, работа при повышенной температуре всей поверхности стенок, приводит, как правило, к полее высокому уровню примесей.

Примеси, образующиеся при каталитических реакциях, поступают в плазму в виде нейтральных молекул. Загрязнение плазмы за счет этого механизма — процесс относительно медленный, определяющийся временем пролета молекул со стенки до границы плазмы (масштаба нескольких десятых миллисекунды). Значительный вклад в поступление примесей указанный процесс дает в квазистационарных системах, с большой длительностью импульсного разряда, порядка миллисекунды или большей. Второй процесс, играющий существенную роль в поступлениеи примесей — микроразряды на стенках, значительно менее инерционен.

3. Поступление примесей из микроразрядов на стенках

Микроразряды («униполярные дуги») приводят к поступлению примесей в плазму в ионизованном состоянии. Ионизация осуществляется в катодном пятне микроразряда, в малом объеме у поверхности стенки, с высокой локальной плотностью газа и высокой плотностью тока (10^5—10^7 а/см^2). Возникающие на стенках катодные пятна микроразрядов становятся локальными источниками плазмы, из которых распространяется квазинейтральная плазма, несущая ионы примесей. Энергия направленного движения ионов в распространяющейся плазме составляет несколько электронвольт. Скорость распространения плазмы из катодных пятен существенно больше тепловых скоростей нейтральных атомов. При распространении плазмы в вакууме, область за передним фронтом облака плазмы является полностью ионизованной в течение промежутка времени, пока точки наблюдения не достигнет нейтральный газ со стенки.

Закономерности распространения плазмы из локальных источников на твердых поверхностях, и механизм возникновения локальных источников плазмы изучались в связи с исследованиями механизма инициирования и развития электрических разрядов в вакууме [9, 10, 11]. Особенности процесса возникновения микроразрядов и распространения из них плазмы в условиях установок с квазистационарными разрядами, изучались на модельной установке ВПС-1 (рис. 6а). Особенности связаны с наличием магнитного поля и распространением плазмы в среде газа с давлением $1\cdot10^{-3}$—$1\cdot10^{-2}$ мм рт.ст.

Первичная плазма в установке ВПС-1 создается линейным разрядом в водороде. Микроразряды возникают на краях апертурной диафрагмы. Компонентный анализ ионов первичной плазмы, и ионов, поступающих из катодных пятен микроразрядов, производится импульсным масс-спектрометром МСХ-1. Ионно-оптический затвор на входе масс-спектрометра позволяет проводить ана-

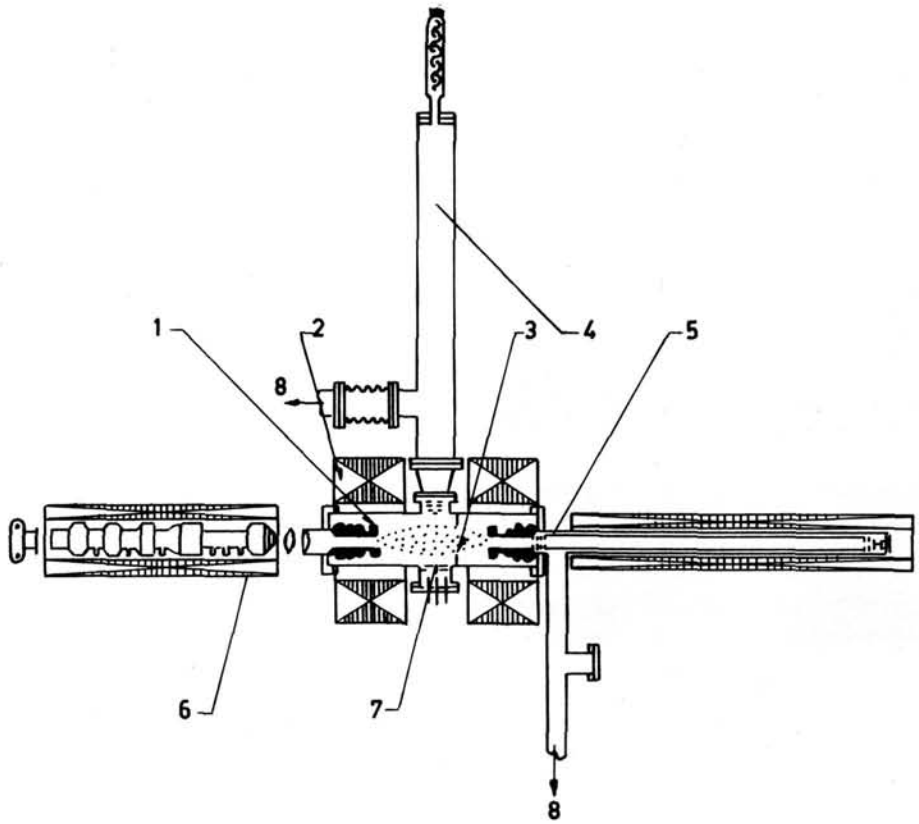

Рис. 6 а Модельная установка ВПС-1 (схематическое изображение). 1 — электроды, 2 — соленоид продольного поля, 3 — апертурная диафрагма, 4 — масс-спектрометр АНК для анализа состава газа, 5 — импульсный масс-спектрометр МСХ-1 для анализа ионов плазмы, 6 — электронно-оптический преобразователь для скоростной фотосъемки, 7 — импульсный манометр.

лиз в определенные моменты времени, с заданной задержкой относительно начала главного разряда или момента возникновения катодного пятна на диафрагме. Длительность открытия ионнооптического затвора при анализе 0,2 мксек. Имеется также возможность получать интегральные спектры масс за интервал времени в 3 мксек. Скоростная фотосъемка плазмы, распространяющейся с краев диафрагмы, производится с помощью электронноптического преобразователя с трехкаскадным усилителем яркости. Затвор электронно-оптического преобразователя управляется от тока в цепи диафрагмы. Выдержка при съемке подбирается так, чтобы первичная водородная плазма не засвечивала снимки. Оптимальная найденная на опыте выдержка составляет 0,05 мксек. Направление съемки совпадает с направлением магнитного поля.

Скоростные снимки облачков плазмы, распространяющихся из катодных пятен микроразрядов вглубь первичной водородной плазмы, приведены на рис. 6б, в, г. При отсутствии продольного магнитного поля и невысоких давлениях газа (ниже $1-2\cdot10^{-3}$ мм рт.ст.), облачко плазмы имеет форму факела, с приблизительно косинусным распределением плотности по углам. Скорость переднего фронта облачка плазмы зависит от компонентного состава ионов плазмы и силы тока в катодном

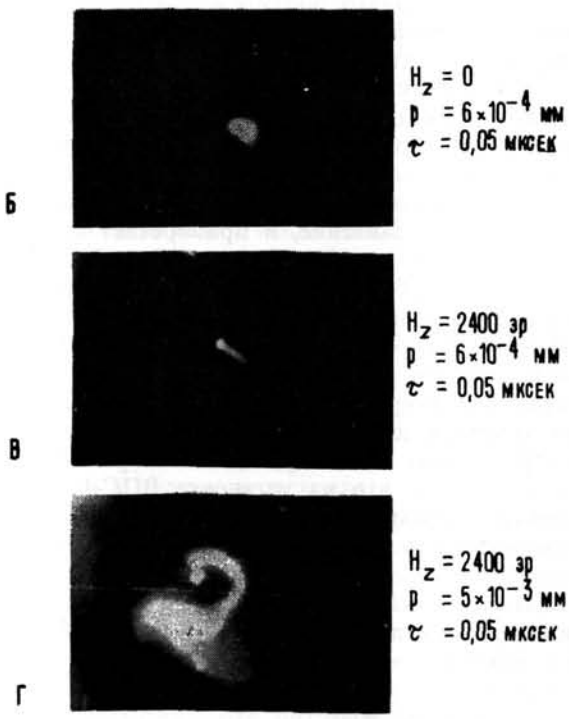

Рис. 6 б—г Скоростные снимки плазмы, распространяющейся из катодных пятен микроразрядов.

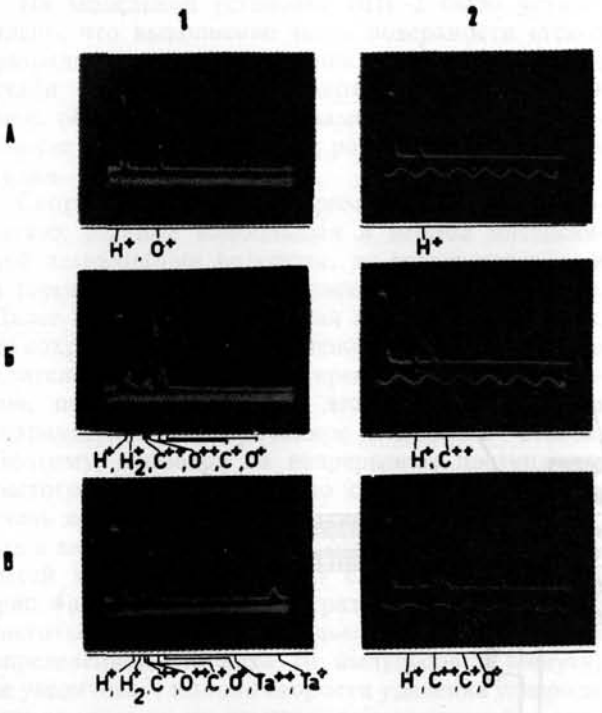

Рис. 7 1 — интегральные масс-спектрограммы ионов примесей, поступающих из микроразрядов при разных режимах. 2 — масс-спектрограммы состава примесей в различные моменты времени после возникновения микроразряда. Время задержки — (а) 3,0 мксек, (б) 4,5 мксек, (в) 6,0 мксек. $\tau = 0{,}2$ мксек.

пятне; в условиях установки ВПС-1 она составляет $1-3\cdot10^6$ см/сек. При наличии магнитного поля напряженностью 2400 эрстед и при низком давлении газа, облачко плазмы имеет форму узкой струи, передний фронт которой перемещается поперек магнитного поля со скоростью $5\cdot10^5-1{,}5\cdot10^6$ см/сек. Вдоль магнитного поля струя расширяется с той же скоростью, что и в отсутствии поля. При более высоком давлении газа ($3\cdot10^{-3}-1\cdot10^{-2}$ мм рт.ст.), и при наличии магнитного поля струя плазмы искривляется, тем более сильно, чем выше давление, и приобретает спиралеобразный характер. Искривленная струя плазмы проникает вглубь первичной водородной плазмы на расстояние около 10 см от края диафрагмы.

Плазма, распространяющаяся из катодных пятен микроразрядов, состоит преимущественно из однократно и двукратно заряженных ионов углерода, или углерода и кислорода [интегральные масс-спектрограммы ионов приведены на рис. 7 (1)]. В связи с тем, что на установке ВПС-1 микроразряды инициируются разрядом в водороде, нет возможности отличить ионы водорода первичной плазмы от водородных ионов, образующихся в катодных пятнах микроразрядов. Из опытов, проведенных в других условиях (при инициировании микроразрядов в вакууме бомбардировкой стенки ионным пучком или плазмой от импульсных источников), известно, что если только стенка не поддерживается при температуре выше 400° С, в плазме микроразрядов содержатся также ионы водорода. Ионы металла — основного материала диафрагмы или стенки, обнаруживаются в плазме не при всех импульсах, и в меньших количествах, чем ионы углерода и кислорода [масс-спектрограмма рис. 7 (1) в]. Эта закономерность соблюдается для большинства употребительных конструкционных материалов (нержавеющая сталь, никель, тантал и т. п.), и не соблюдается для легкоиспаряющихся металлов (серебро, свинец, алюминий), в случае которых в плазме присутствует большое количество ионов металла. Поведение тугоплавких металлов, молибдена и вольфрама, прокаленных при температуре выше 2000° С, имеет особенности, о которых будет сказано дальше.

При распространении плазмы из катодного пятна микроразряда на стенке, ионы в плазме приобретают приблизительно одинаковую энергию направленного движения, так что ионы разных масс движутся с различными скоростями. В области, примыкающей к переднему фронту плазмы, происходит разделение ионов по массам (точнее, по величине отношения m/e). Вблизи переднего фронта распространяющегося облачка движутся наиболее легкие ионы (ионы водорода, двукратно заряженные ионы углерода). Это обстоятельство установлено путем масс-анализа ионов плазмы, достигающих входной щели импульсного масс-спектрометра в различные моменты времени после возникновения микроразряда на стенке. Соответствующие масс-спектрограммы ионов, снятые при задержках 3,0, 4,5 и 6,0 мксек, приведены на рис. 7 (2). Разделение ионов по массам в плазме, распространяющейся из локальных источников на твердых поверхностях, установлено для случаев распространения плазмы в пространстве без магнитного поля, а также в направлении магнитного поля. Закономерности распределения ионов в плазме, распространяющейся поперек магнитного поля, не изучались.

Микроразряды на металлических поверхностях при воздействии плазмы возникают только при отрицательном потенциале стенок относительно плазмы, при поступлении на стенки положительных ионов. Отрицательный потенциал на стенке (или электроде, диафрагме и т.п.) может задаваться искусственно, или устанавливаться естественно, благодаря свойствам плазмы. Условия установления отрицательного потенциала на стенках, соприкасающихся с плазмой, в частности на изолированных электродах, обсуждались в работах [12, 13]. В связи с возможностью существования катодных пятен на изолированных электродах, отрицательный потенциал которых поддерживается поступлением быстрых электронов из плазмы, в названных работах был введен термин «униполярные дуги». В дальнейшем этот термин был распространен на разряды, возникающие и в более общих условиях. Термин «микроразряды», используемый в настоящей работе, имеет тот же смысл.

Возникновение микроразрядов на поверхности металлов, контактирующих с плазмой, зависит от свойств поверхности металла, плотности ионного

тока и длительности облучения поверхности ионами. На поверхностях технических материалов микроразряды возникают легче, и в большем количестве, чем на металлах высокой чистоты. Число возникающих микроразрядов сильно уменьшается при тренировке поверхности разрядами. Для возникновения микроразрядов требуется поступление на единицу поверхности определенного количества электричества; время задержки возникновения микроразрядов обратно пропорционально плотности ионного тока. От абсолютной величины отрицательного потенциала, выше некоторой определенной, время задержки не зависит. Для многих материалов (таких как нержавеющая сталь, никель), при повышенной температуре возникновение микроразрядов ослабляется; катодные пятна возникают при большей плотности ионного тока, чем при нормальной температуре. На поверхности тугоплавких металлов, вольфрама и молибдена, после прогрева до высоких температур (2000—2200° С), микроразряды не возникают при воздействии плазмы с плотностью много большей, чем та, при которой микроразряды возникают на поверхности непрокаленных металлов. Устойчивость поверхности тугоплавких металлов к воздействию плазмы сохраняется в течение сравнительно длительного времени, много большего, чем требуется для образования на поверхности мономолекулярного слоя сорбированных газов. При искусственном нанесении на поверхность диэлектрических пленок, вероятность возникновения микроразрядов возрастает; при напылении на ту же поверхность слоя металла, она вновь снижается. С особо большей вероятностью микроразряды возникают в местах перехода с металла на диэлектрик (на спаях металла со стеклом и т. п.).

Сопоставление перечисленных особенностей условий возникновения микроразрядов с результатами масс-спектрометрического анализа ионов, образующихся в катодных пятнах микроразрядов, позволило сделать определенный вывод о механизме возникновения микроразрядов [9, 10, 11]. При воздействии плазмы на металлические поверхности, микроразряды возникают вследствие наличия на поверхностях микроскопических диэлектрических включений или пленок, в результате зарядки включений положительными ионами, и их пробоя. По химической природе, включения представляют преимущественно карбиды, или другие углеродсодержащие соединения, и окислы. При воздействии плазмы на чисто-металлические поверхности тугоплавких металлов, не содержащие диэлектрических включений и пленок, микроразряды не возникают вплоть до очень больших плотностей плазмы. Наличие мономолекулярной пленки сорбированных газов не приводит к возникновению микроразрядов.

Аналогичный вывод о влиянии диэлектрических включений на возникновение микроразрядов, для специального случая образцов с искусственно нанесенными включениями, сделан в работе [14].

В связи с большой скоростью распространения плазмы из катодных пятен микроразрядов, поступление примесей в первичную плазму за счет микроразрядов является быстрым процессом. Ионы углерода и кислорода попадают во внутренние области первичной плазмы через несколько микросекунд после возникновения катодных пятен на стенках. Время возникновения катодных пятен, в свою очередь, определяется плотностью ионного потока на стенки из первичной плазмы, то есть зависит от степени устойчивости плазмы, и от условий в начальной стадии квазистационарного разряда (пробой газа у стенок, или по оси разрядной камеры).

Распределение участков возникновения микроразрядов по стенкам разрядной камеры зависит от характеристик плазмы и от конструкции разрядной камеры. В установке Такомак-2 микроразряды сосредоточены на краях апертурных диафрагм. На установках с менее устойчивой плазмой, и без применения апертурных диафрагм (например, на установке Зета), катодные пятна располагаются по всей внутренней поверхности камеры.

4. Заключение

Технологические приемы предварительной вакуумной очистки и подготовки разрядных камер, приведшие за последние годы на ряде установок к повышению чистоты плазмы, по существу, не рассчитаны на специфические условия газового разряда и высокотемпературной плазмы. Аналогичная, и даже более жесткая процедура подготовки применяется при производстве многих электровакуумных приборов. Для дальнейшего повышения чистоты плазмы (не рассматривая возможностей, связанных с улучшением удержания ионов), необходимо применение технологических приемов, учитывающих специфику задачи, то есть интенсивное воздействие горячего газа на стенки, приводящее к химическим и электрическим процессам в материале стенок. К числу таких приемов относится, прежде всего, использование рационально выбранных материалов для разрядных камер или их отдельных участков, и, быть может, разработка специальных материалов. Требования к материалам очень сложны. Результаты исследования процессов взаимодействия плазмы со стенками, полученные в настоящей работе, позволяют сформулировать ряд требований к материалам, удовлетворение которых позволит снизить поступление примесей в плазму в системах с квазистационарными разрядами. В химическом составе материалов должно быть минимальное содержание компонент, образующих летучие продукты при каталитических реакциях, активируемых в разряде, то есть углерода и кислорода. На поверхности материалов не должно быть прочных пленок, не удаляемых прогревом, содержащих указанные элементы, в частности, пассивирующих окисных пленок. Поверхность материалов не должна содержать диэлектрических включений, приводящих к возник-

новению микроразрядов. Материал должен быть достаточно тугоплавким, чтобы допускать прогрев, необходимый для удаления случайно образовавшихся поверхностных пленок и включений, подобно вольфраму и молибдену. Целесообразно, чтобы материал не вступал с водородом в химические связи, и не хемосорбировал водород в атомарном и ионизованном состоянии, подобно золоту. Если учесть, что материалы для разрядных камер должны удовлетворять ряду требований по электрическим характеристикам, в частности, по электросопротивлению, то не видно, какие из существующих материалов могли бы удовлетворить всей совокупности требований. При конструировании установок целесообразно итти по линии разграничения функций, выполняемых различными элементами и участками разрядных камер, и использования различных, должным образом выбранных материалов для разных участков. Конкретные решения целиком зависят от типа установки. Для тороидальных систем типа Токамак целесообразно локализовать места выхода положительных ионов из плазмы на стенки с помощью апертурных диафрагм, и материал для диафрагм выбирать с точки зрения повышенной стойкости к образованию микроразрядов (наиболее жесткое из всех требований к материалам, из числа связанных с поступлением примесей). Диафрагмы могут быть выполнены из тугоплавких металлов, с конструкцией, допускающей периодический прогрев до температур порядка 2000° или работу в нагретом состоянии. Для боковых стенок целесообразно опробование материалов типа нержавеющих сталей с пониженным содержанием углерода, прошедших при изготовлении обезгаживание в вакууме или водороде при температурах 800—1100° С. Лучших результатов можно ожидать от применения специальных сплавов высокого сопротивления, не имеющих на поверхности пассивирующей окисной пленки. Целесообразны испытания тонкослойных покрытий боковых стенок металлами, не взаимодействующими с водородом (в частности, золочение). При использовании тонкослойных покрытий трудности могут быть связаны с их разрушением при повторных разрядах, или с напылением поверх них материала диафрагм (в результате катодного распыления).

При использовании для стенок разрядных камер специальных материалов, с улучшенными свойствами по сравнению с применяющимися в настоящее время, более определенные требования должны быть предъявлены к вакуумной откачной аппаратуре. Недостаточно уже откачки до сверхвысокого вакуума прогретой камеры, достижение которого свидетельствует об удалении со стенок пленок легколетучих веществ и сорбированных газов (и о герметичности системы). Потребуется, чтобы в процессе откачки на поверхности не образовывалось труднолетучих налетов. На современном этапе работы, применение паромасляных насосов и безмасляных систем откачки дает не сильно различающиеся результаты в суммарном поступлении примесей, так как углеродные пленки и пленки поверхностных окислов на нержавеющей стали не очень сильно различаются в отношении взаимодействия с водородом и влияния на возникновение микроразрядов. При применении материалов с улучшенными свойствами, образование углеродной пленки, трудно избежимое при использовании масляных насосов, может свести к нулю эффект от замены материалов. Более жесткие требования должны быть предъявлены к вакуумной гигиене и к неотступному соблюдению технологического режима.

Программа работ по получению все более чистой высокотемпературной плазмы в квазистационарных системах проводится на установках Токамак. Программа предусматривает сочетание мер по повышению устойчивости плазмы и технологических мероприятий.

Литература

[1] Knorr, G., *Z. für Naturforschung* **13 a** (1958) 941.

[2] Пост, Р., „Высокотемпературная плазма и управляемые термоядерные реакции". Издательство иностранной литературы. Москва. 1961 г.

[3] Coor, T., Cunningham, S., Ellis, R., Heald, M., Kranz, A.
Доклад № 362 на Второй Международной конференции по мирному использованию атомной энергии. Женева. **32** (1958) 201.

[4] Горбунов Е. П., Долгов-Савельев Г. Г., Муховатов В. С., Стрелков В. С., Явлинский Н. А. *Журнал технической физики*, **30** (1960) 1152.

[5] Васильевский В. С., Муховатов В. С., Стрелков В. С., Явлинский Н. А. *Журнал технической физики* **30** (1960) 1137.

[6] Долгов-Савельев Г. Г., Муховатов В. С., Стрелков Г. Г., Шепелев М. Н., Явлинский Н. А.
Доклад на IV Международной конференции по ионизационным явлениям в газах. Упсала **2** (1959) 947.

[7] Ellis, R., Доклад на IV Международной конференции по ионизационным явлениям в газах. Упсала **2** (1959) 1129.

[8] Афросимов В. В., Гладковский И. П., Гордеев Ю.С., Калинкевич И. Р., Петров М. П., Федоренко Н. В. *Журнал технической физики* **30** (1960) 1469.

[9] Симонов, В. А. Доклад на Межведомственном семинаре по катодной электронике.
Радиотехника и электроника **2** (1957) 666.

[10] Симонов, В. А. Доклад на 8-м Всесоюзном совещании по катодной электронике.
Радиотехника и электроника **3** (1958) 1101.

[11] Симонов, В. А., Кутуков, Г. П. Доклады на 2-й Всесоюзной конференции по газовой электронике. *Радиотехника и электроника* **4** (1959) 1344.

[12] Craston, I., Hancox, R., Robson, A., Kaufman, S., Miles, H.
Доклад № 34 на Второй Международной конференции по использованию атомной энергии. Женева, **32** (1958.) 414

[13] Robson, A., Hancox, R. *Proc. Instn. Elect. Engrs (London)* **A 106,** Suppl. 2 (1959) 47.

[14] Hancox, R. *British Journal of Applied Physics*, **11** (1960) 468.

ПОДДЕРЖАНИЕ СВЕРХНИЗКИХ ДАВЛЕНИЙ НЕЙТРАЛЬНОГО ГАЗА В ПРОЦЕССЕ НАКОПЛЕНИЯ ВЫСОКОТЕМПЕРАТУРНОЙ ПЛАЗМЫ В МАГНИТНЫХ ЛОВУШКАХ С ИНЖЕКЦИЕЙ*

В. А. СИМОНОВ, Г. Ф. КЛЕЙМЕНОВ, А. Г. МИЛЕШКИН, В. А. КОЧНЕВ

АКАДЕМИЯ НАУК СССР, МОСКВА

СОЮЗ СОВЕТСКИХ СОЦИАЛИСТИЧЕСКИХ РЕСПУБЛИК

В стационарных магнитных ловушках с инжекцией (установка Огра и подобные ей) для снижения потерь быстрых ионов на перезарядку в процессе накопления горячей плазмы требуется поддержание сверхнизких давлений нейтрального газа до 10^{-10} мм рт.ст. и устранение примесей многоэлектронных атомов. Нужные для удаления нейтрального газа скорости откачки лежат в диапазоне 1—200 миллионов литров в секунду по водороду. Удаление газа с требуемыми большими скоростями при сверхнизких давлениях возможно только посредством откачных устройств, размещенных непосредственно в рабочем объеме установки, действие которых органически зависит от процессов в высокотемпературной плазме и взаимодействия ее со стенками. В докладе излагаются результаты комплекса работ по исследованию процессов взаимодействия атомов и ионов с поверхностями, определяющих возможности поддержания сверхвысокого вакуума и сохранения чистоты плазмы в рабочих режимах термоядерных установок с магнитными ловушками.

Проведены исследования кинетики сорбции газов при низких давлениях на возобновляемой поверхности химически активных металлов и на поверхности конструкционных материалов; исследования каталических реакций сорбированных газов; измерения газоотдачи поверхностей при бомбардировке быстрыми частицами. Открыты особенности процесса сорбции водорода некоторыми металлами при пониженных температурах, позволившие создать эффективные устройства для сверхвысоковакуумной откачки нейтрального газа с большими скоростями, допускающие работу в условиях бомбардировки сорбирующих поверхностей быстрыми частицами (азотиты). Азотиты, усгановленные в камере Огры, обеспечивают скорость откачки нейтрального газа в 2 миллиона литров в секунду.

Проведены исследования процессов внедрения быстрых ионов водорода и остаточных газов в различные материалы, процессов диффузии внедренных атомов, процессов распыления сорбированных газовых пленок. Определены условия осуществимости ионной откачки газов в магнитных ловушках по методу ускорения вторичных ионов плазмы и внедрения в торцевые элекгроды. (При скоростях откачки масштаба 10—100 миллионов литров в секунду).

Проведены исследования процессов взаимодействия медленных ионов водорода и других газов с поверхностями химически активных металлов при различных температурах. Предложен метод ионной откачки магнитных ловушек, состоящий в поглощении вторичных ионов плазмы без их ускорения, на поверхностях откачных устройств типа азотит, размещенных в зоне выхода вторичных ионов на стенки. Метод позволяет осуществить ионную откачку с большими скоростями при сверхнизких давлениях и исключает возможность лавинообразных процессов загрязнения плазмы, ограничивающих накопление.

1. Введение

В стационарных магнитных ловушках с инжекцией быстрых частиц, для снижения потерь на перезарядку, в процессе накопления горячей плазмы требуется поддержание сверхнизких давлений нейтрального газа и устранение примесей многоэлектронных атомов. В установке Огра (с инжекцией молекулярных ионов и диссоциацией на остаточном газе), для осуществления накопления плотной плазмы, в связи с большой длительностью накопления, при инжекции требуется поддержание давления не выше $1 \cdot 10^{-9}$ мм рт.ст. по водороду, и 10^{-10} мм рт.ст. по примесям [1].

Уже получение начального вакуума требуемого диапазона в установках больших объемов представляет определенные технические трудности. В магнитных же ловушках с инжекцией возникает значительно более сложная вакуумтехническая задача — поддержание сверхвысокого вакуума в условиях поступления в объем больших количеств газа, и интенсивного воздействия на стенки потоков быстрых частиц. В установке Огра поток водорода в камеру создается инжектируемым ионным пучком, нейтрализующимся на стенках магнитного канала. Для удаления только газа, вводимого с пучком, в установке Огра требуются скорости откачки масштаба 10—100 миллионов литров в секунду. Дополнительная газовая нагрузка создается поступлением газа со стенок под воздействием быстрых частиц.

Скорости откачки в миллионы литров в секунду не могут создаваться никакими присоединенными к камере внешними откачными устройствами. Для обеспечения таких скоростей откачки можно идти двумя путями. Первый из них состоит в исполь-

* Доклад CN-10/255, представленный на Конференцию. Докладчик: В. А. Симонов. Дискуссия (на английском языке) по этому докладу дана на стр. 358. Переводы аннотаций находятся в конце этого тома Трудов Конференции.

зовании устройств для откачки газа в нейтральном состоянии, размещаемых непосредственно в рабочем объеме установки, и имеющих большие поглощающие поверхности. Газовыделение с таких поверхностей под воздействием быстрых частиц должно быть малым, по сравнению с количествами поглощаемого ими газа. Второй путь состоит в использовании ионизации газа в накапливаемой горячей плазме, и удалении из объема вторичных ионов. Для осуществления ионной откачки должно быть обеспечено связывание вторичных ионов, выходящих из плазмы. Если возврат в объем газа, образующегося при нейтрализации вторичных ионов, будет меньше ухода ионов из плазмы, то при определенных условиях, в частности, при достаточно большом токе инжекции, может быть осуществлено «выжигание» нейтрального газа в камере и переход к диссоциации инжектируемых ионов на накопленных ионах. При любых методах откачки, для получения сверхвысокого вакуума должна быть предусмотрена вакуумтехнологическая подготовка камеры, снижающая газовыделение со стенок и натекание газа, не связанное с принципиально-необходимым поступлением газа при инжекции.

Необходимые режимы инжекции ионов существенно зависят от применяемых методов удаления нейтрального газа. Если скорости откачки газа в нейтральном состоянии малы (масштаба 100 тысяч литров в секунду), и удаление газа возлагается в основном на ионную откачку, то при наилучших реально возможных условиях связывания вторичных ионов, требуемый ток инжекции (ток перевала), составляет несколько ампер. Инжекция столь больших токов молекулярных ионов в магнитную ловушку представляет трудности, до настоящего времени непреодоленные. Если же в начальных стадиях накопления плазмы нейтральный газ будет откачиваться с большей скоростью, масштаба 1—10 миллионов литров в секунду, то условия осуществимости последующей ионной откачки существенно облегчаются. Требуемый ток инжекции снижается до величины порядка 100 миллиампер.

По мере развития экспериментальных работ на установке Огра, видоизменялись представления о возможных методах поддержания сверхвысокого вакуума в процессе накопления плазмы в ловушках. В первоначальном проекте Огры предусматривалась откачка нейтрального газа с большой скоростью путем поглощения на внутренних стенках камеры напыленным на них слоем химически активных металлов, титана или циркония. Однако, сорбционный метод откачки, в известных его формах, для условий магнитных ловушек оказался неэффективным. Измерения газоотдачи поверхности сорбентов под воздействием быстрых частиц показали, что газовыделения очень велики; в продуктах газоотдачи содержатся большие количества многоэлектронных атомов. Даже при напылении титана только на концевые участки камеры Огры, куда выходят вторичные медленные ионы, повышение давления и поступление примесей при вводе ионного пучка было недопустимо большим. От размещения газопоглощающих поверхностей в рабочем объеме установки пришлось отказаться, и ориентироваться только на ионную откачку.

Связывание вторичных ионов плазмы, уходящих вдоль магнитного поля за пробки, при ионной откачке в Огре может производиться путем ускорения ионов разностью потенциалов, приложенной между плазмой и торцовыми электродами, и внедрения в поверхности торцовых электродов. Исследования процессов внедрения ионов средних энергий в твердые поверхности, и газоотдачи при бомбардировке поверхностей ионами подтвердили принципиальную возможность ионной откачки по методу внедрения ускоренных ионов, и позволили установить требования к материалам вакуумной камеры и режимам вакуумтехнологической обработки. Для установки Огра подготовлена вакуумная система, рассчитанная на начальный вакуум 10^{-10} мм рт.ст., небольшую скорость откачки газов в нейтральном состоянии (100 тысяч литров в секунду по водороду), и осуществление ионной откачки по методу внедрения ионов в торцовые электроды. Главной трудностью при такой схеме накопления плазмы является необходимость инжекции чрезвычайно больших ионных токов, или дальнейшего повышения энергии инжектируемых молекулярных ионов свыше 200 киловольт.

Еще до реконструкции вакуумной системы Огры, при исследованиях кинетики сорбции нейтральных газов на возобновляемых поверхностях металлов, были открыты новые возможности сорбционного метода откачки. При понижении температуры поверхности ниже определенного значения, для ряда металлов происходит изменение механизма сорбции водорода, сопровождающееся возрастанием скорости сорбции, подавлением вторичных химических реакций и снижением газоотдачи при бомбардировке быстрыми частицами. На основе обнаруженного явления, разработаны низкотемпературносорбционные откачные устройства, получившие общее название азотиты, в которых газы сорбируются на возобновляемой поверхности металлов, в частности титана, охлаждаемой до температуры жидкого азота. Существенно меньшая газоотдача охлажденных поверхностей, и более высокая удельная скорость сорбции сделали целесообразным возвращение к системе откачки магнитных ловушек с размещением поверхности, поглощающей нейтральные газы, непосредственно в рабочем объеме установки. Азотиты, размещенные в вакуумной камере Огры, обеспечивают скорость откачи нейтрального газа в 2 миллиона литров в секунду по водороду, при инжекции ионного пучка до 150 миллиампер. Начальный вакуум в камере составляет $5—8 \cdot 10^{-9}$ мм. Высокое начальное давление связано с недостаточной герметичностью существующей камеры, наличием непрогреваемых участков и резиновых уплотнений. Реконструкция вакуумной системы позволит улучшить начальные вакуумные условия и повысить еще в 2—3 раза

скорость сорбции нейтрального газа. При скорости откачки нейтрального газа в процессе накопления плазмы 4—6 миллионов литров в секунду, ток инжекции, необходимый для осуществления ионной откачки, снижается до значений, обеспечиваемых существующим инжектором.

Обнаруженные особенности низкотемпературной сорбции газов на возобновляемых поверхностях металлов дают новые возможности не только для откачки газов в нейтральном состоянии, но и для ионной откачки. Метод связывания вторичных ионов плазмы путем их ускорения и внедрения в твердые поверхности имеет ограничения, связанные с возможностью развития лавинообразных процессов загрязнения плазмы при достижении определенной плотности, в результате того, что в откачиваемых газах присутствуют компоненты (тяжелые атомы), для которых коэффициент газоотдачи больше единицы. Кроме того, задание на торцовые электроды высокого отрицательного потенциала, необходимого для ускорения ионов, приводит к определенным конструктивным трудностям. При исследовании процессов взаимодействия медленных ионов водорода и других газов с поверхностями химически-активных металлов, установлено, что на поверхности азотитов возможно эффективное связывание вторичных ионов плазмы без их ускорения. Существует диапазон энергий ионов и поверхностных концентраций сорбированных газов, в котором суммарный коэффициент газоотдачи для всех ионов меньше единицы. Если максимальная энергия ионов, выходящих из плазмы, не превышает некоторого предела, то поглощение вторичных ионов на поверхности азотитов, размещенных в зоне выхода ионов на стенки, дает эффективный способ ионной откачки, исключающий возможность лавинообразных загрязнений плазмы при высокой плотности.

В докладе излагаются некоторые экспериментальные результаты, полученные при исследовании процессов взаимодействия нейтральных атомов и заряженных частиц с твердыми поверхностями, определяющих возможность поддержания сверхвысокого вакуума в рабочих режимах магнитных ловушек с инжекцией. В цикл работ входит изучение кинетики сорбции газов химически-активными металлами в динамических условиях и сорбции на поверхности конструкционных материалов, исследование процессов внедрения ионов средних энергий в твердые поверхности, газоотдачи поверхностей при бомбардировке ионами, и процессов связывания медленных ионов на возобновляемой поверхности сорбционноактивных металлов.

2. Кинетика сорбции водорода на возобновляемых поверхностях химически-активных металлов, и низкотемпературно-сорбционный метод откачки

Сорбция газов распыляемыми металлами (титаном, молибденом и др.) используется для откачки газов при низких давлениях в сорбционных и сорбционно-ионных насосах, многие разновидности

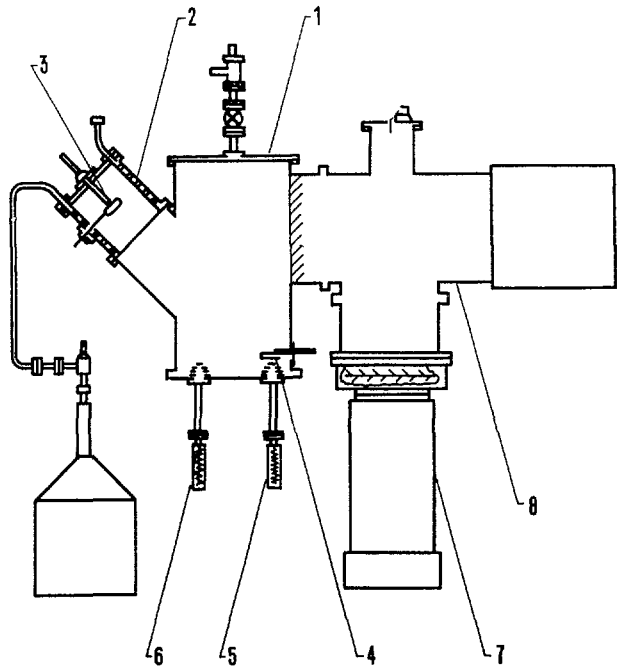

Рис. 1 Установка ИСЭП-1 для исследования кинетики сорбции газов при низких давлениях на возобновляемых поверхностях сорбционно-активных металлов и поверхностях конструкционных материалов. 1 — вакуумная камера, 2 — поверхность конденсации металла, 3 — испаритель металла, 4 — образец исследуемого конструкционного материала, 5 — масс-спектрометр для анализа потока газа, десорбирующегося с поверхности образца, 6 — масс-спектрометр для анализа газа в камере, 7 — парортутный насос, 8 — сорбционно-ионный насос.

которых разработаны за последние годы в ряде стран. В настоящей работе сорбция газов исследовалась с точки зрения ее использования для откачки магнитных ловушек, в которых основной компонентой откачиваемого газа является водород, и главными характеристиками, определяющими применимость метода, является удельная скорость сорбции, величина газоотделения при бомбардировке поверхности быстрыми частицами, и состав продуктов газоотдачи. Исследования проводились на экспериментальных установках ИСЭП-1 и ИСЭП-2 (рис. 1 и 4). Устройство установок ясно из рисунков. Исследуемый металл, испаряемый в непрерывном или периодическом режиме, конденсируется на подложке, температура которой может устанавливаться в пределах от −195° С до +100° С. Состав газа в объеме, и газов, выделяющихся с поверхности исследуемого металла, анализируется с помощью масс-спектрометров хронотрон. Образцы полученных масс-спектрограмм приведены на рис. 2. Для исследования сорбции водорода применяется изотопный метод, с напуском в систему дейтерия, и смесей дейтерия с водородом. Ионная бомбардировка поверхностей производится пучком атомарных или молекулярных ионов дейтерия с энергией от 7 до 25 кэв. Исследование сорбции производилось для титана, циркония, молибдена, никеля, хрома и других металлов. Для названных металлов, харак-

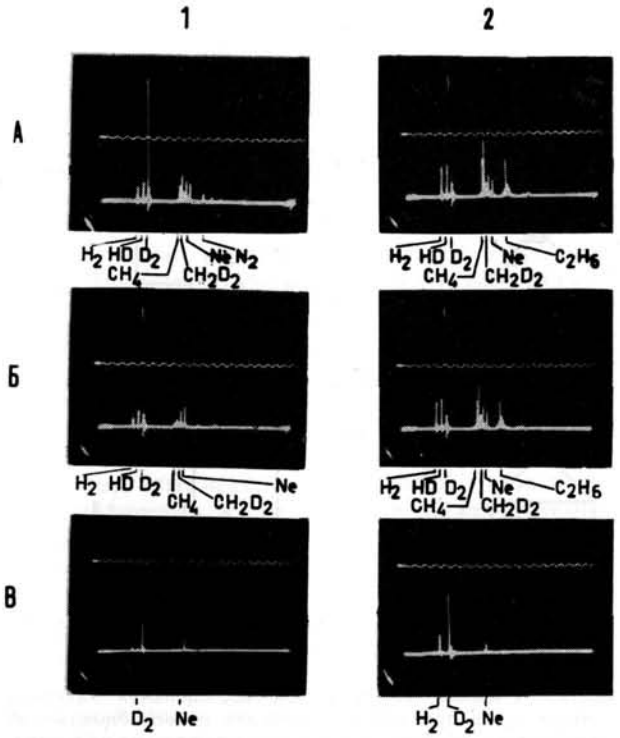

Рис. 2 Сорбция водорода, дейтерообмен, синтез метана на возобновляемой поверхности титана при различных температурах и газоотдача поверхности при бомбардировке ионным пучком. 1 — масс-спектрограммы состава газа в камере при напуске смеси дейтерия и водорода; 2 — масс-спектрограммы состава газа и продуктов газовыделения с поверхности титана при ионной бомбардировке. Температура поверхности: (а) +30° С, (б) −145° С, (в) −190° С. Бомбардировка ионами дейтерия с энергией 20 кэв. Контрольный газ — неон.

теристики сорбции в качественном отношении близки; нижеследующее изложение относится к случаю титана.

Наиболее существенные характеристики сорбции водорода, относящиеся к рассматриваемому вопросу, следующие. При нормальной температуре поверхности металла, молекулы водорода сорбируются с диссоциацией на атомы. Сорбированный атомарный водород активен, мигрирует по поверхности, и легко вступает в каталитические реакции с другими сорбированными атомами и с компонентами металла, образующими летучие соединения с водородом. При практически неизбежном присутствии в металле углерода, протекают реакции образования метиленовых радикалов, синтез метана и этана, с выделением последних в объем (масс-спектрограммы рис. 2 (1) а, б). Над возобновляемой поверхностью металла всегда присутствует атмосфера метана, определяющего предельный вакуум сорбционных насосов. При бомбардировке поверхности ионным пучком, основными компонентами газоотдачи являются метан, этан, водород (масс-спектрограммы рис. 2 (2) а, б, характеристики газоотдачи рис. 3в). При сорбции водорода и дейтерия H_2 и D_2, в продуктах газоотдачи присутствуют молекулы H_2, D_2 и HD. Суммарный коэффициент газоотдачи возрастает с увеличением концентрации сорбированного водорода, и в типичных случаях значительно превышает единицу (рис. 3в). Компоненты газоотдачи — метан и этан, слабо сорбируются, и их выделение с поверхности приводит к сильному повышению давления, зависящему от скорости откачки объема вспомогательными (не сорбционными) насосами.

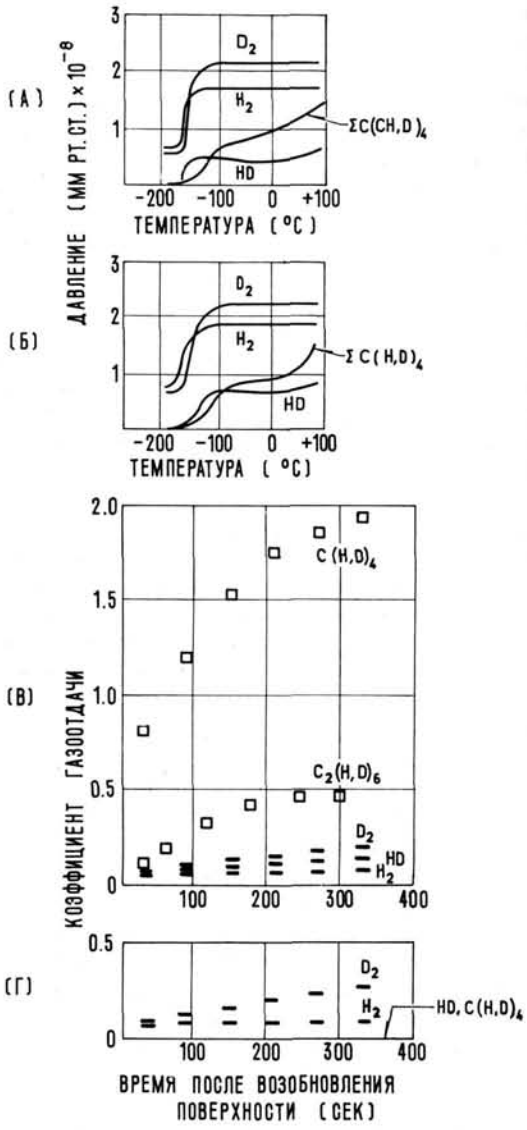

Рис. 3 (А), (Б) — Зависимость скорости сорбции водорода, скорости дейтерообмена и синтеза метана от температуры поверхности металла (в динамическом режиме). (А) никель, (Б) титан. Напуск смеси водорода и дейтерия: (А) 0,05 л/мксек, (В) 0,06 л/мксек; проводимость входного трубопровода 4.000 л/сек. (В), (Г) Газовыделение с поверхности титана при ионной бомбардировке (состав продуктов и коэффициент газоотдачи). Температура поверхности: (В) +30° С, (Г) −190° С. Облучение импульсами по 15 сек., с интервалами 1 мин. (В) — Бомбардировка ионами D^+, $E=20$ кэв, $\delta=2$ мка/см^2, $p=2\cdot10^{-7}$ мм рт.ст. Состав газовой среды: D_2 — $7\cdot10^{-8}$ мм, H_2 — $1\cdot10^{-8}$ мм, HD — $3\cdot10^{-8}$ мм, C (H, D)$_4$ — $7\cdot10^{-8}$ мм, C (H, D)$_4$ — $2\cdot10^{-8}$ мм. (Г) $p=3\cdot10^{-8}$ мм. Состав газовой среды: D_2 — $2{,}5\cdot10^{-8}$ мм, H_2 — $5\cdot10^{-9}$ мм, HD — $<5\cdot10^{-10}$ мм, C (H, D)$_4$ — $5\cdot10^{-10}$ мм.

Удельная скорость сорбции водорода (коэффициент прилипания молекул) сильно зависит от концентрации сорбированных атомов кислорода и азота. Сорбция водорода и кислорода неаддитивна; кислород оказывает отравляющее действие на сорбцию водорода. Для типичных случаев свежевозобновленной поверхности титана, отравление которой связано только с сорбцией газов, выделяемых испарителем, коэффициент прилипания молекул водорода составляет 0,1. По мере сорбции газов на поверхности, коэффициент прилипания сильно снижается. Невысокие значения коэффициента прилипания молекул, и большая чувствительность к степени заполнения поверхности связаны с тем, что для диссоциативной хемосорбции молекулы водорода требуется наличие на поверхности пары рядом расположенных активных участков для сорбции атомов. Число пар активных участков уменьшается при заполнении поверхности быстрее, чем число одиночных активных участков.

Характеристики сорбции водорода распыляемыми металлами, неблагоприятные для использования сорбционного метода откачки в магнитных ловушках и снижающие возможности обычных сорбционных насосов, связаны с диссоциативным характером хемосорбции, приводящим к интенсивному протеканию каталитических реакций с образованием продуктов, слабо связанных с поверхностью. Диссоциативная хемосорбция водорода на чистой поверхности металла не требует энергии активации; ее скорость не зависит от температуры в широком диапазоне, как выше нормальной, так и ниже. Активированный характер сорбции водорода на поверхностях массивных металлов (например, листовых), и сорбционная неактивность при нормальной и пониженных температурах, связаны с наличием на поверхности защитной пленки окислов. Охлаждение металла вплоть до температур $-100 - -130°$ С, практически не изменяет коэффициента прилипания молекул водорода, незначительно ослабляет вторичные химические реакции (дейтерообмен, синтез метана), и мало снижает газоотдачу поверхностей при ионной бомбардировке (рис. 3а, масс-спектрограммы рис. 2 (1,2) б). Положительным эффектом от неглубокого охлаждения является лишь снижение равновесного давления водорода над поверхностью.

В настоящей работе установлено, что при охлаждении поверхностей некоторых металлов до более низких температур (зависящих от рода металла), механизм хемосорбции водорода изменяется, что приводит к существенному изменению характеристик сорбционной откачки — повышению удельной скорости сорбции, подавлению каталитических реакций с образованием летучих продуктов, снижению газоотдачи поверхности при ионной бомбардировке. Изменение характеристик сорбции иллюстрируется графиками рис. 3а, б, для случаев никеля и титана. На графиках приведены парциальные давления водорода и дейтерия, дейтеро-водорода HD, метана и дейтерометана, устанавливающиеся при постоянном напуске смеси водорода и дейтерия в вакуумной системе, откачиваемой за счет сорбции газов на непрерывно возобновляемой поверхности металла, при различных температурах сорбирующей поверхности. При температурах $+100 - -170°$ С для никеля и $+100 - -130°$ С для титана, коэффициент прилипания молекул водорода остается неизменным; каталитические реакции дейтерообмена и синтеза метана протекают со скоростью, не сильно снижающейся при понижении температуры. При дальнейшем охлаждении, в диапазоне температур $-170 - -182°$ С для никеля и $-130 - -170°$ С для титана, коэффициент прилипания молекул водорода (удельная скорость сорбции) возрастает в 4—5 раз. Каталитические реакции резко ослабляются, и на нижней границе указанного диапазона температур, практически подавляются. В газовой среде над поверхностью металла исчезают метан и дейтеровodород (масс-спектрограмма рис. 2 (1) в). Изменяется величина газоотдачи при ионной бомбардировке, и состав продуктов газоотдачи (рис. 3в, г, масс-спектрограммы рис. 2 (2) в). В составе газа, выделяющегося с поверхности при бомбардировке ионами, полностью отсутствует метан и этан, практически отсутствует дейтеровodород. Основными продуктами газоотдачи остаются водород и дейтерий (в молекулярном состоянии), с парциальными коэффициентами газоотдачи, мало отличающимися от их значений при нормальной температуре. При невысоких степенях покрытия поверхности водородом, коэффициент газоотдачи пропорционален степени покрытия. Для типичного соотношения числа атомов металла и числа сорбированных молекул водорода 3—10, суммарный коэффициент газоотдачи не превышает 0,6 (при энергии ионов 15 кэв). В продуктах газоотдачи отсутствуют трудносорбирующиеся молекулы, так что повышение давления в вакуумной системе с сорбционной откачкой при вводе ионного пучка невелико.

Для объяснения причин изменения характеристик сорбции водорода при охлаждении ниже определенных температур, на основе полученных экспериментальных данных, выдвинуто следующее представление. При достаточно низких температурах, на поверхности металлов типа титана, никеля, молибдена, хемосорбция молекул водорода происходит без диссоциации. Молекула связывается с поверхностью одним атомом водорода; для ее сорбции нужен одиночный активный участок. Коэффициент прилипания молекул (удельная скорость сорбции) при бездиссоциативной хемосорбции выше, чем при диссоциативной, потому что число одиночных активных участков на поверхности больше, чем число пар рядом расположенных активных участков. Причиной перехода от диссоциативной к бездиссоциативной сорбции является то, что бездиссоциативная хемосорбция, характеризующаяся несколько меньшей энергией связи водорода с поверхностью, чем диссоциативная, при достаточно низких температурах

становится энергетически возможной, и кинетически преобладающей. Температура перехода тем ниже, и ширина интервала температур, в котором происходит переход, тем меньше, чем ниже теплота сорбции водорода металлом. Малая ширина температурного интервала, в котором происходит переход от диссоциативной к бездиссоциативной сорбции, связана с очень резкой (экспоненциальной) зависимостью от температуры времени жизни сорбированных молекул на поверхности. Невысокие значения коэффициента газоотдачи охлажденной поверхности, содержащей сорбированные молекулы водорода, при ионной бомбардировке, объясняется тем, что связь сорбированных молекул остается прочной, химической, а не слабой физической (Ван-дер-ваальсовой). Сорбированные молекулы водорода неактивны, и не вступают в химические реакции (дейтерообмена, синтеза метана и др.) с образованием непрочно связанных с поверхностью комплексов. Для проверки и уточнения высказанного представления о механизме низкотемпературной сорбции водорода проводится соответствующая экспериментальная работа.

Сорбция кислорода, азота, паров воды, окиси и двуокиси углерода на возобновляемых поверхностях титана и подобных ему металлов при низких температурах происходит со значительной эффективностью; связывание молекул прочное; десорбции при повышении температуры не происходит. При температурах $-195 - -170°$ С происходит также сорбция аргона, с невысоким коэффициентом прилипания. Связь атомов аргона с поверхностью слабая (Ван-дер-ваальсова); коэффициент газоотдачи по аргону высок, так что присутствие аргона в системе и его сорбция являются помехой.

Переход от диссоциативной к бездиссоциативной сорбции для вышеназванных металлов происходит при температурах, выше температуры кипения жидкого азота. Для ряда других химически-активных металлов, например, магния, повышения скорости сорбции водорода вплоть до температуры $-195°$ С не наблюдается. Более низкие температуры не исследовались. Для практического применения, удобнее других металлов титан, из-за сравнительно широкого температурного диапазона перехода к бездиссоциативной сорбции, относительной легкости испарения, и доступности в чистом виде.

При низких температурах диффузия водорода и других газов в толщу металла замедляется. Уменьшение сорбционной емкости, которое с этим может быть связано, компенсируется значительным увеличением истинной поверхности металла при конденсации его паров на охлажденной подложке.

Особенности явления низкотемпературной сорбции позволили создать эффективные сверхвысоковакуумные откачные устройства (азотиты), для магнитных ловушек, и для ряда других вакуумтехнических применений. Азотиты установки Огра обеспечивают скорость откачки в 2 миллиона литров в секунду в рабочем режиме установки. Введение некоторых технических усовершенствований позволит довести скорость откачки до 4—6 миллионов литров в секунду. Вакуумные агрегаты, состоящие из азотитной ловушки и паpортутного насоса, имеют предельный вакуум 10^{-10} мм рт.ст. и значительно большую скорость откачки, чем насосы сверхвысокого вакуума с обычными охлаждаемыми ловушками. Применение азотитов целесообразно в системах дифференциальной откачки установок сверхвысокого вакуума, в различного рода ионопроводах, плазмопроводах (если только откачиваемыми газами не являются инертные). При пропускании через азотитную ловушку струи водородной плазмы, осуществляется эффективный отбор из плазмы нейтральных атомов; степень ионизации в плазме по прохождении ловушки может быть близка к единице. Азотитная ловушка эквивалентна многоступенчатой системе дифференциальной откачки. В связи с малыми значениями коэффициента газоотдачи, азотитные ловушки могут применяться в системах очистки плазмы от посторонних тяжелых ионов.

Особенности явления низкотемпературной бездиссоциативной сорбции на возобновляемых поверхностях металлов могут быть использованы не только для создания устройств сверхвысоковакуумной откачки газов в нейтральном состоянии, но и для ионной откачки. Соответствующие данные приводятся в следующем разделе.

3. Процессы взаимодействия заряженных и нейтральных частиц с твердыми поверхностями, определяющие возможность осуществления ионной откачки в магнитных ловушках

3.1. Внедрение ионов средних энергий в твердые поверхности

В установке Огра для связывания вторичных ионов плазмы, выходящих через пробки, предусмотрен метод ускорения ионов до энергии в несколько десятков килоэлектронвольт, с помощью потенциала, приложенного к торцовым электродам, и внедрения в материал торцовых электродов. Для осуществления ионной откачки необходимо, чтобы суммарный коэффициент газоотдачи при внедрении ионов (отношение числа нейтральных атомов, поступающих в объем с поверхности, к числу падающих ионов) был меньше единицы. Чем ближе к единице коэффициент газоотдачи (усредненный по всем присутствующим ионам), тем менее эффективна ионная откачка, и тем большие токи инжекции требуются для достижения режима перевала.

Газоотдача с поверхностей при внедрении газовых ионов слагается из следующих компонент: рассеяние ионов пучка в объем с нейтрализацией, обратное диффузионное выделение внедренных атомов, катодное распыление металла, распыление сорбированных газовых пленок. Из числа процессов газоотдачи, систематически изучено только катодное распыление металлов. Внедрение

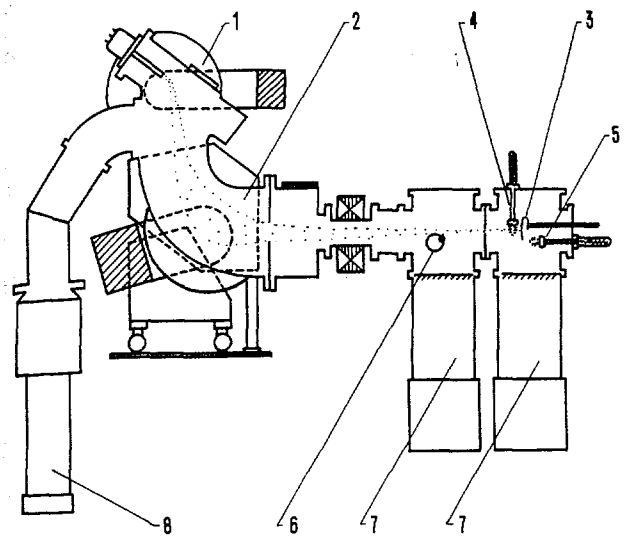

Рис. 4 Установка ИСЭП-2 для исследования процессов внедрения ионов средних энергий в твердые поверхности. 1 — источник ионов, 2 — масс-спектрометр, 3 — мишень, 4 — масс-спектрометр для регистрации потока газоотдачи с мишени, 5 — масс-спектрометр для анализа состава остаточных газов, 6 — модулятор ионного пучка, 7 — сорбционно-ионные насосы, 8 — диффузионный насос.

газовых ионов в материалы исследовалось для нескольких специальных случаев, связанных с электромагнитным разделением изотопов инертных газов, и с методикой приготовления твердых «газовых» мишеней [2, 3]. Количественные характеристики процесса внедрения ионов средних энергий не описаны. Механизм процессов, определяющих насыщение при внедрении ионов, не установлен. Газоотдача за счет распыления сорбированных газовых пленок определяется характеристиками пленок, и должна изучаться для конкретных вакуумных условий, параллельно с исследованием кинетики сорбции газов на поверхностях.

Экспериментальные исследования процессов внедрения ионов проводились на установке ИСЭП-2 (рис. 4). Мишень из исследуемого материала бомбардируется моноэнергетическим пучком ионов, с энергиями в диапазоне 7—25 кэв. Поток газоотдачи с поверхности мишени анализируется масс-спектрометром хронотрон, датчик которого размещен в непосредственной близости у мишени. Регистрация производится в молекулярном пучке, при однократном пролете молекул через датчик. Для выделения потока газоотдачи на фоне остаточных газов, в измерительном объеме поддерживается высокий вакуум (суммарное давление не выше $1-3\cdot10^{-8}$ мм рт.ст.). Для снижения фона от газа, поступающего из источника, применяется двухступенчатая система дифференциальной откачки с сорбционно-ионными насосами. При исследовании внедрения ионов водорода, работа ведется на дейтерии, для уменьшения фона от водорода, содержащегося в остаточных газах. Частицы первичного пучка, рассеянные на поверхности мишени с нейтрализацией и сохранением значительной доли начальной энергии, регистрируются по вторично-электронной эмиссии, с помощью открытого электронного умножителя. Ионный пучок может быть промодулирован по интенсивности с помощью механического или электрического модулятора; частота модуляции — 22 герца. Количество газа, внедренного в материал мишени при ионной бомбардировке в течение заданного времени, определяется путем выделения всего внедренного газа в замкнутом объеме (нагреванием мишени), и измерения количества выделившегося газа с помощью масс-спектрометра, методом сравнения со стандартом. Для измерения ионного тока на мишень, применяется система электродов, подавляющих вторично-электронную эмиссию.

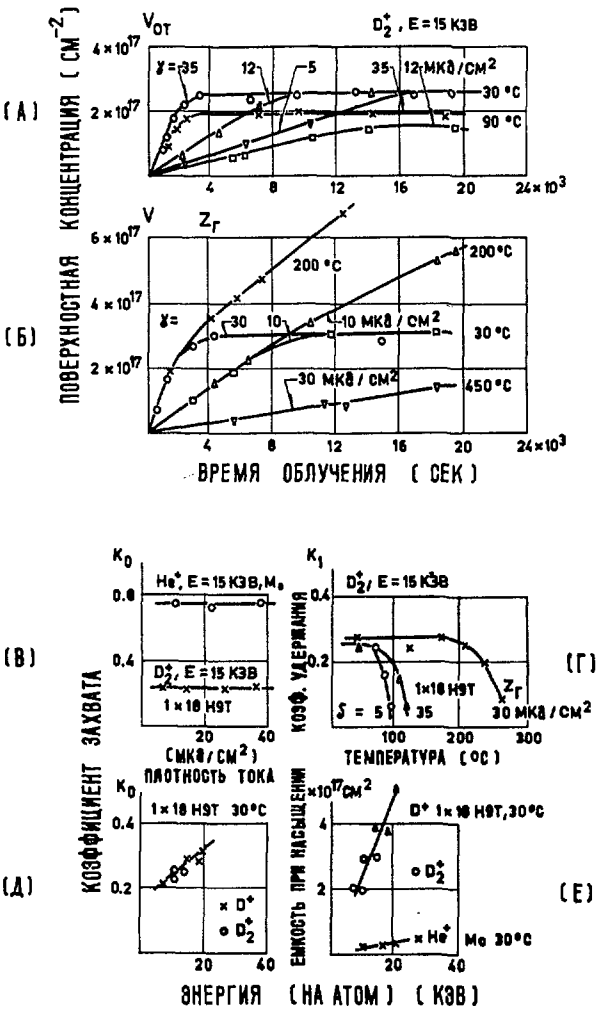

Рис. 5 Характеристики процесса внедрения ионов в поверхности металлов. (А), (Б) — зависимость количества дейтерия, внедренного в поверхности нержавеющей стали и циркония от времени облучения, при разной плотности тока и температуре поверхности; (В), (Д) — зависимость коэффициента захвата ионов от плотности тока и энергии ионов дейтерия и гелия. (Г) — зависимость коэффициента удержания ионов дейтерия от температуры поверхности нержавеющей стали и циркония. (Е) — зависимость газоемкости нержавеющей стали при насыщении от энергии внедряющихся ионов дейтерия и гелия.

Исследование внедрения ионов дейтерия производилось для металлов двух групп: не образующих прочных химических связей с водородом (нержавеющая сталь, никель, молибден, золото), и образующих гидриды (титан, цирконий). Экспериментальные результаты для нержавеющей стали и циркония приведены на графиках рис. 5. Основные закономерности процесса внедрения следующие. При малых концентрациях внедренных атомов, количество внедренного газа линейно возрастает со временем облучения. Коэффициент захвата (отношение количества внедренных атомов к количеству поступивших ионов) не зависит от плотности тока, и при малых временах облучения, не зависит от времени облучения. В исследованном диапазоне энергий ионов, коэффициент захвата для нержавеющей стали возрастает от 0,2 при энергии 7 кэв, до 0,35 при энергии 25 кэв (рис. 5в, д). Для всех исследованных металлов коэффициент захвата при одной и той же энергии ионов различается мало. В отраженном потоке присутствуют преимущественно атомы дейтерия с энергиями значительно выше тепловых (до нескольких десятков электронвольт), образующиеся в результате рассеяния на поверхности ионов, с нейтрализацией и сохранением заметной доли начальной энергии. Выделения атомов с тепловыми скоростями при малых концентрациях внедренного газа не наблюдается.

По мере увеличения длительности облучения, в потоке газоотдачи с поверхности появляются молекулы дейтерия с тепловыми скоростями, выделяющиеся за счет обратной диффузии внедренного газа. При большом времени облучения наступает насыщение, при котором полный поток газа с поверхности равен потоку падающих ионов. Концентрация внедренных атомов при насыщении, согласно измерениям, не зависит от плотности ионного тока и возрастает с энергией ионов (рис. 5а, б, е). Газоемкость при насыщении для разных материалов сильно различается, и возрастает в ряду: нержавеющая сталь, никель, цирконий, молибден, золото. При энергии ионов дейтерия 15 кэв, газоемкость для нержавеющей стали составляет $3 \cdot 10^{17}$ атомов на квадратный сантиметр, для золота — $2 \cdot 10^{18}$ ат/см^2.

Различие между металлами, химически-взаимодействующими и не взаимодействующими с водородом, проявляется в температурной зависимости процесса внедрения ионов. При нормальной температуре, для циркония имеет место такое же насыщение при внедрении ионов, как и для золота или молибдена. При повышенных температурах (200° С), внедрение ионов в цирконий происходит без насыщения, вплоть до полного «пропитывания» материала водородом на всю толщину. Эффективный коэффициент захвата при этом в несколько раз меньше начального (рис. 5 б). Отсутствие насыщения связано со значительной скоростью диффузии газа в толщу материала. При более высоких температурах (450° С) внедрение в цирконий снижается за счет усиливающегося выделения газа в объем. Для материалов, химически не связывающих водород (нержавеющая сталь, молибден, золото), повышение температуры мишени уже до 100—150° С сильно увеличивает обратную диффузию, и уменьшает внедрение (рис. 5г).

Прочность связывания внедренных атомов водорода зависит от химической природы металла. Для металлов, не образующих гидриды, полное выделение внедренного газа происходит при температурах 200—250° С. Выделение внедренного водорода из циркония начинается при температуре 350° С, и при повышении температуры происходит в две стадии. Первая стадия завершается при температурах 600—700° С; вторая стадия проходит при нагревании выше температуры фазового перехода в цирконии (860° С); полное выделение завершается при температуре около 1000° С.

Ионы инертных газов, внедряющиеся в твердые поверхности, связываются более прочно, чем ионы водорода. Коэффициент захвата ионов гелия молибденом, при энергии ионов 15 кэв, составляет 0,75 (рис. 5в). Выделение внедренных ионов гелия происходит при температуре выше 500° С. Газоемкость при насыщении, в связи с меньшей глубиной проникновения ионов, меньше чем для водорода (рис. 5е).

Для изучения механизма захвата ионов водорода при внедрении в твердые поверхности, поставлены опыты с модулированным ионным пучком, и опыты измерения потока диффузионно-выделяющихся атомов в процессе облучения, и по прекращении облучения. В опыте с модулированным пучком, раздельно регистрируется поток отраженных (рассеянных) атомов, с энергиями выше тепловых, и поток газа, выделяющегося с тепловыми скоростями, за счет диффузии. Плотность потоков отраженных и диффузионно выделяющихся атомов отложена по оси ординат на графиках рис. 6а. Мишень, подвергавшаяся до опыта кратковременному облучению (рис. 6а-1), или облучению до насыщения (рис. 6а-2), нагревается в течение нескольких секунд до температуры 250° С. В ходе нагревания, регистрируется переменная и постоянная составляющая потока газа с мишени (при продолжающемся облучении модулированным пучком). Поток отраженных атомов, при всех температурах мишени и длительностях предварительного облучения, остается стопроцентно модулированным; его плотность безинерционно следует за плотностью падающего потока ионов. Обратный диффузионный поток содержит переменную и постоянную составляющие, соотношение которых зависит от температуры мишени и ее предыстории. При малых концентрациях внедренных атомов и низкой температуре мишени, обратный диффузионный поток вообще отсутствует. При повышении температуры мишени, нарастает, и затем спадает до нуля диффузионный поток, содержащий только постоянную составляющую (выделение ранее внедренных атомов за счет тепловой диффузии). При дальнейшем

повышении температуры и продолжающемся облучении модулированным пучком, нарастает, и устанавливается на постоянном значении, зависящем от силы тока в пучке, полностью модулированный диффузионный поток. Скорость обратного диффузионного выделения следует безинерционно (для частоты модуляции 22 герца) за изменениями плотности первичного ионного пучка (рис. 6а-1).

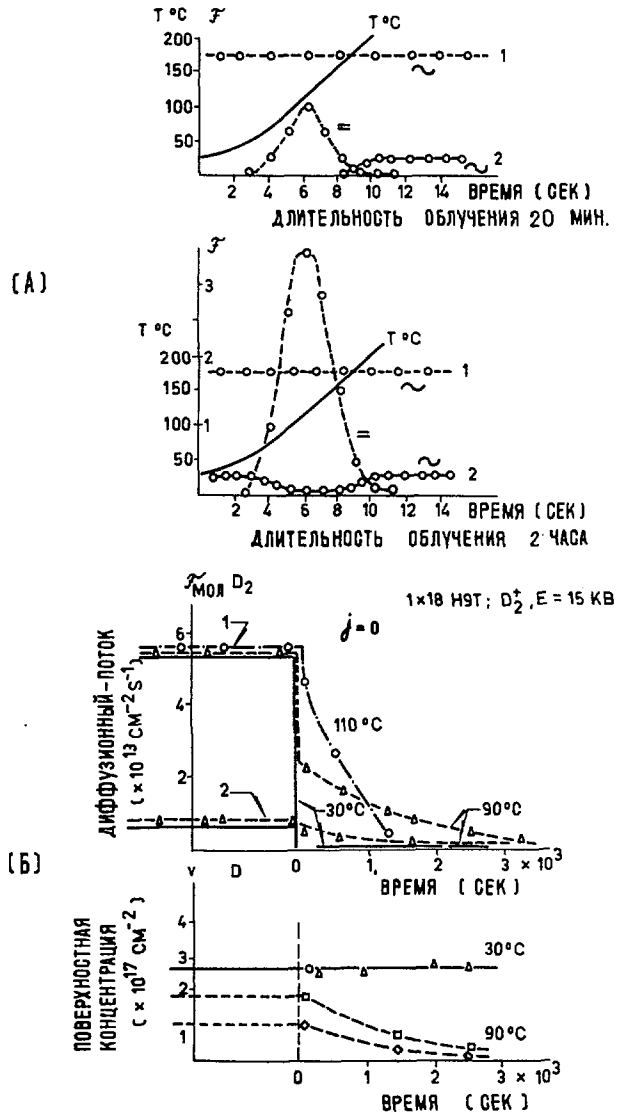

Рис. 6 (А) Соотношение переменной и постоянной составляющей потоков ионов, отражаемых с нейтрализацией, и атомов, диффузионно выделяющихся с поверхности, бомбардируемой модулированным ионным пучком, при повышении температуры мишени. ~ — переменная составляющая, = — постоянная составляющая. 1Х18Н9Т*, D^+, E=16 кв, j=30 мка/см^2, $f_{мод}$=22 гц. 1 — отраженные атомы и ионы, 2 — диффузионные атомы. (Б) — Поток диффузионно-выделяющихся атомов дейтерия, и концентрация внедренных атомов (при облучении до насыщения), в процессе облучения ионным пучком, и после прекращения облучения, для разных температур и разной плотности тока. ○, □ — j=35 мка/см^2, △, ▱ — j=12 мка/см^2, (1) — j=35 мка/см^2, (2) j— =5 мка/см^2. О — момент прекращения облучения.

* Марка нержавеющей стали.

При предварительном облучении мишени до насыщения, уже при низких температурах мишени, наряду с модулированным потоком отраженных атомов, присутствует полностью модулированный поток диффузионно-выделяющихся атомов (в сумме равные потоку падающих ионов). При повышении температуры, происходит нарастание и последующий спад постоянной составляющей диффузионного потока, и спад и последующее нарастание до начального значения переменной составляющей (рис. 6а-2).

Для мишеней, облученных ионным пучком до насыщения, измерения потока диффузионно-выделяющихся атомов по прекращении облучения (рис. 6б), дают следующий результат. При нормальной температуре мишени, диффузионный поток в момент прекращения облучения снижается практически до нуля. При повышенных температурах мишени, в момент прекращения облучения диффузионный поток скачкообразно снижается, но не до нуля, а до конечного значения, меньшего, чем обратный поток при облучении. При выдержке облученной мишени при повышенной температуре, происходит выделение внедренного газа, с постепенно снижающейся скоростью.

Проведенное исследование позволяет составить качественную картину процессов внедрения ионов водорода в твердые поверхности. При малых концентрациях внедренных атомов, внедряющийся ион взаимодействует только с решеткой твердого тела. Ионы, проникшие вглубь решетки, нейтрализуются, рассеиваются на атомах решетки, замедляются, и по достижении некоторой энергии, захватываются решеткой. В исследованном диапазоне средних энергий, рассеяние мало отличается от сферически-симметричного; передача энергии атомам решетки происходит при упругом взаимодействии с атомом, как с целым. В процессе замедления, значительная доля внедряющихся атомов рассеивается на большие углы, и выходит из поверхностного слоя твердого тела обратно в вакуум, сохранив некоторую долю первоначальной энергии. Отступление реального закона рассеяния от закона рассеяния твердых шаров, обнаруживается на опыте в том, что коэффициент захвата ионов с энергией возрастает, тогда как при сферически-симметричном рассеянии он должен слабо снижаться, из-за увеличения числа соударений, требующихся для замедления. Коэффициент захвата ионов в решетку зависит от доли энергии, передаваемой при каждом соударении (что определяет слабую зависимость коэффициента захвата от атомного веса твердого тела), и практически не зависит от химических свойств материала. Расчет коэффициента захвата ионов в решетку может быть сделан с использованием математического аппарата теории замедления нейтронов; получающиеся результаты качественно согласуются с опытом.

При высоких концентрациях газа существенную роль играет взаимодействие внедряющихся ионов с ранее внедренными атомами. Этим взаимодей-

ствием определяется процесс насыщения. Объяснение наблюдаемой на опыте независимости концентрации при насыщении от плотности ионного тока, наличие в обратом диффузионном потоке двух составляющих — безинерционно следующей за изменениями плотности пучка, и инерционной, можно дать на основе следующего представления о механизме явления. Диффузия внедренных атомов в процессе облучения имеет двоякий характер — обычная макроскопическая диффузия, скорость которой зависит от температуры и не зависит от наличия или отсутствия ионного пучка, и диффузия, активируемая облучением. Активированная диффузия внедренных атомов происходит по тепловым клиньям, образующимся вдоль треков внедряющихся ионов. Эффективный коэффициент диффузии, активированной облучением, зависит от истинного коэффициента диффузии в тепловом клине, и пропорционален мгновенной суммарной площади клиньев — среднему сечения клина, времени его существования и числу клиньев, то есть плотности тока. Наблюдаемые на опыте закономерности обратного диффузионного потока при облучении поверхностей ионным пучком с постоянной, или переменной во времени плотностью, качественно описываются диффузионным уравнением вида

$$\frac{\partial c}{\partial t} = q(z) \cdot j - \{D_1(T) + D^* \cdot j \cdot S(z)\} \frac{\partial^2 c}{\partial z^2},$$

где коэффициент диффузии слагается из двух членов:

$D_1(T)$ — нормальный коэффициент диффузии, зависящий от температуры; $D^* j$ — коэффициент активированной диффузии, пропорциональный плотности тока;

c — концентрация внедренных атомов.

$\int_0^d q(z)\,dz = K$ — коэффициент захвата,

$S \cdot (z) = \begin{cases} \sim 1 & 0 < z < a \\ 0 & z > a \end{cases}$

a — глубина внедрения.

Согласно описанному представлению, наибольшую газоемкость при внедрении ионов водорода должны иметь материалы, характеризующиеся наибольшей энергией активации для диффузии внедренных атомов, то есть наиболее трудно растворяющие водород. С этим согласуется то, что наибольшую газоемкость по водороду из числа изученных материалов имеют молибден и золото.

Высказывавшиеся в литературе представления о механизме, определяющем насыщение при внедрении ионов водорода в твердые поверхности — нормальная тепловая диффузия [3], катодное распыление [4], не согласуются с экспериментальными данными.

При практическом использовании внедрения ускоренных ионов, как средства связывания вторичных ионов плазмы при ионной откачке магнитных ловушек, полученные в работе данные позволяют сделать выбор материала для торцовых электродов. Для удобства периодической очистки электродов от внедренного газа, целесообразно применять металлы, не образующие гидридов. Для получения наибольшей газоемкости, целесообразно применять материалы, трудно растворяющие водород, как молибден или золото.

В исследованном диапазоне энергий ионов водорода (7—25 кэв), внедрение, как процесс связывания ионов, характеризуется относительно высоким коэффициентом газоотдачи за счет рассеяния с нейтрализацией (0,6—0,8). С целью увеличения захвата ионов, можно работать при более высоких энергиях. Для того, чтобы суммарный коэффициент газоотдачи не превзошел единицу, должны быть приняты меры к уменьшению других компонент газоотдачи, прежде всего распыления сорбированных газовых пленок.

3.2. Сорбция газов на поверхностях конструкционных материалов при низких давлениях. Распыление сорбированных газовых пленок

Исследование кинетики сорбции газов на поверхностях конструкционных материалов имеет общее значение для техники сверхвысокого вакуума, так как сорбционно-десорбционное равновесие на стенках существенно влияет на достижимый вакуум в динамических системах. В проблеме ионной откачки магнитных ловушек, изучение кинетики сорбции имеет особое значение, так как при наличии на поверхностях сорбированных пленок, ионная бомбардировка приводит к большим значениям газоотдачи, зависящим от плотности сорбированной пленки и ее химической природы. При ионной откачке по методу внедрения, как указывалось выше, не существует значительного запаса по допустимому коэффициенту газоотдачи. В связи с относительно большим значением коэффициента отражения ионов с нейтрализацией, и наличия неизбежного, хотя и небольшого (для ионов водорода) катодного распыления металла, газоотдача за счет распыления сорбированных пленок должна быть сведена к минимуму, чтобы ионная откачка могла осуществляться. Материалы стенок вакуумной камеры и режимы вакуумтехнической подготовки должны выбираться так, чтобы плотность сорбированной газовой пленки на участках ионной бомбардировки была наименьшей.

Коэффициент распыления газовых пленок, при значительной концентрации сорбированного газа, больше чем коэффициент распыления металла. Соответствующие экспериментальные данные, полученные на установке ИСЭП-2 для случая возобновляемой поверхности титана, приводились выше на рис. 3в. Суммарный коэффициент газоотдачи, при типичном режиме возобновления поверхности, составляет 2 атома на ион, главным образом, за счет распыления сорбированных ме-

тана и этана. На рис. 7 приведены значения парциальных коэффициентов газоотдачи с поверхности стенки вакуумной камеры из нержавеющей стали, не подвергавшейся высокотемпературному прогреву. Измерения проведены на установке ИСЭП-2, при непрерывном облучении ионным пучком. На графике показаны компоненты газоотдачи, выделяющиеся с тепловыми скоростями; отраженные с нейтрализацией ионы в график не включены. Основной компонентой газоотдачи являются углеводороды. По мере очистки поверхности ионным пучком, выделение углеводородов со стенки снижается. Количество углеводородов, сбиваемых ионным пучком за время облучения, указывает, что первоначальный сорбированный слой был полимолекулярным. Коэффициент газоотдачи по углеводородам, для непрогретой поверхности превышает единицу.

Коэффициенты распыления ионами водорода сорбированных пленок (порядка единицы), существенно больше, чем коэффициенты катодного распыления металлов, не превышающие величины 0,05, при всех энергиях ионов и для всех металлов. Различие физически связано с тем, что для сбивания сорбированного атома требуется передача ему энергии, порядка энергии связи (не более 3—5 электронвольт). Для выбивания же атома решетки из положения равновесия требуется передача энергии около 25 эв. Передача сорбированному атому импульса, необходимого для разрыва связи с поверхностью, происходит с большей вероятностью, чем аналогичная передача импульса для атомов твердого тела. Механизм распыления сорбированных пленок ближе к термическому; об этом свидетельствует то, что сорбированные молекулы сбиваются при ионной бомбардировке в значительной доле без диссоциации.

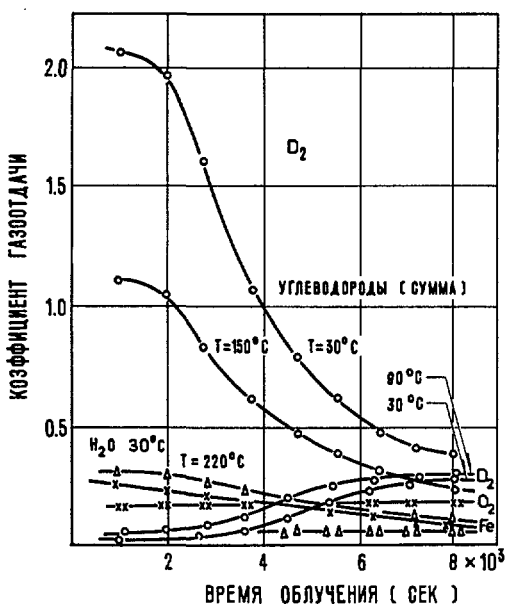

Рис. 7 Газоотдача поверхности стенки вакуумной камеры, не подвергавшейся прогреву, при бомбардировке пучком ионов дейтерия (распыление сорбированных пленок, распыление металла и слоя поверхностного окисла, обратное диффузионное выделение внедренных атомов). 1Х18Н9Т*, D^+, $E=20$ кв, $j=12$ мка/см², $p=4\cdot10^{-8}$ мм рт.ст. Состав газовой среды: D_2 — $2\cdot10^{-8}$ мм, Ar — $8\cdot10^{-9}$ мм, CH_4 — $8\cdot10^{-9}$ мм, CO_2 — $2\cdot10^{-9}$ мм, H_2O — $1\cdot10^{-9}$ мм, углеводороды $1\cdot10^{-9}$ мм, $O_2 < 1\cdot10^{-10}$ мм.

* Марка нержавеющей стали.

В опыте рис. 7, количественно преобладающей компонентой газоотдачи со стенки являются углеводороды, хотя их парциальное давление составляет 2,5% от полного давления в системе. Преобладание углеводородов в поверхностном слое связано со специфическим характером сорбции.

Экспериментальное исследование кинетики сорбции газов при низких давлениях на поверхности конструкционных материалов проводилось на установке ИСЭП-1 (рис. 1). Исследование проведено для сорбции из смесей газов разного состава. В исследовании использован метод вспышки. Образец исследуемого материала выдерживается в течение определенного времени в газовой среде заданного состава, затем быстро нагревается (пропусканием тока) до высокой температуры, при которой все сорбировавшиеся на поверхности газы удаляются. Количество каждой из компонент сорбированных газов, выделяющихся при вспышке, измеряется с помощью масс-спектрометра хронотрон. Датчик масс-спектрометра установлен непосредственно в молекулярном пучке газов, десорбирующихся с образца, и регистрирует выделяющиеся газы при однократном пролете молекул через датчик. Киносъемка с экрана осциллографической трубки масс-спектрометра производится синхронно с записью температуры образца при вспышке.

Сорбционные характеристики некоторых материалов (кинетические кривые и изобары сорбции) приведены на рис. 8. Для вольфрама, при выдержке образца в смеси газов низкого давления, содержащей водород, метан, азот, окись углерода, кислород, аргон, тяжелые углеводороды, на свежеочищенной поверхности сорбируются все компоненты газовой смеси, кроме метана и аргона (рис. 8а). При малых временах выдержки образца в газе после очистки прогревом, количество сорбированных газов линейно возрастает со временем выдержки. При повышении температуры образца в пределах 50—150° С, коэффициент конденсации водорода и тяжелых углеводородов снижается; коэффициент конденсации кислорода, азота и окиси углерода не изменяется. При увеличении времени выдержки, количество сорбирующегося на вольфраме водорода проходит через максимум, и затем снижается в результате понижения коэффициента конденсации и вытеснения водорода с поверхности вольфрама другими сорбирующимися газами. Вытеснение сорбированных молекул водорода начинается при покрытиях, составляющих малую долю мономолекулярного (10%). Сорбция азота и окиси углерода характеризуется насыщением, со степенью покрытия, меньшей единицы.

Сорбция тяжелых углеводородов происходит линейно во времени, с постоянным коэффициентом конденсации, зависящим от температуры. Отклонений от линейного нарастания не наблюдается вплоть до времени выдержки в десятки минут, и степени покрытия в несколько молекулярных слоев. Вытеснения азота, кислорода, окиси углерода тяжелыми углеводородами не происходит; молекулы последних располагаются при сорбции поверх сорбированных слоев кислорода и азота.

Сорбционные характеристики нержавеющей стали сильно отличаются от характеристик вольфрама. Из числа газов, присутствующих в смеси низкого давления, на нержавеющей стали сорбируются тяжелые углеводороды, вода и углекислый газ. Не сорбируются водород, азот, метан, аргон. Сорбция тяжелых углеродородов характеризуется линейным нарастанием во времени, до покрытий, больших мономолекулярного. При сорбции воды и углекислого газа наблюдается равновесное покрытие, меньшее единицы (рис. 8б).

Различие в сорбционных характеристиках нержавеющей стали и свежепрокаленного вольфрама объясняется тем, что на поверхности нержавеющей стали всегда присутствует слой окислов (преимущественно окиси хрома), который не может быть удален нагревом, вплоть до температуры испарения металла. Поверхность окислов сорбционно менее активна, чем поверхность чистых металлов; на поверхности окисного слоя водород и азот при низких давлениях не сорбируются. Поверхность вольфрама, путем высокотемпературного прогрева, может быть сделана чистометаллической, что существенно повышает сорбционную активность. Если вольфрам прогревается до температуры не выше 1000—1200° С, не-

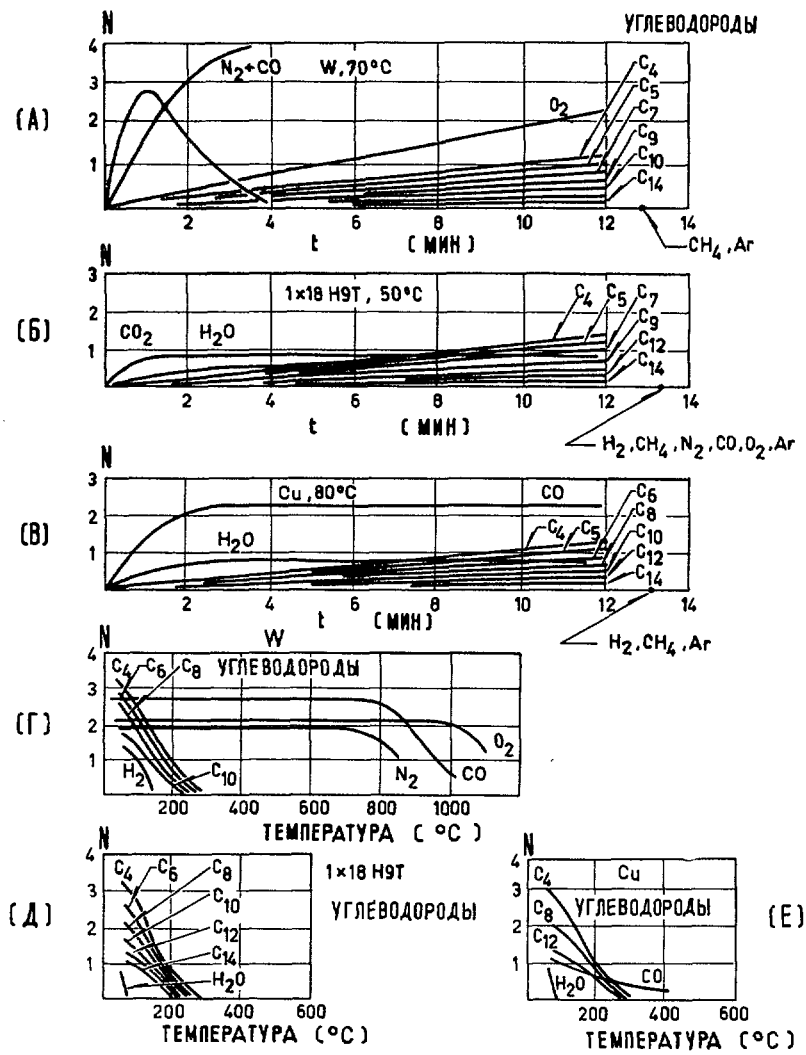

Рис. 8 Характеристики кинетики сорбции газов при низких давлениях на поверхности конструкционных материалов. (А), (Б), (В) — кинетические кривые собрции компонент смеси газов на поверхности вольфрама, нержавеющей стали, меди (зависимость количества сорбированных газов от времени выдержки образца в газе). (Г), (Д), (Е) — изобары сорбции из смеси газов (зависимость количества сорбированных газов от температуры поверхности, при фиксированном времени выдержки). $p = 7 \cdot 10^{-8}$ мм рт.ст. состав газовой среды; H_2 — $2 \cdot 10^{-8}$ мм, CH_4 — $1{,}5 \cdot 10^{-8}$ мм, H_2O — $4 \cdot 10^{-9}$ мм, N_2 — $4 \cdot 10^{-9}$ мм, CO — $1{,}5 \cdot 10^{-8}$ мм, O_2 — $3 \cdot 10^{-10}$ мм, Ar — $1 \cdot 10^{-8}$ мм; углеводороды $3 \cdot 10^{-9}$ мм.

достаточной для удаления кислорода с поверхности, сорбционные характеристики вольфрама становятся подобными характеристикам нержавеющей стали (водород перестает сорбироваться). Сорбционные характеристики меди в условиях опытов близки к характеристикам нержавеющей стали (рис. 8в), в связи с тем, что на поверхности меди присутствует пленка окислов, неудаляемая прогревом.

Температурная зависимость сорбции газов на металлах описывается изобарами, приведенными на рис. 8г, д, е. Для вольфрама сорбция кислорода, азота, окиси углерода является неактивированной хемосорбцией. Коэффициент конденсации не зависит от температуры, при изменении от нормальной до 800—900° С. При повышении температуры свыше 800° С, коэффициент конденсации этих газов снижается и приближается к нулю при температуре около 1500° С. Сорбционные силы, связывающие водород на поверхности вольфрама, слабее, чем силы, связывающие кислород и азот, и, как указывалось выше, резко зависят от степени чистоты поверхности. На чистой поверхности вольфрама, при давлении водорода $\sim 1 \cdot 10^{-8}$ мм рт.ст., равновесное покрытие снижается до нуля при температуре 150° С. Сорбция тяжелых углеводородов имеет характер физической адсорбции; при давлениях $2 \cdot 10^{-9} — 2 \cdot 10^{-8}$ мм рт.ст. тяжелые углеводороды перестают сорбироваться при температуре 300° С.

Изобары сорбции газов на нержавеющей стали указывают на физическую (Ван-дер-Ваальсову) природу сил, связывающих с поверхностью сорбирующиеся на ней газы. В исследованной области низких давлений, сорбция на нержавеющей стали всех компонент остаточных газов, присутствующих в установке, прекращается при температуре 300° С.

Характеристики сорбции газов на поверхности конструкционных материалов при низких давлениях показывают следующие общие черты явления. Сорбция имеет избирательный характер. При нормальной температуре, некоторые газы испытывают хемосорбцию (для вольфрама — кислород, азот); другие газы — физическую сорбцию (вода, углекислота, тяжелые углеводороды). Ряд газов, из числа обычно присутствующих в остаточных газах вакуумных систем (метан, аргон), при нормальной температуре на поверхности металлов не сорбируется. Характер сорбции различен для разных металлов, и зависит как от рода металла, так и от состояния поверхности. При совместной сорбции различных газов, наблюдается явление взаимного влияния сорбированных молекул, включая вытеснение слабо связанных с поверхностью газов, при покрытиях поверхности, меньших мономолекулярного.

Полученные в работе данные о кинетике сорбции газов металлами, позволяют делать выбор конструкционных материалов и режимов вакуумной подготовки поверхностей при осуществлении того или иного из методов сверхвысоковакуумной откачки в рабочем процессе магнитных ловушек.

3.3. Связывание медленных ионов на возобновляемых поверхностях химически-активных металлов при низких температурах

Из приведенных выше экспериментальных данных по внедрению ионов средних энергий в твердые поверхности вытекает, что связывание вторичных ионов плазмы при ионной откачке по методу внедрения, принципиально осуществимо. Необходимые для этого вакуумные материалы и режимы вакуумтехнической подготовки практически доступны. Ионная откачка по методу внедрения имеет, однако, ограничения, связанные с тем, что для ионов тяжелее водорода, при энергиях, необходимых для внедрения, коэффициент катодного распыления металлов больше единицы. Если тяжелые атомы, выбитые с поверхности торцового электрода, будут возвращаться в плазму и ионизоваться раньше, чем связываться на стенках, концентрация тяжелых ионов в плазме будет возрастать. Нарастание примесей может ограничивать накопление плазмы на некотором значении плотности. Снижение влияния примесей с большим коэффициентом катодного распыления может быть достигнуто применением геометрии торцовых электродов, при которой уменьшается возврат в плазму выбитых с поверхности тяжелых атомов.

Указанная трудность отсутствует при другом методе связывания вторичных ионов плазмы, путем их поглощения на возобновляемых поверхностях химически-активных металлов. Возможность практического использования этого метода появилась после открытия особенностей явления низкотемпературной сорбции. При ионной бомбардировке, газовыделение с поверхностей химически-активных металлов при нормальных температурах велико уже при энергиях ионов в несколько электронвольт. Как указывалось выше, это связано с наличием на поверхностях слабо связанных молекулярных комплексов, образующихся в результате каталитических химических реакций.

При достаточно низких температурах металлов, каталитические реакции подавляются, что приводит к снижению газоотдачи. Связывание ионов водорода, кислорода, азота и других химически активных газов, при тепловых энергиях ионов, происходит так же эффективно, как связывание этих газов в атомарном состоянии. Вероятность связывания выше, чем при диссоциативной хемосорбции молекулярных газов, потому что на поверхностях имеется большее число участков, активных для сорбции атомов, чем участков, на которых может происходить сорбция молекул. При энергиях ионов выше тепловых, связывание химическими силами ослабляется, так как при рассеянии иона в поверхностном слое твердого тела, составляющая его энергии для движения в направлении от поверхности в вакуум может превзойти энергию адсорбции. При еще более высоких энергиях ионов, потенциальное связывание заменяется кинетическим (за счет внедрения),

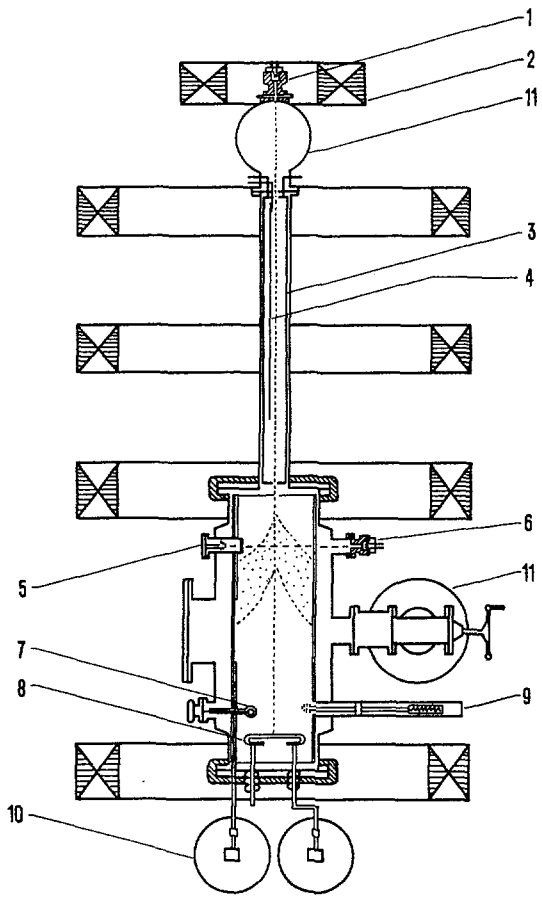

Рис. 9 Установка ВИП-0,4 для исследования кинетики связывания медленных ионов на возобновляемых поверхностях сорбционно-активных металлов. 1 — инжектор плазмы, 2 — катушки продольного магнитного поля, 3 — плазмопровод с трубчатой азотитной ловушкой, 4 — прямонакальный биметаллический испаритель титана, 5, 6 — прибор для зондирования плазмы молекулярным пучком, 7 — испаритель исследуемого металла, 8 — поверхность конденсации металла (мишень для струи плазмы), 9 — масс-спектрометр хронотрон, 10 — дюары с жидким азотом, 11 — паромутные насосы.

описанным выше. Энергия ионов, выше которой потенциальное связывание на химически-активных поверхностях ослабляется, зависит от энергии адсорбции и характеристик металла и иона. Если энергия вторичных ионов плазмы, выходящих за пробки, не превосходит наибольшей энергии, при которой возможно потенциальное связывание (или допускает снижение до этой величины путем торможения), то поглощение ионов на возобновляемых поверхностях химически-активных металлов (титана и др.), охлажденных до температуры жидкого азота, будет эффективным методом ионной откачки.

Характеристики процессов потенциального связывания медленных ионов в настоящее время неизвестны. Для отработки режимов ионной откачки поставлено экспериментальное исследование взаимодействия ионов малых энергий с поверхностями химически-активных металлов.

Экспериментальная установка ВИП-0,4 показана на рис. 9. Возобновляемая поверхность исследуемого металла создается на охлаждаемой подложке (мишени), путем непрерывного или периодического испарения металла. Медленные ионы поступают на мишень из струи плазмы, инжектируемой по силовым линиям магнитного поля из газоразрядного источника (в импульсном режиме, с длительностью импульсов 1 сек). Энергия ионов, поступающих на мишень, регулируется заданием потенциала мишени относительно стенок. Эффективность связывания газовых ионов на поверхности мишени определяется путем измерения повышения парциального давления в объеме за счет газа, десорбирующегося с мишени при вводе струи плазмы. Полный поток газа, приносимого струей плазмы в виде ионов, измеряется по повышению давления при направлении струи плазмы на несорбирующую мишень. Контроль постоянства плотности плазмы от импульса к импульсу осуществляется методом зондирования плазмы молекулярным пучком цезия (по ослаблению молекулярного пучка за счет ионизации в струе плазмы). Уменьшение поступления нейтрального газа из источ-

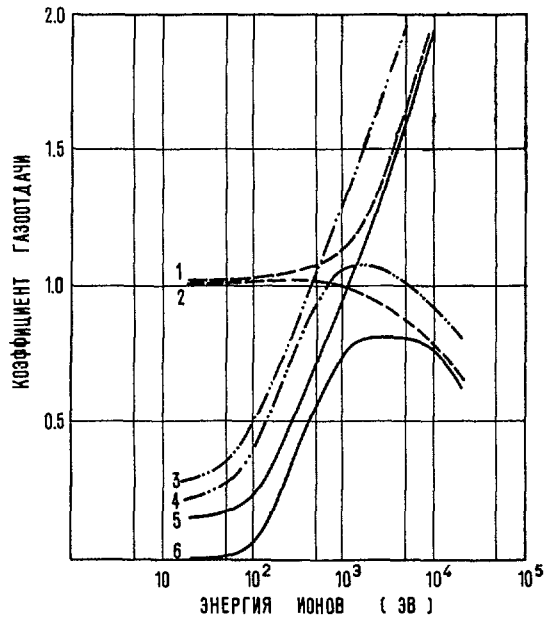

Рис. 10 Зависимость от энергии ионов суммарного коэффициента газоотдачи при бомбардировке твердых поверхностей (возврат в объем нейтрализованных ионов, распыление металла и сорбированных газовых пленок). (1) — ионы азота, поверхность нержавеющей стали, прогретой в вакууме, N^+, 1Х18Н9Т*; (2) — ионы водорода, поверхность нержавеющей стали, прогретой в вакууме, H^+, 1Х18Н9Т*; (3) — ионы азота, поверхность титана при температуре — 190° С, после сорбции газов, со степенью покрытия поверхности 0,2, N^+, Ti (аз.), $S=0{,}2$; (4) — ионы водорода, поверхность титана при температуре —190° С, после сорбции газов, со степенью покрытия поверхности 0,2, H^+, Ti (аз.), $S=0{,}2$; (5) — ионы азота, свежевозобновленная поверхность титана при температуре —190° С, N^+, Ti (аз.), $S=0$; (6) — ионы водорода, свежевозобновленная поверхность титана при температуре —190° С, H^+, Ti (аз.), $S=0$.

* Марка нержавеющей стали.

ника плазмы и поддержание в измерительном объеме высокого вакуума, необходимого для снижения загрязнений плазмы ионами остаточного газа, достигается дифференциальной откачкой. Система дифференциальной откачки состоит из мощного парортутного насоса и трубчатой азотитной ловушки длиной 1,5 метра и диаметром 100 мм. Струя плазмы пропускается по оси ловушки. Слой титана на стенках ловушки возобновляется после каждого импульса инжекции. В описанной простой системе поддерживается давление $1-3\cdot10^{-8}$ мм рт.ст. при инжекции струи плазмы небольшой плотности. Установка допускает также сравнительную оценку эффективности ионной откачки различных газов, путем измерения снижения парциальных давлений компонент остаточных газов, ионизующихся в струе плазмы. Экспериментальная работа находится в стадии отработки методики в направлении уточнения измерений энергии ионов (уменьшения колебаний потенциала плазмы), и повышения чистоты исходной плазмы (снижения загрязнений посторонними ионами, образующимися в инжекторе).

Предварительные экспериментальные результаты показывают высокую эффективность связывания медленных ионов химически-активных газов (водорода, азота) на возобновляемой поверхности титана, охлажденной до температуры жидкого азота. На графике рис. 10 приведены значения суммарного коэффициента газоотдачи при бомбардировке поверхностей ионами водорода и азота разных энергий, от 20 эв до 20 кэв. Экспериментальные данные для низких энергий получены в описываемых опытах на установке ВИП-0,4, для средних энергий — в ранее описанных опытах по внедрению ионов. Коэффициент катодного распыления металлов взят по литературным данным. Для сравнения приведены кривые газоотдачи для несорбирующей поверхности (нержавеющей стали).

На свежевозобновленной охлаждаемой поверхности титана, при энергиях ионов водорода ниже 100 эв, коэффициент газоотдачи ниже 0,1. При повышении энергии ионов до 1000—5000 эв, коэффициент газоотдачи возрастает до 0,8, и при дальнейшем увеличении энергии снижается за счет эффекта внедрения ионов. На поверхности титана, сорбировавшей определенное количество газа (со степенью покрытия около 0,2), газоотдача поверхности больше, за счет распыления сорбированной пленки, но коэффициент газоотдачи остается меньшим единицы до энергии ионов 400—600 эв. Для ионов азота при низких энергиях связывание на поверхности титана и газоотдача аналогичны ионам водорода. При средних энергиях ионов азота, суммарный коэффициент газоотдачи для всех поверхностей больше единицы, из-за сильного катодного распыления металла. Связывание медленных ионов инертных газов на охлажденных поверхностях происходит менее эффективно.

При практическом использовании метода химического связывания медленных ионов, для ионной откачки магнитных ловушек с инжекций, поглощающие поверхности (азотиты) должны размещаться внутри вакуумной камеры установки, за пробками, в зоне выхода вторичных ионов. При этом азотиты будут выполнять двоякую функцию — откачки газов с большими скоростями в нейтральном состоянии, и ионной откачки. Использование азотитов для ионной откачки предусматривается программой экспериментальных работ на установке Огра.

4. Заключение

Проведенные в настоящей работе исследования взаимодействия ионов с твердыми поверхностями, и кинетики сорбции газов металлами, показывают, что задача поддержания сверхнизких давлений нейтрального газа в процессе накопления плазмы в магнитных ловушках с инжекцией, при скоростях откачки масштаба 10—100 миллионов литров в секунду, разрешима, и показывают способы технического решения задачи. Полученные в работе данные имеют общее значение в технике сверхвысокого вакуума динамических систем. Предложенный в работе низкотемпературно-сорбционный метод откачки, и низкотемпературно-сорбционные откачные устройства (азотиты), являются эффективным и широко применимым средством сверхвысоковакуумной откачки с большими скоростями, особенно в системах с присутствием плазмы и потоков заряженных частиц.

Литература

[1] Курчатов, И. В. *Атомная энергия* **5** (1958) 105.
[2] Косн, J., *Nature* **161** (1948) 566.
[3] Fiebiger, K., *Z. für angewandte Physik* **9** (1957) 213.
[4] Кучай, С. А., Родин, А. М. *Атомная энергия* **4** (1958) 202.

EFFET D'UNE PAROI CONDUCTRICE SUR LA STABILITÉ DES CONFIGURATIONS A MIROIRS MAGNÉTIQUES*

M. VUILLEMIN

GROUPE DE RECHERCHES DE L'ASSOCIATION EURATOM-CEA SUR LA FUSION

FONTENAY-AUX-ROSES (SEINE), FRANCE

A l'aide du principe d'énergie de Bernstein, déduit des équations magnétohydrodynamiques de Chew, Goldberger et Low, on étudie la stabilité d'une classe d'équilibres particuliers avec pression anisotrope, dans une configuration à miroirs magnétiques. Dans le cas de la symétrie de révolution sans champ azimuthal, le problème de minimisation de la variation d'énergie peut être conduit d'une manière analogue à celle employée par Bernstein et autres dans le cas d'une pression scalaire.

On montre d'abord qu'en l'absence de parois conductrices, il existe une condition nécessaire de stabilité vis-à-vis des déplacements qui ne modifient pas le champ magnétique.

La présence d'une paroi parfaitement conductrice qui coupe les lignes de champ, en contact avec le plasma, impose aux déplacements de s'annuler sur cette paroi. Cette condition élimine la classe des déplacements responsables de l'instabilité « en flûte ». Dans ce cas, l'étude de la stabilité est ramenée à l'examen du signe des valeurs propres d'une équation de Sturm-Liouville. On établit une condition suffisante de stabilité en cherchant une borne inférieure de la première valeur propre de cette équation: pour que le plasma soit stable. il suffit que cette borne soit positive.

1. Introduction

L'instabilité des configurations à miroirs magnétiques a depuis longtemps été reconnue par différents auteurs [1]. Or, de nombreuses expériences récentes ont mis en évidence une stabilité inattendue [2]. Parmi les raisons que donnent ces auteurs pour justifier ce fait expérimental, la plus satisfaisante semble être la présence d'une paroi conductrice qui interdit aux instabilités, prévues théoriquement, de se développer.

Nous nous proposons d'étudier ici la stabilité d'une classe d'équilibres particuliers avec pression anisotrope, dans une configuration possédant la symétrie de révolution. Nous utilisons pour cela le principe d'énergie de BERNSTEIN [3] étendu à la magnétohydrodynamique de CHEW, GOLDBERGER et LOW.

Dans une première partie, on définit une classe particulière de solutions d'équilibre. On montre dans la deuxième partie que le problème de minimisation de la variation d'énergie peut être conduit comme dans [3]. En l'absence de parois conductrices on en déduit immédiatement une condition nécessaire de stabilité qui généralise celle de ROSENBLUTH et LONGMIRE [1]. En présence de parois conductrices, le problème est ramené à l'examen du signe des valeurs propres d'une équation de Sturm-Liouville. On établit alors une condition suffisante de stabilité en cherchant une borne inférieure de la première valeur propre de cette équation.

2. Solutions d'équilibre

Les équations d'équilibre dans l'approximation C.G.L. s'écrivent:

$$\mathbf{j}\times\mathbf{B} = \nabla\cdot\mathsf{p} \tag{1}$$

$$\nabla\cdot\mathbf{B} = 0 \tag{2}$$

$$\mathbf{j} = \nabla\times\mathbf{B} \tag{3}$$

où p, le tenseur de pression, a la forme:

$$\mathsf{p} = p_\perp(1 - \mathbf{e}\,\mathbf{e}) + p_\parallel \mathbf{e}\,\mathbf{e} \tag{4}$$

$$\mathbf{e} = \mathbf{B}/B$$

Nous nous limitons maintenant aux configurations possédant la symétrie de révolution, sans composante azimuthale du champ magnétique. On utilise alors le système de coordonnées curvilignes, défini dans [3]. Soit $\mathbf{e}_\psi$, $\mathbf{e}_\theta$, $\mathbf{e}_\chi$ le système orthonormé correspondant.

L'élément de volume est $d\tau = J\,d\psi\,d\theta\,d\chi$.

L'opérateur gradient s'écrit:

$$\nabla = rB\,\mathbf{e}_\psi\frac{\partial}{\partial\psi} + \frac{1}{r}\mathbf{e}_\theta\frac{\partial}{\partial\theta} + \frac{1}{JB}\mathbf{e}_\chi\frac{\partial}{\partial\chi}$$

Les équations d'équilibre (1) et (3) deviennent:

$$\frac{\partial N}{\partial\chi} + M\frac{\partial B}{\partial\chi} = 0 \tag{5}$$

$$B\frac{\partial(MB)}{\partial\psi} + N\frac{\partial B}{\partial\psi} + \frac{1}{J}\frac{\partial}{\partial\psi}(JB^2)\left[1 + M - \frac{N}{B}\right] = 0 \tag{6}$$

où l'on a posé

$$M = \frac{P_\perp}{B^2}, \qquad N = \frac{P_\parallel}{B}$$

Les fonctions M et N sont reliées par l'équation (5) et restent donc, dans une large mesure, arbitraires. Nous allons particulariser l'équilibre en imposant une relation supplémentaire entre ces fonctions. Pour cela nous faisons l'hypothèse que les quantités $p_\perp/\varrho B$ et $p_\parallel B^2/\varrho^3$ sont constantes sur une ligne de champ magnétique, soit en éliminant ϱ:

$$N = M^3 g(\psi) \tag{7}$$

On peut justifier l'hypothèse précédente en remarquant que les deux invariants adiabatiques C.G.L.

* Mémoire CN-10/100 présenté par M. VUILLEMIN. La discussion concernant ce mémoire est donnée page 358. Les traductions du résumé se trouvent en fin de volume.

sont liés au mouvement des particules elles-mêmes le long des lignes de champ.

Dans ces conditions, l'équation (5) s'intègre immédiatement à l'aide d'une deuxième fonction arbitraire $h(\psi)$:

$$M = \frac{1}{\sqrt{g}} \left[\frac{2}{3}(h-B)\right]^{\frac{1}{2}} \tag{8}$$

$$N = \frac{1}{\sqrt{g}} \left[\frac{2}{3}(h-B)\right]^{\frac{3}{2}} \tag{9}$$

Nous avons ainsi défini une classe d'équilibres dépendant de deux fonctions arbitraires $g(\psi)$ et $h(\psi)$. L'équation (6) détermine la configuration magnétique. Si les pressions sont faibles, on pourra toujours imposer le type de la configuration par des champs extérieurs.

Nous supposerons dans ce qui suit que la configuration est du type «bouteille magnétique». Dans ce cas les équations (8) et (9) permettent le confinement entre deux miroirs magnétiques.

Les pressions ne sont définies que dans la région

$$0 < g(\psi) < +\infty$$
$$B < h(\psi)$$

Pour avoir un confinement, il suffit de prendre $h(\psi) \leqslant B_{\max}$ sur chaque ligne de champ. Le confinement latéral sera déterminé par la ligne sur laquelle $1/g(\psi)$ s'annule.

3. Etude de la stabilité

Nous allons étudier la stabilité de ces configurations par la méthode du principe d'énergie développée par Bernstein et ses collaborateurs [3].

L'intégrale de volume de la variation d'énergie dans le cas d'une pression anisotrope s'écrit:

$$\begin{aligned}\delta W_F = \frac{1}{2}\int \mathrm{d}\tau \Big\{ & Q^2 - \mathbf{j}\cdot\mathbf{Q}\times\boldsymbol{\xi} + \frac{5}{3}p_\perp(\nabla\cdot\boldsymbol{\xi}) \\ & + \nabla\cdot\boldsymbol{\xi}\,(\boldsymbol{\xi}\cdot\nabla p_\perp) + \frac{1}{3}p_\perp(\nabla\cdot\boldsymbol{\xi} - 3q)^2 \\ & + q\,\nabla\cdot[(p_\parallel - p_\perp)\boldsymbol{\xi}] \\ & + (p_\parallel - p_\perp)[\mathbf{e}\cdot(\mathbf{a}\cdot\nabla)\boldsymbol{\xi} + \mathbf{a}\cdot(\mathbf{e}\cdot\nabla)\boldsymbol{\xi} - 4q^2]\Big\}\end{aligned} \tag{10}$$

où

$$\mathbf{Q} = \nabla\times(\boldsymbol{\xi}\times\mathbf{B})$$
$$\mathbf{a} = (\mathbf{e}\cdot\nabla)\boldsymbol{\xi} - (\boldsymbol{\xi}\cdot\nabla)\mathbf{e}$$
$$q = \mathbf{e}\cdot(\mathbf{e}\cdot\nabla)\boldsymbol{\xi}$$

Nous allons transformer cette expression en utilisant les équations d'équilibres. Après quelques intégrations par parties et en utilisant nos notations, on obtient

$$\begin{aligned}\delta W_F = \frac{1}{2}\int J\,\mathrm{d}\psi\,\mathrm{d}\theta\,\mathrm{d}\chi \Big\{ & (1-\sigma_-)Q_\perp^2 \\ & + (1+2M)\left[Q_\parallel - \frac{B(qM + DM)}{1+2M}\right]^2 \\ & + \alpha B\left[q - \frac{M}{\alpha}\left(DB + \frac{BDM}{1+2M}\right)\right]^2 \\ & + FZ^2 + GXZ + HX^2\Big\}\end{aligned} \tag{11}$$

où

$$X = rB\xi_\psi, \quad Y = \frac{\xi_\theta}{r}, \quad Z = \frac{\xi_\chi}{B}$$

$$Q_\perp^2 = \frac{1}{J^2 r^2 B^2}\left(\frac{\partial X}{\partial\chi}\right)^2 + \frac{r^2}{J^2}\left(\frac{\partial Y}{\partial\chi}\right)^2$$

$$Q_\parallel = -B\left(\frac{\partial X}{\partial\psi} + \frac{\partial Y}{\partial\theta}\right)$$

$$D = \boldsymbol{\xi}\cdot\nabla = X\frac{\partial}{\partial\psi} + \frac{Z}{J}\frac{\partial}{\partial\chi}$$

$$q = \frac{1}{JB}\left[\frac{\partial(ZB)}{\partial\chi} + X\frac{\partial(JB)}{\partial\psi}\right]$$

$$\alpha = 3N - \frac{BM^2}{1+2M}$$

$$\sigma_- = \frac{N}{B} - M$$

$$F = -\frac{B}{J^2\alpha}\left(\frac{\partial B}{\partial\chi} + \frac{B}{1+2M}\frac{\partial M}{\partial\chi}\right)\left(M^2\frac{\partial B}{\partial\chi} + 3N\frac{\partial M}{\partial\chi}\right)$$

$$G = -\frac{2B}{J\alpha}\left(\frac{\partial B}{\partial\psi} + \frac{B}{1+2M}\frac{\partial M}{\partial\psi}\right)\left(M^2\frac{\partial B}{\partial\chi} + 3N\frac{\partial M}{\partial\chi}\right)$$

$$\begin{aligned}H = {} & \frac{1}{J}\frac{\partial(JB)}{\partial\psi}\left(M\frac{\partial B}{\partial\psi} + \frac{\partial N}{\partial\psi}\right) \\ & - \frac{B}{\alpha}\left(\frac{\partial B}{\partial\psi} + \frac{B}{1+2M}\frac{\partial M}{\partial\psi}\right)\left(M^2\frac{\partial B}{\partial\psi} + 3N\frac{\partial M}{\partial\psi}\right)\end{aligned}$$

Dans le cas particulier de nos équilibres, on peut vérifier à l'aide de (5) et (7) que:

$$M^2\frac{\partial B}{\partial\chi} + 3N\frac{\partial M}{\partial\chi} = 0$$

Les coefficients F et G sont donc nuls.

Remarquons d'abord qu'il existe deux conditions nécessaires de stabilité qui doivent être vérifiées en chaque point du plasma [4]:

$$1 - \sigma_- > 0 \tag{12}$$

$$\alpha = 3N - \frac{BM^2}{1+2M} > 0 \tag{13}$$

Si, en effet, ces conditions sont violées dans une petite région du plasma, l'intégrale (11) peut être rendue négative pour des déplacements suffisamment localisés [5]. La condition (12) est toujours vérifiée si $p_\parallel/B^2 < 1$, ce qui est en général le cas pour les machines à miroirs. La condition (13) est, par contre, toujours en défaut au voisinage des miroirs, s'il y a confinement parfait du plasma. En effet, elle s'écrit, en tenant compte de (7)

$$3Mg - \frac{B}{1+2M} > 0$$

Le long d'une ligne de champ $g(\psi)$ reste constant et cette condition est toujours en défaut pour M suffisamment petit. Nous supposerons, pour la suite des calculs, que les pressions ne s'annulent pas rigoureusement aux miroirs (c'est-à-dire qu'il existe une fuite de particules) de façon que la condition (13) reste toujours vérifiée.

Cette hypothèse étant faite nous allons effectuer la minimisation de (11) en suivant la méthode exposée

dans [3] qui s'applique exactement au cas de nos équilibres:

1) Une analyse de Fourier des composantes du déplacement permet d'écrire

$$\delta W_F = \delta W_0 + 2 \sum_m \delta W_m$$

les δW_m étant indépendants, et l'on montre que

$$\text{Min}\,\{\delta W_m\} \geqslant \text{Min}\,\{\delta W_{m+1}\}$$

Il suffit alors de chercher le minimum de δW_∞

2) La minimisation de δW_∞ par rapport à Y est alors algébrique.

3) La minimisation suivante par rapport à Z conduit à l'équation d'Euler que l'on peut intégrer immédiatement.

Tous calculs faits le résultat peut alors se mettre sous la forme:

$$\delta W = \frac{\pi}{2}\int \delta W(\psi)\,\mathrm{d}\psi$$

avec

$$\delta W(\psi) = \int \mathrm{d}\chi \left[\frac{1-\sigma_-}{J r^2 B^2}\left(\frac{\partial X}{\partial \chi}\right)^2 + JHX^2\right] + f^2(\psi)\int \mathrm{d}\chi \frac{JBM^2}{\alpha} \tag{14}$$

$$f(\psi) = \frac{\int JKX\,\mathrm{d}\chi}{\int \frac{JBM^2}{\alpha}\,\mathrm{d}\chi}$$

$$K = \frac{M}{J}\frac{\partial}{\partial \psi}(JB)\left[1 + \frac{MB}{\alpha}\frac{1-\sigma_-}{1+2M}\right]$$

La variable ψ ne figure plus que comme paramètre dans l'expression (14). Le problème de la stabilité au voisinage d'une ligne de champ est donc unidimensionnel.

En l'absence de parois conductrices, on obtient une condition nécessaire de stabilité en écrivant que $\delta W(\psi) > 0$ sur chaque ligne de champ pour les déplacements tels que $\partial X/\partial \chi = 0$.

Dans ce cas le premier terme de (14) disparait et X sort des intégrales dans les autres termes.

$$\delta W(\psi) = X^2 \left\{ \int JH\,\mathrm{d}\chi + \frac{\left(\int JK\,\mathrm{d}\chi\right)^2}{\int \frac{JBM^2}{\alpha}\,\mathrm{d}\chi}\right\} > 0 \tag{15}$$

Si l'on applique ce critère au voisinage de la frontière du plasma où les pressions s'annulent, en tenant compte des relations d'équilibre, il prend la forme:

$$\int \frac{p_\parallel + p_\perp}{r B^2}\frac{\mathrm{d}l}{R} > 0 \tag{16}$$

où l'on a posé

$$\mathrm{d}l = JB\,\mathrm{d}\chi$$

$$\frac{1}{rR} = -\frac{1}{J}\frac{\partial}{\partial \psi}(JB)$$

Le rayon de courbure R est ici défini algébriquement avec la même convention de signe que dans [1]. Le critère (16) est exactement celui trouvé par Rosenbluth et Longmire. Il n'est sans doute jamais vérifié dans une configuration ordinaire où les pressions sont maximum au centre, dans la région où le rayon de courbure est négatif.

Condition suffisante de stabilité en présence de parois conductrices

Lorsqu'une paroi parfaitement conductrice est en contact avec le plasma, le champ de déplacement $\boldsymbol{\xi}$ doit vérifier les conditions aux limites suivantes [3].

$$\mathbf{n}\cdot\boldsymbol{\xi} = 0 \qquad \mathbf{n}\times\mathbf{E} = 0$$

où $\mathbf{n}$ est le vecteur unitaire porté par la normale à la paroi.

Si l'on admet la loi d'Ohm classique

$$\mathbf{E} + \mathbf{v}\times\mathbf{B} = 0$$

la deuxième condition est équivalente à:

$$\mathbf{n}\times(\boldsymbol{\xi}\times\mathbf{B}) = 0$$

$$(\mathbf{n}\cdot\boldsymbol{\xi})\,\mathbf{B} - (\mathbf{n}\cdot\mathbf{B})\,\boldsymbol{\xi} = 0$$

Si la paroi coupe les lignes de champ ($\mathbf{n}\cdot\mathbf{B} \neq 0$) on voit que ces deux conditions imposent $\boldsymbol{\xi} = 0$ sur la paroi.

Dans ce cas, les déplacements définis dans le paragraphe précédent, vérifiant $\partial X/\partial \chi = 0$ ne sont compatibles avec ces conditions aux limites que s'ils sont identiquement nuls.

Pour éliminer ce cas trivial, il suffit d'imposer une normalisation aux déplacements $\boldsymbol{\xi}$. Nous la choisissons de façon à simplifier le plus possible le résultat:

$$\int \frac{J r^2 B^2}{1-\sigma_-} X^2\,\mathrm{d}\chi = 1$$

Nous devons donc chercher une borne inférieure de l'expression:

$$\Lambda = \frac{\int \mathrm{d}\chi \left[\frac{1-\sigma_-}{J r^2 B^2}\left(\frac{\partial X}{\partial \chi}\right)^2 + JHX^2\right] + f^2(\psi)\int \frac{JBM^2}{\alpha}\,\mathrm{d}\chi}{\int \frac{J r^2 B^2}{1-\sigma_-} X^2\,\mathrm{d}\chi}$$

Le deuxième terme du numérateur étant toujours positif, on peut écrire:

$$\Lambda \geqslant \lambda = \frac{\int \mathrm{d}\chi \left[\frac{1-\sigma_-}{J r^2 B^2}\left(\frac{\partial X}{\partial \chi}\right)^2 + JHX^2\right]}{\int \frac{J r^2 B^2}{1-\sigma_-} X^2\,\mathrm{d}\chi}$$

Faisons un changement de variable défini par

$$\mathrm{d}x = \frac{J r^2 B^2}{1-\sigma_-}\mathrm{d}\chi$$

d'où

$$\lambda = \frac{\int \mathrm{d}x \left[X'^2 + \frac{1-\sigma_-}{r^2 B^2} HX^2\right]}{\int X^2\,\mathrm{d}x}$$

Le minimum de cette expression est obtenu par les solutions de l'équation de Sturm-Liouville

$$X'' + \left(\lambda - \frac{1-\sigma_-}{r^2 B^2} H\right) X = 0$$

satisfaisant les conditions aux limites prescrites.

Il existe une borne inférieure de la première valeur propre de cette équation:

$$\lambda_1 \geqslant \frac{\pi^2}{\left(\int \frac{J r^2 B^2}{1-\sigma_-} \mathrm{d}\chi\right)^2} + \mathrm{Min}\left\{\frac{1-\sigma_-}{r^2 B^2} H\right\}$$

L'intégrale doit être prise le long d'une ligne de champ entre les points où cette ligne coupe la paroi conductrice, et le second terme représente la valeur minimum de l'expression sur cette même ligne.

Pour que le plasma soit stable il suffit donc que sur chaque ligne de champ:

$$\frac{\pi^2}{\left(\int \frac{J r^2 B^2}{1-\sigma_-} \mathrm{d}\chi\right)^2} + \mathrm{Min}\left\{\frac{1-\sigma_-}{r^2 B^2} H\right\} > 0 \qquad (17)$$

Une application exacte de ce critère nécessiterait la connaissance de configurations magnétiques par la résolution complète de l'équation (6). Ceci n'étant pas fait, nous nous contenterons de faire quelques hypothèses simplificatrices pour donner quelques résultats qualitatifs.

Remarquons d'abord que ce critère se présente sous forme identique à celle d'un critère énoncé par GRAD [6] dans le cas d'un plasma incompressible en pression scalaire.

Le premier terme positif, donc stabilisant, est dû à la tension des lignes de champ dont les extrémités peuvent être considérées comme attachées à la paroi conductrice.

Ce critère est beaucoup moins sévère que celui de Grad. La raison en est qu'il a été trouvé au dernier stade d'une minimisation rigoureuse de la variation d'énergie. On peut d'ailleurs en trouver un autre tout à fait semblable en pression scalaire, qui se déduit immédiatement des résultats de [3]. L'avantage de ce cas serait de pouvoir s'appliquer à des solutions d'équilibre exactes telles que celles proposées par Grad.

Cependant, moyennant quelques hypothèses simplificatrices, nous allons mettre le critère (17) sous une forme où les paramètres physiques apparaîtront plus clairement. Par analogie avec le cas où il n'y a pas de parois conductrices, nous nous placerons sur une ligne de champ voisine de la frontière du plasma où les pressions s'annulent. D'autre part nous supposerons que la quantité $r^2 B$ est à peu près constante sur une ligne de champ.

Il apparaît alors la quantité $L = \int J B \mathrm{d}\chi$, distance entre les parois comptée le long d'une ligne de champ. Nous pouvons aussi trouver une approximation du second terme contenant H et le critère prend la forme:

$$\frac{\pi^2}{L^2} - \frac{\beta}{r_0 R_m} > 0$$

- r_0 est le rayon du plasma dans le plan médian de la configuration.
- R_m est la valeur minimum du rayon de courbure (en valeur absolue) dans la région où il est négatif.
- β représente une valeur caractéristique du rapport $p_\perp / B^2$ dans la configuration.

Cette relation, sans vouloir donner des résultats numériques corrects, présente l'intérêt de définir l'ordre de grandeur du β critique en fonction des paramètres géométriques d'une configuration magnétique donnée. Elle montre que l'effet stabilisant des parois conductrices diminue lorsque leur distance augmente. D'autre part, un faible rapport de miroir, diminuant la courbure des lignes de champ, facilite la stabilisation.

4. Conclusion

Nous avons mis en évidence l'effet stabilisant dû à la présence de parois conductrices, avec l'hypothèse que le plasma touche effectivement ces parois. Dans une machine à miroirs cela suppose l'existence de fuites permanentes de particules.

Mais nous avons vu que cette condition semble réalisée dans ce type de confinement où le plasma est fondamentalement anisotrope.

L'auteur tient à remercier M. Trocheris pour l'intérêt qu'il a porté à ce travail et les intéressantes suggestions qui l'ont aidé à le réaliser.

Références

[1] ROSENBLUTH, M. N., LONGMIRE, C., *Ann. Phys.* (*N. Y.*) **1** (1957) 120.
[2] POST, R. F., ELLIS, R. E., FORD, F. C., ROSENBLUTH, M. N., *Phys. Rev. Lett.* **4** (1960) 166.
[3] BERNSTEIN, I. B., FRIEMAN, E. A., KRUSKAL, M. D., KULSRUD, R. M., *Proc. Roy. Soc.* **A 244** (1958) 17.
[4] LÜST, R., Risö Report no. 18 (1960) 201.
[5] MERCIER, C., COTSAFTIS, M., *Fusion Nucléaire* **1** (1961) 121.
[6] BERKOWITZ, J., GRAD, H., RUBIN, H., Conférence de Genève, **31** (1958) 177.

AN INVESTIGATION OF ELECTRON HEATING AT THE CYCLOTRON FREQUENCY*

M. C. BECKER, R. A. DANDL, H. O. EASON, JR., A. C. ENGLAND, R. J. KERR, W. B. ARD**

OAK RIDGE NATIONAL LABORATORY

OAK RIDGE, TENNESSEE, UNITED STATES OF AMERICA

A microwave power source feeding a cavity in a magnetic mirror system is employed to heat electrons at the electron cyclotron frequency. The power source is a 1 kW, 13 cm, CW klystron feeding the cavity in transverse electric modes. Two objectives are: to establish environmental plasmas for molecular injection devices, and to form an electrodeless plasma for study.

The plasma is formed by microwave electric field breakdown of the 5×10^{-6} mm Hg background gas. Measured incandescence of metal powder dropped through the plasma indicates electron energy densities in the region of 10^{15} eV/cm^3. Analysis of the bremsstrahlung yields electron temperatures of 10 to 30 keV. The electron temperature estimate is corroborated by measured containment times of 20 to 80 ms. The cyclotron heating of electrons seems to have yielded a plasma worthy of study, and extensions of the experiment are in progress.

1. Introduction

In order to study the properties of a very hot electron gas, several methods by which electrons might be raised to very high temperature have been considered. Although a hot electron gas in a background of cold ions cannot actually be considered a hot plasma, some of its properties should be very nearly the same as a plasma in which the ions are also hot. For instance, the radiation emitted by a plasma is virtually independent of the ion temperature. Since it is essential that the plasma not intercept cold surfaces, heating by absorption of electromagnetic energy is attractive. If one is to feed much energy into the plasma by this method, one has to find a frequency at which the absorption of the plasma is large. An obvious frequency is the electron cyclotron frequency. An additional advantage of this method of heating is that the heating can be applied continuously so that the plasma can come to some equilibrium condition. Also the heating power can be turned off quickly enough so that for a finite length of time the plasma exists completely free of external fields.

Of particular interest is the application of energy at cyclotron resonance to a plasma confined in a magnetic mirror [1, 2]. The energy absorbed by the electrons results in an increase in the components of the electron's velocity vector away from the mirror loss cone.

The following qualitative arguments can be used to arrive at some of the conditions that are necessary for this method of heating to be effective. There are two types of processes by which an assembly of electrons can gain energy from the electromagnetic field. One process can be described as a resonant effect where, if an electron has the same phase in its Larmor orbit as the microwave electric field, it will gain energy from the field during every cycle. The energy gained per cycle is proportional to the Larmor radius of the electron and thus the rate of energy gain increases with increasing electron energy. The energy cannot increase without limit, however, because of the relativistic increase in electron mass which changes the Larmor frequency and takes the electron out of resonance with the heating field. The second process is a stochastic process in which the net result of multiple encounters between a particle and the electromagnetic field is a gain in energy for the particle, even though true line resonance is nonexistent. The rate of energy gain by this type of process is much lower than that gained in a resonant process, but electrons can continue to gain energy by this process after their increased mass prevents them from gaining energy by a resonant process.

Since the resonant process is by far the more effective means of heating, one is interested in the conditions necessary for this process to exist. If one considers that initially a number of electrons are present with random velocities, and random phases in their Larmor orbits, the condition that an appreciable number of them gain energy by a resonant process is that they must be effectively brought into phase with the microwave electric field. The qualitative condition necessary for the electrons to be phased is that they gain an amount of energy between scattering events greater than they had initially. For this condition to be satisfied the following inequality must hold:

$$\frac{1}{2} e \mathcal{E} \lambda > E_i,$$

where $\mathcal{E}$ is the magnitude of the plane polarized microwave electric field intensity, λ is the mean free path of the electrons, and E_i is the initial average

* Conference paper CN-10/158, presented by R. A. Dandl. Discussion of this paper is given on page 358. Translations of the abstract are at the end of this volume of the Conference Proceedings.

** Consultant, University of Florida, Gainesville, Florida, United States of America.

energy. The minimum electric field intensity needed becomes:

$$\mathcal{E} > 2(n\sigma/e)E_i,$$

where λ has been replaced by $1/n\sigma$. The number density of scattering centers is n, and σ is the effective cross-section for a 90° scattering. If this condition is satisfied, an electron with initial energy E_i and 180° out of phase with the applied microwave field will lose an amount of energy E_i, and then gain energy because it will be in phase with the field for the remainder of its free path. Electrons less than 180° out of phase with the field will gain more energy, and electrons starting in phase with the field will have an energy greater than $2E_i$ at the end of a mean scattering time. The average energy of the electrons after one scattering time will thus be greater than E_i.

There is also a condition that must be satisfied if the transverse heating field is to be effective in trapping electrons in the mirror field. In order for the electron's velocity vector to be rotated away from the axis of the field through an appreciable angle, the perpendicular energy gained from the heating field must be of the same order as the initial electron energy. The time in which this energy must be gained is the transit time for the electron in the magnetic mirror.

The scattering time for a given electron density increases rapidly with electron energy so that as the energy increases the less effective stochastic processes might make it possible for the electrons to continue to gain energy after their Larmor frequencies have decreased to such an extent that the resonant process is no longer possible.

2. Electron cyclotron heating apparatus

The basic form of typical experimental apparatus s shown schematically in Fig. 1. The apparatus consisted of a vacuum tank with magnetic mirror coils having a mirror ratio of 2:1. A wave-guide-fed microwave resonator was mounted in the mirror region for containment and heating of the plasma. The magnetic field was adjusted so that the frequency for electrons within the resonator equaled the frequency of the microwave input power. Earlier heating experiments were conducted using a thin tube of plasma supplied by an external axially-mounted cylindrical crossed-field discharge device. The plasma streamed along the static magnetic field lines through annular slots in the ends of the resonator. This external plasma feed was later abandoned in favor of the plasma formed within the resonator itself due to ionization of the residual neutral gas by the microwave fields. The two additional magnetic coils mounted at the ends of the vacuum tank were required for the operation of the external plasma feed, and did not significantly alter the basic mirror field in the region of the resonator.

The power source used in electron cyclotron resonance heating experiments was a Varian Associates Model 802 klystron amplifier having a power output of 1 kW CW. This tube was a four-cavity, air-cooled, permanent-magnet-focussed type with coaxial output, and was tunable over the range from 1.7 to 2.4 kMHz. (1 kMHz = 1000 megahertz.) A standard laboratory signal generator was used to provide the necessary drive power.

A waveguide transmission system was deemed desirable because of component considerations, reduced losses, simplified vacuum seals, and flexibility in resonator excitation for coupling to the plasma. A tunable probe-type transition was employed between the klystron power amplifier and the RG-104/U waveguide system, as shown in Fig. 1. A water-cooled ferrite isolator providing 15 to 20 db isolation was used for protection of the power amplifier under

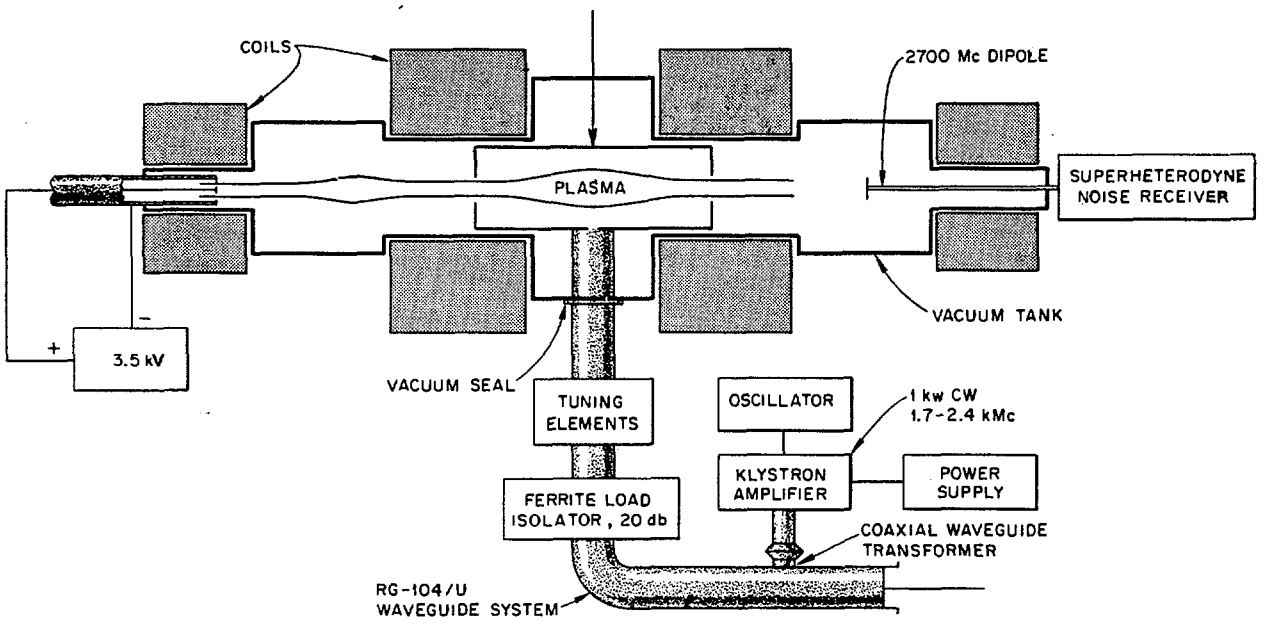

Fig. 1 Physics test facility. Electron heating experiment. Arrow at top indicates cylindrical iris-coupled cavity, TE_{015} mode, 2300 MHz.

the high-VSWR (Voltage Standing Wave Ratio) load condition often encountered in the course of experiments. Isolator characteristics limited the frequencies used in experiments to the region between 2.2 and 2.4 kMHz. Power output of the klystron amplifier and power reflected from the plasma-loaded resonator were monitored with the aid of a bidirectional waveguide coupler of the "Bethe-hole" type. A remote-controlled E-H waveguide tuner having motor-driven shorting plungers was employed to match the plasma load to the waveguide system, using minimum indicated reflected power as a criterion. In some instances, however, monitored plasma parameters were used as criteria for adjustment of the tuner. The vacuum seal for entry of the waveguide into the machine was formed by a quartz plate mounted between waveguide flanges and sealed with teflon "O"-rings.

Several types of resonators have been employed with equal success for coupling to the plasma. Common characteristics of most types included the following:

(1) Cylindrical symmetry about the axis of the magnetic mirror field.
(2) Waveguide excitation arranged so that the microwave electric field was perpendicular to the static magnetic field.
(3) Water-cooled construction of perforated copper to provide for minimum out-gassing and continuous pumping of the enclosed volume, while retaining relatively low-loss characteristics for microwaves.

The earlier resonators were designed to operate in fundamental transverse electric modes as an aid to matching and understanding the behavior of the plasma load. Notable designs included cavities operating in the TE_{011}, TE_{311}, TE_{015} and TE_{315} modes. In a number of instances, matching irises were installed in the waveguide at the cavity wall, but they proved less satisfactory than external tuning. Another permutation involved a cavity with a movable endplate which could be trimmed under load to correct for plasma detuning.

The net effect of considerations of cavity Q, mode, and resonant frequency (for TE modes) was a reduction in input power required for ionization of the residual gas at a given pressure in the high-Q case, as might be expected from the higher microwave fields present. Plasma parameters such as diamagnetism, X-ray production, decay time of cyclotron radiation, etc. were substantially the same for all cavities at given power levels under matched conditions. The results thus demonstrated a lack of preference for either r or θ microwave electric field components.

The logical application of this knowledge was then an expansion of the resonator diameter to approximately three wavelengths, which produced an extremely large number of mode possibilities and reduced practical consideration of resonator parameters to that of empirical load matching. The basic concept was the confinement of the microwave power in a chamber with low-loss reflecting walls. This chamber would also contain the plasma which would in turn provide the principal dissipative element for microwave power through electron cyclotron resonance absorption. The results were encouraging since they were essentially the same as those obtained with cavities operating in fundamental TE modes. It was with this resonator configuration that most of the data presented herein were obtained. Satisfactory operation in the extremely high mode condition is very significant from the practical standpoint in that fundamental restrictions on cavity size at a given magnetic field are considerably relaxed. The method may thus be extended to higher magnetic field strengths, higher densities, and other geometries which are more desirable from the controlled thermonuclear viewpoint.

3. Experimental procedure and results

To study the properties of the plasma produced in the experiment described above, several diagnostic techniques were employed. Microwave noise emitted by the plasma was monitored and used to determine the decay time for the plasma temperature. Measurements were made of X-rays from the cavity and used in an effort to determine the temperature and density of the plasma. The change produced in the external magnetic field by the presence of the plasma was measured and used to determine the diamagnetic properties of the plasma. This provided another measure of the energy density in the plasma.

Other experiments include measurements made of light emitted from fine molybdenum powder dropped through the hot plasma. The details and results of these experiments are discussed below.

3.1. Microwave noise measurements

The apparatus used to observe microwave noise from the plasma consists basically of a dipole antenna placed on the axis of, but outside, the cavity, and coupled through co-axial cable through a transmission cavity to a superheterodyne receiver. (See Fig. 1.) The dipole was oriented perpendicular to the magnetic field so that it would be sensitive to the electron cyclotron radiation [3].

The transmission cavity was tuned to a frequency of 2500 MHz, which was about 200 MHz above the heating frequency. The bandwidth of the cavity was about 6 MHz so that the heating power was prevented from biasing the crystal mixer at the input to the I.F. amplifier.

The antenna factor for the receiver was not known and the receiver was not calibrated so that only relative values could be obtained for the power radiated by the plasma. The chief purpose of these measurements was to determine the decay time of the plasma when the heating power was turned off. The noise measurements are also useful for obtaining relative temperatures for the plasma under different conditions.

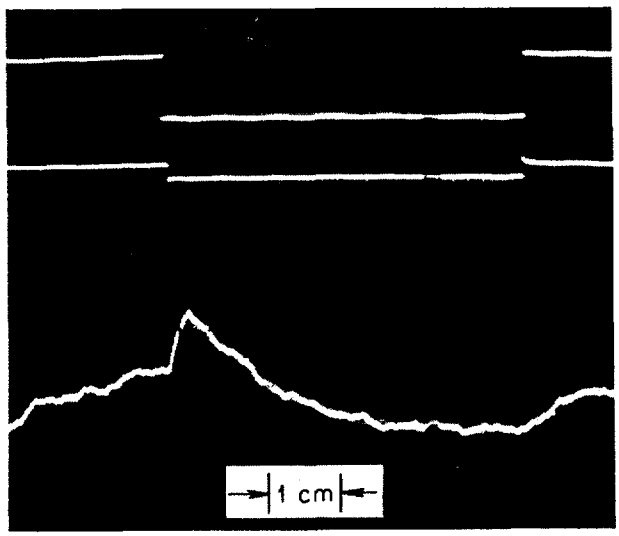

Fig. 2 Decay of electron cyclotron radiation. Sweep speed 25 ms/cm, gas pressure 3.1×10^{-6} mm Hg, heating frequency 2250 MHz, noise receiver tuned to 2500 MHz.

Decay times were measured by turning off the drive to the klystron amplifier and measuring the time required for the microwave noise to decrease to 1/e of its initial value. Fig. 2 is a photograph of a typical oscilloscope trace of the output of the noise receiver while the microwave power was pulsed on and off. The upper trace is the voltage across a crystal coupled to the transmission line and measures the power output from the klystron. The center trace is the triggering pulse applied to the exciter for the klystron amplifier and the lower trace is the d.c. output from the noise receiver. The sweep line for this photograph is 25 ms/cm. It can be seen from the shape of the output signal from the noise receiver that the plasma remains in the machine and remains hot for tens of milliseconds. The apparent rise in temperature after the heating power is turned off is probably due to a greater diffusion rate for the hot plasma along the axis of the mirror when the transverse microwave electric field is not present. Since the receiver is tuned to a frequency higher than the cyclotron frequency of electrons at the midplane of the mirrors, electrons must move away from the midplane into a higher magnetic field before the peak of their noise radiation, which is at their cyclotron frequency, is at the frequency of the receiver.

The long temperature decay times suggested that the trapped electrons were very hot so that coulomb scattering events, which vary as v^{-3}, did not force them rapidly out the mirrors. The electron temperatures required were in the 5-50 keV region.

3.2. Bremsstrahlung measurements

Since the many millisecond microwave noise decay time indicated high electron temperatures, bremsstrahlung experiments were indicated. Measurements of plasma bremsstrahlung radiation in the X-ray region provides a means of determining both density of the electrons and their energy. Allen and Hindmarsh [4] have calculated bremsstrahlung from a thermalized hydrogenic plasma. For energies in the kilovolt region their result may be stated as:

$$I(\nu) = A\, Z^2\, n_i\, n_e\, e^{-h\nu/kT}$$

where A is a constant. Thus a determination of the spectral shape will allow one to determine electron temperature by taking the negative logarithm of intensity as a function of energy.

The total amount of energy radiated in a free-free transition from a thermal distribution of ions is given by Spitzer [5] as:

$$\omega = 1.42 \times 10^{-27}\, Z^3\, n_i^2\, T^{\frac{1}{2}}\, \frac{\text{erg}}{\text{cm}^3}\, \text{s}.$$

Therefore, a measurement of total energy radiated by the plasma in this region together with the electron temperature will give plasma ion density if the atomic number of the constituents is known. Obviously, a prerequisite for such X-ray meaurements is a plasma with very energetic electrons. T.F. Stratton [6] has used bremsstrahlung measurements to determine temperatures of 240 eV for plasma electrons in Scylla. X-ray measurements on the plasma described in this paper have been made with a NaI scintillation spectrometer. A typical spectrum is shown in Fig. 3. The plot of log intensity versus energy from 10 to 60 keV is nearly linear, indicating a Maxwellian distribution. The slope of the distribution indicates a temperature of $\sim$10 keV.

To find what portion of these X-rays were coming directly from the trapped plasma, gas with a high

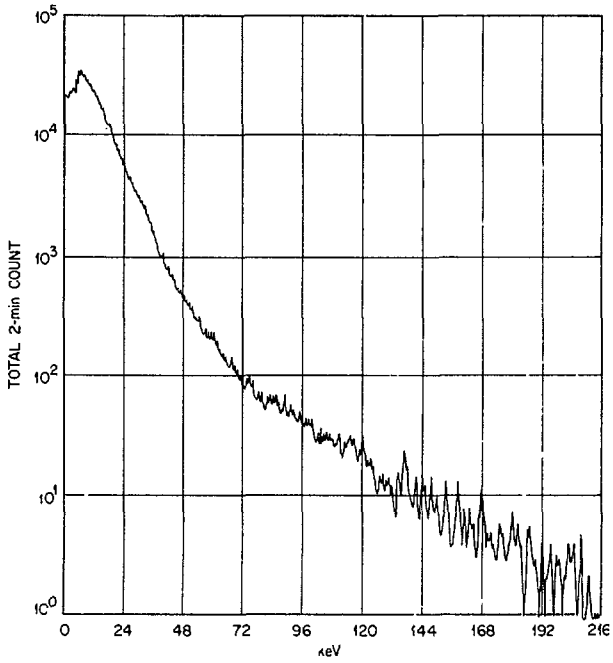

Fig. 3 Bremsstrahlung from electron cyclotron heating. Gas pressure is 5.2×10^{-6} mm Hg, base pressure is 4×10^{-7} mm Hg. Double 1-in. lead collimators spaced 12-in. and having $^1/_2$-in. graded apertures. Axis of spectrometer is midplane.

atomic number (Xe) was let into the plasma region. Since the energy radiated in free-free transitions from an ionized gas is proportional to the cube of the ionic charge, an atom with a Z of 54 should provide a significant increase in radiation efficiency over hydrogen, depending on its charge state. This should have appeared in the spectrum as either an increase intensity or as a decrease in the temperature or both. Neither effect appeared. This means, as was not unexpected, that bremsstrahlung is not at present a significant energy loss mechanism. It means also that most of the radiation detected by the present collimator and crystal assembly is being generated at the copper cavity walls by electrons which diffuse out of the trapped region. The plasma temperature determination by this means is then subject to distortion by diffusion rates across the magnetic and microwave fields and by thick target effects in the 1/16-inch copper wall. Independent measurements of electron energy density, however, point to an energy for the electrons of at least 10 keV.

Most of the higher energy radiation has come into the spectrometer through 3/4-inch of stainless steel or 1/2-inch of lead. This accounts for its higher energy slope of 60 keV. The collimator and crystal assembly have recently been re-designed to see plasma bremsstrahlung above a few keV directly and to discriminate more strongly against X-rays from the cavity walls. Because of alignment difficulties no good spectra have been taken with this device to date.

Integral measurements of X-rays with an ion chamber show a flux of 50 R/hr at a point 36 cm from the center of the plasma looking through a 1/2 cm^2, 30 mil thick, Be window. When corrected for geometrical effects, this number indicates a source strength of $\sim 10^{11}$ sec^{1} of ~ 10 keV X-rays, or $\sim 5 \times 10^{14}$ electrons/sec impinging on the copper cavity walls. We use the measured containment time of 1/20 sec and find $\sim 2 \times 10^{13}$ electrons as the total number trapped. This agrees with the density calculated from the diamagnetic measurement and from metallic powder dropping experiments.

3.3. Experiments with molybdenum powder

An approximate determination of the dimensions of the hot electron gas was obtained by visual observations of the light from molybdenum powder heated to emission when dropped into the plasma, and other preliminary plasma properties were inferred. The powder was contained in a metal can above the microwave cavity and was conveyed to the cavity through a tube. A blow upon the metal can caused a small amount of molybdenum powder to be released through a fine mesh screen and to drop into the plasma. A considerably more refined version of this experiment is being prepared.

The approximate size and shape of the plasma could be inferred from the light emitted by the heated powder as it dropped through the plasma. No light was observed when there was no plasma in the cavity, even when the microwave power was on as the powder was dropped, implying that the microwaves did not interact directly with the powder. Visual observation of the heated powder indicated that the hot electrons formed a ring approximately at the radius at which the magnetic field strength was appropriate for cyclotron resonance.

One could infer the total energy density of the hot electrons by measuring the visible light emission of the molybdenum powder using a silicon solar cell. The silicon cell was calibrated by observing in the identical geometry the radiation from a heated molybdenum wire having the approximate shape of the plasma inside the cavity. The time integral of the silicon cell signal could then be taken as a measure of the hot electron energy in the cavity. The volume of the plasma was estimated from photographs, thus allowing the energy density of the ring to be inferred.

Several assumptions were made as follows: (1) the light emitted was due to powder heated by the hot electrons alone (i.e. microwave power was not also absorbed), (2) all of the electron energy went into heating the powder, (3) the emission spectra of molybdenum wire and powder were identical, and (4) molybdenum wire inserted into the cavity approximated sufficiently well the size and shape of the molybdenum powder glowing under bombardment by the electrons.

The value of the energy density inferred by these measurements is admittedly only approximate, but was, nevertheless, the first reproducible measurement performed. The result was an energy density on the order of 10^{15} eV/cm^3. This measurement appears to agree quite well with the calculated energy density inferred from the diamagnetic measurements described below.

3.4. Diamagnetic measurements

The incandescence of molybdenum powder dropped through the plasma indicated sufficient energy density to warrant a measure of the diamagnetism produced by the plasma [7]. Several devices were considered or employed for the detection of diamagnetism from the electron cyclotron heated plasma. For example, NMR probes were considered but deemed not usable because the non-uniform magnetic field resulting from the mirror geometry severely penalizes the sensitivity. This sensitivity difficulty is emphasized by the remote location of the magnetic sensing probe, a location dictated by the practicalities of removing the probe from the microwave heating cavity. Marshall and Goldstein [8] have reported successful employment of NMR for diamagnetic measurements but the experiments were performed on a low temperature plasma in a very uniform magnetic field with a favorable sensing probe location.

Hall probes were initially found to be useful in our work because they are characterized by response to the magnetic flux φ, rather than to $\mathrm{d}\varphi/\mathrm{d}t$, but their signal-to-noise ratios were not adequate for precise measurement. The double magnetic probe arrangement of Fig. 4 which integrates $\mathrm{d}\varphi/\mathrm{d}t$ proved most satisfactory and was used to take the data presented herein. The difference amplifier front end on the

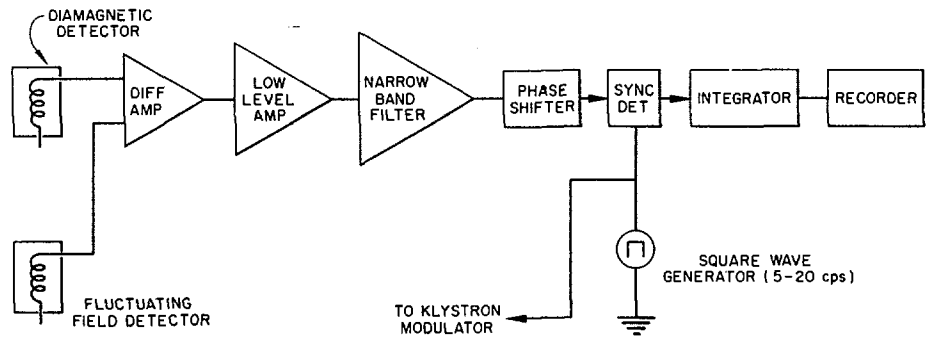

Fig. 4 Block diagram of diamagnetism measurement apparatus.

system was found necessary because of field fluctuations at the rotational frequency of the mirror coil motor generator set. The difference amplifier and low level amplifier are low noise solid state devices, as are the narrow band filter [9] and phase shifter. The amplifier gains are as follows: difference amplifier $G=5$—7, low level amplifier $G=10\,000$, and narrow band filter $Q=50$—200. The synchronous detector was used for accurate quantitative measurements but was not necessary for qualitative observation while tuning the equipment. The magnetic probe and associated electronics were calibrated in a field produced by a 14-inch diameter Helmholtz coil energized by a measured square wave current. The square wave current was passed through low pass filters with time constants from 0.1 to 20 ms in order to check the linearity of integration of the electronics. Considerable experimental difficulty resulted from microwave leakage fields, producing false signals in the low level circuitry. Various techniques, such as low pass filters (providing effective rejection of microwave frequencies) in series with sensitive inputs, and microwave cutoff apertures on the mirror machine eventually eliminated the problem. The test for true signals was the simple expedient of rotating the sensing probe 180° and observing a reversal of polarity of the diamagnetic signal. The conservative noise figure for the system with the d.c. mirror field energized, and with a 13 cycle/sec synchronous rate and a 10 sec integration time is 70 μG peak to peak. This noise figure is for a 1000 turn, 2 cm² pickup coil.

Several kinds of measurement have been made with the diamagnetic detector on the midplane of the apparatus. The magnetic field was varied during the first measurement while the detector was positioned at a constant distance from the axis of 7.3 inches while the microwave power was maintained at a constant level. The resulting diamagnetic signal is shown in Fig. 5 as a function of the midplane axial magnetic field. Also shown is the calculated radius of the resonant heating zone in the midplane (calculated from the known radial field gradient), and the X-ray peak intensity as measured by the pulse height analyzer.

The diamagnetic signal peaks sharply when the resonant heating radius is zero, i.e., the maximum diamagnetic signal occurs for electrons heated on or very near the axis. Some signal is observed for lower magnetic fields indicating that electrons are heated off the midplane at an unspecified distance toward the mirrors. There is a plateau in the diamagnetic signal strength for larger radii of heating which extends out to some critical radius. The structure of this curve is not yet understood in detail and is undergoing further study. For the particular measurements shown in Fig. 5, using an average value for the electron energy of 10 keV, the electron density which gives the peak diamagnetic signal is estimated to be about $3\times10^{11}/\text{cm}^3$. This can be made at least a factor of four higher by increasing the pressure from 6×10^{-6} mm Hg to 3×10^{-5} mm Hg.

This estimation is based on a specific model of the electron plasma. The assumption is made that the plasma is located in a cylinder whose radius is known from observations with molybdenum powder. The equivalent current per unit length (abamp/cm) on the cylindrical surface is $I^1=nE_1/H$ where n is the number per cm³ of electrons, E_1 is their transverse energy in ergs, and H is the magnetic field in oersteds. This geometry is assumed for simplicity in calculations as tables [10] are available relating the field outside finite cylinders to their surface current.

For the second measurement, the diamagnetic detector was moved radially with a constant microwave power input at the magnetic field corresponding to axial heating and the maximum diamagnetic signal

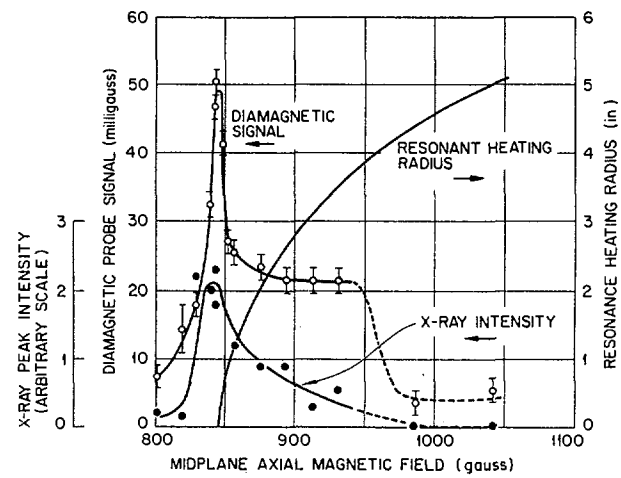

Fig. 5 Diamagnetic signal and X-ray intensity as a function of midplane axial magnetic field.

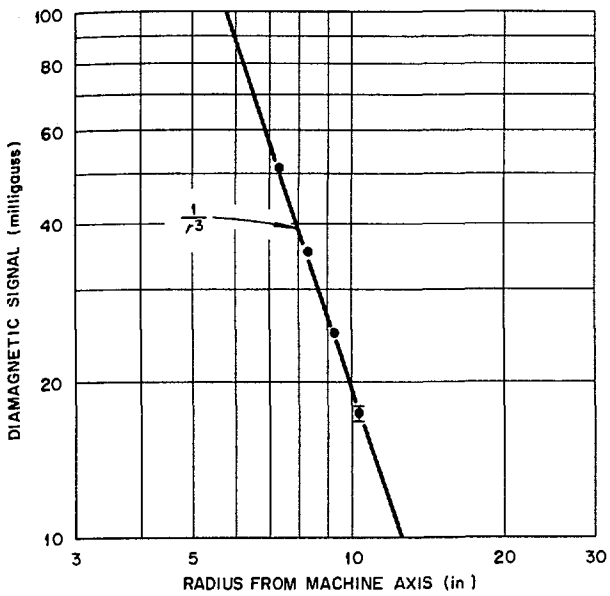

Fig. 6 Radial Decrease of Diamagnetic Signal.

Fig. 6 Radial decrease in diamagnetic signal.

in Fig. 5. The signal shows a drop with radius following an accurate r^{-3} dependence (r=radius) as shown in Fig. 6. It can be concluded from this curve that the plasma contributing to the diamagnetic effect behaves like a dipole or like a finite current loop which has a radius at least 7 times smaller than the distance of the probe to the axis. Deviations from the r^{-3} dependence would allow a better estimation of the radial extent of the plasma, but no deviation is observed inside the experimental errors.

For the third measurement, the diamagnetic detector was held at a constant distance from the axis, the magnetic field was held constant, and the microwave power was held constant while the gas pressure was varied. The resulting variation of the diamagnetic signal with gas pressure is shown in Fig. 7. For pressures higher than 3×10^{-5} mm Hg (not shown in this figure) some new effect takes over which has not been studied extensively. For pressures lower than

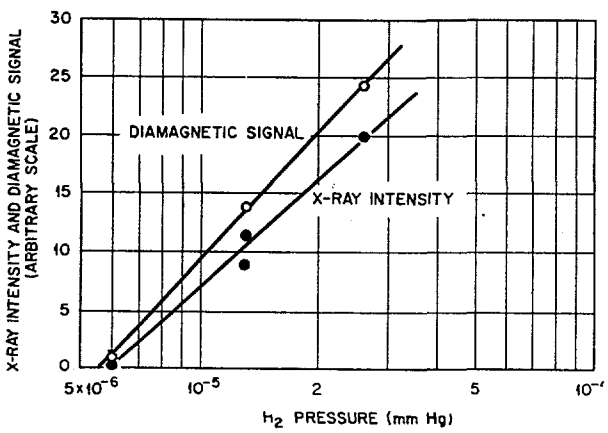

Fig. 7 Diamagnetic signal as a function of H_2 gas pressure.

6×10^{-6} mm Hg the diamagnetic signal was too low to be measured. The interesting fact that the diamagnetic signal varies directly with the logarithm of the pressure in the region between the above limits is unexplained at the present, and further studies are being made of this phenomenon.

It was also observed that when the microwave tuning was optimized by maximizing the X-ray signal, the diamagnetic signal dropped to about one-third of the value for optimized diamagnetic effect.

3.5. Light emission from the plasma

A faint blue light was emitted from the plasma during operation with H_2 gas feed. This light was observed with the aid of a silicon solar cell located in

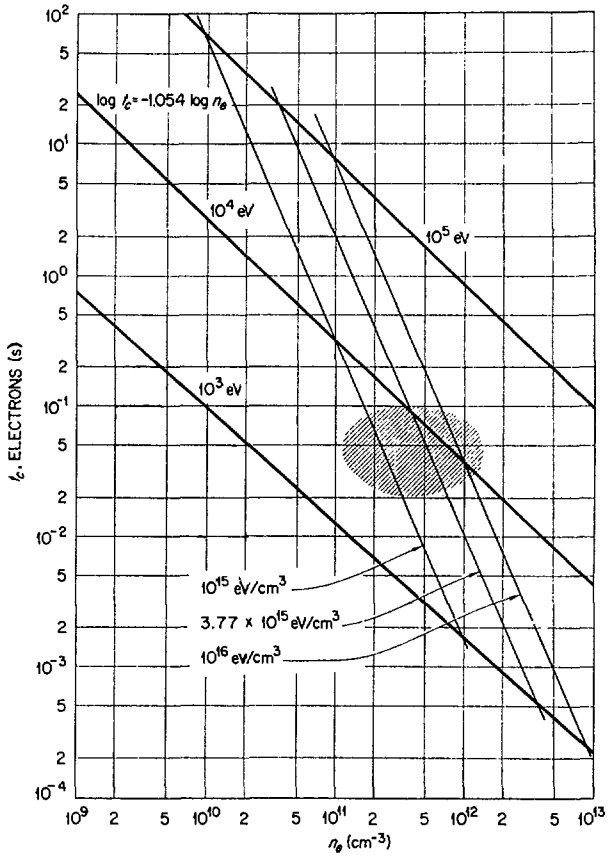

Fig. 8 Self-collision time as a function of electron energy and density.

a port on the midplane of the machine. The output of the silicon cell was recorded on a Sanborn recorder simultaneously with the X-ray signal from a 6292 DuMont phototube and a LiI (Eu) crystal which also viewed the midplane of the machine.

The light intensity was observed to decay with two decay times following the microwave power shut off, and the X-ray signal appeared to decay in a similar manner. The decay waveform of the signals is comprised of two components. A prompt component lasting for approximately one millisecond, and a slow component with a period of from 50 to 100 ms. The

slow decay period is similar (for equivalent conditions) to other decay times, such as those of microwave noise, mentioned previously.

A preliminary density determination involves the curve in Fig. 8, which was calculated from SPITZER'S [5, pages 76—81] treatment of self-collision time. With numbers for any two parameters we can determine the other parameter. The curve provides a convenient method of correlating measurements of temperature, energy density, temperature decay, and density. All of the various measurements give a self-consistent picture of the plasma when compared by means of this curve, namely that it is characterized within the cross-hatched area of Fig. 8.

4. Conclusions

It should be noted that a variety of plasma conditions can be emphasized by adjusting the E-H tuners. For example, one can tune for bremsstrahlung and/or energy density. An additional consideration involves the changes in reflected microwave power as a function of time after turning on the microwave heating power. The stub tuning can be set to achieve maximum energy transfer between 1 ms and 200 ms after turn on, and pass through this point to a less heavily loaded condition. Or the adjustment can be such as to allow the cavity plus plasma to monotonically load the heating source. In general, the approach adopted in this experiment, which necessarily deals with a dynamically nonlinear load, has been essentially an empirical adjustment to arbitrary equilibrium levels of energy density, bremsstrahlung, and/or VSWR.

However, sufficiently strong evidence for the production of a high electron temperature (10—50 keV), reasonably high density (10^{11}—10^{12}cm^{-3}) plasma exists to permit almost unique investigation at this time of several plasma parameters critical to high temperature thermonuclear devices. Synchrotron radiation as a function of temperature and density as well as bremsstrahlung might be mentioned as such parameters.

Plasma produced by this principle of electron heating will soon be investigated at shorter wavelength heating frequencies (3 cm) and higher power (5 kW). Equipment to produce and study this plasma as a function of magnetic field uniformity and self-consistency (because of diamagnetic perturbations) is also being readied.

Cyclotron resonance heating has been used by STIX [11, 12] and others to heat ions to moderate temperatures. There are several reasons why considerably higher temperatures might be achieved by using simultaneous resonance heating of electrons and ions. One reason is that the ion cyclotron frequency is so low that the electrons are able to form sheaths and to a large extent prevent the electric fields from penetrating the plasma, whereas electron cyclotron heating penetrates plasmas at least up to densities corresponding to the electron plasma frequency.

However, it is believed that the very hot electron gas will inhibit sheath formation, thereby enhancing the penetration of ion cyclotron electric fields, and decrease dynamic friction. This adjunct will soon be undertaken ($B=3.9$ kG) in an attempt to raise ion temperatures. Initial attempts at simultaneous ion and electron heating were not seriously undertaken due to the very weak magnetic mirror field required for 13 cm cyclotron heating.

Since experimental evidence also indicates a highly ionized plasma in this device, high power, short wavelength versions of the experiment may shortly be applied as a dissociative medium for one of the high-energy molecular ion injection devices at Oak Ridge. It is hoped that high-temperature electrons will reduce the hot ion energy degradation in these devices, reduce charge exchange losses and possibly contribute to stability.

Acknowledgments

Acknowledgment is made to Dr. A. H. Snell for his continued interest and support. We also wish to acknowledge the conscientious technical assistance of M. W. McGuffin, M. Maskewitz, and R. L. Livesay.

Oak Ridge National Laboratory is operated by Union Carbide Corporation for the United States Atomic Energy Commission.

References

[1] ARD, W. B., DANDL, R. A., EASON, H. O., KERR, R. J., *Bull. Am. Phys. Soc., Ser. II*, **6** (1961) 189.
[2] DELCROIX, J. L., QUEMADA, D., *C. R. Acad. Sci. (Paris)* **24** (1959) 994.
[3] WHARTON, C. W., U.S. Atomic Energy Commission Report UCRL-5129 (Feb. 3, 1958).
[4] ALLEN, J. E., HINDMARSH, W. R., U.K. Atomic Energy Authority Report AERE-GP/R-1761 (Sept. 21, 1955).
[5] SPITZER, L., Physics of Fully Ionized Gases (Interscience Publishers Ltd., London, 1956) 90.
[6] STRATTON, T. F., Optical Spectrometric Measurements of High Temperatures, Ed. by P. J. Dickerman (University of Chicago Press, 1961).
[7] STEENBECK, M., *Wiss. Veröffentl. Siemens-Werke* **15**, 2 (1936) 1.
[8] MARSHALL, T. C., GOLDSTEIN, L., *Phys. Rev.*, **122** (1961) 367.
[9] MAY, F. T., DANDL, R. A., *Rev. Sci. Instr.* **32** (1961) 387.
[10] ALEXANDER, N. B., DOWNING, A. C., U.S. Atomic Energy Commission Report ORNL-2828 (Sept. 29, 1959).
[11] STIX, T., *Phys. Fluids* **1** (1958) 308.
[12] STIX, T., PALLADINO, R. W. *Phys. Fluids* **1** (1958) 446.

DISCUSSIONS (SESSION IV) — DISCUSSIONS (SÉANCE IV) — ДИСКУССИИ (ЗАСЕДАНИЕ IV) — DEBATES (SESIÓN IV)

Paper CN-10/210 *was presented by G. F. Bogdanov* (Union of Soviet Socialist Republics). *The text of the paper is on pages 215 to 225 inclusive. The following discussion took place:*

R. F. Post *(United States of America):* First I would like to congratulate Dr. Bogdanov and his colleagues on this experiment which is obviously of considerable interest to us as well, and I'd like to comment and relate their experimental work to our own and also to relate our own to your previous experiment. First, may I point out that in these experiments the range of plasma densities covered is 10^5 to 10^7. This covers the range between the experiments we have done and those that have been reported here. Also there is a range in these experiments of 10^4 to 10^5 in volume for the plasma, and yet we find only ranges of perhaps a factor of ten in the times of confinement. Now coming first to the evidence from Ogra and from the Ioffe experiments, I would say that these have both demonstrated rather well that something which has the earmarks of the so-called flute instability does occur in this geometry. This is true in their experiments despite the very small value of the plasma density, but this fact is not in disagreement with the theory. There are other effects present too, but I think it is clear that flute-like instabilities seem to have been demonstrated very nicely. Now turning to our own experiments, first those with hot electrons—our oldest experiments,—we have no doubt that we have made plasmas of a density much higher than the low densities reported and yet they have been contained for several tens of milliseconds with no apparent instability effects. In the case of the experiments with hot ions reported yesterday by Coensgen, I personally have no doubt that he has demonstrated that 90 microsecond confinement has been found, apparently limited only by a simple drift of the plasma column as a whole to the wall. This drift seems to be correlated only with a nonuniformity of the field, but this is yet to be shown. In this experiment, in almost all cases, there were no conducting walls—there was no "tying of the magnetic lines", and yet the motion was slow.

Now let me begin then to relate this and summarize. First, I think the Ogra experiments have shown that there exist some means to establish a degree of control of the flute instability. Secondly, our own experiments with hot electrons seem to show that stability is possible; seemingly, this is true when conduction to the walls and to the ends is adequate. Now, bringing this all together, I would say that the flute instability has been shown to be possible in the mirror machine; the theory predicts several entirely different kinds of mechanisms which might remove this instability. (For example, the mechanism discussed by Rosenbluth, which would operate at higher densities, or the use of magnetic shear.) The Ogra experiments and our own have shown the possibility of control through several mechanisms. It seems that we should at this point apply the teachings of theory and experiment. With these we should be able to eliminate the flute instability. In my opinion the most difficult problem in mirror systems is not the flute but the micro-instability. I congratulate the Ogra people on having taken a significant step in controlling plasma instabilities.

G. F. Bogdanov *(Union of Soviet Socialist Republics):* I think that the remark contains no question in itself—this is primarily a commentary. We have no doubts that this is the flute instability although we do not exclude other possible explanations for this instability. As for the mechanism of stabilization, I have mentioned that in addition to using end electrodes we tried to use a "goffered" field in order to provide a negative magnetic drift at which this instability does not develop. We are taking some measures aimed at eventually overcoming this obstacle.

Paper CN-10/212 *was presented by V. I. Pistunovich* (Union of Soviet Socialist Republics). *The text of the paper is on pages 227 to 232 inclusive. The following discussion took place:*

D. Pfirsch *(Federal Republic of Germany):* I would like to mention the observations of Dr. Landauer of our Institute in Munich. He reported on these at the meeting in Munich last week. His observations concern higher harmonics of the electron cyclotron frequency in an ordinary gas discharge, whereas yours concern the ion cyclotron frequency. He found the twenty-fifth harmonic still present. Landauer's idea for an explanation is along the same lines as yours, i.e., in the neighborhood of these harmonics the phase velocity in the plasma is very small so that the electrons behave in a certain sense similar to relativistic electrons, which allow the emission of high harmonics of the cyclotron frequency.

W. Linlor *(United States of America):* Would you please sketch the form and location of the electrodes employed in the experiment?

V. I. Pistunovich *(Union of Soviet Socialist Republics):* If we imagine Ogra as a cylinder, then the electrodes were introduced at the ends of the cylinder. (See Fig. IV-1, next page). An antenna used for measuring the electric field was placed both in the region of enhanced magnetic field or in the center and it was introduced in such a way as to avoid being hit by fast charged particles.

J. L. Tuck *(United States of America):* In your experimental observations on electron-cyclotron radiation it would have been very nice if you could have

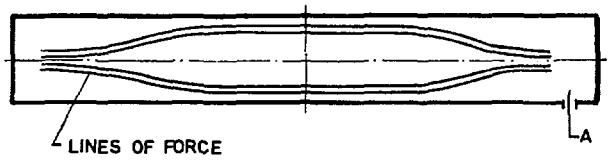

Fig. IV-1 Sketch of disposition of electrodes and dielectric antennas

continued your observations at the harmonic frequencies which even at the low temperature of 100 eV might still have provided some confirmation of the important predictions of Trubnikov and Kondrievtsev. I note that you break off your observations before reaching the first harmonic. Was there nothing to be seen at higher frequencies?

V. I. Pistunovich: In measuring the cylotron radiation we took into account the fact that the refraction coefficient for a given density in this range of frequencies is equal or approximately equal to unity. The electron energy and electron density were too small to permit the detection of the second harmonic, which was probably by a few orders of magnitude smaller than the first. Therefore we measured cyclotron radiation only at the fundamental frequency.

T. H. Stix *(United States of America):* It appears to me that one factor contributing to the production of harmonics of the ion-cyclotron frequency is the variation of cold plasma density over the diameter of the ion Larmor orbit. What was the magnitude of this cold plasma density variation?

V. I. Pistunovich: We have not made detailed radial density measurements, but it can be assumed that, at a distance of the order of the cyclotron radius, the density varies considerably (about a factor of two). We have no experimental evidence that the radial distribution of the density changes considerably with the change of the pressure of the gases. But the electron density measured by the interferometer rises linearly with the pressure. That is why we prefer to explain the origin of the higher harmonics as resulting from the rise of the reflection index of the cold plasma.

Paper CN-10/160 *was presented by J. L. Dunlap* (United States of America). *The text of the paper is on pages 233 to 237 inclusive. The following discussion took place:*

V. I. Pistunovich *(Union of Soviet Socialist Republics):* Tell me, please, when you measured the dependence of the electric field on the injected current, how did the electron density change?

J. L. Dunlap *(United States of America):* We do not have measurements of the electron density at these pressures, so I cannot comment on the variation of this density during these measurements.

V. I. Pistunovich: It is known that in measuring the electric field at the fundamental cyclotron frequency it is necessary to work in such regimes where the density of cold plasma, i.e. electron density, is constant, since the field intensity at the cyclotron frequency may change only because of change in electron density. Therefore I am interested in knowing whether the dependence of the electric field on the injected current is the result of an increase in fast particle density and of the corresponding increase in its electric field or whether it is due in part to cold plasma.

J. L. Dunlap: An electrostatically shielded loop was used as the radiofrequency probe in order to minimize some of the possible effects of the cold plasma. Proper evaluations of those effects which depend specifically on electron density must await measurements of this density. In our apparatus these measurements are complicated by the small plasma volume, approximately one liter, but we hope soon to make determinations of the density.

T. H. Stix *(United States of America):* What changes in the apparatus lead to the reduction in operating pressure, and what was the trapped proton density under these new conditions?

J. L. Dunlap: In answer to your first question—changes in the apparatus included going from a two-region to a three-region vacuum geometry, the addition of pumping by evaporated titanium films in the two inner regions, and operation with liquid nitrogen cooling on the walls of the innermost vacuum region. Concerning the fast proton density, we note that with gas dissociation and proton containment limited only by charge exchange with the background gas, the fast proton density is independent of the pressure but varies linearly with the injected H_2^+ current (for pre-burnout operation). For these conditions 10 mA H_2^+ gave fast proton densities of about 10^8 cm^{-3}.

M. Seidl *(Czechoslovakia):* I have a remark concerning radiofrequency radiation and particle energy-spread observations. There is a striking similarity between the results just reported and the effects of the azimuthal space-charge instability ("negative mass instability") observed on circular accelerators. This instability was theoretically predicted by C. E. Nielsen, A. M. Sessler, K. R. Symon (Proc. International Conference on High Energy Accelerators and Instrumentation, CERN, 1959, page 327) and by A. A. Kolomensky and A. N. Lebedev (*ibid.*, page 115) and experimentally observed at our laboratory during electron injection into a betatron (*ibid.*, page 327 and *Czech. J. Phys.* B11 (1961) 390).

The effect of the instability is an azimuthal bunching of particles into a whole number of rotating bunches and a radial extension of the bunches. The instability sets in at a critical particle density depending on the particle energy spread, the geometry of the beam and on the wall impedance. A higher density causes the development of a higher number of bunches under usual conditions.

To compare the theory of this instability with the results obtained on DCX and Ogra it would be

necessary to know the energy spread *before* the instability sets in. I wonder if this quantity is known.

J. L. Dunlap: The "negative mass instability" suggested by Dr. Seidl is precisely the accelerator instability to which we refer in our paper.

With regard to Dr. Seidl's inquiry, we do not at present know the energy spread before the instability sets in. The reasons for this are as follows:

(1) The rapid fluctuations in the signal from the energy spectrometer (Fig. 8 of our paper) require that these signals be integrated with long time-constant circuits. It has not been possible to measure the distributions during the short time interval that elapses between the turning on of the H_2^+ beam and the appearance of the radiofrequency radiation, which we take to indicate the onset of the instability.

(2) A simplifying assumption is that the energy spread in question is just the spread in the incoming H_2^+ beam. Turning this beam on presented a step-function change in the 600 kV power supply load, and "ringing" in this supply then introduced modulation of the H_2^+ beam which varied with the amount of H_2^+ current and the conditions of the accelerator tube and the power supply. The effects of this modulation in the experiments just described are not completely known. Additional fast-acting regulation has just been added to the supply, and it is possible that the effect of the initial spread in beam energy can be assessed in the experiments now being performed.

In connection with the negative mass instability I wish to mention recent calculations by Dr. T. K. Fowler of O.R.N.L. which have indicated that in DCX-1, operating with a fast proton density of 10^7 cm^{-3}, a few tens of keV initial energy spread are necessary for stability. This result is perhaps more significant if one reverses the arguments and says that, if the instability develops, it will grow until it has caused this amount of energy spread in the trapped ring. Although we are not sure that this is the case, the measured energy spreads are in the order of a few tens of keV under those operating conditions. We do not interpret these results as a definitive evidence in favor of the accelerator instability, partially because of the very qualitative nature of the argument, and also because calculations by Professor Harris have indicated that the instabilities proposed by him could also account for the measured energy spreads.

Papers CN-10/190 *and* 191 *were presented by G. G. Kelley* (United States of America). *The texts of the papers are on pages 239 to 258 inclusive. The following discussion took place:*

A. E. Robson *(United Kingdom):* Have you included the effect of space charge of the injected beam on the path length as calculated by these methods? It seems that in view of the high precision of magnetic field needed to obtain the long path lengths, the space charge of a 400 mA beam might represent a serious disturbance in the calculations.

G. G. Kelley *(United States of America):* Yes, we have considered the question of space charge forces in the circulating injected beam. We do not expect a serious effect on path length. A space potential variation of more than a few kilovolts would be serious but we expect no fluctuations this great from the injected beam because of electron neutralization.

I. N. Golovin *(Union of Soviet Socialist Republics):* Are any special measures taken in the construction of the new machine to permit to change the configuration of the magnetic field in order to prevent growth of flute instability, or do authors think to accomplish stability by some other still not known mechanisms?

G. G. Kelley: We have the facilities for the introduction of stabilizing fields. We have not as yet given serious consideration to a specific configuration or method.

I. N. Golovin: Then, perhaps, you could specify what changes in the form of the magnetic field are provided for achieving stability?

G. G. Kelley: We had not considered this problem in detail.

Paper CN-10/233 *was presented by R. Demirkhanov* (Union of Soviet Socialist Republics). *The text of the paper is on pages 259 to 263 inclusive. The following discussion took place:*

J. L. Tuck *(United States of America):* I am very glad to see that the interesting experiments at Sukhumi on dynamic confinement in cusped geometries ("travelling picket fences" as I would call them) are now being published. I think it is true that in the case of a cusped system travelling around a torus, the inward-along-the-radius confining force arises as a result of a drag-force-inertial for short times, or by connection to the walls of the torus for long times. Thus, a well confined fully ionized plasma would without this force be speeded up till it was stationary with respect to the travelling magnetic field, and confinement would be lost. In your experiments, as I understand it, ionization is variable, so the neutral components provide a steady drag force between the moving plasma and the walls.

Now my question is, do you observe a lessening of confinement, as the degree of ionization becomes complete?

R. Demirkhanov *(Union of Soviet Socialist Republics):* Due to the incomplete ionization, no carrying along of the plasma by the travelling wave has been observed in our experiments. During the transition to the state of full ionization, the plasma will be carried

along after having been separated from the walls. However, the time of acceleration is not very short and the required effect can be achieved during times of the order of a ms. For pulses of longer duration it will be necessary to consider means of slowing down the plasma. This question has been considered by V. N. Starkova in the Proceedings of the Radiotechnical Institute of the U.S.S.R. Academy of Sciences [Trudy Radiotekhnicheskogo Instituta AN SSSR) 2 No. 2 (1960)].

T. Consoli *(France):* I would like to ask two questions:

(1) Did the author observe a heating of the plasma during the application of the high frequency field?

(2) Did the author make measurements of the loss of particles toward the walls? That was his method of measurement?

R. Demirkhanov: Due to the lack of time, I did not dwell on details. The electron temperature in these experiments reached 30 to 40 eV while the ions remain relatively cold. I think that it is so, not because of any fundamental reasons, but because of insufficiently clean conditions in the experiment.

The particle leakage was measured by corresponding probes and was found to decrease, while the lifetime considerably increased. Measurements of leakage were one of the main methods of controlling the behavior of plasma.

Paper CN-10/97 *was presented by F. Prévot* (France). *The text of the paper is on pages 265 to 278 inclusive. The following discussion took place:*

C. Brachet *(France):* The calculation concerning the injection of neutral atoms uses the approximation that the probability of capturing neutrals is very low. [References: Brachet and Vasseur CN-10/105 of the present Conference and report 232 of the Fifth International Conference on Ionization Phenomena in Gases; also *C. R. Acad. Sci.*, Paris **253** (1961) 86 (3 Juillet).] Is it possible to avoid this approximation for considering the case when the probability of capturing the neutral atoms in the plasma is very close to unity? Furthermore, is this condition fulfilled with the experimental device of which you have given the results?

F. Prévot *(France):* Of course, yes. The calculations concerning the injection of molecular ions use values of capture probabilities which are valid in the whole range between 0 and 1. If one can restrict the problem to the case where this probability is 1, the equations are considerably simplified. Similar expressions could be used in the case of neutral injection. However, I do not see today the possibility of building up hot plasma by energetic atom injection with high capture probability.

Paper CN-10/74 *was presented by D. R. Sweetman* (United Kingdom). *The text of the paper is on pages 279 to 287 inclusive. The following discussion took place:*

F. Schwirzke *(Federal Republic of Germany):* Have you considered increasing the number of excited atoms in the neutral beam by irradiation with resonance radiation? What is your opinion of obtaining larger degrees of ionization by such a resonance irradiation method?

D. R. Sweetman *(United Kingdom):* It would certainly be very attractive if one could increase the population of these high excited states by this method. However, resonance radiation of about 13.4 eV is required to excite from the ground state and we do not at the moment know of a suitable source of this photon energy.

J. L. Tuck *(United States of America):* According to this most promising method of particle capture, it seems that a theoretically perfect bottle could be filled, by traversing it with a beam of neutrals. I am not quite sure of this, but does it not follow, from the principle of detailed balancing, that there must exist (be it ever so small) a magnetic-field-enhanced inverse process, i.e. magnetic-field-enhanced recombination?

D. R. Sweetman: One may regard the ionization process as due to a lowering of the potential barrier by the equivalent electric field. It is certainly true that this also enhances the capture probability by penetration of the same barrier. However, the conditions for this capture to occur are so critical that it has no practical effect on the loss probability.

One interesting consequence of the results presented is that the cross-section for ionization of highly excited atoms by the electric field surrounding protons might be expected to be large, and this would cause the transition to trapping by interaction with the plasma particles to set in much earlier than would otherwise be the case.

N. V. Fedorenko *(Union of Soviet Socialist Republics):* I want to ask Dr. Sweetman where in plasma in his opinion are the neutral atoms formed—within plasma or at its boundary? It is believed that during discharges the surface of the chamber emits a great amount of gas, for instance hydrogen. Tell me, please, what is the percentage of highly excited states in the flux of atoms emitted by plasma?

D. R. Sweetman: Since the plasma we are forming at the moment has only a very low density (below 10^7 particles per cm^3), then we may regard the plasma as transparent to the emitted neutral atoms and they therefore come from the body of the plasma.

We have evidence from the low pressures indicated by the decay time of the plasma that a negligible amount of gas is emitted by the chamber walls during the pulse at such low plasma densities.

In answer to the second question: The neutral atoms emitted by the plasma are produced by charge exchange on the argon gas introduced and some of these

are presumably also in excited states. We have not, at the moment, done measurements of the populations after charge exchange on this gas and so I cannot give a quantitative answer to the question.

Paper CN-10/225 *was presented by M. K. Romanovsky* (Union of Soviet Socialist Republics). *The text of the paper is on pages 289 to 298 inclusive. The following discussion took place:*

F. Boeschoten *(Federal Republic of Germany):* Did you find any azimuthal currents in your "Ogrenok" device?

M. K. Romanovsky *(Union of Soviet Socialist Republics):* No, there was practically no azimuthal current, particle current. I did not mention that such oscillations and plasma tongues are found only when currents exceed 300 to 350 μA. But if the current is reduced to say, 300 μA, all these oscillations disappear and there appears a laminar plasma, described by a one-particle model with a classical motion of individual particles including the slow ones. Then there are no oscillations or tongues.

But we were working with currents of a few milliamperes, not more than 5 to 7 mA; therefore it is not of any use to speak about azimuthal current. Are you satisfied with the answer?

R. J. Mackin *(United States of America):* On the basis of your observations, would you comment on the possibility that the "flutes" or "tongues" observed in Ogrenok and Ogra are the result of asymmetry produced by the injection channel?

M. K. Romanovsky: No, this is not connected with the field asymmetry produced by the injector, but it can be due to the space charge field. The frequency of the rotating flutes in our case is almost equal to the double frequency of rotation in an $\mathbf{E}\times\mathbf{H}$ field if we choose the value of the field intensity equal to the very 100 volts I was speaking about. But I would not insist on it. Our plasma is very rarefied; its density is not greater than 3 to $5\cdot10^{7}\,\mathrm{cm}^{-3}$; therefore we cannot, strictly speaking, call it plasma. But the rotation of such tongues we do observe.

Paper CN-10/178 *was presented by J. A. Phillips* (United States of America). *The text of the paper is on pages 299 to 312 inclusive. The following discussion took place:*

A. E. Robson *(United Kingdom):* It may be of interest to report some preliminary results from a somewhat similar magnetic electron trap we are studying at Harwell.

The main parameters of the trap (size, magnetic field, etc.) are not very different from the trap described in this paper, but the field perturbation is axially-symmetric and provided by a set of 10 small coils connected alternately in opposition, after the manner of Sinelnikov's experiment. A pulse of electrons, of 3 μs duration and 800 μA intensity is injected, and the current out of the end mirror measured as a function of time. When the trap is adjusted to satisfy the resonance conditions, we find that ~30% to 50% of the injected electrons are captured during the pulse and then escape with a decay time of the order of 200 μs.

I am grateful to Dr. Phillips for a very interesting discussion on the use of phase-space arguments to estimate the maximum containment times in these traps. Owing to the restriction on the radius at which particles may be injected into our trap, it seems that the "hole in phase space" available for injection into it (and hence for loss from it) may be significantly smaller than in Dr. Phillips' case. This might possibly account for the apparently larger containment of electrons in our trap.

J. A. Phillips *(United States of America):* The results reported by Dr. Robson are very interesting and encouraging. I am surprised that the containment time is ~20 times larger than that observed in our experiment, especially since the range of electron energies accepted by the two systems are about the same. However, the discrepancy could be explained if the acceptance area in the experiment of Dr. Robson is smaller than that in our experiment.

P. Hubert *(France):* Although very ingenious, the method which you describe suffers from the drawback that it is not consistent with axial symmetry. The situation could be remedied by using multipolar coils. In that case injection would have to be outside the axis. Have you made any calculations on this subject?

J. A. Phillips: It is true that this method does not have axial symmetry and as a result there may exist a radial drift of particles on multiple traversals. This has been pointed out by Wingerson. However, in our experiments and orbit calculations we find that radial drifts are small and can be neglected in our present experiments. If the containment times can be increased by an order of magnitude or two, this effect of axial asymmetry could become important.

We have considered other geometries but to date have not made any detailed calculations.

W. Linlor *(United States of America):* Regarding the azimuthal symmetry of non-adiabatic resonance trapping devices, there is a publication in the Aug. 15, 1961, issue of *Physical Review Letters* which shows a non-reciprocal trapping arrangement, using travelling magnetic perturbations.

Taking the Liouville limit to apply, what is your value of trapped density that can be achieved using ion sources with small angular divergence?

J. A. Phillips: In the present experiment with a 1 mA electron beam and a measured confinement time of ~11 μs we calculate an electron density of $\sim10^{7}$ electrons/cm^{3}. Extrapolating these results to 10 keV ions with the assumption that plasma effects do

not become important, an ion density of 10^{10} ions/cm^3 should be reached with a 100 mA beam. From the results reported in the paper the number of traversals through the helix is proportional to its length. As far as the angular divergence of the beam is concerned, the confinement time is on the average independent of the characteristics of the ion source so long as the beam is contained in the acceptance area and solid angle of the magnetic mirror and helix.

B. Safronov *(Union of Soviet Socialist Republics):* What was the maximum density of electrons accumulated in the trap?

J. A. Phillips: We calculate, from the lifetime, the density of 10^7 electrons/cm^3 with a 1 mA electron beam.

B. Safronov: Second question: How do you expect to overcome space charge?

J. A. Phillips: In the present experiment we do not have to worry about space charge. With the beam current that we had with a 11 μs confinement time, the potential of the trapped electrons rises only 30 to 50 eV. However, when one uses large beams of ions, we believe that electrons can be injected from both ends through the mirrors to neutralize space charge potentials.

B. Safronov: One more remark. We performed experiments which are described in a paper not presented orally at this conference. In this paper we describe a method of injecting plasma into an analogous trap, although with not quite symmetrical change of the magnetic field. We obtained results which indicate that we succeeded in transforming more than 50% of the kinetic energy of the plasma jet into its transverse energy.

J. A. Phillips: We have also considered the injection of neutral plasma bunches from hydromagnetic guns into such systems. We feel that the maximum particle density that can be achieved by these methods may be rather low due to plasma effects. Your results are very interesting.

Papers CN-10/254 *and* CN-10/255 *were presented by V. A. Simonov* (Union of Soviet Socialist Republics). *The texts of the papers are on pages 313 to 339 inclusive. The following discussion took place:*

D. J. Grove *(United States of America):* Do you have suggestions for suitable materials not subject to oxide films?

V. A. Simonov *(Union of Soviet Socialist Republics):* There is a suggestion to use for aperture diaphragms of discharge chambers materials such as tungsten which are periodically heated to high temperature. For the side walls of discharge chambers it is appropriate to use high resistance alloys not based on iron or nickel and thin coatings. But in order to use thin coatings it is necessary to perform experiments to determine their rate of evaporation in practical conditions.

Paper CN-10/100 *was presented by M. Vuillemin* (France). *The text of the paper is on pages 341 to 344 inclusive. The following discussion took place:*

R. F. Post *(United States of America):* Could you please amplify your remarks on systems in which the mirrors are short compared with the central uniform field region? You said that this is a delicate matter to calculate.

M. Vuillemin *(France):* The simplified form of the stability conditions does not apply to the systems of which you were speaking. In this case, it would be necessary to define an equivalent radius of curvature by omitting from the configuration the practically uniform part of the field; see Fig. IV-2.

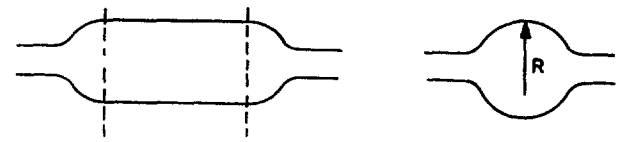

Fig. IV-2 "Equivalent radius of curvature" R defined by omitting the uniform part of the field.

M. S. Ioffe *(Union of Soviet Socialist Republics):* Do you think that your method of stabilization of flute instability has practical perspectives with regard to thermoinsulating plasma in a trap?

M. Vuillemin: Although the method used for this calculation assumes a direct contact between the plasma and the conducting walls, it seems to me that this situation cannot be realized in actual practice. The stabilization can be achieved by walls located outside the magnetic mirrors, if we allow an indirect contact, either by means of the influence of a cold plasma, or by that of the escaping particles. In neither case does our calculation allow computation of the particle density necessary to make this mechanism efficient.

Paper CN-10/158 *was presented by R. A. Dandl* (United States of America). *The text of the paper is on pages 345 to 352 inclusive. The following discussion took place:*

T. Consoli *(France):* I should like to draw attention to an observation of cyclotron heating in the high frequency confinement experiment described in paper CN-10/108.

In this confinement the spherical cavity is traversed by a plasma column varying in density from $10^{12}/cm^3$ to $10^{14}/cm^3$. The resonance frequency of the cavity is 1220 MHz. For the magnetic field value of 320 oersted, corresponding to the resonance $\omega_{ce} = \omega_{resonance}$, a considerable transfer of energy from the oscillator to the plasma is found. This transfer is reflected by a rise in electronic temperature.

R. A. Dandl *(United States of America)*: I don't understand the low temperature. Our densities, we feel, are of the order 10^{11} or $10^{12}/cm^3$. We are fairly confident of the energy density measurements made. So that if one divides these densities into the energy densities, we have to have significantly high temperatures. Also, the decay times observed of the cyclotron radiation are too long for such low temperatures.

NUCLEAR FUSION
FUSION NUCLEAIRE
ЯДЕРНЫЙ СИНТЕЗ
FUSION NUCLEAR

1962 SUPPLEMENT
PART 2

PROCEEDINGS OF THE CONFERENCE ON PLASMA PHYSICS AND CONTROLLED NUCLEAR FUSION RESEARCH, 4—9 SEPTEMBER 1961, SALZBURG, AUSTRIA

LES ACTES DE LA CONFERENCE SUR LA PHYSIQUE DES PLASMAS ET LA RECHERCHE CONCERNANT LA FUSION NUCLEAIRE CONTROLEE, 4—9 SEPTEMBRE 1961, SALZBOURG, AUTRICHE

ТРУДЫ КОНФЕРЕНЦИИ ПО ИССЛЕДОВАНИЯМ В ОБЛАСТИ ФИЗИКИ ПЛАЗМЫ И УПРАВЛЯЕМОГО ЯДЕРНОГО СИНТЕЗА, 4—9 СЕНТЯБРЯ 1961 г., ЗАЛЬЦБУРГ, АВСТРИЯ

LAS ACTAS DE LA CONFERENCIA SOBRE LAS INVESTIGACIONES EN MATERIA DE FISICA DEL PLASMA Y FUSION NUCLEAR CONTROLADA, 4 AL 9 DE SEPTIEMBRE DE 1961, SALZBURGO, AUSTRIA

INTERNATIONAL ATOMIC ENERGY AGENCY • AGENCE INTERNATIONALE DE L'ENERGIE ATOMIQUE • МЕЖДУНАРОДНОЕ АГЕНТСТВО ПО АТОМНОЙ ЭНЕРГИИ • ORGANISMO INTERNACIONAL DE ENERGIA ATOMICA

Selection and Program Committee — Comité de sélection et d'établissement du programme — Комитет по отбору докладов и разработке программы — Comité de Selección y del Programa

P. HUBERT ..... Chef du Service de recherches sur la fusion contrôlée, Commissariat à l'énergie atomique, France

K. V. ROBERTS ..... Theoretical Physics Division, Culham Laboratory, United Kingdom Atomic Energy Authority, United Kingdom

C. VAN ATTA ..... Associate Director, Lawrence Radiation Laboratory, University of California, United States of America

Scientific Secretariat — Secrétariat scientifique — Научный секретариат — Secretaría Científica

B. BURAS ..... *(Co-ordinating Scientific Secretary)* Division of Research and Laboratories, International Atomic Energy Agency

P. A. DAVENPORT .... *(Scientific Secretary)* Culham Laboratory, United Kingdom

C. ETIEVANT ..... *(Secrétaire scientifique)* Association Euratom — CEA, Service de recherches sur la fusion contrôlée, Fontenay-aux-Roses, France

W. F. GAUSTER ..... *(Scientific Secretary)* Oak Ridge National Laboratory, United States of America

Е. В. ПИСКАРЕВ..... *(Ученый секретарь)* Институт атомной энергии им. И. В. Курчатова, Москва, СССР (E. V. PISKAREV)

B. TORKI ..... *(Assistant Scientific Secretary)* Division of Research and Laboratories, International Atomic Energy Agency

I. DRUTMAN ..... *(Technical Secretary)* Division of Research and Laboratories, International Atomic Energy Agency

Editor of "Nuclear Fusion" — Rédacteur de la revue «Fusion Nucléaire»—Редактор журнала «Ядерный синтез» — Redacteur de "Fusión Nuclear"

J. G. BECKERLEY .... Division of Scientific and Technical Information, International Atomic Energy Agency

Executive Secretary — Secrétaire exécutif — Исполнительный секретарь — Secretario Ejecutivo

W. LISOWSKI ..... Division of Scientific and Technical Information, International Atomic Energy Agency

Conference Services — Services linguistiques — Обслуживание конференции — Servicios de la Conferencia

A. BERNSTEIN ..... *(Chief Interpreter)* International Atomic Energy Agency

L. S. LIEBERMAN ..... *(Records Officer)* International Atomic Energy Agency

Public Information — Information — Общественная информация — Información pública

P. FENT ..... *(Press Officer)* International Atomic Energy Agency

MISS M. NAPIER ..... *(Special Media Officer)* International Atomic Energy Agency

FOREWORD — AVANT-PROPOS — ПРЕДИСЛОВИЕ — PREFACIO

In 1958, at the Second United Nations Conference on the Peaceful Uses of Atomic Energy, the results of research on controlled nuclear fusion obtained in a few technically advanced countries were first disclosed to the world at large. Since then, it has become more and more evident that a better understanding of fundamental phenomena is needed before the goal of energy extraction from nuclear fusion may be reached. Consequently, the intensive research undertaken in recent years has been primarily basic research in plasma physics.

The fact that such research is most complex and costly has enhanced the desirability of co-operation and exchange of information and experience between all those engaged in this field of nuclear science and technology. It has become obvious that the International Atomic Energy Agency can play an important part in promoting such co-operation on a world-wide scale.

After consultation with a number of leading scientists, the Agency convened an international conference on Plasma Physics and Controlled Nuclear Fusion Research. The extent of the interest shown by Member States did not merely confirm that such a conference was actually needed at the present time, but greatly exceeded expectations. The quality and volume of the papers submitted, the number of participants and of countries represented, all bore witness to this interest.

Today, plasma physics and controlled thermonuclear fusion research is a more-or-less academic study. All that can be said at this stage is that it should eventually lead to a practical energy source. The day may come when the energy from nuclear fusion will be needed and when the well-being of mankind may depend on the ability to draw on this almost limitless reservoir.

The publication of the conference proceedings is intended to promote international co-operation and accelerate progress in this most important field of scientific endeavor.

INTRODUCTION – ВВЕДЕНИЕ – INTRODUCCIÓN

The Conference on Plasma Physics and Controlled Nuclear Fusion Research was held in Salzburg, Austria, on 4—9 September 1961. More than 500 scientists, representing 29 nations and 6 international organizations, participated in the Conference. The Proceedings are published in three parts as a 1962 supplement to this journal.

Because of the many interconnections between the various problems of plasma physics, it was decided to have no parallel plenary sessions. Accordingly, nine sessions were held during the six days of the Conference. During these sessions, 111 papers were presented. The "free" afternoons and evenings were devoted to at least fourteen informal discussions of topics of special interest to the participants. The present Proceedings do not include the records of these informal discussions (the discussions would have ceased to be "informal" if recorded), although it seems certain that new ideas generated in these discussions will lead to publication of papers elsewhere.

"Part 1" contains the texts (in original language only) of all papers delivered in Sessions I, II and IV of the Conference, the records (in English) of the discussions of these papers, as well as the texts (in English and Russian) of the two concluding speeches by Prof. Artsimovich and Dr. Rosenbluth summarizing the Conference. Translations of the abstracts of each paper (Sessions I, II, IV) are given at the end of this part of the Proceedings. In addition there is an author index.

The remainder of the Proceedings is published in "Part 2" (Sessions III, V, VI, VIII) and in "Part 3" (Sessions VII, IX). The abstracts of those papers accepted but not presented to the Conference, a list of participants, subject and author indexes for the entire Proceedings are included in the third part.

In preparing the Proceedings the Editor gratefully acknowledges the substantial help of B. Buras, P. A. Davenport, C. Etievant, W. F. Gauster, W. A. Newcomb and E. V. Piskarev.

CONTENTS — SOMMAIRE — СОДЕРЖАНИЕ — INDICE

SESSION VI — SÉANCE VI — ЗАСЕДАНИЕ VI — SESIÓN VI

SESSION VIII — SÉANCE VIII — ЗАСЕДАНИЕ VIII — SESIÓN VIII

SESSION III — SÉANCE III

ЗАСЕДАНИЕ III — SESIÓN III

5 SEPTEMBER 1961 — 5 SEPTEMBRE 1961

5 СЕНТЯБРЯ 1961 Г. — 5 DE SEPTIEMBRE DE 1961

Chairman — Le président — Председатель — El Presidente

M. A. Leontovich
[М. А. Леонтович] (*Union of Soviet Socialist Republics*)

Scientific Secretary — Secrétaire scientifique — Ученый секретарь — Secretario Científico

E. V. Piskarev
[Е. В. Пискарев] (*Union of Soviet Socialist Republics*)

[Papers presented: CN-10/43, 73, 87, 88, 132, 152, 164, 199, 220]

ON THE STRUCTURE OF HYDROMAGNETIC SHOCK WAVES WITH TRANSVERSE FIELD AND VISCOUS DISSIPATION*

W. GEIGER**, H. J. KAEPPELER, B. MAYSER

INSTITUT FÜR HOCHTEMPERATURFORSCHUNG DER TECHNISCHEN HOCHSCHULE STUTTGART***

STUTTGART, FEDERAL REPUBLIC OF GERMANY

The problem of hydromagnetic shock waves has recently received increasing interest in connection with experiments carried out to obtain extremely high temperatures for fusion processes. In such experiments a tendency toward appreciable densities (obtained, e.g., by magnetic compression) becomes noticeable.

Theories of hydromagnetic shock structure available at present either neglect the inertial term in the differential equation for the magnetic field if dissipation processes are considered (Marshall, Sen), or if the rigorous equations for the magnetic field are used, a collision-free plasma is considered (Grad, Morawetz).

This paper deals with a study of the effect of viscous dissipation in the rigorous hydromagnetic shock structure equations for the purpose of deriving a theory applicable to relatively high densities. First, the shock structure for a pure hydromagnetic case (neglecting viscosity but considering ohmic resistance as a damping mechanism) is considered in some detail. A stability investigation is carried out and it is shown that there exist two regimes for the shock transition, one characterized by an oscillatory transition, the other by an aperiodic damped transition. Considering viscosity, the range for which this dissipation mechanism becomes appreciable is determined. It can furthermore be shown that whereas solutions for Mach numbers $M < 1$ behind the shock do not exist for the collision-free hydromagnetic case, the inclusion of viscous dissipation in the Navier-Stokes approximation indicates the possibility for such solutions.

1. Hydromagnetic shock structure with ohmic damping

1.1 GENERAL REMARKS AND BASIC EQUATIONS

The structure of a hydromagnetic shock wave as discussed by C. S. MORAWETZ [1] is not based on a truly collision-free theory, as the damping mechanism considered, namely ohmic dissipation, is produced by collisions. For magnetic energy density large compared to thermal energy density (small β values), however, this damping becomes small and in this limit the theory may be regarded as a collision-free one. For appreciable damping, it is very likely that, e.g., viscous dissipation can no longer be neglected, so that for simplicity all those solutions shall be termed "collision-free" where viscous effects can be disregarded, even though a small value of the ohmic resistance is retained for damping purposes.

In our investigations we start with such a collision-free theory for hydromagnetic shock structure. However, unlike C. S. Morawetz, we shall use a definite and concrete equation for the ohmic resistance. The calculations shall furthermore be restricted to the temperature and density range currently of particular interest in hydromagnetic compression experiments, namely from some 10^4 °K to 10^5 °K and particle densities of 10^{16} and 10^{17} cm^{-3}.

As basic equations for the shock structure, the conventional one-fluid equations [1—4] are employed, the equation of continuity and the equation of motion:

$$\varrho u = m, \tag{1}$$

$$\varrho u^2 + p + \frac{B^2}{8\pi\mu} = P, \tag{2}$$

the energy equation,

$$\frac{u^2}{2} + \frac{\varkappa}{\varkappa - 1} \cdot \frac{p}{\varrho} + \frac{c}{4\pi\mu m} E B = Q, \tag{3}$$

and a generalized form of Ohm's law derived from a two-fluid description of the y-momentum equations,

$$\frac{\mathrm{d}^2 B}{\mathrm{d}t^2} + \gamma_e \gamma_i \eta_R \varrho \frac{\mathrm{d}B}{\mathrm{d}t} + \frac{4\pi\mu}{c^2} \gamma_e \gamma_i (\varrho u) \cdot (cE - uB) = 0, \tag{4}$$

together with the Maxwell equation (in gaussian units)

$$j = -\frac{c}{4\pi\mu} \cdot \frac{\mathrm{d}B}{\mathrm{d}x}. \tag{5}$$

With $u = \mathrm{d}x/\mathrm{d}t$, Eq. (4) can also be written in the form

$$\frac{\mathrm{d}^2 B}{\mathrm{d}x^2} + \frac{1}{u}\frac{\mathrm{d}u}{\mathrm{d}x}\frac{\mathrm{d}B}{\mathrm{d}x} + \gamma_e \gamma_i \frac{\varrho}{u} \eta_R \frac{\mathrm{d}B}{\mathrm{d}x} + \frac{4\pi\mu}{c^2} \gamma_e \gamma_i \frac{\varrho}{u} (cE - uB) = 0. \tag{6}$$

In the above equations, u is the x-component of the velocity, ϱ the mass density, p the hydrostatic pressure, B the z-component of the magnetic field, E the y-component of the electric field (E = const.

* Conference paper CN-10/43 presented by H. J. KAEPPELER. Discussion of this paper is given on page 491. Translations of the abstract are at the end of this volume of the Conference Proceedings.

** Recheninstitut der Technischen Hochschule Stuttgart.

*** Prof. Kluge und Prof. Höcker.

due to curl $\mathbf{E}=0$), j the y-component of the current density, η_R the specific ohmic resistance, $\varkappa$ the ratio of the specific heats,

$$\varkappa = c_p/c_v\,, \tag{7}$$

and γ an abbreviation,

$$\gamma_e = e/m_e, \qquad \gamma_i = e/m_i, \tag{8}$$

where e is the elementary charge, m_e the electron mass and m_i the ionic mass.

Assumptions in the above equations are ionic charge $eZ=e$ ($Z=1$) and quasi-neutrality $n_e=n_i$, where n is the particle density.

1.2 Singularities of the differential equation

We consider those states for which the differential equation has singular points, i.e. for which all derivatives vanish (stationary flow). The stationary solution requires that

$$\frac{\mathrm{d}^2 B}{\mathrm{d}x^2} = \frac{\mathrm{d}B}{\mathrm{d}x} = 0;$$

hence,

$$E = \frac{u}{c} B.$$

On the other hand, we find from the conservation laws Eqs. (1) through (3) after elimination of ϱ and p,

$$u^2 - \frac{2\varkappa}{\varkappa+1}\frac{1}{m}\left(P - \frac{B^2}{8\pi\mu}\right)\cdot u - 2\frac{\varkappa-1}{\varkappa+1}\left(\frac{cE}{4\pi\mu m}\cdot B - Q\right) = 0. \tag{9}$$

Inserting $B=cE/u$ into this equation, there follow those values of u for which the flow is steady. There results a third-order equation in u,

$$u^3 - \frac{2\varkappa}{\varkappa+1}\frac{P}{m}\cdot u^2 + 2\frac{\varkappa-1}{\varkappa+1}Q\cdot u + \frac{2-\varkappa}{\varkappa+1}\frac{c^2E^2}{4\pi\mu m} = 0. \tag{10}$$

Expressing m, P and Q by ϱ_0, u_0, p_0 and B_0, there follows that

$$u = u_0$$

is a solution of Eq. (10). Splitting off the factor $(u-u_0)$, there remains a quadratic equation for u,

$$u^2 + \left(u_0 - \frac{2\varkappa}{\varkappa+1}\frac{P}{m}\right)u + \left(2\frac{\varkappa-1}{\varkappa+1}Q + u_0^2 - \frac{2\varkappa}{\varkappa+1}\frac{P}{\varrho_0}\right) = 0. \tag{11}$$

Introducing the new quantities

$$\hat{u} = \frac{u}{u_0}, \quad M_0^2 = \frac{u_0^2}{\varkappa\, p_0/\varrho_0}, \quad \beta_0 = \frac{p_0}{B_0^2/8\pi\mu}, \tag{12}$$

the equation for $\hat{u}$ becomes

$$\hat{u}^2 - \frac{1}{\varkappa+1}\left[\varkappa - 1 + \frac{2}{M_0^2}\left(1+\frac{1}{\beta_0}\right)\right]\cdot\hat{u} - \frac{2}{\varkappa}\frac{2-\varkappa}{\varkappa+1}\frac{1}{\beta_0 M_0^2} = 0,$$

or

$$\hat{u}_{1,(2)} = \frac{1}{2(\varkappa+1)}\left[\varkappa - 1 + \frac{2}{M_0^2}\left(1+\frac{1}{\beta_0}\right)\right] \overset{+}{(-)} \left\{\left[\frac{1}{2(\varkappa+1)}\right]^2\left[\varkappa - 1 + \frac{2}{M_0^2}\left(1+\frac{1}{\beta_0}\right)\right]^2 + \frac{2}{\varkappa}\frac{2-\varkappa}{\varkappa+1}\frac{1}{\beta_0 M_0^2}\right\}^{1/2}. \tag{13}$$

Only the positive sign has a physical meaning, the negative sign results in negative u. If $\hat{u}=1$ designates the singular point in front of the shock, then Eq. (13) yields the singular point behind the shock.

Two special cases for the above Eq. (13) shall be given.

(a) $\varkappa=2$ (two degrees of freedom):

$$\hat{u}_1 = \frac{1}{3}\left[1 + \frac{2}{M_0^2}\left(1+\frac{1}{\beta_0}\right)\right].$$

(b) $\varkappa=5/3$ (three degrees of freedom):

$$\hat{u}_1 = \frac{1}{8}\left[1 + \frac{3}{M_0^2}\left(1+\frac{1}{\beta_0}\right)\right] + \left\{\left(\frac{1}{8}\right)^2\left[1 + \frac{3}{M_0^2}\left(1+\frac{1}{\beta_0}\right)\right]^2 + \frac{3}{20}\frac{1}{\beta_0 M_0^2}\right\}^{\frac{1}{2}}.$$

In both cases, the final velocity is greater than in the gas-dynamic case.

Another way of ascertaining these two singular points is the derivation of the hydromagnetic analogue of the Rankine-Hugoniot relations.

1.3 Solution of the equations in the neighborhood of the singularities

The behavior of the system of equations in the vicinity of the singular points becomes evident from the higher derivatives. Differentiating the differential equation of second order for B, Eq. (6), with respect to x, there follows

$$u\frac{\mathrm{d}^3 B}{\mathrm{d}x^3} + \varrho\gamma_e\gamma_i\eta_R\frac{\mathrm{d}^2 B}{\mathrm{d}x^2} - \frac{4\pi\mu}{c^2}\varrho\gamma_e\gamma_i\frac{\mathrm{d}}{\mathrm{d}B}(uB)\cdot\frac{\mathrm{d}B}{\mathrm{d}x} = 0,$$

where small members of second order were neglected. Inserting the Maxwell Equation (5) results in

$$\frac{\mathrm{d}^2 j}{\mathrm{d}x^2} + \frac{\varrho}{u}\gamma_e\gamma_i\eta_R\frac{\mathrm{d}j}{\mathrm{d}x} - \frac{4\pi\mu}{c^2}\frac{\varrho}{u}\gamma_e\gamma_i\frac{\mathrm{d}}{\mathrm{d}B}(uB)\cdot j = 0. \tag{14}$$

The term $\mathrm{d}(uB)/\mathrm{d}B$ is immediately derived from Eq. (9). This yields

$$\frac{\mathrm{d}}{\mathrm{d}B}(uB) = u\left(1 - \frac{2}{\varkappa\beta}\frac{1}{M^2-1}\right), \tag{15}$$

where M is the gas-dynamic Mach number ($M=u/a$, a=sonic velocity). Substituting (15) into (14), there follows the differential equation for j in the neighborhood of the singularities,

$$\frac{\mathrm{d}^2 j}{\mathrm{d}x^2} + \frac{\varrho}{u}\gamma_e\gamma_i\eta_R\frac{\mathrm{d}j}{\mathrm{d}x} - \frac{4\pi\mu}{c^2}\gamma_e\gamma_i\varrho\left(1 - \frac{2}{\varkappa\beta}\frac{1}{M^2-1}\right)\cdot j = 0. \tag{16}$$

In this neighborhood, the dynamical quantities ϱ, u, etc. may be considered as constants. We thus may write the solution,

$$j = \alpha \cdot e^{\omega x}, \tag{17}$$

where α is a small perturbation. From Eqs. (17) and (16), ω becomes

$$\omega_{1,2} = -\frac{\varrho}{2u} \cdot \gamma_e \gamma_i \eta_R \pm \sqrt{\left(\frac{\varrho}{2u} \cdot \gamma_e \gamma_i \eta_R\right)^2 + \frac{4\pi\mu}{c^2} \gamma_e \gamma_i \varrho \cdot \left(1 - \frac{2}{\varkappa\beta} \frac{1}{M^2 - 1}\right)}. \tag{18}$$

This equation is now used for a discussion of the behavior of the system near the singularities in front of and behind the shock wave.

Singularity in front of the shock wave. In this case we have the hydromagnetic Mach number M^*, expressed by the gas-dynamic Mach number M and the ratio of gas pressure to magnetic pressure β,

$$(M_0^*)^2 = \frac{M_0^2}{1 + 2/\varkappa\beta_0} > 1,$$

and thus

$$1 - \frac{2}{\varkappa\beta_0} \frac{1}{M_0^2 - 1} > 0.$$

The two roots of Eq. (18) yield

ω_1 = positive, real: exponential increase,
ω_2 = negative, real: exponential decrease.

In the low temperature, high density region of our range of interest ($T < 10^5$ °K, $n \geqslant 10^{17}$ cm^{-3}), the first term in the root of Eq. (18) predominates and the "time constant" ω_1 can be represented by

$$\omega_1 = \frac{4\pi\mu}{c^2} \cdot \frac{u_0}{\eta_R} \cdot \left(1 - \frac{2}{\varkappa\beta_0} \cdot \frac{1}{M_0^2 - 1}\right).$$

Example: For $T_0 = 4 \times 10^4$ °K, $n_0 = 10^{17}$ cm^{-3}, $\beta_0 = 1$, $M_0^* = 2$ follows $\omega_1 = 10{,}66$ cm^{-1}.

Singularity behind the shock wave. At the singularity behind the shock wave we have

$$(M_1^*)^2 < 1; \quad 1 - \frac{2}{\varkappa\beta_1} \frac{1}{M_1^2 - 1} < 0.$$

Here, three cases are to be distinguished.

Case (i):

$M_1^2 > 1$;

$$\left(\frac{\varrho_1}{2u_1} \gamma_e \gamma_i \eta_R\right)^2 > \frac{4\pi\mu}{c^2} \cdot \gamma_e \gamma_i \varrho_1 \left(\frac{2}{\varkappa\beta_1} \frac{1}{M_1^2 - 1} - 1\right).$$

The two solutions of Eq. (18) are

ω_1 = negative, real: exponential damping,
ω_2 = negative, real: exponential damping.

The result in this case is an aperiodic damped transition from the singularity in front of the shock to that behind the shock.

Case (ii):

$M_1^2 > 1$;

$$\left(\frac{\varrho_1}{2u_1} \gamma_e \gamma_i \eta_R\right)^2 < \frac{4\pi\mu}{c^2} \cdot \gamma_e \gamma_i \varrho_1 \left(\frac{2}{\varkappa\beta_1} \frac{1}{M_1^2 - 1} - 1\right).$$

Here, ω becomes

$$\omega_{1,2} = -\frac{\varrho_1}{2u_1} \cdot \gamma_e \gamma_i \eta_R \pm i \cdot \sqrt{\frac{4\pi\mu}{c^2} \cdot \gamma_e \gamma_i \varrho_1 \cdot \left(\frac{2}{\varkappa\beta_1} \frac{1}{M_1^2 - 1} - 1\right) - \left(\frac{\varrho_1}{2u_1} \gamma_e \gamma_i \eta_R\right)^2}.$$

The result is a damped oscillatory transition with the damping constant

$$\alpha = \frac{\varrho_1}{2u_1} \cdot \gamma_e \gamma_i \eta_R$$

and the wavelength

$$\lambda = \frac{2\pi}{\sqrt{\frac{4\pi\mu}{c^2} \cdot \gamma_e \gamma_i \varrho_1 \cdot \left(\frac{2}{\varkappa\beta_1} \frac{1}{M_1^2 - 1} - 1\right) - \left(\frac{\varrho_1}{2u_1} \gamma_e \gamma_i \eta_R\right)^2}}.$$

The transition from damped oscillations to a damped aperiodic shock profile is given by the relation

$$\eta_R^2 = 16\pi\mu \cdot \left(\frac{u_1}{c}\right)^2 \cdot \frac{1}{\varrho_1 \gamma_e \gamma_i} \cdot \left(\frac{2}{\varkappa\beta_1} \cdot \frac{1}{M_1^2 - 1} - 1\right). \tag{19}$$

If η_R^2 becomes larger than the right-hand side of Eq. (19), then there exists aperiodic damping. As η_R is a function of temperature T_1, the regime for aperiodic damping can be expressed by temperature, density, Mach number and β-factor.

Case (iii):

$$M_1^2 < 1.$$

For this case the following roots result:

ω_1 = positive, real: exponential increase of a perturbation,
ω_2 = negative, real: exponential decrease.

This means that the solution is unstable near the singularity behind the shock. This will be discussed further in the following section of this paper.

The investigations of behavior near the singularities may be summarized by dividing the entire range of Mach numbers into three regimes:

$0 < M^2 < 1$,	exponential increase of perturbation;
$1 < M^2 < 1 + 2/\varkappa\beta$,	exponential decrease of perturbation (a damped oscillation for the smaller values of M^2, and aperiodic damping for the larger values);
$1 + 2/\varkappa\beta < M^2$,	exponential increase of perturbation.

1.4 Numerical calculations and discussion of damping coefficient, wavelength and entire shock width

The formulae derived above hold only in the vicinity of the singularities. However, they already give a satisfactory picture of the behavior of the

TABLE I. Data of the calculated hydromagnetic shocks

Case	I	II	III	IV
temperature T_0 [°K]	4×10^4	10^5	10^5	10^5
particle density n_0 [cm^{-3}]	10^{17}	10^{17}	10^{16}	10^{16}
† hydromagnetic Mach number $M_0{}^*$	1,4	1,4	1,4	1,4
† pressure ratio β_0	10^{-2}	10^{-2}	6×10^{-3}	10^{-3}
† Mach number M_0	15,4	15,4	19,85	48,5
† pressure ratio β_1	$3{,}13 \times 10^{-2}$	$3{,}13 \times 10^{-2}$	$2{,}9 \times 10^{-2}$	$2{,}34 \times 10^{-2}$
† Mach number M_1	4,72	4,72	4,92	5,44
ϱ_1/ϱ_0	1,503	1,503	1,503	1,503
p_1/p_0	7,06	7,06	10,85	53
T_1/T_0	4,7	4,7	7,2	35

† $M_0{}^* = u_0 / \left(\frac{\varkappa p_0}{\varrho_0} + \frac{B_0{}^2}{4\pi\mu\varrho_0} \right)^{1/2}$, $\beta_0 = \frac{p_0}{B_0{}^2/8\pi\mu}$, $M_0 = \frac{u_0}{(\varkappa p_0/\varrho_0)^{1/2}}$, $\beta_1 = \frac{p_1}{B_1{}^2/8\pi\mu}$, $M_1 = \frac{u_1}{(\varkappa p_1/\varrho_1)^{1/2}}$.

solution. In order to ascertain the extent of their applicability, the shock equations, Eqs. (1) through (6), were solved numerically for certain selected cases. These are presented in Table I and Figs. 1—4. The selection was motivated by interest for actual experimental application.

Case I has almost complete aperiodic damping. The maximum value of the magnetic field B occurs well towards the end of the transition and is approximately 0,05 percent greater than the final value.

Case II also is quite close to aperiodic damping. It seems that the small temperature increase does not change the situation essentially.

In Case III we reduce both β and the density and obtain a pronounced oscillatory transition with good damping. This case will be discussed in detail below.

Case IV shows oscillatory transition with very small damping. The damping per wavelength is approximately 0,73 percent. Comparing this with Case III, the difference between III and IV consists in a lowering of β only, from 6×10^{-3} to 10^{-3}. It seems that the value of β has a decisive influence on the nature of the oscillatory transition.

The following is a more detailed discussion of Case III with respect to damping coefficient, wavelength and entire shock-width.

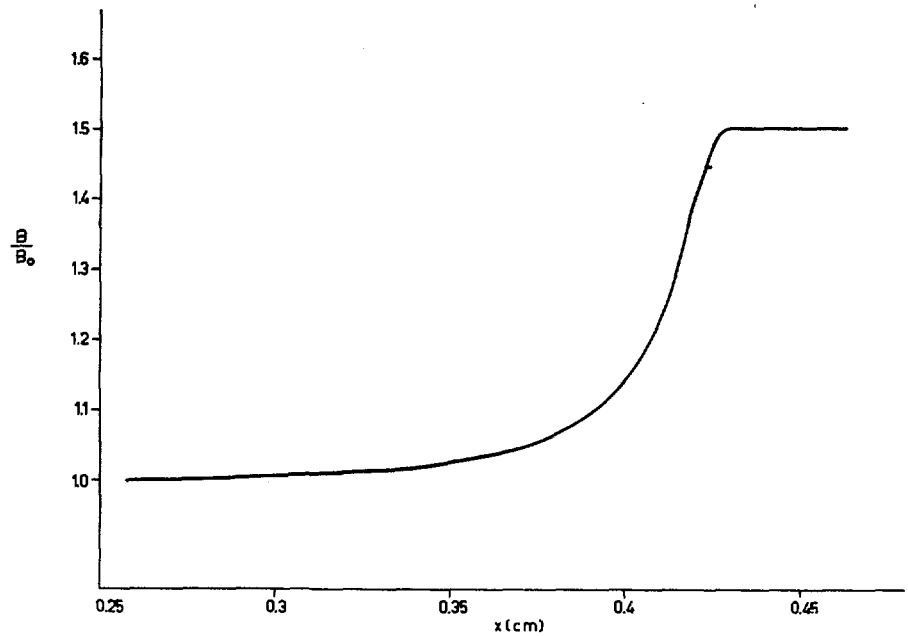

Fig. 1 Shock structure for $M^*{}_0 = 1{,}4$; $\beta_0 = 10^{-2}$; $n_0 = 10^{17}$ cm^{-3}; $T_0 = 4 \cdot 10^4$ °K.

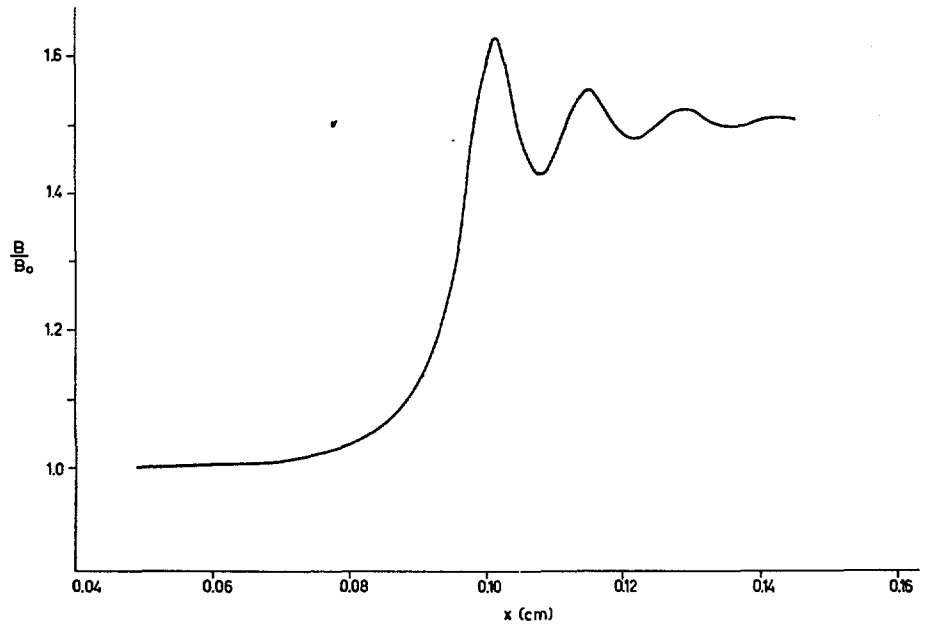

Fig. 2 Shock structure for $M^*_0 = 1{,}4$; $\beta_0 = 10^{-2}$; $n_0 = 10^{17}\ \mathrm{cm}^{-3}$; $T_0 = 10^5\ ^\circ\mathrm{K}$.

Wavelength. If the transition is sufficiently far from being aperiodic, the first term under the root of Eq. (18) may be neglected compared with the second term. This yields for the wavelength,

$$\lambda = \sqrt{\frac{\pi c^2}{\gamma_e \gamma_i \varrho \cdot (C-1)}},$$

where C is an abbreviation

$$C = \frac{2}{\varkappa \beta_1} \cdot \frac{1}{M_1^2 - 1}.$$

The value of C is practically constant in the cases calculated,

$$C = 1.8.$$

The wavelength λ is, from the above equation, essentially proportional to $1/\sqrt{\varrho}$. As ϱ varies quite slowly and $\sqrt{\varrho}$ still more slowly, then λ shows very little variation during the shock transition. Using ϱ_1 (behind the shock) for the calculation of λ, the wavelength is somewhat too small. The calculation yields for Case III

$$\lambda = 4{,}33 \times 10^{-2}\ \mathrm{cm}.$$

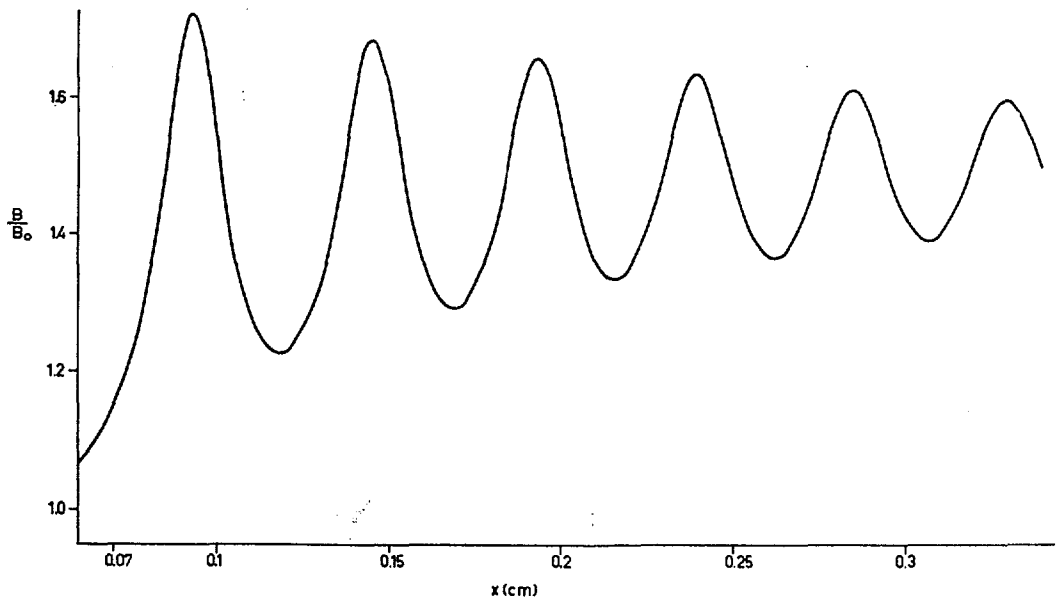

Fig. 3 Shock structure for $M^*_0 = 1{,}4$; $\beta_0 = 6 \cdot 10^{-3}$; $n_0 = 10^{16}\ \mathrm{cm}^{-3}$; $T_0 = 10^5\ ^\circ\mathrm{K}$.

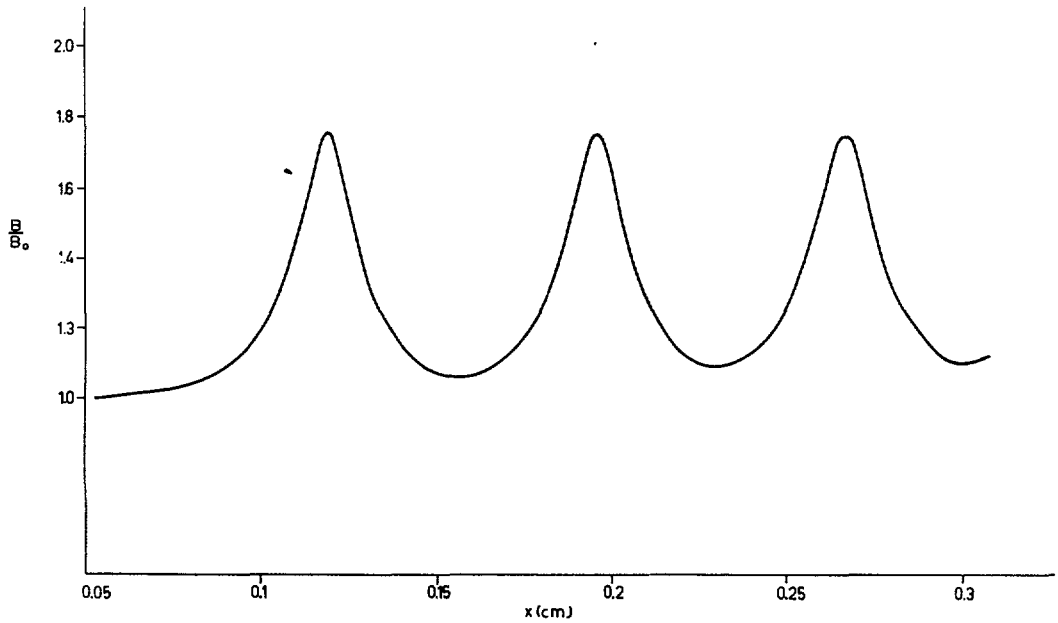

Fig. 4 Shock structure for $M^*_0 = 1{,}4$; $\beta_0 = 10^{-3}$; $n_0 = 10^{16}\,\mathrm{cm}^{-3}$; $T_0 = 10^5\,^\circ\mathrm{K}$.

The numerical solution of the shock equations yields (cf. Fig. 3)

$$5{,}2 \times 10^{-2} \ldots 4{,}2 \times 10^{-2}\,\mathrm{cm}.$$

Damping per wavelength. The damping per wavelength, for relatively small damping, may be expressed by

$$e^{-\alpha\lambda} \approx 1 - \alpha\lambda, \quad \text{for } \alpha\lambda \ll 1.$$

The relative decrease per wavelength thus becomes

$$\alpha \cdot \lambda = \frac{c}{2}\sqrt{\pi\gamma_e\gamma_i}\sqrt{\frac{\varrho u}{C-1}}\frac{\eta_R}{u^{3/2}}$$

$$= 3{,}28 \times 10^{26}\sqrt{\frac{\varrho u}{C-1}}\frac{\eta_R}{u^{3/2}}.$$

The damping per wavelength is essentially proportional to $\eta_R/u^{3/2}$. For Case III there follows from the above equation,

$$\alpha\lambda = 0{,}158 = 15{,}8\,\%.$$

Evaluation of the numerical solution of the shock equations results in

$$\alpha = 16\,\%$$

as the decrease of the current j relative to its value at the beginning of the interval.

Entire shock-width. Defining the shock-width as the distance d along which the amplitude of the oscillation has decreased to 1/10th of its initial value, there follows from

$$e^{-\alpha d} = 0{,}1$$

for the entire shock-width,

$$d = \frac{\ln 10}{\alpha} = \frac{\ln 10}{\varrho/2u \cdot \gamma_e\gamma_i\eta_R} = 3{,}0 \times 10^{-32} \cdot \frac{u}{\varrho \cdot \eta_R}.$$

Using the values behind the shock, there follows from the above formula

$$d = 0{,}62\,\mathrm{cm}.$$

From the numerical solution we find $d = 0{,}58$ cm. The distance from the beginning of the shock until the first maximum of the current is 0,08 cm. In agreement with DAVIS, LÜST and SCHLÜTER [5], we find that the entire shock-width is proportional to the flow velocity; we furthermore find, however, that it is inversely proportional to the specific ohmic resistance.

2. The influence of viscous dissipation on hydromagnetic shock structure

2.1 GENERAL REMARKS AND BASIC EQUATIONS

In the studies presented in the preceding Section of this paper, a certain inconsistency arises from the fact that, while collisions were considered in the damping mechanism (ohmic resistance), all other dissipation mechanisms arising from collisions were neglected. The purpose of the following considerations is to determine in what ranges this is permissible and to what extent viscous dissipation influences the transition through a hydromagnetic shock wave.

For this purpose, the basic equations for a hydromagnetic shock wave with transverse field in a frame of reference moving with the shock shall be given. **B** again is in z-direction, **j** and **E** in y-direction while the flow velocity **u** is in x-direction. Considered are the elements p_{xx} and p_{xy} of the trace-less pressure tensor $p_{ij} = P_{ij} - p\delta_{ij}$. We start from a two-fluid description, where the subscript e denotes the quantities for electrons, the subscript i those for ions. In the derivation we proceed from the conventional differential equations describing a plasma (cf. e.g. [6]).

Demanding quasi-neutrality, $n_e = n_i$, and assuming $T_e = T_i$, the component equations are added to form pseudo-one-fluid equations. There result

(a) the equation of continuity

$$\varrho u = m, \tag{20}$$

(b) the equation of motion

$$\varrho u^2 + p + p_{xx} + \frac{B^2}{8\pi\mu} = P, \tag{21}$$

(c) the energy equation

$$\frac{\varkappa}{\varkappa - 1}\frac{p}{\varrho} + \frac{u^2}{2} + \frac{p_{xx}}{\varrho} + \frac{cE}{4\pi\mu m}B + \frac{1}{2\gamma_e\gamma_i}\frac{j^2}{\varrho^2} - \left(\frac{1}{\gamma_e} + \frac{1}{\gamma_i}\right)\frac{j}{m\varrho}p_{e,xy} = Q, \tag{22}$$

(d) the general Ohm's law,

$$\frac{d^2B}{dx^2} + \frac{1}{u}\frac{du}{dx}\frac{dB}{dx} + \gamma_e\gamma_i\eta_R\frac{\varrho}{u}\frac{dB}{dx} + \frac{4\pi\mu}{c^2}\gamma_e\gamma_i\frac{\varrho}{u}(cE - uB) + \frac{4\pi\mu}{c}(\gamma_e + \gamma_i)\frac{1}{u}\frac{dp_{e,xy}}{dx} = 0. \tag{23}$$

The expressions for the components of the pressure tensor are taken from CHAPMAN and COWLING [7], with the approximation for strong magnetic fields,

$$p_{xx} = -\frac{4}{3}\eta\frac{du}{dx}\left[\frac{1 + (4/9)\,\omega^2\tau^2}{1 + (16/9)\,\omega^2\tau^2}\right], \tag{24}$$

$$p_{xy} = \frac{4}{3}\eta\frac{du}{dx}\left[\frac{\omega\tau}{1 + (16/9)\,\omega^2\tau^2}\right], \tag{25}$$

where

$$\omega = \frac{eB}{mc}, \quad \tau = \frac{3\eta}{2p}, \tag{26}$$

and η is the coefficient of viscosity. In the case of a strong magnetic field $\omega^2\tau^2 \gg 1$.

2.2 Influence of viscosity on shock transition

In order to discuss the influence of viscosity on the shock transition, we derive an equation for du/dx by differentiating Eqs. (20) through (22) and eliminating $d\varrho/dx$ and dp/dx. The result (neglecting the last two terms in the energy equation) is

$$\frac{du}{dx} = \frac{1}{\varrho u\,[1 - (1/M^2) - (\varkappa - 1)\,(p_{xx}/\varrho u^2)]}\left\{\frac{j}{c}\left[\varkappa B - (\varkappa - 1)\frac{\varrho}{\varrho_0}B_0\right] - \frac{dp_{xx}}{dx}\right\}. \tag{27}$$

In the hydromagnetic case without viscosity this equation is

$$\frac{du}{dx} = \frac{1}{\varrho u\,[1 - (1/M^2)]}\cdot\frac{j}{c}\left[\varkappa B - (\varkappa - 1)\frac{\varrho}{\varrho_0}B_0\right]. \tag{28}$$

The influence of viscosity is thus constituted by the term $(\varkappa - 1)\,(p_{xx}/\varrho u^2)$ in the denominator and the second member in brackets in Eq. (27).

It is readily seen that du/dx according to Eq. (28) approaches infinity for the Mach number M approaching unity. This means that the shock becomes a discontinuity and shock-structure solutions are not possible for $M < 1$. This is in agreement with the stability considerations given in the preceding Section of this paper.

In the case of Eq. (27), however, the term $(\varkappa - 1)\,p_{xx}/\varrho u^2$ prevents this singularity at $M = 1$. Hence, the inclusion of viscosity indicates the possibility of solutions for the shock transition with $M < 1$. A stability investigation, however, still has to be carried out.

The second term in brackets in Eq. (27) should essentially influence only the shape of the shock transition. The question as to the magnitude of its influence shall be discussed in the following.

2.3 Comparison of magnitudes of ohmic and viscous dissipation

As an estimate of the influence of viscous dissipation, we may at first assume this influence to be relatively small so that the member p_{xx} can then be treated as a perturbation. This would enable use of the solution with $p_{xx} = 0$ for determining du/dx in the calculation of p_{xx} according to Eq. (24). The conditions for permitting such a procedure are, according to Eqs. (27) and (28)

$$\left|\frac{dp_{xx}}{dx}\right| \ll \left|\frac{j}{c}\left\{\varkappa B - (\varkappa - 1)\frac{\varrho}{\varrho_0}B_0\right\}\right|,$$

$$\left|(\varkappa - 1)\frac{p_{xx}}{\varrho u^2}\right| \ll \left|1 - \frac{1}{M^2}\right|.$$

A further condition, required in using the Newton approximation for the stress tensor, is

$$\frac{p_{xx}}{p} \ll 1.$$

This condition would imply that $p_{xx} \ll B^2/8\pi\mu$ for values of $\beta < 1$. For all cases where the above conditions are fulfilled, neglect of viscous dissipation would definitely be permissible for a relatively simple calculation of hydromagnetic shocks. If it can be shown, however, that for a large range these conditions are violated, then neglect of viscous dissipation would result in an erroneous description of hydromagnetic shock behavior.

Several characteristic points of our four cases were calculated and the quantities are presented in Table II. From these data, it is immediately seen that, for the cases selected, neglect of viscous dissipation is definitely not permissible. In Case I, the influence would become noticeable for the sharp bend towards the end of the shock (not given in Table II).

It is of course difficult to give an accurate picture of the influence of viscosity from such a rough estimate. However, a few definite characteristics can be ascertained.

(1) Viscosity influence always becomes dominating for large values of d^2u/dx^2 and du/dx. This influence increases with increasing temperature.

TABLE II. Comparison of ohmic and viscous dissipation

Case	M_0	T_0 [°K]	β_0	x [cm]	$\frac{\lvert p_{xx}\rvert}{p}$	$\frac{\lvert \mathrm{d}p_{xx}/\mathrm{d}x\rvert}{\left\lvert \frac{j}{c}\left(\varkappa B-(\varkappa-1)\frac{\varrho B_0}{\varrho_0}\right)\right\rvert}$	$1-\frac{1}{M^2}$	$\left\lvert -(\varkappa-1)\frac{p_{xx}}{\varrho u^2}\right\rvert$
I	15,4	4×10^4	10^{-2}	0,4	$2{,}4\times10^{-2}$	$2{,}1\times10^{-3}$	0,992	$7{,}8\times10^{-5}$
II	15,4	10^5	10^{-2}	0,09	$4{,}8\times10^{-1}$	$3{,}35\times10^{-2}$	0,993	$1{,}41\times10^{-3}$
III	19,85	10^5	6×10^{-3}	0,11375	$7{,}3\times10^{-1}$	$2{,}16\times10^{0}$	0,988	$3{,}49\times10^{-3}$
				0,11697	$9{,}8\times10^{2}$	$1{,}11\times10^{2}$	0,963	$1{,}45\times10^{1}$
IV	48,5	10^5	10^{-3}	0,13197	$1{,}23\times10^{3}$	$4{,}19\times10^{1}$	0,986	$7{,}25\times10^{0}$
				0,15447	$2{,}38\times10^{0}$	$4{,}32\times10^{-1}$	0,896	$9{,}9\times10^{-4}$

The values of $\mathrm{d}^2u/\mathrm{d}x^2$ and $\mathrm{d}u/\mathrm{d}x$ tend to increase for comparable points with increasing Mach number M and decreasing β. The effect of viscosity, then, will likely be a smoothing of the oscillation, strongly damping sharp peaks (cf. Case IV).

(2) The total shock-width (cf. e.g. Sec. I. 4.) will probably not be altered essentially as it is mostly determined by the collision mechanism in general. As the collision integral for the pressure tensor approaches zero with increasing temperature more rapidly than the collision integral for the ohmic dissipation (specific resistance η_R), the entire shock-width probably will be essentially determined by η_R.

Stability calculations have shown that for the system of Eqs. (20) through (25), the singularity behind the shock shows unstable behavior. It may well be that in a more rigorous expression for the stress tensor, this instability is retained. However, only if the inclusion of all possible dissipation mechanisms does not remove this instability, will the question as to the physical validity of the equations or the question of a probable general instability of hydromagnetic flows become pertinent.

3. Conclusions

In the case of hydromagnetic shock structure considering ohmic resistance as the only dissipation mechanism, damped aperiodic and damped oscillatory transitions are possible. A criterion giving the limit between the two ranges was derived.

The above case is furthermore characterized by the fact that no shock-structure solutions are possible for Mach numbers smaller than unity in the shock transition. For $M=1$, there results a true discontinuity and it was shown that perturbations increase exponentially for $M<1$.

Numerical estimates showed that viscous dissipation cannot be neglected against ohmic resistance for most cases of practical interest.

If the Mach number in front of the shock becomes sufficiently great and β sufficiently small, large values of $\mathrm{d}u/\mathrm{d}x$ and $\mathrm{d}^2u/\mathrm{d}x^2$ are obtained and viscous dissipation must be considered. This effect then results in a smoothing of the oscillations.

It is intended to carry out detailed calculations of hydromagnetic shock structure with the equations including viscosity (given in this paper) or with a similar system of equations including a more rigorous expression for the stress tensor.

Acknowledgement

This research was in part sponsored by the Aeronautical Research Laboratory, Wright Air Development Center of the Air Research and Development Command, United States Air Force, through its European Office.

References

[1] MORAWETZ, C. S., United States Atomic Energy Commission Report NYO-8677 (January 1959).
[2] GARDNER, C. S., GOERTZEL, H., GRAD, H., MORAWETZ, C. S., ROSE, M. H., RUBIN, H., Second UN International Conference on Peaceful Uses of Atomic Energy **31** (1958) 230.
[3] KAEPPELER, H. J., MAYSER, B., and HÖCKER, K. H., Shock Waves in Partly and Fully Ionized Plasmas. Report AD 235 860 (January 1960).
[4] KAEPPELER, H. J., MAYSER, B., *Raketentechnik und Raumfahrt* **5** (1961) 1.
[5] DAVIS, L., LÜST, R., SCHLÜTER, A., *Z. Naturforschg.* **13a**, (1958) 916.
[6] GRAD, H., United States Atomic Energy Commission Report NYO-6486 (August 1956).
[7] CHAPMAN, S., COWLING, T. G., The Mathematical Theory of Non-uniform Gases (University Press, Cambridge, 1953).

THÉORIE DES ONDES ADIABATIQUES ASSOCIÉES AUX TERMES NON DIAGONAUX DU TENSEUR DE PRESSION DANS LES PLASMAS*

J. L. DELCROIX, J. F. DENISSE,** D. QUÉMADA

LABORATOIRE DE PHYSIQUE DES PLASMAS

ORSAY (SEINE-ET-OISE), FRANCE

La théorie hydrodynamique de la propagation des ondes planes monochromatiques dans un plasma homogène et indéfini, en présence d'un champ magnétique uniforme mais quelconque, est en général développée à l'aide des équations macroscopiques, en admettant que les transformations produites par l'onde satisfont à des conditions d'adiabaticité: $\nabla p_\alpha = \gamma_\alpha \mathrm{k} T_\alpha \nabla n_\alpha$ ($\alpha = \mathrm{e,i}$); mais cela signifie que la pression reste isotrope pendant le passage de l'onde: on sait que cette hypothèse n'est certainement pas vérifiée pour un plasma plongé dans un champ magnétique quelconque.

Les auteurs présentent une théorie où la variation de pression accompagnant le passage de l'onde est représentée par un tenseur, sans aucune hypothèse restrictive. Le système des équations macroscopiques est fermé maintenant par la condition $\nabla \cdot \mathbf{Q} = 0$, qui exprime que le flux de chaleur est nul et, en conséquence, doit être considérée comme une "condition adiabatique" plus générale.

Cette nouvelle théorie conduit à des résultats dont les caractères généraux s'accordent très bien avec ceux obtenus dans la théorie indiquée au premier alinéa, notamment en ce qui concerne les conditions d'existence des modes purement transversaux ou purement longitudinaux; mais, en plus des modes décrits dans la première théorie, les termes non diagonaux du tenseur de pression font apparaître de nouveaux modes. Leur signification physique reste à discuter, mais une telle théorie permet au moins de délimiter, en principe, le domaine de validité de la théorie à pression scalaire. On a étudié plus particulièrement les modes purement longitudinaux, ainsi que les modes purement transversaux en propagation longitudinale.

1. Introduction

Dans un ouvrage récent [1], une théorie hydrodynamique des divers types d'ondes planes monochromatiques pouvant se propager dans un plasma a été présentée; cette théorie a l'avantage de fournir une description générale et systématique des divers types d'ondes.

Dans toute théorie hydrodynamique, la difficulté essentielle consiste à rendre fermé le système des équations macroscopiques (cf. [2] p. 88): en [1], on a fermé le système en admettant que les ondes se propageant sont adiabatiques, et en écrivant pour les électrons et les ions du plasma cette condition sous la forme:

$$\nabla p = \gamma \mathrm{k} T \nabla n \tag{1}$$

où p est la pression et n la densité des particules considérées. Cette écriture suppose donc, à priori, que la pression conserve son caractère scalaire au cours des transformations produites par l'onde.

D'autre part, on est amené dans de nombreux cas à négliger les collisions entre particules; cette hypothèse est raisonnable dans de nombreux cas expérimentaux; elle est d'autre part nécessaire, si l'on veut pousser assez loin les calculs et la description des ondes. Or, il semble que l'existence d'une pression scalaire et l'absence de collisions sont dans une large mesure contradictoires; de plus, la présence d'un champ magnétique implique des anisotropies de pression; il semble donc préférable d'abandonner la condition (1) et de ne faire aucune hypothèse restrictive sur le tenseur de pression $\mathbf{\Psi}$. Il faudra donc, en plus des équations de conservation et de transport de la quantité de mouvement déjà écrites en [1], écrire l'équation de transport de la pression cinétique $\mathbf{\Psi}$ pour chaque espèce de particule:

$$\frac{\partial n}{\partial t} + \nabla \cdot n\mathbf{v} = 0 \tag{2}$$

$$nm\left(\frac{\partial}{\partial t} + \mathbf{v}\cdot\nabla\right)\mathbf{v} = nq(\mathbf{E} + \mathbf{v}\times\mathbf{B}) - \nabla\cdot\mathbf{\Psi} + \mathbf{P} \tag{3}$$

$$\left(\frac{\partial}{\partial t} + \mathbf{v}\cdot\nabla + \nabla\cdot\mathbf{v}\right)\mathbf{\Psi} + \nabla v\cdot\mathbf{\Psi} + (\nabla v\cdot\mathbf{\Psi})^{\mathrm{T}} + \nabla\cdot\mathsf{Q} = \mathsf{H} + \mathsf{R} \tag{4}$$

où l'on fera $\mathbf{P} = \mathsf{R} = 0$ (collisions négligées). Ce système sera fermé par la relation:

$$\nabla\cdot\mathsf{Q} = 0 \tag{5}$$

où Q est le tenseur flux de «chaleur» (cf. [2] p. 67 et 96) et qui semble donc exprimer une condition exacte d'adiabaticité.

Le présent article est consacré à cette théorie "exacte" des ondes adiabatiques dans un plasma; on verra que cette théorie garde les caractères généraux de la théorie «inexacte» faite dans [1], notamment en ce qui concerne les conditions d'existence de modes purement transversaux ou purement longitudinaux; mais les termes non diagonaux du tenseur de pression font apparaître de nouveaux modes.

---

* Mémoire CN-10/87, présenté par J. L. Delcroix. La discussion concernant ce mémoire est donnée page 491. Les traductions du résumé se trouvent en fin de volume.

** Observatoire de Paris, Section astrophysique de Meudon, Laboratoire de radioastronomie, Meudon, France.

La réalité physique des raffinements ainsi introduits dans la théorie hydrodynamique est peut-être sujette à caution; pour la comprendre pleinement, il faudrait déterminer le domaine de validité de la condition d'adiabaticité (5). Il paraît toutefois intéressant de développer cette théorie «exacte», ne serait-ce que parce qu'elle permet, en principe, de délimiter le domaine de validité de la théorie à pression isotrope faite en [1].

2. Équations générales

On étudie la propagation d'une onde plane se propageant parallèlement à **z**; on suppose qu'un champ magnétique d'origine extérieure $\mathbf{B}_0$ situé dans le plan yz (cf. figure 1) est appliqué au plasma; on

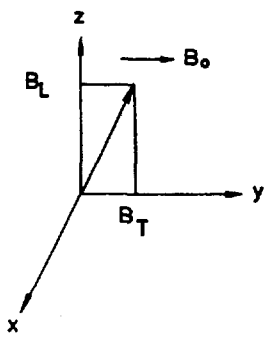

Fig. 1 Un champ magnétique d'origine extérieure $\mathbf{B}_0$ situé dans le plan y—z est appliqué au plasma.

désigne par B_L sa composante longitudinale, et par B_T sa composante transversale. L'état du plasma est caractérisé par les variables suivantes:

densité des électrons $n_e = \bar{n}_e + n_e$
vitesse des électrons $\mathbf{v}_e$
pression cinétique des électrons $\mathbf{\Psi} = \bar{p}_e + \mathbf{p}_e$

et trois variables analogues pour les ions.

Les notations et les méthodes de calcul seront très analogues à celles utilisées dans [1]; pour la commodité du lecteur, nous rappelons ces notations brièvement. Les grandeurs de l'onde varient comme $\exp[\mathrm{j}(\omega t - kz)]$ et on pose:

$$\bar{p}_e = \bar{n}_e \mathrm{k} T_e, \quad \bar{p}_i = \bar{n}_i \mathrm{k} T_i \tag{6}$$

$$\omega_p^2 = \frac{4\pi \bar{n}_e q_e^2 c^2}{m_e}, \quad \Omega_p^2 = \frac{4\pi \bar{n}_i q_i^2 c^2}{m_i},$$

$$\omega_0^2 = \omega_p^2 + \Omega_p^2 \tag{7}$$

$$\omega_b = -\frac{q_e B_0}{m_e}, \quad \omega_L = -\frac{q_e B_L}{m_e}, \quad \omega_T = -\frac{q_e B_T}{m_e} \tag{8}$$

$$\Omega_b = \frac{q_i B_0}{m_i}, \quad \Omega_i = \frac{q_i B_L}{m_i}, \quad \Omega_T = \frac{q_i B_T}{m_i} \tag{9}$$

$$m = \frac{\omega_p^2}{\Omega_p^2} = \frac{\omega_b}{\Omega_b} = \frac{m_i}{Z m_e}, \quad \tau = \frac{T_i}{Z T_e} = m \frac{\varepsilon_e}{\varepsilon_i} \tag{10}$$

$$A = \frac{\omega_p^2 + \Omega_p^2}{\omega_b \Omega_b} \tag{11}$$

$$\left.\begin{aligned} V_e^2 &= \frac{\mathrm{k} T_e}{m_e} \quad V_i^2 = \frac{\mathrm{k} T_i}{m_i} \\ V_s^2 &= \frac{\bar{n}_e m_e V_e^2 + \bar{n}_i m_i V_i^2}{\bar{n}_e m_e + \bar{n}_i m_i} = \frac{\Omega_p^2 V_e^2 + \omega_p^2 V_i^2}{\omega_p^2 + \Omega_p^2} \end{aligned}\right\} \tag{12}$$

$$\varepsilon_e = c^2/V_e^2, \ \varepsilon_i = c^2/V_i^2, \ \varepsilon_s = c^2/V_s^2, \ \varepsilon_a = 1 + A = c^2/V_a^2 \tag{13}$$

$$x = \omega_0^2/\omega^2, \ y = k^2 c^2/\omega^2 \tag{14}$$

$$\left.\begin{aligned} p &= \omega_p/\omega, \ l = \omega_L/\omega, \ t = \omega_T/\omega \\ P &= \Omega_p/\omega, \ L = \Omega_L/\omega, \ T = \Omega_T/\omega \end{aligned}\right\}. \tag{15}$$

Pour plus de détails,* nous renvoyons le lecteur à la référence [1] (chapitres I et II).

Les équations de Maxwell donnent par élimination du champ magnétique de l'onde:

$$\left(\frac{k^2 c^2}{\omega^2} - 1\right) E_x = \frac{4\pi c^2}{\mathrm{j}\omega} (\bar{n}_e q_e v_{ex} + \bar{n}_i q_i v_{ix}) \tag{16}$$

$$\left(\frac{k^2 c^2}{\omega^2} - 1\right) E_y = \frac{4\pi c^2}{\mathrm{j}\omega} (\bar{n}_e q_e v_{ey} + \bar{n}_i q_i v_{iy}) \tag{17}$$

$$E_z = \frac{4\pi c^2}{\mathrm{j}\omega} (\bar{n}_e q_e v_{ez} + \bar{n}_i q_i v_{iz}). \tag{18}$$

Si l'on néglige les collisions, les équations linéarisées de transport de la quantité de mouvement électronique s'écrivent:

$$\mathrm{j}\omega \bar{n}_e m_e v_{ex} = \bar{n}_e q_e (E_x + v_{ey} B_L - v_{ez} B_T) + \mathrm{j} k p_{exz} \tag{19}$$

$$\mathrm{j}\omega \bar{n}_e m_e v_{ey} = \bar{n}_e q_e (E_y - v_{ex} B_L) + \mathrm{j} k p_{eyz} \tag{20}$$

$$\mathrm{j}\omega \bar{n}_e m_e v_{ez} = \bar{n}_e q_e (E_z + v_{ex} B_T) + \mathrm{j} k p_{ezz}. \tag{21}$$

L'équation de transport de la pression cinétique électronique s'écrit, compte tenu de (5):

$$\left(\frac{\partial}{\partial t} + \mathbf{v}\cdot\nabla + \nabla\cdot\mathbf{v}\right)\cdot\mathbf{\Psi} + \nabla\mathbf{v}\cdot\mathbf{\Psi} + (\nabla\mathbf{v}\cdot\mathbf{\Psi})^{\mathrm{T}} = \mathsf{H} \tag{22}$$

avec (cf [2] p. 95):

$$H_{xy} = \frac{q}{m}[(\mathbf{B}\times\mathbf{e}_x)\cdot(\mathbf{e}_y\cdot\mathbf{\Psi}) + (\mathbf{B}\times\mathbf{e}_y)\cdot(\mathbf{e}_x\cdot\mathbf{\Psi})]. \tag{23}$$

L'équation (22) linéarisée (en négligeant les termes d'ordre supérieur) devient:

$$\frac{\partial}{\partial t} p_e + (\nabla\cdot\mathbf{v})\,\bar{p}_e + \nabla\mathbf{v}\cdot\bar{p}_e + (\nabla\mathbf{v}\cdot\bar{p}_e)^{\mathrm{T}} = \mathsf{H}$$

qui s'écrit:

$$j\omega p_e - j k v_{ez}\bar{p}_e - j k \bar{p}_e \begin{vmatrix} 0 & 0 & v_{ex} \\ 0 & 0 & v_{ey} \\ v_{ex} & v_{ey} & 2v_{ez} \end{vmatrix} = \mathsf{H}. \tag{24}$$

Les six composantes de cette équation s'écrivent finalement compte tenu de (4) et de (23):

* La seule différence avec [1] porte sur la formule (12) d'où les coefficients d'adiabaticité γ ont disparu (on avait posé par exemple $v_e^2 = \gamma_e \mathrm{k} T_e/m_e$). Les coefficients γ ne sont plus des données a priori comme le supposait l'utilisation de la formule (1).

$$j\omega p_{ezz} - j k \bar{p}_e v_{ex} = \omega_T (p_{ezz} - p_{exx}) - \omega_L p_{eyz} \quad (25)$$

$$j\omega p_{eyx} - j k \bar{p}_e v_{ey} = -\omega_T p_{exy} + \omega_L p_{ezz} \quad (26)$$

$$j\omega p_{ezz} - j k \bar{p}_e v_{ez} - 2 j k \bar{p}_e v_{ez} = -2 \omega_T p_{ezx} \quad (27)$$

$$j\omega p_{exx} - j k \bar{p}_e v_{ez} = 2 \omega_T p_{exz} - 2 \omega_L p_{exy} \quad (28)$$

$$j\omega p_{exy} = \omega_T p_{eyz} + \omega_L (p_{exx} - p_{eyy}) \quad (29)$$

$$j\omega p_{eyy} - j k \bar{p}_e v_{ez} = 2 \omega_L p_{exy}. \quad (30)$$

Les équations de transport relatives aux ions sont analogues (au signe près des termes faisant intervenir les fréquences gyromagnétiques). Nous ne les écrirons pas mais nous les désignerons par les numéros (19′) à (21′) et (25′) à (30′).

Le système des équations de Maxwell et des équations de transport constitue un système de vingt-et-une équations homogènes par rapport aux vingt-et-une inconnues que sont les composantes de **E**, v_e, v_i, p_e, p_i. Pour que ce système possède une solution non identiquement nulle, il faut que son déterminant soit nul. En écrivant que ce déterminant est nul on obtient une relation entre ω et k: c'est l'équation de dispersion des ondes planes. Le tableau I représente ce déterminant; on a choisi pour classer les équations et les variables l'ordre le plus fructueux pour la discussion physique des propriétés des ondes. Cet ordre est indiqué en marge du tableau dans une première ligne et une première colonne. Les cases laissées en blanc contiennent des zéros que l'on n'a pas écrits pour alléger l'écriture.

E_x	$(v_{ex}/j)(m_e\omega/q_e)$	$(v_{ix}/j)(m_i\omega/q_i)$	$jkp_{exz}/\bar{n}_e q_e$	$jkp_{ixz}/\bar{n}_e q_e$	jE_y	$v_{ey}(m_e\omega/q_e)$	$v_{iy}(m_i\omega/q_i)$	$-kp_{eyz}/\bar{n}_e q_e$	$-kp_{iyz}/\bar{n}_i q_i$	jE_z	$v_{ez}(m_e\omega/q_e)$	$v_{iz}(m_i\omega/q_i)$	$-kp_{ezz}/\bar{n}_e q_e$	$-kp_{izz}/\bar{n}_i q_i$	$-kp_{exx}/\bar{n}_e q_e$	$-kp_{ixx}/\bar{n}_i q_i$	$-jkp_{exy}/\bar{n}_e q_e$	$-jkp_{ixy}/\bar{n}_i q_i$	$-kp_{eyy}/\bar{n}_e q_e$	$-kp_{iyy}/\bar{n}_i q_i$
$1-y$	p^2	P^2																		
1	1		1			$-l$						t								
1		1		1			L						$-T$							
	y/ε_e		1					$-l$						t		$-t$				
		y/ε_i		1					L						$-T$		T			
					$1-y$	p^2	P^2													
	$-l$				1	1		1												
		L			1		1		1											
			$-l$			y/ε_e		1									$-t$			
				L			y/ε_i		1									T		
										1	p^2	P^2								
	t									1	1		1							
		$-T$								1		t		1						
			2t								$3y/\varepsilon_e$		1							
				$-2T$								$3y/\varepsilon_i$		1						
			$-2t$								y/ε_e				1		$-2l$			
				$2T$								y/ε_i				1		$2L$		
								$-t$							$-l$		1	l		
									T							L		1		$-L$
											y/ε_e						$2l$		1	
												y/ε_i						$-2L$		1

	E_x	v_{ex}	v_{ix}	p_{exz}	p_{ixz}	E_y	v_{ey}	v_{iy}	p_{eyz}	p_{iyz}	E_z	v_{ez}	v_{iz}	p_{ezz}	p_{izz}	p_{exx}	p_{ixx}	p_{exy}	p_{ixy}	p_{eyy}	p_{iyy}	
(16)	$j\left[\frac{k^2c^2}{\omega^2}-1\right]$	$-\frac{4\pi c^2\bar{n}_e q_e}{\omega}$	$-\frac{4\pi c^2\bar{n}_i q_i}{\omega}$																			j
(19)	$\bar{n}_e q_e$	$-j\omega\bar{n}_e m_e$		jk			$-\bar{n}_e q_e B_L$					$-\bar{n}_e q_e B_T$										$1/\bar{n}_e q_e$
(19')	$\bar{n}_i q_i$		$-j\omega\bar{n}_i m_i$		jk			$\bar{n}_i q_i B_L$					$-\bar{n}_i q_i B_T$										$1/\bar{n}_i q_i$
(25)		$-jk\bar{p}_e$		$j\omega$					ω_L					$-\omega_T$		ω_T						$k/\bar{n}_e q_e \omega$
(25')			$-jk\bar{p}_i$		$j\omega$					$-\Omega_L$					Ω_T		$-\Omega_T$					$k/\bar{n}_i q_i \omega$
(17)						$j\left[\frac{k^2c^2}{\omega^2}-1\right]$	$-\frac{4\pi c^2\bar{n}_e q_e}{\omega}$	$-\frac{4\pi c^2\bar{n}_i q_i}{\omega}$														-1
(20)		$-\bar{n}_e q_e B_L$				$\bar{n}_e q_e$	$-j\omega\bar{n}_e m_e$		jk													$j/\bar{n}_e q_e$
(20')			$-n_i q_i B_L$			$n_i q_i$		$-j\omega\bar{n}_i m_i$		jk												$j/\bar{n}_i q_i$
(26)				$-\omega_L$			$-jk\bar{p}_e$		$j\omega$									ω_T				$jk/\bar{n}_e q_e \omega$
(26')					Ω_L			$-jk\bar{p}$		$j\omega$									$-\Omega_T$			$jk/\bar{n}_i q_i \omega$
(18)											$j\left[\frac{k^2c^2}{\omega^2}-1\right]$	$-\frac{4\pi c^2\bar{n}_e q_e}{\omega}$	$-\frac{4\pi c^2\bar{n}_i q_i}{\omega}$									-1
(21)		$\bar{n}_e q_e B_T$									$\bar{n}_e q_e$	$-j\omega\bar{n}_e m_e$		jk								$j/\bar{n}_e q_e$
(21')			$\bar{n}_i q_i B_T$								$\bar{n}_i q_i$		$-j\omega\bar{n}_i m_i$		jk							$j/\bar{n}_i q_i$
(27)				$2\omega_T$								$-3jk\bar{p}_e$		$j\omega$								$jk/\bar{n}_e q_e \omega$
(27')					$-2\Omega_T$								$-3jk\bar{p}_i$		$j\omega$							$jk/\bar{n}_i q_i \omega$
(28)				$-2\omega_T$								$-jk\bar{p}_e$				$j\omega$		$2\omega_L$				$jk/\bar{n}_e q_e \omega$
(28')					$+2\Omega_T$								$-jk\bar{p}_i$				$j\omega$		$-2\omega_L$			$jk/\bar{n}_i q_i \omega$
(29)									ω_T							$-\omega_L$		$j\omega$		ω_L		$-k/\bar{n}_e q_e \omega$
(29')										Ω_T							Ω_L		$j\omega$		$-\Omega_L$	$-k/\bar{n}_i q_i \omega$
(30)												$-jk\bar{p}_e$						$-2\omega_L$		$j\omega$		$jk/\bar{n}_e q_e \omega$
(30')													$-jk p_i$						$2\Omega_L$		$j\omega$	$jk/\bar{n}_i q_i \omega$
	1	$j\frac{q_e}{m_e\omega}$	$j\frac{q_i}{m_i\omega}$	$-j\frac{\bar{n}_e q_e}{k}$	$-j\frac{\bar{n}_i q_i}{k}$	$-j$	$\frac{q_e}{m_e\omega}$	$\frac{q_i}{m_i\omega}$	$-\frac{\bar{n}_e q_e}{k}$	$-\frac{\bar{n}_i q_i}{k}$	$-j$	$\frac{q_e}{m_e\omega}$	$\frac{q_i}{m_i\omega}$	$-\frac{\bar{n}_e q_e}{k}$	$-\frac{\bar{n}_i q_i}{k}$	$-\frac{\bar{n}_e q_e}{k}$	$-\frac{\bar{n}_i q_i}{k}$	$j\frac{\bar{n}_e q_e}{k}$	$j\frac{\bar{n}_i q_i}{k}$	$-\frac{\bar{n}_e q_e}{k}$	$-\frac{\bar{n}_i q_i}{k}$	MULTIPLICATEURS

Si un déterminant est nul, il reste nul quand on multiplie les termes d'une même ligne ou d'une même colonne par un même facteur. Il est commode d'utiliser cette propriété pour transformer le déterminant du tableau I en un nouveau déterminant d'écriture plus légère. Nous effectuerons cette transformation en multipliant les lignes par les multiplicateurs indiqués en marge à droite du tableau I et les colonnes par les multiplicateurs indiqués en marge en bas de ce même tableau. Nous obtenons ainsi le déterminant représenté sur le tableau II. Les multiplications effectuées sur les colonnes reviennent à diviser les variables par les mêmes facteurs: dans le tableau II nous avons donc indiqué sur une première ligne les nouvelles variables auxquelles se rapportent les diverses colonnes.

3. Singularités de l'équation de dispersion

L'équation de dispersion obtenue en annulant le déterminant du tableau II a la même structure générale que celle établie dans [1]. Comme dans [1] on voit qu'il existe des cas singuliers correspondant à des ondes de structure particulièrement simples:

Si B_0 est nul, le déterminant se décompose en un produit de trois déterminants selon le schéma suivant:

$$\begin{vmatrix} \Delta_1 & 0 & 0 \\ 0 & \Delta_1 & 0 \\ 0 & 0 & \Delta_L \end{vmatrix}.$$

Au premier terme Δ_1 correspondent des ondes purement transversales polarisées parallèlement à x: de composantes E_x, v_{ex}, v_{ix}, p_{exx} et p_{ixx}.

Au deuxième terme Δ_1 correspondent des ondes identiques aux précédentes mais polarisées parallèlement à y: de composantes E_y, v_{ey}, v_{iy}, p_{eyz} et p_{iyz}.

Enfin, au terme Δ_2 correspondent des ondes purement longitudinales possèdant des composantes E_z, v_{ez}, v_{iz}, p_{ezz}, p_{izz}, p_{exx}, p_{ixx}, p_{exy}, p_{ixy}, p_{eyy} et p_{iyy}.

4. Ondes transversales à polarisation rectiligne (champ magnétique nul)

Si l'on fait $B_0=0$ dans l'équation de dispersion du tableau II, on obtient, comme nous venons de le voir, des ondes polarisées suivant x ou y; en annulant l'un des facteurs Δ_1 leur équation de dispersion s'écrit donc:

$$\begin{vmatrix} 1-y & p^2 & P^2 & 0 & 0 \\ 1 & 1 & 0 & 1 & 0 \\ 1 & 0 & 1 & 0 & 1 \\ 0 & y/\varepsilon_e & 0 & 1 & 0 \\ 0 & 0 & y/\varepsilon_i & 0 & 1 \end{vmatrix} = 0. \qquad (31)$$

En retranchant les lignes 4 et 5 des lignes 2 et 3, puis en multipliant la ligne 2 par p, la ligne 3 par P, la colonne 2 par $1/p$, enfin la colonne 3 par $1/p$, cette équation se réduit à:

$$\begin{vmatrix} 1-y & p & P \\ p & 1-y/\varepsilon_e & 0 \\ P & 0 & 1-y/\varepsilon_i \end{vmatrix} = 0. \qquad (32)$$

Les variables correspondantes sont maintenant:

$$E_x, \quad \frac{v_{ex}}{j} \times \frac{m_e \omega_p}{q_e}, \quad \frac{v_{ix}}{j} \times \frac{m_i \Omega_p}{q_i}.$$

En développant cette équation, on peut la mettre sous la forme:

$$x = \frac{(1-y)\,(1-y/\varepsilon_e)\,(1-y/\varepsilon_i)}{1-y/\varepsilon_s}. \qquad (33)$$

La courbe de dispersion a l'allure représentée sur la fig. 2. Pour les valeurs positives de x (les seules ayant un sens physique), il apparaît trois ondes que nous désignerons par y_0, y_+ et y_- (cf. figure 2).

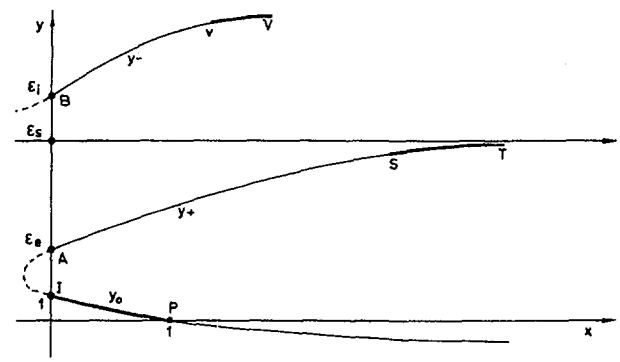

Fig. 2 Courbe de dispersion des ondes transversales à polarisation rectiligne ($\mathbf{B}_0=0$). Pour les valeurs positives de x (les seules ayant un sens physique), il apparaît trois ondes que nous désignerons par y_0, y_+ et y_-. [$y = (kc/\omega)^2$, $x=(\omega_0/\omega)^2$.]

L'onde y_0 est l'onde électro-magnétique transverse classique, avec la fréquence critique classique $\omega=\omega_0$. Sur la branche IP, c'est-à-dire pour des fréquences comprises entre ω_0 et l'infini, les effets de pression tensorielle n'introduisent que des corrections d'ordre $1/\varepsilon_e$ à la théorie simple faite dans [1], négligeables sauf pour des plasmas très chauds.

Les ondes y_+ et y_- sont des ondes lentes qui n'apparaissent pas dans la théorie à pression scalaire. y_+ est caractérisée dans le domaine des basses fréquences par une branche non dispersive au voisinage de l'asymptote $y=\varepsilon_s$. Il faut souligner qu'il ne s'agit pas d'une onde sonore mais d'une onde transversale sans variation de densité.

y_- est caractérisée dans le domaine des basses fréquences par une loi de dispersion de la forme:*

$$y = \left(\frac{\varepsilon_e \varepsilon_i x}{\varepsilon_s}\right)^{\frac{1}{2}}. \qquad (34)$$

* La formule (34) peut s'écrire:

$$\omega = \left(\frac{V_e V_i c}{\omega_0 V_s}\right) k^2$$

et permet de définir une pseudo-particule comme sont définis le phonon [3] et l'hélicon [4].

Pour mieux comprendre la nature de ces trois ondes, il est intéressant de calculer leur «polarisation»; par application dans (32) de la règle des mineurs on obtient:

$$E_x = a\,(1 - y/\varepsilon_e)\,(1 - y/\varepsilon_i) \tag{35}$$

$$\frac{v_{ex}}{j}\,\frac{m_e\,\omega_p}{q_e} = -\,a\,p\left(1 - \frac{y}{\varepsilon_i}\right) \tag{36}$$

$$\frac{v_{ix}}{j}\,\frac{m_i\,\Omega_p}{q_i} = -\,aP(1 - y/\varepsilon_e) \tag{37}$$

a étant un facteur de proportionnalité.

Par combinaison de ces deux dernières équations, on obtient:

$$\frac{v_{ex}}{v_{ix}} = -m\,\frac{1 - y/\varepsilon_i}{1 - y/\varepsilon_e}\,. \tag{38}$$

De manière générale, on en déduit que v_{ex}/v_{ix} est positif pour l'onde y_+ et négatif pour les ondes y_- et y_0.

Il est intéressant d'autre part d'étudier l'expression $-\nabla\cdot\boldsymbol{\Psi}_e/\bar{n}_e q_e \mathbf{E}$ qui caractérise pour les électrons l'importance relative des termes de diffusion et des termes de champ électrique pour le transfert de quantité de mouvement dans une onde.

Dans le cas simple qui nous intéresse, on a:

$$-\nabla\cdot\boldsymbol{\Psi}_e = j\,k\,p_{exx}\,\mathbf{e}_x \tag{39}$$

et d'après (25):

$$\omega\,p_{exx} = k\,\bar{p}_e\,v_{ex} \tag{40}$$

d'où l'on déduit, après un calcul simple utilisant (19):

$$\frac{-\nabla\cdot\boldsymbol{\Psi}_e}{\bar{n}_e\,q_e\,\mathbf{E}} = \frac{y/\varepsilon_e}{1 - y/\varepsilon_e}\,. \tag{41}$$

On voit que ce rapport est positif pour l'onde y_0 et négatif pour les ondes y_+ et y_-.

Le même calcul peut être fait pour les ions et donne:

$$\frac{-\nabla\cdot\boldsymbol{\Psi}_i}{\bar{n}_i\,q_i\,\mathbf{E}} = \frac{y/\varepsilon_i}{1 - y/\varepsilon_i}\,. \tag{42}$$

Le rapport est maintenant positif pour les ondes y_0 et y_+ et négatif pour l'onde y_-.

Par combinaison de (41) et (42) on obtient:

$$\frac{-\nabla\cdot\boldsymbol{\Psi}_e}{-\nabla\cdot\boldsymbol{\Psi}_i} = \frac{1}{\tau}\,\frac{v_{ex}}{v_{ix}}\,. \tag{43}$$

Il est intéressant de particulariser les résultats contenus dans les formules (38), (41) et (42), en étudiant trois cas particuliers limites choisis chacun sur l'une des branches. Ces trois cas sont représentés sur la figure 2 par les arcs IP, ST, et UV. Compte tenu de la condition:

$$1 \ll \varepsilon_e \ll \varepsilon_s < \varepsilon_i \tag{44}$$

on peut faire sur chacun de ces trois arcs une approximation; l'ensemble des résultats obtenus est résumé dans le tableau III, qui appelle les commentaires suivants.

TABLEAU III

	y_0 (arc IP)	y_+ (arc ST)	y_- (arc UV)
$\dfrac{v_{ex}}{v_{ix}}$	$-m$	1	$-\tau$
$\dfrac{-\nabla\cdot\boldsymbol{\Psi}_e}{\bar{n}_e\,q_e\,\mathbf{E}}$	0	-1	-1
$\dfrac{-\nabla\cdot\boldsymbol{\Psi}_i}{\bar{n}_i\,q_i\,\mathbf{E}}$	0	τ	-1
$\dfrac{-\nabla\cdot\boldsymbol{\Psi}_e}{-\nabla\cdot\boldsymbol{\Psi}_i}$	$-\dfrac{m}{\tau}$	$\dfrac{1}{\tau}$	-1

Dans l'onde y_0 les électrons oscillent en opposition de phase avec les ions avec une amplitude très supérieure à celle des ions; les forces de diffusion sont négligeables devant les forces électriques.

Dans l'onde y_+ sur l'arc ST les électrons et les ions s'accompagnent dans leurs mouvements; pour les électrons, la force de diffusion annule presque complètement la force électrique; pour les ions, au contraire, la force de diffusion augmente celle-ci, généralement dans le rapport 2 (pour $\tau = 1$); ces deux conditions sont caractéristiques d'un mouvement de diffusion ambipolaire. On peut appeler l'onde y_+ une onde transversale de diffusion ambipolaire.

Dans l'onde y_-, les électrons et les ions oscillent en opposition de phase avec une amplitude égale pour $\tau = 1$; pour les deux espèces de particules la force de diffusion tend à annuler exactement la force électrique.

Les ondes y^+ et y^- sont des ondes lentes transversales d'un caractère très particulier. Elles ne s'apparentent à aucun type d'onde connu. *La réalité de leur existence physique est sujette à caution*: en effet, comme pour toutes les ondes lentes on peut se demander si la théorie hydrodynamique permet de décrire correctement les phénomènes.

5. Ondes longitudinales (champ magnétique nul ou propagation longitudinale)

Par application de la règle de Laplace, on trouve que le déterminant Δ_L des onze dernières lignes et colonnes qui gouverne l'équation de dispersion des ondes longitudinales se décompose en un produit de deux déterminants:

$$\begin{vmatrix} 1 & p^2 & P^2 & 0 & 0 \\ 1 & 1 & 0 & 1 & 0 \\ 1 & 0 & 1 & 0 & 1 \\ 0 & 3\,y/\varepsilon_e & 0 & 1 & 0 \\ 0 & 0 & 3\,y/\varepsilon_i & 0 & 1 \end{vmatrix} \times D = 0\,, \tag{45}$$

où D est le déterminant formé par les six dernières lignes et colonnes en bas à droite du tableau II; ce déterminant est indépendant de la variable y; il est en général différent de zéro (sauf pour des fréquences

singulières); l'équation de dispersion s'obtient donc en annulant le premier facteur dans (45).

En faisant les mêmes transformations qu'au § 4, on peut donc écrire l'équation de dispersion des ondes longitudinales sous la forme:

$$\begin{vmatrix} 1 & p & P \\ p & 1-3y/\varepsilon_e & 0 \\ P & 0 & 1-3y/\varepsilon_i \end{vmatrix} = 0, \qquad (46)$$

les variables relatives aux trois colonnes étant E_z, $(v_{ez}/j)\,(m_e\,\omega_p/q_e)$, $(v_{ez}/j)\,(m_i\,\Omega_p/q_i)$.

Cette équation se confond identiquement avec celle trouvée dans la théorie à pression scalaire de [1] (cf. chap. 4 p. 37), à condition de prendre, dans cette théorie simple, des rapports d'adiabaticité $\gamma_e=\gamma_i=3$. On voit donc que tous les résultats exposés dans [1] pour les ondes purement longitudinales électroniques et ioniques sont confirmés par la présente théorie.

Pour mieux comprendre la structure de l'onde, il est bon d'examiner comment varient les différentes composantes du tenseur de pression, à partir des équations (25) à (30) et (25′) à (30′).

Le résultat est particulièrement simple pour la pression longitudinale donnée par les équations (27) et (27′), qui sont indépendantes de B_L; (27) donne par exemple:

$$p_{ezz} = 3\,\frac{k}{\omega}\,\bar{p}_e\,v_{ez}.$$

En comparant avec les équations de conservation des particules ([1] p. 11) on obtient:

$$\frac{p_{ezz}}{3\,n_e} = \text{Cte} = \frac{\bar{p}_e}{\bar{n}_e}$$

d'où l'on déduit:

$$\frac{p_{ezz}\cos\omega t}{3\bar{n}_e^2\,n_e\cos\omega t} = \frac{\bar{p}_e}{\bar{n}_e^3} = \frac{\bar{p}_e + p_{ezz}\cos\omega t}{\bar{n}_e^3 + 3\,\bar{n}_e^2\,n_e\cos\omega t} \simeq \frac{\bar{p}_e + p_{ezz}\cos\omega t}{(\bar{n}_e + n_e\cos\omega t)^3}. \qquad (47)$$

On voit, résultat d'ailleurs bien connu ([5] p. 14), que la pression parallèle instantanée $p_{e\parallel}(t) = \bar{p}_e + p_{ezz}\cos\omega t$ est reliée à la densité instantanée $n_e(t) = \bar{n}_e + n_e\cos\omega t$ par une loi de la forme:

$$\frac{p_{e\parallel}(t)}{[n_e(t)]^3} = \text{Cte}. \qquad (48)$$

D'où le rapport d'adiabaticité $\gamma_e=3$, qui apparait dans l'équation de dispersion, où seule la pression longitudinale intervient.

Les autres composantes des pressions devraient dépendre à priori de B_L. Si $B_L=0$, on voit immédiatement que $p_{exy}=p_{ixy}=0$ et $p_{exx}=p_{eyy}=p_{e\perp}$, d'où:

$$\frac{p_{e\perp}(t)}{n_e(t)} = \text{Cte}. \qquad (49)$$

La température transverse $T_{e\perp}$ reste constante, les variations de pression étant dues, ici, uniquement aux variations de densité.

Si $B_L \neq 0$, on montre facilement que ces résultats sont inchangés. Les mêmes conclusions s'appliquent aussi aux ions.

6. Propagation longitudinale ($B_T=0$): ondes transversales à polarisation circulaire

6.1. Ondes ordinaires et extraordinaires

En présence d'un champ magnétique longitudinal, il y a un couplage entre les ondes polarisées suivant x et y; il en résulte des ondes transversales ayant des composantes suivant ces deux directions; leur équation de dispersion s'obtient en annulant le déterminant formé par les dix premières lignes et colonnes du tableau II, soit:

$$\left|\begin{array}{ccccc|ccccc} 1-y & p^2 & P^2 & 0 & 0 & 0 & 0 & 0 & 0 & 0 \\ 1 & 1 & 0 & 1 & 0 & 0 & -l & 0 & 0 & 0 \\ 1 & 0 & 1 & 0 & 1 & 0 & 0 & L & 0 & 0 \\ 0 & y/\varepsilon_e & 0 & 1 & 0 & 0 & 0 & 0 & -l & 0 \\ 0 & 0 & y/\varepsilon_i & 0 & 1 & 0 & 0 & 0 & 0 & L \\ \hline 0 & 0 & 0 & 0 & 0 & 1-y & p^2 & P^2 & 0 & 0 \\ 0 & -l & 0 & 0 & 0 & 1 & 1 & 0 & 1 & 0 \\ 0 & 0 & L & 0 & 0 & 1 & 0 & 1 & 0 & 1 \\ 0 & 0 & 0 & -l & 0 & 0 & y/\varepsilon_e & 0 & 1 & 0 \\ 0 & 0 & 0 & 0 & L & 0 & 0 & y/\varepsilon_i & 0 & 1 \end{array}\right| . \qquad (50)$$

On peut mettre cette équation de dispersion sous une forme plus simple, en effectuant les transformations suivantes:

- On ajoute les lignes 6, 7, 8, 9, 10 respectivement aux lignes 1, 2, 3, 4, 5;
- on soustrait les colonnes 1, 2, 3, 4, 5 des colonnes 6, 7, 8, 9, 10;
- on additionne les colonnes 6, 7, 8, 9, 10, préalablement multipliées par $\frac{1}{2}$, respectivement aux colonnes 1, 2, 3, 4, 5;
- on multiplie les lignes 6, 7, 8, 9, 10 par 2 et les colonnes 6, 7, 8, 9, 10 par $\frac{1}{2}$;
- enfin on soustrait les lignes 1, 2, 3, 4, 5 des lignes 6, 7, 8, 9, 10.

Après ces transformations, l'équation de dispersion s'écrit:

$$\left|\begin{array}{ccccc|ccccc} 1-y & p^2 & P^2 & 0 & 0 & & & & & \\ 1 & 1-l & 0 & 1 & 0 & & & & & \\ 1 & 0 & 1+L & 0 & 1 & & & 0 & & \\ 0 & y/\varepsilon_e & 0 & 1-l & 0 & & & & & \\ 0 & 0 & y/\varepsilon_i & 0 & 1+L & & & & & \\ \hline & & & & & 1-y & p^2 & P^2 & 0 & 0 \\ & & & & & 1 & 1+l & 0 & 1 & 0 \\ & & 0 & & & 1 & 0 & 1-L & 0 & 1 \\ & & & & & 0 & y/\varepsilon_e & 0 & 1+l & 0 \\ & & & & & 0 & 0 & y/\varepsilon_i & 0 & 1-L \end{array}\right| \qquad (51)$$

Au cours des diverses transformations effectuées, les variables relatives aux dix colonnes sont devenues:

$$\mathrm{j}\,E_y + E_x,\quad \frac{m_e\omega}{q_e}\left(v_{ey}+\frac{v_{ex}}{\mathrm{j}}\right),\quad \frac{m_i\omega}{q_i}\left(v_{iy}+\frac{v_{ix}}{\mathrm{j}}\right),$$

$$\frac{k}{\bar{n}_e q_e}(-p_{eyz}+\mathrm{j}\,p_{exz}),\quad \frac{k}{\bar{n}_i q_i}(p_{iyz}+\mathrm{j}\,p_{ixz}) \qquad (52a)$$

$$\mathrm{j}\,E_y - E_x,\quad \frac{m_e\omega}{q_e}\left(v_{ey}-\frac{v_{ex}}{\mathrm{j}}\right),\quad \frac{m_i\omega}{q_i}\left(v_{iy}-\frac{v_{ix}}{\mathrm{j}}\right),$$

$$\frac{k}{\bar{n}_e q_e}(-p_{eyz}-\mathrm{j}\,p_{exz}),\quad \frac{k}{\bar{n}_i q_i}(-p_{iyz}-\mathrm{j}\,p_{ixz}). \qquad (52b)$$

On voit donc que le déterminant (51) se décompose en un produit de deux déterminants à cinq lignes et cinq colonnes; en égalant à zéro le premier de ces deux déterminants, on obtient des ondes dans lesquelles les variables des colonnes 6, 7, 8, 9, 10 sont nulles; dans ces ondes, on a donc:

$$E_y/E_x = -\mathrm{j}. \qquad (53)$$

Ce sont donc des ondes polarisées circulairement; le vecteur électrique de ces ondes tournant dans le sens positif de x vers y, c'est-à-dire dans le même sens que les électrons du plasma sous l'effet du champ B_L. En annulant le deuxième déterminant, on obtient de même des ondes à polarisation circulaire, mais dont le sens de rotation est opposé aux précédentes. Par analogie avec les théories simples, on peut désigner par ondes extraordinaires les ondes qui tournent dans le sens direct, et par ondes ordinaires les ondes qui tournent dans le sens inverse.

6.2. Equation et courbe de dispersion des ondes extraordinaires

L'équation de dispersion des ondes extraordinaires peut se réécrire en soustrayant des colonnes 2 et 3 les colonnes 4 et 5 préalablement multipliées par $1/(1-l)$ et $1/(1+L)$; il vient alors:

$$\begin{vmatrix} 1-y & p^2 & P^2 \\ 1 & 1-l-\dfrac{1}{1-l}\dfrac{y}{\varepsilon_e} & 0 \\ 1 & 0 & 1+L-\dfrac{1}{1+L}\dfrac{y}{\varepsilon_i} \end{vmatrix} = 0. \qquad (54)$$

On peut enfin rendre ce déterminant symétrique en effectuant les mêmes transformations qu'au paragraphe précédent; ceci montre que les trois ondes extraordinaires sont les vecteurs propres d'une matrice symétrique; toutefois, le calcul se présente de façon différente suivant le signe de $1-l$; si $1-l>0$, le déterminant peut finalement s'écrire:

$$\begin{vmatrix} 1-y & p\sqrt{\varepsilon_e(1-l)} & P\sqrt{\varepsilon_i(1+L)} \\ p\sqrt{\varepsilon_e(1-l)} & \varepsilon_e(1-l)^2-y & 0 \\ p\sqrt{\varepsilon_i(1+L)} & 0 & \varepsilon_i(1+L)^2-y \end{vmatrix} = 0 \qquad (55)$$

(55) est l'équation aux valeurs propres d'une matrice réelle et symétrique, donc hermitienne: ses trois racines sont donc toujours réelles.

Quand $1-l<0$, l'équation (54) peut finalement s'écrire:

$$\begin{vmatrix} 1-y & jp\sqrt{\varepsilon_e(l-1)} & P\sqrt{\varepsilon_i(1+L)} \\ jp\sqrt{\varepsilon_e(l-1)} & \varepsilon_e(l-1)^2-y & 0 \\ P\sqrt{\varepsilon_i(1+L)} & 0 & \varepsilon_i(1+L)^2-y \end{vmatrix} = 0 \qquad (56)$$

qui est l'équation aux valeurs propres d'une matrice non hermitienne; on ne peut plus alors affirmer que les trois racines sont réelles. Nous verrons effectivement plus loin qu'il peut y avoir une ou trois racines réelles.

Pour étudier la courbe de dispersion, il est commode de développer l'équation (54); on obtient:

$$(1-y)\,\Gamma_e\,\Gamma_i - p^2(1-l)\,\Gamma_i - P^2(1+L)\,\Gamma_e = 0 \qquad (57)$$

avec:

$$\Gamma_e = (1-l)^2 - \frac{y}{\varepsilon_e}$$

$$\Gamma_i = (1+L)^2 - \frac{y}{\varepsilon_i}.$$

La courbe de dispersion est représentée schématiquement sur la figure 3; sur cette figure on a également

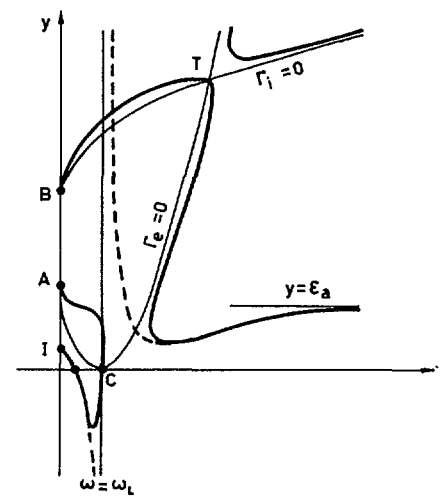

Fig. 3 Courbe de dispersion des ondes transversales extraordinaires ($\mathbf{B}_T=0$). [$y=(kc/\omega)^2$, $x=(\omega_0/\omega)^2$.]

représenté les branches de paraboles $\Gamma_e=0$ et $\Gamma_i=0$ qui permettent de régionner le plan. On montre en effet facilement que la courbe de dispersion ne coupe l'arc $\Gamma_e=0$ qu'aux points C ($\omega=\omega_L$, $y=0$), A ($x=0$, $y=\varepsilon_e$) et T (point de rencontre de $\Gamma_e=0$ et $\Gamma_i=0$) et l'arc $\Gamma_i=0$ qu'aux points B ($x=0$, $y=E_i$) et T.

L'étude détaillée des divers éléments de la courbe de dispersion est développée dans l'appendice, et la discussion physique des propriétés qui en résultent à la fin de ce paragraphe.

6.3. Equation et courbe de dispersion des ondes ordinaires

L'équation de dispersion des ondes ordinaires s'obtient en changeant dans les formules précédentes l en $-l$ et L en $-L$, soit:

$$(1-y)\,\Gamma_e'\,\Gamma_i'-p^2(1+l)\,\Gamma_i'-P^2(1-L)\,\Gamma_e'=0 \quad (58)$$

avec:

$$\Gamma_e'=(1+l)^2-\frac{y}{\varepsilon_c}$$

$$\Gamma_i'=(1-L)^2-\frac{y}{\varepsilon_i}\,.$$

Le même raisonnement que précédemment montre que les trois ondes sont les vecteurs propres d'une matrice hermitienne quand $L<1$ et que par conséquent (58) a alors ses trois racines réelles.

La courbe de dispersion est représentée schématiquement sur la figure 4. Sur cette figure on a également représenté les branches de paraboles $\Gamma_e'=0$ et $\Gamma_i'=0$ qui permettent de régionner le plan. On montre en effet que la courbe de dispersion ne coupe $\Gamma_e'=0$ qu'au point A et $\Gamma_i'=0$ qu'aux points B, T' et C'.

6.4. Discussion

Les figures 3 et 4 sont très trompeuses car avec des échelles linéaires il est impossible de tenir compte des véritables ordres de grandeurs; on a en effet:

$$1 \ll \varepsilon_e \ll \varepsilon_i$$

$$\Omega_L \ll \omega_L\,.$$

On obtient un diagramme plus réaliste en adoptant des échelles qui contractent fortement les coordonnées. La figure 5 est construite avec les coordonnées introduites dans [1] (p. 88) pour un plasma ayant les caractéristiques suivantes:

$$A=10^2 \quad \varepsilon_a=1{,}01\times10^2 \quad \varepsilon_e=1{,}09\times10^5 \quad \varepsilon_i=2\times10^8.$$

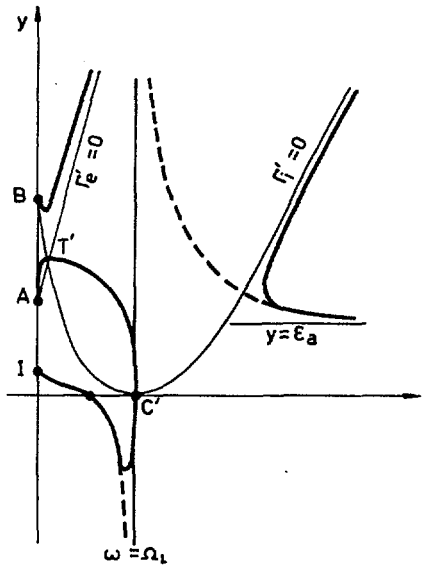

Fig. 4 Courbe de dispersion des ondes transversales ordinaires ($B_T=0$). [$y=(kc/\omega)^2$, $x=(\omega_0/\omega)^2$.]

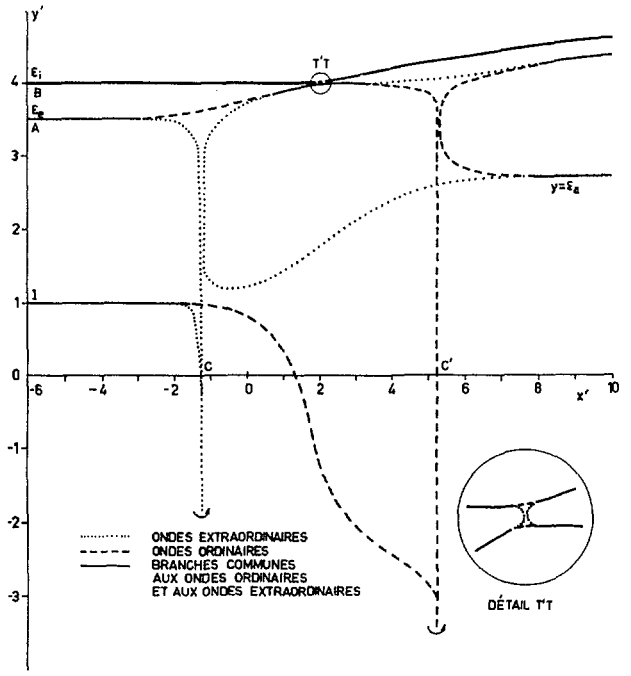

Fig. 5 Ondes transversales. La figure est construite avec les coordonnées introduites dans [1] (p. 88) pour un plasma ayant les caractéristiques suivantes: $A=10^2$, $\varepsilon_a=1{,}01{,}10^2$, $\varepsilon_e=1{,}09\cdot10^5$, $\varepsilon_i=2\cdot10^8$. Le diagramme permet de distinguer des ondes rapides ($y\sim1$ ou $y\sim\varepsilon_a$) et des ondes lentes ($y\sim\varepsilon_e$ ou $y\sim\varepsilon_i$).

On a rassemblé sur ce diagramme les ondes ordinaires (— — —) et extraordinaires (· · · ·); sur certains arcs (————) il y a dégénérescence, c'est-à-dire que les deux espèces d'ondes ont même vitesse. Le diagramme permet de distinguer:

— des ondes rapides ($y\sim1$ ou $y\sim\varepsilon_a$)
— des ondes lentes ($y\sim\varepsilon_e$ ou $y\sim\varepsilon_i$)

Les ondes rapides sont les ondes ordinaires et extraordinaires de la théorie classique ([1] p. 27); elles ne sont pratiquement pas modifiées par les termes de pression non-diagonaux sauf au voisinage des deux résonances cyclotrons. On retrouve notamment les mêmes fréquences critiques et l'asymptote double correspondant aux ondes de Alfvén.

Les ondes transversales lentes (voisinage des points A et B, branches paraboliques) sont au contraire des ondes d'un type nouveau essentiellement liées aux termes de pression non-diagonaux.

L'allure des diagrammes de dispersion est profondément modifiée au voisinage des fréquences cyclotron: dans la théorie classique l'onde ordinaire et l'onde extraordinaire présentaient deux vraies résonances correspondant aux arcs marqués en traits interrompus sur les figures 3 et 4. Ces résonances vraies sont maintenant remplacées par des pseudorésonances; chaque pseudorésonance est une région à forte dispersion reliant l'une des ondes rapides classiques à l'une des ondes lentes introduites par la nouvelle théorie.

Comme conséquence de ce mode de raccordement des ondes, il apparaît au voisinage des fréquences

cyclotrons des intervalles de fréquences dans lesquels l'équation de dispersion possède des racines k^2 complexes. Ceci se produit à la fréquence ω_L pour les ondes extraordinaires et à la fréquence Ω_L pour les ondes ordinaires. Il existe pour les ondes extraordinaires un autre petit intervalle au voisinage de la fréquence mixte $(\omega_L\Omega_L\tau)^{1/2}$ où apparaissent également des racines k^2 complexes.

L'existence de racines k^2 complexes peut correspondre à des ondes évanescentes ou à des ondes autoamplifiées. Du point de vue physique l'existence d'ondes autoamplifiées dans un plasma passif est évidemment absurde. Si de telles ondes étaient prévues par la présente théorie, on devrait en conclure que cette théorie est en défaut, et que l'hypothèse adiabatique est gravement fausse au voisinage des résonances cyclotrons, ce qui semblerait d'ailleurs raisonnable.

En fait STÜRROCK [6] a donné un critère permettant de discerner entre les ondes évanescentes et les ondes autoamplifiées à partir des seules propriétés de l'équation de dispersion. On peut se limiter au cas de la résonance cyclotron électronique; dans ce cas le mouvement des ions est négligeable et on peut, sans changer la nature des phénomènes, supposer m_i infini afin de simplifier les calculs algébriques. On obtient alors les résultats suivants*:

La bande de fréquence $(\omega_\beta < \omega < \omega_\alpha)$ donnant lieu à des valeurs complexes de k^2 se situe autour d'une fréquence légèrement inférieure à la fréquence cyclotron ω_L et définie par la relation:

$$\omega\left(1+\frac{1}{\sqrt{\varepsilon_e}}\right)=\omega_L. \tag{59}$$

La largeur de cette bande de fréquence est d'autant plus grande que le plasma est plus dense; on trouve que les limites de la bande ω_α et ω_β tendent toutes deux vers la valeur définie par (59) quand ω_p^2/ω_L^2 tend vers zéro; dans le cas limite opposé où ω_p^2/ω_L^2 tend vers l'infini ω_α tend vers ω_L et ω_β vers zéro (ce dernier résultat n'a pas de sens, car du côté des basses fréquences il faut tenir compte du mouvement des ions).

Pour appliquer le critère de Stürrock, on recherche dans le plan complexe de la variable $\omega=\omega_r+j\omega_i$ le lieu géométrique des points correspondant à des valeurs réelles de k. On trouve [7] que ce lieu ne comporte pas d'arc enjambant le segment de l'axe réel $(\omega_\alpha, \omega_\beta)$. Par conséquent les ondes de la bande $(\omega_\alpha, \omega_\beta)$ sont des ondes évanescentes.

7. Conclusion

En résumé, les résultats importants obtenus dans cette étude sont:

(*a*) Existence non modifiée des ondes purement longitudinales (oscillations de plasma et ondes pseudosonores);

(*b*) Effets de dispersion anormale et ondes évanescentes pour les ondes transversales au voisinage de la résonance cyclotron électronique*;

(*c*) Apparition d'ondes transversales lentes de types nouveaux dues aux termes non diagonaux du tenseur de pression.

Les résultats (*a*), (*b*), (*c*) sont très intéressants, mais il ne faut peut-être pas se leurrer sur leur validité physique:

Le résultat (*a*) semble le plus solidement établi par son accord avec les résultats de la théorie à pression scalaire [1].

Le résultat (*c*) est probablement le plus incertain: on a montré en effet récemment [10], [11] à propos du tenseur de conductivité que la théorie adiabatique exacte donne les mêmes résultats que la théorie cinétique linéarisée, et que ces résultats doivent représenter correctement les propriétés des plasmas «tièdes» (warm plasmas) au premier ordre en V_e^2/v_φ^2 ou V_i^2/v_φ^2. Les ondes lentes sont donc à priori mal décrites par cette théorie; la tendance actuelle [12] est de considérer qu'elles n'existent pas, essentiellement à cause de phénomènes plus ou moins analogues à l'amortissement de Landau, imprévisibles par une théorie hydrodynamique. On peut toutefois noter que ces critiques s'appliquent même aux ondes pseudosonores et qu'un certain nombre d'expériences récentes [13], [14], [15] semblent avoir mis en évidence ce type d'ondes, à vrai dire dans des conditions géométriques excluant la production d'ondes planes.

Annexe

CRITIQUE DE L'ABSORPTION DE «LANDAU» ET DE L'APPROXIMATION LINÉAIRE DANS L'ÉTUDE DES OSCILLATIONS DE PLASMA ÉLECTRONIQUES

On obtient l'équation de dispersion des ondes électroniques longitudinales de faible amplitude en écrivant la compatibilité de l'équation de Poisson avec l'équation de Boltzmann linéarisée (Landau, Vlasov). Cette procédure conduit à des ondes qui sont toujours atténuées (absorption Landau) avec un coefficient d'absorption qui dépend de la valeur de $\partial F_0/\partial v$ pour $v=u$, où u est la vitesse de l'onde et F_0 la fonction de distribution électronique non perturbée (Landau, Bohm et Gross, Van Kampen).

Quand on considère la solution des équations précédentes non linéarisées on obtient des ondes d'amplitude quelconque non amorties (Bernstein, Greene, Kruskal). Ces deux résultats sont incompatibles.

On se propose d'étudier le processus de linéarisation; pour cela au lieu d'utiliser l'équation de Boltzmann, on utilisera directement le théorème de Liouville de la façon suivante: z et z_0 choisis à priori quelconques; z et z_0 étant choisis ceci relie v et v_0, de façon d'ailleurs non univoque: à une valeur de v_0 peuvent

* Le détail des calculs est développé dans la référence [7].

* On peut d'ailleurs signaler que DOYLE et NEUFELD [8], utilisant une théorie cinétique due à GERSHMAN [9], ont trouvé des valeurs complexes de k au voisinage de la résonance cyclotron ionique.

correspondre deux valeurs de v opposées et réciproquement.

a) On se place dans le repère mobile lié à l'onde ($u=0$); dans ce repère la fonction de distribution f (z, v) est indépendante du temps, et l'existence de l'onde se traduit par une distribution statique de potentiel $\varphi(z)$. Pour chaque électron les équations du mouvement s'écrivent:

$$\begin{cases} v_x = v_{0x} \\ v_y = v_{0y} \\ v_z^2 = v_{0z}^2 - a^2 \end{cases} \tag{A 1}$$

avec

$$a^2 = \frac{2q_c}{m_e}(\varphi - \varphi_0) \tag{A 2}$$

en désignant par φ_0 la valeur du potentiel dans un certain plan de référence z_0 et par v_0 la valeur du vecteur vitesse de l'électron considéré au moment de son passage au plan z_0. Il est commode de placer le plan de référence en un minimum de l'énergie potentielle $q_e\varphi$ (cf. figure 6) et de considérer un plan z situé dans le même creux de potentiel que z_0; alors tous les électrons qui traversent avec la vitesse v, à l'instant t, le plan z, traversent effectivement à un certain instant t' (antérieur ou postérieur) le plan z_0.

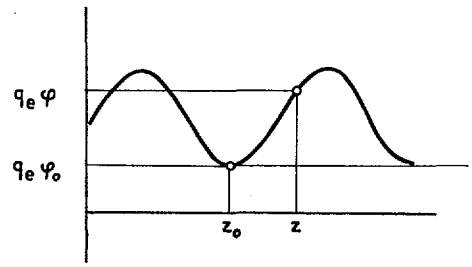

Fig. 6 Le plan de référence est placé en un minimum de l'énergie potentielle $q_e\varphi$.

b) L'application du théorème de Liouville à cette famille d'électrons permet d'écrire:

$$f(z, \mathrm{v}, t) = f(z_0, \mathrm{v}_0, t')$$

ce que nous écrirons simplement puisque les fonctions de distributions sont indépendantes du temps:

$$f(z, \mathrm{v}) = f(z_0, \mathrm{v}_0) \tag{A 3}$$

Par différentiation de (A 1) on obtient:

$$\left.\begin{aligned} \mathrm{d}v_x &= \mathrm{d}v_{0x} \\ \mathrm{d}v_y &= \mathrm{d}v_{0y} \\ v_z\,\mathrm{d}v_z &= v_{0z}\,\mathrm{d}v_{0z} \end{aligned}\right\}. \tag{A 4}$$

Les formules (A 1), (A 3) et (A 4) définissent une transformation associant à toute valeur de v une valeur de v_0 (on choisit évidemment pour v_z et v_{0z} deux valeurs de même signe) et permettant donc de ramener tout calcul relatif au plan z à un calcul relatif au plan z_0. Réciproquement, on ne peut associer une valeur de v à une valeur donnée de v_0 que si $|v_{0z}| \geqslant a$. Les électrons qui dans le plan z_0 ont une vitesse telle que $|v_{0z}| < a$ ne peuvent atteindre le plan z: ce sont des électrons « piégés » avant le plan z.

c) L'équation de Poisson s'écrit dans le plan z:

$$\frac{\mathrm{d}^2\varphi}{\mathrm{d}z^2} = n_i q_i + q_e \int f(v)\,\mathrm{d}v$$
$$= n_i q_i + q_e \int_{-\infty}^{+\infty}\int_{-\infty}^{+\infty} I\,\mathrm{d}v_{0x}\,\mathrm{d}v_{0x} \tag{A 5}$$

avec d'après (A1) et (A4):

$$I = \int_{-\infty}^{+\infty} f_0\,\mathrm{d}v_z = \int_{-\infty}^{-a} \frac{f_0\,v_{0z}\,\mathrm{d}v_{0z}}{-[v_{0z}^2 - a^2]^{1/2}} + \int_{+a}^{+\infty} \frac{f_0\,v_{0z}\,\mathrm{d}v_{0z}}{[v_{0z}^2 - a^2]^{1/2}}.$$

En intégrant par parties on obtient, le terme tout intégré étant identiquement nul:

$$I = \int_{-\infty}^{-a} \sqrt{v_{0z}^2 - a^2}\,\frac{\partial f_0}{\partial v_{0z}}\,\mathrm{d}v_{0z} - \int_{+a}^{+\infty} \sqrt{v_{0z}^2 - a^2}\,\frac{\partial f_0}{\partial v_{0z}}\,\mathrm{d}v_{0z}. \tag{A 6}$$

Cette intégrale est parfaitement définie si f_0 est une fonction de bonne composition.

d) Pour étudier les propriétés des ondes de faible amplitude il est intéressant de chercher le développement de I par rapport à a. I dépend de a par la fonction à intégrer et par les bornes d'intégration. Quand a tend vers zéro, I tend vers

$$I_0 = \int_{-\infty}^{+\infty} -v_{0z}\frac{\mathrm{d}f_0}{\mathrm{d}v_{0z}}\,\mathrm{d}v_{0z} = \int_{-\infty}^{+\infty} f_0\,\mathrm{d}v_{0z} = n_c(z_0). \tag{A7}$$

Il est commode de faire apparaître cette limite en écrivant:

$$I = I_0 - I_1 - I_2$$

avec

$$I_1 = \int_{-a}^{+a} -v_{0z}\,(\mathrm{d}f_0/\mathrm{d}v_{0z})\,\mathrm{d}v_{0z}$$

$$I_2 = \int_{-\infty}^{-a} [-v_{0z} - \sqrt{v_{0z}^2 - a^2}]\,(\mathrm{d}f_0/\mathrm{d}v_{0z})\,\mathrm{d}v_{0z}$$
$$+ \int_{+a}^{+\infty} [-v_{0z} + \sqrt{v_{0z}^2 - a^2}]\,(\mathrm{d}f_0/\mathrm{d}v_{0z})\,\mathrm{d}v_{0z}$$
$$= a^2 \int_{-\infty}^{-a} [-v_{0z} + \sqrt{v_{0z}^2 - a^2}]^{-1}\,(\mathrm{d}f_0/\mathrm{d}v_{0z})\,\mathrm{d}v_{0z}$$
$$+ a^2 \int_{a}^{+\infty} [-v_{0z} - \sqrt{v_{0z}^2 - a^2}]^{-1}\,(\mathrm{d}f_0/\mathrm{d}v_{0z})\,\mathrm{d}v_0.$$

Si a est faible devant la largeur moyenne de la distribution, on peut pour calculer I_1 écrire:

$$\frac{\mathrm{d}f_0}{\mathrm{d}v_{0z}} \simeq \left(\frac{\mathrm{d}f_0}{\mathrm{d}v_{0z}}\right)_0 + v_{0z}\left(\frac{\mathrm{d}^2 f_0}{\mathrm{d}v_{0z}^2}\right)_0.$$

D'où

$$I_1 = -\frac{2a^3}{3}\left[\frac{\mathrm{d}^2 f_0}{\mathrm{d}v_{0z}^2}\right]_{v_{0z}=0} + \mathrm{O}(a^5). \tag{A 8}$$

On peut d'autre part écrire:

$$I_2 = -a^2\left\{\int_{-\infty}^{-a} + \int_{+a}^{+\infty}\right\}\left[\frac{1}{1+[1-(a/v_{0z})^2]^{1/2}}\frac{1}{v_{0z}}\frac{\mathrm{d}f_0}{\mathrm{d}v_{0z}}\mathrm{d}v_{0z}\right]. \tag{A 9}$$

Quand a tend vers zéro, la fonction a intégrée dans (A9) tend vers $(1/2\,\tilde{v}_{0z})$ $(\mathrm{d}f_0/\mathrm{d}v_{0z})$ qui présente un pôle pour $v_{0z}=0$; mais le pôle reste exclus du domaine d'intégration de sorte que l'intégrale qui figure dans (A9) tend vers une limite finie quand a tend vers zéro.

La raison physique de cette exclusion est parfaitement claire: les particules dont les vitesses v_0 sont comprises entre $-a$ et $+a$ ne passent jamais au point z, leur contribution à la charge d'espace en z ne doit pas être comptée.

En résumé le développement de I_1 conduit à des termes de puissance 1/2 entières de $(\varphi-\varphi_0)$ (cf. Bernstein, Bohm et Gross), mais le premier terme en $(\varphi-\varphi_0)^{1/2}$ est nul, on peut donc considérer que l'approximation linéaire est satisfaisante et écrire en conservant I_0 et I_2:

$$I \simeq n_e(z_0) + \frac{1}{2}a^2\,\mathrm{P}\int_{-\infty}^{+\infty}\frac{1}{v_{0z}}\frac{\mathrm{d}f_0}{\mathrm{d}v_{0z}}\mathrm{d}v_{0z}.$$

Cette expression conduit à l'équation de dispersion classique: celle-ci est donc valable, mais on voit que le pôle de $(1/v_0)$ $(\partial f_0/\partial v_0)$, qui conduit à toutes les difficultés d'interprétation et à l'absorption Landau, n'est pas compris dans l'intégration; par suite cette absorption n'existe pas.

On peut vérifier finalement que l'on retrouve bien le terme d'absorption de Landau si l'on calcule la limite, lorsque $a\to 0$, de l'intégrale

$$I_3 = \int_{-a}^{+a}\sqrt{{v_{0z}}^2 - a^2}\,\frac{\mathrm{d}f_0}{\mathrm{d}v_{0z}}\mathrm{d}v_{0z}$$

sur l'intervalle $(-a, +a)$ qui correspond à des valeurs imaginaires du radical, c'est-à-dire à des particules qui ne passent jamais au point (z, φ).

En effet:

$$I_3 = \mathrm{j}\int_{-a}^{+a}\sqrt{a^2 - {v_{0z}}^2}\,\frac{\mathrm{d}f}{\mathrm{d}v_{0z}}\mathrm{d}v_{0z}$$

et

$$\lim_{a\to 0} I_3 = \mathrm{j}\,\frac{\pi}{2}\left(\frac{\mathrm{d}f}{\mathrm{d}v_0}\right)_0 a^2.$$

Ce terme linéaire en $(\varphi - \varphi_0)$ correspond exactement au terme qu'on interprète, incorrectement semble-t-il, depuis Landau comme une atténuation de l'onde.

Références

[1] DENISSE, J. F., DELCROIX, J. L., Théorie des ondes dans les plasmas (Dunod, Paris, 1961).
[2] DELCROIX, J. L., Introduction à la théorie des gaz ionisés (Dunod, Paris, 1958).
[3] KITTEL, C., Introduction to solid state physics (Wiley, New-York, 1959).
[4] AIGRAIN, P., NOZIÈRES, P., Les Hélicons (Conf. Intern. sur la Physique des Semiconducteurs, Prague, 1960).
[5] SPITZER, L. JR., Physics of fully ionized gases (Interscience, New York, 1956).
[6] STÜRROCK, P. A., Amplifying and evanescent waves, convective and non convective instabilities; dans "Plasma physics", J. E. Drummond (Mac Graw Hill, New York, 1961).
[7] DELCROIX, J. L., DENISSE, J. F., PIHAN, J. M., QUÉMADA, D., Théorie des ondes transversales dans les plasmas (Rapport LP 7. Laboratoire des Hautes Energies, Orsay, 1961).
[8] DOYLE, P. H., NEUFELD, J., *Phys. Fluids* **2** (1959) 390.
[9] GERSHMAN, B. N., *Zhur. Eksptl. i Teoret. Fiz.* **24** (1953) 453.
[10] BUNEMAN, O., *Phys. Fluids* **4** (1961) 669.
[11] QUÉMADA, D., *C. R. Acad. Sci. (Paris)* **252** (1961) 3556.
[12] BERNSTEIN, I. B., TREHAN, S. K., *Fusion nucléaire* **1** (1960) 3.
[13] CRAWFORD, F. W., *Phys. Rev. Let.* **6** (1961) 663.
[14] LITTLE, P. F., Acoustic waves in a plasma, A.I.E.A. Conférence sur la physique des plasmas et la recherche concernant la fusion nucléaire contrôlée, Résumé CN-10/59.
[15] GOLDSTEIN, L., Communication privée.

SHOCK WAVES IN COLLISION-FREE PLASMAS*

M. Camac, A. R. Kantrowitz, M. M. Litvak, R. M. Patrick, H. E. Petschek

Avco-Everett Research Laboratory

Everett, Massachusetts, United States of America

Investigation of the structure of a shock wave provides an excellent opportunity for studying the dissipation processes in collision-free plasmas. The thickness of collision-free shock waves was previously obtained from measurements of the light emitted by the plasma in a magnetic annular shock tube. The magnitude of the shock thickness, and its Mach number and density dependence were in agreement with a theoretical estimate based on the concept that the required dissipation in the shock is produced by non-linear interactions between magnetohydrodynamic waves.

Further confirmation of these results has been obtained. A. Measurements of the magnetic field have shown that the magnitude of the field change across the shock agrees with that expected from the conservation equations. Also the distance over which the field changes agrees with the previous shock thickness measurements. B. The electron temperature was estimated to be above 10 eV based on the ultraviolet radiation intensity and the ratio of bound-bound and free-free radiation. C. Measurements of the heat transfer from the plasma to the shock tube wall indicate that less than 1/10 of the gas energy is dissipated to the walls; thus, there is good containment of the shock heated plasma for a time large (50 times) compared with the shock rise transit time. D. The theory of the wave dissipation mechanism has been reformulated so that the distribution of wave action in wave-vector space is described by a Boltzmann equation similar to that for the distribution of phonons in solids. Estimates of relaxation times for the non-linear wave interactions agree with previous predictions. Preliminary results for the shock structure suggest that in the shock front the wave distribution is somewhat concentrated in regions of wave-vector space away from the origin. There are indications that the wave frequency band should be narrow at the shock front and increase going towards the back of the shock. Waves of about ion cyclotron frequency may persist behind the shock while other waves spread to high frequencies by wave-wave collisions and are damped.

1. Introduction

In highly ionized plasmas the cross-section for interparticle collisions decreases with the square of the temperature. When fusion temperatures are approached, the collision processes, which in ordinary gases rapidly dissipate departures from thermodynamic equilibrium, become of negligible importance. The early hopes for the magnetic confinement of high temperature plasmas with extremely small energy loss rates were based on this fact. However, this extremely small collisional dissipation leads to the survival of oscillatory motions for very long times. Furthermore, in many plasma devices the plasma is created in a state of violent motion, and it would be expected that a considerable part of the plasma energy would be in wave motion. It then becomes probable that in many cases non-linear interactions will affect the wave pattern before the linear processes, which are usually considered, have had a chance to act.

We may make a rough comparison of these times in terms of a typical experimental situation corresponding to an electron density $N=10^{16}/\mathrm{cm}^3$, particle temperature $T=300$ eV, magnetic field $B=2\times10^4$ G, a plasma dimension $L=10$ cm, and the ratio of plasma pressure to magnetic pressure $\beta=0.5$. There are three possible linear damping mechanisms. (1) Collisional damping requires a time of the order of the electron mean free time or longer. The electron mean free time varies as $T^{3/2}N^{-1}$ and for the above case is 10^{-7} s. (2) Resonant particle damping depends upon the number of particles which can move at the appropriate velocity to stay in resonance with the wave. Since for some regions of the wave spectrum the required resonant particle velocity can be made arbitrarily large, there would be very few resonant particles for such waves. One may therefore expect that there will be at least some regions of the wave spectrum for which resonant particle damping becomes negligible. (3) Wave energy may be lost to the walls since waves will be only partially reflected at the plasma boundaries. However, even if the walls can be designed to absorb incident wave energy very efficiently over a large range of wavelengths, the time for this absorption process will be larger than the plasma dimension divided by the group velocity. If we take the Alfvén speed as a typical group velocity, this time varies as $L\,\beta^{1/2}\,T^{-1/2}$ and for the above case is 2×10^{-7} s.

The time required for non-linear wave-wave interactions as estimated in our previous papers [1], [2] and as given in Eq. (26) of this paper is

$$\tau \approx \frac{1}{\beta_w \bar{\omega}},$$

where β_w is the ratio of the pressure (roughly energy density) of the wave field to the magnetic pressure and $\bar{\omega}$ is the average angular frequency of waves

* Conference paper CN-10/132, presented by A. R. Kantrowitz. Discussion of this paper is given on page 491. Translations of the abstract are at the end of this volume of the Conference Proceedings.

in the plasma. Assuming somewhat arbitrarily that a typical wave frequency is the geometric mean of the electron and ion cyclotron frequencies, the wave-wave interaction time varies as $B^{-1}\,\beta_w^{-1}$ and for the above case is $10^{-10}/\beta_w$ s.

Comparison of these times suggests that, unless the plasma can be produced so quietly that $\beta_w < 10^{-3}$, wave-wave scattering will be the fastest of these processes. Thus one would expect that non-linear wave phenomena will be of considerable importance in many realistic problems.

Creation of plasmas by shock waves moving at speeds so high that collisional effects play a secondary role provides a fine opportunity for the experimental study of collision-free plasmas and non-linear wave interactions. With the magnetic annular shock tube it has been possible to produce shock waves with speeds (up to 50 cm/μs) which result in temperatures so high that collisions are of secondary importance. Shock waves are particularly interesting for studying the dissipation phenomena for both experimental and theoretical reasons. The conservation laws combined with measured shock velocities provide important information about the average state of the gas both inside and behind the shock wave. Secondly, the inherent planarity of the experimental shock fronts simplifies the overall problem in that overall changes with time and changes in the plane of the shock wave can be neglected. The achievement of thermodynamic equilibrium in a shocked plasma requires the dissipation of a large part of the directed kinetic energy of the incoming gas (referred to a coordinate system moving with a shock wave). When dissipation mechanisms are considered to be absent, an unsteady final state is achieved, and theoretical treatments which do not include dissipation mechanisms simply result in a regular wave pattern in the shocked plasma in which the oscillations contain the energy which must be dissipated. It is clear that such descriptions of a shock wave are subject to possible instabilities of many sorts. For example, ROSENBLUTH [3] pointed out that a large anisotropy in the plasma pressure will lead to the growth of disturbances (non-oscillating growth for sufficiently large anisotropies and growing waves with more moderate anisotropies). He remarked that the resulting instabilities might "play an essential role in producing the entropy necessary for the existence of the shock." The existence of instability mechanisms has led us [1], [2] to investigate the possibility that the collision-free shock would actually dissipate this energy in a random wave field bearing some resemblance to the dissipation of water waves by turbulent wave processes, e.g., breakers at a beach. Our earlier work demonstrated that waves could grow in a compression front, that in strong shocks the wave amplitude which would be required to maintain a constant steepness for the compression front would be large enough so that non-linear effects would be important, and that the scattering of waves on waves could provide the essential dissipating process. In previous papers [4], [5] it was demonstrated experimentally that the thickness of a shock wave was indeed less than the collision-free path when the shock velocity was high enough to make the mean free path in the equilibrium gas behind the shock greater than the ion Larmor radius.

Stimulated by the surprisingly close correspondence between this crude theory and the experimental measurements of the thickness of collision-free shocks [2], PETSCHEK and LITVAK have partially developed a kinetic theory, based on non-linear wave interactions. Although solutions of the shock problem have yet to be obtained, some light can now be shed on the nature of the waves in and behind the shock front. It is to be hoped that this kind of theory, when further developed, will have general application when the non-linear wave interactions become important. Simultaneously, R. M. Patrick has extended his experimental work to the point where magnetic field measurements across the shock front can now be made. M. Camac has developed and applied to the magnetic annular shock tube ("Mast") a heat transfer gauge which measures the rate of deposition of energy on the walls with a resolving time of a fraction of a microsecond.

This paper presents a summary of this program to date, and more detailed results will be published elsewhere.

2. Experiments

The objective of the experiments described in this paper is to create a shock wave which produces a plasma in which (1) the collision mean free path is longer than any length in the apparatus, (2) the ion cyclotron radius is small compared with the size of the container, (3) the plasma behind the shock is completely ionized, and (4) the plasma energy density is of the order of the magnetic energy density. A laboratory experiment which produces this plasma requires a magnetic field strength of the order of 10 to 20 kG, a particle density of the order of 10^{15} particles per cm^3, and a temperature of the order of 10^6 °K. A completely ionized gas is required with high kinetic temperatures; thus, hydrogen was chosen as the working fluid because the simple structure of this atom permits complete ionization at relatively low energies per particle. A temperature of 10^6 °K generated by a shock wave requires a very high shock speed. Therefore, magnetic fields were used to furnish the driving force and containment of the shock heated plasma.

The requirements of magnetic containment and a constant driving force through a uniform channel led to the development of a magnetic annular shock tube, Mast (see Fig. 1). Details of its operation are presented in [4], [6]. The container for the working gas is formed by the annular space between two concentric cylinders [7], [8], [9]. The driving force which produces the shock wave is furnished by the azimuthal magnetic field due to radial currents in the annulus. These radial currents are created by discharging a capacitor bank connected to the

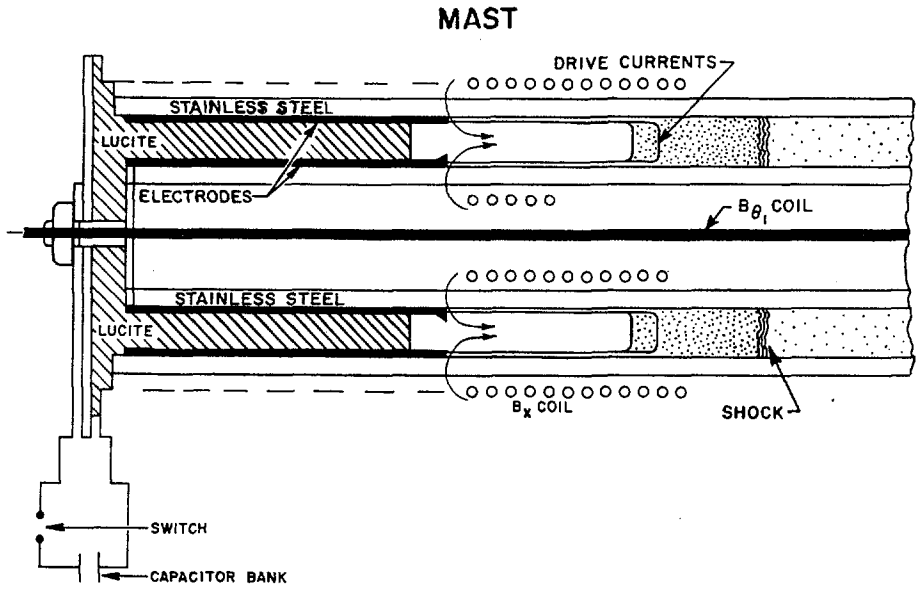

Fig. 1 Cross-section alview of the "Mast". The drawing is not to scale. The B_x coils consist of two concentric solonoids denoted by the small circles. The B_θ bias field is produced by a current in the conductor along the axis.

electrodes. When the gas between the electrodes breaks down, the capacitors are discharged through the gas, and this provides the radial drive current. The space between the two cylinders is evacuated, and during the experiments hydrogen is allowed to pass through an annular passage around an insulating spacer between the electrodes and through the annulus to a pumping system. This flow system provides a means of obtaining a low impurity level (500 parts per million).

For all the experiments described in this paper, there was an initial magnetic bias field ahead of the shock composed of both an azimuthal component, $B_{\theta 1}$, and a small axial component, B_x. The bias fields were furnished by two coil configurations shown in Fig. 1. The magnitude of $B_{\theta 1}$ was sufficient to cause a hydrogen ion moving with the same velocity as the shock to have a gyro-radius that is small compared to the channel width (i.e., annulus spacing). This is an experimentally determined criterion [4] for obtaining high speed shocks in excess of 2.5×10^7 cm/s.

In order to establish experimentally the existence of high speed shocks, measurements were made of the shock velocity, the plasma density and magnetic field jumps across the shock, and heat transfer to the side walls behind the shock. The measurements of the shock velocity and plasma densities have been reported previously [4], and these results agree with the theoretical values [6] based on the measured drive magnetic field intensity and conditions ahead of the shock. Recently, the change in the magnetic field has been measured with a new type of flux coil [10]. These measurements verify that there is a compression of the magnetic field across the shock which checks the calculated value [6] and also gives shock thickness in agreement with the radiation results reported previously. Furthermore, a new type of heat transfer gauge has been developed which has a sufficiently fast response time to measure the wall heat transfer due to the shock heated plasma during the experimental test time (0.5 to 2 μs). The heat transfer measurements show that about 90% of the plasma energy is contained, which verifies the use of the energy conservation across the shock.

The aim of these experiments is to produce a collision-free shock where the mean free path for the shock heated particles is much longer than the shock thickness. The evidence for the production of such a shock can be obtained from the measured shock velocity, plasma density ratio, and containment. For low initial gas pressures in the Mast, the shock velocities were in excess of 45 cm/μs, a condition for which the calculated mean free path for hydrogen ions behind the shock is over 30 cm. This collision-free path calculation is based on the conservation laws and the measured shock velocity, density ratio, and magnetic field jump. The dissipation mechanism in the shock cannot be due to ordinary ion-ion collisions, because such a process would produce a shock wave at least as thick as the ion mean free path.

The shock waves described in this paper are propagating into room temperature hydrogen. The energy invested in dissociation and ionization to completely dissociate and ionize hydrogen is 7.5 eV per particle. This is to be compared to an enthalpy of over 500 eV per particle behind the shock. The ionization process can play a role only in the front portion of such high speed shock waves, since the dissipation energy necessary to cause the jump conditions is much larger than the ionization energy. The major portion of the shock structure must involve a mechanism which is much more energetic than an ionization process.

2.1. Experimental results

2.1.1. *Mast development*

Recently some modifications have been made to the Mast which have improved its performance. The two concentric cylinders which form the annulus have been constructed of stainless (non-magnetic) steel, instead of glass with mylar and brass liners [4]. The stainless steel wall is in contact with the plasma. Higher energy densities in the shock heated plasma can be attained. The electrodes are insulated from the channel walls, thereby causing the initial breakdown to occur at the electrodes.

A larger Mast with a mean diameter of 30 cm has been constructed with a channel spacing equal to 2.1 cm and a 1.5 m useful length. The ratio of the channel width to the mean radius is equal to 0.14 for the 30 cm Mast compared with a ratio of 0.30 for the 15 cm Mast [4].

2.1.2. *Shock velocities*

The shock velocities have been determined by measuring the time interval between the arrival of the shock at several axial stations. The shock was identified by the onset of plasma radiation and more recently by the magnetic field change across the shock and the onset of plasma heat transfer to the side walls. These new results give shock velocities in agreement with the radiation results and further verify the use of the momentum equation to predict the shock velocities.

2.1.3. *Density ratio across shock*

The plasma density behind the shock waves has been obtained by measuring the intensity of the radiation emitted by the shock heated plasma, Fig. 6. Plasma radiation emitted in the direction normal to the shock tube axis was observed. Quartz windows (1.27 cm diameter) were aligned flush with the inside wall of the outer tube. Radiation with wavelengths between 3750 Å and 6600 Å was measured with a photomultiplier interference filter system having a bandwidth of about 80 Å. A spectrograph consisting of two quartz lenses and a water prism was used for measurements from 3400 Å to 4400 Å. Ultraviolet radiation from about 300 Å to 1200 Å was also measured with a tungsten photoelectric detector, see Fig. 2. The known photoelectric conversion efficiency for tungsten [11] was used to calibrate the equipment. A typical oscillogram using this type of detector is shown in Fig. 3. The circuit rise time for these measurements was less than 0.01 μs.

It has been shown [4] that the visible radiation intensity is proportional to N_e^2 where N_e is the electron density, and further, that this intensity is due predominantly to free-free radiation for electron temperatures above 10 eV. The experiments reported previously were carried out for low initial pressures in a Mast where the final equilibrium energy per particle behind the shock is large compared to the energy necessary to ionize and dissociate the hydrogen. Recently, the range of initial gas pressure has been extended to include conditions behind the shock where the energy per particle is not large compared to the ionization energy. A summary of these results showing the measured radiation at 4400 Å is given in Fig. 4. These experiments were carried out with a value of the ratio B_1/B_0 equal to 0.4, so that M_A was 2 and the density ratio across the shock was 2.2.

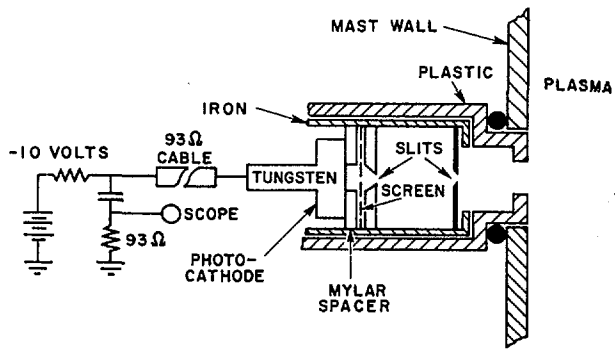

Fig. 2 Schematic view of the tungsten vacuum ultraviolet detector. The slits determine the optical path; the screen is used to furnish a uniform potential over the tungsten surface.

For these conditions the radiation for p_1 below 200 μ is due predominantly to free-free transitions [12]. For higher initial pressures, free-bound radiation [13] makes a significant contribution and must be taken into account. The calculated curve for the intensity was based on equilibrium conditions behind the shock. The drop in the calculated curve for p_1 greater than 400 μ is due to incomplete ionization behind the shock.

These results show that within the scatter of the data the measured radiation agrees with the expected value up to 800 μ. For p_1 greater than 800 μ the calculated plasma conductivity is low enough to allow the magnetic field to diffuse from the interface to the shock during the test time. This indicates that the assumption of infinite conductivity in the shock for p_1 greater than 800 μ is no longer valid.

It should be noted that for low initial pressures the experiments agree with the theoretical prediction and that for these conditions the radiation measurements furnish a good determination of the electron density behind the shock.

2.1.4. ΔB *measurements*

The change in the magnetic field across the shock was measured with small single turn coils [10], [14], see Fig. 5, that were inserted through the outer wall and centered in the annulus. The diameter of the coils ranged from 0.4 mm to 7 mm; the wire size, from 0.085 mm to 0.25 mm. Both insulated and bare coils were used. The output of the insulated coil went directly to an oscilloscope, while the bare coils

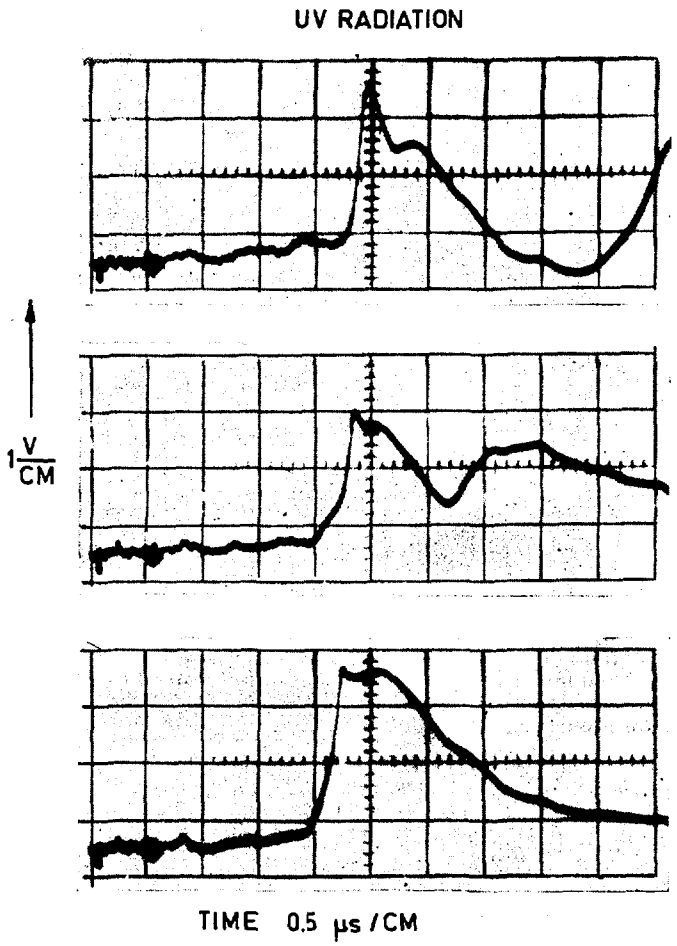

Fig. 3 Three oscillograms obtained with the tungsten ultraviolet detectors. The voltage is proportional to the radiation for wavelengths between 300 Å and 1200 Å. [$p_1 = 40\,\mu$, H_2; $u_s \simeq 25$ cm/μs].

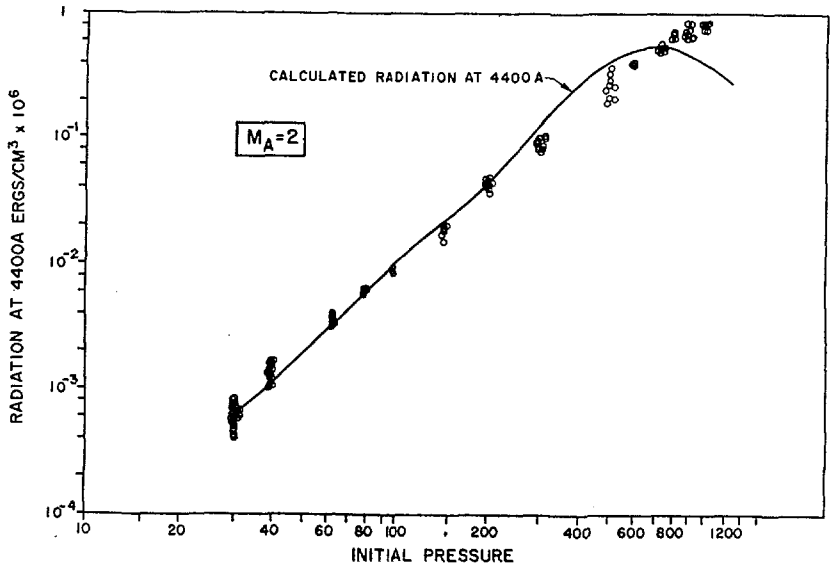

Fig. 4 Measured radiation intensity at 4400 Å *versus* the initial pressure in microns. The Alfvén Mach number was held constant ($M_A = 2$). These results were obtained using the interference-filter and photomultiplier system.

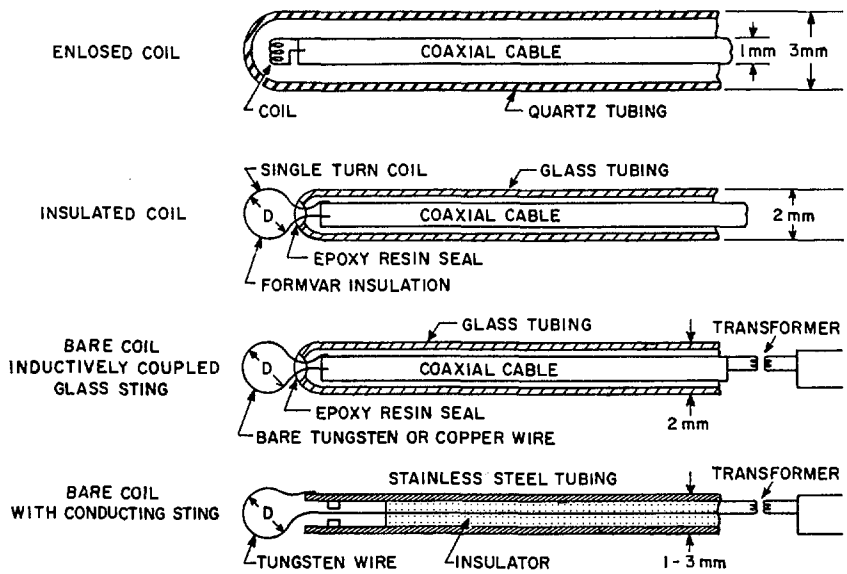

Fig. 5 These coil configurations were used to measure the changes in the magnetic field across the shock. The quartz-enclosed coils (top design) were unsuccessful in measuring this change, because the plasma which flowed outside the quartz was shielded from the coil. The other three diagrams show exposed coils; all of these correctly measured the magnetic field jumps across the shock. The insulated single-turn coil was covered with (three coats of) formvar enamel. The bare coils were in electrical contact with the plasma. The results obtained with both the glass and steel mounting stings were essentially the same. The diameter D of these coils ranged from 0.4 mm to 7 mm; the diameter of the steel tubing for the bottom configurations ranged from 1 do 3 mm.

were inductively coupled to isolate the large plasma potential from the oscilloscope. An oscillogram obtained by using the directly-coupled insulated coil is shown in Fig. 6. The left oscillogram shows both the signal due to the time derivative of the B_θ field in the coil (bottom trace) and the integrated signal showing the compression of the B_θ field across the shock (top trace). The coil frequency response was determined from 5×10^6 to 4×10^8 Hz by using a calibrated sinusoidal magnetic field. The uniform field region of a Helmholtz coil geometry was used, and a known sinusoidal current was passed through the Helmholtz coils. This calibration showed that the coil response in free space was linear for frequencies up to 1.2×10^8 Hz.

The bare coils were used in order to decrease the ablation from the coil surface arising from the intense plasma heat transfer. A series of experiments has been performed which show that the ablation products become ionized presumably in the boundary layer about the coil and electrically shield the coil. In the extreme case where a 1 mm coil was enclosed in a small glass tubing, Fig. 5, there was no reproducible magnetic flux signal at the time of shock passage. The tubing was larger than the size of the loop and could appreciably disturb the flow in the vicinity of the coil. The signal improved as the disturbance of the plasma by the magnetic coil was made smaller. In fact, the best measurements were made with a single turn of wire, either coated or bare, that extended into the plasma, which should produce the smallest disturbance to the flow.

The change in the azimuthal component of magnetic field across the shock, ΔB_θ, was measured with the single turn flux coils. This was done over a wide range of initial pressures at constant Alfvén Mach number, $M_A=2$. The results of these measurements are shown in Fig. 7. The ratio of the measured to the calculated ΔB_θ appropriate for the measured value of M_A is plotted versus the initial pressure, p_1. The initial azimuthal bias field $B_{\theta 1}$ was varied from 2500 to 4200 G, and the coil diameters ranged from 1 mm to 3.5 mm. The data show that for p_1 below 500 μ (which corresponds to shock velocities in excess of 14 cm/μs) the measured change in the field across the shock agrees with the predicted value, assuming no leakage of magnetic flux ahead of the shock. For p_1 above 500 μ, where the shock velocities were less than 14 cm/μs, the measured ΔB_θ is less than the computed value. This shows that for these high densities and lower shock speeds the plasma conductivity behind the shock front is insufficient to prevent appreciable diffusion of the B field ahead of the shock.

The final equilibrium enthalpy behind the shock for values of p_1 above 500 μ is insufficient to totally ionize the plasma. Furthermore, for p_1 above 800 μ the calculated plasma conductivity behind the shock is low enough to allow the B field to diffuse from the interface to the shock during the test time. The data show that for p_1 below 500 μ the plasma properties can be predicted by assuming that there is no leakage of the magnetic field ahead of the shock.

2.1.5. *Heat transfer measurements*

A new type of heat transfer gauge [15] has been employed that is suitable for measurements on shock tubes and other pulsed plasma devices. During recent years, the use of the resistance gauge for measurements of heat transfer in chemical shock tubes has received

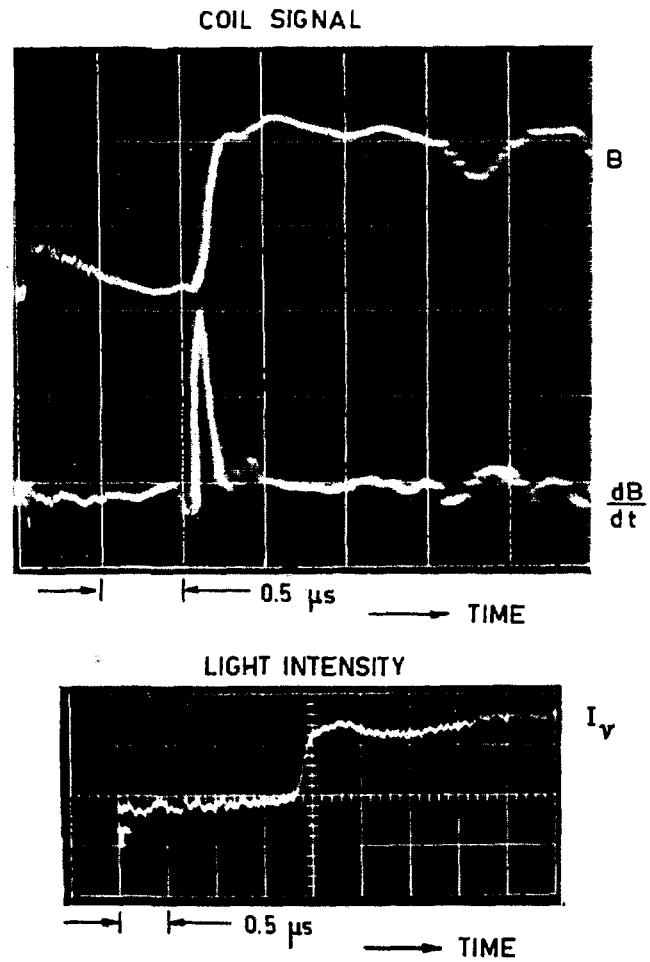

Fig. 6 The upper oscillogram was obtained using an insulated, directly coupled, flux coil. The top trace was obtained by integrating the signal from the coil, and the bottom trace is the coil signal. The initial pressure for this run was 40 μ and the shock velocity was 35 cm/μs. The lower oscillogram was obtained by monitoring the radiation at 4400 Å; the voltage on this trace is proportional to the radiation intensity.

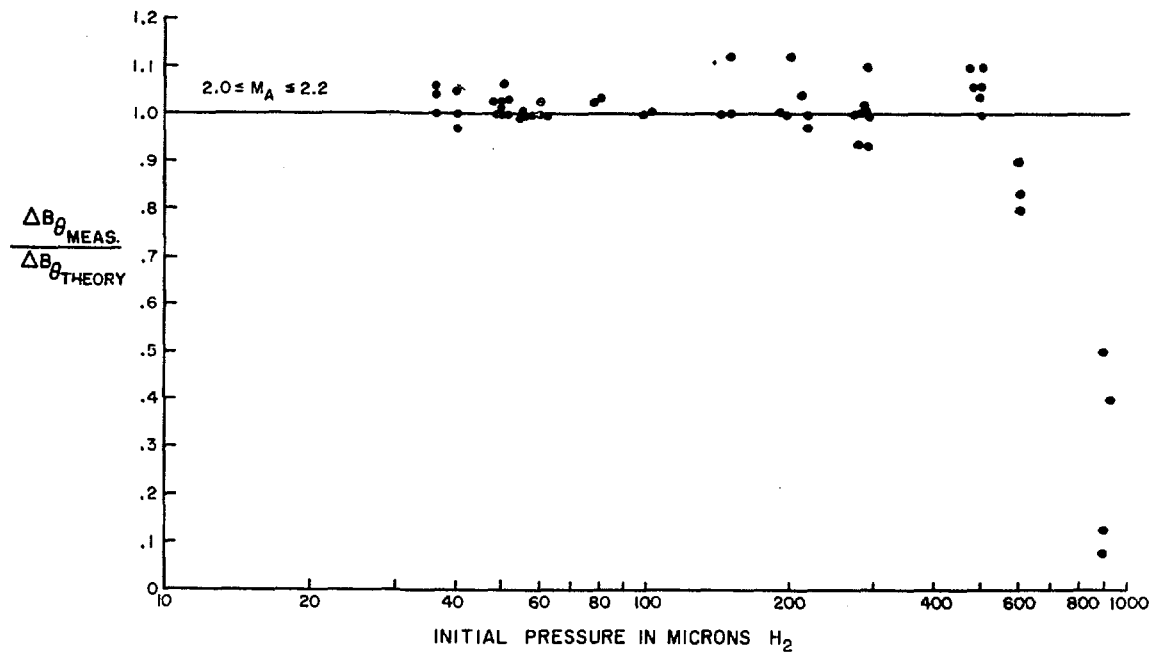

Fig. 7 Plot of the ratio between the measured change in $B\theta$ across the shock to the calculated value for different initial pressures. M_A was constant for these shocks within the accuracy of determining the shock velocity.

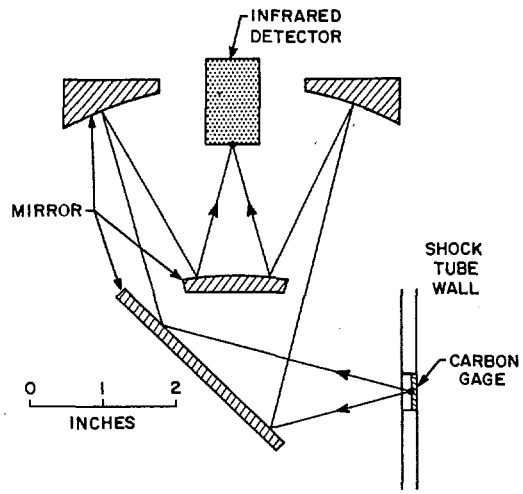

Fig. 8 Infrared gauge experimental arrangement for measurements of heat transfer to the shock tube wall.

wide application. These gauges have sufficient time response and sensitivity but have limited use in plasma devices because of electrical shorting and pickup. The resistance element comes in contact with the plasma and must operate in regions of strong electromagnetic fields. The heat transfer gauge that we have developed is highly suitable for studying plasma heat transfer since it is unaffected by strong electromagnetic fields. The basic idea of the gauge is to use a thin opaque layer of carbon. Plasma heating is applied on one side of the carbon while the temperature of the other side is determined by its infrared emission. The carbon layer is thin enough so that the temperature of the surface in contact with the plasma can be determined within a fraction of a microsecond.

Fig. 8 shows how this gauge is used in shock tubes for heat transfer measurements. A portion of the shock tube wall is replaced with a heat transfer gauge, which consists of a layer of carbon (1000 Å to 8000 Å thickness) deposited on sapphire. Energy from the shock heated gas is transferred to the gauge. Changes in the infrared radiation from the back surface of the carbon are observed with a Westinghouse gold-doped germanium detector. An f:2 Cassegrain optical system using mirrors images the gauge on the infrared detector.

A direct calibration was obtained by measuring the heat transfer rates in shock heated air and showing the results to be in agreement with other experiments [16], [17]. Fig. 9 shows experimental data using an ordinary chemically driven shock tube. The carbon gauge was placed in the end plate and was heated by the air behind the reflected shock. The detector output is shown as a function of time. The gauge signal rises abruptly and levels off. The interaction between the driver gas and the reflected shock appears after 15 μs. The time to reach the final infrared emission was of the order of 0.4 μs. This is the shortest rise time that has been obtained with a plain carbon gauge; thinner gauges become transparent, and the infrared radiation from the surface is swamped by the plasma radiation. In order to reduce the rise time below 0.4 μs a double layer is used in which a thin layer of carbon (optical density of 3) is first deposited on the sapphire which then is coated with an opaque aluminum layer.

Fig. 10 shows a comparison of the experimental data with theory. The lines are the theory and the bars are the experimental points obtained with the present heat transfer gauge. The theory is an extension of the FAY-RIDDELL [17] stagnation heat transfer applied to reflected shock conditions. This extension was made for us by Dr. Kemp. This comparison of the infrared gauge to the work of others using another method gives us confidence in its application for pulsed experiments.

The heat transfer measurements obtained with the Mast are shown in Fig. 11. The carbon was placed flush with the inside wall of the outer tubing. Data for two consecutive runs are shown. The circuit rise time was approximately 0.3 μs, and the aluminum plus carbon coated gauge had 0.1 μs rise time. The peak signal corresponds to a temperature change of 90 °F. Note that the heating stops after about 1/2 μs corresponding to the time of passage of the shock-heated gas. The gauge temperature rise is plotted as a function of the shock velocity in Fig. 12. It should be noted that for shock velocities above 20 cm/μs, the shock-heated gas is in the collision-free regime. Based on these temperature rises, the thermal boundary layer thickness can be computed. This is the equivalent thickness of free stream gas that has the energy equal to that deposited on the wall. This thickness decreases from 2 mm to 1 mm with increasing shock velocity. The free stream gas energy consists of the gas enthalpy and directed kinetic energy (in laboratory coordinates). If the magnetic energy density were included in the free stream energy density, then the thermal boundary layer thickness would be reduced by a factor of 3.

The measured thickness is only an upper limit to the actual boundary layer thickness, since a 6 mm diameter non-conducting gauge was used for the measurements. The magnetic lines can leak into this electrical hole causing additional plasma to flow to the surface. Ablation of material from the shock tube wall might also affect the heat transfer measurements by shielding the plasma from the gauge. These measurements are preliminary, and the effects of holes in the container and wall ablation will be investigated further. It should be noted that the thermal boundary layer thickness is considerably smaller than the annulus spacing of 22 mm that contains the plasma.

2.1.6. *Test time*

The test time is the time required for the shock heated plasma to pass over a fixed axial station in the Mast. The length of the plasma that has been shock heated can be obtained from both the ultraviolet (UV) radiation measurements, Fig. 3, and the side wall heat transfer measurements, Fig. 11. This is taken to be the region for which the radiation or heat transfer is constant behind the shock. Test times of 0.4—0.6 μs have been obtained with the 15 cm diameter Mast

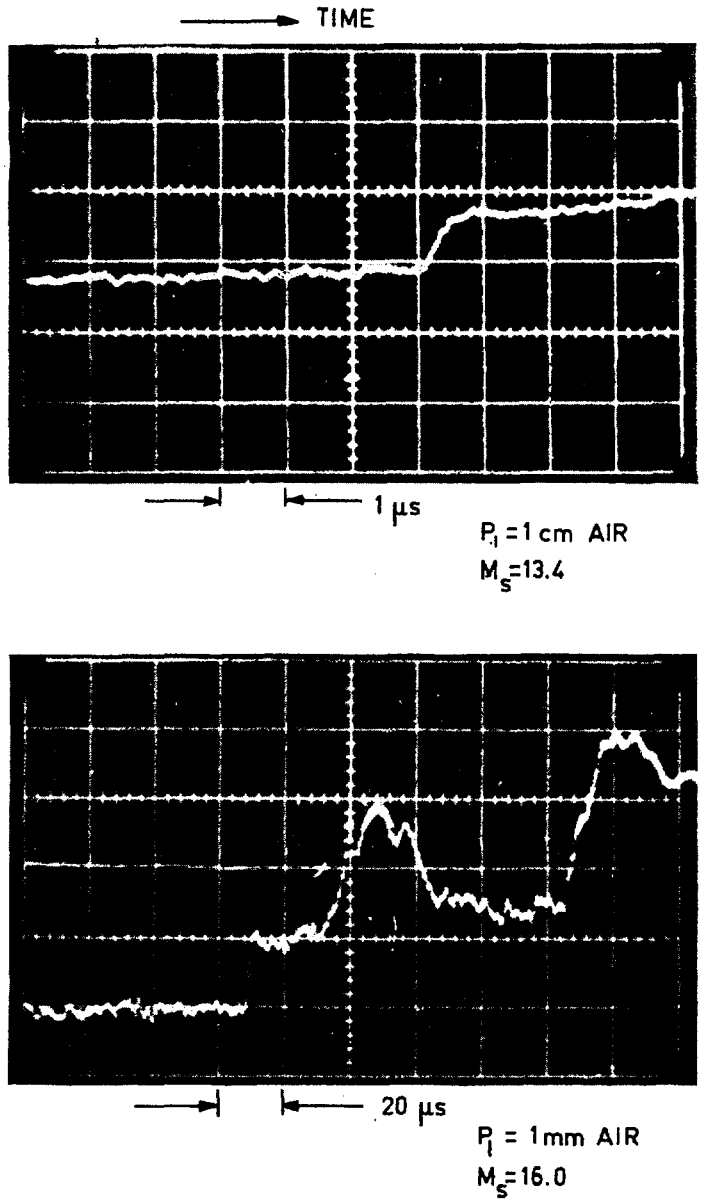

Fig. 9 Heat transfer measurements on the end plate (reflected shock conditions) of a chemically driven shock tube. The oscillograms show the infrared gage output versus time. M_s is the incident normal shock Mach number and p_1 is the initial air pressure.

which has a 2.4 cm annulus spacing. Longer test times with the 30 cm diameter Mast have been obtained, which are proportional to the distance the shock has traveled from the electrodes. The test times obtained using the 30 cm Mast have been as long as 2 μs when the quarter cycle time for the drive field is 6 μs. The length of the uniform plasma in both devices is considerably longer than the shock thickness (up to 50 times using the 30 cm Mast). This indicates that the conditions behind the shock can be measured and that these plasma properties can be distinguished from those in the shock wave.

2.1.7. *Estimation of electron temperature*

The electron temperature for initial pressures less than 200 μ was estimated with two methods. The first was obtained from the UV radiation results and the second from the measurements of the ratio of hydrogen line intensity to the nearby continuum.

An estimation of the electron temperature was obtained with measurements of the UV radiation from about 300 Å to 1200 Å with the tungsten photoelectric detector. The variation of the tungsten gauge output with plasma temperature was obtained by folding the gauge response curve into the plasma radiation intensity. The shock velocity and the Rankine-Hugoniot equations were used to get the electron density behind the shock. This average intensity indicated that the electron temperature was greater than 10 V. This result verifies the use of bremsstrahlung to measure the plasma density in the visible range.

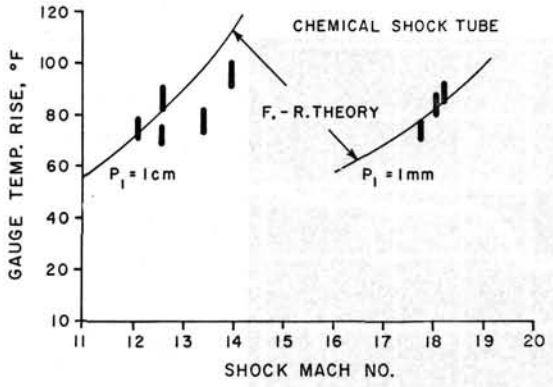

Fig. 10 Comparison of experimental measurements of the heat transfer from air to the theory of Fay and Riddell [17]. The measured temperature rise is plotted as a function of the shock Mach number. Measurements were obtained for initial air pressure of 1 cm and 1 mm.

In addition, the temperature of the electrons can be measured by using the ratio of the H_α (6563 Å) and H_β (4861 Å) line intensities to the nearby continuum, following a method outlined by GRIEM [18]. If the hydrogen plasma is sufficiently dense so that the time between collisions of electrons and excited atoms is shorter than the de-excitation time [19] for the excited state, then the line radiation intensity is proportional to the number of atoms in a particular state. According to the Saha equation, the number of atoms in an excited state is proportional to the square of the electron density and so is the continuum intensity. The ratio of the total line intensity and the nearby continuum intensity is, therefore, only a function of temperature, except for the correction in the ionization potential. For values of T_e approximately equal to 10 V and with $N_e = 10^{16}/cm^3$, this correction due to the decreased ionization potential is very small and the ratio of the total H_α and H_β line intensities to the nearby continuum is inversely proportional to T_e.

If the shock-heated plasma were uniform across the annulus, the method could be used to obtain a close estimate of T_e. The plasma is bounded by two walls, and the hydrogen plasma in contact with either wall will be cooler than the interior; hence, the line radiation from these cool boundary layers will be much more intense compared to the continuum than that coming from the plasma in the interior where T_e is high.

Therefore, the results of these measurements obtained with the Mast can be interpreted as lower limits to the value of T_e. These measurements were made with two photomultipliers, a half silvered mirror, and several interference filters. Two of these filters had their maximum transmission on the H_α and H_β lines. The other filters were used to measure simultaneously the continuum between 4400 Å and 6300 Å. The bandwidth of the filters ranged between 50 Å and 100 Å. These measurements were made with plasma conditions in the Mast such that the initial pressure ranged from 40 μ to 100 μ of H_2, the shock velocity from 25 to 50 cm/μs, and the Alfvén Mach number from 1.8 to 2.8. Both the ratios of H_α and H_β line intensities to the continuum gave values of T_e approximately equal to 10 V. Since small boundary layers with low electron temperatures can effectively reduce the measured T_e with this method, these results cannot be interpreted as a good measure of the shock heated plasma electron temperature; but these results can establish a lower bound of 10 V to T_e, which further confirms the use of bremsstrahlung to measure N_e^2 behind the shock.

2.1.8. *Fine structure magnetic field measurements*

Most of the theoretical descriptions [2], [22—27] of the collision-free shock structure predict the existence of a fine structure to the magnetic field inside the shock. We are attempting to observe the fine structure experimentally. The removal of the quartz envelope around the coil resulted in the successful measurement of the magnetic field jump across the shock. Following this, it was felt that an even smaller disturbance to the plasma would result if the insulat-

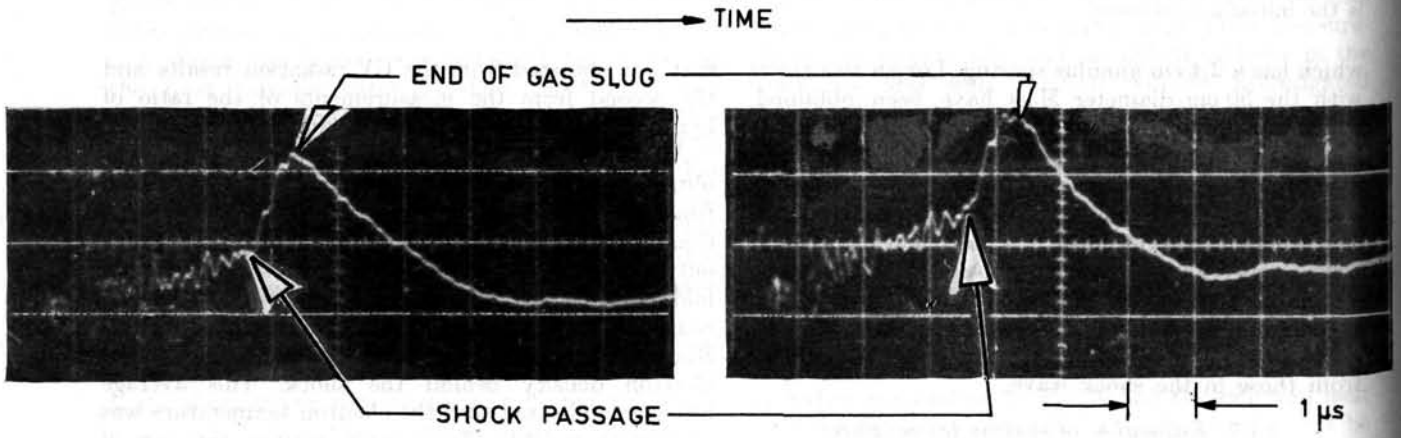

Fig. 11 Heat transfer measurements on the Mast side-well. Oscillograms showing the infrared gauge output versus time for two consecutive runs. $p_1 = 100$ μ H_2; $U_s = 13$ cm/μs; circuit rise time 0.3 μs. The shock arrival time and the end of the heating pulse are indicated.

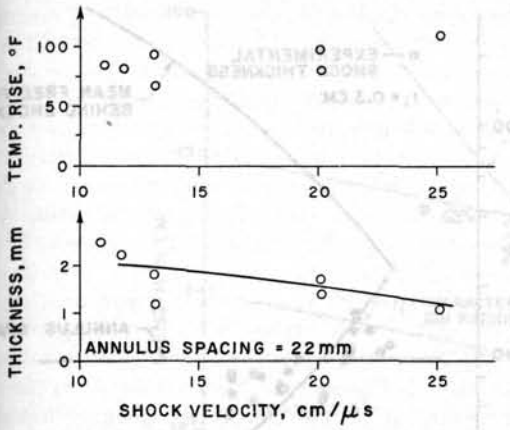

Fig. 12 The top graph presents the experimental results of the gauge temperature rise as a function of the shock velocity. The bottom graph gives the side wall thermal boundary layer thickness after 0.5 μs computed from the gauge temperature rise measurements.

ing layer were removed from the exposed single-turn coils.

We have used the inductively coupled bare coils to attempt to measure high frequency (in the range from 10 to 100 MHz) oscillations of the magnetic field in the shock front. The heat transfer to a surface in the shock heated plasma is of the order of 2×10^6 watts/cm^2. The non-conducting material which covers the insulated, directly coupled coil can be ablated during the time required for the shock to propagate past the coil (10^{-1} μs). This ablated material can form a conducting layer of dense cold plasma around the coil and shield the coil from high frequency changes in the B field. A surface such as copper or tungsten will conduct the heat away from the surface faster than a material such as formvar enamel, which was used to cover the insulated coils. An oscillogram which was obtained with a bare coil is shown in Fig. 13. There is a greater indication of high frequency fluctuations of the B field on this picture, compared with the trace obtained with the insulated coil. This bare coil was constructed as shown in Fig. 5

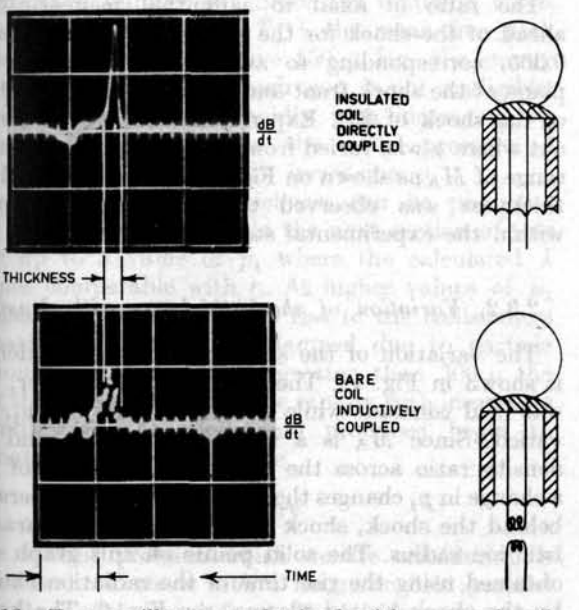

Fig. 13 Two oscillograms obtained with exposed coils showing the time derivative of the azimuthal magnetic field in the shock. The top trace was obtained with an insulated, directly coupled coil, and shows a relatively smooth variation in dB/dt across the shock. The bottom trace was obtained with a small bare inductively coupled coil and shows a noisy variation in dB/dt in the shock.

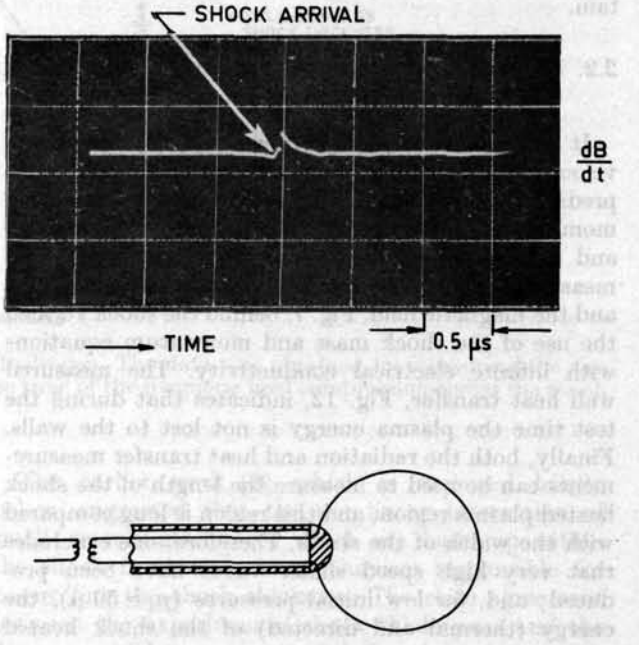

Fig. 14 Oscillogram obtained with a large (diameter 6 mm) inductively coupled bare coil. The signal shows a rapid rise in dB/dt just after the arrival of the shock followed by smooth decay. This signal is typical of those obtained with large bare coils.

with a glass sting, and with a coil diameter of 1.5 mm. Bare coils with metal stings were also used (Fig. 5), but there was no detectable change in the signal with this type of sting. If the signal from the bare coil on Fig. 13 were to be interpreted as giving actual fluctuations of the magnetic field in the plasma, the fluctuating field would be of the order of 3% of the average field. This 3% fluctuation would be an order of magnitude too small to affect the flow.

Larger diameter (3 to 7 mm), bare coils were also tried, and a typical signal from the large coil is shown in Fig. 14. The integrated signal from this coil (area under the dB/dt trace) gives the correct change in B_θ across the shock. The sudden increase in dB/dt followed by the slow decay indicates that there is some non-linear phenomenon associated with the coil signal. A possible explanation of this signal could be that the coil was shielded from the change in the magnetic field across the shock either by a cloud of ablated material from the coil or by an arc between the two leads of the coil where the coil is connected to the sting. The sudden increase in dB/dt then could correspond to a rupture in the shielding due to the

cloud or a break in the arc which allows the compressed field to enter the coil. Furthermore, it must be pointed out that the high frequency oscillations present on the coil signal in Fig. 13 could be due to a series of such effects and not due to a high frequency oscillation in the B field in the shock.

Bare, inductively coupled coils did show some indication of a fine structure to the magnetic field in the shock, but at the present time the interpretation of the high frequency signals from these coils is uncertain.

2.2. Summary of plasma properties to show existence of shock

It has been previously shown [4] that the shock velocity obtained in a Mast is in agreement with that predicted by using the conservation of mass and momentum equations, the known drive field intensity and the initial conditions ahead of the shock. The measurements of both the plasma radiation, Fig. 4, and the magnetic field, Fig. 7, behind the shock verified the use of the shock mass and momentum equations with infinite electrical conductivity. The measured wall heat transfer, Fig. 12, indicates that during the test time the plasma energy is not lost to the walls. Finally, both the radiation and heat transfer measurements can be used to measure the length of the shock heated plasma region, and this region is long compared with the width of the shock. Therefore, one concludes that very high speed shock waves have been produced; and, for low initial pressures ($p_1 \simeq 50$ μ), the energy (thermal and directed) of the shock heated gas is of the order of 10^3 eV per particle.

2.3. Experimental collision-free shock thickness

2.3.1. *Variation of shock thickness with* M_A

The Alfvén Mach number, M_A, of a magnetically driven shock is a function of the ratio of the total azimuthal magnetic field behind the shock to the field ahead of the shock [6], i.e., B_0/B_1. A range of values of M_A was obtained by varying B_1 while keeping constant the drive field and the gas density. The shock thickness was obtained from the rise time of the plasma radiation (see Fig. 6). The results of these experiments are shown in Fig. 15, where the measured ratio of the shock thickness to the characteristic ion radius, r_i, is plotted against M_A. r_i is the gyroradius of a hydrogen ion moving with the Alfvén velocity for conditions ahead of the shock. Note that r_i is only a function of the initial density. The data were obtained for initial hydrogen gas pressure p_1 ranging from 70 to 90 μ Hg and for shock velocities in excess of 30 cm/μs. The ion mean free path λ behind the shock was computed as follows: $\lambda = 1/N_i Q_i$, where $N_i = N_e =$ the measured electron number density behind the shock, Q_i is the Coulomb cross-section for 90° deflections assuming the particles have the equilibrium plasma temperature behind the shock. The equilibrium temperature is obtained by using the energy equation across the shock [6], and the measured

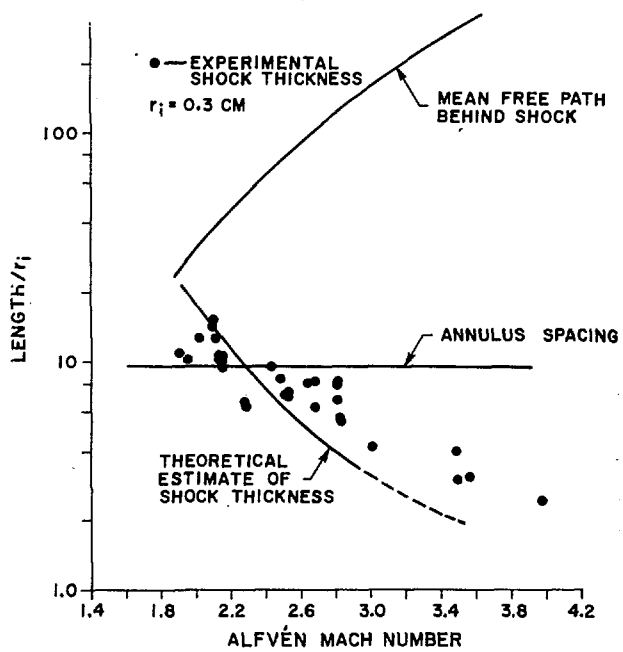

Fig. 15 Shock thickness *versus* Mach number. The experimental shock thickness was obtained by measuring the rise time of the radiation across the shock. This data is shown by the circles. The initial pressure was between 70 μ and 90 μ, the Alfvén Mach number was changed by varying the initial bias field intensity. The characteristic ion Larmor radius, $r_i = 0.3$ cm for these experiments.

shock speeds. Also shown in Fig. 15 is the theoretical estimate [2] of the collisionless shock thickness *versus* M_A. This calculation gives results which are valid within the approximation of the theory for $M_A \gtrsim 3$.

The ratio of axial to azimuthal magnetic field ahead of the shock for the experiments was equal to 0.365, corresponding to an angle, α, between the plane of the shock front and the magnetic field ahead of the shock of 20°. Experiments have been carried out where α was varied from 10° to 35°, over the same range of M_A as shown on Fig. 12. The measured shock thickness was observed to be independent of α within the experimental scatter.

2.3.2. *Variation of shock thickness with density*

The variation of the shock thickness with density is shown in Fig. 16. The Alfvén Mach number, M_A, was held constant while the initial pressure, p_1, was varied. Since M_A is a function of B_0/B_1 and the density ratio across the shock is a function of M_A, a change in p_1 changes the plasma density, temperature behind the shock, shock velocity, and the characteristic ion radius. The solid points on this graph were obtained using the rise time of the radiation emitted by the shock heated plasma, see Fig. 6. The hollow circles denote the results obtained using the single turn flux coils, which measured the rise time of B_θ across the shock. The characteristic ion radius is shown along with a theoretical estimate of the shock thickness [2]. The theoretical shock thickness for

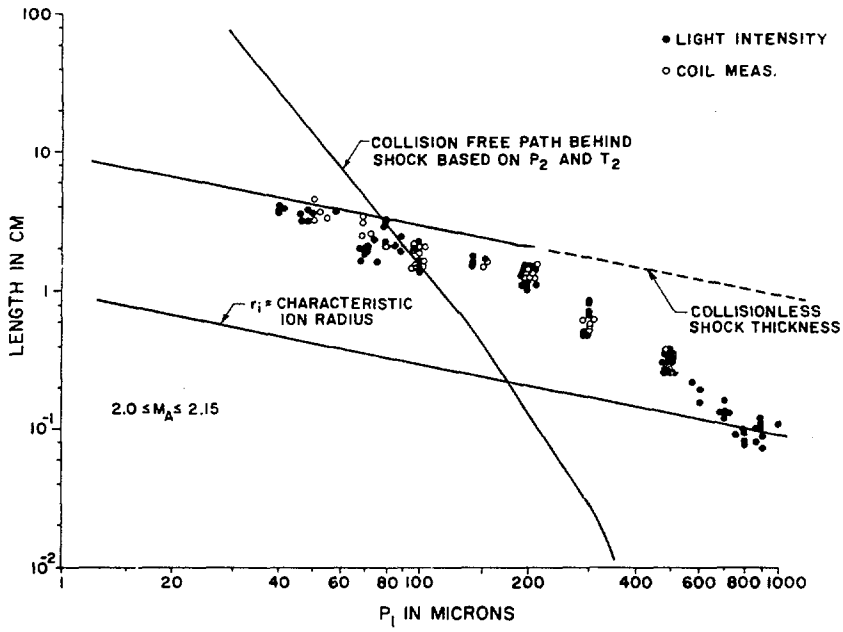

Fig. 16 Measured shock thickness *versus* initial pressure in hydrogen. The data was obtained by measuring the rise time of the radiation across the shock (solid circles) and the rise time of the magnetic field compression across the shock measured with the flux coils (hollow circles).

large mean free paths is equal to $10\,r_i$ for $M_A=2$. Also shown is the ion collision mean free path, λ, based on the same conditions as shown in Fig. 15. For pressure below 150 μ Hg, λ is very nearly proportional to p_1^{-3}. This can be shown as follows: $U_s^2=k_1 B_0^2/p_1$ and $T_2=k_2 U_s^2$, where U_s is the shock velocity, T_2 is the equilibrium temperature behind the shock, and k_1 and k_2 are functions of the Alfvén Mach number [6]. Since the Coulomb cross-section is proportional to T_2^{-2}, the mean free path varies as p_1^{-3}. For p_1 above 150 μ Hg, the energy invested in ionizing the hydrogen is not negligible, and T_2 decreases more rapidly with increasing p_1. Hence, for large values of the initial pressure, λ decreases more rapidly with increasing p_1.

The measured shock thickness can be predicted using the theory reviewed in the next section of this paper up to a value of p_1 where the calculated λ becomes comparable with r_i. At higher values of p_1 the plasma waves which give rise to the collisionless dissipation mechanism are damped due to particle collisions. For values of p_1 greater than 300 μ the shock thickness decreases more rapidly with increasing p_1, indicating that collisional processes begin to dominate the shock structure.

3. Theory

The specific problem which we are considering is that of a shock wave with a magnetic field parallel to the plane of the shock front. The initial temperature is small; that is, the thermal velocities of the ions are much less than the Alfvén speed. However, the gas is hot enough so that the mean free path for particle collisions is much larger than the ion Larmor radius.

The earlier work [2], which is reviewed briefly below, suggested that the non-linear interaction of small wavelength waves which are built up within the shock front was the mechanism responsible for controlling the shock thickness. The close agreement between the experimental shock thicknesses and the distance which a wave moves before interacting with other waves gives strong support to the validity of this suggestion.

In the present paper we attempt to give a somewhat more detailed description of the wave field and its interaction with the flow. First we will derive a relation which describes the motion of a particular wave in terms of the local flow field and the local distribution of other waves. This relation is analogous to the Boltzmann equation in gas kinetic theory which describes the motion of a particle in terms of the local macroscopic fields and the local distribution of other particles. A similar relation for waves has been used for some time to describe the distribution of phonons in solids [20].

Secondly, one must attempt to find a self-consistent solution of this equation. As in the case of ordinary kinetic theory, the complexity of the Boltzmann equation is such that, although it can be derived in a fairly formal and rigorous manner, its solution requires further approximations and will first be carried out with much less rigor. Thus far, we have not obtained even a crude solution to the shock problem. However, a principle will be stated which is based upon the fact that the existence of the wave spectrum in itself requires an extreme departure from equilibrium. This principle determines some features of the wave distribution, in terms of which a more complete qualitative description of the wave pic-

ture can be given. It is also possible to suggest some features of the wave spectrum which may be observable experimentally.

3.1. Review of earlier work

The earlier theoretical discussion [2] which serves as the starting point for this work consisted of four main points:

1. The suggestion that if several scale lengths of the plasma, corresponding to different transport mechanisms, could provide a steady shock structure, the thickest of these is the one that is most likely to occur. If one regards a shock wave as being formed by a steepening of a compression front, this steepening will be stopped by the first dissipative process which can inhibit it. Therefore, the thickest shock will result. On the other hand, if a thinner shock is formed by a sudden pulse, the longer range mechanism may be able to transport energy and momentum across the shock and therefore broaden it. These arguments suggest that one should look for the longest range dissipative mechanisms. For the case of a plasma whose collision mean free path is longer than the ion Larmor radius, it was shown [21] that ion-ion collisions could not provide the required dissipation. The next shorter length which becomes of interest is the ion Larmor radius. Therefore, attention was focused on this rather than the two shorter basic lengths in the plasma, namely, the electron Larmor radius and the Debye length.

2. It was demonstrated that waves which are present in a compressive flow are amplified by the work done by the flow against the wave pressure. Furthermore, waves could be found which would move faster than the flow velocity even at the front of the shock. These waves could, therefore, be present in the shock front and their energy would be built up.

3. It was suggested that the major portion of the dissipation which occurred in the shock front would go into producing such waves. Since the mechanism for producing this wave energy is not highly selective, a large number of such waves should exist with varying wavelengths. These waves would then transport energy and momentum between different places in the shock front. The distance over which they move would be limited by the interactions with other waves. In other words, it was suggested that a kinetic theory of such waves could be formulated. The mean free path for a wave moving through a random distribution of other waves was estimated by considering the diffraction of a wave as it moved through the medium whose magnetic field was disturbed by the presence of the other waves. The change in magnetic field produces a change in the index of refraction of the wave and, therefore, a change in the phase of the wave. The phase changes in going through uncorrelated regions of the disturbing magnetic field were assumed to produce a random walk in the phase of the wave being considered. The mean free path was taken to be the distance a wave had to go before the rms value of its phase change was equal to unity. The resulting mean free path was $\lambda_w = 4/\beta_w k$, where β_w is the ratio of wave pressure to the average magnetic pressure and k is the mean wave number of the spectrum.

4. No serious attempt was made to describe the kinetic theory of the wave distribution for this case. The shock thickness was simply estimated from the statement that the mean free path for these waves was the basic length for dissipation and that a shock which is required to produce a large "temperature" ratio between the subsonic and supersonic streams can be only a few basic dissipation lengths thick. The number of dissipation lengths was somewhat arbitrarily chosen as two. The value of β_w required in the formula for the mean free path is defined by the conservation equations. The value of k was chosen such that waves could propagate to the front of the shock. The values of k required by this criterion are several times the reciprocal of the characteristic ion Larmor radius,

$$r_i = \frac{V_A}{\omega_i} = \sqrt{\frac{Mc^2}{4\pi N e^2}},$$

where V_A is the Alfvén speed; ω_i, the ion cyclotron frequency; M, the ion mass; N, the particle number density; c, the velocity of light; and e, the electron charge. The resulting shock thicknesses are plotted in Figs. 15 and 16 as functions of Alfvén Mach number and density. The density dependence comes from the variation of r_i with density, giving a shock thickness which is inversely proportional to the square root of the density. The decrease of shock thickness with Mach number comes principally from the rapid increase of β_w with the Mach number.

Other theories of collision-free shocks have also suggested turbulent mechanisms for dissipation. Kahn [22] considered a shock wave in the absence of a magnetic field and concluded that the build-up of plasma oscillations would give rise to a characteristic length of the order of a Debye length. Parker [23], on the basis that one should look for the thinnest shock wave, concluded that the Debye length was the relevant length even in the presence of a magnetic field. This is smaller than the experimentally observed thicknesses by a factor of 10^{-5}.

Rosenbluth and Longmire [24] suggested that detailed analysis of the individual particle orbits in the time dependent problem would give rise to density and magnetic field profiles which resembled shock waves and in which the dissipation would appear in the form of oscillatory motions behind the shock front. Because of the complexity of such calculations, they are necessarily limited to the consideration of a one-dimensional approximation to turbulence. Auer, *et al.* [25] have carried out detailed numerical computations. They quote a shock thickness of $3\,r_i$ for an Alfvén Mach number of 5.8 and indicate thicker shock waves at lower Mach numbers. These results are in order of magnitude agreement with the experimental data.

Gardner, *et al.* [26] and Morawetz [27] have suggested a one-dimensional time-independent "lam-

inar" solution for the case of a finite temperature ahead of the shock. The dissipation is produced by the fact that, with an initial spread in particle velocities, the individual particle orbits are not all the same. This is presumed to produce a phase mixing which when viewed on a large scale is equivalent to an entropy increase. No specific statements about the overall shock thicknesses have been made although both the characteristic Larmor radius, r_i, and the characteristic electron Larmor radius, $\sqrt{m_e/m_i}\, r_i$, appear as basic lengths. In view of the instabilities which would be caused by the pressure asymmetry in the shocked gas, it seems highly unlikely that a one-dimensional laminar solution will occur.

DAVIS, *et al.* [28] have suggested that there may be an intermediate temperature range where the fine structure in the shock is not controlled by collisions but the dissipation mechanism is still particle collisions. In this range they predict a fine structure with dimensions of the order of the characteristic electron Larmor radius and an overall shock thickness which is of order of the distance that the gas moves in an electron mean free time. This would give a shock thickness of about one-tenth of the mean free path shown in Figs. 15 and 16. Such a line would cross the experimental data in both figures. However, the dependence on both density and Alfvén Mach number is in sharp disagreement with the experimental results.

3.2. WAVE BOLTZMANN EQUATION

In order to discuss the kinetic theory which was suggested by the previous work, it is necessary to describe the mechanics of the wave motion and its interaction with the flow field in somewhat more detail. This mechanics can be conveniently summarized in terms of a Boltzmann equation for the distribution of wave energy in wave-number and coordinate space. We will do this for the particular wave modes which we expect will be important in the shock wave. However, the generalization of the derivation to other plasma problems where such a description is applicable should not be difficult.

The basic equations from which we set out to describe the plasma are:

$$\frac{\partial}{\partial t} N + \nabla \cdot N \mathbf{V}_i = 0 \tag{1}$$

$$M\left(\frac{\partial}{\partial t} + \mathbf{V}_i \cdot \nabla\right)\mathbf{V}_i = e\left(\mathbf{E} + \frac{\mathbf{V}_i}{c} \times \mathbf{B}\right) \tag{2}$$

$$0 = -e\left(\mathbf{E} + \frac{\mathbf{V}_e}{c} \times \mathbf{B}\right) \tag{3}$$

$$\nabla \times \mathbf{B} = 4\pi N e \frac{\mathbf{V}_i - \mathbf{V}_e}{c} \tag{4}$$

$$\nabla \times \mathbf{E} = -\frac{1}{c}\frac{\partial B}{\partial t} \tag{5}$$

$$\nabla \cdot \mathbf{B} = 0 \tag{6}$$

$$N_i = N_e \equiv N, \tag{7}$$

where $\mathbf{V}_i$ and $\mathbf{V}_e$ are the ion and electron velocities, N_i and N_e are the ion and electron number densities. $\mathbf{E}$ and $\mathbf{B}$ are the electric and magnetic fields.

These are the standard non-linear equations for a plasma with the following approximations: The displacement current and electron Larmor radius have been set equal to zero on the basis of the earlier prediction that the important frequencies in the wave distribution are considerably lower than the electron cyclotron frequency or the plasma frequency. The temperature or velocity spread of the particle distribution function has been taken to be zero on the basis that the energy dissipated in the shock wave is not converted into thermal energy of the particles but remains, at least in the shock front, in wave motion. The mean free time for ordinary particle collisions is infinite. The zero temperature and infinite mean free time assumptions result in the complete neglect of any damping processes for waves. These assumptions will be valid if the actual damping occurs in a time long compared to the times of interest.

Our picture of the plasma is that it consists of an average flow field in which the values of the magnetic field, velocity, etc., vary slowly and a superposed wave field in which there are rapid oscillations in both space and time. The rapid oscillations are described by a perturbation technique and are assumed to exist in a small gradient of the average properties of the medium. The system of equations is closed by considering the reaction of the wave field on the average properties of the medium. In first order, the oscillating field is described by the usual linear waves in a uniform medium. In second order, one must consider corrections due to the non-linear interactions between the waves and due to the spatial gradients in both the wave amplitudes and the average flow properties. Considering the non-linear interactions as perturbations on the linear waves requires that the ratio of the wave energy to the energy of the average magnetic field be small, i.e., that $\beta_w \ll 1$. We have further assumed that the phases of the waves are random. These two assumptions are self-consistent in that the product of the mean free path which is obtained and the wave number is inversely proportional to the energy ratio. This means that a wave moves many times the dimension of a typical wave packet ($1/k$) before interacting with other waves. The interactions may then be considered as occurring between waves which have not interacted previously and are therefore not correlated. The assumption that the gradients through which the waves move is small compared to the wave length is also justified *a posteriori* by the fact that the gradients in the shock wave are of the order of the mean free path, which is long compared to the wave length. The reaction of the waves on the flow is only considered to the lowest order which gives non-trivial results. All of these approximations should be valid in the limit of low Alfvén Mach numbers where the wave energy is small compared to the energy of the average magnetic field. The precise range of validity cannot, of course, be specified;

however, β_w is always less than one for Alfvén Mach numbers less than three.

It should be pointed out that the description in terms of wave amplitude is not merely a Fourier analysis of the problem. The wave amplitudes remain constant over a larger distance than the detailed field variables and therefore are a natural form of analysis.

If we are to describe the flow field in terms of waves, the first step is to linearize the equations and use standard techniques to derive the dispersion relation for the waves and to describe the polarization vectors for the magnetic field, etc., within the waves. For simplicity we will make a further approximation at this point which is based on the earlier conclusion that the wave frequencies are appreciably larger than the ion cyclotron frequencies. In this case the velocity of ions in the waves may be neglected compared to the velocity of electrons, and the linearized equations may be reduced to

$$\frac{\partial \mathbf{B}}{\partial t} - \nabla \times [\mathbf{e}_z \times (\nabla \times \mathbf{B})]\, V_A r_i = 0, \tag{8}$$

where the magnetic field in the undisturbed plasma is in the **z** direction, and $\mathbf{e}_z$ is a unit vector in the **z** direction. The dispersion relation for the resulting waves is

$$\omega_k = V_A r_i k |k_z| \tag{9}$$

if we adopt the convention that the frequency is always positive*. The waves consist of a circularly-polarized magnetic field transverse to the wave vector **k**.

In order to describe the mechanics of the waves in a flow field, we must now consider three separate questions: (1) the effect of the wave distribution on the mean flow field, (2) the changes in the amplitudes of the waves as they move through regions in which the average flow properties change, (3) the changes in wave amplitude due to their non-linear interactions.

3.2.1. *Conservation equations*

The changes in the mean flow field may be derived by substituting the values of the flow variables in terms of their average values and their fluctuating components in Eqs. (1) to (7) and integrating over a region of space which is large compared to the wave lengths but small compared to the changes in the average flow field. By this procedure we obtain the following equations for the case where the average flow properties are functions of the flow direction x only. The shock propagates perpendicular to the average magnetic field B, which is in the **z** direction. Subscripts "1" denote flow properties ahead of the shock. ϱ and u are the ion density and velocity, respectively.

$$\varrho u = \varrho_1 u_1 \tag{10}$$

$$\frac{B}{\varrho} = \frac{B_1}{\varrho_1} \tag{11}$$

$$P_{xx} + \varrho u^2 + \frac{B^2}{8\pi} = \varrho_1 u_1^2 + \frac{B_1^2}{8\pi} \tag{12}$$

$$(\varepsilon + P_{xx})u + q_x + \frac{1}{2}\varrho u^3 + \frac{B^2}{4\pi} u = \frac{1}{2}\varrho_1 u_1^3 + \frac{B_1^2 u_1}{4\pi}, \tag{13}$$

where the quantities P_{xx}, q_x, and ε, which can be interpreted as the pressure, energy flux, and energy density of the waves, have been defined as shorthand notations for the following integrals over the wave distribution:

$$P_{xx} = \int \mathrm{d}^3 k\, n_k\, v_x(k)\, k_x \tag{14}$$

$$q_x = \int \mathrm{d}^3 k\, n_k\, v_x(k)\, \omega_k \tag{15}$$

$$\varepsilon = \int \mathrm{d}^3 k\, n_k\, \omega_k, \tag{16}$$

where n_k is the action density (energy density divided by frequency) in phase space. By analogy with quantum mechanics this may be interpreted as the number of waves with wave vector **k**. ω_k is the wave frequency relative to the ion fluid. $v_x(k) = \partial\omega_k/\partial k_x$ is the group velocity relative to the ion fluid.

The relation that B/ϱ is constant for the average flow is equivalent to the statement that in the presence of the waves the effective electrical conductivity of the plasma is infinite. The relation follows from the fact that we have assumed that the ions move very little in a wave and that the electrons move adiabatically. That B/ϱ is constant is physically reasonable since Joule heating would produce appreciable dissipation for the shock thickness which we are discussing only if the effective mean free time for the electrons were less than the electron cyclotron period. Since all of the frequencies in the wave field are much lower than this, it is unlikely that such a short mean free time appears.

3.2.2. *Motion of waves in a slowly varying medium*

The motion of the waves through the overall flow field can be described rather simply in terms of the action (energy density/frequency) of a wave. Since the gradients in the overall flow field have a characteristic length which is long compared to the wavelength, the motion of a wave packet through the variable medium may be expressed by the simple statement that the action is conserved following the wave packet. This is the well-known result for any oscillator subject to changes that are slow compared to the frequency of oscillation. For example, the action (or in more familiar terms, the magnetic moment) of a charged particle in a slowly-varying magnetic field is a constant.

* Since a real wave consists of the standard exponential factor $e^{i(\mathbf{k}\cdot\mathbf{x} - \omega_k t)}$ and its complex conjugate, we may choose either sign of the frequency as the frequency of the real wave. The above choice is convenient for the description of the phase-independent properties of waves such as energy, action, pressure, etc. In detailed calculations involving phase-dependent properties, proper account must, of course, be taken of the complex conjugate term.

For a steady flow field which is a function of x only the convective derivative following a wave packet trajectory in phase space may be written as:

$$\frac{\mathrm{D}}{\mathrm{D}t} = \frac{\partial}{\partial t} + \frac{\mathrm{d}x}{\mathrm{d}t}\frac{\partial}{\partial x} + \frac{\mathrm{d}x}{\mathrm{d}t}\frac{\mathrm{d}k_x}{\mathrm{d}x}\frac{\partial}{\partial k_x}. \quad (17)$$

The packet trajectory is given by

$$\frac{\mathrm{d}x}{\mathrm{d}t} = u + v_x(k) \quad (18)$$

$$\frac{\mathrm{d}k_x}{\mathrm{d}x} = \frac{-k_x\frac{\mathrm{d}u}{\mathrm{d}x}}{u + v_x(k)}. \quad (19)$$

The second equation follows from the fact that the frequency in the shock-fixed coordinates $\omega_k + k_x u$ is constant and the fact that with B/ϱ constant the frequency ω_k does not depend explicitly on the x coordinate. The conservation of action along a packet path then becomes:

$$\frac{\mathrm{D}n_k}{\mathrm{D}t} = \frac{\partial n_k}{\partial t} + [u + v_x(k)]\frac{\partial n_k}{\partial x} - k_x\frac{\mathrm{d}u}{\mathrm{d}x}\frac{\partial n_k}{\partial k_x} = 0. \quad (20)$$

As might be expected, this equation is quite similar to the Vlasov equation. The third term is to be interpreted as the force term in the above equation, if the wave vector is interpreted as the momentum of a wave.*

It is of interest to examine some of the consequences of this equation, such as, for example, the rate of change of the momentum and energy of a wave packet as it moves through the velocity gradient. If we imagine a wave packet which is reasonably sharply defined in both momentum and position, the rate of change of energy of the whole wave packet is obtained by multiplying the above equation by the frequency ω_k and integrating over all phase space:

$$\frac{\partial}{\partial t}\int\int \omega_k n_k \,\mathrm{d}^3k\,\mathrm{d}^3x = -\int\int\left[\omega_k[u + v_x(k)]\frac{\partial n_k}{\partial x} - k_x\omega_k\frac{\mathrm{d}u}{\mathrm{d}x}\frac{\partial n_k}{\partial k_x}\right]\mathrm{d}^3k\,\mathrm{d}^3x. \quad (21)$$

Using integration by parts we obtain:

$$\frac{\mathrm{d}E}{\mathrm{d}t} = -v_x(k)\,k_x\,n\frac{\mathrm{d}u}{\mathrm{d}x}, \quad (22)$$

where E and n are the total energy and action of the wave packet and $v_x(k)$, k_x, and $\mathrm{d}u/\mathrm{d}x$ are to be evaluated at the center of the wave packet. The total energy of the wave packet therefore changes with time. If the velocity gradient is negative corresponding to a compressive flow, the wave energy increases with time, and conversely for an expanding flow the wave energy decreases. This result is precisely the same as the earlier argument that the wave energy increases because of the work done against the wave pressure by the flow. In terms of that argument, we may see that $v_x(k)\,k_x n$ is to be interpreted as the pressure of a wave packet.

Similarly, in order to obtain the rate of change of momentum of a wave in the velocity gradient, we multiply Eq. (20) by k_x and integrate, obtaining

$$\frac{\mathrm{d}m_x}{\mathrm{d}t} = -m_x\frac{\mathrm{d}u}{\mathrm{d}x}, \quad (23)$$

where m_x is the total x momentum of the packet.

This equation may be interpreted as the velocity gradient producing a force $-m_x\,\mathrm{d}u/\mathrm{d}x$ on the waves. For future reference we may note that this force is in the direction of motion of a wave if the velocity gradient is compressive. Thus, a wave which is moving forward in a shock front will tend to be accelerated forward.

We may summarize the discussion of the motion of the wave through a shallow velocity gradient by:

1. the action is preserved,
2. the momentum is changed by a force $-m_x\,\mathrm{d}u/\mathrm{d}x$,
3. the energy increases in a compressive flow at a rate $-p_{xx}\,\mathrm{d}u/\mathrm{d}x$.

3.2.3. *Wave collisions*

The collisions between waves result from the non-linear terms in the equations of motion of the plasma. The evaluation of these non-linear terms will only be outlined here with particular emphasis on the features which will be of interest to us in discussing the kinetic theory of the waves. The essentials of the method used are the same as those used for the description of phonon collisions in solids (except that in this case we are dealing with a completely classical system). These methods have been applied to the case of plasma oscillations by STURROCK [30]. Since the collisions are a perturbation on the wave motion, we may substitute the linear wave properties into the non-linear terms in the equations of motion. If we consider a case where two waves with wave vectors $\mathbf{p}$ and $\mathbf{q}$ are present, their non-linear interaction will produce a disturbance with a wave vector $\mathbf{k}$ such that $\mathbf{k} = \mathbf{p} + \mathbf{q}$. This disturbance may be regarded as a "force" which tends to produce a wave with a wave vector $\mathbf{k}$. This "force", however, also fluctuates at a frequency which is the sum of the initial frequencies $\omega_p + \omega_q$. If this frequency is not the frequency appropriate to the wave vector $\mathbf{k}$, the disturbing force gives rise only to a forced oscillation but does not feed energy into the $\mathbf{k}$ wave. If, however, the frequency $\omega_p + \omega_q$ is equal to the natural frequency of the $\mathbf{k}$ wave, that is, if $\omega_p + \omega_q = \omega_k$, then the $\mathbf{k}$ wave is being excited at its natural frequency and energy will be fed into it.

The magnitude of the rate at which energy is fed into the $\mathbf{k}$ wave will depend upon the product of the driving "force" and the "velocity" associated with the $\mathbf{k}$ wave. This product is proportional to the product of the amplitudes of the three waves. If we make the assumption, which was justified above, that the initial phases of the waves are random,

* The interpretation of the wave vector as the momentum of a wave is a familiar concept in quantum mechanics. Its justification for the case of classical waves in plasmas has been discussed by P. A. STURROCK [29].

the "velocity" associated with the **k** wave that was present before the interaction may be either in or out of phase with the driving "force". This term will therefore cancel, and the net rate of energy input to the **k** wave will depend upon the in phase component of the "velocity" of the **k** wave, that is, the component which has already been produced by the driving force. This means that the rate of energy transfer is proportional to the square of the driving force or to the product of the energy densities in the **p** and **q** waves.

From this type of analysis [31] the rate of change of action of a particular wave in a random distribution of other waves may be written as

$$\left(\frac{\partial n_k}{\partial t}\right)_{\text{coll}} = \int\int \mathrm{d}^3p\ \mathrm{d}^3q\, |S_{kpq}|^2 \frac{\omega_p\,\omega_q\,\omega_k}{\varrho\, V_A{}^2/2}$$
$$\times \{(n_p n_q - n_k n_p - n_k n_q)\,\delta^{(3)}(\mathbf{p}+\mathbf{q}-\mathbf{k})\,\delta(\omega_p+\omega_q-\omega_k)$$
$$+2(n_p n_q + n_p n_k - n_k n_q)\,\delta^{(3)}(\mathbf{k}+\mathbf{q}-\mathbf{p})\,\delta(\omega_k+\omega_q-\omega_p)\}, \tag{24}$$

where S_{kpq} is a matrix element relating the three waves. For the waves we are discussing, it is the triple scalar product of the three unit polarization vectors.

The frequencies are always defined as positive. The two major terms in the integrand arise, respectively, from the two cases: ω_k greater than either ω_p and ω_q, and ω_k less than at least one of ω_p and ω_q, say ω_p. The factor of two on the latter term accounts for the possibility that ω_q may be the largest frequency and not ω_p, as indicated in the δ-function in frequency in that term. The first, fourth, and fifth terms in the integrand contribute as collisions into the **k** wave at the expense of action in the **p** wave. The second, third, and sixth terms contribute as collisions out of the **k** wave to produce action in the **p** wave.

We may estimate the order of magnitude of the mean free time τ from this expression from the terms corresponding only to collisions out of the **k** wave. If we assume equal contributions from the two major terms in the integrand, we obtain the following expression for τ:

$$\frac{1}{\tau} = -\frac{1}{n_k}\left(\frac{\mathrm{d}n_k}{\mathrm{d}t}\right)_{\text{coll out}}$$
$$= 2\int \mathrm{d}^3q\, \frac{(n_{k-q}+n_q)}{\frac{1}{2}\varrho\, V_A{}^2}\, |S_{k,k-q,q}|^2 \omega_{k-q}\omega_q\omega_k \delta(\omega_{k-q}+\omega_q-\omega_k). \tag{25}$$

Using the rough approximations $n_{\mathbf{k}-\mathbf{q}}+n_{\mathbf{q}} \approx 2\,n_{\mathbf{q}}$, $|S|^2 \approx 1/4$, replacing the frequencies by the average frequency and the δ-function by the reciprocal of the average frequency $\bar{\omega}$, we obtain

$$\tau = \frac{4}{n\,\bar{\omega}^2} \approx \frac{4}{3\beta_{\mathrm{w}}\,\bar{\omega}} \tag{26}$$

$$n = \int \mathrm{d}^3k\, n_k. \tag{27}$$

The previous mean free path estimate, $\lambda_{\mathrm{w}} = 4/\beta_{\mathrm{w}}k$, may be converted into a mean free time by dividing by the group velocity, which for the quadratic dispersion relation that was assumed is approximately $2\,\bar{\omega}/\bar{k}$. This gives a mean free time $2/\bar{\omega}\beta_{\mathrm{w}}$. We see that the two derivations are in substantial agreement.

The requirement that the δ-functions in both the wave vector and the frequency be satisfied restricts the number of waves with which a particular wave may collide, i.e., a particular **p** wave can only interact with **q** waves which lie on a two-dimensional surface in the three-dimensional vector space. However, if the dispersion relation is such that the phase velocity of the waves decreases with increasing frequency, it can be shown [32] that the selection rules cannot be satisfied for the three-wave collisions. In this case one would have to go to higher order in the expansion in powers of wave energy, i.e., β_{w}, in order to obtain collisions involving four waves. For the mode which is of principal interest to us, the phase velocity increases with increasing frequency and, therefore, the three-wave collisions described above can occur. The restriction that a particular wave can only collide with a surface of other waves has important consequences for the kinetic theory of the waves and will be discussed in more detail below.

It is of interest to discuss the rate of change of action associated with such collisions. If we examine a single interaction between three waves, conservation of energy and momentum require that

$$\omega_k \frac{\mathrm{d}n_k}{\mathrm{d}t} + \omega_p \frac{\mathrm{d}n_p}{\mathrm{d}t} + \omega_q \frac{\mathrm{d}n_q}{\mathrm{d}t} = 0 \tag{28}$$

$$\mathbf{k}\frac{\mathrm{d}n_k}{\mathrm{d}t} + \mathbf{p}\frac{\mathrm{d}n_p}{\mathrm{d}t} + \mathbf{q}\frac{\mathrm{d}n_q}{\mathrm{d}t} = 0. \tag{29}$$

Combining this with the restriction imposed by the δ-functions:

$$\omega_k = \omega_p + \omega_q \tag{30}$$

$$\mathbf{k} = \mathbf{p} + \mathbf{q} \tag{31}$$

requires that

$$\frac{\mathrm{d}n_k}{\mathrm{d}t} = -\frac{\mathrm{d}n_p}{\mathrm{d}t} = -\frac{\mathrm{d}n_q}{\mathrm{d}t}. \tag{32}$$

The asymmetry in this relation is caused by the fact that, as the frequencies are all positive, we have selected the **k** wave as the highest frequency wave. The above relations state that in a single collision the same amount of action is involved in each of the three waves that are interacting or, in quantum mechanical language, that the same number of quanta are involved in each state. The net amount of action present is always changed by a collision. Since the sign of the action-change of the two low frequency waves is the same, there is a net loss of action if the two low frequency waves are initially present and produce the high frequency wave. Conversely, there is an action increase if the highest frequency wave and one of the other waves are initially present since only the highest frequency wave loses action in this process. We also note that for action-losing collisions the wave vectors of the initial waves add while for action-producing collisions they subtract.

We may summarize the significant features of the wave collisions as follows:

1. If the dispersion relation of the waves is such that the phase velocity of the waves increases with increasing frequency, collisions between three waves can occur.

2. If the phase velocity decreases, interactions between three waves all of the same mode are not possible and, therefore, collision rates are slower for this mode.

3. In the case of three-wave collisions a wave can only interact with a restricted group of other waves.

4. Energy and momentum are conserved by wave collisions, but the action may be either increased or decreased.

3.2.4. *Boltzmann equation*

The results of the discussion of the wave motion through the average flow fields and the collisions between waves may be summarized in a single equation by setting the rate of change of action due to convection in phase space equal to the rate due to collisions. For the time-independent, one-dimensional case we obtain:

$$[u + v_x(k)]\frac{\partial n_k}{\partial x} - k_x \frac{\mathrm{d}u}{\mathrm{d}x}\frac{\partial n_k}{\partial k_x} = \left(\frac{\partial n_k}{\partial t}\right)_{\text{coll}}, \quad (33)$$

where $(\partial n_k/\partial t)_{\text{coll}}$ is given by Eq. (24). The Boltzmann equation describes the wave distribution in terms of the velocity gradient of the average flow. This equation coupled with Eqs. (10) to (13), which describe the effect of the waves on the average flow, form a complete set of equations to describe the flow.

3.3. Wave distribution

Thus far we have derived the basic equations which govern the kinetic theory of a wave distribution in a plasma. The most promising approach for attempting to solve such a complex relationship would seem to be to assume a parametric form of the wave distribution and then to satisfy only the appropriate number of moments of the Boltzmann equation to determine the parameters. This requires that one first develop a sufficient qualitative description to allow one to choose an appropriate parametric form. In this section we will describe some of the qualitative features.

3.3.1. *Effect of non-equilibrium on kinetic theory*

One of the major differences between the kinetic theory we are considering and ordinary gas kinetic theory is the fact that we are dealing with a situation that is very far from equilibrium. The standard approach in the kinetic theory of gases has been to obtain the equilibrium distribution function and then to derive the small perturbations in this distribution caused by the varying flow field. The fact that there is an equilibrium to which the gas always tends to return is an extremely important basis for the description of gas kinetic theory. In the present case, however, the basic assumption that the wave energy is the largest part of the random energy of the plasma is in itself a statement that the system is very far from equilibrium. We have said in effect that the thermal energy of the plasma has been restricted to the very small number of degrees of freedom associated with the wave motion. For wavelengths of the order of the characteristic ion Larmor radius, $r_i = \sqrt{Mc^2/4\pi Ne^2}$ the fraction of the total number of degrees of freedom of the gas represented by the waves is of the order of $1/Nr_i^3$. For typical gas conditions this is of the order of 10^{-12}. We are therefore, by definition, dealing with a system that is very far from equilibrium.

This raises the question of how such a non-equilibrium situation can maintain itself. The actual requirement in the shock wave is even more stringent since the wave interactions occurring in the shock front must provide the waves which are required to flow out of the back of the shock wave. The wave distribution in the shock front must therefore have interactions which tend to move it *away* from equilibrium in the sense that in spite of the excess of waves which is present the net result of the interactions must be to produce more waves.

Let us first examine a distribution of waves which is a function of frequency only and is confined to low frequencies. Such a distribution function will tend to spread to high frequencies in order to approach the equilibrium distribution. The predominant collisions which occur are, therefore, those in which two low frequency waves produce a high frequency wave. In each such collision action is lost. Since, in the neighborhood of the average frequency of such a distribution, the number of waves at the high frequency is appreciably less than the number of waves at the lower frequencies, the rate of the action-losing collisions will be appreciably larger than the rate of the action-producing collisions. For example, if we take the energy density as decreasing exponentially with frequency $n_k \propto [\exp(-\alpha\omega_k)]/\omega_k$, the ratio of the number of action-losing collisions to the number of action-producing collisions for the interaction of three specified waves is

$$\frac{n_p n_q}{n_k(n_p + n_q)} = \frac{\omega_k}{\omega_q \mathrm{e}^{-\alpha\omega_p} + \omega_p \mathrm{e}^{-\alpha\omega_q}}. \quad (34)$$

This ratio varies between 1 and $\exp(\alpha\omega_k/2)$ depending upon the ratio ω_q/ω_k. In the neighborhood of the mean frequency, $(\omega_q+\omega_p+\omega_k)/3 = 2\omega_k/3 = 1/\alpha$, the number of action-losing collisions is, therefore, about twice as large as the number of action-producing collisions. The total action is then reduced by 1/4 in a single collision.

If this shape were maintained, the same fraction would be lost in the next collision. However, since for constant energy the average frequency is inversely proportional to the action, the mean free time is directly proportional to the action. The resulting rate of action loss is then proportional to the square of the action. This means that the action of the waves

would completely disappear (the high frequency waves that are produced are rapidly damped) in a finite time. For the case given above, it would take four times the original mean free time.

The rapid disappearance of the waves in this relatively symmetric distribution and the requirement that waves actually be produced suggests that we should look for a highly asymmetric distribution which favors action-producing collisions. The possibility of finding a distribution which favors action-producing collisions is afforded us by the fact that not all pairs of waves can collide with each other, i.e., by the restrictions imposed by the δ-functions in both wave vector and frequency.

An action-producing collision occurs when the highest frequency wave and one other wave are initially present. For a dispersion relation where the frequency goes to zero when the wave vector goes to zero, it is possible for two waves with almost the same vector to interact and produce a much lower frequency wave. Two waves with almost the same frequency cannot, however, give rise to action-losing collisions. This would require that two almost parallel wave vectors add to give a third vector which satisfies the frequency relation. This would occur only if the dispersion relation were linear.

We are therefore, led to the suggestion that *the distribution function should consist principally of waves in a restricted region of wave vector space which is away from the origin.* Such "blobs" in the distribution function would have the property that there is no net action change within the blob, since the action change for the two high frequency waves is equal and opposite. The collisions within the blob, however, produce action outside of the blob.

A possible blob configuration in a shock wave is shown in Fig. 17. Two blobs (shaded areas) have been located such that the x component of their group velocity is twice the local Alfvén speed. Two blobs

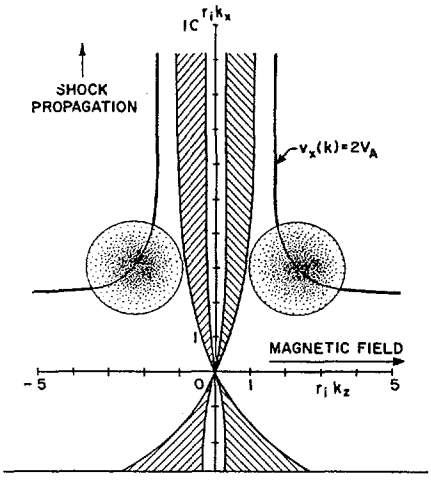

Fig. 17 A possible wave distribution which avoids collisions leading to loss of action. The waves are concentrated in the shaded blobs. Action-losing collisions could only occur with waves in the cross-hatched areas. The locus of wave-vectors such that the x-component of group velocity equals twice the Alfvén speed is also shown.

are required by the fact that the group velocity is never greater than the Alfvén speed on the k_x axis and by the requirement of symmetry in the z direction. The cross-hatched portion of the diagram represents the waves which could give rise to action-losing collisions by interacting with waves in the blobs. The size of the blobs has been chosen for this drawing so that action-losing collisions are completely avoided. We do not, however, mean to imply that the blob actually has sharp boundaries, but only that the action density is appreciably larger in this region. Collisions between waves in the blobs produce waves which are approximately within the cross-hatched area. Such waves would, therefore, also be present in the distribution. However, since these waves have a lower group velocity than the waves in the blob, they move downstream rapidly and their density is kept low.

The concept that highly asymmetric distribution functions are required to avoid rapid action loss is probably applicable to other cases of plasma turbulence. In particular, in those cases in which wave energy is produced adiabatically, the losses of wave action by either damping or convection must be made up for by action-producing collisions. This casts some doubt on the validity of estimates of the electrical conductivity which were made earlier [33] on the assumption that the current produced small asymmetries in the distribution.

3.3.2. *Remarks on shock structure*

We now examine some of the moments of the Boltzmann equation in order to relate some of the properties of the wave distribution to each other and to the flow velocity. The overall conservation Eqs. (12) and (13) have already given two such relations. An additional conservation equation for the wave distribution as a whole may be obtained by multiplying the Boltzmann equation by $\omega_k + k_x u$ and integrating over all k space* [33]. Since both the momentum and energy are conserved in wave collisions, the collision term drops out of this moment and we obtain (after integrating with respect to x)

$$\varepsilon u + q_x + u(P_{xx} + u M_x) = \text{const.} = 0, \quad (35)$$

where ε, q_x and P_{xx} were defined by Eqs. (14) to (16) and

$$M_x = \int \mathrm{d}^3k \, n_k k_x . \quad (36)$$

If we assume no waves ahead of the shock, the integration constant in Eq. (35) is zero. This should be the case in the absence of wave damping since waves which try to propagate ahead of the shock will be slowed down by wave collisions and then overtaken by the shock. In a practical case in which the damping may be appreciable in the colder gas at the front

* Separate consideration of momentum and energy conservation leads only to a relation which is redundant with previous ones.

of the shock one would expect to observe some departure from the above relation.

By algebraic manipulation of Eqs. (10) to (13) and (35) one can show that at the front of the shock $P_{xx} \propto u_1 - u$ and $(P_{xx} + uM_x) \propto (u_1 - u)^2$. The pressure in the wave distribution, therefore, rises linearly with velocity at the front of the shock. The quantity $P_{xx} + u M_x$ must, however, vanish more rapidly at the shock front. The definitions of P_{xx} and M_x would suggest that this could be the case if at the shock front the wave distribution is concentrated along the line $v_x(k) = -u$. Coupled with the previous conclusion that within the shock the wave distribution is concentrated in blobs, this suggests that the blob is highly concentrated at the shock front and that its width increases towards the back of the shock.

A further conservation law may be obtained in terms of the blob picture. If we assume that the blob is sufficiently concentrated so that only action-producing collisions occur, the action within the blob is conserved by collisions. Integration of the Boltzmann equation over the volume of k space occupied by the blob then gives (after integration with respect to x)

$$\int_{\text{blob}} \mathrm{d}^3k\, n_k [u + v_x(k)] = \text{const.} = 0\,, \tag{37}$$

where the integration constant has again been set equal to zero under the assumption that there is no flux of waves ahead of the shock. The mean group velocity of the blob is therefore such that in shock fixed coordinates there is no net flow of action.

Thus far we have considered only relations from which the collision integral vanishes and, therefore, have not obtained a relation which gives any information about the shock thickness. Such a relation can be obtained by considering the conservation of momentum for the blob. Multiplying the Boltzmann equation by k_x and integrating over the volume of k space occupied by the blob, one obtains

$$\frac{\mathrm{d}(P_{xx} + u M_{\mathrm{b}x})}{\mathrm{d}x} + M_{\mathrm{b}x} \frac{\mathrm{d}u}{\mathrm{d}x} = \left(\frac{\partial M_{\mathrm{b}x}}{\partial t}\right)_{\text{coll}}, \tag{38}$$

where the subscript b indicates that the quantity is referred to the blob only and not the entire wave distribution. The first term in this equation may be interpreted as the gradient of a pressure associated with the width of the blob. For small blob size this pressure may be estimated by the first terms in a Taylor expansion of k_x and $v_x(k)$ about the center of the blob. Coupled with Eq. (37) one obtains

$$P_{\mathrm{b}xx} + u M_{\mathrm{b}x} \approx \left(\frac{\partial v_x(k)}{\partial k_x}\right)_c M_{\mathrm{b}x} \frac{(\Delta k_x)^2}{k_{xc}}, \tag{39}$$

where the subscript c indicates that the quantity is to be evaluated at the center of the blob and Δk_x is the width of the blob.

The second term may be interpreted as the force on the blob due to the velocity gradient. The collision term is the loss of momentum from the blob due to the waves which are produced at the low frequencies. A rough estimate of this drag force may be obtained by saying that in one mean free time a wave is moved in k space by roughly the dimension of the blob. It therefore loses a fraction $\Delta k_x/k_{xc}$ of its momentum.

$$\left(\frac{\partial M_x}{\partial t}\right)_{\text{coll}} \approx -\frac{M_x}{\tau} \frac{\Delta k_x}{k_{xc}}. \tag{40}$$

Substituting Eqs. (39) and (40) into Eq. (38) then gives a relation between the width of the blob and the velocity gradient. A further simplification of this relation can be obtained if one assumes that, since the whole process is caused by the velocity gradient, the pressure gradient term is either smaller than or at best comparable to the body force term. By dropping this term one obtains

$$\frac{\mathrm{d}u}{\mathrm{d}x} \approx -\frac{1}{\tau} \frac{\Delta k_x}{k_{xc}}. \tag{41}$$

Since, at present, we have no method for determining the width of the blob, we might use the above relation to give a very rough estimate of the blob width in terms of the measured shock thickness. Assuming a linear velocity profile

$$\frac{\Delta k_x}{k_{xc}} \approx \left(1 - \frac{u_2}{u_1}\right) \frac{u_1 \tau}{L}, \tag{42}$$

where u_2 is the velocity behind the shock. Since $u_1\tau$ is roughly the mean free path defined in the earlier paper and since agreement with experiment was found under the assumption that the shock was two mean free paths thick, this relation gives $\Delta k_x/k_{xc} \approx 1/4$ at the center of the shock. (u_2/u_1 was taken as 0.5 corresponding to a Mach number 2 shock.) This result indicates that the blob picture is not inconsistent with the measured thicknesses.

Although we have not succeeded in deriving a shock thickness, we have obtained some relations between various quantities in the shock. In order to complete the picture one would require a determination of the blob size. This presumably requires a more detailed look at the interactions within the blob.

3.3.3. *Speculation on frequency spectrum*

Some characteristic features of the frequency spectrum which one might expect to observe can be given on the basis of the picture which was developed above. The existence of the blob implies a peak in the frequency spectrum corresponding to waves which are stationary in the shock. Since the blob thickness is probably small at the front of the shock, one would expect to find the most sharply defined frequency at the front. The magnitude of frequency depends upon where on the constant $v_x(k)$ line the blob is sitting. A possible criterion for this position is to choose the minimum frequency point. This is suggested by the fact that collisions in the blob produce low frequency waves from higher frequency ones. For the front of the shock, the point based on this criterion and the approximate dispersion relation, Eq. (9), is given by $k_x/k_z = \sqrt{2}$ and $\omega/\omega_{i1} = (3\sqrt{3}/2)\, M_A^2$, where ω_{i1} is the ion cyclotron frequency ahead of the shock and M_A is the Alfvén Mach number. The

width of the frequency spectrum would increase as one moves toward the rear of the shock.

At the back of the shock wave one would expect that the wave distribution becomes almost symmetric since there is no longer a flow gradient to drive the asymmetry. The waves would then rapidly go to higher frequencies where they would be damped. One would, therefore, not expect the high frequency waves which correspond to the blob in the shock front to persist for many shock thicknesses behind the shock.

There is, however, a wave mode which might be expected to persist for a longer time. As was mentioned previously, the slower of the two magnetohydrodynamic wave modes has a dispersion relation such that three wave collisions within this mode cannot occur and collisions among these waves only occur in higher order. This suggests that they would dissipate themselves more slowly. Since such waves are produced by the higher frequency waves in the shock front, we might look for the persistence of these waves some distance behind the shock front. These waves are restricted to frequencies below the ion cyclotron frequency. The idea that the low frequency waves might persist was suggested to us by satellite observations [34] in the outer regions of the earth's magnetic field. These observations show strong magnetic fluctuations at about one-third the ion cyclotron frequency and exist over a region of several earth radii.

4. Concluding remarks

1. A magnetic annular shock tube, "Mast", has been developed to the point where it produces shocks with speeds ranging up to 50 cm/μs. The shock waves produced are identified in the following ways:

(a) The light intensity behind the shock front agrees with the predicted density behind the shock.

(b) The measured shock velocity agrees with the measured magnetic drive field as is required by conservation of momentum.

(c) The magnetic field compression across the shock wave has been measured, and for all cases where the expected gas temperature behind the shock is high enough so that constancy of B_θ/ϱ is expected, this constancy is observed. For lower shock velocities where lower temperatures are reached behind the shock, smaller field rises are obtained as expected.

2. A preliminary indication has been obtained that only a small fraction of the plasma energy (about 10%) is lost to the walls. At the higher shock velocities (above 26 cm/μs) the kinetic energy of the incoming atoms (or ions) is large enough so that the mean free paths for momentum exchange by particle collision are larger than the apparatus dimensions and the ion cyclotron radius. The existence of a shock wave under these conditions is evidence that processes other than a collisional shock are responsible; i.e., that a collision-free shock has been produced experimentally.

3. The thickness of the collision-free shock waves has been measured by the rise time of the light emission in the visible and ultraviolet and by the rise time in magnetic field as measured with search coils. These thickness are all in agreement and the dependence of this thickness on initial density and Alfvén Mach number has been measured. These measured shock thickneses are smaller than the channel dimensions for small Alfvén Mach numbers and larger than the channel dimensions for larger Alfvén Mach numbers. Further, the hot plasma created by these shock waves is observed to persist for times large (up to 50 times) compared to the time of passage through the shock. These measurements are in agreement with our previously published theory when the characteristic ion cyclotron radius is smaller than the mean free path in the shocked plasma.

4. A somewhat more detailed description of the wave interactions which are responsible for dissipation in a shock wave in a collision-free plasma has been obtained. The rate of collisions between waves has been calculated on the basis of a second order perturbation theory. This rate is in order of magnitude agreement with the previous estimate of the mean free path. An equation, similar to the Boltzmann equation, which relates the changes in the wave distribution function caused by the flow field to the changes caused by the collisions, has been derived.

5. The fact that the existence of the waves represents an extreme departure from equilibrium coupled with the selection rules for the collision term has led to the hypothesis that the wave distribution should be concentrated in a region of k space away from the origin. Based on this hypothesis it is possible to give a partial qualitative description of the wave distribution in the shock and to suggest some characteristic features of the frequency spectrum of waves in and behind the shock which might be easily observable.

Acknowledgment

This work has been supported jointly by the Air Force Office of Scientific Research, Office of Aerospace Research, United States Air Force under Contract AF 49 (638)-61 and the Department of the Navy, Office of Naval Research under Contract Nonr-2524(00).

References

[1] KANTROWITZ, A. R., PATRICK, R. M., PETSCHEK, H. E., Proceedings of Fourth International Conference on Ionization Phenomena in Gases, Uppsala, Sweden (North-Holland Pub., Amsterdam, 1959) p. 1086.

[2] FISHMAN, F. J., KANTROWITZ, A. R., PETSCHEK, H. E., *Rev. Mod. Phys.* **32** (1960) 959.

[3] ROSENBLUTH, M. N., Plasma Dynamics, F. H. Clauser, editor (Addison-Wesley Publ. Co., Reading Mass., 1960) p. 29.

[4] PATRICK, R. M., *Phys. Fluids* **2** (1959) 589.

[5] PATRICK, R. M., *Phys. Fluids* **3** (1960) 323.

[6] KEMP, N. H., PETSCHEK, H. E., *Phys. Fluids* **2** (1959) 599.

[7] MARSHALL, J., "Hydromagnetic Plasma Gun." Fourth Lockheed Symposium on Magnetohydrodynamics, Palo Alto, Calif., Dec. 2, 1959. (Stanford Univ. Press, Stanford, Calif. (1960) 60—72).

[8] ALFVÉN, H., LINDBERG, L., MITLID, P., *J. Nucl. Energy, Part C*, **1** (1960) 116.

[9] PATRICK, R. M., *Bull. Am. Phys. Soc.* **3** (January, 1958) 39.
[10] KECK, J. C., FISHMAN, F., PETSCHEK, H. E., *Bull. Am. Phys. Soc.* **6** (April, 1961) 278.
[11] WALKER, W. C., WAINFAN, N., WEISSLER, G. L., *J. Appl. Phys.* **26** (1955) 1366.
[12] JANES, G. S. and KORITZ, H. E., *J. Appl. Phys.* **31** (1960) 525.
[13] KARZAS, W. J., LATTER, R., "Hydrogenic Bound-Free Gaunt Factors." Rand Corporation Research Memorandum RM-2091-AEC (January, 1958).
[14] PATRICK, R. M., *Bull. Am. Phys. Soc.* **6** (June, 1961) 380.
[15] CAMAC, M., FEINBERG, R., *Bull. Am. Phys. Soc.* **6** (June, 1961) 380.
[16] ROSE, P. H., STARK, W. I., *J. Aero. Sci.* **25** (1958) 86.
[17] FAY, J. A., RIDDELL, F. R., *J. Aero. Sci.* **25** (1958) 73.
[18] GRIEM, HANS R., "Plasma Spectroscopy." Paper presented at the Fifth International Conference on Ionization Phenomena in Gases, Munich. Germany (North-Holland Pub., 1961).
[19] BETHE, H. A., SALPETER, E. E., "Quantum Mechanics of One- and Two-Electron Systems." *Handbuch der Physik*, XXXV/1, Springer-Verlag, Berlin (1957) 88—436.
[20] PEIERLS, R. E., *The Quantum Theory of Solids*, (Oxford at the Clarendon Press, London, 1955) 45—50.
[21] PETSCHEK, H. E., *Rev. Mod. Phys.* **30** (1958) 966.
[22] KAHN, F. D., *J. Fluid Mech.* **2** (1957) 601.
[23] PARKER, E. N., *Astrophys. J.* **129** (1959) 217.
[24] ROSENBLUTH, M. N., LONGMIRE, C. L., United States Atomic Energy Commission Report TID-7520 (1956).
[25] AUER, P. L., HURWITZ, H., JR., KILB, R. W., "Large Amplitude Magnetic Compression of a Collision-Free Plasma, II." (G.E. Report 61-RL-2758 E, June, 1961).
[26] GARDNER, C. S., GOERTZEL, H., GRAD, H., MORAWETZ, C. S., ROSE, M. J., RUBIN, H., Proc. of the Second UN International Conference on the Peaceful Uses of Atomic Energy, **31** (1958) 230.
[27] MORAWETZ, C. S., United States Atomic Energy Commission Report NYO-2885 (Institute of Math. Sciences, NYU, March, 1960).
[28] DAVIS, L., LÜST, R., SCHLÜTER, A., *Z. Naturforsch.* **13a** (1958) 916.
[29] STURROCK, P. A., Nonlinear Effects in Electron Plasmas. M. L. Report No. 654. Stanford U. (October, 1959).
[30] STURROCK, P. A., *Proc. Roy. Soc.* **A 242** (1957) 277.
[31] LITVAK, M. M., "A Transport Equation for Magnetohydrodynamic Waves." Avco-Everett Research Laboratory Research Report 92 (August, 1960).
[32] PEIERLS, R. E., *op. cit.* 43—44.
[33] PETSCHEK, H. E., "Collision-Free Plasmas." *Nuovo Cimento*, to be published.
[34] SONNET, C. P., SMITH, E. J., SIMS, A. R., "Surveys of the Distant Geomagnetic Field. Pioneer I, Explorer VI." *Space Research*, Proc. of the First International Space Science Symposium, Nice, H. K. Bijl, editor (Interscience, New York, 1960) 921.

FORMULATION LAGRANGIENNE DES ÉQUATIONS DE LA MAGNÉTO-HYDRODYNAMIQUE APPLIQUÉE À L'ÉTUDE DE LA STABILITÉ*

M. COTSAFTIS

GROUPE DE RECHERCHES DE L'ASSOCIATION EURATOM-CEA SUR LA FUSION

FONTENAY-AUX-ROSES (SEINE) FRANCE

Dans les approximations magnétohydrodynamiques classique et Chew-Goldberger-Low, toutes les quantités — pression, densité et champ magnétique — sont reliées au mouvement du fluide par des équations du type $dA/dt = 0$. En représentation de Lagrange, celles-ci peuvent être intégrées, du moins formellement. On utilise cette circonstance pour former un Lagrangien dont on déduit par variation l'équation du mouvement du fluide, seule; les autres quantités sont alors connues par les intégrales des équations $dA/dt = 0$.

A partir de ce Lagrangien, on peut obtenir très simplement les équations des petits mouvements, dans le cas le plus général, autour d'un mouvement quelconque. On se limite à l'approximation linéaire. Il est remarquable que ces équations soient formellement identiques à celles données par Hain, Lüst et Schlüter pour le cas particulier des petits mouvements autour d'un état d'équilibre statique; les quantités p, $\mathbf{B}$, ϱ, $\mathbf{j}$ sont liées par des relations différentes.

Pour la stabilité, on retrouve très simplement le principe d'énergie de Bernstein et autres dans le cas particulier de l'équilibre statique et sa généralisation au cas des faibles vitesses, ainsi que les conditions suffisantes de Frieman et Rottenberg dans le cas de vitesses stationnaires quelconques. On étudie une classe particulière de mouvements pour lesquels il existe un principe d'énergie nécessaire et suffisant.

1. Introduction

Ayant en vue l'étude de la stabilité dans les approximations magnétohydrodynamiques classique et Chew-Goldberger-Low (C.G.L.), on cherche un lagrangien dont se déduit l'équation du mouvement du plasma. Cela suffit, car on sait que l'on peut obtenir l'équation de la perturbation du mouvement par variation du lagrangien développé en puissance de la perturbation. Avec les approximations précédentes, cela est possible, car toutes les autres quantités s'expriment en fonction du mouvement dans la représentation de Lagrange. Il résulte du formalisme des propriétés d'hermiticité des opérateurs intervenant dans l'équation des perturbations.

Dans la première partie, on établit un lagrangien dont se déduit l'équation du mouvement du plasma, entouré ou non d'un champ magnétique, dans un récipient à parois fixes et parfaitement conductrices.

Dans la deuxième partie, on obtient l'équation des perturbations autour d'un mouvement quelconque.

On étudie la stabilité dans la troisième partie. En se limitant au cas stationnaire, on retrouve les résultats de FRIEMAN et ROTTENBERG [1]. Il est possible d'écrire un principe nécessaire et suffisant d'énergie dans le cas où deux opérateurs commutent, ce qui redonne le principe de Bernstein et autres quand l'un d'eux est nul.

2. Le lagrangien du mouvement

Le mouvement de fluide sera défini par $x = x\,(a, t)$ en variables de Lagrange [$x\,(a, 0) = a$]. On utilisera le jacobien de la transformation $a \to x$:

$$D = \frac{d\,(x)}{d\,(a)} = \det \frac{\partial x_i}{\partial a_k}. \tag{1}$$

Avec les approximations magnétohydrodynamiques classique et C.G.L., le champ magnétique est gelé dans le fluide, aussi est-il parfaitement connu quand celui-ci l'est. En effet, en variable de Lagrange, les équations:

$$\frac{\partial \varrho}{\partial t} + \operatorname{div} \varrho \mathbf{v} = 0\,, \quad \frac{\mathrm{d}}{\mathrm{d}t}\left(\frac{p}{\varrho^\gamma}\right) = 0\,, \quad \frac{\partial \mathbf{B}}{\partial t} = \operatorname{rot}(\mathbf{v} \times \mathbf{B}) \tag{2}$$

s'intégrent en:

$$\varrho = \varrho_0 \frac{1}{D}\,, \quad p = p_0 \frac{1}{D^\gamma}\,, \quad \mathbf{B} = (\mathbf{B}^0 \cdot \nabla^0)\, x\, \frac{1}{D}\,, \tag{3}$$

$$[\mathbf{B}^0 = \mathbf{B}\,(a, t = 0)].$$

La deuxième équation est remplacée par:

$$\frac{\mathrm{d}}{\mathrm{d}t}\left[\frac{p_\parallel |\mathbf{B}|^2}{\varrho^3}\right] = 0\,, \quad \frac{\mathrm{d}}{\mathrm{d}t}\left[\frac{p_\perp}{\varrho\,|\mathbf{B}|}\right] = 0\,, \tag{4}$$

dans l'approximation C.G.L., et s'intègre immédiatement:

$$p_\parallel = \frac{p_\parallel{}^0}{D} \frac{|\mathbf{B}^0|^2}{|(\mathbf{B}^0 \cdot \nabla^0)\, x|^2}\,, \quad p_\perp = \frac{p_\perp{}^0}{D^2} \frac{|(\mathbf{B}^0 \cdot \nabla^0)\, x|}{|\mathbf{B}^0|}\,. \tag{5}$$

Rappelons rapidement qu'étant donné un lagrangien $\mathcal{L}\,(\varphi, \varphi_\mu, x)$, où $\mu = 1, 2, 3, 4$, x à 4 dimensions, $\varphi = \varphi\,(x)$ étant un champ, la variation de $I = \int \mathcal{L}\,\mathrm{d}^4x$ donne:

$$\delta I = \int_\Omega \left[\partial\mu \frac{\partial \mathcal{L}}{\partial \varphi_\mu} - \frac{\partial \mathcal{L}}{\partial \varphi}\right] \delta\varphi\, \mathrm{d}^4x + \int_\Sigma n_\mu \frac{\partial \mathcal{L}}{\partial \varphi_\mu}\, \delta\varphi\,(\Sigma)\, \mathrm{d}o, \tag{6}$$

d'où $\delta I = 0$ quand

— les équations de Lagrange

$$\partial\mu \frac{\partial \mathcal{L}}{\partial \varphi_\mu} - \frac{\partial \mathcal{L}}{\partial \varphi} = 0 \tag{7}$$

sont vérifiées dans tout le volume;

* Mémoire CN-10/88, présenté par M. Cotsaftis. Les traductions du résumé se trouvent en fin de volume.

— les conditions de surface sont vérifiées:

$$n_\mu \frac{\partial \mathcal{L}}{\partial \varphi_\mu} \delta\varphi(\Sigma) = 0. \tag{8}$$

On pose souvent $\delta\varphi(\Sigma)=0$ sur la surface, mais dans le cas plus général où il y a plusieurs milieux dans chacun desquels il y a une fonction φ il faut préciser les relations entre les $\delta\varphi(\Sigma)$ de deux milieux mitoyens pour avoir un problème entièrement déterminé.

Dans le cas où $\delta x=0$ sur la surface, cherchons le lagrangien pour le mouvement.

Quand $\mathbf{B}=0$ d'abord, on vérifie facilement que

$$\mathcal{L} = \frac{1}{2}\varrho_0\left(\frac{\partial x}{\partial t}\right)^2 - \frac{p_0}{\gamma-1} D^{1-\gamma}, \tag{9}$$

où $D=\det(\partial x_i/\partial a_k)$ donne par variation sur $x(a,t)$ l'équation $\varrho\,\mathrm{d}\mathbf{v}/\mathrm{d}t = -\operatorname{grad} p$ écrite en variables d'Euler.

On a d'ailleurs

$$L=\int \mathcal{L}\,\mathrm{d}^3 a = \int\left(\varrho\frac{v^2}{2} - \frac{p}{\gamma-1}\right)\mathrm{d}^3 x, \tag{10}$$

en variables d'Euler. Quand il y a un champ magnétique, l'équation du mouvement,

$$\varrho\frac{\mathrm{d}\mathbf{v}}{\mathrm{d}t} = -\operatorname{grad} p + (\operatorname{rot}\mathbf{B})\times\mathbf{B}, \tag{11}$$

s'obtient par variation sur $x(a,t)$ du lagrangien:

$$L=\int\left(\varrho\frac{v^2}{2} - \frac{p}{\gamma-1} - \frac{B^2}{2}\right)\mathrm{d}^3 x, \tag{12}$$

écrit en variables d'Euler également. Avec l'approximation C.G.L., on trouve de même le lagrangien:

$$L=\int\left(\varrho\frac{v^2}{2} - p_\perp - \frac{p_\parallel}{2} - \frac{B^2}{2}\right)\mathrm{d}^3 x. \tag{13}$$

Suivant le même processus, il faudra réécrire celui-ci en variables de Lagrange en utilisant les expressions précédentes de $p_\perp$, $p_\parallel$, B et faire la variation sur $x(a,t)$ pour obtenir:

$$\varrho\frac{\mathrm{d}\mathbf{v}}{\mathrm{d}t} = -\operatorname{div}\mathsf{p} + (\operatorname{rot}\mathbf{B})\times\mathbf{B}. \tag{14}$$

On peut introduire également un potentiel extérieur φ, ce qui revient à rajouter aux lagrangiens précédents le terme $-\int \varrho\varphi\,\mathrm{d}^3x$.

A partir des lagrangiens, on peut former des hamiltoniens et rechercher des intégrales premières d'énergie.

Les lagrangiens écrits précédemment permettent également de traiter le cas plus général d'un plasma entouré de champ magnétique dans une enceinte parfaitement conductrice.

En effet, soit:

$$\mathcal{L}_\mathrm{p} = \varrho\frac{v^2}{2} - \frac{p}{\gamma-1} - \frac{B^2}{2}, \tag{15}$$

ou le lagrangien C.G.L., pour le plasma et

$$\mathcal{L}_\mathrm{v} = -\frac{\hat{B}^2}{2}, \tag{16}$$

le lagrangien pour le vide.

Il est facile, en posant $\hat{\mathbf{B}}=\operatorname{rot}\mathbf{A}_0$, de déduire par variation de $\mathcal{L}_\mathrm{v}$ sur $\mathbf{A}_0$ l'équation:

$$\operatorname{rot}(\operatorname{rot}\mathbf{A}_0) = 0. \tag{17}$$

Dans le vide, on a intégré les autres équations de Maxwell. Il est possible de choisir la jauge de manière à ce que:

$$\hat{\mathbf{E}} = -\frac{\partial \mathbf{A}_0}{\partial t}, \qquad \hat{\mathbf{B}} = \operatorname{rot}\mathbf{A}_0, \tag{18}$$

avec $\operatorname{div}\mathbf{A}_0 = 0$.

Lorsqu'on fait la variation sur $x(a,t)$ dans le plasma, sur $\mathbf{A}_0(x,t)$ dans le vide du lagrangien total:

$$L_t = \int \mathcal{L}_t \mathrm{d}^3 x = \int(\mathcal{L}_\mathrm{p} + \mathcal{L}_\mathrm{v})\,\mathrm{d}^3 x = L_\mathrm{p} + L_\mathrm{v}, \tag{19}$$

il y a en plus le terme de surface:

$$\int_\Sigma \left\{n_k\,[T_{ik} + p_{ik}]\,\delta x_i + \frac{\hat{\mathbf{B}}}{2}\cdot \mathbf{n}\times\delta\mathbf{A}_0\right\}\mathrm{d}\sigma \tag{20}$$

où

$$T_{ik} = \frac{1}{2}B^2\delta_{ik} - B_i B_k.$$

On posera la relation, que nous justifierons plus loin:

$$\mathbf{n}\times\delta\mathbf{A}_0 = -(\mathbf{n}\cdot\delta\mathbf{x})\,\hat{\mathbf{B}} \tag{21}$$

qui, avec $\mathbf{n}\cdot\mathbf{B}=0$, donne la contrainte:

$$\left\langle p + \frac{B^2}{2}\right\rangle = 0 \quad \text{ou} \quad \left\langle p_\perp + \frac{B^2}{2}\right\rangle = 0. \tag{22}$$

Dans ce cas sont données non seulement les équations dans le vide et le plasma de toutes les quantités, mais encore les conditions de surface qui en découlent. En particulier:

$$\begin{aligned}
&\frac{\partial \mathbf{B}}{\partial t} = -\operatorname{rot}\mathbf{E} = \operatorname{rot}(\mathbf{v}\times\mathbf{B}), && \text{dans le plasma}\\
&\frac{\partial \hat{\mathbf{B}}}{\partial t} = -\operatorname{rot}\hat{\mathbf{E}}, && \text{dans le vide}\\
&\mathbf{n}\times\langle\mathbf{E}\rangle = (\mathbf{n}\cdot\mathbf{v})\langle\mathbf{B}\rangle, && \text{à la surface.}
\end{aligned} \tag{23}$$

3. Les équations de perturbation

A partir d'un mouvement quelconque, défini par:

$$\mathbf{x}_0 = \mathbf{x}_0(a,t), \qquad \mathbf{A}_0 = \mathbf{A}_0(x,t), \tag{24}$$

on peut définir les perturbations:

$$\mathbf{x} = \mathbf{x}_0 + \boldsymbol{\xi}, \qquad \mathfrak{A} = \mathbf{A}_0 + \mathbf{A} \tag{25}$$

et rechercher les équations auxquelles obéissent $\boldsymbol{\xi}$ et $\mathbf{A}$.

Pour cela, il suffit de développer les lagrangiens précédents en puissance de ces perturbations et écrire les équations de Lagrange sur $\boldsymbol{\xi}$ et $\mathbf{A}$. On utilisera la représentation d'Euler $\xi = \xi(x,t)$, ce qui simplifie les calculs.

A l'ordre zéro, on retrouve les équations non perturbées, et il en est évidemment de même à l'ordre un. C'est sur les termes du deuxième ordre qu'on aura, par variation, les termes linéaires des équations des perturbations. Les autres termes s'obtiennent en développant plus loin.

Par exemple, prenons:

$$L_\mathrm{p}^0 = \int\left(\varrho\frac{v^2}{2} - \frac{p}{\gamma-1} - \frac{B^2}{2}\right)\mathrm{d}^3 x. \tag{26}$$

On a:

$$L_p = L_p^0 + L_p^1 + L_p^2 \tag{27}$$

avec:

$$L_p^1 = \varrho \frac{dx}{dt}\frac{d\xi}{dt} + p\,\mathrm{div}\,\xi - T_{ik}\frac{\partial \xi_i}{\partial x_k}$$

$$L_p^2 = \frac{1}{2}\varrho\left(\frac{d\xi}{dt}\right)^2 + \frac{1}{2}\left(p+\frac{B^2}{2}\right)\left(\frac{\partial \xi_i}{\partial x_i}\frac{\partial \xi_k}{\partial x_k} - \frac{\partial \xi_i}{\partial x_k}\frac{\partial \xi_k}{\partial x_i}\right) - \frac{\gamma p}{2}(\mathrm{div}\,\xi)^2 + B_i B_k \frac{\partial \xi_i}{\partial x_i}\frac{\partial \xi_i}{\partial x_k} - \frac{B_j B_k}{2}\frac{\partial \xi_i}{\partial x_j}\frac{\partial \xi_i}{\partial x_k} - \frac{B^2}{2}(\mathrm{div}\,\xi)^2 . \tag{28}$$

L'équation de Lagrange sur L_p^1 donne l'équation non perturbée, en utilisant l'équation de continuité. Sur L_p^2, elle donne:

$$\varrho \frac{d^2\xi}{dt^2} = \mathbf{F}^{(0)}(\xi) \tag{29}$$

avec:

$$F_i^{(0)}(\xi) = \frac{\partial}{\partial x_j}\left[\left(p+\frac{B^2}{2}\right)\frac{\partial \xi_j}{\partial x_i}\right] + \frac{\partial}{\partial x_k}\left\{[(\gamma-1)p\delta_{ik} + T_{ik}]\frac{\partial \xi_j}{\partial x_j}\right\} - \frac{\partial}{\partial x_i}\left[B_j B_k \frac{\partial \xi_k}{\partial x_j}\right] + \frac{\partial}{\partial x_k}\left[B_k B_j \frac{\partial \xi_i}{\partial x_j}\right], \tag{30}$$

expression qui se trouve être formellement identique à celle donnée par HAIN, LÜST, SCHLÜTER dans le cas statique [2]. Dans le cas présent, ϱ, p, B, v sont liés par les équations du mouvement. Rappelons que:

$$\frac{d}{dt} = \frac{\partial}{\partial t} + \mathbf{v}\cdot\nabla . \tag{31}$$

On trouvera de même par variation sur le lagrangien C.G.L. l'équation des petits mouvements dans ce cas. Elle est très lourde.

Si on avait fait la variation de l'équation du mouvement non perturbé, on aurait trouvé pour ξ une équation différant de l'équation précédente par un terme égal à l'équation non perturbée multipliée par une dérivée convenable de ξ. C'est sous cette forme là qu'est donnée l'équation pour ξ dans le cas scalaire par FRIEMAN et ROTTENBERG par exemple [1].

A partir de L_v^2, on montrera sans difficulté que $\mathbf{A}$ satisfait à l'équation:

$$\mathrm{rot}\,(\mathrm{rot}\,\mathbf{A}) = 0 . \tag{32}$$

La contrainte entre $\boldsymbol{\xi}$ et $\mathbf{A}$ s'obtient en regroupant les termes de surface et en posant entre $\delta\boldsymbol{\xi}$ et $\delta\mathbf{A}$ la relation:

$$\mathbf{n}\times\delta\mathbf{A} = -(\mathbf{n}\cdot\delta\boldsymbol{\xi})\,\hat{\mathbf{B}}; \tag{33}$$

tenant compte de la contrainte non perturbée:

$$\left\langle p + \frac{B^2}{2}\right\rangle = 0 ,$$

on trouve:

$$-\gamma p\,\mathrm{div}\,\boldsymbol{\xi} + \mathbf{B}\cdot[\mathbf{Q} + (\boldsymbol{\xi}\cdot\nabla)\mathbf{B}] = \hat{\mathbf{B}}\cdot[\mathrm{rot}\,\mathbf{A} + (\boldsymbol{\xi}\cdot\nabla)\hat{\mathbf{B}}] \tag{34}$$

où

$$\mathbf{Q} = \mathrm{rot}\,(\boldsymbol{\xi}\times\mathbf{B}).$$

Pour cela, il faut faire attention que, sur la surface, la partie non perturbée du potentiel vecteur $\mathbf{A}_0$ est une fonction de $\mathbf{x} = \mathbf{x}_0 + \boldsymbol{\xi}$. Il revient au même, bien entendu, de développer la contrainte non perturbée au premier ordre en puissance de $\boldsymbol{\xi}$ et $\mathbf{A}$. Il existe entre $\boldsymbol{\xi}$ et $\mathbf{A}$ une autre relation. En effet, la solution des équations de Maxwell dans le vide doit être compatible avec la loi d'Ohm du conducteur parfait $\mathbf{E} + \mathbf{v}\times\mathbf{B} = 0$ dans le plasma [3]. La composante de $\mathbf{E} + \mathbf{v}\times\mathbf{B}$ parallèle à la surface du plasma étant continue à la traversée de celle-ci, il en résulte que cette composante est nulle dans le vide au voisinage de la surface, soit:

$$(\hat{\mathbf{E}} + \mathbf{v}\times\hat{\mathbf{B}})_{\parallel} = 0 . \tag{35}$$

Si $\mathbf{A}$ est la variation sur place du potentiel vecteur et $\boldsymbol{\xi}$ le déplacement de la surface pendant le temps dt, on a:

$$\mathbf{A} = -\hat{\mathbf{E}}\,dt \quad \text{et} \quad \boldsymbol{\xi} = \mathbf{v}\,dt; \tag{36}$$

par suite $\mathbf{A}$ et $\boldsymbol{\xi}$ sont liés par la relation:

$$(-\mathbf{A} + \boldsymbol{\xi}\times\mathbf{B})_{\parallel} = 0 \quad \text{soit} \quad \mathbf{n}\times\mathbf{A} = -(\mathbf{n}\cdot\boldsymbol{\xi})\,\hat{\mathbf{B}} . \tag{37}$$

C'est cette même relation qui a été également choisie entre les variations des fonctions $\mathbf{x}$ et $\mathbf{A}_0$, et $\boldsymbol{\xi}$ et $\mathbf{A}$ pour obtenir les équations du mouvement correctes à partir du lagrangien. Sa justification tient dans le fait que, dans ce formalisme, cette relation est donnée dès que sont données les équations de Maxwell et la loi d'Ohm.

L'hermiticité de $\mathbf{F}^{(0)}$ est alors assurée par les conditions de surface. En effet, de façon générale si:

$$L_p = \frac{1}{2}\varrho\left(\frac{d\xi}{dt}\right)^2 - V^{(0)},$$

on a:

$$\varrho\frac{d^2\xi}{dt^2} = \mathbf{F}^{(0)}(\xi) \tag{38}$$

avec:

$$\mathbf{F}^{(0)}(\xi) = \frac{\partial}{\partial x}\cdot\frac{\partial V^{(0)}}{\partial\left(\frac{\partial \xi}{\partial x}\right)} . \tag{39}$$

Le terme de surface s'écrit, pour la partie plasma:

$$\int_\Sigma \mathbf{n}\cdot\frac{\partial V^{(0)}}{\partial\left(\frac{\partial \xi}{\partial x}\right)}\cdot\delta\boldsymbol{\xi}\,d\sigma . \tag{40}$$

Si on forme maintenant le produit:

$$\int_v \boldsymbol{\eta}^*\cdot\mathbf{F}^{(0)}(\xi)\,d\tau = \int_v \boldsymbol{\eta}^*\cdot\frac{\partial}{\partial x}\frac{\partial V^{(0)}}{\partial\left(\frac{\partial \xi}{\partial x}\right)}\,d\tau = \int_\Sigma \mathbf{n}\cdot\frac{\partial V^{(0)}}{\partial\left(\frac{\partial \xi}{\partial x}\right)}\boldsymbol{\eta}^* d\sigma - \int_v \frac{\partial \boldsymbol{\eta}^*}{\partial x}\cdot\frac{\partial V^{(0)}}{\partial\left(\frac{\partial \xi}{\partial x}\right)}\,d\tau, \tag{41}$$

la partie de volume est une fonction symétrique en $\partial\boldsymbol{\eta}/\partial x$ et $\partial\boldsymbol{\xi}/\partial x$ du fait que $V^{(0)}$ est une fonction quadratique homogène, et l'intégrale de surface est la même que le terme de surface de la variation du lagrangien à condition de poser $\boldsymbol{\eta}^* = \delta\boldsymbol{\xi}$.

Si maintenant on rajoute les termes de vide L_v et si on forme le terme de surface correspondant, on trouvera que le terme de surface total est identique comme écriture à celui qui donne la contrainte entre $\boldsymbol{\xi}$ et $\mathbf{A}$ à condition de remplacer $\delta\boldsymbol{\xi}$ et $\delta\mathbf{A}$ par $\boldsymbol{\eta}^*$ et $\mathbf{A}_0{}^*$.

En leur imposant la relation:

$$\mathbf{n}\times\mathbf{A}_0^*=-(\mathbf{n}\cdot\boldsymbol{\eta}^*)\,\hat{\mathbf{B}} \tag{42}$$

qu'ils doivent vérifier pour être considérés comme des déplacements physiques, on retrouvera la contrainte entre $\boldsymbol{\xi}$ et $\mathbf{A}$; donc le terme de surface total sera nul, et $\mathbf{F}^{(0)}$ sera hermitique. Ceci montre bien qu'il faut toujours considérer les couples $(\mathbf{A}, \boldsymbol{\xi})$, $(\mathbf{A}_0, \boldsymbol{\eta})$ dans ce formalisme.

4. La stabilité dans le cas stationnaire

1) Toutes les quantités ne dépendent pas explicitement du temps. Il est alors possible de chercher pour $\boldsymbol{\xi}$ $(\mathbf{x}, t)$ une solution du type $\boldsymbol{\xi}=\exp(\mathrm{i}\,\omega t)\cdot\boldsymbol{\eta}(\mathbf{x})$. Par exemple, en pression scalaire, on a pour $\boldsymbol{\eta}(\mathbf{x})$ l'équation:

$$-\omega^2\varrho\,\eta+2\mathrm{i}\,\omega\varrho\,\mathbf{v}\cdot\nabla\eta-F(\eta)=0 \tag{43}$$

où:

$$F=F^{(0)}-\varrho\,(\mathbf{v}\cdot\nabla)\,\mathbf{v}\cdot\nabla\,.$$

Multipliant par η^* et intégrant:

$$-\omega^2\int\varrho\,|\eta|^2+2\,\omega\int\mathrm{i}\varrho\,\eta^*(\mathbf{v}\cdot\nabla)\,\eta-\int\eta^*\cdot F(\eta)=0 \tag{44}$$

et on retrouve les deux conditions suffisantes déjà données par Frieman et Rottenberg [1]. L'hermiticité de l'opérateur $\mathrm{i}\,\varrho\,\mathbf{v}\cdot\nabla$ est évidente.

2) On peut trouver une condition nécessaire et suffisante dans le cas simple où les opérateurs: F/ϱ et $\mathrm{i}\mathbf{v}\cdot\nabla$ commutent. Dans ce cas, les modes se découplent. Il existe un système de modes propres et on peut en chercher un commun aux deux opérateurs. F étant aussi hermitique, soit:

$$\begin{aligned} F(\eta_\alpha)&=-\varrho\,\omega_\alpha^2\,\eta_\alpha\\ \mathrm{i}\varrho\,(\mathbf{v}\cdot\nabla)\,\eta_\alpha&=\varrho\,j_\alpha\,\eta_\alpha\end{aligned} \tag{45}$$

un ensemble complet orthonormé.
L'équation aux ω s'écrit:

$$(\omega_\alpha^2-\omega^2+2\,\omega\,j_\alpha)\,a_\alpha=0 \tag{46}$$

pour chaque α. D'où:

$$\omega=j_\alpha\pm\sqrt{\omega_\alpha^2+j_\alpha^2}.$$

On montre, par considération des modes, de façon analogue au cas de l'équilibre pour lequel ici $j_\alpha=0$, que la condition nécessaire et suffisante de stabilité s'écrit:

$$\omega_\alpha^2+j_\alpha^2>0 \tag{47}$$

soit revenant aux opérateurs dont j_α et ω_α^2 sont valeurs propres, l'opérateur:

$$-[F+\varrho\,(\mathbf{v}\cdot\nabla)\,\mathbf{v}\cdot\nabla]=-F^{(0)}$$

doit avoir des valeurs propres toutes positives.
La condition s'écrit donc:

$$-\int\xi^*\cdot F^{(0)}(\xi)\,\mathrm{d}\tau>0\,. \tag{48}$$

Comme par ailleurs $\mathbf{F}^{(0)}$ est identique formellement à l'expression du cas statique (voir 2), cette condition s'écrit exactement comme dans le cas statique. Seules les quantités non perturbées sont liées par des équations différentes.

Les équations de perturbation étant identiques au cas statique, nous allons transformer la quantité précédente en trois intégrales sur le volume du plasma, sa surface et le vide de façon analogue au cas statique. Nous récrivons, dans le cas scalaire, $\mathbf{F}^{(0)}$ sous la forme:

$$\begin{aligned}\mathbf{F}^{(0)}(\boldsymbol{\xi})&=\mathrm{grad}\,(\gamma p\,\mathrm{div}\,\boldsymbol{\xi}+\boldsymbol{\xi}\cdot\mathrm{grad}\,p)+\mathbf{j}\times\mathbf{Q}-\mathbf{B}\times\mathrm{rot}\,\mathbf{Q}\\&+\varrho\,(\mathbf{v}\cdot\nabla)v\,\mathrm{div}\,\boldsymbol{\xi}+(\boldsymbol{\xi}\cdot\nabla)\,(\varrho\,(\mathbf{v}\cdot\nabla)v)-\varrho\,(\mathbf{v}\cdot\nabla)\,\{(\mathbf{v}\cdot\nabla)\xi\}\end{aligned} \tag{49}$$

Nous avons, après quelques calculs:

$$\begin{aligned}\delta W&=-\frac{1}{2}\int\boldsymbol{\xi}^*\cdot\mathbf{F}^{(0)}(\boldsymbol{\xi})\,\mathrm{d}\tau\\&=\delta W_F-\frac{1}{2}\int_S\mathrm{d}\sigma(\mathbf{n}\cdot\boldsymbol{\xi}^*)[\gamma p\,\mathrm{div}\boldsymbol{\xi}+\boldsymbol{\xi}\cdot\mathrm{grad}\,p-\mathbf{B}\cdot\mathbf{Q}],\end{aligned} \tag{50}$$

et, en utilisant le développement de la contrainte au premier ordre:

$$\delta W=\delta W_V+\delta W_S+\delta W_F \tag{51}$$

$$\delta W_V=\frac{1}{2}\int_V\mathrm{d}\hat{\tau}\,|\mathrm{rot}\,\mathbf{A}|^2\,,$$

$$\delta W_S=-\frac{1}{2}\int_S\mathrm{d}\sigma|\mathbf{n}\cdot\boldsymbol{\xi}|^2\mathbf{n}\cdot\left\langle\mathrm{grad}\left(p+\frac{B^2}{2}\right)\right\rangle$$

$$\begin{aligned}\delta W_F=\frac{1}{2}\int_P\mathrm{d}\tau\,\{&|\mathbf{Q}|^2-\mathbf{j}\cdot\mathbf{Q}\times\boldsymbol{\xi}^*+\boldsymbol{\xi}\cdot\mathrm{grad}\,p\,\mathrm{div}\,\boldsymbol{\xi}^*\\&+\gamma p(\mathrm{div}\,\boldsymbol{\xi})^2-\boldsymbol{\xi}^*\cdot\varrho\,(\mathbf{v}\cdot\nabla)\,v\,\mathrm{div}\,\boldsymbol{\xi}\\&-\boldsymbol{\xi}^*\cdot(\boldsymbol{\xi}\cdot\nabla)(\varrho\,(\mathbf{v}\cdot\nabla)v)\}+\boldsymbol{\xi}^*\cdot\varrho\,(\mathbf{v}\cdot\nabla)(\mathbf{v}\cdot\nabla)\boldsymbol{\xi}.\end{aligned} \tag{52}$$

On peut essayer de transformer encore δW_F, comme dans le cas statique, mais le fait que $\mathbf{j}$ n'est plus obligatoirement tracé sur les surfaces du champ magnétique ne permet pas une écriture simple. On a:

$$\begin{aligned}\delta W_F=\frac{1}{2}\int_P\mathrm{d}\tau\,\{&|\mathbf{Q}+\xi_\perp\,\mathbf{j}\times\mathbf{n}|^2-2\,|\boldsymbol{\xi}_\perp|^2\,\mathbf{j}\times\mathbf{n}\cdot(\mathbf{B}\cdot\nabla)\,n\\&+\gamma p\,|\mathrm{div}\,\boldsymbol{\xi}|^2-\varrho\,(\mathbf{v}\cdot\nabla)\,\mathbf{v}\cdot[\boldsymbol{\xi}\,\mathrm{div}\,\boldsymbol{\xi}^*+\boldsymbol{\xi}^*\,\mathrm{div}\,\boldsymbol{\xi}]\\&-\varrho\,|(\mathbf{v}\cdot\nabla)\,\boldsymbol{\xi}|^2+\boldsymbol{\xi}^*\cdot(\boldsymbol{\xi}\cdot\nabla)\,\nabla p\}+\delta W_{F'}\,,\end{aligned} \tag{53}$$

$\delta W_{P'}$ étant une intégrale s'annulant quand $\mathbf{n}\cdot\mathbf{j}=0$, par suite des conditions aux limites. La décomposition précédente s'étend au cas général sans difficulté.

L'auteur tient à remercier Monsieur M. Trocheris et Monsieur C. Mercier de l'aide qu'ils lui ont apportée tout au long de ce travail.

A la fin de ce travail, nous avons appris que Monsieur Frieman avait obtenu des résultats analogues, et nous le remercions de discussions intéressantes.

Références

[1] Frieman, E. A., Rottenberg, A., *Rev. Mod. Phys.* **22** (1960) 898.
[2] Hain, K., Lüst, R., Schlüter, A., *Z. Naturf.* **12 a** (1957) 833.
[3] Blank, A. A., Friedrichs, K. O., Grad, H., United States Atomic Energy Commission Report NYO-6486-MH-V (1 Nov. 1957) p. 116 et suivantes.

LAGRANGIAN AND HAMILTONIAN METHODS IN MAGNETOHYDRODYNAMICS*

WILLIAM A. NEWCOMB

LAWRENCE RADIATION LABORATORY, UNIVERSITY OF CALIFORNIA

LIVERMORE, CALIFORNIA, UNITED STATES OF AMERICA

The Lagrangian and Hamiltonian formulations of classical dynamics are applied to the motion of an infinitely conductive plasma with a frozen-in magnetic field. Two separate cases are considered, one with a scalar plasma pressure and one with a tensor. The treatment of the former is based on the conventional hydromagnetic equations, and that of the latter on the modified hydromagnetic equations of Chew, Goldberger, and Low. In each case the plasma equation of motion is derived, in either the Lagrangian or the Eulerian form, from a variational principle, with the other hydromagnetic equations functioning as holonomic constraints.

The general formalism is applied, for purposes of illustration, to the solution of hydromagnetic stability problems. A simple and concise derivation of the hydromagnetic energy principle is given, and then the energy principle is adapted to steady flows of a certain special type. (It was originally designed only for static equilibria.) Specifically, it is adapted to purely azimuthal steady flows around a symmetry axis, with the frozen-in field either purely toroidal or purely poloidal; and for these it will give the necessary and sufficient condition for $m = 0$ stability (stability against small perturbations that do not destroy the symmetry). This type of steady flow is a hydromagnetic analogue of Couette flow, and the stability conditions are generalizations of Rayleigh's condition.

1. Introduction

As is well known, the nonviscous hydrodynamic equations of motion can be brought into the general scheme of classical mechanics by deriving them from a variational principle [1]. This subject has recently been treated in some detail by ECKART [2], and it has been extended by KATZ [3] to the case of a charged fluid interacting with an electromagnetic field. In Katz's treatment there is no conduction current, but only a displacement current $\partial \mathbf{E}/\partial t$, where $\mathbf{E}$ is the electric field, and a convection current $\eta \mathbf{v}$, where η is the charge density and $\mathbf{v}$ is the fluid velocity. Here we shall treat the opposite case of a perfectly-conducting fluid governed by the conventional hydromagnetic equations, a case in which the displacement and convection currents are negligible under most conditions of interest. We shall first develop the general theory from the Lagrangian and Hamiltonian points of view and then illustrate the usefulness of this approach by solving a few representative problems in hydromagnetic stability theory.

In doing stability problems one examines the behavior of small perturbations away from some specified time-independent state of the system, either a static equilibrium state or a steady flow. For static equilibria the stability criterion is already known: It is the familiar hydromagnetic energy principle [4, 5]. For steady flows, on the other hand, the energy principle is not applicable in general. In fact, we do not know of any general condition that is both necessary and sufficient, although FRIEMAN and ROTENBERG have found one that is sufficient but not necessary [6]. (It reduces to the energy principle when the flow velocity vanishes.) There are, however, special cases where the necessary and sufficient condition is given by some simple modification of the energy principle. One example of this has long been known in the field of hydrodynamics—the Couette flow of an incompressible fluid without viscosity, for which the stability condition was first given by Lord RAYLEIGH [7].

What we shall do is consider steady hydromagnetic flows around an axis of symmetry, assuming that the unperturbed magnetic field is either purely toroidal ($B_r = B_z = 0$) or purely poloidal ($B_\theta = 0$), and ask whether they are stable against those perturbations that maintain the azimuthal symmetry. As we shall see, the answer is given in each case by a modified energy principle. In the toroidal case the energy principle will be derived by eliminating an ignorable coordinate, which will reduce the steady-flow problem to one of static equilibrium; and in the poloidal case the same result will be achieved by means of an appropriate contact transformation.

Returning to the general theory, we shall now state our physical assumptions and write down the basic equations. First, we shall assume that the dissipative effects (viscosity, heat conduction, and finite electrical conductivity) may be neglected. Second, we shall neglect all terms of order v^2/c^2, where v may be either the fluid velocity, the speed of sound, or the Alfvén speed, and where c is the speed of light. Finally, we shall assume that the fluid is a plasma governed by the ideal-gas law with a scalar plasma pressure. (The scalar-pressure requirement will be relaxed later on.) These assumptions lead to the following system of hydromagnetic equations, in which the electromagnetic quantities are expressed in rationalized units with $\mu_0 = \varepsilon_0 = 1$:

* Conference paper CN-10/152, presented by W. A. Newcomb. Discussion of this paper is given on page 492. Translations of the abstract are at the end of this volume of the Conference Proceedings.

$$\frac{\partial \varrho}{\partial t} + \nabla \cdot (\varrho \mathbf{v}) = 0 , \tag{1.1}$$

$$\frac{\partial P}{\partial t} + \mathbf{v} \cdot \nabla P + \gamma P \nabla \cdot \mathbf{v} = 0 , \tag{1.2}$$

$$\frac{\partial \mathbf{B}}{\partial t} - \nabla \times (\mathbf{v} \times \mathbf{B}) = 0 , \tag{1.3}$$

$$\nabla \cdot \mathbf{B} = 0 , \tag{1.4}$$

$$\varrho \left(\frac{\partial \mathbf{v}}{\partial t} + \mathbf{v} \cdot \nabla \mathbf{v} + \nabla \varphi \right) + \nabla \left(P + \frac{1}{2} B^2 \right) - \mathbf{B} \cdot \nabla \mathbf{B} = 0 , \tag{1.5}$$

where ϱ is the mass density, $\mathbf{v}$ is the plasma velocity, φ is the gravitational potential, P is the plasma pressure, $\mathbf{B}$ is the magnetic field, and γ is the adiabatic index (the ratio of specific heats). Equation (1.2) may also be written in the form

$$\frac{\mathrm{d}}{\mathrm{d}t} (P \varrho^{-\gamma}) = 0 , \tag{1.6}$$

which is simply the adiabatic ideal-gas law. The time derivative $\mathrm{d}/\mathrm{d}t$ refers to a point moving with the plasma and is related as follows to the time derivative at a fixed point:

$$\frac{\mathrm{d}}{\mathrm{d}t} = \frac{\partial}{\partial t} + \mathbf{v} \cdot \nabla . \tag{1.7}$$

Equation (1.3) is a direct consequence of Ohm's law with infinite conductivity, as we can see by writing

$$\frac{\partial \mathbf{B}}{\partial t} + \nabla \times \mathbf{E} = 0 , \tag{1.8}$$

$$\mathbf{E} + \mathbf{v} \times \mathbf{B} = 0 . \tag{1.9}$$

(Note that $\mathbf{E} + \mathbf{v} \times \mathbf{B}$ is simply the electric field in a frame of reference moving with the plasma.) The physical content of this equation is that the plasma motion is flux-preserving. That is to say, if C is any closed curve moving with the plasma, then the magnetic flux through C is a constant of the motion. This fact enables us to picture the magnetic field lines as moving with the fluid [8, 9]. We note, incidentally, that the other magnetic-field equation, Eq. (1.4), is not entirely independent of Eq. (1.3), since it must obviously be satisfied for all time whenever it is satisfied initially.

The electrostatic force $\eta \mathbf{E}$ has been neglected in Eq. (1.5), the equation of motion, and so has the displacement current since the magnetic force was evaluated by substituting $\nabla \times \mathbf{B}$ for the plasma current $\mathbf{J}$:

$$\mathbf{J} \times \mathbf{B} = (\nabla \times \mathbf{B}) \times \mathbf{B} = -\nabla \left(\frac{1}{2} B^2 \right) + \mathbf{B} \cdot \nabla \mathbf{B} . \tag{1.10}$$

To justify the neglect of these terms, let us write down the complete expression for the electromagnetic force. (At this point it is convenient to introduce the tensor notation, which we shall use from now on.) Observing the usual convention whereby repeated indices are summed, and making use of all four of Maxwell's equations, we obtain

$$(\mathbf{J} \times \mathbf{B})_i + \eta E_i = -\frac{\partial}{\partial t} (\mathbf{E} \times \mathbf{B})_i - \frac{\partial}{\partial x_i} \left(\frac{1}{2} E^2 + \frac{1}{2} B^2 \right) + \frac{\partial}{\partial x_j} (E_i E_j + B_i B_j) , \tag{1.11}$$

which is simply the law of conservation of electromagnetic momentum. The terms involving $\mathbf{E}$, since $\mathbf{E} + \mathbf{v} \times \mathbf{B} = 0$, are of order B^2/ϱ in comparison with the inertial term $\varrho (\partial \mathbf{v}/\partial t + \mathbf{v} \cdot \nabla \mathbf{v})$ in Eq. (1.5); and the remaining terms, since $\nabla \cdot \mathbf{B} = 0$, reduce to the expression (1.10). But since B^2/ϱ is simply the Alfvén speed squared, it follows that our system of hydromagnetic equations is correct to lowest order in the ratio of Alfvén speed to light speed.

The assumption of a scalar plasma pressure requires a collision frequency large enough to maintain isotropy, which requirement might appear at first sight to be incompatible with that of infinite conductivity. It can be shown, however, that a physically interesting regime exists in which the collision frequency is large enough to maintain a scalar pressure, and at the same time so small that the electrical resistance is negligible [10]. The best examples of this regime are in the field of astrophysics, where characteristic lengths are much larger than the collision mean free path and characteristic times much shorter than the time scale for resistive diffusion [8]. On the other hand, there are many important terrestrial applications, especially in thermonuclear-reactor technology, where the mean free path is extremely large, so that collisions are negligible and a tensor plasma pressure is allowed. But if, at the same time, the mean Larmor radius is small compared with the characteristic dimensions, the situation is again relatively simple: The pressure tensor has only two independent components. In fact, it has the simple form

$$P_{ij} = P_\perp (\delta_{ij} - \tau_i \tau_j) + P_\parallel \tau_i \tau_j , \tag{1.12}$$

where $\boldsymbol{\tau}$ is a unit vector along the field, and where δ_{ij} is the unit tensor:

$$\delta_{ij} = \begin{cases} 1, & \text{if } i = j \\ 0, & \text{if } i \neq j . \end{cases} \tag{1.13}$$

Chew, Goldberger, and Low, the authors of this last result [11], were able, by making the further assumption of zero heat flow, to derive a pair of equations analogous to the adiabatic law (1.6):

$$\frac{\mathrm{d}}{\mathrm{d}t} \left(\frac{P_\perp}{\varrho B} \right) = 0 , \tag{1.14a}$$

$$\frac{\mathrm{d}}{\mathrm{d}t} \left(\frac{B^2 P_\parallel}{\varrho^3} \right) = 0 . \tag{1.14b}$$

By using these equations instead of Eq. (1.6) one obtains another complete system of hydromagnetic equations. At the same time, of course, one must replace the pressure gradient in Eq. (1.5) with the divergence of the tensor pressure:

$$\frac{\partial P}{\partial x_i} \to \frac{\partial P_{ij}}{\partial x_j} = \frac{\partial P_\perp}{\partial x_i} + \frac{\partial}{\partial x_j} [\tau_i \tau_j (P_\parallel - P_\perp)] . \tag{1.15}$$

There is one more qualification to be made: The assumption of zero heat flow is not a very good one, except when the heat flow is required to vanish on grounds of symmetry, because there is nothing to hinder the free transport of thermal energy along the field [9]. It has nonetheless been possible, without making this assumption, to construct an essentially

complete theory of plasma dynamics in the regime we have just described, that of small Larmor radius and large mean free path [10, 12, 13, 14, 15].

Our first task will be to derive Eq. (1.5), the hydromagnetic equation of motion, from a variational principle. Now there are many different variational principles in classical mechanics, and the one we have chosen is Hamilton's principle: The time integral of the Lagrangian is stationary with respect to all variations in the path leaving the initial and final configurations fixed. The equation of motion will appear as the condition for stationarity, and the remaining equations, Eqs. (1.1)—(1.4), will function as holonomic constraints. It will also be possible to treat the tensor-pressure case in accordance with the Chew-Goldberger-Low theory.

2. The variational principle in its Lagrangian form

In the Lagrangian description of a fluid, one considers the position vector $\mathbf{x}$ of a fluid element as a function of time t and initial position $\mathbf{x}_0$:

$$x_i = x_i(\mathbf{x}_0, t); \tag{2.1}$$

and one specifies the initial configuration of the system by giving the mass density, the pressure, and the magnetic field as functions of $\mathbf{x}_0$:

$$\varrho_0 = \varrho_0(\mathbf{x}_0), \tag{2.2}$$

$$P_0 = P_0(\mathbf{x}_0), \tag{2.3}$$

$$B_{0i} = B_{0i}(\mathbf{x}_0). \tag{2.4}$$

These functions are completely arbitrary, except that $\mathbf{B}_0$ must be divergence-free:

$$\frac{\partial B_{0i}}{\partial x_{0i}} = 0. \tag{2.5}$$

We shall write $\dot{x}_i$ for the generalized velocity of the system in configuration space, which is simply the partial derivative of x_i with respect to t. The derivative is taken, of course, with $\mathbf{x}_0$ held fixed and should therefore be identified with the time derivative $\mathrm{d}/\mathrm{d}t$ of Section 1:

$$\dot{x}_i(\mathbf{x}_0, t) = \mathrm{d}x_i/\mathrm{d}t. \tag{2.6}$$

Before proceeding to the variational principle, we must go through a few geometrical preliminaries. Let x_{ij} be an abbreviation for $\partial x_i/\partial x_{0j}$, let J be the Jacobian determinant of $\mathbf{x}$ with respect to $\mathbf{x}_0$, let ε_{ijk} be the unit alternating tensor, and let A_{ij} be the cofactor of x_{ij} in J:

$$x_{ij}(\mathbf{x}_0, t) = \frac{\partial x_i}{\partial x_{0j}}; \tag{2.7}$$

$$J = \det(x_{ij}); \tag{2.8}$$

$$\varepsilon_{ijk} = \begin{cases} +1, & \text{if the subscripts form an even permutation of 1, 2, 3} \\ -1, & \text{if they form an odd permutation} \\ 0, & \text{if any two of them are equal;} \end{cases} \tag{2.9}$$

$$A_{ij} = \frac{1}{2}\varepsilon_{ikl}\varepsilon_{jmn}x_{km}x_{ln}. \tag{2.10}$$

We then have the following identities:

$$J\delta_{ij} = A_{ki}x_{kj}, \tag{2.11}$$

which is simply the standard rule for the expansion of determinants,

$$\frac{\partial J}{\partial x_{ij}} = A_{ij}, \tag{2.12}$$

which follows from the preceding equation because x_{ij} is not contained in any cofactor A_{kj} of the j^{th} column, and

$$\frac{\partial A_{ij}}{\partial x_{0j}} = 0, \tag{2.13}$$

which is obtained by differentiating Eq. (2.10) and making use of the antisymmetry of ε_{ijk}. Now let d^3x, $\mathrm{d}\sigma_i$, and $\mathrm{d}x_i$ be elements of volume, area, and length moving with the fluid. (The vector $\mathrm{d}\sigma_i$ is equal in magnitude to the area of the surface element, and its direction is along the normal.) The time-dependence of these elements is given by

$$\mathrm{d}^3x = J\mathrm{d}^3x_0, \tag{2.14}$$

$$\mathrm{d}\sigma_i = A_{ij}\,\mathrm{d}\sigma_{0j}, \tag{2.15}$$

$$\mathrm{d}x_i = x_{ij}\,\mathrm{d}x_{0j}. \tag{2.16}$$

The first and third of these relations are obvious, and the second follows from them because of Eq. (2.10): One simply considers the cylindrical volume element $\mathrm{d}^3x = \mathrm{d}\sigma_i\,\mathrm{d}x_i$.

As was pointed out in Section 1, the system is subject to holonomic constraints given by Eqs. (1.1)—(1.3). We can easily integrate these constraints by observing that the following quantities are constants of the motion: the mass enclosed within an arbitrary element of volume, the quantity $P\varrho^{-\gamma}$, and the magnetic flux through an arbitrary element of area. We may therefore write

$$\varrho\,\mathrm{d}^3x = \varrho_0\,\mathrm{d}^3x_0, \tag{2.17}$$

$$P\varrho^{-\gamma} = P_0\varrho_0^{-\gamma}, \tag{2.18}$$

$$B_i\,\mathrm{d}\sigma_i = B_{0i}\,\mathrm{d}\sigma_{0i}. \tag{2.19}$$

Using Eqs. (2.11), (2.14), and (2.15), we obtain

$$\varrho = \varrho_0/J, \tag{2.20}$$

$$P = P_0/J^\gamma, \tag{2.21}$$

$$B_i = x_{ij}B_{0j}/J. \tag{2.22}$$

We have thus succeeded in expressing ϱ, P, and $\mathbf{B}$ as functionals of $\mathbf{x}(\mathbf{x}_0)$. (The integration of the magnetic-field constraint was first carried out by WALÉN [16].)

Hamilton's variational principle states that a certain integral is stationary for all variations in the path leaving the initial and final configurations fixed:

$$\delta\int_{t_1}^{t_2}\mathrm{d}t\int L\mathrm{d}^3x_0 = 0, \tag{2.23}$$

where the variation satisfies

$$\delta x_i(\mathbf{x}_0, t_1) = \delta x_i(\mathbf{x}_0, t_2) = 0, \tag{2.24}$$

and where L, the Lagrangian density, is some function of the generalized coordinates and velocities. We shall guess the form of L by analogy with classical mechanics, and then prove it to be the correct form by showing that the variational principle leads to the correct equation of motion. In classical mechanics the Lagrangian has the form

$$L = T - V, \tag{2.25}$$

where T and V are generalized kinetic and potential energies. Here T is simply the kinetic energy of mass flow, whereas V is the sum of three terms—the gravitational energy, the internal thermodynamic energy of the fluid, and the magnetic energy:

$$T = \frac{1}{2}\varrho_0 \dot{x}^2, \tag{2.26}$$

$$V = \varrho_0\left[\varphi + \frac{P}{(\gamma-1)\varrho} + \frac{B^2}{2\varrho}\right]. \tag{2.27}$$

Using Eqs. (2.20)—(2.22), we express the Lagrangian density in terms of x_i, x_{ij}, and $\dot{x}_i$:

$$L = \varrho_0\left[\frac{1}{2}\dot{x}^2 - \varphi(\mathbf{x})\right] - \frac{P_0}{(\gamma-1)J^{\gamma-1}} - \frac{1}{2J}x_{ij}x_{ik}B_{0j}B_{0k}. \tag{2.28}$$

Note that L has an explicit dependence on $\mathbf{x}_0$ through the functions ϱ_0, P_0, and $\mathbf{B}_0$.

Carrying out the variation in Eqs. (2.23), integrating by parts, and using the initial and final conditions (2.24), we obtain

$$\int_{t_1}^{t_2} dt \int d^3x_0\, \delta x_i(\mathbf{x}_0, t)\left[\frac{d}{dt}\left(\frac{\partial L}{\partial \dot{x}_i}\right) + \frac{\partial}{\partial x_{0j}}\left(\frac{\partial L}{\partial x_{ij}}\right) - \frac{\partial L}{\partial x_i}\right] = 0. \tag{2.29}$$

(We are assuming the boundary conditions to be such as to make the surface term vanish in the integration by parts with respect to $\mathbf{x}_0$.) Since δx_i is arbitrary except for the condition (2.24), it is clear that the bracketed expression must vanish identically. In this manner we obtain the hydromagnetic equation of motion in Lagrangian form,

$$\frac{d}{dt}\left(\frac{\partial L}{\partial \dot{x}_i}\right) + \frac{\partial}{\partial x_{0j}}\left(\frac{\partial L}{\partial x_{ij}}\right) - \frac{\partial L}{\partial x_i} = 0, \tag{2.30}$$

or more explicitly,

$$\varrho_0\left(\ddot{x}_i + \frac{\partial\varphi}{\partial x_i}\right) - B_{0j}\frac{\partial}{\partial x_{0j}}\left(\frac{1}{J}x_{ik}B_{0k}\right) + A_{ij}\frac{\partial}{\partial x_{0j}}\left(P_0 J^{-\gamma} + \frac{1}{2J^2}x_{kl}x_{km}B_{0l}B_{0m}\right) = 0, \tag{2.31}$$

where use has been made of Eqs. (2.5), (2.12), and (2.13). An alternative form of this equation is readily obtained with the help of Eq. (2.11):

$$\left[\varrho_0\left(\ddot{x}_j + \frac{\partial\varphi}{\partial x_j}\right) - B_{0k}\frac{\partial}{\partial x_{0k}}\left(\frac{1}{J}x_{jl}B_{0l}\right)\right]x_{ji} + J\frac{\partial}{\partial x_{0i}}\left(P_0 J^{-\gamma} + \frac{1}{2J^2}x_{jk}x_{jl}B_{0k}B_{0l}\right) = 0. \tag{2.32}$$

In the more usual Eulerian description of a fluid, the one that was used in Section 1, we look at a fixed point in space instead of following a fluid element. We can therefore transform the equation of motion from Lagrangian to Eulerian form by changing the independent variable from $\mathbf{x}_0$ to $\mathbf{x}$. For this it will be convenient to have another symbol for the fluid velocity when it is expressed as a function of $\mathbf{x}$. We thus distinguish between the Eulerian velocity $\mathbf{v}$ and the Lagrangian velocity $\dot{\mathbf{x}}$:

$$v_i(\mathbf{x}, t) = \dot{x}_i(\mathbf{x}_0, t). \tag{2.33}$$

Let us write down the identity

$$\delta_{ij} = \frac{\partial x_{0i}}{\partial x_k}\frac{\partial x_k}{\partial x_{0j}} = \frac{\partial x_{0i}}{\partial x_k}x_{kj}, \tag{2.34}$$

and compare it with Eq. (2.11). In this manner we obtain the expression for $\partial x_{0i}/\partial x_k$:

$$\frac{\partial x_{0i}}{\partial x_k} = \frac{1}{J}A_{ki}. \tag{2.35}$$

The Eulerian gradient operator is then given by

$$\frac{\partial}{\partial x_k} = \frac{\partial x_{0i}}{\partial x_k}\frac{\partial}{\partial x_{0i}} = \frac{1}{J}A_{ki}\frac{\partial}{\partial x_{0i}}. \tag{2.36}$$

Another useful operator is obtained by combining Eqs. (2.22) and (2.36), and again making use of Eq. (2.11):

$$B_i\frac{\partial}{\partial x_i} = \frac{1}{J^2}x_{ij}A_{ik}B_{0j}\frac{\partial}{\partial x_{0k}} = \frac{1}{J}B_{0k}\frac{\partial}{\partial x_{0k}}. \tag{2.37}$$

With the help of these relations we can easily put Eq. (2.31) into the Eulerian form:

$$\varrho\left(\frac{dv_i}{dt} + \frac{\partial\varphi}{\partial x_i}\right) - B_j\frac{\partial B_i}{\partial x_j} + \frac{\partial}{\partial x_i}\left(P + \frac{1}{2}B^2\right) = 0, \tag{2.38}$$

which is the same as Eq. (1.5). This completes the proof that the variational principle (2.23), with the Lagrangian density (2.28), leads to the correct equation of motion.

3. Extension of the variational principle to fluids of other types

In this section we shall extend the work of the preceding section to fluids of various types that do not obey the ideal-gas law (1.6). Not every possibility will be considered, but only these three: (1) an arbitrary compressible fluid with a scalar pressure, (2) an incompressible fluid, and (3) a collisionless plasma with a tensor pressure governed by the Chew-Goldberger-Low equations. As before, dissipative processes will be neglected.

Starting with the compressible fluid, let us suppose that the flow takes place adiabatically, in which case we have

$$\frac{ds}{dt} = 0, \quad \text{or } s(\mathbf{x}_0, t) = s_0(\mathbf{x}_0), \tag{3.1}$$

where s is the entropy per unit mass. (This reduces, of course, to Eq. (2.18) when the fluid is an ideal gas.) Now let U be the internal energy per unit mass expressed as a function of s and ϱ^{-1}:

$$U = U(s, \varrho^{-1}). \tag{3.2}$$

The corresponding terms in the Lagrangian density (2.28) and in the Lagrangian equation of motion (2.31) are then modified as follows:

$$-\frac{P_0}{(\gamma-1)J^{\gamma-1}} \to -\varrho_0 U(s_0, J/\varrho_0), \tag{3.3}$$

$$A_{ij}\frac{\partial}{\partial x_{0j}}(P_0 J^{-\gamma}) \to -A_{ij}\frac{\partial}{\partial x_{0j}}\left[\frac{\partial U}{\partial (J/\varrho_0)}\right]. \tag{3.4}$$

This is still the pressure gradient, as is evident from the thermodynamic relation

$$P=-\frac{\partial U}{\partial(\varrho^{-1})}. \tag{3.5}$$

Equations (3.1)—(3.5) are applicable, incidentally, to isothermal as well as adiabatic flow, provided that U and s are reinterpreted as the Helmholtz free energy and the temperature.

The above procedure breaks down when the fluid is incompressible, since the partial derivative in Eq. (3.5) is no longer meaningful; but it can easily be fixed up. We have only to drop the internal-energy term from the Lagrangian and treat the incompressibility as an added constraint. The variational principle is then restricted to variations that satisfy this new constraint condition as well as the initial and final conditions (2.24). The constraint condition is simply

$$J=1, \tag{3.6}$$

and the variational principle may be written as follows:

$$\delta\int_{t_1}^{t_2} dt \int d^3x_0 [L_1+\lambda(\mathbf{x}_0, t)J]=0, \tag{3.7}$$

where λ is an undetermined multiplier and L_1 is the Lagrangian density without the internal-energy term. The Lagrangian equation of motion is then

$$\frac{d}{dt}\left(\frac{\partial L_1}{\partial \dot{x}_i}\right)+\frac{\partial}{\partial x_{0j}}\left(\frac{\partial L_1}{\partial x_{ij}}\right)-\frac{\partial L_1}{\partial x_i}+A_{ij}\frac{\partial \lambda}{\partial x_{0j}}=0, \tag{3.8}$$

from which we see that λ is simply the pressure. Equations (3.6) and (3.8) together form a complete system.

We shall now treat the tensor-pressure case. Let $\boldsymbol{\tau}$ be the unit vector along $\mathbf{B}$, and let Δ be defined as follows:

$$\Delta = x_{ij}\, x_{ik}\, \tau_{0j}\, \tau_{0k}. \tag{3.9}$$

Using Eqs. (2.20) and (2.22), we can solve Eqs. (1.14) for $P_\perp$ and $P_\parallel$, obtaining two equations in the place of Eq. (2.21):

$$P_\perp = \frac{\sqrt{\Delta}}{J^2} P_{\perp 0}, \tag{3.10a}$$

$$P_\parallel = \frac{1}{J\Delta} P_{\parallel 0}. \tag{3.10b}$$

It will also be convenient to have an expression for the vector $\boldsymbol{\tau}$:

$$\tau_i = \frac{1}{\sqrt{\Delta}} x_{ij}\, \tau_{0j}, \tag{3.11}$$

which is readily obtained from Eq. (2.22). The internal energy per unit mass is given by

$$U=\frac{1}{\varrho}\left(P_\perp+\frac{1}{2}P_\parallel\right), \tag{3.12}$$

from which we obtain the Lagrangian density

$$L=\varrho_0\left[\frac{1}{2}\dot{x}^2-\varphi(\mathbf{x})\right]-\frac{1}{2J}x_{ij}\,x_{ik}\,B_{0j}\,B_{0k} - \frac{\sqrt{\Delta}}{J}P_{\perp 0}-\frac{1}{2\Delta}P_{\parallel 0}. \tag{3.13}$$

The Lagrangian equation of motion again has the general form (2.30), which reduces in the present case to

$$\varrho_0\left(\ddot{x}_i+\frac{\partial\varphi}{\partial x_i}\right)-B_{0j}\frac{\partial}{\partial x_{0j}}\left(\frac{1}{J}x_{ik}B_{0k}\right) +A_{ij}\frac{\partial}{\partial x_{0j}}\left[\frac{\sqrt{\Delta}}{J^2}P_{\perp 0}+\frac{\Delta}{2J^2}B_0^2\right] +\frac{\partial}{\partial x_{0j}}\left[x_{ik}\,\tau_{0j}\,\tau_{0k}\left(\frac{1}{\Delta^2}P_{\parallel 0}-\frac{1}{J\sqrt{\Delta}}P_{\perp 0}\right)\right]=0. \tag{3.14}$$

Let us make use of Eqs. (2.11) and (2.13) to write the last term in the more symmetrical form

$$A_{jm}\frac{\partial}{\partial x_{0m}}\left[\frac{1}{\Delta}x_{ik}\,x_{jl}\,\tau_{0k}\,\tau_{0l}\left(\frac{1}{J\Delta}P_{\parallel 0}-\frac{\sqrt{\Delta}}{J^2}P_{\perp 0}\right)\right], \tag{3.15}$$

from which the Eulerian equation of motion is obtainable by inspection. It is simply

$$\varrho\left(\frac{dv_i}{dt}+\frac{\partial\varphi}{\partial x_i}\right)-B_j\frac{\partial B_i}{\partial x_j}+\frac{\partial}{\partial x_i}\left(P_\perp+\frac{1}{2}B^2\right) +\frac{\partial}{\partial x_j}\left[\tau_i\,\tau_j(P_\parallel-P_\perp)\right]=0, \tag{3.16}$$

which agrees with Eq. (1.15).

4. The variational principle in its Eulerian form

In this section we shall state the variational principle in a form that will lead directly to the Eulerian equation of motion, restricting ourselves to the scalar-pressure case treated in Section 2. By analogy with Eq. (2.33), we introduce the Eulerian virtual displacement $\boldsymbol{\epsilon}$:

$$\varepsilon_i(\mathbf{x}, t)=\delta x_i(\mathbf{x}_0, t). \tag{4.1}$$

We change the variables of integration from $\mathbf{x}_0$, t to $\mathbf{x}$, t; and we require the integral of the Lagrangian to be stationary for every Eulerian displacement leaving the initial and final configurations fixed. Thus,

$$\delta\int_{t_1}^{t_2} dt\int d^3x\left(\frac{1}{2}\varrho v^2-\varrho\varphi-\frac{P}{\gamma-1}-\frac{1}{2}B^2\right)=0, \tag{4.2}$$

where the variation satisfies

$$\varepsilon_i(\mathbf{x}, t_1)=\varepsilon_i(\mathbf{x}, t_2)=0. \tag{4.3}$$

The next step, of course, is to express the variations in ϱ, P, $\mathbf{B}$ and $\mathbf{v}$ in terms of the Eulerian displacement. Holding $\mathbf{x}_0$ fixed, let us take the variation of

Eq. (2.33) and the time derivative of Eq. (4.1). The results are

$$\delta v_i + \frac{\partial v_i}{\partial x_j}\varepsilon_j = \delta \dot{x}_i\,, \tag{4.4}$$

$$\frac{\partial \varepsilon_i}{\partial t} + v_j \frac{\partial \varepsilon_i}{\partial x_j} = \delta \dot{x}_i\,. \tag{4.5}$$

Returning now to the vector notation, we obtain the expression for $\delta\mathbf{v}$ as a functional of $\boldsymbol{\epsilon}$:

$$\delta\mathbf{v} = \frac{\partial \boldsymbol{\epsilon}}{\partial t} + \mathbf{v}\cdot\nabla\boldsymbol{\epsilon} - \boldsymbol{\epsilon}\cdot\nabla\mathbf{v}. \tag{4.6}$$

The corresponding expressions for $\delta\varrho$, δP, and $\delta\mathbf{B}$ are obvious:

$$\delta\varrho = -\nabla\cdot(\varrho\,\boldsymbol{\epsilon})\,, \tag{4.7}$$

$$\delta P = -\gamma P\nabla\cdot\boldsymbol{\epsilon} - \boldsymbol{\epsilon}\cdot\nabla P\,, \tag{4.8}$$

$$\delta\mathbf{B} = \nabla\times(\boldsymbol{\epsilon}\times\mathbf{B})\,. \tag{4.9}$$

The variational principle now takes on the explicit form

$$\int_{t_1}^{t_2} dt \int d^3x \left[\varrho\mathbf{v}\cdot\delta\mathbf{v} + \left(\frac{1}{2}v^2 - \varphi\right)\delta\varrho - \frac{\delta P}{\gamma-1} - \mathbf{B}\cdot\delta\mathbf{B}\right]$$
$$= \int_{t_1}^{t_2} dt \int d^3x \left[\varrho\mathbf{v}\cdot\frac{\partial\boldsymbol{\epsilon}}{\partial t} + \varrho\mathbf{v}\cdot\nabla\boldsymbol{\epsilon}\cdot\mathbf{v} - \varrho\boldsymbol{\epsilon}\cdot\nabla\left(\frac{1}{2}v^2\right)\right.$$
$$- \left(\frac{1}{2}v^2 - \varphi\right)\nabla\cdot(\varrho\,\boldsymbol{\epsilon}) + \frac{\gamma P}{\gamma-1}\nabla\cdot\boldsymbol{\epsilon}$$
$$\left. + \frac{1}{\gamma-1}\boldsymbol{\epsilon}\cdot\nabla P - \mathbf{B}\cdot\nabla\times(\boldsymbol{\epsilon}\times\mathbf{B})\right] = 0\,. \tag{4.10}$$

Because of the initial and final conditions (4.3), we can integrate by parts to obtain

$$\int_{t_1}^{t_2} dt \int d^3x\, \boldsymbol{\epsilon}(\mathbf{x},t)\cdot\left[-\frac{\partial}{\partial t}(\varrho\mathbf{v}) - \nabla\cdot(\varrho\,\mathbf{v}\mathbf{v})\right.$$
$$\left. - \varrho\nabla\varphi - \nabla P + (\nabla\times\mathbf{B})\times\mathbf{B}\right] = 0\,. \tag{4.11}$$

The integral vanishes for arbitrary $\boldsymbol{\epsilon}$ if and only if the bracketed expression vanishes identically. We thus obtain the Eulerian equation of motion in the form

$$\frac{\partial}{\partial t}(\varrho\mathbf{v}) + \nabla\cdot(\varrho\,\mathbf{v}\mathbf{v}) + \varrho\nabla\varphi + \nabla P - (\nabla\times\mathbf{B})\times\mathbf{B} = 0\,, \tag{4.12}$$

which is obviously equivalent to Eq. (1.5).

5. The Hamiltonian equations of motion

We now return to the Lagrangian description and introduce the generalized momentum conjugate to $\mathbf{x}$:

$$\pi_i(\mathbf{x}_0,t) = \frac{\partial L}{\partial \dot{x}_i} = \varrho_0\dot{x}_i\,. \tag{5.1}$$

The Hamiltonian density, a functional of $\mathbf{x}$ and $\boldsymbol{\pi}$, is then defined in the usual manner:

$$H = \pi_i\dot{x}_i - L\,. \tag{5.2}$$

This reduces with a scalar pressure to

$$H = \frac{\pi^2}{2\varrho_0} + \varrho_0\varphi(\mathbf{x}) + \frac{P_0}{(\gamma-1)J^{\gamma-1}} + \frac{1}{2J}x_{ij}x_{ik}B_{0j}B_{0k}, \tag{5.3}$$

and with a tensor pressure to

$$H = \frac{\pi^2}{2\varrho_0} + \varrho_0\varphi(\mathbf{x}) + \frac{\sqrt{\Delta}}{J}P_{\perp 0} + \frac{1}{2\Delta}P_{\parallel 0}$$
$$+ \frac{1}{2J}x_{ij}x_{ik}B_{0j}B_{0k}\,. \tag{5.4}$$

The Hamiltonian equations of motions are simply

$$\dot{\pi}_i = -\frac{\partial H}{\partial x_i} + \frac{\partial}{\partial x_{0j}}\left(\frac{\partial H}{\partial x_{ij}}\right), \tag{5.5a}$$

$$\dot{x}_i = \frac{\partial H}{\partial \pi_i}\,. \tag{5.5b}$$

(They would, of course, be completely symmetrical if H depended on the gradient of $\boldsymbol{\pi}$.) We have

$$\frac{d}{dt}\int H\,d^3x_0 = \int d^3x_0\left(\frac{\partial H}{\partial x_i}\dot{x}_i + \frac{\partial H}{\partial x_{ij}}\dot{x}_{ij} + \frac{\partial H}{\partial \pi_i}\dot{\pi}_i\right)$$
$$= \int d^3x_0\left\{\left[\frac{\partial H}{\partial x_i} - \frac{\partial}{\partial x_{0j}}\left(\frac{\partial H}{\partial x_{ij}}\right)\right]\dot{x}_i + \frac{\partial H}{\partial \pi_i}\dot{\pi}_i\right\}$$
$$= \int d^3x_0\,(-\dot{\pi}_i\dot{x}_i + \dot{x}_i\dot{\pi}_i) = 0\,. \tag{5.6}$$

Thus the integrated Hamiltonian is a constant of the motion.

6. The hydromagnetic energy principle

Let us now suppose that the fluid is in a static equilibrium state (one where $\dot{\mathbf{x}}$ and $\dot{\boldsymbol{\pi}}$ vanish identically) and ask whether the equilibrium is stable. The conditions for equilibrium are obtained directly from the Hamiltonian equations of motion. The first of these equations gives

$$\left[\frac{\partial H}{\partial x_i} - \frac{\partial}{\partial x_{0j}}\left(\frac{\partial H}{\partial x_{ij}}\right)\right]_{\mathbf{x}=\mathbf{x}_0} = 0\,, \tag{6.1}$$

which reduces with a scalar pressure to

$$\varrho_0\left(\frac{\partial\varphi}{\partial x_i}\right)_{\mathbf{x}=\mathbf{x}_0} - B_{0j}\frac{\partial B_{0i}}{\partial x_{0j}} + \frac{\partial}{\partial x_{0i}}\left(P_0 + \frac{1}{2}B_0^2\right) = 0\,, \tag{6.2}$$

and with a tensor pressure to

$$\varrho_0\left(\frac{\partial\varphi}{\partial x_i}\right)_{\mathbf{x}=\mathbf{x}_0} - B_{0j}\frac{\partial B_{0i}}{\partial x_{0j}} + \frac{\partial}{\partial x_{0i}}\left(P_{\perp 0} + \frac{1}{2}B_0^2\right)$$
$$+ \frac{\partial}{\partial x_{0j}}\left[\tau_{0i}\tau_{0j}(P_{\parallel 0} - P_{\perp 0})\right] = 0\,. \tag{6.3}$$

The other Hamiltonian equation gives only a trivial result, $\boldsymbol{\pi}=0$.

To get a stability criterion it is necessary to examine the behavior of small displacements from the equilibrium state. We accordingly write

$$x_i = x_{0i} + \xi_i\,, \tag{6.4}$$

treat $\boldsymbol{\pi}$ and $\boldsymbol{\xi}$ as small quantities, and expand the Hamiltonian out to second order. The zero-order part will be dropped, since it has no effect on the Hamiltonian equations of motion; and the first-order part, because of the equilibrium condition, will vanish when integrated over d^3x_0. The second-order part is obviously the sum of two terms, a kinetic energy de-

pending only on $\boldsymbol{\pi}$, and a potential energy depending only on $\boldsymbol{\xi}$:

$$\int H \,\mathrm{d}^3 x_0 = \frac{1}{2}\int \frac{\pi^2}{\varrho_0}\,\mathrm{d}^3 x_0 + W(\boldsymbol{\xi},\boldsymbol{\xi}). \tag{6.5}$$

Each term is a quadratic form in its respective variables, and the kinetic energy is obviously positive-definite. Under these conditions, the equilibrium is stable if and only if the potential energy is also positive-definite (i.e., positive for any nontrivial choice of $\boldsymbol{\xi}$ as a function of $\mathbf{x}_0$.) This result, which is due to BERNSTEIN, FRIEMAN, KRUSKAL and KULSRUD [4], is known as the hydromagnetic energy principle.

To find specific expressions for W we write

$$x_{ij} = \delta_{ij} + \xi_{ij}\,, \tag{6.6}$$

$$J = 1 + \xi_{ii} + \frac{1}{2}(\xi_{ii})^2 - \frac{1}{2}\,\xi_{ij}\,\xi_{ji}\,, \tag{6.7}$$

$$\Delta = 1 + 2\,\tau_{0i}\,\tau_{0j}\,\xi_{ij} + \tau_{0j}\,\tau_{0k}\,\xi_{ij}\,\xi_{ik}\,. \tag{6.8}$$

Substituting these formulas into Eqs. (5.3) and (5.4) we obtain, in the case of a scalar pressure.

$$\begin{aligned} W = \frac{1}{2}\int \mathrm{d}^3 x_0 \Big\{ & \varrho_0 \Big(\frac{\partial^2 \varphi}{\partial x_i\,\partial x_j}\Big)_{\mathbf{x}=\mathbf{x}_0} \xi_i\,\xi_j \\ & + \Big(P_0 + \frac{1}{2}\,B_0^2\Big)\,[\xi_{ij}\,\xi_{ji} - (\xi_{ii})^2] \\ & + (\gamma P_0 + B_0^2)\,(\xi_{ii})^2 + B_{0j}\,B_{0k}\,(\xi_{ij}\,\xi_{ik} - 2\,\xi_{ii}\,\xi_{jk})\Big\}, \end{aligned} \tag{6.9}$$

and in that of a tensor pressure,

$$\begin{aligned} W = \frac{1}{2}\int \mathrm{d}^3 x_0 \Big\{ & \varrho_0 \Big(\frac{\partial^2 \varphi}{\partial x_i\,\partial x_j}\Big)_{\mathbf{x}=\mathbf{x}_0} \xi_i\,\xi_j \\ & + \Big(P_{\perp 0} + \frac{1}{2}\,B_0^2\Big)\,[\xi_{ij}\,\xi_{ji} + (\xi_{ii})^2] \\ & + (B_0^2 + P_{\perp 0} - P_{\parallel 0})\,\tau_{0j}\,\tau_{0k}\,\xi_{ij}\,\xi_{ik} - 2\,(P_{\perp 0} + B_0^2) \\ & \times \tau_{0j}\,\tau_{0k}\,\xi_{jk}\,\xi_{ii} + (4\,P_{\parallel 0} - P_{\perp 0})\,(\tau_{0i}\,\tau_{0k}\,\xi_{ik})^2\Big\}. \end{aligned} \tag{6.10}$$

Expressions of this type for the energy integrals were first given by HAIN, LÜST, and SCHLÜTER [5], but without gravity, and with $P_{\perp 0} = P_{\parallel 0}$. (There is a mistake, though, in their version of Eq. (6.10): They have, as the coefficient of $(\xi_{ii})^2$, $\frac{1}{2}\,B_0^2$ alone instead of $P_{\perp 0} + \frac{1}{2}\,B_0^2$.) One can, by a rather long and tedious calculation, transform the expressions (6.9) and (6.10) into the more familiar ones given by BERNSTEIN *et al.* [4].

Suppose that the plasma pressure is isotropic in the equilibrium state ($P_{\perp 0} = P_{\parallel 0}$). Unless the collision frequency is large, this does not mean that the isotropy will be maintained by a small displacement away from equilibrium; and for this reason we need not expect the two energy integrals (6.9) and (6.10) to be equal in this case. In fact, if we set γ equal to 5/3, the appropriate value for a monoatomic gas, then the tensor-pressure integral will always be larger, and by the amount

$$\frac{1}{2}\int \mathrm{d}^3 x_0\,\frac{1}{3}\,P_0\,(\xi_{ii} - 3\,\tau_{0i}\,\tau_{0j}\,\xi_{ij})^2\,. \tag{6.11}$$

Thus the tensor-pressure energy principle gives a less stringent stability criterion, when the equilibrium pressure is a scalar, than the scalar-pressure energy principle. This result, which again is due to BERNSTEIN *et al.* [4], may be interpreted as follows: Take two equilibrium states, each with a scalar pressure, and differing only in scale. Suppose that their characteristic dimensions are, respectively, large and small compared with the collision mean free path. Then the large system will conform to the scalar-pressure theory, and the small one to the Chew-Goldberger-Low. We may conclude that if the large system is stable, then so is the small. This conclusion, by the way, does not depend on the assumption of zero heat flow in the small system; it remains valid when the Chew-Goldberger-Low theory is replaced by the more elaborate one mentioned in Section 1 [10, 14, 15].

The question of stability is not restricted to static equilibria, but arises in connection with steady flows also. Now in the Eulerian description a steady flow is obviously independent of time; but in the Lagrangian description this is not so, since the position of each fluid element is changing. For this reason the energy principle is not usually applicable to steady flows, and the stability can only be determined by a calculation of the characteristic frequencies. (The flow is unstable if any of these frequencies have imaginary parts corresponding to exponential growth.) We shall see, however, that there are cases in which a steady-flow problem can be reduced to one of static equilibrium; and in those cases the stability criterion will be given by a modified energy principle.

7. Flow with azimuthal symmetry

From now on we shall devote our attention to flows with an axis of symmetry, neglecting gravity ($\varphi = 0$) and considering only the scalar-pressure theory. Introducing cylindrical coordinates r, θ, z, we have

$$\frac{\partial r}{\partial \theta_0} = \frac{\partial z}{\partial \theta_0} = 0\,; \quad \frac{\partial \theta}{\partial \theta_0} = 1\,. \tag{7.1}$$

With this type of flow we can think of the fluid as composed of a doubly infinite set of ring elements encircling the z axis. Each of these elements is identified by its initial coordinates r_0 and z_0, and its instantaneous position is specified by giving the three coordinates r, $\theta - \theta_0$, z as functions of r_0 and z_0. (In order to keep the notation simple, let us write θ instead of $\theta - \theta_0$ from now on, so that θ will be the angular displacement of the ring element as a whole.)

For the initial volume element we now have

$$\mathrm{d}^3 x_0 = 2\pi\, r_0\,\mathrm{d}r_0\,\mathrm{d}z_0\,. \tag{7.2}$$

Consequently, if we again define J as the ratio of $\mathrm{d}^3 x$ to $\mathrm{d}^3 x_0$, we obtain

$$J = \frac{r}{r_0}\Big(\frac{\partial r}{\partial r_0}\,\frac{\partial z}{\partial z_0} - \frac{\partial r}{\partial z_0}\,\frac{\partial z}{\partial r_0}\Big)\,. \tag{7.3}$$

The mass density ϱ and the pressure P are still determined by Eqs. (2.20) and (2.21), but with the new

expression for J. The magnetic-field components are as follows:

$$B_r = \frac{1}{J}\left(\frac{\partial r}{\partial r_0} B_{0r} + \frac{\partial r}{\partial z_0} B_{0z}\right), \tag{7.4 a}$$

$$B_\theta = \frac{r}{J}\left(\frac{\partial \theta}{\partial r_0} B_{0r} + \frac{1}{r_0} B_{0\theta} + \frac{\partial \theta}{\partial z_0} B_{0z}\right), \tag{7.4 b}$$

$$B_z = \frac{1}{J}\left(\frac{\partial z}{\partial r_0} B_{0r} + \frac{\partial z}{\partial z_0} B_{0z}\right), \tag{7.4 c}$$

in which the initial values must satisfy the divergence relation

$$\frac{1}{r_0}\frac{\partial}{\partial r_0}(r_0 B_{0r}) + \frac{\partial B_{0z}}{\partial z_0} = 0. \tag{7.5}$$

Next we have the potential-energy density

$$V = \frac{P_0}{(\gamma-1)J^{\gamma-1}} + \frac{1}{2J}\left[\left(\frac{\partial r}{\partial r_0} B_{0r} + \frac{\partial r}{\partial z_0} B_{0z}\right)^2 + r^2\left(\frac{\partial \theta}{\partial r_0} B_{0r} + \frac{1}{r_0} B_{0\theta} + \frac{\partial \theta}{\partial z_0} B_{0z}\right)^2 + \left(\frac{\partial z}{\partial r_0} B_{0r} + \frac{\partial z}{\partial z_0} B_{0z}\right)^2\right], \tag{7.6}$$

the Lagrangian density

$$L = \frac{1}{2}\varrho_0(\dot{r}^2 + r^2\dot{\theta}^2 + \dot{z}^2) - V, \tag{7.7}$$

and the Lagrangian equation of motion

$$\frac{\mathrm{d}}{\mathrm{d}t}\left(\frac{\partial L}{\partial \dot{q}}\right) + \frac{1}{r_0}\frac{\partial}{\partial r_0}\left(r_0 \frac{\partial L}{\partial(\partial q/\partial r_0)}\right) + \frac{\partial}{\partial z_0}\left(\frac{\partial L}{\partial(\partial q/\partial z_0)}\right) - \frac{\partial L}{\partial q} = 0, \tag{7.8}$$

where q is any one of the three coordinates r, θ, z. Finally, we have the Hamiltonian density

$$H = \frac{1}{2\varrho_0}\left(\pi_r^2 + \frac{1}{r^2}\pi_\theta^2 + \pi_z^2\right) + V, \tag{7.9}$$

in which the canonical momenta are given by

$$\pi_r = \partial L/\partial \dot{r} = \varrho_0 \dot{r}, \tag{7.10 a}$$

$$\pi_\theta = \partial L/\partial \dot{\theta} = \varrho_0 r^2 \dot{\theta}, \tag{7.10 b}$$

$$\pi_z = \partial L/\partial \dot{z} = \varrho_0 \dot{z}. \tag{7.10 c}$$

In the remaining sections we shall consider purely azimuthal steady flows with the magnetic field either purely toroidal or purely poloidal, and investigate their stability against displacements that preserve the azimuthal symmetry ($m=0$ displacements in the usual notation). In both cases (the toroidal and the poloidal) it will be shown that the stability criterion is given by a modified energy principle.

8. Stability of steady azimuthal flow with a toroidal field

Let us now consider an azimuthally symmetric flow, not necessarily a steady one, with $B_{0r} = B_{0z} = 0$, i.e., with a purely toroidal initial field. (Of course, the field will also be purely toroidal at all future times.) For the Lagrangian density in this case we have simply

$$L = \frac{1}{2}\varrho_0(\dot{r}^2 + r^2\dot{\theta}^2 + \dot{z}^2) - \frac{P_0}{(\gamma-1)J^{\gamma-1}} - \frac{r^2}{2r_0^2 J} B_{00}^2, \tag{8.1}$$

which does not contain θ or any of its spatial derivatives. This means that θ is an ignorable coordinate, and that its conjugate momentum is a constant of the motion:

$$\dot{\pi}_\theta = \frac{\mathrm{d}}{\mathrm{d}t}(\varrho_0 r^2 \dot{\theta}) = 0, \tag{8.2}$$

which is simply the conservation of angular momentum for the individual ring elements.

We can eliminate the ignorable coordinate θ with the help of a new function R, the Routhian:

$$R = L - \pi_\theta \dot{\theta} = \frac{1}{2}\varrho_0(\dot{r}^2 + \dot{z}^2) - \frac{1}{2}\frac{\pi_\theta^2}{\varrho_0 r^2} - \frac{P_0}{(\gamma-1)J^{\gamma-1}} - \frac{r^2 B_{00}^2}{2r_0^2 J}. \tag{8.3}$$

By using R as a Lagrangian density (ROUTH's procedure [17]) one obtains equations of motion for the remaining coordinates r and z, the θ motion entering only through the constant π_θ. (Note that in effect we are simply counting the azimuthal kinetic energy as part of the potential energy.)

It is now easy to derive the stability criterion for a steady flow with $v_r = v_z = 0$. With this type of steady flow the only time-dependent coordinate is θ; and since θ has been eliminated, the motion is effectively independent of time in the Lagrangian as well as in the Eulerian description. Furthermore, the Routhian function (8.3) is the sum of two terms, one positive-definite and quadratic in the velocities, and the other depending only on the coordinates. In other words, the Routhian for small displacements from the steady flow has the same form as the Lagrangian for small displacements from a static equilibrium. The steady-flow problem has thus been reduced to one of static equilibrium, and the stability criterion will necessarily be given by an energy principle. The only difference is that the energy integral will now include a centrifugal potential energy.

The procedure described above is an extension of one that is familiar in classical mechanics [18], where it is used to investigate the stability of such steady motions as the regular precession of a top. It should be pointed out, though, that a reduction to static equilibrium cannot always be achieved, since the elimination of ignorable coordinates will often lead to a Routhian with some of its terms linear in the velocities. This occurs, for example, in the problem of the sleeping top.

The equilibrium conditions (which are readily obtained from Eq. (7.8) with R in the place of L) may be reduced to the following:

$$P_0 + \frac{1}{2} B_{0\theta}^2 = F(r_0), \tag{8.4 a}$$

$$B_{00}^2 - \frac{\pi_\theta^2}{\varrho_0 r_0^2} = G(r_0), \tag{8.4 b}$$

where F and G must satisfy

$$G(r_0) + r_0 F'(r_0) = 0. \tag{8.5}$$

Although the combinations F and G can only depend on r_0, we note that the individual terms may depend on z_0 as well.

To describe the small displacements we write

$$r = r_0 + \xi, \tag{8.6 a}$$

$$z = z_0 + \zeta, \tag{8.6 b}$$

and, as in the static-equilibrium case, we expand the potential energy out to second order. The result, if the subscript zeroes are dropped, is

$$W = \pi \int r\,\mathrm{d}r\,\mathrm{d}z \Big[\frac{3\pi_\theta^2}{\varrho} \frac{\xi^2}{r^4} + (\gamma P + B_\theta^2)\,\mathrm{div}^2 - 2\Big(P + \frac{1}{2}B_\theta^2\Big)\Big(\frac{\xi}{r}\frac{\partial \xi}{\partial r} + \frac{\xi}{r}\frac{\partial \zeta}{\partial z} + \frac{\partial \xi}{\partial r}\frac{\partial \zeta}{\partial z} - \frac{\partial \xi}{\partial z}\frac{\partial \zeta}{\partial r}\Big) - B_\theta^2\Big(\frac{2\xi}{r}\frac{\partial \xi}{\partial r} + \frac{2\xi}{r}\frac{\partial \zeta}{\partial z} + \frac{\xi^2}{r^2}\Big)\Big], \tag{8.7}$$

where div is simply the divergence of the vector displacement:

$$\mathrm{div} = \frac{\xi}{r} + \frac{\partial \xi}{\partial r} + \frac{\partial \zeta}{\partial z}. \tag{8.8}$$

The necessary and sufficient condition for stability against azimuthally symmetric displacements is that this integral be positive for every ξ and ζ.

After integrating various terms by parts, and making use of the equilibrium conditions (8.4) and (8.5), we obtain

$$W = \pi \int r\,\mathrm{d}r\,\mathrm{d}z \Big\{ A\,\xi^2 + (\gamma P + B_\theta^2) \Big[\mathrm{div} - \frac{(2r^2 B_\theta^2 - \pi_\theta^2/\varrho)\,\xi}{(\gamma P + B_\theta^2) r^3}\Big]^2 \Big\}, \tag{8.9}$$

where A is a certain function of the equilibrium quantities and their derivatives. We shall prove that W is positive-definite if and only if A is positive for all values of r and z. The "if" part of this statement is obvious; and to prove the "only if" part, let us assume that A is negative at some point and construct a displacement for which W is negative. If at some point we have $A<0$, then, by continuity, that point is surrounded by an entire region Ω in the r, z plane such that A is negative at every point of Ω. Let us pick a ξ that vanishes outside of Ω and that satisfies the following condition for all values of r:

$$\int_{-\infty}^{\infty} \mathrm{d}z \Big[\frac{\partial \xi}{\partial r} + \frac{\xi}{r} - \frac{[2r^2 B_\theta^2 - \pi_\theta^2/\varrho]\,\xi}{(\gamma P + B_\theta^2) r^3}\Big] = 0. \tag{8.10}$$

(It is clear that these two conditions on ξ are compatible.) Comparing Eqs. (8.8) and (8.10), we see that ζ can be chosen so as to make the bracketed term in W vanish. But then, since ξ^2 vanishes wherever A is non-negative, we have $W<0$ for this particular choice of ξ and ζ, which is what we set out to prove. The stability criterion, then, is given by the following inequality, the left-hand side of which is simply the function A written out explicitly:

$$\frac{1}{r^3}\frac{\partial}{\partial r}\Big(\frac{\pi_\theta^2}{\varrho}\Big) - \frac{2}{r} B_\theta \frac{\partial B_\theta}{\partial r} + \frac{2B_\theta^2}{r^2} - \frac{(2r^2 B_\theta^2 - \pi_\theta^2/\varrho)^2}{r^6 (\gamma P + B_\theta^2)} > 0. \tag{8.11}$$

The flow is stable if and only if this inequality holds at every point in the fluid.

Let us briefly consider two special cases, that of magnetostatic equilibrium, where $\pi_\theta = 0$, and that of pure hydrodynamics, where $B_\theta = 0$. (Note that the equilibrium quantities, although they may have a z dependence in the general case, can only depend on r in these special cases.) In the first case ($\pi_\theta = 0$) the stability criterion reduces to

$$\frac{\mathrm{d}\log B_\theta}{\mathrm{d}\log r} < \frac{\gamma P - B_\theta^2}{\gamma P + B_\theta^2}, \tag{8.12}$$

which was first derived by TSERKOVNIKOV [19]; and in the second ($B_\theta = 0$) it reduces to

$$\frac{\mathrm{d}}{\mathrm{d}r}\Big(\frac{\pi_\theta^2}{\varrho}\Big) > \frac{\pi_\theta^4}{\gamma P \varrho^2 r^3}. \tag{8.13}$$

For an incompressible fluid we may take γ infinite and obtain

$$\frac{\mathrm{d}}{\mathrm{d}r}\Big(\frac{\pi_\theta^2}{\varrho}\Big) > 0, \tag{8.14}$$

which will be recognized as Rayleigh's condition for the stability of Couette flow [7]. In its essentials, Lord Rayleigh's derivation of this stability condition was equivalent to the use of an energy principle; and for this reason the material presented here may be regarded as an extension of his work.

9. Stability of steady azimuthal flow with a poloidal field

We shall now consider flows in which the magnetic field is initially poloidal ($B_{0\theta} = 0$). (Note that the field will not, in general, remain poloidal unless the flow is steady, since a nonvanishing B_θ is induced whenever the angular velocity varies from point to point on a single field line.) It will again be possible to reduce the steady-flow problem to one of static equilibrium, but this time the reduction will be carried through by means of a contact transformation. It is therefore appropriate to start with the Hamiltonian, which is now given by

$$H = \frac{1}{2\varrho_0}\Big[\pi_r^2 + \frac{1}{r^2}\pi_\theta^2 + \pi_z^2\Big] + \frac{P_0}{(\gamma - 1) J^{\gamma - 1}} + \frac{1}{2J}\Big[\Big(\frac{\partial r}{\partial r_0} B_{0r} + \frac{\partial r}{\partial z_0} B_{0z}\Big)^2 + r^2\Big(\frac{\partial \theta}{\partial r_0} B_{0r} + \frac{\partial \theta}{\partial z_0} B_{0z}\Big)^2 + \Big(\frac{\partial z}{\partial r_0} B_{0r} + \frac{\partial z}{\partial z_0} B_{0z}\Big)^2\Big]. \tag{9.1}$$

The coordinate θ is no longer ignorable, since it enters the Hamiltonian through its derivatives with respect to r_0 and z_0; and the conjugate momentum π_θ is no longer a constant of the motion. There is, however, an integral of π_θ that is constant. Let B_0

be the magnitude of the initial field, and let dl_0 be the element of arc length in the r_0, z_0 plane. Then, taking the integral of π_θ/B_0 along a magnetic field line (which we assume to be closed), we obtain

$$\frac{d}{dt}\oint\frac{\pi_\theta\,dl_0}{B_0}=\oint\frac{dl_0}{B_0}\left[\frac{1}{r_0}\frac{\partial}{\partial r_0}\left(r_0\frac{\partial H}{\partial(\partial\theta/\partial r_0)}\right)+\frac{\partial}{\partial z_0}\left(\frac{\partial H}{\partial(\partial\theta/\partial z_0)}\right)\right]$$
$$=\oint d\left[\frac{r^2}{J}\left(\frac{\partial\theta}{\partial r_0}B_{0r}+\frac{\partial\theta}{\partial z_0}B_{0z}\right)\right]=0, \quad (9.2)$$

where use has been made of Eq. (7.5). Let us consider the infinitely thin shell between two neighboring flux surfaces. Then, according to Eq. (9.2), the total angular momentum of the fluid within the shell is a constant of the motion. The angular momentum can, however, be transferred by the field from one ring element to another in the same shell, so that an individual ring element need not have a constant angular momentum.

From our present viewpoint there are two respects in which a purely azimuthal steady flow differs from a static equilibrium: The coordinate θ depends on time, and the momentum π_θ does not vanish. What we shall try to do, therefore, is find a contact transformation from the variables θ, π_θ to new variables β, π_β such that $\dot\beta$ and $\dot\pi_\beta$ both vanish when the flow is steady. Let us first note that the field-lines in a steady flow must rotate as rigid bodies (the law of isorotation [20, 21]), which enables us to write

$$B_{0r}\frac{\partial\theta}{\partial r_0}+B_{0z}\frac{\partial\theta}{\partial z_0}=0. \quad (9.3)$$

Now the Hamiltonian has a term proportional to the square of this expression, an expression that has just been seen to vanish when the flow is steady. It is strongly suggested, therefore, that π_β is proportional to that expression. As for the conjugate variable β, we may expect it to be some functional of π_θ, since π_β is a functional of θ; and, since $\dot\pi_\theta$ vanishes when the flow is steady, so will $\dot\beta$.

We now give the generating function of a contact transformation that will lead to variables β, π_β with the desired properties:

$$S(\theta,\beta)=-\beta\,r_0\sqrt{\varrho_0}\left(B_{0r}\frac{\partial\theta}{\partial r_0}+B_{0z}\frac{\partial\theta}{\partial z_0}\right). \quad (9.4)$$

The conjugate momenta are derived from the generating function in the usual manner:

$$\pi_\theta=-\frac{1}{r_0}\frac{\partial}{\partial r_0}\left(r_0\frac{\partial S}{\partial(\partial\theta/\partial r_0)}\right)-\frac{\partial}{\partial z_0}\left(\frac{\partial S}{\partial(\partial\theta/\partial z_0)}\right)$$
$$=B_{0r}\frac{\partial}{\partial r_0}(\beta r_0\sqrt{\varrho_0})+B_{0z}\frac{\partial}{\partial z_0}(\beta r_0\sqrt{\varrho_0}), \quad (9.5a)$$

$$\pi_\beta=-\frac{\partial S}{\partial\beta}=r_0\sqrt{\varrho_0}\left(B_{0r}\frac{\partial\theta}{\partial r_0}+B_{0z}\frac{\partial\theta}{\partial z_0}\right), \quad (9.5b)$$

where use has been made of Eq. (7.5) in the evaluation of π_θ. Let us imagine that Eq. (9.5a) has been solved for β as a functional of π_θ. (The constant of integration must, of course, be chosen independently of time on each field line, or else $\dot\beta$ will not vanish in a steady flow.) If the field lines are closed, then β will generally be multi-valued. It follows from Eq. (9.2), however, that $\dot\beta$ is single-valued; the jump in β is a constant of the motion.

It is easily verified that the new variables β, π_β obey a Hamiltonian system of dynamical equations, or in other words, that the transformation from θ, π_θ to β, π_β is actually a contact transformation. The Hamiltonian of this new system of equations is easily obtained by substituting Eqs. (9.5) into Eq. (9.1):

$$H=\frac{1}{2\varrho_0}\left(\pi_r^2+\frac{r^2}{Jr_0^2}\pi_\beta^2+\pi_z^2\right)+\frac{P_0}{(\gamma-1)J^{\gamma-1}}$$
$$+\frac{1}{2J}\left[\left(\frac{\partial r}{\partial r_0}B_{0r}+\frac{\partial r}{\partial z_0}B_{0z}\right)^2+\left(\frac{\partial z}{\partial r_0}B_{0r}+\frac{\partial z}{\partial z_0}B_{0z}\right)^2\right]$$
$$+\frac{1}{2\varrho_0 r^2}\left[B_{0r}\frac{\partial}{\partial r_0}(\beta r_0\sqrt{\varrho_0})+B_{0z}\frac{\partial}{\partial z_0}(\beta r_0\sqrt{\varrho_0})\right]^2. \quad (9.6)$$

Note that part of the kinetic energy has been counted as potential, and part of the potential energy as kinetic. Specifically, the θ components of the kinetic and magnetic-field energies have been counted, respectively, as potential and kinetic.

We now have a system of canonical variables such that the generalized velocities and momenta all vanish when the flow is steady. Furthermore, the Hamiltonian is the sum of two terms, one positive-definite and quadratic in the momenta, and the other depending only on the coordinates. As before, this means that the steady flow has been reduced to a static equilibrium, and that the stability criterion for azimuthally symmetric displacements will be given by an energy principle.

The conditions for equilibrium are readily obtained by setting $\dot\pi_r$, $\dot\pi_\beta$, and $\dot\pi_z$ equal to zero in the Hamiltonian equations of motion. They are

$$-\frac{\pi_{0\theta}^2}{\varrho_0 r_0^3}+\frac{\partial P_0}{\partial r_0}+B_{0z}\left(\frac{\partial B_{0z}}{\partial r_0}-\frac{\partial B_{0r}}{\partial z_0}\right)=0, \quad (9.7a)$$

$$\frac{\partial P_0}{\partial z_0}+B_{0r}\left(\frac{\partial B_{0r}}{\partial z_0}-\frac{\partial B_{0z}}{\partial r_0}\right)=0, \quad (9.7b)$$

$$B_{0r}\frac{\partial}{\partial r_0}\left(\frac{\pi_{0\theta}}{\varrho_0 r_0^2}\right)+B_{0z}\frac{\partial}{\partial z_0}\left(\frac{\pi_{0\theta}}{\varrho_0 r_0^2}\right)=0, \quad (9.7c)$$

in which $\pi_{0\theta}$ is not regarded as a canonical momentum, but only as an abbreviation for the expression (9.5a) with $\beta=\beta_0$. Note that Eq. (9.7c) is simply the condition for rigid-body rotation of the field lines.

As before, we expand the potential energy to second order in the displacement, which now includes a third component $\eta=\beta-\beta_0$. (Note that η is single-valued even though β itself is not.) The result, if the subscript zeroes are again dropped, is

$$W=\pi\int r\,dr\,dz\left\{\frac{1}{\varrho r^2}\left[\mathbf{B}\cdot\nabla(\eta r\sqrt{\varrho})-\frac{2\pi_\theta\xi}{r}\right]^2-\frac{\pi_\theta^2\xi^2}{\varrho r^4}\right.$$
$$+(\gamma P+B^2)\,\mathrm{div}^2-2\left(P+\frac{1}{2}B^2\right)\left(\frac{\xi}{r}\frac{\partial\xi}{\partial r}+\frac{\xi}{r}\frac{\partial\zeta}{\partial z}\right.$$
$$\left.+\frac{\partial\xi}{\partial r}\frac{\partial\zeta}{\partial z}-\frac{\partial\xi}{\partial z}\frac{\partial\zeta}{\partial r}\right)+(\mathbf{B}\cdot\nabla\xi)^2+(\mathbf{B}\cdot\nabla\zeta)^2$$
$$\left.-2(B_r\mathbf{B}\cdot\nabla\xi+B_z\mathbf{B}\cdot\nabla\zeta)\,\mathrm{div}\right\}, \quad (9.8)$$

where

$$\mathbf{B}\cdot\nabla = B_r\frac{\partial}{\partial r} + B_z\frac{\partial}{\partial z}, \tag{9.9}$$

and where div is defined as before. The stability criterion is that W be positive for all ξ, η, ζ.

Let us now minimize W with respect to η, holding ξ and ζ fixed:

$$W_{\min}(\xi,\zeta) = \mathrm{Min}_\eta\, W(\xi,\eta,\zeta). \tag{9.10}$$

Then the flow is stable if and only if $W_{\min}$ is positive for all ξ, ζ. The minimization condition is

$$\mathbf{B}\cdot\nabla\left[\frac{1}{\varrho r^2}\mathbf{B}\cdot\nabla(\eta r\sqrt{\varrho}) - \frac{2\pi_\theta\xi}{\varrho r^3}\right] = 0, \tag{9.11}$$

or

$$\mathbf{B}\cdot\nabla(\eta r\sqrt{\varrho}) = \varrho r^2 C + 2\pi_\theta\xi/r, \tag{9.12}$$

where C is constant along the field lines. Integrating over the infinitesimal shell between two magnetic surfaces, we obtain

$$0 = C\langle\varrho r^2\rangle + \langle 2\pi_\theta\xi/r\rangle, \tag{9.13}$$

where the brackets indicate a volume average over the shell. Note that the volume average can also be written as follows in terms of line integrals:

$$\langle F\rangle = \frac{\oint F\,\mathrm{d}l/B}{\oint \mathrm{d}l/B}. \tag{9.14}$$

Substituting Eqs. (9.12) and (9.13) into Eq. (9.8), we finally obtain

$$W_{\min} = \pi\int r\,\mathrm{d}r\,\mathrm{d}z\left\{\varrho r^2\frac{\langle 2\xi\pi_\theta/r\rangle^2}{\langle\varrho r^2\rangle^2} - \frac{\pi_\theta^2\xi^2}{\varrho r^4}\right.$$
$$+ (\gamma P + B^2)\,\mathrm{div}^2 - 2\left(P+\frac{1}{2}B^2\right)$$
$$\times\left(\frac{\xi}{r}\frac{\partial\xi}{\partial r} + \frac{\xi}{r}\frac{\partial\zeta}{\partial z} + \frac{\partial\xi}{\partial r}\frac{\partial\zeta}{\partial z} - \frac{\partial\xi}{\partial z}\frac{\partial\zeta}{\partial r}\right)$$
$$\left. + (\mathbf{B}\cdot\nabla\xi)^2 + (\mathbf{B}\cdot\nabla\zeta)^2 - 2(B_r\mathbf{B}\cdot\nabla\xi + B_z\mathbf{B}\cdot\nabla\zeta)\,\mathrm{div}\right\}. \tag{9.15}$$

We shall not go any further into the general case of a poloidal field, but in the next section we shall consider the special case of a purely axial field in detail.

10. The special case of a purely axial field

Let us now suppose that the unperturbed magnetic field has no radial component. Then, if we continue to suppress the subscript zeroes, the equilibrium condition (9.7) reduces to

$$\frac{\mathrm{d}}{\mathrm{d}r}\left(P + \frac{1}{2}B_z^2\right) = \frac{\pi_\theta^2}{\varrho r^3}, \tag{10.1}$$

in which the individual terms can no longer depend on z but only on r. (The stability of a purely azimuthal steady flow in the presence of an axial field has also been treated by CHANDRASEKHAR [22, 23], but under a different, and considerably more difficult, set of conditions. He has taken account of viscosity and finite electrical conductivity, but with an incompressible fluid and a uniform field. We, on the other hand, are neglecting viscosity and assuming infinite conductivity, but we are taking account of compressibility and allowing the field intensity to depend on r.)

Setting B_r equal to zero in Eq. (9.15), integrating various terms by parts, and making use of the equilibrium condition (10.1), we obtain

$$W_{\min} = \pi\int r\,\mathrm{d}r\,\mathrm{d}z\left\{B_z^2\left(\frac{\partial\xi}{\partial r} + \frac{\xi}{r}\right)^2 + \left[\frac{1}{r^3}\frac{\mathrm{d}}{\mathrm{d}r}\left(\frac{\pi_\theta^2}{\varrho}\right)\right.\right.$$
$$\left. - \frac{4\pi_\theta^2}{\varrho r^4} - \frac{\pi_\theta^4}{\gamma P\varrho^2 r^6}\right]\xi^2 + B_z^2\left(\frac{\partial\xi}{\partial z}\right)^2$$
$$\left. + \frac{4\pi_\theta^2}{\varrho r^4}\langle\xi\rangle^2 + \gamma P\left(\mathrm{div} + \frac{\pi_\theta^2\xi}{\gamma P\varrho r^3}\right)^2\right\}. \tag{10.2}$$

Let us define a new integral W_0, in which r is the only variable of integration:

$$W_0 = \pi\int r\,\mathrm{d}r\left\{B_z^2\left(\frac{\partial\xi}{\partial r} + \frac{\xi}{r}\right)^2\right.$$
$$\left. + \left[\frac{1}{r^3}\frac{\mathrm{d}}{\mathrm{d}r}\left(\frac{\pi_\theta^2}{\varrho}\right) - \frac{4\pi_\theta^2}{\varrho r^4} - \frac{\pi_\theta^4}{\gamma P\varrho^2 r^6}\right]\xi^2\right\}. \tag{10.3}$$

We can easily show that $W_{\min}$ is positive for all ξ, ζ if and only if W_0 is positive for all ξ. The "if" part is obvious, since the last three terms of Eq. (10.2) are necessarily positive; and to prove the "only if" part, let $f(r)$ be some function of r such that W_0 is negative when $\xi = f(r)$. Then $W_{\min}$ will be negative when ξ and ζ are chosen as follows:

$$\xi(r,z) = f(r)\cos kz, \tag{10.3a}$$

$$\zeta(r,z) = -\left[f'(r) + \frac{1}{r}f(r) + \frac{\pi_\theta^2}{\gamma P\varrho r^3}f(r)\right]\frac{\sin kz}{k}, \tag{10.3b}$$

where k is very small; for the term $B_z^2(\partial\xi/\partial z)^2$ is negligible when k is small, the next term vanishes because $\langle\xi\rangle = 0$ whenever $k\neq 0$, and the last term vanishes because of the choice of ζ. The necessary and sufficient condition for stability, then, is that W_0 be positive for every $\xi(r)$.

If the magnetic field is so small that we can drop it from the integrand of W_0, then the stability condition is simply

$$\frac{\mathrm{d}}{\mathrm{d}r}\left(\frac{\pi_\theta^2}{\varrho}\right) > \frac{4\pi_\theta^2}{\varrho r} + \frac{\pi_\theta^4}{\gamma P\varrho^2 r^3}. \tag{10.4}$$

Now this condition does not agree with the corresponding condition (8.13) for stability in the presence of a small B_θ. In fact, it is possible for a flow to satisfy the latter condition without satisfying the former; and whenever this happens the flow will be stable in the absence of a field, or in the presence of a small B_θ, but it will be made unstable by an arbitrarily small B_z. (Of course, the growth rate of the instability will be correspondingly small.) What the axial field does is to remove a constraint, the constancy of π_θ, and by so doing it enlarges the class of allowed motions. Suppose, for example, that a particular ring element on a particular flux tube starts to move outward.

Then its angular velocity will decrease; and the axial field, because of its distortion by the nonuniform rotation of the flux tube, will transfer angular momentum from the other ring elements on the flux tube to the one that is moving outward. That element will then be subjected to an increased centrifugal force, tending to push it still further outward and thus to destabilize its radial motion.

If the magnetic field is not small, then the simple condition (10.4) is still sufficient for stability but no longer necessary. To determine the stability when that condition is not satisfied, we may have recourse to a method that has been worked out in connection with the diffuse linear pinch. Here we shall simply give the results, referring to the pinch work for details [24].

We consider the differential equation

$$\frac{\mathrm{d}}{\mathrm{d}r}\left(r B_z^2 \frac{\mathrm{d}\xi}{\mathrm{d}r}\right) - g\xi = 0\,, \tag{10.5}$$

where

$$g(r) = \frac{1}{r^2}\left[\frac{\mathrm{d}}{\mathrm{d}r}\left(\frac{\pi_\theta^2}{\varrho}\right) - \frac{4\pi_\theta^2}{\varrho r} - \frac{\pi_\theta^4}{\gamma P \varrho^2 r^3}\right] + \frac{B_z^2}{r} - \frac{\mathrm{d}B_z^2}{\mathrm{d}r}. \tag{10.6}$$

(This equation is simply the Euler-Lagrange condition for stationary values of W_0). Singularities occur at every value of r for which B_z changes sign, and the solutions $\xi(r)$ may exhibit either of two types of behavior: If r_s is the singular point, then the solutions may have an infinite number of oscillations in the neighborhood of r_s, or they may behave like real powers of $r - r_s$:

$$\xi(r) \sim \begin{cases} (r - r_s)^{-n_1} \\ (r - r_s)^{-n_2}, \quad \text{where } n_1 + n_2 = 1\,. \end{cases} \tag{10.7}$$

The condition for nonoscillatory solutions is that the following inequality be satisfied at the singular point:

$$\left(\frac{\mathrm{d}B_z}{\mathrm{d}r}\right)^2 + \frac{4}{r^3}\left[\frac{\mathrm{d}}{\mathrm{d}r}\left(\frac{\pi_\theta^2}{\varrho}\right) - \frac{4\pi_\theta^2}{\varrho r} - \frac{\pi_\theta^4}{\gamma P \varrho^2 r^3}\right] > 0. \tag{10.8}$$

It can be shown (Corollary 9—1 of Ref. [24]) that instability occurs whenever the solutions are oscillatory; hence the condition (10.8) is necessary for stability.

Now suppose that the flow takes place between concentric cylinders of radius a and b, and that the cylinders are rigid and perfectly conducting. We then have the boundary condition

$$\xi(a) = \xi(b) = 0\,. \tag{10.9}$$

Let the singular points, if any, be r_{s1}, r_{s2}, etc., and divide the interval $a < r < b$ into subintervals $a < r < r_{s1}$, $r_{s1} < r < r_{s2}$, etc. We may assume that the inequality (10.8) holds at each singular point, in which case the solutions of Eq. (10.5) will have the form (10.7), since we already know what happens when it does not hold. We pick out solutions in each subinterval as follows: (1) In the first subinterval let $\xi(r)$ vanish at the left endpoint $r = a$. (2) In every other subinterval let $\xi(r)$, in the neighborhood of the left endpoint, be the smaller of the two expressions (10.7). Except for a multiplicative constant, a unique solution has now been defined in each subinterval, and we can ask whether there are any interior points of the subinterval at which the solution vanishes. It can be shown (Theorem 10 of Ref. [24]) that the flow is stable if and only if there are no such points in any of the subintervals. This result enables us, in any particular case, to determine the stability by solving a second-order differential equation numerically.

Erratum

Consider an upright glass of water, and let the water be subjected to the virtual displacement $\xi_\theta = r$, $\xi_r = \xi_z = 0$, a rigid-body rotation. For this displacement, since $\xi_{ii} = 0$ and $\xi_{ij}\,\xi_{ji} = -2$, the energy integral (6.9) reduces in the absence of a field to

$$W = -\int P_0\,\mathrm{d}^3 x_0 < 0. \tag{E1}$$

Thus, according to our version of the hydromagnetic energy principle, a glass of water is rotationally unstable. It is clear that some mistake has been made.

The trouble arises from an improper definition of $\boldsymbol{\xi}$. Suppose for the sake of definiteness that the fluid is enclosed by a rigid wall, with the magnetic field purely tangential. Then the boundary conditions are

$$B_{0i}\,\mathrm{d}\sigma_{0i} = 0, \tag{E2}$$

$$\xi_i\,\mathrm{d}\sigma_{0i} = 0, \tag{E3}$$

where $\mathrm{d}\boldsymbol{\sigma}_0$ is a surface element of the fluid boundary. These boundary conditions are used in proving that the first-order part of W vanishes. Restricting ourselves temporarily to the scalar-pressure case, we have

$$W^{(1)} = \frac{1}{2}\int \mathrm{d}^3 x_0 \left[\varrho_0\left(\frac{\partial\varphi}{\partial x_i}\right)_{\mathbf{x}=\mathbf{x}_0}\xi_i - \left(P_0 + \frac{1}{2}B_0^2\right)\xi_{ii} + B_{0i}\,B_{0j}\,\xi_{ij}\right]$$

$$= \frac{1}{2}\int \mathrm{d}^3 x_0\,\xi_i\left[\varrho_0\left(\frac{\partial\varphi}{\partial x_i}\right)_{\mathbf{x}=\mathbf{x}_0} + \frac{\partial}{\partial x_{0i}}\left(P_0 + \frac{1}{2}B_0^2\right) - B_{0j}\frac{\partial B_{0i}}{\partial x_{0j}}\right]$$

$$+ \frac{1}{2}\int\left[-\mathrm{d}\sigma_{0i}\,\xi_i\left(P_0 + \frac{1}{2}B_0^2\right) + \mathrm{d}\sigma_{0j}\,B_{0j}\,B_{0i}\,\xi_i\right]. \tag{E4}$$

The volume integral vanishes because of the equilibrium condition, and the surface integral because of the boundary conditions. But, if ξ_i is defined as $x_i - x_{0i}$, then $\xi_i\,\mathrm{d}\sigma_{0i}$ vanishes only to lowest order; and the surface integral, instead of vanishing exactly, reduces to a non-negligible second-order term. What we must do is write

$$x_i = x_{0i} + \xi_i + \frac{1}{2}\eta_i, \tag{E5}$$

where η_i is a second-order term chosen to make ξ_i satisfy the boundary condition (E3) exactly. It is easily shown that $\boldsymbol{\eta}$ must then satisfy the boundary condition

$$\eta_i\,\mathrm{d}\sigma_{0i} = \mathrm{d}\sigma_{0i}\,\xi_{ij}\,\xi_j. \tag{E6}$$

The energy integral will now have a contribution from $\boldsymbol{\eta}$.

From now on, as in Sections 8—10, we shall drop the subscript zeroes from the equilibrium quantities. Proceeding as in Eq. (E4), we find that the contribution of $\boldsymbol{\eta}$ to W is equal to the surface integral

$$-\frac{1}{2}\int \mathrm{d}\sigma_i\, \eta_i\left(P+\frac{1}{2}B^2\right) = -\frac{1}{2}\int \mathrm{d}\sigma_i\, \xi_{ij}\,\xi_j\left(P+\frac{1}{2}B^2\right). \tag{E7}$$

By adding on a term that vanishes as a result of the first-order boundary condition (E3), we can reduce this expression to a volume integral not involving any second derivatives of $\boldsymbol{\xi}$:

$$\begin{aligned}\frac{1}{2}\int \mathrm{d}^3x\,\frac{\partial}{\partial x_i}\left\{\xi_i\frac{\partial}{\partial x_i}\left[\left(P+\frac{1}{2}B^2\right)\xi_j\right]-\left(P+\frac{1}{2}B^2\right)\xi_{ij}\,\xi_j\right\}\\ =\frac{1}{2}\int \mathrm{d}^3x\left\{\xi_i\,\xi_j\frac{\partial^2}{\partial x_i\,\partial x_j}\left(P+\frac{1}{2}B^2\right)+2\,\xi_{ji}\,\xi_i\frac{\partial}{\partial x_i}\left(P+\frac{1}{2}B^2\right)\right.\\ \left.+\left(P+\frac{1}{2}B^2\right)\left[(\xi_{ii})^2-\xi_{ij}\,\xi_{ji}\right]\right\}.\end{aligned} \tag{E8}$$

Finally, by adding this term to Eq. (6.9), we obtain the complete expression for the energy integral:

$$\begin{aligned}W=\frac{1}{2}\int \mathrm{d}^3x\left\{\xi_i\,\xi_j\left[\varrho\,\frac{\partial^2\varphi}{\partial x_i\,\partial x_j}+\frac{\partial^2}{\partial x_i\,\partial x_j}\left(P+\frac{1}{2}B^2\right)\right]\right.\\ +2\,\xi_{ji}\,\xi_i\frac{\partial}{\partial x_i}\left(P+\frac{1}{2}B^2\right)+(\gamma P+B^2)\,(\xi_{ii})^2\\ \left.+B_j\,B_k\,(\xi_{ij}\,\xi_{ik}-2\,\xi_{ii}\,\xi_{jk})\right\}.\end{aligned} \tag{E9}$$

The stability criterion is that this integral be positive-definite relative to the boundary condition (E3).

With a tensor pressure the contribution of $\boldsymbol{\eta}$ is again given by the surface integral (E7), but with $P_\perp$ instead of P. The complete energy integral is then

$$\begin{aligned}W=\frac{1}{2}\int \mathrm{d}^3x\left\{\xi_i\,\xi_j\left[\varrho\,\frac{\partial^2\varphi}{\partial x_i\,\partial x_j}+\frac{\partial^2}{\partial x_i\,\partial x_j}\left(P_\perp+\frac{1}{2}B^2\right)\right]\right.\\ +2\xi_{ij}\,\xi_i\frac{\partial}{\partial x_i}\left(P_\perp+\frac{1}{2}B^2\right)\\ +2\left(P_\perp+\frac{1}{2}B^2\right)(\xi_{ii})^2+(B^2+P_\perp-P_\parallel)\,\tau_j\,\tau_k\,\xi_{ij}\,\xi_{ik}\\ \left.-2\,(P_\perp+B^2)\,\tau_j\,\tau_k\,\xi_{jk}\,\xi_{ii}+(4P_\parallel-P_\perp)\,(\tau_i\,\tau_j\,\xi_{ij})^2\right\}.\end{aligned} \tag{E10}$$

In the case of steady azimuthal flow there is no additional contribution when the wall is a circular cylinder. But if it is a general surface of revolution, as it may well be in Sections 8 and 9, we obtain a surface integral

$$\pi\int r\left(P+\frac{1}{2}B^2\right)\left[\left(\xi\frac{\partial\zeta}{\partial z}-\zeta\frac{\partial\xi}{\partial z}\right)\mathrm{d}z+\left(\xi\frac{\partial\zeta}{\partial r}-\zeta\frac{\partial\xi}{\partial r}\right)\mathrm{d}r\right], \tag{E11}$$

which must be added to Eqs. (8.7), (9.8), and (9.15). This term, when reduced to a volume integral as in Eq. (E8), leads directly to Eqs. (8.9) and (10.2), and for this reason does not affect our final results in any way.

Acknowledgment

This work was performed under the auspices of the United States Atomic Energy Commission.

References

[1] Serrin, J., Handbuch der Physik, **Bd.VIII/1**, Springer-Verlag, Berlin (1959) 145—150, 203—206.
[2] Eckart, C., *Phys. Fluids* **3** (1960) 421.
[3] Katz, S., *Phys. Fluids* **4** (1961) 345.
[4] Bernstein, I. B., Frieman, E. A., Kruskal, M. D., Kulsrud, R. M., *Proc. Roy. Soc. (London)* **A244** (1958) 17.
[5] Hain, K., Lüst, R., Schlüter, A., *Z. Naturforsch.* **12a**. No. 10 (1957) 833.
[6] Frieman, E., Rotenberg, M., *Rev. Mod. Phys.* **32** (1960) 898.
[7] Lin, C. C., The Theory of Hydrodynamic Stability (Cambridge University Press, Cambridge, 1955) pp. 49—52.
[8] Cowling, T. G., Magnetohydrodynamics (Interscience Publishers, Inc., New York, 1957) 5—8.
[9] Newcomb, W. A., *Ann. Phys. (N.Y.)* **3** (1958) 347.
[10] Newcomb, W. A., *Ann. Phys. (N.Y.)* (to be published)
[11] Chew, G. F., Goldberger, M. L., Low, F. E., *Proc. Roy. Soc. (London)* **A236** (1956) 112.
[12] Chandrasekhar, S., Kaufman, A. N., Watson, K. M., *Ann. Phys. (N.Y.)* **2** (1957) 435.
[13] Chandrasekhar, S., Kaufman, A. N., Watson, K. M., *Ann. Phys. (N.Y.)* **5** (1958) 1.
[14] Kruskal, M. D., Oberman, C. R., *Phys. Fluids* **1** (1958) 275.
[15] Rosenbluth, M. N., Rostoker, N., *Phys. Fluids* **2** (1959) 23.
[16] Walén, C., *Arkiv. Mat. Astron. Fysik* **33 A** No. 18 (1946).
[17] Whittaker, E. T., A Treatise on the Analytical Dynamics of Particles and Rigid Bodies (Cambridge University Press, Cambridge, 1960) pp. 54—61.
[18] Whittaker, E. T., *ibid.* pp. 193—207.
[19] Tserkovnikov, Yu. A., Convective Instability of a Rarefied Plasma, Report No. T-2, Division of Theoretical Physics, Mathematical Institute of V. A. Steklov, Academy of Sciences of the U.S.S.R., Moscow (1960).
[20] Ferraro, V. C. A., *Monthly Notices Roy. Astron. Soc.* **97** (1937) 458.
[21] Alfvén, H., *Arkiv. Mat. Astron. Fysik* **29a** No. 19 (1943).
[22] Chandrasekhar, S., *Proc. Roy. Soc. (London)* **A216** (1953) 293.
[23] Chandrasekhar, S., *Mathematika* **1** (1954) 5.
[24] Newcomb, W. A., *Ann. Phys. (N.Y.)* **10** (1960) 232

КВАЗИЛИНЕЙНАЯ ТЕОРИЯ КОЛЕБАНИЙ ПЛАЗМЫ*

А. А. ВЕДЕНОВ, Е. П. ВЕЛИХОВ, Р. З. САГДЕЕВ

ИНСТИТУТ АТОМНОЙ ЭНЕРГИИ ИМ. И. В. КУРЧАТОВА,
АКАДЕМИИ НАУК СССР

МОСКВА, СОЮЗ СОВЕТСКИХ СОЦИАЛИСТИЧЕСКИХ РЕСПУБЛИК

Развивается метод исследования неравновесных процессов в системах с коллективными степенями свободы. Метод позволяет исследовать неравновесные состояния с сильно возбужденными (надтепловыми) колебаниями.

В применении к плазме метод заключается в том, что при рассмотрении неравновесных процессов учитывается воздействие самосогласованного поля колебаний на функцию распределения частиц. Функция распределения представляется в виде суммы медленно и быстро меняющихся частей. В уравнении для «медленной» функции распределения f_0 учитывается квадратичный усредненный эффект колебаний; для описания же самих колебаний используется обычная линейная теория, однако «фоном», на котором развиваются колебания, служит уже усредненная функция распределения f_0.

С помощью квазилинейного метода рассматривается задача о поглощении энергии волн конечной амплитуды в разреженной плазме. Показано, что для надтепловых колебаний затухание значительно уменьшается по сравнению с тем затуханием, которое дается обычной линейной теорией; величина декремента затухания при этом оказывается обратно пропорциональной плотности энергии волн ε. Выражение для декремента затухания γ, справедливое в области $\varepsilon \ll kT$, имеет вид:

$$\gamma = \gamma_0 [1 + A\,(\varepsilon/kT)\,N_D]^{-1}$$

где $A \sim 1$, N_D — число частиц в шаре с радиусом, равным дебаевскому радиусу, а γ_0 — декремент, получающийся в линейной теории.

Приведенная формула для затухания применима лишь в случае достаточно «широкого» пакета волн: $\Delta v_\varphi > (e\varphi_0/m)^{1/2}$ (где Δv_φ — разброс фазовых скоростей в пакете, а φ_0 — амплитуда потенциала). В противоположном предельном случае монохроматической волны «декремент затухания» зависит от амплитуды как $\varepsilon^{-3/4}$. Такая зависимость осуществляется, например, при затухании осцилляций внутри фронта ударных волн в разреженной плазме без магнитного поля. Полученные результаты обсуждаются в связи с задачами диагностики и проблемой высокочастотного нагрева плазмы.

Исследуются колебательные процессы в неустойчивой плазме при не слишком большом удалении от границы устойчивости. В качестве примера находится стационарный спектр шумов в плазме, по которой протекает электрический ток, в условиях, когда имеет место ионная электростатическая неустойчивость. Найдена амплитуда стационарных колебаний. В случае, когда плазма находится в сильном магнитном поле и ток идет вдоль этого поля, форма спектра колебаний дается выражением: $\varepsilon_k \sim x^3 (1-x^2)^{3/2}$, где ε_k — спектральная плотность энергии, $x = \omega_k/ks$, $s^2 = T_e/M$.

Обсуждаются пределы применимости развитой квазилинейной теории, нелинейные эффекты взаимодействия волн и переход к «турбулентному» режиму.

1. Введение

Характернейшей чертой плазмы является наличие семи ветвей спектра колебаний, обычно возбужденных значительно выше равновесного теплового уровня.

В настоящее время хорошо разработана лишь теория малых колебаний плазмы, основывающаяся на линеализованных уравнениях. Эта теория позволяет находить дисперсионные свойства плазмы для различного типа колебаний, а также условия, при которых последние самопроизвольно возрастают (неустойчивости плазмы). Однако, она не дает ответа на вопрос о том, до какой амплитуды раскачиваются колебания и как они влияют на процессы переноса в плазме — важнейший вопрос, возникающий в проблеме магнитной термоизоляции плазмы.

С другой стороны, нелинейные движения плазмы исследовались лишь в ряде частных случаев, при некоторых упрощающих предположениях. Так, например, рассматривались установившиеся плоские волны, когда остается зависимость лишь от одной пространственной координаты. Эти частные решения тем не менее показывают, что даже при малых, но конечных амплитудах, явления протекают иначе, чем их описывает линеаризованная теория. Так обстоит дело с затуханием Ландау, предсказываемым линеаризованной теорией и отсутствующим при нелинейном рассмотрении установившихся волн в плазме без столкновений. Причина этого, как известно, заключается в следующем: ответственными за поглощение волн в плазме являются частицы (ионы, электроны), находящиеся в резонансе с волной; даже при малых амплитудах распределение *из-за* обратного воздействия

* Доклад CN-10/199, представленный на Конференцию. Докладчик: Е. П. Велихов. Дискуссия (на английском языке) по этому докладу дана на стр. 493. Переводы аннотаций находятся в конце этого тома Трудов Конференции.

поля волны будет с течением времени сильно искажаться, чего не учитывает линейная теория. Естественно, что это обратное воздействие играет не меньшую роль и при раскачке колебаний в неустойчивой плазме.

2. Общий формализм квазилинейной теории

Итак, описание явлений при малых, но конечных амплитудах требует учета обратного воздействия колебаний на распределение частиц в пространстве скоростей.

Этот учет можно провести в рамках «квазилинейной» теории, изложению которой и посвящена настоящая статья. В квазилинейном приближении функция распределения частиц по скоростям представляется в виде суммы двух частей: $f_0(\mathbf{v}, t)$ — медленно меняющейся (мы будем называть ее «фоном») и $f_1(\mathbf{v}, t)$ — быстро меняющейся*. Медленное изменение «фона» вследствие обратного воздействия колебаний на частицы обусловлено усредненными квадратичными эффектами малых быстрых осцилляций. В этом смысле здесь имеет место аналогия с известным методом Ван-дер-Поля в нелинейной механике.

Существенно то обстоятельство, что квазилинейное приближение не учитывает взаимодействия между различными «гармониками» и «модами». Поэтому баланс энергии в $\mathbf{k}$-ой гармонике колебаний ($\mathbf{k}$ — волновой вектор) определяется, как и в линейной теории, уравнением $\mathrm{d}\varepsilon_k/\mathrm{d}t = 2\gamma\{f_0\}\varepsilon_k$, где γ — мнимая часть частоты, являющаяся функционалом «фона» f_0.

В качестве простейшего примера выведем уравнение квазилинейной теории для продольных электронных лэнгмюровских колебаний разреженной полностью ионизованной высокотемпературной плазмы. Для описания процессов в такой плазме можно, как известно, пользоваться кинетическим уравнением с самосогласованным полем E, пренебрегая эффектами столкновения частиц друг с другом:

$$\frac{\partial f}{\partial t} + v\frac{\partial f}{\partial x} + \frac{eE}{m}\frac{\partial f}{\partial v} = 0 \qquad (1\,\mathrm{a})$$

$$\frac{\partial E}{\partial x} = 4\pi Ne\left(\int f\,\mathrm{d}v - 1\right). \qquad (1\,\mathrm{b})$$

Разбивая функцию распределения на медленно и быстро меняющуюся части

$$f = f_0 + f_1,$$

(так что среднее значение быстро осциллирующей части равно нулю, $\langle f_1\rangle = 0$ и, следовательно, $\langle f\rangle = f_0$) и полагая

$$f_1 = \frac{1}{\sqrt{V}}\sum_k (f_k \mathrm{e}^{\mathrm{i}kx - \mathrm{i}\omega_k t} + \mathrm{c.c.})$$

$$E = \frac{1}{\sqrt{V}}\sum_k (E_k \mathrm{e}^{\mathrm{i}kx - \mathrm{i}\omega_k t} + \mathrm{c.c.}) \qquad (2)$$

получим, приравнивая справа и слева в уравнениях (1) осциллирующие члены, соотношение между f_1 и E:

$$f_k = \frac{e}{m}\frac{1}{\mathrm{i}(\omega_k - kv)}\frac{\partial f_0}{\partial v}E_k \qquad (3)$$

и обычные выражения для действительной и мнимой части ω_k, следующие из линейной теории,

$$\mathrm{Re}\,\omega_k = \Omega_k\{f_0\} \qquad (4\,\mathrm{a})$$

$$\mathrm{Im}\,\omega_k = \gamma_k\{f_0\}. \qquad (4\,\mathrm{b})$$

Уравнение для медленно меняющейся части функции распределения f_0 мы получим, подставляя выражение (2) для E и f_1 в (1a) и производя усреднение:

$$\frac{\partial\langle f\rangle}{\partial t} + v\frac{\partial\langle f\rangle}{\partial x} + \left\langle\frac{eE}{m}\frac{\partial(f_0 + f_1)}{\partial v}\right\rangle = 0. \qquad (5)$$

Для дальнейшего существенно отметить следующее: мы будем предполагать, что в плазме имеется одновременно много волн с различными волновыми векторами и хаотически распределенными фазами; таким образом, будут рассматриваться волновые пакеты достаточно большой ширины, чтобы можно было пренебречь захватом частиц в «потенциальные ямы» отдельных гармоник пакета. В рассматриваемом случае продольных лэнгмюровских колебаний для этого необходимо, чтобы разброс фазовых скоростей ω/k волн в пакете значительно превышал ту скорость, с которой захваченная волной частица двигалась бы в «потенциальной яме» $e\varphi_0$:

$$\Delta\left(\frac{\omega}{k}\right) \gg \left(\frac{e\varphi_0}{m}\right)^{1/2}. \qquad (6)$$

Если условие (6) выполнено, и, следовательно, захваченные частицы отсутствуют, то мы можем считать усредненную функцию распределения $\langle f\rangle = f_0$ однородной в пространстве, так что $\partial\langle f\rangle/\partial x = 0$. Учитывая, что $\langle Ef_0\rangle = \langle E\rangle f_0 = 0$, получаем из (5) следующее уравнение для «фона» f_0:

$$\frac{\partial f_0}{\partial t} = \frac{\partial}{\partial v}D\frac{\partial f_0}{\partial v}, \qquad (7)$$

где «коэффициент диффузии в пространстве скоростей» D пропорционален квадрату электрического поля волн:

$$D = \frac{e^2}{m^2}\sum_{kk'}\left\langle (E_{k'}\mathrm{e}^{\mathrm{i}k'x - \mathrm{i}\omega_{k'}t} + \mathrm{c.c.}) \times \left(\frac{E_k}{\mathrm{i}(\omega_k - kv)}\mathrm{e}^{\mathrm{i}kx - \mathrm{i}\omega_k t} + \mathrm{c.c.}\right)\right\rangle$$

$$= \frac{e^2}{m^2}2\pi\sum_k |E_k|^2\delta(\omega_k - kv). \qquad (8)$$

С другой стороны, скорость изменения энергии волн в спектральном интервале $(k, k + \mathrm{d}k)$ определяется формулой (4b), которая в случае длин-

* В линейной теории f_0 считается заданной функцией.

новолновых ($kR_D \ll 1$) электронных лэнгмюровских колебаний имеет вид:*

$$\frac{1}{E_k^2}\frac{\mathrm{d}E_k^2}{\mathrm{d}t} = 2\gamma_k\{f_0\} = \frac{\pi\omega^3}{k^2}\left(\frac{\partial F}{\partial v_\parallel}\right)_{v_\parallel=\omega/k} \qquad (9)$$

где $F(v_\parallel) = \int f_0\,\mathrm{d}v_\perp$ — распределение электронов по скорости, параллельной направлению распространения волны. Система уравнений квазилинейной теории (7), (8), (9) является замкнутой; она описывает обратное влияние лэнгмюровских колебаний на функцию распределения частиц. Следует сразу же заметить, что уравнение типа (7) имеет смысл рассматривать лишь в том случае, когда амплитуда колебаний значительно больше амплитуды тепловых шумов плазмы в соответствующем участке спектра, поскольку учет тепловых шумов фактически, как показано в [1], приводит лишь к изменению величины под знаком логарифма в кулоновском члене столкновений (что является превышением точности).

В тех случаях, когда это необходимо, учет столкновений производится нами лишь с логарифмической точностью. Поэтому эффектом тепловых шумов, плотность энергии которых по порядку величины равна NT/N_D, где N_D — число частиц в шаре дебаевского радиуса R_D, мы пренебрегаем, ограничиваясь изучением сильно «надтепловых» колебаний, плотность энергии которых $\varepsilon \gg NT/N_D$.

Следует отметить также то обстоятельство, что область применимости уравнений квазилинейной теории ограничена случаями, когда инкремент (или декремент) колебаний значительно меньше их частоты; если же это условие не выполнено, то разделение функции распределения на быстро осциллирующую и медленно меняющуюся части невозможно и уравнения типа (7), (8), (9) несправедливы.

Из вида уравнения (7) для усредненной функции распределения частиц f_0 ясно, что при возбуждении коллективных степеней свободы — волн — в плазме появляется кроме обычной «столкновительной» дополнительная диффузия в пространстве скоростей. Интересно, что отношение коэффициента «диффузии на волнах» D к коэффициенту «столкновительной диффузии» $D_0 \sim Ne^4/mv$ (где v — средняя тепловая скорость электронов)

$$\frac{D}{D_0} \sim \frac{\omega_e E^2/mN}{Ne^4/mv} \sim \frac{E^2/N}{e^2/R_D} \sim \frac{E^2}{NT}\cdot N_D, \qquad (10)$$

(где $N_D \sim NR_D^3$ — число частиц в шаре дебаевского радиуса R_D) по порядку величины равно отношению энергии волн (в расчете на одну частицу) E^2/N к энергии электростатического взаимодействия (также на одну частицу) e^2/R_D*. Таким образом, эффекты взаимодействия частиц с возбужденными коллективными степенями свободы проявляются тем сильнее, чем меньше неидеальность системы.

* При $kR_D \ll 1$, $\omega \approx \Omega_k = [\omega_e^2 + 3(T/m)k^2]^{1/2}$, $\omega_e^2 = 4\pi Ne^2/m$

** Последняя величина — известная «дебаевская поправка» к термодинамическим потенциалам кулоновской системы.

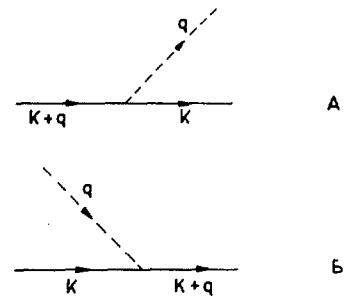

Рис. 1 Излучение (А) и поглощение (Б) волны частицей.

Для того, чтобы выяснить физический смысл квазилинейной теории и обобщить полученные уравнения (7)—(9) на случай произвольной системы с сильно возбужденными коллективными степенями свободы, будем рассматривать такую систему как совокупность двух газов — газа частиц и газа волн — и напишем уравнения сохранения частиц и волн в фазовом пространстве.

Рассмотрим сначала уравнение баланса числа частиц в пространстве скоростей (предполагая, что в координатном пространстве система однородна). Поскольку коллективные моды сильно возбуждены (так что плотность газа волн значительно превышает свое термодинамически равновесное значение), то мы можем учесть, в первом приближении, лишь процессы взаимодействия частиц с волнами. Основным процессом, влияние которого мы должны рассмотреть, является процесс «первого порядка»*: излучение или поглощение волны q частицей k (рис. 1).

Матричные элементы процессов 1А, 1Б пропорциональны, соответственно, $\sqrt{N_q}$ и $\sqrt{N_q+1}$, где N_q — число волн в единице объема фазового пространства;* однако в нашем случае $N_q \gg 1$, и, следовательно, вероятность обоих процессов одинакова и пропорциональна N_q:

$$W(k,q) = N_q W_{k,k+q}\,\delta(\varepsilon_i - \varepsilon_f)$$
$$(W_{k,k+q} = W_{k+q,k}). \qquad (11)$$

В результате излучения или поглощения волн частица меняет свой импульс и переходит в другую точку фазового пространства; изменение числа частиц в точке k фазового пространства складывается из „членов ухода“ вследствие поглощения

$$-\int \mathrm{d}q\, f_k N_q W_{k,k+q}\,\delta(\varepsilon_k + \hbar\omega_q - \varepsilon_{k+q}) \qquad (12a)$$

* Само описание возбужденных состояний системы с помощью двух газов — частиц и волн — предполагает малость взаимодействия между ними. Поэтому можно считать, что процессы высших порядков играют меньшую роль, чем процессы первого порядка по взаимодействию частиц с волнами. В частности, для таких систем с кулоновским взаимодействием, как разреженная плазма или сверхплотная электронная плазма, взаимодействие частиц с волнами имеет электродинамическую природу и пропорционально заряду частицы; слабость взаимодействия частиц с волнами связана в этом случае с малостью параметра $(e^2/\langle\varepsilon\rangle)/r$ (где $\langle\varepsilon\rangle$ — средняя энергия частиц, а r — среднее расстояние между ними), пропорционального квадрату заряда.

** Мы считаем, что волны подчиняются статистике Бозе.

и излучения

$$-\int \mathrm{d}q\, f_k N_q W_{k,k-q}\,\delta(\varepsilon_k - \hbar\omega_q - \varepsilon_{k-q}) \qquad (12\,\text{б})$$

и из аналогичных «членов прихода» из-за поглощения

$$+\int \mathrm{d}q\, f_{k-q} N_q W_{k-q,k}\,\delta(\varepsilon_{k-q} + \hbar\omega_q - \varepsilon_k) \qquad (12\,\text{в})$$

и излучения

$$+\int \mathrm{d}q\, f_{k+q} N q\, W_{k+q,k}\,\delta(\varepsilon_{k+q} - \hbar\omega_q - \varepsilon_k). \qquad (12\,\text{г})$$

Здесь f_k — функция распределения (диагональная часть матрицы плотности в k — представлении частиц), ε_k — кинетическая энергия частицы с волновым вектором $\mathbf{k}$, ε_q — энергия волны q.

Суммируя вклады различных процессов (12), получим для функции распределения частиц f_k уравнение

$$\frac{\partial f_k}{\partial t} = \int \mathrm{d}q\, N_q (\Psi_{k+q,q} - \Psi_{k,q}) \qquad (13\,\text{а})$$

$$\Psi_{k,q} = (f_k - f_{k-q})\, W_{k,k-q}\,\delta(\varepsilon_k - \varepsilon_{k-q} - \hbar\omega_q). \qquad (13\,\text{б})$$

Получим теперь аналогичным образом уравнение для функции распределения волн N_q. Изменение N_q происходит в результате рождения и уничтожения волн частицами,* так что в пространственно однородном случае ($\partial/\partial x = 0$)

$$\frac{\partial N_q}{\partial t} = -\int N_q W_{k,k+q} f_k\,\delta(\varepsilon_k + \hbar\omega_q - \varepsilon_{k+q})\,\mathrm{d}k + \int N_q W_{k+q,k} f_{k+q}\,\delta(\varepsilon_{k+q} - \hbar\omega_q - \varepsilon_k)\,\mathrm{d}k = N_q \int \Psi_{k+q,q}\,\mathrm{d}k. \qquad (14)$$

Уравнения (13) — (14) описывают неравновесные процессы в системах с сильно возбужденными коллективными степенями свободы (в случае, когда отсутствуют внешние силы $\mathbf{F}$ и нет пространственных градиентов**).

Если относительное изменение импульса частицы при рождении или уничтожении волны мало,

$$\frac{q}{k} \ll 1 \qquad (15)$$

то уравнение баланса частиц (13) принимает фоккер-планковский вид: действительно, разлагая в (13) функцию Ψ и разность $\Psi_{k+q,q} - \Psi_{k,q}$ по q, получаем

$$\Psi_{k,q} = q \frac{\partial f_k}{\partial k} W_{k,k-q}\,\delta\left(\frac{\hbar k q}{m} - \hbar\omega_q\right) \qquad (16)$$

и

$$\frac{\partial f_k}{\partial t} = \int \mathrm{d}q\, N_q \cdot q \frac{\partial}{\partial k}\left\{W_{k,k-q}\,\delta\left(\frac{\hbar k}{m} q - \hbar\omega_q\right) q \frac{\partial f_k}{\partial k}\right\}, \qquad (17)$$

т.е. уравнение Фоккер-Планка. В этом же приближении уравнение для N_q можно записать следующим образом:

$$\frac{\partial N_q}{\partial t} = N_q \int \mathrm{d}k\, W_{k,k-q}\,\delta\left(\frac{\hbar k}{m} - \hbar\omega_q\right) q \frac{\partial f_k}{\partial k}. \qquad (18)$$

В частности, для системы частиц с кулоновским взаимодействием — плазмы — относительное изменение импульса электрона при рождении (поглощении) кванта лэнгмюровских колебаний не превышает величины $\hbar\omega_p/\langle\varepsilon\rangle$ и мало в случае разреженной и сверхплотной плазмы, поэтому здесь применимы уравнения (17) — (18); в разреженной плазме

$$W_{k,k-q} = 4\pi^2 e^2 \frac{\hbar\omega_q}{q^2}$$

и (17) совпадает с выведенным ранее уравнением (7), а (18) переходит в обычную формулу линейной теории для инкремента (декремента) волн в плазме (9).

В случае произвольной системы с возбужденными коллективными модами уравнение баланса частиц не имеет Фоккер-Планковского вида; в настоящей работе мы рассмотрим лишь вопросы квазилинейной теории плазмы и поэтому будем пользоваться уравнениями типа (17)—(18) [или (7), (8), (9)].

Способом, использованным при выводе системы уравнений квазилинейной теории (7), (8), (9), можно получить аналогичные уравнения для плазмы в магнитном поле (см., напр., [2]); однако в этой работе мы не будем рассматривать общего случая, а ограничимся анализом ряда конкретных эффектов: развитие колебаний в неустойчивой плазме, поглощение в плазме волн конечной амплитуды и т.п.

3. Развитие неустойчивости

В этом разделе мы рассмотрим в рамках квазилинейной теории задачу о развитии неустойчивости в разреженной плазме. Ограничимся исследованием неустойчивости на лэнгмюровской ветви плазменных колебаний и будем считать, для простоты, задачу одномерной (функция распределения зависит лишь от проекции скорости частиц на одно выделенное направление и продольные лэнгмюровские колебания также происходят в этом направлении).*

Предположим, что в начальный момент времени распределение частиц в пространстве скоростей $f(0, v)$ имеет вид, изображенный на рис. 2А.; тогда в области, где производная $\partial f(0, v)/\partial v$ положительна, начинают раскачиваться лэнгмюровские колебания; спектральная плотность энергии этих колебаний растет по закону, см. (9):

$$\frac{\partial |E_k|^2}{\partial t} = |E_k|^2 \frac{\pi\omega^3}{k^2} \frac{\partial f}{\partial v}\Big]_{v=\omega/k}. \qquad (19)$$

---

* Здесь мы опять учитываем лишь процессы первого порядка и считаем $N_q \gg 1$.

** Для обобщения на случай $\mathbf{F} \neq 0$; $\partial/\partial x \neq 0$ достаточно заменить в левых частях уравнений (13а) и (14) частные производные $\partial f/\partial t$ на полные: $\mathrm{d}f/\mathrm{d}t = \partial f/\partial t + [\mathscr{H} f]$.

* Такая ситуация возникает, например, при наличии сильного магнитного поля, которое и выделяет это направление.

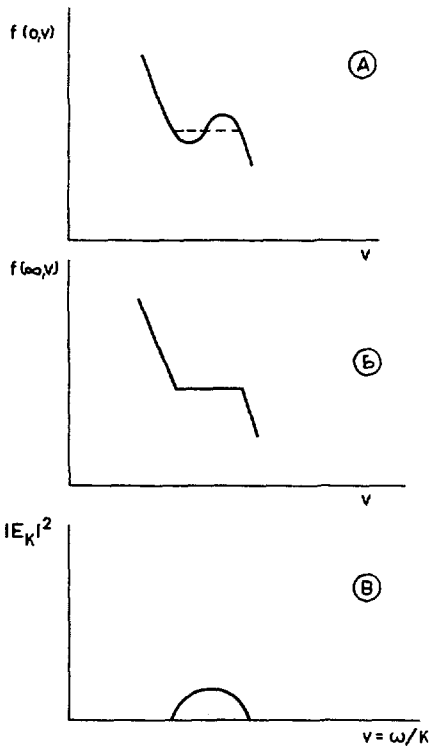

Рис. 2 Образование «плато» на функции распределения частиц (А—Б) и спектр колебаний при $t\to\infty$ (В).

Появление в плазме надтепловых шумов приводит, в свою очередь, к возникновению диффузии частиц в скоростном пространстве:

$$\frac{\partial f}{\partial t}=\frac{\partial}{\partial v}D\frac{\partial f}{\partial v} \tag{20}$$

причем коэффициент диффузии $D(t, v)$ связан в рассматриваемом случае с квадратом поля колебаний соотношением:

$$D=2\pi\frac{e^2}{m^2}\int|E_k|^2\delta(\omega-kv)\frac{dk}{2\pi}=\frac{e^2}{m^2}|E_k|^2\frac{1}{v}, \tag{21}$$

поскольку в рассматриваемом здесь случае длинных волн частота ω совпадает с плазменной частотой $(4\pi N e^2 m)^{1/2}$ и, следовательно, скорость резонансных частци обратно-пропорциональна волновому вектору: $v=\omega/k$.

В результате диффузии начальное распределение частиц сглаживается и в области скоростей $v_1<v<v_2$ появляется «плато» (рис. 2Б) [3]. В то же время в области волновых чисел $\omega/v_2<k<\omega/v_1$ устанавливается стационарный* спектр надтепловых шумов. Форму этого стационарного спектра и величину спектральной плотности энергии можно найти следующим образом.

* Производная по скорости от функции распределения в области плато обращается в нуль, так что колебания не возрастают и не затухают.

Интегрируя (19) по времени и пренебрегая энергией тепловых шумов по сравнению с энергией раскачивающихся колебаний, находим спектральную плотность $|E_k|^2(t)$ надтепловых шумов:

$$|E_k|^2(t)=\frac{\pi\omega^3}{k^2}\int_0^t dt\,|E_k|^2\frac{\partial f}{\partial v}. \tag{22}$$

С другой стороны, интегрируя (20) по времени и по скорости v в пределах от v_1 до v, используя (21) и учитывая еще, что при $v=v_1$ $D\partial f/\partial v=0$, получаем:

$$\int_{v_1}^{v}[f(t,v')-f(0,v')]\,dv'=\frac{e^2}{m^2}\frac{1}{v}\int_0^t|E_k|^2\frac{\partial f}{\partial v}\,dt. \tag{23}$$

Сравнивая (22) с (23), находим спектральную плотность шумов:

$$|E_k|^2(t)=\frac{\pi m^2}{e^2}\omega v^3\int_{v_1}^{v}[f(t,v')-f(0,v')]\,dv'. \tag{24}$$

По окончании процесса выравнивание функции распределения, когда в области $v_1<v<v_2$ устанавливается плато $f(\infty, v)=\text{const}$, искомый стационарный спектр надтепловых лэнгмюровских колебаний полностью определяется начальной и конечной функциями распределения:

$$|E_k|^2(\infty)=\frac{\pi m^2}{e^2}\omega v^3\int_{v_1}^{v}|f(\infty,v')-f(0,v')]\,dv', \tag{25}$$

(вид этого спектра приведен на рис. 2А). Как следует из (25), спектральная плотность шумов обращается в нуль в точках $k_1=\omega/v_1$ и $k_2=\omega/v_2$*, а ее детальная зависимость от k определяется конкретным видом начальной функции распределения частиц по скоростям.

Возникающее в результате развитие неустойчивости и диффузии плазма с «плато» на электронном распределении обладает тем свойством, что возбуждаемые из вне продольные лэнгмюровские волны могут распространяться в ней без затухания, если их фазовая скорость v_f лежит в области плато $v_1<v_f<v_2$.

Плотность энергии надтепловых шумов, устанавливающихся по окончании процесса диффузии, по порядку величины равна

$$E^2=\int 2|E_k|^2\,dk\,(2\pi)^{-1}\sim\delta n\,(mv_2^2-mv_1^2), \tag{26}$$

где δn — плотность той части электронов, которые диффундируют в пространстве скоростей в резуль-

* Интеграл в правой части (25) обращается в нуль при $v=v_2$ в силу закона сохранения числа частиц:

$$\int_{v_1}^{v_2}f(0,v')\,dv'=\int_{v_1}^{v_2}f(\infty,v')\,dv'$$

тате испускания и поглощения коллективных лэнгмюровских колебаний, постепенно изменяя свою кинетическую энергию.

Мы видим, таким образом, что изложенная выше квазилинейная теория позволяет ответить на вопрос о том, в какое состояние переходит неустойчивая в начальный момент плазма в результате развития в ней кинетической неустойчивости, и каковы функция распределения частиц и спектр коллективных колебаний в конечном состоянии. При этом оказывается, что в разреженной плазме релаксационный процесс в пространстве скоростей имеет две стадии: сначала функция распределения частиц $f(v)$ быстро выравнивается вблизи области, где имелась положительная производная $\partial f/\partial v$, и лишь затем, гораздо медленнее, функция распределения стремится к термодинамически равновесной. Квазилинейная теория описывает именно первую стадию — установление «плато» на функции распределения и возникновения надтепловых шумов. Если ширина «плато» невелика, то система уравнений (19)—(21), описывающих этот процесс, может быть приведена к следующему одному уравнению для коэффициента диффузии D:

$$\frac{\partial D}{\partial t} = D\frac{\partial^2 D}{\partial v^2} + \Phi \cdot D \qquad (27)$$

причем функция Φ зависит только от скорости v и с точностью до множителя совпадает с производной $\partial f/\partial v$ в начальный момент времени

$$\Phi(v) = \pi\omega v^3\, \partial f(0, v)/\partial v. \qquad (28)$$

Заметим, что стационарное решение уравнения (27), которое можно получить, положив в нем $\partial/\partial t = 0$, приводит с учетом (28) к формуле для спектральной плотности надтеплового шума (25).

С помощью (27) можно исследовать весь процесс развития колебаний в неустойчивой в начальный момент времени плазме и установление плато на функции распределения частиц $f(v)$. Длительность всего этого процесса τ по порядку величины равна

$$\tau \sim \frac{(v_2 - v_1)^2}{D(\infty)} \sim \left(\frac{v_2 - v_1}{\sqrt{T_e/m}}\right)^2 \cdot \frac{n}{\delta n}\,\frac{T/m}{(v_2 + v_1)^2}\,\frac{1}{\omega_e}. \qquad (29)$$

4. Поглощение волн в плазме

Как известно, линейная теория малых колебаний разреженной плазмы предсказывает наличие «бесстолкновительного затухания» волн, распространяющихся в плазме. Типичным примером такого «бесстолкновительного затухания» является уменьшение амплитуды продольных электронных лэнгмюровских волн, возбуждаемых на границе плазмы внешним электрическим полем частоты $\omega > \omega_e$ и распространяющихся вглубь плазмы перпендикулярно границе. Для длинноволновых колебаний ($k R_D \ll 1$), которые мы только и будем рассматривать, падение амплитуды волны по мере прохождения вглубь плазмы дается следующим выражением:*

$$\frac{|E_k|^{2\prime}}{|E_k|^2} = \frac{\pi}{3}\,\frac{\omega_e^4}{k^3}\,\frac{m}{T}\left(\frac{\partial f}{\partial v}\right)_{v=\omega/k} \qquad (30)$$

здесь ω_e — плазменная частота, k — волновой вектор, $f(v)$ — функция распределения электронов по компоненте скорости, параллельной направлению распространения волн, а штрих означает дифференцирование по координате x.

Таким образом, энергия пакета волн бесконечно малой амплитуды с различными, но близкими частотами (и, соответственно, волновыми векторами) падает экспоненциально с расстоянием от границы, причем пространственный декремент этого затухания определяется формулой (30) с $f = (2\pi T/m)^{-1/2} \exp(-mv^2/2T)$ (рис. 3А).

Если, однако, мы рассмотрим распространение волн малой, но конечной амплитуды, то затухание их коренным образом изменится. Действительно, из уравнения квазилинейной теории разреженной плазмы для усредненной функции распределения электронов f

$$v\frac{\partial f}{\partial x} = \frac{\partial}{\partial v} D \frac{\partial f}{\partial v} \qquad (31\,а)$$

$$D = 2\pi\frac{e^2}{m^2}\sum_k |E_k|^2 \delta(\omega - kv) = \frac{e^2}{m^2}\,\frac{|E_k|^2}{v} \qquad (31\,б)^*$$

следует, что диффузия частиц в пространстве скоростей при испускании и поглощении лэнгмюровских колебаний резко уменьшает производную $\partial f/\partial v$, т.е. по формуле (30) затухание волн по мере прохождения через плазму. В области скоростей резонансных частиц решение системы уравнений (30)—(31) есть

$$f(v, x) = \text{const},$$

$$\frac{\partial}{\partial x}|E_k|^2 = 0, \qquad (32)$$

т.е. волны вообще не затухают (рис. 1Б).

В действительности затухание волн имеет хотя и малую, но конечную величину; это связано с тем,

---

* Это выражение справедливо на расстояниях от границы, больших нескольких длин волн; эффектами пограничной области, где (30) неприменимо, мы не интересуемся. Заметим, что (30) следует из уравнения

$$\frac{\partial N_q}{\partial t} + [\mathscr{H} N_q] = N_q \int dk\, W_{k,k-q}\,\delta\left(\frac{\hbar k q}{m} - \hbar\omega_q\right) q\,\frac{\partial f_k}{\partial q}$$

если учесть, что в рассматриваемом случае $\partial/\partial t = 0$

$$W = 4\pi^2\,\frac{\hbar\omega}{q^2},$$

$$[\mathscr{H} N_q] \equiv \frac{\partial \mathscr{H}_q}{\partial q}\cdot\frac{\partial N_q}{\partial x} - \frac{\partial \mathscr{H}_q}{\partial x}\cdot\frac{\partial N_q}{\partial q} \approx 3\,\frac{k}{\omega}\,\frac{T}{m}\,\frac{\partial N_q}{\partial x}.$$

* Волновой вектор k и скорость резонансной частицы v в рассматриваемом случае связаны однозначно: $v = \omega/k$. Выражение (31б) предполагает, что генератор, создающий на границе волну, не создает в то же время свободно летящих резонансных частиц, т.е. некоторое определенное граничное условие. В обратном случае, при наличии свободно летящих резонансных частиц, результаты качественно не изменяются.

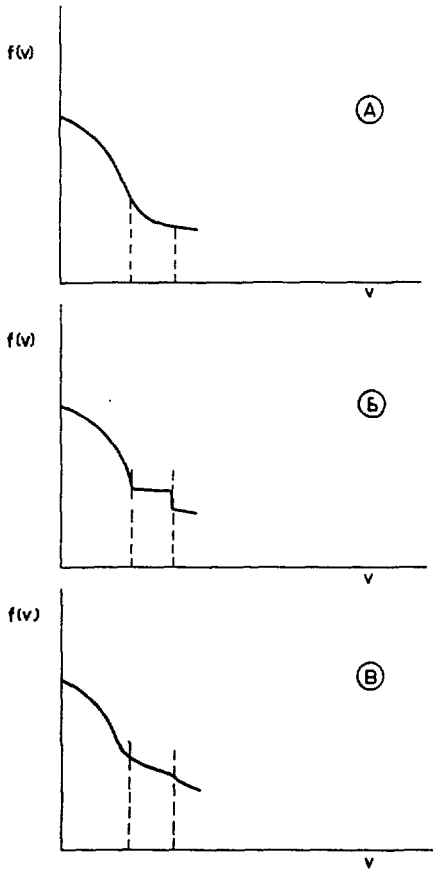

Рис. 3 Искажение функции распределения частиц $f(v)$ под действием пакета лэнгмюровских волн.

что столкновения частиц друг с другом стремятся восстановить термодинамическое равновесие — приблизить функцию распределения электронов к максвелловской, т.е. сделать производную $\partial f/\partial v$ отрицательной (рис. 1В). Для того, чтобы найти величину появляющегося при этом слабого затухания волн нужно ввести в уравнение (2) для усредненной функции распределения f член столкновений. В рассматриваемом случае длинных волн член столкновений имеет вид

$$\mathrm{St}\, f = \frac{\partial}{\partial v} \nu_s \left(v f + \frac{T}{m} \frac{\partial f}{\partial v} \right), \tag{33}$$

где «частота столкновений» ν_s равна

$$\nu_s = S/v^3, \tag{34}$$

где S по порядку величин равно ω_e^4/N.

С учетом столкновений между частицами уравнение для функции распределения электронов плазмы принимает вид

$$v \frac{\partial f}{\partial x} = \frac{\partial}{\partial v} D \frac{\partial f}{\partial v} + \mathrm{St}\, f, \tag{35}$$

где $\mathrm{St}\, f$ дается выражением (33), а D — формулой (31б).

Если амплитуда волн в пакете не слишком мала, так что выполняется неравенство

$$\frac{E^2}{4\pi NT} \gg \frac{1}{(N_D)^{1/2}}, \tag{36}$$

(где $E^2/4\pi$ — плотность энергии волн), то, как показывает оценка, левой частью (35) можно пренебречь. При этом производная функции распределения, как следует из (35), равна

$$\frac{\partial f}{\partial v} = -\nu_s \frac{vf}{D}. \tag{37}*$$

Если ширина пакета не очень велика, $\Delta(\omega/k) \ll \sqrt{T/m}$, то как видно из рис. 3, функция распределения (но не ее производная) изменяется под действием волн незначительно, так что в правой части (37) мы можем заменить f на максвелловскую функцию распределения $f_M = (m/2\pi T)^{1/2} \exp(-mv^2/2T)$ и, подставляя получающееся значение производной $\partial f/\partial v = -\nu_s v f_M/D$ в (35), находим

$$\frac{|E_k|^{2\prime}}{|E_k|^2} = -\frac{\pi}{3} \frac{\omega_e^4}{k^3} \frac{m}{T} \nu_s \frac{v f_M}{D} \tag{38}$$

или, учитывая (31 б), приходим к уравнению, определяющему пространственный ход $|E_k|^2$:

$$\frac{\partial |E_k|^2}{\partial x} = -\frac{\pi}{3} \frac{\omega_e^4}{k^3} v^2 \frac{m^2}{T} \nu_s \frac{f_M}{e^2}. \tag{39}$$

Из (39) следует, что энергия волнового пакета падает линейно по мере удаления от границы по закону (рис. 4)

$$\frac{|E_k|^2(x)}{|E_k|^2(0)} = 1 - \frac{x}{L}, \tag{40}$$

где характерная длина L (на которой происходит затухание волн, возбуждаемых на границе) прямо-

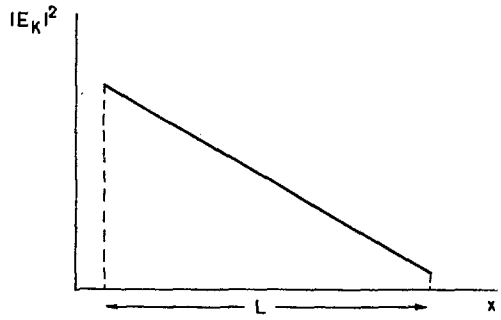

Рис. 4 Затухание лэнгмюровских волн в плазме.

пропорциональна энергии волн на границе и по порядку величины равна

$$L \sim k^{-1} \frac{v^2}{T/m} \frac{NT}{E^2} \frac{1}{N_D}, \tag{41}$$

т.е. значительно превышает длину затухания в линейной теории, если энергия волн превышает энергию тепловых шумов, $E^2/NT \geqslant 1/N_D$ (напомним, что в рассматриваемом случае $E^2/NT \geqslant 1/(N_D)^{1/2}$).

В заключение этого раздела заметим, что рассмотренное уменьшение поглощения волн конечной амплитуды в разреженной плазме (см. также [2]) следует учитывать при расчете нагрева плазмы в. ч. полем.

* т. к. в интересующей нас области скоростей (T/m) $(\partial f/\partial v)$ пренебрежимо мало по сравнению с vf.

5. Плазма в постоянном электрическом поле

В настоящем разделе мы рассмотрим квазилинейную теорию плазмы, находящейся в постоянном электрическом поле E. При включении поля E по плазме протекает ток $j=\sigma E$; удельное сопротивление плазмы σ^{-1} состоит из двух слагаемых: первое определяется столкновениями частиц друг с другом, а второе — взаимодействием носителей заряда с флуктуирующими электрическими полями.

При увеличении электрического поля E средняя направленная скорость электронов v_a увеличивается; при некоторой критической скорости v_c состояние плазмы становится неустойчивым, и в ней раскачиваются низкочастотные колебания — ионный звук [3]. Амплитуда и спектр этих колебаний определяются балансом между потоком энергии, поступающим в колебания от электронов, движущихся в постоянном электрическом поле E, и потоком энергии, диссипируемой в колебаниях. Диссипация энергии может определяться двумя процессами: переносом энергии по спектру колебаний от одних мод к другим (перенос между коллективными степенями свободы) и непосредственным переходом энергии колебаний в тепло при столкновениях частиц. Характерное время переноса энергии по спектру стремится к бесконечности при стремлении амплитуды колебаний к нулю, тогда как характерное время диссипации энергии при столкновениях отдельных частиц остается в этом пределе конечным. Поэтому при небольшой надкритичности (т.е. незначительном превышении v_c) форма спектра колебаний и их уровень определяются балансом между энергией, поступающей от движущихся электронов, и энергией, диссипируемой при парных столкновениях частиц, и могут быть найдены с помощью формализма квазилинейной теории, развитого в § 1.

Для простоты рассмотрим неполностью ионизированную плазму, в которой преобладающую роль играют столкновения носителей заряда с нейтралами. При этом мы ограничимся случаем, когда частота столкновений ν_s значительно меньше частоты колебаний ω, так что в колебаниях нейтралы участия не принимают. Мы будем рассматривать плазму, помещенную в сильное магнитное поле, так что для ионно-звуковой ветви длина волны колебаний будет значительно превышать ларморовский радиус ионов.

Дисперсионное уравнение (42) для ионных колебаний в сильном магнитном поле можно получить с помощью разложения кинетического уравнения для быстроосциллирующей части функции распределения по отношению характерной частоты колебаний к ионной циклотронной частоте:

$$k^2 \equiv \omega_{pe}^2 \int \frac{F_e'(v_\parallel)\,(v_\parallel-\omega/k_\parallel)\,dv_\parallel}{(v_\parallel-\omega/k_\parallel)^2+\nu_e^2/k_\parallel^2} + \omega_{pi}^2 \int \frac{F_i'(v_\parallel)\,(v_\parallel-\omega/k_\parallel)\,dv_\parallel}{(v_\parallel-\omega/k_\parallel)^2+\nu_i^2/k^2}. \qquad (42)$$

Условие баланса потоков энергии (43) имеет вид

$$0 = \omega_{pe}^2 \int \frac{F_e'(v_\parallel)\,\nu_e/k_\parallel\,dv_\parallel}{(v_\parallel-\omega/k_\parallel)^2+\nu_e^2/k_\parallel^2} + \omega_{pi}^2 \int \frac{F_i(v_\parallel)\,\nu_i/k_\parallel\,dv_\parallel}{(v_\parallel-\omega/k_\parallel)^2+\nu_i^2/k_\parallel^2}, \qquad (43)$$

$\omega_{pe}^2 \equiv \omega_e^2 = 4\pi Ne^2/m$; $\omega_{pi}^2 \equiv \omega_i^2 = 4\pi Ne^2/M$.

В уравнениях (42)—(43)

$$F_{e,i}(v_\parallel) = 2\pi \int f_{e,i}(\varepsilon_\perp, v_\parallel)\,d\varepsilon_\perp$$

представляет собой стационарную часть функции распределения электронов (ионов) по скорости $v_\parallel$, параллельной направлению постоянного магнитного поля,* а $k_\parallel$ — проекция волнового вектора на это направление.

Как известно, ионно-звуковые колебания существуют в плазме только в том случае, когда электронная температура T_e значительно превышает температуру ионов T_i; в этом случае уравнения (42) и (43) принимают вид

$$k^2 = \omega_i^2\left(\frac{k_\parallel^2}{\omega^2}-\frac{1}{c^2}\right), \qquad (42')$$

$$F_e'(v_\parallel) = \frac{2}{\pi}\frac{m}{M}\nu_i \frac{1}{v_\parallel^2\,\omega\,(k, v_\parallel)}. \qquad (43')$$

Здесь $$c^2 = -\left\{\frac{M}{m}\int \frac{F_e'(v_\parallel)}{v_\parallel-\omega/k_\parallel}\,dv_\parallel\right\}^{-1} \sim \frac{T_e}{M}$$

представляет собой скорость ионного звука в пределе низких частот ($\omega \to ck_\parallel$, при $\omega \to 0$). Находя из (42′) частоту $\omega\,(k, v_\parallel)$ и подставляя в (43′), получаем условие стационарности для волны, направленной под углом $\vartheta = \arccos k_\parallel/k$ к магнитному полю:

$$F_e'(v_\parallel) = \frac{2}{\pi}\frac{m}{M}\nu_i \frac{1}{v_\parallel^2\,\omega_i\cos\vartheta\sqrt{1-v_\parallel^2/c^2}}. \qquad (44)$$

Правая часть (44) монотонно возрастает с ростом ϑ; поэтому, если для чисто продольных волн ($\vartheta=0$) выполнено условие стационарности

$$F_e'(v_\parallel) = \frac{2}{\pi}\frac{m}{M}\nu_i \frac{1}{v_\parallel^2\,\omega_i\sqrt{1-v_\parallel^2/c^2}}, \qquad (45)$$

то все «косые» ($\vartheta>0$) волны затухают, т.к. для них, в соответствии с (44), диссипация энергии в результате столкновений ионов с нейтралами превышает приток энергии от резонансных электронов. Таким образом, в стационарном состоянии в плазме присутствуют лишь волны, направленные вдоль магнитного поля.

Вид функции распределения электронов, резонирующих со стационарным фоном ионно-звуковых волн, можно определить из уравнения (45); получающееся при этом выражение для функции распределения справедливо в ограниченной области скоростей — там, где дрейф электронов под действием постоянного электрического поля поддерживает стационарный уровень колебаний.

Согласно линейной теории неустойчивость возникает в той области пространства скоростей, где $F_e'(v_\parallel)$ превышает правую часть (45).

* Магнитное поле тока, протекающего по плазме, мы считаем малым и всюду им пренебрегаем.

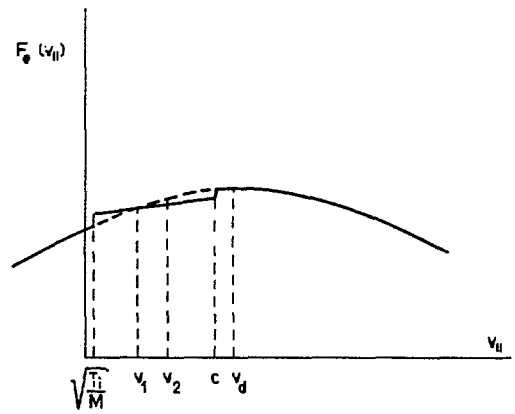

Рис. 5 Функция распределения электронов $F_e(v_\parallel)$ в электрическом поле.

На рис. 5 изображена «первоначальная» область неустойчивости 1—2. Однако, как мы видели в п. 1, за время порядка нескольких периодов колебаний такая неустойчивость распространяется на весь спектр ионных звуковых колебаний, фазовая скорость которых $\omega/k_\parallel$ лежит между средней тепловой скоростью ионов $(T_i/M)^{1/2}$* и скоростью $c\sim(T_e/M)^{1/2}$. В этой области функция распределения электронов по продольным скоростям искажается и принимает вид, изображенный на рис. 5 пунктиром.

Спектр колебаний в этой области можно получить из следующих соображений.

В соответствии с общим формализмом квазилинейной теории (§ 1), учет обратного воздействия колебаний на электроны приводит к уравнению для стационарной функции распределения $F_e(v_\parallel)$

$$\frac{e}{m}E\frac{\partial F_e}{\partial v_\parallel}+\frac{\omega_e^2}{m}\frac{\partial}{\partial v_\parallel}\frac{\varepsilon_k/N}{v_\parallel(1-v_\parallel^2/c^2)}\frac{\partial F_e}{\partial v_\parallel}=0, \quad (46)$$

где $\varepsilon_k=E_k^2/4\pi$, $(k=\omega/v_\parallel)$ — спектральная плотность электростатической энергии. В уравнении (46) первое слагаемое описывает изменение электронного распределения под действием постоянного электрического поля E, а второе слагаемое вызвано обратным воздействием возбужденных волн на резонансные частицы.

Интегрируя (46), получаем выражение для спектральной плотности энергии:

$$\frac{\varepsilon_k/R_D}{NT_e}\frac{v_e}{v_i}\left(\frac{M}{m}\right)^{3/2}=x^3(1-x^2)^{3/2}\sqrt{\frac{T_e}{m}}\times\left\{\int\frac{v_a}{c}F_e\,dv_\parallel+c'\right\}, \quad (47)$$

где «электронный дебаевский радиус» $R_D=\sqrt{T_e/m}/\omega_e$, $x\equiv v_\parallel/c$.

Постоянную интегрирования в (47) мы найдем, налагая требование минимальности полной энергии в спектре колебаний. Требование минимальности заключается в следующем. В том диапазоне пространства скоростей, где выполнено условие (44), могут не затухая распространяться ионно-звуковые волны (например, от какого-то внешнего источника). Если спектр этих волн таков, что

$$\frac{\varepsilon_k}{v_\parallel(1-v_\parallel^2/c^2)}\frac{\partial F_e}{\partial v_\parallel}=\text{const.},$$

то они не дают вклада в диффузию электронов, т.е. вообще не взаимодействуют с плазмой. Поэтому определение спектра возможно лишь с точностью до такого пакета невзаимодействующих, «посторонних» волн. Требование минимальности энергии исключает этот пакет. Чтобы удовлетворить этому требованию, мы должны добавить к монотонно-возрастающей (в рассматриваемой области) функции

$$\frac{v_a}{c}\int F_e'(v_\parallel)\,dv_\parallel=-\alpha\frac{\sqrt{1-x^2}}{x^2},$$

где $\alpha=(2/\pi)(v_a/c)(m/M)(\nu_i/\omega_i)$ постоянное положительное слагаемое

$$c'=\alpha\frac{\sqrt{1-x_0^2}}{x_0}, \quad x_0\cong\sqrt{T_i/T_e}.$$

Следовательно, спектр ионно-звуковых колебаний имеет вид:

$$\frac{\varepsilon_k/R_D}{NT_e}=2\left(\frac{m}{M}\right)^{3/2}\frac{\nu_e}{\omega_e}\times\left\{\frac{\sqrt{1-x_0^2}}{x_0}-\frac{\sqrt{1-x^2}}{x}\right\}\bar{x}\cdot x^3(1-x^2)^{3/2},$$

$$\bar{x}\equiv v_a/c. \quad (48)$$

Как мы уже упоминали, ионный звук существует лишь при $T_i/T_e\ll 1$, т.е. $x_0\ll 1$. Поэтому почти во всей области частот спектральная плотность дается следующей формулой:

$$\frac{\varepsilon_k/R_D}{NT_e}\simeq\left(\frac{m}{M}\right)^{3/2}\frac{T_e}{T_i}(\omega_i\tau_i)\bar{x}\cdot x^3(1-x^2)^{3/2} \quad (\tau_i\equiv 1/\nu_i). \quad (49)$$

Полная плотность электростатической энергии ионно-звуковых колебаний равняется

$$\frac{E^2}{8\pi NT_e}\sim\frac{1}{60\pi^2}\frac{T_e}{T_i}(\omega_i\tau_i)\bar{x}. \quad (50)$$

Из формулы (49) можно найти распределение энергии в низкочастотной части спектра (обычно измеряемое на эксперименте)

$$\varepsilon_\omega=\frac{\varepsilon_k}{d\omega/dk}\approx\frac{\varepsilon_k}{c}=\frac{NT_e}{\omega_i}\left(\frac{m}{M}\right)^{3/2}\frac{T_e}{T_i}(\omega_i\tau_i)\bar{x}\left(\frac{\omega}{\omega_i}\right)^3. \quad (51)$$

Влияние этих колебаний на процессы переноса в однородной плазме мало, так как:

1) Спектр является одномерным ($E_k\parallel H$) поэтому электрические поля колебаний не могут привести к появлению «аномальной диффузии» частиц поперек магнитного поля.

* Вблизи ионной тепловой скорости наступает сильное резонансное поглощение колебаний на ионах, более чем в $\sqrt{M/m}$ раз превышающее раскачку электронами.

2) В пространстве скоростей колебания «занимают» малую область $(c/(T_e/m)^{1/2} \simeq \sqrt{m/M})$. С точки зрения протекания электрического тока электроны можно разбить на две группы: резонансные электроны, тормозящиеся на ионных колебаниях, и нерезонансные электроны, тормозящиеся при столкновениях с нейтралами. Так как во второй группе в $\sqrt{M/m}$ раз больше электронов, влияние дополнительного «коллективного» сопротивления в данном случае мало.

6. Влияние циклотронных волн на время жизни частиц в ловушке с магнитными пробками

Причиной появления неустойчивости и шумов в ловушках с магнитными пробками* может явиться анизотропия функции распределения частиц в пространстве скоростей. Эта анизотропия не только может быть вызвана соответствующей инжекцией или нагревом плазмы, но и органически присуща самому способу удержания: вблизи точек поворота частиц их продольная энергия полностью переходит в поперечную.

Как известно, в результате такой анизотропии в плазме раскачивается электромагнитная волна, поляризованная по кругу [3]. Фазовая скорость волны велика (порядка альфвеновской). Поэтому для того, чтобы в распределении частиц по скоростям оказались резонансные частицы, для которых из-за допплер-эффекта частота волны равна ларморовской частоте, необходимо, чтобы

$$v_\parallel = \frac{\omega \pm \omega_H}{K_\parallel} \sim \sqrt{\frac{T}{m}},$$

поскольку $\omega/k_\parallel \sim H/\sqrt{4\pi N M} > \sqrt{T/M}$, то это возможно лишь при выборе знака минус, который соответствует волне с круговой поляризацией в направлении вращения частиц.

Рассмотрим усредненное влияние такой волны на движение частиц в пространственно-однородной плазме. Для простоты ограничимся случаем чисто продольного распространения. Под действием вращающихся электрического

$$E_- = E_x - \mathrm{i}\, E_y \tag{52}$$

и магнитного

$$H_- = -\frac{\mathrm{i}c}{\omega} k E_- = H_x - \mathrm{i}\, H_y \tag{53}$$

полей волны с волновым числом k изменение функции распределения частиц f_k в пространственно-однородной плазме равно:

$$f_k = \mathrm{i}E_{-k}\frac{1}{\omega_k}\frac{(\omega_k - k v_\parallel)(\partial f_0/\partial v_\perp) + k v_\perp (\partial f_0/\partial v_\parallel)}{\omega - k v_\parallel - \omega_{H\alpha}}\frac{e_\alpha}{2 m_\alpha} e^{\mathrm{i}\varphi} \tag{54}$$

Здесь f_0 — усредненная по многим колебаниям функция распределения частиц по скоростям, $v_\parallel$, $v_\perp$ и φ — цилиндрические координаты в пространстве скоростей, e_α и m_α — заряд и масса частиц.

* В дальнейшем мы всюду предполагаем, что магнитогидродинамическая неустойчивость таких систем устранена соответствующей стабилизацией.

Уравнение для функции f_0 получается путем усреднения уравнения Больцмана по малым осцилляциям, при этом получаем:

$$\frac{\mathrm{d}f_0}{\mathrm{d}t} = \left\langle \sum_{kk'} \left[\left(\mathbf{E}_k + \frac{\mathbf{v}\times\mathbf{H}_k}{c}\right) e^{-\mathrm{i}\omega_k t + \mathrm{i}kz} + \text{c.c.}\right] \times \left[\frac{\partial f_{k'}}{\partial \bar{v}} e^{-\mathrm{i}\omega_k t + \mathrm{i}k'z} + \text{c.c.}\right]\right\rangle . \tag{55}$$

Это приводит к уравнению:

$$\frac{\mathrm{d}f_0}{\mathrm{d}t} = \left\{\left(1 - \frac{k v_\parallel}{\omega_k}\right)\frac{1}{v_\perp}\frac{\partial}{\partial v_\perp} v_\perp + v_\perp \frac{\partial}{\partial v_\parallel}\frac{k}{\omega_k}\right\} D_H \times \left\{\left(1 - \frac{k v_\parallel}{\omega_k}\right)\frac{\partial}{\partial v_\perp} + \frac{k v_\perp}{\omega_k}\frac{\partial}{\partial v_\parallel}\right\} f_0, \tag{55 а}$$

где

$$D_H = \frac{1}{4}\frac{|E_k|^2}{|\mathrm{d}\omega/\mathrm{d}k - v_\parallel|}\frac{e_\alpha^2}{m_\alpha^2},$$

а между $v_\parallel$ и ω_k имеется следующая связь:

$$v_\parallel = \frac{\omega_k - \omega_{H\alpha}}{k}.$$

Таким образом под действием волн изменяется как продольная скорость частиц, так и поперечная, т.е. магнитный момент $\mu_\alpha = m_\alpha v_\perp^2/2H$. Уравнение (55) имеет вид уравнения Фоккер-Планке в пространстве скоростей. В результате «диффузии» функция распределения выравнивается вдоль линий

$$v_\parallel - \frac{v_\perp^2 k}{2\omega_{H\alpha}} = \text{const}.$$

Так как рассматриваются волны малой амплитуды, для которых перенос энергии от одной Фурье-гармоники к другой ничтожно мал по сравнению с потоком энергии от частиц, то изменение энергии волн или пропорционального ей «коэффициента диффузии» D_H определяется из обычной линейной теории:

$$\frac{\mathrm{d}\ln D_H}{\mathrm{d}t} = 2\gamma\{f_0\}, \tag{56}$$

где $\gamma \equiv \mathrm{Im}\,\omega_k$, в свою очередь, может быть найдено из дисперзионного уравнения для малых колебаний:

$$\frac{k^2 c^2}{\omega^2} - 1 = \frac{1}{2}\sum_\alpha \frac{\omega_\alpha^2}{\omega^2}\int \frac{(\omega - k v_\parallel)(\partial f_0/\partial v_\perp) + k v_\perp (\partial f_0/\partial v_\parallel)}{\omega - \omega_{H\alpha} - k v_\parallel} v_\perp \,\mathrm{d}\mathbf{v}. \tag{57}$$

Здесь

$$\omega_\alpha^2 = 4\pi N e_\alpha^2/m_\alpha, \quad \omega_{H\alpha} = e_\alpha H/m_\alpha c.$$

Описанная выше неустойчивость значительно быстрее развивается на электронной ветви колебаний. Однако электроны удерживаются пространственным зарядом ионов. Поэтому уход плазмы, в конце концов, определяется уходом ионов. Если длина волны значительно меньше размеров системы $kL \gg 1$, то для вычисления изменения энергии волны можно воспользоваться приближением геометрической оптики. В этом случае изменение спектральной плотности энергии колебаний ε_k в данной точке определяется уравнением:

$$\frac{\partial \varepsilon_k}{\partial t} + \frac{\partial \omega_k}{\partial k}\frac{\partial \varepsilon_k}{\partial z} - \frac{\partial \omega_k}{\partial z}\frac{\partial \varepsilon_k}{\partial k} = 2\gamma\{f_0\}\varepsilon_k + J_k(z), \quad (58)$$

где $J_k(z)$ — мощность источников теплового шума для данной гармоники k, определяемая по закону Кирхгофа. В уравнении (58) третьим членом в левой части можно, вообще говоря, пренебречь. В результате получаем следующее уравнение для изменения коэффициента диффузии в пространстве:

$$\frac{\partial D_H}{\partial t} + \frac{\partial \omega_k}{\partial k}\cdot\frac{\partial D_H}{\partial x} = 2\gamma D_H + \dot{D}_{H_0}. \quad (59)$$

($\dot{D}_{H_0}$ выражается через равновесные флюктуации электрического поля).

В том же приближении $kL \gg 1$ диффузия частиц под действием волн описывается уравнением (55). Если поле слабо изменяется на размерах порядка размеров ионной орбиты, то в дрейфовом приближении для средней функции распределения f_0 получается следующее уравнение:

$$\frac{\partial f_0}{\partial t} + v_\parallel\frac{\partial f_0}{\partial z} - \frac{\mu_\alpha}{m_\alpha}\frac{\partial H_0}{\partial z}\frac{\partial f_0}{\partial v_\parallel} = \left\{\frac{1}{H}\frac{\partial}{\partial \mu_\alpha} + \frac{\partial}{\partial v_\parallel}\frac{k}{\omega_{H\alpha}}\right\}\frac{2\mu}{H}D_H\left\{\frac{\partial}{\partial \mu_\alpha} + \frac{kH}{\omega_{H\alpha}}\frac{\partial}{\partial v_\parallel}\right\}f_0. \quad (60)$$

В принципе уравнения (57), (59) и (60) позволяют полностью решить задачу об «аномальном» уходе частиц в ловушке. Мы, однако, ограничимся оценкой коэффициента диффузии D_H и времени ухода частиц.

При отсутствии ухода частиц функция их распределения по скоростям в поле, изменяющемся до величины H_m в «пробке», дается следующим выражением:

$$f_0 = f_m(v_\parallel, v_\perp)\,\varepsilon\left(v_\perp\frac{H_m - H}{H} - v_\parallel^2\right), \qquad \varepsilon(x) = \begin{cases} 1 & x > 0 \\ 0 & x < 0 \end{cases} \quad (61)$$

где $f_m(v_\parallel, v_\perp)$ — максвелловская функция распределения. Предположим далее, что эта функция изотропна. При таком распределении (с незаполненным конусом ушедших частиц) из уравнения (57) следует, что:

$$\gamma = -\sqrt{\pi}\frac{k}{\sqrt{2T/M}}v_\parallel^2\,e^{-Mv_\parallel^2/2T}\left(1 + \frac{H_m + H}{H_m - H}\frac{k}{\omega_{Hi}}\frac{v_\parallel^3}{(2T/M)^{3/2}}\right) \quad (62)$$

и

$$k^3 = -\frac{\omega_{Hi}^3}{v_\parallel v_A^2}\sqrt{\frac{H_m - H}{H_m}}; \qquad v_A = \frac{H_m}{\sqrt{4\pi NM}}. \quad (63)$$

В этих выражениях $v_\parallel = (\omega - \omega_{Hi})/k$, т.е. скорость частиц, находящихся в резонансе с волной, имеющей данный волновой вектор k. Направление оси z выбрано так, чтобы магнитное поле расло при $z \to \infty$. Из выражения (63) видно, что нарастающая волна распространяется от пробки вглубь ловушки.

В результате раскачки волн коэффициент диффузии D_H также нарастает по мере удаления от пробки:

$$\ln(D_H/D_{H_0}) \simeq 2\int_0^z \frac{\gamma(z)}{\partial\omega/\partial k}\,dz = \int_0^z \gamma(z)\frac{dz}{v_\parallel}. \quad (64)$$

Величина $\varphi = \int_0^z [\gamma(z)/v_\parallel]\,dz$ достигает максимума для волн, у которых

$$v_\parallel \sim \sqrt{\frac{2T}{M}}\,\beta^{1/2}\left(\frac{14}{3}\right)^{3/2} \quad \text{при} \quad z = 2\beta L.$$

Здесь $\beta = \sqrt{4\pi NT/H_0^2}$, а H_0 — среднее поле.

В результате коэффициент диффузии оказывается по порядку величины равным:

$$\ln(D_H/D_{H_0}) \approx \frac{L}{r_{\Lambda i}}\beta^{4/3},$$

где $r_{\Lambda i}$ — радиус ларморовского вращения иона. Так как диффузия на тепловых колебаниях близка к диффузии из-за парных столкновений, то величина $L/r_{\Lambda i}\beta^{4/3}$ грубо определяет уменьшение времени жизни частиц в ловушке.

В существующих ловушках эта величина весьма мала, так как в них $\beta \sim 10^{-4} - 10^{-5}$, а $z_{\Lambda i} \sim 1 - 0{,}1\,L$.

Величина $\beta_c \sim (r_{\Lambda i}/L)^{3/4}$ определяет критическое значение β, выше которого даже в стабилизированных относительно магнитогидродинамической неустойчивости ловушках с пробками должен наблюдаться аномальный уход.

Отметим, что любое увеличение степени анизотропии функции распределения в результате инжекции или магнитного сжатия должно усилить описываемую диффузию.

7. Заключение

Квазилинейное приближение является полезным методом описания слабо нелинейных процессов в плазме. Для полного описания стационарного состояния плазмы во внешних полях или процесса релаксации в неустойчивой плазме кроме обратного влияния колебаний на распределение частиц необходимо знать и специфические процессы диссипации колебаний в плазме типа «пересечения траекторий», а также законы распада спектра плазменных колебаний. В настоящее время эти процессы изучены лишь для некоторых частных и простых моделей типа одномерных ленгмюровских колебаний электронов. Повидимому, существенный прогресс в этой области может быть достигнут с помощью модельных «машинных экспериментов».

Литература

[1] Давыдов Б. И., Сб. «Физика плазмы и проблема управляемых термоядерных реакций», АН СССР, Москва (1958) т. I, 77.

[2] Веденов А. А., Велихов Е. П., Сагдеев Р. З., *Ядерный синтез* I (1961) 82—100.

[3] Веденов А. А., Велихов Е. П., Сагдеев Т. З. *Успехи физических наук* 73 (1961) 701.

STOCHASTIC METHODS IN THE THEORY OF PLASMA DIFFUSION*

J. B. TAYLOR**

ATOMIC WEAPONS RESEARCH ESTABLISHMENT

ALDERMASTON, BERKSHIRE, ENGLAND

Although the theory of diffusion is fairly complete for thermal plasma (i.e. plasma in local thermodynamic equilibrium), there is almost no information on non-thermal plasma and it may well be that the conventional transport equation approach is not suited to a discussion of this problem. An alternative approach utilising the correlation function of the fluctuating electric field in the plasma as its starting point has therefore been examined. In the first application of this approach, to thermal plasma, Nyquist's theorem played a central role.

In discussing non-thermal plasma Nyquist's theorem cannot be used but instead one can employ equations of motion of the Langevin type. In the present paper the application, and the limitations, of this approach are discussed; it is shown that the diffusion of ions across a magnetic field can be derived simply in terms of the effective dynamic friction coefficient and the significance of this result is discussed. In particular it appears that for given plasma pressure there is a maximum value for the diffusion, related to the controversial "Bohm" diffusion. Comparison of this result with recent measurements on the Stellarator indicates that the maximum is attained in the turbulent plasma resulting from ion-wave instability.

1. Introduction

The conventional approach to the problem of diffusion of plasma across a magnetic field is via a transport equation such as that of Boltzman or Fokker-Planck. In the application to "thermal" plasma (by thermal we mean that the plasma is in local thermodynamic equilibrium) a suitable modification of the Chapman-Enskog method may be used [1–4], to obtain an approximate solution to the transport equation, in powers of a small parameter, and from this one finds the diffusion. In the case of non-thermal plasma such an approach does not seem to be possible and it is therefore of interest to examine other methods of investigating the diffusion problem. In one such approach [5] a fundamental quantity is the correlation function of the fluctuating electric field which is used in conjunction with the stochastic equation for the flux.

$$G = n(x)\langle\Delta x\rangle - \frac{1}{2}\frac{\partial}{\partial x}[n(x)\langle(\Delta x)^2\rangle] \qquad (1)$$

where $\langle\Delta x\rangle$ and $\langle(\Delta x)^2\rangle$ are the first and second moments of the displacement per unit time [6]. In the usual way these are to be evaluated over a time long compared with a fluctuation period but short compared with the time of any macroscopic motion. In the present example such a time would be several cyclotron periods. We note that if one requires the flux correct to first order in the gradient (analogue of Fick's law) then one needs to evaluate $\langle\Delta x\rangle$ to first order, but $\langle(\Delta x)^2\rangle$ is needed only to zero order.

Although the ultimate aim is to deal with non-equilibrium plasma, one naturally first applies these methods to thermal plasma [5]. In doing so it is found convenient to consider the field acting on an ion as made up of two parts, a dynamic friction proportional to the ion velocity and a fluctuating electric field essentially independent of the ion velocity. Then it can be shown that the diffusion is made up of three parts, two of which arise from the friction and the third from the fluctuating field. The contribution due to the fluctuating field is given in terms of the electric field correlation function explicitly, whereas the other contributions are expressed in terms of the coefficient of dynamic friction. However, the fluctuation-dissipation (or Nyquist) theorem provides a relation [7] between the correlation function and the friction coefficient so that the entire diffusion can be expressed in terms of either the friction coefficient or the correlation function as desired.

2. Diffusion in non-thermal plasma

Considering how one might apply these techniques to non-equilibrium (possibly turbulent) plasma it is apparent that the main obstacle lies in the reliance on Nyquist's theorem since this theorem is restricted to systems in thermal equilibrium. However, the introduction of a fluctuating and a frictional component for the force on an ion immediately suggests that the Langevin method might be used in the general non-equilibrium problem, and it is our aim here to discuss this possibility. (The Langevin method referred to is that frequently employed in discussions of Brownian motion [6] to which the present problem is closely analogous.)

We consider specifically a situation in which a density gradient exists only in the x-direction with a uniform magnetic field B in the z-direction. Furthermore the magnetic pressure is dominant ($B^2 \gg 8\pi p$) so that the influence of the plasma on the magnetic

* Conference paper CN-10/73, presented by J. B. Taylor. Discussion of this paper is given on page 494. Translations of the abstract are at the end of this volume of the Conference Proceedings.

** Present address: Culham Laboratory, Abingdon, Berks.

field can be ignored. Singly charged ions and electrons are present in equal numbers and there is no macroscopic electric field. In this situation we wish to examine the diffusion of ions due to the influence of, possibly turbulent, electrons. The ion velocities will generally be much smaller than electron velocities so we resolve the force on an ion into a frictional part, proportional to the difference between its velocity and the mean electron velocity, and a further fluctuating part whose average value is zero and which is independent of the ion motion. The validity of this assumption that there is a fluctuating field independent of the ion motion will be examined later; for the present we merely note that an assumption of this type is involved in any application of the Langevin method.

The frictional term contains a systematic variation since as the ion moves it will encounter regions of different plasma density (i.e. different mean density; the effect of *fluctuations* in density are included as part of the fluctuating force). However we require $\langle \Delta x \rangle$ only to first order in density gradient so we can write the frictional term as

$$F = -\left(\beta + x\frac{\partial \beta}{\partial x}\right)(v - \bar{v}_e) \tag{2}$$

where F is the force per unit mass, β is the friction coefficient evaluated at the average position of the ion under discussion and $\bar{v}_e$ is the mean electron (drift) velocity. This drift velocity is itself of first order in the gradient, being in the y-direction and of magnitude

$$\bar{v}_e = -\frac{c}{eBn}\frac{\partial P_e}{\partial x}, \tag{3}$$

where P_e is the electron pressure, so to the required accuracy:

$$F = -\beta v - (vx)\frac{\partial \beta}{\partial x} + \beta \bar{v}_e. \tag{4}$$

The total force on the ion also includes a fluctuating force independent of ion motion and having zero mean value. The components of this force (per unit mass) are designated $X(t)$, $Y(t)$; then the Langevin type equations of motion can be written

$$\begin{aligned} \dot{u} &= -\beta u + \omega v + \psi(t) \\ \dot{v} &= -\beta v - \omega u + \varphi(t), \end{aligned} \tag{5}$$

where $\omega = eB/Mc$

and

$$\begin{aligned} \psi(t) &= X(t) - ux\frac{\partial \beta}{\partial x} \\ \varphi(t) &= Y(t) - vx\frac{\partial \beta}{\partial x} + \beta \bar{v}_e. \end{aligned} \tag{6}$$

The solution of Eq. (5) yields

$$\begin{aligned} u(t+\tau) = {} & e^{-\beta t}[u(\tau)\cos\omega t + v(\tau)\sin\omega t] \\ & + \int_0^t e^{\beta(s-t)}[\psi(s+\tau)\cos\omega(s-t) \\ & - \varphi(s+\tau)\sin\omega(s-t)]\,ds. \end{aligned} \tag{7}$$

Now the first moment $\langle \Delta x \rangle$ is defined by

$$\langle \Delta x \rangle = \lim \frac{1}{T}\int_0^T \langle u(t+\tau) \rangle\, dt \tag{8}$$

and according to our assumptions about the fluctuating force we have

$$\begin{aligned} \langle \psi \rangle &= -\langle ux \rangle \frac{\partial \beta}{\partial x} \\ \langle \varphi \rangle &= -\langle vx \rangle \frac{\partial \beta}{\partial x} + \beta \bar{v}_e. \end{aligned} \tag{9}$$

In the terms involving $\partial\beta/\partial x$ we make a further approximation, that for $\langle ux \rangle$ and $\langle vx \rangle$ we may insert the average appropriate to an undisturbed circular cyclotron orbit; this leads to:

$$\begin{aligned} \langle \psi \rangle &= 0 \\ \langle \varphi \rangle &= \frac{c\beta}{neB}\left\{\frac{nkT_i}{\beta}\frac{\partial \beta}{\partial x} - \frac{\partial P_e}{\partial x}\right\}, \end{aligned} \tag{10}$$

where kT_i merely denotes the mean ion energy and does not imply a thermal velocity distribution.

By inserting Eq. (7) into (8) and carrying out the necessary integrations (by first inverting the order of integration) we get

$$\langle \Delta x \rangle = \langle \varphi \rangle \frac{\omega}{\omega^2 + \beta^2}$$

or

$$n\langle \Delta x \rangle = \frac{\beta}{\beta^2 + \omega^2}\frac{1}{M}\left\{\frac{nkT_i}{\beta}\frac{\partial \beta}{\partial x} - \frac{\partial P_e}{\partial x}\right\}. \tag{11}$$

This expression is, in general, not zero so that one must be cautious in applying estimates of diffusion based only on consideration of the second moment $\langle (\Delta x)^2 \rangle$. However for thermal plasma β is proportional to n_e and then $\langle \Delta x \rangle$ vanishes if $T_e = T_i$.

We now turn to the evaluation of the second moment $\langle (\Delta x)^2 \rangle$. To do this we first write it in the well known form

$$\langle (\Delta x)^2 \rangle = \lim \frac{1}{T}\int_0^T\int_0^T \langle u(s)\,u(s') \rangle\, ds\, ds'$$

or

$$\frac{\langle (\Delta x)^2 \rangle}{2} = \int_0^\infty \langle u(t+\tau)\,u(\tau) \rangle\, dt. \tag{12}$$

By appealing again to the independence of the velocity and the fluctuating force we find from Eq. (7) that

$$\langle u(t+\tau)\,u(\tau) \rangle = \langle u^2 \rangle e^{-\beta t}\cos\omega t \tag{13}$$

(again neglecting any small corrections involving $\partial\beta/\partial x$ and high order correlations), so that carrying out the integration in Eq. (12) one finds

$$\frac{n\langle (\Delta x)^2 \rangle}{2} = \frac{\beta}{(\omega^2 + \beta^2)}\langle u^2 \rangle = \frac{\beta}{(\omega^2 + \beta^2)} \cdot \frac{1}{M} P_i. \tag{14}$$

The final expression for the flux is therefore

$$\begin{aligned} G = \frac{1}{M}\Bigg[& \frac{\beta}{(\beta^2 + \omega^2)}\left\{\frac{nkT_i}{\beta}\frac{\partial \beta}{\partial x} - \frac{\partial P_e}{\partial x}\right\} \\ & - \frac{\partial}{\partial x}\left\{\frac{\beta}{(\beta^2 + \omega^2)} P_i\right\}\Bigg]. \end{aligned} \tag{15}$$

3. Discussion

Eq. (15) is our final expression for the diffusion of ions across a magnetic field. In the case of thermal plasma the coefficient β is proportional to n_e, as remarked above, and it may be verified that if we ascribe to β the value appropriate to a Maxwellian electron distribution, namely [7]

$$\beta = \frac{n_e}{M}\frac{8\pi^{1/2}e^4}{3kT}\left(\frac{m}{2kT}\right)^{1/2}\log\Lambda,$$

then in the limit $\omega \gg \beta$ we recover from Eq. (15) the accepted classical value for transverse diffusion of thermal plasma in a strong magnetic field. The present method seems a particularly simple way to obtain the more general formula appropriate to arbitrary field strength for which the conventional Chapman-Enskog type of analysis is not suitable.

Of greater interest, however, are the implications of Eq. (15) for the diffusion of non-thermal, possibly turbulent plasma. In this connection one notes the appearance in Eq. (15) of the factor $\beta/(\beta^2+\omega^2)$. In a given magnetic field the value of ω is fixed but the value of β will depend on the electron distribution and the general "state" of the plasma; however, no matter what value β may have, the factor $\beta/(\beta^2+\omega^2)$ can never exceed $1/2\omega$. This implies that for given particle pressures and magnetic field there is a maximum to the transverse diffusion irrespective of the "state" of the plasma [8]. At this point the interpretation of β in a turbulent plasma perhaps calls for some explanation. At a fixed point in the plasma there is a certain fluctuating field $X(t)$ and a slowly moving ion will experience in addition an extra force which can be expanded in powers of v; $-\beta v$ is simply the first term in this expansion. Thus in the case of turbulent plasma there is unlikely to be any proportionality between β and n_e; in fact it will be more accurate to take β as independent of n_e in which case Eq. (15) simplifies to

$$G_{\text{turb}} = -\frac{1}{M}\frac{\beta}{(\beta^2+\omega^2)}\frac{\partial P}{\partial x}, \qquad (16)$$

where P is the total pressure (P_i+P_e). As we have mentioned before, β will certainly depend on the general "state" of the plasma but no matter what its actual value the diffusion flux itself can never exceed

$$G_{\max} = -\frac{1}{4M\omega}\frac{\partial P}{\partial x}$$

or

$$G_{\max} = -\frac{1}{4}\frac{c}{eB}\frac{\partial P}{\partial x}. \qquad (17)$$

This value is four times that suggested several years ago by BOHM [9] as being the value appropriate to diffusion in the presence of fluctuating electric fields. [It may be noted that if we had continued to assume that β was proportional to n_e even in the turbulent case then the formula for the maximum flux would have been only slightly altered—the coefficient becoming e.g. $3\sqrt{3}/16$ instead of $1/4$.]

If one chooses to define a diffusion coefficient by

$$G_i = -D\frac{\partial n_i}{\partial x}$$

then the coefficient corresponding to Eq. (17) can be expressed as

$$D_{\max} = 2.5\times 10^7\frac{(T_e+T_i)}{B}, \qquad (18)$$

where T is measured in electron-volts and B in gauss.

In recent experiments [10] on the Stellarator (where $T_e \gg T_i$) in a regime believed to be subject to ion-wave instabilities [11] so that the plasma is indeed "turbulent", the value of D has been measured and is found to be

$$D' \simeq 2.0\times 10^7\frac{T_e}{B}, \qquad (20)$$

so that in this experiment the diffusion seems to attain its maximum value.

4. Validity of the method

It is inherent in the Langevin method that one introduces a fluctuating force which is regarded as independent of the ion motion. This is a fairly severe restriction and we give below an outline of a proof that the condition for its validity is that the correlation time of the actual field, as seen by the moving ion, must be short compared to a cyclotron period.

We have seen [Eq. (13)] that the assumption of complete independence for the fluctuating field leads to

$$\langle u(t+\tau)\,u(t)\rangle = \langle u^2\rangle e^{-\beta t}\cos\omega t. \qquad (21)$$

If now we introduce $\bar{u}(p)$ as the Fourier transform of $u(t)$ then by the Wiener-Khintchine theorem we may show that

$$\langle|\bar{u}(p)|^2\rangle \sim \int_0^\infty \langle u(t+\tau)\,u(t)\rangle\cos pt.\,dt$$

i.e.

$$\langle|\bar{u}(p)|^2\rangle \sim \left\{\frac{1}{\beta^2+(p+\omega)^2}+\frac{1}{\beta^2+(p-\omega)^2}\right\}. \qquad (22)$$

On the other hand if we take the Fourier transform of Eq. (5)

$$(\beta+ip)\,\bar{u}(p) = \omega\bar{v}(p)+\bar{\psi}(p)$$
$$(\beta+ip)\,\bar{v}(p) = -\omega\bar{u}(p)+\bar{\varphi}(p) \qquad (23)$$

and solve for $|\bar{u}(p)|^2$ we derive the equation

$$[(\beta^2+\omega^2-p^2)^2+4p^2\beta^2]\langle|\bar{u}(p)|^2\rangle = (\omega^2+\beta^2+p^2)\langle|\bar{\varphi}(p)|^2\rangle \qquad (24)$$

where we have utilised the fact that, by symmetry, $\langle|\bar{\varphi}|^2\rangle = \langle|\bar{\psi}|^2\rangle$ and $\langle\bar{\varphi}\bar{\psi}^*\rangle = 0$ etc. If now Eq. (24) is to be consistent with Eq. (22) we must have

$$\langle|\bar{\varphi}(p)|^2\rangle = \text{constant, independent of } p.$$

Therefore the logical conclusion of our assumptions is that the spectrum of the fluctuating field must be flat. Strictly this implies that the correlation function of the fluctuating field must be a δ-function but in reality all that is required is that the correlation should fall to zero in a time short compared with any of the other times of interest such as $1/\beta$ or $1/\omega$. Expressed in this form this condition, for the validity of the "independence" assumption, is almost obvious.

In the case of thermal plasma the "correlation time", i.e. the time for which the correlation of the electric field is significant, is limited by the plasma period so that the condition for validity should be easily satisfied. In the case of turbulent plasma resulting from micro-instability we can estimate the correlation time from the characteristics of the instability. If the fluctuating field in the plasma is $E(x, t)$ then the average correlation time of the field, as seen by an ion moving at speed w along the magnetic field, is

$$\frac{\int \langle E(x, t)\, E(x + w\tau, t + \tau)\, f(w)\, \mathrm{d}w\, \mathrm{d}\tau \rangle}{\langle E(x, t)\, E(x, t) \rangle}, \qquad (25)$$

where $f(w)$ is the velocity distribution. If the dominant modes of the field are grouped around $E \sim \exp[i(kz - pt)]$ then this correlation time can be calculated and expressed as

$$\frac{1}{k} f(p/k) \qquad (26)$$

and the ratio of this to the cyclotron period e.g. is

$$\frac{\omega}{k} f(p/k)\,. \qquad (27)$$

Now $f(p/k)$ is the fraction of particles moving with the wave velocity; for a Maxwellian distribution (27) would be

$$\sim \frac{\omega}{kc} \exp\left(-\frac{p^2}{k^2 c^2}\right), \qquad (28)$$

where c^2 is the mean square ion velocity. In the situation referred to in the Stellarator the unstable ion-waves have a phase velocity given by [11]

$$\frac{p}{k} \simeq \left(\frac{m}{M}\right)^{1/2} c_e\,, \qquad (29)$$

where c_e^2 is the mean square electron speed. As far as the ions are concerned, therefore, the exponential factor in (28) is of order

$$\exp\left(-\frac{\mathrm{k}\, T_e}{\mathrm{k}\, T_i}\right), \qquad (30)$$

which might typically be $\sim\exp(-400)$! We would expect then that the condition for validity would be well satisfied in this case. It should also be well satisfied in situations where other micro-instabilities, such as two-stream instabilities, are present since these tend always to have wave velocities comparable with the mean electron speed rather than with that of the ions.

5. Conclusions

The use of the stochastic approach to plasma diffusion, as discussed in this note, enables one to give a general account of diffusion across a magnetic field in terms of a single parameter β. For plasma in thermal equilibrium β is the well known coefficient of dynamic friction and one can then easily recover the conventional results.

In the more general case when the plasma is not in thermal equilibrium β is not known but one may nevertheless deduce that for any given pressure and magnetic field there is a maximum possible diffusion, this being about four times the value given by the Bohm formula. Experimental data reported from the Stellarator seem to correspond closely with this maximum value.

The condition which must be satisfied in order that the stochastic approach set out here should be valid is that the correlation time of the fluctuating field as seen by an ion should be short compared to the ion cyclotron period. This seems to be well satisfied for thermal plasma and for the turbulent plasma resulting from many forms of micro-instability.

It is hoped that developments such as those given here will be useful in interpreting data on "enhanced diffusion" and in correlating measurements of diffusion with other properties such as noise spectrum or fluctuating microfields.

References

[1] KAUFMAN, A. N., La Théorie des Gaz Neutres et Ionisés, Dewitt C. and Detoeuf J. (Ed.) (Herman, Paris, 1960).

[2] ROSENBLUTH, M. N., KAUFMAN, A. N., *Phys. Rev.* **109** (1958) 1.

[3] BRAGINSKY, S. I., *J. Exptl. Theoret. Phys. USSR* **33** (1957) 459.

[4] FRADKIN, E. S., *J. Exptl. Theoret. Phys. USSR* **32** (1957) 1176.

[5] TAYLOR, J. B., *Phys. Fluids* **4** (1961) 1142.

[6] CHANDRASEKHAR, S., *Rev. Mod. Phys.* **15** (1943) 1.

[7] TAYLOR, J. B., *Phys. Fluids* **3** (1960) 792.

[8] TAYLOR, J. B., *Phys. Rev. Letters* **6** (1961) 262.

[9] BOHM, D., The Characteristics of Electrical Discharges in Magnetic Fields, Guthrie and Wakerling (Ed.) (McGraw-Hill, New York, 1949).

[10] STODIEK, W., ELLIS, R. A. JR., GORMAN, J. G., IAEA Conference on Plasma Physics and Controlled Nuclear Fusion Research, Salzburg, 1961: Paper CN-10/131, page 193 of these Proceedings.

[11] BERNSTEIN, I. B., KULSRUD, R. M. *Phys. Fluids* **3** (1960) 937.

МИКРОСКОПИЧЕСКИЕ НЕУСТОЙЧИВОСТИ ПРОСТРАНСТВЕННО НЕОДНОРОДНОЙ ПЛАЗМЫ В МАГНИТНОМ ПОЛЕ*

Л. И. РУДАКОВ, Р. З. САГДЕЕВ

ИНСТИТУТ АТОМНОЙ ЭНЕРГИИ ИМ. И. В. КУРЧАТОВА,

АКАДЕМИИ НАУК СССР

МОСКВА, СОЮЗ СОВЕТСКИХ СОЦИАЛИСТИЧЕСКИХ РЕСПУБЛИК

Теория устойчивости разреженной плазмы в магнитном поле обычно базируется на уравнениях магнитной гидродинамики с бесконечной проводимостью. Однако такое рассмотрение не обладает полнотой.

На примере простейших геометрий магнитного поля было проведено кинетическое рассмотрение устойчивости разреженной плазмы и показано, что в плазме могут существовать неустойчивости, не описываемые уровнениями магнитной гидродинамики с бесконечной проводимостью. Такие неустойчивости могут быть, когда функция распределения частиц плазмы отличается от термически равновесной максвелловской функции, например в пространственно-неоднородной плазме, плотность n и давление p которой переменны в пространстве.

Хотя в равновесии плазма как целое покоится, но в неоднородном магнитном поле электроны и ионы плазмы дрейфуют поперек силовых линий магнитного поля. Взаимодействуя с возмущениями, частицы, дрейфующие в неоднородном магнитном поле, могут отдавать им свою энергию, раскачивая в плазме электромагнитные волны. Наиболее сильно с волной взаимодействуют частицы, скорость дрейфа которых близка к фазовой скорости волны. Для таких «резонансных» частиц электрическое и магнитное поле волны почти стационарно. Движение резонансных частиц в поле волны в направлении градиента невозмущенной функции распределения и магнитного поля приводит к переносу энергии. Если $\partial (\ln T)/\partial (\ln H) > 1$, то частицы в среднем отдают волне часть своей энергии, запасенной в тепловом движении и магнитном поле. Однако время развития такой неустойчивости велико. Гораздо быстрее может развиваться неустойчивость пространственно-неоднородной плазмы, связанная с переносом тепла в неоднородно нагретой плазме при распространении в ней ионно-звуковых колебаний. Поперечное к магнитному полю $\mathbf{H}_0$ движение частиц в ионно-звуковой волне, распространяющейся под углом к $\mathbf{H}_0$ со скоростью $c\mathbf{E}\times\mathbf{H}/H_0^2$ в неоднородно нагретой плазме, приводит к направленному переносу тепла. Можно выбрать направление распространения волны таким образом, чтобы в фазу «сгущения» плазмы в волне, где возрастает температура T, непрерывно поступал приток тепла из области с большей невозмущенной температурой. Это приводит к раскачке ионно-звуковых колебаний, если $\partial (\ln T)/\partial (\ln n) > 2$ или $\partial (\ln T)/\partial (\ln n) < 0$.

1. Введение

Теория устойчивости плазмы в рамках идеальной магнитной гидродинамики в настоящее время развита с достаточной полнотой. Сформулирован энергетический принцип, позволяющий ответить на вопрос о том, устойчива или нет данная конфигурация плазмы.

Однако описание плазмы с помощью уравнений магнитной гидродинамики приближенно. Более точная теория может предсказать существование неустойчивости там, где магнитогидродинамический анализ дает устойчивость. На это указывает и эксперимент. Так, на «Стеллараторе», установке, где обеспечена гидромагнитная устойчивость, наблюдается аномальный уход частиц из плазмы.

Усовершенствование гидромагнитной теории устойчивости может идти в двух направлениях:

1. Там, где не применим магнитогидродинамической подход к описанию плазмы, надо пользоваться кинетическим уравнением.

2. Плазма представляет из себя смесь двух газов, газа электронов и ионов. Если даже к каждому из газов применимо гидродинамическое описание, то и тогда область применимости магнитной гидродинамики ограничена. В общем случае надо пользоваться так называемым обобщенным законом Ома.

Анализ малых колебаний однородной плазмы в кинетике помимо уточнения значений фазовых скоростей колебаний по сравнению со значениями, полученными из уравнений двухкомпонентной магнитной гидродинамики, показывает, что в разреженной плазме, где столкновения редки, существует резонансное (Черенковское) и циклотронное поглощение волн.

* Доклад С-10/220, представленный на Конференцию. Докладчик: Е. П. Велихов. Переводы аннотаций находятся в конце настоящего тома Трудов Конференцин.

Естественно, что такие же эффекты должны быть и в пространственно неоднородной плазме, но не исключена возможность раскачки колебаний (колебательная неустойчивость) «резонансными» частицами. «Резонансными» частицами мы будет называть частицы, проекция скорости которых на направление распространения волны близка к фазовой скорости волны.

Если градиенты величин, характеризующих плазму, невелики, то естественно искать эффекты пространственной неоднородности плазмы для таких колебаний, которые слабо затухают в однородной плазме. Таким типом колебаний плазмы в магнитном поле являются колебания, распространяющиеся поперек магнитного поля. Они не затухают, так как нет резонансных частиц. В однородной плазме частицы «приклеены» к силовым линиям. Если есть пространственный градиент магнитного поля, то нет и «приклеенности». Частицы плазмы в неоднородном магнитном поле дрейфуют поперек силовых линий H. Скорость дрейфа зависит от энергии частицы, так что при любой фазовой скорости волны найдутся резонансные частицы.

В пункте 2 будет рассмотрен эффект «резонансной» раскачки колебаний, распространяющихся поперек магнитного поля. Можно ожидать, что в неоднородной плазме существует циклотронное поглощение и раскачка волн, распространяющихся поперек магнитного поля. Однако эта задача полностью еще не рассмотрена.

В однородной плазме волна затухает из-за Черенковского поглощения волны резонансными частицами.

В неоднородной плазме механизм взаимодействия резонансных частиц с волной может быть иным. Резонансные частицы, двигаясь в поле волны поперек магнитного поля (для них поле волны медленно меняется во времени) могут приносить энергию из более нагретой области и отдавать ее волне.

В пункте 3 будет показано, что такой эффект может даже превысить Черенковское поглощение волны, распространяющейся под косым углом к магнитному полю.

Полное изучение описанных выше явлений весьма сложно. Поэтому мы ограничились изучением свойств пространственно-неоднородной плазмы в магнитном поле на примере простейшей геометрии магнитного поля. Магнитное поле в плазме может быть неоднородным, но силовые линии его прямые. Будем считать также, что напряженность магнитного поля велика, так что ларморовский радиус иона r_H мал в сравнении с характерными масштабами задачи L, а частота колебаний ω мала в сравнении с циклотронной частотой $\omega_{H\alpha}=eH/m_\alpha c$. В этих предположениях решение кинетического уравнения, в котором опущен интеграл столкновений (разреженная плазма), можно существенно облегчить, разлагая функцию распределения в ряд по обратным степеням магнитного поля. Решение кинетического уравнения не сильно отличается от максвелловской, оказывается для выбранной геометрии магнитного поля дано в приложении. Рассматривается плазма низкого давления, $p \ll H^2/8\pi$.

2. Колебательная неустойчивость плазмы в неоднородном магнитном поле

Рассмотрим магнито-звуковые колебания, распространяющиеся в плазме перпендикулярно магнитному полю. Они описываются системой уравнений

$$\varrho_0 \frac{\partial \mathbf{v}}{\partial t} = -\nabla\left(p_\perp + \frac{HH_0}{4\pi}\right)$$

$$\mathbf{E} + \frac{1}{c}\mathbf{v} \times \mathbf{H}_0 = 0$$

$$\operatorname{rot} \mathbf{E} = -\frac{1}{c}\frac{\partial \mathbf{H}}{\partial t}. \qquad (1)$$

$p_\perp$ — возмущение поперечной составляющей тензора давления плазмы. Для нахождения $p_\perp$ надо решить кинетическое уравнение. Решение кинетического уравнение дано в приложении. Там же приведено выражение для $p_\perp$ [формула (27)]. Исключая из системы уравнений (1) все величины, кроме одной, например E_y, получим одно обыкновенное дифференциальное уравнение второго порядка:

$$\frac{\mathrm{d}}{\mathrm{d}x}\frac{\left(1+\frac{4\pi a}{H_0}\right)E_y' - \mathrm{i}\frac{4\pi b\omega}{cH_0}E_y}{\left(1+\frac{4\pi a}{H_0}\right) - \frac{\omega^2}{k_y^2 V_A^2}} - k_y^2 E_y = 0. \qquad (2)$$

$V_A^2 = H_0^2/4\pi\varrho_0$. Остальные обозначения пояснены в приложении. В квазиклассическом приближении [$E_y \sim \exp\left(\mathrm{i}\int k_x \mathrm{d}x\right)$, где k_x — медленно меняющаяся функция x] получим

$$(k_y^2 + k_x^2)\left(1 + \frac{4\pi a}{H_0}\right) - \frac{\omega^2}{V_A^2} = 0.$$

Действительная часть этого уравнения определяет фазовую скорость колебаний, а мнимая инкремент — ν ($\omega = \omega_1 + \mathrm{i}\nu$). После несложных вычислений находим:

$$\omega_1^2 = (k_x^2 + k_y^2) V_A^2$$

$$\nu = \frac{\pi^2}{2}\omega_1 \cdot \times \left\{\frac{mv_\perp^4}{H_0 H_0'}\left(F_0' + \frac{v_\perp}{2}\frac{\partial F_0}{\partial v_\perp}\frac{H_0'}{H_0}\right)\right\}_{v_\perp^2 = 2\frac{\omega_1}{k_y}\frac{H_0}{H_0'}\omega_H}.$$

Таким образом, критерий неустойчивости $\nu > 0$ имеет вид:

$$\left\{H_0' \cdot \left(F_0' + \frac{v_\perp}{2}\frac{\partial F_0}{\partial v_\perp}\frac{H_0'}{H_0}\right)_{v_\perp^2 = 2\frac{\omega_1}{k_y}\frac{H_0}{H_0'}\omega_H}\right\} > 0 \qquad (3)$$

или для максвелловской функции распределения:

$$\frac{\partial \ln T}{\partial \ln H} > 1. \qquad (3')$$

Время нарастания магнито-звуковых колебаний, когда функция распределения частиц по скоростям

вается экспоненциально велико. Это связано с тем, что при малых градиентах, а только такой случай мы здесь и рассматриваем, экспоненциально мало резонансных частиц.

Чем меньше фазовая скорость колебаний, тем больше резонансных частиц. В пространственно неоднородной плазме могут существовать медленные колебания, фазовая скорость которых пропорциональна градиенту невозмущенного давления. Это так называемые дрейфовые волны [1], [2].

Рассмотрим дрейфовые волны на простой модели. Слой плазмы удерживается магнитным полем в поле силы тяжести $\varrho\mathbf{g}$. Нас интересуют колебания, фазовая скорость которых близка к скорости дрейфа заряженной частицы в неоднородном магнитном поле. При таких колебаниях можно пренебречь инерцией ионов, так что

$$-\nabla\left(p_\perp + \frac{H H_0}{4\pi}\right) + \varrho\,\mathbf{g} = 0 \qquad (4)$$

Это векторное уравнение эквивалентно двум уравнениям:

$$\varrho = 0, \quad p_\perp + \frac{H H_0}{4\pi} = 0\,. \qquad (4')$$

Выражения для плотности и давления приведены в приложении (формулы (26) и (27)).

Система уравнений (4) имеет решение

$$E_y \cdot \sum_\alpha e_\alpha \int\left(F'_{0\alpha} + \frac{v_\perp}{2}\frac{\partial F_{0\alpha}}{\partial v_\perp}\frac{H_0'}{H_0}\right) \times \frac{\mathrm{d}^3 v}{\omega - k_y (v_\perp^2/2\omega_{H\alpha})(H_0'/H_0)} = 0 \qquad (5)$$

В качестве дисперсионного уравнения, связывающего значения частоты ω с параметрами плазмы в окрестности любой точки x_0, возьмем уравнение:

$$d = \sum_\alpha e_\alpha \int\left(F'_{0\alpha} + \frac{v_\perp}{2}\frac{\partial F_{0\alpha}}{\partial v_\perp}\frac{H_0'}{H_0}\right) \times \frac{\mathrm{d}^3 v}{\omega - k_y (v_\perp^2/2\omega_{H\alpha})(H_0'/H_0)} = 0 \qquad (6)$$

Здесь, как и в случае магнито-звуковых колебаний, условие устойчивости определяется скоростью изменения в пространстве функции распределения резонансных частиц.

Для максвелловской функции распределения выражение (6) исследовано в [1]. Критерий неустойчивости имеет вид

$$\frac{\partial \ln T}{\partial \ln H} < -\frac{H^2}{8\pi n T}\,. \qquad (7)$$

Время развития неустойчивости сравнимо с периодом колебаний.

Уравнение (6) алгебраическое. Оно не содержит производной от переменной E_y. Если учесть отброшенный нами инерционный член, то в уравнении (6) добавится член со второй производной $\mathrm{d}^2E_y/\mathrm{d}x^2$. В качестве коэффициента при нем будет стоять малый параметр $\omega^2/k_y g$. Здесь нет необходимости выписывать полное уравнение для E_y. Существенно, что оно имеет вид

$$\frac{\omega^2}{k_y g}\frac{\mathrm{d}^2 E_y}{\mathrm{d}x^2} + A\,\mathrm{d}E_y = 0\,, \qquad (8)$$

где A — размерный множитель.

Это уравнение позволяет найти пространственное распределение полей колебаний, определяемых дисперсионным уравнением (6).

Вблизи точки, где $d=0$, уравнение (8) имеет вид уравнения Эйри от комплексного аргумента. Легко оценить характерный размер «локализации» его решений Δx

$$\Delta x \sim \left(\frac{\omega^2}{k_y g A\, d_{x'}}\right)^{1/3}.$$

Отметим, что величина g не вошла в дисперсионное уравнение.

3. Неустойчивость плазмы с пространственно неоднородным распределением температуры

Рассмотренные в предыдущем разделе колебания казалось бы должны быть наиболее опасными. В однородной плазме они не затухают, поэтому эффекты неоднородности плазмы являются основными. Однако полученные критерии показывают, что колебания достаточно устойчивы.

В этом пункте мы рассмотрим колебания, распространяющиеся под косым углом к магнитному полю. Можно ожидать, что легче всего раскачиваются колебания, слабо возмущающие магнитное поле. В плазме низкого давления, $p_0 \ll H_0^2/8\pi$, это ионные звуковые колебания. Дисперсионное уравнение для ионно-звуковых колебаний легко получить из условия квазинейтральности

$$n_\mathrm{i} = n_\mathrm{e}\,. \qquad (9)$$

Функция распределения $f_{0\alpha}$ и плотности найдены в приложении (формула (28)). В ионно-звуковой волне, распространяющейся почти перпендикулярно к полю $\mathbf{H}_0$, возмущение компоненты H_z магнитного поля пропорционально давлению. Учтем это обстоятельство и опустим в $f_{0\alpha}$ члены с H_z.

Подставляя f_α в уравнение (9) и исключая с помощью уравнения Максвелла H_x, получим

$$E_z \cdot \sum_\alpha \frac{e_\alpha^2}{m_\alpha}\int_{-\infty}^{\infty}\left[\frac{\partial F_{0\alpha}}{\partial v_z} + \frac{k_y v_z}{\omega\omega_{H\alpha}}\frac{\partial F_{0\alpha}}{\partial x}\right]\frac{\mathrm{d}v_z}{\omega - k_z v_z} = 0. \qquad (10)$$

Дисперсионное уравнение

$$\sum_\alpha \frac{e_\alpha^2}{m_\alpha}\int_{-\infty}^{\infty}\left[\frac{\partial F_{0\alpha}}{\partial v_z} + \frac{k_y v_z}{\omega\omega_{H\alpha}}\frac{\partial F_{0\alpha}}{\partial x}\right]\frac{\mathrm{d}v_z}{\omega - k_z v_z} = 0 \qquad (11)$$

определяет в окрестности произвольной точки x_0 зависимость $\omega(k)$. В однородной плазме ($\partial F_0/\partial x = 0$) дисперсионное уравнение (11) описывает затухающие ионные звуковые колебания. Од-

нако, даже при малой неоднородности второй член может стать существенным для возмущений, распространяющихся почти поперек магнитного поля, $k_y \gg k_z$.

Исследуем дисперсионное уравнение (11) в случае Максвелловского распределения частиц по скоростям с переменной плотностью и температурой.

$$F_{0\alpha} = \frac{n(x)}{(2\pi T_\alpha(x)/m_\alpha)^{1/2}} \exp\left(-\frac{m_\alpha v_z^2}{2T_\alpha}\right).$$

В частном интервале $k_z v_{Ti} \ll \omega \ll k_z v_{Te} (v_T = \sqrt{2T/m})$ подинтегральную функцию для ионов можно разложить по малому параметру $k_z v_z/\omega$, а электронную подинтегральную функцию разложить по малой величине $\omega/k_z v_z$. Ограничивая разложение первыми неисчезающими членами, получим после несложных вычислений:

$$\omega^2 - k_z^2 \frac{T_e}{M} + \omega \frac{k_y T_e}{M\omega_{Hi}}\left(\frac{1}{n}\frac{dn}{dx} + \frac{k_z^2}{\omega^2}\frac{1}{Mn}\frac{dnT_i}{dx}\right) - i\pi \frac{\omega^3}{k_z v_{Te}}\left[1 + \frac{k_y T_e}{M\omega_{Hi}}\left(\frac{1}{n}\frac{dn}{dx} - \frac{1}{2T_e}\frac{dT_e}{dx}\right)\right] = 0. \quad (12)$$

Последнее слагаемое в этом выражении — полувычет, возникший при взятии интеграла по малой полуокружности около полюса $v_z = \omega/k_z$ в электронной части формулы (11). Оно учитывает вклад резонансных частиц, тепловая скорость v_z которых близка к фазовой скорости ω/k_z. Так как «резонансных» ионов экспоненциально мало, $\omega/k_z \gg v_{Ti}$, то их можно не учитывать. Поэтому мы опустили ионный полувычет.

Рассмотрим некоторые примеры:

1. $n(x) = \text{const.}$, $T(x) \neq \text{const.}$

В этом случае уравнение (12) может иметь комплексные корни, соответствующие неустойчивости, $\text{Im}\ \omega > 0$. В самом деле, у уравнения

$$\omega^3 - k_z^2 \frac{T_e}{M} + k_z^2 \frac{T_e k_y}{M^2 \omega_{Hi}} \frac{dT_i}{dx} = 0 \quad (13)$$

есть комплексный корень с $\text{Im}\ \omega > 0$, если

$$\frac{k_y^2}{k_z^2}\frac{T_e}{\omega_{Hi}^2}\left(\frac{1}{T_i}\frac{dT_i}{dx}\right)^2 > \frac{2}{27} M \left(\frac{T_e}{T_i}\right)^2.$$

Вдали от границы устойчивости решение уравнения (13) имеет вид

$$\omega = \frac{1-2i}{\sqrt{3}}\left(\frac{k_y}{k_z}\frac{d\ln T_i}{dx} k_z^3 \frac{2T_i T_e}{M^2\omega_{Hi}}\right)^{1/3}.$$

В уравнении (13) опущен член, учитывающий вклад «резонансных» электронов. Хотя таких частиц много, но они несут малую энергию ε

$$\varepsilon \sim \frac{mn\omega^2}{2k_z^2} \ll nT_e$$

Известно, что уравнения двухжидкостной магнитной гидродинамики качественно правильно описывают малые колебания в плазме, если кинетические резонансные эффекты несущественны. Здесь мы имеем именно такой случай, когда неустойчивость не связана с резонансными частицами.

2. $T(x)$ и $n(x)$ зависят от x.

Выпишем дисперсионное уравнение для этого случая.

$$\omega^2 - k_z^2 \frac{T_e}{M} + \omega \frac{k_y T_e}{M\omega_{Hi}} \frac{1}{n}\frac{dn}{dx} - i\pi \frac{\omega^3}{k_z v_{Te}}\left[1 + \frac{k_y T_e}{\omega M \omega_{Hi}}\left(\frac{1}{n}\frac{dn}{dx} - \frac{1}{2T_e}\frac{dT_e}{dx}\right)\right] = 0 \quad (14)$$

Если в этом уравнении не принимать во внимание последний член, то корни его

$$\omega_1 = -\omega_0 \pm \sqrt{\omega_0^2 + k_z^2 (T_e/M)}, \quad \omega_0 = \frac{k_y T_e}{2M\omega_{Hi} n}\frac{dn}{dx} \quad (15)$$

всегда действительны и определяют $\omega(k)$ ионно-звуковых колебаний в пространственно неоднородной плазме. Раскачка и затухание колебаний связаны с резонансными частицами. Найдем инкремент ν, $\omega = \omega_1 + i\nu$, предположив, что он мал ($\nu \ll \omega_1$).

$$\nu = \pi \frac{\omega_1^2}{k_z v_{Te}} \frac{1}{1 + (k_z^2 T_e/M\omega_1^2)}\left[1 - \frac{2 - (\partial \ln T_e/\partial \ln n)}{1 \mp [1 + (k_z^2 T_e/M\omega_1^2)]^{1/2}}\right] \quad (16)$$

ω_1 определена формулой (15).

Если $T(x) = \text{const.}$, то колебания всегда затухают. Колебания раскачиваются с инкрементом ν, если

$$\frac{\partial \ln T_e}{\partial \ln n} > 2 \quad \text{или} \quad \frac{\partial \ln T_e}{\partial \ln n} < 0 \quad (17)$$

Если температура меняется значительно быстрее, чем плотность, то формулы этого пункта не верны. Случай, когда $(\partial \ln T_e/\partial \ln n) \gg 1$, разобран выше.

Резюмируя все сказанное, можно заключить, что плазма с переменной в пространстве температурой может оказаться неустойчивой. Эту неустойчивость можно интерпретировать следующим образом. В пространственно неоднородной плазме ($T(x) \neq \text{const.}$) в косой ионно-звуковой волне ($k_z, k_y \neq 0$) поперечное движение со скоростью $c\mathbf{E} \times \mathbf{H}_0/H_0^2$ резонансных частиц приводит к направленному переносу тепла. Можно выбрать направление распространения волны, знак k_y/k_z таким образом, чтобы в фазу «сгущения» плазмы в волне, где возрастает температура, непрерывно поступал приток тепла из области с большей невозмущенной температурой. Это и будет служить причиной, приводящей к нарастанию колебаний.

Сделаем в заключение следующее замечание. Как и в пункте 2, уравнение (10) определяет зависимость $\omega(k)$, но не дает пространственный ход E_z. Для того, чтобы определить $E_z(x)$, надо в уравнении (9) учесть малые по параметру ω/ω_{Hi} члены, опущенные в наших вычислениях. Тогда E_z будет определяться дифференциальным уравне-

нием второго порядка с малым параметром при старшей производной. Мы приведем это уравнение без вывода:

$$\frac{\mathrm{d}^2 E_z}{\mathrm{d}x^2} = F(\omega, \mathbf{k}, x)\, E_z, \tag{18}$$

где

$$F(\omega,\mathbf{k},x)=4\pi\frac{v_A^2}{c^2}\frac{k_z^2}{\omega-(k_y/M\,\omega_{H1}n)\,(\mathrm{d}/\mathrm{d}x)\,(n\,T_i)}$$
$$\times\sum_\alpha\int\frac{e_\alpha^2}{m_\alpha}\left[\frac{\partial F_{0\alpha}}{\partial v_z}+\frac{k_y v_z}{\omega\omega_{H\alpha}}\frac{\partial F_{0\alpha}}{\partial x}\right]\frac{v_z\,\mathrm{d}v_z}{\omega-k_z v_z}+k_y^2.$$

Оно переходит в уравнение (10), если пренебречь членами со вторыми производными. К уравнению (18) применимы все соображения, высказанные в конце пункта 2.

4. Приложение

Решение кинетического уравнения для малых колебаний пространственно неоднородной разреженной плазмы в сильном магнитном поле.

Невозмущенная (фоновая) функция распределения плазмы F удовлетворяет кинетическому уравнению

$$\mathbf{v}\cdot\nabla F_\alpha+\mathbf{v}\times\boldsymbol{\omega}_{H\alpha}\frac{\partial F_\alpha}{\partial\mathbf{v}}=0 \tag{19}$$

Индекс α обозначает сорт частиц, ионы и электроны.

Пусть силовые линии невозмущенного магнитного поля $\mathbf{H}_0$ прямые, а все величины, характеризующие невозмущенную плазму, переменны в направлении, перпендикулярном к магнитному полю. Введем прямоугольную систему координат с осью z, направленной вдоль $\mathbf{H}_0$, а ось x направим по градиенту функции распределения ($\partial F/\partial x\neq 0$, $\partial F/\partial y=\partial F/\partial z=0$). В пространстве скоростей удобно перейти к цилиндрическим координатам, связанным с магнитным полем.

$$v=v_z\mathbf{h}_z+v_\perp(\mathbf{h}_x\cos\theta+\mathbf{h}_y\sin\theta),\quad \mathbf{h}_z=\frac{\mathbf{H}_0}{H_0}$$

Тогда уравнение (19) запишется в виде

$$v_\perp\cos\theta\frac{\partial F_\alpha}{\partial x}-\omega_{H\alpha}\frac{\partial F_\alpha}{\partial\theta}=0 \tag{20}$$

Если ларморовский радиус иона (электрона) много меньше, чем характерный размер L [$1/L=(1/F)\,\partial F/\partial x$], то уравнение (20) легко решить, разложив его по малому параметру $r_H/L\ll 1$.

Ограничиваясь нулевым и первым членом разложения F, получим

$$F_\alpha=F_{0\alpha}(v_z,v_\perp)+\frac{v_\perp}{\omega_{H\alpha}}\frac{\partial F_{0\alpha}}{\partial x}\sin\theta \tag{21}$$

Поправка f к невозмущенной функции распределения F определяется линеаризованным кинетическим уравнением

$$\frac{\partial f}{\partial t}+\mathbf{v}\nabla f+\mathbf{v}\times\omega_H\frac{\partial f}{\partial\mathbf{v}}=-\frac{e}{m}\left(\mathbf{E}+\frac{1}{c}\mathbf{v}\times\mathbf{H}\right)\frac{\partial F}{\partial\mathbf{v}} \tag{22}$$

Его решение ищем в виде $f(x)\exp[\mathrm{i}(k_z z+k_y y-\omega t)]$ Опять воспользуемся цилиндрическими координатами в пространстве скоростей. Тогда получим

$$-\mathrm{i}(\omega-k_z v_z)f+v_\perp\left(\mathrm{i}k_y\sin\theta+\cos\theta\frac{\partial}{\partial x}\right)f-\omega_H\frac{\partial f}{\partial\theta}$$
$$=-\frac{e}{m}E_z\frac{\partial F}{\partial v_z}-\frac{e}{m}(E_x\cos\theta+E_y\sin\theta)\frac{\partial F}{\partial v_\perp}$$
$$-\frac{\omega_H}{H_0}(H_y\cos\theta-H_x\sin\theta)\left(v_\perp\frac{\partial F}{\partial v_z}-v_z\frac{\partial F}{\partial v_\perp}\right)$$
$$+\frac{1}{v_\perp}\left\{-\frac{e}{m}(E_y\cos\theta-E_x\sin\theta)\right.$$
$$\left.+\frac{\omega_H}{H_0}[v_\perp H_z-v_z(H_x\cos\theta+H_y\sin\theta)]\right\}\frac{\partial F}{\partial\theta}. \tag{23}$$

Функция распределения f периодичная по θ, поэтому ее можно разложить в ряд Фурье

$$f=\sum_{n=-\infty}^{\infty}f_n\,\mathrm{e}^{\mathrm{i}n\theta}$$

Компоненты Фурье f_n удовлетворяют бесконечной зацепляющейся системе уравнений:

$$-\mathrm{i}(\omega-k_z v_z)f_0+\frac{k_y v_\perp}{2}(f_{-1}-f_1)+\frac{v_\perp}{2}\frac{\partial}{\partial x}(f_{-1}+f_1)$$
$$=-\frac{e}{m}E_z\frac{\partial F_0}{\partial v_z}+\left\{\frac{H_x}{H_0}\left(v_z+v_\perp^2\frac{\partial}{\partial v_z}-v_\perp v_z\frac{\partial}{\partial v_\perp}\right)\right.$$
$$\left.+c\frac{E_y}{H_0}\left(1+\frac{v_\perp}{2}\frac{\partial}{\partial v_\perp}\right)\right\}\frac{\partial F_0}{\partial x},$$

$$-\mathrm{i}(\omega-k_z v_z\pm\omega_H)f_{\pm1}\pm\frac{k_y v_\perp}{2}(f_0-f_{\pm2})$$
$$+\frac{v_\perp}{2}\frac{\partial}{\partial x}(f_0+f_{\pm2})=-\frac{e}{2m}(E_x\mp\mathrm{i}E_y)\frac{\partial F_0}{\partial v_\perp}$$
$$+\frac{v_\perp}{2}\left(-\frac{H_z}{H_0}\mp\mathrm{i}\frac{c}{H_0}E_z\frac{\partial}{\partial v_z}\right)\frac{\partial F_0}{\partial x}$$
$$-\frac{\omega_H}{2H_0}(H_y\pm\mathrm{i}H_x)\left(v_\perp\frac{\partial}{\partial v_z}-v_z\frac{\partial}{\partial v_\perp}\right)F_0,$$

$$-\mathrm{i}(\omega-k_z v_z+n\,\omega_H)+\frac{k_y v_\perp}{2}(f_{n-1}-f_{n+1})$$
$$+\frac{v_\perp}{2}\frac{\partial}{\partial x}(f_{n-1}+f_{n+1})=-\frac{c}{4H_0}(E_y\pm\mathrm{i}E_x)v_\perp\frac{\partial}{\partial v_\perp}\frac{\partial F_0}{\partial x}$$
$$+\frac{1}{4H_0}(H_x\mp\mathrm{i}H_y)v_\perp\left(v_\perp\frac{\partial}{\partial v_z}-v_z\frac{\partial}{\partial v_\perp}\right)\frac{\partial F_0}{\partial x},$$
$$n\geqslant 2 \tag{24}$$

Эту систему уравнений легко решить, если мала величина $k_\perp v_\perp/\omega_H$, отношение ларморовского радиуса частицы к «длине волны» колебаний в направлении, перпендикулярном к магнитному полю $\mathbf{H}_0$.

В дальнейшем нам потребуется лишь f_0. Приведем выражения для f_0, полученные из решения

системы уравнений (24) для двух случаев:

1) $$k_z = 0, \quad \omega \sim k_y \frac{v_\perp^2}{2\omega_H} \frac{H_0'}{H_0}$$

$$f_0 = -\frac{v_\perp}{2}\frac{\partial F_0}{\partial v_\perp}\frac{H_z}{H_0} - \frac{\mathrm{i}}{\omega - k_y v_{dp}}\left(c\frac{E_y}{H_0} - \mathrm{i}\frac{v_\perp^2}{2\omega_H}k_y\frac{H_z}{H_0}\right)\left(F_0' + \frac{v_\perp}{2}\frac{\partial F_0}{\partial v_\perp}\frac{H_0'}{H_0}\right) \quad (25)$$

$$n_\alpha = \int f_{0\alpha}\,\mathrm{d}^3v \quad (26)$$

$$p_{\perp\alpha} = \int \frac{m_\alpha v_\perp^2}{2} f_{0\alpha}\,\mathrm{d}^3v = a_\alpha H_x + b_\alpha E_y$$

$$v_{dp} = \frac{v_\perp^2}{2H_0}\frac{H_0'}{\omega_H} \quad (27)$$

2) $$k_z \neq 0, \quad k_z/k_y \gg v_{dp}/v_z$$

$$f_{0\alpha} = -\frac{v_\perp}{2}\frac{\partial F_{0\alpha}}{\partial v_\perp}\frac{H_z}{H_0} - \frac{\mathrm{i}}{\omega - k_z v_z}\left[\left(\frac{c}{H_0}E_y + v_z\frac{H_x}{H_0}\right)F_{0\alpha}' + \left(\frac{e}{m}E_z - \mathrm{i}\frac{v_\perp^2}{2H_0}k_z H_z\right)\frac{\partial F_0}{\partial v_z}\right] \quad (28)$$

$$n_\alpha = \int f_{0\alpha}\,\mathrm{d}^3v. \quad (29)$$

Интегралы по $v_\perp$ в выражении (26), (27) и по v_z в формуле (29) берутся по действительной оси, если $\mathrm{Im}\ \omega > 0$, и по такому контуру, чтобы полюс подинтегрального выражения лежал между действительной осью и этим контуром, если $\mathrm{Im}\ \omega < 0$.

Литература

[1] Церковников Ю. А. *ЖЭТФ* **32** (1957) 67.
[2] Рудаков Л. И., Сагдеев Р. З. *ЖЭТФ* **37** (1959) 1337.

A KINETIC EQUATION FOR SPATIALLY INHOMOGENEOUS SYSTEMS WITH WEAK COUPLING*

EDWARD FRIEMAN

PLASMA PHYSICS LABORATORY, PRINCETON UNIVERSITY

PRINCETON, NEW JERSEY, UNITED STATES OF AMERICA

Prigogine and Balescu recently presented a derivation of the kinetic equation considered here using a diagram technique and operating directly on the Liouville equation. We present here a derivation, similar to Rostoker's, of the same equation which eliminates the need for the diagram technique. The derivation holds for spatially inhomogeneous systems with arbitrary interparticle potentials which satisfy the condition that the maximum value of the potential is small compared to the mean particle thermal energy. Three physically distinct time scales are present in such systems. In increasing order of magnitude they are: τ_1, duration of a collision, τ_2, the time between collisions, and τ_3, the time for a thermal particle to cross the spatial inhomogeneity. We demonstrate that the two-particle distribution function f_2, phase mixes in a time t which satisfies the inequality $\tau_2 \gg t \gg \tau_1$. The phase-mixed value of f_2, when inserted in the collision term in the equation determining the rate of change of the one-particle distribution function f_1, yields the standard Fokker-Planck equation. In principle, the advantage of this derivation is that the "Stosszahlansatz" is demonstrated rather than assumed as in the work of Bogoliubov where f_2 is taken to be a functional of f_1. Similar results have been obtained for short-range forces for which a paper is in the course of preparation.

1. Introduction

Recently, PRIGOGINE and BALESCU [1, 2, 3] have derived kinetic equations for systems of many particles by the use of diagram techniques and summations to all orders. Three separate cases were considered: short range forces, weak coupling, and long range forces. Earlier, BOGOLIUBOV [4] derived kinetic equations for these three cases using assumptions on the functional dependence of the higher order distribution functions. It is the purpose of this paper to illustrate that the recent technique used by ROSTOKER and ROSENBLUTH [5], which is close in spirit to Bogoluibov's procedure, can be extended to the weak coupling case. Further, the presence of spatial inhomogeneities can be taken into account.

The impetus for the present paper is the derivation, by a rigorous technique, of a kinetic equation for a plasma which exhibits no divergences for either small or large impact parameters. The Coulomb potential, of course, takes on the attributes of all three cases mentioned above depending on the magnitude of the impact parameter. A subsequent paper will show that the Boltzmann equation for short range forces can be obtained using the present methods and a completely divergence-free kinetic equation for a plasma derived.

2. The fundamental equations and approximations

We start as usual from the Liouville equation for the N-particle distribution function,

$$\frac{\partial f_N}{\partial t} + \sum_{i=1}^{N} \mathbf{v}_i \cdot \frac{\partial f_N}{\partial \mathbf{x}_i} - \frac{1}{m} \sum_{i \neq j=1}^{N} \frac{\partial \varphi(\mathbf{x}_i - \mathbf{x}_j)}{\partial \mathbf{x}_i} \cdot \frac{\partial f_N}{\partial \mathbf{v}_i} = 0. \quad (1)$$

For simplicity we assume φ to be central and the particles identical. Reduced distribution functions are then defined by

$$f_s(\mathbf{x}_1 \ldots \mathbf{x}_s, \mathbf{v}_1 \ldots \mathbf{v}_s, t) = V^s \int \prod_{j=s+1}^{N} d\mathbf{x}_j \, d\mathbf{v}_j \, f_N, \quad (2)$$

where V is the volume of the system. The Bogoliubov-Born-Green-Kirkwood-Yvon hierarchy is then obtained by integrating over the phase space of $s+1$ particles to yield

$$\frac{\partial f_s}{\partial t} + \sum_{i=1}^{s} \mathbf{v}_i \cdot \frac{\partial f_s}{\partial \mathbf{x}_i} - \frac{1}{m} \sum_{i \neq j=1}^{s} \frac{\partial \varphi(\mathbf{x}_i - \mathbf{x}_j)}{\partial \mathbf{x}_i} \cdot \frac{\partial f_s}{\partial \mathbf{v}_i}$$

$$- \frac{(N-s)}{mV} \int d\mathbf{x}_{s+1} \, d\mathbf{v}_{s+1} \sum_{i=1}^{s} \frac{\partial \varphi(\mathbf{x}_i - \mathbf{x}_{s+1})}{\partial \mathbf{x}_i} \cdot \frac{\partial f_{s+1}}{\partial \mathbf{v}_i} = 0. \quad (3)$$

Following Bogoliubov, we pass to the limit, $N \to \infty$, $V \to \infty$, $N/V = n$ finite, which removes the interaction with the boundary from the problem. The equations governing the time evolution of the one and two particle distributions are then

$$\frac{\partial f_1}{\partial t} + \mathbf{v}_1 \cdot \frac{\partial f_1}{\partial \mathbf{x}_1} - \frac{n}{m} \int d\mathbf{x}_2 \, d\mathbf{v}_2 \frac{\partial \varphi}{\partial \mathbf{x}_1} \cdot \frac{\partial f_2}{\partial \mathbf{v}_1} = 0 \quad (4)$$

and

$$\frac{\partial f_2}{\partial t} + \mathbf{v}_1 \cdot \frac{\partial f_2}{\partial \mathbf{x}_1} + \mathbf{v}_2 \cdot \frac{\partial f_2}{\partial \mathbf{x}_2} - \frac{1}{m} \frac{\partial \varphi}{\partial \mathbf{x}_1} \cdot \frac{\partial f_2}{\partial \mathbf{v}_1} - \frac{1}{m} \frac{\partial \varphi}{\partial \mathbf{x}_2} \cdot \frac{\partial f_2}{\partial \mathbf{v}_2}$$

$$- \frac{n}{m} \int d\mathbf{x}_3 \, d\mathbf{v}_3 \left\{ \frac{\partial \varphi}{\partial \mathbf{x}_1} \cdot \frac{\partial f_3}{\partial \mathbf{v}_1} + \frac{\partial \varphi}{\partial \mathbf{x}_2} \cdot \frac{\partial f_3}{\partial \mathbf{v}_2} \right\} = 0. \quad (5)$$

* Conference paper CN-10/164 presented by E. A. Frieman. Translations of the abstract are given at the end of this volume of the Conference Proceedings.

We now investigate the orders of magnitude of the various terms in Eqs. (4) and (5) and obtain the ratios

$$1 : \frac{v_{\mathrm{th}}\tau}{L_1} : (nr_0^3)\left(\frac{\varphi}{mv_{\mathrm{th}}^2}\right)\frac{v_{\mathrm{th}}\tau}{r_0}$$

for (4) and

$$1 : \frac{v_{\mathrm{th}}\tau}{L_1} : \frac{v_{\mathrm{th}}\tau}{L_2} : \left(\frac{\varphi}{mv_{\mathrm{th}}^2}\right)\frac{v_{\mathrm{th}}\tau}{r_0} : (nr_0^3)\left(\frac{\varphi}{mv_{\mathrm{th}}^2}\right)\frac{v_{\mathrm{th}}\tau}{r_0}$$

for (5). Here r_0 is the range of the potential, τ is the time scale, L_1 and L_2 are the macroscopic length scales, v_{th} the mean thermal velocity, and φ the maximum value of the potential energy.

It is now easy to distinguish the three usual cases:

(a) *Short range forces.* $\varphi/mv_{\mathrm{th}}^2$ is expected to be of order unity since the particles are interacting strongly, while nr_0^3 is expected to be small since we wish to treat binary collisions. In general r_0/L_1 will also be small. If $nr_0^3=\varepsilon$ is chosen to be the parameter of smallness, a formal expansion in ε can then be made.

(b) *Weak coupling.* Here we assume $nr_0^3\sim 1$ but assume $\varphi/mv_{\mathrm{th}}^2\sim\varepsilon$ since the energy of interaction is to be small compared to the kinetic energy. Again r_0/L_1 is assumed small.

(c) *Long range forces.* In this case $(nr_0^3)\sim 1/\varepsilon$ since there are to be many particles in the interaction range. $\varphi/mv_{\mathrm{th}}^2\sim\varepsilon$ since the particles are only weakly interacting due to the long range nature of the force. Again L_1 and L_2 are assumed large compared to r_0.

In all three cases the expansion effectively decouples the equations of the hierarchy so that only a few of the lowest order distribution functions are needed.

3. The weak coupling case

Using the expansion parameter for the weak coupling case, the equations which result are:

$$\frac{\partial f_1^{(0)}}{\partial t} + \mathbf{v}_1\cdot\frac{\partial f_1^{(0)}}{\partial \mathbf{x}_1} = 0, \tag{6}$$

$$\frac{\partial f_1^{(1)}}{\partial t} + \mathbf{v}_1\cdot\frac{\partial f_1^{(1)}}{\partial \mathbf{x}_1} - \frac{n}{m}\int d\mathbf{x}_2\, d\mathbf{v}_2 \frac{\partial\varphi}{\partial \mathbf{x}_1}\cdot\frac{\partial f_2^{(0)}}{\partial \mathbf{v}_1} = 0, \tag{7}$$

$$\frac{\partial f_1^{(2)}}{\partial t} + \mathbf{v}_1\cdot\frac{\partial f_1^{(2)}}{\partial \mathbf{x}_1} - \frac{n}{m}\int d\mathbf{x}_2\, d\mathbf{v}_2 \frac{\partial\varphi}{\partial \mathbf{x}_1}\cdot\frac{\partial f_2^{(1)}}{\partial \mathbf{v}_1} = 0, \tag{8}$$

$$\frac{\partial f_2^{(0)}}{\partial t} + \mathbf{v}_1\cdot\frac{\partial f_2^{(0)}}{\partial \mathbf{x}_1} + \mathbf{v}_2\cdot\frac{\partial f_2^{(0)}}{\partial \mathbf{x}_2} = 0, \tag{9}$$

$$\frac{\partial f_2^{(1)}}{\partial t} + \mathbf{v}_1\cdot\frac{\partial f_2^{(1)}}{\partial \mathbf{x}_1} + \mathbf{v}_2\cdot\frac{\partial f_2^{(1)}}{\partial \mathbf{x}_2} - \frac{1}{m}\frac{\partial\varphi}{\partial \mathbf{x}_1}\cdot\frac{\partial f_2^{(0)}}{\partial \mathbf{v}_1} - \frac{1}{m}\frac{\partial\varphi}{\partial \mathbf{x}_2}\cdot\frac{\partial f_2^{(0)}}{\partial \mathbf{v}_2} - \frac{n}{m}\int d\mathbf{x}_3\, d\mathbf{v}_3\left\{\frac{\partial\varphi}{\partial \mathbf{x}_1}\cdot\frac{\partial f_3^{(0)}}{\partial \mathbf{v}_1} + \frac{\partial\varphi}{\partial \mathbf{x}_2}\cdot\frac{\partial f_3^{(0)}}{\partial \mathbf{v}_2}\right\} = 0, \tag{10}$$

where we have not as yet introduced the fact that the spatial gradients are small.

We note that the system Eqs. (6)—(10) is still formally time reversible. BOGOLIUBOV [4] was the first to point out that one could distinguish widely disparate time scales in the time evolution of kinetic systems and exploit the disparity. For the system under consideration the time scales are, in increasing order of magnitude, τ_0, the duration of a collision, τ_1, the time between collisions, and τ_2, the time for a thermal particle to cross the spatial inhomogeneity. He then postulated that during the time τ_0, while the one particle distribution was changing only slowly, the higher order distributions would change rapidly so as to become functionals of f_1 for all "reasonable" initial conditions. The one particle distribution would then change slowly and approach equilibrium on the time scale τ_1. A point in favor of the ROSTOKER and ROSENBLUTH [5] method is that this can be demonstrated in a sense to be shown below.

For simplicity we first consider the spatially homogeneous case. Eq. (6) then yields

$$f_1^{(0)} = f_1^{(0)}(\mathbf{v}_1) \tag{11}$$

and, in fact, the hierarchy can be satisfied by

$$f_s^{(0)} = \prod_{i=1}^{s} f_1^{(0)}(\mathbf{v}_i). \tag{12}$$

The integral in Eq. (7) then vanishes and we find

$$f_1^{(1)} = f_1^{(1)}(\mathbf{v}_1). \tag{13}$$

The integral in Eq. (8), which is the collision operator, becomes on Fourier analysis:

$$\frac{n}{m}\int d\mathbf{x}_2\, d\mathbf{v}_2 \frac{\partial\varphi}{\partial \mathbf{x}_1}\cdot\frac{\partial f_2^{(1)}}{\partial \mathbf{v}_1} = (2\pi)^3\frac{n}{m}\int d\mathbf{k}\,\varphi(k)\,\mathbf{k}\cdot\frac{\partial}{\partial \mathbf{v}_1}\mathrm{Im}\int d\mathbf{v}_2 f_2^{(1)}(\mathbf{k}, \mathbf{v}_1, \mathbf{v}_2, t). \tag{14}$$

We then solve Eq. (10) by Fourier and Laplace transforms to obtain

$$f_2^{(1)}(\mathbf{k}, \mathbf{v}_1, \mathbf{v}_2, p) = \frac{f_2^{(1)}(\mathbf{k}, \mathbf{v}_1, \mathbf{v}_2, t=0)}{p + i\mathbf{k}\cdot(\mathbf{v}_1 - \mathbf{v}_2)} + \frac{1}{m}\varphi(k)\frac{i\mathbf{k}\cdot\left[\frac{\partial f_1^{(0)}}{\partial \mathbf{v}_1} f_1^{(0)}(\mathbf{v}_2) - \frac{\partial f_1^{(0)}}{\partial \mathbf{v}_2} f_1^{(0)}(\mathbf{v}_1)\right]}{p\,[p + i\mathbf{k}\cdot(\mathbf{v}_1 - \mathbf{v}_2)]}. \tag{15}$$

We see from Eq. (15) that the first term on the right-hand side represents the free particle streaming due to the initial conditions, while the second contains a part which approaches a steady value for long times and represents the effect of the interaction.

For our purposes we only need

$$h(\mathbf{k}, \mathbf{v}_1, t) = \int d\mathbf{v}_2 f_2^{(1)}(\mathbf{k}, \mathbf{v}_1, \mathbf{v}_2, t) \tag{16}$$

and in accordance with the ideas of Bogoliubov consider the limit $t\to\infty$. Using the fact that

$$\lim_{p\to 0} p\,h(\mathbf{k}, \mathbf{v}_1, p) = \lim_{t\to\infty} h(\mathbf{k}, \mathbf{v}_1, t) = h(\mathbf{k}, \mathbf{v}_1),$$

we obtain

$$h(\mathbf{k}, \mathbf{v}_1) = \lim_{p\to 0}\int d\mathbf{v}_2 \frac{f_2^{(1)}(\mathbf{k}, \mathbf{v}_1, \mathbf{v}_2, t=0)\,p}{p + i\mathbf{k}\cdot(\mathbf{v}_1 - \mathbf{v}_2)} + \lim_{p\to 0}\frac{i\varphi(k)}{m}\int d\mathbf{v}_2 \frac{\mathbf{k}\cdot\left[\frac{\partial f_1^{(0)}}{\partial \mathbf{v}_1} f_1^{(0)}(\mathbf{v}_2) - \frac{\partial f_1^{(0)}}{\partial \mathbf{v}_2} f_1^{(0)}(\mathbf{v}_1)\right]}{p + i\mathbf{k}\cdot(\mathbf{v}_1 - \mathbf{v}_2)}. \tag{17}$$

We see that the effect of the initial correlation vanishes in the limit as long as the correlation does not extend over all space (f_2 cannot be a delta function in k space) and thus h does indeed become a functional of f_1. In detail, of course, as $t\to\infty$, $f_2^{(1)}$ becomes a very singular function, and the effect of the initial conditions persists forever. However, all that is ever required for the kinetic equation is an integral over velocity space. All the moments of $f_2^{(1)}$ exhibit fine-scale mixing and approach a steady value.

Introduce the notation

$$\begin{aligned} \mathbf{k}\cdot\mathbf{v}_{1,2} &= k u_{1,2}\,, \\ \mathrm{d}\mathbf{v}_{1,2} &= \mathrm{d}^2\mathbf{v}_{1,2}\,\mathrm{d}u_{1,2}\,, \\ F(u_{1,2}) &= \int \mathrm{d}^2\mathbf{v}_{1,2}\, f_1^{(0)}(\mathbf{v}_{1,2})\,, \end{aligned} \tag{18}$$

and rewrite Eq. (17) as

$$h(\mathbf{k},\mathbf{v}_1) = \lim_{p\to 0}\frac{\varphi(k)}{m}\int \mathrm{d}u_2\,\frac{\left[\dfrac{\partial F}{\partial u_2}f_1^{(0)}(\mathbf{v}_1) - \dfrac{\partial f_1^{(0)}}{\partial u_1}F(u_2)\right]}{u_2 - u_1 + \dfrac{\mathrm{i}p}{k}}. \tag{19}$$

Using the result

$$\lim_{\varepsilon\to 0}\frac{1}{u_2-u_1\pm\mathrm{i}\varepsilon} = \mathsf{P}\frac{1}{u_2-u_1} \mp \mathrm{i}\pi\,\delta(u_2-u_1)\,,$$

we obtain

$$\operatorname{Im} h(\mathbf{k},\mathbf{v}_1) = \pi\frac{\varphi(k)}{m}\left[F(u_1)\frac{\partial f_1^{(0)}}{\partial u_1}(\mathbf{v}_1) - \frac{\partial F}{\partial u_1}f_1^{(0)}(\mathbf{v}_1)\right]. \tag{20}$$

This expression when inserted in Eq. (14) yields the familiar Fokker-Planck collision term.

We now go on to investigate the effect of spatial inhomogeneities. Let us first assume that $r_0/L_1\sim 1$. We then obtain, upon inserting Eq. (12) into Eq. (7),

$$\frac{\partial f_1^{(1)}}{\partial t} + \mathbf{v}_1\cdot\frac{\partial f_1^{(1)}}{\partial \mathbf{x}_1} - \frac{n}{m}\frac{\partial f_1^{(0)}}{\partial \mathbf{v}_1}\int \mathrm{d}\mathbf{x}_2\,\mathrm{d}\mathbf{v}_2\frac{\partial\varphi}{\partial \mathbf{x}_1}f_1^{(0)}(\mathbf{x}_2,\mathbf{v}_2,t) = 0\,. \tag{21}$$

If we define the average force $\mathcal{J}(\mathbf{x}_1,t)$ as

$$\mathcal{J}(\mathbf{x}_1,t) = n\int \mathrm{d}\mathbf{x}_2\,\mathrm{d}\mathbf{v}_2\frac{\partial\varphi}{\partial\mathbf{x}_1}f_1^{(0)}(\mathbf{x}_2,\mathbf{v}_2,t), \tag{22}$$

we recognize that Eq. (21) is just the familiar Vlasov equation. In this case, however, the two time scales r_0/v_{th} and L_1/v_{th} are of the same order of magnitude and no tendency toward the Bogoliubov synchronization process appears. This can be seen formally in that the solution of Eq. (10) contains no $p=0$ pole. Physically this is quite reasonable since we expect that in this case fine-scale mixing will tend to wipe out the large gradients which occur. The distribution function becomes quite singular in the process until collisions finally take over the approach to equilibrium.

We, therefore, are led to consider the case where r_0/L_1 is small initially. The general solution of Eq. (6) is $f_1^{(0)}=f_1^{(0)}(\mathbf{x}_0,\mathbf{v}_0)$ where $\mathbf{x}_0$ and $\mathbf{v}_0$ are the initial position and velocity for the particle trajectory. The solution we require is such that $f_1^{(0)}$ is a slowly varying function of $\mathbf{x}_0=\mathbf{x}_1-\mathbf{v}_1 t$ while its variation with $\mathbf{v}_0$ is arbitrary. We see then that the average force $\mathcal{J}$ will not vanish but in calculating $f_2^{(1)}$ we need not consider the variation with $\mathbf{x}_0$.

4. Summary

The final result of the calculation is then the kinetic equation,

$$\frac{\partial f_1}{\partial t} + \mathbf{v}_1\cdot\frac{\partial f_1}{\partial\mathbf{x}_1} - \frac{1}{m}\frac{\partial f_1}{\partial\mathbf{v}_1}\cdot\mathcal{J} = \frac{8\pi^4 n}{m^2}\frac{\partial}{\partial v_i}\int \mathrm{d}\mathbf{k}\,\varphi^2(k)\frac{k_i k_j}{k}\left\{\frac{\partial f_1}{\partial v_j}I - f_1\frac{\partial I}{\partial v_j}\right\}, \tag{23}$$

where

$$I = \int \mathrm{d}\mathbf{v}'\, f(\mathbf{x}',\mathbf{v}',t)\,\delta\left(\frac{\mathbf{k}\cdot\mathbf{v}}{k} - \frac{\mathbf{k}\cdot\mathbf{v}'}{k}\right) \tag{24}$$

correct to order ε^2. When applied to the Coulomb force it, of course, diverges for both small and large impact parameters. Since the results of Rostoker and Rosenbluth reduce to this form for small impact parameters and the Boltzmann collision integral reduces to this form for small momentum transfers, we see the possibility of removing the divergences at least for all the dominant terms by a consistent method.

The main purpose of the present investigation has been, however, to demonstrate that the procedure of reference [5] applies to the weak coupling case and that spatial inhomogeneities can be included in the formalism.

Acknowledgment

The work reported here was accomplished under the auspices of the United States Atomic Energy Commission.

References

[1] Prigogine, I., Balescu, R., *Physica* **25** (1959) 281.
[2] Prigogine, I., Balescu, R., *Physica* **25** (1959) 302.
[3] Prigogine, I., Balescu, R., *Physica* **26** (1960) 145.
[4] Bogoliubov, N., «Problemy Dinamicheskoi Theorii *i.* Statisticheskoi Fizike» (Moscow, Gostekhizdat, 1947).
[5] Rostoker, N., Rosenbluth, M. N., *Phys. Fluids* **3** (1960) 1.

DISCUSSIONS (SESSION III) — DISCUSSIONS (SÉANCE III) — ДИСКУССИИ (ЗАСЕДАНИЕ III) — DEBATES (SESIÓN III)

Paper CN-10/43 *was presented by H. J. Kaeppeler* (Federal Republic of Germany). *The text of the paper is on pages 403—410. The following discussion took place:*

C. C. Chang *(United States of America):* Comparing terms in the dynamic equations, the thermal conduction is usually more important than the viscous effect in plasma shock. A paper of Y. C. Whang and C. C. Chang based on Grad's thirteen-moment method of two-component plasma, entitled "Structure of Weak Shock Wave in a Plasma", will be published in the *Physics of Fluids.*

H. J. Kaeppeler: We have shown that, for certain points in the shock structure, the effects of viscosity cannot be neglected and also dominate damping by ohmic dissipation. Viscous dissipation results in reducing the first and second derivatives of the velocity, as was pointed out. From our investigations it may be safe to conclude that the importance of the dissipative mechanism for the fine structure of the shock increases with the order of the moments. This would indicate a strong influence of thermal conductivity, in agreement with what Dr. Chang just said.

R. W. Larenz *(Federal Republic of Germany):* I should like to make some remarks about shock-wave calculations we performed at Hannover. We calculated the structure of very strong shock waves in a fully ionized medium with Mach numbers above 30 (related to ordinary sound velocity of a plasma). We took care of the viscosity of ions and electrons and likewise of both heat conductivities. The structure turned out to be essentially stable except for a region ahead of the shock front, which is unstable against electron plasma oscillations.

H. J. Kaeppeler: Is this a mathematical or a physical instability?

R. W. Larenz: The instability is a physical one caused by a steep electron temperature or pressure gradient.

H. J. Kaeppeler: What we found at the singularity behind the shock was a mathematical instability of the differential equations including viscous dissipation. However, we are not saying that there might not also be a physical instability. This is expressed by the last sentence in Section 2 of our paper.

E. P. Velikhov *(Union of Soviet Socialist Republics):* A possible type of electron instability in a shock wave may be connected with a beam instability of the electrons moving along a wave front at a sufficiently high Mach number (see the paper in *Nuclear Fusion* **1** (1961) 87 by A. A. Vedenov, E. P. Velikhov and R. Z. Sagdeev).

H. J. Kaeppeler: I am not familiar with your paper as it came out too recently. I think that this is an interesting point, however.

Paper CN-10/87 *was presented by J. L. Delcroix* (France). *The text of the paper is on pages 411—422. The following discussion took place:*

R. F. Whitmer *(United States of America):* I have two questions: (1) What is the specific form of the pressure tensor, i.e. does the closure condition $\nabla \cdot \mathbf{Q} = 0$ yield a pressure tensor of recognizable form such as the Navier-Stokes form which I used in the paper presented at the Munich conference? (2) Wouldn't collisions broaden the resonance lines?

J. L. Delcroix: (1) We have used in our calculation a pressure tensor which is the sum of two terms:
— the equilibrium scalar pressure $\bar{n}\,k\,T$
— the perturbation in pressure p, written in the form of a symmetric second-order tensor, without any restrictive hypothesis on any of its six components.
We have not yet examined which form of the tensor p is yielded by the closure condition $\nabla \cdot \mathbf{Q} = 0$, or in particular whether this form does or does not resemble that of Navier-Stokes, which you have utilized. But that is a very interesting question.
(2) We are not in a position to say what would be the influence of collisions on the results obtained in our theory in the neighborhood of the resonances. Besides, it is certain that in these regions the hydromagnetic theory breaks down.

O. Buneman *(United States of America):* There is no instability in the full kinetic theory calculation such as that presented by Bernstein (*Phys. Rev.* **109** (1958) 10). It appears that the adiabatic theory breaks down not only at wave velocities less than, or comparable with the velocity of sound, but also in the vicinity of the gyro-resonances. If an adiabatic theory could be completed by introducing Landau damping effects, Delcroix's instability should disappear.

J. L. Delcroix: I quite agree that the adiabatic theory may not work near the cyclotron resonance frequency.

Paper CN-10/132 *was presented by A. R. Kantrowitz* (United States of America). *The text of the paper is on pages 423—445. The following discussion took place:*

C. C. Chang *(United States of America:* If this shock wave is to apply to the regime of thermonuclear fusion, then the temperature would go above 10^8 degrees K. In that case it seems that the radiation term has to be considered. Also, there will be a heat-release term

coming from thermonuclear reactions. Therefore, this mechanism is more similar to a detonation wave than to a shock wave.

A. R. Kantrowitz: No, I do not think that is true. If one extrapolated these results to thermonuclear temperatures, the shock thickness would be many orders of magnitude less than the mean free path. The energy radiated and the thermonuclear energy released during the time a particle spends in the shock transition region will therefore be negligible.

P. L. Auer *(United States of America):* Abstract CN-10/127 ("Numerical Calculations of Strong Magnetic Disturbances" by P. L. Auer, H. Hurwitz, Jr., R. W. Kilb) refers to a calculation performed in the U.S.A. in which numerical integration of the Vlasov equation is performed for a magnetic disturbance travelling perpendicular to the magnetic field. The plasma is initially uniform and cold, with an initial magnetic field. In this highly idealized geometry the waves considered by Kantrowitz do not exist. Nevertheless we observe that for strong enough disturbances micro-turbulence produces a strongly fluctuating shock front followed by a region of compressed plasma containing thermalized ions at elevated temperature. The electrons remain relatively cold. The shock width is of the order of the distance travelled by the disturbance in one-half the ion gyration period.

A. R. Kantrowitz: The shock thicknesses which we have measured are apparently some twenty times or so larger than those you calculate. They are typically of the order of ten times the ion gyro-radius.

P. L. Auer: Well, no, the shock of course travels faster than the Alfvén-wave velocity, so our shock thickness is somewhat larger, say four times the ion gyro-radius, so we would be off from your observation by a factor of about two or three. Is that correct?

A. R. Kantrowitz: Depending upon what the Alfvén-wave Mach number is.

P. L. Auer: Yes, well, the Alfvén-wave Mach number in our calculations is of the order of five or six.

A. R. Kantrowitz: In that case the agreement is probably better than a factor of five. The experimental shock thickness decreases with increasing Alfvén-wave Mach number and is about three times the ion gyro-radius at an Alfvén-wave Mach number of four. I would like to say, the theory that we have proposed will not work for Alfvén-wave Mach numbers larger than about three. For stronger shocks the scattering of waves on waves can no longer be calculated with the random phase approximation which we have used.

J. D. Jukes *(United Kingdom):* I would like to ask Dr. Kantrowitz:

(1) Whether he considers electron gyro-resonance an important damping mechanism for his postulated waves (i.e., $\omega - \mathbf{k}\cdot\mathbf{v}_e \approx \omega_{ce}$)?

(2) If so, whether this represents a powerful electron-heating mechanism?

(3) Whether there is any experimental evidence of an electron temperature consistent with the conservation equations?

A. R. Kantrowitz: I spoke briefly of what I called the ultraviolet catastrophe that happens to these waves when they are not in a blob type distribution. Now some of the waves certainly will be scattered out of that blob distribution and they quickly go to higher frequencies. (It's a process very much like steepening of the longer waves.) In one calculation given in the paper, for example, they go to very high frequencies in times of the order of several times the mean free time, so that these waves would go to electron gyro-frequencies, be damped there by Landau damping, i.e., by a resonance damping process, and would, in fact, heat the electrons. So that would be a powerful heating mechanism. Experimentally we have not determined anything but a lower bound to our electron temperature. This lower bound is between ten and twenty volts. It was measured by comparing the ultraviolet radiation with the visible radiation, but we have made only a few comparisons, so we don't have good measurements for electron temperatures yet.

Paper CN-10/152 *was presented by W. A. Newcomb* (United States of America). *The text of the paper is on pages 451—463. The following discussion took place:*

E. P. Velikhov *(Union of Soviet Socialist Republics):* I have a comment on the problem of the sufficiency of the principle that has just been exposed. I would like to discuss a simple counter-example of the following type: let us consider a magnetic field and an incompressible, perfectly conducting fluid in the magnetic field. The magnetic field is parallel to the wall in the yz-plane, and the fluid is unbounded in the x-direction. We have

$$\sigma = \infty;\ \mathrm{d}\varrho/\mathrm{d}t = 0;\ B = B_0(x) + B^{(1)}$$

Let $\psi = B_{0y}(x)\, B_x^{(1)} \sim \mathrm{e}^{-\mathrm{i}\omega + \mathrm{i}ky}$. The equation for small perturbations of such a medium may be written as follows:

$$\frac{\mathrm{d}}{\mathrm{d}x}\left[\left(\omega^2 - \frac{k^2 B_0^2}{\varrho}\right)\frac{\mathrm{d}\psi}{\mathrm{d}x}\right] = k^2\left(\omega^2 - \frac{k^2 B_0^2}{\varrho}\right)\psi.$$

The boundary conditions are such that ψ should vanish at the wall and at infinity. Multiplying this equation by ψ^*, the complex conjugate of ψ, and integrating by parts, we obtain

$$\omega^2 = \frac{\int (k^2 B_0^2/\varrho)\,(|\psi'|^2 + k^2|\psi|^2)\,\mathrm{d}x}{\int (|\psi'|^2 + k^2|\psi|^2)\,\mathrm{d}x}$$

From this it is clear that ω^2 is greater than zero, i.e. that these perturbations are undamped oscillations.

However, if we solve the original equation exactly, for example in the special case

$$\frac{k^2 B_0^2}{\varrho} = C_1 + C_2 x,$$

where C_1 and C_2 are constants, then we obtain Bessel's equation,

$$\frac{\mathrm{d}}{\mathrm{d}x}\left[\left(\frac{\omega^2}{C_2} - \frac{C_1}{C_2} - x\right)\frac{\mathrm{d}\psi}{\mathrm{d}x}\right] = k^2\left(\frac{\omega^2}{C_2} - \frac{C_1}{C_2} - x\right)\psi,$$

with the general solution

$$\psi = A_1 I_0\left(x - \frac{\omega^2}{C_2} + \frac{C_1}{C_2}\right) + A_2 K_0\left(x - \frac{\omega^2}{C_2} + \frac{C_1}{C_2}\right).$$

The first term vanishes because of the boundary condition at infinity, and the eigenvalue condition,

$$K_0\left(\frac{C_1}{C_2} - \frac{\omega^2}{C_2}\right) = 0,$$

follows from the boundary condition at the wall. But this equation has roots only with ω^2 complex. Thus, in spite of the energy principle, ω^2 has real and imaginary parts. If one were to solve the corresponding initial-value problems, using the Laplace transform, it is obvious that the perturbation would be damped, since there is no physical reason why it should grow. It is possible, however, that there exists a class of perturbations which, even though according to the energy principle there is no instability, might in certain cases be unstable anyway, for I do not know of any proof to the contrary.

What I meant to say is that this example contradicts the energy principle. At the very least it shows it to be insufficient.

W. A. Newcomb: I would of course have to look at this example in more detail before commenting on it with a feeling of confidence. However, I have seen such things before in the theory of Landau damping. It seems that the normal modes in this present case are really singular, as they are in the case of plasma oscillations, and that the solution we have just seen is probably analogous to the asymptotic solution we found by Landau. That solution was not a true normal mode because it was only the electric field that went as exp ($i\omega t$), the other quantities varying as exp ($ikvt$). When different quantities have different frequencies it is not really a normal mode. I don't know whether a similar remark applies here. Now, in the Landau case one can analyze in terms of singular normal modes as van Kampen has done. The result is that, whenever all the normal modes have real frequencies, then you never have anything worse than damping in the Landau motions. If, however, there is a Landau motion which is unstable, or overstable, there will also be a correspondingly unstable normal mode in addition to the singular van Kampen modes; and since the energy principle is concerned with the frequencies of all the normal modes it will detect any such instabilities in the hydromagnetic cases for which it was derived. Therefore I do not believe it could ever happen that the energy principle would lead to stability and yet that there would be some motion of this type with anti-damping rather than damping. It is quite possible though for the energy principle to lead to stability, with all the eigenvalues real, and yet to have something like this come out with a damping term. Namely, this is probably not really an eigenvalue.

(*Editor's note:* This interesting paradox was resolved in the course of subsequent discussions between Drs. Velikhov, Newcomb, Kruskal, and Taylor. The solution is that the Bessel function K_0 is multivalued, and that its zeroes are all located on the wrong branches. That is to say, there is only one branch on which K_0 vanishes at infinity, and on that branch there are no zeroes.)

O. Buneman *(United States of America):* Variational principles were applied to fluids with electromagnetic interaction quite a long time ago. (T. M. Cherry in the mid-forties). The covariant relativistic treatment was given by P. N. Butcher (*Phil. Mag.*, 1954). These treatments are based on the use of the elegant Clebsch variables, in preference to the Lagrangian displacement used in the two previous papers.

Can the variational principle be extended from the case of isotropic or Chew-Goldberger-Low pressures to the case of the general anisotropic pressure as introduced in the paper by Delcroix?

W. A. Newcomb: I have not tried it, but my opinion is that it can. That is only an opinion, however.

Paper CN-10/199 *was presented by E. P. Velikhov* (Union of Soviet Socialist Republics). *The text of the paper is on pages 465—475. The following discussion took place:*

M. Kruskal *(United States of America):* When the plateau is forming it seems that some of the fast particles slow down. What happens to the energy?

E. P. Velikhov: The energy of the particles is completely transformed into oscillations. Fast particles are slowed down and, in this example, the energy goes into plasma oscillations.

M. Kruskal: Yes, but don't you end up eventually with no more oscillations? Do the oscillations persist indefinitely? Don't you get Landau damping, for instance?

E. P. Velikhov: Of course the oscillations are damped, but it takes much greater times than those you are interested in. A more detailed discussion of the damping of these oscillations due to collisions between themselves will be given in Drummond's paper.

M. Kruskal: Well, then eventually the distribution would spread out somewhat.

E. P. Velikhov: Finally, of course, the distribution becomes Maxwellian.

A. Rukhadze *(Union of Soviet Socialist Republics):* As I understand it, the quasi-linear theory is some approximation to the kinetic equation which includes the collision integral in the form given by Rostoker-

Silin (and others), where particle interaction is taken into account by exchange of waves propagating in the plasma.

O. Buneman *(United States of America):* The numerical calculations on the development in the course of time of an initially double humped distribution function do not show the formation of the plateau. Instead, one seems to proceed very rapidly from the double hump to a smooth single hump, a genuine Maxwellian. The plateau does not seem to occur in between. This would be in agreement with Dr. Kruskal's remarks on your paper.

E. P. Velikhov: There are two times: a time for binary collisions, or collisions between waves, which in the case of strong instability cause Maxwellization; and a time for collisions between waves and particles. The time for the latter type is much smaller; and therefore I think that a plateau is formed at the start and that then, after a much longer time, Maxwellization occurs. I am not acquainted with the calculations.

W. Drummond *(United States of America):* What Buneman is referring to is a zero-temperature plasma, and the effects described by Velikhov were for a finite-temperature plasma, which has quite a different behavior until the plateau is formed. After the plateau is formed, the wave-wave collisions will bring about, one thinks, the type of thing that Buneman discussed. However, without particle collisions the final distribution function need not be a Maxwellian, but only a monotonically decreasing function of energy. But that is on a much longer time scale than what Velikhov was discussing here, simply because of the finite temperatures.

Paper CN-10/73 *was presented by J. B. Taylor* (United Kingdom). *The text of the paper is on pages 477—480. The following discussion took place:*

T. Kihara *(Japan):* The relaxation and transport phenomena in a fully ionized gas in a strong magnetic field cannot be treated by the Boltzmann equation or Fokker-Planck equation if the radius of the electron gyration is smaller than the Debye length. In connection with this fact a stochastic method based on the force correlation function has been developed by us at the Physics Department of the University of Tokyo. The method and its application were published in *J. Phys. Soc. Japan* (1959 and 1960) and read at the International Symposium on Magneto-Fluid Dynamics.

J. B. Taylor: Well, I would simply remark that it is perfectly true that the stochastic method can be used for many other forms of transport processes besides diffusion. I merely felt that diffusion was the most interesting one. In connection with the specific points which Dr. Kihara is referring to, I think we should also make reference to the fact that Drs. Rosenbluth and Rostoker have obtained similar results by what I feel is a considerably more rigorous theory.

S. Colgate *(United States of America):* As I understand this maximum diffusion, it corresponds to a random-walk step each Larmor period. Do you have a physical interpretation of why a larger random-walk step at a slightly lower frequency is not physically feasible? Because this would certainly lead to a faster diffusion.

J. B. Taylor: As Dr. Colgate said, it is true that the maximum diffusion corresponds to a random-walk step with a step length equal to a cyclotron radius. Very roughly one can see the result this way: in order of magnitude, the diffusion coefficient—remember regarding it as a random-walk process—is something like the square of the step length divided by the step time. Now if $\omega\tau$ is much greater than one (we are thinking now of a definite collision time τ), then the particle spends most of its time just going around in a Larmor orbit, but every now and then it makes a step. So in this case the step is the Larmor radius, and the diffusion coefficient will be $D \sim v^2/\omega^2\tau$. On the other hand, if $\omega\tau$ is much less than one, the step length is more like the mean free path $v\tau$, so that the diffusion would then go like $v^2\tau$. From this simple argument you see that the magnetic field reduces the diffusion by $\omega^2\tau^2$, which everyone knows, but more interesting is the fact that, if you regard the diffusion as a function of τ, then when $\omega\tau$ is small the diffusion rises with τ, whereas when $\omega\tau$ is large the diffusion falls like τ^{-1}. So by continuity we expect a maximum roughly corresponding with the point Dr. Colgate indicated. Now let me try and answer his question. Why do I think that steps larger than this cannot appear? In order to get them, one would have to have an electric field which was correlated both across the field and along the field over large distances. This would violate the condition that the field as seen by an ion has a short correlation time. If that condition is indeed violated then one can exceed this maximum; and in the case of hydromagnetic instability it might very well be violated. But I do not believe it will be violated by micro-instabilities; and if one believes that the linear theory of micro-instability tells you something about the non-linear regime, then I have in fact proved this point as far as ion-wave instabilities are concerned.

A. R. Kantrowitz *(United States of America):* I should like to point out that waves at frequencies close to the ion cyclotron frequency should be looked for to play an important role in enhanced diffusion for two reasons:

(1) Among waves which can move with group velocities larger than the typical plasma velocity, these waves have the largest wavelength and thus would produce the largest step length.

(2) As was pointed out by Petschek, collisions between these waves result in a transfer of momentum between electrons and ions.

J. B. Taylor: Well, I think that I could only say that now that I have heard Dr. Kantrowitz's paper I realize that there are many points of similarity. Unfortunately, from its title I did not realize this earlier, and therefore I have not been able to explore them.

STUDIES OF STABILITY AND HEATING IN THE SCYLLA MAGNETIC COMPRESSION EXPERIMENT*

E. M. LITTLE, W. E. QUINN, F. L. RIBE, G. A. SAWYER

LOS ALAMOS SCIENTIFIC LABORATORY, UNIVERSITY OF CALIFORNIA

LOS ALAMOS, NEW MEXICO, UNITED STATES OF AMERICA

The Scylla experiment has been extended to higher capacitor bank energies (31 kJ $\leq W \leq$ 180 kJ) and applied magnetic fields (44 kG $\leq B_m \leq$ 145 kG). Various coil lengths (10.6 cm $\leq l \leq$ 26.8 cm) are also used. The stability of the plasma in its compressed state is studied by means of streak and Kerr-cell photographs. Depending upon the values of W and l, the plasma is found to: (a) remain stable throughout the compression; (b) show a growing instability in the form of a rotating elliptical structure; or (c) show a violent instability after an initial period of stability. For small W and large l the plasma is stable; as W is increased or l is decreased, it becomes progressively unstable. The rotating structure appears to correspond to a growing $m=2$ Rayleigh-Taylor flute disturbance, with superimposed rotation of the plasma as a whole. The rate of flute growth is smaller by an order of magnitude than that calculated from the bending of the magnetic mirror lines, and the parameters of the experiment suggest that the stabilizing effects of finite Larmor radii predicted by Rosenbluth, *et al.*, may occur. Electron temperatures T_e are determined by measuring the shape of the soft x-ray continuum with a crystal spectrometer and also with thin absorbers. T_e scales with magnetic field approximately as $B_m^{4/5}$ as would be expected from a model of shock heating followed by adiabatic compression at $\gamma = 5/3$. Time histories of T_e and B during individual compressions show regular behavior of T_e for the stable or weakly unstable cases. The observed slope of ln T_e versus ln B during decompression is smaller than 4/5, corresponding formally to $\gamma \approx 4/3$. For cases with well-developed instability, T_e shows an abrupt decrease at the onset of the instability. There is also an analogous sudden discontinuity in the time distribution of neutron emission when the instability begins. Neutron scaling results show a somewhat slower rise of emission rate R_n versus B_m than would correspond to a two-stage model with adiabatic compression. The scaling curves of T_e and R_n show abrupt decreases for $B_m > 100$ kG which correlates with a large observed increase of soft x-radiation. Large variations of R_n are coupled with much smaller variations of T_e. This tends to confirm an earlier observation in Scylla I [*Phys. Fluids* 4 (1961) 711] that the ions and electrons are to some extent energized independently and that the trapped reversed field exerts a larger effect on the ions.

1. Introduction—summary of previous results

Previously reported results [1—7] of the Los Alamos magnetic compression experiments have dealt exclusively with the Scylla I device. In it a sinusoidal axial magnetic field having a period T of 5.4 μs and an amplitude B_m of 52 kG was applied to a volume of partially ionized deuterium gas at a pressure of approximately 85 μ Hg. The deuterium was contained in a 96 or 99% Al_2O_3 ceramic discharge tube having an inner diameter of 5.4 cm, surrounded by a single-turn compression coil of length 10.6 cm and effective inner diameter 7.5 cm. The coil was excited by a 31-kJ capacitor bank charged to 85 kV, of which 35 kV appeared across the coil initially after switching.

During the first half-cycle of the Scylla I discharge the ionization of the gas is completed, and a small amount B_0 ($\approx$4 kG) of the applied magnetic field is trapped inside the plasma. At the beginning of the second half-cycle a fast ($\approx 10^7$ cm/s) cylindrical shock is driven inward upon the plasma containing the trapped, reversed magnetic field B_0. During a major portion of the 2.7-μs magnetic half-cycle the plasma emits soft x-rays and d-d nuclear reaction products, characteristic of energetic plasma electrons and deuterium ions. Analysis of the soft x-ray continuous spectrum by means of thin absorbers [4] and a Bragg diffraction crystal spectrometer [7] indicates an electron temperature $T_e = 345$ eV. Measurement of the intensity of the visible emission continuum [4] gives a plasma ion density $n = 6 \times 10^{16}$ cm^{-3}. Measurement of the Doppler broadening and shift of the d-d proton and neutron spectra [5], along and transverse to the axis of the discharge, shows the first two moments of the plasma deuteron velocity distribution to be the same as those of a Maxwellian with a deuteron temperature $T_d = 1300$ eV.

It was found [6] that all the above phenomena which occur during the second half-cycle with weak preionization can be made to occur during the first half-cycle by applying strong preionization and a reversed bias field B_0 independently. Excitation of the plasma ions to final kinetic temperatures in the region of 1000 eV occurs only for reversed B_0. However, the electrons attain temperatures of the order of 100 eV even in the absence of B_0. Thus the ion and electron populations appear to be sufficiently decoupled that to some degree they are energized inde-

* Conference paper CN-10/155 presented by F. L. Ribe. Discussion of this paper is given on page 645. Translations of the abstract are at the end of this volume of the Conference Proceedings.

pendently. The calculated electron-ion relaxation time owing to Coulomb collisions [8] is 6 μs, as compared with the magnetic half-cycle $T/2=2.7$ μs.

It is also observed [6] that the reversed B_0 is dissipated from inside the plasma within approximately 0.4 μs after the beginning of the magnetic half-cycle, i.e., during and shortly after the initial shock. An indication of this process (for second half-cycle operation) occurs in the streak camera photographs of Fig. 2 which show the radial extent of the luminous Scylla I plasma as a function of time. The plasma contracts rapidly inward at the beginning of the magnetic half-cycle and reflects outward off the central region containing reversed B_0. Shortly after the second inward contraction the hollow, dark core corresponding to trapped B_0 disappears, leaving a homogeneous luminous plasma. It has been postulated [6, 9] that the interface (sheath) between the plasma and the magnetic field which drives the shock is unstable in the presence of the reversed B_0, causing rapid leakage of magnetic field through the sheath and allowing B_0 to be cancelled by the magnetic field outside the sheath. The magnetic energy which thus disappears is given up to the plasma to enhance the normal heating by the shock. Apparently further plasma heating then occurs largely by means of adiabatic compression by the rising magnetic field during the remainder of the quarter-cycle. However, a question remains as to how long small amounts of B_0 remain in the plasma and contribute to its heating during the magnetic compression.

2. The present experiments—Scylla III

The experiments to be reported here were undertaken to see if by applying larger magnetic fields from more energetic capacitor banks the electron and ion temperatures would be increased in a manner which is consistent with the assumption of adiabatic compression. During the experiments a hydromagnetic plasma instability was observed, and its dependence upon various experimental parameters was studied. The time dependence of the plasma electron temperature during periods of both plasma stability and instability was also measured.

The new apparatus, Scylla III,* utilizes capacitor banks of the same voltage, but having three and six times the stored energy, as the Scylla I experiment. In addition to the 10.6-cm coil length of the former apparatus, coils of greater lengths were also used. The proportions of the longest coil ($l_3=26.8$ cm) are shown in Fig. 1 and those of the shortest (10.6 cm) coil in Fig. 8. They have the same radii as the Scylla I

* The term Scylla II was used to denote an experiment in which the Scylla I coil was "power crowbarred" by switching on a 20-kV capacitor bank at the time of current maximum of the 85-kV bank. Results were reported in References [10] and [11].

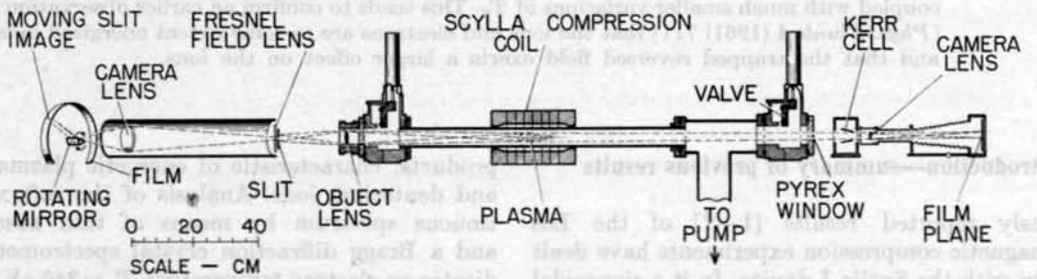

Fig. 1 Apparatus for observing the motion of the plasma. To the left is shown the streak camera whose slit opening is 0.25 mm. The moving slit image has a speed on the film of 0.3 cm/μs. To the right is shown the Kerr-cell and its camera. The Kerr-cell has a transmission of 0.25 when open and its camera has an f/5.6 aperture.

TABLE I. Parameters of Scylla Magnetic Compression Experiments

Capacitor energy W (kJ)	Compression coil length l (cm)	Maximum magnetic field B_m (kG)	Half period $T/2$ (μs)	Voltage on compression coil V_c (kV)	Designation
$W_1=31$	$l_1=10.6$	52	2.70	35	Scylla I
$W_2=93$	$l_1=10.6$	104	3.96	48	Scylla III
	$l_2=16.6$	98	3.62	48	
	$l_3=24.2$	81	3.40	43	
$W_3=180$	$l_1=10.6$	145	5.40	48	Scylla III
	$l_2=18.7$	121	5.04	44	
	$l_3=26.8$	104	4.60	42	

W = energy of capacitor bank when charged to 85 kV.
l = overall length of compression coil.
B_m = maximum vacuum magnetic field in the center of the compression coil during the second half-cycle.
$T/2$ = half period of sinusoidal magnetic field.
V_c = voltage across coil terminals at the beginning of the second half-cycle.
The radius of the coils in their central sections is 4.1 cm and in the end regions ("mirrors") 3.4 cm.

coil. The pertinent parameters of the Scylla III apparatus are given in Table I. The main characteristics of the new apparatus are maximum compression fields as large as 145 kG, longer compression half-cycles, and somewhat higher coil voltages. The latter were a consequence both of the large number of paralleled switched capacitors (30 and 60) and the use of coaxial connecting cables of lower inductance.

In the present experiments weak preionization was used with the consequence that the magnetic shock and the energetic plasma were always obtained during the second half-cycle. Unless otherwise noted, the phenomena to be discussed will always refer to this half-cycle. The compression coils were always short circuited by means of a closely coupled vacuum spark gap at times near the end of the second half-cycle. This is shown in the magnetic field oscillogram of Fig. 3, at the time marked S. The shorting operation was performed so that the capacitor bank energy would not flow into the coil and discharge tube on current half-cycles after the second, causing excessive damage to the tube wall. The discharge tubes were of the same types as those of the Scylla I experiment.

3. Observations of plasma motion—stability

3.1. Apparatus

The gross motion of the plasma, and hence its hydromagnetic stability, was studied by photographing it with streak and Kerr-cell cameras. The apparatus is shown in Fig. 1. The large effective aperture (f/2.9) of the streak camera* [12] shown at the left is essential in order to expose even the most sensitive film (ASA rating 500) from the compressed plasma in these experiments. The plasma light intensity is only a few times greater than that of the deuterium bremsstrahlung continuum [4]. The object lens focuses an image of the plasma on the horizontal slit which is in turn focused by the camera lens on the cylindrical film surface. The rays are reflected from the rotating mirror to provide a rapidly moving image on the film of a narrow section of the plasma near the axis at the central plane of the compression coil. The depth of focus of the streak camera is 1.5 cm.

The Kerr-cell shutter [13] is opened by a high voltage pulse of 0.1 or 1.0 μs duration, which can be made to occur at any desired instant of the discharge cycle. The depth of focus of the Kerr-cell optical system along the axis of the compression coil is 5 cm. Although Fig. 1 shows only the longest compression coil, the experiment involved the use of coils of various lengths.

3.2. Experimental results

Typical photographs of the plasma for the various coil lengths l and capacitor energies W of Table I are shown in Figs. 2 through 6. Depending upon l and W, the behavior of the plasma in its compressed state can be classified observationally in three ways:

(1) The boundary of the luminous plasma is smooth and exhibits only slow motions from side to side as in Figs. 2 (a), 2 (b) and 6 (b). This type of motion will be called *stable* and denoted by the symbol S.

(2) The plasma boundary exhibits growing oscillations of a regular nature as in Figs. 2 (c), 4 (a), 4 (c), 4 (d), 5 (a), and 5 (d). This type of motion is denoted by the symbol O.

(3) The plasma develops fast, irregular motion, its area becomes very small, and it moves completely out of view of the streak camera as in Fig. 3. This type of motion will be called *unstable* and denoted by the symbol U.

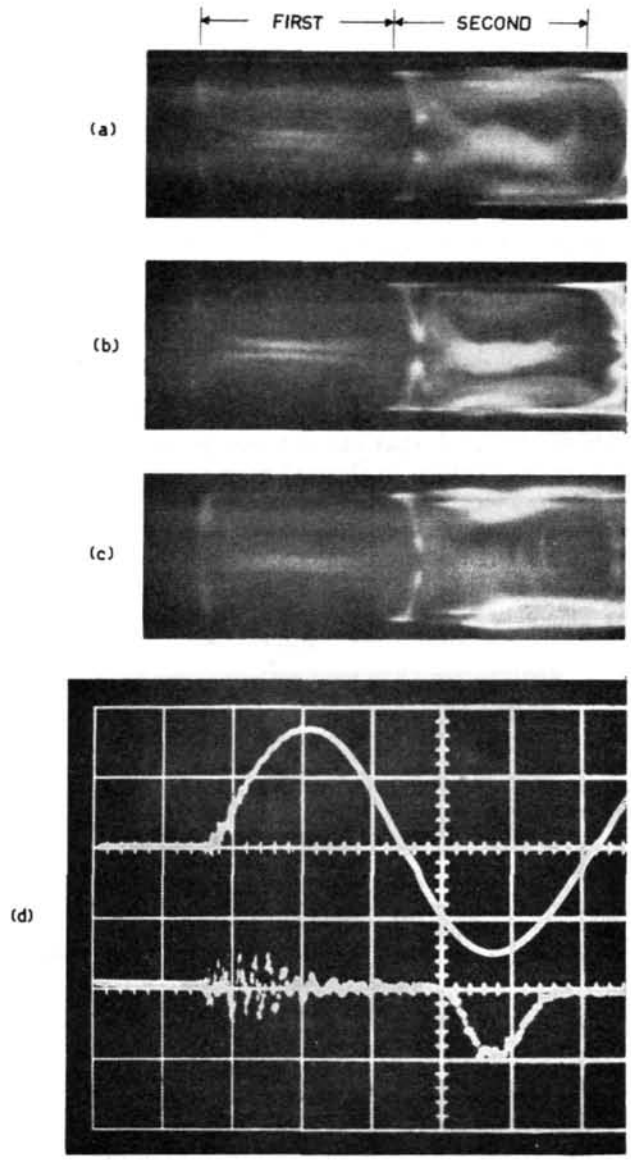

Fig. 2 Typical streak camera photographs of the Scylla I discharge during its first and second half-cycles ((a), (b), (c)). (d) shows oscillograms of the applied magnetic field (upper trace) and the photomultiplier signal arising from neutrons in a plastic scintillation detector. Time scale: 1 μs/division. The streak photographs and oscillograms are aligned on the same time scale.

* We are indebted to A. C. Kolb and collaborators for pointing out the efficacy of this camera for detecting the extremely weak light emission of these magnetically compressed plasmas.

It seems clear that cases (2) and (3) are both examples of a single type of instability. In the former case the instability is in its early stages and in the latter it has grown to violent proportions.

The streak photographs of Fig. 2 show the radial motion of the Scylla I plasma ($W_1 = 31$ kJ, $l_1 = 10.6$ cm) as a function of time. The oscillograms show the applied magnetic field (upper trace) and the neutron detector signal to the same time scale as the streak photographs. During the first half-cycle no shock structure is seen, and the smooth, hollow, luminous image is typical of plasma in which the interior B_θ field is parallel to the applied field [6] because of leakage into the plasma of a portion of the latter. The reflected shock at the beginning of the second half-cycle is somewhat out of focus, probably because it is more luminous in the end mirror regions and the camera was focussed at the central plane. The neutron emission exhibits a smooth structure symmetric about maximum magnetic field. This is the case even in Fig. 2 (c) where the plasma motion becomes oscillatory after maximum magnetic field, rather than remaining stable, as in (a) and (b). The intense light at the outer edge of the plasma in (c) is due to impurities from the discharge tube wall.

With the same short (l_1) compression coil as above, the result of raising the capacitor bank energy from 31 kJ to 93 (or 180) kJ is that the plasma becomes violently unstable near or before maximum magnetic field as shown in Fig. 3. Note that the neutron envelope, instead of continuing to rise smoothly, shows a discontinuity at the time when the plasma be-

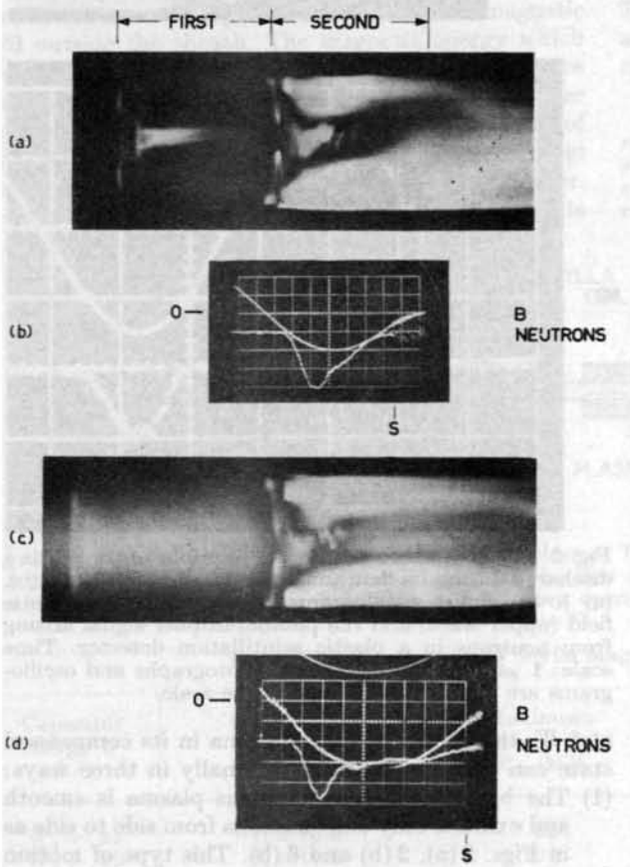

Fig. 3 Streak photographs and oscillograms of Scylla III for the shortest coil ($l_1 = 10.6$ cm) and capacitor bank energies $W_2 = 93$ kJ and $W_3 = 180$ kJ. (a) Typical streak photograph for $W_2 = 93$ kJ. (b) Applied magnetic field (upper trace) and neutron detector signal on the same time scale as (a): 0.5 μs/division. (c) Typical streak photograph for $W_3 = 180$ kJ. (d) Corresponding applied magnetic field and neutron signal on same time scale as (c): 0.5 μs/division. The symbol S denotes the time at which a vacuum spark gap shorted the compression coil. The symbol 0 identifies the base line of the magnetic field oscillogram.

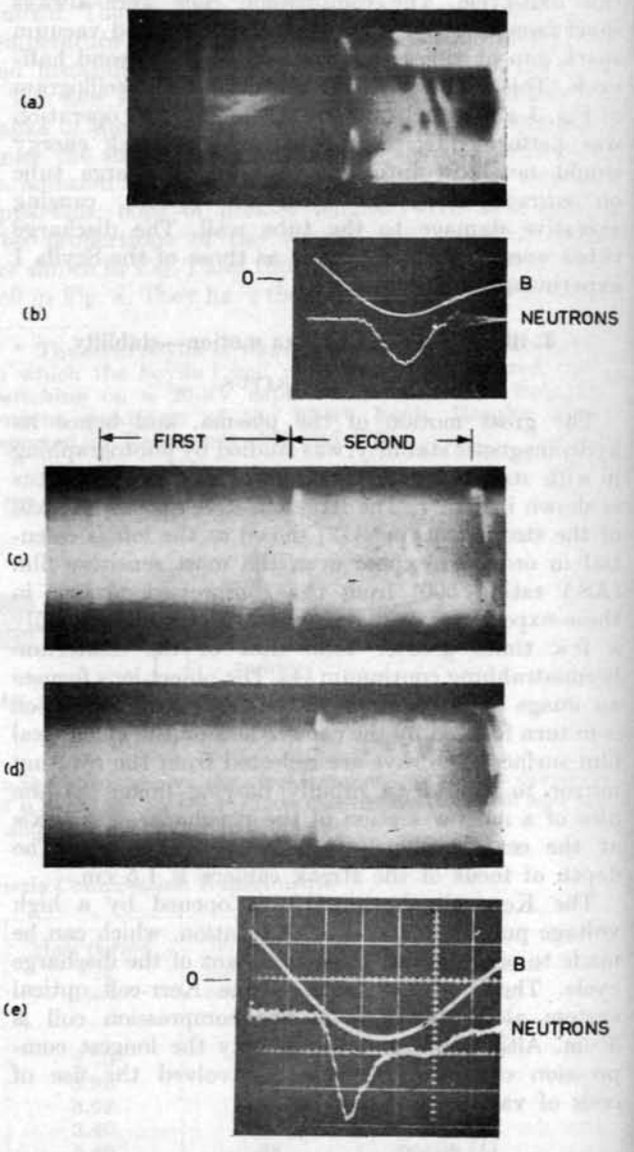

Fig. 4 Streak photographs and oscillograms of Scylla III for compression coils of intermediate lengths $l_2 = 16.6$ and 18.7 cm and corresponding capacitor bank energies $W_2 = 93$ kJ and $W_3 = 180$ kJ. (a) and (b) show a streak photograph and oscillograms of applied magnetic field and neutron signal (lower trace) for the case $W_2 = 93$ kJ. (c), (d), and (e) apply to the case $W_3 = 180$ kJ. In all cases the deuterium pressure was 85 μ Hg, except that of (d) in which it was 105 μ Hg. Time scale of oscillograms 0.5 μs/division.

comes unstable after the initial period of stability. The instability occurs on the average when the magnetic field is 90 kG and 100 kG for the cases $W_2=93$ and $W_3=180$ kJ respectively. In Section 5.4 it will be shown that the electron temperature also undergoes an abrupt discontinuity when the instability occurs.

Figure 4 illustrates the effect of increasing the coil length from its smallest value l_1 to the intermediate value $l_2=16.6$ or 18.7 cm for the same capacitor bank energies W_2 and W_3 as those just discussed. The plasma is now oscillatory, i.e., the instability is in its early stage of growth. In the case of W_2, l_2 the oscillations begin on the average when $B=100$ kG and in the W_3, l_2 case when $B=120$ kG. The neutron envelope is continuous and symmetric in the former case, while in the latter it is discontinuous, as shown in Figs. 4 (b) and 4 (e), respectively.

The shape of the plasma cross section during the growth of the instability is shown by the Kerr-cell photographs of Fig. 5 which were taken at the times indicated on the streak photographs. During the early growth of the instability the plasma cross section becomes elliptical. After further growth of the instability the plasma cross section has a very narrow elliptical shape whose center is off the axis of the discharge tube. This accounts for the occasional disappearance of the plasma image from the streak photographs as in Figs. 4 (a) and 5 (a). In these cases the plasma has moved off axis so that its image sometimes does not lie on the slit of the streak camera.

A case in which the plasma was contaminated with heavy impurity atoms is shown in Fig. 6. The neutron

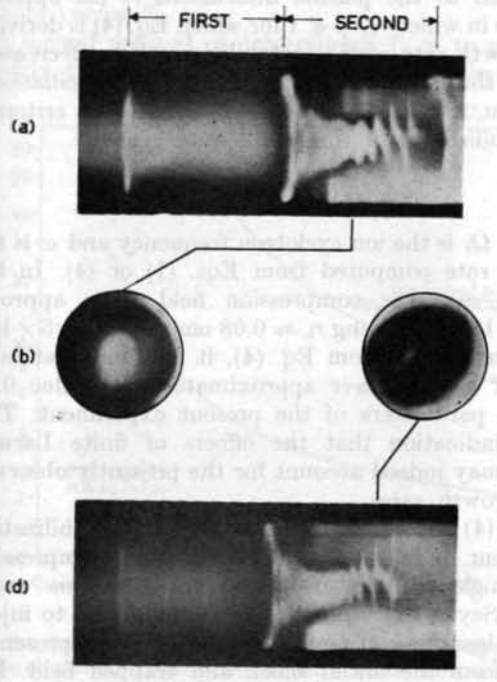

Fig. 5 Streak and Kerr-cell photographs of Scylla III for the longest compression coil ($l_3=26.8$ cm) and largest capacitor bank energy $W_3=180$ kJ. Kerr-cell photographs (b) and (c) were taken with 0.1 μs exposure at the times indicated on the streak photographs (a) and (d).

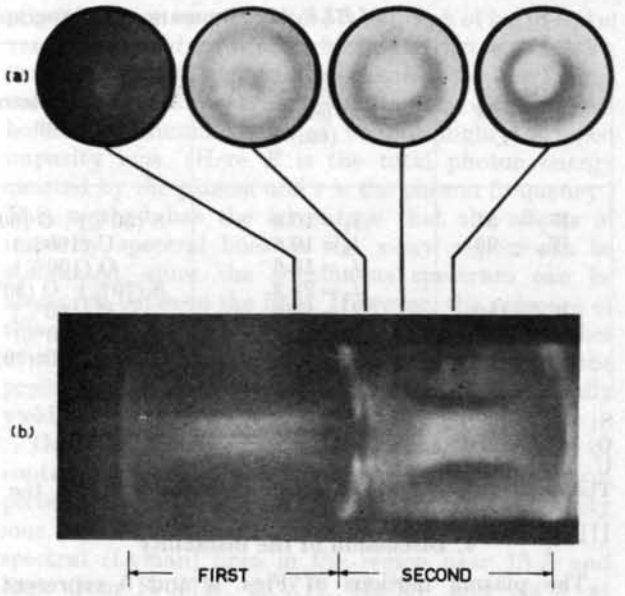

Fig. 6 Streak and Kerr-cell photographs of Scylla III for the longest compression coil ($l_3=26.8$ cm) and largest capacitor bank energy $W_3=180$ kJ. The Kerr-cell exposure time was 1 μs.

emission is small in this case, and the plasma appears to be completely stable. The four Kerr-cell photographs show the hollow plasma during the first half-cycle, the imploding plasma sheath at the beginning of the second half-cycle, and the stable compressed plasma at two instants during the increase of the magnetic compression field. There is an outer band of intense wall impurity light in the last three Kerr-cell photographs which is separated from that of the compressed plasma by a dark annular area.

3.3. Summary of the Results

Evidently the plasma motion observed in these experiments represents a growing elliptical distortion of the plasma cross section, accompanied by rotation of the ellipse about an axis which may pass through the center of the ellipse [Fig. 4 (d)] or lie outside it. The frequency of rotation is about 2×10^6 s^{-1}.

A statistical summary of many streak camera observations is given in Table II. Qualitatively, it is seen that for a given capacitor energy W, an increase in coil length l leads to greater stability. For a given l an increase in W leads to greater instability. Quantitatively, longer coils lead to stability for longer times and to higher values of magnetic field before growth of the instability.

There is a definite correlation of the time history of the neutron emission with the onset of the instability. In all cases neutron emission begins soon after the shock in the second half-cycle. At the onset of violent instability or of the oscillations in some cases the neutron intensity stops rising and falls rapidly, assuming a more or less irregular time variation thereafter.

TABLE II. Summary of photographic observations of the plasma motion

Capacitor energy W (kJ)	Compression coil length l (cm)	Nature of plasma motion	Nature of neutron signal	Magnetic field at onset of oscillation or instability (kG)	Mean time at onset of oscillation or instability (μs)
$W_1 = 31$	$l_1 = 10.6$	S (50%) O (50%)	symmetric	49[a]	1.6[a]
$W_2 = 93$	$l_1 = 10.6$	U (100%)	asymmetric	90	1.3
	$l_2 = 16.6$	O (100%)	symmetric	100	1.8
	$l_3 = 24.2$	S (70%) O (30%)	symmetric	73[a]	2.2[a]
$W_3 = 180$	$l_1 = 10.6$	U (100%)	asymmetric	100	1.3
	$l_2 = 18.7$	O (100%)	asymmetric	120	2.3
	$l_3 = 26.8$	S (30%) O (70)%	symmetric	90[a]	3.0

S: stable
O: oscillatory
U: unstable
The superscript letter "a" denotes cases in which the oscillation occurred after maximum magnetic field.

4. Discussion of the instability

The plasma motions of Figs. 4 and 5 represent elliptical disturbances of the plasma column which grow with an e-folding period of the order of 1 μs. Superimposed on the growth of the instability there is a rotation of the plasma as a whole, having a period of about 0.4 μs. It is instructive to compare this phenomenon with the theoretical model of a developing $m=2$ flute instability. This is a generalization of the Rayleigh-Taylor instability of a two-fluid interface in the presence of a gravitational acceleration, which for a plane interface gives a growth rate [14]:

$$\omega = \tau^{-1} = \sqrt{g\,k}\,, \tag{1}$$

where $k = 2\pi/\lambda$ is the wave number of the instability and τ is the e-folding time. For an $m=2$ flute k is related to the plasma radius r_p as follows:

$$k = 2/r_p\,. \tag{2}$$

The flute growth is assumed to be driven by charge-separation electric fields arising from plasma ion and electron drifts. These are driven by inhomogeneities of the magnetic mirror field, for which the equivalent "gravitational" acceleration is

$$g \approx v^2/R\,. \tag{3}$$

Here v is the thermal speed of the ions and R is the radius of curvature of the lines of the magnetic mirror. Substituting Eqs. (3) and (2) into Eq. (1) gives a growth rate

$$\omega_M \approx \frac{\sqrt{2}\,v}{\sqrt{r_p\,R}}\,. \tag{4}$$

In the present experiments the ions have random energies of about 1.8 keV, corresponding to $v \approx 4\times 10^7$ cm/s. The plasma radius is approximately 1 cm and the radius R not greater than approximately 100 cm. Equation (4) gives a flute growth rate of the order of 0.8×10^7 s^{-1}, or an e-folding time ≈ 0.1 μs. This is too fast by an order of magnitude to account for the observed rate of growth in Scylla III.

The flute growth could also arise from a centrifugal acceleration due to rotation of the plasma as a whole. In this case the growth rate ω would be nearly the same as Ω_D, the angular drift velocity of rotation. Conservation of angular momentum requires that the circular plasma have almost the same angular drift velocity before the flute growth as that of the elliptical plasma after the flute develops. The latter angular velocity is observed to be $\sim 1.6\times 10^7$ s^{-1}. *This would therefore be the predicted rate of flute* growth. Within the uncertainities of the theory it may be in agreement with the observed growth rate. However, the faster mirror growth rate ω_M would be expected to predominate, and it is remarkable that the observed rate is much slower.

ROSENBLUTH, *et al.*, [15] have predicted that for plasmas in which the ion Larmor radii r_L are finite compared to the plasma dimensions r_p (as opposed to those in which $r_L/r_p \ll 1$ for which Eq. (4) is derived) the growth rate of the instabilities will be decreased, even to the extent of their becoming stable oscillations. ROSENBLUTH, *et al.*, provide the following criterion for stabilization of the $m=2$ flute growth:

$$\left(\frac{2r_L}{r_p}\right)^2 \gtrsim \frac{\omega}{\Omega_i}\,. \tag{5}$$

Here Ω_i is the ion cyclotron frequency and ω is the growth rate computed from Eqs. (1) or (4). In the present case the compression field B is approximately 100 kG, giving $r_L \approx 0.08$ cm and $\Omega_i \approx 5\times 10^8$. Substituting ω_M from Eq. (4), it is found that both sides of Eq. (5) have approximately the value 0.02 for the parameters of the present experiment. This is an indication that the effects of finite Larmor radius may indeed account for the presently observed slow growth rates.

Eqs. (4) and (5) predict generally that stabilization will occur in mirror machines with long compression coils, high temperatures, and small plasma radii. In the Scylla experiment it is contemplated to inject hotter, less dense plasmas than those which presently result from the initial shock and trapped field. For such injected plasmas which are then compressed to higher temperatures and lower densities than in the present experiments the stabilizing advantages of larger Larmor radii may be realized.

The present rotating plasma instability is similar to that reported by KOLB and ROSTOKER [16]. However, the "fissioning" of the plasma into two filaments which they observed is not seen in the present experiments.

5. Plasma electron heating

5.1. SOFT X-RAY MEASUREMENTS

Electron temperatures greater than 100 eV are best determined by measuring the shape of the soft x-ray continuous emission spectrum of the plasma. For photon energies comparable to T_e the spectral distribution is proportional to $\exp(-h\nu/kT_e)$, whether the radiation be bremsstrahlung or recombination (free-bound) radiation.

Two methods were previously applied in the Scylla I experiment to determine T_e from the spectral shape (as opposed to absolute intensity). The simplest is the absorber method [4] based on the principle that x-rays of different photon energies are attenuated differently in passing through a given thin foil. Foils of a given material but of different thicknesses will transmit different spectra from a given incident spectrum. This is the basis of the two-absorber method of measuring T_e [17, 18]. The ratio of x-ray intensities through two absorber foils is measured and compared with the ratio calculated (on a digital computer) for assumed incident bremsstrahlung spectra at various T_e, using known absorption coefficients. In the present measurements two combinations of Be and Al foils were used. Figure 7 gives computed calibration curves of the ratio of intensities transmitted by the thin and thick absorbers versus T_e.

A second method of determining T_e is to measure directly the soft x-ray emission spectrum by means of a diffraction spectrometer [7]. A graph of $\log(dE/d\nu)$ versus ν should be a straight line of slope $-h/kT_e$, except for small quantum mechanical (Gaunt factor) corrections and possible discontinuities at the free-bound continuum limits of various highly stripped impurity ions. (Here E is the total photon energy emitted by the plasma and ν is the photon frequency.) This method has the advantage that the effects of impurity spectral lines in the x-ray region can be eliminated, since the continuous spectrum can be measured between the lines. However, the presence of these lines can seriously compromise the two-absorber method, which assumes a pure continuum. In the presence of spectral lines the absorber method generally yields low values of T_e.

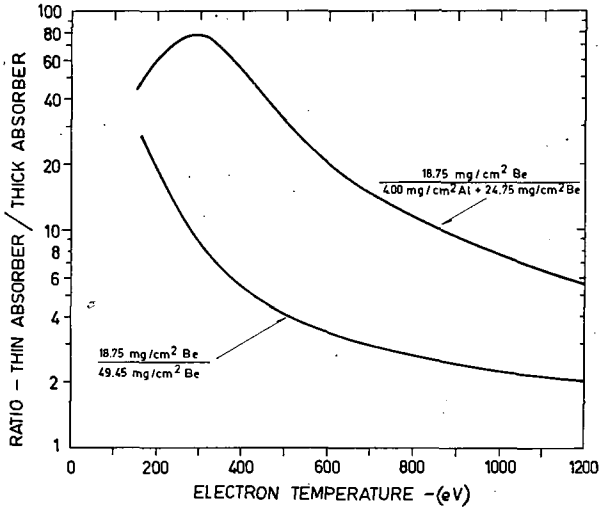

Fig. 7 Calibration curves for the two-absorber apparatus of the electron temperature measurements. The calculated ratio of intensities of bremsstrahlung (or recombination) spectra transmitted through the two absorber foils of Fig. 8 is plotted as a function of temperature of the electrons which give rise to the incident x-ray spectrum. Details of the computational method are given in Ref. [4].

The x-ray spectrum of Scylla I consisted mostly of continuous recombination radiation from a two-percent concentration of O VIII and O IX impurity ions. In addition to the continuum there were O VIII spectral (Lyman) lines in the region near 15 Å and lines from Si XIII, Al XII, Mg XI, and Na X at approximately 7, 8, 9, and 11 Å from traces of these elements in the discharge tube wall. In the present Scylla III experiments thick absorbers were chosen to center the wavelength transmission band at 6 Å for the thinner Be absorber ($T_e = 400$ eV). Thus the observed lines were not readily transmitted by the absorbers and line effects on the temperature measurement were minimized. The shortest wavelength lines at 7 and 8 Å could affect the measurement slightly but it is observed that these lines are not as intense relative to the continuum as they were in Scylla I. The lower intensity is believed to be a result of short-circuiting the compression coil at the end of the second half-cycle of the discharge. This prevents the discharge tube from being heavily eroded by the plasma which would otherwise be released to the wall at the end of the second and later half-cycles. Because of the thick absorbers and the weak impurity lines the two absorber method should yield measurements of T_e which are nearly as dependable as those of the spectrometer. In the present experiments the two techniques do yield the same value of T_e for the same plasma conditions. The two-absorber method then has the advantage of giving a simple measurement of electron temperature on a single discharge.

5.2 APPARATUS

The apparatus for measuring electron temperatures in the Scylla III plasma is shown in Fig. 8. The spectrometer at the left uses as its diffraction element a beryl ($Be_3Al_2Si_6O_{18}$) crystal whose lattice spacing ($d = 7.98$ Å) allows diffraction of x-rays with wavelengths $\lesssim 15.9$ Å. The crystal is mounted in vacuum and is exposed to collimated x-rays from the plasma at the center of the compression coil. The diffracted x-rays are detected by a thin (0.012 cm) plastic scintillator whose time resolved signal is exhibited on an oscilloscope. The grazing angle θ of the crystal and the angle 2θ of the detector arm are adjusted to within 6 seconds of arc by means of precision rotary tables,

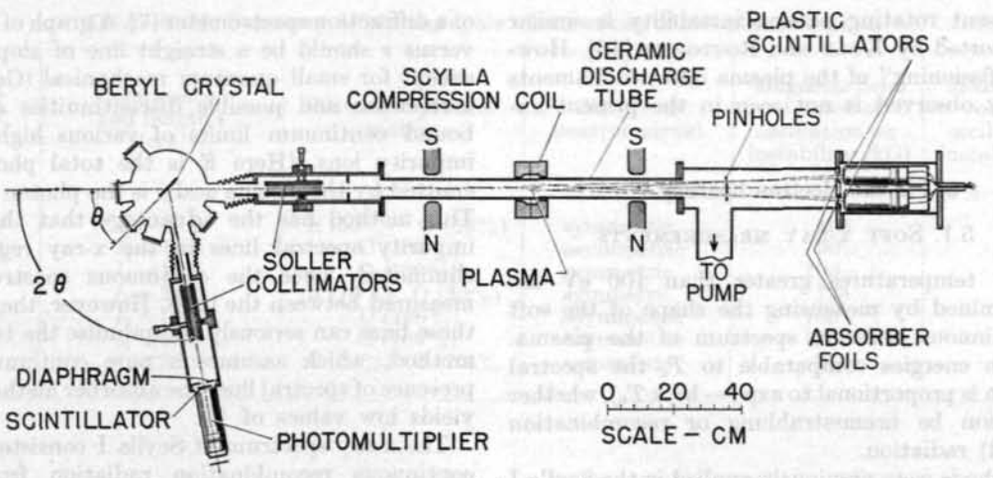

Fig. 8 Apparatus for measuring electron temperatures. The beryl crystal diffraction spectrometer is shown at the left and the two-absorber apparatus at the right. The 10.6 cm compression coil is shown to scale.

and wavelengths are determined by the Bragg relationship for first order diffraction:

$$\lambda = 2\,d \sin\theta\,. \tag{6}$$

The solid angle of the spectrometer, the crystal reflection coefficient as a function of wavelength, and the response of the plastic scintillator were measured. This allows the absolute energy spectrum $\mathrm{d}E/\mathrm{d}\nu$ of the x-radiation to be determined (cf. Ref. [19]).

The two-absorber apparatus is shown at the right of Fig. 8. The two pin-holes form images on each of the two scintillators (thickness = 0.15 cm) of a region near the center of the compression coil having a diameter of about 3 cm. Each absorber foil receives an equal flux of x-rays from the plasma, and the ratio of their transmitted intensities is obtained from the signals of the two photomultipliers. In addition, the photomultiplier signals provide a monitor of the integrated x-ray intensity to which the diffraction spectrometer signal is normalized on each discharge. The permanent magnets at each end of the discharge tube are used to eliminate fast electrons which would otherwise bombard the plastic scintillators.

5.3 Scaling results

One of the main objects of the present experiments was to observe how the plasma electron and ion temperatures would scale with increased magnetic field from the known conditions of Scylla I. Of the two, the electron temperature can be determined more simply, and the measurement does not depend on other plasma quantities such as density and volume.

The instability discussed in Section 3 has a distinct effect on T_e, and two cases can be distinguished, as illustrated by the oscillograms of Fig. 9. For a stable or weakly unstable plasma (small W, large l) the x-ray intensity is a smooth, regular function of time [Fig. 9 (c)]. For an unstable plasma the x-ray intensity is an irregular function of time as shown in Fig. 9 (a), and T_e shows an abrupt decrease at the onset of instability, as will be discussed in the next section.

Spectrometer measurements giving the continuous x-ray energy spectrum $\mathrm{d}E/\mathrm{d}\nu$ versus ν are shown in Fig. 10. Three stable cases (symmetric x-ray signals) are shown. The value $kT_e = 475 \pm 50$ eV for the case $l_2 = 18.7$ cm, $W_2 = 93$ kJ is in agreement with the Be-Al and Be-Be

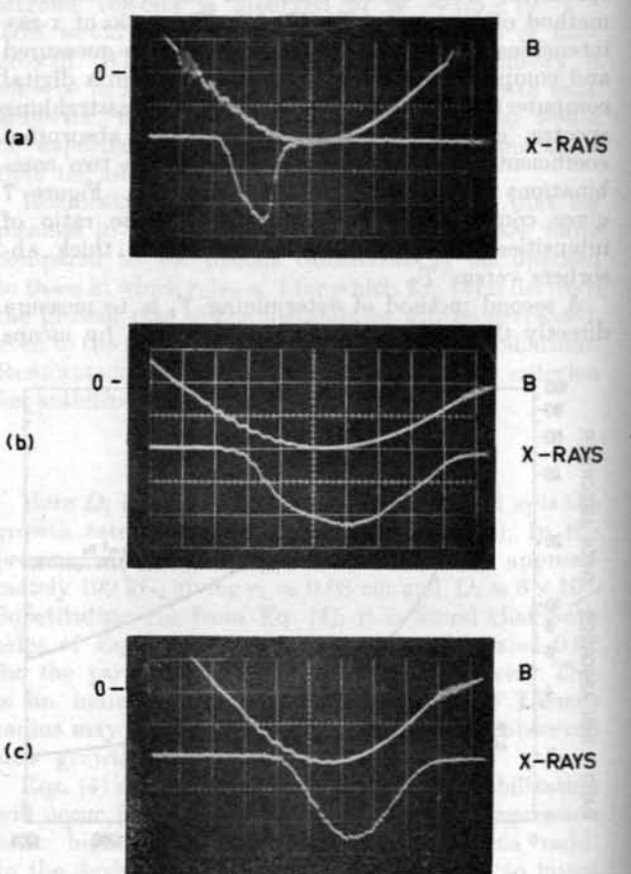

Fig. 9 Oscillograms of the second-half-cycle applied magnetic field and the scintillator signal of the x-rays passing through the thinner Be foil of the two-absorber apparatus. The values of coil length l and capacitor energy W are as follows: (a) $l = 10.6$ cm, $W = 93$ kJ; (b) $l = 26.8$ cm, $W = 180$ kJ; (c) $l = 26.8$ cm, $W = 92$ kJ. Time scale: 0.5 μs/cm.

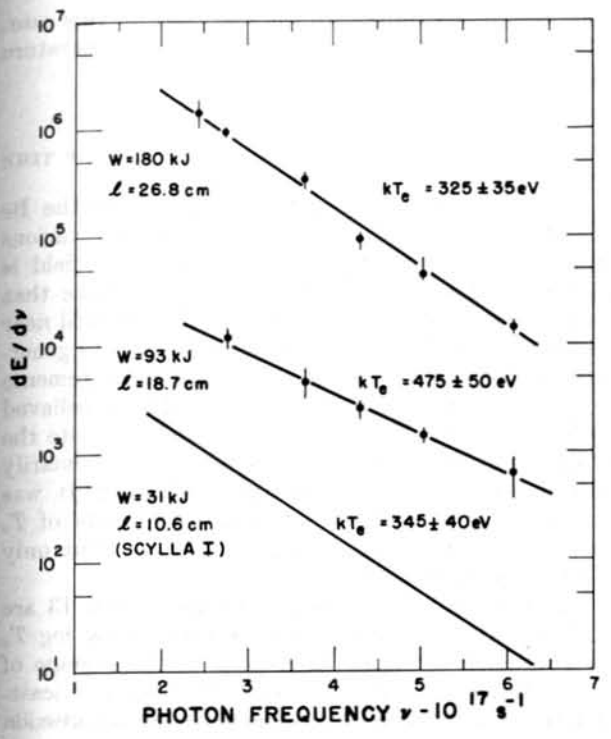

Fig. 10 Continuous x-ray emission spectra as measured with the beryl diffraction spectrometer. Total photon energy per unit frequency interval is plotted against photon frequency. The absolute scale is arbitrary. However, the relative intensities of the various l, W combinations are as shown. The Scylla I curve is from [7].

two-absorber measurements which gave 515 ± 70 and 440 ± 60 eV. The various points of the spectrum of Fig. 10 were measured after the apparatus had been cleaned by repeated discharges until the neutron yield reached a steady value. Also shown on Fig. 10 is the spectrum of [7] for Scylla I. The ordinates of the graphs show the relative intensities of the x-ray continua for the three cases. In the case of the long coil and the largest capacitor energy (l_3 W_3) the intensity of the continuum is larger by an order of magnitude than in the two lower energy cases. The reason for the apparent increase of impurity concentration is not understood. It may be connected with the initial conditions of the reflected shock in this case.

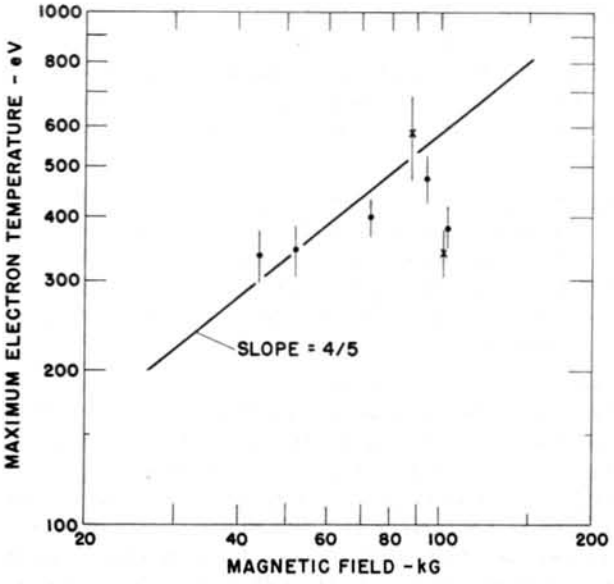

Fig. 11 Scaling curve of electron temperature *vs* the average value of magnetic field at which it was measured for various coil lengths l and capacitor energies W. The circles represent stable cases and the crosses cases where the flute instability interrupts the x-ray signal. See Table III for values of l and W.

Having established satisfactory agreement between the T_e results of the spectrometer and the two-absorber method, the remaining points of the scaling curve were determined by the two-absorber method alone. The average maximum electron temperature was determined for many discharges for each set of l, W values. In the course of these measurements it was found that T_e is only weakly correlated with neutron yield. For an increase in the latter by as much as a factor of 10, after the discharge is clean, T_e increases by only about 10 percent. This tends to confirm the independent excitation of ion and electron energies observed in [6].

The scaling results are presented in Table III and in the graph of Fig. 11. In the graph each point represents a given condition of W and l. The average maximum T_e is plotted against the corresponding average value of magnetic field at the time of maximum T_e. For the stable cases, shown by the circles, this magnetic field is just the maximum of the sine function during

TABLE III. Scaling data for electron temperature

Coil length l (cm)	Energy storage W (kJ)	Magnetic field at maximum T_e B (kG)	Absorbers	Maximum T_e two-absorbers (eV)	T_e from spectrometer (eV)	Average electron temperature T_e (eV)	Stability
10.6	93	88	Be-Be + Al	580 ± 110		580 ± 110	Unstable
18.7	31	44	Be-Be	335 ± 40		335 ± 40	Stable
18.7	93	94	Be-Be + Al	515 ± 70	475 ± 50	475 ± 50	Stable
			Be-Be	440 ± 60			Stable
18.7	180	102	Be-Be	340 ± 35		340 ± 35	Unstable
26.8	93	73	Be-Be	400 ± 35		400 ± 35	Stable
26.8	180	103	Be-Be	430 ± 50	325 ± 35	380 ± 40	Stable

its second half cycle (cf. Table I). For the unstable cases, indicated by the crosses, T_e reaches its maximum at times other than those of maximum magnetic field.

The scaling curve of Fig. 11 can be compared with the adiabatic heating law under the following simple assumptions:

(1) For all conditions of W and l there is a shock of constant energy which leaves the electrons with the same initial temperature.
(2) Following the shock there is magnetic adiabatic compression of the plasma to the state of maximum T_e.

Assumption (1) is plausible since T_e is not a sensitive function of the trapped reversed field as is the neutron yield [6]. The value of T_e after the initial shock should be closely related to the voltage on the compression coil which was nearly constant in the present experiments. If it is further assumed that magnetic compression always starts at the same value of B, then assumptions (1) and (2) lead to the following scaling relation:

$$T_e \propto B^{2(\gamma-1)/\gamma} \propto B^{4/5}, \qquad (7)$$

where the ratio γ of specific heats is taken to be 5/3 for the electrons.

In the log-log plot of Fig. 11 the straight line corresponding to relation (7) gives a reasonably close approximation to the scaling data if the two points corresponding to $B > 100$ kG are excluded. One of these high field cases was shown in Fig. 10 to have very high x-ray emission, and computations of the absolute radiation rate (from a comparison with Scylla I) show that the radiation energy loss is comparable with the energy content of the electrons for this case. This may account for the lower electron temperature at the high B values.

5.4 Electron temperature as a function of time

Figs. 12 and 13 show T_e, as measured by the Be absorbers, plotted as a function of time for various stable conditions of W and l. The magnetic field is plotted on the same graph in each case. Note that measurements of T_e are usually not shown until near peak magnetic field. This is because the x-rays generally did not become intense enough for measurements until near maximum B (cf. Fig. 9 (c)). This is believed to be due to the lapse of time required to excite the O VIII and O IX impurity ions which are primarily responsible for the recombination radiation. It was therefore not possible to obtain measurements of T_e at low magnetic fields during compression, but only during decompression.

The time distribution data of Figs. 12 and 13 are replotted at the right of these figures to show log T_e as a function of log B. Each point is the average of about three runs and the straight lines are least-square fits to the data. Compression and decompression are plotted separately. The compression data are unfortunately based upon so few points that the slopes fluctuate considerably. However, in two cases the curves of kT_e versus B do closely approximate adiabatic compressions at $\gamma = 5/3$ near the end of the compression. The data for the decompressions are much better, owing to the late occurrence of the x-rays, and the log-log plots show definite linear behavior.

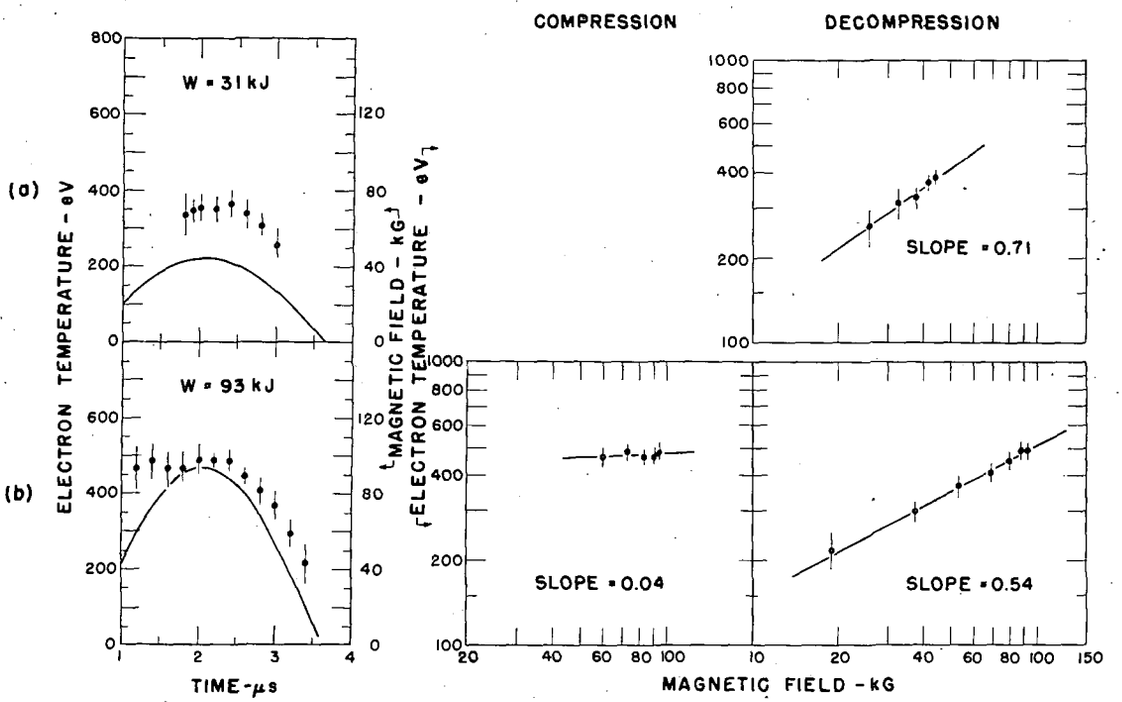

Fig. 12 The graphs at the left show the magnetic field and the plasma electron temperature as functions of time. Those at the right show T_e as a function of the increasing and decreasing magnetic field. The coil length l is 18.7 cm.

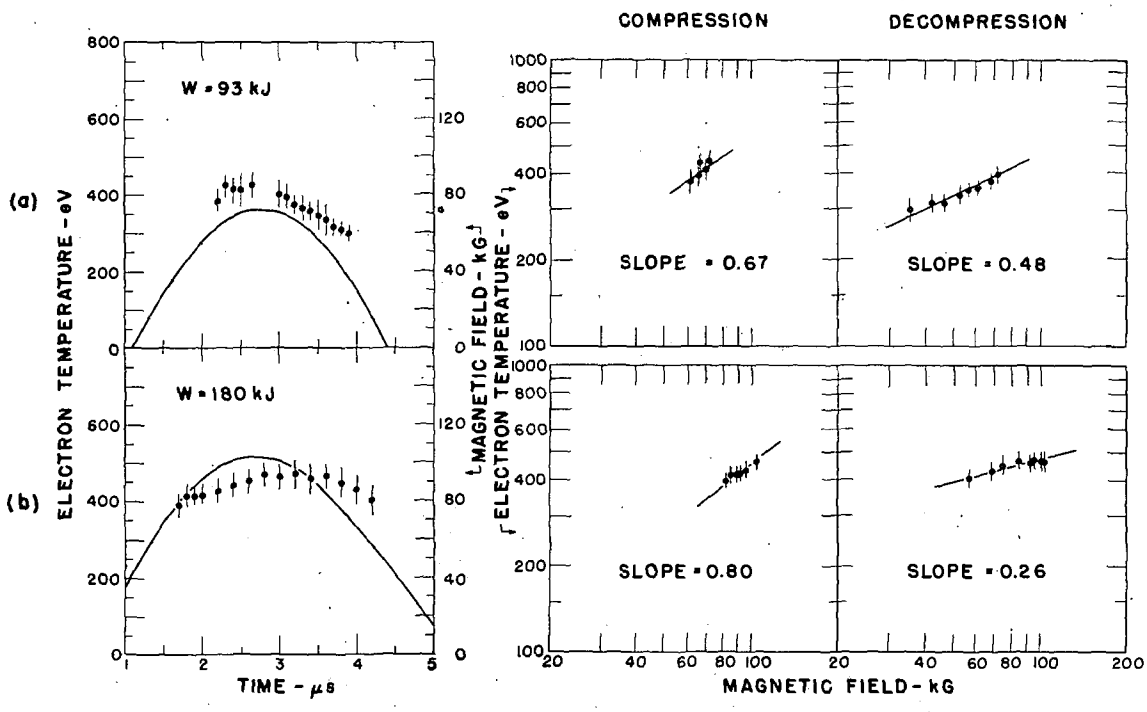

Fig. 13 Electron temperatures as functions of time and magnetic field for $l = 26.8$ cm.

The mean slope, however, would correspond formally to $\gamma \approx 4/3$, rather than the predicted 5/3.

Data for conditions under which the streak photographs show violent growth of the plasma instability are shown in Fig. 14. Each T_e point is the average of two runs, and the graph corresponds to some of the data indicated by one of the crosses in Fig. 11 and to the oscillogram of Fig. 9 (a). The onset of the instability correlates with the sudden decrease of electron temperature, the two events occurring at about the same time on the average. Such a sudden decrease in T_e is only seen in cases which are observed photographically to be unstable. Before the onset of the instability T_e often shows erratic behavior near peak magnetic field, sometimes decreasing with time and sometimes increasing. Even in the stable or weakly unstable cases T_e occasionally shows anamolously high values before maximum magnetic field.

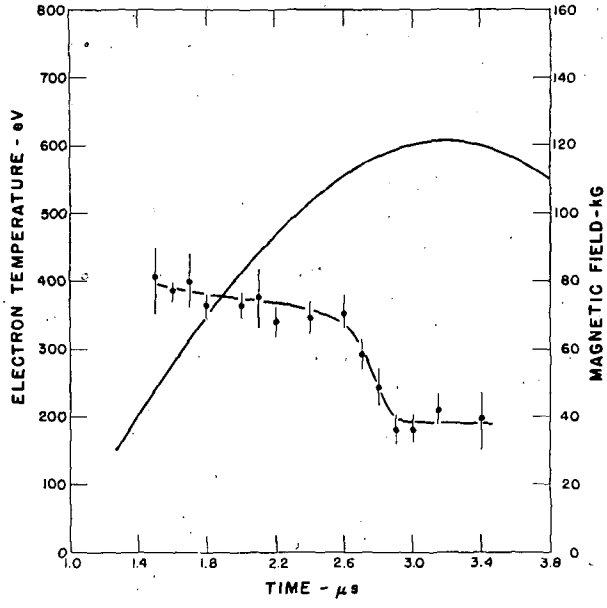

Fig. 14 Electron temperature as a function of time for $l = 10.6$ cm, $W = 93$ kJ.

6. Scaling of neutron emission rate

6.1 Experimental method

It was observed above that the neutron emission is interrupted when the plasma instability grows to violent proportions. It is therefore necessary to measure the instantaneous rate of emission of neutrons in order to make scaling comparisons for both stable and unstable cases. This quantity is denoted by R_n and the total neutron yield during the second half-cycle by Y_n. The total yield is measured by means of a "silver counter" consisting of four Geiger counters in coincidence, each surrounded by a silver foil, and placed in a paraffin moderating geometry. The neutrons from Scylla activate the Ag^{110} 22-s beta rays, and the beta count yields Y_n directly. The silver counter was calibrated absolutely with a known source of d-d neutrons produced by an accelerator. The instantaneous flux of neutrons is measured by observing the "pile-up" signal of proton recoils produced in a plastic scintillator, 9 cm in diameter by 11 cm long. When the area under a scintillator oscillogram is normalized to Y_n, it gives R_n as a function of time.

The procedure followed for each set of l, W values was to clean the apparatus by repeated discharges until Y_n reached a stable value ($\pm 30\%$) and then to determine the maximum value of R_n during the second

TABLE IV. Scaling data for neutron emission rate

Coil length l (cm)	Capacitor energy W (kJ)	Magnetic field at maximum R_n B (kG)	Average neutron yield Y_n (neutrons)	Maximum average neutron rate R_n (neutrons/s)	Normalized rate (10.6 cm/l) R_n (neutrons/s)	Time dependence of R_n
10.6	31	52	$(6.0 \pm 0.4) \times 10^6$	$(7.7 \pm 0.5) \times 10^{12}$	$(7.7 \pm 0.5) \times 10^{12}$	Symmetric
10.6	93	94	$(5.5 \pm 1.0) \times 10^7$	$(4.1 \pm 0.7) \times 10^{13}$	$(4.1 \pm 0.7) \times 10^{13}$	Asymmetric
18.7	31	44	$(6.6 \pm 0.6) \times 10^5$	$(8.4 \pm 0.8) \times 10^{11}$	$(4.7 \pm 0.5) \times 10^{11}$	Symmetric
18.7	93	94	$(7.0 \pm 1.0) \times 10^7$	$(5.5 \pm 1.1) \times 10^{13}$	$(3.1 \pm 0.6) \times 10^{13}$	Symmetric
18.7	180	96	$(1.5 \pm 0.3) \times 10^8$	$(9.2 \pm 1.8) \times 10^{13}$	$(5.2 \pm 1.0) \times 10^{13}$	Asymmetric
24.2	93	81	$(6.3 \pm 1.0) \times 10^7$	$(4.9 \pm 0.8) \times 10^{13}$	$(2.1 \pm 0.3) \times 10^{13}$	Symmetric
26.8	180	103	$(6.7 \pm 1.4) \times 10^7$	$(4.4 \pm 0.9) \times 10^{13}$	$(1.7 \pm 0.4) \times 10^{13}$	Symmetric

half-cycle of B for many dozens of discharges. These were then averaged. For stable or weakly unstable cases R_n reached its maximum when the magnetic field did. For unstable cases (as in Fig. 3) R_n had its maximum during the rise of B, and the corresponding average value of magnetic field was measured on the oscillograms.

Two observed effects are worth noting. For the longer coils and larger capacitor energies larger deuterium pressures (≤ 110 μ Hg) were required to produce maximum Y_n than at smaller l and W values, where 85 μ Hg sufficed. It was also observed in connection with the streak photographs that neutron yields larger by a factor of 2 were associated with well defined reflection of the shock (Fig. 4 (d)) than with barely discernable reflection (Fig. 4 (c)). The condition of strong reflection was also associated with larger deuterium pressures. The effect is attributed to ionization processes during the first half-cycle which cause greater trapping of magnetic field at the higher pressures and consequent strong reflection of the shock and also greater neutron emission.

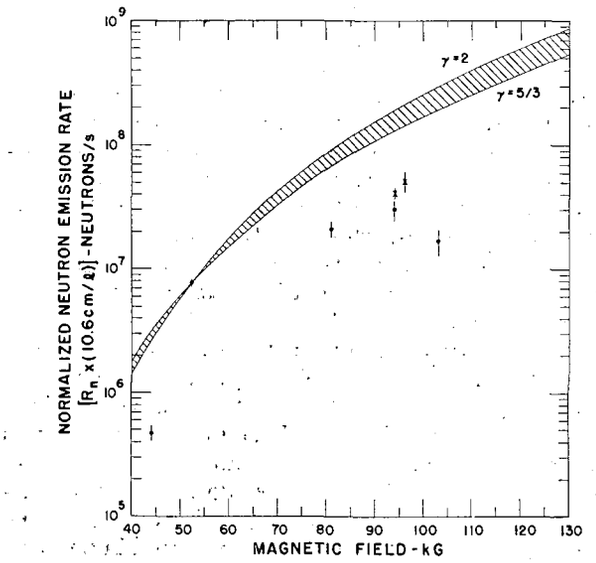

Fig. 15 Scaling data of normalized maximum neutron emission rate (NOTE: ordinate scale should be in neutrons/μs) *versus* the average value of magnetic field at which it occurs for various coil lengths and capacitor energies as given in Table IV. The circles represent stable cases and the crosses cases where the flute instability interrupts the neutron signal. The curves represent ideal adiabatic compression from constant initial conditions.

6.2 Scaling results

The results of the neutron rate measurements are summarized in Table IV. Both Y_n and maximum R_n are given for the various capacitor energies and coil lengths used. There is an order of magnitude increase in Y_n as B is increased from the Scylla I value of 52 kG to the 90—100 kG values of Scylla III. The sixth column gives the scaling quantity which is R_n normalized to a coil length of 10.6 cm. The measured values of this quantity are plotted as a function of B in Fig. 15.

6.3 Discussion of scaling

Measurements of neutron rate can give only a rough indication of the scaling of ion temperature T_i because R_n depends not only upon T_i through the cross-section average over ion velocities $\langle \sigma v \rangle$, but also upon other plasma quantities such as density and volume. The final value of T_i (or equivalently the average random energy of the ions, Maxwellian or not) depends sensitively upon the trapped field effect, so that a scaling assumption of constant "shock" conditions prior to magnetic compression is a tenuous one. Finally R_n depends upon the number of ions in the plasma. In the present case the plasma particle losses are not known, but they may be appreciable.

Nevertheless a scaling model similar to that made for the electron temperatures is used in Fig. 15 for comparison with the data. It assumes constant initial conditions of ion temperature, no particle losses, and adiabatic compression. Then R_n is given by

$$R_n \propto n^2 l A \langle \sigma v \rangle , \tag{8}$$

where A is the mean area of the plasma whose length is assumed in first approximation to be proportional to l. Assuming adiabatic compression, this reduces to

$$\frac{R_n}{l} \propto B^{2/\gamma} \langle \sigma v \rangle , \tag{9}$$

where to good approximation for kT_i in keV,

$$\langle\sigma v\rangle = 150 \times 10^{-16} (kT_i)^{-2/3} \exp[-18.6 (kT_i)^{-1/3}], \quad (10)$$

for the neutron branch of the d-d reaction in the present range of kT_i values. It is necessary to normalize the scaling curve at a single known condition of R_n and kT_i. This is provided by the Scylla I experiment in which both R_n and kT_i were measured. The latter was found from the Doppler broadening of the d-d proton spectrum to be 1.3 keV. With this normalization relations (8), (9), and (10) lead to the curves shown in Fig. 15 for $\gamma=2$ and $\gamma=5/3$. There is no clear choice to be made for the ions, since the Coulomb ion-ion collision time is not greatly smaller than the compression time. Ion temperature is assumed to follow a relation similar to (7).

Comparison of the data with the scaling curve of Fig. 15 shows a slower rise than would be expected under the scaling assumptions. Whether this is due to plasma loss, non-constant initial conditions of trapped field, or non-adiabatic heating of the ions is not known. However, if only the latter is assumed, the lessening of R_n from the ideal scaling law would imply a value of kT_i at 95 kG of about 1.8 keV rather than the ideal 2.2 keV of adiabatic temperature scaling. The fact that both the electron temperature and R_n are anomalously low at magnetic fields >100 kG may have the following significance. As was discussed in Section 5.3, the high x-ray radiation rates in these cases may actually be draining appreciable energy from the electrons. Although the ions and electrons are not closely coupled by Coulomb collisions, there may nevertheless be sufficient coupling that the ions also lose energy through the radiation, via the electrons. More exact knowledge of scaling of the ion temperaoure must await Doppler-broadening measurements of the d-d protons from the Scylla III plasma.

Acknowledgments

We acknowledge with pleasure the support of this work by J. L. Tuck and useful discussions with T. F. Stratton concerning the x-ray measurements. Valuable discussions concerning plasma stability were had with M. N. Rosenbluth and R. C. Mjolsness, and we thank the former for permission to discuss the theory of stabilization of the flute instability prior to its publication. Indispensible technical assistance was given by L. H. McDowell, and the manuscript was typed by Elizabeth J. Pohlmann.

The work was performed under the auspices of the U.S. Atomic Energy Commission.

References

[1] Elmore, W. C,, Little, E. M., Quinn, W. E., Proceedings of the Second U.N. International Conference on the Peaceful Uses of Atomic Energy, Geneva **32** (1958) 337.
[2] Ribe, F. L., Proceedings of the Fourth International Conference on Ionization Phenomena in Gases, Uppsala, Sweden (North Holland Pub. Co., Amsterdam, 1960) **2**, 1032.
[3] Boyer, K., Elmore, W. C., Little, E. M., Quinn, W. E., Tuck, J. L., *Phys. Rev.* **119** (1960) 831.
[4] Jahoda, F. C., Little, E. M., Quinn, W. E., Sawyer, G. A., Stratton, T. F., *Phys. Rev.* **119** (1960) 843.
[5] Nagle, D. E., Quinn, W. E., Ribe, F. L., Riesenfeld, W. B., *Phys. Rev.* **119** (1960) 857.
[6] Little, E. M., Quinn, W. E., Ribe, F. L., *Phys. Fluids* **4** (1961) 711.
[7] Bearden, A. J., *et al.*, *Phys. Rev. Letters* **6** (1961) 257.
[8] Spitzer, L., Jr., Physics of Fully Ionized Gases (Interscience Publishers, Inc., New York, 1956) 80.
[9] Mjolsness, R. C., *et al.*, *Phys. Fluids* **4** (1961) 730.
[10] Quinn, W. E., *et al.*, *Bull. Am. Phys. Soc.* **6** (1961) 202.
[11] Quinn, W. E., in Progress in Nuclear Energy, Series XI, **2** (Pergamon Press, London, 1961). (To be published.)
[12] Brauer, F. L., Hansen, D. F,, *J. Opt, Soc. Am.* **49** (1959) 421.
[13] Zarem, A. M., *et al.*, *Rev. Sci. Instr.* **29** (1958) 1041.
[14] Rosenbluth, M. N., Longmire, C. L., *Ann. Phys. (N.Y.)* **1** (1957) 120.
[15] Rosenbluth, M. N., Rostoker, N., Krall, N. A., Proceedings of this Conference, page 143. Also Private Communication.
[16] Kolb, A. C., Rostoker, N., *Bull. Am. Phys. Soc.* **6** (1961) 203.
[17] Stratton, T. F., *et al.*, *Bull. Am. Phys. Soc*, **6** (1961) 202.
[18] Griem, H. R., *et al.*, *Bull. Am. Phys. Soc*, **6** (1961) 205.
[19] Ribe, F. L., *et al.*, Proceedings of the Fifth International Conference on Ionization Phenomena in Gases, Munich, Germany, 1961 (North Holland Publishing Co., Amsterdam).

RAPID AXIAL CONTRACTION OF A HIGH DENSITY DEUTERIUM PLASMA IN A THETATRON DISCHARGE*

H. A. B. BODIN, T. S. GREEN, G. B. F. NIBLETT, N. J. PEACOCK,
J. M. P. QUINN, J. A. REYNOLDS, J. B. TAYLOR**

ATOMIC WEAPONS RESEARCH ESTABLISHMENT

ALDERMASTON, BERKSHIRE, UNITED KINGDOM

This paper presents experimental observations of the axial contraction of a dense deuterium plasma during the second half-cycle of a high current magnetic compression experiment in which reversed trapped field is left over from the first half-cycle. The reversed field configuration produces a rapid axial contraction and subsequent expansion of the plasma column during which energy in the trapped magnetic field is dissipated. High speed streak and framing cameras and external flux coils are used to monitor the profile of the plasma and to measure the axial velocity of the change in cross-sectional plasma area. Peak axial velocities of 1.2×10^7 cm/sec are recorded. Measurement of the velocity and area ratio of the propagating discontinuity provides a method of determining the ion temperature ahead of and behind the area change.

A theoretical appendix analyses the propagation characteristics of area waves and area shocks and presents solutions of the appropriate conservation equations.

1. Introduction

It is now widely recognised that the characteristics of a high current gas discharge in which deuterium plasma is compressed by a rapidly-rising externally-generated axial magnetic field are strongly influenced by the strength and sign of magnetic field trapped within the plasma and the accompanying paper [1] is an attempt to delineate these characteristics as a function of the trapped field. Of particular importance is the presence of reversed magnetic field which produces, by a mechanism that yet remains obscure, the emission of neutrons and soft x-rays indicative of a high temperature plasma [2, 3, 4, 5, 6]. Magnetic probe measurements [7] have shown that the reversed field results in closure of the field lines round the plasma to form a magnetic field pattern reminiscent of, though not identical to, the unstabilised toroidal pinch configuration. The present paper reports preliminary experimental measurements of the rapid axial contraction of a deuterium plasma on the second half-cycle of a theta pinch discharge and this contraction is likewise attributed to closure of the reversed magnetic field lines and the resultant tension in the lines of force. The contraction velocity has been measured by recording photographically the changing profile of the plasma and by observing the variation of mass per unit length as determined by the frequency of radial oscillations. The axial contraction is accompanied by the propagation of discontinuities in the plasma area. These discontinuities are termed "area shocks" or, for small amplitudes, "area waves". Like the conventional shock, the area shock is an irreversible heating mechanism which increases the entropy of the plasma over which it passes. The propagation of these shocks is a problem of fundamental interest and provides a method of determining the ion temperature ahead of and behind the discontinuity. A theoretical appendix summarises their propagation characteristics.

2. Experimental method

The experiments were carried out in deuterium gas at initial pressures in the range 70—500 microns Hg and a schematic diagram of the experimental equipment is shown in Fig. 1. A bulbous transparent quartz tube is surrounded by a slotted coil 22 cm long of mirror shape. The internal diameter of the coil is 6.9 cm at the centre and 5.6 cm at the ends to give a geometrical mirror ratio R of 1.5. A diagram of the cross-section of the tube and coil is shown in Fig. 2. The coil is connected to a low inductance condenser bank (15 kV, 22.5 kJ, 5.5 mμH) by 100 parallel spark gaps and a corresponding number of cables. Simultaneous closure of the spark gaps provides a lightly-damped oscillating primary current with a peak value of 1.2×10^6 amps and a half-period of 7.7 μs; the corresponding peak magnetic field at the centre of the coil is 62 kilogauss.

High speed streak and framing camera photographs were taken through the side of the coil using a rotating mirror camera designed at A.W.R.E. and described by SKINNER [8]. The framing camera was fitted with 60 lenses staggered with respect to each other to give 60 separate images at speeds of up to 10^7 frames/second. For the majority of experiments the camera was used at a framing rate of 6×10^6 frames/second so that the exposure time for each frame was 0.17 μs.

In addition to high speed photography two search coils in series were used to monitor high frequency

* Conference paper CN-10/70, presented by G. B. F. Niblett. Discussion of this paper is given on page 645. Translations of the abstract are at the end of this volume of the Conference Proceedings.

** Author of Appendix to this paper.

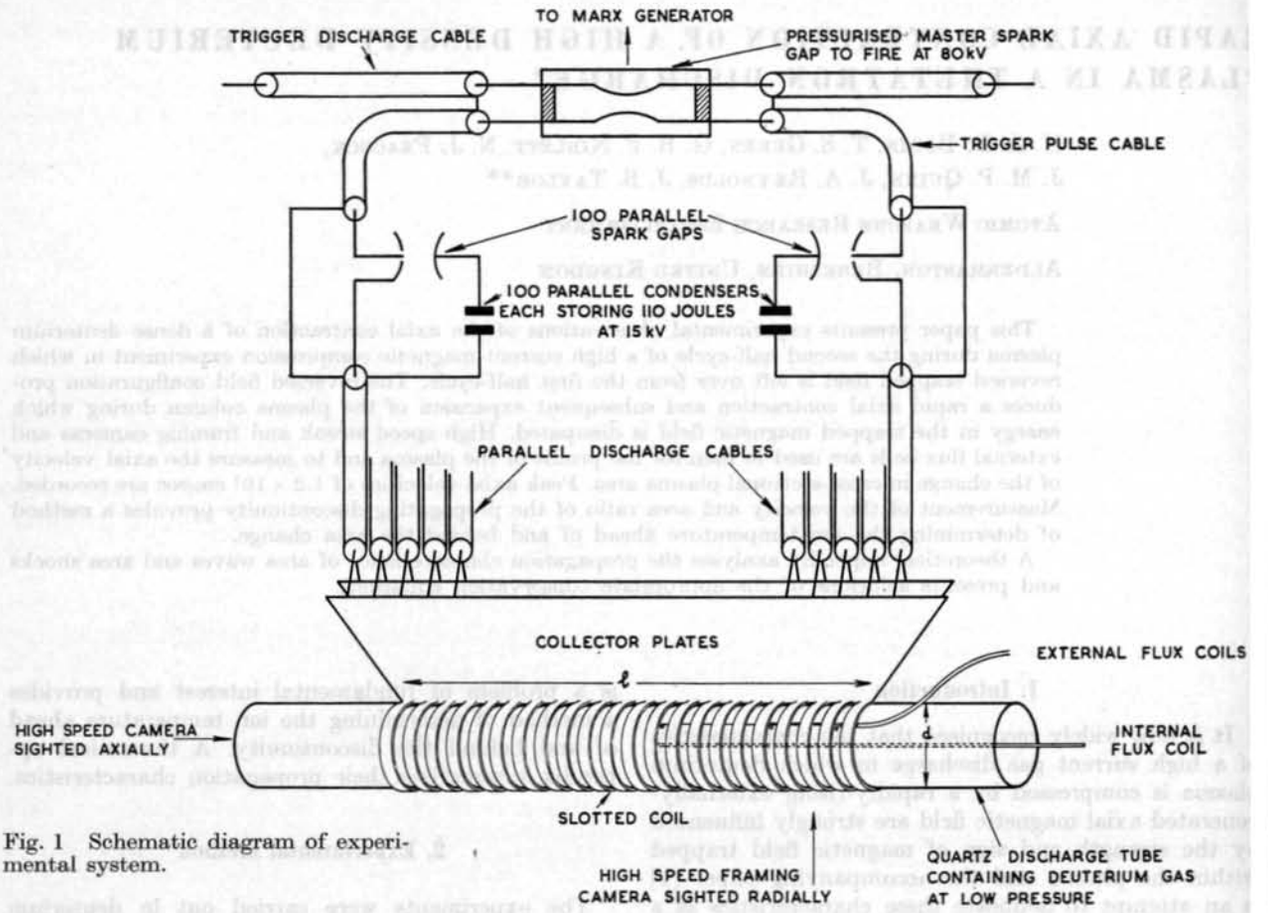

Fig. 1 Schematic diagram of experimental system.

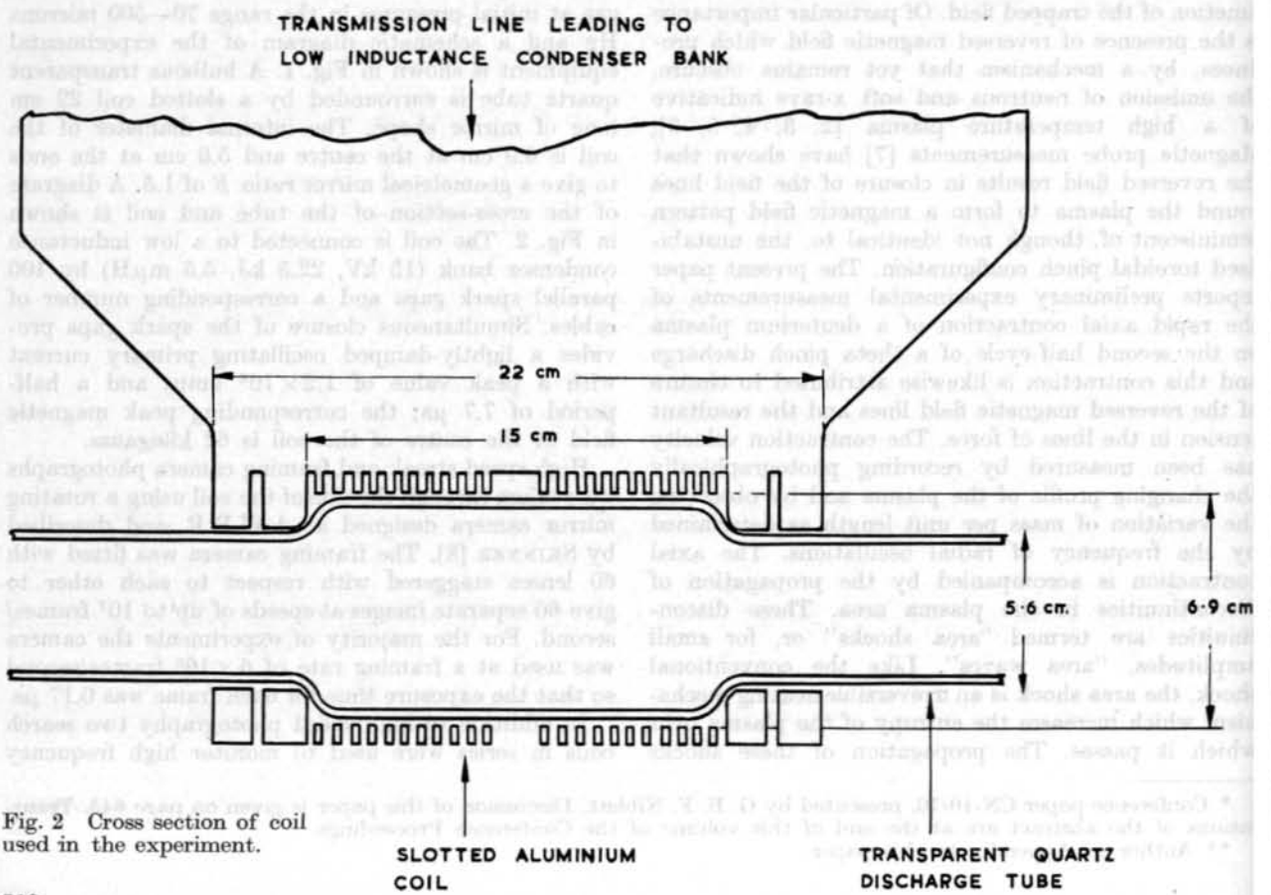

Fig. 2 Cross section of coil used in the experiment.

variations in the magnetic field produced by motion of the plasma. One search coil was positioned so as to respond to variations in flux outside the primary coil whilst the other was mounted between the primary coil and the quartz tube and measured the rate of change of flux inside the coil but external to the plasma. These search coils were connected electrically in series and adjusted to give zero signal when the tube was evacuated. With plasma present the out-of-balance signal records the frequency and amplitude of the plasma oscillations [9]. The period τ is given by

$$\tau = 2\pi \sqrt{\frac{M}{B^2}}, \qquad (1)$$

where M is the mass per unit length and B is the external field. Thus the product τB as a function of time measures the change in mass per unit length.

3. Measurement of the axial contraction

A typical series of radial photographs of a deuterium discharge at 315 microns initial pressure is shown correlated with the driving magnetic field in Figs. 3 and 4. Only half of the coil was photographed since it is symmetrical about its midplane.

The sequence of events is as follows. When the bank is switched on plasma forms at the walls within 10^{-7} second and then implodes radially towards the axis. Axial probes show that on the first half-cycle parallel magnetic field is trapped and the plasma is contained in a hollow annulus. Throughout this half-cycle the plasma exhibits stability and uniformity along its length and there is no evidence of axial contraction. The cylindrical plasma column tapers only slightly towards the mirrors; the plasma area ratio P, i.e. the ratio of area at the centre of the coil to the area at the mirrors, approximates closely to the geometrical mirror ratio R showing that the plasma β (plasma pressure divided by external field pressure) is low*. As the external field falls, the plasma expands to the wall so that at the end of the first half cycle the tube contains ionized, relatively cold plasma permeated with magnetic field.

A new radial implosion occurs at the beginning of the second half-cycle as the driving field changes sign. The photographs afford clear evidence that the presence of reversed trapped field on this half-cycle is accompanied by a rapid axial contraction in which the tension in the circumscribing field lines pulls

* The effect of trapped magnetic field on the relationship between geometrical mirror ratio and plasma area ratio during the effusion of a collision dominated plasma from a magnetic mirror has been analysed by K. V. Roberts [10].

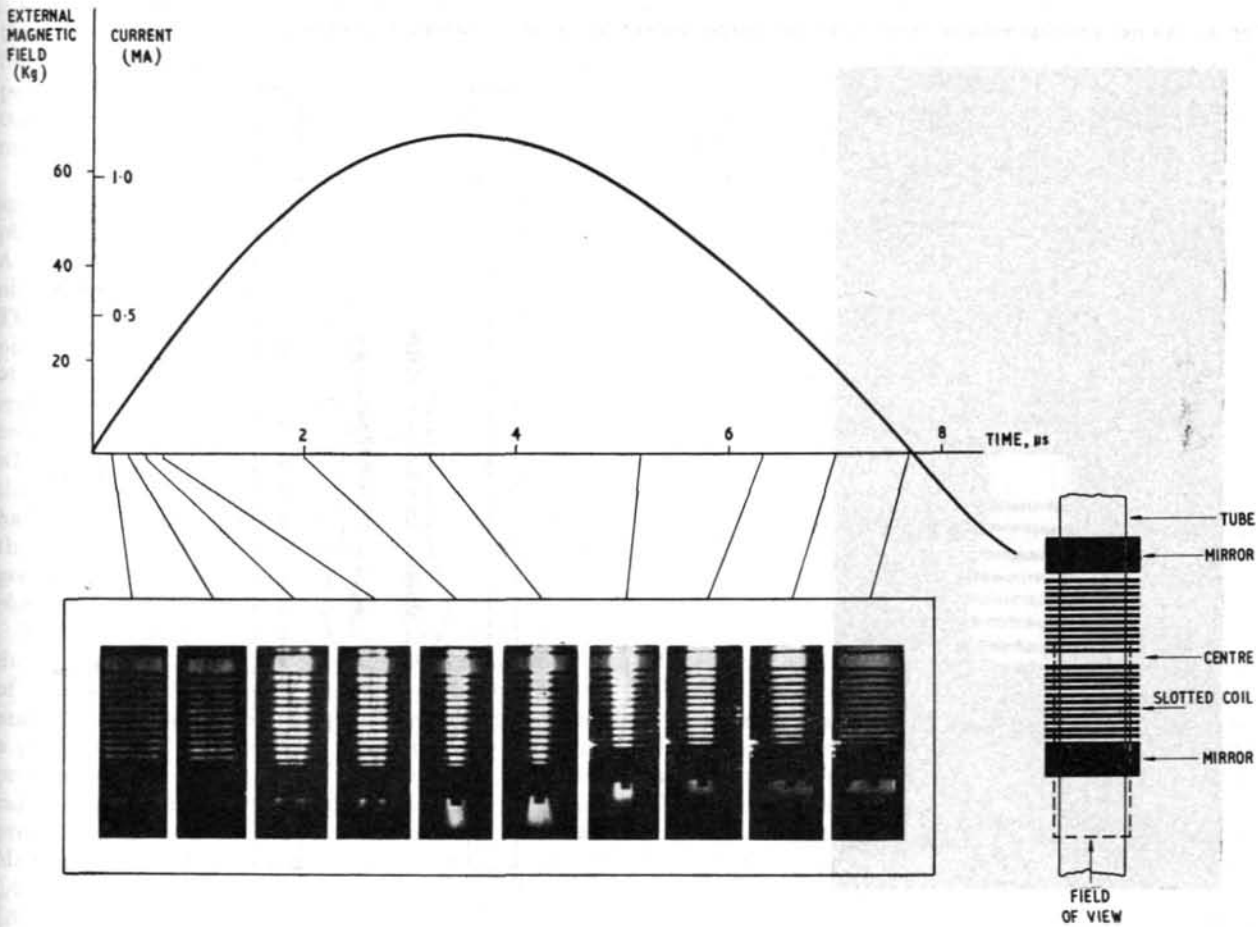

Fig. 3 Radial photographs of deuterium discharge during the first current half-cycle.

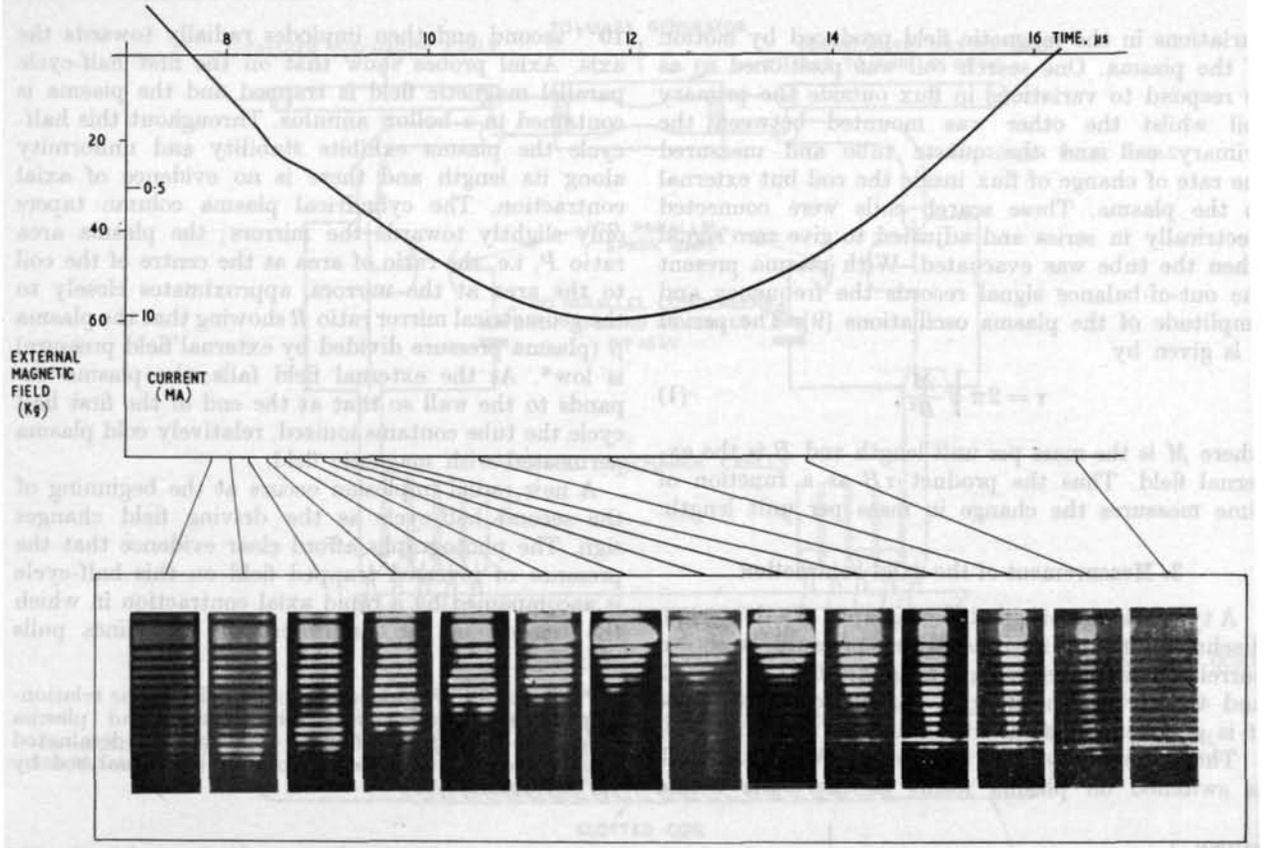

Fig. 4 Radial photographs of deuterium discharge during the second current half-cycle.

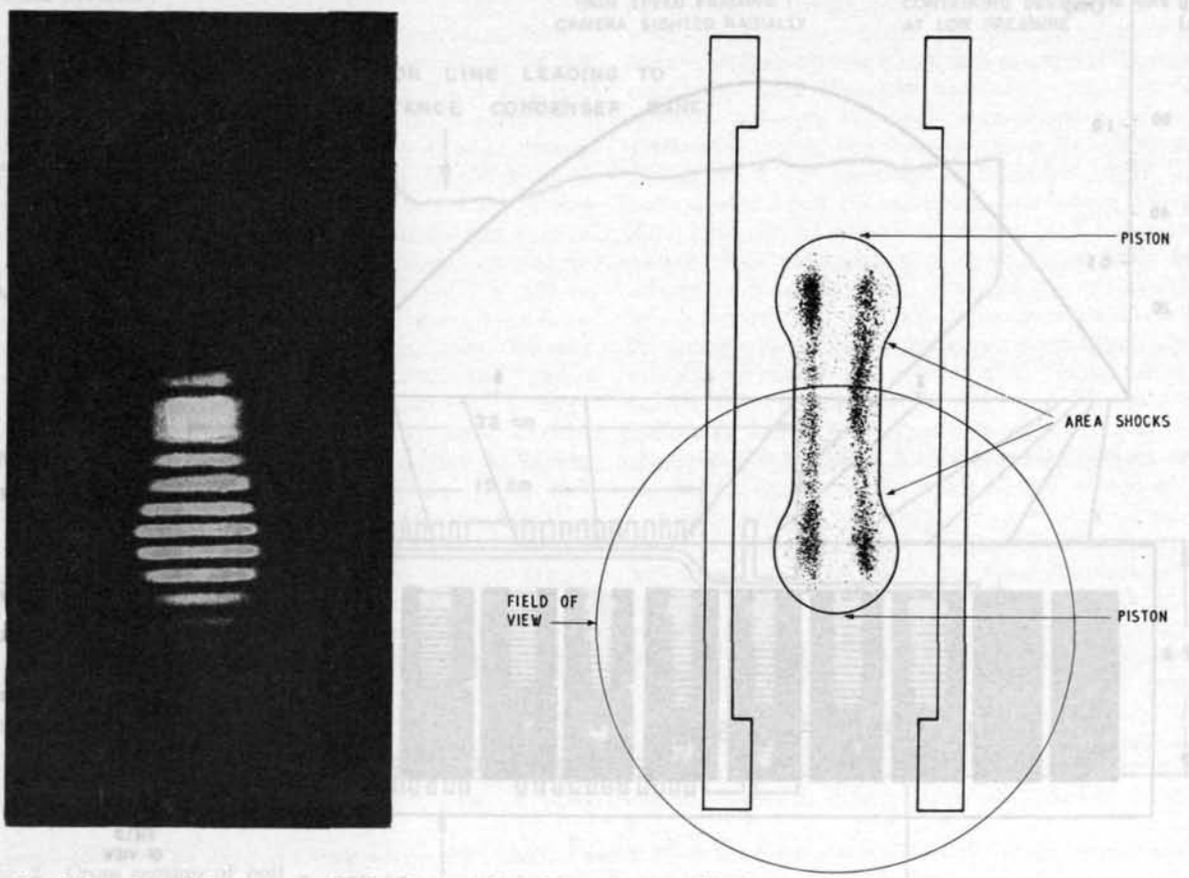

Fig. 5 Enlarged radial photograph showing profile of the area shock.

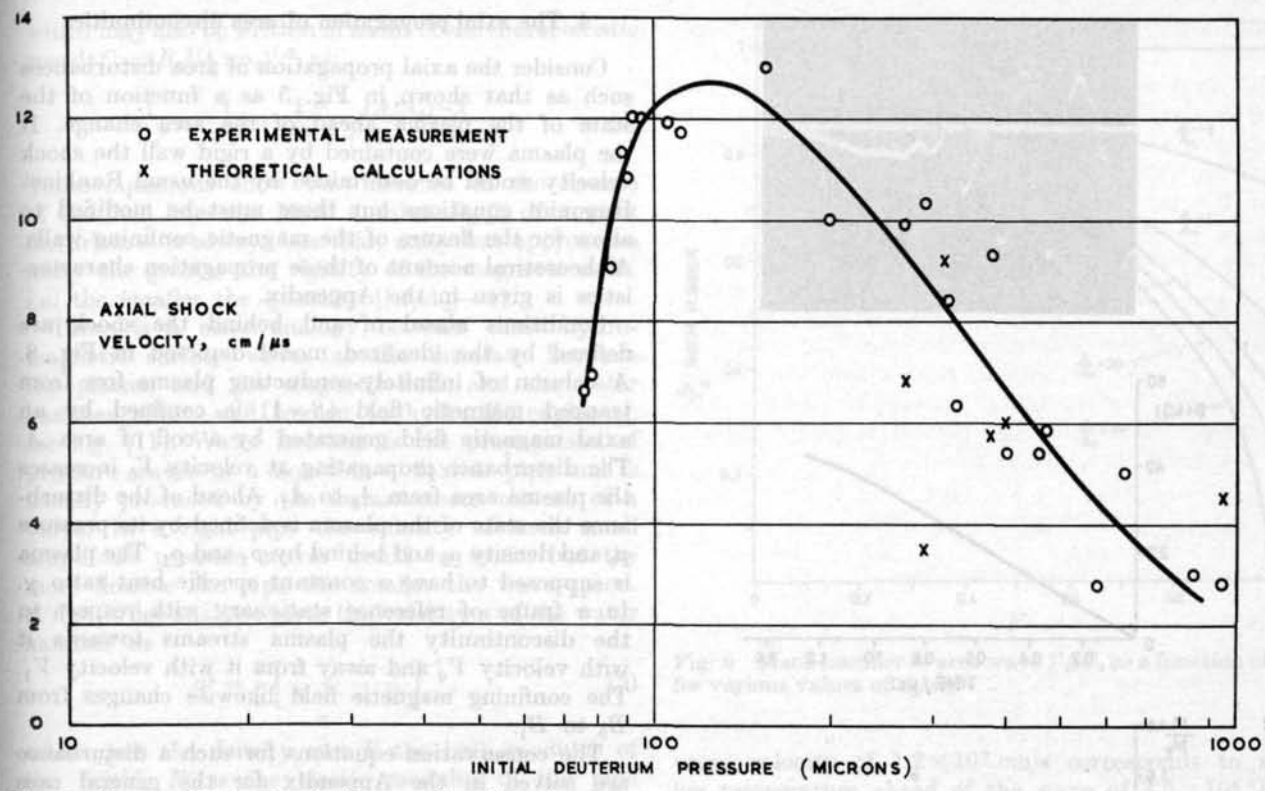

Fig. 6 Mean axial shock velocity as a function of pressure.

the plasma to the centre of the coil. At this stage the field configuration is similar to that of the toroidal pinch and in one sense the axial contraction may be considered as a form of instability in which the wave number k is very small.

The axial contraction is accompanied by the propagation of an increase in area of the undisturbed plasma by a factor which is typically about two. A single frame showing this discontinuous change in plasma area is shown on a larger scale in Fig. 5. This "area shock wave" is driven by the magnetic piston formed by the highly curved lines at the end of the plasma column. The area shocks from both ends collide at the centre to produce a further increase in area. At this stage the reverse field vanishes whilst the plasma expands axially and flows from the ends of the coil. During the remainder of this half-cycle the plasma has a spindle shape in which the plasma mirror ratio P is much greater than the geometrical mirror ratio R, a condition which is characteristic of a high β plasma.

The mean axial velocity of the area discontinuity during the contraction process is plotted as a function of pressure in Fig. 6 using measurements from streak and framing camera photographs. The velocity reaches a peak value of just over 1.2×10^7 cms/s at an initial pressure of 120 microns. The mean velocity decreases rapidly on the low pressure side whilst with increasing pressure the decline in velocity is more gradual. Measurements of the area ratio across the shock (A_1/A_0) and the ratio of coil area to plasma area (A/A_0) are presented in Table I for a series of experiments in deuterium at various initial pressures. Also tabulated are the corresponding measured shock velocities together with theoretical estimates obtained as described in the Appendix. These theoretical values are also plotted in Fig. 6. There is good agreement between theory and experiment.

TABLE I

Initial deuterium pressure (microns)	A_1/A_0	A/A_0	B_0 (kilogauss)	Measured area shock velocity (cm/μs)	Theoretical area shock velocity (See Appendix) (cm/μs)
280	1.5	5.7	21	10.0	6.9
290	2.5	8.3	10	10.4	3.5
315	1.8	4.2	18	8.5	9.3
380	1.7	4.2	13	9.2	5.8
400	2.0	5.7	16	5.5	6.0
980	3.6	8.9	16	2.8	4.6

Confirmatory evidence for axial contraction is afforded by radial oscillation measurements of which typical results at an initial pressure of 100 microns are presented in Fig. 7. The upper diagram shows the output of the two search coils in series from which the variation of the oscillation period τ is obtained. The external driving magnetic field B is plotted in the middle diagram and the graph below displays the calculated ratio of mass per unit length M/M_0 where M_0 refers to the initial condition. Thus the mass per unit length increases rapidly in the first

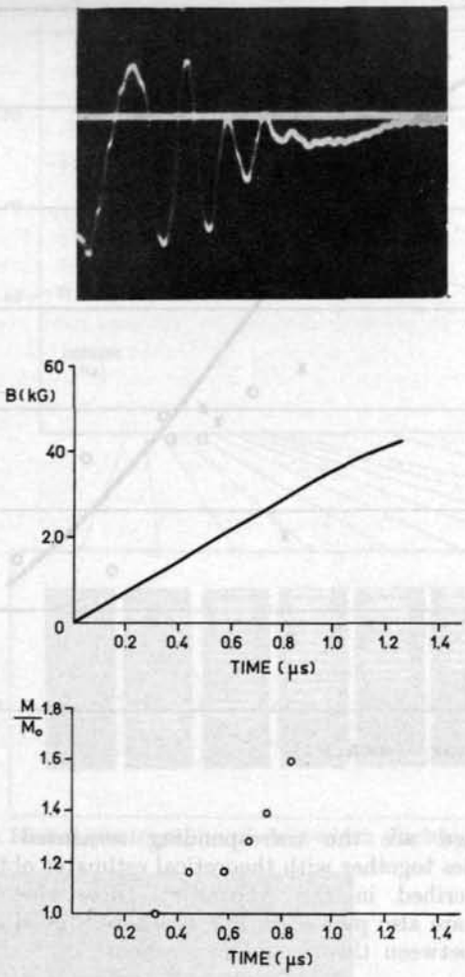

Fig. 7 Increase in mass per unit length from search coil data for a typical discharge at an initial pressure of 100 μ Hg.

microsecond of the second half-cycle. The velocity of contraction calculated approximately from this data is in agreement with the velocity obtained photographically. At Uppsala [5] the increase in the oscillation period on the second half-cycle was attributed to the influx of wall impurities but is now recognised to be an adjunct of the axial contraction.

4. The axial propagation of area discontinuities

Consider the axial propagation of area disturbances such as that shown in Fig. 5 as a function of the state of the plasma ahead of the area change. If the plasma were contained by a rigid wall the shock velocity would be determined by the usual Rankine-Hugoniot equations but these must be modified to allow for the flexure of the magnetic confining walls. A theoretical account of these propagation characteristics is given in the Appendix.

Conditions ahead of and behind the shock are defined by the idealized model depicted in Fig. 8. A column of infinitely-conducting plasma free from trapped magnetic field ($\beta=1$) is confined by an axial magnetic field generated by a coil of area A. The disturbance propagating at velocity V_0 increases the plasma area from A_0 to A_1. Ahead of the disturbance the state of the plasma is defined by its pressure p_0 and density ϱ_0 and behind by p_1 and ϱ_1. The plasma is supposed to have a constant specific heat ratio γ. In a frame of reference stationary with respect to the discontinuity the plasma streams towards it with velocity V_0 and away from it with velocity V_1. The confining magnetic field likewise changes from B_0 to B_1.

The conservation equations for such a disturbance are solved in the Appendix for the general case including trapped magnetic field. When the plasma area is much less than the coil area, the shock wave is near isobaric, i.e. the pressure difference across it is small, and for zero trapped field, i.e. $\beta=1$, its velocity may be written,

$$V_0^2 = C_s^2\left[\frac{1}{\gamma}\frac{A_1}{A_0}\frac{(A_1+A_0)}{A}\right], \tag{2}$$

where C_s is the sound speed in the undisturbed plasma. It is easy to show that there is an increase in entropy across such an area shock and that the area ratio enters into the propagation equations in a similar way to the pressure ratio for conventional shocks.

For a weak shock the area change is small and the speed of the wave is given by

$$\frac{V_0^2}{C_s^2} = \frac{\beta+(1-\beta)\,(A/A_0)}{\beta+(1-\beta)\,(A/A_0)\,(\beta\gamma/2)\,[(A/A_0)-1]}, \tag{3}$$

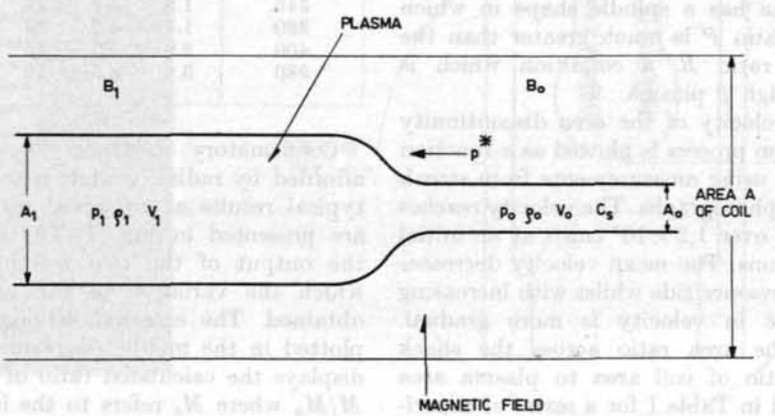

Fig. 8 Conditions ahead of and behind a propagating area shock.

which may also be written in terms of the characteristic speed $C=(B_0^2/4\,\pi\varrho_0)^{1/2}$ as

$$\frac{1}{V_0^2}=\frac{1}{C_s^2}+\frac{1}{C^2}\,\frac{(A/A_0)-1}{\beta+(1-\beta)\,(A/A_0)}. \tag{4}$$

These equations show that because of the flexure of the field lines the Mach number V_0/C_s of a weak disturbance is always less than unity but approaches unity the greater the rigidity of the magnetic walls, i.e. the smaller the quantity $[(A/A_0)-1]$.

There is a close analogy between these hydromagnetic surface waves at the interface between the plasma and the magnetic field, and the water hammer effect well known to hydraulic engineers, see e.g. [11]. Water hammer is the propagation of pressure waves in a liquid in a flexible pipe and is usually produced by the instantaneous closure of a valve. In a rigid pipe the velocity of such small amplitude pressure waves would be sonic, but the more flexible the pipe the smaller the wave speed. A first-order analysis gives the velocity a of the water hammer as

$$a^2=\frac{1}{\varrho}\left[\frac{1}{E}+\frac{d}{e}\,\frac{1}{E'}\right]^{-1}, \tag{5}$$

where ϱ is the density and E the bulk modulus of the liquid, E' is the elastic modulus of the pipe material and d is the diameter and e the thickness of the wall of the pipe. The similarity between water hammer waves and small amplitude magnetohydrodynamic area waves is apparent when the bulk modulus of the plasma is identified as γp, the elastic modulus of the field as $H^2/4\,\pi$ and the ratio d/e with the ratio (A/A_0-1) which determines the flexibility of the magnetic walls.

5. Interpretation of the measurements

Eq. (3) is plotted in Fig. 9 to show V_0/C_s as a function of β for various values of A/A_0 and for a specific heat ratio of 5/3. The measurements of the axial velocity of the area discontinuity can therefore be used to estimate the sound speed and ion temperature ahead of the wave if β and A/A_0 are also measured. Unfortunately, at high β the ion temperature is sensitive to β and the strength of trapped magnetic field is difficult to measure. However, in a reversed field discharge β varies across the plasma from zero at the magnetic field interface to unity at the neutral surface and its average value is probably high. On the assumption that the average value of β is constant as the initial pressure is varied, Fig. 6 shows that the ion temperature ahead of the wave, i.e. at the end of the radial implosion phase, reaches a peak at an initial pressure of 120 microns. This conclusion is consistent with the results of the accompanying paper [1] which shows that the trapped reversed field, the neutron output, and the soft x-ray emission also reach a peak at this initial pressure. Without an exact knowledge of the average β in the plasma the ion temperature cannot be estimated with precision, but for an average β of 0.5 the axial wave velocity of 1.2×10^7 cm/s corresponds to an ion temperature ahead of the wave of 3.5×10^6 °K.

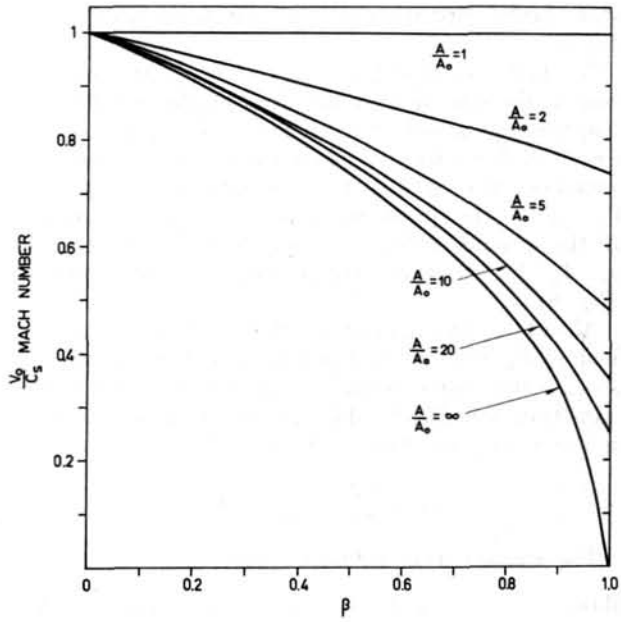

Fig. 9 Mach number of area wave V_0/C_s as a function of β for various values of A/A_0.

6. Conclusion

The rapid axial contraction of plasma on the second half-cycle of a theta discharge has been measured both photographically and from the interpretation of magnetic field variations. The axial propagation of area waves and area shocks is considered on the basis of an infinite conductivity model and solution of the conservation equations is presented. Results for a discharge in deuterium show that the mean wave velocity reaches a peak at an initial pressure of 120 microns. A precise estimate of the ion temperature ahead of the wave requires a knowledge of the strength of trapped magnetic field, and for a β of 0.5 the peak velocity corresponds to a temperature of 3.5×10^6 °K at the end of the radial implosion.

APPENDIX*

A 1. Some propagation characteristics of "Area Waves" and "Area Shocks"

The observations reported above suggest that, in a plasma column confined by an axial magnetic field, changes in the cross-sectional area of the column may be propagated along the column with a characteristic velocity. (In the terminology of instability studies we would refer to small-amplitude waves of this type as the "$m=0$" modes.) The area change may be large and we shall therefore restrict the term "area wave" to mean a small-amplitude disturbance

* The Appendix is by J. B. Taylor.

while larger disturbances will be designated "area shocks".

We first examine the "area shock". We suppose that a discontinuity in the area of the column can propagate at a definite velocity and apply the conservation laws to this phenomenon. In a frame of reference moving with the discontinuity let p_0, A_0, V_0, ϱ_0 be the pressure, area, velocity and density of the plasma column ahead of the "shock" and p_1, A_1, V_1, ϱ_1, the corresponding quantities behind (Fig. 8).

Ahead of the transition the confining magnetic field is B_0 and the trapped field within the plasma is b_0; the corresponding quantities behind the transition are B_1, b_1. The plasma is in equilibrium in the radial direction so that

$$p_0 + \frac{b_0^2}{8\pi} = \frac{B_0^2}{8\pi}, \text{ etc.}$$

The conservation equations are

Mass
$$\varrho_0 V_0 A_0 = \varrho_1 V_1 A_1 = m \tag{A1}$$

Energy
$$p_0 A_0 V_0 - p_1 A_1 V_1 = m\left(\frac{V_1^2}{2} - \frac{V_0^2}{2} + E_1 - E_0\right) \tag{A2}$$

Momentum
$$p_0 A_0 - p_1 A_1 + p^*(A_1 - A_0) = m(V_1 - V_0) \tag{A3}$$

where E_1 is the specific internal energy and the term in p^* represents the effective pressure acting on the plasma over the transition region. In order to determine p^* we require an additional equation obtained by considering the work done on the magnetic field as the shock advances

$$p^*(A_1 - A_0) = \frac{B_1^2}{8\pi}(A - A_1) - \frac{B_0^2}{8\pi}(A - A_0) + \frac{b_1^2}{8\pi}A_1 - \frac{b_0^2}{8\pi}A_0, \tag{A4}$$

where A is the area of the confining coil.

The conservation of flux requires

$$B_0(A - A_0) = B_1(A - A_1)$$
$$b_0 A_0 = b_1 A_1. \tag{A5}$$

As in the case of a conventional (one-dimensional) shock wave, Eqs. (A1)—(A5) are just sufficient to determine the transition completely if the state of the system ahead of the shock is given together with *one* quantity behind it. We shall take this additional given quantity to be the area A_1 since this is directly observable.

The solution of the equations leads in general to unwieldy expressions. Writing for brevity:

$$x = \frac{A - A_0}{A - A_1}; \quad y = \frac{A_0}{A_1}; \quad z = \frac{A}{A_0},$$

the shock speed can be written

$$V_0^2 = \frac{B_0^2}{4\pi\varrho_0}\frac{GH}{K}, \tag{A6}$$

where

$$G = \left[(z-1)(x-1) - \frac{x^2}{y} + 1 + \frac{2b_0^2}{B_0^2}(y-1)\right]$$

$$H = \left[(\gamma-1)\{(z-1)(x-1)+1\} + (\gamma+1)\frac{x^2}{y} - \frac{2b_0^2}{B_0^2}(\gamma+y-1)\right]$$

$$K = 4\left[1 - \frac{x^2}{y} - (\gamma-1)(z-1)(x-1) + \frac{b_0^2}{B_0^2}(2-\gamma)(y-1)\right].$$

In Figs. A1—A3 the variation of V_0/C (where $C^2 = B_0^2/4\pi\varrho_0$) is shown as a function of A_1/A_0 (the "shock strength") and A/A_0 for three values of β (where $1-\beta = b_0^2/B_0^2$). In viewing these curves it should be remembered that the sound speed ahead of the shock is

$$C_s^2 = \frac{\gamma p_0}{\varrho_0} = \frac{\gamma}{2}\beta C^2. \tag{A7}$$

With small values of the "area strength" ($A_1/A_0 \ll A/A_0$) the shock velocity is less than C and, indeed, *is less than the sonic speed* C_s. In this region the pressure change across the "shock" is very small. As the area ratio A_1/A_0 approaches A/A_0 (so that the plasma behind the shock fills most of the tube) the pressure ratio rises and this is reflected in a rapid increase in the shock velocity; the area shock now acquires more of the character of a conventional, pressure-driven, one-dimensional shock.

All the quantities required for a calculation of the shock speed can be directly determined except

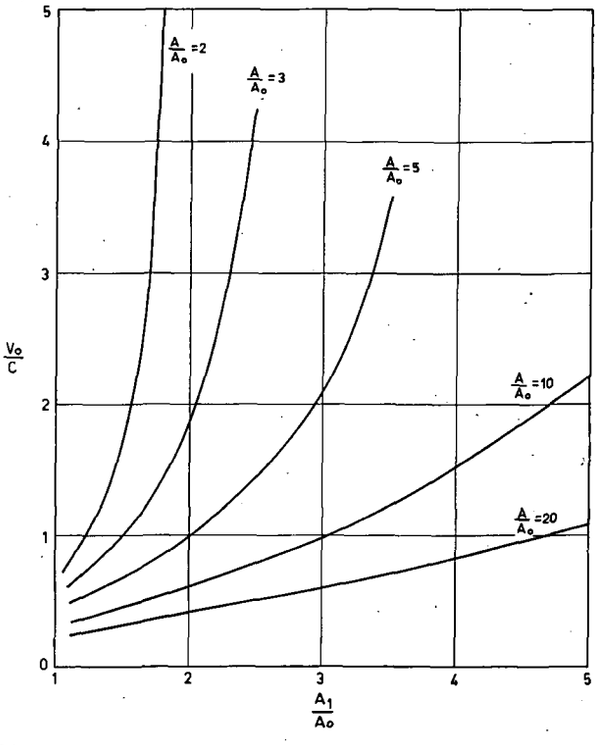

Fig. A1 Variation of shock speed with shock strength A_1/A_0 for $\beta = 1.0$.

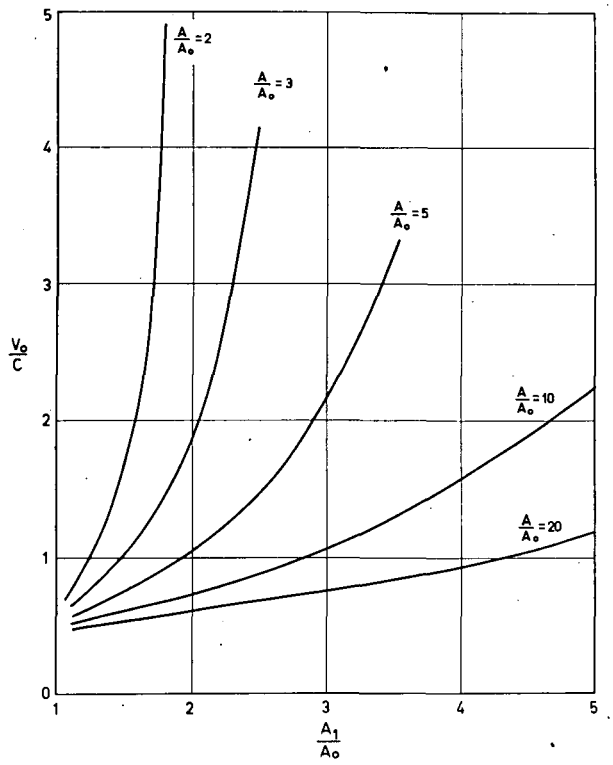

Fig. A 2 Variation of shock speed with shock strength A_1/A_0 for $\beta = 0.5$.

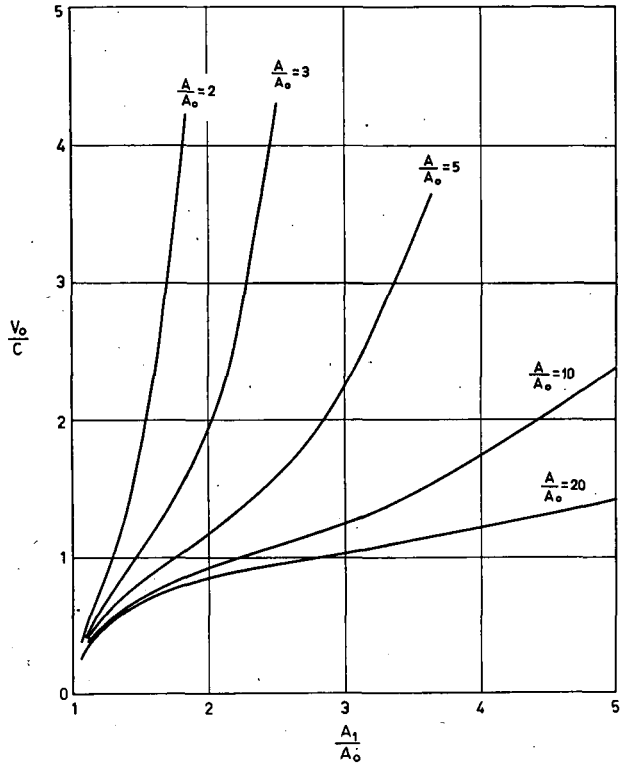

Fig. A 3 Variation of shock speed with shock strengt A_1/A_0 for $\beta = 0$.

g and it is of interest, therefore, to note that the shock speed is insensitive to β when A_1/A_0 and A/A_0 have values in the neighbourhood of those observed experimentally; this is shown in Fig. A4. As a result of this feature we can calculate the shock speed directly from the observations of A_1/A_0, A/A_0, B_0 and ϱ_0 given in Table I and some values deduced in this way have been included in Fig. 6 where they are indicated by the crosses.

In certain limiting cases the shock speed formula simplifies considerably. The most interesting case is that in which the plasma fills only a small fraction of the cross-section of the confining coil (i.e. $A \gg A_0; A_1$) and there is no trapped field. (In this limit only small changes in pressure are possible and we have almost "isobaric" conditions.) The velocity of the "area" shock is then given by:

$$V_0^2 = \left(\gamma \frac{p_0}{\varrho_0}\right)\left[\frac{1}{\gamma}\frac{A_1}{A_0}\left(\frac{A_1+A_0}{A}\right)\right] \qquad \text{(A 8)}$$

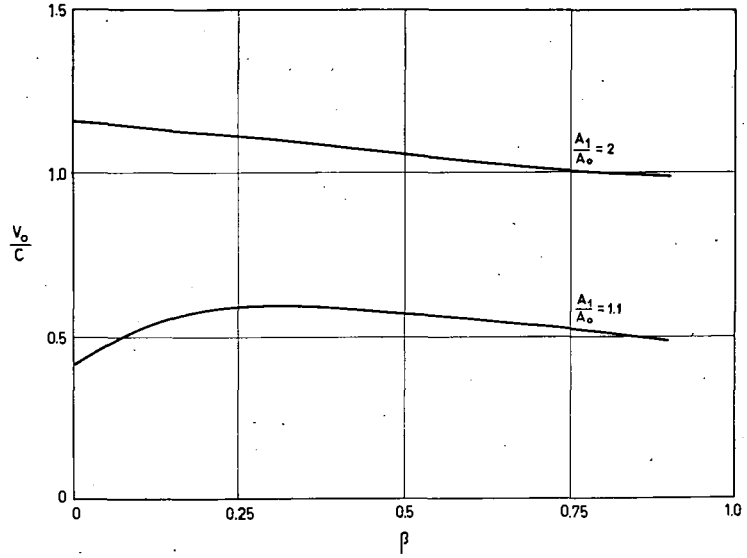

Fig. A 4 Variation of shock speed with β for $A/A_0 = 5$.

These "area shocks" therefore travel more slowly than an ordinary sound wave unless the "shock strength" A_1/A_0 is considerable. The velocity always increases as the shock strength increases.

Another interesting case is that in which the shock strength is small, $A_1 \to A_0$. In this situation the velocity is given by

$$V_0^2 = \left(\frac{\gamma p_0}{\varrho_0}\right)\left[\frac{\beta + (1-\beta)\, z}{\beta + (1-\beta)\, z + (\beta\gamma/2)\,(z-1)}\right], \quad \text{(A 9)}$$

where z again denotes A/A_0. This can be written in the form

$$\frac{1}{V_0^2} = \frac{1}{C_s^2} + \frac{1}{C^2}\left[\frac{(z-1)}{\beta + (1-\beta)\, z}\right]. \quad \text{(A 10)}$$

It will be noted that the velocity of small-amplitude shocks is *always* sub-sonic but approaches sonic speed if the plasma almost fills the confining tube $(z \to 1)$.

The temperature change across an area shock is also of interest. In the near-isobaric limit the temperature ratio is approximately

$$\frac{T_1}{T_0} = 1 + \left(\frac{\gamma - 1}{2\gamma}\right)\left(\frac{1}{p_0 A_0} + \frac{1}{p_1 A_1}\right)\left[p_0 \frac{(A_1^2 - A_0^2)}{A}\right],$$

so that the temperature is always increased, but by *only a small amount.*

A 2. Small amplitude waves

It is clearly of importance to discuss the relationship of these area shocks to the general problem of wave propagation along a plasma column. This can most easily be done from the dispersion equation which is well known from instability studies; see, e.g. [12]. If we consider a cylindrical column confined by axial field then the appropriate dispersion relation for waves $f(r) \exp[\mathrm{i}(kx + \omega t)]$ is:

$$\frac{4\pi[(k^2 b^2/4\pi) - \varrho\omega^2]\, I_0(\varkappa R_0)}{\varkappa I_0'(\varkappa R_0)} = k B^2 \left\{\frac{K_0'(k R)\, I_0(k R_0) - I_0'(k R)\, K_0(k R_0)}{K_0'(k R)\, I_0'(k R_0) - I_0'(k R)\, K_0'(k R_0)}\right\}, \quad \text{(A 11)}$$

where b = internal magnetic field
B = external magnetic field
R_0 = radius of plasma column
R = radius of confining tube

and where

$$\varkappa^2 = \frac{(k^2 - \omega^2/C_A^2)\,(k^2 - \omega^2/C_s^2)}{[k^2 - \omega^2\,(1/C_A^2 + 1/C_s^2)]}. \quad \text{(A 12)}$$

In this expression $C_s^2 = \gamma p/\varrho$; $C_A^2 = b^2/4\pi\varrho$. (This is not to be confused with $C^2 = B^2/4\pi\varrho$.)

There is an infinite number of branches to the dispersion curve given by Eqs. (A11) and (A12). One sequence of branches lies above the line $\omega = C_s k$ and reduces for small kR to the frequencies of the radial oscillations discussed elsewhere [13]. Another sequence lies below $\omega = C_s k$ and approaches

$$\omega = \frac{C_A C_s}{(C_A^2 + C_s^2)^{1/2}} \cdot k$$

for small kR.

However of special significance in the present context is that branch of the dispersion curve corresponding to waves which have *no nodes* in the radial eigenfunction $f(r)$ (the fundamental mode) which separates the two sequences referred to above. Waves corresponding to this fundamental branch have a phase and group velocity which for small kR can be written.

$$C^2 = C_s^2 \left[\frac{\beta + (1-\beta)\,\dfrac{R^2}{R_0^2}}{\beta + (1-\beta)\,\dfrac{R^2}{R_0^2} + \dfrac{\gamma}{2}\left(\dfrac{R^2}{R_0^2} - 1\right)}\right], \quad \text{(A 13)}$$

which is identical with the velocity obtained from the conservation equations for a small-amplitude area shock, Eq. (A10).

It appears then that the same relation exists between area waves on the fundamental branch and area shocks as exists between sound waves and conventional shocks. However a general disturbance of the plasma column would presumably excite waves on all branches so that the initial behaviour of a general area-wave will be complex but, as they correspond to the "smoothest" eigenfunction, one can reasonably expect that after a short transient the fundamental waves would predominate.

References

[1] Bodin, H. A. B., Green, T. S., Niblett, G. B. F., Peacock, N. J., Quinn, J. M. P., Reynolds, J. A., Proceedings of this Conference, page 521.

[2] Kolb, A. C., Dobbie, C. B., Griem, H. R., *Physical Review Letters* **3** (1959) 5.

[3] Kolb, A. C., Griem, H. R., Faust, W. R., Proceedings of the Fourth International Conference on Ionization Phenomena in Gases, Uppsala (North-Holland Pub. Co., Amsterdam) **2** (1959) 1057.

[4] Fay, H., Hintz, E., Jordan, H. L., Proceedings of the Fourth International Conference on Ionization Phenomena in Gases, Uppsala (North-Holland Pub. Co., Amsterdam) **2** (1959) 1046.

[5] Bodin, H. A. B., Green, T. S., Niblett, G. B. F., Peacock, N. J., Proceedings of the Fourth International Conference on Ionization Phenomena in Gases, Uppsala (North-Holland Pub. Co., Amsterdam) **2** (1959) 1061.

[6] Little, E. M., Quinn, W. E., Ribe, F. L., *Physics of Fluids* **4** (1961) 711.

[7] Alidieres, M., Aymar, E., Etievant, C., Jourdan, P., Samain, A., Proceedings of the Fourth International Conference on Ionization Phenomena in Gases, Uppsala (North-Holland Pub. Co., Amsterdam) **2** (1959) 1042.

[8] Skinner, A., Proceedings of the Fourth International Congress on High Speed Photography, Cologne (1958) 172.

[9] Niblett, G. B. F., Green, T. S., *Proc. Phys. Soc.* **74** (1959) 737.

[10] Roberts, K. V., *J. Nuclear Energy* **C 1** (1960) 243.

[11] Davies, C. V. (Editor), The Handbook of Hydraulics, 2nd Edition (McGraw-Hill, 1951): Chapter on "Water Hammer" by C. R. Rich.

[12] Glasstone, S., Lovberg, R. H., Controlled Thermonuclear Reactions (D. Van Nostrand, Princeton, N. J., 1960).

[13] Taylor, J. B., Proceedings of a Conference on Theoretical Aspects of Controlled Fusion Research, Gatlinburg, Tenn.: U.S. Atomic Energy Commission Document TID-7582 (1959).

THE INFLUENCE OF TRAPPED FIELD ON THE CHARACTERISTICS OF A MAGNETICALLY COMPRESSED PLASMA (THETATRON)*

H. A. B. Bodin, T. S. Green, G. B. F. Niblett, N. J. Peacock,
J. M. P. Quinn, J. A. Reynolds

Atomic Weapons Research Establishment

Aldermaston, Berkshire, United Kingdom

Recent results of an experimental investigation of deuterium plasma compressed by a rapidly rising magnetic field are presented and discussed. The discharge which occurred on the second half-cycle of a sinusoidal driving field without preionization was studied and it was found that in the pressure region 50 — 95 μ Hg the trapped flux varied in the range ±25 kilomaxwells. Thus careful control of the initial pressure provided a simple way of varying the trapped flux. In this pressure range the characteristics of the discharge were observed to change markedly, and it is shown that the properties of the plasma are primarily determined by the trapped flux. Three types of discharge are analysed in detail. The first type, trapping maximum parallel flux, has a low β and a low temperature; it is well contained and emits neither neutrons nor soft x-rays although hard x-rays are observed. The second type traps much less parallel flux, has β between 0.2 and 0.8, emits no neutrons and only very small yields of x-rays, and escapes rapidly. The third type traps maximum reversed flux, which is subsequently destroyed. The implosion velocity increases with pressure and the neutron and soft x-ray intensities peak sharply at the pressure at which the trapped reversed field energy and the total energy (field and particle) are a maximum. Soft x-ray measurements lead to an electron temperature between 180 and 400 eV, and total energy measurements show that sufficient energy is available to raise the ions to a temperature of 1 keV. The plasma forms an unstable closed field loop configuration, contracts axially and remains contained away from the walls for about 2.5 μs, after which it normally breaks up following a rapid rotation.

1. Introduction

The heating and containment of a dense plasma by a rapidly rising axial magnetic field has been the subject of much study [1—5]. It has been reported that ion and electron temperatures approaching 10^7 °K can be produced in these discharges [6, 7, 8], and the heating of the plasma has been found to be dependent on the trapped magnetic field [9]. When this field has the opposite sign to the driving field (reversed trapped field) the neutron yield increases sharply [9, 10]. However, the detailed mechanism whereby the trapped field affects the current sheath formation and the subsequent plasma behaviour is not yet fully understood.

In the experiments reported below the effect of trapped field on a discharge which occurred in the second current half-cycle of a sinusoidal driving field without pre-ionization was studied and it has been found that the trapped flux can be varied widely in both sign and magnitude be carefully controlling the initial pressure between 50 and 95 μ Hg. In this relatively narrow pressure range the properties of the discharge are found to vary markedly with pressure and it is the purpose of the present paper to show that this arises due to the variation of trapped flux and that the characteristics of the plasma are predominantly determined by the trapped magnetic field. Measurements of the plasma β (particle pressure/external magnetic pressure), containment time and the radiation emitted are presented and discussed for different trapped field configurations.

2. Apparatus and method of measurement

A 100 μF condenser bank operating at voltages in the range 20—30 kV was used for these experiments. The coil was typically 21 cm long and 5.4 cm in diameter and encircled a quartz or alumina tube of 3.8 cm bore containing deuterium gas at an initial pressure of from 30 to 200 μ Hg. The peak electric field in the gas was about 0.6 kV/cm and the peak magnetic field of 86 kG was reached in 2.5 μs.

A streak camera with a writing speed of 20 mm/μs and a time resolution of 0.05 μs and a framing camera operating at between 5 and 8 frames/μs were used to study the dynamic phases of the discharge and the slower variation of the plasma cross section. The plasma area and the area of the non-luminous core were measured and analysed as described in Section 3.

For escaping plasmas β is estimated from a measurement of the plasma mirror ratio, R_p, (area of the plasma at the middle to that at the end) using the theoretical result* derived by Roberts [11] for systems in which the plasma and field are mixed, that

$$R_p = R(1-\beta)^{-\frac{1}{2}}, \qquad (1)$$

where R is the external mirror ratio (unity in the present experiments).

* This theory assumes that the transverse plasma pressure falls to zero at the ends and recently Taylor [12] has modified Eq. (1) to take into account the finite pressure. Except at high values of β the correction term is small.

* Conference paper CN-10/71, presented by G. B. F. Niblett. Discussion of this paper is given on page 645. Translations of the abstract are at the end of this volume of the Conference Proceedings.

A double magnetic pick-up loop was used to study the plasma diamagnetism. This consisted of two pick-up loops situated in the median plane of the coil, one recording the flux between the coil and the tube wall and the other recording part of the total flux passing through the coil; the outputs were connected in series to give zero signal with no plasma. This technique was used to observe the hydromagnetic oscillations [13]; these have a period given by

$$\tau = 2\pi \sqrt{\frac{M}{B^2}}, \qquad (2)$$

where M is the mass/cm of the plasma and B is the driving field. Hence the value of M found from this equation is compared with the initial mass M_0 to determine the fraction of gas swept up in the implosion and to observe its variation in time.

The sign of the trapped field was measured using an axial magnetic probe.

3. The analysis of the time variation of the plasma cross sectional area

The plasma containment time and β can be determined from a measurement of the plasma area as a function of time. Here the relationship between these quantities is derived using a model in which the luminous area consists of a uniform mixture of field and plasma. Considering first the simple case in which the adiabatic law and pressure balance apply, then

$$\frac{pV^\gamma}{N} = \text{constant}, \qquad (3)$$

where

$$p = \beta \frac{B^2}{8\pi}, \quad V = Al.$$

Therefore

$$\frac{N}{N_0} = \frac{\beta}{\beta_0}\left(\frac{A}{A_0}\right)^\gamma \left(\frac{B}{B_0}\right)^2, \qquad (4)$$

where the symbols have the following meanings:

N = line density
p = particle pressure
B = driving field
A = plasma area
l = length of the coil
γ = ratio of the specific heats of the gas

and the subscript zero refers to the start of the slow compression phase.

The assumption that the adiabatic law holds implies that no work is done on the escaping plasma by the plasma which remains. KOLB [14] has considered escaping plasmas in some detail and from his analysis it can be shown that in the present notation Eq. (3) must be replaced, in the general case, by

$$\frac{pV^\gamma}{N^\alpha} = \text{constant}$$

and the left hand side of Eq. (4) becomes $(N/N_0)^\alpha$, where α is of order 1 and depends on the loss mechanism.

In this paper the approximation $\alpha = 1$ is made and γ is assumed to be 5/3. Eq. (4) can then be rewritten using flux conservation to express β in terms of β_0 as

$$\left(\frac{B}{B_0}\right)^2 \left(\frac{A}{A_0}\right)^{\frac{5}{3}} = \beta_0 \frac{N}{N_0} + (1 - \beta_0)\left(\frac{A}{A_0}\right)^{-\frac{1}{3}}, \qquad (5)$$

from which β can be determined only in the special case of no plasma loss. The left hand side of Eq. (5) is plotted against time and must lie between 1 and the curve of $(A/A_0)^{-1/3}$ for β between 1 and 0 respectively. If it lies outside these limits N/N_0 is varying and the containment time, τ_c, can be determined using Eq. 5 from a plot of $(B/B_0)^2 (A/A_0)^{5/3}$ against time if β_0 is known. However, it can be shown that

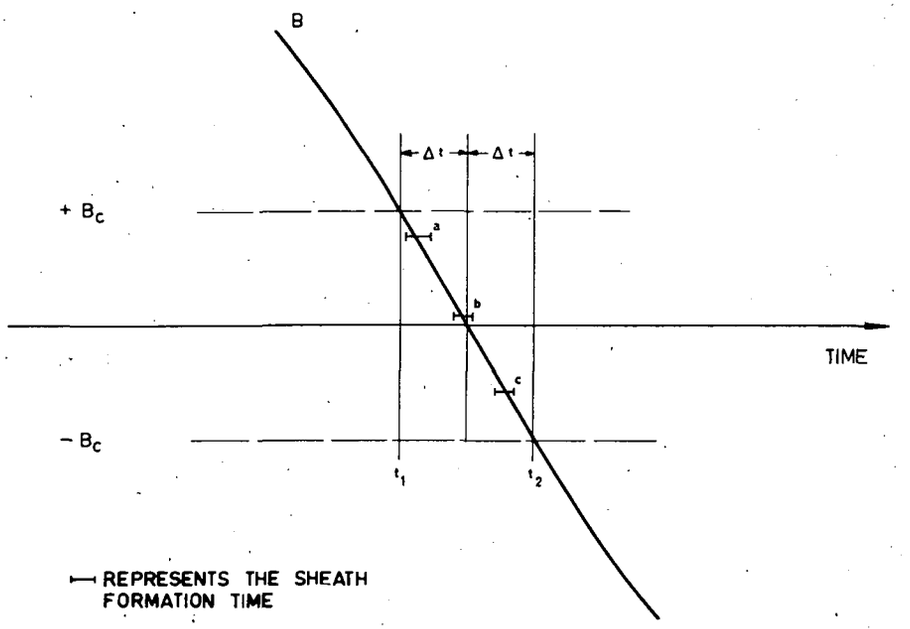

Fig. 1 An illustration of the time and field intervals which are relevant to breakdown and field trapping.

N/N_0 is not very sensitive to β_0, and in this paper τ_c is estimated using the approximation $\beta_0=1$. The error introduced by the two approximations is less than a factor of two.

4. Breakdown and field trapping

The breakdown and current sheath formation [15, 16] in the time varying magnetic field is fundamental to the discharge. In this section breakdown near the second current zero is considered and a simple model is described which can qualitatively account for the observations. The effect of space charge [16] and wall effects and the influence of field diffusion during the implosion [17] are neglected.

It is assumed that ionization can only grow in the crossed electric and magnetic fields when twice the electron drift velocity ($\propto E/B$) exceeds the velocity v corresponding to the ionization potential V_i of the gas ($\frac{1}{2} m_0 v^2 = V_i e$). Thus ionization can only occur when B is less than a critical value, B_c, (~ 1000 gauss for $E \sim 1$ kV/cm and $V_i = 13.6$ eV for deuterium) and therefore a current sheath can only grow within times $\Delta t \sim B_0/\dot{B} \sim 10^{-7}$ sec of current zero (see Fig. 1). The sheath formation time [15] is 10^{-8} sec and so on this model the sheath can form anywhere within the time interval of $\pm\Delta t$ of current zero. At higher pressures ionization proceeds more readily and sheath formation occurs early, for example at "a" in Fig. 1; as the pressure is reduced the ionization rate falls and sheath formation is delayed and can extend over the field zero (b, Fig. 1) or, at still lower pressure, after the zero (c, Fig. 1). There is a critical pressure below which breakdown will be delayed until the next current zero. This is illustrated in Fig. 2 in which the electric field at the plasma surface just after the breakdown is plotted against the pressure. The curve for the first half-cycle breakdown differs from the others, as no ionization occurs before the current zero, but the other curves are repeated when the pressure is reduced as breakdown is delayed until later half-cycles.

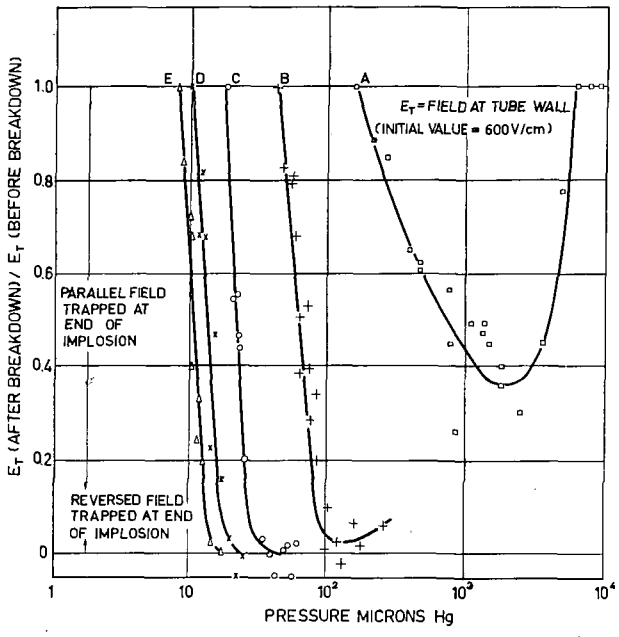

Fig. 2 A plot of the ratio of the electric field at the surface of the plasma before breakdown to that after breakdown against pressure. Breakdown on the first half-cycle is shown by curve (A), and breakdown on the second, third, etc. half-cycles is shown by curves (B), (C), etc.

For cases such as (a) in Fig. 1 the trapped field is reversed in the second half-cycle discharge; for case (b) it can be parallel or reversed; and for case (c) it will be parallel. Fig. 3 illustrates parallel and reversed field configurations. The trapped flux varies from maximum parallel for breakdown at t_2 to maximum reversed for breakdown at t_1 (Fig. 1), i.e. as the pressure is increased. At higher pressures when breakdown at the first current zero takes place the reversed trapped flux in the second half cycle is largely determined by the preceding breakdown and falls off slowly with increasing pressure.

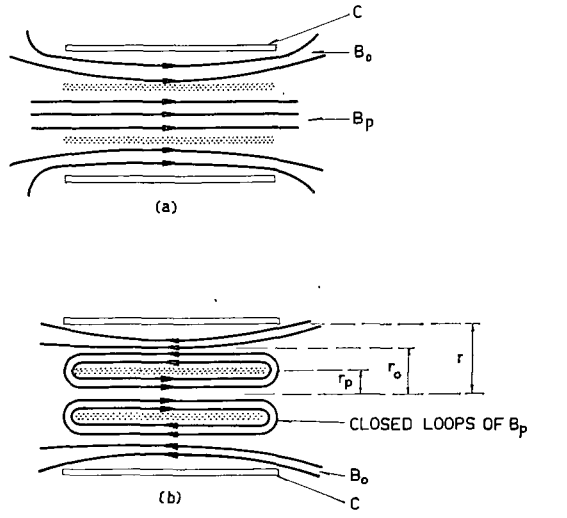

Fig. 3 Parallel and reversed trapped field configurations. (a) parallel trapped field, (b) reversed trapped field (when closed lines have formed). C—coil, B_0—driving field, B_p—trapped field.

Fig. 4 shows the trapped flux determined at the end of the implosion from the area of the non-luminous core measured from streak and framing photographs assuming that the driving field and the trapped field are equal at the equilibrium radius during the oscillations. It is seen that the trapped flux varies from a maximum (parallel field) to a maximum (reversed field) as the pressure is raised from 50 to 95 μ Hg and thereafter it decreases slowly, in agreement with the predictions of the simple model.

5. The dependence of the discharge characteristics on the trapped flux

In the pressure range 50 to 95 μ Hg the characteristics of the discharge are found to change markedly with the trapped flux. To illustrate this three different types of discharge will be discussed.

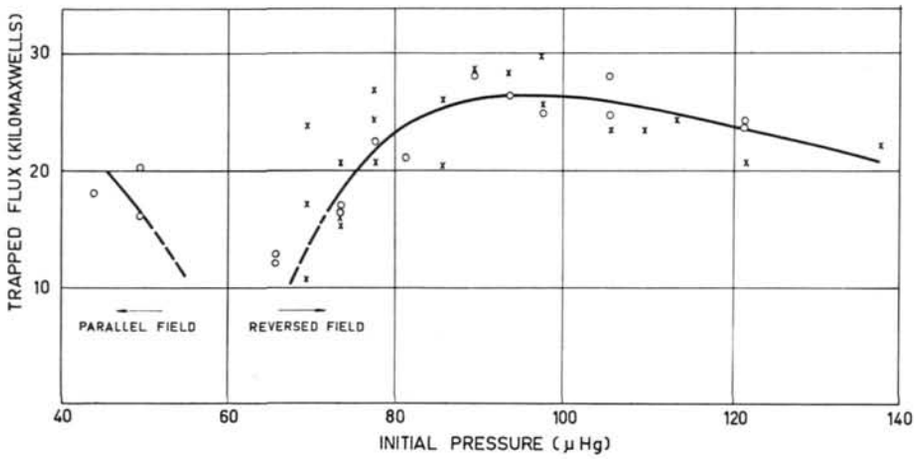

Fig. 4 The trapped flux at the end of the implosion as a function of initial pressure. ×—streak camera measurements, ○—framing camera measurements.

The first type is illustrated in Fig. 5A and occurs at about 50 μ Hg and traps maximum parallel flux, which results in a low compression ratio of about 5 after the implosion. The implosion is followed by adiabatic compression, and the plasma contracts slowly with the driving field and then expands again, remaining in the tube for the duration of the current pulse. During the reversible compression slowly damped radial hydromagnetic oscillations are observed with the double loop and a typical waveform is shown in Fig. 6A; the small amplitude indicates only weak plasma diamagnetism.

The second type (Fig. 5B), defined as the intermediate type, occurs at about 60 μ Hg and traps

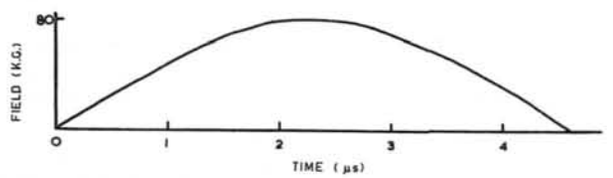

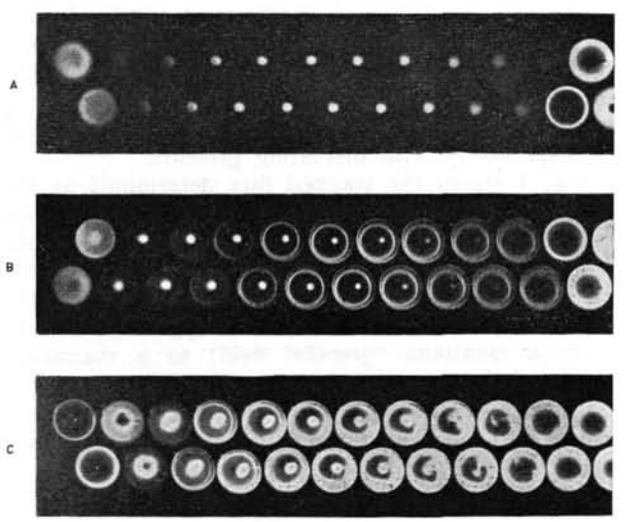

Fig. 5 Framing camera photographs of examples of the three main types of discharge, together with a magnetic field waveform.
(A) Maximum parallel trapped flux: $p_0 \sim 50$ μ Hg, (B) Intermediate trapped flux: $p_0 \sim 60$ μ Hg, (C) Maximum reversed trapped flux: $p_0 \sim 95$ μ Hg.

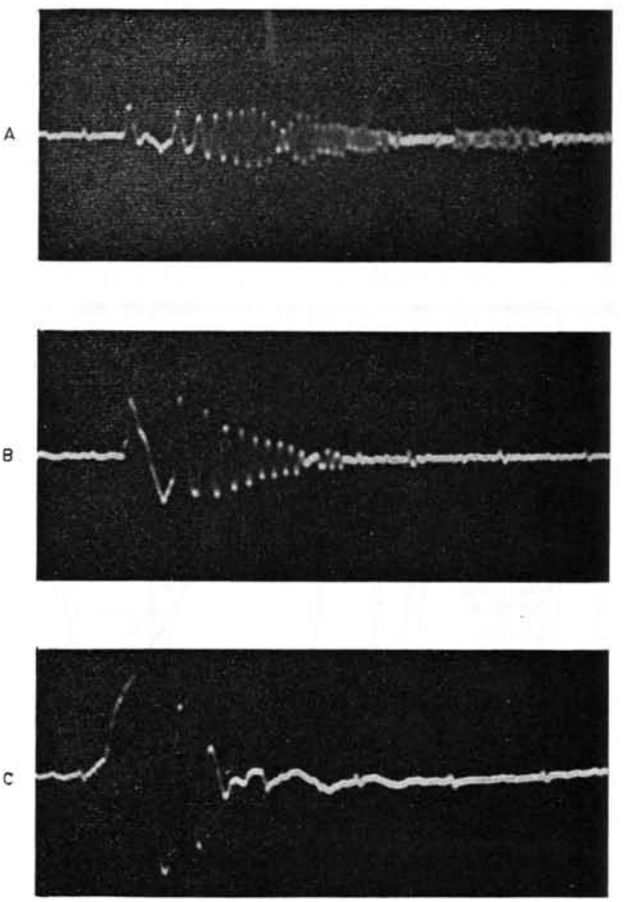

Fig. 6 Double magnetic pickup loop signals for examples of the three main types of discharge. The timing pulses are at half microsecond intervals. (A) Maximum parallel trapped flux: $p_0 \sim 50$ μ Hg, (B) Intermediate trapped flux: $p_0 \sim 60$ μ Hg, (C) Maximum reversed trapped flux: $p_0 \sim 95$ μ Hg.

less than 10 kilomaxwells of parallel flux which results in an increased compression ratio of about 10—20 just after the implosion. More rapidly damped oscillations of larger amplitude (Fig. 6B) follow the implosion and the discharge rapidly contracts and disappears, indicating an axial plasma loss. In the later stages plasma rotation is observed.

The third main type, trapping maximum reversed flux, occurs at about 95 μ Hg (Fig. 5C). The plasma always lies in a clearly defined annulus just after the implosion with a compression ratio of 3 or 4. This annulus is then observed to thicken and to expand while driving field is rising. There are a few large amplitude oscillations which are rapidly damped (Fig. 6C) and after about $\frac{1}{2}$ — 1 μs the non-luminous core has disappeared. The plasma remains contained away from the walls for a further 1 — 2 μs, after which it usually breaks up following a rapid rotation.

In the following sections the data will be analysed quantitatively and the properties of the three types of discharge will be discussed.

6. Discharges trapping maximum parallel flux

The oscillation data obtained from the double loop signal using Eq. (2) are plotted in Fig. 7 and show that the mass of plasma remains constant to within ±10 per cent for the duration of the measurement. The value of M/M_0 of 0.85 is consistent with the observation that sheath does not implode right to the tube axis due to the large trapped flux. The constancy of M/M_0 and the reversibility of the slow compression indicate a containment time of at least 4 μs. It follows that Eq. (5) may be used to determine β and the points in Fig. 7 show the experimental values of $(B/B_0)^2 (A/A_0)^{5/3}$ as a function of time. As shown in Section 3, these must lie between $(A/A_0)^{-1/3}$, the experimental variation of which is shown dotted, and 1, depending on β. It is seen that the distribution of the points is consistent with $\beta \sim 0$. The β can also be estimated from the plasma mirror ratio R_p, using Eq. (1). Direct measurements from radial photographs gave R_p approximately constant and ~ 1 corresponding to $\beta \sim 0$.

The low β and long containment time are mutually consistent on the basis of the model of plasma containment considered theoretically by ROBERTS [11] and arise because the ions are cold and thus have a low escape velocity. Containment and β are further discussed in Section 7.

This type of discharge emits neither neutrons nor soft x-rays, but large yields of hard x-rays with mean energy of several hundred keV are observed. These are interpreted as due to fast electrons produced in the early stages of the sheath formation when the conductivity is poor and the electric field is high. The trapping of a large parallel flux implies that the initial growth of ionization is slow, a conclusion supported by data from the double loop; this would give conditions favourable for the production of fast electrons. Neither of the other two types emit hard x-rays.

7. Intermediate discharges

Typical results from the oscillation data and the area analysis are shown in Fig. 8 and both indicate a rapid loss of plasma. Using Eq. (5) the area analysis gives a containment time of 2 μs which is in fairly good agreement with the values of 1.5 μs obtained from the oscillation data.

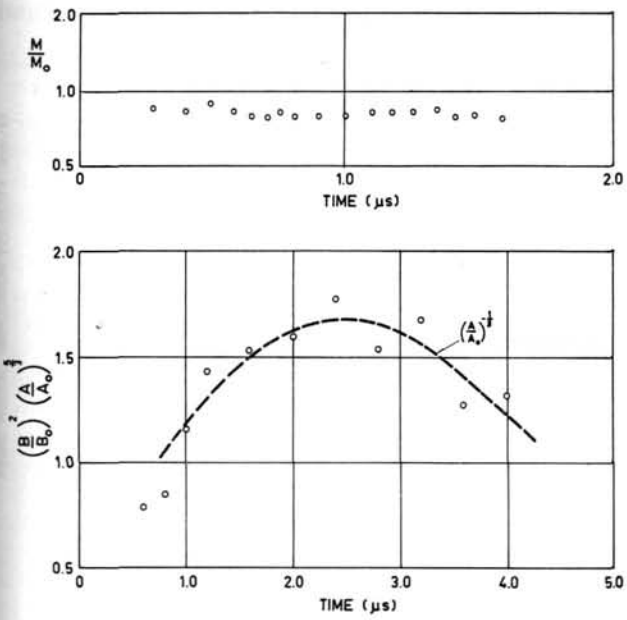

Fig. 7 The time variation of the mass (above) and results from area analyses (below) for a discharge trapping maximum parallel flux.

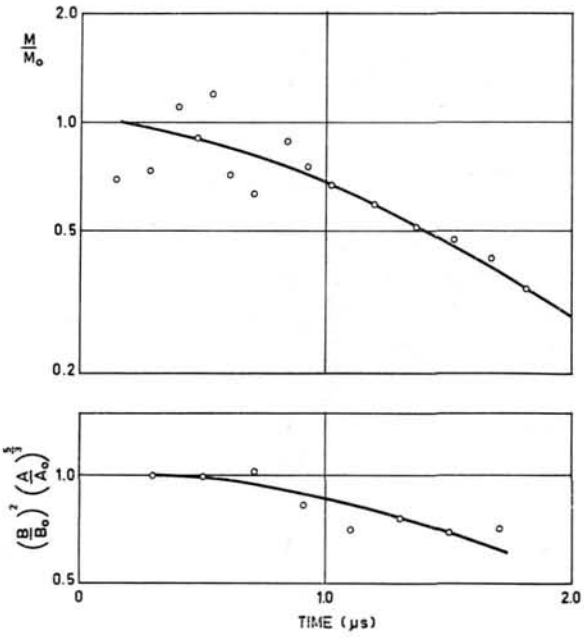

Fig. 8 The time variation of the mass (above) and line density (below) for an intermediate discharge.

The plasma β was estimated from the plasma mirror ratio, which was found to be between 1.2 and 1.7 for this class of discharge, corresponding to β between 0.5 and 0.8; this result is consistent with the observations that the plasma area and trapped flux are both much smaller than for the previous class of discharges and that the amplitude of the double loop signal is larger, indicating greater plasma diamagnetism.

The observation that as the initial pressure is raised the increase in β is accompanied by a decrease in the containment time can be shown to be in agreement with the predictions of theory [11].

The containment time τ_c can be expressed in terms of the driving field B, the mass of gas per cm ϱ and β as follows:

$$\tau_c = \frac{2l}{\bar{v}} \frac{1}{(1-\beta)^{1/2}}, \tag{6}$$

where $\bar{v}$ is the mean velocity of a maxwellian distribution,

$$\bar{v} = \left(\frac{8}{\pi} \frac{kT}{m}\right)^{1/2}.$$

Assuming the ion and electron temperature are equal, pressure balance gives

$$2nkT = \beta \frac{B^2}{8\pi}.$$

Hence
$$\tau_c = \frac{2\sqrt{2}\,\pi l \varrho^{1/2}}{B} \cdot \frac{1}{\beta^{1/2}(1-\beta)^{1/2}}, \tag{7}$$

where
$$\varrho = nm.$$

Using the correction [12] for finite pressure in the neck (see footnote to Section 2)

$$\tau_c = \frac{2\pi\sqrt{2}}{B} l \varrho^{1/2} \frac{[1-f(\gamma)\beta]^{1/2}}{\beta^{1/2}(1-\beta)^{1/2}}, \tag{8}$$

where

$$f(\gamma) = \left(\frac{2}{\gamma+1}\right)^{\gamma/(\gamma-1)}.$$

Numerically, for deuterium with $\gamma = 5/3$,

$$\tau_c = \frac{1.62\times10^{-11}}{B} l n^{1/2} \frac{(1-0.486\beta)^{1/2}}{\beta^{1/2}(1-\beta)^{1/2}} \text{ (seconds)}. \tag{9}$$

In Fig. 9, $B\tau_c/2\pi\sqrt{2}\,l\varrho^{1/2}$ is plotted against β. It is seen that if B and ϱ are constant the containment time will be long when β is small, because the ion escape velocity is low, and also when β approaches unity, because the magnetic constrictions at the end of the plasma become small. It should be noted that the variation of τ_c with β at small and intermediate values of β is the opposite to that for a classical mirror machine with no collisions. In practice β cannot be changed independently of B and ϱ, but in the present experiments the variation of B and ϱ is much less than that of β. Thus the observation of a containment time of greater than 4 μs at low β and of 1.5 — 2 μs at intermediate β is in agreement with the predicted variation. The numerical value of the containment time, calculated at $t = 1.5$ μs, when $B = 62$ kG, $n_i = 5\times10^{16}$ (determined from measurements of the compression ratio and the mass of gas) varies from 2.2 μs at $\beta = 0.6$ to 3 μs at $\beta = 0.2$, in reasonable agreement with experiment.

An upper limit of the temperature can be found using the pressure balance and the upper estimate of $\beta \sim 0.8$; the value found just after the implosion before significant plasma loss is observed to have occurred is about 50 eV for the sum of the ion and electron temperatures. This temperature can be further increased ($\propto B^{4/5}$) as the driving field rises, to a maximum of a few hundred electron-volts. Measurements of the soft x-ray intensity suggest that

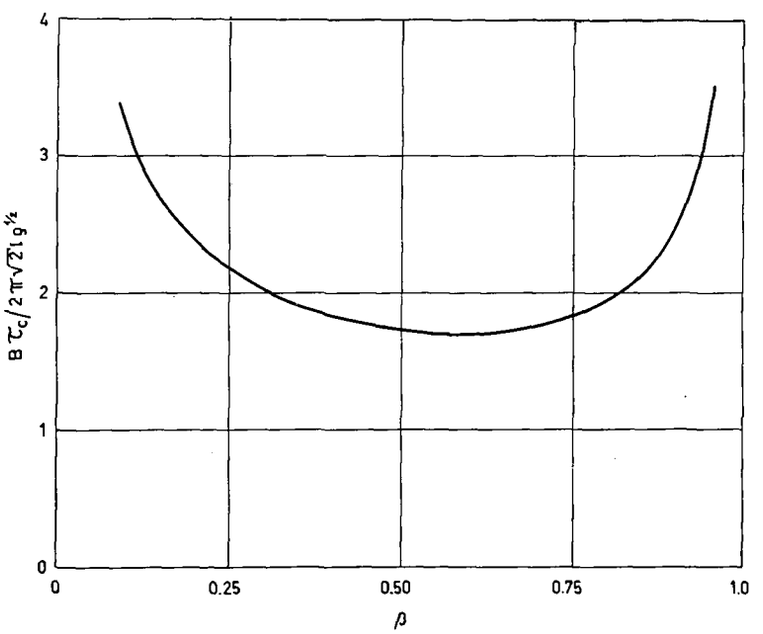

Fig. 9 The theoretical variation of the containment time with β_0. The constant is evaluated for typical conditions of $B \sim 50$ kG and $n_i \sim 10^{17}$/cc.

the electron temperature does not approach this value and, since electrons and ions will thermalise rapidly just after the implosion, the ion temperature is unlikely to be high either. It follows that, for this class of discharge, β is probably considerably less than the upper estimate of 0.8.

Since a conventional model of heating, by an implosion followed by an adiabatic compression, predicts that the temperature falls with increasing pressure, it is necessary to propose a further heating mechanism to account for the greater temperatures observed at higher pressures in discharges trapping reversed field.

8. Discharges trapping maximum reversed flux

8.1. The radial implosion

For discharges trapping maximum reversed flux breakdown occurs very close to t_1 (see Fig. 1) and until the driving field passes through zero the net force on the plasma sheath is outwards. The sheath will implode when the driving field equals the trapped field B_t at time $t_w = (B_t/\dot{B}) \times 10^{-7}$ s; wall hang-up for times of this order is observed on photographs (Fig. 5C). The final radial implosion velocity, measured from streak photographs, is shown as a function of pressure in Fig. 10. It is seen that the maximum velocity increases with pressure, which is at variance with the predictions of simple theory ($v \propto p_0^{-1/4}$). This may be due to wall hang-up which increases the average value of the external magnetic pressure, or to the diffusion of the magnetic field during the implosion, which would tend to reduce the rate of increase of the internal magnetic pressure as the sheath moves inwards. Preliminary measurements of the trapped reversed flux before and after the radial implosion suggest that flux is destroyed during the implosion*, as well as after it (see below). More detailed measurements on these effects and numerical computations of the reversed field implosion are under way; theoretically diffusion can lead to higher velocities.

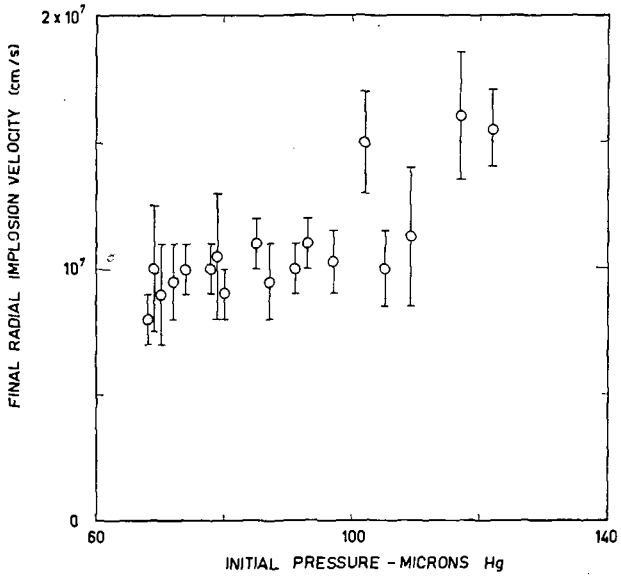

Fig. 10 The final radial implosion velocity as a function of initial pressure.

8.2. The compression phase

Results from the analysis of the plasma area and the oscillations are plotted in Fig. 11 and show a rapid increase in mass and line density; it is seen that N increases by a factor of 10 in 0.5 μs while mass increases by a factor of 7 in 0.5 μs. These observations are interpreted as a consequence of a rapid axial contraction of the plasma resulting from the formation of closed field loops round it (Fig. 3b). The velocity of contraction, measured by streak photography, is of the same order as the radial velocity and varies with pressure in a similar way. Axial contraction is discussed in detail in the accompanying paper [22].

At about peak axial compression (typically 0.5 μs after the end of the radial implosion) the double loop signal is suddenly damped and the non-luminous core is observed to vanish. Fig. 12 shows a plot of the trapped flux against time, with, for comparison, the results for a discharge trapping maximum parallel

* Reynolds and Phillips [17] have recently shown that field diffusion during the implosion is important.

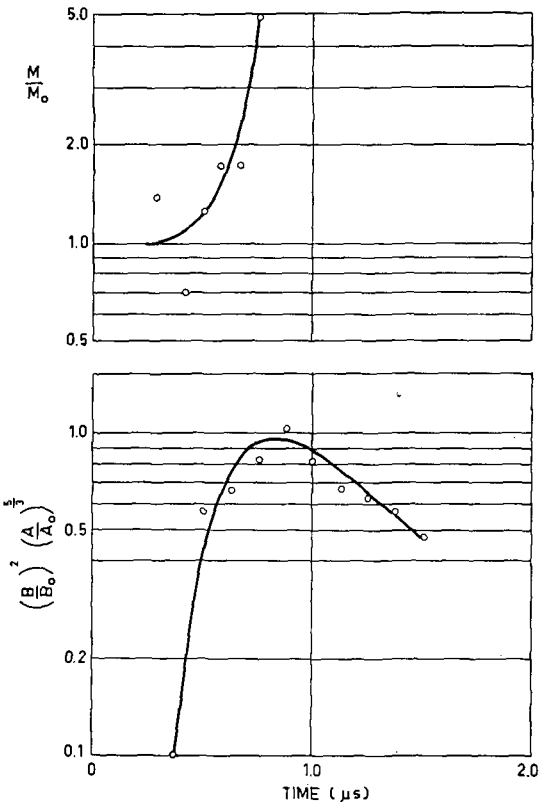

Fig. 11 The time variation of mass (above) and line density (below) for a discharge trapping maximum reversed flux.

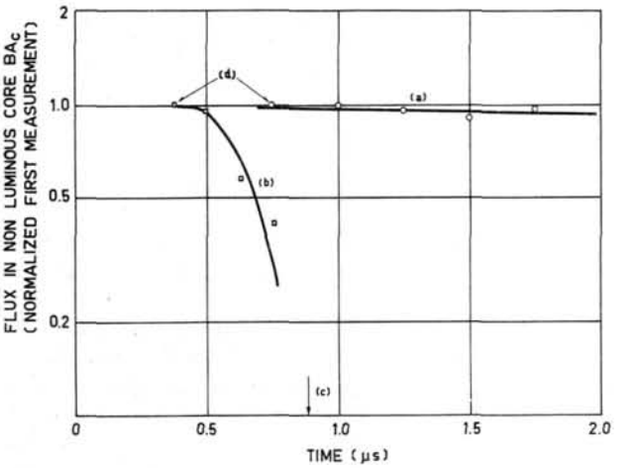

Fig. 12 The conservation of flux in the non-luminous core for discharges trapping maximum parallel and maximum reversed flux. Curve (a) — parallel field; curve (b) — reversed field. The core vanished at $t = 0.875$ μs, indicated by lower arrow at (c). The points labelled (d) indicate first measurement.

flux. Flux is approximately conserved in the core for the parallel field case whilst for the reversed field case flux disappears. Thus the field in the core is destroyed, which confirms early work [7] using magnetic probes and also establishes that field disappearance occurs in the absence of a probe. At the observed electron temperatures (see Section 8.4, below) ordinary resistive diffusion cannot account for these observations, but there may be accelerated diffusion due to collective phenomena in the sheath. It can be shown that such processes can lead to resistivities, several orders of magnitude greater than the Spitzer value, which can account for the disappearance of the field in a few tenths of a microsecond. An alternative interpretation is that the disappearance is due to instabilities in the closed loop field configuration, which is similar to that of the unstabilised toroidal z-pinch, and is subject to the same instabilities. In this case the instabilities will begin at the ends where the curvature of the field lines is greatest, but will rapidly spread over the whole surface as the plasma compresses axially; the growth times of such instabilities is about 10^{-7} second, which is of the right order to account for the observations. There is evidence for structure and flutes in the plasma annulus during the axial contraction consistent with $m = 0$ instabilities, although the whole remains contained away from the walls by the external magnetic field.

In the present experiments a rapid disappearance of reversed field was only found when axial contraction was known to occur. In some associated experiments at low energy where axial contraction was not observed the reversed field did not vanish suddenly; in cases with no axial contraction the fields will presumably mix slowly by ordinary resistive diffusion, heating the electrons. It is suggested that when the reversed field energy vanishes rapidly as a result of axial contraction, preferential ion heating takes place.

8.3. Plasma rotation

Following the axial contraction and the disappearance of the reversed field, plasma rotation [18] is observed on streak photographs. The initial angular velocity of from 3—6×10^7 radians per second is too high to be resolved on the framing camera, which first shows rotation some 0.6 μs later. Fig. 13 shows

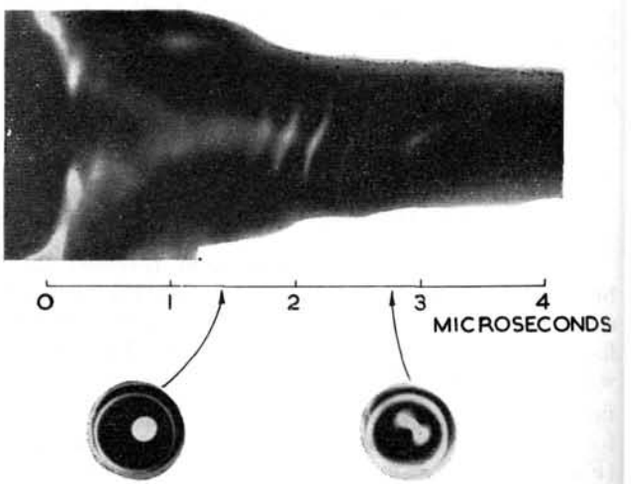

Fig. 13 Streak and framing camera photographs of plasma rotation in the thetatron.

streak photographs of the rotation, together with two framing camera exposures, for a discharge trapping maximum reversed field. Fig. 14 shows two complete sets of framing camera photographs of a rotating plasma; the large amplitude of the flutes in Fig. 14A rules out the possibility of plasma waves as an interpretation, a conclusion supported by the apparent fission in both examples. When the rotation is resolved by the framing camera, two flutes are usually seen and the growth rate of these was shown [19] to be of the order to be expected for a Rayleigh-Taylor instability where the rotation provides the radial acceleration. Although this section is principally concerned with rotation in discharges trapping large reversed flux, where it is most prominent, the plasma is observed to rotate in many conditions and for the trapped flux (measured at the end of the radial implosion) both parallel and reversed. The direction of the rotation is always that of a positive ion in the driving field. In general the onset of rotation appears at about the same time as light from the walls, which is produced by plasma which escapes from the ends and hits the walls; rotation is not observed when β is known to be small and the well contained low-β discharge described in Section 6 is never found to rotate. The angular velocity is observed to decrease rapidly with time, as shown in Fig. 15, and falls to about 5×10^6 radians/s in 1 μs. In ther later stages the plasma usually breaks up into two parts (Fig. 14). In some cases these are initially joined together by a thin filament and rotate about one another (Fig. 14B); ultimately they appear

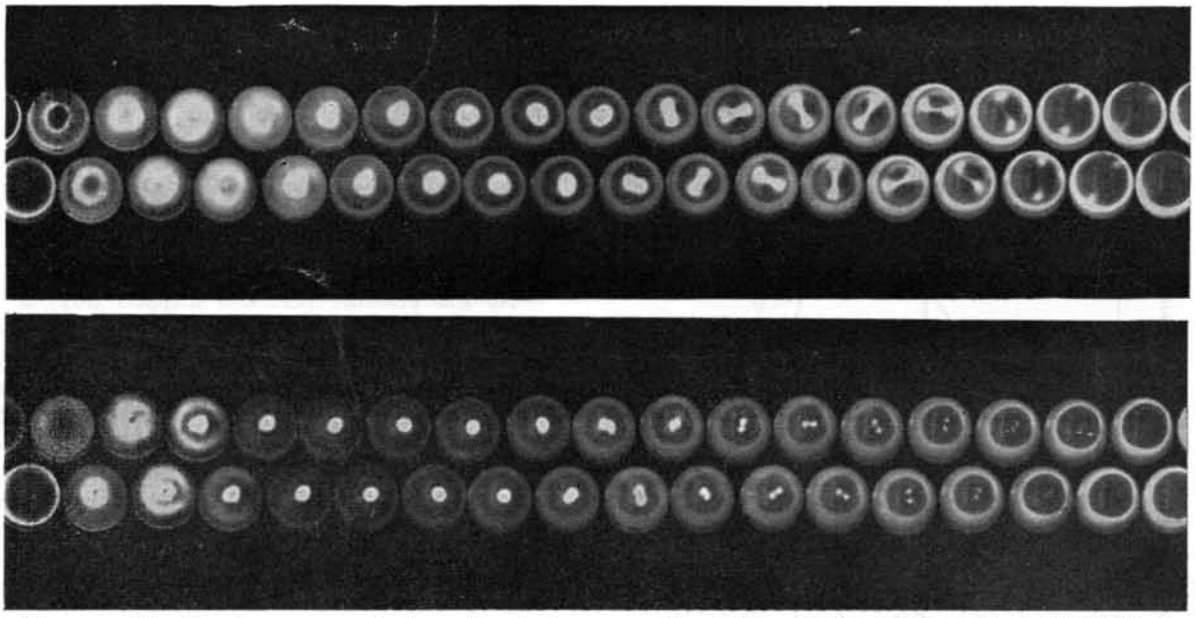

Fig. 14 Two complete framing camera photographs of plasma rotation taken axially at 8 frames/μs. (A) illustrates a case where the plasma shape is seriously perturbed by large amplitude flutes. (B) illustrates plasma fission in a case where this occurs when the amplitude of the flutes is smaller and the two parts remain near the axis of the tube for several frames. In both cases the two parts are initially joined by a thin filament and rotate about one another before complete fission occurs. [In both of the above, 4.9 cm on the printed figures corresponds to 1 μs with zero time at left edge of each figure.]

to fission completely and fly outwards towards the walls.

It has been suggested [20] that the rotation is the direct result of the shorting out of the radial electric field $\mathbf{E}_r$ in the sheath when plasma escapes and makes contact with the walls. When this field is removed there is no radial force to contain the ions, which will then start to rotate with a velocity $\mathbf{v}_i$; the ions are then contained by $\mathbf{v}_i \times \mathbf{B}_z$ instead of by $\mathbf{E}_r$. This mechanism involves the flow of an effective radial current, and predicts the correct direction of rotation, which is independent of the sign of the trapped flux. Initially only a thin skin of ions will rotate and it can be shown [21] that initially the angular velocity is given by

$$W_{\max} = \frac{1}{2}\left[\frac{B^2}{2M}\right]^{1/2}, \tag{10}$$

where M is the mass/cm of the plasma. For a typical case at $p_0 \sim 90\ \mu$ this equation gives $W_{\max} = 4.8 \times 10^7$ radians/s, in agreement with the observed values of from $3 - 6 \times 10^7$ radians/s. The rotating skin of ions will rapidly thicken by dissipative processes and when the whole plasma is rotating the velocity is given by

$$W = \beta \frac{cB}{8eN},$$

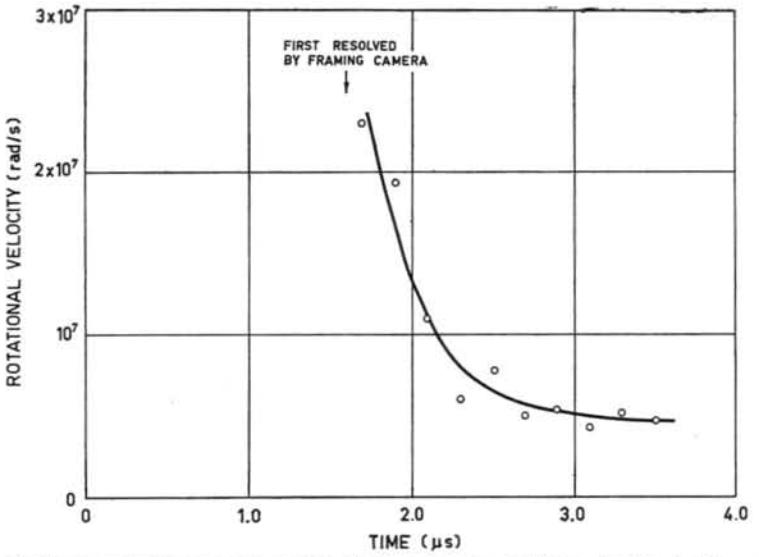

Fig. 15 The frequency of plasma rotation as a function of time (measured from the beginning of the second half-cycle).

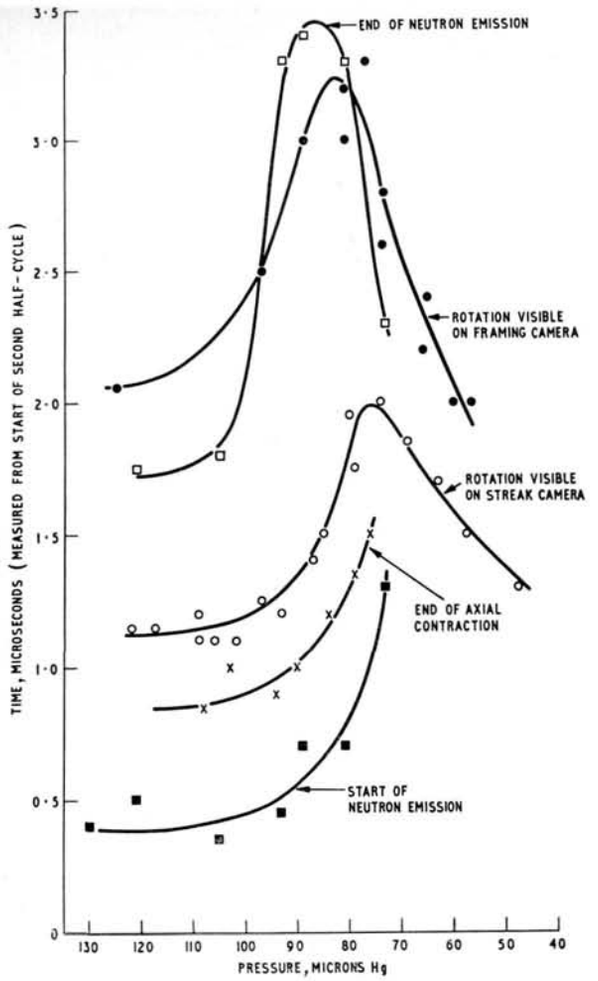

Fig. 16 The time correlation between the axial concentration, the rotation and the neutron emission at different pressures.

where c is the velocity of light and e the electronic charge. At peak field and for $\beta=1$ this gives $W\sim10^7$ s^{-1}, compared with the observed value of about 5×10^6 radians/s.

In this model the onset of rotation and the associated instability can be delayed if the plasma containment time can be lengthened, for example, by increasing the length of the coil or inhibiting the axial contraction which rapidly breaks up the closed field loop configuration.

As the pressure (i.e. the trapped flux) is varied the time of onset of the rotation, the end of the axial contraction, and the beginning and end of the neutron emission all vary in a similar way. This is illustrated in Fig. 16, which shows that at $p_0\sim90$ μ Hg (peak reversed trapped flux) the onset of the rotation is delayed and the neutron pulse is longest. At pressures above 90 μ the start of the neutron emission, the finish of the axial contraction and the onset of rotation follow one another at intervals about 0.5 and 0.3 μs respectively.

8.4. Radiation from reversed field discharges

8.4.1. *Neutron emission*

Neutrons are observed only when the trapped field is reversed. The yield is strongly dependent on the initial pressure and increases from less than 10^3 at an initial pressure of about 65 μ Hg to 7×10^5 at a pressure of 95 μ Hg. Fig. 17 shows the yield and total energy as functions of pressure. The total energy measured just after the radial implosion is the sum of the magnetic energy in the non-luminous core and the particle and magnetic energy in the annulus. About half the energy lies in the core at this stage and, since there is a surface of $\beta=1$ in the plasma, the contribution from the annulus has

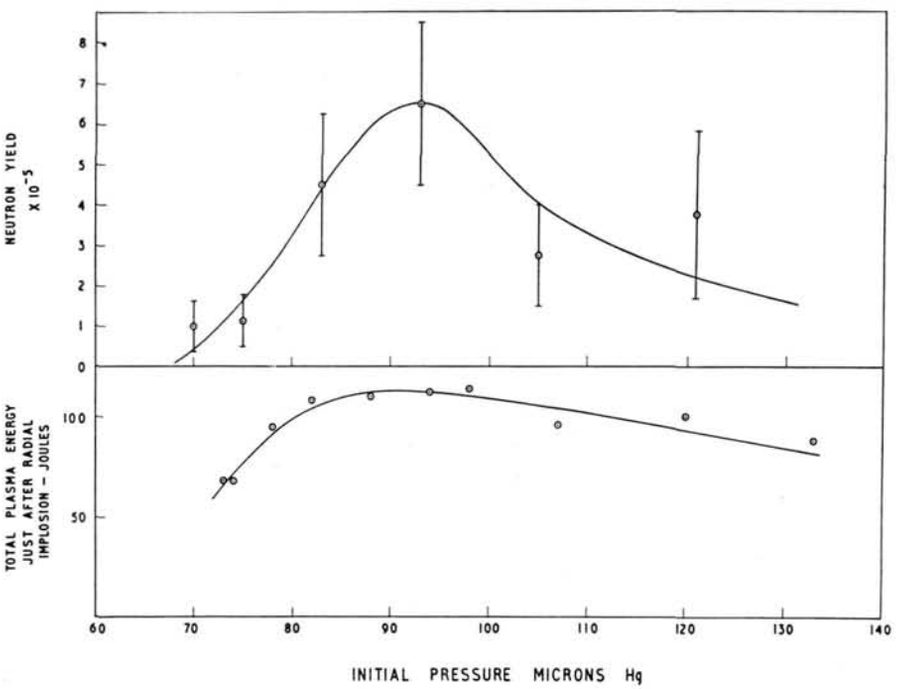

Fig. 17 The neutron yield and total plasma energy just after radial implosion as functions of initial pressure.

been calculated from the data assuming an average β of $^1/_2$. If the $\beta=1$ throughout the annulus the total energy would be increased by 10—15 per cent. The pressure variation of the total energy is similar to that of the trapped flux and both peak at a pressure of 95 μ Hg, as does the neutron yield.

At lower pressures when the yield and total energy are small the neutrons are emitted at about the time of peak field and continue for ~ 0.5 μs. For pressures of 95 μ Hg and greater the emission starts about 0.1 μs after the radial implosion while the plasma is in a grossly stable annulus during the axial contraction, that is before the breakup of the closed field loop configuration has occurred. The pulse at the maximum yield rises and falls slowly and lasts for 2—3 μs, extending over peak driving field; at higher pressures when the yield has fallen but the total energy is still high the emission begins at the same time but only lasts 1 μs. The time correlation between the neutron emission, the axial contraction and the rotation are shown in Fig. 16.

These results suggest that in the present experiments (i) reversed field is necessary for neutron production, (ii) the emission is strongly dependent on the magnitude of the trapped flux and a large value of the total energy is necessary to produce a large yield, (iii) ions can gain energy before the closed field loop configuration is destroyed. The total energy just after the radial implosion which was shown in Fig. 16 will be further increased, as the driving field rises, by B^x where x lies between 4/5 and 1 depending on β. For an initial pressure of 95 μ Hg and at peak driving field there is sufficient energy available to give all the particles initially in the tube an energy of the order of 500 eV, i.e. the sum of the ion and electron temperature could reach 1 keV.

8.4.2. *Soft x-ray emission and electron temperature*

Measurements of the shape of the electromagnetic energy spectrum in the wavelength range < 20 Å provide a means of estimating the electron temperature. As in the experiments of Jahoda, et al. [23], the known absorption cross-sections for photons in this wavelength region have been used to compute the total radiation transmitted through thin foils of Al, C, Ni, assuming the emission spectrum from the plasma to be bremsstrahlung at several temperatures up to 1 keV. The experimental results under conditions of maximum trapped reversed field show a good agreement with the theoretical curves, but predict mean temperatures varying between 180 and 400 eV, the carbon measurement providing the upper value and the aluminium measurement the lower. This wide variation for different absorbers has not yet been adequately explained. The intensity of the x-ray emission is sharply dependent on the electron temperature, electron density, and free-bound continuum from stripped impurities. The latter has been estimated, by observing the effect of adding small known amounts of impurity to the gas, to be of the order of 1 per cent oxygen. Since electron temperature is determined from the shape of the spectral intensity rather than its absolute value, the determination is independent of electron density. Also the free-free and free-bound radiation continua have similar shapes at low wavelengths so neglect of the contribution from impurity radiation will not be serious.

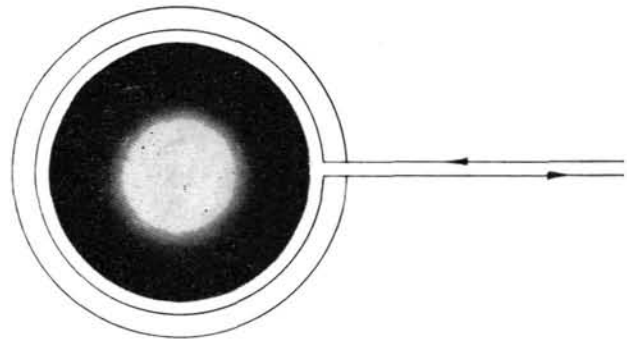

Fig. 18 Axial pin-hole photograph of x-ray emission. Film screened by 135 mg/cm² Al; initial deuterium pressure = 100 μ Hg. Outer edge of film corresponds to internal diameter of the discharge tube = 4.6 cm at the medium plane of the driving coil and the outer rings show the relative dimensions of the coil.

Pin-hole camera x-ray photographs of the discharge, such as that shown in Fig. 18, demonstrate that the plasma is the origin of the x-ray emission. The x-ray emission and driving field are shown in Fig. 19 and at the time of peak intensity there is reasonable agreement between framing and a streak photographs of the plasma in the visible region and the x-ray pin-hole photographs. The latter pictures being time-integrated over a number of discharges predict a lower limit to the compression. With the thinnest

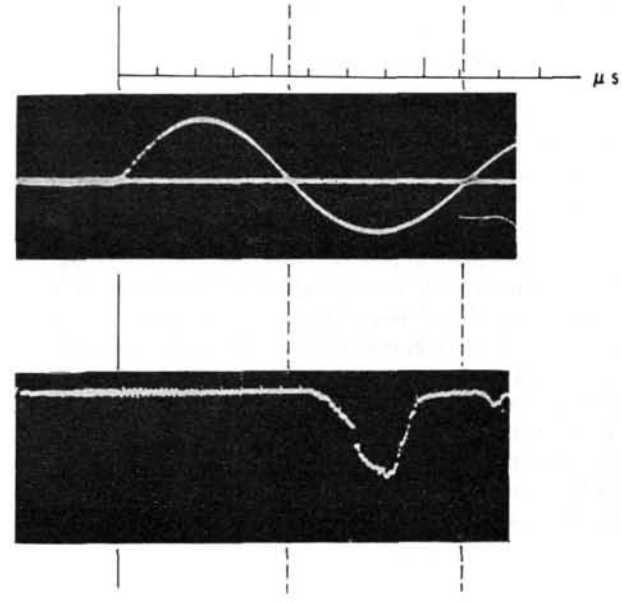

Fig. 19 Waveforms of the driving field and x-ray emission. The lower oscillogram showing the x-ray emission was recorded using a plastic scintillator screened by 1.7 mg/cm² Melinex plus 0.8 mg/cm² carbon. Initial deuterium pressure = 100 μ Hg.

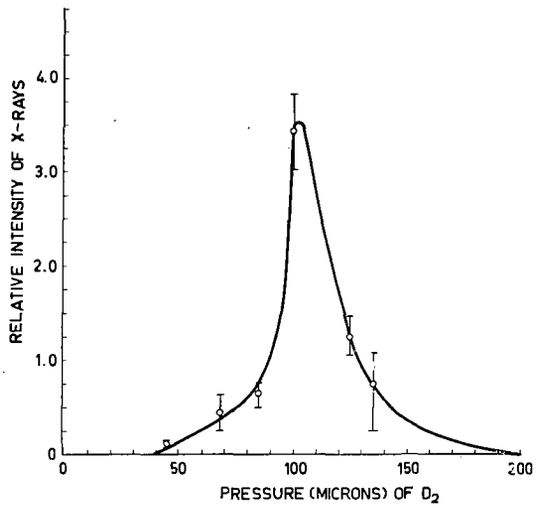

Fig. 20 Variation of x-ray intensity with initial gas pressure.

absorber used, polythene 575 $\mu g/cm^2$ sputtered by 60 $\mu g/cm^2$ Al, a double ring round the central blackened exposed area is observed due to plasma striking the walls of the tube 4 cm outside the ends of thetatron coil.

The variation in the intensity of the x-ray emission with initial gas pressure is shown in Fig. 20. The shape of the curve is the same as for the neutron yield. Peak intensity and maximum duration of the emission occurred at the pressure at which the trapped reversed flux is a maximum.

9. Conclusion

The properties of the plasma are largely determined by the trapped flux and discharges of three main types trapping maximum parallel flux, relatively little flux and maximum reversed flux can all be produced in the range of 50 to 95 μ Hg by carefully controlling the initial pressure. The type trapping maximum parallel field has β less than 0.05, temperatures a few eV and is well contained. The intermediate type has β between 0.2 and 0.8, probably nearer the lower value, and escapes rapidly. The maximum reversed field discharge has electron temperatures of a few hundred eV and energy considerations show that the ion temperature could approach 1 keV. Rapid radial and axial contractions occur and the neutron and soft x-ray intensities both peak at the same pressure as the total plasma energy. An unstable closed field loop configuration is formed, but the plasma is contained away from the walls for 2—3 μs by the external field, after which it breaks up following a rapid rotation.

Acknowledgements

The authors wish to thank A. Skinner and R. J. Abrey for supplying the high speed cameras, N. J. Phillips and J. B. Taylor for many fruitful discussions, and A. A. Newton, who played a major part in carrying out many of the experiments and assisted in the preparation of material for this paper.

References

[1] Boyer, K., Elmore, W. C., Little, E. M., Quinn, W. E., Tuck, J. L., *Phys. Rev.* **119** (1960) 831.
[2] Kolb, A. C., Griem, H. R., Faust, W. R., Proc. Fourth International Conference on Ionization Phenomena in Gases, Uppsala (North-Holland Pub. Co., Amsterdam) **2** (1959) 1037.
[3] Bodin, H. A. B., Green, T. S., Niblett, G. B. F., Peacock, N. J., Proc. Fourth International Conference on Ionization Phenomena in Gases, Uppsala (North-Holland Pub. Co., Amsterdam) **2** (1959) 1061.
[4] Fay, H., Hintz, E., Jordan, H. L., Proc. Fourth International Conference on Ionization Phenomena in Gases, Uppsala (North-Holland Pub. Co., Amsterdam) **2** (1959) 1046.
[5] Kvartskhava, I. F., Karvalidze, K. N., Gvaladze, Yu. S., *Soviet Physics—J.E.T.P.* **11** (1960) 1182.
[6] Nagle, D. E., Quinn, W. E., Ribe, F. L., Riesenfeld, W. B., *Phys. Rev.* **119** (1960) 857.
[7] Griem, H. R., Kolb, A. C., Faust, W. R., *Phys. Rev. Letters* **2** (1958) 281.
[8] Green, T. S., *Phys. Rev. Letters* **5** (1960) 297.
[9] Little, E. M., Quinn, W. E., Ribe, F. L., *Physics of Fluids* **4** (1961) 711.
[10] Kolb, A. C., Dobbie, C. B., Griem, H. R., *Phys. Rev. Letters* **3** (1959) 5.
[11] Roberts, K. V., J. Nuclear Energy **C 1** (1960) 243.
[12] Taylor, J. B., Private communication.
[13] Niblett, G. B. F., Green, T. S., *Proc. Phys. Soc.* **74** (1959) 737.
[14] Kolb, A. C., *Rev. Modern Physics* **32** (1960) 748.
[15] Bodin, H. A. B., Green, T. S., Niblett, G. B. F., Peacock, N. J., Proc. Fourth International Conference on Ionization Phenomena in Gases, Uppsala **2** (1959) 1065.
[16] Treat, R. P., Plasmadyne Corporation Report No. TN-031-655 (15th March, 1961).
[17] Reynolds, J. A. and Phillips, N. J., Proc. Fifth International Conference on Ionization Phenomena in Gases, Munich (Aug. 1961). To be published.
[18] Rostoker, N., Kolb, A. C., *Bull. Am. Phys. Soc. Ser. II* **6** (1961) 203.
[19] Bodin, H. A. B., Newton, A. A., Peacock, N. J., *Nuclear Fusion* **1** (1961) 139.
[20] Roberts, K. V., Private communication.
[21] Taylor, J. B., Private communication.
[22] Bodin, H. A. B., Green, T. S., Niblett, G. B. F., Peacock, N. J., Quinn, J. M. P., Reynolds, J. A., Taylor, J. B., Proceedings of this Conference, page 511.
[23] Jahoda, F. C., Little, E. M., Quinn, W. E., Sawyer, G. A., Stratton, T. F., *Phys. Rev.* **119** (1960) 843.

НЕКОТОРЫЕ НОВЫЕ ДАННЫЕ О САМОСЖАТЫХ РАЗРЯДАХ*

И. Ф. КВАРЦХАВА, К. Н. КЕРВАЛИДЗЕ, Ю. С. ГВАЛАДЗЕ, Б. Н. КАПАНАДЗЕ
ФИЗИКО-ТЕХНИЧЕСКИЙ ИНСТИТУТ АКАДЕМИИ НАУК ГРУЗИНСКОЙ ССР
СУХУМИ, СОЮЗ СОВЕТСКИХ СОЦИАЛИСТИЧЕСКИХ РЕСПУБЛИК

Предсказывая возможность возникновения различного вида нестабильностей, теория самосжатых разрядов не отражает со всей полнотой того многообразия явлений, которое наблюдается на опыте. Используемые теорией модели, по-видимому, не учитывают наличия каких-то процессов в самосжатых разрядах, существенно определяющих реальное поведение плазмы. Проведенные нами опыты выявили ряд таких процессов. Они, в основном, заключаются в неравномерном разгорании разряда у стенок камеры. При этом разрядные токи протекают по нитевидным каналам, которые в θ — пинчах ориентируются преимущественно либо в направлении z, либо направлении θ, а z — пинчах имеют в основном ориентации по z. В процессе сжатия плазмы указанные нитевидные образования получают неодинаковые ускорения. Обладая высокой проводимостью, они способствуют захвату магнитного поля, что затрудняет термализацию кинетической энергии радиального движения плазмы. В результате этого, в стадии максимального сжатия плазма далека от состояния теплового равновесия. Она охвачена движением турбулентного характера.

После максимального сжатия плазмы с поверхности пинча выбрасываются различного вида плазменные образования. Захват магнитного поля в θ — пинчах осуществляется более эффективно, чем в z — пинчах. Вследствие этого, в θ — пинчах наблюдаются более разнообразные виды нестабильностей, чем в z — пинчах.

Метод фотографирования разряда с помощью скоростных камер оказался наиболее удобным и плодотворным для изучения процессов образования и последующего движения плазмы. Рассматриваются фотографии разряда, полученные в режимах непрерывной фоторегистрации и «лупы времени». Приводятся также результаты зондовых измерений магнитных полей и измерений токов с помощью поясов Роговского, дополняющие данные фотоснимков.

1. Введение

В термоядерных исследованиях, как известно, широкое применение находят два основных вида сильноточных самосжатых разрядов, называемых условно θ- и Z-пинчами.

В θ-пинче разряд зажигается под действием вихревого электрического поля в быстро нарастающем во времени аксиально-симметричном магнитном поле. Сжатие плазмы к оси симметрии осуществляется силами отталкивания антипараллельных токов, текущих в газе и в создающем магнитное поле соленоиде. В Z-пинче плазма сжимается силами взаимного притяжения параллельных разрядных токов.

В ранней стадии работ по термоядерным исследованиям предполагалось, что удачное сочетание в самосжатых разрядах интенсивного омического нагрева с быстрым электродинамическим сжатием плазмы позволит, хотя-бы кратковременно, осуществить нагрев достаточно плотной дейтериевой плазмы до термоядерных температур. Как известно, несмотря на использование очень больших мощностей, все попытки такого рода окончились неудачей.

В первых же опытах с Z-пинчем в дейтерии наблюдалось нейтронное излучение. Однако, вскоре было выяснено, что плазма недостаточно нагрета, а нейтронов значительно больше, чем следовало бы ожидать по достигнутым температурам [1—8]. Аналогичная ситуация повторилась и в более поздних опытах, в которых для нагрева и удержания плазмы использовались некоторые модификации θ-пинча [9—16]. Это указывало на существование в самосжатых разрядах другого, нетермоядерного, механизма образования нейтронов. Дальнейшими опытами было установлено, что основной причиной этих неудач является наличие нестабильностей плазмы, нарушающих магнитную термоизоляцию и тем самым ограничивающих достижение высоких температур. С ними же связана возможность возникновения локальных электрических полей, ускоряющих дейтоны и, тем самым, возбуждающих значительную (D, D) реакцию в газе, или на стенках разрядной камеры. Выяснилось также, что с повышением температуры омический нагрев плазмы становится мало эффективным, так как при этом сильно возрастает длина свободного пробега электронов и ослабевает тепловой контакт между электронным газом, получающим основную часть энергии от источника, и ионным газом.

Все это породило серьезные сомнения относительно возможности использования самосжатых разрядов для термоядерных целей. На II Международной конференции по мирному использованию атомной энергии даже было высказано предположение о нецелесообразности продолжения работ в этом направлении.

Тем не менее, самосжатые разряды и до настоящего времени остаются предметом многих иссле-

* Доклад СИ-10/232, представленный на Конференцию. Докладчик: И. Ф. Кварцхава. Дискуссия (на английском языке) по этому докладу дана на стр. 646. Переводы аннотаций находятся в конце этого тома Трудов Конференции.

дований. Это связано с тем, что в таких разрядах наблюдаются тонкие магнито-гидродинамические эффекты, а также большое многообразие нестабильностей плазмы, изучение которых, без сомнения, окажется полезным для решения трудной термоядерной проблемы. Кроме того не исключена возможность, что изучение свойств и природы нестабильностей помогут найти пути борьбы с ними. Этим исследованиям посвящено много работ, как теоретических [17—23], так и экспериментальных. Теория, основанная на идеализированных моделях самосжатых разрядов, предсказывает возможность возникновения различных видов нестабильностей, среди которых наиболее опасными считаются нестабильности типа $m=0$ (пережатия), $m=1$ (извивание пинча вокруг оси) и желобковые нестабильности, связанные с эффектом Релея-Тейлора [24, 25].

На опыте, однако, картина поведения плазмы оказывается более сложной, а нестабильности более интенсивными, чем предсказывается теорией. Это указывает на то, что используемые модели сжатой плазмы не учитывают наличия каких-то процессов, существенно определяющих ее действительное поведение. В опубликованных за последнее время работах было показано, что в отношении выявления таких процессов, а также вызываемых ими видов нестабильностей, наиболее продуктивным и удобным оказался метод фотографирования разряда. Из последующего будет видно, что на соответствующих фотографиях отчетливо выступают характерные магнитогидродинамические эффекты, а также различные виды нестабильностей, среди которых имеются и такие, которые, по-видимому, теорией еще не предсказаны. В конце доклада будут также рассмотрены некоторые предварительные данные, полученные осциллографированием сигналов магнитных зондов и поясов Роговского.

2. Результаты опытов

Принципиальные схемы экспериментальных установок по исследованию самосжатых разрядов хорошо известны, поэтому они здесь не рассматриваются. Необходимые условия опытов будут даны в тексте или в соответствующих таблицах. Отметим лишь некоторые общие данные, относящиеся к этим экспериментам.

Опыты с самосжатыми разрядами обычно проводятся в камерах из изолирующих материалов (кварц, алунд, фарфор, стекло). Чаще всего используются цилиндрические камеры круглого сечения. В отдельных опытах применялись камеры с гранеными стенками. Основной интерес представляет исследование разряда в легких газах (водород, дейтерий, гелий). Некоторые полезные сведения были получены и в опытах с более тяжелыми газами (азот, аргон, криптон). Большинство опытов проводятся при давлениях в пределах 10^{-1} -10^{-3} мм рт. ст.

Для питания разряда обычно используются батареи высоковольтных (несколько десятков кв) конденсаторов с общим запасом энергии до нескольких сот килоджоулей. Конденсаторы соединяются специальной ошиновкой для уменьшения индуктивности системы. Важной характеристикой опытов с самосжатыми разрядами является скорость нарастания тока. В некоторых опытах она была доведена до величины $\sim 10^{12}$ А/сек и выше. Достигнутые скорости сжатия плазмы не превышают нескольких единиц 10^7 см/сек.

Удовлетворительные фотографии разряда удалось получить с помощью скоростной камеры СФР-2М, с вращающимся зеркалом, которая работает или в режиме непрерывной фоторегистрации через узкую щель, со скоростью развертки до нескольких миллиметров в микросекунду, или в режиме «лупы времени», с числом кадров в секунду до $2 \cdot 10^6$ и с экспозицией кадра $\sim 0{,}5$ мксек. В условиях θ-пинча отсутствие торцовых электродов облегчает фотографирование и позволяет получить более полные данные о поведении плазмы в различных стадиях разряда. В случае z-пинча, для получения аналогичных снимков, использовались кольцевые электроды, прилегающие к стенкам камеры.

Рассмотрим несколько групп характерных фотографий разряда.

2.1. Щелевые фотографии

На рис. 1 приведены щелевые фотографии самосжатых разрядов. Снимок (а) относится к z-пинчу с плоскими электродами, остальные — к θ-пинчу. Снимки (а), (в), (г), (д) и (е) получены при фотографировании в аксиальном направлении и ориентации щели вдоль диаметра камеры. Снимок (б) получен при фотографировании в радиальном направлении и ориентации щели на середину пинча, перпендикулярно оси камеры. При этом разряд зажигался двумя параллельными витками, отстоящими друг от друга на расстоянии радиуса камеры. Во всех других случаях для зажигания θ-пинча применялся цилиндрический одиночный виток. В случае снимка (а) в электроде z-пинча просверлены отверстия, расположенные вдоль диаметра, на который наведена щель фотокамеры. Через эти отверстия производилось фотографирование разряда.

На этих снимках можно видеть некоторые интересные особенности самосжатых разрядов. Аксиальный снимок (а) показывает, что в z-пинче, в момент максимального сжатия плазмы, на стенках камеры вторично зажигается разряд. Зажигание происходит в результате испарения тонкого слоя вещества стенок, получившего «тепловой удар» при поглощении обильного излучения плазмы, а также в результате перенапряжения, которое в этот момент обычно возникает на разрядном промежутке. Во второй половине полупериода вся плазма собирается в общий пинч, диаметр которого стал значительно больше. Это объясняется тем,

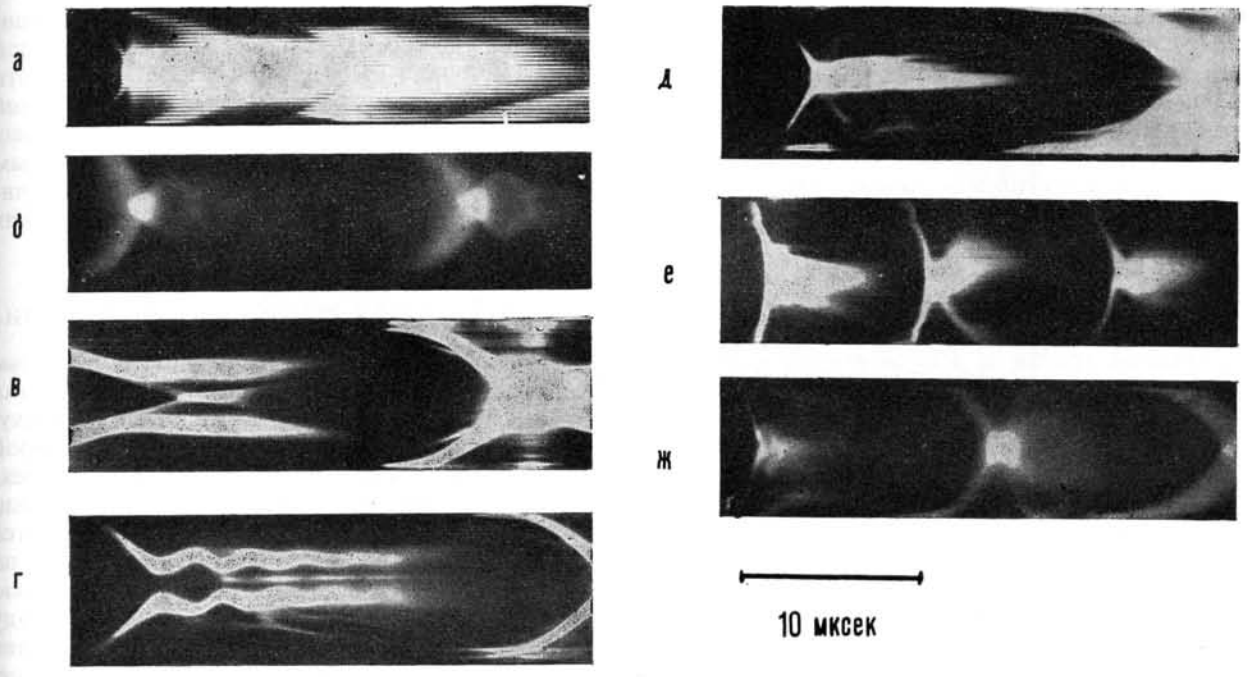

Рис. 1 см. таблицу I.

ТАБЛИЦА I. Таблица к рис. 1

Снимки	Диаметр камеры в см	Длина камеры в см	Длина витка магнитного поля в см	Давление газа в мм рт.ст.	Напряжение на конденсаторах в кв	Емкость батарей конденсаторов в мкф
а	20	20	—	воздух, 10^{-1}	30	60
б	12	30	15	воздух, 10^{-1}	40	13
в	27	90	40	водород, $5\cdot10^{-1}$	30	180
г	27	90	40	водород, 10^{-1}	30	180
д	27	90	40	водород, $4\cdot10^{-2}$	30	90
е	10	100	40	водород, $7\cdot10^{-2}$	40	90
ж	10	100	40	водород, $5\cdot10^{-1}$	40	90

Снимок (а) относится к z - пинчу ($I_{max}=450$ кА), остальные — θ - пинчу.

что в этой части полупериода давление магнитного поля уменьшается, в то время как кинетическое давление возрастает из-за притока вещества со стенок. В последующих полупериодах ток затухает и, как показывает снимок, магнитное поле вообще не может оторвать от стенок плазму, заполнившую к этому времени всю камеру. По плазме начинают распространяться радиальные ударные волны, возбуждаемые омическим нагревом наружного скин-слоя в каждом полупериоде тока. Фронт ударных волн является достаточно гладким, что, по-видимому, указывает на отсутствие крупномасштабных турбулентных движений в плазме. Это означает, что если такие движения и возникают в процессе первого сжатия и расширения плазмы, то они полностью затухают в течение первого полупериода разряда. «Тепловой удар», вызванный поглощением излучения, можно наблюдать и в θ-пинчах, при условии, если мощность разряда достаточно велика и отсутствует «захваченное» магнитное поле, препятствующее быстрому сжатию плазмы.

На радиальном снимке (б) θ-пинча можно видеть зарождение отраженной ударной волны в момент схлопывания плазмы на оси, а также последующее расширение ее фронта к поверхности пинча. Возникновение ударных волн в самосжатом разряде теоретически рассматривалось в работе [26]. Хотя ее автор ограничивается исследованием плоской модели z-пинча, основные его выводы подтверждаются приведенным снимком (б). А именно, скорость расширения отраженного фронта почти постоянна и составляет около половины скорости начального сжатия плазмы. Сразу же после выхода отраженной волны на поверхность пинча (т. е. после завершения сжатия плазмы), скорость расширения наружного слоя плазмы возрастает. Она сравнима со скоростью начального сжатия. В результате торможения в наружном магнитном поле расширение вскоре прекращается и плазма начинает инерциальные радиальные колебания около своего равновесного положения.

Некоторые особенности, связанные с инерциаль-

ными колебаниями плазменной трубки, видны на аксиальном снимке (г) θ-пинча. Снимок показывает, что захваченное магнитное поле препятствует схлопыванию плазмы к оси. Образующаяся при этом плазменная трубка колеблется с частотой ~400 кгц (частота колебаний тока в цепи конденсаторов ~25 кгц). В стадии каждого минимума диаметра трубки, с внутренней ее поверхности отрывается фронт ударной волны, который каждый раз вызывает вспышки свечения газа на оси. Снимок (в) очень наглядно демонстрирует отрыв фронта ударной волны от внутренней поверхности плазменной трубки и его схождение к оси. На снимке (г) можно видеть также несимметричные выбросы каких-то плазменных образований с наружной поверхности трубки, которые происходят в моменты первого, второго и третьего максимумов диаметра трубки. С нижней стороны выбрасывается больше плазмы, чем с верхней. Соответственно трубка получает отдачу и смещается вверх. Снимок (е) демонстрирует наличие сильных несимметричных выбросов в более мощных θ-пинчах. Особенно хорошо это видно во втором полупериоде тока.

Теория инерциальных колебаний плазменных трубок, без учета внутренних ударных волн и отрыва плазменных образований с наружной поверхности, была развита в работе [27]. Результаты качественно согласуются с опытом [27—30].

На снимках (д) и (ж) видны симметричные выбросы, которые, по-видимому, коррелируются с выходом на поверхность плазмы фронта отраженной ударной волны. Следует полагать, что при этом выбрасываются плазменные трубки, коаксиальные с пинчем. Скорость выброса в первом случае (первый полупериод тока) сравнима со скоростью начального сжатия плазмы, а во втором (второй полупериод) она значительно больше. Подобные выбросы редко фиксируются даже на самых чувствительных фотопленках, несмотря на то, что оптическая глубина применяемой аппаратуры превышает длину пинча. Это указывает на слабое свечение плазмы в слое. Корреляция с выходом отраженного фронта наружу наводит на мысль, что выброс слабо светящейся плазменной трубки связан с расширением наружного слоя плазмы, который при этом остывает, делаясь менее проводящим. Уменьшение проводимости приведет к соответствующему уменьшению магнитного давления. В результате, этот слой, обладая радиальной скоростью, может удаляться от поверхности сжатой плазмы. При достаточно большой начальной скорости расширения слой может достигнуть стенок камеры (снимок 3), а при меньшей скорости он тормозится вдали от стенок, совершая радиальные колебания около равновесного положения (снимок д). Относительно низкая частота этих колебаний указывает на слабое взаимодействие слоя с магнитным полем.

Таким образом, щелевые снимки наглядно демонстрируют наличие некоторых магнитогидродинамических эффектов и различных видов нестабильностей плазмы. Однако, ввиду ограниченности поля зрения камеры в режиме непрерывной фоторегистрации через оптическую щель, эти снимки не в состоянии дать достаточно полной пространственной картины исследуемых процессов. Особенно это относится к несимметричным нестабильностям. От такого недостатка в значительной мере свободен метод фотографирования в режиме «лупы времени».

2.2. ФОТОГРАФИИ В РЕЖИМЕ «ЛУПЫ ВРЕМЕНИ»

Фотографии самосжатых разрядов, полученные в этом режиме, были опубликованы в работах [31—35]. Некоторые из них, относящиеся к θ-пинчу, приведены на рис. 2. Они получены с камерой СФР-2М, при фотографировании разряда четырехрядной системой линз в аксиальном направлении. Соответственно на каждом снимке получаются четыре ряда кадров, отстоящих друг от друга на 0,5 мксек (~время экспозиции кадров). С целью экономии места, здесь приводится по одному ряду кадров из каждого снимка. Поэтому расстояние между соседними кадрами составляет ~2 мксек. В качестве примера дается также четырехрядный снимок (к).

В рассматриваемых опытах применялись фарфоровые камеры круглого сечения и кварцевые камеры восьмиугольного и квадратного сечения. Нарастающие во времени аксиальные магнитные поля создавались круглыми одиночными витками разной длины. Снимки показывают неожиданно сложную картину образования, сжатия и последующего расширения плазмы. Обращает на себя внимание возникновение неоднородностей распределения плазмы в начальной стадии разгорания разряда. Они до некоторой степени сохраняются и в процессе сжатия. Начальные неоднородности, по-видимому, в значительной мере определяют дальнейшее поведение плазмы. В стадии расширения, в некоторых случаях, наблюдаются желобкообразные деформации поверхности пинча (снимки (в), (з), (и) и (к)). Принято считать, что они связаны с нестабильностями типа Релея-Тейлора [33—35]. Авторы работы [35], изучавшие θ-пинч в дейтерии и гелии, в камере малого диаметра, рассматривают эти нестабильности как желобковые и высказывают некоторые теоретические соображения по этому поводу. Однако, снимки рис. 2 показывают, что желобковые нестабильности далеко не исчерпывают наблюдаемое поведение плазмы.

На снимке (а) слой плазмы в стадии начального сжатия претерпевает значительные деформации, в то время как в стадии максимального сжатия и дальнейшего расширения желобковые деформации поверхности пинча очень слабо выражены. На снимке (в) плазма сжимается в виде двух приблизительно коаксиальных слоев, соединенных между собой светящимися перемычками. После сжатия из пинча выбрасывается одна кумулятивная струя, вызывающая вспышку при ударе об стенку. На-

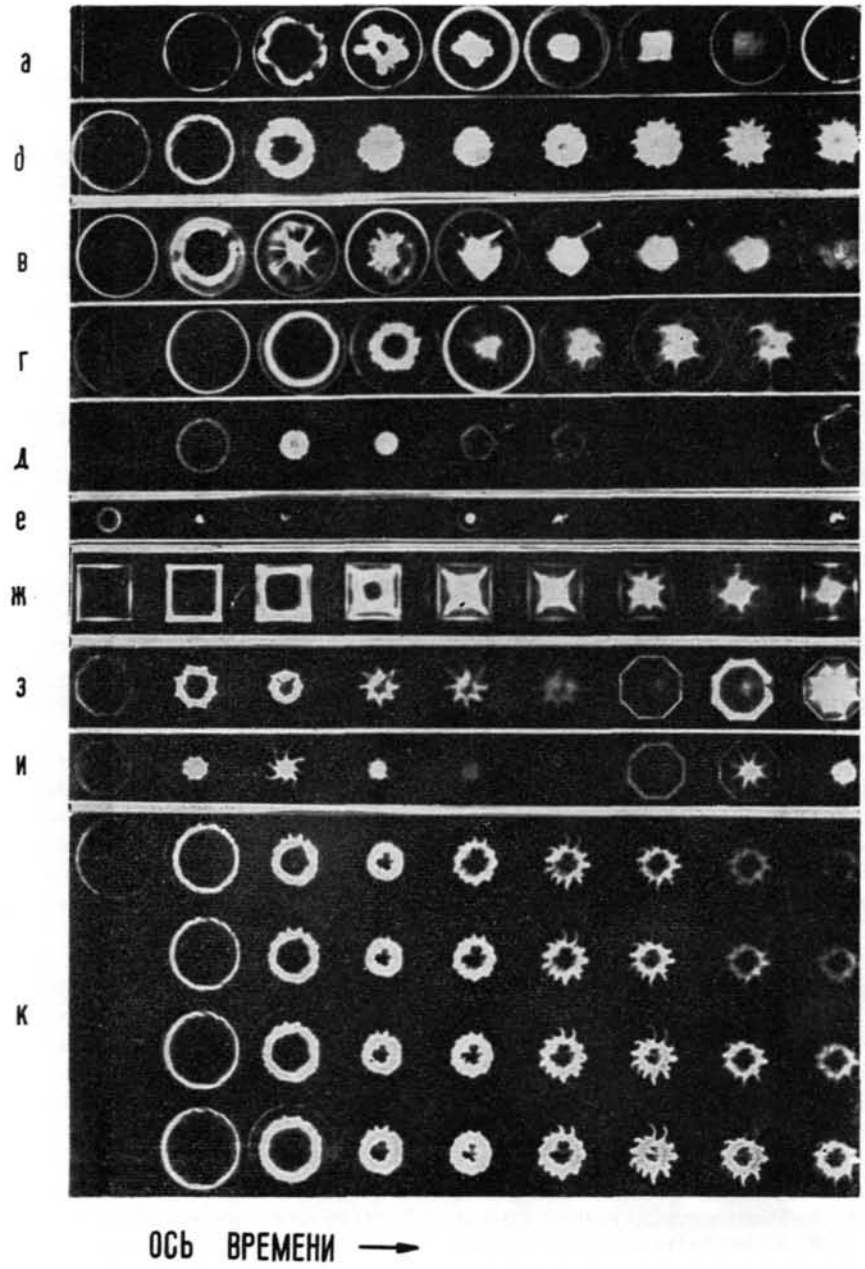

Рис. 2
см. таблицу II.

ТАБЛИЦА II. Таблица к рис. 2

Снимки	Размеры сечения камеры	Длина камеры в см	Длина витка магнитного поля в см	кгаусс	№ полупериода тока	Давление газа в мм рт. ст.
а	⌀ 27 см	100	55	12	1	воздух 10^{-1}
б	⌀ 27 см	100	15	35	1	Kr 10^{-1}
в	⌀ 27 см	100	15	35	2	He $7\cdot10^{-1}$
г	⌀ 27 см	100	55	18	2	He $5\cdot10^{-2}$
д	⌀ 27 см	100	55	10	1	He 10^{-1}
е	⌀ 5 см	100	15	70	1—2	He $5\cdot10^{-2}$
ж	квадрат с площадью $S=490$ см^2	50	15	25	2	воздух 10^{-1}
з	восьмигранник с площадью $S=200$ см^2	50	12	45	1	He 10^{-1}
и	—"—	50	12	45	1	He $5\cdot10^{-2}$
к	⌀ 27 см	100	15	35	1	N $2\cdot10^{-1}$

правление этой струи составляет с радиусом довольно большой угол. На снимке (г) начальное сжатие осуществляется достаточно гладко, однако, в стадии расширения происходит бурный развал плазмы, даже отдаленно не напоминающий желобковой нестабильности.

Как показывает снимок (е), в камерах малого диаметра характер движения плазмы и формы нестабильностей становятся менее сложными; в то же время интенсивность нестабильностей остается высокой.

В камерах круглого сечения формы движения плазмы плохо воспроизводятся не только от опыта к опыту, но часто и от полупериода к полупериоду разрядного тока. В отличие от этого, в граненых камерах наблюдается полная их воспроизводимость. При этом упрощаются формы нестабильностей. Опыты показывают, что в θ-пинчах, возбуждаемых в граненых камерах, наблюдаются лишь желобковые нестабильности. Их происхождение можно объяснить следующим образом.

Как это видно, например, на снимках (ж), (з) и (и), в граненых камерах сжимающийся слой плазмы сохраняет форму, подобную форме камеры. Передние фронты граней плазмы представляют собой плоские фронты ударных волн, в которых частицы приобретают перпендикулярные к ним, и одинаковые по величине, скорости направленного движения. Слои плазмы, которые накапливаются на диагональных плоскостях (на стыках соседних ударных волн) движутся к оси со скоростью, меньшей скорости фронтов. В результате они отстают от остального слоя плазмы, образуя диагональные плазменные «языки». Величина скорости плазмы в «языке» определяется параллельными диагональной плоскости компонентами скоростей соседних ударных волн. Перпендикулярные компоненты скоростей увеличивают плотность плазмы в «языке». К концу процесса сжатия плоские струи плазмы от этих «языков» должны сталкиваться с «захваченным» магнитным полем. При этом они будут расщепляться на два потока, обтекающих поле в противоположных направлениях. При встрече потоков от соседних «языков» произойдет резкое повышение кинетического давления плазмы. В результате возникнут «языки», прорастающие в наружное поле по плоскостям, перпендикулярным соответствующим граням и содержащим ось камеры.

Снимки, получаемые в граненых камерах, показывают, что ширина желебков зависит от давления газа. При малых давлениях возникают преимущественно узкие желобки.

Узкие желобки всегда более глубоко прорастают в наружное поле, чем широкие. Часто с острой вершины широкого желобка начинает прорастать узкий. Эти особенности могут быть объяснены, в основном, влиянием скин-слоя. Если ширина желобков превышает толщину скина, их прорастание будет тормозиться давлением наружного магнитного поля. При более тонких желобках, ввиду проникновения магнитного поля во внутрь слоя плазмы, его тормозящее действие уменьшается, что способствует более быстрому просачиванию желобка. Таким образом, с точки зрения нестабильности, наиболее опасными являются тонкие желобки. По-видимому, для подавления этого вида нестабильности могут быть эффективно использованы высокочастотные электромагнитные поля, уменьшающие толщину скин-слоя.

В шестигранной камере наблюдаются случаи, когда скорость выброса плазмы в желобках превышает максимальную начальную скорость сжатия плазмы.

Трудно найти какие-либо простые соображения, объясняющие возникновение других, более сложных нестабильностей в камерах круглого сечения. Приведенные снимки показывают, что они связаны с наличием в сжимающихся слоях плазмы значительных неоднородностей, возникающих с начала разгорания разряда. По понятной причине аксиальные снимки не в состоянии дать картину пространственного распределения этих неоднородностей. Поэтому возникает необходимость торцевого фотографирования разряда по возможности под большим углом к оси камеры. При этом будет видно распределение плазмы по значительной части поверхности сжимающегося слоя. Для этих опытов была использована камера большого диаметра. Опыты проводились как с θ-пинчем, так и с z-пинчем. В последнем случае, для облегчения фотографирования, электроды пинча были изготовлены в виде колец.

Полученные снимки приведены на рис. 3. Каждый содержит по два ряда кадров, один из которых снимался в аксиальном направлении, а другой — одновременно с ним, под углом 10° к оси камеры. Эти снимки позволяют сравнивать аксиальную картину распределения плазмы с ее поверхностным распределением. Снимки (а), (б), (в), (г) и (д) относятся к θ-пинчу, а снимки (е) и (ж) — к z-пинчу.

Эти снимки указывают на наличие нового обстоятельства, на которое обычно не обращалось внимания. А именно, как в θ, так и в z-пинче, в начальной стадии разгорания разряда, токи протекают в основном по извилистым тонким волокнам, которые в случае θ-пинча ориентируются преимущественно или в направлении θ, или в направлении z, а в z-пинча имеют, в основном, ориентацию по z. В то же время характер искривления волокон, их распределение и ориентация носят случайный характер. Нет какой-либо определенной зависимости и от природы газа в пределах давлений 10^{-1}—10^{-3} мм рт. ст.

Токовые волокна должны являться каналами высокой проводимости, в которых накапливается плазма в стадии разгорания разряда. Их возникновение обусловлено притяжением параллельных токов и может быть связано с процессами флюктуационного характера, которые сильнее должны проявляться именно в стадии разгорания разряда. Разветвлению токов может способствовать увеличение поперечного магнитного поля, вызванное нарастанием общего тока. С наличием дискретных

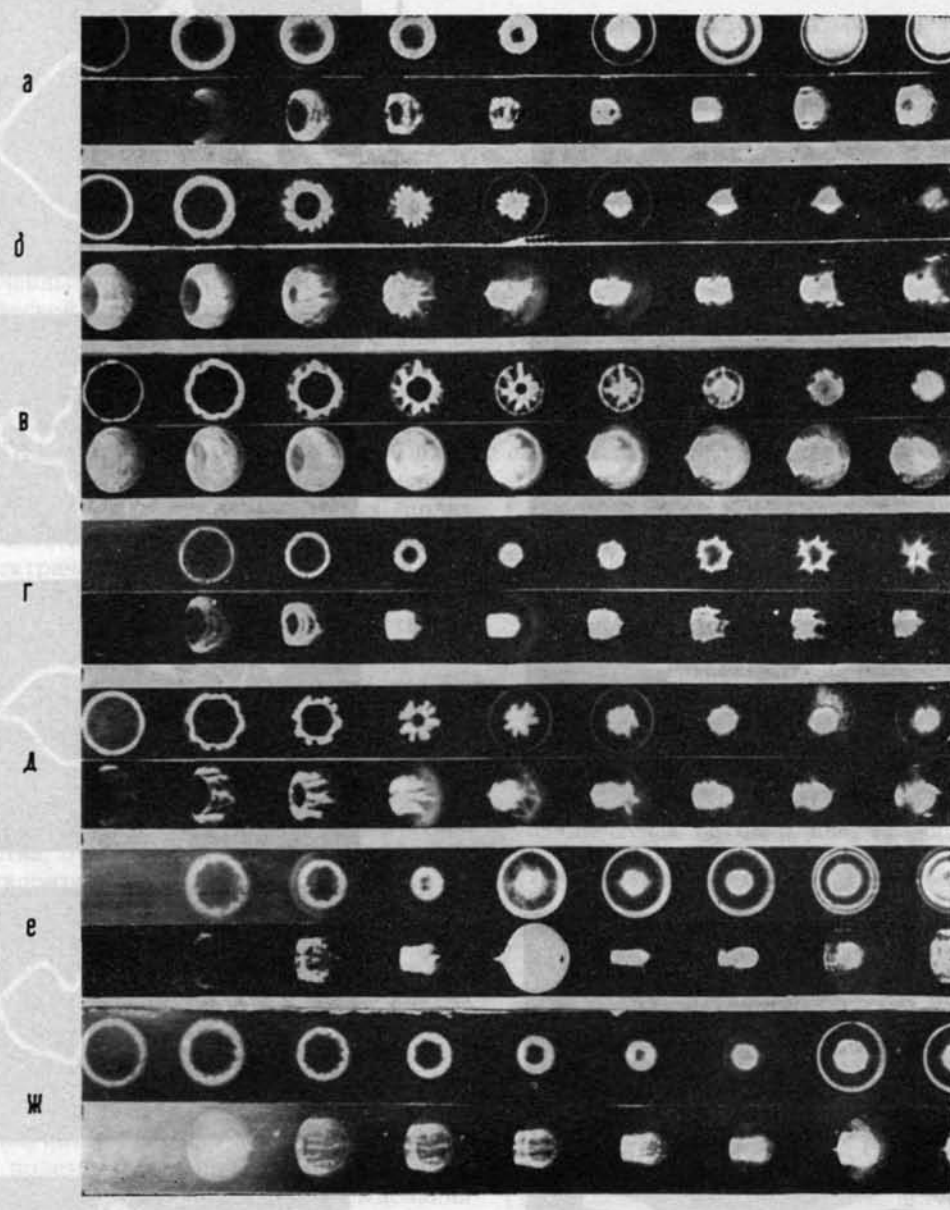

Рис. 3 см. таблицу III.

ТАБЛИЦА III. Таблица к рис. 3

Снимки	Давление в мм рт.ст.	H_{max} кгаусс	I_{max} кА	№ полупериода разрядного тока	Вид пинча
а	Kr, $5 \cdot 10^{-2}$	6	—	1	*0* — пинч
б	Kr, $2 \cdot 10^{-2}$	15	—	2	*0* — пинч
в	Kr, $1{,}5 \cdot 10^{-2}$	15	—	2	*0* — пинч
г	He, $1{,}5 \cdot 10^{-1}$	15	—	1	*0* — пинч
д	He, $1{,}5 \cdot 10^{-1}$	15	—	2	*0* — пинч
е	He, $5 \cdot 10^{-2}$	—	240	1	*z* — пинч
ж	Kr, $2 \cdot 10^{-2}$	—	240	1	*z* — пинч

В этих опытах применялась фарфоровая камера ⌀ 36 см и длиной 74 см. Длина витка магнитного поля — 48 см.

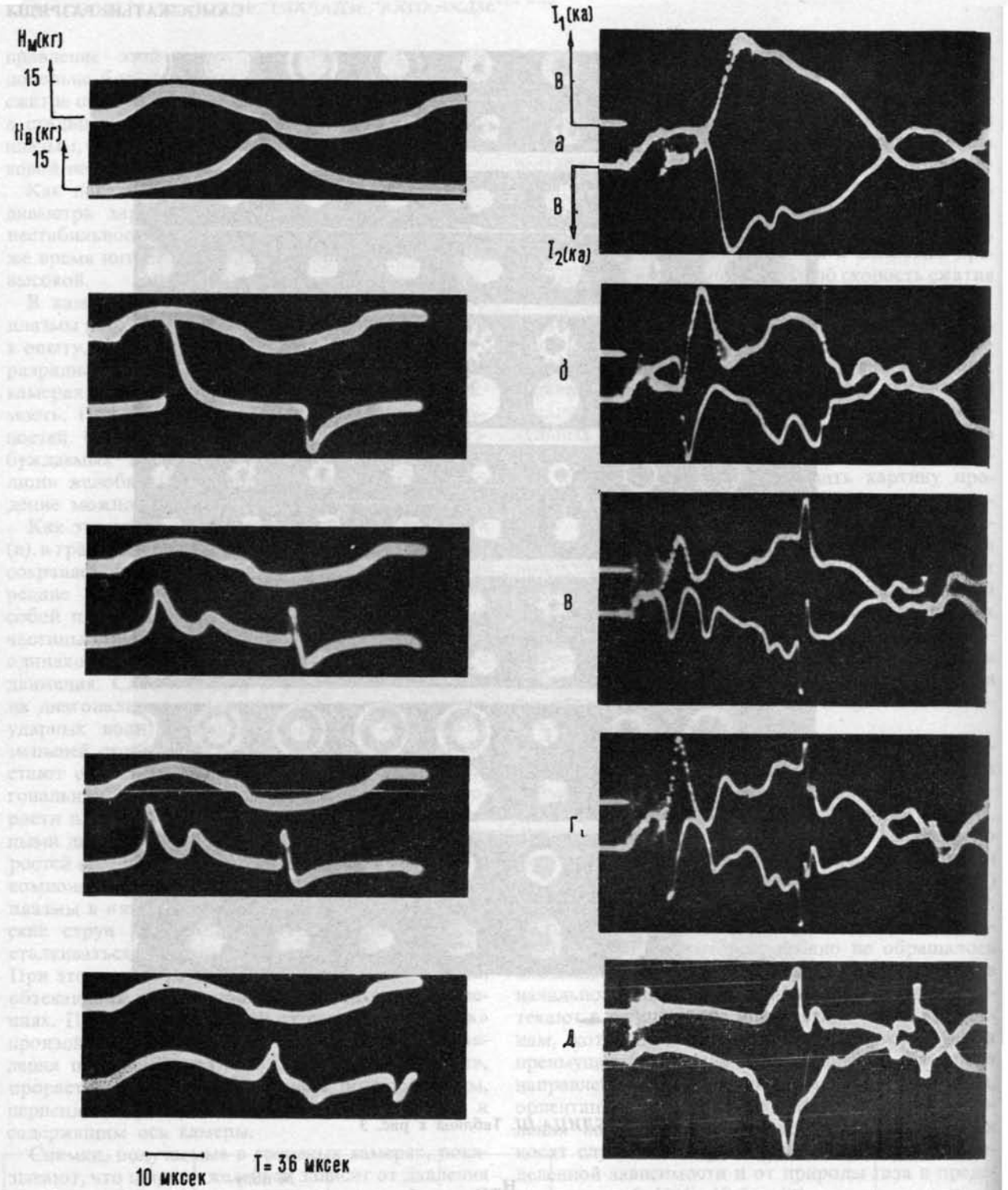

Рис. 4 см. таблицу IV.

ТАБЛИЦА IV. Таблица к рис. 4

Емкость батарей конденсаторов 90 мкф, начальное напряжение 30 кв,
⌀ камеры 36 см, длина 74 см,
⌀ катушки 46,5 см, длина 48 см,
$H_м$ — магнитное поле у стенки камеры,
$H_в$ — магнитное поле на оси камеры,
I_1 — ток в плазме у края витка,
I_2 — ток в плазме в средней части витка.

Снимки	Газ	Давление	Снимки	Газ	Давление
а	Kr	10^{-1}	г	He	10^{-1}
б	Kr	$1{,}5\cdot10^{-2}$	д	He	$1{,}5\cdot10^{-1}$
в	He	$2\cdot10^{-1}$			

токовых волокон, являющихся по своей природе как бы элементарными z-пинчами, связаны наблюдаемые на опыте неравномерности движения плазмы в процессе ее сжатия. На рассматриваемом снимке видно, что токовые волокна ускоряются неодинаково. Это в большей степени относится к θ-пинчу. Обладая высокой проводимостью и разными скоростями движения к оси пинча, эти волокна могут эффективно захватывать магнитные поля. Захваченные поля препятствуют термализации кинетической энергии радиального движения плазмы. Это приведет к возникновению нестабильностей, связанных с существованием направленных потоков плазмы и возможностью их столкновения между собой, и отражения от захваченных магнитных полей. При удачных стечениях потоков может произойти кумулятивный выброс плазменной струи. Движение потоков в магнитных полях должно способствовать также возникновению локальных электрических полей.

В θ-пинче возникает более сложное разветвление токовых волокон, чем в z-пинче. Соответственно в нем наблюдается большее многообразие нестабильностей.

Таким образом, удается показать, хотя бы качественно, что основная причина интенсивных нестабильностей сильноточных самосжатых разрядов заключается в неравномерностях разгорания разряда. Теория пинчей, не учитывающая этого обстоятельства, очевидно, не может претендовать на удовлетворительное согласие с опытом. В настоящее время процесс разгорания сильноточных разрядов совершенно не изучается, особенно экспериментально. Известна лишь одна работа [36], в которой дается теоретическая постановка этого вопроса.

Для надлежащего исследования сложных процессов разгорания разряда, очевидно, совершенно недостаточно использование лишь метода фотографирования, хотя, как было показано, он может дать много полезных сведений. Необходимо привлечение и других известных методов исследования плазмы. Нами начаты измерения в θ-пинчах с помощью магнитных зондов и поясов Роговского. На рис. 4 показаны некоторые предварительные результаты таких измерений.

Левая группа кривых представляет собой осциллограммы изменения магнитного поля около стенки (верхние кривые) и на оси камеры (нижние кривые). θ-пинч зажигался при различных давлениях газа в криптоне (кривые а и б) и в гелии (кривые в, г и д). На этих осциллограммах видны скачкообразные изменения магнитного поля при прохождении мимо зондов сжимающегося слоя плазмы (верхние кривые), и колебания захваченного поля в соответствии с радиальными колебаниями сжатой плазмы (нижние кривые). Во втором полупериоде, при больших скоростях сжатия плазмы, наблюдается почти мгновенное исчезновение захваченного от первого полупериода обратного магнитного поля. При этом на соответствующих фотоснимках наблюдается некоторое усиление нестабильностей плазмы. На правой группе снимков представлены осциллограммы сигналов от поясов Роговского. Пояса прямоугольной формы (размеры 18×5 см) располагались в середине камеры (нижние кривые) или были сдвинуты к краю катушки магнитного поля (верхние кривые). Они фиксировали токи, текущие в направлении θ. Осциллограммы показывают, в основном, изменения суммарного разрядного тока в процессе сжатия плазмы. Однако, помимо этих изменений, связанных с колебаниями плазмы как целого, на осциллограммы часто накладываются нерегулярные колебания тока малой амплитуды. Последние, по-видимому, связаны с отмеченным выше неравномерным распределением токовых волокон в сжимающемся слое плазмы.

Литература

[1] Курчатов И. В. *Атомная энергия* **1**, № 3 (1956).
[2] Арцимович Л. А. *Труды второй Международной конференции по мирному использованию атомной энергии.* Женева, 1958 г. т. **1**, стр. 5, М. 1959.
(Proc. Second U.N. International Conference on Peaceful Uses of Atomic Energy, Geneva, **31** (1958).
[3] Андрианов А. И. и др. там же стр. 31.
[4] Комельков В. С. и др. там же стр. 53.
[5] Головин И. Н. и др. *Атомная энергия* **1**, № 5 (1956) 26.
[6] Anderson, O. A., Baker, W. R., Colgate, S. A., Ise, J. Jr., Pyle, R. V., Proc. Third International Conference on Ionization Phenomena in Gases, Venice (1957).
[7] Colgate S. A., Furth, H. P., *Science* **128** (1958) 337.
[8] Burkhardt, L. C., Dunaway, R. E., Mather, J. W., Philips, J. A., Sawyer, G. A., Stratton, T. F., Stovall, E. J. Jr., Tuck, J. L., *J. Appl. Phys.* **28** (1957) 519.
[9] Осовец С. М. и др. Доклад на второй Женевской конференции по мирному использованию атомной энергии. Женева, 1958 г. М. 1959.
(Proc. Second U.N. International Conference on Peaceful Uses of Atomic Energy, Geneva, **32** (1958) 311.
[10] Tuck, J. L., Доклад № 1860, Женева, 1958 г. (Proc. Second U.N. International Conference on Peaceful Uses of Atomic Energy, Geneva, **32** (1958) 311.
[11] Elmore, W. C., Little, E. M., Quinn, W. E., Proc. Second U.N. International Conference on Peaceful Uses of Atomic Energy, Geneva, **32** (1958) 337. (Доклад № 356)
[12] Tuck, J. L., Proc. Fourth International Conference on Ionization Phenomena in Gases, Uppsala (North-Holland, Pub. Co., Amsterdam) **2** (1959) 920.
[13] Kolb, A. C., Доклад № 345, Женева, 1958 г. Proc. Second International U.N. Conference on Peaceful Uses of Atomic Energy, Geneva, **31** (1958) 328.
[14] Kolb, A. C., Dobbie, C. B., Griem, H. R., *Phys. Rev. Letters* **3**, 1 (1959) 5.
[15] Kolb, A. C., Griem, H. R., Faust, W. R., Proceedings of Fourth International Conference on Ionization Phenomena in Gases (North-Holland Pub. Co., Amsterdam) **2** (1959) 1037.
[16] Kolb, A. C., *Phys. Rev.* **112** (1958) 291.
[17] Леонтович М. А., Шафранов В. Д., Физика плазмы и проблема управляемых термоядерных исследований т. 1, стр. 207. М. 1958.
[18] Трубников В. А. Физика плазмы и проблема управляемых термоядерных исследований. т. 1, стр. 289, М. 1958.
[19] Шафранов В. Д. то же т. 1, стр. 130.
[20] Kruskal, M. D., Schwarzschild, M., *Proc. Roy. Soc.* **A 223** (1954) 348.

[21] TAYLER, R. J., *Proc. Phys. Soc.* (*London*), **B 70** (1957) 31.
[22] TAYLER, R. J., *Proc. Phys. Soc.* (*London*) **B 70** (1957) 1049.
[23] ROSENBLUTH, M. N., Proc. 3rd Intern. Conf. on Ionization Phenomena in Gases, Venice, 1957.
[24] ROSENBLUTH, M. N., LONGMIRE, C. L., *Ann. Phys.* (*N. Y.*) **1** (1957) 120.
[25] TAYLER, G. J., *Proc. Roy. Soc.* **A 201** (1950) 192.
[26] ALLEN, J. E., *Proc. Phys. Soc.* (*London*) **B 70** (1957) 24.
[27] NIBLETT, G. B. F., GREEN, T. S., *Proc. Phys. Soc.* (*London*) **74** (1959) 737.
[28] BODIN, H. A. B., GREEN, T. S., NIBLETT, G. B. F., PEACOCK, N. J., Proceedings of Fourth International Conference on Ionization Phenomena in Gases, Uppsala (North-Holland Pub. Co., Amsterdam) **2** (1959) 1061 and 1965.
[29] ТОЛОК В. Т. и др. *ЖТФ* **30** (1960) 769.
[30] КВАРЦХАВА И. Ф., КЕРВАЛИДЗЕ К. Н., ГВАЛАДЗЕ Ю. С., *ЖТФ* **30** (1960) 297.
[31] КВАРЦХАВА И. Ф., КЕРВАЛИДЗЕ К. Н., ГВАЛИДЗЕ Ю. С., *ЖТФ* **38** (1960) 1641.
[32] КВАРЦХАВА И. Ф., КЕРВАЛИДЗЕ К. Н., ГВАЛИДЗЕ Ю. С., *ЖТФ* **30** (1960) 1321.
[33] LATHAM, R., NATION, J. A., CURZON, F. L., FOLKERSKI, A., *Nature* **186** (1960) 624; *Proc. Roy. Soc.* (*London*) **A227** (1960) 386.
[34] GREEN, T. S., NIBLETT, G. B. F., *Nuclear Fusion* **1** (1960) 42.
[35] BODIN, H. A. B., NEWTON, A. A., PEACOCK, N. S., *Nuclear Fusion* **1** (1961) 139.
[36] БРАГИНСКИЙ С. И., БУДКЕР Г. И. Физика плазмы и проблема управляемых термоядерных реакций т. 1, стр. 186, М. 1959.

MEASUREMENTS OF ELECTRON DENSITIES AND TEMPERATURES AND OTHER PLASMA PARAMETERS IN MAGNETIC COMPRESSION EXPERIMENTS*

H. R. GRIEM**, A. C. KOLB, W. H. LUPTON, D. T. PHILLIPS

U.S. NAVAL RESEARCH LABORATORY

WASHINGTON, D.C., UNITED STATES OF AMERICA

A high energy plasma is produced in preionized deuterium (0.1 mm Hg) that has been preheated with an electrodeless discharge to 1.0 eV by a current pulse through a single-turn coil (length 70 cm, inner diameter 5.7 cm, mirror ratio 2:1, peak current 5.5 MA, H_{max} 80 kG in 5 μs, coil voltage 9 kV, bank voltage 17 kV). Time-resolved measurements of the soft x-ray intensities transmitted by various absorber foils yield an electron temperature which rises rapidly from 1 keV at 3 μs to 2.5 keV at peak current and persists at this level through most of the first half-cycle. This electron temperature is higher than the temperature expected from shock heating and adiabatic compression by a factor of ~3 — 6. The additional heating is due to the dissipation of an initially trapped reverse field of 6 kG opposite in direction to the main confining field. From the visible bremsstrahlung follows an electron density of $7 \pm 2 \times 10^{16}$ cm^{-3} at the time of maximum current, indicating a high β. Streak camera observations show that the plasma is macroscopically stable through most of the first half-cycle of the discharge and that end losses are small. Towards the end of the first half-cycle, the plasma splits into two filaments rotating around each other, and the end losses increase sharply. For the first 2 μs the radial electron density distribution has a minimum on the axis, due to some remaining trapped (reserve) field. The upper limit for impurities during the first half-cycle is about 1% since within the experimental error no excessive x-ray radiation could be observed, and otherwise rapid radiation cooling would dominate the electron temperature. (During the second half-cycle the electron temperature stays below 300 eV.) Similar experiments (PHAROS) with a larger plasma volume (length 180 cm, bore 9.6 cm, mirror ratio 2:1) and comparable fields (80 kG at 11.5 MA in 10 μs) yield electron temperatures of 350 ± 50 eV, which is lower than before, possibly because of the longer times required for the reverse field to dissipate with a larger plasma diameter. However, the impurity concentration is not yet known and this could account for the difference.

1. Introduction

1.1. EARLIER OBSERVATIONS AND SPECULATIONS

In an earlier series of experiments [1] with high density plasmas (10^{16}—10^{17} particles/cm^3), observations of the confinement and compression of preionized deuterium in a rapidly rising B_z (axial) magnetic field (60—120 kG maximum) showed that end losses were a controlling factor and decreased with increasing coil length. With short coils (10—15 cm having a mirror ratio of 2 to 3) the confinement time was determined to be about 3 μs from streak camera photographs, which coincided approximately with the duration of the neutron emission. With longer coils (30—50 cm) the plasma could be contained and the time of neutron emission prolonged by about a factor of two. (In these experiments the half-period of the discharge ranged between 11 and 15 μs, depending on the particular coil inductance.)

It was also found [1, 2] that the overall macroscopic stability of the plasma column was abruptly terminated by the sudden onset of an apparent "radial oscillation" which led to a rapid loss of plasma and sharp decline in the neutron emission rate. The onset of this instability could be delayed by using longer coils and was found to be connected with the dissipation of a reverse magnetic field whose direction is opposite to the main confining field. (See the discussion of this instability in Section 3.1 and in the following paper.)

The preliminary experiments discussed briefly above all pointed to the importance of the reverse magnetic field in the heating of the plasma. However, the nature of the mechanism for the reverse field dissipation remained obscure; it was not known whether the energy went directly into the ions or electrons (or both). It was speculated [3, 4] that a plasma wave instability in the current sheet which reverses the plasma magnetic field led to turbulence and preferential heating of the ions, or that perhaps a hydromagnetic-ion cyclotron resonance occurred which heated the ions (a self-excited magnetic pumping effect) and that the apparent "radial oscillations" were a manifestation of such a phenomenon [4].

1.2. EXPERIMENTS FOLLOWING 1959 UPPSALA CONFERENCE

To obtain further information on the factors which influence the heating, confinement time and nature of the instability, the above experiments were repeated with a longer (70 cm) coil having the same bore (6 cm)

* Conference paper CN-10/192 presented by A. C. Kolb. Discussion of this paper is given on page 647. Translations of the abstract are at the end of this volume of the Proceedings.

** Physics Department, University of Maryland, College Park, Maryland, U.S.A.

as before. Because of the low value of the coil inductance (~4 mμH), the 285 kJ capacitor bank was rebuilt so that the external inductance was comparable to the coil inductance and ~9 kV could be applied at the gap which feeds current to the coil. With these modifications the current was increased from 2.5 MA (at the time of the 1959 Uppsala Conference [1]) to the present maximum of 5.5 MA with a quarter period of 5 μs and a peak magnetic field of 80 kG. (The other parameters of the experiment are tabulated in an accompanying paper by HAIN and KOLB [5], where a theoretical description of the experiment based on the full set of magnetohydrodynamic equations is given.)

The initial conditions and purity of the plasma before the start of the main compression are of paramount importance. The method of preheating is similar to that studied in detail by the Jülich (Germany) group and reported at this conference [6]. The first part of the present paper is concerned with techniques for the spectroscopic measurement of the initial conditions established by discharging a 17 kV, 130 μF slow capacitor bank (14 μs half-period) with a 20 kV, 0.6 μF, 500 kHz discharge superimposed. These two capacitor banks are discharged into the main coil and are connected in parallel with the large capacitor bank, using spark gaps [7]. The slow bank produces a quasi-static reverse field of up to —7 kG and the high frequency discharge (opposite polarity to the slow bank) breaks down the gas and joule heats it to 1.0 eV with ~50% ionization. (The initial preheating discharge is very reproducible and is also discussed further in another paper [8] for a discharge tube 180 cm long having a 10 cm bore.)

To obtain information on the heating mechanisms with a reverse field present in the plasma, time-resolved measurements of the electron temperature from the emission of soft x-rays were made for initial fields between —3 and —7 kG (most of the data reported here are for $B_z = -6$ kG). The measurements discussed in the second part of this paper lead to the conclusion that the transfer of energy from the reverse field to the plasma provides a powerful mechanism for heating the electron component to temperatures as high as 3 keV (average 2.5 keV) and certainly does not result in preferential ion heating as was presumed to be the case in the interpretation [3] of similar observations with a faster discharge, where the electron temperature (~400—500 eV) was reported to be lower than in the present experiments. It is likely that the low impurity level (possibly due to the method of preionization) in our experiments [9] is responsible for the different results.

Calculations [5] do not rule out ordinary collisional dissipation (ordinary plasma resistance) as having a major influence on the observed heating rate. Because of the small plasma radius the dissipation time is not exceedingly long, in spite of the high conductivity. Another observation which supports this hypothesis is that the ion "temperatures" from neutron emission seem to be about a factor of 2 to 3 lower than the electron temperatures for the highest (—6 kG) reverse field case and are comparable with the electron temperatures for reverse fields of —3 to —4 kG [9]. At the high final electron temperatures of 2 to 3 keV and for densities of about 5×10^{16} cm^{-3}, the electron-electron collision time (0.06 μs) is short compared to the experimental times, while the time to transfer energy from the electrons to the ions is much longer. If the plasma contained a few percent of impurities, the electrons could radiate away their internal energy in a few tenths of a microsecond (see Section 3.4). Consequently, there would be a temperature barrier at a few hundred electron volts, as is observed here during the second half-cycle of the discharge after the plasma hits the walls at the end of the first half-cycle.

Recent streak camera observations of the radial density distribution show that the plasma seems to be contained quite well in the 70 cm coil until the appearance of the instability (Section 3.1). It is doubtful whether the confinement can be described simply in terms of plasma streaming out the ends [4], as was implied by the Uppsala experiments [1] with short coils, because of the closed field lines at the ends. The factors which influence the end losses still remain obscure but further information on this point should be forthcoming in a larger experiment with considerably longer coils (typically 2 meters with a 10 cm bore), utilizing parallel and anti-parallel initial fields, with and without magnetic mirrors [10].

The radial density distribution during the first few microseconds shows a density minimum near the axis (Section 3.1). From this observation the existence of a trapped magnetic field can be inferred, without the use of probes. This region of low density near the center of the compressed plasma fills in during the observed time of rapid heating, implying that the energy in the trapped field is being fed into the plasma.

1.3. PHAROS — A LARGE MAGNETIC COMPRESSION EXPERIMENT

A 20 kV, 2 MJ capacitor bank having a very low inductance (~1 mμH) is nearing completion and is now operating with 714 kJ at 11.5 MA. This system is described further in the following paper [10] together with a discussion of preliminary observations of the heating rate, compression and stability, with and without an initial reverse magnetic field.

Because of the larger plasma diameter (relative to the earlier experiments) it is expected that the characteristic time for the reverse field dissipation will be increased if collisions determine the conductivity. This is borne out by measurements of the electron temperature by the same methods as used in the 285 kJ experiment. Now, the electron temperature rises to 350 eV in 10 μs, compared to 2.5 keV in 3 μs for the smaller discharge tube. In both cases the peak magnetic field (80 kG), initial voltage gradient at the walls (~500 V/cm), pressure (100 microns D_2) and initial conditions were essentially the same. However, the plasma radius is larger than before so that the characteristic time for the reverse field relaxation may be increased.

These experiments with the large capacitor bank are only in a preliminary stage but early indications are that the mechanisms for the plasma heating are similar to those in the smaller apparatus, with the scaling (plasma diameter, heating rate, implosion time, etc.) roughly as was expected (see the following paper). The possibility of microinstabilities in the plasma which contribute to the heating (in both experiments) are not ruled out, but it is not necessary to invoke their occurrence to explain the observations reported here and in the accompanying paper on the larger experiment.

2. Measurements in the preheated plasma

2.1. Electron densities

There are two standard methods to determine electron densities exceeding 10^{14} cm^{-3} in plasmas in the 10^4 °K range which either involve a measurement of absolute continuum intensities or of the Stark broadening of spectral lines. The first method requires a knowledge of the optical path, i.e., of the plasma diameter for side-on observations. This radius is difficult to obtain in the preheater phase, and cannot be assumed equal to the tube diameter because of the possibility of a slow magnetic compression by the B_z field [8, 10].

Therefore, time-resolved measurements of the Stark profiles of deuterium Balmer lines were undertaken. The most suitable line turned out to be D_δ, which is about twice as broad as the two preceding lines in the series, but still well separated from the neighboring lines. Also, it is the last line for which detailed Stark profiles have been calculated, including the electron broadening [11].

The measurements were done with two Bausch and Lomb grating monochromators (50 cm focal length), equipped with photomultipliers. One instrument monitored the total line intensity, the other the intensity from a narrow wavelength band in the line core. Both signals were displayed on a dual-beam oscilloscope. From the ratio of the signals a value for the electron density is obtained which is practically independent of the (electron) temperature. (Only the broad band signal had to be corrected for the continuum contribution, which was measured between D_γ and D_δ.)

In Fig. 1 some calculated curves are shown for the narrow to broad band signal ratio as function of electron density for the band widths (4 and 40 or 80 Å) used in this experiment. It is seen that the temperature dependence is indeed very small, so that errors in the measured temperature (see the following Section) only cause negligible errors in the electron density determination. The velocity distribution of the emitting hydrogen atoms should be characterized by a temperature that is not much larger than the electron temperature because of the high density. Therefore, by neglecting the Doppler broadening only negligible errors are introduced compared to those stemming from uncertainties in the measured intensity ratio

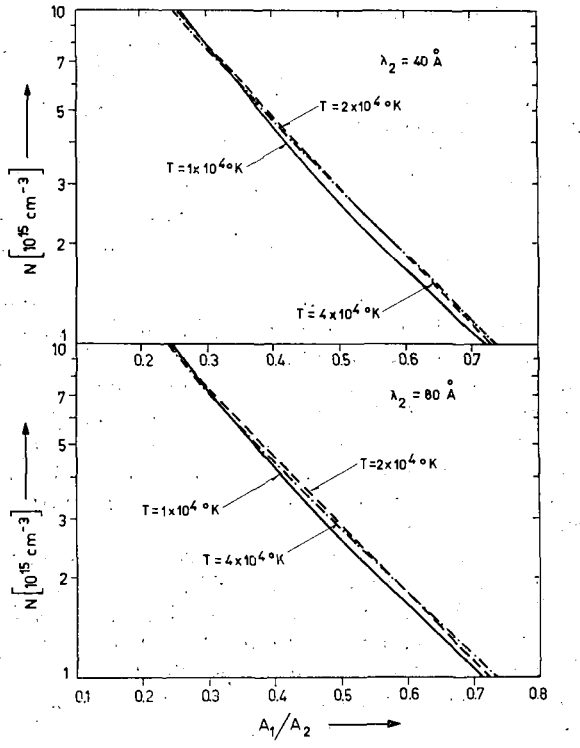

Fig. 1 Ratio of the intensities A_1/A_2 in a 4 Å and a 40 Å (or 80 Å) wavelength band, both centered at the deuterium D_δ line, as function of electron density for various temperatures.

(~10%) and the remaining uncertainties in the theory of Stark broadening, which may cause comparable errors in the electron density [12, 13].

At an initial pressure of 0.1 mm Hg D_2 the electron densities determined with this method were $N = 3.5 \times 10^{15}$ cm^{-3} with an estimated precision within 20%. (Results are given here only for the preheating of the gas in the 285 kJ experiment. The preheating in the PHAROS experiment is discussed in [8] (see also the following paper [10]).) If the total density is close to the initial density, this would correspond to 50% ionization or an ionization (Saha) temperature of 1.0 eV with an experimental error of 5%. For hydrogen at electron densities of this order the Saha equation should still be applicable, because three-body recombination into excited states and subsequent radiative decay is a very important recombination mechanism [14, 15, 16]. (Estimates [17] of the limit of the validity of Saha's equation neglecting excited states lead to a minimum electron density that may be too small by two or more orders of magnitude.)

2.2. Electron temperatures

There is little doubt that with the measured electron densities and low temperatures in the preheater phase the velocity distribution of the electrons is very nearly maxwellian. Furthermore, detailed calculations of the collisional excitation (ionization) and de-excitation (recombination) processes indicate that for an optically thin plasma of this kind the relative populations

in excited bound (free) states are described quite accurately by the electron (kinetic) temperature [17]. More specifically, one can relate the populations of the various excited states with the electron density by the appropriate Saha equations, using the electron temperature.

Therefore, this temperature can be obtained, in principle, from most of the well-known spectroscopic methods. However, for a pure hydrogen plasma, there appears to be only one *sensitive* method which does not require absolute intensity measurements and a knowledge of the optical path. This method is based on the measurement of the ratio of total line intensities and continuum intensities in adjacent wavelength bands. Such ratios are practically independent of the electron density, which only enters in the correction to the ionization potential of the free atom due to plasma effects. (For a detailed discussion, see [18].)

Again, the D_δ line was chosen for the temperature measurement together with a 100 Å continuum band on the long wavelength side of this line. As in case of the line broadening measurement, a small correction for the underlying continuum at the line had to be applied. The experimental error in the ratio is again ~10%.

The measured ratio was 18, which corresponds to an electron temperature of 1.0 eV (Fig. 2). The estimated experimental error results in a temperature error of only 5%. The agreement with the (calculated) Saha temperature (previous Section) then serves as a further indication that the assumption of local thermal equilibrium is indeed justified in this analysis.

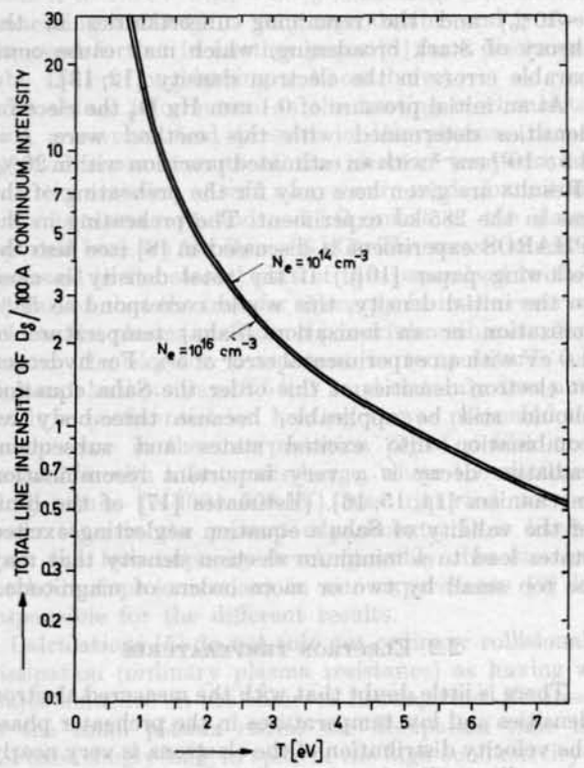

Fig. 2 Ratio of the total intensity of the deuterium D_δ line and the continuum in an adjacent 100 Å wavelength band as function of temperature for $N = 10^{14}$ and 10^{16} cm^{-3}. Gaunt corrections are included.

The results given here and in the last section are for a time of 5 μs after the switching of the preheater and B_z capacitor banks, at which time the main capacitor bank was fired in the subsequent experiments. However, the preheater conditions are quite stationary in the time-scale of this experiment, except for the first one or two microseconds. The e-folding time for the decay of the electron density is about 30—100 μs, depending on the magnitude of the initial B_z field (if the main bank is not discharged).

2.3. Magnetic fields

Only the total flux through the coil was measured in the experiment described here so that probe coils were not introduced into the plasma. However, reliable values for the magnetic field trapped in the preheated plasma are obtained because its conductivity is so poor that a practically homogeneous field is established in a few microseconds. (The slow B_z bank dominates this field at the time the main bank is discharged, i.e., the field from the preheater bank damps and is negligible after 5 μs.) The magnetic pressure of the initial reverse field is two orders of magnitude larger than the pressure of the preheated plasma.

To summarize: As a result of radiofrequency preionization and a fast (preheater) and a slow (B_z) discharge through the coil, a large volume (~2 liters) of deuterium at an initial pressure of 0.1 mm Hg is ~50% ionized and heated to 1.0 eV in the presence of a slowly rising, nearly homogeneous magnetic field of —6 kG.

3. Measurements in the magnetically compressed plasma

3.1. Plasma geometry and confinement

Streak camera photographs of the dense plasma produced behind the shock waves generated by the rapidly rising currents from the main bank and of the magnetic compression following the shock phase yield much qualitative information of the time-development of the high energy plasma.

All observations were made side-on with the slit of the streak camera at right angles to the coil axis. At the onset of the main discharge one first sees an imploding shock front with velocities up to 8 cm/μs (Fig. 3) which is then reflected near the axis on the compressed reverse field. (This field is separated from the external field by a current sheet formed initially near the walls.) For about a microsecond the plasma remains dynamic, i.e., there is a series of reflected shock waves, but these "oscillations" damp out, and the plasma is compressed further in the second microsecond by the rising main field.

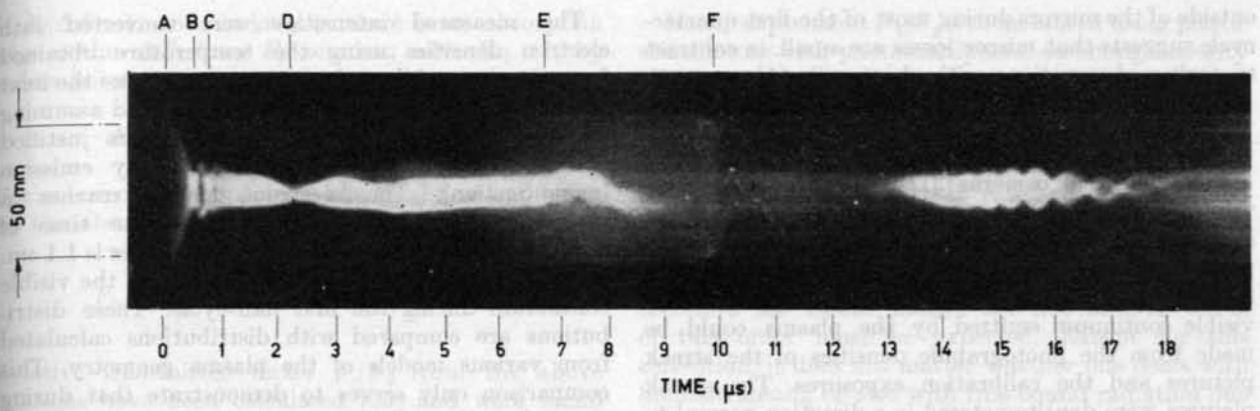

Fig. 3 Streak camera photograph of the high energy plasma taken at right angles to the (horizontal) axis of the plasma through a vertical slit in the center of the magnet. (A) start of the discharge; (B) plasma shock reflects off axis; (C) dynamic bouncing; (D) sudden contraction and expansion as discussed in text; (E) fission instability; (F) beginning of second half-cycle.

Detailed discussion of this phase is contained in another Conference paper [5]. After this there is a sudden collapse in some cases and then a sudden increase in the plasma luminosity and diameter (see Fig. 3). In other photographs this effect is not so pronounced (Fig. 4). Further discussion is found in the following paper. From then on the radius decreases only very slowly until a fission instability (referred to in earlier papers as "radial oscillations") occurs, even though the field decreases in the second quarter-cycle. These observations are certainly not expected for a simple adiabatic compression and de-compression.

Towards the end of the first half-cycle the plasma in nearly all cases breaks up into two filaments (fission instability) which, as shown by stereoscopic streak camera pictures, rotate around each other. This rotation and the fission instability seem to depend on the dissipation of the reverse field and are discussed elsewhere [10, 19, 20]. Simultaneous streak camera pictures were also obtained through slits near the center of the coil and near the magnetic mirrors, either just inside or just outside of the magnet. Just inside the mirror region the plasma behaves very much as in the center of the coil, except that after about 3 μs the plasma radius tends to be smaller by about a factor of two than that in the central plane, reducing the aperture for end losses. But on the outside of the coil no plasma radiation could normally be seen in the first 3 to 5 μs. Near the onset time of the fission instability mentioned in the preceding paragraph an intense flash of light is observed outside the mirrors (Fig. 4), presumably at a time when end losses increase sharply.

These observations indicate that most of the time the plasma is approximately cylindrical with an effective length that is somewhat shorter than the distance between the magnetic mirrors and apparently well confined even as the main field decreases during the second quarter-cycle. The absence of plasma just

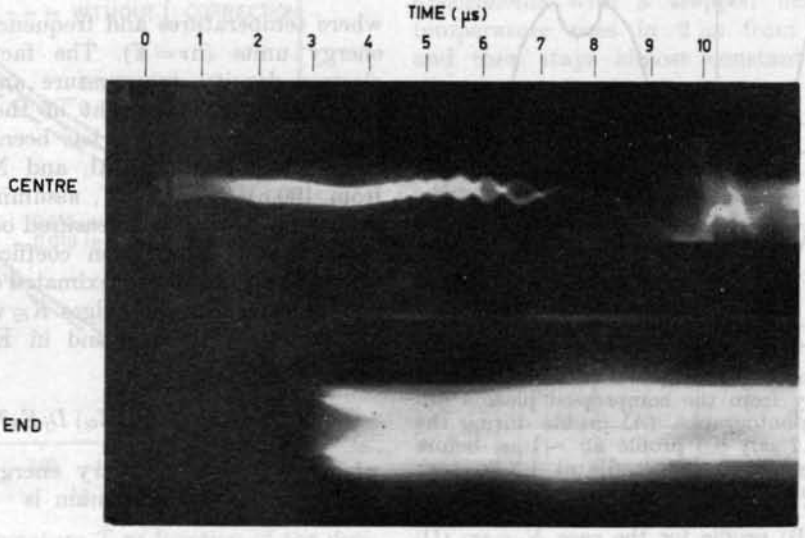

Fig. 4 Simultaneous streak camera photographs of the high energy plasma taken through a slit in the center of the magnet and a slit just outside of one of the magnetic mirrors, showing end losses. Comparing the compression in the center with Fig. 3 shows the contraction and expansion (at D) is not nearly so evident here.

outside of the mirrors during most of the first quarter-cycle suggests that mirror losses are small, in contrast to earlier observations with short coils [1].

3.2. Electron densities

The f/2.9 streak cameras [21] used in the experiment were calibrated with a tungsten ribbon lamp as an absolute intensity standard and a xenon flash to produce relative H and D curves by means of a step filter. In this way an absolute measurement of the visible continuum emitted by the plasma could be made from the photographic densities of the streak pictures and the calibration exposures. The streak pictures were densitometered in a direction normal to the coil axis. The resulting intensity distributions could then be unfolded into radial density distributions, using the Abel integral inversion or by assuming various models for the density distribution and comparing with the observations as in Fig. 5.

The observed (not yet unfolded) intensity distribution was doubly peaked first and then tended to be quite flat until ~ 2 μs, which implies that little light is emitted near the coil axis. Since it is quite unlikely that very large temperature gradients exist near the axis [5], this suggests that the density is a minimum there, which in turn implies that there is a trapped magnetic field at these times. The trapped magnetic field which is indicated by the density distribution can serve as an energy reservoir which heats the plasma as it dissipates.

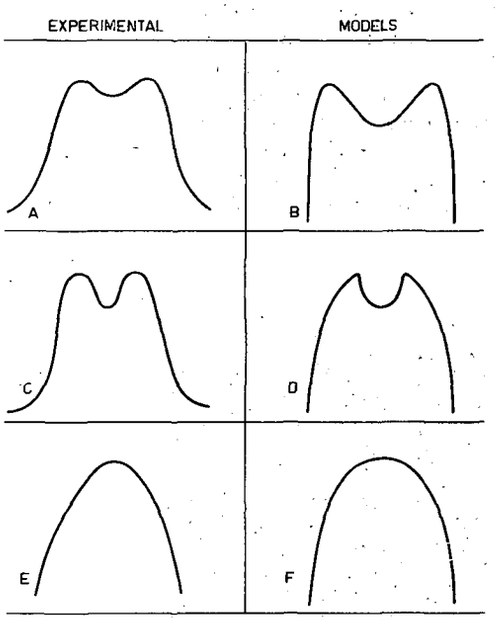

Fig. 5 Shown at the left above are radial profiles of visible light intensity from the compressed plasma obtained from streak photographs. (A) profile during the first implosion (~ 0.2 μs); (C) profile at ~ 1 μs, before the trapped field dissipates; (E) profile at 4.5 μs, near the peak of coil current. The profiles on the right are based on simple models of plasma geometry, assuming a uniform temperature. (B) profile for the case $N_e = \alpha r$; (D) profile for a hollow plasma cylinder, $N_e = 0$ $(0 < r < r_1)$, $N_e = K$ $(r_1 < r < R)$; (F) profile for a plasma of constant density, $N_e = K$.

The measured intensities were converted into electron densities using the temperature obtained from the slope of the soft x-ray spectrum (see the next Section), calculated Gaunt factors [22], and assuming a pure deuterium plasma, which appears justified because there is no excessive soft x-ray emission (next Section). The electron density reaches a maximum of $7 \pm 2 \times 10^{16}$ cm^{-3} near the time of maximum current when the plasma diameter is 1.1 cm.

Figure 5 shows the radial distribution of the visible continuum during the first half-cycle. These distributions are compared with distributions calculated from various models of the plasma geometry. This comparison only serves to demonstrate that during the early stages of the compression there is a density minimum on the axis which fills in at the time of rapid heating. This behavior is expected if the reverse field dissipates.

3.3 Electron temperatures

At high temperatures, much of the continuum radiation from a plasma is emitted in the soft x-ray region. If the plasma consists of pure deuterium or of completely stripped heavier ions, and if the electrons have a maxwellian velocity distribution, then the shape of the spectrum on the high frequency side of all absorption edges is essentially determined by $\exp(-h\nu/kT)$, because the Gaunt factors do not depend strongly on the photon energy. A measurement of the slope of the spectrum will therefore directly yield a value for the electron temperature.

However, it is much easier to measure relative x-ray fluxes transmitted by suitable absorber foils, which will be given by

$$F_j = A \int_0^\infty \mathrm{d}E \exp\left(-\frac{E}{T} - K_{Ej} D_j\right), \qquad (1)$$

where temperatures and frequencies are expressed in energy units ($h\nu = E$). The factor A depends on electron density, temperature and geometry. K_{Ej} is the absorption coefficient of the foil and D_j is its thickness. This integral has been performed numerically [23] for C, Be, Al, and Ni for temperatures from 100 eV to 1400 eV, assuming various absorber thicknesses and using measured or theoretically interpolated x-ray absorption coefficients [24], but can also be analytically approximated quite accurately [25].

Between absorption edges K_{Ej} varies approximately as E^{-3}, i.e., the integrand in Eq. (1) has a sharp maximum at

$$E_j = [3 K_E(E_{0j}) D_j E_{0j}^3 T]^{1/4}, \qquad (2)$$

where E_0 is an arbitrary energy close to E_j. The 1/e width of this maximum is

$$\Delta E_j = \left(\frac{E_j T}{2}\right)^{1/2}. \qquad (3)$$

If $E_j/\Delta E > 1$, and as long as there is no absorption edge within ΔE_j from E_j, one can solve Eq. (1) by saddle-point integration, which leads to

$$F_j \approx \sqrt{\pi}\, A\, \Delta E_j \exp\left(-\frac{4}{3}\frac{E_j}{T}\right). \tag{4}$$

For an exponential spectrum the total flux impinging on the absorber foil is

$$F_0 = A \int_0^\infty \exp(-E/T)\, \mathrm{d}E = AT. \tag{5}$$

Relative transmitted fluxes F_j/F_0 from the above relations have been calculated [25] and were found to be in satisfactory agreement with the results of the numerical integrations [23].

By measuring the relative transmitted flux as a function of absorber thickness or through different absorber materials, the temperature can be obtained by curve-fitting with the calculated values [23]. However, time-resolution can only be achieved if the fluxes through at least two different foils are measured simultaneously. Then the flux ratio F_1/F_2 transmitted by the two foils $j=1$ and 2 can be used to determine the temperature, for which a double application of Eqs. (3) and (4) yields

$$T \approx \frac{(4/3)\,(E_2 - E_1)}{\ln(F_1/F_2) - \ln(g_1/g_2) + (1/2)\ln(E_2/E_1)}. \tag{6}$$

Here the Gaunt factors [22] are included and they should be chosen to correspond to the two values E_1 and E_2 of the maximum of the integrand in Eq. (1), which can be obtained from Eq. (2) by iteration. (Since both $E_{1,2}$ and $g_{1,2}$ depend on T, Eq. (6) must also be solved by iteration.) Equation (6) yields temperatures that are within 1% of those calculated numerically [26].

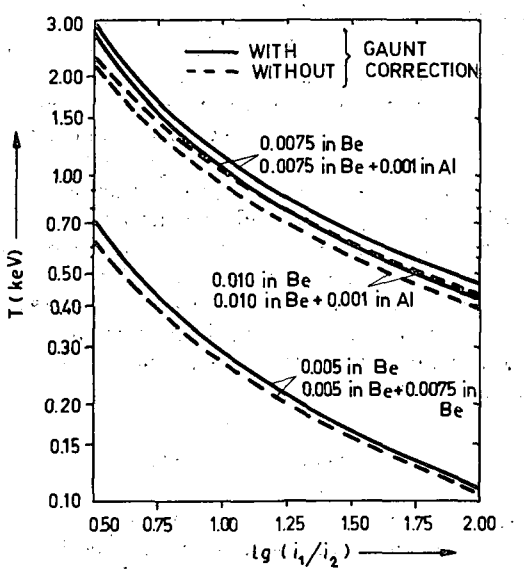

Fig. 6 Electron temperature T as function of the decimal logarithm lg (i_1/i_2) of the ratio of the detector currents for x-rays transmitted by various absorber foil combinations.

In our experiment F_1/F_2 was measured using plastic scintillators with photomultipliers, assuming linearity (E_2/E_1 rarely exceeds 3). Figure 6 shows some calculated calibration curves for actually used absorber foil combinations with the photomultiplier current ratio as the independent variable. Also shown are the temperature vs. current ratio curves calculated without the Gaunt corrections, which would indicate temperatures that are typically 10% too low. In cases where the composition of the plasma and therefore the Gaunt factors are not known, errors of this order must be expected. Except for this correction, it does not matter whether one deals with bremsstrahlung or also with free-bound radiation due to high-Z impurities, as long as one is not close to an absorption edge.

More serious uncertainties are introduced by the possibility of line radiation from impurities [27, 28], which would tend to be more important at low x-ray energies, i.e., cause a reduction in the apparent x-ray temperature. However, in our experiment only x-ray energies exceeding 2 keV could be transmitted through the absorber foils and a typical charge for spectral line-producing impurities would therefore be $Z=14$, corresponding to the hydrogen-like silicon spectrum. But according to theoretical estimates [29], the population of this species can hardly follow the rapid rise of the observed temperatures. Furthermore, measurements with foils cutting off at higher energies (>5 keV) yielded essentially the same temperatures, and the absolute x-ray intensities are consistent with a pure deuterium plasma.

It is therefore believed that these uncertainties do not contribute significantly to the experimental error in the x-ray temperatures, which is estimated to be always less than 20%.

Figure 7 gives the average x-ray temperature history of 5 discharges. The shot-to-shot variations (20% in T_e) are of the order of the experimental uncertainty in a particular determination. In these experiments with a trapped field of -6 kG the temperature rises in 2 μs from 1 keV to 2.5 keV and then stays almost constant until the plasma

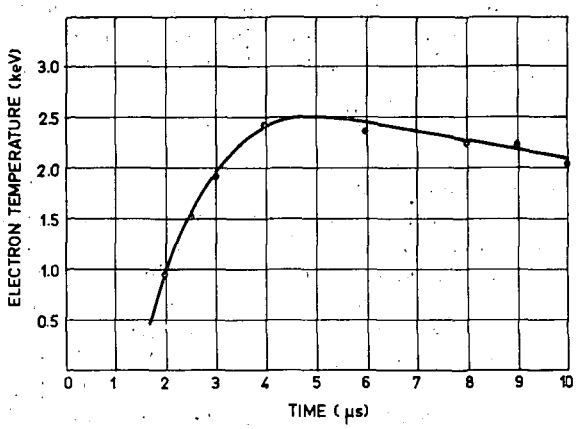

Fig. 7 Electron (x-ray) temperatures of the high energy plasma as function of time (measured points are averaged over 5 discharges).

disappears at the onset of the instability. This contrasts with earlier observations [9] with $B_z = -4$ kG, where the x-ray temperature rose to 1.1 keV at the peak of the main field and then dropped with decreasing field strength, and also with time-resolved electron temperature measurements in the Scylla experiments [30] where the temperature remains below 400 keV, possibly due to radiation losses from impurities.

After the plasma hits the walls at the end of the first half-cycle, impurities are introduced into the discharge. As a result, in the second half-cycle the soft x-ray intensity through the Be absorber remains comparable to that during the first half-cycle, even though the temperature drops below 300 eV. Because of the lower temperature and the influx of high-Z impurities during later half-cycles, the visible radiation (lines and continuum) also increases greatly in intensity.

3.4. Impurity concentrations

With photographic x-ray films it was found in earlier experiments that measured and calculated x-ray pulses agreed within the experimental accuracy of about a factor of two, if a pure deuterium plasma was assumed.

If N_z impurity ions of charge z were present, the corresponding free-bound and free-free continuum would cause an increase in the x-ray intensity by a factor

$$1 + \frac{N_z}{N} z^2 \left[1 + 2\,\frac{E_z}{\mathrm{k}T} \exp\left(\frac{E_z}{\mathrm{k}T}\right)\right]$$

over that of a pure deuterium plasma (see, e.g., [25]), N being the electron density and E_z the ionization potential of the ion in question. In this experiment ($\mathrm{k}T = 2.5$ keV), completely stripped oxygen is the most likely impurity ion ($z = 8$), and already a relative concentration of $N_8/N = 0.01$ would increase the x-ray continuum by a factor 2.3, or 2.6 if the proper Gaunt factors are inserted, whereas the visible continuum increases only by 1.6. One can therefore conclude that the impurity concentration is about or below 1%.

The sensitivity of the absolute x-ray method is much less if the effective z of impurities is smaller. Then the electrons in the hot plasma would lose their energy at a relative rate $1/T\,(\mathrm{d}T/\mathrm{d}t)$ of the order

$$\sum_z E_z N_z \langle \sigma_z v \rangle / \mathrm{k}T$$

by exciting and ionizing the impurities, $\sigma_z \approx 10^{-16}/z^2\,(\mathrm{cm}^2)$ being an estimate for the relevant total cross-sections at temperatures $\mathrm{k}T \approx E_z$. Most of this energy would immediately escape in the resonance lines, which are optically thin in this experiment due to Doppler broadening, as long as impurity concentrations remain in the percent range. With $E_z \approx 10\,z^2$ [eV], $\langle \sigma_z v \rangle \approx 10^{-7}/z^2$ [cm^3 sec^{-1}] and $\mathrm{k}T \approx 2.5 \times 10^3$ [eV] one therefore estimates the relative rate at which electrons would lose their energy to be $4 \times 10^{-10} \sum N_z$ [sec^{-1}].

The long duration of the high x-ray temperatures implies that this rate is 10^5 sec^{-1} or smaller, i.e., that $\sum N_z$ is below 2.5×10^{14} cm^{-3}, which is 0.5% of the electron density. (It should be noted that $\sum N_z$ is the total concentration of incompletely stripped ions with z sufficiently large to justify the above assumption for the cross-sections.)

From the absence of excessive x-ray radiation *and* of significant impurity radiation cooling, it therefore follows that the total impurity concentration is about or below 1%, regardless of the degree of ionization. Since the relative rate of radiation loss is much larger at lower temperatures, the impurity level should be still lower during the time of rapid heating.

3.5. Neutron yield

The neutron emission was recorded with silver counters, scintillators and with BF_3 counters. The duration of the scintillator signals is practically equal to the time during which energetic (>6 keV) x-rays are observed, i.e., from about the third microsecond to the onset of the instability, which typically occurs after 8 μs. The relative neutron yields are well correlated with the small shot-to-shot variations in the peak x-ray temperatures. But the absolute yields ($\sim 10^5$) are much smaller than those calculated from measured electron densities, x-ray temperatures and plasma volume. (The "neutron yield temperatures" are slightly below 1 keV.)

3.6. Magnetic fields

Reliable probe measurements can only be made for the first two or three microseconds of the main discharge, when the plasma radius is larger than the probe diameter. They clearly indicate the compression of the reverse field which is comparable to the external field after the reflection of the shock waves near the coil axis. Trapped fields of up to 30 kG were measured. Later on the probe signals show a sudden field reversal, but the signals are no longer reproducible. It may be that the presence of the probe drastically affects the behavior of plasma and field at later times, and that the very sudden reversal may not occur without the probe. At 2 μs after the start of the discharge, the reverse B_z field would occupy a volume with a radius of 5 mm if the field dissipation is due to joule heating, while the probes used here had a diameter of 3 mm.

Acknowledgments

The assistance of T. H. DeRieux in operating the 285 kJ capacitor bank and preparing the instrumentation is greatly appreciated.

The work reported here was jointly supported by the U.S. Atomic Energy Commission and the Office of Naval Research.

References

[1] KOLB, A. C., GRIEM, H. R., FAUST, W. R., Proceedings of the Fourth International Conference on Ionization Phenomena in Gases (North-Holland Publishing Company, Amsterdam) **2** (1959) 1037.

[2] KOLB, A. C., Proceedings Second U.N. Conference on Peaceful Uses of Atomic Energy, Geneva, **31** (1958) 328.

[3] LITTLE, E. M., QUINN, W. E., RIBE, F. L., *Phys. Fluids* **4** (1961) 728.

[4] KOLB, A. C., *Rev. Modern Phys.* **32** (1960) 755.

[5] HAIN, K., KOLB, A. C., page 561 of these Proceedings.

[6] One of us (A. C. K.) would like to acknowledge several conversations and communications with E. HINTZ concerning the preheating discharge.

[7] LUPTON, W. H., Proceedings of the Fifth International Conference on Ionization Phenomena in Gases, Munich (1961), to be published.

[8] LUPTON, W. H., MCLEAN, E. A., PHILLIPS, D. T., Proceedings of the Fifth International Conference on Ionization Phenomena in Gases, Munich (1961), to be published.

[9] GRIEM, H. R., KOLB, A. C., LUPTON, W. H., PHILLIPS, D. T., *Bull. Am. Phys. Soc.*, Ser. II, **6** (1961) 205.

[10] KOLB, A. C., GRIEM, H. R., LUPTON, W. H., PHILLIPS, D. T., RAMSDEN, S. A., MCLEAN, E. A., FAUST, W. R., SWARTZ, M., page 553 of these Proceedings.

[11] GRIEM, H. R., SHEN, K. Y., KOLB, A. C., U.S. Naval Research Laboratory Report 5455 (1960).

[12] GRIEM, H. R., KOLB, A. C., SHEN, K. Y., *Phys. Rev.* **116** (1959) 4.

[13] GRIEM, H. R., KOLB, A. C., SHEN, K. Y., *Astrophys. J.* **135** (1962) 272.

[14] D'ANGELO, N., *Phys. Rev.* **121** (1961) 505.

[15] BATES, D. R., KINGSTON, A. E., *Nature* **189** (1961) 652.

[16] MCWHIRTER, R. W. P., *Nature* **190** (1961) 902.

[17] DEWAN, E. M., *Phys. Fluids* **4** (1961) 759.

[18] GRIEM, H. R., Proceedings of the Fifth International Conference on Ionization Phenomena in Gases, Munich (1961), to be published.

[19] ROSTOKER, N., KOLB, A. C., *Bull. Am. Phys. Soc.*, Ser. II, **6** (1961) 203.

[20] ROSTOKER, N., KOLB, A. C., "Fission of a Hot Plasma", *Phys. Rev.* **124** (1961) 965.

[21] BRAUER, F. L., HANSEN, D. F., *J. Opt. Soc. Am.* **49** (1959) 421.

[22] KARZAS, W. J., LATTER, R., U.S. Atomic Energy Commission Report AECU-3703 (rev. 1958); RM-2091-AEC (1958), The Rand Corporation, Santa Monica, California; *Astrophys. J.*, Suppl. No. 55, **6** (1961) 167.

[23] JAHODA, F. C., LITTLE, E. M., QUINN, W. E., SAWYER, G. A., STRATTON, T. F., *Phys. Rev.* **119** (1960) 843.

[24] VICTOREEN, J. A., *J. Appl. Phys.* **20** (1959) 1141; GILMORE, F. R., The Rand Corporation Report RM-2367 AEC, *preliminary version* (1959, unpublished).

[25] GRIEM, H. R., Proceedings of the 4th Symposium on Temperature, Its Measurement and Control in Science and Industry, Columbus, Ohio (1961), to be published.

[26] SAWYER, G. A., private communication.

[27] STRATTON, T. F., Proceedings of the 4th Symposium on Temperature, Its Measurement and Control in Science and Industry, Columbus, Ohio (1961), to be published.

[28] BEARDEN, A. J., RIBE, F. L., SAWYER, G. A., STRATTON, T. F., *Phys. Rev. Letters* **6** (1961) 257.

[29] KNORR, G., *Z. Naturforschung* **13a** (1958) 941.

[30] STRATTON, T. F., LITTLE, E. M., QUINN, W. E.; QUINN, W. E., LITTLE, E. M., STRATTON, T. F., *Bull. Am. Phys. Soc.* II, **6** (1961) 202.

A HIGH ENERGY MAGNETIC COMPRESSION EXPERIMENT*

A. C. KOLB, H. R. GRIEM**, W. H. LUPTON, D. T. PHILLIPS, S. A. RAMSDEN***, E. A. McLEAN, W. R. FAUST, M. SWARTZ

U.S. NAVAL RESEARCH LABORATORY

WASHINGTON 25, D.C., UNITED STATES OF AMERICA

To investigate the production of large volumes ($\sim$500 cm^3) of collision-dominated plasma at densities of $\sim 10^{17}$ cm^{-3} with temperatures in the kilovolt range, a large 2 MJ, 20 kV capacitor bank with 2.5 m μH external inductance was put into operation in April 1961. The entire system, PHAROS, can produce 20 MA in a 13 liter single turn coil, 180 cm long with a 10.5 cm bore and 2:1 mirror ratio (inductance 5.4 m μH) corresponding to peak fields $\sim$150 kG in $\sim$14 μs. Initial experiments are reported with 11 MA and 80 kG using 714 kJ for an initial pressure of 100 microns Hg D_2.

The heating is accomplished by a sequence of RF; joule heating to $\sim$1.2 eV ($N_e = 10^{16}$ cm^{-3}, 50—95 percent ionization) by I_0 currents (250 kA); shock heating by the initial implosion when the main bank voltage is applied; dissipation of an initial trapped reverse field which is between 0—10 kG (3.8 kG at present) initially (generated by a 190 kJ slow capacitor bank); and finally slow adiabatic compression by the rising field of the large bank.

An important feature of magnetic compression experiments is the onset of an instability (observed in smaller coils). This is caused by plasma rotation at high compression ratios, which seems to be caused by the relaxation of the reverse field. This instability has not yet been observed in PHAROS, probably because of the relatively long characteristic time for the reverse field relaxation with a plasma diameter of 1.7 cm.

Evidence is presented (for 1/3 of the PHAROS bank) which indicates that end losses are small; reverse field relaxation is not complete; the effective β is high with $\bar{N}_e = 4 \pm 1.5 \times 10^{17}$ (from the visible continuum) and $T_e = 350 \pm 50$ eV. Under these conditions the mean-free-paths are small (≤ 1 cm) so that the plasma pressure should be isotropic and a hydromagnetic description may be expected to have some validity. The total number of confined particles is 10^{20} with a volume compression of 30.

1. Introduction

As described in the preceding paper [1], electron temperatures up to $2—3 \times 10^7$ °K at densities of $7 \pm 2 \times 10^{16}$ electrons/cm^3 have been reached for times of about 5 μs with a 285 kJ capacitor bank. Investigations of the heating rate and confinement time showed that they depended strongly on the coil length and on the dissipation of an initially reverse magnetic field. In high density (collision-dominated) magnetic compression experiments without a trapped reverse field (no closed field lines at the ends), the confinement time is expected [2, 3] to be determined by a parameter $RL/\bar{v}$ (sec); where R is the effective mirror ratio, L the coil length, and $\bar{v}$ the average ion velocity. The detailed dependence of the loss rate on these parameters has not yet been determined, and the factors which determine the effective mirror ratio remain obscure, especially with closed field lines when there is a trapped reversed field. Therefore, experiments with longer coils are desirable.

Also, with long coils ($\sim$2 m) the compression for the first $\sim$5 μs should not be influenced greatly by end effects, for, at temperatures of a few hundred electron volts, sound speeds are of the order 20 cm/μs. It is possible to compute the radial compression and plasma state for an infinite cylinder confined by a pulsed B_z (axial) field from the numerical solution of the full set of hydromagnetic equations [4, 5]. Experiments designed to test the validity of these equations can be made to comply with the assumptions used in the theory. It will be possible to work at higher densities ($\gtrsim 10^{17}$ cm^{-3}) than before, thus assuring that collision times of both ions and electrons will be short compared to the compression time. In that case the plasma pressure should be nearly isotropic throughout the compression, as is assumed in the theoretical analysis. Furthermore, at densities of $\sim 10^{17}$ cm^{-3}, with longer confinement time, the ion and electron temperatures are expected to be nearly equal [5] if the impurity level is not so high as to cause radiation cooling of the electrons (see the discussion in [1]).

The confinement time was limited in practice by an instability that caused the plasma to break up into filaments (Section 3.2), as well as by the loss of particles out the ends. This instability was observed to occur only at high compression when the plasma radius was a few times larger than the calculated ion Larmor radius. In order to increase the plasma diameter and to investigate its influence on the stability, it is

* Conference paper CN-10/189, presented by A. C. Kolb. Discussion of this paper is given on page 647. Translations of the abstact are at the end of this volume of the Conference Proceedings.

** Physics Department, University of Maryland, College Park, Md., U.S.A.

*** On one year's leave of absence from Atomic Energy Research Establishment, Harwell, England.

necessary to increase both the area and length of the coil (because of the end losses).

These considerations led to the design of the much larger PHAROS system, having a load current capability of ~20 MA (compared to the previously available 5.5 MA). With these high currents, magnetic fields in the 100—150 kG range can be produced within magnet volumes of ~15 liters, and the duration of the discharge can be increased to 30 μs. In addition to the main capacitor bank, several auxiliary banks are used to break down and preheat the plasma and provide for an initial quasi-static field. Each of these banks can be operated independently of the others, to study the influence of each component on the compression.

2. Experimental apparatus and operation

2.1. Method of heating

The preionization, initial joule heating, establishment of an initial B_z field and main compression are accomplished by a series of programmed discharges. A low power (1 kW, 20 MHz) RF discharge is capacitively coupled to the ends of the tube and establishes a low level of ionization before any of the capacitor banks are discharged. The low-power preionizing discharge is pulsed for a relatively short time (800 μs) to avoid introducing impurities into the gas.

Following the RF discharge, a 190 kJ slow capacitor bank with a quarter period of 40 μs is discharged into the coil through a 65 mμH isolating inductance. Only 100 kJ were used in the preliminary experiments reported here. (See Table I for the other bank parameters.) This bank is used to produce an initial quasi-static magnetic field up to 10 kG which may be parallel or antiparallel to the main confining field.

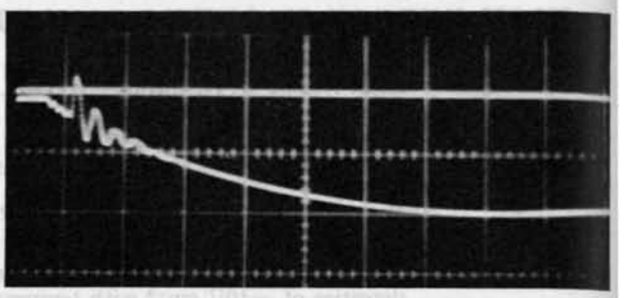

Fig. 1 Oscilloscope traces of preheater and reverse B_z fields. (10 μs/cm and 2.5 kG/cm).

Following the discharge of the slow bank, a 5 μF preheater capacitor bank is discharged after a selected interval of a few microseconds; this produces ~250 kA and fields of ~2 kG in 0.4 μs. The relative timing of the preheater and slow B_z is chosen so that the B_z field is reversed (Fig. 1). As the field goes through zero during the first quarter-cycle, the voltage applied on the coil from the preheater discharge breaks the gas down. Later cycles heat the plasma to 1.1—1.3 eV, giving a high degree of ionization. The breakdown is observed from the voltage waveform and spectroscopic observations of the Balmer lines and continuum radiation, using photoelectric detection (Section 3.1).

The main capacitor bank is discharged after the initial joule heating and in the presence of a quasi-static B_z field. The rapidly-rising field produces an imploding shock wave followed by a slower compression, as in the previous experiments. For the preliminary experiments reported in this paper, one-third of the bank (714 kJ) was used to produce a magnetic field of 80 kG with 11 MA in 10 μs. Typical voltage and current waveforms are shown in Fig. 2.

TABLE I. Capacitor bank parameters with 5.4 mμh load coil (180 cm, 10.5 cm bore, 2:1 mirror ratio)

	2 MJ compression bank	714 kJ (presently)	Preheater	Slow B_z bank
Energy (kilojoules)	2000	714	0.5—1.5	190
Voltage (kilovolts)	20	19	15—25	6
Capacity (microfarads)	10000	3570	5	10500
Quarter period (microseconds)	14	9	0.4	40
Maximum current (megamperes)	~20	11	0.250	1.4
Maximum field (kilogauss)	~150	80	~2	10
External inductance (millimicrohenries)	~3**	4.5	9	65
Number of sections	12	4	2	6
Number of switches	390	140	60*	70

* Pressurized.
** Includes 2 m μH inductance of current collector plate.

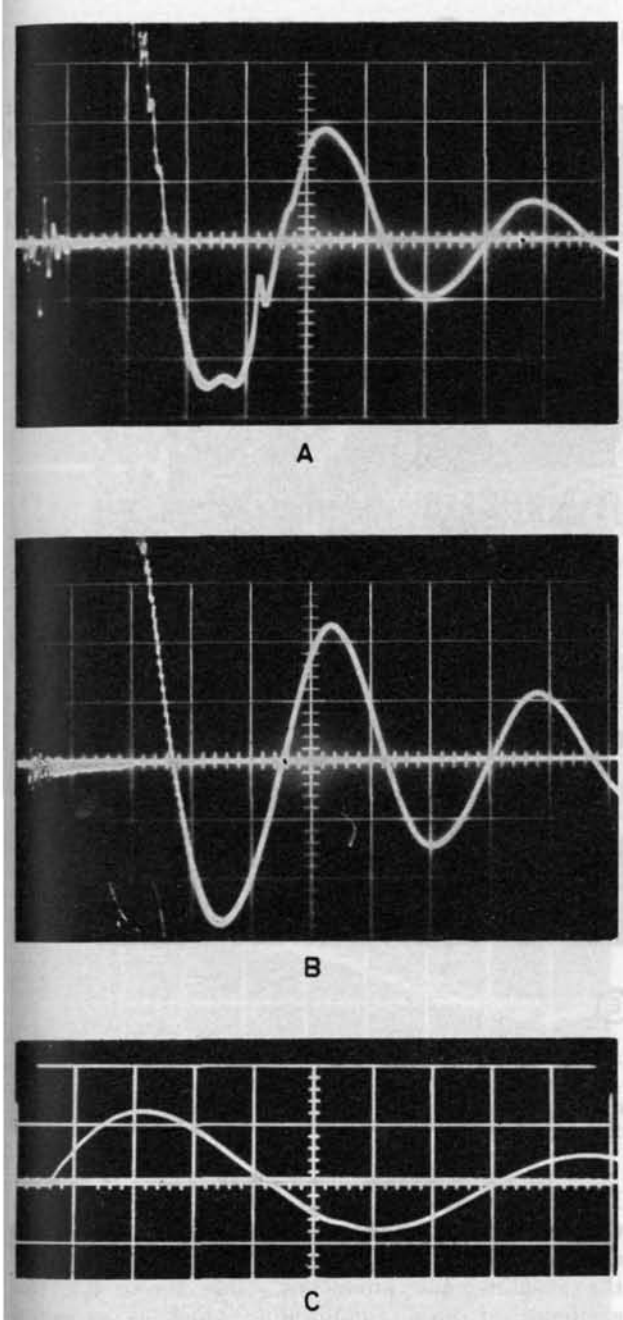

Fig. 2 Oscilloscope traces of the coil voltage and current. (A) Preheater and 714 kJ bank with plasma (3 kV/cm, sweep 10 μs/cm). (B) 714 kJ bank voltage with evacuated tube. (C) Current (9.2 MA/cm, sweep 5 μs/cm).

2.2. Some features of the construction

The coil presently used has a length of 180 cm with a bore of 10 cm. It is constructed of nine separated sections to facilitate side-on spectroscopic and photographic observations. The single-turn copper coils have a wall thickness of 5 cm, except the beryllium-copper end coils which produce a 2:1 mirror ratio within a 20 cm tapered section.

Because of the high mechanical forces, a 16 ft × 4 ft collector plate has been constructed with 142, 1.5-inch diameter bolts, spaced each 8 to 16 inches. To limit the motion of the plates to 0.3 mm (calculated), which is roughly half the thickness of the Mylar insulation, 60 tons of lead are coupled to the top and bottom of the current-carrying copper plates, which are backed up with 2 inches of steel. The copper plates are terminated by a 2-inch thick section of beryllium-copper (8 inches wide and extending over the 16-ft width), which is then connected to the coil. Beryllium-copper is used because of the high fields in the mirror region. The coil and collector system is shown in Fig. 3. This collector assembly has an inductance of 2 mμH (including cable connections) when feeding a 2 m coil.

2.3. Instrumentation

Spectroscopic methods have been employed to determine the initial conditions before the discharge of the main capacitor bank. Three Bausch and Lomb monochromators (f/5, 16 Å/mm) with photoelectric detectors are used to measure electron densities from the line widths of D_β and D_δ and to measure impurity concentrations during the preheater discharge. A 1.8 m, f/26 Bausch and Lomb Littrow Spectrograph with quartz or glass optics is used for the determination of the absolute intensities of the Balmer lines and continuum from which the temperature can be calculated. This spectrograph is presently equipped with 5 photoelectric channels.

Two f/2.9 streak cameras [6] are used for stereoscopic observations of the radial compression in the central plane of the coil, and for comparing observations at different axial positions. These cameras can be calibrated to determine the radial distribution of the electron density [1] during the main compression, when the visible radiation is mainly a continuum. The existence of a trapped magnetic field can be inferred from the radial density distribution without the use of probes.

Four absorber-foil scintillator detectors are used to measure the soft x-ray distribution and electron temperature by the methods described in the previous paper [1]. Conventional BF_3, silver activation and scintillator detectors are employed for the observation of neutrons.

3. Preliminary results

3.1. Preheater-B_z discharge

The joule heating during the preheater discharge is observed to be very reproducible. (The details are given in another paper [7].) Fig. 4 shows three superimposed voltage and D_α, D_γ light intensity waveforms together with the voltage with a vacuum in the tube. Comparison of the voltages with and without plasma shows that the gas discharge begins during the first quarter cycle and damps the preheater appreciably.

A streak photograph (Fig. 5) shows that the rising B_z field compresses the plasma to some extent, and one can estimate the optical path for density measurements from the absolute intensity of the lines and continuum.

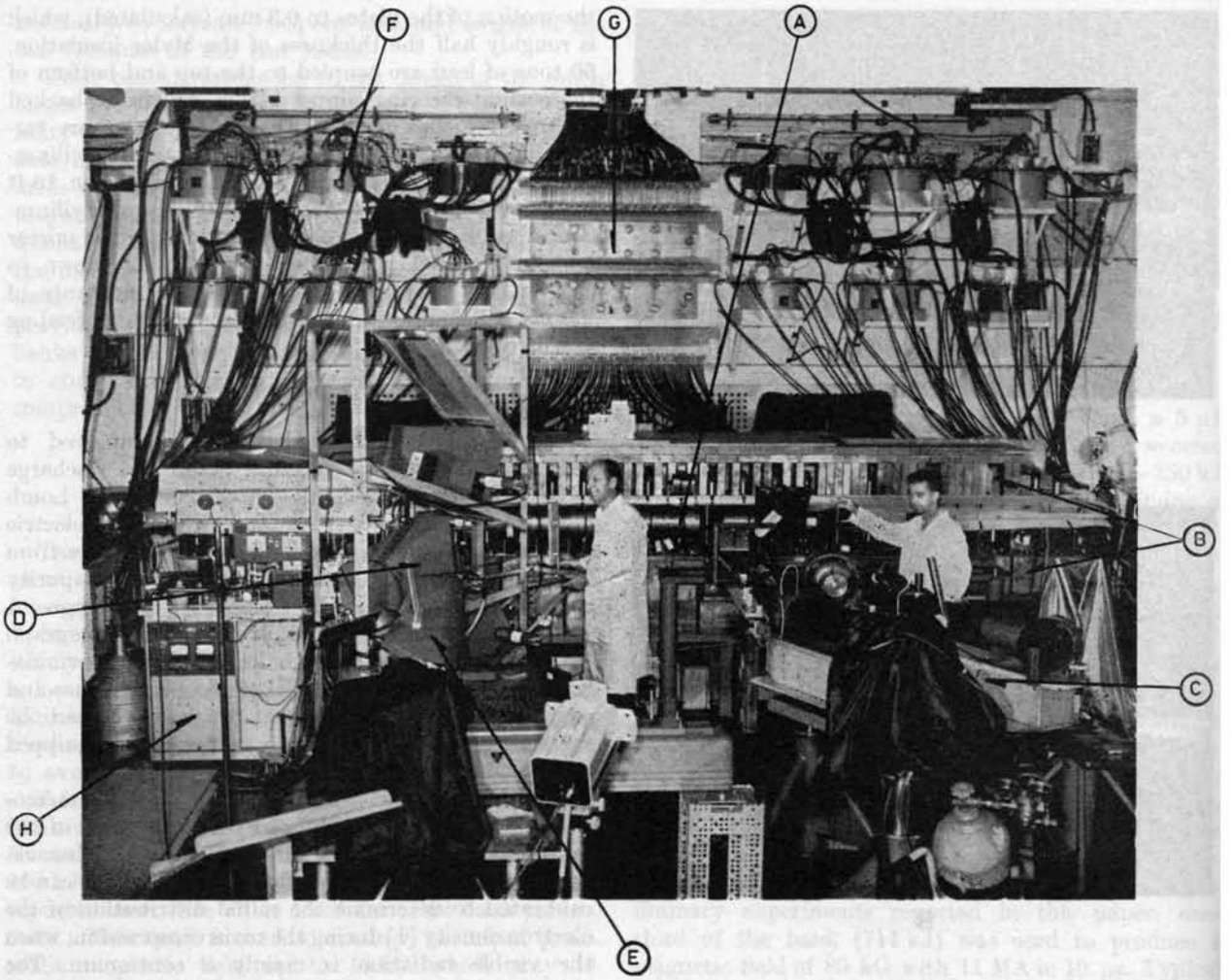

Fig. 3 PHAROS experimental area. Letters designate: A — coil, B — current collector plate, C — streak cameras, D — three monochromators, E — Littrow spectrograph, F — fast preheater capacitor, G — current collector plate for slow B_z bank, H — vacuum system. The main capacitor bank is located in a room behind the collector assembly.

Eight microseconds after the beginning of the preheater discharge, the electron density is 8×10^{15} cm^{-3} (95% ionization) and stays nearly constant for the next 10 μs. However, in this time the number of neutrals increases by a factor of about 5, and the degree of ionization drops to about 80%. Since the plasma radius remains quite constant during this period, this observation shows that the total number of particles in the compressed plasma increases continuously, finally approaching the line density corresponding to the initial pressure (100 microns Hg) at 17 μs. The compressed plasma column, which is formed in the first few microseconds, apparently acts as a pump for the neutrals remaining outside.

Temperatures calculated [8] from the measured line to continuum ratio show a variation of only 5% for 25 discharges (1.3 eV at 8 μs and 1.1 eV at 17 μs), using the Balmer lines. Also, the electron density determined from the absolute continuum intensities, using the measured temperatures, and Stark-broadened line profiles agree with one another to within 8%. Furthermore, the number of neutrals calculated from the Saha equation agrees within the experimental errors (~30%) with those measured directly from the absolute line intensities, thus confirming the existence of local equilibrium, which is expected because of the high electron densities. From the internal consistency of the data, it appears that the initial conditions can be determined with considerable accuracy.

With an initial electron temperature of about 1 eV, the conductivity and β (~0.04) are so low that the quasi-static field at the time the main bank is discharged is nearly homogeneous. However, the conductivity is sufficiently high so that a current sheet can be formed by the fast-rising external field, and the initial field is trapped in the plasma, producing an imploding shock wave.

The moderate compression by the slow B_z field also serves to isolate the plasma from the walls and reduces the possibility of contamination by impurities during the initial ohmic heating.

3.2. Stability

In the 285-kJ compression experiments, the plasma is observed [1, 9, 10] to rotate and then break up into two filaments which usually rotate about each other with an angular frequency $\omega \sim 10^7$ sec^{-1}. For a cylindrical plasma column confined by a B_z field with zero initial angular momentum, there is a balance between

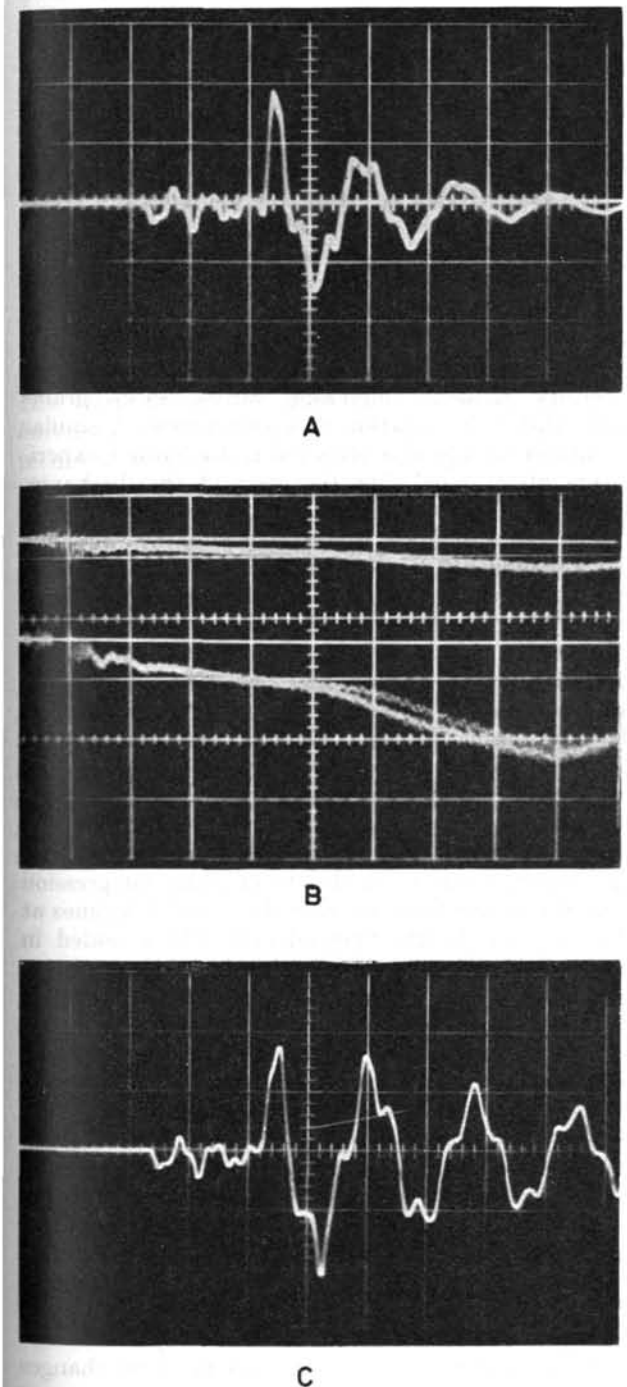

Fig. 4 Superimposed oscilloscope traces obtained from three shots of preheater and reverse B_z banks. (A) Coil voltage (3 kV/cm, sweep 1 μs/cm); (B) photomultiplier outputs from the D_α and D_γ lines; (C) coil voltage with vacuum in the tube.

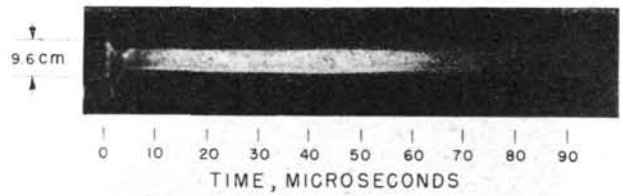

Fig. 5 Streak photographs of the plasma compression produced by the preheater and reverse B_z banks. $N_e = 10^{16}$ cm^{-3}, $T_e = 1.0$—1.25 eV, degree of ionization 90% at 11 μs at and 50% at 20 μs.

the angular momentum due to the guiding center drift and the angular momentum connected with the diamagnetic ion current [10]. If there is an initial trapped reverse field in the plasma which relaxes due to some dissipation process, then the angular momentum associated with the diamagnetic currents, which support the trapped field, appears in the guiding center drift, and the plasma will rotate. These considerations lead to an expression (due to N. Rostoker) for the angular velocity, based on the Vlasov equation using a power series expansion [11] in the ratio of the Larmor radius to the plasma radius

$$\Omega = \frac{4}{\beta}\left(\frac{a_i}{r_0}\right)^2\left(\frac{r_1}{r_0}\right)^2, \tag{1}$$

where β has its usual meaning, a_i is the ion Larmor radius, r_0 is the plasma radius and $r_1 < r_0$ is the location of the current sheet which causes the field reversal. The direction of the rotation is in the direction of the ion current, as is observed.

The stability of a rotating plasma column in an axial magnetic field has also been worked out [10,12]. This shows that the centrifugal forces upset the usual neutral stability for modes $m=2$ and higher. The modes for $m \geq 2$ are stable if

$$\frac{1-\sqrt{m}}{2} < \frac{\Omega}{\Omega_0} < \frac{1+\sqrt{m}}{2}, \tag{2}$$

where $\Omega_0 = 2\,(a_i/r_0)^2\,\omega_i$. Estimates of Ω_0 for the 285-kJ experiments, using the measured value of Ω, show that the observed $m=2$ (fission) mode should be unstable. It is also expected that the fission modes will not develop which result in fragments of the plasma which are smaller than the ion Larmor radius. (The diameters of the fission fragments are close to the ion Larmor radius computed from the measured field strength for kilovolt ions.)

Consideration of Eqs. (1), (2) indicates that one can always expect this instability in magnetic compression experiments with a reverse trapped field *if* this field transfers its energy to the plasma by some dissipative process, but is unlikely to occur if there is no initial reverse field. The fission instability has never been observed in the latter case but is always evident in the (285-kJ experiment) streak photographs with a reverse field.

Numerical solutions of the magnetohydrodynamic equations [5] for the experiments described in the preceding paper [1] show that ordinary collisional

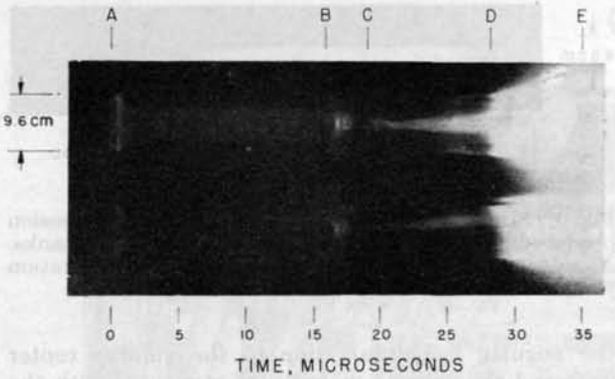

Fig. 6 Stereoscopic streak photographs of the main compression. (A) Preheater fired; (B) 714 kJ bank discharged; (C) sudden increase in luminosity as discussed in text; (D) light from plasma hitting tube wall; (E) end of first half-cycle of current.

dissipation (joule heating) is not inconsistent with the observations of the heating rate and seems to account for the disappearance of the trapped field during the first half-cycle of the discharge. The reverse field relaxation time will depend roughly on r_0^2/η, where η is the resistivity. It was speculated [10] that this instability could be delayed in time by scaling up the characteristic dimensions of the apparatus, as has been done in PHAROS. In the streak camera photographs (Fig. 6) of the main compression with —3.8 kG initial field, this instability has not yet been seen. This supports the assumption that the field dissipation is due to ordinary plasma resistance and not an instability in the plasma current sheet which supports the reverse field. The absence of the fission instability in PHAROS may also indicate that a portion of the reverse field remains trapped during most of the first half-cycle.

This tentative conclusion is supported by measurements of the heating rate from the soft x-ray emission (next Section) and also from the streak camera observations. In the earlier experiments [1] a bright flash of light was seen outside the mirrors, shortly after the sudden heating indicated the relaxation of the trapped field. This light was not seen in PHAROS, thus implying that the closed field lines in the plasma prevented rapid end losses.

Although the macroscopic stability of the plasma seems to be good, a slow drift toward the slot in the coil ($\sim$0.3 cm/μs) causes the plasma to hit the wall after 12 μs. Attempts to improve the cylindrical symmetry of the fields at the ends may reduce this drift. However, streak photographs without an initial B_z field do not show this drift. There have not been enough observations to tell whether or not the slow drift observed in some of the discharges with a reverse field is typical.*

To summarize: there is a marked improvement in the macroscopic stability and confinement in the larger PHAROS coil, which also serves to suggest that internal instabilities do not result in the rapid relaxation of the trapped fields.

3.3. Electron temperatures and density

The electron density was measured from the absolute intensity of the continuous radiation over a 100 Å band at 4340, 4600, and 5700 Å. The optical path was found from the streak camera photograph. The three density determinations yield a maximum value of $\bar{N}_e=(4\pm1.5)\times10^{17}$ cm^{-3} at 8 μs after the start of the discharge when the plasma diameter was 1.7 ± 0.2 cm. With 9.6 cm as the initial diameter, the volume compression is about 32. For an initial density of 7×10^{15} cm^{-3}, the expected density is $2.2\pm0.5\times10^{17}$ cm^{-3}, which is within the experimental error. However, some axial contraction could cause an increase in line density in the central plane of the coil.

However, there is a curious feature in the streak photograph (Fig. 6) which is not explained. Between 3 and 4 μs after the beginning of the implosion little light is emitted from the plasma, after which the intensity suddenly increases. Streak spectrograms show that this radiation is a continuum. A similar phenomenon was also observed in the earlier experiments about 2 μs after the start of the discharge. From the observed plasma radius and intensity of visible radiation one would conclude that the line density suddenly increased to the initial line density; but the question remains, where did the plasma come from? One possibility is that for some reason the electron velocity distribution is non-maxwellian during the initial rapid heating, and one cannot apply the usual continuum formula. Then, because of the high density, the electron gas equilibrates and the luminosity increases to the expected level. Another possibility is that there are neutrals left behind during the compression, which diffuse into the plasma column, raising its density. Or alternatively, an increase in line density could occur due to an axial compression from the mirror fields or from the closed field lines at the ends due to the trapped field. [Note added in proof: This effect could also be due to a resistive instability which causes the plasma column to separate into pieces along the axis [14]. This refers in particular to the phenomena at D, Fig. 3 on page 547, which may or may not be similar to dimming of radiation at C, Fig. 6 above. We refer to these questions as the "Salzburg dilemma".]

The electron temperature reaches a maximum of 350 eV at the time of the current maximum. With the measured electron density and $B_z=80$ kG, one obtains a β of the order unity. The error in estimating β is difficult to determine since only average values of T_e and N_e are obtained. It is interesting, however, that with a reverse field the highest temperature and density occur in the region where the field changes direction, and the β is unity [5].

The observed electron temperature is roughly consistent with the expected heating due to an adiabatic compression of a shock preheated plasma [13] without the dissipation of the reverse field.

* Note added in proof: Subsequent experiments show this drift is a characteristic of the present experimental arrangement.

All the present observations in PHAROS of the stability, temperature, density, compression, and confinement seem to *indicate* that with larger plasma diameters the reverse field relaxation time is longer than 15 μs. This conclusion is by no means definitive because the impurity concentrations are not yet known, and it could be that the density measurement from the visible radiation is in error, and the electron temperature is held low because of radiation losses. However, it appears that in spite of some theoretical objections it is possible to produce a dense plasma with high ion and electron temperatures and local regions of high β in mirror geometries.

Finally, one calculates that increasing the discharge energy by about a factor 3 to 2 MJ should result in temperatures of 700—1000 eV with densities near 10^{17} cm^{-3}, even if the residual reverse trapped field does not dissipate completely.

Acknowledgments

We should like to express our appreciation to Drs. R. M. Page, W. C. Hall and C. V. Strain for their encouragement and for providing the financial and technical assistance which made possible the construction of the PHAROS system. The additional support of the U.S. Atomic Energy Commission and the cooperation of Dr. A. Ruark in this venture were of considerable importance. The many people at the U.S. Naval Research Laboratory who contributed to the project deserve much of the credit. In particular, we would like to express our gratitude to P. Shifflett, G. F. Wall, M. P. Young and C. B. Dobbie (electrical engineering); J. M. Frame (general engineering and collector plate design); C. Martin and B. Taubersmith (design drafting); W. Andrews for providing help with the control system; G. Seaver, S. Leo, J. P. Deverin, F. Ridgeway, J. A. Piatt for help in planning and supervising the construction; T. De Rieux, L. Melhart, E. C. Turbyfill, E. Laiken, W. Byrnes, J. Meeks, J. Perry, E. Vincent, J. Robinson, R. L. Grant, G. E. Holloway, T. L. Lockhart and R. L. Borkey (technical assistance); L. B. Clark and M. Fink for their work with the large quartz tubes; R. C. Elton and F. D. Harrington for assistance with the optical instrumentation; C. E. Thompson for photographic assistance; and J. V. Moran for his help in the general planning and coordination.

The work reported here was jointly supported by the U.S. Atomic Energy Commission and the Office of Naval Research.

References

[1] Griem, H. R., Kolb, A. C., Lupton, W. H., Phillips, D. T., page 543 of these Proceedings.
[2] Kolb, A. C., Griem, H. R., Faust, W. R., Proceedings of Fourth International Conference on Ionization Phenomena in Gases, Uppsala (North-Holland Publishing Co., Amsterdam) **2** (1959) 1037.
[3] Kolb, A. C., *Rev. Modern Phys.* **32** (1960) 755.
[4] Hain, K., Hain, G., Roberts, K. V., Roberts, S. J., *Z. f. Naturf.* **15** (1960) 12.
[5] Hain, K., Kolb, A. C., page 561 of these Proceedings.
[6] Brauer, F. L., Hansen, D. F., *J. Opt. Soc. Am.* **49** (1959) 421.
[7] Lupton, W. H., McLean, E. A., Phillips, D. T., Proceedings of the Fifth International Conference on Ionization Phenomena in Gases, Munich (1961), to be published.
[8] Griem, H. R., Proceedings of the Fifth International Conference on Ionization Phenomena in Gases, Munich (1961), to be published.
[9] Rostoker, N., Kolb, A. C., *Bull. Am. Phys. Soc.* II, **6** (1961) 203.
[10] Rostoker, N., Kolb, A. C., *Phys. Rev.* **124** (1961) 965.
[11] Rosenbluth, M. N., Rostoker, N., *Phys. Fluids* **2** (1959) 23.
[12] Rosenbluth, M. N., Rostoker, N., Krall, N., page 143 of these Proceedings.
[13] Kolb, A. C., Faust, W. R., Anderson, A. D., *Nuclear Fusion* **1** (1961) 257.
[14] Furth, H. P., private communication and *Bull. Am. Phys. Soc. II* **7** (1962) 405.

FAST THETA-PINCH*

K. HAIN

INSTITUT FÜR PLASMAPHYSIK, GARCHING BEI MÜNCHEN

FEDERAL REPUBLIC OF GERMANY

A. C. KOLB

U.S. NAVAL RESEARCH LABORATORY

WASHINGTON, D.C., UNITED STATES OF AMERICA

A fully ionized plasma with cylindrical symmetry is assumed. The hydromagnetic theory should be valid, that is, the two-fluid model with charge neutrality including electrical resistivity and thermal conductivity. The ion and electron temperatures are treated separately. As an initial condition a fully ionized homogeneous plasma with magnetic fields is assumed. To this plasma B_z-fields are applied. The resulting partial differential equations are solved numerically. The numerical methods for solution are discussed in a separate paper. The effects of different initial B_z-fields — parallel, zero, reversed — are discussed.

In all cases there are types of shock waves running into the undisturbed plasma. With parallel fields a simple consideration shows that the Mach-number has to exceed 3/2 to get an ion temperature higher than electron temperature. In the zero field case, because of high thermal conductivity in absence of magnetic fields, a heat wave of electrons runs in front of the shock front. The reversed field case shows the highest ion temperature.

The results are compared with experiments done in the Naval Research Laboratories, Washington, D. C.

1. Introduction

It has now been established experimentally in a number of laboratories that high temperature plasmas can be produced in a fast theta-pinch. In these experiments a low temperature plasma is first formed by an auxiliary discharge or by the first half-cycle of the main discharge. After the preheating phase, the plasma is then compressed rapidly by a fast rising magnetic field. In experiments where the electron density is high enough so that the mean free path of the ions and electrons is less than the length of the apparatus [1, 2], one expects the particles to have a random velocity distribution and the plasma to behave as a three-dimensional $\gamma=5/3$ fluid. Furthermore, during the implosion phase the particle mean free paths are of the order of millimeters, which is small compared to the tube diameter, and the shock waves which are produced should be collision-dominated. One of the main objects of the present paper is to see whether the observed phenomena (compression, heating rate, dissipation of a reversed-trapped magnetic field, etc.) can be accounted for in the hydromagnetic approximation, taking into account the characteristics of the external circuit which produces the magnetic field.

2. Theoretical assumptions

The full magnetohydrodynamic equations for a neutral, fully ionized plasma having a cylindrical symmetry have been solved numerically for certain pinch experiments [3]. Results will be given here for the case where the magnetic field is directed along the axis of the discharge tube (E_θ, B_z configuration of the "theta-pinch"). Earlier difficulties connected with the numerical stability in cases of high magnetic fields (high Alfvén velocities) have been overcome by using an implicit method.

The assumption of cylindrical symmetry implies that end losses are not taken into account. However, numerical calculations [4] of the adiabatic compression of a finite plasma cylinder containing a trapped magnetic field show that the final temperature is not greatly influenced by end losses (there are variations of perhaps 25%) and that the observed [5] electron temperatures are at least a factor 2 higher than predicted by the adiabatic theory if field dissipation is not taken into account. A program which will take into account end losses will be prepared in the future. Inany case, the present computer program is expected to give accurate results for times shorter than l/v_s, where l is the tube length and v_s is the velocity of sound. For tubes longer than about 50 cm (see Section 4), this time is several microseconds, and might be longer if the closed field lines at the ends inhibit the flow of plasma out the ends for the reverse field case.

Initially, at $t=0$, the plasma is assumed to fill a cylindrical tube of radius R, have a homogeneous density ϱ_0, trapped magnetic field B_{z0} (of either polarity relative to the main confining field) and electron and ion temperatures T_{e0}, T_{i0}. At the

* Conference paper CN-10/28, presented by K. Hain. Discussion of this paper is given on page 635. Translations of the abstract are at the end of this volume of the Conference Proceedings.

time $t=0$, a voltage V_θ is applied to the single-turn coil by discharging a capacitor bank charged to V_c with a capacitance C and external inductance L_1. The inductance L_2 of the insulating discharge tube is approximately given by

$$L_2 = \frac{4\pi\,(R_1^2 - R^2)}{l}\,, \tag{1}$$

where R_1 is the coil radius.

The voltage V_θ around the plasma column is determined by the rate of change of magnetic flux

$$V_\theta = \frac{\mathrm{d}\Phi}{\mathrm{d}t}\,, \tag{2}$$

where

$$\Phi = 2\pi \int_0^R E_z(r)\, r\, \mathrm{d}r\,. \tag{3}$$

The total current is expressed in terms of the magnetic field in the single-turn solenoid

$$B_z(R) = \frac{4\pi}{10}\,\frac{I}{l}\,. \tag{4}$$

If the coil ends are constricted to produce a mirror field, Eqs. (1) and (4) are multiplied by an appropriate constant determined by separate inductance calculations. The current is found from the circuit equation

$$(L_1 + L_2)\,\frac{\mathrm{d}I}{\mathrm{d}t} = V_c - V_\theta - I\,r\,; \quad \frac{\mathrm{d}V_c}{\mathrm{d}t} = -\frac{I}{C}\,, \tag{5}$$

where r is the external resistance which damps the discharge.

2.1. Equations of motion

The hydromagnetic equation gives the flux Φ at each time, whereas the circuit equation gives the total current. Therefore, $B_z(R)$ is evaluated with Eq. (4) and serves as a boundary condition for the solution of the partial differential equations. The other boundary conditions are discussed later.

The conservation of mass and momentum are described by the usual set of partial differential equations, with gas flow only in the radial direction

$$\frac{\mathrm{d}\varrho}{\mathrm{d}t} + \varrho\,\mathrm{div}\,v = 0 \tag{6}$$

$$\frac{\mathrm{d}v}{\mathrm{d}t} + \frac{1}{\varrho}\,\frac{\partial}{\partial r}\,(P_e + P_i + \varrho\, q_i) + \frac{1}{\varrho}\,B\,\frac{\partial B}{\partial r} = 0\,, \tag{7}$$

where $B_z \equiv B$, $v_r \equiv v$ and

$$\frac{\mathrm{d}}{\mathrm{d}t} = \frac{\partial}{\partial t} + v\,\frac{\partial}{\partial r}\,; \quad \mathrm{div} = \frac{1}{r}\,\frac{\partial}{\partial r}\,r\,. \tag{8}$$

The von Neumann term is applied only to the ions and is taken to be

$$\begin{aligned} q_i &= L^2\,(\mathrm{div}\,v)^2 \text{ if } \mathrm{div}\,v < 0\,; \\ &= 0 \text{ if } \mathrm{div}\,v \geq 0\,. \end{aligned} \tag{9}$$

This artificial term conserves mass, momentum and energy across the shock front having a width L, which is arbitrarily taken to be approximately 1/10 the radius R. One of the main difficulties in the theory is the correct calculation of the structure of the shock front, with the proper relative heating of ions by the shock wave and ohmic heating of the electrons. The theoretical viscosity of a fully ionized plasma is much too small to be of any practical use in the numerical computation. Attempting to widen the shock artificially but maintaining the correct structure has led to numerical instabilities*.

The internal energy $\mathscr{E}$ and equation of state are taken to be

$$\mathscr{E} = P/(\gamma - 1)\,; \quad P = \varrho\, T\,; \tag{10}$$

and the energy equations for ions and electrons are

$$\begin{aligned} &\frac{\mathrm{d}T_e}{\mathrm{d}t} + (\gamma - 1)\,T_e\,\mathrm{div}\,v \\ &= \mathrm{div}\left(\varkappa_e\,\frac{\partial T_e}{\partial r}\right) + \frac{\mu}{\varrho}\,(\gamma - 1)\left(\frac{\partial B}{\partial r}\right)^2 - \frac{T_e - T_i}{t_{eq}}\,, \end{aligned} \tag{11}$$

$$\begin{aligned} &\frac{\mathrm{d}T_i}{\mathrm{d}t} + (\gamma - 1)\,(T_i + q_i)\,\mathrm{div}\,v \\ &\qquad = \mathrm{div}\left(\varkappa_i\,\frac{\partial T_i}{\partial r}\right) + \frac{T_e - T_i}{t_{eq}}\,, \end{aligned} \tag{12}$$

where μ is the Spitzer resistivity expressed in $\mathrm{cm}^2/\mu\mathrm{s}$ and $t_{eq} \sim T_e^{3/2}/\varrho$ is the ion-electron energy equipartition time. The energy equation for the electrons allows for ohmic heating while the von Neumann shock heating term q_i appears only in the ion energy equation. $\varkappa_e$, $\varkappa_i$ are the heat diffusion coefficients

$$\varkappa \sim \frac{T^{5/2}}{1 + (\omega\tau)^2} = \frac{T^{5/2}}{1 + \alpha\, B^2\, T^3/\varrho^2}\,, \tag{13}$$

with $\alpha = \text{constant}$ [6].

The equation for B expresses Ohm's law and flux conservation

$$\mathrm{d}B/\mathrm{d}t + B\,\mathrm{div}\,v = \mathrm{div}\,(\mu\,\partial B/\partial r)\,. \tag{14}$$

2.2. Boundary conditions

The solution of the above set of equations requires boundary conditions at $r=0$, R; the conditions $r=0$ are trivial and at $r=R$, B is given by Eq. (4) as discussed above.

The temperature at the wall is held constant

$$T_e(R) = T_i(R) = T_{e0} = T_{i0} = \text{constant}, \tag{15}$$

and the radial gradient of T_e and T_i may not exceed a certain value (once the plasma has detached itself from the walls these temperature boundary conditions do not have any influence on the state of the compressed plasma, i.e. the rapid heating soon masks the influence of the initial conditions as well as the temperature boundary condition). The boundary condition for the density is

$$\varrho(R) \geq \varrho_{\min}, \text{ if } v(R) < 0\,, \tag{16}$$

and the density piles up at the wall if $v(R) \geq 0$, as is the case when the external field is less than the

* One of us (K. H.) would like to thank K. V. Roberts (Harwell) for clarifying discussions on this point.

internal field during the time it takes to trap a reverse magnetic field in the plasma. This boundary condition makes the wall a source of plasma to avoid extremely low densities, high Alfvén velocity and accompanying numerical difficulties. The boundary condition for the radial flow velocity v is given by momentum balance at the last mesh point used in the solution of the difference equations.

2.3. Numerical considerations

This set of partial differential equations together with the boundary conditions is solved by an implicit method which will be described by one of us [7]. The main difficulty is connected with the very high velocities of Alfvén waves in the low density region outside the main column of compressed plasma. In the implicit method the time step is not limited by the characteristics, but with high magnetic fields small fluctuations in B give rise to rather violent velocity fluctuations with a complicated wave structure and this leads to fluctuations in V_θ and eventual numerical instabilities. Experience has shown that after the first bounce (following the initial implosion of the plasma) an artificial damping term in the low density region near the wall can be used to smooth these fluctuations. Accordingly, a term was added to the resistivity in Eq. (14)

$$\mu_j \to \overline{\mu}_j = \mu_j + A\,\frac{(B_j - B_{j-1})^2}{j}\,Y^{-\varrho j/\varrho_{\max}}, \qquad (17)$$

where $A \sim 0.2$, $Y \sim 2000$ and j numbers the mesh point. The factor involving Y and the maximum density makes the added term small where the density is high even if there are large gradients in B, i.e. near the current sheet causing field reversal. The energy connected with the waves smoothed by this term is lost from the system. The smoothing term leads to numerical stability; however, in some cases the time step became very small. The time step could be increased by adding an additional constant term to the resistivity which is large only in regions where the density is less than 1/50 the maximum density. Such a term tends to prevent the development of any fluctuation in B and v in the outside regions.

2.4. Shock structure and heating

The other difficulty mentioned earlier is in the computation of the relative heating of ions and electrons in a shock wave carrying currents and moving into a magnetic field. This problem has not yet been solved satisfactorily but some theoretical estimates of the relative heating rates can be given. If L is the shock width, the ohmic heating rate $\mathscr{E}_j$ for strong shock waves becomes

$$\mathscr{E}_j = \int \mu \left(\frac{\partial B}{\partial x}\right)^2 \mathrm{d}x \approx \mu \left(\frac{2}{\gamma - 1}\right)^2 \frac{B_0^2}{L}. \qquad (18)$$

The jump in the magnetic field across strong shock fronts is $B_1 - B_0 = B_0\,[(\gamma+1)/(\gamma-1) - 1]$. The index "0" designs the value in front of the shock front.

The gain in thermal energy by shock heating is of the order

$$\mathscr{E}_s = \varrho_0\, v^2\, v_s\, \frac{\gamma + 1}{\gamma - 1}, \qquad (19)$$

v_s being the velocity of the shock front relative to the velocity of the plasma in front of the shock.

Introducing the Alfvén Mach-number

$$M^2 = \frac{v_s^2}{B_0^2/\varrho_0} \qquad (20)$$

and taking the ratio of the two heating rates, yields

$$\frac{\mathscr{E}_s}{\mathscr{E}_j} \approx \frac{(\gamma+1)\,(\gamma-1)}{4}\,\frac{\varrho\, v^2}{B^2}\,\frac{L v_s}{\mu}. \qquad (21)$$

One finds with $\gamma = 5/3$ and introducing $L_r \approx \mu/v_s$, the shock width determined by resistivity, that

$$\frac{\mathscr{E}_s}{\mathscr{E}_j} \approx \frac{4}{9}\,M^2\,\frac{L}{L_r}. \qquad (22)$$

If $L = L_r$, then the ions gain more energy than the electrons for $M > 3/2$.

The next question is whether the Larmor radius r_L can be considered as small compared to L. Diffusion processes connected with finite Larmor radius have a diffusion constant μ_L of the order

$$\mu_L \approx r_L\, v_s \approx \frac{m\sqrt{\overline{v^2}}\; c}{e\,B}\, v_s, \qquad (23)$$

with

$$v_s \sim \sqrt{\frac{B_0^2}{\varrho}}$$

for strong shocks,

$$\mu_L \approx \lambda_D\, c, \qquad (24)$$

where λ_D is the Debye length.

Therefore, if the ratio

$$\frac{\mu_L}{\mu} \approx \frac{c\,\lambda_D}{L_r\, v_s} \qquad (25)$$

is small compared to unity, the shock width is determined mainly by the resistivity. For $\lambda_D \sim 10^{-5}$ cm, $T_e \sim 2$ eV and $\mu \sim 1$ cm$^2/\mu$s

$$\frac{\mu_L}{\mu} \sim 0.3.$$

For much higher temperatures the shock width L is determined by the Larmor radius and, according to Eq. (22), the ions gain more energy from the passage of the shock wave than the electrons. Therefore, the introduction of the shock heating term q_i only into the energy equation for the ions seems to be justified.

3. Discussion of numerical results

To illustrate the evolution of the plasma during the fast magnetic compression in a theta-pinch, three cases were run for a proposed typical large experiment (Figs. 1—8). The initial plasma conditions were held constant ($n_e = n_i = 5 \times 10^{15}$ cm^{-3}, $T_e = T_i = 1$ eV) and

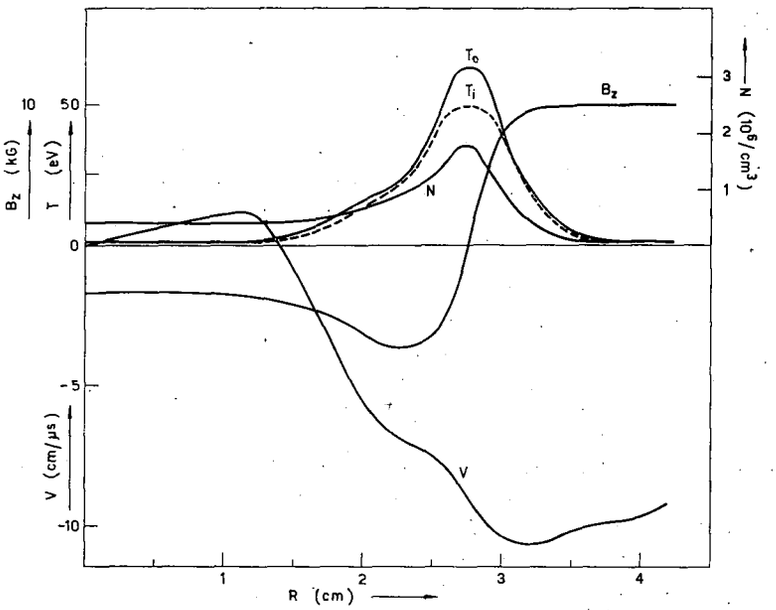

Fig. 1 B_z, T_e, T_i, N, and V as functions of the radius at about half the bounce time for $B_{z0} = -5$ kG, $t = 0.3640$ μs.

the trapped magnetic field was varied $B_0 = (-5, 0, +5)$ kilogauss. The other parameters were:

Tube length	100 cm
Tube bore	10 cm
L_1	3 mμH
L_2	1.8 mμH
C	3300 F
r	0
V_c	30 kV

In Figs. 1—6 the various quantities are plotted as a function of radius at two different times. Figures 1—3 show the configuration at about one-half the implosion time. One sees already the characteristic differences in the density distribution. For the reversed field case the density distribution shows a hump in the $\beta = 1$ region where there is a current sheet which causes the reversal. In the parallel field case, however, the density distribution is quite flat because there the Alfvén velocity is high and the Mach number of the imploding shock wave is low. This general behavior is observed in streak camera photographs where, in the reverse field case, the density hump appears as a bright luminous line moving toward the axis. In the parallel field case the imploding luminous front is not observed to be well defined, as one would expect from these calculations. The compression time with the reverse field is about one-half that for the parallel field, which is also in rough agreement with photographic observations [8, 9].

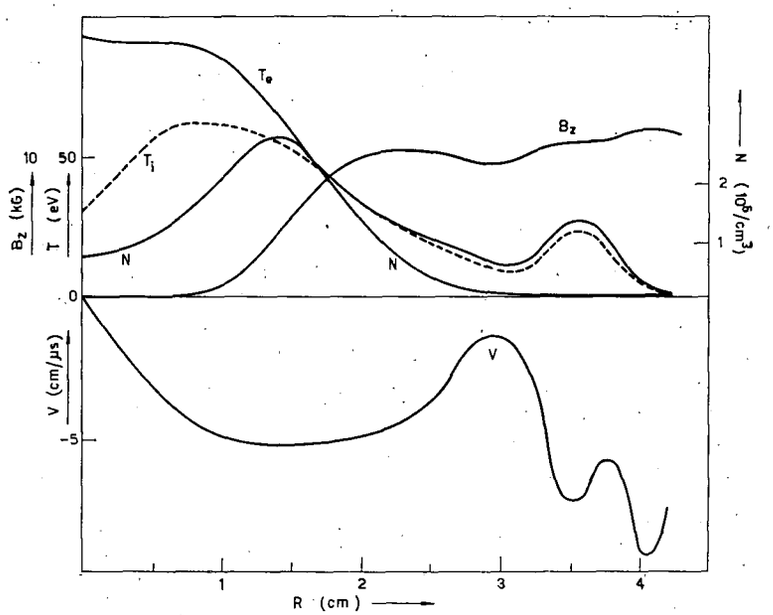

Fig. 2 B_z, T_e, T_i, N, and V as functions of the radius at about half the bounce time for $B_{z0} = 10^{-4}$ kG, $t = 0.3243$ μs.

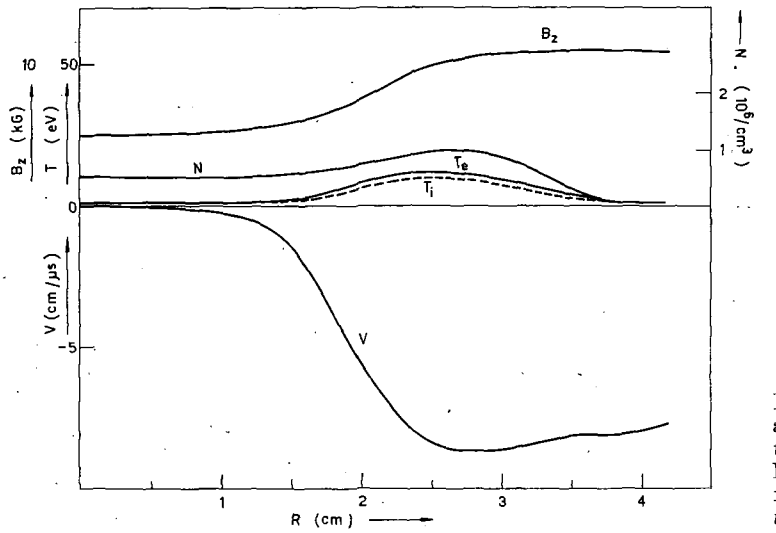

Fig. 3 B_z, T_e, T_i, N, and V as functions of the radius at about half the bounce time for $B_{z0} = +5$ kG, $t = 0.16$ μs.

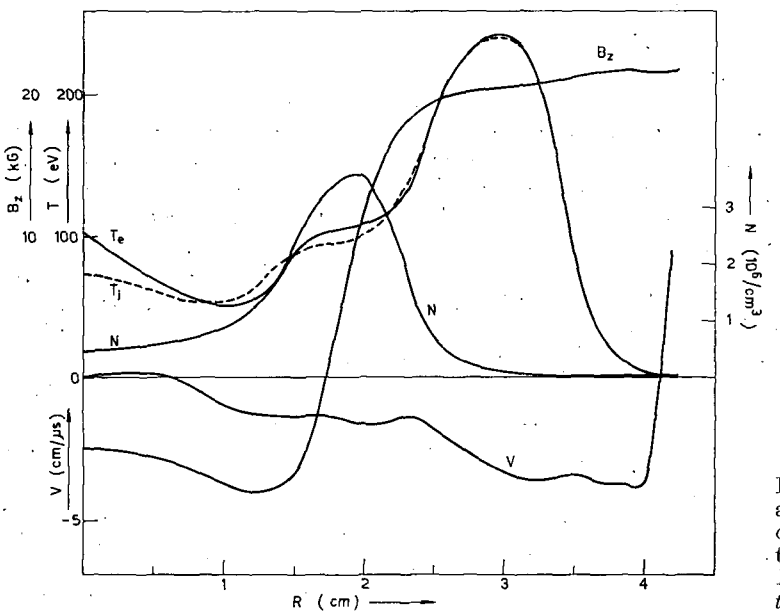

Fig. 4 B_z, T_e, T_i, N, and V as functions of the radius at about the bounce time for $B_{z0} = -5$ kG, $t = 0.7343$ μs.

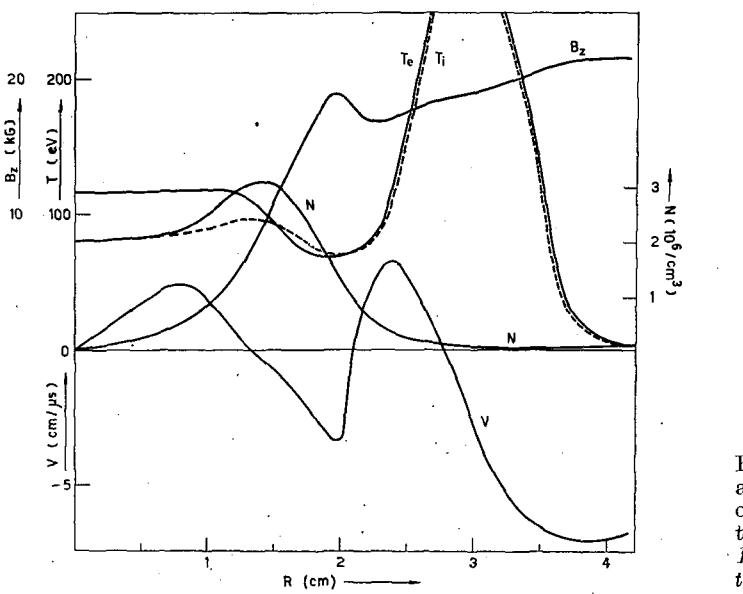

Fig. 5 B_z, T_e, T_i, N, and V as functions of the radius at about the bounce time for $B_{z0} = 10^{-4}$ kG, $t = 0.5873$ μs.

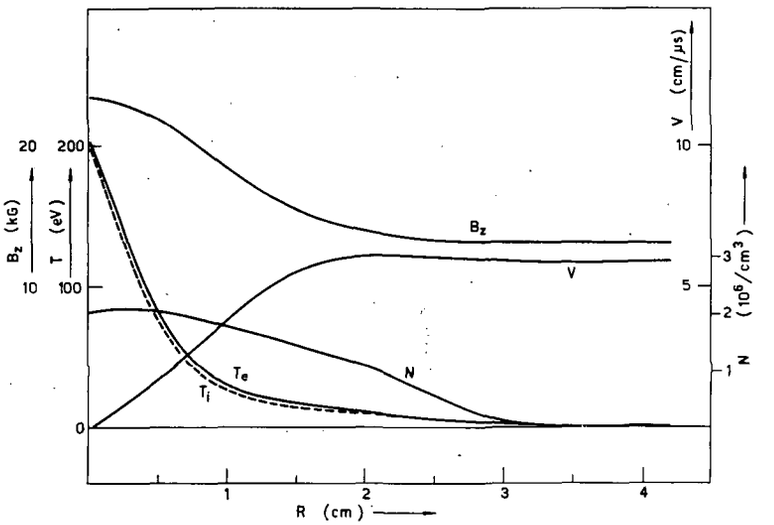

Fig. 6 B_z, T_e, T_i, N, and V as functions of the radius at about the bounce time for $B_{z0} = +5$ kG, $t = 0.275$ μs.

In the zero field case an electron heat wave moves ahead of the shock front because of the high heat conductivity of the electrons in the zero field region. The plasma energy produced by ohmic heating is transported to the center by this mechanism, which is important if the initial trapped magnetic field is less than about 500 gauss. The temperatures reached at the time the first shock wave reflects off the axis are comparable in all three cases. However, after long times the highest temperatures are reached in the reversed field case because of the ohmic heating in the current sheet which separates the internal and external magnetic fields (Figs. 4—6).

The rising temperature in the center of the pinch is caused by three combined effects. As a result of the first compression of the trapped magnetic field, there are high current densities near the center of the order 5 kA/cm², which heats the electrons. The ions are heated by the converging shock wave and by electron-ion relaxation. Secondly, the temperature rises due to heat conduction, which is big enough to be important because of the small dimensions even though the heat conductivity is small. Thirdly, the temperature rises by adiabatic compression.

Figure 7 shows the variation of B_z with time for the reverse field case at $r=0$, 2 cm. Because of the rapid rise of the magnetic field, the trapped magnetic field rises to more than twice the value of the external field due to dynamic effects.

The motion of the current sheet as it moves toward the axis is shown in Fig. 8 for the reverse field case. The region of maximum density moves with this current sheet and one can see clearly the shock front

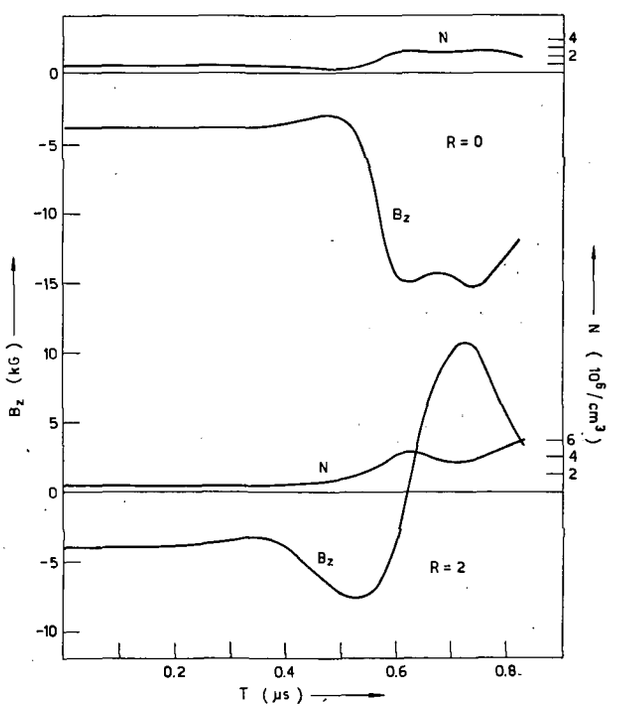

Fig. 7 B_z and N as functions of time at $r=0$ and $r=2$. Parameters slightly different from those in Figs. 1—6 have been used, but the characteristic features are the same.

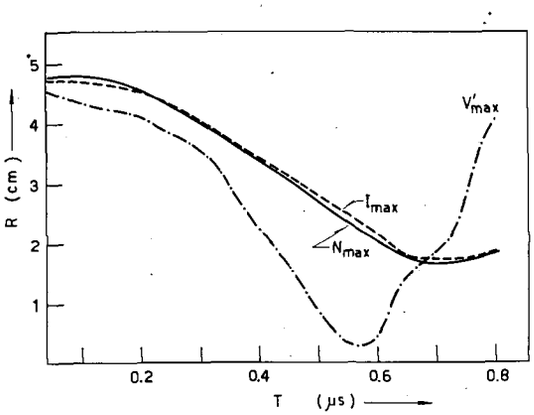

Fig. 8 Shock and current sheet position as a function of time. Parameters slightly different from those in Figs. 1—6 have been used, but the characteristic features are the same.

(characterized by the point at which the velocity gradient is a maximum) being driven ahead of the highest current region.

After the first bounce there are outward moving shock waves which travel with approximately the Alfvén velocity in the outside region, i.e. about 100 cm/s. These waves move back and forth between the main pinch and the wall. These waves hitting the wall may be responsible for the impurity radiation observed near the wall in certain experiments [10] with high coil voltages and very fast implosion velocities. Experimentally, one should also find fluctuations in the coil voltage because of the waves which carry field lines along with them. If such fluctuations are not observed experimentally, then it is likely that the plasma density near the wall is higher than assumed in the calculation ($\sim 1/20$ the ambient density). If this is the case, then the wall may be emitting gas as is apparently the case in ordinary z-pinches [11].

There is also another physical explanation why the computed fluctuations do not appear. In the numerical calculation cylindrical symmetry is assumed; therefore the Alfvén waves are theoretically coherent, whereas experimentally there is not a smooth cylindrical surface of the plasma. There are Rayleigh-Taylor instabilities [12]. Therefore, the emitted waves are in fact incoherent. Therefore such wild fluctuations caused theoretically by coherent Alfvén waves should not exist*. Theoretically one should introduce either a high electrical resistivity, as has been done in this paper, or a high artificial viscosity in low density regions outside the main pinch. This will be tried in further calculations.

4. Comparison with experiment

Experiments have been carried out at the Naval Research Laboratory [5] with relatively long coils so that the influence of end losses on the plasma in the central region should not be serious for several microseconds. The size of the capacitor bank, voltage and tube volume are smaller than for the previous example. The experimental parameters were:

V_c	17 kV
C	1140 μF
L_1	5 mμH
L_2	1.2 mμH
r	7×10^{-4} ohm
l	70 cm
R	2.5 cm
R_1	3 cm
I_{max}	5.5 MA
quarter-period	5 μs
P_0	100 microns Hg
B_{z0}	—3 kG
maximum field	80 kG.

* One of us (K. H.) would like to point out that this explanation had been proposed to him first by H. Jordan in a discussion.

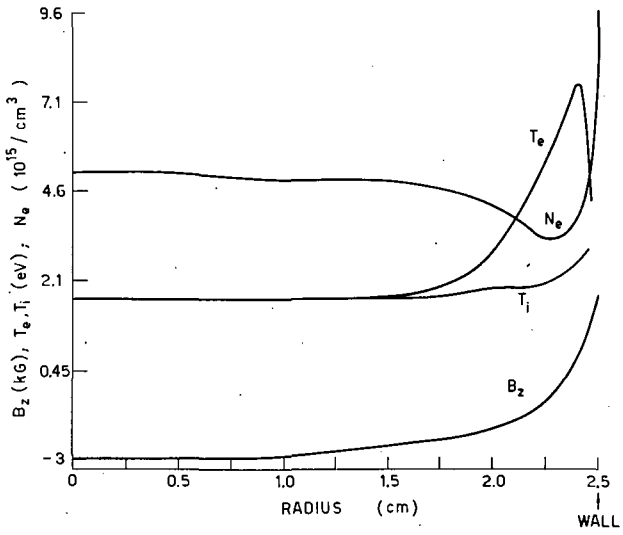

Fig. 9 Theoretical distribution of physical quantities as functions of the radius for $t = 0.12$ μs. The scaling was done automatically by the computer according to the maximum and minimum values.

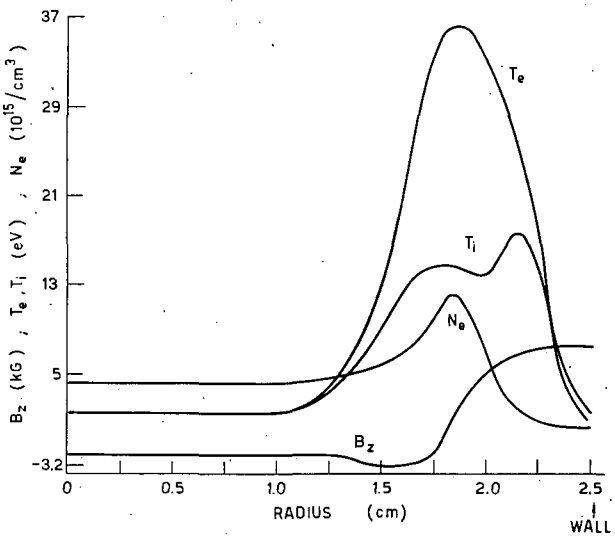

Fig. 10 Same as Fig. 9 except for $t = 0.3$ μs.

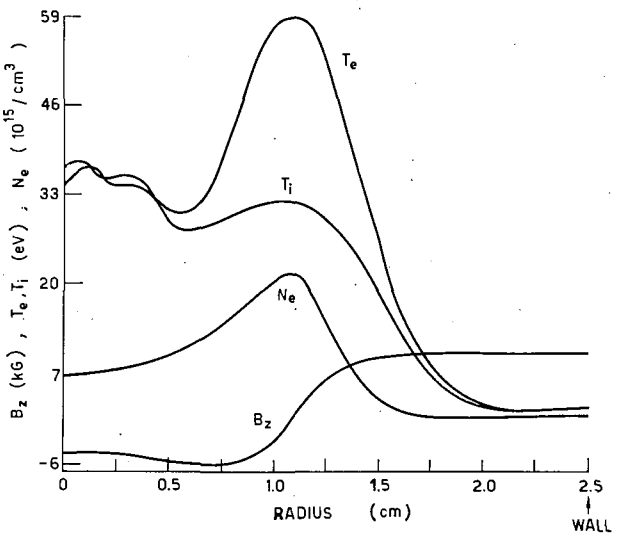

Fig. 11 Same as Fig. 9 except for $t = 0.4$ μs.

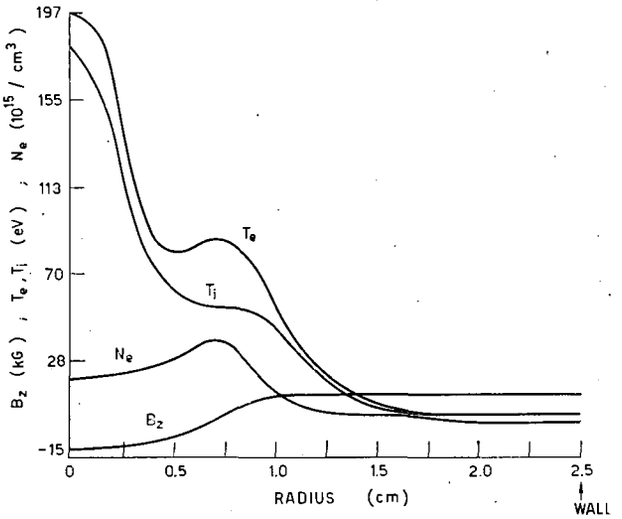

Fig. 12 Same as Fig. 9 except for $t = 0.5$ μs.

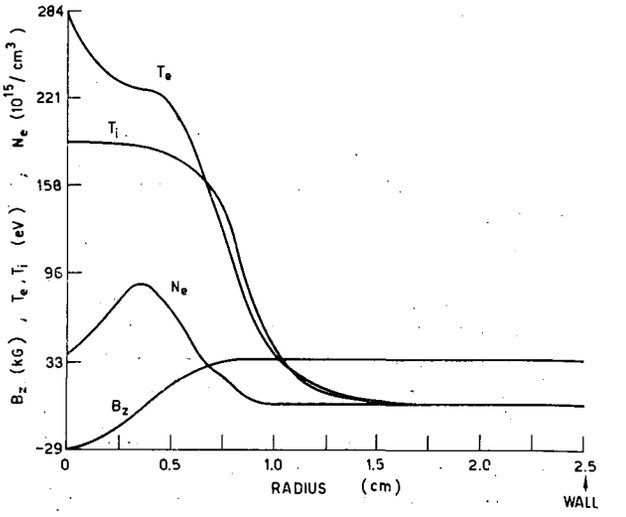

Fig. 14 Same as Fig. 9 except for $t = 1.5$ μs.

The voltage appearing on the coil when the bank is switched is about 9 kV. The plasma was preheated to 1.0 eV (50% ionization) by discharging a small capacitor bank into the coil (20 kV, 0.6 μF, with 4 kV appearing on the coil).

Figures 9—15 show the calculated plasma state and field configuration for times between 0.12 and 1.85 μs. At 0.12 μs the external field is less than the initial quasi-static internal field of —3 kilogauss. Consequently, the plasma expands and piles up at the wall. The electron temperature rises rapidly to 8 eV by ohmic heating due to field interdiffusion and a thin current sheet is formed. The ion temperature remains low because a shock wave has not yet been formed and there has not been sufficient time for ion-electron relaxation. At 0.3 μs the plasma is away from the walls and moving rapidly toward the axis with a velocity of ~7 cm/μs, which is observed. At this time the electron density has the characteristic maximum in the zero field region of the current sheath. The ion temperature has increased rapidly to ~15 eV from the shock heating and the electron temperature is 37 eV. At 0.4 μs the shock front has reached the axis and there is a sudden rise in the electron and ion temperatures in the central region. The observed time to the first bounce is 0.35 μs, which is in excellent agreement with the calculation. The temperature now rises very rapidly near the axis for a short time (Fig. 13) and then falls somewhat during the expansion at the first bounce. As time proceeds (Figs. 12, 13), the two maxima in the temperature at the axis and in the $B = 0$ region smooth out but the density maximum remains. The streak camera photographs show a less luminous region near the axis which corresponds to the calculated dip in density, with the observed region of maximum luminosity close to the predicted value.

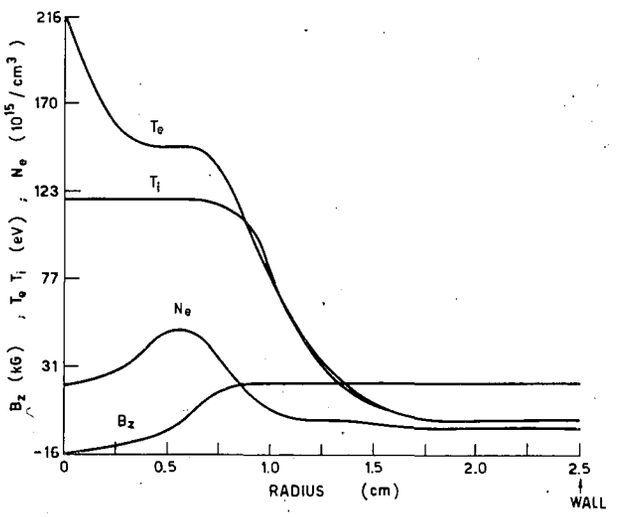

Fig. 13 Same as Fig. 9 except for $t = 1.0$ μs.

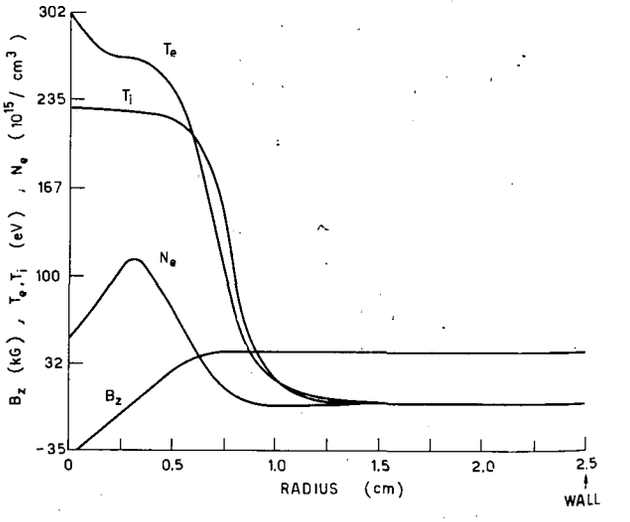

Fig. 15 Same as Fig. 9 except for $t = 1.9$ μs.

At 1.85 μs the electron and ion temperatures lie between 200 and 300 eV and the mean electron density is $\sim 5\times10^{16}$ cm^{-3}. The electron temperature has been measured [5] from the spectral distribution of soft x-rays, using various absorber-foil combinations and scintillators. The measured electron temperature at 2 μs after the start of the discharge was 300 ± 50 eV, which is in close accord with the numerical results. Also, the measured plasma radius of 5 ± 1 mm is very close to expectations from Fig. 15. The numerical solutions have not yet been carried out for longer times but it appears that the dynamic behavior, compression and heating rate are very nearly those expected from the two-fluid hydromagnetic approximation. It remains to be seen whether the final electron temperature of 1100 eV at 5 μs will appear as a solution of the magnetohydrodynamic equations; however, one can conclude from the present results that the theory certainly has some validity in predicting the behavior of a fast theta-pinch in deuterium.

The fact that the electron temperature is close to the predicted value implies also that impurity radiation does not constitute a serious mechanism for energy loss. This is in agreement with measurements of the absolute intensity of soft x-rays which puts an upper limit on the impurity concentration 1% [13].

One concludes finally that the heating due to the dissipation of a trapped reversed magnetic field can be accounted for by ordinary resistive processes in this particular experiment, at least for early times. At later times the characteristic time for the diffusion is of the order $R_s^2/n=10^{-14}\,R_s^2T_e^{3/2}$, where R_s is the position of the reverse current sheet. From Figs. 14 and 15 $R_s\sim0.3$ cm and $T_e\sim3000$ eV, so that $R_s^2/n\sim5$ μs. Therefore, one can expect that during the next 8 μs of the first half-cycle of the discharge that the remaining trapped field will be dissipated into the plasma by collisional processes, leading to high final temperatures.

Acknowledgments

The authors would like to express their thanks to Mrs. G. Hain, whose help in coding has been invaluable for the calculations. She and K. Hain also thank the Office of Naval Research for enabling them to work for a short period in Washington, D. C.

The authors also thank Mrs. Sally Peavy and Mrs. Ruth Varna at the National Bureau of Standards, Washington, D. C. (U.S.A.), for their assistance with the coding and operation of the IBM 704.

The work reported here was jointly supported by the U.S. Atomic Energy Commission and the Office of Naval Research.

References

[1] Kolb, A. C., Griem, H. R., Faust, W. R., Proceedings of Fourth International Conference on Ionization Phenomena in Gases, Uppsala, (North-Holland Publ. Co., Amsterdam) **2** (1959) 1037.
[2] Kolb, A. C., *Rev. Modern Phys.* **32** (1960) 748.
[3] Hain, K., Hain, G., Roberts, K. V., Roberts, S. J., *Z. Naturforschg.* **15a** (1960) 1039.
[4] Kolb, A. C., Faust, W. R., Anderson, A. D., *Nuclear Fusion* **1** (1961) 257.
[5] Griem, H. R., Kolb, A. C., Lupton, W. R., Phillips, D. T., see page 543 of these Proceedings.
[6] Spitzer, L. Jr., Physics of Fully Ionized Gases (Interscience, New York, 1956).
[7] Hain, K. (to be published).
[8] Janes, G. S., Patrick, R. M., Conference on Extremely High Temperatures (John Wiley, New York, 1958) 3—12.
[9] Kolb, A. C., Proceedings of Fourth International Conference on Ionization Phenomena in Gases, Uppsala (North-Holland Publ. Co., Amsterdam) **2** (1959) 1029.
[10] Little, E. M., Quinn, W. E., Ribe, F. L., *Phys. Fluids* **4** (1960) 716.
[11] Roberts, K. V., private communication.
[12] Bodin, H. A. B., Newton, A. A., Peacock, N. J., *Nuclear Fusion* **1** (1961) 139.
[13] Griem, H. R., Kolb, A. C., Lupton, W. H., Phillips, D. T., *Bull. Am. Phys. Soc.* Ser. II, **6** (1961) 205.

A COMPARISON BETWEEN NUMERICAL CALCULATIONS OF A LINEAR z-PINCH DISCHARGE AND MEASUREMENTS BY MAGNETIC PROBES*

H. FISSER

MAX-PLANCK-INSTITUT FÜR PHYSIK UND ASTROPHYSIK

MÜNCHEN, FEDERAL REPUBLIC OF GERMANY

J. SCHLÜTER

KERNFORSCHUNGSANLAGE JÜLICH DES LANDES NORDRHEIN-WESTFALEN E. V.

JÜLICH, FEDERAL REPUBLIC OF GERMANY

We compared distributions of the axial B_z (r, t) and the azimuthal B_θ (r, t) magnetic fields in an argon linear, stabilized z-pinch discharge, obtained from magnetic probe measurements, with numerical calculations. Ionization of Ar II was taken into account and brought about an essential improvement in the B_θ distributions compared with calculations without Ar III production, so that there is now good agreement with the measurements. The results give rise to the hope that a more exact treatment of the motion of the Ar III particles—we tied them to the Ar II ions for simplification—will also improve the theoretical B_z distributions, since B_z is more affected by the dynamics of the discharge than B_θ. The consideration of Ar IV, observed in the discharge, and of excitation phenomena may remove the remaining deviations in B_θ from the measured values.

We conclude that z-pinch discharges with a ratio of about 1 cm/μs between tube radius and bounce time can be described accurately by the magnetohydrodynamic equations up to times shortly after the first compression.

1. Theoretical assumptions

The numerical calculations were based on the magnetohydrodynamic equations for a fully-ionized plasma, i.e. neutral particles were not considered. Since the second ionization potential of argon is $\chi=27.6$ eV, Ar III ions should be taken into account. This was done in an approximate manner. The ions of Ar II and Ar III were assumed to have identical momenta and temperatures. The assumption of temperature equilibrium should be a good approximation because the equal masses bring about an effective energy exchange. It is a restriction, however, to equalize the hydrodynamic velocities of the two ion species, since for Ar III the Lorentz forces—and the corresponding accelerations—are twice as large as for Ar II.

Under these premises, we obtain a system of seven partial differential equations for the quantities:

v	the radial flow velocity;
n	the number density of the atomic nuclei;
α	the ratio n_2/n_1, where n_2 is the number density of Ar III ions;
T_e, T_i	the electron and ion temperatures;
B_θ, B_z	the azimuthal and axial magnetic fields.

All these quantities are assumed to depend only on the time t and the distance r from the axis of the cylindrical pinch tube. Therefore, $\mathbf{j}\times\mathbf{B}$ and grad p have only r-components, and $v_\theta=v_z=0$ is a compatible boundary condition. Neglecting the inertia of the electrons, Ohm's law becomes

$$\mathbf{E}+\mathbf{v}\times\mathbf{B}=\mathbf{E}^m=\frac{1+3\alpha}{1+\alpha}\eta_1\mathsf{Q}\,\mathbf{j}+\frac{1}{en_e}(\mathbf{j}\times\mathbf{B}-\operatorname{grad}p_e)-\mathbf{E}_r,$$

where η_1 is the electrical resistivity taken from Spitzer's formula with the charge number $Z=1$. The Hall and pressure diffusion terms are cancelled out by $\mathbf{E}_r$, a radial electrical field, which is produced by slight deviations from quasi-neutrality.
Q is the tensor

$$\mathsf{Q}=\begin{pmatrix}1+0.97\frac{B_z^2}{B^2}, & -0.97\frac{B_z B_\theta}{B^2}\\ -0.97\frac{B_z B_\theta}{B^2}, & 1+0.97\frac{B_\theta^2}{B^2}\end{pmatrix}$$

with $B^2=B_z^2+B_\theta^2$; the tensor takes into account the difference in perpendicular and parallel resistivity.

The main effect we considered in addition to those in the previous code developed by HAIN [2] was the energy loss of the electrons due to the ionization of Ar II ions by collisions with subsequent radiative recombination. The photo-ionization can be neglected.

With $\gamma=c_p/c_v=5/3$, $n_1\cdot n_e\cdot S_{12}=$ the number of ionizations per cm^{3}sec, $n_1=n(1-\alpha)=$density of Ar II

* Conference paper CN-10/36 presented by K. Hain. Discussion of this paper is given on page 648. Translations of the abstract are at the end of this volume of the Conference Proceedings.

ions, and $n_e = n(1+\alpha)$ = electron density, the energy equation for the electrons is

$$\frac{dT_e}{dt} = -(\gamma-1)\, T_e \operatorname{div} v + \frac{T_i - T_e}{t_{eq}} + \frac{\gamma-1}{k n_e}\varepsilon_F + \frac{1}{n_e}\operatorname{div} \varkappa_e \operatorname{grad} T_e - n(1-\alpha) S_{12}\left[\frac{(\gamma-1)}{k} + T_e\right],$$

where ε_F is the ohmic heating term, k the Boltzmann constant, t_{eq} the equipartition time [1], and $\varkappa_e$ the coefficient of heat conductivity [2]. The last term on the right hand side describes the energy loss due to ionization processes, each of which involves the ionization energy χ and $kT_e/(\gamma-1)$, the kinetic energy of the stripped electron.

If $n_e\, n_2\, Q_{21}$ is the number of photo-recombinations per cm³sec, the differential equation for α is:

$$\frac{d\alpha}{dt} = n(1+\alpha)\left[(1-\alpha) S_{12} - \alpha Q_{21}\right].$$

The equations for n, B_z, B_θ, T_i are the same as given in the paper by HAIN *et al.* [2]. In the momentum equation the electron pressure is $p_e = n(1+\alpha)\, kT_e$.

As the initial state at $t=0$ we assumed a homogeneous plasma:

$$v = \alpha = B_\theta = 0,$$

the stabilizing field $B_z = B_0$,

$$n = n_0,$$

$$T_i = T_e = T_0.$$

At the wall of the tube containing the plasma, $r=R$, we applied the following boundary conditions:

$$T_e(R) = T_i(R) = T_0,$$

$$\alpha(R) = 0 \text{ for a sufficiently low } T_0;$$

for $n(R)$, no boundary condition can be imposed if $v(R) \geq 0$, but for $v(R) < 0$ the ordinary differential equation $\dot{n}(R) = [v(R)/l]\ [n(R) - n_M]$ was solved, so that $n(R)$ approaches some minimum density n_M in a time determined by $v(R)$ and the parameter l. This was necessary to limit the Alfvén velocities near the boundary, but the precise values of n_M, l do not influence the calculated quantities in the region of high densities.

The velocity is calculated at points which are displaced by half a mesh spacing from those of the other variables. Hence the outer endpoint of v is located at $r = R[1-(1/2N)]$, where N is the number of mesh intervals, and $\dot{v}$ at $R + R/2N$ arising from $(v \cdot \nabla)\, v$ was set = 0. We dropped the pressure forces at the wall because the momentum transfer with small n_M is negligible, i.e. grad p is very small near the wall.

The plasma tube is enclosed within an infinitely conducting metal cylinder, which provides a further stabilization and a return current path from one of the electrodes. The conservation of the magnetic flux within this cylinder gives an ordinary differential equation for the boundary value $B_z(R)$:

$$\pi(R_a^2 - R^2)\, \dot{B}_z(R) = 2\pi R \cdot E_\theta(R),$$

where R_a is the inner radius of the conductor.

$B_\theta(R)$ is governed by the equation

$$\left(DR \ln \frac{R_a}{R}\right) \cdot \dot{B}_\theta(R) = V - DE_z(R),$$

with an electrode separation D. The voltage is found from the circuit equation

$$V = V_c - L\dot{I} - R_{el} I$$

with

$$V_c = V_0 - \frac{1}{C}\int_0 I\, dt.$$

V_0 is the initial condenser bank voltage, C the capacity, L the inductance, and R_{el} is the electrical resistance of the external circuit, $I = 5 \cdot R \cdot B_\theta(R)$ is the total current. The electrical fields $E_\theta(R)$ and $E_z(R)$ are calculated from Ohm's law by solution of the plasma equations.

It may be noted that the bound-bound radiation is not yet considered; however, it is not expected that there will be large corrections because of the relatively low temperatures. Also the experiments with heavier gases such as argon are not sensitive to impurities, because their own radiation will predominate.

2. Comparison between calculations and experiments

The system of partial differential equations described above was solved numerically by an explicit difference scheme developed by K. Hain, which was extended for our purposes to include ionization effects. For the comparison we selected the fastest of the Jülich experiments; it had the largest ratio V_0^2/n_0, which is proportional to the energy available per particle.

The external circuit had the following parameters: $C = 4950\ \mu F$, $L = 0.060 \cdot 10^{-6}$ H and $R_{el} = 10^{-3}\ \Omega$. The pinch tube had the following dimensions: $R = 9.5$ cm, $D = 93$ cm and $R_a = 11.2$ cm.

The initial conditions are $n_0 = 0.33 \cdot 10^{16}$ cm^{-3}, $B_0 = 270$ G with an assumed temperature of $T_0 = 1.25$ eV.

The voltage of the capacitor bank was applied without preionization of the gas. The quantities $dB_z(t)/dt$ and $dB_\theta(t)/dt$ were measured by magnetic probes (single-coil probes) and integrated numerically to get $B_z(r, t)$ and $B_\theta(r, t)$.

Two different calculations have been made. In the first, the coefficient S_{12} was taken to be zero; hence $\alpha = 0$. In the second run, we used the ionization and recombination coefficients S_{12} and Q_{21} as given by ELWERT [3]. It is very instructive to compare the different calculations and to study the effects produced by the ionization and recombination terms.

In the first stage of the discharge its bounce time is about 12 μs – the total current rises with $\dot{I} \approx V_0/L^*$, where L^* is the total inductance.

In Fig. 1 the profiles of B_z, B_θ and n^* are plotted over r at a fixed time; n^* is a normalized number

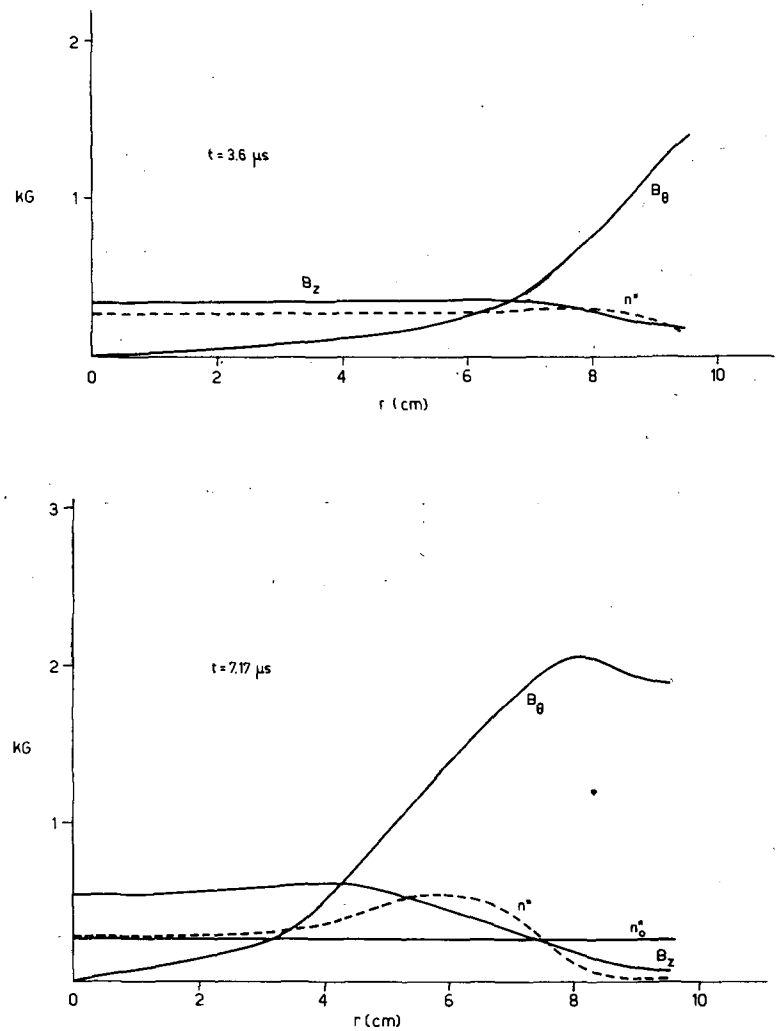

Fig. 1 B_θ, B_z, and n^* as functions of r at $t=3.6$ μs and at $t=7.17$ μs.

density with $n^*=(B_0/n_0)\,n$; the deviations of B_z from n^* show the effect of field diffusion.

For $t<2.2$ μs the number density n changes less than 3%; B_z, however, begins to rise immediately from the beginning of the discharge, except in the outer region of the tube, where it must decrease because the total B_z-flux is conserved. This growth is caused by the so-called "paramagnetic effect", due to the off-diagonal elements in the resistivity tensor $\mathbf{Q}$. The resistivity is so low that B_z increases uniformly inside the compression region (Fig. 1).

At later times—$t\sim 10-13$ μs—(Figs. 2, 3)** the influences of compression and convection have become dominant. It is obvious that the curve "b", calculated with ionization, approximates the experimental curve much better than curve "a" obtained without ionization. Curve "a" is not steep enough near $r=0$ and is concave at $r\sim 2.5$ cm contrary to the measurements. These differences arise because without ionization the gas near the axis is heated to a higher temperature than with ionization. Therefore, the gas pressure remains lower and the compression is higher. Accordingly, the maximum values of n (with respect to time at $r=0$) $n^a{}_{max}$ and $n^b{}_{max}$ are given by the relation $n^b{}_{max}/n^a{}_{max}\approx 2$. Consequently the B_z and B_θ fields are higher in case "b". Furthermore, it is noted that B_z is more affected by compression than B_θ because of the cylindrical geometry.

For $t>14$ μs the differences between calculation "b" and the measurements become appreciable (Fig. 4): the $B_\theta{}^b(r)$ values are larger than the experimental ones. This happens where α has reached 1, and therefore the ionization term in the energy equation for the electrons goes to zero. The three-body recombinations into excited states, which were omitted in our calculations, will delay the time at which the Ar II ions die out; in addition there will be Ar IV ions present even at lower temperatures. Therefore the temperatures will be also kept down and the resistivity will grow by a factor $\sim 3/2$, so that eventually the peaks of the $B_\theta{}^b$-curves may vanish (Figs. 5, 6).

** Note on figures: The curves obtained from calculations without ionization of Ar II are assigned the letter "a", those with ionization "b". The label "exp" relates to the measured curves.

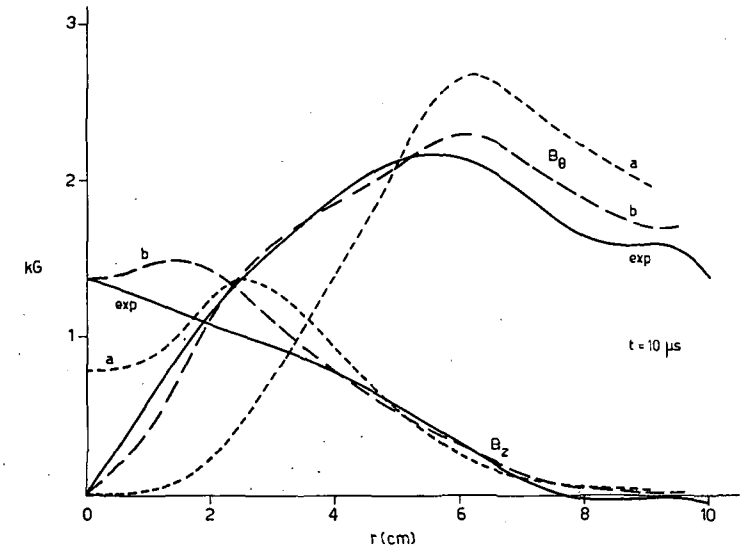

Fig. 2 B_θ and B_z as a function of r at $t=10\mu s$. (a) — calculated without ionization of Ar II; (b) — calculated with ionization of Ar II; (exp) — measured experimentally.

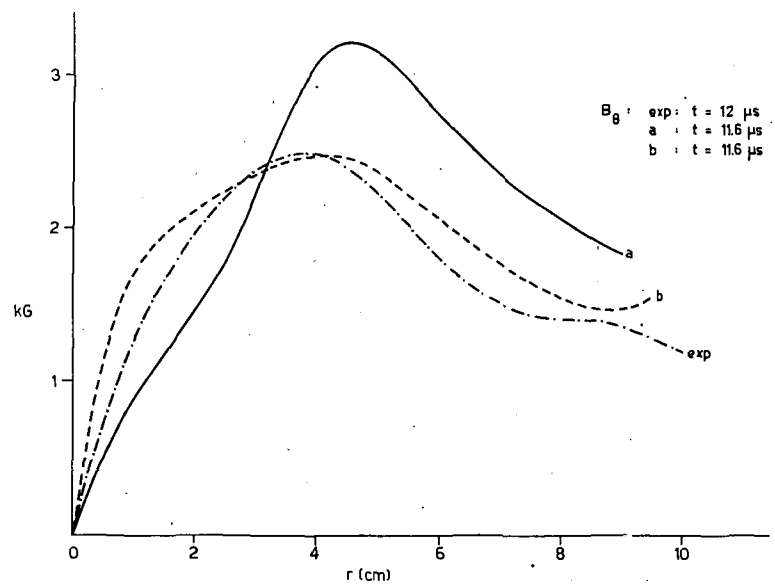

Fig. 3 B_θ as a function of r at $t=12$ μs. (a) — calculated at $t=11.6$ μs without ionization of Ar II; (b) — calculated at $t=11.6$ μs with ionization of Ar II; (exp) — measured experimentally at $t=12$ μs.

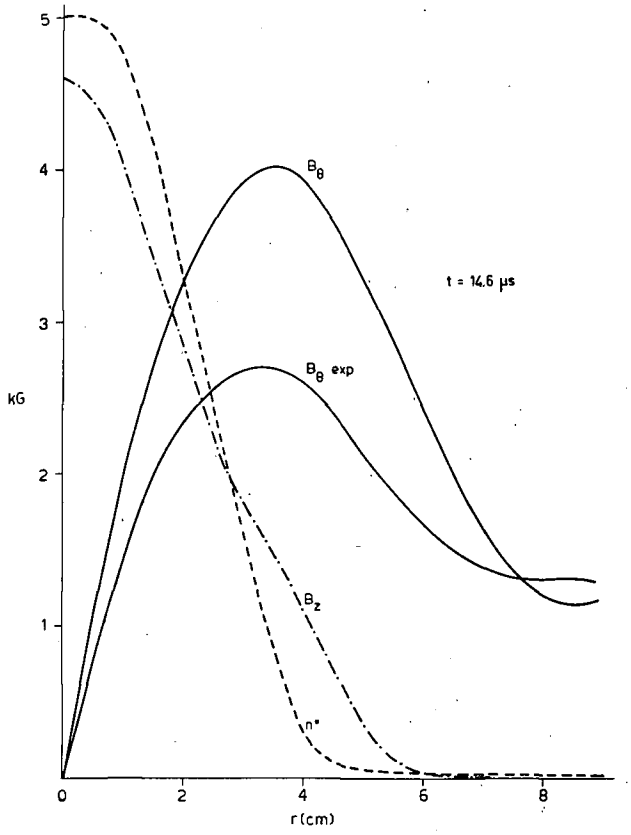

Fig. 4 B_θ and B_z as a function of r at $t = 14.6$ μs. (a)—calculated without ionization of Ar II; (b)—calculated with ionization of Ar II; (exp) — measured experimentally.

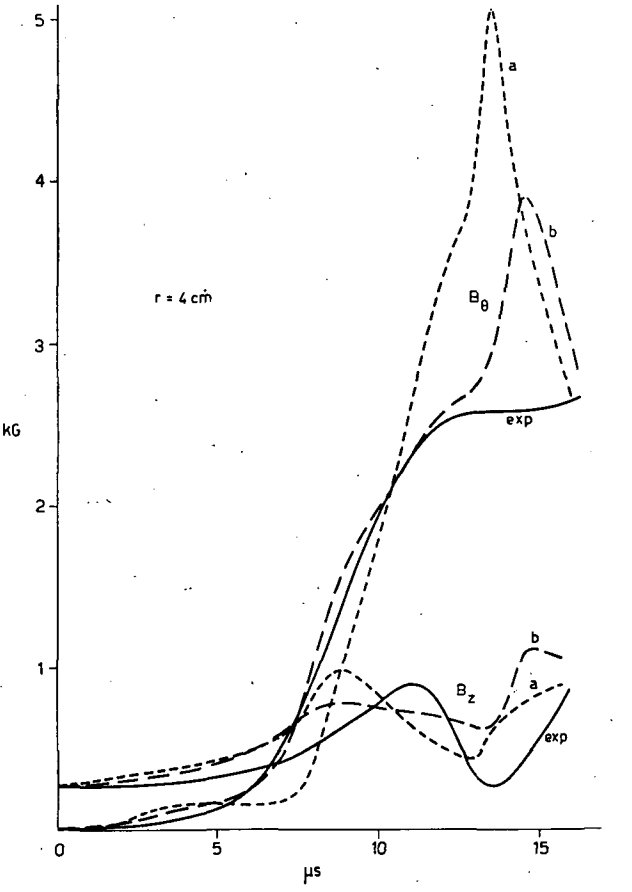

Fig. 5 B_θ and B_z as a function of time at $r = 4$ cm. (a) — calculated without ionization of Ar II; (b) — calculated with ionization of Ar II; (exp) — measured experimentally.

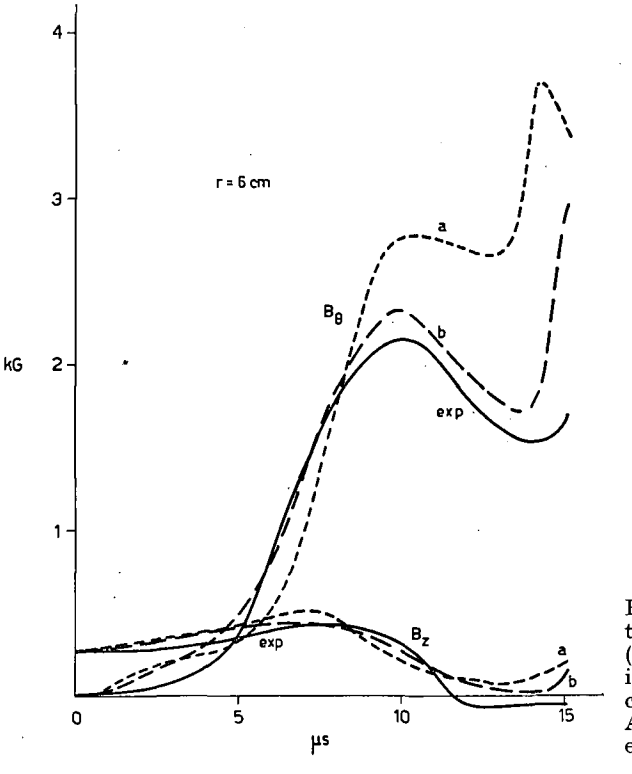

Fig. 6 B_θ and B_z as a function of time at $r = 6$ cm. (a) — calculated without ionization of Ar II; (b)—calculated with ionization of Ar II; (exp) — measured experimentally.

With regard to the B_z field distribution, the "a"-calculations showed a rather good agreement with the measurements if the $B_z^{a}(t)$-curves were delayed in time by ~ 2 μs. While the B_θ distributions were improved essentially in the "b"-calculation, this cannot be said for the $B_z^{b}(t)$-curves; some of them are even worse than the "a"-curves, as Fig. 5 shows. We hope that a more exact treatment of the momenta of the different ion species will bring about a better approximation of the B_z traces. It turns out that almost all the "b"- and experimental curves can be fitted better if the "b"-graphs are delayed in time by 0.5 μs, i.e. all changes occur a bit later in experiment; this time interval is about 2 μs if the "a"- and measured curves are compared. We suppose that the ionization of Ar I requires about 0.5 μs here. Similarly we ascribe the 1.5 μs delay between "a" and "b"-curves to the ionization of Ar II.

The n^* and B_z traces plotted in Fig. 4 show an interesting phenomenon near the axis concerning the field diffusion. The diffusion equations for the magnetic fields are:

$$\frac{\partial B_z}{\partial t} = \frac{1}{r}\frac{\partial}{\partial r} r \left\{ \eta_{\theta\theta} \frac{\partial B_z}{\partial r} - \eta_{\theta z} \frac{1}{r} \frac{\partial (r B_\theta)}{\partial r} \right\}$$

$$\frac{\partial B_\theta}{\partial t} = \frac{\partial}{\partial r} \left\{ \eta_{zz} \frac{\partial (r B_\theta)}{r \partial r} - \eta_{\theta z} \frac{\partial B_z}{\partial r} \right\}$$

(η_{ik} is the resistivity tensor $\mathbf{Q} \cdot \eta$)

According to Fig. 1 the ratio B_z/n^* at $r=0$ grows by the paramagnetic effect in the first stage of the discharge. Later B_z is lowered by field diffusion, since the term $(1/r)(\partial/\partial r)(r\eta_{\theta\theta}\partial B_z/\partial r)$ becomes negative by compression. Now in case "b" the minimum value of η at $r=0$ is six times as large as in case "a", due to a factor of 2.1 in the electron temperatures and a factor 2 caused by $Z=2$. As a result of this enlarged resistivity B_z decreases to less than n^*. This does not occur in case "a", since B_z/n^* decreases too slowly.

Acknowledgments

One of the authors (H. F.) is indebted to the United Kingdom Atomic Energy Authority for the kind permission to perform these calculations on the computer IBM 7090 at Aldermaston, Berks. He particularly thanks Dr. K. V. Roberts and Miss S. J. Roberts, A.E.R.E. Harwell, Berks., for arranging the calculations; he thanks Dr. K. Hain for many helpful suggestions and Mrs. G. Hain for her assistance in the numerical calculations.

References

[1] SPITZER, L. Jr., Physics of Fully Ionized Gases (Interscience, New York, 1956) 80.
[2] HAIN, K., *et al.*, *Z. Naturforschung* **15a** (1960) 1040.
[3] ELWERT, G., *Z. Naturforschung* **7a** (1952) 703.

ПЛОТНАЯ ВЫСОКОТЕМПЕРАТУРНАЯ ПЛАЗМА В ОБЛАСТИ НЕЦИЛИНДРИЧЕСКОЙ КУМУЛЯЦИИ *z*-ПИНЧА*

Н. В. ФИЛИППОВ, Т. И. ФИЛИППОВА, В. П. ВИНОГРАДОВ

АКАДЕМИЯ НАУК СССР

МОСКВА, СОЮЗ СОВЕТСКИХ СОЦИАЛИСТИЧЕСКИХ РЕСПУБЛИК

Из предшествующих работ по изучению мощного импульсного разряда в камере с металлическими боковыми стенками следовало, что сжатие токовой оболочки не является цилиндрическим, а имеет фокус на оси камеры вблизи анода, служащий резко локализованным источником интенсивного нейтронного излучения. Особенностью разряда является то, что токовая оболочка формируется в газе, не участвующем в последующем сжатии к оси.

В данной работе основное внимание было обращено на изучение свойств плазмы в момент максимального сжатия.

Применены следующие методы исследования:

Магнито-зондовые измерения.

Оптические измерения в видимой области спектра:

a) снятие интегрального по времени спектра,

b) получение развертки спектра во времени на плоском пленочном диске,

c) фотоэлектрическое измерение абсолютной интенсивности континуума,

d) определение размеров светящейся области методом «оптического трансформатора».

Измерения в области мягкого рентгеновского излучения:

a) определение методом фильтров жесткости излучения,

b) определение полного числа рентгеновских квантов,

c) фотографирование камерой-обскурой,

d) измерение фазы и длительности излучения фотоэлектрическим методом с помощью тонкого сцинтиллятора,

e) исследование тонкой структуры пинча одновременным фотографированием через три отверстия с различными фильтрами,

f) развертка рентгеновского изображения на вращающейся пленке с временным разрешением $1 \cdot 10^{-7}$ сек,

g) применение монохроматора для проверки характера спектра.

Наблюдение нейтронно-протонного излучения:

a) измерение интегрального выхода нейтронов за разряд с одновременной сцинтилляционной регистрацией во времени,

b) регистрация треков протонов из D (d, p) T — реакции ядерной эмульсией.

Измерение давления по оси разряда выполнено с помощью мембранного датчика.

В результате экспериментов обнаружено, что пинч-эффект приводит к образованию области сжатия диаметром около 0,5 см и средней плотностью порядка 10^{19} см$^{-3}$. За счет кумуляции внутри этой области возникает зона диаметром $1 \div 1{,}5$ мм, имеющая приблизительно такую же плотность и температуру $0{,}8 \div 1{,}2$ кэв. Наблюдаемое время существования области кумуляции ($0{,}2 \cdot 10^{-6}$ сек) значительно больше необходимого для максвелизации дейтонов и для выравнивания электронной и ионной температур.

Благодаря большому выходу протонов (d—d) — реакции впервые удалось получить распределение протонов по энергии за один разряд. Максимальный зарегистрированный нейтронный выход равен $0{,}5 \cdot 10^{10}$.

Полученные данные согласуются с расчетом, сделанным по теории Брагинского и др. с учетом эффекта кумуляции ударных волн в области с размерами порядка длины свободного пробега для этих параметров.

Данная работа является продолжением исследований мощного импульсного разряда в дейтерии в камере с металлическими боковыми стенками [1, 2].

В обычных цилиндрических камерах, применяемых для исследования *z*-пинч-эффекта, токовая оболочка формируется у изолирующей стенки камеры, и газ, сжимающийся к оси, загрязняется атомами примесей.

На рис. 1 показана конструкция камеры, в значительной мере свободной от этого недостатка. Камера состоит из медного корпуса и введенного через изолятор положительного электрода. С помощью кольцевого вакуумного разрядника на камеру разряжалась батарея конденсаторов ИМ-2,7-50 общей емкостью 40 мкф. Рабочее напряжение 32 кв, давление дейтерия 1 мм рт. ст., максимальный ток около 500 ка.

Ранее отмечалось, что при наличии боковой металлической стенки, развитие разряда и характер сжатия обладают следующими особенностями:

* Доклад CN-10/226, представленный на Конференцию. Докладчик: К. А. Разумова. Дискуссия (на английском языке) по этому докладу дана на стр. 648. Переводы аннотаций находятся в конце этого тома Трудов Конференции.

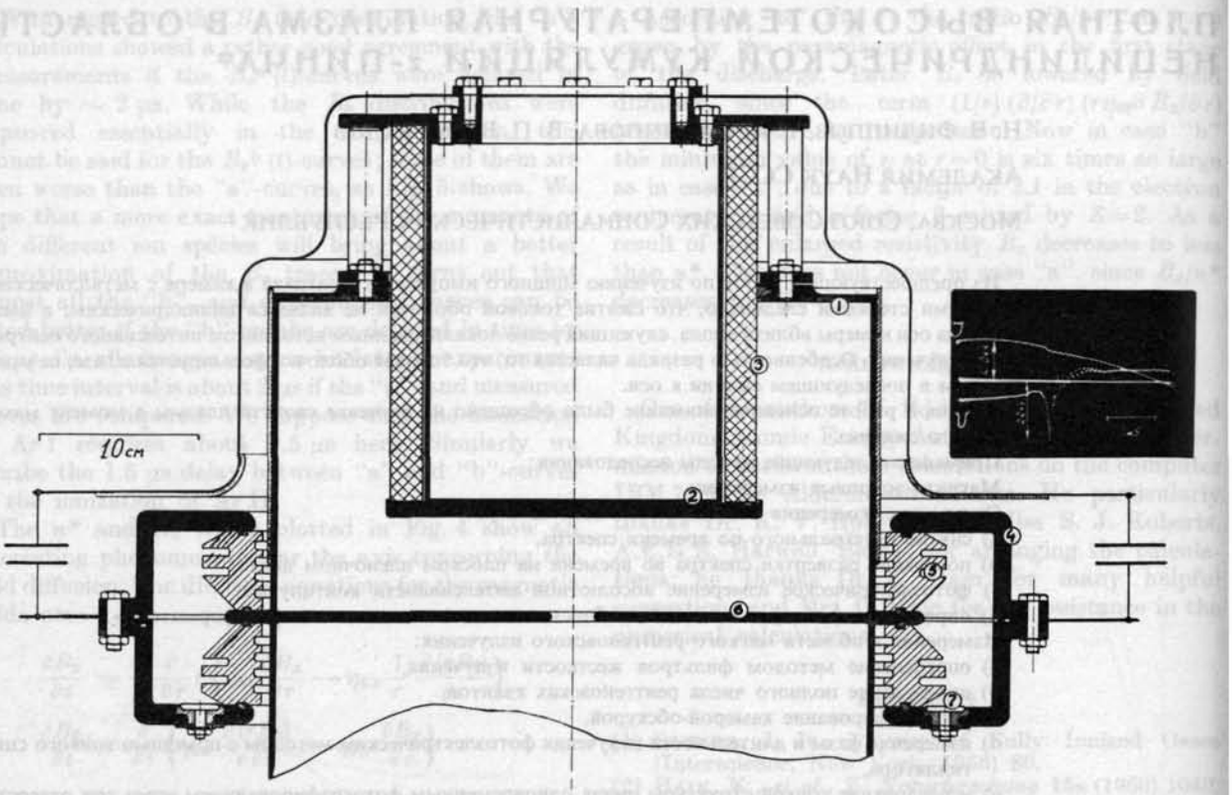

Рис. 1 Первый вариант газоразрядной камеры. 1 — медный корпус, 2 — внутренний электрод (анод), 3 — фарфоровый изолятор, 4 — корпус кольцевого вакуумного разрядника, 5 — изолятор из органического стекла, 6 — перегородка, разделяющая камеру на две симметричные части, 7 — инициирующие электроды. В правом верхнем углу приведен участок осциллограммы тока и напряжения разряда.

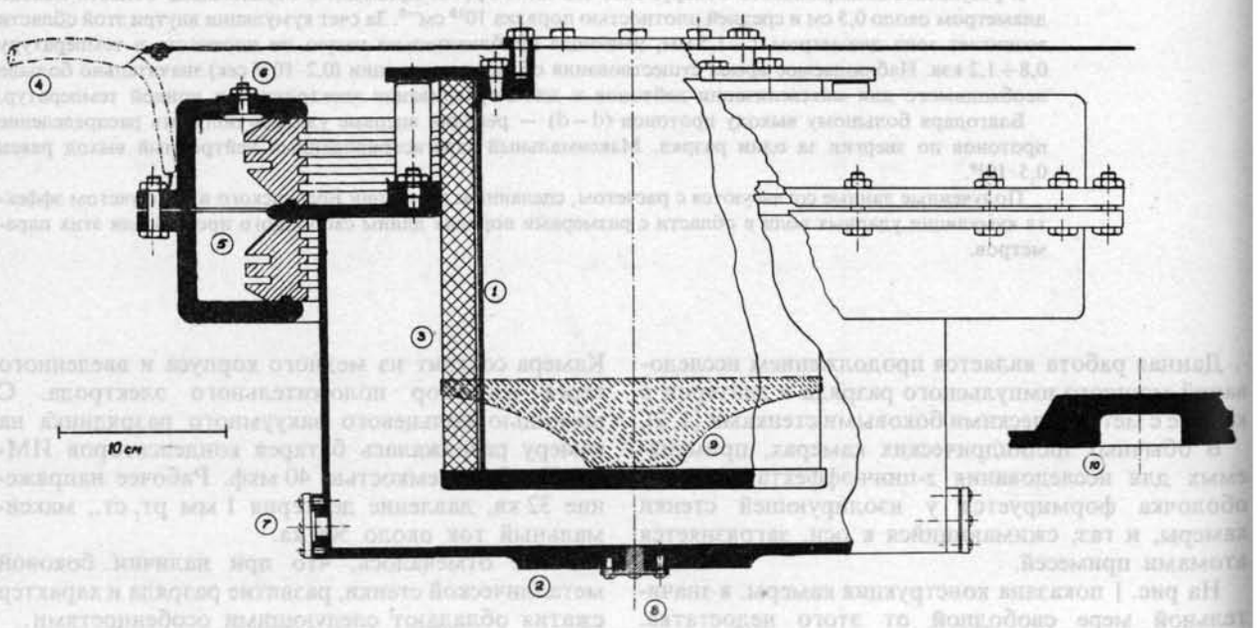

Рис. 2 Второй вариант газоразрядной камеры. 1 — внутренний электрод (анод), 2 — медный корпус, 3 — фарфоровый изолятор, 4 — кабельная подводка, 5 — вакуумный разрядник, 6 — инициирующие электроды, 7, 8 — окошки для наблюдения, 9 — конический вариант внутреннего электрода, 10 — внутренний электрод с углублением в центре.

а) Плазма не загрязняется атомами материала изолятора. На начальной стадии разряда токовая оболочка формируется, как обычно, у поверхности изолятора, но затем движется *не к оси, а к боковым стенкам камеры.*

Движение газа к центру камеры происходит вдоль поверхности внутреннего электрода и начинается тогда, когда ток дорос почти до максимума, при этом газ, в котором протекала начальная стадия развития разряда, в сжатии не участвует.

б) Сжатие токовой оболочки носит нецилиндрический характер и имеет на оси камеры вблизи анода фокус, служащий резко локализованным источником нейтронов с интенсивностью до $0{,}5 \cdot 10^{10}$ нейтронов за разряд.

в) Оптимальные режимы соответствуют бóльшим начальным давлениям дейтерия при тех же параметрах установки, чем в камерах с изолирующими стенками.

г) Так как сжатие происходит неодновременно по оси камеры, то можно было предположить, что оно носит конический характер, приводящий к образованию плазменных струй.

Конструкция камеры, показанная на рис. 1, предусматривала возможность одновременной работы двух идентичных частей камеры с целью проверки возможного эффекта столкновения плазменных струй. В этом случае общая емкость двух батарей составляла 80 мкф.

Результаты работы двойной камеры показали, что образующаяся область максимального сжатия пинча имеет гораздо меньшие размеры, чем предполагалось раньше и поэтому вероятность столкновения струй при данном техническом исполнении камеры мала.

В процессе исследования сжатого состояния плазмы основная часть работ производилась на одной половине камеры с батареей 40 мкф или 80 мкф, а также на конструктивно улучшенной и более простой в работе камере II-го типа, показанной на рис. 2. В этой камере при сохранении основных размеров варьировалась форма положительного электрода для того, чтобы:

а) удалить фокус сжатия от поверхности электрода, придав оболочке составляющую скорости вдоль оси z (случай конического электрода),

б) убрать из непосредственной близости к фокусу сжатия поверхность электрода, сделав углубление в центральной его части.

Одновременно с усовершенствованием разрядной камеры развивались экспериментальные методики, позволившие получить сравнительно полное представление о параметрах образующегося сжатого состояния плазмы.

Результаты экспериментов. Оптические измерения

Большое место в изучении сжатого состояния плазмы на установках I и II занимали оптические методы исследования в видимой области спектра.

Интегральный во времени спектр видимого излучения, снятый по оси камеры, характеризуется мощной вспышкой сплошного фона и сравнительно слабым свечением линий примесей. В основном это медь и цинк.

Развертка спектра во времени была получена путем замены приемной кассеты спектрографа пневматической турбиной, вращающей диск из фотопленки высокой чувствительности. Пленка вращалась в откачиваемом объеме с окружной скоростью до 300 м/сек. Временное разрешение при этом достигало 0,15 мксек.

Серия типичных спектральных разверток приведенных рис. 3а, 3б, 3в, получена при наблюдении

Рис. 3а Развертка спектра между D_α и D_β со спектральной щелью 0,02 мм и развертывающей — 0,05 мм для камеры первого варианта.

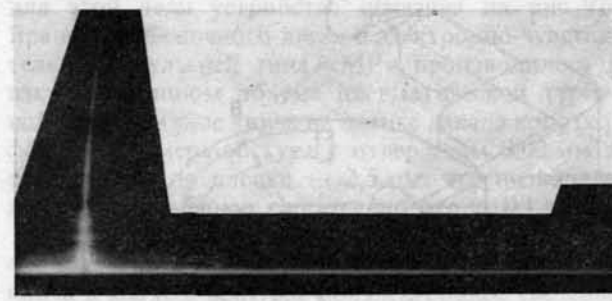

Рис. 3б Развертка спектра между D_α и D_β со спектральной щелью 0,1 мм и развертывающей — 0,05 мм для камеры первого варианта.

вдоль оси камеры. Все фотографии характеризуются яркой вспышкой сплошного фона и длительно светящейся линией D_α, ширина которой меняется во времени. Спектрограмма на рис. 3б снята со значительно увеличенной против рис. 3а входной щелью. Стала заметной сильно уширенная линия D_β и слабые линии примесей, не видимые на рис. 3а. Самопоглощение дейтериевых линий можно объяснить тем, что свет пинча проходит через толстый слой нейтрального газа, возбужденного излучением разряда.

Спектрограмма на рис. 3в — пример развертки с максимальным разрешением по времени (соответствующая фотоэлектрическая запись показана на рис. 6).

На интегральных спектрах и развертках был выбран участок континуума, свободный от линейчатого спектра, и в этом интервале длин волн

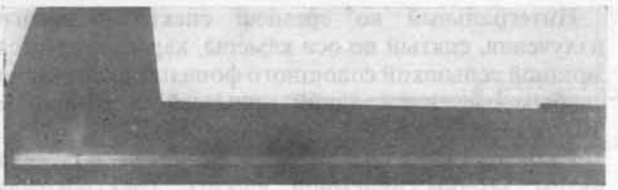

Рис. 3в (см. рис. 3а, 3б) Пример максимального разрешения во времени (0,26 мм/мксек на пленке на радиусе D_α). Время между двумя вспышками континуума ~0,8 мксек.

проводились последующие измерения абсолютной интенсивности континуума и определение размеров излучающей области.

Поскольку сжатие имеет нецилиндрический характер и недостаточно ограничиться временной разверткой одного какого-либо сечения пинча, был создан специальный «оптический трансформатор» см. рис. 4 превращавший двумерную картину пинча в одномерную и позволявший наблюдать ее в узком спектральном интервале с разрешением по времени ~ 0,1 мксек.

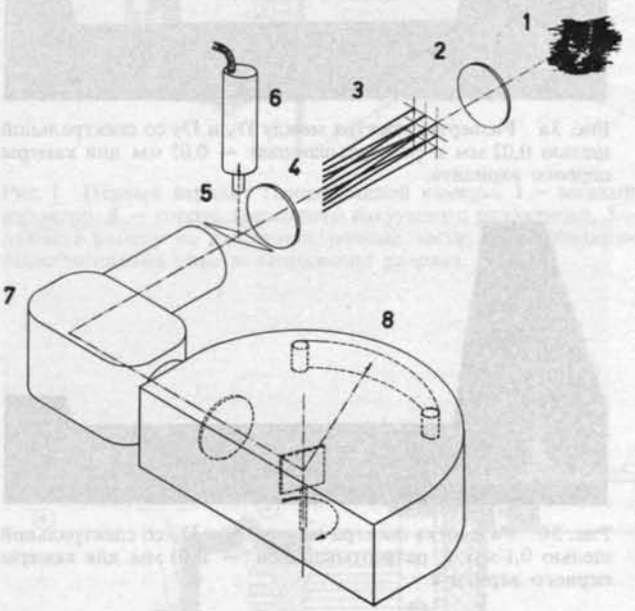

Рис. 4 Схема оптического трансформатора. 1 — объект, 2 — объектив, 3 — система световодов, 4 — промежуточный объектив, 5 — стеклянная пластинка, 6 — фотоэлектронный умножитель, 7 — монохроматор, 8 — фоторегистратор.

Источник света — 1 объективом — 2 изображается на передней поверхности оптического трансформатора — 3, представляющего собой систему из 77 стеклянных световодов (⌀ 0,15 мм), разбивающих изображение пинча на 77 элементов. Входные полированные концы световодов лежат в одной плоскости и расположены чаще в середине предполагаемого места изображения и реже на краях. Выходные концы всех световодов сведены в одну прямую линию и фокусируются объективом — 4 в плоскости входной щели монохроматора УМ-2 в масштабе 1:5. Выходная щель монохроматора одновременно служила входной щелью фоторегистратора типа СФР.

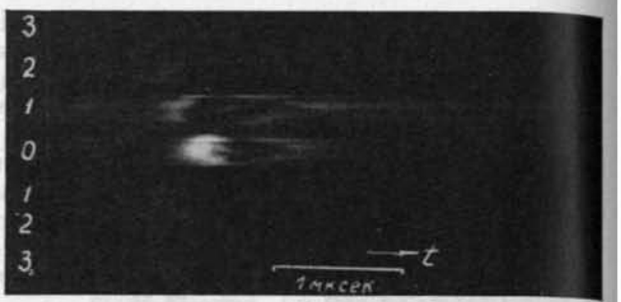

Рис. 5а Примеры светограмм, полученных с помощью оптического трансформатора: в свете линии D_α.

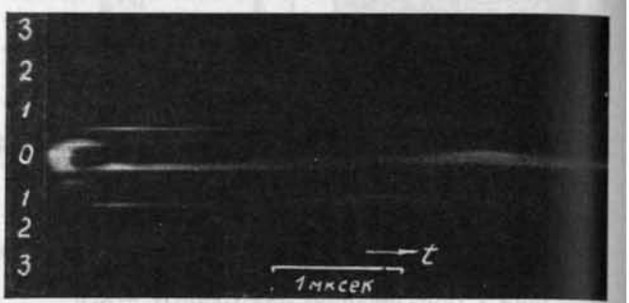

Рис. 5б Примеры светограмм, полученных с помощью оптического трансформатора: в свете континуума (λ = = 5853 Å). Полосы 0, 1, 2, 3 — вертикальные сечения пинча через 0,7 см.

Полученные светограммы для II-го варианта камеры приведены на рис. 5. Рис. 5а — фотография в свете линии D_α ($\Delta\lambda$=40 Å), а рис. 5б — фотография в свете континуума ($\Delta\lambda$=30 Å; λ = 5853 Å). Полосы 0; 1; 2; 3 соответствуют вертикальным сечениям пинча через 0,7 см. Каждая такая полоса разбита световодами на 11 элементов.

На рис. 5а видно, что движение светящейся оболочки к центру происходит со скоростью более 10^7 см/сек. (Найденная более точно из зондовых измерений скорость близка к $(2—3)\cdot 10^7$ см/сек).

На светограмме рис. 5б видна нецилиндричность сжатия. Оцененный диаметр области, испускающей континуум ~ 0,5 см, длительность свечения около 0,2—0,4 мксек.

На рис. 5б видно, как возникающее у электрода свечение паров меди со скоростью $1{,}5\cdot 10^6$ см/сек распространяется вдоль оси камеры. Свечение паров имеет вид узкого факела, возникшего вследствие мгновенного выделения энергии на электрод из области сжатия пинча.

Абсолютное измерение интенсивности континуума в выбранном участке длин волн было произведено по методике, подробно описанной в работе Лукьянова С. Ю. и др. [3].

Практическая независимость интенсивности тормозного излучения плазмы в видимой области спектра от температуры, если последняя больше 30 эв, позволяет таким методом находить усредненную по высоте и диаметру пинча плотность электронов.

В нашем случае плотность электронов с учетом объема излучателя оказалась $(0{,}7—1{,}2)\cdot 10^{19}$ см$^{-3}$,

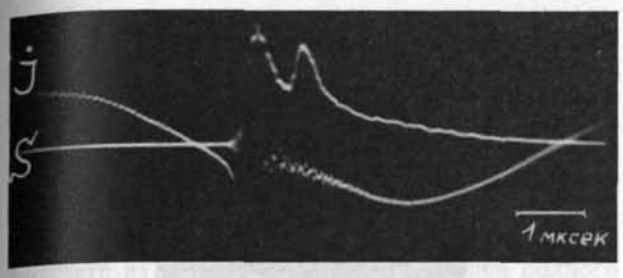

Рис. 6 Осциллограмма интенсивности континуума ($\lambda = 5853$ Å).

что в предположении равенства плотности ионов и электронов, соответствует приблизительно стократному сжатию частиц.

На рис. 6 показана осциллограмма фотоэлектрической записи интенсивности континуума совместно с производной тока разряда.

Измерения в области мягкого рентгеновского излучения

Тонкая структура сжатого состояния пинча была обнаружена при переходе к наблюдению более коротковолнового излучения в области мягкого рентгена с длиной волны меньше 15 Å. В мягком рентгеновском излучении выявилась резкая неоднородность структуры пинча в приосевой области, которая раньше не выделялась на фоне равномерно светящегося в видимом континууме пинча диаметром 0,5 см. Осевая область, излучающая мягкий рентген, составляет часть длины пинча и имеет диаметр ~1,5 мм. Это значение диаметра находится на границе разрешения примененной аппаратуры, т.е. можно утверждать, что он меньше или равен 1,5 мм. Вне этой области интенсивность излучения плавно спадает.

На рис. 7 приведена одна из фотографий пинча в собственном рентгеновском излучении, полученная камерой-обскурой (рис. 8) с экраном из 6 мк фольги Al (разряд в камере I-го варианта). Масштаб изображения 1:1; горизонтальная полоса на рис. 7 соответствует свечению на поверхности электрода. Специальными опытами по развертке рентгеновского изображения во времени с помощью вращающегося пленочного диска с эмульсией типа «МР» удалось установить, что объемное свечение пинча и свечение поверхности электрода разнесены во времени. Схема применявшегося для этой цели устройства показана на рис. 9б. Вращение пленочного диска с электронно-чувствительной эмульсией типа «МР» производилось в вакуумированном объеме пневматической турбиной. Изображение пинча на пленке давала короткофокусная камера-обскура с отверстием 0,02 мм и расстоянием до пленки — 2,5 мм, что позволяло получить временное разрешение около 0,1 мксек.

Рис. 7 Фотография пинча в свете мягкого рентгеновского излучения. Масштаб 1:1; (разрядная камера первого варианта). Горизонтальная полоса — свечение поверхности внутреннего электрода. Вертикальный столб — объемное свечение пинча.

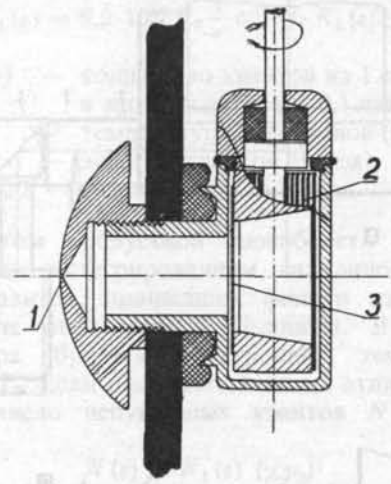

Рис. 8 Конструкция рентгеновской камеры-обскуры для первого варианта газоразрядной камеры. 1 — отверстие диаметром 0,15 мм, 2 — катушка с пленкой на 20 кадров, 3 — 6 мк алюминиевый экран.

В тех случаях, когда центральная часть электрода «убиралась» из области сжатия, на фотографиях пинча в мягком рентгене приэлектродное свечение значительно ослаблено.

Пример фотографии через фильтр из алюминия в 6 мк показан на рис. 10 (II-ой вариант камеры).

Для получения сведений о распределении электронной температуры по пинчу производилось фотографирование разряда камерой-обскурой с тремя отверстиями 0,15 мм, закрытым различными бериллиевыми и алюминиевыми фильтрами. (Бериллий от 12 до 150 мк, алюминий 6, 12, 18 мк и т. д.)

Схематический чертеж камеры-обскуры для этого случая показан на рис. 9в. Оцененная методом фильтров максимальная жесткость объемного излучения мягкого рентгена соответствует энергии квантов, равной 1 кэв.

Электронно-чувствительная эмульсия с размером зерна 0,3 мк допускала количественную оценку числа квантов, испущенных разрядом в данной области пинча, путем подсчета числа зерен на участке изображения с известным почернением. По данным Бромли и др. [4] квантовый выход эмульсий такого типа в нашем интервале энергий

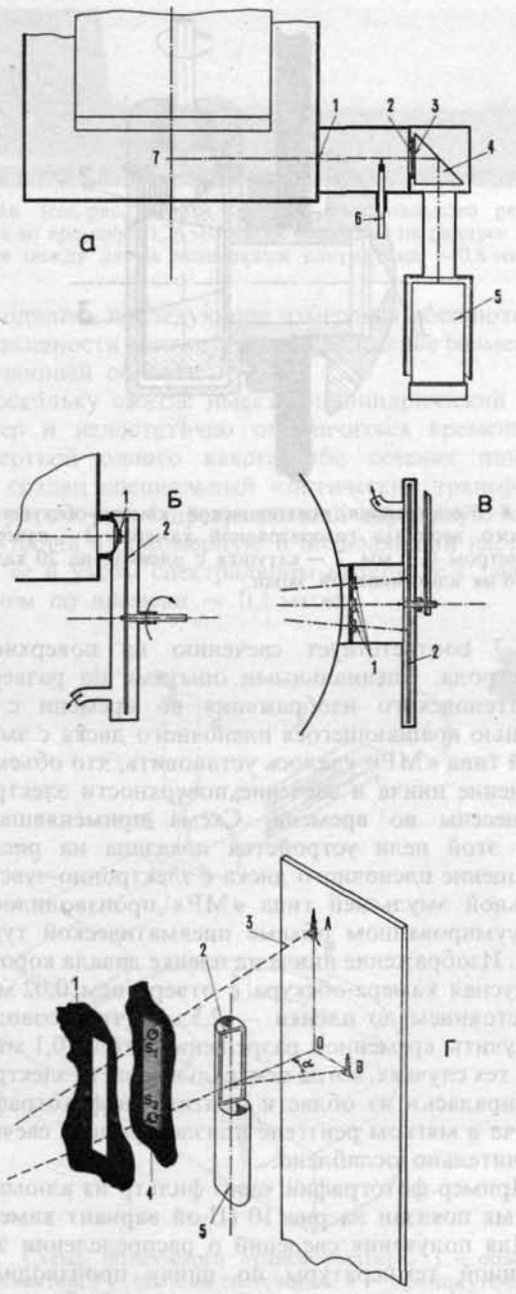

Рис. 9 Аппаратура для наблюдения мягкого рентгеновского излучения в камере второго варианта.
(а) Фотоэлектрическая регистрация. 1 — отверстие в стенке камеры, 2 — защитная фольга 6 мк Al, 3 — сцинтиллятор толщиной 0,2 мм, 4 — стеклянная призма, 5 — фотоэлектрическое устройство, 6 — маска, 7 — разрядная камера.
(а) Фотоэлектрическая регистрация. 1 — отверстие в стенке камеры, 2 — защитная фольга 6 мк Al, 3 — сцинтиллятор толщиной 0,2 мм, 4 — стеклянная призма, 5 — фотоэлектрическое устройство, 6 — маска, 7 — разрядная камера.
(б) Развертка изображения во времени. 1 — отвертстие диаметром 0,02 мм, закрытое 12 мк Be, 2 — диск из фотопленки, вращающейся на расстоянии 2 мм от отверстия.
(в) «Трехобъективная» камера-обскура. 1 — три отверстия диаметром по 0,15 мм, закрываемые разными фильтрами, 2 — диск из фотопленки, поворачиваемый для смены кадров. Расстояние от отверстий до пленки — 20 мм.

(Продолжение на правой стороне)

Рис. 10 Такая же фотография, как на рис. 7, но для разрядной камеры второго варианта с углублением в центре. Видно слабое свечения поверхности электрода у краев углубления. Основное свечение пинча оторвано от поверхности электрода.

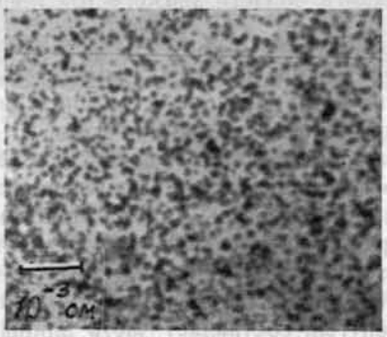

Рис. 11а Микрофотографии рентгеновского изображения пинча, полученного камерой-обскурой на эмульсии «МР». Увеличение 1000×. Участок изображения с измеренной плотностью почернения.

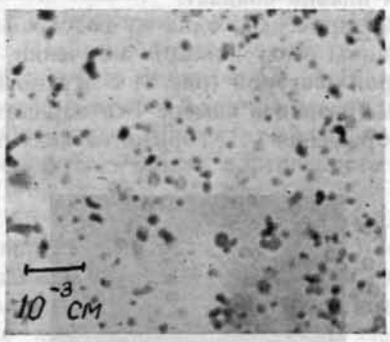

Рис. 11б Микрофотографии рентгеновского изображения пинча, полученного камерой-обскурой на эмульсии «МР». Увеличение 1000×. Фон.

(г) Макет монохроматора. 1 — коллимирующая щель. S_1, S_2 — отверстия для получения прямого изображения и отраженного от слюды, соответственно, 2 — диспергирующий элемент — слюда, 3 — фотопластинка с эмульсией «МР», A — Прямое изображение пинча, B — отраженное от слюды изображение пинча, α — удвоенный угол Вульфа-Брегга, 4 — фольга 12 мк Be, 5 — поворачиваемая колонка.

рентгеновских квантов равен единице, одновременно этот значит, что кривая «освещенность-почернение» имеет вид прямой, проходящей через начало координат. Зерна считались на микрофотографиях при увеличении в 1000×. На рис. 11а показан участок изображения пинча с небольшим почернением, на рис. 11б — фон.

Измеренное число квантов, приведших к данному почернению, служит исходным числом для подсчета из геометрических соображений полного числа квантов, испущенных единицей объема плазмы за время излучения.

Временная характеристика вспышки мягкого рентгеновского излучения была получена фотоэлектрическим методом с помощью тонкого (0,2 мм) органического сцинтиллятора, нечувствительного к нейтронам и жесткому излучению. Во избежание прямого попадания жестких излучений на катод и диноды ФЭУ была применена стеклянная призма. Видимое излучение разряда задерживалось тонкой (6 мк) алюминиевой фольгой, а от приэлектродного рентгеновского излучения люминофор экранировался подвижной маской. Аппаратура приведена на рис. 9а. Из этих измерений было найдено, что вспышка мягкого рентгена, длящаяся около 0,15—0,25 мксек (типичная осциллограмма на рис. 12), происходит одновременно с

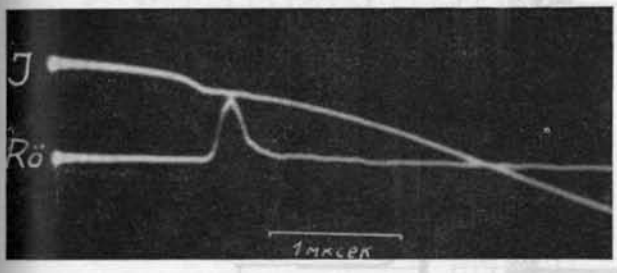

Рис. 12 Осциллограммы тока через разрядную камеру и импульс мягкого рентгеновского излучения, регистрируемого с помощью устройства, показанного на рис. 9 (а).

максимумом оптического континуума (моментом появления нейтронов) и соответствует моменту максимального сжатия пинча.

Общее число квантов, прошедших данный фильтр, определяется температурой электронов и плотностью плазмы.

В сочетании с относительными измерениями почернений за различными фильтрами можно попытаться определить температуру и менее точно — плотность. Можно значительно уточнить экспериментальные данные, измерив плотность независимым путем.

В предположении температурной природы наблюдаемого тормозного излучения были проделаны соответствующие численные расчеты интенсивности излучения для 1 см³ плазмы при плотности $n_0 = 7 \cdot 10^{16}$ см$^{-3}$ как функции квантов и температуры электронов.

Вычисления проводились в борновском приближении по формуле:

$$N_1(\varepsilon) = 8{,}2 \cdot 10^{17}\, T_e \frac{1}{\varepsilon} e^{-\varepsilon/2T_e} K_0(\varepsilon/2T_e), \quad (1)$$

где $N_1(\varepsilon)$ — количество квантов из 1 см³ в 1 сек в интервале $(\varepsilon,\ \varepsilon + 0{,}1$ кэв),
T_e — температура электронов (в кэв),
ε — энергия квантов (в кэв),
$K_0\, \varepsilon/2T$ — функция Макдональда.

С учетом пропускной способности фильтров численным интегрированием находилось общее число квантов, прошедших фильтр из данного материала определенной толщины. В качестве параметра бралась электронная температура плазмы T_e. Если плотность плазмы отличается от n_0, то число испущенных квантов $N(\varepsilon)$ будет равно:

$$N(\varepsilon) = N_1(\varepsilon) \cdot (\gamma p_0)^2 \quad (2)$$

где $\gamma = n/n_0$ — степень сжатия,
p_0 — начальное давление в мм рт.ст.

Объем области находился из фотографий пинча.

Сравнение экспериментальных данных с численными расчетами показало, что плотность частиц в области, испускающей мягкий рентген, такого же порядка ($n \sim 10^{19}$ см$^{-3}$), чти и в области видимого континуума, а электронная температура лежит в интервале (0,8—1,2) кэв.

Вопрос о правильности интерпретации наблюдаемого рентгеновского излучения как температурного можно с уверенностью решить, измерив распределение квантов по спектру. С этой целью нами был построен миниатюрный макет монохроматора с диспергирующим элементом — слюдой (плоскость спайности 001, $d = 9{,}9$ Å), работающем при углах Вульфа-Брэгга от 10° до 30°.

Схема монохроматора показана на рис. 9г. Такой прибор мог дать только качественные результаты, однако они позволяют с уверенностью считать наблюдаемый спектр сплошным, а не линейчатым, как это могло быть в случае глубокой ионизации атомов примесей с большим атомным номером. К сожалению, трудности печатного размножения не позволяют привести здесь слабоэкспонированные фотографии.

Измерение давления

Измерить газокинетическое давление плазмы в таком разряде пьезоэлектрическим датчиком оказалось невозможным, так как механический удар в момент максимального сжатия разрушает защитный колпачок и чувствительный элемент — титанат бария. Поэтому был использован применявшийся ранее [5] диафрагменный датчик с диафрагмой из нержавеющей стали толщиной 0,1 мм. Датчик располагался по оси камеры в углублении на расстоянии 0,8 см от поверхности внутреннего электрода. На рис. 13 показаны фотографии плоских диафрагм, побывавших в разряде на расстоянии 1,5 см от фокуса сжатия. Значительная пластическая деформация возникает уже после

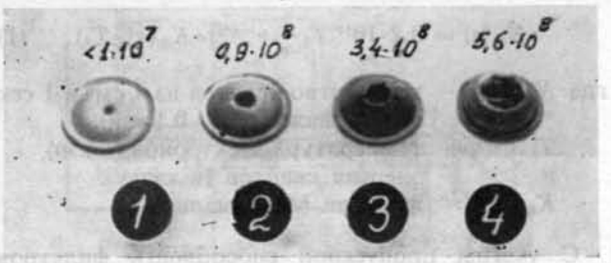

Рис. 13 Фотографии диафрагм (0,1 мм нержавеющая сталь) мембранного датчика импульса давления плазмы после регистрации одного разряда каждой. Центральное отверстие — результат удара диафрагмы об острие контакта датчика. Около каждой диафрагмы приведен нейтронный выход, зарегистрированный при данном разряде.

того, как осциллографически измерена начальная скорость мембраны.

Степень разрушения диафрагм коррелирует с наблюдавшимся нейтронным выходом для данного разряда.

Замена мембран производилась вакуумным шлюзованием.

Амплитудное значение давления было оценено в предположении, что длительность импульса давления Δt совпадает с длительностью вспышки оптического континуума, а форма импульса достаточно точно аппроксимируется полупериодом синусоиды. Эти предположения основаны на неопубликованной работе авторов по пьезоизмерениям в цилиндрических камерах. Оцененное таким образом давление в случае диафрагмы № 2 (рис. 13) для $\Delta t = 0{,}5$ мксек равно $2{,}2 \cdot 10^3$ кг/см². Из рис. 13 видно, что в случае диафрагмы № 4 давление было значительно больше. Условия регистрации давления на некотором расстоянии от центра сжатия и принятое значение времени $\Delta t = 0{,}5$ мксек, очевидно, дают заниженное давление, т. к. высокотемпературная область, излучающая мягкий рентген, существует, например, лишь 0,15—0,25 мксек.

Протонные измерения

Нейтронное излучение в исследуемом разряде возникает в момент максимального сжатия синхронного со вспышкой мягкого рентгена и запазды-

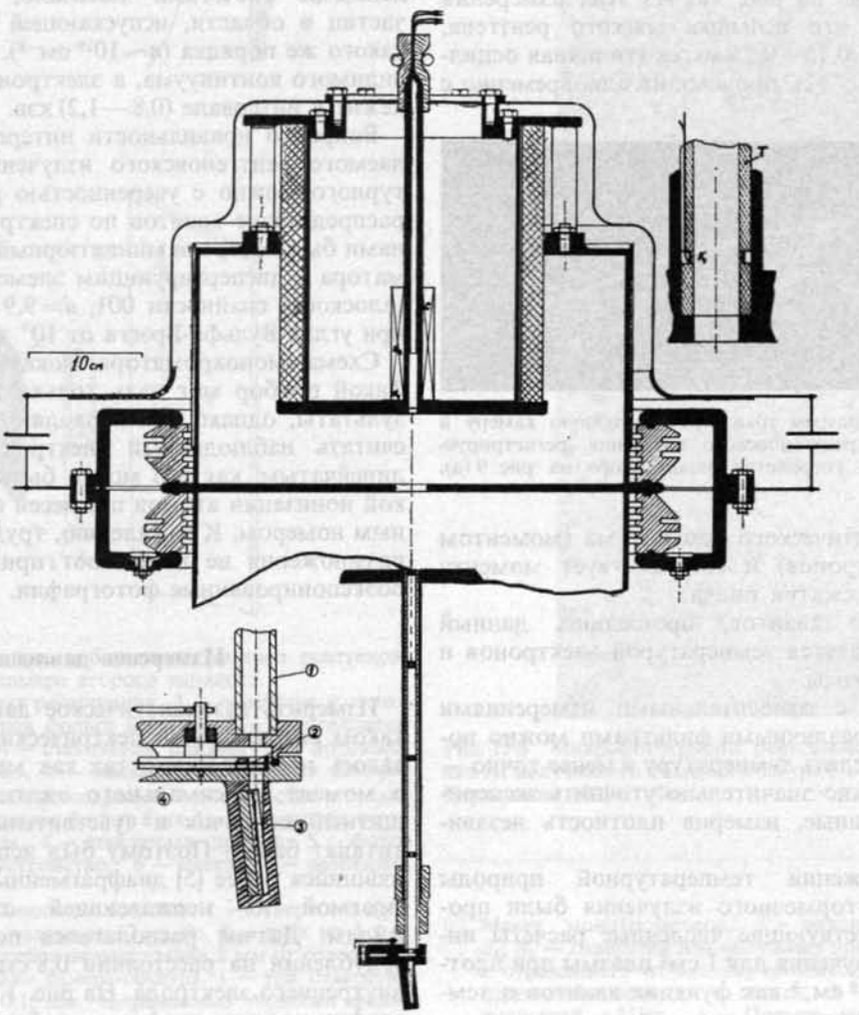

Рис. 14 Схема расположения аппаратуры для исследования протонного излучения разряда. 1 — «Глушитель» — трубка с рядом диафрагм для ослабления ударной волны, 2 — окошко закрытое 6 мк алюминиевой фольгой, 3 — кассета с пластинкой «Ilford C-2», 4 — револьверный диск для замены рабочего участка фольги.

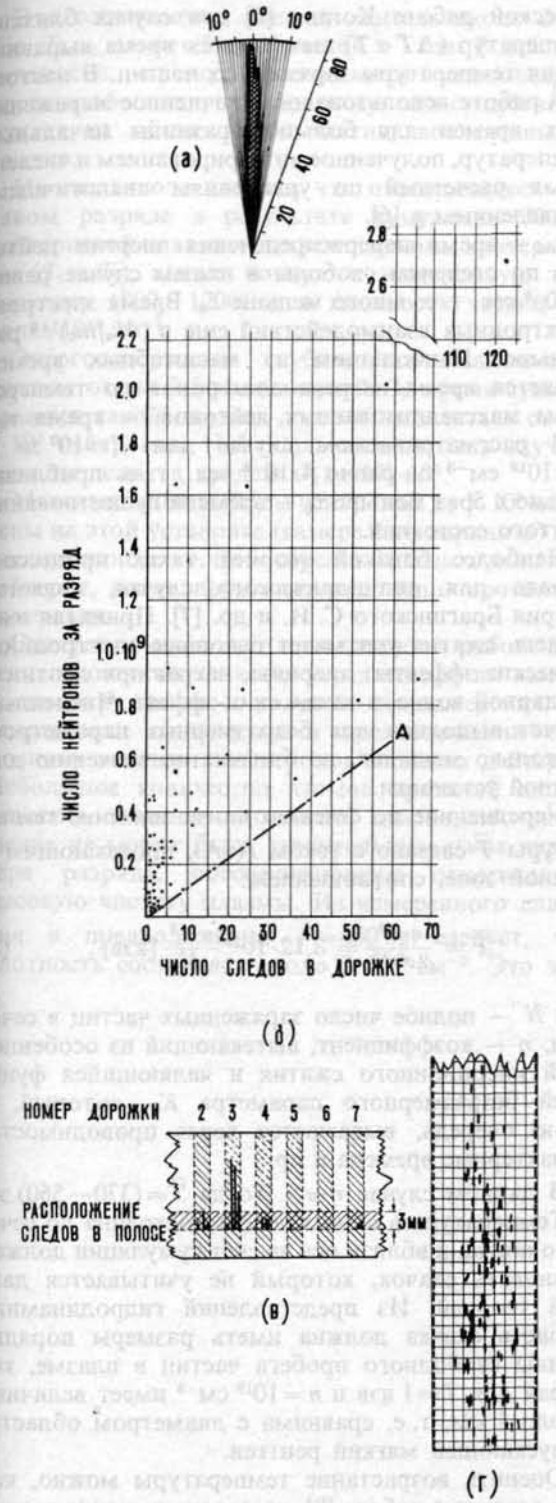

Рис. 15 Результаты протонных измерений. (а) Угловое распределение треков протонов за один разряд. (б) Зависимость полного числа треков протонов от нейтронного выхода. (в) Контроль эффективности регистрации протонного излучения. Вертикальные заштрихованные полосы соответствуют облученным участкам пластинки («дорожкам»). Нейтронный выход и количество следов указаны в следующей таблице (в промежутках между дорожками треков нет):

Продолжение на правой стороне)

вает на 0,2—0,3 мксек относительно скачка напряжения на камере.

Благодаря высокой интенсивности нейтронного излучения и резкой локализации источника удалось провести определение энергии протонов из второй ветви (d—d) — реакции.

Для этого протонное излучение выпускалось вдоль оси разряда и регистрировалось ядерной эмульсией «Ilford C-2». Угол падения протонов 6°. Схема расположения кассеты с пластиной показана на рис. 14. От видимого излучения эмульсия защищалась алюминиевой шестимикронной фольгой, которая заменялась на новую после каждого разряда. Высокая эффективность регистрации протонов позволила получить спектр протонов за один разряд, что практически невозможно для нейтронной методики, а также для установок с меньшим выходом (d—d) — реакций.

Результаты протонных измерений показаны на рис. 15. Рис. 15а — угловое распределение треков за один разряд для выхода $2{,}7\cdot10^9$ нейтр./разряд.

Рис. 15б — зависимость полного числа зарегистрированных треков протонов от нейтронного выхода для отдельных разрядов. Симметричность сжатия, т. е. сжатие у геометрической оси, характеризуется близостью точек к прямой OA.

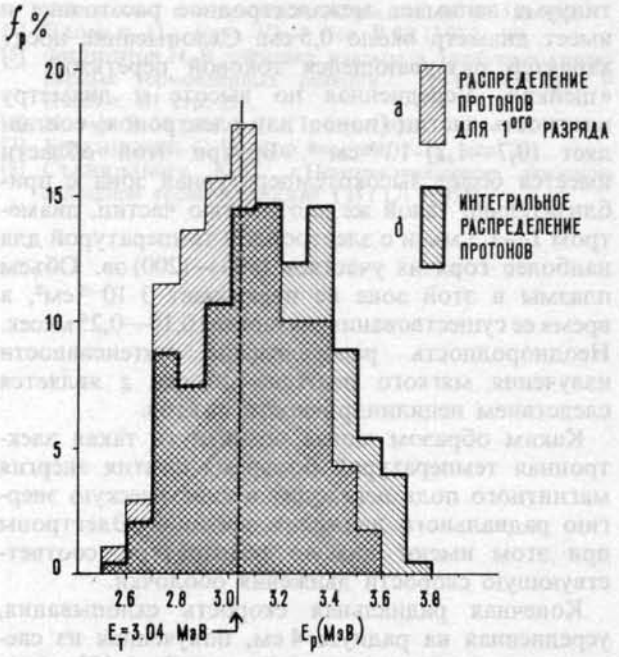

Рис. 16 Распределение протонов по энергии. (а) Распределение, полученное за один разряд. Общее число треков — 122, нейтронный воход $2{,}7\cdot10^9$, (б) интегральный спектр за 25 разрядов. Общее число треков — 529.

номер дорожки	2	3	4	5	6	7
нейтронов за разряд	$4\cdot10^8$	$27\cdot10^8$	$9\cdot10^8$	$1{,}7\cdot10^8$	$2\cdot10^8$	$4{,}7\cdot10^8$
полное число следов в дор.	24	122	23	15	0	11
количество следов в полосе	5	33	6	1	0	2

(г) Распределение треков протонов по «дорожке» для разряда с нейтронным выходом $2{,}7\cdot10^9$.

Рис. 15в — контроль эффективности регистрации протонного излучения. Вертикальные заштрихованные полосы соответствуют участкам пластин, подвергавшимся облучению — «дорожки».

Рис. 15г — схематическое расположение треков на дорожке для разряда с нейтронным выходом $2{,}7 \cdot 10^9$. Выдержаны координаты и углы треков. Полное число треков 122.

На рис. 16 штриховкой показан спектр протонов для того же разряда, что и на рис. 15г. Жирная линия — интегральный спектр протонов за несколько десятков разрядов, значительная часть которых имела небольшой нейтронный счет. В первом случае в пределах точности измерения максимум распределения лежит без сдвига относительно энергии 3,04 Мэв, что соответствует энергии дейтонов 0—2,5 кэв. Во втором случае максимум лежит в интервале (2,5—15) кэв. Точность измерения недостаточна, чтобы пытаться как-то интерпретировать форму спектра, и для уточнения кривых необходимы масспектрометрические измерения.

Обсуждение результатов

Таким образом, вследствие схлопывания токовой оболочки на оси образуется область максимального сжатия плотности, которая в видимом континууме занимает межэлектродное расстояние и имеет диаметр около 0,5 см. Схлопывание носит характер развивающейся токовой перетяжки — «шейки». Усредненная по высоте и диаметру плотность частиц (ионов или электронов) составляет $(0{,}7—1{,}2) \cdot 10^{19}$ см$^{-3}$. Внутри этой области имеется более высокотемпературная зона с приблизительно такой же плотностью частиц, диаметром 1—1,5 мм и с электронной температурой для наиболее горячих участков (800—1200) эв. Объем плазмы в этой зоне не превышает $3 \cdot 10^{-2}$ см^3, а время ее существования составляет 0,15—0,25 мксек. Неоднородность распределения интенсивности излучения мягкого рентгена по оси z является следствием нецилиндричности сжатия.

Каким образом могла возникнуть такая электронная температура? Во время сжатия энергия магнитного поля переходит в кинетическую энергию радиального движения дейтонов. Электроны при этом имеют низкую температуру, соответствующую скорости движения оболочки.

Конечная радиальная скорость схлопывания, усредненная на радиусе 4 см, полученная из световых и зондовых измерений равна $2—3 \cdot 10^7$ см/сек. Скорость разлета плазмы после сжатия вдоль оси, измеренная методом вытесненного магнитного потока, тоже близка к $3 \cdot 10^7$ см/сек.

Тип сжатия инерционный, сопровождающийся образованием сходящейся к оси ударной волны. Высокая электронная температура могла возникнуть благодаря обмену энергией с дейтонами, если за время существования сжатого состояния τ_0 энергия радиального движения успеет перераспределиться по 3-м степеням свободы и электроны нагреются до температуры ионов. В теоретической работе Когана [6] для случая близких температур ($\Delta T < T$) вычисляется время выравнивания температуры заряженных частиц. В настоящей работе использовалось уточненное выражение этих времен для большой разницы начальных температур, полученное интегрированием и численными расчетами по уравнениям аналогичным, приведенным в [6].

τ_{dd} — время перераспределения энергии дейтонов по степеням свободы в нашем случае равно $5 \cdot 10^{-9}$ сек, т. е. много меньше τ_0. Время электрон-электронных взаимодействий еще в $(M_\alpha/m_e)^{1/2}$ раз меньше. Наибольшим из масштабных времен является время нагрева электронов до температуры максвеллизованных дейтонов — время τ_{ed}.

В рассматриваемом случае для $T = 10^3$ эв и $n \approx 10^{19}$ см$^{-3}$ τ_{ed} равно $4 \cdot 10^{-8}$ сек., т. е. приблизительно в 5раз меньше τ_0 — времени существования сжатого состояния.

Наиболее близкой теорией таких процессов, правда для цилиндрического случая, является теория Брагинского С. И. и др. [7]. Принятая ими модель сжатия учитывает основные электродинамические эффекты: инерцию, нагрев при сжатии и в ударной волне, а также скин-эффект. Численный расчет выполнен для безразмерных параметров, несколько меньших, но близких по значению для данной установки.

Усредненное по сечению пинча значение температуры $\overline{T}$ связано с током I(кА), протекающим в данной зоне, соотношением:

$$\overline{T} = \frac{\eta \cdot I^2}{2c^2 N} = 3{,}12 \cdot 10^{12} \frac{\eta \cdot I^2}{N} \text{ [кэв]}, \qquad (3)$$

где N — полное число заряженных частиц в сечении, η — коэффициент, вытекающий из особенностей инерционного сжатия и являющийся функцией безразмерного параметра K_σ, который, в свою очередь, выражается через проводимость, характерные времена и пр.

В данном случае $\eta \approx 5$. Тогда $\overline{T} = (370—560)$ эв.

Температура в самом деле непостоянна по сечению пинча, и вблизи оси за счет кумуляции должен возникать скачок, который не учитывается данной теорией. Из представлений гидродинамики область скачка должна иметь размеры порядка длины свободного пробега частиц в плазме, которая для $T = 1$ кэв и $n = 10^{19}$ см$^{-3}$ имеет величину около 1 мм, т. е. сравнима с диаметром области, испускающей мягкий рентген.

Оценить возрастание температуры можно, как это сделано в работе [8], на основе решения задачи о сходящейся автомодельной ударной волне.

$T_{макс.}$ связано со средней температурой соотношением:

$$T_{макс.} = \overline{T} : \left(\frac{d}{\lambda}\right)^{2\alpha} \qquad (4)$$

где d — диаметр области с температурой $\overline{T}$,
λ — длина свободного пробега,
$\alpha = 0{,}2—0{,}23$.

Это соотношение дает множитель около 2—3, т. е. $T_{макс.}$ может быть близкой к 1 кэв. В действительности, процесс осложняется нецилиндричностью оболочки, по-видимому, это существенно влияет на общее число частиц, вовлеченных в сжатие.

Из сказанного следует, что образующиеся при таком разряде в результате кумуляции 30 мм³ дейтериевой плазмы максвеллизованы, изотермичны ($T_i = T_e$), имеют ионную и электронную температуру (800—1200) эв и плотность частиц порядка 10^{19} см$^{-3}$.

Энергосодержание кубического сантиметра плазмы около 3,5 килоджоулей. За время существования такой плазмы должно выделиться около $3 \cdot 10^7$ нейтронов. Наблюдавшиеся в этих случаях выходы лежат в пределах $(1—10) \cdot 10^7$.

Максимальные выходы нейтронов до $5 \cdot 10^9$ получены на этой установке (камера 1-го варианта) при увеличенной емкости батареи и большем давлении дейтерия, когда производились лишь протонные измерения.

Следует помнить, что приведенное в работе значение плотности является усредненным по высоте и диаметру пинча и получено из измерения интенсивности континуума в предположении тормозного излучения электронов на ионах дейтерия. Небольшое количество атомов примесей может завысить значение плотности, однако, это завышение не может быть значительным из-за характера разряда, обеспечивающего относительно высокую чистоту плазмы. Из измеренного давления в предположении $\overline{T} = 400$ эв следует, что плотность составляет около $2 \cdot 10^{18}$ см$^{-3}$. Это значение является сильно заниженным и поэтому может служить уверенной низшей оценкой для плотности.

В данной работе использовались разнообразные методы измерения, позволившие обнаружить некоторые качественные особенности сжатого состояния пинча. Очевидно, что каждая из методик может быть развита с целью получения более точных количественных результатов.

Авторы признательны Л. А. Арцимовичу, А. М. Андрианову, С. И. Брагинскому, В. И. Когану, В. Д. Шафранову за полезное обсуждение экспериментальных результатов и благодарят Сулковскую М. М., Овсянникову М. И. за обработку ядерных эмульсий и тщательно выполненные измерения протонных треков, а также Комиссарова В. В. и Иванова В. Д. за техническую помощь в проведении экспериментов.

Литература

[1] Петров Д. П., Филиппов Н. В. и др. «Физика плазмы и проблема управляемых термоядерных реакций». Из-во АН СССР (1958) т. IV, стр. 170—181.
[2] Андрианов А. М. и др. Доклад на Женевской конференции № 2301. «Мирное использование атомной энергии ООН, Ядерная физика, стр. 31.
[3] Лукьянов С. Ю., Синицын В. И. *Журнал экспериментальной и теоретической физики* **34** (1958) 849.
[4] Bromley, D., *Proc. Phys. Soc.* **B 63** (1950) 90.
[5] Филиппов Н. В. «Физика плазмы и проблема управляемых термоядерных реакций». Из-во АН СССР (1958) т. III стр. 231.
[6] Коган В. И. там же, т. I, стр. 130.
[7] Брагинский С. И. и др. там же, т. IV, стр. 201.
[8] Станюкович К. П. «Неустановившееся движение сплошной среды», Москва ГИТТЛ (1954).

METHODS FOR THE PRODUCTION OF HIGH DENSITY, HIGH TEMPERATURE PLASMAS BY MAGNETIC COMPRESSION UNDER CONTROLLED INITIAL CONDITIONS*

H. L. JORDAN

INSTITUT FÜR PLASMAPHYSIK DER KERNFORSCHUNGSANLAGE JÜLICH DES LANDES NORDRHEIN-WESTFALEN E. V.

JÜLICH, FEDERAL REPUBLIC OF GERMANY

In earlier magnetic compression experiments, main physical phenomena were observed in the second or later half-cycles of the compression field. Plasma conditions at the beginning of the compression were essentially determined by breakdown properties in the previous half-cycle. Uncontrolled values and distributions of internal magnetic fields, rather high amounts of impurities from wall contamination and inhomogeneity of plasma properties were observed.

A general experimental technique has been developed which allows the formation of a plasma with controlled amounts of internal magnetic field, and the subsequent compression of this plasma. The method uses three capacitor banks which can be switched with a high precision consecutively on the same compression coil. As the same compression coil is used in all stages of the experiment, this technique preserves symmetry and can therefore be applied for different field configurations and coil dimensions, in contrast to other methods for preheating.

Measurements on a small scale experiment were made over a large range of parameters and are described in detail in other reports at this Conference. The essential results are that in the preheating phase an almost fully ionized, uniform plasma with low impurity content and controlled amount of internal magnetic field is formed. By the subsequent fast compression of this initial plasma, a high density and high temperature plasma is obtained in a fully reproducible way. The ratio β of kinetic pressure to external magnetic pressure can be made small or close to 1. The pilot experiment has proved the effectiveness of the method. Based on the same principles, a larger compression experiment is now under construction at Jülich.

1. Heating of plasma by magnetic compression

Magnetically confined plasmas can be heated by enlarging the strength of the confining field. The external magnetic pressure grows and the plasma is compressed. This method is generally called magnetic compression. Depending on the time elapsed from start to peak compression compared to other characteristic times, such as particle collision times, energy transfer time, transit times for small and large amplitude disturbances through the plasma region, field diffusion time and characteristic times for various types of losses, the temporal and spatial development of the plasma compression differs greatly. A large number of phenomena have been observed, which show that under very similar external conditions plasmas with greatly differing configuration and distribution of internal magnetic field, with greatly varying degrees of wall contamination, of thermalization and of density distribution can be obtained. Electron and ion temperatures, stability properties, and losses show great variations. As a whole, the physical picture is usually complex and rather confusing. A number of idealized cases can be considered theoretically, but actual experiments are at best a mixture of these models:

(a) Two-dimensional adiabatic compression of an initially homogeneous thermal plasma with or without internal magnetic field. Collision and diffusion times are large compared to the compression time, while transit times are small. The plasma can be treated as collision-free and energy transfer to the third degree of freedom of the translational motion can be disregarded.

(b) Three-dimensional adiabatic compression of an initially homogeneous thermal plasma with or without internal magnetic field. Transit times are small compared to compression time, while collision times are comparable. Depending on field diffusion time, the initial ratio β of the kinetic energy density of the plasma to the external magnetic energy density is more or less preserved during compression. The final temperature and homogeneity in both cases depend on the compression ratio and the exponent of the adiabatic law, the β of the plasma and on the rate of field diffusion.

(c) Fast (non-adiabatic) compression of an initially homogeneous thermal plasma. In this case transit times for small and large amplitude disturbance are comparable to the compression time. Compression waves and in some cases shock waves influence the heating of the plasma. Two- and three-dimensional cases can again be considered.

(d) Compression of an initially homogeneous non-thermal plasma with or without internal magnetic field, whereby a plasma with given (e.g.

* Conference paper CN-10/184, presented by H. L. Jordan. Discussion of this paper is given on page 649. Translations of the abstract are at the end of this volume of the Conference Proceedings.

singular) non-thermal velocity distributions of ions and electrons is compressed either adiabatically or non-adiabatically, two- or three-dimensionally, depending again on the ratios of characteristic times.

The simpler cases can more or less be described by different plasma models, such as collision-free models, snow-plow models, one- or two-fluid hydromagnetic models, and kinetic models.

In order to improve the understanding of physical processes and to make theory applicable, experiments should aim at reaching if possible the simplest of the cases mentioned. This means specifically a high degree of homogeneity of all plasma properties, a low percentage of neutrals and impurities, and thermal velocity distributions of ions and electrons, if possible with equal ion and electron temperatures. Initial plasmas before compression should have a high conductivity, so that a thin sheath is formed which separates for the time of compression the external field from the plasma.

2. Experiments on magnetic compression

A large number of experiments on the magnetic compression of plasmas have been reported [e.g. 5—14]*. In these experiments various configurations of the compression field were used, such as magnetic fields produced by straight homogeneous cylindrical coils, mirror and cusp fields, and toroidal fields. While in earlier experiments these fields are applied to an initially cold neutral or weakly ionized gas, some experiments reported lately are performed on initially highly ionized plasmas.

These initial plasmas are either produced outside of the compression region by plasma sources or plasma guns and shot into the compression coil, or are produced by a number of different preheating techniques inside the compression region. In particular high power RF discharges, pinch discharges, oscillating electrodeless ring discharges and reflex discharges were used, as reported e.g. in several contributions to this Conference.

In non-preheated experiments an oscillating compression field is used, whereby the first half-cycle or some later half-cycle serves as a preheating phase. A common feature of these experiments is the existence of a trapped internal magnetic field, which depending on breakdown conditions and conductivity can reach large values in particular antiparallel to the external field during the second (or the effective) half-cycle compression. A rather large concentration of impurities is then found in the plasma, which have been detached from the wall of the enclosing tube at the end of the preheating cycle. The amount and the spatial distribution of the trapped internal field is strongly dependent on the initial gas pressure, on the impurity concentration, and on a number of other parameters. Although some of these experiments seem to have produced large mean ion energies of probably thermal origin and relatively quiescent plasmas of high density, the interpretation of the physical processes underlying is still rather difficult. This is due to the fact that during the preheating cycle an initial plasma is formed, but its physical state is unknown and uncontrolled. Breakdown conditions for the originally neutral or weakly ionized gas depend on the density, on the rate of rise of the external magnetic field, on the value and rate of rise of the induced electric field, and on the initial degree of ionization.

These parameters can be varied by varying gas pressure, voltage and energy content of the capacitor bank, the ratio of internal to external inductance of the experiment, the dimensions of the compression coil, and the power, voltage, and coupling of the preionizing RF-circuit. The common experience shows that the variation of one external parameter changes practically all internal parameters of the plasma in such a way that a systematic study of plasma properties during the compression and a comparison between different experiments is difficult.

Regarding the possibility of a larger volume compression experiment the first half-cycle preheating is in addition to this uneconomical as a rather considerable part of the initially stored electric energy is used up by damping in this first half-cycle.

3. Preheated experiments

Essential progress has been made in a number of preheated experiments. In these experiments magnetic compression and formerly observed second half-cycle phenomena occur already in the first half-cycle and considerably smaller impurity concentrations can be reached [5, 9]. Since in earlier experiments the initial state of the plasma before compression was neither known in detail nor too well reproducible, the physical information obtained was again limited.

4. Magnetic bias field experiments

A number of authors [9, 10, 11] have observed that the most critical parameters for a compression experiment are strength, sign, and spatial distribution of the initially trapped magnetic field. These parameters can be varied to some extent by the addition of a static magnetic bias field of variable sign and amplitude. Experiments reported on this technique [12, 13] have proved the fundamental importance of trapped fields and show characteristic differences in plasma behaviour during compression for the cases of parallel and antiparallel internal field. Under reverse field conditions, high mean ion energies and neutrons from D-D reactions are now observed already in the first compression half-cycle [18]. Calculations by HAIN [15] on the compression of a low-β plasma with internal strong parallel or antiparallel fields indicate in the antiparallel case sharp fronts, in the parallel case a more homogeneous radial density distribution. Again a comparison between theory and experiments is difficult, as long as the initial state of the plasma is not sufficiently known.

* See also the next four Conference papers following this one.

5. Preheating under controlled conditions

These considerations have led during the past two years at the Plasma Physics Institute, Jülich, Germany, to the development of experimental and diagnostic techniques for the production and subsequent magnetic compression of an almost fully ionized initial plasma with a known and reproducible state.

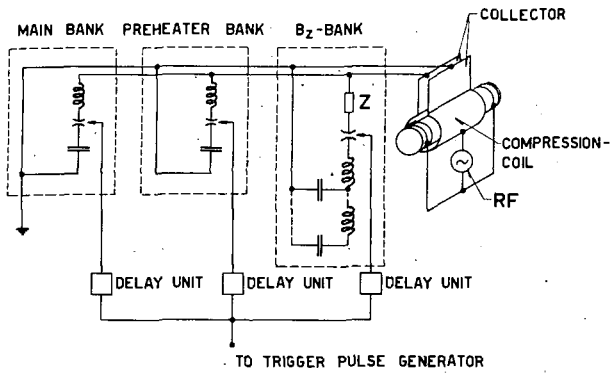

Fig. 1 Block diagram of circuit.

The method is generally characterized by the use of three capacitor banks, which can be switched with a high precision of timing consecutively on the same compression coil (Fig. 1):

(a) A slow, or square wave, bank for the generation of a quasistatic initial magnetic bias field.

(b) A high resonance-frequency bank for the production of a highly ionized, magnetically isolated plasma.

(c) A larger low inductance bank for the main compression field.

A fourth bank may be necessary for the forming of the boundary layer before the main compression.

A fundamental advantage of this method is that in contrast to other methods of preheating and producing bias fields, the same compression coil is used for all stages of the experiment. Shape and symmetry are therefore preserved for all magnetic fields used in sequence.

Some of the construction techniques for these low inductance banks have been described in earlier reports [10, 16, 17].

6. Pilot experiment

A pilot experiment for the study of this method was constructed by HINTZ and FAY. An important contribution to the switching technique was given by BEERWALD and HINTZ [16]. HINTZ, BOGEN and others have made with this experimental facility extensive studies on the breakdown, formation of the initial plasma and on the subsequent magnetic compression. These compression experiments have been made with hydrogen, deuterium, and with added impurities, for a range of initial densities and for different values and polarity of the trapped internal field. Measurements on the breakdown, preheating, and compression phase were made with small steel shielded magnetic probes, time and space resolved spectroscopy in the visible and ultraviolet, smear camera photographs and microwave interferometry.

Some results of these measurements are reported at this Conference [1, 2, 3] and a comparison between these results and theoretical calculations on the dynamic behaviour of the compression of an axially symmetric plasma with trapped internal magnetic field has been made by KEVER [4]. These calculations use a free particle reflection model, a snow-plow model and an adiabatic model for the description of different phases of the plasma compression.

The general data of this experiment are:

(a) RF preionizing with a 500 W, 10 MHz generator, capacitively coupled to the discharge tube.

(b) Magnetic bias field up to 3 kG produced by a matched square wave pulsed delay line with 100 μs duration and 4 μs rise time.

(c) Preheating discharge with a pulsed oscillating, magnetic field of 5 kG maximum amplitude and 0.9 MHz frequency, weakly damped.

(d) Main compression field ≈ 50 kG, 2 μs half-period, produced by a bank of thirty 25 kV, 0.5 μF capacitors. Each capacitor is separately switched. The total bank inductance is $5 \cdot 10^{-9}$ henry.

(e) Straight and homogeneous single turn cylindrical compression coil of 15 cm length and 4 cm inner diameter. Inside the coil is a closely fitted quartz tube, which contains the gas.

The experiment is operated in the followig way. After the generation of the magnetic bias field, the weakly RF-preionized gas is ionized and preheated by a rapidly oscillating electrodeless ring discharge, induced by switching one or more high resonance frequency capacitors on the compression coil. The gas becomes thereby highly ionized, and in subseqeunt half-cycles of the preheater discharge further heating and thermalization of the plasma takes place, mainly by the interdiffusion of antiparallel magnetic fields (field mixing). This effect can be shown by magnetic probe measurements, spectroscopic observations and smear camera photographs [1].

The timing of the main compression bank with respect to the firing of the preheater bank has a precision of $5 \cdot 10^{-8}$ sec. The main compression can thus be made reproducibly in a chosen part of any half-cycle of the preheating discharge. Observations show that the plasma properties are radially inhomogeneous during the first few half-cycles. In later half-cycles (10 and later) the plasma becomes more and more homogeneous and the outer radius expands until the plasma reaches the tube walls. Up to this time the plasma is practically isolated from the walls, due to its inertia, by the oscillating magnetic field, and has a high degree of purity. Spectroscopic measurements give impurity concentrations below 0.05% at densities around 10^{16} electrons/cc and temperatures of 2—3 eV. At these temperatures and densities, collision and energy transfer times are short compared to the pulse time, so that the plasma can be assumed to be in thermal equilibrium.

Basic conditions for a simple case are therefore fulfilled; the initial plasma is thermal and magnetically isolated from the tube walls for such a length of time that it becomes radially homogeneous. Density, temperature, and the distribution of the internal magnetic field can be measured as functions of time. By chosing the time of compression, the value and the polarity of the bias field and the initial density, one can realize the compression of a fully ionized, pure, thermal, and almost homogeneous plasma of sufficient conductivity with and without internal field, parallel or antiparallel to the compression field, with known and reproducible initial conditions over a wide range of parameters.

The clearest experimental results are obtained when the main compression field is applied in later half-cycles [2] of the preheating discharge, when the plasma almost fills the tube. In this case the stray inductance in the coil is a minimum and the coupling of the compression field to the plasma best (Fig. 2).

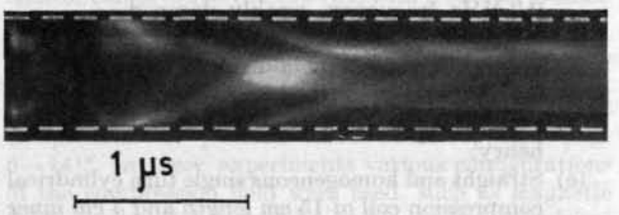

Fig. 2 Smear camera picture of preheating discharge. Initial pressure 230 μ, D_2.

In summarizing the results of papers [2—4] describing the compression phase, it could be shown for the range of parameters used that:

(a) Physical phenomena occurring during the compression and containment time are reproducible within the accuracy of measurements.

(b) The compressed plasma is stable and quiescent during the pulse time at least for the case of weak or strong parallel internal field. No instabilities are observed under preheated conditions, while instabilities clearly develop under non-preheated conditions.

(c) A comparison of streak photographs and magnetic probe measurements shows that magnetic flux inside the plasma is conserved during the implosion and during the compression at least up to current maximum. At current maximum, the period of small amplitude oscillations of the plasma column check with calculated ones for the initial line density, showing conservation of line density. Amplitudes of the radial magnetic field component are small compared to the axial one. These observations indicate high conductivity and exclude small scale instabilities or turbulence.

(d) Both the initial and the compressed plasmas have a very low content of wall impurities. Spectroscopic measurements give impurity concentrations below 0.05% for both cases.

(e) A high density, high temperature thermal plasma can be produced even in the case of parallel internal field. At line densities of $1.8 \cdot 10^{17}$ particles/cm in the case of parallel internal field, temperatures above $1 \cdot 10^6$ °K are observed at the relatively high density of $3 \cdot 10^{17}$ particles/cm. As collision and energy transfer times are short compared to the pulse time of 2 μs, the compressed plasma should become thermalized during the pulse time.

(f) A number of characteristic differences are observed for the cases of strong parallel, weak parallel, and for the case of strong antiparallel internal field (Figs. 3—5). The parallel case shows a conservation of the spatial distributions during the compression for both weak and strong internal fields. In the case of a strong antiparallel field, a hollow cylinder of high density plasma is initially formed and collapsed. After the first compression, this hollow cylinder first oscillates, compressing and decompressing the reverse field trapped inside. As shown by both magnetic probes and smear pictures, the central hole then suddenly disappears, simultaneously with the reverse trapped field on the axis.

(g) For the parallel field case, implosion times calculated by a snow-plow model with internal magnetic field check with observed ones. Plasma energy calculated from the same model can account for about two-thirds of the plasma energy observed at current maximum.

(h) In addition to the results stated in papers [2—4], 10^5 neutrons per pulse are observed at low (50—120 μ Hg) initial pressures in deuterium under reverse field conditions. Space resolved Doppler-broadening measurements of C V lines both side on and end on indicate a spatially symmetric distribution with mean ion energies ≈ 1 keV. Time resolved line profiles have not yet been obtained. Since both radial and axial shock waves are observed, it cannot be excluded

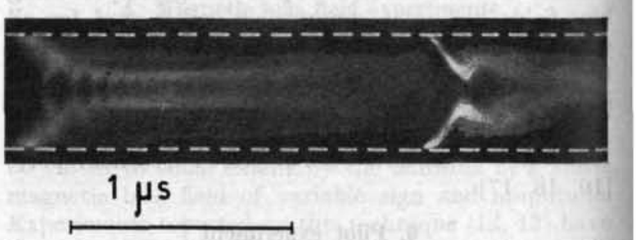

Fig. 3 Smear camera picture of plasma compression in the case of strong parallel internal magnetic field. Initial pressure 230 μ, D_2; $B_0 = +2.5$ kG.

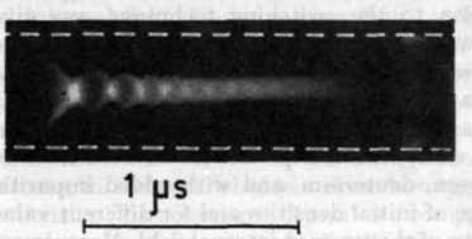

Fig. 4 Smear camera picture of plasma compression in the case of weak parallel internal magnetic field. Initial pressure 300 μ, D_2; $B_0 < 0.5$ kG.

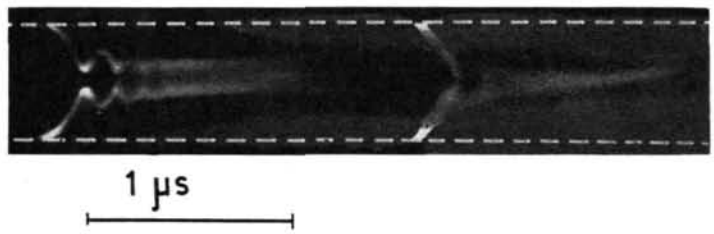

Fig. 5 Smear camera picture of plasma compression in the case of strong antiparallel internal magnetic field. Initial pressure 230 μ, D_2; $B_0 = -2.5$ kG.

that the associated velocity distribution is non-thermal.

Hard x-rays appear only at low densities and at breakdown during the preheating phase. The time of appearance depends on the line density. These x-rays can therefore be attributed to highly accelerated electrons striking the walls, which have been produced during the breakdown phase.

7. Large scale experiment

For the purpose of the magnetic compression of a larger volume of plasma and for longer containment times a larger energy storage is necessary. In a joint effort between a group at this laboratory (Anger, Bohn, Fay, Friedrich, Hopmann, Jelinek) and the Brown-Boveri Co., Mannheim, a large scale compression experiment with magnetic bias field and controlled preheating is under construction at Jülich. The general data of this experimental facility are for the first stage:

(a) Magnetic bias field 5 kG maximum, charging voltage 20 kV, inductance 1 μH, 96×7.7 μF capacitors.
(b) Preheating bank 40×0.3 μF capacitors max. charging voltage 40 kV.
(c) Main compression bank 384×7.7 μF capacitors, charging voltage 20 kV, stored energy 600 kJ.
(d) Compression coil 1 m length, maximal 1.5 m, 10 cm diameter.
(e) Peak field 120 kG.
(f) Half period 20 μs.

8. Further applications

The technique described can be applied to other magnetic field geometries. Experiments on the production of plasma pulses by a plasma gun with an inhomogeneous driving coil are being undertaken at the laboratory along the same general lines. Studies on the production and compression, on stability and losses of plasmas in cusped geometries should be possible using the same method, but require rather large low inductance capacitor banks.

Although this method has been applied only to fast magnetic compression experiments, it could equally well be applied to slower purely adiabatic compression experiments.

Acknowledgements

The author is grateful to W. Fucks, H. Fay, H. Kever, E. Hintz, H. Beerwald, P. Bogen, Miss T. El-Khalafawy and many other members of the laboratory for valuable discussions, advice, and cooperation.

A close contact with A. C. Kolb of the Naval Research Laboratory in Washington, D.C., and interesting discussions with F. L. Ribe and W. E. Quinn of the Los Alamos Scientific Laboratory, New Mexico, and K. Hain of the Max-Planck Institut für Physik, München, have helped to clarify many points.

References

[1] Beerwald, H., Bogen, P., El-Khalafawy, T., Hintz, E., Kever, H., see page 595 of these Proceedings.
[2] Hintz, E., see page 601 of these Proceedings.
[3] Bogen, P., Hintz, E., see page 607 of these Proceedings.
[4] Kever, H., see page 613 of these Proceedings.
[5] Kolb, A. C., Proc. Second U.N. International Conference on Peaceful Uses of Atomic Energy, Geneva, **31** (1958) 328.
[6] Elmore, W. C., Little, E. M., Quinn, W. E., Proc. Second U.N. International Conference on Peaceful Uses of Atomic Energy, Geneva, **32** (1958) 337.
[7] Boyer, K., Little, E. M., *et al.*, *Phys. Rev. Letters* **2** (1959) 279.
[8] Nagle, D. L., Quinn, W. E., *et al.*, *Phys. Rev. Letters* **3** (1959) 318, *Phys. Rev.* **119** (1960) 857.
[9] Kolb, A. C., Fourth Int. Conf. on Ionization Phenomena in Gases, Uppsala (North-Holland Pub. Co., Amsterdam) **2** (1959) 1021.
[10] Fay, H., Hintz, E., Jordan, H. L., Fourth Int. Conf. on Ionization Phenomena in Gases, Uppsala (North-Holland Pub. Co., Amsterdam) **2** (1959) 1046.
[11] Kolb, A. C., Dobbie, C. B., Griem, H. R., *Phys. Rev. Letters* **3** (1959) 5.
[12] Quinn, W. E., Little, E. M., Ribe, F. L., *Bull. Am. Phys. Soc.* **5** (1960) 341.
[13] Goldman, L. M., *et al.*, Div. of Plasma Phys. American Physical Society, Monterey Conference B 5 (1959).
[14] Bodin, H. A. B., Green, T. S., *et al.*, Fourth Int. Conf. on Ionization Phenomena in Gases, Uppsala (North-Holland Pub. Co., Amsterdam) **2** (1959) 1065.
[15] Hain, K., private communication.
[16] Hintz, E., Beerwald, H., Fourth Int. Conf. on Ionization Phenomena in Gases, Uppsala (North-Holland Pub. Co., Amsterdam) **1** (1959) 468.
[17] Jordan, H. L., Rendiconti S.I.F. XIII Corso p. 97.
[18] Little, E. M., Quinn, W. E., Ribe, F. L., *Phys. Fluids* **4** (1961) 711.

PRODUCTION OF A HIGHLY IONIZED DEUTERIUM PLASMA, OF LOW IMPURITY LEVEL, WITH AND WITHOUT MAGNETIC BIAS FIELDS, FOR MAGNETIC COMPRESSION EXPERIMENTS*

H. BEERWALD, P. BOGEN, T. EL-KHALAFAWY, H. FAY, E. HINTZ, H. KEVER

INSTITUT FÜR PLASMAPHYSIK DER KERNFORSCHUNGSANLAGE JÜLICH DES LANDES NORDRHEIN-WESTFALEN E. V.

JÜLICH, FEDERAL REPUBLIC OF GERMANY

Magnetic compression experiments require a well defined, highly ionized initial plasma. Otherwise main effects occur during the second compression half-cycle in a plasma of comparatively high impurity, and under rather uncontrolled conditions.

Investigations have been made on the production of plasma by a pulsed, rapidly oscillating electrodeless ring discharge in RF-preionized gas, and within a straight magnetic compression coil. The amount of trapped internal magnetic field is controlled by an initial axial magnetic bias field. The breakdown mechanism can be theoretically and experimentally shown to depend on the direction and strength of the bias field with respect to the pulsed field, and the initial electron density. Ionization growth has been determined by microwave techniques. The results explain typical phenomena of non-preheated compression experiments.

Full ionization in deuterium at electron temperatures around 2 eV is reached. It is observed that heating is due to interdiffusion of magnetic fields of opposite polarity. The plasma has very low impurity content and reaches both thermal equilibrium and a homogeneous density distribution at the end of the preheating pulse. Electron densities are measured by Stark broadening of H_β.

The amplitude of trapped magnetic field can be varied from 0—3000 G. The measured field distribution is homogeneous at the end of the pulse. The method produces a fully ionized clean plasma with known and uniform initial parameters such as temperature, density and internal magnetic field, which can be varied in a reproducible way.

1. Introduction

For the compression of a cylindrical plasma by fast rising axial magnetic fields the initial state of this plasma is of critical importance [1]. For this reason experiments with a preheating discharge for the production of an initial plasma with known and reproducible properties were started at this laboratory simultaneously with the first experiments on the compression of a weakly preionized deuterium gas.

An electrodeless ring discharge was chosen. The absence of electrodes makes a high degree of purity of the plasma possible. KOLB's experience [2, 3] with a preheating discharge for magnetic compression experiments confirmed this conception and gave further impulse to the work.

Early experiments were made with a RF-transmitter as current generator, in pulsed as well as in stationary operation. Due to the low inductance of the compression coil considerable difficulties are met in coupling the RF power to the discharge. The maximum available power is limited to some hundred kilowatts.

By discharging a low inductance condenser on the compression coil a damped RF pulse with a power of 100 megawatts is easily obtained. To avoid prefiring of the main condenser bank, the voltage of the coil must be limited. With the spark gaps used at this laboratory the maximum permissible voltage at the coil was about 5 kV. This voltage, however, is sufficient to start an electrodeless ring discharge in hydrogen.

Investigations on this electrodeless ring discharge were made with and without a steady magnetic bias field in a wide pressure range. Preliminary results are reported here concerning the breakdown of the gas, the formation of a highly ionized plasma and the subsequent decay of the plasma due to end losses and recombination.

2. Diagnostic methods

For the formation and the decay of the plasma, electron temperature and electron density are of main interest. The appropriate diagnostic method for the measurement of these quantities depends on the range of temperatures and densities expected.

Between 10^{10} and 10^{13} electrons/cm^3, electron density and density changes were measured with an 8.5 mm microwave interferometer [4]. Above 10^{15} electrons/cm^3 the electron density was determined by Stark broadening of H_β. The profile of H_β is well known from theoretical [5] and experimental work [6]. The easiest method for the experimental determination of n_e is the measurement of the half width of the line. This can be done by measuring the intensity as a

* Conference paper CN-10/185, presented by H. L. Jordan. Discussion of this paper is given on page 649. Translations of the abstract are at the end of this volume of the Conference Proceedings.

function of time at various distances from the line centre at consecutive discharges.

Above 2 eV the electron temperature was determined by the relative intensities of C II (4267 Å) and C III (2297 Å) spectral lines, as described elsewhere [7]. Below 2 eV an estimate of the electron temperature can be obtained at the intensity maximum of H_β if the plasma is not being compressed.

Magnetic probe measurements give additional information on the heating mechanism and on the homogeneity of the plasma. From the measured magnetic field distributions one gets the skin-depth and the magnetic pressure gradient, from which the electron temperature and the particle density can be derived.

3. Experimental arrangement

A single-turn, cylindrical compression coil of 40 mm inner diameter and 150 mm length is used for the generation of both the alternating magnetic field and the steady magnetic field. The discharge tube of 2 mm wall thickness and 600 mm length is closely fitted to the coil.

A diagram of the electrical circuit is shown in Fig. 1. The current generator for the steady magnetic field is an artificial delay line, terminated by its impedance, which produces a nearly rectangular current pulse. The duration of the pulse is about 100 μs, the risetime

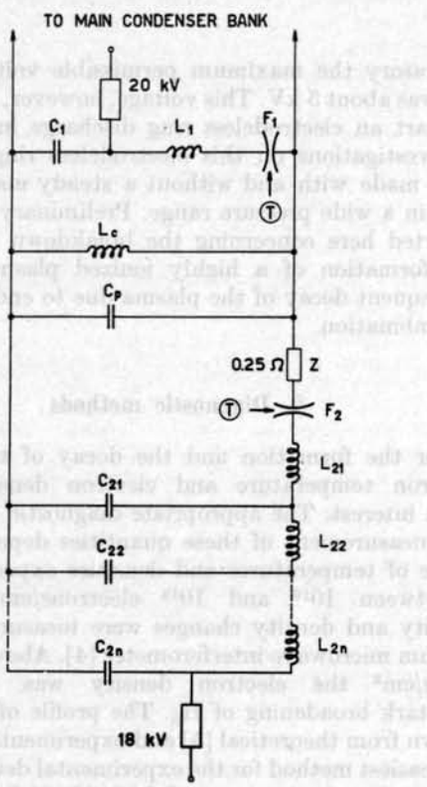

Fig. 1 Electrical circuit diagram. C_p—collector plate capacitance, C_1—capacitance of preheat condenser, L_c—inductance of discharge coil, $C_{21} \ldots C_{2n}$—capacitances of artificial delay-line, $L_{21} \ldots L_{2n}$—inductances of artificial delay-line, T—trigger pulse.

4 μs and the maximum current 35000 A, the maximum field correspondingly 3000 G. By discharging C_1 an oscillating magnetic field with a maximum amplitude of 5000 G, an oscillation frequency of 900 kHz and a damping constant of 2.6 μs can be produced.

4. Results

4.1. Growth of ionization

In an electrodeless ring discharge the electrons are moving in crossed electric and magnetic fields, in contrast to other types of gas discharges. This strongly influences ionization growth, in particular at low pressures. Assuming $\nu_e < \nu_c$ (ν_e = electron-atom collision frequency, ν_c = electron cyclotron frequency) $\omega \ll \nu_e$ (ω = resonance frequency of the discharge circuit), and plane geometry, the energy transfer to the electrons can be calculated for times of the order $1/\nu_c$ [8].

Assuming a sinusoidal magnetic field, two time intervals can be distinguished:

$$(a)\ \frac{1}{\nu_c}\frac{1}{B}\frac{\mathrm{d}B}{\mathrm{d}t} > 1, \qquad (b)\ \frac{1}{\nu_c}\frac{1}{B}\frac{\mathrm{d}B}{\mathrm{d}t} < 1.$$

Case (*a*): The electron obtains a maximum velocity of $V_m \approx 1.6 \cdot r/2\,\dot{\omega}_c^{1/2}$, at a time of $t_m = 2\,\dot{\omega}_c^{-1/2}$, where $\omega_c = 2\,\pi\,\nu_c$. The corresponding energy of the electron is $E \approx (1/10)\,U$ (eV), where U is the voltage at the coil. From this relation one gets an estimate for maximum ionization growth due to this mechanism

$$n_e \approx n_{e0}\,\frac{U}{30\,U_i},$$

where n_{e0} is the initial electron density and U_i the ionization energy.

Case (*b*): Two critical cases can be distinguished:

(b.1) $\omega_c(T) > \omega_p$; ω_p = plasma frequency and T = time since the start of the discharge.

The maximum velocity is $2\,E/B$, which means that the electron energy can exceed the ionization energy only for times of the order 10^{-8} sec in the experiment described.

(b.2) $\omega_c\,(T) < \omega_p$.

The electron velocity tends to $(1/2)\,\dot{\omega}_c\,r \sim Et$. It is remarkable that the velocity increases linearly with time. As a consequence ionization can proceed as long as the E-field is high enough.

The main conclusion from these results is that good preionization of the gas, which results in a high initial electron density and plasma frequency, is really an essential point for the fast growth of ionization.

4.2. Breakdown with superimposed magnetic field

For the breakdown of the gas with a steady magnetic bias field the sign and the magnitude of the ratio $K = B$ (steady)$/B$ (pulsed) are of importance. In order

to obtain favourable conditions for the breakdown in the first half-cycle, it is necessary

(1) to choose the negative sign for K,

(2) to choose K smaller than 1, because E/B stays small for $K \geqslant 1$ and a rapid ionization will not occur in either of the two cases (b.1), (b.2).

This can be confirmed by measurements. Fig. 2 shows oscilloscope traces of the microwave signal for two typical cases at 50 μ D_2.

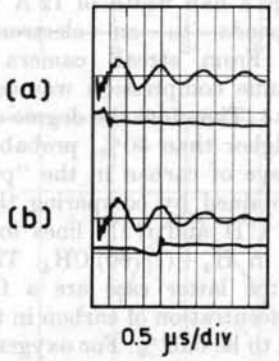

Fig. 2 Ionization growth at 50 μ, D_2. Upper trace: voltage at the coil, lower trace: microwave interferometer signal. (a) $K = -1/2$; $\omega_p = 10^{10}$ electrons/cm^3; (b) $K = 0$, $\omega_p \ll 10^{10}$ electrons/cm^3.

The first is for $K = -1/2$ and $\omega_p = 10^{10}$ sec^{-1}. About 0.1 μs after the maximum of E_θ the cyclotron frequency of the electrons becomes smaller than the plasma frequency and a short time later the magnetic field goes through zero. In this time interval there should be a rapid increase in electron density. This is in good agreement with the experimental results. Within $2 \cdot 10^{-7}$ sec the electron density increases by a factor of 100.

The second case is for $K = 0$ and $\omega_p \ll 10^{10}$ sec^{-1}. This picture shows the importance of a high initial electron density for the breakdown of the gas. The first two half-cycles of the discharge are used to build up an electron density of about $5 \cdot 10^{10} - 10^{11}$ cm^{-3}, which in the other case exists already at the start of the discharge. At the following fourth voltage maximum the gas breaks down.

4.3. Development of the plasma after breakdown

Most of the measurements have been made at an initial pressure of 230 μH_2 without a magnetic bias field, this being the most interesting case for present compression experiments at this laboratory. It could be shown, however, that with other interesting sets of initial parameters the maximum electron temperature and ionization degree in the plasma are not much different.

Fig. 3 shows photomultiplier traces of the C II and C III lines and the temporal development of the electron temperature derived from their relative intensities at 230 μ H_2. The plotted curve gives a minimum value of T_e. The true electron temperature is probably

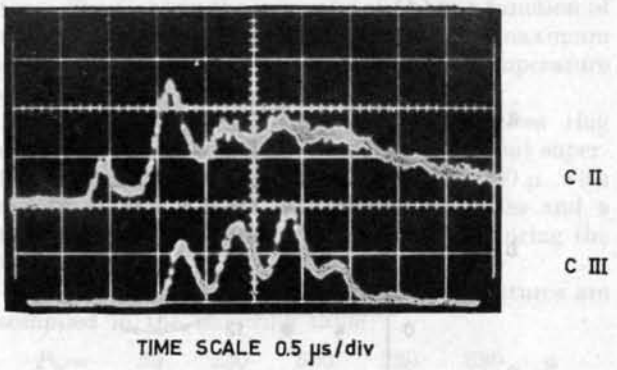

Fig. 3a C II (4267 Å) and C III (2297 Å) spectral line intensity as a function of time.

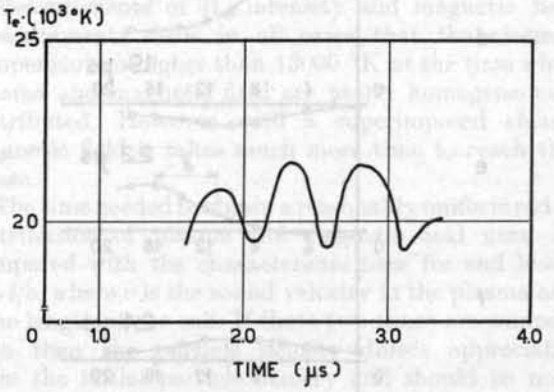

Fig. 3b Electron temperature as a function of time. $p_0 = 230$ μ, $H_2 + (1/760)$ CH_4.

higher due to incomplete equilibrium and nonuniform distribution of the electron temperature.

Magnetic field measurements can give information on the homogeneity of the plasma. Fig. 4 shows the internal and external field at 230 μ and at 120 μ D_2. The magnetic field signals at these two pressures are very similar and show clearly that during the third current half-cycle internal and external fields are of opposite sign, with high magnetic field gradients in between. These are produced by strong currents giving a sudden increase of electron temperature.

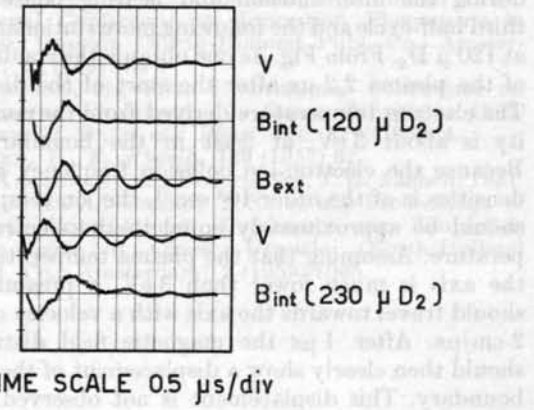

Fig. 4 B_{int} (t) and B_{ext} (t) at 230 μ, D_2 and 120 μ, D_2. V—voltage at the coil.

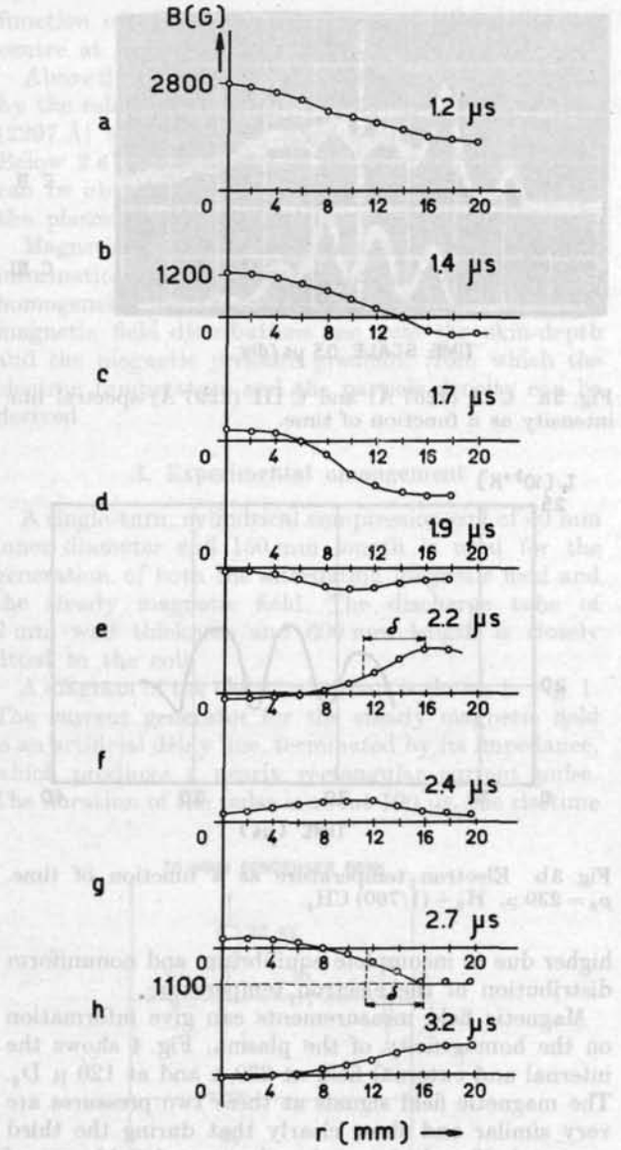

Fig. 5 Radial magnetic field distribution at different times. $p_0 = 120\ \mu$, D_2.

Fig. 5 shows a set of magnetic field distributions during the interdiffusion and heating phase in the third half-cycle and the following more stationary phase at 120 μ D_2. From Fig. 5e one obtains the conductivity of the plasma 2.2 μs after the start of the discharge. The electron temperature derived from the conductivity is about 3 eV, at least in the boundary zone. Because the electron-ion collision frequency at these densities is of the order $10^8\ \mathrm{sec}^{-1}$, the ion temperature should be approximately equal to the electron temperature. Assuming that the plasma temperature near the axis is much lower than 3 eV, a pressure front should travel towards the axis with a velocity of about 2 cm/μs. After 1 μs the magnetic field distribution should then clearly show a displacement of the plasma boundary. This displacement is not observed.

Smear camera pictures likewise show that in this time interval velocity changes of the plasma boundary are negligible. Therefore inertial effects can be neglected and the external magnetic pressure is balanced by the kinetic pressure. Assuming the particle density to be 10^{16} particles/cm³, one derives a plasma temperature of about 18000 °K from Fig. 5g.

At 230 μ H_2 the electron density was measured by Stark broadening of H_β. Fig. 6 shows a photomultiplier trace at the centre of H_β and at $\Delta\lambda = 5$ Å. The half width of H_β and the calculated electron density as a function of time are shown in Fig. 7. 3 μs after the start of the discharge a half width of 12 Å was measured, which corresponds to an electron density of $1.4 \cdot 10^{16}\ \mathrm{cm}^{-3}$. From streak camera pictures the maximum volume compression was estimated to be smaller than 2:1. Therefore the degree of ionization at that time is higher than 50%, probably near 100%.

The percentage of carbon in the "pure" hydrogen plasma was obtained by comparing the photomultiplier traces of C II and C III lines in initially pure hydrogen and in $H_2 + (1/760)\ CH_4$. The carbon line intensities in the latter case are a factor of three higher. The concentration of carbon in the plasma was then estimated to be 0.02%. For oxygen a value of the same order of magnitude was obtained. The impurity

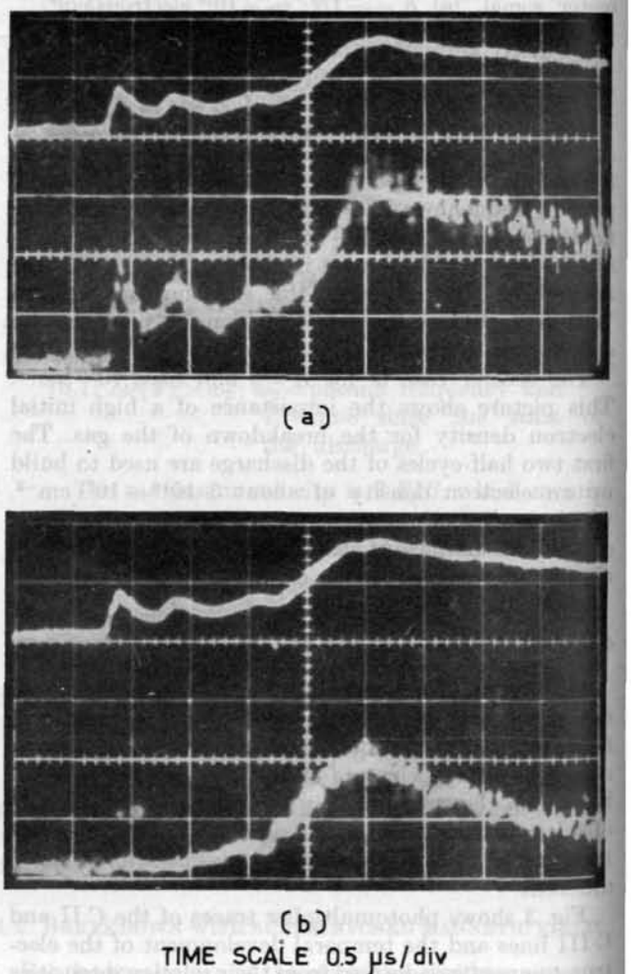

Fig. 6 H_β line intensity (a) at the line center and (b) at $\Delta\lambda = 5$ Å.

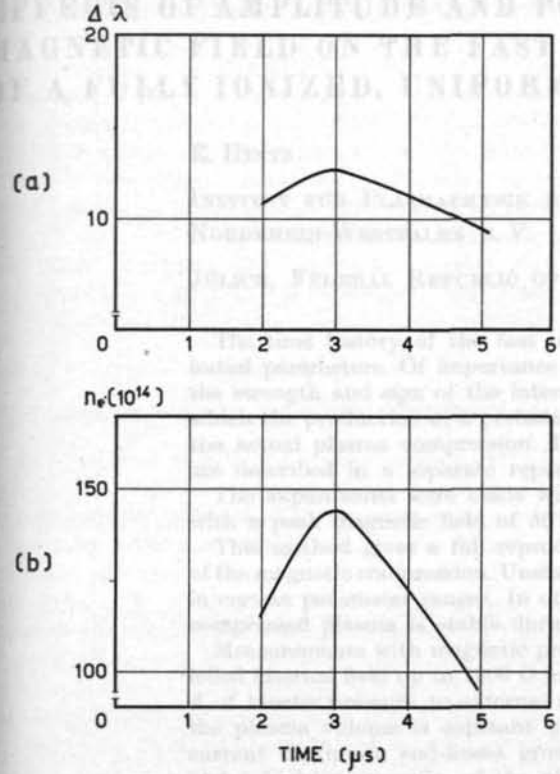

Fig. 7 (a) Half-width of $H\beta$ ($\Delta\lambda$) and (b) electron density (n_e) as functions of time.

degree was not constant but always below a value of 0.05%.

Both streak camera and magnetic field measurements indicate that the plasma is fairly uniformly distributed after about 5 μs. With the assumption that at this time the degree of ionization is above 50% one would expect a maximum of $H\beta$ after some time. Fig. 8 shows the intensity of $H\beta$ as a function of time at an initial pressure of 230 μ. The maximum appears after about 11 μs, indicating a temperature of about 13000 °K at this time.

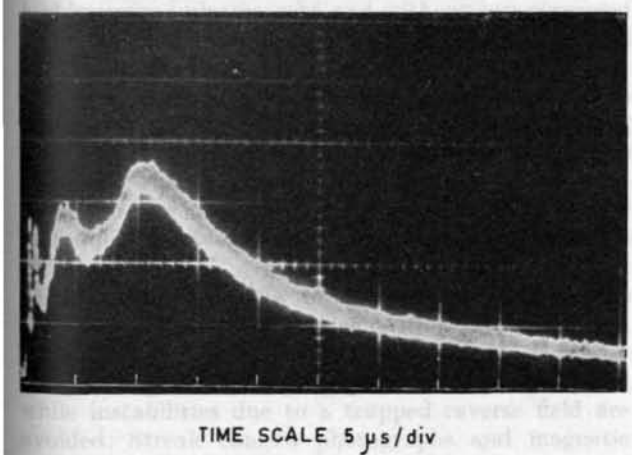

Fig. 8 $D\beta$ intensity as a function of time.

Further investigations on the electrodeless ring discharge were made at 60 μ and 500 μ without superimposed steady magnetic field and at 230 μ with steady magnetic fields of various amplitudes and a field direction opposite to the pulsed field during the first half-cycle.

The measured maximum electron temperatures are compiled in the following table:

$P_0 =$	50	230	500	230	230	μ
$B_0 =$	0	0	0	1200	2400	Gauss
$T_e =$	27000	22000	16000	32000	27000	°K

Measurements of $H\beta$ intensity and magnetic field measurements show in all cases that the electron temperature is higher than 13000 °K at the time when plasma and magnetic field are nearly homogeneously distributed. However with a superimposed steady magnetic field it takes much more time to reach this phase.

The time needed to obtain a reasonably uniform radial distribution of plasma and magnetic field must be compared with the characteristic time for end losses $\tau \sim l/v$, where v is the sound velocity in the plasma and l the length of the coil. If these two times are comparable then the particle density differs appreciably from the initial particle density and should be non-uniform along the axis. This is demonstrated in Fig. 7 which shows the change in electron density due to end losses.

Experiments also show that end losses are influenced by the presence of an internal field. To fix the initial conditions for a magnetic compression experiment, the particle density for each set of initial conditions therefore must be measured separately at the appropriate time.

References

[1] Jordan, H. L., see page 589 of these Proceedings.
[2] Kolb, A. C., Proceedings of Second U.N. International Conference on Peaceful Uses of Atomic Energy **31** (1958) 328.
[3] Kolb, A. C., *et al.*, Proceedings of Fourth International Conference on Ionization Phenomena in Gases, Uppsala (North-Holland Publ. Co., Amsterdam) **2** (1959) 1037.
[4] Beerwald, H., Fifth International Conference on Ionization Phenomena in Gases, München, 1961.
[5] Griem, H. R., *et al.*, *Phys. Rev.* **116** (1959) 4.
[6] Bogen, P., *Z. Physik*, **149** (1957) 62.
[7] El-Khalafawy, T., Dissertation, T. H. Aachen, 1961.
[8] Bodin, H. A., Green, T. S., *et al.*, Proceedings of Fourth International Conference on Ionization Phenomena in Gases, Uppsala (North-Holland Publ. Co., Amsterdam) **2** (1959) 1065.

EFFECTS OF AMPLITUDE AND POLARITY OF INTERNAL MAGNETIC FIELD ON THE FAST MAGNETIC COMPRESSION OF A FULLY IONIZED, UNIFORM PLASMA*

E. HINTZ

INSTITUT FÜR PLASMAPHYSIK DER KERNFORSCHUNGSANLAGE JÜLICH DES LANDES NORDRHEIN-WESTFALEN E. V.

JÜLICH, FEDERAL REPUBLIC OF GERMANY

The time history of the fast magnetic compression of a plasma depends critically on the initial parameters. Of importance are density, conductivity, degree of ionization and especially the strength and sign of the internal magnetic field. An experimental technique is described by which the production of a preheated plasma with controlled initial parameters is decoupled from the actual plasma compression. Diagnostic techniques and properties of this preheating phase are described in a separate report by H. Beerwald *et al.*

The experiments were made with a single-turn, cylindrical compression cell without mirrors, with a peak magnetic field of 50 kG and a quarter period of 1 μs.

This method gives a full reproducibility of all measurable quantities during the stable phase of the magnetic compression. Unstable behaviour is observed in later stages (near current maximum) in certain parameter ranges. In other ranges of values of density and internal magnetic field the compressed plasma is stable during the whole first half-cycle of the compression.

Measurements with magnetic probes and smear camera pictures show that in the case of parallelled internal field up to 1000 G magnetic flux is conserved during compression and that the ratio β of kinetic pressure to external magnetic pressure is above 0.8. The line density of particles in the plasma volume is constant up to current maximum and equal to the initial value. After current maximum end-losses grow rapidly. The case of negligible internal field gives a $\beta \approx 1$ and a high compression of the plasma.

The case of antiparallel internal field shows in contrast to the parallel configuration a very sharp defined transition zone between external and internal field. During compression this transition zone smears out gradually and disappears near current maximum. At the same time probe signals indicate the break-through of the external field, while smear pictures show no difference when the probe is inserted.

1. Introduction

This paper gives a report on experimental investigations concerning the fast magnetic compression of a highly ionized plasma with and without superimposed magnetic fields. A straight cylindrical compression coil without mirrors was chosen to avoid axial shock waves. In order to study the influence of important initial parameters such as density, amplitude, and direction of a magnetic bias field, an experimental technique was used which made it possible to vary these parameters independently. Details on this experimental technique are given in other papers of this Conference [1, 2].

The main effort was directed to the study of the temporal behaviour of a plasma during compression with low but parallel initial magnetic field. This way a high temperature, high β plasma can be produced while instabilities due to a trapped reverse field are avoided. Streak camera photographs and magnetic field measurements show that the theoretical concepts regarding the properties of such a high β plasma are valid.

Further experiments deal with effects caused by an antiparallel magnetic bias field. Characteristic differences from the case of a parallel field are observed and partly explained.

2. Experimental arrangement

The electrical circuit diagram is shown in Fig. 1. The compression coil ($l = 15$ cm, diameter $d = 4$ cm) is connected to three separate current generators. Preheater- and B_z-bank are described in detail in [2]. They serve to provide a preheated plasma with or without a superimposed steady magnetic field. The main bank, consisting of thirty 0.5 μF low inductance condensers, each with its own spark gap, can be switched on the coil with a time delay arbitrarily chosen with respect to the discharge of the preheater bank. A typical oscilloscope trace of the voltage at the collector is also shown in Fig. 1. The maximum magnetic field in the coil is 46 500 G and the half period of the discharge 1.7 μs. A quartz tube of 700 mm length and a wall thickness of 2 mm is closely fitted inside the coil. The base pressure reached in the tube is $1—2 \cdot 10^{-6}$ mm Hg.

With a plasma of 1—2 eV inside the tube the maximum dB/dt of the magnetic field pulse amounts to $2 \cdot 10^{11}$ G/sec. For constant dB/dt the characteristic

* Conference paper CN-10/186, presented by H. L. Jordan. Discussion of this paper is given on page 649. Translations of the abstract are at the end of this volume of the Conference Proceedings.

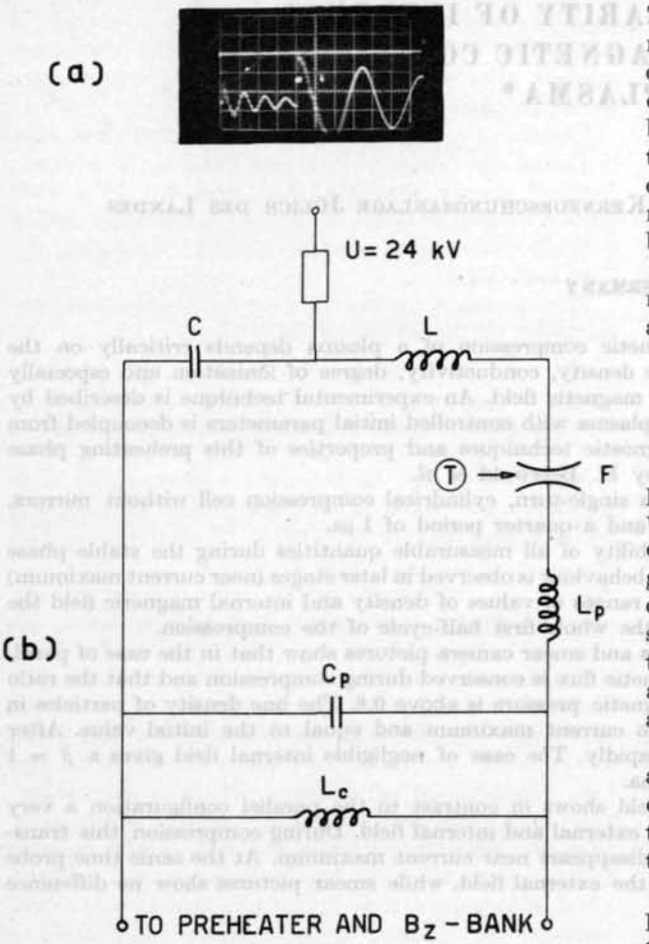

Fig. 1 (a) Voltage at the coil. (b) Electrical circuit diagram. C — $30 \times 0{,}5$ μF, L — $1/30 \times 50$ mμH, F-30 trigatrons, L_p (inductance of collector plate) — 3 mμH, C_p — capacitance of collector plate, L_c (inductance of compression coil) — 10 mμH.

time to build up a magnetic pressure equal to the plasma pressure at a particle density of 10^{16} cm^{-3} would be $t_P = 5 \cdot 10^{-9}$ sec. Due to the finite switching time, the initial dB/dt is much smaller. A better estimate for t_P is therefore $t_P \approx t_s \approx 2 \cdot 10^{-8}$ sec, (t_s = switching time).

3. Methods of measurement

A streak camera and magnetic probes have been used to get information on the temporal behaviour of the plasma. By an appropriate combination of these two diagnostic methods one obtains data on the energy density of the plasma, on particle density, and density distributions during time.

The discharge was photographed with a Beckmann and Withley 339b streak camera both side-on and end-on. The entrance slit was normal to the tube axis and the time resolution between 1—$2 \cdot 10^{-8}$ sec. Further experimental details regarding streak camera pictures are discussed in another paper of this conference [3].

In order to determine the magnetic field distribution in the plasma a small size magnetic probe was used. The pick up coil of 0.5 mm length and 0.4 mm diameter is shielded by a stainless steel tube of 1 mm diameter and 0.1 mm wall thickness. Time resolution can theoretically [4] and experimentally be shown to be about $5 \cdot 10^{-8}$. The probe is radially inserted into the plasma and can be moved along a diameter of the discharge tube. The possibilities and limits of probe measurements under our experimental conditions have been discussed elsewhere [5].

From these results we can conclude that the magnetic field measurements described in this paper are reliable.

4. Results

4.1. Investigations on a high β-plasma

All experiments described in this section have been performed at an initial pressure of 250 μ H_2 or D_2 without a superimposed magnetic field. Measurements of plasma properties during the preheating phase are given in [2]. Fig. 7b of that paper shows the electron density n_e as a function of time. About 3 μs after the start of the discharge, n_e has a maximum; the density then decreases, mainly due to end losses. Between 3 and 10 μs the ionization degree is higher than 50% and the electron temperature higher than 13000 °K.

At 3 μs, the internal magnetic field amounts to about 900 G. The external field decays with a time constant of 2.6 μs. Due to the low plasma conductivity the internal field decays with approximately the same time constant.

An attempt has been made to study plasma compression with a β between 0.8 and 0.95, at several densities, by varying the delay time between the preheater discharge and the main bank discharge. Some of the results shall now be discussed.

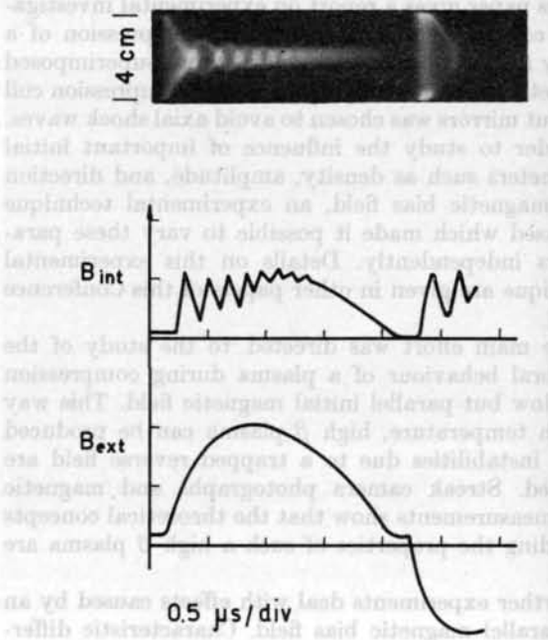

Fig. 2 Streak photo of plasma compression. $B_{int}(t)$ and $B_{ext}(t)$ at an initiale line density of $N_0 = 1{,}8 \times 10^{17}$ cm^{-1} and an initial magnetic field of $B_0 = 900$ G.

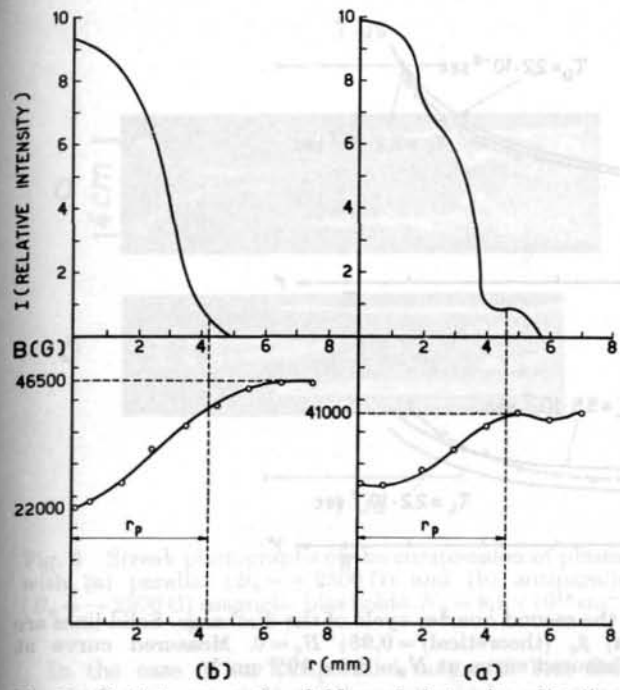

Fig. 3 Radial magnetic field and intensity distribution during plasma compression of deuterium gas. $N_0 = 1{,}75—10 \times 10^{17}$ cm^{-1}. (a) $B(r)$ and $I(r)$ at the second maximum compression of the plasma cylinder and (b) $B(r)$ and $I(r)$ at the current maximum.

A general result is that with this experimental procedure streak photos, magnetic probe signals, and photoelectric signals of a C V line show a high degree of reproducibility if the tube has once been cleaned up by about 40 discharges. This makes the measurement of B-distributions possible.

Fig. 2 shows a side-on streak photo of plasma compression at $t=3$ μs together with B_{int} and B_{ext}. The dynamics of plasma compression under these conditions are discussed in detail by H. KEVER [6].

A comparison of $(B_{max}/B_{min})^{1/2}$ with r_{max}/r_{min} shows [5] that these ratios are equal, within the accuracy of measurement, in the time interval from the first maximum compression of the plasma cylinder up to current maximum. This means that the magnetic flux is constant during this time.

The radial magnetic field distribution in a cross section of the coil 2 cm away from the symmetry plane has been determined at the second maximum compression and at current maximum. The results are shown in Fig. 3 together with the radial intensity distribution.

The magnetic field on the axis at current maximum agrees within the accuracy of measurement with the initial magnetic field at the start of the compression multiplied by the compression ratio. This means that in the region near the axis magnetic flux is also constant during the first implosion.

However, it is to be expected that magnetic field penetrates into the boundary zone before the plasma starts moving. When the plasma temperature suddenly increases, this distribution is frozen in. This is shown by a comparison of the magnetic field distributions in Figs. 3a and 3b. Both figures also show a remarkable agreement of plasma radii determined by intensity (density) distributions or magnetic field distributions, although probe measurement and streak photographs were taken in directions perpendicular to each other. Rotational symmetry of the plasma can therefrom be concluded.

Near current maximum velocity changes of the plasma boundary are negligible. The reproducibility of measurements, the observed rotational symmetry, and the fact that a radially inserted probe shows no effect on the plasma argue against a fast rotation of the plasma. Therefore inertial terms can be neglected in the pressure balance equation, and the external magnetic pressure should balance the internal magnetic pressure plus the kinetic pressure.

Radial magnetic fields were not detected although a probe with high sensitivity was used. Therefore it is not likely that plasma turbulence gives a significant contribution to the kinetic pressure.

From Fig. 3a $\beta = nkT/(B^2/2\,\mu_0) = 0.8$ is obtained in the vicinity of the axis.

The measured oscillation period at current maximum gives a line density of $N = 1.8 \cdot 10^{17}$ cm^{-1}. This value is in agreement with the initial line density, which indicates effective particle trapping and negligible end losses up to this time.

With a β of 0.8 and a particle density of $3 \cdot 10^{17}$ cm^{-3} one obtains $T_e + T_i = 2 \cdot 10^6$ °K.

Fig. 4 shows magnetic field signals and a streak photo of the plasma when the main bank is fired

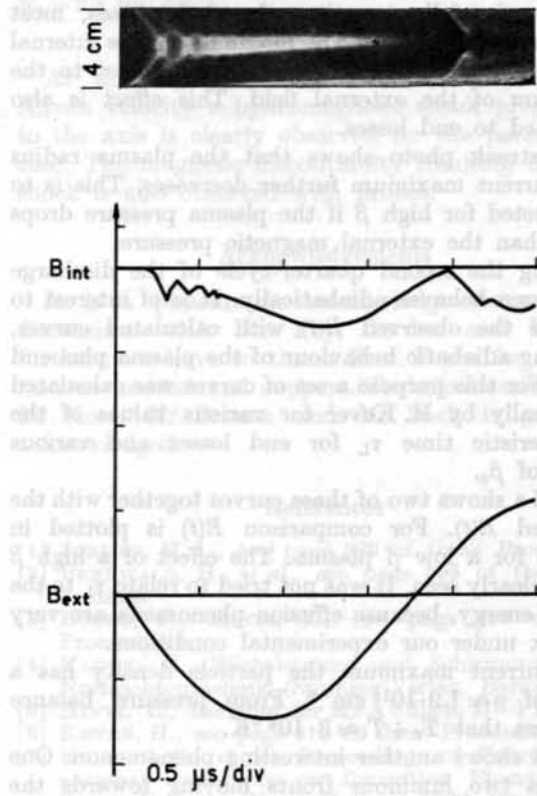

Fig. 4 Streak photo of plasma compression, $B_{int}(t)$ and $B_{ext}(t)$ at an initial line density of $N_0 = 1 \times 10^{17}$ cm^{-1}.

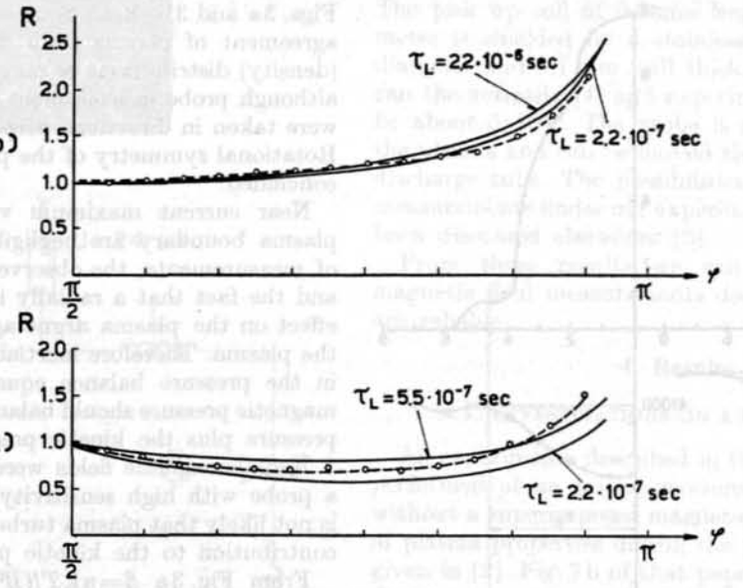

Fig. 5 $R(t)$ plotted theoretically and experimentally during the second quarter-cycle of the discharge. Solid lines are theoretical curves, broken lines are measured curves. (a) β_0 (theoretical) = 0,95; $B_0 = 0$. Measured curve at $N_0 = 1 \times 10^{17}$ cm^{-1}. (b) β_0 (theoretical) = 0,1; $B_0 = 2500$ G. Measured curve at $N_0 = 8{,}8 \times 10^{16}$ cm^{-1}.

with a delay of 8 μs. In this case the initial line density N is about $1 \cdot 10^{17}$ cm^{-1}, and the initially trapped field is appreciably lower than with a delay of 3 μs. The oscillations of the plasma cylinder are damped out very soon and a more stationary state is reached about 0.4 μs after the start of the main discharge. At this time the β has a value of about 0.95. In the following time the β decreases, most likely due to end losses. The maximum of the internal magnetic field is clearly shifted with respect to the maximum of the external field. This effect is also attributed to end losses.

The streak photo shows that the plasma radius after current maximum further decreases. This is to be expected for high β if the plasma pressure drops faster than the external magnetic pressure.

During the second quarter-cycle of the discharge the plasma behaves adiabatically. It is of interest to compare the observed $R(t)$ with calculated curves, assuming adiabatic behaviour of the plasma plus end losses. For this purpose a set of curves was calculated numerically by H. Kever for various values of the characteristic time τ_L for end losses and various values of β_0.

Fig. 5 a shows two of these curves together with the measured $R(t)$. For comparison $R(t)$ is plotted in Fig. 5 b for a low β plasma. The effect of a high β can be clearly seen. It was not tried to relate τ_L to the plasma energy, because effusion phenomena are very complex under our experimental conditions.

At current maximum the particle density has a value of $n \approx 1.9 \cdot 10^{16}$ cm^{-3}. From pressure balance it follows that $T_e + T_i \approx 3 \cdot 10^6$ °K.

Fig. 4 shows another interesting phenomenon. One observes two luminous fronts moving towards the tube centre. It can be shown that the second front arises from cold gas near the walls [3], which is relatively late ionized and conducting. If the time between the firing of the preheating bank and the main bank is too long, the ionization degree near the walls gets very low. When the compression pulse is applied, the magnetic field penetrates through the cold gas layer and the plasma implosion starts somewhat away from the walls. At a later time a second sheath follows.

At higher densities and consequently higher ionization frequencies the time delay for the formation of the second sheath is less and the distance of the two fronts should be smaller. With a superimposed antiparallel field, ionization should be favoured [2] in comparison to the parallel field case. This is in agreement with observations (Figs. 7 and 8).

4.2. Compression of low β plasma with internal magnetic fields parallel or antiparallel to the driving field

Experiments described in this section were performed at initial pressures of 250 μ D_2 and 500 μ D_2. A steady B_z field of 2500 G was superimposed on the plasma, and the main bank was fired with a delay of 8 μs with respect to the preheater discharge.

Fig. 6 shows streak photographs of plasma compression at a line density of $8.8 \cdot 10^{16}$ cm^{-1} with parallel and antiparallel magnetic bias fields. In Fig. 7 the corresponding oscilloscope traces of the external and internal magnetic field are given. The influence and significance of field polarity is clearly demonstrated. With an antiparallel magnetic field the start of plasma implosion is delayed and the development of the plasma boundary velocity is different from the parallel field case. This can be attributed to the different temporal behaviour of $B^2(t)$ at the plasma boundary which results in an initial plasma flow towards the walls.

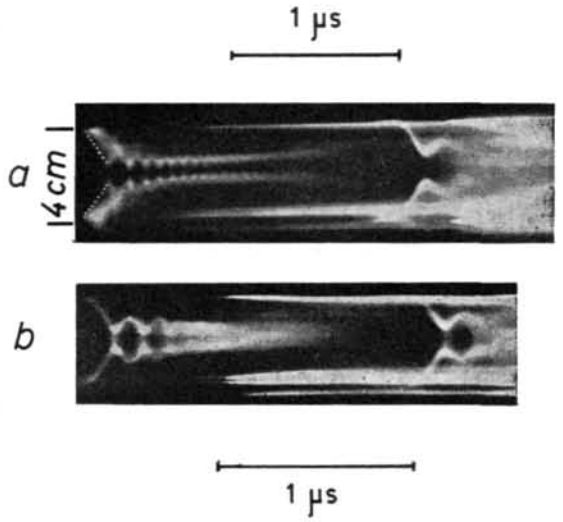

Fig. 6 Streak photographs of the compression of plasma with (a) parallel ($B_0 = +2500$ G) and (b) antiparallel ($B_0 = -2500$ G) magnetic bias fields. $N_0 = 8{,}8 \times 10^{16}\,\mathrm{cm}^{-1}$.

In the case of an antiparallel magnetic bias field the high magnetic field gradients should be connected with high density and temperature gradients, which is also observed. The intensity distributions are discussed in more detail in [3].

The internal magnetic field during plasma compression with a parallel magnetic bias field (Fig. 7) shows no remarkable effect. From the ratio of the internal to the external field, the β is estimated to be 0.3. With an antiparallel magnetic bias field the internal field changes its sign after about 0.5 μs. This sudden reversal of the trapped [7, 8] field coincides with the disappearance of the hole in the intensity distribution observed in Fig. 6. The field reversal is not attributed to the presence of the probe. At higher densities the trapped field stays antiparallel throughout the first half-cycle. In this case the intensity distributions likewise show a minimum on the axis up to the end of the first half-cycle. This is demonstrated in Fig. 8 which shows streak camera photos at a line density of $2 \cdot 10^{17}\,\mathrm{cm}^{-1}$.

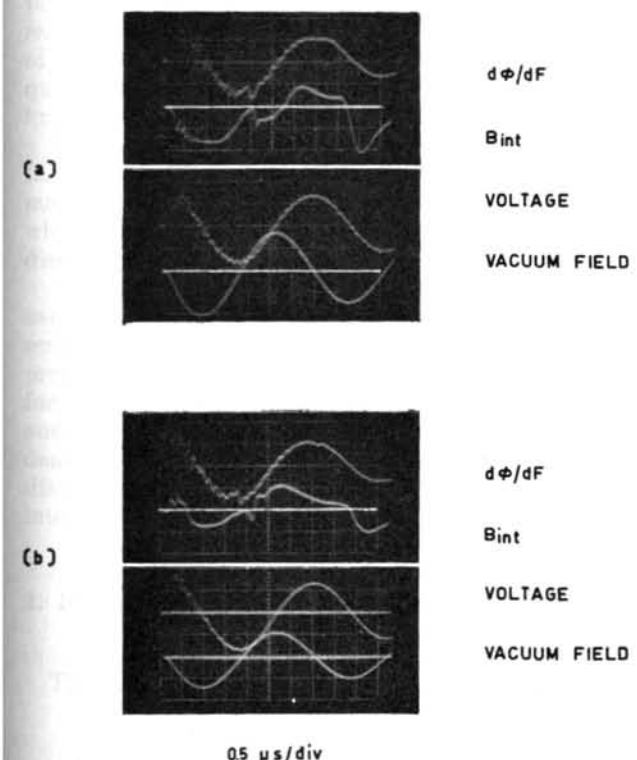

Fig. 7 Magnetic field on the axis during magnetic compression with (a) parallel ($B_{z0} = +2500$ G) and (b) antiparallel ($B_{z0} = -2500$ G) magnetic bias fields. $N_0 = 8.8 \times 10^{16}\,\mathrm{cm}^{-1}$. [Note: The labels "$\mathrm{d}\varphi/\mathrm{d}F$" should be "$\mathrm{d}\varphi/\mathrm{d}t$".]

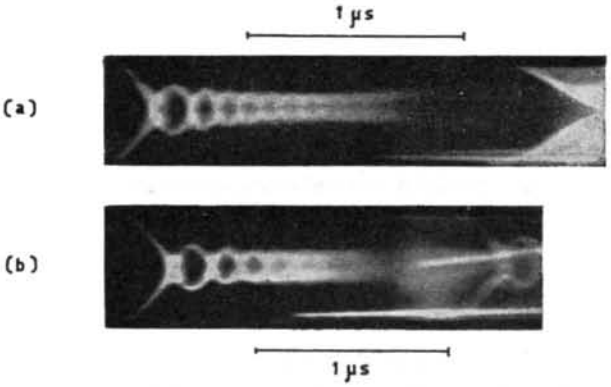

Fig. 8 Streak photographs of the compression of plasma with (a) parallel ($B_0 = +2500$ G) and (b) antiparallel ($B_0 = -2500$ G) magnetic fields at high line densities. $N_0 = 2 \times 10^{17}\,\mathrm{cm}^{-1}$.

At this higher density and consequently lower Alfvén velocity a hydromagnetic shock propagating to the axis is clearly observed for the parallel field case. The magnetic discontinuity resulting from the shock is also observed with probes.

Acknowledgements

It is a pleasure to acknowledge many helpful discussions with Drs. Fay, Jordan and Kever. I furthermore have to thank Prof. Fucks for his continuous interest and support. Technical assistance of Mr. Korr, Mr. Braune and Mr. Bach is gratefully acknowledged.

References

[1] Jordan, H. L., see page 589 of these Proceedings.
[2] Beerwald, H., *et al.*, see page 595 of these Proceedings.
[3] Bogen, P., Hintz, E., see page 607 of these Proceedings.
[4] Kaden, H., Wirbelströme und Schirmung in der Nachrichtentechnik (Springer-Verlag, Berlin, 1959).
[5] Hintz, E., Berichte der KFA Jülich, B—PP
[6] Kever, H., see page 613 of these Proceedings.
[7] Kolb, A. C., *et al.*, Proceedings of Fourth International Conference on Ionization Phenomena in Gases, Uppsala (North-Holland Publ. Co., Amsterdam) **2** (1959) 1037.
[8] Little, E. M., *et al.*, *Phys. Fluids* **4** (1960) 711.

DENSITY DISTRIBUTION FROM RADIATION MEASUREMENTS DURING THE FAST MAGNETIC COMPRESSION OF A PLASMA*

P. BOGEN, E. HINTZ

INSTITUT FÜR PLASMAPHYSIK DER KERNFORSCHUNGSANLAGE JÜLICH DES LANDES NORDRHEIN-WESTFALEN E. V.

JÜLICH, FEDERAL REPUBLIC OF GERMANY

Smear camera pictures of radially compressed plasmas are generally used for the determination of the radii of luminous fronts such as current carrying layers, shock fronts, etc., as functions of time. More quantitative results can be obtained from densitometer plots. These film density plots can be transformed into light intensity distributions when the film is standardized with a Pt filter and a short-time light source.

Observations have been made on magnetic compression experiments in preheated hydrogen and deuterium. The observed radiation may be composed of impurity radiation (both continuous and line radiation), line radiation, free-bound radiation and free-free radiation. The influence of impurity radiation can be excluded by experimental evidence. At higher temperatures (>10 eV) the light intensity comes mainly from free-free radiation. This intensity is proportional to

$$(N_i N_e/\sqrt{kT_e}) \exp(-h\nu/kT_e).$$

For temperature distributions not strongly inhomogeneous, the observed intensity can therefore be interpreted in terms of particle density distributions. These density distributions have been determined and are discussed for typical cases of plasma compression without and with internal magnetic fields in axial geometry.

1. Introduction

For the fast magnetic compression of a deuterium plasma, as described in another paper of this Conference [1], the compression ratio and end losses are of special interest. For the determination of these quantities the radial density distribution must be known as a function of time.

Present theoretical calculations, concerned with the fast compression of plasma with parallel or reverse magnetic bias field, are in need of experimental data, which also can be taken from density and intensity distributions [2].

This information can partly be obtained from smear camera pictures. For this purpose the film density must be transformed into light intensity. The interpretation of the intensity distribution requires information on the composition of plasma radiation and on the dependence of the intensity on plasma density and temperature. In some cases the density distributions can be derived from the observed intensity.

2. Determination of densities from intensity measurements

The observed radiation may be composed of

Impurity radiation
Line radiation
Free-bound radiation
Free-free radiation

A calculation of the impurity radiation was believed to be impossible. Therefore an experimental determination was used. Pure hydrogen was mixed with methane or oxygen.

From the increase of the intensity of C or O spectral lines as functions of the added amount of impurity one can determine the concentration of C and O in the "pure" hydrogen plasma. The contribution of impurities to the total visible radiation was estimated in a similar way.

The line radiation intensity is given by

$$I = (1/4\pi) A_{nm} h\nu N_i N_e \frac{h^3}{(2\pi m kT)^{3/2}} n^2 \exp(U_n/kT),$$

where

A_{nm} = transition probability,
T = electron temperature,
n = quantum number of the upper level,
U_n = ionisation energy from the upper level,
N_i = ion density,
N_e = electron density.

The free-bound radiation intensity is given by

$$I = C \int g_{fb} \frac{2U_0}{(kT)^{3/2}} N_i N_e \left[\sum_n \frac{1}{n^3} \exp(U_n/kT)\right] \times \exp(-h\nu/kT)\, d\nu$$

g_{fb} = free-bound Gaunt factor, $C = 6.36 \times 10^{-47}$ cgs units.

The free-free radiation intensity is given by

$$I = C \int g_{ff} \frac{N_i N_e}{(kT)^{1/2}} \exp(-h\nu/kT)\, d\nu.$$

* Conference paper CN-10/187, presented by H. L. Jordan. Discussion of this paper is given on page 649. Translations of the abstract are at the end of this volume of the Conference Proceedings.

These equations show that the intensities of different kinds of hydrogen radiation are proportional to $N_i N_e$, but they depend on the temperature in a different way. In all cases the exponential is close to one if T is higher than 10 eV. Furthermore, at these temperatures the intensity of free-free radiation is higher than that of the free-bound and line radiations together. Therefore, the ion density $N_i = N_e$ can be calculated for $T > 10$ eV by

$$N_i = \left(\frac{I}{C}\right)^{1/2} \cdot (kT)^{1/4}.$$

As N_i is only weakly dependent on T, the assumption that the temperature across the diameter of the plasma is nearly constant can often be used for the quantitative interpretation of smear camera pictures.

As will be shown later, this assumption is not correct in all cases. At low temperatures (1—10 eV) a simple test can be made. The discharge can be photographed one time in the light between 3700 Å—6400 Å and another time in the light between 5100 Å and 6400 Å. Caused by hydrogen line radiation, the region between 3700 and 5100 Å is very sensitive to temperature changes. If no strong temperature gradient exists, the pictures must be identical in both spectral regions.

3. Methods of measurement

The smear camera pictures were taken from the discharge with a Beckmann 339b streak camera. Observations have been made both side-on and end-on. Distributions taken from side-on pictures can be transformed into radial intensity distributions in the case of rotational symmetry by Abel's integral equation. As this symmetry is not always completely given, the interpretation of results has to be done carefully.

End-on pictures give directly the intensity distribution $I(r)$. But this intensity is integrated over inhomogeneous zones parallel to the axis of the plasma cylinder. The plasma region not focused gives a broadening of the observed diameter.

Because both side-on and end-on observations have their advantages and disadvantages, in one case the plasma was photographed by both methods under identical conditions. Unfortunately, at lower densities side-on observations were impossible because the intensity was too low.

The standardization of the films was performed by a Pt filter at the slit of a quartz spectrograph. As light source a spark with a duration of about 0.2 μs was used. This way the error caused by the Schwarzschild exponent was made as low as possible. The standardization could be obtained for all wavelengths between 3700 and 6400 Å. But the error in the intensity distribution caused by neglecting wavelength dependence was lower than 10% if the standardization at 5000 Å was taken.

The intensity distributions obtained from the densitometer curves were plotted in a logarithmic scale. If the numbers on the scale are divided by two, the density distributions are obtained.

At low film densities errors must be expected from stray light, caused by the camera, by low temperature plasma in front of the high temperature zone, and by light from the hot quartz tube. This results in the measured intensity differences being lower than in reality.

4. Results

The observed impurity radiation belongs to oxygen and carbon. Fig. 1 shows the intensity of a C V spectral line as a function of the added amount of

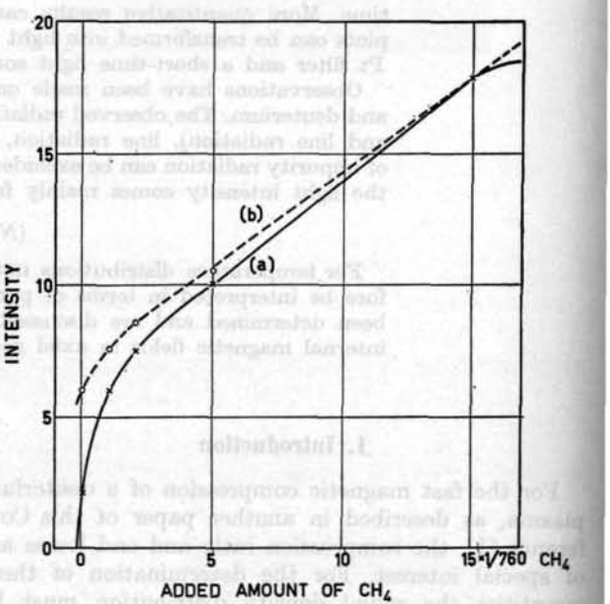

Fig. 1 (a) Intensity of a C V 2271 Å spectral line and (b) the total visible radiation 0,7 μs after firing of the main bank as a function of the added amount of CH_4 at a pressure of 230 μ, H_2.

methane. Extrapolating the plot to zero intensity a concentration of 0.02% carbon in the "pure" hydrogen is estimated. From the second curve of this figure a contribution of carbon to the visible radiation below 10% was concluded.

In the same way the percentage of oxygen in the "pure" hydrogen was estimated to be lower than 0.04%. Fig. 2 shows the intensity of an O V line in a discharge in "pure" hydrogen and in 230 μ (H_2 +(1/760) O_2). In the second half-cycle both amplitudes are equal, whereas in the first half-cycle the amplitude in pure gas is much lower than with oxygen added. It follows that the impurities come mainly from the walls at the end of the first half-cycle, caused by interaction of plasma with the walls and not by high electric fields at the start of the first half-cycle.

As was shown, the plasma is of high purity in the first half-cycle, and it is possible to neglect the impurity radiation in the visible region. Therefore the observed radiation can belong only to hydrogen and is proportional to $N_i N_e$.

In Figs. 3, 4 end-on and side-on intensity distributions of the discharge without a magnetic bias field

at a line density of $2.2 \cdot 10^{17}$ cm are given. The observed side-on intensity distribution was transformed by Abel's integral equation.

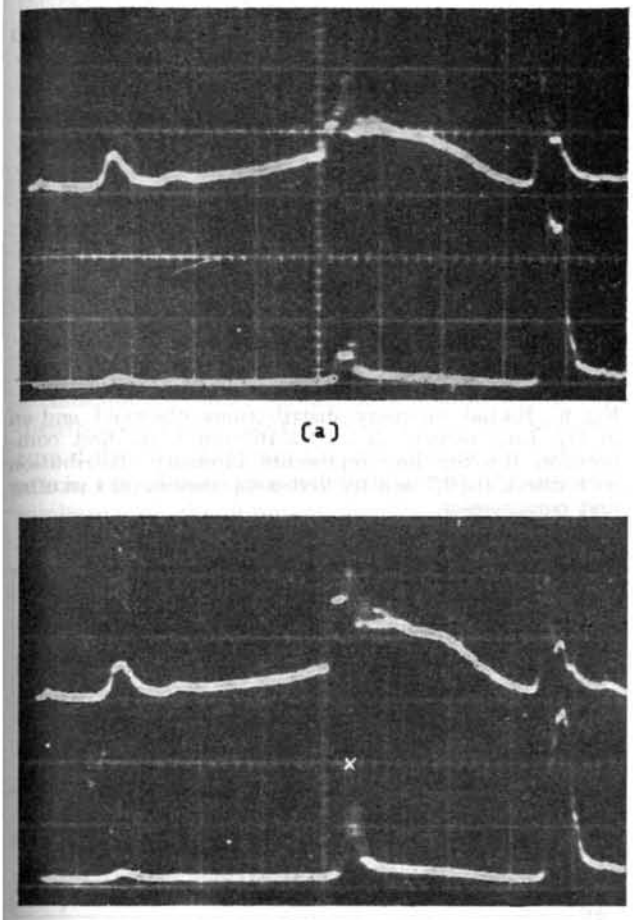

Fig. 2 Total visible radiation (upper trace) and OV 2781 Å spectral line (lower trace) as a function of time at a pressure of (a) 230 μ, H_2 and (b) 230 μ, $H_2 + (1/760)\ O_2$. × indicates maximum intensity.

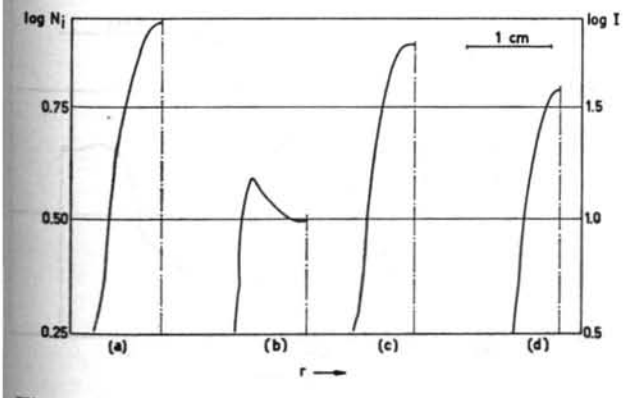

Fig. 3 Radial intensity distributions observed end-on in D_2. Line density $N = 2{,}2 \times 10^{17}\ \mathrm{cm}^{-1}$. (a) first compression, (b) first expansion, (c) second compression, (d) 1 μs after first compression.

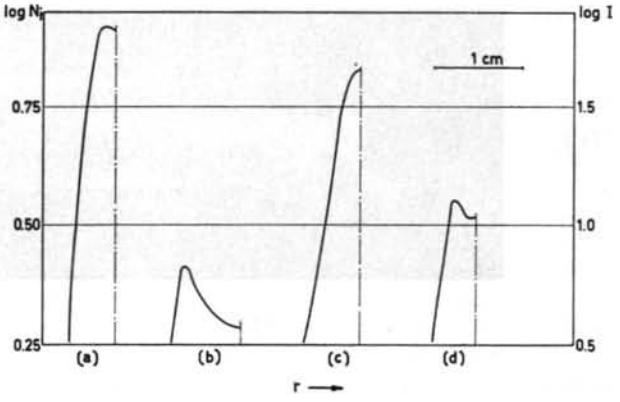

Fig. 4 Radial density distribution observed side-on in D_2 after transformation with Abel's integral equation. Line density $N = 2{,}2 \times 10^{17}\ \mathrm{cm}^{-1}$. (a) first compression, (b) first expansion, (c) second compression, (d) 1 μs after first compression.

From this figure the following conclusions can be drawn:

(1) The intensity distributions obtained end-on and side-on are not exactly equal. The half-width observed side-on has a maximum deviation of 30% from the "end-on" measurement. The plasma diameter can be defined by the half-width of the density distribution. Then one obtains from side-on observation a volume compression of 1:20 at the first maximum compression and of 1:26 at the second maximum compression. From end-on observation much lower ratios are calculated.

(2) At the first compression the intensity has its maximum in the centre of the tube. But in the following expansion the intensity in the centre amounts to 60% of the maximum intensity corresponding to 75% of the maximum density.

(3) The intensity side-on decreases faster than the intensity end-on, which may be caused by density variations along the axis.

(4) An upper limit for the end losses can be obtained by comparing the line densities at the second compression maximum and 0.8 μs later. The integration across the radius must be interrupted at a certain value to reduce the contribution from stray light. The integration is terminated both times at the same value of r to obtain the volume mass-losses. Assuming that the temperature is only increasing, we obtain a mass loss lower than 30%.

As mentioned before, at lower pressures only end-on photographs were possible. In Fig. 5 the smear camera pictures of the discharge without magnetic field at a line density of 1.1×10^{17}/cm and with parallel or antiparallel magnetic bias field at a line density of 8.8×10^{16}/cm are given. From these photographs the intensity distributions were evaluated (Figs. 6—8).

The dynamic behaviour of the plasma without a magnetic bias field at a line density of 1.1×10^{17}/cm is similar to that at higher density. The average plasma diameter between compression and expansion

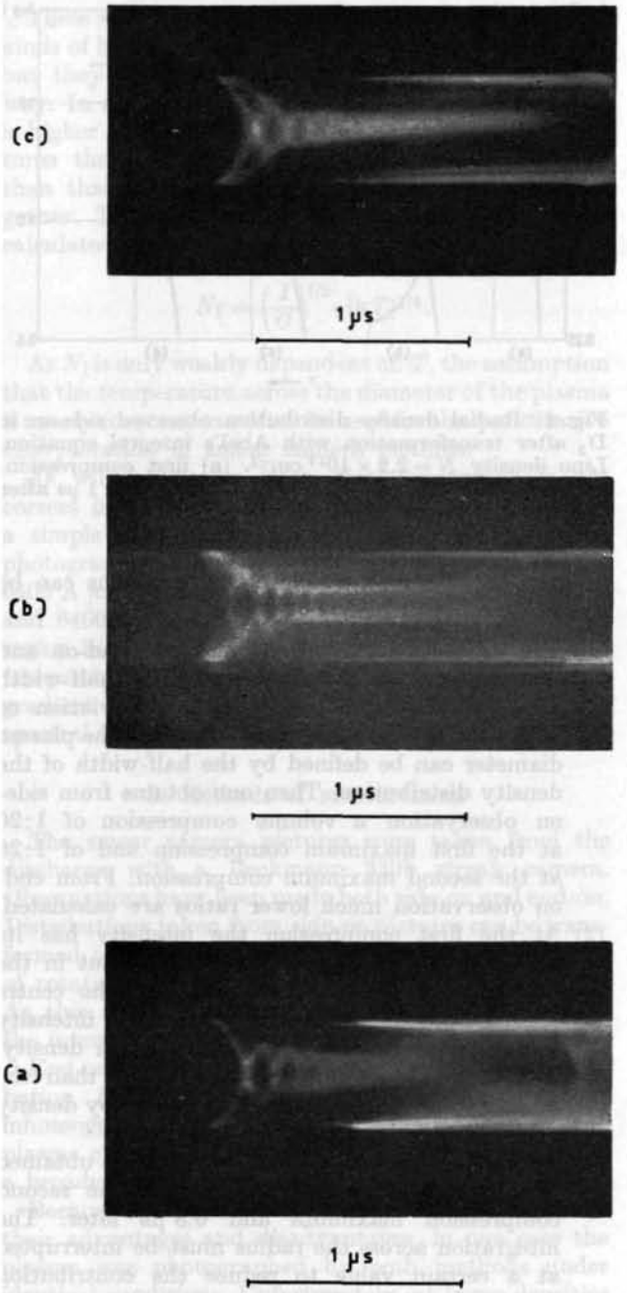

Fig. 5 Smear camera pictures with and without a steady magnetic field of 2500 G. (a) $B_{z0} = -2500$ G, $N = 8.8 \times 10^{16}$ cm^{-1}; (b) $B_{z0} = +2500$ G, $N = 8.8 \times 10^{16}$ cm^{-1}; (c) $B_{z0} = 0$, $N = 1.1 \times 10^{17}$ cm^{-1}.

decreases with increasing field as expected. But at the low line densities used in Fig. 6, even with decreasing field, the diameter decreases. This phenomenon can be explained by assuming that the kinetic pressure decreases faster than the magnetic pressure.

The interpretation of intensity distributions of plasma with trapped magnetic field is much more difficult than without field, because temperature inhomogeneities must be expected caused by the low thermal conductivity across the magnetic field.

With a steady magnetic field parallel to the external field the intensity distribution has two maxima at the first compression. But the picture in the light between 5100 and 6400 Å shows only one maximum. As mentioned before, the second maximum therefore is due to the low plasma temperature in that region.

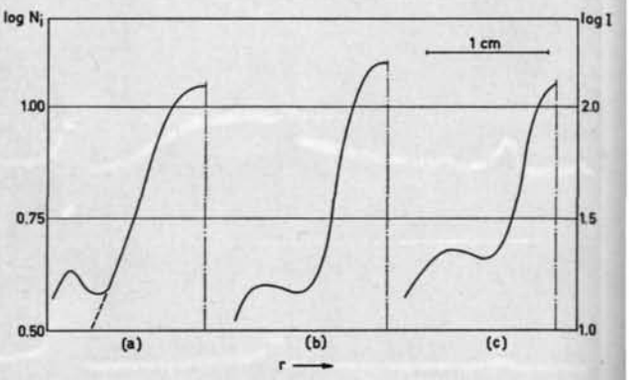

Fig. 6 Radial intensity distributions observed end-on in D_2. Line density $N = 1.1 \times 10^{17}$ cm^{-1}. (a) first compression (broken line represents intensity distribution with filter), (b) 0.7 μs after first compression, (c) 1 μs after first compression.

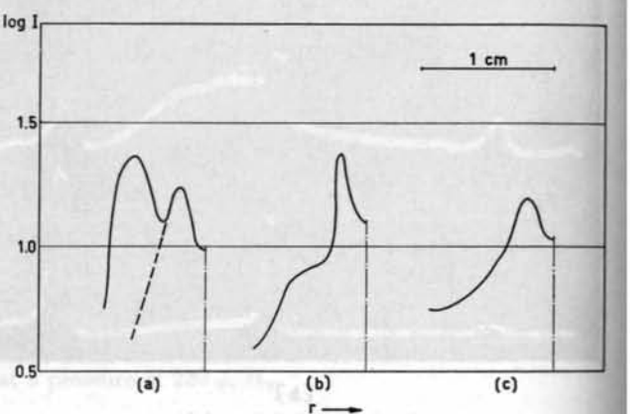

Fig. 7 Radial intensity distributions observed end-on in D_2. Line density is 8.8×10^{17} cm^{-1}, $B_{z0} = +2500$ G. (a) first compression (broken line represents intensity distribution with filter), (b) 0.7 μs after first compression, (c) 1 μs after first compression.

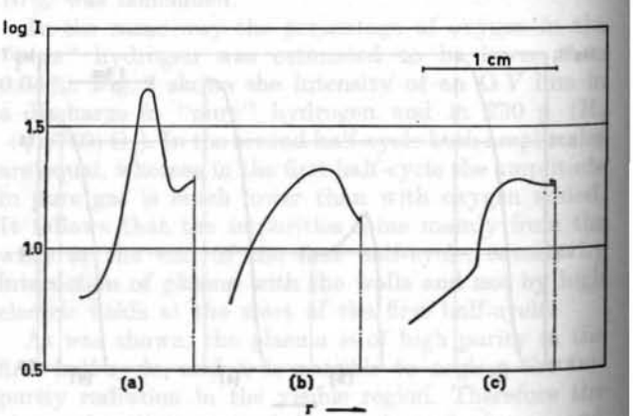

Fig. 8 Radial intensity distribution observed end-on in D_2. Line density is 8.8×10^{16} cm^{-1}, $B_{z0} = -2500$ G. (a) first compression, (b) second compression, (c) 0.7 μs after first compression.

The intensity minimum in the axis can not be understood by a density effect, because the magnetic field measurements give a homogeneous distribution. But as shown by theoretical calculations [3] an increase of the electron temperature is to be expected in the centre, causing a minimum in the intensity distribution.

In the following oscillations this intensity distribution is frozen in. This is to be expected due to the low field diffusion. Probably the temperature distribution will likewise be unchanged due to low thermal conductivity.

In the case of antiparallel magnetic bias fields, there is a high magnetic field gradient caused by high currents in the sheath between parallel and antiparallel fields. Because a part of the antiparallel field is dissipated in this layer, a mass flow results from the central part to the plasma boundary. As a consequence, there should be a hole in the density distribution at the centre. In this case the temperature differences between the centre and the intensity maximum seem to be not very high [3]. The observed minimum of the intensity in the centre can then only be understood by a density minimum.

As can be seen from the following plots, the sheath broadens rapidly, and the hole disappears after about three oscillations. At higher densities it can be observed during the whole discharge.

5. Summary

Since the plasma observed has low impurity concentration, only the hydrogen radiation has to be taken into account for the interpretation of smear camera pictures. This radiation is proportional to N_i^2. Without steady magnetic field it seems possible to neglect the radial temperature inhomogeneity for the calculation of the density distribution.

Side-on and end-on photographs do not give exactly the same results for the radius of the plasma and for the intensity as function of time. The differences are probably caused by inhomogeneity of the density along the axis. Side-on observations have the disadvantage, that for the calculation of the radial intensity distribution, radial symmetry is necessary. In the case discussed above this seems to be allowed because no eruptions, etc., were observed.

In this way it could be shown in one case that particle losses are lower than 30%. At lower pressures end losses seem to be higher. The plasma radius decreases even after the magnetic field has reached its maximum.

This can be understood by mass losses because a rapid temperature decrease is not expected by theory. Furthermore, in this case an increase of the intensity should be observed which is not the case.

For an accurate calculation of densities from intensities in the case of strong trapped magnetic fields, a measurement of the radial temperature distribution is necessary. Without this only a rough estimate for a plasma with trapped antiparallel field is possible. A comparison with theoretical calculations [3] shows that the intensity minimum observed on the axis cannot be attributed to temperature differences alone. A density minimum must be therefore in the centre.

References

[1] Hintz, E., see page 601 of these Proceedings.
[2] Hain, K., private communication.
[3] Hain, K., private communication.

THEORY OF DYNAMICAL BEHAVIOUR OF PLASMAS WITH INTERNAL MAGNETIC FIELDS DURING MAGNETIC COMPRESSION: COMPARISON WITH EXPERIMENTS*

H. KEVER

INSTITUT FÜR PLASMAPHYSIK DER KERNFORSCHUNGSANLAGE JÜLICH DES LANDES NORDRHEIN-WESTFALEN E. V.

JÜLICH, FEDERAL REPUBLIC OF GERMANY

Application of the free particle reflection model to the process of magnetic compression of axial-symmetric plasmas without internal magnetic fields gives analytical solutions for the time of maximum compression and for the energy gained by the plasma during the first compression period. More general results to the dynamics of plasma compression are obtained when internal magnetic fields are included. Two approximations to the magnetic-hydrodynamic equations are deduced and solved. In the first approximation the thickness of the shocked region is assumed to be small as compared to the plasma radius, leading to the Rosenbluth-Garwin snow-plow-equation with inclusion of trapped magnetic fields and finite kinetic pressure. Plasma radius, internal magnetic field and the kinetic energy of plasma at maximum compression are calculated as functions of initially trapped magnetic field and ratio of coil inductivity to external inductivity. The results are compared with magnetic probe measurements and streak camera photographs of a fast magnetic compression experiment. In a second adiabatic approximation to the flow problem in magnetic compression experiments the magnetic flux inside the plasma is assumed to be constant and the magnetic field is assumed to be self-similar, as indicated by magnetic probe measurements.

The resulting equation of motion and the equation for the current are solved numerically as a set of simultaneous equations, showing the effect of finite oscillation period of the external current on the plasma motion. Results are again compared with experimental observations by streak camera photographs.

1. Introduction

Magnetic compression experiments described in preceding papers [1, 2] have shown the possibility of obtaining plasmas in which, at current maximum, the pressure of trapped internal magnetic fields is small compared to the kinetic pressure of the plasma. In the period of first implosion, however, trapped internal magnetic fields may play the dominant part in determining the rate and degree of compression, especially in the case of plasmas with low β-values. As we have been interested primarily in the dependence of the radius of the plasma column and of magnetic field strength on time in order to interpret experimental results and to obtain information about the scaling of quantities such as plasma energy, elementary models [3, 4, 5] have been adapted to the case of magnetic compression of plasmas with trapped magnetic fields and are used to determine the quantities in question.

From the free-particle reflection model the time from beginning of compression to the first compression maximum is given by

$$\tau_c = 1.4\left(1+\frac{2}{3}\Lambda\right)^{1/2}, \tag{1}$$

where τ_c is the value of the dimensionless time variable $\tau=t/t_c$ at maximum compression.

$$t_c = \left[\frac{2\,a_0\,l\,L_a\,\varrho_0^{1/2}}{\mu_0^{1/2}\,V_0}\right]^{1/2}, \tag{2}$$

where a_0=initial radius of plasma, l=length of compression coil, L_a=external inductance, V_0=charging voltage of condenser bank, and ϱ_0=initial density of plasma. The parameter Λ is the ratio of vacuum coil inductance $L_c=\mu_0\pi a_0^2/l$ to external inductance L_a, where the external inductance is the total inductance of circuit minus the vacuum coil inductance (which by the definition used here is the inductance connected to the magnetic flux inside the discharge tube).

For the energy imparted to the plasma during compression, that is, the work done by the magnetic pressure, one obtains from the free-particle reflection model an expression

$$W=\overline{W}\,(1+\Lambda)\,\frac{1+2y^3-3y^2}{1+\Lambda\,(1-y^2)}, \tag{3}$$

where $y=a/a_0$ is the radius of the plasma column in units a_0. $\overline{W}$ denotes the value of W at $y=0$; if $y\leq 0.25$, $W\geq 0.8\,\overline{W}$ for all possible values of Λ. The scaling of plasma energy is given by

$$\overline{W}=\frac{2}{3\,\mu_0^{1/2}}\,a_0\varrho_0^{1/2}V_0\,\frac{\Lambda}{1+\Lambda}. \tag{4}$$

2. Application of the snow-plow model

Considering first the basic assumption of this model, we write the magneto-hydrodynamic equation of motion in the form

$$\frac{\partial}{\partial t}(\varrho v_r)+\frac{1}{r}\frac{\partial}{\partial r}(r\varrho v_r^2)=-\frac{\partial}{\partial r}p_m, \tag{5}$$

where v_r is the radial velocity of plasma and $p_m=B^2/2\,\mu_0$. Integration of Eq. (5) over the cylindrical area between the limits a_1 and $a_2=a_1+d$ gives, with an integration by parts on the right side,

* Conference paper CN-10/188, presented by H. L. Jordan. Discussion of this paper is given on page 649. Translations of the abstract are at the end of this volume of the Conference Proceedings.

$$2\pi\int_{a_2}^{a_2}\left[r\frac{\partial}{\partial t}(\varrho v_r)+\frac{\partial}{\partial r}(r\varrho v_r^2)\right]\mathrm{d}r = -2\pi[r\,p_m]_{a_1}^{a_2}+2\pi\int_{a_1}^{a_2}p_m\,\mathrm{d}r.$$

The second term in the first integral gives $a_2\varrho_2 v_2^2 - a_1\varrho_1 v_1^2$. If a_2 denotes a point outside the plasma, $\varrho_2=0$, and a_1 a point inside the plasma before the shocked region where $v_r=0$, one obtains by neglecting on the right side terms of the order d/a_2

$$2\pi\int_{a_1}^{a_2} r\frac{\partial}{\partial t}(\varrho v_r)\,\mathrm{d}r = -2\pi a_2(p_2-p_1). \qquad (6)$$

The remaining integral can be written

$$\frac{\partial}{\partial t}\left(\int_{a_1}^{a_2} r\varrho v_r\,\mathrm{d}r\right)+\dot{a}_1(\varrho a v_r)_1-\dot{a}_2(\varrho a v_r)_2,$$

for the same reasons as mentioned before the last two terms vanish. With v_r inside the shocked region assumed to be approximately equal to the velocity $\dot{a}_2$ of the plasma boundary, Eq. (6) leads to

$$\frac{\mathrm{d}}{\mathrm{d}t}[\pi\varrho_0(a_0^2-a^2)\dot{a}] = -2\pi a(p_2-p_1), \qquad (7)$$

whereby the subscript of the symbol for the radius of the plasma boundary has been omitted. For finite kinetic pressure Eq. (7) would apply with p_1 equal to the total pressure inside the plasma ahead of the shock wave.

It follows from the derivation that Eq. (7) holds if the extension of the region where the momentum ϱv_r per unit volume of the plasma attains large values remains small in comparison to the radius of the plasma column. From the distributions of plasma density and radial velocity calculated by numerical solution of the complete set of magneto-hydrodynamic equations [6] it can be seen that, in the beginning of plasma compression, the distribution of the product of these quantities is peaked near the plasma boundary. In addition to this, there is direct experimental evidence for the assumption of a higher plasma density within a small region in the vicinity of the plasma boundary, since the observed luminosity must be partly attributed to the enlarged density of radiating plasma at the boundary [2].

Solutions of Eq. (7) have been calculated numerically under the assumptions:

(1) constancy of voltage at the condenser,
(2) constancy of magnetic flux inside the plasma cylinder.

Within the accuracy of probe measurements, the second assumption has been proved to hold approximately during the time of first implosion for the magnetic field in the vicinity of the axis.

It is convenient to express the strength of magnetic field in units $\hat{B}$, where $\hat{B}$ is given by

$$\hat{B}=\mu_0\frac{V_0 t_c}{l L_a}$$

and to introduce the dimensionless quantity b by $B/\hat{B}$. The initial value B_0 of the internal magnetic field in units $\hat{B}$ shall in the following be denoted by b_0. Figure 1 is a plot of the dependence of the plasma

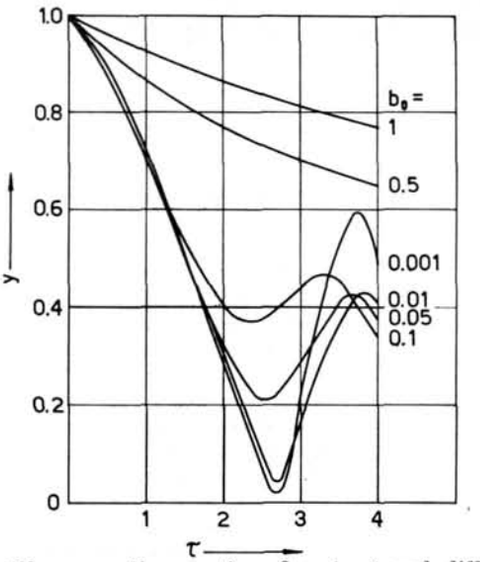

Fig. 1 Plasma radius vs time for $\Lambda=5$ and different values b_0 of initial magnetic field.

radius on time τ for different values of b_0 and $\Lambda=5$. For large values of b_0 the plasma moves monotonously inwards, while for small values of b_0 the curves approximate the case $b_0=0$ up to small values of y. The deviations are shifted to later times and increase in magnitude for decreasing values of b_0.

Under the conditions of the experiment described in [1, 2] Λ equals 2 and the value of B is about 2.5×10^4 G. Theoretical curves with $b_0=0.05$ (Fig. 2) and $b_0=0.1$ (Fig. 3) therefore correspond to initial magnetic fields $B_0=1250$ G and $B_0=2500$ G. Fig. 4 shows for comparison a streak camera photograph of a discharge in deuterium with 0.9×10^{16} cm^{-3} initial density, for which the compression time t_c is 0.09 μs. The observed times of the first and second compression maximum are respectively 0.17 μs and 0.3 μs, corresponding to $\tau=1.9$ and $\tau=3.3$. For a discharge in deuterium at 2×10^{16} cm^{-3} the absolute time of the different maxima would theoretically be a factor 1.2 larger, in agreement with the observations, see Fig. 2 of [2]. The measured B_z is about 1 kG so that Fig. 2 should apply. The calculated times of compression maxima and minima agree within the limit of resolution with the observed ones. The observed compression ratios are only accounted for by the theoretical curves with $b_0=0.1$. The same holds for the compression of the internal magnetic field given by the magnetic probe signal [2]. The conclusion is to be drawn that at and after the first compression maximum the plasma motion is not determined by the pressure of the trapped magnetic field alone.

The energy imparted to the plasma can be calculated by numerical integration of the solution for y and $\dot{y}$. Table I contains the values of energy W^* of disordered motion at first compression maximum in units $\overline{W}$. For the range of parameter values Λ, b_0 listed here the ratio $W^*/\overline{W}$ is only a slowly varying

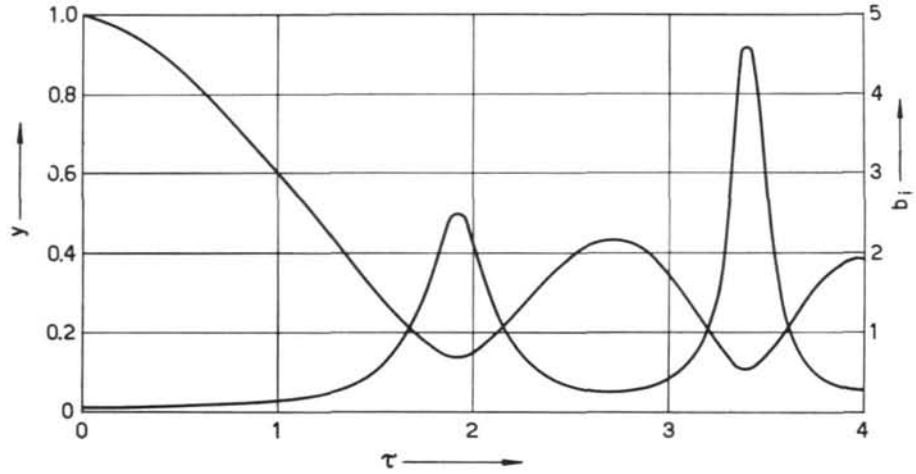

Fig. 2 Dependence of plasma radius and internal magnetic field on time for $\Lambda = 2$, $b_0 = 0{,}05$.

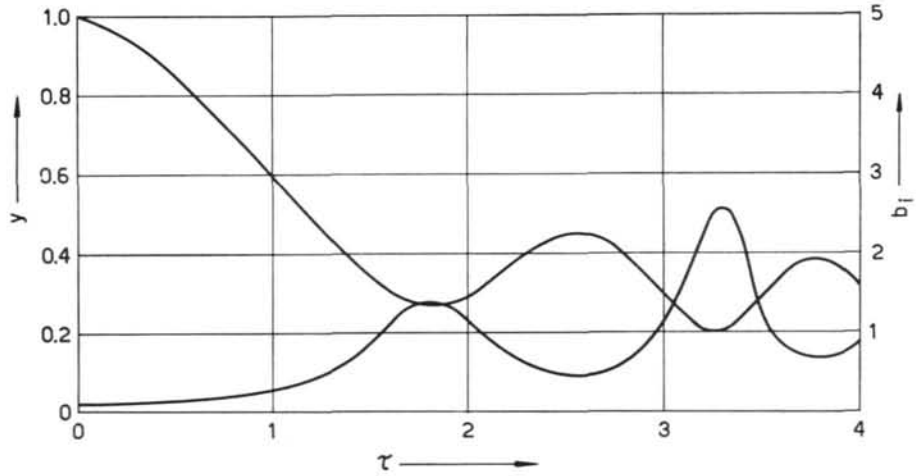

Fig. 3 Dependence of plasma radius and internal magnetic field on time for $\Lambda = 2$, $b_0 = 0{,}1$.

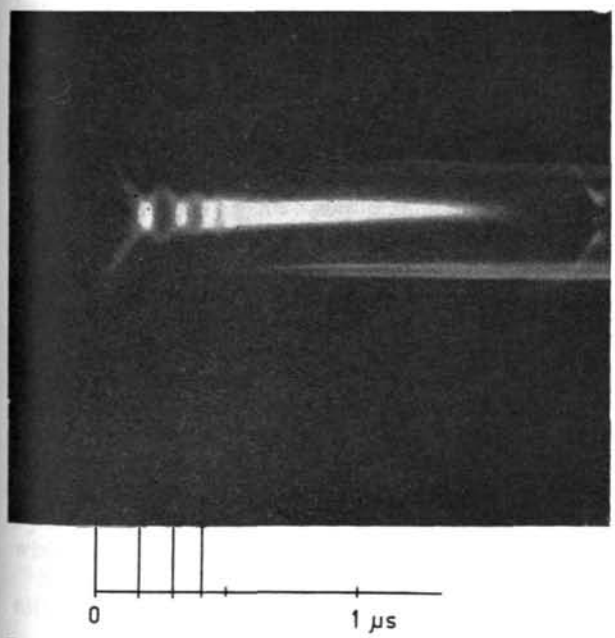

Fig. 4 Streak camera photograph of compression of deuterium plasma with line density of 10^{17} cm^{-1} and $B_0 = 1$ kG.

TABLE I. Dependence of $W^*/\overline{W}$ on Λ, b_0

b_0	$\Lambda=1$	$\Lambda=2$	$\Lambda=3$	$\Lambda=4$	$\Lambda=5$
0.1	0.229	0.220	0.208	0.206	0.179
0.05	0.267	0.270	0.266	0.262	0.257
0.01	0.286	0.299	0.301	0.297	0.308
0.005	0.291	0.300	0.307	0.310	0.312
0.001	0.292	0.301	0.308	0.311	0.313

function of Λ and b_0, so that for these values the plasma energy W^* gained by shock heating during the first implosion scales as $\overline{W}$ does in the case without internal magnetic fields. Comparison of the theoretical result with the value of the plasma energy estimated from the plasma β at maximum current [1] indicates that the quantity W^* can account for about 2/3 of the actual plasma energy.

3. Adiabatic approximations

Since in later stages of magnetic compression experiments the magnetic flux is preserved to a high degree within the plasma [1], the electrical conductivity of the plasma must be very high and the induced electrical fields are balanced by the Lorentz-

force on the electrons. Assuming the magnetic field to be self-similar, $B = B(t)\,g(r/a)$ with an arbitrary function $g(x)$ of the relative radius $x = r/a$, one concludes that the plasma velocity must be proportional to r, i.e. $v_r = (\dot{a}/a)\,r$. Conversely, if $v_r \sim r$ holds, the magnetic field becomes self-similar at high conductivities. Hence at any point within the plasma the magnetic field scales as a^{-2}:

$$B(r,t) = B_0\, g\left(\frac{r}{a}\right)\left(\frac{a_0}{a}\right)^2,$$

where B_0 is the value of B_z at time $t = 0$ on the axis. Inserting $v_r = (\dot{a}/a)r$ into the equation for the adiabatic change of state

$$\frac{\partial}{\partial t}\left(\frac{p}{\varrho^\gamma}\right) + v_r \frac{\partial}{\partial r}\left(\frac{p}{\varrho^\gamma}\right) = 0,$$

the existence of solutions of the form

$$p(r,t) = p_0\left(\frac{r}{a}\right)\left(\frac{a_0}{a}\right)^{2\gamma}$$

can be shown. Substituting v_r in the equation of motion and integrating over the radius of the plasma column leads to

$$mN\ddot{a} = -2\pi a\left\{\frac{B_a^2}{2\mu_0} - \left[\bar{p}\left(\frac{a_0}{a}\right)^{2\gamma} + \frac{\bar{B}_i^2}{2\mu_0}\left(\frac{a_0}{a}\right)^4\right]\right\} \qquad (8)$$

where $mN = 2\pi\int_0^a \varrho r\,\mathrm{d}r$ is the line density of moving particles, bars denoting values on the axis of the discharge tube.

Equation (8) has been solved numerically together with the differential equation for the current taking into account the finite capacity of the condenser bank. Fig. 5 shows results for the set of parameter values assigned to the plot. $T_{1/4}$ denotes the quarter-period of the current oscillations when the coil inductance is neglected. The quarter-period of the actual solution is longer as a part of the coil inductance becomes effective during the compression. For larger values of $T_{1/4}/t_c$ and lower b_0 the number of oscillations increases. In the limit of small changes of external magnetic field the half period of the radial hydromagnetic oscillations [7] in units t_c is given by $\tau_{1/2} = \pi y^{*2}/4b_0$ where y^* denotes the value of y at the equilibrium of external and internal pressure. If the compression is two dimensional b_0 denotes an effective field strength including the contribution of the kinetic pressure at equilibrium.

In contrast to experimental observation, Fig. 4, the plasma motion is theoretically symmetric with respect to current maximum. Radial oscillations with increasing amplitude are necessarily connected to the solutions of Eq. (8) in the case of decreasing current. Obviously the adiabatic model without losses used here is, under the conditions of the considered experiment, not applicable after the current maximum.

Acknowledgements

The author wishes to express his gratitude to Dr. H. L. Jordan and E. Hintz for helpful discussions.

References

[1] Hintz, E., KFA Jülich, Bericht Nr. 13, 1961.
[2] Hintz, E., see p. 601 of these Proceedings.
[3] Rosenbluth, M., Garvin, R., U. S. Atomic Energy Commission Report LA-1850 (1954).
[4] Leontovich, M. A., Osovets, S. M., *J. Nucl. Energy* 4 (1957) 209.
[5] Osovets, S. M., Plasma Physics and the Problem of Controlled Thermonuclear Reactions (Pergamon Press, London, 1959) Vol. III., p. 193.
[6] Hain, K., private communication.
[7] Niblett, G. F. B., Green, T. S., *Proc. Phys. Soc.* 74 (1959) 737.

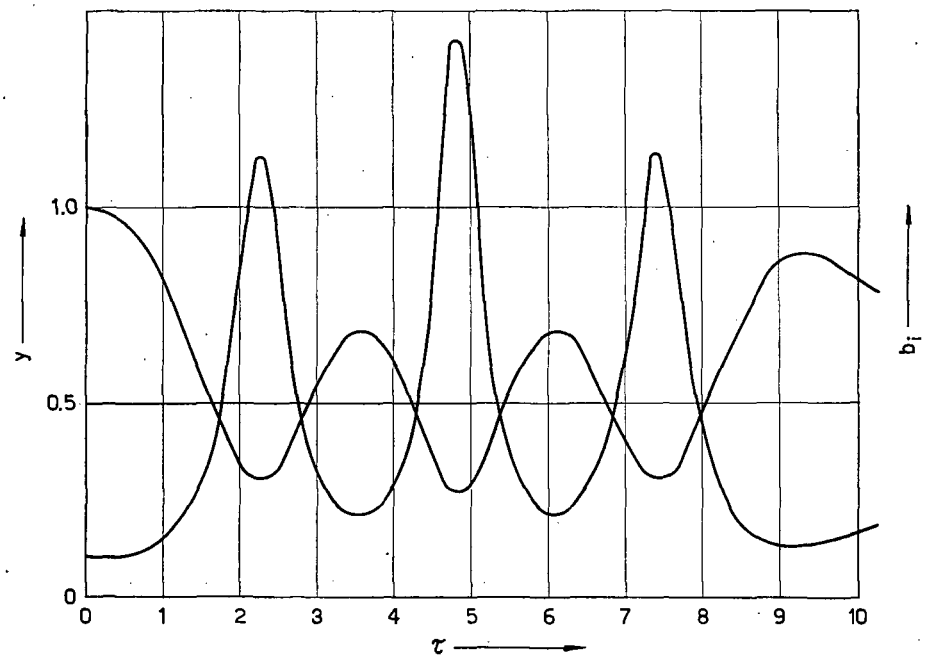

Fig. 5 Plasma radius and internal magnetic field as given by the adiabatic model for a finite oscillation period of external current with $T_{1/4} = 2.5\,t_c$, $\Lambda = 5$, $b_0 = 0.1$.

MEASUREMENTS ON AN ORTHOGONAL PINCH DISCHARGE*

J. E. ALLEN, M. U. MARTONE, S. E. SEGRE

LABORATORIO GAS IONIZZATI (EURATOM-C.N.E.N.)

FRASCATI, ROME, ITALY

Measurements on an orthogonal pinch discharge are reported, the discharge being produced by a condenser bank of 11.25 μF at 20 kV with a period of oscillation of 35 μs.

Above a certain pressure (~250 μ Hg in A) a converging shock is produced at each half cycle of the exciting current. Below this pressure the discharge has a complicated behaviour; a luminous sheet is observed, which may be interpreted as an ionization wave, and a high-frequency oscillation of the magnetic field takes place.

1. Introduction

The present report describes a continuation of previous work [1] on the orthogonal pinch in which the distribution of the magnetic field was obtained as a function of time. New measurements have been made, using magnetic probes of higher frequency response [2] and high-speed photography has been carried out using a rotating-mirror (streak) camera and an image converter. The results obtained using the magnetic probes reveal a high-frequency oscillation of the magnetic field. At low pressures, the high speed photography shows an inwardly moving luminous region, which may represent a wave of ionization, whereas at high pressures shock-wave propagation and reflection is observed.

2. Apparatus

The experimental set-up has been described previously [1]. It consists essentially of a condenser bank of 11.25 μF at 20 kV, which is connected via a spark gap to a 10-turn coil of 30 cm in length; the latter surrounds a cylindrical pyrex tube of inner diameter of 42.4 mm, and 75 cm in length. Between the coil and the tube there is a hollow copper cylinder, of the same length as the coil. It is split longitudinally into two semicylinders which are insulated with teflon foil. The purpose of these semicylinders is to increase the uniformity of the fast-rising magnetic field inside the tube. Before the discharge of the condenser bank a weak preionization is provided by a 2 ms pulse of radio frequency at 40 MHz. The current in the coil is oscillatory with a period of 35 μs.

The distribution of the magnetic field is measured by means of a magnetic probe [3] which is inserted radially through a vacuum seal. The attenuation of the probe used in the present work is flat (to within 1%) up to 20 MHz [2]. The signal of the probe is integrated by a passive *RC* integrator whose attenuation is linear with frequency from 20 kHz to 20 MHz.

Streak photographs are obtained with a rotating mirror camera; the maximum aperture is f:7, the maximum writing speed is 10 mm/μs (at 5000 rev/s) and the minimum resolving time, due to diffraction, is 1×10^{-9} s. The photographs were obtained at a writing speed of ~ 1 mm/μs and a resolving time of 7×10^{-8} s.

Single-shot photographs are obtained with an image converter using a Mullard ME 1201 tube. The minimum exposure time is 0.1 μs with a resolution of 500 line pairs per frame and a maximum effective aperture of f:2.

3. Results

Measurements have been made in argon and xenon. It was not found possible to obtain breakdown in hydrogen or helium. The magnetic probe measurements and the fast photography, using a streak camera and an image converter, show that discharge is reproducible.

The streak photographs were taken through a slit in the side of the tube, the slit being perpendicular to the tube axis. Below a pressure of about 250 μ Hg in argon the behaviour of the discharge is quite different from its behaviour at higher pressures. Above about 250 μ Hg, at each half-cycle a converging shock propagates to the axis and is then reflected (Fig. 1). The results obtained with the magnetic probes show that the currents in the gas are small compared with the exciting current.

Below the "transition pressure" the streak photographs (Fig. 2) show at each half-cycle an inward moving luminous sheet and also a detailed structure. Examination of the latter yields propagation velocities between 5×10^5 cm/s and 5×10^6 cm/s. The corresponding magnetic probe measurements (Fig. 7) show that strong currents flow in the gas, the maximum current density being about 2 kA/cm².

The behaviour of xenon (Fig. 3) is quite similar to that of argon but the pressure at which the discharge changes character is about 60 μ Hg. A streak record of the discharge in argon at the intermediate pressure of 260 μ Hg is shown in Fig. 4.

Image converter photographs taken in the axial direction (Fig. 5) show the luminous sheet as it moves

* Conference paper CN-10/8, presented by J. E. Allen. Translations of the abstract are at the end of this volume of the Conference Proceedings.

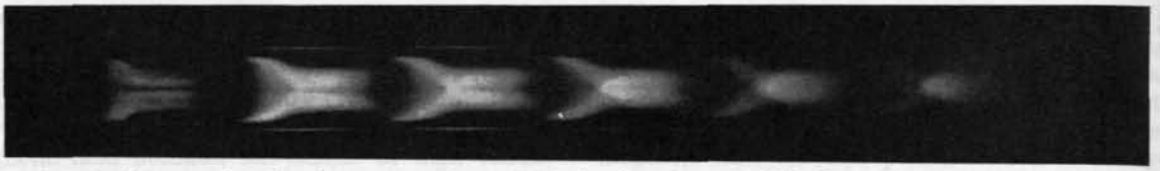

Fig. 1 Streak photograph taken in argon at 0.5 mm Hg, bank voltage 18 kV, $T/2 = 17.5$ μs.

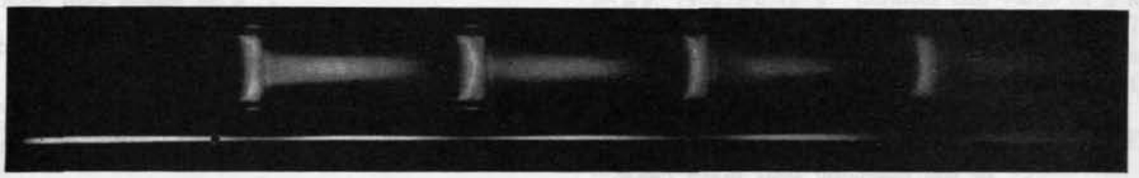

Fig. 2 Streak photograph taken in argon at 75 μ Hg, bank voltage 16 kV, $T/2 = 17.5$ μs.

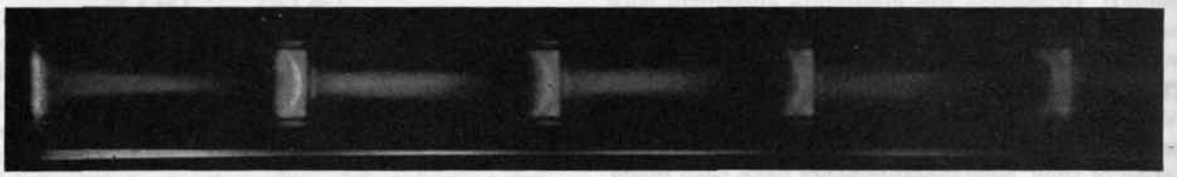

Fig. 3 Streak photograph taken in xenon at 16 μ Hg, bank voltage 17 kV, $T/2 = 17.5$ μs.

Fig. 4 Streak photograph taken in argon at 260 μ Hg, bank voltage 18 kV, $T/2 = 17.5$ μs.

Fig. 5 Image converter photographs: argon at 44 μ Hg, bank voltage 17 kV; exposure time 0.1 μs. The times in μs after the beginning of the third half-cycle are as follows: (from left to right) 1, 1.2, 1.7, 2.2, 2.2.

inwards. A magnetic probe, which is seen as a dark shadow, is inserted radially and the records show that it does not alter the appearance of the discharge. This is also confirmed by the streak photography. Streak photographs taken in the axial direction are similar to those discussed above.

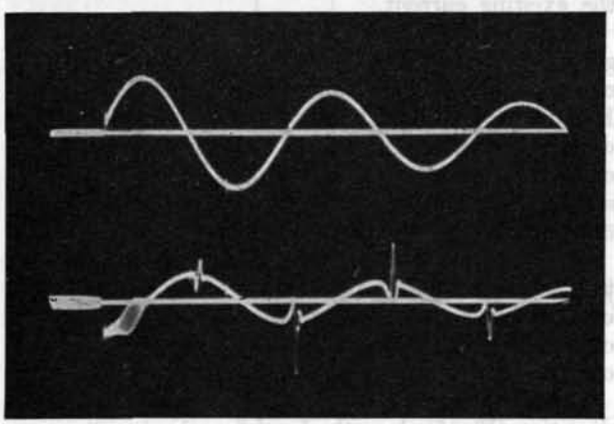

Fig. 6 Upper trace: current in the coil; lower trace: unintegrated probe signal. Argon at 44 μ Hg, bank voltage 18 kV, $T/2 = 17.5$ μs. The distance of the probe from the tube axis is 9 mm.

The distribution of the axial magnetic field as a function of radius has been derived from the probe measurements and is shown in Fig. 7. Each curve is labelled with a number indicating the time (in μs) after the beginning of the third half-cycle. A typical unintegrated signal from the magnetic probe is shown in Fig. 6. Successive half-cycles show a similar behaviour with decreasing magnitude. The plots show that the current builds up near the wall and then moves inwards at a speed of about 1.5×10^6 cm/s. There follows an over-all oscillation of the magnetic field which is strongly damped and which has a period of about 1.2 μs.

4. Discussion

The streak records at high pressures can easily be interpreted in terms of a simple shock theory [4] in which a shock wave leaves the boundary of the plasma and propagates to the centre while the boundary itself moves inwards with a slower speed. The shock is reflected on the axis and returns to the boundary of the ionized gas.

At low pressures the phenomena are more complicated. The luminous sheet, which appears as a crescent

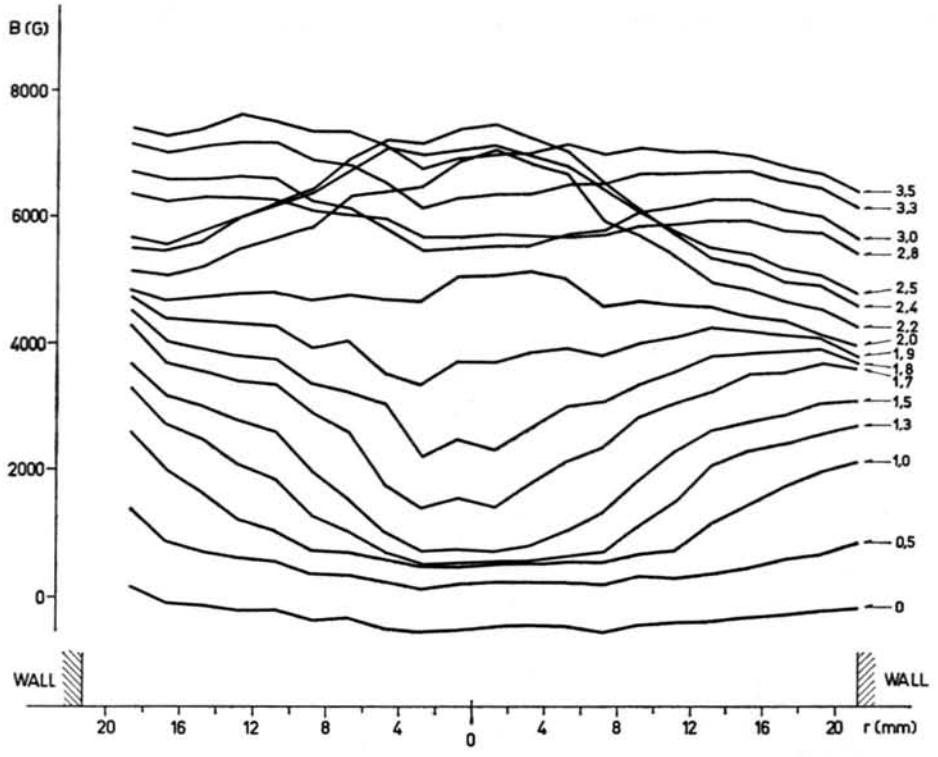

Fig. 7 The magnetic field as a function of radius at different times. The number labelling each curve indicates the time, in μs, after the beginning of the third half-cycle. Argon at 50 μ Hg, bank voltage 18 kV.

shape on the streak photographs, does not seem to be associated with any inertial effects. It is possible to interpret it as a wave of ionization. An ionization wave could be produced by ambipolar diffusion, by photo-ionization or by the gradual penetration of the electric field into the gas, the latter process being associated with the inward diffusion of the magnetic field. At intermediate pressures (Fig. 4) the luminous sheet is seen to precede the shock wave.

Probe signals very similar to those obtained in the present work (Fig. 6) have been reported in other orthogonal pinch experiments [5, 6]. Oscillations of the magnetic field have been discussed by NIBLETT and GREEN [7] in order to explain certain rotating-mirror photographs. In the model used by these authors, however, the current flowing in the plasma is concentrated in a narrow sheet. In the present case, the measurements (see Fig. 7) show that the current is not localized in a narrow sheet during the oscillation. There seems to be an over-all oscillation more in the nature of a standing wave, which may also involve the axial direction.

Acknowledgements

The authors wish to thank Prof. B. Brunelli for his interest in this work.

The image converter equipment was built by Mr. G. H. Lunn of A.W.R.E. (Aldermaston, Berks., England).

References

[1] ALLEN, J. E., SEGRE, S. E., Proc. 4th Int. Conf. on Ionization Phenomena in Gases, Uppsala (North-Holland Publ. Amsterdam) **2** (1959) 1073.
[2] SEGRE, S. E., ALLEN, J. E., *J. Sci. Inst.* **37** (1960) 369.
[3] LOVBERG, R. H., *Ann. Phys. (New York)* **8** (1959) 311.
[4] ALLEN, J. E., *Proc. Phys. Soc.* **B 70** (1957) 24.
[5] KVARTSKHAVA, I. F., KERVALIDZE, K. N., GVALADZE, J. S., Proc. 4th Int. Conf. on Ionization Phenomena in Gases, Uppsala (North-Holland Publ. Co., Amsterdam) **2** (1959) 876.
[6] ALIDIERES, M., AYMAR, R., ETIEVANT, C., JOURDAN, P., SAMAIN, A., Proc. 4th Int. Conf. on Ionization Phenomena in Gases, Uppsala (North-Holland Publ. Co., Amsterdam) **2** (1959) 1043.
[7] NIBLETT, G. B. F., GREEN, T. S., *Proc. Phys. Soc.* **74** (1959) 737.

OBSERVATIONS ON AN ORTHOGONAL PINCH DISCHARGE (CARIDDI)*

J. E. Allen, C. Bartoli, B. Brunelli, J. A. Nation, B. Rumi, R. Toschi

Laboratorio Gas Ionizzati (Euratom-C.N.E.N.)

Frascati, Rome, Italy

Observations are reported of an orthogonal pinch produced by means of a six-sector device. The discharge has been photographed using a rotating-mirror (streak) camera and also with an image converter. Measurements have been made of the coil current and of the voltage per turn, the latter being about 60 kV. Magnetic probe measurements have also been made and are compared with the optical data.

1. Introduction

The apparatus "Cariddi" [1] has been designed to investigate the rapid compression of a plasma by a magnetic field. One of the objects of the work is the study of the shock waves [2] which can be set up in a plasma which contains a magnetic field. These shock waves have many features which are not associated with ordinary shock waves, due to the interaction between the charged particles (which constitute the plasma) and the magnetic field [3, 4]. The study of the characteristics of such waves constitutes one of the most important problems in plasma physics. In addition, it is quite possible that the rapid compression of a plasma is the best way to obtain astronomical temperatures in plasmas of reasonable density.

In the present work the "orthogonal pinch effect" is employed to compress the gas. A rapidly rising axial magnetic field induces circulating (diamagnetic) currents in the plasma which then interact with the magnetic field to give an inwardly directed magnetic force. In this case the lines of current flow are circles and the magnetic field lines are straight, whereas the reverse is the case in the ordinary well-known "pinch effect".

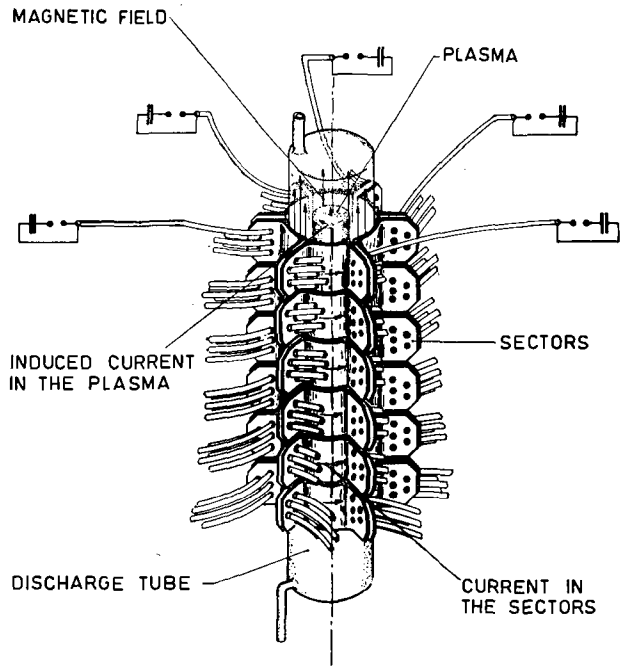

Fig. 1a Schematic diagram of "Cariddi".

2. Apparatus

2.1. Cariddi

Experiments in a number of laboratories have been carried out using a single-turn coil; the apparatus known as Scylla (at Los Alamos [5]) is of this type. In the present case a different procedure is adopted in which the coil is split into a number of sectors, each sector being fed by a low inductance condenser bank [6]. The device can be thought of as a transformer in which the turns ratio is greater than unity, even though the secondary (the gas) has only one turn. A schematic diagram of the apparatus is shown in Fig. 1a, where it is seen that the coil is also divided into horizontal sections. The figures for the apparatus are given in Table I; these data refer to the "open-circuit" conditions, i.e. without plasma.

A second condenser bank, which is nearing completion, will be used to provide an initial magnetic field within the discharge tube. This magnetic field has a maximum value of 8000 G and is produced by the circuit shown in Fig. 1b. The resonant frequency of the circuit is about 1 kHz and L_0 represents a single-turn coil, of length 1 metre, which fits inside the sectors of Cariddi.

The sectors have a length of 16.7 cm and an internal diameter of 23 cm. Two sections of the coil are being used at present and these are separated by a distance of about 2.5 cm for viewing purposes. The discharge

* Conference paper CN-10/12, presented by J. E. Allen. Translations of the abstract are at the end of this volume of the Conference Proceedings.

TABLE I. Data on Cariddi (under "open-circuit" conditions)

	Complete Cariddi	Present work
Number of sectors	6	6
Number of sections	6	2
Number of condensers per sector per section	5	4
Total capacitance	180 μF	48 μF
Charging voltage	40 kV	25 kV
Inductance of discharge tube	52 mμH	150 mμH*
Inductance of external circuit	57.4 mμH	216 mμH*
Period	4.6 μs	4.4 μs*
Voltage per turn	114 kV	60 kV*
Maximum value of dI/dt	2.2×10^{12} amp/sec	4×10^{11} amp/sec*

* Values calculated from the frequency measurement; these values are in general agreement with those obtained from direct measurements.

tube is of pyrex and has an internal diameter of about 18 cm. Each condenser is connected via a cable and a four-electrode spark-gap; details of the latter are given elsewhere [7].

2.2. Streak camera; image converter

A rotating mirror streak camera is used which has an aperture of f/7 and a maximum writing speed of 1 cm/μs (at 5000 rev/sec); the minimum resolution time, due to diffraction, is 10^{-9} sec. The present photographs were obtained using a writing speed of 1 mm/μs and a resolution time of 8×10^{-8} sec.

The image converter employs a Mullard ME 1201 tube and is used to obtain single photographs with an exposure time of 9×10^{-8} sec. A resolution of 500 line pairs per frame is obtained and the maximum effective aperture is f/2.

2.3. Current and voltage measurements

The current flowing in the lower section of the coil is measured by means of a Rogowsky coil. The signal from the coil is integrated using an RC network which has a linear frequency response from 50 kHz to 11 MHz. If it is assumed that the two sections of the coil are very closely coupled, then it can easily be shown that they must carry the same current. This would be the case even if the plasma were very non-uniform in the axial direction.

The voltage developed around the coil is measured by means of a resistive loop which is placed around the tube inside the sectors (of the upper section). The loop has a total resistance of 180 kΩ and two tapping

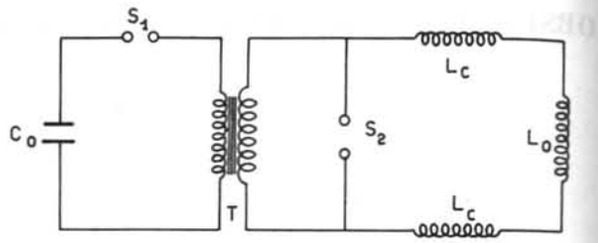

Fig. 1b The circuit for the production of an initial magnetic field. C_0—capacitor bank with rating of 120 kJ at 40 kV, T—transformer with 20:1 step-down ratio, S_1—6 pressurized spark gaps, S_2—crow-bar vacuum spark gap, $2L_c$—0.5 μH choke coil, L_0—52 mμH single-turn coil.

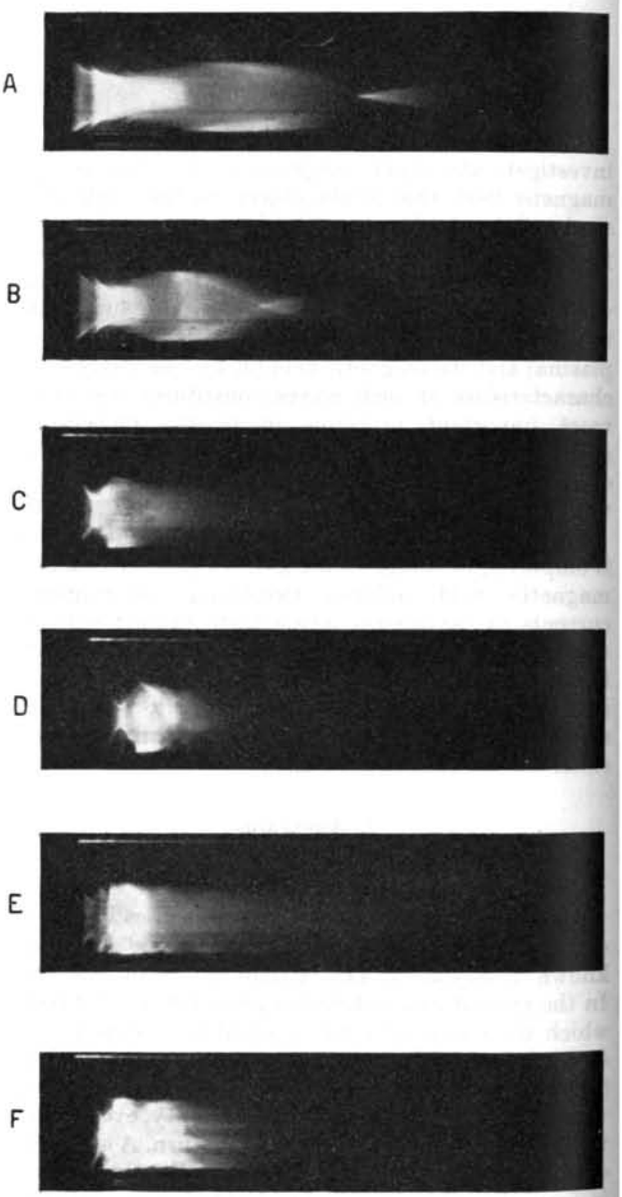

Fig. 2 Streak photographs taken through the side of the tube. (A) argon at 500 μ Hg, (B) argon at 250 μ Hg, (C) helium at 500 μ Hg, (D) helium at 250 μ Hg, (E) hydrogen at 500 μ Hg, (F) hydrogen at 250 μ Hg. The length of the background corresponds to a time of 80 μs.

points are used which are 67 Ω apart. A matched 75 Ω cable is used, however, and so the tapping points are effectively 35.4 Ω apart.

The coil is electrostatically screened by two other resistive loops, one inside and one outside, each of which has a resistance of 30 kΩ. Such electrostatic screens are satisfactory if the time constant $R_s C_s$ is small in comparison with the times of interest, where R_s is the resistance of the screen and C_s is the capacitance between the screen and the sectors (or that between the screen and the plasma). In the present case $R_s C_s$ is estimated to be about 6×10^{-8} sec. There may be a small error associated with capacitive currents flowing between the resistive loops in the region of the tapping points.

Another criterion is that L_s/R_s must be small compared with the times of interest, where L_s is the inductance of the screen. This criterion, however, is very easily satisfied and L_s/R_s is of the order of 10^{-11} sec in the present case.

2.4. Magnetic probe

The magnetic probe, which is inserted in the top end of the discharge tube, consists essentially of a coil of 4.8 mm diameter having 5 turns at a spacing of 2.5 mm. The coil is connected to a twisted pair of wires which form a transmission line having roughly the same characteristic impedance as the external measuring circuit. The latter consists of a matched cable (75 Ω), followed by an RC integrator which has a time constant of 80 μs.

The wires are within a glass tube which is coated (with carbon) in order to form an electrostatic screen. This screen, in turn, is surrounded by two further screens of silver coating. These outer screens are slit lengthwise and are necessary because the carbon screen has an appreciable resistance in the axial direction (the length is 75 cm).

3. Results

Measurements have been made using argon, hydrogen and helium at various pressures. Typical results are shown in Figs 2—10. A description of the results for several different discharge conditions is given below.

3.1. Argon at 50 μ Hg

Streak photographs show that breakdown and compression occur during the first half-cycle. The electrical measurements (see Fig. 8) also indicate that a contraction takes place during this time. The quantity $\int_0^t V\,\mathrm{d}t/I$ would represent the inductance if the plasma were a perfect conductor and on this basis one can calculate that the radius decreases to 60% of its original value during $\frac{1}{2}$ μs. Since resistive effects are present, however, the quantity $(1/I)\int_0^t V\,\mathrm{d}t$ has no simple geometrical interpretation but depends on the history of the discharge.

At the second half-cycle a further implosion takes place. An image converter photograph taken during this phase (at 2.4 μs) is shown in Fig. 3 left. This record is somewhat similar to those taken by Albares, Krall and Oxley [8], who investigated the Rayleigh-Taylor instabilities which developed during the compression in a stabilized linear pinch tube. The probe measurements show an internal magnetic field at this time (flux which has been trapped during the first half-cycle) so that the present photograph may well represent a Rayleigh-Taylor instability which develops on the inner surface of a collapsing shell of gas. Another possibility, however, is that the break-

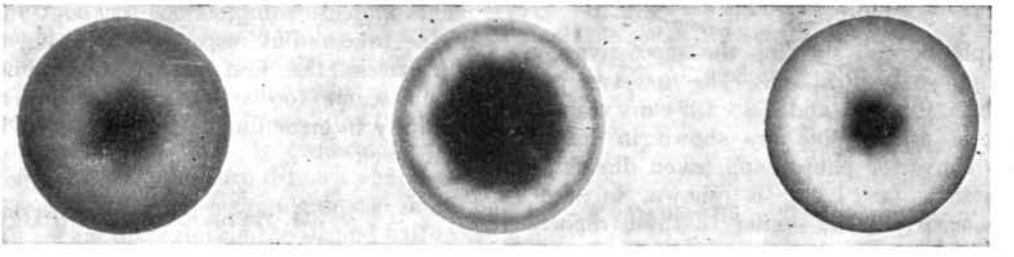

Fig. 3 Image converter photographs (exposure time 90 m μs) of an argon discharge taken at 50 μ Hg. Left photograph, 2.4 μs; centre, 4.7 μs; right, 14.8 μs.

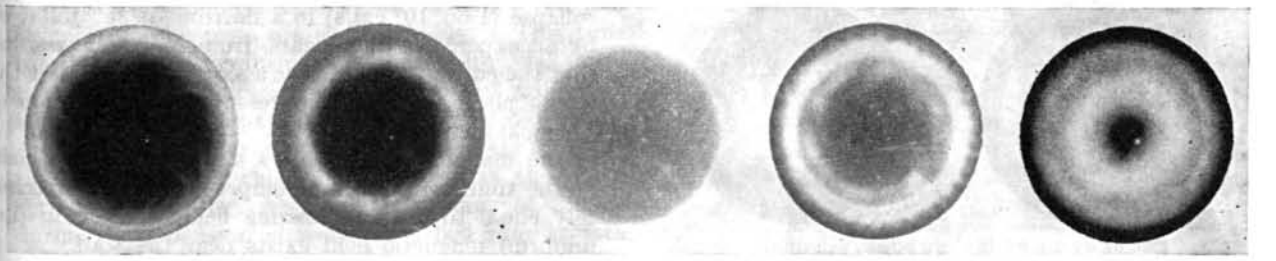

Fig. 4 Image converter photographs (exposure time 90 m μs) of an argon discharge taken at 250 μ Hg. From left to right, times are: 1.0 μs, 2.7 μs, 3.5 μs, 3.6 μs and 11.1 μs, respectively.

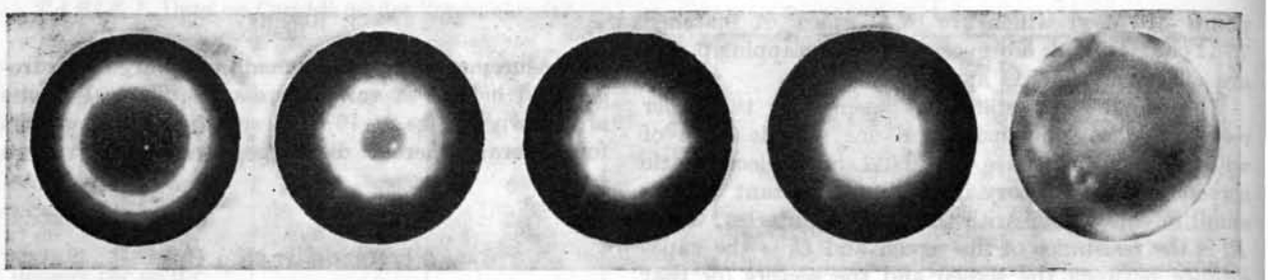

Fig. 5 Image converter photographs (exposure time 90 mμs) of a hydrogen discharge taken at 50 μ Hg. From left to right, times are: 2.9 μs, 3.15μs, 3.3 μs, 3.55 μs and 5.2 μs, respectively.

down occurs in a non-uniform manner, thereby producing a shell of non-uniform density which is subsequently compressed. This mechanism has been discussed by KVARTSKAVA, KERVALIDZE and GVALADZE [9]. A six-pointed star is seen in Fig. 3, left, and the "inner points" of this star are in line with the six gaps between the sectors. Electrostatic fields are set up between the sectors [10] and may be important in determining the breakdown. In the present experiment these fields are screened out in the upper section (by the voltage-measuring loop), but not in the lower section.

An image converter photograph taken at 4.7 μs is shown in Fig. 3, centre. A hexagonal shape is clearly seen and the photograph probably shows an expansion of the previous picture. At this time the magnetic probe measurements show a uniform magnetic field (the original trapped flux) within a certain radius (~5 cm).

A photograph taken at a much later time (14.8 μs) is shown in Fig. 3, right, where it is seen that the centre is still dark. A number of successive implosions have taken place by this time and some trapped field still exists in the central region.

3.2. ARGON AT 250 μ Hg

A streak photograph showing the successive contractions is shown in Fig. 2 (B). The first two have velocities of 2×10^6 cm/s and 2.8×10^6 cm/s respectively. Magnetic probe plots are shown in Fig. 10.

An image converter photograph taken during the first contraction (at 1 μs) is shown in Fig. 4 "Wisps" are clearly seen, similar to those reported by KVARTSKAVA *et al.* (loc. cit). It was suggested by these authors that the "wisps" are produced by run-away electrons. Further evidence is required before this hypothesis can be tested; x-ray measurements have not yet been made.

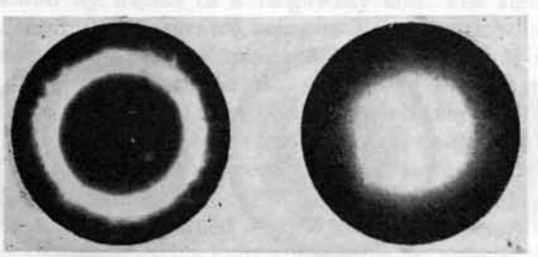

Fig. 6 Image converter photographs (exposure time 90 mμs) of a hydrogen discharge at 250 μ Hg. Left photograph, 3.05 μs; right, 4.0 μs.

Later photographs are shown in Fig. 4. The photograph at 3.6 μs is of interest in that the outer surface of the plasma has a structure which is probably due to a Rayleigh-Taylor instability. Such instabilities have already been observed in orthogonal [11, 12] and ordinary [13] pinched discharges.

3.3. ARGON AT 500 μ Hg

A streak photograph is shown in Fig. 2 (A) and magnetic probe plots are shown in Fig. 10. The first two contractions have velocities of 1.4×10^6 cm/s and 2×10^6 cm/s respectively. Image converter photographs (not shown) are similar in type to those taken at 250 μ in that they show the "wispy" type of record and also the external Rayleigh-Taylor instability.

The magnetic field in the inner regions always has the same sign and is fairly uniform in space indicating that the currents flow in the outer regions of the discharge. The probe results do not indicate thin current shells but rather a distribution of current over several centimetres. The external electrical measurements indicate compressions to about 70% and 60% of the tube radius respectively, during the first two half-cycles; the first compression time is 0.4 μs, which seems too small, but these deductions are certainly in error due to the resistive effects already mentioned.

3.4. HYDROGEN AT 50 μ Hg

Breakdown occurs just before the end of the first half-cycle, as shown by the magnetic probes. The streak photograph (not shown) shows a very rapid collapse (1.6×10^7 cm/s) to a narrow "neck" followed by an expansion. It appears, from the probe results, that the current advances at a slower rate, so that the streak photograph may represent the propagation of a shock wave.

The magnetic probe shows a trapped field which, at the time of maximum compression, is approximately equal to the compressing field. A vacuum (i.e. uniform) magnetic field exists near the wall.

The external electrical measurements (Fig. 8) show that breakdown does not occur until late in the first

half-cycle. They then indicate that a compression takes place, followed by an expansion.

A series of image converter photographs is shown in Fig. 5. The centre photograph refers to the maximum compression (examination of the original film shows that less light is emitted from the centre). The first two show that the luminous region has an irregular outer surface and the final photograph (5.2 μs) shows a complicated structure which corresponds to a new plasma just leaving the walls.

3.5. Hydrogen at 250 μ Hg

A streak photograph is given in Fig. 2 (F) and magnetic probe plots are shown in Fig. 9. Again breakdown occurs just before the end of first half-cycle. Compression then takes place, at a velocity of 5×10^6 cm/s and is followed by an expansion of comparable velocity. Fig. 6 shows two image converter photographs,

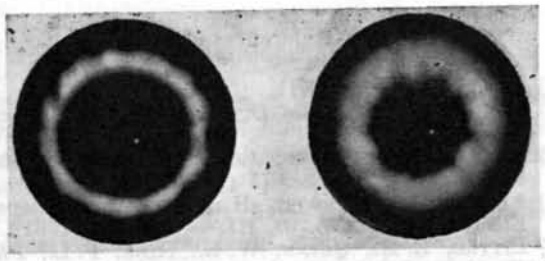

Fig. 7 Image converter photographs (exposure time 90 mμs) of a hydrogen discharge taken at 500 μ Hg. Left photograph, 1.2 μs; right, 2.1 μs.

the second being at the instant of maximum compression (4.0 μs); the earlier one (3.05 μs) shows an irregular outer surface with no obvious periodicity. The trapped magnetic field inside the luminous region is fairly constant in space and reaches its maximum value at maximum compression. In this case the currents seem to flow immediately behind the luminous region, according to the magnetic probes. The general appearance of the streak photograph is in agreement with this suggestion since the luminous region does not contract to a very narrow "neck" (as in the case of hydrogen at 50 μ), which is consistent with it being the edge of the plasma and not a shock wave.

The external electrical measurements also show the compression taking place during the second half-cycle.

3.6. Hydrogen at 500 μ Hg

A streak photograph is shown in Fig. 2 (E) and magnetic probe plots are shown in Fig. 9. This time breakdown occurs during the first half-cycle. Compression then follows, at a velocity of 3.2×10^6 cm/s followed by an expansion at about 2.8×10^6 cm/s. An image converter photograph taken at 1.2 μs is shown in Fig. 7, where it is seen that the outer surface is irregular. A photograph taken at 2.1 μs, during the expansion, shows a perturbed inner surface (see Fig. 7); this may be an instability associated with acceleration outwards.

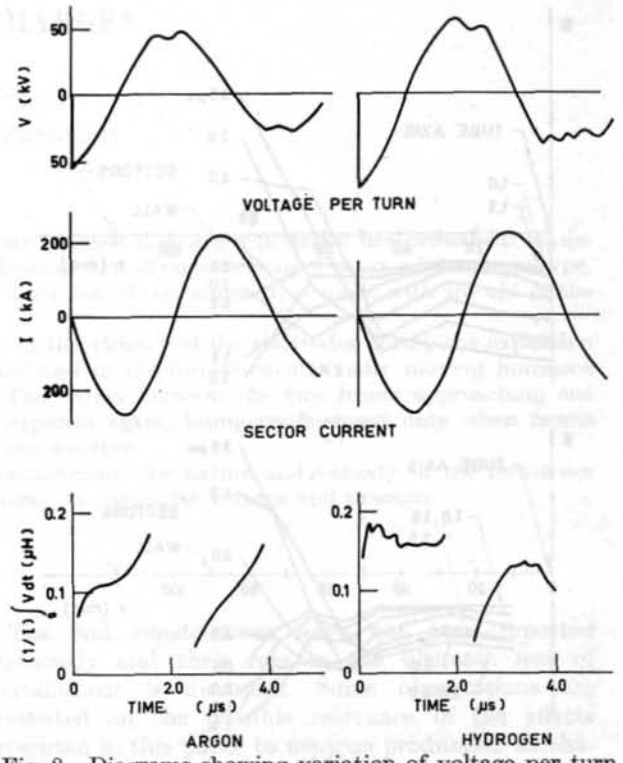

Fig. 8 Diagrams showing variation of voltage per turn at sector radius, current flow in sectors, and the "effective" tube inductance as functions of time for argon and hydrogen. $V_c = 25$ kV, $C = 48$ μF, pressure = 50 μ Hg.

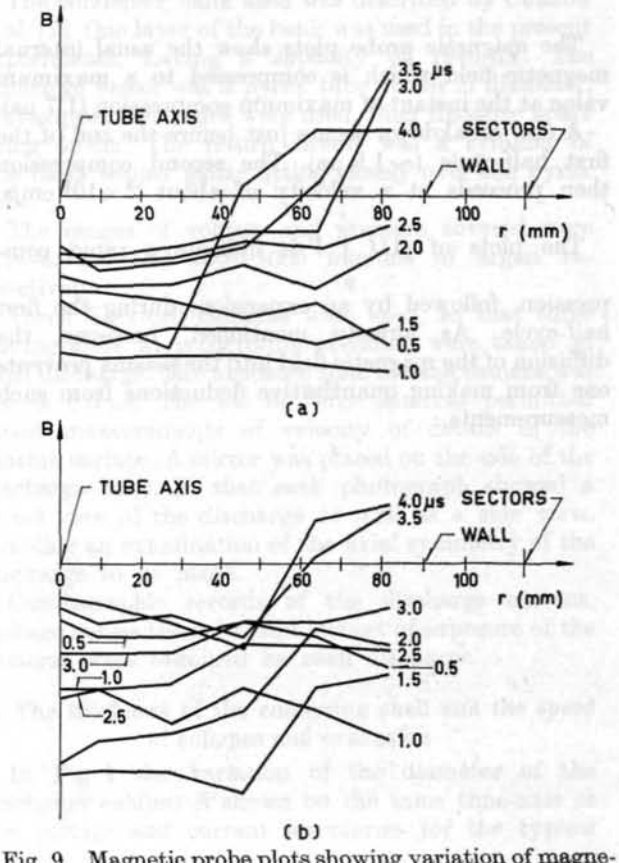

Fig. 9 Magnetic probe plots showing variation of magnetic field with radius and time (in μs) for hydrogen at (a) 250 μ Hg, (b) 500 μ Hg.

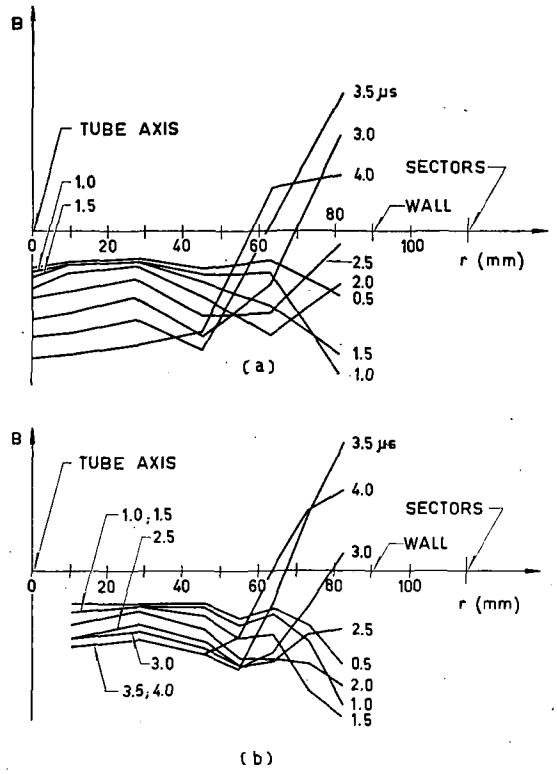

Fig. 10 Magnetic probe plots showing variation of magnetic field with radius and time (in μs) for argon at (a) 250 μ Hg, (b) 500 μ Hg.

The magnetic probe plots show the usual internal magnetic field which is compressed to a maximum value at the instant of maximum compression (1.7 μs).

A new breakdown occurs just before the end of the first half-cycle (~1.9 μs). The second compression then proceeds at a velocity of about 2×10^6 cm/s.

The plots of $(1/I \int_0^t V \mathrm{d}t$ indicate a rapid compression, followed by an expansion, during the first half-cycle. As already mentioned, however, the diffusion of the magnetic field into the plasma prevents one from making quantitative deductions from such measurements.

4. Conclusions

The measurements described in this paper are of a preliminary nature and will be repeated and extended. In addition the initial magnetic field will be used in the future experiments.

Since high velocities of compression can undoubtedly be attained, it will be of particular interest to study the degree of randomization which exists in the plasma.

Acknowledgements

The authors wish to thank Dr. M. U. Martone and Dr. S. E. Segre for their assistance with the image converter photography.

The image converter equipment was built by Mr. G. H. Lunn of A.W.R.E. (Aldermaston).

References

[1] Homer, Ὀδυσσεύς, XII.
[2] Alighieri Dante, La Divina Commedia, Inferno, Canto VII, 22.
[3] Adlam, J. H., Allen, J. E., *Phil. Mag.* **3** (1958) 448; *Proc. Phys. Soc.* **75** (1960) 640.
[4] Auer, P. L., Hurwitz, H., Kilb, R. W. General Electric Report No. 61, RL — (2663 E) (1961).
[5] Little, E. M., Quinn, W. E., Ribe, F. L., *Phys. Fluids* **4** (1961) 711.
[6] Allen, J. E., Segre, S. E., Proc. 4th Int. Conf. on Ionization Phenomena in Gases, Uppsala (North-Holland Publ. Co. Ltd., Amsterdam) **2** (1959) 1073.
[7] Rumi, B., Trautteur, G., Gambirasio, G., to be published; see also Notiziario del C.N.E.N., 1961, No. 4.
[8] Albares, D. J., Krall, N. A., Oxley, C. L., General Atomic Report No. 1962 (1961).
[9] Kvartskava, I. F., Kervalidze, K. N., Gvaladze, Yu. S., *Zhur. Eksptl. Teoret. Fiz.* **38** (1960) 1641.
[10] Allen, J. E., Segre, S. E., 1961, *Il Nuovo Cimento*, **21** (1961) 980.
[11] Green, T. S., Niblett, G. B. F., *Nuclear Fusion* **1** (1960) 42.
[12] Bodin, H. A. B., Newton, A. A., Peacock, N. J., *Nuclear Fusion* **1** (1961) 139.
[13] Curzon, F. L., Folkierski, A., Latham, R., Nation, J. A., *Proc. Roy. Soc.* **A 257** (1960) 386.

END EFFECTS IN A LINEAR PINCHED DISCHARGE*

A. FOLKIERSKI, P. G. FRAYNE, R. LATHAM

IMPERIAL COLLEGE OF SCIENCE AND TECHNOLOGY

LONDON, UNITED KINGDOM

Kerr-cell photographs of unstabilized linear pinched discharges in argon are presented. A detailed study of the onset of instabilities, the development of constrictions of the $m = 0$ (sausage) type, and the manner in which these lead to the final loss of containment, is made with the aid of the photographs.

It is found that $m = 0$ constrictions occur in the vicinity of the electrodes during the expansion of the discharge after the first pinch. They lead to the formation of axially moving luminous fronts, which are probably shock waves. The region between the two fronts approaching one another collapses to a second pinch and expands again, losing confinement only when fronts advancing from $m = 0$ constrictions meet one another.

In view of the effect of the fronts on containment, the nature and velocity of the fronts are studied as a function of discharge parameters—in particular voltage and pressure.

1. Introduction

The over-all behaviour of the unstabilized linear pinched discharge is well known and has been discussed experimentally and theoretically by many authors.

It is found that the discharge in its early stages has the form of a conducting cylindrical shell which collapses on to the axis at the time of the first pinch. Next the discharge expands radially and, depending on conditions, it may subsequently collapse again to a second pinch. The repetition of this cycle, which would ultimately lead to radial dynamic equilibrium, is interrupted by the onset and rapid growth of instabilities.

One type of instability, the Rayleigh-Taylor [1], was studied in detail by CURZON, FOLKIERSKI, LATHAM and NATION at Imperial College [2]. Photographic studies in argon, with the use of Kerr cells, showed that these instabilities develop in the time interval between the first and second pinches, while the plasma surface is subject to an acceleration directed radially towards the axis.

In the present paper the photographic observations are extended to include:

(a) The measurements of the thickness of the current shell during the first collapse;
(b) The details of the structure of the first pinch;
(c) The formation, under certain conditions, of an outer boundary or sheath surrounding the original discharge column;
(d) The occurrence—in all cases—of constrictions near the electrodes; these constrictions grow to large amplitudes, while the main body of the discharge is only slightly perturbed by the Rayleigh-Taylor instability;
(e) The occurrence of similar constrictions in the body of the discharge at a later stage.

The end constrictions have not been reported previously and their role in the ultimate loss of containment is discussed. Some observations are presented on the possible relevance of the effects presented in this paper to neutron production mechanisms in deuterium discharges.

2. Experimental technique

The condenser bank used was described by CURZON *et al.* [2]. One layer of the bank was used in the present experiments, having a capacity of 1940 μF. The discharge vessel was a pyrex tube 15 cm in diameter. Flat copper electrodes were used, their distance apart being 45 cm. The return circuit was a cylinder of fine mesh copper gauze fitting closely over the pyrex tube.

The ranges of voltage and pressure covered were 1.5—4.0 kV and 200—1000 microns of argon respectively.

Three Kerr-cell cameras were used, so that three photographs, at predetermined times, were taken on each discharge. The exposure time of each camera was set at 0.5 μs. The use of three cameras permitted direct measurements of velocity of details of the plasma surface. A mirror was placed on the side of the discharge tube, so that each photograph showed a direct view of the discharge as well as a side view, enabling an examination of the axial symmetry of the discharge to be made.

Oscillographic records of the discharge current, voltage across the tube, and instant of exposure of the cameras were obtained on each discharge.

3. The thickness of the collapsing shell and the speed of collapse and expansion

In Fig. 1 the variation of the diameter of the discharge column is shown on the same time-axis as the voltage and current waveforms for the typical

* Conference paper CN-10/48, presented by A. Folkierski. Discussion of this paper is given on page 650. Translations of the abstract are at the end of this volume of the Conference Proceedings.

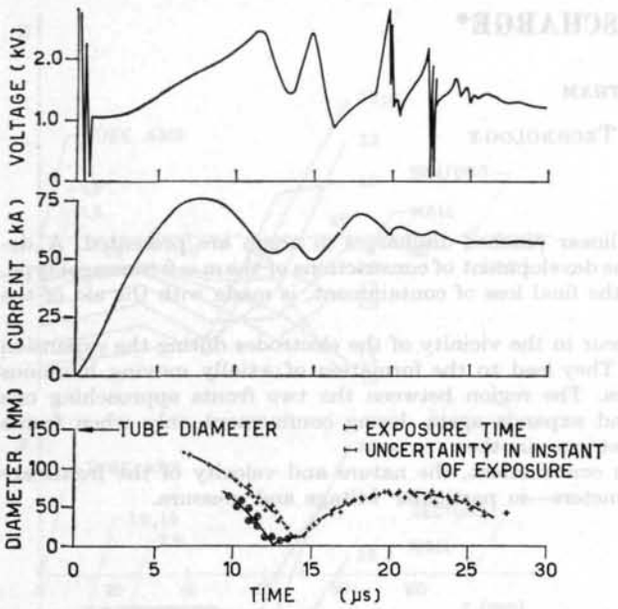

Fig. 1 Voltage, current and the diameter of the discharge column as a function of time. $V = 2.5$ kV; $p = 200$ μ Hg.

case of a discharge in argon at 200 μ pressure, with a bank voltage of 2.5 kV.

It is seen that the shell structure becomes visible when the outer diameter is about 90 mm, that is some 60% of the tube diameter (see also Fig. 2). The thickness of the shell appears to increase slightly towards the pinch, though this may be an illusion; clearly, when the inside diameter of the shell becomes very small the inside boundary may not be visible from outside.

Fig. 2 The collapsing shell. Conical electrodes are used and a bright line can be seen where the shell is in contact with the cathode (top of the picture). $V = 2.5$ kV; $p = 200$ μ Hg.

The discharge develops a bright core when the inner boundary of the shell reaches the axis ($t = 12.5$ μs in Fig. 1). This core then expands while the outside of the shell is still collapsing (see Fig. 3). Minimum over-all diameter occurs when the two boundaries meet ($t = 14.0$ μs). The column then begins to expand radially, and it is at this stage that Rayleigh-Taylor instabilities develop.

The measurements of diameter presented in Fig. 1 were taken in the central part of the length of the discharge column. Where Rayleigh-Taylor perturbations of the surface were present an average value of the diameter was taken. At times later than $t = 25$ μs large perturbations of the surface occurred, and consequently it was not feasible to measure diameters.

Fig. 3 The discharge showing the expanding central core surrounded by the collapsing shell during the formation on the first pinch. $V = 2.5$ kV; $p = 500$ μ Hg.

The current waveform of Fig. 1 exhibits a local minimum when the bright core develops. Under different conditions of voltage and pressure this minimum becomes just a change of slope of the waveform. The principal minimum of current and the simultaneous rise of voltage are not in this case associated with any special feature of the diameter curve.

The finiteness of the exposure time (0.5 ± 0.1 μs) introduced a small uncertainty in the drawing of the graph of Fig. 1. The abscissae plotted are the times at which exposures began. But it may be presumed that the photographs show the maximum diameter, occurring during an exposure, for the outer edge and the minimum diameter for the inner edge. This would lead to the conclusion that the shell is in fact thinner than shown. For the same reason the diameter of the pinch may be slightly smaller than shown.

The degree to which the discharges are repetitive is shown by the fact that points obtained on an individual discharge and on different discharges fit well on the same curve.

4. The formation of an outer boundary or sheath

At voltages in excess of 3 kV a new phenomenon, the formation of an outer sheath which surrounds the original discharge column, is observed. This occurs when the discharge reaches its maximum expansion after the first pinch and begins to collapse to the second pinch. A sequence of photographs showing the development and collapse of the sheath is shown in Fig. 4.

The appearance of the photographs suggests strongly that the sheath is formed out of plasma which has escaped from the original column through the pointed tips of the characteristic cusp pattern of the Rayleigh-Taylor instability. The cusps bend towards the anode that is in the direction of electron flow; then the sheath appears, the position of its boundary coinciding initially with the positions of the tips of the cusps at the time of maximum expansion of the column.

The original column then collapses quite rapidly to the second pinch, which is somewhat irregular in shape, and expands again. Meanwhile the outer sheath begins to collapse and an over-all minimum of diameter is reached when the two boundaries meet, in analogy with the situation at the first pinch. Thereafter the discharge remains quiescent until the arrival of disturbances due to end-effects.

5. Constrictions of the $m=0$ type

As already mentioned, Rayleigh-Taylor instabilities are observed to grow soon after the first pinch.

The characteristic cusps occur at random positions on the plasma surface and do not exhibit cylindrical symmetry, at least not to any marked degree. As they grow larger, however, the neighbouring depressions of the surface grow by joining one another until they acquire the character of a constriction and develop a measure of cylindrical symmetry. This process can be observed in discharges at voltages at which the outer sheath does not form; it occurs shortly before the second pinch. Once a constriction is formed it collapses rapidly to a small diameter (see Fig. 5) and can be considered as an example of the $m=0$ instability predicted by the conventional theory of the steady state cylindrical plasma column [1, 3, 4].

It must be emphasized, however, that the constrictions are not spatially periodic, so that it is not possible to ascribe a wavelength to them. On the other hand individual constrictions have a characteristic length which increases during their growth. The positions at which the constrictions occur are not obviously correlated from one discharge to another.

The last remark is not true of constrictions occurring near each of the electrodes. These constrictions are present under all conditions and constitute a major feature of the discharge. They form quite early, while the body of the discharge is expanding after the first pinch. They arise a few centimetres away from the electrode surfaces and constrict to minimum diameter about the time of the maximum expansion of the column after the first pinch. They give rise to end-effects described later.

Similar constrictions in the body of a deuterium discharge are discussed by ANDERSON *et al.* [5, 6] and by TRUBNIKOV [7] with reference to photographs obtained at Los Alamos and by Orlinskii respectively.

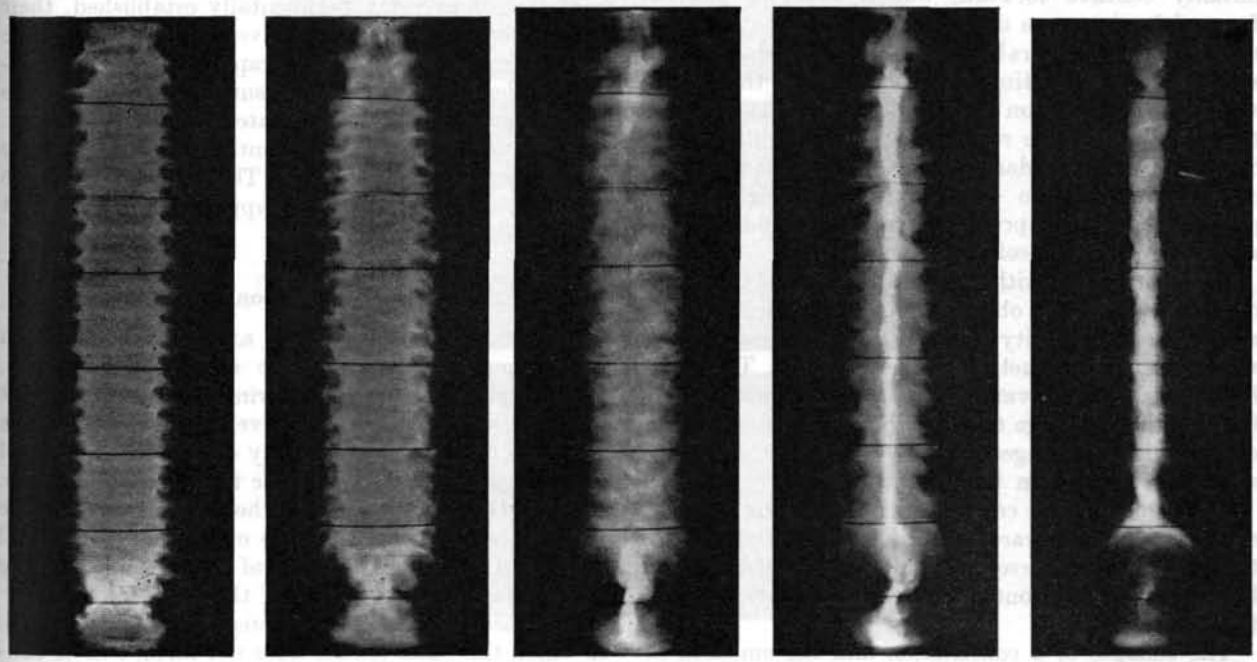

Fig. 4 Sequence showing the development and collapse of the outer sheath. $V=3.5$ kV; $p=200$ μ Hg. Times (in microseconds) with reference to the onset of current flow are (from left to right): 14.5, 16.0, 17.5, 19.0, 20.5.

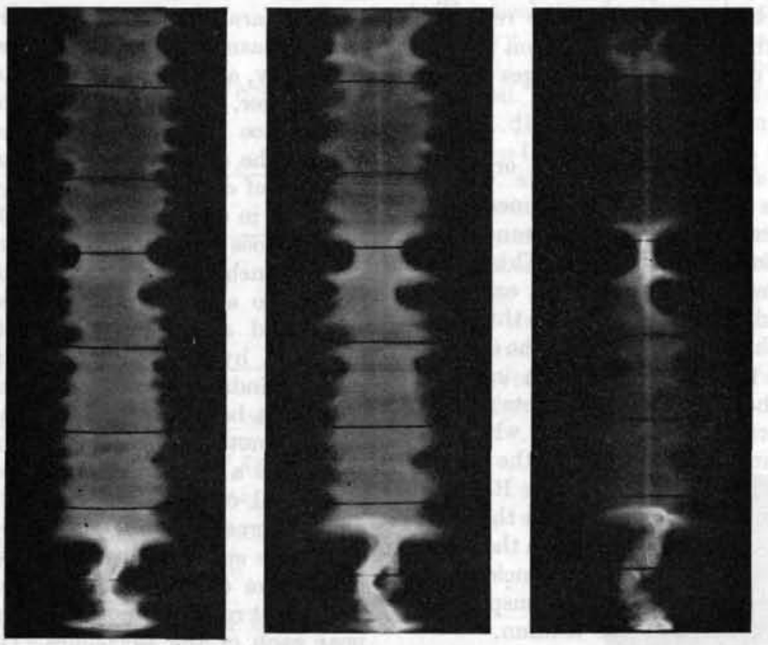

Fig. 5 Sequence showing the collapse of an $m = 0$ constriction in the body of the discharge. $V = 2.5$ kV; $p = 200$ μ Hg. Times are (from left to right) 18.0, 19.0, 20.0 μs, respectively.

6. End constrictions

End-constrictions invariably form a few centimetres from the electrodes while the discharge is expanding after the first pinch. The diameter of the constricted part falls rapidly to about 1 cm or 5% of the tube diameter, and a local bright core forms. From this bright core a disturbance is propagated axially towards the body of the discharge. This disturbance has the form of a luminous front which is initially concave forward, but it becomes convex forward in the space of about 1—2 μs. The shape is now similar to a paraboloid and the boundary quite sharp. At the same time the luminosity of the region where the constriction was formed drops rapidly and the boundary of the region becomes difficult to see. Sometimes the boundary reforms with the appearance of the characteristic cusps of the Rayleigh-Taylor perturbation, appropriate to an expanding region subject to radial acceleration inwards.

The front moves with an initial velocity of the order of 1 cm/μs. It can be observed for several microseconds and it loses its identity only when it starts interacting with some other structure in the discharge. This may be a similar front advancing from a constriction in the body of the discharge towards the electrode or, in the case of higher voltages, it may be the second pinch which has formed in the meantime.

Sometimes a front can be seen propagating from an end-constriction towards the neighbouring electrode. Observation is, however, difficult because of the short life-time of such a front, which very soon hits the electrode surface.

The collapse of a constriction and the emission of an axial luminosity front are found to be correlated in time with a dip in the current waveform and a very sudden increase in the voltage followed by a sharp drop often accompanied by rapid fluctuations similar to noise. This can be seen in Fig. 1 at $t = 20.0$ μs and $t = 22.5$ μs.

A sequence of photographs showing the final stage of a collapsing constriction and the emission of a front is shown in Fig. 6. The position of the two fronts proceeding towards the centre of the discharge column is plotted against time in Fig. 7.

While the nature of the propagating luminosity fronts is not as yet experimentally established, their appearance is strongly suggestive of shock fronts. The process envisaged is that the rapid collapse of a constriction leads to an excess pressure in the centre of the constriction, possibly accentuated by Joule heating. This gives rise to two shock fronts propagating axially away from the constriction. The velocity of these decreases in time since the supply of energy is not maintained.

7. The effect of fronts on containment

The effect of the supposed axial shock waves on containment of the discharge column is profound.

The trailing edge of a moving paraboloidal front does not appear to be effectively contained by the magnetic field. This is probably due to the high local value of β, the ratio of kinetic to magnetic pressure. The kinetic pressure behind the shock front can be expected to be large, while the magnetic field is small in view of the large diameter of the current carrying region at the trailing edge of the front.

Two cases have to be distinguished. At low voltages, at which the outer sheath does not form, loss of containment occurs when fronts moving from the electrodes meet fronts advancing from constrictions in the

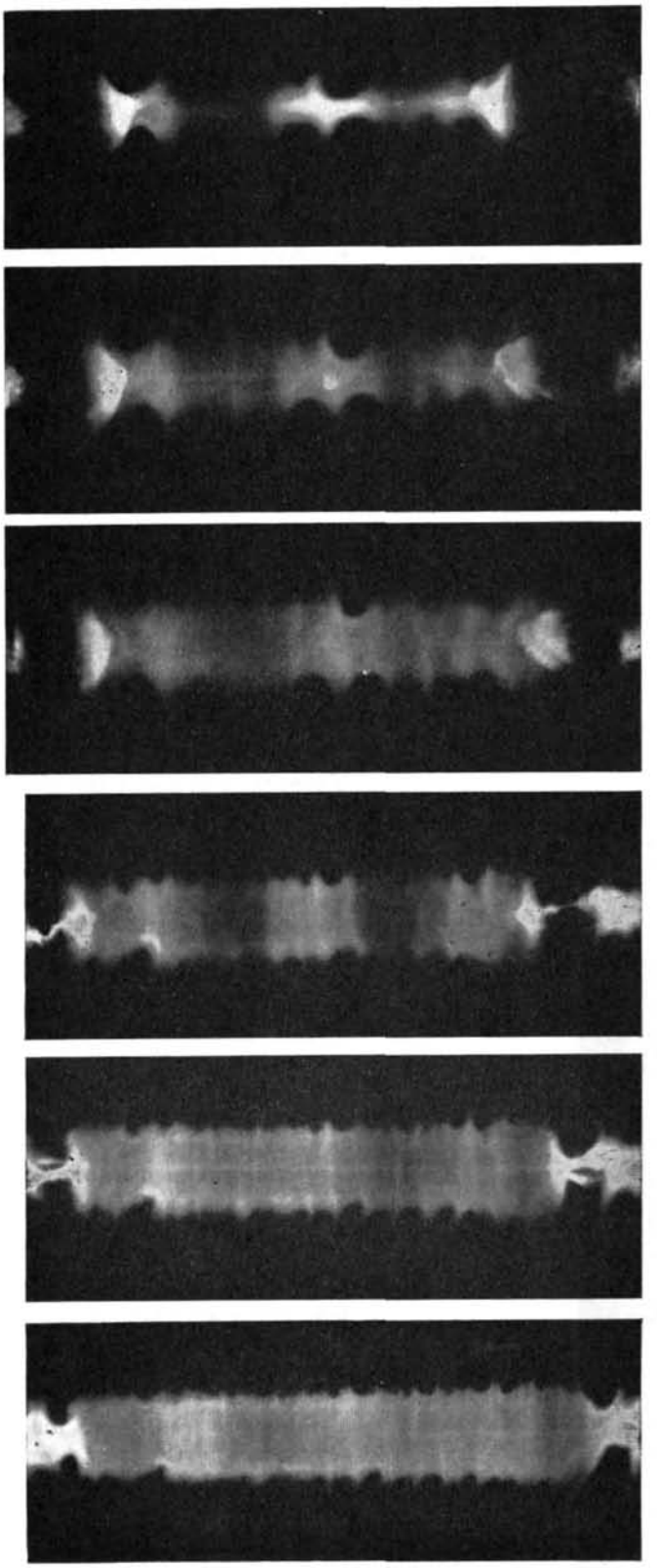

Fig. 6 Sequence showing the collapse of the end constrictions, the formation of fronts and their propagation. Anode at the top. $V = 2.5$ kV; $p = 200$ μ Hg. Times are (from left ro right): 19.0, 20.1, 21.5, 22.7, 23.8, 25.2 μs.

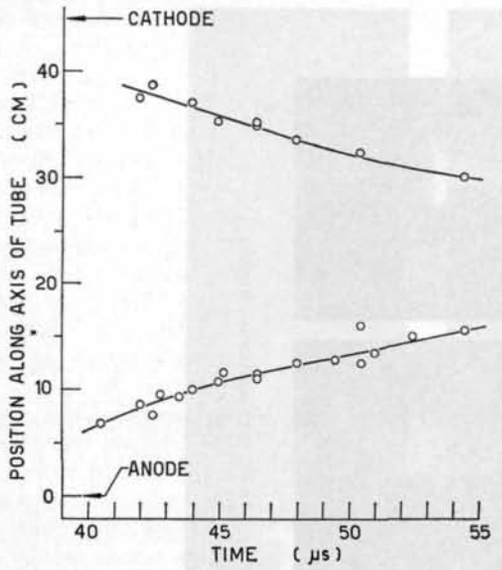

Fig. 7 Position of fronts as a function of time. $V = 2.5$ kV; $p = 1000$ μ Hg.

body of the discharge. When two such fronts meet the region increases in luminosity, expands and acquires a turbulent appearance.

For higher voltages, at which the collapse of the outer sheath impedes the formation of constrictions in the body of the discharge, loss of containment occurs gradually as the fronts from the electrode regions approach one another (Fig. 8).

In an attempt to modify the behaviour of the discharge near the anode and cathode, the flat electrodes were replaced by conical ones, having a half-angle of 45° and a slightly rounded tip. The results showed that the end-constrictions formed in a manner quite similar to that observed with flat electrodes, no first order change being observed. The outer boundary of the sheath present at higher voltages was, however, found to be curved so as to terminate at the electrode tips.

Fig. 8 Loss of containment when anode and cathode fronts approach one another. Photograph taken with conical electrodes. $V = 4$ kV; $p = 200$ μ Hg.

8. Relevance to emission of neutrons from deuterium discharges

The broad similarity of behaviour of pinched discharges in deuterium and argon indicates that the efficiencies of trapping of particles by the collapsing shell are comparable, while the collapse times are not seriously influenced by various assumptions regarding the role of shock waves. Thermal conduction and radiation do not appear to play a major role and the current shell once formed does persist for a time relevant to the interpretation of results.

It thus appears possible to select conditions in which an argon discharge may be considered as a model of a deuterium discharge as regards plasma dynamics and electrical behaviour. Such a model has the advantages that the discharge is bright and therefore suitable for photography and that the time scale is slowed down.

The observations presented in this paper may be relevant to a number of mechanisms proposed for the production of neutrons. These include the $m=0$ instability considered by ANDERSON *et al.* [5, 6], the formation of breaks in the discharge discussed by TRUBNIKOV [7], and the shock mechanism proposed by PHILLIPS [8].

Neutrons have been reported at the time of the second pinch in deuterium discharges, by Anderson *et al.* as due to the acceleration of deuterons in $m=0$ constrictions. Such constrictions are observed to form in the body of the argon discharge around the time of the second pinch. In their initial stages these constrictions arise as a result of the merging of Rayleigh-Taylor perturbations. The process appears to be inhibited at higher voltages, which may be relevant to the decrease in the intensity of instability neutrons observed when the discharge voltage is increased beyond the optimum value.

Voltage transients observed when end-constrictions form indicate that caution is necessary in interpreting discontinuities of the voltage waveform as signs of successive pinches in absence of direct diameter measurements. In the present experiments soon after the first pinch a voltage maximum is observed which is not correlated with any particular change in the diameter of the discharge column, and is probably due to a rise in the resistivity of the plasma.

Trubnikov considered the breaks in the discharge reported by Orlinskii as giving rise to local electric fields responsible for deuteron acceleration. On the basis of the present photographs it would appear that the breaks are not complete, and that weakly luminous plasma exists even where a photograph obtained with a camera of lower aperture would indicate a break.

The observations in argon show the existence of shock fronts moving axially both near the electrodes

and at random positions along the discharge. As suggested by Phillips, these could give the kind of ordered motion necessary to explain the neutron results. It would be interesting to see if similar fronts occur in deuterium discharges and if so to measure their velocity.

It must be emphasized that different conditions may well obtain in argon and in deuterium discharges and the above comments should only be regarded as tentative until confirmed or otherwise by experiment.

Acknowledgements

The authors wish to thank Prof. P. M. S. Blackett, F.R.S., for his constant encouragement of this work.

The condenser bank used in the experiments was provided by a special grant from the Department of Scientific and Industrial Research. One of the authors (P.G.F.) is indebted to the Department of Scientific and Industrial Research for a maintenance grant.

References

[1] KRUSKAL, M., SCHWARZSCHILD, M., *Proc. Roy. Soc. (London)*, **A 233** (1954) 348.

[2] CURZON, F. L., FOLKIERSKI, A., LATHAM, R., NATION, J. A., *Proc. Roy. Soc. (London)*, **A 257** (1960) 386.

[3] TAYLER, R. J., *Proc. Phys. Soc. (London)*, **B 70** (1957) 31.

[4] SHAFRANOV, V. D., *J. Nuclear Energy*, **5** (1957) 86.

[5] ANDERSON, O. A., BAKER, W. R., COLGATE, S. A., ISE, J., PYLE, R. V., Proceedings of the Third International Conference on Ionisation Phenomena in Gases, Venice (1957) 62.

[6] ANDERSON, O. A., BAKER, W. R., COLGATE, S. A., ISE, J., PYLE, R. V., *Phys. Rev.* **110** (1958) 1375.

[7] TRUBNIKOV, B. A., Plasma Physics and the Problem of Controlled Thermonuclear Reactions (Pergamon Press, London, 1960), Vol. IV, p. 101.

[8] TUCK, J. L., Proceedings of Second U.N. Conference on Peaceful Uses of Atomic Energy, Geneva, **32** (1958) 3.

О МЕХАНИЗМЕ СИЛЬНОТОЧНОГО ГАЗОВОГО РАЗРЯДА В СЛАБОМ МАГНИТНОМ ПОЛЕ*

А. П. Бабичев, А. И. Карчевский, Ю А. Муромкин, В. В. Сокольский

Академия Наук СССР

Союз Советских Социалистических Республик

Конфигурация магнитных полей в тороидальном сильноточном разряде изучалась на установках «Зета», «Скептр», «Альфа» и др. Нами были выполнены аналогичные исследования, но при большем разнообразии внешних условий: в одной серии измерений в сечении разрядной камеры сохранялся постоянным поток продольного магнитного поля, в другой — напряженность поля на краю разрядной камеры и, наконец, в третьей — внешнее магнитное поле менялось в течение разряда. Было установлено, что все наблюдаемые явления могут быть как качественно, так и количественно объяснены с единой точки зрения. Эксперименты проводились на тороидальной камере, имеющей толстостенный (10 мм) алюминиевый кожух с диаметрами 750 и 250 мм. Внутри кожуха размещалась разрядная камера (лайнер) диаметром 160 мм. Исследовался разряд в водороде при давлении $10^{-3} \div 5 \cdot 10^{-4}$ мм рт. ст. длительностью 600 мксек.

Следует заметить, что в первой серии опытов конфигурация разряда при заданном магнитном потоке в сечении лайнера определяется только величиной тока, протекающего по плазме в данный момент времени, независимо от того, в какой фазе разряда этот ток достигается. Во второй и третьей серии опытов конфигурация разряда полностью определяется величинами тока и внешнего магнитного поля на краю разряда и не зависит от скорости их изменения. Из этого следует, что время диффузии магнитного поля в плазме мало по сравнению с периодами изменения внешних магнитных полей, т. е. отсутствует вмороженность магнитного поля в плазме. Это согласуется с низкой проводимостью плазмы и незначительной ее температурой.

Все наблюдаемые явления описываются квазистационарной бессиловой моделью. Сопоставление результатов, вычисленных по этой модели, дает хорошее качественное согласие для всех трех серий экспериментов. Отсутствие токов, перпендикулярных направлению магнитного поля, с микроскопической точки зрения может быть объяснено в рамках механизма конвективной неустойчивости.

1. Введение

Радиальное распределение магнитных полей в тороидальном сильноточном разряде изучалось в ряде работ [1 ÷ 5].

Для выяснения свойств газоразрядной плазмы в слабых магнитных полях нами были проведены исследования распределения магнитных полей в тороидальном разряде при следующих условиях: 1) в сечении разрядной камеры сохранялся постоянным поток продольного магнитного поля; 2) сохранялась постоянной напряженность магнитного поля на поверхности разрядной камеры и, наконец, 3) внешнее магнитное поле менялось в течение времени разряда. Было установлено, что все наблюдаемые явления могут быть как качественно, так и количественно объяснены с единой точки зрения.

2. Экспериментальная установка

Эксперименты проводились на тороидальной камере, имеющей толстостенный (10 мм) алюминиевый кожух со средним диаметром тора 750 мм и диаметром отверстия 250 мм. Кожух имел два поперечных разреза, что позволяло возбуждать в нем продольное электрическое поле при помощи трансформатора с железным сердечником. Внутри кожуха размещалась разрядная камера (лайнер) с диаметром 160 мм. Все опыты проводились на водороде. Схематический чертеж разрядной камеры представлен на рис. 1.

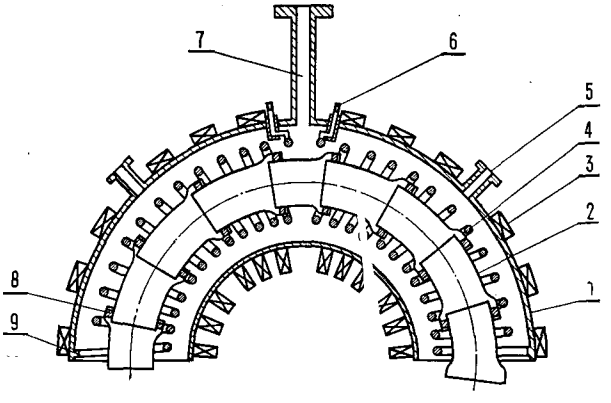

Рис. 1 Схема тороидальной разрядной камеры. 1 — толстостенный алюминиевый кожух камеры с диаметром трубы 250 мм; 2 — внутренняя секционированная разрядная камера (лайнер) с диаметром отверстия 160 мм; 3 — катушки постоянного продольного магнитного поля; 4 — спиральная дополнительная обмотка для создания переменного продольного магнитного поля; 5 — отвертстие для откачки камеры; 6 — выводы обмотки, создающей переменное магнитное поле; 7 — смотровая щель в разрядной камере; 8 — изолирующие тефлоновые прокладки между отдельными секциями лайнера; 9 — место крепления второго вывода обмотки дополнительного переменного поля.

* Доклад CN-10/215, представленный на Конференцию. Докладчик: Б. Б. Кадомцев. Дискуссия (на английском языке) по этому докладу дана на стр. 651. Переводы аннотаций находятся в конце этого тома Трудов Конференции.

В первой серии опытов лайнер был собран из шестнадцати алюминиевых секций, изолированных друг от друга тефлоновыми прокладками. Толщина стенок лайнера составляла 4 мм, что обеспечивало сохранение магнитного потока в сечение лайнера в течение всего времени разряда. В каждом опыте регистрировались полный ток разряда, напряжение на обходе камеры и сигналы от магнитных зондов, введенных в плазму. Масштаб величин, которыми характеризуется разряд, следующий: напряжение на обходе — 1,2 кв, начальное магнитное поле — 500 эрстед, длительность первого полупериода тока — 600 мксек, рабочее давление водорода $7\cdot10^{-4}$—10^{-3} мм рт.ст., амплитуда разрядного тока — 60 ка. Проводимость плазмы, измеренная в максимуме тока на оси камеры, составила $6\cdot10^{14}$CGSE. Распределение магнитных полей существенно не отличается от полученного на установках «Зета», «Скептр» и др. Азимутальная компонента магнитного поля достигает максимума примерно на половине радиуса лайнера и затем спадает к периферии. Это отвечает формированию токового канала, «оторванного» от стенок.

Во второй серии опытов был применен лайнер такой же конструкции, но его секции были изготовлены из немагнитной стали, толщиной 0,1 мм. В этом случае магнитное поле из зазора между кожухом и лайнером могло проникать внутрь камеры за времена, малые по сравнению с длительностью изучаемых процессов. Так как площадь сечения указанного зазора того же порядка, что и площадь сечения лайнера, напряженность поля на его периферии в течение разряда оставалась примерно постоянной. Амплитуда разрядного тока при прочих равных условиях оказалась примерно в 1,5, а проводимость в 8 раз меньше, чем в опытах с толстостенным лайнером. Азимутальная компонента магнитного поля линейно возрастала от центра разряда до стенок лайнера, т. е. аксиальный ток протекал по всему сечению разряда с практически постоянной плотностью.

3. Влияние переменного магнитного поля на тороидальный разряд

В третьей серии опытов описанный выше тонкостенный лайнер был окружен дополнительной обмоткой, которая была расположена в зазоре между лайнером и кожухом (см. рис. 1). Через эту дополнительную обмотку разряжалась батарея конденсаторов, в результате чего создавалось аксиальное поле, с периодом $2{,}4\cdot10^{-4}$ сек, т. е. примерно в четыре раза меньшим периода основного разряда.

Амплитуда переменного магнитного поля варьировалась в пределах от 0,5 до 4,0 кэ. Знак и время включения этого дополнительного поля могли по желанию меняться. Наложение переменного магнитного поля вызывает в разряде ряд характерных явлений, которые частично были наблюдены в работах [6, 7]. В качестве примера опишем поведение разряда для случая, когда переменное продольное поле вводилось одновременно с началом разряда, и его первая полуволна усиливала начальное поле постоянное H_{z0}. Для этого случая осциллограммы тока I_2 и поля H_z (0) на оси разряда представлены на рис. 2, из которого следует, что в первой четверти периода тока, питающего дополнительную обмотку, продольное поле в центральной области разряда изменяется синфазно с током. Эта синфазность сохраняется и при спадающем токе в обмотке, но только до того момента t_1, когда аксиальная и азимутальная компоненты поля на периферии разряда становятся приблизительно равными. С этого момента t_1 поле в центральной области разряда остается постоянным или несколько увеличивается. Второй характерный момент t_2 в поведении разряда наступает спустя

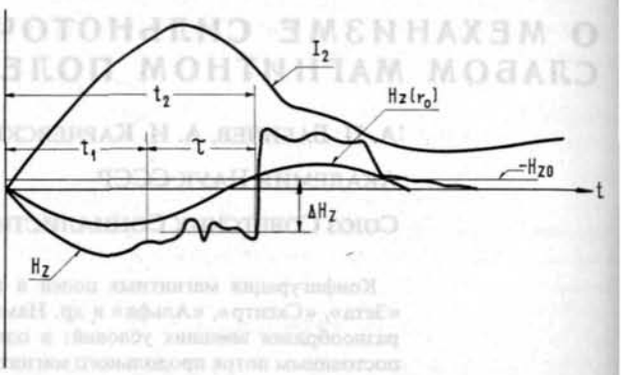

Рис. 2 Типичная осциллограмма тока I_2 и поля H_z (0) на оси разряда при наложении переменного магнитного поля.

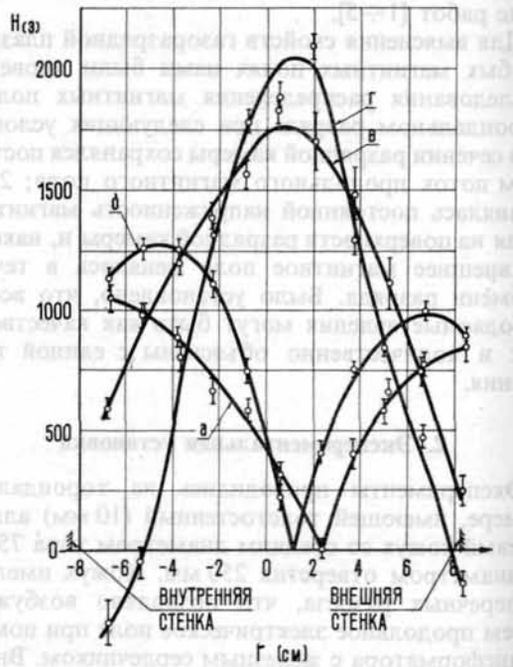

Рис. 3 Формирование токового канала в разряде между моментами времени t_1 и t_2. $H_{z0}=230$ э; $H_{доп}=1000$ э; $E_0=4$ в/см; $I_2=40$ ка. (а) H_φ, $t=100$ мксек, (б) H_φ, $t=128$ мксек, (в) H_z, $t=100$ мксек, (г) H_z, $t=128$ мксек.

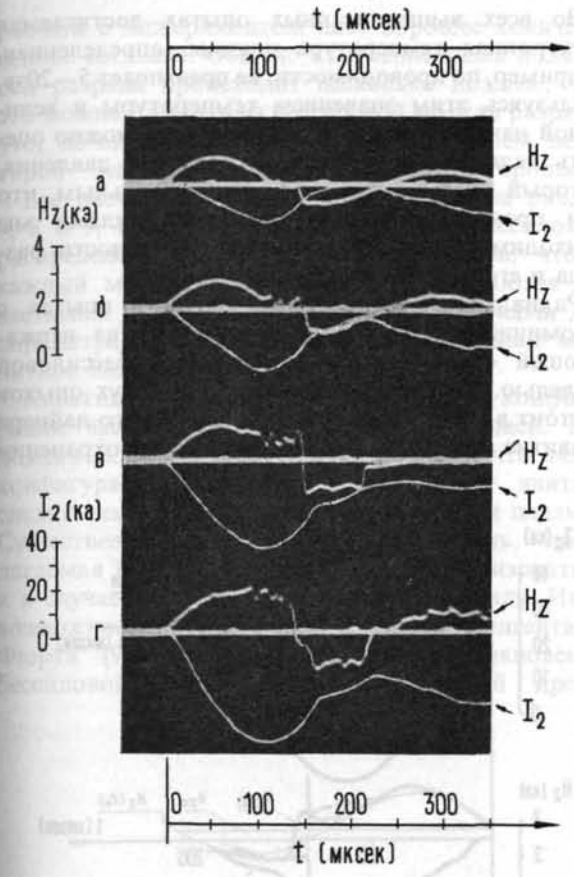

Рис. 4 Осциллограммы $H_z(0)$ и I_2 при постоянной амплитуде переменного магнитного поля.

несколько микросекунд (10—15) после того, как внешнее поле на периферии разрядного столба (радиус лайнера) изменит свой знак. В момент t_2 аксиальное поле внутри плазмы скачкообразно (за 2—4 мксек) изменяется с переменой знака (см. рис. 2).

Измерения азимутальной компоненты поля показывают, что в течение времени $\tau = t_2 - t_1$, в разряде успевает сформироваться токовый канал, радиус которого примерно равен половине радиуса лайнера. На рис. 3 представлено радиальное распределение полей H_φ и H_z и плазме в моменты $t_1 = 100$ мксек и $t_2 = 128$ мксек.

Для выяснения характера разряда в переменном магнитном поле были поставлены две серии экспериментов, в одной из которых изменялась амплитуда разрядного тока (при постоянной амплитуде переменного магнитного поля), а в другой — изменялась амплитуда переменного магнитного поля, вводимого в плазму (при одинаковой величине разрядного тока).

На рис. 4 показана серия осциллограмм поля $H_z(0)$ в центре камеры и разрядного тока I_2, в которой неизменным параметром была амплитуда переменного магнитного поля, определяющая скорость изменения внешнего магнитного поля.

Амплитуда разрядного тока изменялась в этой серии экспериментов от 15 до 50 ка.

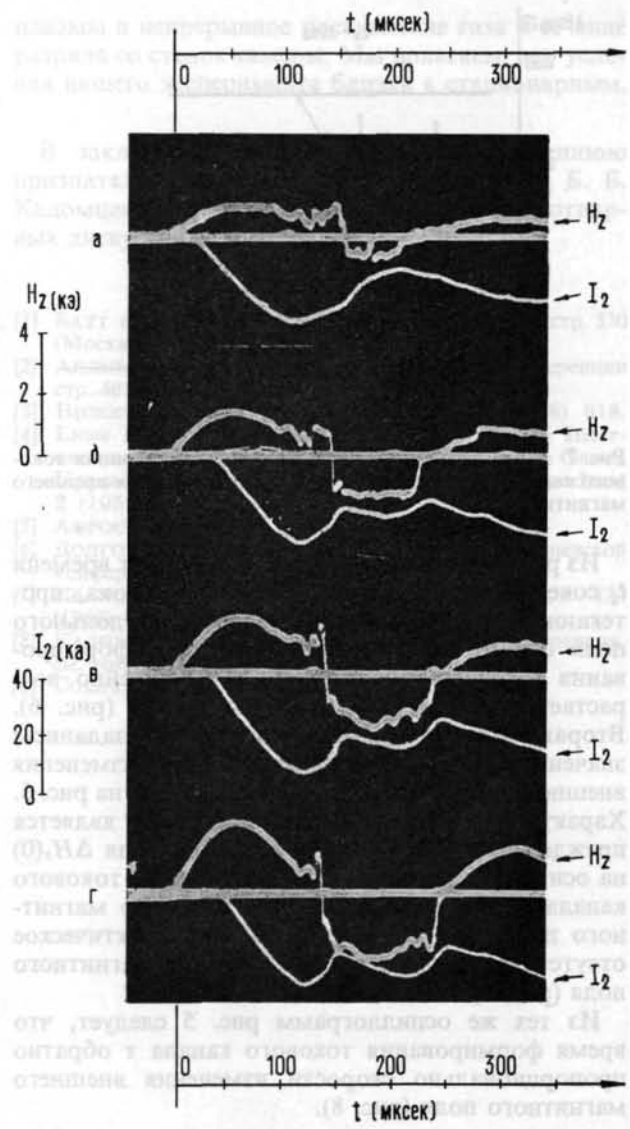

Рис. 5 Осциллограммы H_z (0) и I_2 при постоянной величине тока I_2 в момент времени t_2.

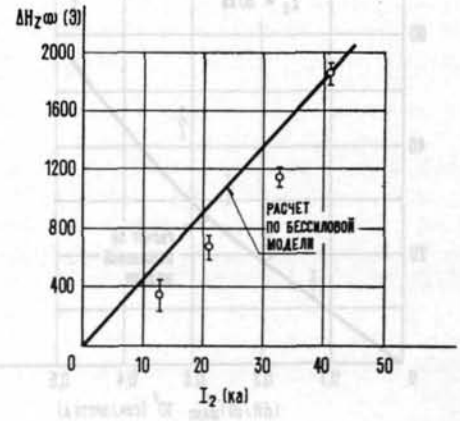

Рис. 6 Зависимость поля на оси разряда ΔH_z (0) во время формирования токового канала от величины разрядного тока.

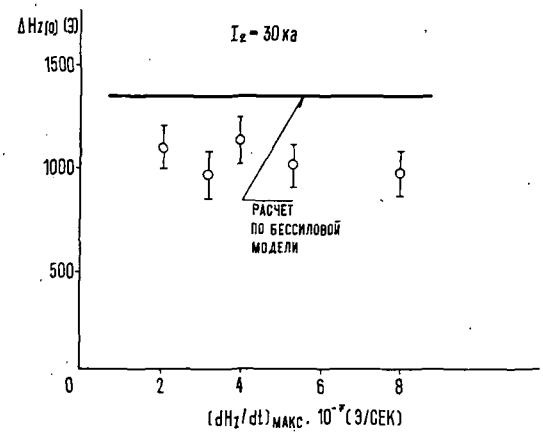

Рис. 7 Поле на оси разряда в период формирования токового канала в зависимости от скорости изменения внешнего магнитного поля.

Из рис. 4 легко обнаружить, что момент времени t_2 совершенно не зависит от величины тока, протекающего по плазме, и что величина продольного поля $\Delta H_z(0)$ на оси разряда во время формирования токового канала (от t_1 до t_2) линейно возрастает с амплитудой разрядного тока (рис. 6). Вторая серия опытов, поставленная при заданном значении тока I_2 и различных скоростях изменения внешнего магнитного поля, представлена на рис. 5. Характерным для этих осциллограмм является прежде всего независимость величины поля $\Delta H_z(0)$ на оси разряда в период формированния токового канала от скорости изменения внешнего магнитного поля, что четко указывает на практическое отсутствие «вмороженного» в плазму магнитного поля (рис. 7).

Из тех же осциллограмм рис. 5 следует, что время формирования токового канала τ обратно пропорционально скорости изменения внешнего магнитного поля (рис. 8).

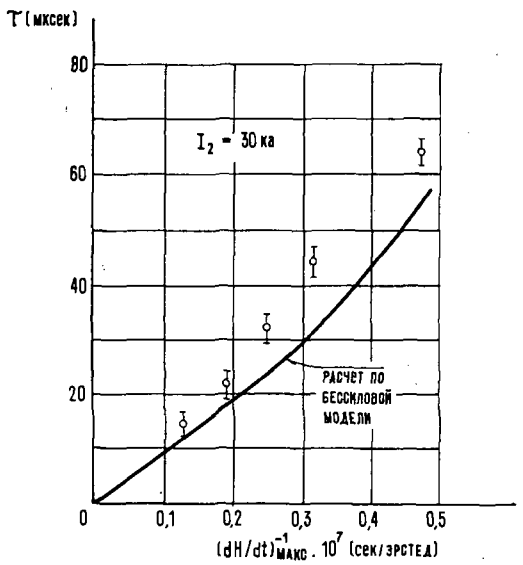

Рис. 8 Зависимость времени формирования токового канала от обратной величины максимальной скорости изменения внешнего магнитного поля.

Во всех вышеописанных опытах достигаемая электронная температура плазмы, определенная, например, по проводимости, не превышает 5—20эв. Пользуясь этим значением температуры и величиной начального давления водорода, можно оценить величину радиального градиента давления, который оказывается столь незначительным, что при пренебрежении инерционными силами мы приходим к принятию квазистационарности разряда и его бессиловой конфигурации.

Радиальное распределение полей в опытах с алюминиевым лайнером и лайнером из нержавеющей стали хорошо описывается бессиловой моделью. Физическое различие этих двух опытов состоит в том, что в случае алюминиевого лайнера развитие разряда происходит при сохранении

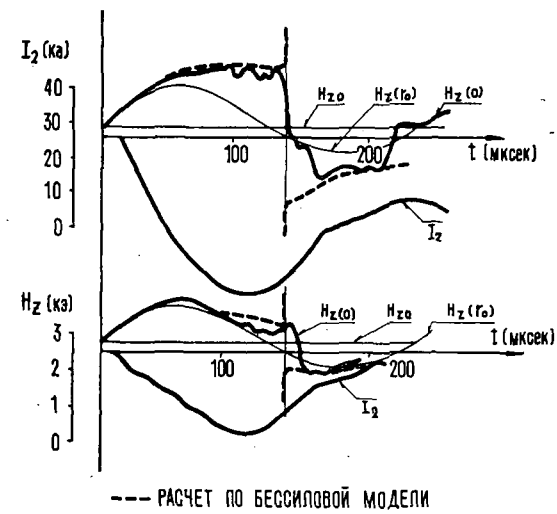

Рис. 9 Сравнение расчетных кривых и реальных осциллограмм поля в разряде с переменным продольным магнитным полем.

магнитного потока в сечении, а в случае тонкостенного лайнера возбуждение тока в плазме производится при искусственном сохранении величины продольного поля на периферии разряда.

Все основные явления, наблюдающиеся в разряде с переменным магнитном полем, также хорошо интерпретируются, если принять, что разряд квазистационарен и обладает бессиловой конфигурацией.

В частности, скачкообразное изменение поля в центре разряда с переменой знака естественно объясняется в рамках этой модели изменением направления внешнего магнитного поля, т.к. знак поля на оси разряда определяется направлением полного продольного поля на периферии в любой момент времени разряда, а величина поля на оси разряда в период от t_1 до t_2 полным током, протекающим по плазме (рис. 6). Пользуясь, например, данными рис. 4, можно рассчитать по бессиловой модели поле на оси разряда, считая разрядный ток и продольное поле на периферии разряда заданными в каждый момент времени. Результаты расчета приведены на рис. 9. Сопоставление результатов

расчета с экспериментом дает хорошее количественное согласие. Обычно изменение знака поля на оси разряда происходит несколько позднее, чем это можно ожидать из бессиловой модели разряда, что, по-видимому, связано с проявлением некоторой нестационарности реального процесса.

Все расчетные кривые, приведенные на рис. 6, 7, 8 и 9, получены из стационарных бессиловых распределений полей, причем полагалось, что в каждый момент времени разряда считаются известными и заданными внешними условиями два параметра — продольный ток и аксиальное магнитное поле на периферии разряда.

Кинетика установления бессиловой конфигурации экспериментально не исследовалась. Кадомцев Б. Б. [8] теоретически показал, что такая конфигурация полей в разряде может явиться следствием конвективной неустойчивости плазмы. Существенно подчеркнуть, что модель, предлагаемая Б. Б. Кадомцевым, может реализоваться и в случае стационарного газового разряда. Иная возможность обсуждается в статье Колгейта и Фюрта [9], привлекающих для возникновения бессиловой конфигурации, радиальный дрейф плазмы и непрерывное поступление газа в сечение разряда со стенок камеры. Мы полагаем, что условия нашего эксперимента близки к стационарным.

В заключение авторы выражают искреннюю признательность академику И. К. Кикоину, Б. Б. Кадомцеву и В. Д. Шафранову за ряд плодотворных дискуссий.

Литература

[1] Батт и др. Труды 2-й Женевской конференции стр. 370 (Москва, 1959).
[2] Аллибон и др. Труды 2-й Женевской конференции стр. 485 (Москва, 1959).
[3] Bickerton R. J. *Proc. Phys. Soc.* **72** (1958) 618.
[4] Lees D. J., Rusbridge M. G., Proc. Fourth International Conference on Ionisation Phenoma in Gases, Uppsala (North-Holland Publ. Co., Amsterdam) **2** (1959) 955.
[5] Афросимов В. В. и др. *ЖТФ* **30** (1960) 1381.
[6] Долгов-Савельев Г. Г. и др. Труды 2-й Женевской конференции стр. 85 (Москва, 1959).
[7] Иванов Д. П., Кириллов В. Д. *ДАН СССР* **133** (1960) 793.
[8] Кадомцев Б. Б. Доклад на настоящей конференции, см. том 3.
[9] Colgate S. A., Furth H. P., **3** (1960) 982.

EXPERIMENTAL AND THEORETICAL INVESTIGATIONS OF THE CURRENT-ONSET IN LINEAR PULSE DISCHARGES*

W. Frie, A. Michel

Forschungslaboratorium der Siemens-Schuckert-Werke, A.G.

Erlangen, Federal Republic of Germany

Probe measurements demonstrate the existence of a current channel near the axis immediately after the breakdown. This current is interpreted as a consequence of the transition from a glow discharge to an arc due to thermal instability. Theoretical considerations, using Maxwell's equations, the balance of energy and Ohm's law, deal with the variation of current density, electric field strength, and conductivity in space and time. Theoretical and experimental results are compared.

1. Introduction

The inductance of a linear pulse discharge, usually measured under the assumption that current flows only in a thin sheet, shows a steep decrease immediately after breakdown [1]. This decrease points out that the magnetic field inside of the skin layer cannot be neglected, at least at the beginning of the discharge; this means that the current flows more or less uniformly distributed over the cross-section at this stage. The presented paper deals with experimental and theoretical investigations on this matter.

2. Experimental

For measuring the space and time variation of magnetic field strength during current-onset of the discharge, a probe of high sensitivity, high resonance frequency, and high signal-to-noise ratio is needed. With coil probes, high sensitivity can be achieved either by a large turn-area or by a small time constant of the integrating *RC*-network. A large turn-area implies a low resonance frequency. A small time constant shortens the measuring time.

An integrating network is not needed, when a Hall probe [2] is used. The Hall voltage being proportional to the control current, the sensitivity can be raised by increasing the control current. The increase in sensitivity is limited by control current heating of the probe, for the Hall coefficient decreases with increasing temperature. Furthermore, the increase of resistance with increasing magnetic field limits the applicability of the Hall probe. This change in resistance causes an additional heating and a decrease of control current which however can be kept sufficiently low by a large series resistor. For these reasons it is suitable to pulse the probe, choosing the pulse height as high and the pulse length as short as possible.

To avoid noticeable noise due to fast changes in the magnetic field, the probe inductance has to be kept as low as possible; consequently the resonance frequency is very high.

With a pulsed InSb-probe (size 4×2 mm^2, thickness 17 μ) a Hall-sensitivity of 168 G/V and a resonance frequency of 240 MHz has been reached. With this probe the normal component of the magnetic field has been measured as a function of axial distance and time immediately after breakdown. The discharge chamber was a quartz cylinder of 38 cm inner diameter through which a previously described condensor battery [1] of 1030 μF, 4 nH and 15 kV had been discharged. The results are given in Fig. 1. The pictures were taken on successive single shots. The assumption of axial symmetry however could not be confirmed as is demonstrated in Fig. 2. The pictures taken under the same conditions on two successive

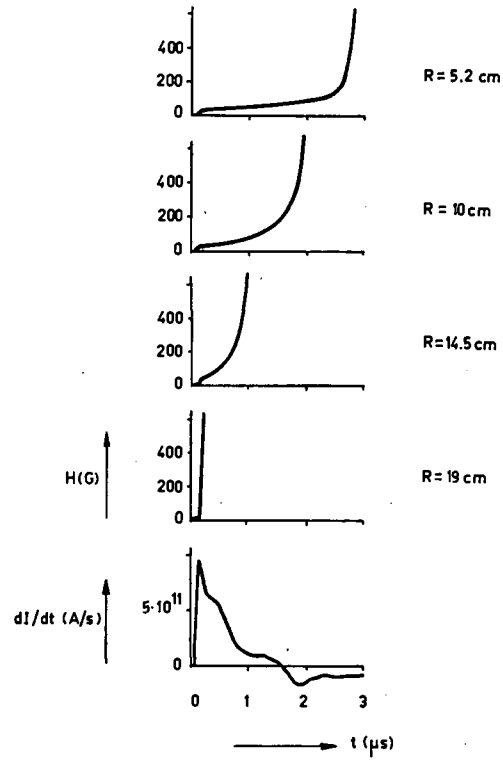

Fig. 1 Magnetic field component perpendicular to the diameter versus time measured by a Hall probe at various axial distances; initial pressure $p_0 = 0{,}15$ mm Hg H_2; charging voltage $U_0 = 15$ kV.

* Conference paper CN-10/46 presented by A. Michel. Translations of the abstract are at the end of this volume of the Conference Proceedings.

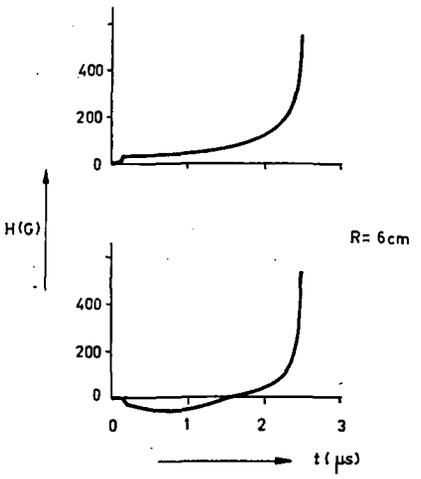

Fig. 2 Magnetic field component perpendicular to the diameter versus time measured by a Hall probe at a fixed distance, taken with two successive shots. $p_0 = 0{,}15$ mm Hg H_2; $U_0 = 15$ kV.

shots exhibit at first in the upper part a positive, in the lower part a negative magnetic field. The common steep positive rise corresponds to the moment at which the contracting current layer reaches the probe. The change of sign leads to the supposition that the center of gravity of the onset-current lies off the axis of the discharge chamber. This can be investigated by measuring the magnetic field simultaneously at various distances from the axis. This can be done in principle by means of pulsed Hall-probes; the required equipment however is considerable; therefore it seemed to be appropriate to return to probe coils. Six coils had been arranged equally spaced along the diameter and symmetrical to the axis, each having 5.25 cm² turn area, and a resonance frequency of 9 MHz. The probe signals were integrated by means of RC-networks with a time-constant of 10^{-5} sec. Two typical results are given in Fig. 3, showing the component of the magnetic field perpendicular to the diameter as a function of time. It can be seen that the current is not centered on the axis. If the field component is plotted against the distance from the axis (Fig. 4), it appears that the current is confined into a region near the axis and increases with time. This confinement to a channel is somewhat surprising, but can be understood if the current is considered as the result of breakdown due to thermal instability, representing the transition from a glow discharge to an arc. A similar phenomenon can be observed as sudden change from the stationary high-current glow discharge to an arc [3].

3. Theory

The theory to be developed has to describe the skin effect and the different heating of plasma connected with it. This problem is treated by means of Maxwell's equations, the balance of energy, and Ohm's law. Cylindrical symmetry is postulated, heat dissipation is neglected. In order to derive unique initial conditions, Ohm's law in differential form shall be expanded by adding the inertia of the charge carriers from the plasma equations [4]. Then the initial current density can be zero. The further development of the current onset however is not influenced by the inertia of the charge carriers, if it is small enough.

The following symbols are used:

E = electric field strength
j = current density
I = electric current
T = temperature
σ = electric conductivity
$\varrho_D c_p$ = specific heat per unit volume
$\overline{\varrho_D c_p}$ = mean value of the specific heat
m_e = electron mass
b = mobility
e_0 = electronic charge
l = length of the discharge gap

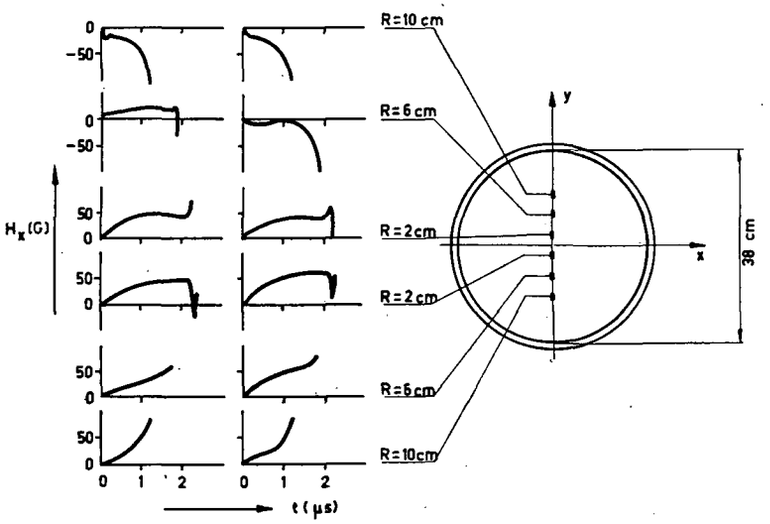

Fig. 3 Magnetic field component perpendicular to the diameter versus time, simultaneously measured by coil probes at various axial distances. Two independent measurements are reproduced. $p_0 = 0{,}15$ mm Hg H_2; $U_0 = 15$ kV.

R = radius of the discharge gap
R_2 = inner radius of the return conductor
V_0 = charging voltage
L_a = outer inductivity.
U_i = ionization potential
$T^* = e_0 U_i/k$
k = Boltzmann's constant
σ_∞ = conductivity in the final state

Now the problem is described by the following equations:

$$\frac{1}{r}\frac{\partial}{\partial r}\left(r\frac{\partial E}{\partial r}\right) = \mu\frac{\partial j}{\partial t} \tag{1}$$

$$\frac{\partial T}{\partial t} = \frac{1}{\varrho_0 c_p} E j \tag{2a}$$

with:

$$\sigma = \sigma_\infty e^{-T^*/2T}; \quad \sigma_0 = \sigma_\infty e^{-T^*/2T_0} \tag{2b}$$

$$E = \frac{j}{\sigma} + \frac{m_e b}{e_0}\frac{\partial}{\partial t}\left(\frac{j}{\sigma}\right) \tag{3}$$

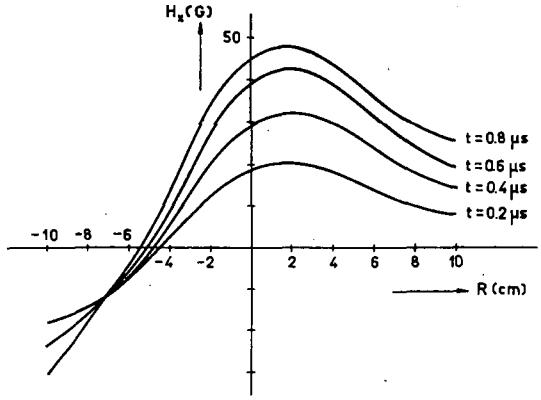

Fig. 4 Magnetic field components versus radius at successive times.

Combining (2a) and (2b) yields for the temporal increase of the electrical conductivity:

$$\frac{\partial \sigma}{\partial t} = \frac{2}{T^*\sqrt{\varrho_0 c_p}}\sigma E j\left(\ln\frac{\sigma}{\sigma_\infty}\right)^2 \tag{2c}$$

The specific heat per unit volume is replaced by a constant mean value. The boundary condition of the outer circuit is the following:

$$E(R)\,l + \left(L_a + \frac{\mu}{2\pi} l \ln\frac{R_2}{R}\right)\frac{\partial I}{\partial t} = V_0 \tag{4a}$$

From Eq. (1) follows:

$$\frac{\partial I}{\partial t} = \frac{2\pi}{\mu} R\left(\frac{\partial E}{\partial r}\right)_R \tag{4b}$$

Therefore Eq. (4a) can be written:

$$E(R) + \lambda R\left(\frac{\partial E}{\partial r}\right)_R = \frac{V_0}{l} = E_0 \tag{5a}$$

with:

$$\lambda = \ln\frac{R_2}{R} + \frac{2\pi}{\mu}\frac{L_a}{l}. \tag{5b}$$

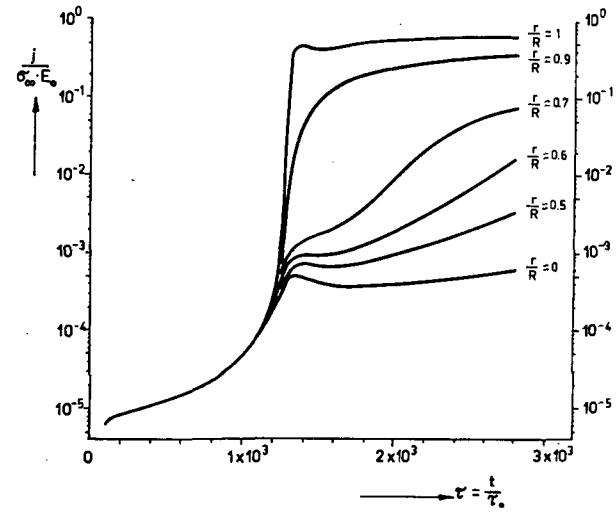

Fig. 5 Calculated current density versus time in normalized units; R = radius of the discharge chamber.

By means of the following nondimensional quantities:

$$\tau_0 = \frac{\overline{\varrho c_p}\,T^*}{2\sigma_\infty E_0^2}; \quad \alpha = \frac{\mu\sigma_\infty R^2}{\tau_0}; \quad \alpha_1 = \frac{m_e b}{e_0}\frac{1}{\tau_0}; \tag{6}$$

$$\varrho = \frac{r}{R}; \quad \tau = \frac{t}{\tau_0}; \quad \psi_1 = \frac{1}{E_0}\frac{j}{\sigma}; \quad \psi_2 = \frac{\sigma}{\sigma_\infty}; \quad \psi_3 = \frac{E}{E_0}$$

the problem can be reduced to:

$$\frac{1}{\varrho}\frac{\partial}{\partial\varrho}\varrho\frac{\partial\psi_3}{\partial\varrho} = \alpha\frac{\partial\psi_1\psi_2}{\partial\tau} \tag{7a}$$

$$\frac{\partial\psi_2}{\partial\tau} = \psi_1\psi_3\psi_2^2(\ln\psi_2)^2 \tag{7b}$$

$$\psi_3 = \psi_1 + \alpha_1\frac{\partial\psi_1}{\partial\tau} \tag{7c}$$

with the initial and boundary conditions:

$$\psi_3(\varrho = 1;\tau) + \lambda\left(\frac{\partial\psi_3}{\partial\varrho}\right)_{\varrho=1;\tau} = 1 \tag{8a}$$

$$\psi_2(\varrho;\tau=0) = \psi_{20} = \text{const.} \tag{8b}$$

$$\left(\frac{\partial\psi_3}{\partial\varrho}\right)_{\varrho=0;\tau} = 0;\ \psi_1(\varrho;\tau=0) = 0 \tag{8c}$$

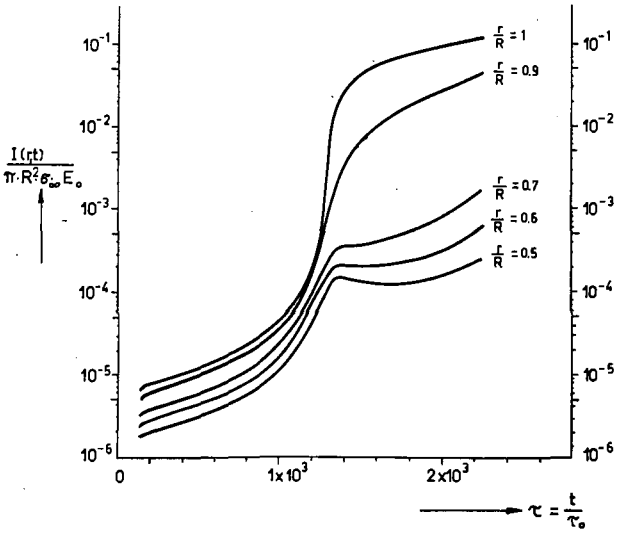

Fig. 6 Calculated enclosed current versus time in normalized units; R = radius of the discharge chamber.

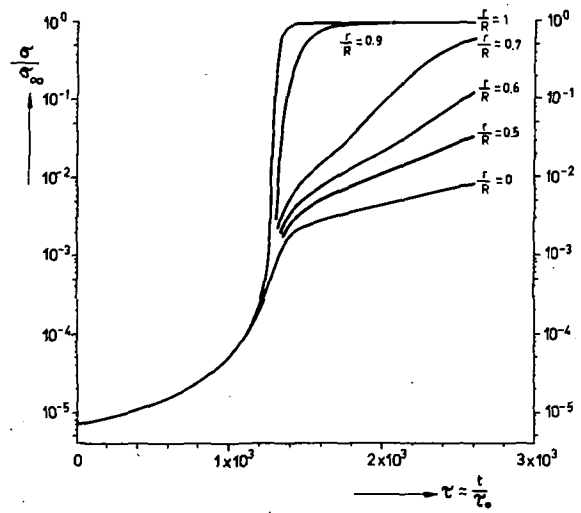

Fig. 7 Calculated electrical conductivity versus time in normalized units; R = radius of the discharge chamber.

Using $\alpha_1 \neq 0$, the differential equation, Eq. (7a), can be transformed to a normal differential equation, namely:

$$\frac{1}{\varrho}\frac{\partial}{\partial\varrho}\varrho\frac{\partial\psi_3}{\partial\varrho} - \psi_3\,\alpha\left[(\psi_1\psi_2\ln\psi_2)^2 + \frac{1}{\alpha_1}\psi_2\right] + \frac{\alpha}{\alpha_1}\psi_1\psi_2 = 0. \quad (9)$$

If $\psi_1(\varrho)$ and $\psi_2(\varrho)$ are known for $\tau=\tau'$, then $\psi_3(\varrho)$ can be calculated. After this, new values of $\psi_1(\varrho)$ and $\psi_2(\varrho)$ for $\tau=\tau'+\Delta\tau$ can be obtained, $\partial\psi_1/\partial\tau$ and $\partial\psi_2/\partial\tau$ following from (7c) and (7b). The step $\Delta\tau$ is limited by the condition:

$$\Delta\tau \ll \alpha_1.$$

The numerical calculations have been done by a Siemens digital computer. Figures 5, 6, 7, 8 show current density, the enclosed current, that means the current flowing within a circle of radius r, electrical conductivity and electric field strength versus time in normalized units with $\varrho=r/R$ as parameter. This example has been calculated, using the values:

$$\alpha=10^5; \quad \lambda=0.119; \quad \psi_{20}=0.71\cdot10^{-5}.$$

4. Discussion

The above mentioned assumptions made in theory are not completely confirmed by the experiment: namely the current flows only in a channel near but not centered to the axis. Furthermore the theory does not deal with the contraction; therefore comparison with experiment is possible only up to the moment when the contracting sheet reaches the probe.

On the other hand, there is qualitative agreement between the observed and calculated time development of the confined current. The slope of the current versus time decreases with decreasing radius and exhibits the tendency to bend downwards. This can be explained by the decay of field strength which overcompensates the rise of conductivity resulting in a temporal decrease of current density.

References

[1] FRIE, W. *et al.*, *Z. Naturforschg.* **16a** (1961) 121.
[2] MICHEL, A., Progress Report, European Study Group on Fusion, Rome, 1961 (CERN/FSG/14).
[3] WEIZEL, W. *et al.*, Forschungsberichte des Wirtschafts- und Verkehrsministeriums Nordrhein-Westfalen, Nr. 267 (1956), Westdeutscher Verlag Köln und Opladen.
[4] MAECKER, H. *et al. Z. Physik* **144** (1956) 605.

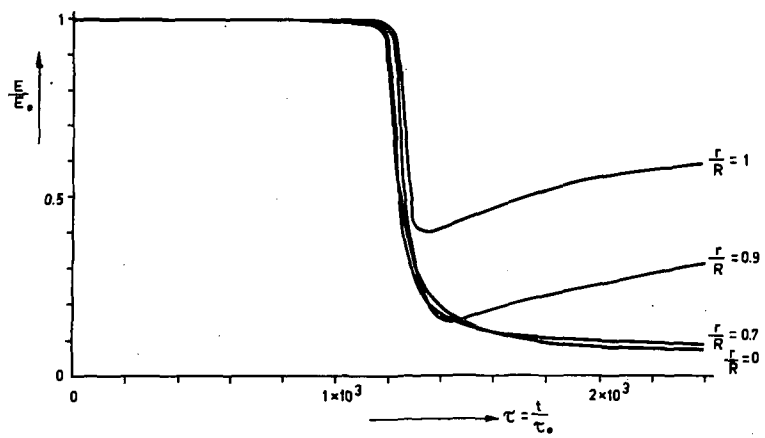

Fig. 8 Calculated electrical field-strength versus time in normalized units; R = radius of the discharge chamber.

DISCUSSIONS (SESSION V) — DISCUSSIONS (SÉANCE V) — ДИСКУССИИ (ЗАСЕДАНИЕ V) — DEBATES (SESIÓN V)

Paper CN-10/155 *was presented by F. L. Ribe* (United States of America). *The text of the paper is on pages 497—509. The following discussion took place.*

A. C. Kolb *(United States of America):* You stated that the electron temperature scarcely depends on B_z. You also said that earlier you postulated an unstable sheath, and that you believe that this behavior is characteristic of the fast shock apparatus. Obviously it is characteristic—do you mean that low electron temperatures are a general characteristic of any plasma with one or two percent impurity?

F. L. Ribe: No, I don't mean that. Reading your paper I gather that it is quite possible to observe a loss of the trapped field by simple Coulomb collision diffusion, in which case most of the energy goes to the electron and some may or may not go to the ions. I am not talking about the subject of radiation temperature limitation here—I'm simply talking about the mechanism of heating in this machine. If the ion energy depends very strongly on the trapped field and the electron temperature does not, it is suggestive of the fact that when the reverse field somehow gives its energy up to the plasma, it gives it up preferentially to the ions; this would most likely occur when one had a process in which the sheath broke up turbulently so that there was a velocity imparted both to electrons and ions. This is perhaps more characteristic of a fast shock such as ours, with an 85 kV bank, than with the slower shock of the other experiments simply because it seems to be in contrast with the two observations. In some cases there seems to be a joule heating diffusion of the trapped field. In ours we can only infer that there is a more violent micro-instability diffusion through the sheath.

H. A. B. Bodin *(United Kingdom):* I would like to ask a question on the curve showing the scaling of the electron temperature T_e with the field B. It has been observed that the radiation, in particular the neutrons and the soft x-rays, is a very sensitive function of the initial gas pressure; this is almost certainly associated with the fact that the trapped field varies with the gas pressure. I would like to ask, when you performed measurements of the electron temperature, did you keep the pressure constant as you varied the different parameters or did you optimize on the x-ray or on the neutron emission or on the reversed trapped field for all values of B?

F. L. Ribe: We optimized on the neutron yield which I consider to be identical with optimizing on the reverse trapped field. The pressure in these experiments varied very little from one set of conditions to another—it may have gone from 90 to 110 microns of deuterium.

H. R. Griem *(United States of America):* I would like to make a comment on the estimates of the radiation losses due to impurity radiation. Assuming a quasi-stationary degree of excitation and ionization and an impurity concentration of two percent, one obtains for an electron density $N_e \simeq 5 \times 10^{16}$ cm^{-3} and temperature $T_e = 300$ eV, a cooling time of one microsecond using procedures described, for example, by Wolley and Stibbs in "The outer layers of a star" (Oxford University Press, 1953). I consider this to be an over-estimate because in the short times of the experiment the quasi-stationary approximation will not be valid, i.e., intermediate-Z impurities with large cross-sections are more abundant than has been assumed in this estimate.

F. L. Ribe: In our experiment the absolute energy lost by line and continuum radiation for $\lambda < 16$ Å are measured. Furthermore, the absolute continuum is rather closely equal to that from oxygen as predicted by the Elwert (coronal) equation. The radiated energy during the compression time for $\lambda = 16$ Å is less by two orders of magnitude than that of the electrons of the plasma. It is also unlikely that species other than O-VIII and O-IX contribute greatly to our radiation. Therefore, there is some indication that our electron temperature is not radiation limited. A final answer depends upon measurement for $\lambda > 16$ Å. The scaling of T_e and neutron yield with magnetic field does not indicate a radiation limit.

Paper CN-10/70 *and* 71 *were presented by G. B. F. Niblett* (United Kingdom). *The text of the papers is on pages 511—532. The following discussion took place.*

R. D. Medford *(United Kingdom):* I would like to draw attention to a paper to be published in the *Journal of Nuclear Energy (Part C)* by Wright, Chambers and myself, in which we study the stability of long tubular plasmas with reversed trapped magnetic field and show that there will be an axial contraction of the plasma cylinder for certain conditions on the geometry. Secondly, I'd like to draw attention to a paper by the same authors presented at the Munich conference in which we do the theory for longitudinal shocks in theta-pinches, linear Z-pinches and stabilized linear Z-pinches. The results for the theta-pinches confirm the experimental evidence of Dr. Niblett. This theory does not have the algebraic approximation given in Dr. Taylor's paper.

G. B. F. Niblett: Thank you for those comments. In a long coil it is possible to find an equilibrium position of the reversed field configuration in which the radial magnetic pressure at the middle of the coil balances the tension at the ends. Under these conditions the plasma does not contract axially to sufficiently small dimensions for the instability which I described to develop. In a short coil the axial contraction does

take place and the instability follows. This is a simple explanation of the greater stability observed in long coils for which the plasma ratio is large.

J. B. Taylor *(United Kingdom):* In papers CN-10/70 and 71 there has been reference to theoretical instability growth-rates and to comparison of these with experiment. I would merely like to point out that the theory refers to the small amplitude phase of the instability whereas it is clear that the experiments are in the phase when the amplitude is large. In those cases where the large amplitude (non-linear) phase can be calculated, the growth rate is very much less than that in the small amplitude phase and indeed is of a quite different character.

A. A. Ware *(United Kingdom):* Plasma rotation has been observed in several different experiments—in theta-type pinches, in mirror machines, in the Stellarator and in the Sceptre III toroidal pinch discharge. In all these experiments there are magnetic lines of force which pass from the plasma region to the walls. The lines go to the end walls in theta-pinches and mirror machines, to the limiter in the Stellarator and to the copper liners in Sceptre III. In all these cases the correct direction of rotation can be explained by the preferential loss of electrons along these lines to the walls. The positive charge left in the plasma causes a radial electric field (E_r) which crossed with B causes the rotation. (Currents flow radially across the field and the circuit is closed via the field lines going to the walls, and via the cold plasma in the vicinity of the walls.) This mechanism also explains the correct z-motion in the case of Sceptre III, since in that case E_r is crossed with B_θ as well as with B_z.

G. B. F. Niblett: I agree that the mechanism you are suggesting is essentially the same as the one described in our paper.

W. H. Bostick *(United States of America):* I would like to make a comment concerning the first type of rotation which was mentioned—the rotation which occurs when the plasma shell contracts into a loop which is short along the axis and which, as the speaker has indicated, is responsible for a break-up because the magnetic moment of this loop is aligned anti-parallel to the impressed magnetic field.

At Stevens Institute of Technology a similar flipping or rotation of a plasma loop has been observed by Dickinson and Di Marco by means of Kerr cell photographs. In this experiment a small plasma loop from a two-wire button plasma gun is projected across a magnetic field that is anti-parallel to the magnetic moment of the plasma loop current. The loop is unstable against rotation in the magnetic field and flips. This process is field mixing by rotation. The original energy of orientation of the plasma loop in the magnetic field is converted to the kinetic energy of rapid expansion of the plasmoid along the field.

F. L. Ribe *(United States of America):* I don't quite understand what you mean by the damping of this rotation. I'm aware that the rotation becomes somewhat slower and I would take this opportunity to advance an alternative explanation that in all these cases the moment of inertia of the plasma about the axis is becoming larger and larger and, since its angular momentum is conserved, it has to slow down.

G. B. F. Niblett: Thank you for those pertinent comments. Experimentally we observe a rapid decay of the rotational velocity and, at least in the early stages, this decay cannot be explained by an increase in moment of inertia of the plasma. Indeed, in one example that we have analyzed, the rotational velocity decreases whilst the plasma is still being compressed. However, during the later stages, when the flutes develop, the decrease in velocity might well be explained by the conservation of angular momentum as the moment of inertia of the rotating plasma increases.

Paper CN-10/232 *was presented by I. F. Kvartskhava* (Union of Soviet Socialist Republics). *The text of the paper is on pages 533—542. The following discussion took place.*

H. Jordan *(Federal Republic of Germany):* In the pictures of the Z-pinch the threads you mentioned looked very similar to the plasma jets one gets in inhomogeneous fields (e.g. plasma guns). In the theta-pinch case where these threads do not occur, this could be explained by the fact that in the theta-pinch case the field distribution is homogeneous. Could it be that the threads observed are not due to the instabilities, but to plasma jets in inhomogeneous fields because they are so regular and stable in behavior?

I. F. Kvartskhava: No, those threads are not plasma jets. In Z-pinches they extend from one electrode to the other and in theta-pinches they are oriented mainly in the theta direction and are closed. The main reason for the separation of the total current into individual threads is that under conditions of a high-current discharge at low gas density and for comparatively large cross-section of the conducting zone, uniform distribution of the current is unstable. Even before the mutually attracting forces of the currents succeed in assembling the plasma into a single total pinch, Z-pinch elements are formed along which the total current flows. These pinch elements will develop in those places where the current density is randomly higher (e.g. as a result of fluctuations). Assuming a high plasma conductivity in the threads, it is easy to explain the effective trapping of the magnetic field in the theta-pinch during the first half-period of the current. In Z-pinches there are no conditions for trapping the field; this is the reason for some differences in the behavior of these pinches. In particular the theta-pinch is characterized by a greater variety of kinds of instabilities than the Z-pinch.

J. A. Reynolds *(United Kingdom):* In a theta-pinch experiment the possibility of sheath break-up into

droplets during the implosion should depend on the sign of the internal field. With parallel field the currents flowing on the inside and outside surfaces of the sheath are opposed and droplets can form without changing the internal field. However, with an anti-parallel field, the currents flow in the same direction, there is a neutral plane and droplets cannot form. I would like to know the sign of the trapped field for the results you give.

I. F. Kvartskhava: By using small Rogovsky belts and probes one finds in the theta-pinch that the average value of the current density is usually greater in the center and decreases towards the ends regardless of the sign of the trapped field. In the second half-period of the current where the trapped field is directed oppositely to the external field, the formation of threads is also observed. In this case they often cross each other and form a net.

A. C. Kolb *(United States of America):* My first comment is that your measurements seem to show the importance of good pre-ionization to eliminate the threads which you observe. A second comment: your photographs of instabilities with theta-pinches in hexagonal chambers show that the form of the instability depends on the shape of the chamber. Now a question—everyone here seems to be talking about rotation in theta-pinches—do you observe a rotation also under any circumstances? Also, what gas was used to obtain these photographs of theta-pinches?

I. F. Kvartskhava: The first comment concerns the possibility of preventing thread formation by means of good pre-ionization of the gas. This is probably not true because the first half-period yields fairly good pre-ionization for the second half-period, and in the second half-period one observes the formation of well-developed current threads.

The second question: In photographs of the theta-pinch one often observes a right or a left rotation of the ejected plasma "tongues". This is possibly connected with the direction of the discharge current. We have not observed any other kinds of rotation.

The third question: We used different gases, from hydrogen to xenon. Qualitatively the picture remains the same. In case of high molecular weight gases the process is correspondingly slower and the luminescence of the discharge becomes brighter. In xenon one can easily find such plasma jets whereas in hydrogen or helium one can only do so with difficulty.

W. H. Bostick *(United States of America):* The tendency of plasma in a magnetic field to form two-dimensional droplets or shreds by the action of surface forces is now well known. Although the processes occurring in Dr. Kvartskhava's polygonized theta-pinches are a complicated mixture of reflecting shocks and Rayleigh-Taylor instability, the geometry is so arranged that plasma islands or shreds are formed at locations which are arranged in an orderly fashion.

Paper CN-10/189 *and* 192 *were presented by A. C. Kolb* (United States of America). *The text of the papers is on pages 543—559. The following discussion took place.*

H. A. B. Bodin *(United Kingdom):* I would like to make some comments on the disappearance of the reversed trapped field. I think there is evidence for two mechanisms here and the first one is associated very strongly with the axial contraction of the plasma. This mechanism will take place in short coils, which is the case in our own experiments and probably in the Scylla experiments. I think that in this mechanism you get preferential ion-heating—in fact the ion temperature is higher than the electron temperature. Now if you prevent the axial contraction—and, among other methods, you can do this by lengthening the coil—then this dissipation process which depends on the axial contraction will be stopped and so eventually you must reach a stage where ordinary field diffusion will take over. I would suggest that this is the regime of the experiment described by the last speaker. If you don't get the axial contraction then you will get ordinary resistive diffusion and in this case you will get preferential electron-heating.

Some evidence which I have noticed in a paper by Hintz (CN-10/186) bears out the point about the axial contraction. Photographs shown in his paper were obtained under slightly different conditions of pressure both with parallel and with reversed trapped field. In one of these cases, from the frequency of radial hydromagnetic oscillations which are determined by the plasma mass per cm length, you can see that strong axial contraction takes place and in this case the reversed field is observed to disappear rapidly. In the other case, from the radial oscillations you see no axial contraction; it is pointed out in the paper that the reversed field does not disappear. So we have evidence that the rapid disappearance does result from the axial contraction. The mechanism of this was mentioned in the paper by Dr. Niblett.

Now regarding this enhanced stability against rotation, described in Dr. Kolb's paper, this is consistent with the model of rotation due to the end losses shorting out the space charge field, that is, the model proposed by Roberts. In the experiments with the long coil you do not get the axial contraction. Therefore, the reversed field lines will remain for a longer time and, while the reversed field lines remain closed, you get no loss of the plasma out of the ends of the tube; consequently, you cannot get the shorting-out of the space charges and you get no rotation. So the observation that the longer coil is more stable can be explained simply on that basis, and you can also achieve stability if you prevent the axial contraction in other ways.

A. C. Kolb: I would like to congratulate you on the longest comment in the history of physics. First, with reference to the differences between these experiments and others—namely the very high electron temperature: we calculate that this could be explained

on the basis of our low impurity level. It may be that there is also an instability in experiments with shorter coils which leads to preferential heating of the ions, but I don't believe this point will be settled until someone does a short-coil experiment at high purity. Also, since you chose to mention the experiment of Hintz and Bogen which will be reported later in this session, it was my understanding that they also showed that impurities changed the field dissipation times remarkably and that the electron temperatures were limited by radiation losses. I think this was correct.

Now concerning the axial contraction as a mechanism for the instability—this is certainly a possibility and would tend to explain the better stability that we get with longer coils. Concerning the rotational instability there is the possibility, as discussed in a paper from Los Alamos, that the flutes are driven by mirror fields. There is another possibility that the flutes are caused primarily by the centrifugal forces connected with the observed rotation. Now there is the argument of what would cause this rotation. We heard one explanation in the paper from England. Another possibility is that the angular momentum connected with the diamagnetic currents, associated with the ion current in the reverse current sheet, could transfer angular momentum to a guiding-center drift. This also gives the correct order of magnitude of the angular velocity which is sufficient to cause the observed instability. One consequence of the latter explanation, which also tends to explain our results with larger apparatus, is that if the instability is connected primarily in our case with the dissipation of the reverse field and if the dissipation of the reverse field is connected with an ordinary plasma resistance, then the characteristic time for the field diffusion will increase with the dimensions of the system. These are all consistent notions, but I do not believe that there is enough data from any labotarory to distinguish in detail between the various explanations.

N. Christofilos *(United States of America):* How much is the plasma length decreased during the time the magnetic lines are closed? And secondly, what is the ratio of the duration of the first half-cycle to the expected instability time for $m=2$?

A. C. Kolb: The observations of the plasma were made through slots in the coil placed every twenty centimeters. Hence, with the present arrangements it was impossible to obtain data to answer your question in detail. However, from a finite number of streak photographs it appears that the plasma length is between 1 and 1.5 meters for a coil 1.8 m long. One can see that the plasma has a large diameter in the center and a smaller one near the ends. But we do not know the detailed shape as yet.

N. Christofilos: And the second question, what is the stability time?

A. C. Kolb: If one connects the expected instability time with the characteristic time for the propagation of disturbances across a diameter, then the confinement time is some orders of magnitude longer than this. If the expected instability time is connected with, say, the propagation time of sound waves along the length of the apparatus, the quarter-period (nine microseconds) is comparable to this time for a 300 eV plasma. Since the plasma column is observed to be microscopically stable for times of 12—15 μs (except for the slow drift) it may be possible to extend the confinement time, although the theoretical reasons are not clear.

Paper CN-10/28 *and* 36 *were presented by K. Hain* (Federal Republic of Germany). *The text of the papers is on pages 561—576. The following discussion took place.*

F. L. Ribe *(United States of America):* I would like to mention the following by way of adding to the comparison of the results of this code with experiment. At Los Alamos we have run the code for a few cases and, in particular for the case of our Scylla I parameters, with a positive (parallel) trapped field. The agreement between the predictions of this code for the variation of the magnetic field on the axis of the pinch and the probe measurements for a parallel field, with a probe reported in the June 1961 issue of *Physics of Fluids* is very good. All of the details of the probe time variation are reproduced by the code. I would state tentatively that for the reversed field the code is a little more difficult to apply in this case and it is harder to get through a complete quarter-cycle of the applied field. But there is an indication that the experimental probe pulses of reverse trapped field damp out faster than would be indicated by this code.

Paper CN-10/226 *was presented by A. K. Razumova* (Union of Soviet Socialist Republics). *The text of the paper is on pages 577—587. The following discussion took place.*

S. Colgate *(United States of America):* I would like to ask if you have any evidence that the neutrons come from a thermal plasma rather than from an instability acceleration of a small fraction of the deuterons? What is the deuteron energy corresponding to the observed shift in the reaction product distribution?

K. A. Razumova: The energy distribution of protons measured in one discharge corresponds to a deuteron energy of 0 to 2.5 keV. In the case of averaging over many discharges it is necessary to assume some accelerating mechanism, since the energy was between 2.5 keV and 15 keV.

F. L. Ribe *(United States of America):* Did I hear you say that the density was something times 10^{19} cm^{-3}?

K. A. Razumova: Yes, the authors estimate the density to be of the order of 10^{19}. It has been estimated by different methods and the results agree.

F. L. Ribe: Let me check some more parameters. How much did you say that the volume of this plasma was?

K. A. Razumova: The diameter of this formation was of the order of 1 to 1.5 mm. There is probably some distribution of density, naturally, but the authors estimate the volume as several decades of cubic millimeters.

F. L. Ribe: And the ion temperature was 800 eV to 1 keV?

K. A. Razumova: The authors estimate the ion temperature to be of the order of 1 keV, 800 to 1200 eV.

F. L. Ribe: What was the neutron yield?

K. A. Razumova: The neutron yield varied in different experiments. Each discharge could be different from the other. The neutron yield was varying from 3×10^7 to 10×10^7. But there were also experiments with more powerful discharges performed in order to obtain the proton distribution in one discharge. In these discharges no other measurements have been made but the neutron yield amounted to about 0.5×10^{10}.

F. L. Ribe: My comment was going to be that at this very large density one would get a very large neutron yield which would have to be about 10^{10}.

A. C. Kolb *(United States of America):* I have a practical question. At the highest power of these discharges with densities of 10^{19} cm^{-3} and temperatures of a keV, the gas pressures are perhaps 50 000 atmospheres. Does your apparatus "live" for more than one discharge?

K. A. Razumova: The chamber was made of copper and was sufficiently strong but the diaphragm pressure detectors were destroyed in a single discharge. The same would happen to the piezo-electric detectors; the authors could not use these detectors because the destructive force of the discharge was very great.

J. G. Linhart *(Italy):* If I may impose one question myself. Have you observed any instabilities, i.e. instabilities of form in the plasma shell collapsing towards the center of convergence?

K. A. Razumova: No instabilities were observed.

G. von Gierke *(Federal Republic of Germany):* What was the duration and the shape of the neutron pulse?

K. A. Razumova: Neutrons appear at the moment of maximum compression and are delayed by 0.2 to 0.3 μs relative to the voltage rise. The pulse duration is about 0.2 to 0.3 μs.

Papers CN-10/184, 185, 186, 187, 188 *were presented by H. L. Jordan* (Federal Republic of Germany). *The text of the papers is on pages 589—616. The following discussion took place.*

R. D. Medford *(United Kingdom):* I would like to congratulate Drs. Bogen and Hintz on their ingenuity in measuring density distribution from radiated light. But I would like to point out that there is a more direct method, described by Hunt, Wright and myself at the recent conference in Munich, which uses an optical interferometer. The technique consists of superimposing streak and optical interference fringe photographs of the motion of the plasma on the same emulsion. Such photographs yield the spatial distribution of electron density with time in a fast discharge. If, at the same time, polarized light is transmitted through the wall of the discharge tube and possibly an optical insert, the driving and trapped magnetic fields can also be obtained from the same streak photograph. (This method of measuring the magnetic field is also being used by Dr. Nesterikhin of the Union of Soviet Socialist Republics for other geometries.) These methods can be extended to two dimensions by using a single white fringe and high speed color photography to give radial distributions of line integrated electron density and longitudinal magnetic fields.

H. L. Jordan: It is certainly well known that density measurements, both of electrons and ions can be made with interferometers. Accordingly at our laboratory such methods are being investigated, e.g. by Beerwald (Munich 1961) in the microwave region and by Dippel in the visible region. However, up to now we have not observed any measured density distributions during the fast magnetic compression of a plasma, especially in the case of longer coils.

R. F. Post *(United States of America):* I want to comment on some similarities that appear in listening to these papers; first the one by Dr. Kolb and then this very interesting paper. It appears that the effects observed relate, at least superficially, to our own work on this question of the apparently "quiescent plasma" with a slow drift. The drift is associated apparently in each case with the current leads of the coil system. The significance of this is that in the special cases described by these authors they have apparently been able to make a quiescent plasma suffering only from the $m=1$ instability.

In the case of this last paper, could an estimate of the ratio of what he would call the quiescent time of the plasma to the characteristic hydromagnetic instability time be given to see just how much significance we can draw from these experiment when taken all together?

H. L. Jordan: The observation times of the plasma are about 2 μs at densities around 10^{17} particles/cm^3. Nothing can be said about the behavior for longer times.

H. R. Griem *(United States of America):* In one of your figures, the electron temperature of the preheated plasma seems to follow the period of the preheated discharge but the electron density does not. Do you consider this modulation of the temperature to be a real effect, or could it be connected with the only approximate validity of either the corona or the Saha equations in the analysis? These difficulties

would be considerably reduced if one would determine the temperature from ratios of hydrogen line to continuum intensity.

P. Bogen *(Federal Republic of Germany):* The observed small temperature changes of about 10% presumably are not due to plasma compression but to joule-heating of the plasma, especially of the boundary zone. With regard to the validity of the corona equation our calculations indicate that the equilibrium is determined by electron collisions and three-body recombination and, therefore, the Saha equation is a better approximation, Finally, the temperature obtained from the ratio of hydrogen line to continuum intensity is about 20% lower than the temperature measured by relative intensities of C II and C III lines, which may be attributed to the inhomogeneous optical layer.

M. B. Gottlieb *(United States of America):* May I ask a question—this is directed to several of the previous speakers who have spoken about drifts essentially due to the feed lines. In the case of a very long solenoid (long compared with its diameter), if the feed lines are in the form of a plane, it is not clear to me that one can get much effect except at the very ends of the system. But in an infinitely long solenoid this effect would disappear entirely. Therefore, I ask if the feed was in the form of a sheet?

H. L. Jordan: The feed was in sheet form, but the coil was not long compared to its diameter (15 cm long, 4 cm diameter).

A. C. Kolb *(United States of America):* In our particular case where the coil length was of the order of two meters, no special care was taken to make the field homogeneous at the end. In fact, you can see that it cannot be homogeneous because of the large mass of metal at the feed point just outside the mirror. This metal is used to hold the collector plate together. However, I think it is reasonable that by proper design one can also make the magnetic field at the ends uniform. In answer to your question, most likely these effects are connected with end effects. This is an opinion. We don't know for sure.

J. L. Tuck *(United States of America):* The disturbing effect of the current leads to a single-turn compression coil can of course be reduced by reducing the feed point gap spacing. As reported in our early Scylla paper [*Phys. Rev.* **119** (1960) 831] using a counter telescope to determine the contours of the small (1.5 cm diameter) neutron-emitting region or fireball, this, with a normal feed point gap spacing of 2 mm was displaced 5 mm from the axis towards the feed point. Unpublished measurements showed that when the feed point gap was reduced (at the cost of increasing the dielectric stress in the feed point gap insulator to the point of breakdown) the fireball duly moved close to the axis.

P. Hubert *(France):* I want only to point out that I recently wrote a report about a method of designing coils having a very high degree of axial symmetry. This method can be particularly useful for single-turn coils.

Paper CN-10/48 *was presented by A. Folkierski* (United Kingdom). *The text of the paper is on pages 627—633. The following discussion took place.*

J. A. Nation *(Italy):* Do you have any magnetic probe results which indicate whether the current-carrying and luminous regions coincide, particularly in the vicinity of the "end" constrictions?

One of the principal parameters which determine the velocity of propagation of the axial disturbances is the square of the ratio of the magnetic field in the end constriction to that at the main column edge. This parameter will be large even for small disturbances when the column radius is small. Do you have, or know of, any information on whether such disturbances propagate in tubes of *large* radius when the discharge radius might not get to such small values as you observe, and hence the strength parameter $[B\ (\text{constriction})/B\ (\text{column})]^2$ would be much smaller? Under such conditions it might well be possible that these axial disturbances would not occur or else be so weak that they would not lead to loss of plasma containment.

A. Folkierski: With respect to the second question, I also do not have information on tubes of much larger diameter. With respect to the first question, the values of the diameter of the discharge determined by photography and by magnetic probes are reasonably similar, though the probe measurements were not performed in the region and at the time of constriction.

J. L. Tuck *(United States of America):* Dr. Folkierski reports a phenomenon which is new to me. Did I understand correctly, that a disappearance of these violent pinch fluctuations of voltage was observed as the voltage was increased?

A. Folkierski: What I meant was that $m=0$ constrictions in the main body of the discharge are inhibited by the collapse of the outer shell as we go to higher voltages.

H. Zwicker *(Federal Republic of Germany):* We have made some measurements about two years ago with helium in a tube of 20 cm diameter and found similar results at low pressures. However, with increasing pressure, instabilities became more and more weak and at pressures of about 4 mm Hg and higher, instabilities couldn't be found either photographically or by magnetic probes and the confined plasma column expanded symmetrically.

P. Hubert *(France):* The experiments which you describe can be of assistance in understanding the experiments of Meunier *et al.* [published in *J. Phys. Rad.* **18** (1957) 585], which show production of neutrons during explosions of wires containing deuterium.

These experiments were done at a time when diagnostic techniques were rudimentary. Nevertheless, photography has shown that the production of neutrons was associated with a discharge of globular appearance.

It therefore appears possible that there exists a mechanism of acceleration by instabilities of the $m=0$ type, even in a discharge with materials of high atomic number.

W. A. Bostick *(United States of America):* Dr. Folkierski is to be congratulated on his excellent photographs of Rayleigh-Taylor instabilities. We (Dickinson, Di Marco, Koslov, Bostick) have Kerr cell photographs at Stevens Institute of Technology of Rayleigh-Taylor flutes in plasma which break off at the end into droplets. These two-dimensional droplets are to be expected from the surface forces in plasma in a magnetic field which are analogous to the surface forces in a conventional fluid. The formation of the second layer, as observed by Folkierski in his pinch, by the breakup of the flutes near their extremities is due very likely to the interplay of these surface forces. Perhaps in his case the situation is so violent that a kind of spray of foam is formed instead of individual resolvable droplets.

A. Folkierski: I would like to comment on this as I did not really concentrate on Rayleigh-Taylor instabilities here since they are the subject of another paper [*Proc. Roy. Soc.* XXX (1961) XXX] and there we do in fact present measurements of the growth rate of the Rayleigh-Taylor instability. We have never observed the breaking off of plasma droplets from the flutes.

I. F. Kvartskhava *(Union of Soviet Socialist Republics):* It could be expected from the photographs shown that there would be a higher voltage drop at the ends of the discharge (in the vicinity of electrodes). Did you try to measure it?

A. Folkierski: We did not measure local electric field. The only voltage measurements we have are of over-all voltage between the electrodes.

I. F. Kvartskhava: The so-called Rayleigh-Taylor flutes seen on your photographs are at an angle with respect to the magnetic field H_0. The same effect is seen in our photographs of a fast pinch. This would mean that the flutes are encircling the pinch as a kind of a helix with a small pitch. Do you not suppose that in this case the mechanism of deformation of the pinch surface differs from that of Rayleigh-Taylor?

A. Folkierski: Three Kerr-cell photographs were taken on each discharge; a mirror was used so as to obtain a stereoscopic picture. In the early stages of the discharge the cusps are local. There is no spatial correlation between cusps observed on the right-hand side, left-hand side, front and back of the discharge column. At later stages the cusps develop into ridges whose orientation with respect to the magnetic field fluctuates in time. Still later, when the perturbations grow sufficiently large in amplitude and wavelength, they join up to form constrictions of $m=0$ type. We have looked for spiral perturbations, but never observed them.

Paper CN-10/215 *was presented by B. B. Kadomtsev* (Union of Soviet Socialist Republics). *The text of the paper is on pages 635—639. The following discussion took place.*

G. S. Murty *(India):* In calculating the distribution of the magnetic field, by assuming that the field is force-free, is any assumption made regarding the electric conductivity of the medium? In particular, was it assumed to be a tensor?

B. B. Kadomtsev: In the force-free model I used to compare with experimental results, the longitudual conductivity was assumed to be constant ($\sigma_{\parallel}=$ const.) and $\sigma_{\perp}$ arbitrary. In this model it makes no difference whether transverse conductivity is scalar or tensor, since almost all current flows along the lines of force and transverse conductivity is of no importance.

A. A. Ware *(United Kingdom):* I wish to report that effects similar to those reported in this paper were found in experiments on the torus at General Atomic (U.S.A.). On the outside of a pinch discharge containing a positive B_z-field, the field was reversed in an attempt to produce a more stable configuration. However, magnetic probe measurements showed that the reversed field region propagated inwards with a velocity of about 10^6 cm/s. The transition between positive and negative B_z became more rapid with decreasing radius. At the walls the circuits changed B_z in 4 μs; near the center of the discharge, fields of about $+5$ kG changed to about -5 kG in 1 μs. My explanation of this phenomena was identical with that reported by the above paper, but I am afraid it has not been published.

This theory, which is based on the assumption that instabilities and other effects keep ∇p, and hence $j_{\perp}$, and $\sigma_{\perp}$ small, could explain the rapid disappearance of the reversed field in theta-pinch discharges. If this is correct an appreciable B_θ field should be generated near the region where B_z passes through zero. It would be of interest if magnetic probes were used to look for such a field in theta-pinch discharges.

SESSION VI — SÉANCE VI

ЗАСЕДАНИЕ VI — SESIÓN VI

7 SEPTEMBER 1961 — 7 SEPTEMBRE 1961

7 СЕНТЯБРЯ 1961 Г. — 7 DE SEPTIEMBRE DE 1961

Chairman — Le président — Председатель — El Presidente

E. Nagy *(Hungary)*

Scientific Secretary — Secrétaire scientifique — Ученый секретарь — Secretario Científico

C. Etievant *(France)*

[Papers presented: CN-10/4, 7, 10, 11, 18, 103, 156, 197, 218, 221, 222]

ИЗЛУЧЕНИЕ ПРИМЕСЕЙ В РАЗРЕЖЕННОЙ ГОРЯЧЕЙ ВОДОРОДНОЙ ПЛАЗМЕ*

А. П. Васильев, Г. Г. Долгов-Савельев, В. И. Коган

Академия наук СССР

Москва, Союз Советских Социалистических Республик

Произведены численные расчеты интенсивности излучения примесей ряда элементов в разреженной водородной плазме, для интервала температур от нескольких эв до 10 кэв.

Глубины ионизации атомов примесей определяются исходя из стационарного состояния разреженной плазмы, которое характеризуется равновесием между ионизацией электронным ударом и излучательной рекомбинацией («эльвертовское» равновесие). Для некоторых из рассмотренных элементов вычислены отдельно вклады в полную интенсивность излучения за счет связанно-связанных, свободно-связанных и свободно-свободных переходов. Эффективные сечения возбуждения ионов примесей берется в борновском приближении или его полуэмпирических модификациях.

Температурный ход интенсивности излучения примеси обнаруживает несколько максимумов и минимумов (в соответствии с числом электронных оболочек данного элемента). В наибольшем из максимумов интенсивность излучения на один атом примеси более чем в 10^5 раз превосходит интенсивность излучения на один атом водорода.

Там, где это возможно, производится сравнение результатов с результатами расчетов Кнорра и Поста и в этой связи критикуется часть результатов Кнорра. Обсуждаются границы применимости проведенных расчетов, а также предложенной ранее оценочной формулы. Оценивается роль излучения примесей при переходных эффектах (начальная стадия процессов конечной длительности), в связи с чем дискутируются некоторые выводы Макуиртера.

Рассчитаны времена установления ионизационного равновесия для различных ступеней ионизации в зависимости от температуры. Обсуждается роль метастабильных состояний в потерях на излучение примеси.

Полученные результаты используются для оценки роли излучения примесей в уходе энергии из конкретных экспериментальных систем.

Излучение примесей, являющееся одним из важных механизмов потерь энергии горячей водородной плазмы, рассматривалось в ряде теоретических [1]—[7] и экспериментальных [8]—[11] работ. Настоящая работа посвящена расчетам излучения примесей ряда элементов в стационарном состоянии, а также оценке роли переходных эффектов.

1. Расчет по ионизационному равновесию примесей

Ионизационное состояние малых примесей в разреженной водородной плазме определяется равновесием процессов ионизации электронным ударом и фоторекомбинации [12], [3]; равновесие этого типа будем называть «эльвертовским равновесием». Сама возможность такого равновесия связана со «встречным» изменением сечений ионизации и рекомбинации по мере роста глубины обдирки $Z_{эф}$ примесных ионов ($\sim Z_{эф}^{-4}$ и $\sim Z_{эф}^{4}$ соответственно).

Изменение плотности $n_i^{(k)}$ k-кратно ионизованных атомов описывается уравнением

$$\frac{dn_i^{(k)}}{dt} = -n_i^{(k)} \cdot n_e \langle v\sigma_и^{(k)} \rangle + n_i^{(k+1)} n_e \langle v\sigma_р^{(k+1)} \rangle - n_i^{(k)} n_e \langle v\sigma_р^{(k)} \rangle + n_i^{(k-1)} n_e \langle v\sigma_и^{(k-1)}, \quad (1)$$

где n_e — полная плотность электронов, v — скорость электрона; $\sigma_и^{(k-1)}$, $\sigma_и^{(k)}$, $\sigma_р^{(k)}$, $\sigma_р^{(k+1)}$ — сечения ионизации и рекомбинации ионов соответствующей кратности ($k=0,1,2 \ldots Z$); угловые скобки означают усреднение по распределению электронных скоростей (ниже оно считается максвелловским). В стационарном состоянии ($dn_i^{(k)}/dt=0$ для всех k) (1) сводится к системе однородных взаимно зацепляющихся уравнений, из которой рекуррентным образом следует попарная взаимная компенсация членов в каждой из строк правой части (1), так что

$$\frac{n_i^{(k+1)}}{n_i^{(k)}} = \frac{\langle v\sigma_и^{(k)} \rangle}{\langle v\sigma_р^{(k+1)} \rangle}. \quad (k = 0,1, \ldots, Z) \quad (2)$$

Как видно, переход от (1) к (2) отнюдь не связан с пренебрежением второй парой членов в (1) по сравнению с первой, как это утверждается в [6].

Расчет ионозационного равновесия примесей в данной работе производился на основе аналитического вида системы (2), полученного в [12]. Графики, удобные для оценок ионизационного равновесия, приведены в [7].

Интенсивность тормозного и рекомбинационного излучений

Принимаем, что излучение примесей, складывающееся из тормозного, рекомбинационного и линейчатого излучений, свободно выходит из объема плазмы.

* Доклад CN-10/197, представленный на конференцию. Докладчик: Г. Г. Долгов-Савельев. Переводы аннотаций находятся в конце этого тома Трудов Конференции.

Интенсивности тормозного и рекомбинационного излучений равны, соответственно, (см. напр. [1], [2]):

$$Q_т \simeq 1{,}5 \cdot 10^{-25} T_e^{1/2} n_e \sum_k Z_{k,эф}^2 n_i^{(k)}, \text{ (эрг см}^{-3} \text{ сек}^{-1}) \quad (3)$$

$$\left.\begin{aligned} Q_{p,n_0}^{(k)} &= 2{,}1 \cdot 10^{-24} T_e^{-1/2} n_e n_i^{(k)} Z_{k,эф}^4 \frac{\overline{\zeta_{n_0}^{(k)}}}{n_0^5}, \\ &\qquad \text{(эрг см}^{-3} \text{ сек}^{-1}) \\ Q_p &= \sum_k Q_{p,n_0}^{(k)} (1 + v_k' + v_k''). \end{aligned}\right\} \quad (4)$$

Здесь T_e — электронная температура в эв; $Z_{k,эф}$ — эффективный заряд k — кратно ионизованного атома; $Q_{p,n_0}^{(k)}$ — энергия, излучаемая при захвате электрона прямо на основной уровень наинизшей незаполненной оболочки с главным квантовым числом n_0; $\overline{\zeta}_{n_0}$ — число свободных мест в этой оболочке. Члены v_k' и v_k'' учитывают соответственно излучение при рекомбинации на верхние оболочки ($n > n_0$) и линейчатое излучение при последующих переходах $n \to n_0$.

Численный коэффициент в формуле (3) несколько отличен от принятого в [2] и отвечает квазиклассическому приближению $2\pi Z_{эф} e^2/\hbar v \gg 1$, справедливому в большей части рассматриваемого интервала T_e (см. напр. [13]). Выражения для v' и v'', приведенные в [2], основаны на формуле Крамерса и потому, например, не учитывают зависимость v' от T_e; однако они не сильно отличаются от более точных, которые можно получить из [14].

Величина $Z_{k,эф}$ является растущей функцией от T_e, которая, однако, ввиду резкого различия потенциалов ионизации последовательных электронных оболочек, «замораживается» перед вскрытием каждой новой оболочки; следствием этого являются провалы на кривых $Q_т$ (T_e) и, особенно, Q_p (T_e); см. рис. 6, 7. Этот эффект, естественно, наиболее сильно выражен при переходе к «гелиевой» оболочке $n = 1$. Равенство $Q_т = Q_p$ наступает уже после полной обдирки атома ($Z_{эф} = Z$), при $T_e \approx 35 Z^2$ эв. (ср. [14]).

Интенсивность линейчатого излучения

Интенсивность линейчатого излучения $Q_л$ возбужденных ионов примеси в разреженной плазме может быть рассчитана в предположении «мгновенного резонансного высвечивания» такого иона сразу же после его образования и, следовательно, определяется скоростью поступления электронов на возбужденные уровни (в отличие от случая термодинамического равновесия, когда $Q_л$ определяется просто «больцмановской» заселенностью уровней и интенсивностью высвечивания, пропорциональной ω^4).

Скорость поступления электронов на возбужденные уровни складывается из скорости возбуждения ионов электронным ударом и скорости рекомбинации электронов на эти уровни. Второй из этих механизмов, вклад которого в излучение уже учтен выше членом $Q_{p,n_0} \cdot v''$ в (4), играет второстепенную роль. Действительно, скорость рекомбинации на возбужденные уровни при эльвертовском равновесии заведомо не превосходит скорости ионизации с основного уровня, а эта скорость, в свою очередь, меньше скорости возбуждения электронным ударом (особенно для переходов на уровни, близкие к основному, дающих главный вклад в $Q_л$). Таким образом:

$$Q_л \simeq \sum_k \sum_s n_e n_i^{(k)} \cdot \chi_в^{(k,s)} \langle v \sigma_в^{(k,s)} \rangle \text{ (эрг см}^{-3} \text{ сек}^{-1}), \quad (5)$$

где $\sigma_в^{(k,s)}$, $\psi_в^{(k,s)}$ — сечение и энергия возбуждения; суммирование производится как по всем переходам s при данной кратности ионизации k, так и по всем k.

Для вычисления сечений возбуждения многозарядных ионов не существует точной теории, и разные авторы используют различные аппроксимации, основанные большей частью на приближении Борна-Бете. Наиболее известные из этих аппроксимаций можно свести к единообразному виду:

$$\sigma_в = \frac{\pi e^4}{\chi_в^2} f_{погл} \cdot F\left(\frac{E}{\chi_в}\right) \text{ (см}^2\text{)}, \quad (6)$$

где e — заряд электрона, $f_{погл}$ — сила осциллятора для рассматриваемого перехода, E — энергия

Таблица 1. Безразмерные сечения возбуждения $F(E/\chi_в) \equiv F(u)$ и скорости возбуждения $\Psi(\chi_в/T_e) = \Psi(x)$ для различных аппроксимаций сечения возбуждения $\sigma_в$

№№	Источник	$F(u) = \frac{\sigma_в}{\pi e^4 f_{погл}/\chi_в^2}$	$\Psi(x) = \frac{\langle v \sigma_в \rangle}{\pi e^4 f_{погл}[8/(\pi m \chi_в^3)]^{1/2}}$
1	Аллен [15]	$3(u-1)/u^2$	$3\sqrt{x}\, e^{-x}[1 - x e^x \mathrm{Ei}(x)]$
2	Кнорр [2]	$(0{,}45 \ln u)/(u-1)$	$0{,}225\, e^{-x} G(x)$, где $G(x)$ графически представлено в [2]
3	Пост [6]	$(2{,}72 \ln u)/u$	$2{,}72\sqrt{x}\, \mathrm{Ei}(x)$
4	Эльверт [1]	$[\ln(\sqrt{u} + \sqrt{u-1})]/u$	$\frac{1}{2}\sqrt{x}\, e^{-x/2} K_0(x/2)$

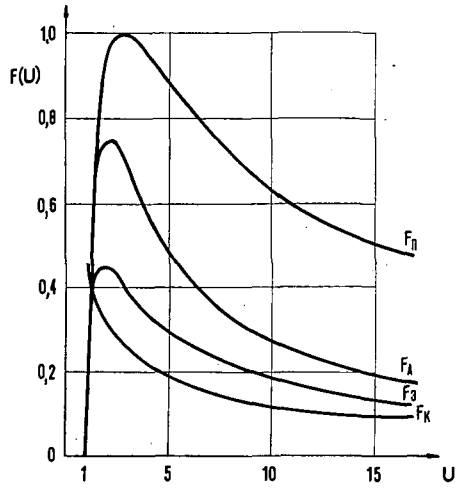

Рис. 1 Безразмереные сечения возбуждения $F(E/\chi_B)\equiv F(U) = \sigma_B/(\pi e^4 f_{погл}/\chi_B^2)$ в зависимости от отношения энергии электрона к энергии возбуждения χ_B для различных аппроксимаций сечения σ_B, используемых Постом ($F_П$), Эльвертом ($F_Э$), Алленом (F_A) и Кнорром ($F_К$).

электрона; различные варианты безразмерной функции F сведены в таблицу 1. Усредненные по Максвеллу величины $\langle v\,\sigma_в\rangle$ равны

$$\langle v\sigma_в\rangle = \pi e^4 f_{погл}\sqrt{\frac{8}{\pi m \chi_в^3}}\,\Psi\left(\frac{\chi_в}{T_e}\right)(\text{см}^3\,\text{сек}^{-1}). \qquad (7)$$

Соответствующие варианты функции Ψ также приведены в табл. 1. Рисунки 1 и 2 наглядно иллюстрируют различия между используемыми аппроксимациями $\sigma_в$, а, следовательно, и между рассчитанными по ним величинам $Q_л$. Как видим, даже для тех умеренных требований, которые можно предъявить к точности расчетов по примесям, эти различия довольно значительны. В настоящей работе сечения $\sigma_в$ вычислялись в соответствии с [15]. При этом ионные переходы и соответствующие значения $X_в$ брались из [16], а силы осцилляторов f получались с помощью таблиц [17]; для ступеней ионизации и переходов, дающих наибольший вклад в излучение, эти значения f не сильно отличаются от «водородоподобных» значений [18], [1]. При данном k основной вклад в $\sum_s$, см. (5), дает переход на уровень, ближайший к основному.

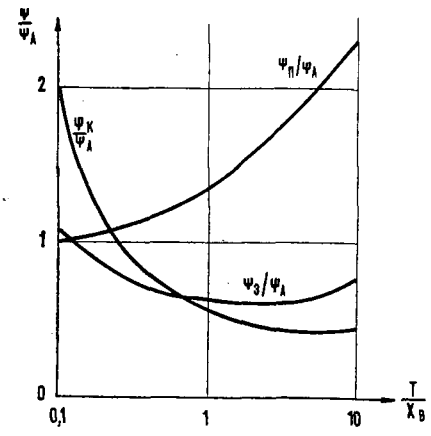

Рис. 2 Отношение безразмерных скоростей возбуждения $\Psi(\chi_B/T_e)=\langle v\sigma_B\rangle/\pi e^4 f_{погл}(8/\pi m\chi_B^3)^{1/2}$, соответствующих аппроксимациям Поста ($\Psi_П$), Эльверта ($\Psi_Э$) и Кнорра ($\Psi_К$), к скорости возбуждения, соответствующей аппроксимации Аллена (Ψ_A) — в функции от T_e/χ_B.

Равновесная ионизация частиц примеси

Обычно в (5) подставляют значения $n_i^{(k)}$, отвечающие эльвертовскому равновесию, что дает стационарную мощность излучения примесей; соответствующие потери энергии плазмы W растут пропорционального времени t. Однако для процессов конечной длительности значительный вклад в полные потери энергии может давать излучение ионов примеси в ходе установления самого эльвертовского равновесия. Этот переходный эффект дает некоторый «разовый вклад в цену равновесной ионизации частицы примеси» ε (эв/ион). Для нахождения ε нужно решить систему уравнений (1) и полученные $n_i^{(k)}(t)$ подставить в $\int_0^{t^*} Q_л(t)\,dt$, где t^* — время установления эльвертовского равновесия для ступеней ионизаций, наиболее существенных в излучении. В общем случае процесс обдирки примесных ионов происходит параллельно с изменением $T_e(t)$, однако обычно можно ограничиться рассмотрением более простого случая, когда обдирка происходит при заданной температуре; это соответствует мгновенному поступлению атомов примеси в плазму (например, со стенок). Для данного элемента «разовый вклад» ε, очевидно, зависит только от T_e (но не от n_e). Грубая оценка ε дана в [4]; более аккуратное рассмотрение переходного эффекта произведено в [7] и особенно [в 6]; впрочем, даже и в последнем случае, ввиду пренебрежения рекомбинацией, результаты имеют, на наш взгляд, лишь оценочную точность.

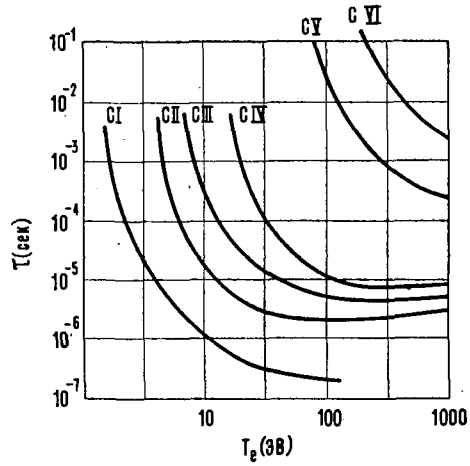

Рис. 3 Времена ионизации $\tau=1/n_e\,\langle v\sigma_и$ для последовательных ступеней ионизации углерода в функции T_e; $n_e=10^{14}$ см$^{-3}$.

Для ε имеем приближенное выражение:

$$\varepsilon \simeq \sum_{k=0}^{k^*} \chi_{\text{в}}^{(k)} \cdot \frac{\langle v\,\sigma_{\text{в}}^{(k)}\rangle}{\langle v\,\sigma_{\text{и}}^{(k)}\rangle} \text{ (эв/ион)}, \qquad (8)$$

где k^* — наибольшая из «пройденных» кратностей ионизации для эльвертовского равновесия при данном T_e. В случае, если длительность процесса $t_{\text{пр}}$ меньше времени t^*, в качестве k^* надо брать, очевидно, кратность ионизации, наибольшую из пройденных за время $t_{\text{пр}}$. В суммах (8) обычно наиболее значительны последние слагаемые, так что значения ε чувствительны к выбору k^*, что лишний раз подчеркивает оценочный характер формулы (8). На рис. 3 ,4 и 5 представлены вычисленные значения времен ионизации τ для $n_e = 10^{14}$ см$^{-3}$ и «разового вклада» ε. Последние относятся к случаю $t_{\text{пр}} > t^*$; если ступень ионизации пройдена лишь частично, то она учитывалась в сумме с соответствующим множителем <1.

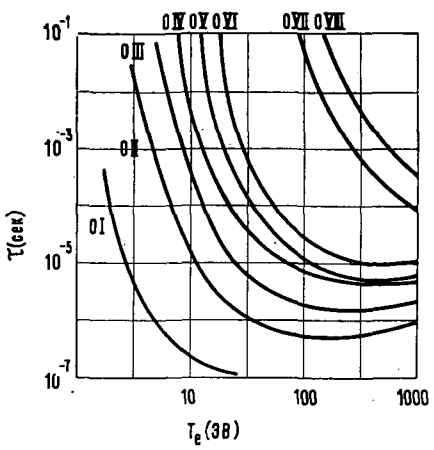

Рис. 4 Времена ионизации τ для ступеней ионизации кислорода в функции T_e; $n_e = 10^{14}$ см$^{-3}$.

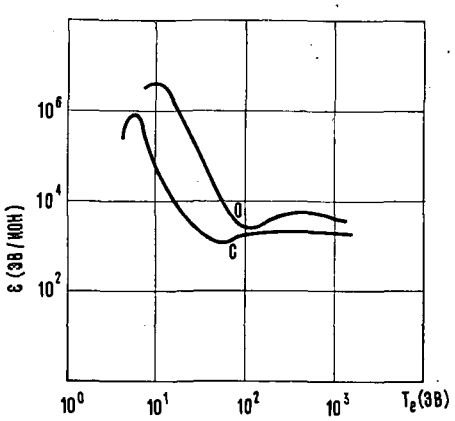

Рис. 5 «Разовый вклад в цену равновесной ионизации»

$$E = \sum_{k=0}^{k^*} [\chi_{\text{в}}^{(k)} \langle v\sigma_{\text{в}}^{(k)}\rangle / \langle v\,\sigma_{\text{и}}^{(k)}\rangle] \text{ эв/ион.}$$

для кислорода и углерода в функции T_e.

Численные расчеты

На рис. 6—10 приведены результаты численных расчетов излучения примесей, находящихся в эльвертовском равновесии. По оси абсцисс отложена электронная температура T_e в эв, по оси ординат — мощность излучения примеси, отнесенная к одному атому примеси и одному электрону,

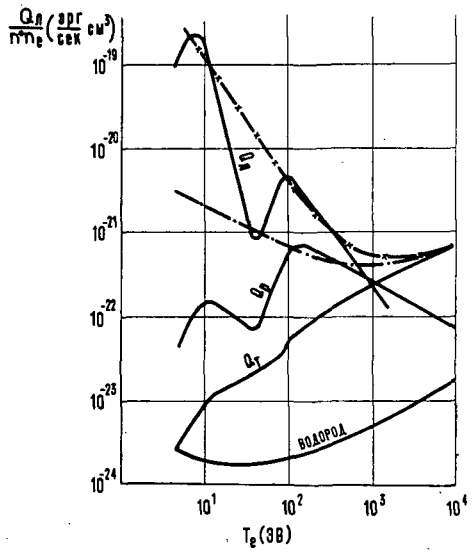

Рис. 6 Мощность линейчатого (q_Λ), рекомбинационного (q_P) и тормозного (q_T) излучения углерода на один электрон и один атом С. Для сравнения нанесена кривая суммарного рекомбинационного и тормозного излучения водорода (на один электрон и один ион Н). Кривые —.— и —×— описывают суммарную мощность излучения, вычисленную соответственно по формуле, предложенной в [4], и по формуле (9) данной работы.

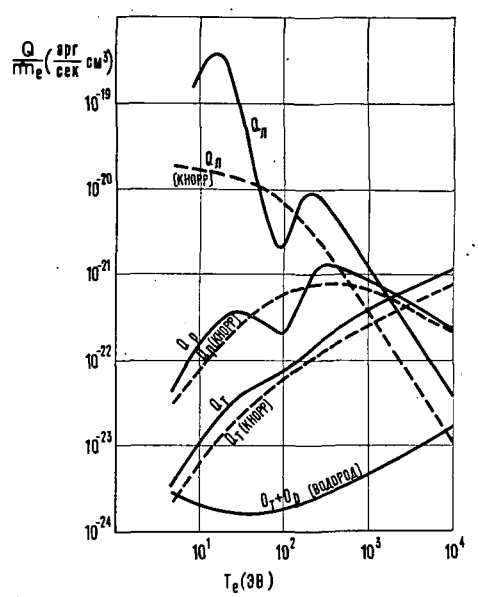

Рис. 7 Мощность линейчатого (q_Λ), рекомбинационного (q_P) и тормозного (q_T) излучения кислорода на один электрод и один атом О. Для сравнения нанесены кривая суммарной мощности рекомбинационного и тормозного излучения водорода и штрихпунктирные кривые, представляющие результаты Кнорра.

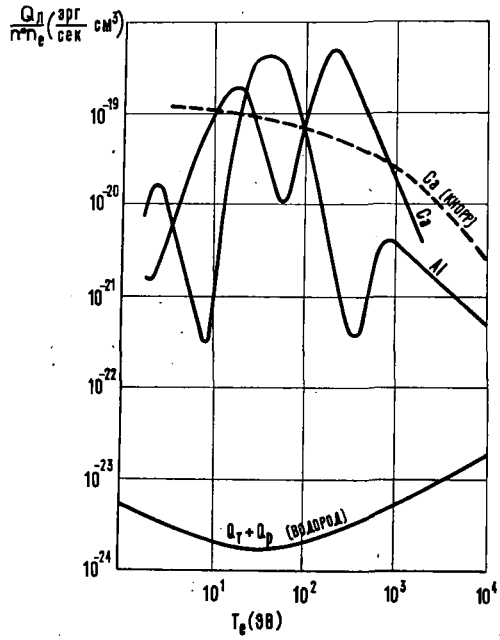

Рис. 8 Мощность линейчатого излучения q_Λ для Al и Ca, отнесенная к одному электрону и одному атому. Для сравнения даны кривая излучения водорода и штрихпунктирная кривая, результаты Кнорра [2].

т. е. $Q/n^*n_e \equiv q$ (эрг см^3 сек.$^{-1}$), где n^* — полная плотность частиц примеси. Для всех рассмотренных элементов приведены кривые $q_л$, а для углерода и кислорода — также и кривые $q_т$, $q_р$. На рис. 7 и 8 приведены для сравнения (пунктиром) соответствующие результаты Кнорра [2]. Для линейчатого излучения различие оказывается весьма значительным. Это вызвано тем, что в [2] не учтены, во-первых, резкие скачки энергий ионизации и возбуждения при переходе от одной электронной оболочки к другой (отсюда — плавный ход кривых), и, во-вторых, легко возбуждаемые переходы типа nS→np, дающие основной вклад в линейчатое излучение (отсюда — существенное занижение главных максимумов $q_л$). Ожидаемый характер кривых $q_л$ был отмечен в [4] и качественно подтвержден на эксперименте [10].

Кривые рис. 9, 10 иллюстрируют вклад отдельных ступеней ионизации углерода и кислорода в суммарное линейчатое излучение. Из них виден, в частности, определяющий вклад в $q_л$ излучения литиеподобных ионов C IV и O VI; он обусловлен переходами 2S→2p с $\psi_в = 2(Z-2)$ эв. Эти же переходы 2S→2p ответственны за главные максимумы в излучении и других элементов (рис. 8). Местоположение главного максимума может быть оценено по формуле $T_{max} \approx 0{,}5\ (Z-2)^2$ эв. Высота главного максимума мало изменяется от элемента к элементу и составляет $\sim(2-4)\cdot 10^{-19}$ эрг см^3 сек$^{-1}$.

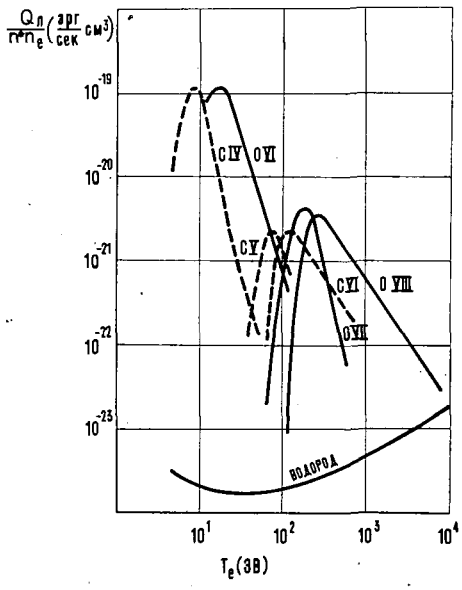

Рис. 9 Мощность линейчатого излучения некоторых (соответственных) ионизационных состояний углерода и кислорода на один электрон и один атом. Для сравнения нанесена кривая интенсивности излучения водорода.

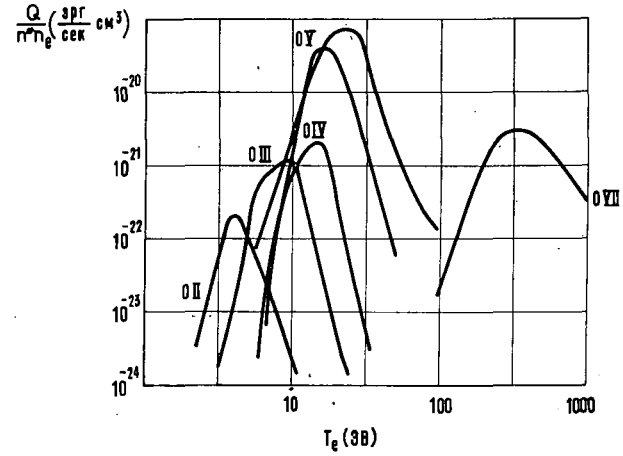

Рис. 10 Мощность линейчатого излучения последовательных ионизационных состояний кислорода и функции T_e. (На один электрон и один атом.)

(По порядку величину это значение можно найти из самой грубой оценки, подставляя в $q_л = \psi_в \langle v\,\sigma_в \rangle$ типичные значения $v \sim 10^8$ см/сек, $\sigma \sim 10^{-16}$см^2, $\psi_в \sim 10$ эв). Примерное постоянство главного максимума (несмотря на постепенный спад $q_л$ литиеподобного иона начиная с некоторого Z) связано с большей «комбинаторикой» ионизационных ступеней и переходов с ростом Z. Значительный вклад в $q_л$ дает также излучение бериллиеподобных ионов типа C III, OV и т. п., см. рис. 10. Небольшое численное отличие данных рис. 9 и 10 объясняется использованием в последнем случае иного вида $\sigma_в$.

Сравнение результатов, представленных на рис. 6—10, с результатами Поста [3] для $q_л$ литиеподобных и водородоподобных ионов дает вполне удовлетворительное согласие — в том смысле, что имеющиеся численные различия целиком объясняются различием, использованным Постом и нами, сечений $\sigma_в$. В этом легко убедиться, применяя

данные рис. 2 к соответствующим значениям T/ψ_B. (Отметим еще, что в [3], в отличие от данной работы, представлены не абсолютные значения $q_л$, а их отношения к $q_т$ водорода).

Из рис. 6—8 видно, что излучение на одну частицу примеси может превышать суммарное тормозное и рекомбинационное излучение на один атом водорода более чем в 10^5 раз.

На рис. 6 изображены (штрих-пунктиром) еще две кривые: нижняя — предложенная в [4] для мощности суммарного излучения, но оказывающаяся, как видно, скорее границей снизу, и верхняя — грубая огибающая сверху суммарных потерь на излучение, выражаемая формулой:

$$\frac{Q_{\text{сумм}}}{n^* n_e} \equiv q_{\text{сумм}} = 8\cdot 10^{-23} Z^6 T_e^{-3/2} + 6\cdot 10^{-24} Z^4 T_e^{-1/2} + 1{,}5\cdot 10^{-25} Z^2 T_e^{1/2} \text{ (эрг см}^3\text{ сек}^{-1}\text{)}, \quad (9)$$

где Z — порядковый номер элемента, T_e — в эв. формула (9) хорошо описывает огибающую также и для кислорода.

Отметим, что в районе минимумов кривых $q_л$, когда преобладают ионы с замкнутой электронной оболочкой (например, гелиевой), даже малая доля ионов с одним оптическим электроном (C IV и т. п.), составляющая всего $\sim 10^{-3}$ от общего числа ионов, дает определяющий вклад в полное излучение.

Оценка переходных эффектов

При оценке роли переходных эффектов следует помнить, что кривые рис. 5 имеют асимптотический (по времени) смысл, т. е. они справедливы лишь для процессов, длительность которых $t_{пр}$ превышает время установления эльвертовского равновесия t^*. Если ввести $t_{пр}$ в качестве дополнительного параметра и извлекать максимальные глубины ионизации k^* (для данного $t_{пр}$) из рис. 3, 4, то каждая из кривых рис. 5 расщепится в своей низкотемпературной части на семейство кривых для разных $t_{пр}$, имеющее вид «метелки». Поэтому, например, при $T_e \sim 10$ эв и $t_{пр} \sim 10^{-3}$ сек ε будет гораздо меньше своего «асимптотического» значения $\varepsilon \sim 10^6$ эв, которое могло бы реализоваться лишь при очень большом $t_{пр}$.

Потери энергии на излучение примесей с учетом «разового вклада» ε даются формулой:

$$W = n^* (\varepsilon + q\, n_e t'_{пр}) \quad \text{(эрг см}^{-3}\text{)},$$

$$t'_{пр} = t_{пр} - t^* \quad (10)$$

где ε выражено в эргах. Условие преобладания стационарных потерь над «разовым вкладом», т. е. условие того, что переходный эффект установления ионизационного равновесия малосуществен, имеет вид:

$$n_e t'_{пр} \gg \frac{\varepsilon}{q} \quad \text{(см}^{-3}\text{ сек)}. \quad (11)$$

Полагая $q \cong q_л$ и беря значения ε и $q_л$ с кривых рис. 5—7, получаем следующий, не очень сильно зависящий от T_e, критерий:

$$n_e t'_{пр} \gg (10^{12}—10^{13}) \text{ см}^{-3} \text{ сек}. \quad (12)$$

Этот критерий близок к полученному в [7].

Дискуссия по результатам

Приведенные выше результаты справедливы в предположении, что плазма разрежена настолько, что возбужденный ион примеси успевает высветиться до тушащего столкновения с электроном. Оценка частоты ударов второго рода показывает, что это предположение справедливо для иона C IV при $n_e \ll 1.10^{-16}$ см$^{-3}$, для иона O VI — при $n_e \ll 4.10^{16}$ и т. п. При относительном содержании примесей порядка нескольких процентов эти ограничения сравнимы по жесткости с условием малости эффектов самопоглощения излучения, полученным Постом [5]: $n^* \ll (10^{14}—10^{15})$ см$^{-3}$. Впрочем, вопрос о количественной достоверности последнего условия неясен в свете критики, высказанной Томасом [19].

При возрастании n_e и, соответственно, частоты ударов второго рода в плазме начинает устанавливаться распределение ионов по уровням энергии, более близкое к больцмановскому, что должно привести, в частности, к снижению потерь на излучение за счет переходов 2S→2p по сравнению с приведенными выше в несколько раз (помимо эффекта тушащих столкновений). Разумеется, этот эффект необходимо рассчитывать одновременно с эффектом самопоглощения.

Выводы

Из изложенных результатов ясно видно существование своего рода «радиационного барьера» (как для q, так и для ε), обусловленного излучением примесей, при $T_e \geqslant 10$ эв. Высота этого барьера позволяет объяснить наблюдаемый порядок величины потерь на излучение [10], не прибегая к каким-либо дополнительным предположениям, при содержании примесей порядка всего лишь нескольких процентов. Наличие примесей нескольких сортов приводит, очевидно, к сглаживанию провалов на суммарной кривой q и к уширению «радиационного барьера». С учетом полученной выше высоты этого барьера оценки роли примесей, полученные в [4] для плазменного шнура, заметно ужесточаются.

Авторы благодарят Л. А. Арцимовича и М. А. Леонтовича за интерес к работе и стимулирующее обсуждение.

Литература

[1] Elwert, G., *Z. Naturf.* **9a** (1954) 637.
[2] Knorr, G., *Z. Naturf.* **13a** (1958) 941.
[3] Post, R., *Ann. Rev. Nucl. Sci.* **9** (1959) 378. (Имеется русский перевод «Высокотемпературная плазма и управляемые термоядерные реакции» ИЛ, 1961 г.).

[4] Коган, В. И., ДАН СССР, **128**, 702 (1959).
[5] Post, R., Symposium of Plasma Dynamics, Ed. F. H. Clauser, 30 (1960).
[6] Post, R., International Summer Course in Plasma Physics, Riso (Denmark) Report Nr. 18 (1960).
[7] McWhirter, R. W. P., *Proc. Phys. Soc.* (London) **75** (1960) 520.
[8] Кириллов, В. Д., *ЖТФ* **30** (1960) 320.
[9] Долгов-Савельев, Г. Г., Муховатов, В. С., Стрелков, В. С., Шепелев, М. Н., Явлинский, Н. А., *ЖЭТФ* **38** (1960) 394.
[10] Karr, H. J., Knapp, E. A., Osher, J. E., *Phys. Fluids* **4** (1961) 424.
[11] Dimock, D., Fourth International Conference on Ionization Phenomene in Glases, Uppsala, 18 (1959).
[12] Elwert, G., *Z. Naturf.* **7** (1952) 432.
[13] Коган, В. И., Мигдал, А. Б., Сборник «Физика плазмы и проблема управляемых термоядерных реакций» т. 1, стр. 172 (1958).
[14] Коган, В. И., Сборник «Физика плазмы и проблема управляемых термоядерных реакций», т. 3, стр. 99 (1958).
[15] Аллен, К. У., «Астрофизические величины» ИЛ, 1960 г.
[16] Landolt-Börnstein, "Zahlenwerte und Funktionen aus Physik, Chemie, Astronomie, Geophysik und Technik", Bd. I.
[17] Bates, D. R., Damgaard, A., *Phil. Trans. Roy. Soc.* **242** (1949) 101.
[18] Бете, Г., Солпитер, Э., «Квантовая механика атомов с одним и двумя электронами» ИЛ, 1960 г.
[19] Thomas, R., Symposium of Plasma Dynamics, Ed. F. H. Clauser, 46 (1960).

THE COLLISION OF TWO PLASMAS*†

JOHN MARSHALL, T. F. STRATTON

LOS ALAMOS SCIENTIFIC LABORATORY, UNIVERSITY OF CALIFORNIA

LOS ALAMOS, NEW MEXICO, UNITED STATES OF AMERICA

Two coaxial guns inject hydrogen or deuterium plasmas into opposite ends of an evacuated drift space containing an axial magnetic field. With simultaneous firing of deuterium plasmas, the fast fronts of the plasmas ($\sim 10^8$ cm/s) superimpose to produce an extended region of plasma in which the transverse energy density is approximately 2 J per cm length, the transverse ion temperature is ~ 3 keV, and the particle density is $\sim 10^{14}/\text{cm}^3$. Following the fast plasma component, there is a slower component, observable by Coulomb scattering of the ions in one plasma by the ions in the other. The temperature is considerably smaller (~ 100 eV) than that of the fast component, but the density is high ($\sim 10^{16}/\text{cm}^3$) and the particles are presumably well randomized in direction. No evidence has been obtained for a two-stream instability in the plasma collision. Unexplained phenomena take place in the entry of the plasma into the guide field. The fast component appears to penetrate the magnetic field without regard to its strength, and the slow plasma component enters the field with practically no energy in the transverse degrees of freedom.

1. Introduction

We report here an experiment involving the collision of two plasmas. The plasmas, which are derived either from deuterium or hydrogen gas, move in opposite directions along a magnetic guide field in an evacuated drift space. Coaxial guns [1, 2] are used as the sources, and obviously everything which is observed depends on the characteristics of the guns and on the phenomena involved in the injection of the gun plasmas into the ends of the guide field.

The experiment was undertaken with two main purposes. One was that the interaction of the two fast plasmas might produce a relatively hot stationary plasma in the impact region which would serve as the charge of a thermonuclear machine. The other was that it might be possible to observe a two stream instability [3] in the collision, and this would be interesting in itself.

2. Apparatus

The equipment consists of two coaxial guns mounted so as to fire against one another into opposite ends of an evacuated drift tube. The drift tube is wound with a solenoid which provides an axial magnetic guide field in the region between the gun muzzles. A simplified general view is given in Fig. 1.

The design of the guns is shown in Fig. 2. The two coaxial copper electrodes are about 60 cm long with diameters of approximately 3.2 cm and 8.3 cm. Deuterium or hydrogen gas is admitted from a fast valve halfway along the inner electrode. The two gun valves are opened simultaneously by a mechanical hammer through a pair of sonic transmission lines. Each valve is provided with a small plenum, filled through a capillary leak between shots and emptied nearly completely when the valve is opened. The plenum volume is about 0.4 cm^3 and it is usually filled with gas to about 2.5 atmospheres pressure so that one cm^3 atmosphere of gas is admitted when the valve is opened.

The insulator at the gun breach is a Pyrex disk with a hole drilled in it. "O" rings make vacuum seals between the Pyrex and the brass gun flanges. The design is such as to provide a long surface path on the back side of the insulator, difficulty having been had in the past with electrode erosion at the point where the insulator meets the central electrode. Mechanical force is applied to the insulator through phenolic washers to reduce danger of breakage, and the washers are provided with skirts to increase the surface breakdown path between flanges while keeping the inductance low.

The gun flanges are connected to the capacitor bank (45 μF) through eighteen 80 cm lengths of low impedance coaxial cable ($Z_0 = 13$) in parallel, three ignitrons in parallel being used on each of the three capacitors. The ignitrons are fired with a controlled delay after the hammer blow. It is computed from the velocity of sound in the steel sonic transmission lines that the valves cannot open sooner than 750 μs after the hammer blow. Electrical contact between the hammer and the anvil starts a time delay circuit which fires the guide field capacitor bank and the gun banks after the appropriate delays. Normal gun delay with deuterium is 975 μs, which corresponds to a delay of 225 μs after the sound wave from the hammer blow reaches the valves. At this time the gas admitted to the system extends in a symmetrical roughly triangular distribution of density for about 40 or 50 cm along the gun barrel. A coaxial choke

* Conference paper CN-10/156, presented by John Marshall. Discussion of this paper is given on page 747. Translations of the abstract are at the end of this volume of the Conference Proceedings.

† The authors of the addendum to this paper are E. M. Little, J. Marshall, W. E. Quinn and T. F. Stratton, all of Los Alamos Scientific Laboratory.

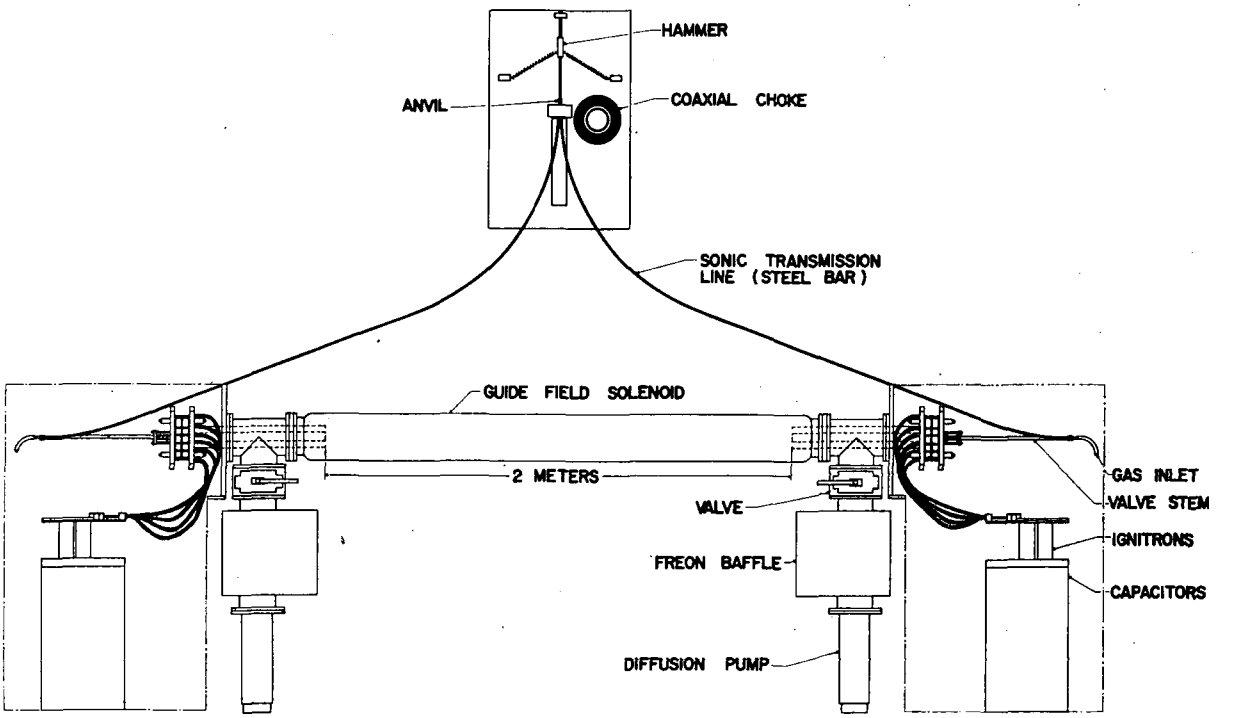

Fig. 1 General view of colliding plasma experiment.

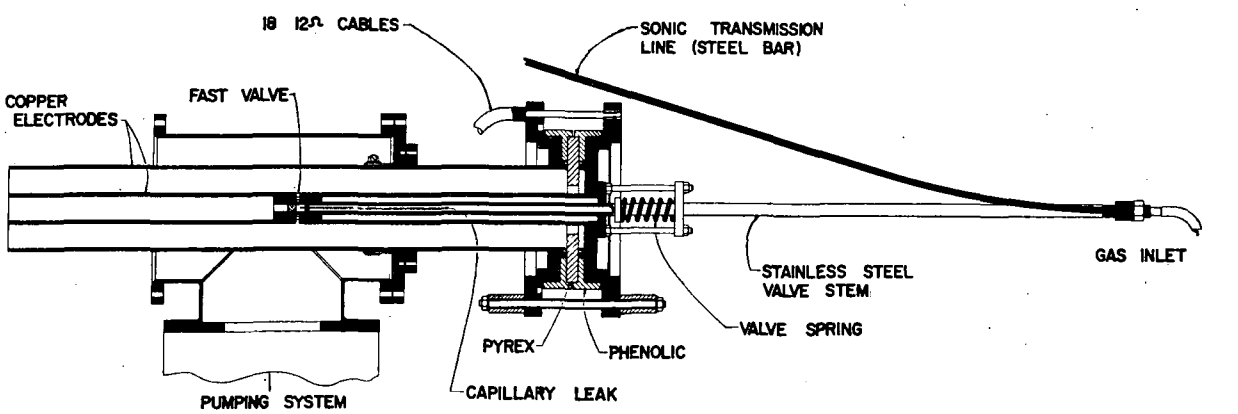

Fig. 2 Coaxial plasma gun assembly.

is used to isolate the hammer contact from the input to the delay circuits. This prevents destruction of the delay circuits by the high voltage which is applied to the hammer and the guns upon firing. The ignitrons of the gun capacitor banks are fired by a single trigger ignitron common to the entire system. It is arranged to connect the igniters of all 18 ignitrons to ground, each one through its own 50 Ω resistor. With the bank charged to 14 kV this amounts to 280 A per igniter. In the absence of a gas breakdown the bank is discharged partly through the igniters and partly through the coaxial choke.

The sonic transmission line provides an unintentional electrical connection between the center electrodes of the two guns. It might be thought that this would cause interference between the guns, making it impossible for instance, to fire one alone. The inductance of the transmission line, however, is very large compared to that of the guns and their associated circuitry and it turns out that, if the capacitor bank and ignitron trigger of only one gun are energized, that gun behaves quite normally and no plasma comes from the other one. It is possible to remove the gas supply from either of the guns, in which case that gun can certainly not fire, but this appears to make no difference in operation of the other gun.

Two separate pumping systems are used on the equipment, each one pumping through an annular space around a gun muzzle. Freon cooled baffles at about —30° C prevent pump oil from contaminating the system. Each baffle consists of a 15 cm diameter section of tubing with four overlapping internal vanes arranged alternately from the two sides. External

cooling makes impossible the migration of oil through the baffle along warm surfaces. The base pressure appears to be about 3×10^{-7} torr, and normally between shots the pressure falls to about 10^{-6} torr. Most of the vacuum seals are made with lightly greased neoprene "O" rings. The total pumping speed on the system is about 300 liters/s.

Each gun with its pumping system and capacitor bank is mounted on wheels so that it can be pulled away from the end of the experimental tube in which the plasma is observed. The capacitor bank is in a shielded box with ground connections made at the gun flange to reduce ground loop interference. The sonic transmission line and hammer assembly cannot easily be shielded. It appears, however, that the currents in the transmission line are small enough not to introduce serious interference with measurements.

The solenoid which provides the axial magnetic guide field in the drift space between the two guns is energized by a capacitor bank normally run at 2.5 kV or less and capable of storing up to 200 kJ of energy. It is wound with welding cable, convenient during winding because of its flexibility, and is covered with glass tape and epoxy resin which supplies adequate support against magnetic forces. Originally in one-gun experiments a solenoid wound on glass was tried. It appears that rather serious difficulties in interpretation of magnetic diagnostics were introduced by interaction between the plasma and the solenoid. Emf's induced in the solenoid were large enough to produce significant changes in the magnetic field long before any plasma arrived at the place where measurements were being made. Accordingly all subsequent solenoids have been wound on a stainless steel tube 16.8 cm in diameter and with a 3.2 mm wall thickness. The L/R penetration time of such a conducting shell is short enough for magnetic field from the slow solenoid circuit to get in, but long enough so that it can be considered a perfect flux-conserving surface during plasma measurements. Interaction between the plasma and the conductors surrounding it is reasonably well localized, and rather simple boundary conditions are imposed on the field. The inductance of the solenoid can be reduced to reasonable values by winding several cables in parallel. The rise time of the magnetic field is arranged to be comfortably less than the 975 μs delay between hammer blow and gun firing time. Thus by appropriate timing of solenoid switching, the magnetic field can be made approximately constant during the time of interest for plasma collision.

During measurement with one gun it was found that appreciable currents sometimes flowed between the plasma and the conducting walls of the drift space. These produced violent fluctuations in magnetic fields as measured with probes, and accordingly an insulating glass cylinder was inserted between the plasma and the wall. The glass cylinder interferes with the insertion of probes, but provides a convenient surface on which to support magnetic pick-up loops. These pick-up loops provide a considerable amount of averaging when, for some reason, the plasma moves from side to side of the tube, and thus give more nearly reproducible signals than probes.

The muzzles of the two guns are two meters apart, this rather long distance being chosen to allow the faster parts of the plasma to separate from the slow parts and to allow room between the guns for attempts at trapping portions of the plasma with magnetic mirrors and the like. This distance has tended to become rather inflexible because of the inconvenience of changing the lengths of the sonic transmission lines.

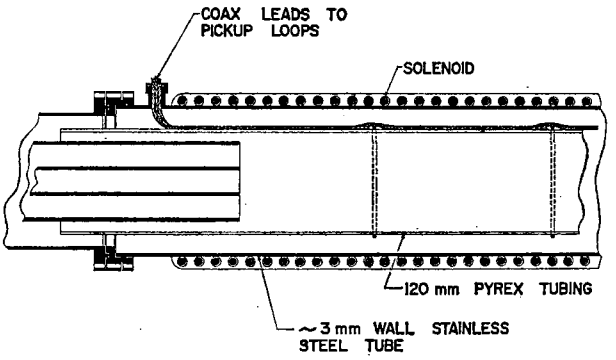

Fig. 3 Arrangement of gun muzzle and evacuated drift space with axial magnetic field and magnetic pick-up loops.

An alternate arrangement to that shown in Figs 1 and 3 has been used in which the insulating glass tube has formed the vacuum wall with the solenoid on its stainless steel tube split in two to allow optical observation in the plane midway between the guns. A probe can be inserted through a glass tubulation in this plane.

3. Operation

One gun and two gun experiments have been carried out over a considerable range of parameters such as gun voltage, gas load, delay between gas admission and firing, and guide field strength. The operation of the system is sensitive to all of these and unfortunately to some additional uncontrolled ones. The uncontrolled parameters result in an unexplained variation from time to time of the operation of the system. There is considerably more variation than is explainable by adsorbed gas which must always be removed from the walls of the system by a few preliminary discharges at the beginning of a run.

3.1 One gun

The operation of a gun with the particular design we are using, and with our particular set of controllable parameters set as we set them, can be summarized as follows: Enough time is allowed after opening the fast valve for the gas to be spread well along the gun barrel. The ignitrons are then fired so that the capacitor bank (45 μF charged to 14 kV) is connected to the gun terminals. The voltage across the gun terminals rises surprisingly slowly at first, taking about 0.2 μs to charge the cable capacity to

5 kV. At this voltage the gun breaks down, the voltage drops nearly to zero and then rises more rapidly than before as the ignitron resistance drops. The current rises nearly linearly to about 5×10^5 amperes in 1.5 μs while the voltage comes up to a maximum of 9.2 kV in 0.4 μs. During this time the radial discharge between the electrodes is driving rapidly away from its initial position near the gun terminals and the inductance is rising rapidly so that the current behavior is violently non-sinusoidal, requiring 5 μs to return to zero from peak current. Just before zero current another breakdown occurs near the gun terminals, and another discharge is driven along the gun. The second and subsequent half cycles are much reduced in amplitude, most of the bank energy having been dissipated during the first (See Fig. 4).

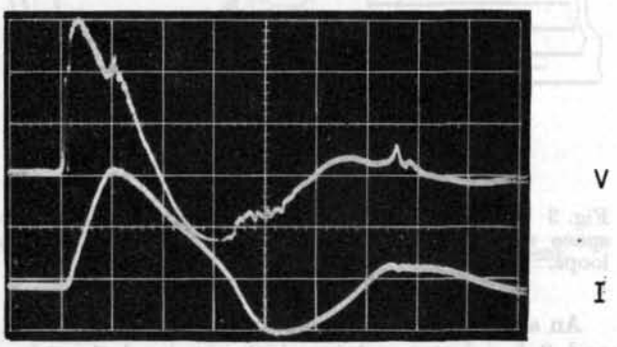

Fig. 4 Gun voltage (V) and current (I) as a function of time. Sweep, 2 μs/cm; V_{max}, 9.2 kV; I_{max}, $\sim 5 \times 10^5$ A.

The first plasma emerges from the gun muzzle 2.5 to 3 μs after gun breakdown. It has a high velocity front, with speeds as great as 10^8 cm/s, depending strongly on gun parameters, followed by a large burst of plasma moving at about 10^7 cm/s. Most of the plasma appears to originate at the end of the initial gas load in the gun at about the time that a current sheath moving at 2×10^7 cm/s would arrive there. The high velocity front may be due to some phenomenon associated with the transmission of a hydromagnetic shock wave inside the gun through the gas surface into vacuum.

Some effort was made to diagnose magnetically the behavior of the plasma from a single gun as it moved along a guide field. This work was done before the two gun system was completed, and so unfortunately the conditions were different from those which later appeared to be of most interest for the two gun experiment. The magnetic guide field was approximately 2500 G and the gun bank voltage was 12.5 kV. Hydrogen gas was used. The magnetic measurements are capable, as is explained in the appendix, of giving values of the line density of transverse plasma energy. It was found that at a position 35 cm from the muzzle the diamagnetic signal rose to a value corresponding to a transverse plasma energy of 2 to 3 J per cm, remained roughly constant for about 5 μs, and then fell off to zero in another 4 μs. The front of the diamagnetic signal was due to the high velocity plasma front, the later parts coming from plasma of continuously diminishing velocities.

The total transverse energy flux, injected by the gun into the guide field, could be estimated by multiplying the line density of transverse energy, as a function of time, by velocity, also as a function of time, and integrating. Velocities for this purpose were determined from streak camera photographs. Analysis of one set of data gave a total transverse energy of 360 J injected by the gun into the guide field. An analysis of this sort depends on the assumption that the plasma simply streams past the point of measurement with velocity as measured. This appears to be true at small guide field values. At higher fields, however, a large part of the plasma is stopped by the field, some of it presumably being reflected and some apparently leaking into the field as a low β plasma.

An attempt was made to measure calorimetrically the total energy of the plasma injected into the guide field. Difficulties were encountered, caused by the fundamental incompatibility of a good calorimeter with a pulsed magnetic field. Conditions which gave an estimated transverse energy total of 360 J delivered only about 200 J to a graphite disk. A part of the discrepancy may be due to errors in the transverse energy measurement, but some part is probably caused by reradiation from the hot graphite surface before the heat has had an opportunity to spread throughout the disk.

3.2 Two guns

The measurements employed on the two-gun experiment have made use of magnetic pick-up loops, magnetic probes, spectroscopic observations, both time resolved and integrated, and neutron measurements, also time resolved and integrated.

3.3 Hydrogen

The first experiments were performed with hydrogen plasmas which were observed with magnetic pick-up loops. The loops involved were placed at various positions along the drift space between the guns. The signals from only two of them are shown in Fig. 5, those two being 10 cm apart symmetrical to the midplane. For the discharges shown in the figure the guide field was 6800 G and the gun banks were charged to 12.5 kV. One-gun discharges showed a diamagnetic signal, associated mostly with the fast plasma component, moving away from the gun which was fired, and falling in amplitude with distance. The two-gun shots showed an initial diamagnetic signal which, within the reproducibility of the measurements, was a linear addition of the signals from the two guns fired separately. This was followed by a relatively large signal which reached its peak ~ 10 μs later. The amplitude of this signal was larger than that of the two guns separately at that time by a large factor, approximately 20. Loops at other

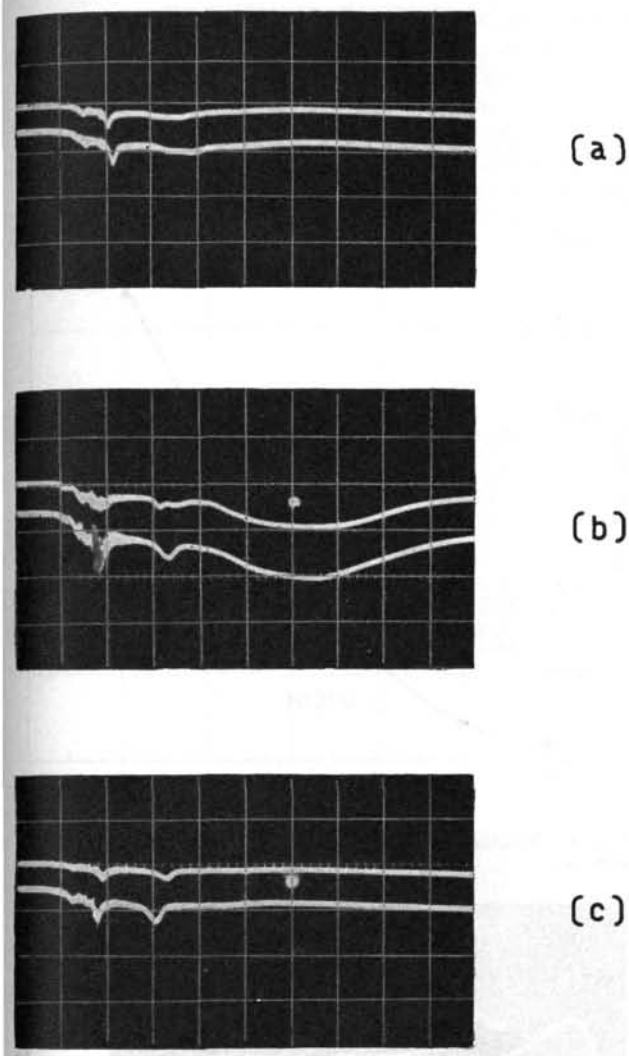

Fig. 5 Time dependence of signal from magnetic pick-up loops for one and two gun operation with hydrogen. Sweep, 2 μs/cm; 1 cm vertical deflection corresponds to 2.5 J/cm total transverse energy increment. (a) Gun 1, (b) Gun 1 and 2, (c) Gun 2.

positions show that the slow late signal is spread out along most of the length of the drift space. In the figure a deflection of 1 cm on the oscilloscope corresponds to a transverse line energy density of 2.5 J per cm length.

We infer that in this experiment the plasma injected by a single gun into the guide field had a fast front with a transverse energy density near the center of the drift space (~ 100 cm from the gun muzzle) of about one joule per cm, but with a particle density too small to produce an appreciable interaction when the two plasmas collided. The fast front is followed by a slower component (velocity $\sim 10^7$ cm/s) having a very small transverse energy and a particle density large enough to produce a large interaction between the two plasmas which causes conversion of axial into transverse particle energy. A crude estimate of the number of particles involved can be made by combining the estimated axial particle energy before collision with the measured transverse energy density after collision. The axial particle energy is assumed to be randomized by the collision into all three degrees of freedom. A total transverse energy of 3 J/cm, with a reasonable value of β, implies a transverse particle energy density of ~ 2 J/cm. At an average particle energy of 50 eV (10^7 cm/s protons), this would require a line density of 2.5×10^{17} particles per cm. If we assume the plasma after collision to occupy 25 cm^2 of area, this means a particle density of 10^{16}/cm^3. Such an area does not appear to be unreasonable when we remember that a magnetic field of 6800 G has an energy density of $B^2/8\pi = 0.184$ J/cm^3, so that the minimum possible plasma area ($\beta = 1$) is 11 cm^2.

We have found no means of measuring the area occupied by the low-β, slow plasma component. The signal from a magnetic probe which intersects the two-gun fast plasma component is clearly perturbed seriously by the foreign plasma derived from the probe itself. Loop measurements near the muzzle of either gun appear to indicate the presence at reasonably high fields of a tongue of high energy density plasma which extends some distance into the guide field (~ 50 cm), and in which the slow component appears to be stopped. The low-β, slow plasma which we observe in collision may be derived from mirror leakage of the stopped plasma into the field. Whatever the mechanism may be, it must be rather efficient, since after collision the slow component occupies approximately one meter of length which, at the density inferred above, would give a total of 2.5×10^{19} particles. This is approximately one quarter of the total number of protons admitted to the guns by the fast valves. To account for the interaction between the slow plasma components, large angle scattering cross-sections of 10^{-17} cm^2 are required. Such cross-sections appear to be compatible with the particle energies assumed. Actually, of course, the plasma does not in reality consist of two definite components, but must contain a continuous gradation of densities and energies covering the entire range. This introduces an element of fiction into the particle density computed above.

3.4. Deuterium

Immediately after the experiments described above, two gun operation was repeated with deuterium instead of hydrogen. Neutrons were observed with a silver radioactivity counter. With operating parameters adjusted as they had been for hydrogen, no neutrons were seen, but it was found that with a somewhat higher gun bank voltage, together with a critical adjustment of delay between gas admission and firing, a considerable number of neutrons per discharge could be made. Figs 6, 7, and 8 show the dependence of neutron yield on delay, strength of guide field, and gun bank voltage. Any inconsistancies from curve to curve reflect changes with time in system behavior.

With the system adjusted to produce the maximum number of neutrons, the slow component has a dia-

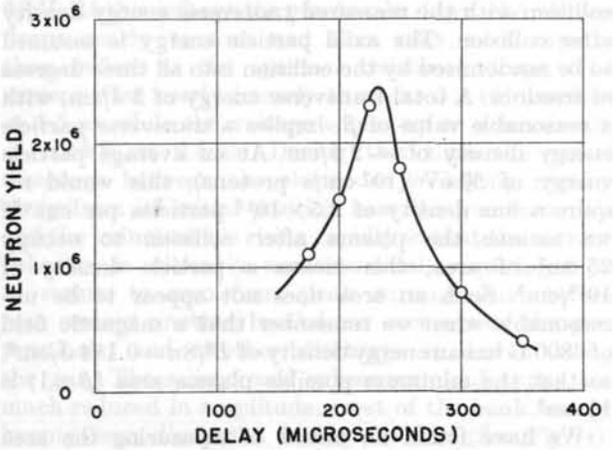

Fig. 6 Neutron yield *vs* delay between gas admission and firing of guns. Two guns; gun bank voltage, 14 kV; B_z, 8000 G.

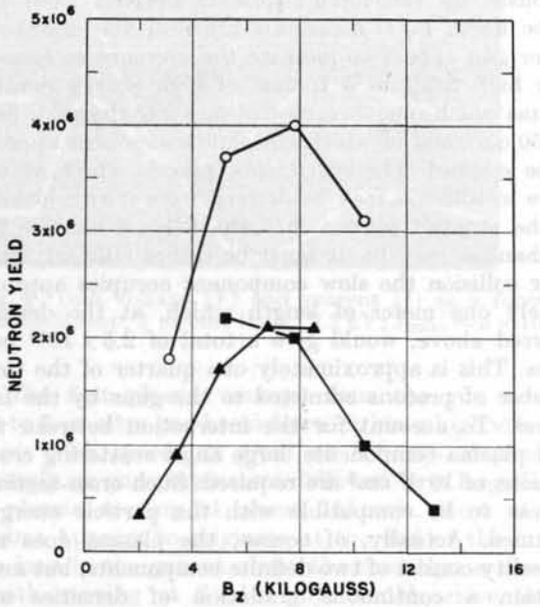

Fig. 7 Neutron yield *vs* strength of guide field. Two guns; gun bank voltage, 14 kV.

magnetic signal relatively smaller than it was before, and, in fact, with deuterium we have never been able to reproduce the traces shown in Fig. 5. The slow component is still present; it is simply less pronounced relative to the fast component.

The neutrons furnish a powerful diagnostic tool in this experiment, both qualitative and quantitative. First of all, it is possible to obtain some idea of the region over which collisions are taking place by the spatial distribution of the neutrons. Normally we place the silver counter close to the tube surrounding the drift space and midway between the guns. This is the position in which the intensity is largest. By measuring the neutron intensity as a function of the distance between the tube and the silver counter we are able to establish that the intensity falls off less rapidly than the inverse square law which would correspond to a concentrated source in the center of the drift space. The variation with distance is in fact consistent with a line source roughly a meter long.

Using a plastic scintillator and a photomultiplier we are able to make time resolved measurements of the fast neutrons from the plasma collision. By moving the scintillator from one position to another we have been able to establish the approximate positions from

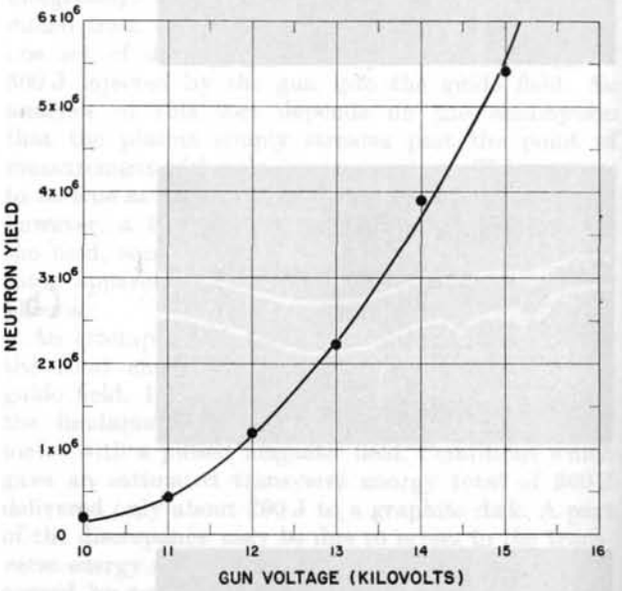

Fig. 8 Neutron yield *vs* bank voltage. Two guns; B_z, 8000 G.

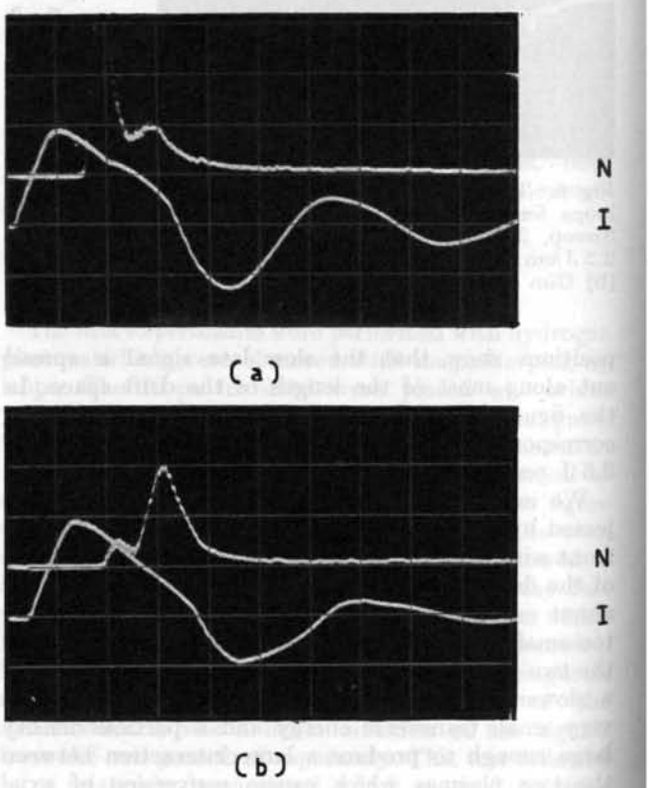

Fig. 9 Time dependence of neutron pulse on B_z. Scintillation detector near end of solenoid. Two guns; sweep, 2 μs/cm. N—neutrons, I—current; (a) $B_z = 1300$ G. (b) $B_z = 8500$ G.

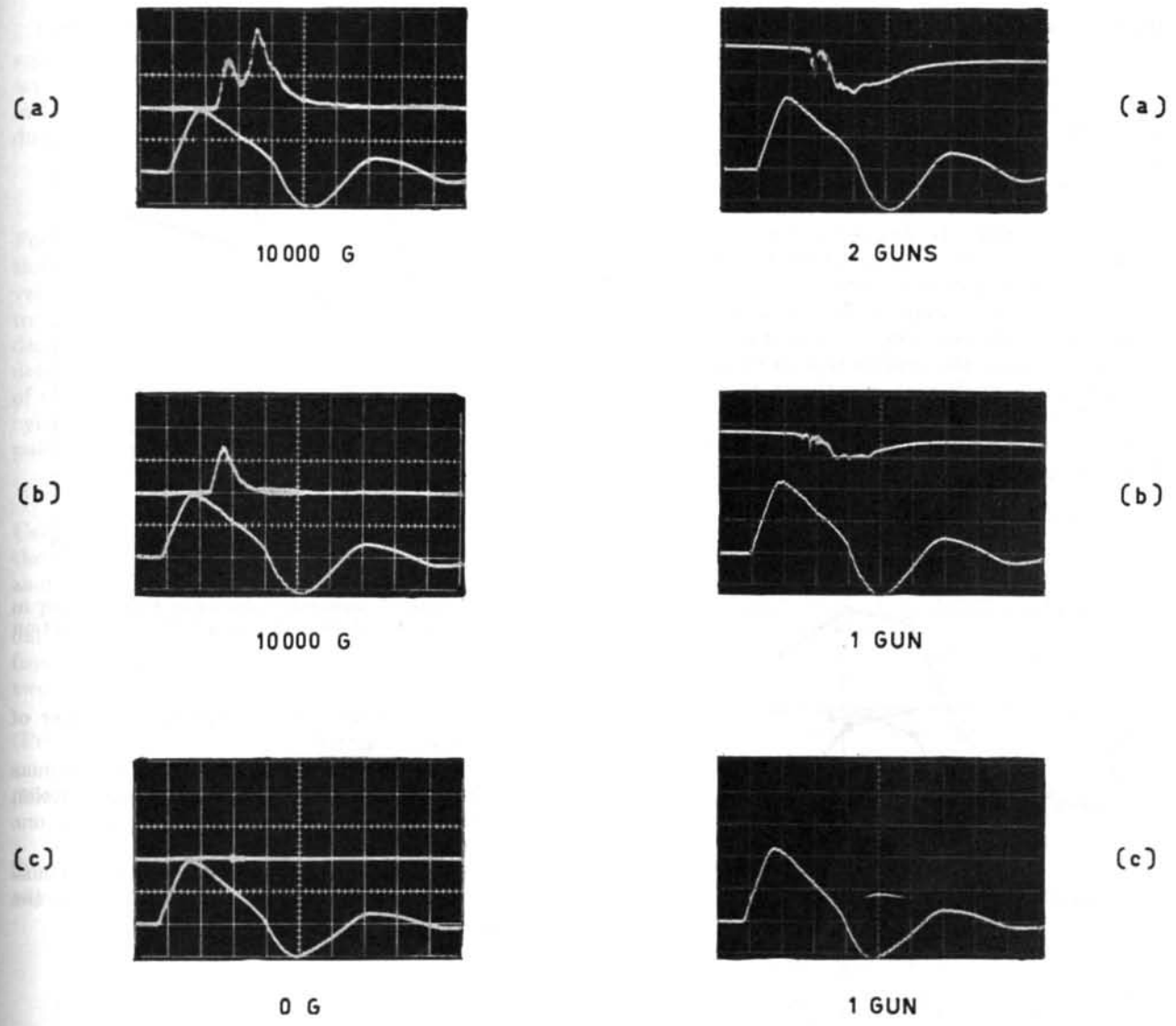

Fig. 10 Time dependence of neutron yield and diamagnetic signal with one and two guns at 10 kG. Sweep, 2 μs/cm. (a) 10 kG, 2 guns; (b) 10 kG, 1 gun; (c) 0 G, 1 gun. (Note: The labels are ambiguous. *Both* top curves are for "10000 G, 2 guns", *both* middle curves for "10000 G. 1 gun", etc.)

which neutrons come at various times. We find that at low and medium fields the neutron production begins, as we would expect, when the fast plasma fronts first intersect, as shown by their diamagnetic signals. The neutron intensity then rises to a maximum and decreases again to zero, making an approximately triangular pulse of full width one to two μs depending on conditions. This is what would be expected from two uniform rods of plasma passing through each other, the two rods moving in opposite directions at a constant velocity. We do not wish to imply that this is what actually happens, but the model is so simple and easily analyzed that it is an attractive one to use provisionally.

We find that, as the magnetic field is raised toward our limit of 13 kG, an earlier neutron peak appears. It occurs just when the fast plasma front enters the guide field. By moving the detector we have established that the neutrons originate from just inside the end of the guide field, and we infer that this represents the fast plasma component colliding with a portion of itself which has been stopped by the end of the guide field. These neutrons are present with one or two guns and are not present in the absence of guide field (See Fig. 10).

The silver counter is one which has been used on other experiments in the past, and which was calibrated with D-D neutrons from a Cockcroft-Walton machine. We have used that calibration, suitably adjusted for the different spatial extent of our source. We are thus able to measure absolute numbers of neutrons with sufficient accuracy for the analysis which appears below.

From the diamagnetic signal we can obtain a measure of the total transverse energy density of our plasma, and from the neutron yield we can derive information about the number of deuterons involved in the collision between the fast plasma components

from the two guns. However, we still need to know the areas of the two colliding plasmas, since these are involved in the number of neutrons. An attempt was made to obtain such information with a magnetic probe. One of our guide field coils is provided with a gap in the median plane, and it was possible thus to insert a probe from the side there. Measurements were made of the value of B_z seen by such a probe as a function of radius. It was found immediately that, inside the plasma, the readings of the probe were quite unreliable. The magnetic perturbation observed was considerably larger than it should have been to be compatible with loop signals, and had a different time dependence. We assume this to be due to large amounts of energy deposited on the probe surface from the two moving plasmas, this producing a local plasma of high energy content composed of material coming from the quartz probe envelope. However, although

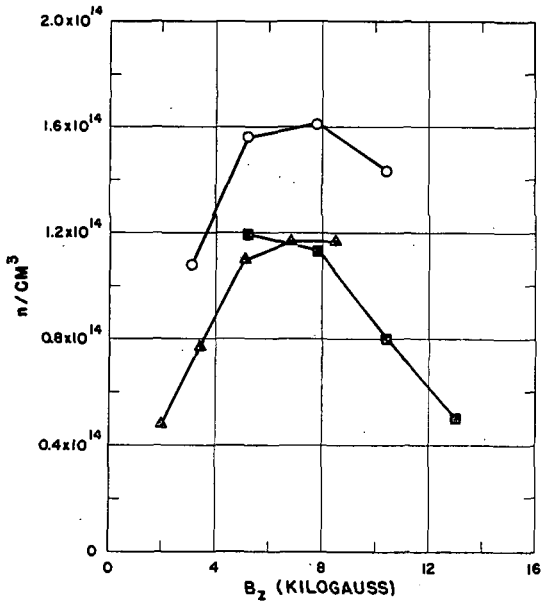

Fig. 11 Computed deuteron density in collision region of fast plasma components as a function of B_z.

the probe is unreliable inside the plasma, it is quite reliable outside, and we believe that we have been able to establish a reasonably accurate boundary for the plasma. We find that the fast plasma has an area almost independent of the strength of the guide field and that its diameter is approximately equal to that of the gun. Clearly unexplained phenomena are occurring in the entry of the plasma into the field.

With the various bits of information discussed above we are able to obtain a considerable amount of quantitative information about the colliding plasmas. We have found it necessary to make a number of simplifying assumptions in order to obtain results. We do not intend to claim these assumptions to be really true, but they represent a close enough approximation to the fact that we believe the results have some validity. The assumptions are as follows:

1. The fast plasma component moves all with one velocity.

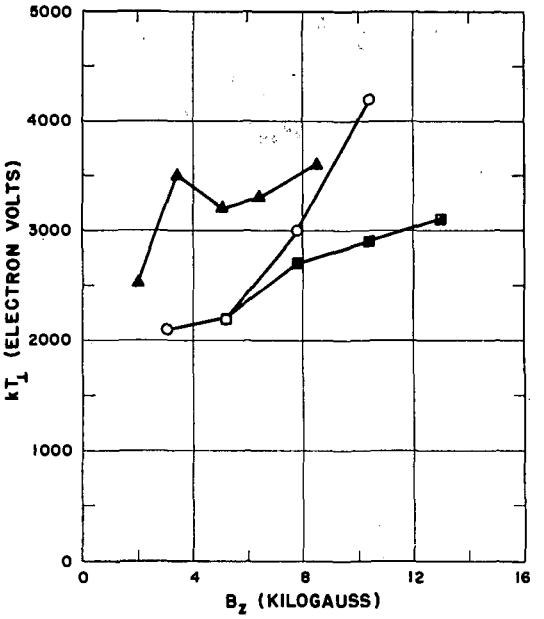

Fig. 12 Computed transverse deuteron temperature in collision region of fast plasma components as a function of B_z.

2. Its density is uniform throughout a cylinder of area α and length l.
3. The interaction consists solely of the two plasmas passing through each other, a negligible fraction of the deuterons being scattered upon one another.
4. As they pass through each other the two plasmas have the same speed and density, and occupy the same area α.

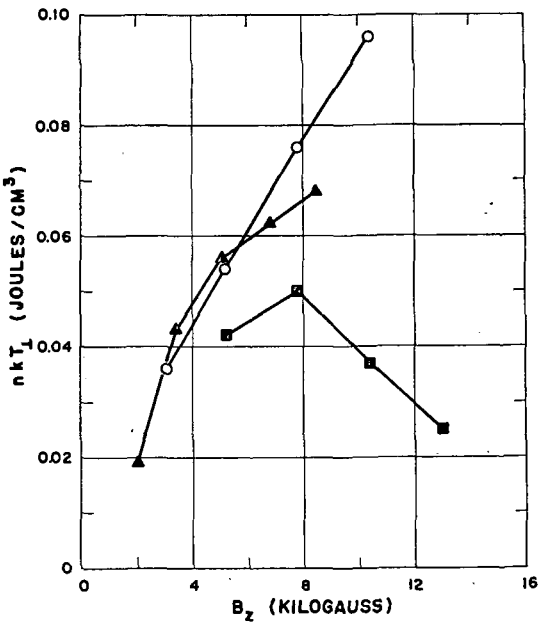

Fig. 13 Computed transverse plasma energy density in collision region of fast plasma components as a function of B_z.

Under these assumptions the neutron yield Y_n is equal to the total number of deuterons N in one plasma, multiplied by the number of deuterons per square cm in the other plasma, multiplied by the neutron production cross-section

$$Y_n = \frac{N^2 \sigma}{\alpha}$$

For the data we have analyzed, we have taken for σ the value corresponding to a deuteron (plasma) velocity of 7.5×10^7 cm/s. The plasma area α is taken to be constant at 50 cm^2. To obtain the local plasma density we divide the total number of deuterons determined from the above equation by the volume of the cylinder of plasma. The length l of the plasma cylinder is taken to be the full duration of the neutron pulse multiplied by the assumed plasma velocity:

$$l = (1.6 \times 10^{-6}\,\text{s}) \times (7.5 \times 10^7\,\text{cm/s}) = 120\,\text{cm}.$$

Using this value of l we are able to obtain a value for n, the plasma density, from the total number of deuterons as determined above.

To determine the transverse temperature and β of our plasma we use the diamagnetic signal information from the flux loops together with the density. We have two equations which must be obeyed simultaneously.

(Pressure balance) $$n\,\mathrm{k}\,T_\perp = \beta \frac{B^2}{8\pi} \qquad (1)$$

(Flux conservation) $$B_0 A = B(A-\alpha) + \sqrt{1-\beta}\,B\alpha. \qquad (2)$$

The symbols used are defined in the appendix. Eliminating β we obtain

$$n\,\mathrm{k}\,T_\perp = \frac{B^2}{8\pi} - \frac{[B_0 A - B(A-\alpha)]^2}{8\pi\alpha^2}. \qquad (3)$$

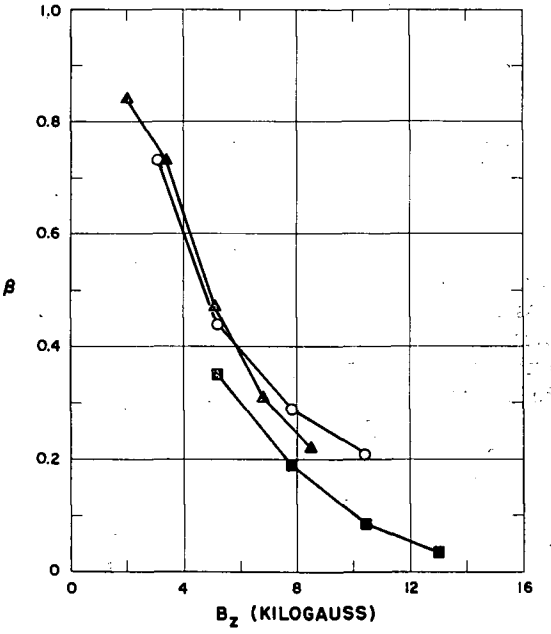

Fig. 14 Computed value of β ($8\pi n\,\mathrm{k}\,T_\perp/B^2$) in collision region of fast plasma components as a function of B_z.

Experimentally the quantities used are B_0 and $\Delta B = B - B_0$, where ΔB is the flux change in the pick-up loop divided by the area outside the loop into which the flux is compressed, i.e. $\Delta B = \Delta\Phi/(A-a)$. From this we get

$$n\mathrm{k}T_\perp = B_0 \Delta B \frac{2A}{8\pi\alpha} + \frac{\Delta B^2}{8\pi}\left[2\frac{A}{\alpha} - \frac{A^2}{\alpha^2}\right] \qquad (4)$$

$$\beta = \left[\frac{2B_0 \Delta B + [2-(A/\alpha)]\Delta B^2}{(B_0 + \Delta B)^2}\right]\frac{A}{\alpha}. \qquad (5)$$

In each case ΔB is used as measured near the center of the drift space at the peak of the neutron pulse indicated by the scintillation detector. The total number of neutrons is measured with the silver counter. A number of runs at different times are combined in the results shown in Figs. 11, 12, 13, and 14. Different points taken during one run are averaged, but the results from different runs are plotted separately.

3.5. Spectroscopic observations

A considerable amount of effort was spent on spectroscopic observation with a relatively meager return. The results for two-gun operation can be summarized as follows: Without time resolution the strongest lines are those of the deuterium Balmer series, but in addition numerous lines of silicon, oxygen, calcium and sodium are observed, some of these showing an obvious maximum of intensity in the vicinity of the walls. Presumably these impurities all come from Pyrex, but it has not been definitely established whether they all come from the glass tube between the plasma and the stainless steel wall of the drift space, or whether some of the material comes from the glass insulator in the breech of the gun. No copper is observed, although the electrodes are of copper, and although the surface of the tip of the central electrode is apparently melted slightly under some operating conditions. Carbon lines have been observed. Some of the impurity lines appear only away from the wall. Generally these are of multiply ionized states, but none require an electron temperature of more than a few volts.

Time-resolved spectroscopy has been performed to a limited extent and shows that the light of most impurities has an initial intensity envelope which matches rather closely the diamagnetic signal. This is taken as indicating that the impurity radiation is excited by a bombardment of the walls which is roughly proportional to the energy content of the plasma. Whether this is particle bombardment or some other type of radiation we do not know, but the fact, now known, that the plasma boundary is not far from the wall makes it seem plausible that particle bombardment could be occurring. Many impurity lines, notably the sodium D lines, persist longer than the diamagnetic signal, with a later intensity maximum lasting for varying lengths of time occurring after the end of the diamagnetic signal.

The Balmer light falls into two categories. Initially light is emitted with a time behavior like that of most

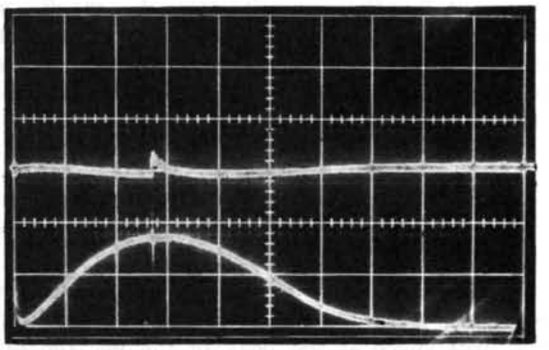

1 GUN

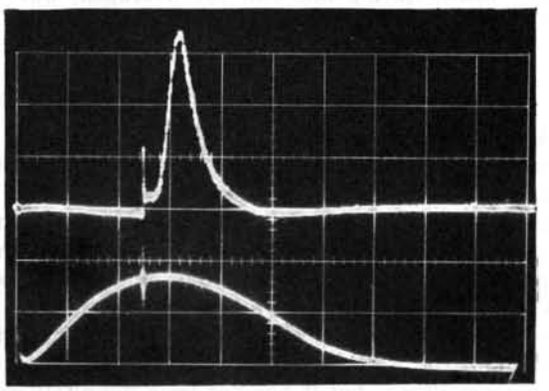

2 GUNS

Fig. 15 Intensity of D_β line as a function of time for one gun and two gun operation. Sweep, 200 μs/cm. The lower trace shows B_z *vs* time.

impurities, i.e., the intensity is roughly proportional to the diamagnetic signal. At the end of the diamagnetic signal the Balmer intensity, which has decreased to perhaps one quarter of its maximum so far, starts to increase again, rises for about 100 μs to a value 2 to 5 times its initial maximum and then falls off again reaching zero after another 250 μs. This is the behavior with two guns. With one gun alone, the long persistance signal is missing entirely. A possible explanation of the Balmer light behavior is that the initial light is actually from deuterium absorbed on the wall, which is blasted off by plasma particles or radiation just like any other wall impurity. This deuterium is never highly ionized but radiates immediately after excitation. The initial plasma is fully ionized and has electron temperatures too high for any appreciable amount of Balmer light to be emitted. At the end of the diamagnetic signal, however, this plasma has either cooled off or has gone away, recombination can occur, and Balmer light is given off. Oscillograms of the time history of D_β light are reproduced in Fig. 15.

We find a strong qualitative difference between the impurity content of the plasma for short and long delays of gun discharge time. If the guns are fired early the plasma has a white appearance to the eye, and the impurity lines are stronger than the Balmer lines. At the delay for optimum neutron intensity, and for all later delays the plasma has the pink appearance of a hydrogen discharge and the Balmer lines are relatively strong as seen with the spectrograph. We have not analyzed spectra taken with short time delays.

4. Conclusions

No evidence so far has been established for a two-stream instability in the plasma collision. Within the reproducibility of the diamagnetic measurements the transverse energy in the collision region of the fast plasma fronts is just the sum of the transverse energies from the guns fired separately.

The guns as described here are capable, when fired against one another, of producing from the fast components in the collision region a plasma with a transverse temperature of ~ 3 keV and a density of $\sim 10^{14}/\text{cm}^3$. This plasma occupies a volume of several liters and has axial particle energies larger than the transverse energies by a factor 2 or 3. Such a plasma is not ideal for loading a thermonuclear machine, but there is a good chance of capturing a part of it between the mirrors of a fast compression device such as Scylla [4], and, if this can be done, rather substantial temperatures and energies may be attainable.

Following the fast plasma component there is a slower component, observable by Coulomb scattering of the ions in one plasma by the ions in the other. The temperature is considerably smaller (~ 100 eV) than that of the fast component, but the density is high ($\sim 10^{16}/\text{cm}^3$) and the particles are presumably well randomized in direction. It may be that this dense, relatively cool plasma may provide a more practical charge for a thermonuclear machine than does the fast component. Plans are being made for an attempt at injection of Scylla with the guns used for these experiments. With the system as planned it should be easy to try either component.

Unexplained phenomena take place in the entry of the plasma into the guide field. The fast component appears to disregard the magnetic field over a wide range of field strengths. Its area and density are roughly independent of field from about 3000 to 10000 gauss. At higher guide field strengths a part of the fast plasma component is stopped by the field, but we do not understand why the plasma is not compressed into a smaller area by entry into larger fields. The slow plasma component enters the field with practically no energy on the transverse degrees of freedom. This may well be due to rejection by the magnetic mirror, formed at the boundary between the plasma and the field, of all but those particles moving nearly exactly along a field line. The particles presumably are scattered many times in the dense plasma piled up beyond the gun muzzle until they fall within the loss cone of the mirror. The fraction of particles injected appears, however, to be much larger than

would be expected ($\sim 1/4$ of the number of particles admitted to the gun). It is conceivable that a substantial fraction of the gas load of a gun is held between discharges as an absorbed layer on the gun electrode surfaces. There is support for this hypothesis since there is some neutron production for the first 2 or 3 discharges after the gun feed is changed from deuterium to hydrogen.

Acknowledgement

The work reported here* was performed under the auspices of the United States Atomic Energy Commission.

APPENDIX

Magnetic Diagnosis

Magnetic probing inside the plasma of a single gun can be done with some reliability, so long as one realizes that conditions downstream from the probe may be drastically changed by foreign plasma, blasted off the probe, and carried along by the moving plasma. Since the foreign plasma is carried away from the probe it may not affect very much the conditions just there. In a plasma collision experiment, however, the foreign plasma may not be carried away and may therefore interfere strongly. It is not necessary to insert a probe into the plasma itself to obtain a considerable amount of information regarding it. If the plasma is surrounded by a plasma-free magnetic field which in turn is surrounded by a flux conserving surface, the diamagnetic effect of the plasma can be measured by observing the increase of magnetic field strength near the wall when the plasma is introduced.

Attempts were made to diagnose the plasma from a single gun by probes between the plasma and the wall. Reproducibility from shot to shot was poor, but could be improved by using wire loops on the glass insulator between plasma and wall to measure the change of magnetic field. Such loops are advantageous in that their areas can be measured directly with reasonable accuracy and that their self inductance is much lower than that of probes for equal area.

We shall define here the symbols to be used in the discussion of magnetic diagnosis.

A = area of flux conserving tube.
a = area of pick-up loop.
α = area of plasma.
B_0 = magnetic field (axial) before introduction of plasma.
B = magnetic field measured outside of the plasma.
B_p = magnetic field inside the plasma.
$\beta = 8\pi n k T_\perp / B^2$ = the ratio of the plasma pressure to the pressure of the exterior magnetic field.
$T_\perp$ = temperature in the transverse degrees of freedom.
$K = (B - B_p)/B$ = the fraction of magnetic field excluded by the plasma. K is related to β by the equation $(1-K)^2 = 1-\beta$.
U = line density of energy inside the flux conserving wall. It is the total magnetic and transverse plasma energy per cm length.
U_p = the line density of transverse plasma energy.

Magnetic measurements between plasma and wall, with either loop or probe are capable of giving an indication of the transverse energy of the plasma. The equation of pressure inside the plasma to that outside

$$\frac{B^2}{8\pi} = n k T_\perp + (1-\beta)\frac{B^2}{8\pi}$$

is also an energy density equation. The total energy in a one cm length of tube is then simply the energy density of the magnetic field near the wall multiplied by the area of the tube.

$$U = A\frac{B^2}{8\pi}.$$

The line density of energy in the tube is increased by the introduction of the plasma, and its increment can be computed directly from the measured increase of field.

$$\Delta U = A\frac{B^2}{8\pi} - A\frac{B_0^2}{8\pi} = \frac{A}{8\pi}(2B_0\Delta B + \Delta B^2).$$

The increase of energy so measured is due partly to the transverse energy of the plasma and partly to magnetic energy increment coming from compression of the original field. If the plasma is assumed to be uniform over an area α and to have a magnetic field in it

$$B_p = B(1-K)$$

then the transverse energy of the plasma is a fraction

$$\frac{U_p}{\Delta U} = \frac{2-K}{2-K(\alpha/A)}$$

of the total energy increment. This fraction is always larger than 1/2. For reasonable values in our case ($K = 1/2$, $\alpha/A = 1/4$), it becomes ~ 0.8.

ADDENDUM

Injected Magnetic Compression Experiment

Since the submission of the above paper, further work has been done using the same guns for the injection of plasma into the Scylla III fast compression magnetic mirror machine [5]. The arrangement is similar to that of the colliding plasma experiment except that the magnetic compression coil is interposed midway between the guns. Auxiliary coils and slow capacitor banks are arranged to produce a nearly uniform guide field in the evacuated space between the guns. The time of initiation of the fast compression field can be adjusted to any desired delay after gun firing so as to trap the various plasma components. The compression coil is approximately 40-cm in length

* Including material presented in the Appendix and Addendum.

with the field strengthened at the ends so as to give a mirror ratio of 1.2. The field rises to 70 kG in 2.5 μs.

It has been found possible to capture and compress deuterium plasma from the fast and the slow components with the compression field parallel or anti-parallel to the guide field. Energetic trapped plasma is indicated in each case by a pulse of neutrons with its peak near the time of maximum compression field. Neutron yields are highest with anti-parallel fields (up to 6×10^7 neutrons per shot), but perhaps it is significant that there are neutron yields also with parallel fields where there is no possibility of heating by reversed trapped field. With parallel fields neutrons are produced at two distinct delay times, one corresponding to the fast plasma with high transverse deuteron energies as inferred above, and one corresponding to the slow component which produces initial transverse energies by Coulomb collisions. With anti-parallel fields neutrons are produced for intermediate delays also. Successful injection has also been obtained with one gun, all plasma components leading to neutron yields with reversed fields, but only the fast component with parallel fields. It appears that with anti-parallel fields initial transverse ion energy is unnecessary for injection, but that it must be present with parallel fields.

References

[1] MARSHALL, J., *Phys. Fluids*, **3** (1960) 134.
[2] MARSHALL, J., "Plasma Acceleration", Proceedings of the 4th Lockheed Symposium on Magnetohydrodynamics, (Stanford University Press, California, 1960) 60.
[3] BUNEMAN, O., *Phys. Rev.* **115** (1959) 503.
[4] BOYER, K. *et al.*, *Phys. Rev.* **119** (1960) 831.
[5] LITTLE, E. M., QUINN, W. E., RIBE, F. L., SAWYER, G. A., these Proceedings, page 497.

ELECTRODELESS PLASMA GUN*

F. WAELBROECK, C. LELOUP, J. P. POFFÉ, P. EVRARD, R. DER AGOBIAN, D. VÉRON

GROUPE DE RECHERCHES DE L'ASSOCIATION EURATOM-CEA SUR LA FUSION

FONTENAY-AUX-ROSES (SEINE), FRANCE

The discharge of a condenser bank (< 3 kJ) into a single turn conical coil encircling a tube injects a deuterium plasma consisting of $\leqslant 10^{19}$ particles (ions + electrons) into a longitudinal magnetic guide field ($B_z \leqslant 4000$ G). For various experimental conditions, velocities in the range 3×10^6 to 3×10^7 cm/s have been observed. For most of the experiments described here, the energy stored in the gun condenser bank was low (720 J); a set of experimental parameters were varied within rather broad limits.

The only identified impurity lines in the visible spectrum are weak C-lines. The velocity and longitudinal shape of the plasma were measured by magnetic loops, microwave techniques and photomultipliers, its momentum and radial distribution by ballistic pendula. The variation of the D_β line broadening as a function of time is being studied by means of a 10 channel (0.19 Å/channel) analyser. For guide fields $B_z \leqslant 1000$ G, the collimation of the plasma beam appears satisfactory. The plasma puff is slowed down, and its luminosity enhanced, when the delay between the opening of the quick-acting valve (injecting the D_2) and the discharge of the gun is too long; a large number of neutral molecules is then on the beam trajectory. The effect of these neutrals increases when the guide field intensity decreases. The use of a crowbar on the discharge has confirmed the fact that little plasma is ejected during the first half-cycle of the discharge current (period = 6 μs). During the second half-cycle, the amount of plasma ejected is large when the gun and guide fields are parallel; when they are antiparallel, the amount of plasma ejected decreases as the guide field intensity increases. It is quite small for high guide field values. When the amount of D_2 introduced into the tube is small, the ejection occurs later: at the third, fourth or fifth half-cycle of the gun current. Small amplitude oscillations are usually detected on the magnetic loop signals. These frequencies are almost those of the ion cyclotron rotation in the guide field.

An approximate model predicts satisfactorily the shapes and amplitudes of the four magnetic loop signals (oscillations excepted) from hypotheses on the average ion and electron temperature, on the average velocity of the plasma, and on its initial shape.

1. Introduction

This article presents some results obtained by means of an electrodeless plasma accelerator [1, 2]. Its operation is analogous to that of the plasma gun described by J. MARSHALL [3]. Such accelerators [4] are found to produce fairly pure plasma puffs. But, in order to avoid perturbation of the gun operation and, above all, to avoid an alteration of the plasma purity, the fast valve used to inject the gas had to be situated a certain distance from the accelerator. A fraction only of the injected gas is transformed into plasma and the fast plasma puff is followed by some slow, neutral gas. This implies that a rather long distance must separate the accelerator from the bottle in which the capture of the puff will be attempted, since purity with respect to the neutrals has to be an objective. Fortunately, our plasma puffs ($n_e \geqslant 10^{15}$ cm^{-3}) are found to be guided by a longitudinal magnetic field; particle losses and wall-interactions are small.

We have not yet attempted to reach the limiting performances of the gun: the results presented here have almost all been obtained when only one-fourth of the maximum possible energy was stored in the gun condenser bank. We have rather tried to understand the influence of various experimental parameters on the properties of the ejected plasma puffs. Such a study requires a sufficient reproducibility of the gun. This has been attained through the almost complete automatisation of the experiment, the use of pre-ionization, and of a crowbar system on the gun. The reproducibility is illustrated on Fig. 1: each curve consists of three superimposed magnetic loop signals under the same experimental conditions.

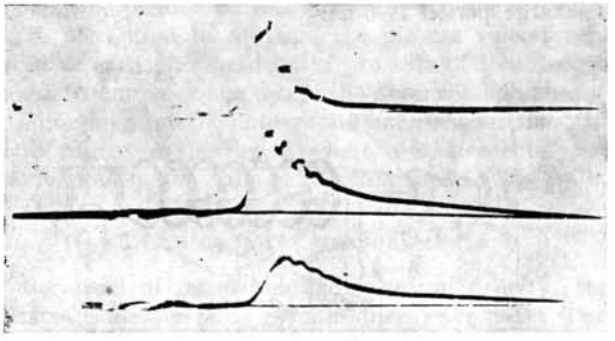

Fig. 1 Reproducibility test: 4 superimposed experiments, 3 with and 1 without gas. Experimental conditions: $\tau = 700$ μs; $Q = 0.3$ cm^3-atm; C I; $E_0 = 12$ kV; $B_z = 1300$ G.

* Conference paper CN-10/103, presented by F. Waelbroeck. Discussion of this paper is given on page 748. Translations of the abstract are at the end of this volume of the Conference Proceedings.

2. Description of the accelerator

The experimental apparatus is illustrated on Fig. 2. A quick-acting valve injects some deuterium at one end of an evacuated tube. The gas is slightly pre-ionized. A short time later, the discharge of a condenser bank in a conical loop completes the ionization, compresses the resulting plasma and ejects it into a parallel magnetic field, which guides it, and minimizes its interaction with the walls.

The fast valve is entirely metallic, with the exception of a teflon gasket which separates the tube from a 0,3 cc plenum. D_2 is admitted into the plenum through a needle valve; its pressure can be varied between 0,1 and 2 atm; the filling time is about 1 s. A hammer falling from a constant height produces a blow which opens the valve for about 1 ms. The emptying time of the plenum is much shorter. Above a certain threshhold, the amount of gas injected is independent of the amplitude of the blow; for a given amplitude, the opening time of the valve can be reproduced to within ± 20 μs or less.

Except for the above-mentioned teflon gasket, all the apparatus is built of metal and glass (indium gasket). The base pressure is of the order of 10^{-7} mm Hg (100 litre/s oil diffusion pump and liquid N_2 trap).

The D_2 is slightly pre-ionized ($\approx 10^{10}$ electrons cm^{-3}) by means of four capacitively coupled electrodes, placed symmetrically around the tube, and fed by a 20 MHz, 200 W oscillator. The weak initial degree of ionization is sufficient to produce reproductible results.

The voltage E_0 on the accelerator condenser bank (10 μF) can be varied between 6 and 25 kV. The length of the conical loop is 5 cm; its extreme diameters are 7 and 9 cm; its inductance is about 65 mμH. The main parasitic inductance (≈ 25 mμH) is concentrated in the single spark gap used for the switching. The discharge period is 6 μs.

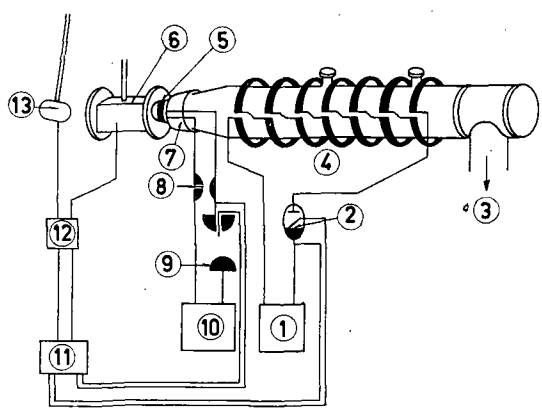

Fig. 2 Electrodeless plasma gun. Diagram of the apparatus. 1—guide field condensers, 2—ignitron, 3—pumping system, 4—guide field solenoid, 5—preionization electrodes, 6—fast valve, 7—conical coil, 8—crowbarring spark gap, 9—spark gap, 10—accelerator condensers, 11—delay lines, 12—pulse generator, 13—hammer. D_2 is admitted through needle valve (at left of 6 in above figure).

For small E_0 values, a succession of two or three plasma puffs, produced during different half-cycles of the gun current, are observed in the tube. This complicates the interpretation of the measurements. A crowbarring spark gap [5] is used to suppress all the puffs except the first. It can be operated at any desired time.

The discharge of a 480 μF condenser bank into a 12 μH solenoid produces the guiding field. Its period (550 μs) is much longer than the plasma transit time ($\leqslant 10$ μs) through the tube. The plasma, injected a few microseconds before the guiding field reaches its maximum value, moves along a stationary magnetic field. The solenoid is calculated to produce a homogeneous ($\pm 2\%$) field over a length of 45 cm. This was checked experimentally. The magnetic field intensity can be varied between 370 and 4050 G.

A pilot unit ensures that all the voltages of the various condenser banks can be reproduced from experiment to experiment with an accuracy of better than $\pm 0{,}5\%$ and that the pre-ionization operates for the same length of time before the discharge and is cut off just as the gun is fired, to reduce the noise level.

3. Diagnostic techniques

3.1. Ballistic pendula

The total momentum of the plasma puff has been measured by a large ballistic pendulum (8 cm diameter) and its radial distribution by a small pendulum (1 cm^2) placed at different vertical positions on a diameter of the tube. The pendula (teflon, mica or glass) hang at a distance of 41 cm from the conical coil. The magnetic field at this point is homogeneous, and it is not perturbed appreciably by the discharge of the accelerator. The pendulum deviations are read by a sighting telescope, with an eye-piece micrometer.

The plasma puff contains about 10% of the injected gas. Its momentum is calculated from the difference between the observed deviations when the valve is opened, and the gun is or is not fired. This last deviation is small.

When the small pendulum is located below the plasma puff, its suspension wires (0,2 mm diameter) receive still some momentum. A small correction was estimated, assuming the pendulum and wires to form a rigid body.

The compensated magnetic loops (see below) show that the plasma velocity after reflection from the large ballistic pendulum (Fig. 3) is roughly 30% of the incident velocity. We have used this value, and assuming that the masses of the incident and reflected beams are equal, have calculated the plasma momentum.

It was further confirmed that the observed momentum is independent of the nature (glass or teflon) of the pendulum material and that the small ballistic pendula results, integrated over the tube cross-section, yield a value of the total momentum which agrees which the large pendula measurements.

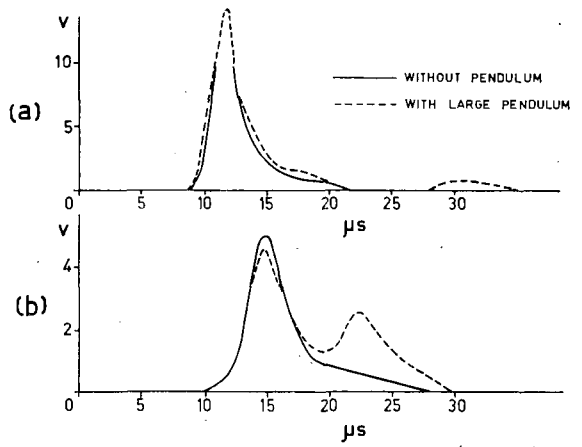

Fig. 3 Evidence of plasma reflection on the large ballistic pendulum. Experimental conditions: C.I.; $E_0 = 12$ kV; $B_z = 1300$ G; $Q = 0.3$ cm³-atm; crowbar used at the end of the 2nd half-cycle. (a) Compensated magnetic loop No. 1. (b) Compensated magnetic loop No. 2. ("C.I." = "Cusp I", see Section 4.3.3.)

3.2. Compensated magnetic loops

The plasma puff, moving along the guide field, induces an electrical signal in a loop encircling the tube. The advantage of this measurement, is that it hardly perturbes the plasma. In our set-up, the loop is parallel to the conical coil and to the windings producing the guide field. The addition of a compensating element to the loop reduces the effects of the oscillating currents in these coils. This "compensating element" is a winding (situated outside the tube, but inside the guiding solenoid) whose equivalent area is equal to that of the loop. The loop and the compensating element are wound in opposite directions. We have considered elsewhere [6] the advantages and drawbacks of this technique:

1) The compensated loop measures the longitudinal plasma shape more accurately than the uncompensated loop.
2) For rather long plasma puffs, the integrated signal V of the compensated magnetic loop is a fairly direct measure of the magnetic flux variation $\Delta \Phi_p$ within the plasma cross-section*:

$$V = \frac{1}{RC}\left[1 + \frac{r_p^2}{r_3^2 - r_p^2}\right] \Delta \Phi_p . \qquad (1)$$

r_p and r_3 are the plasma and the guiding solenoid radii. R and C are the resistance and capacity of the integrator circuit. For such a puff, moreover, $\Delta \Phi_p$ is related to the line density of transverse energy $N_i' \, k \, (T_e + T_i)$

$$\Delta \Phi_p = 2\pi B_0 \int \frac{\beta}{1 + \sqrt{1-\beta}} \, r \, dr \approx \frac{2\mu_0}{1 + \sqrt{1-\beta}} \frac{N_i' \, k \, (T_e + T_i)}{B_0} . \qquad (2)$$

B_0 is the magnetic induction, outside the plasma, β is conventionally defined as $\beta = 2\mu_0 p / B_0^2$ and N_i' is the ion line density.

* Giorgi units.

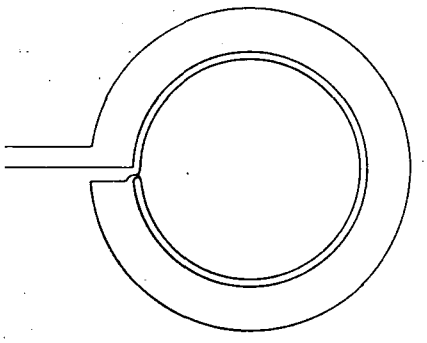

Fig. 4 Compensated magnetic loop. The geometry shown has a bandpass of over 10 MHz. Note: The crossing of conductors in the figure is somewhat ambiguous. The connections are such that the two inner conductors have parallel currents.

3) The compensating element increases the inductance of the system, and reduces its frequency response. The geometry shown on Fig. 4 has, however, a band-pass of over 10 MHz.

Four compensated magnetic loops, placed at various distances from the accelerator, yield useful information on the plasma shape, its velocity, its time of ejection from the gun, and its transverse energy.

3.3. Optical measurements

A "Huet 20" spectrograph (4000—6500 Å) has been used to survey the main impurity lines in the visible.

The time variation of the D_β and D_γ line broadenings is being investigated: The light coming out of a grating monochromator (4 Å/mm in the D_β region) is split up by a 10 channels glass-fibre analyser, and brought to appropriate photo multipliers. Each channel covers 0,19 Å.

Two photomultipliers (51 AVP Radiotechnique), looking perpendicularly towards the axis of the tube, have been used to measure the plasma velocity. In front of each photomultiplier two slits of 1 cm length and 0.01 cm thickness define the observed light beam.

Time-integrated photographs have shown that the light source in the region where measurements were made, was in the tube centre, and not at the walls.

3.4. Microwave measurements

Becaused of its rather high electron density, the plasma is opaque to an 8.6 mm microwave beam. Two methods have been used to measure the plasma velocity: the transverse method and the longitudinal method.

The transverse method is based on the fact that it is possible to observe the arrival of the plasma puff at a point on the axis of the gun by measuring the cut-off time of a microwave beam. This measurement, performed in two points sufficiently apart along the axis, gives the velocity of the puff between those two

* This experiment was described at the Fifth International Conference on Ionisation Phenomena in Gases, Munich, August 1961.

points (time-of-flight method). These velocities check fairly well with the values obtained by other devices. They are, generally speaking, from 30 to 50% higher. This is probably due to the fact that microwaves are already perturbed by rather low electron densities. The method yields the velocity of the fastest particles.

The longitudinal method has the advantage of giving the velocity variations as a function of time. In the absence of guiding field, or for small values of this field, the plasma front may be considered as a practically flat moving reflector. A horn-lens system radiates a plane wave along the tube axis. A small fraction of the incident wave energy is reflected by the plasma creating a periodic varying field of standing waves. The measurement of the frequency of this phenomenon gives practically the plasma front velocity along the whole tube. The first results are in good agreement with previously obtained data, see Table I.

4. Experimental results

4.1. Impurity lines in the visible spectrum

The plasma is not very luminous. It takes about 50 to 100 discharges to produce a reasonable exposure of D_β on a photographic plate. These plates show:

1) the D_α, D_β, D_γ lines;
2) a C^+ line and a C^{++} doublet which are faint when 10 discharges are produced before the plate is exposed and when the liquid nitrogen trap is used;
3) a single unidentified impurity line at about 4662 Å, which appears whenever the high frequency pre-ionization is used.

4.2. Influence of delay between valve opening and accelerator discharge

The performance of the plasma accelerator is a function of the D_2 distribution in the tube when the gun is fired. If the discharge occurs soon after the valve is opened, the D_2 pressure in the conical loop is small. If one waits too long, a large amount of plasma is ejected, but it is slowed down and cooled by collisions and charge-exchange reactions with the neutral molecules beyond the conical coil.

We have studied the distribution of the D_2 molecules as a function of time and of space, by means of a fast ionization gauge described by J. Marshall [7]. The absolute calibration of the ion current as a function of pressure still presents some difficulties in the high pressure range (~0.1 mm Hg). The deuterium arrives at the centre of the coil about 400 μs after the hammer blow. The pressure increase is rapid until 700 μs, then it is slower. A pressure maximum occurs between 1000 and 1200 μs. At 700 μs, when 0.3 cc atm of D_2 is injected, the pressure is somewhat above 0.1 mm Hg at the entrance of the coil and about 5×10^{-2} mm Hg at the exit. It decreases progressively beyond this point, to a value of 6×10^{-3} mm Hg at a distance of 25 cm from the coil, it is less than 10^{-3} mm Hg 10 cm further.

These measurements are in agreement with our interpretation [1] of previous experimental results. The optical measurements are quite sensitive to the presence of neutral molecules on the beam trajectory: the intrinsic plasma luminosity is weak. The D_2 molecules encountered act as scintillators, emitting strongly in the front of the puff. For small values of τ (the time interval between the hammer blow and the accelerator discharge) the signals observed on our

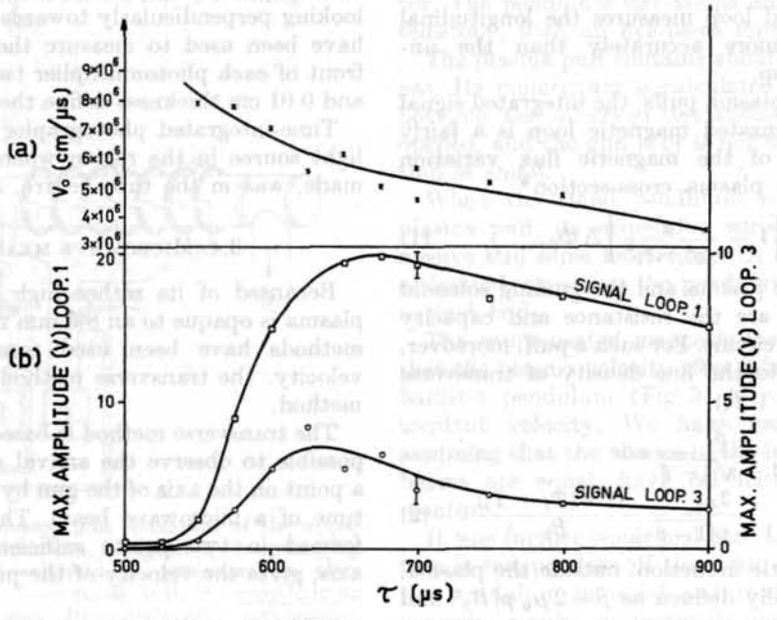

Fig. 5 Influence of the delay τ on the plasma velocity and on the amplitude of the compensated magnetic loop signals. Experimental conditions: C.I.; $E_0 = 12$ kV; $B_z = 1300$ G; $Q = 0.3$ cm³-atm; crowbar used at the end of the 2nd half-cycle.

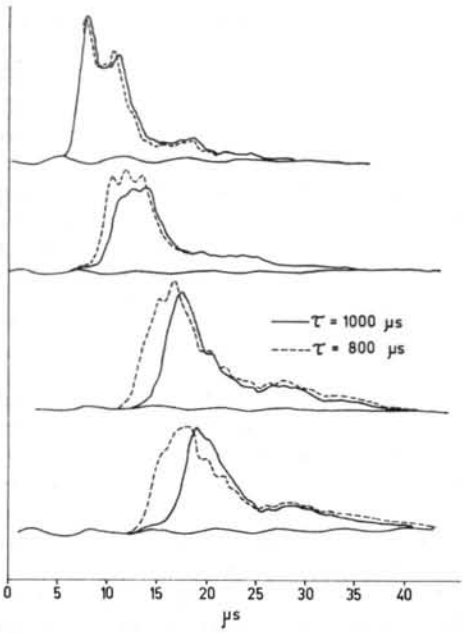

Fig. 6 Influence of the delay τ on the compensated magnetic loop signals. These experiments, without crowbar, show the complexity of interpretation when several puffs are ejected. Experimental conditions: C.I.; $E_0 = 12$ kV; $B_z = 1300$ G; $Q = 0.3$ cm³-atm.

photomultipliers are similar to those of the compensated magnetic loops. When τ increases, the signal of the first photomultiplier, 22 cm from the coil, is distorted: its front edge becomes much sharper, and its amplitude increases. The shape of the second photomultiplier signal, 50 cm from the coil, changes only for large τ values. We have checked that this distortion is caused by the presence of neutrals in front of the photomultiplier by ejecting a plasma puff in a stationary D_2 pressure of 4×10^{-3} mm Hg. The spectroscopic measurements further confirm this interpretation. For large τ values (1000 μs) one observes, 50 cm from the gun, a strong D_β emission in the front of the puff. The half-width of this line is more than 2 Å. The plasma seems cold and quite dense. For $\tau = 700$ μs the luminous peak in front of the puff has disappeared, the D_β emission is approximately 20 times weaker, and the line is thinner.

Fig. 5 indicates how the velocity and the maximum amplitude of the magnetic loop signals vary with τ. The measurements with large ballistic pendula yield a curve similar to those of Fig. 5b. The maximum is flatter, and displaced towards the larger τ values (800 μs).

For $\tau > 800$ μs the velocity, calculated between two consecutive magnetic loops, is no longer constant (Fig. 6). For $\tau < 650$ μs, the total plasma momentum, and the amplitude of the magnetic loop signals decrease sharply with decreasing τ. We have chosen the value $\tau = 700$ μs for most of our experiments. For this value, the effect of the neutrals is reduced, but not negligible (cf. Fig. 5a and Section 4.3.4). The plasma is probably slowed down before its arrival at the first compensated magnetic loop.

4.3. Influence of guide field intensity and polarity

4.3.1. *Focussing effect*

Three techniques have been used to study the efficiency of the guide field: time-integrated photographs, the darkening of a teflon plate* placed on the beam trajectory (see Fig. 7) and small ballistic pendula for measuring the radial distribution of the plasma momentum.

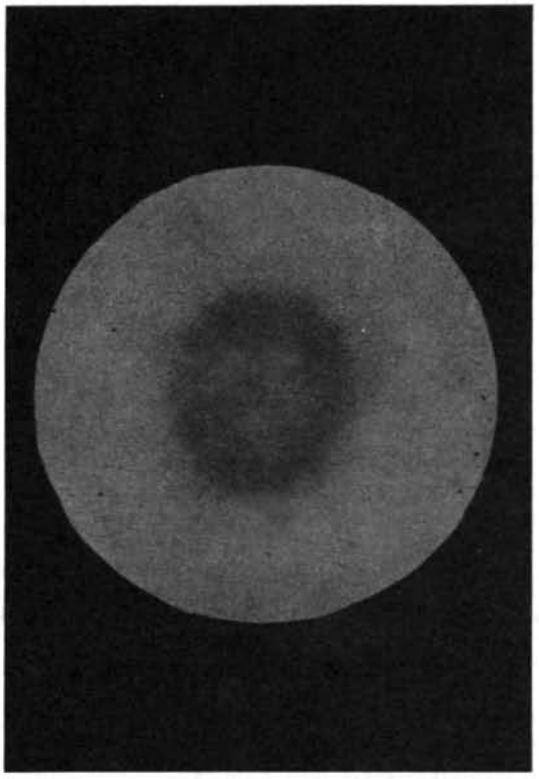

Fig. 7 Darkening of a teflon plate placed on the beam trajectory. About 40 discharges are required to produce a measurable darkening.

The axial variation of the plasma radius is plotted on Fig. 8. The experiments shown on this figure were carried out without crowbar and without the end-corrections of the guide field. Two phenomena at least are expected to cause a variation of the plasma radius as a function of distance: the inhomogeneity of the magnetic field at the ends, and the non-negligible initial β of the plasma such that, as time increases, the plasma expands longitudinally, the density and plasma pressure decrease, leading to a radial contraction of the puff. The latter effect masks the radial diffusion of the plasma.

Fig. 9 shows some recent results obtained with the small pendulum** 41 cm away from the coil; the

* About 40 discharges are required to produce a measurable darkening.

** The momentum values plotted on these figures are those observed by our small pendula. The curves would have had somewhat steeper edges if pendula of infinitesimal area had been used.

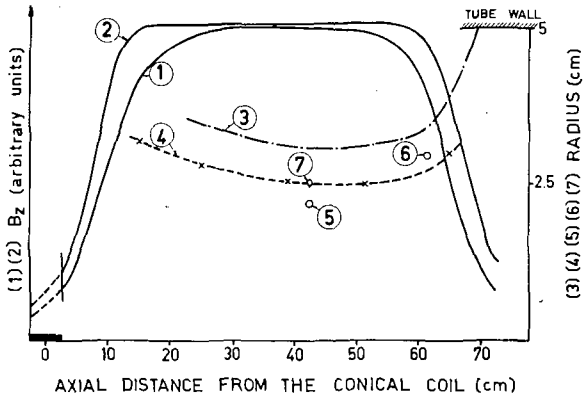

Fig. 8 Axial variation of the guide field and of the plasma radius. Curve 1—Guide field without end correction. 2—Guide field with end correction. 3—Plasma radius measured from time integrated photograph. 4, 5, 6—Plasma radius obtained from the darkening of teflon plates. 7—Plasma radius from small ballistic pendulum measurements. Experimental conditions: C.I.; $E_0 = 12$ kV; $\tau = 700$ μs; $Q = 0.6$ cm³-atm; $B_z = 2680$ G.

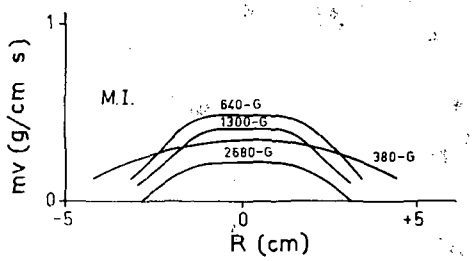

Fig. 9a Radial distribution of plasma momentum in the guide field. (Small ballistic pendulum measurements.) Experimental conditions: $\tau = 700$ μs; $E_0 = 12$ kV; $Q = 0.3$ cm³-atm; crowbar used at the end of the 2nd half-cycle. ("M.I." configuration, see p. 681.)

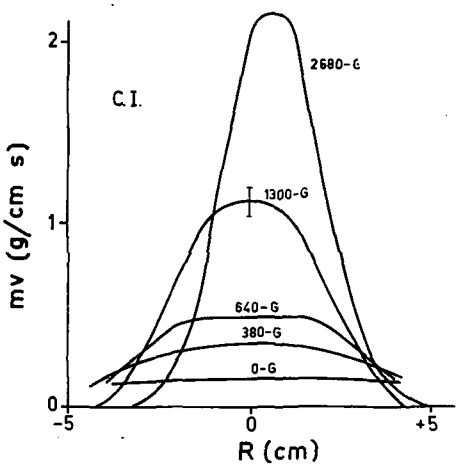

Fig. 9b Radial distribution of plasma momentum in the guide field. (Small ballistic pendulum measurements.) Experimental conditions: $\tau = 700$ μs; $E_0 = 12$ kV; $Q = 0.3$ cm³-atm; crowbar used at the end of the 2nd half-cycle. ("C.I." configuration, see p. 681.)

puff is well separated from the wall when the guide field intensity is larger than 1000 G. It may, however, have interacted with the walls in the region between the conical coil and the guiding solenoid. We believe indeed that the difference between the radial distances of the centres of gravity of the puffs observed at 1300 and 2680 G is due to a small misalignment, and to an asymetric wall interaction as the plasma penetrated into the 1300 G guide field. The wall interactions increase when the guide field decreases below 1000 G, and probably dominate the behaviour of the plasma puffs when $B_z = 370$ G. The small dispersion of the measurements, even in the regions where the plasma momentum varies rapidly as a function of radius, indicates the reproducibility of the plasma trajectory.

4.3.2. *Ejection time*

An analysis of the magnetic loop signals yields both the plasma velocity and its time of ejection from the gun. When the characteristic times of the loop signals are plotted versus the axial distance between the loop and the coil (Fig. 10), they usually fall on straight lines whose slopes are the inverse of the corresponding velocities. When the microwave result, (transverse time-of-flight method) or the beginning of the photomultiplier signal are plotted on such a graph, the points fall on the line corresponding to the velocity of the front of the puff.

For a given experiment, and for a sufficient guide field intensity, the lines generally converge towards a common time of ejection from the coil. This time is approximately that of maximum current in the conical coil at a certain half-cycle. (In some other cases, as shown on Fig. 6, two or more successive puffs can be distinguished at the first magnetic loop).

We have never observed a plasma puff ejected during the first half-cycle of the gun current. Fig. 10 presents the results of three experiments, carried out under quite different experimental conditions, which have produced plasma puffs during the second, third, and fourth half-cycles. This method of determining

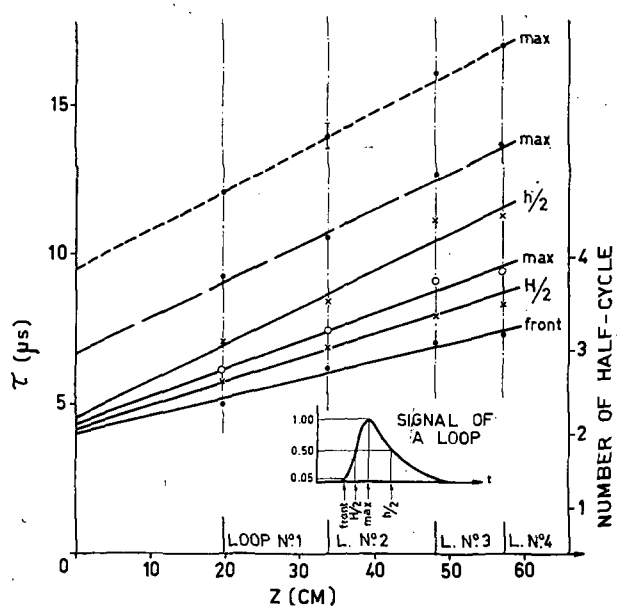

Fig. 10 Velocity and time of ejection analysis for three experimental conditions having produced plasma puffs at the 2nd, 3rd and 4th half-cycle.

the time of ejection of the puffs has been verified by the use of the crowbarring switch: by crowbarring the discharge between successive half-cycles, the ejection time can be determined unambiguously.

4.3.3. *Influence of the initial configuration*

We subdivide our experiment in two groups according to the initial mutual orientation of the gun and guide (B_z) magnetic fields during the first half-cycle of the discharge in the conical coil. In the first case which we call "Mirror I" (M.I.) the two fields are parallel during the first and all the odd-numbered half-cycles, and anti-parallel during the even numbered half-cycles. In the second case, designated "Cusp I" (C.I.), the situation is the opposite.

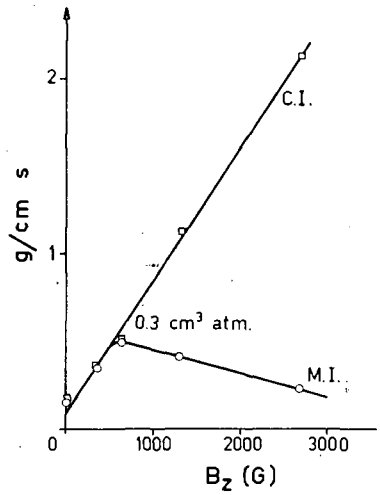

Fig. 11a Plasma momentum *vs* intensity of the guide field for the two initial configurations. Experimental conditions: $E_0 = 12$ kV; $\tau = 700$ μs; crowbar used at the end of the 2nd half-cycle. Small pendulum on the axis.

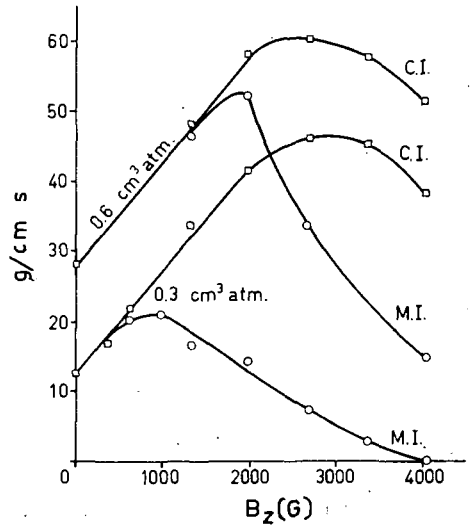

Fig. 11b Plasma momentum *vs* intensity of the guide field for the two initial configurations. Experimental conditions: $E_0 = 12$ kV; $\tau = 700$ μs; crowbar used at the end of the 2nd half-cycle. Large pendulum.

Figures 9 and 11 present some measurements on plasma puffs ejected during the second half-cycle (the discharge was crowbarred before the end of this half-cycle). For small B_z values, the behaviour of the plasma is almost independent of the initial configuration, the velocities, the loop signals, the total momentum and its radial distribution are practically identical. For large B_z values, the momentum and especially the amplitude, of the loop signals are much smaller in M. I. than in C. I. When 0,3 cc atm of D_2 is injected, the loop signal is unobservable for fields equal to, or larger than 2000 G, and the momentum decreases by a factor 4.

We consider at the present two possible explanations of this effect, which is still being investigated experimentally:

1) The intensity of the guide field, inside the conical coil, is about 15 % of its value inside the solenoid. It is known [8] that fast magnetic compressions are strongly dependent on the presence and polarity of an initial magnetic field. In particular, a parallel initial field has a negative effect on the subsequent behaviour of the compressions. According to this hypothesis, an initial parallel field of 300 G would inhibit almost entirely the operation of our gun, when 0,3 cc atm are injected. For 0,6 cc atm, it would take about 600 G to produce the same effect.
2) In C. I., the second half-cycle ejection occurs in a mirror configuration; the plasma must enter the guide field without difficulties. In M. I., the plasma, as it is ejected during the second half-cycle, expands violently out of the conical coil. It crosses there a region of zero magnetic field, where it probably interacts with the walls, before it can penetrate in the strongly convergent guide field. It is known [9] that a plasma puff penetrates with some difficulty in such a field. In first approximation, there should exist a critical field B_c value, beyond which the penetration is no longer possible. For an ion density of 10^{15} cm^{-3} and a velocity of the order of 10^7 cm/s, B_c would be of the order of 2500 G.

4.3.4. *Influence of the guide field intensity on the plasma velocity*

The velocities v deduced from the maxima of the four magnetic loop signals in the "Cusp I" configuration are given on Table I. If one assumes that the plasma consists only of D^+ ions and of electrons, the momentum measurement (Fig. 11) and those velocities yield the total number of ions striking the pendulum, see Table I.

The velocity is almost constant for small guide field intensities. It increases almost linearly with B_z between 1000 and 4000 G. If the fast-ion gauge calibrations, obtained in a static pressure, can be applied without correction to a dynamical system, we have about 6×10^{17} D_2 molecules within the conical coil when the gun is fired. We observe more

TABLE I. Plasma velocities, obtained from the maxima of the magnetic loop signals, as a function of the B_z guide field intensity, and number of D^+ ions striking the large ballistic pendulum, 41 cm from the conical coil. ["Cusp I" configuration (the 2nd half-cycle is a mirror), $E_0 = 12$ kV, 0,3 cc atm of D_2 injected, $\tau = 700$ μs.]

B_z (gauss)	0	370	520	640	845	1000	1300	1660	1970	2330	2680	3380	4050
V (10^6 cm/s)	3,8[a]	4,5 4,5[a]	4,5	4,5 5,0[a]	4,6	4,8	4,7[b] 5,3[b]	6,15	6,5	7,45	8,1	9,8	11,6
$\mathcal{N}$ (10^{18} ions)		1,35	1,50	1,65	1,8	1,9	2,1	2,1	2,15	2,0	1,9	1,5	1,05

[a] Values obtained from Döppler microwave measurements.
[b] Two sets of measurements, two months apart.
Note: In the "Mirror I" configuration, the observed velocities are somewhat lower: 3,5 and $3,6 \times 10^6$ cm/s for $B_z = 640$ and 1300 G, respectively.

than $1,2 \times 10^{18}$ D^+ ions at the pendulum. This increase in mass and decrease in velocity are probably caused by the interaction of the plasma puff with the neutral molecules whose pressure decreases from about 5×10^{-2} mm Hg beyond the gun; those neutrals, ionized by the puff, could produce the two effects. For larger B_z values, the plasma cross-section is smaller (Fig. 9), and the number of particles collected decreases. Part of the velocity increase may also result from the initial antiparallel field in the coil.

In the case of the "Mirror I" configuration, it is difficult to measure the velocity for intermediate B_z values, where the signals shapes are irregular, particularly on the first loop; for high guide field intensities, as mentioned above, the signals vanish entirely.

4.4. Influence of the amount Q of gas injected by the fast valve and of the voltage E_0 on the accelerator condenser bank

The effect of these two interconnected parameters has not yet been thoroughly studied. Some preliminary measurements, in C. I. configuration, without crowbar, have shown [1] that the momentum received by the large ballistic pendulum, varies almost linearly with Q, between 0,01 and 0,3 cc atm. Between 0,3 and 0,6 cc atm, the increase is slower. For $Q = 0,6$ cc atm, and large τ values, slow plasma containing as much as 10^{19} particles (ions + electrons) have been observed. The compensated magnetic loops and the microwaves techniques have since shown that the dependence on Q is complex: when Q decreases, the ejection occurs later; for example, when $Q = 0,03$ cc atm, and without pre-ionization, the plasma is formed reproducibly during the fifth half-cycle of the gun current. The maximum current, which determines the energy available for the acceleration, decreases by about 14% per half-cycle. Two experiments carried out at different pressures are thus not strictly comparable. Even with our pre-ionization system, the amount ejected by the accelerator during the second half-cycle is small, when $Q = 0,1$ cc atm.

Another preliminary experiment [1], without crowbar, has shown that the momentum measured by the large ballistic pendulum is a quadratic function of E_0 for $Q = 0,1$ cc and $10 \text{ kV} \leqslant E_0 \leqslant 18$ kV. But the phenomena are again complex, since a variation of E_0 may have changed the ejection time from a "cusp" to a "mirror" half-cycle, or even by two half-cycles. As expected, the plasma moves faster when E_0 increases, and Q decreases. For $E_0 = 20$ kV, $Q = 0,06$ cc atm, and $\tau = 700$ μs (Mirror I configuration), the puff ejection occurs only at the fifth half-cycle but the average velocity is $2,5 \times 10^7$ cm/s, and that of the front $3,5 \times 10^7$ cm/s.

4.5. Oscillations observed on the magnetic loop signals

An oscillation (Fig. 1) appears on the magnetic loop signals when the guide field intensity $B_z \geq 800$ G

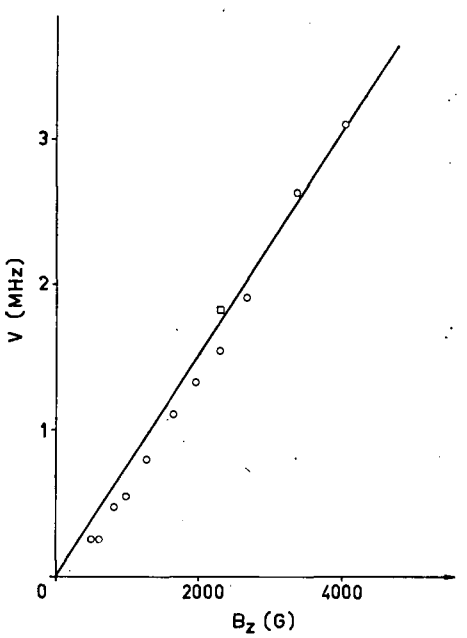

Fig. 12 Frequencies of the oscillations observed on the magnetic loop signals as a function of the guide field intensity. ○—Values observed in the vicinity of the signal maximum (loop number 3). □—Value observed at the end of the sweep. The straight line is the ion cyclotron frequency. Experimental conditions: C.I.; $E_0 = 12$ kV; $\tau = 700$ μs; $Q = 0.3$ cm³-atm; crowbar used at the end of the second half-cycle.

and when the delay $\tau \leqslant 800$ μs. For a given experimental condition, this oscillation is reproducible from one discharge to the next; the frequency is about 10—20% smaller at the maximum of the signal (where the density is large) than at the end of the sweep. The observed frequency varies linearily as a function of the guide field, (Fig. 12). The straight line drawn on this figure represents the variation of the D^+ cyclotron frequency as a function of the external guide field.

The maxima of these oscillations, observed on different loops, occur at identical times, within experimental errors, indicating that they correspond probably to a pulsation, or "radial breathing" of the whole puff.

5. Discussion of the observed loop signals

We have seen that, for sufficiently long plasma puffs, the magnetic flux variation $\Delta\Phi_p$ on the plasma cross-section is related to the line density of transverse energy by the equation:

$$\Delta\Phi_p = N_i' \frac{k(T_e + T_i)}{B} \frac{2\mu_0}{1 + (1-\beta)^{1/2}}, \qquad (2)$$

where N_i' is the line density of the ions in the plasma. In the case of a collisionless plasma, the transverse energy and the parallel velocity of each particle is constant and one must have for any magnetic loop encircling the plasma

$$\int \Delta\Phi_p \, dt = \text{constant}. \qquad (3)$$

Consider a low-β collisionless plasma, guided by a longitudinal magnetic field and moving with an average velocity v_0. If, initially, the plasma length is small, and the thermal energy of the particles is given by a Maxwell-Boltzmann distribution function, the plasma will lengthen along the magnetic lines of force; its shape becomes rapidly a gaussian, which flattens out progressively. One shows that such a plasma should produce a magnetic loop signal whose shape is analogous to those observed on our oscillograms.

The predicted amplitude ratio, from one loop to the next, does not agree with the experimental observations. This collisionless model satisfies Eq. (3), whereas the experimental values of this integral decrease in the ratio 6:1 from the first to the last loop.

This decrease could be due to a particle loss, or to a reduction of the perpendicular temperature. The first hypothesis could hardly be responsible for the whole of the observed effect, in view of the large number of particles striking the pendulum 41 cm away from the gun, and of the efficiency of the guide field (Fig. 9). On the other hand [1], the lengthening of the plasma puff, decreasing the parallel temperature, and the collisions*, which tend to maintain the equilibrium $T_\parallel = T_\perp$, lead to a decrease of the transverse energy. The plasma radiation may enhance this effect.

We have examined the consequences of the hydrodynamic equations under the following hypotheses:

1) The guiding magnetic field, parallel to the z axis, does not affect the z motion of the particles ($\beta \ll 1$), but stops all radial diffusion.
2) At a time t, and for a given z, all the plasma properties are independent of r, up to the boundary.
3) The collision number is such that, at every point, $T_\parallel = T_\perp$.
4) The plasma is electrically neutral; $n_i = n_e$, and the ion mass m_i is much larger than the electron mass m_e.
5) One assumes finally that, for every time t, one has:

$$n_i(z,t) = \frac{N_i}{\sqrt{\pi}\,\lambda(t)} \exp\left(-\frac{z^2}{\lambda^2(t)}\right), \qquad (4)$$

where N_i is the number of ions in a cylinder of infinite length along z and of unit cross-section; λ is a function of time only, and z is the distance between a volume element and the centre of mass of the puff.

The continuity equation is

$$\frac{\partial n_i}{\partial t} + \frac{\partial}{\partial z}(n_i v) = 0.$$

v is the relative velocity of the volume element and of the centre of mass. Using (4), the only antisymmetrical solution in z is

$$v = \frac{z}{\lambda}\lambda'. \qquad (5)$$

The equation of motion can be written as

$$\frac{\partial p}{\partial z} + n_i m_i \frac{\partial v}{\partial t} + n_i m_i v \frac{\partial v}{\partial z} = 0.$$

Since $p=0$ for $z=\pm\infty$, we obtain, by means of Eqs. (4) and (5),

$$p = n_i \frac{m_i}{2} \lambda\lambda''. \qquad (6)$$

The third hypothesis justifies the use of the equation of state, whence

$$k(T_e + T_i) = \frac{m_i}{2}\lambda\lambda''. \qquad (7)$$

The hypotheses imply, thus, that average temperature of the ions and electrons is uniform in space and that it is only a function of time. The conservation of energy W of the system is written as:

$$\frac{W}{S} = \frac{3}{2}\int_{-\infty}^{+\infty} n_i k(T_i + T_e)\,dz + \frac{1}{2}\int_{-\infty}^{+\infty} n_i m_i v^2\,dz$$
$$= \frac{3}{4} N_i m_i \lambda\lambda'' + \frac{1}{4} N_i m_i (\lambda')^2 = \text{constant}. \qquad (8)$$

S is the plasma cross-section. Let us use as initial time $t_0 = 0$ the instant when λ is minimum, and let

* The plasma density is almost certainly of the order of 10^{15} cm^{-3}, and the ion temperature 20 eV or less: The D^+,D^+ collision time is then smaller than 0,1 μs.

the subscript zero characterize the values of the variables at this instant. Thus

$$\frac{W}{S} = \frac{3}{2} N_i k (T_e + T_i)_0 .$$

We define two reduced parameters:

$$\Lambda = \frac{\lambda}{\lambda_0}, \qquad \tau = \left[\frac{6k(T_e + T_i)}{m \lambda_0^2}\right]^{1/2} t = \frac{t}{\xi}. \tag{9}$$

Eq. (8) becomes

$$3\Lambda \frac{d^2\Lambda}{d\tau^2} + \left(\frac{d\Lambda}{d\tau}\right)^2 = 1. \tag{10}$$

The solution of this equation is

$$\tau = (\Lambda^{2/3} - 1)^{1/2} (\Lambda^{2/3} + 2). \tag{11}$$

Eqs. (7), (10) and (11) yield

$$\frac{(T_i + T_e)_t}{(T_i + T_e)_0} = \frac{1}{\Lambda^{2/3}} = \left(\frac{\lambda_0}{\lambda}\right)^{2/3}. \tag{12}$$

This equation expresses the fact that the expansion is adiabatic, with $\gamma = 5/3$.

Finally, the line density of transverse energy at a distance of Z cm from the position occupied by the centre of mass of the plasma puff at time $t_0 = 0$ is given by the equation:

$$N_i' k (T_e + T_i) = \frac{\mathcal{N}_i m_i v_0}{6\sqrt{\pi}\alpha\xi} \frac{1}{\Lambda^{5/3}} \exp\left\{-\frac{[(Z/\lambda_0) - \alpha\tau]^2}{\Lambda^2}\right\}. \tag{13}$$

$\mathcal{N}_i$ is the total number of ions in the plasma puff, v_0 is the average velocity of the plasma puff, and

$$\alpha = \left(\frac{m_i v_0^2}{6k(T_e + T_i)}\right)^{1/2}. \tag{14}$$

Eqs. (1), (2) and (13) link some of our experimental results ($\mathcal{N}_i m_i v$, the plasma momentum measured by the large ballistic pendulum; the shape and amplitude of the magnetic loop signals) to a set of four characteristic parameters:

λ_0, which measures the puff length at time t_0;
v_0, average velocity of the puff;
$(T_e + T_i)_0/2$, average ion and electron temperature at time t_0;
Z_0, the distance between the centre of mass of the puff at time t_0, and the centre of the conical coil.

Note: Z_0 is probably not equal to zero, since the magnetic forces act upon the ions during a length of time which varies according to the initial position of the ion in the coil: the ions formed downstream are ejected earlier, but with a smaller velocity. The effect of the collisions with the neutrals is to enhance the tendency of the puff to "bunch" around a point which we choose as the origin of the expansion.

By successive eliminations, one shows that the values of the four parameters which predict reasonably well the shapes and amplitudes of the four magnetic loop signals fall within rather narrow limits. For example: for a plasma puff ejected in "Cusp I" configuration into a guide field of 3380 G, one finds

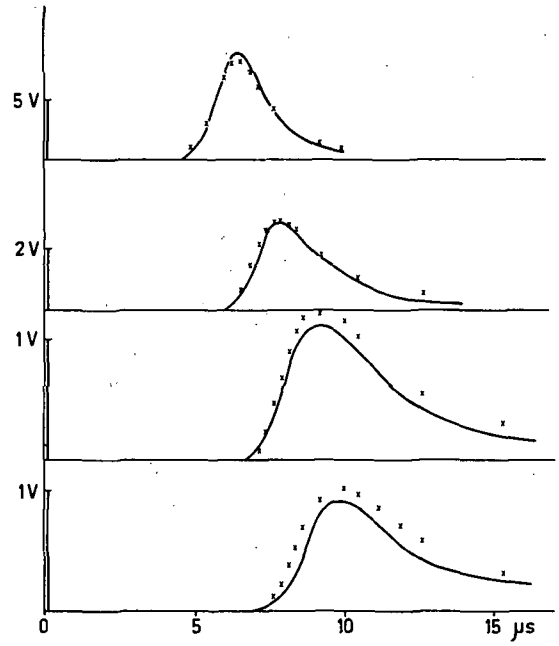

Fig. 13 Comparison of the observed signals of the four compensated magnetic loops (each loop consists of four turns in series) and of points calculated from the equations of Section 5. Experimental conditions: C.I.; $E_0 = 12$ kV; $\tau = 700$ μs; $B_z = 3380$ G; $Q = 0.3$ cm³-atm; crowbar used at the end of the second half-cycle. Parameters used for the calculation: $\frac{1}{2}(T_e + T_i)_0 = 2 \cdot 10^5$; $v_0 = 6 \cdot 10^6$ cm/s; $\lambda_0 = 8$ cm; $z_0 = 10$ cm.

$\lambda_0 = 10 \pm 2$ cm; $(T_e + T_i)_0/2 = (2 \times 10^5 \pm 4 \times 10^4)°$K; $v_0 = (7 \pm 1) \times 10^6$ cm/s. The choice of Z_0 is somewhat less critical: the results agree for 5 cm $\leqslant Z_0 \leqslant 15$ cm Fig. 13 indicates the type of agreement that one finds for a reasonably good set of parameters. The signal shapes fit rather accurately; the amplitude ratio is predicted within an accuracy of 15%. Even though this is slightly more than the uncertainty in the measuring circuit calibrations, the agreement is satisfactory considering the hypotheses made. Part of this agreement may result from the fact that the magnetic loops [6] and the ballistic pendulum do not measure the fine structure of the plasma.

Acknowledgements

We wish to express our most sincere thanks to Dr. P. Hubert, head of the "Service de Recherches sur la Fusion Contrôlée", for the constant interest with which he followed this work, and for useful guidance.

Let Professor D. Palumbo, from the Euratom Commission, Brussels, and Mr. and Mme Lafleur, S.T.G.I., Fontenay-aux-Roses, find here the expression of our gratitude for fruitful discussions.

The skillful technical assistance of MM. J. P. Moussy, J. Godaert and M. Vleminckx is gratefully acknowledged.

Several aspects of these problems have been clarified during conversations with Professor W. Fucks, Dr. H. L. Jordan and members of their team.

We also thank Dr. J. Marshall, from Los Alamos Scientific Laboratory and Dr. F. R. Scott from the John Jay Hopkins Laboratory, San Diego, for their cordial welcome during our interesting visits.

References

[1] WAELBROECK, F., LELOUP, C., POFFÉ, J. P., "Canon à plasma sans électrode avec champ de guidage" Rapport Interne N° 57 — Association EURATOM-CEA sur la Fusion — Juin 1960.

[2] LELOUP, C., POFFÉ, J. P., VÉRON, D., WAELBROEK, F., *Bull. Am. Phys. Soc.*, **6** (1961) 187.

[3] MARSHALL, J., Proceedings of the Second United Nations International Conference on the Peaceful Uses of Atomic Energy, **31** (1958) 341.

[4a] ALIDIERES, M., AYMAR, R., JOURDAN, P., SAMAIN, A., "Microstriction I & II" — Rapport Interne N° 110 — Association EURATOM-CEA sur la Fusion. — Juin 1961.

[4b] KVARTSKHAVA, I. F., MELADZE, R. D., SULADZE, K. V., Proceedings of the International Conference on High Energy Accelerators and Instrumentation. (CERN, 1959) p. 178.

[4c] HÖGBERG, L., VOGEL, K. — *Nucl. Instr. Meth.* **10** (1961) 95.

[5] ANDRÉ, T., "Eclateur de court-circuit à basse impédance" — Rapport Interne N° 79 — Association EURATOM-CEA sur la Fusion. — Décembre 1960.

[6] LELOUP, C., LUC, H., POFFÉ, J. P., WAELBROECK, F., "Discussion du diagnostic des boucles magnétiques compensées" Rapport Interne N° 112 — Association EURATOM-CEA sur la Fusion. Juillet 1961.

[7] MARSHALL, J., Plasma Acceleration (S. W. KASH, Ed.: Stanford University Press, 1960) p. 61.

[8a] KOLB, A. C., DOBBIE, C. B., GRIEM, H. R., *Phys. Rev. Letters* **3** (1959) 5.

[8b] LITTLE, E. M., QUINN, W. E., RIBE, F. L., *Phys. Fluids* **4** (1961) 711.

[8c] JORDAN, H. L., these Proceedings, page 589; HINTZ, E., these Proceedings, page 601.

[9] TUCK, J. L., *Phys. Rev. Letters* **3** (1959) 313.

ЭКСПЕРИМЕНТЫ ПО ВЗАИМОДЕЙСТВИЮ ПЛАЗМЫ С ЭЛЕКТРОМАГНИТНЫМ ПОЛЕМ ОБЪЕМНОГО РЕЗОНАТОРА*

Ю. И. Арсеньев, В. М. Глаголев, Г. А. Елисеев, Н. С. Чеверев

Академия наук СССР,

Москва, Союз Советских Социалистических Республик

В вакуумном цилиндрическом резонаторе, питаемом от импульсного магнетрона десятисантиметрового диапазона, возбуждены колебания типа H_{111} с амплитудой высокочастотного магнитного поля ~250 эрстед при длительности импульса 1,2 мсек. В резонатор инжектировалась плазма, создаваемая импульсным высокочастотным плазменным источником. Плотность плазмы превышала 10^{12} см$^{-3}$. Вся система находилась в постоянном магнитном поле (H_0~1500 эрстед). Исследовалось взаимодействие плазмы с электромагнитным полем объемного резонатора. Установлено, что давление электромагнитной волны препятствует входу плазмы в резонатор.

Обсуждаются полученные результаты.

Введение

Известно, что термоизоляция плазмы в системах со стационарными магнитными полями в значительной степени затрудняется различными видами неустойчивостей, присущих этим системам (токовые, пучковые, конвективные и др.).

Использование высокочастотных полей открывает новые пути в создании более совершенных плазменных ловушек, свободных от некоторых видов этих неустойчивостей.

Удержанию отдельных заряженных частиц высокочастотным электромагнитным полем посвящены работы [1, 2].

Удержание плазмы исследовалось в работах [3, 4, 5, 6].

Основным недостатком высокочастотных методов удержания плазмы является то, что вследствие скин-эффекта для создания высокочастотных полей требуются значительно большие энергетические затраты, чем для создания стационарных полей. Однако, успехи радиоэлектроники и недавно выполненные работы по созданию сверхпроводников с большим критическим магнитным полем [7] могут при дальнейшем их развитии в значительной степени устранить этот недостаток.

Использование комбинации стационарных и высокочастотных удерживающих полей расширит наши возможности в исследовании физических процессов в высокотемпературной плазме.

Простейшим примером комбинированной плазменной ловушки является система, в которой удержание плазменного шнура в радиальном направлении осуществляется аксиально-симметричным магнитным полем, а в направлении магнитных силовых линий — давлением, создаваемым высокочастотными полями резонаторов [4].

Высокочастотные поля могут также использоваться для стабилизации неустойчивостей плазмы, в частности для стабилизации конвективной неустойчивости в неоднородном магнитном поле. Такая неустойчивость присуща многим системам с удержанием плазмы стационарным магнитным полем. В работе [8] показано, что, используя высокочастотные поля, можно устранить указанную неустойчивость.

В настоящем докладе рассматриваются вопросы, связанные с взаимодействием электромагнитных полей резонаторов с плазмой. Первая часть доклада посвящена экспериментам по удержанию плазмы электромагнитным полем вакуумного резонатора. Во второй части изложены предварительные результаты экспериментов, проводимых в направлении использования высокочастотных полей для стабилизации плазменных неустойчивостей.

1. Эксперименты по удержанию

1.1. Описание установки

Экспериментальная установка (рис. 1) представляет собой вакуумную цилиндрическую камеру (1) длиной ~1 метр, на одном из торцов которой установлен вакуумный цилиндрический резонатор (2), а на другом — высокочастотный плазменный источник (3).

Камера и вакуумный резонатор откачивались паромасляными насосами до давления ~10^{-6} мм рт. ст. С помощью системы катушек создавалось продольное магнитное поле, регулируемое от 0 до 2000 эрстед.

Плазменный источник состоял из кварцевой трубки (⌀10 мм), в которой возбуждался высокочастотный разряд от магнетронного генератора десятисантиметрового диапазона (4) мощностью 100 квт.

Длительность импульса регулировалась в пределах 10—1000 мксек. Второй магнетронный генератор (5) использовался для возбуждения в вакуумном цилиндрическом резонаторе (2) с высокой добротностью (Q=30000) электромагнитных коле-

* Доклад CN-10/218, представленный на конференцию. Докладчик: В. М. Глаголев. Дискуссия (на английском языке) по этому докладу дана на стр. 748. Переводы аннотаций находятся в конце этого тома Трудов Конференции.

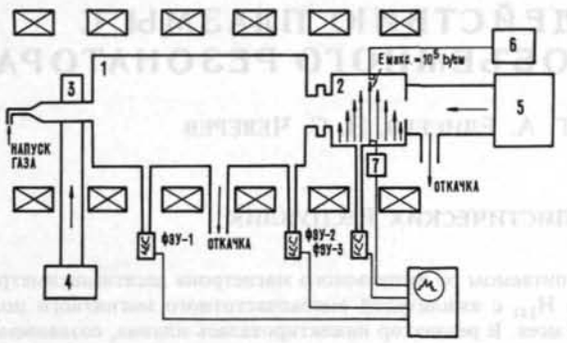

Рис. 1 Схема установки:
1) вакуумная цилиндрическая камера
2) вакуумный цилиндрический резонатор
3) высокочастотный плазменный источник
4) магнетронный генератор
5) магнетронный генератор
6) измерительный генератор стандарт-сигналов
7) волномер.

баний типа H_{111}. Длительность импульса этого генератора составляла 1 мсек.

Максимальная амплитуда высокочастотного магнитного поля в резонаторе достигала ~250 эрстед (амплитуда электрического поля ~100 кв/см). Такое высокочастотное поле не вызывало пробоя до давлений порядка 10^{-3} мм рт. ст. как в воздухе, так и в H_2, He и Ar.

Скорость поступления газа, подаваемого в плазменный источник, устанавливалась такой, чтобы получить достаточно плотный плазменный шнур и вместе с тем не вызвать пробой в вакуумном резонаторе.

В оптимальном режиме плазменного источника давление газа (N_2) в камере составляло $1-2\cdot10^{-4}$мм рт. ст. и $1-4\cdot10^{-5}$ мм рт.ст. в резонаторе.

В этих условиях при включении магнетрона (4) в камере создавался резко очерченный плазменный шнур, диаметром около 20 мм, который инжектировался в резонатор. Оценка скорости распространения светового фронта плазменного шнура и фиксация момента инжекции плазмы в резонатор производились с помощью 3-х фотоумножителей (ФЭУ-1, ФЭУ-2; ФЭУ-3).

Специальная схема позволяла изменять момент инжекции плазмы в резонатор относительно начала импульса магнетронного генератора (5).

Измерение концентрации электронов плазменного шнура производилось по известной резонаторной методике [9].

Для этого в резонаторе (2) от измерительного генератора стандарт-сигналов (6) возбуждались колебания типа E_{010}.

Оценка концентрации производилась также по перестройке частоты колебаний типа H_{111}.

Амплитуда высокочастотного поля в резонаторе измерялась с помощью петли, соединенной с ламповым детектором.

Для контроля за частотой магнетронного генератора (5) сигнал из резонатора (2) мог быть подан на осциллограф через волномер (7) (резонатор с $Q=30000$).

1.2. Результаты измерений

Первоначально были измерены параметры плазмы, инжектируемой в резонатор.

С помощью фотоумножителей ФЭУ-1 и ФЭУ-3 определялась скорость распространения светового фронта плазменного шнура от источника.

Из этих экспериментов выяснилось, что световой фронт плазменного шнура достигает резонатора за время порядка нескольких мксек, которое значительно меньше длительности высокочастотного ионизирующего импульса.

Столь большая скорость светового фронта

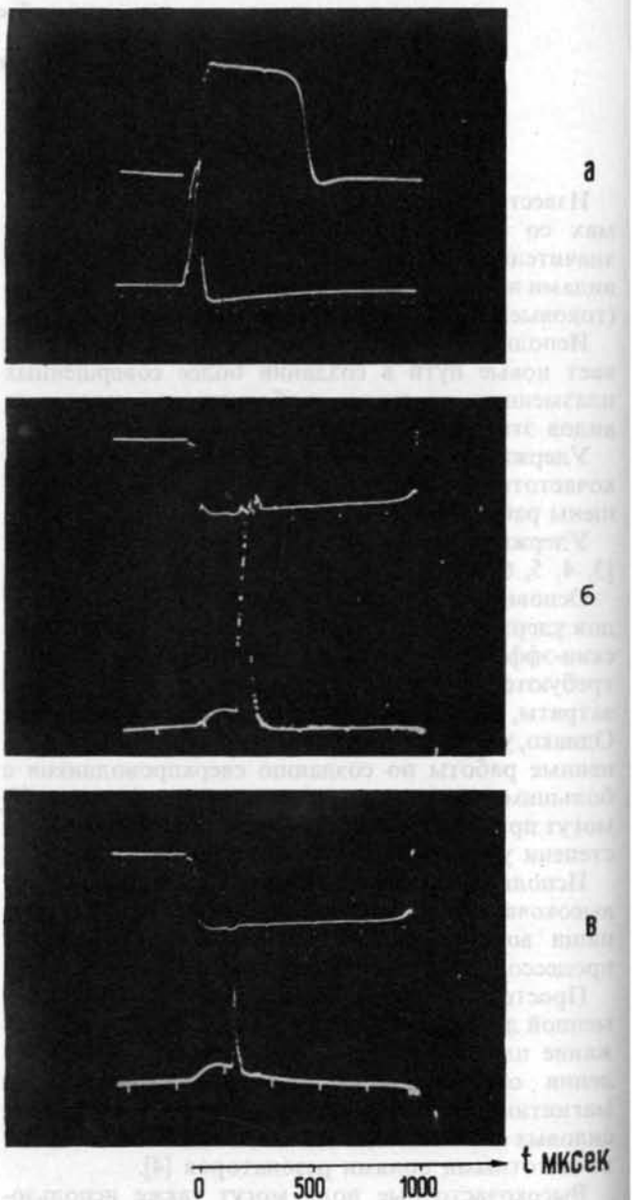

Рис. 2 Расстройка резонатора:
а) на верхней кривой приведен сигнал из резонатора, на нижней кривой — сигнал с ФЭУ-2
б) осциллограмма: верхняя кривая — сигнал из резонатора, нижняя кривая — сигнал с ФЭУ-2
в) удержание плазмы за счет снижения мощности магнетронного генератора.

плазменного шнура может быть, повидимому, объяснена ионизацией газа электромагнитной волной, бегущей по шнуру.

В резонаторе (2) с помощью генератора (6) были возбуждены колебания типа E_{010} и по смещению собственной частоты резонатора определена концентрация электронов в плазменном шнуре.

В результате этих измерений выяснилось, что в резонатор инжектируется плазма с максимальной концентрацией электронов $\sim 10^{12}$ см$^{-3}$, спустя ~ 300 мксек после конца импульса ионизирующего магнетрона (4) концентрация падает до $\sim 10^{8}$ см$^{-3}$.

Затем в резонаторе (2) с помощью генератора (6) возбуждались колебания типа H_{111} и в него инжектировался плазменный шнур с указанными выше параметрами. При этом резонатор расстраивался и поле в нем исчезало (рис. 2а). На верхней кривой рис. 2а приведен сигнал из резонатора (2), а на нижней — сигнал с ФЭУ-2.

Поле в резонаторе вновь возникало, когда концентрация электронов в плазменном шнуре становилась настолько малой, что смещение собственной частоты резонатора делалось меньше его полосы пропускания.

Далее в резонаторе (2) магнетронным генератором (5) возбуждались колебания типа H_{111} с большой амплитудой высокочастотного магнитного поля и в него инжектировался плазменный шнур, параметры которого определены выше. На рис. 2б представлена полученная осциллограмма. Верхняя кривая — сигнал из резонатора (2), поданный через волномер (7), нижняя — сигнал с ФЭУ-2 (максимальная плотность инжектируемой плазмы $\sim 10^{12}$ см$^{-3}$, продольное магнитное поле ~ 1500 эрстед, амплитуда высокочастотного магнитного поля ~ 150 эрстед).

Из осциллограммы видно, что в отличие от случая малой амплитуды высокочастотного поля [питание резонатора генератором (7)] при большой амплитуде поля практически не наблюдается расстройки резонатора инжектируемой плазмой в течение всего импульса магнетронного генератора (5), частота которого остается постоянной. Это означает, что плазма с $\sim 10^{12}$ см$^{-3}$ не входит в резонатор.

Расстройка резонатора (2) меньше его полосы пропускания. Зная его добротность ($Q = 30000$) можно оценить верхний предел «степени просачивания плазмы» в резонатор (2). Концентрация «просачиваемой плазмы» в нашем случае составляет не более 0,01% от концентрации инжектируемой плазмы.

Эта величина указывает на высокую степень изоляции плазмы электромагнитным полем в этих условиях. Так как концентрация инжектируемой плазмы изменяется в широких пределах во время импульса магнетрона (5), то, как это видно из осциллограммы, эффект удержания имеет место в широком диапазоне концентраций.

Удержание сохраняется и при уменьшении плотности инжектируемой плазмы за счет снижения мощности магнетронного генератора (4) (рис. 2б).

2. Эксперименты по выяснению принципа стабилизации

Как известно, высокочастотное поле, не проникающее в плазму, создает электромагнитное давление на ее поверхность. Если при этом плазма находится в сильном магнитном поле ($\widetilde{H}^2 \ll H_0^2$), то под действием этого давления в плазме возникает стационарный ток, перпендикулярный магнитным силовым линиям и градиенту высокочастотного давления. При взаимодействии этого тока с магнитным полем появляется лоренцова сила, препятствующая смещению плазмы поперек магнитных силовых линий. Направление тока таково, что магнитное поле внутри плазмы увеличивается, т. е. создается своеобразный паромагнитный эффект в плазме. Как показано в [8], этот ток может быть использован для стабилизации неустойчивостей плазмы конвективного типа.

Величину магнитного поля в плазме можно найти из условия равновесия, т. е. равенства давлений на внешнюю и внутреннюю поверхности плазмы. При условии, что высокочастотное поле проникает в плазму на небольшую глубину [порядка скинслоя для высокой частоты $\simeq c/\omega_0 = c\, m^{1/2}/(4\pi n e^2)^{1/2}$], величину магнитного поля за скинслоем H_i можно найти из условия равенства внешнего и внутреннего давлений на скинслой, т.е.

$$\frac{\widetilde{H}^2}{8\pi} + \frac{H_0^2}{8\pi} = \frac{H_i^2}{8\pi} + P_0.$$

Если давление плазмы мало ($8\pi P_0/\widetilde{H}^2 \ll 1$), то увеличение поля внутри плазмы должно определяться формулой:

$$\Delta H = H_i - H_0 = \frac{\widetilde{H}^2}{H_i + H_0} \simeq \frac{\widetilde{H}^2}{2H_0}. \qquad (1)$$

Таким образом при наличии высокочастотного давления на плазму внутри ее, согласно формуле

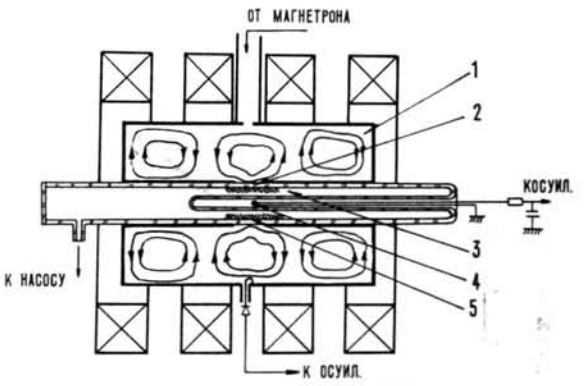

Рис. 3 Схема установки:
1) вакуумный коаксиальный резонатор
2) внутренний цилиндр коаксиального резонатора
3) кварцевая труба
4) катушка для измерения магнитного поля
5) свечение разряда.

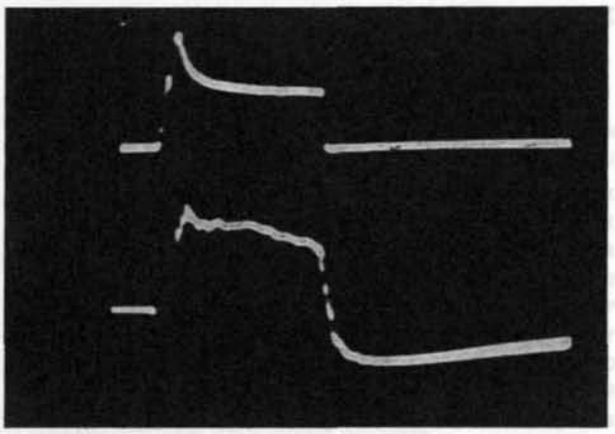

Рис. 4 Верхняя кривая — высокочастотное поле резонатора, нижняя кривая — сигнал с измерительной катушки.

(1) должно наблюдаться увеличение статического магнитного поля.

Эксперименты по обнаружению этого явления проводились на установке, изображенной на рис. 3.

Высокочастотные поля колебаний типа H_{013} с амплитудой поля $\sim$100 эрстед создавались в вакуумном коаксиальном резонаторе (1). Колебания возбуждались с помощью импульсного магнетрона частоты ω (в 10 см диапазоне длин волн) с длительностью импульса 20 мксек. Внутренний цилиндр коаксиального резонатора имел разрез (2) шириной 15 мм, в который провисало высокочастотное электромагнитное поле. Конфигурация магнитных силовых линий этого поля дана на рисунке. В центральную часть резонатора вставлялась кварцевая труба (3) диаметром 50 мм, внутри которой помещалась катушка (4) для измерения магнитного поля. Сигнал с катушки после интегрирования подавался на осциллограф.

Откачка из резонатора и кварцевой трубки производилась независимо. Вся установка помещалась в продольное магнитное поле, которое могло регулироваться от 0 до 1500 эрстед. Рабочее давление газа (воздух) в кварцевой трубке составляло $2\cdot10^{-2}$ мм рт.ст., в резонаторе -10^{-5} мм рт.ст. В этих условиях при возбуждении колебаний в резонаторе в кварцевой трубке (3) зажигался высокочастотный разряд [в провисающих высокочастотных полях в районе разреза (2)]. Свечение разряда (5) наблюдалось в тонком слое ($\sim$0,5 см) вблизи внутренних стенок трубки и было равномерным по углу. Отсутствие свечения разряда внутри кварцевой трубки свидетельствует о достаточно хорошей экранировке высокочастотного поля плазмой. При этом разряд в резонаторе не возникал.

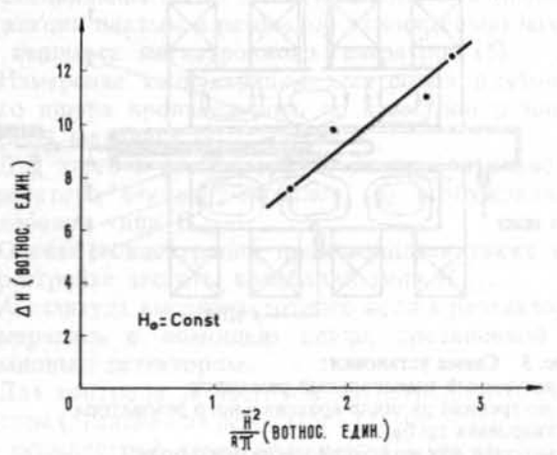

Рис. 5 Зависимость ΔH от высокочастотного давления.

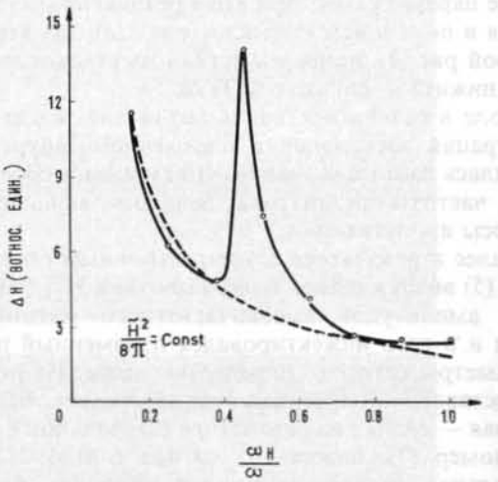

Рис. 6 Зависимость ΔH от статического магнитного поля H_0.

На экран двухлучевого осциллографа подавался продетектированный сигнал высокочастотных колебаний в эндовибраторе (пропорциональный $\widetilde{H}^2$) и сигнал с измерительной катушки (пропорциональный ΔH).

На рис. 4 верхняя кривая — высокочастотное поле резонатора, нижняя кривая — сигнал с измерительной катушки. Все измерения производились в районе разреза (2).

Было установлено, что при включении высокочастотных полей и образовании плазмы магнитное поле на оси кварцевой трубки увеличивается, т.е. действительно имеет место парамагнитный эффект.

Экспериментально определялась зависимость ΔH от высокочастотного давления и статического магнитного поля. На рис. 5 представлена зависимость ΔH от высокочастотного давления (в относительных единицах) при H_0=const. Из графика следует, что в пределах точности измерений зависимость ΔH от $\widetilde{H}^2$ получается линейной, что находится в соответствии с формулой (1).

На рис. 6 представлена зависимость ΔH от статического магнитного поля H_0 ($\omega_H/\omega = eH_0/mc\omega$) при

$\widetilde{H}^2 = \text{const}$. Из этого графика следует, что зависимость ΔH от ω_H/ω согласуется с расчетной кривой (пунктирная кривая). Исключение составляет область магнитных полей близких по величине к полям, соответствующим параметрическому резонансу ($\omega_H/\omega = 0{,}5$).

Ведется дальнейшая работа по изучению описанных явлений.

В заключение приносим искреннюю благодарность доктору технических наук А. П. Федосееву за ряд ценных советов по высокочастотной электронике.

Литература

[1] Гапонов, А. В., Миллер, М. А., *ЖЭТФ*, **34** (1958) 242.
[2] Self, S. A., Boot, H. A. H., *J. Electronics Control* **6** (1959) 527.
[3] Knox, F. B., *Austral. J. Phys.* **10** (1957) 228.
[4] Веденов, А. А. и др., Труды второй Международной конференции по применению атомной энергии в мирных целях, 1958, доклад № 2501.
[5] Сагдеев, Р. З., «Физика плазмы и проблема управляемых термоядерных реакций», 1958, том III, 346.
[6] Волков, Т. Ф., *тоже*; том III, 336.
[7] Kunzler, J. E. *et al.*, *Phys. Rev. Letters* **6** (1961) 89.
[8] Волков, Т. Ф., Глаголев, В. М., Кадомцев, Б. Б., Доклад на данной конференции (Аннотация CN-10/228).
[9] Brown, S. C., Rose, D. J., *J. Appl. Phys.* **23** (1952) 711.

THE STABILITY OF AN ALTERNATING PINCH DISCHARGE*

P. C. T. VAN DER LAAN, L. H. TH. RIETJENS

FOM-INSTITUUT VOOR PLASMA-FYSICA

RIJNHUIZEN, JUTPHAAS, NETHERLANDS

Experiments have been carried out to study the stability of an alternating pinch discharge. In the discharge, a plasma column is confined by B_z- and B_θ-fields, oscillating with the same frequency and with a phase difference of 90°. The confining fields are induced by two primary helical windings, wound with opposite pitch around a torus. The primary windings are connected to charged capacitors by means of spark-gaps, triggered with an adjustable time delay. Resonant frequencies of the LC circuits are 80 kHz; the primaries are wound so as to give a low magnetic coupling. In any point of the surface of the plasma, the alternating pinch fields can, in first order, be thought of as a magnetic field which is constant in magnitude and rotating in a plane tangential to the plasma column. The field is penetrating into the plasma, and if the applied frequency ω is smaller than the collision frequency ν_c, a shear is produced in the magnetic field lines in the skin of the plasma.

A necessary condition for stability in cylindrical geometry is derived from the Suydam criterion, assuming the skin depth to be small compared to the radius of the plasma column, r_0. For a given r_0, this stability criterion, together with the requirement $\omega \ll \nu_c$ and the Bennett relation, yields combinations of electron temperatures and electron densities, where experiments can verify the validity of this theory.

Experiments are described by which the z-pinch, the θ-pinch, and the alternating pinch are compared. The choice between these different pinch configurations can be made by means of the adjustable time-delay.

1. Introduction

The confinement of a plasma by means of a magnetic field, constant in magnitude and rotating in a plane tangential to the surface of the plasma, has been discussed by several authors [1, 2, 3]. The major part of these discussions deals with a plasma of infinite conductivity. For a plane plasma surface, and assuming an infinite sound velocity v_s, BERKOWITZ [1] has found certain regions for the rotation frequency ω in which particular modes of instability are suppressed. Similar results have been obtained in cylindrical geometry. A stabilizing effect has also been found in the case ω goes to infinity [2, 4].

In the case of finite conductivity, a skin is formed and the magnetic field lines take on a lamellar structure. It has been pointed out by TUCK that this shear is qualitatively most encouraging for stability [3, 5].

In the present work the penetration of a rotating magnetic field into a cylindrical plasma column has been calculated (compare [3]). Results are obtained for a plasma with an electron density distribution $n_e(r)$ and a uniform conductivity under the assumption that the applied frequency ω is small compared with the collision frequency ν_c. The substitution of the solution into a slightly modified version of the SUYDAM criterion [6] yields a necessary stability criterion for an alternating pinch. However, in Suydam's criterion a steady field is assumed. Therefore, the results obtained are only applicable to instabilities which might develop in a time short compared to the period.

An experimental arrangement has been built to produce a toroidal alternating pinch discharge. Measurements are carried out to compare z-, θ-, and alternating pinch discharges.

2. A necessary stability criterion for alternating pinch discharges

In this section cylindrical symmetry is assumed. A plasma column of radius r_0 is given with an electron density distribution $n_e(r)$ and an electron temperature T_e independent of r. The rotating field at $r=r_0$ has a constant magnitude B_0.

Starting from Maxwell's equations,

$$\operatorname{rot} \mathbf{B} = \mu_0 \mathbf{j} \qquad \operatorname{div} \mathbf{B} = 0$$

$$\operatorname{rot} \mathbf{E} = -\partial \mathbf{B}/\partial t \qquad \operatorname{div} \varepsilon_0 \mathbf{E} = e(n_i - n_e),$$

the pressure balance,

$$\mathbf{j} \times \mathbf{B} = \operatorname{grad} p,$$

and Ohm's law,

$$\mathbf{E} + \frac{1}{e n_e} \operatorname{grad} p_e - \frac{1}{e n_e} \mathbf{j} \times \mathbf{B} - \eta \mathbf{j} = 0,$$

the following equations for $B_z(r)$ and $B_\theta(r)$ can be derived:

$$\frac{\partial^2 B_z}{\partial r^2} + \frac{1}{r}\frac{\partial B_z}{\partial r} - \frac{i\omega\mu_0}{\eta} B_z = 0,$$

$$\frac{\partial^2 B_\theta}{\partial r^2} + \frac{1}{r}\frac{\partial B_\theta}{\partial r} - \left(\frac{i\omega\mu_0}{\eta} + \frac{1}{r^2}\right) B_\theta = 0.$$

* Conference paper CN-10/18, presented by L. H. Th. Rietjens. Discussion of this paper is given on page 749. Translations of the abstract are at the end of this volume of the Conference Proceedings.

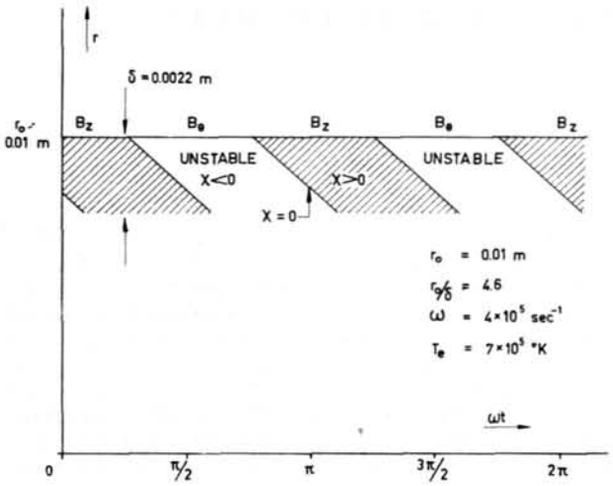

Fig. 1 The stability criterion for the given alternating pinch arrangement.

In Ohm's law, $\omega m_e/n_e e^2$ has been neglected with respect to η, which is equivalent to $\omega \ll \nu_c$.

The solution for B_z and B_θ is given by:

$$B_z(r,t) = \mathrm{Re}\left\{\frac{B_0}{J_0(\sqrt{-2\mathrm{i}}\, r_0/\delta)} \cdot J_0(\sqrt{-2\mathrm{i}}\, r/\delta) \cdot \mathrm{e}^{\mathrm{i}(\omega t+\pi/2)}\right\},$$

$$B_\theta(r,t) = \mathrm{Re}\left\{\frac{B_0}{J_1(\sqrt{-2\mathrm{i}}\, r_0/\delta)} \cdot J_1(\sqrt{-2\mathrm{i}}\, r/\delta) \cdot \mathrm{e}^{\mathrm{i}\omega t}\right\},$$

in which J_0 and J_1 are the zero and first-order Bessel functions, and $\delta = (2\eta/\mu_0\omega)^{1/2}$ is the skin depth.

After substitution of the pressure balance, the Suydam criterion can be written as (cylindrical symmetry):

$$\left(B_z B_\theta - r B_z \frac{\partial B_\theta}{\partial r} + r \frac{\partial B_z}{\partial r} B_\theta\right)^2 - 8 B_\theta^2 \left(r B_z \frac{\partial B_z}{\partial r} + r B_\theta \frac{\partial B_\theta}{\partial r} + B_\theta^2\right) \geqslant 0.$$

With the solution for $B_z(r,t)$ and $B_\theta(r,t)$ one arrives at a condition which, in a zero-order approximation with respect to δ/r_0, yields:

$$\chi \equiv r_0/\delta - 8\cos^2\{\omega t + (r - r_0)/\delta\} \geqslant 0.$$

This is satisfied at any time if $r_0/\delta \geqslant 8$, which expresses, therefore, in a zero-order approximation, a necessary condition for magnetohydrodynamic stability. Higher-order approximations are being worked out.

This result can be applied to our experiment, in which $\omega = 5.4 \times 10^5$ radians/s. Taking $r_0 = 0.01$ m and $T_e = 7 \times 10^5$ °K, and calculating the resistivity from Spitzer's formula [7], one finds in one period two unstable regions in the vicinity of the I_z-current maxima (see Fig. 1).

In Fig. 2, some of the requirements for confining a plasma by alternating pinch fields are summarized in a N_e (number of electrons per unit length) versus T_e diagram.

(a) The stability criterion yields:

$$\frac{r_0}{\delta} = r_0\sqrt{\frac{\mu_0\omega}{2\eta}} \geqslant 8,$$

or numerically:

$$\omega r_0^2\, T_e^{3/2} \geqslant 8.3 \times 10^{10}\,(T_e \text{ in } {}^0\mathrm{K}).$$

For a given ωr_0^2 a plasma is unstable for temperature on the left side of the vertical line.

(b) The condition to attain shear:

$$\omega < \nu_c.$$

This inequality is strengthened to $\omega \ll \nu_c$, because of the radial dependence of the electron density and because of the assumption made in Ohm's law.

Or numerically:

$$\frac{\omega r_0^2\, T_e^{3/2}}{N_e} \ll 7.3 \times 10^{-6}.$$

In Fig. 2, lines are drawn for $10\ \omega = \nu_c$, where ν_c is taken at a density $n_e = N_e/\pi r_0^2$. The allowed regions lie on the left side of these lines.

(c) The pressure balance, given by the Bennett relation:

$$I_z^2 = 0.55 \times 10^{-15} N_e T_e,$$

is shown for two different values of I_z. For the maximum value of I_z, attainable in a particular experiment, the allowed region lies to the left of the corresponding line.

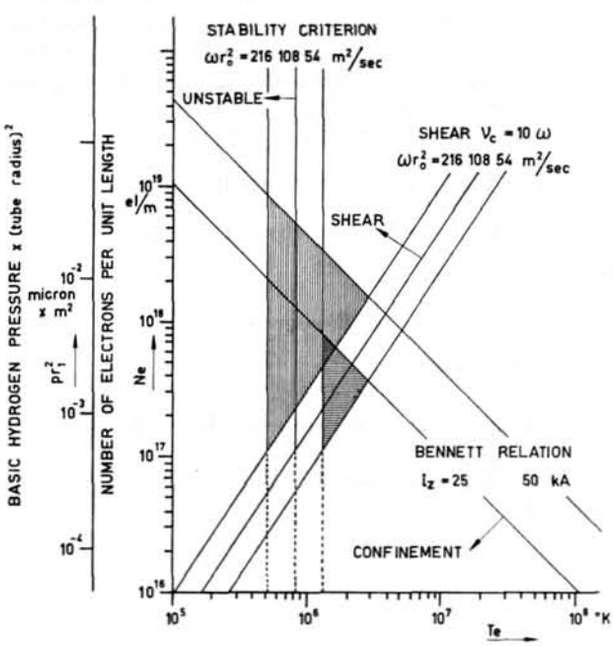

Fig. 2 Stability criterion, condition for shear in magnetic field lines, and Bennett relation for alternating pinch discharges.

The horizontally hatched area represents the region in which, for the experiment described in this paper, these three requirements are fulfilled (the pinch

radius is taken as 0.01 m). The figure shows that the discharge has to be struck in a hydrogen gas with a pressure of about 1 micron, which meets with experimental difficulties.

The advantage of increasing r_0 and I_z appears from the vertically hatched area in Fig. 2, which represents an arrangement in which both the dimensions of the torus and the plasma current are increased by a factor 2. It can be seen that the gas pressure can be increased to about 10 microns, while the lower limit of the electron temperature is decreased to 5×10^5 °K.

3. The experimental arrangement

The experiments are carried out in a pyrex glass torus with a major and a minor diameter of $2R=0.32$ and $2r_1=0.08$ m, respectively. The torus is covered with a layer of silver, having four radial gaps and one azimuthal gap. Around the tube, two helical coils with opposite pitch are wound. Each coil consists of 8 parallel wires making n_θ turns in the θ-direction and only one in the z-direction. The torus with the helical windings is shown in Fig. 3.

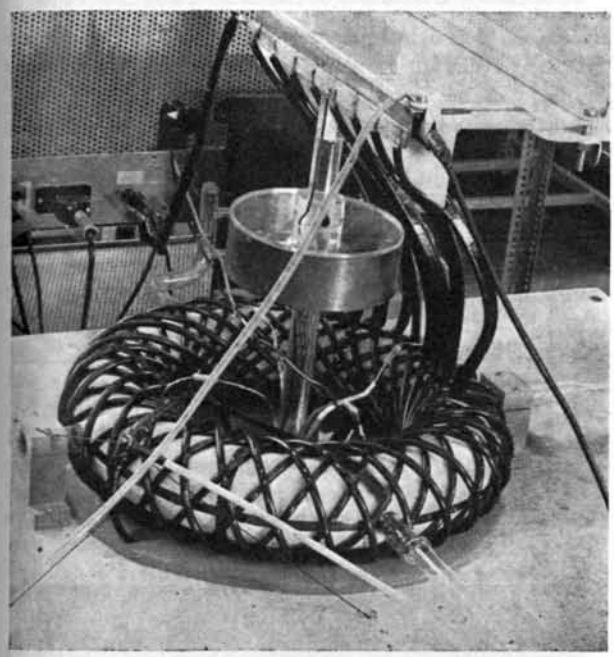

Fig. 3 Torus and helical windings of the alternating pinch arrangement.

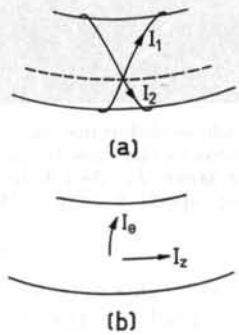

Fig. 4 Definition of the currents. (a) Currents in the helical coils: $I_1=\hat{I}\cos\omega t$, $I_2=\hat{I}\cos(\omega t+\varphi)$. (b) Equivalent currents on the torus: $I_z=I_1+I_2=2\hat{I}\cos(\varphi/2)\cos(\omega t+\varphi/2)$; $I_\theta=n_\theta(I_1-I_2)=2n_\theta\hat{I}\sin(\varphi/2)\sin(\omega t+\varphi/2)$.

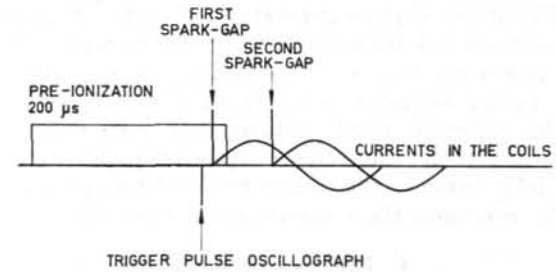

Fig. 5 Timing sequence.

A low-inductance plate system with a built-in triggered spark-gap connects each coil with a 7.5 μF, 18 kV condenser. In this way, two equal LC circuits with resonant frequencies of 80 kHz are obtained. The two spark-gaps are triggered with an adjustable time delay between the trigger pulses. This results in a phase difference φ between the two alternating currents I_1 and I_2 (see Fig. 4). The angle φ determines the amplitudes of the corresponding equivalent currents I_z and I_θ on the surface of the torus. With $\varphi=0$, a toroidal z-pinch can be expected. With $\varphi=180°$, the θ-current on the surface will induce a pure θ-pinch. With an intermediate value of φ, the resulting z- and θ-currents are 90° out of phase. They produce a rotating magnetic field at the surface of the plasma column. To keep the magnitude of this field constant, as is required for an alternating pinch, $\hat{I}_\theta/\hat{I}_z$ should be equal to pR/r_0, in which p is the ratio of the secondary to the primary z-current.

In an alternating pinch discharge, the ratio of the amplitudes and the phase difference of I_z and I_θ may be disturbed by an energy transfer between the two oscillating systems, due to the mutual inductance of the coils. However, the mutual inductance can be made sufficiently small by adjusting the above-mentioned number n_θ. An additional variation of the mutual inductance can be achieved with a conducting ring or a ferrite core in the centre of the torus.

Without a discharge, n_θ follows from the approximate formula $n_\theta=(L_z/L_\theta)^{1/2}$, where L_z and L_θ are the self-inductions of a conducting layer on the torus for z- and θ-currents, respectively. With a plasma column in the torus, the mutual inductance is changed, and the choice of n_θ has to be made experimentally. It turns out that in the experiment, a negligible energy transfer during about one period is found with $n_\theta=4$. After that time the phase difference changes rapidly, presumably by instabilities of the discharge.

All experiments are carried out with hydrogen, admitted through a heated nickel tube. The gas is pre-ionized by a 200 μs pulse of a radio-frequency oscillator.

The pulses which are fed into the trigger units of the spark-gaps, the start and stop pulses of the radio-frequency oscillator, and the trigger pulse of the oscillograph are provided by a time control unit. This

unit contains a pulse generator for cyclic operation, transistorized delay circuits, and output stages where the pulses are fed into long matched coaxial cables. The timing sequence is shown in Fig. 5.

The different pinch-configurations can easily be compared under the same circumstances by varying the delay between the trigger pulses of the spark-gaps or by reversing the connections of one coil.

4. The measurements

4.1. Electrical measurements

Rogowski coils are used to measure the currents in the helical coils and the total z-current in the coils and the plasma. The equivalent I_z- and I_θ-currents on the torus and the z-current in the plasma are found by linear combinations of the integrated signals from these Rogowski coils.

More detailed information has been obtained with a magnetic probe. A symmetrical coil of 40 turns in a quartz tube of 3 mm outer diameter is used. B_z- and B_θ-fields can be measured as a function of r in the median plane of the torus.

Typical results of these measurements in a z-pinch are shown in Fig. 6. As five signals have been superimposed, the onset of instabilities in the first half period, and more clearly in the second one, can be seen. Some of the results obtained from the analysis of this picture are given in Fig. 7. After 2.0 μs a pinch has developed, which subsequently breaks up. At 4.0 μs the signals are again fairly reproducible. At this time, large fields still exist, although the net

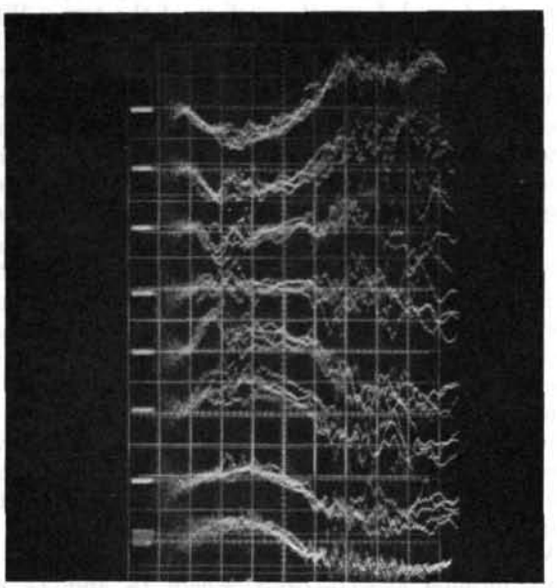

Fig. 6 $B_\theta\,(r, t)$ field in z-pinch (0.17 Wb/m² div). Lower trace: I_z current in plasma (60 kA/div). Sweep speed 1 μs/div. Hydrogen pressure 9.5 microns. Each trace is obtained from five successive discharges. The signals from top to bottom are taken at probe positions ranging from inner to outer wall.

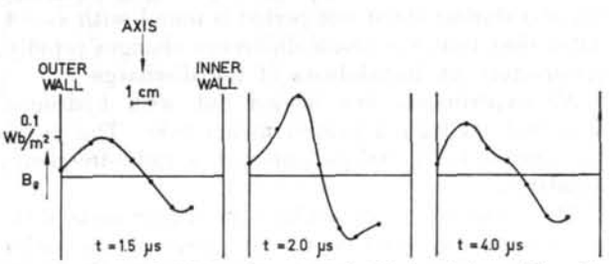

Fig. 7 $B_\theta\,(r)$ field in the z-pinch (derived from Fig. 6). $t = 0$ firing moment of the spark-gaps.

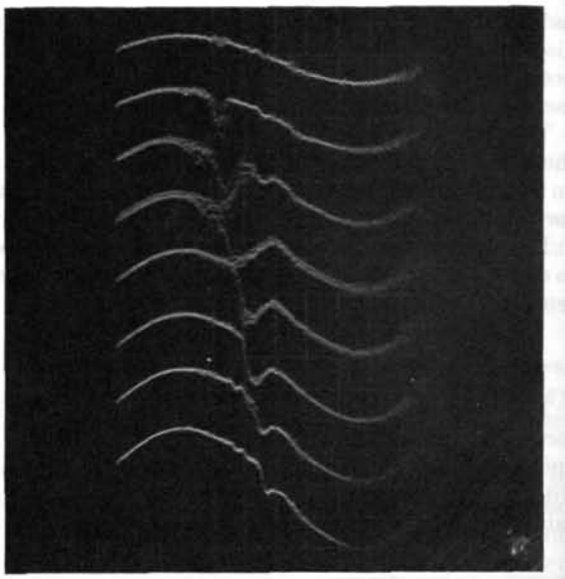

Fig. 8 $B_z\,(r, t)$ field in θ-pinch (0.43 Wb/m² div). Lower trace: I_θ current on the torus (680 kA/div). Sweep speed 1 μs/div. Hydrogen pressure 9.5 microns. Each trace is obtained from five successive discharges. The signals from top to bottom are taken at probe positions ranging from inner wall to outer wall.

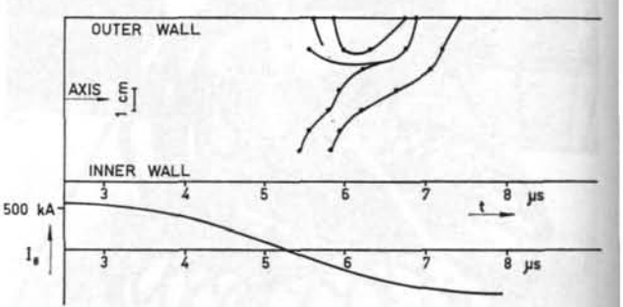

Fig. 9 "Streak"- picture of the current carrying plasma layer in the θ-pinch (derived from Fig. 8).

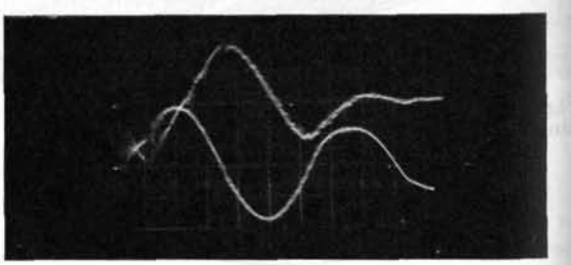

Fig. 10 The 90° phase difference between the I_z and I_θ currents on the torus in the case of an alternating pinch discharge. (Upper trace I_z, 34 kA/div, lower trace I_θ, 270 kA/div). Sweep speed 2 μs/div. Hydrogen pressure 8 microns.

current in the plasma is almost zero. This indicates the existence of z-currents flowing in opposite directions (compare [8]).

Probe measurements of the B_z-field in a θ-pinch are shown in Fig. 8. As the B_z-field in vacuum will vary proportional to I_θ, that is as a sine wave, each departure of this waveform is caused by current-carrying plasma layers. The discharge starts near the wall just before the primary I_θ-current drops to zero. The probe signal shows the compression of the still existing B_z-field, until the inward moving plasma layer passes the probe. The moments at which these passages begin and end can be measured at different probe positions. With these results, a graph resembling a "streak" picture can be drawn (Fig. 9). The picture shows that, after compression, the plasma moves rapidly to the outer wall. This outward movement, which is caused by the difference in the magnetic pressures at the inner and outer wall, occurs in a time of the same order of magnitude as the compression time.

The I_θ-currents in the plasma layer can be derived from the magnitudes of the magnetic fields inside and outside the plasma layer. Currents up to 600 kA have been observed. Due to the presence of the trapped field from the previous half-period, this secondary current exceeds the primary one.

Preliminary experiments to demonstrate the existence of an alternating pinch have been performed. In Fig. 10, a picture of the I_z- and I_θ-current is given which shows, during about one period, the required 90° phase difference. This indicates a low magnetic coupling between the two oscillating systems. Magnetic probe measurements in an alternating pinch discharge have been performed. A pinch with a vaguely defined radius of about 0.03 m has been found. A large B_z-field is trapped inside. Due to this trapped field, the measured configuration does not yet permit a comparison between theory and experiment.

4.2. Spectroscopical measurements

Measurements of the spectra emitted by the different pinch discharges have been made with a Fuess spectrograph for the visible light and a Hilger medium quartz spectrograph for the ultra-violet region. The photographic plates are scanned by means of a microdensitometer. Parts of the spectra are shown in the diagram of Fig. 11. The wavelengths of the lines are given in Table I [9, 10].

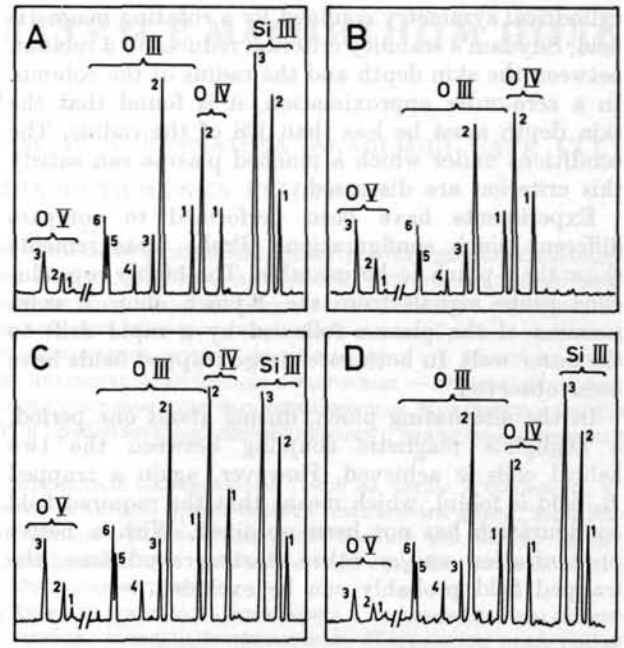

Fig. 11 Micro-densitometer diagrams of spectral lines in the U.V. region. A: z-pinch discharge, B: θ-pinch discharge, C: alternating pinch type I and D: alternating pinch type II. The two types of alternating pinch discharges have different starting conditions. The spectra are integrated over 50 discharges. For identification of spectral lines see Table I.

Again, the z-, θ-, and the alternating pinch have been compared. In the alternating pinch, two different starting conditions have been used. In type I, the first current maximum is in the z-direction, whereas in type II, the first maximum is in the θ-direction.

In all spectra O V has been observed. By comparing the relative intensities of the O V and O IV or the O IV and O III lines, an indication can be found that the θ-pinch and the alternating pinch of type I have higher electron temperatures than the z-pinch and the alternating pinch of type II. In the θ-pinch only very weak Si and B lines are observed. (See the Si III lines in Fig. 11.) This means that in this configuration the contamination by wall materials is smaller than in the other configurations.

5. Discussion

At the present stage of this work, the following conclusions can be drawn. For a plasma column of

Table I. Wavelengths of spectral lines shown in Fig. 11.

O III	O IV	O V	Si III
1) 3059.30 Å	1) 3071.66 Å	1) 2789.9 Å	1) 3096.786 Å
2) 3047.13	2) 3063.46	2) 2787.1	2) 3093.423, 93.613
3) 3043.02		3) 2781.0	3) 3086.225, 86.429, 86.620
4) 3035.43			
5) 3024.57			
6) 3023.45			

cylindrical symmetry confined by a rotating magnetic field, Suydam's stability criterion reduces to a relation between the skin depth and the radius of the column. In a zero-order approximation, it is found that the skin depth must be less than 1/8 of the radius. The conditions under which a pinched plasma can satisfy this criterion are discussed.

Experiments have been performed to compare different pinch configurations. Probe measurements show the z-pinch to be unstable. The highly reproducible probe signals from the θ-pinch show a compression of the plasma followed by a rapid drift to the outer wall. In both cases large trapped fields have been observed.

In the alternating pinch, during about one period, a negligible magnetic coupling between the two helical coils is achieved. However, again a trapped B_z-field is found, which means that the required field configuration has not been obtained. With a better pre-ionization and/or other starting conditions, the trapped field probably can be excluded.

Acknowledgement

This work was performed as a part of the programme of the "Stichting voor Fundamenteel Onderzoek der Materie" (FOM) with financial support from the "Nederlandse Organisatie voor Zuiver-Wetenschappelijk Onderzoek (ZWO).

The authors are indebted to Dr. C. M. Braams for his stimulating interest and to Dr. M. P. H. Weenink for valuable discussions. The technical collaboration of Sj. van der Meulen and the spectroscopical evaluation by R. Mewe and R. F. de Vries is sincerely acknowledged.

References

[1] BERKOWITZ, J., GRAD, H., RUBIN, H., Proceedings of Second U.N. International Conference on Peaceful Uses of Atomic Energy, Geneva, **31** (1958) 177.
[2] TAYLER, R. J., United Kingdom Atomic Energy Research Establishment, Report T/R 2263 (1957).
[3] TUCK, J. L., Proceedings of Second U.N. International Conference on Peaceful Uses of Atomic Energy, Geneva, **32** (1958) 3.
[4] BRINKMAN, H. C., Private Communication.
[5] ALLEN, J. E., see reference [2].
[6] SUYDAM, B. R., Proceedings of Second U.N. International Conference on Peaceful Uses of Atomic Energy, Geneva, **31** (1958) 157.
[7] SPITZER, L., Jr., Physics of Fully Ionized Gases (Interscience Pub., New York, 1956) 84.
[8] BURKHARDT, L. C., LOVBERG, R. H., *Nature* **181** (1958) 228.
[9] MOORE, C. E., A Multiplet Table of Astrophysical Interest (Princeton Observatory, 1945).
[10] MOORE, C. E., Atomic Energy Levels, Circular No. 467, National Bureau of Standards (Washington, D. C., 1949).

ПОПЕРЕЧНОЕ ДВИЖЕНИЕ ПЛАЗМЫ В МАГНИТНОМ ПОЛЕ*

Л. И. ЕЛИЗАРОВ, А. В. ЖАРИНОВ

ИНСТИТУТ АТОМНОЙ ЭНЕРГИИ ИМ. И. В. КУРЧАТОВА АКАДЕМИИ НАУК СССР, МОСКВА, СОЮЗ СОВЕТСКИХ СОЦИАЛИСТИЧЕСКИХ РЕСПУБЛИК

Изучалось влияние напряженности магнитного поля на зондовые характеристики разряда с накопленным катодом. Зонды были установлены в плоскости анода вне пучка первичных электронов. Обнаружено, что отношение I_e/I — электронного тока насыщения к ионному изменяется немонотонно с увеличением магнитного поля. При некотором критическом значении поля происходит скачкообразное увеличение I_e/I приблизительно на порядок. Осциллографирование характеристик показало, что вблизи критического магнитного поля в разряде возникают интенсивные колебания с частотами $\sim 10^4$ герц, размывающие как электронную, так и ионную ветвь осциллограмм зондовых характеристик. Критическое магнитное поле зависит от рода газа (H_2, N_2, Ar) и приблизительно линейно растет с давлением в интервале 10^{-3}—10^{-2} мм рт.ст.

При изучении фазовых соотношений в переменной составляющей токов на зонды установлено, что при критическом магнитном поле образуется устойчиво вращающийся плазменный факел, вырывающийся из первичного пучка. Концентрация плазмы в факеле существенно больше, чем вне его. Период вращения факела согласуется с величиной дрейфовой скорости и уменьшается с ростом магнитного поля в интервале 100—300 мксек при H 1 до 3 кэрст соответственно.

С целью более детального и наглядного изучения процессов образования и движения плазмы поперек магнитного поля нами был разработан прибор, названный плазмоскоп. Плазмоскоп представляет собой плоскую электронно-оптическую систему, состоящую из двух параллельных мелкоячеистых сеток и люминесцирующего экрана. Первая сетка плазмоскопа является анодом разряда. На экране поверх слоя люминофора нанесена алюминиевая пленка толщиной 200—500 миллимикрон — непрозрачная для света.

Плазмоскоп может работать в двух режимах. В режиме «электронного» изображения 2-я сетка имеет потенциал анода и является электростатическим экраном. Электроны из плазмы, проходящие сквозь обе сетки, ускоряются в зазоре между 2-й сеткой и экраном положительным импульсным напряжением и вызывают свечение люминофора. В режиме «ионного» изображения на 2-ю сетку прикладывается отрицательный импульс, а экран имеет потенциал анода. Свечение люминофора вызывается вторичными электронами, выбитыми ионами из второй сетки.

Плазмоскоп работает в условиях регулярно повторяющихся импульсов с частотой от 0 до 50 герц. На катод разряда подается отрицательный импульс с амплитудой 0 до 500 в и длительностью от 10 до 1000 мксек. С произвольно регулируемой задержкой после включения разрядного импульса на экран или 2-ю сетку подается импульс подсветки амплитудой 10 кв и длительностью 1 до 3 мксек. Полярность импульса изменяется в зависимости от режима. Этим способом мы наблюдаем последовательные стадии развития разряда и поперечного движения плазмы с замедлением в 10^6 или более раз.

В нашей работе изучается поперечное движение плазмы в разряде с накаленным катодом в продольном магнитном поле. Более 10-ти лет назад Д. Бом и его сотрудники [1] обнаружили в разряде такого же типа аномально большую скорость поперечного перемещения электронов, на несколько порядков превышающую диффузионную. Несмотря на большой срок, прошедший с тех пор, механизм аномального движения электронов в соответствующих условиях продолжает оставаться неясным. Поэтому новые экспериментальные результаты, касающиеся этого вопроса, по-прежнему представляют значительный интерес.

1. Критическое магнитное поле

Ранее [2], при изучении влияния напряженности магнитного поля на характер зондовых характеристик вторичной плазмы, было обнаружено скачкообразное увеличение отношения электронного тока на зонд к ионному при некотором критическом значении магнитного поля. Последующие измерения показали, что критическое магнитное поле зависит от рода газа (H_2, N_2, Ar) и приблизительно линейно растет с давлением в интервале 10^{-3}—10^{-2} тора.

Скачкообразное увеличение отношения токов на зонд сопровождается возникновением интенсивных колебаний как в электронной, так и в ионной ветви осциллограмм зондовых характеристик с частотой 10—20 килогерц.

После скачка, в надкритическом режиме, отношение токов на зонд значительно медленнее уменьшается с удалением от первичного электронного пучка, чем в докритическом режиме. Благодаря этому отношение токов на зонд увеличивается при критическом магнитном поле тем в большее число раз, чем дальше находится зонд от первичного пучка.

* Доклад CN-10/221, представленный на конференцию. Докладчик: Е. П. Велихов. Дискуссия (на английском языке) по этому докладу дана на стр. 749. Переводы аннотаций находятся в конце этого тома Трудов Конференции.

2. Вращающийся плазменный факел

С помощью серии зондов, расположенных в плоскости анода, изучались фазовые соотношения в колебаниях плотности плазмы в различных точках сечения разряда [3]. Было установлено, что при критическом магнитном поле образуется плазменный факел, устойчиво вращающийся в ионную сторону. Концентрация плазмы в факеле существенно больше, чем вне его. В момент прохождения факела над зондом можно наблюдать отчетливые максимумы как в ионном, так и в электронном токе на зонд. (При отрицательном и положительном по отношению к аноду потенциале зонда соответственно.)

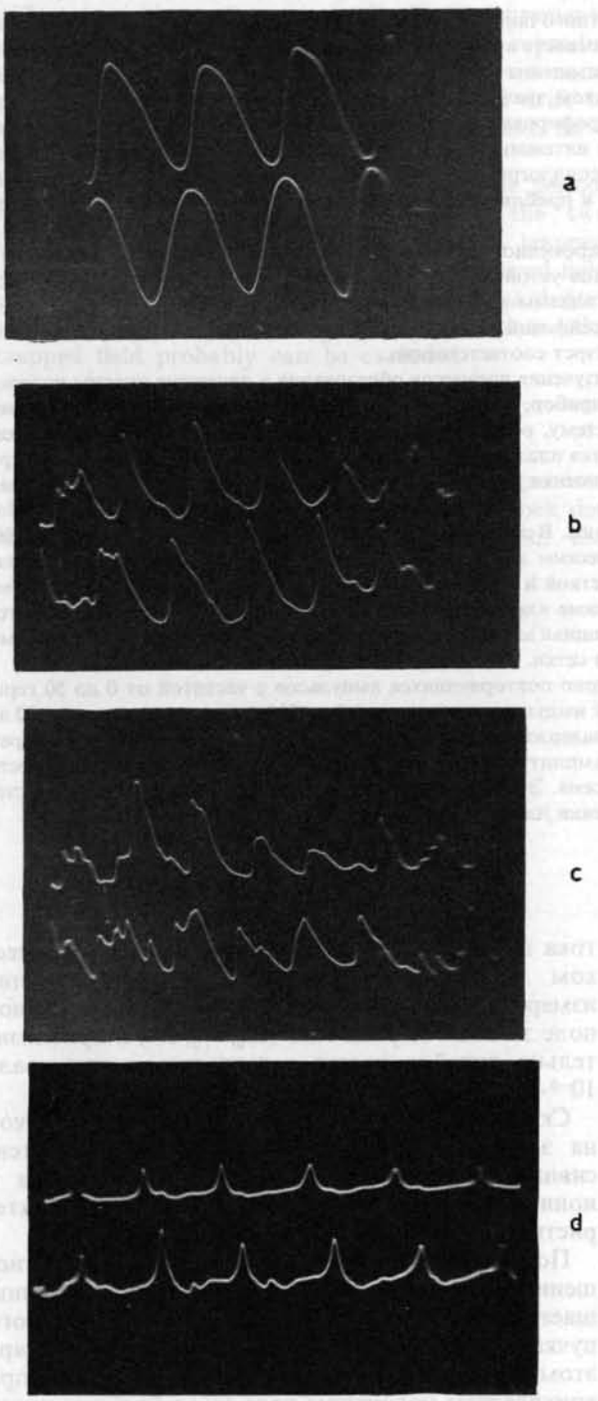

Рис. 1 Осциллограммы ионных токов на зонды, установленные по разные стороны от первичного пучка. Аргон. $V_p = 150$ в, $I_p = 0{,}4$ а, $p = 10^{-2}$ тор. (a) $H = 2000$ эрст, $T = 80$ мксек. (b) $H = 2800$ эрст, $T = 65$ мксек. (c) $H = 3300$ эрст, $T = 55$ мксек. (d) $V_p = 150$ в, $I_p = 0{,}6$ а, $p = 1{,}4 \cdot 10^{-2}$ тор., $H = 3700$ эрст, $T = 65$ мксек.

Характерные осциллограммы ионных токов на 2 зонда, регистрируемые одновременно, представлены на рис. 1. Можно видеть, что форма факела и период его вращения зависят от напряженности магнитного поля. Вблизи критического магнитного поля (1a) факел широкий, осциллограмма близка к синусоидальной. При дальнейшем увеличении магнитного поля (1в, 1c) факел сужается, период его вращения уменьшается и наблюдается тенденция к нарушению регулярности. Сравнение осциллограмм в, c и d показывает, что давление и величина разрядного тока также существенно влияют на форму факела.

Аналогичные явления наблюдались в работе [4], доложенной на 2-ой Женевской конференции. Однако, как отмечают авторы, вращение плазменного сгустка возникало лишь при большом продольном градиенте давления газа. В условиях наших опытов давление практически равномерно по объему разрядной камеры.

3. Плазмоскоп

С целью дальнейшего, более наглядного и детального изучения различного типа неустойчивостей плазмы и ее движения в направлении, перпендикулярном магнитному полю, нами был разработан прибор, названный плазмоскопом.

Плазмоскоп позволяет получать мгновенные фотографии распределения плотности плазмы по сечению разряда, отвечающие экспозиции около одной микросекунды. В зависимости от режима работы с помощью плазмоскопа можно получить либо неподвижное изображение регулярно вращающегося факела, либо на одном кадре, — несколько последовательных стадий движущегося факела.

В основу этой методики положено преобразование потока электронов или ионов из плазмы в поток света, так же, как это делается в электронно-оптических преобразователях.

Для того, чтобы свести до минимума возмущения плазмы электрическими полями, электрод, сквозь который производится наблюдение, выполнен из металлической сетки с возможно меньшими размерами ячеек. В нашем распоряжении была сетка с ячейками 70×70 микрон из никелевой проволоки диаметром 30 микрон. Эта первая сетка, натянутая специальными пружинами на круглой металлической оправе диаметром 130 мм, одновременно служила анодом разряда. На расстоянии 2 мм от нее установлена вторая, которую мы будем условно называть ионной. Далее, на расстоянии не более 2 мм от ионной сетки, расположен люминесцентный, алюминированный экран. Лю-

минофор нанесен на стекло, сквозь которое и производится наблюдение. Так как мощность, рассеиваемая сетками и экраном, ограничена, то разряд питается прямоугольными отрицательными импульсами напряжения длительностью от 10 до 1000 микросекунд и амплитудой до 500 вольт, прикладываемыми к катоду. Частота повторения разрядных импульсов может изменяться от 0 до 50 герц.

4. Разрядный прибор

Газоразрядный прибор представляет собой цилиндрическую медную вакуумную камеру диаметром 20 см, служившую одновременно каркасом соленоида. Соленоид состоял из 10 секций и имел длину 54 см.

На одном торцевом фланце смонтирован прямонакальный танталовый катод в виде тонкого диска, диаметром 0,4 см, нормального к магнитному полю. Катод нагревался с помощью нефильтрованного однополупериодного выпрямителя, сфазированного так, чтобы в момент приложения разрядного импульса ток накала равнялся нулю. Непосредственно перед катодом, на расстоянии около 1 мм, расположена анодная диафрагма с отверстием диаметром 5 мм. В начальном варианте катод устанавливался наподвижно на аксиально расположенной изолированной штанге длиной 15 см, заключенной в электростатический экран. В усовершенствованном варианте — катод можно перемещать вдоль магнитного поля и вращать вокруг оси штанги.

На противоположном фланце устанавливался плазмоскоп. Расстояние между катодом и анодной сеткой плазмоскопа 30 см. В усовершенствованном варианте — от 30 см до 10 см.

5. Режим электронного изображения

В режиме электронного изображения вторая, ионная, сетка не играет принципиального значения. На люминесцирующий, алюминированный экран подается в желаемый момент времени один или несколько положительных прямоугольных импульсов подсветки (И. П.) длительностью 1—8 микросекунд и амплитудой до 10 киловольт. Плазменные электроны, прошедшие сквозь обе сетки, ускоряются в зазоре между ионной сеткой и экраном и, пробивая алюминиевую пленку (толщина 200—500 миллимикрон), вызывают свечение люминофора. Для увеличения срока службы экрана кроме И. П. к нему прикладывается постоянное отрицательное смещение, препятствующее попаданию первичного электронного пучка на протяжении разрядного импульса. При выбранных параметрах ускоряющего зазора и напряжения роль объемного заряда электронов пренебрежимо мала вплоть до плотностей тока в несколько ампер на квадратный сантиметр. Поэтому изображение получается вполне четким. Ионная сетка в электронном режиме может использоваться для регулировки яркости изображения с помощью постоянного смещения.

Очевидно при достаточно малых размерах ячеек сетки, плотность потока j_1, электронов из плазмы, проходящих сквозь анодную сетку, близка к величине потока j_a на сплошной металлический анод, умноженной на проницаемость γ:

$$j_1 \approx \gamma \cdot j_a = \gamma \cdot \frac{n v_e}{4} e^{-\varphi/T_e} \qquad (1)$$

где φ — потенциал плазмы относительно анода; T_e — температура электронов; n — концентрация.

Таким образом, при линейной зависимости яркости свечения от плотности тока, электронное изображение определяется не только распределением концентрации плазмы, но и распределением потенциала и температуры в плазме.

На рис. 2 приведено семейство электронных плазмограмм, иллюстрирующих образование и движение плазменного факела в водородном разряде. (Магнитное поле — нормально к плоскости рисунка и направлено от наблюдателя.) Масштаб плазмограмм 1:2.

Эти плазмограммы получены в стробоскопическом режиме, при длительности разрядного импульса (И. Р.) 250 мксек и частоте повторения 50 герц. Длительность И. П. составляла 6 мксек. Фотографирование производилось с экспозицией 1/50 сек.

При постоянной задержке И. П. относительно переднего фронта И. Р. изображение получалось неподвижным. Это объясняется случайной ассиметрией прибора, которая систематически проявлялась при каждом И. Р. и регулярно инициировала возникновение факела в одном и том же месте. Последнее подтверждается возможностью повернуть плазмограмму на произвольный угол путем поворота катода на соответствующий угол. В случае устойчиво фиксированного начального азимута факела все стадии его развития можно проследить путем плавного изменения задержки И. П.

Разумеется, далеко не при всех условиях удается получить неподвижное изображение. Поэтому более универсальным является фотографирование сдвоенных или строенных плазмограмм, которые получаются при работе с двумя или тремя, соответственно сдвинутыми, И. П.

При рассмотрении плазмограмм 1—7, отвечающих одинаковым параметрам разряда, можно заметить, что факел возникает в пучке первичных электронов, в начальной стадии разряда. С течением времени он приобретает сравнительно устойчивую спиральную форму и вращается с периодом около 100 мксек. (неясно, следует ли в данном случае говорить об одном или двух факелах). Отметим также, что в этом опыте вращение происходит в электронную сторону, тогда как в другом [3] направление вращения было обратным. При длине разрядного промежутка 30 см ни изменение формы магнитного поля путем раздельного питания секций соленоида, ни изменение параметров разряда не позволило получить ионное направле-

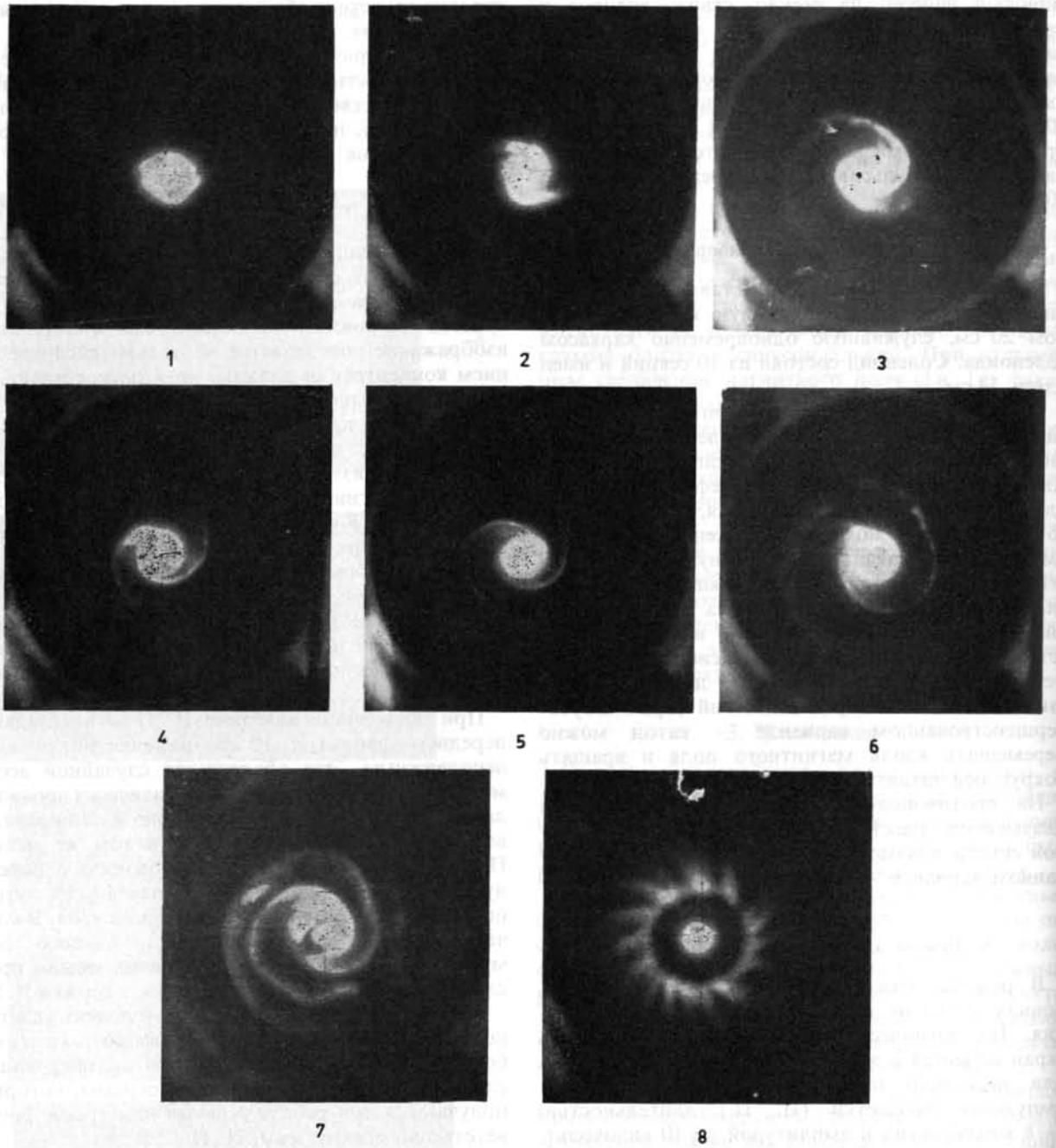

Рис. 2 Электронные плазмограммы. Направление $\mathbf{H}\oplus$, $V_p = 210$ в, $p = 8 \cdot 10^{-3}$ тор., $H = 900$ эрст. Длительность И. Р. 250 мксек. Длительность И. П. 6 мксек. Длительность задержки И. П. (мксек): (1) — 20; (2) — 45; (3) — 75; (4) — 115; (5) — 150; (6) — 175; (7) > 250; (8) > 250 при $H = 200$ эрст.

ние вращения. И лишь при длине разряда около 10 см, наряду с электронным, можно было получить и ионное направление вращения. Полученные плазмограммы по форме напоминают мгновенные фотографии струйки воды, вытекающей из трубочки, тангенциально расположенной на ободе диска, вращающегося под действием реактивной силы (Сегнерово колесо). Действительно, сравнение плазмограмм 1, 2, 3 подтверждает, что передний фронт факела обладает не только радиальной, но и тангенциальной скоростью, направленной в сторону, противоположную вращению. Причем, тангенциальная скорость = приблизительно $4 \cdot 10^4$ см/сек и по порядку величины соответствует дрейфовой скорости cE/H при $E \approx 0{,}5$ в/см и $H \approx 10^3$ эрст.

Видно также, что электронное изображение факела имеет сложную структуру с яркими спиральными линиями. Яркость этих линий убывает с удалением от первичного пучка.

Плазмограмма № 7, полученная после выключения разрядного напряжения, показывает, что при

распаде плазмы сохраняется сложная спиральная форма факела и наблюдается выравнивание яркости свечения вдоль него. Следует отметить, что центральное пятно на этой плазмограмме (и на плазмограмме № 8) объясняется наличием отверстия в первой сетке, проплавленного первичными электронами в одном из опытов. Таким образом, при распаде плазмы в центре плазмограммы, под первичным пучком, образуется темное пятно, увеличивающееся с течением времени. Одновременно сжимается к центру и периферийная темная область.

Плазмограмма № 8 относится к другому режиму разряда, в более слабом магнитном поле, и должна рассматриваться как иллюстрация многообразия и сложности наблюдаемых процессов поперечного движения плазмы.

6. Режим ионного изображения

В ряде случаев электронное изображение невозможно получить (например, пенинговский разряд), или оно недостаточно полно отображает топографию распределения концентрации плазмы по сечению. Поэтому, наряду с электронным был также отработан режим ионного изображения.

В этом режиме на ионную сетку прикладывается отрицательный И. П. Ускоренные ионы выбивают из ионной сетки вторичные электроны, которые и вызывают свечение люминофора, ускоряясь в зазоре между сеткой и экраном. Таким образом, в ионном режиме свечение люминофора пропорционально концентрации плазмы.

Роль объемного заряда в ускоряющих зазорах существенно сказывается на качестве ионного изображения. Однако при выбранных параметрах плазмоскопа (амплитуда И. П. — 10 кв, зазоры — 2 мм, ячейки 70 × 70 микрон) — изображение вполне удовлетворительно, если плотность ионного тока соответствует условию:

$$j_+ \ll \frac{1}{9\pi}\sqrt{\frac{2e}{M}}\,\frac{U^{3/2}}{\alpha^2}, \qquad (2)$$

где U — амплитуда И. П., α — большее расстояние между электродами плазмоскопа (сетки, экран). В частности, для разряда в водороде должно быть: $j_+ \ll 1$ А/см².

На рис. 3 приведена серия ионных плазмограмм. Они также получены в стробоскопическом режиме

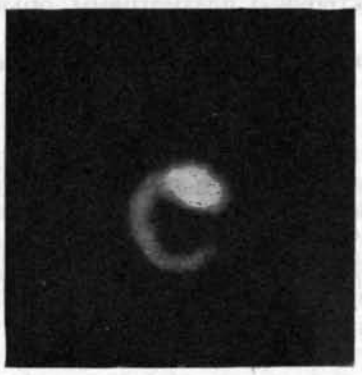

1

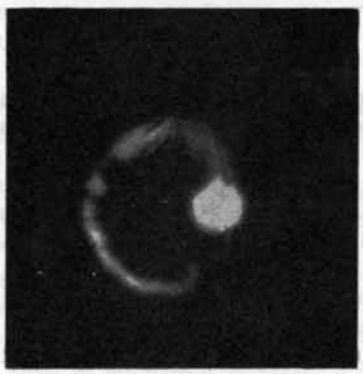

2

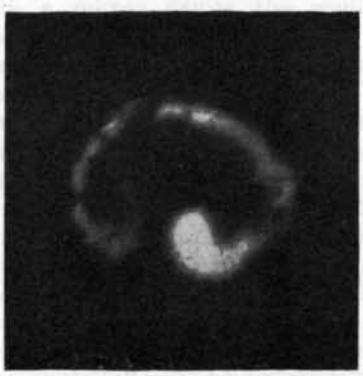

3

4

Рис. 3 Ионные плазмограммы. Направление **H** ○, $V_p = 280$ в; $p = 6 \cdot 10^{-3}$ тор., $H = 1000$ эрст. Длительность И. Р. 250 мксек. Длительность И. П. 8 мксек. Длительность задержки И. П. (мксек): (1) — 75; (2) — 100; (3) — 125; (4) — 150.

(масштаб 1:2). Предварительно качество ионного изображения проверялось с помощью контрольной решетки, устанавливаемой поверх анодной сетки.

Длина разрядного промежутка была равна 12 см. Магнитное поле, соответствующие этому рисунку, направлено на наблюдателя. Таким образом, в данном случае, наблюдалось ионное направление вращения факела с периодом около 80 мксек. Сравнивая плазмограммы 1 и 2, можно заметить, что отдельные участки факела двигаются не с одинаковой скоростью. Например, передний фронт (т.е. наиболее удаленный от первичного пучка участок) почти не переместился, тогда как промежуточный участок удалился от центра приблизительно на 4 см. (Клеточки, различимые на плазмограммах, являются изображением масштабной сетки с ячейкой 1 см $\times$ 1 см.) Таким образом, скорость поперечного движения плазмы оказывается порядка 10^5 см/сек при напряженности магнитного поля 10^3 эрст.

7. Заключение

Приведенные результаты имеют предварительный, несистематический характер и не позволяют составить четкое представление о наблюдаемых процессах.

С помощью плазмоскопа пока изучался лишь разряд в водороде, причем, в основном, как объект для испытания и отработки новой методики. Вследствие этого наблюдения, естественно, носят отрывочный характер, имеется ряд противоречивых обусловленных, по-видимому, различием условий. Например, при зондовых измерениях надежно установлено, что факельная структура распределения плазмы возникает при определенном критическом магнитном поле, а с помощью плазмоскопа пока не удалось наблюдать соответствующей скачкообразной перестройки плазмы. Всегда, даже в сравнительно слабых магнитных полях ($H \sim 80$ эрстед) и высоких давлениях ($p \sim 10^{-2}$ тор) наблюдались факельные плазмограммы, причем их многообразие и сложность далеко не исчерпываются приведенными иллюстрациями.

Пока остаются также неясными факторы, определяющие направление вращения факела и его регулярный, устойчивый характер.

Вполне очевидно, однако, что наблюдаемые процессы поперечного движения не имеют ничего общего с диффузией, а являются проявлением неустойчивости конфигурации плазмы. Возможно, что в наших условиях эта неустойчивость обусловлена поляризацией плазмы в пучке первичных электронов вследствие неравномерного распределения плотности по азимуту и центробежного дрейфа ионов. Скорость движения переднего фронта факела несомненно указывает на дрейфовый характер движения электронов из первичного пучка, т.е. что факел — поляризован. Это подтверждается также неравномерностью свечения электронных плазмограмм, объясняющейся главным образом соответствующей структурой потенциального рельефа факела (см. формулу (1) § 5).

Литература

[1] Вонм, D., "The Characteristics of Electrical Discharges in Magnetic Fields" A. Guthrie, R. K. Wakerling (Eds.) Ch. 1, 2, 9 (New York, 1949).
[2] Жаринов, А. В., *Ат. Энерг.* **7** (1959) 215.
[3] Жаринов, А. В., *Ат. Энерг.* **10** (1961) 368.
[4] Найдай, Унвер. Избр. докл. иностр. ученых. т. 1 стр. 327. Москва. Атомиздат. 1959.

EXPERIMENTS ON THE ENERGY BALANCE AND CONFINEMENT OF A MAGNETIZED PLASMA*

J. BERGSTRÖM, S. HOLMBERG, B. LEHNERT

ROYAL INSTITUTE OF TECHNOLOGY

STOCKHOLM, SWEDEN

In order to achieve a fully ionized plasma of high temperature by energy amounts which do not exceed the heat content of the plasma by many orders of magnitude, a strong particle confinement has to be established. Particle losses along and across the field lines of a magnetic bottle should then be kept at the lowest possible level.

The purpose of the present experiments is to investigate the interaction between a rotating plasma and a wall which is placed across the field of the magnetic bottle. The position of the wall can be changed and, within the same experimental device, it is then possible to compare conditions which closely correspond to the Homopolar, Ixion and current loop configurations. For the latter, radial ratios of about 3.4 and mirror ratios of about 7.7 are obtainable in the present apparatus.

The results show that the energy losses, the radiation from impurities and the gas released by interaction with the movable wall are reduced considerably when the conditions are changed from those corresponding to a Homopolar to those prevailing in a current loop device. For the latter the kinetic energy of the rotation can be kept at a slow rate of decay, from 135 to 15 joules within 0.6 milliseconds.

From the results is concluded that the interaction between the plasma and its container walls can be reduced very much in a configuration with high radial and mirror ratios. The long containment times observed also indicate that the plasma is stable, at least with respect to the large losses of particles which would occur from the rapidly growing flute instabilities predicted by earlier hydrodynamic theories.

1. Introduction

A fully ionized plasma of high temperature can be produced by moderate amounts of energy only if a good confinement is established. This implies that particle losses along and across the field of a magnetic "bottle" have to be kept at the lowest possible level and that the configuration should be stable. In a number of earlier reports [1—4] it was suggested that the particle leakage could be reduced by using the magnetic field generated by a current loop.

There are a number of mechanisms which can be applied to heat the plasma in a magnetic field of this kind. One possibility is provided by a discharge which takes place in the crossed electric and magnetic fields of a rotating plasma [2]. When the latter is contained in a mirror device the confinement is improved by the centrifugal force [5, 6]. The large radial extensions of the current loop configuration are of special advantage when a strong centrifugal confinement has to be realized. This can be seen both from a theory on particle motion [3] and from a macroscopic approach including the energy balance [4].

So far, the confinement of charged particles in the field of a ring current has been investigated experimentally with electrons [7] and with a plasma (as demonstrated recently in a brief report [8]).

The purpose of the present experiments is to study how the energy balance and the confinement of a rotating plasma are influenced by particle losses along the magnetic field lines. The mass motion of the plasma is easy to detect by relatively simple methods and gives a considerable amount of information about the conditions of the plasma itself.

For the purpose of the experiments the apparatus has been provided with a movable, non-conducting wall (Fig. 1) which can be placed across the field of the magnetic bottle at different distances from the "equatorial" plane, i.e., the central plane of the main coil. By this arrangement the radial extensions and the mirror ratio of the magnetic bottle can be changed continuously. Within the same experimental device it is then possible to realize conditions which closely correspond to both the Homopolar [5], Ixion [6] and the current loop configurations.

The present investigations constitute a first stage in the study of the end losses along the field lines where the current loop is enclosed in a cylindrical box. In a later stage the losses should be reduced further by suspending the loop by a number of leads [1, 2].

2. Experimental arrangement

2.1. THE MAGNETIC FIELD

An outline of the magnetic field **B** inside the discharge chamber is given in Fig. 1. The field is produced by a ring-shaped main coil and by two external auxiliary coils. At full power supply the mean field strength in the equatorial plane has the value $B_0 = 0.44$ Vs/m^2 (4400 G) and at the insulator surfaces (b) and (c), which constitute the ends of the magnetic bottle, the

* Conference paper CN-10/4, presented by B. Lehnert. Discussion of this paper is given on page 750. Translations of the abstract are at the end of this volume of the Conference Proceedings.

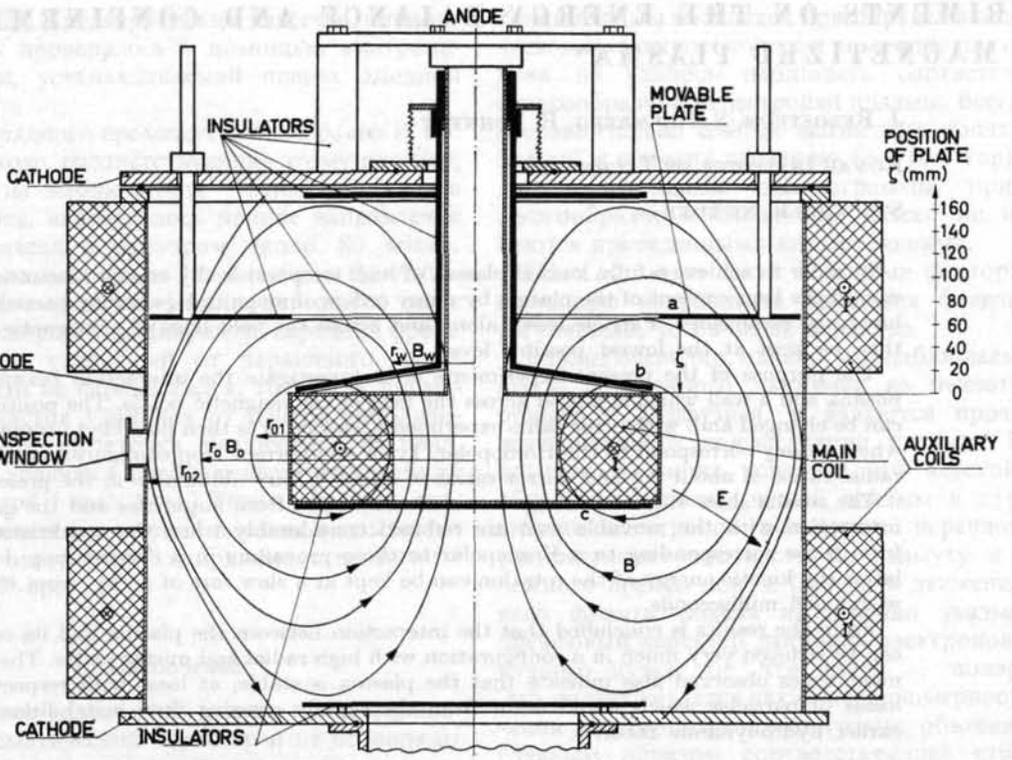

Fig. 1 The discharge chamber. A main coil and two auxiliary coils produce the magnetic field **B**. A voltage is applied between the shield of the main coil and the walls of the vacuum chamber to give an electric field **E**, essentially at right angles to **B**. The coordinate ζ of the movable plate is indicated at the right hand edge of the figure. Outer radius of vessel is $r_{02} = 0.25$ m.

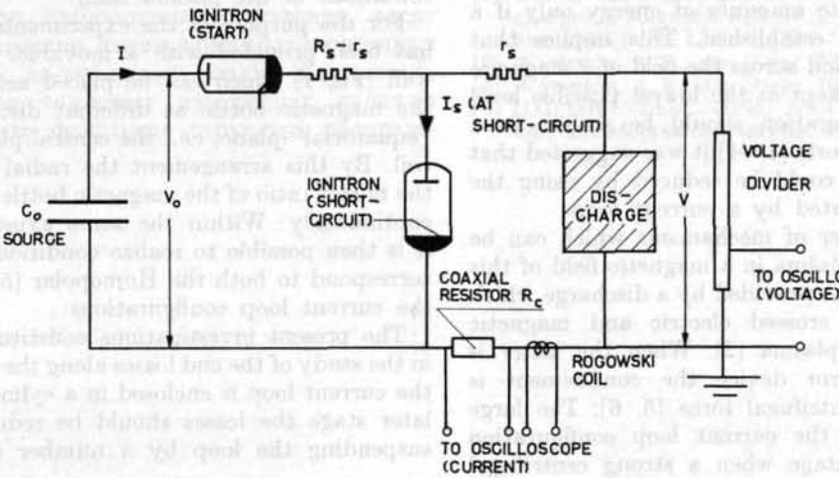

Fig. 2 The discharge circuit. Energy is supplied from a condenser bank C_0 which is connected to the discharge through a timed ignitron and a series resistance R_s. A short-circuit can be applied across the discharge by means of a second ignitron.

value is $B_w = 3.4$ Vs/m². This corresponds to a mirror ratio of about 7.7. Of special importance to the centrifugal confinement and the energy balance [3, 4] is the *radial ratio* r_0/r_w which in the present apparatus has a mean value of about 3.4.

The data just mentioned apply to a situation where the movable, ring-shaped plate (a) of Fig. 1 is in its upper position ($\zeta = 165$ mm) and full use is made of the bottle produced by the magnetic field. With the plate in its lower position ($\zeta = 0$) the radial and mirror ratios are reduced to values only slightly greater than unity when the main part of the plasma is situated near the equatorial plane.

A current pulse of about 0.2 s duration is used for the magnetization of the coils. The main coil is enclosed in a box of stainless steel and is cooled by circulating transformer oil which also improves the electric insulation.

2.2 The discharge

When the magnetic field has reached its maximum value a voltage is applied between the shield surrounding the main coil and the walls of the vacuum chamber. This gives an electric field **E**, essentially at right angles to **B**, which ionizes the gas and sets it into rotation around the axis of symmetry. The insulators shown in Fig. 1 are placed in a way such as to prevent a short-circuit across the metal surfaces.

Fig. 2 shows the arrangement of the discharge circuit. The energy source consists of a condenser bank of capacity $C_0 = 330$ μF, charged to about 5 kV. It is connected with the discharge chamber through a timed ignitron switch and a total series resistance R_s which has been varied in the range from about 10^{-2} to 10 ohms. A short-circuit can be applied across the discharge by a second timed ignitron. Different loads r_s from about 10^{-2} to 0.4 Ω have been present at short-circuit. A coaxial resistor and a Rogowski coil have been used in the measurements of the discharge current I and of the "crowbar"-current I_s from the back-pulses which arise at a short-circuit. No measurable difference has been observed in the current oscillograms obtained with these two arrangements.

The discharges have been run mainly with hydrogen and nitrogen.

2.3 The vacuum system

Between the discharges the vessel is pumped down to a basic pressure of about 7×10^{-6} mm Hg. A water-cooled baffle and a non-creep liquid-air trap have been placed between the pump and the vessel. The insulators shown by the heavy black lines in Fig. 1 are all made of plexi-glass. This is more sensitive to damage by the discharge than ordinary glass—an advantage in the present experiment where the interaction between the plasma and the walls is to be studied.

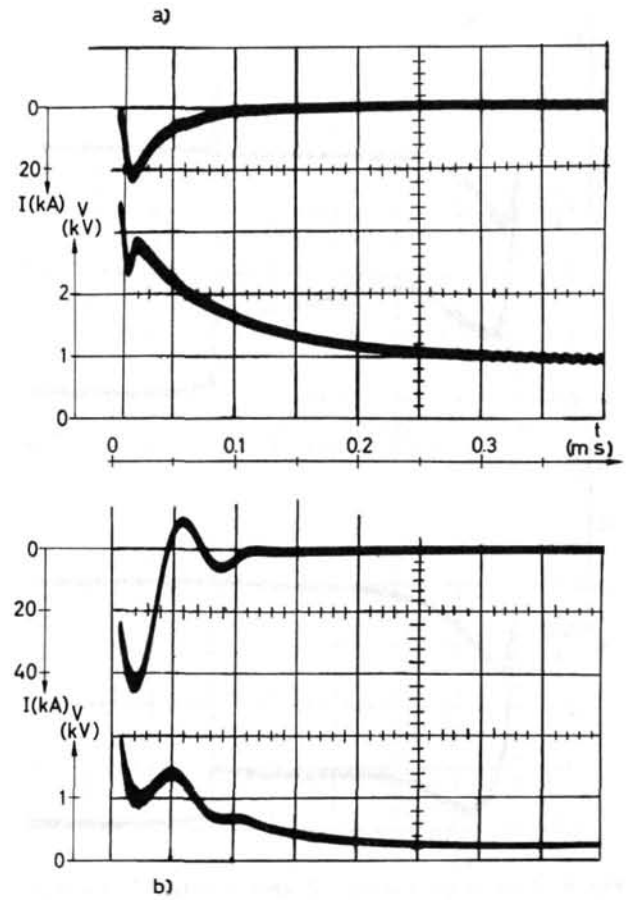

Fig. 3 Oscillogram on discharge current I and voltage V as functions of time t for hydrogen at an initial density corresponding to a pressure $p_0 = 40 \times 10^{-3}$ mm Hg. Initial voltage $V_0 = 4.5$ kV, series resistance $R_s = 0$ Ω and $\bar{B}_0 = 0.40$ Vs/m². (a) Plate in upper position, (b) Plate in lower position.

3. Results

3.1. Voltage and current characteristics

The voltage and current characteristics have been investigated in a range of different series resistances R_s which limit the maximum current extracted from the energy source at the start. When R_s is practically zero and the plate is in its upper position (Fig. 3a), the discharge starts with a current pulse during the later phases of which the voltage decreases gradually. It still remains above a rather high level for a considerable time. When the plate is moved to its lower position (Fig. 3b), however, the current starts with a large peak and oscillates violently like at a short-circuit of the condenser bank. The voltage breaks down to a low value.

With the series resistance increased to $R_s = 0.4$ Ω and the plate in upper position (Fig. 4a) the discharge starts with a current pulse during which ionization and acceleration mainly take place. The voltage then reaches a maximum about 0.2 ms from the start. This is followed by a period during which the voltage is decaying slowly and the current remains at a low level of a few hundred amperes. The short-circuit applied 0.5 ms after the start in Fig. 4 will be discussed later. With the plate in lower position (Fig. 4b) the acceleration period requires a somewhat larger current which slowly returns to zero at the same time as the energy of the plasma is dissipated. The voltage is much lower in Fig. 4b than in Fig. 4a and reaches a constant level about 0.2 ms from the start.

From the current and voltage traces a diagram can be drawn as shown in Fig. 5. With the plate in lower position the voltage becomes constant within a large range of discharge currents. The constant levels obtained for a number of discharges with hydrogen and nitrogen are demonstrated in Fig. 6. This seems to be the same levels as earlier found by Block and Fahleson [9]. When the plate is changed to its upper position Fig. 5 shows that the voltage level is raised and is no longer constant. In this case an increase of the source voltage V_0 gives a slow increase in the observed maximum of the plasma voltage V somewhat like the saturation phenomenon earlier observed in the Ixion [10].

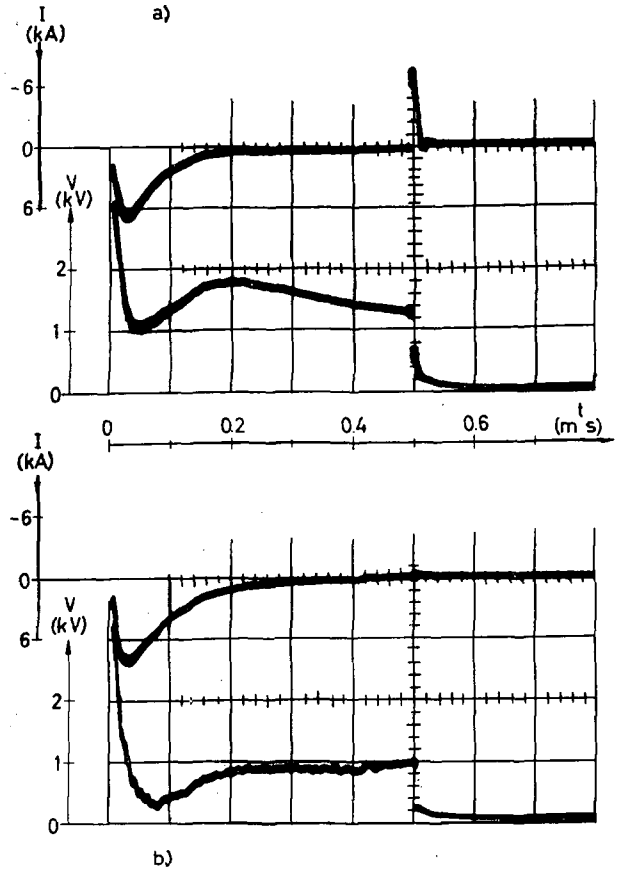

Fig. 4 Discharge current I and voltage V as functions of time t for hydrogen at $p_0 = 45 \times 10^{-3}$ mm Hg, $V_0 = 4.5$ kV, $R_s = 0.4$ Ω and $\bar{B}_0 = 0.44$ Vs/m². A short-circuit is applied at $t_s = 0.5$ ms from the start and $r_s \approx 0$. (a) Plate in upper position, (b) Plate in lower position.

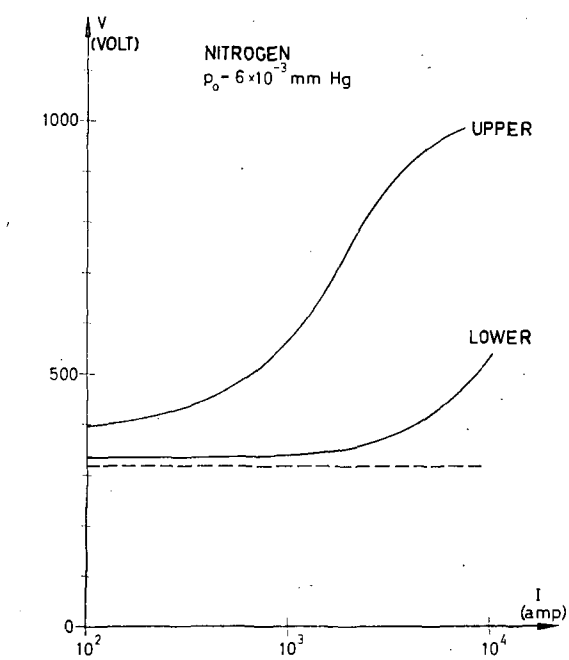

Fig. 5 Associated values of voltage and current taken from oscillograms on discharge in nitrogen. $p_0 = 6 \times 10^{-3}$ mm Hg, $V_0 = 4.0$ kV, $R_s = 0.1$ Ω and $\bar{B}_0 = 0.30$ Vs/m². Plate in upper and lower positions. Dashed line gives constant level calculated from Eq. (1).

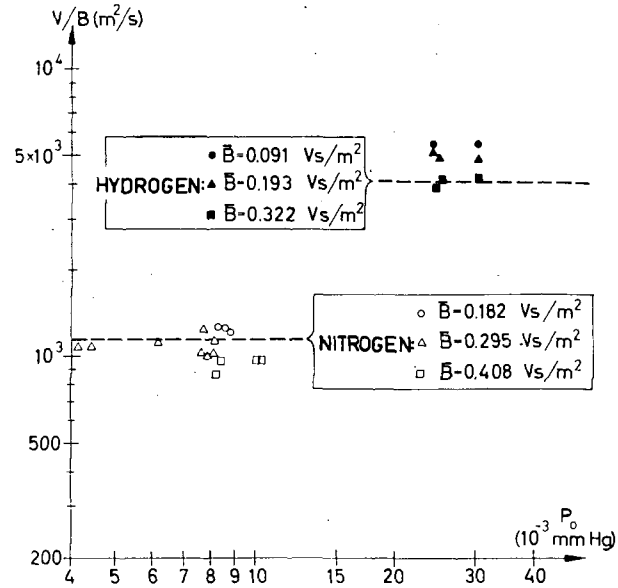

Fig. 6 Constant voltage levels obtained with plate in lower position for discharges in hydrogen and nitrogen. $V_0 = 4.0$ kV and $R_s = 0.1$ and 1 Ω for hydrogen and nitrogen, respectively. Dashed lines give levels calculated from Eq. (1).

Finally, when the series impedance is increased still more, the difference between the oscillograms obtained with the plate in different positions gradually disappears. For $R_s = 10$ ohms a number of measurements with hydrogen at $p_0 = 30 \times 10^{-3}$ mm Hg, $V_0 = 5.0$ kV and $B_0 = 0.091$, 0.194 and 0.323 Vs/m² gave exactly the same levels as obtained in Fig. 6, both with the plate in the upper and the lower positions.

Generally the present experiments indicate that the voltage traces contain a considerable amount of hash (noise) when the plate is in lower position (cf Fig. 4 b) but that the hash decreases very much when the plate is moved to its upper position (cf Fig. 4 a).

3.2. Back-pulses

When a short-circuit is applied at some time t_s after the start, a reserved current pulse will be observed in the branch of the coaxial resistor (Fig. 2), provided that the plasma contains a measurable amount of kinetic energy. One example is given in Fig. 4 which shows a back-pulse at $t_s = 0.5$ ms when the plate is in upper position and no such pulse when the plate is moved to its lower position. In the former case a highly ionized plasma containing considerable amounts of kinetic energy is present at the time t_s. However, in the latter case, only a discharge of low ionization degree is burning at the same time. In Fig. 7 the peak values $(I_s)_{max}$ of the back-pulses have been plotted as a function of t_s for the upper and lower plate positions. Both the pulse strength and the time interval during which pulses can be detected are seen to be much larger for the plate in upper than in lower position. Back-pulses received at times t_s closer to the start

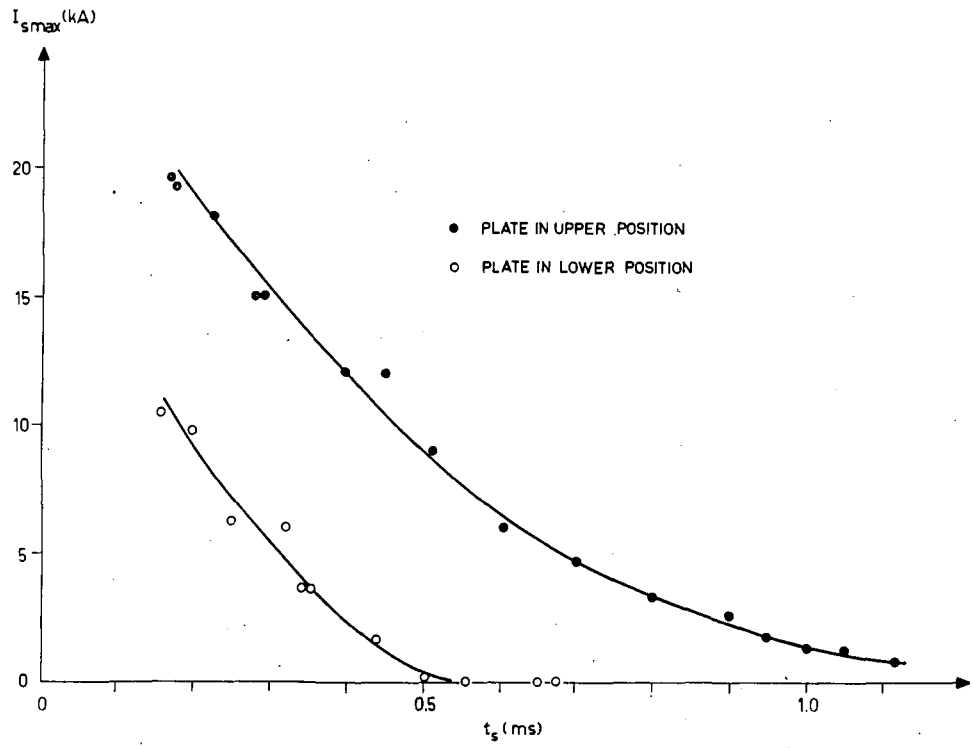

Fig. 7 Peak value $I_{s(max)}$ of the back-pulse current as a function of the time t_s of short-circuit for a hydrogen discharge. $p_0 = 40 \times 10^{-3}$ mm Hg, $V_0 = 4.5$ kV, $R_s = 0.4\ \Omega$, $r_s \approx 0$ and $\overline{B}_0 = 0.44$ Vs/m². Plate in upper and lower positions.

than 0.15 ms are shown in Fig. 8 for the plate in upper position. The figure also gives the general behaviour of the current and voltage during the different phases of the discharge as discussed later in this paper. The maximum back-pulse current $(I_s)_{max}$ is roughly proportional to the recovered charge.

Fig. 9 shows the peak value $(I_s)_{max}$ as a function of plate position ζ at two different times $t_s = 0.2$ and 0.45 ms. In both cases the pulses increase rapidly with ζ, at least in the range from $\zeta = 0$ to 110 mm. Observe that for positions where $\zeta \geqslant 110$ mm (see Fig. 1) almost the entire magnetic bottle is free from bounding walls except the surfaces (b) and (c).

Further, the series resistance r_s in the back-pulse branch was varied from 0 to 0.3 Ω. The peak value $(I_s)_{max}$ was then reduced from 21 to 5.3 kA whereas the duration of the back-pulse was increased such as to give a nearly constant recovered charge. The latter was about 0.16 coulombs, i. e., about 1/5 of the total charge extracted from the energy source at the time of short-circuit. In this particular experiment R_s was kept at the constant value of 0.4 Ω, t_s at 0.2 ms, B_0 at 0.44 Vs/m² and the plate in upper position.

The extracted charge from the capacitor bank was found to be rather insensitive to the strength of the magnetic field as long as there was no breakdown and the plate was in upper position. However, the strength of the back-pulses and the relative magnitude of the recovered charge were found to increase rapidly with the field at the same time. Thus, a change of the current $(I_s)_{max}$ from 0.5 to 6.3 kA was observed at $t_s = 0.45$ ms when the field was increased from 0.10 to 0.44 Vs/m².

Finally, the back-pulses appeared in the form of oscillations with a period of about 10 μs and were damped after about three periods when $r_s \approx 0$. This occurred when the plate was in upper position and t_s was less than about 0.4 ms. If the resistance r_s was increased and the short-circuit was applied at later times t_s or the plate was kept in lower positions the oscillations disappeared and the back-pulses became aperiodic.

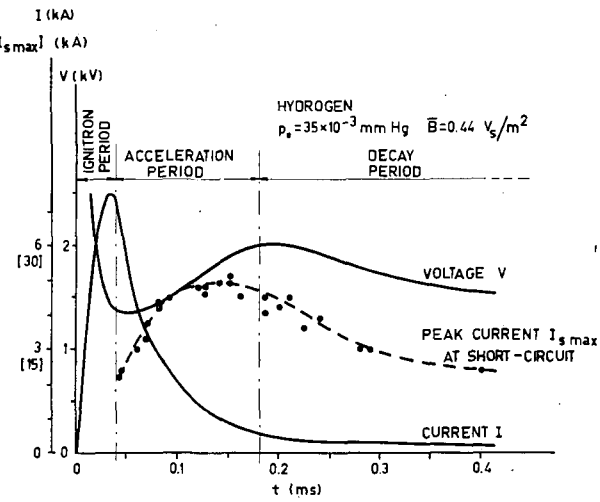

Fig. 8 The three phases of a discharge in hydrogen. $p_0 = 35 \times 10^{-3}$ mm Hg, $V_0 = 4.5$ kV, $R_s = 0.4\ \Omega$, $r_s \approx 0\ \Omega$ and $\overline{B}_0 = 0.44$ Vs/m². Plate in upper position. The maximum back-pulse current $I_{s(max)}$ is roughly proportional to the recovered electric charge.

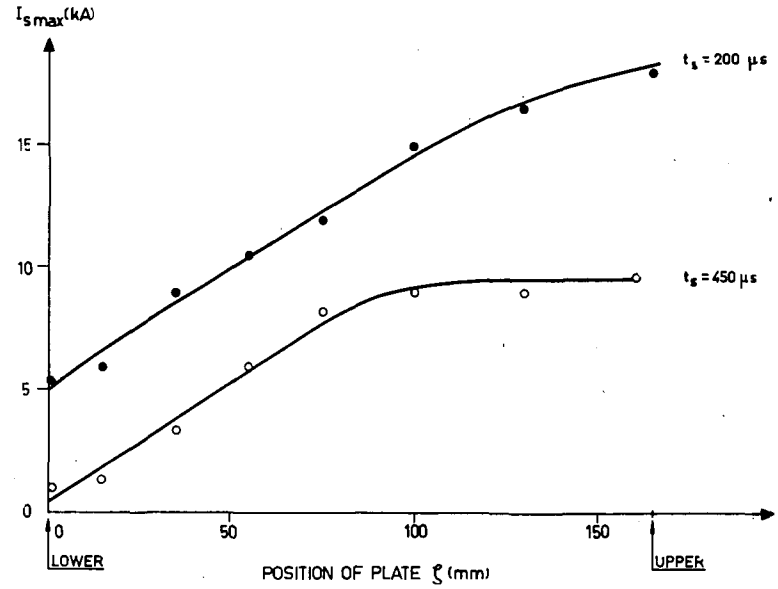

Fig. 9 Peak value $I_{s(\max)}$ as a function of plate position ζ for hydrogen. $p_0 = 45 \times 10^{-3}$ mm Hg, $V_0 = 4.5$ kV, $R_s = 0.6\ \Omega$, $r_s \approx 0$ and $\overline{B}_0 = 0.44$ Vs/m². Times of applied short-circuit are $t_s = 0.2$ and 0.45 ms from start.

3.3. Light intensity

Photometric measurements with hydrogen indicated a relatively weak pulse of light of rather long duration when the plate was in upper position (Fig. 10a).

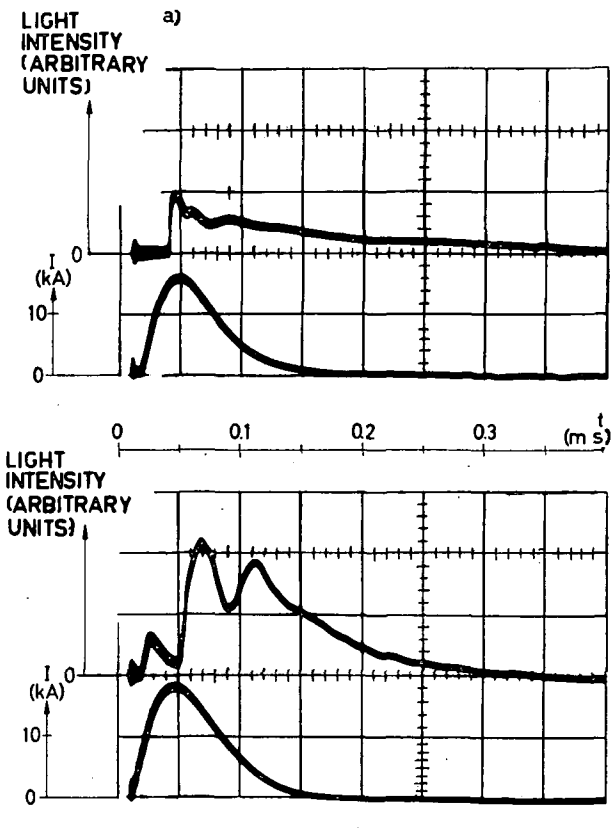

Fig. 10 Traces on light intensity and discharge current I for hydrogen at $p_0 = 43 \times 10^{-3}$ mm Hg, $V_0 = 4.5$ kV, $R_s = 0.1\ \Omega$ and $\overline{B}_0 = 0.32$ Vs/m². (a) Plate in upper position, (b) plate in lower position.

When it was moved to the lower position, the light pulse became much stronger during the early stages of the discharge, but its duration was shorter (Fig. 10b). The oscillations in light intensity at the early stages of the discharge might be due to some "spoke formation" at the start.

A preliminary study of spectra obtained from the discharge indicates an increase in the impurity lines when the plate is moved from the upper to the lower position.

3.4. Gas production and wall constitution

Measurements were made of the pressure in the vessel immediately before and after a discharge had taken place. The recorded increase in pressure was used to determine the relative increase $\Delta n/n_0$ of the particle density by gas released from the walls. Fig. 11 shows a very steep reduction in the gas production from about 190% to about 3% when the plate is moved from the lower to the upper position.

The condition of the insulator surfaces is demonstrated by Fig. 12a which shows the top insulator (b) after about 1000 shots and the movable plate (a) after half as many shots. Fig. 12b gives the bottom insulator (c) after about 300 shots and the movable plate after half the number of shots. The surfaces (b) and (c) have very small signs of contamination compared to (a) which is heavily damaged by the discharge.

4. Discussion

4.1. Voltage levels

When full charge transfer has taken place between the energy source and the plasma the current drops to a low value. The plasma has then been set into rotation with the velocity v_φ around the axis of symmetry.

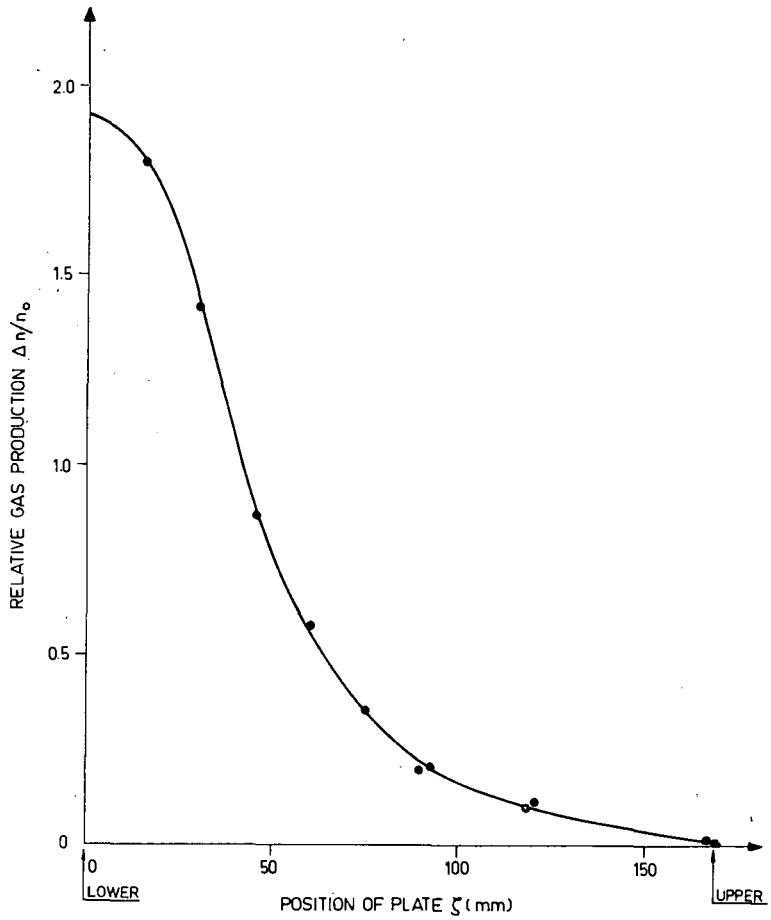

Fig. 11 Relative increase $\Delta n/n_0$ of gas released from walls as a function of plate position in a nitrogen discharge. $p_0 = 9 \times 10^{-3}$ mm Hg, $V_0 = 4.0$ kV, $R_s = 0.1\ \Omega$ and $\overline{B}_0 = 0.41$ Vs/m².

The macroscopic equations of motion give a potential difference (cf ref. [11])

$$V = \int_{r_{01}}^{r_{02}} E_r \, \mathrm{d}r = \int_{r_{01}}^{r_{02}} \left\{ -v_\varphi B_0 + \frac{m_i - m_e}{er} v_\varphi^2 - \frac{m_i}{e\varrho} \frac{\partial p_i}{\partial r} + \frac{m_e}{e\varrho} \cdot \frac{\partial p_e}{\partial r} \right\} \mathrm{d}r \tag{1}$$

between the electrodes at radial distances r_{01} and r_{02} when integration is performed in the equatorial plane of Fig. 1. In Eq. (1) m_i, m_e and p_i, p_e are the ion and electron masses and pressures, respectively, ϱ is the mass density; dissipation has been neglected. When the radius of gyration of an ion is much smaller than the radial dimensions r of the configuration, the angular velocity of rotation v_φ/r is much smaller than the gyro-frequency eB_0/m_i of an ion and the thermal velocity at least does not exceed v_φ too much, the three last terms within the bracket of Eq. (1) can be neglected with good approximation. For moderate deformations of the magnetic field B_0 by the centrifugal force, the voltage V can then be taken as a measure of the velocity v_φ of rotation. Figs. 4 and 5, therefore, indicate that the velocity with the plate in upper position is much greater than that in the lower position. Thus, in the latter case the plate has a strong braking action on the rotation of the plasma.

In their experiments with a Homopolar device BLOCK and FAHLESON have observed a constant voltage level which is proportional to the magnetic field strength [9]. They assume that interaction between the plasma and the neutral gas keeps the velocity at a constant value $v_{\varphi i} = (2e\Phi_i/m_i)^{1/2}$, where Φ_i is the ionization potential, as earlier suggested by ALFVÉN [12]. With the approximations just mentioned v_φ can then be taken out of the integral sign of Eq. (1) and the voltage level V can be calculated from an integration of B_0 between r_{01} and r_{02}. The dashed lines in Figs. 5 and 6 give the values obtained from Eq. (1) which are seen to agree well with the observed levels obtained with the plate in lower position. Thus, the present results are consistent with those obtained by Block and Fahleson.

When the conditions are changed to those prevailing in a low current discharge by increasing the series resistance to $R_s = 10\ \Omega$ the results do not change noticeably with the plate position. This may be due to the slow start of the discharge by which only a small

a

Fig. 12a Photograph of insulator surfaces. Top insulator (b) after about 1000 shots and moving plate (a) after half as many shots.

fraction of the gas has time to become ionized and to be set into rotation. The energy input is very small and the ionization process is slow enough for the neutrals to establish an interaction between the plasma and the container walls, no matter whether the magnetic confinement of the charged constituents is good or not. One may ask why the levels obtained in this case with the plate in upper position should just be equal to those calculated from Eq. (1) for the equatorial plane. At a first sight, there seem to be good reasons for the integration to be performed along any path between the electrodes which is not situated in the equatorial plane. However, due to the form of the magnetic field, this would give higher values of V for any path off this plane. With the condition of co-rotation of the plasma on a certain field line [13, 4, 14] the velocity v_φ would then have to exceed $v_{\varphi i}$ in the equatorial plane if V is determined by $v_\varphi = v_{\varphi i}$ along a path off the same plane. From the conditions of constant velocity and co-rotation the voltage V, therefore, becomes uniquely determined by the field in the equatorial plane. This is also suggested by the experimental results.

The tendency for the maximum voltage to saturate when the plate is in upper position can be understood from the deformation of the magnetic field by the centrifugal pressure. According to an earlier investigation [11] a noticeable deformation will take place when the parameter

$$x_0 = Q\left(\frac{\mu_0}{2\varrho_0}\right)^{1/2}\frac{1}{2\pi r_{02}} \qquad (2)$$

becomes comparable to unity. In Eq. (2), Q is the electric charge transmitted to the plasma per unit length of the magnetic field direction, ϱ_0 is the mass density of the plasma in the equatorial plane and μ_0 is the permeability in vacuo. In the experiments these quantities have the approximate values $Q \approx 1$ coulomb/m and $\varrho_0 \approx 3 \times 10^{-6}$ kg/m^3 for hydrogen which gives $x_0 \approx 0.3$. Thus, with the plate in upper position the centrifugal deformation should be noticeable in the present high-current experiments.

4.2. Energy balance

From the plots of the voltage, current and back-pulses (Fig. 8), the development of the discharge is seen to pass through three phases. When the energy source is connected to the electrodes, a discharge starts during which the current increases steeply and the voltage across the plasma device drops rapidly to a minimum (in this particular case about 40 μs after the start). At the end of this period the back-pulses

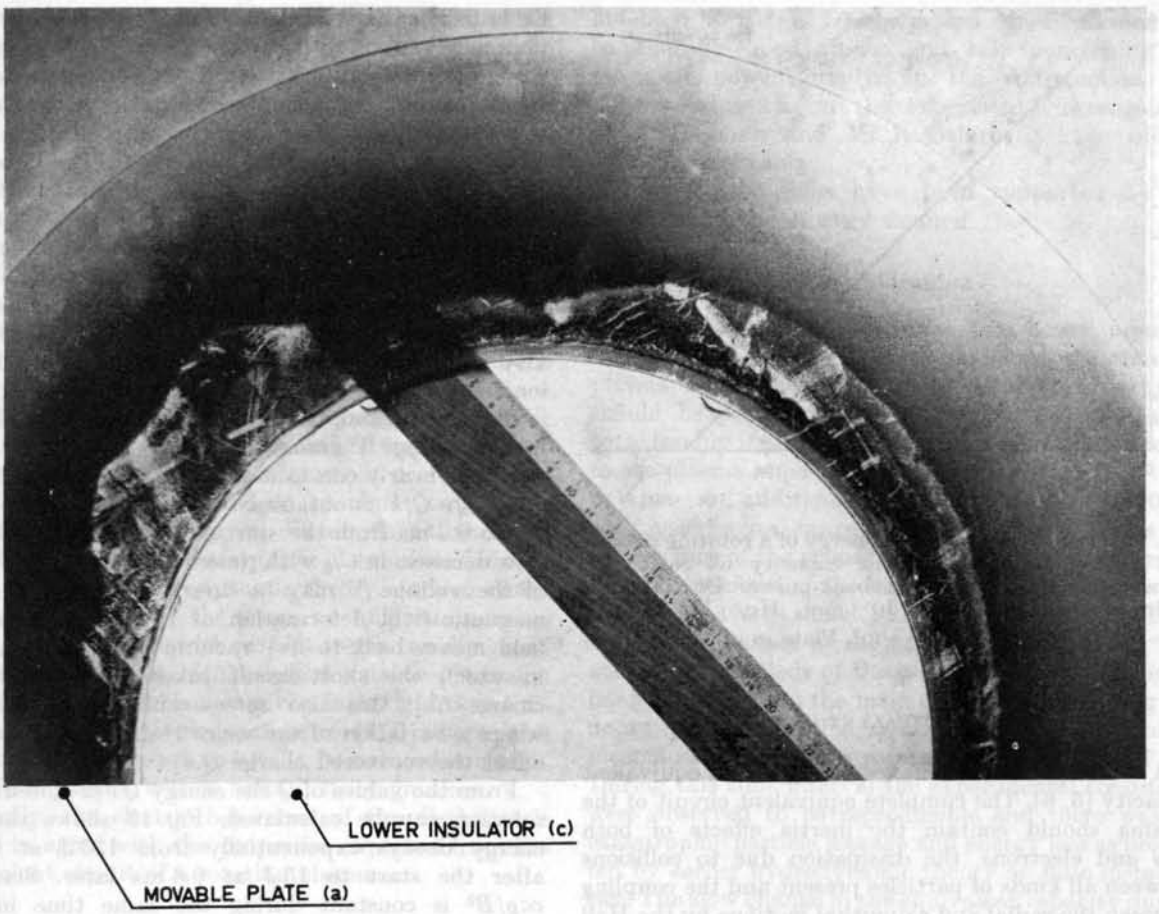

Fig. 12b Photograph of insulator surfaces. (c) Bottom insulator after about 300 shots and (a) plate after half as many shots.

are found to be small; it is, therefore, concluded that, during the ignition period indicated in Fig. 8, the energy input mainly goes into ignition and ionization of the gas and into some type of dissipation.

The charge recovered by the back-pulses at the end of the ignition period is about one-third the total charge fed into the device at this time. Therefore, a loss of angular momentum to the walls must take place during this period. What determines the loss is not fully clear at this stage. It is possible that it is caused by neutrals which have not had time to become ionized at an early stage and which pick up momentum from the ions and are thrown out to the chamber walls. The lack of centrifugal confinement at small angular velocities also increases the interaction with the insulator surfaces.

After the ignition period the voltage increases as well as the strength of the back-pulses whereas the current decreases exponentially; the behaviour resembles the charging of an electric condenser. At the end of this acceleration period full transfer of charge and energy has taken place between the source and the plasma and the voltage and the back-pulses approach their maxima as given by Fig. 8. About one-fifth the total input of charge can be recovered at this time. A mechanism which gives momentum losses during later stages of the discharge is provided by the centrifugal deformation of the magnetic field. Because of the deformation, part of the rotating plasma will be "scraped off" at the chamber walls and momentum is lost [11].

When the acceleration has been completed a slow decay of voltage and back-pulses starts where the current remains at a low level. The impedance of the plasma is relatively high and the dissipation is balanced by a moderate power input of about 500 kW. At the same time the ionization seems to be complete and a considerable amount of rotational energy is accumulated in the plasma as indicated by Fig. 13, which shows a decay of this energy from 135 to 15 J within 0.6 ms. In addition, the plasma will also contain thermal energy the magnitude of which has not yet been estimated. The mean lifetime of each charged particle is then about 200 μs or more, which implies that every particle will make more than 16 turns around the axis of the apparatus before being lost to the walls. From the earlier hydrodynamic theory on flute instabilities one would expect the particles to move across the magnetic field with their full velocity (10^5 m/s) and the escape time would become of the order of one microsecond, which is much smaller than the time estimated above.

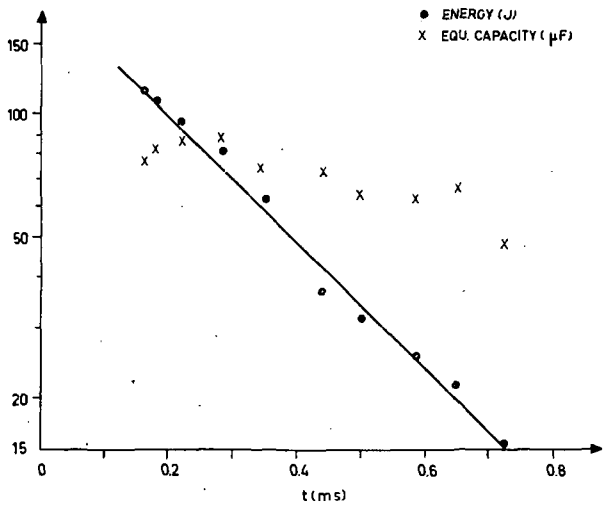

Fig. 13 Decay of the kinetic energy of a rotating plasma and corresponding equivalent capacity as calculated from the measurements on back-pulses. Discharge in hydrogen with $p_0 = 40 \times 10^{-3}$ mm Hg, $V_0 = 4.5$ kV, $R_s = 0.4\ \Omega$ and $\overline{B}_0 = 0.44$ Vs/m^2. Plate in upper position.

4.3. Equivalent circuit

A rotating plasma behaves mainly as an equivalent capacity [5, 6]. The complete equivalent circuit of the plasma should contain the inertia effects of both ions and electrons, the dissipation due to collisions between all kinds of particles present and the coupling between the radial and azimuthal motions by the Hall current. Fig. 14 gives the circuit of a unit cube of plasma obtained for a thin cylindrical sheet at small

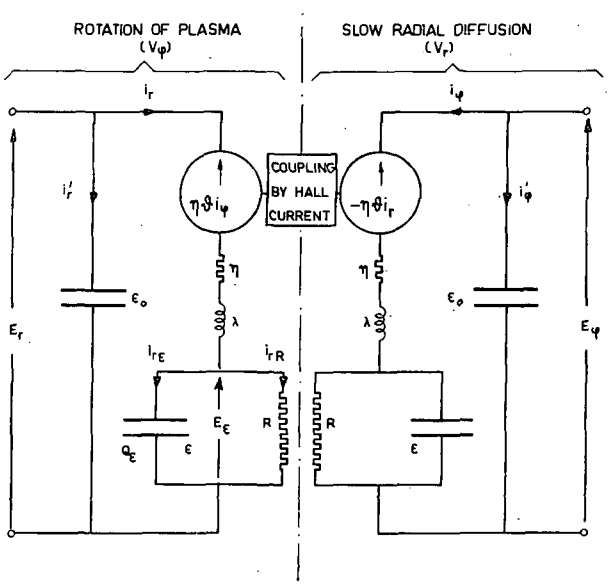

Fig. 14 Equivalent circuit of a unit cube of a rotating plasma [14]. The voltage V between the electrodes of Fig. 1 gives rise to an electric field E_r and a velocity v_φ of rotation. A Hall coupling exists between the radial and azimuthal currents i_r and i_φ. An electric field E_φ is generated in the azimuthal direction by induced magnetic fields. ε_0 is the dielectric constant in vacuo.

field deformations [14]. A detailed discussion of all parameters involved is beyond the scope of the present paper. It shall only be pointed out here that the inertia of the rotating plasma, which has to be accelerated to a velocity v_φ, is given by a specific equivalent capacity ϱ/B^2 and a specific inductivity λ. The latter can be left out when the inertia of electrons is neglected. The leakage of charge is given by the resistance R which corresponds to frictional losses of momentum. The left circle in Fig. 14 represents an electric field due to the Hall current which mainly determines the series impedance of the plasma, because the resistivity η is usually quite a small quantity in a highly ionized gas.

If the recovered charge Q in a back-pulse is divided by the voltage V across the plasma just before short-circuit, a nearly constant value of an equivalent capacity $C_{eq} = Q/V$ is obtained within a range from about 0.2 to 0.7 ms from the start as shown in Fig. 13. The slow decrease in C_{eq} with time during the decay period of the voltage V may be due to a reduction of the magnetic field deformation as v_φ decreases and the field moves back to its "vacuum position". The way in which the short-circuit takes place should not change C_{eq}; this also agrees with the experiments where a variation of the series resistance r_s does not affect the recovered charge Q.

From the values of Q the energy $QV/2$ stored in the rotation can be calculated. Fig. 13 shows that the energy decays exponentially from 135 J at 0.1 ms after the start to 15 J at 0.6 ms later. Since $C_{eq} \propto \varrho/B^2$ is constant during the same time interval this suggests that the plasma has a nearly constant density for about 0.6 ms. The reason for decay of the back-pulses is, then, that the rotation is being braked slowly by a weak interaction between the plasma and its surroundings. This is represented by a leakage resistance, which in the present experiments is of the order of 4 Ω, as given by the voltage-current characteristics. For further discussion of the frictional forces generated by circulating neutral gas and charge-exchange collisions, reference is made to some earlier reports [4].

4.4 Interaction with walls

All the electric measurements discussed so far give a very clear indication that the interaction between the plasma and the movable wall decreases gradually when the latter is moved upwards. There are also other more direct confirmations of this, such as the increase in released gas and in the light intensity which probably originates from impurities when the plate is moved towards its lower position. The damage to the plate (a) shown in Fig. 12 also gives indications in the same direction.

When the series resistance R_s is reduced to zero and the power input at the start becomes very high, there is a sudden and violent breakdown, see Fig. 3b. This may be due to a strong production of gas by the surface of the moving plate followed by a breakdown across the surface as observed earlier in the Ixion [10].

In all the measurements made so far the hash in the voltage was found to be much stronger with the plate in the lower than in the upper position. Whether this is due to currents across the plate cannot yet be decided.

5. Conclusions

The present experiments show that the interaction between a highly ionized rotating plasma and its container walls can be suppressed considerably in a magnetic bottle which has large radial and mirror ratios. This is consistent with the predictions made in earlier theoretical investigations on the confinement and the energy balance [1—4].

A highly ionized plasma containing considerable amounts of energy has been sustained by a moderate power input. The mean containment time of each individual particle is found to be about two orders of magnitude longer than the containment time which would result in the presence of flute instabilities deduced from the earlier hydrodynamic theory. As also observed earlier [6, 15, 16], the present configuration seems to be stable, at least with respect to the rapidly growing instabilities just mentioned. A further discussion of the stability problem is given in an additional report submitted to this conference [17], where it is shown that the growth rates can be reduced considerably in a plasma with a finite density gradient.

Finally, the electric behaviour of the discharge is found to agree with the properties expected from the equivalent circuit of a rotating plasma.

6. Acknowledgements

The authors are indebted to Prof. H. Alfvén, Dr. B. Bonnevier and Mr. U. Fahleson for valuable discussions on the present investigations. We are also indebted to Dr. E. Djurberg and Mr. R. Ekman for considerable good advice and help concerning the magnetic power supply. In the construction and mechanical work on the experidental arrangement Mr. L. Hagman and Mr. K. Österberg have offered valuable assistance.

The investigations have been supported by the Swedish Atomic Energy Council.

7. Addendum

As pointed out in Section 4.2, a power input of about 500 kW is required to maintain the rotating plasma during the decay period. This suggests that it should be possible to prolong the state of rotation considerably if an additional energy source is matched to the plasma impedance during this period.

When an additional capacitor bank of 1320 μF with a series resistance of 3.8 Ω is placed across the connections of the primary bank C_0 of Fig. 2, the equivalent capacity and the kinetic energy of the rotating plasma behave as shown in Fig. 15. The primary bank still supplies most of the energy to the ignition and acceleration periods of the plasma, but the additional bank now becomes the main energy source during the decay period. By this arrangement a fully ionized plasma can be kept in rotation for more than 7 ms. During this time interval the experimental conditions were observed to be reproducible and there was no catastrophic particle leakage and energy loss as predicted by earlier hydrodynamic theory on flute instabilities. The slow change in the equivalent capacity during this interval suggests that the particle density is nearly constant and that the leakage of particles is very small. As far as can be judged at this stage there seems to be no principal difficulty in prolonging the state of rotation for times far beyond 7 ms.

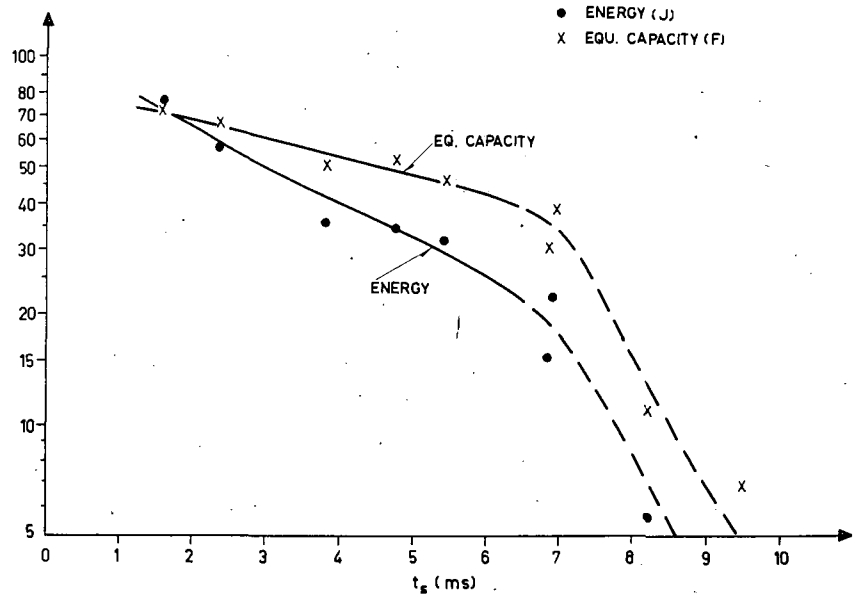

Fig. 15 Equivalent capacity and kinetic energy of rotation as calculated from back-pulses applied at different times t_s from start. Additional bank has capacity 1320 μF and series resistance 3.8 Ω. Discharge in hydrogen with $p_0 = 23 \times 10^{-3}$ mm Hg, initial voltage across both condenser banks 5 kV, $R_s = 0.6$ Ω and $\overline{B}_0 = 0.43$ Vs/m².

References

[1] LEHNERT, B., *Nature*, **181** (1958) 331.
[2] LEHNERT, B., *J. Nuclear Energy*, **C 1** (1959) 40; *Arkiv f. Fysik*, **15** (1959) 579.
[3] BONNEVIER, B., LEHNERT, B., *Arkiv f. Fysik*, **16** (1960) 231.
[4] LEHNERT, B., *Arkiv f. Fysik*, **17** (1960) 177; **18** (1960) 251; *Rev. Mod. Phys.*, **32** (1960) 1012.
[5] ANDERSON, O. A., BAKER, W. R., BRATENAHL, A., FURTH, H. P., ISE, J., KUNKEL, W. B., STONE, J. M., Proc. Second U.N. International Conference on Peaceful Uses of Atomic Energy, **32** (1958) 155.
[6] BOYER, K., HAMMEL, J. E., LONGMIRE, C. L., NAGLE, D., RIBE, F. L., RIESENFELD, W. B., *ibid.* **31** (1958) 319.
[7] BONNEVIER, B., *Arkiv f. Fysik*, **18** (1960) 421.
[8] BERGSTRÖM, J., HOLMBERG, S., LEHNERT, B., *Phys. Rev. Letters*, **6** (1961) 525.
[9] FAHLESON, U., *Phys. Fluids*, **4** (1961) 123; see also ALFVÉN, H., *Rev. Mod. Phys.*, **32** (1960) 710.
[10] BAKER, D. A., HAMMEL, J. E., *Bull. Amer. Phys. Soc., Ser. II*, **5** (1959) 314.
[11] LEHNERT, B., *Nuclear Fusion*, **1** (1961) 125.
[12] ALFVÉN, H., On the origin of the solar system (Oxford, Clarendon Press, 1954).
[13] FERRARO, V. C. A., *Mon. Not. Roy. Astr. Soc.*, **97** (1937) 458.
[14] LEHNERT, B., Progress in Nuclear Energy: Series XI: Vol. **2**, "Plasma Physics and Thermonuclear Research", J. L. TUCK (Ed.) (Pergamon Press, Oxford, 1961).
[15] POST, R. F., ELLIS, R. E., FORD, F. C., ROSENBLUTH, M. N., *Phys. Rev. Letters*, **4** (1960) 166.
[16] VAN ALLEN, J. A., *J. Geophys. Res.*, **64** (1959) 1683.
[17] LEHNERT, B., *Phys. Fluids*, **4** (1961); 525, 847; and paper submitted to this conference, see p. 135 of these Proceedings.

CONTRIBUTION A LA THÉORIE DES CHOCS CONVERGENTS DANS UN PLASMA*

J. P. SOMON, J. G. LINHART, H. KNOEPFEL

LABORATORIO GAS IONIZZATI (EURATOM-C.N.E.N.)

FRASCATI (ROME), ITALY

Les auteurs présentent les résultats des calculs effectués sur de fortes ondes de choc cylindriques convergentes et de choc sphériques convergentes dans le plasma. Ceci leur permet d'évaluer la production maximum de neutrons que l'on peut obtenir à partir d'ondes de choc convergentes dans un plasma de (D, T).

1. Introduction

On suppose qu'on a pu obtenir dans une géométrie cylindrique ou sphérique une assemblée de particules initialement contenue dans un grand volume et possédant une énergie cinétique dirigée vers le centre de symétrie.

Les effets d'inertie dans cette géométrie permettent de concentrer dans un petit volume une partie notable

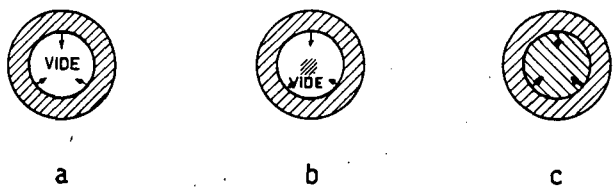

Figure 1 (a) Les particules occupent une couche extérieure à un espace vide et convergent vers le centre de symétrie. (b) On place au centre de symétrie un petit groupe de particules séparé de la couche de particules extérieure par du vide ou par un champ magnétique de confinement. (c) La couche de particules entoure un milieu continu et qu'une onde de choc converge vers le centre.

de l'énergie initiale des particules. Les trois principaux cas suivants peuvent être alors distingués selon la disposition initiale du milieu:

a) Les particules occupent une couche extérieure à un espace vide et convergent vers le centre de symétrie (figure 1a); elles se trouvent ainsi focalisées au voisinage de ce centre où une partie de leur énergie du mouvement radial se transforme en chaleur.

b) On place au centre de symétrie un petit groupe de particules séparé de la couche de particules extérieure par du vide ou par un champ magnétique de confinement (figure 1b). Au cours de son mouvement, la couche extérieure communique de l'énergie au groupe central.

c) Finalement on peut imaginer que la couche de particules entoure un milieu continu et qu'une onde de choc converge vers le centre (figure 1c). Le transfert d'énergie s'effectue des couches extérieures vers les couches centrales.

Les cas *a*) et *b*) sont analysés dans d'autres articles [1, 2]. On s'attache ici au cas *c*) du choc convergent. Il est connu qu'un choc convergent, en géométrie cylindrique ou sphérique, permet d'accroître la température et la densité d'un plasma [4—11]. La production par ce procédé de réactions thermonucléaires contrôlées a même été envisagée [5, 11]. Les considérations approximatives qui suivent réduisent cet espoir quant au cas traité.

On étudie le cas très idéal d'un milieu continu, totalement ionisé, sans perte de radiation et d'ionisation, sans instabilités, en supposant essentiellement qu'un tel plasma obéit à une équation d'état de la forme $(\mathrm{d}/\mathrm{d}t)\,(p/\varrho^{\gamma})=0$, avec $\gamma=5/3$.

Une solution connue du choc convergent est la solution de similitude [12—17]. On choisit cette solution pour des raisons de simplicité et également parce qu'elle paraît optimiste. Après avoir étudié l'allure générale des solutions de similitude on donne les courbes relatives à la solution singulière [12] calculées numériquement dans les cas cylindriques et sphériques. A partir de cette solution on peut calculer d'une façon certainement très grossière, mais qu'on peut croire optimiste, le taux de réaction pour un milieu fusionable. Ce taux est relativement faible.

Afin de s'assurer de la valeur de la solution de similitude on a exécuté des calculs purement numériques [18] qui se rapportent à une situation plus physique; les premiers résultats sont exposés dans l'appendice 3.

2. Les solutions de similitude

On considère un milieu fluide indéfini, originellement homogène et au repos, dans lequel se propage un front de choc convergent. Les équations sont les équations habituelles qui comprennent l'équation d'état classique:

$$\begin{aligned} &\frac{\partial \varrho}{\partial t}+\frac{\partial \varrho v}{\partial r}+\alpha\frac{\varrho v}{r}=0\\ &\frac{\partial v}{\partial t}+v\frac{\partial v}{\partial r}+\frac{1}{\varrho}\frac{\partial p}{\partial r}=0\\ &\frac{\partial}{\partial t}(p/\varrho^{\gamma})+v\frac{\partial}{\partial r}(p/\varrho^{\gamma})=0 \end{aligned} \qquad (1)$$

($\alpha = 1$, cas cylindrique; $\alpha = 2$, cas sphérique).

* Mémoire CN-10/7 présenté par J. G. Linhart. Les traductions du résumé se trouvent en fin de volume.

Les notations sont évidentes. On suppose de plus que le front de choc est raide et que le choc est fort. C'est-à-dire qu'en désignant par les indices respectifs 1 et 2 le milieu au repos et le milieu après le passage de l'onde, par R la position du front de choc, on a:

$$p_2 = \frac{2}{\gamma+1}\varrho_1 \dot{R}^2$$
$$\varrho_2 = \frac{\gamma+1}{\gamma-1}\varrho_1 \qquad (2)$$
$$v_2 = \frac{2}{\gamma+1}\dot{R}$$

sur le front de choc.

Les solutions de similitude sont telles que [12]

$$p = \overline{p}(\xi)\, r^{-2x}$$
$$v = \pm\, \overline{v}(\xi)\, r^{-x} \qquad x > 0 \qquad (3)$$
$$\varrho = \overline{\varrho}(\xi)$$

avec le paramètre de similitude

$$\xi = \frac{r}{(\mp t)^{1/1+x}}\,. \qquad (4)$$

Le déplacement du front de choc obéit à la loi:

$$R^x \dot{R} = \text{Cte} < 0 \qquad (5)$$

soit

$$R/(\mp t)^{1/1+x} = \xi_0 = \text{Cte}. \qquad (6)$$

On prend pour instant initial $t=t_0<0$ (formules avec le signe —); le front de choc arrive sur l'axe (sur le centre) à $t=0$, puis se réfléchit ($t>0$, formules avec le signe +).

Le système (1) se transforme grâce aux équations (3), en un système d'équations différentielles ordinaires donné dans l'appendice 1.

On adopte dans tout ce qui suit la valeur $\gamma=5/3$. Deux paramètres restent libres si l'on connaît le milieu 1: ξ_0 et x. ξ_0 est déterminé par la position et la vitesse initiales du front de choc. Le paramètre x qui, d'après (5), donne la variation de la vitesse du front, reste à fixer. Pour ce faire on a calculé l'allure des diverses solutions selon les valeurs de x.

On peut suivre sur la figure 2 la variation, selon x, des courbes qui représentent p, ϱ, v en fonction de r, en un instant déterminé $t<0$, c'est-à-dire avant la réflexion de l'onde. Les courbes restent évidemment semblables quand t varie (équation 3). Les flèches indiquent le sens de variation des courbes lorsque x décroît. Les valeurs remarquables de x sont:

x	x_0	x_1	x_2
$\alpha=1$	0,226	0,416	2/3
$\alpha=2$	0,453	0,832	1

Quand x est grand, p et ϱ (et la vitesse du son) deviennent infinis à distance finie ($x>x_2$). Puis, x décroissant, p et ϱ (et la vitesse du son), ne sont plus infinis qu'à l'infini ($x_0<x<x_2$). La vitesse v est aussi infinie à l'infini; la valeur $x=x_1$ sépare simplement les solutions pour lesquelles v possède ou non un minimum.

La solution $x=x_0$ est singulière [12]; ceci se voit sur la figure où l'on a porté les solutions $x_0\pm(\varepsilon)$. Pour $x<x_0$ les solutions peuvent avoir plusieurs allures différentes, mais elles sont toutes multiformes et

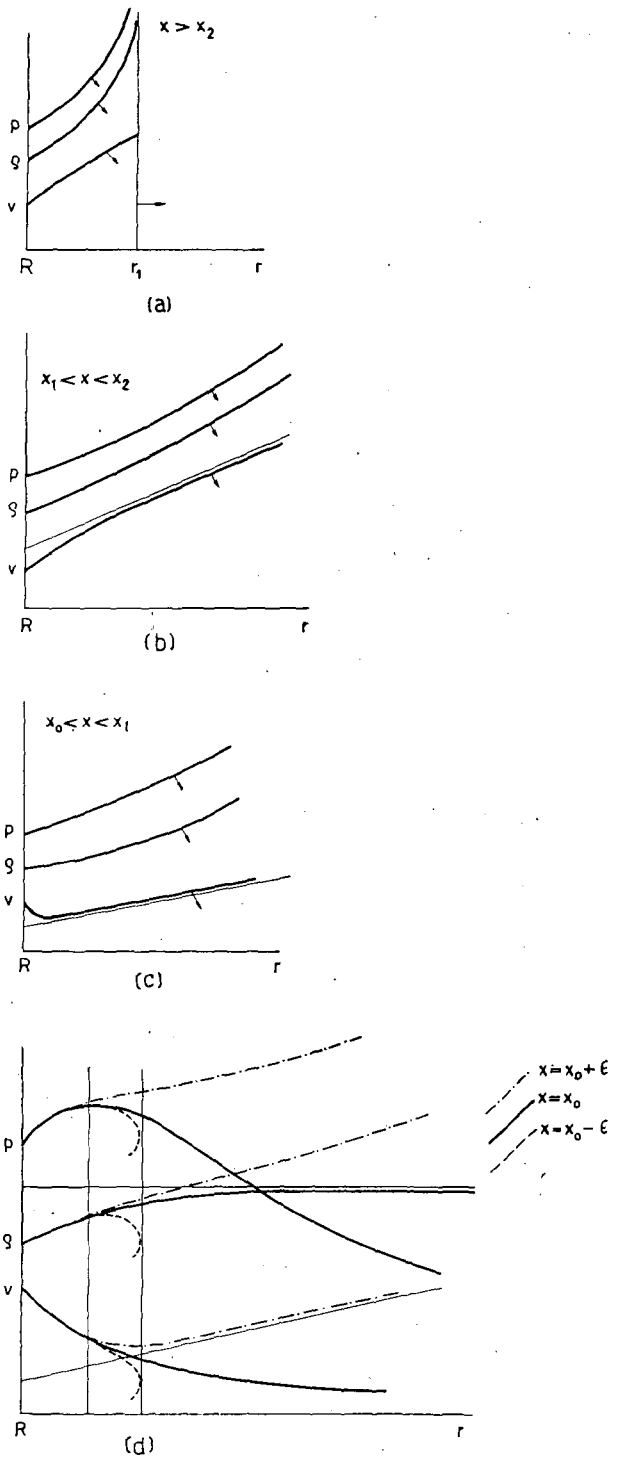

Figure 2 La variation, selon x, des courbes qui représentent p, ϱ, v en fonction de r, en un instant déterminé $t<0$. (a) cf Figure 6a et b, (b) cf Figure 6c, (c) cf Figure 6c à d, (d) cf Figure 6d.

on les élimine. Les cas $x > x_0$ de compression forte pourraient être physiquement réalisés à l'aide d'un piston; mais l'on voit de toute manière qu'ils sont très défavorables du point de vue de la concentration de l'énergie. Reste donc la solution singulière $x = x_0$ dont l'allure paraît acceptable. Par ailleurs cette solution a une certaine stabilité [7, 17].

3. La solution singulière

Un gros effort de calcul numérique est nécessaire pour élaborer cette solution, tant pour calculer la valeur x_0 que pour calculer la solution elle-même. Guderley a étudié le cas $\gamma = 7/5$ et Aikin le cas $\gamma = 5/3$ sphérique, donnant les courbes p, ϱ, v en fonction du temps en un point déterminé. On complète ici ces études en donnant pour $\gamma = 5/3$, les deux cas, sphérique et cylindrique, avec les courbes de p, ϱ, v en un point déterminé en fonction de t, ou en un instant déterminé en fonction de r. On ajoute une autre quantité, la densité d'énergie:

$$w = \frac{1}{2}\varrho v^2 + \frac{p}{\gamma - 1}.$$

Les valeurs de x_0 sont [13]

$$0{,}226 \ldots \quad \text{pour} \quad \alpha = 1$$
$$0{,}452 \ldots \quad \text{pour} \quad \alpha = 2$$

Les figures 3 et 4 donnent respectivement les résultats du calcul pour le cas cylindrique et le cas sphérique. L'échelle des grandeurs physiques p, ϱ, v, w est telle que ces grandeurs physiques sont toutes égales à l'unité sur le front du choc direct dans le

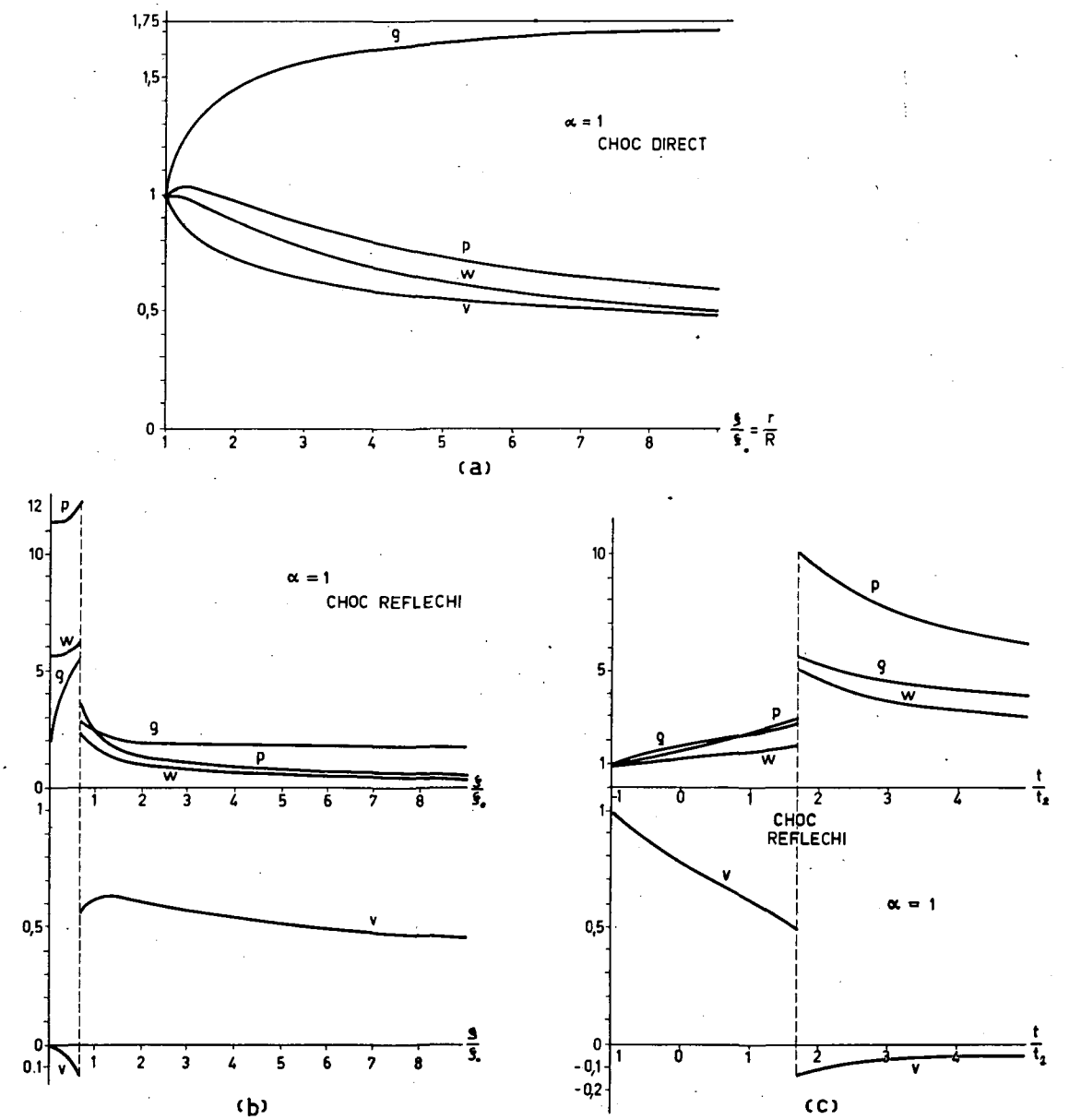

Figure 3 Les résultats du calcul pour le cas cylindrique. $\alpha = 1$. (a) choc direct, (b) choc réfléchi, (c) l'évolution au cours du temps en un point fixe. (Mettre ϱ pour g partout dans cette figure.)

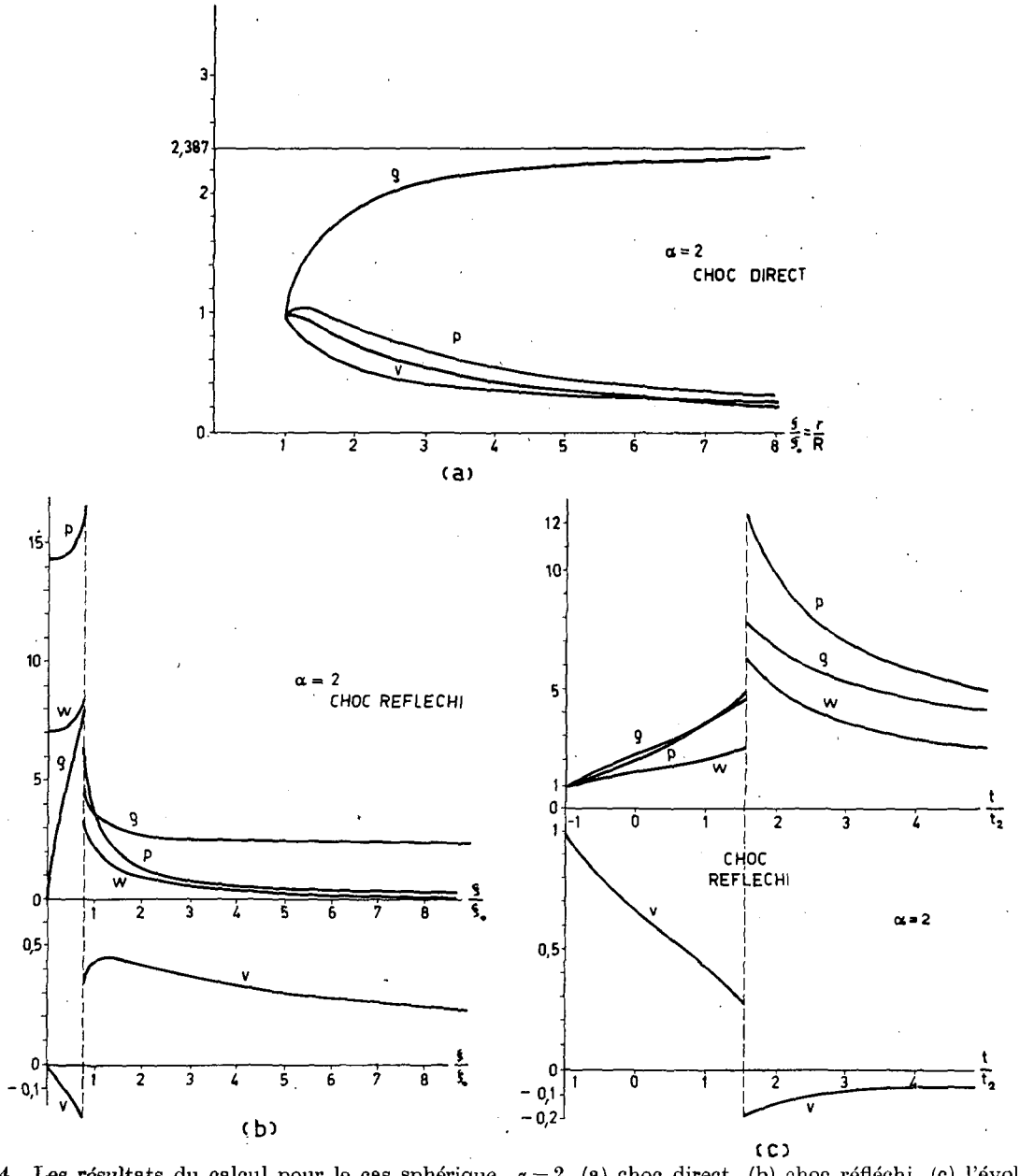

Figure 4 Les résultats du calcul pour le cas sphérique. $\alpha = 2$. (a) choc direct, (b) choc réfléchi, (c) l'évolution au cours du temps en un point fixe. (Mettre ϱ pour g dans cette figure.)

milieu 2; les grandeurs elles-mêmes sont alors obtenues avec les équations (2) et (5). On voit leur variation dans l'espace en un instant déterminé (alors $r/R = \xi/\xi_0$) sur les figures 3a, 4a pour le choc direct ($t<0$) et sur les figures 3b, 4b pour le choc réfléchi ($t>0$). Leur évolution au cours du temps en un point fixe est donnée par les figures 3c, 4c; le temps est rapporté au temps t_2 de passage du choc direct au point considéré, temps déterminé par les équations (5) ou (6) et la donnée des conditions initiales:

$$t = t_0;\ R = R_0;\ \dot{R} = \dot{R}_0. \tag{7}$$

Le déplacement du front de choc réfléchi obéit à la loi (6) mais avec une constante $\xi_0{}^*$ différente de la constante ξ_0 du choc direct; on lit directement $\xi_0{}^*$ sur la figure 3b, 4b (ou 3c, 4c).

A titre d'illustration, on montre sur la figure 5 l'allure de la variation de la pression en fonction de l'espace et du temps.

Ces courbes, avec l'aide des formules (2) à (7), permettent de déterminer entièrement le comportement du choc. On complètera facilement les courbes des figures 3a, b et 4a, b pour une valeur élevée de ξ/ξ_0 sachant que p, v, w, ϱ atteignent pratiquement leur comportement asymptotique pour $\xi/\xi_0 > 10$. Ce comportement est:

$$\begin{aligned} p &\propto (\xi/\xi_0)^{-2x_0} \\ w &\propto (\xi/\xi_0)^{-2x_0} \\ v &\propto (\xi/\xi_0)^{-x_0} \\ \varrho &\propto \mathrm{Cte} \end{aligned} \tag{8}$$

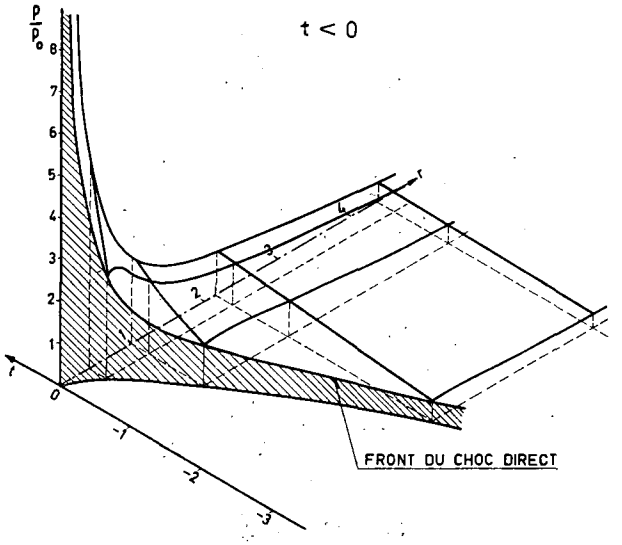

Figure 5a L'allure de la variation de la pression en fonction de l'espace et du temps. L'echelle est telle que le front de choc passe par le point (1, —1, 1). $t<0$.

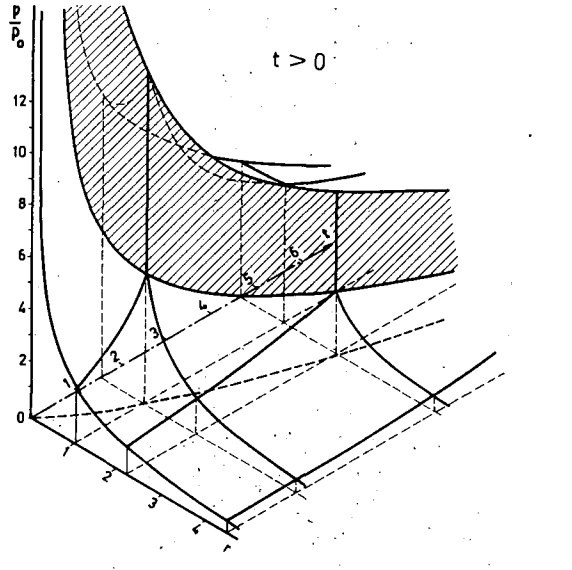

Figure 5b L'allure de la variation de la pression en fonction de l'espace et du temps. $t>0$.

On remarquera enfin (figures 3c et 4c) que si en un point donné la pression et la densité augmentent entre le passage du choc direct et celui du choc réfléchi, la température $T_2 \propto p_2/\varrho_2$ reste presque constante.

Ce calcul est mathématique et, même si l'on suppose que les équations (1) sont capables de représenter le phénomène physique, cette représentation devient forcément mauvaise au temps $t\sim 0$ où le front de choc arrive au voisinage de l'axe (ou du centre). Les grandeurs p, w, v, T deviennent très grandes et tendent vers l'infini lorsque t tend vers zéro. C'est que l'on doit limiter la valeur de R à un rayon R_1 minimum de l'ordre de grandeur du libre parcours moyen relatif aux collisions responsables de l'établissement du front de choc. Il est évidemment difficile d'analyser les phénomènes qui se produisent pour un rayon $r<R_1$ entre le passage de l'onde directe et de l'onde réfléchie au point $r=R_1$; mais si l'on admet que les particules deviennent alors libres puisqu'elles ne subissent plus de collisions, on peut montrer que la température pour $r<R_1$ ne s'élève pratiquement plus et se stabilise à une valeur peu différente de la valeur atteinte en $r=R_1$ au passage du choc direct; de plus on peut voir qu'un choc réfléchi se forme et que les valeurs des grandeurs physiques relatives à ce choc sont, ainsi calculées, en bon accord avec les valeurs données par le calcul mathématique pour $r>R_1$. Ceci suppose qu'aucune instabilité ne se produit.

Par ailleurs, la solution du choc réfléchi montre que, si la température reste très élevée près de l'axe, cet effet s'exerce sur un milieu de densité évanescente (figures 3b et 4b; le comportement de ϱ est, lorsque r tend vers 0:

$$\varrho \propto r^{0,315} \quad \text{pour} \quad \alpha = 1,$$

$$\varrho \propto r^{0,662} \quad \text{pour} \quad \alpha = 2.$$

4. Application à un cas physique

Le calcul précédent est évidemment très grossier si on veut l'appliquer par exemple à l'onde de choc créée initialement par une grande masse d'explosif placée autour d'un plasma. Il suppose en particulier la validité de l'équation d'état avec un γ égal à 5/3. Mais on peut espérer qu'il surestime les températures finales obtenues; on a en effet négligé toutes les pertes d'énergie et les instabilités qui sont des facteurs défavorables; la pression en un point déterminé croît toujours avec le temps, ce qui semble difficile à réaliser avec un explosif; cet explosif devrait d'ailleurs occuper un très grand volume. Malgré ces facteurs optimistes, on peut voir sur les figures a ou b et le comportement asymptotique (8) que le processus de concentration de l'énergie n'est pas très bon.

Sur le front de choc la température $T_2(t)$ en un instant $t<0$ est donnée, en fonction de la température initiale $T_2(t_0)$ par:

$$\frac{T_2(t)}{T_2(t_0)} = \left(\frac{R(t)}{R_0}\right)^{-2x}.$$

Si on prend comme libre parcours moyen entre particules chargées:

$$\lambda(\text{cm}) \sim \frac{2\cdot 10^4 [T(^\circ\text{K})]^2}{n(\text{cm}^{-3})}$$

et que l'on égale à λ le rayon minimum R_1 on obtient une température maximum:

$$T = [T_2(t_0)]^{1/1+4x} \left(\frac{R_0 n}{2.10^4}\right)^{2x/1+4x},$$

soit en prenant

$$T_2(t_0) = 10^4\,^\circ\text{K},$$

$$R_0 = 50\ \text{cm},$$

$$T \sim \begin{cases} 30\, n^{0,25} & \text{cas cylindrique}, \\ 3{,}8\, n^{0,32} & \text{cas sphérique}. \end{cases}$$

Les températures de 10^7 °K pour le cas cylindrique et 10^8 °K pour le cas sphérique sont les températures tout à fait extrêmes que l'on pourrait atteindre.

Cependant ce calcul dépend beaucoup de l'expression adoptée pour le libre parcours moyen, ou rayon minimum R_1. Aussi peut-on plutôt estimer directement le nombre des réactions thermonucléaires en fonction du rayon minimum et en avoir une borne supérieure.

On calcule, dans l'appendice 2, le nombre de réactions produit par le choc direct dans un plasma formé d'un mélange de deuterium et de tritium en parties égales. Les approximations faites surestiment un peu le taux de réaction; on prend pour conditions initiales, dans le milieu 2, au rayon R_0:

$$\dot{R}_0 = 10^6 \text{ cm/s},$$

$$T = 10^4 \text{ °K}.$$

Le nombre N de réactions est donné par la formule (A8).

Il dépend d'une facon critique du rayon minimum R_1 atteint par le choc. Sa valeur maximum s'obtient pour un rayon $R_1 = 0$. On a [formule (A12)]:

$$N(R_1) \leqslant N(0) \sim \begin{cases} 10^{-39} R_0^4 n_1^2 \text{ cas sphérique}, \\ 10^{-46} R_0^3 n_1^2 \text{ cas cylindrique (par unité de longueur)}. \end{cases}$$

Cette valeur maximum est faible dans tous les cas pratiques; l'évaluation numérique de l'intégrale de la formule (A8) montre que $N(R_1)$ peut être encore considérablement inférieur à la valeur maximum $N(0)$, même pour un rayon R_1 très petit (appendice 4, figure 9). On sait d'ailleurs que les instabilités ou les irrégularités géométriques viennent précisément limiter le choc direct à un rayon minimum grand par rapport à l'épaisseur réelle du front de choc [6, 9].

Bien que le choc réfléchi ait alors un sens physique très douteux, on a calculé de la même manière le nombre de réactions produit par ce choc. On obtient une valeur maximum de ce nombre; cette valeur est tout au plus égale à quelques dizaines de fois la valeur maximum précédente, compte tenu d'approximations optimistes.

5. Conclusion

Il est visible, d'après ces calculs, que le transfert de l'énergie par un choc convergent est peu efficace bien que la densité de l'énergie augmente avec la convergence. A cet égard les deux autres mécanismes mentionnés dans l'introduction sont préférables de beaucoup. Il est par ailleurs peu probable que les chocs convergents puissent atteindre le rendement énergétique intéressant pour la fusion contrôlée.

Remerciements

Les auteurs remercient vivement le Docteur Turrin (C.N.E.N., Laboratorio Nazionali di Frascati) et les Docteurs Guerri et Di Cola (Euratom-Ispra), qui se sont chargés des calculs numériques.

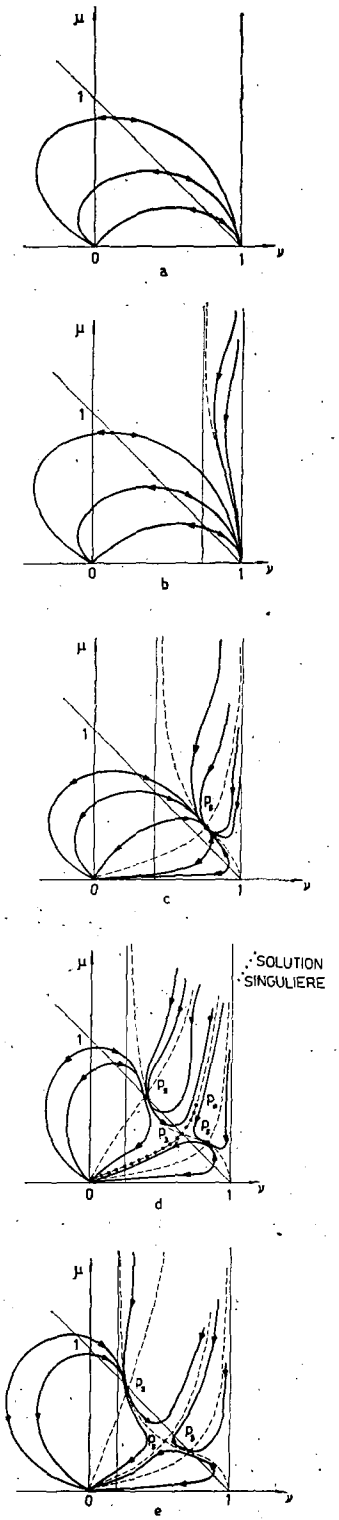

Figure 6 Il existe plusieurs points singuliers qui dépendent du paramètre x. En ces points $N = D = 0$. Les courbes montrent les divers cas possibles. x décroit de ∞ à 0 de la figure (a) à (e).

Appendice 1.

On obtient un système d'équation différentielles ordinaires en portant (3) dans (1). En introduisant de plus les grandeurs:

$$\bar{a}^2(\xi) = \gamma \frac{\bar{p}}{\bar{\varrho}},$$

$$\mu = \frac{\bar{a}\,(1+x)}{\xi^{1+x}},$$

$$v = \mp \frac{\bar{v}\,(1+\xi)}{\xi^{1+x}},$$

une des équations se découple et le système devient:

$$\frac{\mathrm{d}\mu}{\mathrm{d}v} = \frac{\mu}{2(v-1)} \cdot \frac{N}{D}$$

avec

$$N = 2\mu^2[\gamma(v-1)-x] + \gamma(v-1)\{-[2+\alpha(\gamma-1)]v^2 + [(3-\gamma)(1+x)+1+\gamma+\alpha(\gamma-1)]v - 2(1+x)\},$$

$$D = \mu^2[\gamma v(1+\alpha) - 2x] - \gamma v(v-1)(v-x-1),$$

$$\frac{\mathrm{d}L_n\xi}{\mathrm{d}v} = \frac{\gamma - 1 + N/D}{2(x+1) - [\gamma + 1 + \alpha(\gamma-1)]v}$$

$$= -\frac{\gamma}{D}[\mu^2 - (v-1)^2],$$

$$\frac{\mathrm{d}L_n\bar{\varrho}}{\mathrm{d}v} = -\frac{1}{v-1} \cdot \left[1 + (1+\alpha)v \frac{\mathrm{d}L_n\xi}{\mathrm{d}v}\right].$$

La discussion se fait sur l'équation en (μ, v). La solution passe par le point initial indépendant de x:

$$\mu_2^2 = \frac{2\gamma(\gamma-1)}{(\gamma+1)^2}$$

$$v_2 = \frac{2}{\gamma+1}$$

Il existe plusieurs points singuliers qui dépendent du paramètre x. En ces points $N = D = 0$. Les courbes de la figure 6 montrent les divers cas possibles.

On remarquera que les équations ne fixent pas l'échelle des grandeurs $\bar{\varrho}$ et ξ. L'échelle de $\bar{\varrho}$ est déterminée par la condition initiale (2), celle de ξ par la constante de l'équation (5) ou (6). ξ possède un extrêmum aux points d'intersection d'une courbe solution avec la droite $\mu + v = 1$ (sauf points singuliers).

On n'entrera pas dans les détails de la discussion des solutions qui permet de passer des figures 6 aux figures 2. Guderley donne une analyse des singularités et s'intéresse au cas de la figure 6d.

Appendice 2.

Les équations simples des solutions de similitude permettent de faire un calcul approximatif facile du nombre maximum de neutrons produit par la compression (choc direct).

A l'instant initial t_0, on se donne la position R_0 et la vitesse $\dot{R}_0$ du front de choc; on se donne aussi la température $T_2(0)$ et le nombre de particules par cm^3 $n_2(0)$ dans le milieu 2 sur le front de choc. Le milieu est un mélange de deutérium et de tritium en parties égales.

Les lois de similitude apprennent que:

$$n_2 = n_2(0)\bar{n}\left(\frac{\xi}{\xi_0}\right),$$

$$T_2 = T_2(0) f\left(\frac{\xi}{\xi_0}\right)\left[\frac{r}{R_0}\right]^{-2x}. \qquad (A\,1)$$

C'est-à-dire qu'à l'instant t, en posant:

$$\eta = \frac{\xi}{\xi_0} = \frac{r}{R} \qquad (A\,2)$$

on a:

$$n_2 = n_2(0)\,\bar{n}(\eta)$$

$$T_2 = T_2(0) f(\eta)\left[\frac{R_0}{R}\right]^{2x} \eta^{-2x}. \qquad (A\,3)$$

En désignant par $N(t)$ le nombre de neutrons produits par le choc, entre l'instant t_0 et l'instant t dans le milieu 2, du front de choc au rayon R_0 on a:

$$\frac{\mathrm{d}N}{\mathrm{d}t} = \frac{1}{4}\int_R^{R_0} n_2^2 \langle\sigma v\rangle_{\mathrm{DT}} \frac{\mathrm{d}\omega}{\mathrm{d}r}\,\mathrm{d}r \qquad (A\,4)$$

avec $\langle\sigma v\rangle_{\mathrm{DT}} = F(T_2)$, $\mathrm{d}\omega/\mathrm{d}r = \pi(2r)^\alpha$ (par unité de longueur pour $\alpha = 1$), d'où:

$$\frac{\mathrm{d}N}{\mathrm{d}t} = 2^{\alpha-2}\pi R^{\alpha+1}\int_1^{\eta_1} [n_2(0)\,n(\eta)]^2 \cdot F\left[T_2(0) f(\eta)\left(\frac{\eta}{\eta_1}\right)^{-2x}\right] \cdot \eta^\alpha\,\mathrm{d}\eta\,. \qquad (A\,5)$$

Cette formule peut être simplifiée en surestimant un peu le taux de neutrons. La fonctions $n(\eta)$ varie entre 1 et une certaine borne supérieure (figures 3a et 4a); on remplacera cette fonction par sa borne supérieure. En désignant par n_1 le nombre de particules par cm^3 dans le milieu au repos on sait d'après les conditions de choc que $n_2(0) = 4\,n_1$. Ceci revient donc à remplacer la fonction $[n_2(0)\,n(\eta)]^2$ par la constante

$$b\,n_1^2 \quad \text{avec} \quad b \sim \begin{cases} 50 & \alpha = 1 \\ 100 & \alpha = 2 \end{cases}$$

Pour la température T_2 on remplacera la fonction f par la valeur 1. Ceci revient à dire que la température est constante en un point déterminé après le passage du choc. On a vu (figures 3c et 4c) que ceci est pratiquement réalisé. L'approximation revient à surestimer la température (et donc le nombre de neutrons) avec une erreur inférieure à 10%.

On adopte [3] pour la réaction D-T la formule:

$$\langle\sigma v\rangle \equiv F(T) = \frac{10^{-11}}{T^{2/3}}\,10^{-19{,}7/T^{1/3}} \qquad (A\,6)$$

$$\frac{\mathrm{d}N}{\mathrm{d}t} = 3 \cdot 2^{\alpha-3}\,10^{-11}\frac{\pi}{x} R_0^{\alpha+1} b\,[T_2(0)]^{-2/3} n_1^2\, I[(R_0/R)^{-2x/3}] \qquad (A\,7)$$

avec

$$I(v) = \int_v^1 u^{(3/2x)(\alpha+1)+1}\,10^{-19{,}7[T_2(0)]^{-1/3}u}\,\mathrm{d}u.$$

(T en 10^6 °K.)

On intègre ensuite entre t_0 et t_1; ou encore entre R_0 et R_1 en utilisant la relation suivante donnée par l'équation (5) et les conditions initiales:

$$\mathrm{d}t = \frac{R_0}{|\dot{R}_0|}\frac{\mathrm{d}\eta_1}{(\eta_1)^{x+2}}, \quad \eta_1 = R_0/R_1.$$

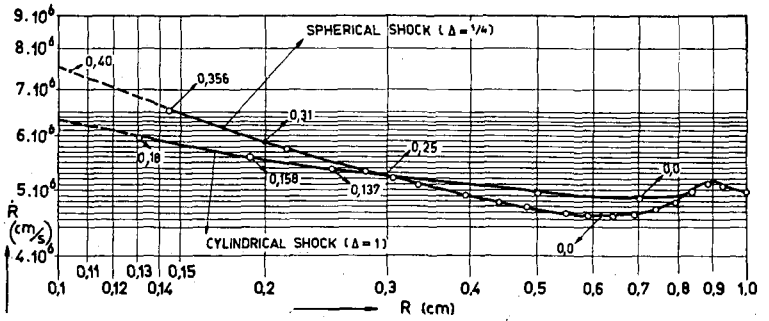

Figure 7 Cette figure montre que, lorsque le choc s'approche de l'axe, la vitesse du choc tend à suivre la loi $\dot{R}R^x = \text{Cte}$ de la solution de similitude. Les nombres attachés aux courbes correspondent à x. Pour la solution de similitude: $x = 0{,}226$ cas cylindrique, $x = 0{,}452$ cas sphérique.

On obtient ainsi:

$$N(R_1) = 3^2 \cdot 2^{\alpha-4}\, 10^{-11} \frac{\pi}{x^2} R_0^{\alpha+2} |\dot{R}_0|^{-1} [T_2(0)]^{-2/3} b n_1^2 K[(R_1/R_0)^{2x/3}] \quad \text{(A 8)}$$

avec

$$K(w) = \int_w^1 v^{(x+3)/2x} I(v)\, dv.$$

Le rayon minimum R_1 est fixé par un libre parcours moyen ou une condition de stabilité. Lorsque R_1 tend vers 0 la température tend vers l'infini mais dans un volume infinitésimal: la formule (A 6) n'est plus valable mais elle surestime $\langle \sigma v \rangle$. $N(0)$ est une valeur maximum du nombre de neutrons produits par le choc direct et cette valeur est facile à calculer.

On a pour $x = x_0$:

	$\alpha = 1$	$\alpha = 2$
$\frac{3}{2x}(\alpha+1)+1$	14,25	10,92
$\frac{x+3}{2x}$	7,15	3,80

En prenant pour conditions initiales les valeurs compatibles:

$$\left.\begin{aligned} &T_2(0) \sim 10^4\,°\text{K (soit } 10^{-12} \text{ dans les unités utilisées)} \\ &\dot{R}_0 \sim 10^6 \text{ cm/s,} \end{aligned}\right\} \text{(A 9)}$$

valeurs encore optimistes, on a:

$$10^{-19{,}7} [T_2(0)]^{-1/3} u = e^{-210u}.$$

Dans le cas sphérique par exemple:

$$K(0) = \int_0^1 v^{3{,}80}\, dv \int_v^1 u^{10{,}92} e^{-210u}\, du.$$

ou en intégrant par partie:

$$K(0) = \frac{1}{4{,}8} \frac{1}{(210)^{16{,}7}} \int_0^{210} y^{15{,}7} e^{-y}\, dy$$

$$\sim \frac{1}{4{,}8} \frac{1}{(210)^{16{,}7}} \int_0^{\infty} y^{15{,}7} e^{-y}\, dy$$

$$= (1/4{,}8)\, \Gamma(16{,}7)/(210)^{16{,}7}$$

soit

$$K(0) \sim 10^{-27}, \qquad \text{cas sphérique.} \quad \text{(A 10)}$$

On calcule de même:

$$K(0) \sim 10^{-34}, \qquad \text{cas cylindrique.} \quad \text{(A 11)}$$

Appliquant ces résultats au cas considéré on trouve ainsi:

$$N(0) \sim \begin{cases} 10^{-39} R_0^4 n_1^2 & \text{cas sphérique,} \\ 10^{-46} R_0^3 n_1^2 & \text{cas cylindrique (par unité de longueur).} \end{cases} \quad \text{(A 12)}$$

(L'unité de longueur partout utilisée est le cm.)

Les résultats numériques du calcul de $N(R_1)$, parvenus tardivement, sont exposés en appendice 4.

Appendice 3.

La solution de similitude du cas convergent représente un choc provenant de l'infini. Afin de s'approcher d'un cas plus physique, on a calculé numériquement [18]

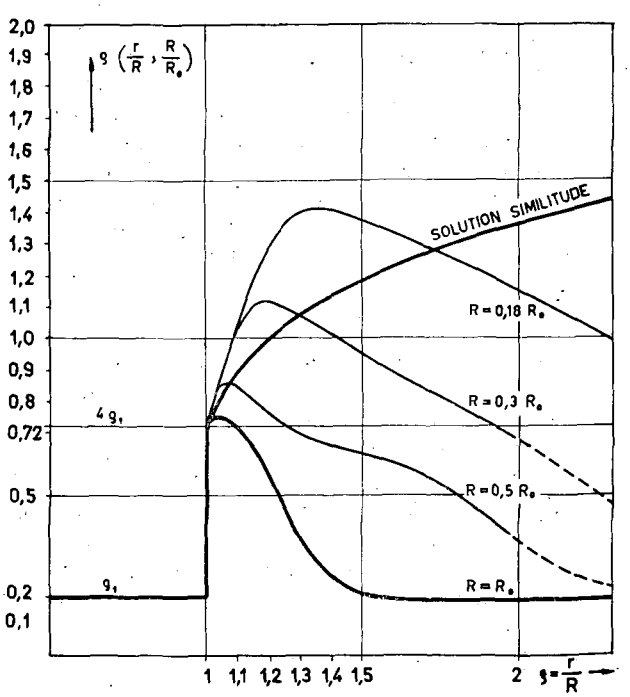

Figure 8 D'après cette figure on voit que la distribution de densité $\varrho(t, r/R)$ du choc convergent réel s'approche de plus en plus au cours du temps de la distribution ϱ de la solution de similitude.

le comportement d'un choc dont les distributions initiales de pression, densité et vitesse sont les suivantes:

$$p_2 = \frac{3}{4}\varrho_1 \dot{R}_0^2 \left(\frac{r}{R_0}\right)^a \exp\left[-\left(\frac{r-R}{\Delta}\right)^2\right],$$

$$v_2 = \frac{3}{4}\dot{R}_0 \left(\frac{r}{R_0}\right)^{-b} \exp\left[-\left(\frac{r-R}{\Delta}\right)^2\right],$$

$$\varrho_2 = 4\,\varrho_1 \left(\frac{r}{R_0}\right)^c \exp\left[-\left(\frac{r-R}{\Delta}\right)^2\right],$$

avec $a=0{,}67$, $b=0{,}43$, $c=1{,}72$.

Les coefficients a, b et c ont été choisis de telle façon que ces distributions sont tangentes sur le front de choc aux distributions correspondantes dans la solution de similitude; elles sont ainsi semblable aux solutions de similitude dans la région $(R_0,\ R_0+\Delta)$ mais coupées exponentiellement pour $r>R_0+\Delta$.

D'après la figure 8 on voit que la distribution de densité $\varrho\,(t, r/R)$ du choc convergent réel s'approche de plus en plus au cours du temps de la distribution ϱ de la solution de similitude. Un autre diagramme (figure 7) montre que, lorsque le choc s'approche de l'axe, la vitesse du choc tend à suivre la loi $\dot{R}R^x = \text{Cte}$ de la solution de similitude.

Appendice 4.

On a calculé numériquement la double intégrale K de la formule (A 8).

Cette intégrale dépend des deux paramètres R_1/R_0 et $T_2(0)$. Dans tous les cas pratiques ces paramètres sont tels que l'on peut remplacer les bornes supérieures d'intégration par l'infini; K s'écrit alors:

$$K\left[\frac{R_1}{R_0},\ T_2(0)\right] = \text{Cte}\cdot[T_2(0)]^d \cdot F\left\{\frac{R_1}{R_0}\cdot[T_2(0)]^{-1/2x}\right\}, \tag{A 13}$$

avec

$$\text{Cte} = \begin{cases} 5{,}45\cdot 10^{-34} \\ 1{,}39\cdot 10^{-27} \end{cases} \qquad d = \begin{cases} 7{,}8 \text{ cas cylindrique} \\ 5{,}6 \text{ cas sphérique.} \end{cases}$$

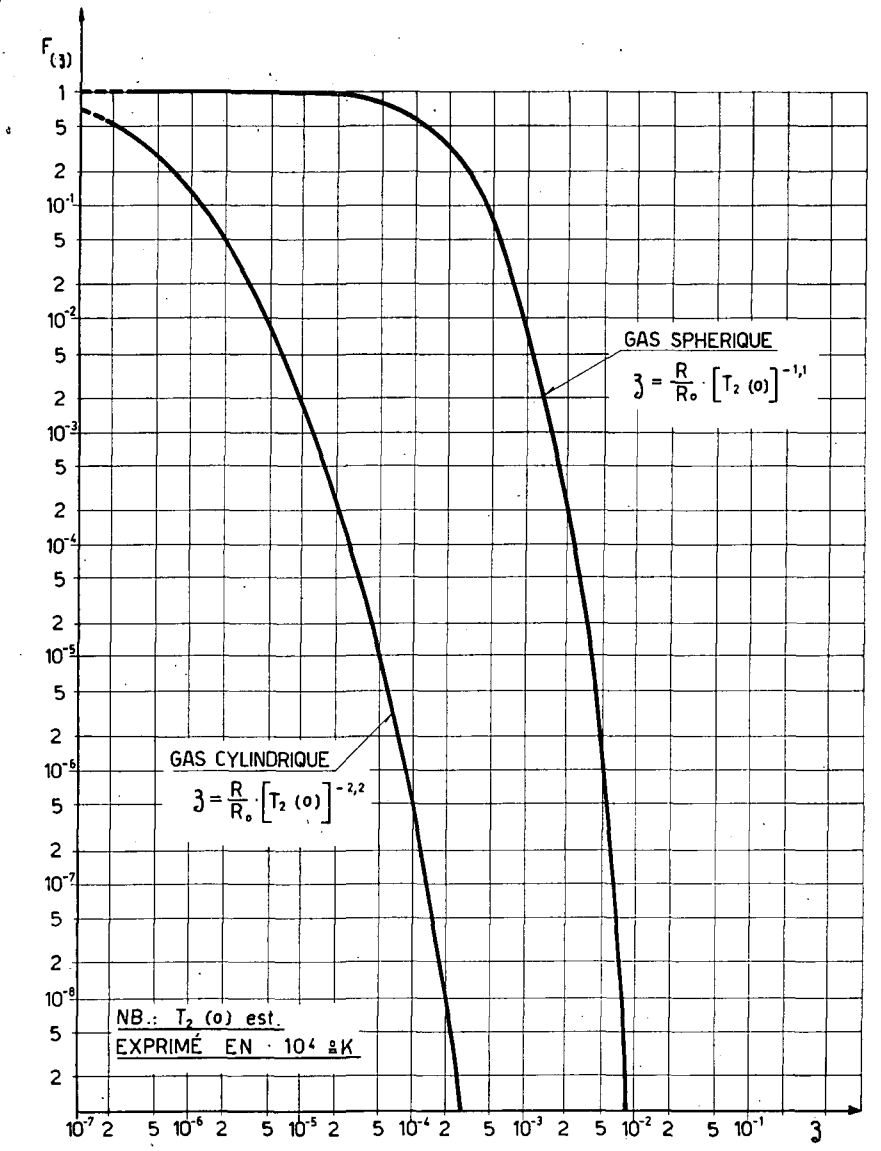

Figure 9 Les variations de F dans les cas cylindrique et sphérique. Unité de température est 10^4 °K. (Mettre R_1 pour R dans cette figure.)

F est une double intégrale qui ne dépend plus que d'une variable et la constante est telle que $F(0)=1$; le calcul numérique de F a été effectué en employant une série double et en remplaçant les coefficients du tableau (page 724) par les entiers les plus proches. La figure 9 montre les variations de F dans les cas cylindrique et sphérique; on a pris ici comme unité de température 10^4 °K.

On obtient une expression condensée du nombre de réactions N en reportant (A13) dans (A8) et en notant que pour un choc fort:

$$T_2(0) = \text{Cte} \cdot \dot{R}_0^2.$$

La constante est déterminée par (A9). En éliminant ainsi $\dot{R}_0$ de la formule (A8) on obtient:

$$N(R_1) = \begin{cases} 4 \cdot 10^{-46} R_0^3 n_1^2 [T_2(0)]^{6,5} \cdot F\left\{\frac{R_1}{R_0} \cdot [T_2(0)]^{-2,2}\right\} \\ \qquad \text{cas cylindrique (par unité de longueur)} \\ 10^{-39} R_0^4 n_1^2 [T_2(0)]^{4,5} \cdot F\left\{\frac{R_1}{R_0} \cdot [T_2(0)]^{-1,1}\right\} \\ \qquad \text{cas sphérique.} \end{cases}$$

(L'unité de longueur est le cm; l'unité de température est 10^4 °K.)

Références

[1] Maisonnier, Ch., Linhart, J. G., Haegi, M., Comptes rendus de cette Conférence, voir page 727.
[2] Linhart, J. G., Knoepfel, H., Gourlan, C., Compte rendus de cette Conférence, voir page 733.
[3] Linhart, J. G., Plasma Physics (North-Holland Pub. Co. Amsterdam, 1960).
[4] Perry, R. W., Kantrowitz, A., *J. Appl. Phys.* **22** (1951) 878.
[5] Sänger, E., *Z. Naturforschung* **6a** (1951) 302.
[6] Butler, D. S., ARDE Report 18/56 (1956).
[7] Morawetz, C. S., Thesis, New York University, (1957).
[8] Zaidel, R. M., Lebedev, V. S., *Doklady Akad. Nauk SSSR* **135** (1960) 1166.
[9] Whitham, G. B., *J. Fluid Mech.* **2** (1957) 145.
[10] Aikin, A. W., Metropolitan-Vickers Research Report 5090 (1956).
[11] Völcker, H., *Atomkernenergie* **5** (1960) 209, 262.
[12] Guderley, G., *Z. Luftfahrtforschung* **19** (1942) 302.
[13] Butler, D. S., ARDE Report 54/54 (1954).
[14] Calkin, J. W., U. S. Atomic Energy Commission Report LASL-242 (1954).
[15] Hide, R., U.K. Atomic Energy Authority Report AERE-GP/M-191 (1956).
[16] Stanyukovich, K. P., Unsteady Motion of Continuous Media (Pergamon Press, Oxford, 1960).
[17] Häfele, W., *Z. Naturforschung* **11a** (1956) 183.
[18] von Neumann, J., Richtmyer, R. D., *J. Appl. Phys.* **21** (1950) 232.

GENERATION OF SHOCKS IN A COLLAPSING CYLINDRICAL PLASMA SHELL*

CH. MAISONNIER, J. G. LINHART, M. HAEGI

LABORATORIO GAS IONIZZATI (EURATOM-C.N.E.N.)

FRASCATI, ROME, ITALY

A theory is presented of the development of a cylindrical shock produced by the radial collapse of a thin cylindrical shell of plasma. The expected neutron flux from the shocked region is calculated. Experimental arrangement is described. This consists of an electrostatic injector producing a thin, annular beam of $LiAlD_4$ powder within a cylindrical evacuated chamber. This beam is first ionized and later accelerated radially by the discharge of a 40 kV, 50 kJ condenser bank.

1. Introduction

All schemes studied up to now, with controlled production of fusion power as an ultimate goal, require long-term confinement of the reacting plasma. One of us has proposed recently [1] an alternate possibility, the use of an unconfined plasma, thermonuclear energy being produced during the assembly and the free expansion of a plasma column. The present paper deals with some theoretical considerations related to such a system, as well as the description of an experimental apparatus designed to test the soundness of the principles involved.

2. Energy release during the free expansion of a cylindrical plasma

Let r_0 be the initial radius (in cm) of an infinitely long cylindrical column of a (50% deuterium, 50% tritium) plasma having a Maxwellian velocity distribution corresponding to a temperature T_0 such

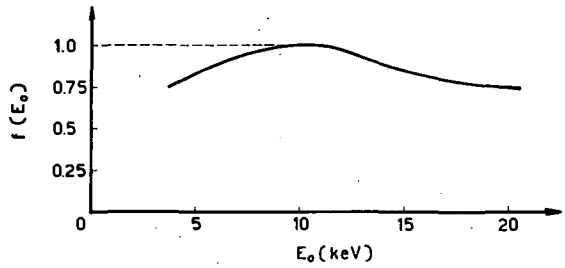

Fig. 1 The function $f(E_0)$. See Eq. (1) and the discussion in the Appendix.

that $kT_0 = E_0$. The thermal energy stored per unit length in the column is called W_s. In Appendix 1, it it is shown that the fusion energy W_F released per unit length during the free expansion of the plasma in vacuum is:

$$W_F = 6{,}4 \cdot 10^{-8} \frac{W_s^2}{r_0} f(E_0). \qquad (1)$$

in which $f(E_0)$ is given in Fig. 1 and is equal to unity for $E_0 = 11$ keV. We shall assume that approximately the same energy is generated during the focalisation and assembly of the plasma into the volume of radius r_0.

Supposing that the optimum initial temperature of 11 keV is obtained and, neglecting all losses, a net energy gain ($W_F > W_s$) in joules per centimetre can be reached if:

$$W_s > 0{,}8 \cdot 10^8 r_0 \qquad (2)$$

where r_0 is in cm. It is evident that very small pinch radii are necessary in order to avoid impracticably large stored energies. A further decrease in the required minimum stored energy could be achieved if during the expansion a portion of the plasma energy could be recuperated.

3. Generation of a thin plasma core

In a normal linear dynamic pinch, the production of large compression ratios is precluded owing to the current carrying layer being slowed down by the gas inside it, this gas being either incorporated to the plasma layer (snow-plough model) or reflected towards the axis creating then an increasing internal pressure.

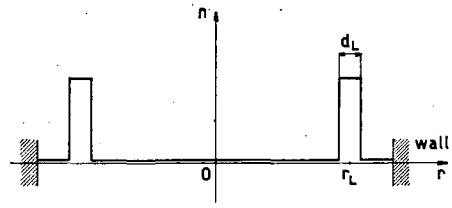

Fig. 2 Desired initial plasma density as a function of radius.

It is clear that the situation is different if one starts from a cylindrical plasma layer having a density n whose variation with radius is shown in Fig. 2. If the thickness of the layer $d_i \ll r_i$, the analysis of a simple model shows [1] that, driven by pinch forces, the tubular plasma structure collapses towards the axis creating there a plasma column of high density, high temperature and having a very small diameter. Physically, the system can be described as a cylindrical plasma gun in which, along a path of length r_i, the

* Conference paper CN-10/10, presented by J. G. Linhart. Translations of the abstract are at the end of this volume of the Conference Proceedings.

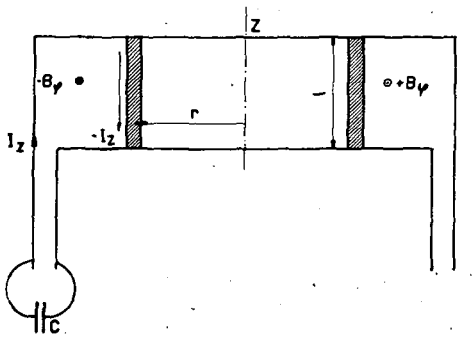

Fig. 3 Schematic representation of a cylindrical plasma gun.

energy $(1/2)\,C\,V_0^2$ stored in a condenser bank is mainly converted into a kinetic energy $(1/2)\,lNM\dot{r}^2$ of the plasma shell. (l is the length of the plasma column, N the number of proton-neutron pairs per unit length and M the deuteron mass). This energy of a radial motion can be transformed into thermal energy at the end of the acceleration process through collisions occurring near the axis.

3.1. Dynamics of a cylindrical plasma gun

The motion of the plasma layer in the system shown on Fig. 3 has been studied previously [2]. Calling L_0 the inductance (in henries) of the bank, including switch and leads, a simple manipulation of the results obtained in [2] shows that, if one puts:

$$a_1 = \frac{(C\,V_0)^2}{100\,M\,N\,r_i^2}, \quad a_2 = \frac{L_0}{2.10^{-9}\cdot l},$$

$$\omega^2 = \frac{1}{2.10^{-9}\,l\,C},$$

where C is in farads, V in volts, MN in grams per cm and l, r_i in cm, the velocity $\dot{r}$ of the shell just before it reaches the axis (more exactly at $r/r_i = 1/10$) is $\dot{r} = \dot{x}\,\omega\,r_i$. The normalized velocity $\dot{x}$ can be obtained from a diagram in Fig. 4, where it is plotted as a function of a_1.

The transfer of energy from the condenser bank to the kinetic energy of the plasma is easily shown to occur with an efficiency

$$\eta = \frac{\dot{x}^2}{2\,a_1}.$$

The variation of η as a function of a_1 and a_2 is as indicated in Fig. 5. From Fig. 5, it is clear that a reasonable energy transfer, say larger than 50%, requires simultaneously:

$$a_1 < 10, \tag{3}$$

$$a_2 < 0{,}5. \tag{4}$$

3.2. Thermalization near the axis

It is possible to show that when ions are thermalized during the interaction near the axis a reasonable equipartition of energy between ions and electrons will occur. Then, for one-electron atoms, the optimum temperature for neutron production ($kT_0 = E_0 = 11$ keV) will be obtained if each incoming ion brings about $3\,E_0$; thus one obtains for the total kinetic energy

$$Nl \cdot 3\,E_0 \cdot 1{,}6 \cdot 10^{-9} = \tfrac{1}{2}\eta\,CV_0^2;$$

or, putting $\eta \simeq 0{,}7$,

$$Nl \simeq 6{,}8 \cdot 10^{13}\,CV_0^2. \tag{5}$$

In order that a cylindrical shock of final thickness d be thermalized near the axis, one needs:

$$\frac{\langle(\Delta w_\perp)^2\rangle}{(2\,w)^2} > \frac{2\,w}{d},$$

w being the velocity of the incoming particles corresponding to a deuteron energy of $3\,E_0$. Taking into account interaction between both electrons and ions, and supposing that only binary collisions are of importance, this formula reduces to:

$$N > 10^{22}\,d. \tag{6}$$

As the reactor criterion (2) is equivalent to (see Appendix 1):

$$N > 2{,}96 \cdot 10^{22}\,r_0,$$

and as r_0 is of the order of $d/2$ it follows that thermalization and power production will take place above a common threshhold for N.

It should be noted that, as far as neutron yield is concerned, thermalization is not an essential feature: if it is not obtained, the interaction time will be slightly smaller, but the energy will not be shared with the electrons, so that the number of reactions

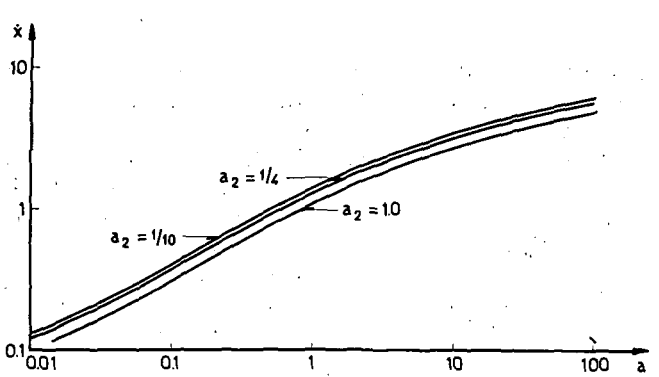

Fig. 4 Normalized velocity $\dot{x}$ as a function of a_1.

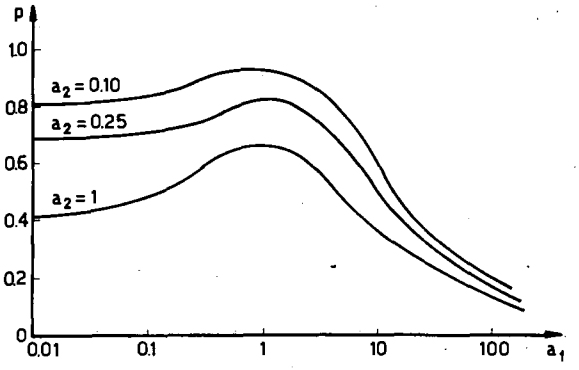

Fig. 5 Variation of $\eta = \dot{x}^2/2\,a_1$ as a function of a_1 and a_2. (Note: axis of ordinates should be labelled η.)

remains of the same order of magnitude. The optimum energy is now of the order of 20 keV per deuteron so that (5) is replaced by:

$$N l \simeq 4 \cdot 10^{13}\, C V_0^2. \tag{7}$$

3.3. Conclusion

The radial plasma gun should be designed in such a way that Eqs. (3), (4) and (7) are satisfied. Thermalization will not occur if (6) is not satisfied.

4. Role of impurities

If a large percentage of impurities exists, the following phenomena will occur.

(a) During the contraction of the cylindrical shell, the temperature of the plasma will be kept low (a few 10^5 °K) because of excitation radiation [3].

(b) If the temperature is low enough, the magnetic field diffuses appreciably in the plasma and impedes the development of a Halley distribution of density in the shell, thus increasing the thickness d and consequently the minimum radius r_0. The criterion for magnetic field not being troublesome is:

$$\frac{\omega_c}{2\pi} \ll \nu_{DD}, \tag{8}$$

where ω_c is the deuteron cyclotron frequency and ν_{DD} the collision frequency between deuterons.

(c) If (8) is satisfied, the heavy impurities will tend to sediment at the external driven plasma boundary. Preliminary calculations seem to show that sedimentation will effectively occur in most cases of interest. This is consistent with experimental results observed in existing plasma guns.

(d) Bremsstrahlung should be negligible when thermalization does not take place, because of the low electron temperature at all times.

(e) The impurity ions will have the same radial velocity as the deuterons and tritons and, therefore, the kinetic energy of any ion will be proportional to its mass. Consequently the energy W_H transferred to the hydrogen plasma is

$$W_H = \frac{M_H}{M_i + M_H}\, W, \tag{9}$$

M_H and M_i being the total mass of hydrogen and impurities and W the total kinetic energy of the shell. This repartition of kinetic energy and inertia may contribute to an inertial confinement [4].

5. Stability considerations

The hydromagnetic dynamic stability of a conducting cylindrical shell driven by an azimuthal magnetic field has been studied elsewhere [5]. The conclusions were that sausage-type perturbations are unstable, flutes are not, and helical perturbations go from unstable to stable during the contraction, with the exception of the kink which is always unstable. The e-folding times of all the unstable modes were shown to be of the order of the collapse time of the shell, so that these instabilities would not be dangerous provided the initial configuration possesses a high degree of symmetry.

Recently, E. Harris* has shown that instabilities of the Rayleigh-Taylor type would grow faster than the above mentioned hydromagnetic ones, the e-folding time being equal to $1/(g\,k)^{1/2}$ (g is the acceleration and k the wave-number). An effort will be made to observe these growing perturbations.

6. Experimental apparatus

6.1. General description

The initial density distribution shown in Fig. 2 cannot be obtained using a direct injection of plasma in vacuum by an annular gun, because a thin and homogeneous plasma layer is required, whilst no guiding magnetic field can be used (it would be trapped inside the shell and create a back-pressure). Consequently the following problems must be solved:

(1) production in vacuum of a layer of neutral material with the required density [criteria (3), (4), and (7)] and geometry;

(2) transformation of such a layer into a plasma without altering its shape, in absence of any magnetic field.

To solve point 1, density requirements do not allow one to start from a solid structure such as a thin foil or grid whilst the stringent requirements on the uniformity and sharp boundaries of the layer lead one to reject gas injection, e.g. supersonic streams. It was found convenient to start from a tubular curtain of powder consisting of a material having a large content of hydrogen, the other components having small atomic numbers; LiH and $LiAlH_4$ seem particularly convenient.

* On leave of absence from the University of Tennessee (private communication).

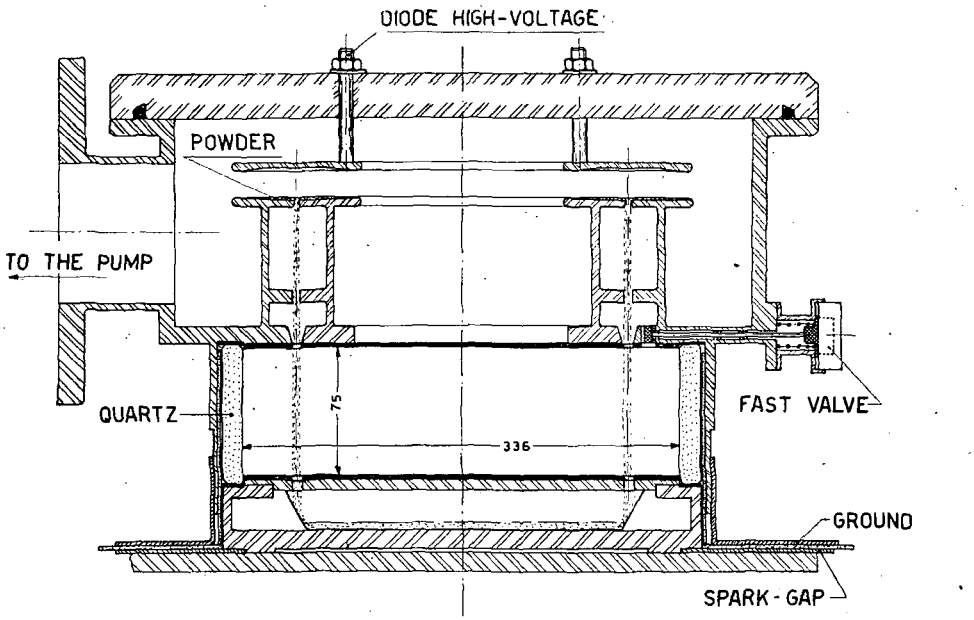

Fig. 6 Diagram of experimental chamber.

Vaporization and ionization of this powder layer appear to be rather difficult. This is because a large amount of energy is required for this transformation in a time during which the first particles that are vaporized cannot move appreciably. Considering that the surrounding medium is a gas at a pressure lower than a few microns of mercury, it was decided to start a normal dynamic pinch in the pre-ionized residual gas. It is expected that the immersion of the grains in the hot plasma produced that way results in a transfer of energy to the powder at a rate sufficient for its conversion into a plasma state. The apparatus then consists of a condenser bank, feeding through a spark-gap, a discharge struck in a linear experimental chamber in which a thin annular layer of $LiAlH_4$ powder is injected previously. Fig. 6 is a schematic view of the experimental chamber which has been built. The different components are briefly described in the following sub-sections.

6.2. Condenser bank

This is a conventional 60 μF, 40 kV, 48 kJ fast bank, connected to the load by only one vacuum spark-gap [6]. Considering that the transfer of energy to the accelerated layer is strongly dependent upon L_0 (see Fig. 5), great care has been taken to reduce the total inductance L_0 of the bank, of the connections and of the spark-gap as much as possible. Using parallel plates as connections an inductance of $4 \cdot 10^{-9}$ Henry has been obtained.

6.3. Experimental chamber

The length of the chamber is chosen to be 7.5 cm, in order to satisfy criterion (4). For practical reasons, the initial radius r_i of the plasma shell has been taken to be 13.5 cm. Eq. (3) shows then that the number N of neutron proton pairs per cm length of the discharge should be of the order of $8 \cdot 10^{18}$. From Fig. 5, $\eta \simeq 0.5$, so that the estimated energy per incoming deuteron is about 3 keV. As this is below the optimum energy of 20 keV, (7) is not satisfied, and the neutron yield will not be maximum. The end electrodes are made out of copper; thin annular slits are used for introduction and elimination of the powder beam, injected from above. Quartz and pyrex are being used for the cylindrical inner wall. It is hoped that, owing to the very short collapse time, the end effects will not be troublesome.

6.4. Injection of the powder

It has been found convenient to inject the powder by electrostatic means, using a microparticle diode. This diode works as follows: a voltage difference is applied between two parallel plates, of which at least one is covered by a thick layer of conducting powder. A current flows in the system, carried by the particles which are charged when in contact with one electrode and accelerated subsequently by the electric field between the electrodes. In the steady state, current is space-charge limited. If a slit is made in one electrode, a parallel beam of particles is emitted, the density and velocity of which depend on the diameter of the grains, the accelerating voltage and the distance between the electrodes. Theory and experiment, described elsewhere [7], have shown that beams of $LiAlH_4$ powder having the required properties can be injected in the manner described above for feasible values of the parameters (diameter of the grains 10^{-3} cm, distance between electrodes 2 cm, accelerating voltage of the order of 30 kV). The profile of the electrodes in the diode is such that particles are confined and cannot escape side-wise. The arrangement of the annular

diode, of the annular slit for the collimation of the powder-beam and of the experimental chamber is shown in Fig. 6.

6.5. Transformation of powder into plasma

This has been briefly described in Section 6.1. The current layer, starting from the walls of the tube, proceeds inwards with a large velocity due to the small mass accelerated (region I, Fig. 7) and stops when it reaches the external boundary of the powder layer. It then progresses very slowly up to the internal boundary of that layer (region II, Fig. 7) as the grains buried in the plasma are being decomposed and continuously emit vapours which are ionized and carry the current (this latter remaining outside by skin-effect). Finally, it moves inwards with a rather slow

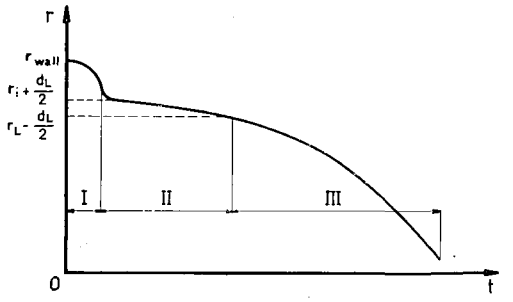

Fig. 7 Transformation of powder into plasma. In region I the current layer proceeds inward from the wall at relatively high velocity (mass accelerated is small). In region II the powder is being picked up, decomposed, etc. In region III the relatively large resulting mass moves slowly inward.

velocity (region III), corresponding to the large mass in motion. The pre-ionization at a low pressure of the background gas is achieved by multi-packing effect, produced by a radiofrequency electric field (14 MHz, a few hundred volts peak-to-peak and power of the order of 1 kW). The gas is admitted by a fast valve just before the pre-ionization is applied, in order that a breakdown should not occur in the powder diode during the previously made injection of powder. The decomposition of the powder is due to a thermal effect: each grain, when immersed in the plasma, acts as a small floating probe whose voltage is of the order of the maximum electron energy. The grain is then bombarded by positive ions accelerated by this voltage difference appearing across the sheath surrounding the grain. Calculations show that grains of 10^{-3} cm diameter made out of $LiAlH_4$ (decomposition temperature 100° C) should be vaporized and ionized completely in a time of the order of 1 μs provided a non negligible portion of the electron population in the low pressure discharge has directed energies larger than about 100 eV. Auxiliary experiments to study this plasma powder interaction have been set up.

6.6. Diagnostics

Magnetic probes are inserted in the discharge so that the current density can be measured versus space and time. Conventional high speed cinematography is used to photograph the driven plasma shell. As the central core will have a very short life-time, short exposure times and high repetition rate are necessary. It is planned to use a S.T.L. image converter camera, capable of taking a sequence of three pictures having exposure times of $5 \cdot 10^{-3}$ μs and separated by intervals of $50 \cdot 10^{-3}$ μs.

Acknowledgements

We wish to thank Prof. B. Brunelli, Director of the "Laboratorio Gas Ionizzati", for his encouragement and support. We are indebted to Prof. E. Harris for his contribution to the study of the stability of accelerated plasma-layers and to Ing. C. Gourlan who built the condenser bank. One of us (M. H.) would like to express his gratitude to the "Fond National Suisse de la Recherche Scientifique" of Switzerland for granting him a fellowship.

Appendix 1

Let us consider an infinitely long plasma column of radius r_0 in which the plasma density and temperature are initially uniform. The plasma is composed of equal parts of deuterons and tritons and of a corresponding number of neutralizing electrons. In absence of any constraining forces the column will expand radially. For sufficiently high densities, quasi-neutrality is always preserved and collisions between electrons and positive ions cause the difference in temperature between the two gases to be small as compared with the average plasma temperature. An expansion of the column follows during which the random velocities of the particles in the plasma are steadily converted in the energy of radial plasma flow away from the axis. This behaviour can be expressed approximately by an equation of state:

$$\frac{T}{T_0} = \left[\frac{r_0}{r}\right]^{4/3}, \tag{A 1}$$

where $T_e = T_p = T$, and an equation of motion:

$$N M \ddot{r} = 2\pi r k T n, \tag{A 2}$$

where n is the density and N is the linear density of positive ions, M is the mean ion mass. Substituting from Eq. (A 1) into Eq. (A 2) it follows that

$$\ddot{r} = \frac{2 k T_0}{M} \frac{r_0^{4/3}}{r^{7/3}} \tag{A 2a}$$

or

$$\dot{r} = \left\{\frac{3 k T_0}{M}\left[1 - \left(\frac{r_0}{r}\right)^{4/3}\right]\right\}^{1/2}. \tag{A 2b}$$

From this it follows that after an expansion of the plasma column to $r = 4 r_0$ the velocity of the radial flow reaches about 90% of the maximum attainable value. The original step-distribution of plasma density will diffuse, during the expansion, into a more gradual one. We have neglected this feature in our approximate model; however, this does not alter our main conclusions about the expansion process. Let us now calculate the energy W_F generated per unit length of

the column by DT reactions during the expansion of the plasma. This can be written formally as

$$W_F = N P Q/2, \tag{A 3}$$

where P is the probability that a deuteron will be involved in a DT reaction during the expansion. Q is the energy released in a single reaction and is $2.8 \cdot 10^{-5}$ erg.

P can be expressed using the expression $\langle w\sigma_n \rangle$ for the mean value of the rate of the DT reaction. Thus

$$P = \int_{r_0}^{\infty} \frac{n}{2} \langle w\sigma_n \rangle \frac{dr}{\dot{r}} = \int_{r_0}^{\infty} \frac{N}{2\pi r^2} \langle w\sigma_n \rangle \frac{dr}{\dot{r}} \tag{A 4}$$

Then

$$W_F = \frac{N^2}{4\pi} Q \int_{r_0}^{\infty} \frac{\langle w\sigma_n \rangle}{r^2} \frac{dr}{\dot{r}}. \tag{A 5}$$

The thermal energy stored per unit length of the initial plasma column (N ions and N electrons per unit length) is

$$W_s = 3 N k T_0.$$

Then,

$$N = \frac{W_s}{3 k T_0} \tag{A 6}$$

and (A5) can be written, making use of Eq. (A2b) and putting $r/r_0 = x$

$$W_F = \frac{W_s^2 Q M^{1/2}}{4\pi (3 k T_0)^{5/2} r_0} \int_I^{\infty} \langle w\sigma_n \rangle x^{-2} \frac{dx}{(1 - x^{-4/3})^{1/2}} \tag{A 7}$$

in which $\langle w\sigma_n \rangle$ is a function of T alone, and then of x alone, as $T = T_0 x^{-4/3}$.

Using the numerical values of $\langle w\sigma_n \rangle$ given in [8], it can be shown that, for values of $E = kT$ between 2,5 and 40 keV, the expression (E is in keV and $w\sigma_n$ in cm³/s)

$$\langle w\sigma_n \rangle = 7{,}41 \cdot 10^{-20} \cdot E^{3,5} \cdot e^{-0{,}0935 E}$$

fits quite accurately the experimental curve. Then, putting $x^{-4/3} = y$ one obtains

$$W_F = \frac{W_s^2 Q M^{1/2}}{4\pi (3 k T_0)^{5/2} r_0} 7{,}41 \cdot 10^{-20} \cdot (3/4) \int_0^1 E_0^{3,5} \cdot \exp[-0{,}0935 E_0 y] \frac{y^{13/4}}{(1-y)^{1/2}} dy \tag{A 8}$$

In this formula, c.g.s. units are used except for E_0 which is expressed in keV.

As E_0 is proportional to T_0, it is clear that, for a given energy input W_s, the energy production W_F will be proportional to

$$I = \int_0^1 E_0 \cdot e^{-0{,}0935 E_0 y} \cdot y^{13/4} \cdot [1 - y]^{1/2} dy.$$

The variation of I versus E_0 is shown in Fig. 1 in which, for reasons of normalization, $f(E_0) = 0{,}253\ I$. The energy release will be maximum for $E_0 = 11$ keV which corresponds to $T_0 = 1{,}28 \cdot 10^8$ °K, and $I_{max} = 3{,}95$. Inserting numerical values into Eq. (A8) and noting that M is the mean value of the deuteron and triton masses, one gets (c.g.s. units):

$$(W_F)_{max} = 6{,}4 \cdot 10^{-16} \frac{W_s^2}{r_0} \tag{A 9}$$

If one neglects all losses, but at the same time assumes that no recuperation of the final kinetic energy of the plasma is made, a net energy gain would be obtained if $(W_F)_{max} > W_s$, which means:

$$W_s > 1{,}56 \cdot 10^8 r_0 \text{ (J/cm, cm)}. \tag{A 10}$$

From Eq. (A6), one can see that (A10) is equivalent to another criterion

$$N > 2{,}96 \cdot 10^{22} r_0. \tag{A 11}$$

Eq. (A10) has to be compared to Eq. (9) of [1] where a simplified analysis led to the more stringent condition:

$$W_s > 2{,}5 \cdot 10^9 \cdot r_0 \text{ (J/cm, cm)}.$$

References

[1] LINHART, J. G., *Nuovo Cimento* **17** (1960) 850.
[2] LINHART, J. G., *Nuclear Fusion* **1** (1961) 78.
[3] POST, R. F., Risö Report No. 18 (1960) 313.
[4] LINHART, J. G., KNOEPFEL, H., GOURLAN, C., these Proceedings, page 733.
[5] LINHART, J. G., *J. Appl. Phys.* **32** (1961) 500.
[6] BAKER, W. R., *Rev. Sci. Instr.* **30** (1959) 700.
[7] MAISONNIER, CH., HAEGI, M., *J. Appl. Phys.* (submitted for publication).
[8] HESSELBERG-JENSEN, T., *et al.* Risö Report No. 2. (4 May 1958) 23 p.
[9] POST, R. F., *Revs. Mod. Phys.* **28** (1956) 338.

AMPLIFICATION OF MAGNETIC FIELDS AND HEATING OF PLASMA BY A COLLAPSING METALLIC SHELL*

J. G. LINHART, H. KNOEPFEL, C. GOURLAN

LABORATORIO GAS IONIZZATI (EURATOM-C.N.E.N.)

FRASCATI, ROME, ITALY

The principle is described of inertial confinement of plasma in which a cylindrical metallic shell compresses a magnetic field and plasma in a "soft-core" geometry. The shell transforms a part of its kinetic energy into the thermal energy of the compressed plasma and into the stored magnetic energy. The source of the kinetic energy of the shell can be either a condenser bank or an annular explosive charge. Two experiments, each using one of these energy-sources, are described.

1. Introduction

It has been mentioned elsewhere [1, 2] that unconfined plasma, such as a freely expanding cylinder of plasma, can be of interest in controlled thermonuclear research. In order that the fusion output W_F from such a plasma be larger than its initial thermal energy W_0 one must have for a 50/50 mixture of deuterium and tritium plasma:

$$W_0(\mathrm{J/cm}) > 8 \times 10^7 r_0, \tag{1}$$

where

$$W_0 = 3 N \mathrm{k} T_0, \tag{2}$$

$$T_0 \sim 1.3 \times 10^8\ ^\circ\mathrm{K}. \tag{3}$$

Therefore,

$$N(\mathrm{electrons/cm}) > 1.5 \times 10^{22} r_0. \tag{4}$$

A free expansion of a plasma column from a radius r_0 to radius $2r_0$ is accomplished with a mean speed approximately equal to $[2\,\mathrm{k}T_0/\langle M\rangle]^{1/2}$ where $\langle M\rangle$ is the mean ionic mass. The effective lifetime τ_0 (in seconds) of such a column is therefore:

$$\tau_0 \sim \frac{2 r_0}{[2\,\mathrm{k}T_0/\langle M\rangle]^{1/2}}. \tag{5}$$

It is evident that if one could reduce the speed of expansion v_{exp} of the column by a factor $\varkappa$ the nuclear output would be increased by $\varkappa$. Let us assume that the total energy loss will remain equal to W_0; then the reactor criterion becomes:

$$W_0 > 8 \times 10^7 \frac{r_0}{\varkappa}(\mathrm{J/cm}), \tag{6}$$

$$N > 1.5 \times 10^{22} \frac{r_0}{\varkappa}(\mathrm{electrons/cm}), \tag{7}$$

$$T_0 \sim 1.3 \times 10^8 (^\circ\mathrm{K}). \tag{8}$$

For example, if $r_0 = 0.1$ cm and $\varkappa = 20$, then $W_0 = 400$ kJ/cm, $N > 0.75 \times 10^{20}$ electrons per cm and $\tau = \varkappa\tau_0 \sim 4.25 \times 10^{-8}$ seconds. The duration of such a confinement is obviously limited by the appearance of all the known instabilities of a linear pinch, by the end-losses and by the emission of radiation (see Appendix 1). In order to obviate these difficulties a confinement factor $\varkappa$ smaller than 20 will probably have to be considered.

It can be shown that such a short confinement cannot be achieved by static means. The plasma pressure during the confinement is

$$p = 2 n \mathrm{k} T_0 = 1.7 \times 10^8 r_0^{-1} \varkappa^{-1}(\mathrm{atm, cm}) \tag{9}$$

from which it follows that the pressure is typically of the order of 10^7 atmospheres.

Such pressure can only be balanced, for a short time, by the inertial forces of a medium surrounding the hot plasma column. Let us consider, as an example, a cylinder of hot plasma located inside and thermally insulated from a thin metallic shell. Let the kinetic energy of the system be initially equal to zero. Let us also assume that the mass of the shell M_s is much larger than that of the plasma M_p.

The equation of motion of the shell becomes:

$$M_s \ddot{r} = (2\pi r)\, 2 n \mathrm{k} T. \tag{10}$$

For adiabatic expansion one has

$$T = T_0 \left[\frac{r_0}{r}\right]^{4/3}; \tag{11}$$

the equation of motion then becomes:

$$\ddot{r} = \left[\frac{4 N \mathrm{k} T_0 r_0^{4/3}}{M_s}\right] r^{-7/3}.$$

Integrating, we get

$$\dot{r} = \left\{\frac{6 N \mathrm{k} T_0}{M_s}\left[1 - \left(\frac{r_0}{r}\right)^{4/3}\right]\right\}^{1/2}. \tag{12}$$

The expansion velocity at $r = 2r_0$ is, therefore,

$$\dot{r}(r = 2r_0) = 1.9 \left[\frac{N \mathrm{k} T_0}{M_s}\right]^{1/2}, \tag{12 a}$$

whereas the expansion velocity for an unconfined plasma column at $r = 2r_0$ is approximately [1]

* Conference paper CN-10/11, presented by J. G. Linhart. Translations of the abstract are at the end of this volume of the Conference Proceedings.

$1.35\,(k\,T_0/\langle M\rangle)^{1/2}$. The confinement factor $\varkappa$ is thus

$$\varkappa \cong 0.7\sqrt{\frac{M_s}{M_p}}. \qquad (13)$$

In order to achieve $\varkappa \sim 20$ the mass M_s of the shell must be about 1000 times the mass M_p of the compressed plasma (for the criterion limiting the mass M_s see Appendix 2).

Inertial confinement has often been used to augment the efficiency of combustion of chemical explosives; the outer shell being known as "the tamper". In our case it is obvious that the applicability of this method depends on our ability to insulate thermally the plasma from the surrounding tamper during the time $\varkappa\tau_0$. As, in most cases of interest to us, the mean free path of the hydrogen nuclei is commensurable with the radius r_0, the thermal insulation can be achieved only by means of a magnetic field.

The value of the magnetic field corresponding to the plasma pressure, given by Eq. (9), becomes

$$B = \frac{65}{\sqrt{r_0\,\varkappa}}\,(\mathrm{MG, cm})$$

Thus if, e.g., $r_0 = 0.1$ cm and $\varkappa = 20$, then $B = 46$ megagauss. Fields of 15 MG have already been generated by shells imploding on a magnetic field [3].

2. Basic considerations of energy transfer

This defines a model (Fig. 1), which we shall try to realize experimentally, in which a cylindrical metallic shell implodes on a magnetic field surrounding a central column of plasma.

Another feature of our model that has to be decided is the geometry of the magnetic field. The choice is, effectively, between an axial (B_z) field and an azimuthal (B_φ) field. As it appears [4] that a heavy shell collapsing on a B_φ field (a "soft core" geometry) is more stable than a shell collapsing on a B_z field (orthogonal pinch) and that up to the first pinch all plasmas are stable, we have decided to do our first experiments with a B_φ field.

Let us consider the system in which a collapsing cylindrical liner compresses a plasma cylinder through an azimuthal magnetic field. The initial quantities at $t = t_0$ are denoted by an index, 0, whereas the values referring to the plasma and the liner are symbolized, respectively, by an additional index 1 and 2. We wish to study in which manner the initial kinetic energy of the liner E_{0k} is transferred to the plasma, to the magnetic field and to the compressed liner. These transfers will be expressed as functions of the compression ratio $X = r_1/r_{01}$.

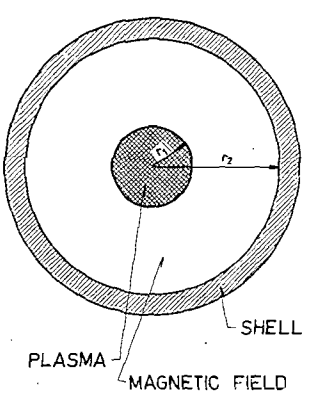

Fig. 1 Diagram of basic geometry of experiment.

2.1. Plasma energy

Let us assume that the compression of the plasma is adiabatic and is, therefore, governed by the equation of state

$$\frac{T_{01}}{T_1} = \left[\frac{r_1}{r_{01}}\right]^{2(\gamma-1)}.$$

Let us further assume that at the plasma boundary the magnetic field pressure is equal to the plasma pressure:

$$2\,n_1\,k\,T_1 = \frac{B_1^2}{8\pi}.$$

It follows, that

$$B_{01}/B_1 = (r_1/r_{01})^\gamma = X^\gamma.$$

The thermal energy of the plasma is

$$E_P = 3\,N_1\,k\,T_1,$$

where $N_1 = n_1 \cdot \pi r_1^2$ is the linear density of ions.

The energy increase during the compression can thus be written:

$$\Delta E_P = E_P - E_{0P} = E_{0P}\,[X^{2(1-\gamma)} - 1].$$

2.2. Magnetic field energy

The conservation of flux of an azimuthal magnetic field $B_\varphi = (r_1/r)\,B_1$ is expressed by

$$r_{01}\,B_{01}\ln(r_{02}/r_{01}) = r_1\,B_1\ln(r_2/r_1),$$

where the index 1,2 indicates that the field is evaluated at r_1, r_2 respectively.

The energy stored in the magnetic field being

$$E_M = (1/4)\,B_1^2\,r_1^2\ln(r_2/r_1),$$

the energy increase during the compression becomes

$$\Delta E_M = E_M - E_{0M} = E_{0M}\,(X^{1-\gamma} - 1)$$

2.3. Liner energy

The elastic energy of the liner compressed by pressures of the order of a few megabars is roughly

$$E_L = \tfrac{1}{2}\,0.11\,V_0\,p,$$

(see Appendix 2), where we have assumed that the pressure decreases linearly from p at the inside of the linear to zero at the outside. From the condition of flux conservation and the radial dependence of the azimuthal magnetic field, the equation

$$\frac{B_2}{B_{02}} = \frac{B_1}{B_{01}}\left(\frac{r_{01}}{r_{02}}\right)^{(r_{01}/r_1)\,(B_{01}/B_1-1)}$$

can be found, allowing the energy increase,

$$\Delta E_L = E_L - E_{0L} = E_{0L}\left[\frac{B_2^2}{B_{02}^2} - 1\right],$$

to be written more conveniently in the form:

$$\Delta E_L = E_{0L}\left\{X^{-2\gamma}\left[\frac{r_{01}}{r_{02}}\right]^{2X^{\gamma-1}-2} - 1\right\}.$$

2.4. The three basic energy equations

It has been shown that magnetic fields larger than 10 megagauss are necessary to contain our plasma. Experimentally such fields can be produced only by large amplification, implying that X is small. Introducing $\gamma = 5/3$ we can then write with good approximation:

$$\Delta E_L = E_{0L}\left[\frac{r_{02}}{r_{01}}\right]^2 X^{-10/3},$$

$$\Delta E_P = E_{0P} X^{-4/3},$$

$$\Delta E_M = E_{0M} X^{-2/3},$$

where

$$E_{0L} = (1/2)\, 0.11\, V_{02}\, B_{01}^2\, (r_{01}/r_{02})^2,$$

$$E_{0P} = 3\, N_{01}\, k\, T_{01},$$

$$E_{0M} = (1/4)\, B_{01}^2\, r_{01}^2 \ln (r_{02}/r_{01}).$$

The comparison of the three energy equations shows that ΔE_L is increasing most rapidly with decreasing X.

It remains now to find the source of kinetic energy for our imploding shell. If one could obtain plasma radii smaller than 1 mm, the kinetic energy of a correspondingly thin shell could be provided by a condenser bank. As an example, consider

$r_0 = 0.02$ cm, $\varkappa = 20$ then $W_0 > 80$ kJ/cm,

$N > 1.5 \times 10^{19}$ electrons/cm and $\varkappa\, \tau_0 \sim 0.85 \times 10^{-8}$ s.

However, if such a high concentration of energy proved unattainable then the chemical energy liberated by high explosives might be used, in which case the explosive energy per unit length of the system could be as high as 1 MJ/cm. This corresponds closely to the example given following Eq. (8).

We have decided to use both these systems of propulsion. They will be described in the next two sections.

3. Experiment I

An experiment has been set up in which a cylindrical metallic shell is imploded by an external azimuthal magnetic field, the latter being generated by a current drawn from a battery of condensers. We would like to realize and study the following sequence of processes: (a) the conversion of the energy of the condenser battery into the kinetic energy of radial motion of the shell; (b) the slowing down of the collapsing shell and its eventual stopping by the rapidly increasing pressure of an internal B_φ field and plasma; (c) the conversion of the kinetic energy of the shell into thermal energy of the plasma and into stored energy of the magnetic field (see Fig. 2).

We shall first describe the type of plasma we wish to study. From this follow the properties of the metallic shell and the corresponding characteristics of the condenser bank.

Or aim is to study a cylindrical plasma compressed to densities higher than 10^{22} electrons/cm^3 and to temperatures in excess of 10^7 °K. Owing to the lack of experience with cylindrical systems in which energy dissipated per unit length exceeds 10 kJ/cm we assume that, at the moment of maximum compression,

$$3 N k T < 10^{11}$$

or

$$r_0 < 0.03 \text{ cm}.$$

The linear mass density of such a plasma will be of the order of 10^{-3} g/cm. If $\varkappa \sim 20$ is to be achieved, the mass of the shell will have to be of the order of 1 g/cm. It was decided to use aluminium, soft copper and lead foils. The initial radius R_0 of the shell is partly dictated by the requirement that the electrical skin depth δ_e should be smaller than the thickness of the shell δ_s. Thus we get for copper

$$\delta_s \sim \frac{1}{2\pi R_0 \times 8.5} > \frac{6.6}{\sqrt{f}}. \qquad (15)$$

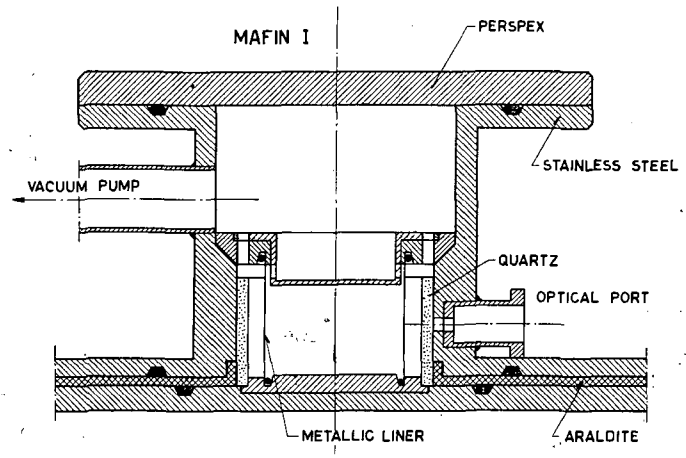

Fig. 2 Experimental set-up for study of implosion of a cylindrical metallic shell by a pulsed external azimuthal magnetic field.

The ringing frequency of the system cannot be an order of magnitude different from 10^5 Hz and consequently $R_0 < 1$ cm. For aluminium foils one gets $R_0 < 3$ cm.

Considerations of inductance and of the symmetry of the current flow suggest that the length l of the system should be about equal to the radius R_0. We have chosen

$$R_0 = 3 \text{ cm}, \; l = 3.2 \text{ cm}.$$

These order-of-magnitude considerations determine the size and type of condenser bank to be used.

The bank consists of 27 condensers with maximum voltage of 10 kV. The short-circuit frequency is 120 kHz and the maximum stored energy 27 kJ. It is connected to the load by a single switch. The switching is achieved by perforating a 50 μ thick layer of Mylar by means of a small detonator [5]. The relatively slow repetition rate of this system is consistent with the time it takes to replace the metal foil within the experimental chamber. The construction of the switch is simple and its inductance is very low (about 0.3 nH). During the first tests the maximum current obtained was about 2×10^6 A and the total inductance about 15 nH, of which about 5 nH correspond to the experimental chamber.

The motion of metallic shell can be described by the adiabatic approximation [6]. In order that this approximation be valid one must have

$$\frac{C^2 V^2}{100 M_s R_0^2} < 0.05 \, (\text{F, V, g, cm}).$$

Inserting in this criterion the characteristics of our bank and taking a typical value for M_s, we see that this condition is satisfied. In that case

$$\frac{1}{2} M_s \dot{R}^2 = \frac{CV^2/2}{10^{-7} l} \left[1 - \left(1 + \frac{2 \times 10^{-9} l}{L_0} \ln \frac{R_0}{R} \right)^{-1/2} \right].$$

The efficiency of conversion of electrical energy into the kinetic energy of the shell will be

$$\eta (R/R_0) = \left[1 - \left(1 + \frac{2 \times 10^{-9} l}{L_0} \ln \frac{R_0}{R} \right)^{-1/2} \right].$$

The mean radius of a fully collapsed shell is about 0.3 cm; also in our case $l = 3.2$ cm and $L_0 \sim 12$ nH. Then $\eta \sim \eta \, (0.1) = 0.33$. It follows, therefore, that the kinetic energy of the shell will be about 10 kJ, or about 3 kJ/cm.

4. Experiment II

4.1. Energy sources

We have mentioned in the introduction that one of the possible sources of kinetic energy for an imploding shell is high explosives. It is interesting to make a comparison of different energy sources covering the energy range of several MJ. Such a comparison is reviewed in Table I.

Table I. Energy storage systems whose time of discharge is in the range of a few microseconds

Storage system	Energy density (J/cm³)	Price per energy release of 1 MJ
electrical (conventional condensers)*	10^{-2}	\$ 0.50—\$ 2.00
electrical (ferroelectric condenser)	1	larger than for conventional condensers
plasma (homopolar device)	$\gtrsim 1$	?
explosive	10^4	\$ 0.50—\$ 1.50

* Taking 10^5 as a mean number of discharges at full voltage.

The high density explosives exhibit several advantages over a conventional condenser bank. However, many technical difficulties have to be overcome. The application of solid organic explosives requires above all an experience in their preparation and handling. A great difficulty is encountered in starting a detonation wave simultaneously at different points of the high explosive charge. Even more difficult is the problem of containing chemical explosions within vessels, without the solution of which one could not use explosives in the laboratory.

The principle of the experiment to be described here is nearly the same as the one already mentioned in Section 3. The cylindrical liner is now driven towards its axis of symmetry and against an internal azimuthal magnetic field B_φ by an annular charge. About 30% of the chemical energy is transferred to the imploding shell. The liner gradually transforms all its kinetic energy into the energy of the compressed magnetic field and of the plasma and into its own internal energy.

The comparison of the two experiments, one using electrical condensers, the other explosives as energy source, may throw some interesting light on the practical use of chemical stored energy in the megajoule and microsecond range. In addition, experiments on containment of large energy bursts in a converging geometry and its related problems are of quite general interest in our approach to the problem of controlled nuclear fusion.

4.2. Apparatus

Fig. 3 shows a cut through the central part of the apparatus which was used for the confinement experiments.

4.3. Explosives

The type of explosive used is "Composition B" (60% RDX, 40% TNT). It is a solid explosive, which can be cast homogeneously and worked to high

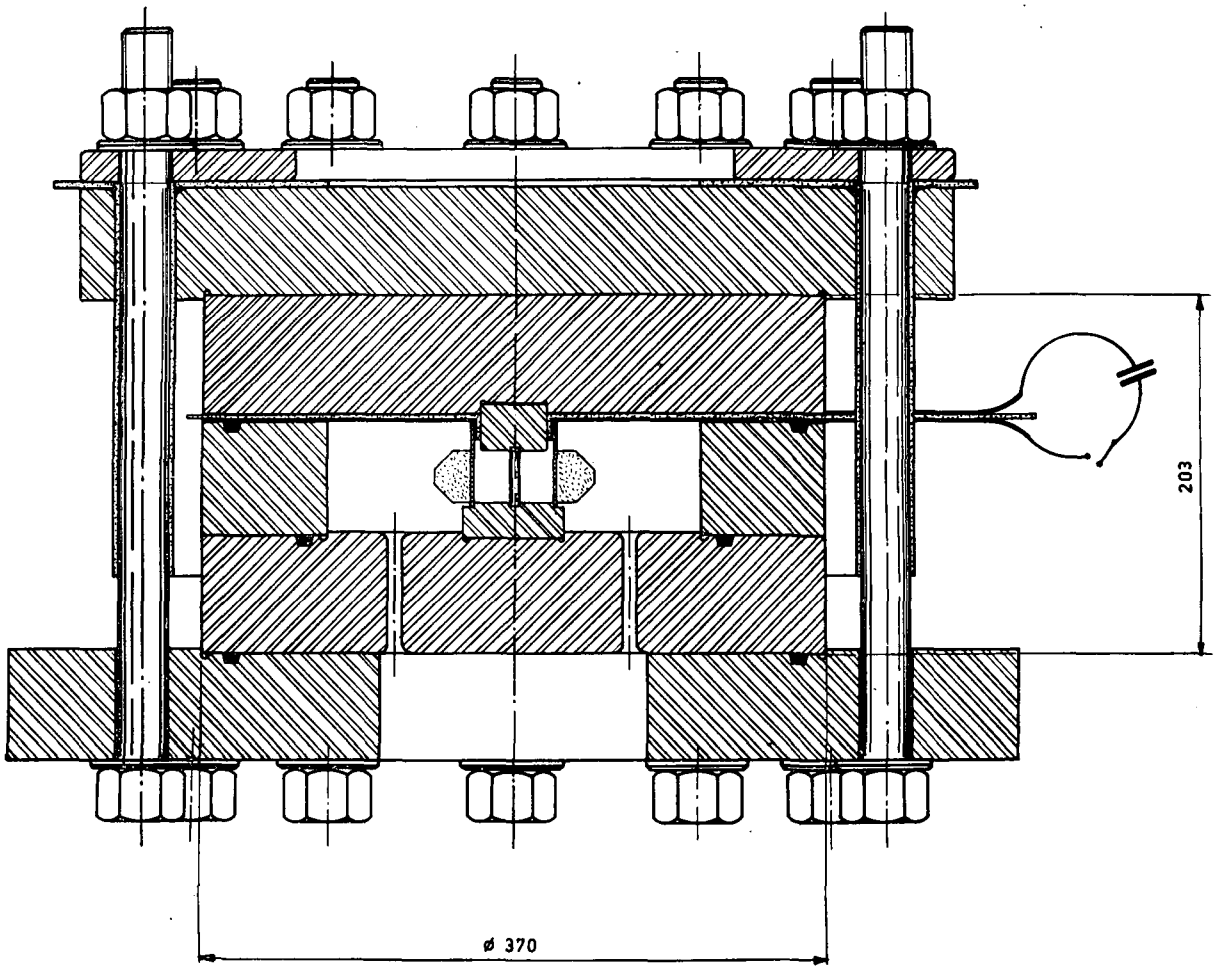

Fig. 3 Experimental set-up for study of implosion of a cylindrical metallic shell by explosives. This chamber has been used for the containment experiments (Fig. 5). The main diameter is 370 mm. In the centre one can see the liner which supports the annular charge. Also sketched in the drawing is the electrical circuit which would be necessary to build up an initial B_φ field.

precision [7]. Its main characteristics are: detonation speed 0.8×10^6 cm/s, density 1.7 g/cm^3, pressure in the detonation front 250 000 atm and energy density 5 kJ/g. A typical annular charge used for this experiment has the following characteristics: inner diameter 50 mm, height 30 mm, outer diameter from 72 mm at the ends to 94 mm at the centre, weight 164 g. Including the explosive of the detonators this charge then represents about 1 MJ of stored energy.

In order to achieve a regular converging detonation wave, a ring of 20 electrical detonators is fired. The mean time jitter of these detonators is less than 0.1 μs. By conveniently shaping the secondary explosive, one can produce regular implosions. (The history of one of these is imprinted on the steel end-pieces, see Fig. 4.)

4.4. Liners

The materials mostly used for our liners were copper and aluminium. The explosive was formed directly on the external cylindrical surface of the liner. The high explosive charges used by us were able to impart a speed of 0.5 cm/μs to the metallic shell, which implies that more than 30% of the chemical energy is converted into the kinetic energy of the liner.

4.5. Containment of chemical explosions

A container must withstand the momentum impact of the explosion, without reaching anywhere the rupture limit of its elastic-plastic response characteristic.

If the pressure pulse $p\,(t)$ on the cylindrical container wall is short compared to the oscillation period, as it is in fact in our case, and if the transferred momentum

$$I = 2\pi r \int_0^t p(t)\,\mathrm{d}t$$

is known, then one can easily compute the resulting dilatation in the case of a "thin container"*. In

* One neglects radial strains and stresses and assumes the tangential forces constant through the thickness of the wall.

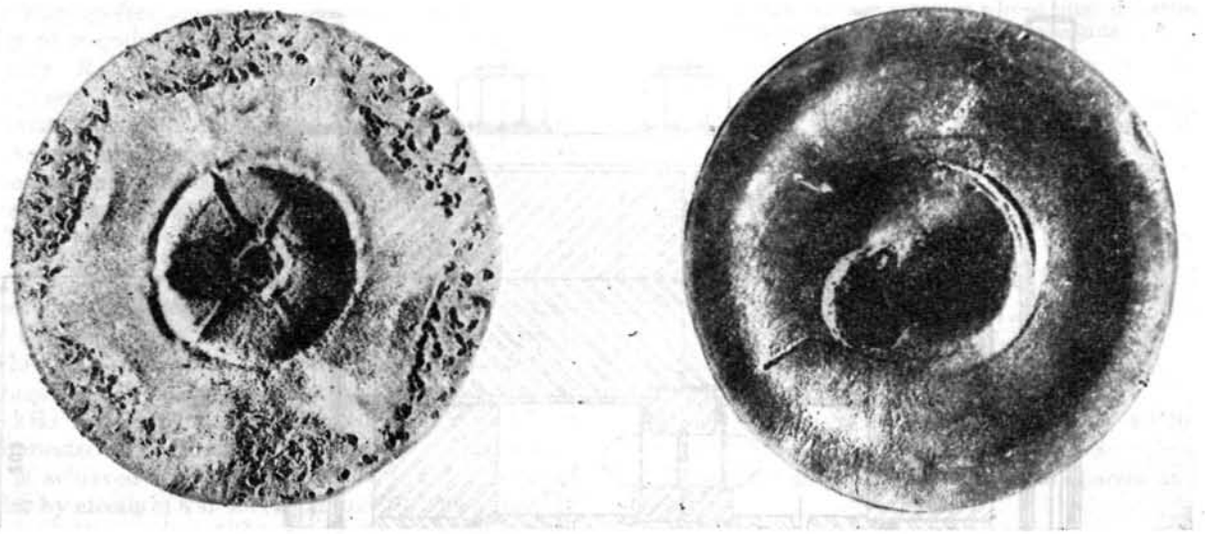

Fig. 4 The end-plates which support the explosive ring (see Fig. 3) are shown after implosion. The plate shown at the left is damaged in such a way that one can recognize many details of the implosion history. In particular, one sees the good simultaneity of the six detonators.

fact, it is

$$\frac{I^2}{2M} = \int_0^{2\pi\Delta r} \sigma e \, \mathrm{d}x,$$

which gives

$$I = r\,\omega\,M\,(\Delta r/r),$$

with $\sigma = Ex/2\pi r$ being the tangential strain, E the Young's modulus, ϱ the density, r the radius, e the thickness, M the mass of the container, $\omega = (1/r)\,(E/\varrho)^{1/2}$ the circular frequency of the radial mode of oscillations. One sees that the permissible momentum transfer in the vessel is proportional to the mass of the shell.

Experimentally it has been shown [8] that the pressure on the wall is, with good approximation, proportional to the explosive mass so that one can write

$$K \cdot \frac{\Delta r}{r} = \frac{M_{\text{explosive}}}{M_{\text{vessel}}},$$

where K is a value depending essentially on the geometry of the arrangement and also on the type of explosive and on the wall material.

The elastic behaviour of a thick container is more complicated as infinitely many radial frequency modes can be excited. However, the elastic response of even a relatively thick shell can be adequately described using the thin shell assumptions.

Our containment results of radially imploding annular charges are plotted in Fig. 5. They apply to the apparatus shown in Fig. 3. The ring has the following dimensions: outer radius $r_e = 18.5$ cm, inner radius $r_i = 11$ cm, height $l = 6.5$ cm, mass $= 35$ kg, mass of an equivalent sphere $M_{\text{eq. sph.}} = 157$ kg, maximal loading factor 0.03. The mean K value for the two different charges reduced for equivalent sphere mass and for $\Delta r/r$ measured at the outside of the container is $K = 0.7 \pm 0.2$. The measured frequency at the same point is $\nu = 5.9 \pm 0.1$ kHz.

The rest of the container, i.e. the two covers held together by the screws, represents another oscillating system, for which one finds

$$\frac{\Delta l}{l} = \frac{M_{\text{explosive}}}{K_1} \frac{1}{(M_{\text{total}}\,M_{\text{screws}})^{1/2}},$$

where $\Delta l/l$ is related to the screws, and the various M's are the masses of the explosive, of the screws and the total mass of the system. Measurements give $K_1 = 0.8 \pm 0.2$ and $\nu_1 = 0.8 \pm 0.1$ kHz.

Frequencies and elongations have been measured at different points with strain gauges.

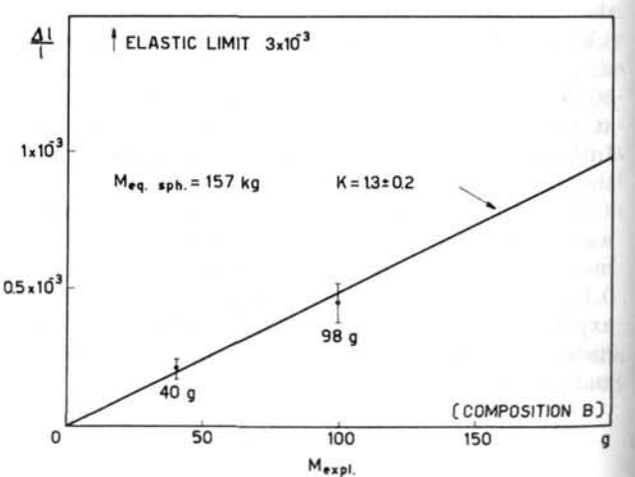

Fig. 5 Mass of explosive versus the strain $\Delta l/l$ (see text). (Note: The value of K indicated on graph should be 0.7 ± 0.2. The strain scale is incorrect and should be labelled 1.0×10^{-3}, 2.0×10^{-3} instead of 0.5×10^{-3}, *etc.*)

4.6. Conclusion

The experiments indicate that it is possible to contain chemical explosions up to 200 g of explosive (1 MJ equivalent) within our chamber and that this could be extended to about 1 kg after some modification of the apparatus. However, there is still an appreciable and uncomfortable amount of energy transmitted by shock waves and oscillations through the container to the surrounding air. This difficulty can be solved by different acoustical shieldings, best of which is an evacuated space.

Acknowledgement

We would like to thank Dr. F. Herlach for his help with the evaluation of the energy loss in the liner and to the Bombrini Parodi-Delfino Company for preparing the explosive charges.

Appendix 1

End-losses. One of the simplest criteria limiting the value of $\varkappa$ follows from considering the end-losses of the system.

Let us assume that the hot plasma flows towards the end-electrodes with its mean thermal speed. The energy loss during the confinement time $\tau_0 \varkappa$ will then be

$$\Delta W \sim 2 \times 3 N \mathrm{k} T \cdot \sqrt{\frac{2 \mathrm{k} T}{\langle M \rangle}} \cdot \tau_0 \varkappa .$$

This energy loss must be much smaller than the total plasma energy, which is $l \times 3 N \mathrm{k} T$.

Thus

$$\varkappa \ll \frac{l}{4 r_0} .$$

Example: a typical case is $r_0 = 0.1$ cm, $l = 4$ cm then $\varkappa \ll 100$; thus one may accept $\varkappa = 20$.

This criterion represents a pessimistic estimate as the actual thermal diffusion towards the electrodes occurs at a speed lower than $(2 \mathrm{k} T/\langle M \rangle)^{1/2}$ [9].

Bremsstrahlung. If all the bremsstrahlung radiation could escape from the plasma column and if the nuclear reaction products do not heat the plasma, $\varkappa$ would not be limited at all. This follows directly from the corresponding equation for a plasma cooled by bremsstrahlung:

$$\frac{\mathrm{d} T}{\mathrm{d} t} = 0.35 \times 10^{-11} \times n \sqrt{T} .$$

Integrating from T to αT one gets

$$n \tau = 6 \times 10^{11} \sqrt{T} (1 - \sqrt{\alpha}) .$$

Using Eq. (7) one sees that $\varkappa$ cancels in the term $n\tau$ and one gets

$$1 - \alpha \sim 2 \times 10^{-2} .$$

Consequently during the confined period, whatever $\varkappa$, in a zero-energy-gain reactor only 2% of the plasma energy is carried away by bremsstrahlung.

The same should be true about the cyclotron radiation, of which one could hope to reabsorb a good portion owing to the high densities and to the reflection on the inner wall of the shell.

Instabilities. The most severe limitation on $\varkappa$ will be the appearance of instabilities. This is difficult to predict analytically. An estimate could be obtained for the simple sausage instability where two adjacent bulges may be regarded as "ends" and the $\varkappa$ may then be evaluated from the end-loss formula

$$\varkappa < \frac{\lambda/2}{4 r_0} ,$$

where λ is the wavelength of maximum instability growth.

Example: λ determined by viscosity is given by [10]

$$\lambda_\mathrm{m} = 3 \times 10^6 \frac{T^{5/3}}{g^{1/3} n^{2/3}} .$$

Using Eqs. (7) and (8) we get $\lambda \sim 2 \varkappa^{2/3} r_0^{1/3}$ (cm). Thus $\varkappa \ll (1/2) r_0^{-2}$, for $r_0 = 0.1$ cm one gets $\varkappa \ll 50$. Again a value of $\varkappa$ not exceeding 20 is being suggested.

Appendix 2

Energy absorption by the metallic liner

When the imploding "tamper" is stopped by the pressure p of the internal magnetic field and of the plasma a certain portion of its kinetic energy is transformed into its own internal energy W_s where

$$W_s = \int_{V_1}^{V_0} p \, \mathrm{d} V .$$

The $p\,(V)$ diagrams for several metals are available up to 4 Mbar. We have used those for lead, copper and aluminium given by Altshuler *et al.* [11]. The internal energy W_s was determined by graphical integration of the p, V curves. It appears that in the range from 0.5 to 4 Mbar the relation between pressure and energy can be approximated by the simple formula

$$\frac{W_s}{V_0 p} = 0.11 \pm 0.01 ,$$

where V_0 is the initial volume of the shell.

Putting in the densities $\varrho_0\,(\mathrm{Al}) = 2.7$ g cm^{-3}, $\varrho_0\,(\mathrm{Cu}) = 8.9$ g cm^{-3}, $\varrho_0\,(\mathrm{Pb}) = 11.3$ g cm^{-3}, one obtains for the energies:

$W_s\,(\mathrm{Pb}) = 1.0$ kJ/g Mbar,
$W_s\,(\mathrm{Cu}) = 1.3$ kJ/g Mbar,
$W_s\,(\mathrm{Al}) = 4.2$ kJ/g Mbar.

Discussion in terms of $\varkappa$ and r_0

From Eq. (13) we get

$$\varrho_0 V_0 = M_s = 2 \varkappa^2 \langle M \rangle N ,$$

which combined with Eq. (4) and assuming $\langle \mathrm{M} \rangle = 4 \times 10^{-24}$ g gives

$$V_0 > 1.2 \times \frac{r_0 \varkappa}{\varrho_0} .$$

Using this formula and Eq. (9) we get for the internal energy*

$$W_s > \frac{2.5\times10^5}{\varrho_0}\,(\mathrm{J/cm^3},\ \mathrm{g/cm^3}),$$

and combining this with Eq. (3), there is

$$\frac{W_0}{W_s} < 4\times10^{-4}\,\frac{r_0}{\varkappa}\,\varrho_0.$$

For copper $\varrho_0 = 8.9\ \mathrm{g/cm^3}$ and, therefore,

$$\frac{W_0}{W_s} < 4\times10^{3}\,\frac{r_0}{\varkappa}.$$

Evidently for $r_0 = 0.1$ cm and $\varkappa = 100$ about 30% of the available kinetic energy is used up in compressing the liner.

* Actually W_s is somewhat smaller on account that the pressure in the temper is not constant. It drops to zero on the outer cylindrical boundary.

References

[1] LINHART, J. G., *Nuovo Cimento* **17** (1960) 850.
[2] MAISONNIER, CH., LINHART, J. G., HAEGI, M., these Proceedings, page 727.
[3] FOWLER, C. M., *J. Appl. Phys.* **31** (1960) 588.
[4] LINHART, J. G., *J. Appl. Phys.* **32** (1961) 500.
[5] GABRIEL, H. A., *et al.*, *J. Sci. Instr.* **38** (1961) 136.
[6] LINHART, J. G., *Nuclear Fusion* **1** (1961) 78.
[7] JAMES, E., Second Office of Naval Research Symposium on Detonation (Washington D.C., February 1955) p. 1.
[8] HOFFMAN, A. J., MILLS, S. N., BRL Report 988 (July 1956).
[9] ALFVÉN, H., *Nature* **188** (1960) 801.
[10] GREEN, T. S., NIBLETT, G. B., *Nuclear Fusion* **1** (1961) 42.
[11] ALTSHULER, X., *et al.*, *Soviet Phys. JETP* **11** (1960) 573.

ИССЛЕДОВАНИЕ ТОРОИДАЛЬНОГО РАЗРЯДА В ПЕРЕМЕННОМ ПРОДОЛЬНОМ МАГНИТНОМ ПОЛЕ*

Д. П. Иванов, К. А. Разумова

Академия наук СССР,

Москва, Союз Советских Социалистических Республик

В докладе обсуждаются результаты экспериментов, проведенных на тороидальной камере с сильным продольным магнитным полем. Конструкция камеры позволяла в некоторый произвольный момент разряда накладывать дополнительное переменное продольное магнитное поле. Все эксперименты проводились в камере, обезгаженной длительной тепловой тренировкой.

Сжатие и расширение плазмы, наблюдаемые, соответственно, в нарастающем и убывающем продольном магнитном поле, позволяют утверждать, что плазма существенно замагничена. Оценка минимальной величины поперечной проводимости дает $\sigma \simeq 1 \cdot 10^{14}$ CGSE, в то время как средняя по сечению разряда продольная проводимость составляет $\sigma \simeq 1 \cdot 10^{15}$ CGSE.

Процессы в плазме характеризуются появлением резких колебаний в некоторый момент времени и связанным с ними уменьшением тока. В докладе приводятся зависимости момента появления колебаний от различных параметров. Показано, что колебания могут трактоваться как магнитогидродинамические неустойчивости 1-ой моды, если предположить, что радиус тока не равен радиусу диафрагм, ограничивающих апертуру камеры, а убывает со временем со скоростью $\sim 10^4$ см/сек.

Эксперименты с переменным продольным магнитным полем хорошо согласуются с такой трактовкой.

В докладе проводится сравнение описанных экспериментальных результатов с опубликованными ранее.

Введение

В работах [1, 2] показано, что на поведение разряда с большим током, стабилизированным сильным продольным магнитным полем, в чистых вакуумных условиях оказывают существенное влияние возникающие в таком разряде неустойчивости. Представляет большой интерес выяснение природы этих неустойчивостей, а также вопрос о том, как велика скорость диффузии плазмы поперек магнитного поля до и после развития неустойчивости.

Методом, дающим возможность ответить на эти вопросы, может служить изучение поведения плазмы в присутствии дополнительного продольного магнитного поля, изменяющегося за времена меньшие, чем длительность тока разряда. Правда, возможности этого метода ограничены, вследствие крайней нежелательности введения внутрь разряда каких-либо измерительных органов, т.к. они могут сильно возмущать плазму в условиях тщательно обезгаженной камеры. Тем не менее, даже на основании изучения общих характеристик разряда при изменении продольного магнитного поля удается получить некоторые интересные результаты.

1. Установка

Эксперименты проводились на тороидальной камере, конструкция и размеры которой приведены на рис. 1. В камере можно было создать практически постоянное за время разряда продольное магнитное поле напряженностью до 7,5 кэрст. Кроме того, конструкция камеры позволяла накладывать дополнительное переменное магнитное поле напряженностью до 8 кэрст. Длительность

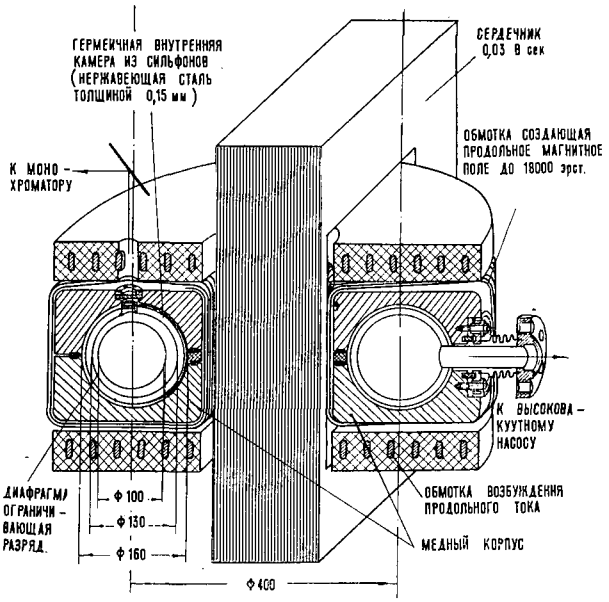

Рис. 1 Схема тороидальной разрядной камеры, на которой проводились эксперименты.

первого полупериода тока разряда составляла от 500 до 700 мксек, длительность полупериода изменяющегося магнитного поля — от 200 до 500 мксек. Разрядная камера тщательно обезгаживалась прогревом и специальной тренировкой разрядом. Апертура разряда ограничивалась двумя симметрично расположенными тонкими диафрагмами из нержавеющей стали.

Результаты экспериментов показывают, что состояние стенок существенно сказывается на

* Доклад CN-10/222, представленный на конференцию. Докладчик: К. А. Разумова. Дискуссия (на английском языке) по этому докладу дана на стр. 751. Переводы аннотаций находятся в конце этого тома Трудов Конференции.

характере развития разряда. Если в «грязной» камере средняя по сечению проводимость для максимума тока ни в одном режиме не превышает 2.10^{14} CGSE, то в чистой камере эта величина в режимах с сильными продольными магнитными полями достигает 2.10^{15} CGSE. Кроме того, для осциллограмм различных параметров разрядов в чистых условиях характерно возникновение колебаний значительной амплитуды. Однако, даже после тщательного обезгаживания камеры, интегральные спектры разряда содержат много линий примесей.

Рабочим газом в экспериментах служил водород при давлении от 5.10^{-4} до 5.10^{-3} мм. рт. ст. Напряженность электрического поля менялась от 0,3 до 1,2 в/см.

2. Эксперименты в постоянном продольном магнитном поле

На рис. 2 приведены типичные осциллограммы для режима с постоянным продольным магнитным полем.

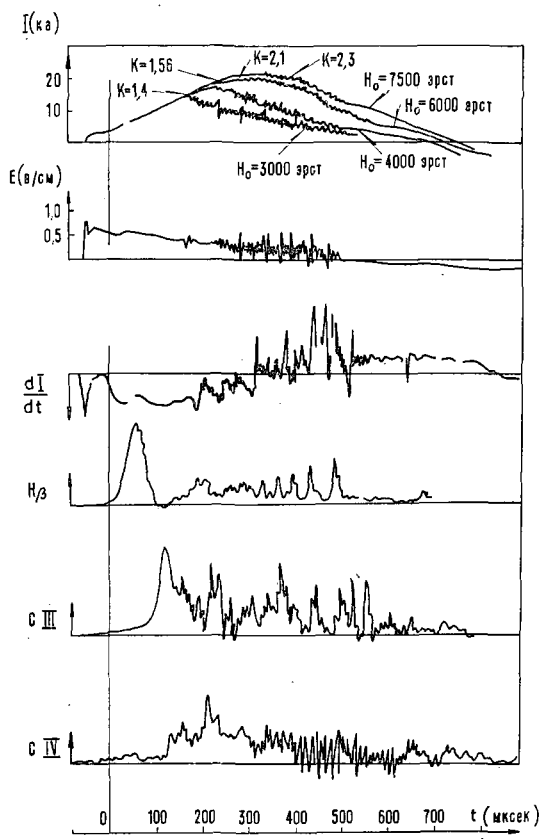

Рис. 2 Типичные осциллограммы тока, напряженности электрического поля, производной тока, интенсивности спектральной линии водорода $H\beta$ (4859 Å) и углерода C III (4650 Å) и C IV (2530 Å).
Для всех осциллограмм напряженность постоянного магнитного поля составляла $H_z = 6$ кэрст.
На верхнем рисунке приведены также осциллограммы тока для полей $H_z = 3$ кэрст, $H_z = 4$ кэрст, $H_z = 7{,}5$ кэрст и отмечены величины $\kappa = cH_z a^2/2IR$ для момента появления неустойчивостей. Здесь a — радиус тока, принятый равным внутреннему радиусу диафрагмы. R — большой радиус тора. Давление водорода $p = 1 \cdot 10^{-3}$ мм рт. ст.

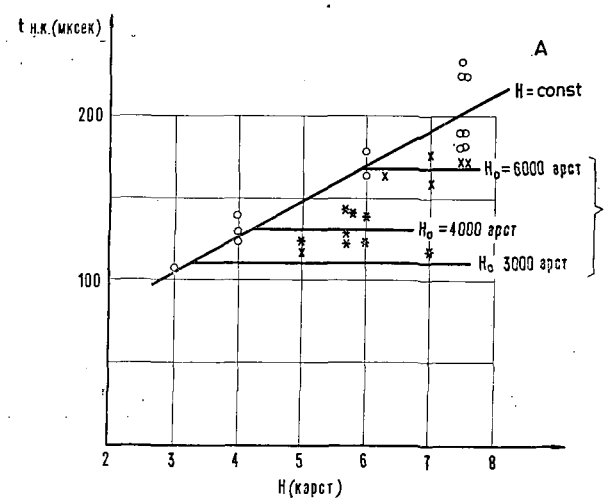

Рис. 3 Зависимость момента появления колебаний от величины продольного магнитного поля: (A) для разряда в постоянном магнитном поле; (B) для разряда в нарастающем продольном магнитном поле, причем нарастающее поле накладывалось на еще устойчивую плазму. По оси абсцисс отложена суммарная величина магнитного поля в момент начала колебаний.
⊙ — только постоянное магнитное поле,
× — начальное постоянное магнитное поле $H_0 = 6$ кэрст,
* — начальное постоянное магнитное поле $H_0 = 4$ кэрст.
Учтите: точка обозначенная звездочкой (*) при $H = 7$ кэрст, 120 мксек — начальное постоянное магнитное поле $H_0 = 3$ кэрст. Точка обозначенная × при $H = 5$ кэрст должна обозначаться *.

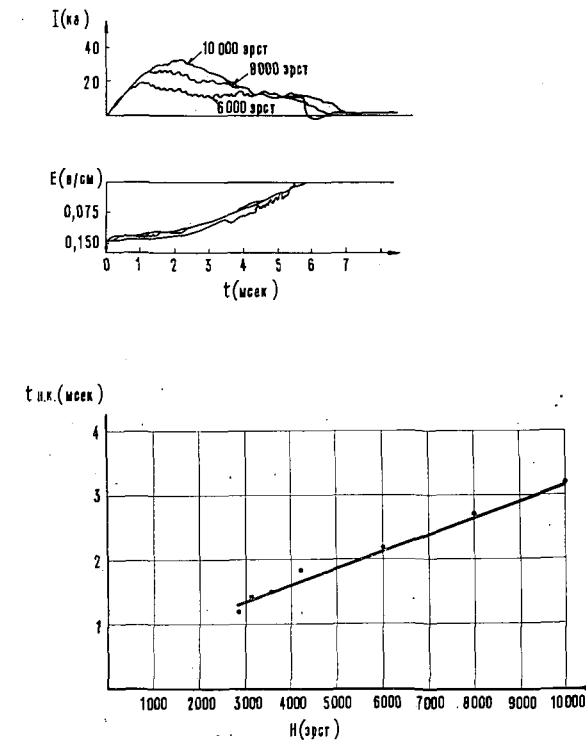

Рис. 4 Осциллограммы тока и напряженности продольного электрического поля для различных постоянных продольных магнитных полей, и зависимость момента появления колебаний от величины продольного магнитного поля, измеренные на установке Токамак-2 [1].
Давление водорода $p = 5 \cdot 10^{-4}$ мм рт. ст.

Затухание линии водорода, а также наблюдаемая последовательность зажигания линий углерода говорят о достижении высокой степени ионизации и росте электронной температуры. На производной тока в некоторый момент времени появляются резкие колебания, характерные для разряда в чистых вакуумных условиях. Они хорошо коррелируют с колебаниями, возникающими приблизительно в то же время на осциллограммах напряжения обхода и интенсивности спектральных линий. Появление колебаний сопровождается замедлением роста тока, а в случае небольших продольных магнитных полей даже спадом тока. На рис. 2 приведены осциллограммы тока разряда при четырех различных магнитных полях. Видно, что до появления колебаний ток разряда развивается одинаково для всех магнитных полей, однако, в меньших магнитных полях колебания развиваются раньше, они больше по амплитуде и приводят к более сильному ограничению величины тока. На рис. 3 приведена зависимость момента появления колебаний от постоянного магнитного поля (кривая А). Кроме того можно отметить, что колебания появляются тем раньше, чем больше начальная напряженность электрического поля и чем меньше давление газа. Зависимости, совершенно аналогичные описанным выше, наблюдались в экспериментах на установке Токамак-2 [1]. На рис. 4 приведены осциллограммы тока для различных магнитных полей и зависимость момента появления колебаний от величины постоянного продольного магнитного поля для этой установки.

3. Эксперименты с переменным продольным магнитным полем

Если кроме постоянного магнитного поля приложить переменное магнитное поле, то поведение разряда существенно изменяется как в том случае, если переменное поле накладывается до момента появления колебаний, так и тогда, когда переменное поле накладывается на уже потерявшую устойчивость плазму. На рис. 5 приведены типичные осциллограммы для режима первого типа. Резкое спадание производной тока при включении нарастающего магнитного поля (момент времени t_1) может быть объяснено сжатием плазменного шнура. Действительно, в тороидальной системе с хорошей связью контуров остается практически постоянной величина напряжения обхода, которая задается внешним контуром:

$$U_{\text{обх}} = U_{\text{ак}} + L\frac{\mathrm{d}I}{\mathrm{d}t} + I\frac{\mathrm{d}L}{\mathrm{d}t}$$

где I — ток, L — индуктивность газового витка, а $U_{\text{ак}}$ — падение напряжения на активном сопротивлении разряда. Трудно предположить, чтобы скачком изменялась $U_{\text{ак}}$, т.е. проводимость плазмы. Тогда должно выполняться равенство

$$L\left[\left(\frac{\mathrm{d}I}{\mathrm{d}t}\right)_1 - \left(\frac{\mathrm{d}I}{\mathrm{d}t}\right)_2\right] = -I\left[\left(\frac{\mathrm{d}L}{\mathrm{d}t}\right)_1 - \left(\frac{\mathrm{d}L}{\mathrm{d}t}\right)_2\right]$$

где индексы 1 и 2 относятся, соответственно, к моментам до и после включения нарастающего поля. Таким образом из уменьшения величины производной тока $\Delta(\mathrm{d}I/\mathrm{d}t)$ можно оценить $\mathrm{d}L/\mathrm{d}t$, т.е. скорость сжатия плазмы. На рис. 6 приведена зависимость величины скачка производной тока

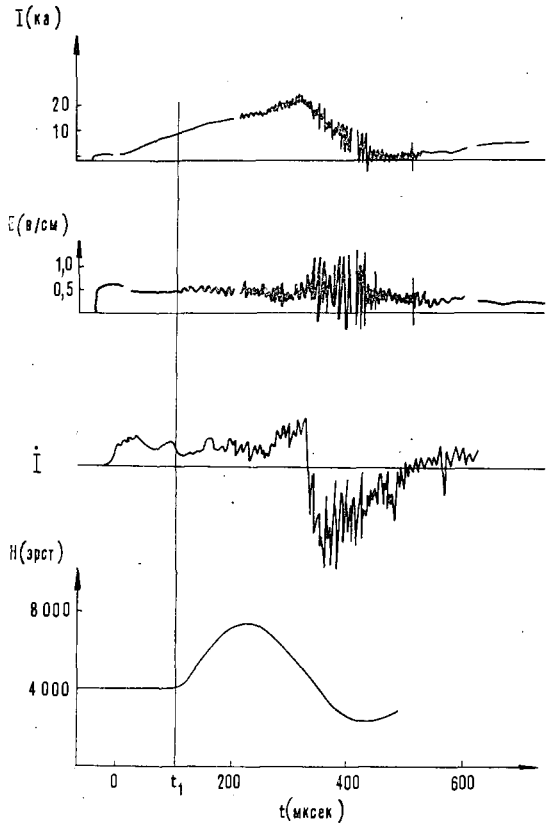

Рис. 5 Типичные осциллограммы тока, напряженности электрического поля, производной тока и магнитного поля для режима с нарастающим продольным магнитным полем. Давление водорода $p = 1\ 10^{-3}$ мм рт. ст.

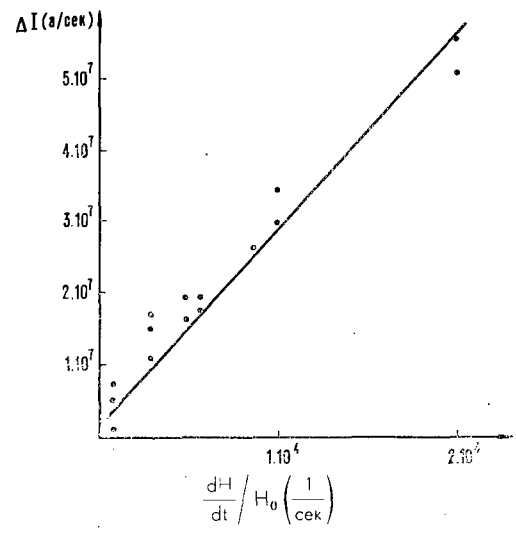

Рис. 6 Зависимость величины скачка производной тока от отношения производной нарастающего магнитного поля $\mathrm{d}H/\mathrm{d}t$ к постоянному магнитному полю H_0. Ток разряда составлял 8 ка, давление водорода $1{,}5 \cdot 10^{-3}$ мм рт. ст.

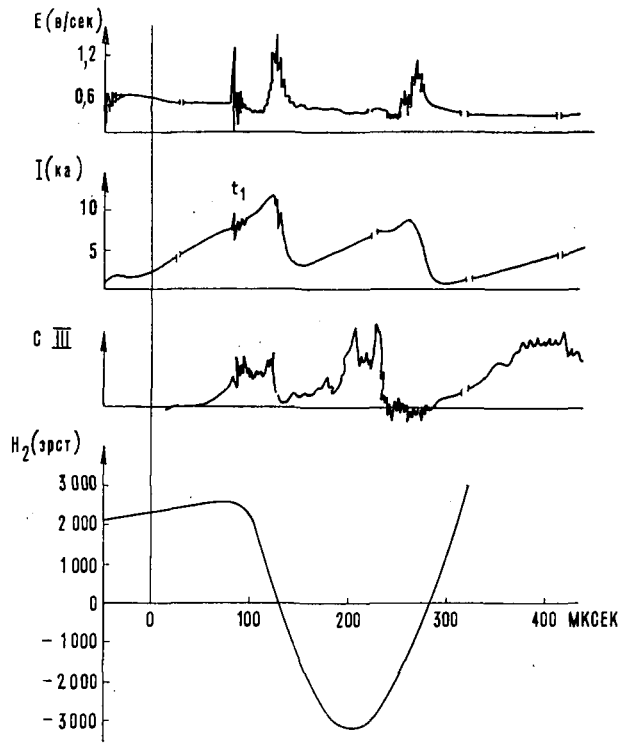

Рис. 7 Осциллограммы напряженности электрического поля, тока, интенсивности линии C III (4650 Å) и магнитного поля для случая убывающего по величине продольного магнитного поля. Давление водорода $p = 1 \cdot 10^{-3}$ мм рт. ст.

от отношения $(dH/dt)/H_0$. Скорость сжатия, подсчитанная таким способом, оказывается очень близкой к той величине, которая должна была бы наблюдаться при полном сохранении потока продольного магнитного поля внутри плазмы. Оценка проводимости, сделанная из соображения, что скорость сжатия должна превышать скорость диффузии плазмы наружу, позволяет сказать, что поперечная проводимость во всяком случае больше, чем $1 \cdot 10^{13}$ CGSE для всех наблюдаемых режимов.

После максимума суммарного продольного магнитного поля наблюдается, наоборот, увеличение производной тока, соответствующее расширению плазмы в спадающем продольном магнитном поле. В некоторый момент времени, когда магнитное поле становится приблизительно равным по величине начальному постоянному магнитному полю, ток начивает резко падать и на всех осциллограммах появляются колебания большой амплитуды, свидетельствующие о сильном взаимодействии плазмы со стенкой. Скорость затухания тока в широком диапазоне пропорциональна скорости уменьшения поля и может трактоваться как уход плазмы на стенку вместе с магнитными силовыми линиями. Если переменное магнитное поле с самого начала имеет знак, обратный постоянному, сразу после его включения наблюдается возрастание производной тока, т.е. расширение плазмы (момент времени t, рис. 7).

Если нарастающее поле включается после начала колебаний плазмы, трудно дать количественную оценку скачка производной тока, т.к. в это время dI/dt определяется не только индуктивностью шнура, но и другими более сложными процессами взаимодействия плазмы со стенкой. Можно только сказать, что в этом случае также происходят некоторые сжатия и расширения в нарастающем и спадающем поле соответственно, кроме того колебания производной тока в нарастающем поле

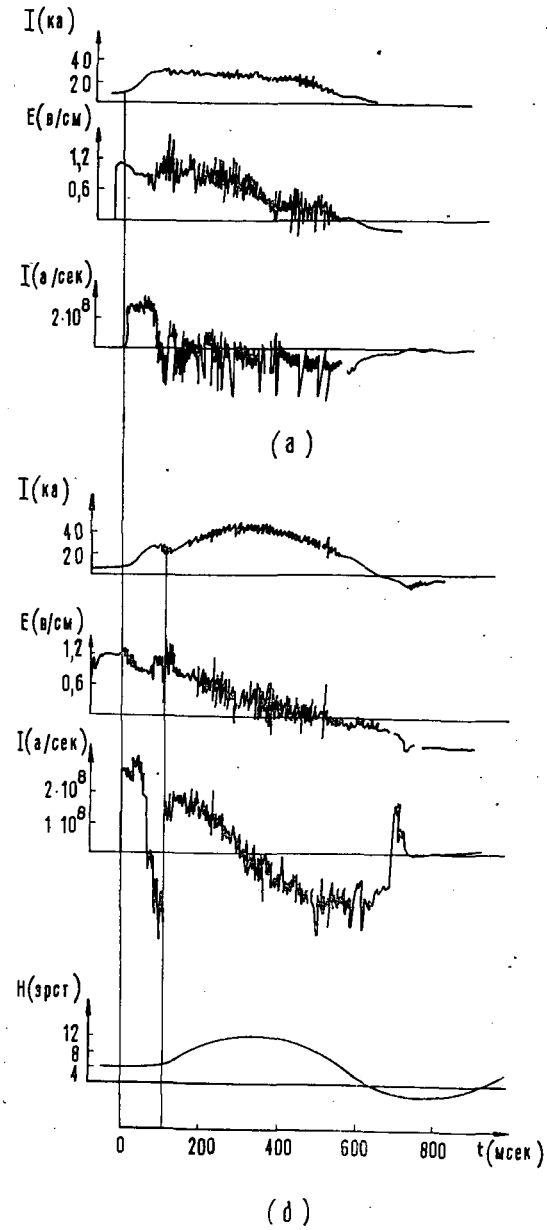

Рис. 8 Осциллограммы тока, напряженности электрического поля и производной тока: а) для режима с постоянным магнитным полем $H_0 = 4$ кэрст. На осциллограмме тока величина $K = 1{,}1$ для момента появления колебаний; б) для режима с начальным постоянным полем $H_0 = 4$ кэрст и нарастающим магнитным полем, включенным после начала неустойчивости. Внизу — осциллограмма магнитного поля. Усиление на верхней и нижней осциллограммах производной тока отличается в 2 раза. t — время в мксек.

меньше по амплитуде, чем в постоянном магнитном поле. Причем амплитуда колебаний тем меньше, чем больше отношение амплитуды нарастающего поля к величине постоянного магнитного поля. Как видно из рисунка 8, ток после включения нарастающего поля растет и максимальная проводимость оказывается гораздо больше, чем была бы в режиме с постоянным магнитным полем.

4. Обсуждение результатов

Из описанных выше экспериментов и из экспериментов, проведенных на установке Токамак-2 [1], мы знаем, что ток разряда практически не может превосходить предельного тока Шафранова-Крускала, или, другими словами, величина K должна быть меньше единицы, где $K=c\,H_z a^2/2IR$, H_z — продольное магнитное поле, I — ток разряда, R — большой радиус тора и a — радиус тока, принимаемый, в данном случае, равным внутреннему радиусу диафрагмы, (рис. 8а). Поэтому был сделан вывод, что при $K=1$ развивается неустойчивость первой моды [2], [3], ограничивающая дальнейшее возрастание тока. Однако, при меньших напряженностях электрического поля, а также при больших магнитных полях неустойчивость появляется значительно раньше, при $K>1$, причем тем больших, чем больше продольное магнитное поле или чем меньше электрическое (рис. 2, верхняя осциллограмма), но характер ограничения тока и появления колебаний остается тем же. Это, а также явная зависимость момента появления колебаний от магнитного поля, наводит на мысль о том, что и тут мы также имеем дело с магнитогидродинамической неустойчивостью 1-й моды. Действительно, критерий устойчивости для пучковых нестабильностей может зависеть от магнитного поля только косвенно, например, через электронную температуру, коэффициент диффузии и т.п., однако, как мы видели из рис. 2, до начала колебаний при различных магнитных полях и одинаковых прочих параметрах ток развивается одинаково. То же можно сказать об интенсивности спектральных линий. Мало вероятно, что физические процессы, происходящие в плазме в этом отрезке времени, заметно различаются. А тогда, в момент появления неустойчивости для разряда в слабом магнитном поле должны быть те же электронная температура и плотность заряженных частиц, что и для разряда в сильном магнитном поле в тот же момент времени, хотя последний остается устойчивым еще по крайней мере 100 мксек.

Если принять, что во всех режимах мы имеем дело с нарушением условия устойчивости Шафранова-Крускала, то необходимо отказаться от предположения о том, что разряд занимает всю площадь отверстия диафрагмы или какую-то неизменную часть ее, как это делалось в предыдущих работах. Можно оценить эффективный токовый радиус разряда, который для большинства режимов оказывается меньше внутреннего радиуса

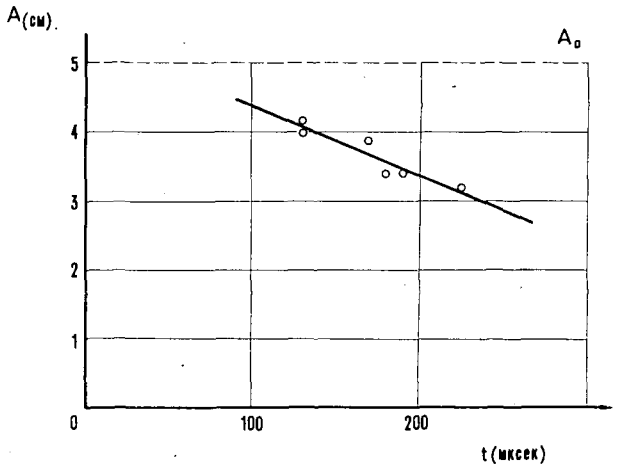

Рис. 9 Изменение во времени эффективного токового радиуса, подсчитанное из осциллограмм тока для различных продольных магнитных полей по формуле $a^2=2IR/cH_z$, где I — величина продольного тока в момент появления колебаний. a_0 — внутренний радиус диафрагмы. Начальное электрическое поле 0,4 в/см. Давление водорода $p=1\cdot10^{-3}$ мм рт. ст. (Учтите: A и A_0 на рисунке должно быть a, a_0.)

диафрагмы (рис. 9) и убывает со временем со скоростью порядка 10^4 см/сек. Чем можно объяснить такое уменьшение радиуса? В разряде в сильном продольном магнитном поле при малом отношении $8\pi p/H^2$ радиус плазмы за рассматриваемые времена практически изменяться не может. Поэтому можно говорить только о перераспределении тока по сечению. Если в плазме с самого начала имеются неустойчивости, скажем типа описанных в работе Кадомцева [4], то, в результате больших потоков энергии на стенку, может, вообще говоря, получиться некоторое концентрирование тока. Однако, при отмеченной выше значительной проводимости поперек магнитного поля трудно ожидать больших энергетических потерь такого типа. Другой причиной перераспределения тока может быть, так называемая, «тепловая концентрация», заключающаяся в том, что в плазме с малой теплопроводностью поперек магнитного поля сильнее греются участки с большей проводимостью. Кроме того, потери энергии на излучение атомов углерода в рассматриваемой области температур падают с ростом температуры электронов [5]. Все это при начальном неоднородном распределении температур может привести к концентрированию тока со временами порядка наблюдаемых (скиновые времена).

Итак, мы приходим к следующей картине: ток разряда концентрируется со скоростью $\sim10^4$ см/сек до тех пор, пока не нарушается условие Шафранова-Крускала за счет уменьшения радиуса, причем момент этот наступает в больших полях позднее, а следовательно при меньших радиусах.

Что должно в свете такой картины наблюдаться в нарастающем поле? Так как нарастающее поле сжимает плазму, следует ожидать, что неустойчивости в этом случае появятся раньше, чем в ре-

жиме с таким же по величине постоянным полем H_0, т.е. колебания должны появляться в тот же момент, что и при одном постоянном начальном магнитном поле, ибо нарастающее поле во столько же раз ухудшает условие устойчивости из-за уменьшения радиуса, во сколько улучшает его из-за увеличения абсолютной величины продольного магнитного поля (если считать, что при сжатии продольный магнитный поток внутри шнура остается приблизительно постоянным). Из рис. 3 (прямые В) следует, что это действительно так. Таким образом, опыты с нарастающим магнитным полем подтверждают решающую роль уменьшения эффективного токового радиуса в механизме потери устойчивости, хотя, конечно, оба приведенных заключения, как замагниченность плазмы, так и уменьшение эффективного радиуса, приводящее к неустойчивости первой моды, нуждаются в дальнейшей тщательной экспериментальной проверке.

Как показал Б. Б. Кадомцев, после нарушения условий устойчивости шнур должен закручиваться в спираль, радиус которой порядка ее токового радиуса. Если при этом шнур начнет задевать края диафрагмы и терять энергию и частицы, на осциллограммах появятся колебания, причем регулярный характер наблюдаемых в эксперименте колебаний хорошо согласуется с этой картиной.

Ясно, что чем меньше радиус тока, а это должно иметь место в сильных магнитных полях, тем меньше будет радиус спирали после нарушения устойчивости и тем меньше будет потеря энергии, а, следовательно, и амплитуда колебаний.

Нарастающее продольное магнитное поле сжимает как плазменный шнур, так и спираль, в которую он искривлен, поэтому при достаточной амплитуде нарастающего магнитного поля амплитуда колебаний становится очень маленькой, что способствует росту проводимости плазмы.

Спадающее магнитное поле заставляет спираль раскручиваться и выбрасывает плазму на диафрагму и стенки камеры. Это сопровождается резкими колебаниями и загасанием тока (рис. 5).

Итак, подводя итог сказанному выше, делаем вывод, что плазму в описанных условиях можно считать замагниченной, а наблюдаемые неустойчивости трактовать, как результат нарушения критерия Шафранова-Крускала.

В заключение авторы приносят благодарность Л. А. Арцимовичу, В. Д. Шафранову и Н. А. Явлинскому за ценные дискуссии, своим товарищам по работе — Б. А. Гальперину и А. А. Кондратьеву, а также коллективу физиков, работающих на установке Т-2, за материалы, представленные для сравнения.

Литература

[1] Горбунов, Е. П. и др. *ЖТФ* **30** (1960) 1152.
[2] Coor, T., Cunningham, S. P., Ellis, R. A., *et al.*, *Phys. Fluids* **1** (1958) 411.
[3] Долгов-Савельев, Г. Г. и др. *ЖЭТФ* **38** (1960) 394.
[4] Кадомцев, Б. Б., Турбулентные утечки частиц из разряда в сильном продольном магнитном поле. *ЖТФ* — в печати.
[5] Васильев, А., Долгов-Савельев, Г. Г., Коган, В. И. См. стр. 655 этого тома Трудов Конференции.

DISCUSSIONS (SESSION VI) — DISCUSSIONS (SÉANCE VI) — ДИСКУССИИ (ЗАСЕДАНИЕ VI) — DEBATES (SESIÓN VI)

Paper CN-10/156 *was presented by J. Marshall* (United States of America). *The text of the paper is on pages 663 to 674 inclusive. The following discussion took place:*

N. J. Phillips *(United Kingdom):* I think one of the most interesting possibilities with this experiment is that the two plasmas may in fact collide by means of waves which arise from an instability of the two streams. Have you any information on the relative velocity of your two plasmas in relation to the Alfvén velocity? This question is of importance in determining whether the streams may interact by instability waves. This instability does not have to be microscopic in origin, but may be a hydromagnetic instability.

J. Marshall: We were hoping that we would observe such a thing but we were not able to observe any interaction that appeared to come from this.

N. J. Phillips: At high β, unstable hydromagnetic surface waves will scatter the streams. Are your β values close to unity or are they always low? The fact that you do not seem to have seen such an instability may be due to the rather low β obtained?

J. Marshall: We can get a high β with the fast plasma only when we have low field. When we have a high field, the β is quite low. The slow plasma —(10^7 cm/s)—has an exceedingly low β, but in all cases I think that the electron velocities are considerably larger than the relative ion velocities and this may explain why there is no interaction between the two streams.

J. L. Tuck *(United States of America):* In view of the fact that the number of neutrons and their time dependence resemble those of the original Scylla experiment, but the density is an order of magnitude lower, could you give a rough indication of what the approximate temperature would be?

J. Marshall: I can just say what I think. In the high-energy plasma case the initial transverse energy of the particles as they enter the compression field is about 3 keV. It is very hard to imagine that they can be trapped unless they have their transverse energy raised to a large value as they go through the coil. Probably in the first pass they must get up to something like 20 keV and probably go even higher afterwards, but no measurement has been made of this.

A. Dattner *(Sweden):* What is the B_θ field in the "diamagnetic" region?

One could think of two explanations of the "diamagnetic effect" other than diamagnetism of plasma:

(1) a cork-screw instability in the current path connecting the inner conductor of the gun with the plasma; and

(2) the radial electric field due to diffusion together with the longitudinal magnetic field.

J. Marshall: In the case of the collision of two plasmas we have looked for this field in the middle of the machine and have seen very little. I think that mostly it has decayed by the time it reaches the collision region (about one meter from the end of the gun).

A. A. Rukhadze *(Union of Soviet Socialist Republics):* Prof. Marshall, please repeat what were the temperatures of electrons and ions in the plasma bunch shot by the gun?

J. Marshall: The electron temperature we do not know, but we assume that it is quite low. We have made some spectroscopic observations to see if we could tell something about the electron temperature. The plasma is too hot to give the Balmer series of hydrogen during the collision, but very shortly after, the Balmer series appear. We believe that the electron temperature is not very large. The ion temperature is hard to evaluate. Probably it is not exactly a temperature. In the case of the fast plasma, the transverse energy per particle appears to be about 3 keV and for the slow plasma something of the order of 100 eV.

A. A. Rukhadze: Was the electron temperature greater than the ion temperature?

J. Marshall: No, the electron temperature is certainly much lower than that of the ions.

O. Buneman *(United States of America):* The two-stream instability would require the mutual velocity of the plasmas to exceed the random electron velocity. Was this the case?

J. Marshall: The electron random velocity probably exceeded the mutual plasma velocity.

O. Buneman: Moreover, the plasmas would have to interpenetrate for a long enough interval so that the instability could build up and take effect. Was the interpenetration long enough?

J. Marshall: Interpenetration occurred over approximately 1 meter.

A. C. Kolb *(United States of America):* You remarked at one point that there was a 3 keV transverse energy. Was this the transverse energy from the gun or was this the transverse energy as a result of the plasma penetrating the magnetic field of the Scylla coil? If the latter was the case, what was the mechanism of the transfer of energy from axial to transverse components?

J. Marshall: There are two cases—one is the slow plasma and the other one is the fast plasma. The fast plasma gets a 3 keV transverse energy approximately when it penetrates into the end of the guide field, not into the compression coil. There is a guide field that runs through the whole system first. The randomiza-

tion occurs only in the case of the slow plasma—in this case the transverse energy is very low as it leaves the gun.

Paper CN-10/103 *was presented by F. Waelbroeck* (France). *The text of the paper is on pages 675 to 685 inclusive. The following discussion took place:*

A. Dattner *(Sweden):* Did you make any attempts to obtain a gross analysis of the dynamics of the plasma puff and energy exchange between the condenser bank and the plasma?

F. Waelbroeck: The model discussed deals exclusively with the plasma puff behavior after it has entered the guide field. It is assumed that at the bunching time t_0 the puff is already in the constant homogeneous field. This is consistent with the analysis of the magnetic loop signals. We have not yet tried to analyse the dynamics of the energy exchange and momentum variation during the acceleration phase and we believe that a detailed analysis would be premature until the effect of the reversed trapped magnetic field, which appears during the acceleration, is better understood and until, in particular, the time at which it disappears has been measured.

A. Dattner: Does the circulating, driving current become affected by the collision of the plasma with the pendulum?

F. Waelbroeck: The answer to your second question is as follows. The ballistic pendulum is at a distance of 41 cm from the accelerating coil. When the plasma collides with it, the discharge current is usually crowbarred. No effect was observed on its wave-form due to the presence of the pendulum. Nor can one expect a noticeable effect, caused by the currents circulating in the acceleration coil, on the plasma puff which is reflected from the pendulum.

A. Dattner: Do you see any difference between the primary current curve when you have vacuum in the system compared with the case when the tube is full of plasma, i.e. what is the efficiency of the gun?

F. Waelbroeck: Experimentally, the analysis of our data shows that, although the number of particles in the plasma puff, their average directed velocity and their random thermal energy vary by factors of 2 to 3 depending upon experimental conditions, the total energy of the beam (concentrated on a 3—12 cm^2 cross-section, 70 cm away from the gun) is nearly the same: 30—40 joules. This is about 5% of the initial energy (720 joules) stored in the capacitor bank. From the current wave-form a value of 10—12% energy transfer to the plasma is deduced, but this is rather inaccurate and, moreover, includes energy transfer to particles situated at the neck or upstream from the coil, which are ejected backwards and not found in the beam.

One could increase the efficiency of such a gun by reducing its parasitic inductance, lengthening the coil and decreasing the taper angle. The efficiency would then about equal that of a fast magnetic compression device. However, our present aim is essentially to accelerate pure plasma, if possible, with emphasis on dense and short puffs. This is a necessary condition for some trapping experiments which we are starting. Energy efficiency has been a secondary preoccupation.

A. Dattner: One would expect the guns of this type to have low efficiency because of the very short time of interaction between the energy source and the plasma.

J. Marshall *(United States of America):* I made some measurements once, which were similar to yours, on the conservation of transverse energy as the puff moves along the field. I found no loss of transverse energy, but this was probably because the plasma was much more extended in space and had higher particle energy and lower density in that part of the plasma which produced a diamagnetic signal.

Paper CN-10/218 *was presented by V. M. Glagolev* (Union of Soviet Socialist Republics). *The text of the paper is on pages 687 to 691 inclusive. The following discussion took place:*

S. C. Brown *(United States of America):* What is the power fed into the electromagnetic plug?

V. M. Glagolev: The power used in our experiments was about 100 kW.

S. C. Brown: What is the Q of the plug cavity?

V. M. Glagolev: The Q value of the circuit was about 30 000.

S. C. Brown: What was the pressure in the plug cavity?

V. M. Glagolev: Gas pressure in those experiments was about 10^{-5} mm Hg, but the electric strength of the cavity was conserved to very high values of pressure. For different gases we obtain different values up to about 10^{-3} mm Hg and for He up to almost 10^{-2} mm Hg. Such a cavity was able to work with up to 100 kV/cm which corresponds to the amplitude of the magnetic field of about 300 Oersteds. The fact that the electrical strength of the cavity was preserved up to such high values could be explained only by assuming that there was a high frequency barrier which instantly pushed electrons to the walls before they could start ionizing the gas. Estimates of that effect are in a good agreement with theory.

H. Motz *(United Kingdom):* Have you carried out experiments on confinement with microwaves in a resonator without magnetic fields?

V. M. Glagolev: We performed experiments on plasma confinement with an axial magnetic field, since from the high frequency plasma source we could obtain a bounded plasma rod only when the axial

magnetic field was on. But if analogous experiments on plasma confinement were to be performed without magnetic field, I would have no doubt that we would obtain the same results.

J. L. Tuck *(United States of America):* In connection with your favorable remark on the use of the delightful new high-current superconductors (Matthias, Kunzler *et al.*) I feel I ought to warn you that their low losses probably only apply for dc. Their properties are explicable in terms of filaments in the superconducting state imbedded in a matrix of ordinary conductor. A changing magnetic field in the latter involves dissipation. Ordinary soft superconductors, Pb for instance, retain their superconductivity at high frequencies but, having much lower critical magnetic field (~1000 gauss), cannot confine much pressure. I am confident that these new high field superconductors are going to be of decisive importance for the production of steady magnetic fields in dc confinement however.

V. M. Glagolev: I do not agree with you. I am not a specialist in superconductivity but I believe that, although the superconductivity for high frequency is different from that for static fields, still it is possible to produce superconductors applicable to high frequency resonators.

T. Consoli *(France):* Do you have an explanation for the resonance (page 690, Fig. 6) which you mention you have observed at one-half the electron cyclotron frequency?

I would add a comment. In our experiments with confinement by a high frequency field, which is described in paper CN-10/108, we have observed at this particular frequency a minimum in the radial leakage flux of ions and a maximum of the ionic temperature in this region of magnetic field.

V. M. Glagolev: We do not have as yet sufficient experimental data to explain this resonance. I can only make some assumptions: 1) The paramagnetic current may be increased due to collisions of electrons with the wall. This effect becomes stronger when the resonance is present because of the higher electron energies. 2) The additional paramagnetic current may exist if the gas pressure outside the plasma is higher than that inside.

N. Christofilos *(United States of America):* Commenting on Dr. Tuck's remarks on superconductors, I would like to say that soft superconductors are suitable for radiofrequency. Experiments in this direction were conducted by Sanford *et al.* at Harwell.

What is the ratio of the electromagnetic field pressure to the plasma pressure?

V. M. Glagolev: In our experiment the pressure exerted by the high frequency field on the walls of the resonator exceeded the pressure of the plasma. The pressure of the high frequency field on the plasma was naturally equal to the pressure of the plasma.

Paper CN-10/18 *was presented by L. H. Th. Rietjens* (Netherlands). *The text of the paper is on pages 693 to 698 inclusive. The following discussion took place:*

H. E. Wilhelm *(Federal Republic of Germany):* Did you take into account the effect of a stabilizing B_z field in your calculations with respect to the produced shear and the stability of the column?

L. H. Th. Rietjens: In our experiment no stabilizing B_z field is present. As has been pointed out, the shear is produced by the real part in wave number of the penetrating rotating magnetic field.

H. E. Wilhelm: What is the effect of applying the Suydam criterion, which is derived for a steady state, to your non-steady-state configuration?

L. H. Th. Rietjens: In case the period of the alternating pinch field is long compared with the time that instabilities may grow, the magnetic field configuration can be considered as quasi-stationary. However, other time-dependent effects have to be considered. There will occur oscillations in the plasma column as the magnetic pressure cannot be made constant at all radii. This results from the difference in penetration of the B_z and B_θ fields in the cylinder.

Moreover, $m=1$ oscillations of the whole column will be present, due to the outward force from the gradient in B_z and the counterforce from the B_θ field which is compressed against the metal wall.

I would like to make a comment regarding the difference between z- and θ-pinch discharges in a torus. Results similar to those described by the authors have been observed for a z-pinch and a θ-pinch by Remy and co-workers in a very similar experimental arrangement. It was found that if the phase angle between the two currents is chosen so as to give a pure θ-pinch, the plasma behaves rather nicely, namely, it contracts and subsequently drifts to the (outer) wall without showing instabilities. Whereas, when the phase angle is chosen so that the discharge is a pure z-pinch one observes strong irregularities.

Paper CN-10/221 *was presented by E. Velikhov* (Union of Soviet Socialist Republics). *The text of the paper is on pages 699 to 704 inclusive. The following discussion took place:*

B. Lehnert *(Sweden):* Does your observed instability have anything to do with the abnormal diffusion observed in the positive column at higher pressures and with relatively large electric fields? Is the electric field along the magnetic field lines negligible?

E. Velikhov: It is still difficult to state the reasons for this instability since the direction of plasma rotation has not been determined, but it is very likely that this instability is connected with plasma rotation.

In response to your second question, Kadomtsev's theory assumes that there is an electric field. There is practically no electric field inside the electron column;

this field is extremely weak. Therefore Kadomtsev's theory is hardly applicable here.

W. I. Linlor *(United States of America):* Did I understand that you have an explanation for the difference in the direction of rotation between a short cylinder and a long cylinder? Because, if you do not, I would like to venture one. I would like to suggest that, for a short cylinder, the electrons diffuse out the ends more rapidly than the ions, giving one sign of charge to the plasma and therefore giving a corresponding electric field. If you have a long cylinder, then the ions diffuse across the lines of force more rapidly than the electrons, giving the opposite sign of charge to your plasma and therefore the reverse direction of rotation. Have you checked whether the plasma takes different potentials depending on whether you have a long or a short plasma?

E. Velikhov: Unfortunately, such experiments were not made. But I do not understand why such a decrease of cylinder dimensions would change the plasma potential. The plasma potential is determined by the fact that electron mobility is greater than that of ions. Therefore, apparently the potential should be positive.

G. von Gierke *(Federal Republic of Germany):* Did a change of the strength of the magnetic field have any influence on the direction of rotation of your spiral? In a radiofrequency discharge experiment carried out at the Max-Planck Institut at Munich a standing spiral could be produced at a certain magnetic field.

E. Velikhov: A change in the magnetic field intensity in the plasmascope experiments did not cause a change in the direction of rotation.

C. Brachet *(France):* The results presented here give direct evidence for a spiral plasma loss mechanism, such as suggested, for PIG discharges, by Backus* and supported by Miyagawa's observations** on cathode marks in this type of discharge in relation with plasma rotation induced by the local radial electric field.

Does Fig. 3 (page 702, plasmagraph 8), which shows a tubular shape, represent a transitory state of instability or a steady state? Does it confirm the existence under certain conditions of a hollow discharge described by many authors?

E. Velikhov: Unfortunately I am not the author. I do not know what the author thinks with regard to Fig. 3. In the paper it is stated that this plasmagraph belongs to a different regime of the discharge in the weaker magnetic field and that it should be considered as an illustration of multiple and complex characteristics of motion across a magnetic field. I don't know any other details.

W. H. Bostick *(United States of America):* I don't know whether this effect is applicable to the experiment which the speaker has reported, but the spiralling of jets of plasma as they proceed across a magnetic field has, of course, been observed before. If the plasma goes across a cold background plasma there are retarding effects due to induced currents; retarding effects produce Hall effects and so the jets will not only be retarded but they will be deflected into spiral trajectories. I think this method of producing the deflection of a jet of plasma should at least be considered in the interpretation of the present experiment.

E. Velikhov: These experiments were performed under different pressure conditions, in particular when the mean free path was much greater than the dimensions of the machine.

Paper CN-10/4 *was presented by B. Lehnert* (Sweden). *The text of the paper is on pages 705 to 716 inclusive. The following discussion took place:*

S. Colgate *(United States of America):* The implication of centrifugal containment for as long as milliseconds requires that the centrifugal stress be balanced by a magnetic stress. Have you any diamagnetic signals corresponding to this containment?

B. Lehnert: We have not as yet any final results for publication. However, there are indications that the centrifugal pressure expands the magnetic field and that part of the flux leaks out of the wall which is made of stainless steel.

F. G. Insinger *(Netherlands):* Could you indicate whether the presence of the plate which you could lower has an effect upon the rotating plasma? Are there viscous effects by which the plasma is stopped from rotating or are the impurities which it produces responsible for braking the rotating action?

B. Lehnert: I think that there is a direct contact between the plasma and the plate. There are, of course, also viscous effects in both the transverse and longitudinal directions which tend to stop the rotation. In any case I think that the most important loss of momentum comes from the escape of charged particles along the magnetic field as long as the flux of such particles is not reduced considerably. In fact, this is what the experiments with the movable plate show.

F. G. Insinger: You mean that if you were not to use plexiglass plates, then you would have a different action?

B. Lehnert: No. We have made experiments with glass insulators and the electric properties of the discharge are quite the same. The particles are lost to the surface of the plate when it is in the lower position and this puts a brake on the rotation.

F. G. Insinger: It is not the impurities which enter?

B. Lehnert: There will be impurities generated from the contact between the plasma and the plate, espe-

* Backus, J. in "The Characteristics of Electrical Discharges in Magnetic Fields" (McGraw-Hill, New York, 1949) 345—369.

** N. Miyagawa: "On the Mechanism of the Philips Ionization Gauge" *Sci. Papers IPCR* **54** (1960) 6—15.

cially when it is in the lower position; the measurements of gas production show this very clearly. However, when the plate is in the upper position there is hardly any gas production and this shows that the amount of impurities then becomes strongly reduced. Just in order to get a sensitive indicator of the plasma-wall interaction we have used plexiglass insulators in some of our experiments.

E. Velikhov *(Union of Soviet Socialist Republics):* I should like to observe that, apparently, the process in Dr. Lehnert's system constitutes a stationary process of current flow, in which the average lifetime of the particle is a few tens of microseconds, as is evident from the decay characteristics. For this reason, all that the author can assert is that no instability developed during periods of the order of microseconds.

W. B. Kunkel *(United States of America):* The comment made by Mr. Velikhov that you are dealing essentially with a steady-state discharge is certainly correct. The duration of rotation is simply given by an RC time constant where R is the effective resistance of the discharge and C is the total capacity in the circuit. This is not to be confused with the containment time. Actually, what you have shown is that your rotating plasma discharge represents a remarkably large impedance, i.e. is characterized by relatively low losses when compared with many other power discharges.

B. Lehnert: The power input into the plasma is about 5×10^5 watts and the energy content of the mass motion is about 100 joules. Thus, particles have to stay at least for 200 μs within the confinement region. This is a long time, at least compared to that for flutes to develop (about 1 μs for a particle velocity of 10^5 m/s at distances of about 10 cm), as predicted by the earlier theory of Rosenbluth and Longmire. What I mean by a stable confined plasma which is kept in rotation for more than 7 ms is simply that during this interval of time no such flutes could develop which would drain off the rotational energy for a time of the order of microseconds. Measurements of the equivalent capacity show that the particle density is nearly constant but not necessarily that the same particles are present; this has not been claimed in our report.

There might also exist instabilities with slow growth rates, of the order of 100 μs and more. This is just what I have discussed in Paper CN-10/3 of this Conference (see page 135 of these Proceedings).

Paper CN-10/222 *was presented by K. Razumova* (Union of Soviet Socialist Republics). *The text of the paper is on pages 741 to 746 inclusive. The following discussion took place:*

S. Colgate *(United States of America):* Have you made any magnetic probe measurements that might demonstrate turbulent magnetic fields?

K. Razumova: In the present set-up we did not make probe measurements since we did not want to introduce impurities into the plasma. In another case where the chamber was not clean we performed probe measurements.

M. B. Gottlieb *(United States of America):* Was the confinement time of your particles comparable in this experiment to that in the other experiment?

K. Razumova: In this experiment the electron density was not measured, but it should be mentioned that all oscillograms obtained with this small machine are similar—at any rate in the initial stages of the process—to the oscillograms obtained with the big machine except for the second current maximum which can be seen with the big machine when the process is long. I did not mention that in our case the duration of the process was only 500 to 600 μs. Confinement time was not measured, but since all results are similar, it can be inferred from the data obtained with "Tokamak".

SESSION VIII — SÉANCE VIII

ЗАСЕДАНИЕ VIII — SESIÓN VIII

8 SEPTEMBER 1961 — 8 SEPTEMBRE 1961

8 СЕНТЯБРЯ 1961 Г. — 8 DE SEPTIEMBRE DE 1961

Chairman — Le président — Председатель — El Presidente

L. Spitzer, Jr. *(United States of America)*

Scientific Secretary — Secrétaire scientifique — Ученый секретарь — Secretario Científico

C. Etievant *(France)*

[Papers presented: CN-10/35, 89, 95, 162, 166, 243, 245]

О ЦИКЛОТРОННОМ ПОГЛОЩЕНИИ ЭЛЕКТРОМАГНИТНЫХ ВОЛН В ПЛАЗМЕ*

Л. С. Богданкевич, А. А. Рухадзе, В. П. Силин

Академия наук СССР,

Москва, Союз Советских Социалистических Республик

Магнитотормозное излучение и поглощение плазмы существенно как для энергетического баланса плазмы, так и для распределения частиц по скоростям. На сегодняшний день вопрос о форме линий магнитотормозного поглощения все еще недостаточно изучен. В настоящей работе исследуется форма линий поглощения в нерелятивистской электронно-ионной плазме при весьма общих предположениях о виде функций распределения частиц по скоростям. Показано, что учет релятивистских эффектов теплового движения частиц может привести к значительному поглощению волн, распространяющихся поперек магнитного поля, даже в случае нерелятивистских температур плазмы. Так как коэффициенты поглощения $\varkappa$ и показатели преломления электромагнитных волн выражаются через функцию распределения частиц, эксперименты по измерению n и $\varkappa$ могут быть использованы для определения функции распределения.

Обсуждается вопрос об использовании ионного циклотронного резонанса для нагрева ионов в плазме. Показано, что электромагнитные волны с частотой, равной удвоенной резонансной частоте ионов, могут быть эффективно использованы для нагрева ионов плазмы.

1. Введение

Вопросу о магнитотормозном излучении и поглощении плазмы посвящен целый ряд работ (см. [1], где приведена подробная библиография). Чрезвычайно интересными являются работы Кудрявцева и Трубникова [2—4], показавшие, что магнитотормозное поглощение существенно как для энергетического баланса горячей плазмы, так и для распределения частиц по скоростям. На сегодняшний день нам представляется все еще недостаточно изученным вопрос о форме линий магнитотормозного поглощения плазмы и связи формы линий поглощения с функцией распределения частиц. В настоящей работе исследуется форма линий поглощения в нерелятивистской электронно-ионной плазме при весьма общих предположениях о виде функций распределения частиц по скоростям. Показано, что для правильного описания формы линий, антиэрмитовскую часть тензора диэлектрической проницаемости, ответственную за поглощение электромагнитных волн в плазме, следует вычислять с учетом релятивистских эффектов теплового движения частиц. Коэффициенты поглощения $\varkappa$ и показатели преломления n электромагнитных волн в плазме выражены через функции распределения; это позволяет из экспериментов по измерению n и $\varkappa$ восстановить функции распределения частиц в плазме.

В работе также кратко обсуждается вопрос о нагреве плазмы с помощью ионных циклотронных волн.

2. Форма линий магнитотормозного поглощения в электронной плазме

Для построения теории формы линий магнитотормозного поглощения в плазме будем исходить из дисперсионного уравнения электромагнитных волн:

$$\left| k^2 \delta_{ij} - k_i k_j - \frac{\omega^2}{c^2} \varepsilon_{ij}(\omega, \mathbf{k}) \right| = 0 \qquad (1)$$

где $\mathbf{k}$ — волновой вектор, а $\varepsilon_{ij}(\omega, \mathbf{k})$ — тензор диэлектрической проницаемости с учетом пространственной дисперсии. Ниже мы в основном будем интересоваться нерелятивистской плазмой, в которой $k\langle v_{e,i}\rangle/\omega = n\langle v_{e,i}\rangle/c \ll 1$, где $\langle v_{e,i}\rangle$ — тепловая скорость электронов и ионов, а n — показатель преломления. При этом ограничении, однако, исследование формы линий поглощения все еще остается сложным, т.к. в дисперсионном уравнении (1) существенными оказываются как диагональные, так и все недиагональные члены тензора диэлектрической проницаемости плазмы. В связи с тем, что форма линий магнитотормозного поглощения определяется тепловым движением частиц, можно надеяться на упрощение в условиях, когда тепловое движение дает либо малый эффект, либо напротив, оно является основным. Действительно, в двух предельных случаях, когда

$$\frac{k_z\langle v_{e,i}\rangle}{\omega - m\Omega_{e,i}} = \frac{\omega}{\omega - m\Omega_{e,i}} \frac{n\langle v_{e,i}\rangle}{c} \cos\vartheta \ll 1, \qquad (а)$$

или когда

$$\frac{k_z\langle v_{e,i}\rangle}{\omega - m\Omega_{e,i}} = \frac{\omega}{\omega - m\Omega_{e,i}} \frac{n\langle v_{e,i}\rangle}{c} \cos\vartheta \gg 1 \qquad (б)$$

положение существенно упрощается ($\Omega_{e,i}$ — гирочастота электронов и ионов). В этих случаях при исследовании дисперсионного уравнения (1) можно пользоваться следующим выражением для тензора диэлектрической проницаемости:

$$\varepsilon_{ij}(\omega, \mathbf{k}) = \varepsilon_{ij}^{s} + \varepsilon_{ij}^{a} = \begin{pmatrix} \varepsilon_1 & -ig & 0 \\ ig & \varepsilon_1 & 0 \\ 0 & 0 & \varepsilon_2 \end{pmatrix} \qquad (2)$$

* Доклад CN-10/243, представленный на Конференцию. Докладчик: А. А. Рухадзе. Дискуссия (на английском языке) по этому докладу дана на стр. 815. Переводы аннотаций находятся в конце этого тома Трудов Конференции.

где $\varepsilon_{ji}^{э}$ и $\varepsilon_{ij}^{а}$ — соответственно эрмитовская и антиэрмитовская часть тензора $\varepsilon_{ij}(\omega, \mathbf{k})$. Общее выражение для диэлектрической проницаемости плазмы приведено в [1]. Заметим, что компоненты $\varepsilon_{13}=\varepsilon_{31}$ и $\varepsilon_{23}=-\varepsilon_{32}$, строго говоря, отличны от нуля, однако в рассматриваемой области частот, когда выполняется условие (а) или (б), их вклад в дисперсионном уравнении (1) оказывается пренебрежимо малым. Подставляя выражение (2) в уравнении (1) получим следующее уравнение для обыкновенной и необыкновенной волны:

$$n^2 = \frac{(\varepsilon_1^2-g^2-\varepsilon_1\varepsilon_2)\sin^2\vartheta+2\varepsilon_1\varepsilon_2 \mp \sqrt{(\varepsilon_1^2-g^2-\varepsilon_1\varepsilon_2)^2\sin^4\vartheta+4g^2\varepsilon_2^2\cos^2\vartheta}}{2(\varepsilon_1\sin^2\vartheta+\varepsilon_2\cos^2\vartheta)} \tag{3}$$

Переходя к исследованию электромагнитных волн вблизи резонансных частот $\omega\sim m\Omega_{e,i}$ заметим, что при условии (а) антиэрмитовская часть тензора диэлектрической проницаемости экспоненциально мала по сравнению с эрмитовской, причем $\varepsilon_1^{а}\approx g^{а}$, а $\varepsilon_2^{а}\ll\varepsilon_1^{а}$. В области же частот, определяемой условием (б), антиэрмитовская часть тензора диэлектрической проницаемости по порядку величины отличается от эрмитовской на величину $(n\sim\langle v_{e,i}\rangle/c)^{2m-1}$. Отсюда следует, что вблизи первой резонансной частоты, $m=1$, антиэрмитовская часть тензора $\varepsilon_{ij}(\omega, \mathbf{k})$ больше эрмитовской; вблизи же резонансных частот с $m>1$, $\varepsilon_{ij}^{а}\ll\varepsilon_{ij}^{э}$. Поглощение электромагнитных волн вблизи первой резонансной частоты при условии (б) так велико, что при рассмотрении распространения волн в этой области частот, строго говоря, следует решать граничную задачу [5, 6]. Поэтому этой областью частот мы не будем заниматься.

В тех областях частот, в которых антиэрмитовская часть тензора диэлектрической проницаемости мала по сравнению с эрмитовской (при условии (а) это имеет место для всех: m, а при условии (б) — лишь для $m>1$) в уравнении (3) для определения показателей преломления волн в первом приближении антиэрмитовской частью тензора диэлектрической проницаемости можно пренебречь. Учет малой антиэрмитовской части $\varepsilon_{ij}(\omega, \mathbf{k})$ в уравнении (3) позволяет определить коэффициент поглощения волн в виде линейной функции $\varepsilon_{ij}^{а}(\omega, \mathbf{k})$. В свою очередь тензор $\varepsilon_{ij}^{а}(\omega, \mathbf{k})$ выражается через функции распределения частиц по скоростям. Это позволяет определить функции распределения частиц в плазме из экспериментов по измерению показателей преломления и коэффициентов поглощения электромагнитных волн.

В случае электронной плазмы формулы для n и $\varkappa$ для волн, распространяющихся под произвольным углом ϑ к постоянному магнитному полю, весьма громоздки. Здесь рассмотрим лишь наиболее простые случаи. Так в области частот, определяемой условием (а), вблизи первой резонансной частоты и при $\vartheta\approx 0$ для обыкновенной и необыкновенной волн получаем:

$$n_{1,2} = 1 - \frac{\omega_{0e}^2}{\omega(\omega\pm\Omega_e)}, \quad \varkappa_{1,2} = -i\frac{\varepsilon_1^{а}\mp g^{а}}{2n_{1,2}}, \tag{4}$$

где

$$\begin{pmatrix}\varepsilon_1^{а}\\ g^{а}\end{pmatrix} = -i\frac{4\pi^3 e^2 m_e c}{\omega^2 n}\left[F_{1e}\left(\frac{m_e c^2(\omega-\Omega_e)^2}{2\omega^2 n^2}\right) \pm F_{1e}\left(\frac{m_e c^2(\omega+\Omega_e)^2}{2\omega^2 n^2}\right)\right]$$

$$\omega_{0e} = -\frac{4\pi e^2}{3}\int \mathbf{dp}\, v^2 \frac{\partial f_{0e}(E)}{\partial E}$$

$$\frac{\partial F_{1e}(E)}{\partial E} = f_{0e}(E) \tag{5}$$

Для определения функции распределения электронов этими формулами можно пользоваться лишь в той области частот, где $n^2>0$ (т.е. когда волна может распространяться в плазме). Из выражений (4) следует, что для обыкновенной волны $n^2>0$ при $\omega_{0e}^2<2\Omega_e^2$, т.е. в случае достаточно разреженной плазмы, а для необыкновенной волны $n^2>0$ при $\omega<\Omega_e$. Заметим, что формулы (5) для $\varepsilon_1^{а}$ и $g^{а}$ являются нерелятивистскими, т.е. не учитывают релятивистских эффектов теплового движения электронов. Учет последних в рассматриваемом случае при $\vartheta=0$ приводит к несущественным поправкам. Напротив, для волн, распространяющихся под углом $\vartheta=\pi/2$ к магнитному полю, поглощение целиком обусловлено релятивистскими эффектами теплового движения электронов. При нерелятивистском рассмотрении поглощение волн в плазме при $\vartheta=\pi/2$ полностью отсутствует. Вблизи первой линии поглощения для обыкновенной и необыкновенной волн, распространяющихся под углом $\vartheta\approx\pi/2$ к магнитному полю, получаем

$$n_1^2 = \frac{1-(\omega_{0e}/\omega)^2}{1+(\langle v_e^2\rangle/c_2^2)[\omega_{1e}\omega/\Omega_e^2(\omega-\Omega_e)]}$$

$$\varkappa_1 = \frac{-in\varepsilon_2^{а}}{2[1-(\omega_{0e}/\omega)^2]}$$

$$n_2^2 = \frac{1-[\omega_{0e}^2/(\omega^2-\Omega_e^2)][2-(\omega_{0e}/\omega)^2]}{1-\omega_{0e}^2/(\omega^2-\Omega_e^2)} \tag{6}$$

$$\varkappa_2 = -i\frac{\varepsilon_1^{а}}{2n_2}\left(1+\frac{\Omega_e}{\omega}\frac{\omega_{0e}^2}{\omega^2-\Omega_e^2-\omega_{0e}^2}\right),$$

где

$$\omega_{1e}^2 = -\frac{4\pi e^2}{5}\frac{1}{\langle v_e^2\rangle}\int \mathbf{dp}\, v^4\frac{\partial f_{0e}}{\partial E}, \qquad \langle v_e^2\rangle = \int \mathbf{dp}\, v^2 f_{e0},$$

$$\varepsilon_1^{а} = g^{а} = \begin{cases} -i\dfrac{8}{3}\dfrac{\pi^3\Omega_e^3 m_e^2 e^2 c^5}{\omega^5}\left(1-\dfrac{\omega_e^2}{\omega^1}\right)^{3/2} f_{0e}'\left(m_e c^2\dfrac{\Omega_e}{\omega}\right) & \text{при } \omega<\Omega_e \\ 0 \text{ при } \omega>\Omega_e, \end{cases} \tag{7}$$

$$\varepsilon_2^{а} = \begin{cases} -i\dfrac{8}{15}\dfrac{\pi^3\Omega_e^3 m_e^2 e^2 c^5}{\omega^5}\left(1-\dfrac{\omega^2}{\Omega_e^2}\right)^{5/2} f_{0e}'\left(m_e c^2\dfrac{\Omega_e}{\omega}\right) & \text{при } \omega<\Omega_e \\ 0 \text{ при } \omega>\Omega_e. \end{cases}$$

Из формулы (6) следует, что при $\omega\sim\Omega_e$ показатель преломления обыкновенной волны мал и меняет знак. Для необыкновенной же волны $n^2>0$ лишь в случае разреженной плазмы, когда $\omega_{0e}^2<2\Omega_e^2$.

Для того, чтобы из экспериментов по измерению величин n и $\varkappa$ можно было восстановить функцию распределения частиц, необходимо, чтобы поглощение волн в плазме было достаточно интенсивным. Покажем, что учет релятивистских эффектов теплового движения электронов, содержащийся в формулах (7), даже в области нерелятивистских температур может привести к значительному поглощению волн в плазме. Так, в Максвелловской электронной плазме при $\omega=\Omega_e/2$ имеем

$$|\varepsilon_1^a| \approx \frac{10^{19} N_e}{B^2 T_e^{5/2}} e^{-10^{10}/T_e}, \quad |\varepsilon_2^a| \approx \frac{2\cdot 10^{18} N_e n^2}{B^2 T_e^{5/2}} e^{-10^{10}/T_e}$$

При $T_e\sim 10^9$, $B\sim 10^4$ и $N_e\sim 10^{13}$ для обеих волн $n\sim 1$. Для обыкновенной волны при этом $\varkappa_1\sim 10^{-3}$, а для необыкновенной волны $\varkappa_2\sim 10^{-2}$, т.е. обыкновенная волна полностью поглощается в плазме на длине $\delta\sim 100$ см (при этом $\lambda\sim 1$ см), а необыкновенная на длине $\delta\sim 10$ см ($\lambda\sim 1$ см). Заметим, что магнитотормозное поглощение волн при $\vartheta=\pi/2$ превышает поглощения, обусловленные столкновениями частиц в плазме, при условии

$$10^{30} B e^{-10^{10}/T_e} \gg 1$$

При $T_e \gtrsim 3.10^3$ это условие хорошо выполняется в широкой области изменения величин B и N_e ($B\sim 10^3 \div 10^5$, $N_e\sim 10^{13}\div 10^{15}$).

Исследование распространения электромагнитных волн в области частот, определяемой условием (а) при $m>1$, с точки зрения определения функции распределения электронов в нерелятивистской плазме интереса не представляет. Дело в том, что в этой области частот антиэрмитовская часть тензора диэлектрической проницаемости наряду с экспоненциально малым множителем содержит множитель порядка $(\langle v_e\rangle/c)^{2m}$. Поэтому магнитотормозное поглощение волн в плазме в этой области частот практически всегда пренебрежимо по сравнению с поглощением, обусловленным столкновениями частиц.

С помощью уравнений (3) легко исследовать электромагнитные волны вблизи резонансных частот с $m>1$ и при выполнении условия (б). В этом случае антиэрмитовская часть тензора диэлектрической проницаемости мала по сравнению с эрмитовской и при определении показателей преломления волн ею можно пренебречь, подставляя в формулы (3) выражения

$$\varepsilon_1 = 1 - \frac{\omega_{0e}^2}{\omega^2 - \Omega_e^2}, \quad g = -\frac{\omega_{0e}^2 \Omega_e}{\omega(\omega^2 - \Omega_e^2)},$$

$$\varepsilon_2 = 1 - \frac{\omega_{0e}^2}{\omega^2} \qquad (8)$$

Учитывая далее малую антиэрмитовскую часть диэлектрической проницаемости, определяем коэффициенты поглощения волн. Так как условие (б) выполняется в области углов не очень близких к $\pi/2$, то при вычислении коэффициентов волн можно пользоваться нерелятивистскими формулами для $\varepsilon_{ij}(\omega, \mathbf{k})$:

$$\varepsilon_1^a = g^a = i\frac{8\pi^3 e^2 m_e c}{\omega^2 |n\cos\vartheta|}\frac{(-1)^m}{2^m} m\left(\frac{n\omega\sin\vartheta}{\sqrt{m_e}\, e\Omega_e}\right)^{2m-2} F_{me}(0),$$

$$\varepsilon_2^a = 0, \quad \frac{\partial^m F_{me}}{\partial E^m} = f_{0e}(E). \qquad (9)$$

Для коэффициентов поглощения обыкновенной и необыкновенной волн получаем

$$\varkappa_{1,2} = -i\varepsilon_1^a \frac{1}{4n_{1,2}(\varepsilon_1\sin^2\vartheta + \varepsilon_2\cos^2\vartheta)} \{[\sin^4\vartheta(\varepsilon_1 - g)^2 + 2\sin^2\vartheta\cos^2\vartheta\,\varepsilon_2(\varepsilon_1 - g) + \cos^2\vartheta(1+\cos^2\vartheta)\varepsilon_2^2] \times \sqrt{(\varepsilon_1^2 - g^2\varepsilon_1\varepsilon_2)^2\sin^4\vartheta + 4\varepsilon_2^2 g^2\cos^2\vartheta}$$
$$\mp [\sin^4\vartheta(\varepsilon_1^2 - g^2 - \varepsilon_1\varepsilon_2)(\sin^2\vartheta(\varepsilon_1 - g)^2 + \cos^2\vartheta\,\varepsilon_2(2\varepsilon_1 - 2g - \varepsilon_2)) + 4g\varepsilon_2^2\cos^2\vartheta(\varepsilon_1\sin^2\vartheta - g\sin^2\vartheta + \varepsilon_2\cos^2\vartheta)]\}.$$

Наибольший интерес представляет область частот вблизи второй резонансной линии поглощения. В этой области частот с одной стороны вследствие малости антиэрмитовской части тензора диэлектрической проницаемости следует ожидать достаточно хорошего проникновения волн в плазму. С другой стороны, вблизи второй резонансной линии поглощения при выполнении условия (б) антиэрмитовская часть тензора диэлектрической проницаемости не является экспоненциально малой величиной; она всего лишь на величину $\sim n\langle v_e\rangle/c$ меньше эрмитовской части. Это в свою очередь обуславливает достаточно интенсивное поглощение волн в этой области частот. Так в разреженной Максвелловской плазме, в которой $\omega_{0e}^2 \lesssim 4\Omega_e^2$ (в плотной плазме, в которой $\omega_{0e}^2 \gg 4\Omega_e^2$ электромагнитные волны с частотой $\omega\sim 2\Omega_e$ распространяться не могут, т.к. при этом $n^2<0$), в области углов $\vartheta\sim 1$ для обеих волн $n\sim 1$, а $\varkappa\sim 0{,}1\langle v_e\rangle/c$. При $T_e\sim 10^7$ имеем $\varkappa\sim 0{,}003$, т.е. в такой плазме электромагнитные волны полностью поглощаются на длине $\delta\sim 30$ см (принимая $B\sim 10^4$).

Заметим, что при условии (б) вблизи второй резонансной линии поглощения столкновениями частиц можно пренебречь, если выполняется неравенство

$$\frac{\lambda_B}{nl} \sim \frac{0{,}1 N_e}{n T_e^2 B} \ll 1,$$

где $\lambda_B = c/\omega_B$, а l — длина свободного пробега электронов. Это условие хорошо выполняется в широкой области изменения величин B, N_e и T_e как в лабораторной плазме, так и в ионосферной (например, в F-слое ионосферы [7]).

3. Ионный циклотронный резонанс в плазме

Исследование электромагнитных волн в области частот ионного циклотронного резонансов представляет большой практический интерес также и с точки зрения нагрева ионов в плазме. Естественен поэтому тот интерес, который уделяется этому вопросу в литературе (см. [1] и приведенную там библиографию). Исследование электромагнитных

волн в области частот ионного циклотронного резонансов проводится также, как и в области частот электронного циклотронного резонансов. В этой области частот, однако, имеется одно существенно упрощающее обстоятельство, позволяющее относительно просто исследовать распространение электромагнитных волн под произвольным углом к магнитному полю, а именно выполняется неравенство $\varepsilon_1^2 - g^2 \ll \varepsilon_1 \varepsilon_2$.

Вблизи первой резонансной частоты при выполнении условия (а) из уравнения (11) получаем показатели преломления обыкновенной и необыкновенной волн в виде:

$$n_1^2 = \frac{\omega_{0e}^2}{\omega^2} \frac{1 + \cos^2\vartheta}{(\omega_{0e}/\omega_{0i})^2 (\Omega_i^2 - \omega^2/\omega^2)\cos^2\vartheta - \sin^2\vartheta}, \quad (11)$$

$$n_2^2 = -\frac{\omega_{0i}^2}{\omega^2} \frac{1}{1 + \cos^2\vartheta}, \quad (12)$$

где $$\omega_{0i}^2 = -\frac{4\pi e^2}{3} \int \mathrm{d}\mathbf{p}\, v^2 \frac{\partial f_{0i}}{\partial E}.$$

Отсюда следует, что необыкновенная волна вблизи первой резонансной частоты в плазме не распространяется, т.к. $n_2^2 < 0$. Что же касается обыкновенной волны, то $n_1^2 > 0$ при $\mathrm{tg}^2\vartheta < (\omega_{0e}/\omega_{0i})^2 (\Omega_i^2 - \omega^2/\omega^2)$. Это условие выполняется при $\omega < \Omega_i$ и практически для всех углов ϑ, не слишком близких к $\pi/2$. Учет малой антиэрмитовской части тензора диэлектрической проницаемости в уравнении (11) приводит к следующему выражению для коэффициентов поглощения обыкновенной волны

$$\varkappa_1 = \frac{n_1^3}{2(1 + \cos^2\vartheta)} \left[\frac{-i\varepsilon_1^a \cos^2\vartheta}{(\omega_{0i}^2/\omega^2 - \Omega_i^2)^2} + \frac{-i\varepsilon_2^a \sin^2\vartheta}{(\omega_{0e}^2/\omega^2)^2} \right], \quad (13)$$

где

$$\varepsilon_1^a = -i \frac{4\pi^3 e_i^2 M c}{\omega^2 |n \cos\vartheta|} F_{1i}\left(\frac{M c^2 (\omega - \Omega_i)^2}{2\omega^2 n^2 \cos^2\vartheta}\right),$$

$$\varepsilon_2^a = i \frac{8\pi^3 e^2 m_e^2 c^3}{\omega^2 |n \cos\vartheta|^3} f_{0e}\left(\frac{m_e c^2 \omega^2}{2n^2 \cos^2\vartheta}\right),$$

$$\frac{\partial F_{1i}(E)}{\partial E} = f_{0i}(E) \quad (14)$$

Здесь мы воспользовались нерелятивистскими формулами для антиэрмитовской части тензора диэлектрической проницаемости. В рассматриваемой области частот ионного циклотронного резонансов такое приближение практически всегда является достаточным.

Из полученных формул (11)—(14) следует, что с помощью измерений показателя преломления n_1 коэффициента поглощения $\varkappa_1$ обыкновенной волны при $\vartheta = 0$ можно восстановить функцию распределения ионов в плазме. Заметим, что в горячей плазме поглощение обыкновенной волны происходит достаточно интенсивно. Так, например, в Максвелловской плазме при $T_i \sim 10^7$, $B \sim 10^4$, $N \sim 10^{14}$ и $|(\omega - \Omega_i)/\omega| \sim 0{,}3$ для волны, распространяющейся под углом $\vartheta = 0$ к магнитному полю, имеем $n_1 \sim 100$, а $\varkappa_1 \sim 1$. Это означает, что такая волна полностью поглощается ионами плазмы на длине $\delta \sim 10^2$ см (при этом $\lambda \sim 1$ см). Количество тепла, выделяемое в единицу времени и в единице объема плазмы, при этом равно $Q/V \sim 10^9 |E|^2$, т.е. энергия, передаваемая волной одному иону в 1 мсек порядка $\sim 10^{-8} |E|^2$. Если $E \sim 100$, то прирост энергии иона за 1 мсек равен 1 кэв. Из этих оценок следует, что обыкновенная волна вблизи первой резонансной частоты может быть использована для нагрева ионов плазмы.

Магнитотормозное поглощение ионами плазмы в области частот, определяемой условием (а) при $m > 1$ практически всегда меньше поглощения, обусловленного столкновениями частиц. Поэтому эту область частот мы не будем здесь рассматривать.

В области частот, определяемой условием (б), с точки зрения нагрева плазмы наибольший интерес представляют волны с удвоенной резонансной частотой $\omega \sim 2\,\Omega_i$. В этой области частот электромагнитные волны хорошо проникают в плазму, но вместе с тем достаточно интенсивно поглощаются ионами плазмы. В наиболее интересном случае плотной плазмы, когда $\omega_{0i}^2 > 3\,\Omega_i^2$, для обыкновенной волны $n_1^2 < 0$, т.е. такая волна в плазму не проникает. Что же касается необыкновенной волны, то из уравнения (3) получаем:

$$n_2^2 = \frac{\omega_{0i}^2}{6\,\Omega_i^2} \cdot \frac{(\sin^4\theta + 16\cos^2\theta)^{1/2} - (1 + \cos^2\theta)}{\cos^2\theta},$$

$$\varkappa_2 = -i \frac{3 n_2}{2} \cdot \frac{\Omega_i^2}{\omega_{0i}^2} \varepsilon_1^a \frac{1 + \cos^2\theta}{(\sin^4\theta + 16\cos^2\theta)^{1/2}}, \quad (15)$$

где

$$\varepsilon_1^a = i \frac{4\pi^3 e_i^2}{c\Omega_i^2} \frac{n \sin^2\vartheta}{|\cos\vartheta|} F_{2i}(0), \qquad \frac{\partial^2 F_{2i}(E)}{\partial E^2} = f_{0i}(E)$$

Отсюда видно, что при $\omega_{0i}^2 > 3\,\Omega_i^2$ необыкновенная волна проникает в плазму, т.к. при этом $n^2 > 0$. В случае Максвелловской плазмы $\varepsilon_1^2 = i\sqrt{\pi/8}\,(\omega_{0i}/\Omega_i)^2 \langle v_i \rangle / c\,(n \sin^2\theta)/|\cos\theta|$. Для рассмотренных выше параметров плазмы ($T_i \sim 10^7$, $N \sim 10^{14}$, $B \sim 10^4$) и при $|\omega - \Omega_i| \sim 0{,}1$ имеем $n_2 \sim 100$, а $\varkappa_2 \sim 10$. Такая волна полностью поглощается ионами плазмы на длине $\delta \sim 10$ см (длина волны при этом равна $\lambda \sim 1$ см). Энергия, выделяемая в единицу времени и в единице объема плазмы в такой волне, равна $Q/V \sim 10^{11} |E|^2$. При $E \sim 10$ в/см прирост энергии иона за 1 мсек порядка 10 кэв. Достаточно интенсивный нагрев происходит и при более низких температурах плазмы, начиная с $T_i \sim 10^5$. Приведенные оценки свидетельствуют о том, что необыкновенная волна с удвоенной резонансной частотой $\omega \sim 2\,\Omega_i$ может служить эффективным средством нагрева ионов плазмы.

4. Циклотронные волны в плазме в области больших показателей преломления

При рассмотрении электромагнитных волн вблизи циклотронных частот электронов и ионов нами принималось выполненным неравенство $n\langle v_{e,i}\rangle/c \ll 1$. В области больших показателей преломления, когда нарушается это условие, полученные выше результаты очевидно перестают быть справедливыми. При этом, как указали Ю. Н. Днестровский и Д. П. Костомаров [8], для анализа распространения электромагнитных волн в плазме необходимо пользоваться численными или качественными методами решения дисперсионных уравнений. Однако, в области больших показателей преломления, когда выполнено обратное неравенство $n\langle v_{e,i}\rangle/c \gg 1$, можно легко получить аналитические решения дисперсионных уравнений электромагнитных волн. Покажем это на примере нерелятивистской Максвелловской электронно-ионной плазмы. Также как и выше будем считать выполненным одно из двух условий (а) или (б). Можно показать, что в области частот, определяемой условием (б), тензор диэлектрической проницаемости плазмы $\varepsilon_{ij}(\omega, \mathbf{k})$ мало отличается от единичного тензора δ_{ij}, а показатели преломления волн порядка единицы, что противоречит предположению $n\langle v_{e,i}\rangle/c \gg 1$. В области частот, определяемой условием (а), при исследовании дисперсионного уравнения (1) существенными оказываются лишь компоненты ε_{11}, ε_{22} и ε_{33} тензора диэлектрической проницаемости $\varepsilon_{ij}(\omega, \mathbf{k})$. При этом условии уравнение (1) распадается на три уравнения, представляющие собой дисперсионные уравнения соответственно, обыкновенной, необыкновенной и плазменной волн:

$$n^2 \sin^2\vartheta = \varepsilon_{33}, \quad n^2 = \varepsilon_{22}, \quad \varepsilon_{11} = 0 \tag{16}$$

Учитывая малость антиэрмитовской части тензора диэлектрической проницаемости определяем показатели преломления и коэффициенты поглощения электромагнитных волн в области прозрачности, находящихся в резонансе с гирочастотой одного определенного сорта частиц $\omega \sim m\Omega_i$ ($\alpha = e,i$):

$$n_1 = \left(\frac{\omega_{0\alpha}^2 \sqrt{m_\alpha}\,\Omega_\alpha c}{\sqrt{2\pi}\,\omega^2 (m\Omega_\alpha - \omega)\sqrt{\varkappa T_\alpha}} \frac{1}{\sin^3\vartheta}\right)^{1/3},$$

$$\varkappa_1 \approx -\sqrt{\frac{\pi}{2}}\, n_1 \beta_{m_\alpha}{}^3 e^{-\beta m_\alpha^2/2},$$

$$n_2 = \left(\frac{\omega_{0\alpha}^2\, \Omega_\alpha c \sqrt{m_\alpha}}{\sqrt{2\pi\varkappa T_\alpha}\,\omega^2 (m\Omega_\alpha - \omega)} \frac{1}{\sin\vartheta}\right)^{1/3},$$

$$\varkappa_2 \approx -\sqrt{\frac{\pi}{2}}\, n_2 \beta_{m_\alpha} e^{-\beta m_\alpha^2/2}, \tag{17}$$

$$n_3 = \left(\frac{\omega_{0\alpha}^2\, \Omega_\alpha{}^3 c^3 m_\alpha{}^{3/2} m^2}{\sqrt{2\pi}\,(\varkappa T_\alpha)^{3/2}\,\omega^4 (\omega - m\Omega_\alpha)} \frac{1}{\sin^3\vartheta}\right)^{1/3},$$

$$\varkappa_3 \approx \frac{1}{3}\sqrt{\frac{\pi}{2}}\, n_3 \beta_{m_\alpha} e^{-\beta m_\alpha^2/2},$$

где

$$\beta_{m_\alpha} = \frac{\omega - m\Omega_\alpha}{n\omega|\cos\vartheta|} \frac{c\sqrt{m_\alpha}}{\sqrt{\varkappa T_\alpha}} \gg 1$$

Из полученных формул следует, что для обыкновенной и необкновенной волн плазма прозрачна при $\omega < \Omega_\alpha m$, а для плазменной волны при $\omega > m\Omega_\alpha$. Это результат согласуется с качественным исследованием, приведенным в работе [8].

В заключение заметим, что область углов, в которой справедливы формулы (17), определяется из условия (а) и неравенства $(n\langle v_{e,i}\rangle/c)\sin\vartheta \gg 1$. Легко видеть, что эти условия выполняются в узком интервале углов $\vartheta \sim \pi/2$.

Литература

[1] Силин, В. П., Рухадзе, А. А., «Электромагнитные свойства плазмы и плазмоподобных сред» (М. Атомиздат, 1961 г.)

[2] Трубников, Б. А., Сб. «Физика плазмы и проблемы термоядерных реакций» т. 3, стр. 104 и т. 4, стр. 305 (Изд. АН СССР, 1958).

[3] Кудрявцев, В. С., Сб. «Физика плазмы и проблемы термоядерных реакций», т. 3, стр. 114 (Изд. АН СССР, 1958).

[4] Кудрявцев, В. С., Трубников, Б. А., Тр. П-Конференции по мирному использованию атомной энергии. Докл. Советских ученых (Ядерная физика) 165 (1959); Proceedings of Second U.N. International Conference on Peaceful Uses of Atomic Energy, Geneva, **31** (1958) 93.

[5] Силин, В. П., *Тр. ФИАН СССР* **6** (1955) **200**.

[6] Степанов, К. Н., *ЖЭТФ* **36** (1959) 1457.

[7] Гершман, Б. Н., *ЖЭТФ* **37** (1959) 695; **38** (1960) 912.

[8] Днестровский, Ю. Н., Костомаров, Д. П., доклад CN-10/257 на Конференции в Зальцбурге (1961).

FOKKER-PLANCK COEFFICIENTS FOR A PLASMA INCLUDING CYCLOTRON RADIATION*

NORMAN ROSTOKER, ALBERT SIMON**

GENERAL ATOMIC DIVISION OF GENERAL DYNAMICS CORPORATION

SAN DIEGO, CALIFORNIA, UNITED STATES OF AMERICA

Kinetic equations for a plasma have previously been obtained by starting with the Liouville equation and making an expansion in powers of the discreteness parameters. To the lowest order in this expansion the Vlasov equations are obtained. In first order a Fokker-Planck equation is obtained where the coefficients come from the time-asymptotic solutions of integro-differential equations for the pair correlation functions.

Solutions have been published for an infinite plasma with Coulomb forces, Coulomb forces and a constant magnetic field, the complete electromagnetic field and no constant magnetic field. In the present paper the complete electromagnetic field and a constant magnetic field are included. The new feature of this problem is that electromagnetic radiation obtains which was absent in all of the cases previously treated.

At the outset, the system consists of a large number of "bare" particles that interact with each other and a denumerably infinite number of vacuum oscillators. The present statistical treatment leads to a kinetic equation for the one-body function that has a physical interpretation in terms of "dressed" particles and renormalized oscillators. A shield cloud of charge and current density envelopes a particle and the radiation takes place in terms of oscillators that satisfy the plasma dispersion relation instead of the vacuum dispersion relation.

In the low-density limit, or when $k \gg \omega_p/c$, the result agrees with the vacuum radiation formula employed by Trubnikov. If terms of order $(\omega_p/kc)^2$ are retained, the principal effect is the renormalization of the oscillators. In the exact radiation formula longitudinal and transverse waves are coupled, i.e., the normal modes do not have a simple polarization. The virtue of the present treatment is that it indicates the terms that represent electromagnetic radiation and the proper particle dressing under these circumstances.

1. Introduction***

It is assumed that the plasma consists of N electrons of charge $-e$ and mass m in a volume V. The ions are assumed to have infinite mass and to be randomly distributed. The radiation field is represented by a denumerably infinite set of oscillators with periodic boundary conditions. Oscillators are treated like particles so that the phase space of the system consists of particle coordinates $(\mathbf{x}_n, \mathbf{v}_n)$ with $n=1, 2 \ldots N$ and oscillator coordinates $q_\lambda p_\lambda$ with $\lambda=1, 2 \ldots \infty$. By taking moments of the Liouville equation an infinite chain of equations is obtained that is a simple generalization of the B-B-K-G-Y chain. The discreteness parameters are e, m and $1/n_0 \leqq V/N$ for the particles and $1/V$ for the oscillators. In the continuum limit e, m, $1/n_0$, $1/V \to 0$ there is no correlation between particles or between particles and oscillators. The one-body particle function obeys the Vlasov equations. To first order in the discreteness parameters the one-body particle function obeys an equation of the form:

$$\frac{\partial f}{\partial t} + \mathbf{v} \cdot \frac{\partial f}{\partial \mathbf{x}} - \frac{e}{mc}(\mathbf{v} \times \mathbf{B}) \cdot \frac{\partial f}{\partial \mathbf{v}} = \mathrm{St}\{f\} \qquad (1)$$

where the collision operator $\mathrm{St}\{f\}$ is determined by the two particle correlation function $g(\mathbf{x}, \mathbf{v}; \mathbf{x}', \mathbf{v}')$ and the particle-oscillator correlation function $g'(\mathbf{x}\ \mathbf{v}; q_\lambda p_\lambda)$. The integro-differential equations for g and g' have previously been obtained [6] when the external magnetic field $\mathbf{B}=0$. After indicating the appropriate generalization when $\mathbf{B} \neq 0$ we shall assume these equations as a starting point of the present paper.

The analysis in this problem is sufficiently overwhelming to obscure the physical content. In order to provide some perspective we consider a sequence of problems as follows:

(1) *Inconsistent Test Particle Problem:* In this case only one particle is considered to be discrete. All oscillators and field particles are treated in the continuum limit. This problem serves to introduce the mathematical apparatus.

(2) *Superposition of Dressed Test Particles:* A simple procedure has previously been devised for deriving the collision operator [8]. It is known to give correct results when only Coulomb forces are considered. Applied to the present problem, this procedure does not constitute a legitimate derivation, but indicates the expected result with the least effort.

(3) *Consistent Test Particle Problem:* Initially all particles but one and all photons are considered

* Conference paper CN-10/162, presented by N. Rostoker. Discussion of this paper is given on page 815. Translations of the abstract are at the end of this volume of the Conference Proceedings.

** Oak Ridge National Laboratory, Oak Ridge, Tennessee, U.S.A.

*** The earlier work referred to in the abstract is given in references [1—4].

to be in thermal equilibrium. All particles and oscillators are treated to first order in the discreteness parameters. A Fokker-Planck equation is obtained for the test particle.

(4) *Oscillators and Particles at Different Temperatures:* Initially it is assumed that oscillators and particles have thermal distributions at different temperatures. The resultant collision operator has only a radiation term that is proportional to the temperature difference.

Throughout the paper we assume infinite ion mass and non-relativistic particles for convenience. The appropriate generalization to eliminate these restrictions will be given for some of the results.

2. Inconsistent test-particle problem

The equations for the problem are as follows:

$$\frac{\partial}{\partial t}\delta f + \mathbf{v}'\cdot\frac{\partial}{\partial \mathbf{x}'}\delta f - \frac{e}{mc}(\mathbf{v}'\times\mathbf{B})\cdot\frac{\partial}{\partial \mathbf{v}'}\delta f = \frac{e}{m}\left(\delta\mathbf{E}+\frac{1}{c}\mathbf{v}'\times\mathbf{B}\right)\cdot\frac{\partial f}{\partial \mathbf{v}'} \quad (2)$$

$$\nabla\times(\nabla\times\delta\mathbf{E})+\frac{1}{c^2}\frac{\partial^2\delta\mathbf{E}}{\partial t^2} = -\frac{4\pi}{c^2}\frac{\partial}{\partial t}\delta\mathbf{J}, \quad (3)$$

where

$$\frac{\partial}{\partial t}\delta\mathbf{B} = -c\nabla\times\delta\mathbf{E},$$

$$\delta\mathbf{J} = -e\,\mathbf{v}(t)\,\delta[\mathbf{x}'-\mathbf{x}(t)] - en_0\int\delta f\,\mathbf{v}'\,d\mathbf{v}'.$$

The z-direction is taken in the direction of $\mathbf{B}$. Cylindrical coordinates $(v_\perp', \theta', v_z')$ and $(k_\perp, \alpha, k_z)$ are employed for $\mathbf{v}'$ and the Fourier transform vector $\mathbf{k}$. $f=f(v_\perp', v_z')$ is independent of θ'. The prescribed test-particle orbit is

$$\mathbf{x}(t) = \mathbf{x}_0 + \mathbf{e}_x a[\sin(\theta_0+\omega_c t)-\sin\theta_0] - \mathbf{e}_y a[\cos(\theta_0+\omega_c t)-\cos\theta_0] + \mathbf{e}_z v_z t, \quad (4)$$

$$\mathbf{v}(t) = d\mathbf{x}(t)/dt.$$

$(\mathbf{e}_x, \mathbf{e}_y, \mathbf{e}_z)$ are unit vectors. $a=v_\perp/\omega_c$ is the Larmor radius and $\omega_c=eB/mc$ is the cyclotron frequency.

The first step is to take Fourier and Laplace transforms of all the perturbed quantities in Eq. (2). For example,

$$\delta f(\mathbf{x}', \mathbf{v}'; t) = \int\frac{d\mathbf{k}}{(2\pi)^3}e^{i\mathbf{k}\cdot[\mathbf{x}'-\mathbf{x}(t)]}\int\frac{dp}{2\pi i}e^{pt}\delta f(\mathbf{k}, p, \mathbf{v}'). \quad (5)$$

We shall only be concerned with the asymptotic solution

$$\lim_{p\to 0} p\,\delta f(\mathbf{k}, p, \mathbf{v}').$$

This quantity will depend on the test particle velocity $\mathbf{v}$ and we shall denote it by $\delta f_k(\mathbf{v}, \mathbf{v}')$. Similarly

$$\delta\mathbf{E}_k(\mathbf{v}) = \lim_{p\to 0} p\,\delta\mathbf{E}(\mathbf{k}, p).$$

In addition, we shall make a Bessel function transformation as follows:

$$\delta\mathbf{E}_k(\mathbf{v}) = \exp[ik_\perp a\sin(\theta-\alpha)]\sum_{n=-\infty}^{\infty}\exp[-in(\theta-\alpha)]J_n(k_\perp a)\,\delta\mathbf{E}_n(v_\perp, v_z), \quad (6)$$

$$\delta f_k(\mathbf{v}, \mathbf{v}') = \exp[ik_\perp a\sin(\theta-\alpha)-ik_\perp a'\sin(\theta'-\alpha)] \times\sum_{ns}\exp[is(\theta'-\alpha)-in(\theta-\alpha)] \times J_s(k_\perp a')J_n(k_\perp a)\,\delta f_{ns}(v_\perp, v_z; v_\perp', v_z').$$

$\delta\mathbf{E}_n$, δf_{ns} will be referred to as "Fessel-space components". Similarly we can find Fessel-space components for vectors such as $\mathbf{v}$, $\mathbf{k}$. For example,

$$\mathbf{v} = \exp[-ik_\perp a\sin(\theta-\alpha)]\sum_n\exp[in(\theta-\alpha)]J_n(k_\perp a)\,\mathbf{v}_n, \quad (7)$$

where

$$\mathbf{v}_n = \mathbf{e}_1\frac{(k_z v_z+n\omega_c)}{k}+\mathbf{e}_2\left(\frac{k_\perp v_z}{k}-\frac{k_z n\omega_c}{k k_\perp}\right)+\mathbf{e}_3 i v_\perp\frac{J_n'(k_\perp a)}{J_n(k_\perp a)}.$$

$\mathbf{e}_1=\mathbf{k}/k$, $\mathbf{e}_2=\mathbf{k}\times(\mathbf{B}\times\mathbf{k})/kk_\perp B$, $\mathbf{e}_3=(\mathbf{k}\times\mathbf{B})/k_\perp B$, are unit vectors. Similarly $\mathbf{k}_n=k(\mathbf{e}_1)_n=k_z\mathbf{e}_z+(n/a)\mathbf{e}_\varrho$ where $(\mathbf{e}_\varrho, \mathbf{e}_\theta, \mathbf{e}_z)$ are cylindrical unit vectors determined by $\mathbf{v}$. Similarly Fessel-space components can be obtained for tensors like $\mathbf{vv}$, $\mathbf{kk}$, and operators like $(\partial/\partial\mathbf{v})$, $\mathbf{v}\times\mathbf{B}\cdot(\partial/\partial\mathbf{v})$.

Equations (2) and (3) can be replaced by equations for their Fessel-space components:

$$\lim_{\lambda\to 0}\{i[k(u_s'-u_n)-i\lambda]\,\delta f_{ns}\} = \frac{e}{m}\left[\delta\mathbf{E}_n+\frac{1}{c}(\mathbf{v}_s'\times\delta\mathbf{B}_n)\right]\cdot\frac{\partial f}{\partial \mathbf{v}_s'}, \quad (8)$$

$$k^2\left(1-\frac{u_n^2}{c^2}\right)\delta\mathbf{E}_n-\mathbf{k}(\mathbf{k}\cdot\delta\mathbf{E}_n) = 4\pi i\frac{ku_n}{c^2}\delta\mathbf{J}_n, \quad (9)$$

where

$$\delta\mathbf{B}_n = \frac{c\mathbf{k}\times\delta\mathbf{E}_n}{ku_n+i\lambda},$$

$$\delta\mathbf{J}_n = -e\,\mathbf{v}_n^*-n_0 e\int d\mathbf{v}'\sum_s J_s^2(k_\perp a')\,\mathbf{v}_s'^*\,\delta f_{ns}(v, v'),$$

$$u_n = \frac{\mathbf{k}\cdot\mathbf{v}_n}{k} = \frac{\mathbf{k}_n\cdot\mathbf{v}}{k} = \frac{k_z v_z+n\omega_c}{k}.$$

The point of the transformation is that these equations are formally the same as the equations for the simpler test-particle problem when $\mathbf{B}=0$. This technique succeeds in transforming away the magnetic field in all of the problems considered to date. It is now a simple matter to express δf_{ns} in terms of $\delta\mathbf{E}_n$, calculate $\delta\mathbf{J}_n$, substitute into Eq. (9) and solve for $\delta\mathbf{E}_n$. The result is

$$\delta\mathbf{E}_n = \frac{4\pi e i}{k(u_n+i\lambda)}\mathbf{Y}^{-1}(\mathbf{k}, -iku_n)\cdot\mathbf{v}_n^*, \quad (10)$$

where

$$\mathbf{Y}(\mathbf{k}, p) = \mathbf{I}\left[1+\frac{\omega_p^2}{p^2}\right]+\frac{k^2c^2}{p^2}\mathbf{I} + \frac{\omega_p^2}{p^2}\int d\mathbf{v}\sum_n\frac{J_n^2(k_\perp a)[i\mathbf{k}_n\cdot\partial f/\partial\mathbf{v}]\,\mathbf{v}_n^*\,\mathbf{v}_n}{p+iku_n}. \quad (11)$$

$\mathbf{I}$ is the unit dyadic: $\mathbf{I} = \mathbf{e}_2\,\mathbf{e}_2 + \mathbf{e}_3\,\mathbf{e}_3$; $\boldsymbol{\Upsilon} \cdot \boldsymbol{\Upsilon}^{-1} = \mathbf{I}$; $\omega_p = (4\pi n e^2/m)^{1/2}$ is the plasma frequency. For subsequent problems it is convenient to calculate

$$\mathbf{F}(X, X') = \delta\mathbf{E}(\mathbf{x}') + \frac{1}{c}\mathbf{v}' \times \delta\mathbf{B}(\mathbf{x}'),$$

which is the force on a field particle at $\mathbf{x}'$ moving with velocity $\mathbf{v}'$ due to an asymptotic or fully dressed test particle at $\mathbf{x}$ moving with velocity $\mathbf{v}$. The result is

$$\mathbf{F}(X, X') = 4\pi i e \int \frac{d\mathbf{k}}{(2\pi)^3} \exp[i\mathbf{k}\cdot(\mathbf{x}' - \mathbf{x})] \cdot$$

$$\exp[i k_\perp a \sin(\theta - \alpha)] \cdot \sum_n \exp[-in(\theta - \alpha)] J_n(k_\perp a)$$

$$\times \left\{ \frac{\boldsymbol{\Upsilon}^{-1}(\mathbf{k}, -ik u_n)\cdot \mathbf{v}_n^*}{(k u_n + i\lambda)} + \frac{\mathbf{v}' \times [\mathbf{k} \times (\boldsymbol{\Upsilon}^{-1}\cdot \mathbf{v}_n^*)]}{(k u_n + i\lambda)^2} \right\} \quad (12)$$

3. Superposition of dressed test particles

The general form of the collision operator previously derived for the case of pure Coulomb interactions [8] is

$$\mathrm{St}\{f\} = \frac{e}{m}\frac{\partial}{\partial \mathbf{v}} \cdot \left\{ \mathbf{E}(X, x) f(v) + \left(\frac{e}{m}\right)^2 \frac{\partial}{\partial \mathbf{v}} \cdot \int_0^\infty d\tau\, \mathbf{C}(\tau) \cdot \frac{\partial f}{\partial \mathbf{v}} \right\}. \quad (13)$$

$\mathbf{E}(\mathbf{X}, \mathbf{x}')$ means the electric field at $\mathbf{x}'$ due to a test particle at $\mathbf{x}$ with velocity $\mathbf{v}$.

$$\mathbf{C}(\tau) = \langle \mathbf{E}(\mathbf{x}, t)\, \mathbf{E}[\mathbf{x}(t+\tau), t+\tau] \rangle, \quad (14)$$

where the bracket means the ensemble average and $\mathbf{x}(t)$ is given by Eq. (4). According to the superposition principle [8]

$$\langle \mathbf{E}(\mathbf{x}, t)\, \mathbf{E}(\mathbf{x}', t') \rangle$$

$$= \frac{n_0}{V} \int \mathbf{E}(X_1, \mathbf{x})\, \mathbf{E}(X_1', \mathbf{x}')\, W_{11}^{(0)}(X_1 t; X_1', t')\, dX_1\, dX_1',$$

where

$$W_{11}^{(0)} = V f(v_1)\, \delta[x_1' - x_1(t')]\, \delta[\mathbf{v}_1' - v_1(t')].$$

That is, the correct result is obtained by assuming that the fields derive from dressed test-particles that are statistically independent. The obvious generalization of this to include the complete electromagnetic field is to replace $\mathbf{E}(X, \mathbf{x})$ by $\mathbf{F}(X, X)$ in Eq. (12) and assume

$$\mathbf{C}(\tau) = \langle \mathbf{F}(\mathbf{x}, \mathbf{v}; t)\, \mathbf{F}[\mathbf{x}(t+\tau); \mathbf{v}(t+\tau); t+\tau] \rangle.$$

This procedure leads to the following collision operator:

$$\mathrm{St}\{f\} = -\frac{(2\pi e \omega_p)^2}{m} \int \frac{d\mathbf{k}}{(2\pi)^3} \sum_n \frac{\mathbf{k}_n}{k} \cdot \frac{\partial}{\partial \mathbf{v}} \frac{J_n^2(k_\perp a)}{u_n^4} \times$$

$$\left\{ [\mathbf{v}_n \cdot \mathbf{H}_1(u_n) \cdot \mathbf{v}_n^*] f - [\mathbf{v}_n \cdot \mathbf{H}_2(u_n) \cdot \mathbf{v}_n^*] \frac{\mathbf{k}_n}{k} \cdot \frac{\partial f}{\partial \mathbf{v}} \right\}. \quad (15)$$

$\mathbf{H}_1$ and $\mathbf{H}_2$ are Hermitian tensors defined as follows:

$$\mathbf{H}_1(u) = [\boldsymbol{\Upsilon}^{-1}(u)] \cdot \mathbf{G}'(u) \cdot [\boldsymbol{\Upsilon}^{-1}(u)]_H$$

$$\mathbf{H}_2(u) = [\boldsymbol{\Upsilon}^{-1}(u)] \cdot \mathbf{G}(u) \cdot [\boldsymbol{\Upsilon}^{-1}(u)]_H.$$

$\boldsymbol{\Upsilon}^{-1}(u)$ denotes the inverse of $\boldsymbol{\Upsilon}(\mathbf{k}, iku)$; $[\boldsymbol{\Upsilon}^{-1}(u)]_H$ denotes the Hermitian conjugate.

$$\mathbf{G}(u) = \int d\mathbf{v}\, f(v) \sum_n J_n^2(k_\perp a)\, \mathbf{v}_n^*\, \mathbf{v}_n\, \delta(u - u_n), \quad (16)$$

$$\mathbf{G}'(u) = \int d\mathbf{v} \sum_n \frac{\mathbf{k}_n}{k} \cdot \frac{\partial f}{\partial \mathbf{v}} J_n^2(k_\perp a)\, \mathbf{v}_n^*\, \mathbf{v}_n\, \delta(u - u_n). \quad (17)$$

Two points about Eq. (15) may be noted. If $f(v) = (m/2\pi\Theta)^{3/2} \exp(-mv^2/2\Theta)$, $\mathrm{St}\{f\} = 0$. Also if f is an arbitrary function of $v_\perp$ and v_z, then

$$\frac{\partial T}{\partial t} = \int d\mathbf{v}\, \frac{1}{2} m v^2\, \mathrm{St}\{f\} = 0, \quad (18)$$

i.e., the collision operator does not produce any change in the mean kinetic energy of the particles.

4. Consistent test-particle problem

The equations for the particle pair correlation function and certain moments of the oscillator-particle correlation function have previously been derived and are given by Eqs. (2.11), (2.12), and (2.13) of [6]. These equations apply only when $\mathbf{B} = 0$. When $\mathbf{B} \neq 0$ the equations for the "Fessel-space" components are almost identical. They are as follows:

$$[k(u_s' - u_n) - i\lambda]\, g_{ns}(\mathbf{v}, \mathbf{v}')$$

$$= \left\{ \frac{\omega_p^2}{k^2} \mathbf{k}_s \cdot \frac{\partial f}{\partial \mathbf{v}'} \int d\mathbf{v}'' \sum_r J_r^2(k_\perp a'')\, g_{nr}(\mathbf{v}, \mathbf{v}'') + \frac{\omega_p^2}{n_0 k^2} \mathbf{k}_s \cdot \frac{\partial f}{\partial \mathbf{v}'} f(\mathbf{v}) \right.$$

$$\left. - [\mathbf{F}_n(\mathbf{v}) + \mathbf{v}_s' \times \mathbf{k} \times \mathbf{E}_n(\mathbf{v})] \cdot \frac{\partial f}{\partial \mathbf{v}_s} \right\} - \left\{ \begin{matrix} n \to s \\ s \to n \\ \mathbf{v} \to \mathbf{v}' \\ \mathbf{v}' \to \mathbf{v} \end{matrix} \right\}^*. \quad (19)$$

The particle correlation function depends only on $(v_\perp, v_z)$ and $(v_\perp', v_z')$. It has the symmetry property $g_{ns}(\mathbf{v}, \mathbf{v}') = g_{sn}^*(\mathbf{v}', \mathbf{v})$. $\mathbf{E}_n(\mathbf{v})$, $\mathbf{F}_n(\mathbf{v})$ are moments of the particle oscillator correlation function $g'(\mathbf{x}, \mathbf{v}; q_\lambda p_\lambda)$. They are independent of θ and are determined by the equations;

$$(k u_n + i\lambda)\, \mathbf{E}_n(\mathbf{v}) - \mathbf{F}_n(\mathbf{v})$$

$$= \frac{\omega_p^2}{k^2} \mathbf{k}_n \cdot \frac{\partial f}{\partial \mathbf{v}} \int d\mathbf{v}' \sum_l J_l^2(k_\perp a')\, \mathbf{E}_l(\mathbf{v}')$$

$$- \frac{\omega_p^2}{n_0 m} \frac{\partial f}{\partial \mathbf{v}_n} \cdot [\mathbf{v}_n^* \times (\mathbf{k} \times \mathbf{Q}_0)], \quad (20)$$

$$(k u_n + i\lambda)\, \mathbf{F}_n(\mathbf{v}) - k^2 c^2\, \mathbf{E}_n(\mathbf{v})$$

$$= \frac{\omega_p^2}{k^2} \mathbf{k}_n \cdot \frac{\partial f}{\partial \mathbf{v}} \int d\mathbf{v}' \sum_l J_l^2(k_\perp a')\, \mathbf{F}_l(\mathbf{v}')$$

$$- \omega_p^2 \int d\mathbf{v}' \sum_s J_s^2(k_\perp a')\, \mathbf{I} \cdot \mathbf{v}_s'^*\, g_{ns}(\mathbf{v}, \mathbf{v}')$$

$$- \frac{\omega_p^2 k^2 c^2}{n_0 m} \frac{\partial f}{\partial \mathbf{v}_n^*} \cdot \mathbf{Q}_0 - \frac{\omega_p^2}{n_0} f(\mathbf{v})\, \mathbf{I} \cdot \mathbf{v}_n^*. \quad (21)$$

$$\mathbf{Q}_0 = \sum_{\nu=2,3} \mathrm{e}_\nu\, \mathrm{e}_\nu \int q_\nu^2\, f_0(p_\nu, q_\nu)\, \mathrm{d}p_\nu\, \mathrm{d}q_\nu$$

is proportional to the oscillator energy. For example, a thermal distribution for the oscillator is:

$$f_0(p_\nu, q_\nu) = \text{const.} \times \exp\left[-\frac{p_\nu^2 + c^2k^2q_\nu^2}{2\Theta'}\right],$$

in which case $\mathbf{Q}_0 = \Theta' \mathbf{I}/c^2k^2$ where Θ' is the oscillator temperature. For the consistent test-particle problem we assume that, at $t=0$, the oscillators have the above distribution and all particles but one have the distribution $f(\mathbf{v}) = (m/2\pi\Theta)^{3/2} \exp(-mv^2/2\Theta)$ with $\Theta = \Theta'$. The test particle is assumed to have the distribution $W(\mathbf{v})$ which is an arbitrary function of $(v_\perp, v_z)$. The particle correlation function for two field particles is initially and remains

$$g_{sr}(\mathbf{v}', \mathbf{v}'') = -\frac{1}{n_0} \frac{f(\mathbf{v}')\, f(\mathbf{v}'')}{1 + (k L_\mathrm{D})^2}$$

where $1/L_\mathrm{D}^2 = 4\pi n e^2/\Theta$. The correlation between any field particle and any oscillator is initially and remains zero, i.e., $\mathbf{E}_s(\mathbf{v}') = \mathbf{F}_s(\mathbf{v}') = 0$. It remains to solve for $g_{ns}(\mathbf{v}, \mathbf{v}')$ the correlation function for the test particle and a field particle and $\mathbf{E}_n(\mathbf{v})$, $\mathbf{F}_n(\mathbf{v})$ which are moments of the test particle-oscillator correlation function. For this, Eqs. (14), (20), and (21) are employed; these simplify considerably because we can place:

$$\mathbf{E}_s(\mathbf{v}') = \mathbf{F}_s(\mathbf{v}') = 0,$$

$$g_{sr}(v', v'') = -\frac{1}{n_0} \frac{f(v')\, f(v'')}{1 + (k L_\mathrm{D})^2}.$$

The procedure is to define the field variable

$$\delta\mathbf{E}_n(\mathbf{v}) = -\mathrm{i}\frac{m}{e}\mathbf{F}_n(\mathbf{v}) + 4\pi\,\mathrm{i}\,e\,\frac{\mathbf{k}}{k^2}\left[W(\mathbf{v}) + n_0 \int \mathrm{d}\mathbf{v}'' \sum_r J_r^2(k_\perp a'')\, g_{nr}(\mathbf{v}, \mathbf{v}'')\right], \tag{22}$$

which combines longitudinal and transverse quantities. Equations (20) and (21) are combined and moments of $g_{ns}(v, v')$ are expressed in terms of $\delta\mathbf{E}_n(\mathbf{v})$ by carrying out appropriate integrations of Eq. (19). This leads to a field equation identical to Eq. (9) where now

$$\delta\mathbf{J}_n(\mathbf{v}) = -e\mathbf{v}_n^* W(v) + \frac{\mathrm{i}k u_n}{4\pi}\left[1 - \mathbf{Y}(\mathbf{k}, -\mathrm{i}k u_n) - \frac{c^2}{(u_n + \mathrm{i}\lambda)^2}\mathbf{I}\right] \cdot \delta\mathbf{E}_n(\mathbf{v}) - \frac{e\Theta}{mk^2}\mathbf{k}\mathbf{k}_n \cdot \frac{\partial W}{\partial \mathbf{v}} + \frac{e\Theta}{mk^2}\frac{(k L_\mathrm{D})^2}{1 + (k L_\mathrm{D})^2}(\mathbf{Y}\cdot\mathbf{k})\,\mathbf{k}_n \cdot \frac{\partial W}{\partial \mathbf{v}} - \frac{e\Theta}{mk(u_n + \mathrm{i}\lambda)}\mathbf{I}\cdot\mathbf{v}_n\mathbf{k}_n \cdot \frac{\partial W}{\partial \mathbf{v}}. \tag{23}$$

It is now a simple matter to solve for $\delta\mathbf{E}_n(\mathbf{v})$ and calculate

$$\mathrm{St}\{f\} = \frac{e}{m}\int \frac{\mathrm{d}\mathbf{k}}{(2\pi)^3} \sum_n \mathbf{k}_n \cdot \frac{\partial}{\partial \mathbf{v}} J_n^2(k_\perp a)\, \mathrm{Re}\left[\frac{\mathbf{v}_n\, \delta\mathbf{E}_n(\mathbf{v})}{k(u_n + \mathrm{i}\lambda)}\right]. \tag{24}$$

The result is that already anticipated in Eq. (15) with $f(\mathbf{v})$ replaced by $W(\mathbf{v})$ except in the expressions for $\mathbf{H}_1(u)$, $\mathbf{H}_2(u)$, where the Maxwell distribution obtains.

5. Oscillators and particles at different temperatures

The collision operator of Eq. (15) does not change the mean particle energy and as such must be incomplete. It contains only the interactions of dressed particles and no real radiation. The simplest problem in which radiation appears is where we assume $f(\mathbf{v})$ and $f_0(p_\lambda q_\lambda)$ are Maxwell distributions at temperatures Θ and Θ'. Equations (19), (20), and (21) apply to this case. We subject them to a treatment similar to the previous section and ultimately obtain a field equation like Eq. (9). The solution is of the form $\delta\mathbf{E}_n(v) = \mathbf{S}(u_n)\cdot\mathbf{v}_n^* f(\mathbf{v})$ where $\mathbf{S}(u)$ satisfies the singular integral equation:

$$u^2\mathbf{Y}(u)\cdot\mathbf{S}(u) = \frac{4\pi\,\mathrm{i}\,e\,u}{k}\left\{\left[1 + \frac{1}{(k L_\mathrm{D})^2}\right]\mathbf{e}_1\mathbf{e}_1 + \frac{\Theta - \Theta'}{\Theta}\mathbf{I}\right\} - \frac{u}{(k L_\mathrm{D})^2}\int \frac{\mathrm{d}u'}{u' - u - \mathrm{i}\lambda}\mathbf{G}(u')\cdot\mathbf{S}_\mathrm{H}(u') - \frac{4\pi\,\mathrm{i}\,u}{k}\mathbf{C}_1 - \frac{4\pi\,\mathrm{i}}{k}\mathbf{C}_2. \tag{25}$$

$\mathbf{S}_\mathrm{H}$ means the Hermitian adjoint and $\mathbf{C}_1$, $\mathbf{C}_2$ are constant tensors defined as follows:

$$\mathbf{C}_1 = \frac{\mathrm{i}k}{4\pi(k L_\mathrm{D})^2}\int \frac{\mathrm{d}u}{u}\{\mathbf{e}_1\mathbf{e}_1\cdot\mathbf{G}(u)\cdot\mathbf{S}_\mathrm{H}(u) + \mathbf{S}(u)\cdot\mathbf{G}(u)\cdot\mathbf{e}_1\mathbf{e}_1\} - \frac{\mathrm{i}k}{4\pi(k L_\mathrm{D})^4}\int \frac{\mathrm{d}u'\,\mathrm{d}u''}{u'' - u' - \mathrm{i}\lambda}\left\{\mathbf{e}_1\cdot\mathbf{G}(u'') \cdot \frac{[\mathbf{S}(u') + \mathbf{S}_\mathrm{H}(u'')]}{u'\,u''}\cdot\mathbf{G}(u'')\cdot\mathbf{e}_1\right\}\mathbf{e}_1\mathbf{e}_1, \tag{26}$$

$$\mathbf{C}_2 = -\frac{\mathrm{i}k}{4\pi(k L_\mathrm{D})^2}\int \mathrm{d}u\,\mathbf{S}(u)\cdot\mathbf{G}(u)\cdot\mathbf{e}_1\mathbf{e}_1 - \frac{\mathrm{i}k}{4\pi(k L_\mathrm{D})^4}\int \frac{\mathrm{d}u'\,\mathrm{d}u''}{u'' - u' - \mathrm{i}\lambda} \cdot \left\{\mathbf{G}(u'')\cdot\frac{[\mathbf{S}(u') + \mathbf{S}_\mathrm{H}(u'')]}{u'}\cdot\mathbf{G}(u')\cdot\mathbf{e}_1\mathbf{e}_1\right\}. \tag{27}$$

Consider first the case where $\mathbf{B}=0$ in which case the same equations apply except that

$$\mathbf{G}(u) = G_{11}(u)\,\mathbf{e}_1\mathbf{e}_1 + G_\perp(u)\,\mathbf{I},$$

$$\mathbf{Y}(u) = Y_{11}(u)\,\mathbf{e}_1\mathbf{e}_1 + Y_\perp(u)\,\mathbf{I},$$

where

$$G_{11}(u) = u^2\sqrt{\frac{m}{2\pi\Theta}}\exp\left(-\frac{mu^2}{2\Theta}\right)$$

$$G_\perp(u) = \frac{\Theta}{m}\sqrt{\frac{m}{2\pi\Theta}}\exp\left(-\frac{mu^2}{2\Theta}\right)$$

$$Y_{11}(u) = 1 + \frac{1}{(k L_\mathrm{D})^2 u}\int \frac{\mathrm{d}u'}{u' - u - \mathrm{i}\lambda}G_{11}(u').$$

$$Y_\perp(u) = 1 - \frac{c^2}{u^2} + \frac{1}{(k L_\mathrm{D})^2 u}\int \frac{\mathrm{d}u'}{u' - u - \mathrm{i}\lambda}G_\perp(u').$$

The solution is of the form $\mathbf{S}(u)=S_{11}(u)\,\mathbf{e}_1\mathbf{e}_1+S_\perp(u)\,\mathbf{I}$, where

$$S_{11}(u)=\frac{4\pi i e}{k(u+i\lambda)}\,\frac{(kL_D)^2}{1+(kL_D)^2}$$

and $S_\perp(u)$ satisfies the equation

$$uY_\perp(u)\,S_\perp(u)=\frac{4\pi i e}{k}\,\frac{\Theta-\Theta'}{\Theta}$$
$$-\frac{1}{(kL_D)^2}\int\frac{du'}{u'-u-i\lambda}\,G_\perp(u')\,S_\perp{}^*(u'). \quad (28)$$

The constants $\mathbf{C}_1$, $\mathbf{C}_2$ are absent because it is clear from Eqs. (26) and (27) that they only have $\mathbf{e}_1\mathbf{e}_1$ components. Making use of the property that $Y_\perp(u)$ has no poles in the upper half of the u-plane we can show by contour integration that $\mathrm{Re}\,S_\perp(u)$ satisfies the sum rule

$$\int_{-\infty}^{\infty}\mathrm{Re}\,S_\perp(u)\,du=\frac{4\pi^2 e}{k}\,\frac{\Theta-\Theta'}{\Theta}. \quad (29)$$

Similarly, it follows that $S_\perp(u)$ satisfies the dispersion relation

$$\int_{-\infty}^{\infty}\frac{S_\perp(u')}{u'-u+i\lambda}\,du'=0. \quad (30)$$

Since

$$\mathrm{Im}\,S_\perp(u)=-\frac{1}{\pi}\,\mathsf{P}\int\frac{du'}{u'-u}\,\mathrm{Re}\,S_\perp(u'),$$

we can eliminate $\mathrm{Im}\,S_\perp(u)$ from Eq. (28). Substituting for $\mathrm{Im}\,S_\perp(u)$ and interchanging orders of integration with the Poincaré-Bertram formula, Eq. (28) is transformed to

$$\frac{1}{\pi i}\int\frac{du'}{u'-u-i\lambda}\,u'\,Y_\perp(u')\,\mathrm{Re}\,S_\perp(u')=0. \quad (31)$$

$\mathrm{Re}\,S_\perp(u)=0$ is not an acceptable solution because it does not satisfy the sum rule. The solution must be of the form

$$uY_\perp(u)\,\mathrm{Re}\,S_\perp(u)=\frac{1}{Y_\perp{}^*(u)}\sum_{n=1}\frac{\Gamma_n}{u^n},$$

where Γ_n are constants. Since $u^nY_\perp{}^*(u)\to 0$ as $u\to 0$ for $n>2$, in order to satisfy Eq. (31) $\Gamma_n=0$ for $n>2$. From Eq. (30) we can infer that $\int\mathrm{Re}\,S_\perp(u)\,du/u=0$. Since $|Y_\perp(u)|^2$ is an even function of u, $\Gamma_2=0$. The solution is, therefore,

$$\mathrm{Re}\,S_\perp(u)=\frac{\Gamma_1}{|uY_\perp(u)|^2}. \quad (32)$$

The constant Γ_1 follows from the sum rule:

$$\Gamma_1=\frac{4\pi^2 e}{k}\,\frac{(\Theta-\Theta')/\Theta}{\int|uY_\perp(u)|^{-2}du}.$$

The solution when $\mathbf{B}\neq 0$ is the tensor analog with some minor differences. $\mathbf{S}(u)=\mathbf{H}(u)+\mathbf{A}(u)$ where the Hermitian part $\mathbf{H}(u)$ and the anti-Hermitian part $\mathbf{A}(u)$ are related by Hilbert transformation. That is

$$\mathbf{A}(u)=\frac{1}{\pi i}\,\mathsf{P}\int\frac{du'}{u'-u}\,\mathbf{H}(u'). \quad (33)$$

The result for $\mathbf{H}(u)$ is

$$\mathbf{H}(u)=\frac{4\pi^2 e}{k}\,\frac{(kL_D)^2}{1+(kL_D)^2}\,\mathbf{e}_1\mathbf{e}_1\,\delta(u)$$
$$+[\mathbf{Y}^{-1}(u)]\cdot\left[\frac{\Gamma_1}{u^2}+\frac{\Gamma_2}{u^3}\right][\mathbf{Y}^{-1}(u)]_{\mathrm{H}}. \quad (34)$$

Substituting Eq. (34) into Eqs. (26) and (27) it can be demonstrated that

$$e\left[1+\frac{1}{(kL_D)^2}\right]\mathbf{e}_1\mathbf{e}_1-\mathbf{C}_1=\frac{e}{1+1/(kL_D)^2}$$

and $\mathbf{C}_2=0$.

The constants $\mathbf{\Gamma}_1$ and $\mathbf{\Gamma}_2$ are Hermitian tensors determined by the sum rule:

$$\int\mathbf{H}(u)\,du=\frac{4\pi^2 e}{k}\left\{\frac{(kL_D)^2}{1+(kL_D)^2}\,\mathbf{e}_1\mathbf{e}_1+\frac{\Theta-\Theta'}{\Theta}\,\mathbf{I}\right\} \quad (35)$$

and

$$\int\frac{du}{u}\left\{\mathbf{H}(u)-\frac{4\pi^2 e}{k}\,\frac{(kL_D)^2}{1+(kL_D)^2}\,\mathbf{e}^1\mathbf{e}^1\,\delta(u)\right\}=0. \quad (36)$$

$\mathbf{\Gamma}_2\neq 0$ in this case because $u^{-3}\,[\mathbf{Y}^{-1}(u)]\cdot\mathbf{\Gamma}_1[\mathbf{Y}^{-1}(u)]$ is not an odd function of u. The only obvious properties are $\mathbf{e}_1\cdot\mathbf{\Gamma}_1\cdot\mathbf{e}_1=\mathbf{e}_1\cdot\mathbf{\Gamma}_2\cdot\mathbf{e}_1=0$. This is essential because

$$\lim_{u\to 0}\mathbf{Y}^{-1}(u)=\frac{1}{1+1/(kL_D)^2}\,\mathbf{e}_1\mathbf{e}_1+\mathrm{O}(u^2)$$

and we know that the sum-rule integral exists.

6. Radiation formulae

The collision operator takes the form

$$\mathsf{St}\{f\}=\frac{e}{m}\int\frac{d\mathbf{k}}{(2\pi)^3}\sum_n\mathbf{k}_n$$
$$\cdot\frac{\partial}{\partial v}\,J_n{}^2(k_\perp a)\,\frac{[\mathbf{v}_n\cdot\mathbf{H}(u_n)\cdot\mathbf{v}_n{}^*]}{ku_n}\,f(v).$$

$\mathbf{H}(u_n)$ is given by Eq. (34) in which the first term may be omitted. The rate of change of particle kinetic energy per unit volume is

$$\frac{\partial T}{\partial t}=\int d\mathbf{v}\,\frac{1}{2}\,mv^2\mathsf{St}\{f\}$$
$$=-n_0 e\int\frac{d\mathbf{k}}{(2\pi)^3}\int du\,\mathrm{tr}\,[\mathbf{H}(u)\cdot\mathbf{G}(u)].$$

An approximate calculation will be made in which ω_p/kc is regarded as a small quantity. If we retain terms of order $(\omega_p/kc)^2$ but neglect higher orders the off-diagonal elements of the matrix $\mathbf{Y}(u)$ disappear. In carrying out the u-integration to determine $\mathbf{\Gamma}_1$ and $\mathbf{\Gamma}_2$ and in Eq. (38), the main contribution comes from the resonance at

$$(ku_0)^2=(kc)^2+\omega_p{}^2\left[1+\mathrm{O}\left(\frac{\Theta}{mc^2}\right)\right]$$

and we assume $\Theta/mc^2\ll 1$ in the present calculation. With these approximations

$$\mathbf{\Gamma}_1=\frac{4\pi^2 e}{k^3 L_D{}^2}\left(\frac{\Theta-\Theta'}{\Theta}\right)[G_{22}(u_0)\,\mathbf{e}_2\mathbf{e}_2+G_{33}(u_0)\,\mathbf{e}_3\mathbf{e}_3] \quad (39)$$

$$\mathbf{\Gamma}_2=0$$

Equation (38) can thus be reduced to

$$\frac{\partial T}{\partial t} = -4\pi^2 e^2 n_0 \left(\frac{\Theta - \Theta'}{\Theta}\right) \int \frac{\mathrm{d}\mathbf{k}}{(2\pi)^3} \frac{1}{k} \mathrm{tr}\left[\mathbf{I} \cdot \mathbf{G}(u_0)\right]. \quad (40)$$

For an optically thin plasma we can assume that the oscillator temperature $\Theta' = 0$. In the low-density limit $u_0 = c$ and Eq. (40) is just the vacuum radiation formula [7]. Equation (40) describes the radiation of oscillators that satisfy the plasma dispersion relation $\omega^2 = (ku_0)^2 = \omega_p^2 + k^2c^2$. Although this has only been demonstrated approximately, it is apparent from the exact formula that the resonance is always characteristic of the plasma. The calculation commenced with vacuum oscillators and ends with plasma oscillators. Much of the complicated analysis of this problem corresponds to the oscillators struggling for re-normalization and could be avoided with a systematic procedure that starts with plasma oscillators.

In the exact radiation formula longitudinal and transverse waves are coupled which makes detailed calculation laborious. In this case the normal modes do not have a simple polarization and it is not even apparent which modes constitute radiation. The definition of radiation under these circumstances is accomplished by Eq. (38) although detailed calculations have not yet been carried out.

7. Kinetic equation

We have thus far considered only the case where $f(\mathbf{v})$ and $f_0(q, p)$ are Maxwellian. When this is not the case, the methods developed in this paper can still be carried through, although details will not be given here. The result is

$$\mathrm{St}\{f\} = -\frac{4\pi^2 e}{m} \int \frac{\mathrm{d}\mathbf{k}}{(2\pi)^3} \frac{1}{k^2} \times \sum_n \mathbf{k}_n \frac{\partial}{\partial \mathbf{v}} \frac{J_n^2(k_\perp a)}{u_n^2} \left\{ \mathrm{Im}\left(\mathbf{v}_n \cdot \mathbf{Y}^{-1}(u_n) \cdot \mathbf{v}_n^*\right) f(\mathbf{v}) + \frac{\pi\omega_p^2}{u_n^2} \left[\mathbf{v}_n \cdot \mathbf{H}_2(u_n) \cdot \mathbf{v}_n^*\right] \mathbf{k}_n \cdot \frac{\partial f}{\partial \mathbf{v}} + \pi \left[\mathbf{v}_n \cdot \mathbf{H}(u_n) \cdot \mathbf{v}_n^*\right] \mathbf{k}_n \cdot \frac{\partial f}{\partial \mathbf{v}} \right\}. \quad (41)$$

Although in a somewhat different form, the first two terms are identical to those predicted by the superposition principle in Eq. (15). In the last term

$$u^2 \mathbf{H}(u) = \left[\mathbf{Y}^{-1}(u)\right] \cdot \left[\boldsymbol{\Gamma}_1 + \frac{\boldsymbol{\Gamma}_2}{u}\right] \cdot \left[\mathbf{Y}^{-1}(u)\right]_{\mathrm{H}},$$

where $\boldsymbol{\Gamma}_1$ and $\boldsymbol{\Gamma}_2$ must be obtained by solving the equations

$$\int \mathbf{H}(u)\, \mathrm{d}u = \frac{1}{k} \left\{ \frac{k^2 c^2}{m} Q_0 \mathbf{I} - \frac{\omega_p^2}{k^2} \int \frac{\mathrm{d}u}{u^2} \left[\mathbf{H}_2(u) - \mathbf{e}_1 \mathbf{e}_1 (\mathbf{e}_1 \cdot \mathbf{H}_2(u) \cdot \mathbf{e}_1)\right] \right\}$$

$$\int \mathbf{H}(u) \frac{\mathrm{d}u}{u} = 0,$$

where

$$\mathbf{H}_2(u) = \left[\mathbf{Y}^{-1}(u)\right] \cdot \mathbf{G}(u) \cdot \left[\mathbf{Y}^{-1}(u)\right]_{\mathrm{H}}.$$

The generalization to include finite mass ions is accomplished as follows:

When they appear explicitly e, m, a, ω_p, and $f(v)$ are replaced by e_i, m_i, a_i, ω_{pi}, and $f_i(v)$, the corresponding quantities for particles of species i. The appropriate modification of $Y(u)$ is

$$\mathbf{Y}(u) = \mathbf{I}\left[1 - \sum_j \frac{\omega_{pj}^2}{(ku)^2}\right] - \frac{c^2}{u^2}\mathbf{I} - \frac{1}{(ku)^2} \sum_j \omega_{pj}^2 \int \mathrm{d}\mathbf{v}' \sum_n \frac{J_n^2(k_\perp a_j') \left(\mathbf{k}_n \cdot \partial f_j / \partial \mathbf{v}'\right) \mathbf{v}_n'^* \mathbf{v}_n'}{k u_n' - k u - \mathrm{i}\lambda}. \quad (42)$$

The additional sum is over particle species j. In the expression for $\mathbf{H}_2(u)$, $\mathbf{G}(u)$ is replaced by $\sum_j \mathbf{G}_j(u)$.

The generalization to make the results relativistic involves the following recipe:

i) replace $\partial/\partial \mathbf{v}$ by $\partial/\partial \boldsymbol{\xi}$ and $\mathrm{d}\mathbf{v}$ by $\mathrm{d}\boldsymbol{\xi}$ where $\boldsymbol{\xi} = \mathbf{v}[1-(v/c)^2]^{-1/2}$;

ii) replace $f(v_\perp, v_z)$ by $f(\xi_\perp, \xi_z)$ such that $\int f(\xi_\perp, \xi_z)\, \mathrm{d}\boldsymbol{\xi} = 1$;

iii) for the cyclotron frequency substitute $\omega_c = (eB/mc)[1-(v/c)^2]^{1/2}$, where m is the rest mass;

iv) for the operator $\mathbf{k}_n \cdot \partial/\partial \mathbf{v}$, as it appears immediately after the summation symbol in the collision integral in Eqs. (15), (24), (37), and (41) substitute

$$k_z \frac{\partial}{\partial \xi_z} + \frac{n\omega_c}{\xi_\perp} \frac{\partial}{\partial \xi_\perp} \frac{\xi_\perp}{\mathbf{v}_\perp};$$

v) for the tensor $\mathbf{Y}(u)$ substitute

$$\mathbf{Y}(u) = \mathbf{I} - \frac{c^2}{u^2}\mathbf{I} + \frac{\omega_p^2}{(ku)^2} \int \mathrm{d}\boldsymbol{\xi} \sum_n J_n^2(k_\perp a)\, v_n \frac{\partial f}{\partial \xi_n} - \frac{\omega_p^2}{(ku)^2} \int \mathrm{d}\xi' \sum_n \frac{J_n^2(k_\perp a') \left(\mathbf{k}_n \cdot \partial f / \partial \boldsymbol{\xi}'\right) \mathbf{v}_n'^* \mathbf{v}_n'}{\mathbf{k} \cdot \mathbf{v}_n' - k u - \mathrm{i}\lambda}.$$

Acknowledgements

We should like to express our appreciation to Professor Marshall Rosenbluth for constructive criticism.

This work was carried out under a joint General Atomic—Texas Atomic Energy Research Foundation program on controlled thermonuclear reactions. The contribution of one of the authors (A.S.) was based on work performed while associated with the Oak Ridge National Laboratory (operated by Union Carbide Corporation for the United States Atomic Energy Commission).

References

[1] Rostoker, N., Rosenbluth, M. N., *Phys. Fluids* **3** (1960) 1.
[2] Simon, A., Harris, E. G., *Phys. Fluids* **3** (1960) 245.
[3] Lenard, A., *Ann. Phys. (N. Y.)* **10** (1960) 390.
[4] Balescu, R., *Phys. Fluids* **3** (1960) 52.
[5] Rostoker, N., *Phys. Fluids* **3** (1960) 922.
[6] Simon, A., *Phys. Fluids* **4** (1961) 586.
[7] Trubnikov, B., Kudryavtsev, V., Proceedings of Second U.N. International Conference on Peaceful Uses of Atomic Energy, Geneva, **31** (1958) 93.
[8] Rostoker, N., *Nuclear Fusion* **1** (1961) 101.

NEUTRALISATION D'UN FAISCEAU D'IONS PAR INJECTION D'ÉLECTRONS*

J. M. DOLIQUE

COMPAGNIE GÉNÉRALE DE TÉLÉGRAPHIE SANS FIL

ORSAY (SEINE-ET-OISE), FRANCE

La réalisation d'un faisceau d'ions, neutralisé par injection d'électrons, est susceptible d'un grand nombre d'applications pratiques extrêmement intéressantes: propulsion des fusées, injection dans une bouteille magnétique — en vue de la fusion thermonucléaire —, accélérateurs à plasma, etc.

Expérimentalement, l'obtention d'un faisceau mélangé stable, à grande intensité, offre de très grosses difficultés; d'où l'intérêt qui s'attache à l'étude théorique du problème; on développe ici une étude théorique.

1. Hypothèses

Des ions, provenant d'une source S (figure 1), sont accélérés par une grille G; ils forment au delà un faisceau homogène (densité n_i), dans lequel les vitesses $\mathbf{w}_i$ des ions sont distribuées (dans les trois dimensions) autour d'une vitesse moyenne $\mathbf{v}_i = \langle \mathbf{w}_i \rangle$ parallèle à Oz, avec des températures longitudinale et transversale, $T_{i\parallel}$ et $T_{i\perp}$.

On se propose d'étudier la possibilité de neutraliser un tel faisceau par mélange à des électrons, issus d'une cathode K et accélérés (ou ralentis) entre K et G.

On suppose que le faisceau mélangé est de révolution autour de Oz ($\partial/\partial\theta = 0$) et indéfini radialement ($\partial/\partial r = 0$): les grandeurs physiques introduites ne dépendront que de la cote z et éventuellement du temps t. La mobilité des ions étant beaucoup plus petite que celle des électrons, on admet que le faisceau d'ions conserve, après le début du mélange ($t > 0$), ses caractéristiques antérieures (n_i, v_i, T_i).**

Les électrons possèdent, dans le faisceau mélangé, une densité $n_e(z, t)$ et des vitesses $\mathbf{w}_e(z, t)$ distribuées (dans les trois dimensions) autour d'une vitesse moyenne $\mathbf{v}_e(z, t) = \langle \mathbf{w}_e(z, t) \rangle$ parallèle à Oz, avec des températures longitudinale et transversale, $T_{e\parallel}$ et $T_{e\perp}$. (Le temps d'équipartition de l'énergie entre électrons et ions est beaucoup plus long que les temps de relaxation en vitesse: $T_{i\parallel}$, $T_{i\perp}$, $T_{e\parallel}$, $T_{e\perp}$ sont considérés comme constants).

Les données sont n_i, v_i, $T_{i\parallel}$, $T_{i\perp}$, $T_{e\parallel}$, $T_{e\perp}$, $n_e(0, t)$ (lié au chauffage de K), et la densité de courant totale au niveau de l'injection ($z = 0$):

$$j_0(t) = e\,[n_i v_i - n_e(0, t)\, v_e(0, t)]$$

** L'étude des oscillations ioniques montre que cette hypothèse est justifiée en petits signeaux [$n_e(0, t) \simeq n_i$, $v_e(0, t) \simeq v_i$]. En grands signaux, des oscillations ioniques samplifiant peuvent appairaître (instabilité à 2 faisceaux, cf. [2]).

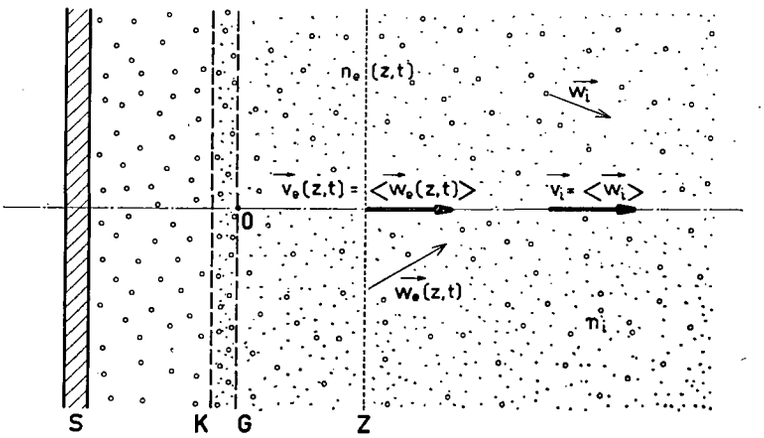

Figure 1 Géométrie du mélange.

* Mémoire CN-10/89 présenté par J. M. Dolique. La discussion concernant ce mémoire est donnée page 816. Les traductions du résumé se trouvent en fin de volume.

(lié à la différence de potential K — G). Les inconnues sont $n_e(z, t)$ et $v_e(z, t)$.

La neutralisation idéale correspondrait à $n_e(z, t) \equiv n_i$. Mais dans les applications pratiques, une neutralisation approchée: $u(z, t) \equiv [n_e(z, t) - n_i]/n_i \ll 1$ suffit généralement. Ce sont les conditions de cette neutralisation approchée qu'on va rechercher. On va étudier pour cela, dans quelques cas particuliers importants, la forme des solutions $[n_e(z, t), v_e(z, t)]$ du système d'équations aux dérivées partielles ($\mathfrak{S}$) formé par les équations de Maxwell et l'équation de transport de la quantité de mouvement de Fokker-Planck (ν désignera la fréquence des collisions électron-ion, calculée en [1] pour des gaz électronique et ionique à des températures différentes).

2. Phénomènes linéaires (petits signaux)

On va supposer d'abord qu'au niveau de l'injection les écarts relatifs à la neutralité, en densité:

$$u_0(t) \equiv u(0, t) \equiv \frac{n_e(0, t) - n_i}{n_i},$$

et en courant:

$$i_0(t) \equiv \frac{j_0(t)}{n_i e v_i} \equiv \frac{n_i v_i - n_e(0, t) v_e(0, t)}{n_i v_i}$$

sont petits: $u_0(t) \ll 1$, $i_0(t) \ll 1$ (et donc $[v_e(0, t) - v_i]/v_i \ll 1$); et on va chercher dans quelles conditions l'écart relatif à la neutralité en densité $u(z, t) \equiv n_e(z, t)/n_i - 1$ reste petit dans le faisceau mélangé. $u(z, t)$ est donc traité en perturbation et le système différentiel ($\mathfrak{S}$) (Fokker-Planck-Maxwell) linéarisé. Les résultats sont donnés, d'abord, pour le cas particulier très important du régime permanent ($\partial/\partial t = 0$), puis pour le cas général.

2.1. Régime permanent

Les données, $u_0(t)$ et $i_0(t)$ sont alors des constantes u_0 et i_0. Une condition nécessaire d'existence d'un régime permanent est $i_0 = 0$.

Un paramètre essentiel qui apparaît est:

$$\alpha = \frac{\sigma_e}{v_i} = \frac{1}{v_i}\left(\frac{kT_{e\parallel}}{m_e}\right)^{1/2} \tag{2.1}$$

rapport entre l'écart-type $\sigma_e = (1/v_i)\,(kT_{e\parallel}/m_e)^{1/2}$ de la distribution des vitesses électroniques, et la vitesse moyenne ionique v_i.

Il y a d'abord, autour de $\alpha = 1$, une bande très étroite: $1 - \nu/2\,\omega_p < \alpha < 1 + \nu/2\,\omega_p$. ($\omega_p = [n_i e^2/\varepsilon_0 m_e]^{1/2}$, pulsation plasma; on a toujours $\nu \ll \omega_p$), où la théorie linéaire n'est pas valable.

Si $\alpha < 1$, $u(z)$ est une fonction sinusoïdale amortie, ayant pour période

$$\lambda = \frac{2\pi v_i}{\omega_p}\sqrt{1 - \alpha^2} \tag{2.2}$$

et pour distance d'amortissement $[u(l/2\pi) = (1/e)\,u_0]$

$$l = \frac{4\pi v_i}{\nu}(1 - \alpha^2). \tag{2.3}$$

On a un régime de neutralisation «libre». [Les écarts à la neutralité en charge ou en courant, au niveau de l'injéction, se propagent le long du faisceau, atténuées seulement par les collisions. Le faisceau mélangé est neutre: *a*) en moyenne, rigeureusement ($\langle n_i(z)\rangle = \langle n_e(z)\rangle$), et *b*) en tout point, de manière approchée ($n_e(z) \simeq n_i(z)$.] Si $u_0 = 0$, $u(z) \equiv 0$: il y a neutralisation idéale.

Si $\alpha > 1$, $u(z)$ est une exponentielle décroissante avec une distance d'attenuation $(u(\lambda'/2\pi) = e\,u_0)$:

$$\lambda' = \frac{2\pi v_i}{\omega_p}\sqrt{\alpha^2 - 1}. \tag{2.4}$$

On a un régime de neutralisation «forcée». [Les écarts à la neutralité en charge, ou en courant, au niveau de l'injection, sont très rapidement atténués.]

Dans les problèmes d'injection d'ions à grande énergie dans une bouteille magnétique, on se trouve dans la région $\alpha < 1$: on a neutralisation libre. Ainsi, dans les premières expériences faites au département atomistique de la C.S.F., le faisceau d'ions, extrait d'un duoplasmatron sous une tension pouvant varier de 5 à 50 kV, avait les caractéristiques suivantes: protons, $n_i = 10^{14}$ m^{-3}, $T_{i\perp} = 230\,000°$ K (20 eV), $T_{e\perp} = 1500°$K. On a, pour ce faisceau, $\alpha \ll 1$, $\lambda = 3{,}4$ cm, $l = 640$ m.

En propulsion ionique au contraire, les électrons doivent en général être ralentis entre K et G; on a $\alpha > 1$, et neuralisation forcée; ainsi pour un faisceau d'ions césium de densité $n_i = 10^{17}$ m^{-3}, accélérés à 1 keV, on a (avec encore $T_{e\perp} = 1500°$K): $\alpha = 2{,}3$, $\lambda' = 16\ \mu$: la neutralisation se produit avec une extrême rapidité.

2.2. Régimes dépendant du temps

u_0 et i_0 sont maintenant de certaines fonctions (qu'on se donne) du temps, $u_0(t)$ et $i_0(t)$, l'écart relatif à la neutralité en densité, u (qu'on cherche), une fonction de z et de t, $u(z, t)$. En introduisant les notations sans dimensions suivantes $\varkappa = \nu/2\omega_p$, $Z = (\omega_p/v_i)\,z$, $T = \omega_p\,t$, et les fonctions auxiliaires:

$$I_0(T) = \frac{1}{1 - \alpha}\left\{\int_0^T i_0(T)\,dT + 2\varkappa i_0(T) + i_0'(T)\right\} \tag{2.5}$$

$$L_0(T) = e^{-\varkappa T}\int_0^T e^{\varkappa T} I_0(T)\,dT \tag{2.6}$$

$$\varphi(T) = \frac{1 + \alpha}{2\alpha}u_0(T) + \frac{1 - \alpha}{2\alpha}L_0(T) \tag{2.7}$$

$$\psi(T) = -\frac{1 - \alpha}{2\alpha}[u_0(T) + L_0(T)] \tag{2.8}$$

On trouve pour $u(Z, T)$ (solution du système différential (Ⓢ)-Fokker-Planck-Maxwell-linéarisé)

$$u(Z,T) = e^{-\varkappa Z/(1-\alpha)}\varphi\left(T - \frac{Z}{1-\alpha}\right) + e^{-\varkappa Z/(1+\alpha)}\psi\left(T - \frac{Z}{1+\alpha}\right) - \frac{Z}{2\sqrt{1-\alpha^2}}\, e^{-\varkappa Z/(1-\alpha^2)} \times \int_0^{\pi} e^{\varkappa[\alpha Z/(1-\alpha^2)]\cos\theta} J_1\left(\frac{Z}{\sqrt{1-\alpha^2}}\sin\theta\right) \times \left[(1-\cos\theta)\varphi\left(T - \frac{Z}{1-\alpha^2} + \frac{\alpha Z}{1-\alpha^2}\cos\theta\right) + (1+\cos\theta)\psi\left(T - \frac{Z}{1-\alpha^2} + \frac{\alpha Z}{1-\alpha^2}\cos\theta\right)\right] d\theta \quad (2.9)$$

(J_1: fonction de Bessel de première espèce d'ordre 1; au voisinage immédiat de $\alpha = 1$, les phénomènes non-linéaires sont essentiels, cette formule n'est plus valable.)

$u(Z, T)$ apparaît comme somme d'une onde φ, de vitesse de phase $V_1 = 1 - \alpha$ (dans l'espace des Z, soit $v_1 = v_i(1 - \alpha)$ dans l'espace réel), d'une onde ψ de vitesse de phase $V_2 = 1 + \alpha$, et de deux ondes dont les composantes spectrales — paramètre θ — ont des vitesses de phase V, $V_1 < V < V_2$.

On va examiner maintenant les cas particuliers les plus importants.

2.2.1. Le cas: $u_0(T) \equiv u_0$, $i_0(T) \equiv 0$.

On a alors $L_0(T) \equiv 0$; on peut montrer que la formule ci-dessus redonne bien les solutions $u(Z)$, indépendantes du temps, étudiées au paragraphe 2.1.

2.2.2. Le cas: $u_0(T) \equiv u_0$, $i_0(T) \equiv i_0 \neq 0$.

On obtient pour $u(Z, T)$ une fonction de Z et de T qui n'est pas bornée. Le faisceau mélangé se détruit donc. Mais l'hypothèse $i_0(T) \equiv i_0 \neq 0$ n'est pas réaliste physiquement, car on a alors en $Z = 0$ (au niveau de la grille accélératrice des électrons) un champ électrique $E(0, T) = -(1/e)\, v_i\, m_e\, \omega_p\, i_0\, T$, qui tend, quand T croît, à accélérer davantage les électrons et par conséquent à réduire i_0. On a là un mécanisme auto-oscillateur.

2.2.3. L'influence d'oscillations (pulsation ω)

Pour connaître l'influence d'oscillations (pulsation ω) au niveau de l'injection sur le comportement ultérieur du faisceau, on est amené à étudier le cas où $u_0(T)$ [ou $i_0(T)$] est une fonction sinusoïdale $u_0(T) = u_0 \cos \Omega T$ ($\Omega = \omega/\omega_p$). C'est d'ailleurs là le cas particulier le plus simple et le plus intéressant après $u_0(T)$ [ou $i_0(T)$] constant.

Par transformation de Fourier on pourra toujours y réduire les cas plus généraux, où $u_0(T)$ est une fonction quelconque du temps (les équations en u ont été linéarisées). Par la considération de la fonction de corrélation on pourra en déduire la réponse du faisceau mélangé à des fluctuations aléatoires de densité (ou de vitesse électronique moyenne) au niveau de l'injection.

Les résultats sont résumés par la figure 2.

Dans la zone de neutralisation $u(Z, T)$ résulte de la superposition de deux ondes (ondes de charge d'espace électroniques), amorties par les collisions, de vitesses de phase V_1 et V_2 (vitesses réduites = $(1/v_i)$ × vitesses réelles):

$$V_1 = \frac{\Omega}{\Omega^2 - 1}\left[\Omega + \sqrt{1 - \alpha^2 + \alpha^2\Omega^2}\right],$$
$$V_2 = \frac{\Omega}{\Omega^2 - 1}\left[\Omega - \sqrt{1 - \alpha^2 + \alpha^2\Omega^2}\right]. \quad (2.10)$$

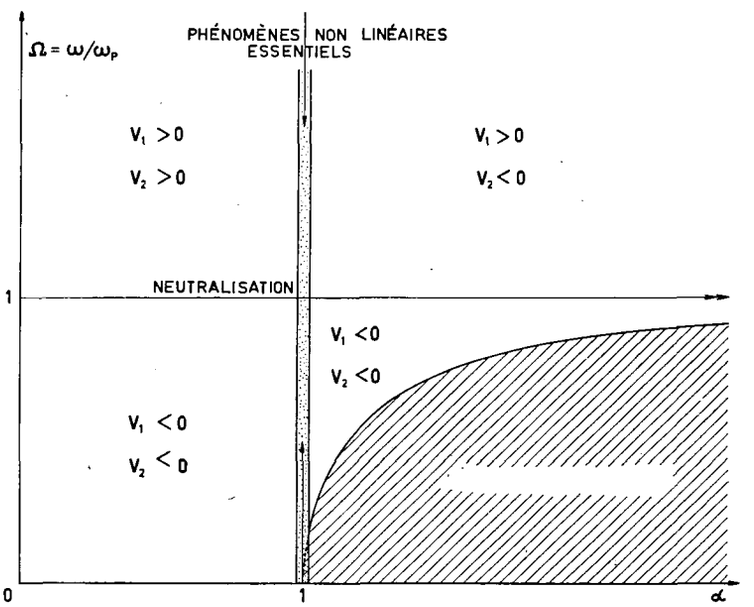

Figure 2 Domaine de la neutralisation libre, en régime sinusoïdal [$u_0(T) = u_0 \cos \Omega T$] (petits signaux). La zone hachurée: neutralisation «forcée». (Au lieu de «neutralisation» sur la figure, lire: «neutralisation libre».)

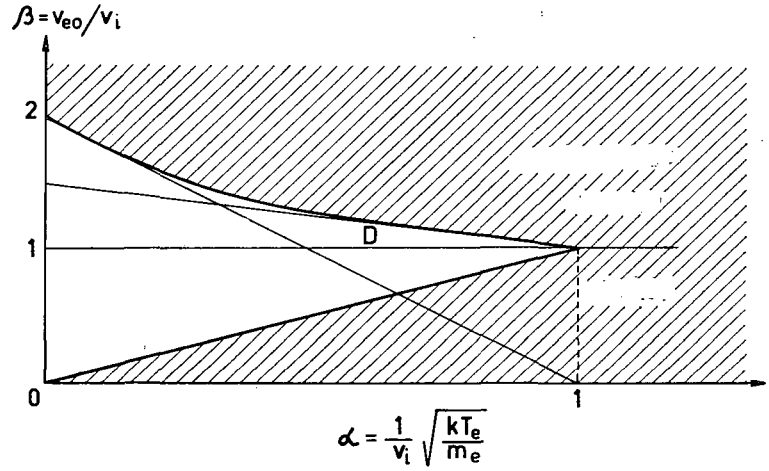

Figure 3 Domaine de la neutralisation libre, en régime permanent (grands signaux).

Pour $\Omega=0$, $V_1=V_2=0$ et on retombe sur la solution $u(Z)$ indépendante du temps du paragraphe 2.1. Pour $\alpha=0$ (électrons à la température 0), on retrouve la formule de RAMO [2]: $V_{1,2}=\omega/(\omega\pm\omega_p)$.

3. Phénomènes non linéaires (grands signaux)

On suppose maintenant qu'au niveau de l'injection, les écarts relatifs à la neutralité, en densité $u_0=n_{e0}/n_i-1$ et en courant $i_0=j_0/n_i\ ev_i=1-n_{e0}v_{e0}/n_iv_i$, ne sont plus petits, mais quelconques. (La vitesse moyenne d'injection des électrons v_{e_0} est donc quelconque également par rapport à v_i.)

Le système différentiel (℘)(Fokker-Planck-Maxwell), désormais non-linéaire, n'est plus justiciable d'un traitement analytique. On l'a étudié sur un calculateur analogique ANALAC (A. 101), dans le cas du régime permanent ($\partial/\partial t=0$; $i_0=0$). Les résultats sont les suivants:

3.1. Domaine de la neutralisation libre

Les deux paramètres qui conditionnent l'allure des solutions sont α (défini plus haut: $\alpha=\sigma_e/v_i=(1/v_i)(k\,T_e/m_e)^{1/2}$) et $\beta=v_{e0}/v_i$. Dans le plan (α, β), il apparaît (figure 3) un domaine $\mathfrak{D}$ à l'intérieur duquel $u(Z)$ est une fonction pseudo-périodique amortie alternative (moyenne nulle sur une pseudo-période): on a neutralisation libre le faisceau mélangé est neutralisé en moyenne.

A l'extérieur de $\mathfrak{D}$, il y a neutralisation forcée. $\mathfrak{D}$ est un triangle mixtiligne, graphe de la relation:

$$\alpha<\beta<\frac{2}{1+\alpha},\quad \text{ou}\quad \alpha v_i<v_{e0}<\frac{2}{1+\alpha}v_i. \tag{3.1}$$

La droite $\beta=v_{e0}/v_i=1$ (sur laquelle on a également $n_{e0}/n_i=1$, puisque $i_0=0$) correspond à la neutralisation idéale. Dans le cas particulier $\alpha=0$ (injection d'électrons monocinétiques) on retrouve la condition $0<v_{e0}/v_i<2$ indiquée en [3].

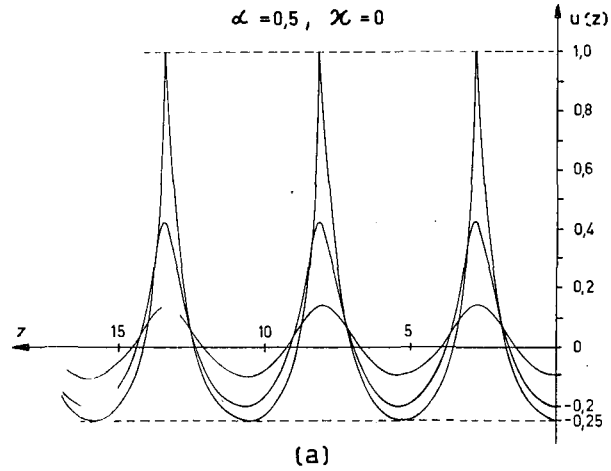

Figure 4a Variation de l'écart relatif à la neutralité en densité $u=n_e/n_i-1$, en fonction de la distance z au niveau d'injection des électrons, pour $\alpha=0{,}5$ et $\varkappa=0$ où $\alpha=(1/v_i)(k\,T_{e\parallel}/m_e)^{1/2}$ (agitation thermique des électrons) et $\varkappa=\nu/2\ \omega_p$ (collisions électron-ion). cf. texte.

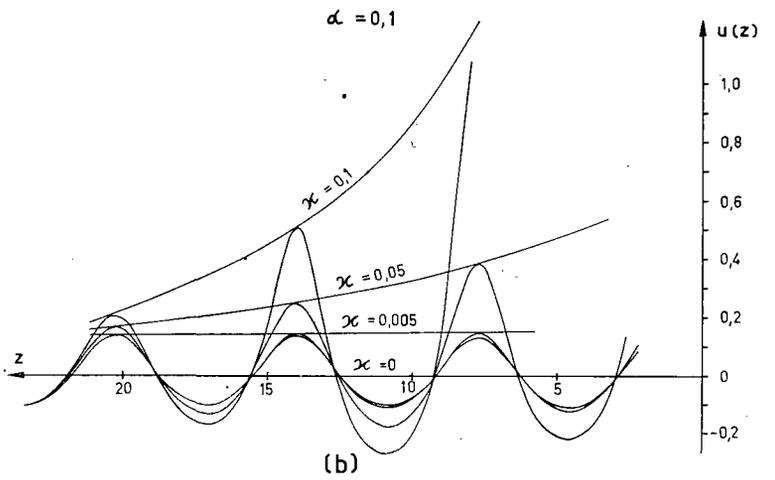

Figure 4b Voir légende de la figure 4a. Cas $\alpha = 0{,}1$ et $0 \leq \varkappa \leq 0{,}1$.

3.2. Variation de la densité électronique dans le faisceau mélangé en l'absence de collisions

Lorsque les collisions sont négligeables ($\varkappa = 0$) la variation de u (et donc de la densité électronique $n_e = n_i(1+u) = n_i + n_i u$) en fonction de Z dans le faisceau mélangé [pour $(\alpha, \beta) \in \mathfrak{D}$] a l'allure représentée sur la figure 4a (cas particulier $\alpha = 0{,}5$). Pour $|u_0| \ll 1$ on retrouve la sinusoïde de la théorie linéaire. Lorsque u_0 croît en valeur absolue, se rapprochant de l'une de ses bornes, supérieure, positive $u_{0m} = (1/\alpha) - 1$ (qui correspond à $v_{e0} = 2v_i/1+\alpha$) ou inférieure, négative $u_{0m} = -(1-\alpha)/2$ (qui correspond à $v_{e0} = \alpha v_i$) la courbe $u(Z)$ présente des maxima de plus en plus aigus et des minima de plus en plus plats. La période décroît légèrement avec u_0 pour α donné.

3.3. Rôle d'amortissement des collisions

La figure 4b montre pour $\alpha = 0{,}1$ et de petites valeurs de u_0 l'amortissement introduit par les collisions. $\varkappa = 0{,}005$ correspond à

$$T_e = 1000\,°\mathrm{K},\ n_i = 10^{17}\,m^{-3}\,[T_i \ll (m_i/m_e)\,T_e].$$

Les figures 4c et 4d* montrent que le rôle des collisions devient plus important quand, à α constant, u_0 croît, ou quand, à u_0 constant, α se rapproche de 1, donc, d'une manière générale, quand les phénomènes non-linéaires deviennent plus importants.

* La programmation du système différentiel ($\mathfrak{S}$) ne se faisait commodément qu'avec $dz/dt < 0$ (t temps de la machine): toutes les courbes sont tracées de gauche à droite (vers les $Z < 0$) et ont donc même ordonnée finale (en Z) et non même ordonnée initiale u_0.

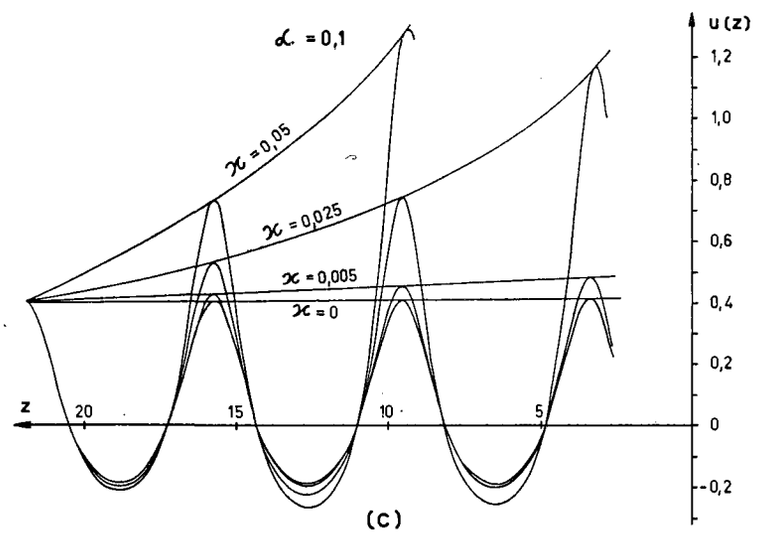

Figure 4c Voir légende de la figure 4a. Cas α constant, u_0 croît. (Voir texte.)

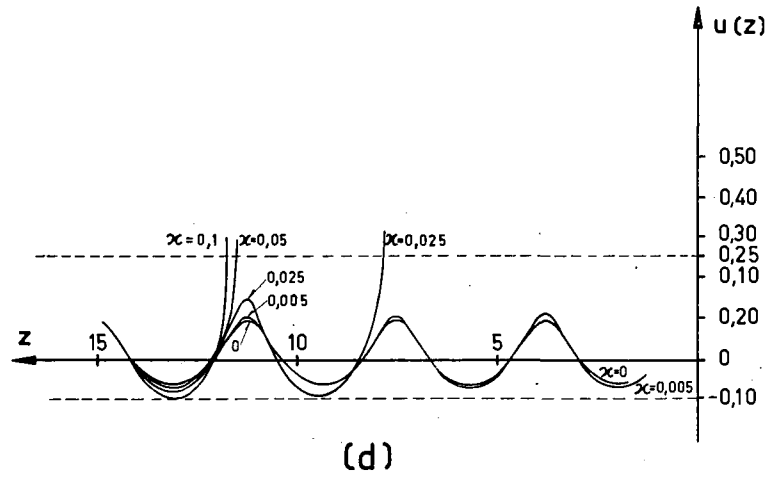

Figure 4d Voir légende de la figure 4a. Cas u_0 constant, α se rapproche de 1. (Voir texte.)

3.4. Instabilité à deux faisceaux

L'étude précédente ne concerne que les oscillations électroniques. En fait, pour $v_e \neq v_i$, on n'a plus le droit de négliger le couplage entre oscillations électroniques et ioniques. Des instabilités à deux faisceaux apparaissent.*

4. Conclusion

Cette étude théorique montre la possibilité de réaliser, dans certaines conditions, une neutralisation approchée, ou en moyenne, d'un faisceau d'ions par injection d'électrons.

Appendice

En fonction des températures θ_i et θ_e des ions et des électrons dans la source d'ions S, et dans la cathode K, et des tensions, d'accélérations des ions V_i, et d'accélération (ou de ralentissement) des électrons V_e, on a [4]:

$$T_{i\perp} = \theta_i$$

$$T_{i\parallel} = \theta_i \left\{ 2\,\tau_i^2 + 1 - \frac{2}{\pi}\,[1 + \mathfrak{K}_0(\tau_i^2/2)]^2 \right\}$$

où

$$\tau_i = (e V_i / k\theta_i)^{1/2}, \quad \mathfrak{K}_0(x) = \int_0^x \exp(t) \cdot K_0(t)\,dt,$$

(K_0 fonction de Bessel modifiée de 2e espèce, d'ordre 0.)

$$T_{e\perp} = \theta_e$$

$$T_{e\parallel} = \theta_e \times \begin{cases} 2[1 - \frac{\pi}{4}\,e^{2\tau_e^2}(1 - \operatorname{erf}\tau_e) - \sqrt{\pi}\tau_e e^{\tau_e^2}(1 - \operatorname{erf}\tau_e)] \\ \qquad \text{(électrons accélérés)} \\ 2\,e^{-\tau_e^2}[1 - (\pi/4)\,e^{-\tau_e^2}] \\ \qquad \text{(électrons ralentis),} \end{cases}$$

où $\tau_e = (e V_e / k\theta_e)^{1/2}$, erf: fonction d'erreur,

$$v_i = (2/\pi)^{1/2}\,(k\theta_i/m_i)^{1/2}\,[1 + \mathfrak{K}_0(\tau_i^2/2)]$$

$$v_e = \begin{cases} \sqrt{2}\,(k\theta_e/m_e)^{1/2}\ \tau_e + \frac{\sqrt{\pi}}{2}\,e^{\tau_e^2}\,[1 - \operatorname{erf}(\tau_e)] \\ \qquad \text{(électrons accélérés)} \\ (\pi/2)^{1/2}\,(k\theta_e/m_e)^{1/2}\,e^{-\tau_e^2} \\ \qquad \text{(électrons ralentis).} \end{cases}$$

Pour les ions, on aura pratiquement toujours $e V_i \gg k\,\theta_i$; qu'on envisage les applications à l'alimentation d'une bouteille magnétique ou à la propulsion ionique, $k\,\theta_i$ ne dépassera jamais en effet quelques dizaines d'électron-volts tandis que $e V_i$ ne sera jamais inférieur à quelques keV. On a alors $\tau_i \gg 1$ et:

$$v_i(\tau_i \gg 1) \sim (2 e V_i / m_i)^{1/2},$$

$$T_{i\parallel} \to 0\,.$$

Pour les électrons, il faut distinguer les deux types d'applications. Pour la neutralisation d'un faisceau d'ions à grande énergie (quelques dizaines ou une centaine de keV) en vue de l'injection dans une bouteille magnétique, l'égalité des vitesses moyennes sera réalisé pour des v_{e0} de quelques dizaines de eV. On a alors $e\,V_e \gg k T_e$ ($1000°\,K \simeq 0{,}09$ eV), $\tau_e \gg 1$, et

$$v_{e0}(\tau_e \gg 1) \sim (2\,e V_e / m_e)^{1/2},$$

$$T_{e\parallel} \to 0.$$

* Editor's note: The publication schedule did not permit modification of Fig. 3 to indicate this region of instability. The region would consist of two wedge-shaped regions formed by $\alpha = 0$ and a line radiating upward from $\alpha = 0$, $\beta = 1$, and a similar line radiating downward from $\alpha = 0$, $\beta = 1$. The apex angle of each wedge would be $\ll 1$.

Dans les applications à la propulsion ionique, les ions sont lourds, par example ^{133}Cs, et leur énergie en général plus faible (de l'ordre de la dizaine de keV). Les électrons doivent être ralentis (entre K et G); τ_e est de l'ordre de l'unité, et il faut utiliser les formules générales ci-dessus.

Références

[1] Dolique, J. M., *C. R. Acad. Sci.* (*Paris*) **251** (1960) 1163.
[2] Ramo, S., *Phys. Rev.* **56** (1939) 276.
[3] Staff of the Ramo-Woolridge Research Laboratory, *Proc. Inst. Radio Engrs.* **48** (1960) 477.
[4] Dolique, J. M., Thèse de Doctorat des Sciences, Paris (1962).

ASYMPTOTIC THEORY OF HAMILTONIAN AND OTHER SYSTEMS WITH ALL SOLUTIONS NEARLY PERIODIC*

MARTIN KRUSKAL

PRINCETON UNIVERSITY, PLASMA PHYSICS LABORATORY

PRINCETON, NEW JERSEY, UNITED STATES OF AMERICA

Consider a system of N ordinary first-order differential equations in N dependent variables and let the independent variable s not appear explicitly. Let the system depend on a small parameter ε and possess a formal infinite power series expansion in ε, and suppose that the limiting system for $\varepsilon = 0$ exists and has only periodic solutions. Then a formal solution can be constructed involving infinite power series in ε and satisfying the equations over large domains of s (of order $1/\varepsilon$). The true solutions of the system exist over such domains and are asymptotically represented as $\varepsilon \to 0$ by the formal solutions. The construction is based on the standard type of formal series solution of a "reduced" system of $N-1$ equations in $N-1$ dependent variables and with the new independent variable $\sigma = \varepsilon s$; the omitted variable is essentially an angle variable φ describing the phase around the simple closed curves. If the original system is Hamiltonian, then one can define the usual action integral $J = \int \mathbf{p} \cdot \mathrm{d}\mathbf{q}$ to all orders; the integral is taken around the phase ring. It is proved that J is an integral of the system and that the Poisson bracket of φ with J is unity, both to all orders. The usefulness of this particular integral is that it is computable locally. The reduced system, after elimination of another dependent variable by means of the constancy of J, can itself be put in Hamiltonian form; if its solutions are nearly periodic, the whole procedure can be reapplied. The present theory encompasses previous proofs of adiabatic invariance to all orders for particular systems such as the harmonic oscillator, the nonlinear oscillator, the charged particle gyrating tightly in a given electromagnetic field, and the longitudinal back-and-forth motion of such a particle trapped between two "magnetic mirrors" in a weak electric field. There are many other applications.

1. Introduction

1.1. HISTORICAL PERSPECTIVE

The phenomenon of adiabatic invariance (constancy of an action integral under slow change of external parameters) has long been known in classical mechanics, receiving prominence because of its role in the so-called quantum conditions and of their importance during the transition from classical to quantum mechanics. Although the invariance was recognized to be only approximate and was only demonstrated to the lowest significant order [1], the question whether the constancy might be valid to higher order seems not to have been considered at that time or in that connection. For this there were perhaps two reasons: the first, that the question probably appeared to be of only academic interest and the second, that not all adiabatic invariants are constants beyond lowest order.

The question apparently first became of significance for applications in connection with the magnetic moment of gyration of a charged particle gyrating tightly in a strong magnetic field, which was shown to be an adiabatic invariant by ALFVÉN [2]. On the one hand, the theory of virtually every prospective device for the production of useful energy from controlled thermonuclear fusion [3] has leaned very heavily on the constancy of this magnetic moment, and in those cases for which more or less steady operation was envisioned (stellarator, mirror machine, etc.) it was seen that the requirement that particles remain confined for periods of time encompassing many millions of gyrations could generally be met only if the magnetic moment were in fact constant to a much higher approximation. In connection with the stellarator several other related approximate results were proved to hold to all orders [4, 5], which made it seem both fitting and somewhat more likely that the constancy of the magnetic moment would follow suit. On the other hand, astrophysical theories (e.g. the Fermi mechanism [6] for cosmic ray production) led to precisely the same question, in response to which HELLWIG [7] proved the constancy of the magnetic moment to the next order beyond the lowest. KULSRUD [8] considered the simpler problem of a harmonic oscillator with slowly changing coefficient of elasticity and proved that its adiabatic invariant (ratio of energy to frequency) was constant to all orders, seemingly the first result of the kind. In quick succession after this breakthrough KRUSKAL [9] proved the analogous result for the gyrating particle and LENARD [10] for the anharmonic oscillator. BERKOWITZ and GARDNER [11] stiffened the results with unwonted (but wanted!) mathematical rigor by proving that the formal expansions employed to describe the motion of the gyrating particle really were correct asymptotic series for the true trajectory.

Another adiabatic invariant whose degree of constancy has become of practical importance recently is the so-called longitudinal adiabatic invariant of

* Conference paper CN-10/166, presented by M. Kruskal. Discussion of this paper is given on page 816. Translations of the abstract are at the end of this volume of the Conference Proceedings.

the gyrating particle. This obtains under more restrictive conditions than the magnetic moment invariant, namely, if the tightly gyrating particle moves back and forth along a magnetic line of force and returns periodically nearly to its initial state. It seems to have been first employed (to lowest order) by ROSENBLUTH [12]. It became of interest again (and to higher order) in connection with the VAN ALLEN belt [13]. GARDNER [14] has settled the matter by proving the invariance to all orders.

1.2. Significance and arrangement of present paper

In the present paper a unification and simplification of all these preceding treatments of adiabatic invariance to higher order is achieved. The significant common element has turned out to be that each was concerned with a Hamiltonian system whose solutions are all nearly periodic. Lest this appear too like a truism, it may be pointed out that there are other types of adiabatic invariant associated with Hamiltonian systems whose solutions to lowest order are ergodic over surfaces of constant energy in phase space. (Incidentally, LENARD [10] has shown that descriptions and results valid to all orders can be obtained even for a system all of whose solutions are nearly only "multiply periodic" so long as it is linear.)

These two characteristics, of being Hamiltonian and of having all solutions nearly periodic, may largely be treated independently of each other, although their amalgamation (coined "almost-mechanics" by E. Gerjuoy) leads to interesting consequences (Section 5). Since the theory of Hamiltonian systems is already extremely well developed, everything we need is at hand, except perhaps for the result proved in Section 6.2. We therefore devote the major portion of the paper to discussing systems of differential equations with all solutions nearly periodic, which is of great independent interest in any case. We first derive the appropriate formal series solutions (Sections 2.5 to 2.9). This treatment is in essence very similar to the method of KRYLOFF and BOGOLIUBOFF [15], but seems to be a slight generalization inasmuch as the latter method is confined to quasi-linear second order systems.

Following the determination of the formal series we prove (Sections 2.10, 2.11) that the given system has exact solutions for an appropriately large range of the independent variable and that the formal series solutions represent the exact solutions asymptotically. The method seems simpler and more natural than that given by BERKOWITZ and GARDNER [11] for the special case of the gyrating particle. An interesting feature is the "bootstrap" argument (Section 2.11) by which the two items are linked together and proved simultaneously, thereby avoiding a certain duplication to be found in their treatment.

Section 3 starts with the theorem of phase independence, the importance and utility of which for this paper can hardly be overestimated: it is fair to say that Sections 3, 4 and 5 consist of almost nothing but its systematic exploitation. The full power of this ridiculously simple theorem can probably only be appreciated by those who, like the author, have spent tremendous amounts of effort and time in attempting (often unsuccessfully) to obtain various results to all orders.

1.3. Notation and conventions

We shall consistently employ vector and dyadic notation in dealing with arrays of quantities and shall often indulge in the geometric terminology which accompanies it so naturally. Vectors are designated by bold-face letters ($\mathbf{A}$, $\mathbf{B}$, ...) throughout, and polyadics are designated by bold-face block letters (A, B, ...). The number of components (array elements) of every vector (etc.) will of course be announced (if it is definite) when that vector is first introduced, but that number will not be indicated thereafter by any special notational feature. The unit dyadic in any number of dimensions will be denoted by I. The inner ("dot") product of two vectors is defined only if they have the same number of components, and the double inner product is to be understood in the sense that $\mathbf{ab}:\mathbf{cd}=\mathbf{a}\cdot\mathbf{d}\,\mathbf{b}\cdot\mathbf{c}$.

Differentiation, whether ordinary or partial, will be consistently denoted by attaching as a subscript the variable with respect to which the derivative is taken. Moreover, the use of subscripts is reserved exclusively for this purpose. To maintain the correct vector ordering, it is convenient in a few places to put the subscript before the symbol to which it is attached; thus ${}_{\mathbf{x}}\mathbf{f}$ denotes the gradient of the vector field $\mathbf{f}$ and the transpose of the dyadic $\mathbf{f}_{\mathbf{x}}$.

When one set of variables (coordinates) is transformed into another, which will be symbolized by a double-headed arrow $\longleftrightarrow$, the new variables will be denoted by symbols entirely distinct from the old ones. Therefore (in contrast, for instance, with the conventional notation in thermodynamics), there can arise no possible ambiguity as to what is being held fixed during a partial differentiation.

We will have mostly to do with formal infinite series in increasing integral powers of an expansion parameter ε, and we generally omit any indication of ε in the notation. If $\mathbf{f}$ denotes such a series, $\mathbf{f}^{(n)}$ denotes the coefficient of ε^n, and $\mathbf{f}^{[n]}$ denotes the sum of all the terms of $\mathbf{f}$ up to and including $\varepsilon^n\mathbf{f}^{(n)}$. As usual, $O(\varepsilon^n)$ denotes any quantity which, as $\varepsilon\to 0$, approaches zero at least as fast as ε^n.

A variable will be called *angle-like* if it is determined up to and only up to an additive integer, so that it is like an angle variable measured in units of a complete revolution. (As here, defined terms will regularly be italicized when they are introduced.)

1.4. Local dependence and useful integrals

For a full exposition of the significance of the results to come, it is necessary to discuss here the concept of local dependence. A function $\eta(\mathbf{x})$ on a

space of points $\mathbf{x}$ which is a functional of (i.e. depends on) another such function $\xi(\mathbf{x})$ depends *locally* on $\xi(\mathbf{x})$ if the value of η at any given point $\mathbf{x}$ is independent of the values of ξ outside of arbitrarily small neighborhoods of that point. (Here ξ and η can stand indifferently also for sets of independently many functions.) In practice this usually means that the value of η at $\mathbf{x}$ is a function of $\mathbf{x}$ and of the values at $\mathbf{x}$ of ξ and its derivatives (and often in fact only a finite number of them). We shall use this definition only "metamathematically" and so may modify it or use it loosely on occasion.

To see why local dependence is significant, let us observe that one of the later results is the derivation of an approximate integral or "constant of motion" J (Section 5.2) for certain systems of differential equations. How can this be important, in view of the fact that such systems commonly have not merely one but a complete set of exact integrals? The answer is that J is a "useful" integral. There are two ways in which an integral of a system may fail to be useful. The first is that it may fail to be a so-called isolating integral (see WINTNER [16]), the second that it may not be locally computable.

To illustrate the first possibility (without really going into the subject or even giving the definition of isolating integral) by means of a really trivial example, let us take the system which consists of two independent subsystems

$$\alpha_s = a, \quad \beta_s = b, \tag{1.1}$$

where α and β are angle-like variables, s is the independent variable, and a and b are given constants. The subsystems have each one integral, namely

$$\alpha - as, \quad \beta - bs \tag{1.2}$$

respectively. If we now ask for integrals which are independent of s, we see that the subsystems have none, but the combined system has the s-independent integral

$$b\alpha - a\beta. \tag{1.3}$$

This integral, however, is multivalued. If a and b are commensurable (a/b rational) it is an isolating integral and is useful: knowing the value of the integral (from initial conditions, for example) and, say, of β, we can say something about the value of α; in fact, writing a/b in standard form as m/n (m and n relatively prime integers and n positive), we can tell that α must have one of n (essentially distinct) values all of whose pairwise differences are multiples of $1/n$. On the other hand, if a and b are incommensurable, the integral is not isolating, and is clearly not useful in the same way.

The second possibility is of more direct concern. For illustration consider the motion of a particle in a given static three-dimensional potential field. To guarantee the existence of a complete set of isolating integrals let us agree to accept time-dependent integrals. (In various special cases this can be guaranteed even for time-independent integrals, for instance if the potential has a translational invariance, so that the corresponding spatial coordinate is ignorable, grows linearly in time, and can serve in effect as the time.) In such a case it is sometimes said that the energy is the only integral. Strictly speaking, this is nonsense, since we know that there is a complete set of integrals (for instance, the values of the dynamical variables taken on at $t=0$, viewed as functions of the free dynamical variables). But there is no question about the exceptional status of the energy integral: it plays in countless physical arguments a unique role denied to the other integrals. The reason for this is that the energy depends only locally on the potential and there is no other integral (functionally independent of the energy) with that property. The point is that, although in every particular case (i.e. for every particular potential function) the other integrals exist, and can be perfectly well defined mathematically, the problem of finding them is equivalent to the problem of integrating the equations of motion of the particle. Only the energy integral is useful because it alone is known *a priori*, without integrating the system completely, and because it alone remains unaffected (in its functional form) in one region by a change in the potential elsewhere along the orbit of the particle.

1.5. AUTONOMOUS SYSTEMS

Throughout this paper we shall be dealing with systems of ordinary differential equations. Primarily for notational convenience we do not permit the functions expressing the derivatives to depend on the independent variable, but this is no essential restriction, for there is no objection to such a dependence *de facto* (so long as appearances are preserved *de nomine*) by way of the existence of a dependent variable which always equals the independent variable, i.e. has derivative unity. Denoting the dependent variables collectively by $\mathbf{x}$ and the independent variable by s, we may write a general system in the form

$$\mathbf{x}_s = \mathbf{f}(\mathbf{x}). \tag{1.4}$$

This may be interpreted as a first-order differential equation in the space of points $\mathbf{x}$. We call it an *autonomous* system for short and as a faint reminder that the rate of change of $\mathbf{x}$ depends only on $\mathbf{x}$ itself. When $\mathbf{f}(\mathbf{x})$ is a formal series in powers of ε, we shall say that Eq. (1.4) is in *standard form* if $\mathbf{f}$ starts with a term of zeroth order which nowhere (as a function of $\mathbf{x}$) vanishes (in all components simultaneously).

We assume that $\mathbf{f}$ is as smooth as needed, so all the standard theory of systems of ordinary differential equations applies. A most fundamental teaching of that theory is that for every specified "initial condition", i.e. specification of $\mathbf{x}$ at (say) $s=0$, there exists a solution $\mathbf{x}(s)$ of Eq. (1.4) which may be continued indefinitely so long as $\mathbf{x}$ stays within the domain of definition of $\mathbf{f}$. Another fundamental teaching is that such a solution is unique: any two functions satisfying the same autonomous system

and equal for $s=0$ are equal for all values of s (in any interval which contains zero and over which both functions are defined); this is in fact a special case of the fundamental approximation theorem for ordinary differential equations (Section 6.1).

Let $\mathbf{X}(\mathbf{x}, s)$ denote the unique solution of (1.4) which passes through $\mathbf{x}$ at $s=0$, i.e. let $\mathbf{X}$ be defined by the conditions

$$\mathbf{X}_s(\mathbf{x}, s) = \mathbf{f}[\mathbf{X}(\mathbf{x}, s)], \tag{1.5}$$

$$\mathbf{X}(\mathbf{x}, 0) = \mathbf{x}. \tag{1.6}$$

An important property of the solutions of autonomous systems is that the one-parameter family of mappings of the form $\mathbf{x} \to \mathbf{X}(\mathbf{x}, s)$ (between parts of $\mathbf{x}$ space) constitute a group, and furthermore that the group operation on $\mathbf{X}(\mathbf{x}, s')$ and $\mathbf{X}(\mathbf{x}, s)$ is $\mathbf{X}(\mathbf{x}, s'+s)$, so that the group is isomorphic to the additive group of real numbers s. [Indeed, (1.6) already states that $s=0$ represents the identity.] To show this, one must establish that

$$\mathbf{X}[\mathbf{X}(\mathbf{x}, s'), s] = \mathbf{X}(\mathbf{x}, s + s'). \tag{1.7}$$

This follows from the uniqueness theorem, since the two sides are equal for $s=0$ by (1.6), and satisfy the same autonomous system because the left-hand side is obtained from $\mathbf{X}(\mathbf{x}, s)$ merely by substituting $\mathbf{X}(\mathbf{x}, s')$ for $\mathbf{x}$ and the right-hand side by substituting $s+s'$ for s, neither of which substitutions invalidates (1.5).

A further property we shall use in the next Section is now easily obtained. Using (1.5) with $s=0$ and (1.6) we have

$$\mathbf{X}(\mathbf{x}, 0) = \mathbf{f}(\mathbf{x}). \tag{1.8}$$

Differentiating (1.7) with respect to s', setting $s'=0$, and using (1.6) and (1.8) gives

$$\mathbf{X}_{\mathbf{x}}(\mathbf{x}, s) \cdot \mathbf{f}(\mathbf{x}) = \mathbf{X}_s(\mathbf{x}, s). \tag{1.9}$$

1.6. Recurrent systems

If all solutions of Eq. (1.4) are periodic (not necessarily with equal periods) we call (1.4) a *recurrent* system. We also call the vector field $\mathbf{f}$ in $\mathbf{x}$-space *recurrent* under the same circumstances, namely when its integral curves (curves which at each of their points are tangent to the field) are closed, forming topological circles; we call them *loops*. For each $\mathbf{x}$ there is then a least positive value of s for which the initial value $\mathbf{x}$ recurs; we denote this period by $S(\mathbf{x})$ and have

$$\mathbf{X}[\mathbf{x}, S(\mathbf{x})] = \mathbf{x}, \tag{1.10}$$

$$\mathbf{X}(\mathbf{x}, s) \neq \mathbf{x} \text{ for } 0 < s < S(\mathbf{x}). \tag{1.11}$$

We next show by a formal argument the obvious fact that the period $S(\mathbf{x})$ is constant along a solution of (1.4). We first take the s-derivative of (1.10) as $\mathbf{x}$ varies in accordance with (1.4), or in other words we take the $\mathbf{x}$-derivative, on the right, say, and then dot on the right with $\mathbf{f}(\mathbf{x})$; using (1.9) with $s=S(\mathbf{x})$ the result may be written

$$\mathbf{X}_s[\mathbf{x}, S(\mathbf{x})] + \mathbf{X}_s[\mathbf{x}, S(\mathbf{x})]\, S_{\mathbf{x}}(\mathbf{x}) \cdot \mathbf{f}(\mathbf{x}) = \mathbf{f}(\mathbf{x}). \tag{1.12}$$

But setting $s=S(\mathbf{x})$ in (1.5) we have

$$\mathbf{X}_s[\mathbf{x}, S(\mathbf{x})] = \mathbf{f}(\mathbf{x}) \tag{1.13}$$

in view of (1.10). Therefore the extreme terms in (1.12) cancel, and, furthermore, since $\mathbf{f} \neq 0$, we have

$$S_{\mathbf{x}}(\mathbf{x}) \cdot \mathbf{f}(\mathbf{x}) = 0, \tag{1.14}$$

which is the desired result; to be entirely explicit,

$$\begin{aligned} \{S[\mathbf{X}(\mathbf{x}, s)]\}_s &= S_{\mathbf{x}}[\mathbf{X}(\mathbf{x}, s)] \cdot \mathbf{X}_s(\mathbf{x}, s) \\ &= S_{\mathbf{x}}[\mathbf{X}(\mathbf{x}, s)] \cdot \mathbf{f}[\mathbf{X}(\mathbf{x}, s)] = 0 \end{aligned} \tag{1.15}$$

in view of (1.5) and of (1.14) with $\mathbf{x}=\mathbf{X}(\mathbf{x}, s)$, so that the period evaluated at all points of the solution $\mathbf{X}(\mathbf{x}, s)$ is the same (independent of s). This result may be written

$$S[\mathbf{X}(\mathbf{x}, s)] = S(\mathbf{x}). \tag{1.16}$$

Another hardly surprising result, a generalization of (1.10), is

$$\mathbf{X}[\mathbf{x}, s + S(\mathbf{x})] = \mathbf{X}(\mathbf{x}, s), \tag{1.17}$$

which follows from (1.7) by setting $s'=S(\mathbf{x})$ and using (1.10).

It is now obvious that $\mathbf{X}(\mathbf{x}, s)$ has the same value for two different values of s if and only if they differ by an integral multiple of $S(\mathbf{x})$; the "if" follows by induction from (1.17) and the "only if" part since otherwise a contradiction to (1.11) could be similarly obtained.

1.7. Splittable systems

An important property of some systems of differential equations is the possession of an autonomous subsystem. Suppose that, of the set of N dependent variables denoted collectively by $\mathbf{x}$, there are some M (where $1 \leq M \leq N-1$) whose s-derivatives as given by (1.4) are independent of the remaining $N-M$ variables. The M variables then satisfy an autonomous subsystem of their own and we call the original system *split*. More generally, we call a system *splittable* if by a local change of dependent variables it can be transformed into a split system, i.e. if there are local definitions of M new variables, functions of $\mathbf{x}$ whose derivatives, computed using (1.4), are expressible as functions of the M new variables themselves alone. These variables then satisfy a *new autonomous* system of fewer variables.

By a local change of variables is meant one whose defining formulas depend locally on $\mathbf{f}(\mathbf{x})$ (see Section 1.4). The requirement of localness is essential to the definition; without it, for instance, every system with a complete set of isolating integrals would be

not merely splittable but completely splittable into N independent autonomous subsystems of one dependent variable each.

The problem of solving a system of order N may, if the system is splittable, be split up into the problems of first solving a system of order M and then one of order $N-M$.

2. Nearly recurrent systems

2.1. Formulation and description

Consider the system of first-order ordinary differential equations

$$\mathbf{x}_s = \mathbf{F}(\mathbf{x}, \varepsilon), \tag{2.1}$$

where $\mathbf{x}$ and $\mathbf{F}$ are vectors of N components. We suppose that $\mathbf{F}$ is defined in a suitable domain of its arguments, with properties to be described shortly, and that it and all its derivatives of all orders exist and are continuous. Let the domain be the product of a domain in $\mathbf{x}$-space with a closed interval of values for ε among which occurs zero. Let (2.1) be a recurrent system for $\varepsilon=0$, so that $\mathbf{F}(\mathbf{x}, 0)$ is a nowhere vanishing vector field with all integral curves closed. (When we speak of loops in connection with (2.1), we shall always mean these, even if it should happen, most atypically, that (2.1) is also recurrent for $\varepsilon \neq 0$.) We require finally that the domain of points in $\mathbf{x}$-space for which $\mathbf{F}(\mathbf{x}, \varepsilon)$ is defined be closed, bounded, and N-dimensional and be made up of loops.

As ε approaches zero any solution of (2.1) gets closer and closer to a loop, so long as the range of values of s considered remains bounded (independently of ε). We may say that the solutions of system (2.1) are all *nearly periodic** for small ε. The distance in $\mathbf{x}$-space (in any reasonable sense) by which a solution misses its initial point after one *gyration*, namely after approximately following one closed loop around, is of order ε; in general it is to be expected that these small deviations will accumulate, so that after a large number of gyrations (a large change in s) of order $1/\varepsilon$, the solution will have *drifted* a finite amount and will be gyrating in a different region of $\mathbf{x}$-space from where it started. The curve in $\mathbf{x}$-space traversed by a solution in its entirety may be suggestively thought of as the distorted image of a helix of small pitch, as shown in Fig. 1.

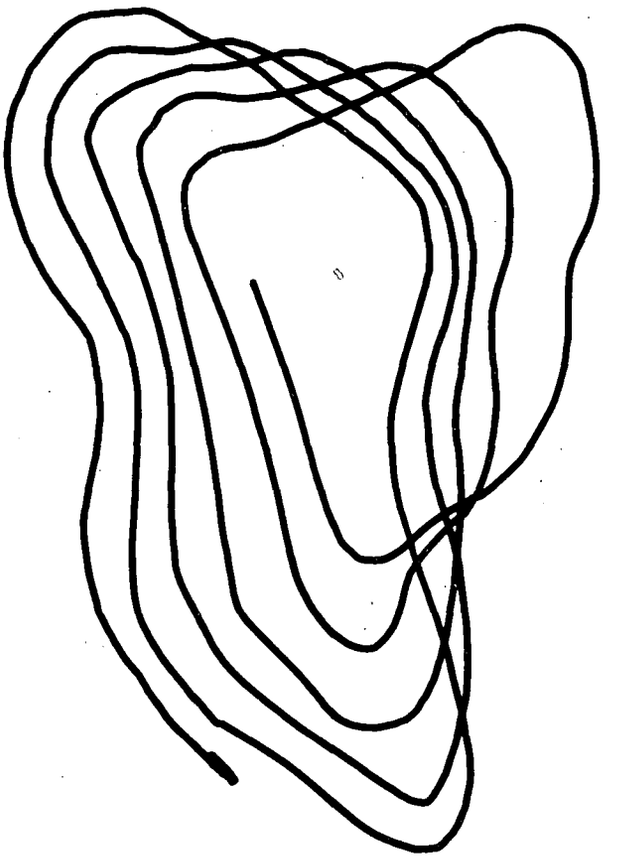

Fig. 1 Curve traversed by a solution of Eq. (2.1). The curve cannot cross itself; the apparent crossings are due to projection.

2.2. Inadequacy of obvious series solution

Our first task is to find some kind of formal solution of (2.1), in terms of infinite power series in ε, which is asymptotically valid uniformly over large ranges of s and shows explicitly its nearly periodic nature. The obvious approach at first sight seems to be to represent $\mathbf{x}$ directly by a series,

$$\mathbf{x} \approx \mathbf{u}^{(0)}(s) + \varepsilon \mathbf{u}^{(1)}(s) + \varepsilon^2 \mathbf{u}^{(2)}(s) + \dots, \tag{2.2}$$

and to determine the $\mathbf{u}^{(i)}$ by substituting this series into (2.1), expanding the function on the right-hand side in a formal double Taylor series around its zeroth order arguments $(\mathbf{u}^{(0)}, 0)$, and collecting and separately equating like powers of ε. This leads to the equations

$$\mathbf{u}_s^{(0)} = \mathbf{F}(\mathbf{u}^{(0)}, 0)$$

$$\mathbf{u}_s^{(1)} = \mathbf{F}_{\mathbf{x}}(\mathbf{u}^{(0)}, 0) \cdot \mathbf{u}^{(1)} + \mathbf{F}_{\varepsilon}(\mathbf{u}^{(0)}, 0), \dots, \tag{2.3}$$

which do indeed determine the $\mathbf{u}^{(n)}$ if some initial values are given, say at $s=0$. (And, in fact, if $\mathbf{F}$ is analytic then the series in (2.2) converges to an analytic solution of (2.1) for sufficiently small ε.) Of course $\mathbf{u}^{(0)}$ runs periodically around a loop. But (2.2) obviously can represent a solution asymptotically only so long as the solution stays within $O(\varepsilon)$ of $\mathbf{u}^{(0)}$, which in general means only for bounded values of s: for larger s the solution will have drifted farther from its initial loop. Therefore (2.2) is not useful for our purpose.

2.3. Standardization

Before proceeding any further let us replace (2.1) by

$$\mathbf{x}_s = \mathbf{f}(\mathbf{x}), \tag{2.4}$$

where $\mathbf{f}(\mathbf{x})$ denotes the Taylor expansion

$$\mathbf{f}(\mathbf{x}) = \sum_{n=0}^{\infty} \varepsilon^n \frac{1}{n!} \left[\frac{\partial^n \mathbf{F}}{\partial \varepsilon^n} \right]_{\varepsilon=0} \tag{2.5}$$

* This concept is not to be confounded with that of almost periodic functions [17], which we are not concerned with here.

of $\mathbf{F}$ around $\varepsilon=0$, and is therefore an infinitely differentiable formal infinite series of non-negative powers of ε. We have two reasons for doing this: first, since we are seeking a formal solution (which will later be proved to represent the true solution asymptotically, but which does not in general converge to it, nor indeed at all—see the next Section) we must switch over to formal series at some point anyway, and it is simplest to do so at the start; second, the theory about to be developed can be applied not only to true systems of differential equations, but also to merely formal systems (and in particular to the "reduced" system resulting from the first application of the theory—see Section 5.6).

However, a warning is in order. Certainly (2.4) is the formal analogue of (2.1); and indeed, the formal solutions of (2.4) which we shall obtain, when taken up to terms of order n, do provide approximations up to that order of the true solutions of (2.1) (as do also the true solutions of the system $\mathbf{x}_s=\mathbf{f}^{[n]}(\mathbf{x})$), as we see from the basic approximation theorem of Section 6.1. But this is only for ranges of s bounded independently of ε; due to the exponential in the estimate, no matter how large we take n we could not expect these formal approximations to remain at all close to the true solutions for ranges of s of order $1/\varepsilon$ (or of order $1/\varepsilon^\alpha$, $\alpha>0$; but we could, for instance, for ranges of order $\log \varepsilon$). Or rather, we could not expect so except for the near periodicity assumed; one of our conclusions (Section 2.10) will be that the approximations are in fact good for ranges of order $1/\varepsilon$. (But not quite so good: two orders in ε get lost in the shuffle.)

2.4. An example

An extremely simple but doubly illuminating example is provided by the harmonic oscillator with slowly varying rest point. As our basic equation we take

$$\varepsilon^2 u_{tt} + u = r(t), \tag{2.6}$$

where u is the displacement of the oscillator and $r(t)$ the rest point, a given function of its argument (and allowably a series in powers of ε). If r were constant, every solution of (2.6) would oscillate sinusoidally around r with periodic $2\pi\varepsilon$; as it is, r is nearly constant during a period, so it should be possible to put (2.6) into the form this paper deals with.

To render the period finite we introduce $s\equiv t/\varepsilon$, so (2.6) becomes

$$u_{ss} + u = r(\varepsilon s), \tag{2.7}$$

a version of the equation we might have started with; here the right-hand side varies slowly because of the factor ε in the argument. To render (2.7) as a formally first order system we introduce $v\equiv u_s$. To eliminate the dependence (of r) on the independent variable s we bring back t, but now as a new dependent variable. (It wouldn't do to introduce a new dependent variable equal to s itself, because s does not recur, even to lowest order.) Altogether, we end up with a system in standard form (2.4) with

$$\mathbf{x} \equiv (u, v, t),$$
$$\mathbf{f} \equiv [v, r(t) - u, \varepsilon]. \tag{2.8}$$

This system is nearly recurrent because to zeroth order t remains constant and u and v oscillate periodically.

Having used this example to illustrate how a given system may be transformed as required by the theory, we now use it to illustrate why the formal series we are led to are, in general, only asymptotic and not convergent as one might have hoped (when $\mathbf{f}$ is convergent, i.e. analytic). For this we need only the original form (2.6). Since the corresponding homogeneous equation has the general solution

$$u = \alpha \cos(t/\varepsilon) + \beta \sin(t/\varepsilon), \tag{2.9}$$

we may confine ourselves to a particular solution of (2.6). One particular solution, for that matter, may be singled out as "oscillation-free" (a concept which may be rendered precise by interpreting it to mean the vanishing of J; see Section 5.2). This is a unique characterization to all orders, though ill-defined for finite ε. The oscillations referred to are naturally those of small period $2\pi\varepsilon$, and are excluded by requiring that t-differentiation not affect (not lower) the order in ε, in obvious contrast to its effect on the general solution (2.9). Thus $\varepsilon^2 u_{tt}$ is regarded as small, and (2.6) is solvable recursively to yield

$$u = r - \varepsilon^2 u_{tt}$$
$$= r - \varepsilon^2 r_{tt} + \varepsilon^4 r_{tttt} - \cdots. \tag{2.10}$$

This formal development differs from the Taylor series for $r(t+\varepsilon)$ in two respects unimportant for present purposes (the absence of odd powers of ε and the alternation of sign among the even powers) and in one important respect, the absence of $n!$ in the denominator of the ε^n term. It is thus clear that even the analyticity of $r(t)$ is insufficient to assure the convergence of (2.10). For (2.10) to have a radius of convergence greater than zero, the development of $r(t+\varepsilon)$ must have an infinite radius of convergence, i.e. $r(t)$ must be an entire function. And even this is not quite enough, as can be seen by Fourier analysis of (2.6).

2.5. More appropriate variables

Let us start our search for an asymptotic solution of (2.4) by introducing a new coordinate system more appropriate than $\mathbf{x}$ for describing a nearly periodic but slowly drifting trajectory. To this end observe that the loops form an $(N-1)$-dimensional family, so that there exist $N-1$ independent functions of $\mathbf{x}$ each of which is constant on every loop; these can obviously also be chosen infinitely differentiable, since $\mathbf{f}^{(0)}$ is. (For instance, we may pick an infinitely differentiable $(N-1)$-dimensional hypersurface in $\mathbf{x}$-space which is nowhere tangent to $\mathbf{f}^{(0)}$, then pick any set of $N-1$ independent infinitely differentiable coordinates $\mathbf{Y}$ on the hypersurface, and then extend $\mathbf{Y}$ to the rest of

$\mathbf{x}$-space so as to be constant on every loop.) Denote some arbitrary fixed set of such functions collectively by a vector function $\mathbf{Y}(\mathbf{x})$ with $N-1$ components. Thus each loop is characterized uniquely by the constant (vector) value assumed on it by $\mathbf{Y}(\mathbf{x})$.

Next, let $\Upsilon(\mathbf{x})$ be any infinitely differentiable angle-like function which varies monotonically around each loop; for definiteness, say it increases with s. We then change variables from $\mathbf{x}$ to $\mathbf{y}$ and $v\Upsilon$ by the transformation

$$\mathbf{y} = \mathbf{Y}(\mathbf{x}),\ v = \Upsilon(\mathbf{x}). \tag{2.11}$$

Of course v is determined only up to an arbitrary additive integer. The transformation clearly possesses an infinitely differentiable inverse which we denote by

$$\mathbf{x} = \mathbf{X}(\mathbf{y}, v), \tag{2.12}$$

where $\mathbf{X}$ is of course periodic in v (with period unity).

In terms of our new variables the system (2.4) takes the form

$$\mathbf{y}_s = \varepsilon\, \mathbf{g}(\mathbf{y}, v),\ v_s = \psi(\mathbf{y}, v), \tag{2.13}$$

where (omitting the arguments $\mathbf{y}$, v consistently)

$$\varepsilon \mathbf{g} \equiv \mathbf{Y}_{\mathbf{x}}(\mathbf{X}) \cdot \mathbf{f}(\mathbf{X}), \tag{2.14}$$

$$\psi \equiv \Upsilon_{\mathbf{x}}(\mathbf{X}) \cdot \mathbf{f}(\mathbf{X}); \tag{2.15}$$

here $\mathbf{g}$ and ψ are infinitely differentiable formal series, their leading terms are O (1) and that of ψ is definitely positive, and $\mathbf{g}$ is written accompanied by the factor ε because, by construction, $\mathbf{y}_s$ must vanish to zeroth order. These equations exhibit the gyration clearly: to zeroth order, as s increases $\mathbf{x}$ stays on a loop (since y is constant) and runs periodically around it (since v increases monotonically); to first order the loop may drift (since $\mathbf{y}$ may vary).

We can hardly rest content with our system in the form (2.13), however. For the gyration it pictures may be very uneven, full of sudden accelerations and decelerations, since ψ may fluctuate wildly; further, and in fact more serious, the net rate of drift is not at all in evidence, since in the course of one gyration $\mathbf{g}$ may point in all different directions, even quite opposite to the direction that $\mathbf{y}$ is effectively drifting in, which can only be obtained by some sort of integration around a loop. Using a previous metaphor, we might say that we have introduced coordinates $\mathbf{y}$, v in terms of which every trajectory does indeed look like a helix of small pitch (if we think of v as the angle of a point on a circle), but only to zeroth order, and even there s does not increase uniformly around the loops.

But these defects can be remedied. As for one minor issue, it is not hard to see that if Υ had been chosen judiciously, $\psi^{(0)}$ would have come out independent of v. It would only have been necessary to take

$$\Upsilon(\mathbf{x}) = \left\{\int_{\mathbf{x}'}^{\mathbf{x}} d\mathbf{x}/\mathbf{f}^{(0)}\right\} \Big/ S(\mathbf{x}'), \tag{2.16}$$

where $\mathbf{x}'$ is some definite point on the loop through $\mathbf{x}$ (say the intersection with the hypersurface suggested before), S is the period (Section 1.6), and the line integral is taken along the loop (so that the ratio of vectors under the integral sign is well defined and scalar and, to be sure, nothing but ds). In carrying out our procedure in particular problems, it is in fact very desirable to start with such an Υ. We have not specified this to-be-so-called *judicious choice*, however, since for our abstract purposes it would make little difference, and that of dubious advantage; but we shall occasionally note where it would affect matters.

2.6. Nice variables

The defects we have noticed in (2.13) are all due to the dependence of $\mathbf{g}$ and ψ on v. We therefore ask whether we can find an infinitely differentiable formal transformation to new variables which are similar to $\mathbf{y}$ and v and satisfy equations similar to (2.13), but without the odious dependence on the angle-like variable—and not only to lowest order but to all orders. We shall see that the answer is yes.

Denote the new sought variables by a vector $\mathbf{z}$ of $N-1$ components and an angle-like variable φ, related to the old variables by

$$\mathbf{z} = \mathbf{Z}(\mathbf{y}, v),\ \varphi = \Phi(\mathbf{y}, v), \tag{2.17}$$

where $\mathbf{Z}$ and Φ are to be determined. Let the system (2.13), and indirectly therefore (2.4), transform into

$$\mathbf{z}_s = \varepsilon\, \mathbf{h}(\mathbf{z}),\ \varphi_s = \omega(\mathbf{z}), \tag{2.18}$$

analogous to (2.13) but without φ appearing as an argument on the right-hand sides; $\mathbf{h}$ and ω are also to be determined. Naturally $\mathbf{h}$ and ω, like $\mathbf{g}$ and ψ, will be infinite power series in ε, and it is only natural that $\mathbf{Z}$ and Φ be so too. Thus the transformation (2.17), unlike (2.11), depends on the expansion parameter ε. But this is of no concern, especially since $\mathbf{Z}$ and Φ, as for that matter $\mathbf{h}$ and ω, are to be O(1).

We must impose on $\mathbf{Z}$ and Φ periodicity conditions which express that v is an angle-like variable and that φ is to be a similar one, namely

$$\mathbf{Z}(\mathbf{y}, v+1) = \mathbf{Z}(\mathbf{y}, v),\ \Phi(\mathbf{y}, v+1) = \Phi(\mathbf{y}, v) + 1. \tag{2.19}$$

It turns out that we may specify the dependence of $\mathbf{Z}$ and Φ on $\mathbf{y}$ for $v=0$ with great freedom; for definiteness and simplicity we choose the initial conditions

$$\mathbf{Z}(\mathbf{y}, 0) = \mathbf{y},\ \Phi(\mathbf{y}, 0) = 0. \tag{2.20}$$

These express that $\mathbf{z}$ and φ are to equal $\mathbf{y}$ and v at one definite point on each loop, where $v=0$.

With conditions (2.18), (2.19) and (2.20) we now claim not only the existence but also the uniqueness of the formal transformation we are seeking.

2.7. Determination of recursion relations

The first step in determining $\mathbf{Z}$, Φ, $\mathbf{h}$, and ω is to substitute (2.17) in (2.18), use the chain rule of differentiation, and eliminate $\mathbf{y}_s$ and v_s by (2.13), which yields

$$\varepsilon\, \mathbf{Z}_{\mathbf{y}} \cdot \mathbf{g} + \mathbf{Z}_v \psi = \varepsilon\, \mathbf{h}(\mathbf{Z}), \tag{2.21}$$

$$\varepsilon\, \Phi_{\mathbf{y}} \cdot \mathbf{g} + \Phi_v \psi = \omega(\mathbf{Z}). \tag{2.22}$$

Let us assume temporarily that we know $\mathbf{h}$ and ω as functions of their arguments. These equations may then be construed, thanks to the factor ε appearing in the first term of each of them, as determining, order by order, the derivatives of $\mathbf{Z}$ and Φ with respect to v in terms of known quantities, while $\mathbf{y}$ plays the role of a parameter. Accordingly, we transfer the first terms to the right-hand side, divide by ψ, and integrate; in view of the initial conditions (2.20) the results may be written

$$\mathbf{Z} = \mathbf{y} + \varepsilon \int_0^v dv\, [\mathbf{h}(\mathbf{Z}) - \mathbf{Z}_\mathbf{y} \cdot \mathbf{g}] \frac{1}{\psi}, \tag{2.23}$$

$$\Phi = \int_0^v dv\, [\omega(\mathbf{Z}) - \varepsilon \Phi_\mathbf{y} \cdot \mathbf{g}] \frac{1}{\psi}. \tag{2.24}$$

On these we next wish to impose the periodicity conditions (2.19), which it suffices to use only for $v=0$ (for, assuming that (2.19) are satisfied in the previous orders, the integrands of (2.23) and (2.24) are periodic functions of v). We obtain

$$\int_0^1 dv\, [\mathbf{h}(\mathbf{Z}) - \mathbf{Z}_\mathbf{y} \cdot \mathbf{g}] \frac{1}{\psi} = 0, \tag{2.25}$$

$$\int_0^1 dv\, [\omega(\mathbf{Z}) - \varepsilon \Phi_\mathbf{y} \cdot \mathbf{g}] \frac{1}{\psi} = 1. \tag{2.26}$$

These are the conditions we shall employ to determine the functions $\mathbf{h}$ and ω, which we previously assumed known.

To this end, denote the integral in (2.23) by $\mathbf{K}$, substitute $\mathbf{y} + \varepsilon\mathbf{K}$ for the argument of $\mathbf{h}$ in (2.25) and of ω in (2.26), and expand $\mathbf{h}$ and ω in Taylor series around the argument $\mathbf{y}$. The factors $\mathbf{h}(\mathbf{y})$ and $\omega(\mathbf{y})$ in the leading terms of these expansions, being independent of v, come out of the integrals, and we obtain

$$\mathbf{h}(\mathbf{y}) \int_0^1 dv \frac{1}{\psi} = \int_0^1 dv \left\{ \mathbf{Z}_\mathbf{y} \cdot \mathbf{g} - \varepsilon \left[\frac{\mathbf{h}(\mathbf{y} + \varepsilon \mathbf{K}) - \mathbf{h}(\mathbf{y})}{\varepsilon} \right] \right\} \frac{1}{\psi}, \tag{2.27}$$

$$\omega(\mathbf{y}) \int_0^1 dv \frac{1}{\psi} = 1 + \varepsilon \int_0^1 dv \left\{ \Phi_\mathbf{y} \cdot \mathbf{g} - \left[\frac{\omega(\mathbf{y} + \varepsilon \mathbf{K}) - \omega(\mathbf{y})}{\varepsilon} \right] \right\} \frac{1}{\psi}; \tag{2.28}$$

the expressions enclosed in curly brackets are to be thought of as expanded in the obvious way, and are clearly O(1). The factor $\int_0^1 dv/\psi$ can be developed as a series with a leading term which is O(1) and definitely positive, due to the nature of ψ. Thus (2.27) and (2.28) provide recursion formulas for $\mathbf{h}(\mathbf{y})$ and $\omega(\mathbf{y})$.

2.8. Recursive construction of desired functions

We are now prepared to prove the existence and uniqueness of formal series $\mathbf{Z}(\mathbf{y}, v)$, $\Phi(\mathbf{y}, v)$, $\mathbf{h}(\mathbf{y})$, and $\omega(\mathbf{y})$ satisfying Eqs. (2.17) to (2.20). (Since it is $\mathbf{h}$ and ω as functions that are sought, it is of no account that we now denote their arguments by $\mathbf{y}$ instead of $\mathbf{z}$.) We proceed by induction. It suffices to prove, for each non-negative integer n, that if the series exist and are unique up to terms of order n—1, then they do and are so up to terms of order n. (For they certainly exist and are unique up to order minus one, since they are required to start with terms of order zero!)

The argument is easy; we need merely appeal to the determining Eqs. (2.23), (2.24), (2.27), (2.28) we have derived, making sure to find $\mathbf{Z}$ before Φ or $\mathbf{h}$, and ω before Φ. Thus, we may first uniquely determine $\mathbf{Z}$ to order n by (2.23), noting that the right-hand side can be obtained to that order in terms of lower order quantities, already known according to the induction hypothesis. Of course it is supposed that $\mathbf{h}(\mathbf{Z})$ has been expanded in a Taylor series around its zeroth order argument $\mathbf{y}$, the products and quotients expanded out, and the integration performed. Similarly, we may then uniquely obtain $\mathbf{h}$ from (2.27), ω from (2.28), and finally Φ from (2.24).

As a matter of fact, since (2.23) and (2.27) do not involve Φ or ω, we can find $\mathbf{Z}$ and $\mathbf{h}$ to all orders before finding Φ and ω at all.

The construction of $\mathbf{Z}$ and Φ guarantees trivially that they satisfy the initial conditions (2.20) to order n. At the same time, the construction of $\mathbf{h}$ and ω guarantees that (2.25) and (2.26) are satisfied to order n, and therefore likewise the periodicity conditions (2.19) for $v=0$. But $\mathbf{Z}_v$ as determined by (2.21) is clearly periodic in v up to order n, since $\mathbf{Z}$ is periodic up to order $n-1$ by induction hypothesis, and so the first periodicity condition holds in general. It then follows similarly that also Φ_v is periodic up to order n and hence that the second periodicity condition holds in general. This completes the proof.

It is obvious by our construction that the formal series transformation from $\mathbf{y}$ and v to $\mathbf{z}$ and φ expressed by (2.17) is infinitely differentiable, and we can easily show that it possesses an infinitely differentiable inverse transformation. It is only necessary to obtain recursion relations for finding $\mathbf{y}$ and v order by order, and the proof proceeds like the one just completed. The formula for $\mathbf{y}$ is merely (2.23) with its last term shifted to the other side, and with the judicious choice we could have obtained the one for v equally simply. As it is, we observe from (2.24) and (2.28) and from the positiveness of ψ that the function which gives φ to zeroth order as a function of $\mathbf{y}$ and v can be inverted to give v to zeroth order as a function of φ and $\mathbf{y}$ and hence of φ and $\mathbf{z}$; applying this inverse function to (2.24) (i.e. using each side of (2.24) in turn as argument of this inverse function and equating the results) and expanding leads to an equation whose only term of zeroth order on the right is just v, which may then be solved for trivially to give the desired recursion relation.

2.9. Restatement of formal result

Let us restate what has been achieved, omitting the intermediate variables $\mathbf{y}$, v and redefining $\mathbf{Z}$, Φ, and $\mathbf{X}$ accordingly. We have shown that, given the

original infinitely differentiable system (2.4) with all solutions nearly periodic, it is possible to find a transformation

$$\mathbf{z} = \mathbf{Z}(\mathbf{x}),\ \varphi = \Phi(\mathbf{x}) \tag{2.29}$$

and functions $\mathbf{h}(\mathbf{z})$, $\omega(\mathbf{z})$ such that the new variables satisfy (2.18); moreover, the transformation possesses an inverse

$$\mathbf{x} = \mathbf{X}(\mathbf{z}, \varphi), \tag{2.30}$$

and $\mathbf{Z}$, Φ, $\mathbf{h}$, ω, and $\mathbf{X}$ are infinitely differentiable infinite series of non-negative powers of ε (the zeroth order term of ω being definitely positive).

2.10. Proof that series represents true solution asymptotically

We now wish to prove that the solutions of (2.18) provide asymptotically correct solutions of (2.4) and also of any true system (2.1) of which (2.4) is the formal expansion. What this means, roughly speaking, is that if we are seeking the solution of (2.1) or (2.4) with a prescribed initial value at $s=0$, and are content with an approximation to within some particular positive power of ε, then we may solve correspondingly approximate versions of (2.18) instead, with initial values for $\mathbf{z}$ and φ obtained from that for $\mathbf{x}$ by a correspondingly approximate version of the transformation (2.29), and convert the solutions so obtained into $\mathbf{x}$-space by a correspondingly approximate version of the inverse transformation (2.30). And the claim is that we thereby obtain the desired approximate solution of (2.1) or (2.4), not only for s bounded but even for $s=\mathrm{O}(\varepsilon^{-1})$.

Owing to our desire for results valid for such large s, we must initially employ approximations up to two orders better than that of our conclusion, and also than we would have needed to obtain the same conclusion restricted to bounded values of s. This is because we lose an order of accuracy, so to speak, in integrating over a large range of s, which we do twice. It is the estimation of the mobile phase angle that necessitates much of the extra accuracy; the drift of $\mathbf{z}$ alone is easier to follow, as will become clear.

To state precisely what we shall prove, let $\hat{\mathbf{x}}(s)$ be a solution of (2.1) or alternatively of the system obtained from (2.4) by truncating the formal series at order $n+1$ ($n \geq 0$), so that

$$\hat{\mathbf{x}}_s = \mathbf{F}(\hat{\mathbf{x}}, \varepsilon) \text{ or } \hat{\mathbf{x}}_s = \mathbf{f}^{[n+1]}(\hat{\mathbf{x}}); \tag{2.31}$$

these are of course genuine systems of differential equations, and not merely formal. Define $\mathbf{z}'(s)$ and $\varphi'(s)$ as those solutions of the equations obtained from (2.18) by appropriate analogous truncations of $\mathbf{h}$ and ω which have at $s=0$ the values obtained from $\hat{\mathbf{x}}(0)$, by an appropriately truncated version of transformation (2.29); specifically, $\mathbf{z}'(s)$ and $\varphi'(s)$ are uniquely defined by the conditions

$$\mathbf{z}'_s = \varepsilon\, \mathbf{h}^{[n]}(\mathbf{z}'),\ \varphi'_s = \omega^{[n]}(\mathbf{z}'), \tag{2.32}$$

$$\mathbf{z}'(0) = \mathbf{Z}^{[n]}[\hat{\mathbf{x}}(0)],\ \varphi'(0) = \Phi^{[n]}[\hat{\mathbf{x}}(0)]. \tag{2.33}$$

Next, transform to obtain a curve in $\mathbf{x}$-space, defining $\mathbf{x}'(s)$ as the result of applying the appropriately truncated version of transformation (2.30) to $\mathbf{z}'(s)$ and $\varphi'(s)$:

$$\mathbf{x}' = \mathbf{X}^{[n-1]}(\mathbf{z}', \varphi'). \tag{2.34}$$

The claim now is that $\mathbf{x}'$ is a good approximation to $\hat{\mathbf{x}}$, specifically that

$$\hat{\mathbf{x}}(s) = \mathbf{x}'(s) + \mathrm{O}(\varepsilon^n), \tag{2.35}$$

for s within a range of order $1/\varepsilon$, so long as $\hat{\mathbf{x}}$ and $\mathbf{x}'$ stay in the domain of definition of $\mathbf{f}$. (For all we know yet this might limit s more severely, but in the next Section it will be shown that they do stay in for $s=\mathrm{O}(1/\varepsilon)$.)

The proof proceeds in three stages. First, we show that $\mathbf{Z}^{[n+1]}(\hat{\mathbf{x}})$ is close to $\mathbf{z}'$; then, that $\Phi^{[n]}(\hat{\mathbf{x}})$ is close to φ', and finally, that $\mathbf{x}'$ is close to $\hat{\mathbf{x}}$, as desired. We need the three formal identities in $\mathbf{x}$:

$$\mathbf{Z}_{\mathbf{x}} \cdot \mathbf{f} = \varepsilon\, \mathbf{h}(\mathbf{Z}), \tag{2.36}$$

$$\Phi_{\mathbf{x}} \cdot \mathbf{f} = \omega(\mathbf{Z}), \tag{2.37}$$

$$\mathbf{x} = \mathbf{X}(\mathbf{Z}, \Phi), \tag{2.38}$$

the first two of which express that (2.29) transforms (2.4) into (2.18), and the last that (2.30) inverts (2.29). Or rather, we need their approximate versions

$$\mathbf{Z}_{\mathbf{x}}^{[n+1]} \cdot \mathbf{f}^{[n+1]} = \varepsilon\, \mathbf{h}^{[n]}(\mathbf{Z}^{[n+1]}) + \mathrm{O}(\varepsilon^{n+2}), \tag{2.39}$$

$$\Phi_{\mathbf{x}}^{[n]} \cdot \mathbf{f}^{[n+1]} = \omega^{[n]}(\mathbf{Z}^{[n]}) + \mathrm{O}(\varepsilon^{n+1}), \tag{2.40}$$

$$\mathbf{x} = \mathbf{X}^{[n-1]}(\mathbf{Z}^{[n-1]}, \Phi^{[n-1]}) + \mathrm{O}(\varepsilon^n), \tag{2.41}$$

the last of which, for instance, may be shown as follows: The difference between the left-hand side and the first term on the right is a well defined infinitely differentiable function of $\mathbf{x}$ and ε. Its Taylor expansion around $\varepsilon=0$ vanishes identically up to terms of order $n-1$, since it contains exactly the same terms up to that order as occur in the formal identity (2.38). Thus, the quotient of the difference by ε^n is a continuous function of $\mathbf{x}$ and ε on a closed bounded domain and is therefore bounded independently of $\mathbf{x}$ and ε, which completes the proof. The same argument, but with n replaced everywhere by $n+2$ or $n+1$, applies to (2.39) and (2.40).

If we temporarily restrict ourselves to the second alternative in (2.31), then (2.39) evaluated at $\hat{\mathbf{x}}$ may be written

$$\{\mathbf{Z}^{[n+1]}(\hat{\mathbf{x}})\}_s = \varepsilon\, \mathbf{h}^{[n]}[\mathbf{Z}^{[n+1]}(\hat{\mathbf{x}})] + \mathrm{O}(\varepsilon^{n+2}). \tag{2.42}$$

We now wish to compare this with the first equation (2.32), and invoke the approximation theorem of Section 6.1. The crux of the proof is to change the independent variable first, setting

$$\sigma = \varepsilon s. \tag{2.43}$$

The two equations we wish to compare become thereby (after division by ε)

$$\{\mathbf{Z}^{[n+1]}(\hat{\mathbf{x}})\}_\sigma = \mathbf{h}^{[n]}[\mathbf{Z}^{[n+1]}(\hat{\mathbf{x}})] + \mathrm{O}(\varepsilon^{n+1}), \tag{2.44}$$

$$\mathbf{z}'_\sigma = \mathbf{h}^{[n]}(\mathbf{z}'). \tag{2.45}$$

Thus $\mathbf{Z}^{[n+1]}(\hat{\mathbf{x}})$ and $\mathbf{z}'$ satisfy the same autonomous system of differential equations within $O(\varepsilon^{n+1})$, and since by (2.33) they have the same initial values also within $O(\varepsilon^{n+1})$, according to the approximation theorem

$$\mathbf{Z}^{[n+1]}(\hat{\mathbf{x}}) = \mathbf{z}' + O(\varepsilon^{n+1}) \tag{2.46}$$

for bounded σ, i.e. for $s = O(1/\varepsilon)$. (In this we might as well replace the truncation index $n+1$ on the left by n.) This completes the first stage, except for the remark that the case of the first alternative in (2.31) may be treated in exactly the same way by using, instead of (2.39), the obviously equally valid formula obtained from it by replacing the factor $\mathbf{f}^{[n+1]}$ by $\mathbf{F}$.

The second stage is even simpler. Restricting ourselves again to the second alternative (with the same trivial modification to cover the first alternative), we evaluate (2.40) at $\hat{\mathbf{x}}$ and write it in the form

$$\begin{aligned}[\Phi^{[n]}(\hat{\mathbf{x}})]_s &= \omega^{[n]}[\mathbf{Z}^{[n]}(\hat{\mathbf{x}})] + O(\varepsilon^{n+1}) \\ &= \omega^{[n]}(\mathbf{z}') + O(\varepsilon^{n+1}) = \varphi'_s + O(\varepsilon^{n+1}),\end{aligned} \tag{2.47}$$

where we have used (2.46) and the second equation (2.32). In view of the common initial values, asserted in the second equation (2.33), a simple integration immediately yields

$$\Phi^{[n]}(\hat{\mathbf{x}}) = \varphi' + O(\varepsilon^n) \tag{2.48}$$

for $s = O(1/\varepsilon)$. (Again, we might as well replace the truncation index n on the left by $n-1$.)

The third stage is the simplest of all. Evaluating (2.41) at $\hat{\mathbf{x}}$ and using (2.46) and (2.48) yields

$$\hat{\mathbf{x}} = \mathbf{X}^{[n-1]}(\mathbf{z}', \varphi') + O(\varepsilon^n), \tag{2.49}$$

which in view of (2.34) is precisely (2.35). The proof is complete.

2.11. Proof that true solution remains long in domain

We can now demonstrate that $\hat{\mathbf{x}}(s)$ actually remains interior to the given domain of x-space over a large range in s of order $1/\varepsilon$. For (2.45) shows that there is some finite range of σ over which $\mathbf{z}'$ stays interior to the corresponding domain of z-space. This corresponds by (2.43) to some definite large range of s, to which we restrict the discussion from now on. [Since φ' is an angle-like variable it is subject to no restriction in magnitude, and to be sure it varies by $O(1/\varepsilon)$, as we see from (2.32).] From (2.34) it is then clear that $\mathbf{x}'$ is defined and interior to the domain, so (2.35) holds so long as $\hat{\mathbf{x}}$ stays inside. On the other hand, so long as (2.35) holds, $\hat{\mathbf{x}}$ does in fact stay in. Pulling ourselves up by the bootstraps in this way, we arrive at the conclusion that $\hat{\mathbf{x}}$ stays inside as long as $\mathbf{x}'$ does (at least very nearly, though naturally one may reach the boundary a little before the other).

If this argument does not appear immediately convincing (as may well be the case), it can be elaborated as follows. Knowing that $\mathbf{x}'$ stays well within the domain for some range of s of order $1/\varepsilon$, that is, stays a finite distance δ away from the boundary, let us assume (for the sake of a *reductio ad absurdum*) that $\hat{\mathbf{x}}$ leaves the domain during that range. Consider the value of s nearest to zero for which $\hat{\mathbf{x}}$ and $\mathbf{x}'$ are at a distance of $\delta/2$. Since $\hat{\mathbf{x}}$ and $\mathbf{x}'$ are both within the domain up to that point, (2.35) applies and shows that they are separated by only $O(\varepsilon^n)$, which is much less than $\delta/2$. This contradiction proves that $\hat{\mathbf{x}}$ in fact could not have left the domain during the range of interest.

3. Rings and the reduced system

3.1. Theorem of phase independence

At this point we introduce a simple but powerful tool, which we shall apply repeatedly to establish that functions are independent of the phase angle φ. Let $\mathbf{W}(\mathbf{z}, \varphi)$ be a vector with any finite number M of components, a formal infinite series in powers of ε, $O(1)$, and a function of its indicated arguments $\mathbf{z}$ and φ, periodic in the latter (of course with period unity). Let $\mathbf{W}$ satisfy a formal differential equation

$$\mathbf{W}_\varphi = \mathbf{A}(\mathbf{z}) + \varepsilon \mathbf{B}(\mathbf{z}, \mathbf{W}, \mathbf{W}_\mathbf{z}), \tag{3.1}$$

where $\mathbf{A}(\mathbf{z})$ and $\mathbf{B}(\mathbf{z}, \mathbf{w}, \mathbf{v})$ are vectors of M components, formal infinite series in powers of ε, and functions of their indicated arguments ($\mathbf{w}$ being a generic variable with M components, and $\mathbf{v}$ one with $M(N-1)$ components), and where $\mathbf{B}$ is $O(1)$, but no such assumption is made about $\mathbf{A}$. Then $\mathbf{W}$ is in fact independent of φ to all orders.

To prove this *theorem of phase indepence*, we merely form the indefinite integral of (3.1),

$$\mathbf{W}(\mathbf{z}, \varphi) = \mathbf{W}(\mathbf{z}, 0) + \int_0^\varphi d\varphi\, [\mathbf{A}(\mathbf{z}) + \varepsilon \mathbf{B}(\mathbf{z}, \mathbf{W}, \mathbf{W}_\mathbf{z})]; \tag{3.2}$$

impose the periodicity condition on $\mathbf{W}$, whence

$$\int_0^1 d\varphi\, [\mathbf{A}(\mathbf{z}) + \varepsilon \mathbf{B}(\mathbf{z}, \mathbf{W}, \mathbf{W}_\mathbf{z})] = 0; \tag{3.3}$$

and proceed by induction. Up to order minus one $\mathbf{W}$ vanishes and so is independent of φ. Suppose $\mathbf{W}$ is independent of φ up to terms of order $n-1$. Up to order n, then, the integrand of (3.3) is independent of φ, and so equals its own integral, which vanishes. Therefore (3.2) may be written

$$\mathbf{W}(\mathbf{z}, \varphi) = \mathbf{W}(\mathbf{z}, 0) + O(\varepsilon^{n+1}), \tag{3.4}$$

which shows that $\mathbf{W}$ is independent of φ up to terms of order n, and thereby completes the induction. (And we have as a side result that $\mathbf{A} = O(\varepsilon)$, and in fact that $\mathbf{A} + \varepsilon \mathbf{B} = 0$ to all orders.)

It is clear that we could have allowed $\mathbf{B}$ to depend on higher derivatives of $\mathbf{W}$ with respect to $\mathbf{z}$, with no change in the argument or the conclusion. Of this we shall make no use, but there is a slight modification of the theorem which we shall use very frequently. Namely, let us specialize by assuming that $\mathbf{B}$ is a linear function of its last two arguments.

We can then trivially generalize by allowing $\mathbf{W}$ to start with any (e.g. a negative) power of ε, instead of being O(1), and obviously the same conclusion holds.

Another slight but useful modification is obtained by replacing $\mathbf{W}_\varphi$ by $\mathbf{W}_s$ in (3.1). Since

$$\mathbf{W}_s = \mathbf{W}_\varphi\, \omega(\mathbf{z}) + \varepsilon \mathbf{W}_\mathbf{z} \cdot \mathbf{h}(\mathbf{z}), \tag{3.5}$$

the resulting equation can be immediately put back in the same form as (3.1) with $\mathbf{A}$ and $\mathbf{B}$ appropriately modified, so the conclusion still holds.

It is convenient to observe here, what will be needed later and is obvious from (3.5), that the operators of differentiation with respect to s and to φ commute with each other.

3.2. Arbitrariness of nice variables

It is clear that the nice variables $\mathbf{z}$ and φ obtained in Section 2 are far from unique. For, the process by which we determined them involved some arbitrary choices, namely of the functions $\mathbf{Y}$ and Υ in Section 2.5 and of the form of the initial conditions Eqs (2.20). We address ourselves now to the investigation of exactly how much freedom there is finally in the choice of such desirable coordinates.

Suppose that we were to introduce new variables $\hat{\mathbf{z}}$ and $\hat{\varphi}$, expressed as infinitely differentiable formal infinite series in non-negative powers of ε, with coefficients depending on $\mathbf{z}$ and φ, such that $\hat{\mathbf{z}}$ is periodic in φ and $\hat{\varphi}$ changes by unity with φ, and such that the transformation is formally invertible to give similar expressions for $\mathbf{z}$ and φ in terms of $\hat{\mathbf{z}}$ and $\hat{\varphi}$. We then may ask, first, under what reasonably general conditions $\hat{\mathbf{z}}$ and $\hat{\varphi}$ will necessarily satisfy equations analogous to Eqs (2.18).

An answer is easy to find. For $\mathbf{z}$ satisfies an autonomous system of equations, and this will certainly transform into an autonomous system for $\hat{\mathbf{z}}$ so long as $\hat{\mathbf{z}}$ is obtained by a transformation from $\mathbf{z}$ alone, i.e. so long as

$$\hat{\mathbf{z}}_\varphi = 0. \tag{3.6}$$

(Indeed, it is then immediate that $\hat{\mathbf{z}}_s = \varepsilon \hat{\mathbf{h}}(\hat{\mathbf{z}})$, where $\hat{\mathbf{h}}(\hat{\mathbf{z}}) = \hat{\mathbf{z}}_\mathbf{z} \cdot \mathbf{h}(\mathbf{z})$.) Furthermore, φ may be thought of as satisfying the trivial first order differential equation $\varphi_s = \omega(\mathbf{z})$ if $\mathbf{z}$ is considered a parameter, and $\hat{\varphi}$ will certainly satisfy a similar trivial equation so long as it differs from φ by only a "constant", which may of course depend on the "parameter" $\mathbf{z}$ (we cannot take $\hat{\varphi}$ to be a more general linear function of φ, since the two angle variables must change by unity together), namely so long as

$$\hat{\varphi}_\varphi = 1. \tag{3.7(}$$

(Indeed, it is then immediate that $\hat{\varphi}_s = \hat{\omega}(\hat{\mathbf{z}})$, where $\hat{\omega}(\hat{\mathbf{z}}) = \varepsilon \hat{\varphi}_\mathbf{z} \cdot \mathbf{h}(\mathbf{z}) + \omega(\mathbf{z})$; note that $\hat{\varphi}_\mathbf{z}$ depends on $\mathbf{z}$ alone, since $\hat{\varphi}_{\varphi\mathbf{z}} = 0$.)

We next may ask, conversely, whether every transformation from $\mathbf{z}$, φ to new nice variables $\hat{\mathbf{z}}$, $\hat{\varphi}$ in fact satisfies (3.6) and (3.7). The answer is yes; the conditions we have found are necessary as well as sufficient to preserve the form of Eqs (2.18). For to begin with, suppose there exists a function $\hat{\mathbf{h}}$ such that

$$\hat{\mathbf{z}}_s = \varepsilon \hat{\mathbf{h}}(\hat{\mathbf{z}}); \tag{3.8}$$

then we may apply the theorem of phase independence and deduce (3.6). And suppose also that there exists a function $\hat{\omega}$ such that

$$\hat{\varphi}_s = \hat{\omega}(\hat{\mathbf{z}}); \tag{3.9}$$

to this we cannot directly apply the theorem of phase independence (even though we know that $\hat{\mathbf{z}}$ depends on $\mathbf{z}$ only), because $\hat{\varphi}$ is not periodic in φ, but we may rewrite it as

$$[\hat{\varphi} - \varphi]_s = \hat{\omega}(\hat{\mathbf{z}}) - \omega(\mathbf{z}), \tag{3.10}$$

to which we can, because $\hat{\varphi} - \varphi$ is periodic; we thereby deduce that

$$[\hat{\varphi} - \varphi]_\varphi = 0, \tag{3.11}$$

which is equivalent to (3.7).

3.3. Rings, phase differences, and the reduced system

The necessary and sufficient conditions (3.6) and (3.7) that new variables $\hat{\mathbf{z}}$, $\hat{\varphi}$ be as nice as $\mathbf{z}$, φ enable us to introduce some simple concepts connected with the original system in $\mathbf{x}$, Eq. (2.4), which are based on the existence of nice variables, but are independent of which ones they specifically are. These concepts will of course be defined only to all orders, and not in general exactly.

Consider the set of all points in $\mathbf{x}$-space which correspond to a common value of $\mathbf{z}$. Since φ is an angle variable, this set is a topological circle which we call a *ring*. Two points in $\mathbf{x}$-space with the same $\mathbf{z}$ we call *ringmates*. Now (3.6) has the simple interpretation that $\hat{\mathbf{z}}$ is constant around any ring, which shows that the concept of rings and ringmates is invariant with respect to the choice of nice variables.

The particular value of the phase variable φ corresponding to a point $\mathbf{x}$ has of course no invariant significance. But if two points are ringmates, then their *phase difference* $\Delta\varphi$ does have, for, by (3.7),

$$\Delta\hat{\varphi} = \int \mathrm{d}\,\hat{\varphi} = \int \hat{\varphi}_\varphi \mathrm{d}\varphi = \int \mathrm{d}\,\varphi = \Delta\varphi, \tag{3.12}$$

where the integrals are extended over a portion of the ring between the two points. Of course this phase difference is only defined modulo unity.

It is also clear that the knowledge of which points are ringmates and of the phase differences between those that are is all the information inherent in knowing some nice variables but independent of which ones they are. For from that knowledge one can construct nice variables.

Since $\mathbf{z}$ satisfies an autonomous system, it is obvious that if two solutions $\mathbf{x}(s)$ of the original system are ringmates at any one value of s, then they are so

at every value of s. Also, their phase difference is always the same, since $(\Delta\varphi)_s = \omega(\mathbf{z}) - \omega(\mathbf{z}) = 0$. It is therefore meaningful to apply the invariant concepts of rings and of phase difference not only to points in x-space but also to entire solutions $\mathbf{x}(s)$ of Eq. (2.4).

The ring constitutes a sophisticated or refined version of the loop, which is indeed a zeroth order approximation to it. Each ring is characterized by its value of $\mathbf{z}$, just as each loop was characterized (in Section 2.5) by its value of $\mathbf{y}$. That is, the rings form an $(N-1)$-dimensional space, and their slow drift as s varies is governed by the formal autonomous system

$$\mathbf{z}_\sigma = \mathbf{h}(\mathbf{z}), \tag{3.13}$$

where we have reintroduced the change of independent variable, Eq. (2.43), to $\sigma = \varepsilon s$ in order that what we shall call the *reduced system* (3.13) might be in the same general form as the original system, Eq. (2.4) (though not necessarily in standard form). The phase now plays a subordinate role (in contrast to its previous rather dominant one), since it has no effect (to any finite order) on the drift.

Among other things, we have shown that the nearly recurrent system, Eq. (2.4), is splittable. The new autonomous system $\mathbf{z}_s = \varepsilon\,\mathbf{h}(\mathbf{z})$ contains one less variable.

If (3.13) should itself happen to be nearly recurrent and in standard form, we can reapply the whole procedure to it and obtain a doubly reduced system, and so on. The arguments of Section 2.11 can then be extended to show that the true solution $\hat{\mathbf{x}}(s)$ of Eq. (2.31) remains in the relevant domain of x-space for a range of s even larger than $O(1/\varepsilon)$.

3.4. Roto-rate

It should at this point be apparent that all the information contained in knowledge of the rings and of phase differences on them is contained, in "capsule" form, in knowledge of $\mathbf{x}_\varphi$. For, as we shall show in detail shortly, the rings are obtainable from it by integration of an autonomous system whose independent variable is the phase. It is noteworthy that in terms of $\mathbf{x}_\varphi$ as a function* of $\mathbf{x}$ we may express our results entirely within x-space, even though it was convenient to transform to other variables in deriving them; so expressed, furthermore, the results take on an esthetically satisfying uniqueness, since for any other nice variables $\hat{\mathbf{z}}$, $\hat{\varphi}$ we have

$$\mathbf{x}_\varphi = \mathbf{x}_{\hat{\mathbf{z}}} \cdot \hat{\mathbf{z}}_\varphi + \mathbf{x}_{\hat{\varphi}}\,\hat{\varphi}_\varphi = \mathbf{x}_{\hat{\varphi}} \tag{3.14}$$

by (3.6) and (3.7). The function merits a specific name and symbol, and so we define the *roto-rate* $\mathbf{R}(\mathbf{x})$ by

$$\mathbf{R} \equiv \mathbf{x}_\varphi, \tag{3.15}$$

the name being supposed to suggest the defining characteristic of $\mathbf{R}$ as the rate of change (with respect to phase) of the point at $\mathbf{x}$ in rotating around its ring.

We next derive four properties of $\mathbf{R}$ which can be expressed independently of nice variables, rings, and phases, and show afterward that these properties characterize it uniquely. The first property is that the autonomous system (3.15) is recurrent; this is obvious because every solution in fact runs around a ring. The second property (also obvious) is that the initial value recurs (for the first time) when the independent variable φ has increased by unity; this may be expressed by writing

$$\oint d\mathbf{x}/\mathbf{R} = 1, \tag{3.16}$$

where the line integral is taken once around any integral curve of $\mathbf{R}$, and the ratio of vectors is defined, since precisely on such a curve the vectors are parallel (and in fact $d\mathbf{x} = \mathbf{x}_\varphi\, d\varphi = \mathbf{R}\, d\varphi$). The third property is that to lowest (zeroth) order $\mathbf{R}$ is parallel to $\mathbf{f}$ and unequal to zero, as seen immediately from Eq. (2.4) and from Eq. (3.5) with $\mathbf{W}$ replaced by $\mathbf{x}$. Finally, the fourth property is that

$$\mathbf{f}_\mathbf{x} \cdot \mathbf{R} = \mathbf{R}_\mathbf{x} \cdot \mathbf{f}, \tag{3.17}$$

which expresses the consistency of Eq. (2.4) with Eq. (3.15) and is in fact a trivial rewriting of

$$\mathbf{f}_\varphi = \mathbf{x}_{s\varphi} = \mathbf{x}_{\varphi s} = \mathbf{R}_s, \tag{3.18}$$

in which we have used the observation at the end of Section 3.1.

To show that the roto-rate is uniquely characterized by these four properties, it suffices to show that for any (infinitely differentiable formal series) function $\mathbf{R}$ with these properties we can find nice variables $\mathbf{z}$ and φ such that (3.15) holds. This is because for any other function $\hat{\mathbf{R}}$ with the four properties we could then find nice variables $\hat{\mathbf{z}}$ and $\hat{\varphi}$ such that $\hat{\mathbf{R}} = \mathbf{x}_{\hat{\varphi}}$, whereupon (3.14) would show immediately that $\mathbf{R} = \hat{\mathbf{R}}$.

We may construct the desired nice variables as solutions of

$$\mathbf{z}_\mathbf{x} \cdot \mathbf{R} = 0, \tag{3.19}$$

$$\varphi_\mathbf{x} \cdot \mathbf{R} = 1; \tag{3.20}$$

that is, the $\mathbf{z}$ are constructed to be (of course independent) constants on the closed (first property!) integral curves of $\mathbf{R}$, and φ to be multivalued. That φ is an angle variable, i.e. that its branches differ by integers, follows from (3.16) (second property!),

$$\oint d\varphi = \oint \varphi_\mathbf{x} \cdot d\mathbf{x} = \oint \varphi_\mathbf{x} \cdot \mathbf{R}\, d\mathbf{x}/\mathbf{R} = 1. \tag{3.21}$$

The variables are indepedent since the $\mathbf{z}$ were chosen independent and, if φ were expressible as a function of $\mathbf{z}$, we would have $\varphi_\mathbf{x} \cdot \mathbf{R} = 0$ as a consequence of (3.19), contradicting (3.20). We may therefore employ a standard representation of the unit dyadic in the derivation

$$\mathbf{R} = \mathbf{I} \cdot \mathbf{R} = (\mathbf{x}_\mathbf{z} \cdot \mathbf{z}_\mathbf{x} + \mathbf{x}_\varphi \varphi_\mathbf{x}) \cdot \mathbf{R} = \mathbf{x}_\varphi, \tag{3.22}$$

* Of course, $\mathbf{x}$ is to be treated as a function of φ and $\mathbf{z}$ through the transformation Eq. (2.30) when the differentiation is performed, but the derivative may then be treated as a function of $\mathbf{x}$ by the inverse transformation, Eq. (2.29).

which verifies (3.15). It is now fairly easy to establish one of the main properties of nice variables, that z_s and φ_s are functions of $\mathbf{z}$ only*:

$$\begin{aligned}(z_s)_\varphi &= (z_x \cdot f)_x \cdot R = z_{xx}\colon f\, R + z_x \cdot f_x \cdot R \\ &= z_{xx}\colon R\, f + z_x \cdot R_x \cdot f \\ &= (z_x \cdot R)_x \cdot f_x = 0\,,\end{aligned} \tag{3.23}$$

using successively Eqs. (2.4), (3.15), the symmetry of the triadic z_{xx} in its last two vector positions, (3.17) (fourth property!), and (3.19); and the same for φ_s. This already shows that φ_s may be written as $\omega(\mathbf{z})$; to show that z_s may be written as $\varepsilon\, h(\mathbf{z})$ it remains only to note that $z_x \cdot f = O(\varepsilon)$, in view of (3.19) (third property!).

It does not appear obvious whether an explicit recursion formula to determine R in terms of f can be found. If so, the whole theory of this paper might be simplified and rendered less deep.

4. Hereditary properties

4.1. Definition

We now have a systematic formal procedure which we can apply to any nearly recurrent formal system in N dependent variables, enabling us to "take out the fast gyration" and find a reduced system in $N-1$ dependent variables which describes the drift of rings to all orders. There are, as we shall see, a number of properties of systems of differential equations which, if possessed by the original system Eq. (2.4), are carried over or *inherited* by the reduced system Eq. (3.13). We shall call a property of systems of differential equations *hereditary* if, whenever it holds for the original system (at least in the formal sense of expansions to all orders), it also holds for the reduced system. This definition, like that of local dependence, is metamathematical and need not be used with great strictness.

4.2. Inheritance of splittability

As a first, fairly trivial, example of an hereditary property consider that of being splittable (Section 1.7). If Eq. (2.4) is splittable, and if the functionals which depend locally on $f(\mathbf{x})$ and define the M new variables satisfying the new autonomous system are expansible in power series in ε, with zero order leading terms, then the new autonomous system obviously also has all solutions nearly periodic and can be put into standard form by an appropriate change of variables. Introducing new nice variables, it can be seen by the methods of Section 3 that the new angle variable is essentially the same as (and could have been chosen to be in fact the same as) the original angle variable φ; and thus that the reduced system of the new autonomous system is the new autonomous system of the original reduced system (3.13). Therefore the original reduced system is splittable, and the decrease in number of dependent variables as a result of the splitting is the same as for the given splittable system (2.4).

4.3. Inheritance of an integral (constant of motion)

An important and simple hereditary property is the possession of an integral (independent of s). To see this let $I(\mathbf{x})$ be an (expansible) integral of Eq. (2.4); that is, let

$$I_s = I_x \cdot f = 0\,, \tag{4.1}$$

so that I is constant on every solution of Eq. (2.4). By the theorem of phase independence we immediately deduce that I is a function of $\mathbf{z}$ only, and is therefore also an integral of the reduced system Eq. (3.13).

It follows from this that Eq. (2.4) cannot possess a complete set of integrals (N functionally independent integrals) all of which are expansible. For Eq. (3.13) can of course have only $N-1$ independent integrals. Any integral of (2.4) which distinguishes between ringmates is inexpansible.

4.4. Inheritance of invariant measure

Another interesting hereditary property is possession of an invariant measure. Let $\varrho(\mathbf{x})$ be the measure density of a measure which is invariant under the "flow" represented by Eq. (2.4); that is, the measure of any region in $\mathbf{x}$-space is the integral of ϱ over that region, and the measures of the images of that region for different values of s under the "motion" are all equal. The mathematical expression of this invariance is just the "time-independent" equation of continuity

$$\mathbf{I}\colon (\varrho\, f)_x = 0\,, \tag{4.2}$$

where the left-hand side is nothing but the divergence of $\varrho\, f$, written in accordance with our subscript-differentiation notation. This may also be written

$$\varrho_s + \varrho\ \mathbf{I}\colon f_x = 0\,. \tag{4.3}$$

Such an invariant measure is intrinsically independent of coordinate system. In $\mathbf{z}$, φ space it has the measure density $\tau(\mathbf{z}, \varphi)$ obtained from ϱ by multiplying by the Jacobian of $\mathbf{x}$ with respect to $\mathbf{z}$, φ. We then have (4.2) and (4.3) in the forms

$$\mathbf{I}\colon (\tau\, \varepsilon\, h)_z + (\tau\, \omega)_\varphi = 0\,, \tag{4.4}$$

$$\tau_s + \varepsilon\, \tau\ \mathbf{I}\colon h_z = 0\,. \tag{4.5}$$

If ϱ is expansible in a power series then of course so is τ (since the Jacobian certainly is), hence by the theorem of phase independence τ is a function of $\mathbf{z}$ alone. Thus $(\tau\omega)_\varphi = 0$, and (4.4) becomes for the reduced system the precise analogue of (4.2) for the original system, which proves the inheritance.

* In this paragraph we cannot appeal to the commutativity of the differentiations, which would enable us to bypass several intermediate steps in (3.23), because we do not yet know that $\mathbf{z}$, φ are nice variables, that being, indeed, what we wish to establish.

4.5. General integral invariants

The last two hereditary properties discussed are essentially special cases of a more general one, possession of an integral invariant* of any degree m. They correspond, in fact, to the extreme cases $m=0$ and $m=N$, whose particular simplicity seemed to merit separate treatment. We confine ourselves in this section to the case $m=2$, which is perhaps uniquely characterized as being enough like the general case to permit immediate generalization** of all concepts, results, and non-notational features, yet simple enough to permit handling in our index-free notation with no further special conventions and no particular clumsiness. However, we consider not only absolute integral invariants but also relative integral invariants.

Let $\mathbf{A}(\mathbf{x})$ be an antisymmetric dyadic*** field in $\mathbf{x}$-space. Then $\mathbf{A}:d\mathbf{x}\,d\mathbf{x}$ is a second order differential form**** whose integral over any surface imbedded in $\mathbf{x}$-space constitutes a sort of measure for such surfaces. The rate of change of this measure with respect to s, as (each point of) the surface varies with s according to Eq. (2.4), is another measure similarly associated with the differential form

$$(\mathbf{A}:d\mathbf{x}\,d\mathbf{x})_s=\mathbf{A}_s:d\mathbf{x}\,d\mathbf{x}+\mathbf{A}:(d\mathbf{f}\,d\mathbf{x}+d\mathbf{x}\,d\mathbf{f})$$
$$=(\mathbf{A}_s+\mathbf{A}\cdot\mathbf{f}_{\mathbf{x}}+{}_{\mathbf{x}}\mathbf{f}\cdot\mathbf{A}):d\mathbf{x}\,d\mathbf{x}. \qquad (4.6)$$

The condition that $\mathbf{A}:d\mathbf{x}\,d\mathbf{x}$ be a *relative integral invariant* is that (4.6) vanish upon integration over every closed surface, the condition for which in turn is that there exist a single-valued vector field $\mathbf{V}(\mathbf{x})$ satisfying

$$\mathbf{A}_s+\mathbf{A}\cdot\mathbf{f}_{\mathbf{x}}+{}_{\mathbf{x}}\mathbf{f}\cdot\mathbf{A}=\mathbf{V}_{\mathbf{x}}-{}_{\mathbf{x}}\mathbf{V}, \qquad (4.7)$$

where the right-hand side is just the curl of $\mathbf{V}$. In this case the measure of any closed surface stays constant as the surface flows. The condition that $\mathbf{A}:d\mathbf{x}\,d\mathbf{x}$ be an *absolute integral invariant* is that (4.6) vanish upon integration over every (not necessarily closed) surface, namely that the left-hand side of (4.7) vanish. In this case the measure of any surface at all stays constant as the surface flows.

4.6. Inheritance of relative invariants

Transforming to nice variables we have

$$\mathbf{A}:d\mathbf{x}\,d\mathbf{x}=\mathbf{A}:(\mathbf{x}_{\mathbf{z}}\cdot d\mathbf{z}+\mathbf{x}_\varphi\,d\varphi)(\mathbf{x}_{\mathbf{z}}\cdot d\mathbf{z}+\mathbf{x}_\varphi\,d\varphi)$$
$$=\mathbf{B}:d\mathbf{z}\,d\mathbf{z}+\mathbf{C}\cdot(d\mathbf{z}\,d\varphi-d\varphi\,d\mathbf{z}), \qquad (4.8)$$

where there can of course be no $d\varphi\,d\varphi$ term (and its coefficient would vanish anyway), and where

$$\mathbf{B}\equiv{}_{\mathbf{z}}\mathbf{x}\cdot\mathbf{A}\cdot\mathbf{x}_{\mathbf{z}},\quad \mathbf{C}\equiv\mathbf{x}_\varphi\cdot\mathbf{A}\cdot\mathbf{x}_{\mathbf{z}}. \qquad (4.9)$$

The condition that (4.8) be a relative invariant, obtainable in the same way as (4.7) or by transforming (4.7), is that there exist single-valued $\mathbf{W}(\mathbf{x})$ and $T(\mathbf{x})$ such that

$$\mathbf{B}_s+\mathbf{B}\cdot\varepsilon\,\mathbf{h}_{\mathbf{z}}+\varepsilon\,{}_{\mathbf{z}}\mathbf{h}\cdot\mathbf{B}-\mathbf{C}\,\omega_{\mathbf{z}}+\omega_{\mathbf{z}}\,\mathbf{C}=\mathbf{W}_{\mathbf{z}}-{}_{\mathbf{z}}\mathbf{W}, \qquad (4.10)$$

$$\mathbf{C}_s+\mathbf{C}\cdot\varepsilon\,\mathbf{h}_{\mathbf{z}}=T_{\mathbf{z}}-\mathbf{W}_\varphi. \qquad (4.11)$$

Let us denote the complete integral over phase (equivalently, the closed line integral around a ring, or the average value with respect to φ) by an overhead bar. Then from (4.11) we have immediately (since differentiations and integrations with respect to φ and to s commute)

$$\bar{\mathbf{C}}_s+\bar{\mathbf{C}}\cdot\varepsilon\,\mathbf{h}_{\mathbf{z}}=\bar{T}_{\mathbf{z}}. \qquad (4.12)$$

This is just the condition (analogous to (4.7), but of order one less) that $\bar{\mathbf{C}}\cdot d\mathbf{z}$ be a relative integral invariant of the reduced system. If $\mathbf{A}$ and $\mathbf{V}$ are expansible in ε then so are $\mathbf{C}$ and T and so also $\bar{\mathbf{C}}$ and $\bar{T}$. Thus the inheritance of a relative invariant is proved.

Of course $\bar{\mathbf{C}}\cdot d\mathbf{z}$ might happen to be a trivial relative invariant, in the sense of its integral having a constant value independent of the closed path it is taken over. This is the case only if $\bar{\mathbf{C}}$ is a gradient (i.e. a $\mathbf{z}$-derivative), so that its curl vanishes,

$$\bar{\mathbf{C}}_{\mathbf{z}}-{}_{\mathbf{z}}\bar{\mathbf{C}}=0. \qquad (4.13)$$

But then we are amusingly compensated in that the phase integral of Eq. (4.10) can be written

$$\bar{\mathbf{B}}_s+\bar{\mathbf{B}}\cdot\varepsilon\mathbf{h}_{\mathbf{z}}+\varepsilon\,{}_{\mathbf{z}}\mathbf{h}\cdot\bar{\mathbf{B}}=(\bar{\mathbf{W}}+\bar{\mathbf{C}}\omega)_{\mathbf{z}}-{}_{\mathbf{z}}(\bar{\mathbf{W}}+\bar{\mathbf{C}}\omega), \qquad (4.14)$$

which is just the condition (analogous to (4.7)) that $\bar{\mathbf{B}}:d\mathbf{z}\,d\mathbf{z}$ be a relative integral invariant of the reduced system.

4.7. Inheritance of absolute invariants

There was an element of humbug in the just described inheritance of relative invariants. The fact is that any relative invariant of a system yields lower order relative invariants upon integration over closed sub-manifolds, so that if the system is splittable, then

---

* See De Donder [18] for the definitions, for a clear exposition of the general theory of integral invariants, and accordingly for a justification of some of the steps in this section. Strictly speaking, the hereditary property is possession of an integral invariant whose degree is less than the order of the system by a definite integer, since an invariant of degree m of the original system induces one of degree $m-1$ of the reduced system. The word "essentially" above is to indicate that from this point of view the property of Section 4.3 is slightly anomalous.

** The important case $m=1$ may be even more immediately obtained by the opposite process (here "degradation" rather than specialization), and moreover is illustrated by the theory of Hamiltonian systems in Part 5 (as also is the case $m=2$ for a relative invariant), where the invariant has the special form $\mathbf{p}\cdot d\mathbf{q}$.

*** In the general case it should be a completely antisymmetric m-adic, which changes sign under the transposition of any two "vector locations" (in index notation a tensor of order m which changes sign under the interchange of any two indices).

**** It should be noted that $d\mathbf{x}\,d\mathbf{x}$ (often written $d\mathbf{x}\wedge d\mathbf{x}$ in the literature) is, despite appearances, neither symmetric nor a dyad, but rather an antisymmetric dyadic. Indeed, since $\mathbf{A}$ is antisymmetric, any symmetric component of $d\mathbf{x}\,d\mathbf{x}$ would contribute nothing to the differential form. The interchange of vector order reverses the orientation of the surface element $d\mathbf{x}\,d\mathbf{x}$ and with it the sign. In fact, on any surface determined by giving $\mathbf{x}$ as a function of two parameters u and v, we have $d\mathbf{x}\,d\mathbf{x}=(\mathbf{x}_u\mathbf{x}_v-\mathbf{x}_v\mathbf{x}_u)\,du\,dv$.

when the non-autonomous variables are integrated out, a relative invariant of the new autonomous subsystem is obtained. That the "niceness" of the nice variables was really irrelevant is apparent in that the theorem of phase independence was not invoked. With the inheritance of absolute invariants the situation is otherwise, and we are back in our subject proper.

If $\mathbf{A}:\mathrm{d}\mathbf{x}\,\mathrm{d}\mathbf{x}$ is an absolute invariant, then transforming to nice variables and introducing $\mathbf{B}$ and $\mathbf{C}$ by (4.9) as before, we have Eqs. (4.10) and (4.11) with the right-hand sides replaced by zero. From the latter we see, first, by the theorem of phase independence, that $\mathbf{C}$ depends only on $\mathbf{z}$, and second, as a consequence, that $\mathbf{C}\cdot\mathrm{d}\mathbf{z}$ is an absolute invariant of the reduced system. From the former, we then see that $\mathbf{B}$ depends only on $\mathbf{z}$, but it is not apparent what more can be deduced, unless $\mathbf{C}\cdot\mathrm{d}\mathbf{z}$ is a trivial invariant, in which case $\mathbf{B}:\mathrm{d}\mathbf{z}\,\mathrm{d}\mathbf{z}$ is easily seen as before to be a relative invariant (or unless either of the very special cases $\mathbf{C}=0$ or $\omega_{\mathbf{z}}=0$ obtains, when $\mathbf{B}:\mathrm{d}\mathbf{z}\,\mathrm{d}\mathbf{z}$ is of course even an absolute invariant).

5. Hamiltonian systems

5.1. Preparatory transformations

The hereditary property with the perhaps most important applications is that of being in Hamiltonian form. Let the dependent variables consist of the $N=2M$ canonically conjugate coordinates $\mathbf{q}$ and $\mathbf{p}$, and let the Hamiltonian $H(\mathbf{q},\mathbf{p})$ be single-valued and time-independent. (Time-dependent systems, such as those with "slowly changing external parameters", are not excluded by this, since they can be converted to time-independent form by the well known device of treating time and energy as a new additional pair of conjugate coordinates. See also Section 2.4). The $\mathbf{q}$ and $\mathbf{p}$ jointly satisfy the autonomous system constituted by Hamilton's equations

$$\mathbf{q}_t = H_{\mathbf{p}}\,, \quad \mathbf{p}_t = -H_{\mathbf{q}}\,. \tag{5.1}$$

In order to allow the widest latitude in applications, we do not require that (5.1) be in standard form, but merely that there exist some (monotonic) transformation of the independent variable

$$t \longleftrightarrow s \tag{5.2}$$

and some transformation of the dependent variables

$$\mathbf{q},\mathbf{p} \longleftrightarrow \mathbf{x} \tag{5.3}$$

which take the system into the standard form, Eq. (2.4), with all solutions nearly periodic. (The only reason for permitting the former transformation is to normalize the magnitude of $\mathbf{f}$; therefore t and s will generally differ at most by a factor which is some power of ε.) Applying now our general theory, we make a further transformation of dependent variables

$$\mathbf{q},\mathbf{p} \longleftrightarrow \mathbf{x} \longleftrightarrow \mathbf{z},\varphi \tag{5.4}$$

to nice variables satisfying Eq. (2.18). Here $\mathbf{x}$ has been a mere intermediary and is of no further interest.

5.2. The action integral

It is well known that $\mathbf{p}\cdot\mathrm{d}\mathbf{q}$ is a relative integral invariant (see Section 4.5) of every Hamiltonian system; indeed, this property may be used to define Hamiltonian systems. In other words, the line integral $\oint \mathbf{p}\cdot\mathrm{d}\mathbf{q}$ taken around any closed curve remains constant in the course of time if (every point of) the curve varies in accordance with the equations of motion (5.1). In this way one may construct any number of constants of motion, which, however, are for the most part not useful, because not locally computable (see Section 1.4). There is no way of telling what the family of closed curves chosen at one time will have become at a later time, except of course by fully solving the equations of motion, the very task to avoid or (to help) to effect which one would like to know constants of motion in the first place.

In the present situation there is, nevertheless, a family of curves admirably suited to the construction of a useful constant of motion; these are the rings, which as a family remain invariant (since rings flow into rings; see Section 3.3), and which are to an adequate degree locally computable (not local to a point, but local to the loop through a point). Accordingly we define the *phase integral of action*

$$J(\mathbf{z}) \equiv \oint_{\text{ring } \mathbf{z}} \mathbf{p}\cdot\mathrm{d}\mathbf{q} = \int_0^1 \mathrm{d}\varphi\, \mathbf{p}\cdot\mathbf{q}_\varphi, \tag{5.5}$$

in which $\mathbf{q}$ and $\mathbf{p}$ are to be thought of as functions of $\mathbf{z}$ and φ in accordance with (5.4). It is perhaps worth giving the trivial direct proof of the constancy of J to all orders: since differentiation with respect to s commutes with differentiation or integration with respect to φ, so does differentiation with respect to t, whence

$$\begin{aligned} J_t &= \oint (\mathbf{p}_t\cdot\mathrm{d}\mathbf{q} - \mathbf{q}_t\cdot\mathrm{d}\mathbf{p}) \\ &= -\oint (H_{\mathbf{q}}\cdot\mathrm{d}\mathbf{q} + H_{\mathbf{p}}\cdot\mathrm{d}\mathbf{p}) = -\oint \mathrm{d}H = 0\,, \end{aligned} \tag{5.6}$$

where in the first step we have integrated the second term by parts and in the next we have used (5.1). (Incidentally, J is obviously also invariant under canonical transformations.)

The constancy of J to all orders clearly holds for ranges of the independent variable of order ε^{-n} for any n, so long as J remains defined.

5.3. Poisson Brackets

Let $\mathbf{A}$ and $\mathbf{B}$ be any polyadic functions of the state of our physical system, i.e. of $\mathbf{q}$, $\mathbf{p}$. Their *Poisson bracket* is defined (as usual) by

$$[\mathbf{A},\mathbf{B}] = \mathbf{A}_{\mathbf{q}}\cdot{}_{\mathbf{p}}\mathbf{B} - \mathbf{A}_{\mathbf{p}}\cdot{}_{\mathbf{q}}\mathbf{B}\,. \tag{5.7}$$

We shall need the formula

$$[\mathbf{A},\mathbf{B}]_s = [\mathbf{A}_s,\mathbf{B}] + [\mathbf{A},\mathbf{B}_s]\,, \tag{5.8}$$

which is immediately equivalent to its analogue with t-derivatives in place of s-derivatives (multiply by

t_s or s_t to go back or forth), a well known formula easily derived by straightforward calculation using nothing more than (5.1).

Now, by (5.8), (2.18), and (5.7) we have

$$[\mathbf{z}, \mathbf{z}]_s = [\varepsilon \mathbf{h}, \mathbf{z}] + [\mathbf{z}, \varepsilon \mathbf{h}] = \varepsilon \mathbf{h}_{\mathbf{z}} \cdot [\mathbf{z}, \mathbf{z}] + \varepsilon [\mathbf{z}, \mathbf{z}] \cdot {}_{\mathbf{z}}\mathbf{h}, \tag{5.9}$$

so that by the theorem of phase independence the (obviously antisymmetric) dyadic $[\mathbf{z}, \mathbf{z}]$ is a function of $\mathbf{z}$ alone,

$$[\mathbf{z}, \mathbf{z}]_\varphi = 0. \tag{5.10}$$

(Note that although there is no reason to suppose that $[\mathbf{z}, \mathbf{z}]$ is O (1), the theorem is applicable anyway because (5.9) is linear.) In the same way we have

$$[\varphi, \mathbf{z}]_s = [\omega, \mathbf{z}] + [\varphi, \varepsilon \mathbf{h}] = \omega_{\mathbf{z}} \cdot [\mathbf{z}, \mathbf{z}] + \varepsilon [\varphi, \mathbf{z}] \cdot {}_{\mathbf{z}}\mathbf{h}, \tag{5.11}$$

so that, again by the theorem of phase independence, which applies in view of (5.10),

$$[\varphi, \mathbf{z}]_\varphi = 0. \tag{5.12}$$

We need the two formulas

$$[\mathbf{z}, \mathbf{z}] \cdot ({}_{\mathbf{z}}\mathbf{p} \cdot \mathbf{q}_\varphi - {}_{\mathbf{z}}\mathbf{q} \cdot \mathbf{p}_\varphi) = 0, \tag{5.13}$$

$$[\varphi, \mathbf{z}] \cdot ({}_{\mathbf{z}}\mathbf{p} \cdot \mathbf{q}_\varphi - {}_{\mathbf{z}}\mathbf{q} \cdot \mathbf{p}_\varphi) = 1. \tag{5.14}$$

The short way to establish them is to observe that their common parenthetical factor is the Lagrange bracket of $\mathbf{z}$ and φ and to exploit the well known relationship between the Poisson and the Lagrange brackets, in view of the fact that the summation indicated by the left-most dot in each of them runs over a set of variables complete except for the omission of φ, for which the Lagrange bracket would vanish anyway. Of course (5.13) and (5.14) can also be easily established by direct calculation. It is only necessary to expand them out by (5.7) and the distributive law and then to make use of relations (coming from the chain rule for differentiation) between the derivatives of $\mathbf{q}$ and $\mathbf{p}$ with respect to $\mathbf{z}$ and φ and vice versa, namely

$$\mathbf{q}_{\mathbf{z}} \cdot \mathbf{z}_{\mathbf{q}} + \mathbf{q}_\varphi \varphi_{\mathbf{q}} = \mathbf{q}_{\mathbf{q}} = \mathbf{I} \tag{5.15}$$

and similar relations based on two-sided evaluations of $\mathbf{q}_{\mathbf{p}}$, $\mathbf{p}_{\mathbf{q}}$, $\mathbf{p}_{\mathbf{p}}$, $\mathbf{z}_\varphi$, and φ_φ. (The two remaining similar relations coming from $\mathbf{z}_{\mathbf{z}}$ and $\varphi_{\mathbf{z}}$ are not needed.)

We are now prepared to evaluate two particular Poisson brackets of interest. One is

$$[\mathbf{z}, J] = [\mathbf{z}, \mathbf{z}] \cdot J_{\mathbf{z}} = [\mathbf{z}, \mathbf{z}] \cdot \int_0^1 \mathrm{d}\varphi \, ({}_{\mathbf{z}}\mathbf{p} \cdot \mathbf{q}_\varphi - {}_{\mathbf{z}}\mathbf{q} \cdot \mathbf{p}_\varphi) = 0, \tag{5.16}$$

where the first equation is seen to hold by (5.7) and the fact that J depends on $\mathbf{z}$ alone, the second by direct differentiation of (5.5) followed by an integration by parts, and the last by (5.13) after $[\mathbf{z}, \mathbf{z}]$ has been brought inside the integral by virtue of (5.10). The other is

$$[\varphi, J] = 1, \tag{5.17}$$

as seen in the same way using (5.14) and (5.12).

5.4. Nontriviality of action integral

We digress momentarily to point out that J can hardly be a trivial constant of motion. It certainly cannot be completely trivial, in the sense of being an outright constant, for then its Poisson bracket with any other quantity would vanish, contradicting (5.17). But suppose that J can be expressed as a function of H alone, which is obviously a kind of triviality since H is of course automatically a constant of motion. Now J_H cannot vanish, else we would have $[\varphi, J] = [\varphi, H] J_H = 0$, contradicting (5.17) as before, so we may invert the relationship and express H as a function of J. Then

$$\mathbf{z}_t = [\mathbf{z}, H] = [\mathbf{z}, J] H_J = 0, \tag{5.18}$$

where the first equation is well known and obvious, and the last is a consequence of (5.16). Thus the $\mathbf{z}$ provide a complete set of integrals of the system. Only in this extremely special case can J be a function of H alone.

5.5. Reduced Hamiltonian system

We continue with our program of showing the hereditary character of being Hamiltonian. To this end we wish to put the reduced system into Hamiltonian form. Through the reduction process itself we have gotten rid of (or "left behind") one variable, φ, and now that we have the nontrivial constant of motion J, we may use it to eliminate another variable. Thus we may hope to put the remaining system of $2M-2$ variables into the form of a Hamiltonian system of $M-1$ degrees of freedom.

Our actual procedure for obtaining this *reduced time-independent Hamiltonian* system is to make a canonical transformation from our original set of M pairs of canonically conjugate coordinates $(\mathbf{q}, \mathbf{p})$ to a new set of which one pair is (φ, J) and of which the remaining $M-1$ pairs, to be denoted collectively by $(\mathbf{Q}, \mathbf{P})$, are also locally computable. Now the necessary and sufficient condition that the transformation to a new set of pairs of coordinates be canonical is that the Poisson bracket of any two new coordinates be zero if they come from different pairs and unity if they constitute a pair (in the right order). Because of (5.17) it is not immediately excluded that we can find a canonical transformation of the kind described, but it is also not immediately obvious that we can. In Section 6.2 it is shown* that whenever one knows some

* A very similar theorem is demonstrated by Nordheim and Fues [19], who assume that an integral is known and show how this can be used to reduce to a Hamiltonian system of one less degree of freedom; one finds a canonical transformation to new coordinates one of which is the known integral, in which case its conjugate coordinate obviously is ignorable. In our present application the ignorable coordinate, φ, has come first. It is not on account of this minor difference that a separate discussion is appended, but rather partly to keep this paper as self-contained as possible and partly because the method is so simple and seems to offer a slightly unconventional insight into the nature of the Poisson bracket conditions.

of the new coordinates of a proposed prospective canonical transformation, and these coordinates satisfy all the requisite Poisson bracket conditions among themselves and have linearly independent derivatives with respect to the old coordinates, then one can indeed define the missing coordinates (in a way locally dependent on the Hamiltonian) so as to form a complete canonical transformation; furthermore the whole construction is obviously valid order by order when the coordinates involved are construed as series.

The condition of linear independence of the derivatives is certainly satisfied, for if we had, say,

$$J_{\mathbf{q}} = k\varphi_{\mathbf{q}}, \quad J_{\mathbf{p}} = k\varphi_{\mathbf{p}}, \tag{5.19}$$

we could immediately deduce

$$[\varphi, J] = k[\varphi, \varphi] = 0,$$

once again contradicting (5.17). Accordingly, we may assume that we now have the sequence of transformations

$$\varphi, \mathbf{z} \longleftrightarrow \mathbf{q}, \mathbf{p} \longleftrightarrow \Phi, J, \mathbf{Q}, \mathbf{P}, \tag{5.20}$$

where in view of the discussion in Section 1.3 we have introduced the new symbol Φ (not to be confused with the Φ of Section 2) for φ in its role as a member of the new set of variables, so that the equation

$$\Phi = \varphi \tag{5.21}$$

may be used freely except to substitute one subscript for another (but see below!). The new variables $\mathbf{Q}$ and $\mathbf{P}$ have been so constructed as to satisfy the correct bracket conditions

$$[\mathbf{Q}, \mathbf{Q}] = 0, [\mathbf{P}, \mathbf{P}] = 0, [\mathbf{Q}, \mathbf{P}] = \mathbf{I} \tag{5.22}$$

among themselves and also the "cross-conditions"

$$0 = [\mathbf{Q}, \Phi] = [\mathbf{Q}, \varphi] = \mathbf{Q}_{\mathbf{z}} \cdot [\mathbf{z}, \varphi], \tag{5.23}$$

$$0 = [\mathbf{Q}, J] = \mathbf{Q}_{\varphi}[\varphi, J] + \mathbf{Q}_{\mathbf{z}} \cdot [\mathbf{z}, J] = \mathbf{Q}_{\varphi}, \tag{5.24}$$

and the same with $\mathbf{Q}$ replaced throughout by $\mathbf{P}$. From (5.24) we see that $\mathbf{Q}$ and $\mathbf{P}$ actually are independent of φ, like J, so the transformation $\mathbf{z} \longleftrightarrow J, \mathbf{Q}, \mathbf{P}$ is wholly independent of φ, and we may (and from now on do) obliterate completely the distinction between Φ and φ.

The new Hamiltonian is of course just the old one H itself, naturally expressed now as a function of the new canonical coordinates through the transformation (5.20). In the new coordinates, Hamilton's equations take the form

$$\varphi_t = H_J, \tag{5.25}$$

$$J_t = -H_{\varphi}, \tag{5.26}$$

$$\mathbf{Q}_t = H_{\mathbf{P}}, \quad \mathbf{P}_t = -H_{\mathbf{Q}}. \tag{5.27}$$

Since $\varphi_t = \varphi_s s_t = \omega s_t$, (5.25) yields the familiar sort of relation between the frequency and the derivative of the Hamiltonian with respect to the action variable. Since $J_t = 0$, (5.26) shows that H is independent of φ, which we might have known anyway from the fact that H is an integral of the system (see Section 4.3). It is now clear that (5.27) constitutes a one-parameter family (parametrized by J) of autonomous Hamiltonian systems.

5.6. Possibility of repetition and further invariants

As a consequence of our ability to put the reduced system back into Hamiltonian form, we see immediately that if the reduced system itself has all solutions nearly periodic (naturally with a period longer than the period of the original system at least by an order of ε), then there exists also another constant of motion

$$J' \equiv \oint_{\text{ring } z'} \mathbf{P} \cdot \mathrm{d}\mathbf{Q} = \int_0^1 \mathrm{d}\varphi' \, \mathbf{P} \cdot \mathbf{Q}_{\varphi'}, \tag{5.28}$$

where $\mathbf{z}'$ and φ' are the new nice variables for the reduced system,

$$\mathbf{z} \longleftrightarrow J, \mathbf{Q}, \mathbf{P} \longleftrightarrow \mathbf{z}', \varphi'. \tag{5.29}$$

As one should expect, it is by no means necessary to go through the complicated integration process involved in finding $\mathbf{Q}$ and $\mathbf{P}$ in order to compute J', for

$$J' = \int_0^1 \mathrm{d}\varphi' \, (\mathbf{P} \cdot \mathbf{Q}_{\varphi'} + J\varphi_{\varphi'}) = \int_0^1 \mathrm{d}\varphi' \, \mathbf{p} \cdot \mathbf{q}_{\varphi'}, \tag{5.30}$$

since $\varphi_{\varphi'} = 0$ (the transformation (5.29) being independent of φ) and the differential form $\mathbf{p} \cdot \mathrm{d}\mathbf{q}$ is a canonical invariant.

Because $\mathbf{Q}$ and $\mathbf{P}$ are locally computable, so is J'. Furthermore, J' cannot depend only on J, nor even only on J and H except in the very trivial special case that we can find a complete set of integrals. Incidentally it may be noted that there is no chance here of finding still another integral by the well known device of forming the Poisson bracket of two already known, since by a further canonical transformation we can introduce a set of canonical coordinates among which are the conjugate pairs (φ, J) and (φ', J'), which demonstrates that

$$[J, J'] = 0 \tag{5.31}$$

in addition to three other such relations.

If the new reduced system should itself happen to have all solutions nearly periodic we can find still another integral J'' and ignore another angle variable φ'', and so on indefinitely, till the successive near periodicities run out. If the internal degrees of freedom run out first, we end up with a complete (asymptotic) description of the system in terms of M ignorable angle variables and their M locally determined conjugate action variables.

6. Appendices

6.1. Fundamental approximation theorem

For the sake of completeness we give here a brief outline of the well known proof that two functions

which satisfy nearly identical autonomous systems and have nearly equal initial values are themselves nearly equal for a bounded range of the independent variable. Let $\mathbf{x}(s)$ and $\hat{\mathbf{x}}(s)$ satisfy

$$\mathbf{x}_s = \mathbf{f}(\mathbf{x}), \quad \hat{\mathbf{x}}_s = \mathbf{f}(\hat{\mathbf{x}}) + \boldsymbol{\gamma}(\hat{\mathbf{x}}), \tag{6.1}$$

$$\mathbf{x}(0) = \hat{\mathbf{x}}(0) + \boldsymbol{\delta}, \tag{6.2}$$

where $\boldsymbol{\gamma}$ and $\boldsymbol{\delta}$ are small quantities whose norms (maximized over x-space in the case of $\boldsymbol{\gamma}$) we denote by γ and δ. (Any reasonable norm may be employed, and will be denoted by absolute value signs.) In the region of interest in x-space $\mathbf{f}$ satisfies a Lipschitz condition,

$$|\mathbf{f}(\mathbf{x}') - \mathbf{f}(\mathbf{x}'')| \leq c\,|\mathbf{x}' - \mathbf{x}''| \tag{6.3}$$

for an appropriate positive constant c and any $\mathbf{x}'$ and $\mathbf{x}''$ (if only because $\mathbf{f}_\mathbf{x}$ exists and is continuous on a closed bounded domain and therefore has all components bounded). To estimate the difference we have

$$|\hat{\mathbf{x}} - \mathbf{x}| = \left|\hat{\mathbf{x}}(0) - \mathbf{x}(0) + \int_0^s \mathrm{d}s\,[\mathbf{f}(\hat{\mathbf{x}}) + \boldsymbol{\gamma}(\hat{\mathbf{x}}) - \mathbf{f}(\mathbf{x})]\right|$$

$$\leq \delta + \int_0^s \mathrm{d}s\,[c\,|\hat{\mathbf{x}} - \mathbf{x}| + \gamma], \tag{6.4}$$

for simplicity restricting ourselves to non-negative values of s. Now the maximum value $\mu(s)$ of $|\hat{\mathbf{x}} - \mathbf{x}|$ in the range from 0 to s satisfies

$$\mu \leq \delta + \int_0^s \mathrm{d}s\,[c\,\mu + \gamma]$$

$$\leq \delta + s\,[c\,\mu + \gamma], \tag{6.5}$$

so that for $s \leq 1/(2c)$ (for instance) we have

$$\mu \leq \frac{\delta + \gamma s}{1 - cs} \leq 2\delta + 2\gamma s. \tag{6.6}$$

In order to obtain an estimate for larger values of s we could apply (6.6) over and over again, proceeding in steps of size $1/(2c)$ and using the final estimate at each step as the initial estimate corresponding to (6.2) for the next step. In this way we would obtain an exponential estimate, which is, however, more elegantly and perhaps simply obtained by noting that an upper bound for $|\hat{\mathbf{x}} - \mathbf{x}|$ is provided by the function $\nu(s)$ which satisfies the equation obtained from (6.4) by replacing $|\hat{\mathbf{x}} - \mathbf{x}|$ by ν and $\leq$ by $=$. Indeed, the difference $D \equiv \nu - |\hat{\mathbf{x}} - \mathbf{x}|$ satisfies

$$D \geq c \int_0^s \mathrm{d}s\,D, \tag{6.7}$$

$$\left(\mathrm{e}^{-cs} \int_0^s \mathrm{d}s\,D\right)_s \geq 0, \tag{6.8}$$

whence upon integration from 0 to s it follows that the right-hand side of (6.7) and *a fortiori* D are non-negative. But it is trivial to solve explicitly for ν, and we find that

$$|\hat{\mathbf{x}} - \mathbf{x}| \leq \nu = \left(\delta + \frac{\gamma}{c}\right)\mathrm{e}^{cs} - \frac{\gamma}{c}. \tag{6.9}$$

That there can be no estimate radically better than this is obvious from even the simplest examples. The standard uniqueness theorem is of course obtained as the special case $\boldsymbol{\gamma} = \boldsymbol{\delta} = 0$.

6.2. Completion of canonical transformation

The necessary and sufficient conditions that a transformation

$$\mathbf{q}, \mathbf{p} \longleftrightarrow \hat{\mathbf{q}}, \hat{\mathbf{p}} \tag{6.10}$$

be canonical are of course the fundamental Poisson bracket relations

$$[\hat{\mathbf{q}}, \hat{\mathbf{q}}] = 0, \quad [\hat{\mathbf{q}}, \hat{\mathbf{p}}] = \mathbf{I}, \quad [\hat{\mathbf{p}}, \hat{\mathbf{p}}] = 0. \tag{6.11}$$

A consequence of these relations is that the derivatives of the components of $\hat{\mathbf{q}}$ and $\hat{\mathbf{p}}$ are linearly independent (and *a fortiori* that the components themselves are functionally independent), since for any linear combination of these derivatives which vanishes,

$$\mathbf{a} \cdot \hat{\mathbf{q}}_\mathbf{q} + \mathbf{b} \cdot \hat{\mathbf{p}}_\mathbf{q} = 0, \quad \mathbf{a} \cdot \hat{\mathbf{q}}_\mathbf{p} + \mathbf{b} \cdot \hat{\mathbf{p}}_\mathbf{p} = 0, \tag{6.12}$$

we have, by (11) and (12), that

$$\mathbf{a} = \mathbf{a} \cdot [\hat{\mathbf{q}}, \hat{\mathbf{p}}] = -\mathbf{b} \cdot [\hat{\mathbf{p}}, \hat{\mathbf{p}}] = 0 \tag{6.13}$$

and similarly that $\mathbf{b} = 0$.

Suppose now that we are given, as functions of $\mathbf{q}$ and $\mathbf{p}$, some but not all of the components of $\hat{\mathbf{q}}$ and $\hat{\mathbf{p}}$ in a proposed transformation (6.10). We wish to prove that we can construct the remaining components. Let $\mathbf{q}$, $\mathbf{p}$, $\hat{\mathbf{q}}$, $\hat{\mathbf{p}}$ each have M components. We denote the $N < 2M$ given components (of both $\hat{\mathbf{q}}$ and $\hat{\mathbf{p}}$, not necessarily paired) collectively by $\boldsymbol{\alpha}$, and require them to have linearly independent derivatives and to satisfy those components of relations (6.11) which involve them alone. Since we can proceed by mathematical induction, it suffices to construct one of the remaining components of $\hat{\mathbf{q}}$ or $\hat{\mathbf{p}}$, say of $\hat{\mathbf{q}}$. We denote this component by q' and its conjugate by p'. We must construct q' to satisfy those components of relations (6.11) which involve it and the $\boldsymbol{\alpha}$. These conditions on q' have in fact the form

$$[\boldsymbol{\alpha}, q'] = \mathbf{c}, \tag{6.14}$$

where $\mathbf{c}$ is constant and, to be sure, has all components zero except for at most one of them, which equals -1 (that component, if it is among the $\boldsymbol{\alpha}$, which corresponds to p').

Conditions (6.14) amount to a prescription of the directional derivative of q' in each of a number of directions, one for each component of $\boldsymbol{\alpha}$. These directions are linearly independent, since the derivatives of the components of $\boldsymbol{\alpha}$ are. We next inquire into the conditions for the compatibility of (6.14), namely the conditions that the second derivatives of q' be the same independently of the order of differentiation. The dyadic second directional deriv-

ative of q' (which, if expanded out, contains first as well as second derivatives of q') is

$$[\boldsymbol{\alpha}, [\boldsymbol{\alpha}, q']] = [\boldsymbol{\alpha}, \mathbf{c}] = 0, \tag{6.15}$$

since $\mathbf{c}$ is constant. Taking the directional derivatives in the reverse order gives

$$-[[\boldsymbol{\alpha}, q'], \boldsymbol{\alpha}] = 0 \tag{6.16}$$

(which happens to be the transpose of (6.15)). This has the same second derivatives of q', so we obtain the consistency conditions by taking the difference

$$[\boldsymbol{\alpha}, [\boldsymbol{\alpha}, q']] + [[\boldsymbol{\alpha}, q'], \boldsymbol{\alpha}] = 0\,. \tag{6.17}$$

Now, Jacobi's identity, written for two vectors and a scalar with due regard to the dyadic order, is

$$[\boldsymbol{\alpha}, [\boldsymbol{\alpha}', q']] + [[\boldsymbol{\alpha}, q'], \boldsymbol{\alpha}'] + [q', [\boldsymbol{\alpha}, \boldsymbol{\alpha}']] = 0\,, \tag{6.18}$$

the middle term being the transpose of $[\boldsymbol{\alpha}', [q', \boldsymbol{\alpha}]]$. Taking $\boldsymbol{\alpha}'$ to be $\boldsymbol{\alpha}$, we see that (6.17) is equivalent to

$$[[\boldsymbol{\alpha}, \boldsymbol{\alpha}'], q'] = 0\,, \tag{6.19}$$

which is explicitly devoid of second derivatives of q'. But $[\boldsymbol{\alpha}, \boldsymbol{\alpha}']$ is a constant dyadic, all of whose components are 0 or ± 1, in view of (6.11), so (6.19) holds identically.

Since the compatibility conditions are satisfied (tautologously), it follows from the general theory of partial differential equations that (6.14) has a general solution q' with the freedom of an arbitrary function of $2M - N$ variables. From the geometrical point of view, indeed, we have shown that the N-dimensional vector space determined at each point by the directions of the directional derivatives $[\boldsymbol{\alpha}, \ldots]$ there, is the tangent space of a $(2M - N)$-dimensional family of N-dimensional hypersurfaces*. In (6.14) we have a complete prescription of the derivatives of q' as a function on each hypersurface, but no restriction on the variation of q' from one hypersurface to another. Clearly q' is determined up to a constant (its "initial value" at any given point) on each hypersurface.

It remains only to show that the arbitrariness in q' permits us to choose it in such a way that the derivatives of q' and the $\boldsymbol{\alpha}$ will be linearly independent. This is merely a matter of counting dimensions, for suppose contrarily that

$$q'_{\mathbf{q}} = \mathbf{k} \cdot \boldsymbol{\alpha}_{\mathbf{q}}, \quad q'_{\mathbf{p}} = \mathbf{k} \cdot \boldsymbol{\alpha}_{\mathbf{p}}. \tag{6.20}$$

If p' is among the $\boldsymbol{\alpha}$, then since $[\boldsymbol{\alpha}, q']$ vanishes in all except that component, and since by (6.20)

$$0 = [q', q'] = \mathbf{k} \cdot [\boldsymbol{\alpha}, q'], \tag{6.21}$$

it follows that the corresponding component of $\mathbf{k}$ vanishes. Similarly, if any (other) two conjugate coordinates q'', p'' are among the $\boldsymbol{\alpha}$, the corresponding components of $\mathbf{k}$ must both vanish, else by means of (6.20) we could solve for and eliminate the derivatives of either q'' or p'' and by (6.11) obtain the contradiction

$$1 = [q'', p''] = 0.$$

Let the number of such pairs be L, so that the number of unpaired components of $\boldsymbol{\alpha}$ is $N - 2L$. Obviously

$$N - L = (N - 2L) + L \leq M, \tag{6.22}$$

the right-hand equality holding only if p' is among the $\boldsymbol{\alpha}$. The number of possibly nonzero components of $\mathbf{k}$ is

$$N - 2L = 2(N - L) - N \leq 2M - N \tag{6.23}$$

or $N-2L-1$ if $\mathbf{p}'$ is among the $\boldsymbol{\alpha}$; thus in either case it is strictly less than $2M - N$. But q' has the freedom of an arbitrary function of $2M - N$ variables, so its derivatives span a $(2M - N)$-dimensional linear space, contradicting (6.20).

6.3. Iterated near-identity mappings

There is a strong and intimate connection between the asymptotic theory of nearly recurrent systems and the asymptotic theory of iterated near-identity mappings, which has previously been treated less satisfactorily by Kruskal [5] and applied by Spitzer [4]. In this section we describe the latter theory and explore the connections.

A *near-identity mapping* of a space of vectors $\boldsymbol{\xi}$ into itself is a function, $\mathbf{T}(\boldsymbol{\xi})$ say, which can be written in the form

$$\mathbf{T}(\boldsymbol{\xi}) = \boldsymbol{\xi} + \varepsilon \mathbf{D}(\boldsymbol{\xi}), \tag{6.24}$$

where, $\mathbf{D}(\boldsymbol{\xi})$ may be a series in powers of ε and is required to be $\mathrm{O}(1)$. Associated with such a transformation (as with any) is the sequence of its iterates, the transformations $\mathbf{T}^n(\boldsymbol{\xi})$ defined recursively by

$$\mathbf{T}^1(\boldsymbol{\xi}) \equiv \mathbf{T}(\boldsymbol{\xi}), \quad \mathbf{T}^{n+1}(\boldsymbol{\xi}) \equiv \mathbf{T}^n[\mathbf{T}(\boldsymbol{\xi})], \tag{6.25}$$

where n runs over the positive integers.* We then ask for an asymptotic description (as $\varepsilon \to 0$) of the discrete "trajectory" of a point $\boldsymbol{\xi}$ under iteration of $\mathbf{T}$, i.e. of the sequence of points $\mathbf{T}^n(\boldsymbol{\xi})$, $n = 0, 1, 2, \ldots$

Obviously as $\varepsilon \to 0$ the points get closer and closer together. For any fixed n, of course $\mathbf{T}^n(\boldsymbol{\xi}) \to \boldsymbol{\xi}$, but this does not imply that the trajectory as a whole collapses into the initial point, since for n taken approximately equal to c/ε (where c is a constant) we may expect $\mathbf{T}^n(\boldsymbol{\xi})$ to remain distinctly away from $\boldsymbol{\xi}$ and indeed to converge to a limit** different from $\boldsymbol{\xi}$. Rather, the discrete trajectory approximates better and better to a continuous (and smooth) curve denoted by $\boldsymbol{\Xi}^{(0)}(\sigma)$ and determined by

$$\boldsymbol{\Xi}^{(0)}(0) = \boldsymbol{\xi}, \quad \boldsymbol{\Xi}^{(0)}{}_{\sigma} = \mathbf{D}(\boldsymbol{\Xi}^{(0)}), \tag{6.26}$$

the latter being obtained from (6.24) by replacing $\boldsymbol{\xi}$

---

* See Newcomb [20] for a heuristic description of the theory of such questions. In his terminology, we have shown that the "cross-bracket" of any two directions of differentiation is zero.

* Obviously (6.24) can be formally inverted to yield an inverse transformation $\mathbf{T}^{-1}$, with iterates $\mathbf{T}^{-2}$, $\mathbf{T}^{-3}$, etc. With $\mathbf{T}^0(\boldsymbol{\xi}) \equiv \boldsymbol{\xi}$, (6.25) becomes valid for all integers n.

** This limit can in fact be expressed as $\boldsymbol{\Xi}^{(0)}(c)$, see (6.28).

by $\mathbf{T}^n(\boldsymbol{\xi})$ and then going to the limit after making the identifications

$$\sigma \equiv n\varepsilon, \tag{6.27}$$

$$\boldsymbol{\Xi}^{(0)}(\sigma) \equiv \lim_{\varepsilon=0} \mathbf{T}^n(\boldsymbol{\xi}). \tag{6.28}$$

Except to zeroth order the points $\mathbf{T}^n(\boldsymbol{\xi})$ naturally need not lie on $\boldsymbol{\Xi}^{(0)}$. This suggests (what we have already presaged by the notation) that we seek a formal series $\boldsymbol{\Xi}(\sigma)$ such that the representation

$$\mathbf{T}^n(\boldsymbol{\xi}) = \boldsymbol{\Xi}(\sigma) \tag{6.29}$$

will be valid to all orders under the identification (6.27), which there is no need to modify. And it is indeed easy to obtain the appropriate conditions (differential equation and initial condition) determining $\boldsymbol{\Xi}$ to higher orders. We could then develop a rigorous theory, with analogues of the results in the main body of this paper. It is simpler, however, to reduce the problem to the one that we have already exhaustively analyzed.

The crucial step is to imbed the sequence $\mathbf{T}^n(\boldsymbol{\xi})$ in a continuous trajectory satisfying an autonomous system of differential equations. That is, we seek a function $\boldsymbol{\eta}(\boldsymbol{\xi})$ such that the curve $\hat{\boldsymbol{\xi}}(\boldsymbol{\xi}, \sigma)$ defined as the solution of the system

$$\hat{\boldsymbol{\xi}}_\sigma = \boldsymbol{\eta}(\hat{\boldsymbol{\xi}}) \tag{6.30}$$

determined by the initial condition

$$\hat{\boldsymbol{\xi}}(\boldsymbol{\xi}, 0) = \boldsymbol{\xi} \tag{6.31}$$

passes through the points in the sequence for σ given by (6.27):

$$\hat{\boldsymbol{\xi}}(\boldsymbol{\xi}, n\varepsilon) = \mathbf{T}^n(\boldsymbol{\xi}). \tag{6.32}$$

We shall show that $\boldsymbol{\eta}$ is determined (and uniquely) as a series to all orders by this condition (required to hold for arbitrary $\boldsymbol{\xi}$).

Obviously it suffices to determine $\boldsymbol{\eta}$ merely so that (6.32) holds with $n=1$,

$$\hat{\boldsymbol{\xi}}(\boldsymbol{\xi}, \varepsilon) = \mathbf{T}(\boldsymbol{\xi}), \tag{6.33}$$

since it will then automatically hold for all larger n by an induction based on the calculation

$$\begin{aligned}\hat{\boldsymbol{\xi}}(\boldsymbol{\xi}, n\varepsilon + \varepsilon) &= \hat{\boldsymbol{\xi}}[\hat{\boldsymbol{\xi}}(\boldsymbol{\xi}, \varepsilon), n\varepsilon] \\ &= \hat{\boldsymbol{\xi}}[\mathbf{T}(\boldsymbol{\xi}), n\varepsilon] = \mathbf{T}^n[\mathbf{T}(\boldsymbol{\xi})] = \mathbf{T}^{n+1}(\boldsymbol{\xi}),\end{aligned} \tag{6.34}$$

where the first equation is an instance of Eq. (1.7), the second will follow from (6.33), the third will be an instance of the induction hypothesis (6.32), and the fourth is part of (6.25). Now by a Taylor expansion

$$\begin{aligned}\hat{\boldsymbol{\xi}}(\boldsymbol{\xi}, \varepsilon) &= \hat{\boldsymbol{\xi}}(\boldsymbol{\xi}, 0) + \varepsilon\, \hat{\boldsymbol{\xi}}_\sigma(\boldsymbol{\xi}, 0) + \tfrac{1}{2}\varepsilon^2\, \hat{\boldsymbol{\xi}}_{\sigma\sigma}(\boldsymbol{\xi}, 0) + \ldots \\ &= \boldsymbol{\xi} + \varepsilon\boldsymbol{\eta}(\boldsymbol{\xi}) + \tfrac{1}{2}\varepsilon^2\, \boldsymbol{\eta}_{\boldsymbol{\xi}}(\boldsymbol{\xi}) \cdot \boldsymbol{\eta}(\boldsymbol{\xi}) + \ldots,\end{aligned} \tag{6.35}$$

which by (6.24) and (6.33) may be written in the form

$$\boldsymbol{\eta} + \tfrac{1}{2}\varepsilon\boldsymbol{\eta}_{\boldsymbol{\xi}} \cdot \boldsymbol{\eta} + \ldots = \mathbf{D}, \tag{6.36}$$

omitting the argument $\boldsymbol{\xi}$ everywhere. Inverting this we have immediately

$$\boldsymbol{\eta} = \mathbf{D} - \tfrac{1}{2}\varepsilon\, \mathbf{D}_{\boldsymbol{\xi}} \cdot \mathbf{D} + \ldots \tag{6.37}$$

The desired representation (6.29) is now obviously obtained merely by taking

$$\boldsymbol{\Xi}(\sigma) \equiv \hat{\boldsymbol{\xi}}. \tag{6.38}$$

It is at last a trivial matter to bring this theory under that of the main body of the paper. Treating n as a continuous variable and calling it s now, or in other words defining

$$s \equiv \sigma/\varepsilon, \tag{6.39}$$

and introducing a redundant angle variable θ equal to s up to an arbitrary additive integer, and finally defining*

$$\mathbf{x} \equiv (\boldsymbol{\xi}, \theta), \tag{6.40}$$

we have a system in standard form:

$$\mathbf{x}_s = \mathbf{f} \equiv (\varepsilon\boldsymbol{\eta}, 1). \tag{6.41}$$

This is nearly recurrent, since to zeroth order $\boldsymbol{\xi}$ is constant and θ increases uniformly, returning to its initial value (up to an integer, which is all that has meaning for an angle value!) each time s increases by unity. Therefore the general theory applies. The introduction of nice variables is of course utterly trivial, being given by

$$\mathbf{z} = \boldsymbol{\xi}, \quad \varphi = \theta. \tag{6.42}$$

And the reduced system is just (6.30), which we started from. The only point to this otherwise rather farcical merry-go-round is that the further developments of the theory, and especially the proof that the formal series is really an asymptotic representation of the true solution, is secured thereby.

We close with a brief description of the reverse procedure. Had we chosen to develop the mapping theory in full, we could have based the theory of nearly recurrent systems on it by choosing for $\boldsymbol{\xi}$-space a hypersurface in $\mathbf{x}$-space cutting across the loops. The mapping would then be obtained by starting from any point $\boldsymbol{\xi}$ in the hypersurface and following the solution of Eq. (2.4) around until it first again intersects the hypersurface in a point to be called $\mathbf{T}(\boldsymbol{\xi})$. Thus we see that the two theories are completely equivalent.

Acknowledgments

This work was accomplished largely under the auspices of the U.S. Atomic Energy Commission. Some of it was accomplished while the author was a guest at the Max-Planck-Institut für Physik und Astrophysik (Munich) as a National Science Founda-

* Thus $\mathbf{x}$-space is topologically the product of $\boldsymbol{\xi}$-space with a circle.

tion Senior Postdoctoral Fellow, to both of which organizations he is very grateful.

It is a pleasure to acknowledge the helpful discussions and suggestions of a number of scientists, especially E. Gerjuoy, J. Moser, and the author's colleagues at the Princeton Plasma Physics Laboratory, mainly I. Bernstein, E. Frieman, R. Kulsrud, A. Lenard, C. Oberman, and L. Spitzer, Jr.

References

[1] BORN, M., FOCK, V., *Zeits. f. Physik* **51** (1928) 165.
[2] ALFVÉN, H., Cosmical Electrodynamics (Clarendon Press, Oxford, 1950).
[3] BISHOP, A., Project Sherwood (Addison-Wesley, Reading, Mass., 1958).
[4] SPITZER, L., *Phys. Fluids* **1** (1958) 253.
[5] KRUSKAL, M., U.S. Atomic Energy Commission, Report NYO-998 (PM-S-5), 1952 and NYO-996 (Appendix to PM-S-3), 1951.
[6] FERMI, E., *Astrophys. J.* **119** (1954) 1.
[7] HELLWIG, G., *Zeits. Naturforschung* **10a** (1955) 508.
[8] KULSRUD, R., *Phys. Rev.* **106** (1957) 205.
[9] KRUSKAL, M., Rendiconti del Terzo Congresso Internazionale sui Fenomeni D'Ionizzazione nei Gas tenuto a Venezia (Societá Italiana di Fisica, Milan, 1957).
[10] LENARD, A., *Ann. Phys. (NY.)* **6** (1959) 261.
[11] BERKOWITZ, J., GARDNER, C., *Comm. on Pure and Applied Math.* **12** (1959) 501.
[12] ROSENBLUTH, M., U.S. Atomic Energy Commission Report LA-2030 (1956).
[13] VAN ALLEN, J., *J. Geophys. Res.* **64** (1959) 1683.
[14] GARDNER, C., *Phys. Rev.* **115** (1959) 791.
[15] KRYLOFF, N., BOGOLIUBOFF, N., Introduction to Non-Linear Mechanics (Annals of Mathematics Studies, No. 11, Princeton University Press, Princeton, 1947).
[16] WINTNER, A., Analytical Foundations of Celestial Mechanics (Princeton University Press, Princeton, 1941), Section 128.
[17] BOHR, H., Fastperiodische Funktionen, Ergebnisse der Mathematik und ihrer Grenzgebiete (Julius Springer, Berlin, 1932), Vol. 1, No. 5.
[18] DE DONDER, TH., Théorie des Invariants Intégraux (Gauthier-Villars, Paris, 1927).
[19] NORDHEIM, L., FUES, E., Handbuch der Physik (Julius Springer, Berlin, 1927), Vol. 5, Chap. 3.
[20] NEWCOMB, W., *Ann. Phys. (NY.)* **3** (1958) 347.

ТРАНСПОРТИРОВКА И УДЕРЖАНИЕ ДВИЖУЩИХСЯ ПЛАЗМЕННЫХ СГУСТКОВ (В. Ч. И МАГНИТНЫЕ ПЛАЗМОВОДЫ)*

Г. А. АСКАРЬЯН, М. Л. ИОВНОВИЧ, М. Л. ЛЕВИН, М. С. РАБИНОВИЧ

АКАДЕМИЯ НАУК СССР

МОСКВА, СОЮЗ СОВЕТСКИХ СОЦИАЛИСТИЧЕСКИХ РЕСПУБЛИК

В работе показаны широкие возможности стабилизации формы и орбиты плотных плазменных сгустков, быстро двигающихся через систему пространственно неоднородных и в.ч. полей. В системе координат движущегося сгустка пространственно неоднородные поля воспринимаются как высокочастотные.

Для теоретического рассмотрения выбрана модель абсолютно проводящего сгустка с резкой границей, размеры которого малы по сравнению с характерным размером полей.

В комбинации гофрированного поля с амплитудой H_0 и первой гармоники винтового поля с амплитудой H_1 условия равновесия, устойчивости и фокусировки к оси выполняются при $H_0/(1-M) = H_1(1+M)$, где M — фактор размагничивания сфероидального сгустка.

Если вместо гофрированного поля в предыдущем случае использовать H_0-волну, то условия устойчивости и фокусировки выполняются при

$$\lambda/\lambda_B < 1/8 \text{ и } L \ll 2\sqrt{2}\,\lambda\lambda_B/\sqrt{4\lambda_B^2-3\lambda^2} \text{ (для } M=1/3),$$

где λ, λ_B — длины волн в свободном пространстве и в волноводе, а L — период винтового поля.

Кроме этих случаев, рассмотрены также сочетания кругополяризованной E_1-волны с гофрированным или стелларатором полем.

Приведены оценки условий, при которых справедливы принятые упрощающие предположения (малый размер сгустка, экранировка полей, возможность усреднения воздействия полей).

Полученные результаты могут быть использованы для создания магнитных и в.ч. плазмоводов, предназначенных для транспортировки, ускорения и инжекции плазменных сгустков с сохранением концентрации их энергии. Возможен одновременный нагрев движущихся сгустков при пролетании через неоднородные магнитные поля (токами Фуко или пульсациями) или в.ч. полями.

1. Введение

Цель настоящего сообщения — обратить внимание на возможность стабилизации формы и орбиты быстро двигающихся плотных плазменных сгустков в системе постоянных и увч полей. При движении с достаточной скоростью в пространственно неоднородных магнитных полях сгусток может быть стабилизован этими полями. Действительно, в системе координат движущегося сгустка эти пространственно неоднородные поля воспринимаются как высокочастотные, причем с плотностью энергии, значительно превышающей в.ч. плотности, достижимые в лабораторной системе. Такие устройства можно рассматривать как плазмоводы, предназначенные для транспортировки, инжекции, ускорения или нагрева сгустков плазмы. Если плазмовод сделать замкнутым, то такие системы представляют интерес и для более длительного удержания и накопления сгустков.

Еще более широкие возможности открываются при рассмотрении комбинации в.ч. и постоянных пространственно неоднородных полей. В этом случае в.ч. поля могут быть использованы как для удержания, так и для предложенного В. И. Векслером радиационного ускорения сгустков плазмы. Несколько лет тому назад Левин М. Л. [1, 2] нашел комбинацию из двух (в этом случае одна из волн медленная) или трех типов волн разных частот, обеспечивающих осевую фокусировку (устойчивость орбиты), устойчивость формы (относительно основных гармоник возмущения) малого сгустка плотной плазмы.

Для теоретического исследования была выбрана довольно грубая модель абсолютно проводящего сгустка с резкой границей. Некоторые соображения о поведении отдельных частиц будут приведены ниже. Кроме того, предполагалось, что размеры сгустка малы по сравнению с неоднородностями поля, а постоянные и в.ч. поля не проникают внутрь сгустка, т.е. скин-слой в.ч. полей, а также постоянных неоднородных полей, воспринимаемых как в.ч. в системе центра инерции сгустка, мал по сравнению с его размерами. (В случае постоянных однородных полей это означает, что полученные результаты применимы лишь для времен, меньше скиновых.)

Вычисление условий равновесия и устойчивости велось обычным образом путем вычисления усредненных по времени t и по пролетной координате z давления и энергии сгустка. При вычислении первых гармоник возмущения усредненная энергия зависела от координаты r и факторов размагничения сгустков M_i.

* Доклад CN-10/245 представленный на Конференцию. Докладчик: А. А. Рухадзе. Переводы аннотаций находятся в конце этого тома Трудов Конференции.

В настоящей работе рассматривается ряд конкретных систем, удобных для транспортировки сгустков без изменения их формы.

2. Равновесие и устойчивость сгустка

Рассмотрим проводящий сгусток, размеры которого малы по сравнению с неоднородностями полей. Будем, как было сказано, считать, что постоянные, а также в.ч. поля не проникают внутрь сгустка.

Энергия малого эллипсоидального плазменного сгустка в квазиоднородных полях, как известно, равна (оси x, y, z совдапают с осями эллипсоида)

$$u = \frac{V}{8\pi}\sum\left(\frac{H_i^2(r,\varphi,z,t)}{1-M_i} - \frac{E_i^2(r,\varphi,z,t)}{M_i}\right), \quad (1)$$

где M_i — нормированные факторы размагничивания

$$M_1 + M_2 + M_3 = 1. \quad (2)$$

Если считать, что средние значения разных компонент электромагнитного поля в точке нахождения сгустка равны нулю

$$\overline{E_i E_k} = \overline{H_i H_k} = 0 \qquad i \neq k \quad (3)$$

то из уравнения (1) можно получить все условия равновесия и устойчивости плазменных сгустков.

Пусть, например, сгусток движется в направлении оси z. Усредняя выражение для энергии по времени t и координате z, получим условия равновесия

$$\frac{\partial \bar{u}}{\partial r} = \frac{\partial \bar{u}}{\partial \overline{M_k}} = 0, \quad \bar{u} > 0 \quad (4)$$

при этом при дифференцировании по M_k мы должны учесть условие (3). Требование положительности $\bar{u}$ эквивалентно требованию положительности среднего электромагнитного давления, так как при выполнении условий равновесия

$$\bar{u} = P_{\text{ср}} V, \quad (5)$$

где $P_{\text{ср}}$ — среднее давление, а V — объем сгустка.

Условия устойчивости получаются из уравнения (1) при рассмотрении соответствующих вторых производных.

Мы рассмотрим неоднородные магнитные поля трех типов: «гофрированное» поле с потенциалом

$$\Psi_{m0} = H_c z + \frac{1}{\alpha_0} H_0 I_0(\alpha_0 r)\sin\alpha_0 z \quad (6\,\text{а})$$

(как было показано [3], такое поле фокусирует движущийся сгусток к оси) и две первых гармоники винтового поля с потенциалами

$$\Psi_{mn} = \frac{1}{\alpha_n} H_n I_n(n\alpha_n r)\sin n(\varphi - \alpha_n z) \quad (6\,\text{б})$$

(осефокусирующее действие винтовых полей на сгусток было показано А. И. Морозовым).

В качестве дополнительных будут рассмотрены в.ч. поля следующих мод: H_0-волна и кругополяризованная E_1-волна. Для этих усредненных полей равновесной конфигурацией является сфероид, для которого

$$M_3 = M, \quad M_1 = M_2 = \frac{1}{2}(1-M).$$

3. Плазменный сгусток в поле кругополяризованной E_1-волны и гофрированного постоянного поля

Рассмотрим гофрированное поле следующего вида (вблизи оси)

$$H_r = \frac{1}{2} H_0 \alpha_0 r \sin\alpha_0 z$$

$$H_z = H_c + H_0\left(1 + \frac{\alpha_0^2 r^2}{4}\right)\cos\alpha_0 z \quad (7)$$

и кругополяризованную волну E_1 с амплитудой A и продольным волновым числом h. Усредненная энергия для этого случая равна вблизи оси плазмовода (с точностью до r^2)

$$\frac{\bar{u}\cdot 16\pi}{V} = \left|\frac{K}{\varkappa}A\right|^2\left[\frac{1}{1-M}\left(\frac{1-M}{1+M} - \frac{h^2}{K^2}\right) + \frac{(1+M)^2h^2 - (1+2M-3M^2)\varkappa^2}{4M(1-M^2)}r^2\right] + \frac{2H_c^2 + H_0^2}{1-M} + \frac{\alpha_0^2 r^2 H_0^2}{1-M^2}, \quad (8)$$

где K — волновое число в вакууме и $\varkappa^2 = K^2 - h^2$. Из уравнения (8) получаем условие равновесия

$$2H_c^2 + H_0^2 = \left|\frac{K}{\varkappa}A\right|^2\left[\left(\frac{1-M}{1+M}\right)^2 + \frac{h^2}{K^2}\right]. \quad (9)$$

Условия устойчивости формы

$$\frac{h^2}{K^2} < \left(\frac{1-M}{1+M}\right)^3 \text{ и } \frac{h^2}{K^2} < \frac{M(3-M)}{(1+M)^2}. \quad (10)$$

Для сферического сгустка $M = 1/3$ условие (10) эквивалентно

$$\frac{h^2}{K^2} < \frac{1}{8}. \quad (11)$$

Осевая устойчивость имеет место

$$h^2(1+M)^2 + \frac{4M_K^2\alpha_0^2}{\varkappa^2[1+(2H_c^2/H_0^2)]}\left[\left(\frac{1-M}{1+M}\right)^2 + \frac{h^2}{K^2}\right] > (1+2M-3M^2)K^2. \quad (12)$$

Для сферического сгустка и при малом h должно быть (если $H_c = 0$) $\alpha_0 > (8/3)^{1/2}K$, т.е. шаг гофра $L < \lambda/(8/3)^{1/2}$, где λ — длина волны в.ч. поля. Следовательно, шаг гофра должен быть достаточно мал. Практически, это оказывается неудобным.

4. Сгусток в поле H_0-волны и первой гармоники винтового поля

Рассмотрим первую гармонику винтового поля вблизи оси плазмовода

$$H_r = \frac{1}{2}H_1\left[1 + \frac{3}{8}\alpha_1^2 r^2\right]\sin(\varphi - \alpha_1 z)$$

$$H_\varphi = \frac{1}{2}H_1\left[1 + \frac{1}{8}\alpha_1^2 r^2\right]\cos(\varphi - \alpha_1 z) \quad (13)$$

$$H_z = -\alpha_1 r H_\varphi$$

и H_0-волну с амплитудой A. В этом случае условия устойчивости, по-видимому, можно выполнить не только для первых гармоник возмущений, но и для более высоких, т.к. электрическое поле на оси волновода равняется нулю.

Производя вычисления точно также как в предыдущем случае, получим условие равновесия, зная

$$\frac{\overline{u}\cdot 16\pi}{V} = A^2\left[\frac{1}{1-M} + \frac{h^2-(1+M)K^2}{1-M^2}r^2\right] + H_1^2\left(\frac{1}{1+M} + \frac{3-M}{4(1-M^2)}\alpha_1^2 r^2\right) \quad (14)$$

$$\frac{\partial \overline{u}}{\partial M} = \frac{A^2}{(1-M)^2} - \frac{H_1^2}{(1+M)^2} = 0\,. \quad (15)$$

Условия устойчивости выполняются автоматически при выполнении условия (15). Для обеспечения фокусировки к оси необходимо, чтобы выполнялось условие

$$h^2 + \frac{(1+M)^2(3-M)\alpha_1^2}{4(1-M)^2} > (1+M)K^2 \quad (16)$$

Для шарового сгустка условие фокусировки

$$L < \frac{2\sqrt{2}\,\lambda\,\lambda_B}{\sqrt{4\lambda_B^2 - 3\lambda^2}} \quad (17)$$

где λ, $\lambda_в$ — длины волн в вакууме и волноводе, а L — шаг винтового поля.

В этом случае шаг винтового поля можно выбрать довольно большим.

5. Сгусток плазмы в стелларапторном поле и в поле E_1-волны

Рассмотрим кругополяризованную волну типа E_1 и вторую гармонику стелларапторного поля вблизи оси волновода

$$\begin{aligned} H_r &= H_2\,\alpha_2\, r \sin 2(\varphi - \alpha_2 z) \\ H_\varphi &= H_2\,\alpha_2 \cos 2(\varphi - \alpha_2 z) \\ H_z &= H_c - H_2\,\alpha_2^2\, r^2 \cos 2(\varphi - \alpha_2 z) \end{aligned} \quad (18)$$

Интересно отметить, что в квазистелларапторном поле, т.е. при не очень большом значении продольного поля H_c [$H_c < H_2(1+M)/(1-M)$] осевая устойчивость имеет место и для неподвижных сгустков.

Условия равновесия определяют значения постоянного продольного поля

$$H_c^2 = \frac{1}{2}\left|\frac{K}{\varkappa}A\right|^2\left[\left(\frac{1-M}{1+M}\right)^2 + \frac{h^2}{K^2}\right] \quad (19)$$

В этом случае условия устойчивости формы совпадают с приведенными в 3, а условие фокусировки

$$h^2 + 8\left(\frac{H_2}{H_c}\right)^2 \frac{M(1-M)K^2}{\varkappa^2(1+M)^2}\left[\left(\frac{1-M}{1+M}\right)^2 + \frac{h^2}{K^2}\right]\alpha_2^2 > \frac{1+2M-3M^2}{(1+M)^2}K^2 \quad (20)$$

Для шарового сгустка при $h^2/K^2 = 1/8$ или $h^2/K^2 = 0$ условие (20) принимает следующий вид

$$L < \frac{\lambda H_2}{\sqrt{35/24}\,H_c} \quad \text{или} \quad L < \frac{\lambda H_2}{\sqrt{3}\,H_c}\,;$$

6. Движение сгустка в пространственно неоднородных полях ψ_{m0} и ψ_{m1}

Для целого ряда задач представляет большой интерес транспортировка плазменных сгустков без ускорения, но при сохранении их компактности.

Рассмотрим комбинацию гофрированного поля ψ_{m0} и первой гармоники винтового поля ψ_{m1}. Из полученных выше выражений для энергии в (1) и (2) легко получить условие равновесия

$$\frac{H_0}{1-M} = \frac{H_1}{1+M} \quad (21)$$

При выполнении условия (21) автоматически будут выполнены условия устойчивости формы и осевой фокусировки. Равномерное усреднение давления, оказываемое постоянным пространственно неоднородным полем на сгусток, равно

$$p = \frac{H_1^2}{4\pi(1+M)^2}\,, \quad (22)$$

а фокусирующая сила, отнесенная к единице объема, равна

$$f = -\frac{H_1^2}{8\pi(1+M)^2}\left\{\alpha_0^2\left(\frac{1-M}{1+M}\right) + \frac{(1+M)(3-M)}{4(1-M)}\alpha_1^2\right\} \quad (23)$$

Легко найти условия, которым должны удовлетворять сгустки плазмы, чтобы пространственно-неоднородные поля обеспечивали их компактность. Во-первых, плотность плазмы сгустков и их скорость должны быть настолько велики, чтобы скин-слой в системе центра инерции и амплитуды деформации были значительно меньше размеров сгустка. Во-вторых, средняя тепловая скорость ионов в сгустке должна быть значительно меньше средней направленной скорости. При выполнении этих условий легко подобрать амплитуды полей H_0 и H_1 так, чтобы они с одной стороны были достаточно велики, чтобы создавать большее давление P и препятствовать растеканию сгустка, а с другой стороны были бы достаточно малы, чтобы сгусток без отражения проходил через систему гофрированных полей. В частности, в этом случае можно поворачивать сгусток по орбите радиуса R, где

$$R \approx \frac{W_H}{W_T \alpha^2 r} \quad \text{при} \quad \alpha r \ll 1\,,$$

а W_H и W_T — направленная и тепловая энергия плазмы.

Можно легко оценить, что при направленных скоростях сгустков более чем 10^7 см/сек, а тепловых порядка 10^6 см/сек и плотностям более чем 10^{13} см$^{-3}$ указанные условия будут выполняться.

7. Заключение

Из приведенных примеров видно, что имеется большое число различных возможностей для транспортировки и удержания и ускорения малых сгустков плазмы. По-видимому, с точки зрения практики наиболее удобно воспользоваться H_0-вол-

ной в сочетании с первой гармоникой винтового поля.

Однако, естественно возникает вопрос о границах применимости данных расчетов. Условия применимости в рамках магнитной гидродинамики сформулированы в § 1. Здесь мы хотим обратить внимание на поведение отдельных частиц, которое существенно для любых систем, использующих удержание плазмы в.ч. полями. Как известно, высокочастотное поле действует на электроны, а уходу ионов препятствует кулоновское поле. Поэтому естественно ожидать, что уход отдельных частиц не будет играть существенного значения, если сгусток заряжен отрицательно. И наоборот, естественно ожидать распада сгустка, если он будет заряжен положительно. Для оценки этого эффекта было рассмотрено методом А. В. Гапонова и М. А. Миллера [4] поведение отдельных частиц в в.ч. поле при наличии сгустков плазмы с резкой границей. Оказывается, что в волне типа E_1 для электронов существует барьер высотой $(h^2/2\varkappa^2)\,A^2$. Наоборот, волны типа H_1 уносят отдельные электроны на стенку, в поле E_0-волны электроны уходят вдоль оси волновода. В поле H_0-волны в направлении оси силы, действующие на частицы, равны нулю. С этой точки зрения волна типа E_1 должна препятствовать развалу сгустка из-за ухода отдельных частиц.

Другой неприятный эффект связан с выбросом частиц из сгустка из-за нестационарности действующего в.ч. поля вследствие малости времени пролета скин-слоя по сравнению с периодом в.ч. поля. Действительно, в этом случае энергия направленного движения частицы, вышедшей из сгустка, будет зависеть от фазы в.ч. поля в момент ее выхода из сгустка и может быть сравнимой с энергией осцилляции. Это обстоятельство будет препятствовать возвращению электронов обратно в сгусток в.ч. барьером.

Следует также обратить внимание на устойчивость оболочки сгустка из-за нерезкости границы. Для устойчивости также могут оказаться существенными электрические поля, возникающие при поляризации сгустка из-за неоднородности постоянного поля и из-за индукции движением (при достаточно больших скоростях).

Вся совокупность возникающих здесь вопросов требует дальнейшего теоретического рассмотрения. Конечно, для того, чтобы двигаться в теории дальше, желательно проверить исходные данные на эксперименте.

Литература

[1] Левин, М. Л., *Научные Труды РТИ АН СССР*, том 1, Вып. 2 (1959) стр. 36.
[2] Левин, М. Л., Рабинович, М. С., Аскарьян, Г. А., Proc. of Inter. Conf. CERN (1959)
[3] Аскарьян, Г. А., *Атомная энергия*, **4** (1958) 71.
[4] Гапонов, А. В., Миллер, М. А., *ЖЭТФ* **34** (1958) 242.

CRITÈRE DE STABILITÉ D'UN SYSTÈME TOROÏDAL HYDROMAGNÉTIQUE EN PRESSION SCALAIRE*

C. MERCIER

GROUPE DE RECHERCHES DE L'ASSOCIATION EURATOM-CEA SUR LA FUSION

FONTENAY-AUX-ROSES (SEINE), FRANCE

A l'aide du principe d'énergie de Bernstein et autres, on étudie les conditions de stabilité d'un plasma vis-à-vis des déplacement localisés. Un critère a déjà été ainsi trouvé dans le cas de la symétrie de révolution, qui se réduit au critère du Suydam en symétrie cylindrique.

Dans ce travail, on établit un critère nécessaire et suffisant pour les déplacements locaux s'appliquant à un plasma toroïdal quelconque.

La condition de stabilité doit être vérifiée sur chaque ligne magnétique fermée dans le plasma; ces lignes sont tracées sur les surfaces à pression constante caractérisées par l'invariant de surface $\iota(p)/2M = \delta\bar{\psi}/\delta\psi$ prenant des valeurs rationnelles m/n. $\delta\bar{\psi}$ est le flux de **B** entre deux surfaces p voisines le long d'une ligne fermée faisant un petit tour et pas de grand tour; et $\delta\psi$ est le flux de **B** entre deux surfaces p voisines le long d'une ligne fermée faisant un grand tour. m et n sont les nombres de grands et de petits tours que fait la ligne magnétique avant de se refermer. La condition de stabilité s'écrit $Q_{n,m} > 0$. (L'expression complète est donnée dans le mémoire.)

Sauf pour un cas particulier (symétrie de révolution), cette expression prend des valeurs différentes pour les lignes magnétiques fermées tracées sur la même surface S à pression constante. Cependant, quand les nombres m et n tendent vers l'infini, la condition de stabilité s'exprime à l'aide d'intégrale de surface et les valeurs de $Q_{\infty,\infty} > 0$ pour les différentes surfaces voisines sont continues.

1. Introduction

Le principe d'énergie développé par BERNSTEIN et autres [1] fournit une méthode puissante pour étudier la stabilité d'un plasma magnétohydrodynamique en équilibre. En symétrie de révolution, l'étude des déplacements localisés a permis de trouver un critère [2] généralisant celui de SUYDAM [3] obtenu en géométrie cylindrique. Dans ce travail nous démontrerons un critère nécessaire et suffisant pour les déplacements localisés, applicable à un plasma de forme toroïdale quelconque [7]. En géométrie de révolution, il se réduit au critère précédemment trouvé [2] qui était donc non seulement nécessaire mais aussi suffisant pour la classe particulière des déplacements locaux. Nous n'envisagerons que le cas d'une pression scalaire. La généralisation à des pressions anisotropes dans l'approximation Chew-Goldberger-Low déjà étudiée en symétrie de révolution [4] ne présenterait pas de difficultés nouvelles mais une complexité accrue.

2. Lignes magnétiques et transformation rotationelle

Soit un champ de vecteur **B** de divergence nulle et tel que les lignes magnétiques soient tracées sur des surfaces toriques emboitées. Le tore le plus interne étant réduit à une courbe, l'axe magnétique.

Définissons les surfaces $\eta = \text{constantes}$, par la fonction η, multiforme, continue partout sauf sur l'axe magnétique, augmentant d'une unité sur toutes courbes qui tournent une fois autour de l'axe magnétique. Elles définissent sur les surfaces **S** des lignes $c_{1,0}$ que nous dirons de classe (1,0) (un grand tour, pas de petit tour). Soit

$$\psi = \int_v \mathrm{d}t \cdot \mathbf{B} \cdot \operatorname{grad}\eta\,, \tag{1}$$

l'intégration étant étendue sur le volume intérieur à un tore **S**.

Cette fonction est une fonction uniforme et constante sur les surfaces **S**. Elle est égale, à une constante près, au flux à travers toute surface dont la limite est formée par une courbe de la classe (1,0).

On peut alors toujours définir le champ **B** par

$$\mathbf{B} = \operatorname{grad}\chi \times \operatorname{grad}\psi\,, \tag{2}$$

le flux étant alors donné par $\mathrm{d}\varphi = \mathrm{d}\chi\,\mathrm{d}\psi$. χ est une fonction multiforme constante sur les lignes magnétiques. Le flux à travers la surface $\eta = \text{const.}$ entre deux surfaces **S** voisines s'écrit:

$$\mathrm{d}\psi = \int_{C_{1,0}} \mathrm{d}\chi\,\mathrm{d}\psi\,,$$

ce qui fournit la condition:

$$\int_{C_{1,0}} \mathrm{d}\chi = 1\,.$$

Choisissons alors des surfaces $\bar{\theta} = \text{constantes}$, définies par la fonction $\bar{\theta}$ multiforme continue partout et augmentant d'une unité quand on parcourt l'axe magnétique. Elle définissent sur les surfaces **S** des

* Mémoire CN-10/95 présenté par C. Mercier. La discussion concernant ce mémoire est donnée page 817. Les traductions du résumé se trouvent en fin de volume.

lignes $c_{1,0}$ de la classe (0,1) (un petit tour, pas de grand tour).

Le flux à travers la surface $\bar{\theta}=$ entre deux surfaces S voisines $\mathrm{d}\bar{\psi}$, constant sur S, est donné par

$$\mathrm{d}\bar{\psi} = \int_{C_{0,1}} \mathrm{d}\chi \, \mathrm{d}\psi,$$

ce qui fournit une deuxième condition sur χ:

$$\int_{C_{0,1}} \mathrm{d}\chi = \mathrm{d}\bar{\psi}/\mathrm{d}\psi = -\iota/2\pi, \tag{3}$$

ι étant une fonction constante sur les surfaces S et que nous appellerons angle de transformation rotationnel*. Si les surfaces S sont désignées par la fonction continue ψ, constante sur elles, la fonction $\chi(\eta, \bar{\theta}, \psi)$ devra satisfaire aux conditions:

$$\chi(\eta, \bar{\theta}+1) = \chi(\eta, \bar{\theta}) + 1,$$

$$\chi(\eta+1, \bar{\theta}) = \chi(\eta, \bar{\theta}) - (\iota/2\pi)\, p.$$

Elle doit donc s'écrire:

$$\chi = \bar{\theta} - (\iota/2\pi)\,\eta + \hat{\chi}(\bar{\theta}, \eta, \psi),$$

$\hat{\chi}$ étant une fonction uniforme. On voit facilement alors que les lignes magnétiques sont fermées ou ergodiques selon que $\iota/2\pi$ est rationnel ou non. Si $\iota/2\pi = (k/m)\cdot k$ représente le nombre de grands tours et m le nombre de petits tours avant la fermeture de la courbe.

Au lieu des variables η, $\bar{\theta}$, ψ, il sera commode d'utiliser les variables η, χ, ψ. Ceci est possible si la transformation est biunivoque ce qui exige que $\partial\chi/\partial\bar{\theta}$ ne s'annule pas. Supposons

$$\frac{\partial\chi}{\partial\bar{\theta}} > 0;$$

or

$$\mathbf{B}\,\mathrm{grad}\,\eta = (\mathrm{grad}\,\chi \times \mathrm{grad}\,\psi)\,\mathrm{grad}\,\eta$$

$$= \frac{\partial\chi}{\partial\bar{\theta}}(\mathrm{grad}\,\eta \times \mathrm{grad}\,\bar{\theta})\,\mathrm{grad}\,\psi.$$

Si η, $\bar{\theta}$, ψ forme un système direct en tout point:

$$(\mathrm{grad}\,\eta \times \mathrm{grad}\,\bar{\theta})\,\mathrm{grad}\,\psi > 0.$$

La condition pour que la transformation soit biunivoque s'écrit alors

$$\mathbf{B}\,\mathrm{grad}\,\eta > 0. \tag{4}$$

La même condition permet de passer du système η, $\bar{\theta}$, ψ au système η, $\theta = \bar{\theta} + \hat{\chi}(\theta, \eta, \psi)$, ψ. Ce qui permet d'écrire

$$\chi = \theta - (\iota/2\pi)\,\eta. \tag{5}$$

* Ces définitions sont semblables mais non identiques à celles introduites par KRUSKAL et KULSRUD [5]. En particulier la quantité $\iota/2\pi$ ici définie est l'inverse de celle introduite par ces auteurs.

3. Équilibre magnétohydrodynamique

Un système magnétohydrodynamique à l'équilibre en pression scalaire est régi par les équations suivantes:

$$\mathrm{div}\,\mathbf{B} = 0, \tag{6}$$

$$\mathbf{J} \times \mathbf{B} = \mathrm{grad}\,p, \tag{7}$$

$$\mathbf{J} = \mathrm{rot}\,\mathbf{B}. \tag{8}$$

Les lignes magnétiques et les lignes de courant sont tracées sur les surfaces à pression constante qui sont les tores S. Par conséquent:

$$p = p(\psi). \tag{9}$$

Evidemment

$$\mathbf{B}\cdot\mathrm{grad}\,\chi = 0 \tag{10}$$

et

$$\mathbf{J}\times\mathbf{B} = \mathrm{grad}\,p = \mathbf{J}\times(\mathrm{grad}\,\chi\times\mathrm{grad}\,\psi)$$

$$= -(\mathbf{J}\cdot\mathrm{grad}\,\chi)\,\mathrm{grad}\,\psi.$$

D'où

$$\mathbf{J}\cdot\mathrm{grad}\,\chi = -p'. \tag{11}$$

En désignant par $\mathrm{grad}_{\|}\,\chi$ la composante de grad χ sur les surfaces S, on a

$$\mathrm{grad}_{\|}\,\chi = \mathrm{grad}\,\chi - (\mathbf{n}\cdot\mathrm{grad}\,\chi)\,\mathbf{n},$$

$$\mathbf{B} = \mathrm{grad}_{\|}\,\chi \times \mathrm{grad}\,\psi,$$

$$\mathbf{n} = \frac{\mathrm{grad}\,p}{|\mathrm{grad}\,p|},$$

d'où

$$\mathrm{grad}_{\|}\,\chi = \frac{p'(\mathbf{n}\times\mathbf{B})}{|\mathrm{grad}\,p|}, \tag{12}$$

avec

$$p' = \frac{\mathrm{d}p}{\mathrm{d}\psi}. \tag{13}$$

D'une façon générale, on désignera par $V_{\|}$ et $V_{\perp}$ les composantes parallèle et perpendiculaire à la surface S d'un vecteur V quelconque.

Calculons alors:

$$\mathrm{grad}\,p \times \mathrm{grad}\,\frac{\mathbf{n}\cdot\mathrm{grad}\,\chi}{|\mathrm{grad}\,p|} = (\mathbf{J}\times\mathbf{B}) \times \mathrm{grad}\,\frac{\mathbf{n}\cdot\mathrm{grad}\,\chi}{|\mathrm{grad}\,p|}$$

$$= \mathrm{rot}\,(\mathrm{grad}_{\|}\,\chi).$$

Ainsi

$$\mathrm{rot}\,\mathrm{grad}_{\|}\,\chi = \mathrm{grad}\,p \times \mathrm{grad}\,\frac{\mathbf{n}\cdot\mathrm{grad}\,\chi}{|\mathrm{grad}\,p|}. \tag{14}$$

Une fonction de point dans le système η, χ, p; $F(\eta, \chi, p)$ doit être une fonction doublement périodique de périodes 1 en η et $\theta = \chi + (\iota/2\pi)\,\eta$. Donc

$$F(\eta, \chi, p) = \sum_{m,k} f_{m,k}(p) \exp 2\mathrm{i}\pi(m\chi + V_{k,m}\eta), \tag{15}$$

où

$$V_{k,m} = k + m(\iota/2\pi)\,p. \tag{16}$$

Les fonctions ψ et χ doivent satisfaire aux équations suivantes:

$$\mathbf{J}\cdot\mathrm{grad}\,\psi = 0$$

$$\mathbf{J}\cdot\mathrm{grad}\,\chi = -p',$$

système qui peut s'écrire

$$\operatorname{div} |\operatorname{grad} \psi|^2 \operatorname{grad}_{\parallel} \chi = 0 \tag{17}$$

$$\operatorname{div} |\operatorname{grad}_{\parallel} \chi|^2 \operatorname{grad} \psi + (\operatorname{rot} \operatorname{grad}_{\parallel} \chi \times \operatorname{grad}_{\parallel} \chi) \cdot \operatorname{grad} \psi = -p'. \tag{18}$$

4. Etude de la stabilité

Nous étudierons la stabilité à l'aide du principe d'énergie de Bernstein pour des perturbations localisées. Seul le terme δW pour le plasma intervient dans ces calculs. Nous l'écrirons sous la forme suivante où les perturbations $\boldsymbol{\xi}$ sont complexes

$$\boldsymbol{\xi} = \xi_{\perp} \mathbf{n} + u \mathbf{n} \times \mathbf{B} + v \mathbf{B} \tag{19}$$

$$\delta W = \frac{1}{2} \int \mathrm{d}t \{ [\mathbf{Q}(\boldsymbol{\xi}) + \xi_{\perp}(\mathbf{J} \times \mathbf{n})] [Q(\boldsymbol{\xi}^*) + \xi_{\perp}^*(\mathbf{J} \times \mathbf{n})] - 2 \xi_{\perp} \boldsymbol{\xi}^* (\mathbf{J} \times \mathbf{n}) (\mathbf{B} \nabla \mathbf{n}) + \gamma p \operatorname{div} \boldsymbol{\xi} \operatorname{div} \boldsymbol{\xi}^* \}, \tag{20}$$

où

$$\mathbf{Q} = \operatorname{rot} (\boldsymbol{\xi} \times \mathbf{B}). \tag{21}$$

Posons

$$U = \frac{|\operatorname{grad} p|}{p'} \xi_{\perp},$$

$$\boldsymbol{\xi} \times \mathbf{B} = U \operatorname{grad}_{\parallel} \chi - \frac{u B^2}{|\operatorname{grad} p|} \operatorname{grad} p,$$

$$\mathbf{Q} = U \operatorname{rot} \operatorname{grad}_{\parallel} \chi - \operatorname{grad}_{\parallel} \chi \times \operatorname{grad} U + \operatorname{grad} p \times \operatorname{grad} \frac{u B^2}{|\operatorname{grad} p|}.$$

En utilisant les relations du paragraphe précédent, on trouve:

$$\mathbf{Q} = Q_{\perp} + Q_{\parallel}, \tag{22}$$

$$Q_{\perp} = \frac{p'}{|\operatorname{grad} p|} (\mathbf{B} \cdot \operatorname{grad} U) \mathbf{n}, \tag{23}$$

$$Q_{\parallel} = \operatorname{grad} p \times \left[\operatorname{grad}_{\parallel} A + \frac{\mathbf{n}}{|\operatorname{grad} p|} \times (\operatorname{grad} \chi \times \operatorname{grad} U) \right], \tag{24}$$

où

$$A = U \frac{\mathbf{n} \cdot \operatorname{grad} \chi}{|\operatorname{grad} p|} + \frac{u B^2}{|\operatorname{grad} p|}. \tag{25}$$

En remarquant que

$$\xi_{\perp} (\mathbf{J} \times \mathbf{n}) = -\operatorname{grad} p \times \frac{p' U \mathbf{J}}{|\operatorname{grad} p|^2},$$

on obtient:

$$\mathbf{Q} + \xi_{\perp} (\mathbf{J} \times \mathbf{n}) = Q_{\perp} + \operatorname{grad} p \times [\operatorname{grad}_{\parallel} A + \mathbf{c}], \tag{26}$$

$$\mathbf{c} = \frac{\mathbf{n}}{|\operatorname{grad} p|} \times (\operatorname{grad} \chi \times \operatorname{grad} U) - \frac{p' U \mathbf{J}}{|\operatorname{grad} p|^2}. \tag{27}$$

$\mathbf{c}$ est un vecteur parallèle aux surfaces $\mathbf{S}$.

Avec ces nouvelles notations, δW s'écrit:

$$\delta W = \frac{1}{2} \int \mathrm{d}t \left\{ \frac{p'^2}{|\operatorname{grad} p|^2} |\mathbf{B} \cdot \operatorname{grad} U|^2 + |\operatorname{grad} p|^2 (\operatorname{grad}_{\parallel} A + \mathbf{c}) (\operatorname{grad}_{\parallel} A^* + \mathbf{c}^*) - \frac{2 p'^2}{|\operatorname{grad} p|^2} |U|^2 (\mathbf{J} \times \mathbf{n}) (\mathbf{B} \nabla \mathbf{n}) + \gamma p |\operatorname{div} \boldsymbol{\xi}|^2 \right\}. \tag{28}$$

Le terme en $|\operatorname{div} \boldsymbol{\xi}|^2$ est le seul à contenir la fonction v.

Nous montrerons que $(\operatorname{div} \boldsymbol{\xi})_{\min} = d_{\min}$ peut être pris aussi petit que l'on veut pour des perturbations localisées; plus précisément, si les déplacements sont différents de zéro dans un interval en p autour de p_0 de l'ordre de ε, $d_{\min}$ peut être pris de l'ordre ε et le terme $\gamma p |\operatorname{div} \boldsymbol{\xi}|^2$ ne contribuera pas au critère.

En effet:

$$\operatorname{div} \boldsymbol{\xi} = \mathrm{d}_{\min},$$

s'écrit:

$$\mathbf{B} \cdot \operatorname{grad} v = -\operatorname{div} [\xi_{\perp} \mathbf{n} + u (\mathbf{n} \times \mathbf{B})] + d_{\min}.$$

Cette équation n'a de solution uniforme que si

$$\oint \operatorname{div} [\xi_{\perp} \mathbf{n} + u (\mathbf{n} \times \mathbf{B})] \frac{\mathrm{d}l}{B} = \int d_{\min} \frac{\mathrm{d}l}{B},$$

sur toutes lignes fermées. (Voir NEWCOMB, W. A. [6].)

Or, en désignant par m le nombre de petits tours de la ligne magnétique:

$$\oint \operatorname{div} [\xi_{\perp} \mathbf{n} + u (\mathbf{n} \times \mathbf{B})] \frac{\mathrm{d}l}{B} = -m \int_S \operatorname{div} [\xi_{\perp} \mathbf{n} + u (\mathbf{n} \times \mathbf{B})] \frac{\mathrm{d}\mathbf{S}}{|\operatorname{grad} \psi|} + m \mathrm{O}(\varepsilon).$$

(Voir Annexe.)

Mais

$$\int_S \operatorname{div} [\xi_{\perp} \mathbf{n} + u (\mathbf{n} \times \mathbf{B})] \frac{\mathrm{d}\mathbf{S}}{|\operatorname{grad} \psi|} = \frac{\mathrm{d}}{\mathrm{d}\psi} \int_S \xi_{\perp} \mathrm{d}\sigma + \int_V \operatorname{div} \left(\mathbf{B} \times \operatorname{grad} \frac{u}{|\operatorname{grad} \psi|} \right) \mathrm{d}t = \frac{\mathrm{d}}{\mathrm{d}\psi} \int_S \xi_{\perp} \mathrm{d}\sigma. \tag{29}$$

Cette dernière expression n'est différente de zéro que pour la partie constante sur les surfaces $\mathbf{S}$ du développement de $\xi_{\perp}(\eta, \chi, \psi)$ en série de la forme (15). Nous verrons par la suite que ce terme doit être choisi nul pour les déplacements localisés. Ainsi $d_{\min}$ doit satisfaire à la condition

$$\frac{1}{m} \oint d_{\min} \frac{\mathrm{d}l}{B} = \mathrm{O}(\varepsilon),$$

qui est compatible avec

$$d_{\min} = \mathrm{O}(\varepsilon). \tag{30}$$

5. Déplacements localisés

Les déplacements localisés sont des perturbations $\boldsymbol{\xi}$, centrées autour d'une surface $\mathbf{S}_0$ définie par p_0 (ou ψ_0), continues ainsi que leurs dérivées, nulles pour $p = p_0 \pm \varepsilon$ et à l'extérieur de l'intervalle $(p_0 - \varepsilon, p_0 + \varepsilon)$, ε étant aussi petit que l'on veut.

Une composante quelconque de ce déplacement, par exemple $\xi_{\perp}$ (ou U) s'écrira donc

$$U(p, \eta, \chi) = \sum_{k,m} f_{k,m} \left(\frac{p - p_0}{\varepsilon} \right) \exp 2\mathrm{i}\pi [m \chi + V_{k,m}(p) \eta] = \sum_{k,m} f_{k,m}(t) \exp 2\mathrm{i}\pi [m \chi + V_{k,m}(p_0 + \varepsilon t) \eta], \tag{31}$$

en posant

$$\frac{p-p_0}{\varepsilon} = t$$

$$V_{k,m} = k + m\frac{\iota}{2\pi}(p). \tag{32}$$

Les fonctions $f_{k,m}(t)$ sont telles que

$$f_{k,m}(t) = 0 \text{ pour } |t| \geqslant 1.$$

Calculons les diverses expressions intervenant dans δW

$$\operatorname{grad} U = \frac{\partial U}{\partial \eta}\operatorname{grad}\eta + \frac{\partial U}{\partial \chi}\operatorname{grad}\chi + \frac{1}{\varepsilon}\frac{\partial U}{\partial t}\operatorname{grad} p, \tag{33}$$

$$\mathbf{B}\cdot\operatorname{grad} U = \frac{\partial U}{\partial \eta}\mathbf{B}\cdot\operatorname{grad}\eta, \tag{34}$$

$$\mathbf{C} = \frac{1}{\varepsilon}\frac{\partial U}{\partial t}\operatorname{grad}_{\parallel}\chi + \frac{1}{|\operatorname{grad} p|}\frac{\partial U}{\partial \eta}\mathbf{n}\times(\operatorname{grad}\chi\times\operatorname{grad}\eta) - \frac{p' U \mathbf{J}}{|\operatorname{grad} p|^2} \tag{35}$$

$\mathbf{c}$ augmente indéfiniment quand ε décroit et par conséquent δW deviendra toujours positif si la partie croissante de $\mathbf{c}$ contenue dans le terme $(1/\varepsilon)\ (\partial v/\partial t)\ \operatorname{grad}_{\parallel}\chi$ ne peut être compensée par $\operatorname{grad}_{\parallel} A$.

Posons $U = U_0 + \varepsilon U_1$; U_0 et U_1 sont des fonctions de points d'ordre 0 en ε et seront précisées par la suite.

Pour que $(1/\varepsilon)\ (\partial U_0/\partial t)\ \operatorname{grad}_{\parallel}\chi$ soit un gradient parallèle, il faut que

$$\mathbf{n}\cdot\operatorname{rot}\frac{\partial U_0}{\partial t}\operatorname{grad}_{\parallel}\chi = 0,$$

soit

$$\mathbf{B}\cdot\operatorname{grad}\frac{\partial U_0}{\partial t} = 0.$$

Ainsi $\partial U_0/\partial t$ doit être constant le long des lignes magnétiques, c'est-à-dire ne pas dépendre de η à des termes d'ordre ε près. Il en est de même de U_0 car $U_0 = 0$ pour $t = \pm 1$.

Pour satisfaire à cette condition nous sommes conduits à définir U_0 par un développement ne contenant que des termes en $m_0\ k_0$ tels que

$$V_{m_0,k_0}(p_0) = k_0 + m_0\frac{\iota(p_0)}{2\pi} = 0, \tag{37}$$

ce qui oblige à choisir pour S_0 une surface où les lignes magnétiques sont fermées.

Dans ces conditions

$$V_{m_0,k_0}(p) = k_0 + m_0\frac{\iota(p)}{2\pi} = \left[\frac{\iota(p)}{2\pi} - \frac{\iota(p_0)}{2\pi}\right]m_0,$$

$$\frac{\partial U_0}{\partial \eta} = 2\pi\,\mathrm{i}\sum_{m_0,k_0} f_{m_0,k_0} V_{k_0,m_0}(p)\exp 2\mathrm{i}\pi(m\chi + V_{k_0,m_0}\eta),$$

$$\frac{\partial U_0}{\partial \eta} = \left[\frac{\iota(p)}{2\pi} - \frac{\iota}{2\pi}(p_0)\right]\frac{\partial U_0}{\partial \chi} = \varepsilon\left(\frac{\iota}{2\pi}\right)_0' t\frac{\partial U_0}{\partial \chi} + \mathrm{O}(\varepsilon^2). \tag{38}$$

Par conséquent

$$\mathbf{B}\cdot\operatorname{grad} U = \left(\frac{\partial U_0}{\partial \eta} + \varepsilon\frac{\partial U_1}{\partial \eta}\right)\mathbf{B}\cdot\operatorname{grad}\eta = \varepsilon\left[\left(\frac{\iota}{2\pi}\right)_0' t\frac{\partial U_0}{\partial \chi} + \frac{\partial U_1}{\partial \eta}\right]\mathbf{B}\cdot\operatorname{grad}\eta = \mathrm{O}(\varepsilon), \tag{39}$$

et

$$\operatorname{grad}_{\parallel} A + \mathbf{c} = \operatorname{grad}_{\parallel}\left(\frac{\mathrm{u}\,B^2}{|\operatorname{grad} p|} + U_0\frac{\mathbf{n}\cdot\operatorname{grad}\chi}{|\operatorname{grad} p|}\right) + \frac{1}{\varepsilon}\frac{\partial U_0}{\partial t}\operatorname{grad}_{\parallel}\chi - \frac{p' U \mathbf{J}}{|\operatorname{grad} p|^2} + \frac{\partial U_1}{\partial t}\operatorname{grad}_{\parallel}\chi + \mathrm{O}(\varepsilon). \tag{40}$$

Remarquons que pour une fonction de point F quelconque, développée sous la forme (15):

$$\frac{\partial F}{\partial t} = \sum_{m,k} f'_{m,k}\exp 2\mathrm{i}\pi(m\chi + V_{k,m}\eta) + 2\pi\,\mathrm{i}\,\eta\sum_{m,k} f_{m,k}\left(\frac{\mathrm{d}}{\mathrm{d}t}V_{k,m}\right)\exp 2\mathrm{i}\pi(m\chi + V_{k,m}\eta),$$

$$= \left(\frac{\partial F}{\partial t}\right)_p + \varepsilon\eta\left(\frac{\iota}{2\pi}\right)\frac{\partial F}{\partial \chi}. \tag{41}$$

$(\partial F/\partial t)_p$ indique la partie doublement périodique de $\partial F/\partial t$, c'est-à-dire représente une fonction de point sur les surfaces S. Dans l'expression (40), la quantité $n\cdot\operatorname{grad}\chi/|\operatorname{grad} p|$ n'est pas une fonction doublement périodique.

$$\frac{\mathbf{n}\cdot\operatorname{grad}\chi}{|\operatorname{grad} p|} = \left(\frac{\mathbf{n}\cdot\operatorname{grad}\chi}{|\operatorname{grad} p|}\right)_p + \left(\frac{\mathbf{n}\cdot\operatorname{grad}\chi}{|\operatorname{grad} p|}\right)_{n\cdot p}.$$

Or

$$\left(\frac{\mathbf{n}\cdot\operatorname{grad}\chi}{|\operatorname{grad} p|}\right)_{n\cdot p} = -\left(\frac{\iota}{2\pi}\right)'\eta. \tag{42}$$

En effet $\mathbf{n}\cdot\operatorname{grad} F/|\operatorname{grad} p|$ est une fonction périodique (F fonction de point quelconque) ainsi que $\mathbf{n}\cdot\operatorname{grad}\eta/|\operatorname{grad} p|$.

Par conséquent

$$\left(\frac{\mathbf{n}\cdot\operatorname{grad} F}{|\operatorname{grad} p|}\right)_{n\cdot p} = 0 = \frac{\partial F}{\partial \eta}\left(\frac{\mathbf{n}\cdot\operatorname{grad}\eta}{|\operatorname{grad} p|}\right)_{n\cdot p} + \frac{\partial F}{\partial \chi}\left(\frac{\mathbf{n}\cdot\operatorname{grad}\chi}{|\operatorname{grad} p|}\right)_{n\cdot p} + \frac{1}{\varepsilon}\left(\frac{\partial F}{\partial t}\right)_{n\cdot p},$$

soit en utilisant (41)

$$\frac{\partial F}{\partial \chi}\left[\left(\frac{\mathbf{n}\cdot\operatorname{grad}\chi}{|\operatorname{grad} p|}\right)_{n\cdot p} + \left(\frac{\iota}{2\pi}\right)'\eta\right] = 0,$$

ou

$$\left(\frac{\mathbf{n}\cdot\operatorname{grad}\chi}{|\operatorname{grad} p|}\right)_{n\cdot p} + \left(\frac{\iota}{2\pi}\right)'\eta = 0.$$

En utilisant les résultats ci-dessus (38), (40) on peut écrire:

$$\frac{1}{\varepsilon}\frac{\partial U_0}{\partial t}\operatorname{grad}_{\parallel}\chi = \operatorname{grad}_{\parallel}\frac{1}{\varepsilon}\int^{\chi}\frac{\partial}{\partial t}U_0\,\mathrm{d}\chi - \frac{1}{\varepsilon}\frac{\partial}{\partial \psi}\int^{\chi}\frac{\partial U_0}{\partial \eta}\,\mathrm{d}\chi\operatorname{grad}_{\parallel}\eta$$

$$= \operatorname{grad}_{\parallel}\frac{1}{\varepsilon}\int^{\chi}\frac{\partial}{\partial t}U_0\,\mathrm{d}\chi - \left(\frac{\iota}{2\pi}\right)_0'\frac{\partial}{\partial t}(tU_0)\operatorname{grad}_{\parallel}\eta + \mathrm{O}(\varepsilon)$$

et

$$\operatorname{grad}_\parallel A + \mathbf{c} = \operatorname{grad}_\parallel Y - \left(\frac{\iota}{2\pi}\right)_0' \frac{\partial}{\partial t}(t U_0)\operatorname{grad}_\parallel \eta - \frac{p' U_0 \mathbf{J}}{|\operatorname{grad} p|^2} + \frac{\partial U_1}{\partial t}\operatorname{grad}_\parallel \chi + \mathbf{O}(\varepsilon),$$

où

$$Y = \frac{u B^2}{|\operatorname{grad} p|} + U_0 \frac{\mathbf{n}\cdot\operatorname{grad}\chi}{|\operatorname{grad} p|} + \frac{1}{\varepsilon}\int^{\chi} \frac{\partial}{\partial t} U_0 \, \mathrm{d}\chi .$$

Pour compenser le terme en $1/\varepsilon$ par la composante u du déplacement il faut que Y soit une fonction de point. Or d'après (41), (42)

$$\frac{1}{\varepsilon}\int^{\chi} \frac{\partial}{\partial t} U_0 \, \mathrm{d}\chi = \frac{1}{\varepsilon}\int^{\chi}\left(\frac{\partial}{\partial t} U_0\right)_p \mathrm{d}\chi + \left(\frac{\iota}{2\pi}\right)' \eta U_0 = \frac{1}{\varepsilon}\int^{\chi}\left(\frac{\partial}{\partial t} U_0\right)_p \mathrm{d}\chi - U_0\left(\frac{\mathbf{n}\cdot\operatorname{grad}\chi}{|\operatorname{grad} p|}\right)_{n\,.\,p}$$

donc

$$Y = \frac{u B^2}{|\operatorname{grad} p|} + U_0\left(\frac{\mathbf{n}\cdot\operatorname{grad}\chi}{|\operatorname{grad} p|}\right)_p + \frac{1}{\varepsilon}\int^{\chi}\left(\frac{\partial}{\partial t} U_0\right)_p \mathrm{d}\chi .$$

Y sera donc une fonction de point si le développement de $[(\partial/\partial t)\, U_0]_p$

$$\left(\frac{\partial}{\partial t} U_0\right)_p = \sum_{m_0,\, k_0} f'_{m_0, k_0} \exp 2\mathrm{i}\pi\,(m_0\chi + V_{k_0, m_0}\eta),$$

ne contient pas de terme $m_0 = k_0 = 0$ soit $f_{0,0}' = 0$. On en déduit en particulier que $(\mathrm{d}/\mathrm{d}\psi)\int_S \xi_\perp \, \mathrm{d}\sigma = 0$ ce qui justifie l'élimination du terme $\gamma p\,|\operatorname{div}\boldsymbol{\xi}|^2$.

Nous pouvons alors écrire, à des termes en ε près

$$\delta W = \frac{1}{2}\int \mathrm{d}t \left\{ |\operatorname{grad} p|^2 \, \mathbf{E}\cdot\mathbf{E}^* - \frac{2p'^2}{|\operatorname{grad} p|^2}|U_0|^2 (\mathbf{J}\times\mathbf{n})(\mathbf{B}\nabla\mathbf{n})\right\}, \quad (43)$$

$$\mathbf{E} = \operatorname{grad}_\parallel A + \mathbf{c}.$$

En utilisant l'identité de Lagrange:

$$\mathbf{E}\cdot\mathbf{E}^* = \frac{|\mathbf{B}\cdot\mathbf{E}|^2}{B^2} + \frac{(\mathbf{B}\times\mathbf{E})(\mathbf{B}\times\mathbf{E}^*)}{B^2} = \frac{|\mathbf{B}\cdot\mathbf{E}|^2}{B^2} + \frac{|\mathbf{V}\cdot\mathbf{E}|^2}{B^2|\operatorname{grad} p|^2},$$

avec $\mathbf{V} = \operatorname{grad} p \times \mathbf{B}$, nous séparerons δW en deux termes:

$$\delta W = \delta W_1 + \delta W_2,$$

$$\delta W_1 = \frac{1}{2}\int \mathrm{d}t \left\{ \frac{|\operatorname{grad} p|^2}{B^2} \times \left| \mathbf{B}\cdot\operatorname{grad} Y - \left(\frac{\iota}{2\pi}\right)_0' \frac{\partial}{\partial t}(t U_0)\,\mathbf{B}\cdot\operatorname{grad}\eta - \frac{p' U_0 \mathbf{B}\cdot\mathbf{J}}{|\operatorname{grad} p|^2}\right|^2 - \frac{2p'^2}{|\operatorname{grad} p|^2}|U_0|^2(\mathbf{J}\times\mathbf{n})(\mathbf{B}\nabla\mathbf{n})\right\}, \quad (44)$$

$$\delta W_2{}^2 = \frac{1}{2}\int \frac{\mathrm{d}t}{B^2}\left| \mathbf{V}\cdot\operatorname{grad}_\parallel Y - \left|\frac{\iota}{2\pi}\right|_0' \frac{\partial}{\partial t}(t U_0)\,\mathbf{V}\cdot\operatorname{grad}\eta - \frac{p' U_0 \mathbf{V}\cdot\mathbf{J}}{|\operatorname{grad} p|^2} + \frac{\partial U_1}{\partial t}\mathbf{V}\cdot\operatorname{grad}_\parallel\chi\right|^2. \quad (45)$$

La suite du calcul consistera à minimiser δW_1, seul et nous constaterons que pour $\delta W_{1\min}$, δW_2 peut être choisi nul et par conséquent que $\delta W_{\min} = \delta W_{1\min}$ exactement.

6. Minimisation de δW_1

Les fonctions Y et U_0 sont des fonctions de point indépendantes, s'annulant à $t = \pm 1$.

Posons $\mathbf{B}\cdot\operatorname{grad} Y = f$ et minimisons d'abord sur f pour U_0 donnée. D'après NEWCOMB [6] f doit vérifier la condition

$$\oint f \frac{\mathrm{d}l}{B} = 0, \quad (46)$$

sur toutes lignes magnétiques fermées.

Selon l'annexe, à ε près nous pouvons remplacer pour $t \neq 0$ ces conditions par

$$\int_S f \frac{\mathrm{d}S}{|\operatorname{grad}\psi|} = 0.$$

Pour $t = 0$, surface où les lignes de force sont fermées, la condition reste

$$\oint f \frac{\mathrm{d}l}{B} = 0.$$

Choisissons comme système de coordonnées (l, χ, t), l étant l'abscisse curviligne sur les lignes magnétiques;

$$\frac{\mathrm{d}l}{B} = \frac{\mathrm{d}\eta}{\mathbf{B}\cdot\operatorname{grad}\eta}.$$

Avec ces coordonnées

$$\mathrm{d}\tau = \frac{\varepsilon}{p' B}\mathrm{d}t\,\mathrm{d}\chi\,\mathrm{d}l,$$

$$\mathrm{d}S = \frac{|\operatorname{grad}\psi|}{B}\mathrm{d}\chi\,\mathrm{d}l.$$

Une intégrale sur les surfaces S peut s'écrire (voir figure 1):

$$\int_S I\,\mathrm{d}\mathbf{S} = \frac{1}{k}\int_0^{\frac{\iota}{2\pi}(p)} \mathrm{d}\chi \int_0^{l(\chi)} \frac{I}{B}|\operatorname{grad}\psi|\,\mathrm{d}l, \quad (47)$$

et une intégrale de volume entre les surfaces $p_0 \pm \varepsilon$:

$$\int_V I\,\mathrm{d}t = \frac{1}{k}\int_{-1}^{+1}\mathrm{d}t \int_0^{\frac{\iota}{2\pi}(p)}\mathrm{d}\chi \int_0^{l(\chi)} \frac{I}{|p'|B}\,\mathrm{d}l, \quad (48)$$

où

$$l(\chi) = \int_0^{k\cdot\frac{2\pi}{\iota}} \frac{B}{\mathbf{B}\cdot\operatorname{grad}\eta}\,\mathrm{d}\eta,$$

et k un nombre entier quelconque.

A ε près, on peut remplacer $\iota(p)/2\pi$ par $\iota(p_0)/2\pi = k_0/m_0$ et $l(\chi)$ par $l_0(\chi) = \int_0^{m_0} (B/\mathbf{B}\cdot\operatorname{grad}\eta)\mathrm{d}\eta$ en choisissant $k = k_0$.

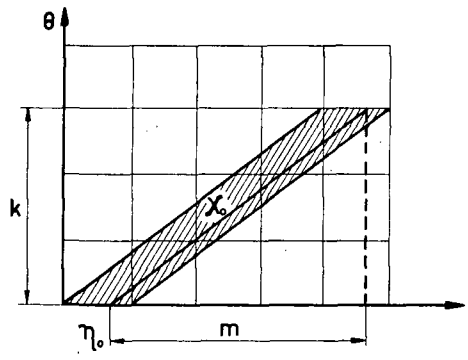

Figure 1 Domaine d'intégration choisi pour une surface S définie par $\iota/2M = k/m$. Ce domaine représente k fois la surface elle-même.

La condition sur f s'écrira alors

$$\int_0^{(\iota/2\pi)_0} v(t,\chi)\,\mathrm{d}\chi = 0 \quad \text{pour} \quad t \neq 0,$$

$$v(0,\chi) = 0 \quad \text{pour} \quad t = 0,$$

où

$$v(t,\chi) = \int_0^{l_0} f \frac{\mathrm{d}l}{B}.$$

Mais

$$v(t,\chi) = \int_{\eta_0}^{\eta_0+m_0} f \frac{\mathrm{d}\eta}{\mathbf{B}\cdot\operatorname{grad}\eta} = Y(\eta_0+m_0) - Y(\eta_0) = \mathrm{O}(\varepsilon). \tag{49}$$

Dans δW toutes les quantités sauf $U_0 Y$ et $\partial U_1/\partial t$ sont régulières en t et nous pourrons prendre leurs valeurs à $t=0$.

Une première minimisation sur f soumis à la condition $\int_0^{l_0} f\,(\mathrm{d}l/B) = v\,(t,\chi)$ conduit pour δW_1 à l'expression

$$\delta W_1 = \frac{\varepsilon}{2k_0|p_0'|}\int_{-1}^{+1}\frac{\mathrm{d}t}{|p'|}\int_0^{(\iota/2\pi)}\mathrm{d}\chi\left\{\frac{1}{\int_0^{l_0} B\,\mathrm{d}l/|\operatorname{grad}p|^2}\times\right.$$

$$v - \left(\frac{\iota}{2\pi}\right)_0'\frac{\partial(tU_0)}{\partial t}\int_0^{l_0}\mathbf{B}\cdot\operatorname{grad}\eta\,\frac{\mathrm{d}l}{B} - p'U_0\int_0^{l_0}\frac{\mathbf{B}\cdot\mathbf{J}}{|\operatorname{grad}p|^2}\frac{\mathrm{d}l}{B}\Big|^2$$

$$\left. - 2p'^2|U_0|^2\int_0^{l_0}\frac{(\mathbf{J}\times\mathbf{n})(\mathbf{B}\nabla\mathbf{n})}{|\operatorname{grad}p|^2}\frac{\mathrm{d}l}{B}\right\},$$

ou, à ε près, et en tenant compte de

$$\int_0^{l_0}\mathbf{B}\cdot\operatorname{grad}\ \eta\,(\mathrm{d}l/B) = m_0,$$

$$\delta W_1 = \frac{\varepsilon}{2k_0|p_0'|}\int_0^{(\iota/2\pi)_0}\mathrm{d}\chi\int_{-1}^{+1}\mathrm{d}t\left[\int_0^{l_0} B\,\mathrm{d}l/|\operatorname{grad}p|^2\right]^{-1}$$

$$\times\left\{\left|\left(\frac{\iota}{2\pi}\right)_0' m_0\frac{\partial}{\partial t}(tU_0) + p'U_0\int_0^{l_0}\frac{\mathbf{B}\cdot\mathbf{J}}{|\operatorname{grad}p|^2}\frac{\mathrm{d}l}{B}\right|^2\right.$$

$$\left. - 2p'^2|U_0|^2\int_0^{l_0}\frac{(\mathbf{J}\times\mathbf{n})(\mathbf{B}\nabla\mathbf{n})}{|\operatorname{grad}p|^2}\frac{\mathrm{d}l}{B}\right\}.$$

Posons

$$A = \left(\frac{\iota}{2\pi}\right)_0' m_0,$$

$$B = p'\int_0^{l_0}\frac{\mathbf{B}\cdot\mathbf{J}}{|\operatorname{grad}p|^2}\frac{\mathrm{d}l}{B} + \left(\frac{\iota}{2\pi}\right)_0' m_0$$

$$= p'\oint\frac{\mathbf{B}\cdot\mathbf{J}}{|\operatorname{grad}p|^2}\frac{\mathrm{d}l}{B} + \left(\frac{\iota}{2\pi}\right)_0' m_0,$$

$$C = \int_0^{l_0}\frac{B\,\mathrm{d}l}{|\operatorname{grad}p|^2} = \oint\frac{B^2}{|\operatorname{grad}p|^2}\frac{\mathrm{d}l}{B},$$

$$D = -2p'^2\int_0^{l_0}\frac{(\mathbf{J}\times\mathbf{n})(\mathbf{B}\nabla\mathbf{n})}{|\operatorname{grad}p|^2}\frac{\mathrm{d}l}{B}$$

$$= -2p'^2\oint\frac{(\mathbf{J}\times\mathbf{n})(\mathbf{B}\nabla\mathbf{n})}{|\operatorname{grad}p|^2}\frac{\mathrm{d}l}{B}.$$

En développant le terme carré et en intégrant par partie le double produit on obtient

$$\delta W_1 = \frac{\varepsilon}{2k_0|p_0'|}\int_0^{(\iota/2\pi)_0}\mathrm{d}\chi\int_{-1}^{+1}\mathrm{d}t\left\{\frac{A^2}{C}t^2\left|\frac{\partial U_0}{\partial t}\right|^2\right.$$

$$\left. + \left(\frac{B^2}{C} + D - \frac{AB}{C}\right)|U_0|^2\right\}. \tag{50}$$

Jusqu'à présent U_0 était supposé d'ordre 0 en ε et sa norme était d'ordre ε. Sans changer le signe de δW nous pouvons prendre la norme suivante:

$$\int_0^{(\iota/2\pi)_0}\mu(\chi)\,\mathrm{d}\chi = 1 \quad \text{avec} \quad \int_{-1}^{+1}|U_0|^2\,\mathrm{d}t = \mu(\chi)/\varepsilon,$$

d'où

$$\delta W_1 = \frac{1}{2k_0|p_0'|}\int_0^{(\iota/2\pi)_0}\mu(\chi)\,d\chi$$

$$\left\{\frac{A^2}{C}\frac{\int_{-1}^{+1}t^2|\partial U_0/\partial t|^2\,\mathrm{d}t}{\int_{-1}^{+1}|U_0|^2\,\mathrm{d}t} + \frac{B^2}{C} + D - \frac{AB}{C}\right\}.$$

Or

$$\frac{\int_{-1}^{+1}t^2|\partial U_0/\partial t|^2\,\mathrm{d}t}{\int_{-1}^{+1}|U_0|^2\,\mathrm{d}t} \geqslant \frac{\int_{-1}^{+1}t^2|\partial|U_0|/\partial t|^2\,\mathrm{d}t}{\int_{-1}^{+1}|U_0|^2\,\mathrm{d}t} \geqslant \frac{1}{4}, \tag{51}$$

d'après un résultat démontré dans [2]. $\mu(\chi)$ peut être choisi aussi concentré que l'on veut autour d'une ligne magnétique. Par conséquent on peut exprimer le critère nécessaire et suffisant de stabilité vis-à-vis des déplacements localisés sous la forme: l'expression

$$(1/4\,C)\,(A-2\,B)^2+D$$

doit être positive sur chaque ligne magnétique fermée, à condition que l'expression δW_2 puisse être choisie nulle.

En explicant la condition, on obtient:

$$\mathfrak{C}=\left[4\frac{1}{m_0}\oint\frac{B^2\,\mathrm{d}l}{|\mathrm{grad}\,\psi|^2\,B}\right]^{-1}\times\left[\frac{\mathrm{d}}{\mathrm{d}\psi}\left(\frac{\iota}{2\pi}\right)+\frac{2}{m_0}\oint\frac{\mathbf{J}\cdot\mathbf{B}}{|\mathrm{grad}\,\psi|^2}\frac{\mathrm{d}l}{B}\right]^2-\frac{2}{m_0}\oint\frac{(\mathbf{J}\times\mathbf{n})\,(\mathbf{B}\,\nabla\,\mathbf{n})}{|\mathrm{grad}\,\psi|^2}\frac{\mathrm{d}l}{B}>0\,. \qquad (52)$$

δW_2 sera nulle si

$$\mathbf{V}\cdot\mathrm{grad}_{\parallel}\,Y-\left(\frac{\iota}{2\pi}\right)'_0\frac{\partial}{\partial t}\,(t\,U_0)\,\mathbf{V}\,\mathrm{grad}_{\parallel}\,\eta-p'\,U_0\,\frac{\mathbf{V}\cdot\mathbf{J}}{|\mathrm{grad}\,p|^2}+\frac{\partial\,U_1}{\partial t}\,\mathbf{V}\cdot\mathrm{grad}_{\parallel}\,\chi=0\,,$$

U_1 étant une fonction de point arbitraire.

La condition de possibilité de cette équation s'écrit en intégrant sur t de -1 à $+1$

$$\int_{-1}^{+1}\mathbf{V}\cdot\mathrm{grad}_{\parallel}\,Y-p'\,\frac{\mathbf{V}\cdot\mathbf{J}}{|\mathrm{grad}\,p|^2}\int_{-1}^{+1}U_0\,\mathrm{d}\,t=0\,.$$

Or on peut choisir par exemple pour U_0 des fonctions antisymétriques en τ sans changer le résultat (51). Y, définie par la minimisation sur f, sera aussi antisymétrique et la condition ci-dessus est alors vérifiée.

Les valeurs de $\mathfrak{C}$ pour des lignes magnétiques fermées voisines ne sont pas en général voisines. On peut obtenir une expression seulement nécessaire mais qui a l'avantage d'être continue en cherchant la limite de $\mathfrak{C}$ pour des lignes magnétiques presque ergodiques. D'après l'annexe cette limite est

$$\overline{\mathfrak{C}}=\left[4\int_{\mathrm{S}}\frac{B^2}{|\mathrm{grad}\,\psi|^3}\,\mathrm{d}\,\mathbf{S}\right]^{-1}\times\left[\frac{\mathrm{d}}{\mathrm{d}\psi}\left(\frac{\iota}{2\pi}\right)+2\int_{\mathrm{S}}\frac{\mathbf{J}\cdot\mathbf{B}}{|\mathrm{grad}\,\psi|^3}\,\mathrm{d}\,\mathbf{S}\right]^2-2\int_{\mathrm{S}}\frac{(\mathbf{J}\times\mathbf{n})\,(\mathbf{B}\,\nabla\,\mathbf{n})}{|\mathrm{grad}\,\psi|^3}\,\mathrm{d}\,\mathbf{S}\,. \qquad (53)$$

Au voisinage d'une surface S quelconque on peut trouver des lignes magnétiques qui se ferment après un nombre de tours arbitrairement grands et par conséquent une valeur de $\mathfrak{C}$ arbitrairement voisine de $\overline{\mathfrak{C}}$ donc $\overline{\mathfrak{C}}\geqslant 0$, est un critère nécessaire.

Ce critère a été développé au voisinage de l'axe magnétique [8].

En symétrie de révolution $\overline{\mathfrak{C}}=\mathfrak{C}$ et ce critère se réduit au critère donné dans [2] qui est ainsi non seulement nécessaire mais suffisant pour les déplacements localisés.

En symétrie cylindrique, on obtient le critère de Suydam.

* * *

En terminant je tiens à remercier Messieurs M. Trocheris et M. Cotsaftis pour leurs suggestions au cours de nos discussions.

Références

[1] Bernstein, I. B., Frieman, E. A., Kruskal, M. D., Kulsrud, R. M., *Proc. Roy. Soc. (London)* **A 244** (1958) 17.
[2] Mercier, C., *Nuclear Fusion*, **1** (1960) 47.
[3] Suydam, B. R., *Proceedings of Second U.N. International Conference on Peaceful Uses of Atomic Energy*, **31** (1958) 157.
[4] Mercier, C., Cotsaftis, M., *Nuclear Fusion* **1** (1961) 121.
[5] Kruskal, M. D., Kulsrud, R. M., *Proceedings of Second U.N. International Conference on Peaceful Uses of Atomic Energy* **31** (1958) 213.
[6] Newcomb, W. A., *Phys. Fluids* **2** (1959) 362.
[7] Mercier, C., *C. R. Acad. Sci. (Paris)* **252** (1961) 1577.
[8] Mercier, C., Cotsaftis, M., *C. R. Acad. Sci. (Paris)* **252** (1961) 2203.

Annexe

Expression des intégrales sur les lignes magnétiques fermées dans le cas des lignes asymptotiques presque ergodiques.

C'est le cas où $\iota/2\pi=k/m$ avec k et m nombres entiers très grands, premiers entre eux.

Soit $K=(1/m)\oint V\,\mathrm{d}l/B$, V étant une fonction de point sur la surface S rapportée aux lignes de coordonnée η et χ. Dans ce système (voir figure 1):

$$\mathrm{d}\,t=\frac{\mathrm{d}\eta\,\mathrm{d}\chi\,\mathrm{d}\psi}{(\mathrm{grad}\,\eta\times\mathrm{grad}\,\chi)\cdot\mathrm{grad}\,\psi}$$

$$\mathrm{d}\,\mathbf{S}=\frac{\mathrm{d}\eta\,\mathrm{d}\chi}{\mathbf{B}\cdot\mathrm{grad}\,\eta}\,|\mathrm{grad}\,\psi|$$

$$\frac{\mathrm{d}l}{B}=\frac{\mathrm{d}\eta}{\mathbf{B}\cdot\mathrm{grad}\,\eta}$$

D'où

$$K=\frac{1}{m}\int_{\eta_0}^{\eta_0+m}F\,(\eta,\chi_0)\,\mathrm{d}\eta$$

où $F=V/\mathbf{B}\cdot\mathrm{grad}\,\eta$ est une fonction de point, ce qui permet d'écrire

$$K=\frac{1}{m}\int_0^m F\,(\eta,\chi_0)\,\mathrm{d}\eta\,.$$

F restant inchangé dans la transformation

$$\eta\to\eta+p$$

$$\chi_0\to\chi_0-(\iota/2\pi)\,p+q=\chi_m$$

il est possible d'ajuster les entiers p et q de façon que

$$\chi_m = \frac{\mu}{m}, \quad 0 \leqslant \mu \leqslant 1 .$$

Alors

$$K = \frac{1}{m}\int_0^m F\left(\eta, \frac{\mu}{m}\right) \mathrm{d}\eta = \frac{1}{m}\int_0^m F(\eta, 0)\,\mathrm{d}\eta + \mathbf{O}\left(\frac{1}{m}\right).$$

Par conséquent

$$\int_S \frac{V\,\mathrm{d}\mathbf{S}}{|\operatorname{grad}\psi|} = \frac{1}{k}\int_0^{\iota/2\pi} \mathrm{d}\chi_0 \int_0^m \mathrm{d}\eta\, \frac{V}{\mathbf{B}\cdot\operatorname{grad}\eta}$$

$$= \frac{1}{k}\int_0^{\iota/2\pi} \mathrm{d}\chi_0 \int_0^m F(\eta, \chi_0)\,\mathrm{d}\eta = K + \mathbf{O}\left(\frac{1}{m}\right).$$

Soit

$$\frac{1}{m}\oint V\,\frac{\mathrm{d}l}{B} = \int_S \frac{V\,\mathrm{d}\mathbf{S}}{|\operatorname{grad}\psi|} + \mathbf{O}\left(\frac{1}{m}\right). \qquad \text{(A 1)}$$

Application:

Soit une surface $S_0\,(p_0)$ où $\iota/2\pi\,(p_0) = k_0/m_0$ et envisageons toutes les surfaces $\mathbf{S}$ où $\iota/2\pi$ est rationnel comprises entre p_0 et $p_0+\varepsilon$

$$\frac{\iota}{2\pi}(p) = \frac{\iota}{2\pi}(p_0) + \varepsilon\left(\frac{\iota}{2\pi}\right)' \qquad \varepsilon \leq \varepsilon_0$$

$$= \frac{k_0}{m_0} + \frac{p}{q} = \frac{k_0 q + p m_0}{m_0 q} \text{ où } \frac{p}{q} < \varepsilon_0 \left|\left(\frac{\iota}{2\pi}\right)'\right|$$

p et q premiers entre eux.

Le dénominateur de la fonction irréductible égale à $\iota(p)/2\pi$ étant toujours supérieur ou égal à q/m_0; on pourra dans la famille des surfaces $\mathbf{S}$ définies ci-dessus remplacer les intégrales curvilignes $\oint$ par les intégrales de surface à des termes en m_0/q près, soit en prenant pour q une borne inférieure $q \sim 1/\varepsilon_0\,|(\iota/2\pi)'|$

$$\frac{1}{m}\oint V\,\frac{\mathrm{d}l}{B} = \int_S \frac{V\,\mathrm{d}\mathbf{S}}{|\operatorname{grad}\psi|} + \mathbf{O}(\varepsilon_0). \qquad \text{(A 2)}$$

STABILITÉ HYDROMAGNÉTIQUE D'UN PLASMA TOROÏDAL*

M. BINEAU**

EURATOM-MAX-PLANCK-INSTITUT FÜR PHYSIK UND ASTROPHYSIK

MUNICH, FEDERAL REPUBLIC OF GERMANY

Le problème variationnel de la recherche des minimums de l'intégrale d'énergie donnée dans le principe d'énergie [Bernstein, Frieman, Kruskal, Kulsrud: *Proc. Roy. Soc.* **A244** (1958) 17] est traité pour un plasma toroïdal.

1. Introduction

Par le principe d'énergie de BERNSTEIN et coauteurs [1] l'étude de la stabilité hydromagnétique d'un plasma revient à l'étude variationnelle de la forme quadratique:

$$W(\boldsymbol{\xi}) = -\int \boldsymbol{\xi} \cdot \mathbf{F}(\boldsymbol{\xi})\, \mathrm{d}\tau, \tag{1.1}$$

$$\mathbf{F}(\boldsymbol{\xi}) = \mathbf{j} \times \mathbf{Q} - \mathbf{B} \times \operatorname{rot} \mathbf{Q} + \nabla(\gamma p \operatorname{div} \boldsymbol{\xi} + \boldsymbol{\xi} \cdot \nabla p), \tag{1.2}$$

$$\mathbf{Q} = \operatorname{rot} \boldsymbol{\xi} \times \mathbf{B}.$$

Le volume d'intégration de (1.1) est le volume du plasma. Nous supposerons que le plasma remplit entièrement l'enceinte métallique Σ_0 qui le contient.

Désignons par ξ_n la composante de $\boldsymbol{\xi}$, normale à la surface magnétique Σ. Les déplacements $\boldsymbol{\xi}$ pour lesquels on recherche le signe de l'énergie $W(\boldsymbol{\xi})$ obéissent à la condition:

$$\xi_n = 0 \quad \text{sur} \quad \Sigma_0. \tag{1.3}$$

En tenant compte de (1.3), des intégrations partielles transforment (1.1) en la forme:

$$W(\boldsymbol{\xi}) = \int [(\mathbf{Q} + \xi_n \mathbf{j} \times \mathbf{n})^2 + \gamma p (\operatorname{div} \boldsymbol{\xi})^2 - 2\, \mathbf{j} \times \mathbf{n} (\mathbf{B} \cdot \nabla n)\, \xi_n^2]\, \mathrm{d}\tau. \tag{1.4}$$

Le plasma en équilibre considéré dans l'étude présente a une géométrie toroïdale. Les surfaces magnétiques Σ entourent un axe magnétique.

2. Description de l'équilibre

2.1. CHOIX DES COORDONNÉES

On définit un système de coordonnées η, θ, ψ dont les surfaces $\psi = \text{const.}$ sont les surfaces magnétiques ou surfaces à pression constante. Un système de surfaces $\eta = \text{const.}$ qui contiennent l'axe magnétique est choisi de telle sorte que η prenne des valeurs de 0 à 1 lorsque les surfaces font un tour complet autour de l'axe magnétique. On définit alors ψ par:

$$\psi = \int \mathbf{B} \cdot \nabla \eta\, \mathrm{d}\tau \tag{2.1}$$

volume intérieur à Σ

Ayant choisi une surface $\theta = 0$ on définit θ sur chaque ligne $\eta = \text{const.}$; $\psi = \text{const.}$ par:

$$\theta\, \mathrm{d}\psi = \int_S \frac{\nabla \eta}{|\nabla \eta|} \cdot \mathbf{B}\, \mathrm{d}S, \tag{2.2}$$

où la surface S est définie sur la surface $\eta = \text{const.}$ par les intervalles ψ, $\psi + \mathrm{d}\psi$; 0, θ. θ a la période 1 sur la surface $\psi = \text{const.}$

On suppose positive la quantité:

$$J = \frac{1}{(\nabla \eta \times \nabla \theta) \cdot \nabla \psi}.$$

2.2 GRANDEURS DE L'ÉQUILIBRE

Pour écrire l'équation des lignes magnétiques on définit

$$\alpha(\eta, \psi)\, \mathrm{d}\psi = \int_S \frac{\nabla \theta}{|\nabla \theta|} \cdot \mathbf{B}\, \mathrm{d}S, \tag{2.3}$$

où la surface S est définie sur la surface $\theta = \text{const.}$ par les intervalles ψ, $\psi + \mathrm{d}\psi$; 0, η. L'équation des lignes magnétiques est:

$$\psi = \text{const}; \quad \theta = \alpha(\eta, \psi) + \text{const.} \tag{2.4}$$

On utilise les notations:

$$\mu = \frac{\partial \alpha}{\partial \psi}, \quad i(\psi) = 2\pi [\alpha(\eta + 1, \psi) - \alpha(\eta, \psi)], \tag{2.5}$$

$$v(\eta, \theta, \psi) \equiv \theta - \alpha(\eta, \psi). \tag{2.6}$$

Avec ces définitions le champ magnétique a pour expression:

$$\mathbf{B} = \nabla v \times \nabla \psi. \tag{2.7}$$

Les dérivées le long du champ magnétique sont données par l'identité:

$$J \mathbf{B} \cdot \nabla = \frac{\partial}{\partial \eta} + \mu \frac{\partial}{\partial \theta}. \tag{2.8}$$

L'équation de l'équilibre $\mathbf{j} \times \mathbf{B} = \nabla p$ donne les relations: $\nabla \psi \cdot \operatorname{rot} \mathbf{B} = 0$ ou $\nabla \cdot \nabla \psi \times \mathbf{B} = 0$ et $\mathbf{j} \cdot \nabla v = -p'(\psi)$. On peut donc écrire $\mathbf{j} = \operatorname{rot} \mathbf{B}$ avec une quantité w:

$$\mathbf{j} = \nabla \psi \times \nabla w, \quad \mathbf{B} \cdot \nabla w = -p'(\psi) \tag{2.9}$$

La projection d'un vecteur sur la surface $\psi = \text{const.}$ sera désignée par l'indice s. Par exemple, $\boldsymbol{\xi} = \boldsymbol{\xi}_s + \xi_n \mathbf{n}$.

---

* Mémoire CN-10/35 présenté par M. Bineau. La discussion concernant ce mémoire est donnée page 817. Les traductions du résumé se trouvent en fin de volume.

** Nouvelle adresse: Laboratorio Gas Ionizzati (Euratom-C.N.E.N.), Roma (Frascati), Italy.

3. Définition des minimales

Les déplacements qui rendent $W(\boldsymbol{\xi})$ minimum appartiennent à la classe des déplacements qui satisfont les équations d'Euler. Les équations d'Euler relatives aux intégrales (1.1) et (1.4) s'écrivent:

$$\mathbf{F}(\boldsymbol{\xi}) = 0. \tag{3.1}$$

$\mathbf{F}$ est défini en (1.2). On utilise les deux coordonnées X et U pour définir les composantes de $\boldsymbol{\xi}$ dans un plan perpendiculaire au champ magnétique:

$$X = \boldsymbol{\xi} \cdot \nabla\psi \quad \text{et} \quad U = \boldsymbol{\xi} \cdot (\nabla\theta - \mu\nabla\eta). \tag{3.2}$$

Remarquons les relations:

$$\mathbf{Q} = \mathbf{Q}_s + \mathbf{Q}_\perp,$$

avec

$$\mathbf{Q}_\perp = \mathbf{B} \cdot \nabla X \frac{\nabla\psi}{|\nabla\psi|}$$

$$\mathbf{Q}_s = \mathbf{Q}_s(X) + \nabla\psi \times \nabla U,$$

$$\xi_n \mathbf{j} \times \mathbf{n} = X \nabla_s w. \tag{3.3}$$

3.1. Equations $\mathbf{F}_s(\boldsymbol{\xi})=0$

De $\mathbf{B}\cdot\mathbf{F}(\boldsymbol{\xi}) = \gamma p \mathbf{B}\cdot\nabla \operatorname{div}\boldsymbol{\xi}$ on obtient une des équations $\mathbf{F}_s(\boldsymbol{\xi})=0$ sous la forme:

$$\mathbf{B} \cdot \nabla \operatorname{div} \boldsymbol{\xi} = 0. \tag{3.4}$$

Cette équation a pour solution:

$$\operatorname{div}\xi = \frac{1}{\omega(\psi)} \frac{\mathrm{d}}{\mathrm{d}\psi} \int X \frac{\mathrm{d}S}{|\nabla\psi|}, \text{ où } \omega(\psi) = \int \frac{\mathrm{d}S}{|\nabla\psi|}. \tag{3.5}$$

(Dans les expressions du type $\int f \,\mathrm{d}S/|\nabla\psi|$ la surface d'intégration est la surface Σ, $\psi=$const.) En tenant compte de (3.4) la seconde équation $\mathbf{F}_s(\boldsymbol{\xi})=0$ s'écrit:

$$\nabla\psi \cdot \operatorname{rot}(\mathbf{Q} + \xi_n \mathbf{j} \times \mathbf{n}) = 0, \tag{3.6}$$

c'est-à-dire

$$\nabla \cdot [(\nabla\psi)^2 \nabla_s U + \mathbf{Q}(X) \times \nabla\psi - X\,\mathbf{j}] = 0.$$

Sur chaque surface magnétique, pour X donné, l'équation (3.6) détermine U à une constante près. Il est commode de représenter cette détermination implicite par celle de la fonction Z, définie par:

$$\nabla_s Z = -(\mathbf{Q}_s + X \nabla_s w). \tag{3.7}$$

(Dans le vide Z serait: moins le potentiel de la perturbation magnétique.)

$\nabla_s Z$ uniforme sur la surface $\psi=$const. (c.à.d. périodique en η et θ) et continu est défini de façon unique par l'équation:

$$\nabla \cdot \nabla_s Z = -\nabla \cdot (\mathbf{Q}_s(X) + X \nabla_s w), \tag{3.8}$$

avec des conditions qui expriment la périodicité de U en η et θ; par exemple:

$$\int \mathbf{B} \cdot (\nabla_s Z + \nabla v \times \nabla X - X \nabla_s w) \frac{\mathrm{d}S}{|\nabla\psi|} = 0, \tag{3.9a}$$

$$\int \nabla_s v \cdot (\nabla_s Z + \nabla v \times \nabla X - X \nabla_s w) \frac{\mathrm{d}S}{|\nabla\psi|} = 0. \tag{3.9b}$$

Les résultats énoncés jusqu'à présent signifient que pour $X = \boldsymbol{\xi}\cdot\nabla\psi$ donné, l'équation $\mathbf{F}_s(\boldsymbol{\xi})=0$ définit $\boldsymbol{\xi}_s$ en fonction de X. La détermination n'est pas unique mais l'énergie correspondante est unique et représente le minimum de l'énergie pour X donné. La forme (1.4) de l'énergie pour un volume compris entre ψ_1 et ψ_2 a pour minimum si X est donné:

$$W(\psi_1, \psi_2, X) = \int \mathrm{d}\tau \left\{ (\nabla_s Z_X)^2 + [\mathbf{Q}_\perp(X)]^2 - 2KX^2 + \frac{\gamma p}{\omega} \frac{\mathrm{d}}{\mathrm{d}\psi} \int X \frac{\mathrm{d}S}{|\nabla\psi|} \right\} \tag{3.10}$$

où Z_X représente une solution de (3.8) avec les conditions (3.9) et $K = \mathbf{j}\times\mathbf{n}\cdot(\mathbf{B}\cdot\nabla\dot{n})/|\nabla\psi|^2$.

3.2. Equation des minimales $X(\eta, \theta, \psi)$

L'équation $\nabla\psi\cdot\mathbf{F}(\boldsymbol{\xi})=0$ qui représente la condition pour annuler la variation de (3.10) s'écrit:

$$\operatorname{div}(\nabla_s Z_X \times \nabla v) + \nabla_s w \cdot \nabla_s Z_X + \operatorname{div}[\nabla v \times \mathbf{Q}_\perp(X)] + 2KX + \frac{\mathrm{d}}{\mathrm{d}\psi} \frac{\gamma p}{\omega} \frac{\mathrm{d}}{\mathrm{d}\psi} \int X \frac{\mathrm{d}S}{|\nabla\psi|} = 0. \tag{3.11}$$

Nous appellerons minimales les solutions $X(\eta, \theta, \psi)$ de cette équation. Pour la définition des minimales on peut donc remplacer le système initial $\mathbf{F}(\boldsymbol{\xi})=0$ par le système noté symboliquement

$$\begin{aligned} EZ &= fX \text{ et conditions (3.9)} \\ gZ &= -HX, \end{aligned} \tag{3.12}$$

avec les définitions:

$$EZ \equiv \nabla \cdot \nabla_s Z$$

$$\begin{aligned} fX &\equiv -\nabla \cdot [\mathbf{Q}_s(X) + X \nabla_s w] \\ &\equiv \frac{1}{J} \frac{\partial}{\partial\psi} J\mathbf{B} \cdot \nabla X - \nabla \cdot X \nabla_s w - \nabla \cdot [\mathbf{B} \cdot \nabla X (\mathbf{r}_\psi)_s] \end{aligned}$$

$$\begin{aligned} gZ &\equiv \nabla \cdot (\nabla_s Z \times \nabla v) + \nabla_s w \cdot \nabla_s Z \\ &\equiv \mathbf{B} \cdot \nabla \frac{\partial Z}{\partial\psi} + \nabla_s w \cdot \nabla_s Z - \mathbf{B} \cdot \nabla (\mathbf{r}_\psi \cdot \nabla_s Z) \end{aligned}$$

$$\begin{aligned} HX &\equiv \nabla v \cdot \operatorname{rot} \mathbf{Q}_\perp(X) + 2KX + \frac{\mathrm{d}}{\mathrm{d}\psi} \frac{\gamma p}{\omega} \frac{\mathrm{d}}{\mathrm{d}\psi} \int X \frac{\mathrm{d}S}{|\nabla\psi|} \\ &\equiv \mathbf{B} \cdot \nabla \frac{\mathbf{B}\cdot\nabla X}{|\nabla\psi|^2} + 2KX + \frac{\mathrm{d}}{\mathrm{d}\psi} \frac{\gamma p}{\omega} \frac{\mathrm{d}}{\mathrm{d}\psi} \int X \frac{\mathrm{d}S}{|\nabla\psi|}. \end{aligned} \tag{3.13}$$

L'équation $\mathbf{B}\cdot\nabla f = g$ qui apparait dans le système (3.12) a été étudiée par Newcomb [2].
Remarquons une autre expression de (3.10):

$$W(\psi_1, \psi_2, X) \equiv -\int \mathrm{d}\tau\, X F X - \left[\int \frac{\mathrm{d}S}{|\nabla\psi|} X G X \right]_{\psi_1}^{\psi_2}$$

où $\quad FX \equiv -gZ_X - HX$

et $\quad GX \equiv -\mathbf{B}\cdot\nabla Z_X - \dfrac{\gamma p}{\omega} \dfrac{\mathrm{d}}{\mathrm{d}\psi} \displaystyle\int X \frac{\mathrm{d}S}{|\nabla\psi|}.$ (3.14)

F est hermitique pour les fonctions X nulles aux

extrémités de l'intervalle de ψ, d'après la relation:

$$\int \frac{dS}{|\nabla\psi|}(X_1 F X_2 - X_2 F X_1) + \frac{d}{d\psi}\int \frac{dS}{|\nabla\psi|}(X_1 G X_2 - X_2 G X_1) = 0. \quad (3.15)$$

4. Propriétés des minimales

4.1. Les conditions initiales sont données

Sur une surface magnétique à lignes magnétiques ergodiques on peut choisir arbitrairement pour X et $\mathbf{B}\cdot\nabla Z$ des valeurs initiales $X=\varphi(\eta,\theta)$, $\mathbf{B}\cdot\nabla Z = \sigma(\eta,\theta)$, qui satisfont à la condition (3.9b). A tout choix de ces valeurs initiales correspond une minimale unique déterminée par son développement en série de Taylor en ψ.

4.2. Les conditions aux limites sont données

Les équations d'Euler transforment par une transformation linéaire et continue un système de fonctions initiales $\varphi_0(\eta,\theta)$ et $\sigma_0(\eta,\theta)$ correspondant à une solution X et $\mathbf{B}\cdot\nabla Z$ pour $\psi=\psi_0$ en un système de fonctions finales $\varphi_1(\eta,\theta)$ et $\sigma_1(\eta,\theta)$ correspondant à la même solution X et $\mathbf{B}\cdot\nabla Z$ pour $\psi=\psi_1$.

Remarquons que deux minimales sont liées par la relation:

$$\frac{d}{d\psi}\int\frac{dS}{|\nabla\psi|}\left\{X_1\left(\mathbf{B}\cdot\nabla Z_2 + \frac{\gamma p}{\omega}\frac{d}{d\psi}\int X_2\frac{dS}{|\nabla\psi|}\right) - X_2\left(\mathbf{B}\cdot\nabla Z_1 + \frac{\gamma p}{\omega}\frac{d}{d\psi}\int X\frac{dS}{|\nabla\psi|}\right)\right\} = 0. \quad (4.1)$$

Cette relation peut être utilisée pour exprimer les coefficients du développement d'une solution quelconque X, Z en série de solutions X_i, Z_i choisies pour constituer un système complet.

On peut utiliser ces remarques pour étudier l'application $X(\eta,\theta,\psi_0)\to X(\eta,\theta,\psi_1)$ pour les minimales nulles en ψ_0, c'est-à-dire satisfaisant $X(\eta,\theta,\psi_0)=0$.

Le résultat s'énonce ainsi:

Pour qu'à deux fonctions arbitraires $\varphi_0(\eta,\theta)$ et $\varphi_1(\eta,\theta)$ corresponde une et une seule minimale égale à $\varphi_0(\eta,\theta)$ pour $\psi=\psi_0$ et à $\varphi_1(\eta,\theta)$ pour $\psi=\psi_1$, il est nécessaire et suffisant qu'il n'existe pas de minimale nulle à la fois pour $\psi=\psi_0$ et $\psi=\psi_1$.

4.3. Minimales singulières

Pour toute valeur $\psi_{k,m}$ de ψ où les lignes magnétiques sont fermées $[i(\psi_{k,m})=2k\pi/m]$, l'opérateur $J\mathbf{B}\cdot\nabla$ appliqué à des fonctions périodiques de η et θ a une valeur propre nulle. On peut donc s'attendre à trouver des solutions singulières au système (3.12).

On cherche ces solutions en écrivant les équations (3.12) au moyen du système de coordonnées x, y, ψ défini par

$$x = \int_{\psi=\psi_{k,m}} \mathbf{B}\cdot d\mathbf{r} \quad \text{et} \quad y(\eta,\theta) = \theta - \alpha(\eta,\psi_{k,m})$$

Si le système (3.12) a des solutions singulières, X et $\nabla_s U$ singuliers sont équivalents au voisinage de $\psi_{k,m}$ à X_0 et $\nabla_s U_0$ de la forme:

$$X_0(y,\psi) = \varphi(y)\,|\psi-\psi_{k,m}|^{-n(y)} \quad (4.2)$$

$$\nabla_s U_0 = \frac{\partial X_0}{\partial\psi}\nabla_s y,$$

qui vérifient en outre les conditions suivantes:

$$\operatorname{div}\xi_0 = 0, \text{ et}$$

$$U_0 \text{ périodique sur la surface } \psi = \text{const.} \quad (4.3)$$

L'exposant $n(y)$ peut prendre 2 valeurs fonctions de y définies comme les solutions de l'équation:

$$a(n^2-n) - b(y) = 0. \quad (4.4)$$

Les coefficients a et $b(y)$ sont donnés par des intégrales le long des lignes magnétiques:

$$a = \left(\oint\frac{1}{J}\frac{\partial\mu}{\partial\psi}\frac{dl}{B}\right)^2 = \left(\frac{m}{2\pi}i'(\psi)\right)^2$$

$$b = \oint\frac{\mathbf{j}\cdot\mathbf{B}}{|\nabla\psi|^2}\frac{dl}{B}\left\{\frac{m}{2\pi}i'(\psi) + \oint\frac{\mathbf{j}\cdot\mathbf{B}}{|\nabla\psi|^2}\frac{dl}{B}\right\} - \oint\frac{B^2}{|\nabla\psi|^2}\frac{dl}{B}\oint 2K\frac{dl}{B}. \quad (4.5)$$

Lorsqu'il n'y a pas de symétrie il n'existe aucune fonction $\varphi(y)$ vérifiant les conditions (4.3). Les conditions (4.3) sont donc incompatibles avec la forme (4.2) et il n'existe pas de minimales singulières.

En symétrie de révolution $n(y)$ est une constante. Les deux conditions (4.3) sont identiquement vérifiées pour les perturbations des modes $m\neq 0$. Les modes $m\neq 0$ ont donc deux solutions singulières.

D'après (4.4) les exposants des solutions singulières sont réels ou imaginaires selon que $a+4b$ est positif ou négatif.

Remarquons que le critère local dit critère de Suydam en symétrie cylindrique et obtenu par Mercier en géométrie toroïdale [4] s'écrit $a+4b>0$ pour toutes les lignes magnétiques fermées.

5. Condition suffisante pour l'existence d'une énergie négative

Si une minimale est connue pour $\psi\leqslant\psi_1$, et si $\psi_1=$const. est une surface à lignes magnétiques ergodiques, la minimale se poursuit de façon unique pour $\psi>\psi_1$ et la dérivée $\partial X_1/\partial\psi$ est continue en ψ_1.

Pour une valeur de ψ où les lignes magnétiques sont fermées il y a un paramètre d'indétermination pour $\partial X/\partial\psi$.

Soit ψ_A ψ_B l'intervalle de variation de ψ, ψ_B représentant la paroi et ψ_A l'axe magnétique. Pour ces deux valeurs de ψ les déplacements $\boldsymbol{\xi}$ vérifient $\boldsymbol{\xi}\cdot\nabla\psi = 0$. On désignera par X_0 la minimale triviale, $X_0\equiv 0$. Supposons qu'une minimale $X_1\neq X_0$, nulle en ψ_B, s'annule en ψ_1 entre ψ_A et ψ_B. Définissons la fonction Y par $Y=X_1$ pour $\psi_1\leqslant\psi\leqslant\psi_B$ et $Y=X_0$ pour $\psi_A\leqslant\psi\leqslant\psi_1$. Y n'est pas une minimale, sauf dans le cas très exceptionnel expliqué ci dessus et dans lequel il conviendrait de ne pas distinguer Y de X_0.

Or:

$$W(\psi_A, \psi_B; Y) = 0.$$

S'il existe une minimale X_1 nulle pour $\psi=\psi_B$ et $\psi=\psi_1$, il existe donc des fonctions X obéissant aux conditions aux limites qui rendent l'énergie négative.

6. Invariant intégral de Hilbert

6.1. Constitution d'un champ de minimales

Supposons qu'aucune minimale non triviale et nulle en ψ_B ne s'annule à nouveau entre ψ_A et ψ_B. Par application des résultats du paragraphe 4 relatif aux conditions aux limites, on peut associer à toute fonction $Y(\eta, \theta, \psi)$ et à une relation biunivoque $\psi=\psi(t)$ un champ de minimales à 1 paramètre t au moyen des conditions:

$$X(\eta, \theta, \psi_B, t) = 0; \quad X[\eta, \theta, \psi(t), t] = Y[\eta, \theta, \psi(t)]. \tag{6.1}$$

6.2. Définition de l'invariant intégral

Soit $$W(t) = W[\psi(t), \psi_B; X(t)] \tag{6.2}$$

selon (3.10). L'expression de $dW(t)/dt$ contient $\partial X/\partial t$. En utilisant (6.1) pour définir une fonction Y on peut exprimer $\partial X/\partial t$ en $\psi=\psi(t)$ par la relation:

$$\frac{\partial X}{\partial t} = \frac{\partial (Y-X)}{\partial \psi}\frac{\partial \psi}{\partial t}. \tag{6.3}$$

Des intégrations partielles donnent à $dW(t)/dt$ la forme:

$$\frac{dW(t)}{dt} = \left[\frac{d\psi}{dt}\int \frac{ds}{|\nabla\psi|}\left\{(\nabla_s Z_y)^2 + \frac{\gamma p}{\omega^2}\left(\frac{d}{d\psi}\int Y\frac{ds}{|\nabla\psi|}\right)^2 + Q_\perp{}^2(Y) - 2KY^2 - [\nabla_s(Z_y - Z_x)]^2 - \frac{\gamma p}{\omega^2}\left[\int\left(\frac{\partial Y}{\partial\psi} - \frac{\partial X}{\partial\psi}\right)\frac{ds}{|\nabla\psi|}\right]\right\}\right]_{\psi(t)}^{\psi_B}, \tag{6.4}$$

où Z_x et Z_y sont définis en fonction de X et Y par (3.8) et (3.9).

Soit $Y(\eta, \theta, \psi)$ une fonction qui permette de définir un champ de minimales à 1 paramètre, par exemple selon (6.1).

On définit la fonctionelle $I(Y)$ par

$$I(Y) = \int_{\psi_I}^{\psi_B} d\tau\left\{(\nabla_s Z_y)^2 + \frac{\gamma p}{\omega^2}\left(\frac{d}{d\psi}\int Y\frac{ds}{|\nabla\psi|}\right)^2 + Q_\perp{}^2(Y) - 2KY^2 - [\nabla_s(Z_x - Z_y)]^2 - \frac{\gamma p}{\omega^2}\left[\int\left(\frac{\partial X}{\partial\psi} - \frac{\partial Y}{\partial\psi}\right)\frac{ds}{|\nabla\psi|}\right]^2\right\}. \tag{6.5}$$

D'après (3.10) la définition (6.5) peut s'écrire:

$$W(Y) - I(Y) = \int d\tau\left\{[\nabla_s(Z_y - Z_x)]^2 + \frac{\gamma p}{\omega^2}\left[\int\left(\frac{\partial Y}{\partial\psi} - \frac{\partial X}{\partial\psi}\right)\frac{ds}{|\nabla\psi|}\right]^2\right\}. \tag{6.6}$$

$I(Y)$ a les propriétés:

1. $I(Y)$ ne dépend que des valeurs de Y aux limites ψ_I et ψ_B de l'intégration en ψ. Si $Y=0$ en ψ_I et ψ_B, $I(Y)=0$;
2. Si Y n'est pas une minimale, $W(Y)>I(Y)$;
3. Si Y est une minimale, $W(Y)=I(Y)$.

7. Condition nécessaire et suffisante de stabilité

Dans le paragraphe 5 on a vu une condition nécessaire de stabilité à savoir qu'il n'existe pas de minimale nulle en ψ_B qui s'annule pour une valeur de ψ entre ψ_A et ψ_B.

La théorie de l'invariant intégral permet de montrer la réciproque. La condition à imposer aux fonctions X sur l'axe magnétique dépend de la forme de l'équilibre du plasma au voisinage de l'axe. On peut éviter cette question en considérant des intervalles $\psi_I\,\psi_B$ avec $\psi_I \to \psi_A$ et en imposant en ψ_I la condition $X=0$.

Si aucune minimale nulle en ψ_B ne s'annule en une valeur ψ comprise entre ψ_A et ψ_B, pour toute fonction Y nulle en ψ_I et ψ_B on peut définir l'invariant $I(Y)$. D'après ses propriétés $I(Y)=0$ et si $Y \not\equiv X_0$, c'est-à-dire si $Y \not\equiv 0$, $W(\psi_I, \psi_B; Y)$ est positif; donc $W(\psi_A, \psi_B; Y)$ est positif ou nul.

En résumé, en incluant le cas de stabilité marginale dans les cas de stabilité, la condition nécessaire et suffisante de stabilité est qu'il n'existe pas de minimale nulle en ψ_B et s'annulant pour une seconde valeur ψ de l'intervalle $\psi_A\,\psi_B$ ($\psi_A<\psi<\psi_B$).

8. Propriétés de la symétrie de révolution

En symétrie de révolution on peut choisir comme coordonnée θ l'angle azimuthal et choisir les surfaces $\eta=$ const. de telle sorte que $\eta\,\theta\psi$ forment un système droit.

Si on représente le déplacement ξ comme la partie réelle de $\Sigma_m \xi_m e^{im\theta}$ l'énergie est décomposée en $\Sigma_m W_m(\xi_m)$. Pour les modes $m\neq 0$,

$$\int X_m\, e^{im\theta}\frac{ds}{|\nabla\psi|} = 0,$$

et le déplacement minimal est à divergence nulle.

Considérons les modes $m\neq 0$. D'après le paragraphe 4 au voisinage des points ψ_k tels que $i(\psi_k) = 2k\pi/m$ il existe deux minimales singulières de la forme

$$X = |\psi - \psi_k|^{-n}\{\varphi_0(\eta) + (\psi - \psi_k)\varphi_1(\eta) + \ldots\}$$
$$Z = |\psi - \psi_k|^{-n}\{\lambda\varphi_0(\eta) + (\psi - \psi_k)\sigma_1(\eta) + \ldots\}. \tag{8.1}$$

Les exposants n sont les solutions d'une équation

$$a(n^2 - n) - b = 0 \tag{8.2}$$

Si $a+4b<0$ les solutions singulières oscillent au voisinage de ψ_k et d'après le paragraphe 5 le plasma est instable. $a+4b>0$ est donc une condition nécessaire de stabilité. Supposons $a+4b>0$ et soient n_1 et n_2, $n_1<n_2$ les solutions de (8.2). D'après (8.2)

$n_1<1/2$ et $n_2>1/2$. Soient X_{k,n_1} et X_{k,n_1} les minimales singulières en ψ_k. On peut montrer les propriétés suivantes:

1. Pour $\psi\to\psi_k$ avec la définition (3.14) $W(\psi_0, \psi; X_{k,n_1})$ est convergent et $W(\psi_0, \psi; X_{k,n_2})$ est divergent.
2. Soit Y une fonction continue telle que $W(Y)$ soit fini; la fonction égale pour $\psi<\psi_k$ et $\psi>\psi_k$ respectivement à $Y+\lambda_1 X_{n_1}$ et $Y+\lambda_2 X_{n_1}$ peut être rendue finie et continue par une déformation effectuée dans un intervalle infiniment petit $\psi_k-\delta\psi$, $\psi_k+\delta\psi$ qui modifie l'énergie d'une quantité infiniment petite.

Par suite de ces propriétés, on doit admettre que les fonctions Y avec lesquels on vérifie le signe de l'expression $W(Y)$ (3.14) aient au voisinage des points ψ_k des divergences et des discontinuités de la forme $\lambda X_{k,n_1}$.

On constitue donc les champs de minimales selon le paragraphe 6 en ajoutant la condition:

En tout point singulier ψ_k chaque minimale $X(\eta, \psi, t)$ n'est pas équivalente à X_{k,n_2} mais a en ce point une discontinuité de la forme $\lambda X_{k,n_1}$.

Remarquons comment une minimale $X(\eta, \psi)$ se poursuit de façon unique à travers un point singulier. Cette minimale, pour $\psi<\psi_k$, a une partie continue $X_c(\eta, \psi)$ et une partie singulière:

$$X(\eta, \psi) = X_c(\eta, \psi) + \lambda X_{k,n_1}(\eta, \psi).$$

Au voisinage de ψ_{k+1},

$$X_c(\eta, \psi) \sim \alpha X_{k+1,n_2}(\eta, \psi)$$

et

$$X_{k,n_1}(\eta, \psi) \sim \beta X_{k+1,n_2}(\eta, \psi).$$

Entre ψ_k et ψ_{k+1} la minimale $X(\eta, \psi)$ est donc:

$$X_c(\eta, \psi) - \frac{\alpha}{\beta} X_{k,n_1}(\eta, \psi).$$

9. Application à un plasma toroïdal à couche mince de courant

On peut appliquer cette théorie à un plasma à couche mince de courant en tenant compte de la structure de la couche dans la limite où l'épaisseur de la couche tend vers zéro.

Un plasma toroïdal se distingue essentiellement d'un plasma cylindrique étudié par NEWCOMB [3] par l'impossibilité de séparer complètement les variables. Par suite, les surfaces singulières $\psi=\psi_{k,m}$ du système minimal ne séparent pas le volume en sous-volumes indépendants et le critère de stabilité ne peut pas se séparer en plusieurs critères.

L'intégration du système (3.12) a été faite dans le cas d'une couche mince de courant d'un plasma toroïdal ayant la symétrie de rotation. Si la composante normale du déplacement minimal est $(\xi_n)_e$ et $(\xi_n)_i$ à l'extérieur et à l'intérieur de la couche respectivement, on trouve lorsque l'épaisseur tend vers zéro,

1. $|(\xi_n)_e - (\xi_n)_i| \to 0$;
2. l'énergie minimum tend vers l'expression

$$\int |\xi_n|^2 \Delta\left[n \cdot \nabla\left(p + \frac{B^2}{2}\right)\right] \mathrm{d}S$$

c'est-à-dire l'expression de l'énergie de surface donnée dans l'étude de BERNSTEIN et coauteurs [1].

* * *

Un exposé plus complet des arguments et des calculs présentés dans cet article est en préparation.

Références

[1] BERNSTEIN, I. B., FRIEMAN, E. A., KRUSKAL, M. D., KULSRUD, R. M., *Proc. Roy. Soc. (London)*, **A 244** (1958) 17.
[2] NEWCOMB, W. A., *Phys. Fluids* **2** (1959) 362.
[3] NEWCOMB, W. A., *Ann. Phys. (N. Y.)* **10** (1960) 232.
[4] MERCIER, C., comptes rendus de cette conférence, voir page 801.

Paper CN-10/243 *was presented by A. Rukhadze* (Union of Soviet Socialist Republics). *The text of the paper is on pages 755 to 759 inclusive. The following discussion took place:*

T. H. Stix *(United States of America):* I would just like to mention, from the point of view representing the experimenters, that this technique of analyzing the ion distribution in the plasma has already been used by the group at Princeton. Dr. Hooke and his colleagues have used this technique. Dr. Hooke reported on it at the Montreal meeting of the American Physical Society in June, a little more than a year ago, and the same work will appear in the current issue of the *Physics of Fluids*. If I may make one point, it is important from an experimental point of view to consider more than just these dispersion relations, which are accurate only for a homogeneous plasma. In general, the experimenter has to work with an inhomogeneous plasma and then it is important to study the variation of the amplitude factor in front of the exponential as well as the value of the exponent itself.

A. Rukhadze: I regretfully did not know of Dr. Hooke's work, and can therefore say nothing. I am very happy that someone else is also interested in this problem. As regards the inhomogeneous plasma, the theory is more difficult by an order of magnitude. But, considering the large number of skillful and powerful theoreticians, I think that in the next few years the problem of the propagation of electromagnetic waves in an inhomogeneous plasma will also be solved and that the effect of inhomogeneity on the attenuation of the wave amplitude will be found.

Paper CN-10/162 *was presented by N. Rostoker* (United States of America). *The text of the paper is on pages 761 to 766 inclusive. The following discussion took place:*

B. Bertotti *(Italy):* I wonder if you can comment on the validity of Kirchhoff's principle in a plasma which is not in thermodynamic equilibrium.

N. Rostoker: According to Kirchhoff's law the emission per unit volume is equal to the absorption coefficient times the energy density. In the presence of a magnetic field a more general expression is involved because we do not have a single scalar absorption coefficient. Instead, we must consider an absorption tensor defined as follows. Consider the Vlasov equations where the electric and magnetic fields are specified to be proportional to $\exp i(\omega t + kx)$; suppose that the fields were applied adiabatically at $t = -\infty$. We can calculate the current density and the power absorption:

$$P = \frac{1}{2}\,\mathrm{Re}\,(\mathbf{J}\cdot\mathbf{E}^*)$$

$$= \mathrm{tr}\,(\boldsymbol{\sigma}_H\cdot\mathbf{E}\,\mathbf{E}^*)\,.$$

$\boldsymbol{\sigma}_H(\mathbf{k},\omega)$ is the Hermitian conductivity tensor; for the problem stated the result would be

$$\boldsymbol{\sigma}_H(\mathbf{k},\omega) = -\frac{\omega_p^2}{4}\,\mathbf{G}'(-\omega/k)\,,$$

where $\mathbf{G}'(u)$ has been defined in our paper.

Emission is calculated by multiplying the collision operator by $mv^2/2$ and integrating. The result may be expressed in the form

$$\frac{\partial T}{\partial t} = \int \mathrm{d}\mathbf{v}\,(m\,v^2/2)\,\mathsf{St}\,\{f\} = \int \frac{\mathrm{d}\mathbf{k}\,\mathrm{d}\omega}{(2\pi)^4}\,\varepsilon(\mathbf{k},\omega)\,.$$

Now consider the contributions from the three terms in the collision operator of Eq. (41)*. The first term that involves the frictional drag force produces

$$\varepsilon(\mathbf{k},\omega) = 8\pi\,\mathrm{tr}\,\{\boldsymbol{\sigma}_H(\mathbf{k},\omega)\cdot\mathbf{W}(\mathbf{k},\omega)\}\,, \qquad (1)$$

$$\mathbf{W}(\mathbf{k},\omega) = \frac{4\pi n_0 e^2}{\omega^2}\,\frac{\pi}{k}\{[\mathbf{Y}^{-1}(u)]\cdot\mathbf{G}\cdot[\mathbf{Y}^{-1}(u)]_H\}_{u=-\omega/k}.$$

We note that

$$\int \frac{\mathrm{d}\mathbf{k}\,\mathrm{d}\omega}{(2\pi)^4}\,\mathbf{W}(\mathbf{k},\omega) = \left\langle \frac{\mathbf{E}(xt)\,\mathbf{E}(xt)}{8\pi} \right\rangle,$$

where $\langle\rangle$ denotes the ensemble average, and

$$\int \mathbf{W}(\mathbf{k},\omega)\,\frac{\mathrm{d}\omega}{2\pi} = \frac{\Theta}{2}\,\frac{\mathbf{e}_1\,\mathbf{e}_1}{1+(k l_D)^2} + \frac{\Theta}{2}\,\mathbf{I}\,,$$

if the one-body particle function is Maxwellian. Thus Eq. (1) above is a generalized form of Kirchhoff's law. The formal expression is valid for any stable one-body function of the form $f(v_\perp, v_z)$.

Now the second term in the collision operator produces $-\varepsilon(\mathbf{k},\omega)$ so that together the first two terms produce no change in the particle energy. These two terms describe emission and absorption by the particles for which there is detailed balance. The last term produces the result

$$\varepsilon(\mathbf{k},\omega) = 8\pi\,\mathrm{tr}\,[\boldsymbol{\sigma}_H(\mathbf{k},\omega)\cdot\mathbf{W}(\mathbf{k},\omega)]\,,$$

where

$$\mathbf{W}(\mathbf{k},\omega) = \pi m\,\mathbf{H}(-\omega/k)\,.$$

Making use of the sum rule of our paper (page 765 of these Proceedings):

$$\int \mathbf{W}(\mathbf{k},\omega)\,\frac{\mathrm{d}\omega}{2\pi} = \left(\frac{\Theta-\Theta'}{2}\right)\mathbf{I}\,,$$

* See page 766 of these Proceedings.

in the case that the particles and oscillators both have Maxwell distributions at temperatures Θ and Θ'. In our treatment radiation is defined as a change in the mean oscillator energy, that is obtained at the expense of the particle kinetic energy. The emission formula can evidently be placed in the form anticipated by Kirchhoff's law. The energy density involves the difference between the energy per mode implied by the particle temperature and the energy per mode assigned to the oscillators. Alternately, the net emission is the difference between emission determined by the particle temperature and absorption determined by the oscillator temperature.

Paper CN-10/89 *was presented by J. M. Dolique* (France). *The text of the paper is on pages 767 to 774 inclusive. The following discussion took place:*

P. Auer *(United States of America):* Could the speaker kindly give a brief sketch of the physical experiment to which his calculations refer? That is, how is this neutralization performed in one dimension?

J. M. Dolique: I think that, to answer this question correctly, I would be driven to excessively long developments and I would rather that the person who asked this question should refer to Paper CN-10/92, which describes the experimental aspect of this neutralization, or if he prefers, engage in private discussions with Dr. Régnier, who has directed these experiments, or with me.

W. I. Linlor *(United States of America):* I have a very brief comment and a question. My comment is that at Hughes Research Laboratory we are engaged in producing a neutralized beam of ions for use in propulsion and have accomplished this experimentally.

My question is: when you refer to your beam as being destroyed do you consider the space-charge sheath which occurs at the far end of the beam when the two components of plasma tend to separate? Let me say it perhaps slightly differently. In your calculation have you considered any tendency of the ions and electrons to become separated when they are far away from the source?

J. M. Dolique: We have considered space-charge forces, but for a radially infinite beam. This hypothesis of an infinite extension of the beam is only given to simplify the mathematical description. We are not taking into account many phenomena which are certainly not negligible, in particular: (*a*) a possible divergence (by space-charge) of a poorly neutralized beam and (*b*) the edge effects.

The theory developed here is only the first step. We are presently working on a model of an ideal axial beam ($\partial/\partial\theta=0$), but radially bounded ($\partial/\partial r\neq 0$), where the two effects mentioned above occur.

F. Boeschoten *(Federal Republic of Germany):* Do you think that your results are strongly modified if the electron and ion beams are shot along converging magnetic field lines, for example, along the field which exists at the neck of a magnetic bottle?

J. M. Dolique: I believe your question has two aspects and calls for two answers.

If you ask if the conditions of mixing electrons with an ionic beam—which is the subject of this study—are generally preserved when introducing the mixing zone into a longitudinal magnetic field with converging lines of force, the answer is yes. We create a magnetic focussing which acts essentially on the radial extension of two beams—electronic and ionic—which are to be mixed; but this does by no means fundamentally modify the mixing conditions described in this paper which depend on the longitudinal velocities (or on the densities).

If you ask if the theory developed here can furnish some indication of the behavior of the mixed beam when it penetrates into a magnetic bottle, the answer is no, if we consider penetration that is transverse or along the neck. These are totally different problems on which we are presently working at the Département Atomistique de la Compagnie Générale de Télégraphie Sans Fil.

F. Boeschoten: Do you think, as a first guess, that the modification will be great or do you think it is not too important?

J. M. Dolique: I think that the theory and the experiment would be completely different in the presence of magnetic fields.

Paper CN-10/166 *was presented by M. Kruskal* (United States of America). *The text of the paper is on pages 775 to 795 inclusive. The following discussion took place:*

K. Husimi *(Japan):* I would like to ask if your theory can be applied as well to the case of multidimensional dynamics as to the one-dimensional case. As far as I have examined the theory of Lenard for the case of anharmonic oscillations, it seems to work only with the condition of one-dimensionality. I would like to ask if it is possible to treat the adiabatic invariant of a multidimensional system.

M. Kruskal: That's a very pertinent question. The answer is yes, the method applies to systems of any number of dimensions—for instance, to the charged particle gyrating in a given electromagnetic field, a a three-dimensional case treated in my Venice paper. However, it does not apply to just any system whatsoever: since the trajectories must be closed curves (to lowest order), the system must resemble the case of one degree of freedom in having a single frequency in common for the recurrence of all the coordinates (of phase space). Thus a system with two degrees of freedom each of which is (nearly) periodic but with different (and independently varying) frequencies does not come under the theory; but if the system is

linear, invariants to all orders can be found anyway, as shown by Lenard in that same paper.

L. Spitzer *(United States of America):* The condition that the two frequencies of motion in the successive adiabatic invariants be very different—is that the same thing as the condition that each be separately almost periodic?

M. Kruskal: The two frequencies are automatically of different orders because the reduced system had an extra ε factor so that everything occurred more slowly there; more slowly by a different order in the expansion parameter E. So they are incommensurable because they are infinitely far apart.

Paper CN-10/95 *was presented by C. Mercier* (France). *The text of the paper is on pages 801 to 808, inclusive. The following discussion took place:*

R. S. Pease *(United Kingdom):* You have drawn a distinction between the case when the rotational transform is a rational fraction of 2π and the case when it is not. Do you expect there to be any physically observable consequences of this possible difference? Observations in both the Stellarator and in Zeta strongly suggest that there are effects associated with integral values of the rotational transform.

C. Mercier: The constant-pressure surfaces on which $\iota/2\pi = k/m$ (k and m relatively prime) form an infinite class of surfaces, difficult to detect physically, within the much more important class of surfaces where the magnetic lines are ergodic. However, the surfaces with small k and m are clearly separated from each other and can have properties distinct from those of neighboring surfaces where $\iota/2\pi$ is irrational or rational with k and m very large. For example, the criterion varies in a discontinuous manner for neighboring magnetic lines and probably the more so when one places oneself in the neighborhood of a surface on which k and m are small. It could be that sources of detectable turbulent motion are to be found there.

R. J. Tayler *(United Kingdom):* Is it true that your criterion is (1) necessary and sufficient for localized perturbations and (2) dependent only on perturbation helices which are parallel to the magnetic field helix?

C. Mercier: My criterion is effectively necessary and sufficient for perturbations localized in the neighborhood of the constant-pressure surfaces. Among these displacements, the worst ones are, in addition, localized in the neighborhood of the helices of the magnetic field. The general criterion reduces, in the case of axial symmetry, to the criterion given in a previous paper of mine [*Nuclear Fusion* **1** (1960) 47] which was, therefore, not only necessary but also sufficient for the localized perturbations, even though the demonstration in that paper did not prove that aspect of the criterion.

Paper CN-10/35 *was presented by M. Bineau* (Federal Republic of Germany). *The text of the paper is on pages 809 to 813 inclusive. The following discussion took place:*

M. Kruskal *(United States of America):* How much of this work is known from the classical theory of variations? Some of it is similar, isn't it?

M. Bineau: Yes, there is a similarity to classical theory. I do not know the theory of integrals having many functions of many variables. But it is a property of the energy integral to be reducible to a functional of a single function of the kind to which the classical method is applicable. The criterion described is in reality Jacobi's criterion of envelopes, applicable to integrals: $\int f(x, y, z, v, \partial v/\partial x, \partial v/\partial y, \partial v/\partial z)\, d\tau$.

Newcomb's studies have nevertheless shown that the energy integral for one variable $\int_a^b f(x, y, y')\, dx$ leads to the singular case of the classical theory where $f_{y'y'}$ goes to zero in the interval a, b. From this point of view the variational problem posed by the energy integral for many variables is singular. The problem posed by this singularity can be solved by the classical method of the integral invariant of Hilbert.

R. J. Tayler *(United Kingdom):* This isn't a question —it's just a comment. As somebody who has unsuccessfully tried to prove this same result, I'd like to congratulate Dr. Bineau on his success.

M. Bineau: Thank you, Dr. Tayler. I am grateful to you for your comments.

W. A. Newcomb *(United States of America):* I would like to make the same remark as Dr. Tayler, since I also decided beforehand that this problem could not be done.

NUCLEAR FUSION
FUSION NUCLEAIRE
ЯДЕРНЫЙ СИНТЕЗ
FUSION NUCLEAR

1962 SUPPLEMENT

PART 3

PROCEEDINGS OF THE CONFERENCE ON PLASMA PHYSICS AND CONTROLLED NUCLEAR FUSION RESEARCH, 4—9 SEPTEMBER 1961, SALZBURG, AUSTRIA

LES ACTES DE LA CONFERENCE SUR LA PHYSIQUE DES PLASMAS ET LA RECHERCHE CONCERNANT LA FUSION NUCLEAIRE CONTROLEE, 4—9 SEPTEMBRE 1961, SALZBOURG, AUTRICHE

ТРУДЫ КОНФЕРЕНЦИИ ПО ИССЛЕДОВАНИЯМ В ОБЛАСТИ ФИЗИКИ ПЛАЗМЫ И УПРАВЛЯЕМОГО ЯДЕРНОГО СИНТЕЗА, 4—9 СЕНТЯБРЯ 1961 г., ЗАЛЬЦБУРГ, АВСТРИЯ

LAS ACTAS DE LA CONFERENCIA SOBRE LAS INVESTIGACIONES EN MATERIA DE FISICA DEL PLASMA Y FUSION NUCLEAR CONTROLADA, 4 AL 9 DE SEPTIEMBRE DE 1961, SALZBURGO, AUSTRIA

INTERNATIONAL ATOMIC ENERGY AGENCY · AGENCE INTERNATIONALE DE L'ENERGIE ATOMIQUE · МЕЖДУНАРОДНОЕ АГЕНТСТВО ПО АТОМНОЙ ЭНЕРГИИ · ORGANISMO INTERNACIONAL DE ENERGIA ATOMICA

Selection and Program Committee — Comité de sélection et d'établissement du programme — Комитет по отбору докладов и разработке программы — Comité de Selección y del Programa

P. HUBERT ..... Chef du Service de recherches sur la fusion contrôlée, Commissariat à l'énergie atomique, France

K. V. ROBERTS ..... Theoretical Physics Division, Culham Laboratory, United Kingdom Atomic Energy Authority, United Kingdom

C. VAN ATTA ..... Associate Director, Lawrence Radiation Laboratory, University of California United States of America

Scientific Secretariat — Secrétariat scientifique — Научный секретариат — Secretaría Científica

B. BURAS ..... (*Co-ordinating Scientific Secretary*) Division of Research and Laboratories, International Atomic Energy Agency

P. A. DAVENPORT ..... (*Scientific Secretary*) Culham Laboratory, United Kingdom

C. ETIEVANT ..... (*Secrétaire scientifique*) Association Euratom — CEA, Service de recherches sur la fusion contrôlée, Fontenay-aux-Roses, France

W. F. GAUSTER ..... (*Scientific Secretary*) Oak Ridge National Laboratory, United States of America

Е. В. ПИСКАРЕВ ..... (*Ученый секретарь*) Институт атомной энергии им. И. В. Курчатова, Москва, СССР (E. V. PISKAREV)

B. TORKI ..... (*Assistant Scientific Secretary*) Division of Research and Laboratories, International Atomic Energy Agency

I. DRUTMAN ..... (*Technical Secretary*) Division of Research and Laboratories, International Atomic Energy Agency

Editors of "Nuclear Fusion" — Rédacteurs de la revue «Fusion Nucléaire» — Редакторы журнала «Ядерный синтез» — Redactores de "Fusión Nuclear"

J. G. BECKERLEY* ....
R. HOBART ELLIS, JR. ... } Division of Scientific and Technical Information, International Atomic Energy Agency

* Present address: MIT, Nuclear Engineering, 138 Albany St., Cambridge 39, Mass., USA

Executive Secretary — Secrétaire exécutif — Исполнительный секретарь — Secretario Ejecutivo

W. LISOWSKI ..... Division of Scientific and Technical Information, International Atomic Energy Agency

Conference Services — Services linguistiques — Обслуживание конференции — Servicios de la Conferencia

A. BERNSTEIN ..... (*Chief Interpreter*) International Atomic Energy Agency

L. S. LIEBERMAN ..... (*Records Officer*) International Atomic Energy Agency

Public Information — Information — Общественная информация — Información pública

P. FENT ..... (*Press Officer*) International Atomic Energy Agency

MISS M. NAPIER ..... (*Special Media Officer*) International Atomic Energy Agency

FOREWORD — AVANT-PROPOS — ПРЕДИСЛОВИЕ — PREFACIO

In 1958, at the Second United Nations Conference on the Peaceful Uses of Atomic Energy, the results of research on controlled nuclear fusion obtained in a few technically advanced countries were first disclosed to the world at large. Since then, it has become more and more evident that a better understanding of fundamental phenomena is needed before the goal of energy extraction from nuclear fusion may be reached. Consequently, the intensive research undertaken in recent years has been primarily basic research in plasma physics.

The fact that such research is most complex and costly has enhanced the desirability of co-operation and exchange of information and experience between all those engaged in this field of nuclear science and technology. It has become obvious that the International Atomic Energy Agency can play an important part in promoting such co-operation on a world-wide scale.

After consulation with a number of leading scientists, the Agency convened an international conference on Plasma Physics and Controlled Nuclear Fusion Research. The extent of the interest shown by Member States did not merely confirm that such a conference was actually needed at the present time, but greatly exceeded expectations. The quality and volume of the papers submitted, the number of participants and of countries represented, all bore witness to this interest.

Today, plasma physics and controlled thermonuclear fusion research is a more-or-less academic study. All that can be said at this stage is that it should eventually lead to a practical energy source. The day may come when the energy from nuclear fusion will be needed and when the well-being of mankind may depend on the ability to draw on this almost limitless reservoir.

The publication of the conference proceedings is intended to promote international co-operation and accelerate progress in this most important field of scientific endeavor.

INTRODUCTION – ВВЕДЕНИЕ – INTRODUCCIÓN

The Conference on Plasma Physics and Controlled Nuclear Fusion Research was held in Salzburg, Austria on 4—9 September 1961. More than 500 scientists, representing 29 nations and 6 international organizations, participated in the Conference. The Proceedings are published in three parts as a 1962 supplement to this journal.

Because of the many interconnections between the various problems of plasma physics, it was decided to have no parallel plenary sessions. Accordingly, nine sessions were held during the six days of the Conference. During these sessions, 111 papers were presented. The "free" afternoons and evenings were devoted to at least fourteen informal discussions of topics of special interest to the participants. The present Proceedings do not include the records of these informal discussions (the discussions would have ceased to be "informal" if recorded), although it seems certain that new ideas generated in these discussions will lead to publication of papers elsewhere.

"Part 1" contains the texts (in original language only) of all papers delivered in Sessions I, II and IV of the Conference, the records (in English) of the discussions of these papers, as well as the texts (in English and Russian) of the two concluding speeches by Prof. Artsimovich and Dr. Rosenbluth summarizing the Conference. Translations of the abstracts of each paper (Sessions I, II, IV) are given at the end of this part of the Proceedings. In addition there is an author index.

The remainder of the Proceedings is published in "Part 2" (Sessions III, V, VI, VIII) and in "Part 3" (Sessions VII, IX). The abstracts of those papers accepted but not presented to the Conference, a list of participants, subject and author indexes for the entire Proceedings are included in the third part.

In preparing the Proceedings the Editors gratefully acknowledge the substantial help of B. Buras, P. A. Davenport, C. Etievant, W. F. Gauster, W. A. Newcomb and E. V. Piskarev.

CONTENTS — SOMMAIRE — СОДЕРЖАНИЕ — INDICE

SESSION VII — SÉANCE VII — ЗАСЕДАНИЕ VII — SESIÓN VII

SESSION IX — SÉANCE IX — ЗАСЕДАНИЕ IX — SESIÓN IX

(Contents continued, next page)

SESSION VII — SÉANCE VII

ЗАСЕДАНИЕ VII — SESIÓN VII

8 September 1961 — 8 septembre 1961

8 сентября 1961 г. — 8 de septiembre de 1961

Chairman — Le président — Председатель — El Presidente

P. C. Thonemann (*United Kingdom*)

Scientific Secretary — Secrétaire scientifique — Ученый секретарь — Secretario Científico

P. A. Davenport (*United Kingdom*)

[Papers presented: CN-10/38, 47, 54, 57, 58, 60, 63, 68, 91, 96, 106, 150, 223, 224, 227, 238, 239, 241]

COMPARISON BETWEEN THEORY AND EXPERIMENT FOR THE STABILITY OF THE TOROIDAL PINCH DISCHARGE*

A. A. WARE

RESEARCH LABORATORY, ASSOCIATED ELECTRICAL INDUSTRIES

ALDERMASTON COURT, ALDERMASTON, BERKSHIRE, UNITED KINGDOM

A summary is given of the experimental observations which are relevant to the stability of the toroidal pinch discharge. This includes recent measurements on the wave velocity of fluctuations in the "Sceptre" experiments and the recent observation of steps on the magnetic field oscillograms with the torus at General Atomic. These results are first compared with the stability predictions based on the magneto-hydrodynamic (MHD) approximations (the energy principle). The experimental results indicate that of the MHD modes, only the interchange mode can be occurring with large amplitude in practice. Secondly, the stability predictions based on more accurate plasma equations are compared with experiment. These include the entropy waves discovered by Tserkovnikov and Kadomtsev and my prediction that the MHD modes move as waves. Lastly, it is shown that if instabilities keep $|\nabla p| \ll |\sigma_{\|} E_{\|} B|$, the rapid penetration of B_θ into the pinch discharge and the enhancement of B_z can be explained.

1. Introduction

The toroidal pinch discharge has been intensively studied over the past few years and many of its properties are now well known. A survey of these properties has been given elsewhere [1]; here (in Section 2 below) a summary is given of the properties relevant to stability.** Most notable of these is the gross stability of the discharge column, the discharge preserving itself in an approximately steady state for as long as the electric field is applied. Also included in the summary are the recent measurements [2, 3] of the propagation velocities of fluctuations in the discharge, and the discovery of steps on the magnetic field waveforms at the Kruskal limit and its harmonics [4].

Most treatments of the MHD stability of the pinch discharge assume that the currents are confined to a thin skin. Their results are not relevant to the toroidal pinch, since after the first few microseconds there is no skin effect. The maximum current density is, in fact, at the centre of the discharge. The more general energy principle [5] can be applied and in Section 3 its predictions are compared with experiment.

Since there are discrepancies between MHD theory and experiment, more accurate plasma equations must be considered. When higher-order terms are retained, two modifications to the stability predictions result. First, the MHD modes of instability will no longer be stationary but will propagate as waves [6]. Second, new modes of instability are possible [7, 8, 9] which have little effect on the magnetic field. KADOMTSEV [8] has given these modes the name "entropy waves." In Sections 4.1 and 4.2 these predictions are compared with the experimental results.

Among other unexplained properties of the toroidal pinch are the rapid penetration of B_θ into the plasma at the onset of the discharge, and the enhancement of B_z flux within the discharge. In Section 5 it is shown that if instabilities are assumed to keep the pressure gradient small so that $|\nabla p| \ll |\sigma_{\|} E_{\|} B|$, both these effects can be explained.

Throughout this paper all but one of the effects of the toroidal curvature are neglected, and cylindrical co-ordinates r, θ, z will be used to describe the discharge, the z-axis being taken parallel to the discharge tube. The one effect retained is the boundary condition that requires all properties of the discharge to be periodic in the z-direction with the torus circumference as the fundamental length.

2. Experimental properties of the toroidal pinch discharge

A summary is given below of the main properties of the toroidal discharge relevant to stability. The results refer in general to discharges for which the initial values of the toroidal field, namely B_{z_0}, lie within the approximate range from about a quarter to unity times the maximum value of B_θ generated at the tube wall. Above this range little pinch effect occurs and with B_{z_0} much below this range, if not before, the discharge is grossly unstable.

2.1 PENETRATION OF B_θ INTO THE DISCHARGE

Magnetic probe measurements have shown that B_θ penetrates into the discharge much more rapidly than predicted by electromagnetic theory [4, 10]. Kinks or steps are observed on the magnetic probe oscillograms [4], and it has been found that these occur

* Conference paper CN-10/47, presented by A. A. Ware. Discussion of this paper is given on page 1017. Translations of the abstract are at the end of this volume of the Conference Proceedings.

** This paper is restricted to instability frequencies ω small compared with the ion cyclotron frequency and to wavelengths comparable with or greater than the tube radius. Instabilities with higher frequencies and shorter wavelengths, such as ion waves and electron oscillations, have been the subject of considerable theoretical interest recently, but as yet there is no evidence for their existence (or absence) in the toroidal pinch discharge.

when the pitch of the magnetic lines of force, namely $\lambda_B = 2\pi r B_z / B_\theta$, satisfies $\lambda_B \approx L/n$ or $2L/n$ where n is an integer and L is the torus circumference. These steps appear to be associated with the penetration of B_θ, since during the time B_θ is remaining approximately constant over an outer region of the discharge, it is simultaneously increasing at smaller radii. Steps for a given value of λ_B occur later at smaller radii.

2.2 The steady state magnetic field configuration

The axial field B_z is enhanced in the discharge and its radial profile exhibits a characteristic bell shape [11, 12, 13] with a maximum at the centre of the discharge. (Since the enhancement persists for such long times with little change, it cannot be due to trapping of the field in the initial discharge constriction, and it is not explained by the paramagnetic effect of the anisotropic conductivity [11]. The corresponding profile for B_θ, when converted to axial current density, shows that j_z is a maximum at the centre of the discharge and falls off slowly with radius [11, 12, 13.] At a radius which is often about half the tube radius dB_θ/dr changes sign, and j_z is much smaller beyond this radius although j_θ is often still large.

Over the centre of the discharge the pitch of the magnetic lines of force is approximately constant [11] or varies only slowly with radius (see the published field profiles for Zeta [11], Perhapsatron S4 [14] and TA 2,000 [13], but near the walls B_z falls too rapidly with radius to maintain this condition (and sometimes goes negative), so that the pitch decreases appreciably in this region.

Among the slow toroidal pinch discharges, only in the case of Sceptre III has the plasma pressure deduced from the magnetic probes measurements been published [12]. The pressure is a maximum in the centre of the discharge and falls off with radius throughout the main core of the discharge. At approximately half the tube radius the pressure passes through a minimum and then rises towards the walls. A somewhat similar pressure profile was obtained for the faster discharge in Perhapsatron S4, except that the central maximum has a dip in it [14].

2.3 Discharge stability

With zero or low applied axial magnetic fields, the pinch discharge exhibits violent kink instability and large magnetic field fluctuations. Within the magnetic field range considered here this large amplitude kink instability no longer occurs [11, 15]. However, smaller magnetic field fluctuations remain whose amplitudes are usually in the range 10-20% of the unperturbed field [11, 12], and whose mean frequency is usually in the range $10^4 - 10^5$ Hz. On streak photographs light intensity variations are observed which sometimes show helical patterns and sometimes "bars" [15], these variations being correlated with the field fluctuations [16].

In the outer regions of the discharge the magnetic fluctuations often have a regular nature, and these have been identified as an $m=1$ perturbation [2]. (Discharge perturbations of the form $\exp i\,(\omega t - m\theta - kz)$ are considered.) These fluctuations generally propagate in the z direction with a velocity [2] of the order $+10^6$ cm/s. (The positive direction is taken parallel to the current). Observation of the fluctuations of light emitted from these regions (spectral lines from unionised atoms and singly-ionised impurities) showed similar velocities (see Table 3). This $m=1$ instability resembles the moving $m=1$ perturbations observed throughout the whole discharge at much lower currents by Allen [17], Baker *et al.* [18] and Rusbridge *et al.* [19]. In the first two of these references, Doppler shift measurements are reported which showed that a wave motion was involved and not a mass motion.

In the central region of the discharge the magnetic fluctuations were small and irregular, and no wave motion could be ascertained. Light from highly ionised particles in this region, however, showed fluctuations [3] with a wave velocity of about -5×10^6 cm/s.

3. Magnetohydrodynamic stability of the discharge core

The predictions of the MHD energy principle [5] regarding the stability of the discharge core, after field penetration is complete, have been considered by Ware [1]. Since the magnetic field has a constant

TABLE I. Properties of kink and interchange types of instability

	Interchange modes $(mB_\theta + krB_z = 0)$		*Kink modes* $(mB_\theta + krB_z \neq 0)$	
Condition for minimum change in potential energy (δW)	$\nabla \cdot \boldsymbol{\xi} = \dfrac{2B_\theta^2 \xi_r}{r(B^2 + \gamma p)}$	(1)	$\nabla \cdot \boldsymbol{\xi} = 0$	(5)
Stability condition	$\dfrac{dp}{dr} \geqslant -\dfrac{2\gamma p B_\theta^2}{\gamma(B^2 + \gamma p)}$	(2)	$\dfrac{dp}{dr} > \alpha^2 > 0$	(6)
Magnetic-field fluctuations	$\delta B_\theta \ll \xi_r \dfrac{r\,d(B_\theta/r)}{dr}$	(3)	$\delta B_\theta \approx r\xi_r \dfrac{d(B_\theta/r)}{dr}$	(7)
	$\delta B_z \ll \xi_r \dfrac{dB_z}{dr}$	(4)	$\delta B_z \approx \xi_r \dfrac{dB_z}{dr}$	(8)

(p is the pressure, γ the ratio of the specific heats (5/3) and α^2 is an undetermined positive quantity)

pitch, two types of MHD instability are possible, namely interchange modes and kink modes, depending on whether the helical perturbation has the same or a different pitch to the magnetic field. The properties of these two types of instability are summarised in Table 1 below. Normal mode displacements of the form $\xi = \xi\ (r)\ \exp i\ (\omega t - m\theta - kz)$ are considered.

The wavelength in the z direction for an interchange mode is λ_B/m, where λ_B is the pitch of the magnetic field, namely $2\pi r B_z/B_\theta$. For the kink modes the most unstable m value is 1 and the unstable wavelengths lie in a range extending above and below λ_B, the growth rate going to zero at the singular point within this range where $2\pi/k = \lambda_B$.

Since the experimental results show a substantial negative pressure gradient for the core of the discharge [12], the relation (6) of Table I predicts that the core should exhibit a gross kink instability. In the case of the interchange mode, to compare the predicted stability criterion, Table I, Eq. (2), with experiment it is necessary to know the plasma pressure. Since there is an unknown integration constant in the pressure deduced from the observed pressure gradient, it is more convenient to compare observed and predicted pressures in this case.

TABLE II. Comparison between experimental and theoretical pressures

Radius (cm)	Pressure observed by ALLEN and LILEY [12] (p_0 is the integration constant) (10^5 dynes/cm^2)	Pressure from (2) using observed pressure gradient, etc. (10^5 dynes/cm^2)	Percentage error with $p_0 = 1.3 \times 10^5$ dynes/cm^2 (%)
1	$1.04 + p_0$	2.9	+24
2	$0.84 + p_0$	2.19	+2
3	$0.56 + p_0$	2.28	+23
4	$0.30 + p_0$	1.32	+17
5	$0.10 + p_0$	0.68	−51
−1	$1.05 + p_0$	2.68	+14
−2	$0.90 + p_0$	2.33	+6
−3	$0.72 + p_0$	2.07	+2
−4	$0.52 + p_0$	1.66	−9
−5	$0.33 + p_0$	1.1	−32

In Table II, the second column shows the plasma pressures obtained experimentally by ALLEN and LILEY [12] for the discharge core. p_0, the integration constant, is the value of the pressure at $r = 6$ cm, the position of the pressure minimum. The third column shows the pressures calculated from the equality in (2) (of Table I) using the observed values for dp/dr, B_θ and B_z. The last column shows the percentage difference between the two pressures if p_0 is taken as 1.3×15^5 dynes/cm^2, the value for best fit. Assuming that this is the correct value for p_0, the agreement between theory and experiment is as good as can be expected, since dp/dr will have a large experimental error.

The range of other values which could be taken for p_0 is limited from other considerations. Thus, the lowest possible value for p_0 is zero; this would make the observed negative pressure gradients twice (at $r = 2$ cm) to six times (at $r = 5$ cm) the allowable gradient for interchange stability. The upper limit for p_0 cannot be much higher than the value taken, since the integral $\int 2\pi r p\ dr$ already leads to a value of N which is several times the initial gas filling [12] even if the mean ion temperature is taken as high as $10^{6\circ}$K. (N is the number of particles per unit length of the discharge.) These considerations, therefore, suggest that the plasma pressure must be such that the negative pressure gradient is of the same order as, or somewhat greater than, the value for marginal interchange stability.

In the experimental results [12] for Sceptre III, dB_z/dr is approximately $-B_z/r$ at $r = 6$ cm and hence the expected percentage fluctuation for B_z in a kink mode instability is $100\ \xi_r/r$. Since the observed fluctuations are only 15%, this means ξ_r cannot be greater than about $0.15r \approx 1$ cm or about 6% of the tube radius. On the other hand, the interchange instability, which produces only small changes in the magnetic field, could be occurring with large amplitude. Since other workers with slow pinch discharges have observed only small fluctuations, this last conclusion must be general for such discharges.

The above results indicate that the kink instability either is not occurring in the pinch-discharge core or, at most, is occurring with only small amplitude. This reveals an apparent discrepancy between experiment and the predictions of MHD stability theory. Secondly, the observed pressure gradient suggests that the interchange instability is occurring and is limiting the negative pressure gradient to a value close to that for marginal stability with these modes.

Some possible causes for the small (or zero) amplitude of the kink mode have been discussed elsewhere [1]. These include (a) the higher-order terms omitted from the MHD equations, since the ion Larmor radius is not negligible compared with the discharge radius, and (b) the possible presence in the discharge of a large number of deuterons moving with high velocities parallel to the magnetic field so that they experience a frequency just above their cyclotron frequency. Such particles would have a stabilising effect on kink modes.

It should be noted that the above results and discussion refer only to the discharge core. In the annular region between the core and the walls an $m = 1$ perturbation has been observed [2], which could be a kink instability which has grown to a limited amplitude and then been stabilised by higher-order effects.

The steps observed on the magnetic probe oscillograms during the growth and decay of the current could be due to either changes in wavelength of an interchange instability or a kink instability. A study of the work of TAYLER [20] indicates that a discharge with uniform j_z and B_z which fills the whole tube is unstable to an $m = 1$ kink mode only for a narrow range of wavelengths $2\pi/k$ immediately above λ_B. Wavelength transitions would therefore be expected

at values of λ_B which are just below L/n. For interchange modes to occur, the field must have approximately constant pitch and the lines of force must join on themselves. The latter condition is satisfied when $\lambda_B = mL/n$, when an m type interchange is possible. It seems likely that an interchange mode would tend to keep the magnetic pitch constant over the annular region in which it was occurring. Hence steps would occur on the magnetic field waveforms for $\lambda_B = mL/n$. The annular region in which a given interchange is occurring might move radially inwards as the current is increased. This would explain why the steps are observed later at smaller radii. This latter property suggests that the interchange modes are the cause rather than kink modes.

4. The stability predictions of more accurate plasma equations

4.1 MHD instability waves

In the case of a plasma whose particle-collision frequencies are greater than the instability frequency ω (so that the particle pressures are approximately isotropic) and whose electron-collision frequency is small compared with the electron cyclotron frequency, the electric conduction equation [21] is

$$\mathbf{E} + \mathbf{V} \times \mathbf{B} - \frac{\mathbf{j} \times \mathbf{B}}{ne} - \frac{\nabla p_e}{ne} = 0 \qquad (9)$$

($\mathbf{E}$ is the electric field, $\mathbf{V}$ the plasma velocity, n the particle density, $\mathbf{j}$ the current density and p_e the electron pressure).

If
$$\varrho/L \ll 1 \qquad (10)$$

and
$$\omega^2 L^2 \gtrsim \mathrm{k}\, T_i/M, \qquad (11)$$

where ϱ is the ion Larmor radius, L is the characteristic length of the discharge or the instability, T_i the ion temperature and M the ion mass, the third and fourth terms in Eq. (9) are small compared with either of the first two terms [5]. Because of this, the approximate equation $\mathbf{E} + \mathbf{V} \times \mathbf{B} = 0$ has been widely used in stability theory. When it is combined with the other plasma equations involving the MHD approximations, the predicted values for ω^2 are always real [5], and an instability perturbation ($\omega^2 < 0$) will grow continuously in time with no oscillations or wave motion involved.

However, neither of the conditions (10) and (11) are good approximations for many pinch discharge experiments. When the last two terms are retained in Eq. (9) ω^2 is no longer always real, and an instability perturbation will move as a wave [6]. A physical picture of this wave motion can be obtained by considering the "freezing-in" of magnetic lines of force in the plasma. By combining Eq. (9) with Maxwell's equation for $\nabla \times \mathbf{B}$ and the appropriate continuity equation, assuming $T_e \ll T_i$, the magnetic field is found to be frozen to the electrons [6] and not to the mean motion of the plasma. Both the unperturbed and the fluctuating components of the electron velocity will, in general, cause the instability magnetic field fluctuations to propagate, but experimentally there is evidence that the effect of the unperturbed electron motion predominates [6]. If this is the case, the wave velocity with which a helical instability will propagate in the z direction is

$$V_w \approx -\frac{1}{ne}\left(j_z - \frac{m j_\theta}{kr}\right) \qquad (12)$$

(The assumption has been made that there is no mass motion in the discharge, so that the mean electron velocity is given approximately by $\mathbf{j}/ne$.)

In the special case where the instability crests are parallel to $\mathbf{B}$, as in the case of an interchange mode or a kink mode with small δk, the wave velocity reduces to [6]

$$V_w = \frac{1}{ne B_\theta}\frac{\mathrm{d}p}{\mathrm{d}r} \qquad (13)$$

In Table III, the next-to-last column shows the velocity in the z-direction with which fluctuations have been observed to propagate in various toroidal discharge experiments and in the straight tube Columbus T. In order to obtain a theoretical propagation velocity from Eq. (12) or Eq. (13), it is necessary to know the wave numbers m, k, the density n and either the current densities j_θ and j_z, or the pressure gradient and B_θ. Where these are known, or where a rough estimate can be made, the values are shown in the appropriate columns in Table III and the last column shows the theoretical propagation velocity deduced from them. For the discharge core in Sceptres III and IV the instability is assumed to be an interchange mode (see Section 3 above) and the pressure gradient is taken from Allen and Liley [12]. In the case of the outer region of Sceptre IV the fluctuations were very irregular and were observed to propagate sometimes in one direction and sometimes in the opposite direction. As in the case of the core fluctuations for Sceptres III and IV the values of m and k were not obtained because of the irregularity of the fluctuations.

It can be seen from Table III that the present theory gives the correct direction of propagation in every case where a theoretical value was possible, and also the right order of magnitude for the velocity.

4.2 Entropy waves

By using plasma equations which retain higher order terms in the parameter ϱ/L, several Russian workers (Tserkovnikov [7], Kadomtsev [8] and Rudakov and Sagdeev [9]) have shown that, in addition to the MHD modes, new modes of instability are possible. They have taken a simple pinch discharge with $B_z = 0$ and considered only $m = 0$ perturbations. In particular Kadomtsev has used Eq. (9), together with thermal-energy equations which are more accurate than the simple adiabatic relation of the MHD approximation, and has found an instability whose growth rate has an order of magnitude which is ϱ/L times the MHD growth rates. If the negative

TABLE III

Experiment	Region of discharge	Particle density (cm^{-3})	$2\pi/k$ (cm)	m	Mean value of $j_z - mj_\theta/kr$ (amp)	$\frac{dp}{dr}$ (dynes/cm^3)	B_θ (G)	Propagation velocity of fluctuations (cm/s)	
								Experiment	Theory
Glass torus	Whole[a]	—	15	1	—	—	—	-10^6	—
Columbus T	Whole[b]	$\sim 4\times10^{14}$	15	1	+26	—	—	-2×10^5	-4×10^5
Sceptre III	Core[c]	$\sim 5\times10^{14}$	λ_B/m (assumed)	—	—	-2×10^4	10^3	-3×10^5 to -3×10^6	-2×10^6
	Outer region[d]	$\sim 5\times10^{14}$	67	1	−390	—	—	$+5\times10^5$ to $+4\times10^6$	$+5\times10^6$
Sceptre IV	Core[c, e]	$\sim 5\times10^{14}$	λ_B/m (assumed)	—	—	-2×10^4	10^3	-10^6 to -4×10^6	-2×10^6
	Outer region[c, f]	—	—	—	—	—	—	$\pm5\times10^5$ to $\pm4\times10^6$	—
Mark IV	Whole[g]	2×10^{13}	50	1	+2.2	—	—	-4×10^5	-7×10^5

(a) ALLEN, T. K. [17]; (b) BAKER, *et al.* [18]; (c) WILLIAMS, R. V. [22]; (d) ALLEN, N. L. [2]; (e) WILLIAMS, R. V. [3]; (f) ALLEN, N. L. [23]; (g) RUSBRIDGE, *et al.* [19].

pressure gradient exceeds that given by Eq. (2) with B put equal to B_θ, the stability condition is

$$\frac{d\ln T}{d\ln r} \geqslant 1 + \left(\frac{7}{10} + \frac{\beta}{4}\right)\frac{d\ln p}{d\ln r}, \qquad (14)$$

where $\beta = 8\pi p/B_\theta^2$.

This instability involves different displacements (ξ_i, ξ_e) for the ions and the electrons, and these occur in such a manner that the fluctuations in p, **B** and **j** are small. The main quantities which vary in first order are n, T_e and T_i, hence these instabilities have been given the name "entropy waves". Kadomtsev has taken the unperturbed values of T_e and T_i to be equal, and in this case the fluctuations propagate with half the velocity given by Eq. (13). (Eq. (13) was derived assuming $T_e \ll T_i$.)

It can be shown [24] that in the case of a discharge with B_z, and with constant-pitch lines of force, the equations for instability modes with the same pitch as the field are very similar to those for the particular case considered by Kadomtsev with $m=0$, $B_z=0$. The only differences are that the wave number k is replaced by $[k^2+m^2/r^2]^{1/2}$ and one term contains the extra factor B_θ^2/B^2. It is believed that a stability condition similar to (14) will result with $\beta = 8\pi p/B^2$.

The stability condition (14) is not very enlightening; however, if the faster-growing MHD interchange modes are assumed to have reduced the pressure gradient to the value for marginal stability [Eq. (2)], the condition (14) reduces to the more transparent form

$$\frac{1}{T}\frac{dT}{dr} \geqslant \frac{2}{5}\frac{1}{p}\frac{dp}{dr} \quad \text{or} \quad \frac{1}{T}\frac{dT}{dr} \geqslant \frac{2}{3}\frac{1}{n}\frac{dn}{dr} \qquad (15)$$

This is the same condition as the well known stability condition for thermal convection in a gravitational field. This and other considerations suggest that the entropy waves are a form of thermal convection.

Since the marginal stability condition (2) for the MHD interchange modes can be rewritten in the form

$$\frac{1}{p}\frac{dp}{dr} = \frac{5}{3}\frac{1}{B_z}\frac{dB_z}{dr} \qquad (16)$$

the marginal stability conditions for both entropy waves and MHD interchange modes, and the constant pitch condition can be summarised as follows

$$\frac{r}{B_\theta}\frac{d(B_\theta/r)}{dr} = \frac{1}{B_z}\frac{dB_z}{dr} = \frac{3}{5}\frac{1}{p}\frac{dp}{dr} = \frac{3}{2}\frac{1}{T}\frac{dT}{dr}\left(=\frac{1}{n}\frac{dn}{dr}\right). \qquad (17)$$

A preliminary study suggests that in the case when the unperturbed electron and ion temperatures are unequal, each temperature gradient must satisfy relation (15) separately.

Lastly a strange coincidence in the constants of nature must be pointed out. In a discharge in a steady state such that $E_\theta = 0$ and E_z is a constant with respect to radius, from Maxwell's equation for $\nabla\times\mathbf{B}$, and the relation $j_\parallel = \sigma_\parallel E_\parallel$ (where σ is the electrical conductivity and the subscripts refer to the components parallel to **B** in each case) it follows that constant pitch requires

$$\frac{1}{B_z}\frac{dB_z}{dr} = \frac{1}{\sigma_\parallel}\frac{d\sigma_\parallel}{dr} \qquad (18)$$

and hence for completely ionised hydrogen

$$\frac{1}{B_z}\frac{\mathrm{d}B_z}{\mathrm{d}r} = \frac{3}{2}\frac{1}{T_e}\frac{\mathrm{d}T_e}{\mathrm{d}r} \tag{19}$$

This is identical with the condition for marginal stability for the entropy wave. It is a coincidence since here the factor 3/2 arises from Coulomb scattering, whereas in the stability condition it arises because of the ratio of the specific heats. It suggests that the constant-pitch configuration may arise as a result of the entropy waves. Also, provided the MHD kink instability does not occur, it suggests that a discharge satisfying equations (17) will maintain itself in a steady state indefinitely as long as the electric field is applied.

5. Field penetration and enhancement

5.1 The conductivity of a plasma perpendicular to a magnetic field

In a plasma in equilibrium, currents flow perpendicular to the magnetic field only if there is a pressure gradient, since $\mathbf{j}\times\mathbf{B}=\nabla p$. If, therefore, instabilities in a discharge prevent the generation of an appreciable pressure gradient, $j_\perp$ will remain small. In particular if the pressure gradient is limited such that

$$\left|\frac{\mathrm{d}p}{\mathrm{d}r}\right| \ll |\sigma_\parallel E_\parallel B| \tag{20}$$

then

$$|j_\perp| \ll |j_\parallel| \tag{21}$$

and the plasma will behave approximately as if it has zero conductivity perpendicular to the magnetic field. In the case of the experimental pressure gradient considered in Section 3 the highest value of $|\,\mathrm{d}p/\mathrm{d}r\,|$ was about a quarter of $|\,\sigma_\parallel E_\parallel B\,|$.

When condition (21) is satisfied the components of Maxwell's curl **B** equation for a cylindrically symmetric discharge reduce to

$$\frac{1}{r}\frac{\partial(rB_\theta)}{\partial r} = 4\pi\sigma_\parallel\left(E_z\frac{B_z^2}{B^2}+E_\theta\frac{B_\theta B_z}{B^2}\right) \tag{22}$$

$$-\frac{\partial B_z}{\partial r} = 4\pi\sigma_\parallel\left(E_z\frac{B_\theta B_z}{B^2}+E_\theta\frac{B_\theta^2}{B^2}\right) \tag{23}$$

5.2 The enhancement of B_z

The solution of Eqs. (23) and (24) for the conditions corresponding to the steady-state pinch discharge at peak current will be considered first. Since the components of $\partial\mathbf{B}/\partial t$ are small, E_z is approximately constant with respect to radius and $E_\theta \ll E_z$. Eqs. (22) and (23) have therefore been solved on a computer for E_z = constant, $E_\theta = 0$ and also $\sigma_\parallel$ assumed constant. Example solutions for B_θ and B_z are shown in a dimensionless form in Fig. 1. The scaling factor $B_{\theta w}$ is the value of B_θ at the edge of the discharge and the pairs of curves are for various values of B_z at the tube wall (B_{zw}).

The enhancement of B_z within the discharge for low values of B_{zw} at the wall is very marked. Secondly, it should be noted that for low B_{zw} there is a fairly abrupt change of $\mathrm{d}B_\theta/\mathrm{d}r$ within the discharge, indicating a small j_z beyond this radius. In the past, experimenters have been inclined to interpret such a change of slope as the edge of the discharge. The present theory shows that it could be due to the anisotropic conductivity in a uniform plasma.

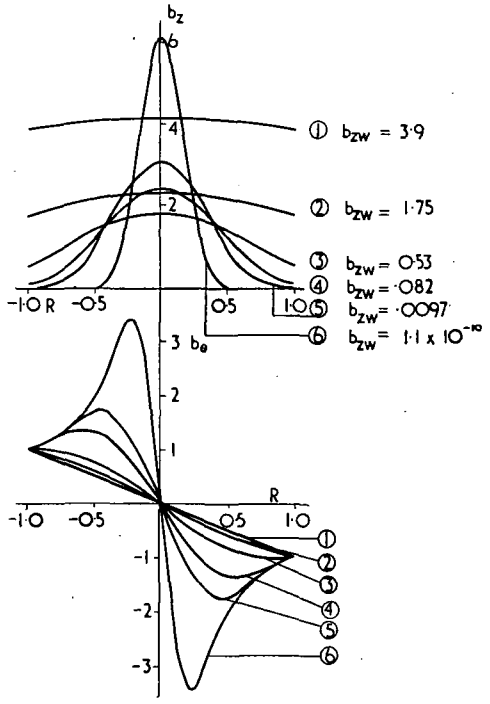

Fig. 1 Example solutions of Eqs. (22) and (23) for the values of b_{zw} indicated ($b_z = B_z/B_{\theta w}$, $b_\theta = B_\theta/B_{\theta w}$, $R = 4\pi\sigma_\parallel E_z r/B_{\theta w}$ and the subscript w denotes the value at the tube wall).

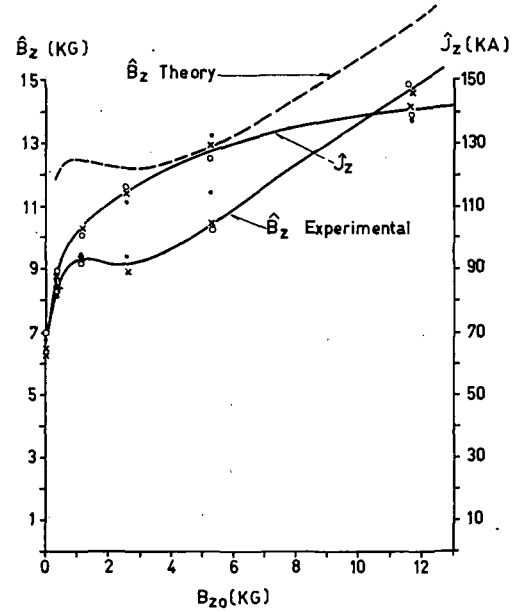

Fig. 2. Comparison between theoretical and experimental values for $\hat{B}_z$, which is the value of B_z at the centre of the discharge. The abscissa B_{z0}, is the value of B_z at the tube wall since in these experiments this field remained approximately equal to the initial field. The peak gas current, J_z, is shown for comparison.

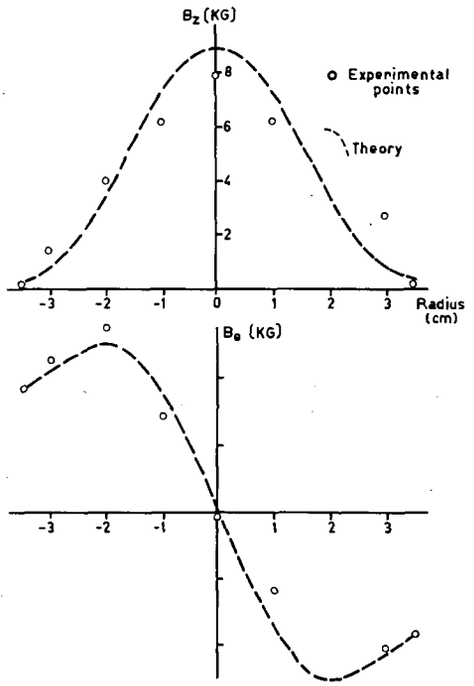

Fig. 3 Comparison between theory and experiment for the radial variation of B_z and B_θ.

In Fig. 2 the enhancement of B_z is compared with the experimental results of WARE *et al.* [4]; the observed and theoretical values of B_z at the centre of the discharge (namely B_z) are plotted against B_{z0}, the initial field. (In this experimental work the coil producing the initial B_z had a high-impedance source, and the value of B_z at the tube wall (B_{zw}) remained approximately equal to the initial value B_{z0}.) Qualitatively, the shape of the theoretical curve agrees very well with experiment; even the small bump at $B_{z0}=1$ kG is reproduced. Quantitatively the predicted fields are higher than the observed fields, the error varying from 13% at 12 kG to 40% at 300 G.

In Fig. 3 theoretical profiles for B_z and B_θ are compared with the experimental measurements of B_z and B_θ across the tube for a low B_{zw} case. It can be seen that there is reasonably good agreement in the magnitude of both B_θ and B_z at all radii.

Since the theoretical values of B_z exceed the observed values, the theory is an adequate explanation of the enhancement of B_z. The fact that the observed enhancement of B_z is less than that predicted by theory is probably due to the fact that $\mathrm{d}p/\mathrm{d}r$ and $\mathrm{d}\sigma_\parallel/\mathrm{d}r$ are not accurately zero, as assumed in the theory, but have small negative values.

In experiments where the metal sheath is continuous in the θ-direction, the general shape of the magnetic-field profiles is again given, as has been pointed out by LEES and RUSBRIDGE [10], but the fact that B_z goes negative close to the tube wall is not explained.

5.3 THE PENETRATION OF B_θ

To predict the rate of penetration of B_θ Eqs. (22) and (23) must be solved simultaneously with Maxwell's equation for curl **E**. This has not yet been carried out, but the following qualitative discussion shows that a more rapid penetration is predicted for low B_{z0}.

First, for $B_z \gg B_\theta$ the term containing E_θ in Eq. (22) will be small and the first term will be approximately equal to $4\pi\sigma_\parallel E_z$. In this case, therefore, B_θ will penetrate at the same rate as into a normal conductor with isotropic conductivity $\sigma_\parallel$. At low B_z, however, the effective conductivity in the first term in Eq. (22) will be reduced by the factor $B_z^2/B^2 \approx B_z^2/B_\theta^2$ and hance as far as this term is concerned the penetration will be more rapid. Further, since B_z is increasing in the discharge, E_θ will have a negative value and will make the second term in Eq. (22) negative. Hence, at any instant of time when the values of B_θ, B_z and $\partial B_\theta/\partial r$ are given, E_z must have a larger value in order to satisfy Eq. (22). That is, the effect of the second term is to make $\partial B_\theta/\partial t$ larger. Both terms, therefore, have the effect of causing a more rapid penetration of B_θ.

6. Conclusions

1. The value of the pressure gradient, and the smallness of the magnetic fluctuations, in the core of the high current toroidal discharge, are evidence that only the interchange mode of MHD instability can be occurring with large amplitude, although MHD theory predicts that the kink modes should be unstable.

2. In the outer regions of the discharge there is an $m=1$ kink distortion which has reached a certain amplitude and ceased to grow, but moves along the tube.

3. More accurate plasma equations than the MHD approximations show that for $T_e \ll T_i$ the magnetic field is trapped to the electrons and, in general, instabilities will propagate as waves. Observations on the propagation of fluctuations in the discharge, and the $m=1$ distortion in particular, show that the correct direction of propagation and the right order of magnitude for the wave velocity are predicted.

4. The Russian workers have shown that the more accurate plasma equations lead to new modes of low-frequency instabilities (entropy waves). If the pressure gradient is close to the value for marginal stability against interchange modes [$\mathrm{d}\ln p/\mathrm{d}r = \gamma\,\mathrm{d}\ln B_z/\mathrm{d}r$] the new modes are stable when $\mathrm{d}\ln T/\mathrm{d}r \geqslant (2/5)\,\mathrm{d}\ln p/\mathrm{d}r$ [i.e. $\mathrm{d}\ln T/\mathrm{d}r \geqslant (2/3)\,\mathrm{d}\ln B_z/\mathrm{d}r$] which is identical with the well-known stability condition for thermal convection.

5. The marginal stability condition for the entropy waves is the same as the condition for a constant-pitch magnetic field in a steady-state discharge for which the electrical conductivity parallel to **B** is proportional to $T_e^{3/2}$. The entropy waves may therefore be the cause of the observed constant configuration in the discharge core.

6. If instabilities keep $|\nabla p| \ll |\sigma_\parallel E_\parallel B|$, the plasma will behave approximately as if it has zero electrical conductivity perpendicular to **B**, and the enhancement of B_z and the rapid penetration of B_θ can be explained.

Acknowledgements

The work reported in Sections 3, 4.2 and 5 was undertaken while the author was on leave of absence at the John Jay Hopkins Laboratory for Pure and Applied Science, General Atomic Division of General Dynamics Corporation, San Diego, California, and the author gratefully acknowledges the assistance of discussions with Marshall Rosenbluth, Donald Kerst, Norman Rostoker and other colleagues at that laboratory. The author also thanks Bruce Liley and other colleagues at Associated Electrical Industries Research Laboratory, for helpful discussions, Norman Allen and Roy Williams for permission to include unpublished results in Table III, and Dr. T. E. Allibone, C.B.E., F.R.S., Director of the Laboratory, for permission to publish this paper. Part of the work at the Associated Electrical Industries Research Laboratory was done under contract to the Atomic Energy Research Establishment, Harwell.

References

[1] WARE, A. A., *Phys. Rev.* **123** (1961) 19.
[2] ALLEN, N. L., *Nature* **187** (1960) 279.
[3] WILLIAMS, R. V., *J. nucl. Energy, Part C* **3** (1961) 31.
[4] WARE, A. A., FORSEN, H. K., SCHUPP, A. A., *Phys. Rev.* **125** (1962) 417.
[5] BERNSTEIN, I. B., FRIEMAN, E. A., KRUSKAL M. D., KULSRUD, R. M., *Proc. Roy. Soc.* (*London*) **A244** (1958) 17.
[6] WARE, A. A., *J. nucl. Energy, Part C*, **3** (1961) 93.
[7] TSERKOVNIKOV, Yu. A., *Zh. exp. teor. Phys.* (*USSR*) **32** (1957) 67.
[8] KADOMTSEV, B. B., *Zh. exp. teor. Phys.* (*USSR*) **37** (1959) 1096.
[9] RUDAKOV, L. I., SAGDEEV, R. Z., *Zh. exp. teor. Phys.* (*USSR*) **37** (1959) 1337.
[10] LEES, D. J., RUSBRIDGE, M. G., Proc. 4th Conf. Ionisation Phenomena in Gases (Uppsala 17—21 Aug. 1959) **2** North Holland Publ. Co., Amsterdam (1960) 876.
[11] BUTT, E. P., *et al.*, in Proc. 2nd U.N. Intern. Conf. PUAE **32** United Nations, Geneva (1958) 42.
[12] ALLEN, N. L., LILEY, B. S., in proceedings of Ref. 10, **2**, 937.
[13] ETIEVANT, C., *et al.*, in proceedings of Ref. 10, **2**, 967.
[14] CONNOR, J. P., *et al.*, in proceedings of Ref. 11, **32**, 297.
[15] ALLIBONE, T. E., CHICK, D. R., THOMSON, G. P., WARE, A. A., in proceedings of Ref. 11, **32**, 169.
[16] WARE, A. A., in proceedings of Ref. 10, **2**, 931.
[17] ALLEN, T. K., in Proc. 3rd Intern. Conf. Ionisation Phenomena in Gases, (Venice, 11—15 June 1957), **1**, North Holland Publishing Co., Amsterdam (1959) 40.
[18] BAKER, D. A., SAWYER, G. A., STRATTON, T. E., in proceedings of Ref. 11, **32**, 34; SAWYER, G. A., SCOTT, P. L., STRATTON, T. F., *Phys. Fluids* **2** (1959) 47.
[19] RUSBRIDGE, M. G. *et al.*, *J. nucl. Energy, Part C*, **3** (1961) 98.
[20] TAYLER, R. J., *Proc. Phys. Soc.* (*London*) **70** (1957) 1049.
[21] SPITZER, L., Jr., Physics of Fully Ionised Gases (Interscience, New York, 1956) 21.
[22] WILLIAMS, R. V., to be published.
[23] ALLEN, N. L., to be published.
[24] WARE, A. A., to be published.

THE INFLUENCE OF THE HALL EFFECT ON A SIMPLE HYDROMAGNETIC STABILITY PROBLEM*

R. J. TAYLER

CULHAM LABORATORY

CULHAM, BERKSHIRE, UNITED KINGDOM

One factor that is commonly neglected in hydromagnetic stability problems is the Hall effect. It has been pointed out that, with the introduction of this term in the generalized Ohm's law, the differential equations governing the problem are no longer self-adjoint. Thus complex growth rates can be expected to occur, and ordinary instabilities may be replaced by instability waves (overstability). However, most of the arguments have been qualitative rather than quantitative.

In the present paper an exact solution is given for one very simple problem in which the Hall current is included. This is the stability of an incompressible conducting fluid containing a uniform axial magnetic field and a uniform axial current density and filling a conducting tube. For this problem it is shown that overstability does occur but that the system including the Hall effect is never overstable when the system without the Hall effect is stable. In addition, when overstability occurs, the real part of the growth rate is smaller than it is when the Hall effect is absent; thus the instability waves grow more slowly than the original instabilities. If the ion gyration frequency is much less than the characteristic hydromagnetic frequency the band of unstable wavenumbers becomes very small.

1. Introduction

Recently WARE [1] has suggested that an important factor that has been overlooked in many stability investigations is the Hall effect. He suggests that when the Hall effect is included, the pure instability predicted by the idealized hydromagnetic equations will be replaced by an instability wave (overstability). Furthermore he suggests that the approximate wave velocity will be the component of the electron drift velocity perpendicular to the instability. He points out that in many experiments such instability waves are observed and that their wave velocities are in reasonable agreement with simple theory.

The simplest argument for waves of this type is that the equation

$$\mathbf{E}+\mathbf{v}\times\mathbf{B}/c=0\,, \tag{1.1}$$

is not an adequate approximation to Ohm's law. This equation predicts that the magnetic field lines are tied to the motion of the material whereas the equation

$$\mathbf{E}+\mathbf{v}\times\mathbf{B}/c-\mathbf{j}\times\mathbf{B}/n\,e\,c=0 \tag{1.2}$$

which is the next approximation to Ohm's law in a low-pressure plasma, implies that the magnetic field is tied to the motion of the electrons. Thus, if an equilibrium is considered in which a current flows so that the electrons have an appreciable zero-order drift velocity relative to the ions, there is a probability that any perturbations in the magnetic field will be convected with the drift velocity of the electrons.

In Ware's paper no problem is solved exactly. It seems worthwhile to give a complete solution of one very simple problem for which the equations can be solved and that is the object of the present paper. The configuration considered is a very simple one which has been much studied previously [2, 3]. A conducting fluid fills a conducting cylindrical tube and contains a uniform axial magnetic field and a uniform axial current density. To obtain exact results the conducting fluid is taken to be incompressible; this should not be serious as it should be possible to study the effects of compressibility and the Hall effect independently.

The results obtained in the present paper are as follows:

1. If the system was previously stable, it is not made unstable by the introduction of the Hall effect.

2. If the system was previously unstable it may now be stable; otherwise the pure instability is replaced by an instability wave. The band of unstable wavenumbers rapidly becomes very small when the ion gyration frequency is much less than the characteristic hydromagnetic frequency (c_H/r_0).

3. As long as overstability occurs, the ratio of the phase velocity of the wave to the electron drift velocity is independent of the ion gyration frequency. An upper limit to the phase velocity is half the electron velocity but this is not usually attained. At the moment detailed numerical results have only been obtained for axisymmetric perturbations; further results are being obtained and will be reported in detail elsewhere. It must be stressed that results have only been obtained for one specially simple problem and have not been shown to have greater generality.

Although the problem as posed has been completely solved, the range of validity of the solutions is not clear. It will be seen later that the condition for the Hall-effect term to be of any importance is that the

* Conference paper CN-10/63, presented by R. J. Tayler. Translations of the abstract are at the end of this volume of the Conference Proceedings.

ion gyration frequency is relatively small; this is to be expected because Eq. (1.1) can be derived from the collisionless Boltzmann equation as a first approximation when the gyration frequency is large (see e.g. [4]). When the gyration frequency is low, the derivation of hydrodynamic equations is much more difficult and a complete treatment must involve much more than the mere introduction of the Hall effect. However, it may be that some of the qualitative effects of finite gyration frequency are included in the present paper; for example result 2 (above) suggests that the introduction of the Hall effect has a strong stabilizing influence on low-density systems.

2. Derivation of dispersion relation

The set of hydromagnetic equations including the Hall effect is

$$\varrho \frac{\mathrm{d}\mathbf{v}}{\mathrm{d}t} = -\nabla p + \frac{\mathbf{j}\times\mathbf{B}}{c}, \tag{2.1}$$

$$\nabla\cdot\mathbf{v}=0, \tag{2.2}$$

$$\mathbf{E} + \frac{\mathbf{v}\times\mathbf{B}}{c} - \frac{1}{ne}\nabla p_\mathrm{i} - \frac{M}{e}\frac{\mathrm{d}\mathbf{v}}{\mathrm{d}t} = 0, \tag{2.3}$$

$$\nabla\times\mathbf{B} = \frac{4\pi}{c}\mathbf{j}, \tag{2.4}$$

$$\nabla\times\mathbf{E} = -\frac{1}{c}\frac{\partial\mathbf{B}}{\partial t}, \tag{2.5}$$

$$\nabla\cdot\mathbf{B}=0, \tag{2.6}$$

$$\nabla\cdot\mathbf{E}=4\pi\varepsilon, \tag{2.7}$$

where $\mathbf{E}$, $\mathbf{B}$, $\mathbf{j}$ and $\mathbf{v}$ are the electric field, magnetic field, current density and fluid velocity. p is the total pressure, p_i the ion pressure and ϱ the density of the fluid. M is the ion mass, e the magnitude of the electronic charge and n is the density of either species of particle; their difference in density, which is small, is determined by Eq. (2.7), ε being the electric charge density. Displacement currents and the force exerted by the electric field are neglected. An alternative form of Eq. (2.3) is

$$\mathbf{E} + \frac{\mathbf{v}\times\mathbf{B}}{c} - \frac{\mathbf{j}\times\mathbf{B}}{nec} + \frac{1}{ne}\nabla p_\mathrm{e} = 0, \tag{2.8}$$

where p_e is the electron pressure.

In equilibrium an incompressible fluid of density ϱ_0 (particle densities n_0) fills a tube of radius r_0. The fluid contains a magnetic field $(0, B_0\, r/r_0, B_0 b)$. The pressure profile is

$$p = p_1 - B_0^2\, r^2/4\pi\, r_0^2 \tag{2.9}$$

and there is a radial electric field balanced by the ion pressure gradient. There is no need to specify the relation between the electron and the ion pressure for purposes of the stability problem. It is, however, necessary that the radial electric field and the resultant charge density should be small enough to be neglected in the equation of motion (2.1).

Perturbations are now considered in which any physical variable has the form

$$q = q_0 + q_1 \exp \mathrm{i}\,(m\theta + kz + \nu t). \tag{2.10}$$

The full set of linearised equations is

$$\mathrm{i}\nu\varrho_0\mathbf{v}_1 = -\nabla p_1 + (\nabla\times\mathbf{B}_1)\times\frac{\mathbf{B}_0}{4\pi} + (\nabla\times\mathbf{B}_0)\times\frac{\mathbf{B}_1}{4\pi}, \tag{2.11}$$

$$\nabla\cdot\mathbf{v}_1 = \nabla\cdot\mathbf{B}_1 = 0, \tag{2.12}$$

$$\nabla\times\mathbf{E}_1 = -\mathrm{i}\nu\mathbf{B}_1/c, \tag{2.13}$$

$$\mathbf{E}_1 + \frac{\mathbf{v}_1\times\mathbf{B}_0}{c} - \frac{M\nabla p_{\mathrm{i}_1}}{e\varrho_0} - \frac{\mathrm{i}\nu M\mathbf{v}_1}{e} = 0. \tag{2.14}$$

Taking the curl of Eq. (2.11) leads to

$$\mathrm{i}\nu\,\varrho_0\nabla\times\mathbf{v}_1 = \frac{\nabla\times[(\nabla\times\mathbf{B}_1)\times\mathbf{B}_0]}{4\pi} + \frac{\nabla\times[(\nabla\times\mathbf{B}_0)\times\mathbf{B}_1]}{4\pi}, \tag{2.15}$$

and Eq. (2.13) and (2.14) combine to give

$$\mathrm{i}\nu\mathbf{B}_1 = \nabla\times(\mathbf{v}_1\times\mathbf{B}_0) - \frac{\mathrm{i}\nu Mc}{e}\nabla\times\mathbf{v}_1. \tag{2.16}$$

With the special form for $\mathbf{B}_0$, expressions for $\nabla\times[(\nabla\times\mathbf{B}_1)\times\mathbf{B}_0]$, $\nabla\times[(\nabla\times\mathbf{B}_0)\times\mathbf{B}_1]$ and $\nabla\times(\mathbf{v}_1\times\times\mathbf{B}_0)$ can be obtained and these can be substituted into Eq. (2.13) and (2.14) to yield

$$\mathrm{i}\nu\varrho_0\nabla\times\mathbf{v}_1 = \frac{\mathrm{i}B_0(m+bkr_0)}{4\pi r_0}\nabla\times\mathbf{B}_1 - \frac{\mathrm{i}kB_0}{2\pi r_0}\mathbf{B}_1, \tag{2.17}$$

$$\mathrm{i}\nu\mathbf{B}_1 = \frac{\mathrm{i}B_0(m+bkr_0)}{r_0}\mathbf{v}_1 - \frac{\mathrm{i}\nu Mc}{e}\nabla\times\mathbf{v}_1. \tag{2.18}$$

It is now clear that Eqs. (2.12) are implied by (2.17) and (2.18). $\mathbf{B}_1$ can now be eliminated from equations (2.17) and (2.18) and there results

$$\frac{Mc\nu r_0}{eB_0}(m+bkr_0)\nabla\times\nabla\times\mathbf{v}_1 + \left[\frac{4\pi\varrho_0\nu^2 r_0^2}{B_0^2} - (m+bkr_0)^2 - \frac{2Mc\nu kr_0}{eB_0}\right]\nabla\times\mathbf{v}_1 + 2k(m+bkr_0)\mathbf{v}_1 = 0. \tag{2.19}$$

This equation is rewritten

$$(a_2/k^2)\nabla\times\nabla\times\mathbf{v}_1 + (a_1/k)\nabla\times\mathbf{v}_1 + a_0\mathbf{v}_1 = 0, \tag{2.20}$$

where

$$a_2 = kr_0\,\nu(m+bkr_0)/\omega_\mathrm{i}, \tag{2.21}$$

$$a_1 = 4\pi\varrho_0\nu^2 r_0^2/B_0^2 - (m+bkr_0)^2 - 2kr_0\nu/\omega_\mathrm{i}, \tag{2.22}$$

$$a_0 = 2(m+bkr_0). \tag{2.23}$$

and $\omega_\mathrm{i} = eB_0/Mc$ is the ion gyration frequency in the field B_0.

The solutions of equations (2.20) are Bessel functions of argument $(\lambda^2-1)^{1/2}kr$ where

$$a_2\lambda^2 + a_1\lambda + a_0 = 0. \tag{2.24}$$

The equation can be factorized

$$(\nabla\times - \lambda^\mathrm{I}k)(\nabla\times - \lambda^\mathrm{II}k)\mathbf{v}_1 = 0 \tag{2.25}$$

and the solution of the equation

$$\nabla \times \mathbf{v}_1 = \lambda k \mathbf{v}_1$$

is known [3] to be

$$v_{1r} = \frac{i(\lambda^2-1)^{1/2}}{2(\lambda+1)} J_{m+1}[(\lambda^2-1)^{1/2} kr] - \frac{i(\lambda^2-1)^{1/2}}{2(\lambda-1)} J_{m-1}[(\lambda^2-1)^{1/2} kr],$$

$$v_{1\theta} = -\frac{(\lambda^2-1)^{1/2}}{2(\lambda+1)} J_{m+1}[(\lambda^2-1)^{1/2} kr] - \frac{(\lambda^2-1)^{1/2}}{2(\lambda-1)} J_{m-1}[(\lambda^2-1)^{1/2} kr],$$

$$v_{1z} = J_m[(\lambda^2-1)^{1/2} kr]. \tag{2.26}$$

From Eq. (2.18) expressions for $\mathbf{B}_1$ can also be obtained. If the above expression for v_{1r} is written as

$$v_{1r} = \varphi(\lambda, m, kr),$$

the complete solution for v_{1r} is

$$v_{1r} = A\varphi(\lambda^{\mathrm{I}}, m, kr) + B\varphi(\lambda^{\mathrm{II}}, m, kr). \tag{2.27}$$

The corresponding expression for B_{1r} can be shown to be

$$B_{1r} = \alpha^{\mathrm{I}} A \varphi(\lambda^{\mathrm{I}}, m, kr) + \alpha^{\mathrm{II}} B \varphi(\lambda^{\mathrm{II}}, m, kr), \tag{2.28}$$

where

$$\alpha = \frac{B_0(m+bkr_0)}{\nu r_0} - \frac{Mc\lambda k}{e}. \tag{2.29}$$

A and B are constants to be determined by the boundary conditions.

The boundary conditions implied by Eqs. (2.1) to (2.7) at an interface between two fluids are four in number; this is consistent with the order of the differential equation (2.20). Thus Eqs. (2.2) and (2.6) imply that the normal components of magnetic field and velocity must be continuous; Eq. (2.1) implies that $(p+B^2/8\pi)$ must be continuous and (2.3) shows that p_i must be continuous. In the present problem where the fluid is contained by rigid walls, the pressure can be supported by the walls, and the only conditions are that the radial components of both velocity and magnetic field should vanish at the wall.

If v_{1r} and B_{1r} both vanish at $r=r_0$, the following possibilities arise

$$\begin{aligned} &\text{(a)} \quad A=0, \quad \varphi(\lambda^{\mathrm{II}}, m, kr_0)=0, \\ &\text{(b)} \quad B=0, \quad \varphi(\lambda^{\mathrm{I}}, m, kr_0)=0, \\ &\text{(c)} \quad \alpha^{\mathrm{I}}=\alpha^{\mathrm{II}}. \end{aligned} \tag{2.30}$$

The third possibility can be ruled out because $\alpha^{\mathrm{I}}=\alpha^{\mathrm{II}}$ is equivalent to $\lambda^{\mathrm{I}}=\lambda^{\mathrm{II}}$. In this case, if B_{1r} and v_{1r} vanish at $r=r_0$, they vanish everywhere, and so do all the other perturbed quantities. Thus this case corresponds to an identically zero perturbation.

The dispersion relation thus takes the form

$$\varphi(\lambda, m, kr_0)=0, \tag{2.31}$$

where λ is related to ν by Eq. (2.24).

3. Solution of dispersion relation

Before proceeding further, dimensionless variables are introduced. Thus write

$$X_0 = kr_0, \tag{3.1}$$

$$\mathcal{Y}_0^2 = \nu^2 r_0^2/c_{\mathrm{H}}^2 = -Y_0^2, \tag{3.2}$$

$$Z_0 = \omega_i r_0/c_{\mathrm{H}}, \tag{3.3}$$

where

$$c_{\mathrm{H}}^2 = B_0^2/4\pi\varrho_0. \tag{3.4}$$

It may be noted that an alternative expression for Z_0 is $\omega_{\mathrm{pi}} r_0/c$ where ω_{pi} is the ion plasma frequency. The dispersion relation can then be written

$$\varphi(\lambda, m, X_0)=0 \tag{3.5}$$

and Eq. (2.24) becomes

$$\mathcal{Y}_0^2 + \frac{X_0 \mathcal{Y}_0 [\lambda(m+bX_0)-2]}{Z_0} + \frac{(m+bX_0)[2-\lambda(m+bX_0)]}{\lambda} = 0. \tag{3.6}$$

If m and X_0 are specified, Eq. (3.5) can be solved, and there is an infinite discrete set of roots λ_n. The dimensionless frequencies $\mathcal{Y}_{0n}$ corresponding to these roots are then given by Eq. (3.6) when b and Z_0 are specified.

At this stage it is perhaps worthwhile to compare the present equations with those obtained if the Hall effect is neglected. Equation (3.5) is again obtained for λ_n but $\mathcal{Y}_{0n}$ satisfies the equation

$$\mathcal{Y}_0^2 + (m+bX_0)[2-\lambda(m+bX_0)]/\lambda = 0. \tag{3.7}$$

Equation (3.7) can be obtained from Eq. (3.6) by allowing the ion gyration frequency to tend to infinity.

Two facts are immediately apparent. If $\mathcal{Y}_0$ is real before the Hall effect is introduced, it remains real. Thus the region of unstable wavenumbers cannot be increased by the introduction of the Hall effect, and it may be reduced. In the event that complex roots, $\mathcal{Y}_0 = x \pm iy$, occur where previously the roots, $\mathcal{Y}_0 = \pm iy_0$, were pure imaginary, then

$$x^2 + y^2 = y_0^2. \tag{3.8}$$

Thus if overstability does occur, the growth rate is reduced.

In each case the least stable solutions correspond to the solutions for λ_n of lowest modulus; whether the negative or positive solution for λ is the more important depends on the relative signs of m, X_0 and b. Thus it can be seen from Eq. (3.7) that instability can only occur if

$$0 < \lambda(m+bX_0) < 2. \tag{3.9}$$

The smaller the value of $|\lambda|$, the larger the possible unstable range of X_0.

If Eq. (3.6) has complex roots so that overstability occurs, the real part of $\mathcal{Y}_0$ is given by

$$\mathcal{Y}_{0R} = [2-\lambda(m+bX_0)] X_0/2Z_0 \tag{3.10}$$

and the phase velocity of the instability wave is

$$v_p = \mathcal{Y}_{0R}\, c_H/X_0 \qquad (3.11)$$
$$= [2 - \lambda(m + bX_0)]\, c_H/2Z_0 .$$

It may be noted that, provided overstability does occur, the ion gyration frequency does not enter into the relation between the phase velocity of the instability wave and the zero-order electron drift velocity, for the latter can be obtained from the equation

$$j_z = n\, e\, v_- = 2B_0\, c/4\pi\, r_0 , \qquad (3.12)$$

which leads to

$$v_- = 2\, c_H/Z_0 . \qquad (3.13)$$

Then
$$v_p/v_- = [2 - \lambda(m + bX_0)]/4. \qquad (3.14)$$

This equation shows that the phase velocity has a maximum possible value of half the zero-order electron drift velocity, but this value will not normally be attained.

For small enough values of Z_0, the range of unstable wavenumbers is reduced by the introduction of the Hall effect. This is demonstrated in the next section where results are given for axisymmetric perturbations.

4. Numerical results—Axisymmetric perturbations

The results are especially simple in this case. The equation $\varphi = 0$ reduces to

$$J_1[(\lambda^2 - 1)^{1/2} X_0] = 0 \qquad (4.1)$$

and $\mathcal{Y}_0$ satisfies the equation

$$\mathcal{Y}_0^2 + \frac{X_0 \mathcal{Y}_0 [\lambda b X_0 - 2]}{Z_0} + \frac{bX_0[2 - \lambda bX_0]}{\lambda} = 0 . \qquad (4.2)$$

Equation (4.1) has solutions

$$\lambda_n^2 = 1 + j_n^2/X_0^2 , \qquad (4.3)$$

where j_n is any zero of the first-order Bessel function (other than $j_n = 0$). The least stable case occurs for $j = j_1$ where

$$j_1 = 3.83 \qquad (4.4)$$

and the results are calculated for this case.

Results are first calculated for the case in which the Hall effect is neglected. This problem has already been considered in [3] though there the fluid had a free surface. The new results are qualitatively similar though the conducting wall exerts a stabilizing influence. Equation (4.2) becomes

$$\mathcal{Y}_0^2 = b^2 X_0^2 [1 - 2/\lambda bX_0] . \qquad (4.5)$$

Instability can only occur if

$$0 < \lambda bX_0 < 2 \qquad (4.6)$$

and, combining Eqs. (4.3), (4.4) and (4.6), one can easily see that no instability can occur if

$$b^2 > 4/(3.83)^2 = 0.273 . \qquad (4.7)$$

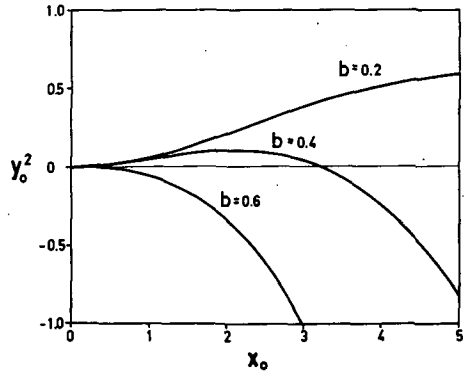

Fig. 1 Axisymmetric perturbations in the absence of the Hall effect. The square of the dimensionless growth rate ($Y_0^2 = -4\pi\, \varrho_0\, r_0^2\, \nu^2/B_0^2$) is shown as a function of the dimensionless wavenumber ($X_0 = kr_0$) for several values of the axial magnetic field ($B_0\, b$).

The corresponding criterion when the fluid has a free surface is

$$b^2 > 4/(2.4)^2 = 0.694 . \qquad (4.8)$$

The solutions of Eq. (4.5) are shown in Fig. 1 for three values of b (0.2, 0.4, 0.6). The quantity plotted as a function of X_0 is $Y_0^2 = -\mathcal{Y}_0^2$; this facilitates comparisons with previous papers. Instability occurs when Y_0^2 is positive.

Solutions of the full dispersion relation including the Hall effect have been obtained for one value of b only. Real roots of Eq. (4.2) occur if

$$\lambda X_0 (2 - \lambda bX_0)^2 > 4Z_0^2\, b\, (2 - \lambda bX_0) . \qquad (4.9)$$

As shown previously this is obviously satisfied if $2 - \lambda bX_0$ is negative. If $2 - \lambda bX_0$ is positive, inequality (4.9) becomes

$$4Z_0^2 < \lambda X_0 (2 - \lambda bX_0)/b . \qquad (4.10)$$

If this inequality is satisfied in the neighbourhood of $X_0 = 0$, there is a new range of stable wavenumbers that did not exist in the absence of the Hall effect. The condition for it to be satisfied at $X_0 = 0$ is

$$4Z_0^2 < j_1 (2 - j_1 b)/b . \qquad (4.11)$$

Thus, given a value for b, there will be a value of Z_0 below which a new region of stability occurs. For $b = 0.4$, this critical value of Z_0 is

$$Z_0 = 1.06 . \qquad (4.12)$$

As soon as Z_0 is appreciably less than this value, the range of unstable wavenumbers becomes very small. Thus the moment the ion gyration frequency is a few times less than the characteristic hydromagnetic frequency the band of unstable wavenumbers is negligibly small. It would be interesting to know whether this finite-gyration-frequency effect also occurs in a more rigorous treatment.

The numerical results are shown in Figs. 2 and 3 for several values of Z_0 and for wavenumbers for which overstability occurs. The real part of Y_0 (growth rate) is shown in Fig. 2 and the imaginary part in Fig. 3.

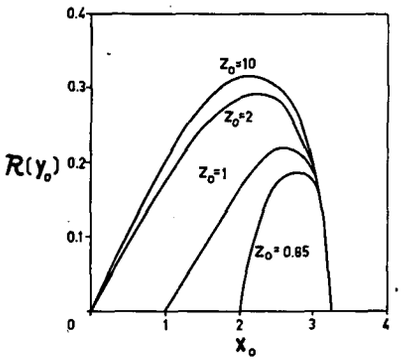

Fig. 2 Axisymmetric perturbations; $b = 0.4$. The real part of the dimensionless growth rate is shown as a function of the dimensionless wavenumber for several values of the dimensionless ion gyration frequency ($Z_0 = \omega_i r_0/c_H$).

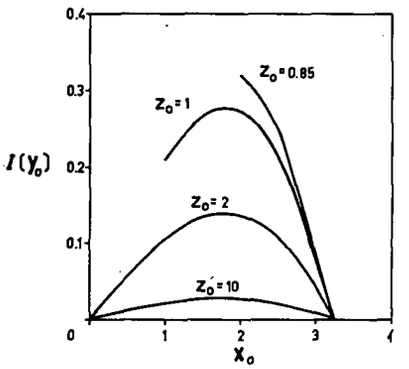

Fig. 3 Axisymmetric perturbations; $b = 0.4$. The imaginary part of the dimensionless growth rate is shown as a function of the dimensionless wavenumber for several values of the dimensionless ion gyration frequency ($Z_0 = \omega_i r_0/c_H$). The curves are drawn only for values of the wavenumber for which overstability occurs.

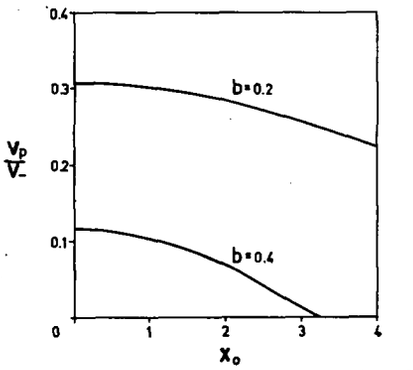

Fig. 4 Axisymmetric perturbations; relation between phase velocity and electron drift velocity. The ratio of phase velocity to electron drift velocity is shown as a function of the dimensionless wavenumber for two values of the axial magnetic field. These curves apply to the values of Z_0 for which overstability occurs at the wavenumber considered.

For cases in which overstability occurs, the ratio of phase velocity to electron drift velocity is shown in Fig. 4. It can be seen from these figures that, if Z_0 is appreciably greater than unity, the growth rate is virtually unaltered by the introduction of the Hall effect term, and the imaginary part of Y_0 is very small.

Acknowledgement

I am grateful to A. A. Ware for making available to me a preprint of his paper [1].

References

[1] Ware, A. A., *J. nucl. Energy, Part C*, **3** (1961) 93.
[2] Tayler, R. J., *Proc. Phys. Soc. (London)* **70** (1957) 1049.
[3] Tayler, R. J., *Rev. mod. Phys.* **32** (1960) 907.
[4] Chew, G. F., Goldberger, M. L., Low, F. E., *Proc. Roy. Soc.* **A236** (1956) 112.

SPECTROSCOPIC INVESTIGATION OF PLASMA IN THE WAVELENGTH RANGE 0.1—2.0 MM*

G. N. HARDING

ATOMIC ENERGY RESEARCH ESTABLISHMENT

HARWELL, BERKSHIRE, UNITED KINGDOM

V. ROBERTS

ROYAL RADAR ESTABLISHMENT

MALVERN, WORCESTERSHIRE, UNITED KINGDOM

The radiation emitted by Zeta in the wavelength range 0.1-2.0 mm has been measured with a vacuum grating spectrograph. The detector was either a carbon bolometer or an indium antimonide photo-conductor, giving time-integrated and time-resolved measurements, respectively.

Continuous spectra were obtained that can be explained on the basis of free-free emission and absorption. At short wavelengths the plasma is optically thin, and at long wavelengths a blackbody spectrum is obtained. Thus both electron temperature and density can be found.

Measured values of these parameters obtained under varying conditions of pressure and magnetic field are presented and their significance discussed.

1. Introduction

Measurements depending on the interaction between electromagnetic radiation and plasma have proved to be an important method of investigating conditions in plasmas with the advantage over probe methods that the plasma is not affected by the measurement. Most of the work reported has been in one of three regions of the spectrum: (a) visible, ultra-violet and vacuum ultra-violet, (b) microwave and (c) soft X-ray. The experiments reported here have been made in the far infrared region (wavelength 0.1—2.0 mm) which has the advantage over (a) that no detailed knowledge of atomic processes is needed since the radiation interacts strongly only with free electrons. Moreover, the frequencies used can be well above the plasma frequency for electron densities of interest in thermonuclear research; thus one avoids one of the most serious drawbacks of microwaves in the present stage of technology.

In a previous publication [1], we presented results of the measurement of radiation emitted by Zeta in this wavelength region and showed that they could be accounted for on the basis of free-free emission and absorption. In this paper we make use of this fact in interpreting some new observations of the emission spectrum from Zeta, most of which have been made with a new fast photo-conductive detector.

2. Apparatus

The radiation entering a 10-cm-diameter hole in the median plane of the Zeta torus was transmitted by means of a tapered tube with a finely machined internal surface to a grating spectrometer that covered the wavelength range 0.1–2.0 mm by means of three interchangeable gratings. The gratings had rulings spaced at 0.5, 1.25 and 3.4 mm. The passband was about 10 % of the wavelength to which the instrument was set. Further details will be found in Ref. [1].

Two detectors were used: (a) a carbon bolometer [2], which had a resolving time of a few milliseconds, and gave measurements integrated over the time of the Zeta pulse; (b) a photo-conductive detector consisting of a block $1.0 \times 0.5 \times 0.5$ cm of InSb of very high purity with electrodes soldered on two opposite faces and placed in a magnetic field of 6000 G. Such a detector has been shown by PUTLEY [3] to be extremely sensitive at wavelengths up to 4 mm and to have a resolving time of the order of a microsecond. Both detectors were operated in liquid helium at 1.7° K. The output from the fast detector was amplified, displayed on an oscilloscope and photographed.

3. Analysis of the Spectra

In Fig. 1 are shown two spectra obtained with the slow detector. The quantity actually observed was the energy per pulse, and the power has been calculated by assuming a pulse length of 2 ms. This pulse length was subsequently confirmed with the fast detector. Each point represents the average of readings from 3-10 pulses. The errors shown are the resultant of scatter in the observations and calibration errors. The Zeta running conditions were as shown on the figures and differed in the two cases only in the value of the applied axial magnetic field. The lines drawn through the points are theoretical curves obtained by choosing values of the appropriate parameters

* Conference paper CN-10/54, presented by R. S. Pease. Discussion of this paper is given on page 1017. Translations of the abstract are at the end of this volume of the Conference Proceedings.

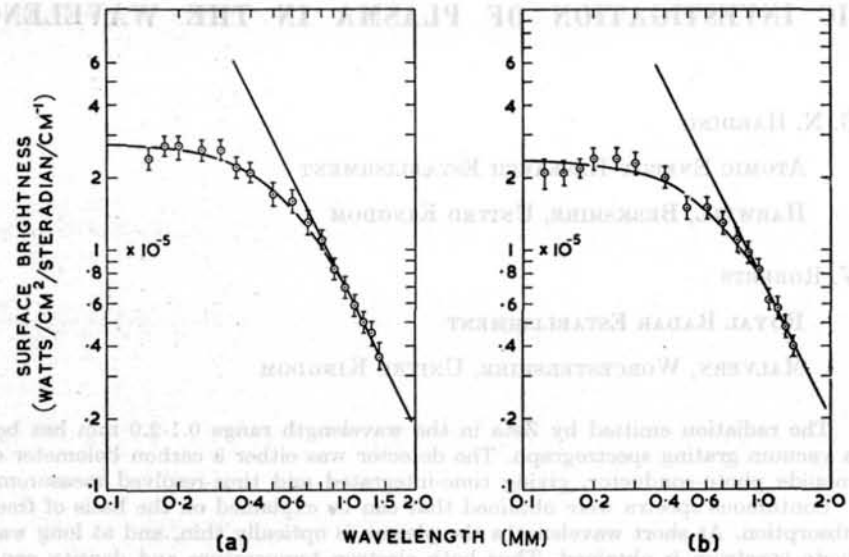

Fig. 1 Time-integrated far-infrared spectra of Zeta deuterium plasma. (a) $p = 5$ mtorr, $V_c = 10$ kV, $B_z = 560$ G. (b) $p = 5$ mtorr, $V_c = 10$ kV, $B_z = 1120$ G.

(see below) that give the best fit. By plotting the spectra on log-log paper, the essential features are emphasised. The emission at all wavelength is due to free-free transitions; at short wavelengths absorption is small, and the surface brightness per unit frequency interval is independent of wavelength. As the wavelength increases, the absorption becomes appreciable, and the surface brightness falls until absorption is so strong that the plasma behaves as a black body and the points lie on a straight line of slope -2. The surface brightness per unit frequency interval over the whole spectrum is given by the expression [4 – 8]

$$\frac{16}{3}\left(\frac{\pi}{6m^3}\right)^{1/2}\frac{e^6Z^2}{c^3}(kT)^{-1/2}\,g\,n_e\,n_i\,\frac{1-e^{-Kd}}{K}$$

with the absorption coefficient (including stimulated emission) given by

$$\frac{8}{3}\left(\frac{\pi}{6m^3}\right)^{1/2}\frac{e^6Z^2}{c}(kT)^{-3/2}\nu^{-2}g\,n_e\,n_i$$

Here g is the Gaunt factor; n_e, n_i are the electron and ion densities, respectively; d is the depth of the plasma and the other symbols have their usual meanings.

In the above expressions the approximation $h\nu/kT \to 0$ has been made; the electrons have been assumed to have a Maxwellian velocity distribution, and the plasma has been assumed uniform. The parameters that can be adjusted to give the theoretical curve that best fits the experimental points are the electron temperature T_e and the product $n_e n_i d$ of the electron and ion densities and the depth of the plasma. Thus, if the depth is known, the product $n_e n_i$ can be found, which for a pure hydrogen or deuterium plasma is equal to n_e^2. The depth d could in principle be measured by scanning across a diameter of the torus, but with the existing windows on Zeta this was not possible and to obtain the results given below we have calculated d from measurements of the gas current and the applied axial magnetic field, using the magnetic probe results of LEES and RUSBRIDGE [9]. The analysis of the measurements shown in Fig. 1 is given in Table I.

If we compare these values of line density with the values obtained on the assumption that all the gas is singly ionized (2.75×10^{18} cm^{-1}), there appears to be a considerable discrepancy. On the other hand, the temperature values agree, within the absolute calibration accuracy of $\pm 35\%$, with values obtained on Zeta using different methods [10, 11]. One possible explanation of this, advanced in our earlier publication [1], is that multiple reflections occur inside the metal torus of Zeta, which would increase the emission in the optically thin case but not the optically thick. Another possible explanation is that the expressions used for emission and absorption both give a value

TABLE I Analysis of time-integrated measurements at pressure 5 mtorr in deuterium

Applied axial magnetic field (G)	Elecron temperature (°K)	$n_e n_i d$ (cm^{-5})	d (cm)	$n_e n_i$ (cm^{-6})	n_e (cm^{-3})	Line density $\frac{\pi}{4} d^2 n_e$ (cm^{-1})
560	8.5×10^4	1.16×10^{32}	64	1.82×10^{30}	1.35×10^{15}	4.35×10^{18}
1120	9.7×10^4	1.06×10^{32}	81	1.31×10^{30}	1.15×10^{15}	5.9×10^{18}

that is too low by the same amount so that their ratio and hence the black-body emission are not affected. In the absence of absolute measurements of the emission from a plasma of known temperature, density and effective size, we conclude that the absolute values of density cannot at present be relied on, within a factor of 2 or 3. In either case, all determinations of density, being based on the emission from an optically thin plasma, would be affected by the same amount; the relative densities are therefore considered reliable within the internal accuracy of the observation, which was of the order of $\pm 10\%$.

4. Time-Resolved Measurements

In the experiments using the photo-conductive detector, the resolving time (limited not by the detector but by its associated very-low-noise amplifier, to about 10 μs), was short compared with the Zeta pulse of about 2 ms, so that the variation in time of the emission could be studied. The method used was to photograph a number of consecutive pulses on the same film (as a check for reproducibility), and to make the measurements from the photographs. A number of the original records are reproduced in Fig. 2. Using the method of analysis outlined above, density and, where possible, temperature have been calculated at intervals of 100 or 200 μs. and are plotted in Figs. 3–7. Details of the measurements and calculations are as follows: —

1. Zeta conditions: pressure, 5 mtorr deuterium; 11000-μF capacitor bank charged to 10 kV; applied axial magnetic field, 560 G. The emission was measured at seven wavelengths, between 0.15 and 1.0 mm. The calculated temperature and density are shown in Fig. 3. Comparing these results with values calculated by McWhirter [10] from measurements of the intensities of spectral lines in the visible region, the shape of the curves is similar, but the temperature given by the infrared measurements is some 20% higher, and the density is greater by a factor of 2.3. This is of the same order as the discrepancy between the measured and calculated line densities in Table I.

2. Pressure, 4, 3 and 2 mtorr; capacitor, 10 kV; field, 560 G. In these conditions insufficient data were obtained to enable temperatures to be calculated, and in calculating the density we have assumed a constant electron temperature of 10^5 °K. As explained below, this is unlikely to make the density values seriously in error. The densities are plotted in Fig. 4.

3. Pressure, 0.5 and 1 mtorr; capacitor, 10 kV; axial magnetic field, 160, 240, 320, 560 and 800 G. At these pressures the emission was so low that readings were only possible when the grating was replaced by a plane mirror. The spectrometer then accepted radiation in the wavelength range 0.1—1.0 mm, approximately, determined by the filters and the detector. Since at these pressures the plasma is optically thin over the whole of this wavelength range, the density can be determined from the expression given above by setting $K=0$ if the temperature is known. For a given rate of emission

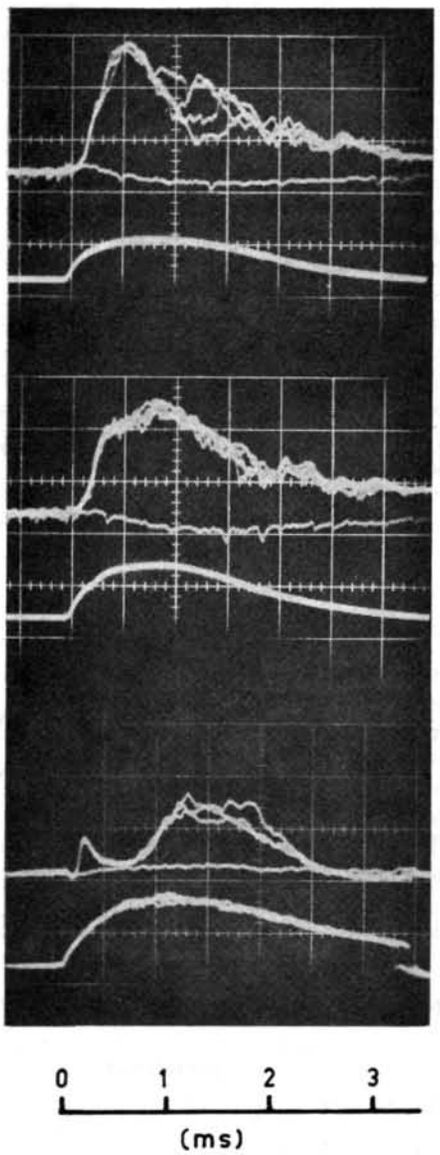

Fig. 2 Oscilloscope traces of signals from the fast detector. Upper trace, infrared signal (one exposure with shutter in); lower trace, gas current.

(a) $p=5$ mtorr, $V_c=10$ kV, $B_z=$ 560 G, $\lambda=0{,}4$ mm, 4 pulses.
(b) $p=5$ mtorr, $V_c=10$ kV, $B_z=1120$ G, $\lambda=0{,}4$ mm, 5 pulses.
(c) $p=5$ mtorr, $V_c=10$ kV, $B_z=$ 160 G, $\lambda=0.1$-1 mm, 3 pulses.

the density is proportional to the fourth root of the temperature; so the choice of temperature is not very critical. To illustrate this point, in Fig. 5 we show the calculated density for one set of measurements with three different assumptions about the temperature: (a) constant at 10^5 °K, (b) constant at 2×10^5 °K, (c) rising linearly to 2×10^5 °K at 500 μs and then constant at that value. On the same figure we have plotted the density calculated from the expressions given above assuming that the plasma is fully ionized and determining its diameter from the gas current

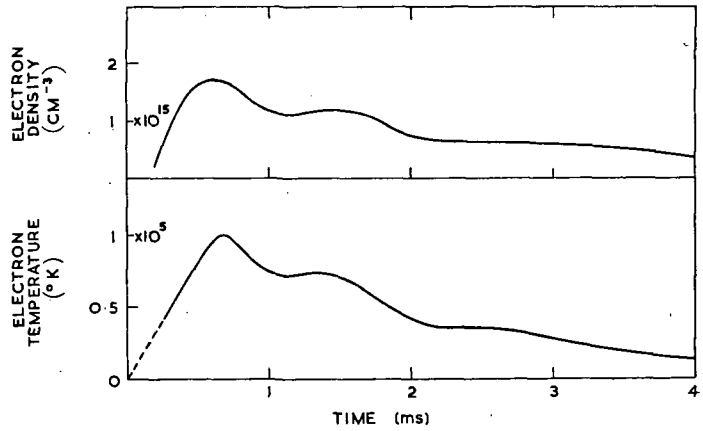

Fig. 3 Time-resolved electron temperature and density calculated from the infrared spectra. $p = 5$ mtorr, $V_c = 10$ kV, $B_z = 560$ G.

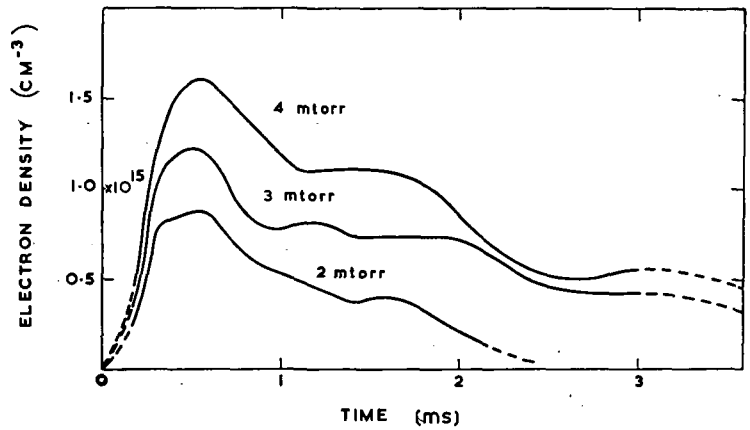

Fig. 4 Electron density vs time for deuterium pressure of 2, 3 and 4 mtorr. $V_c = 10$ kV, $B_z = 560$ G.

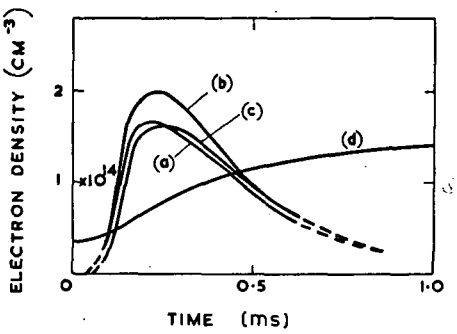

Fig. 5 Electron density deduced from the infrared spectra with different assumptions about electron temperature. (a) T_e constant at 10^5 °K. (b) T_e constant at 2×10^5 °K. (c) T_e rising linearly to 2×10^5 °K at 500 μs, then constant. Curve d shows calculated density assuming gas is fully ionized and total number of electrons remains constant.

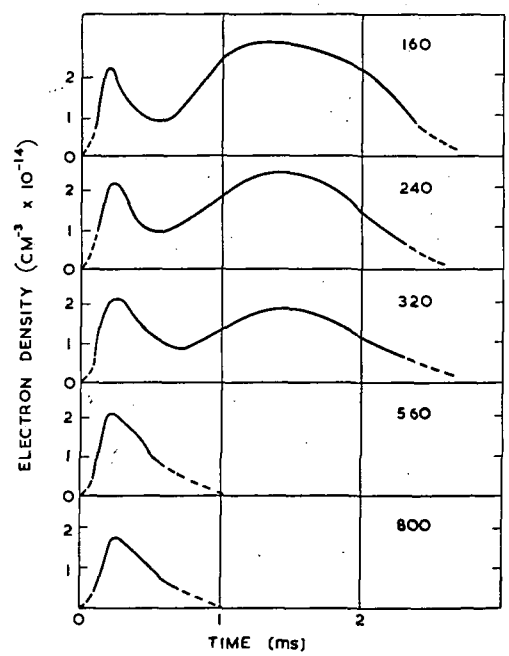

Fig. 6 Electron density vs time. $p = 0.5$ mtorr, $V_c = 10$ kV. Numbers on curves show B_z in gauss.

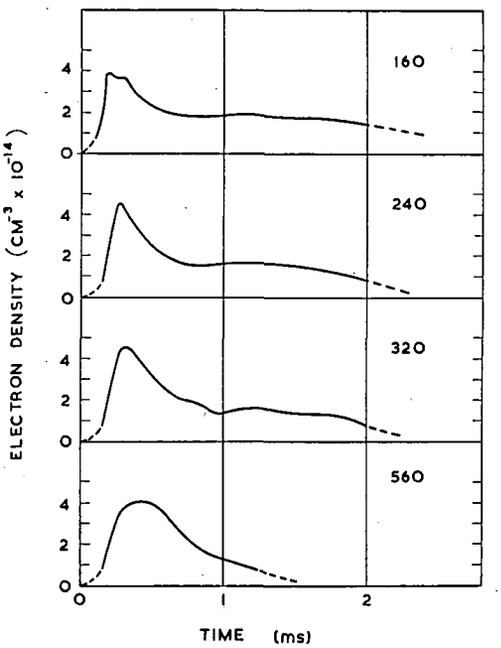

Fig. 7 Electron density vs time. $p = 1$ mtorr, $V_c = 10$ kV. Numbers on curves show B_z in gauss.

and axial magnetic field. Since the choice of temperature affects the calculated density only to a small extent, we have assumed a constant temperature of 2×10^5 °K for the remainder of these results, which are plotted in Figs. 6 and 7.

5. Discussion

Probably the most interesting feature of the density measurements, in particular those at 0.5 and 1 mtorr, is that they show direct evidence of the phenomena of "particle loss" and "injection" found by WILSON and BURTON [12] from a study of the time-variation of intensity of spectral lines of highly ionized impurity atoms. The present observations confirm that the particle-loss rate is not affected by the applied magnetic field while the injection rate is reduced by increasing the field. It can also be seen that these processes occur at pressures up to 5 mtorr, although the effect is not so pronounced at the higher pressures.

An attempt was made to measure the density under conditions in which the current in Zeta suddenly falls by a very large amount, but because this effect occurs at a relatively low density, the infrared emission had fallen to a value well below the limit of sensitivity of the present apparatus.

It was observed that at wavelengths for which the plasma was behaving as a black body, the traces obtained were quite reproducible from pulse to pulse, showing that the temperature followed the same pattern each time. In contrast to this, the traces at short wavelengths under certain conditions exhibited striking non-reproducibility, showing that random variations in density were occurring. This effect was found at all the pressures investigated. In general the irregularities started about 500 μs after the start of the current pulse and increased in amplitude to a maximum value (sometimes about one-half of the total emission) at about 1500 μs. The frequency spectrum ranged from about 1 to 100 kHz the upper limit being set up by the amplifier. It was found that the irregularities were reduced by increasing the axial magnetic field (see Fig. 2). This observation supports the hypothesis that the density in the latter half of the pulse is increased by injection of atoms from the walls by arcs or some other spasmodic process and that the injection is inhibited by the presence of an axial magnetic field. Rough calculation shows that a rate of injection from the walls of 10^{22}—10^{23} electrons/s would be needed to account for the observed radiation. It has been shown by ROBSON [13] that from a unipolar arc the rate is about 10^{19} particles/s. Thus either a very large number of unipolar arcs, or some other process would appear to be occurring.

6. Conclusions

The measurement of far-infrared radiation emitted from a hot plasma promises to be a very useful method of determining the space-averaged electron density and temperature. The ability to obtain time resolution is an important feature of the method, and the time resolution obtainable is likely to improve as techniques and detectors are developed. The clarification of the uncertainty in the absolute intensity of emission from an optically thin plasma is an essential task for the future, in which direct absorption measurements could play an important part.

References

[1] HARDING, G. N., et al., *Proc. phys. Soc.* (*London*) **77** (1961) 1069.
[2] BOYLE, W. S., RODGERS, K. F., *J. opt. Soc. Amer.* **49** (1959) 66.
[3] PUTLEY, E. H., *Proc. phys. Soc.* (*London*) **76** (1960) 802.
[4] GAUNT, J. A., *Phil. Trans. roy. Soc.* **A229** (1930) 163.
[5] CILLIÉ, G., *Monthly Notes roy. Astron. Soc.* **92** (1932) 820.
[6] ALLEN, J. E., HINDMARSH, W. R., U. K. AERE Report GP/R 1761 (1955).
[7] SMERD, S. F., WESTFOLD, K. C., *Phil. Mag.* **40** (1949) 831.
[8] MARTYN, D. F., *Proc. roy. Soc.* **A193** (1948) 44.
[9] LEES, D. J., RUSBRIDGE, M. G., in Proc. 4th Intern. Conf. Ionization Phenomena in Gases (Uppsala, 17-21 Aug. 1959) **2**, North Holland Publishing Co., Amsterdam (1960) 954.
[10] HOBBS, G. D., et al., "The temporal variation of line radiation from impurities in Zeta," in Proc. 5th Intern. Conf. Ionization Phenomena in Gases (Munich, 28 Aug.-1 Sept. 1961) **2**, North Holland Publishing Co., Amsterdam (1962) 1965.
[11] BURTON, W. M., et al., "Plasma loss in Zeta," *Nuclear Fusion*: 1962 Supplement, Part 3, 903.
[12] WILSON, R., BURTON, W. M., *Proc. phys. Soc.* (*London*) **78** (1961) 1516.
[13] ROBSON, A. E., HANCOX, R., *Proc. Inst. elec. Eng.* **106A**, Supplement 2 (1959) 47.

SPECTROSCOPIC STUDIES OF ION ENERGIES IN ZETA*

B. B. JONES, R. WILSON

ATOMIC ENERGY RESEARCH ESTABLISHMENT

HARWELL, BERKSHIRE, UNITED KINGDOM

The energies of trace ions in a Zeta deuterium plasma are determined from measures of the Doppler widths of spectral lines emitted in the vacuum ultraviolet. The instrument used is a normal-incidence, 3-metre, vacuum spectrograph giving a reciprocal linear dispersion of 2.8 Å/mm. The inert gases neon, argon, krypton and xenon are added to act as trace elements and give a selection of spectral lines that embrace a considerable range in ion charge and mass. Several new lines due to the more highly ionized species have been identified for this purpose. Photographic-plate calibration is achieved by an aperture restriction system located at the Sirks focus. This gives a step distribution in the focal plane with an intensity ratio of 2:1.

A simple analysis of the motion of ions in time-varying electric fields in a magnetically constrained plasma shows that their energies depend on their charge and mass and the characteristic frequency of the perturbing field. This is used as a guide in interpreting the observations. It is shown that the ion energies vary with time of appearance, and conclusions concerning the heating mechanism are based on observations of different ionic species made at the same time. The ion energies E_i, can be represented by a constant energy plus an energy corresponding to a common velocity system, the directed motion being perpendicular to the magnetic field. The heating mechanism is interpreted as a low-frequency perturbation, perpendicular to the magnetic field lines showing a marked degree of relaxation towards thermalization. For one specific condition, $E_i = 102 + 2.3\,M_i/M_D$ (eV). This is used to deduce the deuteron energies and a relaxation time of 13 μs is calculated for the directed mode. This agrees well with the ion-ion relaxation time. Calculation of the equivalent electric field driving the directed mode gives a value of the same order as that observed with electrostatic probes. The ion energies and electrostatic fluctuations are consistent with each other.

1. Introduction

The profiles of spectral lines emitted by impurity ions in a Zeta deuterium plasma, are broadened by a Doppler effect. Other types of broadening due to the statistical Stark effect, electron impact and radiation trapping are negligible because of the low density and small optical depth of the plasma. Measurements of line widths can therefore be used to determine the kinetic energies of ions, and observations presented at the Geneva conference [1, 2] gave values of the order of a few hundred electron volts for ions of carbon, nitrogen and oxygen, of which small quantities (<1%) are normally present in the plasma. On the other hand, determinations of the electron temperature, made from measurements of microwave noise and the intensity of C V 2271 Å [2], and more recently by means of an electron detector [3], all give values of the order of a few tens of electron volts. The ion energies are therefore far in excess of the electron temperature and some plasma process must be operating that preferentially heats the ions. An investigation has been started to determine the form of this ion-heating mechanism, and the purpose of this paper is to report the state of this work.

2. Method

It has been proposed by PEASE [4] and THONEMANN [5] that plasma perturbations in the form of fluctuating electric fields may be the dominant mode for ion heating. If the power spectrum of the electric fields is $A(\omega, t)$ the equation of motion for a particle of charge Zq and mass M may be written

$$\frac{d\mathbf{v}}{dt} = \frac{Zq}{M}[\mathbf{A}(\omega, t) + \mathbf{v} \times \mathbf{B}] = \beta \mathbf{v} \qquad (1)$$

where β is the collision frequency. Collisions are introduced as a "dynamical friction" and hence no account is taken, in this equation, of any relaxation of the mode towards thermalization. Since the power spectrum is unknown, we make the simple assumption that the heating effects can be described by an equivalent monochromatic field; i.e.

$$\mathbf{A}(\omega, t) = \mathbf{A}_0 e^{i\omega t} \qquad (2)$$

and solve Eq. (1) for a uniform plasma with constant magnetic field B. The mean kinetic energy E is then calculated for fluctuations parallel and perpendicular to the magnetic field—

$$\mathbf{A} \parallel \mathbf{B}, \text{ all } \omega, : E = \frac{q^2 {A_0}^2}{4(\omega^2 + \beta^2)} \frac{Z^2}{M} \qquad (3)$$

$$\mathbf{A} \perp \mathbf{B}, \begin{cases} \omega \gg \omega_c : E = \dfrac{q^2 {A_0}^2}{4(\omega^2 + \beta^2)} \dfrac{Z^2}{M} & (4) \\ \omega \ll \omega_c : E = \dfrac{{A_0}^2}{4(1 + \beta/\omega_c)^2 B^2} M & (5) \end{cases}$$

where the cyclotron frequency $\omega_c = ZqB/M$.

* Conference paper CN-10/57, presented by R. S. Pease. Discussion of this paper is given on page 1017. Translations of the abstract are at the end of this volume of the Conference Proceedings.

These equations presuppose that all particles see essentially the same electric fields as a function of time. If the amplitude of motion of the particles are widely different, this may not be true, and deductions based on this model will be unsound. A self-consistent condition is $2\,(E/M)^{1/2} \ll \lambda\,\omega$, where λ is the distance over which the electric field extends.

For the case of electron plasma oscillations, Eq. (3) would apply for all particles, but since it implies strong preferential heating of the electrons, it must be discarded. For the case of ion sound waves, the condition is not satisfied for the electrons, but Eq. (3) might apply to heavy trace ions. For the cases $\mathbf{A} \perp \mathbf{B}$, the electron motion is limited by the magnetic field, and Eqs. (4) and (5) both give preferential ion heating. For the Zeta conditions to be investigated, we generally have $\omega_c \gg \beta$ and the effect of collisions on the directed energies in the mode is therefore small. For the domain which obviously results in a preferential ion heating, we therefore have—

$$\mathbf{A} \perp \mathbf{B},\ \omega \ll \omega_{ce} \begin{cases} \omega \gg \omega_{ci} : E_i \propto \dfrac{Z^2}{M} & (6) \\ \omega \ll \omega_{ci} : E_i \propto M & (7) \end{cases}$$

where the subscripts e and i refer to the electron and ion respectively. The physical reason for the difference in ion-energy spectrum is that the plasma reacts as a fluid to low-frequency fields and as a system of particles to high-frequency fields. The low-frequency energy represents a system of velocities that is common to all particles.

3. Experimental

In applying the above treatment to an experimental test, two additional parameters must be considered—space and time. The observed variations of line intensity with time in the Zeta spectrum are now well understood [6]. This work demonstrated the effect of loss and injection processes due to lack of plasma confinement and showed that the intensity distributions could be divided into two parts, an "initial transient" of relatively short duration due to those atoms initially present in the plasma, followed by a "tail," which persisted throughout the current pulse, due to the injection process. This injection tail could be made negligible by using high B_z fields or the inert gases as impurity elements, and the experimental conditions were selected so as to meet these conditions. Each spectral line is therefore formed by ions that were initially present in the discharge. Although there will be a spatial distribution associated with the emission, two ions appearing at the same time will be strictly comparable in this respect. Hence the measurements of the ion energies can be analysed in terms of a single parameter—time of appearance—in addition to the parameters that identify the ion.

To cover the range of ions required for the experiment, the observations were made in the vacuum ultra-violet region of the spectrum using a normal-incidence vacuum spectrograph designed and built at Harwell. The optical length is 3 meters, the aperture f/30 and the reciprocal linear dispersion 2.78 Å/mm in the first order. Temporal intensity distributions were measured with a 1-meter vacuum monochromator equipped with photoelectric recording. The plasma was viewed across its diameter and therefore the observed velocities were necessarily perpendicular to **B**.

To cover the range of mass required, the inert gases neon, argon, krypton and xenon were used as added trace elements to the deuterium gas. Knowledge of the spectra of these elements in multiply ionized form is extremely limited and presented an identification problem that was solved for the purpose of this investigation. Several new lines have been classified [7] that enabled the observations to be extended to Ne VIII, Ar VIII, Kr VIII and Xe IX.

Initially the photometric calibration of the photographic emulsion (Ilford Q 2) was achieved by photographing successive spectra in which the total exposure (in terms of number of discharges) was varied by factors of two and then assuming no intermittency effects or reciprocity failure. This was found to be inadequate for the accuracy ultimately required for the experiment and the problem of plate calibration was tackled and solved. An aperture-restriction device built at the Sirks focus was designed so as to give a stepped variation in the final image of the spectral line with a standard intensity ratio of 2:1 [8]. The spectrograms were measured with a recording microphotometer and Doppler widths read off directly by measuring the width of the intense component at the density corresponding to the peak of the fainter component. The mean ion kinetic energy was then calculated after making allowance for the instrumental width.

4. Results

The observations have been made for a "standard" discharge condition specified by

Bank voltage:	10 kV (Stored energy: 0.5 MJ)
Peak current:	320 kA
B_z:	800 G ($\theta_p = 1.7$)
Gas pressure:	0.5 mtorr
Gas:	deuterium + selected trace elements

The first experiments were carried out with 5% additions of neon, argon, krypton and xenon separately. The measurements of ion energy gave a correlation with Z^2/M as is shown by the results for Ne IV to VIII plotted in the upper part of Fig. 1. The values for the heavier inert gases also gave, within the errors of measurement, this same correlation, indicating that there was no large mass component in the measured energies. However, since the ionization potential scales roughly as Z^2/M, this latter parameter is also correlated with the time of appearance. Hence there is also a correlation between ion energy and time, as shown by the neon results plotted against time in the bottom half of Fig. 1.

The problem is now to determine which of the two correlations represents a true physical relationship. This requires the determination of second-order effects,

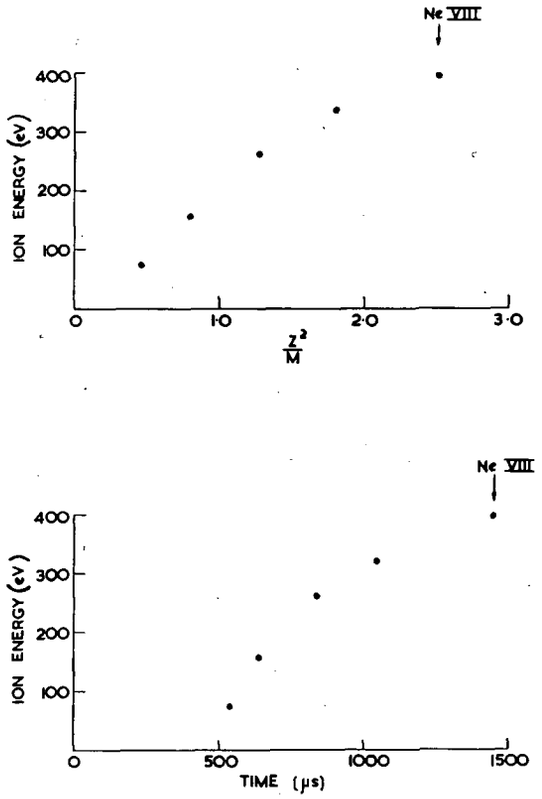

Fig. 1 Measured energies of neon ions against Z^2/M (upper) and time of appearance (lower). I_g, 320 kA; B_z, 800 G; 0.5 mtorr deuterium with 5% neon.

and it was at this point that the accurate calibration system was designed and installed. Further, the observations were now made in the second order of the spectrum and careful checks were made on the determination of the instrumental profile. On the average, about 15 independent measurements were made, giving mean energies with an internal standard error of ± 6 eV. This corresponds to a fractional error of $\pm 4\%$ in the ion energies to be analysed.

Experiments were then carried out with two trace elements simultaneously present in the discharge, in particular a combination of 9% oxygen and 2% argon. At this high value of B_z, the injection of oxygen is negligible, and this gas was used in preference to an inert gas in order to compare the ions O VI and A VIII. O VI appears ealier in time than Ar VIII, but it has a higher value of Z^2/M. Hence the observed energy ratio Ar VIII/O VI will be less than unity for a Z^2/M effect and greater than unity for a time effect. The mean value of several measures is 1:6 indicating a time effect, and this is supported by similar measurements of other pairs of ions. The correlation of E_i with Z^2/M is therefore accidental and it should be noted that this could also be expressed as a correlation with Z as observed in Alpha [9].

The effect of a time parameter must therefore be removed before tests of the form of the energy spectrum can be made. This was done by using pairs of trace elements, plotting the measured ion energies

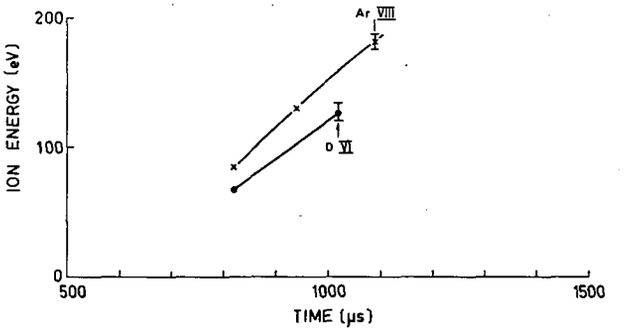

Fig. 2 Measured energies of argon and oxygen ions against time of appearance. I_g, 320 kA; B_z, 800 G; 0.5 mtorr deuterium with 2% argon and 9% oxygen. Mean square errors are indicated.

as functions of time, and reading off energies at any one time. Such a plot is shown for the sequences Ar VI, VII, VIII and O V, VI in Fig. 2.

TABLE I. Observed ratios of ion energies compared with theoretical ratios for different forms of heating

Energy ratio	Z^2/M	Thermal	M	Observed
$\frac{\text{Ar VIII}}{\text{O VI}}$	0.8	1.0	2.5	1.3 ± 0.1
$\frac{\text{Ar VIII}}{\text{Ne VI}}$	1.0	1.0	2.0	1.1 ± 0.1
$\frac{\text{Ar VII}}{\text{Ne V}}$	1.1	1.0	2.0	1.2 ± 0.1
$\frac{\text{Kr VIII}}{\text{Ar VII}}$	0.6	1.0	2.1	1.3 ± 0.1
$\frac{\text{Kr VIII}}{\text{Ne V}}$	0.7	1.0	4.1	1.6 ± 0.1

The results for several pairs of ions are shown in Table I. The theoretical ratios expected according to a $Z/^2M$ or M relation are given together with the thermal ratio. The observed ratios refer to the time of appearance of the heavier ion. It is clear that the ion energies do not fit well with any one simple model and that allowance should be made for relaxation towards thermal equilibrium. A correlation with Z^2/M is now absent. All the observed ratios are intermediate between the mass and thermal ratios, and none occur between the Z^2/M and thermal ratios. It is concluded that a fluctuation with frequency $> \omega_{ci}$ is not effective as an ion-heating mechanism and that the results indicate the presence of a low-frequency mode that shows a considerable degree of relaxation towards thermalization.

We introduce the effects of relaxation on the energy spectrum by making the simple assumption that each energy has two components, a constant energy plus an energy corresponding to a common-directed-velocity system; i.e.

$$E_i = E_0 + \frac{M_i}{M_D} e \tag{8}$$

where e is the directed energy per deuteron mass and M_D is the deuteron mass. Solving this equation for the argon and oxygen measurements given in Fig. 2 for the time of appearance of O VI, gives

$$E_i = 104 + 2.8 \frac{M_i}{M_D} \text{(eV)} \tag{9}$$

To test the validity of Eq. (8), an experiment was carried out with three trace elements simultaneously present in the plasma *viz* 6% neon, 1% argon and 3% krypton. The measured ion energies are plotted against time of appearance in Fig. 3. The latest time

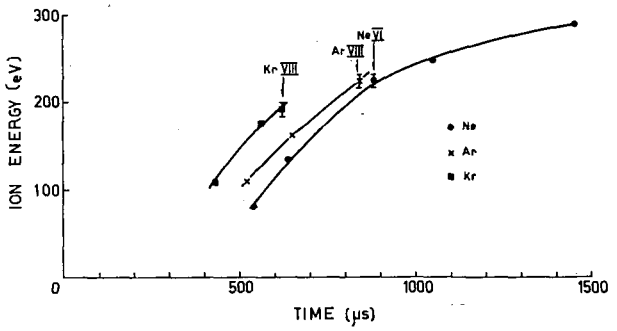

Fig. 3 Measured energies of neon, argon and krypton ions against time of appearance. I_g, 320 kA; B_z, 800 G; 0.5 mtorr deuterium with 6% neon, 1% argon, and 3% krypton. Mean square errors are indicated.

at which simultaneous measurements of the three trace elements can be made is limited by the appearance of Kr VIII. For this time, the three measured energies were used to solve Eq. (8), giving

$$E_i = 106 + 2.2 \frac{M_i}{M_D} \text{(eV)} \qquad \text{[Ar, Kr]}$$

$$E_i = 101 + 2.3 \frac{M_i}{M_D} \text{(eV)} \qquad \text{[Ne, Kr]}$$

$$E_i = 100 + 2.5 \frac{M_i}{M_D} \text{(eV)} \qquad \text{[Ne, Ar]}$$

with an average solution

$$E_i = 102 + 2.3 \frac{M_i}{M_D} \text{(eV)} \tag{10}$$

The small differences among the three solutions are consistent with the errors of measurement and the results confirm the validity of Eq. (8) in representing the energies of the trace ions. The similarity of Eq. (9) and (10) is not surprising since the energies are measured for ions with similar ionization potentials in similar discharges. We will now confine our discussion to Eq. (10).

5. Discussion

We have arrived at a model of a low-frequency perturbation that is relaxing towards thermalisation. The directed energy is given by Eq. (5). Equating this to the mass term in Eq. (10) and putting in the relevant numbers, we can calculate the equivalent electrostatic amplitude of the fluctuation. This gives $A_0 \approx 30$ volts/cm. Probe measurements by MASON [3] have detected electrostatic fluctuations with an amplitude of about 20 volts/cm and a frequency of about 5×10^4 Hz. This represents good agreement in amplitude and a frequency in the required domain. These electrostatic-probe measurements are discussed in reference to plasma loss in the accompanying Zeta paper [10].

To infer the deuteron energies, we make the simplest assumption possible at this stage, i.e., that Eq. (10), determined for the trace ions, also applies to the deuterons. This gives a directed energy that is much less than the total deuteron energy. The relaxation effects can now be treated in a power-balance equation. The spectroscopic measurements of plasma containment [6] showed that for the discharge being studied, most of the energy is carried to the walls by escaping plasma. Assuming the energy is deposited in the directed mode and then relaxes by collisions towards the random mode, a power balance equation can be formed:

$$\sum \frac{e M_i / M_D}{t_r} = \frac{\Sigma E_i}{\tau_c} \tag{11}$$

where the summations are over all ions, τ_c is the ion-containment time and t_r is the energy-relaxation time for the directed mode. Using Eq. (10) and the value of $\tau_c = 200$ μs determined from the observed spectral-line-intensity distributions gives $t_r = 13$ μs. From the Spitzer relaxation formulae [11] the deuteron-deuteron and ion-deuteron relaxation times are calculated to be about 20 and 10 μs, respectively. Thus the observed energy distributions are consistent with the interparticle relaxation times. If we imagine the directed velocities as a system of "eddies" then the thermalization time will be roughly the sum of the inter-eddy collision time and the interparticle relaxation time. The results would then indicate that the former time is negligible compared to the latter. This may be experted since the random velocities are much greater then the directed velocities, and heavy intermixing between perturbed regions may occur, particularly along the magnetic field lines.

Because of the mass effect, most of the directed energy (2/3) is carried by the trace ions. It is planned to reverse this in future experiments by reducing the amounts of trace elements.

The observation of a large random component in the ion energies makes it necessary to consider the in-phase correlation distance L along the magnetic field lines. For the ion energies to have the form shown in Eq. (8), ions moving along the field lines must see fluctuation frequencies much less than the cyclotron frequency. The condition for this is

$$\frac{1}{3} \frac{\langle v \rangle}{L} \ll \frac{\omega_{ci}}{2\pi}$$

where $\langle v \rangle$ is the mean random velocity. For the conditions of Eq. (10), this gives $L \gg 2$ cm. Electrostatic-probe measurements give $L > 10$ cm. This gives

direct support to the assumption involved in the ion-energy analysis.

Future work will include an investigation of the relationship between the ion heating mechanism and the plasma loss process. If the observed directed velocities are random in space with a mean free collision time given by t_r, a containment time can be calculated on the basis of a two-dimensional random walk, and compared with the spectroscopic value [6]. For the conditions of Eq. (10) this gives

$$\tau_c \approx \frac{D^2}{\langle v^2 \rangle t_r} \approx 300\ \mu s \qquad (12)$$

where D is the dimension of the plasma and $\langle v^2 \rangle$ is the mean square directed velocity. This shows a reasonable agreement with the spectroscopic value of 200 μs.

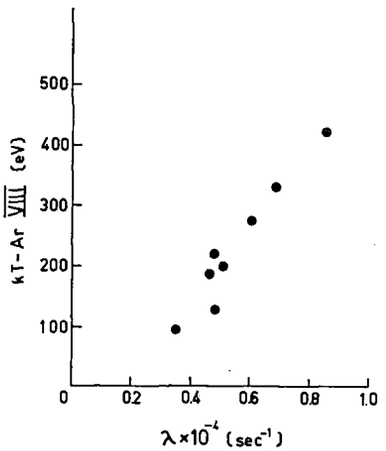

Fig. 4 Measured energies of Ar VIII ions against the inverse containment time λ. Various discharge conditions.

This possible link of the ion-heating mechanism and plasma-loss process has been investigated for only one particular discharge condition. It is planned to extend the work to cover a range of containment times and some preliminary results are given in Fig. 4, where the energy of one ion (Ar VIII) is plotted against the inverse containment time λ (sec^{-1}). λ was varied by changing the gas density and trace element concentrations. The measures show a definite correlation; the energy of Ar VIII increases with increasing plasma-loss rate. However, the time of appearance of Ar VIII is determined by λ as well as the electron temperature, and there are therefore secondary effects in the observed correlations.

6. Conclusions

It is shown that the ion energies vary with time of appearance. This is supported by time-resolved photoelectric measurements of a parent ion (He^+) in a similar discharge (Mark IV) by HEARN *et al.* [12]. Conclusions concerning the heating mechanism are based on observations of different ionic species made at the same time. The ion energies can be represented by the sum of a constant energy and an energy corresponding to a common motion (Eq. (8)), the directed motion being perpendicular to the magnetic field lines. This is interpreted as being due to a perturbation perpendicular to **B** with a frequency well below the ion cyclotron frequency, producing a mass motion that is relaxing towards thermal equilibrium. It is proposed that the energy is deposited in the directed mode and then heats the ions by relaxation due to collisions. A power-balance equation on this basis gives a relaxation time of the same order as the ion-ion relaxation time. Calculation of the amplitude of the equivalent electric field driving the directed mode gives a value of the same order as observed with electrostatic probes. From the data given by RUSBRIDGE *et al* [13] it can be shown that the electrostatic fluctuations should give ion energies about ten times greater than the magnetic-field fluctuations. It is thus clear that the ion energies and electrostatic fluctuations are consistent with each other.

This work is still in progress. The aim is to determine the behaviour of the ion heating mechanism as a basis for understanding the detailed physics of the perturbations.

Acknowledgements

We are grateful to R. H. White and F. F. Freeman for assistance with the experiments and to the Zeta Operations Group for their co-operation. The investigation has benefited from many fruitful discussions with R. S. Pease and P. C. Thonemann.

References

[1] HARDING, G. N., et al, in Proc. 2nd U.N. Intern. Conf. PUAE **32**, United Nations, Geneva (1958) 365.
[2] BUTT, E. P., et al, in proceedings of ref. 1, **32**, 42.
[3] GIBSON, A., MASON, D. W., *Proc. phys. Soc.* (*London*) **79** (1962) 326.
[4] PEASE, R. S., unpublished lecture delivered at Varenna School of Physics (1959).
[5] THONEMANN, P. C., U. K. AERE Report R 3340 (1960).
[6] BURTON, W. M., WILSON, R., *Proc. phys. Soc.* (*London*) **78** (1961) 1416.
[7] FAWCETT, B. C. et al, *Proc. phys. Soc.* (*London*) **78** (1961) 1223.
[8] JONES, B. B. *Applied Optics* **1** (1962) 239.
[9] ZAIDEL, A. N., et al, *Zh. tek. Fiz.* **30** (1960) 1422.
[10] BURTON., W. M., BUTT, E. P., et al, *Nuclear Fusion*: 1962 Supplement, Part 3, 903.
[11] SPITZER, L., Jr., Physics of Fully Ionized Gases, Interscience Publishers, New York (1956).
[12] HEARN, A. G., et al, *J. nucl. Energy, Part C*, **4** (1962) 23.
[13] RUSBRIDGE, M. G., et al, *Nuclear Fusion*: 1962 Supplement, Part 3, 895.

ELECTRIC AND MAGNETIC FIELD FLUCTUATIONS IN HIGH-CURRENT TOROIDAL DISCHARGES*

M. G. RUSBRIDGE, D. J. LEES, P. A. H. SAUNDERS

ATOMIC ENERGY RESEARCH ESTABLISHMENT

HARWELL, BERKSHIRE, UNITED KINGDOM

Electric-field probes and magnetic search coils have been used to observe low-frequency fluctuations in discharges in Zeta and a similar torus of smaller bore. The amplitude of the fluctuations has been measured as a function of discharge conditions and the results are summarized briefly. A simple ideal hydromagnetic model is introduced which fits the observed magnetic field fluctuations closely; this shows that the principal perturbation has a long wavelength and azimuthal symmetry number $m = 1$. The rms plasma displacement is less than 10% of the discharge tube radius under normal conditions.

The origin of the observed electric-field fluctuations is discussed, and an equation is derived that in principle relates the electric- and magnetic-field fluctuations. The observed electric-field amplitudes are shown to be consistent with this result, but the coefficient of correlation between the electric- and magnetic-field fluctuations is small. A characteristic frequency for the fluctuations is estimated by counting the number of maxima per unit time. This frequency varies approximately inversely as the square root of gas pressure and directly with the magnetic field at the centre of the discharge; this is consistent with the hydromagnetic model described above.

The form of the dispersion relation for hydromagnetic waves in a cylindrical discharge is discussed in the light of these results, and theoretical results on the stability of a particular model of the discharge are given. The origin and maintenance of the fluctuations and their significance for the diffusion of plasma across containing magnetic fields are discussed.

1. Introduction

The stability of the pinched discharge has been the subject of several investigations [1-5] based on the ideal hydromagnetic approximation, which have in general led to the conclusion that such discharges are theoretically unstable unless stringent conditions are met. The random fluctuations that are known to occur in these discharges [6, 7] are usually taken to indicate that they are in fact unstable, but it is not known how these fluctuations are related to the predicted instabilities. In fact the theory predicts that unstable perturbations should grow exponentially with time whereas the observations show that the fluctuations are oscillatory with an amplitude that remains constant on the average over times long compared with the theoretical growth rate.

In this paper we summarize the general behaviour of the fluctuations of electric and magnetic fields observed in discharges in Zeta and the Mark IV torus [8] under conditions in which the mean magnetic fields are fully diffused. We introduce a simple hydromagnetic model of the perturbations and show that the magnetic field fluctuations agree with the model closely while the electric fields do not. The magnetic-field fluctuations are found to correspond to modes that are probably stable, while the predicted instabilities make only a small contribution to the fluctuation level.

We define a fluctuation as any departure of the measured quantity from its mean value over many discharges. Experimental limitations set an upper limit to the frequency of the fluctuations we can observe at about 2 MHz; however, we shall show experimentally that a characteristic frequency exists in the region of 50-100 kHz, and the fluctuations in which we shall be interested lie below this limit. By the use of special techniques fluctuations have been observed at frequencies of up to 25 MHz, but their importance is not yet known.

2. Experimental methods

Magnetic fields were measured in Zeta using search coils of 500 turns and electronic integrators with over-all frequency response of about 300 kHz; for higher frequencies a small coil of 50 turns was used with a simple RC integrating circuit, which responded up to 2 MHz. These coils were placed in a 7/8-in.-diameter quartz tube silvered on the inside that served as a vacuum envelope. The frequency response of the small coil was measured inside the silvered tube.

With the low-frequency coils, the field was recorded simultaneously at 17 points in the discharge using a multi-channel oscilloscope. By superposing records from different shots a measure of the relative amplitude of fluctuation in different coils was obtained, but the number of shots was in general too small to give an accurate measure of the absolute fluctuation level. This was measured with greater accuracy with one coil only at the centre of the discharge.

Electric fields were measured by observing the voltage developed between two platinum probes, each 4 mm long by 2 mm in diameter placed 1.6 cm apart.

* Conference paper CN-10/58, presented by R. S. Pease. Discussion of this paper is given on page 1017. Translations of the abstract are at the end of this volume of the Conference Proceedings.

Since the potential at the centre of the discharge may rise to several kilovolts (D. MASON, private communication) the voltage was measured through a pulse transformer [9]. The frequency response of this system extended from about 100 to 300 kHz.

In the Mark IV the same methods were used, but the pulse transformer was not necessary for the electric-field measurements, and magnetic-field measurements were made principally with two search coils that could be moved relative to each other along a diameter. The high pulse repetition frequency of 1 discharge/s. which could be obtained in the Mark IV allowed the use of electrical averaging to obtain the mean amplitude of fluctuations. The fluctuating signal was filtered to remove any d.c. level, and the positive and negative parts were separately sampled by rectifiers over a sampling time of 50 μs and integrated over many discharges in a long-period integrator. This system, which will be described more fully elsewhere, has been used principally for measurements in the frequency band 14-25 kHz. It can be shown that for this frequency band and sampling time we obtain about 2.1 effectively independent measurements per discharge. The method of full-wave rectification gives a probable error of $\pm 51/N^{1/2}\,\%$ where N is the number of independent measurements. Thus for 100 discharges we obtain a probable error of $\pm 3.5\,\%$. A correction can be applied to the results to take account of the non-linear characteristics of the rectifiers, but this has been found to be small and has usually been neglected.

From measurements of the amplitudes of the sum and difference of two signals the normalized correlation coefficient between them can be obtained with a probable error of ± 0.05 or less.

It has not yet been possible to use this system on Zeta, and here measurements are made from film records in the usual way; this restricts us in practice to about 30 independent measurements, giving a probable error of about 10%.

3. General behaviour of fluctuations

To indicate the orders of magnitude with which we have to deal, we give here some results of a survey carried out in Zeta of the dependence of the rms level and characteristic frequency of the fluctuations on the discharge parameters. The characteristic frequency is determined by counting the number of maxima per unit time; we denote this by N_m. RICE [10] has shown that for a signal whose power spectrum is constant up to a frequency limit f_c, N_m is given by

$$N_m = 0.775\, f_c \qquad (1)$$

Since we do not know the detailed form of the power spectrum, we have not attempted to calculate the actual limiting frequency, but we note that it will not be much greater than N_m.

Measurements were restricted to periods of 100 or 200 μs around peak gas current; within this period conditions are sensibly constant. Table I shows the over-all ranges of discharge parameters covered. The filling gas is deuterium.

TABLE I. Over-all ranges of discharge parameters

Capacitor-bank energy	0.75 MJ (at 25 kV)
Capacitor-bank voltage	5—15 kV
Peak gas current	50—230 kA
Applied axial field	150—750 G
Gas pressure	0.2—15 mtorr
θ	1.0—3.0

The quantity θ given in Table I is the parameter shown by LEES and RUSBRIDGE [11] to determine the magnetic-field configuration; it is defined by $\theta = 2I/aB_0$ where I is the gas current, a the tube radius, and B_0 the applied axial field.

Some of the results are shown in Figs. 1 to 4. The rms electric field was measured as a function of gas current I and pressure p for approximately constant θ and was found to be proportional to a single parameter I^2/p; this is shown in Fig. 1. The rms field ranges up to 30 V/cm with occasional peaks up to 150 V/cm.

The rms level of the magnetic field fluctuations, normalised by dividing by the initial axial field B_0, is proportional to θ^2 for $\theta \lesssim 3.0$. This is shown in Fig. 2. For higher values of θ the fluctuations in-

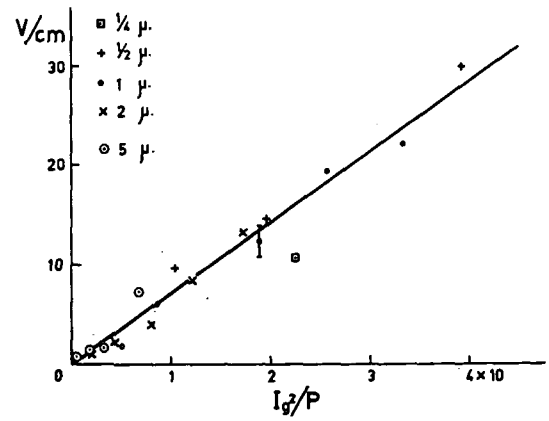

Fig. 1 Rms electric-field fluctuations as a function of I_g^2/p where I_g is gas current in kiloamperes and p is pressure in mtorr (μ).

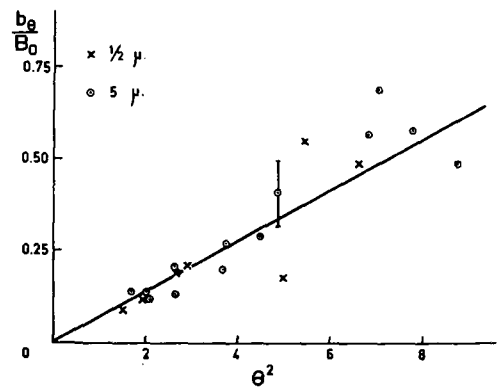

Fig. 2 Normalized rms magnetic-field fluctuations as a function of θ^2.

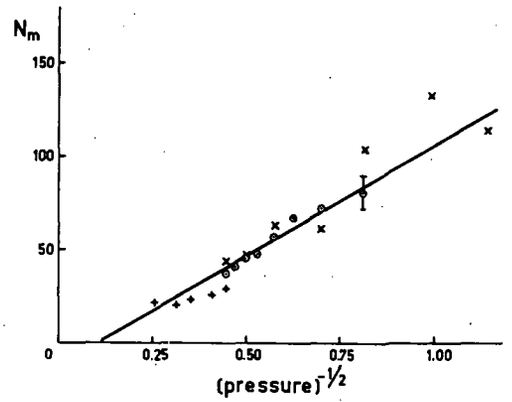

Fig. 3 Average number of maxima per millisecond as a function of $p^{-1/2}$ where pressure p is in mtorr. The different points distinguish measurements with different coil and integrator systems.

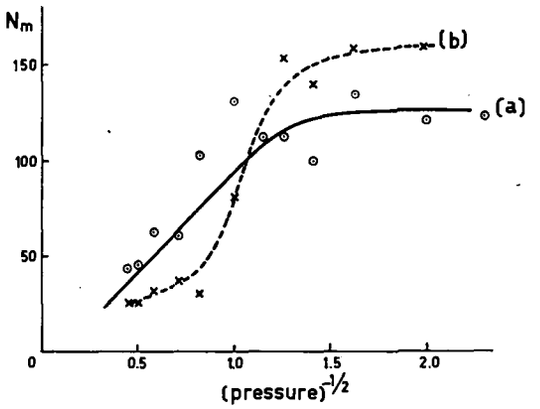

Fig. 4 Average number of maxima per millisecond as a function of $p^{-1/2}$ where pressure p is in mtorr. X's are for capacitor-bank potential of 10 kV, 220 G, ~130 kA; circles are for 15 kV, 220 G, ~170 kA.

crease rather more rapidly, but even so do not exceed 20% of the maximum field of the discharge. The rms level is approximately independent of pressure; results are shown for two pressures, 0.5 and 5 mtorr.

The number of maxima per unit time is shown in Figs. 3 and 4 as a function of $p^{-1/2}$ where p is pressure and is measured in millitorrs, for the magnetic-field fluctuations. Fig. 3 shows that at high pressures, above 1 millitorr, the relation between N_m and $p^{-1/2}$ is approximately linear, but the best straight line does not pass through the origin. The different points in this figure distinguish measurements made with different coil and integrator systems of different frequency response to demonstrate that the frequency limit is not related to that of the apparatus. Figure 4 shows that the linear relation does not hold for lower pressures; the frequency reaches a limiting value of between 100 and 200 kHz. These measurements were made with the small coil with a frequency response of 2 MHz. The frequency limit is greater for the smaller gas current; this confirms that the frequency limit is not due to the apparatus.

The characteristic frequency of the electric field is somewhat greater than that of the magnetic field, but no detailed measurements have been made.

All these measurements were made at the geometric centre of the discharge, measuring fields normal to the discharge axis.

4. Comparison of theory and experiment

4.1 Magnetic field fluctuations

We consider an infinitely long cylindrical discharge of radius a, bounded by infinitely conducting walls. We assume the plasma to be cold, compressible, and of uniform density, and the magnetic-field configuration to be force-free. These assumptions represent a first approximation to the properties of the plasma in Zeta and the Mark IV torus. By comparison with experiment we hope to determine how far these assumptions need modification.

We use the usual set of linearized ideal hydromagnetic equations [12] and assume that all fluctuating quantities can be represented in the form

$$A = A(r) \exp i(m\theta + kz - \omega t) \tag{2}$$

$A(r)$ is some function of radius to be determined. In particular we require to determine $A(r)$ for the fluctuating components of magnetic and electric fields and the phase relations between them. We define $\mathbf{B}$ as the mean magnetic field, $\mathbf{b}$ as the amplitude of the fluctuating component, and $\boldsymbol{\xi}$ as the amplitude of plasma displacement. Since $B_r = 0$ by symmetry, we may write

$$\boldsymbol{\xi} = B_{z0}(0, f, g) \tag{3}$$

where B_{z0} is the value of B_z for $r = 0$ and f and g are functions of r alone. From the condition that the plasma is tied to the lines of force it may be shown that

$$\mathbf{b} = \nabla \times (\boldsymbol{\xi} \times \mathbf{B}) \tag{4}$$

Since the plasma is pressureless there is no force acting parallel to the field lines, thus

$$\boldsymbol{\xi} \cdot \mathbf{B} = 0 \tag{5}$$

Using Eqs. (3) and (5) we may write the components of Eq. (4) in the following forms

$$b_r = \frac{iB_{z0}}{a} \xi_r \left(\frac{mf}{x} - Kg \right) \tag{6}$$

$$b_\theta = \frac{B_{z0}}{a} [\xi_r f' + \xi_r' f - K\eta] \tag{7}$$

$$b_z = \frac{B_{z0}}{a} \left[\xi_r \left(g' + \frac{g}{x} \right) + \xi_r' g - \frac{m\eta}{x} \right] \tag{8}$$

where $x = r/a$, $K = -$ ka and

$$\eta = -i\xi_0 \frac{f^2 + g^2}{g} \tag{9}$$

(we have defined K in this way since it will normally be positive with this definition). From Eqs. (6)-(8) and the linearized equations of motion we obtain the relation

$$\eta = \frac{(f^2+g^2)[\xi_r(mg - Kxf) + \xi_r' x(mg + Kxf)]}{(f^2+g^2)(m^2 + K^2x^2) - \Omega x^2} \tag{10}$$

where

$$\Omega = \frac{4\pi\varrho\,\omega^2 a^2}{B_{z0}^2} \tag{11}$$

and ϱ is the plasma density, together with a further relation between ξ_r and η. The solution of these coupled equations, subject to the boundary conditions that ξ_r should be finite on the axis and vanish at the walls, gives ξ_r and η as functions of x and the relation between Ω, K, and m, i.e., the dispersion relation. These equations have not been solved; conventional hydromagnetic stability calculations, however, determine the sign of Ω and the values of K for which $\Omega=0$. From these results and comparison with simpler cases where the dispersion relation can be obtained exactly [13], a reasonable guess at the form of the dispersion relation can sometimes be made. As an example we consider a configuration similar to that given by the paramagnetic model [14] but with vanishing conductivity across the lines of force and with the total axial flux chosen so that $\theta=1.64$. This configuration has been tested for stability by WHITEMAN (private communication) using the criterion

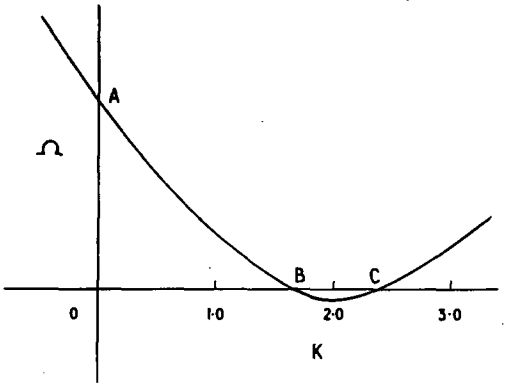

Fig. 5 Conjectural form of dispersion relation for $m=1$. BC is region of instability; observed fluctuations appear to lie in region AB.

due to NEWCOMB [5]. He finds that it is stable for $m=0$, and unstable for $m=1$ only in the range $K=1.65$ to 2.35, surrounding the point $K=2.0$ at which the perturbation and magnetic-field helices coincide at the centre of the discharge. On this basis we suggest that the dispersion relation for $m=1$ has a form similar to that shown in Fig. 5. Here BC represents the range of instability ($\Omega<0$).

We now consider some more detailed predictions from the model and compare them with experiment. The equations giving η and ξ_r, mentioned above, have real coefficients so that η and ξ_r themselves are real. Inspection of Eqs. (6)-(8) then shows that the components of $\mathbf{b}$ are either real or purely imaginary, which implies that no phase change (except possibly a change of sign) occurs along a radius of the discharge.

An experiment to test this prediction was carried out in the Mark IV; the correlation coefficients between b_θ at the centre and $\mathrm{d}b_\theta/\mathrm{d}t$ near the wall, in the frequency band 14—25 kHz were measured. A small phase shift was found but could be attributed entirely to phase lags in the circuits; an estimate of the residual phase shift in the plasma gave 0.02 ± 0.04 radians at 20 kHz.

In this simple model the frequency enters only in the combination Ω defined by Eq. (11) above, provided that the frequency is much lower than the ion cyclotron frequency, which in our conditions in Zeta is typically 1.5 MHz. Thus, in particular, any characteristic frequencies should be proportional to $B_{z0}/\varrho^{1/2}$ if the parameter θ, which determines the functions f and g, is constant.

In the high-pressure region above 1 mtorr the variation of N_m with density shown in Fig. 3 is approximately correct (though not exactly since the best straight line does not pass through the origin); the dependence on B_{z0} has not been measured in detail but is qualitatively correct; and the frequency given by $\Omega=1$, which should give the order of any characteristic frequency, is of the same order as the observed N_m. At low pressures, however, the results, shown in Fig. 4, clearly do not fit the simple theory.

To proceed further we must make some approximations. We note that by simple symmetry argument, ξ_r, η and b_θ must vanish on the axis unless $m=1$; also b_z must vanish on the axis except for $m=0$. Results to be presented below show immediately that at low frequencies there is a large contribution from $m=1$. For this case we assume that ξ_r may be represented by a simple parabolic form:

$$\xi_r = \xi_0\,(1-x^2) \tag{12}$$

Further, in the conditions for which the results of Figs. 9 and 10 below were obtained we find $\Omega\lesssim 0.1$ for frequencies less than 20 kHz; as a first approximation therefore we neglect Ω in Eq. (10). Equations (6)-(8), (10) and (12) can then be used to calculate $\mathbf{b}/\xi_0$ as function of r with K as the only parameter for any given configuration. This has been done for the force-free paramagnetic model mentioned above; the results for three values of K are shown in Figs. 6 and 7. We see that the amplitude decreases in general as K increases; at the centre, the amplitude vanishes

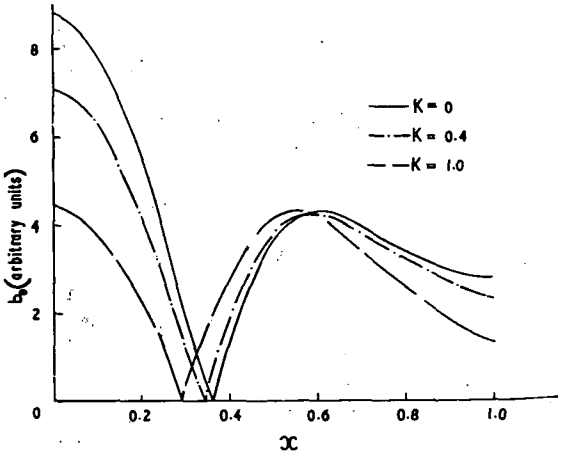

Fig. 6 b_θ as a function of x for the force-free paramagnetic model with $\theta=1.70$ for various values of K. Zeros correspond to changes of phase by π.

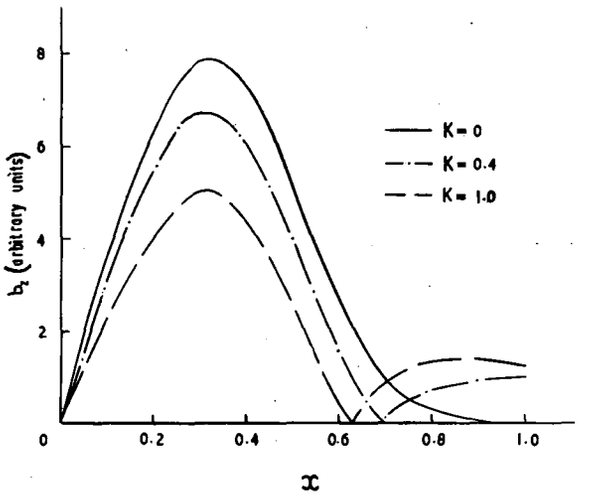

Fig. 7 b_z as a function of x for the force-free paramagnetic model with $\theta = 1.70$ for various values of K. Zeros correspond to changes of phase by π.

for $K = 2.0$ and increases again for higher values of K. Since the magnetic-field perturbations give rise to the plasma restoring force, this behaviour is consistent with the form of the dispersion relation given in Fig. 5. However, it also implies that fluctuations lying in the unstable region BC will be difficult to detect in the presence of fluctuations with other values of K.

The radial distribution of b_θ and b_z has been measured in Zeta under the following conditions: pressure 2 mtorr, gas current 94 kA, and applied axial field 220 G, corresponding to $\theta = 1.70$. No frequency discrimination was used in these measurements, the total shot-to-shot variation being measured from the multi-channel oscilloscope records. Figure 8 shows the mean configuration, and the peak-to-peak amplitudes of b_θ and b_z are shown in Figs. 9 and 10. The solid curves are derived from the mean configuration using the theory outlined above; the best fit was obtained for $K = 0.4$, corresponding to a wavelength of 750 cm. (The total length of the toroidal tube is 1160 cm). This value was chosen by fitting the ratio of the central peak of b_θ to the peaks at

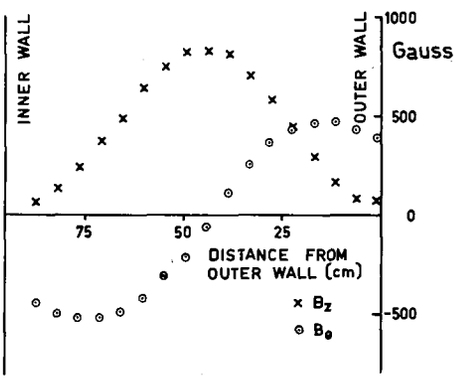

Fig. 8 Mean-magnetic-field configuration at 94 kA, 220 G, 2 mtorr of deuterium measured along a horizontal diameter of the torus.

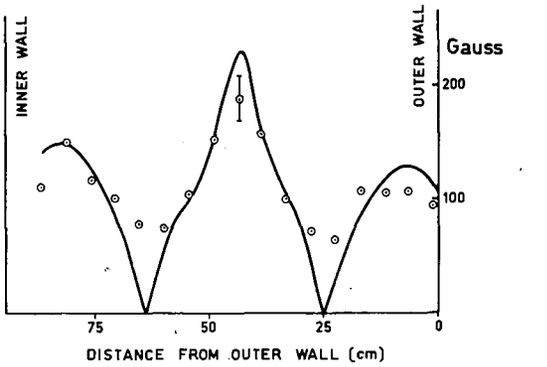

Fig. 9 Experimental results for b_θ under conditions of Fig. 7 compared with theoretical curve deduced from Fig. 7 for $K = 0.4$.

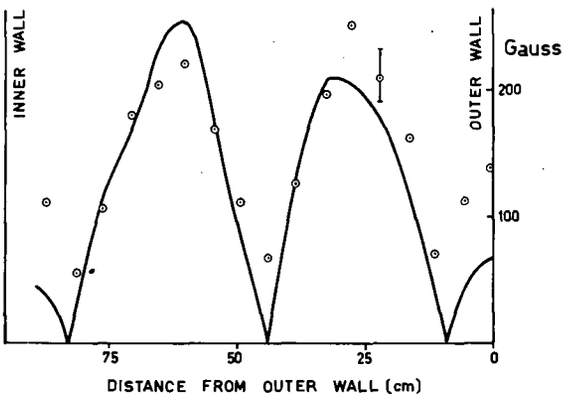

Fig. 10 Experimental results for b_z under conditions of Fig. 7 compared with theoretical curve deduced from Fig. 7 for $K = 0.4$.

10 and 80 cm. With this value of K the theoretical curves have been normalized independently to the experimental points for b_θ and b_z since they were derived from different sets of discharges. We see that the general shape of the curves agrees excellently with experiment, and in particular the positions of all the minima agree with predicted zeros to within a few centimeters.

Since there was no frequency discrimination in this experiment, the value of K must represent some average over the frequency distribution. Measurements made in a restricted frequency band in the Mark IV have yielded essentially similar results; they clearly indicate a small positive value of K, but their analysis is not yet complete.

The force-free paramagnetic-model configuration is essentially similar to the experimental configuration shown in Fig. 8, though rather more compressed. If the dispersion relation for the experimental configuration is similar to that shown in Fig. 5, then it seems that the principal magnetic field fluctuations correspond to perturbations lying on the stable branch AB.

This tentative conclusion justifies our comparison of N_m and the frequency given by $\Omega = 1$, which rests on the implicit assumption that the observed modes are stable.

The deep minimum observed in b_z at the centre in Fig. 10 shows that fluctuations with $m=0$ make only a small contribution. We cannot exclude contributions from $m \geq 2$, but the good fit obtained suggests that it is unnecessary to consider such contributions. Further, the measurements in the Mark IV referred to above gave a correlation coefficient between b_θ at the centre and at the wall of -0.95 ± 0.07, which also suggests that only one mode contributes.

We see therefore that the magnetic-field fluctuations appear to fit our simple theory satisfactorily and give hope that a more refined analysis on these lines will be worth while.

4.2 Electric field fluctuations

Provided the impedance of the voltage-measuring circuit is large, the signal obtained from an electric probe is a measure of the potential difference between two points in the plasma, together with the induced EMF in the circuit formed by the probe and plasma. The probe is constructed so as to reduce this induced EMF as far as possible; the area of the loop is not well defined but is about 10 cm^2, which gives an induced signal usually about 10-20% of the observed fluctuations. Since this is only of the same order as the experimental error, we shall ignore the induced voltage.

A general electric field distribution $\mathbf{E}$ can always be decomposed into an irrotational part $\mathbf{e}$ and a solenoidal part $\mathbf{E}_s$ which are defined by

$$\begin{aligned} \nabla \times \mathbf{e} &= 0 \\ \nabla \cdot \mathbf{E}_s &= 0 \\ \mathbf{E}_s + \mathbf{e} &= \mathbf{E} \end{aligned} \tag{13}$$

Then $\mathbf{e}$ is the field distribution that would be observed by a probe whose loop area is zero. (We are grateful to D. Mason for pointing this out to us.) Equations (13) are sufficient to determine $\mathbf{e}$; for e_θ we find

$$\frac{\mathrm{d}^2 e_\theta}{\mathrm{d}r^2} + \frac{3}{r}\frac{\mathrm{d}e_\theta}{\mathrm{d}r} - \frac{m^2 - 1 + k^2 r^2}{r^2} e_\theta = \mathrm{i}\frac{m}{r}\nabla \cdot \mathbf{E} \tag{14}$$

For $m=1$ this reduces to

$$\frac{\mathrm{d}^2 e_\theta}{\mathrm{d}r^2} + \frac{3}{r}\frac{\mathrm{d}e_\theta}{\mathrm{d}r} - k^2 e_\theta = \frac{\mathrm{i}}{r}\nabla \cdot \mathbf{E} \tag{15}$$

with the boundary conditions that e_θ should vanish at the wall and remain finite on the axis. This equation can be solved if k^2 is small enough to be neglected. The electric field $\mathbf{E}$ is given for a cold plasma by

$$\mathbf{E} + \mathbf{V} \times \mathbf{B} = 0 \tag{16}$$

and we find that e_θ on the axis is given by

$$e_{\theta_0} = (0.55 + 0.05\,K)\; V_0\, B_{z_0} \tag{17}$$

for the model configuration used above, where $\mathbf{V}$ is the plasma velocity given by $\mathbf{V} = \mathrm{i}\omega\xi$, and $V_0 = \mathrm{i}\omega\xi_0$. The numerical coefficients will of course depend on the configuration but those of Eq. (17) should be typical.

In Eq. (17) V_0 can be obtained from the observed value of $\partial b_\theta/\partial t$ at the centre using the theory developed in the previous section, and assuming $K=0$. The phase relations are such that e_{θ_0} is in phase with $\partial b_\theta/\partial t$; this relation is independent of the direction of propagation of the wave. An experiment to test these predictions was carried out in Zeta; e_{θ_0} and $\partial b_\theta/\partial t$ were measured simultaneously in restricted frequency bands 7-14 kHz and 14-25 kHz. The axial field was 220 G in all cases. The results are shown in Table II.

In this table F is the measured correlation coefficient; the probable error is about ± 0.1. We have assumed that Eq. (17) is approximately correct for this configuration also, so that the expected value of e_{θ_0} is about $0.5\; V_0 B_{z_0}$. (The mean configuration was not measured at 2 mtorr; so no value for $0.5\, V_0 B_{z_0}$ can be given for these cases.)

We see immediately from the values of F that the greater part of the observed electric field cannot be accounted for on our model. The part of the electric field associated with the magnetic-field fluctuations will be given by Fe_{θ_0}; this is shown in the last column. The agreement between this and $0.5\, V_0 B_{z_0}$ is probably as good as can be expected on our simplified assumptions. When the plasma is not assumed cold, a number of additional effects associated with temperature and density fluctuations contribute to the voltage measured by the probe and could account for the discrepancy; these have been considered by Rusbridge *et al* [8] for a particular case but no estimate of them has yet

TABLE II. Correlation between e_{θ_0} and $\partial b_\theta/\partial t$

Gas current (kA)	Pressure (mtorr)	e_{θ_0} observed (V/cm)	$\partial b_\theta/\partial t$ observed (10^6 G/s)	F measured	$0.5\; V_0 B_{z_0}$ calculated (V/cm)	Fe_{θ_0} observed (V/cm)
7–14 kHz						
195	0.5	1.0	1.35	+0.06	0.17	0.06
170	2	0.8	1.85	+0.09		
160	5	0.4	1.5	+0.13	0.15	0.05
14–25 kHz						
195	0.5	1.1	2.35	+0.16	0.3	0.18
170	2	0.65	2.5	+0.08		
160	5	0.6	3.0	+0.06	0.3	0.04

been made in Zeta. All these effects produce voltages in phase with $\partial b_\theta/\partial t$; there may in addition be a resistive field if the conductivity is finite, which will be in phase with b_θ. The correlation coefficient between e_{θ_0} and b_θ was measured for one of the conditions of Table II and found to be 0.06; so at least one can say that the resistive fields are not greater than the other terms.

At the centre the electric field components obey the same symmetry rules as the magnetic fields; thus the absence of $m=0$ fluctuations leads us to expect a small value of e_z at the centre. When no frequency discrimination is used this expectation is fulfilled; but both in the Mark IV and in Zeta it appears that in the frequency band 14-25 kHz e_z and e_θ at the centre are very nearly equal, and the radial variation is inconsistent with the equation $\nabla \times \mathbf{e}=0$, if only a single mode is present. These latter results are preliminary; if they are confirmed, they would possibly suggest that the electric field fluctuations have a short correlation distance across the lines of force. This is consistent with the conclusion that the electric field is not associated with gross motions of the discharge, and agrees with results obtained by GIBSON and MASON [15] who measured fluctuations of the potential of the discharge with respect to the wall and showed that these were uncorrelated over distances greater than about 10 cm across the lines of force.

5. Discussion

We have shown that it is likely that the observed magnetic field fluctuations are stable in the hydromagnetic approximation. Their growth to their observed finite amplitude therefore cannot be explained on the simple theory given here. Nevertheless this growth may be due to small terms that are omitted from the equations in the ideal hydromagnetic approximation such as finite conductivity [16] or the Hall effect [17]; such terms may affect the properties of the oscillatory modes very little apart from making Ω complex.

We cannot exclude the possibility that theoretically unstable modes are present, but they must be stabilized by non-linear effects; the amplitude of the plasma perturbation could, however, be appreciably larger than that corresponding to the stable modes, which is no greater than a few centimeters. Some of the observed electric field fluctuations could be associated with these modes. Apart from this possibility, however, the origin of the electric field fluctuations is not known. However, unless they are largely due to the effects discussed by RUSBRIDGE *et al* [8], they will be associated with a drift of plasma across lines of force and hence with plasma loss. BURTON and WILSON [18] have shown that the Zeta plasma suffers loss and injection processes and have determined the dependence of the loss and injection rate coefficients on discharge parameters, while GIBSON and MASON [15] have discussed the loss process and come to the conclusion that it can be accounted for by electric-field fluctuations. The injection rate, however, increases with θ although the loss rate is independent of θ; this suggests that the injection may be associated with the magnetic-field fluctuations which also increase with θ. This suggests that injection occurs when the bulk of the plasma comes into contact with the wall; the proportion of time for which this occurs will increase with the amplitude of plasma motion and hence with θ.

6. Conclusions

We have shown that the behaviour of the magnetic field fluctuations in Zeta and the Mark IV agree well with a simple hydromagnetic model; the fluctuations have $m=1$ and probably correspond to perturbations that are stable in the ideal hydromagnetic approximation. The electric fields associated with these fluctuations have been calculated, but the observations show that these fields are masked by much larger electric-field fluctuations of unknown origin. If these fluctuations are not due to effects associated with electron-temperature and density fluctuations they may be responsible for the loss of plasma across the magnetic field that is known to occur in Zeta.

Acknowledgements

We are grateful to K. J. Whiteman for carrying out the stability calculations for us and to D. Mason and R. S. Pease for helpful discussions.

References

[1] ROSENBLUTH, M. N., in Proc. 3rd Intern. Conf. Ionization Phenomena in Gases (Venice, 11-15 June 1957) **2**, North Holland Publishing Co., Amsterdam (1959) 903.
[2] SHAFRANOV, V. D., Atom. Energiya **5** (1957) 709.
[3] TAYLER, R. J., *Proc. phys. Soc.* (*London*) **B 70** (1957) 31.
[4] SUYDAM, B. R., in Proc. 2nd U.N. Conf. PUAE **31**, United Nations, Geneva (1958) 157.
[5] NEWCOMB, W. A., *Ann. Phys.* **10** (1960) 232.
[6] BUTT, E. P., et al, in proceedings of ref. 4 **32**, 42.
[7] COLGATE, S. A., FURTH, H. P., *Phys. Fluids* **3** (1960) 982.
[8] RUSBRIDGE, M. G., et al, *J. nucl. Energy, Part C*, **3** (1961) 98.
[9] JONES, H. W., SAUNDERS, P.A.H., *J. sci. Instr.* **37** (1960) 457.
[10] RICE, S. O., *Bell System Tech. J.* **24** (1945) 46.
[11] LEES, D. J., RUSBRIDGE, M. G., in Proc. 4th Intern. Conf. Ionization Phenomena in Gases (Uppsala, 17-21 Aug. 1959) **2**, North Holland Publishing Co., Amsterdam (1960) 954.
[12] TAYLER, R. J., *Proc. phys. Soc.* (*London*) **B 70** (1957) 1049.
[13] NEWCOMB, W. A., in Magnetohydrodynamics, (R.K.M. Landshoff, ed.), Stanford University Press (1957) 109.
[14] BRAGINSKY, S. I., SHAFRANOV, V. D., in Plasma Physics and the Problem of Controlled Thermonuclear Reactions, (M. A. Leontovich, ed.), Pergamon Press **2** (1959) 39.
[15] GIBSON, A., MASON, D., *Proc. phys. Soc.* (*London*) **79** (1962) 326.
[16] JUKES, J. D., *Phys. Fluids* **4** (1961) 1527.
[17] WARE, A. A., *J. nucl. Energy, Part C*, **3** (1961) 93.
[18] BURTON, W. M., WILSON, R., *Proc. phys. Soc.* (*London*) **78** (1961) 1516.

PLASMA LOSS IN ZETA*

W. M. BURTON, E. P. BUTT, H. C. COLE, A. GIBSON, D. W. MASON, R. S. PEASE, K. WHITEMAN, R. WILSON

ATOMIC ENERGY RESEARCH ESTABLISHMENT

HARWELL, BERKSHIRE, UNITED KINGDOM

Observations are presented on the Zeta discharge, in deuterium at initial pressures of 0.25-20 mtorr and in other gases, at currents of 100-900 kA. The observations are interpreted in terms of energy loss and of plasma loss and injection. The phenomena observed depend on a number of parameters, of which the loss process appears to be governed mainly by the energy input per unit mass of plasma ε. At values of $\varepsilon > 1$ keV per proton mass the energy loss is due to a plasma loss-and-injection process. Plasma containment times of about 100 μs have been measured by spectroscopic, energy-balance and electric-field-fluctuation methods. The plasma mass motions required agree with those measured spectroscopically. There is a net pump-out of plasma during the discharge and measurements show that when the line density falls to about 6×10^{16} cm^{-1}, there is a catastrophic runaway process in which the energy is carried to the walls by runaway electrons. At values of $\varepsilon \lesssim 1$ keV, the energy is mainly radiated, and plasma containment times of about 10^{-3} s with β values of 5% can be inferred; under those conditions, however, the temperatures are $< \sim 10$ eV.

The loss of plasma is associated with an excess resistance, whose presence is established by comparison of observed resistance with resistance calculated from electron-temperature measurements. This excess resistance corresponds to the energy used in driving the plasma to the walls and heating the ions to the high temperature. The diffusion loss process is therefore likely to be driven by the electromagnetic forces rather than by Joule heating of the plasma.

The nature of the mechanism is not clear, but evidence suggests a possible connection with discontinuities in the current waveforms, which may be associated with integral numbers of helices formed by the magnetic field configuration in the torus.

1. Introduction

Extensive reports on attempts to produce hot contained plasma in the toroidal pinch geometry were given at the Geneva Conference in 1958 [1-5]. The conditions theoretically required were discussed by ROSENBLUTH [6], BICKERTON [7] and others. These calculations showed that the pinch geometry is a possible basis for a controlled fusion device. It is obvious, however, that the theoretically required conditions were not all met in the experiments described, and the energy balance achieved indicated a serious failure of energy containment in many conditions. However, neither the observations nor their interpretation were sufficiently detailed for it to be obvious that the poor containment was solely due to the failure to meet the theoretical conditions. For this reason we have pursued experimental studies on pinch systems with the aim of establishing and interpreting the predominant plasma physics phenomena.

The Zeta apparatus is essentially a 1-m-bore torus, of 12-m circumference round the centre line of the bore, in which pulse currents of several hundred kiloamperes are passed through low-pressure gas in the presence of a stabilizing magnetic field B_0, for times of 1-3 ms. The main characteristics of the discharge reported in 1958 [1] were: a confinement time of the plasma energy of about 100 μs; impurity-ion energies corresponding to temperatures of about 5×10^6 °K; electron temperatures in the range $0.1\text{-}0.5 \times 10^6$ °K; the diffuse nature of the magnetic field distributions, including the absence of a skin effect at the start of the pulse; the presence of fluctuations in the magnetic fields and in the total current; the abrupt termination of the current pulse; the emission of X-rays and of neutrons. Since 1958 the apparatus has been modified to give considerable extensions of the operating parameters, and these modifications are briefly described herein. The extensions of operating parameters have not revealed drastically new phenomena, and the studies carried out have been concerned with these main characteristics. Details of many of these studies are given elsewhere [8-14]. It is the purpose of this paper to survey the observations related to the key problems of plasma loss, and their interpretation.

The paper starts from the well-known problem of energy-loss mechanisms, and the results presented in Section 3 show that radiation does not account for the energy loss at deuterium pressures below about 5 mtorr. In Section 4 three types of observations are described, all giving strong evidence of plasma loss and quantitatively accounting for the energy loss. The methods used are (a) spectroscopic measurement, (b) the measurement of plasma at the walls and (c) the measurement of electric fields corresponding to plasma movement. The spectroscopic measurements also give an estimate of the injection rate of gas throughout the pulse. These results go far to explaining the occurence of runaway electrons towards the

* Conference paper CE-10/60. presented by R. S. Pease. Discussion of this paper is given on page 1017. Translations of the abstract are at the end of this volume of the Conference Proceedings.

end of the pulse due to a net pump-out, and these runaway electron effects are described in Section 5. In Section 6 evidence on the relation of plasma loss to excess resistivity is presented. The possibility that the loss processes are associated with current discontinuities is discussed in Section 7. Finally, the loss processes are discussed in terms of hydromagnetic stability theory and observations on Zeta given in other papers.

2. Apparatus

2.1 Modifications to the torus assembly

The torus assembly used in these experiments is largely as described by Mitchell and co-workers [15]. The main features of this are the use of a corrugated stainless steel liner with a resistance of 0.022 ohms in place of the original segmented arrangement and the considerably improved configuration of the initial stabilizing field. Further to these modifications the liner system has been extended into the diagnostic ports and vacuum manifolds to provide virtually complete vacuum and electrical isolation of the region between the liner and the outer shell from the main discharge region within the liner. The overall pumping speed of the system has perforce been reduced to about 1000 lusec, but the increased isolation and the bake-out facility provided by the liner give a system with typical operating base pressures between 5×10^{-7} and 10^{-6} torr. Apart from a small reduction of bore to 97 cm, the dimensions of the apparatus are as described previously.

2.2 Modifications to the power supplies

The main capacitor bank now consists of 1.1×10^{-2} F, which can be charged to 24 kV to give 3 MJ stored energy. The bank is subdivided into four equal sections each with a 'make', 'clamp' and 'dump' ignitron (BK 194) feeding the primary winding in parallel. The original 0.5-MJ capacitor bank is used as a preionizing bank when required. A further 1.5-MJ bank has been used both for experiments to prolong the pulse length with an 'active clamp' circuit and as a fast-start bank. The stabilizing field supply has been increased so that approximately 1800 G can be obtained.

The primary winding has been reassembled as close as possible to the torus and for the present experiments has been operated with a turns ratio of 4:1. In this condition the total external circuit impedance (referred to the secondary at 4:1) consists of a resistance of 0.8 milliohms and an inductance of 1.35 μH. The secondary circuit is now complicated by the shunting effect of the liner as discussed by Tosswill and Hope [16]. The L/R time of the liner circuit is about 80 μs, and the time to gas current peak is about 1 ms with the full capacitor bank.

The gas current I_g is measured with Rogowski coils placed just inside the stainless-steel liner. The total secondary current is measured by external Rogowski coils, and by iron-cored current transformers. The mean emf V_L at the liner is obtained by difference measurement of the liner current and the known liner resistance and also by a primary voltage potentiometer corrected for the potential drop due to current changes in the leakage inductance and resistance of the primary winding. The power input and energy supplied to the gas are measured by multiplying V_L by I_g and integrating to obtain energy. A comprehensive system of electronic units has been developed [17] to improve the oscillograph recording and monitoring equipment and to perform elementary computing operations on the input signals. The accuracy of individual measurements of current and voltage is about 5%.

2.3 Performance characteristics

In this present form the machine has operated for several hundred thousand discharges at currents in the range of 200-600 kA with only minor technical difficulties and no electrical breakdowns in the torus-liner assembly. Experiments are normally carried out in deuterium.

Various detailed tests on the effects of slots in the metal shell and on the stabilizing field configuration, the comparison of observations on the various forms of Zeta, the effect of preheat, and the comparison of our observations with those of workers on other toroidal discharges, strongly suggest that the main phenomena encountered do not depend sensitively on accidental constructional features of the apparatus. As discussed below, the parameters of greatest experimental significance are:

(a) the magnetic configuration parameter θ. This is the ratio of the azimuthal pinch field B_θ at the walls to the initial stabilizing field B_0. It determines the main features of the magnetic field distribution [8].

(b) the energy input per unit mass of plasma ε. This corresponds somewhat to the characteristic energy per particle $B^2/8\pi n$ used by Colgate [18], but we have found the mass effect to be important. The energy input is integrated over the pulse.

(c) the number of electrons per unit length. This determines the runaway condition and, together with the impurity content, the radiation losses.

Studies of the minimum operating gas pressure for initiating discharges indicate that these are determined by the mean free path for ionizing collisions; the phenomena observed are consistent with a maximum in the ionization cross-section. Operation below about 0.25 mtorr in deuterium in a pinch condition is limited by excessive mean free paths for electron-ion scattering, that is, essentially by a runaway condition. Attempts to operate below about 0.25 mtorr give no current or give a grossly unreproducible current waveform or give strong evidence that the effective pressure is enhanced by evolution of gas from the liner.

A limited number of discharges have been carried out at full energy when gas currents of about 900 kA were reached. Such currents placed a severe mechanical strain on the primary winding assembly and the torus

was not fully conditioned at these currents. However, the observation of resistance, current waveform and neutron yield suggested no major qualitative difference in the plasma phenomena occurring, and detailed experimentation has been carried out only up to currents of about 700 kA. At a current of 500 kA neutron energy measurements by WARD [26] show axial energy anistropies at low pressures similar to those discovered at lower currents.

2.4 ELECTRICAL ENERGY SUPPLIED

The energy supplied to the gas $\int V_L I_g \, dt$ is between 20% and 60% of the capacitor bank energy according to experimental conditions, and is illustrated in

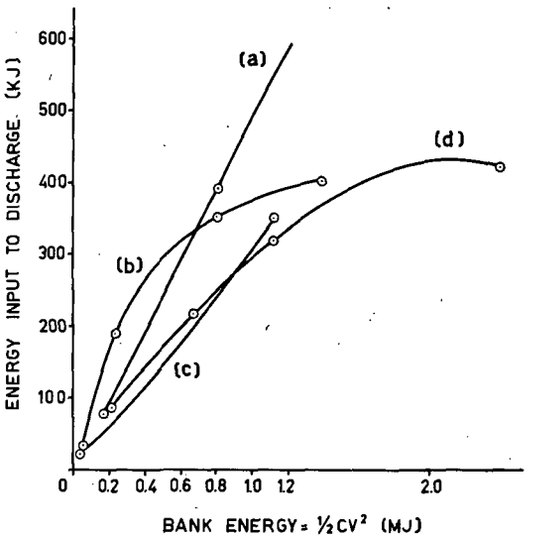

Fig. 2.1 Energy supplied to deuterium discharge as a function of energy stored and gas pressure. (a) 15 mtorr, $\theta_{max} = 1.35$. (b) 0.5 mtorr, $\theta_{max} = 1.35$. (c) 2.0 mtorr, $\theta_{max} = 1.35$. (d) 2.0 mtorr, $\theta_{max} = 1.95$.

Fig. 2.1. The remainder of the energy is dissipated in the liner and external circuit. Losses in the liner account for 5-15% of the energy stored and the remainder occurs in the damping and load-sharing resistors in the primary circuit.

The relationship between the discharge resistance and energy input at various pressures is shown in Fig. 2.2 for discharges of constant θ. At low pressures (~0.5 mtorr) gas resistance increases with increasing energy input. At high pressures (15 mtorr) and in argon, the resistance is virtually independent of energy. At 2 mtorr resistance falls with increasing energy over the range studied.

3. Radiation loss

3.1 METHOD

Total-radiation-loss measurements have been made with a radiation thermopile whose current output was measured with a galvanometer having a time constant of 1 sec. The sensitive element has uniform response from approximately 10^{-4} to 20 mtorr. It

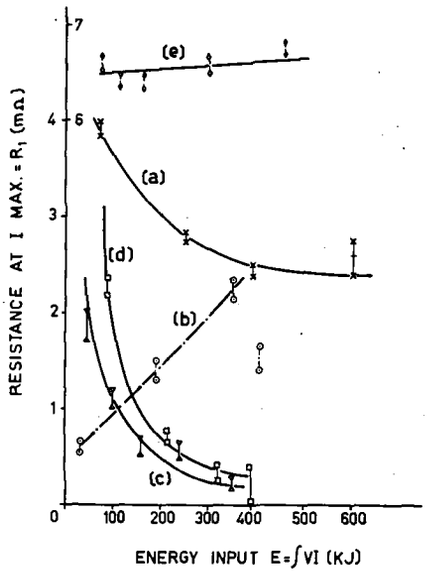

Fig. 2.2 Resistance at peak current as a function of energy input and gas pressure for discharges in deuterium and argon. (a) D_2, 15 mtorr, $\theta_{max} = 1.35$. (b) D_2, 0.5 mtorr, $\theta_{max} = 1.35$. (c) D_2, 2 mtorr, $\theta_{max} = 1.35$. (d) D_2, 2 mtorr, $\theta_{max} = 1.95$. (e) Ar, 2 mtorr, $\theta_{max} = 1.60$. (Inside ordinate scale is for argon.)

has an area of 0.1 cm² and views the plasma from about 10 cm outside the torus walls.

To pass from the energy incident on the thermopile to the energy radiated by the discharge it is necessary to know the geometry of the radiating channel. Thus for a given amount of energy falling on the thermopile 6.5 times as much energy would be radiated, in total, by a uniform source filling the discharge tube as by a line source on its axis. The radiation geometry has been estimated by taking pinhole photographs of the discharge through suitable filters.

3.2 RESULTS FOR DEUTERIUM DISCHARGES

The radiation emitted by a deuterium discharge in Zeta varies between 10% and 100% of the input energy depending on the operating conditions. The

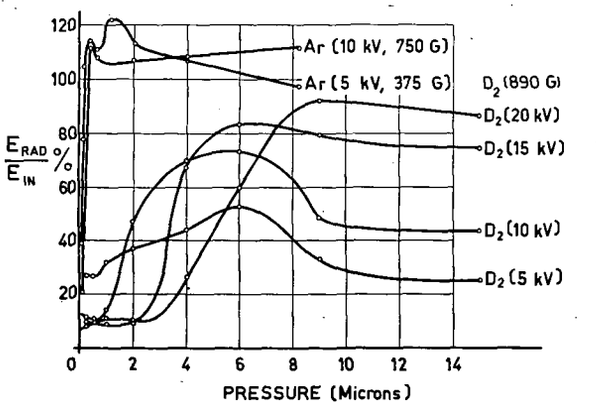

Fig. 3.1 Energy radiated as a function of gas pressure and capacitor-bank potential for discharges in deuterium and argon.

variation of radiation loss with pressure and capacitor-bank voltage for discharges in a conditioned torus is shown in Fig. 3.1. The radiation level increases rapidly over the range 1-5 mtorr and with 1 MJ or more stored in the capacitor bank approaches 100% of the total energy input. The curves are quite reproducible when the machine has been conditioned by a large number of discharges, but in contaminated conditions the radiation level is increased.

The two curves obtained at lower energy inputs (5 kV and 10 kV) exhibit maxima, but by the addition of impurity elements (argon, carbon and nitrogen were used) the plasma is once again completely radiation cooled. In view of the low electron temperature at these high pressures and low energy inputs, incomplete ionization and hence charge-exchange losses may explain the observed maxima. Assuming a charge exchange cross section of 10^{-15} cm^2 and an ion temperature of 5 eV, calculations suggest that 1-5% of neutral atoms could account for this loss.

At high pressures the radiation losses were, within the experimental accuracy (15%), independent of θ. At low pressures (0.5 mtorr), however, the radiation loss increased as the stabilizing field was reduced. Thus a three fold increase in radiation was observed as θ varied from one to five.

3.3 Argon discharges

Observations show that argon discharges are radiation cooled above 0.25 mtorr but that the radiation loss is reduced to 20% of the input energy at about 0.05 mtorr. Thus a similar dependence on pressure to that for deuterium discharges is observed but at much reduced pressures (0.05-0.25 mtorr compared to 0.5-5 mtorr).

3.4 Theoretical radiated power

Measurements with filters show that all but a few percent of the radiation is in the vacuum ultraviolet range below 1600 Å. The obvious source is line radiation from impurities.

For low-density plasmas, spectral-line emission is determined by the processes of collisional excitation followed by radiative decay. In this regime one may calculate the power P radiated by a hydrogen plasma containing impurities, the result being approximately [19]

$$P = \frac{10^{-24}\, n_e\, n_i}{(k\,T_e)^{1/2}} \text{ watts/cm}^3$$

(n_i = density of impurity ions — cm^{-3}; n_e = electron density — cm^{-3}; kT_e is in electron volts).

The observed radiation power loss agrees to within a factor two over the range of conditions considered, with this predicted power loss with an assumed n_i of 0.5×10^{11} cm^{-3}. The required density of impurity atoms is comparable with that obtained experimentally by Griffin (unpublished) of about 10^{11} oxygen and nitrogen ions/cm^3.

We conclude that the observed impurity density can readily account for the radiation emitted from the plasma, and that the increase with pressure is accounted for by the increase in electron density. The increase with θ may be partly the increased compression but may also be associated with an increase in n_i.

4. Plasma loss

4.1 Plasma at walls

The density and energy spectrum of electrons at the wall of Zeta have been measured with an electrostatic analyser [10]. The opening of the analyser was about 2 cm in from the wall. Figure 4.1 shows

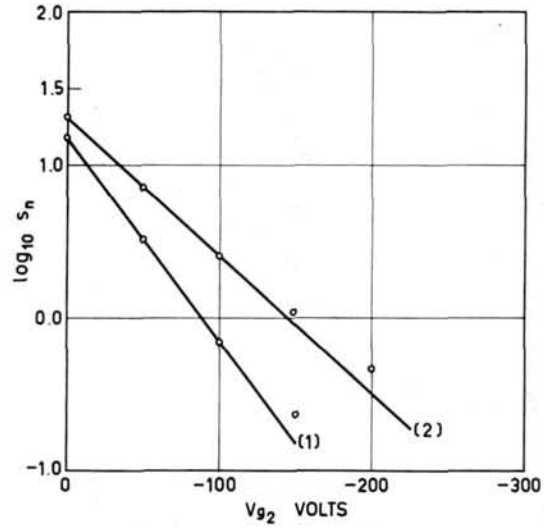

Fig. 4.1 Energy spectrum of electrons measured at the wall of Zeta with the electron energy analyser. S_n is proportional to electron flux. Curve 1: measurement during 750-μs interval before peak current. Curve 2: measurement during 750-μs interval after peak current. Analyser directed downstream with respect to electron drift velocity.

the Maxwellian energy spectrum obtained, giving a good estimate of electron temperature T_e. The electron density is obtained to within 20% from the intercept at zero voltage assuming the full Langmuir sheath potential is developed. The results show that over the range of pressures investigated (0.5-2 mtorr) the electron density close to the wall is $\sim 3 \times 10^{13}$ cm^{-3} and the electrons have mean energies between 50 and 15 eV depending on the pressure and degree of contamination. The high electron temperature is obtained at the low pressures. The field lines near the wall intersect it [15] and thus plasma may diffuse to the wall at the regions of intersection. Calculations show that the consequent energy flux is quite sufficient to account for the energy loss at high values of ε. At high pressures (5 mtorr) the electrons detected have energies of only a few electron volts and are indistinguishable from photo-electrons. They are moreover of too low an energy to transfer more than a few percent of the energy input to the walls.

4.2 Spectroscopic evidence of plasma loss

Evidence on plasma loss has been provided by observations of the time variation of impurity-ion spectral-line intensities [9]. These have been interpreted with a theoretical model of a partially contained plasma and show that in the absence of any injection process the duration of the light from very highly ionized ions is primarily determined by the containment time rather than by the characteristic time of the atomic processes of ionization and recombination.

A vacuum ultraviolet monochromator is used to select resonance lines of highly ionized impurity atoms in a deuterium plasma. Some of the observed ions are normally present in the discharge (e.g., N V, O V, O VI) and a few percent of argon is also added to provide additional ions (e.g., Ar VI, Ar VII, Ar VIII). The impurity atoms are ionized during the Zeta discharge pulse and successive ionization states are formed in sequence. Figure 4.2 shows the observed time variation of spectral line intensities of the argon ion sequence Ar I to Ar VIII. The intensities and the ion populations rise to a maximum value and then decrease as the next ion is produced. For a fully confined plasma only atomic processes are involved, and since the ionization rates decrease rapidly along an ionic sequence, the duration of the transients should increase rapidly from less than 100 μs for Ar I to several milliseconds for Ar VIII. However, the observed traces show that the transient lifetime Δt_n for the nth ionization state reaches a limiting value of about 300 μs at Ar VI, and this value is not exceeded. The limiting value is the result of a loss process, and the ion containment time t_c (defined by $t_c\, dN_i/dt = -N_i$) is predicted by theoretical analysis of a simplified model to be given by $t_c \approx \Delta t_{n\,max}/2.7$. In given discharge conditions the observed limit on Δt_n is independent of the charge and mass of the tracer ion selected for the measurement, and it is therefore assumed that the method can be used to determine the deuterium ion containment time.

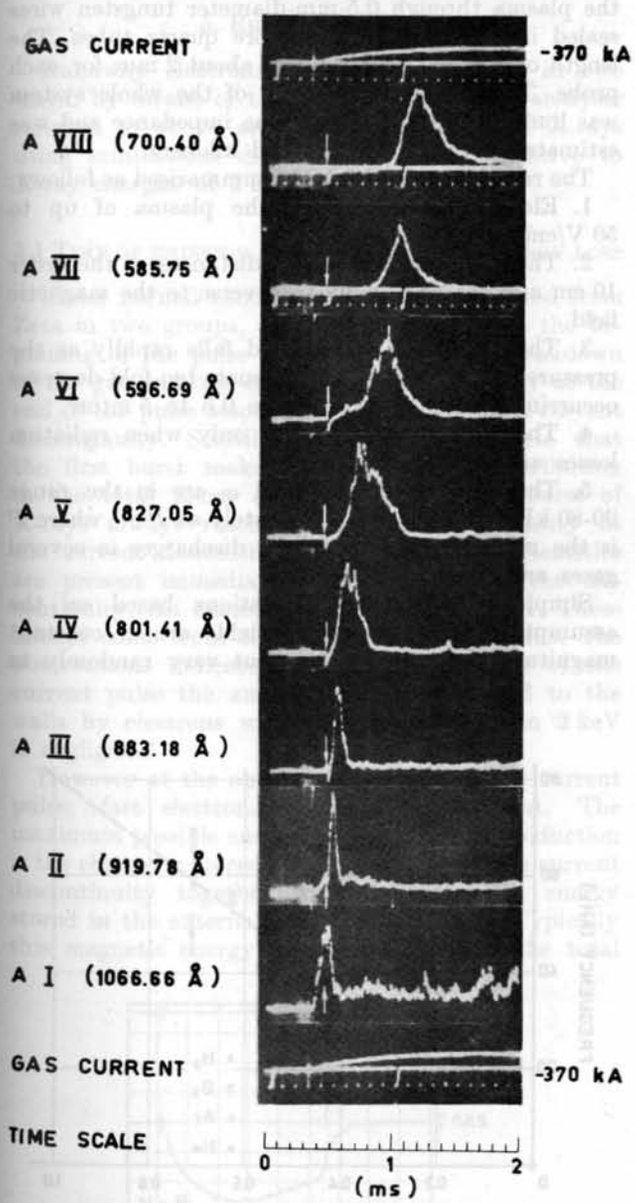

Fig. 4.2 Time variation of spectral-line intensity in Zeta 1A for the sequence of argon ions Ar I to Ar VIII showing transient lifetime limit. (0.5 mtorr $D_2 + 10\%$ Ar, 10 kV, 800 G, 3-MJ bank, no pre-heat.)

With this technique and allowance for injection, t_c has been measured over a wide range of Zeta operating conditions. The results are summarised in Fig. 4.3 where $1/t_c$ is plotted against the parameter ε, the energy input per unit mass of gas in the discharge. The points, which form a linear plot, refer to the discharge conditions listed. At high ε, the ion containment time is about 100 μs, which is of the same order as the energy-containment time deduced from the energy input [10]. A more detailed energy-balance calculation based on the measured loss rate in a particular case shows that at the high-energy-input conditions ($\varepsilon = 3$ keV/proton mass) about 80% of the energy input is lost by escape of plasma to the tube wall. The remaining 20% of the energy input is accounted for by radiation loss.

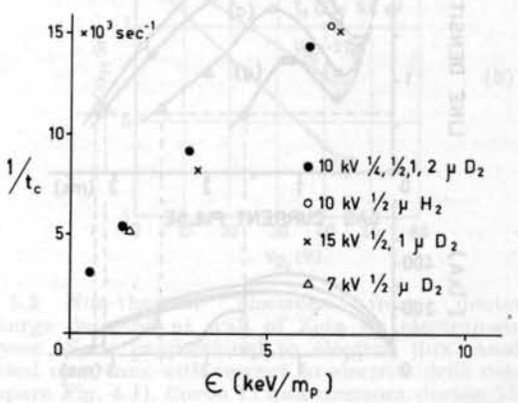

Fig. 4.3 Loss-rate coefficient $1/t_c$ determined spectroscopically as a function of ε for all observed discharge conditions. (ε = energy input per unit mass of gas.)

Another result shown by these measurements is that the loss rate in a hydrogen plasma is almost double that in a deuterium plasma at similar discharge conditions. When the parameter ε is reduced by increasing the concentration of heavy impurity atoms to 10%, the radiation losses increase, and the measured ion loss rate falls to a value which is predictable from Fig. 4.3 by using a new ε value corrected for the radiated energy. The ion containment time t_c is largely independent of the configuration parameter θ and appears to be approximately constant throughout the pulse. At sufficiently high pressures ($\gtrsim$5 mtorr) the ion containment time becomes comparable with the length of the discharge pulse and the measurement of containment times by this method then becomes impossible. A detailed study of this high pressure case, in which recombination predominates, has been made by HOBBS et al [37].

4.3 PUMP-OUT

The spectroscopic observations have also demonstrated the presence of an injection process. Essentially the injection causes a persistence of emitted light after the initial transient; an injection rate is obtained from the ratio of the persistent intensity to the peak intensity at the transient. The injection varies with time and depends on θ and t_c. If one defines the injection rate Λ in terms of the initial line density N_0 by $dN/dt = \Lambda N_0$, the peak current value of Λ is given by $t_c \Lambda = 0.2\ \theta_{max}$. The measurements of the loss rate and injection rate have provided estimates of the variation of the deuterium plasma line density with time throughout the Zeta discharge pulse. Results for four different discharge conditions are shown in Fig. 4.4. These curves are calculated from the measured loss and injection rates after making several assumptions. The results are, however, confirmed by infrared radiation measurements [11]. Moreover a microwave-transmission measurement by D. J. Wort showed that the plasma density decreased to the critical value for transmission of 8.7-mm radiation (1.5×10^{13} cm^{-3}) at a time when the spectroscopic observations gave a density of 1.3×10^{13} cm^{-3}.

4.4 ELECTRIC FIELDS

The rapid diffusion of plasma both to and from the walls may arise through non-thermal fluctuating electric fields in the plasma [20]. Electric fields below the ion cyclotron frequency produce the well-known $\mathbf{E} \times \mathbf{B}$ drifts of the plasma as a whole. Preliminary electric field measurements have been made on Zeta using simple probes which made electric contact with the plasma through 0.5-mm-diameter tungsten wires sealed in the ends of 7-mm-bore quartz tubes. The length of exposed tungsten was about 2 mm for each probe. The frequency response of the whole system was limited by the probe-plasma impedance and was estimated to be a few hundred kiloherz.

The results obtained may be summarised as follows:

1. Electric fields exist in the plasma of up to 50 V/cm.
2. They are correlated over distances of the order 10 cm and are principally transverse to the magnetic field.
3. The amplitude of the field falls rapidly as the pressure is increased, an approximate ten fold decrease occurring in the pressure range 0.5 to 5 mtorr.
4. The amplitudes are large only when radiation losses are small.
5. The frequencies observed ω are in the range 20-80 kHz, and vary approximately as $P^{-1/2}$ where P is the mass of gas. Results for discharges in several gases are given in Fig. 4.5.

Simple random-walk calculations based on the assumption that the electric fields are of constant magnitude E for a time $1/\omega$, but vary randomly in

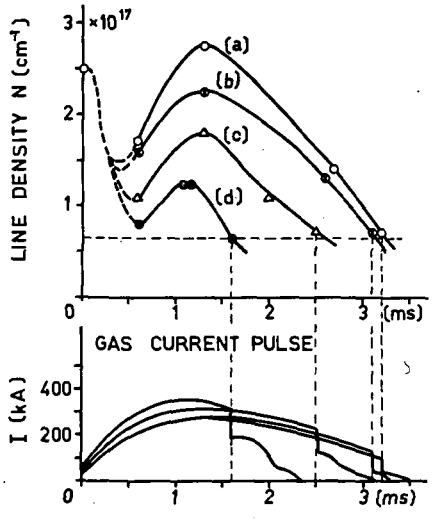

Fig. 4.4 Variation of line density during Zeta pulse determined from spectroscopic observations showing effect of pump-out (0.5 mtorr D_2, 10 kV, 3-MJ bank). (a) $\theta_p = 4.9$. (b) $\theta_p = 3.8$. (c) $\theta_p = 3.0$. (d) $\theta_p = 1.9$.

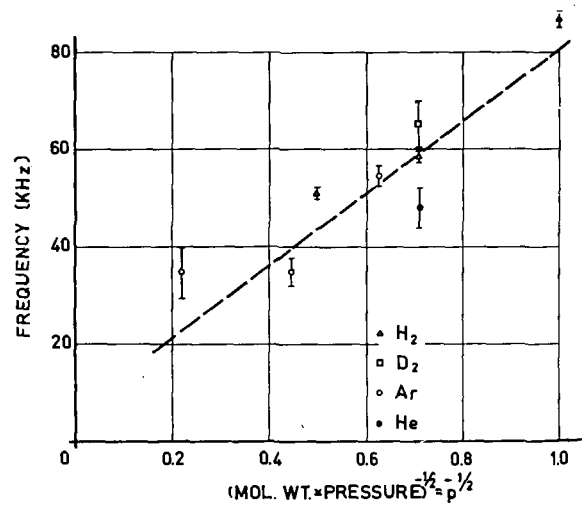

Fig. 4.5 Frequency of electric-field fluctuations as a function of the square root of the effective mass of gas in the discharge.

direction from one period to another yield for the containment time

$$t_c = a^2 \omega \left(\frac{B}{E}\right)^2 \qquad (1)$$

The observed electric fields can well account for the plasma loss required by energy-balance considerations and the spectroscopic observations. In addition they are consistent with the mass-motion component of the Doppler widths of ionic spectra [14].

As pointed out by Spitzer, because of the thermal motion of the electrons, the model may require that the plasma potential should be constant for long distances along the lines of force. Further studies on fluctuating fields are reported in an accompanying paper [12].

5. Runaway electrons

Runaway electrons have been observed in two ways: by means of the electrostatic energy analyser referred to above and by the detection of X-rays using scintillation detectors and films sensitive to X-ray energies of 2 keV and upwards.

5.1 Time of emission and magnitude of energy loss

Under normal conditions X-rays are emitted from Zeta in two groups, one of low intensity at the beginning of the pulse associated with the breakdown of the gas and one of much greater intensity at the end of the pulse associated with the terminal current discontinuity. Scintillation detectors indicate that the first burst makes no appreciable contribution to the total X-ray intensity. The second burst of X-rays always reaches its maximum intensity at the current discontinuity; much smaller intensities are present immediately before and after the discontinuity. An example is shown in Fig. 5.1. These X-rays come from electrons striking the walls. The observations indicate that during the bulk of the current pulse the amount of energy carried to the walls by electrons with energy greater than 2 keV is negligible.

However at the abrupt termination of the current pulse, fast electron loss can be important. The maximum possible energy for fast-electron production is the change in stored magnetic energy at the current discontinuity together with the inductive energy stored in the external circuit at this time. Typically this magnetic energy is about 20-30% of the total input energy. A direct estimate of the energy carried to the walls by fast electrons has been made by comparing films exposed at the Zeta liner with films exposed to an X-ray set in the laboratory. This estimate is not very accurate because there is a wide shot-to-shot variation arising from a local deposition of electrons on the wall. The results obtained [10], however, are entirely compatible with the major part of the total energy present in the tube at the current discontinuity being lost as fast electrons.

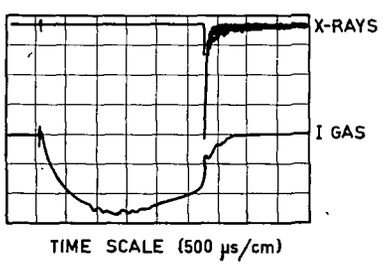

Fig. 5.1 Observed X-ray emission during Zeta pulse. (0.5 mtorr D_2, 10 kV, 375 G.)

The mean energy of the fast electrons giving the X-rays has been measured by measuring the transmission of the X-rays through a selection of filters and calibrating the absorption curves with an X-ray tube. The Zeta X-rays give absorption curves that are experimentally indistinguishable from those of the X-ray set operated at a fixed potential between 7 and 10 keV, the exact value depending on discharge conditions and being accurate to about ± 0.5 keV.

5.2 Low-energy runaways during the pulse

The electrostatic electron energy analyser can receive electrons only within a limited acceptance angle with respect to the lines of force. When it is directed downstream with respect to the electron-drift velocity, it cannot detect runaways, but directed

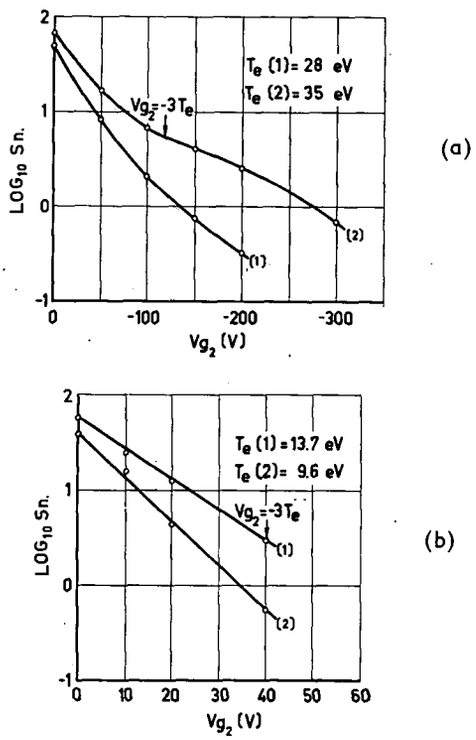

Fig. 5.2 Non-thermal electrons from deuterium discharge detected at wall of Zeta by electron-energy analyser. S_n is proportional to electron flux. Analyser directed upstream with respect to electron drift velocity (compare Fig. 4.1). Curve 1: measurement during 750-μs interval before peak current. Curve 2: measurement during 750-μs interval after peak current. (a) 0.5 mtorr, 5 kV, B_0=185 G. Curvature of curve 2 is reproducible. (b) 2 mtorr, 10 kV, B_0=370 G.

upstream, it will detect both the Maxwellian spectrum and any runaways. Comparisons of the observed energy spectrum in the two directions are shown in Figs. 4.1 and 5.2. Low-energy runaways are plainly indicated for the case of a discharge at low pressures (high ε) but not at high pressures. Typically these runaways are observed at low pressures from about peak current onwards and increase in number and energy towards the end of the pulse. However, it does not appear that they have sufficient energy to affect the discharge drastically until just before the current discontinuity.

The runaway calculation [21] gives in effect an extremely sharp boundary condition between no electrons running away and a sufficient number to short out the normal resistive field. In places where this occurs the electrons must be expected to have mean energies of about $B^2/8\,\pi\,n_e$ in agreement both with the low mean energies observed during the pulse and with the increase of energy as pump-out proceeds.

5.3 NATURE OF ABRUPT CURRENT TERMINATION

The runaway condition may be expressed in terms of line density by using the modified Bennett relation [1]

$$\beta I_g^2 = 4 N_e \langle kT \rangle \tag{2}$$

where N_e is the line density of electrons, and $\langle kT \rangle$ an average thermal energy of the particles. The runaway criterion [22] can be expressed as a limiting ratio ξ of the drift velocity $\langle V \rangle$ to the thermal velocity $(\langle kT \rangle/m)^{1/2}$. Simple substitution then gives, for the runaway condition to be satisfied *on average* throughout the plasma

$$N_e \leqslant 4 \frac{mc^2}{e^2} \frac{1}{\beta \xi^2} \tag{3}$$

where e and m are the electron charge and mass and c the velocity of light. Assuming a constant value of β, runaway should occur at fixed values of N_e.

Support for this view is provided by the spectroscopic analysis of line density, for, as shown in Fig. 4.4, the current discontinuity is found to occur, regardless of the initial conditions, at the same line density, 6×10^{16} cm^{-1}. This corresponds to a value of $\beta\,\xi^2$ of 2.5×10^{-4}, which is compatible with runaway conditions. A more detailed argument based on the actual densities, electron temperature and electric fields is given elsewhere [10].

If the effects were due to ion wave instabilities [23], the critical value of N_e would be expected to depend on ion mass. Comparison of the spectroscopic results in hydrogen with those in deuterium show the same value of N_e in both cases within experimental accuracy of 15%, supporting the view that the phenomenon is due to runaway electrons.

The product of the critical value of N_e with the mean measured X-ray energy yields an estimate of the energy carried by runaway electrons to the walls. The figures obtained (Table I) suggest that only about half the electrons present at the discontinuity reach the walls with the mean energy.

TABLE I. Fast electron energy loss.

Initial conditions			Electron energy (kV)	Change in magnetic energy per electron at current discontinuity (keV)
Condenser bank voltage (kV)	B_0 field (G)	Pressure (mtorr)		
5	225	0.5	7	2
10	375	0.5	8.4	4
10	375	1.0	8.4	—
10	525	0.5	9.3	6
10	750	0.5	10	6

We thus conclude that the current termination and the appearance of X-rays coincide with pump-out to a critical line density, at which point the magnetic energy of the discharge is catastrophically converted to runaway electron energy and conveyed to the walls. All our evidence on the conditions for producing X-rays and the abrupt current termination is consistent with this view.

The characteristic duration of the catastrophic process would be expected to be about $a/(kT/M)^{1/2}$, with $kT \approx 5$ keV, where M is the ion mass and a is the radius of the tube. This is calculated to be 1 μs, which agrees well with 1-2 μs observed.

6. Discharge resistance

6.1 RELATION OF RESISTANCE TO RESISTIVITY

The resistance observed R_1 is V_L/I_g at current maximum. This is averaged over a number of shots to eliminate fluctuation effects. The possible change of inductance is neglected because the measured average field configurations are very largely a function of θ only [8].

The observed resistance R_1 is related to resistivity $\eta_\parallel$ along the lines of force by a configuration function $F(\theta, K)$ defined by

$$R_1 = R_0 F(\theta, K) \tag{4}$$

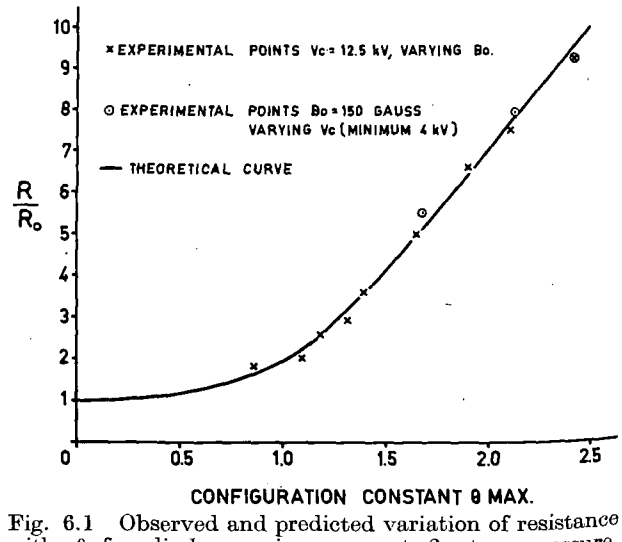

Fig. 6.1 Observed and predicted variation of resistance with θ for discharges in argon at 2-mtorr pressure.

Here R_0 is $l\,\eta_{\parallel}/\pi\,a^2$, a is the tube radius, l is the major circumference of the torus, θ is the magnetic configuration parameter, and K is the ratio of resistivities along and across the lines of force. Values of $F(\theta, K)$ have been evaluated from the Bessel-function model of the configuration [8] for the force-free condition $K=0$. $F(\theta)$ is not sensitive to the exact form of the diffuse distribution assumed and the neglect of $\eta_{\perp}$ leads to underestimates of $\eta_{\parallel}$.

The validity of this procedure has been checked with discharges in argon at 2 mtorr. The resistance observed (see Fig. 2.2) is constant at constant θ_{max} over a wide range of power inputs, and it is inferred that the resistivity is constant due to radiation cooling. The observed variation of R_1 with θ is compared with the calculated value in Fig. 6.1, and supports this method of dealing with the discharge configuration. The absolute value of resistivity, 11×10^{-3} ohm-cm, is also in good agreement with estimated plasma parameters.

6.2 Resistivity in deuterium discharges

This technique has been applied to measure the resistivity of deuterium discharges as a function of initial pressure and energy input and to compare these with resistivities calculated from independent measurements of electron temperature using the classical binary collision theory given by Spitzer [24], viz

$$\eta_{\parallel} = \frac{6.53\times10^{3}\log\Lambda}{T_e^{3/2}}\ \text{ohm-cm}\ (T_e \text{ in } ^\circ\text{K}) \qquad (5)$$

Results in hydrogen at 5 mtorr are shown in Table II where the observed resistivities are compared with values calculated from the electron temperature obtained by McWhirter from measurements of the Balmer continuum [37]. The agreement of the two resistivities is within experimental error of about 10%. Similar agreements have been obtained at 20 mtorr of hydrogen, and also with 2-mm microwave noise measurements at low values of ε (<0.5 keV/m_p).

TABLE II. Comparison of resistivities*

Discharge conditions		Temperature measurements		Resistance measurements		Pressure correction	
V_c (kV)	θ	T_e (eV)	η (milliohm-cm)	R_1	η (milliohm-cm)	β	η** (milliohm-cm)
4	0.73	3.0	8.4	1.6	8.0		
6	1.07	3.7	6.3	2.05	6.4	0.16	7.5
8	1.35	3.9	5.7	1.95	4.0	0.1	4.4
10	1.57	4.1	5.3	2.3	3.5	0.08	3.7
12	1.78	5.2	3.8	2.45	2.9	0.09	3.1
14	2.0	7.6	2.2	2.6	2.5	0.09	2.7

* From resistance and temperature measurements at 5 mtorr of hydrogen, $B_0=750$ G. T_e measurements obtained from Balmer continuum. Error on resistance measurements: $\pm5\%$. Error on spectroscopic measurements: 2 eV, $\pm5\%$; 5 eV, $\pm10\%$; 10 eV, $\pm20\%$.

** In column 8 the effect of finite gas pressure has been allowed for by adjusting the given θ to a value $\theta_1=(1-\beta)^{1/2}\theta$ and estimated β from the modified Bennett relation, taking N_e to be the initial line density.

A comparison has also been made at low pressures. Here, however, independent estimates of electron temperature are much more limited. Values have been obtained from the electrostatic electron-energy analyser, and from rough estimates made spectroscopically from the intensities of impurity spectral lines. The results are summarized in Table III, and show marked excess resistivity measured electrically, which increases as the energy input per unit mass ε. Such discrepancies might conceivably be due to impurities, which would have to give an average charge per positive ion of between 3 and 4. The effect of added impurities on resistance is entirely different from that predicted by this type of argument, and is illustrated in Fig. 6.2. Here an addition of 5% argon to deuterium at 0.5 mtorr initial pressure

TABLE III. Comparison of resistivities obtained from resistances and temperature measurements at 0.5 mtorr D_2

Experimental conditions			Resistance measurements		Temperature measurements		
V_c (kV)	B_0 (G)	θ	R_1 (milliohms)	η (milliohm-cm)	Method of measurement	T_e (10^4 °K)	η (milliohm-cm)
5.0	188	2.8	1.4*	0.9 1.3	Electron analyser	46 (±5)	0.25
10.0	750	1.7	1.5	1.9 $\pm10\%$	Spectroscopic impurity-ion line intensity	23.0^{+10}_{-6}	0.6
3.5 7.0 10.0	375 750 1125	1.35 1.35 1.35	0.6 1.4 2.3	1.1 2.8 4.5	Estimates from Ar VIII	18—40	0.9—0.26

* Assuming $\beta=0.4$ from T_e measurement.

reduced the resistance to approximately half the value in pure deuterium.

This evidence for an excess resistivity obtained from R_1, is confirmed by using measurements of average resistance $\langle R\rangle = \int V_L I_g \, dt \Big/ \int I_g^2 \, dt$, where the integrations are taken between points of equal current. Measurements of $\langle R\rangle$ and R_1 are shown in Figs. 6.3 and 6.4. The same general trend is shown, and the excess resistance appears to be responsible for the marked minimum in resistance at 2 mtorr and the increase of resistance as the pressure is lowered below this point. To account for such curves classically would require a maximum in the electron temperature at 2 mtorr, whereas all the independent evidence points to a monotonic increase of electron temperature as ε is increased.

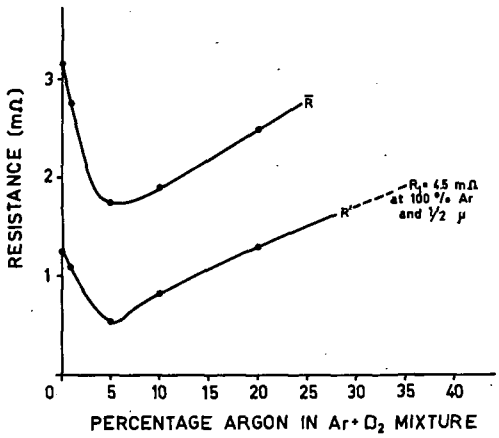

Fig. 6.2 Variation of resistance with gas composition for discharges in deuterium with argon impurity. (0.5 mtorr D_2, 10 kV, 750 G, 3-MJ bank.)

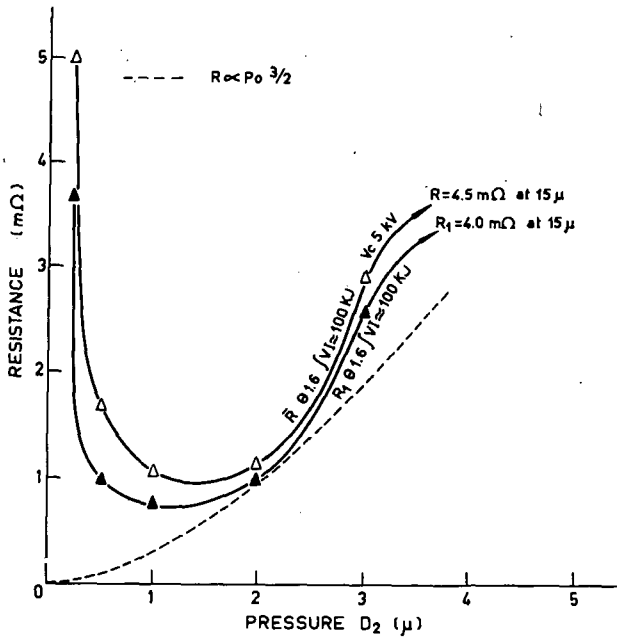

Fig. 6.3 Variation of impedance at peak current R_1 and mean resistance $\langle R\rangle$ ($= \bar{R}$) with pressure in deuterium for $V_c = 5$ kV, $\theta = 1.6$.

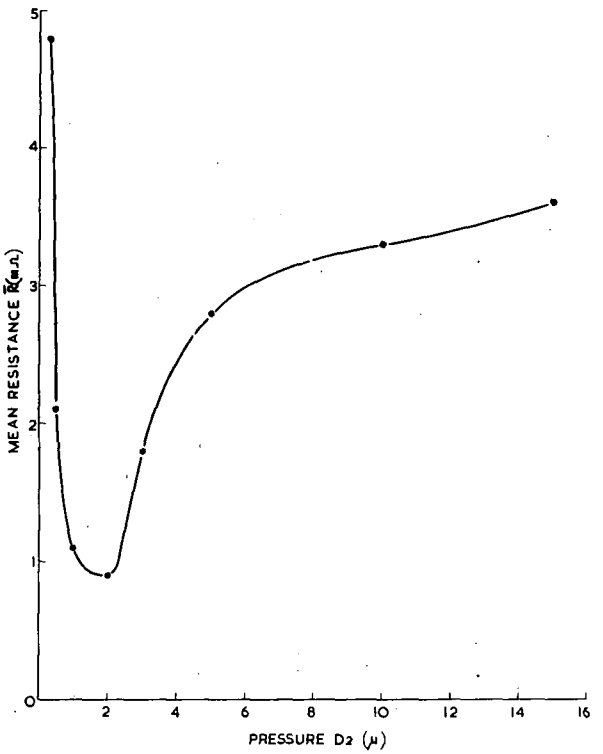

Fig. 6.4 Variation of mean resistance $\langle R\rangle$ with pressure in deuterium for $V_c = 10$ kV, $B_0 = 750$ G, $\theta \approx 2$.

6.3 Excess resistance

The variation of resistance with pressure is summarised semi-empirically as follows: The resistance consists of two terms: $\langle R_c\rangle$, the classical binary collision term, and an excess term due to cooperative interaction, $\langle R_i\rangle$. In a fully contained preionized

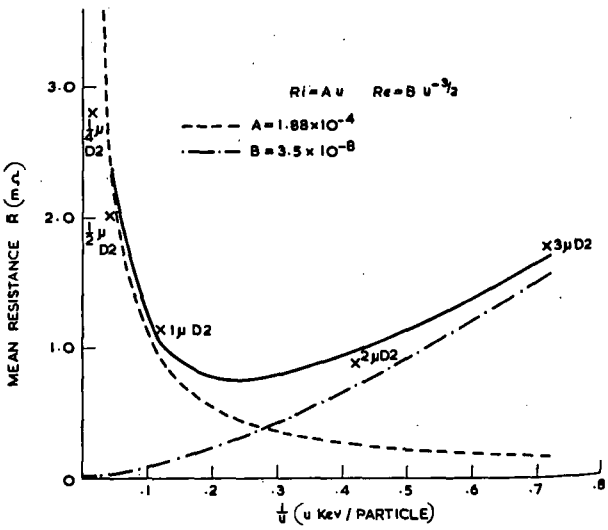

Fig. 6.5 Mean resistance $\langle R\rangle$ as a function of $1/U$. U is energy input less that radiated in keV per particle.

TABLE IV. Containment times by different methods

Energy input less energy radiated (keV/proton mass)	Pressure (mtorr)	Capacitor potential (kV)	Resistance[a] t_c/β (ms)	Spectroscopic[b] t_c (ms)	Electrostatic analyser[c] t_c(ms)	Electric field fluctuations[d] t_c (ms)	Infrared[e] t_c (ms)
0.23	3.0	10	1.2	—	—	—	—
0.3	2.0	10	1.8	0.33	0.28	—	—
0.53	1.0	7	—	—	0.33	—	—
0.7	0.5	5	—	—	0.39	0.1 (to within a factor of 3)	—
1.2	1.0	10	0.77	0.18	0.14	—	—
3.1	0.5	10	0.46	0.11	—	—	0.18 ($\pm$0.06)
6.0	0.25	10	—	0.07	—	—	—
9.0	0.25	12	0.34	—	—	—	—

(a) obtained from Eq. (6). (b) obtained from the measured ion lifetimes. (c) obtained from the measured T_e by dividing the thermal energy by the rate of energy input less that radiated. (d) obtained from Eq. (1). (e) obtained from intensity of infrared emission [11].

plasma $\langle R_e \rangle \propto U^{-3/2}$ where U is the energy supplied per particle less the radiated energy. There is no *a priori* way of estimating $\langle R_i \rangle$, but it is observed that at low pressure it decreases linearly with pressure. Consequently the total resistance $\langle R \rangle$ is expected to be given approximately by:

$$\langle R \rangle = A\,U^{-3/2} + B\,U$$

where A and B are constants for a given gas.

Such a relation obviously is of roughly the right form to fit the observed variation with pressure. An analysis of a specific case is shown in Fig. 6.5, where $\langle R \rangle$ is plotted as a function of U, and a good fit is obtained.

It is clear that there is an excess resistance which is roughly proportional to the energy fed into the gas less that radiated. In these studies, the molecular weight of the gas has not been altered. At present the only direct evidence that energy per unit mass is important in the excess term is provided by Fig. 6.2, where the added argon doubled the average molecular weight and halved the resistance in conditions where the excess resistance dominates and the radiation and ionic charge effects are estimated to be small.

In a pinched plasma to which the modified Bennett relation can be applied and where the energy loss is due only to radiation and to loss and injection of plasma, the plasma containment time is given roughly by [1]

$$t_c = \frac{3\beta}{4\Omega}\left(1 - \frac{P_R}{\Omega I^2}\right)^{-1} \qquad (6)$$

where P_R is the power radiated per unit length, Ω is the resistance per unit length and β is defined by Eq. (2). For constant β these relations require $t_c \propto \beta U^{-1}$ compared to $t_c \propto \varepsilon^{-1}$ observed spectroscopically. A comparison of the containment times deduced from resistance using Eq. (6) and from spectroscopic measurements is shown in Table IV.

7. Current steps

7.1 Integral helices in the magnetic field

In earlier work [1] attention was drawn to current steps and voltage transients observed during the discharges in Zeta 1. A significant part of the energy input could be associated with them, and they might be associated both with energy loss and with ion heating. These effects are still observed in the modified machine although the external voltage transients are attenuated by the conducting liner, which is in parallel with the plasma circuit.

Examples of these fluctuations are shown in Figs. 7.1-7.3. They occur during both the rise and fall of the current. The frequency of the steps is governed mostly by the rate of change of current. In contrast with the normal current-pulse conditions of Fig. 7.1, Fig. 7.2 shows results with the rate of change of current greatly reduced by the use of a powered

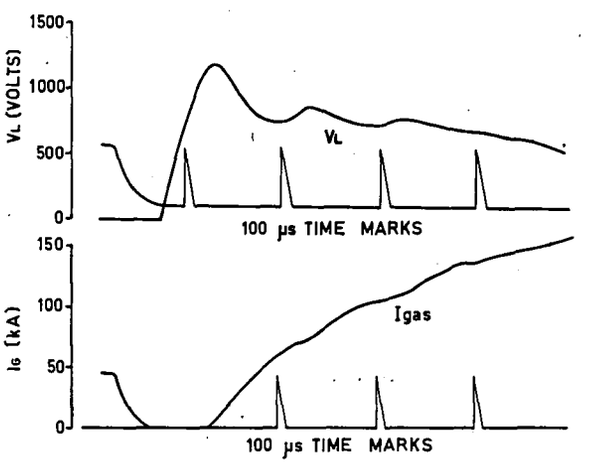

Fig. 7.1 Current and voltage waveforms illustrating impedance changes during the current rise.

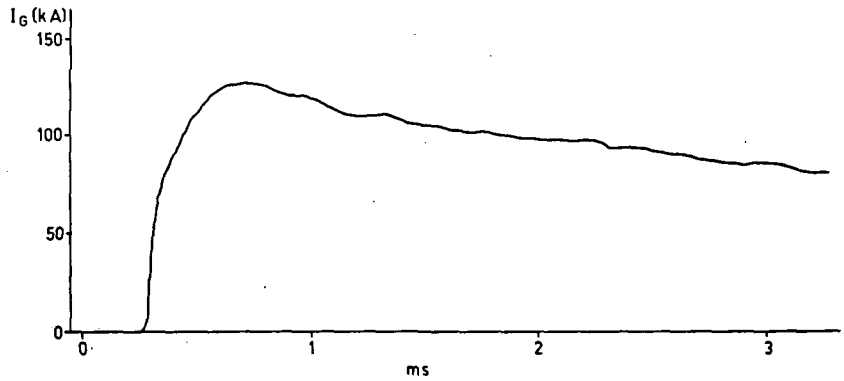

Fig. 7.2 Current steps during a current pulse with the rate of fall considerably decreased by a power clamp. (Power clamp 5.4 kV, 2 mtorr Ar, 14 kV, 300 G.)

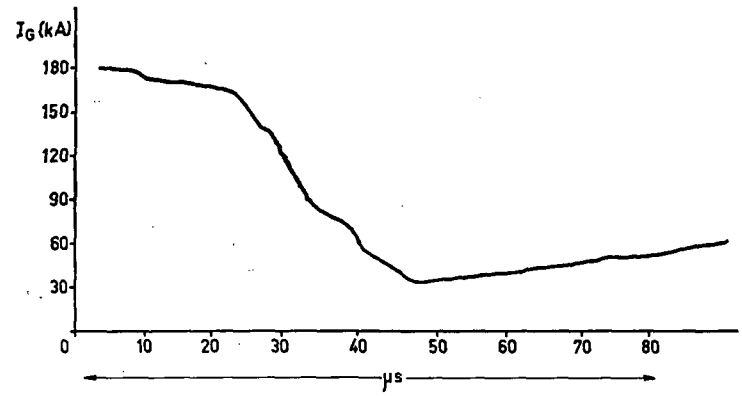

Fig. 7.3 Current steps during the terminal current discontinuity. (D_2, 0.5 mtorr, 10.5 kV, 370 G.)

clamp circuit, and Fig. 7.3 shows the steps occurring during a rapid decrease of current at the abrupt termination of the current pulse. Moreover these steps occur both at various pressures and in different gases at approximately the same time intervals for given electrical conditions. It thus appears that the steps are not associated with any dynamic oscillation, and analysis suggests that they are associated with particular values of the configuration parameter θ. A histogram of the discontinuities as a function of θ is shown in Fig. 7.4. A detailed analysis of the curves of Fig. 7.1 is shown in Fig. 7.5.

The impedance changes have also been studied by measuring the resistance R_1 at peak current as a function of θ. Fluctuations on this impedance are found, as illustrated in Fig. 7.6. The impedance changes do not occur always at exactly the same value of θ; the actual values observed depend somewhat on conditions, a situation that may occur because the actual discharge configuration is determined by plasma pressure as well as by the parameter θ.

The values of θ at which the discontinuities are found strongly suggest a relation with an integral number of helices that can occur in the magnetic field round the torus. The important parameter is thus the characteristic length d of a complete turn of the helix, where $d=2\pi r B_z/B_\theta$. Since the value of rB_z/B_θ varies with r on the Lees and Rusbridge Bessel-function model [8] and this model is itself only a cylindrical approximation, it is only possible to calculate rough values of θ at which integral numbers of helices should occur. A comparison with observation is shown in Table V using observations taken under various conditions and assuming a helix pitch obtained from (a) the value at the centre of the discharge and (b) a value averaged over the radius.

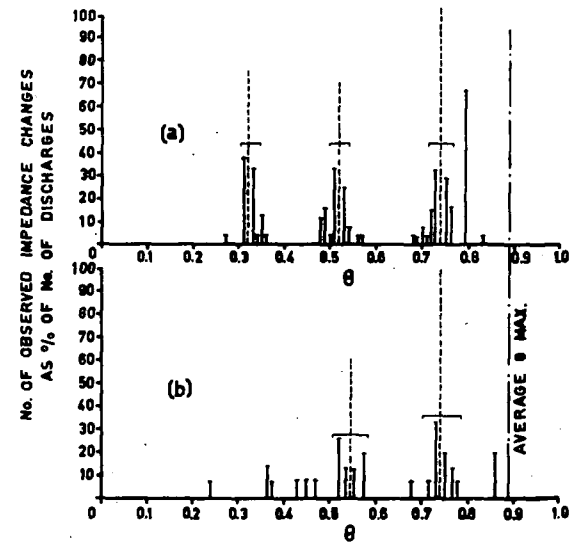

Fig. 7.4 Histogram of impedance discontinuities in Zeta 1A2. (D_2, 0.5 mtorr, 7.5 kV, 750 G, 0.75-MJ bank.) (a) Gas current rising. (b) Gas current falling.

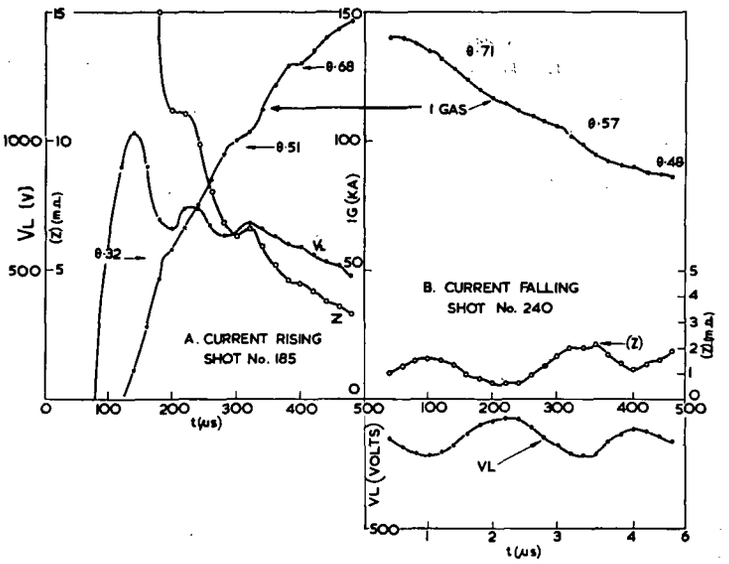

Fig. 7.5 Impedance changes in Zeta 1A2 during steps similar to those of Fig. 7.1. (7.5 kV, 750 G, 0.75-MJ bank.)

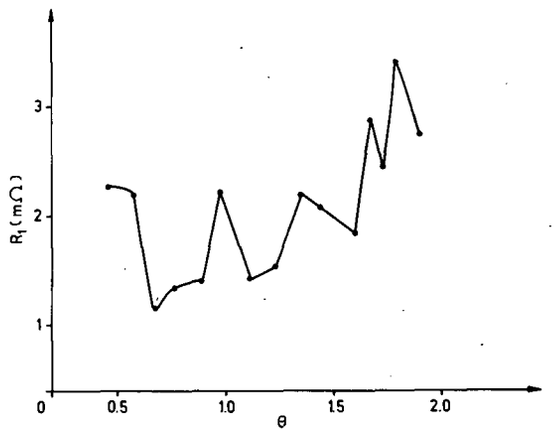

Fig. 7.6 Fluctuations of the resistance R_1 at peak current as a function of θ. (0.5 mtorr, 5.0 kV, varying B_0, 0.75-MJ bank.)

The numerical agreement obtained is within limits expected of this crude approach. The calculated value of $\theta = 0.27$ corresponds to the Kruskal limit, and there is an obvious analogy between these results obtained above the Kruskal limit with those obtained below it in the B1 Stellarator [25].

A more accurate evaluation of the pitch length has been attempted by analysing search-coil measurements obtained with a 36-channel probe. This has yielded some evidence that the pitch can become constant near the critical values of θ and with closely the correct value of pitch. However both this and actual configuration changes require further observation.

7.2 Energy associated with current steps

The energy associated with these steps can only be obtained semi-quantitatively. Previous estimates [1] suggested that at low ε, about 30% of the input

TABLE V. Comparison of θ values giving magnetic resonance from calculation and experiment

Number of complete turns in helix	θ calculated from Bessel-function model		Observed impedance changes			
			Current rising	Peak current		Current falling
	B_z/B_θ at $r = 0$	Mean value*	0.5 mtorr D_2 (Fig. 7.4)	0.5 mtorr D_2 (Fig. 7.6)	5.0 mtorr Ar	0.5 mtorr D_2 (Fig. 7.4)
1	0.27	0.27	0.32	—	0.3	0.23
2	0.53	0.52	0.52	0.6	0.6	0.37 0.45
3	0.84	0.73	0.74	0.8	0.7	0.54 0.73
4	1.1	0.92	0.79	1.0	1.0	0.87
5	1.4	1.09	—	1.4	—	—

* $\frac{1}{a}\int_0^a (r\, B_z/B_\theta)\mathrm{d}r$

energy was associated with them. An estimate can be obtained from the fluctuation of resistance R_1 as a function of θ. These fluctuations are about equal to the resistance itself and suggest that at low pressures perhaps 50% of the impedance is associated with the steps. Some results are presented in Table VI.

TABLE VI. Impedance changes at peak current

Experimental condition			ΔR_1 (milliohms)	$R_{1\min}$ (milliohms)	$\frac{\Delta R_1}{R_{1\min}}$
P_0 (mtorr)	B_0 (G)	θ_1 (average)			
0.25	1125	1.35	3.5	1.8	1.9
0.25	750	1.3	2.9	3.0	0.9
0.5	1125	1.3	2.8	2.6	1.0

As pressure is increased, the magnitude of this form of energy is decreased. It is also rather better defined. An analysis of the case of Fig. 7.5 where $\varepsilon=0.8$ keV per proton mass has been carried out by evaluating $\int I_g \Delta V \, dt$ over the pulse. ΔV is in the excess voltage associated with the steps. This gave 18 kJ, about 20% of the total energy supplied. The excess resistance for this condition from analysis of Section 6 is estimated to be 16%.

8. Hydromagnetic stability

The hydromagnetic stability of the magnetic field configuration has been investigated [27] with a computer programme based on Newcomb's [26] necessary and sufficient conditions. These calculations are necessarily approximate because the criterion is based on a cylindrical model whereas the Zeta configuration is toroidal; moreover because of the presence of magnetic field fluctuations, the configuration is not well defined experimentally, and it is to be expected that under conditions of observed plasma loss, the average configuration is determined in part by the dynamic processes rather than the strict static equilibrium assumed in the theory.

To simplify this problem, an analytical cylindrical model has been used, which is force free. The differential equations of this model are

$$\frac{db_z}{d\gamma} = \frac{\Theta b_\theta b_z}{b_\theta^2 + b_z^2}$$

$$\frac{1}{r}\frac{d(r b_\theta)}{dr} = \frac{\Theta b_z^2}{b_\theta^2 + b_z^2} \qquad (7)$$

where b_θ and b_z are the field components divided by the (axial) field B_{z0} on the discharge axis, r is the radial coordinate divided by the tube radius, a. The parameter Θ is given by:

$$\Theta = \frac{4\pi a \sigma_\parallel E_z}{B_\theta} \qquad (8)$$

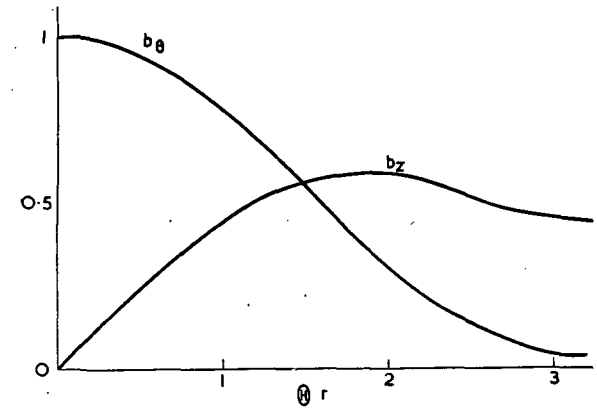

Fig. 8.1 Force-free field configuration used for stability calculation.

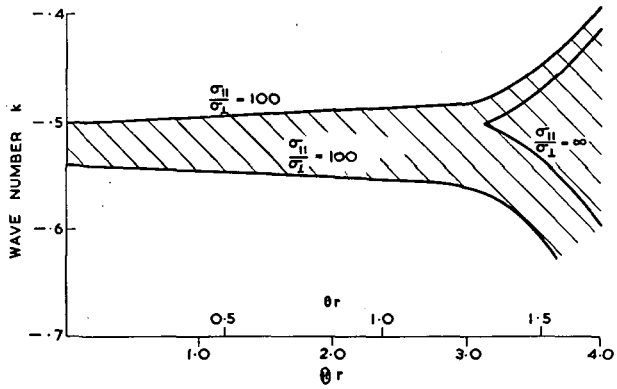

Fig. 8.2 Stability diagram for force-free configuration.

where E_z is the (constant) z component of the electric field and $\sigma_\parallel$ is the (constant) conductivity along the field lines.

The solution of these equations satisfying the conditions $b_z=1$, $b_\theta=0$ when $r=0$ depends only on Θ, (Fig. 8.1). This model is similar but not identical to the Bessel-function model and represents the characteristics of the configuration at low values of θ. The relation between the parameter Θ and the standard magnetic configuration parameter θ, is indicated in Fig. 8.2.

Results of stability computations for this field are shown in Fig. 8.2 for $m=1$ modes. The configuration is unstable for a narrow range of wave numbers, $k=2\pi a/\lambda$ near the value $^1/_2$ that corresponds to the pitch of the field helix on the discharge axis. As Θ decreases, the width of the unstable region diminishes until at $\Theta=3$ it vanishes within the mesh of the computation. The value $\Theta=3$ corresponds to $\theta=1.27$.

It is obviously possible to modify these equilibria by adding a small amount of plasma pressure. When this is done by adding a small constant component of transverse conductivity, the discharge becomes unstable according to the Suydam criterion [26], although apparently over a very narrow range of wave numbers for small values of β.

9. Discussion

9.1 General interpretation

It is first necessary to distinguish three phases of the discharge. At the start the field configurations can show a skin current [13] and the energy absorbed is associated with ionization, radiation in the Balmer continuum and heating from the diffusing fields. This skin phase shows anomalous diffusion [28], which in conditions of high energy per unit mass can exceed ten times that calculated from the electron temperature estimated spectroscopically. The second phase corresponds to fully diffused fields with a quasi-thermal plasma. This lasts for the bulk of the discharge period and is the phase with which the main observations reported herein are concerned. In the third phase the discharge ends abruptly with the evidence pointing strongly to a catastrophic runaway process. The duration of these phases and their predominance depends on a number of factors, of which the most important appears to be the energy input per unit mass ε.

The energy loss processes are complex and can be due predominantly to radiation, to plasma loss or to runaway electrons, depending on conditions. At low values of the pressure and high energy inputs ($\varepsilon \gtrsim 1$ keV per proton mass over the pulse length) the energy fed in is lost by plasma getting to the walls at a rate that is largely independent of the magnetic configuration parameter θ and of time throughout the discharge pulse. Various methods have been used to estimate the plasma containment time, and a comparison of results is given in Table IV. The loss of plasma is to some extent counteracted by injection of material from the walls which varies throughout the pulse. At high ε and $\theta > 1$ there is a net over-all pump-out, and when the plasma line density falls to a critical line density of 6×10^{16} cm^{-1}, catastrophic runaway sets in, and the energy in the torus is lost to the walls by runaway electrons. When this happens early in the pulse, a large part of the total energy must be dissipated by runaway electrons.

At low energies (< 1 keV per proton mass) the loss and injection processes become less important; energy is increasingly lost by radiation in the vacuum ultraviolet. The radiation is due to impurities present to the extent of about 0.1%. The radiated energy rises to 100% of the input energy in argon at 0.5 mtorr and in deuterium at 5 mtorr (for more than 1 MJ stored energy). However, at high pressures of deuterium the radiated energies measured at lower currents are only about 60% of the total. Although this may be due to experimental errors in the geometrical factors, it is quite possible that charge-exchange processes are responsible for some of the energy loss in these very-high-density regions. We have no direct evidence to support such a suggestion, but charge exchange has been observed by Russian workers [29].

With radiation cooling the plasma is better contained, and plasma containment times of about 1 ms at densities of about 10^{15} deuterons/cm^3 may be inferred. However, the electron temperatures under these conditions are only about 10 eV or less, and the ion temperatures are probably low as well. The values of β are about 5×10^{-2}.

9.2 Plasma loss

The plasma is lost apparently by a coarse diffusion process in which mass motion of the plasma at velocities of about 10^6 cm/s take place for times of the order 10 μs, giving a step length of 10 cm, and roughly 10 steps to diffuse to the walls. Such motion could well be a circular eddy motion such as is discussed by Kadomtsev [30]. If the kinetic energy of the mass motion is degenerated into thermal motion of the ions at the end of each step, the observed ion temperature of ~100 eV can be achieved within the containment time, and the energy absorbed is about the same as the excess energy measured electrically.

The cause of the loss process is not yet established. A pinch system involves an inward diffusion of plasma with a velocity of about $(\mathbf{E}_z \times \mathbf{B}_\theta)/B^2$ where $\mathbf{E}_z$ is the applied electric field; in the steady state this is balanced by an outward diffusion due to ion-electron collisions. If an indefinite rise of temperature is prevented by radiation and the configuration is stable, containment should continue indefinitely. The pinch is liable to a large variety of instabilities (see for example W. B. Thompson [31]. The calculations on the hydromagnetic model given above suggest that the observed configuration may be marginally stable for zero plasma pressure, and low values of θ but becomes unstable for small pressure, particularly when there is a pressure maximum at the centre.

These predicted instabilities may be the source of plasma loss; in particular, the plasma loss is associated with frequencies well below the ion-cyclotron frequency, and the ion containment time is observed to be independent of the charge and mass of the tracer ions. The velocity of the plasma motion observed both spectroscopically and by electric-field probes is of the same order but less than the velocity of sound and the Alfvén velocity.

On the other hand, the plasma loss does not appear to be correlated with magnetic-field fluctuations, and the plasma containment is good at low values of ε when such fluctuations are still present. Moreover the spectroscopic observations of t_c suggest the containment time is almost independent of θ, while the stability criterion is very sensitive to this parameter. In addition, results on hardcore pinches [18, 32, 33] show that instabilities occur that are not predicted by hydromagnetic theory.

It seems unlikely that the excess resistance can arise solely from the Joule heating of cold gas to a point at which the internal energy of the gas is converted into the mass motion of instability. For not only is the excess resistance deduced from the *observed* electron temperature, but in addition, the greater part of the internal pressure is due to the ion temperature, which itself appears to be produced by the mass motion. It is, of course, possible that

electrostatic instabilities due to flow of current along the lines of force are responsible for the excess resistivity. At low pressures and high current densities, excess drift velocities can cause runaway electrons and also ion-wave instabilities. However, the runaway tails do not appear to develop until rather late in the pulse; JUKES [34] has shown that runaways must be expected to appear before ion wave instabilities in a hydrogen plasma; and the processes involved suggest that either an excessive electron temperature should develop or the ion heating should be predominantly due to oscillating electric fields which would give rise to Z^2/M effects in the Doppler widths. These are not observed [14].

Consequently present data favour the view that the instabilities are driven directly by the electromagnetic energy fed into the configuration. This view has been advocated strongly by Colgate [18, 32]. The details of the process must be the subject of further study. The discontinuities in the current and associated coherence phenomena are likely to be closely involved. The presence of these discontinuities suggests that the magnetic-field configuration can, with the present rather rapid change of current, change significantly in times comparable with the energy loss time, and experiments under conditions when these times are widely different are needed. The current discontinuities appear to involve energy inputs of the same order as that associated with the excess resistivity deduced from the analysis of resistance.

Another feature requiring further study is the good plasma containment observed at high pressures. For example measurements at 8 mtorr and 20 kV suggest β values of 5-10% contained for $\sim$1 ms. This containment time can be compared to the times $a/(kT_e/M)^{1/2}$ and $a(4\pi\varrho)^{1/2}/H$ — 22 μs and 4.0 μs, respectively. Although such effects might be due to the exact nature of the loss mechanism at the walls, the small values of electric fields observed under radiation-cooled conditions and decrease of Doppler widths with increase of pressure suggests an absence of the driven diffusing mechanisms under these circumstances.

This may be due to the transport properties of the plasma across the lines of force. These depend [35] on the quantity $(\omega_c\tau)^{-2}$ where ω_c is the cyclotron frequency and τ a collision time. In the conditions mentioned above, taking $n=4\times10^{15}$ cm^{-3}, $T=10$ eV; $H=5000$ G; $\omega\tau$ for electrons$=40$; $\omega\tau$ for ions$=1.1$. On the other hand for severe plasma-loss conditions, for example, $n=10^{14}$, $T=20$ eV (corresponding to an assumed quiescent initial condition) and $H\approx2000$ G (corresponding to 0.5 mtorr of deuterium initial pressure, $\theta=2$ and $I\approx250$ kA) $\omega\tau$ for electrons$=1600$; $\omega\tau$ for ions$=48$.

The figures suggest that the collisional transport of the ions is large in the quiescent case and small in the turbulent case. The ratio of the perpendicular and parallel electrical conductivities is $(\omega\tau)^{-2}$. The conductances that are important are those of paths right round the torus ($\sim$1160 cm) and across the lines of force. Taking the observed radial scale length r of 10 cm, the ratio, which scales as $(r/L)^2\approx(1/100)^2$. Consequently it appears as if the radial electrical isolation may depend predominantly in the one case on cross conduction and in the other on conduction round the torus. Such "round the torus" conduction will, of course, be ineffective if the magnetic configuration forms an integral number of helices in the torus, as it is suggested occurs near particular values of θ.

10. Conclusions

1 Energy balance measurements, spectroscopic measurements and the infrared measurements have demonstrated the presence of plasma loss and injection in Zeta.

2 This plasma loss is responsible for the major part of the energy loss at high energies per unit mass ($\gtrsim$1 keV per proton mass).

3 When the plasma density is reduced by pump-out to a value of about 6×10^{16} particles per centimeter of length in hydrogen and deuterium, the discharge stops abruptly, apparently due to an electron runaway process.

4 The plasma loss is associated with an excess resistance; both increase apparently linearly with the parameter ε, energy per unit mass, where ε is the total energy absorbed over the discharge pulse less that radiated. A similar excess resistivity, with qualitatively the same dependence on ε has been found in the skin-diffusion measurements [28].

5 Measurements of the electric fields, together with spectroscopic analysis of Doppler widths, yield mass motion of the plasma with the required velocities and frequencies to account for the plasma loss by a random-walk process. The frequencies involved are between 10 and 50 times less than the ion cyclotron frequency, and the observations give no evidence of significant disturbance in high frequency modes, such as the whistler mode, or plasma oscillations.

6 The stability of the configuration of fields in Zeta, as calculated on the cylindrical hydromagnetic approximation, is likely to be limited to very low values of β.

7 The excess resistance, together with the excess ion energies, suggests that the outward and inward diffusion of plasma is driven by electromagnetic forces acting directly rather than indirectly by Joule heating. Observations suggest it is involved with particular values of the magnetic field configuration parameter θ, which themselves are probably connected with integral numbers of the pitch lengths of the helices formed by the magnetic line of force around the torus. But this matter requires further study.

8 At low values of ε ($<$1 keV per proton mass) the energy is predominantly radiated, and in some conditions long particle containment times (up to 1 ms) can be inferred with β values of 5%. The magnetic field fluctuations are observable with approximately the same amplitude (depending on θ) but lower frequency (as $(NM)^{1/2}$) when the electric fields are absent. It is concluded that magnetic-field

fluctuations (at these low temperatures) are not in themselves a cause of plasma loss.

9 These dense plasmas are relatively cold ($\lesssim$10 eV), and the absence of driven diffusion may be connected with the low values of the product of the cyclotron frequency and collision time, particularly of the ions. These must necessarily be large in an ultimate non-explosive reactor.

10 Further progress in the pinch containment system depends on elucidation of the plasma-loss mechanism.

11. Acknowledgements

We wish to thank E. M. Jackson and the Zeta operations and engineering team for their indispensable contribution to this work.

References

[1] BUTT, E. P., et al, in Proc. 2nd U.N. Conf. PUAE **32**, United Nations, Geneva (1958) 42.
[2] ALLIBONE, T. E., et al, in proceedings of ref. 1, **32**, 169.
[3] COLGATE, S. A., et al, in proceedings of ref. 1, **32**, 129.
[4] CONNER, J. P., et al, in proceedings of ref. 1, **32**, 297.
[5] DOLGOV-SAVELEV, G. G., et al, in proceedings of ref. 1, **32**, 82.
[6] ROSENBLUTH, M. N., et al, in proceedings of ref. 1, **31**, 85.
[7] BICKERTON, R. J., *Proc. Inst. elect. Eng.* **A106**, Supplement 2 (1959) 148.
[8] LEES, D. J., RUSBRIDGE, M. G., in Proc. 4th Intern. Conf. Ionization Phenomena in Gases (Uppsala, 17-21 Aug. 1959) **2**, North Holland Publishing Co., Amsterdam (1960) 954.
[9] BURTON, W. M., WILSON, R., *Proc. phys. Soc. (London)* **78** (1961) 1516.
[10] GIBSON, A., MASON, D. W., *Proc. phys. Soc. (London)* **79** (1962) 326.
[11] HARDING, G. N., ROBERTS, V., *Nuclear Fusion:* 1962 Supplement, Part 3, 883.
[12] RUSBRIDGE, M. G., et al, *Nuclear Fusion:* 1962 Supplement, Part 3, 895.
[13] LEES, D. J., et al, (to be published) abstract in *Nuclear Fusion:* 1962 Supplement Part 3, 1120.
[14] JONES, B. B., WILSON, R., *Nuclear Fusion:* 1962 Supplement, Part 3, 889.
[15] MITCHELL, J. T. D., et al, *Proc. Inst. elec. Eng.* **A106**, Supplement 2 (1959) 74.
[16] TOSSWILL, C. H., HOPE, E. L. V., *Proc. Inst. elect. Eng.* **A106**, Supplement 2 (1959) 101.
[17] BUTT, E. P., GILLESPIE, A. B., in Proc. 5th Intern. Instruments Measurements Conf. **2** (Stockholm, 13-16 Sept. 1960), Academic Press Publishers, New York, London (1961) 938.
[18] COLGATE, S. A., FURTH, H. P., *Phys. Fluids* **3** (1960) 982.
[19] WOOLLEY, R. v. d. R., STIBBS, D. W. N., The Outer Layers of a Star, Oxford University Press, London (1953) 120.
[20] SPITZER, L., *Phys. Fluids* **3** (1960) 659.
[21] DREICER, H., in proceedings of ref. 1, **31**, 57.
[22] GIBSON, A., in Proc. 3rd Intern. Conf. Ionization Phenomena in Gases (Venice, 11-15 June 1957) **1**, North Holland Publishing Co., Amsterdam, 365.
[23] BERNSTEIN, I. B., KULSRUD, R. M., *Phys. Fluids* **3** (1960) 937.
[24] SPITZER, L., The Physics of Fully Ionized Gases, Interscience Publishers, New York (1956).
[25] BERNSTEIN, W., et al, *Phys. Fluids* **3** (1960) 1019.
[26] NEWCOMB, W. A., *Ann. Phys.* **10** (1960) 232.
[27] COPLEY, D. M., WHITEMAN, K. J., U. K. AEA Report AERE R 3407 (1960).
[28] LEES, D. J., RUSBRIDGE, M. G., *Phys. Fluids* **4** (1961) 653.
[29] AFROSIMOV, V. V., et al, *Soviet Phys. Tech. Phys.* (translation) **5** (1961) 1389.
[30] KADOMTSEV, B. B., *Soviet Phys. J. exp. theor. Phys.* (translation) **13** (1961) 223.
[31] THOMPSON, W. B., in Riso Report 18, Danish Atomic Energy Commission (1960) 237.
[32] COLGATE, S. A., U. S. AEC Report UCRL 5888 (1961).
[33] AITKEN, K., et al, *Nuclear Fusion:* 1962 Supplement, Part 3, 979.
[34] JUKES, J. D., *J. nucl. Energy, Part C*, **3** (1961) 140.
[35] MARSHALL, W., U. K. AEA Report AERE T/R 2419 (1958).
[36] WARD, B. A., *J. nucl. Energy, Part C.*
[37] HOBBS, G. D., et al, in Proc. 5th Intern. Conf. Ionization Phenomena in Gases (Munich, August 1961), North Holland Publishing Co., Amsterdam (1962) 1965.

ИССЛЕДОВАНИЕ ПОТОКА АТОМНЫХ ЧАСТИЦ, ИСПУСКАЕМЫХ ПЛАЗМОЙ*

В. В. Афросимов, И. П. Гладковский, И. Ф. Калинкевич, М. П. Петров, Н. В. Федоренко

Физико-технический Институт имени А. Ф. Иоффе, Академия Наук СССР

Ленинград, Союз Советских Социалистических Республик

Разработан новый метод диагностики плазмы, основанный на исследовании потока нейтральных атомных частиц, испускаемых плазмой. Метод позволяет определять величину потока нейтральных частиц с энергией выше 100 эв, исследовать энергетическое распределение частиц и распределение их потока во времени, а также производить анализ частиц по массе. Для измерения параметров потока используется регистрация отдельных частиц после их превращения в ионы посредством обдирки при столкновениях в газе и ускорения напряжением 10-20 кв.

Метод был применен для исследованния потока нейтральных частиц с энергией от 100 эв до 10 кэв, испускаемых плазмой, на установке «Альфа» [1]. Найдено, что поток нейтральных частиц состоит, главным образом, из атомного водорода. Энергетическое распределение атомов не имеет максимума в области энергий, превышающих 100 эв, и не соответствует максвелловскому распределению. Полученные данные показывают, что наличие потока атомов в установке «Альфа» является одной из основных причин энергетических потерь плазмы.

На основании экспериментальных данных высказываются соображения о механизме нейтрализации ионов в плазме. Рассматривается также вопрос о связи между энергетическим распределением атомов, испускаемых плазмой, и энергетическим распределением ионов в плазме.

1. Введение

Как хорошо известно, протоны или дейтроны, являясь основной компонентой высокоионизованной водородной плазмы, не дают оптического излучения, в связи с чем анализ их энергии не может быть проведен спектроскопическим путем. Поэтому необходимо искать другие возможности для выяснения этого фундаментального вопроса. Ценные результаты может дать, например, исследование потока нейтральных частиц, испускаемых плазмой, предложенное в качестве одного из методов ее диагностики в 1958 г. Б. П. Константиновым. Применение такого метода преследует две основные цели. Одна из них состоит в получении сведений об энергетическом распределении ионов в плазме и, прежде всего, ионов водорода; другая — заключается в выяснении роли, которую играют нейтральные частицы в энергетических потерях плазмы. Для достижения этих целей прежде всего необходимо иметь возможность измерять величину потока нейтральных частиц, определять его энергетические и временные характеристики, а также производить анализ частиц по массе.

2. Методика исследования потока атомных частиц

2.1. Краткое описание прибора

Для исследования параметров потока нейтральных частиц, обладающего широким спектром кинетических энергий от электронвольт до десятков килоэлектронвольт, методы механической селекции по скоростям и сцинтилляционной спектрометрии оказываются мало пригодными. Кроме того, существенную трудность представляет собой сама регистрация нейтральных частиц. Наиболее рациональным способом, по-видимому, является ионизация атомов с последующим анализом по энергии и регистрацией образующихся при этом вторичных ионов. В разработанном нами приборе (рис. 1) пучок нейтральных частиц, испускаемых плазмой, коллимировался и очищался от заряженных частиц с помощью конденсатора. Далее пучок пропускался через газ при давлении $1\text{-}2 \times 10^{-4}$ мм рт ст, в котором часть атомов пучка при столкновениях с молекулами газа превращалась в ионы в результате обдирки. Вторичные ионы анализировались по энергии в электрическом поле и отклонялись в детектор. В детекторе применялось ускорение ионов напряжением $I_M = 10\text{-}20$ кв и регистрация их по электронам вторичной эмиссии с помощью сцинтилляционного счетчика. Помимо простоты, достоинством использованного способа является то, что отклонение ионов при анализе их по энергии позволяет практически полностью устранить при измерениях помехи, связанные с электромагнитным излучением плазмы, поступающим в прибор вместе с потоком нейтральных частиц. Регистрация ионов в режиме счета отдельных частиц обеспечивает высокую чувствительность прибора.

Для определения масс-состава потока нейтральных частиц используется либо анализ по времени пролета с одновременной (панорамной) регистрацией масс-спектра, либо анализ частиц в магнит-

* Доклад CN-10/238, представленный на Конференцию. Докладчик: Н. В. Федоренко. Дискуссия (на английском языке) по этому докладу дана на стр. 1019. Переводы аннотаций находятся в конце тома.

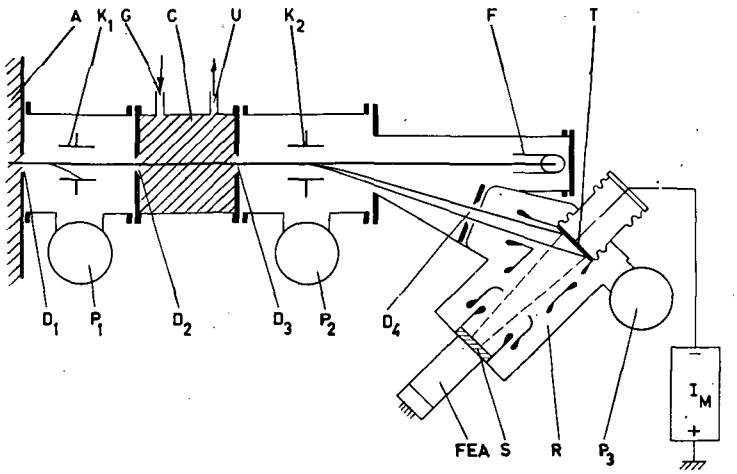

Рис. 1 Схема прибора для исследования потока атомных частиц: A — объем, в котором создается плазма; D_1 — входная щель прибора; K_1 — конденсатор для очистки пучка атомов от заряженных частиц; C — камера с газом для обдирки атомов; D_2 и D_3 — входная и выходная щели камеры обдирки; G и V — трубки для впуска газа и измерения давления; K_2 — конденсатор для анализа по энергии; D_4 — входная щель детектора; R — детектор; T — мишень для ионов; I_M — источник напряжения, ускоряющего ионы; S — сцинтиллятор; FEA — фотоумножитель; P_1, P_2, P_3 — диффузионные насосы; F — вспомогательный фарадеев приемник.

ном поле, обладающий большей светосилой и разрешающей способностью по массе. В первом случае пучок вторичных ионов модулируется с помощью конденсатора, помещаемого для этой цели на выходе из камеры обдирки (на рис. 1 этот конденсатор не показан). Время пролета ионов от камеры обдирки до детектора измеряется по запаздыванию импульсов детектора, регистрирующего ионы различных масс, относительно импульсов напряжения, модулирующего пучок ионов. Во втором случае между конденсатором для анализа ионов по энергии и детектором устанавливается магнитный масс-анализатор.

Естественно, что с помощью прибора, показанного на рис. 1, можно также исследовать поток ионов, испускаемых плазмой и достигающих входной щели прибора. При этом камера обдирки откачивается до предельного вакуума и ионы, прошедшие коллиматор, анализируются по энергии и отклоняются в детектор.

2.2. Аппаратура для регистрации электрических импульсов

Счет числа импульсов фотоумножителя, возникающих при регистрации частиц, производится с помощью радиотехнической аппаратуры для интегрального и дифференциального счета импульсов с временным разрешением 1,5 мксек. Для исследования зависимости потока частиц от времени применяется пятиканальный временной анализатор, позволяющий производить счет частиц в заданные интервалы времени в течение разряда в плазменной установке. Средняя длительность разряда в установке «Альфа» составляет 2,5 мсек.

В ряде случаев более удобным оказывается осциллографирование временных или энергетических характеристик потока нейтральных частиц. Для этого импульсы, возникающие на выходе детектора при регистрации ионов, интегрируются, и сигнал фотографируется с экрана осциллографа. Исследование потока в течение отдельных временных интервалов производится путем изменения момента запуска осциллографа и длительности развертки.

2.3. Калибровка аппаратуры

Определение оптимальных условий работы прибора и калибровка аппаратуры производились с помощью установки, позволяющей получать монокинетические пучки ионов и атомов заданной массы и известной интенсивности. Энергия частиц могла регулироваться в пределах 100 эв-40 кэв.

Было установлено, что благодаря ускорению в детекторе эффективность регистрации ионов не зависит от их начальной энергии и близка к 100%. Эффективность регистрации атомов определяется коэффициентом их обдирки в газе. При наполнении камеры обдирки азотом до давления 10^{-4} мм рт ст эффективность регистрации атомов водорода изменяется от 0,001% при энергии 100 эв до 2% при энергии 10 кэв. Исследования показали, что для регистрации легких атомов, таких как атомы водорода, обдирка их в газе оказывается более удобным и эффективным методом, чем ионизация электронным ударом при всех энергиях, превышающих 100 эв.

Градуировка аппаратуры при осциллографировании производилась путем регистрации модулированного пучка известной интенсивности.

Подробное описание определения эффективности регистрации частиц и калибровки аппаратуры дано в работе [2].

3. Результаты измерения потока атомных частиц, испускаемых плазмой

Первые же опыты, предпринятые на установке «Альфа», показали, что существует поток атомов, кинетическая энергия которых составляет сотни и

тысячи электронвольт. Поток атомов, испускаемых плазмой, измерялся в направлении большого радиуса тороидальной камеры; он оказался на 3—4 порядка больше минимального потока, который может быть зарегистрирован и исследован с помощью описанного выше прибора.

Благодаря тщательной экранировке измерительного прибора электрические и магнитные поля, возникающие в непосредственной близости от установки «Альфа», не влияли на его работу. Это было проверено путем контроля за регистрацией ионов от вспомогательного ионного источника, помещенного перед камерой обдирки внутрь измерительного прибора.

Наряду с потоком атомов было установлено наличие потока ионов, испускаемых плазмой и обладающих энергиями до нескольких десятков килоэлектронвольт. Однако вследствие влияния магнитных полей на пути от плазмы до входа в измерительный прибор этот поток сильно «обеднен» ионами малых энергий и легких масс и поэтому не отражает концентрации, состава и энергетического распределения ионов в плазме. Представляет интерес лишь сам факт существования потока ионов, испускаемых плазмой, и зависимость его от времени, т. к. сведения о потоке ионов могут быть использованы для интерпретации механизма взаимодействия частиц плазмы со стенками камеры, в которой она образуется.

3.1. Анализ масс нейтральных частиц

С помощью масс-анализа было установлено, что поток атомов, испускаемых плазмой, во всех режимах установки «Альфа» состоит в основном из атомного водорода. Поток атомов примесей не превышает 5-15% от потока атомов водорода.

3.2. Распределение атомов в потоке по энергии

Энергетическое распределение атомов в потоке $\mathrm{d}J/\mathrm{d}E$, испускаемом с единицы площади поверхности плазмы, может быть найдено из соотношения

$$\frac{\mathrm{d}J}{\mathrm{d}E} = \frac{2\pi\nu j_+(E)}{\langle\Omega\rangle S_{\text{эфф}} E\,\alpha_0(E)} \qquad (1)$$

где E — энергия атомов, ν — разрешающая способность прибора по энергии, $\langle\Omega\rangle$ — средний телесный угол, вырезаемый коллиматором, $S_{\text{эфф}}$ — эффективная площадь поверхности плазмы, с которой испускаемые частицы могут попадать в прибор, $\alpha_0(E)$ — эффективность регистрации атомов с энергией E, $j_+(E)$ — поток вторичных ионов с энергиями от $E\,[1+(1/2\,\nu)]$ до $E\,[1-(1/2\,\nu)]$, одновременно регистрируемых детектором. Множитель $2\pi/\langle\Omega\rangle$ учитывает долю частиц, выделяемых коллиматором прибора из общего числа частиц, при изотропном распределении их скоростей.

Типичное энергетическое распределение $\mathrm{d}J/\mathrm{d}E = f(E)$, усредненное во времени за период разряда, приведено на рис. 2. Из рис. 2 видно, что энергетическое распределение атомов не имеет максимума в области энергий, превосходящих 100 эв. Поток атомов быстро и монотонно падает с увеличением их энергии. Измерения показали, что энергетические распределения для различных режимов установки «Альфа» не имеют качественных различий. Однако относительное количество быстрых атомов несколько возрастает при увеличении энергии, вводимой в разряд W, и при уменьшении напряженности внешнего магнитного поля H_z и начального давления водорода в камере «Альфы» p_{H}.

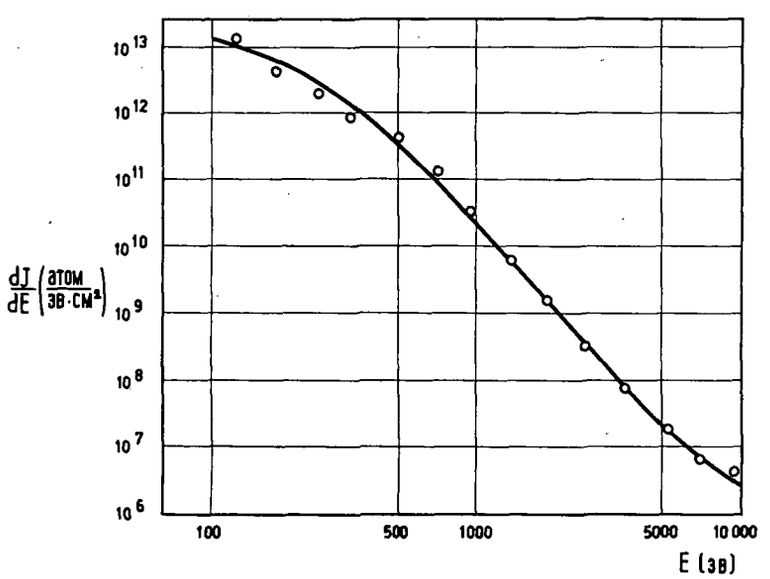

Рис. 2 Энергетическое распределение атомов в потоке, усредненное во времени за период разряда. $W = 230$ кдж; $H_z = 360$ э; $p_{\text{H}} = 2 \times 10^{-4}$ мм рт ст.

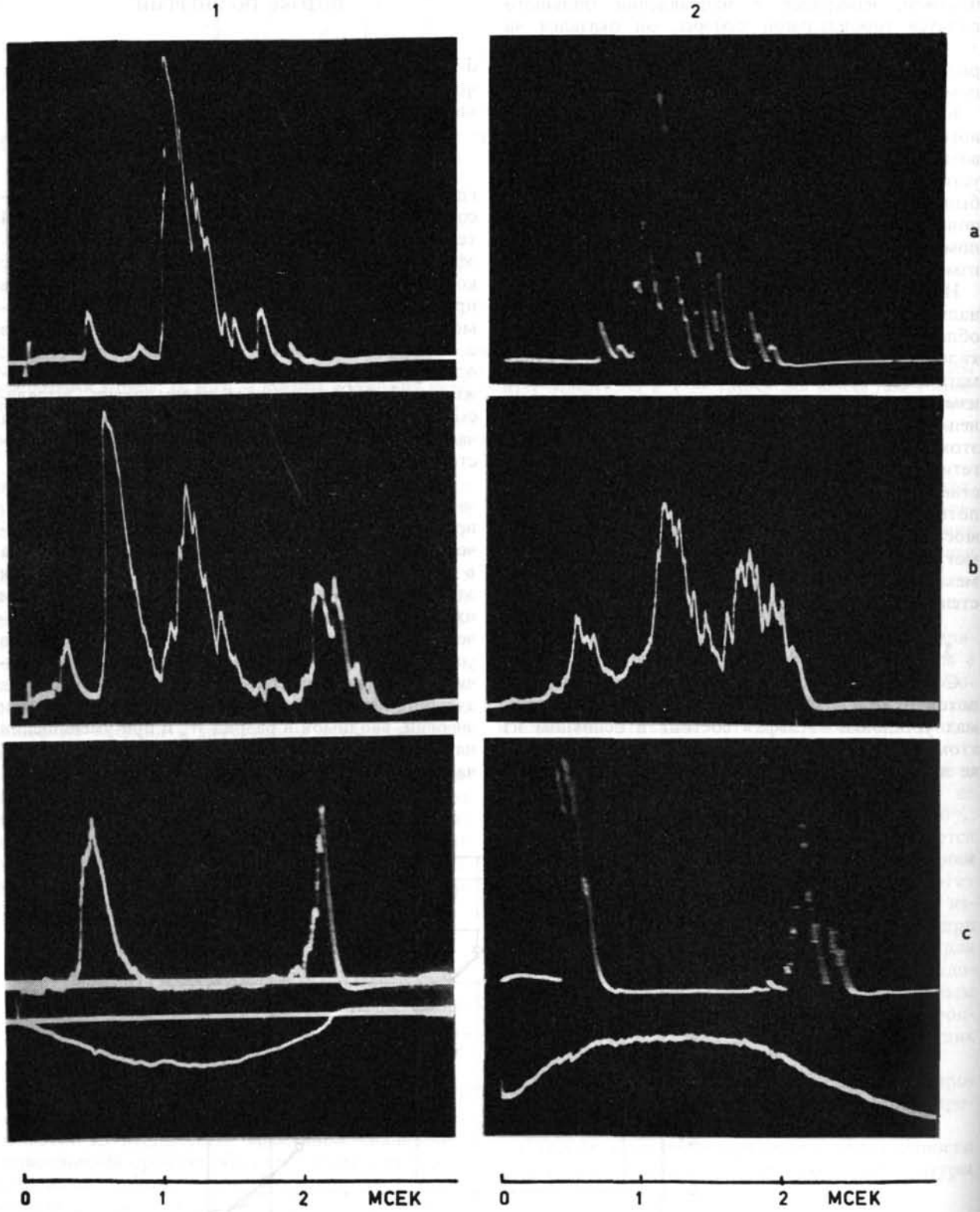

Рис. 3 Зависимость потока атомов и ионов от времени при различной вводимой в разряд энергии: 1 — атомы; 2 — ионы. W (кдж): a — ~30, b — 130, c — 230; $H_z = 360$ э; $p_H = 2 \times 10^{-4}$ мм рт ст.

3.3. Зависимость величины потока атомных частиц от времени

Временные характеристики потока атомных частиц наиболее сильно зависят от величины энергии, вводимой в разряд. Эта энергия может быть определена по осциллограммам тока и напряжения разряда. Несколько временных характеристик потока атомов и ионов приведено на рис. 3. Осциллограммы на рис. 3 свидетельствуют о резких изменениях потока атомов и ионов, испускаемых плазмой, на протяжении разряда. При этом для потока ионов характерны более быстрые колебания, чем для потока атомов. При изменении напряженности внешнего магнитного поля или начального давления водорода изменяется главным образом величина потока и продолжительность его существования, характер же зависимости потока от времени сохраняется.

3.4. Плотность потока, концентрация атомов и энергия, уносимая потоком атомов из плазмы

Исследование энергетических распределений и временных характеристик позволяет определить абсолютную величину плотности потока атомов

$$J = \int_{E_1}^{E_2} \frac{\mathrm{d}J}{\mathrm{d}E}\,\mathrm{d}E \qquad (2)$$

(E_1 и E_2 — границы исследованного интервала энергии, составляющие в настоящей работе соответственно 100 эв и 10 кэв), концентрацию атомов в объеме

$$n_0 = 2\,(2M)^{1/2} \int_{E_1}^{E_2} \frac{\mathrm{d}J}{\mathrm{d}E}\,\frac{\mathrm{d}E}{E^{1/2}} \qquad (2)$$

(M — масса атома) и энергию, уносимую потоком атомов из плазмы

$$\mathscr{E} = \int_{E_1}^{E_2} \frac{\mathrm{d}J}{\mathrm{d}E}\,E\,\mathrm{d}E \qquad (4)$$

Ввиду того, что величина $\mathrm{d}J/\mathrm{d}E$ быстро уменьшается с увеличением энергии атомов, величины, даваемые формулами (2) — (4) для $E_2 = 10$ кэв должны практически совпадать с величинами для $E_2 = \infty$.

Измерения показали, что плотность потока атомов с энергией, превышающей 100 эв, составляет в среднем 1,0-1,4 $\times 10^{15}$ см$^{-2}$ за разряд. Концентрация атомов этих энергий в объеме изменяется в течение разряда в пределах от 1×10^9 до 6×10^{11} см$^{-3}$, т.е. не превосходит 4% от полной концентрации ионов, составляющей около $1{,}5 \times \times 10^{13}$ см$^{-3}$. Энергия, уносимая потоком атомов с $E \geqslant 100$ эв из плазмы, оказывается в среднем равной 15 кдж, что заметно превышает величины, полученные нами в работе [3] для потока атомов с энергией, более 300 эв. Относительная величина потери энергии плазмой, связанной с потоком атомов, оказывается наибольшей при малых значениях энергии, вводимой в разряд (~50 кдж), и достигает при этом 30%.

На рис. 4 представлен график потока энергии $\mathrm{d}\mathscr{E}/\mathrm{d}E = E\,\mathrm{d}J/\mathrm{d}E$, уносимой из плазмы атомами с различной энергией. Из рис. 4 следует, что поток энергии, уносимой атомами из плазмы, возрастает с уменьшением их энергии. И хотя рост кривой в сторону малых энергий атомов замедляется, она не имеет максимума в области $E \geqslant 100$ эв. Последнее обстоятельство дает основание считать, что на установке «Альфа» энергия, уносимая полным потоком атомов, включая атомы с $E < 100$ эв, может являться одной из главных причин энергетических потерь плазмы.

4. Интерпретация экспериментальных данных

4.1. Представления о механизме образования потока атомов, испускаемых плазмой

Основным процессом, приводящим к образованию потока атомов с энергией в сотни электронвольт, испускаемых плазмой, на установке «Альфа» является перезарядка ионов на ней-

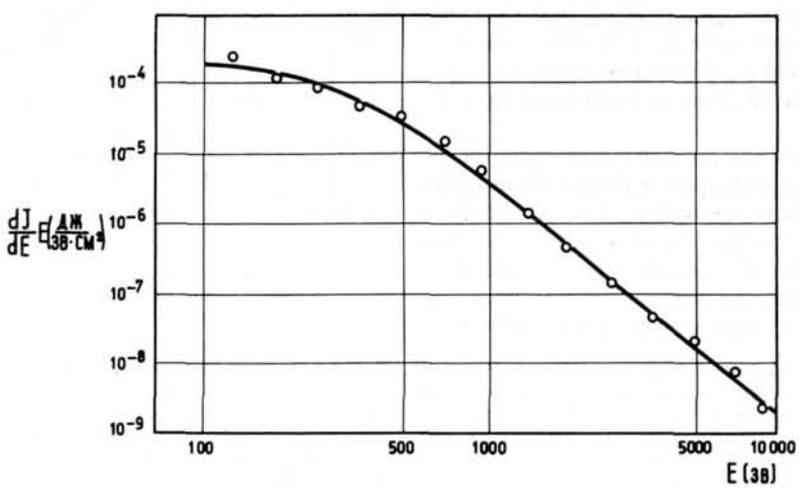

Рис. 4 Поток энергии, уносимой из плазмы атомами с различной энергией. Режим тот же, что и для рис. 2.

тральных частицах, поступающих в плазму со стенок. Объемная рекомбинация протонов и электронов обладает значительно меньшими сечениями и не может приводить к наблюдаемым экспериментально значениям концентрации таких атомов. Атомы, возникающие в результате нейтрализации ионов на стенках, как показывают оценки их энергии [3] и расчеты по данным работы [4], сами практически не проходят через плазму и играют лишь роль мишени для перезарядки ионов плазмы. Поток нейтральных частиц, поступающих в плазму, может возникать как в результате нейтрализации ионов на стенках, так и при десорбции газа. В образовании потока атомов водорода, испускаемого плазмой, наиболее существенную роль играет, по-видимому, резонансная перезарядка протонов на атомах водорода.

Картина образования потока атомов, испускаемых плазмой, может быть качественно описана следующим образом. Поступающий в плазму со стенок поток атомов, который для краткости можно называть «входящим», ослабляется в результате ионизации атомов электронами и перезарядки с ионами плазмы. Относительная вероятность перезарядки и ионизации атомов входящего потока определяется отношением соответствующих средних частот столкновений $\langle \nu_п \rangle$ и $\langle \nu_и \rangle$

$$\eta = \frac{\langle \nu_п \rangle}{\langle \nu_и \rangle} = \frac{\langle \sigma_п v \rangle}{\langle \sigma_и v_э \rangle} \qquad (5)$$

где $\sigma_п$ — сечение перезарядки, $\sigma_и$ — сечение ионизации, v и $v_э$ — скорости ионов и электронов в плазме.

Средняя длина свободного пробега атомов, образующихся при перезарядке в плазме, должна превышать среднюю длину пробега атомов входящего потока, имеющих меньшую энергию, чем ионы плазмы. Поэтому при изотропном распределении ионов по скоростям почти половина атомов, образующихся при перезарядке ионов плазмы на атомах входящего потока, сразу же попадет на стенки. Другая половина атомов, возникших при перезарядке, двигаясь вглубь плазмы, будет частично ионизована, а частично в результате последующих актов перезарядки также попадет на стенки. Атомы, испускаемые плазмой, отдают стенкам свою энергию и затем в составе входящего потока поступают в плазму, где все явление повторяется.

Численные оценки по данным для сечений из работ Файта [5, 6] и Далгарно и Ядава [7] показывают, что для атомов водорода, поступающих в водородную плазму, перезарядка оказывается более вероятной, чем ионизация ($\eta > 1$) при всех температурах плазмы, не превышающих нескольких кэв*. Поэтому атомы водорода сравнительно слабо поглощаются водородной плазмой, и для них существует вероятность возникновения механизма последовательного во времени, «эстафетного» выхода нескольких атомов на стенки, прежде чем произойдет ионизация. Напротив, для примесей относительная вероятность перезарядки должна быть значительно меньше и они будут в основном сразу поглощаться водородной плазмой вследствие ионизации электронами, не вызывая появления потока атомов, испускаемых плазмой.

4.2. О СВЯЗИ МЕЖДУ ЭНЕРГЕТИЧЕСКИМИ РАСПРЕДЕЛЕНИЯМИ АТОМОВ И ИОНОВ

В работе [4] было показано, что энергетическое распределение ионов в плазме $\varphi(E)$ связано с энергетическим распределением испускаемых ею атомов $\mathrm{d}J/\mathrm{d}E$ соотношением

$$\varphi(E) = I\,C(v)\,\frac{1}{v\,\sigma_п(v)}\,\frac{\mathrm{d}J}{\mathrm{d}E} \qquad (6)$$

где v и $\sigma_п(v)$ — имеют прежнее значение, а I — плотность входящего потока атомов и $C(v)$ — функция, учитывающая вероятность того, что на пути атома, образующегося при перезарядке, к стенке может произойти его ионизация или повторная перезарядка. Численные оценки с использованием данных работ [5, 6, 7] показывают, что в интервале энергий атомов водорода 100 эв — 10 кэв величина $C(v)/v\,\sigma_п(v)$ уменьшается всего в 3,7 раза. На рис. 5 представлено энергетическое распределение атомов в потоке $\mathrm{d}J/\mathrm{d}E$, измеренное экспериментально, и рассчитанные из него энергетические распределения атомов $\mathrm{d}n_0/\mathrm{d}E$ и ионов $\varphi(E)$ в объеме камеры «Альфы». Ввиду того, что численное значение плотности входящего потока

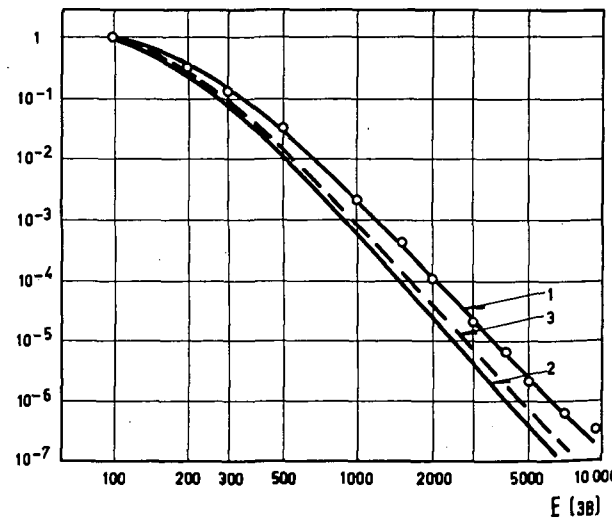

Рис. 5 Энергетические распределения атомов и ионов: 1 — экспериментальная кривая энергетического распределения атомов в потоке $\mathrm{d}J/\mathrm{d}E$; 2 — энергетическое распределение атомов в объеме $\mathrm{d}n_0/\mathrm{d}E$, рассчитанное из кривой 1; 3 — энергетическое распределение ионов в объеме $\varphi(E)$, рассчитанное из кривой 1. $W = 230$ кдж; $H_z = 360$ э; $p_{\mathrm{H}} = 2 \times 10^{-4}$ мм рт.ст.

* Оценки величины $\langle \nu_и \rangle$ производились для максвелловского распределения электронов плазмы по скоростям. Для оценки $\langle \nu_п \rangle$ распределение ионов также принималось максвелловским. Последнее допущение оправдывается тем, что вид функции распределения ионов вообще мало влияет на результат, ввиду слабой зависимости произведения $\sigma_п v$ для резонансной перезарядки от скорости ионов.

неизвестно, энергетические распределения в объеме даны в относительных единицах. Для удобства сравнения все кривые совмещены в точке $E = 100$ эв. Из рис. 5 видно, что энергетические распределения атомов и ионов мало отличаются друг от друга. Обработка данных о потоке атомов, произведенная для различных режимов «Альфы», показала, что ни одно из полученных энергетических распределений ионов в плазме не может быть аппроксимировано распределением Максвелла.

4.3. О РОЛИ НЕЙТРАЛЬНЫХ ЧАСТИЦ В ЭНЕРГЕТИЧЕСКИХ ПОТЕРЯХ ПЛАЗМЫ

Нейтральные частицы, поступающие в плазму, приводят к ее «охлаждению» как из-за потери энергии электронами на их возбуждение и ионизацию, так и из-за передачи энергии стенкам камеры потоком атомов, образующихся при перезарядке ионов. При этом, как отмечалось ранее, в водородной плазме эффективность ионизации оказывается наибольшей для примесей, а эффективность перезарядки — для атомов водорода. Количественные оценки показывают, что поступление в плазму потока атомов водорода, образующихся при нейтрализации ионов на стенках или диссоциации десорбированных молекул водорода, ($I_{\text{ст}}$) должно сопровождаться появлением потока атомов, испускаемых плазмой (J), который обладает примерно такой же интенсивностью. Так как атомы, испускаемые плазмой, возвращаются в нее после отражения от стенок, величина J может быть найдена из соотношения

$$J = A\,(J + I_{\text{ст}})$$

откуда

$$J = \frac{A}{1-A}\, I_{\text{ст}} \qquad (7)$$

здесь A — альбедо плазмы для атомов, выражение для которого было получено в работе [4]. В работе [3] нами было найдено, что энергия частиц, отраженных от стенки, составляет в среднем менее 0,1 от их начальной энергии. При этом альбедо плазмы может быть представлено как

$$A \approx 1 - \left(\frac{1}{\eta + 1}\right)^{1/2} \qquad (8)$$

где величина η определяется приведенным выше выражением (5). Численный расчет показывает, что альбедо атомов водорода в области температур плазмы до $T \approx 1$ кэв составляет $A \approx 0{,}5$, откуда согласно (7) $J \approx I_{\text{ст}}$. Лишь в области $T = 30$-100 эв, соответствующей максимуму сечения ионизации атомов водорода электронами, альбедо уменьшается до $A \approx 0{,}3$, что дает $J \approx 0{,}4\, I_{\text{ст}}$.

В заключение следует отметить, что большая величина потока атомов в установке «Альфа» связана, по-видимому, с большим потоком ионов на стенки. Однако возможность возникновения интенсивного обмена нейтральными частицами между плазмой и стенками должна существовать и при удовлетворительном удержании заряженных частиц во всех установках, камеры которых наполняются водородом. Предварительное обезгаживание стенок и улучшение начальных вакуумных условий не может полностью исключить образование потока десорбированного газа в плазму в течение разряда. Количество водорода даже в мономолекулярном слое на стенках камеры, наполненной водородом до давления $\sim 10^{-4}$ мм рт ст, в несколько раз превышает количество водорода в объеме. В то же время именно поток атомов и молекул водорода, диссоциирующих в плазме, представляет собой наиболее эффективную мишень для перезарядки ионов водородной плазмы.

Литература

[1] Афросимов В. В. и др, *Ж. техн. Физ.* **30** (1960) 1381.
[2] Афросимов В. В. и др, *Ж. техн. Физ.* **30** (1960) 1456.
[3] Афросимов В. В. и др, *Ж. техн. Физ.* **30** (1960) 1469.
[4] Константинов О. В., Перель В. И., *Ж. техн. Физ.* **30** (1960) 1485.
[5] Fite, W. L., Brackmann, R. T., Snow, W. R., *Phys. Rev.* **112** (1958) 1161.
[6] Fite, W. L., Brackmann, R. T., *Phys. Rev.* **112** (1958) 1141.
[7] Dalgarno, A., Iadav, H. N., *Proc. Phys. Soc. (London)* **A66** (1953) 173.

СПЕКТРАЛЬНЫЕ ИССЛЕДОВАНИЯ НА УСТАНОВКЕ «АЛЬФА»*

А. Б. Березин, А. Н. Зайдель, Г. М. Малышев, Г. Т. Раздобарин, В. В. Скидан

Академия Наук СССР

Москва, Союз Советских Социалистических Республик

1. На установке Альфа с помощью нескольких фотоумножителей одновременно регистрировались интенсивности линий кислородных ионов разной кратности (O III, O IV, O V), а также разных ионов одной кратности (N IV, O IV).

Длительность свечения всех линий возрастает при увеличении напряжения на конденсаторной батарее.

При малых напряжениях (10 кв) свечений линий O III, O IV, N IV и O V имеет один максимум в средине импульса, а при больших (15 кв) все линии имеют два максимума в начале и в конце импульса. Ход интенсивности линий, принадлежащих ионам разной кратности, показывает, что появление двух максимумов не может быть объяснено только увеличением степени ионизации вблизи максимума тока в средней части импульса разряда.

Исследование частот колебания интенсивности показало, что до нескольких десятков кгц изменения интенсивностей всех линий примерно одинаковы. Колебания более высоких частот, по-видимому, не коррелируют между собой. Следует отметить, что частоты колебания интенсивности спектральных линий больше частот колебания разрядного тока.

Исследовалось также свечение линии N IV испускаемое различным участками разряда. Установлено, что ход интенсивности этой линии, испускаемой двумя объемами плазмы, отстоящими, примерно, на 1 м друг от друга, одинаков в области низких частот (до 10 кгц). В области более высоких частот характер свечения обоих объемов независим. При расстояниях между светящимися объемами в несколько сантиметров имеется полная корреляция свечения на частоте до 100 кгц и различный детальный ход на более высоких частотах.

2. Для обнаружения коллективных движений в плазме одновременно регистрировался ход интенсивностей длиноволновой и коротковолновой половин линии N IV, которая разделялась с помощью оптического устройства.

Когда допплеровские смещения линий малы и соответственно мал вклад коллективных движений в уширение линий, количественная обработка экспериментального материала оказывается достаточно простой. В этом случае отношение сдвига линии $\Delta\lambda$ к ее полуширине α приближенно выражается соотношением $\Delta\lambda/\alpha=\beta/2$, где β — отношение разности регистрируемых световых потоков к их сумме.

Результаты обработки экспериментального материала показывают, что относительный сдвиг спектральных линий, соответствующий коллективным движениям в исследовавшемся режиме работы установки «Альфа», не превышает 15%, а общий вклад коллективных движений в уширение линии N IV за время импульса значительно меньше этой верхней границы.

Из рассмотрения полученного материала делается вывод, что скорости коллективных движений не превосходят 10^6 см/сек, т.е. того же порядка, что и скорости направленного движения вдоль электрического поля, измеренные ранее.

1. Введение

Одновременная регистрациия интенсивностей различных участков спектра импульсного разряда является удобным средством исследования процесса развития разряда и изменения его параметров в течение импульса. Такое исследование разряда в камере установки «Альфа» [1] проводилось с помощью многоканального регистрирующего устройства.

Для спектрального разложения служил спектрограф ДФС-8, снабженный выходными щелями, имеющий дисперсию 6 Å/мм при разрешающей способности 60000. Регистрация велась с помощью фотоумножителей ФЭУ-18А и двухлучевых осциллографов. Регистрирующая система имела полосу пропускания от 50 гц до 2 мгц.

2. Коллективные движения

2.1. Метод измерений

Исследование вклада коллективных движений ионов N IV в наблюдающееся допплеровское уширение линии N IV ($\lambda=3479$ Å) проводило с помощью оптического устройства, состоящего из увеличивающей системы и зеркал, отбрасывающих длинноволновую и коротковолновую половины этой линии на два фотоумножителя [2]. Хаотическое движение, а так же симметричные пульсации плазмы, не изменяют относительной величины сигналов обоих фотоумножителей, в то время как коллективное направленное движение излучающих ионов вдоль линии наблюдения вызывает в результате допплеровского смещения изменение отношения сигналов, даваемых обоими

* Доклад CN-10/239, представленный на конференцию. Докладчик: А. Б. Березин. Дискуссия (на английском языке) по этому докладу дана на стр. 1019. Переводы аннотаций находятся в конце тома.

фотоумножителями. От наблюдаемых относительных изменений интенсивности можно перейти к вкладу коллективных движений в уширение линий.

2.2. Эксперимент

Для увеличения ширины изображения спектральной линии применялась цилиндрическая кварцевая линза с фокусным расстоянием 12 мм, установленная параллельно выходной щели прибора, дающая изображение последней с десятикратным увеличением. В плоскости изображения этой линзы помещалось ребро призмы, алюминированные грани которой служили зеркалами. Юстировка системы проводилась так, чтобы ребро призмы возможно точно совпадало с положением максимума линии NIV. Примеры осциллограмм, записанных с помощью этого устройства, приведены на рис. 1. На осциллограмме рис. 1а отчетливо видно, что амплитуды колебаний интенсивности, соответствующие двум половинам линии, различны, а максимумы свечения, вообще говоря, сдвинуты друг относительно друга.

Для проверки того, что такого рода относительные колебания интенсивности не обусловлены инструментальными ошибками (например флуктуационным явлениями или электрическими наводками) в тех же условиях было проведено осциллографирование при широкой входной щели спектрального прибора (рис. 1б). В этих условиях на оба зеркала попадает свет всех частот в интервале спектральной ширины исследуемой линии. Вследствие этого относительного изменения величины

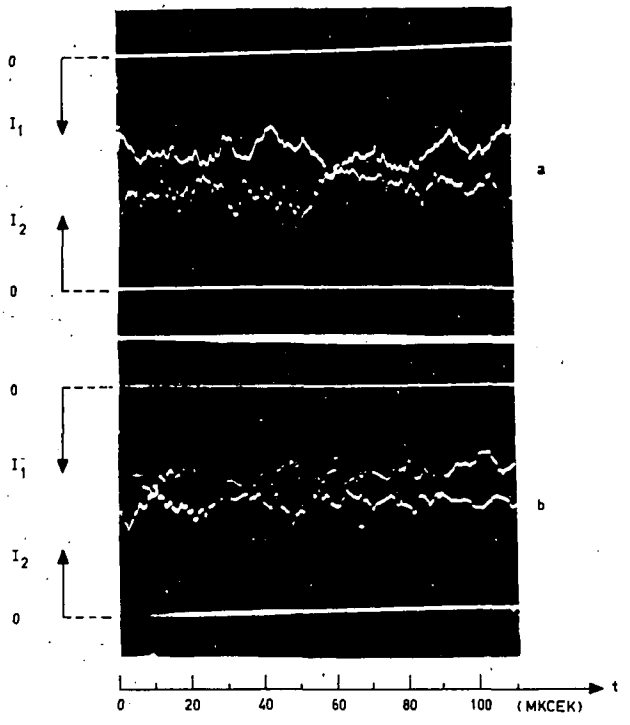

Рис. 1 Осциллограммы световых потоков от длинноволновой (I_1) и коротковолновой (I_2) частей линии NIV ($\lambda = 3479$ Å) при узкой (а) и широкой (б) входной щели спектрографа.

сигналов, даваемых фотоумножителями, не должно быть. Это и иллюстрируется на рис. 1 б. В случае «а» спектральная ширина входной щели составляла 0,2-0,3 Å, в случае «б» 2-3 Å.

2.3. Обсуждение результатов

Обработка полученных результатов производилась на основании следующих соображений: контур линии в данный момент времени можно представить в следующем виде (имеется ввиду контур получающийся в результате усреднения вдоль линии наблюдения и по малому промежутку времени соответствующему границе полосы пропускания аппаратуры со стороны высоких частот):

$$F(t,\lambda) = A(t)\varphi\left(\frac{\lambda-\lambda_0}{\alpha} - \frac{\Delta\lambda}{\alpha}\right) \qquad (1)$$

Здесь $A(t)$ — интегральный световой поток от всей линии;
$\alpha = \alpha(t)$ — ширина линии;
$\Delta\lambda = \Delta\lambda(t)$ — сдвиг линии, возникающий в результате коллективного движения;
λ_0 — длина волны, соответствующая максимуму несмещенной линии.

Световые потоки от длинноволновой и коротковолновой частей спектральной лиинн записываются как

$$I_1 = \int_{-\infty}^{\lambda_0} F(\lambda,t)\,d\lambda$$

$$I_2 = \int_{\lambda_0}^{\infty} F(t,\lambda)\,d\lambda \qquad (2)$$

Эти величины λ_0 пропорциональны ординатам осциллограмм на рис. 1. Если ввести относительную разность потоков

$$\beta = \frac{I_1 - I_2}{I_1 + I_2} \qquad (3)$$

то можно показать, что относительный сдвиг контура линии

$$\frac{\Delta\lambda}{\alpha} = \Phi(\beta) \qquad (4)$$

где функция Φ не зависит от ширины контура, но различна для контуров разной формы.

Таким образом для определения вклада коллективных движений в уширение линий необходимо задать на основании тех или иных соображений вид контура линии. Однако, если величина сдвига составляет не более 25-30% от ширины линий, то для оценки вклада можно считать, что результаты вычислений не зависят от формы контура и для всех контуров применять соотношение

$$\frac{\Delta\lambda}{\alpha} = \frac{\beta}{2} \qquad (5)$$

Для оценки вклада надо получить относительные сдвиги по всему импульсу разряда или, во всяком случае, для всех тех моментов времени, когда

интегральная интенсивность линии $A(t)$ достаточно велика.

Из выражения (5) можно получить скорость направленного движения:

$$v_{\text{H}} = v_{1/2}\beta \qquad (6)$$

где $v_{1/2}$ — скорость, соответствующая половине полуширины контура спектральной линии.

Если считать, что полуширина линии мало меняется за время интенсивного свечения и в течение этого времени мало отличается от полуширины результирующего контура, то $v_{1/2}$ можно найти обычным фотографическим методом. Тогда соотношение (6) даст значение направленной скорости в данный момент времени.

Для получения нужного разрешения во времени период развертки осциллографа был выбран в 150 мксек. Нужный интервал импульса вырезался с помощью временной задержки, так что каждый раз регистрировалось примерно $^1/_{10}$ всего импульса. Окончательный результат получался путем статистической обработки осциллограмм, полученных для различных участков импульса.

По ряду осциллограмм были измерены потоки I_1 и I_2 и получены их относительные сдвиги $\Delta\lambda/\alpha$ по всем промежуткам времени, где интегральное свечение линии достаточно велико. Измерения на осциллограммах производилось в точках на расстояниях, соответствующих примерно 3 мксек. Выбор такого интервала для измерений обусловлен тем, что частоты колебаний интенсивности, дающие заметную величину β, не превосходят 300-400 кгц.

Оказалось, что относительные сдвиги для всех моментов времени не превосходят ~20%, а как правило они меньше. Это позволяет сделать вывод, что коллективные движения ионов N IV не дают заметного вклада в уширение спектральных линий. Во всяком случае он меньше 20%.

Приведенные результаты относятся к работе камеры в течение декабря—января 1961 г. при задаваемом напряжении на конденсаторной батарее $U=12{,}5$ кв, напряженности продольного магнитного поля $H_z=360$ э и давлении водорода $p=2\times10^{-4}$ мм рт ст.

3. Интенсивности линий примесей

3.1. Эксперимент

На спектрографе ДФС-8 были установлены три выходные щели с фотоумножителями ФЭУ-18А, которые позволяли одновременно регистрировать с помощью двух двухлучевых осциллографов интенсивности трех произвольно выбранных линий, а также ток разряда. Система имела полосу пропускания от 50 гц до 2 мгц. С помощью этой установки исследовался ход интенсивности свечения линий ионов O III ($\lambda=3265$ Å); O IV ($\lambda=3386$ Å); O V ($\lambda=2781$ Å), а также ионов N IV ($\lambda=3479$ Å) и линии H_β.

Время развертки могло меняться от 2,5 мсек до 0,1 мсек, так что регистрировалось свечение в течение всего импульса, либо отдельных его частей. Исследование проводилось в различных режимах работы установки, но при одном и том же начальном давлении водорода, равном 2×10^{-4} мм рт ст.

3.2. Результаты и их обсуждение

Установлено, что длительность свечения по мере увеличения напряжения на конденсаторной батарее от 10 до 15 кв растет примерно от 1,5 до 3 мсек для линий O IV, N IV, O V и от 2 до 3 мсек для линии O III.

Из полученных осциллограмм видно, что при напряжении на конденсаторной батарее $U=10$ кв и напряженности продольного начального магнитного поля $H_{z0}=360$ э интенсивности всех линий имеют максимум в середине импульса разряда (рис. 2). При напряжении на конденсаторной батарее $U=12{,}5$ кв в некоторых импульсах разряда имеется один максимум, а в некоторых два максимума (рис. 3). (На этом рисунке и далее осциллограммы, снятые в течение одного и того же импульса, соединены вместе.) При напряжении

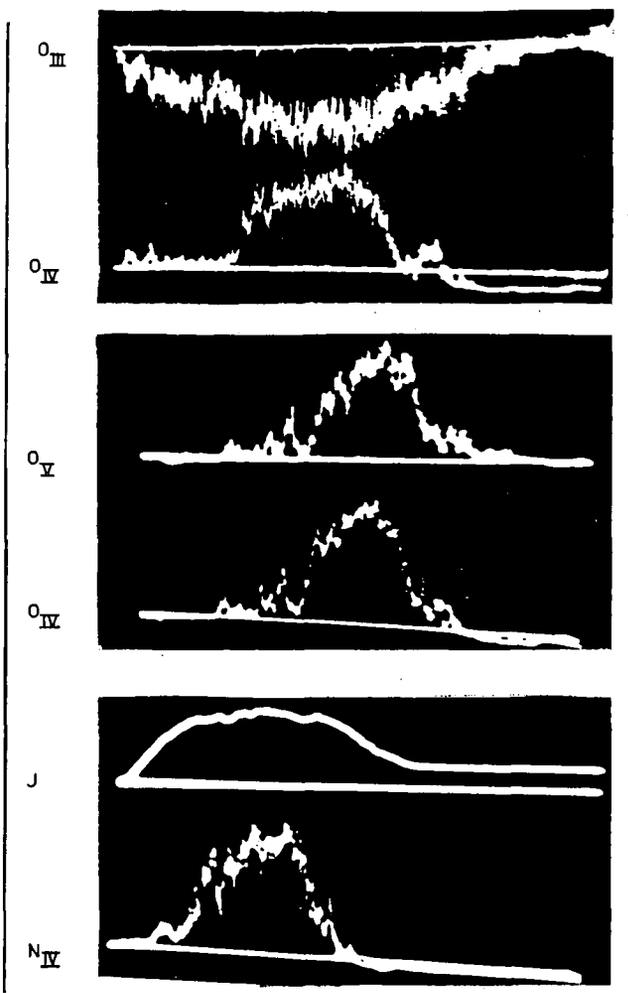

Рис. 2 Интенсивности линий O III ($\lambda=3265$ Å); O IV ($\lambda=3386$ Å); N IV ($\lambda=3479$ Å); O V ($\lambda=2781$ Å) и ток разряда (J). Время развертки $T_{\text{р}}=2{,}5$ мсек. Режим: $U=12{,}5$ кв; $H_z=360$ э.

$U=15$ кв интенсивность линий имеет, как правило, два максимума в начале и в конце импульса, а иногда один максимум в конце его.

Аналогичные результаты были получены ранее [2] для линии N IV ($\lambda=3479$ Å).

В редких случаях даже при $U=15$ кв наблюдаются линии N IV, O IV и O V с одним максимумом в середине разряда.

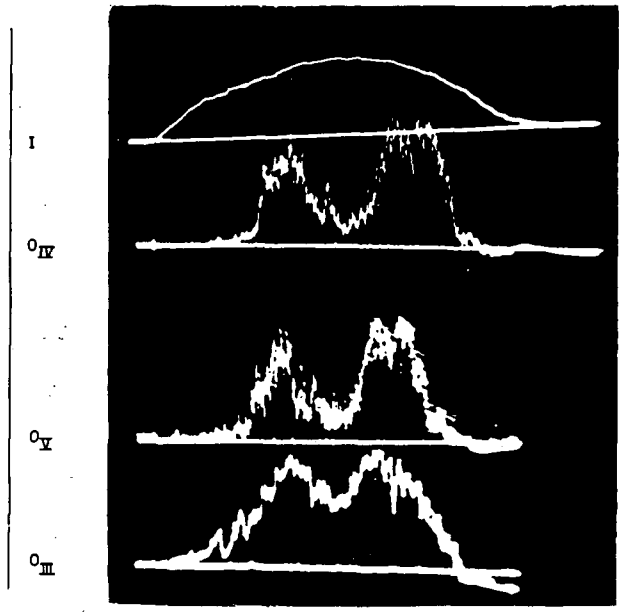

Рис. 3 Интенсивности линий: O III ($\lambda=3265$ Å); O IV ($\lambda=3386$ Å); O V ($\lambda=2781$ Å) и разрядный ток, соответствующие одному и тому же импульсу разряда. $T_p=2{,}5$ мсек. Режим: $U=12{,}5$ кв; $H_z=360$ э.

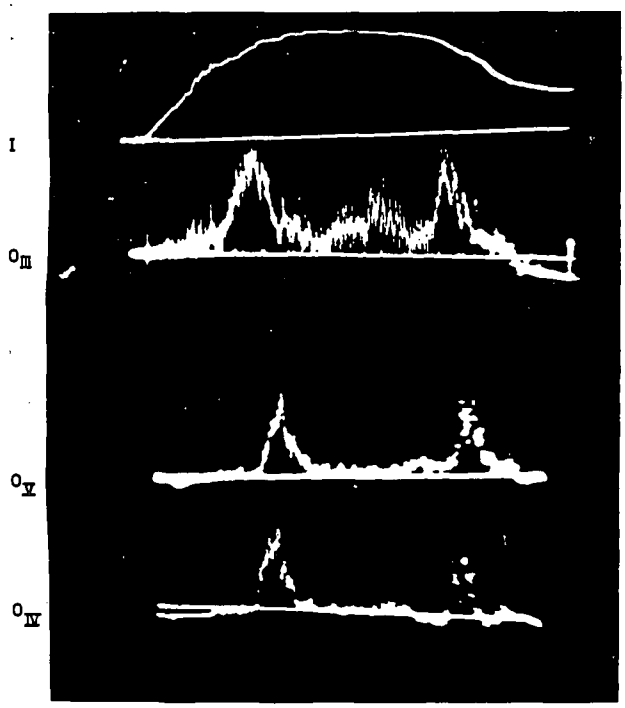

Рис. 4 Интенсивности линий: O III ($\lambda=3265$ Å); O IV ($\lambda=3386$ Å); O V ($\lambda=2781$ Å) и разрядный ток. Эти осциллограммы сняты за один и тот же импульс разряда. $T_p=2{,}5$ мсек. Режим: $U=15$ кв; $H_z=360$ э.

Обращает на себя внимание тот факт, что общий ход интенсивности линий O III, O IV, N IV и O V примерно одинаков. Характерное отличие свечения высоких степеней ионизации (O IV, N IV, O V) от более низких (O III) состоит в том, что интенсивность линий многозарядных ионов нарастает и спадает быстрее, чем у двухзарядных. Провал между двумя максимумами интенсивности линий принадлежащих ионам высокой степени ионизации выражен более резко (рис. 3 и 4).

Такой ход интенсивности не может быть объяснен просто увеличением степени ионизации вблизи максимума тока, так как в этом случае провал интенсивности, наблюдаемый в середине импульса, должен быть более глубоким для линий, принадлежащих ионам более низких степеней ионизации.

Пока не представляется возможным дать простое объяснение такому ходу интенсивностей спектральных линий. Вероятно он определяется совокупным действием ряда факторов связанных как с процессом развития разряда, так и взаимодействия его со стенками камеры.

Частоты колебания интенсивности

На всех осциллограммах, наряду с относительно медленными изменениями интенсивности спектральных линий, наблюдаются также колебания с

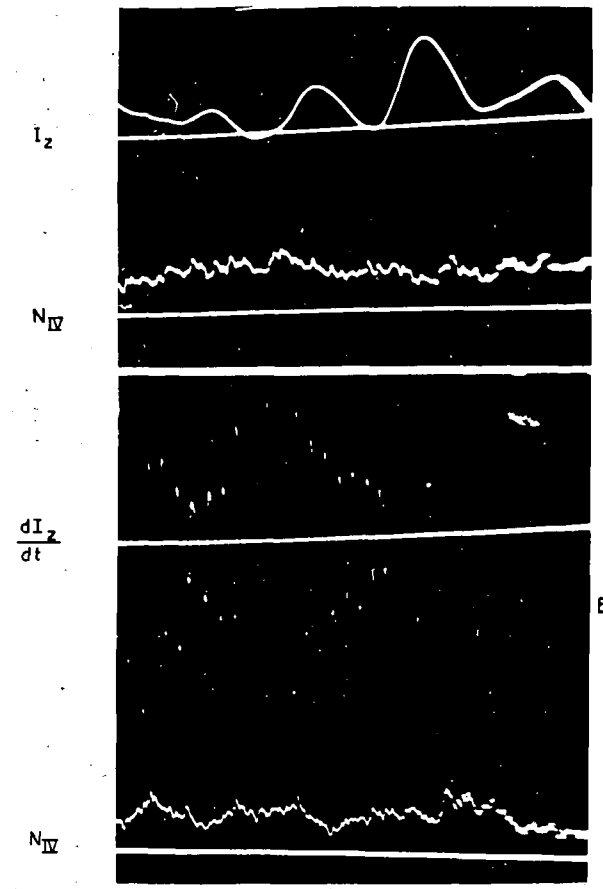

Рис. 5 Ток вдоль оси камеры (I_z); производная тока (dI_z/dt) и интенсивность линии N IV ($\lambda=3479$ Å). Время задержки от начала разряда $T_з=1{,}5$ мсек; $T_p=150$ мсек. Режим: $U=10$ кв; $H_z=360$ э.

частотами порядка сотен кгц. Была сделана попытка сопоставить эти колебания с колебаниями силы тока, текущего вдоль оси камеры. Для измерения тока служил небольшой пояс Роговского, расположенный внутри камеры на ее оси. На осциллограммах (рис. 5) видно, что частоты колебаний тока значительно ниже, чем частоты колебаний интенсивности (рис. 5а). С другой стороны последние имеют тот же порядок величины, что и частоты производной тока, текущего вдоль оси разряда.

5. Свечение различных участков разряда

Для изучения корреляций свечения, испускаемого различными участками плазмы, применялись два идентичных спектральных прибора, расположенных напротив радиальных окон, отстоящих друг от друга на расстоянии 1 м по оси разряда.

Изучалось свечение линии NIV. Исследование показало, что при развертках длительностью 2,5 мсек, т. е. когда высокочастотные колебания

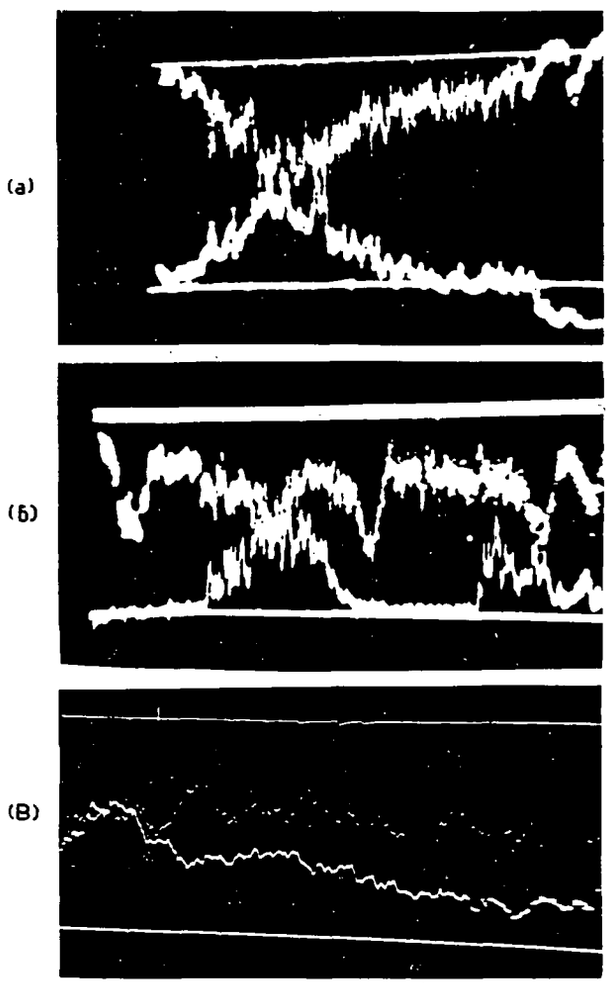

Рис. 6 Интенсивность линии NIV ($\lambda = 3479$ Å) для объемов плазмы находящихся на расстоянии 1 м друг от друга. Режим: $U = 15$ кв; $H_z = 360$ э. (а) $T_з = 500$ мксек, $T_р = 2{,}5$ мсек; (б) $T_з = 1{,}5$ мсек, $T_р = 2{,}5$ мсек; (в) $T_з = 900$ мксек, $T_р = 150$ мксек.

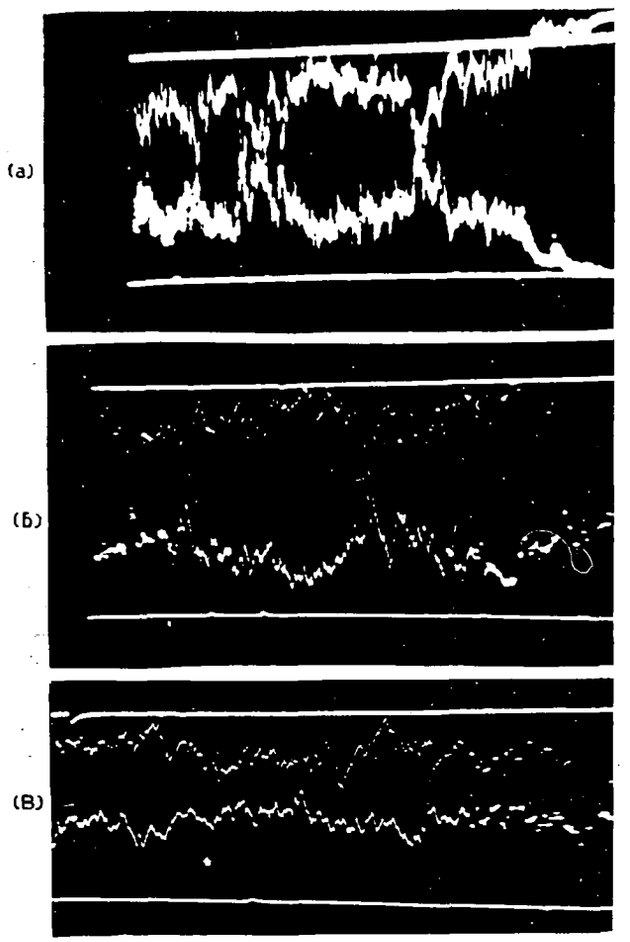

Рис. 7. Интенсивность линии: NIV ($\lambda = 3479$ Å) для объемов плазмы находящихся на расстоянии около 1 см друг от друга. (а) $T_з = 1$ мсек, $T_р = 2{,}5$ мсек, Режим: $U = 15$ кв; $H_z = 360$ э; (б) $T_з = 1$ мсек, $T_р = 1$ мсек, Режим: $U = 10$ кв; $H_z = 360$ э; (в) $T_з = 2$ мсек, $T_р = 150$ мсек, Режим: $U = 12{,}5$ кв; $H_z = 540$ э.

интенсивности не могут наблюдаться, общий ход свечения примерно одинаков, хотя и в этом случае максимумы свечения не всегда точно совпадают друг с другом (рис. 6). При развертках меньшей длительности (т.е. в области частот от десятков килогерц и выше, свечения исходящие из этих двух объемов совершенно не коррелируют между собой. Конструкция камеры не позволила нам наблюдать свечение от участков, расположенных на расстоянии нескольких десятков сантиметров один от другого, что дало бы возможность проследить за скоростью распространения волн в плазме, подобно тому, как это было сделано на установке «Септр IV» [3]. По-видимому на протяжении 1 м возмущение успевает деформироваться настолько, что за ним не удается проследить по свечению разряда.

Была сделана также попытка проследить за свечением двух близко расположенных объемов плазмы. С этой целью свет от двух участков окна (диаметр окон 3 см) расположенных друг от друга на расстоянии одного сантиметра проектировался

на входную щель прибора. За выходной щелью были помещены два фотоумножителя, регистрировавшие свечение, выходившее из верхнего и нижнего участков окна. Рассмотрение осциллограмм (рис. 7) показывает, что колебания интенсивности частотой в десятки килогерц полностью соответствуют друг другу (рис. 7а и б). В области частот в сотни килогерц имеет место нарушение строгой корреляции свечения даже для столь близко расположенных (и частично перекрывающихся) участков плазмы.

Литература

[1] Афросимов В. В. и др, *Ж. техн. Физ.* **30** (1960) 1381.
[2] Зайдель А. Н. и др, *Ж. техн. Физ.* **30** (1960) 1437.
[3] Williams, R. W., *J. nucl. Energy, Part C* **3** (1961) 31

ИССЛЕДОВАНИЕ ШУМОВОГО ИЗЛУЧЕНИЯ ГОРЯЧЕЙ ПЛАЗМЫ В ДИАПАЗОНЕ САНТИМЕТРОВЫХ И МИЛЛИМЕТРОВЫХ ВОЛН*

М. М. ЛАРИОНОВ

АКАДЕМИЯ НАУК СССР

МОСКВА, СОЮЗ СОВЕТСКИХ СОЦИАЛИСТИЧЕСКИХ РЕСПУБЛИК

Для определения электронной температуры плазмы по мощности шумового излучения ее в диапазоне СВЧ необходимо знать коэффициент поглощения плазмы в этом диапазоне. Опытное определение коэффициента полощения часто трудно осуществить. Поэтому важно знать условия, при которых плазма является абсолютно черным телом для этих частот.

Проведены расчеты коэффициента поглощения реальной горячей плазмы (концентрация электронов — 10^{12}—10^{14} см$^{-3}$, электронная температура более 10^5 °К) для волн 10 см — 2 мм. Для плазмы, находящейся в свободном пространстве, коэффициент поглощения почти всегда много менее единицы. При этом коэффициент поглощения поддается лишь очень грубым оценкам. Однако имеются условия, когда коэффициент поглощения близок к единице в широком диапазоне частот. Это значительно облегчает измерения электронной температуры по шумам.

Если плазма окружена замкнутой металлической оболочкой и через введенную внутрь антенну излучается СВЧ-сигнал, то он испытывает внутри оболочки многократные отражения. При этом он много раз взаимодействует с плазмой, проходя сквозь нее или отражаясь от нее. Такой сигнал будет в конце концов поглощен в плазме, так как коэффициент поглощения при однократном отражении от металла гораздо меньше, чем при однократном взаимодействии с плазмой.

Если рассматривать излучение плазмы, заключенной в оболочке, то оно будет находиться в тепловом равновесии с электронами плазмы, так как поглощение в стенках мало.

Измеряя плотность такого излучения антенной, введенной внутрь оболочки, можно определить электронную температуру плазмы.

Пользуясь изложенными представлениями, проводился анализ шумового излучения мощного тороидального разряда, возникающего в металлической камере установки «Альфа». Наблюдалось шумовое излучение, а также прохождение сквозь плазму и отражение от плазмы сигналов на волнах 8,2, 16 и 32 мм.

По наблюдениям прохождения и отражения сигналов установлено, что камера с плазмой обладает в некоторых режимах коэффициентом поглощения, близким к единице. Произведены измерения шумовой температуры плазмы в различных режимах работы установки. Получены осциллограммы шумовой температуры за время разряда.

При измерении на волнах 8,2 и 16 мм зарегистрирована шумовая температура от $1{,}5 \times 10^5$ до $1{,}2 \times 10^6$ °К. При измерении на волне 32 мм обнаружено в некоторых случаях весьма мощное излучение из плазмы. Происхождение этого излучения выясняется в настоящее время.

1. Введение

Один из методов определения электронной температуры плазмы основан на исследовании излучения плазмы в диапазоне сверхвысоких частот. Этот метод был применен для изучения горячей плазмы в работах УОРТОНА и др. [1, 2] и ДЕЛЛИСА [3]. Источником излучения плазмы служит тепловое движение электронов. При соударениях электронов с ионами и атомами возникает тормозное излучение, имеющее непрерывный спектр. Оно может быть легко зарегистрировано в диапазоне миллиметровых и сантиметровых волн. По мощности этого излучения определяется так называемая шумовая температура источника. Она связана с мощностью излучения следующей зависимостью: $P_ш = kT_ш \cdot \Delta f$, где $P_ш$ — мощность излучения, регистрируемая приемником, Δf — рабочая полоса частот приемника, k — постоянная Больцмана, $T_ш$ — шумовая температура объекта.

В ряде работ [3-6] показано, что если в плазме распределение электронов по энергиям является максвелловским, то электронная температура плазмы связана с шумовой соотношением: $T_e = T_ш/A$, в котором A — коэффициент поглощения плазмы в условиях опыта, T_e — электронная температура плазмы. Эта зависимость является выражением закона Кирхгофа для плазмы. Таким образом, для определения электронной температуры необходимо знать коэффициент поглощения СВЧ-сигнала плазмой в условиях опыта. Так как измерение коэффициента поглощения обычно трудно осуществить, важно знать условия, при которых этот коэффициент равен единице, то-есть плазма может рассматриваться, как абсолютно черное тело.

2. Условия поглощения СВЧ-сигнала плазмой

Анализ показывает [3, 6], что плазма эффективно поглощает электромагнитные колебания при следующих условиях:

1. Частота соударений велика по сравнению с частотой поля. Этот случай не реализуется в высокотемпературной плазме.

* Доклад CN-10/241, представленный на Конференцию. Докладчик: А. Б. Березин. Дискуссия (на английском языке) по этому докладу дана на стр. 1019. Переводы аннотаций находятся в конце тома.

2. Частота сигнала близка к электронной циклотронной частоте в замагниченной плазме.

В этом случае возникают узкие пики поглощения на циклотронных частотах и их гармониках.

3. Частота сигнала близка к плазменной частоте. При этом коэффициент поглощения в реальных случаях не слишком велик. Кроме того, это условие может быть выполнено лишь в малых объемах, так как концентрация плазмы изменяется по сечению разряда.

Нами произведены расчеты коэффициента поглощения плазмы для условий, когда плазменная частота, соответствующая максимальной концентрации в разряде, ниже и выше частоты сигнала. Вычисление производилось для плазмы с электронной температурой более 10^5° К (10 эв) и с концентрацией 10^{12}-10^{14} $см^{-3}$. При этом отношение частоты соударений электронов к плазменной частоте не превышает 10^{-5}. Влияние магнитного поля не учитывалось, поэтому результаты расчетов справедливы, если циклотронная частота значительно меньше частоты сигнала.

Если частота сигнала выше плазменной, то сигнал распространяется сквозь плазму, и толщина слоя поглощения составляет 10^3-10^5 λ_0 (λ_0 — длина волны сигнала в пустоте) [7]. Размеры плазмы в экспериментальных установках обычно оказываются гораздо меньше толщины слоя поглощения.

Если частота сигнала ниже максимальной плазменной частоты, то сигнал отражается от слоя плазмы, в котором плазменная частота близка к частоте сигнала.

Для этого случая можно вычислить коэффициент поглощения при отражении сигнала от плазмы [7]. Для возможных в экспериментальных установках градиентов концентраций коэффициент поглощения оказывается равным 10^{-3}-10^{-1}.

Таким образом, плазма почти всегда, за исключением условий электронного циклотронного резонанса, оказывается или прозрачной, или отражающей. Коэффициент поглощения ее много меньше единицы, и измеряемая шумовая температура должна быть много ниже электронной.

Однако в ряде случаев зарегистрировано интенсивное шумовое излучение плазмы в областях, далских от циклотронного резонанса [3]. Шумовая температура при этом оказывается близкой к электронной температуре, определенной другими методами. Нами установлено, что условия приема излучения плазмы связаны с влиянием окружающей ее металлической оболочки. Это влияние ранее не учитывалось.

3. Влияние металлической оболочки на условия поглощения

Имеется разница в величине коэффициента поглощения плазмы, находящейся в свободном пространстве, и плазмы, окруженной металлической оболочкой. При наличии такой оболочки любой СВЧ-сигнал, вошедший внутрь ее, испытывает многократные отражения от стенок. При этом

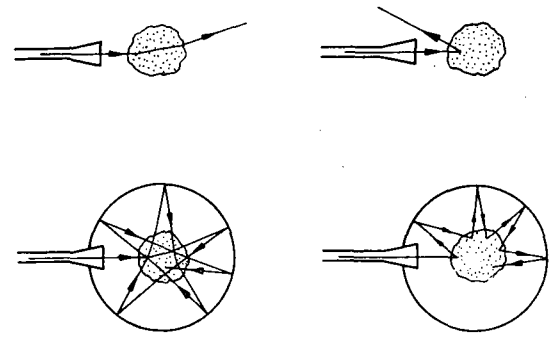

Рис. 1 Схема, поясняющая влияние металлической оболочки на коэффициент поглощения плазмы. Слева — частота сигнала выше плазменной, справа — частота сигнала ниже плазменной.

сигнал много раз проходит сквозь плазму, если она прозрачна, или много раз отражается от нее в противном случае. В результате сигнал полностью поглощается внутри оболочки. Так как коэффициент поглощения при однократном отражении от металла имеет порядок 10^{-4}, а коэффициент поглощения при однократном прохождении сигнала сквозь плазму или отражении от плазмы обычно гораздо больше (см. выше), то поглощение происходит главным образом в плазме. Рис. 1 иллюстрирует этот механизм поглощения.

Тормозное излучение электронов в результате многократных отражений накапливается внутри оболочки, пока не будет достигнуто равновесие его с электронами плазмы. Поглощением излучения в стенках часто можно пренебречь. Измеряя плотность излучения небольшой антенной, введенной внутрь оболочки, можно определить температуру электронов. При этом не нужно учитывать коэффициент поглощения, так как оболочка с плазмой представляет собой абсолютно-черное тело для широкого диапазона частот в области СВЧ, имеющее температуру электронов.

Справедливость описанного механизма подтверждена простым опытом. Трубка с тлеющим разрядом, электронная температура в котором равна 18000° К, помещалась перед рупорной антенной радиометра. При этом регистрировалась шумовая температура 2000° К. Затем, при том же расположении трубки с разрядом и антенны, они окружались металлическим экраном. При этом шумовая температура, регистрируемая приемником, возрастала до 16000° К.

4. Исследования излучения плазмы на установке «Альфа»

На основе изложенных представлений производился анализ шумового излучения, возникающего во время разряда на установке «Альфа» [8, 9]. Установка представляет собой тороидальную металлическую камеру со слабым продольным магнитным полем. Диаметр камеры — 1000 мм, диаметр тора — 3200 мм. Разряд возбуждается индуктивно. Ток разряда доходит до 300 ка, при длительности разряда 2 мсек.

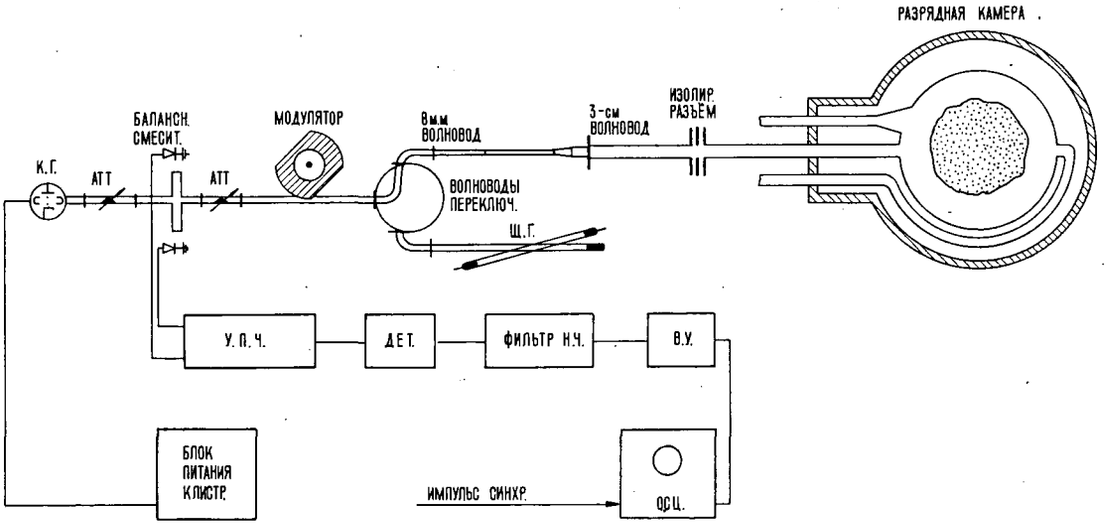

Рис. 2 Блок-схема аппаратуры для измерения шумового излучения плазмы.

Роль металлической оболочки выполняет лайнер внутри разрядной камеры установки, изготовленный из нержавеющей стали. Внутрь лайнера введены волноводы и рупорные антенны, которые служат для приема шумового излучения плазмы, а также для наблюдения прохождения СВЧ-сигналов сквозь плазму и отражения их от плазмы.

Приемная аппаратура состоит из супергетеродинного радиометра и устройства для калибровки его.

Для этого используется газоразрядный шумовой генератор соответствующего диапазона и механический модулятор. Схема аппаратуры приведена на рис. 2. Определение электронной температуры плазмы производится путем сравнения шумового сигнала от разряда с известным сигналом от шумового генератора. Радиометр позволяет регистрировать тепловое излучение с постоянной времени 10 мксек. Чувствительность радиометра по температуре составляет 2500° К.

Кроме наблюдений шумового излучения разряда, изучалось прохождение СВЧ-сигнала сквозь плазму и отражение его от плазмы. По величине отраженного от плазмы сигнала можно было оценить коэффициент поглощения камеры с плазмой. Кроме того, по наблюдениям за прохождением сигналов можно было судить о концентрации плазмы в центре камеры, а по наблюдениям за отражением — о концентрации у стенок камеры. Измерения проводились на длинах волн 8,2, 16 и 32 мм. Осциллограммы сигналов приведены на рис. 3 и 4.

Были проведены измерения шумовой температуры разряда при различных режимах работы установки «Альфа». Зарегистрированы максимальные за время разряда шумовые температуры от 150×10^3° К (13 эв) до $1{,}2 \times 10^6$° К (100 эв). Результаты измерений, выполненных на волне 8,2 мм, представлены в виде графиков на рис. 6, 7 и 8. Следует отметить падение шумовой температуры с ростом давления в камере установки. Одновременно растет величина отраженного от плазмы сигнала, то-есть растет электронная концентрация у стенок камеры.

Были также произведены измерения на длинах волн 16 и 32 мм. Если принимаемое излучение

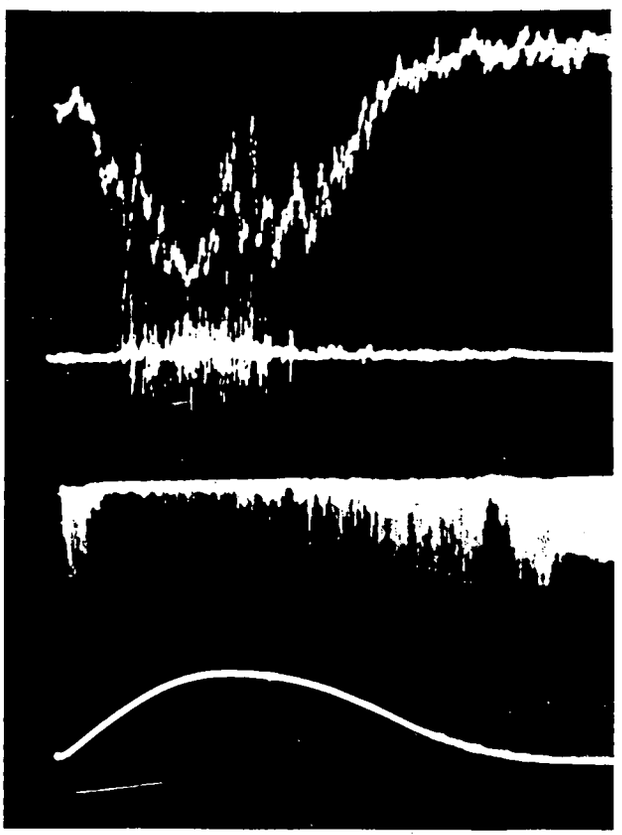

Рис. 3 Осциллограммы сигналов на волне 8,2 мм. Сверху вниз: шумовое излучение плазмы; сигнал отраженный от плазмы; сигнал проходящий сквозь плазму; ток разряда.

является тормозным излучением электронов и верно предположение о равновесном характере излучения плазмы, то шумовая температура не должна зависеть от частоты, на которой производятся измерения.

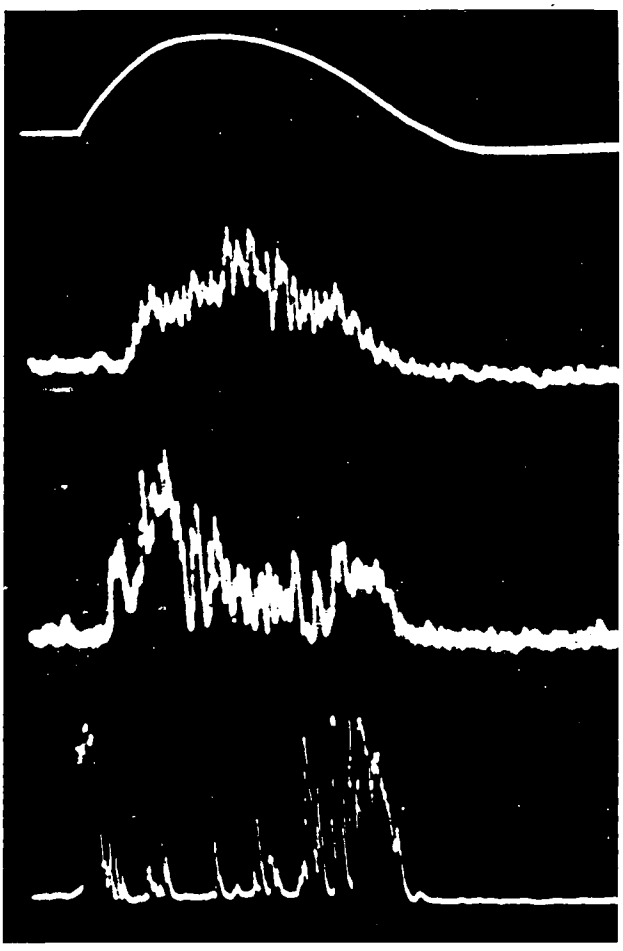

Рис. 4 Осциллограммы шумового излучения плазмы на различных длинах волн. Сверху вниз: ток разряда; волна 8,2 мм; волна 16 мм; волна 32 мм.

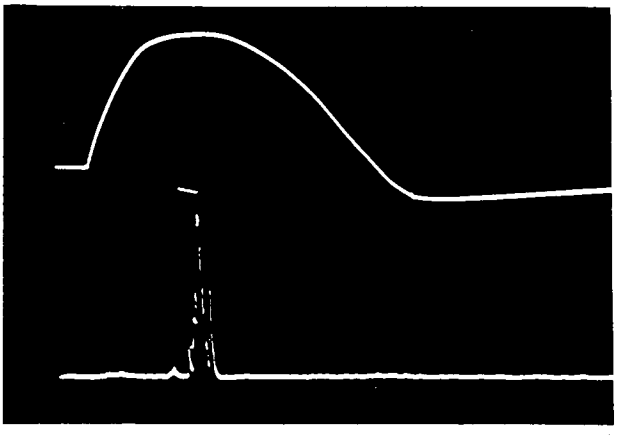

Рис. 5 Нетепловое излучение плазмы на волне 32 мм. Усиление приемника на 20 дб ниже, чем на рис. 4. Сверху вниз: ток разряда; всплеск излучения.

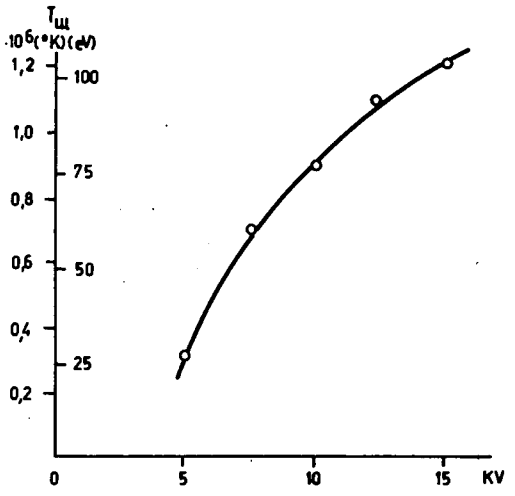

Рис. 6 Зависимость шумовой температуры разряда от напряжения на конденсаторной батарее установки.

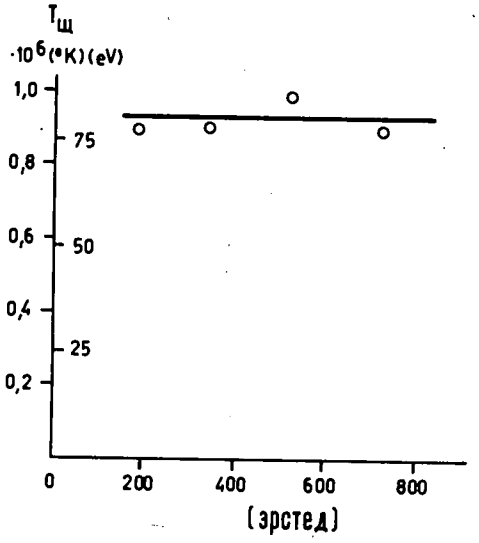

Рис. 7 Зависимость шумовой температуры разряда от начального магнитного поля в камере установки.

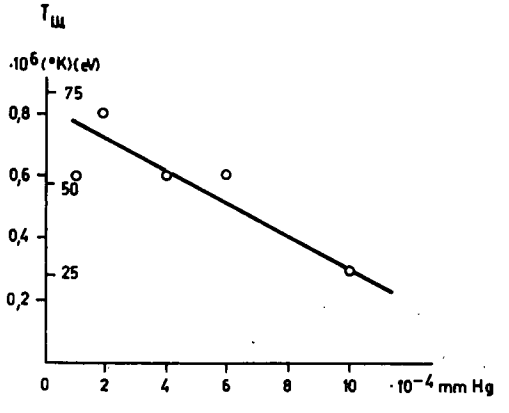

Рис. 8 Зависимость шумовой температуры разряда от давления водорода в камере установки.

Действительно, в то время, когда камера с плазмой имеет коэффициент поглощения, близкий к единице, шумовые температуры, измеренные на всех трех длинах волн, близки (рис. 4). Провалы на осциллограммах 16 и 32-мм сигналов в области максимума тока соответствуют увеличению отражений от плазмы на этих длинах волн. При этом коэффициент поглощения оказывается существенно меньшим единицы. Электронная температура, измеренная по шумовому излучению, не совпадает с температурой, вычисленной по проводимости плазменного шнура. В режиме, когда зарегистрирована шумовая температура $1{,}2 \times 10^6$° К, температура по проводимости равна 3×10^5° К. Причиной такого расхождения может быть отклонение от максвелловского распределения электронов плазмы. При этом шумовая температура может не соответствовать средней энергии электронов. С другой стороны, при вычислении температуры по проводимости не было учтено влияние магнитного поля на проводимость шнура в целом.

В ряде случаев при измерениях на волне 32 мм зарегистрировано излучение значительной мощности, имеющее вид отдельных узких всплесков длительностью около 100 мксек (рис. 5). Амплитуда их превосходит уровень теплового излучения в 100 и более раз. На других длинах волн такие всплески излучения не обнаружены. Следует отметить, что в процессе разряда в плазме возникают магнитные поля напряженностью до 3 килоэрстед. Поэтому наблюдаемые всплески излучения могут быть связаны с излучением быстрых электронов плазмы на циклотронной частоте. Возможно также, что это явление связано с генерацией колебаний в плазме во время разряда.

В заключение автор считает своим долгом выразить благодарность О. Н. Щербинину и Б. П. Полоскину, совместно с которыми выполнены измерения на установке «Альфа», и В. Е. Голанту за постоянный интерес к работе и ряд ценных советов.

Литература

[1] Wharton, C. B., Howard, J. C., Heinz, O., "Plasma diagnostic developments in the UCRL Pyrotron program", in Proc. 2nd U.N. Conf. PUAE **32**, United Nations, Geneva (1958) 388.
[2] Wharton, C. B., "Microwave radiation measurements of very hot plasmas," in Proc. 4th Intern. Conf. Ionization Phenomena in Gases (Uppsala, 17—21 Aug. 1959) **2**, North Holland Publishing Co., Amsterdam (1960) 737 (Paper No. 6).
[3] Dellis, A. N., "Microwave measurements in low pressure discharges," in Proc. 3rd Intern. Conf. Ionization Phenomena in Gases (Venice, 11—15 June 1957) **1**, North Holland Publishing Co., Amsterdam (1959) 228 (Paper No. 3).
[4] Parzen, P., Goldstein, L., *Phys. Rev.* **79** (1950) 190.
[5] Parzen, P., Goldstein, L., *Phys. Rev.* **82** (1951) 724.
[6] Drummond, J. E., "Theory of microwave diagnostics of hot plasmas," in Proc. 2nd U.N. Intern. Conf. PUAE **32**, United Nations, Geneva (1958) 379.
[7] Гинзбург В. Л., Распространение Электромагнитных Волн в Плазме, Государственное издательство физико-математической литературы, Москва (1960).
[8] Глухих В. А. и др, «Конструктивные данные и основные параметры установки ‚Альфа'», *Ж. техн. Физ.* **30** (1960) 1394.
[9] Глухих В. А. и др, «Исследование электрических и магнитных характеристик разряда на установке ‚Альфа'», *Ж. техн. Физ.* **30** (1960) 1404.

ЭКСПЕРИМЕНТЫ ПО ДЖОУЛЕВУ НАГРЕВУ ПЛАЗМЫ В СИЛЬНОМ МАГНИТНОМ ПОЛЕ*

Е. П. ГОРБУНОВ, Г. Г. ДОЛГОВ-САВЕЛЬЕВ, К. Б. КАРТАШЕВ, В. С. МУХОВАТОВ, В. С. СТРЕЛКОВ, М. Н. ШЕПЕЛЕВ, Н. А. ЯВЛИНСКИЙ

АКАДЕМИЯ НАУК СССР

МОСКВА, СОЮЗ СОВЕТСКИХ СОЦИАЛИСТИЧЕСКИХ РЕСПУБЛИК

Изучался импульсный безэлектродный разряд в дейтерии длительностью 5—7 мсек в сильном продольном магнитном поле. Показано, что на первой стадии разряда имеют место аномально быстрые потери заряженных частиц из плазмы. Среднее время удержания электронов при этом обычно составляло $\sim$ 600 мксек. На электрических характеристиках разряда наблюдаются колебания. Амплитуда этих колебаний заметно увеличивается, когда кривая плотности электронов проходит через максимум. Обсуждаются возможные механизмы возникновения таких колебаний и механизмы потерь заряженных частиц. Ионная температура, определенная по допплеровскому уширению спектральных линий углерода, возрастает в течение первой стадии процесса и достигает к началу второй стадии $\sim$20 эв (по уширению CIII $\lambda = 4647$ Å). Температура электронов, измеренная по соотношению интенсивностей спектральных линий OIV и OV, имеет примерно ту же величину.

Во время второй стадии разряда концентрация заряженных частиц в центральной области шнура сохраняется примерно постоянной (в типичных режимах разряда $\sim 10^{13}$ см$^{-3}$) или несколько подрастает. При этом плотность электронов на периферии плазменного столба меньше, чем 10^{12} см$^{-3}$. В то же время наблюдается рост электронной температуры, определяемой по электропроводности плазмы.

Специальные обмотки позволяли изменять конфигурацию продольного магнитного поля в области диафрагм. Исследовалось влияние этого возмущения на характеристики разряда в различных стадиях процесса.

1. Введение

Предыдущие исследования [1] на установке «Токамак-1» показали, что при выполнении условия Шафранова-Крускала плазменный шнур макроскопически устойчив и значительная часть энергии теряется из плазмы за счет линейчатого излучения примесей.

Улучшение вакуумных условий и чистоты стенок разрядной камеры на установке «Токамак-2» привело к повышению температуры плазмы, увеличению амплитуды колебаний на электрических характеристиках разряда и к появлению второго максимума разрядного тока [2].

В настоящей работе излагаются результаты дальнейших исследований на установке «Токамак-2».

2. Экспериментальная установка

Установка «Токамак-2» представляет собою медный тор с внутренней камерой из нержавеющей стали. Большой диаметр тора 125 см, внутренний диаметр разрядной камеры 40 см. Внутри разрядной камеры расположены две диафрагмы с диаметром отверстия 20 см. На диафрагмах установлены специальные обмотки, позволявшие изменять величину продольного магнитного поля в районе диафрагм. Максимальная величина продольного магнитного поля в описываемых экспериментах составляла 6 кэ. Начальная напряженность электрического поля E_0 изменялась о 0,1 до 0,25 в/см. Длительность разряда определялась насыщением железного сердечника, и при $E_0 = 0{,}15$ в/см составляла 6 мсек. В большинстве экспериментов в качестве рабочего газа использовался дейтерий при начальном давлении 5×10^{-4}—$1{,}4 \times 10^{-3}$ мм рт ст.

Разрядная камера очищалась путем длительного прогрева при температуре 450° С и последующей тренировкой разрядом. Для откачки использовались паромасляные насосы, отделенные от камеры двумя ловушками, охлаждаемыми до температуры жидкого азота.

Более подробно конструкция установки, вакуумная система и электрическая схема описаны в [3].

3. Результаты экспериментов

3.1. ЭЛЕКТРИЧЕСКИЕ ХАРАКТЕРИСТИКИ

Напряжение на обходе тора создавалось разрядом батареи конденсаторов через обмотку, расположенную на поверхности тора. На рис. 1 показаны типичные осциллограммы напряжения, разрядного тока и его производной. Ток в газе имеет характерную форму с двумя максимумами. Величина тока в первом максимуме обычно составляла 10-20 ка и не превышала критического значения, определяемого критерием устойчивости Шафранова-Крускала.

* Доклад CN-10/223, представленный на Конференцию. Докладчик: Г. Г. Долгов-Савельев. Дискуссия (на английском языке) по этому докладу дана на стр. 1019. Переводы аннотаций находятся в конце тома.

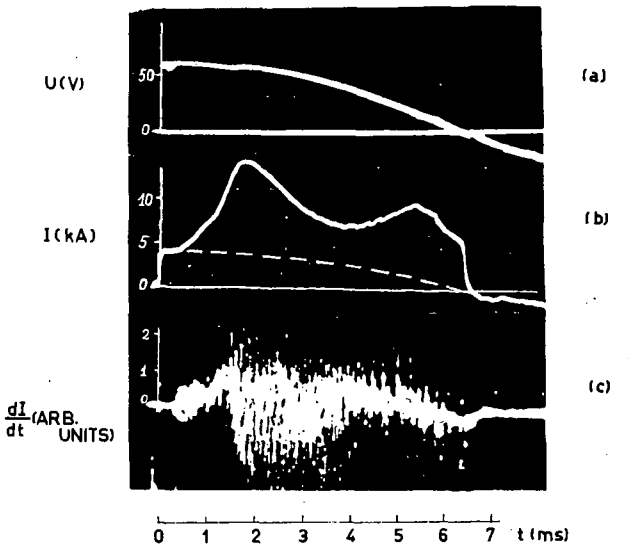

Рис. 1 (а) Напряжение на обходе тора; (б) суммарный ток. Разность суммарного тока и тока, текущего по внутренней камере (пунктирная кривая), дает величину тока в плазменном шнуре; (с) производная разрядного тока. Начальное давление дейтерия $P_0 = 7 \times 10^{-4}$ мм рт ст, напряженность магнитного поля $H_0 = 5400$ э.

3.2. ПЛОТНОСТЬ ЭЛЕКТРОНОВ

Для определения концентрации электронов в разряде был использован радиоинтерферометр, собранный по схеме, примененой Уортоном для исследования плазмы [4]. Расположение излучающих и приемных рупоров показано на рис. 2. Таким образом имелась возможность определять среднюю концентрацию электронов в плазме вдоль луча, проходящего через центр плазменного шнура, и вдоль луча, смещенного относительно центра на половину радиуса шнура.

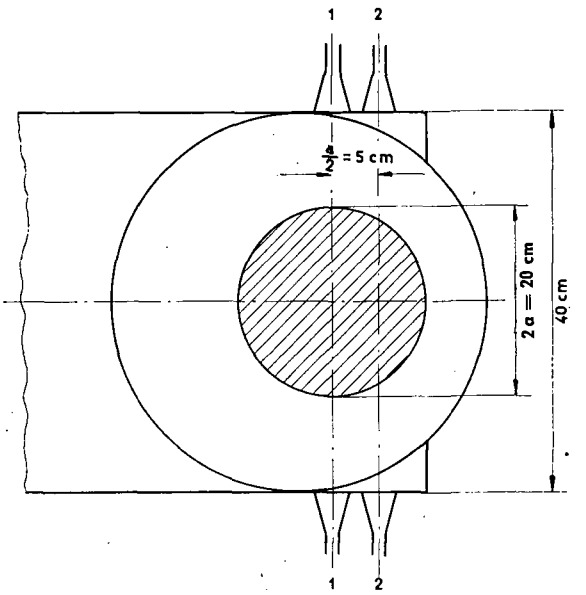

Рис. 2 Схема расположения излучающих и приемных рупоров для микроволнового зондирования плазмы. Ось симметрии тора расположена слева. Заштрихованная область соответствует отверстию в диафрагме.

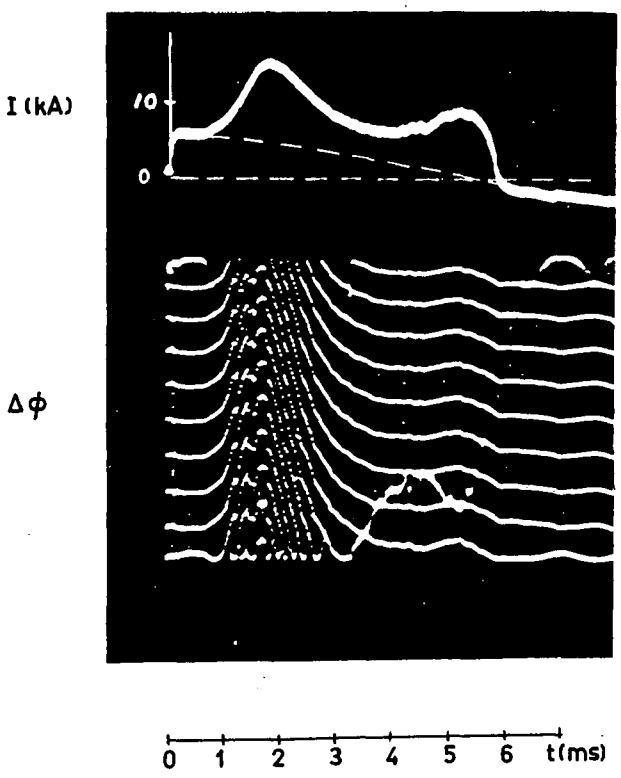

Рис. 3 Осциллограмма изменения фазы сигнала, прошедшего через плазму. Вверху — ток разряда. ($E_0 = 0{,}15$ в/см, $H_0 = 5400$ э, $P_0 = 7 \times 10^{-4}$ мм рт ст).

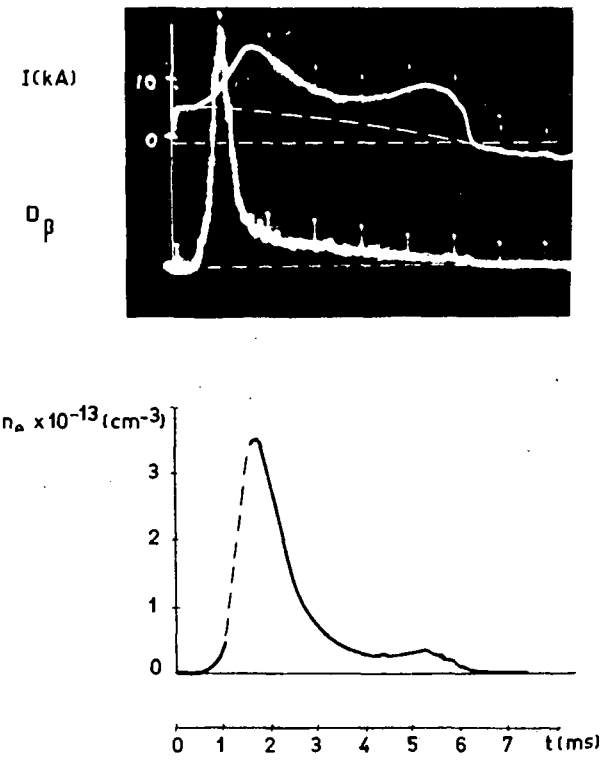

Рис. 4 Изменение во времени средней по сечению плазменного шнура плотности электронов. Вверху — ток разряда и интенсивность линии $D\beta$. ($E_0 = 0{,}15$ в/см, $H_0 = 5400$ э, $P_0 = 7 \times 10^{-4}$ мм рт ст.)

На рис. 3 показана осциллограмма, полученная с помощью такого интерферометра. Смещение горизонтальных полос на осциллограмме пропорционально изменению фазы сигнала, прошедшего через плазму, причем изменению фазы на 2π соответствует перемещение, равное расстоянию между двумя соседними полосами. Вверху в том же временном масштабе приведена осциллограмма тока в разряде.

На рис. 4 представлена кривая, показывающая изменение во времени средней по сечению шнура плотности электронов $\langle n_e \rangle$, построенная по этим осциллограммам. При вычислении предполагалось, что шнур ограничен диаметром отверстий в диафрагмах. Начальная плотность нейтральных атомов в разрядном объеме для этого случая составляла $n_0 = 5 \times 10^{13}$ см$^{-3}$.

После пробоя газа величина плотности электронов увеличивается и спустя примерно 1 мсек достигает максимума, причем в большинстве случаев $\langle n_e \rangle_{max}/n_0 = 0{,}5\text{-}1{,}0$. Максимум плотности опережает первый максимум тока на 200-300 мксек. Затем плотность электронов уменьшается и через 2,5-3 мсек составляет около 0,1 максимальной. После этого дальнейший спад плотности прекращается и во время второго максимума тока $\langle n_e \rangle$ остается примерно постоянной, либо в ряде режимов немного подрастает. В режимах с малой величиной H_0 или большой величиной E_0 плотность продолжает падать, однако скорость спадания в это время уменьшается. Измерения сдвига фаз сигнала, прошедшего вдоль оси 1-1 и вдоль оси 2-2 (рис. 2), позволяют получить некоторые сведения о распределении плотности электронов по сечению разряда. Изменение фазы сигнала,

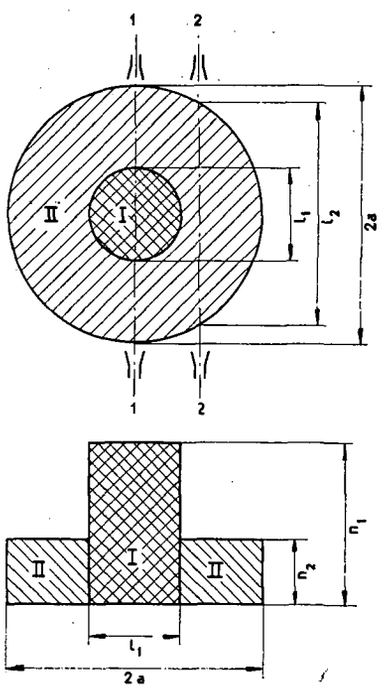

Рис. 5 Схема, поясняющая вычисление n_1 и n_2.

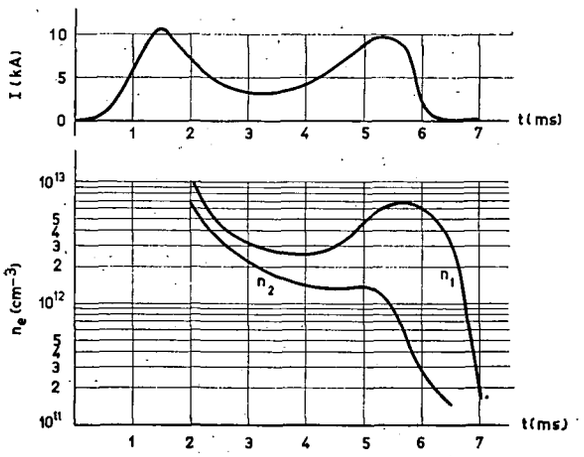

Рис. 6 Зависимость от времени тока в плазменном шнуре (верхняя кривая) и концентрации электронов в центральной (n_1) и внешней (n_2) зонах шнура. $H_0 = 5600$ э; $E_0 = 0{,}15$ в/см; $P_0 = 5 \times 10^{-4}$ мм рт.ст.

прошедшего через смещенный канал (2-2) равно

$$\Delta\varphi_2 \approx \frac{\pi l_2}{\lambda} \frac{n_2}{n_{кр}}$$

где n_2 — средняя плотность электронов на длине l_2, (рис. 5), $n_{кр}$ — критическая плотность для используемой длины волны λ. Если плотность электронов в разряде имеет цилиндрически-симметричное распределение, то без большой ошибки можно положить среднюю плотность в периферической области II равной n_2. Тогда изменение фазы сигнала, прошедшего через центральный канал, можно представить в виде:

$$\Delta\varphi_1 \approx \frac{\pi}{\lambda n_{кр}} [l_1 n_1 + (2a - l_1) n_2]$$

где n_1 — средняя плотность электронов в центральной области разряда диаметром l_1, a — радиус шнура, принятый равным радиусу отверстия в диафрагме.

Зная $\Delta\Phi_1$ и $\Delta\Phi_2$, можно определить n_1 и n_2. На рис. 6 представлены величины n_1 и n_2 и осциллограмма разрядного тока. После 1-го максимума тока средняя плотность электронов в центральной области превышает среднюю плотность на периферии примерно в 1,5 раза, причем это соотношение мало меняется вплоть до минимума тока. Затем отношение n_1/n_2 начинает возрастать сначала за счет увеличения концентрации электронов в центральной области, а в конце процесса за счет более быстрого спада плотности на периферии.

Величина n_1 во втором максимуме тока при увеличении продольного магнитного поля линейно возрастает.

3.3. Оптические измерения

Изучался временной ход интенсивности ряда спектральных линий кислорода и углерода: OIV, $\lambda = 3071{,}7$ Å; $3s^2\,S - 3p^2\,P$; OV, $\lambda = 2781$ Å; $3s^3\,S - 3p^3\,P$; CIII, $\lambda = 4647$ Å; $3s^3\,S - 3p^3\,P$.

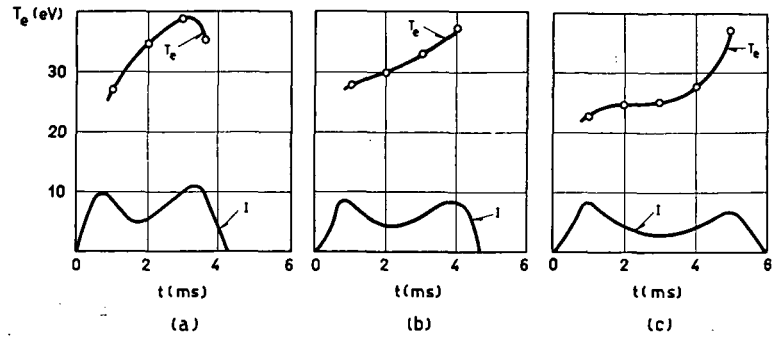

Рис. 7. Зависимость от времени электронной температуры, вычисленной по относительным интенсивностям спектральных линий ионов кислорода OIV, $\lambda = 3071$ Å и OV, $\lambda = 2781$ Å для трех значений напряженности электрического поля: (а) $E_0 = 0{,}25$ в/см; (б) $E_0 = 0{,}2$ в/см; (с) $E_0 = 0{,}15$ в/см. $H_0 = 5400$ э, $P_0 = 7 \times 10^{-4}$ мм рт.ст. Нижние кривые — ток разряда.

В предположении, что ионизационное равновесие определяется процессами ионизации электронным ударом и парной рекомбинацией с излучением, а заполнение верхних уровней описывается формулой Больцмана, по соотношению интенсивностей линий ионов различной кратности ионизации можно определить температуру электронов в плазме. Применимость этого метода обоснована тем, что время установления ионизационного равновесия $\tau = 1/n_e \langle \sigma_i v \rangle$ в условиях наших экспериментов составляло около 200 мксек, в то время как длительность разряда равнялась 4-6 мсек. Следует однако иметь ввиду, что точность данного способа определения температуры не высока, т.к. при этом не учитывается гибель ионов на стенках камеры, а формула Больцмана дает несколько завышенное значение числа атомов на верхних уровнях. Кроме того свечение спектральных линий ионов различной кратности ионизации может происходить из разных областей плазменного шнура.

На рис. 7 приведена зависимость от времени T_e, определенной по отношению интенсивностей линий OIV и OV. Величина T_e возрастает со временем и во втором максимуме тока достигает значений, близких к 40 эв.

Для измерения временного хода температуры ионной компоненты плазмы использовался интерферометр Фабри-Перо. Метод измерения описан в работе [5]. На рис. 8 приведена измеренная таким способом температура ионов по линии CIII, $\lambda = 4647$ [5]. Как видно из этого рисунка, температура ионов растет со временем и спустя 2-3 мсек после начала разряда достигает 20 эв.

Для того, чтобы выяснить, является ли измеренная температура результатом нагрева ионов плазмы или результатом действия механизмов ускорения, подобных тем, которые наблюдаются на установках «Альфа» и «Зета» [6, 7], где температура ионов растет линейно с увеличением заряда иона, в разряд добавлялся гелий ($n_{He} = (0{,}05\text{-}0{,}06) \cdot n_{D_2}$), что не сказалось сколько-нибудь существенно на макроскопических характеристиках разряда. Как видно из рис. 8, температура ионов, измеренная по уширению линии HeII, $\lambda = 4686$ Å хорошо совпадает с температурой, измеренной по уширению линии CIII, $\lambda = 4647$ Å.

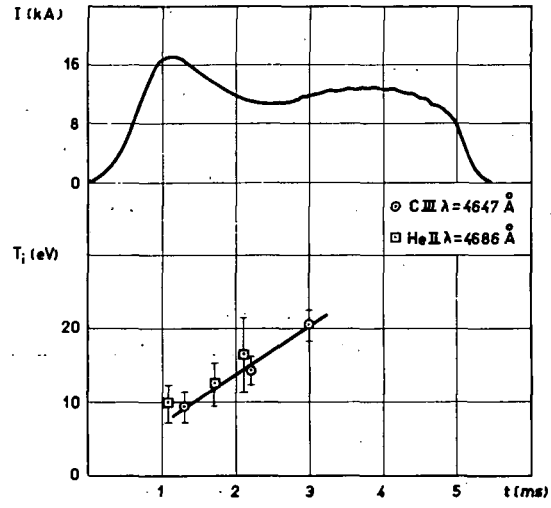

Рис. 8. Зависимость от времени ионной температуры, вычисленной по допплеровскому уширению спектральных линий углерода и гелия. Верхняя кривая — ток разряда.

3.4. Колебания на электрическом зонде

В верхней части камеры был помещен электрический зонд. Имелась возможность устанавливать зонд на различных расстояниях от оси шнура. Зонд соединялся со стенкой разрядной камеры через высокоомное сопротивление. Колебания потенциала зонда анализировались с помощью стандартного измерителя помех и фиксировались на осциллографе. Этот прибор позволяет выделять из всего спектра частот фиксированные интервалы в диапазоне 0,15-25 мгц. На рис. 9 приведена одна из таких осциллограмм.

При регистрации потенциала зонда непосредственно осциллографом удается обнаружить колебания с частотой, близкой к 10 кгц.

Измерения показывают, что плазма заряжена положительно относительно стенок камеры и величина радиального электрического поля на границе шнура достигает 30 в/см.

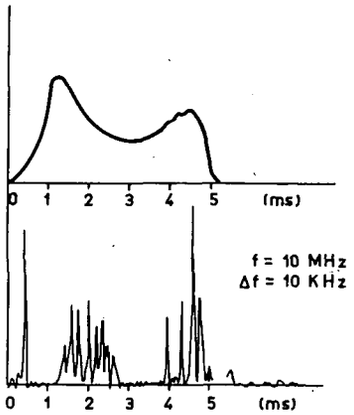

Рис. 9 Зависимость от времени интенсивности колебаний на электрическом зонде, расположенном на границе плазменного шнура. Вверху — ток разряда. $E_0 = 0{,}2$ в/см, $P_0 = 6 \times 10^{-4}$ мм рт ст, $H_0 = 5600$ э.

4. Опыты с магнитными диафрагмами

В наших экспериментах плазма активно взаимодействует с диафрагмами. Это подтверждает внешний вид диафрагм после большого числа импульсов разряда [1].

Для того, чтобы уменьшить взаимодействие плазмы с диафрагмами была сделана попытка воздействовать на плазменный шнур импульсным магнитным полем. Для этой цели внутри диафрагмы (рис. 10а) располагалась обмотка. Разряжая конденсаторную батарею на эту обмотку, мы могли создавать в районе диафрагмы дополнительное магнитное поле. Максимальная величина этого поля в центре диафрагмы достигала 2,5 кэ, при длительности полупериода 3 мсек. Магнитные диафрагмы могли включаться в любой момент времени относительно начала разряда.

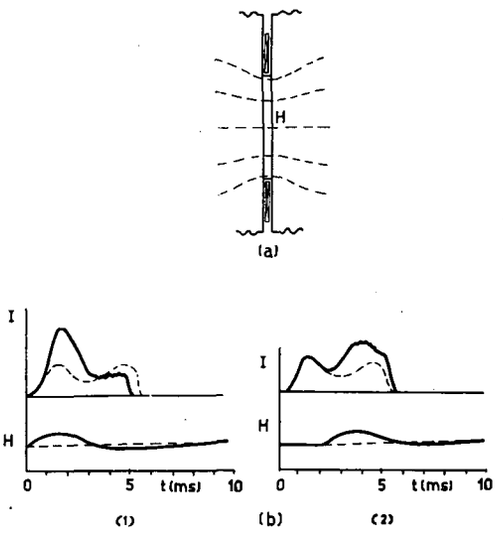

Рис. 10 (а) Магнитная диафрагма. (б) Осциллограммы разрядного тока и магнитного поля внутри диафрагмы. Магнитное поле диафрагмы включено: (1) в начале процесса; (2) в середине процесса. Пунктиром показаны значения тока и магнитного поля в обычном разряде (магнитные диафрагмы не включены).

Из приведенных на рис. 10б осциллограмм видно, что местное усиление магнитного поля вызывает возрастание тока разряда.

На рис. 11 приведена зависимость $J/J_0 = f(H/H_0)$, где J_0 и H_0 — ток разряда и продольное магнитное поле без включения магнитных диафрагм, J и H — значения тока и поля внутри диафрагмы при включенных магнитных диафрагмах. Магнитные диафрагмы включались вначале процесса. Максимум дополнительного поля совпадал во времени с I-м максимумом тока. Приведенные на графике величины соответствуют этому моменту времени.

Локальное усиление магнитного поля в районе диафрагм приводит к искривлению силовых линий магнитного поля и тем самым дает возможность шнуру плазмы занимать вдали от диафрагм большее сечение. Если плотность тока остается прежней, то в этом случае ток разряда увеличивается в H/H_0 раз. Прямая $J = J_0 H/H_0$ на рис. 11 показывает возрастание тока за счет искривления силовых линий. Для объяснения более быстрого по сравнению с этой прямой роста тока необходимо допустить наличие какого-то дополнительного механизма. В частности, можно предположить, что местное усиление магнитного поля, изменяя условия взаимодействия плазмы с краями диафрагмы, приводит к увеличению температуры шнура. Это предположение находится в согласии с результатами измерения относительных интенсивностей спектральных линий кислорода.

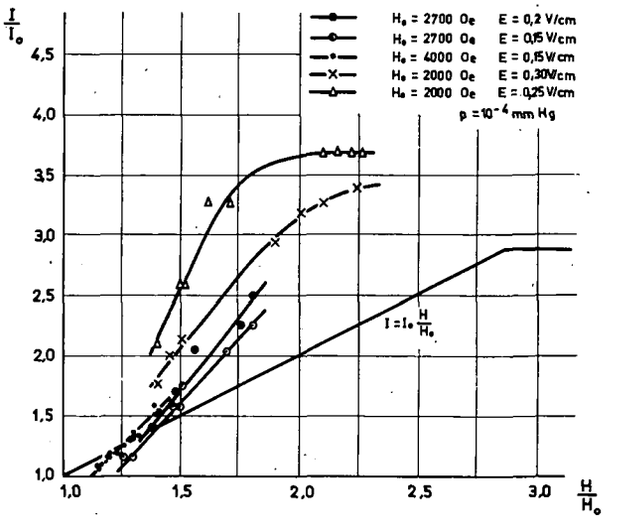

Рис. 11 Зависимость $I/I_0 = f(H/H_0)$.

Допустимо и другое предположение: магнитные диафрагмы, создавая местные усиления магнитного поля, могут приводить к «закреплению» шнура в двух точках и тем самым препятствовать развитию гидромагнитных возмущений с $m = 1$ и $\lambda = L$, где L — длина шнура. Если рост тока ограничивается гидромагнитными неустойчивостями, то это повышает значение критического тока вдвое, т.к. в этом случае наибольшая длина волны уменьшается в 2 раза.

Казалось бы, что гидромагнитные неустойчивости с $m=1$ в наших экспериментах не должны проявляться, так как максимальные токи не достигали критических значений, если считать, что плотность тока постоянна по всему сечению шнура.

Однако, если происходит перераспределение тока к центру, то шнур может потерять устойчивость.

5. Обсуждение результатов

Анализируя зависимость от времени средней плотности электронов в шнуре и сопоставляя ее с другими характеристиками разряда, представляется возможным разделить весь процесс на три существенно различающиеся стадии.

Первая стадия охватывает промежуток времени от начала пробоя газа до 1-го максимума плотности электронов; вторая стадия соответствует спадающему участку на кривой плотности, третья стадия охватывает область, где плотность электронов меняется слабо (вблизи 2-го максимума тока).

Рассмотрим более подробно каждую из этих стадий.

5.1. Первая стадия

Как видно из рис. 4, в течение этой стадии плотность электронов нарастает. Интенсивность спектральной линии D_β за это время достигает максимума и к моменту достижения максимальной плотности уменьшается примерно в 10 раз. Это свидетельствует о том, что степень ионизации в шнуре близка к полной.

В условиях наших экспериментов разрядный шнур окружен оболочкой из нейтрального газа, находящегося в тени диафрагм. Механизм ионной откачки нейтральных атомов шнуром плазмы должен был привести, при условии отсутствия потерь частиц из разряда, к превышению максимума плотности электронов над плотностью нейтрального газа приблизительно в 4 раза. В то же время измеренная величина $\langle n_e\rangle_{max}$ обычно составляет 50-100% от начальной плотности нейтрального газа. Это значит, что в процессе ионизации происходят потери частиц из разряда.

Есть основания полагать, что на этой начальной стадии процесса являются существенными потери из разряда нейтральных атомов. Так как отношение вероятностей диссоциации молекулы дейтерия и образования молекулярного иона в плазме $\langle\sigma_d v\rangle/\langle\sigma_i v\rangle\approx 10$ [8], то вначале происходит в основном диссоциация молекул. При этом атомы приобретают скорость, близкую к 10^6 см/сек. Пробег атома до столкновения в наших условиях порядка размеров системы, а среднее время пролета атома до стенки камеры составляет около 30-50 мксек. Время жизни атома до ионизации во время развития разряда превышает 10^3 мксек. Поэтому часть атомов дейтерия после диссоциации молекул уходит из разряда и попадает на стенку камеры. Так как атомарный водород легко сорбируется стенками, то этот механизм может привести к значительным потерям частиц из разряда в процессе ионизации.

Измерения с электрическим зондами показывают, что на этой стадии процесса в тени диафрагм имеет место слабая ионизация. В силу сказанного выше о соотношении вероятностей ионизации и диссоциации молекулы дейтерия, можно полагать, что газ в тени диафрагм также в значительной степени диссоциирован, а поэтому подвержен этому же механизму потерь.

С другой стороны, в промежутках между импульсами стенки камеры покрываются слоем молекул дейтерия, которые во время разряда под влиянием бомбардировки нейтральными атомами, а также под воздействием ультрафиолетового излучения попадают в разрядный объем. Таким образом, на начальной стадии процесса между областью разряда и стенкой должен происходить интенсивный газообмен.

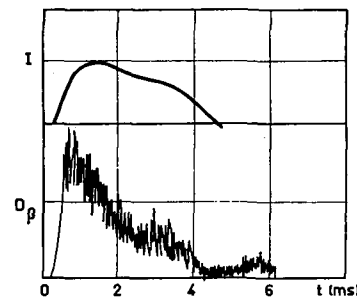

Рис. 12 Ток в плазме и интенсивность линии D_β при разряде в гелии.

О том, что сорбированный стенками дейтерий во время разряда поступает в разрядный объем, говорит следующий эксперимент. Камера после большого числа разрядов в дейтерии откачивалась и наполнялась гелием. Затем производился разряд в гелии. При этом наблюдалось свечение линии D_β. На рис. 12 показана осциллограмма тока в гелии и осциллограмма интенсивности линии D_β. Линия D_β появляется практически одновременно с разрядным током. Ее интенсивность в какой-то мере характеризует приток в плазму нейтрального дейтерия.

5.2. Вторая стадия

Время удержания плазмы в нашей системе, вычисленное в предположении, что потери частиц обусловлены только классической замагниченной диффузией, должно составлять около 0,2 сек.

На самом деле, как видно из рис. 4, плотность электронов после достижения максимума уменьшается значительно быстрее. Спадающий участок кривой $\langle n_e(t)\rangle$ может быть апроксимирован экспонентой. Распределение плотности по сечению разряда в это время меняется мало (рис. 6), поэтому постоянная времени экспоненты τ характеризует среднее время жизни электрона в разряде.

Величина τ близка к 600 мксек и является слабо меняющейся функцией продольного магнитного поля, электрического поля и начального давления газа.

Определенное таким способом время жизни электронов в разряде, по-видимому, несколько завышено, так как наряду с потерями заряженных частиц идет обратный процесс пополнения плазмы за счет ионизации поступающих в плазму нейтральных атомов.

Минимальное время жизни электрона в шнуре можно оценить, предположив, что вся энергия, выделяющаяся в плазме, уносится уходящими из плазмы электронами. Если принять, что каждый электрон в среднем уносит энергию, равную kT_e, где T_e определяется по электропроводности плазмы, то для τ_{min} получаем величину $\sim$15 мксек. На самом деле значительная доля энергии теряется из плазмы за счет излучения примесей. Поэтому действительное время жизни электронов должно намного превышать τ_{min}.

Аномально быстрые потери заряженных частиц из разряда при джоулевом нагреве плазмы впервые были обнаружены на установках типа «стелларатор» [9]. Время удержания электронов в этих экспериментах составляло около 100 мксек.

Обращает на себя внимание то обстоятельство, что время удержания электронов в Токамаке превышает время удержания электронов в стеллараторе в сходных режимах разряда примерно в отношении квадратов радиусов шнура. Так как принципы удержания плазмы в обеих системах подобны, то, по-видимому, процессы, приводящие к аномально большим потерям частиц в этих системах, имеют одинаковую природу.

5.3. Третья стадия

Если во время второй стадии процесса распределение плотности электронов по сечению шнура менялось мало, то для третьей стадии характерным является быстрое изменение распределения плотности в шнуре. На периферии шнура плотность продолжает падать, в то время как в центральной области плотность сохраняется постоянной или несколько увеличивается. Таким образом, в центральной области шнура образуется «керн» с более высокой плотностью электронов.* Это подтверждается фотографиями разрядного шнура, полученными с помощью вакуумной камеры-обскуры [2]. Одновременно происходит возрастание температуры электронов в плазме, о чем свидетельствует рост электропроводности, а также измерение температуры по относительным интенсивностям спектральных линий кислорода (рис. 7). Учитывая, что энергия, выделяющаяся в плазме, при этом уменьшается (за счет спадания электрического поля), можно сделать вывод о том, что потери энергии на этой стадии разряда снижаются.

Мы считаем, что основной причиной малого изменения плотности электронов в «керне» является снижение скорости ухода заряженных частиц из плазмы.

К аналогичному результату могло бы привести также поступление в разряд атомов примесей с их последующей ионизацией.

Однако есть основания полагать, что скорость поступления примесей со стенок камеры в это время значительно снижается, так как, во-первых, уменьшается поток заряженных частиц, бомбардирующих стенку (по крайней мере, пропорционально n_e), во-вторых, примерно на порядок величины ослабляется мощность ультрафиолетового излучения плазмы. Кроме того поток примесей, поступающий со стенок камеры, должен приводить к обогащению электронами главным образом наружного слоя плазмы, в то время как в экспериментах наблюдается обратный эффект: в центре плотность убывает медленнее, чем снаружи.

Температура электронов, определенная оптическими методами, обычно превышает температуру, рассчитанную по средней электропроводности плазмы. При этом отношение интенсивностей спектральных линий ионов с большей кратностью ионизации дает величину температуры более высокую, чем отношение интенсивностей линий, принадлежащих ионам с меньшей кратностью ионизации. Эти факты согласуются с предположением о том, что температура электронов в центральных областях шнура выше, чем в среднем по сечению.

Температура ионов, определенная по допплеровскому уширению спектральных линий, одинакова для ионов с различным зарядом (CIII и HeII) и несколько меньше электронной температуры, определенной по отношению интенсивностей линий OIV и OV. Следует однако иметь ввиду, что определяемые таким способом величины T_e и T_i могут характеризовать различные области плазмы и различие между температурой электронов и ионов в действительности может быть несколько больше, чем дают эти измерения.

Энергия, вкладываемая в плазму в наших опытах, достаточна для того, чтобы нагреть электроны и ионы до температуры, во много раз превышающей измеренную. Потери энергии из плазмы могут быть связаны с неустойчивостями, которые, во-первых, приводят к потерям заряженных частиц из разряда и, во-вторых, увеличивают взаимодействие плазмы со стенками разрядной камеры. Последнее приводит к поступлению в плазму атомов примесей.

Уменьшение плотности электронов в шнуре происходит в то время, когда колебания на производной тока (рис. 1), а также на сигналах электрических (рис. 9) и магнитных зондов имеют максимальную величину. Зарегистрированы колебания в

* Внесенное в гранки примечание: Как показано в работе Л. А. Арцимовича, К. Б. Карташева (*Докл. Акад. Наук* **146** (1962) 1305), во время разряда происходит перемещение плазменного шнура под влиянием поперечной компоненты магнитного поля. Двугорбая форма разрядного тока и характер изменения фазы микроволнового сигнала в значительной степени объясняются этим обстоятельством.

области частот 10 кгц—25 мгц, причем верхний предел измеряемых частот определялся параметрами приемника. Низкочастотные колебания перед вторым максимумом тока несколько ослабляются, высокочастотные исчезают совсем, а затем вновь появляются вблизи второго максимума тока и на спаде тока.

Одной из возможных причин потерь частиц может быть токовоконвективная неустойчивость, рассмотренная Б. Б. Кадомцевым [10]. Эта неустойчивость возникает в плазме с градиентом температуры при наличии продольного электрического поля. Инкремент нарастания этой неустойчивости равен

$$\frac{k_y}{k_z}\frac{E}{H}\frac{c}{\sigma}\frac{d\sigma}{dx} - \chi k_z^2$$

Здесь χ — коэффициент температуропроводности плазмы, σ — электропроводность, E — напряженность электрического поля в плазме, k_z и k_y — волновые векторы возмущения вдоль магнитного поля и перпендикулярно ему. Если первое слагаемое больше второго, то такое возмущение будет нарастать во времени.

Оценки показывают, что такая неустойчивость может привести к значительным утечкам частиц и энергии поперек силовых линий магнитного поля, причем времена удержания электронов в плазме, полученные из этих оценочных расчетов, хорошо согласуются с наблюдаемыми экспериментально.

Особенностью этой неустойчивости является существование критической температуры электронов, выше которой эта неустойчивость развиваться не может. Для плазмы с параметрами, наблюдаемыми на установке «Токамак», эта температура оценивается в 30 эв.

В области первого максимума тока потери энергии столь велики, что энергия, выделяющаяся в плазме, оказывается недостаточной для того, чтобы температура электронов стала выше этого предела. Однако, по мере уменьшения плотности плазмы, величина E/p возрастает, и температура электронов может достичь критического значения. Такая картина хорошо согласуется с ходом электронной температуры, определенной по относительным интенсивностям спектральных линий (рис. 7). К началу третьей стадии T_e составляет 30 эв, причем ее величина меньше при меньших E. Последнее находится в соответствии с приведенным выше условием нарастания таких неустойчивостей.

Электростатические неустойчивости не могут являться причиной потерь частиц из плазмы в наших экспериментах ввиду того, что $T_e \approx T_i$.

6. Заключение

Приведенные экспериментальные результаты, позволяют сделать следующие выводы:

1. Аномально высокий уход частиц из плазмы приводит к перераспределению плотности по сечению шнура. В результате этого в центральной области плазменного витка в конце процесса наблюдается «керн» с плотностью, обеспечивающей эффективную передачу энергии от электронов к ионам.

2. Температура ионов в центральном «керне» мало отличается от температуры электронов и в наших условиях к концу процесса превышает 20—30 эв.

3. Одинаковые температуры однозарядных ионов гелия и двухзарядных ионов углерода, определенные по допплеровскому уширению спектральных линий, показывают, что в нашей системе мала роль коллективных процессов, приводящих к ускорению отдельных частей плазмы, подобных тем, которые наблюдаются на установках «Альфа» и «Зета».

4. Использование магнитных диафрагм может привести к уменьшению прямого взаимодействия плазменного шнура с диафрагмами.

Авторы пользуются возможностью поблагодарить Л. А. Арцимовича за систематические и плодотворные обсуждения наших опытов.

В измерениях ионной температуры участвовал В. Г. Колошников, которому авторы приносят свою благодарность.

В проведении опытов принимали участие А. И. Воробьев, Л. С. Ефремов. В. С. Горячкин, А. С. Капралов, А. Д. Кургузов, Ю. А. Розанов и В. П. Иринархов.

Литература

[1] Долгов-Савельев Г. Г. и др, «Исследование тороидального разряда в сильном магнитном поле», *Ж. эксп. теор. Физ.* **38** (1960) 394.

[2] Горбунов Е. П. и др, «Исследование тороидального разряда в сильном магнитном поле», *Ж. техн. Физ.* **30** (1960) 1152.

[3] Васильевский В. С. и др, «Тороидальная установка с сильным магнитным полем Токамак-2», *Ж. техн. Физ.* **30** (1960) 1137.

[4] Wharton, C. B., Howard, J. C., Heinz, O. "Plasma diagnostic developments in the UCRL Pyrotron program," in Proc. 2nd U.N. Conf. PUAE **32**, United Nations, Geneva (1958) 388.

[5] Колошников В. Г., Мандельштам С. Л. «Измерение температуры ионов на установке Токамак», *Ядерный Синтез*: Дополнение 1962, Часть 3, стр. 1232.

[6] Зайдель А. Н. и др, «Спектральные исследования на установке Альфа», *Ж. техн. Физ.* **30** (1960) 1422.

[7] Butt, E. P. et al. "The design and performance of ZETA," in Proc. 2nd U.N. Conf. PUAE **32**, United Nations, Geneva (1958) 42.

[8] Мэсси Г. С. В., Бархоп Е. Г. С. Электронные и Ионные Соударения, Издательство Иностранной Литературы, Москва (1958).

[9] Spitzer, L., "The Stellarator Program," in Proc. 2nd U.N. Conf. PUAE **32**, United Nations, Geneva (1958) 181.

[10] Кадомцев Б. Б., «Турбулентная утечка частиц из разряда в сильном магнитном поле». *Ж. техн. Физ.* **31** (1961) 1209.

ВЛИЯНИЕ ПРИМЕСЕЙ НА ИОНИЗАЦИЮ И НАГРЕВАНИЕ ДЕЙТЕРИЕВОЙ ПЛАЗМЫ*

Г. Г. ДОЛГОВ-САВЕЛЬЕВ, В. С. МУХОВАТОВ, А. М. САВЕНКОВ, Н. А. ЯВЛИНСКИЙ

АКАДЕМИЯ НАУК СССР

МОСКВА, СОЮЗ СОВЕТСКИХ СОЦИАЛИСТИЧЕСКИХ РЕСПУБЛИК

Получение чистой полностью ионизированной дейтериевой плазмы представляет большие экспериментальные трудности. Тщательное тепловое обезгаживание стенок приводит к значительному снижению оклюдированных газов на поверхности. Однако наличие масляных насосов всегда приводит к оседанию на стенках камеры углеводородов и продуктов их распада.

Использование систем откачки, в которых не применяются органические вещества как на насосах высокого вакуума, так и на форвакуумных устройствах, позволяет сделать вывод, что основным источником поступления углерода в плазму является крекинг тяжелых углеводородов, оседающих на стенках камеры.

Приводятся сравнительные данные, характеризующие плазму, полученную в обезгаженной камере с безмасляной системой откачки и в камере, откачиваемой паромасляными насосами. Эти результаты показывают, что в первом случае удается значительно снизить содержание углерода в разряде.

Проведенные измерения мощности излучения в вакуумной области спектра показывают, что на первых стадиях разряда даже в этих условиях значительное количество вкладываемой энергии в плазму уносится в виде излучения. В последующих стадиях разряда потери на излучение значительно снижаются.

Измерения интенсивности линий углерода при разряде в чистом дейтерии и в смеси дейтерия с дозированными количествами метана показывают, что в системах с паромасляной откачкой концентрация атомов углерода в разряде спустя 1—2 мсек после начала разряда составляет около 20%.

Для выяснения механизма потерь энергии из плазмы были проведены модельные расчеты джоулева нагрева на электронной счетной машине. Расчеты согласуются с предположением о том, что в первой стадии развития разряда энергия теряется за счет излучения примесей. Вычислена скорость поступления примесей в разряд, при которой сходится баланс энергии, поступающей в разряд и уносимой излучением.

Обсуждаются другие возможные механизмы потери энергии.

1. Введение

В настоящее время, по-видимому, можно утверждать, что линейчатое излучение атомов примесей, например углерода и кислорода, которые в значительных количествах попадают в разряд, уносят из плазмы большую часть вкладываемой энергии.

Паромасляные диффузионные насосы, применяемые для откачки рабочих камер, и ротационные форвакуумные насосы являются источниками поступления углерода в разряд.

Для того, чтобы выяснить роль системы откачки в загрязнении камер углеродом проведены сравнительные исследования на установках «Токамак-2» и «Токамак-1а».

Система откачки «Токамак-2» подробно описана в работе [1]. Она состоит из высоковакуумных и форвакуумных насосов, использующих масла.

На установке «Токамак-1а» используются ртутные диффузиионные насосы и водоэжекторный насос для откачки форвакуумных линий.

В настоящей работе приведены некоторые сравнительные характеристики разряда, полученные при исследовании плазмы на камерах с различными системами откачки.

2. Электрические характеристики разряда

Исследование разряда производилось в двух камерах с тождественными параметрами с тем отличием, что в одном случае («Токамак-2») использовалась масляная система откачки, а в другом («Токамак-1а») в качестве насосов высокого вакуума использовались ртутные диффузионные насосы, и в форвакуумной системе применялись водоструйные насосы. Конструкция диффузионных насосов как масляных, так и ртутных, позволяла прогревать их до температуры 400—450° С. Подробное описание конструкции камеры приведено в работе [1]. Отметим только некоторые отличия в конструкции камер. Для ограничения апертуры в камере «Токамак-2» были установлены две диафрагмы с диаметром отверстия 20 см, а в камере «Токамак-1а» одна диафрагма с диаметром отверстия 25 см. Однако, как нам кажется, это обстоятельство не должно было существенно сказаться на геометрии разряда, приводя только к увеличению диаметра разрядного шнура с 20 до 25 см.

На рис. 1 приведены кривые напряжения на обходе тора и средней по сечению шнура плотности тока, полученные при одинаковых значениях начального давления дейтерия и магнитного поля на

* Доклад CN-10/224, представленный на Конференцию. Докладчик: Г. Г. Долгов-Савельев. Дискуссия (на английском языке) по этому докладу дана на стр. 1019. Переводы аннотаций находятся в конце тома.

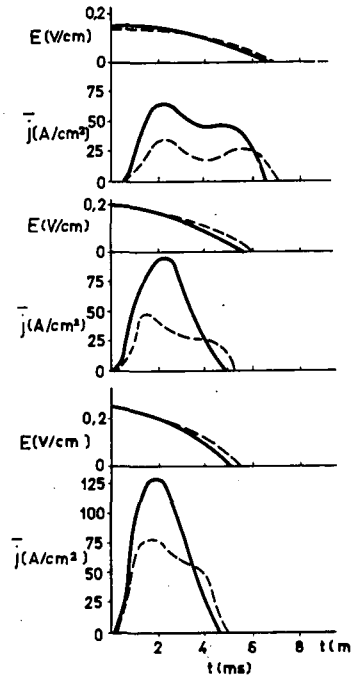

Рис. 1 Напряженность электрического поля E и средняя по сечению шнура плотность тока j для значений $E_0=0{,}15$; 0,20 и 0,25 в/см. $H_0=5600$ э, $P_0=7\times10^{-4}$ мм рт ст. Рабочий газ дейтерий. Сплошные линии — ток в системе с ртутной откачкой, пунктирная — в системе с масляной откачкой.

обеих камерах для трех значений электрического поля. Как видно из этих кривых, средняя по сечению шнура плотность тока в системе с ртутной откачкой («Токамак-1а») несколько больше, чем в системе с масляной откачкой («Токамак-2»).

3. Спектроскопические характеристики разряда

Рассмотрим, прежде всего, как изменилась интенсивность линий примесей относительно интенсивности линии D_β. В табл. 1 приведены отношения

ТАБЛИЦА I

Установка	$I_{D\beta}(\lambda=4860\text{Å})$ / $I_0^{III}(\lambda=4650\text{Å})$	$I_{D\beta}(\lambda=4860\text{Å})$ / $I_0V\ (\lambda=2781\text{Å})$	$I_0V\ (\lambda=2781\text{Å})$ / $I_0^{III}(\lambda=4560\text{Å})$
«Токамак-2»	0,25	6	0,04
«Токамак-1а»	2	2	1

амплитуд интенсивностей соответствующих линий.

Как видно из таблицы, относительное содержание примесей в «Токамаке-1а» несколько понизилось и, кроме того, существенно изменился их качественный состав.

По относительным интенсивностям линий O V ($\lambda=2781$ Å) и O IV ($\lambda=3071$ Å) была вычислена электронная температура плазмы в различные моменты времени. На рис. 2 показано изменение температуры во времени для двух систем. Обращает на себя внимание тот факт, что для «Токамака-1а» наблюдается резкий рост в начале процесса.

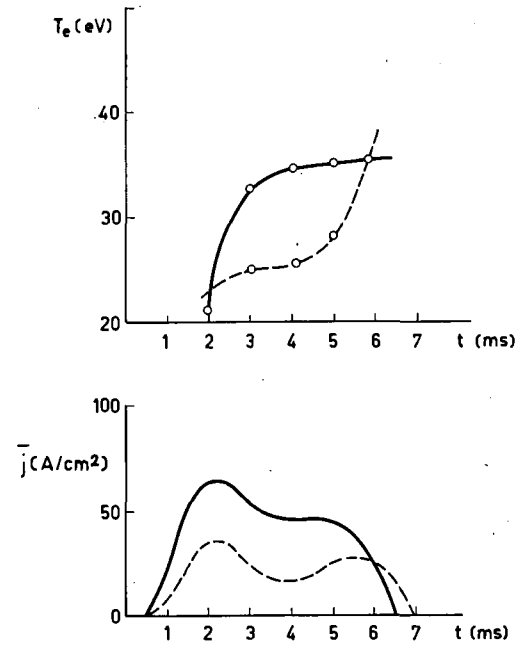

Рис. 2 Зависимость от времени электронной температуры в системах с ртутной (сплошная линия) и масляной (пунктир) откачкой. Внизу плотности тока в плазме. $H_0=5{,}6$ кэ, $E_0=0{,}15$ в/см, $P_0=7\times10^{-4}$ мм рт ст. Рабочий газ — дейтерий.

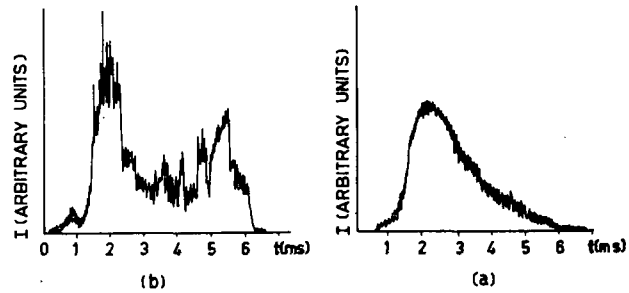

Рис. 3 Осциллограммы временного хода интенсивности линии O V $H_0=5{,}6$ кэ, $E_0=0{,}15$ в/см, $P_0=7\times10^{-4}$ мм рт ст в системе с ртутной (а) и масляной (б) откачкой. Рабочий газ дейтерий.

На рис. 3 приведены типичные осциллограммы линии O V($\lambda=2781$ Å) в двух различных системах при напряженности магнитного поля 5,6 кэ и электрического поля $E_0=0{,}15$ в/см.

4. Потери энергии из разряда

Несмотря на меры, принятые для уменьшения загрязнения разряда примесями, нам пока не удалось нагреть плазму до сколь-нибудь значительных температур, хотя на один атом дейтерия вкладывается 2000—3000 эв. Поэтому вопрос об источниках потерь до сих пор остается чрезвычайно важным. Нами была предпринята попытка измерить потери энергии, уносимые из разряда излучением.

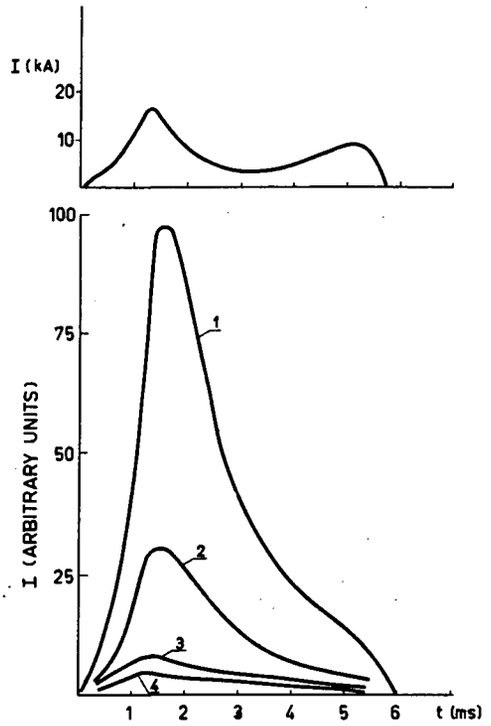

Рис. 4 Сигнал фотоэлемента при различных фильтрах: 1 — без фильтра; 2 — LiF, 3 — кварц; 4 — стекло. Вверху ток разряда. Режим работы: $H_0 = 5{,}6$ кэ, $E_0 = 0{,}15$ в/см, $P_0 = 7 \times 10^{-4}$ мм рт ст.

Для этой цели был использован фотоэлемент, окно которого было покрыто слоем салицилового натра. На рис. 4 показан сигнал с фотоэлемента при трех различных фильтрах, помещаемых на пути светового пучка, а также сигнал, когда фильтры отсутствовали. Как видно из этого рисунка, наибольшая часть энергии уносится излучением с длинами волн меньше, чем 2000 Å. Доля энергии, уносимая излучением с $\lambda > 2000$ Å, составляет не более 5% от всей энергии, уносимой излучением из разряда. Так как основной примесью в разряде в «Токамаке-2» является углерод, то можно предположить, что энергия уносится с излучением иона C IV $\lambda = 1550$ Å. Зависимость от времени отношения мощности, измеренной фотоэлементом W_1, к вкладываемой в разряд мощности W_2 приведена на рис. 5. При определении W_1 считалось, что вся энергия излучения связана с линией C IV $\lambda = 1550$ Å.

К сожалению, подобные эксперименты не были проделаны для системы с ртутной откачкой, поэтому мы не имеем возможности судить о том, уменьшились ли потери на излучения в этом случае.

5. Измерение количественного состава примесей

Для определения количественного состава примесей использовался метод добавок подобно тому, как это было описано в работе [2]. На рис. 6 показаны осциллограммы линий C II $\lambda = 4267$ Å в чистом дейтерии и с добавкой 5,6% метана в разряд. Два максимума свечения линии соответствуют двум различным процессам. Первый максимум соответствует объемному свечению углерода, напущенного в камеру. Второй максимум соответствует поступлению углерода в разряд со стенок камеры. Сравнивая осциллограммы с добавкой метана и без нее, можно определить содержание углерода в разряде. Содержание углерода в плазме, спустя 1,5 мсек после начала разряда, не превышает 10% от общего числа частиц.

6. Обсуждение результатов

Сравнивая осциллограммы токов для двух различных систем откачки, можно отметить, что электропроводность плазмы в первом максимуме тока в системе с ртутной откачкой несколько выше, чем в системе с масляной откачкой.

Это, возможно, объясняется несколько меньшим поступлением примесей в первой стадии разряда.

Рассмотрим теперь вопрос о содержании примесей в разряде.

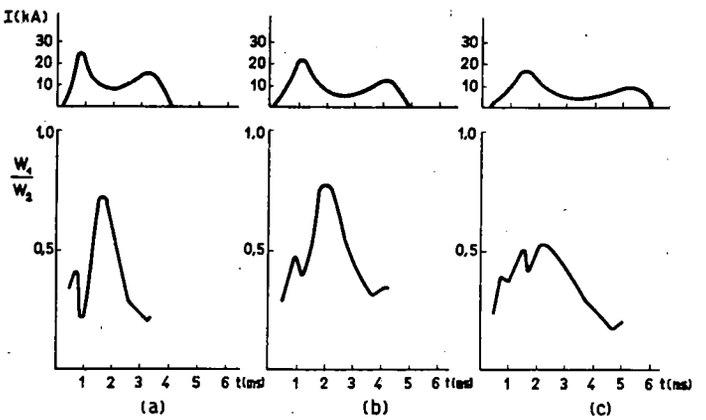

Рис. 5 Отношение мощности потерь на излучение W_1, к вкладываемой в разряд мощности W_2. $H_0 = 5{,}6$ кэ, $P_0 = 7 \times 10^{-4}$ мм рт ст, напряженность электрического поля E_0: (а) 0,25 в/см, (б) 0,20 в/см, (с) 0,15 в/см. Рабочий газ — дейтерий.

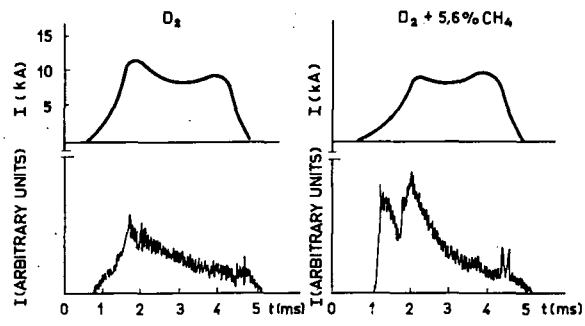

Рис. 6 Осциллограммы линии CII в чистом дейтерии и с добавкой метана.

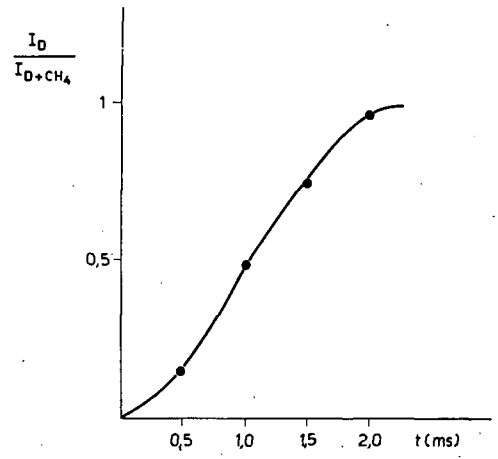

Рис. 7 Отношение интенсивности линии CII 4267 в чистом дейтерии и при разряде с добавкой 5,6% метана.

Кривая, приведенная на рис.7, характеризует отношение интенсивностей линий CII $\lambda=4267$ Å при разряде в чистом дейтерии и при разряде в дейтерии с добавкой 5,6% молекул метана. Как видно из рисунка, величина этого отношения через 1,5-2 мсек достигает единицы. Это означает, что углерод, добавленный искусственно в разряд, быстро ионизируется, и оставшееся свечение обусловлено поступлением примесей в плазму со стенок камеры во время разряда. Как уже указывалось, при определении потерь на излучение мы считали, что вся энергия уносится с излучением резонансной линии CIV $\lambda=1550$ Å. Абсолютное значение энергии, уносимой из плазмы в первом максимуме тока, равно $2{,}5\times10^7$ эрг/сек·см^3. Воспользовавшись данными для мощности излучения приведенными в работе [3], можно оценить концентрацию углерода в разряде. По этим оценкам концентрация углерода составляет около 10%.

Мощность излучения плазмы в области вакуумного ультрафиолета в отдельные моменты времени достигает 70—80% от мощности, выделяемой в плазме.

Потери энергии из плазмы в установках, где не предпринималось специальных мер для обезгаживания стенок разрядных камер в значительной мере обусловлены потерями с линейчатым излучением примесей [4, 5, 6].

Наши эксперименты показывают, что даже в том случае, когда камера очищалась длительным прогревом и тренировкой разрядами, роль примесей в балансе энергии плазмы все еще остается существенной.

Для выяснения влияния примесей на характеристики разряда нами были предприняты модельные расчеты на быстродействующей вычислительной машине. В этих расчетах учитывались следующие элементарные процессы:

$$1\quad H_2+e \rightarrow H+H+e$$
$$2\quad H_2+e \rightarrow H_2^++2e$$
$$3\quad H_2^++e \rightarrow H+H^++e$$
$$4\quad H_2^++e \rightarrow H^++H^++2e$$
$$5\quad H+e \rightarrow H^++2e$$

Так как эти расчеты имеют чисто ориентировочный характер, то нами не учитывались более детально процессы взаимодействия электрона с молекулой водорода, а также взаимодействие атомов и молекул со стенками разрядной камеры и между собой. Кроме того, принимая во внимание, что первая стадия разряда до окончания ионизации водорода длится около 0,5 мсек и дает сравнительно малый вклад в энергетический баланс разряда, то детальный учет этих процессов, по-видимому, не влияет сколько-нибудь существенно на характеристики разряда.

Нагрев электронов плазмы, осуществляемый джоулевым теплом, описывается уравнением вида:

$$j^2/\sigma = \frac{3}{2}\frac{\mathrm{d}}{\mathrm{d}t}(n_e T_e) + Q_{ie} + Q_H + Q_{пр}$$

и для j имеем уравнение:

$$\frac{\mathrm{d}}{\mathrm{d}t}(LI) + \frac{l}{\sigma S} I = lE,$$

где $\sigma = AT_e^{3/2}$ — электропроводность плазмы;
Q_{ie} — описывает нагрев ионов за счет электронно-ионных соударений;
Q_H — потери энергии на ионизацию, диссоциацию и возбуждение водорода;
$Q_{пр}$ — потери энергии на ионизацию и возбуждение примесей.

Результаты этих расчетов приведены на рис. 8. На этом рисунке сплошными линиями показаны расчетные значения плотности токов при различном содержании примесей в разряде (0, 5, 10 и 20% углерода), пунктирной линией показано экспериментальное значение плотности тока, причем в этом случае считалось, что плотность тока по сечению разряда была постоянной. Как видно из этого рисунка, для первых двух миллисекунд наблюдается достаточно хорошее совпадение между теоретическими расчетами и экспериментальными данными, когда концентрация примесей принималась равной 5—10%. Эти цифры хорошо согласуются с оценкой, сделанной на основании экспериментальных данных. Расхождение между теоретическим и экспериментальным значением

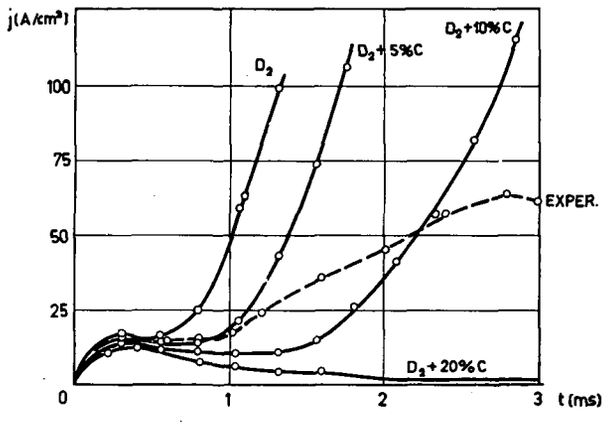

Рис. 8 Результаты расчета плотности электрического тока в газе для различного процентного содержания примесей. Пунктиром показана экспериментальная плотность тока.

тока после 2 мсек может быть объяснено непрерывным поступлением примесей в плазму во время разряда, причем, как показывают расчеты, скорость поступления примесей должна равняться примерно 5×10^{14} см$^{-3}$ сек$^{-1}$, что составляет около 1,5% за 1 мсек.

7. Заключение

Применение ртутно-водяной системы откачки позволяет несколько понизить содержание примесей в дейтериевой плазме. Однако необходимо провести детальные исследования и разработать методы обезгаживания рабочих камер для того, чтобы существенно снизить величину энергии, излучаемой тяжелыми атомами.

Расчеты на вычислительной машине показали, что если в уравнениях принять, что содержание примесей составляет 7% от числа частиц дейтерия, то можно получить удовлетворительное совпадение с опытом для начальной стадии разряда (2 мсек от начала процесса).

Авторы считают своим приятным долгом выразить глубокую благодарность Л. А. Арцимовичу за постоянный интерес к работе.

Вычисления на электронной счетной машине проводились Г. С. Исаковой. В проведении экспериментов авторам большую помощь оказали Н. В. Краснов, Г. А. Егоренков, Л. С. Ефремов. Всем этим товарищам авторы выражают свою глубокую благодарность.

Литература

[1] Васильевский В. С. и др, «Тороидальная установка с сильным магнитным полем ‚Токамак-2'», *Ж. техн. Физ.* **30** (1960) 1137.

[3] Dimock, D., "The spectroscopy of impurities in the stellarator plasma," in Proc. 4th Inter. Conf. Ionization Phenomena in Gases (Uppsala, 17—21 Aug. 1959) **2**, North Holland Publishing Co. Amsterdam (1960) 1136.

[3] Васильев А. И., Долгов-Савельев Г. Г., Коган В. И., *Ядерный Синтез*: Дополнение 1962, Часть 2, 655.

[4] Долгов-Савельев Г. Г. и др, *Ж. эксп. теор. Физ.* **38** (1960) 394.

[5] Кириллов В. Д., *Ж. техн. Физ.* **30** (1960) 320.

[6] Karr, H. I., Knapp, E. A., Osher, I. E., Univ. of Calif. Los Alamos, New Mexico Report (1961).

PARTICLE MOTION ON MAGNETIC FLUX SURFACES IN STABILIZED AND HARDCORE PINCHES*

D. H. BIRDSALL,**, S. A. COLGATE, H. P. FURTH, C. W. HARTMAN, R. L. SPOERLEIN***

LAWRENCE RADIATION LABORATORY, UNIVERSITY OF CALIFORNIA

LIVERMORE, CALIFORNIA, UNITED STATES OF AMERICA

High-power "stabilized pinches" are subject to magnetic disturbances and leakage of energetic particles. A diffusion theory describing the leakage in terms of interconnection of flux surfaces is consistent with the experimental data. Direct observation of the leakage phenomenon has been realized in a 4-in., 100-kA linear pinch tube, along which is passed a 200-kV, 10-mA electron beam of 0.1-μs duration. Prior to onset of magnetic disturbances, the beam delineates regular nested magnetic-flux surfaces at the phosphor end-window. When the beam is injected on a flux surface where magnetic disturbances have begun, the trace becomes erratic, and subsequently all transmission ceases. The loss of beam containment within the pinch begins at the current layer and propagates inward.

By addition of a hard core to the pinch tube, suppression of magnetic disturbances can be achieved in "inverse stabilized pinches." Correspondingly, regular beam traces are obtainable throughout the pinch cycle, at levels of current density where transmission through stabilized pinches cannot be maintained at all. The successful containment of particles in hard-core geometry is being given a further test by means of a newly completed 400-kA levitron (toroidal pinch with ring core) of 12-in. minor diameter.

The electron-beam probe has proved highly useful for diagnosis of the magnetic structure of pinch discharges even in their stable state. The magnetic pitch on a flux surface can be derived from the angle rotation of the beam image about the pinch axis. The time rate of rotation measures the interdiffusion of magnetic-field components. The magnetic shear can be derived directly from the elongation of the beam image along the flux surface.

Experimental tests of this measurement of shear confirm that the results are nearly independent of beam energy and duration, and of absolute magnetic field strength. In stabilized pinches regions of low shear are found prior to onset of the magnetic disturbances. In inverse stabilized pinches substantial shear can be maintained at all radii.

1. Introduction

The prospect of using a conventional pinch for thermonuclear containment has received a series of setbacks corresponding to the discovery of an ascending hierarchy of instabilities. The kink and sausage modes destroyed the containment of the dynamic pinch within a few traversals of sound [1]. The manifestations of instability in the "stabilized pinch" (axial-field centered pinch) have been more subtle but equally disastrous [2, 3]. First, the observed resistivity was inconsistently large in terms of expectations based on collision theory; second, magnetic probe measurements demonstrated the presence of turbulent magnetic fields; and third, in the highest-powered pinch discharges, a large flux of energetic electrons managed to escape from confinement and "dump" an appreciable part of the pinch energy at the tube wall [2]. At least two of these manifestations of instability have been suppressed in recent hard-core pinch experiments [4, 5]. This improvement is consistent with the favorable prospects held out by the hydromagnetic stability theory for configurations having a large magnetic shear throughout.

Until now a sensitive direct measure of the particle-confinement properties of pinch fields has been lacking. In the present experiments, passage of an externally produced electron beam along the pinch discharge provides us with a technique for determining the time-dependent properties of the magnetic surfaces of various pinch configurations. The results confirm our speculations on the structure of turbulent fields and visibly demonstrate how the observed turbulence leads to enhanced diffusion and rapid loss of particles. In addition the comparatively quiescent behavior of the magnetic flux surfaces of the hard-core pinch encourages optimistic expectations for particle confinement in the toroidal hard-core pinch or "levitron." (See [4] for a discussion of the principle of the levitron.)

2. Apparatus

The apparatus for electron-beam probing of the hard-core pinch is shown in Fig. 1. The tube can also be operated with the hard core removed, and with a conventional cathode having a radial slit for the beam entrance. The electron beam is formed by an electron gun pulsed negative to 100–300 kV by a pulse transformer. The effective on-time of the beam is 0.1 μs, as determined by the x-ray pulse in a scintillator. (A few measurements were made with a pulse of 0.2μs in order to test the time dependence

* Conference paper CN-10/150, presented by S. Colgate. Discussion of this paper is given on page 1020. Translations of the abstract are at the end of this volume of the Conference Proceedings.
** Co-author in Sections 9, 10. *** Co-author in Sections 1-8.

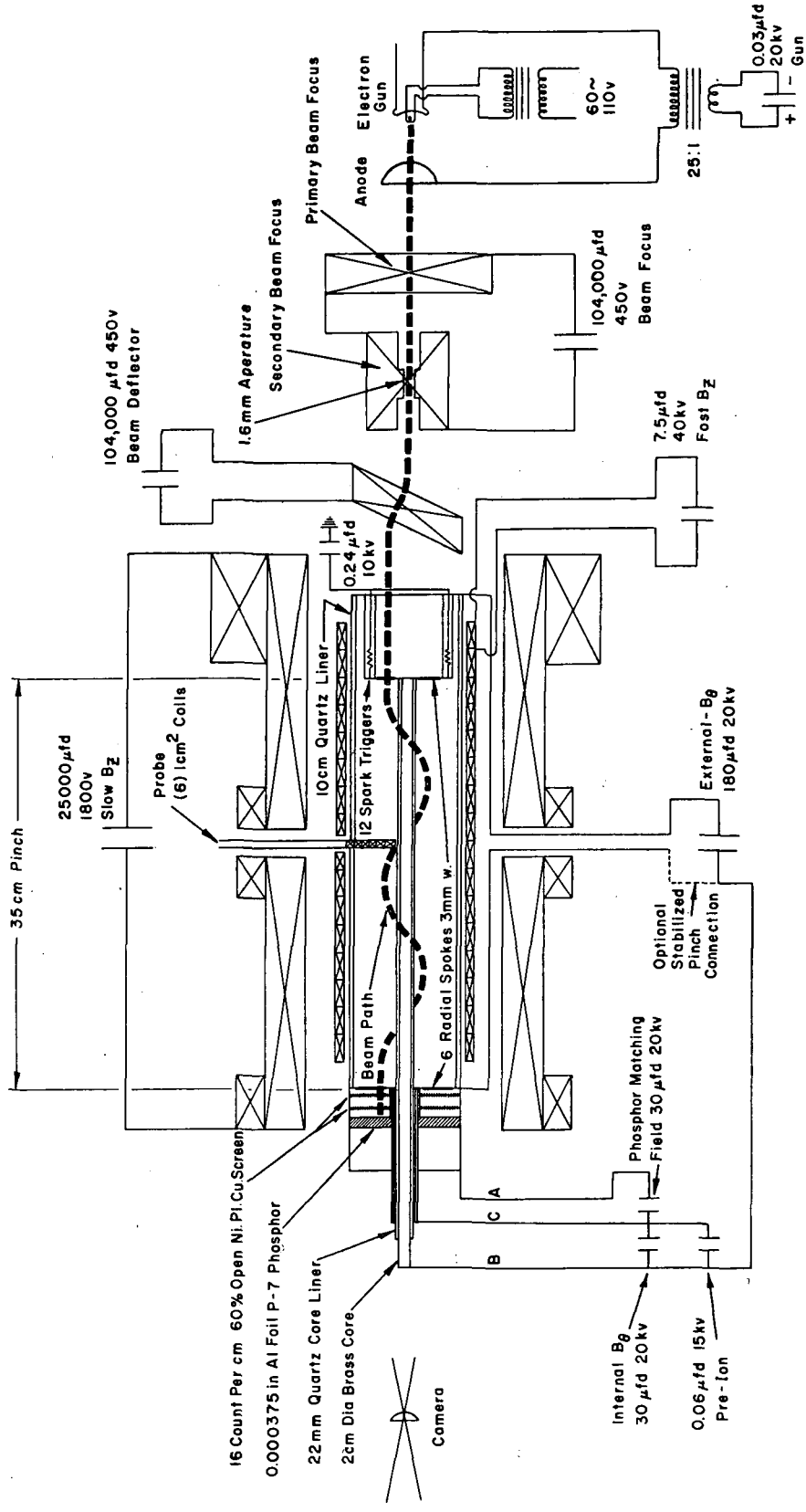

Fig. 1 Electron-beam probe and pinch apparatus.

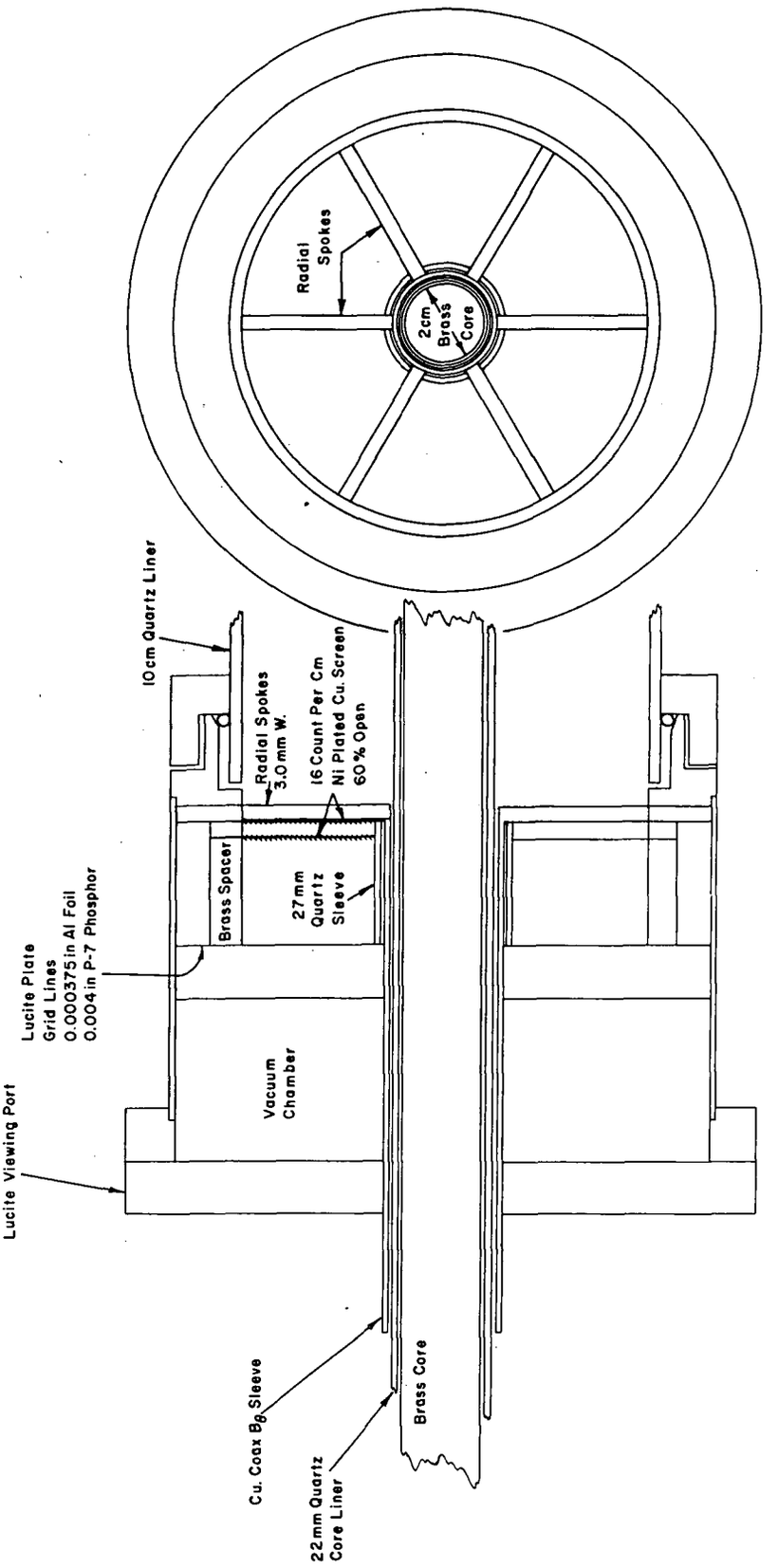

Fig. 2 Electron-beam exit electrode.

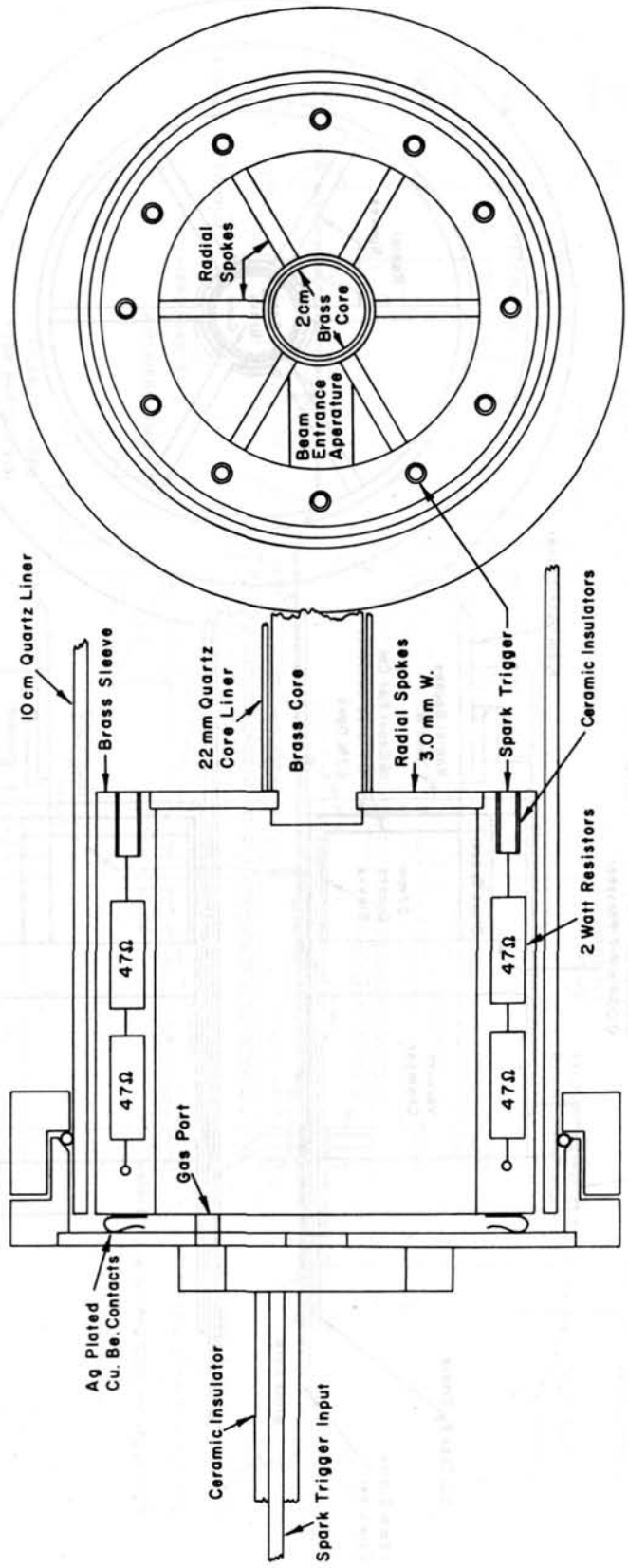

Fig. 3 Electron-beam entrance electrode with spark triggers.

of beam phenomena.) The total beam current is about 1 A, but a small fraction, of the order of 10 mA, is selected from the focussed beam by a $^1/_{16}$-in. aperture in the center of the secondary focus coil. (The beam is, therefore, a trivial perturbation to the pinch whose current density is at least 1000 times as great.) The purpose of this aperture is not only to limit the beam size, but also to afford vacuum isolation between the high-voltage gun and the pinch discharge. Following the aperture is a radial-deflection coil that places the beam on any desired flux surface within the pinch tube. The beam trajectory, after passage through the pinch, terminates at a phosphor screen of lucite, which is protected from the pinch by a series of two 16-mesh/cm etched-nickel screens (Fig. 2), and finally by a 0.00037-in. aluminum foil. The rear of the phosphor screen is viewed through a vacuum-seal window by a Landback camera. The over-all resolution of camera and phosphor is sufficient to make the 16-mesh/cm protection screens clearly visible by the shadow appearing in the beam spot. The beam spot itself is 0.1 to 0.2 cm in diameter for axial fields greater than 1 kG.

The pinch discharge is similar to many linear pinches previously reported, aside from somewhat greater-than-usual precautions taken to provide uniform initial ionization. Special "matching fields" are also used at the ends to permit exit and entrance of the electron beam.

The 10-cm-diameter, 33-cm-long quartz tube is tightly surrounded by a B_z winding to provide the fast changes of the axial field ($\sim$5 μs, which is the period of the pinch). The main B_z field is established by a large external coil of slow rise time ($\sim$50 ms), to permit the field to penetrate the massive end electrodes. The B_θ fields are generated by three condenser banks to give, respectively, an initial vacuum B_θ field, internal (unpinch) B_θ near the hard-core, or external (pinch) B_θ.

The end electrodes (Figs. 2 and 3) of the pinch must be transparent to the electron beam, yet still carry the pinch and hard-core currents with sufficient uniformity so that the entrance and exit distortion of the beam is small. Six 1/8-in. diameter radial tungsten rods have proved satisfactory (whereas a thinner conductor, e.g., the fine mesh screens, caused too sudden and nonadiabatic a change in direction of the beam).

3. Pre-ionization and formation of arc spots

The most difficult requirement for successful electron-beam diagnostics proved to be that of highly uniform initial ionization. Early experiments with a standard "stabilized pinch" (no hard-core) demonstrated that the initial current density was strongly concentrated along one or two asymmetric "streamers." This occurred regardless of the degree of initial ionization. A number of powerful techniques, including pulsed r.f., continuous r.f., high-voltage capacitor discharges, and use of hot-filament cathodes, were tried unsuccessfully. The behavior was consistent with the formation at the cathode of one or two arc spots whose non-symmetric position distorted the configuration of the entire pinch. The formation of these arc spots was clearly shown by direct Kerr-cell photography of the cathodes. A special cathode was finally constructed (Fig. 3) consisting of 12 uniformly spaced spark triggers located around the outer circumference of the entrance electrode. Resistors divide the current ($\sim$200 A) to each trigger so that, initially, 12 symmetric arc spots are formed. The resultant pinches are symmetric, as can be determined by injecting the electron beam on axis (without hard-core) and observing that the phosphor spot remains centered during the initial current rise.

The presence of arc spots at the cathode might lead one to suspect that these localized sources of current might represent the dominant perturbation of the electron-beam trajectory through a pinch. In order to test this hypothesis, a more detailed investigation of arc spots was made using a "stabilized pinch" discharge.

Using the photographic technique of M. Sterns, General Atomic (unpublished) 0.1-μs exposure-time Kerr-cell photographs of the cathode were taken for various gases at 2, 5 and 7 μs (Fig. 4). The initial B_z is 1500 G, and the current reaches a peak value of 125 kA at 6 μs. The photographs shown were thus taken at I=60, 110, and 110 kA respectively. The ring of triggers is clearly seen in the helium, 5-μs photo. The main discharge light appears in the foreground. The trigger assembly and pinch light are also seen reflected in the tube wall.

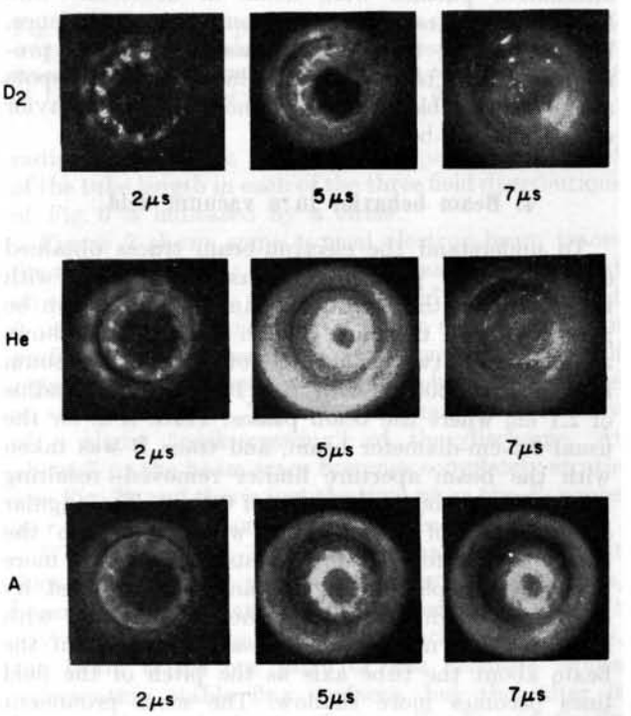

Fig. 4 0.1-μs Kerr-cell photographs of pinch cathode for deuterium, helium and argon gases, taken 2, 5, and 7 μs after pinch initiation.

Comparison of the three gases indicates a predominance of arc spots with deuterium, some arc spots with helium late in the cycle, and almost no arc spots with argon. The surprising lack of arc spots with high-Z gases (air has no arc spots either) suggests a new discharge regime is encountered, somewhat analogous to a high-pressure, thermionic cathode discharge. It appears plausible that suppression of arc spots can be attributed to intense photoemission supplying the necessary current at a much lower cathode potential drop than that required to maintain an arc.

The possibility of motion of the arc spots (in deuterium), as current is redistributed at the cathode, has been examined. It is observed that the spots generally do not move but rather that changes in the current distribution are accompanied by the formation of fresh spots.

The general filamentary character of the pinch, induced by the method of triggering, is observed most clearly in the argon photos. Some indication of this azimuthal periodicity has also been observed with the electron beam.

A study was made of the possibility that arc spots are responsible for the observed random fluctuations of the electron beam trace, either directly, by means of local magnetic field perturbations at the cathode, or indirectly, by inducing turbulence in the discharge. To test the former possibility a very short discharge tube was used. In that case very little erratic behavior of the beam was found even though the arc-spot phenomenon was the same as always. To test whether arc spots might be a causative agent for turbulence alternative pinches were made in deuterium and helium. In both cases there was comparable turbulence, but in helium, the arc-spots were much less pronounced. It is tentatively concluded that arc spots are not responsible for the occurence of erratic behavior of the electron-beam probe.

4. Beam behavior in a vacuum field

To understand the electron-beam traces obtained during various pinches it is useful to begin with trajectories in the helical vacuum fields that can be generated with the hard core in place. Fig. 5 shows a composite of two beam traces obtained in a vacuum field of $B_z=2600$ G, with $B_\theta=1600$ G at the radius of 2.1 cm where the beam passes. Trace A is for the usual 0.2-cm-diameter beam, and trace B was taken with the beam aperture limiter removed, resulting in an effective beam diameter of 0.4 cm. The angular displacement of these traces with respect to the beam position for $B_\theta=0$ amounts to somewhat more than one complete turn, as can be ascertained by raising B_θ gradually (during successive shots), with fixed B_z, and noting the increasing rotation of the beam about the tube axis as the pitch of the field lines becomes more shallow. The most prominent feature of the beam traces is the azimuthal smear. Experimentally this smear is found to be proportional to the beam diameter and to the beam rotation about the tube axis. To first order the smear is found independent of beam energy, beam on-time, and absolute field strength. These results exclude as possible explanations of the beam smear the change in time of the field, the occurence of nonadiabatic effects, and the presence of large electron drifts in the magnetic field.

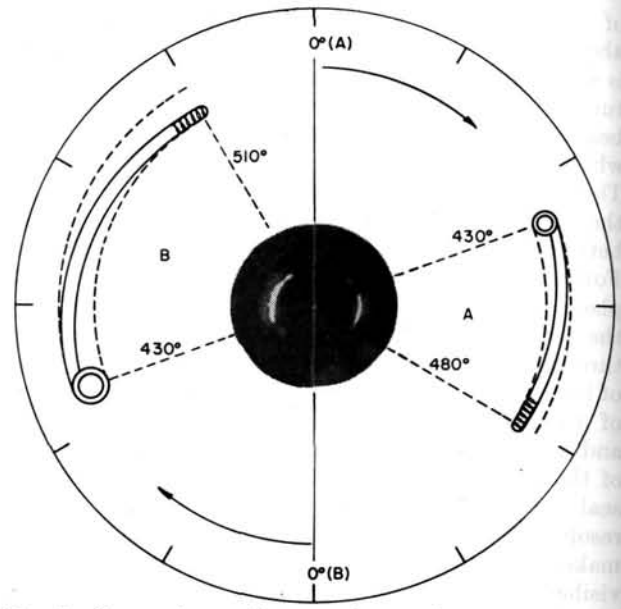

Fig. 5 Comparison of two electron-beam traces in identical helical vacuum fields for beams of different initial diameter. The total angle of rotation in the field is indicated at each end of the beam smear.

The observed smear can be readily explained on the basis of ordinary optical considerations. The beam enters the helical field on flux lines distributed over a finite extent in radius from the axis of the tube. As is well known, a helical vacuum field has substantial shear; i.e., there is a difference in pitch for field lines on flux surfaces at different radii. The beam smear therefore represents the different amount of rotation about the tube axis for beam particles near the inner (small-radius) edge of the beam spot, relative to particles near the outer edge. The beam smear can be regarded simply as a mapping of a flux tube that is cylindrical in cross-section at the beam-input end and acquires a highly elongated cross-section farther down the tube. Since the smear of the beam is proportional to the shear of the field, it provides a convenient tool for determining the local shear of magnetic-field distributions in pinches and, therefore, a useful indication of theoretical hydromagnetic stability.

Among the second-order perturbations of the beam trajectory is the drift associated with the acceleration of the electrons during passage from the initial rectilinear trajectory to the helical path imposed by the pinch fields. The drift velocity $\mathbf{u}$, which describes motion of the guiding center to a neighboring line, is given by

$$\mathbf{u}=\frac{\mathbf{n}}{B}\times\left(-c\mathbf{E}+v_\perp{}^2\frac{mc}{2eB}\nabla\mathbf{B}+v_\parallel{}^2\frac{mc}{e}\frac{\partial\mathbf{n}}{\partial s}\right) \quad (1)$$

($v_\perp$ and $v_\parallel$ are the velocity components perperdicular and parallel to **B**, **n** is the unit vector along **B**, and s is the coordinate along **B**).

In the present experiment the first two terms, involving the electric-field drift and the gradient-of-**B** drift, are small compared with the third term, which describes the drift due to the centrifugal force on a particle of velocity **n** $v_\parallel$. Eq. (1) can thus be written approximately as

$$\mathbf{u} = \frac{a_\parallel v_\parallel}{R^2}(\mathbf{R}\times\mathbf{n}) \tag{2}$$

where $a_\parallel$ is the gyro-radius that a particle of parallel velocity $v_\parallel$ would have if it were gyrating perpendicular to **B**, and R is the local radius of curvature of the field line.

On entering the pinch tube, the electron beam is turned through an angle $\varphi=\tan^{-1} B_\theta/B_z$ and a radial drift occurs, leading to a displacement

$$\Delta r = \int u_r \,\mathrm{d}t \tag{3}$$

where

$$\int \frac{v_\parallel}{R}\,\mathrm{d}t = \varphi \tag{4}$$

so that

$$\Delta r = a_\parallel \varphi \tag{5}$$

A radial drift of this order has been observed, with a reversal in sign for a reversal in B_θ.

Besides the initial radial drift, there is also a continuous axial and azimuthal drift, due to the centrifugal force on the beam as it follows the helical field in the pinch tube. This drift causes the beam to emerge with an azimuthal displacement

$$\Delta\theta = \frac{\Delta x}{r}\frac{B_z}{B} \tag{6}$$

(r=radius from the axis, and Δx is total distance of drift normal to **B**). From Eq. (2) one can derive

$$\Delta x = \theta\frac{B_\theta}{B}a_\parallel \tag{7}$$

where θ is the angle of beam revolution around the axis, so that $\Delta\theta$ becomes

$$\Delta\theta = \theta\frac{a_\parallel}{r}\frac{B_\theta B_z}{B^2} \tag{8}$$

5. Beam behavior in the stabilized pinch

The stabilized-pinch magnetic-field distribution of Fig. 6 was obtained with a 0.1-torr deuterium filling and with the hard core removed. From the field distributions and the attached B_θ-probe signals taken at four different radii, one can see that the irreprodicibility phenomenon starts earliest at $r=\sim 3$ cm, which is the region of maximum current density. The instability-onset times are seen to be roughly: $r=0$, $t=7.3$; $r=1.5$, $t=4.5$; $r=3.0$, $t=3.8$; $r=4.5$, $t=4.8$ (units of cm and μs, respectively). The electron beam is introduced either on center or at a radius $r_0=2.7$ cm at the cathode end, which corresponds to a B_z-flux surface including 10^5 G-cm². The

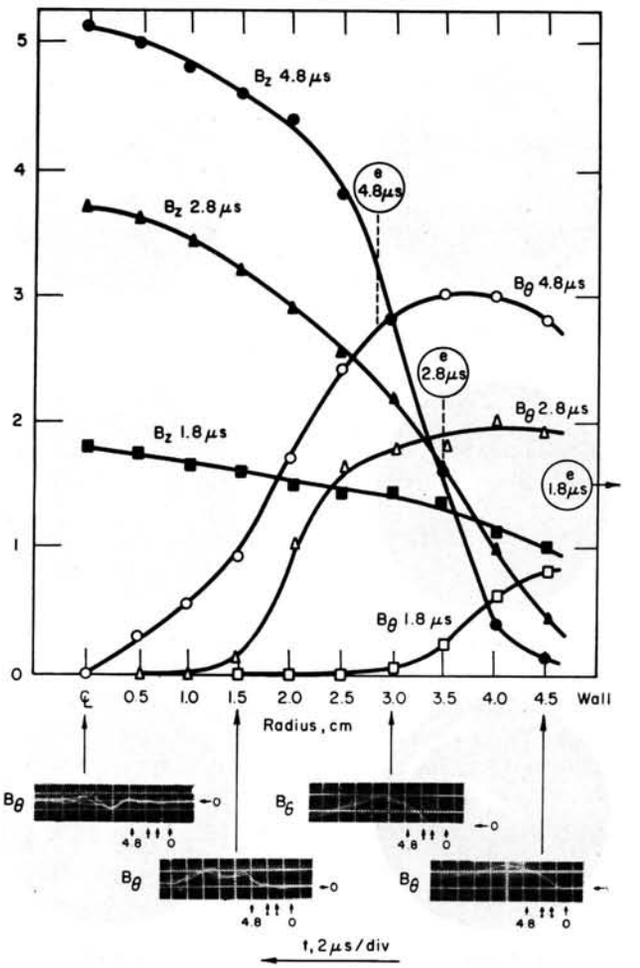

Fig. 6 "Stabilized pinch" magnetic field distributions without hard core taken at times corresponding to beam traces. Overlay magnetic-probe traces taken near radius of beam passage show typical probe flutter.

radius at which the beam actually passes down most of the tube length in each of the three field distributions of Fig. 6 is indicated by a circle.

Figure 7 shows some typical electron-beam traces for the pinch of Fig. 6. When the beam is introduced on center, it is only slightly deflected during the first 6 μs or so of the pinch. The minor departures from perfect centering seem to correspond to the small *reproducible* asymmetries indicated by the B_θ-probe at $r=0$ (see Fig. 6). These features may be indicative of a slight "cork-screwing" of the discharge. At about 7 μs the beam trace becomes completely erratic (see Fig. 7), and this is just the time when the B_θ-probe at $r=0$ shows the onset of irreproducibility.

When the beam is introduced at $r_0=2.7$ cm, it does not appear on the phosphor until about 2.2 μs, because prior to that the B_z-flux surface on which it moves intersects the tube wall. Until about 3.5 μs, the beam traces out more or less accurate circles representing stable flux surfaces, but thereafter it becomes increasingly erratic (see Fig. 7) and finally disappears altogether from the phosphor screen. The early onset of B_θ-probe-signal irreproducibility in the

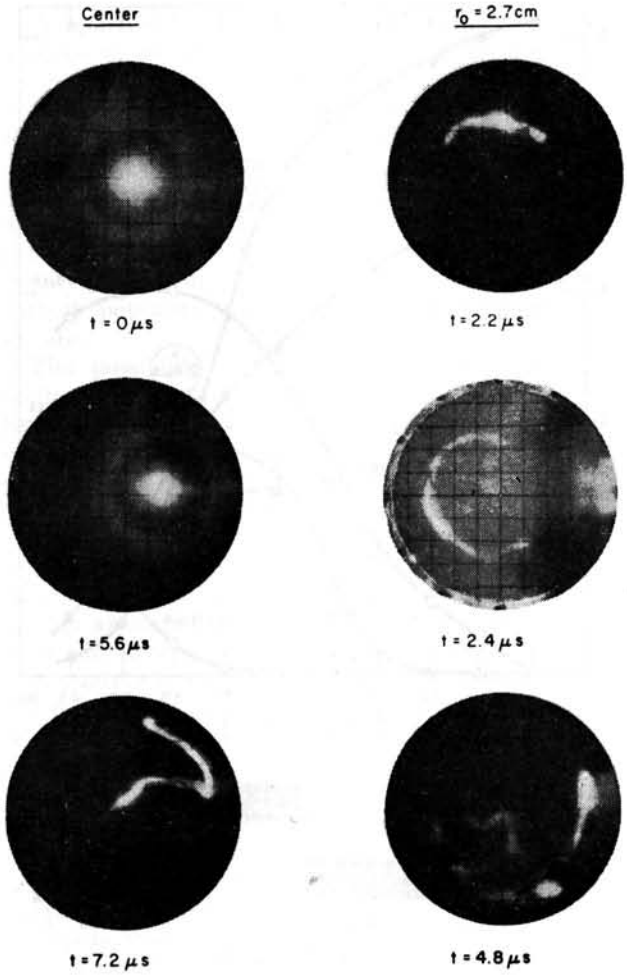

Fig. 7 Electron-beam traces for field distributions of Fig. 6.

current-carrying region is seen to be perfectly correlated with the onset of electron-beam fluctuations in the same region.

The substantial angular extent of the traces for $r_0 = 2.7$ cm indicates large local shear of the pinch field. One finds, however, that slight variations of the radial beam position are sufficient to give traces of little or no angular extent, i.e., little or no shear.

6. Beam behavior in hard-core pinches

The behavior of the electron beam in a helical vacuum field has been shown in Fig. 5. With the addition of a fairly "weak" unpinch current (50 kA), the magnetic probe traces remain reproducible, and the electron beam traces out the expected stable flux surface (see top of Fig. 8). The small jogs in the circular beam trace can be correlated with the periodic magnetic perturbation caused by the six radial spokes at each end of the pinch.

For purposes of direct comparison with this "inverse stabilized pinch," a stabilized pinch was made with the same plasma current and with the hard-core in place (see bottom of Fig. 8). The erratic and irreproducible beam pattern is evidence of gross fluctuations in the magnetic-flux surfaces. The time at which the trace was taken (3.7 μs) was the latest time in the pinch cycle at which any beam transmission could be observed at all whereas in the comparable inverse stabilized pinch the trace could be observed throughout the cycle.

Inverse stabilized pinches of sufficient current density can be made to show a certain turbulence and irreproducibility of magnetic probe traces despite their theoretical hydromagnetic stability [5].

In Fig. 9, the field distribution of such a pinch is given, with attached multiple-overlay B_z-probe traces taken at the radii at which the beam passes. The turbulence in the magnetic probe traces correlates with the erratic beam behavior shown in Fig. 10. The maximum turbulence is observed with both means of detection at small radii where the current density is highest. Indeed the erratic excursions of the beam trace are so strictly and reproducibly confined to a limited tubular zone at small radii (see Fig. 10) that one suspects the presence of effective particle containment within the outer stable zone in spite of the pronounced turbulence in the inner zone. If this effect actually takes place, it will be of prime importance in the formation and heating of plasma in toroidal hard-core pinches, where a local region of instability may arise before the plasma has had a chance to become hot.

7. Interpretation

The observation that the surface of particle motion can become grossly distorted over a length of a few pinch diameters is in complete agreement with predictions based on the observed fluctuations of the magnetic probe signals. These signals indicate random local field directions, and hence define field lines that lead in a random-walk manner across the turbulent zone.

For frequency components of the turbulence that are not much greater than the maximum frequency observed by magnetic probes ($\sim\omega_{ci}$, the ion cyclotron frequency), and for a radius of curvature of field distortion that is not much smaller than a_i (the ion gyro-radius at Alfvén speed), an electron moves adiabatically (i.e., is bound to a line of force), provided its energy is less than about kT_cM/m, where $kT_c = B^2/8\pi N$ is the magnetic energy per particle.

The observed probe-signal flutter indicates that in very turbulent pinches the local magnetic field is distorted randomly with an autocorrelation length $L_c \approx 2a_i$ [3] and a mean energy density of distortion that is comparable to the mean field energy density. Accordingly the local magnetic vector contains a random radial component that causes it to make an angle α with the pinch axis ranging from 0 to 45°.

A fast electron following a line of force sees a random orientation of magnetic field from point to point on its path and in an axially symmetric system will undergo a radial random walk process, with a mean radial step, $a_i \sin \alpha$, occurring for each auto-

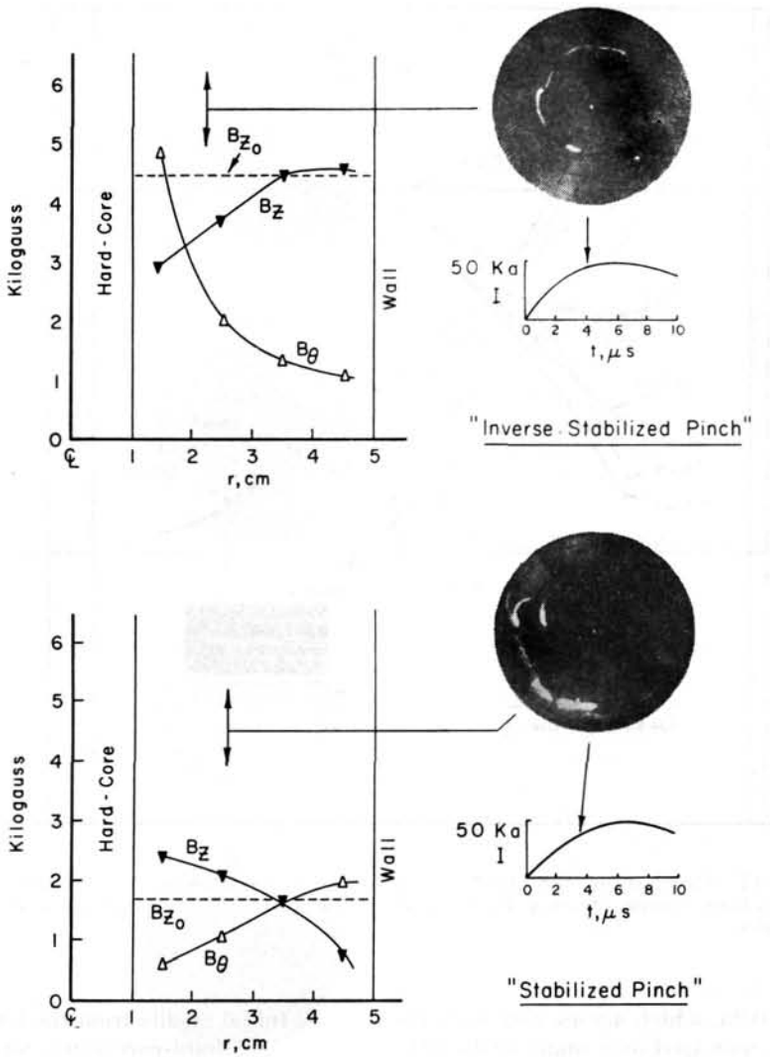

Fig. 8 Comparison of an "inverse stabilized pinch" and a "stabilized pinch" with core present, but electrically disconneted, showing stable circular flux surface (with slight distortion due to spokes) for the B_θ-centered pinch and usual turbulence for B_z-centered version. The current density was small ($\sim$1 kA/cm^2).

correlation length along the line of force. The path length before a line starting from radius r reaches the wall at radius R becomes:

$$\lambda_d = \left(\frac{R-r}{2\,a_i \sin\alpha}\right)^2 L_c \tag{9}$$

and so we have for the ideal case of extreme turbulence (where $L_c \approx 2\,a_i$)

$$\lambda_d = \frac{(R-r)^2}{2\,a_i \sin^2\alpha} \tag{10}$$

A decrease in the relative amplitude A of the turbulent field implies a reduction in the mean radial step roughly in proportion to A while the autocorrelation length becomes greater. If one takes L_c proportional to $1/A$, the path length becomes proportional to $(1/A)^3$.

In a toroidal stabilized pinch experiment [2] where the magnetic energy per ion was extremely high (T_c=4 keV) and the turbulence quite pronounced, a path length of about 200 cm for runaway electrons to reach the wall was determined experimentally from the energy of x-rays emitted upon impact, and from the electric field in the plasma.

For the parameters R=5 cm, r=1 cm, α=45°, and $L_c = 2a_i$=2 cm, the diffusion path length calculated from Eq. (10) is 65 cm. The appropriate choice of the parameter A, characterizing the degree of turbulence, is therefore $A \approx 0.7$, which is consistent with the observed amplitude of flutter on the magnetic-probe traces.

In the electron-beam pinch experiment, for the unstable-inverse-stabilized-pinch case (Fig. 10), the beam is erratic over a radial zone of $\sim$0.7 cm. For $R - r$=0.7 cm, a_i=0.4 cm (5000 G, 0.1 torr initial deuterium pressure), and the length, λ_D, of the electron trajectory from cathode to anode=80 cm, the indicated amplitude, A, of the turbulent field

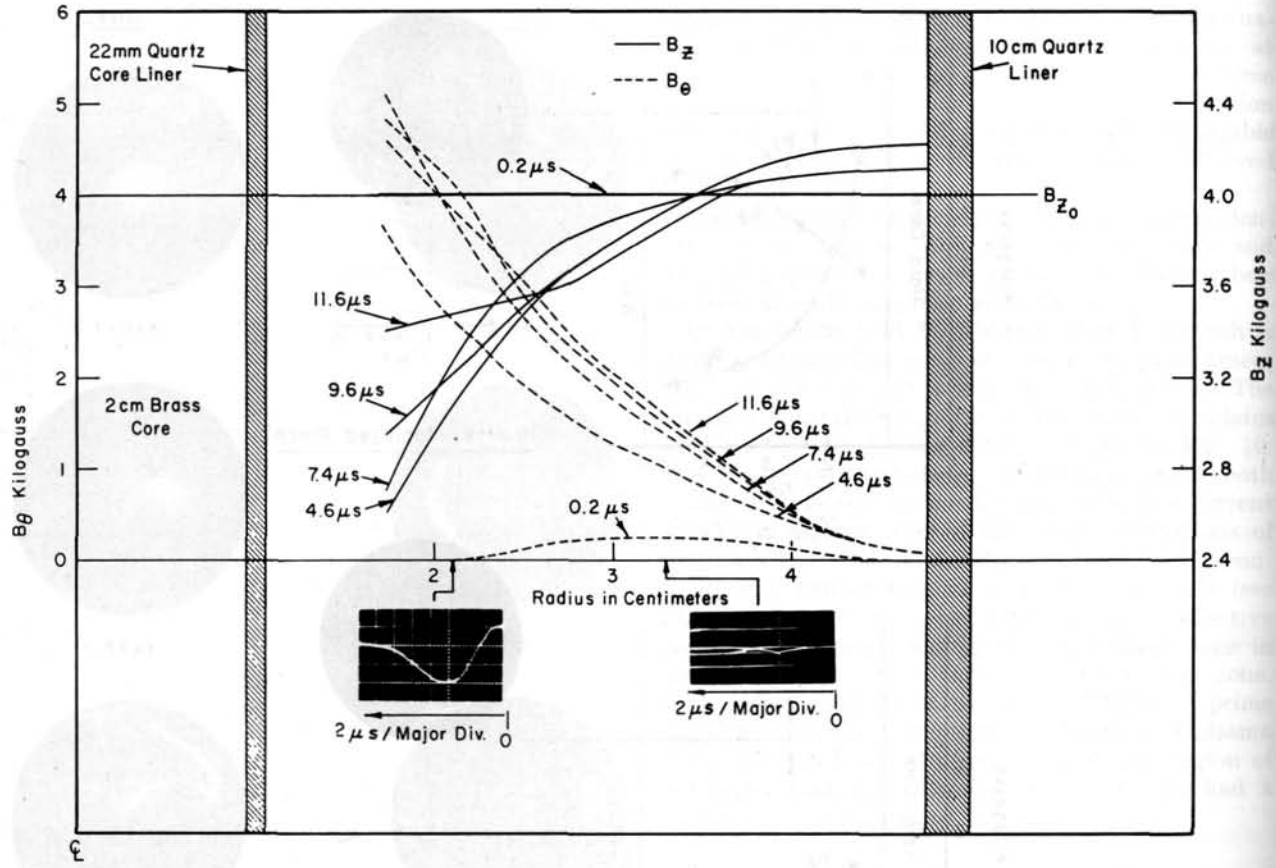

Fig. 9 Magnetic field distribution for high-current-density (~2 kA/cm²) "inverse stabilized pinch" at times corresponding to beam traces. Overlay B_z magnetic-probe traces taken near radii of beam passage indicate partially turbulent field.

component is about 0.25, which agrees well with the magnetic-probe data, averaged over many shots. (The magnitude of "flutter" on the particular traces shown in Fig. 8 is below average.)

8. Conclusion

The relationship between irreproducibility of magnetic probe traces, occurrence of instabilities, and leakage of particles from the pinch is strongly confirmed by the present experiment. The nature of this relationship is understandable on the above simple theoretical basis.

However, the mechanism by which the pinch instabilities are excited, even in configurations where the shear should be sufficient to guarantee stability, remains to be determined. A plausible phenomenological description involves cyclical feed-back, where turbulence causes enhanced "resistivity," with the corresponding "resistive dissipation" serving to maintain the turbulence. A detailed mapping of the turbulent field by the electron-beam technique will help contribute to the clarification of the instability mechanism by providing information about frequency spectra and autocorrelation lengths without disturbing the discharge in the region of measurement.

9. Initial results from the levitron — a toroidal hard-core-pinch construction*

The levitron is a toroidal version of the hard-core pinch in which the hard core—now a ring core—remains transiently centered in the toroidal chamber without mechanical support. This permits plasma experiments utilizing the endless magnetic lines that form the helical nested magnetic surfaces surrounding the hard core. Any possible support rod, current-carrying or otherwise, intersects all surfaces and destroys single-particle containment and possibly also plasma stability properties [4]. Hence the requirement of transient levitation. The torus (Fig. 11) has been constructed with a bakeable inner liner to obtain sufficiently clean vacuum conditions to demonstrate —or refute—the expected improved containment of plasma in the hydromagnetically more stable pinch configuration achievable with a hard core [5].

In Fig. 11, the hard core is a 10-cm-o.d. and 6.8-cm-i.d. copper ring with a 120-cm major diameter, surrounded by corrugated stainless-steel liner 0.019 cm thick, with a 30-cm i.d. This liner is supported inside an insulated 0.6-cm-thick copper vacuum vessel.

* Sections 9 and 10 were submitted to the conference as an addendum to the originally submitted paper.

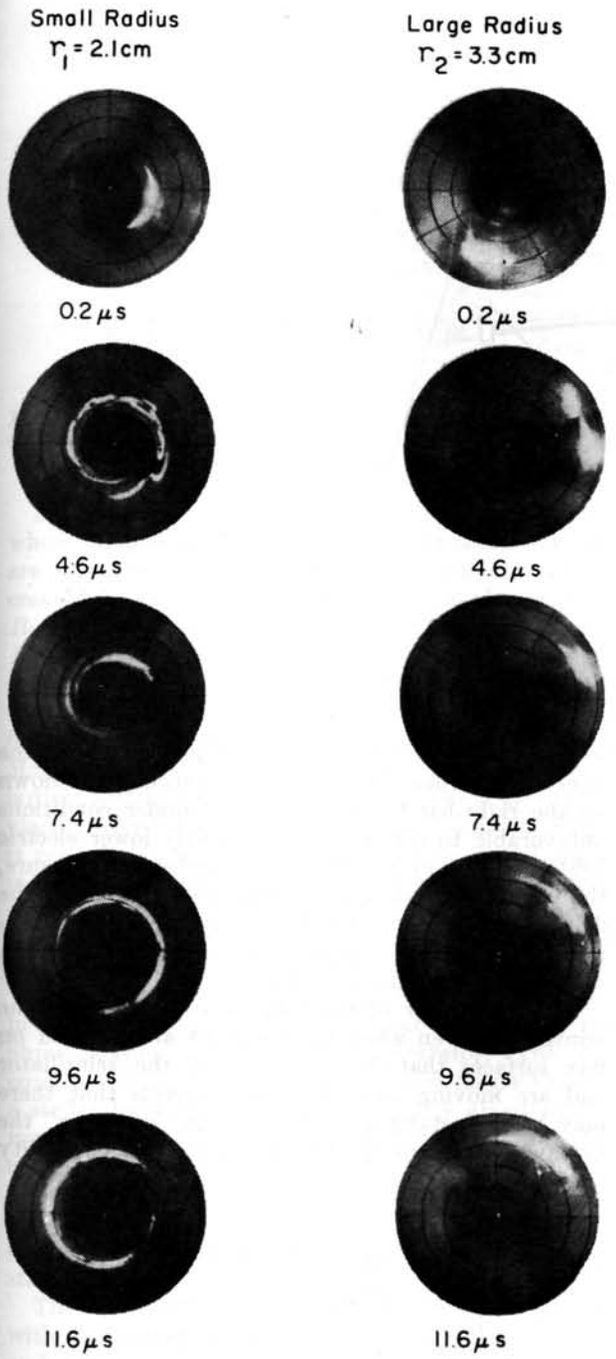

Fig. 10 Electron-beam traces for passage at small and large radii in the pinch of Fig. 9.

The copper shell has electrically insulated toroidal and poloidal slits, to permit rapid change of both orthogonal magnetic-field components. Surrounding the copper vacuum shell (which also acts as a flux concentrator) are two magnetic field coils for generating B_z- and B_θ-field components. The minimum rise time of these fields, (50 μs) is limited by liner resistivity, and the maximum pulse duration is limited by the inductive decay time (30 ms) of the external coils and ring core. The 1-megajoule condenser bank can be switched so as to give any desired rise time or composite rise times within this range, resulting in peak magnetic fields of 15 000 to 20 000 G. The ring core is normally supported on rods that are withdrawn from the inner volume in 10 ms immediately prior to the formation of a discharge and are then returned following the discharge so as to support the ring before it has fallen appreciably from its original position.

10. Operation

More than 500 successful operations of levitation in vacuum with pulsed magnetic fields have been achieved; however, neither the fields (5000 G maximum) nor the vacuum (10^{-6} torr minimum) have yet been optimized. The liner has been baked at 450° C but no "clean" discharge experiments have been performed as yet.

10.1 Experimental Results

The observation of single-particle containment was the objective of the first experiments performed. Paradoxically, the single-particle containment when both B_z and B_θ components are present has proved so effective as to make difficult the achievement of vacuum-field conditions. For the lowest magnetic-field rise times used (3 ms, 0.1 V/cm) and the lowest pressures (10^{-6} torr) the containment is sufficient to "break down" the residual gas and give rise to a major plasma current. Only for substantial initial pressure of air or deuterium (10^{-3} torr) can vacuum-field conditions be achieved for the purpose of carrying out aperture-testing electron-beam experiments.

An electron gun is inserted at the end of a probe, a 40-kV accelerating voltage is applied for 0.2 μs, and a 10-100 mA electron current is injected into the levitron during rising vacuum fields. The scientillator crystal, which is located 90° downstream, registers a prompt signal for helical fields, and a slightly delayed signal for pure B_θ field, where only the inhomogeneous field drift acts to carry the electrons along the torus. If either the gun or the scintillator protrudes less than $^1/_4$ in. beyond the liner, the signal is weakened, which weakening indicates that the magnetic aperture of the levitron is quite satisfactory. (The ring core tends strongly to produce regular and well centered surfaces in spite of any irregularities in the outer windings.)

In the course of these electron-gun experiments, a remarkable phenomenon was discovered. Under certain conditions the scientillator recorded not only the prompt signal at the time of firing of the gun, but also a delayed signal of 10^2-10^3 times greater integrated magnitude, coming 0.1-1 ms after the gun firing.

The interpretation of this phenomenon is evidently that at values of neutral density and electric field just sufficient to keep *thermal* electrons from starting a general avalanche, the injection of energetic electrons will start a limited avalanche consisting of those secondary electrons (produced by electron-neutral

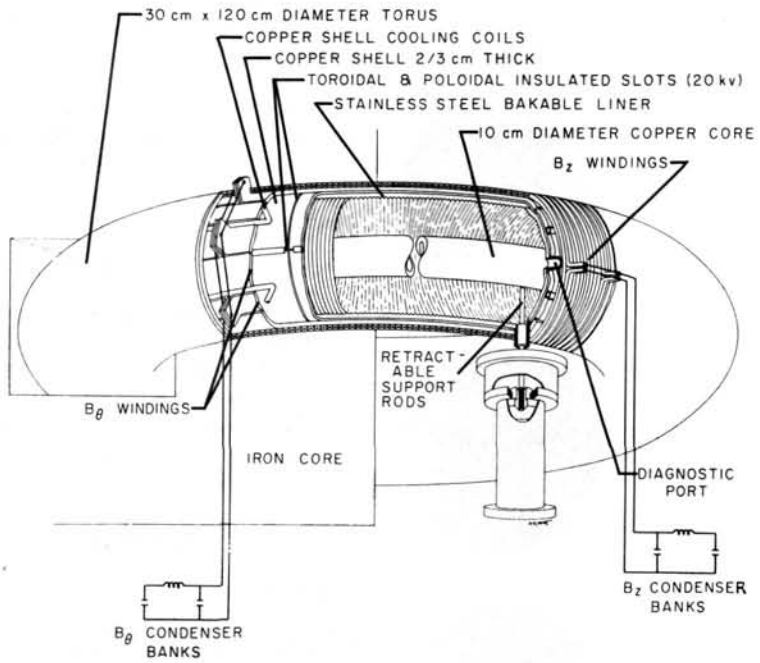

Fig. 11 Hard core is copper ring surrounded by corrugated stainless-steel liner.

collisions) that have sufficient initial energy to run away in the electric field.

The x-ray signals shown at the top of Fig. 12 were obtained for two different timings of the B_θ field relative to the gun firing (which is indicated by an arrow on the trace). In each case there is a very faint x-ray signal at the time of gun firing and a large delayed signal with a delay time inversely related to the E_z field at the time of gun-firing. The total absence of x-ray signals between the initial and delayed spikes is due to the time required for secondary electrons to gain 20 keV (the minimum energy that is detectable) by running away in the electric field. This process is readily calculated to involve about 10^3-10^4 transits around the levitron (depending on E_z), corresponding to a delay of a fraction of a millisecond.

The large initial spike (which is barely visible) and other sharp features of the delayed signal on the left-hand side of Fig. 12 are characteristic of traces obtained under conditions favoring run-away: relatively high electric field and low gas pressure (close to break-down conditions) and high energy of the injected electrons. The broad bell-shaped pulse shown on the right-hand side is obtained under conditions unfavorable to run-away. For slightly lower electric field or energy of injection or for higher gas pressure, the phenomenon disappears altogether. Similarly, the delayed pulse cannot be obtained without the simultaneous presence of appreciable components of both B_z and B_θ, or without levitation.

The appearance of the delayed x-ray signal at the scintillator, even when the electrons are injected on flux surfaces that do not intersect the scintillator and are moving away from it, suggests that there may be an instability mechanism for "dumping" the run-away electrons. Further studies of this possibility are under way.

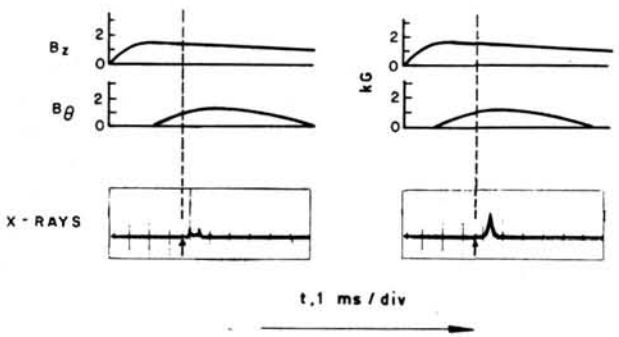

Fig. 12 X-ray signals for different timings of B_θ field relative to gun firing (arrow).

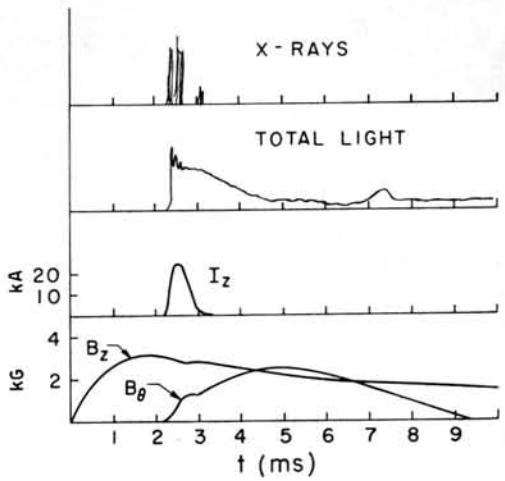

Fig. 13 Large plasma currents occur at low pressures for which breakdown occurs. Both B_θ and B_z must be present.

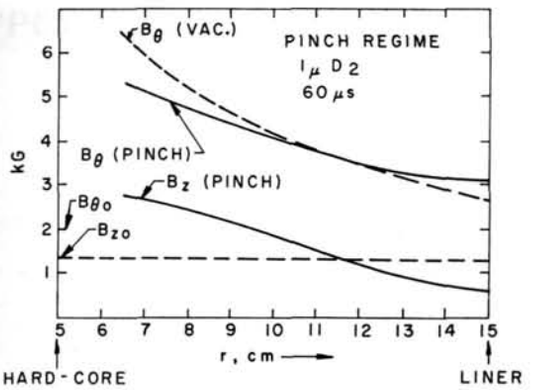

Fig. 14 With fast-rising fields B_z field is compressed toward core and relaxation times are $\sim$100 μs.

At lower pressures (10^{-5} torr residual gas), where breakdown occurs, substantial plasma currents are measured (Fig. 13). The plasma current can be created by a B_θ pinch with an initial B_z or by a B_z pinch with an initial B_θ or by a simultaneous B_z and B_θ pinch, but components of both fields must be present for breakdown to occur. Flux loops show that the plasma current induced by one time-rising field component compresses the orthogonal component. Magnetic probe measurements show that the current is distributed throughout the volume. The approximate plasma resistivity is given by $\varrho = 10^{-3}$ ohm-cm, which is remarkably low considering that the initial gas is mostly air. Without levitation the resistivity increases somewhat, but the effect is not large since an average electron can travel 100 meters before striking a levitator rod.

The parameters of operation and the results obtained in these discharges are quite similar to those for the ohmic-heating cycle in the stellarator. The gas current can, of course, be made much larger than in a stellarator since there is no difficulty about hydromagnetic instabilities, which tend to keep the current in the stellarator below the Kruskal limit. The appearance of x-rays at the beginning and end of the gas current flow appears to correspond to the dumping of energetic electrons by an instability, just as in the stellarator.

The levitron has also been used to make pinches with fast-rising fields. For this purpose initial B_z and B_θ fields are set up, and a B_θ field of 50-μs rise-time ($\sim$3 kG at the liner) is then applied. At pressures of about 0.001 torr deuterium, quite satisfactory pinches are obtained without preionization. The B_z field is compressed towards the core with resultant departures of about 50% from the vacuum-field distribution and relaxation times of about 100 μs (Fig. 14). The magnetic-probe traces are smooth and substantially reproducible—in marked contrast with traces obtained for configurations of this kind in linear, hard-core pinch experiments. This finding suggests that the presence of electrodes in linear-pinch experiments contributes to the erratic behavior of the magnetic-field distribution.

At lower initial pressures, the fast rising B_θ does not couple as well to the plasma (as determined from the light output) or to the B_z field (as determined from magnetic probes). Large x-ray bursts are observed during the rise of the fast B_θ. At low pressures, part of these x-rays are above 100 keV, and can be detected at some distance outside the levitron. At pressures of about 0.001 torr, where good coupling is obtained, the hard-x-ray component disappears.

The difference in breakdown behavior for the stellarator regime (better coupling at low pressure) and the conventional pinch regime (better coupling at high pressure) is probably related to the dumping phenomenon previously discussed. At the very high electric fields of the pinch regime it is not the collisional mean free path but the mean path before dumping that appears to limit the motion of the conduction electrons. The ability of the levitron to operate continously in the range between the stellarator and the pinch regime will permit us to investigate this point more closely.

The work reported here was performed under the auspices of the U.S. Atomic Energy Commission.

References

[1] Anderson, O. A., Baker, W. R., Colgate, S. A., Ise, J., Jr., Pyle, R. V., *Phys. Rev.* **110** (1958) 1375.
[2] Colgate, S. A., Ferguson, J. P., Furth, H. P., in Proc. 2nd. U. N. Intern. Conf. PUAE **32**, United Nations, Geneva (1958) 129.
[3] Burkhardt, L. C., Lovberg, R. H., in proceedings of Ref. 2, **32**, 29.
[4] Birdsall, D. H., Colgate, S. A., Furth, H. P., in Proc. 4th Intern. Conf. Ionization Phenomena in Gases (Uppsala, 17-21 Aug. 1959) **2**, North Holland Publishing Co., Amsterdam (1960) 888, 892.
[5] Colgate, S. A., Furth, H. P., *Phys. Fluids* **3** (1960) 982.

ТУРБУЛЕНТНЫЙ РАЗРЯД В ПРОДОЛЬНОМ МАГНИТНОМ ПОЛЕ*

Б. Б. КАДОМЦЕВ

АКАДЕМИЯ НАУК СССР

МОСКВА, СОЮЗ СОВЕТСКИХ СОЦИАЛИСТИЧЕСКИХ РЕСПУБЛИК

Настоящий доклад посвящен рассмотрению турбулентной конвекции плазмы в газовом разряде с умеренным продольным полем.

Показано, что при нарушении условия устойчивости Сайдема в плазме возникает конвекционное движение, состоящее в выталкивании трубок с более горячей плазмой на стенку. Конвекционный перенос тепла поперек магнитного поля приводит к снижению давления плазмы до нескольких процентов от давления магнитного поля, так что конфигурация магнитного поля становится практически бессиловой. Распределение продольного и азимутального магнитных полей в такой конфигурации может быть приближенно получено из условия обращения в нуль поперечной проводимости. Это распределение определяется единственным параметром $y=4\pi\sigma Ea/H_0$, где a — радиус кожуха, σ — продольная проводимость, E — продольное электрическое поле, H_0 — продольное магнитное поле на оси разряда. Если параметр y превышает некоторое критическое значение, то разряд теряет цилиндрическую симметрию и становится винтовым. С учетом нелинейности и конечной проводимости найдены шаг и амплитуда винтового искривления разряда при небольшом превышении y над критическим значением.

Далее в работе сравнительно подробно рассматривается механизм турбулентного переноса энергии и перемешивания полей, и в частности, обсуждается вопрос о возникновении обратного продольного поля на периферии разряда.

В заключение кратко рассмотрен вопрос о том, как возникает и видоизменяется турбулентная конвекция плазмы по мере увеличения продольного тока в интервале экспериментальных условий от положительного столба тлеющего разряда до сильноточного разряда с умеренным продольным полем.

1. Введение

Разряд с умеренным продольным полем, рассмотрению которого посвящен настоящий доклад, был использован для исследования высокотемпературной плазмы сначала в установке «Зета» [1, 2], а затем в целом ряде аналогичных установок [3—5]. Такой разряд обнаруживает целый ряд особенностей, которые нельзя объяснить в рамках ламинарной теории, исходящей из предположения об аксиальной симметрии движения плазмы. К таким особенностям относится, прежде всего, наличие сильного «парамагнетизма»: при достаточно сильном продольном токе все продольное магнитное поле оказывается сосредоточенным внутри шнура с током, а при дальнейшем увеличении тока магнитный поток внутри шнура дополнительно возрастает одновременно с возникновением снаружи от шнура магнитного поля в обратном направлении.

При этом разряд оказывается практически квазистационарным: вторая четверть периода в точности воспроизводит первую в обратном порядке [2, 5]. Следовательно, сжатие продольного поля к оси нельзя объяснить эффектом скинового захвата поля. Так как давление плазмы в таком разряде значительно меньше давления магнитного поля, то можно предположить [6], что вся энергия уносится излучением, и вследствие гажения стенок создается непрерывный поток плазмы к оси разряда. Однако такое объяснение находится в прямом противоречии с экспериментально наблюдаемым переносом энергии на стенки самой плазмой и связанными с этим переносом довольно сильными колебаниями магнитного поля с частотой $\sim 10^4$—10^5 Hz. Поэтому такой разряд фактически является турбулентным с развитыми пульсациями различных масштабов.

Поскольку плазма в магнитном поле часто бывает неустойчива по отношению к самым различным типам возмущений, то при изучении тех последствий, к которым эти неустойчивости приводят, разумно пользоваться упрощенными моделями, в которых предполагается наличие только одного из видов колебаний. В настоящей работе рассматривается одна из таких моделей, в которой учитывается только локальная конвективная неустойчивость, исследованная в линейном приближении Сайдемом [7]. Можно думать, что этот механизм будет преобладающим в достаточно плотной и хорошо проводящей плазме.

В пар. 2 показано, что возникающая вследствие этой неустойчивости конвекция естественно приводит к бессиловой конфигурации магнитного поля, хорошо согласующейся с наблюдаемой на опыте. В пар. 3 исследуется извивание токового шнура, которое возникает при увеличении продольного тока. В пар. 4 качественно обсуждается механизм турбулентного переноса энергии.

В настоящей работе мы ограничиваемся рассмотрением только квазистационарного разряда, в котором внешнее электрическое поле считается постоянным.

---

* Доклад CN-10/227, представленный на Конференцию. Докладчик: Б. Б. Кадомцев. Дискуссия (на английском языке) по этому докладу дана на стр. 1020. Переводы аннотаций находятся в конце тома.

2. Приближение продольной проводимости

Как показал Сайдем [7], для устойчивости шнура с распределенным током необходимо, чтобы было выполнено условие

$$-8\pi p' < \frac{H_z^2 r}{4}\left(\frac{\mu'}{\mu}\right)^2 \qquad (1)$$

где $\mu = H_\theta / r H_z$ — величина, характеризующая шаг силовых линий, H_z — продольное, H_θ — азимутальное магнитные поля, а штрих обозначает производную по радиусу r. Если это условие не выполнено, то в плазме начнет развиваться конвекционное движение, состоящее в выталкивании к периферии разряда магнитных трубок с более горячей плазмой. Время развития такого движения довольно мало: оно порядка времени пролета ионов с тепловой скоростью v_i поперек шнура, т.е. порядка $t_i = a/v_i$, где a — радиус камеры. При достаточно высокой проводимости σ это время может оказаться значительно меньше скинового $t_s = \pi\sigma a^2/c^2$, которое характеризует скорость нагрева плазмы за счет джоулева тепла. В этом случае возникающий за счет неустойчивости конвекционный перенос тепла на стенки может значительно превосходить энерговыделение за счет джоулевых потерь. Поэтому любой избыток давления над устойчивым будет немедленно «сброшен» на стенки, и давление плазмы будет целиком определяться условием устойчивости (1), в котором знак $<$ следует заменить на знак $=$.

С другой стороны, давление плазмы связано с распределением магнитного поля по радиусу условием равновесия:

$$\nabla p = \frac{\mathbf{j}\times\mathbf{H}}{c} \qquad (2)$$

Так как условие (1) содержит в правой части малый множитель, то мы можем воспользоваться разложением по малому параметру, полагая в первом приближении $p = 0$, $\mathbf{j}\times\mathbf{H} = 0$. Это означает, что приближенно магнитное поле считается бессиловым.

Чтобы найти распределение магнитного поля по радиусу, следует воспользоваться законом Ома, который мы запишем в виде

$$\frac{\mathbf{j}}{\sigma} = \frac{\mathbf{v}\times\mathbf{H}}{c} + \mathbf{E} \qquad (3)$$

пренебрегая градиентом давления и анизотропией проводимости. Ради простоты будем, кроме того, считать проводимость σ постоянной по сечению разряда.

Строго говоря, при наличии хаотического турбулентного движения все величины в (2), (3), как то: магнитное и электрическое поля, скорость плазмы и ее давление, следует считать случайными величинами, и для определения усредненных величин нужно построить цепочку усредненных уравнений. Однако в рассматриваемом здесь случае хорошо проводящей плазмы можно произвести некоторые упрощения. Поскольку локальная конвективная неустойчивость связана с такой перестановкой соседних силовых трубок, при которой искажение магнитного поля минимально, то в приближении $p \sim 0$ следует пренебречь и флуктуациями магнитного поля, так что в уравнениях (2), (3) под $\mathbf{H}$ можно подразумевать среднее поле.

В этом приближении уравнение (3) является линейным относительно флуктуирующих величин, поэтому при усреднении оно не изменяет своего вида, и под входящими в (3) величинами можно понимать их средние значения (следует однако иметь в виду, что входящая в уравнение (3) средняя скорость $\mathbf{v}$ не совпадает с гидродинамической скоростью плазмы, определяющей перенос вещества).

Умножая (3) на $\mathbf{H}$ и учитывая, что в бессиловом поле ток направлен по силовым линиям, получим:

$$\operatorname{rot}\mathbf{H} = \frac{4\pi\mathbf{j}}{c} = \frac{4\pi\sigma}{c}\frac{\mathbf{E}\cdot\mathbf{H}}{H^2} \qquad (4)$$

Формально это уравнение совпадает с уравнением равновесия анизотропно проводящей плазмы [8], у которой проводимость $\sigma_\perp$ поперек магнитного поля равна нулю. Поэтому такой приближенный метод рассмотрения равновесия шнура с током мы будем называть приближением продольной проводимости. Следует однако подчеркнуть, что условие $\sigma_\perp = 0$ ни в коей мере не относится к «истинной» проводимости плазмы, связанной с «микроскопическим» взаимодействием электронов и ионов: в рамках используемого здесь гидродинамического подхода мы считаем эту проводимость заданной и никак не связанной с интенсивностью турбулентных пульсаций. Приближение $\sigma_\perp = 0$ означает лишь, что в плазме возникает такое движение, что первый член в правой части уравнения (3) в точности компенсирует поперечную компоненту электрического поля и приводит к исчезновению градиента давления.

Для прямого шнура с цилиндрической симметрией удобно ввести безразмерные величины: $H_z = H_0 v(x)$, $H_\theta = H_0 u(x)$, $x = 4\pi\sigma E_0 r/H_0$, где $E_0 = \text{const}$ — продольное электрическое поле, H_0 — магнитное поле на оси шнура. Для такого шнура векторное уравнение (4) можно записать в виде двух скалярных, которые в безразмерных переменных имеют вид:

$$\frac{1}{x}\frac{\mathrm{d}}{\mathrm{d}x}(xu) = \frac{v^2}{v^2+u^2} \qquad (5)$$

$$\frac{\mathrm{d}v}{\mathrm{d}x} = -\frac{uv}{v^2+u^2} \qquad (6)$$

Результат численного интегрирования этих уравнений при начальных условиях $u(0) = 0$, $v(0) = 1$ представлен на рис. 1. На этом же рисунке приведено распределение давления плазмы, вычисленное из условия устойчивости (1). Как мы видим, при данном распределении магнитного поля давление устойчиво удерживаемой плазмы не превосходит 4% от давления магнитного поля, что свидетельствует о хорошей точности приближения продольной проводимости.

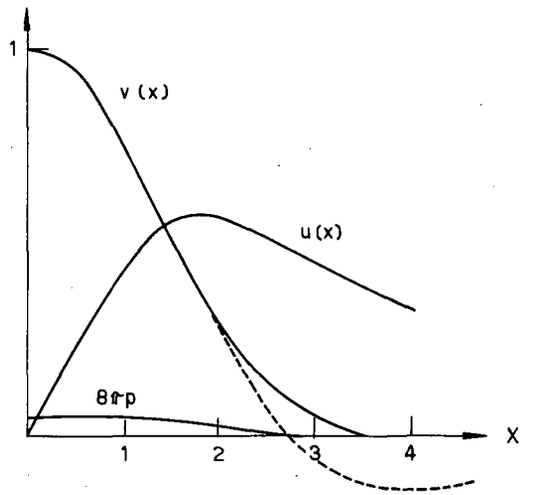

Рис. 1 Распределение магнитного поля и давления плазмы по радиусу в разряде с умеренным продольным полем.

Приведенное на рис. 1 распределение магнитного поля очень хорошо согласуется с экспериментально измеренным. Оно характеризуется единственным параметром $y=4\pi\sigma E_0 a/H_0$, представляющим собой безразмерный радиус кожуха. Увеличение y соответствует перемещению положения кожуха на рис. 1 в сторону больших x, т.е. концентрации тока к оси разряда. Согласно рис. 1 плотность тока убывает с удалением от оси разряда, так что основная часть тока ($\sim 85\%$) протекает в области $x<2$. Это означает, что при $y>2$ токовый шнур практически отрывается от стенок, и его радиус перестает зависеть от радиуса камеры a.

Вместо параметра y удобно ввести другой параметр $\eta=4\pi I a/\varphi c$, который выражается непосредственно через измеряемые на опыте величины — полный ток I и продольный магнитный поток φ, заключенный внутри токового шнура. Ток I определяется соотношением $I=c\,a\,H_0\,u(y)/2$, а магнитный поток равен

$$\varphi=\frac{H_0 a^2}{y^2}\int_0^y 2\pi x v\,\mathrm{d}x$$

Численный расчет показывает, что величина y/η является медленно меняющейся функцией y: $y/\eta=1$ при $y<2$, $y/\eta=1{,}2$ при $y>4$, а в интервале $2<y<4$ y/η изменяется с y приблизительно линейно. Таким образом, с точностью до 20% можно положить

$$y\equiv\frac{4\pi\sigma E_0 a}{H_0}\approx\eta\equiv\frac{4\pi I a}{\varphi c} \tag{7}$$

Таким образом, зная только полный ток I и продольный поток φ, по формуле (7) можно определить безразмерный радиус кожуха y, поле на оси разряда

$$H_0=\frac{2I}{cau(y)} \tag{8}$$

а следовательно, и полное распределение полей.

Если положить $\varphi=\varphi_0=\pi a^2 H_{z0}$, где H_{z0} — продольное магнитное поле перед началом разряда, то такой расчет приводит к хорошему согласию с данными экспериментальных измерений, но только для значений параметра $\eta<3$. При дальнейшем же увеличении тока и параметра $\eta_0=4\pi I a/\varphi_0 c$ величина $\eta=4\pi I a/\varphi c$ остается практически постоянной, так что магнитный поток внутри шнура φ линейно возрастает с током. При этом снаружи от шнура появляется продольное магнитное поле в обратном направлении. Это обстоятельство было отмечено в работе Лиза и Разбриджа [9], в которой было произведено сопоставление экспериментальных данных относительно распределения магнитного поля по радиусу с бессиловой моделью. Качественное обсуждение того, почему параметр η замораживается на значении $\eta\approx 3$, будет дано в пар. 4.

3. Винтовой разряд

Как известно [10, 11], токовый шнур, достаточно тонкий по сравнению с диаметром проводящего кожуха, неустойчив по отношению к извиванию. Поэтому естественно возникает мысль, что рассмотренный в пар. 2 бессиловой цилиндрически симметричный разряд существует только при достаточно большом продольном поле. Если же $\eta_0=4\pi I a/\varphi_0 c$ превысит некоторое критическое значение, то шнур с током потеряет устойчивость и превратится в винтовой. Чтобы убедиться в этом, необходимо, во-первых, определить условие устойчивости шнура по отношению к извиванию, а во-вторых, показать, что винтовой разряд может существовать стационарно.

Как известно [12], векторное уравнение равновесия (2) при винтовой симметрии приводится к одному единственному уравнению

$$\Delta^*\psi+4\pi\frac{\mathrm{d}p}{\mathrm{d}\psi}+\frac{I}{k^2r^2+m^2}\frac{\mathrm{d}I}{\mathrm{d}\psi}+\frac{2kmI}{(k^2r^2+m^2)^2}=0 \tag{9}$$

где

$$\Delta^*=\frac{1}{r^2}\frac{\partial^2}{\partial\zeta^2}+\frac{1}{r}\frac{\partial}{\partial r}\left(\frac{r}{k^2r^2+m^2}\frac{\partial}{\partial r}\right)$$

$\zeta=kz-m\vartheta$, ϑ — азимутальный угол, $k=2\pi/\lambda$, λ — период изменения p и $\mathbf{H}$ вдоль оси z. Функция ψ, являющаяся вместе с p и I постоянной на магнитных поверхностях, представляет собой комбинацию $\psi=m\psi_\vartheta-k\psi_z$ из продольного

$$\psi_z=\frac{1}{2\pi}\int_0^{2\pi}\int_0^{r(\psi)}H_z\,r\,\mathrm{d}r\,\mathrm{d}\vartheta$$

и азимутального

$$\psi_\vartheta=\frac{1}{\lambda}\int_0^{\lambda}\int_0^{r(\psi)}H_\vartheta\,\mathrm{d}r\,\mathrm{d}z$$

магнитных потоков, I — аналогичная комбинация из азимутального и продольного токов внутри заданной магнитной поверхности.

Компоненты магнитного поля при винтовой симметрии полностью определяются через ψ и $I(\psi)$:

$$H_r = \frac{1}{r}\frac{\partial \psi}{\partial \zeta}$$

$$H_\vartheta = \frac{1}{k^2r^2+m^2}\left(m\frac{\partial \psi}{\partial r} + krI\right)$$

$$H_z = \frac{1}{k^2r^2+m^2}\left(-kr\frac{\partial \psi}{\partial r} + mI\right) \qquad (10)$$

Если амплитуда винтового искривления мала, то уравнение (9) можно попытаться решать методом разложения по малому параметру, причем естественно ограничиться случаем $m=1$.

В нулевом приближении имеем: $\psi=\psi_0(x)$, $I=I_0(x)$, причем $\mathrm{d}\psi_0/\mathrm{d}x = H_0(u-kxv)$, $I=H_0(v+kxu)$. Полагая в уравнении (9) $\psi=\psi_0(x)+\psi_1(x)\cos\zeta$, $I=I_0(\psi)=I_0(x)+\psi_1\cos\zeta\,\mathrm{d}I_0/\mathrm{d}\psi_0$, и ограничиваясь только членами первого порядка малости, получим в пренебрежении давлением плазмы следующее уравнение для ψ_1:

$$\frac{\mathrm{d}^2\psi_1}{\mathrm{d}x^2} + p\frac{\mathrm{d}\psi_1}{\mathrm{d}x} + Q\psi_1 = 0$$

где

$$p = \frac{1-k^2x^2}{1+k^2x^2}$$

$$Q = -k^2 - \frac{1}{x^2} + \frac{(v^2-u^2)}{(v^2+u^2)^2} - \frac{2kv}{(u^2+v^2)(1+k^2x^2)} - \frac{2uv^2}{x(u^2+v^2)^2} + \frac{u(1-2kv)}{(u-kxv)(u^2+v^2)} \qquad (11)$$

Заметим, что если ввести смещение ξ магнитной поверхности в радиальном направлении, то возмущения ψ_1, I_1 можно выразить через ξ: $\psi_1 = -\xi\,\mathrm{d}\psi_0/\mathrm{d}x$, $I_1 = -\xi\,\mathrm{d}I_0/\mathrm{d}x$, и после такой замены уравнение (11) в точности совпадает с уравнением, определяющим границу устойчивости шнура с распределенным током (см. например, [7]).

Решая уравнение (11) для различных значений k при начальном условии $\psi_1(0)=0$, $\psi_1'(0)=1$, можно определить то значение $x=y_c$, где ψ_1 второй раз обращается в нуль. Эта точка определяет положение проводящего кожуха, при котором шнур нейтрально устойчив по отношению к извиванию.

При решении уравнения (11) следует учесть, что оно имеет особенность в точке $x=x_s$, где $u-kxv=0$, т.е. шаг возмущения совпадает с шагом невозмущенных силовых линий. В этой точке $\mathrm{d}\psi_0/\mathrm{d}x = H_0(u-kxv)$ также обращается в нуль. Поэтому при бесконечной проводимости, когда смещение магнитной поверхности ξ совпадает с реальным смещением вещества и поэтому не может иметь особенностей, $\psi_1 = -\xi\,\mathrm{d}\psi_0/\mathrm{d}x$ в этой точке должно обращаться в нуль.

Это значит, что по отношению к колебаниям, происходящим с инерционными временами, цилиндр $x=x_s$ при хорошей проводимости сам играет роль кожуха, разбивающего шнур на две не связанные между собой области $x<x_s$ и $x>x_s$, причем в самой точке x_s $\psi_1=0$ (см. например, [13]).

При конечной проводимости магнитные поверхности могут перемещаться относительно вещества, и поэтому на ее смещение ξ никаких ограничений не накладывается, в соответствии с чем $\psi_1 = -\xi\,\mathrm{d}\psi_0/\mathrm{d}x$ в точке $x=x_s$ может быть произвольной, и единственным граничным условием является $\psi_1(0)=0$.

При таком граничном условии уравнение (11) было решено численно для нескольких значений k. Найденные отсюда значения y_c, соответствующие положению проводящего кожуха, приведены в табл. 1. Интерполированием находим, что минимальное значение $y_c \approx 2{,}8$ достигается примерно при $k=0{,}7$, и что для возмущения с $k=0{,}5$, шаг которого равен максимальному шагу силовых линий, $y_c \approx 3{,}4$.

ТАБЛИЦА I

k	0,3	0,4	0,45	0,62	0,85
$y_c(k)$	5,11	4,13	3,72	2,86	3,27

Таким образом, если параметры разряда таковы, что безразмерный радиус кожуха y становится больше 2,8, то шнур оказывается неустойчивым по отношению к извиванию. Если $2{,}8<y<3{,}4$, то к неустойчивости приводят лишь такие возмущения, у которых шаг оказывается меньше шага невозмущенных силовых линий около оси разряда, т.е. шаг возмущения совпадает с шагом силовых линий в некоторой точке $x=x_s$. В этом случае возмущение имеет особенность в точке x_s.

Задача о скорости нарастания таких возмущений представляет значительные трудности, а сам интервал значений Δy, в котором эта задача представляет интерес, является сравнительно малым ($\Delta y/y \approx 0{,}2$), поэтому мы откажемся от ее строгого решения. Так как возмущениям с $\psi_1(x_s)=0$ соответствуют гораздо большие значения y_c, то можно думать, что время нарастания возмущений с особенностью должно быть порядка скинового.

Такие возмущения имеют локальный характер: амплитуда возмущения поля имеет в точке x_s резкий максимум (в линейном приближении она даже обращается в бесконечность) и быстро спадает в обе стороны от этой точки. Именно такого типа возмущения были обнаружены на установке Скептр [14] в режиме, соответствующем примерно $y \approx \eta_0 = 4$.

При $y>3{,}4$ извивание шнура может происходить со скоростью порядка альфвеновской, причем шаг такого инерционного извивания больше максимального шага силовых линий (т.е. волновое число $k<0{,}5$).

Если продольное электрическое поле E_0 не намного превосходит критическое значение $E_c = H_0 y_c/4\pi\sigma a$, то нарастание амплитуды винтового извивания довольно быстро прекратится за счет нелинейных эффектов, и установившуюся амплитуду можно найти по теории возмущений, учитывая только квадратичные члены (квазилинейное приближение). Такой расчет, детали которого изложены в Приложении, был проведен для $k=0{,}4$ и

$k=0{,}45$. Как показывает расчет, при увеличении продольного электрического поля выше критического значения E_c амплитуда извивания A растет пропорционально $[(E_0/E_c)-1]^{1/2}$: для $k=0{,}4$ $A=0{,}18$ $[(E_0/E_c)-1]^{1/2}$, для $k=0{,}45$ $A=0{,}09$ $[(E_0/E_c)-1]^{1/2}$.

Отсюда видно, что даже при довольно большом превышении E_0 над критическим значением E_c амплитуда извивания оказывается все еще малой. Тем не менее, такое извивание оказывает сильное влияние на распределение средних полей. При малой амплитуде винтового искривления среднее поле опять оказывается бессиловым и близко соответствует профилю рис. 1. для цилиндрически симметричного шнура. Это распределение снова можно характеризовать единственным параметром $\eta=4\pi\, a\, I/\varphi c$. Оказывается, что при $E_0>E_c$ параметр η не только перестает возрастать с E_0, но и начинает даже несколько уменьшаться: для $k=0{,}4$ $\eta/\eta_c\approx 1{,}3-0{,}3\, E_0/E_c$, для $k=0{,}45$ $\eta/\eta_c=1{,}1-0{,}1\, E_0/E_c$.

Таким образом, согласно этим расчетам при увеличении E_0 выше критического значения ток в шнуре должен практически замораживаться на уровне критического $I_c=c\,\varphi\,\eta_c/4\pi.a$, что можно интерпретировать как результат уменьшения эффективной проводимости шнура за счет его извивания (напомним, что проводимость поперек магнитного поля в бессиловой модели равна нулю). Следовательно, в приближении продольной проводимости увеличение $E_0>E_c$ должно просто увеличивать амплитуду винтового искривления при постоянном полном токе I.

Как показывает анализ, проведенный в работе [9], на эксперименте действительно наблюдается «замораживание» параметра η на значении $\eta\approx 3$, так что при дальнейшем увеличении E_0 радиус токового шнура остается практически постоянным. Однако при этом ток I продолжает возрастать за счет увеличения магнитного потока φ внутри шнура и появления снаружи от шнура обратного потока.

Винтовой разряд с большой амплитудой извивания наблюдался СОЙЕРОМ и др. [15] на установке Колумбус, разрядная камера которой представляла собой прямую металлическую трубу радиуса $a=8$ см. При начальном магнитном поле $H_{z0}=100$ гс и токе $I=10$ ка, что соответствует значению параметра $\eta_0=5$, наблюдалось извивание токового шнура с шагом $\lambda\approx 2a$, т.е. $ky=3$.

Обнаруженное этими авторами сравнительно медленное вращение токового шнура побудило их сделать предположение, что извивание разряда представляет собой бегущую альфвеновскую волну. Однако эта гипотеза оказалась ошибочной, что видно из приведенных в этой же работе оценок, показывающих, что вращение шнура является практически безинерционным. Кроме того, как это было отмечено в заметке [16], альфвеновская волна при той низкой проводимости, какую имела плазма в установке Колумбус, затухла бы за один период колебаний. Следовательно, винтовой разряд в Колумбусе является квазистационарным, а

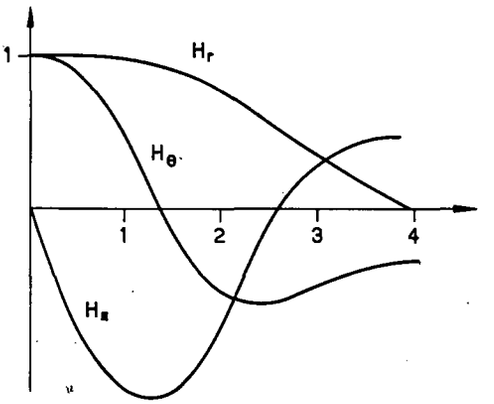

Рис. 2 Магнитное поле в винтовом разряде.

его вращение связано с медленными диффузионными процессами. Как мы видим, довольно большое числовое значение параметра η_0 как раз соответствует наличию заметного извивания шнура, а длина волны оказывается того же порядка, что и полученная из рассмотрения неустойчивости.

На рис. 2 приведено распределение магнитного поля, возникающего вследствие извивания шнура, для значения $k=0{,}4$. Чтобы получить полное распределение поля в пространстве, представленые на этом рисунке H_z и H_θ следует умножить на $A\cos(\vartheta-kz)$, H_z — на $A\sin(\vartheta-kz)$, где A — амплитуда извивания, и сложить со средним полем рис. 1. К сожалению, в работе [15] приведены лишь данные о распределении тока и поэтому прямое сравнение распределения рис. 2 с экспериментальным провести нельзя.

4. Турбулентная конвекция плазмы

Рассмотрим теперь более подробно сам механизм конвекционного переноса энергии на стенки. Мы ограничимся здесь лишь случаем достаточно хорошей проводимости, когда скиновое время значительно больше инерционного. При этом давление плазмы относительно быстро выравнивается вдоль силовых линий, и поэтому перенос плазмы на стенку должен быть связан с искривлением силовых линий. Его можно представить себе в виде «вышячивания» отдельных силовых трубок

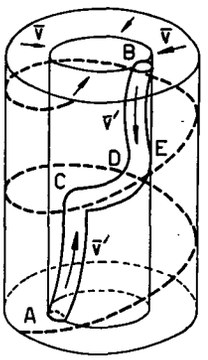

Рис. 3 Искривление силовой трубки с плазмой вследствие конвективной неустойчивости.

(рис. 3). Так как при любом искривлении силовых трубок энергия магнитного поля несколько увеличивается, то к неустойчивости в первую очередь будут приводить такие возмущения, которые минимально искажают силовые линии. Искажение поля минимально, когда смещенная трубка ADB имеет форму одного витка такой винтовой линии, чтобы ее наиболее выдвинувшийся участок CDE совпадал по направлению с невозмущенным магнитным полем в той точке, куда он сместился.

При достаточно большом искривлении трубка соприкоснется со стенкой в точке D. Поскольку тепловая скорость электронов много больше ионной, то трубка с плазмой сразу же приобретает потенциал относительно стенки порядка нескольких электронных температур, так чтобы скорость утечки на стенку ионов и электронов была одинаковой. При достаточно большой температуре электронов эта разность потенциалов может привести к зажиганию униполярной дуги [17] и быстрому охлаждению электронов.

Наряду с этим из плазмы начнут уходить быстрые ионы, т.е. вся плазма как по каналу начнет вытекать на стенку вдоль искривленных силовых линий, и давление плазмы в этой трубке начнет быстро уменьшаться. Вследствие этого все остальные участки плазмы будут немного сжиматься к оси (см. рис. 3). Как только давление в трубке ADB станет меньше давления окружающей ее плазмы, то она будет вытеснена внутрь разряда другими более горячими трубками, стремящимися выйти к стенке. При этом трубка ADB захватит с собой часть газа со стенки, который затем нагреется, и весь процесс повторится снова.

Таким образом, движение плазмы можно разложить на две составляющие: более или менее равномерное сжатие к оси со скоростью $\mathbf{v}$ и пульсационный выброс плазмы на стенку по «каналам», образованным искривленными силовыми линиями. Именно скорость $\mathbf{v}$ и приводит к компенсации поперечной составляющей электрического поля в законе Ома (3).

При наличии пульсационного движения скорость $\mathbf{v}$ не совпадает с гидродинамической скоростью движения плазмы $\mathbf{v}_0$, которая определяет поток вещества $\mathbf{j}_n=n\mathbf{v}_0$. А именно, $\mathbf{j}_n=n\mathbf{v}+\langle n'\mathbf{v}'\rangle$, где второе слагаемое учитывает перенос вещества за счет пульсаций. Таким образом, поток вещества $\mathbf{j}_n$ не связан непосредственно с v и может иметь любой знак в зависимости от того, какие процессы происходят на стенках (т.е. в зависимости от интенсивности гажения стенок).

Итак, картина движения плазмы в разряде с умеренным продольным полем может быть представлена как наложение движения отдельных трубок. При этом для переноса плазмы из центральной области не требуется, чтобы центральные трубки испытывали сильное искривление и непосредственно соприкасались со стенкой. Процесс конвекции может иметь и эстафетный характер: на поверхности искривленной силовой трубки с давлением, превышающим давление окружающей плазмы, в свою очередь могут возникнуть небольшие пульсации и т.д. вплоть до пульсаций настолько малого масштаба, что силовые линии уже не будут вморожены в вещество. В результате соседние трубки получают возможность эффективного обмена плазмой.

При таком движении с пульсациями самых различных масштабов силовые линии в разряде будут иметь очень сложный вид. Пульсации магнитного поля приведут к разрушению магнитных поверхностей, и любая силовая линия рано или поздно выйдет на стенку. В результате электроны получают возможность выходить на стенку вдоль силовых линий, вследствие чего вся плазма должна зарядиться относительно стенки до потенциала в несколько электронных температур. А поскольку давление плазмы спадает к стенкам, то и внутри шнура появится радиальное электрическое поле, направленное наружу. О наличии такого поля можно судить по экспериментально наблюдаемому вращению плазмы.

Произведем теперь некоторые оценки. Пусть l — есть эффективный масштаб конвективных пульсаций. Поскольку обычно разряд бывает окружен лайнером, расположенным на некотором расстоянии от проводящего кожуха, то кожух не оказывает стабилизирующего действия на мелкомасштабные пульсации. Вследствие этого масштаб l не изменяется существенно при приближении к стенке, и приближенно можно положить $l/a=\text{const}$ (по аналогии с турбулентностью затопленных струй можно ожидать $l/a\approx 10^{-1}$).

Пульсацию давления p' можно представить как $p'\approx l\,\mathrm{d}p/\mathrm{d}r\approx lp/a$, а поток энергии на стенки $q=\langle p'v'\rangle\approx \nu p\, l^2/a^2$, где $v'\approx l\nu$ — пульсация скорости, ν — эффективная частота пульсаций. Частота пульсаций ν может быть найдена из условия баланса энергии $2\pi qa=Q_s$, где Q_s — разность между джоулевым теплом и излучением на примесях. Если энергия, уносимая плазмой на стенки, сравнима с энергией излучения на примесях, то приближенно $Q_s\approx\pi a^2 j^2/\sigma\approx c^2 H_\theta^2/4\pi\sigma$, откуда получаем:

$$\nu\approx\frac{c^2}{\pi\sigma l^2}\frac{H_\vartheta^2}{8\pi p} \tag{12}$$

Пульсация скорости v' определяется работой, которая совершается пульсацией градиента избыточного давления $p_1'/a\approx l/a^2\, p_1$, на длине l: $\mu n(v')^2\approx\approx l^2 p_1/a^2$. Отсюда следует: $p_1\approx\mu n(\nu a)^2$. Подставляя сюда вместо ν выражение (12), получим:

$$\left(\frac{p_1}{p}\right)^{1/2}\approx\frac{H_\vartheta^2}{8\pi p}\frac{ac^2}{v_i\pi\sigma l^2}\approx\frac{H_\theta^2 a^2}{8\pi p l^2}\frac{c^2}{\pi\sigma v_i a} \tag{13}$$

где $v_i=(T/\mu)^{1/2}$ — тепловая скорость ионов, μ — их масса.

Отсюда видно, что при очень хорошей проводимости, когда инерционное время $t_i=a/v_i$ значительно меньше скинового $t_s=\pi\sigma a^2/c^2$, избыточное давление p_1 действительно мало. При уменьшении проводимости условие $p_1/p<1$ будет нарушено, и тогда можно считать $p_1\approx p>p_0$. В

этом случае $\nu = v_i/a$, и из соотношения (13) получим:

$$\frac{8\pi p}{H_\phi^2} \approx \left(\frac{a}{l}\right)^2 \frac{c^2}{\pi\sigma v_i a} \qquad (14)$$

Таким образом, если бы в шнуре не было других механизмов раскачки колебаний, то при заданном токе и продольном магнитном поле можно было бы ожидать следующий характер изменения параметров разряда при увеличении плотности частиц n. При малой плотности $p_1 \ll p \approx p_0$, и уменьшение плотности должно было бы приводить к возрастанию температуры и проводимости, а следовательно, к уменьшению частоты пульсаций. При этом распределение полей должно быть бессиловым. Затем должен быть некоторый интервал плотностей, в котором конфигурация полей является еще бессиловой ($p_0 < p < H^2/8\pi$), а частота пульсаций $\nu \approx v_i/a = \text{const}$. При дальнейшем увеличении n температура плазмы должна быстро падать, а ее давление приближаться к давлению магнитного поля.

Хотя в настоящее время и есть намеки на изменение характера разряда при увеличении плотности, (см. [9]), однако для полного выяснения этого вопроса необходимы дополнительные исследования.

В заключение этого параграфа мы обсудим еще вопрос об обратном поле. Как мы уже упоминали выше, при увеличении тока разряда продольное поле снаружи от токового шнура меняет знак. Особенно сильно этот эффект был выражен на Зете [2], где величина обратного поля составляла примерно $^1/_4$ от поля на оси разряда.

Это явление нельзя объяснить ни скиновым захватом поля, ни анизотропией проводимости. Более того, как было показано экспериментально [9], его нельзя объяснить и винтовым искривлением всего шнура как целого. К этому же выводу приводит и теоретическое рассмотрение извивания шнура в квазилинейном приближении: как было отмечено в пар. 2, среднее поле при малом извивании по-прежнему сохраняет вид рис. 1 и не обнаруживает тенденции к изменению знака на периферии разряда.

Качественно эффект генерации обратного поля можно понять на основе механизма турбулентной конвекции. Заметим прежде всего, что в тороидальной камере токовый шнур всегда немного сдвинут в направлении к наружной стенке. Поэтому внутри лайнера, между его внутренней стенкой и токовым шнуром, образуется серповидная область, силовые линии в которой проходят через лайнер. Как правило, именно в этой области и наблюдается появление обратного поля. Так как все процессы переноса вдоль магнитного поля происходят значительно эффективнее, чем поперек, то можно думать, что плазма в этой области является холодной и плохо проводящей. Поэтому, казалось бы, ток в этой области должен отсутствовать, и продольное поле должно быть постоянным.

Но на самом деле это было бы так, если бы длина перемешивания l была ничтожно мала. В турбулентном разряде в область между шнуром и лайнером все время выбрасываются трубки с хорошо проводящей плазмой из внутренних частей разряда. При этом отдельная трубка ADE (рис. 3) искривляется таким образом, что только ее небольшая часть CD оказывается на периферии, а концы остаются внутри разряда. Поэтому даже в том случае, когда периферийная силовая линия CD оказывается наклоненной в обратную сторону, по отношению к E_0, ток по этому участку будет по-прежнему итти в ту же сторону от C к D, так как полная ЭДС, приложенная между A и B, сохраняет свой знак при таком искривлении. Таким образом, за счет этого эффекта ток в области обратного поля должен течь против внешней ЭДС, что и наблюдается в действительности.

Можно сказать, что с учетом конечности l ток в некоторой точке пространства будет определяться не только проводимостью в данной точке, но и проводимостью и направлением магнитного поля в соседних точках, что приближенно можно учесть заменой величины $\sigma E_0 H_z$ в уравнении (6) на $(1/2)\,[\sigma E_0 H_z)_{z+e} + (\sigma E_0 H_z)_{z-e}]$. Отсюда видно, что при конечном l производная $\mathrm{d}H_z/\mathrm{d}z$ может быть отличной от нуля при $H_z = 0$, так что распределение продольного поля должно принять вид, качественно представленный на рис. 1 пунктирной кривой.

В предыдущем параграфе мы установили, что при увеличении E_0 выше критического значения E_c шнур в приближении продольной проводимости теряет осевую симметрию, а параметр y замораживается. Но в приближении продольной проводимости мы искусственно разбиваем движение шнура на пульсационное, с масштабом $l \ll a$, и макроскопическое, описываемое посредством средних величин. В действительности такое разбиение носит чисто условный характер, и можно думать, что при приближении к критическому радиусу масштаб и амплитуда пульсационных движений также возрастают, что облегчает генерацию обратного поля. Как мы уже отмечали, на эксперименте генерация поля имеет место как раз при замороженном значении y.

5. Заключение

Итак, рассмотренная здесь модель турбулентного разряда позволяет дать качественное объяснение многим особенностям разряда в продольном магнитном поле. В частности, она устраняет кажущееся противоречие между парамагнитизмом шнура, который может поддерживаться только за счет движения плазмы к оси разряда, и экспериментально наблюдаемым выбросом горячей плазмы на стенки. (Впрочем, это противоречие может быть устранено и при учете других механизмов конвекции. Для бессиловой модели достаточно лишь, чтобы большая утечка энергии из шнура не была связана с сильными колебаниями магнитного поля.)

В реальном разряде наряду с рассмотренным здесь механизмом конвекции могут присутство-

вать другие, в частности, обусловленные неустойчивостью плазмы с конечной проводимостью. Поэтому для полного выяснения динамики плазмы в турбулентном разряде требуются еще дополнительные исследования, прежде всего экспериментальные.

В заключение приношу глубокую благодарность акад. М. А. Леонтовичу, В. Д. Шафранову и А. И. Карчевскому за обсуждение затронутых здесь вопросов. Численные расчеты были выполнены А. Е. Бажановой, которой автор выражает свою искреннюю признательность.

Приложение

ВИНТОВОЙ ШНУР В КВАЗИЛИНЕЙНОМ ПРИБЛИЖЕНИИ

Пользуясь уравнением (9) и выражениями (10), нетрудно проверить, что в бессиловом поле при винтовой симметрии

$$\operatorname{rot}\mathbf{H}=-\frac{dI}{d\psi}\mathbf{H} \tag{15}$$

Сравнивая это выражение с (4), находим:

$$\frac{dI}{d\psi}=-\frac{4\pi\sigma}{c}\frac{\mathbf{E}\cdot\mathbf{H}}{H^2} \tag{16}$$

Электрическое поле в винтовом шнуре складывается из продольного $\mathbf{E}_0$ и безвихревого поля, возникающего за счет неоднородности магнитного поля, так что $\mathbf{E}=\mathbf{E}_0-\nabla\varphi$. Поставляя это выражение в (16) и учитывая винтовую симметрию, получим:

$$\frac{dI}{d\psi}=-\frac{4\pi\sigma}{cH^2}\left\{E_0H_z+\frac{1}{r}\frac{D(\psi,\varphi)}{D(r,\zeta)}\right\}. \tag{17}$$

Это соотношение можно рассматривать как уравнение для φ. Оно должно удовлетворять условиям разрешимости, которое можно получить, умножая обе части уравнения (17) на rH^2 и усредняя его затем по поверхности $\psi=\text{const}$. Из полученного таким образом условия разрешимости находим:

$$\frac{dI}{d\psi}=-\frac{4\pi\sigma E_0}{c}\frac{\langle rH_z\rangle_{\psi=\text{const}}}{\langle rH^2\rangle_{\psi=\text{const}}}.$$

Подставляя это выражение в (15) и усредняя его затем по ζ, мы получим два уравнения для средних полей $\bar{H}_z$ и $\bar{H}_\theta$:

$$\frac{d\bar{H}_z}{dr}=-\frac{4\pi\sigma E_0}{c}\left\langle\frac{H_\vartheta\langle H_z r\rangle_{\psi=\text{const}}}{\langle H^2 r\rangle_{\psi=\text{const}}}\right\rangle_{r=\text{const}} \tag{18}$$

$$\frac{1}{r}\frac{d}{dr}(r\bar{H}_\vartheta)=\frac{4\pi\sigma E_0}{c}\left\langle\frac{H_z\langle H_z r\rangle_{\psi=\text{const}}}{\langle H^2 r\rangle_{\psi=\text{const}}}\right\rangle_{r=\text{const}}. \tag{19}$$

Допустим, что продольное электрическое поле E_0 немного превышает критическое значение E_c для винтового возмущения с определенным шагом. Введем безразмерный радиус $x=4\pi\sigma E_c/H_0$ и величину $\varepsilon=(E_0/E_c)-1$. При $\varepsilon\ll 1$ среднее поле можно представить в виде:

$$\frac{\bar{H}_\theta}{H_0}=u(x)+\delta(x)$$

$$\frac{\bar{H}_z}{H_0}=v(x)+\gamma(x) \tag{20}$$

где δ, γ — малые величины порядка ε, H_0 — среднее магнитное поле при $x=0$. Если $k<0{,}5$, то шаг силовых линий всюду меньше шага возмущения, и ψ_1 нигде не имеет особенности. В этом случае ψ_1 равномерно непрерывно зависит от ε, и при малых значениях ε можно считать, что от ε зависит только амплитуда A винтового возмущения, а зависимость ψ_1 от радиуса остается неизменной.

Чтобы найти A, следует прежде всего определить δ и γ. Для этого в ур. (18), (19) подставим выражения для средних полей (20) и произведем разложение правых частей (18), (19) по A до второго порядка включительно. При разложении по A следует учесть, что

$$\langle f(r,\zeta)\rangle_{\psi=\text{const}}=\frac{\int f(r,\zeta)\,\delta(\psi-\text{const})\,dr\,d\zeta}{\int\delta(\psi-\text{const})\,dr\,d\zeta}=\frac{\int\frac{f(r(\psi)\,\zeta)}{|\partial\psi/\partial r|}\,d\zeta}{\int\frac{d\zeta}{|\partial\psi/\partial r|}}. \tag{21}$$

Так как это разложение не представляет принципиальных трудностей, но очень громоздко, то мы приведем здесь лишь окончательный результат. Если δ, γ разложить на две части $\delta=A^2\delta_1+\delta_2$, $\gamma=A^2\gamma_1+\gamma_2$, где $\delta_2=\varepsilon x\,du/dx$, $\gamma_2=\varepsilon x\,dv/dx$, то вытекающие из (18), (19) уравнения для δ_1, γ_1 примут вид:

$$\frac{1}{x}\frac{d}{dx}(x\delta_1)+\frac{2uv^2}{(u^2+v^2)^2}\delta_1+\frac{2u^2v}{(u^2+v^2)^2}\gamma_1=fv-g\left(\frac{v}{u^2+v^2}\psi_1{}^2+kx\psi_1\frac{d\psi_1}{dx}\right) \tag{22}$$

$$\frac{d\gamma_1}{dx}+\frac{v(v^2-u^2)}{(u^2+v^2)^2}\delta_1-\frac{u(v^2-u^2)}{(u^2+v^2)^2}\gamma_1=-fu+g\left(\frac{kxv}{u^2+v^2}\psi_1{}^2-\psi_1\frac{d\psi_1}{dx}\right) \tag{23}$$

где

$$f=\frac{1}{2x^2(u^2+v^2)^2}\left\{\frac{kx^2}{1+k^2x^2}\frac{d\psi_1}{dx}+\frac{2x(u-kxv)}{1+k^2x^2}\frac{v}{u^2+v^2}\frac{d\psi_1}{dx}+\psi_1\left[\frac{xv}{(1+k^2x^2)(u^2+v^2)}-\frac{uv(2u-x)}{(u^2+v^2)(u-kxv)}-\frac{2xv^2(v+kxu)}{(u^2+v^2)^2(1+k^2x^2)}\right]\right\}\times\left\{\frac{2x(u-kxv)}{1+k^2x^2}\frac{d\psi_1}{dx}\right.$$

$$+\psi_1\left[\frac{v^2-u^2}{u-kxv}-\frac{2xv(v+kxu)}{(u^2+v^2)(1+k^2x^2)}\right]\Bigg\}$$
$$-\frac{v}{2(u^2+v^2)^2}\left\{\frac{1}{1+k^2x^2}\left(\frac{d\psi_1}{dx}\right)^2+\psi_1^2\left[\frac{1}{x^2}\right.\right.$$
$$\left.\left.+\frac{v}{(u^2+v^2)^2(1+k^2x^2)}\right]\right\}+\frac{v}{2(u^2+v^2)(u-kxv)^2}$$
$$\times\left\{\frac{u(2u-x)}{x^2(u^2+v^2)}\left[\psi_1^2-x\psi_1\frac{d\psi_1}{dx}\right]\right.$$
$$\left.+\frac{x-3u}{x^2(u^2+v^2)}\left[\frac{2u}{x}-\frac{v^2-u^2}{v^2+u^2}\right]\psi_1^2\right\} \quad (24)$$

$$g=\frac{uv}{2(u-kxv)(1+k^2x^2)(u^2+v^2)^2}\left(\frac{2u}{x}-\frac{v^2}{u^2+v^2}\right) \quad (25)$$

Вместо u и v подставим в ур. (11) средние поля $\bar{H}_\theta/H_0$, $\bar{H}_z/H_0$, разложим Q по δ, γ, умножим полученное уравнение на $\psi_1 x\,dx/(1+k^2x^2)$ и проинтегрируем по x. Вследствие самосопряженности ур. (11) и того обстоятельства, что ψ_1 удовлетворяет этому уравнению, мы получим соотношение

$$A^2\int\left[\frac{\partial Q}{\partial u}\delta_1+\frac{\partial Q}{\partial v}\gamma_1\right]\psi_1^2\frac{x\,dx}{1+k^2x^2}$$
$$+\varepsilon\int\left[\frac{\partial Q}{\partial u}\frac{du}{dx}+\frac{\partial Q}{\partial v}\frac{dv}{dx}\right]\frac{\psi_1^2x^2\,dx}{1+k^2x^2}=0 \quad (26)$$

определяющее величину амплитуды A.

Если решение ур. (22), (23) с начальными условиями $\delta_1(0)=\gamma_1(0)=0$ подставить в (26), то получим:

$$A=S\varepsilon^{1/2}=S(k)\left(\frac{E_0}{E_c(k)}-1\right)^{1/2} \quad (27)$$

где S — некоторая функция k. Численный расчет показал, что для $k=0{,}4$ $S=0{,}18$, для $k=0{,}45$ $S=0{,}09$.

То обстоятельство, что $S(k)$ быстро убывает при $k\to 0{,}5$, указывает на плохую точность квазилинейного приближения, когда при извивании появляется особенность у магнитного поля.

Численный расчет показывает, что распределение средних полей H_θ и H_z опять оказывается близким к бессиловому, которое задается значением только одного параметра $\eta=4\pi Ia/\Phi c$. Этот параметр можно определить как

$$\frac{\eta}{\eta_c}=\frac{1+\varepsilon\left(\frac{1}{u}\frac{du}{dx}\right)_{x=x_c}+S^2\varepsilon\left(\frac{\delta_1}{u}\right)_{x=x_c}}{1+\varepsilon\int_0^{x_c}\left(\frac{dv}{dx}+S^2\gamma_1\right)x\,dx\left[\int_0^{x_c}vx\,dx\right]^{-1}} \quad (28)$$

При $\varepsilon\ll 1$ это выражение можно разложить по ε, и подстановка результатов численного интегрирования дает:

$$\frac{\eta}{\eta_c}=1-0{,}3\varepsilon \quad \text{для} \quad k=0{,}4$$

$$\frac{\eta}{\eta_c}=1-0{,}1\varepsilon \quad \text{для} \quad k=0{,}45$$

Отсюда следует, что при $E_0>E_z$ распределение поля по радиусу практически замораживается и соответствует примерно $\eta\approx 3$.

Литература

[1] Thonemann, P. C., et al, *Nature* **4604** (1958) 218.
[2] Butt, E. P., et al, in Proc. 2nd U.N. Inter. Conf. PUAE **32** United Nations, Geneva (1958) 42.
[3] Allibone, T. E., Chick, D. R., Thomson, G. P., in Proc. 2nd U.N. Inter. Conf. PUAE **32** United Nations, Geneva (1958) 169.
[4] Афросимов В. В. и др, *Ж. техн. Физ.* **30** (1960) 1383.
[5] Бабичев А. П. и др, *Ядерный синтез:* Дополнение 1962, Часть 2, 635.
[6] Colgate, S. A., Furth, H., U.S. AEC Report UCRL-S862 (1960).
[7] Suydam, B., in Proc. 2nd U.N. Inter. Conf. PUAE **31** United Nations, Geneva (1958) 157.
[8] Брагинский С. И., Шафранов В. Д., в Физике Плазмы и Проблеме Управляемых Термоядерных Реакций **2** (Леонтович, М. А., ред.) Академия Наук СССР, Институт атомной энергии, Москва (1958) 26.
[9] Lees, D. J., Rusbridge, M. G., in Proc. 4th Inter. Conf. Ionization Phenomena in Gases (Uppsala, 17—21 Aug. 1959) **2**, North Holland Publishing Co. Amsterdam (1960) 954.
[10] Шафранов В. Д., *Ат. Энерг.* **5** (1956) 38.
[11] Tayler, R., *Proc. phys. Soc. (Lond.)* **870** (1957) 1049.
[12] Johnson, J., et al, *Phys. Fluids* **1** (1958) 281.
[13] Newcomb, W. A., *Ann. Phys.* **10** (1960) 232.
[14] Allen, W. L., *Nature* **4734** (1960) 279.
[15] Sawyer, G. A., Scott, P. L., Stratton, T. E., *Phys. Fluids* **2** (1959) 47.
[16] Wilcox, J. M., Boley, F. I., *Phys. Fluids* **3** (1960) 141.
[17] Робсон А. Е., *Радиотехн. Электр.* **4** (1959) 1299.

PINCH STABILITY: THEORY AND EXPERIMENT*

K. AITKEN, R. BICKERTON, R. HARDCASTLE, J. JUKES, P. REYNOLDS, I. SPALDING

ATOMIC ENERGY RESEARCH ESTABLISHMENT

HARWELL, BERKSHIRE, UNITED KINGDOM

Experimental observations on the stability of various linear hard-core and pinch systems are presented. Although theoretically stable on the ideal hydromagnetic approximation the experimental hard core exhibits instabilities similar to those seen in the pinch. The effect of including finite electrical conductivity is considered theoretically in the two limits of large and small conductivity. In both cases the result is to make the hard-core system unstable. The results of the low conductivity approximation are compared with the behaviour of a model hard-core experiment using liquid mercury. The plasma observations are discussed in the light of these extensions to the stability theory.

1. Introduction

A well known result of ideal (non-dissipative) hydromagnetic theory is that the linear hard-core pinch is stable if $B_\theta \, \mathrm{d}(r B_\theta)/\mathrm{d}r \leq 0$ at all radii [1]. This simple, easily satisfied condition is in sharp contrast to the complex criteria for the stabilized pinch [2]. Nevertheless experimental hard-core pinches have displayed instabilities [3, 4] similar to those seen in stabilized pinches [5]. In this paper we present new experimental observations on the nature of these instabilities, discuss the theoretical effect on stability of allowing for finite electrical conductivity in the two limits of very large and very small conductivity, compare the results of the small-conductivity approximation with the behaviour of a model hard-core experiment using liquid mercury and finally discuss the plasma results in the light of these extensions to stability theory.

2. Plasma experiments

The hard-core apparatus is shown in Fig. 1. The current flows down the central rod (in negative direction) and returns through the plasma which forms near the central rod and subsequently expands radially, compressing the initially applied axial magnetic field against the outer (flux conserving) brass cylinder. Under typical operating conditions the tube is filled with hydrogen gas at a pressure of 50 millitorr, the applied axial magnetic field is 2000 G and the discharge current rises to 150 kA in 8 μs. Energy input during the first half cycle amounts to about 10 eV per proton. Before the firing of the main discharge the gas is pre-ionized by an auxiliary damped oscillatory discharge of 10 kA, with a period of 140 μs and a decay time of 1 ms. The symmetry of breakdown of the main discharge, as judged by the magnitude of the azimuthal field (B_θ) at the outer wall (zero for absolute symmetry) is found to be greatest if the firing of the main discharge is delayed until 200 μs after the end of this pre-heating pulse. Figure 2

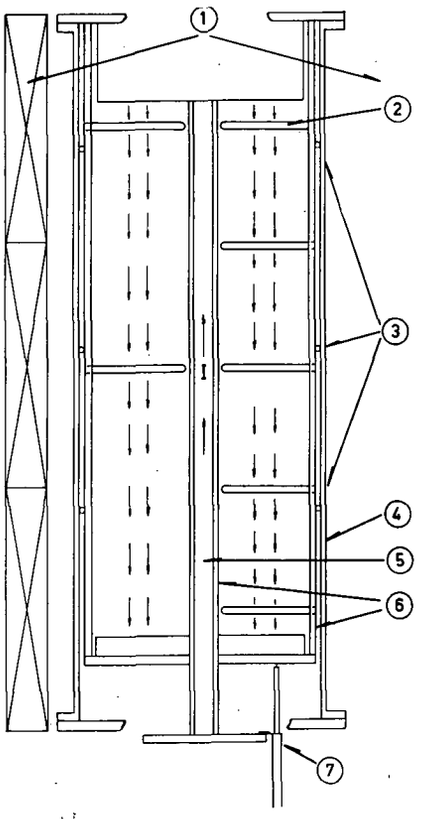

Fig. 1 Hard-core apparatus showing 80-cm tube, 30-cm i. d. 1—B_z coils, 2—quartz probe tubes, 3—12 external B_θ probes, 4—brass flux shield, 5—copper tube, 3.4-cm i. d., 6—silica tubes, 7—cables 3.4-cm i. d.

shows an overlay of magnetic probe measurements of B_θ versus time made at the radius 8.5 cm for ten successive discharges. The traces are reproducible for 3.5 μs after which irreproducible fluttering occurs. In Fig. 3 the radial distributions of azimuthal (B_θ) and axial (B_z) magnetic fields are shown for single discharges, the measurements being made with a multiple magnetic probe. Also shown dashed on the same

* Conference paper CN-10/68, presented by R. Bickerton. Discussion of this paper is given on page 1020. Translations of the abstract are at the end of this volume of the Conference Proceedings.

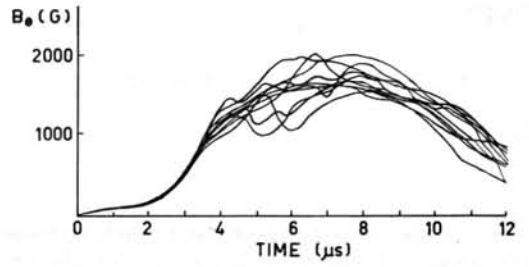

Fig. 2 B_θ magnetic-probe signal at $r = 8.5$ cm. Overlay of 10 shots.

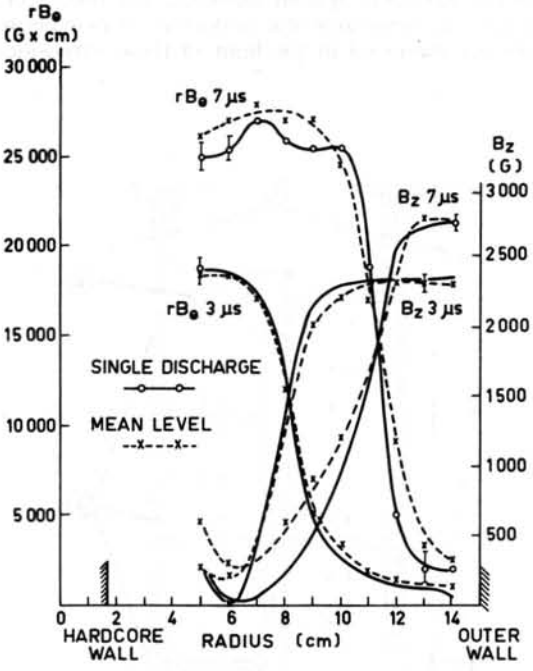

Fig. 3 Field distributions of 80-cm hard-core tube. Hydrogen pressure, 50 mtorr, $B_{z0} = 1900$ G, $I_{max} = 150$ kA at $t = 7.5$ μs.

diagram are the field distributions averaged over 40 discharges. Confirming the overlay results it can be seen that the single discharge distributions at 3 μs are very close to the average ones, whilst at 7 μs considerable deviations occur. Further it can be seen that during the reproducible period the criterion $B_\theta \, \mathrm{d}(r B_\theta)/\mathrm{d}r \leq 0$ is satisfied at all radii within the experimental error. During the later "fluttering" period this is not so, but, as will be shown later, the discharge is not then azimuthally symmetric.

Earlier work on this tube [4] had implied that the instabilities started at the cathode and propagated along the tube at the Alfvén speed. This suggested the curvature of the axial field lines near the electrodes as one possible origin of the instability. Later measurements have shown that the instabilities start at approximately the same time along the tube length and further that changing the field curvature at the ends by varying the axial dependence of the applied longitudinal magnetic field has no significant effect on the instability behaviour.

Since at this stage the randomness of magnetic probe signals was the only evidence for instability, the question as to whether the presence of the probes inside the discharge caused the fluctuation was crucial. To answer this, measurements were made with two monochrometers, both looking at the 3261-Å O III impurity line, one accepting light from a narrow cone including in its path part of a probe tube, the other taking light from a similar cone directed away from the probe tube. These observations together with the magnetic probe signals are shown for two different discharges in Fig. 4. Clearly there is a random emission of impurities from the probe surface and this emission causes variations in the probe signals. Similar but less marked results were obtained by looking at silicon and copper lines. Strong impurity emission from the probe surface occurred on approximately one discharge in three. A calibration of the monochrometer system by putting known amounts of oxygen into the filling gas showed the observed emission to be consistent with the presence of 10^{15}-10^{16} oxygen atoms/cm^3 in the probe region. The impurities are thought to affect the magnetic probe signal primarily through their inertia, the ionized atoms forming a local volume of plasma with anomalously high density.

To investigate the stability of the system without inserting probes, external pick-up coils close to the outer wall and oriented so as to detect B_θ fluctuations were used. If the volume between the current sheath and the wall is insulating, the perturbed azimuthal field due to an instability of axial wave number k and azimuthal mode number m in cylindrical (r, θ, z) co-ordinates is

$$\Delta B_\theta = \frac{C\, m\, F\,(m, k, \Lambda)}{r} \, \mathrm{e}^{\mathrm{i}(m\theta + kz)} \qquad (1)$$

(C is an arbitrary constant; F is a combination of Bessel functions; and Λ is the ratio of radii of the outer conducting wall and of the plasma). In the event of the space between the wall and the current channel being filled with highly conducting plasma then only those plasma displacements that do not vanish at the wall will be detected; nevertheless the dependence on the m and k values of these perturbations will be similar to that shown above. Evidently external coils measuring B_θ cannot detect $m = 0$ instabilities. Experimentally, 12 coils were used, disposed in annular groups of four at three different axial positions. The signals from these wall coils show fluctuations whether there are probes inside the discharge or not. In general, the amplitudes are smaller with probes removed, detail results depending on the relative position of the probes and wall coils. Thus there are residual magnetic-field variations inside the plasma not excited by the presence of probes.

Information about the type of instability has been obtained using statistical correlation techniques. The correlation R between the field fluctuations ΔB (1) at position 1 and fluctuations ΔB (2) at position 2 is given by,

$$R = \left[\frac{\langle \Delta B(1) \Delta B(2) \rangle}{\langle \Delta B(1)^2 \Delta B(2)^2 \rangle^{1/2}} \right]_t \qquad (2)$$

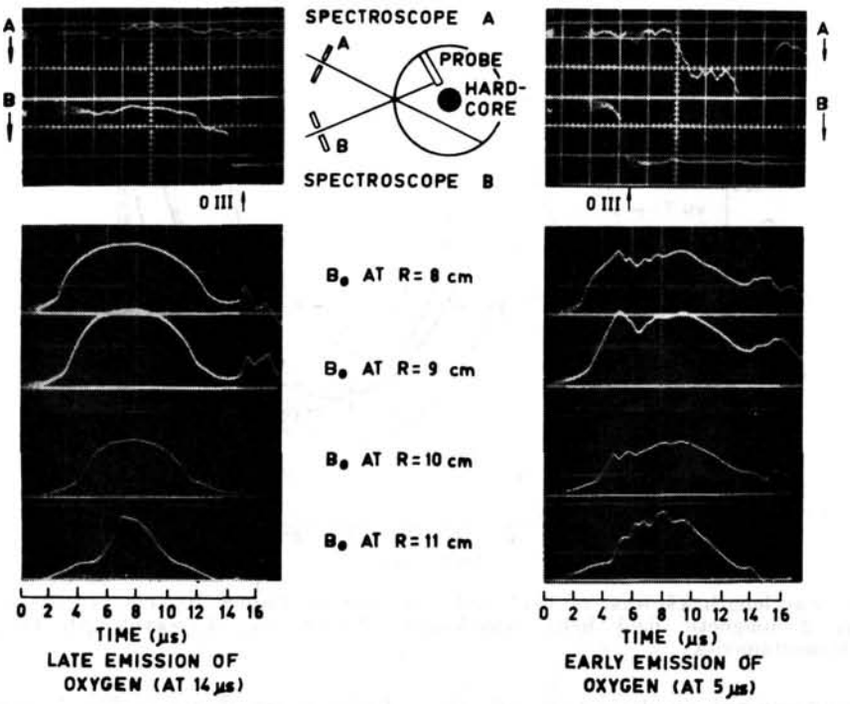

Fig. 4 Impurity emission from probes. Connection between shape of magnetic-probe signal (B_θ) and emission of O III light. ($\lambda = 3261$ Å.)

where $\langle\ \rangle$ denotes averaging over a large number (N) of individual discharges; the fluctuations in each case are the deviations from the average value for the N discharges at time t after the start of each discharge. Consider for example the correlation between coils disposed azimuthally round the discharge at one axial position; suppose that the fluctuations are represented by the Fourier sum,

$$\Delta B(1) = \sum_m a_m \cos m\,(\theta_1 + \varphi)\,,$$

$$\Delta B(2) = \sum_m a_m \cos m\,(\theta_2 + \varphi)\,,$$

where θ_1 and θ_2 are the angular position of the two probes and φ represents the arbitrary phases of the instabilities for individual discharges. If we average over a large number of discharges and assume that the phase φ is random, then,

$$R\,(\theta_2 - \theta_1) = \frac{\sum a_m^2 \cos m\,(\theta_2 - \theta_1)}{\sum_m a_m^2} \qquad (3)$$

Hence from a Fourier analysis of the curve R as a function of $\theta_2 - \theta_1$ the amplitude factors for successive m numbers can be obtained. Similar considerations show that for correlations between axially separated probes distance z apart, the coefficient R is given by,

$$R\,(z) = \frac{\int_0^\infty a_k^2 \cos kz\,\mathrm{d}k}{\int_0^\infty a_k^2 \mathrm{d}k} \qquad (4)$$

where the continuum of k values permissible leads to an integral in place of a sum. The correlation R is of significance only if it exceeds $N^{-1/2}$. Experimentally the random phase assumption receives support from the high azimuthal symmetry of the mean field configuration and from the approximate constancy of the mean square fluctuation level on surfaces of constant radius.

The correlation found for five magnetic probes disposed in a line down the tube at radius 10.5 cm and detecting B_θ fluctuations is shown in Fig. 5. Over 80 discharges were used to obtain the data. With only five coils the measurements are necessarily crude

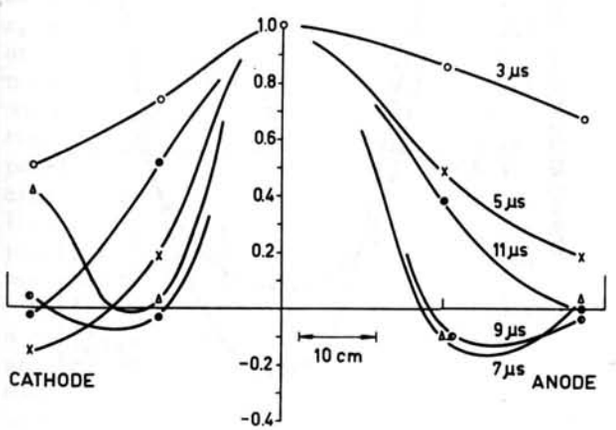

Fig. 5 Axial correlation of B_θ field at $r = 10.5$ cm with five in-line magnetic probes for hard-core tube.

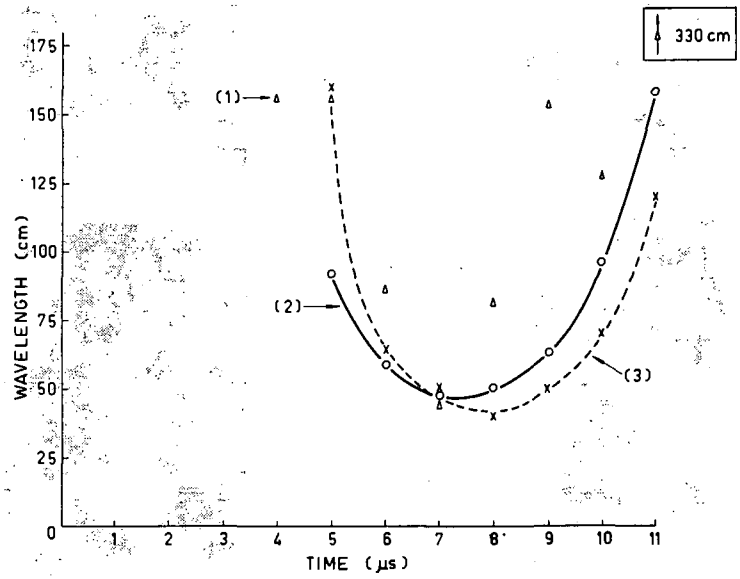

Fig. 6 Instability wavelength vs time of field and j pitches at radius 10.5 cm. 1—gas current helix wavelength $= 2\ \pi\ r\ j_z/j_\theta$, 2—magnetic field helix wavelength $= 2\ \pi\ r\ B_z/B_\theta$, 3—wavelength of perturbation from probe-correlation measurements.

and they may be interpreted simply in terms of only two modes, one with $k=0$ (represented by the mean level) and one with finite wavelength. The amplitude of the effectively infinite wavelength ($k=0$) component is likely to be overestimated since experimental fluctuations in charging voltage, filling pressure and timing errors all contribute preferentially to this mode. The wavelength of the other mode deduced from these measurements is shown versus time in Fig. 6. Also shown is the pitch of the magnetic field helix at the same radius. It is seen that within the experimental error the instability wavelength is equal to the field pitch; certainly the temporal behaviour of the lengths is similar. Similar correlation measurements made at other radii show that although the field pitch is a sharp function of radius, the instability wavelength is not; it always corresponds roughly with the field pitch in the centre of the current sheath. Axial correlation measurements made with three external wall coils and *with no probes in the discharge* are shown in Fig. 7. These yield the same order of wavelengths and the same time dependence as the internal measurements showing once again that there are fluctuations in the discharge not excited by the insertion of probes. Azimuthal correlations obtained with four external coils each separated by 90° are shown in Fig. 8. They give a clear indication that the dominant azimuthal mode is $m=1$. To determine the sign of the perturbation helix represented by $m\theta + kz =$ constant, we need to know the relative signs of m and k. This requires correlations between skewed probes, i.e., probes separated both axially and azimuthally. Such measure-

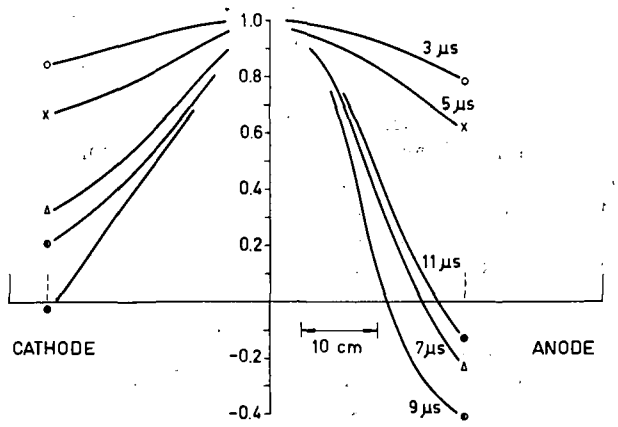

Fig. 7 Axial correlation of external B_θ coils $R = 16.5$ cm with three in-line probes.

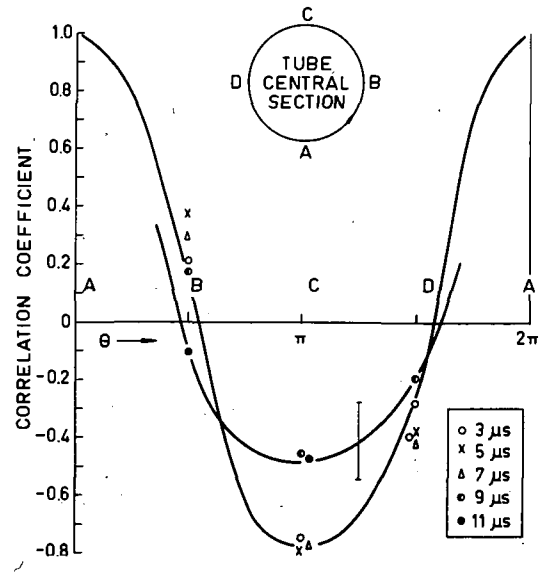

Fig. 8 Azimuthal correlations in external B_θ from probe A (44 shots). Four external coils.

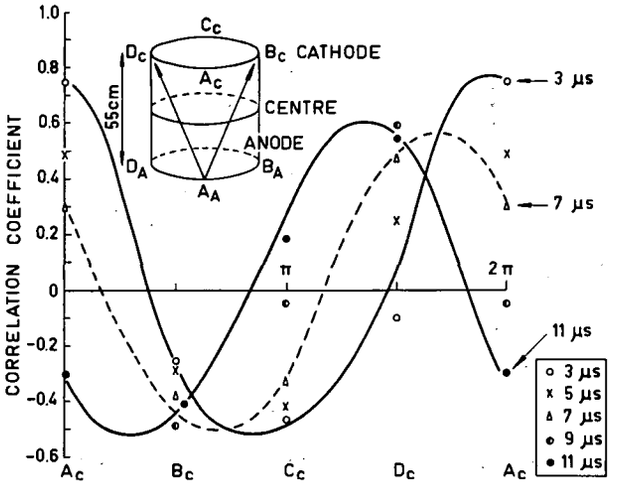

Fig. 9a Skewed correlations. External B_θ field, anode probe to cathode probe group, 55 cm.

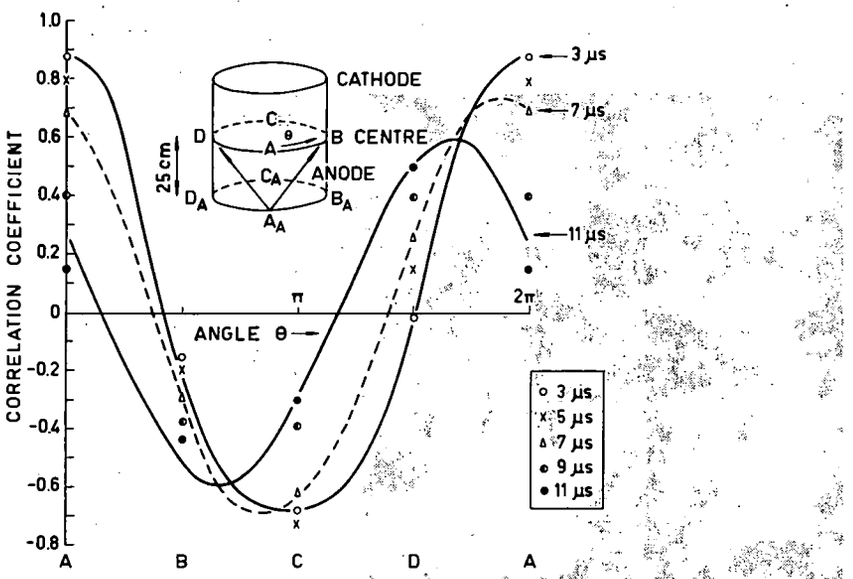

Fig. 9b Skewed correlations. External B_θ field, anode probe to centre probe group, 25 cm.

ments are shown in Fig. 9. If the axial separation between the probes is z_0, the correlation should go as cos $(m\theta + kz_0)$; results are given for two values of z_0. At early times (e.g. 3 μs) the value of kz_0 is small and the results are almost equivalent to the azimuthal measurements at one axial position. Later the wavelength shortens (k increases) and the cosine function is seen to move to the left corresponding to a positive sign for k. The equivalent angular shift is approximately proportional to the separation z_0. Under the operating conditions of the experiment this positive-k result means a perturbation helix of the same sign as the field helix.

Correlations obtained in the radial direction with a multiple magnetic probe inserted into the discharge are shown in Fig. 10. These show that the magnetic-field fluctuations at a radius of 15.5 cm, (i.e. where wall coils are placed) are significantly correlated with the fluctuations in the main current sheath at a radius of 11 cm.

Since $\Delta B_\theta \approx \xi_r (\partial B_\theta / \partial r)_0$ where ξ_r is the radial displacement of the plasma and $(\partial B_\theta / \partial r)_0$ is the unperturbed field gradient (negative at all radii in these discharges), the change in sign of the correlation as one moves inwards or outwards from the current sheath at ~11 cm implies differential (and apparently compressional) radial motions; that is, if the plasma at 11 cm moves outwards, that at 14 cm moves inwards, and that at 8 cm inwards.

Finally, in connection with these instability observations in general, it should be emphasized that the plasma motions involved are extremely small, e.g. of the order 5-10 mm in the current sheath. Thus it is not obvious that they will have any significant effect on particle containment. Measurements of plasma density made with a biased Langmuir double probe located at the outer wall are shown in Fig. 11. With no applied axial magnetic field, plasma with a density of the order $3 \times 10^{14}/\text{cm}^3$ is detected as soon as the discharge is fired, but with 3 kG initial field,

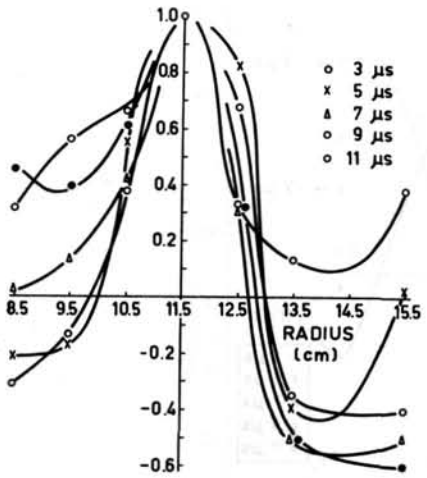

Fig. 10 Multiple probe radial correlations in B_θ field for hard-core tube.

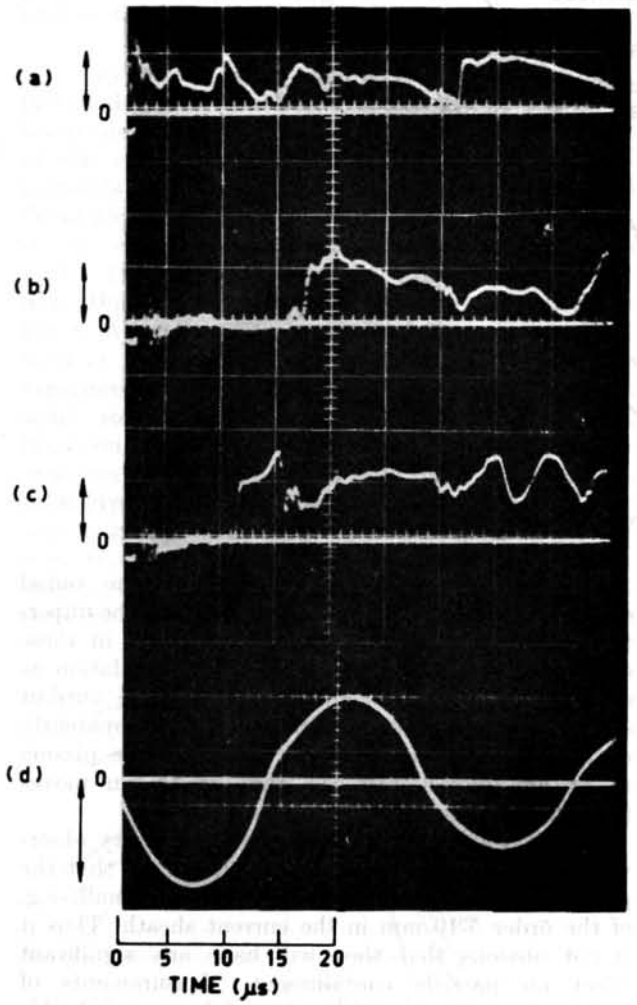

Fig. 11 Langmuir double-probe measurements. Hydrogen pressure, 50 mtorr. (Arrow represents density n.) (a) $n = 3 \times 10^{14}$ ions/cm^3, $B_z = 0$; (b) $n = 3 \times 10^{14}$ ions/cm^3, $B_z = 3$kG; (c) $n = 1.5 \times 10^{13}$ ions/cm^3, $B_z = 3$ kG; (d) gas current (Arrow represents 150 kA.).

plasma of such density is not detected until 4 μs after the first current zero. Even with 20 times the sensitivity, plasma is not detected until 12 μs after the start of the pulse, i.e. 8 μs after the onset of fluttering instabilities. This shows that there is no sudden loss of particle containment concurrent with the start of instability. Nevertheless, until the instabilities are understood and the scaling laws known, their ultimate importance cannot be assessed.

3. Stability theory with finite electrical conductivity

In the above experiments we have a clear contradiction with the predictions of stability theory based on the ideal hydromagnetic approximation. It is natural to question some of the simplifying assumptions made in the theory. Here we consider the effect of permitting the plasma to have finite rather than infinite conductivity. We do this in the two limits of very large and very small conductivity σ. In both cases the energy equation is ignored so that only effects due to the slipping of the plasma relative to the magnetic field will appear; phenomena associated with plasma heating are excluded.

The equations used include the generalized Ohm's law (in e.m. units)

$$\mathbf{j} = \sigma(\mathbf{E} + \mathbf{V} \times \mathbf{B}) \tag{5}$$

combined with Maxwell's equations

$$\text{curl } \mathbf{E} = -\frac{\partial \mathbf{B}}{\partial t} \tag{6}$$

and

$$\text{curl } \mathbf{B} = 4\pi \mathbf{j} \tag{7}$$

These give an equation for the perturbed field $\mathbf{B}_1$ in terms of the perturbed velocity $\mathbf{V}_1$. For perturbations varying as $e^{\omega t}$ it becomes

$$\text{curl } (\mathbf{V}_1 \times \mathbf{B}_0) - \omega \mathbf{B}_1 = -\frac{\text{curl curl } \mathbf{B}_1}{4\pi\sigma} \tag{8}$$

3.1 Large conductivity theory

Models of the stabilized pinch and the hard-core pinch are considered in which the current is confined to a thin layer of thickness δ and conductivity σ, where $\delta \ll r$, the radius of the current sheath. It is further assumed that the radial perturbation ξ_r is constant across the layer, and that the gas between the axis and the layer in the pinch case (layer and the wall in hard-core case) has zero conductivity and hence is decoupled from the magnetic field. This model makes the same approximation for ξ_r as that used in the early treatment of the stabilized pinch where only surface currents were considered [6—8], but now Eq. (8) is used, instead of (5) with the right-hand bracket zero. In the limit of infinite conductivity the present treatment yields the same stability criterion. Effectively an expansion in inverse powers of the magnetic Reynolds number $S \equiv 4\pi C_s \sigma r (\delta/r)^2$ is made, where C_s is the sound speed in the plasma. The inclusion of finite conductivity in these models

is found to make both the stabilized pinch and the hard-core pinch overstable with growth rates of the order 0.1 $\omega_0 S^{-1/2}$, ω_0 being the frequency of the oscillatory mode given by the dispersion relation for infinite conductivity. Only those perturbations whose defining helices are approximately orthogonal to the mean magnetic-field helix in the layer are unstable in this way. These are perturbations which cause most disturbance to the magnetic field, in contrast to the interchange modes usually considered most dangerous on infinite conductivity theory. The overstable growth rate is proportional to the geometric mean of the acoustic frequency ($\sim C_s/r$) and the rate of diffusion of the current layer $1/4\pi\sigma\delta^2$. A consequence of this result is that the effective lifetime of the stabilized pinch is reduced from the time for the skin to thicken sufficiently to become unstable on infinite conductivity theory to the e-folding time for the new overstable modes. With typical thermonuclear parameters ($T_e = 10$ keV, $r = 20$ cm, $\delta/r = 0.1$) this means a reduction in lifetime by a factor of the order 10^2. For the hard-core system, where a thin current-carrying sheath is not a necessary requisite for stability, no comparable deduction can be made from the present theory.

3.2. Small conductivity theory

The calculation follows closely the method used by Tayler to treat a similar pinch problem [9]. In Eq. (8) for the case of small conductivity (i.e. $4\pi\sigma\omega L^2 \ll 1$ were L is the characteristic length in the problem) the approximation,

$$\text{curl curl } \mathbf{B}_1 = 0 \tag{9}$$

is made. The equilibrium considered is one in which a current εI_0 ($\varepsilon \geq 1$) flows through an infinitely conducting central rod of radius a, and I_0 returns with uniform current density through an annular shell of *incompressible* plasma, inner radius r_0, outer radius b There is a uniform axial magnetic field, strength. $2\varphi\ I_0/a$, at all radii; i.e., there are no zero-order azimuthal currents in the plasma. To maintain equilibrium there is a non-conducting gas with pressure p extending from radius b to infinity. The residual return current $(\varepsilon - 1)\, I_0$ is supposed to return at infinity. If one considers perturbations of the form $e^{i(kz + m\theta) + \omega t}$ with the appropriate boundary conditions, from the equations of motion for the two free surfaces at r_0 and b the dispersion relation of Eq. 10 (on this page) is obtained. In this equation $\gamma = kb$, $\alpha = kr_0$, $\beta = ka$. L, M, N, O, P, S are combinations of Bessel functions of these three parameters. The equation is a quadratic in ω^2 so that for each value of m and k there are two values for ω^2. It is clear from the equation that the axial magnetic field has no effect on the stability of $m = 0$ modes. Numerical calculations of $\chi\omega^2$ vs kr_0 have been made for a system with the proportions $b/r_0 = 1.2$, $a/r_0 = 0.4$ with some modifications to the dispersion relation to allow for the fact that in a later liquid-metal experiment the frequencies involved are low so that the perturbed magnetic field penetrates the central copper rod. With $m = 0$ and 1 these calculations show the system to be stable for all wave numbers. The solutions for $m = 1$ and various values of $B_z(\theta)$ are shown in Fig. 12. One of the roots corresponds to instability for all wave numbers. The effect of increasing the axial field is to increase the instability growth rate, the increase being greater for positive wave numbers, i.e., those corresponding to perturbation helices opposite in sign to that of the magnetic field. The effect of increasing the current in the central rod (ε) is also shown. It is always stabilizing. In general the

$$\frac{-\chi\omega^2 + \gamma\dfrac{O}{N} + \dfrac{M}{L}\left\{\dfrac{m^2+\gamma^2}{\gamma} + \dfrac{\gamma^2-\alpha^2}{2\gamma\beta}\left[(\varepsilon-1)\beta - m\varphi\right]\right\} + 1 + \dfrac{K_m(\gamma)}{LK_{m'}(\beta)}\cdot\left[\dfrac{m^2 MS}{\gamma} + \dfrac{m^2}{\alpha\gamma}P\right]}{\dfrac{\gamma}{\alpha N} - \dfrac{1}{L}\left\{\dfrac{m^2+\alpha^2}{\alpha^2} + \dfrac{\gamma^2-\alpha^2}{2\alpha^2\beta}\left(\varepsilon\beta - m\varphi\right)\right\} + \dfrac{K_m(\gamma)}{LK_{m'}(\beta)}\ P\left\{\dfrac{m^2 M}{\alpha} - \dfrac{m^2}{\alpha^2}\dfrac{K_m(\alpha)}{K_m(\gamma)}\right\}}$$

$$= \frac{\dfrac{1}{L}\left\{\dfrac{m^2+\gamma^2}{\gamma^2} + \dfrac{\gamma^2-\alpha^2}{2\gamma^2\beta}\left[\beta(\varepsilon-1) - m\varphi\right]\right\} + \dfrac{K_m(\gamma)}{LK_{m'}(\beta)}\left(\dfrac{m^2}{\gamma^2}\,S - \dfrac{m^2 OP}{\gamma}\right) - \left(\dfrac{\varepsilon\gamma^2 + (2-\varepsilon)\alpha^2}{2\alpha\gamma N}\right)}{-\chi\omega^2 + \left(\dfrac{\varepsilon\gamma^2 + (2-\varepsilon)\alpha^2}{2\alpha}\right)\dfrac{M}{N} + \dfrac{O}{L}\left(\dfrac{m^2+\alpha^2}{\alpha} + \dfrac{\gamma^2-\alpha^2}{2\alpha\beta}(\beta\varepsilon - m\varphi)\right) + 1 + \dfrac{K_m(\gamma)}{LK_{m'}(\beta)}\,P\left(\dfrac{m^2}{\alpha\gamma} + \dfrac{m^2}{\alpha}\dfrac{OK_m(\alpha)}{K_m(\gamma)}\right)} \tag{10}$$

$$L = I_{m'}(\gamma)\,K_{m'}(\alpha) - I_{m'}(\alpha)\,K_{m'}(\gamma)$$
$$M = K_m(\gamma)\,I_{m'}(\alpha) - I_m(\gamma)\,K_{m'}(\alpha)$$
$$N = K_m(\gamma)\,I_m(\alpha) - K_m(\alpha)\,I_m(\gamma)$$
$$O = K_{m'}(\gamma)\,I_m(\alpha) - I_{m'}(\gamma)\,K_m(\alpha)$$
$$P = I_{m'}(\beta)\,K_m(\alpha) - I_m(\alpha)\,K_{m'}(\beta)$$
$$S = I_m(\gamma)\,K_{m'}(\beta) - I_{m'}(\beta)\,K_m(\gamma)$$
$$\chi = \pi\varrho\,(b^2 - r_0^2)^2/4\,I_0^2$$

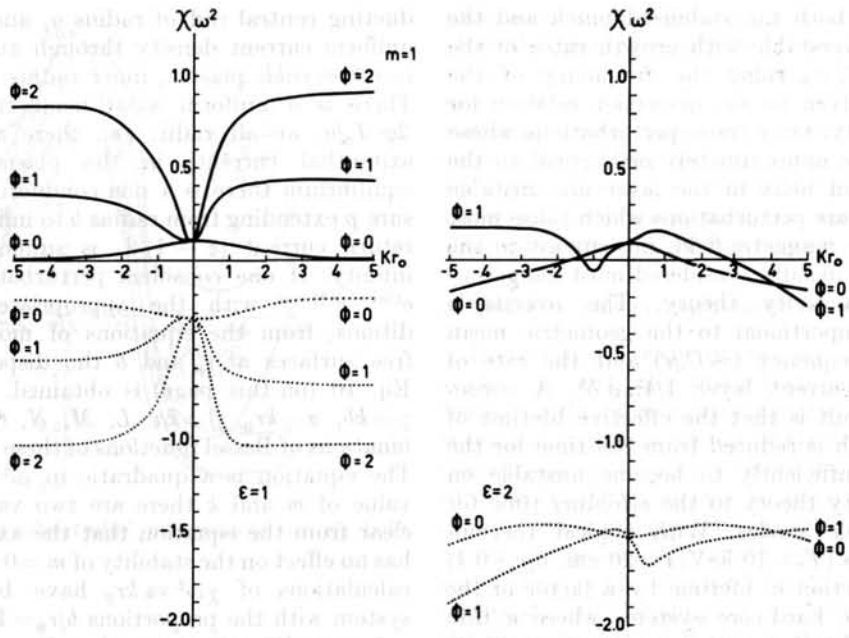

Fig. 12 Dispersion relation: solutions for various values of axial magnetic field (φ) for the cases $\varepsilon=1$ and $\varepsilon=2$.

behaviour of the system may be represented by the relation,

$$\omega^2=\alpha I_0^2-\beta I_0 I_1+\gamma r_0 B_z I_0 \qquad (11)$$

where αI_0^2 represents instability arising from the interaction of the current in the plasma with its own self-field (normal pinch instability), $\beta I_0 I_1$ the stabilizing effect of the interaction of the plasma current I_0 with the vacuum field of the current I_1 in the central rod and $\gamma r_0 B_z I_0$ the destabilizing interaction between the plasma current and the axial magnetic field. The physics of this latter interaction is made clearer by solving the dispersion equation for the two cases in which (a) the inner surface of the plasma is fixed (e.g., by a solid insulating surface) and (b) the outer surface is fixed. The two solutions for $m=1$ are shown in Fig. 13. In the case where the outer surface is free, increasing the axial magnetic field (φ) stabilizes those perturbations with helices of the same sign as the magnetic field (negative k) and destabilizes those opposite to the field spiral. With the inner surface free the reverse happens. Figure 14 shows diagrammatically the hard core with an $m=1$ perturbation on the external surface; the axial field penetrates the plasma and interacts with the radial components of current to give azimuthal forces F_θ. With perturbation helices opposite to the field spiral F_θ is directed so as to increase the perturbation, but with helices parallel to the field the forces are stabilizing. Similar arguments applied to a free inner surface show opposite effects, in agreement with the dispersion relations.

Finally we can insert coupling terms into the equations of motion for the two free surfaces which force them to move together, an assumption almost equivalent to that used in the high conductivity model, namely that the radial displacement ξ_r is constant across the layer. The dispersion relation obtained for the case $m=1$ and for various axial fields is shown in Fig. 15. Perturbation spirals opposite to the field spirals are unstable so that in this approxi-

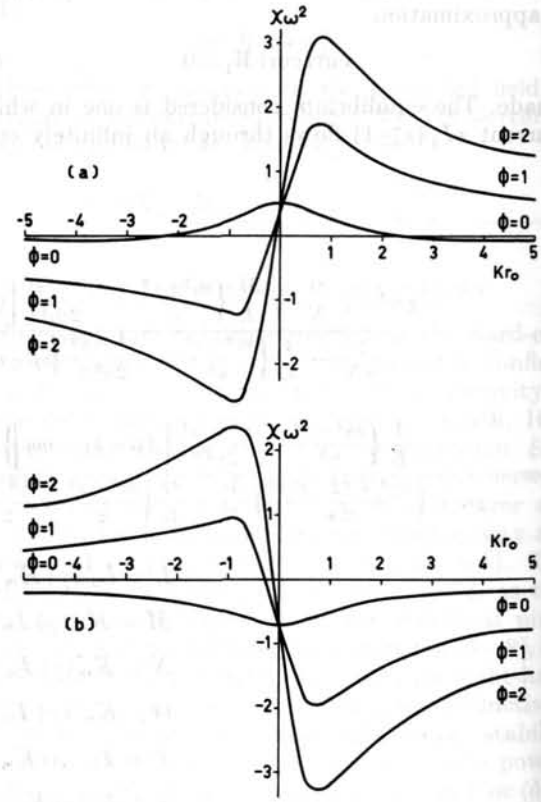

Fig. 13 Dispersion relations for one free surface. $m=1$ (a) inner boundary fixed, (b) outer boundary fixed.

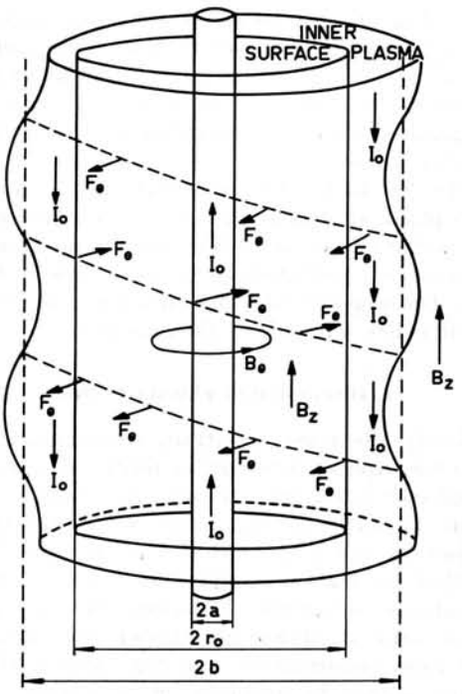

Fig. 14 Forces on buckled outer free surface of plasma in hard-core tube due to axial-magnetic-field penetration.

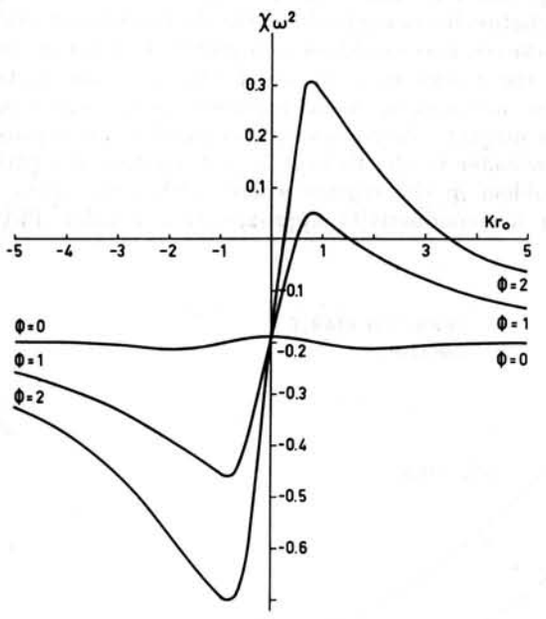

Fig. 15 Dispersion relation for the two surfaces coupled together. $m = 1$.

mation the high- and the low-conductivity models give similar results.

A general feature of the low-conductivity dispersion relation is that the growth rate of unstable modes increases as the azimuthal mode number m increases. The viscosity of a real plasma, neglected in the present theory, would stabilize these higher-m modes.

4. Liquid-mercury experiment

A free-falling annular cylinder of liquid mercury has been used to simulate a plasma in the low-conductivity approximation. The apparatus is shown in Fig. 16. Currents of the order 300 A were passed up the central conductor and returned through the mercury column. A pressure balance was maintained by suitably adjusting the air pressure on the outer surface of the mercury. Instabilities developed when an axial field of about 900 G was applied, and these

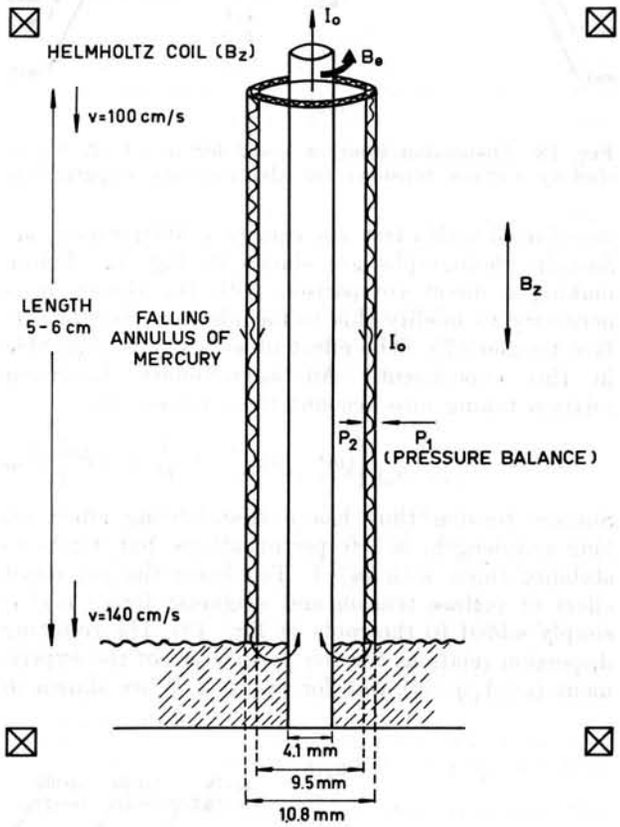

Fig. 16 Arrangement of mercury experiment.

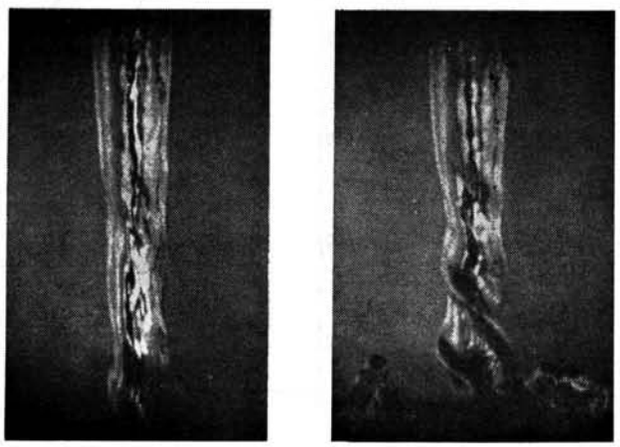

Fig. 17 Photographs of mercury column. Ciné stills show instabilities developing in mercury shell.

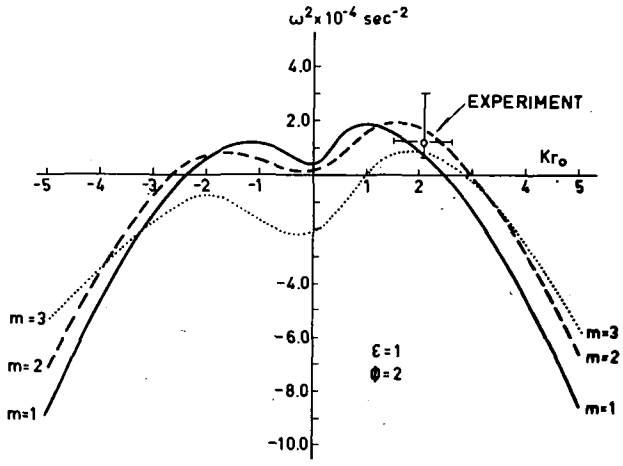

Fig. 18 Dispersion relation $\varphi = 2$ for $m = 1$, 2, 3 (*including* surface tension) for the mercury experiment.

were filmed with a fast cine camera at 4000 frames/sec. Sample photographs are shown in Fig. 17. Before making a direct comparison with the theory it is necessary to modify this to include the effect of surface tension (T). (The effect of viscosity is negligible in this experiment.) An approximate dispersion relation taking into account these forces only is

$$\omega_T{}^2 = -\frac{T}{\varrho\,(b-r_0)}\left[(m^2-1)\frac{1}{r_0{}^2}+\frac{1}{b^2}+2k^2\right] \quad (12)$$

Surface tension thus has a destabilizing effect on long-wavelength, $m=0$ perturbations but tends to stabilize those with $m \geq 1$. To obtain the combined effect of surface tension and magnetic forces $\omega_T{}^2$ is simply added to the roots of Eq. (10). The resulting dispersion relations for the parameters of the experiment ($\varepsilon = 1$, $\varphi = 2$) and for $m = 1$, 2, 3 are shown in Fig. 18. The most unstable modes are seen to be $m = 1$ and $m = 2$ with perturbation helices opposite to the field spiral. This agrees with the experimental observation (cf. Fig. 17.) The observed growth rate also agrees, within the experimental error, with the theoretical value.

Figure 19 shows the experimental points on the $I_0 - B_z$ plane at which the column is observed to be either stable or unstable. Also shown are theoretical contours of constant growth rate for various instability modes. The experimental line dividing stability from instability lies parallel to these contours.

5. Discussion of plasma results

Probably the most important consequence of the plasma measurements is that the fluttering instabilities are well correlated over considerable axial distances and in azimuth so that in no sense can they be described as fine-scale turbulence. The good $m=1$ azimuthal correlation would also seem to rule out explanations involving break-up of the current channel into a series of filamentary discharges.

The finite-conductivity theories predict that the discharge should be unstable with e-folding times of the order 10 μs for the high-conductivity approximation (taking $kT_e = 10$ eV) and ~1 μs for the low-conductivity case. In direct contrast to the experimental result the first theory gives only perturbation helices opposite to the field spiral as unstable. However, this would seem in part to be a consequence of the model used in which the two free surfaces were assumed to move together. In the experiment the magnetic Reynolds number (used as an expansion parameter in the theory) is ~2, putting the plasma problem in the regime where neither the high- nor the low-conductivity approximation is valid. Physic-

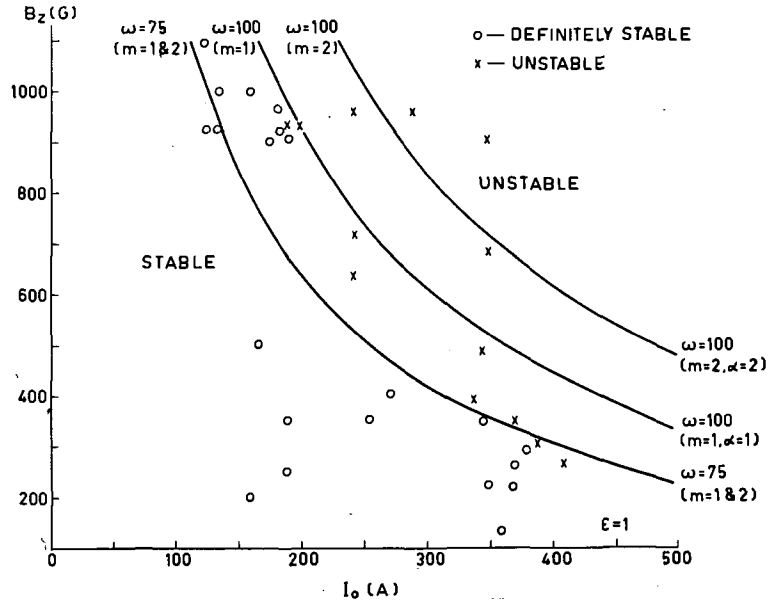

Fig. 19 Instability/stability points in $I_0 - B_z$ plane, contours of constant growth rate (ω, sec^{-1}) for the $m = 1$ and 2 modes.

ally the growth rates given by the low-conductivity theory would be expected to be reduced by a factor $1/4\,\pi\,\omega_0\,\sigma\,\delta^2$ where ω_0 is the frequency of the oscillatory mode (imaginary part of ω). This frequency will be greatest for those modes which distort the magnetic field the most so that the net effect would be to stabilize these perturbations with helices opposite in sign to the field helix and to leave the interchange modes as overstable, (see Fig. 12). This point can only be proved rigorously by solving the high-conductivity case with two independent free surfaces.

The possibility that the instabilities are due to the radial acceleration of the plasma (Rayleigh-Tayler) must be considered. These would be expected to follow the mean magnetic field as observed. The growth rate ν calculated assuming that there is no shear in the magnetic field is given by [10]

$$\nu^2 = r''\left(\frac{m^2}{r^2}+k^2\right)^{1/2} \tag{13}$$

where r'' is the plasma acceleration. In this case the sign of r'' is not of basic importance; it simply determines whether the instabilities are on the outside or the inside of the current sheath. From the measured time dependence of the current sheath radius it is inferred that r'' starts with a value of $\sim 4\times 10^{11}$ cm/sec^2 which then falls to about one tenth of this 3 μs after the start of the discharge, remaining low for the remaining times of interest. Substitution into (13) together with the measured values of m and k gives

$$\nu\,(\text{maximum}) \approx 2\times 10^5\ \text{sec}^{-1}$$

Since the maximum acceleration lasts only for about 2 μs and since the presence of considerable shear in the magnetic field should reduce the growth rate still further, this type of instability cannot grow fast enough to account for the experimental results.

6. Conclusions

As a result of this work we conclude that:

1 The emission of impurities from the surface of a magnetic probe tube in a plasma causes fluctuations in the local magnetic field.

2 Information about the fluctuations within the discharge can be obtained by external magnetic-field measurements.

3 There are residual magnetic-field fluctuations in the hard-core pinch not excited by the presence of probes in the plasma.

4 These instabilities are predominantly $m=1$ with a perturbation helix parallel to the mean magnetic-field spiral.

5 There is no sudden loss of particle containment when instability starts.

6 The inclusion of finite electrical conductivity in hydromagnetic stability theory shows both the hard-core and the stabilized pinches to be unstable; this instability could seriously affect their potentialities as containment systems for plasma at thermonuclear temperatures.

7 Some features of the low-conductivity stability theory have been confirmed by a model hard-core experiment using liquid mercury.

8 The instabilities seen in the plasma hard-core experiments have not yet been proved to be those due to finite electrical conductivity.

References

[1] Laing, E. W., AERE Report T/M 161 (1958).
[2] Rosenbluth, M., in Proc. 2nd U. N. Intern. Conf. PUAE **31**, United Nations, Geneva (1958) 85.
[3] Colgate, S. A., et al, in Proc. 4th Intern. Conf. Ionization Phenomena in Gases (Uppsala, 17-21 Aug. 1959) **2**, North Holland Publishing Co., Amsterdam (1960) 888.
[4] Aitken, K., et al, in proceedings of ref. 3, **2**, 896.
[5] Burkhardt, L. C., Lovberg, R. H., in proceedings of ref. 2, **32**, 29.
[6] Shafranov, V. D., *Atomnaja Energija* **5** (1957) 709.
[7] Rosenbluth, M., U. S. AEC Report LA-2030 (1957).
[8] Tayler, R. J., *Proc. phys. Soc. (London)* B**70** (1957) 314.
[9] Tayler, R. J., AERE Report R-3229 (1960).
[10] Kruskal, M., Schwarzschild, M., *Proc. roy. Soc.* A**223** (1954) 348.

ACTION DE CHAMPS ÉLECTRIQUE ET MAGNÉTIQUE EXTÉRIEURS SUR UN PLASMA*

P. BERTRAND, G. BRIFFOD

CENTRE D'ÉTUDES NUCLÉAIRES DE SACLAY

SERVICE DE PHYSIQUE APPLIQUÉE, SECTION D'IONIQUE GÉNÉRALE

GIF-SUR-YVETTE (S.-ET-O.), FRANCE

La fonction de distribution des vitesses f_0 caractérisant l'état stationnaire d'un plasma soumis à l'action de champs magnétique et électrique statiques est calculée au premier ordre, par résolution de l'équation de Boltzmann dans l'hypothèse du gaz de Lorentz. La fonction de distribution f_0 ainsi obtenue est anisotrope.

A partir de cet état stationnaire, l'étude du système formé par l'équation de Boltzmann linéarisée et par les équations de Maxwell conduit à une relation de dispersion.

L'étude de cette relation de dispersion permet d'examiner les conditions d'existence de l'état stationnaire ainsi que les domaines de propagation des instabilités.

1. Introduction

L'expérience montre que la plupart des plasmas de laboratoire sont soumis à l'action de champs magnétique et électrique. L'effet diamagnétique étant absolument négligeable pour des plasmas froids, le champ magnétique appliqué et le champ magnétique dans le plasma sont identiques.

En ce qui concerne le champ électrique, sa valeur est essentiellement variable en fonction des différents points d'observation selon qu'il s'écoule localement du courant ou non et sa présence a pour effet de modifier le comportement local du plasma.

Le but de cette étude est d'analyser l'influence de ce champ électrique sur le comportement du plasma et plus spécialement sur l'évolution des phénomènes oscillatoires. Nous nous limiterons dans ce travail au cas de champs magnétique et électrique perpendiculaires.

2. Principe de l'étude

La connaissance de la fonction de distribution des vitesses des particules d'espèce h dans le plasma suppose la résolution de l'équation de Boltzmann. Dans le cas où le plasma est soumis à l'action de champs $\mathbf{E}$ et $\mathbf{B}$, cette équation s'écrit

$$\frac{\partial f_h}{\partial t} + \mathbf{v}\cdot\nabla_r f_h + \frac{\mathbf{Z}e}{m}(\mathbf{E}+\mathbf{v}\times\mathbf{B})\cdot\nabla_v f_h = \sum_l J_{hl} \qquad (1)$$

où Ze est la charge des particules d'espèce h et J_{hl} désigne la variation de f_h due aux collisions des particules d'espèce h avec les particules d'espèce l.

Dans le cas où le gaz est faiblement ionisé, la densité n des particules chargées est beaucoup plus faible que la densité N des particules neutres. Le mouvement des électrons est essentiellement fixé par les collisions électrons-molécules. Comme de plus la masse m_e des électrons est beaucoup plus petite que la masse m_i des ions, le modèle du gaz de Lorentz est bien adapté au problème proposé et permet d'avancer la résolution de (1) en utilisant des méthodes de développement [1, 2, 3].

Pour l'étude des oscillations, nous admettrons l'existence d'un état stationnaire $f=f_0$ solution de (1), et nous supposerons que le système s'écarte très peu de cet état, ce qui permet d'écrire dans ce cas

$$f=f_0+f_1$$
$$\mathbf{E}=\mathbf{E}_0+\mathbf{E}_1$$
$$\mathbf{B}=\mathbf{B}_0+\mathbf{B}_1$$

où $\mathbf{E}_0$ et $\mathbf{B}_0$ sont les champs stationnaires appliqués.

En reportant ces expressions dans l'équation de Boltzmann et en ne retenant que les termes du 1er ordre, nous obtenons

$$\frac{\partial f_1}{\partial t} + \mathbf{v}\cdot\nabla_r f_1 + \frac{e}{m}(\mathbf{E}_0+\mathbf{v}\times\mathbf{B}_0)\cdot\nabla_v f_1 = -\frac{e}{m}(\mathbf{E}_1+\mathbf{v}\times\mathbf{B}_1)\cdot\nabla_v f_0 \qquad (2)$$

Cette équation peut être résolue par transformation de Fourier dans l'espace des positions et de Laplace sur le temps.

Toutefois, dans l'étude de la stabilité, il est équivalent de raisonner sur l'équation de dispersion obtenue en prenant pour f_1, $\mathbf{E}_1$ et $\mathbf{B}_1$ des dépendances de la forme $e^{i(\omega t+\mathbf{k}\cdot\mathbf{r})}$ [4, 5]. Nous utiliserons cette seconde méthode.

f_1 étant connue, les équations de Maxwell sont déterminées et s'écrivent

$$\nabla\cdot\mathbf{E}_1 = \frac{e}{\varepsilon_0}\int f_1 \,\mathrm{d}\,\mathbf{v} \qquad (3)$$

$$\nabla\cdot\mathbf{B}_1 = 0 \qquad (4)$$

$$\nabla\cdot\mathbf{E}_1 = -\frac{\partial \mathbf{B}_1}{\partial t} \qquad (5)$$

$$c^2\nabla\cdot\mathbf{B}_1 = \frac{\partial \mathbf{E}_1}{\partial t} + e\int \mathbf{v} f_1 \,\mathrm{d}\,\mathbf{v} \qquad (6)$$

L'équation (5) dans ces hypothèses s'écrit $\mathbf{B}_1 = -\mathbf{k}\times\mathbf{E}_1/\omega$ et permet d'éliminer le champ magnétique

* Mémoire CN-10/106, présenté par G. Briffod. La discussion concernant ce mémoire est donnée page 1021. Les traductions du résumé se trouvent en fin de volume.

dans les autres équations. L'étude de l'existence de l'onde se trouve ramenée à l'étude de l'existence de **E** solution du système.

$$(c^2k^2-\omega^2)\,\mathbf{E}_1-c^2(\mathbf{k}\cdot\mathbf{E}_1)\,\mathbf{k}=-\frac{i e\omega}{\varepsilon_0}\int \mathbf{v} f_1 \,d\mathbf{v} \qquad (7)$$

$$i\mathbf{k}\cdot\mathbf{E}_1=\frac{e}{\varepsilon_0}\int f_1\,d\mathbf{v} \qquad (8)$$

3. Calcul de f_1

3.1. Choix de l'etat stationnaire f_0

Comme nous l'avons indiqué (par. 2), f_0 peut être approché par un développement. En particulier, il est intéressant d'utiliser un développement en série de fonctions sphériques dans l'espace des vitesses de la forme

$$f_0=\alpha_{00}+\sum \alpha_{lm}\,C_{lm}+\beta_{lm}\,S_{lm}$$

ou C_{lm} et S_{lm} sont des fonctions réelles telles que

$$C_{lm}+i\,S_{lm}=v^l\,Y_l^m$$

En suivant cette méthode et les calculs explicités par Bayet, Delcroix et Denisse [6], les premiers coefficients du développement pour un plasma homogène soumis à des champs stationnaires $\mathbf{E}_0$ et $\mathbf{B}_0$ s'écrivent dans un système de coordonnées où Oz est dirigé selon $\mathbf{B}_0$ et Ox est dirigé selon $\mathbf{E}_0$.

$$\alpha_{11}=-\frac{\nu}{\nu^2+\Omega_c^2}\frac{1}{v}\frac{\partial\alpha_{00}}{\partial v}\frac{eE_0}{m}$$

$$\alpha_{10}=0$$

$$\beta_{11}=-\frac{\omega_c}{\nu^2+\omega_c^2}\frac{1}{v}\frac{\partial\alpha_{00}}{\partial v}\frac{eE_0}{m}$$

avec ν=fréquence de collision électron-molécule; ω_c=fréquence cyclotronique des électrons; α_{00} =partie isotrope de la fonction de distribution.

Si le champ électrique est faible ($eE_0/\nu m \ll v_{th}$), ou si le temps de Maxwellianisation des électrons entre eux est plus petit que le temps d'échange d'énergie entre les électrons et les molécules, la partie isotrope α_{00} est sensiblement Maxwellienne et la fonction de distribution se met sous la forme

$$f_0=k\,(1+\boldsymbol{\alpha}\cdot\mathbf{v})\,e^{-v^2/u^2}$$

$$\alpha_x=-\frac{2}{u^2}\frac{\nu}{\nu^2+\omega_c^2}\frac{eE_0}{m}$$

$$\alpha_y=\frac{2}{u^2}\frac{\omega_c}{\nu^2+\omega_c^2}\frac{eE_0}{m} \qquad (9)$$

$$\alpha_z=0$$

$$k=\frac{n}{\pi^{3/2}u^3}$$

3.2. Forme explicite de f_1 pour $\mathbf{k}\|\mathbf{B}_0$

L'hypothèse $\mathbf{E}_0\perp\mathbf{B}_0$ nous permet d'écrire l'équation (2) sous la forme

$$i\,(\omega+\mathbf{k}\cdot\mathbf{v})f_1+\frac{e}{m}\left[\left(\mathbf{v}-\frac{\mathbf{E}_0\times\mathbf{B}_0}{\mathbf{B}_0^2}\right)\times\mathbf{B}_0\right]\cdot\boldsymbol{\nabla}_v f_1$$
$$=-\frac{e}{m}\,(\mathbf{E}_1+\mathbf{v}\times\mathbf{B}_1)\cdot\boldsymbol{\nabla}_v f_0 \qquad (10)$$

Par le changement de variable $\mathbf{V}=\mathbf{v}-\mathbf{E}_0\times\mathbf{B}_0/\mathbf{B}_0^2$ $=\mathbf{v}+\mathbf{v}_D$ et le passage en coordonnées cylindriques d'axe parallèle à $\mathbf{B}_0$, l'éq. (10) devient

$$i\,[\omega+\mathbf{k}\,(\mathbf{V}+\mathbf{v}_0)]\,f_1-\frac{e}{m}\,\mathbf{B}_0\frac{\partial f_1}{\partial\varphi}$$
$$=\frac{e}{m}\,[\mathbf{E}_1+(\mathbf{V}+\mathbf{v}_D)\times\mathbf{B}_1]\cdot\boldsymbol{\nabla}_v f_0$$

La solution de cette équation périodique en φ et nulle pour $\mathbf{E}_1=\mathbf{B}_1=0$ s'écrit [7]

$$f_1(U,W,\varphi)=$$
$$\frac{1}{\exp\left(-2i\pi\dfrac{\omega+kU}{\omega_c}\right)-1}\int_{\varphi}^{\varphi+2\pi} b(\varphi')\,G(\varphi,\varphi')\,d\varphi'$$

avec les notations

$$b(\varphi')=\frac{e}{m\omega_c}\,[\mathbf{E}_1+(\mathbf{V}+\mathbf{v}_D)\times\mathbf{B}_1]\cdot\boldsymbol{\nabla}_v f_0$$

$$G(\varphi,\varphi')=\exp i\left(\frac{\omega+kU}{\omega_c}\right)(\varphi-\varphi')$$

En prenant pour l'état stationnaire f_0 l'expression (9), le calcul de f_1 conduit à une expression linéaire en E_{1x}, E_{1y}, E_{1z}

$$f_1=F_xE_{1x}+F_yE_{1y}+F_zE_{1z} \qquad (11)$$

$$F_x=\frac{K'}{u^2}\exp-\left(\frac{U^2+W^2+v_D^2}{u^2}\right)\sum_{-\infty}^{+\infty} i^n\,I_n\left(\frac{2Wv_D}{u^2}\right)$$
$$\times\left\{-A_{n-2}\frac{W^2}{2}(\alpha_x+i\alpha_y)-A_{n-1}W\gamma+A_n\left[\alpha_x(u^2-W^2)\right.\right.$$
$$\left.\left.+\alpha_x\frac{ku^2}{\omega}U\right]-A_{n+1}W\gamma+A_{n+2}\frac{W^2}{2}(-\alpha_x+i\alpha_y)\right\}$$

$$F_y=\frac{K'}{u^2}\exp-\left(\frac{U^2+W^2+v_D^2}{u^2}\right)\sum_{-\infty}^{+\infty} i^n\,I_n\left(\frac{2Wv_D}{u^2}\right)$$
$$\times\left\{A_{n-2}(\alpha_y-i\alpha_x)\frac{W^2}{2}-A_{n-1}W[(\alpha_x+i\alpha_y)v_D+i\gamma]\right.$$
$$+A_n\left[\alpha_y(u^2-W^2)-2\gamma v_D+\alpha_y u^2\frac{kU}{\omega}\right]$$
$$\left.+A_{n+1}W[(-\alpha_x+i\alpha_y)v_D+i\gamma]+A_{n+2}[\alpha_y+i\alpha_x]\frac{W^2}{2}\right\}$$

$$F_z=\frac{K'}{u^2}\exp-\left(\frac{U^2+W^2+v_D^2}{u^2}\right)\sum_{-\infty}^{+\infty} i^n\,I_n\left(\frac{2Wv_D}{u^2}\right)\times$$
$$\left\{-A_{n-1}W(\alpha_x+i\alpha_y)U-2\gamma UA_n-A_{n+1}W(\alpha_x-i\alpha_y)U\right\}$$

avec les conventions

$$K'=\frac{Ke}{m\omega_c}\exp i\left(\frac{\omega+kU}{\omega_c}\right)\varphi$$

$$A_n=\frac{\exp i\left(n-\dfrac{\omega+kU}{\omega_c}\right)\varphi}{i\left(n-\dfrac{\omega+kU}{\omega_c}\right)}$$

I_n=fonction de Bessel modifiée

$\gamma=1+\alpha_y v_D$

4. Equation de dispersion

f_1 étant connue, pour former l'équation de dispersion il suffit d'expliciter le système d'équations (7) et (8) reliant $\mathbf{E}_1$ à f_1. En fait, (7) et (8) ne sont pas indépendantes comme le montre l'intégration sur $\mathbf{v}$ de l'équation (10).

Nous ne conserverons donc pour l'équation de dispersion que les trois composantes de (7).

Le courant $\mathbf{j}$ se calcule à partir de f_1 par

$$\mathbf{j} = \frac{e}{\varepsilon_0}\int \mathbf{v} f_1 \,\mathrm{d}\,\mathbf{v} = \frac{e}{\varepsilon_0}\int (\mathbf{V}+\mathbf{v}_\mathrm{D}) f_1 W \,\mathrm{d}W \,\mathrm{d}U \,\mathrm{d}\varphi$$

En utilisant les résultats de l'appendice pour l'intégration sur φ et W, on obtient pour $\mathbf{j}$, une relation linéaire en E_{1x}, E_{1y}, E_{1z} donnée par les éqs. (12), (13), (14) (cette page) avec $b=(\omega+k\,U)/\omega_\mathrm{c}$.

$$\left.\begin{aligned}
\frac{\partial j_x}{\partial E_{1x}} &= -\mathrm{i}\,\pi\,\frac{K u^2}{2}\,\frac{e^2}{m\omega_\mathrm{c}}\int_{-\infty}^{\infty}\left[\left(\frac{1}{1+b}-\frac{1}{1-b}\right)+\mathrm{i}\left(\frac{1}{1+b}+\frac{1}{1-b}\right)\alpha_y\, v_\mathrm{D}\,\frac{kU}{\omega}\right]\mathrm{e}^{-(U/u)^2}\,\mathrm{d}U\\
\frac{\partial j_x}{\partial E_{1y}} &= \pi\,\frac{K u^2}{2}\,\frac{e^2}{m\omega_\mathrm{c}}\int_{-\infty}^{\infty}\left(\frac{1}{1+b}+\frac{1}{1-b}\right)\left(1+\alpha_y\, v_\mathrm{D}\,\frac{kU}{\omega}\right)\mathrm{e}^{-(U/u)^2}\,\mathrm{d}U\\
\frac{\partial j_x}{\partial E_{1z}} &= \pi\,\frac{K u^2}{2}\,\frac{e^2}{m\,\omega_\mathrm{c}}\int_{-\infty}^{\infty}\left[\left(\frac{1}{1+b}+\frac{1}{1-b}\right)\left(\alpha_y-\frac{2U}{u^2}\right)U-\mathrm{i}\left(\frac{1}{1-b}-\frac{1}{1+b}\right)\alpha_x U\right]\mathrm{e}^{-(U/u)^2}\,\mathrm{d}U
\end{aligned}\right\}\qquad(12)$$

$$\left.\begin{aligned}
\frac{\partial j_y}{\partial E_{1x}} &= \pi\,\frac{K u^2}{2}\,\frac{e^2}{m\,\omega_\mathrm{c}}\int_{-\infty}^{\infty}\left[-\left(\frac{1}{1+b}+\frac{1}{1-b}\right)+\left(\frac{1}{1-b}-\frac{1}{1+b}\right)\mathrm{i}\,\alpha_x\,\frac{kU}{\omega}\,v_\mathrm{D}+\frac{2\mathrm{i}\,\alpha_x v_\mathrm{D}}{b}\,\frac{kU}{\omega}\right]\mathrm{e}^{-(U/u)^2}\,\mathrm{d}U\\
\frac{\partial j_y}{\partial E_{1y}} &= \pi\,\frac{K u^2}{2}\,\frac{e^2}{m\,\omega_\mathrm{c}}\int_{-\infty}^{\infty}\left[\mathrm{i}\left(\frac{1}{1-b}-\frac{1}{1+b}\right)\left(1+\alpha_y\, v_\mathrm{D}\,\frac{kU}{\omega}\right)+\frac{2\mathrm{i}\,\alpha_y v_\mathrm{D}}{b}\,\frac{kU}{\omega}\right]\mathrm{e}^{-(U/u)^2}\,\mathrm{d}U\\
\frac{\partial j_y}{\partial E_{1z}} &= \pi\,\frac{K u^2}{2}\,\frac{e^2}{m\,\omega_\mathrm{c}}\int_{-\infty}^{\infty}\left[\mathrm{i}\left(\frac{1}{1-b}-\frac{1}{1+b}\right)\left(-2\frac{v_\mathrm{D}}{u^2}U+\alpha_y U\right)-\left(\frac{1}{1-b}+\frac{1}{1+b}\right)\alpha_x U-\mathrm{i}\,\frac{4\,v_\mathrm{D}\,U}{bu^2}\right]\mathrm{e}^{-(U/u)^2}\,\mathrm{d}U
\end{aligned}\right\}\qquad(13)$$

$$\left.\begin{aligned}
\frac{\partial j_z}{\partial E_{1x}} &= \pi\,\frac{K u^2}{2}\,\frac{e^2}{m\,\omega_\mathrm{c}}\int_{-\infty}^{\infty}\mathrm{i}\,\alpha_x\,\frac{ku^2}{\omega}\,\frac{U^2}{b}\,\mathrm{e}^{-(U/u)^2}\,\mathrm{d}U\\
\frac{\partial j_z}{\partial E_{1y}} &= \pi\,\frac{K u^2}{2}\,\frac{e^2}{m\,\omega_\mathrm{c}}\int_{-\infty}^{\infty}\mathrm{i}\,\alpha_y\,\frac{ku^2}{\omega}\,\frac{U^2}{b}\,\mathrm{e}^{-(U/u)^2}\,\mathrm{d}U\\
\frac{\partial j_z}{\partial E_{1z}} &= \pi\,\frac{K u^2}{2}\,\frac{e^2}{m\,\omega_\mathrm{c}}\int_{-\infty}^{\infty}-2\,\frac{U^2}{b}\,\mathrm{e}^{-(U/u)^2}\,\mathrm{d}U
\end{aligned}\right\}\qquad(14)$$

$$\begin{vmatrix}
\mathrm{i}\,\dfrac{\omega}{\varepsilon_0}\dfrac{\partial j_x}{\partial E_{1x}}+c^2k^2-\omega^2 & \dfrac{\mathrm{i}\omega}{\varepsilon_0}\dfrac{\partial j_x}{\partial E_{1y}} & \dfrac{\mathrm{i}\omega}{\varepsilon_0}\dfrac{\partial j_x}{\partial E_{1z}}\\
\dfrac{\mathrm{i}\omega}{\varepsilon_0}\dfrac{\partial j_y}{\partial E_{1x}} & \dfrac{\mathrm{i}\omega}{\varepsilon_0}\dfrac{\partial j_y}{\partial E_{1y}}+c^2k^2-\omega^2 & \dfrac{\mathrm{i}\omega}{\varepsilon_0}\dfrac{\partial j_y}{\partial E_{1z}}\\
\dfrac{\mathrm{i}\omega}{\varepsilon_0}\dfrac{\partial j_z}{\partial E_{1x}} & \dfrac{\mathrm{i}\omega}{\varepsilon_0}\dfrac{\partial j_z}{\partial E_{1y}} & -\omega^2+\dfrac{\mathrm{i}\omega}{\varepsilon_0}\dfrac{\partial j_z}{\partial E_{1z}}
\end{vmatrix}=0\qquad(15)$$

$$\begin{vmatrix}
\omega^2-c^2k^2+\dfrac{\omega_p^2}{u\,\pi^{1/2}}\displaystyle\int\varphi_-(1-\alpha_{1x}v_\mathrm{D})\,\mathrm{d}U & -\mathrm{i}\,\dfrac{\omega_p^2}{u\,\pi^{1/2}}\displaystyle\int\varphi_+(1+\alpha_{1y}v_\mathrm{D})\,\mathrm{d}U & -\mathrm{i}\,\dfrac{\omega_p^2}{u\,\pi^{1/2}}\displaystyle\int\varphi_+\alpha_{1z}\,U\,\mathrm{d}U\\
\dfrac{i\,\omega_p^2}{u\,\pi^{1/2}}\displaystyle\int\varphi_+(1-\alpha_{2x}v_\mathrm{D})\,\mathrm{d}U & \omega^2-c^2k^2+\dfrac{\omega_p^2}{u\,\pi^{1/2}}\displaystyle\int\varphi_-(1+\alpha_{2y}v_\mathrm{D})\,\mathrm{d}U & \dfrac{\omega_p^2}{u\,\pi^{1/2}}\displaystyle\int\varphi_-\alpha_{2z}\,U\,\mathrm{d}U\\
\dfrac{2\,\omega_p^2}{u\,\pi^{1/2}}\displaystyle\int\psi\,\alpha_x k\,U^2\,\mathrm{d}U & \dfrac{2\,\omega_p^2}{u\,\pi^{1/2}}\displaystyle\int\psi\,\alpha_y k\,U^2\,\mathrm{d}U & \omega^2-\dfrac{4\omega_p^2}{u\,\pi^{1/2}}\displaystyle\int\psi\,\omega\,U^2\,\mathrm{d}U
\end{vmatrix}=0\qquad(16)$$

En reportant ces expressions dans (7) et en annulant son déterminant on obtient l'équation de dispersion (15), indiquée page 993.

Discussion

En explicitant l'équation de dispersion (15), en fonction des expressions $\partial j_i/\partial E_i$ (12), (13), (14) précédemment calculées, et en regroupant les termes en fonction du champ électrique nous obtenons l'éq. (16) (page 993) avec les notations

$$\varphi_+ = \left(\frac{\omega}{\omega+\omega_c+k\,U} + \frac{\omega}{\omega_c-\omega-k\,U}\right)\exp-\left(\frac{U}{u}\right)^2$$

$$\varphi_- = \left(\frac{-\omega}{\omega+\omega_c+k\,U} + \frac{\omega}{-\omega-kU+\omega_c}\right)\exp-\left(\frac{U}{u}\right)^2$$

$$\alpha_{1x} = \mathrm{i}\,\alpha_x\frac{\omega_c}{\omega}\frac{kU}{\omega+k\,U} \qquad \alpha_{1y} = \alpha_y\frac{k\,U}{\omega}$$

$$\alpha_{1z} = \alpha_y - \frac{2v_D}{u^2} + \alpha_x\frac{\omega+k\,U}{\omega_c}$$

$$\alpha_{2x} = \alpha_{1x} \qquad \alpha_{2y} = \alpha_{1y}\frac{\omega_c^2}{(\omega+k\,U)^2}$$

$$\alpha_{2z} = \alpha_y - \frac{2v_D}{u^2} + \mathrm{i}\,\alpha_x\frac{\omega_c}{\omega+k\,U}$$

$$\psi = \frac{1}{\omega+k\,U}\exp-\left(\frac{U}{u}\right)^2$$

$v_D = \dfrac{E_0}{B_0}$ vitesse de dérive

Pour discuter ce déterminant examinons les deux cas suivants:

(1) Si le champ électrique est nul, $E_0=0$, $\alpha=0$ $v_D=0$, le déterminant se simplifie et donne deux relations de dispersions indépendantes, l'une pour les ondes électromagnétiques et l'autre pour les ondes électrostatiques.

Ces deux relations s'écrivent

$$c^2k^2-\omega^2 = \frac{{\omega_p}^2}{u\,\pi^{1/2}}\int_{-\infty}^{+\infty}\frac{\omega}{\omega\pm\omega_c+k\,U}\exp-\left(\frac{U}{u}\right)^2\mathrm{d}\,U$$

$$1 = \frac{2\,{\omega_p}^2}{k u^3\pi^{1/2}}\int_{-\infty}^{\infty}\frac{U}{\omega+k\,U}\exp-\left(\frac{U}{u}\right)^2\mathrm{d}\,U$$

(2) Si le champ électrique n'est pas nul, $E_0\neq 0$ $\alpha\neq 0$ $v_D\neq 0$, tous les termes du déterminant sont différents de zéro; les relations de dispersion des ondes électrostatiques et des ondes électromagnétiques ne sont plus indépendantes; il y a couplage.

Appendice

Nous donnons ici les valeurs de certaines intégrales apparaissant dans le calcul du courant **j** à partir de f_1.

(a) Dans l'intégration sur φ nous voyons apparaître les trois expressions

$$B_1 = \int_0^{2\pi}\cos\varphi\,\mathrm{e}^{\mathrm{i}\,b\varphi}\,A_n\,\mathrm{d}\,\varphi$$

$$B_2 = \int_0^{2\pi}\sin\varphi\,\mathrm{e}^{\mathrm{i}\,b\varphi}\,A_n\,\mathrm{d}\,\varphi$$

$$B_3 = \int\mathrm{e}^{\mathrm{i}\,b\varphi}\,A_n\,\mathrm{d}\,\varphi$$

avec $$A_n = \frac{\mathrm{e}^{-2\,\mathrm{i}\,\pi b}-1}{\mathrm{i}\,(n-b)}\,\mathrm{e}^{\mathrm{i}(n-b)\,\varphi}$$

Le calcul conduit à

$$B_1 = -\mathrm{i}\,\pi(\mathrm{e}^{-2\,\mathrm{i}\,\pi b}-1)\left(\frac{\delta_{n,1}}{1-b}-\frac{\delta_{n,-1}}{1+b}\right)$$

$$B_2 = \pi\,(\mathrm{e}^{-2\,\mathrm{i}\,\pi b}-1)\left(\frac{\delta_{n,1}}{1-b}+\frac{\delta_{n,-1}}{1+b}\right)$$

$$B_3 = 2\,\mathrm{i}\,\pi(\mathrm{e}^{-2\,\mathrm{i}\,\pi b}-1)\,\frac{\delta_{n,0}}{b}$$

$$\delta_{ij} = \begin{cases} 0 & \text{si } i\neq j \\ 1 & \text{si } i=j \end{cases}$$

(b) Dans l'intégration sur W les intégrales intervenant sont

$$\Lambda^{(n)} = \int_0^{\infty} W^{n+1}\,I_n\left(\frac{2v_D}{u^2}\,W\right)\mathrm{e}^{-W^2/u^2}\,\mathrm{d}\,W$$

$$\Lambda_1 = \int_0^{\infty} W^3\,I_0\left(\frac{2v_D}{u^2}\,W\right)\mathrm{e}^{-W^2/u^2}\,\mathrm{d}\,W$$

$$\Lambda_2 = \int_0^{\infty} W^4\,I_1\left(\frac{2v_D}{u^2}\,W\right)\mathrm{e}^{-W^2/u^2}\,\mathrm{d}\,W$$

Ces intégrales sont connue sous le nom d'«Intégrales de Weber» [8]

$$\Lambda^{(n)} = \frac{u^2}{2}\,{v_D}^n\mathrm{e}^{-{v_D}^2/u^2}$$

Une intégration par partie donne

$$\Lambda_1 = \frac{u^2}{2}\,(u^2+{v_D}^2)\,\mathrm{e}^{{v_D}^2/u^2}$$

et l'égalité $(u^2/2)\,(\mathrm{d}\Lambda_1/\mathrm{d}v_D)=\Lambda_2$ entraîne

$$\Lambda_2 = \frac{u^2}{2}\,(2\,u^2\,v_D+{v_D}^3)\,\mathrm{e}^{{v_D}^2/u^2}$$

Références

[1] CHAPMAN, S., COWLING, T. G., The Mathematical Theory of Non-Uniform Gases, Cambridge University Press, London (1960).

[2] ALLIS, W. P., in Handbuch der Physik **21** (S. Flügge. ed.) Springer-Verlag, Berlin (1956) 404.

[3] JANCEL, R., KAHAN, T., in Proc. 3rd Intern. Conf. Ionization Phenomena in Gases (Venice, 11-15 June 1957) **2**, North Holland Publishing Co., Amsterdam (1959) 569.

[4] BERTRAND, P., BRIFFOD, G., Rapport Technique 113 P.A. — C.E.N. Saclay.

[5] HARRIS, E. G., *J. nucl. Energy, Part C*, **2** (1961) 138.

[6] BAYET, M., DELCROIX, J. L., DENISSE, J. F., *J. Phys. Radium* **15** (1954) 795; **16** (1955) 274; **17** (1956) 923.

[7] BERNSTEIN, I., *Phys. Rev.* **109** (1958) 10.

[8] WATSON, G. N., Theory of Bessel Functions, 2nd edition, Cambridge University Press, London (1944).

ÉTUDE DE LA DIFFUSION PERPENDICULAIRE AU CHAMP MAGNÉTIQUE*

J. F. Bonnal, G. Briffod, M. Grégoire, C. Manus

Centre d'Etudes Nucléaires de Saclay

Service de Physique Appliquée, Section d'Ionique Générale

Gif-sur-Yvette (S-et-O), France

Une étude de la diffusion d'un plasma perpendiculairement au champ magnétique a été effectuée dans un milieu faiblement ionisé. Les observations mettent en évidence trois régimes différents du flux de fuite, chacun étant caractérisé par une certaine plage du champ magnétique:

(1) Pour une valeur de champ magnétique inférieure à un certain champ critique, le flux diminue avec le champ magnétique et augmente avec la pression, selon les lois classiques de la diffusion par collision binaire.

(2) Le flux de fuite passe par un minimum au champ critique. Au-delà de cette valeur, des instabilités apparaissent, et le flux se met à augmenter. L'effet de la pression dans ce régime se manifeste de façon différente sur le flux, qui est d'autant plus faible que la pression est élevée, à l'inverse de ce qui a été décrit au paragraphe 1.

(3) Le flux, après être passé par un maximum pour une certaine valeur élevée du champ magnétique, se met à diminuer progressivement pour des valeurs plus grandes du champ. La dépendance du flux à l'égard de la pression reste semblable au deuxième régime. L'amplitude des instabilités diminue avec le champ magnétique. Il s'agit encore d'une diffusion anormale, dominée par les champs électriques fluctuants.

L'étude du bruit dans le régime instable — (2 et 3) — met en évidence des composantes à une fréquence supérieure à la fréquence plasma. Cette dernière remarque et l'ensemble des observations ont suggéré aux auteurs une tentative d'explication théorique à caractère microscopique (voir le mémoire CN-10/106, page 991, ce volume).

1. Introduction et principe de la mesure

L'étude de la diffusion que nous vous présentons a été effectuée sur des plasmas produits par des décharges "PIG REFLEX" plongées dans un champ magnétique longitudinal. Les plasmas créés dans de telles décharges ont des caractéristiques physiques nettement différentes des plasmas obtenus dans les décharges à colonne positive. Après avoir rappelé brièvement le principe des mesures effectuées par B. Lehnert [1, 2] ainsi que T. K. Allen et al [3, 4] sur les colonnes positives, nous décrirons la méthode utilisée dans nos expériences.

B. Lehnert s'est servi de la mesure du champ électrique longitudinal E_z pour suivre l'évolution du flux de fuite. En effet, on peut montrer qu'une augmentation de champ magnétique correspond à une diminution de la température électronique ainsi que du flux de fuite. Comme le champ électrique est lié à la valeur de la température électronique, une augmentation du champ magnétique doit se traduire par une réduction de E_z; si tel n'est pas le cas, on peut en déduire que le flux de fuite a été altéré par une autre cause, l'apparition de phénomènes oscillatoires par exemple.

Il est évident que ce principe de mesure n'est pas applicable dans une décharge reflex [5] où E_z est très faible sur presque toute la longueur. Nous nous sommes tournés vers une méthode différente, inspirée par A. Simon [6] d'une part et G. Ecker [7] de l'autre.

Ce dernier a montré que le coefficient de diffusion perpendiculaire au champ magnétique est donné par

$$D_\perp = \frac{D_+\mu_- + D_-\mu_+}{\varepsilon\mu_+ + \mu_-} \times \frac{1}{1 + \dfrac{\mu_+\mu_- B^2}{1+(\sigma_+ + \sigma_-)} \dfrac{\mu_+ + \varepsilon\mu_-}{\mu_- + \varepsilon\mu_+}} \quad (1)$$

D = coefficient de diffusion; μ = mobilité; ε est défini par $\Gamma_{r-} = \varepsilon\Gamma_{r+}$ [2]; Γ_r est le flux radial; ε est un paramètre qui permet de caractériser le type de diffusion envisagé; $\varepsilon = 0$: diffusion proposée par Simon due aux effets de court circuit; $\varepsilon = 1$: diffusion ambipolaire; σ caractérise l'effet des interactions dans le plasma).

L'expression (1) montre nettement que l'apparition d'un terme d'interaction σ, qui pourrait être produit par exemple par un certain régime oscillatoire, a pour effet d'augmenter le coefficient de diffusion perpendiculaire.

On sait par les travaux de Simon [8] que la distribution de densité radiale permet de déterminer le coefficient de diffusion ambipolaire perpendiculaire. En particulier, la valeur n_{ext}/n_0, quotient de la densité extérieure du plasma (c'est-à-dire la densité mesurée en dehors du cordon du plasma) par la densité intérieure, diminue pour les valeurs croissantes du champ magnétique. Si pour une certaine valeur du champ le plasma devient le siège d'un régime oscillatoire, celui-ci peut éventuellement être associé à une augmentation du terme $\sigma_+ + \sigma_-$ entraînant une augmentation de $D_\perp$, soit une modification de la valeur de la densité radiale.

* Mémoire CN-10/91, présenté par G. Briffod. La discussion concernant ce mémoire est donnée page 1021. Les traductions du résumé se trouvent en fin de volume.

La mesure de la densité radiale est effectuée au moyen d'une sonde polarisée négativement par rapport au plasma. Si la différence de potentiel entre plasma et sonde est suffisante, le courant mesuré est alors proportionnel à la densité locale. Il convient néanmoins de prendre un certain nombre de précautions que nous ne détaillerons pas ici. Notons cependant un point important. L'étude de la densité intérieure du plasma, effectuée par sondes et par hyperfréquences, montre qu'elle dépend légèrement des paramètres tels que la pression et le champ magnétique. C'est donc toujours le rapport n_{ext}/n_0 qui figure dans les courbes que nous avons relevées.

2. Premiere partie experimentale

2.1. Résultats de mesure sur une décharge réflex de petite dimension ($L=110$ mm)

La figure (1) nous montre la variation de la densité extérieure en fonction du champ magnétique pour différentes valeurs de la pression, soit de la fréquence de collision entre particules chargées et neutres, dans l'hydrogène. La densité du plasma est de l'ordre de quelques 10^{10} particules/cm^3 (voir le par. 2.2 pour l'influence du degré d'ionisation).

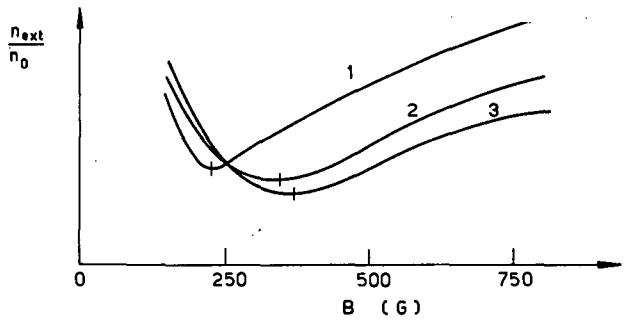

Fig. 1 Variation du rapport n_{ext}/n_0 (quotient de la densité extérieure du plasma par la densité intérieure) en fonction du champ magnétique dans l'hydrogène. $0<B<1000$ G; $L=110$ mm; $D=30$ mm; $V=400$ V; $I=200$ mA. (1) $p=1{,}6\times10^{-2}$ torr; $B_c=230$ G. (2) $p=2{,}4\times10^{-2}$ torr; $B_c=320$ G. (3) $p=3\times10^{-2}$ torr; $B_c=360$ G.

Examinons la courbe 1. On constate que, pour les faibles valeurs du champ magnétique, le rapport des densités diminue lorsque le champ magnétique augmente selon les prévisions théoriques. Pour la B_{c1} (dite champ critique), ce rapport passe par un minimum, puis il se met à augmenter pour les valeurs plus élevées du champ magnétique. Nous diagnostiquons donc en B_{c1}, un changement du régime de diffusion.

Examinons la courbe 2, établie pour une pression plus élevée. Le comportement est le même, la seule différence réside dans le fait que la valeur de B_{c2} est plus élevée que B_{c1}. Il en est de même pour la courbe 3, $B_{c3}>B_{c2}$. Ainsi, nous constatons que le champ critique croît avec la pression.

L'examen plus attentif des courbes révèle une particularité intéressante reliant le comportement de n_{ext}/n_0 en-dessus et en-dessous du champ critique.

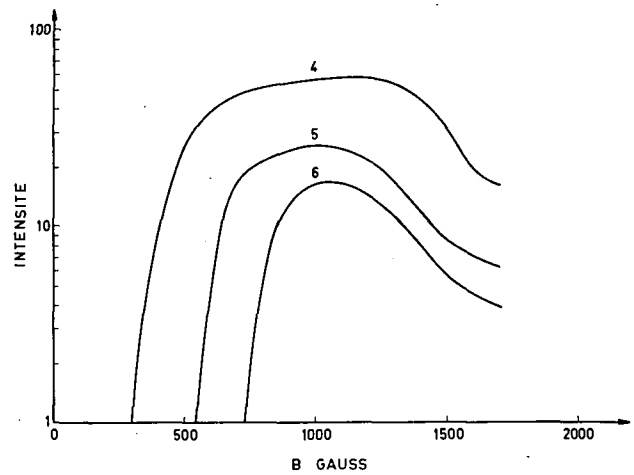

Fig. 2 Valeurs relatives de l'intensité du bruit rayonée à 1000 MHz en fonction du champ magnétique pour trois pressions differentes. $L=110$ mm; $D=15$ mm; $V=400$ V; $I=200$ mA. (4) $p=8\times10^{-3}$ torr; $B_c=440$ G. (5) $p=10^{-2}$ torr; $B_c=460$ G. (6) $p=1{,}6\times10^{-2}$ torr; $B_c=530$ G.

Pour des valeurs telles que $B<B_c$, n_{ext}/n_0 croît avec la pression, ce qui correspond à un régime de diffusion normal.

Pour les valeurs telles que $B>B_c$, c'est l'inverse qui se produit, la densité est d'autant plus faible que la pression est élevée; nous reviendrons sur ce point à la lumière des courbes de bruit (fig. 2).

2.2. Étude en fonction de la densité des particules chargées

Si l'on procède à des mesures analogues à un courant de décharge plus élevé, l'allure des courbes reste la même et l'on ne décèle pas de déplacement important de la valeur du champ critique, quand bien même la densité des particules chargées varie de près d'un ordre de grandeur. En fait on observe, plus exactement, une très légère augmentation du champ critique en fonction de la densité des particules chargées, il n'est guère possible actuellement de chiffrer avec précision cet effet.

2.3. Étude en fonction du diamétre du plasma

Nous avons modifié le diamètre du plasma en agissant sur le diamètre de la cathode et des anodes. On constate que le champ critique est affecté par la valeur du diamètre de telle façon que le produit $B_c \times$ *diamètre* soit sensiblement constant.

Nous avons effectué ces mesures pour les diamètres suivants: $D=10$, 15, 20, 30 mm.

2.4. Étude du bruit

Si l'on oscillographie le potentiel d'une sonde flottante plongée dans le plasma, on constate une augmentation très importante du niveau du bruit pour des valeurs de champ magnétique: $B>B_c$.

Nous avons étudié le bruit à une fréquence beaucoup plus élevée (1000 MHz) au moyen d'un radiomètre que nous allons décrire brièvement. Le réflecteur est constitué par un secteur d'ellipse dont le plasma occupe un des foyers; à l'autre foyer, on a disposé une antenne quart d'onde. Un système de double hétérodynage permet d'effectuer une mesure directe sur galvanomètre. La sensibilité actuelle du dispositif n'est pas suffisante pour permettre l'observation du bruit thermique du plasma (qui est très en dessous des valeurs représentées dans la fig. 2).

La première courbe (fig. 2) a été relevée à une pression de 8×10^{-3} torr. Le bruit à 1000 MHz est nettement observable à un champ magnétique de 500 G, alors que le champ critique est de 440 G; il passe par un maximum pour une valeur de champ plus élevée et décroît ensuite en intensité au fur et à mesure que le champ augmente.

Les deux autres courbes relevées respectivement à une pression de 10^{-2} torr et $1{,}6 \times 10^{-2}$ torr présentent la même allure générale. Elles sont caractérisées par leur amplitude plus faible.

L'écart entre la valeur du champ critique et le champ magnétique à partir duquel le bruit devient observable peut être probablement expliqué par la sensibilité relativement faible du dispositif. Il est évident en effet qu'une plus grande sensibilité nous permettrait d'observer le bruit à une valeur plus faible du champ magnétique, c'est-à-dire plus proche du champ critique.

On constate que la pression des neutres joue un rôle modérateur sur l'amplitude du rayonnement. Les collisions semblent correspondre à un facteur d'amortissement du régime oscillatoire. Cette remarque suggère une comparaison avec les courbes de la fig. 1. On a signalé que le rapport n_{ext}/n_0 est d'autant plus élevé au-dessus du champ critique que le pression est faible; on peut rapprocher ce fait des courbes de rayonnement qui montrent une dépendance analogue de l'énergie rayonnée en fonction de la pression.

2.5. Conclusions

Ainsi, certains des résultats que nous venons de signaler semblent s'apparenter de façon étroite aux observations effectuées sur des décharges à colonne positive [1-4]. (Les études que nous avons faites avec des gaz de différentes natures renforcent encore ce rapprochement). Celà ne peut manquer de surprendre, puisque les caractéristiques des plasmas produits dans notre décharge sont très différentes.

En effet

(1) Le critère de Simon fixant les conditions d'ambipolarité de la diffusion n'est pas satisfait dans nos expériences; nous sommes toujours dans le cas où

$$\frac{L}{R} < \left(\frac{q}{R}\right)^{1/2} \Omega_- \tau_- ; \quad \frac{1}{q} = \frac{1}{n}\frac{\mathrm{d}n}{\mathrm{d}r} \qquad (3)$$

(L=longueur; R=rayon; Ω=pulsation cyclotronique; τ=temps entre deux collisions électron-molécule).

(2) Le plasma à proprement parler, soit la région comprise entre les anodes, est une région dans laquelle le champ électrique longitudinal est extrêmement faible, comme en témoigne l'étude théorique et expérimentale de Salz et al [9]... Ceci n'est évidemment pas le cas dans une décharge à colonne positive.

2.6. Étude de la densité à champ magnétique plus élevé

Les courbes de la fig. 3 montrent le comportement du plasma à des champs magnétiques nettement supérieures au champ critique. Nous voyons que le rapport n_{ext}/n_0 ne croît pas indéfiniment. Il passe par un maximum et décroît pour des valeurs plus élevées du champ. A noter que la valeur du champ correspondant au maximum B_m dépend de la pression.

Notons également que la diffusion n'est pas redevenue normale dans cette région puisque n_{ext}/n_0 est toujours d'autant plus élevé que la pression est faible.

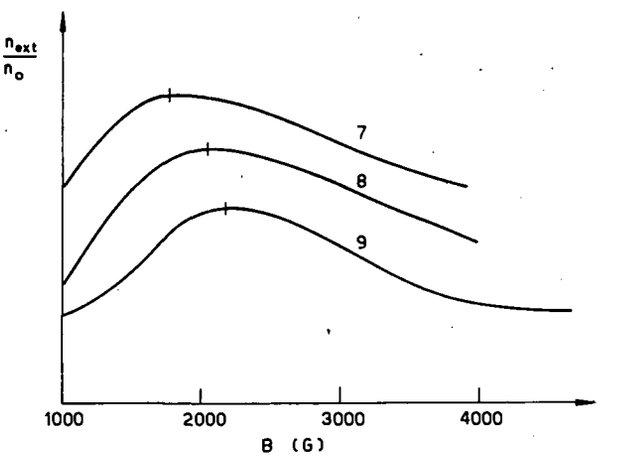

Fig. 3 Variation du rapport n_{ext}/n_0 en fonction du champ magnétique dans l'hydrogène. $1000 < B < 4000$ G; $L = 110$ mm; $D = 15$ mm; $V = 400$ V; $I = 200$ mA. (7) $p = 2{,}1 \times 10^{-2}$ torr; $B_{max} = 1800$ G. (8) $p = 2{,}5 \times 10^{-2}$ torr; $B_{max} = 2100$ G. (9) $p = 3 \times 10^{-2}$ torr; $B_{max} = 2150$ G.

3. Deuxième partie de l'étude experimentale

(décharge reflex de plus grandes dimensions: L= 100 cm, φ=5 cm)

Il nous a paru utile de reprendre ces mesures sur un plasma de dimensions nettement plus importantes. Le schéma de l'installation est donné dans la figure 4.

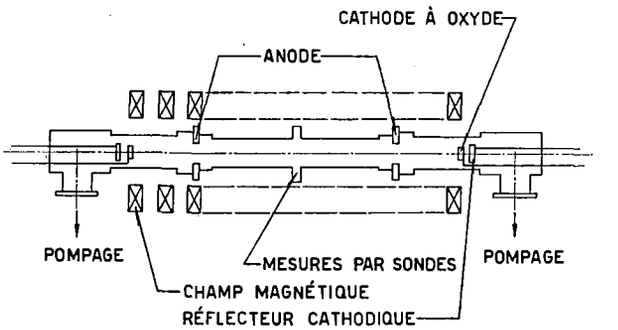

Fig. 4 Dispositif expérimental. Longeur entre cathodes est 1 mètre; diamètre du tube est 100 mm.

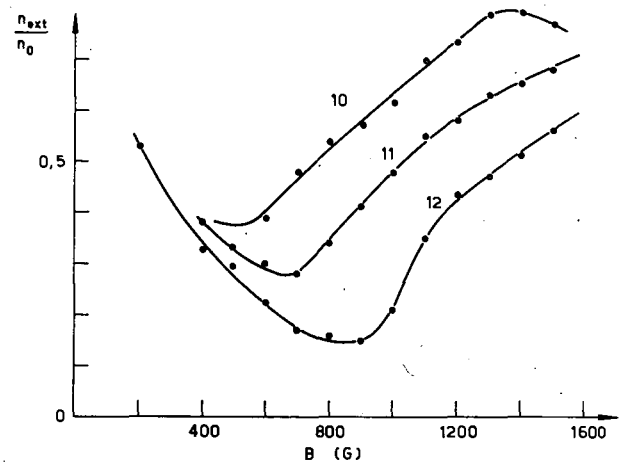

Fig. 5 Variation du rapport n_{ext}/n_0 en fonction du champ magnétique dans l'hydrogène. $L = 1$ mètre; $D = 50$ mm; $V = 650$ V; $I = 500$ mA. (10) $p = 1{,}6 \times 10^{-3}$ torr; $B_c = 480$ G. (11) $p = 2{,}9 \times 10^{-3}$ torr; $B_c = 650$ G. (12) $p = 6{,}2 \times 10^{-3}$ torr; $B_c = 850$ G.

Cette installation fait l'objet d'une communication à la Conférence de Munich; nous nous contenterons donc de signaler uniquement les résultats sur la diffusion.

Mesures de densité. Les courbes de la fig. 5 ont été établies pour l'hydrogène; leur allure est comparable à celle de la fig. 1. La densité est de l'ordre de $10^{11}/cm^3$. Une remarque s'impose: bien que la diamètre du plasma soit plus important, les champs critiques (définis par le minimum des courbes) sont plus élevés. Quant aux courbes de la fig. 6, elles ont été mesurées dans l'azote. Sur cette figure on remarque que les courbes 15 et 16 ne présentent pas de minimum dans le domaine de champ exploré.

Nous ne donnerons pas les courbes du bruit rayonné à 1000 MHz. Leur allure s'apparente à celle de la fig. 2.

4. Discussion

Les mesures de PAULIKAS et al [10] semblent avoir prouvé que, dans une décharge à colonne positive, l'existence d'un champ critique peut être expliqué par la théorie de B. B. KADOMTSEV et A. V. NEDOSPASOV [11] basée sur l'existence d'une instabilité magnéto-hydrodynamique à caractère hélicoïdal. La théorie de F. C. HOH [12] est également en accord raisonnable avec les valeurs expérimentales bien qu'elle soit établie sur une base tout-à-fait différente. Des photographies effectuées au moyen d'une «streak camera» ainsi que des études de la lumière émise par la décharge ont confirmé l'existence d'un tel mouvement.

En ce qui concerne les plasmas que nous avons étudiés, nous n'avons pas, jusqu'à maintenant, observé un tel phénomène de rotation hélicoïdal (bien que nous nous servions des mêmes techniques d'observation).

Examinons néanmoins si le critère de B. B. Kadomtsev et A. V. Nedospasov est susceptible de s'appliquer à nos expériences.

La condition d'existence de ce mode hélicoïdal est donnée par

$$K x^4 + F x^2 + G \leqslant m B v^* x \frac{b_c}{b_i} \qquad (4)$$

Sans rappeler la définition des différents termes entrant dans cette relation, si v^*, qui est la vitesse de dérive des électrons est voisine de 0, c'est-à-dire si le champ longitudinal est très faible, cette condition devient impossible à satisfaire, car tous les termes de gauche sont positifs. Or, le seul domaine dans lequel il règne un champ longitudinal important dans nos plasmas est de toute évidence localisé dans la région comprise entre la cathode et l'anode, c'est-à-dire sur une distance très faible par rapport à la longueur totale de la colonne et située à chacune de ses extrémités.

Il est donc essentiel de diagnostiquer la région dans laquelle se manifestent les phénomènes que nous

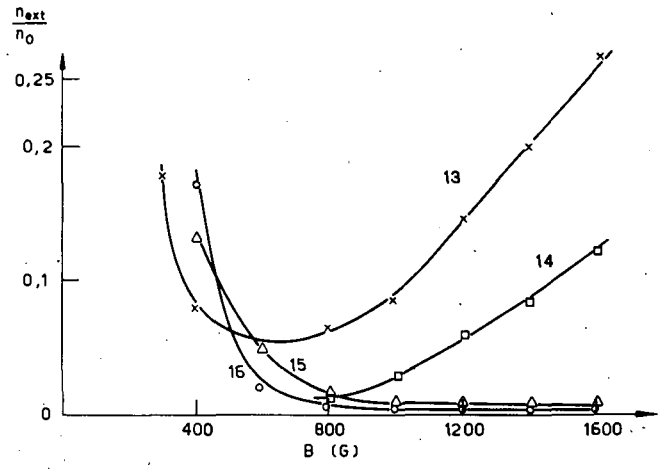

Fig. 6 Variation du rapport n_{ext}/n_0 en fonction du champ magnétique dans l'azote. $L = 1$ mètre; $D = 50$ mm; $V = 800$ V; $I = 500$ mA. (13) $p = 2{,}3 \times 10^{-3}$ torr. (14) $p = 3{,}2 \times 10^{-3}$ torr. (15) $p = 4{,}5 \times 10^{-3}$ torr. (16) $p = 9 \times 10^{-3}$ torr.

avons décrits. Des mesures sont en cours pour élucider ce point.

Nous terminerons par les remarques suivantes:

(1) L'apparition de bruit à fréquence élevée (1000 MHz) peut difficilement être interprétée dans le cadre d'une théorie magnétohydrodynamique.

(2) Nous avons pu, dans certaines conditions expérimentales, réduire de façon importante la partie basse fréquence du spectre de bruit observé. Les courbes de densité radiale n'en ont pas été affectées; la valeur du champ critique est restée inchangée.

(3) Nous n'avons pas observé de mouvements hélicoïdaux dans les plasmas que nous avons étudiés.

Ces différentes remarques nous ont incité à chercher une explication à caractère microscopique. Celle-ci fait l'objet d'une communication de MM. P. BERTRAND et G. BRIFFOD [15].

Remerciements

Nous remercions MM. G. Lecomte, M. Dagai et Nguyen pour la réalisation du radiomètre qui a servi aux mesures de bruit à 1000 MHz. Le concours de MM. J. Morellec et J. Legrand nous a été précieux au cours des mesures.

References

[1] LEHNERT, B., dans Proc. 2nd U. N. Conf. PUAE **32**, United Nations, Geneva (1958) 349.
[2] HOH, F. C., LEHNERT, B., *Phys. Fluids* **3** (1960) 600.
[3] ALLEN, T. K., PAULIKAS, G. A., PYLE, R. V., *Phys. Rev. Letters* **5** (1960) 409.
[4] ALLEN, T. K., PAULIKAS, G. A., PYLE, R. V., U. S. AEC Rapport UCRL-9110 (May 1960).
[5] BONNAL, J. F., BRIFFOD, G., MANUS, C., *C. R. Acad. Sci.* **250** (1960) 2859; *Phys. Rev. Letters* **6** (1961) 665.
[6] SIMON, A., *Phys. Rev.* **98** (1955) 317.
[7] ECKER, G., *Phys. Fluids* **4** (1961) 127.
[8] SIMON, A., dans Proc. 2nd U. N. Conf. PUAE **32**, United Nations, Geneva (1958) 366.
[9] SALZ, F., MEYERAND, R. G., JR., LARY, E. C., WALCH, A. P., *Phys. Rev. Letters*, **6** (1961) 523.
[10] PAULIKAS, G. A., U. S. AEC Rapport UCRL-9588 (27 Feb. 1961).
[11] KADOMTSEV, B. B., NEDOSPASOV, A. V., *J. Nuclear Energy, Part C*, **1** (1960) 230.
[12] HOH, F. C., *Phys. Rev. Letters* **4** (1960) 559.
[13] JOHNSON, R. R., Boeing Scientific Research Laboratories Rapport Dl-82-0101.
[14] ZHARINOV, A. V., *J. nucl. Energy, Part C*, **1** (1960) 271.
[15] BERTRAND, P., BRIFFOD, G., *Fusion Nucléaire*, Supplement 1962, Partie 3, 991.

ÉTUDE EXPÉRIMENTALE D'UNE DÉCHARGE DE STRICTION TUBULAIRE*

J. ADAM**, P. GINOT***, P. H. REBUT****, A. TOROSSIAN***

CENTRE D'ÉTUDES NUCLÉAIRES DE FONTENAY-AUX-ROSES

FONTENAY-AUX-ROSES, FRANCE

Les idées qui ont motivé cette étude sont les suivantes:

- étude des perturbations naissantes dans une configuration «unpinch» malgré la stabilité magnétohydrodynamique
- étude de la corrélation entre le niveau de turbulence du champ magnétique et l'énergie des ions
- étude de la validité de la relation de linéarité rB_θ—B_z décrite par P. Rebut.

On forme un plasma tubulaire (longueur: 1,20 m, diamètres: 16 et 10 cm), de 10^{15} ions/cm^3, confiné par deux décharges simultanées: l'une du type «unpinch» (7 kJ, 125 kA, 4 kV), l'autre du type "thétatron" (6 kJ, 125 kA, 3 kV). La période est de 150 μs.

La position moyenne d'équilibre est en bon accord avec celle que l'on peut déduire par le calcul de l'égalité des pressions magnétiques et des périodes des deux décharges.

Les signaux de sondes magnétiques montrent deux zones de stabilité pendant une demi-période. De légères oscillations naissent ensuite.

Le β (pression cinétique/pression magnétique) apparent est de 0,4. La densité de courant atteint 0,8 kA/cm^2.

A la précision des mesures, la relation linéaire rB_θ—B_z est vérifiée.

1. Les idées

Le projet MEST (Machine pour l'Étude de la Striction Tubulaire) a été adopté en Janvier 1960 pour l'étude des points suivants:

(1) validité du modèle d'équilibre décrit par P. REBUT [1] selon lequel un magneto plasma homogène sans collision en géométrie cylindrique voit chaque assemblée de ses particules identiques (ions et électrons) se mouvoir les unes par rapport aux autres avec un mouvement hélicoïdal comme un corps solide.

Cette propriété se traduit par l'existence d'une relation linéaire entre la composante longitudinal du champ magnétique (B_z) et le produit de sa composante azimuthale par le rayon (rB_θ).

(2) nature des instabilités décrites par S. COLGATE [2] et P. REYNOLDS [3] dans les décharges de type "unpinch", stables en géométrie cylindrique indéfinie selon la magnetohydrodynamique.

(3) corrélation entre le confinement et l'énergie des ions et un niveau variable de turbulence. Cette étude est orientée vers la mise au point et l'exploitation d'un mode d'extraction et d'analyse des particules.

2. La machine

Deux décharges simultanées "unpinch" et "thétatron" forment un plasma annulaire dans une chambre cylindrique (figs. 1 et 2).

Le courant I_{HC} circulant dans le conducteur central se répartit entre le plasma I_p et un conducteur

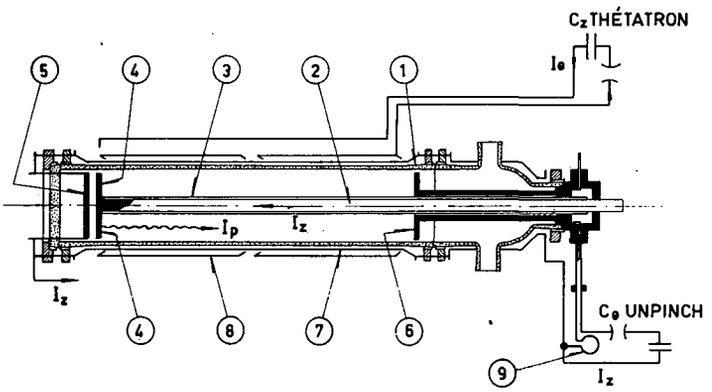

Fig. 1 La machine MEST. 1, Pyrex, diamètre 22 cm, longeur 120 cm; 2, conducteur central, diamètres 4 et 4,4 cm, laiton; 3, Pyrex, diamètre 5,8 cm; 4, 5, 6, électrodes; 7, conducteur longitudinal; 8, conducteur azimuthal; 9, spire.

* Mémoire CN-10/96, présenté par P. Ginot. La discussion concernant ce mémoire est donnée page 1022. Les traductions du résumé se trouvant en fin de volume.

** Euratom. *** Commissariat à l'Energie Atomique, Service de recherches sur la Fusion Contrôlée. **** Commissariat à l'Energie Atomique, Section de Théorie des Gaz Ionisés.

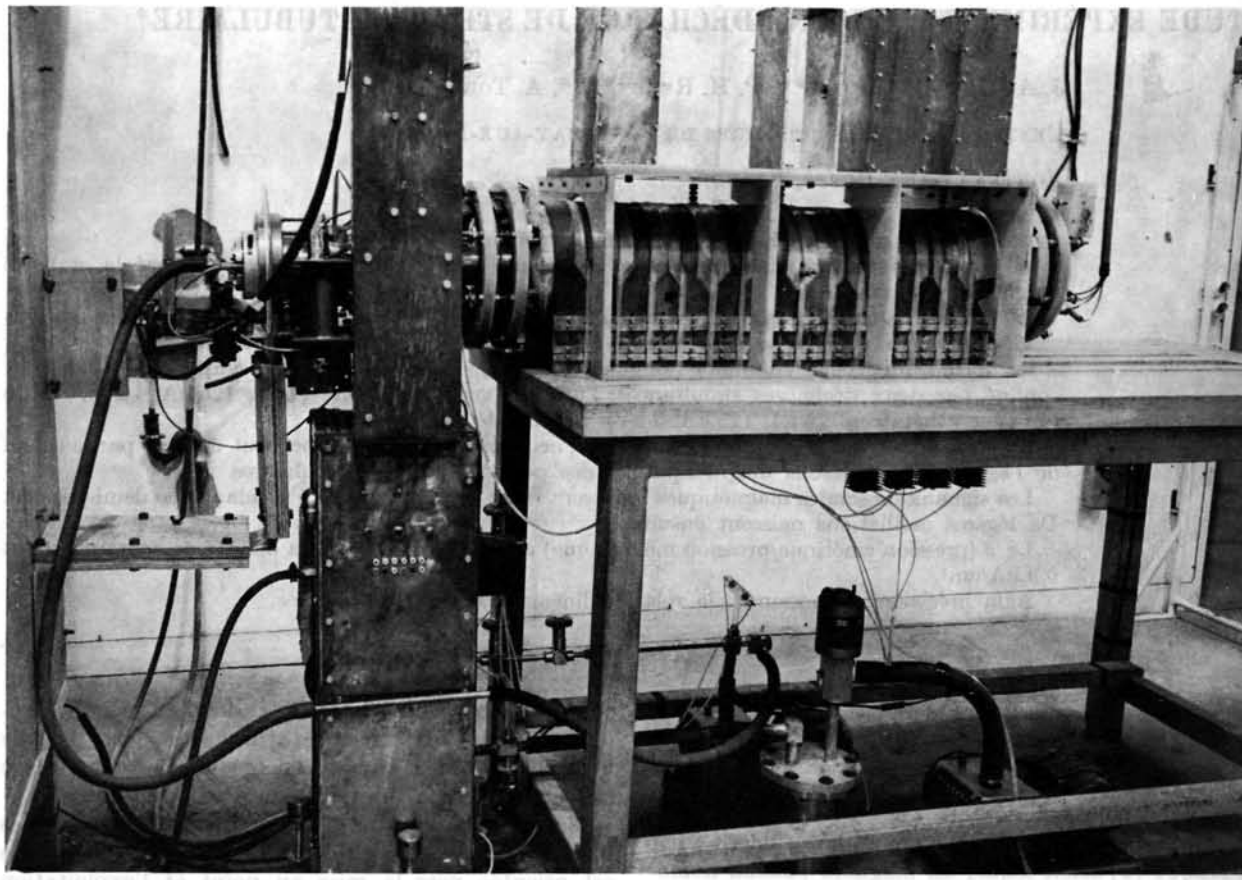

Fig. 2 Photographie de la machine.

extérieur I_E suivant l'impédance d'une spire placée sur I_p.

Les électrodes sont composées de rayons (fig. 3) afin de permettre la pénétration des lignes de forces magnétiques et d'éviter ainsi toute courbure nuisible.

La décharge peut être mise en court-circuit si l'on veut prolonger la première alternance.

Une prédécharge de type "unpinch" ionise le gaz avant la décharge principale, guidée par un champ longitudinal lent pré-établi.

diamètre du conducteur central:	4 cm
diamètre du conducteur extérieur:	25 cm
longueur de la chambre:	120 cm
pression de travail:	10^{-2} torr dans H_2
champ longitudinal lent:	7.5 kJ; t = 1400 μs; 500 G
prédécharge:	500 J; t = 40 μs; 20 kA
décharge "unpinch":	12 kJ (5 kV); t = 150 μs
décharge "thétatron":	15 kJ (5 kV); t = 150 μs

3. Les diagnostics

Sondage magnétique. Des lignes de sondes comportant 16 bobines, d'axes alternativement azimutaux et longitudinaux, plongent suivant un rayon dans la

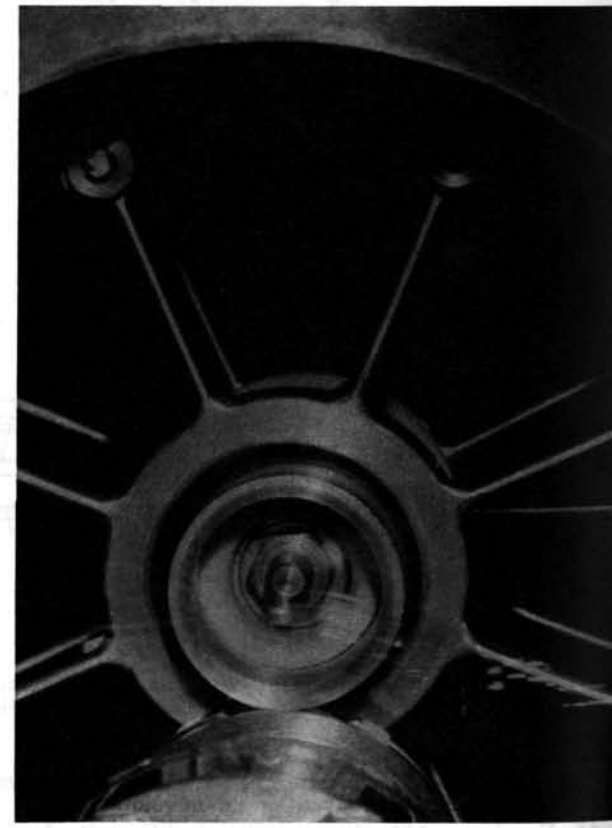

Fig. 3 Electrode composée de rayons.

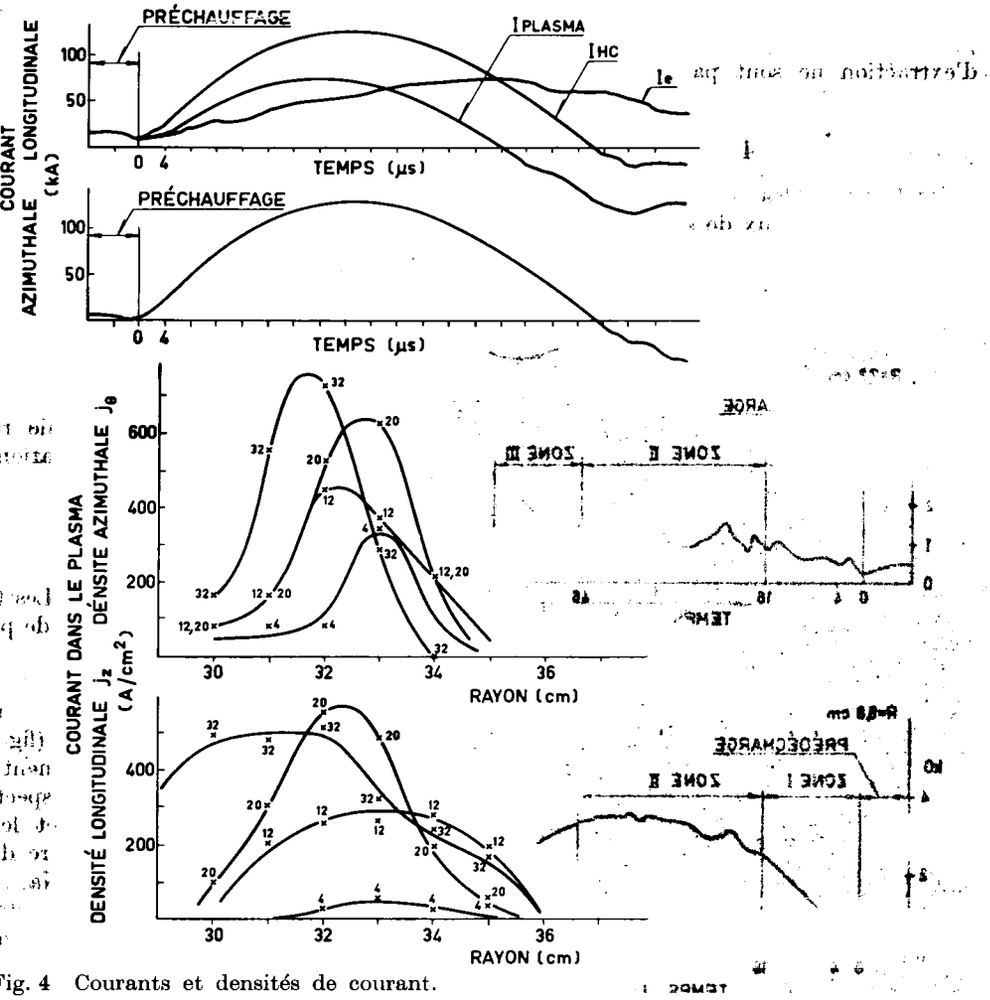

Fig. 4 Courants et densités de courant.

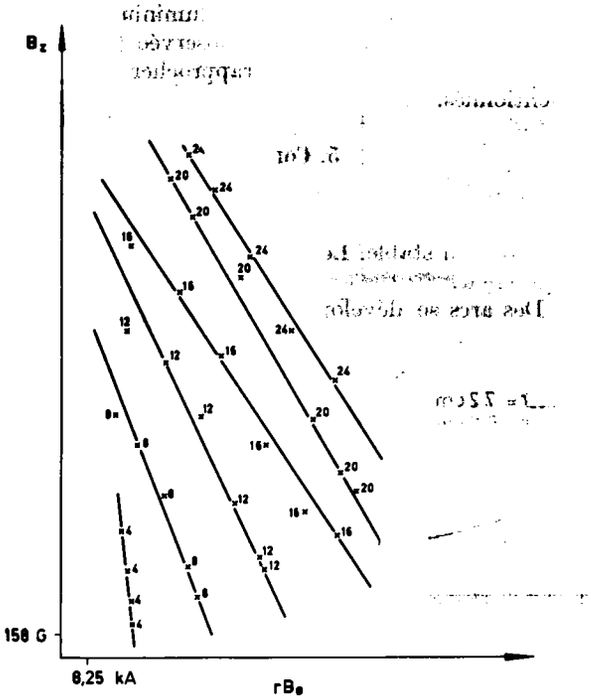

Fig. 5 Vérification de la relation linéaire décrit dans réf. [1].

cavité annulaire. On peut les placer en diverses positions le long et autour de la chambre.

Cinématographie rapide. La caméra LCA-CI1 à activité totale (120 images à la vitesse maximum de 2 images/µs) a été utilisée visant le gaz à travers les électrodes. Une adjonction d'hélium (50%) est nécessaire pour rendre le plasma suffisamment lumineux.

Spectrographie optique. Une caméra Beaudoin munie d'un prisme peu dispersif (le visible en 37 mm) permet de résoudre les principales raies dans le temps en visant à travers les électrodes.

Un spectrographe Réosc (3800-6500 Å) à réseaux croisés (a: 60 traits/mm ordre 35 à 60; b: 600 traits/mm ordre 1) donne une dispersion de 3 Å/mm dans le visible. Muni d'un photomultiplicateur il permet de suivre l'évolution des raies en visant soit à travers les électrodes soit suivant un rayon.

Spectroscopie d'énergie. Un analyseur sépare les particules suivant leur énergie (50 eV-1 keV) à l'aide d'un condensateur cylindrique. Le pouvoir de résolution est de 100 et la sensibilité de 10^{-11} A grâce à un multiplicateur d'électrons. Un cône blindé muni d'un champ magnétique guide extrait les particules

du sein du plasma. Cet ensemble entre dans sa phase préliminaire d'exploitation. Les premiers résultats d'extraction ne sont pas totalement incohérents.

4. Les résultats

(1) Lorsque les conditions initiales sont convenables les signaux de sonde magnétiques montrent une configuration de type "unpinch-thétatron". La fig. 4 donne le courant total dans le conducteur central (I_{HC}), dans le plasma (I_p), dans le conducteur

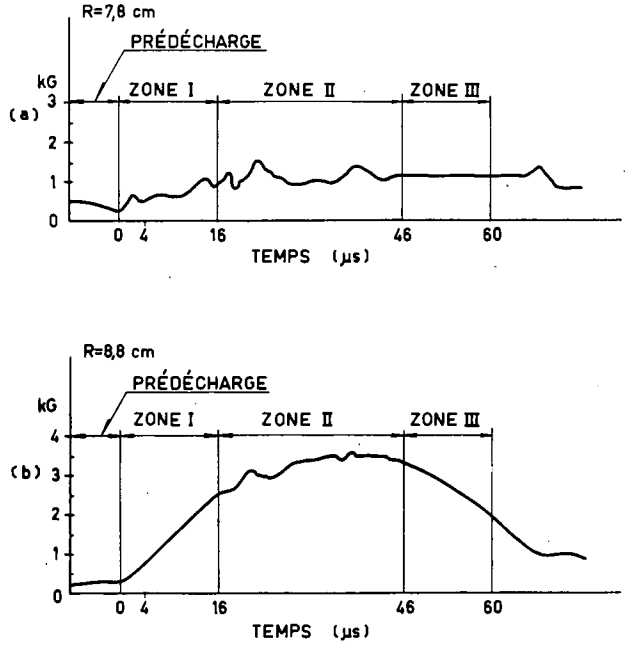

Fig. 6 Signaux de sondes magnétiques. (a) Sonde orientée suivant θ. (b) Sonde orientée suivant z.

extérieur de retour (I_c) et dans la spire azimutale (I_{th}) ainsi que la distribution des densités de courant dans le gaz suivant un rayon. Le β observé est de 0,3 au moins.

La relation linéaire entre B_z et rB_θ décrite dans la réf. 1 est vérifiée (fig. 5).

Les signaux de sonde sont successivement (fig. 6)

Zône I 0-10 μs peu sinueux et reproductibles
Zône II 16-46 μs sinueux et irréproductibles
Zône III 46-60 μs peu sinueux et reproductibles

On en déduit une configuration tour à tour stable, puis turbulente et de nouveau stable au sens habituel. En mettant la décharge en court circuit après le maximum de courant et en utilisant un gaz très propre on garde la décharge confinée pendant les deux premières zônes et une bonne partie de la troisième. Les composantes du champ magnétique longitudinal et azimutal s'interpénètrent lentement tandis que le plasma diffuse. La figure 7 donne l'évolution de la composante longitudinale en divers points d'un rayon de la chambre.

(2) La cinématographie rapide à travers l'anode met en évidence la formation d'un anneau de lumière partant du conducteur central, confiné et stable pendant la première zone magnétique — 15% d'hélium est ajouté habituellement pour que l'on puisse localiser le plasma. L'anode et les conducteurs de retour apparaissent en ombre. Les taches lumineuses situées entre les rayons de l'anode proviennent de la cathode à l'autre bout du tube.

Des arcs se développent à l'anode après 15 μs.

(3) La résolution dans le temps de H_β indique, un haut degré d'ionisation (fig. 8). Cette mesure est en accord avec l'élargissement Stark observé sur H_β également à l'aide du spectrographe Réosc. L'intégration dans l'espace et le temps réduit toutefois l'intérêt de cette dernière donnée.

Les impuretés (C, Na, ...) n'apparaissent pas pendant la première zone stable. Elles se manifestent ensuite (fig. 9), le maximum de l'emission arrivant à la fin de la demi période lorsque l'on laisse la décharge osciller.

Une nette progression de l'aluminium le long du tube à partir de l'anode est observée (fig. 10). Cette émission est sans doute à rapprocher des arcs déjà mentionnés.

5. Conclusion

En résumé on observe un plasma fortement ionisé, stable au sens usuel pendant 15 μs, puis turbulent et de nouveau stable. Les champs magnétiques diffusent lentement.

Des arcs se développent à l'anode vers 15 μs. La

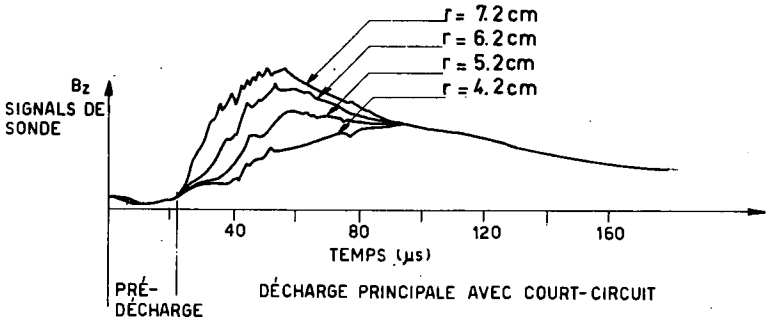

Fig. 7 Evolution dans le temps du champ magnétique longitudinal en divers points, le long d'un rayon.

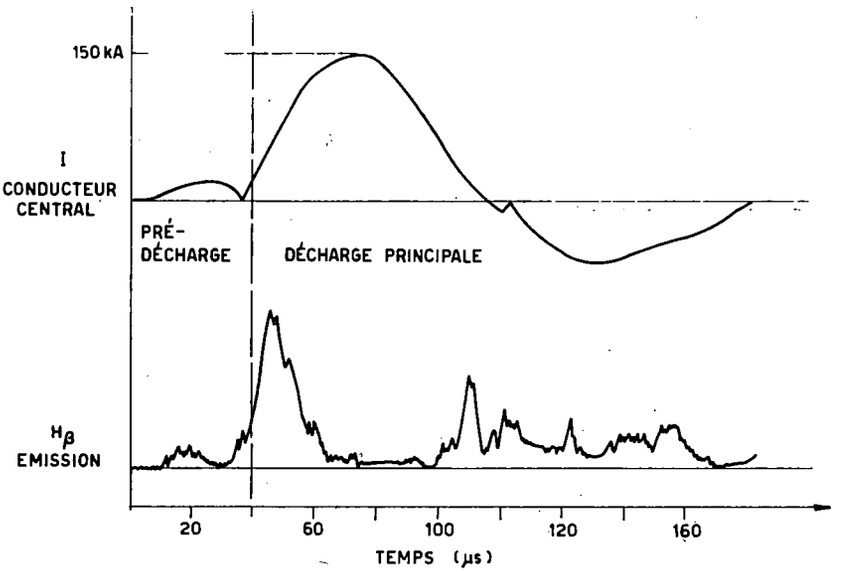

Fig. 8 Evolution de H_β dans le temps.

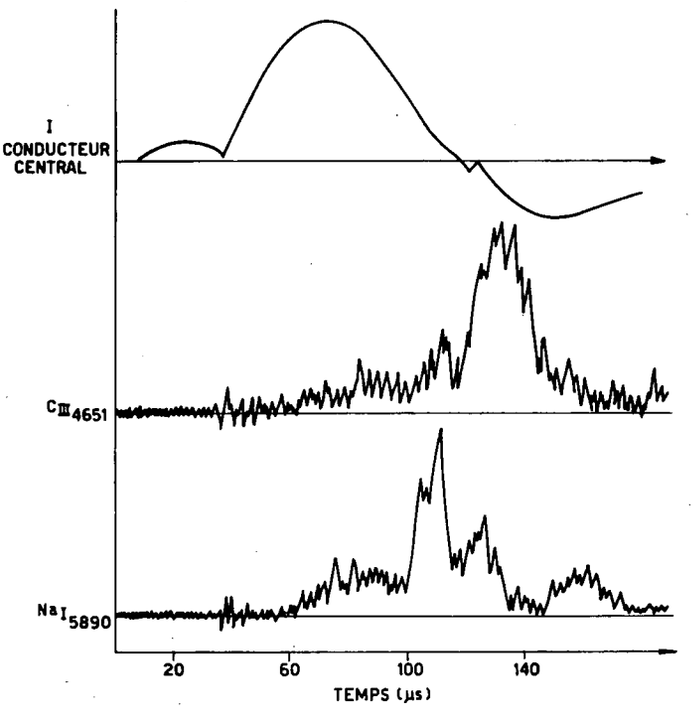

Fig. 9 Evolution des impuretés dans le temps.

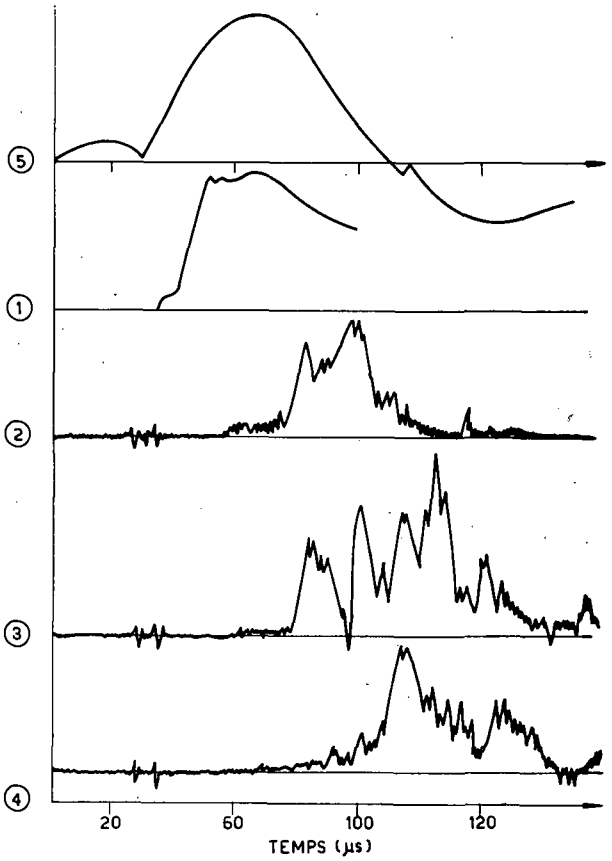

Fig. 10 Evolution dans le temps et progression de Al III (4450 Å) le long du tube. 1, camera visant à travers l'anode; 2, PM à 30 cm de l'anode; 3, PM à 50 cm de l'anode; 4, PM à 90 cm de l'anode; 5, conducteur central.

dissymétrie entre les électrodes et les perturbations importantes à l'anode signalé par S. COLGATE [2] sont confirmées.

6. Remarques

L'apparition des arcs au début de la période turbulente est un fait. On peut en déduir qu'ils sont la cause de l'instabilité. Le raisonnement inverse est possible toutefois: lorsque le plasma devient turbulent des champs électriques apparaissent et provoquent la naissance des arcs.

Une interprétation de la nature des instabilités observées est proposée par P. REBUT [4]. Pour certaines valeurs des paramétres faisant intervenir la proximité de la paroi extérieure, la densité longitudinale du courant, l'épaisseur du plasma... des états d'équilibre hélicoïdaux peuvent exister en plus de l'état d'équilibre cylindrique. Ce point de branchement des équilibres indique la limite de la stabilité. Les déformations épousent le pas des lignes de courant et le plasma se divise en filaments.

Références

[1] REBUT, P., *J. nucl. Energy, Part C*, **3** (1961) 22.
[2] COLGATE, S., U.S. AEC Rapport UCRL-5862; *Phys. Fluis* **3** (1960) 982.
[3] AITKEN, K. L., BURCHAM, J. N., REYNOLDS, P., in Proc. 4th Intern. Conf. Ionisation Phenomena in Gases (Uppsala, 17-21 Aug. 1959) **2**, North Holland Publishing Co., Amsterdam (1960) 896.
[4] REBUT, P., *Fusion Nucléaire*, Supplément 1962, Partie 3, 1167 (seulement résumé).

RUNAWAY ELECTRONS IN A TOROIDAL Z-PINCH DISCHARGE IN HYDROGEN*

U. GROSSMANN-DOERTH, J. JUNKER

MAX-PLANCK-INSTITUT FÜR PHYSIK UND ASTROPHYSIK

MUNICH, FEDERAL REPUBLIC OF GERMANY

The x-rays produced by runaway electrons in the toroidal discharge experiment T-1 have been investigated. The intensity of the radiation as a function of time and energy was measured with the discharge parameters having the following values: electric field strength 5-15 V/cm, pressure 0.02-0.1 torr (hydrogen), B_z-field strength 0-800 G. A burst of radiation was found to appear at the beginning of the discharge with main quantum energy of about 10-20 keV. The radiation during the main part of the discharge is appreciably softer, and the intensity is several orders of magnitude smaller. Similar phenomena were observed in other experiments and are reported in the literature. An attempt was made to explain the burst by the rapidly changing particle densities at the beginning of the discharge leading to complete ionization and by the different values of transport cross-section of hydrogen molecules and protons. Whereas the initial burst could be explained in these terms, the small rate of runaway at later times in the discharge as well as the small energies of the electrons seem to call for a process which suppresses the runaway of electrons. Different kinds of instabilities as possible explanation are discussed.

1. Introduction

It is well known that under the action of an applied electric field electrons in a plasma have a tendency to leave their thermal velocity distribution and gain high energies by following the electric field lines without being scattered. Several authors have dealt theoretically with this phenomenon [1-3] which has been dubbed "runaway" of electrons. The bremsstrahlung produced by these electrons when they hit dense material has been detected in a number of gas-discharge experiments [4-10]. This paper represents the results of the measurements of the x-rays that are emitted from the T-1 discharge. We also made an attempt to explain these observations, particularly the striking feature of an initial radiation burst which has been observed in similar discharge experiments too [4-7, 10].

2. Apparatus

The gas-discharge device called "T-1" consists essentially of a Pyrex torus (major diameter 100 cm, minor diameter 4 cm) enclosed by a copper torus which serves as stabilizing wall and as primary of a transformer the secondary of which is the gas in the glass torus. A number of iron cores improve the electromagnetic coupling. A stabilizing magnetic field ("B_z-field") is produced by the discharge of a condenser through a solenoid that is wound around the copper envelope. A detailed description of the discharge apparatus will be found in Ref. 11.

The experiments to be described here were all made with hydrogen. The discharge parameters had the following values:

pressure of the gas filling	$P_0 = 0.02-0.1$ torr
capacitor voltage	$V_c = 6$ kV
B_z-field strength	$B_z = 0$-800 G

The x-rays emitted from the discharge with energies above ~5 keV were measured with a scintillation counter. The window through which the quanta

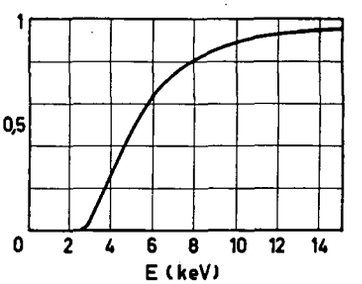

Fig. 1a Fraction of photons that penetrate both beryllium windows and 7 cm of air.

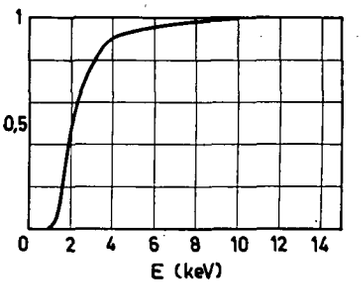

Fig. 1b Fraction of photons that penetrate both Mylar windows.

leave the torus as well as the cover of the scintillation crystal were made of beryllium foils (0.18 mm thick). To extend the range of possible measurements down to ~2 keV a proportional counter (flow counter) was installed. The window of the torus and the entrance window of the counter were in this case made from thin organic foils (Mylar, 0.006 mm).

* Conference paper CN-10/38, presented by U. Grossmann-Doerth. Discussion of this paper is given on page 1022. Translations of the abstract are at the end of this volume of the Conference Proceedings.

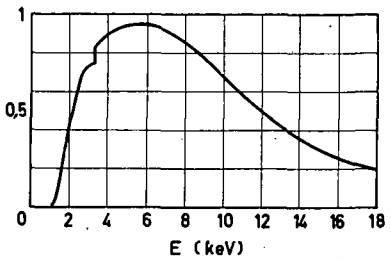

Fig. 2 Probability for a photon to penetrate two Mylar foils and be absorbed in the gas counter.

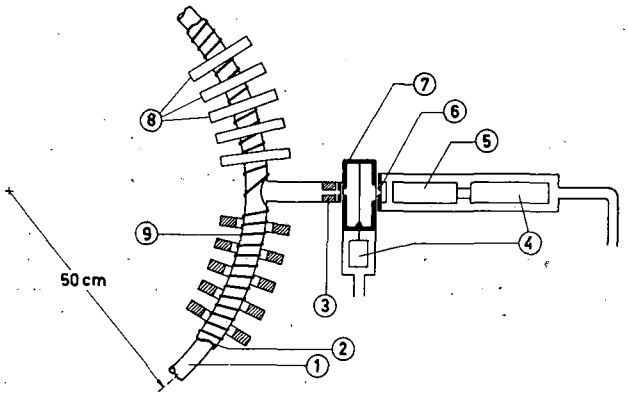

Fig. 3 Experimental setup. 1, Pyrex torus; 2, copper torus; 3, lead collimator; 4, preamplifier; 5, multiplier; 6, scintillation crystal; 7, flow proportional counter; 8, iron cores; 9, B_z field winding.

Figure 1 shows for both cases the absorption by the material the quanta have to penetrate before being counted. By using a collimated beam of x-rays which intercepts the proportional counter first before it enters the crystal, we made it possible to measure both parts of the spectrum simultaneously. Figure 2 shows the probability for a quantum to penetrate both windows and be absorbed in the gas counter. The entire experimental set-up is shown in Fig. 3.

3. Experimental results

During the first microseconds after initiation of the discharge there appears a strong burst of x-rays which is surprisingly reproducible in its amplitude and time dependence (under clean conditions, the mean deviation of the amplitude from the average value is about 20%). Figure 4 is a reproduction of an oscillogram of the x-ray intensity as measured with the scintillation counter and the plasma current. We used a sodium-iodide-crystal for the measurement of the amplitude of the burst and a fast organic crystal for the determination of its time dependence. Table 1 gives a survey of the times that characterize the burst as measured with the scintillator.

The spectra of the quanta emitted with the burst were determined by the absorption method. The absorption curves were evaluated graphically. Figure 5 shows the spectrum of the burst for two specific cases.

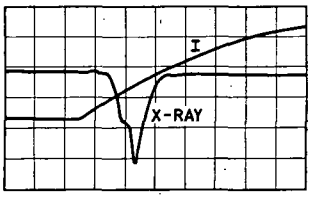

Fig. 4 Reproduction of an oscillogram of x-ray intensity and plasma current I (5 kA/div.) Sweep 1 μs/div.

TABLE I. Characteristic times of the burst

P_0 (torr)	B_z (G)	t_1* (μs)	t_2** (μs)	t_3*** (μs)	I† (kA)
0.02	160	0.65	1.15	0.28	3.6
0.02	800	1.15	2.0	0.4	7.7
0.05	0	0.53	0.9	0.13	1.4
0.05	160	0.5	1.3	0.3	3.2
0.05	800	0.7	1.9	0.5	6.2
0.1	0	0.6	1.0	0.25	1.3
0.1	160	0.5	1.3	0.3	2.7
0.1	800	0.5	1.8	0.4	5.5

* t_1 is the time from start of plasma current to the start of the scintillator signal.

** t_2 is the time from start of current to burst maximum.

*** t_3 is the time in which the burst decreased again to 1/3 of the maximum value.

† I is the magnitude of plasma current at burst maximum. (Reproducibility about 20%.)

The intensity of the x-radiation following the burst is several orders of magnitude smaller and practically constant during the remainder of the discharge. This radiation was measured by counting single quanta. We found that the energy of virtually none of these quanta exceeds 5 keV. It is necessary, therefore, to measure these quanta with the proportional counter. Since the gas counter has only recently been installed, these measurements have not been completed yet. From preliminary scintillator measurements we determined the number of single quanta with energies between ~3 and 5 keV.

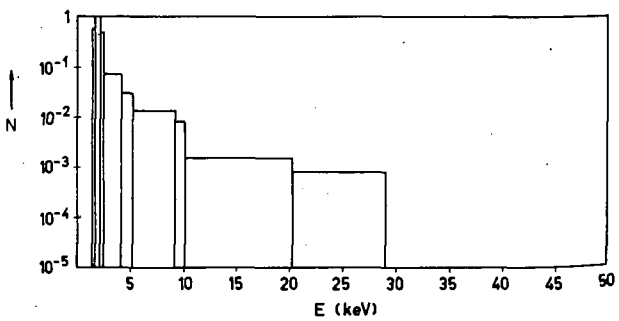

Fig. 5a Burst spectrum as measured with proportional counter. N is number of quanta per energy interval in arbitrary units. $P_0 = 0.05$ torr. $B_z = 0$.

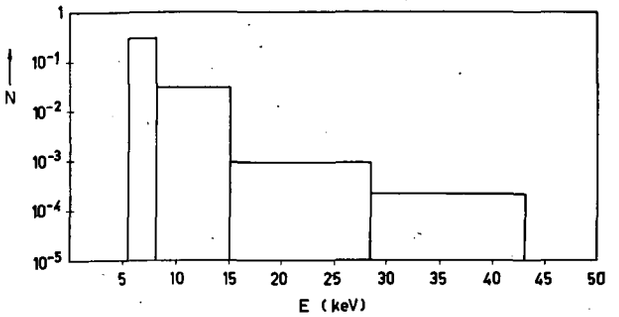

Fig. 5b Burst spectrum as measured with scintillation counter. Same conditions as in Fig. 5a.

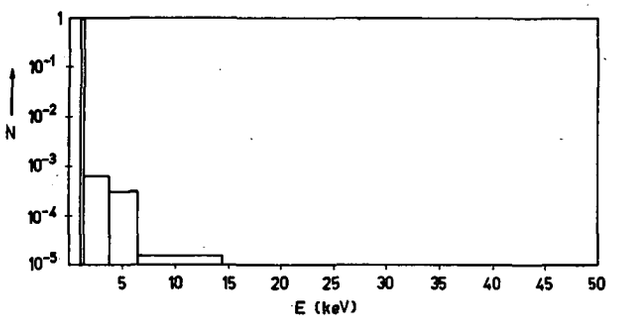

Fig. 5c Burst spectrum as measured with proportional counter. N is the number of quanta per energy interval in arbitrary units. $P_0 = 0.05$ torr. $B_z = 800$ G.

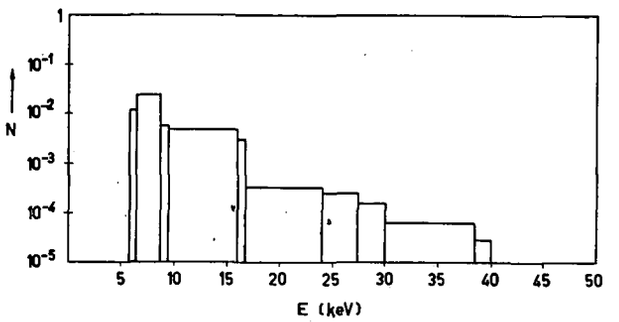

Fig. 5d Burst spectrum as measured with scintillation counter. Same conditions as Fig. 5c.

A schematic drawing of x-ray emission and plasma current during the discharge is shown in Fig. 6.

To compare the experimental results with theory we have to relate the x-ray quanta to the electrons producing them. This was done with consideration of the geometry and the efficiency of the production of bremsstrahlung by electrons. In addition we assumed all the electrons that produce the burst quanta to have 20-keV energy when they hit the wall. Since we are mainly interested in the order of magnitude of the flux of runaway electrons to the wall, this simplifying assumption seems compatible with the measured spectra. Table 2 represents the measured numbers of quanta and the corresponding values of the flux of runaway electrons φ which we define as the number of runaway electrons that hit the wall per second and per square centimeter. The

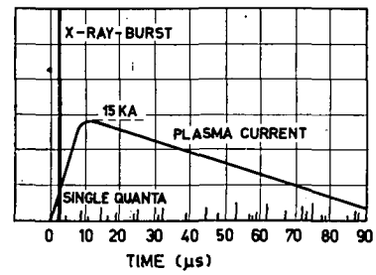

Fig. 6 Plasma current and x-ray emission as functions of time.

data representing the radiation after the burst refer to the preliminary scintillator measurements in the energy region between 3 and 5 keV as mentioned above.

When we calculated the flux of the runaway electrons to the wall, we made the assumption that this quantity does not depend on position. For energies above 25 keV this assumption seems to be correct since we found experimentally that at least the intensity of the burst radiation penetrating 2 mm glass is the same all around the (major) circumference of the torus.

4. Discussion

4.1. Energy of the run-away electrons

The question arises whether the measured energy of the runaway electrons is compatible with the idea of electrons being accelerated by the electric field until their Larmor radius has become too large for them still to be confined in the torus. In order to answer this question the energy ε of electrons with Larmor radius of 2 cm was calculated as a function of the distance r from the axis for different conditions. Table 3 gives the results of these calculations. B_θ is the magnetic field produced by the plasma current I at the time of burst maximum.

Quantum energies much greater than 100 keV cannot be expected to appear with the burst since the acceleration time of the corresponding electrons would be longer than the time elapsed between the beginning of the current and burst maximum (see Table 1).

The influence of drift movements across the magnetic field due to centrifugal forces and inhomogeneity of the magnetic field was estimated. The latter does not play any role. The drift due to the centrifugal force in a pure B_z field, however, is large enough to prevent the runaway electrons from gaining more than $\sim$10 keV. So the additional B_θ field is needed to understand why we measured quantum energies up to 60 keV and more.

By and large the measured energy spectra of the burst seem to agree with our concept of electrons being accelerated in the axial electric field until they hit the wall because of their large Larmor radius or drift movements across the magnetic field. It cannot be easily understood, however, why the energy

TABLE II. Fluxes of photons, and runaway electrons

P_0 (torr)	B_z (G)	n_q (burst)	$\langle E\rangle$**(burst) (keV)	n_q* (single)	φ*** (burst) (cm^{-2} sec^{-1})	φ*** (single) (cm^{-2} sec^{-1})
0.05	0	9×10^3	8	5	10^{15}	5×10^{11}
	160	2×10^5	13	5×10^2	2×10^{16}	5×10^{13}
	800	10^6	16	4×10^2	10^{17}	4×10^{13}
0.1	0	8×10^2	10	—	10^{14}	—
	160	9×10^4	8	30	10^{16}	3×10^{12}
	800	7×10^4	13	10^2	10^{16}	10^{13}

* n_g = numbers of quanta as measured by the scintillation counter. ** $\langle E\rangle$ is the average quantum energy. *** φ = the corresponding flux of runaway electrons to the wall.

TABLE III. Magnetic field strength and corresponding energy of electrons with 2 cm Larmor radius

r (cm)	0.5	1.0	1.5	2.0	Remarks
B_θ (G)	40	75	120	150	$I = 1.5$ kA (current density independent of position)
ε (keV)	0.6	2	6	8	$B_z = 0$
B_θ (G)	600	300	200	150	$I = 1.5$ kA (volume current of constant density, constricted to 1 cm diameter)
ε (keV)	150	40	15	9	$B_z = 0$
B (G)	190	250	340	430	$I = 4$ kA (current density independent of position)
ε (keV)	12	17	32	52	$B = (B_\theta^2 + B_z^2)^{1/2}$ $B_z = 160$ G
B (G)	810	850	920	1000	$I = 6$ kA (current density independent of position)
ε (keV)	260	290	340	400	$B_z = 800$ G

of the runaway electrons that appear after the burst is so low. Both electric and magnetic fields increase during about 10 μs after the burst. One would expect a marked increase in quantum energy.

4.2. Possible explanations

Whereas the increase in x-ray intensity up to the maximum of the burst can easily be explained by the increase of the electron density during that time, the subsequent sudden decrease by several orders of magnitude seems mysterious. The following is a list of possible explanations of this phenomenon:

a The variation of the degree of ionization during the first microseconds could be responsible for a decrease of the number of runaway electrons if electrons are scattered by protons more efficiently than by neutral molecules. An essential part of this paper will consist of a quantitative pursuit of this idea.

b An increase of contamination of the discharge by particles from the wall with large momentum transfer cross-section could make the rate of runaway of electrons smaller. The relative contamination was estimated from spectroscopic measurements to be of the order of 10^{-2}. It consists mainly of oxygen ions with some carbon and silicon ions present. At present, however, our scanty knowledge of the densities of all impurities as functions of time as well as their cross-sections as functions of energy seems to rule out a quantitative treatment of this possibility.

c Abrupt movements of the plasma as a consequence of suddenly occurring instabilities can produce strong electric fields in which electrons are accelerated. However, smear-camera pictures of the discharge show more plasma movements during the main part of the discharge than at the beginning when the burst appears.

d As well as a runaway-electron-producing mechanism, gross plasma instabilities could work as a mechanism that suppresses runaway. It is very conceivable that distortions of the magnetic fields caused by such instabilities reduce the free path of electrons drastically. Essentially, then, runaway electrons would, regardless of their energy, hit the wall before gaining enough energy to produce detectable x-ray quanta.

e So-called "microscopic" instabilities in connection with plasma oscillations (e.g. two-stream-instabilities) have been predicted by several authors [12-15]. Oscillations of this kind could scatter the runaway

electrons out of the plasma. Since a two-stream instability in a plasma occurs if the anisotropy of the electron velocity distribution exceeds a certain value, it is possible that plasma oscillations start to rise if the electric current reaches a critical value. In fact it turned out that the magnitude of the plasma current at the time of burst maximum was approximately the same as the critical value predicted by BERNSTEIN [14]. Also high-frequency radiation (between 10 and 50 MHz) is emitted during the discharge in a somewhat regular pattern. However, the value of the critical current depends on the ratio of electron to ion temperature [15], which has been assumed to be very large in our application of Bernstein's theory. However, we don't have a good knowledge of this ratio which might in reality be much closer to unity. An application of microscopic instability theory seems to require a much better knowledge of the distribution functions of electrons and ions than we have at the present. We therefore do not want to make a decision now as to whether such processes have an influence on the runaway phenomena in our discharge or not.

4.3. THE DENSITY OF RUN-AWAY ELECTRONS IN A MULTICOMPONENT PLASMA

To find out more about the mechanism that produces the burst it is necessary to calculate the "normal" rate of runaway in our plasma; that means, the density of runaway electrons as functions of the degree of ionization with none of the other processes listed in the last section playing any role. For a completely ionized plasma the number of runaway electrons has already been calculated by DREICER [1] to whose results we will refer later.

4.31. *General relations*

If the electric field in a plasma is larger than a critical value E_c (which depends on temperature and pressure) the electrons runaway instantaneously. For electric fields smaller than E_c electrons have to diffuse in velocity space into a certain region before they actually become decoupled from the thermal velocity distribution and run away. In a completely ionized plasma, for instance, the drift velocity of an electron v_D has to become larger than the average thermal velocity v_{th} for the electron to run away [1]. In this case Dreicer has calculated the rate of diffusion into the critical region and by that the rate of runaway. The calculations can be considerably simplified by neglecting the statistical distributions of velocities and free paths. So in the following we will assume all particles to have the same thermal and drift velocities v_{th} and v_D respectively, and the same free path $\lambda(v)$. The flux of runaway electrons will then be found as follows:

q_{tr} shall be the so-called "momentum transfer cross-section", that is, the cross-section for a complete exchange of momentum of an electron moving through a plasma. If n is the density of particles to which the electron may lose momentum and ε_{th} its thermal energy, and if an electric field E is applied to the plasma, the probability W for the electron to travel a distance s without being scattered is given by

$$\ln W(\varepsilon) = -\frac{n}{E}\int_{\varepsilon_{th}}^{\varepsilon} q_{tr}(\varepsilon)\,\mathrm{d}\varepsilon \tag{1}$$

$\varepsilon = Es$ is the energy gained by the electron on its way. (This is the formula for a radioactive decay with time-dependent decay "constant".)

The time between two collisions of a thermal electron is $\tau = \lambda(v_{th})/v_{th}$. By definition, electrons lose their entire extra momentum parallel to the electric field in this collision. But the fraction $W(\varepsilon)$ fails to collide and instead keeps travelling until it reaches the energy ε. Therefore, the number $\varphi(\varepsilon)$ of electrons reaching the energy ε per cubic centimeter per second is given by

$$\varphi(\varepsilon) = \frac{1}{\tau} n_e W(\varepsilon) = \gamma_{th} n_e W(\varepsilon) \tag{2}$$

(n_e is the number density and γ_{th} the collision frequency of thermal electrons; $\varphi(\varepsilon)$ shall be called "flux density of runaway electrons"). If ε is the largest electron energy that be confined by the magnetic field in the torus and if one assumes that all runaway electrons reach this energy before being lost to the wall, the number of runaway electrons hitting the wall per square centimeter per second is given by

$$\Phi(\varepsilon) = \frac{V}{F}\varphi(\varepsilon) = \frac{V}{F}\gamma_{th} n_e W(\varepsilon) \tag{3}$$

where V is the volume of the torus and F its surface. Φ shall be called flux of runaway electrons. It is assumed that the "rain" of runaway electrons to the wall is homogeneous over its surface.

It is easy to see that for a mixture of different particles with which the electrons can collide (3) becomes

$$\Phi(\varepsilon) = \frac{V}{F} n_e \sum \gamma_k(v_{th}) \prod W_k(\varepsilon) \tag{4}$$

(γ_k = frequency of collisions of thermal electrons with particles of the kind k; $W_k(\varepsilon)$ = probability of electrons not to collide with k-particles until having reached a certain energy).

We will now apply this equation to three different cases, practically neutral hydrogen, completely ionized hydrogen plasma and an incompletely ionized hydrogen plasma.

4.32. *Runaway of electrons in hydrogen gas*

In order to apply (2) we have to know q_M, the momentum transfer cross-section of electrons colliding with hydrogen molecules as a function of energy. No exact measurements or calculations of this quantity over the entire energy range from 5 eV up to 10 keV are available. We therefore make use of an approximation proposed by ROBERTS [16]:

$$q_M\,[\mathrm{cm}^2] = \frac{1.5\times 10^{-12}}{\varepsilon^{1/2}\,(750+\varepsilon^{3/2})} \qquad (5)$$

(ε in eV)

This formula interpolates between the measured values at low energy and those that can be reliably calculated for high energy (see Fig. 7).

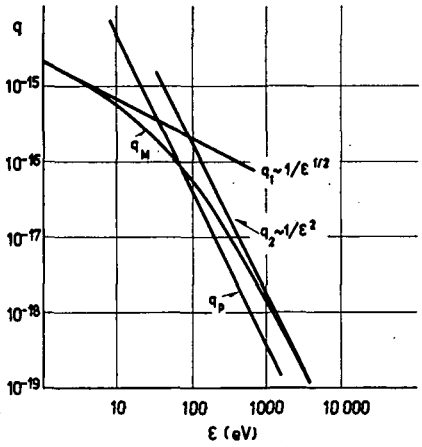

Fig. 7 Momentum-transfer cross-section of electrons colliding with hydrogen molecules.

The values of the integral were determined to be:

$$\int_{\varepsilon_{th}}^{10^4} q_M(\varepsilon)\,d\varepsilon\ [\mathrm{cm}^2\text{-eV}] = \begin{cases} 3.8\times 10^{-14} & \varepsilon_{th} = 5\,\mathrm{eV} \\ 3\times 10^{-14} & \varepsilon_{th} = 10\,\mathrm{eV} \end{cases} \qquad (6)$$

They are practically independent of the upper limit as long as it is larger than several keV.

Hence we have for the probability W_M for an electron at a temperature of 5 eV in hydrogen (density n_M) to gain at least several keV under the influence of an applied electric field E

$$W_M = \exp\left(-3.8\times 10^{-14}\, n_M/E\right) \qquad (7)$$

If we assume $\gamma_{th} = 1.3\times 10^{-7}\, n_M$ for the collision frequency we finally obtain the flux density of runaway electrons in practically neutral hydrogen (electron temperature 5 eV)

$$\varphi\,[\mathrm{cm}^{-3}\,\mathrm{sec}^{-1}] = 1.3\times 10^{-7}\, n_e \exp\left(-3.8\times 10^{-14}\, n_M/E\right) \qquad (8)$$

4.33. *Runaway of electrons in a completely ionized hydrogen plasma*

The electric resistivity ϱ of a completely ionized plasma as given by SPITZER [17]

$$\varrho\,[\mathrm{ohm-cm}] = 6.5\times 10^{-3}\, T^{3/2} \ln \Lambda$$

(T in °K)

yields the momentum transfer cross-section for the electrons (with $\ln \Lambda = 11$)

$$q_p\,[\mathrm{cm}^2] = 3.7\times 10^{-13}\,\varepsilon^2 \qquad (9)$$

(cf. Fig. 7)

Hence we have

$$\int_{\varepsilon_{th}}^{10^4} q_p(\varepsilon)\,d\varepsilon\ [\mathrm{cm}^2\text{-eV}] = \begin{cases} 7.4\times 10^{-14} & \varepsilon_{th} = 5\,\mathrm{eV} \\ 3.7\times 10^{-14} & \varepsilon_{th} = 10\,\mathrm{eV} \end{cases} \qquad (10)$$

$$W_p = \begin{cases} \exp\left(-7.4\times 10^{-14}\, n_e/E\right) & \varepsilon_{th} = 5\,\mathrm{eV} \\ \exp\left(-3.7\times 10^{-14}\, n_e/E\right) & \varepsilon_{th} = 10\,\mathrm{eV} \end{cases}$$

From this we obtain the flux density of the runaway electrons ($T_e = 10$ eV)

$$\varphi\,[\mathrm{cm}^{-3}\,\mathrm{sec}^{-1}] = n_e\,\gamma_{th} \exp\left(-3.7\times 10^{-14}\, n_e/E\right) \qquad (11)$$

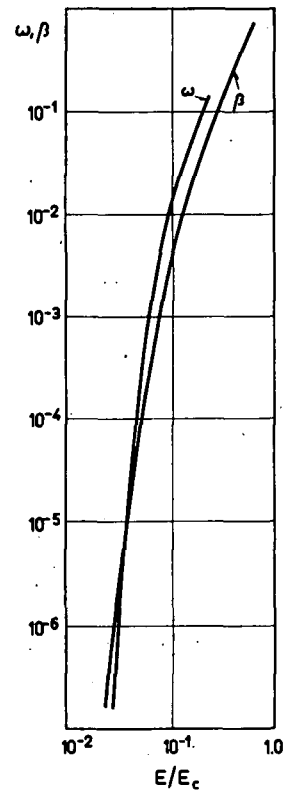

Fig. 8 Probability of runaway of electrons.

To compare this with DREICER's results [1] we make use of an approximation formula given by this author according to which the probability of an electron to run away within the time t is given by $P(t) = 1 - e^{-\beta t/\tau}$ where β is a function of n_e, T_e, E and $1/\tau$, the collision frequency. This yields the flux density of runaway electrons in a stationary state

$$\varphi = n_e \left(\frac{dP}{dt}\right)_{t=0} = n_e\,\beta/\tau = n_e\,\gamma_{th}\,\beta \qquad (12)$$

Evidently the function β (which DREICER called λ) is identical with our $W(\varepsilon)$ [see eq. (2)]. A numerical comparison of both quantities is possible taking into account that $\beta = \beta(E/E_c)$ where $E_c \approx n_e/T_e$ and hence

$\beta = \beta\,(E\,T_e/n_e)$. On the other hand, if $A = \text{const.}$ (independent of n_e, T_e, E) we can write

$$W = \exp\left(-\frac{n_e}{E}\int_{T_e}^{\varepsilon}\frac{A}{\varepsilon^2}\,\mathrm{d}\,\varepsilon\right)$$

$$\approx \exp\left(-\frac{n_e}{E}\int_{T_e}^{\infty}\frac{A}{\varepsilon^2}\,\mathrm{d}\,\varepsilon\right) = \exp\left(-\frac{A\,n_e}{E\,T_e}\right) \quad (13)$$

To compare β and W we keep n_e and T_e constant and vary E. This has been done in Fig. 8 where β as given by DREICER is plotted together with $W = \exp(-3.7\times10^{-14}\,n_e/E)$ ($n_e = 3\times10^{15}$ cm^{-3}, $T_e = 10$ eV, E between 7 and 40 V/cm). The agreement seems satisfactory.

4.34. *Runaway of electrons in an incompletely ionized hydrogen plasma*

Equation (4) when applied to a mixture of protons (density n_p), molecules and electrons yields the flux density of runaway electrons in such a plasma

$$\varphi = n_e\,(\gamma_P + \gamma_M)\,W_P\,W_M \quad (14)$$

W_P and W_M are given by Eqs. (10) and (7), respectively. The collision frequencies follow from

$$\gamma_P = n_P\,v_{th}\,q_P\,(v_{th}) = 2.2\times10^{-5}\,\varepsilon^{-3/2}\,n_e\,[\text{sec}^{-1}]$$

$$\gamma_M = n_M\,v_{th}\,q_M\,(v_{th}) = 1.3\times10^{-7}\,n_M\,[\text{sec}^{-1}] \quad (15)$$

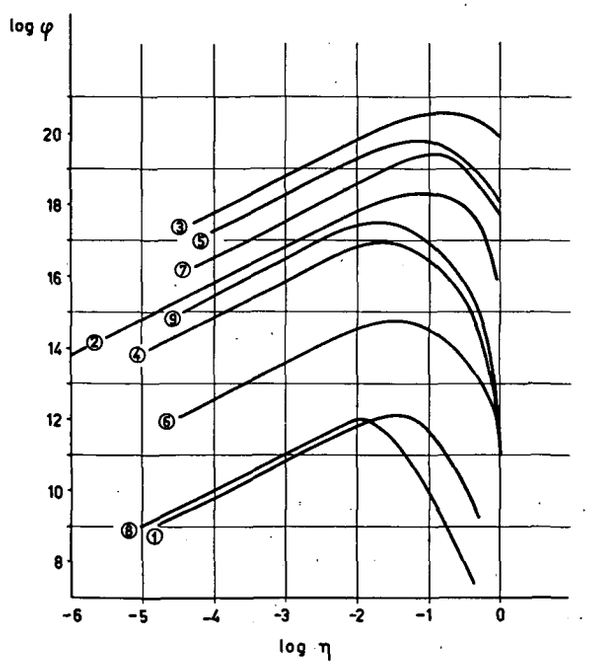

Fig. 9 Calculated flux density of runaway electrons (φ) in hydrogen as function of the degree of ionization (η). φ in cm^{-3} sec^{-1}. Parameters: P_0, filling pressure; T_e, electron temperature; E, electric field strength.

No.	1	2	3	4	5	6	7	8	9
P_0 (torr)	0.05	0.05	0.05	0.05	0.05	0.1	0.1	0.1	0.1
T_e (eV)	10	10	10	5	5	10	10	5	5
E (V/cm)	2	5	10	5	10	5	10	5	10

Equation (14) was solved numerically for a number of different cases. The results are shown in Fig. 9. It can be seen that there is a maximum in the flux of the runaway electrons if the degree of ionization η increases from small values up to values in the neighbourhood of unity. Since such an increase takes place at the beginning of the discharge it has been shown that the difference in cross-section between molecules and protons may actually be responsible for the burst phenomenon.

4.35. *Electric field strength and degree of ionization in the discharge*

A more detailed application of the results of the last section to our discharge requires the knowledge of the electric field strength, the particle densities involved and the electron temperature as functions of time and space. The electron density was measured spectroscopically [18] and was found to correspond to $\eta \approx 1$ a few microseconds after initiation of the discharge. With a time resolution of several microseconds no spatial distribution could be observed. The electron temperature has been deduced from spectroscopic and conductivity measurements. Depending on discharge parameters it lies between 4 and 6 eV. The electric field strength E is not well known from experiments during the first period of the discharge since the measured secondary voltage is mainly inductive at that time. However, the course of a discharge with its main features was calculated on an electronic computer [11]. Fig. 10 shows the results of these calculations for a specific case. φ_{theor} is the flux density of runaway electrons as calculated from Eq. (14) where we used for E and η the values presented by the respective curves. There is also plotted φ_{exp}, the measured flux density of runaway electrons and I_{exp}, the measured plasma current. It must be pointed out that the magnitude of the first maximum and minimum of E_{theor} is larger than in reality due to the simplifying assumption of a constant ionization cross section. A correction would shift the maximum of φ_{theor} to later times. Correcting for the finite acceleration time of the runaway electrons would have the same effect.

With the sensitive dependence of φ on temperature, densities and electric field strength in mind one could consider the order of magnitude agreement of φ_{theor} and φ_{exp} during the first microseconds as satisfactory. There is a strong discrepancy, however, between both quantities at later times: Whereas the measured flux of runaway electrons drops by several orders of magnitude to about 10^{14} cm^{-3} sec^{-1} one would expect φ to rise to about 10^{20} cm^{-3} sec^{-1} due to the increasing electric field strength. The increase of E between 3 and 10 μs is a well established fact. It must be concluded, therefore, that at least for times later than the burst a mechanism is at work that suppresses the runaway of electrons. It is conceivable then that this mechanism is also of importance for the burst phenomenon even though the burst could be explained in terms of cross-sections and a varying degree of ionization.

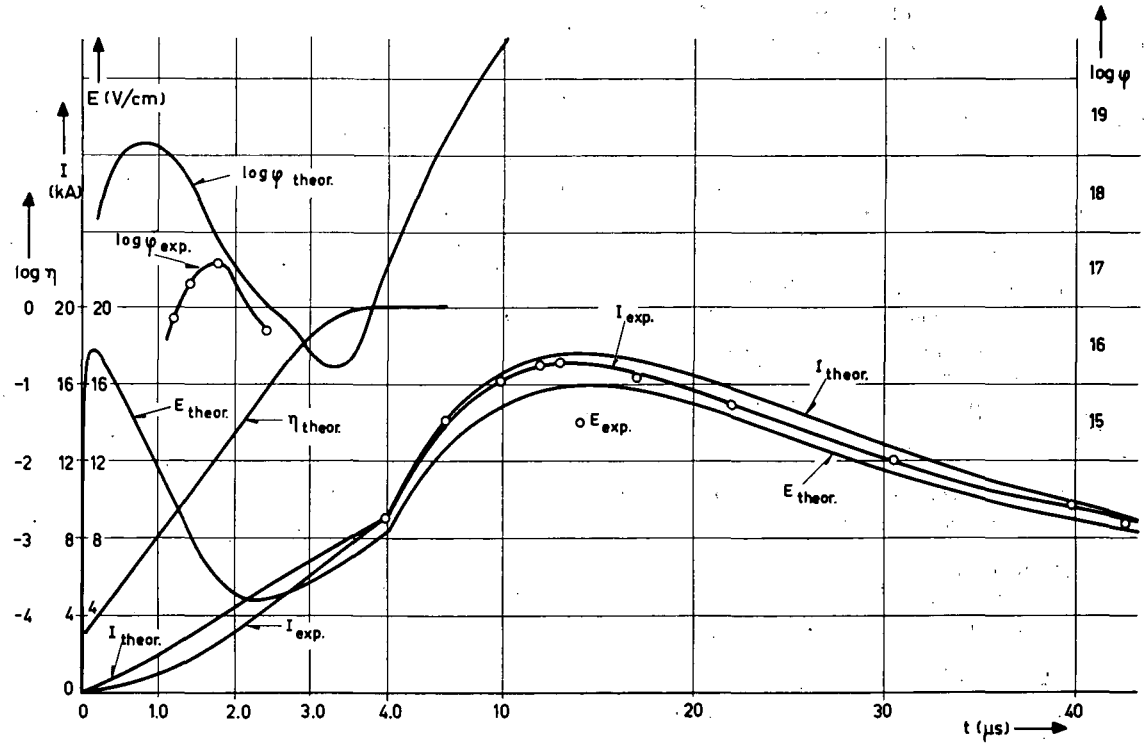

Fig. 10 Plasma current (I), electric field strength (E), degree of ionization (η) and flux density of runaway electrons (φ) as functions of time. Hydrogen 0.05 torr; capacitor voltage 6 kV; B_z field strength 800 G. φ in $cm^{-3}\ sec^{-1}$.

5. Conclusions

The extremely strong dependence of the flux of runaway electrons in a plasma on temperature, densities, and electric field makes it difficult to reach definite conclusions regarding the mechanisms that produce or suppress the runaway of electrons. However, considering the relatively good agreement of the theoretical with the experimental results at the beginning of the discharge and the discrepancy of about six orders of magnitude during a long time afterwards it seems justified to make the following statement: During the first few microseconds when the ionization is not yet complete, electrons run away at a rate that can be explained in terms of a simple model that only takes into account the scattering power of the most important particles. Afterwards, however, during the main part of the discharge a process is operating that suppresses the runaway of electrons or, at least, prevents runaway electrons from gaining more than about 1 keV. It is not quite clear whether this process is also responsible for the decrease of the flux of runaway electrons after burst maximum.

In accordance with this statement, we are able to rule out plasma instabilities *producing* runaway electrons as being responsible for the burst. It also seems unlikely that scattering by impurity atoms is the process we are looking for because it would not explain the low energies of the x-rays after the burst. Once a runaway electron has reached about 1 keV, its cross-section for Coulomb scattering is so low that a collision has become very improbable (cf. Fig. 7).

From our list given above only plasma instabilities reducing the flux of runaway electrons with energies above approximately 2 keV remain as a possible explanation for the behaviour of the runaway electrons in our discharge.

Acknowledgements

The authors wish to thank D. Pfirsch for helpful discussions on the subject of microscopic plasma instabilities.

References

[1] Dreicer, H., "On the theory of runaway electrons", in Proc. 2nd U.N. Conf. PUAE **31**, United Nations, Geneva (1958) 67.

[2] Bernstein, I. B., et al, "The velocity distribution of plasma electrons in an external electric field", in Proc. 4th Intern. Conf. Ionization Phenomena in Gases (Uppsala, 17-21 Aug. 1959) 2, North Holland Publishing Co., Amsterdam (1960) 634.

[3] Harrison, E. R., "Runaway and suprathermal particles", *J. nucl. Energy, Part C*, **1** (1960) 105.

[4] Burkhardt, L. C., et al, "X-rays from Perhapsatron", in Proc. Conf. Thermonuclear Reactions (Livermore, 7-9 Feb. 1955), Report no. WASH-289, 49.

[5] Conner, J. P., et al, "Operational characteristics of the stabilized toroidal pinch machine, Perhapsatron S-4", in proceedings of Ref. 1, **32**, 297.

[6] Aymar, R., et al, "Experimental studies on the striction phenomenon", in proceedings of Ref. 1, **32**, 92.

[7] Etievant, C., et al, "Experiments with T. A. 2000", in proceedings of Ref. 2, **2**, 967.

[8] COLGATE, S. A. et al, "A toroidal stabilized pinch", in proceedings of Ref. 1, **32**, 134.
[9] WARE, A. A., "Sceptre IIIA", *Proc. Instn. elect. Eng.* **A 106**, Suppl. 2 (1959) 30.
[10] ETIEVANT, C., "Etudes expérimentales sur le rayonnement x d'une décharge annulaire à forte intensité", Centre d'Etudes Nucléaires de Saclay Rapport 1111 (1959).
[11] GROSSMANN-DOERTH, U., "Aufbau und quasi-stationärer Zustand einer leistungsstarken toroidalen Pinch-Entladung in Wasserstoff", *Z. Naturforsch.* **16a** (1961) 1290.
[12] BUNEMAN, O., "The dissipation of currents in ionized media", *Phys. Rev.* **115** (1959) 503.
[13] JACKSON, J. D., "Plasma oscillations", Space Technology Laboratories, Inc., Report GM-TR-0165-00535 (1958).
[14] BERNSTEIN, I. B., et al, "Ion wave instabilities", *Phys. Fluids* **3** (1960) 136.
[15] JACKSON, E. A., "Drift instabilities in a Maxwellian plasma", *Phys. Fluids* **3** (1960) 786.
[16] ROBERTS, K. V., unpublished laboratory report, Harwell (1959).
[17] SPITZER, L., Jr., Physics of Fully Ionized Gases, Interscience, New York (1956).
[18] BERGSTEDT, K., WULFF, H., "Spectroskopische Messungen am T-1", unpublished laboratory report, Max-Planck-Institut (1961).

DISCUSSIONS (SESSION VII) — DISCUSSIONS (SÉANCE VII) — ДИСКУССИИ (ЗАСЕДАНИЕ VII) — DEBATES (SESIÓN VII)

Paper CN-10/47 *was presented by A. A. Ware* (United Kingdom). *The text of the paper is on pages 869—876. The following discussion took place:*

R. J. Tayler *(United Kingdom):* I would like to ask Dr. Ware three questions. The first one refers to general aspects of pinch discharges. Does he feel that all slow toroidal pinches are going to reach the diffuse state described in his paper and does that make him pessimistic about their future in controlled thermonuclear research? Secondly, in his pressure calculations has he taken fully into account the effects of toroidal geometry and, bearing in mind that the plasma pressure is low, can he happily deduce the pressure from his differences in magnetic field measurements? Thirdly, although there is a fortuitous agreement between the criteria for entropy waves and interchange instabilities, am I correct in thinking they are quite different phenomena? Entropy waves depend essentially on the presence of fast particles that can get across the field lines and are essentially related to a velocity-space effect, unlike interchanges which involve the whole plasma.

A. A. Ware: I think that all pinch discharges which are free from disturbing magnetic fields, due to gaps and so on, will probably end up satisfying these Eqs. (17) over the central core. I think most toroidal discharges up to now have suffered from large disturbing fields, which may prevent this constant-pitch condition appearing. In particular Sceptre IV has suffered from disturbing fields which we didn't know about when we made it. We have only recently discovered them. I think this is also true of many earlier experiments. Secondly, I have ignored toroidal effects completely. To have an interchange instability in toroidal geometry one needs an integral number of wavelengths of the magnetic field pitch around the torus. One observes this in practice, as the magnetic field changes rather abruptly in steps at the Kruskal limit and its harmonics.

R. J. Tayler: The toroidal effect that I was referring to was only the toroidal effect in calculating the pressure. In giving your results you show a rather good agreement between calculated pressure and theoretical pressure, but if toroidal effects were not taken into account and (bearing in mind that the pressure is low compared to the magnetic field energy) isn't this agreement fortuitous?

A. A. Ware: Toroidal effects have been taken into account partially, but one that has been ignored is the effect due to radial component of magnetic field. I don't think this is a very large error in the case where the discharge cross-section is roughly circular. Secondly, although the pressure gradient was small enough to satisfy Eq. (20), it was not insignificant. The difference between $j_z B_\theta$ and $j_\theta B_z$, for the Sceptre III results quoted, was between 30 and 50% of the larger component.

In reply to Dr. Tayler's other questions, the entropy wave instability is a different phenomenon from the interchange instability, but it is not a velocity space effect. In Kadomtsev's treatment he assumed isotropic pressures. Lastly, the diffuse pinch may have a future if a constant pitch configuration can be achieved with short pitch and with no kink instability.

S. A. Colgate *(United States of America):* One brief question. Do you feel this theory applies to the hard core configurations?

A. A. Ware: No, the hard core has a great deal of magnetic shear, whereas I have considered a discharge with no magnetic shear, that is, constant pitch.

Papers CN-10/54, 57, 58 *and* 60 *were presented by R. S. Pease* (United Kingdom). *The texts of the papers are on pages 883—919. The following discussion took place:*

L. Spitzer *(United States of America):* I would like to make a brief comment and ask two questions. It is very gratifying to see the marked progress that has been made in the last three years in understanding the kinematics of the plasma processes in Zeta. I hope that within the next three years similar progress will be made in understanding the underlying dynamical processes, which present an even more challenging problem. My first question concerns the transfer of energy to the wall. Do you have any measurements or estimates of the relative energy flux carried to the wall by electrons and by positive ions when the pressure is low and only 10% of the energy is carried to the wall by radiation?

Secondly, do you have any comment on the physical processes responsible for the injection of impurities into the Zeta plasma? In particular, the lack of dependence of the injection rate on the amount of energy reaching the wall is most remarkable. Do you have any theories to account for this effect, or any plans to test such theories experimentally?

R. S. Pease: The ion energy in the plasma is estimated to be about 5-10 times as great as the electron energy. Consequently if ions and electrons have the same containment time, the majority of the energy is carried by ions. We can measure the ion-containment time directly, and it is found to be the same as the energy-containment time (less the radiation effects) within experimental error. The electron-containment time could be perhaps half the ion-containment time, the electrostatic balance being retained by injection of electrons through unipolar arcs. However, the measurements on mass motion suggest that within the bulk of the discharge, the diffusion process is a mass-motion effect which transfers the plasma as a whole, and on this picture any difference

between ion- and electron-containment times arises solely from break-down of the Langmuir-sheath conditions when the plasma reaches the walls.

There is little direct evidence on the processes at the wall responsible for injection. However, we know that unipolar arc spots occur, and rough estimates of the rates of injection which could be expected have been made. These calculations suggest that unipolar arcs could account for the observed rate of injection without absorbing an amount of energy large compared to that associated with plasma loss. Some details are given in a report* on spectroscopic measurements of ion loss and injection. These spectroscopic measurements indicate that the injection rate is proportional to the loss rate, but is not solely a function of this. Apart from conditioning effects, it also appears to be a function of the magnetic configuration parameter θ, while the particle-loss rate is not. If we work at constant θ but vary the loss rate by varying other parameters, then the injection rate (as far as experiments have gone) varies in the same way. Thus there is a direct connection between loss and injection, and the known variation of the frequency of arc-spot formation with conditions [+] [‡] [§] might account for the other aspects of the variation of injection rate. But we have no reliable evidence on this latter point.

A. A. Ware *(United Kingdom):* The speaker has reported some excellent experimental work showing that the ion energies lie between those expected for a true temperature and those for simple mass motion. He then concluded that the heating mechanism for the ions was mass motion. I do not understand how mass motion can heat the ions. I would like to point out that in an impure hydrogen plasma such as this, ohmic heating will cause a direct heating of the deuterons. The electric fields causing the currents in the plasma will produce relative motion between the deuterons and the impurity ions. Collisions between ions and deuterons will generate thermal energy, which goes initially to the deuterons but will be shared with the impurity ions by other collisions. (A. A. WARE, B. Y. WESSON, *Proc. Phys. Soc. (Lond.)* **77** (1961) 801.)

R. S. Pease: We have no direct experimental evidence on the relaxation, if any, of the mass motion to thermal energy. The discussions in Section 9.2 of Paper CN-10/60 and Section 5 of Paper CN-10/57 show that *if we assume* that the mass-motion energy relaxes to thermal energy at the end of each step of the mass motion, then the energy absorbed is of the right order to account both for the excess resistance of the plasma and also for the observed ion temperatures. Estimates of relaxation times supposing there are collisions or that the randomizing process is due to motion of the ions along the lines of force both suggest that such a relaxation is possible in the time available. However, our experimental evidence, so far taken in rather limited discharge conditions, does not conclusively exclude other heating mechanisms. As regards impurity heating, this may be a contributor to the heating, particularly in the circumstances of the present experiments where comparatively large amounts of impurities were added and two thirds of the mass energy is carried by impurities. However, we have not studied this in detail, and we note that the theory referred to by Dr. Ware requires an unspecified electron cooling mechanism and additional hypotheses to accommodate the observations on Sceptre III which contradict simple predictions of the theory.

M. B. Gottlieb *(United States of America):* I have two questions: (1) Have you examined the ratio of electric field to electron density at the time of current discontinuity? (2) Is it possible that the low-frequency signals seen by the probes are due to rotation?

R. S. Pease: (1) As you will see in our paper, we have treated the runaway problem in terms of the ratio of drift velocity to thermal velocity, averaged over the discharge radius. This is, of course, a rough treatment, but it is equivalent to an examination in terms of the electric field and the electron density. Such an analysis suffers from the fact that no direct information on the electric field is available at the current discontinuity. The whole matter is discussed by A. GIBSON and D. W. MASON, (*Proc. Phys. Soc. (Lond.)* **79**, Part 2, (1962) 326.)

(2) The preliminary measurements on electric fields were carried out to establish that fields exist of roughly the magnitude and frequency to account for diffusion. There is a d.c. component in the fluctuating fields that might be associated with rotation. Further analysis of the fields and correlation lengths is needed to establish this.

L. Artsimovich *(Union of Soviet Socialist Republics):* About runaway electrons, since the pitch of the resultant magnetic field lines increases as one moves from the centre of the plasma column to the outside, surely the effective electric field per unit length of the electron path is weaker towards the outside.

Secondly, since measurement shows that a considerably fraction of the energy is associated with the ions, can't you calculate the strength of the fluctuating electric field needed to account for that portion of the energy which is proportional to Z^2/m?

R. S. Pease: As regards the first question, we have tried to avoid analysing the runaway conditions in terms of the applied electric field. It seems to me that such terminology is misleading because the electric fields observed by the electrons in the plasma are resistive ones given by the Spitzer formula. What matters is the ratio of the drift velocity to the thermal velocity, and therefore the conditions responsible for runaways are not given by the simple analysis which is suggested by Professor Artsimovich, but by the ratio of current densities and particle densities.

* BURTON, W. M., WILSON, R., *Proc. Phys. Soc. (Lond.)* **78** (1961) 1516.

[+] ROBSON, A. E., THONEMANN, P. C., *Proc. Phys. Soc. (Lond.)* **73** (1959) 508.

‡ CRASTON, J. L., *et al*, Proc. 2d U.N. Conf. PUAE **32**, United Nations, Geneva (1958) 414.

§ HANCOX, R., WALKER, C. N., AERE Report R 3245 (1960).

I am not quite sure that I understood the second question about ion heating. From results that we have obtained, we do not believe that there is any high-frequency-electric-field heating. The results of our analysis suggest that the heating is solely by mass motion and not by high-frequency electric fields. Therefore, the question of measuring these electric fields and deducing the ion energy becomes irrelevant. We have measured the electric field which suggests that the mass motion is of the right order. We have also put in high-frequency probes with a response up to about ten times the ion cyclotron frequency and we have found some fluctuations there, but we are not at all willing to present them in public at this stage until we check everything there.

Paper CN-10/238 *was presented by N. Fedorenko* (Union of Soviet Socialist Republics). *The text of the paper is on pages 921—927. The following discussion took place:*

R. S. Pease *(United Kingdom):* The excellent work on the energy spectrum of the ions directly suggests the connection between the excess ion energies seen spectroscopically and the very high energies of a small component that is likely to be responsible for the neutron yield (ROSE *et al*, *Nature* 181 (1958) 1630, and WARD, to be published). Have you estimated the neutron yield to be expected from your ion energy spectrum? Secondly, have you looked for any relation between this spectrum and the ion energies obtained by optical spectroscopy?

N. Fedorenko: Those atoms which we detect have, no doubt, arisen from the protons which constitute part of the plasma, because the atoms which come from the walls due to ion bombardment possess low energies and our device will not record them at all. Besides, we did a control experiment which showed that if a flux of ions (protons) is fired at a metallic wall of stainless steel, then we obtain an overwhelming quantity of slow atoms and protons of very low energies. I would like to stress once more that the neutral particles which we observe come from the protons from the plasma and not from the walls.

Papers CN-10/239 *and* 241 *were presented by A. Berezin* (Union of Soviet Socialist Republics). *The texts of the papers are on pages 929—939.* The *following discussion took place:*

L. Spitzer *(United States of America):* What wavelength was used in obtaining these results?

A. Berezin: We have used a wavelength of 8 mm.

R. S. Pease *(United Kingdom):* The first point I want to make is that we have done a rather similar experiment with photomultipliers examining line profiles and this is now in the course of publication (A. G. Hearn, B. B. Jones, S. A. Ramsden, *J. nucl. Energy, Part C* 4 (1962) 23).

Secondly, what is the frequency response of the photomultipliers used? The time resolution of the experiment is a crucial feature of an attempt to disentangle mass motion from thermal motion.

A. Berezin: We used sweeps of about 150 μs on which we noticed oscillations with a resolution of about 1 μs. The band width of the apparatus was from 100 Hz to 6 MHz. The photomultiplier time constant was 10^{-8} s.

G. N. Harding *(United Kingdom):* I would like to comment on the second paper on the microwave measurements. We have made very similar measurements on Zeta and have also found very high values of electron temperature at low pressures. We have also compared these measurements with measurements made at a wavelength of 2 mm and also with the infrared measurements, and we find that at 2 mm and in the infrared we do not obtain such high values of temperature. We have proved, I think conclusively, that for the infrared measurements the plasma is behaving as a black body and we therefore concluded that the 8-mm radiation was non-thermal in character. I would like to ask Mr. Berezin what proof he has that the plasma was behaving as a black body in these measurements.

A. Berezin: The validity of the assumption expressed has been confirmed by a simple experiment. A glow discharge tube, the electron temperature of the discharge being 18 000° K, was placed in front of the horn antenna of the radiometer. A noise temperature of 2 000° K was recorded. Then, with the discharge tube and the antenna in the same position, both were surrounded by a metal screen. The noise temperature recorded by the receiver increased to 16 000° K.

Papers CN-10/223 *and* 224 *were presented by G. Dolgov-Savelev* (Union of Soviet Socialist Republics). *The texts of the papers are on pages 941—953. The following discussion took place:*

A. Kuckes *(United States of America):* I note in your Fig. 6 where you consider the electron density in the central and outer regions that the electron density lost from the central region is initially characterized by a time constant of 1 ms, whereas very late in the discharge it is characterized by a time of several hundred microseconds. Do you have any physical explanation or interpretation for this?

G. Dolgov-Savelev: As could be seen from this slide, in the central region of the discharge the loss of particles takes place only after the discharge current stops when the plasma is not stable and the particles simply fall quickly to the walls.

A. Kuckes: Would it be correct to interpret the slow loss of density initially to continued ionization of neutral hydrogen gas?

G. Dolgov-Savelev: We feel that this is not correct because the neutral gas can only flow the walls of the discharge and no increase of the density in the peripheral regions of the discharge has been observed. Besides, we should have observed an increase of the luminescence of the spectral lines at that time. This process has also not been observed.

L. Spitzer *(United States of America):* Since the Tokomak device is very similar to the Model C Stellarator in its present form, I was particularly interested in these results. As I spent most of yesterday asking questions of Dr. Dolgov, I will confine myself now to one minor question: what is the ratio of the base pressures, that is, the impurity levels in the gas, before the discharge with the mercury pumping system and the oil pumping system?

G. Dolgov-Savelev: The pressure of the residual gas was 10^{-8} mm Hg, both in the case of oil and of mercury pumping.

Paper CN-10/150 *was presented by S. Colgate* (United States of America). *The text of the paper is on pages 955—967. The following discussion took place:*

A. Torossian *(France):* I would like to ask Dr. Colgate whether he made measurements of the escape of plasma across the magnetic field.

S. Colgate: No, our measurements are entirely preliminary and we have established only single-particle confinement. Unfortunately we burned a hole in the stainless-steel liner, terminating our initial experiments.

Paper CN-10/227 *was presented by B. Kadomtsev* (Union of Soviet Socialist Republics). *The text of the paper is on pages 969—977. The following discussion took place:*

R. J. Taylor *(United Kingdom):* Does Dr. Kadomtsev feel that he can introduce the concept of a single turbulent mixing length in a medium like a plasma which is highly anisotropic? Or, in other words, does hydromagnetic turbulence resemble hydrodynamic turbulence?

B. Kadomtsev: Of course, due to the strong anisotropy the turbulence of the plasma differs noticeably from the isotropic case and is two-dimensional. The concept of the mixing length is introduced merely for the transverse motion.

P. H. Rebut *(France):* What is the value of the critical field E_c in the formula $[(E/E_c)-1]^{1/2}$ which relates the amplitude of the deformation to the experimental conditions of the Zeta-type discharge?

B. Kadomtsev: The field is calculated from the value $\theta_c=3$ and is dependent on conductivity.

A. A. Ware *(United Kingdom):* Is the helical distortion occurring above $\theta=3$ the normal kink instability? If so, what makes the pinch discharge stable for values of $\theta<3$? The energy principle gives kink instability for all values of θ.

B. Kadomtsev: Yes, this is the usual instability with respect to the kink. For the case $\beta=0$ it appears only for $\theta>3$.

A. Kuckes *(United States of America):* I would like to ask Prof. Kadomtsev whether there is a simple physical explanation for the instability depending on the square root of H for the Stellarator case of low β.

B. Kadomtsev: I can suggest no simple explanation for this dependence.

T. Consoli *(France):* Did you find that when the instability appeared it was accompanied by increased high-frequency noise?

B. Kadomtsev: No, I have considered only low-frequency pulsations.

Paper CN-10/68 *was presented by R. Bickerton* (United Kingdom). *The text of the paper is on pages 979—989. The following discussion took place:*

S. A. Colgate *(United States of America):* Some years ago we performed a hard-core experiment using sodium in which the growth of the instability correspond to a shredding of the current layer. Similarly, the electron-beam equipment shows a breaking up into current filaments at the moment of incipient instability. To what extent does your correlation data agree with these observations?

R. Bickerton: Well, as I have said, we can't distinguish between the current helix and the magnetic field helix very well, and I would have thought that the $m=1$ instability is a fairly gross distortion and not the sort of thing one might expect to see from this shredding instability. This is just an opinion.

P. H. Rebut *(France):* I would like to point out that the theoretical studies that I have undertaken can offer a relatively satisfactory explanation for the instabilities observed in the hard-core (unpinch) type configuration. Moreover, in these calculations, the pitch of the instabilities is the pitch of the currents. This is summarized in Paper CN-10/101.

G. S. Murty *(India):* In connection with the hard-core mercury equipment I want to take a remark. When the current flows in opposite directions along the wire and the annular mercury jet, the jet may not be in equilibrium and so the stability question will not arise.

E. Velikhov *(Union of Soviet Socialist Republics):* In your calculation, did you take into account the dependence of the conductivity on temperature?

R. Bickerton: In the mercury experiment a differential gas pressure is maintained across the falling annulus to give static equilibrium. This equilibrium is observed to be stable in the absence of any applied axial magnetic field. The dependence of conductivity on temperature is not taken into account. In both calculations the fluid (plasma) is effectively assumed to be incompressible. Thus the only physical effect of finite conductivity treated here is the slipping of magnetic field lines relative to the plasma. The so-called "heating instabilities" are not included. Regarding Dr. Rebut's comment all I would say is that his theory assumes a collisionless plasma; ours is collision-dominated ($\nu > 10^{10}$).

Papers CN-10/91 *and* 106 *were presented by G. Briffod* (France). *The texts of the papers are on pages 991—999. The following discussion took place:*

C. Brachet *(France):* In the reflex discharge of the classical type, used by the authors, the ionization rate is limited, and the discharge gives rise to two opposing effects in the particle balance. These two effects, which depend on the gas pressure used, are the losses by normal or anomalous diffusion of the plasma and gas feeding of the discharge, which compensates for the diffusion losses. This gas feeding of the discharge is provided by the neutral atoms arriving from the external gas in the chamber, by recombinations and by ions neutralized at the cathodes. At high intensities, this latter mechanism becomes important in a classical reflex discharge. The diffusion measured can be influenced by the effect of these feeding mechanisms in the classical reflex discharge.

The two opposing effects of diffusion and gas feeding can be separated and made independent if one feeds the gas discharge from the centre of the cathodes, as we have reported in our paper at the Munich conference and in our paper CN-10/105 at this conference. It appears in this case, according to our observations, that in the operation at high axial density, the diffusion coefficient decreases when the magnetic field is increased.

Have the authors made some experiments with an axial gas feed or do they plan to perform such experiments?

The decrease of the diffusion with increasing magnetic field observed with axial feeds, appears in Paper CN-10/91 with results for pressures of the order of 9×10^{-3} with nitrogen (Fig. 6, curves 15 and 16).

G. Briffod: I wish to say that we have worked on a discharge which is fed in the centre by a gas system. We have worked with an arc in a low-pressure gas, the pressure of which was very much lower than that shown here, which was of the order of 10^{-4}-10^{-5}. One can observe that also in these arcs there are some instabilities and that in certain cases the arc dies out. So much for centre feeding of a discharge. Now, we have also worked on a more strongly ionized medium but we have not yet evaluated all the results.

I wish to point out that the method of measurement by ratios of the density or by recording of radial density profiles enables one to have direct control over the phenomena to which you refer.

A matter which seems much more important to us is the observation of these phenomena at higher ionization rates. Preliminary results have been obtained and studies are at present under way.

F. Schwirzke *(Federal Republic of Germany):* The critical magnetic field was found, as shown in your pictures, by measurement of n_{ex}/n_o. Do you find the critical field too, if you plot the inverse e-folding length of the logarithmic radial density distribution, as shown in your first slide, against the magnetic field? As it is shown in the paper described in Abstract CN-10/33, an exponential decay of the density with a constant e-folding length across the whole discharge radius need not necessarily exist.

Did you measure the radial potential distribution? At these low pressures, changes of the radial potential take place and this may influence the diffusion.

G. Briffod: I will answer in the affirmative to your first question. In effect, we have been able to show the existence of a critical field by plotting the radial density curves; in other words, the trend of the coefficient of perpendicular diffusion is identical to those curves which give (n_{ex}/n_o as a function of the magnetic field. This is made possible by the fact that the theoretical form of the radial distribution law is maintained in anomalous diffusion.

As regards your second question, we have in fact made radial potential measurements which will be published later.

F. Boeschoten *(Federal Republic of Germany):* In your experiments the Larmor radius of the ions may be estimated to be about 1 cm at a magnetic field strength of 150 G. In the kind of analysis which you used all characteristic lengths (like tube diameter and e-folding length of the density) should be large compared to the Larmor radius of the ions. In tubes of 3-cm and 5-cm diameter this condition is only fulfilled if the magnetic field strength is at least 500 or 1000 G.

How large is your axial electric field strength E_z compared with the E_z field in positive columns?

G. Briffod: The Larmor radii of the electrons and ions in the two experiments were always smaller than the discharge radius. This was particularly true in the second arrangement (a discharge of 1-meter length and 5-cm diameter) where the critical field was of the order of 500 G. It should be remembered that the degree of ionization was weak and the ion temperature was low.

The longitudinal electric field in the central part of the plasma where the measurements were taken is of an order of magnetude less than that which characterized the positive column. Measurements are presently under way to clarify this matter.

A. Simon *(United States of America):* I wish to point out that in these low-pressure discharges it is possible to obtain the Kadomtsev type of instability without the application of a longitudinal electric field. The instability is caused by the slightly different velocities with which the electrons and ions stream out of the plasma in the longitudinal direction. In this regard, I wish to ask whether you have obtained any direct experimental evidence of the existence of such a spiral mode of instability within your discharge and if so, what was the wavelength in the longitudinal direction?

G. Briffod: Despite our attempts to detect a helical mode in the column of the plasma, no effect of this kind has been observed up till now.

Paper CN-10/96 *was presented by P. Ginot* (France). *The text of the paper is on pages 1001—1006. The following discussion took place:*

S. Colgate *(United States of America):* I wish to congratulate you on these very fine results and comment that I entirely agree with you that arc apots are not necessary condition for turbulence. With argon-gas pinches we have no arc spots but do have equivalent turbulence as determined by the electron beam and magnetic probes.

R. J. Tayler *(United Kingdom):* In this paper a theory by Rebut was described in which a linear relation between B_θ and B_z (not involving the electric field) replaces Ohm's law.

Have any stability calculations been made using this equation, and if so, does this mean that stability can be determined without considering the induced electric field?

P. Ginot: Well, I think it would be better for Dr. Rebut to answer this question as he has performed studies on this stability problem using this relation.

P. H. Rebut *(France):* In my work, new equilibria, that is, helical, are considered. For certain discrete positions of the external conducting wall, a "junction" of the cylindrical and helical equilibria may exist showing a limit for the stability of the cylindrical ones. For these calculations it is not necessary to know the dynamics of the plasma and the induced electric field.

Paper CN-10/38 *was presented by U. Grossmann-Doerth* (Federal Republic of Germany). *The text of the paper is on pages 1007—1015. The following discussion took place:*

M. B. Gottlieb *(United States of America):* Did you try varying amounts of pre-ionization?

U. Grossmann-Doerth: The measurements reported in our paper were carried out without pre-ionization. Very recently we started to investigate the influence of a pre-ionizing pre-discharge on the burst. Preliminary results are: the initial burst of X-rays is suppressed by the pre-discharge. However, the X-ray burst at the beginning of the main discharge reappears if the main discharge is struck about 150 μs after the pre-discharge.

M. B. Gottlieb: Was the peak X-ray energy equal to the time integral of the electric field?

U. Grossmann-Doerth: The peak X-ray energy is about 2-3 times less than the time integral of the electric field.

M. B. Gottlieb: Did you measure the electron density as a function of time?

U. Grossmann-Doerth: Yes, but with 5-μs time resolution. However, the course of the discharge was computed numerically (see our Ref. 11). As is explained in our paper, we used these calculated values of particle densities when we compared theoretical with experimental values.

SESSION IX — SÉANCE IX

ЗАСЕДАНИЕ IX — SESIÓN IX

9 SEPTEMBER 1961 — 9 SEPTEMBRE 1961

9 СЕНТЯБРЯ 1961 Г. — 9 DE SEPTIEMBRE DE 1961

Chairman — Le président — Председатель — El Presidente

R. S. Pease *(United Kingdom)*

Scientific Secretary — Secrétaire scientifique — Ученый секретарь — Secretario Científico

E. V. Piskarev
[Е. В. Пискарев] *(Union of Soviet Socialist Republics)*

[Papers presented: CN-10/94, 134, 163, 165, 169, 171, 207, 209, 230, 231, 262]

EXPÉRIENCE D'INTERACTION FAISCEAU-PLASMA EN PRÉSENCE DE CHAMP MAGNÉTIQUE*

C. ETIEVANT

CENTRE D'ÉTUDES NUCLÉAIRES DE FONTENAY-AUX-ROSES

FONTENAY-AUX-ROSES, FRANCE

Le but de l'expérience est d'étudier en présence d'un champ magnétique les modes d'instabilité excités dans un plasma par le passage d'un courant d'électrons.

Deux séries d'expérience sont décrites, l'une avec un seul faisceau, l'autre avec deux faisceaux en sens inverse. Cette dernière disposition permet en principe de faire apparaître des systèmes d'ondes stationnaires notamment pour les ondes longitudinales électroniques et pour les ondes cyclotroniques des ions.

Les observations ont porté sur l'étude des fluctuations de densité, sur l'analyse du spectre et l'amplitude relative des ondes excitées.

1. Introduction

Le problème des interactions d'un faisceau de particules avec un plasma s'est posé dans des domaines très différents: tubes hyperfréquences à faisceaux d'électrons, radioastronomie, recherches sur la fusion contrôlée, etc.

Depuis PIERCE en 1948, BOHM, AKHIEZER et FAINBERG en 1950, de nombreux auteurs ont développé la théorie de ces interactions [1-8]. Simultanément le développement d'expériences portant sur l'excitation d'ondes longitudinales à l'aide d'un faisceau d'éléctrons en l'absence de champ magnétique [9-12] ont permis d'arriver ces dernières années à un certain accord entre la théorie et l'expérience.

Lorsqu'un champ magnétique est présent, la situation est notablement plus compliquée par suite des couplages possibles entre modes transversaux et longitudinaux. Dans le cas des ondes à propagation parallèle au champ magnétique les modes longitudinaux et transversaux sont alors indépendants et obéissent respectivement aux équations de dispersion [5, 6]:

$$1 = \sum \omega_{pj}^2 \int f_0 \frac{d^3 \mathbf{v}_j}{(\omega + k v_j)^2} \tag{1}$$

$$\omega^2 = k^2 c^2 + \sum \omega_{pj}^2 \int f_0 \left[\frac{\omega + k v_j}{\omega + k v_j \pm \omega_{cj}} + \frac{k^2 v_{\perp j}^2/2}{(\omega + k v_j \pm \omega_{cj})^2} \right] d^3 \mathbf{v}_j \tag{1'}$$

en appellant

$\omega_{pj}^2 = 4\pi\, n\, e^2 c/m_j$ — la fréquence plasma de l'espèce j
$\omega_{cj} = e\, B/m_j$ — la fréquence cyclotronique de l'espèce j
f_0 = fonction de distribution non perturbée
K = la constante de propagation de l'onde
v_j = la vitesse des particules de l'espèce j

Plusieurs auteurs [6, 16] ont montré à partir de l'équation de dispersion (1'), la possibilité d'instabilité pour des ondes transversales de basse fréquence, notamment à la fréquence cyclotronique des ions.

Un cas intéressant est celui où le plasma est traversé par deux faisceaux en sens inverse. En faisant l'hypothèse de températures nulles, l'éq. (1') prend alors la forme

$$\omega^2 = c^2 k^2 + \omega_p^2 \left(\frac{\alpha\, \omega\, (1 + 2\varepsilon)}{\omega - \omega_{ci}} + \frac{\omega}{\omega + \omega_{ce}} + \frac{\varepsilon\, (\omega - kv)}{\omega + \omega_{ce} - kv} + \frac{\varepsilon\, (\omega + kv)}{\omega + \omega_{ce} + kv} \right) \tag{2}$$

($\alpha = m_e/m_i$; ε = le rapport de la densité électronique d'un faisceau à la densité électronique du plasma).

On remarque que l'instabilité à la fréquence cyclotronique des ions subsiste. On trouve deux ondes instables possédant la même polarisation et se propageant en sens inverse, ce qui doit en principe permettre l'établissement d'un système d'ondes cyclotroniques stationnaires assez analogue à celui mis en évidence par Kofoid [18] dans le cas des interactions électrostatiques.

Le calcul montre que le coefficient de croissance de cette instabilité cyclotronique n'est appréciable que lorsque la densité d'énergie dirigée des faisceaux est de l'ordre de la densité d'énergie magnétique.

La décomposition en ondes longitudinales et transversales n'est plus rigoureuse lorsque la propagation est oblique. Cependant dans l'hypothèse $\omega/k \ll c$, il est possible de montrer que des ondes quasi-électrostatiques peuvent se développer, vérifiant l'équation de dispersion:

$$1 = \sum_j \left[\frac{\omega_{pj}^2 \cos^2 \theta}{(\omega - k_{\|} v_j)^2} + \frac{\omega_{pj}^2 \sin^2 \theta}{(\omega - k_{\|} v_j)^2 - \omega_{ce}^2} \right] \tag{3}$$

(θ = angle de $\mathbf{k}$ et $\mathbf{B}$)

Ici encore des systèmes d'ondes stationnaires peuvent être excités avec deux faisceaux opposés, ce qui rend possible la mesure des longueurs d'onde.

L'expérience décrite ci-dessous a pour but l'étude de ces mécanismes. Le paragraphe 5 rassemble les observations effectuées avec un seul faisceau. Dans le paragraphe 6, nous donnons quelques récentes observations avec deux faisceaux en sens inverse.

* Mémoire CN-10/94, présenté par C. Etievant. La discussion concernant ce mémoire est donnée page 1107. Les traductions de résumé se trouvent en fin de volume.

2. Dispositif expérimental

Une vue d'ensemble et un schéma du dispositif expérimental sont représentés dans les figs. 1 et 2.

Nous avons été conduits à fractionner l'appareil en plusieurs enceintes.

- La chambre 1 renferme le canon à électrons. Elle est munie d'une pompe à diffusion de 500 l/s.
- La chambre 2 est destinée à produire un pompage différentiel à l'aide d'une pompe à diffusion de 500 l/s.

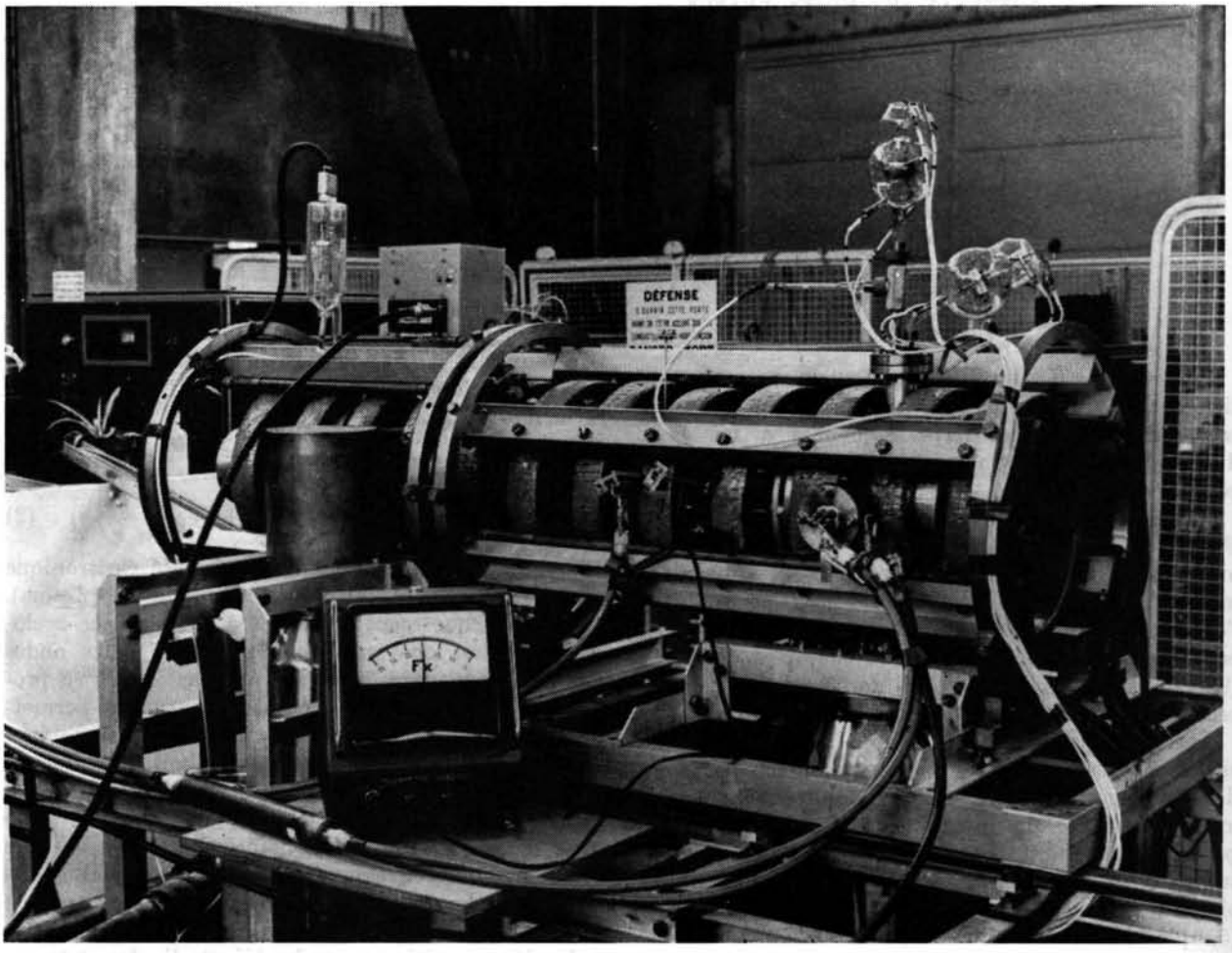

Fig. 1 Photographie du dispositif expérimental.

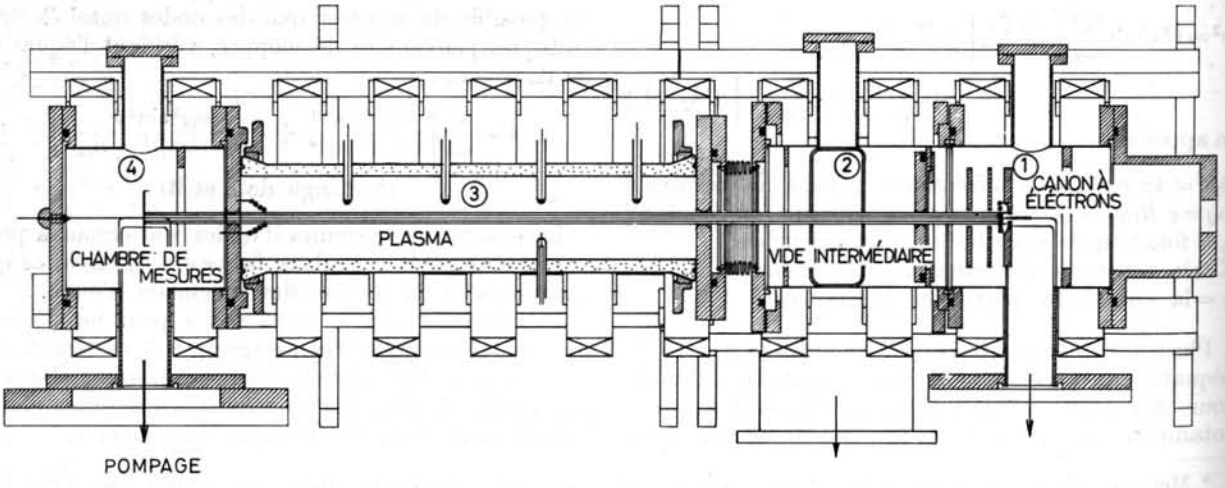

Fig. 2 Schéma. La chambre 3 constitue la zone d'interaction.

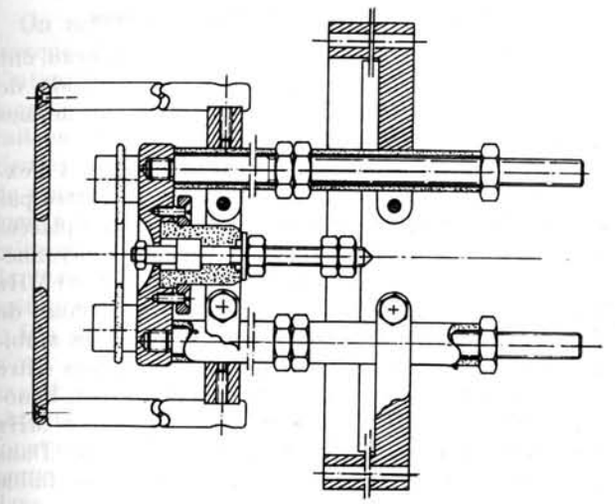

Fig. 3 Le canon à électrons donne un intensité maximum de 1 A pour une tension accélératrice de 10 kV.

- La chambre 3 constitue la zone d'interaction.
- La chambre 4 permet d'effectuer des mesures sur le faisceau émergeant. Elle est également maintenue sous vide à l'aide d'une pompe de 1000 l/s. (Dans cette chambre est logé le deuxième canon dans le cas des expériences à deux faisceaux).

Des orifices circulaires de diamètre 1 cm permettent le passage du faisceau. Cette disposition permet de maintenir dans l'enceinte contenant le canon une pression environ 200 fois plus faible que dans la chambre 3, de façon à éviter l'amorçage d'arcs entre les électrodes du canon.

Le canon à électrons (fig. 3) a été décrit dans un précédent rapport [14]. La cathode est une spirale plane de tungstène. Le diamètre du faisceau est 10 mm. L'intensité maximum débitée pour une tension accélératrice $V=10\,\text{kV}$ est $I=1$ A. Les mesures décrites ci-dessous correspondent à $V<3$ kV, et la densité électronique du faisceau est de l'ordre de 10^8 électrons/cm^3.

Un système de bobines permet de réaliser un champ magnétique uniforme parallèle à la direction du faisceau. La zone couverte est 0-1500 G. Une étude sur calculateur analogique, a montré que les inhomogénéités de champ dues à la périodicité des bobines, sont inférieures à 1 %, au voisinage de l'axe, dans la zone occupée par le faisceau.

La coïncidence des différents axes (champ magnétique, diaphragmes, faisceau) est contrôlée à l'aide d'une cible à quatre secteurs placée dans la chambre 4. Le réglage est réalisé, lorsque les courants collectés par les quatre secteurs sont identiques.

Nous avons pensé souhaitable d'éliminer les perturbations du plasma résultant de champs électriques imposés de l'extérieur. Ceci est rendu possible en utilisant le plasma produit par l'ionisation du gaz sur le trajet du faisceau. Les densités du plasma réalisées par cette méthode ont varié entre $n_e=10^8$ et 10^{11} électrons/cm^3, pour des pressions variant entre 10^{-4} et 10^{-2} torr. La colonne de plasma ainsi obtenue possède une longueur d'environ 50 cm et un diamètre sensiblement égal à celui du faisceau. La température électronique évaluée d'après les caractéristiques de sondes de Langmuir est comprise entre 5 et 7 eV.

3. Mesure de la densité électronique

La colonne de plasma traverse axialement une cavité hyperfréquence cylindrique, oscillant suivant le mode TM_{020}, à la fréquence $f_0=9000$ MHz. Le plasma se comporte comme un diélectrique de permittivité relative $\varepsilon_r<1$ et produit de ce fait un désaccord Δf dont la mesure permet, suivant une méthode mise au point par S.C. Brown [15] de déterminer la densité électronique du plasma.

La fréquence du plasma $\omega_P^2=4\pi ne^2c^2/m_e$ étant ici très inférieure à la fréquence de la cavité, la densité de plasma est sensiblement proportionelle au désaccord Δf.

La cavité fonctionne en réflexion: le klystron destiné à l'exciter est modulé en fréquence à l'aide d'une tension en dents de scie appliquée sur le réflec-

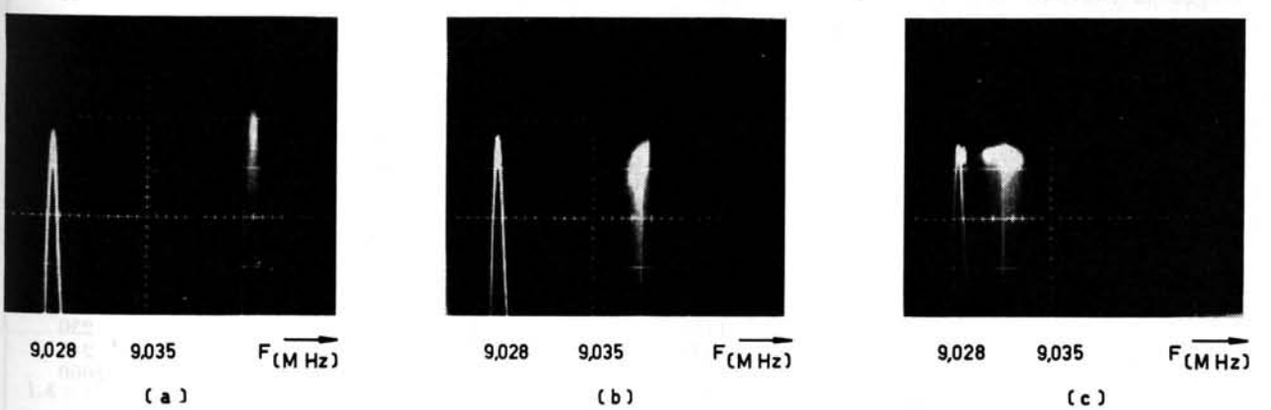

Fig. 4 Courbes de résonance de la cavité mettant en évidence les fluctuations de la densité. (Le pic à 9.028 MHz correspond à l'absence de plasma.) (a) Faibles fluctuations ($V_f=3$ kV, $B=438$ G, $n_e=2{,}54\times10^{10}$ électrons/cm^3). (b) Fluctuations plus importantes ($V_f=3$ kV, $B=438$ G, $n_e=1{,}3\times10^{10}$ électrons/cm^3). (c) Zone de forte instabilité ($V_f=2$ kV, $B=438$ G). Un régime très instable est observé pour n_e—$3{,}5\times10^9$ électrons/cm^3. Après destruction du plasma, la densité retombe à $n_e=6\times10^8$ électrons/cm^3.

teur. La figure 4 représente des relevés oscillographiques de l'absorption de la cavité au voisinage de la résonance avec et sans plasma. Ces mesures fournissent simultanément une indication sur la stabilité de la colonne de plasma. D'importantes fluctuations de densité sont en effet rendues visibles (figs. 4b et 4c).

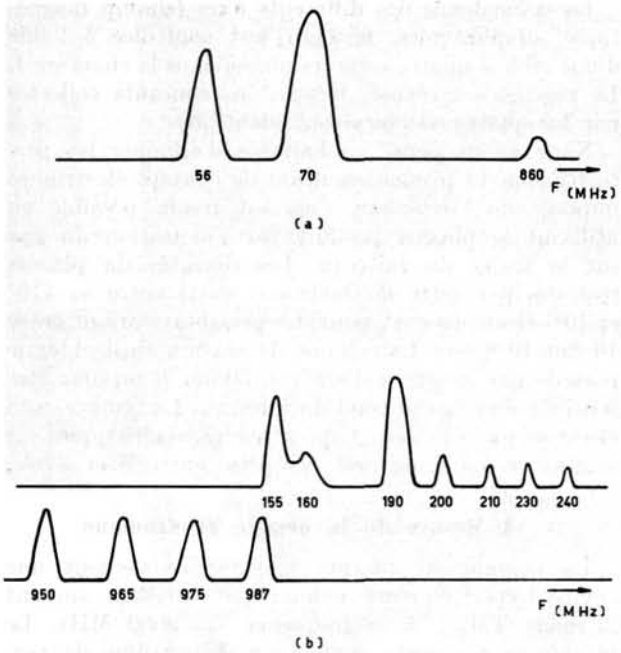

Fig. 5 Spectres types des radiofréquences excitées. (a) $V_f = 2$ kV, $B = 548$ G, pression $D_2 = 3 \times 10^{-4}$ torr. (b) $V_f = 3$ kV, $B = 370$ G, pression $D_2 = 4 \times 10^{-4}$ torr.

4. Etude du spectre des ondes excitées

Les ondes excitées par le passage du faisceau ont d'abord été détectées dans le plasma à l'aide de sondes de Langmuir et de sondes magnétiques munies d'un blindage électrostatique.

L'intensité du rayonnement de ces ondes à l'extérieur du plasma a été suffisante pour permettre par la suite de substituer aux sondes, des antennes placées à l'extérieur de la chambre. L'analyse de ce rayonnement a été effectuée dans la bande de 10 à 4000 MHz à l'aide d'un analyseur de spectre, Polarad, muni de filtres passe-bande appropriés pour éliminer les ambiguités de lecture. Pour les fréquences comprises entre 1 et 10 MHz, nous avons utilisé l'analyseur Panoramic SPA 25. Les fréquences inférieures à 1 MHz ont été analysées au moyen d'un oscilloscope. Dans plusieurs autres expériences d'interaction, la faible durée de passage du faisceau dans le plasma a rendu difficile l'étude détaillée du spectre des oscillations. Afin de faciliter l'emploi d'un analyseur du spectre, nous avons opéré en régime continu.

5. Résultats expérimentaux avec un seul faisceau

5.1. Spectre des oscillations dans le cas d'un plasma peu dense

La figure 5 montre deux spectres typiques d'oscillations excitées par le faisceau. Le rayonnement présente un certain nombre de raies. Nous donnons dans le tableau I, les valeurs des fréquences de ces raies. La zone de paramètres explorée correspond à $\varepsilon < 1/20$. (ε = ratio de densité électronique du faisceau à la densité électronique du plasma).

TABLEAU I. Fréquence des raies excitées*

Champ magnétique (G)	438	438	548	548	657	657
Pression (torr)	$2{,}6 \times 10^{-4}$	4×10^{-4}	$2{,}6 \times 10^{-4}$	4×10^{-4}	$2{,}6 \times 10^{-4}$	4×10^{-4}
Densité éléctronique du plasma (électrons/cm³)	3×10^{8}	10^{10}	3×10^{8}	$1{,}2 \times 10^{10}$	3×10^{8}	8×10^{8}
Fréquences des raies (MHz)	55 69	100 120 135 145 187 190 193 200 900 920 970 1050 1100 1120 1140 1300 1350 1370	56 70	18 80 157 175 187 200 210 220 233 245 900 975 1190 1250 1300 1350 1370 1380 1400	50 54 134 145 155 175 185 197 210 290	18 24 35 40 135 145 155 175 187 197 210 220 230 245 1000

* Energie du faisceau: $V = 2$ kV; densité du faisceau: $nf = 7 \times 10^{7}$ électrons/cm³.

On notera que le nombre de ces raies augmente lorsque l'on fait croître la densité du plasma et l'intensité du champ magnétique. Simultanément la largeur des raies augmente. Une série de raies apparait en général pour des fréquences légèrement inférieures à la fréquence du plasma. Il est important de remarquer que dans certains cas le spectre s'étend bien au delà de F_p une autre série de raies apparaissant au voisinage de F_{ce}. Les fréquences correspondantes sont souvent reliées par une progression arithmétique (cf. tableau I, colonne 6).

Les densités de plasma figurant dans le tableau I n'ont pu être mesurées directement à l'aide de la cavité, étant donné leur faible valeur. Elles ont été obtenues par extrapolation des courbes de densité en fonction de la pression. La relation entre les différentes raies d'émission parait relativement compliquée; il ne semble pas qu'elle puisse être expliquée à partir de l'équation de dispersion (1). Il sera probablement nécessaire de faire appel à une théorie plus précise tenant compte des conditions aux limites et éventuellement des couplages dus aux modes à propagation oblique.

5.2. Instabilités conduisant à la destruction de la colonne de plasma

Lorsque l'on augmente la densité de plasma au delà des valeurs enregistrées dans le tableau I, on observe, pour des valeurs suffisantes du champ magnétique, des régimes particulièrement instables se traduisant par la destruction périodique de la colonne de plasma. La figure 6 représente l'intensité du faisceau à la sortie du plasma et l'intensité du bruit collecté par une sonde de Langmuir au cours d'un tel régime. L'oscillogramme d'intensité montre des fluctuations

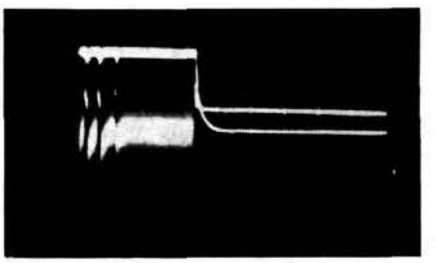

Fig. 6 Instabilités conduisant à la destruction de la colonne de plasma (100 ms/cm). En haut: courant du faisceau après la région d'interaction En bas: enregistrement du bruit basse fréquence à l'aide de sondes de Langmuir.

du courant d'environ 20%, ce qui prête à penser qu'une diffusion importante du faisceau se produit dans la zone d'interaction. La figure 4c montre nettement que la densité retombe à une très faible valeur après l'éclatement de la colonne de plasma.

Le tableau II donne la zone de paramètres où nous avons observé cette situation.

Une "destruction" du plasma a été prévue théoriquement par Buneman [7] en l'absence de champ magnétique, lorsque la vitesse de dérive des électrons devient notablement supérieure à la vitesse d'agitation thermique.

J. E. Drummond [17] et Kofoid [18] signalent avoir observé, dans une expérience d'interaction de deux faisceaux, cette instabilité prévue par Buneman.

Dans notre cas, en présence de champ magnétique, le mécanisme est certainement très différent et nous avons observé que la "destruction" du plasma apparait beaucoup plus nettement pour des champs magnétiques plus élevés. Cette observation est à rapprocher de nos mesures de la densité de plasma. L'intensité

TABLEAU II. Fluctuations de la densité électronique*

Pression (torr) \ B (G)	325	565	730	820	1060
$7{,}5 \times 10^{-4}$	$n_e = 3{,}5 \times 10^8$ $\frac{\Delta n}{n} = 0{,}46$	$n_e = 28 \times 10^9$ $\frac{\Delta n}{n} = 0{,}3$	$n_e = 37 \times 10^9$ $\frac{\Delta n}{n} = 0{,}65$	$n_e = 55 \times 10^9$ $\frac{\Delta n}{n} = 0{,}71$	$n_e = 55 \times 10^9$ $\frac{\Delta n}{n} = 1$
9×10^{-4}	$n_e = 12 \times 10^9$ $\frac{\Delta n}{n} = 0{,}46$	$n_e = 30 \times 10^9$ $\frac{\Delta n}{n} = 0{,}28$	$n_e = 30 \times 10^9$ $\frac{\Delta n}{n} = 0{,}5$	$n_e = 55 \times 10^9$ $\frac{\Delta n}{n} = 0{,}71$	$n_e = 55 \times 10^9$ $\frac{\Delta n}{n} = 1$
10^{-3}	$n = 14 \times 10^9$ $\frac{\Delta n}{n} = 0{,}53$	$n_e = 30 \times 10^9$ $\frac{\Delta n}{n} = 0{,}3$	$n_e = 30 \times 10^9$ $\frac{\Delta n}{n} = 0{,}5$	$n_e = 55 \times 10^9$ $\frac{\Delta n}{n} = 0{,}71$	$n_e = 55 \times 10^9$ $\frac{\Delta n}{n} = 0{,}91$
$1{,}4 \times 10^{-3}$	$n_e = 17 \times 10^9$ $\frac{\Delta n}{n} = 0{,}53$	$n_e = 30 \times 10^9$ $\frac{\Delta n}{n} = 0{,}43$	$n_e = 55 \times 10^9$ $\frac{\Delta n}{n} = 0{,}7$	$n_e = 55 \times 10^9$ $\frac{\Delta n}{n} = 0{,}67$	$n_e = 55 \times 10^9$ $\frac{\Delta n}{n} = 0{,}91$

* Le degré d'instabilité de la colonne de plasma est représenté dans le tableau par l'amplitude des fluctuations de la densité électronique: $\Delta n/n$. On remarque que dans certains cas très instables $\Delta n/n$ atteint la valeur 1. Paramètres: Energie du faisceau $V = 2$ kV; densité faisceau $nf = 7 \times 10^7$ électrons/cm^3; gaz, deutérium.

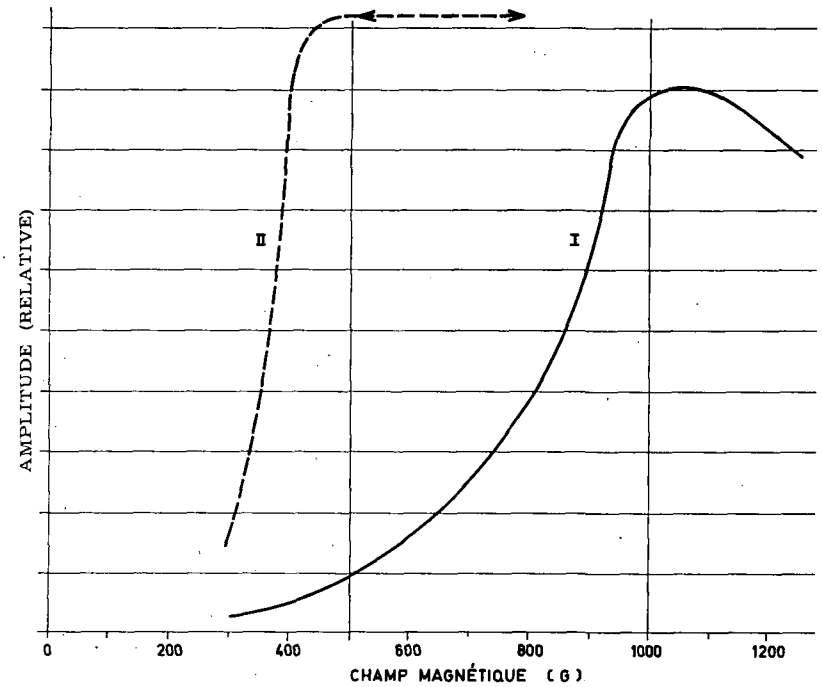

Fig. 7 Amplitude des oscillations basse fréquence en fonction du champ magnétique. Courbe I, $p = 10^{-3}$ torr H_2. Courbe II, $p = 9 \times 10^{-3}$ torr H_2.

du faisceau et la pression étant maintenues constantes, les mesures indiquent une décroissance de la densité lorsque le champ magnétique augmente (pour $<7 \times 10^{-4}$ torr). Ces faits amènent à conclure que le champ magnétique joue un rôle important dans les mécanismes de destruction du plasma.

5.3. Oscillations de basse fréquence

Des oscillations basse fréquence ($F < 1$ MHz) ont été observées et étudiées dans l'intervalle de variation des paramètres où une colonne de plasma stationnaire a pu être produite. La figure 7 montre les variations de l'amplitude de ce bruit en fonction du champ magnétique. On remarque des augmentations rapides de l'amplitude pour différentes valeurs critiques du champ magnétique. Une interprétation possible de ces valeurs critiques consiste à faire appel à des modes d'oscillations de grande longueur d'onde liés aux conditions aux limites de la colonne de plasma. Pour vérifier ce point de vue, nous avons fait varier la longueur de la colonne de plasma en déplaçant une plaque métallique le long de la chambre. Nous avons noté (figure 8), une augmentation des valeurs critiques du champ lorsque la longueur de la chambre est diminuée.

6. Expériences avec deux faisceaux

Dans une autre série d'expériences, un deuxième canon à électrons a été placé dans l'enceinte 4, ce qui a permis de réaliser pour les électrons une fonction de distribution symétrique avec des courants en sens inverse. Malgré une certaine analogie, cette géométrie diffère du celle des décharges réflex, parce que les électrons sont émis et accélérés dans des chambres où un vide suffisamment poussé peut être maintenu, ce qui permet de contrôler leur énergie.

Les résultats obtenus dans le cas d'un seul faisceau ont été retrouvés avec cette disposition. En particulier nous avons retrouvé l'existence d'un rayonne-

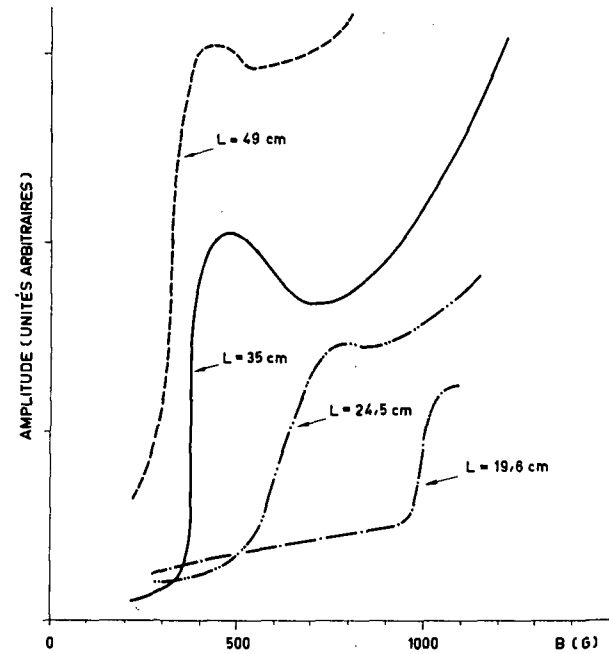

Fig. 8 Variations de l'intensité des oscillations basse fréquence en fonction du champ magnétique pour différentes longeurs de la colonne de plasma. On note une diminution du champ critique lorsque la longueur augmente.

ment haute fréquence présentant un spectre de raies. Un groupe de raies apparait en général au voisinage de ω_p et un autre au voisinage de ω_{ce}.

Des mesures de longueur d'onde actuellement en préparation, permettront une comparaison entre les modes excité set les solutions des équations (1), (2) et (3).

Conclusion

Les mesures que nous venons de décrire, ont montré qu'en présence d'un champ magnétique, le spectre des ondes excitées dans un plasma par un faisceau d'électrons est relativement complexe et comporte un grand nombre de raies. Pour des champs élevée ces raies peuvent se situer bien au delà de la fréquence propre du plasma.

Les instabilités qui se développent conduisent dans certains cas à la destruction de la colonne de plasma.

Nous tenons à remercier M.M. Hubert et Vendryes pour l'intérêt qu'ils ont toujours porté à ce travail et les facilités qu'ils ont mis à notre disposition pour réaliser l'expérience.

Références

[1] Pierce, J. R., *J. appl. Phys.* **20** (1949) 1060.
[2] Bohm, D., Gross, E., *Phys. Rev.* **75** (1949) 1864.
[3] Bohm, D., Gross, E., *Phys. Rev.* **79** (1950) 992.
[4] Akhiezer, A. I., Fainberg, Ya. B., *Zh. eksp. teor. Fiz.* **21** (1951) 1262; *Doklady Akad. Nauk SSSR* **69** (1949) 559.
[5] Bernstein, I. B., Trehan, S. K., *Fusion Nucléaire* **1** (1960) 3.
[6] Harris, E. G., *J. nucl. Energy, Part C*, **2** (1961) 138.
[7] Buneman, O., *Phys. Rev. Letters* **1** (1958) 8.
[8] Neufeld, J., Doyle, P. H., *Phys. Rev.* **121** (1961) 654.
[9] Merril, H. J., Webb, H. W., *Phys. Rev.* **55** (1959) 1191.
[10] Looney, H., Brown, S. C., *Phys. Rev.* **93** (1955) 965.
[11] Boyd, G. D., Field, L. M., Gould, R. W., *Phys. Rev.* **109** (1958) 1393.
[12] Demirkhanov, et al, dans Proc. 4th Int. Conf. Ionization Phenomena in Gases, (Uppsala 17-21 Aug. 1959) **2**, North-Holland Publishing Company, Amsterdam 655; *Zh. tek. Fiz.* **30** (1960) 315.
[13] Bernstein, I. B., Kulsrud, R. M., *Phys. Fluids* **3** (1960) 937.
[14] Etievant, C., Rapport SRFC No. 55.
[15] Buchsbaum, S. J., Mower, L., Brown, S. C., *Phys. Fluids* **3** (1960) 806.
[16] Dawson, J., Bernstein, I. B., in Proc. Controlled Thermonuclear Conf. (Washington, 3-5 Feb. 1958) U.S. AEC Report TID-7558 (1958) 360.
[17] Drummond, J. E., Boeing Scientific Research Laboratories Report Dl-82-0108.
[18] Kofoid, M. J., *Phys. Rev. Letters* **4** (1960) **556**.
[19] Kino, G. S., *Phys. Rev. Letters* **6** (1961) 163.

INVESTIGATION OF THE DOUBLE-STREAM INSTABILITY*

J. DAWSON

PLASMA PHYSICS LABORATORY, PRINCETON UNIVERSITY

PRINCETON, NEW JERSEY, UNITED STATES OF AMERICA

The development of the double-stream instability and the resultant breakup of the two streams was investigated by following the motion of a one-dimensional plasma (sheet plasma) on a high speed computing machine. The initial state of the plasma was one of two cold interpenetrating electron streams of equal average density on which were superposed random density fluctuations. All Fourier modes were present in the initial density fluctuations so that all unstable modes were excited. It was found that the linearized theory and estimates of when it would break down give a reasonably accurate picture of the initial development of the unstable modes and the level to which they grow. After the modes become nonlinear there is a rapid break up of the two streams and a large part of the energy is converted to random motion. However, the low Fourier modes are found to retain several times the average thermal energy for quite long times after the breakup of the two streams.

1. Introduction

There are a large number of instabilities that can occur in a plasma. It is natural to ask: To what amplitudes will these grow before they are limited by nonlinear effects, and what will happen to them after they reach this limiting amplitude?

Among the instabilities that can occur are the electrostatic oscillations that arise when there are several streams of electrons passing through a plasma. As a start in the investigation of the nonlinear behavior of such oscillations the double-stream instability was investigated on the one-dimensional plasma model [1].

The one-dimensional plasma is composed of identical charge sheets imbedded in a fixed neutralizing background. The sheets are allowed to pass freely through each other. The plasma is made finite by putting perfectly reflecting boundaries at positions $x=0$ and L. This is equivalent to having an infinite plasma in which the conditions are periodic functions of position; the motion of the plasma between $-L$ and 0 and L and $2L$ being the mirror image of what happens between 0 and L. The plasma as a whole is taken to be neutral.

This model is sufficiently simple that the motions of a large number (1000 or more) of sheets can be followed in detail on a high-speed computer. (All computations were made on an IBM 704).

The situation that was investigated was the following: A system of 1000 sheets was started out so that initially the sheets were equally spaced and had velocities either $+V$ or $-V$, the positive or negative velocity being chosen at random. Thus the distribution of velocities over the sheets was a random sequence of plus and minus V. No bias was given to either velocity so that on the average there were as many positive as negative velocities. However, these numbers were not forced to be the same so that there were small differences in the number with each velocity. A number of runs (five complete and two incomplete) were made. Each run had a different set of V's so that averages could be taken and some idea could be obtained of the extent to which the results depend on the initial conditions.

The initial conditions correspond to two cold beams travelling through each other. The mean density of the streams was the same, but there were random density fluctuations superposed on them. All modes are initially excited to some extent. All unstable modes will grow until they are limited by nonlinear effects.

A problem similar to this has been investigated by Buneman [2]. He followed the breakup of an electron stream passing through heavy but movable ions. He started his system with the most unstable mode already strongly excited, and all other modes were not excited. Also, only one wavelength of the most unstable mode fitted in his system.

In analyzing the results of these calculations, we are interested in explaining as much of the system's behavior as possible. Initially the amplitudes of all modes are small and we can expect the linearized theory to apply. It is natural, therefore, to see what behavior we would predict from this theory. We can also estimate the time when the theory will break down and something about the state of the plasma at the time of breakdown. We will, therefore, proceed according to the following outline:

(a) develop the linearized theory of the longitudinal oscillations of two electron streams

(b) give the boundary conditions appropriate to the problem considered

(c) estimate the initial excitation of the modes

(d) estimate when the linearized theory will break down and the conditions that will exist in the plasma at that time

(e) compare the computed results with the predictions of the linearized theory, including estimated time of breakdown and conditions at breakdown.

* Conference paper CN-10/163, presented by J. Dawson. Discussion of this paper is given on page 1107. Translations of the abstract are at the end of this volume of the Conference Proceedings.

2. The linearized theory

The linearized theory of the longitudinal oscillations of several electron beams has been given in an earlier paper [3]. However, for completeness and clarity, the theory of two beams will be given here. The linearized equations of motion are given in Eqs. (1-3).

$$\frac{\partial v_\pm}{\partial t} \pm V \frac{\partial v_\pm}{\partial x} = -\frac{eE}{m} \tag{1}$$

$$\frac{\partial n_\pm}{\partial t} \pm V \frac{\partial n_\pm}{\partial x} + N \frac{\partial v_\pm}{\partial x} = 0 \tag{2}$$

$$\frac{\partial E}{\partial x} = -4\pi e (n_+ + n_-) \tag{3}$$

Here $n_\pm$ and $v_\pm$ are the perturbations in number density and velocity for the beams with positive and negative velocities; N is the average number density and is the same for both streams; E is the electric field.

We look for normal modes where all quantities vary as $e^{i(\omega t - kx)}$.

$$\begin{Bmatrix} n_\pm(x,t) \\ v_\pm(x,t) \\ E(x,t) \end{Bmatrix} = \begin{Bmatrix} n_\pm \\ v_\pm \\ E \end{Bmatrix} e^{i(\omega t - kx)} \tag{4}$$

Substituting in Eqs. (1-3) leads to Eqs. (5-7).

$$i(\omega \mp kV) v_\pm = -\frac{eE}{m} \tag{5}$$

$$(\omega \mp kV) n_\pm - kN v_\pm = 0 \tag{6}$$

$$ikE = 4\pi e (n_+ + n_-) \tag{7}$$

Eliminating E and $v_\pm$ gives

$$(\omega \mp kV)^2 n_\pm = \omega_p^2 (n_+ + n_-) \tag{8}$$

$$\omega_p^2 = \frac{4\pi N e^2}{m}.$$

The amplitude of the wave is arbitrary so we may choose $n_\pm$ so as to satisfy the normalizing condition (9).

$$n_+ + n_- = 1 \tag{9}$$

Any multiple of a solution will also be a solution. With this condition, Eqs. (5), (6), (7) and (8) lead to (10-12) for E, $n_\pm$ and $v_\pm$.

$$E = -\frac{i 4\pi e}{k} \tag{10}$$

$$n_\pm = \frac{\omega_p^2}{(\omega \mp kV)^2} \tag{11}$$

$$v_\pm = \frac{4\pi e^2}{m} \frac{1}{k(\omega \mp kV)} \tag{12}$$

Equations (9) and (11) lead to the dispersion relation (13) which ω and k must satisfy [4].

$$\omega^4 - 2(k^2V^2 + \omega_p^2)\omega^2 + k^2V^2(k^2V^2 - 2\omega_p^2) = 0 \tag{13}$$

Equation (13) is a biquadratic in ω. There are four ω's ($\pm\omega_1$, $\pm\omega_2$) which satisfy it for each value of k. We may solve (13) for ω^2 and thus find (14).

$$\omega^2 = (k^2V^2 + \omega_p^2) \pm (4k^2V^2\omega_p^2 + \omega_p^4)^{1/2} \tag{14}$$

For $|k|$ less than $2^{1/2}\omega_p/V$ (14) gives one positive and one negative value for ω^2. The negative value leads to one growing and one damped mode. The most rapid growth rate

$$\omega = -i\omega_p/2 \tag{15}$$

occurs for

$$k = \left(\frac{3}{4}\right)^{1/2} \frac{\omega_p}{V} \tag{16}$$

For small kV the growth rate is approximately given by

$$\omega = -ikV \tag{17}$$

For short wave lengths and hence large k, we find for ω

$$\omega^2 \approx (kV \pm \omega_p)^2$$

$$\omega \approx \pm (kV \pm \omega_p)$$

The $+kV$ term gives a mode in which mainly the positively moving stream is oscillating while the $-kV$ term gives a mode in which the negatively moving stream oscillates. Inserting ω in Eqs. (11) and (12) for $n_\pm$ and $v_\pm$ shows this. In a frame moving with the positively moving stream, its oscillations will be at the plasma frequency. The same is true for the oscillations of the negatively moving stream for the frame in which it is at rest.

The modes found above satisfy an orthogonality relation. Since the orthogonality on k is standard, we omit that part of the calculation. Let ω and ω' be two roots of the dispersion relation for the same k. Multiply (8) by $n_\pm'$ and (8') (Eq. (8) with primed quantities) by $n_\pm$. Subtract and add the results for both the positively and negatively moving streams. This gives

$$(\omega - \omega')\sum_\pm (\omega + \omega' \mp 2kV) n_\pm n_\pm'$$

$$= \omega_p^2 \sum_\pm [n_\pm'(n_+ + n_-) - n_\pm(n_+' + n_-')] = 0 \tag{18}$$

If $\omega' \neq \omega$

$$\sum_\pm (\omega + \omega' \mp 2kV) n_\pm n_\pm' = 0 \tag{19}$$

If $\omega' = \omega$ then this sum need not equal zero and we set it equal to $H(\omega, k)$.

$$H(\omega,k) = 2\sum_\pm (\omega \mp kV) n_\pm^2$$

or by (11)

$$H(\omega,k) = 4\omega_p^4 \frac{\omega^3 + 3k^2V^2\omega}{(\omega^2 - k^2V^2)^3} \tag{20}$$

With the aid of this orthogonality relation we may solve the general initial-value problem. Again since the Fourier analysis in k is straightforward we will omit it. Suppose that at $t=0$ the amplitudes of the

kth Fourier components of $n_\pm$ and $v_\pm$ are $n_\pm(k)$ and $v_\pm(k)$. The time development of these modes may be expanded in terms of the normal modes.

$$n_\pm(k,t) = \sum_\omega C(\omega,k)\, n_\pm(\omega,k)\, e^{i\omega t} \tag{21}$$

$$v_\pm(k,t) = \sum_\omega C(\omega,k)\, \frac{(\omega \mp kV)\, n_\pm(\omega,k)\, e^{i\omega t}}{Nk} \tag{22}$$

Set $t=0$ in (21) and (22) and then multiply (21) by $(\omega' \mp kV)\, n_\pm$ and (22) by $Nkn_\pm$. Subtracting the two results, summing over both signs, and making use of the orthogonality relations gives

$$C(\omega',k) = \frac{1}{H(\omega',k)} \sum_\pm [(\omega' \mp kV)\, n_\pm(k)\, n_\pm(\omega',k) + kN v_\pm(k)\, n_\pm(k,\omega')] \tag{23}$$

We are now in a position to analyze the motion of the two streams.

3. The boundary conditions

Since the plasma is neutral as a whole, the boundary conditions on E are

$$E = 0 \quad \text{at} \quad \begin{cases} x = 0 \\ x = L \end{cases} \tag{24}$$

To satisfy these boundary conditions we must take

$$E(\omega,k) = -E(\omega,-k) \tag{25}$$

Since ω takes on the same values for $-k$ as it does for $+k$, this is possible. Furthermore, we must restrict k to the values

$$k = \frac{j\pi}{L}, \quad \text{j an integer.} \tag{26}$$

An integral number of half wavelengths must fit in the system. Equation (25) implies that

$$C(\omega,k) = C(\omega,-k) \tag{27}$$

since by (10)

$$E(k) = -\frac{i\pi e}{k} \sum_\omega C(\omega,k). \tag{28}$$

The boundary conditions on n and v are

$$n_+ = n_- \quad \text{at} \quad x = 0, L$$

$$v_+ = -v_- \quad \text{at} \quad x = 0, L \tag{29}$$

These relations come from the fact that at $x=0$, the negatively moving stream is converted into the positively moving one and vice versa at $x=L$. These conditions are automatically satisfied if relation (27) holds between the C's.

Finally, it should be remarked that we require all quantities $E, n_\pm, v_\pm$ be real. One can show from Eqs. (10), (11), and (12) for these quantities and relation (27) between the C's, that when $C(\omega,k)$ is chosen so as to make E real, all other quantities are also real.

4. The initial conditions

To find the initial excitation of the various modes we must analyze the initial state of the beams in terms of the normal modes. Since the initial state is chosen at random, we cannot predict exactly what this excitation will be, but we can predict certain averages.

Because $C(\omega,k)$ is equal to $C(\omega,-k)$ we will work with the sum of these two terms. From Eq. (23) for the C's, and Eqs. (11) and (20) for $n_\pm(\omega,k)$ and $H(\omega,k)$, plus the fact that $v_\pm(k)$ is initially zero (all particles belonging to a stream have the same velocity) we find (30).

$$C(\omega,k)+C(\omega,-k) = \frac{(\omega^2-k^2V^2)^3}{4\omega_p^2\,\omega(\omega^2+3k^2V^2)} \left[\frac{n_+(k)}{\omega-kV} + \frac{n_-(k)}{\omega+kV} + \frac{n_+(-k)}{\omega+kV} + \frac{n_-(-k)}{\omega-kV}\right] \tag{30}$$

Fourier analyzing the density, which is a series of delta functions, we have

$$\frac{n_\pm(k)}{\omega \mp kV} + \frac{n_\pm(-k)}{\omega \pm kV} = \frac{1}{L} \sum_{l_\pm}^{N} \left(\frac{2\omega}{\omega^2-k^2V^2} \cos k\delta l_\pm \pm \frac{2ikV}{\omega^2-k^2V^2} \sin k\delta l_\pm \right) \tag{31}$$

where $l_\pm$ means the sum is to be carried over the particles with positive velocity for l_+ and over particles with negative velocity for l_-; δ is the initial spacing between sheets and $(N+1)\,\delta = L$.

Substituting (31) in (30) gives (32).

$$\begin{aligned} A(\omega,k) &= C(\omega,k) + C(\omega,-k) \\ &= \frac{1}{L} \frac{(\omega^2-k^2V^2)^3}{4\omega_p^2\,\omega(\omega^2+3k^2V^2)} \sum_{l=1}^{N} \left(\frac{2\omega}{\omega^2-k^2V^2} \cos k\delta l \pm \frac{2ikV}{\omega^2-k^2V^2} \sin k\delta l_\pm \right) = \\ &\frac{1}{L} \frac{(\omega^2-k^2V^2)^2}{2\omega_p^2\,\omega(\omega^2+3k^2V^2)} \sum_{l=1}^{N} (\omega \cos k\delta l \pm ikV \sin k\delta l_\pm) \\ &\approx \frac{1}{L} \frac{ikV(\omega^2-k^2V^2)^2}{2\omega_p^2\,\omega(\omega^2+3k^2V^2)} \sum_{l=1}^{N} \pm \sin k\delta l_\pm \end{aligned} \tag{32}$$

The last approximate equality is derived from the following identity in which use is made of the facts that

$$(N+1)\,\delta = L, \qquad k = \frac{j\pi}{L}$$

$$\sum_{l=1}^{N} \cos k\delta l = \frac{1}{2} \left(\frac{e^{ik\delta} - e^{ik\delta(N+1)}}{1-e^{ik\delta}} + \frac{e^{-ik\delta} - e^{-ik\delta(N+1)}}{1-e^{-ik\delta}} \right)$$

$$= \frac{1}{2}[-1 + (-1)^{j+1}] = \begin{cases} 0 & \text{j odd} \\ -1 & \text{j even} \end{cases} \tag{33}$$

We will see in a moment that the sum over the sine terms is of the order of $N^{1/2}$ and so in our case where N is 1000, (33) is negligible. This also requires that kV be not too small compared to ω, but this is true for all but the very lowest mode.

To find the expected value of $A(\omega, k)$ we take ensemble averages. First the average value of $A(\omega, k)$ is zero since the lth particle is equally likely to have a positive or negative velocity in any given run. Formally

$$\left\langle \sum_{l=1}^{N} \pm \sin k\delta l_{\pm} \right\rangle = \sum_{l=1}^{N} \langle \pm \rangle \sin k\delta l_{\pm} = 0$$

since $\langle \pm \rangle$ for a given l is zero.

The average value of the square of the sum over the sine terms is given by the following expression since the velocities of different particles are not correlated.

$$\sum_{l,m} \langle (\pm \sin k\delta l_{\pm})(\pm \sin k\delta m_{\pm}) \rangle = \sum_{l} \sin^2 k\delta l = \frac{N}{2}$$

Thus we find the average value of $|A|^2$ is given by (34).

$$|A|^2 = \frac{1}{L^2} \left| \frac{kV(\omega^2 - k^2V^2)^2}{2\omega_p{}^2\omega(\omega^2 + 3k^2V^2)} \right|^2 \frac{N}{2} \tag{34}$$

For the most unstable mode

$$kV = \left(\frac{3}{4}\right)^{1/2} \cdot \omega_p$$

$$\omega = \mathrm{i}\frac{\omega_p}{2^{1/2}}$$

and we find

$$|\mathrm{A}|^2 = 0.15 \frac{N}{L^2}$$

or

$$(|\mathrm{A}|^2)^{1/2} = 0.387 \frac{N^{1/2}}{L} \tag{35}$$

Since all modes are excited initially, the very high modes will have some energy. To a certain extent this will look like a temperature since it will cause a random motion of the particles within a stream. We can estimate the energy in this random motion as follows. From Eq. (34) we find that for large k, $\langle |A|^2 \rangle$ is given by

$$\langle |\mathrm{A}|^2 \rangle = \frac{N}{8L^2}$$

or

$$\langle |\mathrm{A}|^2 \rangle^{1/2} = \frac{1}{2L}\left(\frac{N}{2}\right)^{1/2} \tag{36}$$

By Eqs. (11) and (21) the contribution of the kth mode to the initial density fluctuations is on the average given by (37).

$$\langle |n_{\pm}|^2 \rangle = \frac{1}{L}\frac{N}{2}\cos kx \tag{37}$$

Of course, due to the initial conditions the density fluctuations on the negatively moving stream are the negative of those on the positively moving stream since the total density is constant. Now the very high modes look like simple plasma oscillations of the two different streams. Initially there is a density perturbation, but no velocity. Associated with the density perturbation is an electric field. Initially the electric field associated with the waves on the negative stream cancels the field due to the waves on the positive stream. It develops rapidly, however, in a time of the order of $1/kV$. We can ignore the initial cancellation and compute the energy of the oscillations as if they went on independently. Initially all the energy is in the electric field and the electric field is equal to

$$\langle |E_{k\pm}|^2 \rangle^{1/2} = -\frac{4\pi e}{Lk}\left(\frac{N}{2}\right)^{1/2} \sin kx \tag{38}$$

Since energy is conserved and it is all electric to begin with, we have

$$W_k = \int_0^L \frac{\langle E_k{}^2 \rangle}{8\pi}\,\mathrm{d}x = \frac{\pi e^2}{Lk^2}\frac{N}{2} = \frac{\omega_p{}^2}{4k^2}m \tag{39}$$

The total random energy on one beam is given by

$$W = \sum_{k_{\min}}^{k_{\max}} \frac{\omega_p{}^2 m}{4k^2} \approx \frac{m\omega_p{}^2 L^2}{4\pi^2} \int_{j_{\min}}^{j_{\max}} \frac{\mathrm{d}j}{j^2}$$

$$\approx \frac{m\omega_p{}^2 L^2}{4\pi^2 j_{\min}} \tag{40}$$

If $j_{\min}$ is set equal to $2^{1/2} L\omega_p/\pi V$ corresponding to a minimum k of the order of $2^{1/2}\omega_p/V$ (the last unstable Fourier mode) then we find

$$W = \frac{m\omega_p L V}{4\pi 2^{1/2}} \tag{41}$$

or per particle

$$\frac{W}{N/2} = \frac{m\omega_p L V}{N 2\pi 2^{1/2}} = \frac{m\omega_p \delta V}{2\pi 2^{1/2}} \tag{42}$$

This is very small compared to the streaming energy per particle $mV^2/2$ since in the case computed V is 35 ω_p. It would correspond to a Debye length of the order of 2 δ.

5. Breakdown of the linearized theory

We can expect the linearized theory to break down when the perturbed density of one of the beams becomes of the order of its unperturbed density. We can estimate the time at which this will happen by estimating the time at which the perturbed density due to the most unstable mode is equal to the unperturbed density. In reality many modes contribute to the perturbed density, but mainly a few modes in the vicinity of the most unstable one will be important at the time the theory breaks down. The various modes will have different wavelengths and hence will reinforce each other at various points throughout the plasma. This will cause the theory to break down somewhat earlier than predicted. Also the theory will break down before the perturbed density equals the unperturbed density. However, due to the exponential character of the growths, the breakdown should occur only slightly earlier than predicted, perhaps one or two e-folding times earlier.

Setting the root-mean-square density perturbation* due to the most unstable mode equal to the unperturbed density we have by Eqs. (11), (15), (16), (33), and (35)

$$|C(\omega_{\max}, k_{\max})\, n_+(\omega_{\max}, k_{\max}) + C(\omega_{\max}, -k_{\max})\, n_+(\omega_{\max}, -k_{\max})|\, e^{\omega_p t/2}$$
$$= (|A_{\max}|^2)^{1/2}\, |n_+(\omega_{\max}, k_{\max})|\, e^{\omega_p t/2}$$
$$= \frac{0.387 N^{1/2}}{L} e^{\omega_p t/2} = \frac{N}{2L} \quad (43)$$

or

$$t = \frac{2}{\omega_p} \ln \frac{N^{1/2}}{0.774} \quad (44)$$

For our case where $N=1000$

$$t \approx 7.42/\omega_p \quad (45)$$

At the time the linearized theory breaks down the energy in the electric field,

$$\varphi = \int_0^L \frac{E^2}{8\pi}\, dx, \quad (46)$$

can also be estimated from the linearized theory. Again approximating the situation as if the most unstable mode were the only important one, setting the maximum perturbed density of one of the streams at $N/2L$, and making use of Eqs. (10), (11), (15), (16), and (27), we find

$$\varphi = \frac{N m V^2}{6} = \frac{W_{\text{tot}}}{3} \quad (47)$$

where W_{tot} is the total energy.

Here also several modes will be important at the time the theory breaks down. They will interfere constructively at certain places throughout the plasma so that the breakdown will occur at a smaller amplitude than was used in computing (47). On the other hand, since several modes will contribute to φ, the smaller amplitude is offset to a certain extent. Actually the maximum potential was found to be about 25% of W_{tot} which agrees rather well with (47). This maximum potential is found to occur somewhat after the linearized theory has broken down. Equation (47) is probably something like an upper limit on φ.

6. The results of the calculation

Some of the pertinent parameters which entered the calculations are given in the following list.

$N=1000$	
$\omega_p=1/2^{1/2}$	ω_p for a single stream
$L=1$	
$V=0.025$	
$j_{\max}\approx 8$	most unstable mode, $j=Lk/\pi$. j is the number of half wavelengths that fit in the system.
$j_{\text{last}}=12$	last unstable mode
$n_{\max}\approx 280$	number of particles per wavelength in the most unstable mode.
$t_b\approx 7-10$	estimated time for the breakdown of the linearized theory.
$\varphi_{\max}\approx 0.3\, W_{\text{tot}}$	estimated maximum value of $\int_0^L E^2\, dx/8\pi$.

A total of seven runs were made with different initial conditions. Of these, five runs were carried from $t=0$ to $t=40$ while the other two were incomplete, one going up to $t=13$ and the other to $t=6$. Some of the results of these calculations are shown in Figs. 1 through 9.

Figures 1, 2, and 3 show plots of the amplitudes of three of the Fourier modes vs time for one of the runs. Figure 1 is a plot for the lowest mode, $j=1$. The curve is that predicted by a fit of the linearized theory to the initial data. The curve is a superposition of the four normal modes corresponding to the four ω's that exist for this j or k. The fit is not bad out to $t=20$, at which time the envelope for the linearized theory starts curving up although the computed points do not. This curving up of the envelope for the linearized theory is due to the growth of the unstable mode whose e-folding time is 12 time units. The oscillations of the stable modes cause the amplitude to oscillate about this ever increasing value.

The explanation of the fit for such a long time appears to be the following: The double streaming is destroyed at about $t=10$ as we will see shortly. This destroys the unstable normal mode. In fact, the two-cold-stream description is no longer valid. One should probably use a distribution-function description. Nevertheless, even if the streaming were completely thermalized, the stable modes would still exist and have essentially the same frequency ($\pm 2^{1/2}\,\omega_p$). It is reasonable to assume that the stable modes are only slightly affected by the breakup and continue to oscillate as before.

Figure 2 shows a similar plot for the fourth Fourier mode. Again the curve is the theoretical fit to the initial data and is a superposition of four normal

* NOTE ADDED IN PROOF:

We should set

$$\sum_k \langle n_k^2(t)\rangle \approx m_k \langle n_k^2{}_{\max}(t)\rangle = n_0^2$$

where m_k is the number of modes in the vicinity of the most unstable one that make a significant contribution to the perturbation density. The time at which the linearized theory breaks down then becomes independent of the size of the system for large systems. For these experiments m_μ is of the order of 2 or 3 and the breakdown time changes only slightly (0.5 log 2). For runs with 3000 particles in a system three times as large but with everything else the same, the breakdown of the linearized theory was found to occur at the same time, and the fraction of the energie in the electric field (Fig. 8) was reproduced within the statistical accuracy. This showed that the system was in effect a large system.

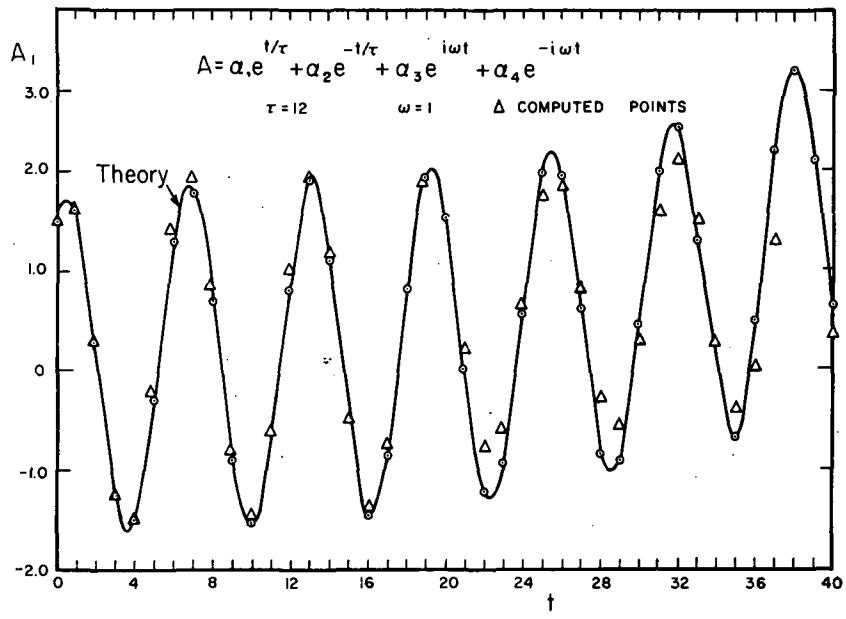

Fig. 1 Amplitude of mode 1 vs time for run 1.

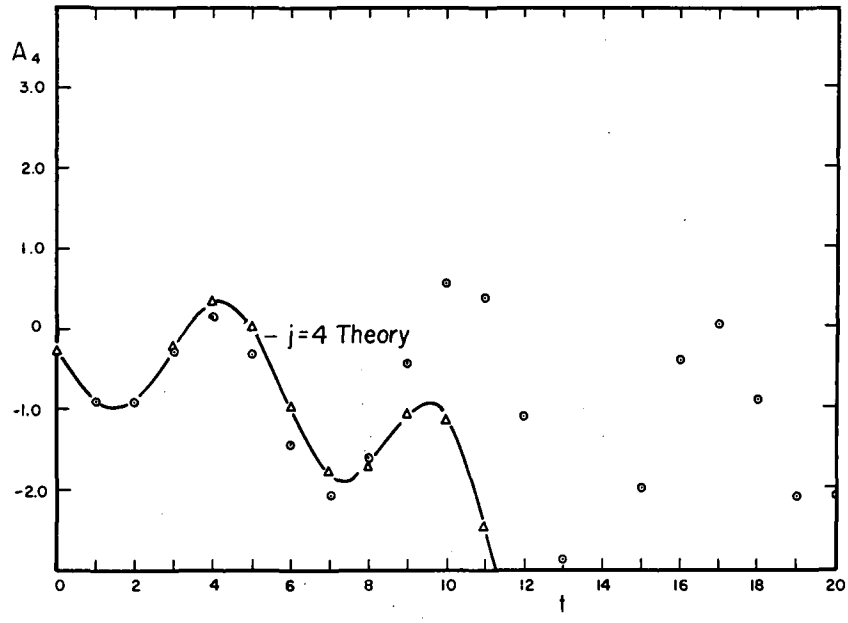

Fig. 2 Amplitude of mode 4 vs time for run 1.

modes. The e-folding time for the unstable mode is equal to 3.75 time units. Here the agreement is good out to about $t=7$ or 8.

Figure 3 is a plot for the seventh Fourier mode. The maximum growth rate occurs for a k which corresponds to a j between 7 and 8, 7.8 to be exact. This mode roughly corresponds to the most unstable mode. The e-folding time is 1.4. The computed points start to deviate appreciably from the linearized theory at about $t=5$.

In general, it was found that the computed points started to deviate from the linearized theory in the vicinity of $t=6$. It appears that the double streaming starts to break up shortly after this. This is shown in Figs. 4, 5, and 6. These figures show the velocity distribution function, $N(V)$, averaged over all runs and over x, for a number of different times. Figure 4 shows the velocity distribution at $t=0$, 3 and 6. At $t=0$, $N(V)$ is two delta functions centered about $\pm V$. At $t=3$ and 6 the delta functions have spread but still form two well defined peaks. The width at these two times does not represent a true temperature of the two streams but is mainly due to the wave motions added to the streaming motion. The averaging process makes this motion appear like a velocity distribution. The results on the Debye cloud

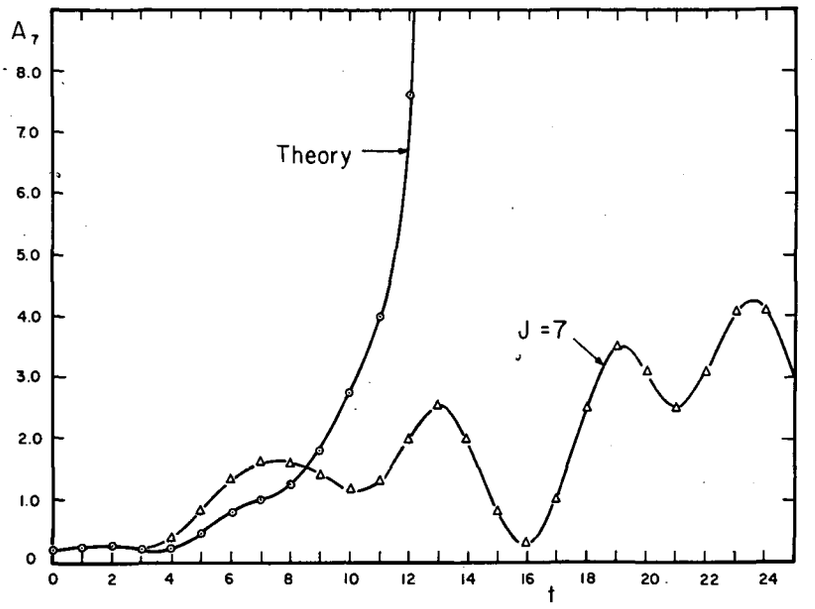

Fig. 3 Amplitude of mode 7 vs time for run 1.

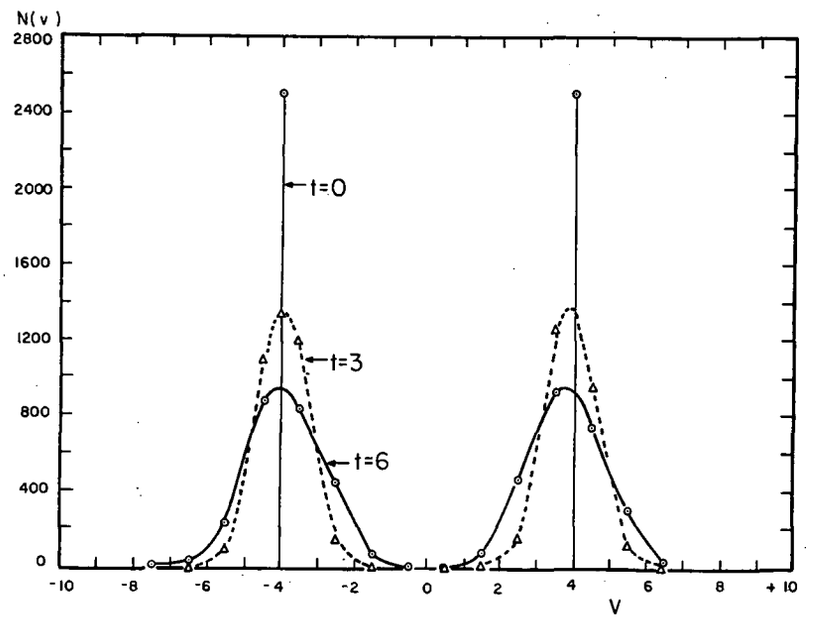

Fig. 4 Velocity distribution for $t=0$, 3 and 6. Average of all runs.

which will be presented shortly verify this interpretation.

Figure 5 shows the velocity distribution for $t=9$, 12 and 15. Between $t=6$ and 9 the region between the two peaks fills in and the double streaming is largely destroyed. At $t=12$ there has been an over compensation in the center and there are more particles with low velocities than a Maxwell distribution would have. By $t=15$ the distribution has come back towards the Maxwellian and as shown by Fig. 6, it does not deviate very much from this at $t=25$ and 39.

An interpretation of these results is the following: Between $t=6$ and 9 the unstable waves have grown to such large amplitudes that they are able to stop particles and reverse their motions. This breaks up the streams and rapidly fills in the center of the distribution.

The correctness of this interpretation is borne out by the results shown in Fig. 7. This figure shows the effective shielding distance D, or Debye length, vs time. What is plotted is the reciprocal of twice the depression of the density in the vicinity of a sheet. If the plasma were in thermal equilibrium, this would be the Debye length. For very short times the density in the vicinity of a sheet is more or less a square

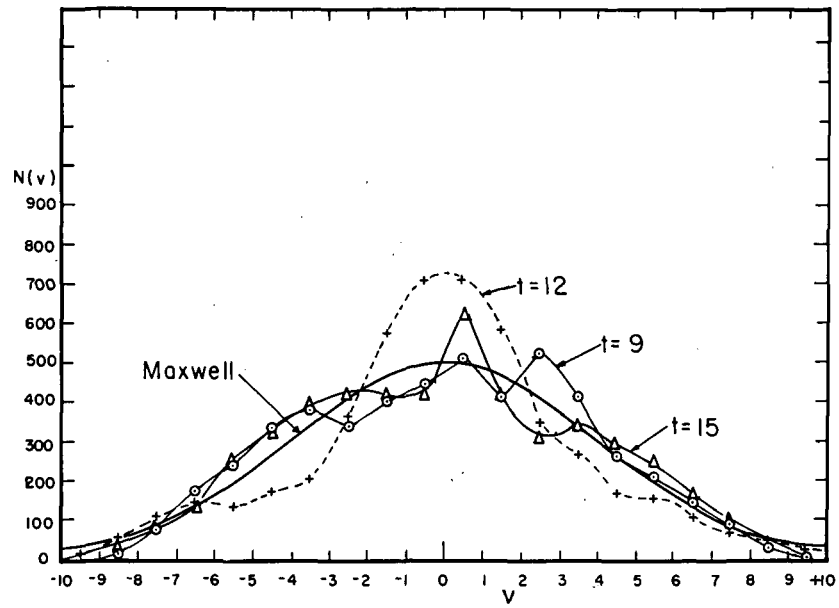

Fig. 5 Velocity distribution for $t=9$, 12 and 15. Average of all runs.

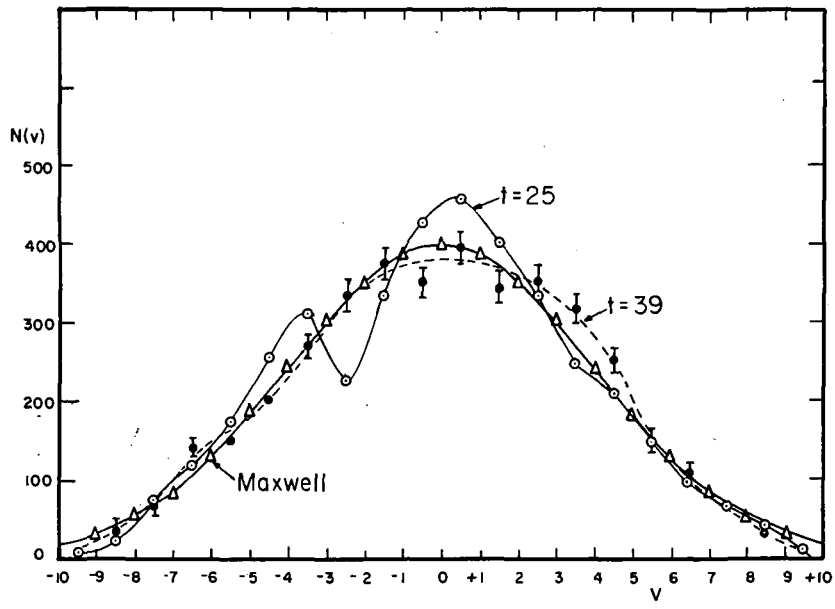

Fig. 6 Velocity distribution for $t=25$ and 39. Average for all runs.

wave which has the following shape if we take the test sheet to be at x_0

$$n = \frac{N}{L} \text{ for } |x - x_0| > \text{one intersheet spacing}$$

$$n = \frac{N}{2L} \text{ for } |x - x_0| < \text{one intersheet spacing} \quad (48)$$

The explanation of this is the following: Initially the streams are cold, and the sheets in one stream repel each other so that they tend to space themselves equally. Due to the random way that the system was started out, this is only a tendency and is not absolutely correct. As pointed out earlier the particles within a stream will develop some random motion with respect to one another because all modes are excited initially. This motion is, however, small as Eq. (42) indicates. The sheets belonging to the test sheets' stream will thus contribute little to the density in its vicinity and contribute $N/2L$ to the density at distances greater than an intersheet spacing. On the other hand, the sheets belonging to the other stream are moving so fast with respect to the test sheet that they hardly feel its electric field and hence contribute $N/2L$ to the density in its vicinity. As the sheets in a stream pick up some random motion with respect to each other, they can start to penetrate the fields around particles in the same stream and contribute to the density. Thus this

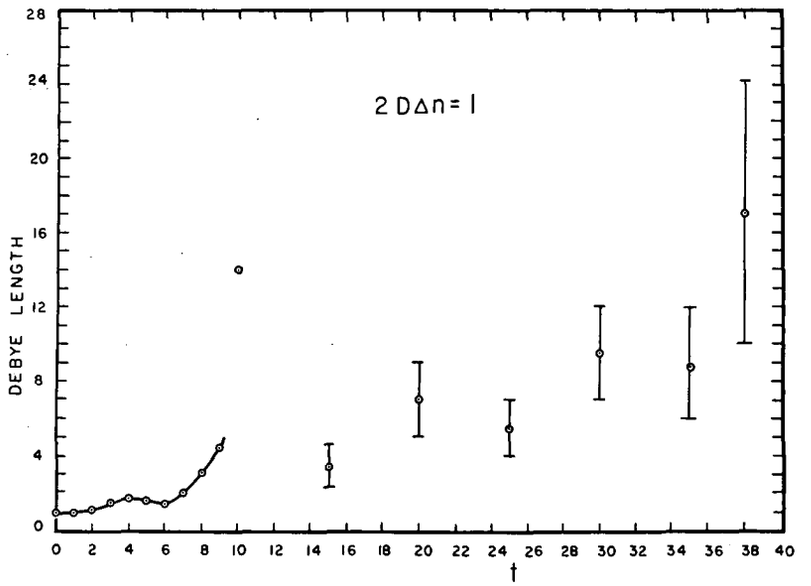

Fig. 7 Debye length vs time. Average over all runs.

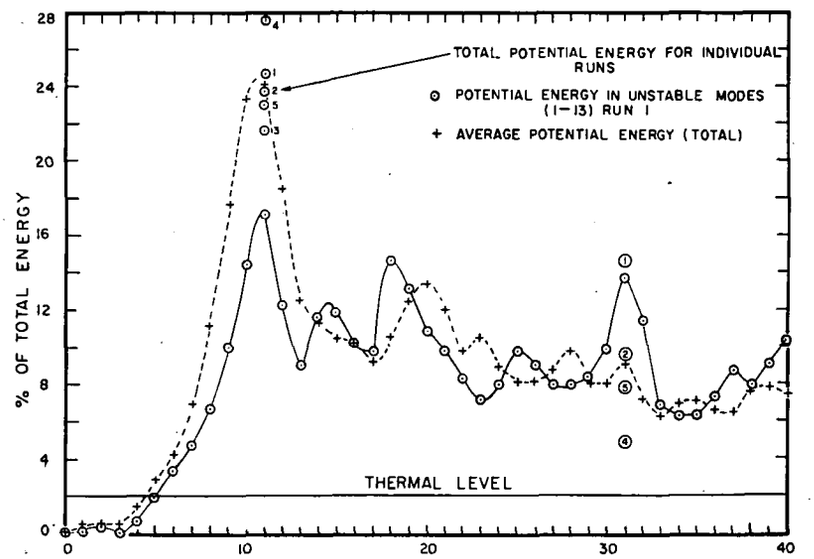

Fig. 8 Potential energy vs time averaged over all runs and the potential energy of the unstable modes vs time for run 1. Potential energy $= \int E^2 \, dx/8\pi$.

depression in density is a measure of the random motion within a stream.

Figure 7 shows that at $t=0$, D is one intersheet spacing. It does not change much up to the time $t=7$, at which time it changes very rapidly and, in fact, goes off the graph at $t=11$. This shows that at $t=11$, the particles within a stream are penetrating one another's clouds to a very great extent and are certainly crossing one another. This is consistent with the picture of the breakup of the stream at this time. D comes back to a value around three intersheet spacings at $t=15$ and then starts to rise towards its thermal equilibrium value of 25. The whole breakup takes roughly one plasma period, $2\pi/\omega_p$.

During the time from $t=9$ to 15, the concept of a shielding cloud is probably not very meaningful. The state of the plasma is changing so fast during this time that a true shielding cloud can probably not be defined, since it takes of the order of one plasma period to form. The error bars are estimated uncertainties in D. They become large at the later t's because Δn is very small there and small density fluctuations can throw the calculations way off.

While the breakup of the streams is quite a catastrophe, the thermalization is not quite so complete as the averaged velocity distribution function might indicate. The return of D to a small value after the breakup indicates this as well as the fact that

large-amplitude waves persist for quite long times as is shown by Fig. 8.

Figure 8 shows the total potential energy $\left(\int_0^L E^2 \mathrm{d}x/8\pi\right)$ averaged over all runs as a function of time, and also the potential energy in the unstable Fourier modes* ($j=1$ to 12) for one run vs time. The individually numbered points show the total potential for various runs at $t=11$ and 31 and thus indicate the scatter in the results. The line labeled "thermal level" at 2% is the total potential energy that all Fourier modes would have if the system were in thermal equilibrium.

Both the total potential and the potential energy in the unstable Fourier modes show a rather sharp peak between $t=10$ and 11. At this time the total potential energy is 25% of the total energy while the potential in the unstable modes amounts to 17% of the total. By $t=15$, the total potential energy has dropped to around 10% of the total energy. It then oscillates about this value with a slight tendency towards lower values, ending up at around 7-8% at $t=40$.

The potential energy in the unstable modes also drops to about 10% of the total by $t=13$ and oscillates about this value as time goes on. As can be seen, the potential energy in the unstable modes can pretty well account for the total potential energy between $t=15$ and 40.

The time of the breakdown of the linearized theory and the estimated maximum value of the total potential energy are in rough quantitative agreement with the predictions of the linearized theory. That the maximum total potential agrees so well with the crude estimate given by Eq. (47) is perhaps fortuitous since there are many processes going on such as harmonic generation and the interference of the various modes which were not taken into account. Nevertheless, this estimate probably gives an upper limit to the potential and this is probably the reason for the agreement.

At the time of maximum wave activity ($t=11$) it appears that a considerable amount of interaction is taking place between the low modes. This is evident from Table 1 where average energies (averaged over the runs) in the low modes are given for several different times. As can be seen, modes which were initially stable, $j>12$, have energies comparable to the unstable modes. Harmonic generation is probably the cause of this. Also, as the beams slow down, the last unstable mode moves towards shorter wavelengths. The short-wavelength modes rapidly dissipate their energy as is shown by the column for $t=15$. This is probably the cause of the rapid drop in potential energy after $t=11$. Waves of short wavelength are strongly subject to breaking [5] or phase mixing.

If the plasma was thermalized, $j=13$ corresponds to a k of $1/D$ (D is the Debye length and is 25 intersheet spacings for thermal equilibrium). Waves much shorter than this should rapidly dissipate as soon as a little random motion develops.

One further point should be made here: While there is a large dissipation at around $t=10$ the initially unstable Fourier modes or low-j modes retain much more than their share of the energy even out to $t=40$. One might think that these modes simply gain a lot of energy during the unstable phase and do not give it back to the plasma after the beams break up. This is undoubtedly true, but estimates of the rate at which the Fourier modes should come to equilibrium based on Landau [6] theory, indicate that they should have thermalized in times short compared to the observed time. For example, Landau theory would indicate that the thermalization time for mode 6 should be of the order of seven time units whereas from beam breakup to the end of the run amounts to 25 time units. Further, Fig. 9 shows the energy in some of the low modes vs time for one of the runs. As can be seen after $t=10$, the energy in an individual Fourier mode is not constant. There appears to be an exchange of energy between the

TABLE 1. Average energy in the fourier modes at various times*

Mode, j	$t=6$	$t=11$	$t=15$	$t=40$
1	0.506	0.501	0.823	1.111
2	0.585	0.160	0.695	3.529
3	1.758	0.984	3.385	8.951
4	0.563	2.122	21.371	12.693
5	0.764	6.176	8.858	5.180
6	8.993	7.892	18.313	14.182
7	4.375	2.607	16.192	3.886
8	1.018	3.095	6.460	3.355
9	22.240	14.838	9.326	2.566
10	0.977	4.953	3.238	7.669
11	1.957	13.352	3.972	5.750
12	1.818	30.409	2.051	1.218
(last unstable mode)				
13	2.581	13.969	7.944	2.185
14	1.492	14.491	2.149	0.745
15	0.433	5.208	3.561	5.943
16	1.598	6.409	1.067	1.073
17	0.135	8.341	1.572	1.147
18	0.333	40.356	2.460	0.684
19	0.076	3.888	1.176	2.100
20	0.585	6.653	1.565	0.779
21	0.729	6.217	2.266	0.399
22	0.295	8.195	0.694	0.528
23	0.135	5.144	2.672	0.489
24	0.127	3.629	0.641	0.800
25	0.442	0.653	1.962	0.276
Number of runs averaged over	7	6	5	5

* The energy is in arbitrary units. At thermal equilibrium $\mathrm{k}T/2=0.313$.

* Fourier modes should be distinguished from normal modes. As long as the two streams are intact, the motion of a Fourier mode can be decomposed into four normal modes. After the breakup of the beams the normal modes are no longer significant. The Fourier modes are still meaningful. Here unstable Fourier modes mean Fourier modes which contained one unstable normal mode initially. In some places just the world "mode" is used, but it should be clear from the text whether it is a Fourier mode or a normal mode.

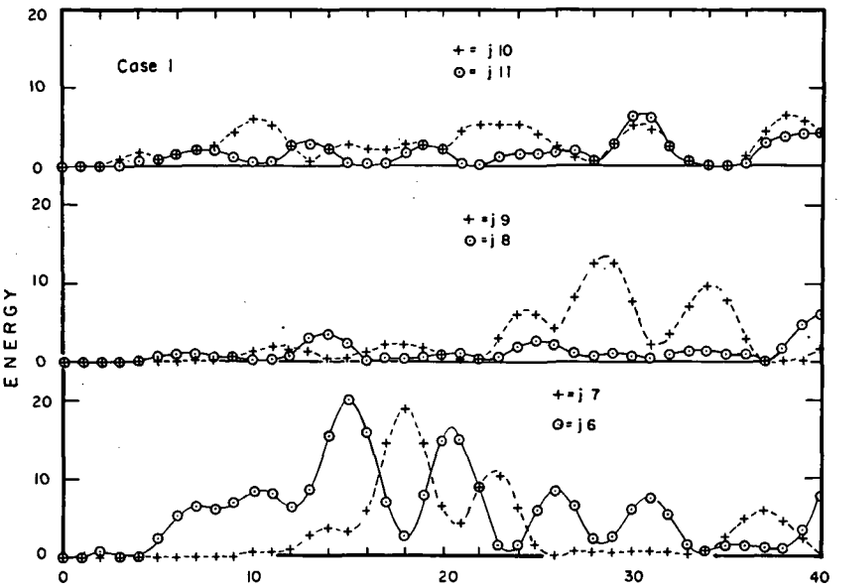

Fig. 9 The energy in some of the unstable modes vs time for run 2.

modes. These modes have such large amplitudes that the usual linearized theory almost certainly does not apply. However, the mechanism of energy exchange is also not clear. It is not clear whether this phenomenon would exist for a system containing more particles and hence more unstable modes with each one having less energy.

One final point should be made. In earlier work [1] on the one-dimensional plasma in thermal equilibrium, it was found that due to graininess there was a relaxation time or thermalization time for small disturbances from equilibrium. It is caused by random fluctuations or collisions due to sheets crossing each other. For the case run, this relaxation time would be 100 units, or more than twice the length of a total run.*

Thus, it is reasonable to describe this is a "collisionless" situation.

7. Conclusions

The early stages of the double-stream instability can be accurately predicted by the linearized theory. Estimates of when the theory should break down are reasonably accurate. The maximum energy in the electric field agrees well with what one would predict at the time the streams break up.

Large-amplitude oscillations of the low modes persist for long times after breakup. Though the energy in the low modes is roughly constant after breakup, there is an exchange of energy between these modes.

This work was accomplished under the auspices of the United States Atomic Energy Commission.

* NOTE ADDED IN PROOF: The relaxation times given in [1] are test-particle relaxation times. Recently ELDRIDGE and FEIX [7] have shown that the distribution function does not relax at the rate given by the test-particle calculations because the test particle in essence simply exchanges velocities with other particles in the distribution. The relaxation time for the total distribution is much longer and appears to be due to three-body interactions. Recent calculations [8] show that this relaxation goes as D^2 and for the case run would be several thousand time units. This makes the thermalization due to the unstable waves even more impressive.

References

[1] DAWSON, J., "A one-dimensional plasma model", *Phys. Fluids* **5** (1962) 445.
[2] BUNEMAN, O., *Phys. Rev.* **115** (1959) 503.
[3] DAWSON, J., *Phys. Rev.* **118** (1960) 381.
[4] KAHN, F. D., *J. Fluid Mech.* **2** (1957) 601.
[5] DAWSON, J., "The breaking up of large amplitude plasma oscillations", Plasma Physics Laboratory Report, MATT-31 (February 1960).
[6] LANDAU, L., *J. Phys.* (*USSR*) **10** (1946) 25.
[7] ELDRIDGE, O. C., FEIX, M., *Phys. Fluids* **6** (1963) 398.
[8] DAWSON, J., *Bull. Am. Phys. Soc.*, Series II, 8 (1963) 160.

НЕКОТОРЫЕ НОВЫЕ РЕЗУЛЬТАТЫ ПО УДЕРЖАНИЮ ПЛАЗМЫ В МАГНИТНОЙ ЛОВУШКЕ*

Ю. В. Готт, М. С. Иоффе, В. Г. Тельковский

Академия Наук СССР

Москва, Союз Советских Социалистических Республик

Для того, чтобы не допустить ухода плазмы, о котором я говорил в моем предыдущем докладе (CN-10/216), была предпринята попытка так видоизменить конфигурацию поля, чтобы напряженность поля нарастала (от центра ловушки) не только в продольном, но и в радиальном направлении, не нарушая при этом адиабатических свойств ловушки. Мы наложили на основное поле другое поле от системы проводников. Поскольку токи в соседних проводниках пропускаются в противоположных направлениях, то поле имеет геометрию такого же типа как и в гиперболических ловушках. Поле такой системы возрастает по радиусу, однако силовые линии, которые проходят дальше оси, искривляются так, что они пересекают боковую стенку камеры. Поэтому необходимо создать «стеночные пробки», делая поле проводников настолько большим, чтобы частицы отражались как они отражаются на концах ловушки. Эти результаты носят сугубо предварительный характер и показывают, что, изменяя конфигурацию магнитного поля, можно существенным образом влиять на те нестабильности, которые имели место в наших прежних опытах.

(*Аннотация редактора*)

Я хочу рассказать о некоторых экспериментах с новой конфигурацией магнитного поля ловушки с пробками. Эти эксперименты были начаты совсем недавно, поэтому полученные результаты носят лишь предварительный характер.

Как я уже говорил здесь в своем докладе во вторник,** в наших прежних опытах отчетливо наблюдается уход плазмы из ловушки поперек магнитного поля. Имеющиеся по этому поводу экспериментальные данные дают основание считать, что этот уход обусловлен неустойчивостью желобкового типа, которая может иметь место в полях, убывающих при удалении от границы плазмы наружу.

В связи с этим была предпринята попытка так видоизменить конфигурацию поля, чтобы напряженность поля нарастала от центра ловушки не только в продольном направлении, но и в радиальном, не нарушая при этом существенным образом адиабатические свойства ловушки.

Среди возможных способов создания такого поля нами был выбран способ, который схематически изображен на рис. 1. Имеются катушки, создающие основное продольное поле с пробками на концах. На него накладывается поле от системы проводников с током, которые расположены вдоль силовых линий основного поля вокруг оси ловушки. Ток через соседние проводники пропускается в противоположных направлениях так, что создаваемое ими поле имеет геометрию того же типа, что и в гиперболических ловушках (рис. 2).

Я хочу здесь отметить, что подобные схемы полей рассматривались в различное время различными авторами, например, Градом и др. [1] в

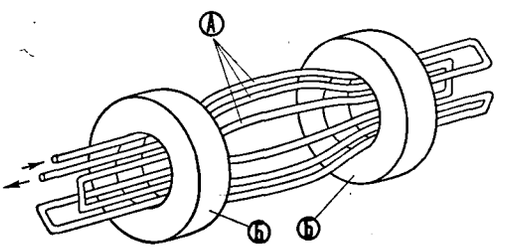

Рис. 1 Схема создания магнитного поля.

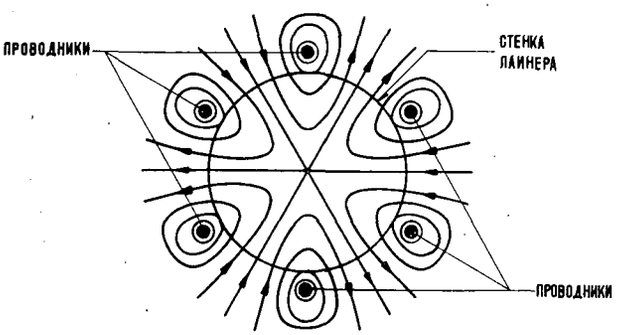

Рис. 2 Геометрия магнитного поля.

докладе на второй Женевской конференции, Головиным — в его статье в журнале УФН за 1961 год [2], Арцимовичем — в недавно выпущенной им книге [3] (помещенные здесь рисунки взяты из этой книги).

Так как поле такой системы проводников нарастает от оси по радиусу, то, пропуская через проводники достаточно большой ток, можно скомпенсировать радиальный спад напряженности ос-

* Доклад CN-10/262, представленный на конференцию докладчиком М. С. Иоффе, печатался по звукозаписи. Дискуссия (на английском языке) по этому докладу дана на стр. 1108. Переводы аннотаций находятся в конце тома.

** Доклад CN-10/216: М. С. Иоффе, Е. Е. Юшманов, «Экспериментальное изучение нестабильности плазмы в ловушке с магнитными пробками», *Ядерный Синтез*, Дополнение 1962, Часть 1, 177.

новного поля и сделать поле возрастающим по радиусу.

При этом, однако, следует иметь в виду следующее обстоятельство. Когда поле проводников накладывается на основное продольное поле, силовые линии суммарного поля приобретают довольно сложную форму. Только сравнительно узкий пучок силовых линий вблизи оси будет проходить по-прежнему через всю ловушку, не пересекая ее боковых стенок. Силовые линии, которые проходят дальше оси, искривляются так, что они пересекают боковую стенку камеры. Поэтому, чтобы частицы, движущиеся вдоль этих силовых линий, не попадали на стенки, необходимо, очевидно, создать с помощью проводников так называемые «стеночные пробки», т.е. сделать поле проводников настолько большим, чтобы частицы, приближаясь к стенке, отражались от областей усиленного поля подобно тому, как они отражаются от областей усиленного поля на концах ловушки.

По аналогии с обычным пробочным отношением $\alpha = H_m/H_0$ можно ввести понятие стеночного пробочного отношения, определив его следующим образом:

$$\alpha_{cT} = \frac{(H_0^2 + H_g^2)^{1/2}}{H_0}$$

(H_0 — напряженность поля в центре ловушки; H_g — напряженность поля, создаваемого проводниками, в местах пересечения силовыми линиями боковой стенки ловушки).

Это выражение показывает во сколько раз абсолютное значение суммарного поля вблизи стенки больше, чем поле в центре ловушки.

Эксперименты проводились на той же установке, о которой я говорил в прошлый раз (рис. 3).

Проводники питались током до 100 ка от ударного генератора. Ток имеет форму затухающей синусоиды с периодом 40 мсек. Максимальная напряженность поля в зазоре между проводниками 3500—4000 гаусс.

Были проведены измерения зависимости времени жизни плазмы от напряженности дополнительного поля при всех остальных постоянных параметрах. Такими параметрами являются: H_0, U, p и режим плазменного источника (U — амплитуда импульса ускоряющего напряжения, p — давление водорода в камере).

Время жизни находилось по убыванию во времени потока быстрых нейтральных частиц, которые получаются при перезарядке ионов в нейтральном газе.

На рис. 4 показаны осциллограммы потока нейтральных частиц на стенку при различных значениях H_g.

На рис. 5 приведена зависимость времени жизни от H_g, полученная после обработки приведенных выше осциллограмм.

Здесь видно, что увеличение дополнительного поля вызывает возрастание времени жизни, которое достигает затем насыщения при достаточно

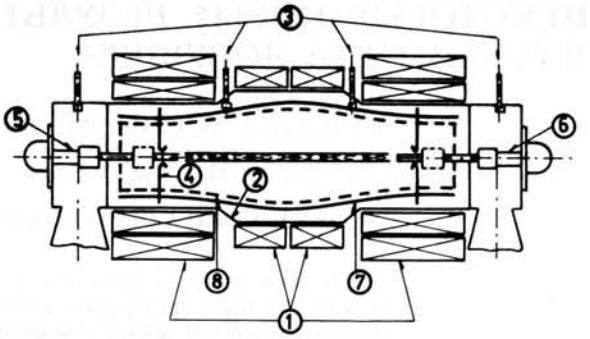

Рис. 3 Схема установки: 1 — катушка для создания магнитного поля; 2 — вакуумная камера; титановые испарители; 4 — диафрагма; плазменный источник; 6 — приемный электрод; 7 — проводники для создания дополнительного поля; 8 — лайнер.

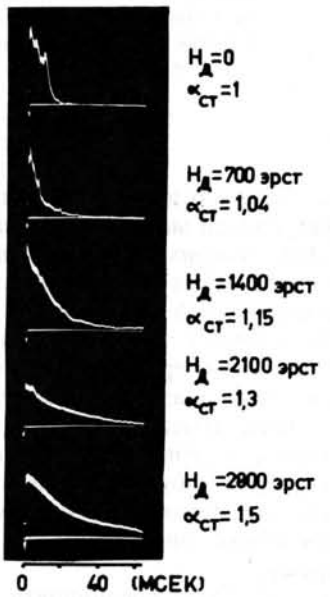

Рис. 4 Осциллограммы потока нейтральных частиц.

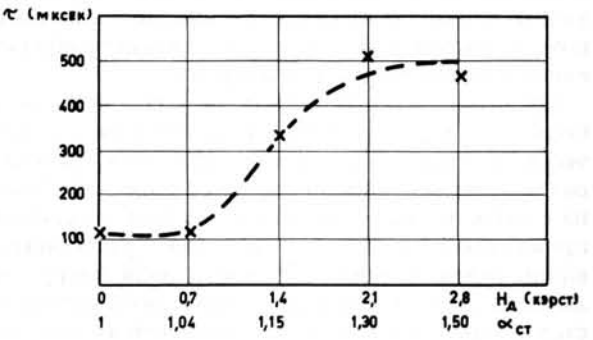

Рис. 5 Кривая зависимости времени жизни от дополнительного поля.

больших полях. Можно думать что величина τ, достигаемая на участке насыщения, определяется теперь уже только механизмом перезарядки, а не уходом плазмы из ловушки из-за неустойчивости. На это указывает зависимость времени жизни от давления водорода.

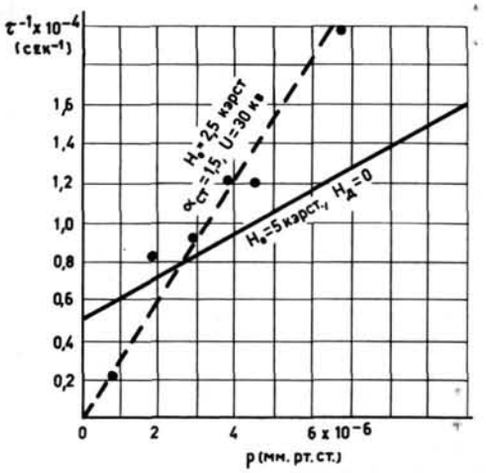

Рис. 6 Зависимость обратного времени жизни от давления водорода.

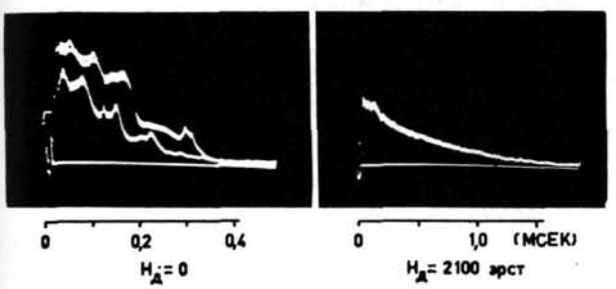

Рис. 7 Осциллограммы потока нейтральных частиц с дополнительным полем и без него.

На рис. 6 приведена зависимость обратного времени жизни от давления водорода в интервале $9\times10^{-7}-6\times10^{-6}$ мм рт ст. Как следует из рис. 6, экспериментальные значения $1/\tau$ лежат около прямой, которая при экстраполяции к нулевому давлению проходит близко от начала координат (пунктирная прямая). Это означает, что потери, не обусловленные перезарядкой, если таковые и остаются, малы по сравнению с перезарядочными потерями. На том же рисунке приведена для сравнения зависимость $1/\tau$ от давления при $H_0=5000$ эрстед в отсутствии дополнительного поля.

Наконец можно еще привести сравнительный вид осциллограмм потока нейтральных частиц без дополнительного поля и с дополнительным полем (рис. 7).

В первом случае видны колебания, которые отражают собой глубокие пульсации плотности плазмы, которые имеют место вблизи стенки ловушки.

Во втором случае кривая достаточно гладкая, и это указывает на отсутствие таких пульсаций.

Таковы те экспериментальные факты, которые можно привести в настоящее время. Они показывают, что, изменяя конфигурацию магнитного поля, можно существенным образом влиять на те нестабильности, которые имели место в наших прежних опытах.

В заключение я хотел бы еще раз подчеркнуть, что эти результаты носят сугубо предварительный характер, и на основании их можно сделать сейчас, пожалуй, лишь один определенный вывод, а именно, что имеет смысл вести работу в этом направлении.

Авторы считают своим долгом выразить благодарность академику Л. А. Арцимовичу за интерес к настоящей работе, ценные советы и обсуждение.

Литература

[1] Grad, H., et al, in Proc. 2nd U.N. Conf. PUAE **31**, United Nations, Geneva (1958) 230.
[2] Головин И. Н., *Усп. физ. Наук* **73** (1961) 685.
[3] Арцимович Л. А., Управляемые Термоядерные Реакции, Физикоматематическое Государственное Издательство, Москва (1961 г.).

NON-LINEAR STABILITY OF PLASMA OSCILLATIONS*

W. E. DRUMMOND, D. PINES**

JOHN JAY HOPKINS LABORATORY FOR PURE AND APPLIED SCIENCE, GENERAL ATOMIC DIVISION OF GENERAL DYNAMICS CORPORATION

SAN DIEGO, CALIFORNIA, UNITED STATES OF AMERICA

The collective behavior of a fully ionized plasma in which the number of particles in a sphere of radius a, the Debye length, is very large compared to one is governed by the collisionless Boltzmann or Vlasov equation. In an infinite homogeneous plasma of this type, it is well known that in the "linearized" theory a velocity distribution $f_0(v)$ consisting of a main part that is a monotonically decreasing function of energy plus a small gentle bump on the tail of the main part (e.g. a Maxwellian plus runaway electrons) leads to unstable (growing) plasma oscillations, and that the unstable oscillations are those for which $v\,\partial f_0(v)/\partial v > 0$ for $v = \omega/k$ (ω is the frequency and k the wave number).

After a sufficient time these waves grow to such an amplitude that the non-linear terms in the Vlasov equation are important and the linearization is no longer valid. The question then arises as to the behavior of these waves in the non-linear region and it is this question which we consider.

The method is to divide the non-linear terms into two groups, one of which combined with the linear terms yields a non-linear dispersion relation, while the other provides a weak coupling between the different modes. The non-linear dispersion relation leads to the establishment of an equilibrium spectrum, which then decays slowly to zero due to the mode-coupling terms. The limiting of the wave amplitudes to the equilibrium spectrum is due to flattening of the bump in the velocity distribution by non-linear effects. The slow decay of the equilibrium spectrum leads to further changes in the velocity distribution so that asymptotically the distribution function is a monotonically decreasing function of energy and hence stable. Analytic expressions for the equilibrium spectrum and the equilibrium velocity distribution are obtained. An approximate value for the maximum energy in the equilibrium electric field is given by the geometric mean of the thermal energy and the drift energy of the particles in the bump.

1. Introduction

The collective behavior of a fully ionized plasma in which the number of particles in a sphere of radius a, the Debye length, is very large compared to one is governed by the collisionless Boltzmann or Vlasov equation. In an infinite homogeneous plasma of this type it is well known that certain velocity distributions lead to unstable (growing) oscillations. The frequencies and growth rates of these oscillations are obtained by linearizing the Vlasov equation about the unperturbed distribution function, and this leads to exponentially damped (stable) or exponentially growing (unstable) solutions. After a sufficient time the unstable solutions evidently grow to such an amplitude that the non-linear terms become important and the linearizing of the Vlasov equation is no longer valid. The question then arises as to the ultimate fate of such unstable oscillations. It is this question that we wish to consider.

It will be shown that the development in the non-linear regime for certain types of unstable modes can be followed in considerable detail for long times. This is illustrated for the case of unstable electron-plasma oscillations. The result is that these waves, which are initially unstable, grow in a short time to an equilibrium spectrum (in k space) and then decay slowly to zero. The limiting of these waves to an equilibrium spectrum is a result of a diffusion in the velocity distribution due to non-linear effects and cannot be obtained in the magnetohydrodynamic (MHD) approximation. The decay of this spectrum is due to a combination of non-linear changes in the distribution function and MHD effects.

The method is to divide the non-linear terms into two groups. One of these, combined with the linear terms, yields a non-linear dispersion relation, and leads to the establishment of an equilibrium spectrum. The other group of non-linear terms provides coupling between the different modes, and it is this coupling that leads to the eventual damping of the spectrum. In practical cases, this decay time may be so long that collision effects will dominate the damping process.

The instabilities to which the theory applies are those for which the growth rate depends on the velocity gradient of the distribution function, and the dispersion relation is such that the interaction between modes is non-resonant.

In Section 2 the linearized solutions are discussed, and the non-linear dispersion relations are developed in Section 3. In Section 4 the non-linear dispersion relations are applied to a one-dimensional example. The damping due to mode coupling is discussed in Section 5, and the results are discussed in Section 6.

* Conference paper CN-10/134, presented by W. E. Drummond. Discussion of this paper is given on page 1109. Translations of the abstract are at the end of this volume of the Conference Proceedings.

** PERMANENT ADDRESS: Departments of Physics and Electrical Engineering, University of Illinois, Urbana, Ill.

2. Linearized theory

In treating the dynamics of the electrons we shall treat the ions as a uniform background of positive charge. In so doing we neglect the influence of the ionic polarizability, an approximation which is valid for phenomena occurring at frequencies large compared to characteristic ionic frequencies. We study the Vlasov equation which governs the time rate of change of the single-particle distribution function, $F(\mathbf{r}, \mathbf{v}, t)$, according to

$$\frac{\partial F}{\partial t} + \mathbf{v}\cdot\nabla F - \frac{e\mathbf{E}}{m}\cdot\nabla_{\mathbf{v}} F = 0 \tag{2.1}$$

Here $\mathbf{E}$ is the electric field produced by the particles, and is determined by Poisson's equation

$$\nabla\cdot\mathbf{E} = +4\pi e(n-\varrho) = +4\pi e\left[n - \int \mathrm{d}^3\mathbf{v}\, F(\mathbf{v})\right] \tag{2.2}$$

where $\varrho(\mathbf{r}, t)$ is the local electron density, and n is the average electron and ion density, and e and m are the electronic charge and mass respectively.

The use of Eq. (2.1) represents an approximation of the following kind [1, 2]. First, it is valid only when

$$n a^3 \gg 1 \tag{2.3}$$

where a is the Debye length,

$$a^2 = \mathrm{k}T/4\pi n e^2 \tag{2.4}$$

and T is the electron temperature. This approximation is well satisfied in all classical plasmas of physical interest. Next we remark that in general the right-hand side of (2.1) should not be zero but should contain Fokker-Planck-type collision terms, which are themselves non-linear functions of F. These collision terms give rise to relaxation phenomena in the electron gas which are characterized by a time

$$\tau = n a^3/\omega_{\mathrm{p}} \tag{2.5}$$

when $\omega_{\mathrm{p}} = (4\pi n e^2/m)^{1/2}$ is the plasma frequency. Our use of Eq. (2.1) is therefore only valid as long as the phenomena we consider take place in a time short compared to τ.

The solution of Eqs. (2.1) and (2.2) is obtained by splitting F into two parts

$$F(\mathbf{r}, \mathbf{v}, t) = F_0(\mathbf{v}) + f(\mathbf{r}, \mathbf{v}, t) \tag{2.6}$$

Here $F_0(\mathbf{v})$ is the unperturbed homogeneous time-independent distribution function, while $f(\mathbf{r}, \mathbf{v}, t)$ represents the correction to $F_0(\mathbf{v})$ brought about by the Coulomb interaction between the electrons. If we expand f in a Fourier series in a box of size L^3,

$$f(\mathbf{r}, \mathbf{v}, t) = \sum_{k} f_{\mathbf{k}}(\mathbf{v}, t)\, \mathrm{e}^{\mathrm{i}\mathbf{k}\cdot\mathbf{r}}$$

$$f_{\mathbf{k}}(\mathbf{v}, t) = \frac{1}{L^3}\int \mathrm{d}^3\mathbf{r}\, f(\mathbf{r}, \mathbf{v}, t)\, \mathrm{e}^{-\mathrm{i}\mathbf{k}\cdot\mathbf{r}} \tag{2.7}$$

we obtain

$$\frac{\partial f_{\mathbf{k}}}{\partial t} + \mathrm{i}\mathbf{k}\cdot\mathbf{v} f_{\mathbf{k}} = +\frac{e}{m}\mathbf{E}_{\mathbf{k}}\cdot\nabla_{\mathbf{v}} F_0 + \frac{e}{m}\sum_{\mathbf{q}} \mathbf{E}_{\mathbf{k}-\mathbf{q}}\cdot\nabla_{\mathbf{v}} f_{\mathbf{q}} \tag{2.8}$$

and

$$\mathbf{E}_{\mathbf{q}}(t) = \frac{4\pi e}{q^2}\mathrm{i}\mathbf{q}\int \mathrm{d}^3\mathbf{v}\, f_{\mathbf{q}}(t) \tag{2.9}$$

where we have made use of the fact that we consider only longitudinal electric fields.

In this section we consider the perturbation series solution of Eqs. (2.8) and (2.9), in which $f(\mathbf{v}, t)$ is regarded as representing a small correction to the initial velocity distribution, $F_0(\mathbf{v})$. Our motivation in doing so is, first, to bring out the nature of the difficulties that arise when $F_0(\mathbf{v})$ is such as to yield growing plasma waves; and second, to provide a framework within which to view the non-perturbation solution discussed in the following section.

The perturbation-theoretical solution consists in expanding $f_{\mathbf{k}}$ and $\mathbf{E}_{\mathbf{k}}$ as follows

$$f_{\mathbf{k}} = f_{\mathbf{k}}^{(1)} + f_{\mathbf{k}}^{(2)} + f_{\mathbf{k}}^{(3)} + \ldots$$

$$\mathbf{E}_{\mathbf{k}} = \mathbf{E}_{\mathbf{k}}^{(1)} + \mathbf{E}_{\mathbf{k}}^{(2)} + \mathbf{E}_{\mathbf{k}}^{(3)} + \ldots \tag{2.10}$$

while regarding $F_0(\mathbf{v})$ as a zero-order quantity. The first three equations are

$$\frac{\partial f_{\mathbf{k}}^{(1)}}{\partial t} + \mathrm{i}\mathbf{k}\cdot\mathbf{v} f_{\mathbf{k}}^{(1)} = \left(\frac{e}{m}\right)\mathbf{E}_{\mathbf{k}}^{(1)}\cdot\nabla_{\mathbf{v}} F_0 \tag{2.11}$$

$$\frac{\partial f_{\mathbf{k}}^{(2)}}{\partial t} + \mathrm{i}\mathbf{k}\cdot\mathbf{v} f_{\mathbf{k}}^{(2)} = \left(\frac{e}{m}\right)\left[\mathbf{E}_{\mathbf{k}}^{(2)}\cdot\nabla_{\mathbf{v}} F_0 + \sum_{\mathbf{q}} \mathbf{E}_{\mathbf{k}-\mathbf{q}}^{(1)}\cdot\nabla_{\mathbf{v}} f_{\mathbf{q}}^{(1)}\right] \tag{2.12}$$

$$\frac{\partial f_{\mathbf{k}}^{(3)}}{\partial t} + \mathrm{i}\mathbf{k}\cdot\mathbf{v} f_{\mathbf{k}}^{(3)} = \left(\frac{e}{m}\right)\left\{\mathbf{E}_{\mathbf{k}}^{(3)}\cdot\nabla_{\mathbf{v}} F_0 + \sum_{\mathbf{q}}\left[\mathbf{E}_{\mathbf{k}-\mathbf{q}}^{(2)}\cdot\nabla_{\mathbf{v}} f_{\mathbf{q}}^{(1)} + \mathbf{E}_{\mathbf{k}-\mathbf{q}}^{(1)}\cdot\nabla_{\mathbf{v}} f_{\mathbf{q}}^{(2)}\right]\right\} \tag{2.13}$$

and

$$\mathbf{E}_{\mathbf{q}}^{(1)} = \frac{4\pi e}{q^2}\mathrm{i}\mathbf{q}\int \mathrm{d}^3\mathbf{v}\, f_{\mathbf{q}}^{(1)}(\mathbf{v}) \tag{2.14}$$

with corresponding equations connecting $\mathbf{E}_{\mathbf{q}}^{(2)}$ and $f_{\mathbf{q}}^{(2)}$, $\mathbf{E}_{\mathbf{q}}^{(3)}$ and $f_{\mathbf{q}}^{(3)}$. One then finds, from (2.11) and (2.14) that a non-zero solution of $\mathbf{E}_{\mathbf{q}}^{(1)}$ with a time dependence of the form $\exp -\mathrm{i}\Omega t$ exists only for frequencies Ω which satisfy the dispersion relation

$$\varepsilon^{(1)}(\mathbf{q}, \Omega) = 1 + \frac{4\pi e^2}{m q^2}\int \mathrm{d}^3\mathbf{v}\, \frac{\mathbf{q}\cdot\nabla_{\mathbf{v}} F_0(\mathbf{v})}{\Omega - \mathbf{q}\cdot\mathbf{v}} = 0 \tag{2.15}$$

Here $\varepsilon^{(1)}(\mathbf{q}, \Omega)$ is the first-order dielectric constant of the plasma, and Im $\Omega > 0$. $\varepsilon^{(1)}(\mathbf{q}, \Omega)$ is thus defined only for Ω in the upper half of the complex Ω plane and is to be continued analytically into the lower half plane where necessary to obtain solutions for which Im $\Omega \leq 0$.

In the present paper we confine our attention to distribution functions $F_0(\mathbf{v})$ which are such that one will find for certain values of $\mathbf{q}$ growing plasma oscillations with

$$\Omega(\mathbf{q}) = \omega_{\mathbf{q}}^{(1)} + i\gamma_{\mathbf{q}}^{(1)} \tag{2.16}$$

such that the growth rate $\gamma_{\mathbf{q}}^{(1)}$ is small compared to the oscillation frequency, $\omega_{\mathbf{q}}^{(1)}$, the latter being given by its long wavelength expansion

$$\omega_{\mathbf{q}}^2 \approx \omega_p^2 + 3\int d^3\mathbf{v}\, F_0(\mathbf{v})(\mathbf{q}\cdot\mathbf{v})^2 + \cdots \tag{2.17}$$

In addition we require $\gamma_q/q\Delta v \ll 1$ where Δv is the characteristic velocity increment in which $F_0(\omega_p/q)$ changes. The growth rate $\gamma_{\mathbf{q}}^{(1)}$, is then given by

$$\frac{\gamma_{\mathbf{q}}^{(1)}}{\omega_{\mathbf{q}}^{(1)}} = \frac{2\pi^2 e^2}{m q^2}\int d^3\mathbf{v}\, \mathbf{q}\cdot\nabla_{\mathbf{v}} F_0(\mathbf{v})\,\delta(\omega_{\mathbf{q}}^{(1)} - \mathbf{q}\cdot\mathbf{v}) \ll 1 \tag{2.18}$$

In the second order one finds, on substituting the appropriate first-order solutions for $f_{\mathbf{k}}^{(1)}$ and $\mathbf{E}_{\mathbf{k}}^{(1)}$ into (2.12), that $\mathbf{E}_{\mathbf{k}}^{(2)}$ (and $f_{\mathbf{k}}^{(2)}$) oscillate at the sum and difference frequencies $\omega_{\mathbf{q}} \pm \omega_{\mathbf{k}-\mathbf{q}}$ as one might expect. These solutions, when substituted into the equation for $f_{\mathbf{q}}^{(3)}$ (2.13) will yield corrections to the dispersion relation (2.15). There is also in second order a correction to $F_0(\mathbf{v})$ arising from $f_0^{(2)}(\mathbf{v})$. The equation for the time rate of change of $f_0^{(2)}(\mathbf{v})$ reads

$$\frac{\partial f_0^{(2)}(\mathbf{v})}{\partial t} = \sum_{\mathbf{q}} \frac{8\pi}{q^2}\left(\frac{e}{m}\right)^2 \mathscr{E}_{\mathbf{q}}(t)\,\mathbf{q}\cdot\nabla_{\mathbf{v}} \frac{\gamma_{\mathbf{q}}^{(1)}}{(\omega^{(1)} - \mathbf{q}\cdot\mathbf{v})^2 + (\gamma_{\mathbf{q}}^{(1)})^2} \times \mathbf{q}\cdot\nabla_{\mathbf{v}} F_0(\mathbf{v}) \tag{2.19}$$

where we have introduced $\mathscr{E}_{\mathbf{q}}(t)$, the electrostatic energy in the $\mathbf{q}$th plasma mode

$$\mathscr{E}_{\mathbf{q}}(t) = \frac{|E_{\mathbf{q}}(t)|^2}{8\pi} \tag{2.20}$$

According to (2.16), one further has

$$\frac{\partial \mathscr{E}_{\mathbf{q}}}{\partial t} = 2\gamma_{\mathbf{q}}^{(1)}\mathscr{E}_{\mathbf{q}} \tag{2.21}$$

Plasma waves that are damped (and which possess an initial energy level $\mathscr{E}_{\mathbf{q}}$ not much greater than the thermal level, kT) do not make a sizeable contribution to $f_0^{(2)}(\mathbf{v})$. Their contribution is such that $f_0^{(2)}(\mathbf{v})$ will be of order $1/na^3$ compared to $F_0(\mathbf{v})$ and therefore represent a small correction consistent with the assumptions underlying the use of perturbation theory. In fact, under these circumstances, the terms on the right-hand side of (2.19) are of the same order as certain of the Fokker-Planck terms we have neglected. Again, for damped plasma waves, it is necessary to consider corrections to (2.21) that are contained in the more complete Fokker-Planck equation, which correspond to spontaneous emission of plasma waves, and which we have neglected.

In third order one finds corrections to the dispersion relation (2.15) the most important of which comes from $f_0^{(2)}(\mathbf{v})$ and is of the form

$$\frac{\delta\gamma_{\mathbf{q}}}{\omega_{\mathbf{q}}} = \frac{2\pi^2 e^2}{m_{\mathbf{q}}^2}\int d^3\mathbf{v}\, \mathbf{q}\cdot\nabla_{\mathbf{v}} f_0^{(2)}(\mathbf{v},t)\,\delta(\omega_{\mathbf{q}} - \mathbf{q}\cdot\mathbf{v}) \tag{2.22}$$

This correction term $\delta\gamma_{\mathbf{q}}$ is of order $(1/na^3)\gamma_{\mathbf{q}}$ for damped waves or waves with energies $\mathscr{E}_{\mathbf{k}}(t)$ near the thermal level kT. Similar behavior is found for the other third-order terms; so for these circumstances the use of perturbation-theory is well justified.

For growing plasma waves the situation is quite different. If one begins with a thermal level of energy kT in such a wave, after a few e-folding times ($t \gtrsim 1/\gamma_{\mathbf{q}}$), the corrections to (2.19) and (2.21) arising from the Fokker-Planck collision terms will be small. Moreover, as the energy in these growing plasma modes increases, the correction to $\gamma_{\mathbf{q}}$ arising from $f_0^{(2)}(\mathbf{v})$ will eventually become comparable to $\gamma_{\mathbf{q}}$. Further inspection shows that at this point the corrections to $\gamma_{\mathbf{q}}$ from $f_0^{(4)}$, $f_0^{(6)}$, etc., are also comparable to $\gamma_{\mathbf{q}}$ and thus the perturbation-theory solution breaks down. One is forced, then, to search for a more accurate set of equations to describe this time-dependent interrelationship between the spatially homogeneous part of the distribution function

$$g(\mathbf{v},t) = F_0(\mathbf{v}) + f_0(\mathbf{v},t) \tag{2.33}$$

and the growth rate, now also time dependent $\gamma(\mathbf{q},t)$.

3. Non-linear theory

The breakdown in the perturbation-theoretical solution of (2.8) and (2.9) for plasmas in which growing waves exist leads us to consider an alternative set of solutions in which the spatially homogeneous part of the distribution function $g(\mathbf{v},t)$ plays a special role. From among the terms in the sum over $\mathbf{q}$ on the right hand side of Eq. (2.8) we single out the term with $\mathbf{q}=0$ so that the non-linear Vlasov equation becomes

$$\frac{\partial f_{\mathbf{K}}}{\partial t} + i\mathbf{K}\cdot\mathbf{v} f_{\mathbf{K}} = +\frac{e}{m}\mathbf{E}_{\mathbf{K}}\cdot\nabla_{\mathbf{v}} g + \frac{e}{m}\sum_{\mathbf{q}}{}' \mathbf{E}_{\mathbf{K}-\mathbf{q}}\cdot\nabla_{\mathbf{v}} f_{\mathbf{q}} \tag{3.1}$$

where $g(\mathbf{v},t) = F_0(\mathbf{v}) + f_0(\mathbf{v},t)$ and the prime in the summation indicates that the term with $q=0$ is to be deleted. For $\mathbf{K}=0$, $\partial f_0/\partial t = \partial g/\partial t$, we likewise have

$$\frac{\partial g}{\partial t} = +\frac{e}{m}\mathbf{E}_0\cdot\nabla_{\mathbf{v}} g + \frac{e}{m}\sum_{\mathbf{q}}{}' \mathbf{E}_{-\mathbf{q}}\cdot\nabla_{\mathbf{v}} f_{\mathbf{q}} \tag{3.2}$$

In the term $\mathbf{E}_0\cdot\nabla_{\mathbf{v}} g$ in Eq. (3.2), $\mathbf{E}_0$ is determined by the boundary conditions. If the different boundaries are held at different fixed potentials $\mathbf{E}_0$ is non-zero. However, if we apply periodic boundary conditions (to the potential), $\mathbf{E}_0=0$. We shall take $\mathbf{E}_0=0$ for the sake of simplicity.

The non-linear terms in the second term on the right-hand side of (3.1) represent an interaction between different modes whereas the non-linear part of $\mathbf{E}_{\mathbf{K}}\cdot\nabla_{\mathbf{v}} g$ combined with (3.2) leads to a slow variation of the frequency and growth rate with time.

Our procedure is first to solve Eqs. (3.1) and (3.2) neglecting the mode-coupling terms and then to treat these terms as a perturbation. The justification for this is that when we neglect mode coupling we

find that the energy $\mathscr{E}_{\mathbf{q}}$ in the unstable modes does not grow indefinitely as in the linearized theory but instead comes rapidly to an equilibrium spectrum the amplitude of which is of order $\gamma_{\mathbf{q}}^{(1)}/\omega_{\mathbf{q}}$ and hence small. Since the equilibrium amplitude is small, the non-linear mode coupling can be treated by perturbation-theoretical methods and leads to a rather slow decay of the equilibrium spectrum.

The basic equations which we consider with (2.9), are therefore

$$\frac{\partial f_{\mathbf{K}}}{\partial t} + \mathrm{i}\,\mathbf{K}\cdot\mathbf{v} f_{\mathbf{K}} = \frac{e}{m}\mathbf{E}_{\mathbf{K}}\cdot\nabla_{\mathbf{v}} g \tag{3.3}$$

$$\frac{\partial g}{\partial t} = + \frac{e}{m}\sum_{\mathbf{q}}{}' \mathbf{E}_{\mathbf{q}}\cdot\nabla_{\mathbf{v}} f_{\mathbf{q}} \tag{3.4}$$

Our solution is based on the fact that the frequency and growth rate determined from these equations are slowly varying functions of time. Thus we wish to assume that the change in γ (or ω) during a time of interest (γ^{-1} or ω^{-1}) is small compared to γ (or ω) and then demonstrate that this assumption is consistent. The derivation is based on a type of WKB approximation, and is given in the appendix. The resulting equations are

$$\frac{\partial g(\mathbf{v})}{\partial t} = \sum_{\mathbf{q}}{}' \frac{8\pi e^2 \mathscr{E}_{\mathbf{q}}(t)}{m^2 q^2}\mathbf{q}\cdot\nabla_{\mathbf{v}} \frac{\gamma(\mathbf{q},t)}{(\omega_{\mathbf{q}} - \mathbf{q}\cdot\mathbf{v})^2 + \gamma^2}\mathbf{q}\cdot\nabla_{\mathbf{v}} g(\mathbf{v},t) \tag{3.5}$$

$$\gamma(\mathbf{q},t) = \frac{2\pi^2 e^2}{m q^2}\omega_{\mathbf{q}}\int \mathrm{d}^3\mathbf{v}\,\mathbf{q}\cdot\nabla_{\mathbf{v}} g(\mathbf{v},t)\,\delta(\omega_{\mathbf{q}} - \mathbf{q}\cdot\mathbf{v}) \tag{3.6}$$

$$\frac{\partial \mathscr{E}_{\mathbf{q}}}{\partial t} = 2\gamma(\mathbf{q},t)\,\mathscr{E}_{\mathbf{q}} \tag{3.7}$$

It is instructive to compare these equations with their perturbation-theoretical counterparts. We remark that (3.5) differs from (2.19) in that $g(\mathbf{v},t)$ now relaxes toward itself rather than toward $F_0(\mathbf{v},t)$. Equation (3.6) (there is an analogous equation for $\omega_{\mathbf{q}}(t)$ of which we shall not have need) states that the growth rate is determined by the total spatially homogeneous distribution function existing at the time t rather than the initial value $F_0(\mathbf{v})$. This result seems eminently reasonable since one would expect the plasma dispersion relation to follow $g(\mathbf{v},t)$ adiabatically provided the latter changed slowly over characteristic plasma times. Indeed one is so naturally led on intuitive grounds to write down (3.5) and (3.6) that it is hardly surprising that their derivation is possible.

We may further remark that from the point of view of a perturbation-theoretical approach, we have essentially summed a whole class of higher-order terms (those corresponding to $f_0^{(4)}$, $f_0^{(6)}$, $f_0^{(8)}$, etc.) in writing down these basic equations. We also note that these equations may be obtained by means of a quantum treatment based on the explicit introduction of collective coordinates, a plasmon distribution function and the random phase approximation [3].

We consider some general properties of (3.5) and (3.6). First we note that (3.5) resembles the diffusion term in a Fokker-Planck equation. Thus we may write

$$\frac{\partial g(\mathbf{v},t)}{\partial t} = \sum_{i,j}\frac{\partial}{\partial v_i} T_{ij}\frac{\partial}{\partial v_j} g(\mathbf{v},t) \tag{3.8}$$

where the diffusion coefficient T_{ij} is given by

$$T_{ij}(\mathbf{v}) = \sum_{\mathbf{q}}{}' \frac{8\pi e^2 \mathscr{E}_{\mathbf{q}}(t)}{m^2 q^2}\frac{\gamma(\mathbf{q},t)}{(\omega_{\mathbf{q}} - \mathbf{q}\cdot\mathbf{v})^2 + \gamma_{\mathbf{q}}^2} q_i q_j \tag{3.9}$$

$T_{ij}(\mathbf{v})$ possesses a rather different character depending on whether or not $\mathbf{v}$ is such that $\mathbf{q}\cdot\mathbf{v} \approx \omega_{\mathbf{q}}$. Where $\mathbf{q}\cdot\mathbf{v} \approx \omega_{\mathbf{q}}$, since $\gamma \ll \omega_{\mathbf{q}}$, the denominator displays a characteristic resonance behavior, and we have

$$\frac{\gamma(\mathbf{q},t)}{(\omega_{\mathbf{q}} - \mathbf{q}\cdot\mathbf{v})^2 + \gamma_{\mathbf{q}}^2} \approx \pi\,\delta(\omega_{\mathbf{q}} - \mathbf{q}\cdot\mathbf{v})$$

We thus find an explicit plasma-oscillation diffusion coefficient

$$T_{ij}^{p'}(\mathbf{v}) = \sum_{\mathbf{q}}{}' \frac{8\pi^2 e^2}{m^2 q^2} q_i q_j \delta(\omega_{\mathbf{q}} - \mathbf{q}\cdot\mathbf{v})\,\mathscr{E}_{\mathbf{q}} \tag{3.10}$$

These equations have a physical significance which is most easily understood in a one-dimensional case. In this case particles traveling slightly slower than the phase velocity of a particular wave are accelerated by the wave and thus take energy from the wave, whereas particles traveling slightly faster than the wave are slowed down and give up energy to the wave. Thus if there are more particles going slightly faster than the wave than there are particles going slightly slower than the wave, i.e., if $\partial f/\partial v > 0$ for $v = \omega_{\mathbf{q}}/q$, then there is a net energy transfer to the wave. In three dimensions it is the projection of the particle velocity in the direction of wave propagation that determines the growth or damping, and thus if $\int \mathrm{d}^3\mathbf{v}\,\mathbf{q}\cdot\nabla_{\mathbf{v}} g(\mathbf{v},t)\,\delta(\omega_{\mathbf{q}} - \mathbf{q}\cdot\mathbf{v}) > 0$, the wave grows. This is the physical significance of Eq. (3.6). The accompanying diffusion of the particle distribution function is given by Eq. (3.8) and is such as to reduce the growth rate.

This process continues until the particle distribution function is readjusted such that $\int \mathrm{d}^3\mathbf{v}\,\mathbf{q}\cdot\nabla_{\mathbf{v}} g(\mathbf{v},t)\,\delta(\omega_{\mathbf{q}} - \mathbf{q}\cdot\mathbf{v}) = 0$ for those particles which interact with the waves. The waves then have reached an equilibrium spectrum and their amplitude no longer changes. This process is discussed in detail for a one-dimensional example in the next section.

Next on a time scale longer compared to that of the above process the mode-coupling terms act to distort and damp the equilibrium spectrum. This process is considered in detail in Section 5. Before going to that, we wish to discuss the question of energy conservation as determined by Eqs. (3.5)-(3.7).

Particle energy U is given by

$$U = \int \mathrm{d}^3\mathbf{v}\,\frac{m v^2}{2} g(\mathbf{v}) \tag{3.11}$$

We have, using (3.5)

$$\frac{dU}{dt} = \sum_{\mathbf{q}}{}' \frac{8\pi e^2}{m^2 q^2} \mathscr{E}_{\mathbf{q}}(t) \int d^3\mathbf{v} \frac{mv^2}{2} \times \left[\mathbf{q}\cdot\nabla_{\mathbf{v}} \frac{\gamma(\mathbf{q},t)}{(\omega_{\mathbf{q}} - \mathbf{q}\cdot\mathbf{v})^2 + \gamma_{\mathbf{q}}^2} \mathbf{q}\cdot\nabla_{\mathbf{v}} g(\mathbf{v},t) \right] \quad (3.12)$$

From the integral over velocities, there will be two distinct contributions to dU/dt, according to whether or not one has resonant transfer of energy to plasma waves at $\mathbf{q}\cdot\mathbf{v} \approx \omega_p$.

We consider the resonant contribution first. We then have

$$\left(\frac{dU}{dt}\right)_{res} = \sum_{\mathbf{q}}{}' \frac{4\pi^2 e^2}{m^2 q^2} \mathscr{E}_{\mathbf{q}}(t) \int d^3\mathbf{v}\, m v^2 (\mathbf{q}\cdot\nabla_{\mathbf{v}}) \times [\delta(\omega_{\mathbf{q}} - \mathbf{q}\cdot\mathbf{v})\, \mathbf{q}\cdot\nabla_{\mathbf{v}} g(\mathbf{v},t)] \quad (3.13)$$

If we integrate by parts, we find

$$\left(\frac{dU}{dt}\right)_{res} = -\sum_{\mathbf{q}}{}' \frac{8\pi^2 e^2}{m q^2} \mathscr{E}_{\mathbf{q}}(t) \times \int d^3\mathbf{v}\, \mathbf{q}\cdot\mathbf{v}\, \delta(\omega_{\mathbf{q}} - \mathbf{q}\cdot\mathbf{v})\, \mathbf{q}\cdot\nabla_{\mathbf{v}} g(\mathbf{v},t) \quad (3.14)$$

The integrated part vanishes since $\mathbf{q}\cdot\nabla_{\mathbf{v}} g(\mathbf{v},t)$ vanishes for the limits at which growing waves no longer occur. We then see, on comparing (3.14) and (3.6) (and making use of the replacement of $\mathbf{q}\cdot\mathbf{v}$ in the integrand by $\omega_{\mathbf{q}}$ according to the properties of the δ function), that

$$\left(\frac{dU}{dt}\right)_{res} = -\sum_{\mathbf{q}} 4\gamma(\mathbf{q},t)\, \mathscr{E}_{\mathbf{q}} = -2\sum_{\mathbf{q}} \frac{\partial \mathscr{E}_{\mathbf{q}}}{\partial t} \quad (3.15)$$

Thus where the resonances occur, the particle energy is transferred directly to the plasma waves, as we might expect.

There is also the non-resonant contribution to (3.12). The major contribution to this comes from small $\mathbf{v}$. After integrating by parts twice we obtain

$$\left(\frac{dU}{dt}\right)_{non\text{-}res} \approx \sum_{\mathbf{q}}{}' \frac{8\pi e^2}{m} \mathscr{E}_{\mathbf{q}}(t)\, \gamma(\mathbf{q},t) \times \bar{\int} d^3\mathbf{v} \frac{1}{(\omega_{\mathbf{q}} - \mathbf{q}\cdot\mathbf{v})^2 + \gamma_{\mathbf{q}}^2} g(\mathbf{v},t) \quad (3.16)$$

The bar over the integral denotes that principal parts are to be taken, and we neglect a term of order $(qa)^2$. If we now make use of the dispersion relation

$$1 = \frac{4\pi e^2}{m} \bar{\int} d^3\mathbf{v} \frac{1}{(\omega - \mathbf{q}\cdot\mathbf{v})^2 + \gamma_{\mathbf{q}}^2} g(\mathbf{v},t) \quad (3.17)$$

we see that

$$\left(\frac{dU}{dt}\right)_{non\text{-}res} \approx \sum_{\mathbf{q}}{}' 2\gamma(\mathbf{q},t)\, \mathscr{E}_{\mathbf{q}}(t) = \sum_{\mathbf{q}} \frac{\partial \mathscr{E}_{\mathbf{q}}}{\partial t} \quad (3.18)$$

This result possesses a simple physical interpretation. Those particles with velocities near the phase velocity of the waves give up an energy $2\Sigma_{\mathbf{q}} \mathscr{E}_{\mathbf{q}}$ to the waves. Half of this, $\Sigma_{\mathbf{q}} \mathscr{E}_{\mathbf{q}}$, goes to potential energy and the other half goes into the kinetic energy of oscillation of the bulk of the particles. The over-all energy transfer is therefore given by

$$\frac{d}{dt}\left(U + \sum_{\mathbf{q}}{}' \frac{|E_{\mathbf{q}}|^2}{8\pi}\right) = 0 \quad (3.19)$$

4. Application to one-dimensional case

We now specialize to the one-dimensional case and examine in detail the development of the equilibrium spectrum. We take $g(v,0) = F_0(v)$ to consist of a main part which is a monatonically decreasing function of energy plus a small gentle bump on the tail of the main part (see Fig. 1).

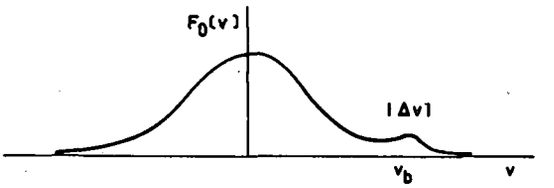

Fig. 1 Initial velocity-distribution function for one-dimensional case has bump on tail of monotonically decreasing main part.

The mean drift velocity of the bump is denoted by v_b and the width of the bump by Δv. The number of particles in the bump is denoted by n_b, and it is assumed that $n_b/n \ll 3\bar{v}^2(\Delta v)^2/v_b^4$, $\frac{\gamma^{(1)}}{\omega_p}\frac{v_b}{\Delta v} \ll 1$ and $n_b v_b^2 \ll n\bar{v}^2$ where $\bar{v}$ is the root-mean-square velocity of the main part, so that the approximations made in Section 3 are satisfied.

Denoting $\mathscr{E}_q(t)$ by $\mathscr{E}(v,t)$ where $v = \omega_q/q$, Eqs. (3.5) to (3.7) become, for v near v_b,

$$\frac{\partial \mathscr{E}(v,t)}{\partial t} = \alpha(v)\, \mathscr{E}(v,t) \frac{\partial g(v,t)}{\partial v} \quad (4.1)$$

$$\frac{\partial g(v,t)}{\partial t} = \frac{\partial}{\partial v}\left[\beta(v)\, \mathscr{E}(v,t) \frac{\partial g(v,t)}{\partial v}\right] \quad (4.2)$$

where $\alpha(v) = 4\pi^2 e^2 v^2/m\omega_p$, $\beta = 8\pi L e^2/m^2 v$, and we have neglected $(ka)^2 \approx (\bar{v}/v_b)^2 \ll 1$.

The temporal behavior of this pair is described as follows: If $\partial g/\partial v$ is positive at v, then $\mathscr{E}(v)$ increases in time. However $\beta\, \mathscr{E}(v)$ plays the role of a diffusion coefficient in Eq. (4.2) and hence as $\mathscr{E}(v)$ increases, $g(v)$ diffuses in such a way as to reduce $\partial g/\partial v$ at v. Thus the behavior of the pair of equations is such as to limit the amplitude of $\mathscr{E}(v)$.

To determine the resulting equilibrium spectrum we combine Eqs. (4.1) and (4.2) to obtain

$$\frac{\partial g}{\partial t} = \frac{\partial}{\partial v}\beta \mathscr{E} \frac{\partial g}{\partial v} = \frac{\partial}{\partial v}\frac{\beta}{\alpha}\frac{\partial \mathscr{E}}{\partial t}$$

and therefore

$$\frac{\partial}{\partial t}\left(g - \frac{\partial}{\partial v}\frac{\beta}{\alpha}\mathscr{E}\right) = 0 \quad (4.3)$$

We assume that $\frac{\beta}{\alpha}\frac{\partial \mathscr{E}}{\partial v}$ is negligible at $t=0$ and thus

$$\frac{\beta}{\alpha}\frac{\partial \mathscr{E}}{\partial v} = g(v) - F_0(v) \quad (4.4)$$

We seek a solution as $t\to\infty$ for which $\partial\mathscr{E}/\partial t = \partial g/\partial t = 0$. This is given by

$$\frac{\beta}{a}\mathscr{E}_\infty(v) = \int_{v_0}^{v}[g_\infty - F_0(v)]\,dv, \qquad v_0 < v < v_1 \tag{4.5}$$
$$= 0 \qquad v < v_0;\ v > v_1$$

where g_∞ is a constant which together with v_0 and v_1 is determined by

$$\int_{v_0}^{v_1} g_\infty\,dv = g_\infty(v_1 - v_0) = \int_{v_0}^{v_1} F_0(v)\,dv \tag{4.6}$$

This result is illustrated in Fig. 2. It is worth noting that the equilibrium spectrum is independent of the initial data, provided only that the initial data are smooth enough so that the sum in Eq. (3.9) can be evaluated by replacing $\gamma/((\omega_q - qv)^2+\gamma^2$ by $\pi\delta(\omega_q - qv)$. From Fig. 2 we also note that the energy given up to the plasma waves is of the order of $|g_\infty - F_0(v)|_{\max}$ for $v_0 < v < v_1$ times $mv_b\Delta v$ and is thus much less than the drift energy of the particles in the bump.

The development of this equilibrium spectrum in time has been calculated numerically for a typical

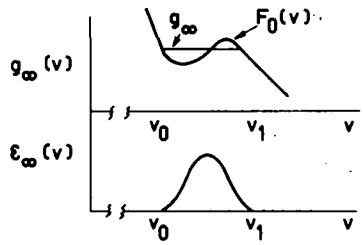

Fig. 2 Equilibrium velocity distribution and electric field spectrum from one-dimensional calculation.

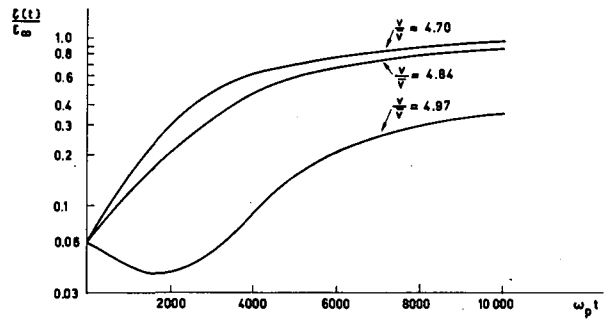

Fig. 3 Development in time of $\mathscr{E}(v)$ for several values of v.

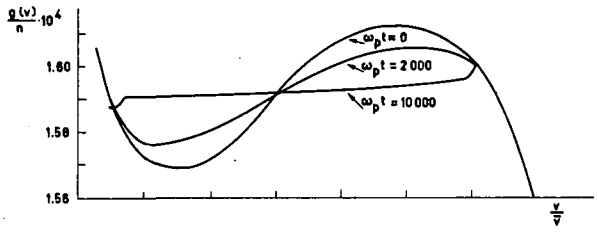

Fig. 4 Diffusion of $g(v)$.

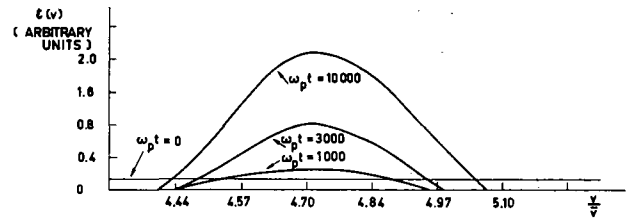

Fig. 5 Spectrum of $\mathscr{E}(v)$ at different times.

case and is illustrated in Figs. 3, 4, and 5. $F_0(v)$ was taken to be

$$\frac{n}{(2\pi)^{1/2}\bar{v}}\left\{\exp\left[-\frac{1}{2}\left(\frac{v}{\bar{v}}\right)^2\right] + 4\times10^{-4}\exp\left[-\frac{1}{2}\left(\frac{v}{\bar{v}}-5\right)^2\right]\right\}$$

and the initial data were taken to be constant in the region of interest and of such a magnitude that equilibrium was reached after a few e-folding times. Fig. 3 shows the development in time of $\mathscr{E}(v)$ for several values of v, and we note that the linear theory is valid for small times even for the relatively large initial data used. Figure 5 shows the spectrum of $\mathscr{E}(v)$ at different times while Fig. 4 shows the accompanying diffusion of $g(v)$.

From Eq. (4.5) we can estimate the amplitude of the equilibrium spectrum. We have

$$\mathscr{E}_\infty \approx \frac{\alpha}{\beta}(g_\infty - F_0)\Delta v \approx \frac{\alpha}{\beta}\frac{\partial F_0}{\partial v}(\Delta v)^2 \approx \frac{(\Delta v)^2}{\beta}\gamma^{(1)}$$

and the total electrostatic energy in the equilibrium spectrum is approximated by

$$\sum_q \mathscr{E}_q = \frac{2L}{2\pi}\int_0^\infty dq\,\mathscr{E}_q \approx \frac{L}{\pi}\mathscr{E}_q\Delta_q$$
$$\approx \frac{1}{2\pi}\left(\frac{\Delta v}{v_b}\right)\left(\frac{\Delta v}{\bar{v}}\right)^2\frac{\gamma^{(1)}}{\omega_p}\,n\,m\bar{v}^2 \ll \frac{n\,m\bar{v}^2}{2}$$

Thus the amplitude of the equilibrium spectrum is in fact of order $\gamma^{(1)}/\omega_p$, which is extremely small. As discussed in the next section, the mode-coupling terms that affect the equilibrium spectrum are of order $\mathscr{E}_q$, $\mathscr{E}^2$, etc., compared to the terms of the non-linear dispersion relation. Thus we may view the non-linear dispersion relation as the lowest order result of an expansion in powers of $\gamma^{(1)}/\omega_p$, and the mode-coupling terms can be safely treated by perturbation-theoretical methods.

5. Mode coupling

We now wish to consider for the one-dimensional case the effect of the non-linear mode-coupling terms in Eq. (3.1) on the equilibrium spectrum. We first note that the equilibrium spectrum is relatively narrow and f_q and E_{k-q} are large only if $|q|$, $|k-q| \approx |k_0|$, where k_0 denotes the center of the spectrum. It follows that k must lie near 0 or $\pm 2k_0$. Thus to second order (in E) the mode coupling terms lead to waves near

$k=0$ or $\pm 2k_0$, and to no change in the amplitude near k_0. Moreover, since the natural frequency of these waves $\omega_k \approx \omega_p$ is very different from $\omega_{k-q}+\omega_q \approx 0$ or $2\omega_p$, there are no "time proportional" transitions to these waves. In third order (in E) we find that the mode-coupling terms introduce an additional time dependence of the waves near k_0 which is given by

$$\frac{\partial E_k}{\partial t} = -\frac{i\omega_k}{2}\sum_{q,q'}{}' H(k,q,q')\,E_{k-q}(t)\,E_{q-q'}(t')\,E_{q'}(t) \qquad q \ll k_0 \tag{5.1}$$

The prime on the sum denotes that the terms with $q=0$ are to be deleted. In what follows only Im $[H(k,\ q,\ k)+H(k,\ q,\ q-k)]$ for $q \ll k_0$ is needed and this is given, after some tedious algebra, by

$$\begin{aligned}\mathrm{Im}\,[H(k,q,k) + H(k,q,q-k)] &= 9\left(\frac{k}{q}\right)^2 \frac{k^2}{\omega_p{}^4}\left(\frac{e}{m}\right)^2\left(1-\frac{q}{k}\right)^2 \mathrm{Im}\,\frac{1}{\varepsilon(q,\ \omega_{q-q'}+\omega_{q'})} \qquad q \ll k_0 \\ &= \frac{9\pi k^4}{\omega_p{}^2}\left(\frac{e}{m}\right)^2 \frac{\left(1-\frac{q}{k}\right)^2}{q^3|q|}\,\frac{1}{|\varepsilon|^2}\,\frac{\partial q}{\partial v}\bigg|_{v=v_0}\end{aligned} \tag{5.2}$$

where $v_0 = 3|k|[1-(2q/k)]\,a\bar{v} \ll \bar{v}$.

We consider first the terms in Eq. (4.1) that are in phase with E_k. These have $q'=k$ or $q-q'=k$, and it is only the imaginary parts of these that give a change in amplitude. Thus

$$\frac{\partial E_k}{\partial t} = \frac{\omega_k}{2}\,\mathrm{Im}\sum_q [H(k,q,k)+H(k,q,q-k)]\,E_k|E_{q-k}|^2 \qquad q \ll k_0 \tag{5.3}$$

and the in-phase coupling terms yield

$$\frac{\partial |E_k|^2}{\partial t} = |E_k|^2\,\omega_k\,9\pi k^4\left(\frac{e}{m}\right)^2\frac{1}{\omega_p{}^2} \times \sum_q \frac{\left(1-\frac{q}{K}\right)^2}{q^5}\,\frac{|q|}{|\varepsilon|^2}\,\frac{\partial q}{\partial v}\bigg|_{v_0}|E_{k-q}|^2 \qquad q \ll k_0 \tag{5.4}$$

This term arises from the fact that in second order in E the waves interact with the distribution function at $v=v_0$. For $k \geq k_0$ this interaction is such as to damp the waves while for $k \leq k_0$ this interaction leads to growth. However, it is easy to show that $\Sigma_k \partial|E_k|^2/\partial t = 0$ and thus there is no net transfer of energy between the particles and the waves, and the interaction simply distorts the equilibrium spectrum towards the lower k values. It should be noted that formally this "in-phase" mode coupling is of the same order in γ/ω_p as terms in the non-linear dispersion relation and might have been considered as part of the non-linear dispersion relation. However, for the problem considered it is numerically small and can thus be treated as a perturbation.

To estimate the size of this interaction we note that

$$\frac{1}{|\varepsilon|^2} \approx (qa)^4 \text{ and } \left(\frac{\partial f}{\partial v}\right)_{v_0} \propto -\frac{3ka}{\bar{v}^2}$$

Thus

$$\left|\frac{\partial \mathscr{E}}{\partial t}\right| \approx \left|\frac{27\pi(ka)^5}{v^2}\left(\frac{e}{m}\right)^2\frac{1}{\omega_p{}^2}\,\frac{L}{2\pi}\int dq\,\frac{q}{|q|}\left(1-\frac{q}{k}\right)^2 \times (E_{k-q})^2\right| \mathscr{E}_q \approx 2\gamma^{(1)}\mathscr{E}_q\left[\frac{27}{2}\,(ka)^5\left(\frac{\Delta v}{\bar{v}}\right)^2 M\right] \qquad (M<1) \tag{5.5}$$

Thus the in-phase mode-coupling terms have a time scale long compared to that of the initial growth. For the example considered in Section 4, it is longer by a factor of about 10^3.

The out-of-phase terms in Eq. (4.1) lead to time-proportional transitions and can be treated by the familiar methods of quantum mechanics. For these terms we obtain for the transitions to the kth mode

$$\begin{aligned}|E(k,t+\tau)|^2 - |E(k,t)|^2 &= \left(\frac{\omega_K}{2}\right)^2 \sum_{\substack{q,\,q' \\ p,\,p'}} H(k,q,q')\,H^*(k,p,p') \\ &\times \left(\frac{\exp[i(\omega_k-\omega_{k-q}-\omega_{q-q'}-\omega_{q'})\tau]-1}{i(\omega_k-\omega_{k-q}-\omega_{q-q'}-\omega_{q'})}\right) \\ &\times \left(\frac{\exp[i(\omega_k-\omega_{k-p}-\omega_{p-p'}-\omega_{p'})\tau]-1}{i(\omega_k-\omega_{k-p}-\omega_{p-p'}-\omega_{p'})}\right) \\ &\times \mathfrak{E}_{k-q}\,\mathfrak{E}_{q-q'}\,\mathfrak{E}_{q'}\,\mathfrak{E}_{k-p}\,\mathfrak{E}_{p-p'}\,\mathfrak{E}_{p'}\end{aligned} \tag{5.6}$$

where the * denotes complex conjugate and $E_{k-q} = \mathfrak{E}_{k-q}\exp -i\omega_{k-q}t$, $E_{q-q'} = \mathfrak{E}_{q-q'}\exp -i\omega_{q-q'}t$, etc.

We assume that the phases of the initial data are random and since no phase correlation is introduced by the non-linear dispersion relation the only terms which survive the q, q', p, p' summation are those for which the phases cancel. The result is

$$\begin{aligned}|E(k,t'+\tau)|^2 - |E(k,t)|^2 &= \left(\frac{\omega_k}{2}\right)^2 \sum_{q,\,q'} |E_{K-q}|^2|E_{q-q'}|^2|E_{q'}{}^2| \\ &\times \left|\frac{\exp[i(\omega_k-\omega_{k-q}-\omega_{q-q'}-\omega_{q'})\tau]-1}{i(\omega_k-\omega_{k-q}-\omega_{q-q'}-\omega_{q'})}\right|^2 \\ &\times H^*(k,q,q')\{H^*(k,q,q') + H^*(k,q,q-q') \\ &+ H^*(k,k+q'-q,q) + H^*(k,k+q'-q,k-q) \\ &+ H^*(k,k-q',q-q') + H^*(k,k-q',k-q)\}\end{aligned} \tag{5.7}$$

The term

$$\times \left|\frac{\exp[i(\omega_k-\omega_{k-q}-\omega_{q-q'}-\omega_{q'})\tau]-1}{i(\omega_k-\omega_{k-q}-\omega_{q-q'}-\omega_{q'})}\right|^2$$

has resonances at $q'=k$, $q-k$, for $q \ll k_0$, $q \approx 2k$ and at $q=0$ for $q' \approx \pm k_0$. Evaluating the q, q' sum at these

resonances thus yields for the transition rate to the kth mode

$$\left(\frac{\partial |E_k|^2}{\partial t}\right)_{\lambda \to K} = \frac{\omega_p L}{12 a^2} |E_k|^2 \sum_\lambda \frac{|E_\lambda|^4}{|k-\lambda|} |\mathscr{H}_{k,\lambda}|^2 \quad (\lambda \approx k) \tag{5.8}$$

where

$$\mathscr{H}_{k,\lambda} = H(k, k-\lambda, k) + H(k, k-\lambda, -\lambda) + H(k, k+\lambda, k) + H(k, k+\lambda, \lambda) + H(k, 0, -\lambda) + H(k, 0, \lambda) \tag{5.9}$$

Similarly the transitions from the kth mode to all other modes are given by

$$\left(\frac{\partial |E_k|^2}{\partial t}\right)_{K \to \lambda} = \frac{\omega_p L}{12 a^2} |E_k|^4 \sum_\lambda \frac{|E_\lambda|^2 |\mathscr{H}_{\lambda k}|^2}{|k-\lambda|} \quad (\lambda \approx k) \tag{5.10}$$

and the net change of the kth mode is given by

$$\frac{\partial |E_k|^2}{\partial t} = \frac{\omega_p L}{12 a^2} |E_k|^2 \sum_\lambda \frac{|E_\lambda|^4 |\mathscr{H}_{k\lambda}|^2 - |E_k|^2 |E_\lambda|^2 |\mathscr{H}_{\lambda k}|^2}{|k-\lambda|} \quad \lambda \approx k \tag{5.11}$$

This term arises from the scattering of waves from each other and we note that for those k's for which $|E_k|^2$ is less than the average $\partial |E_k|^2/\partial t > 0$ while for k's near the peak of the spectrum $\partial |E_k|^2/\partial t < 0$. Thus the scattering of waves tends to flatten the spectrum.

$\mathscr{H}_{k\lambda}$ is relatively complicated but since this term turns out to be extremely small the exact form of $\mathscr{H}_{k\lambda}$ is unimportant. However, it is worth noting that the leading term of $\mathscr{H}_{k\lambda}$ is proportional to $(k^2/\omega_p{}^4)$ $(e/m)^2$ $(ka)^2$.

Estimating $\partial \mathscr{E}/\partial t$ we obtain

$$\left|\frac{\partial \mathscr{E}}{\partial t}\right| \approx 2\gamma \mathscr{E} \frac{\gamma}{\omega} (ka)^6 \left(\frac{\Delta v}{V}\right)^4 M \tag{5.12}$$

Thus, the out-of-phase mode-coupling terms have a time scale longer than that of the initial growth. For the example of Section 4, it is longer by a factor of about 10^8, and we can neglect the out-of-phase-mode-coupling terms compared to in-phase terms.

The damping due to the in-phase mode-coupling terms arises from the distortion of the spectrum towards the lower values of k. This feeds energy into those modes that have phase velocities greater than v_1 and hence for which $\partial g/\partial v < 0$. However since these modes are naturally damped, their amplitude will be small and the rate of energy transfer will be correspondingly small. On the other hand the Fokker-Planck terms, which we have neglected, may have a time scale comparable to that of the in-phase mode-coupling terms and these will tend to drive $\partial f/\partial v$ negative over the entire range of interest, and the ultimate decay may actually be dominated by collisions.

6. Conclusions

The basic requirements for validity of the theory described above are two fold. First, the solution of the linearized problem must yield a growth rate γ, which depends on the velocity gradient of the distribution function and $\gamma/\omega \ll 1$. This is necessary in order that the non-linear dispersion relation lead to a diffusion of the distribution function. Second, the dispersion relation is such that neither the sum nor difference of the frequencies of two of the unstable modes is equal to the natural frequency of another mode. It is this requirement that keeps the energy of the unstable modes from being fed into harmonics.

These restrictions apply to a large class of waves in a plasma with a magnetic field and the method can be generalized in a straightforward way to these waves. The result as in the case illustrated above will be a non-linear dispersion relation that leads to the establishment of an equilibrium spectrum of waves. This result represents a special type of turbulence in which the wave spectrum is confined to a relatively narrow band of wave-lengths.

Although there are no "time-proportional" transitions to waves outside of the equilibrium spectrum, the second order interaction between waves in the equilibrium spectrum do produce a stationary spectrum of very-small-amplitude [$\mathscr{E}_q$ of order $(\gamma/\omega)^2$] waves near $q=0$. These waves will interact with the bulk of the particles and produce a diffusion of the bulk of the particles, an effect which is important for the case of a plasma with a magnetic field.

Acknowledgments

The authors would like to thank M. N. Rosenbluth and N. Rostoker for many stimulating discussions during the course of this work, and Miss Margaret Johnson for assistance with the computing.

This work was done under a joint General Atomic-Texas Atomic Energy Research Foundation program on controlled thermonuclear reactions.

References

1. Rostoker, N., Rosenbluth, M. N., *Phys. Fluids* **3** (1960) 1.
2. Balescu, R., *Phys. Fluids* **3** (1960) 52.
3. Pines, D., Schrieffer, *Phys. Rev.* **125** (1962) 804.

Appendix

We wish to show that for $\gamma/\omega \ll 1$, Eqs. (3.3), (3.4) and (2.9) reduce to Eqs. (3.5), (3.6) and (3.7).

Integrating Eq. (3.3) along the unperturbet orbits yields

$$f_{\mathbf{K}} = \frac{e}{m} \int_{-\infty}^{t} \mathrm{d}t' \, G_{\mathbf{K}}(t-t') \, \mathbf{E}_{\mathbf{K}}(t') \cdot \nabla_{\mathbf{v}} g(t') \tag{A1}$$

where we have set the lower limit to $-\infty$ and neglected $f_K(v, 0)$—a good approximation for growing waves. Integrating over velocities then yields

$$E_{\mathbf{K}}(t) = -\frac{4\pi e^2}{i m K} \int \mathrm{d}^3 \mathbf{v} \int_{-\infty}^{t} \mathrm{d}t' \, G_{\mathbf{K}}(t-t') \, \mathbf{E}_{\mathbf{K}}(t') \cdot \nabla_{\mathbf{v}} g(t') \tag{A2}$$

We expect the solution of Eq. (A2) to have the same general form as the solution of the linearized problem except that the frequency and growth rate will be slowly varying functions of time. We then take $E_{\mathbf{K}}(t')$ to be of the form

$$\begin{aligned}\mathbf{E}_{\mathbf{K}}(t') &= E_{\mathbf{K}}(0)\exp\left\{\int_0^{t'} S_{\mathbf{K}}(\tau)\,\mathrm{d}\tau\right\}\\ &= E_{\mathbf{K}}(t)\exp\left\{-\int_{t'}^{t} S_{\mathbf{K}}(\tau)\,\mathrm{d}\tau\right\}\\ &= E_{\mathbf{K}}(t)\exp\{-S_{\mathbf{K}}(t)(t-t')\}\\ &\quad\times\left\{1+\frac{1}{2}\frac{\partial S_k}{\partial t}(t-t')^2+\ldots\right\} \qquad \text{(A3)}\end{aligned}$$

and $g(v, t')=F_0(v)+f_0(v, t)+(\partial f_0/\partial t)(t'-t)+\ldots$

We shall assume and verify later that $S_{\mathbf{K}}(\tau)$ changes slowly in a period of oscillation and that the change in frequency and of growth rate are of the same order of magnitude. In particular we make use of the result, Eq. (A8), that $S_{\mathbf{K}}$—$S_{\mathbf{K}_0}/S_{\mathbf{K}}$ depends linearly on $f_0(v, t)$ and that $\partial f_0/\partial t\approx 2\gamma f_0$ so that

$$\frac{1}{S_{\mathbf{K}}{}^2}\frac{\partial S_{\mathbf{K}}}{\partial t}\approx\frac{2\gamma}{S_{\mathbf{K}}}\frac{S_{\mathbf{K}}-S_{\mathbf{K}_0}}{S_{\mathbf{K}_0}}\ll\frac{S_{\mathbf{K}}-S_{\mathbf{K}_0}}{S_{\mathbf{K}}} \qquad \text{(A4)}$$

where $S_{\mathbf{K}_0}$ is the solution of the linearized problem.

Using Eqs. (A3) and (A4), Eq. (A2) yields

$$\begin{aligned}E_{\mathbf{K}}(t) &= E_{\mathbf{K}}(t)\left\{1-\frac{1}{2}\frac{\partial S_{\mathbf{K}}}{\partial t}\frac{\partial^2}{\partial S_{\mathbf{K}}{}^2}+\ldots\right\}\\ &\quad\times\left\{\frac{4\pi e^2}{mK^2}\int \mathrm{d}^3\mathbf{v}\,\frac{\mathrm{i}\mathbf{K}\cdot\nabla_{\mathbf{v}}}{S_{\mathbf{K}}(t)+\mathrm{i}\mathbf{K}\cdot\mathbf{v}}[F_0+f_0]\right.\\ &\quad\left.+\frac{4\pi e^2}{mK^2}\frac{\partial}{\partial S_{\mathbf{K}}}\int \mathrm{d}^3\mathbf{v}\,\frac{\mathrm{i}\mathbf{K}\cdot\nabla_{\mathbf{v}}}{(S_K+\mathrm{i}\mathbf{K}\cdot\mathbf{v})}\frac{\partial}{\partial t}f_0(t)\right\} \qquad \text{(A5)}\end{aligned}$$

The term involving $F_0(v)$ has the same form as in the linearized theory and thus we have

$$\begin{aligned}&E_{\mathbf{K}}(t)\left\{1-\frac{1}{2}\frac{\partial S_{\mathbf{K}}}{\partial t}\frac{\partial^2}{\partial S_{\mathbf{K}}{}^2}+\ldots\right\}\varepsilon[\mathbf{K}, S_{\mathbf{K}}(t)]\\ &\quad=\left\{1-\frac{1}{2}\frac{\partial S_{\mathbf{K}}}{\partial t}\frac{\partial^2}{\partial S_{\mathbf{K}}}\right\}\frac{4\pi e^2}{mK^2}\int \mathrm{d}^3\mathbf{v}\,\frac{\mathrm{i}\mathbf{K}\cdot\nabla_{\mathbf{v}}f_0}{S_{\mathbf{K}}(t)+\mathrm{i}\mathbf{K}\cdot\mathbf{v}}\\ &\quad+\frac{4\pi e^2}{mK^2}\frac{\partial}{\partial S_{\mathbf{K}}}\int \mathrm{d}^3\mathbf{v}\,\frac{\mathrm{i}\mathbf{K}\cdot\nabla_{\mathbf{v}}}{S_{\mathbf{K}}(t)+\mathrm{i}\mathbf{K}\cdot\mathbf{v}}\frac{\partial f_0}{\partial t}+\ldots \qquad \text{(A6)}\end{aligned}$$

Now $(S_{\mathbf{K}}(t)$—$S_{\mathbf{K}_0})/S_{\mathbf{K}_0}\ll 1$ and thus we can expand $\varepsilon[\mathbf{K}, S_{\mathbf{K}}(t)]$ about $S_{\mathbf{K}_0}$ to obtain

$$\begin{aligned}\varepsilon[\mathbf{K}, S_{\mathbf{K}}(t)] &= \varepsilon(\mathbf{K}, S_{\mathbf{K}_0})+\frac{\partial\varepsilon}{\partial S_{\mathbf{K}_0}}(S_{\mathbf{K}}-S_{\mathbf{K}_0})+\ldots\\ &\approx\frac{\partial\varepsilon}{\partial S_{\mathbf{K}_0}}(S_{\mathbf{K}}-S_{\mathbf{K}_0})\approx-2\frac{\omega_p{}^2}{S_{\mathbf{K}_0}{}^3}[S_{\mathbf{K}}(t)-S_{\mathbf{K}_0}]\\ &\approx 2\frac{[S_{\mathbf{K}}(t)-S_{\mathbf{K}_0}]}{S_{\mathbf{K}_0}}\end{aligned}$$

since $\varepsilon(\mathbf{K}, S_{\mathbf{K}_0})=0$. The correction term on the left-hand side of Eq. (A6) is, since $\varepsilon\approx 1+\omega_p{}^2/S_{\mathbf{K}}{}^2$, of the order of

$$\frac{\partial S_{\mathbf{K}}}{\partial t}3\frac{\omega_p{}^2}{S_{\mathbf{K}}{}^4}\approx\frac{3}{\omega_p{}^2}\frac{\partial S_{\mathbf{K}}}{\partial t}\ll\frac{S_{\mathbf{K}_0}-S_{\mathbf{K}}}{S_{\mathbf{K}_0}}$$

and can thus be neglected.

$f_0(v, t)$ is non zero only in the small neighborhood Δv. Defining (for simplicity we consider only the one-dimensional case)

$$I=\int\frac{\mathrm{d}v\,(\partial f_0/\partial v)}{S_K(t)+iK\cdot v}=\mathrm{i}\,P\int\frac{(\partial f_0/\partial v)\,\mathrm{d}v}{(\omega-Kv)}+\frac{\pi}{K}\frac{\partial f_0}{\partial v}\bigg|_{v=\omega_K/K} \qquad \text{(A7)}$$

$\partial^2 I/\partial S^2$ is thus of the order of $I/(K\Delta v)^2$ and the first correction term on the right-hand side of Eq. (A6) is of order

$$I\frac{\partial S}{\partial t}\frac{1}{(K\Delta v)^2}=I\left(\frac{v_b}{\Delta v}\right)^2\frac{\partial S}{\partial t}\frac{1}{(Kv_b)^2}\ll\frac{S_K-S_{K_0}}{S_K}$$

where $Kv_b\approx\omega_p$. Similarly since $\partial f_0/\partial t\approx 2\gamma f_0$, the second correction term on the right-hand side of Eq. (A6) can be neglected.

The result, neglecting $(Ka)^2\ll 1$, is

$$S_K(t)-S_{K_0}=\frac{2\pi e^2}{mK}\omega_{K_0}\left\{\frac{\pi}{K}\frac{\partial f_0}{\partial v}\bigg|_{v=\omega_K/K}+\mathrm{i}\,P\int\frac{\mathrm{d}v\,\partial f_0/\partial v}{(\omega-Kv)}\right\} \qquad \text{(A8)}$$

Using $S_{\mathbf{K}}(t)=-\mathrm{i}\,\omega_{\mathbf{K}}(t)+\gamma_{\mathbf{K}}(t)$ we obtain

$$\omega_K(t)=\frac{K}{|K|}\omega_{K_0}\left[1-\frac{2\pi e^2}{mK}P\int\frac{\partial f_0/\partial v\,\mathrm{d}v}{(\omega-Kv)}\right] \qquad \text{(A9)}$$

$$\frac{\gamma_K}{\omega_K}=\frac{2\pi^2 e^2}{K^2 m}\frac{\partial g(v,t)}{\partial v}\bigg|_{v=\omega_K/\omega}$$

and the three-dimensional result is given by Eq. (3.6).

The change in $\omega_{\mathbf{K}}(t)$ is of the same order as the change in $\gamma_{\mathbf{K}}$ and since $\gamma_{\mathbf{K}}/\omega_{\mathbf{K}}\ll 1$ we can neglect the correction to $\omega_{\mathbf{K}}$. The change in $\gamma_{\mathbf{K}}$ is however significant.

The energy in the Kth mode thus grows according to

$$\frac{\partial|E_K|^2}{\partial t}=2|E_K|^2\gamma_K(t) \qquad \text{(A10)}$$

In the same way Eq. (A1) can be integrated to obtain

$$f_K=-\frac{e}{m}\frac{E_K}{S_K+\mathrm{i}Kv}\frac{\partial g}{\partial v} \qquad \text{(A11)}$$

and thus

$$\frac{\partial g}{\partial t}=\left(\frac{e}{m}\right)^2\frac{\partial}{\partial v}\sum_{q=-\infty}^{\infty}\frac{|E_q|^2}{(Sq+\mathrm{i}qv)}\frac{\partial g}{\partial v} \qquad \text{(A12)}$$

and the three-dimensional result is given by Eq. (3.5).

EXPERIMENTAL STUDY OF THE DAMPING OF LONGITUDINAL PLASMA ELECTRON OSCILLATIONS*

M. J. KOFOID

BOEING SCIENTIFIC RESEARCH LABORATORIES

SEATTLE, WASHINGTON, UNITED STATES OF AMERICA

Landau damping is a well-known function of the product $k\lambda_D$, where k is the wave number and λ_D the Debye length. Test results have been obtained which are consistent with a statement that the maximum value of $k\lambda_D$ with which oscillations can still be sustained is independent of the plasma electron temperature. This is for constant excitation-energy input and for fixed geometry.

The test was performed by observing the minimum plasma wavelength with which standing waves of longitudinal electron oscillations could be maintained with different electron temperatures. The waves were excited in different gases by instabilities produced by oppositely directed coincident 1.0-mm-diameter electron beams passing through a plasma having a Langmuir frequency of 500 MHz [1, 2]. The electron mean free path was several times the 2.0-cm separation of the beam-emitting electrodes. The damping was produced by a loss of electrons possessing oscillatory energy from the regions of coherent oscillations; this was effected by thermal electron motion. The loss was due to both Landau-type damping in the axial direction and simple removal of electrons by thermal motion in the radial directions.

From the finite-diameter beam data the minimum wavelength for oscillations in an infinitely wide beam was calculated for four different plasma electron temperatures. This was done on the assumption of a Maxwellian gas and a Landau damping unit volume loss in the infinite beam equal to the total unit volume loss from the region of coherent oscillation in the finite beam. The results give $1/k\lambda_D = \lambda/\lambda_D \approx 2$ for all temperatures.

In the progress of this work, with particular beam energies and with no background plasma present, "bursting" of the two interpenetrating excitation beams was observed. Perhaps this was an example of the destruction of directed electron velocities predicted by Buneman [3].

1. Introduction

Landau damping is a function of the product $k\lambda_D$ where k is the wave number and λ_D the Debye length [4]. Test results have been obtained which are consistent with a statement that the maximum value of $k\lambda_D$ with which longitudinal electron oscillations still can be sustained is independent of the plasma electron temperature.

The test was performed by observing the minimum plasma wavelength with which standing waves of longitudinal electron oscillations could be excited with different electron temperatures under conditions which could be considered as reasonably collisionless. The geometry was fixed and the excitation-energy input was roughly constant.

In a one-dimensional theoretical picture the damping of electron-oscillation travelling waves in a collisionless gas is commonly attributed to a phase-mixing process referred to as "Landau damping". The phase mixing effects a loss of coherent-oscillation energy. Any phase-mixing phenomenon must arise basically because of thermal motion of the charged particles. Standing waves of electron oscillations are assumed to exist as the resultant of two potential waves, associated with electron pressure waves, traveling in opposite directions. Then the damping phenomenon in standing waves should be theoretically explainable in terms of the damping of the oppositely directed component waves.

The actual case in the laboratory is three-dimensional with the electron oscillations generated in the volume occupied by the streams of electrons that are passed through the plasma to give rise to the oscillations. It is believed that in the experiment performed the effective loss of oscillatory energy, and hence the damping, may have taken place largely through phase mixing regardless of the direction in which the electrons escaped. For the purpose of a crude comparative analysis of the test data the oscillatory energy of the frequency of the coherent oscillations of any electron escaping from the region due to thermal motion is treated simply as totally lost without question as to the mechanism. However, later in the paper results are included from a very recent analysis by J. E. DRUMMOND [5] in which the damping due to phase-mixing in three-dimensional space is treated.

In a large region of uniform oscillation it is immaterial with regard to the electrostatic effects and damping whether the individual electrons move about in this region as long as they do not leave it. But if in the production of oscillations the regions of uniformity produced are small, the thermal movement of the electrons can cause them to move away after a short time; the result is to carry oscillatory energy

* Conference paper CN-10/169, presented by M. J. Kofoid Discussion of thisp aper is given on page 1110. Translations of the abstract are at the end of this volume of the Conference Proceedings.

of the coherent oscillation frequency out from the region, thereby effecting damping. Electrons at various velocities carry oscillatory energy from places of one phase to places of different phase, producing general phase mixing.

It becomes of particular interest to consider a region so small that electrons traveling, say, along the z axis with an effective thermal velocity $u_z = (kT_e/m)^{1/2}$ (the symbols have the usual meaning) travel across it in a length of time comparable to the reciprocal of the plasma angular frequency, i.e. $1/\omega_p$. Then the electron space charge tending to form the vibrational field will lose coherent energy so rapidly that a distinct eigen vibration can no longer get started.

The extent Λ_e of a uniformly vibrating region in the plasma must therefore be appreciably larger than u_z/ω_p. This requires

$$\Lambda_e > \frac{u_z}{\omega_p} = \frac{(kT_e/m)^{1/2}}{(4\pi e^2 N/m)^{1/2}} = \left(\frac{kT_e}{4\pi e^2 N}\right)^{1/2} = \lambda_D$$

It appears that in all directions the vibrating region must be perhaps several times larger than λ_D.

If a vibration has been started in some manner, it will be damped due to the gradual separation of the charge carriers caused by the thermal movement. On a physical basis it seems reasonable to conclude that the damping should be a function of λ_D/Λ_e and should become severe when $\Lambda_e \to \lambda_D$. Rompe and Steenbeck commented on these points relating to a small oscillating region years ago [6].

If with this simple picture the minimum length Λ_e of the uniform oscillation region, which is depicted as basically dependent on the velocity $u \approx T_e^{1/2}$, is expressed in terms of $\lambda_D \approx T_e^{1/2}$, the ratio Λ_e/λ_D should be independent of the electron temperature T_e. Then, also, the equivalent expressions

$$\frac{\lambda_{p\infty}}{2\pi}\frac{1}{\lambda_D} = \frac{1}{k\lambda_D} = \frac{\lambda\!\!\!^{-}_{\infty}}{\lambda_D} = \frac{m_1\Lambda_e}{\lambda_D} = \frac{m_2\lambda_D}{\lambda_D}$$

should be independent of temperature. Here m_1 and m_2 are constants and $\lambda_{p\infty}$ is the wavelength in the plasma. (The symbol ∞ is used in the subscripts to denote quantities pertaining to the case of infinitely wide oscillating regions, i.e. the one-dimensional case, in contrast to the experimental case. The symbols λ_p and $\lambda\!\!\!^{-}$ will be used to refer to the experimental quantities.)

The objects of the experimental study were to obtain data with which to verify this independence of temperature and to approximately evaluate $\lambda\!\!\!^{-}_{\infty}/\lambda_D$ for the particular experimental arrangement used, under steady-state conditions with anticipated constant fractional energy loss per period. (It was assumed that with λ_p the minimum with which experimental standing waves could be excited, the fractional loss would be constant with the different gases used.) The results have also served as comparison data for the recent generalized Landau damping analysis.

No appreciable region with true uniformity of oscillation intensity and phase existed in the standing waves produced. Although conveniently described as sinusoidal, in actuality the shape of the standing waves was typically that of a fundamental with considerable third-harmonic content, in the sense of the central region being augmented. However, with accuracy satisfactory for the purpose at hand, the central section of each loop of an arbitrary, but considered, section length $\lambda\!\!\!^{-} = \lambda_p/2\pi$ will be treated in the analysis as one of quasi-uniform oscillations, making Λ_e (experiment) $= \lambda\!\!\!^{-}$. ($\lambda\!\!\!^{-}$ will always refer to the minimum wavelength.)

The laboratory task was then to establish the minimum λ_p, hence the minimum $\lambda\!\!\!^{-}$, obtainable with different electron temperatures with as nearly as possible constant excitation energy input.

2. Experimental work

The determination of the maximum number of half-wavelength loops of standing-wave potential that could be produced in plasma between plane parallel electrodes established the minimum λ_p. Data at different T_e were obtained from experiments performed in different noble gases and in mercury vapor.* Although the minimum-wavelength data might have been established more exactly if the electrode separation as well as the temperature had been made a variable parameter, to do so was not deemed worthwhile in view of the difficulties involved. The writer believes that in each case with noble gases the operation was quite close to the limit of operation for the number of loops stated—especially with argon, insofar as could be judged by the experimental difficulty in exciting them. If in the work with mercury vapor the limit was not so closely approached, the error should not be serious because of the large number of loops excited.

The standing waves of coherent longitudinal electron oscillations were excited in a plasma by two independent oppositely directed electron beams, with no sheaths on the flat parallel electrodes from which the electron streams entered the plasma [1]. The axes of the two beams were coincident.

The principal elements of the experimental arrangement are shown in Fig. 1. Each beam of closely mono-energetic electrons entered the plasma through a 1.0-mm-diameter aperature in an electrode A_2. The electrodes faced each other across 2.0 cm of plasma whose electron density permitted electron oscillations at 500 MHz. The beam electrodes were both held at the potential of the plasma to prevent sheath formation. The beam currents were of the order of 0.5 mA, non-critical, and adjusted for maximum oscillation amplitude. The beam velocities were usually equal; the range of beam electron energies was 35-90 V. The beam velocities were specific and critical as dictated by the requirements for a high

* The included result for mercury vapor was deduced from data obtained by Looney [7]. The experimental arrangements differed in that Looney used one, rather than two, excitation beams and that in the Looney experiment there was a positive ion sheath on each electrode.

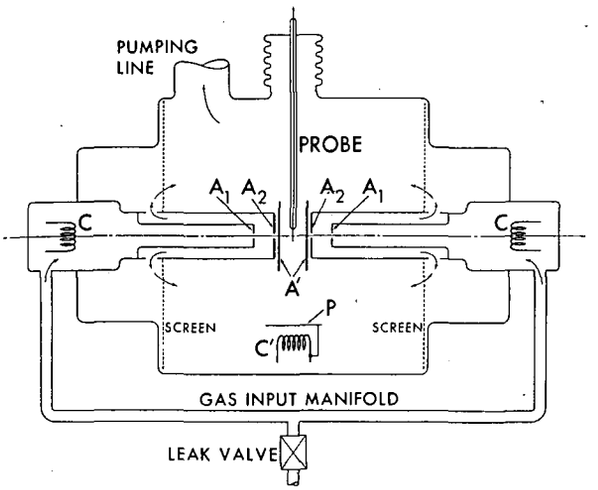

Fig. 1 Principal elements of experimental arrangement. Electron beams enter plasma through aperture in electrode A_2.

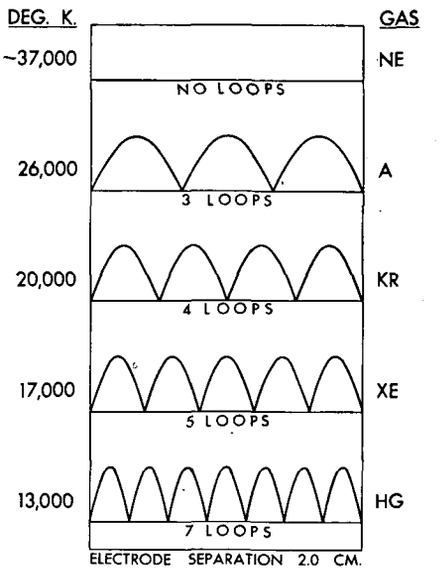

Fig. 2 Maximum number of loops in standing wave and electron temperature at optimum operating pressure.

degree of energy transfer from the beam to the oscillating plasma [2]. The pressure p was that at which the maximum amplitude of oscillation could be obtained; oscillations could not be readily excited at pressures more than about 25% higher or lower than the optimum value.

The standing-wave loops were detected by a 0.20-mm-diameter movable probe located 1 mm out from the visible edge of the interpenetrating beams. The gas densities were low enough that the electron mean free paths were several times the separation of the beam electrodes. However, the densities were high enough to afford sufficient positive-ion focusing of the beams so that in no case did the diameter of the visible beam increase from the initial 1.0 mm to more than 1.5 mm after traveling through the 2.0 cm of plasma.

The electron temperatures were determined by probe measurements at the center of the region between the gun electrodes without the beams present. Although not taken at extremely short times after cleaning, the probe measurements were made with good care in identical manners soon after cleaning; therefore the temperature determinations for the noble gases should be consistent among themselves.

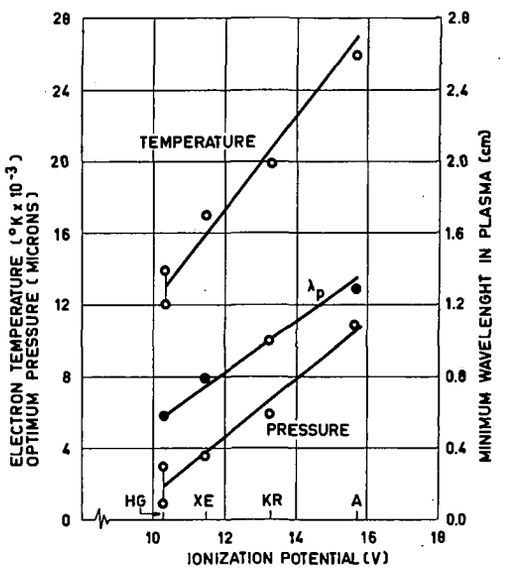

Fig. 3 Electron temperature, minimum plasma wavelength excited and optimum gas pressure in electron-oscillation standing-wave experiment as functions of ionization potential.

3. Experimental results

The use of xenon, krypton, argon and neon gases satisfactorily provided the spread in T_e essential to the experiment. With a particular geometry and gas density T_e is an increasing function of the ionization potential E_i; with all other conditions fixed, it is a decreasing function of gas density. Although the optimum pressure was greater for the higher E_i gases, they had higher measured values of T_e.

The principal experimental results are shown graphically in Fig. 2. (As has been indicated, the mercury data were secured from Looney's results.) That the obtained spread in T_e of from 13000° K for mercury to 26000° K for argon caused sufficient differences in the electron random thermal velocities to produce appreciable differences in the loss situations in the oscillatory plasmas is evidenced by the differences in the maximum number of loops excited. While seven loops of electron longitudinal oscillation standing wave could be excited in mercury, only three loops could be excited in the higher-temperature argon, and none in the still-higher temperature neon gas. (T_e for neon was estimated.)

For showing the degree of smoothness of the data and the compatibility of Looney's data, and for general interest, the values of T_e, p and λ_p are plotted against the values of E_i in Fig. 3. With mercury

a pair of points is used to indicate the probable range of uncertainty.

The experimentally established minimum wavelengths λ_p and the corresponding values of $\lambda\!\!\!^{-}/\lambda_D$ are listed in Table I.

TABLE I. Data for Experiments with Standing Waves of Minimum Plasma Wavelength*

Gas	T_e ($10^{3\circ}$K)	λ_D (cm)	Maximum number of loops excited	Minimum λ_p(cm)	$\lambda\!\!\!^{-}$ (cm)	$\frac{\lambda\!\!\!^{-}}{\lambda_D}$
Hg	13	0.014	7	0.57	0.09	6.5
Xe	17	0.016	5	0.80	0.13	8.0
Kr	20	0.018	4	1.0	0.16	9.1
Ar	26	0.020	3	1.3	0.21	10.0
Ne	~37	~0.024	0			

* Electrode separation, 2.0 cm; frequency 500 MHz; 1.0-mm-diameter electron beams.

The operating conditions desired were ones of equal excitation energy to the plasma; those obtained were ones of optimized gas density, beam velocities and beam current. How well the conditions obtained met those desired cannot be solidly stated. Limited analogue-computer studies showed the beam-to-plasma energy transfer to differ but little with different permissible phase-velocity-to-electron-velocity modes of operation; experimental observations appear to be consistent with this conclusion. With considerable caution the excitation has been considered constant. The fact that the data for mercury, deduced from Looney's results, appear compatible with the data for the noble gases may offer support for an argument that the excitation level is not significantly important to the establishment of the minimum λ_p.

From these finite-diameter-beam data were sought the answers to the several principal questions stated earlier.

4. Analysis and discussion

Only an approximate comparative analysis was attempted by the writer. The effort was limited because of the recognized uncertainties in the data and because of the lack, at the time, of applicable theoretical expressions for the damping. For instance only the visible, rather than the effective, diameter of the beams was well known. Further, a proper expression for the quantitative evaluation of the Landau-type damping believed to have been taking place must be valid for the three-dimensional case of a small finite-diameter beam with neither $k\to\infty$ nor $k\to 0$, but with k between these limits. As mentioned, a method of extending Landau's expression to this case has now been developed.

The comparative analysis was started with a consideration of the electron oscillating energy lost in one period from the central region due to thermal motion. (The electron oscillatory travel was estimated to be small compared to the central-volume dimensions and was therefore ignored.) The study was based on the assumption that on the average an electron that escaped in the beam's axial direction from a central uniform volume permanently removed as much coherent oscillation energy as an electron escaping through the side of the beam. With every electron leaving the region treated as having an identical amount of oscillatory energy, it was possible to calculate the loss in terms of ratios of the number of electrons that escaped with a positive or a negative velocity in each one of the three coordinate directions to the total number of electrons N_0 in the volume. The losses were thereby found effectively on a unit-volume basis. The energy input was taken as a constant per unit length of beam, hence per unit volume. The analysis was further simplified by assuming the beam to have a 1-mm square cross section rather than a circular one with a 1-mm diameter.

The loss ratios were evaluated in the following manner: First, an expression was found for the number of electrons escaping with positive velocities in the time τ of a period of oscillation from a region bounded by two parallel infinite imaginary planes with a separation s; for example, with z taken as the beam's axial direction, for finding the number escaping in the positive z direction from a central region volume with $s=\lambda\!\!\!^{-}$. In a plasma with a Maxwellian electron-velocity distribution the total number of electrons of all velocities passing through a plane of any orientation is $nc/4$ per square centimeter per second or $nc\tau/4$ per square centimeter per period, where n is the electron density and c is the average random thermal velocity. Let the plane be one of the surfaces of the volume, which has sides x and y and length z. The number of electrons escaping with a positive velocity in a period through a surface, say specifically in the axial z direction, is $N_z'/2=nc\tau xy/4$. The sum of those escaping with either a positive or a negative velocity will be $N_z'=nc\tau xy/2$. This electron loss, expressed in terms of the volume population $N_0=nxy\lambda\!\!\!^{-}$, is found to be

$$\frac{N_z'}{N_0}=\frac{nc\tau xy/2}{nxy\lambda\!\!\!^{-}}=\frac{c\tau}{2\lambda\!\!\!^{-}}$$

Similarly,

$$\frac{N_x'}{N_0}=\frac{c\tau}{2x}\text{ and }\frac{N_y'}{N_0}=\frac{c\tau}{2y}$$

The loss ratio was evaluated for each of the three coordinate directions for each gas used. The total of the loss ratios was compluted as

$$\frac{N'}{N_0}=\frac{N_x'}{N_0}+\frac{N_y'}{N_0}+\frac{N_z'}{N_0}$$

The N'/N_0 quantities gave a comparative measure of the electrons lost in all directions in one period from a finite-diameter volume of assumed uniform coherent oscillation. The component and total losses are tabulated in Table II and are plotted as a function of temperature in Fig. 4. It is to be noted that in all cases the total numbers of electrons that escaped in different periods were about equal.

TABLE II. Loss Ratios Calculated from Finite-Diameter Beam Experimental Data

Gas	c^* (10^8 cm/sec)	$c\tau$ (cm)	$\frac{c\tau}{2}$ (cm)	Side loss ratio**	Axial loss ratio***	Total loss ratio†
Hg	0.72	0.144	0.072	0.72	0.80	2.24
Xe	0.81	0.163	0.081	0.81	0.62	2.24
Kr	0.88	0.176	0.088	0.88	0.55	2.31
Ar	1.01	0.202	0.101	1.01	0.48	2.50

* $c=(8\ kT_e/\pi m)^{1/2}$; ** $N_x'/N_0=N'_y/N_0$; *** N_z'/N_0; † N'/N_0

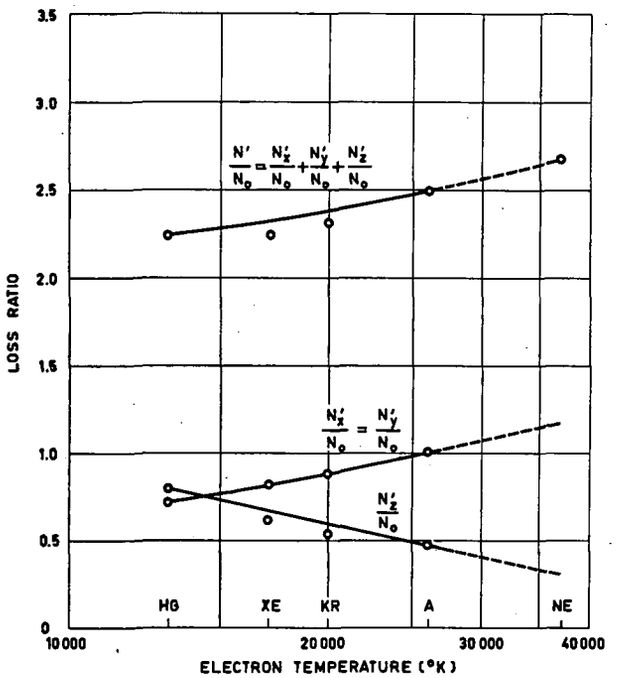

Fig. 4 Component and total-loss ratios calculated from finite-diameter-beam experimental data.

Since the beam diameter was taken as a constant for the purpose of computation, the losses out of the sides of the beam, which were given by the ratios $N_x'/N_0=N_y'/N_0$, increased linearly as a function of $T_e^{1/2}$. In the axial z direction the trend toward increased losses with increased T_e was more than offset by the diminishing effect on the loss of the experimentally found increases in λ. It was anticipated the decrease in the N_z'/N_0 ratio would exactly offset, at the minimum—λ_p operating condition, the increases in N_x'/N_0 plus N_y'/N_0 as the temperature was increased, leaving the ratio for the total loss N'/N_0 a constant for all gases tested. From the N'/N_0 curve of Fig. 4 it would appear that the total losses did increase some with temperature. However, it is believed more probable that the actual total losses did not increase. The beam diameter was observed to increase due to space-charge-repulsion spreading—the degree being negligible with xenon, slight with krypton and increasingly appreciable for the lighter argon and neon gases, which had the higher temperatures. The use of a larger value of beam diameter with the higher T_e gases would decrease their N_x'/N_0 and N_y'/N_0 loss ratios. The total loss ratio N'/N_0 for each of the gases would have been closely the same if the average beam diameter were increased 10% for argon, less for krypton and xenon, and not at all for mercury; the visible beam-diameter increase was at least this much for argon.

The values of the curves of Fig. 4 are not inconsistent with an explanation of why no standing waves could be excited in neon, which would have had an estimated temperature $T_e\approx 37000°$ K. The extrapolation of the N_z'/N_0 curve to 37000° K gives a value of about 0.30 for neon. If the oscillations were to be excited, it appears that N_z'/N_0 would have had to have been about 0.30 or less. In the experiment the minimum λ_p could be no larger than 4.0 cm, i.e. one loop in 2 cm; correspondingly, $\lambda=0.64$ cm and $N_z'/N_0=0.2$, or slightly less than the supposedly allowable value. But, were the temperature just a little greater than estimated, which, considering the roughness of the estimate, could easily have been the case, the experimental losses would have been the greater and oscillations would not have built up. Much effort was expended on trying to establish standing waves in neon, without success.

The data illustrate that the total radial losses can be large relative to the axial losses for small-diameter beams, ranging in these experiments from a factor of 1.8 for mercury to 4.2 for argon. That this should be so was suggested by K. G. Emeleus several years ago.

If the excited volume were of infinite diameter or width, what would be the length of a central region of uniform oscillation λ_∞? Values of λ_∞ were computed from the finite-diameter-beam data on the assumption that the one-dimensional unit-volume losses in the infinite case should equal the sum of the unit-volume losses in the three dimensions of the finite case. The length of the uniform region for each gas was computed as

$$\lambda_\infty=\lambda\frac{N_z'/N_0}{\frac{N_x'}{N_0}+\frac{N_y'}{N_0}+\frac{N_z'}{N_0}}$$

The results for λ_∞, and also the values of $\lambda_\infty/\lambda_D=1/k\lambda_D$, calculated from the data for beams with equal finite diameters, are presented in Table III. In Fig. 5 the values of λ_p and $1/k\lambda_D$ for the infinite case are plotted. The magnitudes of the quantity $1/k\lambda_D$ are seen to be close to constant for the different-temperature gases.

When these calculations based on the finite-beam data were repeated with adjusted beam diameters to give a constant total loss ratio as discussed above the values of $\lambda_\infty/\lambda_D=1/k\lambda_D$ were found to be close to 2.3 for all the gases, i.e., for all temperatures.

TABLE III. Minimum Wavelength Excited by Infinitely Wide Beams*

Gas	Total-to-axial loss ratio in finite beam	$\bar{\lambda}$ for finite width beam (cm)	$\bar{\lambda}_\infty$ for infinite width beam (cm)	$\frac{\bar{\lambda}_\infty}{\lambda_D}$
Hg	2.8	0.09	0.032	2.3
Xe	3.6	0.13	0.036	2.2
Kr	4.2	0.16	0.038	2.2
Ar	5.2	0.21	0.041	2.0

* As calculated from finite-width-beam data; beam diameters, 1.0 mm.

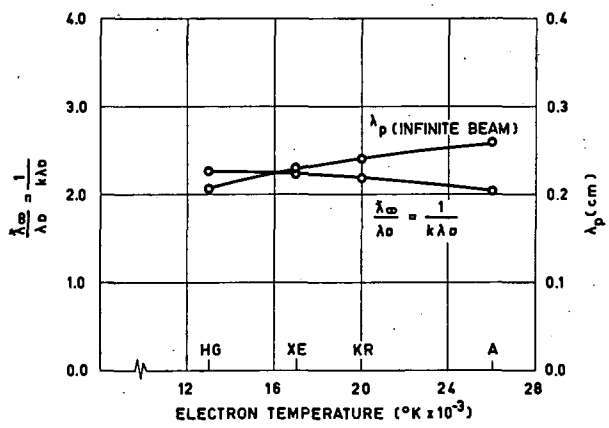

Fig. 5 Minimum wavelengths and relationships for standing waves of electron oscillations calculated for infinite-width beam from finite-beam data.

These results for the infinite case, based on steady-state* condition data, are consistent with Landau's expression for damping by phase mixing which requires that with constant loss $k\lambda_D$ must be invariant with temperature.

It was noted that, since the analysis was largely a comparative one, the choice of the length of the quasi-uniform oscillating region Λ_e (experiment) $=\bar{\lambda}$ turned out to be not critical.

A qualitative value of λ_∞/λ_D can be roughly deduced from a simple inspection of the phase mixing. Consider at the center of one of the regions of uniform oscillation in a standing wave in an infinite plasma a group of electrons initially in a volume element of thickness Δz. At time $t=0$ let their phase angle be ψ_0. Due to random thermal velocity u, after the time of one period τ the electrons will have diffused into a volume of thickness $\pm u\,\tau$. They will have passed from the region Δz, where the phase of the standing wave was ψ_0, into a region where at $t=\tau$ the phase lies in the range $\Delta\psi=\psi_0\pm ku\,\tau$. The phases will have become mixed and some of the energy of coherent electron oscillation will have been lost. Linhart [9] has pointed out that with a rate of phase diffusion making $\langle\Delta\psi^2\rangle$ per second approximately equal to $(ku)^2\,\tau$ the electric field of the ω component of the oscillation becomes damped out when $\langle\Delta\psi^2\rangle$ becomes comparable with $(2\,\pi)^2$, where $\langle\Delta\psi^2\rangle$ is a mean square value. Under this condition for complete damping

$$ku\tau \approx 2\pi = k\lambda_{p\infty}$$

$$u\tau \approx \lambda_{p\infty}$$

or

$$2\pi\,\lambda_D \approx \lambda_{p\infty},$$

and

$$\frac{\bar{\lambda}_\infty}{\lambda_D} \approx 1$$

But for oscillation to build up $\bar{\lambda}_\infty/\lambda_D$ must be somewhat greater than this value; the critical ratio of 2.3 found from the experiments therefore appears to be reasonable.

In the crude comparative analysis, the total number of electrons calculated to leave the central oscillating volume in a period was about twice its population, suggesting an unrealistically large loss rate. In the actual situation, immediately upon leaving the region of the hypothesized central volume electrons are yet in a region of strong oscillation although one of decreasing amplitude. Their oscillatory energy is not immediately totally lost from the oscillatory field. Further, some energy is continuously transferred into the central volume by electrons entering it from outside. The actual rate of net loss in the central region is therefore more properly pictured to be moderate.

The oscillations could be detected at distances up to several beam diameters from the edge of the visible beam. The more general accounting required of the Landau-type damping phenomena in the experiment should involve phase mixing in three dimensions and in a more general type of wave in the vicinity of the beams that excite the standing waves. The damping may be by phase mixing regardless of the direction in which electrons move between regions of different phase. This accounting is facilitated by noting that the conductivity of a warm plasma (with no magnetic field) is the same for all electric ($\nabla\times\mathbf{E}=0$) waves of a given total wave number [10] ($\nabla^2\,\mathbf{E}+k^2\mathbf{E}=0$), and consequently the damping is the same for all waves of the same total wave number k. Therefore Landau's damping formula is immediately generalized by using the total k. These justifications and the following approximate evaluation of the general Landau damping produced by radial as well as axial thermal electron motions are due to J. E. Drummond [5] (a comprehensive treatment of the generalized damping in the three-dimensional case has been made [11]).

The total wave number to be used in Landau's formula is $k=(k_z^2+k_\perp^2)^{1/2}$, where k_z is the wave

* Although Landau developed his damping decrement expression for a transient condition, it has been shown [8] that it is valid to consider Landau damping to occur for low-amplitude steady-state oscillations if even only a small collision frequency exists.

number in the axial direction determined from the experimental λ_p and $k_\perp$ is an effective wave number for the group of transverse waves generated. It is necessary to obtain an estimate of $k_\perp$; this is provided by the uncertainty principle for (J_0) Hankel transforms:

$$\Delta k_\perp \, \Delta r_\perp \gtrsim 1$$

where Δr pertains to the effective radial extent of the oscillations, which is assumed to be approximately the diameter of the beams exciting the oscillations. Since large values of $k_\perp$ will be most rapidly damped by Landau damping, the group of wave numbers will assume the smallest values possible consistent with this expression. Thus, $k_\perp \approx C/D$ where D is the beam diameter and C is a constant near unity.

Interesting results which were computed for the conditions of the present experiments are reproduced in Table IV. Values of $k_z \lambda_D$ are listed to emphasize

TABLE IV. Landau and Collisional Damping Logarithmic Decrements*

Gas	k_z (cm)	$k_z \lambda_D$	$k\lambda_D$	$\gamma(k\lambda_D)\tau$ ($\times 10^2$)	$\gamma(k^+\lambda_D)\tau$ ($\times 10^2$)	$\frac{\nu_c \tau}{2}$ ($\times 10^2$)
Hg	11.0	0.15	0.21	0.3	1.1	3.1**
Xe	7.7	0.13	0.20	0.2	0.7	1.6
Kr	6.2	0.11	0.21	0.4	3.0	1.4
Ar	4.8	0.10	0.22	1.0	2.8	2.6
Ne***	$\geqslant 1.6$	$\geqslant 0.04$	0.22	$\geqslant 3.3$***	—	—

* Three-dimensional Landau-damping and collisional-damping logarithmic decrements calculated for experimental conditions and an estimated $k_\perp = 1/D = 10$ cm^{-1}.
** P_c taken to be 200.
*** Based on estimated $T_e \approx 37000$ °K and under the experimentally unattained oscillation condition of one loop of standing wave.

that they are not independent of T_e. The Landau damping computed using these k_z values alone has been found entirely negligible. However, upon including the $k_\perp$ component in the wave number, the computed $k\lambda_D$ products are found nearly temperature independent. The generalized Landau damping decrement multiplied by the time τ of one period, $\gamma(k\lambda_D)\tau$ was evaluated by interpolation from the tables of FRIED and CONTE [12]. This logrithmic decrement was found considerably larger for argon than for mercury, xenon or krypton. Since oscillations in argon were the most difficult, and indeed very difficult, to excite, the value computed for it of $\gamma(k\lambda_D)\tau = 0.01$ might be looked upon as the critical allowable value in the tests. Because the value for the hypothetical situation of a single loop in neon is much larger, oscillations would not be expected; experimentally none could be produced. Further consistency in the results of the analysis is noted in the values of the logrithmic decrement $\gamma(k^+\lambda_D)\tau$ computed with a total wave number k^+ for the hypothetical situation of the existence of one more loop than could be experimentally excited. In every case the Landau damping was markedly increased; except for xenon, it always exceeded the maximum value which apparently could be tolerated, i.e., the 0.01 value for argon, although the difference in the case of xenon and, in particular, of mercury may be too small to be significant.

It must be borne in mind that these agreements are only semiquantitative at best because of the objectionable use of the parameter C in estimating $k_\perp$. The point is that this parameter can be chosen continuously between 0.9 and 1.2, within the range of values required by the uncertainty principle, to obtain results that show the generalized Landau damping to be consistent with the experimental results and to increase significantly with the addition of a single loop of standing wave beyond the maximum found experimentally. Thus a generalized form of Landau damping has been compared with observations of oscillations that were sensitive to changes in both wavelength and temperature. The results do suggest that the Landau or a closely related mechanism must have been operative.

Included in Table IV for comparison are also collisional damping logrithmic decrements, taken as equal to $\nu_c \tau/2$ where ν_c is the collision frequency. These values are based on the simple assumption that, on the average, every electron loses all its coherent oscillatory energy in a collision. This assumption and the additional assumption implicit in the calculations that electrons with high thermal velocities possess as much oscillatory energy as those with lower velocities lead to values of damping that are believed to be too large, possibly by a very considerable amount. In each gas the waves were long compared to the Debye length, i.e. $\lambda_p/\lambda_D \approx 30$, and the electron temperature was much greater than the ion temperature with ratios of from about 35 to 70; these are conditions under which damping by collisions is often viewed as negligible [13]. Because the entire series of values for collisional damping may be excessively high, and because all values of each series of Landau damping can be rapidly made higher or lower by the adjustment of an estimated constant, one is cautioned against drawing conclusions based on close numerical cross comparisons between decrement values for the two types of damping. As calculated, the collisional damping logarithmic decrements are several times larger than the $\gamma(k\lambda_D)\tau$ values for Landau damping based on experimental data; they approach equality with the $\gamma(k^+\lambda_D)\tau$ values. This latter comparison is perhaps the more important as it is for the case where the total damping exceeded the allowable.

The desirability of experiments with larger-diameter beams is evident. Not only should they provide better experimental guidance as to the damping in an infinitely wide beam but also they should permit the excitation of standing waves in gases with higher temperatures.

In the progress of this work, with particular beam energies and with no background plasma present, complete "bursting" of the two interpenetrating

excitation beams was observed in the inter-interaction region although each existed, normal in appearance, back of the beam-emitting electrodes. (The interaction region was the space between the two A_2 beam-emitting electrodes of Fig. 1). Perhaps this was an example of the destruction of directed electron velocities predicted by Buneman [3].

6. Acknowledgements

I wish to state my appreciation to P. Zieske for assistance in making the analysis of the experimental results and to H. Cleva for his careful continuous help in the laboratory. It is a pleasure to thank J. Drummond for inspiring discussions of the damping problem, for valued criticism of this manuscript, and for the privilege of including in it certain results obtained by him in his theoretical analysis of Landau damping in three-dimensions.

References

[1] KOFOID, M. J., *Phys. Rev. Letters* **4** (1960) 541.
[2] KOFOID, M. J., Abstracts 13th Annual Gaseous Electronics Conf. (Monterey, Calif., 1960).
[3] BUNEMAN, O., *Phys. Rev. Letters* **1** (1958) 8.
[4] LANDAU, L., *J. Phys. (USSR)* **10** (1946) 25.
[5] DRUMMOND, J. E., private communication.
[6] ROMPE, R., STEENBECK, M., *Ergebnisse der exakten Naturwissenschaften* **18** (1939) 257.
[7] LOONEY, D. H., "A study of the oscillations in low pressure gas discharges", Ph. D. thesis, Massachusetts Institute of Technology (1953).
[8] PLATZMAN, P. M., BUCHSBAUM, S. J., *Bull. Am. Phys. Soc.* **6** (1961) 290.
[9] LINHART, J. G., Plasma Physics, North-Holland Publishing Co., Amsterdam (1960) 111-112.
[10] DRUMMOND, J. E., *Phys. Rev.* **110** (1958) 300.
[11] DRUMMOND, J. E., "Beam power development in a plasma", Boeing Scientific Research Laboratories (Seattle, Wash.) Report D1—82—0125 (July 1961).
[12] FRIED, B. D., CONTE, S. D., "The plasma dispersion function", Space Technology Laboratories Report (1960).
[13] GROSS, E. P., KROOK, M., *Phys. Rev.* **102** (1956) 597.

ЭКСПЕРИМЕНТАЛЬНОЕ ИЗУЧЕНИЕ МАГНИТНО-ЗВУКОВОГО РЕЗОНАНСА*

А. В. БАРТОВ, Е. К. ЗАВОЙСКИЙ, И. А. КОВАН, Б. И. ПАТРУШЕВ, В. Д. РУСАНОВ, Д. А. ФРАНК-КАМЕНЕЦКИЙ

АКАДЕМИЯ НАУК СССР

МОСКВА, СОЮЗ СОВЕТСКИХ СОЦИАЛИСТИЧЕСКИХ РЕСПУБЛИК

Эксперименты ставились в линейных и существенно нелинейных условиях. В линейных экспериментах, проводимых на плазме, приготовленной внешним источником, резонанс возбуждался маломощным измерительным генератором, воздействием которого на концентрацию плазмы можно было пренебречь. При этом параметры плазмы (концентрация, размер шнура, магнитное поле) были постоянны в пределах опыта, либо строго контролируемые, что существенно для выяснения физической картины явления. Опыты проводились при значениях концентраций плазмы от 10^{10} до 4×10^{13} см$^{-3}$, магнинтное поле в большинстве опытов составляло $1-2\times10^3$ э. Резонанс возбуждался в диапазоне частот от нескольких мегагерц до ~200 мгц, контурами в форме удлиненного витка, и регистрировался: (1) по изменению добротности измерительного контура и (2) по показаниям магнитных зондов. С помощью магнитных зондов измерялось также пространственное распределение переменных магнитных полей в плазме в момент резонанса. Эти измерения позволяют определить значения K_r и K_z, а также обнаруживают усиление переменного магнитного поля в плазме при резонансе. Контроль за концентрацией в плазме осуществлялся с помощью СВЧ-методов, а также двойными электрическими зондами. Экспериментально наблюдаемые при этом зависимости резонансной частоты от концентрации плазмы и величины напряженности магнитного поля подтверждают выводы теории. Измерение добротности плазмы, однако, показывает, что, по-видимому, диссипация энергии не объясняется простейшими механизмами столкновений.

Нелинейный эксперимент, в котором создание плазмы производилось тем же самым контуром, в котором изучался резонанс, является сложным (резонанс наблюдается при меняющихся параметрах плазмы: концентрация, размер шнура), но имеет практический интерес прежде всего как эффективный способ создания плазмы.

Исследование резонанса в нелинейных условиях позволило определить величину поглощаемой плазмой мощности и температуру электронов плазмы. Так, при возбуждении резонанса генератором, имеющим частоту $\nu=100$ мгц и номинальную мощность 300 кв, поглощаемая мощность составляла около 180 кв. При этом $H_{\text{рез}}=7\times10^3$ э и концентрация заряженных частиц $n\approx2\times10^{13}$ см$^{-3}$.

В этих опытах оценка электронной температуры по интенсивности линий $\lambda=4713$ Å и $\lambda=5016$ Å дает значение $T_e=15-20$ эв. Эти величины подтверждаются спектральными измерениями, показавшими наличие примесных линий O^+ и N^+ и отсутствие линий He^+, с потенциалом возбуждения выше 50 эв. Степень ионизации при резонансе была близка к 100%.

Измеренная добротность плазмы при этом оказалась равной ~20, в то время как теоретическая оценка дает $Q=240$. Это показывает, что в данном случае учет лишь простейших механизмов диссипации энергии является недостаточным.

1. Постановка проблемы

Предсказанное теорией плазмы [1—3] явление магнитно-звукового резонанса представляет научный и прикладной интерес с ряда точек зрения. Для термоядерной проблемы магнитно-звуковой резонанс интересен прежде всего как перспективный метод нагрева плазмы. В сочетании с черенковским поглощением, этот метод применим при сколь угодно высоких температурах. В то же время магнитный звук, как явление простое в теоретическом отношении и удобное для экспериментального исследования, представляется очень подходящим объектом для экспериментальной проверки выводов теории плазмы, и в частности для изучения таких сложных явлений, как диссипация энергии в плазме. Строгая теория этих явлений может быть развита только в линейном приближении. Между тем, как видно хотя бы из аналогии с обычной турбулентностью, для диссипативных процессов нелинейные явления могут иметь фундаментальное значение. Поэтому, от экспериментального исследования диссипативных процессов можно ждать новых результатов, важных для всех областей физики плазмы. Исходя из всех этих задач, нами и были поставлены работы, излагаемые в настоящем докладе.

2. Общее описание экспериментов

Эксперименты ставились в линейных и в существенно нелинейных условиях. В линейных экспериментах на плазме, приготовленной внешним источником, резонанс возбуждался маломощным измерительным генератором, воздействием которого на концентрацию плазмы можно было пренебречь. При этом параметры плазмы (концентрация, размер шнура, магнитное поле) были постоянны в

* Доклад CN-10/207, представленный на конференцию. Докладчик: Е. К. Завойский. Переводы аннотаций находятся в конце тома.

пределах опыта, либо строго контролируемы, что существенно для выяснения физической картины явления. Линейные эксперименты разделяются на опыты с малым и с большим погонным числом электронов. В опытах с первым плазма приготовлялась в осциллирующем разряде типа Пеннинга, и концентрации были в пределах $10^{10}-10^{12}$ см$^{-3}$. В этой серии экспериментов резонансная частота была близка к гибридной. Здесь было обнаружено и исследовано явление максимума резонансной частоты в зависимости от концентрации, позволившее обосновать магнитно-звуковой метод приготовления плазмы, к которому мы пришли эмпирически еще ранее, в нелинейных экспериментах. В опытах с большим погонным числом электронов удалось осуществить предсказанный теорией эффект пространственного усиления переменных магнитных полей: в резонансных условиях амплитуда поля внутри плазменного столба оказывается значительно выше чем вне его, или в отсутствие плазмы.

Опыты в нелинейных условиях показали возможность получения магнитно-звуковым методом плазмы с высокой степенью ионизации и температурой электронов 15—20 эв, при концентрации заряженных частиц до 2×10^{13} см$^{-3}$. В этих опытах непосредственно показано поглощение энергии. Мощность, поглощаемая плазмой, доходила до 180 квт и была на порядок больше, чем если бы поглощение происходило только в результате столкновений между частицами плазмы.

3. Линейные эксперименты при большом погонном числе электронов

Для проведения этих опытов был сконструирован магнитно-звуковой источник плазмы, который позволял получать в постоянном магнитном поле плазменный шнур диаметром $\sim$5 см с концентрацией заряженных частиц $\sim10^{13}$ см$^{-3}$ при высокой степени ионизации. Установка состояла из стеклянной трубы, разделенной на ионизационный объем диаметром 10 см и измерительный объем диаметром 6 см (рис. 1). Напряженность постоянного магнитного поля в ионизационном объеме могла достигать 1000 э, в измерительном — 3000 э. Переменное поле в ионизационном объеме возбуждалось мощным импульсным генератором (150 квт) при частоте 50 мгц. Плазма, созданная импульсным в. ч. разрядом в ионизационном объеме, вытекала вдоль силовых линий магнитного поля в измерительный объем, где на нее накладывалось переменное поле малой амплитуды (10^{-5} от постоянного магнитного поля) от генератора стандартных сигналов с интервалом частот от 2 до 25 мгц. Переменное магнитное поле было направлено параллельно постоянному магнитному полю. Разряд происходил в водороде при началь-

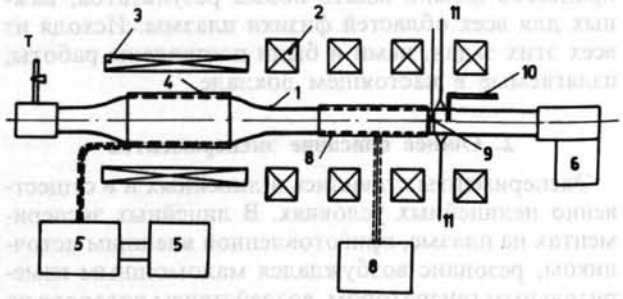

Рис. 1 Схема установки: 1 — стеклянная труба; 2 — катушки магнитного поля измерительного объема; 3 — соленоид магнитного поля источника; 4 — в.ч. контур источника; 5 — генератор и модулятор ($P_{max}=150$ квт); 6 — диффузионный насос; 7 — газовый натекатель; 8 — измерительный генератор и контур; 9 — магнитный зонд; 10 — двойной электрический зонд; 11 — 8 мм зондирующие антенны.

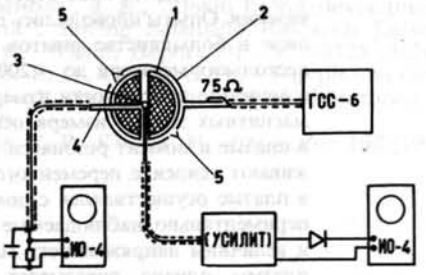

Рис. 2 Схема возбуждения и индикации резонанса: 1 — стеклянная труба; 2 — возбуждающий виток; 3 — магнитный зонд; 4 — двойной электрический зонд; 5 — 8 мм зондирующие антенны.

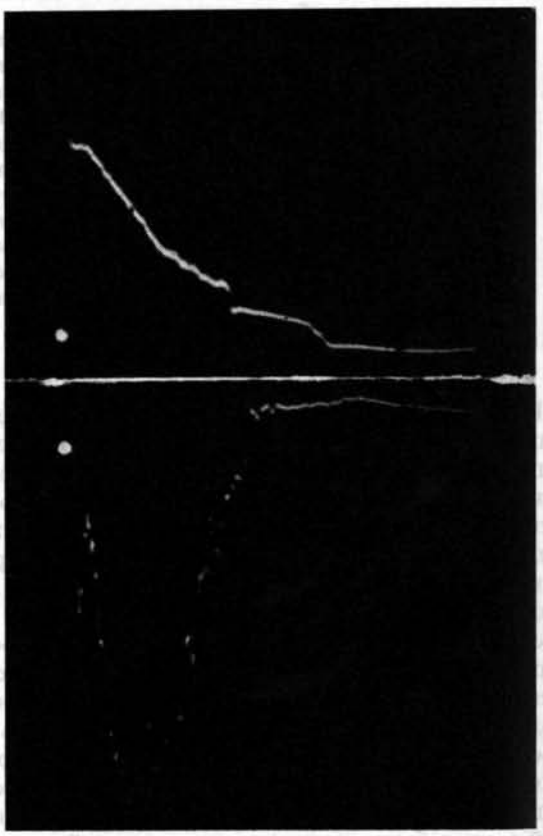

Рис. 3 Осциллограмма тока двойного электрического зонда и э.д.с. с магнитного зонда: I — осциллограмма тока двойного зонда; II — э.д.с. с магнитного зонда. $H_0=1500$ э; $P_0=2\times10^{-3}$ мм рт ст; $n_{max}=1{,}6\times10^{13}$ см$^{-3}$; $f=17$ мгц длительность развертки — $\sim$15 мсек.

ном давлении порядка 10^{-3} мм рт ст. Радиальное распределение переменных полей измерялось магнитным зондом, который мог перемещаться в стеклянной трубочке вдоль радиуса. Зонд защищался от электрических полей электростатическим экраном. Схема измерений представлена на рис. 2. Изменение концентрации плазмы в ходе опыта определялось по показаниям двойного электрического зонда. Ионизация производилась генератором, дающим экспоненциально спадающий импульс с временем затухания 10 мсек. В соответствии с этим, концентрация плазмы также убывала во времени. На рис. 3 сверху дана осциллограмма сигнала с двойного электрического зонда, показывающая спад концентрации плазмы в ходе ионизующего импульса. Снизу дана осциллограмма магнитного зонда, помещенного на оси цилиндра. Эта кривая показывает изменение амплитуды переменного поля внутри плазмы при изменении концентрации. На рисунке амплитуда возрастает книзу. Из осциллограммы видно, что в определенной области концентрации (зависящей от частоты и от напряженности постоянного поля) возникает резонанс: амплитуда переменного поля внутри плазмы возрастает в несколько раз в сравнении с начальной. В стадии затухания разряда плазма с нерезонансной концентрацией экранирует переменное поле: амплитуда его в нерезонансной плазме оказывается меньше, чем без плазмы. В стадии нарастания концентрации эффект экранировки заметить не удается, т.к. ионизация происходит слишком быстро. Измерение концентрации двойным электрическим зондом контролировалось посредством 8 мм микроволнового интерферометра, собранного по схеме Уортона [4]. На рис. 4 показания зонда сопоставлены с показаниями интерферометра и видно, что в диапазоне концентраций от 2×10^{12} до 10^{13} см$^{-3}$ оба прибора дают практически совпадающие данные. Этот результат свидетельствует, в частности, и о том, что распределение концентрации по сечению не слишком отличается от равномерного.

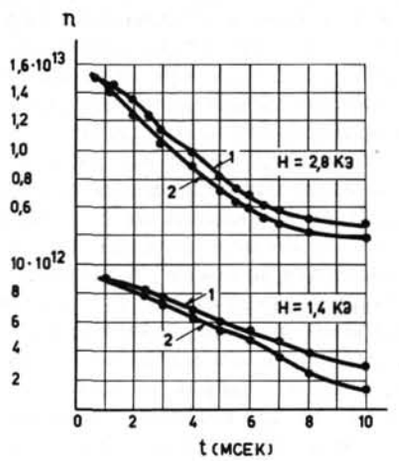

Рис. 4 Калибровка двойного электрического зонда микроволновым интерферометром: 1 — показания интерферометра; 2 — показания двойного электрического зонда.

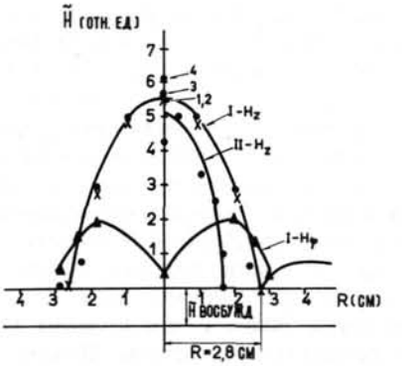

Рис. 5 Распределение $H_z\sim$ и $H_\varphi\sim$ — компонент магнитного поля по радиусу для двух значений диаметра плазменного столба; кривая I — соответствует $D=5{,}6$ см; кривая II — соответствует $R=3{,}4$ см.

С помощью магнитного зонда были получены радиальные распределения осевой и азимутальной компонент переменного магнитного поля для двух значений радиуса плазменного столба. Эти распределения представлены на рис. 5. Как видно из рисунка, кривые при разных радиусах подобны. Распределение осевой компоненты близко к функции Бесселя нулевого, азимутальной — первого порядка. Такой характер радиальной зависимости наблюдается только в резонансной области; в области экранировки азимутальная компонента отсутствует.

Резонансные кривые, полученные при изменении концентрации, снимались для разных частот в диапазоне от 2 до 25 мгц и были перестроены в резонансную кривую зависимости H_z от частоты, представленную на рис. 6. Кривая отражает зависимость амплитуды переменного магнитного поля от частоты при фиксированных значениях концентрации $1{,}3\times10^{-13}$ см$^{-3}$, радиуса плазменного столба 2,8 см и напряженности постоянного магнитного поля 1500 э. На кривой отчетливо видны два резонансных максимума.

На основании полученных экспериментальных данных была сделана попытка идентификации типа колебаний. Измеренные радиальные распределения соответствуют типу колебаний с азиму-

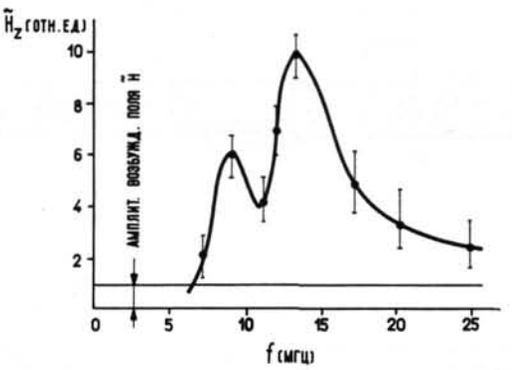

Рис. 6 Зависимость H_z в центре плазменного столба от частоты возбуждения $H_0=1500$, $P_0=9\times10^{-4}$ мм рт ст; $n=1{,}3\times10^{13}$ см$^{-3}$.

тальным числом $m=0$ и радиальным числом $n=1$ для цилиндра со свободной границей. Измеренные значения концентрации и радиуса шнура дают эффективное погонное число электронов $П \approx 30$. Отсюда с помощью приближенной формулы для длинного цилиндра [5] можно подсчитать ожидаемое значение резонансной частоты магнитного звука для заданных условий эксперимента и принятого продольного числа l. Для плазмы с концентрацией 10^{13} см$^{-3}$ при радиусе шнура 2,8 см и напряженности постоянного поля 1500 э расчет дает при длине 50 см и продольном числе $l=1$ значение резонансной частоты 16 мгц. Экспериментальное значение для этих условий 17 мгц. Таким образом, в эксперименте, по-видимому, возбуждался тип колебаний с $m=0$, $n=1$, $l=1$.

Полученное в этом эксперименте усиление амплитуды поля внутри плазмы в 5—7 раз против начальной свидетельствует, что магнитно-звуковой резонанс действительно является резонансом раскачки [5] и обеспечивает хорошую связь генератора с плазмой.

4. Линейные эксперименты при малом погонном числе электронов

В этих опытах плазма создавалась осциллирующим разрядом типа Пеннинга между двумя вольфрамовыми катодами в установке, изображенной на рис. 7. При подаче напряжения между катодами образуется цилиндрический плазменный столб диаметром около 2 см.

Разрядная трубка находилась в постоянном продольном магнитном поле напряженностью до 3000 э. Концентрация плазмы задавалась силой разрядного тока и менялась в пределах от 6×10^{9} до 10^{12} см$^{-3}$. Для измерения концентрации использовались два метода: сдвиг собственной частоты резонатора в области низких концентраций и 8-миллиметровый микроволновой интерферометр в области более высоких концентраций.

В области, где оба метода применимы, второй дает значения примерно в 1,5 раза выше первого,

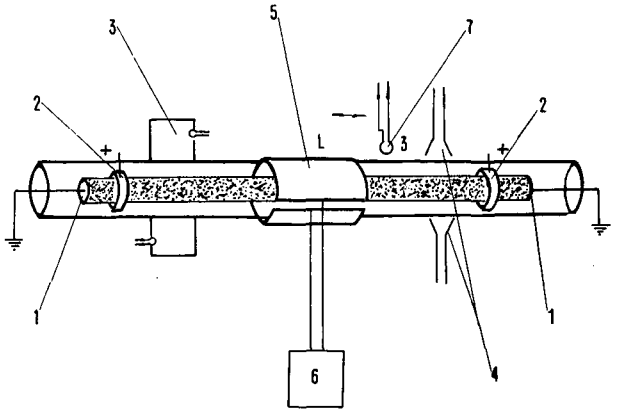

Рис. 7 Схема установки: 1 — катоды; 2 — аноды осциллирующего разряда; 3 — резонатор ($\lambda=10$ см, тип колебаний TM_{010}); 4 — антенны интерферометра; 5 — индуктивность измерительного контура; 6 — измеритель добротности контуров; 7 — магнитный зонд.

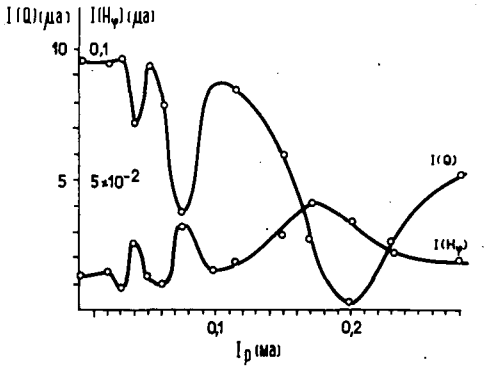

Рис. 8 Зависимость показаний прибора, регистрирующего добротность контура $I(Q)$ и тока зонда $I(H_\varphi)$ от величины разрядного тока, для гелия, $P_0=1{,}3\times10^{-2}$ мм ртст; рабочая частота $\nu=158$ мгц, поле $H=800$ э.

что может служить мерой неточности, вносимой неоднородностью концентраций и полей. Для возбуждения магнитно-звуковых колебаний на трубу надевался контур в виде удлиненного витка. Используемые частоты лежат в диапазоне 100—150 мгц. На небольшом расстоянии от контура вне разрядной трубки располагались магнитные зонды, измерявшие азимутальную и осевую составляющие переменного магнитного поля. Зонды могли передвигаться вдоль трубки на постоянном расстоянии от оси. Добротность Q контура вместе с плазмой измерялась Q — метром.

Магнитно-звуковой резонанс регистрировался по резкому падению добротности контура при некоторых значениях тока разряда (т.е. концентрации плазмы). Одновременно возрастает амплитуда переменного поля, измеряемая магнитным зондом. Типичные резонансные кривые показаны на рис. 8. По горизонтальной оси отложен ток разряда. Верхняя кривая представляет величину, пропорциональную добротности Q контура, нижняя — амплитуду азимутальной составляющей переменного магнитного поля.

Посредством перемещения магнитного зонда вдоль трубы были измерены распределения азимутальной и осевой составляющих переменного магнитного поля вдоль оси плазменного цилиндра. Полученные результаты представлены на рис. 9. По этим кривым можно непосредственно определить продольное число l, т.е. число полуволн, укладывающихся на длине плазменного столба. Для большинства наблюдавшихся резонансов значения оказались в пределах от 4 до 6. То, что в этой серии опытов возбуждались высшие гармоники, объясняется высоким диапазоном рабочих частот. Концентрации плазмы, получавшиеся в осциллирующем разряде, соответствуют погонным числам электронов меньше единицы. Опыты велись при таких напряженностях постоянного магнитного поля, при которых электронная циклотронная частота того же порядка величины, что и плазменная. В этих условиях теория [6] предсказывает своеобразные особенности магнитно-звукового резонанса, которые в полной мере обнаружи-

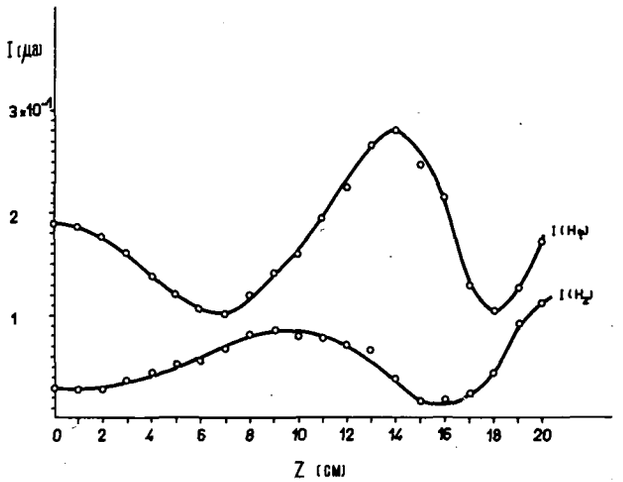

Рис. 9 Зависимость тока магнитных зондов, регистрирующих амплитуды азимутальной ($I(H_\varphi)$) и осевой ($I(H_z)$) составляющих высокочастотного поля от расстояния зондов от одного из катодов, для гелия, давление $P_0 = 1{,}5 \times 10^{-2}$ мм ртст, рабочая частота $\nu = 158$ мгц, постоянное поле $H = 800$ э, величина тока разряда $I_p = 0{,}12$ ма. ($n = 0{,}8 - 1{,}0 \times 10^{10}$ см$^{-3}$).

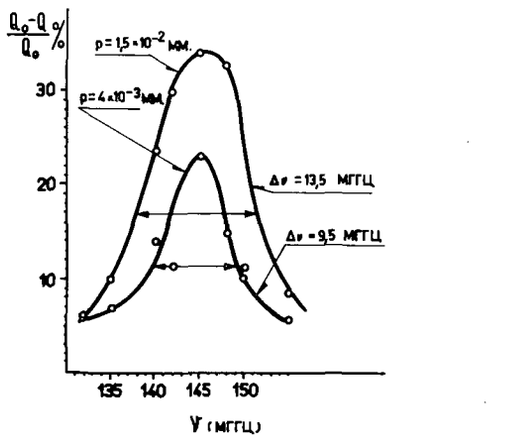

Рис. 10 Зависимость относительного уменьшения добротности измерительного контура Q от рабочей частоты, для гелия, для двух значений давления P_0. Поле $H = 1{,}1 \times 10^3$ э, ток разряда $I_p = 0{,}28$ ма ($n = 0{,}9 - 1{,}1 \times 10^{10}$ см$^{-3}$).

ваются на опыте: резонансная частота перестает зависеть от массы иона и обнаруживает максимум в зависимости от концентрации. При концентрациях ниже точки максимума зависимость резонансной частоты от концентрации обращается: чем меньше концентрация, тем ниже основная резонансная частота. В соответствии с этим, в эксперименте при фиксированной частоте с уменьшением концентрации возрастало продольное число l.

Для выяснения характера диссипативных процессов в плазме, были построены кривые, показывающие измение добротности контура с плазмой в зависимости от частоты. Эти кривые показаны на рис. 10 для двух различных начальных давлений. На них непосредственно видна ширина резонанса. Она заметно больше, чем подсчитанная по простейшей теории затухания магнитного звука, учитывающей только диссипацию, вызванную столкновениями.

5. Эксперименты в нелинейном режиме

Работа в нелинейном режиме проводилась с мощным генератором (номинальная импульсная мощность около 1 мгвт), на частоте 100 мгц. Максимальная длительность импульса в.ч. поля 40 мсек. Вместо постоянного магнитного поля в этих экспериментах использовалось квазистатическое, создаваемое разрядом конденсаторной батареи с полупериодом 28 мсек и амплитудой 12 кэ. Контур, создающий в плазме переменное поле, представлял собой удлиненный виток длиной 60 см, диаметром 12 см. Работа проводилась с водородом, гелием и смесью водорода с гелием. В качестве разрядных камер использовались стеклянные или кварцевые трубы длиной 250 см, с диаметрами от 8 до 10 см. Начальное давление газа бралось в пределах $5 \times 10^{-4} - 10^{-3}$ мм ртст. В экспериментах исследовался нагрев электронов плазмы и отбор в.ч. мощности генератора. Концентрация плазмы контролировалась по запиранию 8 мм сигнала, отбор мощности — по сеточному току генератора. Для оценки электронной температуры использовались спектроскопические измерения как в интегральном спектре, так и с разверткой по времени. Сравнение интенсивности гелиевых линий 5016 Å и 4713 Å в предположении максвелловского распределения дает значение электронной температуры в максимуме резонанса порядка 15—20 эв. Эта оценка согласуется с наличием в интегральном спектре примесных линий N II и O II (потенциал возбуждения около 30 эв) и отсутствием линии He II (потенциал возбуждения свыше 50 эв).

Отбор мощности генератора, измеряемый по сеточному току, достигал 180 кв, что дает оценку добротности плазмы $Q \sim 20$ (для ненагруженного генератора $Q \sim 150$). Затухание, вызванное кулоновскими столкновениями, при электронной температуре, оценной по спектру, давало бы $Q \sim 240$. Роль перезарядочных столкновений еще меньше. Таким образом, интенсивность диссипативных процессов в плазме на порядок выше, чем при учете столкновений. В затухании магнитного звука основное значение видимо имеют процессы диссипации без столкновений.

В смеси водорода с 5—10% гелия наблюдалось практически полное исчезновение линий серии Бальмера в момент, когда линии гелия достигали максимальной интенсивности. Это позволяет сделать вывод, что в максимуме магнитно-звукового резонанса достигается практически полная ионизация плазмы.

Литература

[1] Ахматов А. П. и др, *Ж. экспер. теор. Физ.* **39** (1960) 536.
[2] Русанов В. Д. и др, *Ж. экспер. теор. Физ.* **39** (1960) 1497.
[3] Завойский Е. К. и др, *Ж. тех. Физ.* **31** (1961), 513.
[4] Уортон, Говард, Гейнц, в Сб. «Физика Горячей Плазмы и Термоядерные Реакции», Атомиздат, Москва (1959) 675—685.
[5] Франк-Каменецкий Д. А., *Ж. эскпер. теор. Физ.* **39** (1960), 669.
[6] Бартов А. В. и др, *Ж. экспер. теор. Физ.* **41** (1961) 588.

ПОГЛОЩЕНИЕ ПЛАЗМОЙ ЭНЕРГИИ ПЕРЕМЕННЫХ ЭЛЕКТРОМАГНИТНЫХ ПОЛЕЙ БОЛЬШОЙ АМПЛИТУДЫ*

М. В. БАБЫКИН, Е. К. ЗАВОЙСКИЙ, Л. И. РУДАКОВ, В. А. СКОРЮПИН

АКАДЕМИЯ НАУК СССР

МОСКВА, СОЮЗ СОВЕТСКИХ СОЦИАЛИСТИЧЕСКИХ РЕСПУБЛИК

Переменные электромагнитные поля, возбуждаемые в плазме, индуцируют в ней электрические токи. Если относительная токовая скорость v заряженных частиц плазмы превышает их тепловую скорость, то в плазме может развиться неустойчивость, которая приводит к торможению электронной компоненты плазмы ионами. Это хорошо известная неустойчивость «пучка» электронов. Такого рода коллективный эффект должен сказаться в том, что токовая скорость не может сильно превышать тепловую скорость электронов. Благодаря этому, энергия поля будет необратимо передаваться электронам плазмы. Этот эффект пороговый. Для возникновения неустойчивости в лучшем случае необходимо, чтобы плотность электромагнитной энергии превышала давление плазмы $H_{\sim}^2/8\pi > nT$.

Для проверки изложенных соображений был поставлен эксперимент. Плазма приготовлялась прямым разрядом, а высокочастотное магнитное поле напряженностью до 750 эрстед создавалось колебательным контуром, состоящим из одновитковой катушки индуктивности и емкости. Плотность плазмы достигала 2×10^{13} см$^{-3}$, а частота контура изменялась от 8 до 13 мгц.

При выбранных параметрах время ионизации было больше $0{,}5\times10^{-6}$ сек. Обнаружено поглощение плазмой энергии контура за время порядка периода колебаний. Рост концентрации плазмы после срабатывания контура можно объяснить, лишь допустив, что за время работы контура (10^{-7} сек) электроны плазмы запасли энергию, достаточную для последующей ионизации.

1. Введение

Одно из основных затруднений на пути получения высокотемпературной плазмы состоит в том, что скорость обычной столкновительной диссипации электромагнитной энергии в плазме невелика и быстро падает с ростом ее температуры.

В настоящем докладе излагаются результаты экспериментов по исследованию поглощения плазмой энергии переменных электромагнитных полей. Показано, что при достаточно большой напряженности переменного электромагнитного поля существует аномальное поглощение плазмой энергии поля со скоростью, значительно превосходящей скорость столкновительной диссипации.

Это поглощение связано с возбуждением мелкомасштабных неустойчивостей при больших значениях скорости направленного движения электронов относительно ионов в переменном электромагнитном поле. Скорость движения электронов плазмы относительно ионов определяется значением пространственной производной магнитного поля

$$\mathrm{rot}\,\mathbf{H} = \frac{4\pi}{c} e n (\mathbf{v}_i - \mathbf{v}_e) \qquad (1)$$

Относительная скорость электронов $\mathbf{u}=\mathbf{v}_e-\mathbf{v}_i$ не может быть очень большой. Начиная с некоторого значения $\mathbf{u}$ в плазме будут возникать неустойчивости.

В отсутствии магнитного поля «пучковая» неустойчивость возникает, если относительная скорость электронов u превышает скорость электронного звука $c_s=(\gamma P_e/nm)^{1/2}$. Наиболее быстро за время $(M/m)^{1/3}/\omega_{pe}$ нарастают возмущения масштаба u/ω_{pe}, где $\omega_{pe}=4\pi ne^2/m$. Если эта длина меньше ларморовского радиуса электрона u/ω_{He}, $\omega_{He}=eH/mc$, то можно пренебречь влиянием магнитного поля на развитие таких возмущений. В настоящих экспериментах $\omega_{pe}\gg\omega_{He}$, время развития и масштаб неустойчивости много меньше периода и длины волны колебаний, возбуждаемых контуром в плазме. Поэтому воспользуемся результатами рассмотрения устойчивости «пучка» электронов в однородной плазме без магнитного поля. Строгое решение этой задачи можно найти в работе [1].

Макроскопический эффект от возбуждения мелкомасштабных неустойчивостей состоит в том, что электроны будут тормозиться под действием силы коллективного трения об ионы, а энергия упорядоченного движения пойдет на «нагрев» электронов. Здесь следует отметить, что такой механизм поглощения энергии упорядоченного движения впервые был использован Р. З. Сагдеевым в развиваемой им теории ударных волн в разреженной плазме. Поглощение будет продолжаться до тех пор, пока энергия беспорядочного движения электронов не сравняется с их упорядоченной энергией, т.е. нарушится условие возникновения «пучковой» неустойчивости.

В эксперименте высокочастотный контур возбуждал в плазме цилиндрическую волну, распространяющуюся поперек постоянного магнитного поля H. Частота контура ω равнялась 6×10^7 гц и всегда удовлетворяла условию $\omega_{Hi}\ll\omega\ll\omega_{He}$. В

* Доклад CN-10/209, представленный на конференцию. Докладчик: Е. К. Завойский. Дискуссия (на английском языке) по этому докладу дана на стр. 1110. Переводы аннотаций находятся в конце тома.

такой волне скорость электронов связана с переменным магнитным полем $H_\sim$ соотношением

$$v_e = \omega\left(\frac{Mc^2}{4\pi n e^2}\right)^{1/2}\frac{H_\sim}{H}\left(1-\frac{\omega^2}{\omega_{Hi}\omega_{He}}\right)^{-1/2} \quad (2)$$

Подставляя это значение скорости в критерий возникновения неустойчивости, получим

$$\frac{H_\sim^2}{8\pi p_e} > \gamma\frac{|\omega_{Hi}\omega_{He}-\omega^2|}{\omega^2} \quad (3)$$

Это соотношение определяет предельное давление электронов плазмы p_m. При заданной частоте контура p_m зависит только от отношения напряженностей переменного и постоянного магнитных полей. Если p_m меньше начального давления, которое определяется условиями приготовления плазмы в эксперименте, то «пучковой» неустойчивости не будет. В эксперименте источник давал плазму с плотностью, большей чем $1{,}7\times10^{13}$ см$^{-3}$ и температурой электронов порядка 5 эв. В этих условиях аномальное поглощение должно наблюдаться, если

$$\frac{H_\sim}{H} \gtrsim \frac{1}{2} \quad (4)$$

Из приведенной оценки видно, что в области значений $H_\sim/H$, где существует аномальное поглощение, может быть существенной нелинейность. Нелинейность может привести к искажению формы волны. Форма волны, распространяющейся от края цилиндра радиуса R к центру успеет исказиться из-за нелинейности, если

$$\frac{H_\sim}{H} > \frac{\pi H}{(4\pi n M)^{1/2}\omega R} \quad (5)$$

Из формулы (3) следует, что максимальное поглощение должно наблюдаться когда среднегеометрическая частота $\Omega=(\omega_{Hi}\omega_{He})^{1/2}$ близка к частоте контура.

2. Описание эксперимента

Схема установки показана на рис. 1.

В первоначальных опытах установка состояла из катушек Гельмгольца, создающих поле до 3000 эрстед и одновиткового высокочастотного контура с частотой 10 мгц и добротностью $Q=60$, ударно возбуждаемого первичным контуром с разрядником. Начальная амплитуда переменного магнитного поля равнялась 170 эрстед. Внутри контура находилась кварцевая труба с внутренним диаметром 3,6 см, соединенная одним концом с вакуумной системой и наполняемая исследуемым газом. С другого конца трубы в плазму вводилась запаянная кварцевая трубка с наружным диаметром 4 мм, в которую вставлялся магнитный зонд. Поглощение энергии контура плазмой, образующейся при срабатывании контура, определялось по затуханию контура, измеряемому как магнитным зондом, помещенным внутри плазмы, так и зондом, помещенным снаружи. Концентрация заряженных частиц измерялась по прохождению микроволнового сигнала ($\lambda=8$ мм) у края контура.

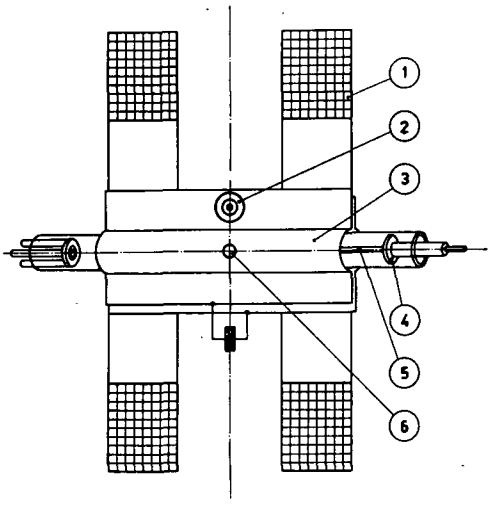

Рис. 1 Схема установки. 1 — катушки Гельмгольца, 2 — разрядник, 3 — контур, 4 — электроды прямого разряда, 5 — магнитный зонд, 6 — отверстие для пропускания микроволнового сигнала $\lambda=8$ мм.

Для того, чтобы отделить поглощение энергии за счет эффекта «пучковой» неустойчивости от поглощения энергии на ионизацию были поставлены эксперименты при меньших давлениях с предварительной ионизацией газа прямым разрядом до концентрации заряженных частиц, большей чем $1{,}7\times10^{13}$ см$^{-3}$. В этом случае использовался обычный контур с управляемым разрядником, имеющий частоту от 8 до 13 мгц и максимальную амплитуду высокочастотного магнитного поля до 750 эрстед. Энергия, запасенная в контуре, достигала 2—5 дж. Сдвиг по времени между включением прямого разряда и контура задавался управляющей схемой и мог быть установлен от 0 до 100 мксек.

В середине контура имелось отверстие для определения концентрации заряженных частиц по прохождению сигнала $\lambda=8$ мм. Поглощение энергии контура определялось по показаниям магнитного зонда внутри плазмы, зонда, расположенного между плазмой и контуром и по напряжению на емкости контура. В этих опытах производилось также измерение скорости волны по временному сдвигу показаний внутреннего и внешнего магнитных зондов на различных полупериодах колебаний.

3. Обсуждение результатов эксперимента

1 Для проверки изложенных во введении соображений об аномальном поглощении энергии необходимо было выбрать такие условия эксперимента, чтобы исключить столкновительные механизмы поглощения энергии: ионизацию, возбуждение, джоулев нагрев, перезарядку.

В подготовительных экспериментах использовался высокодобротный контур. Плазма предварительно не готовилась, а создавалась самим рязрядом контура. Минимальное рабочее давление газа определялось давлением, при котором начи-

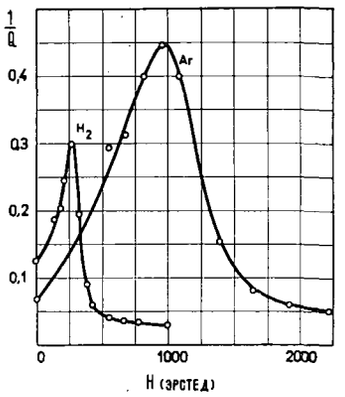

Рис. 2. Поглощение высокочастотной энергии для водорода $P=1{,}8\times10^{-2}$ мм ртст и аргона $P=9\times10^{-3}$ мм ртст в зависимости от постоянного магнитного поля. $H_{\sim}=170$ э.

нался пробой. В этих опытах оно составляло 2×10^{-2} мм Hg для водорода и 4×10^{-3} мм для аргона. Скорость поглощения энергии мерилась по затуханию колебаний в контуре.

На рис. 2 приведены экспериментальные кривые, изображающие зависимость скорости поглощения плазмой высокочастотной энергии контура в зависимости от напряженности постоянного магнитного поля. $H_{\sim}$ составляла 170 эрстед, частота колебаний 10 мггц. Концентрация заряженных частиц измерялась у края контура и всегда достигала значений, больших чем $1{,}7\times10^{13}$ см$^{-3}$.

Кривые поглощения имеют резко выраженные максимумы при магнитных полях H, для которых среднегеометрическая частота $\Omega=(\omega_{\mathrm{Hi}}\,\omega_{\mathrm{He}})^{1/2}$ близка к частоте контура. Этот экспериментальный факт легко объяснить тем, что скорость электронов в периодически меняющемся электромагнитном поле зависит от значения постоянного магнитного поля и растет, когда среднегеометрическая частота приближается к частоте колебаний (формула (2)).

В районе среднегеометрической частоты энергия, запасенная в контуре, поглощается водородной плазмой за время порядка 4×10^{-7} сек.

2 Экспериментальные результаты, приведенные в предыдущем разделе, из-за больших столкновительных потерь не дают возможности ответить на вопрос, существует ли аномальное поглощение энергии переменных электромагнитных полей большой амплитуды.

Для того, чтобы исключить ионизационные потери, а также потери на джоулев нагрев, перезарядку и возбуждение были поставлены эксперименты при давлениях нейтрального газа на два порядка меньшем, чем в опытах без предварительной ионизации. Плазма с концентрацией выше $1{,}7\times10^{13}$ см$^{-3}$ готовилась предварительно отдельным источником. Так как время развития «пучковой» неустойчивости очень мало и, следовательно, поглощение высокочастотной энергии идет очень быстро, то в этой серии опытов был взят контур с малой добротностью. В отсутствии плазмы контур затухал за 3—4 периода, что составляло 0,3—0,4 мксек. Так как в этих опытах давление нейтрального газа (водорода) отличалось на два порядка в сравнении с опытами без предварительной ионизации, то запас по времени на два порядка гарантировал нам, что за время работы контура столкновительного поглощения не могло быть.

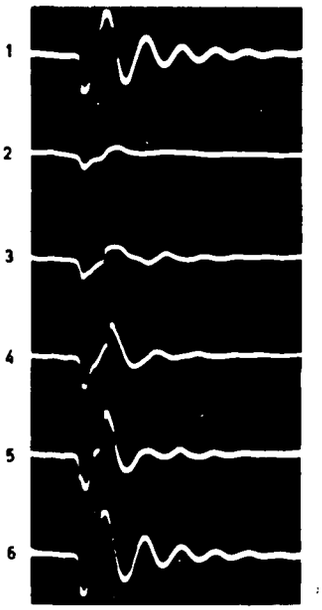

Рис. 3 Форма сигнала магнитного зонда внутри плазмы, при различных значениях постоянного магнитного поля. $H_{\sim}=600$ э. 1 — без плазмы, 2 — 120 э, 3 — 300 э, 4 — 480 э, 5 — 900 э, 6 — 1800 э.

Давление нейтрального газа менялось от 2×10^{-4} до 2×10^{-2} мм. В широком интервале давлений поглощение энергии не зависит от давления. Это исключает возможность привлечения ионизации, упругих столкновений, перезарядки и возбуждения для интерпретации поглощения энергии, обнаруженного в этих экспериментах. При давлениях больше чем 10^{-2} мм Hg, где роль столкновений в поглощении энергии уже не вызывает сомнений, поглощение энергии несколько увеличивается.

Регистрация переменных полей производилась с помощью магнитных зондов. Внешний зонд помещался между плазмой и контуром, внутренний зонд на оси цилиндра. Была снята серия осциллограмм сигналов с внутреннего и внешнего зондов при разных значениях напряженности переменного и постоянного полей. Наиболее типичные осциллограммы приведены на рис. 3.

При больших значениях постоянного магнитного поля как и следовало ожидать сигналы на внутреннем и внешнем зондах совпадают и повторяют сигнал, снятый без плазмы. Начиная с некоторого значения постоянного поля при фиксированной амплитуде переменного поля $H_{\sim}$, первоначальная форма сигнала на внутреннем зонде, затухающая косинусоида, начинает искажаться, затягивается полупериод колебаний, падает амплитуда. При дальнейшем уменьшении поля H искажение сигнала и уменьшение его амплитуды увеличиваются.

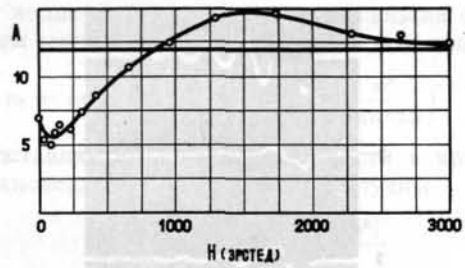

Рис. 4 Показания магнитного зонда в центре плазмы при $H_{\sim}=200$ э.

Максимум искажений и минимум амплитуды лежит в районе 200 эрстед постоянного поля. Искажаются лишь первые 2—3 полупериода сигнала. Последующие полупериоды, амплитуда которых невелика, не искажаются. Форма сигнала на внешнем зонде оставалась неизменной. Слегка менялась лишь его амплитуда в зависимости от напряженности постоянного магнитного поля. На рис. 4 приведены результаты обработки осциллограмм сигналов с внутреннего зонда, снятых для различных значений постоянного магнитного поля H. В этом опыте напряженность переменного магнитного поля в контуре без плазмы составляла 200 эрстед. Некоторое увеличение показаний на зонде в районе 1200 эрстед постоянного поля можно объяснить тем, что при таком значении поля на радиусе плазменного цилиндра укладывается четверть длины волны колебаний и отраженная волна усиливает сигнал на зонде. Сигнал минимален, когда постоянное поле порядка 150—200 эрстед и составляет менее 50% от сигнала на внешнем зонде. Это свидетельствует о том, что волна существенно поглотилась, пока шла от периферии к центру. При большей напряженности переменного поля относительное уменьшение амплитуды растет. Изучение осциллограмм сигналов на внутреннем зонде позволило определить граничное значение $H_{\sim}/H$, начиная с которого появляются искажения формы сигнала. Из всех осциллограмм, снятых при разных значениях $H_{\sim}$, с хорошей повторяемостью следовало, что $H_{\sim}/H$ близко к $^1/_2$. Это соответствует значению $H_{\sim}/H$, полученному теоретически (формула (4)) в предположении, что может существовать «пучковая» неустойчивость. Если бы искажение формы сигнала определялось в основном нелинейностью, то зависимость значения $H_{\sim}$ от граничного значения H, начиная с которого сказываются искажения формы из-за нелинейности, была бы иной, а именно $H_{\sim}\approx H^2$ (формула (5)), что противоречит эксперименту.

По временному сдвигу показаний внутреннего и внешнего зондов измерялась скорость волны при различных значениях напряженности постоянного магнитного поля. Эта зависимость для начала первой полуволны, снятая в опытах, где $H_{\sim}=400$ эрстед (в отсутствии плазмы), изображена на рис. 5. Для сравнения на этом рисунке нанесена прямая, изображающая зависимость скорости линейной волны от магнитного поля, вычисленная в предположении, что плотность плазмы равна $1{,}7\times10^{13}$ см$^{-3}$. Расхождение экспериментальной и теоретической кривой появляется при постоянных магнитных полях, меньших 800 эрстед. При этих же полях появляется искажение сигнала на внутреннем зонде. Скорость прихода искаженного сигнала оказывается выше скорости линейной волны. В этих же опытах были проделаны измерения скорости прихода сигналов на последних полупериодах колебаний магнитного поля, которые искажаются мало. Полученные значения скорости близки к расчетной альфвеновской скорости. Это свидетельствует о том, что изменение скорости сигнала в области малых напряженностей постоянного магнитного поля не связано с изменением плотности плазмы. Слабую зависимость скорости сигнала от напряженности постоянного магнитного поля можно было бы объяснить двояко: во-первых, причиной этому может быть нелинейность сигнала, во-вторых, увеличение скорости может быть связано с возникновением «пучковой» неустойчивости. При $H_{\sim}/H>1/2$ скорость электронов в волне не может сильно отличаться от тепловой скорости электронов, а это ограничивает значение тока, экранирующего переменное магнитное поле. Поэтому скорость сигнала может быть больше, чем в случае, когда при том же значении H нет «пучковой» неустойчивости. В пользу последнего объяснения говорит то, что расхождение расчетной и экспериментальной зависимости скорости сигнала начинается одновременно с искажением его формы.

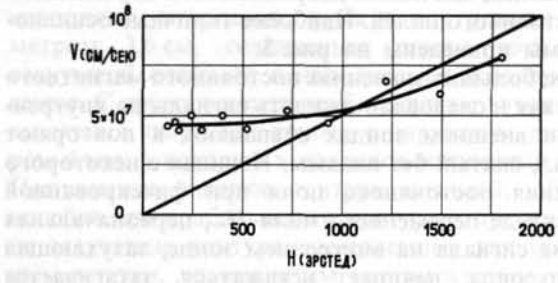

Рис. 5 Скорость распространения фронта сигнала в зависимости от постоянного магнитного поля. $H_{\sim}=400$ э. Прямая, проведенная из начала координат — скорость линейной волны в плазме с плотностью $1{,}7\times10^{13}$ см$^{-3}$.

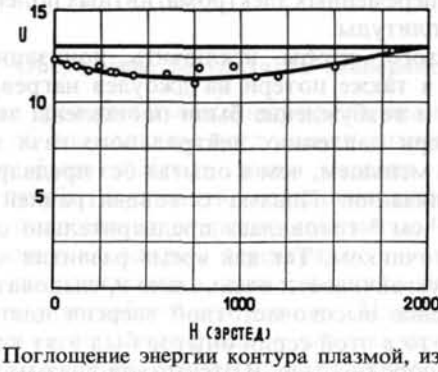

Рис. 6 Поглощение энергии контура плазмой, измеренное по напряжению на емкости контура на втором полупериоде колебаний. $H_{\sim}=600$ э.

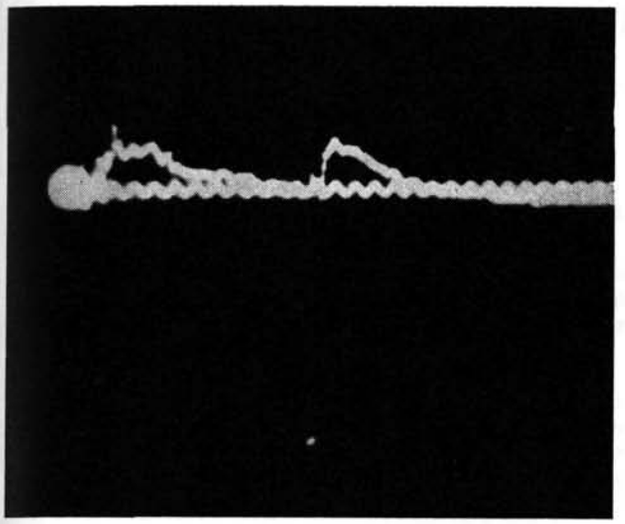

Рис. 7 Рост концентрации заряженных частиц после срабатывания высокочастотного контура. На второй луч подан сигнал калибровки $f = 0{,}5$ мггц. В начале осциллограммы видно запирание микроволнового сигнала плазмой прямого разряда. Затем концентрация плазмы постепенно падает и после срабатывания контура (в центре рисунка) вновь достигает $1{,}7 \times 10^{13}$ см$^{-3}$.

Помимо наблюдений с помощью магнитных зондов снимались осциллограммы напряжений на контуре при различных значениях напряженности постоянного магнитного поля. Сравнивая амплитуды напряжений на контуре с плазмой и без плазмы можно судить о величине поглощенной энергии переменного электромагнитного поля. На рис. 6 приведены значения амплитуды напряжения на контуре, измеренные по второму полупериоду колебаний в зависимости от постоянного магнитного поля. Напряженность переменного магнитного поля составляла 600 эрстед.

Непосредственным доказательством факта поглощения высокочастотной энергии является увеличение концентрации плазмы после срабатывания контура. После выключения устройства для приготовления плазмы концентрация ее в объеме медленно падала. В некоторый момент времени концентрация плазмы становилась меньше, чем $1{,}7 \times 10^{13}$ см$^{-3}$, что регистрировалось по прохождению восьмимиллиметрового сигнала. После включения высокочастотного контура наблюдается рост концентрации плазмы. Типичная осциллограмма зондирующего сигнала показана на рис. 7. Такие измерения были сделаны при различных значениях $H_\sim/H$. Когда H превосходило $H_\sim$ больше чем в два-три раза, роста концентрации не наблюдалось. За время работы высокочастотного контура ионизация не может произойти. Однако, «нагретые» в результате аномального поглощения энергии электроны могут ионизовать нейтральный газ уже после затухания контура. Граничное значение $H_\sim/H$, совпадающее с полученными из измерений магнитными зондами, убеждает нас, что аномальное поглощение высокочастотной энергии связано с возникновением в плазме «пучковой» неустойчивости.

4. Заключение

Приведенные результаты свидетельствуют о существовании аномального поглощения энергии переменных электромагнитных полей большой амплитуды и о том, что оно связано с возникновением в плазме «пучковой» неустойчивости. Таким способом можно получать сравнительно легко плазму с горячими электронами. Интересно продолжить эти эксперименты с целью выяснения возможности нагрева ионов. Для этого надо приготовить плазму с двумя сортами ионов. В переменном электромагнитном поле их скорости будут отличаться друг от друга. При большой относительной скорости такое двухскоростное движение неустойчиво. В результате часть энергии упорядоченного движения уйдет на нагрев ионов плазмы.

Таким образом, мы обнаружили, что в плазме есть эффективная бесстолкновительная диссипация энергии и имеются основания считать, что она вызвана мелкомасштабной «пучковой» неустойчивостью.

Мы хотим отметить, что подобный механизм, возможно, будет эффективным и для ионов, если плазма содержит ионы разных масс.

Литература

[1] Веденов А. А., Велихов Е. П., Сагдеев Р. З., *Ядерный Синтез* **1** (1961) 88.

ИССЛЕДОВАНИЕ ИОННЫХ ЦИКЛОТРОННЫХ ВОЛН*

Н. И. НАЗАРОВ, А. И. ЕРМАКОВ, А. С. ЛОБКО, В. А. БОНДАРЕВ, В. Т. ТОЛОК, К. Д. СИНЕЛЬНИКОВ

АКАДЕМИЯ НАУК УССР

ХАРЬКОВ, СОЮЗ СОВЕТСКИХ СОЦИАЛИСТИЧЕСКИХ РЕСПУБЛИК

В работе выяснялись условия резонансного возбуждения ионных циклотронных волн в плазме, созданной мощным высокочастотным разрядом, и исследовалось распространение этих волн вдоль магнитного поля. Проведены измерения поляризации волны, распределения высокочастотных полей волны по сечению разрядной колбы и исследовано затухание волны при наличии неоднородности магнитного поля.

Показано, что волна имеет круговую поляризацию и направление вращения вектора поля совпадает с направлением вращения иона в магнитном поле. Из исследования поведения волны в областях неоднородного магнитного поля установлено, что волна имеет значительное затухание только в непосредственной близости от циклотронного резонанса для исследуемого сорта ионов. Измеренная длина волны в плазме находится в хорошем соответствии с длиной волны внешней возбуждающей секции.

В работе изучался мощный в.ч. разряд в водороде и дейтерии, в области близкой к ионному циклотронному резонансу. Выяснены условия вынужденного резонансного возбуждения ионных циклотронных волн и распространения последних вдоль магнитного поля.

Проведено измерение поляризации волн, распределения в.ч. полей по сечению разряда в колбе и исследовано затухание волны на неоднородности магнитного поля.

Одним из возможных способов нагрева плазмы до высоких температур является передача ей энергии электромагнитного поля. Суть этого метода заключается в вынужденном возбуждении высокочастотным полем собственных колебаний плазменного столба в продольном магнитном поле с последующим необратимым переходом энергии этих колебаний к заряженным частицам плазмы. Получить большую амплитуду высокочастотных полей в плазме возможно не на всех собственных частотах плазменного столба. Так, например, если частота внешнего возбуждающего поля совпадает либо с ионной циклотронной, либо с электронной циклотронной частотой, то из-за сильного поглощения на этих частотах невозможно значительно раскачать плазму большой плотности. Поэтому наиболее интересными являются те резонансы, которые не связаны с сильным поглощением. Примером такого типа резонанса может служить альфвеновская волна, которая вблизи области аномальной дисперсии переходит в ионную циклотронную волну и испытывает сильное поглощение на гирочастоте ионов.

Примером реализации такого резонанса для нагрева плотной плазмы является система, в которой пространственно разделены область возбуждения колебаний и область, где эти колебания затухают.

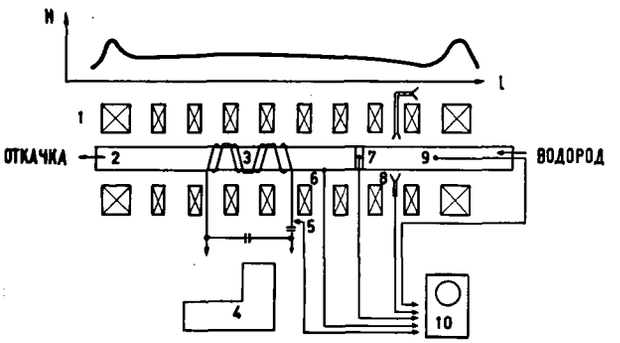

Рис. 1 Схема установки для изучения свойств циклотронных волн. 1 — катушки магнитного поля; 2 — разрядная труба; 3 — возбуждающая катушка; 4 — спектрограф, ИСП-51 с ФЭП; 5 — электрический в.ч. зонд; 6, 7, 9 — магнитные зонды; 8 — антенны с.в.ч.; 10 — осциллограф.

Первые эксперименты по наблюдению возбуждения и распространения ионных циклотронных волн были описаны в работах [1, 2].

В данной работе проводилось дальнейшее изучение вопроса возбуждения ионных циклотронных волн и их поглощения.

Изучение свойств ионных циклотронных волн проводилось на установке, схема которой представлена на рис. 1. Источником плазмы служил мощный высокочастотный разряд в водороде. Разряд создавался в трубе из молибденового стекла длиной 2 м и диаметром 60 мм. Разрядная труба помещалась на оси соленоида, создающего квазипостоянное магнитное поле пробочной конфигурации ($k=1{,}5$) с различной геометрией «магнитного берега». Тем самым создаются две области магнитного поля, в одной из которых происходит резонансное генерирование ионных циклотронных волн (однородный участок магнитного поля), в другой создаются условия для затухания

* Доклад CN-10/231, представленный на конференцию. Докладчик: В. Т. Толок. Дискуссия (на английском языке) по этому докладу дана на стр. 1110. Переводы аннотаций находятся в конце тома.

волн и передачи их энергии ионной компоненте плазмы («магнитный берег»).

Соленоид для создания магнитного поля составлялся из отдельных десятивитковых катушек с внутренним диаметром 150 мм, намотанных медной трубкой 10×8 мм. Для увеличения механической прочности катушки запекались в эпоксидной смоле с кварцевым наполнителем. Общая длина соленоида равнялась 1,5 м. Катушки соленоида охлаждались проточной водой. Конфигурация поля определялась с точностью до 1% зондовыми измерениями при питании соленоида переменным током промышленной частоты. Абсолютное значение магнитного поля определялось с помощью электронного циклотронного резонанса на частоте 10000 мггц. Магнитное поле создавалось разрядом батареи конденсаторов общей емкостью $2{,}25 \times 10^{-2}$ фарады, которая могла заряжаться до 5 кв. За время 5 мсек магнитное поле достигало своего максимального значения 20—25 кгс и затем спадало по экспоненте.

Возбуждающим элементом служила надетая на разрядную трубку катушка, создающая электромагнитное поле с пространственной периодичностью $\lambda = 16$ см. Необходимость пространственной периодичности электромагнитного поля обусловлена тем, что для резонансного возбуждения ионной циклотронной волны необходимо соблюдение равенства частоты и длины этой волны с частотой и длиной волны внешнего возбуждающего поля.

Резонансный контур, образованный возбуждающей катушкой и вакуумными конденсаторами, обладал добротностью $Q = 400$. Контур запитывался от генератора, отдающего в нагрузку до 80 квт высокочастотной мощности на частоте от 3 до 30 мггц. В проведенной работе частота генератора равнялась 10 мггц. Длительность высокочастотного импульса могла изменяться от нескольких сотен мксек до десятков мсек. Максимальное высокочастотное напряжение на контуре достигало 30 кв.

Вакуумная система имела ряд ловушек, надежно защищающих разрядную трубу от попадания в нее паров масла. Предельное разрежение в трубе достигало 1×10^{-6} мм рт ст. Работа проводилась на проточном водороде, напуск которого осуществлялся через палладиевый натекатель. Рабочее давление газа составляло 10^{-2}—10^{-4} мм рт ст.

Контроль за поглощением высокочастотной мощности и за распространением ионных циклотронных волн производился: (1) по измерению в.ч. напряжения на контуре; (2) по сигналам с высокочастотных магнитных зондов; (3) по изменению интенсивности спектральных линий водорода во времени; (4) зондированием плазмы *СВЧ* сигналом.

Все измерения проводились после длительной тренировки системы в.ч. разрядом.

Система запуска генератора позволяла производить включение в.ч. импульса при различных значениях магнитного поля.

При исследовании зависимости передачи в.ч. мощности в плазму от величины магнитного поля, наблюдается поглощение энергии электромагнитного поля как на гирочастоте ионов, так и при магнитных полях большого циклотронного значения (H_{ci}). При этом следует отметить, что наибольшая в.ч. мощность поступает в плазму при полях больших H_{ci}, и характер поглощения имеет резонансный вид рис. 2.

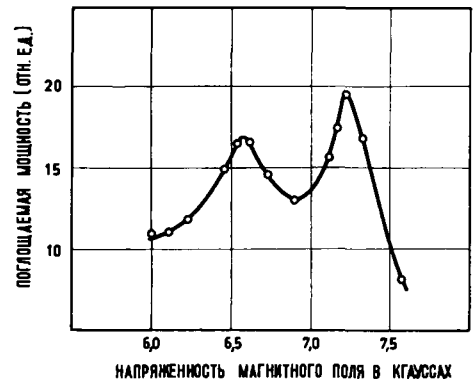

Рис. 2 Кривая характера поглощения.

На следующих осциллограммах (рис. 3) показано изменение положения этого резонансного пика поглощения при различных уровнях в.ч. мощности, подводимой к плазме. Осциллограммы относятся к спадающей части магнитного поля во времени. При небольших уровнях мощности, подводимой к плазме, имеется поглощение только при $H \approx H_{ci}$. С увеличением мощности появляется также резонансная нагрузка при полях больших H_{ci}. Смещение этой резонансной нагрузки в сторону больших магнитных полей происходит, очевидно, до тех пор, пока плотность в момент резонанса перестает зависеть от подводимой мощности, т.е. наступает глубокая ионизация. Как уже отмечалось [2], в этот момент интенсивность спектральных линий водорода практически равна нулю. Проведенная оценка плотности по запиранию 4 мм СВЧ сигнала дает значение плотности не менее 6×10^{13} см$^{-3}$ на расстоянии 30 см от края возбуждающей секции.

Как уже отмечалось ранее [3, 4], наличие поглощения при полях больших H_{ci} обусловлено генерированием и поглощением ионных циклотронных волн.

Изучение ионных циклотронных волн проводилось магнитными зондами, которые могли измерять все компоненты в.ч. магнитного поля волны. Зонд представлял собой виток диаметром 3 мм. Все подводящие провода помещались в двойной экран для устранения наводок.

На рис. 4 приведена осциллограмма сигнала от магнитного зонда ($\tilde{H}_z$), расположенного в центре разрядной трубы на расстоянии 25 см от края возбуждающей секции. Верхняя кривая — сигнал с зонда, нижняя — напряжение на контуре.

Как видно из этих осциллограмм, действительно, в момент резонансной нагрузки, соответствующей

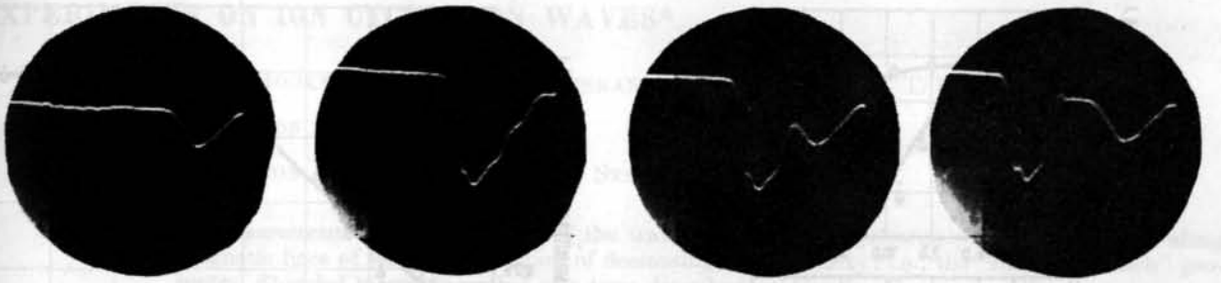

Рис. 3 Изменение резонансного пика поглощения.

генерированию волн, имеется распространение волны вдоль постоянного магнитного поля.

Распределение по радиусу магнитных полей этой волны приведено на рис. 5. Хотя исследования проводились для нелинейного случая, распределение электромагнитных полей качественно совпадает с распределением для ионных циклотронных волн.

Из сравнения амплитуд и фаз сигналов с двух зондов, расположенных в плоскости, перпендикулярной оси разрядной трубы, под углом 90°, с помощью кольцевого фазового детектора было показано, что исследуемая волна имеет круговую поляризацию. Направление вращения вектора поля совпадает с направлением вращения свободного иона в магнитном поле.

Рис. 4 Осциллограмма сигнала от магнитного зонда.

На рис. 6 приведены результаты измерения фазовой скорости волны, распространяющейся в области, где магнитное поле уменьшается в направлении распространения. Изменение амплитуды фазового детектора от положительной до отрицательной означает изменение фазы на 180°. Измеренная таким образом начальная длина волны $\lambda = 15$ см хорошо совпадает с длиной волны внешней возбуждающей секции. Фазовая скорость из этих измерений изменяется от $1{,}5 \times 10^8$ см/сек до 6×10^7 см/сек. Затухание циклотронных волн является необходимым условием для данного способа нагрева плазмы. Учет столкновений электрон-ион (считая, что влияние другого рода столкновений незначительно) приводит к обычному столкновительному затуханию волны. Учет же теплового движения приводит к циклотронному затуханию. Циклотронное затухание экспоненциально нарастает в области гирочастоты ионов.

В данном эксперименте исследовалось затухание волны, распространяющейся в область магнитных полей, равных циклотронному. На рис. 7 показано изменение амплитуды волны (верхний график) при

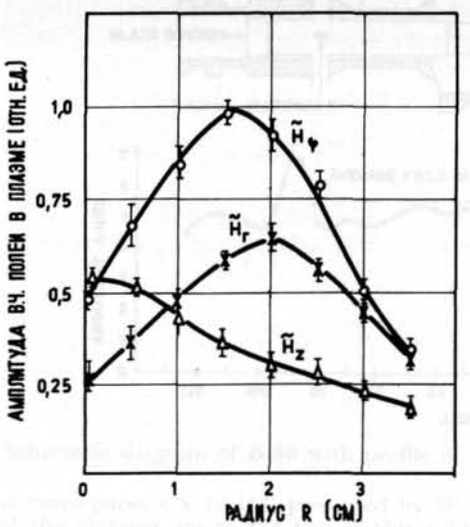

Рис. 5 Кривые распределения по радиусу магнитных полей.

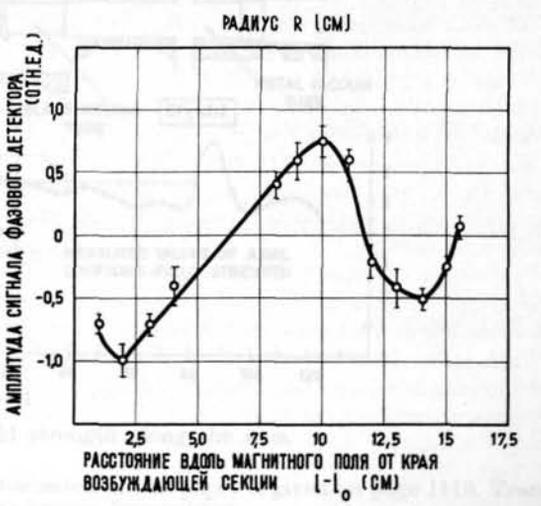

Рис. 6 Результаты изменения фазовой скорости волны.

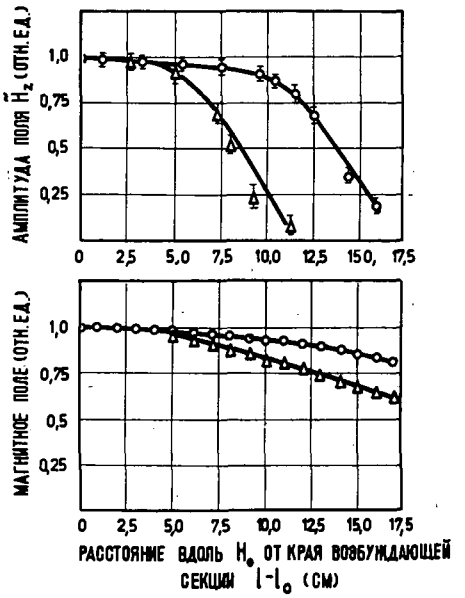

Рис. 7 Изменение амплитуды (верхний график) при распространении ее вдоль уменьшающегося по величине магнитного поля для двух разных конфигураций (нижний график).

распространении ее вдоль уменьшающегося по величине магнитного поля для двух разных конфигураций его (нижний график). Как видно из этих графиков, волна затухает на определенном расстоянии для различной геометрии магнитного поля. При этом основное затухание волны происходит на длине, которую нельзя объяснить учетом затухания только за счет столкновений. На рис. 8 показано изменение амплитуды волны в зависимости от магнитного поля, где видно, что основное затухание происходит в области магнитного поля, равного циклотронному для ионов водорода.

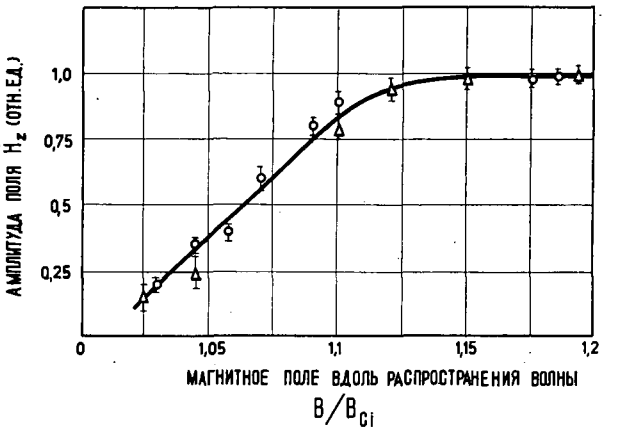

Рис. 8 Изменение амплитуды волны в зависимости от магнитного поля.

Таким образом, говоря о затухании циклотронной волны, можно прийти к следующему выводу: при больших фазовых скоростях основной вклад в затухание вносят столкновительные механизмы. Но это затухание незначительно, длина затухания, обусловленная этим механизмом, равна 60 см. В области $H \approx H_{Ci}$, наряду со столкновительным механизмом начинает действовать циклотронный механизм затухания, причем более эффективно, и длина затухания резко сокращается до 3 см.

Литература

[1] Stix, T. H., Palladino, R. W., Report on Project Matterhorn No. 32 (29 Feb. 1960).
[2] Назаров Н. И. и др, *Ж. техн. Физ.* **31** (1961) 254.
[3] Stix, T. H., Palladino, R. W., in Proc. 2nd U.N. Inter. Conf. PUAE **31**, United Nations, Geneva (1958) 360.
[4] Синельников К. Д. и др, *Ж. техн. Физ.* **30** (1960) 283.

EXPERIMENTS ON ION CYCLOTRON WAVES*

W. M. HOOKE, P. AVIVI**, M. BRENNAN***, M. A. ROTHMAN, T. H. STIX

PRINCETON UNIVERSITY

PRINCETON, NEW JERSEY, UNITED STATES OF AMERICA

Measurements have been made of the wavelengths of ion cyclotron waves propagating along magnetic lines of force into a region of decreasing field intensity; i.e., the "magnetic beach" geometry. Shielded magnetic probes of a type described previously [1] were used for these measurements. Simultaneous measurement of the wavelength, frequency of oscillation, electron density and magnetic field have allowed a comparison of experimental results with the theoretical dispersion relations [2]. The free electron density ranged from around 3×10^{12} cm^{-3} to 3.5×10^{13} cm^{-3} and the magnetic field from 22 to 27 kG. The measured wavelengths varied from around 15 cm to 60 cm. These results appear to be consistent with the theoretical dispersion relations. In addition, the magnetic probes have been used to measure the power carried by the ion cyclotron waves along the lines of force, yielding a flux of 100 kW.

1. Introduction

A number of experiments on hydromagnetic waves at frequencies near the ion cyclotron frequency have been reported previously [1, 3—8]. In the present experiment, the predictions of the dispersion relation for these waves have been compared with experiment by the simultaneous measurement of frequency and wavelength, together with the magnetic field and plasma density.

This work has been done on the B-66 machine, which has been operating in a linear mirror geometry, as described previously [8]. An induction coil [9] at the center of the mirror generates waves in the plasma at a frequency of 16 MHz. These waves propagate toward a region of decreasing magnetic field (the magnetic beach). Figure 1 shows a schematic diagram of the apparatus and a profile of the axial magnetic field strength.

In the previous experiments with this apparatus [8] production of ion cyclotron waves and the damping of these waves on the magnetic beach were inferred from the detection of neutrons generated in the beach region and from the amplitude of signals induced in a magnetic probe. The qualitative results were consistent with theory [2, 9] but there were certain quantitative discrepancies.

In the present experiment, these discrepancies have been reduced by direct measurement of the wavelength.

A dispersion relation for waves in a cylindrical plasma is given by Eq. (10) of Ref. [2]. This gives the relationship between the longitudinal wave number k and the radial wave number h for waves of a given

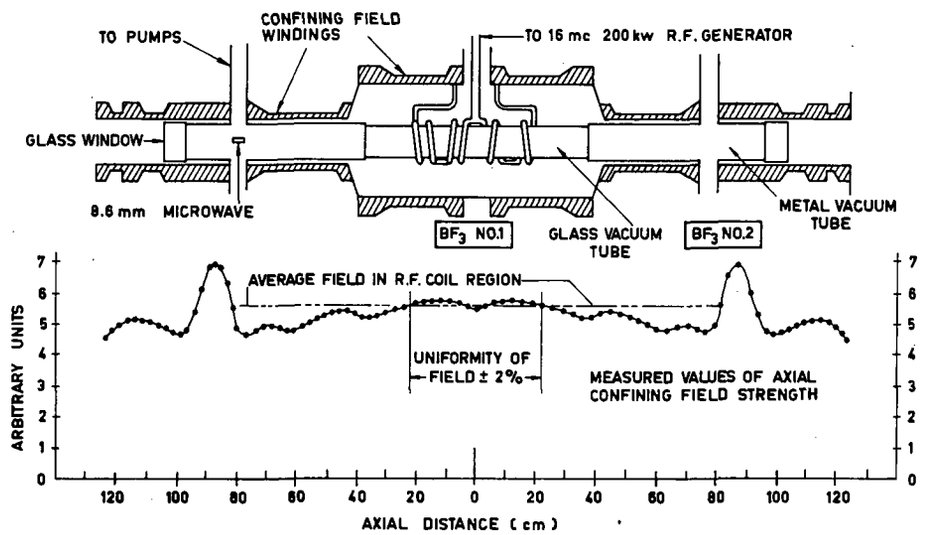

Fig. 1 Schematic diagram of B-66 with profile of magnetic field strength along the axis.

* Conference paper CN-10/165, presented by W. M. Hooke. Discussion of this paper is given on page 1110. Translations of the abstract are at the end of this volume of the Conference Proceedings.

** On leave from the Hebrew University of Jerusalem, Israel. *** Now at the University of Sydney, Australia.

frequency ω in a plasma of uniform density n_e in a longitudinal magnetic field B_0 as follows

$$h^2 = \frac{(\omega/c)^4(\alpha^2 - \Omega^2) - 2k^2(\omega/c)^2(\alpha - \Omega^2) + k^4(1-\Omega^2)}{(\omega/c)^2(\alpha - \Omega^2) - k^2(1-\Omega^2)} \tag{1}$$

$$\alpha = \frac{4\pi n_e m_i c^2}{B_0^2} + 1 = \left(\frac{\omega_{pi}}{\omega}\right)^2 \Omega^2 + 1$$

(α is plasma dielectric constant; $\omega_{pi} = (4\pi e^2 n_i/m_i)^{1/2}$ is the plasma ion frequency; $\Omega = \omega/\omega_{ci}$; $\omega_{ci} = eB_0/m_i c$ is ion cyclotron frequency).

In the present work the frequency is fixed by the oscillator at 16 MHz so that $\omega = 1.005 \times 10^8$ Hz. The relative frequency Ω is a function of B_0, which in turn is a function of z, the distance along the axis.

Upon making approximations based on $(\omega_{pi}/\omega)^2 \gg 1$ and $(\omega_{pi}/\omega)^2 \Omega^2 = (\omega_{pi}/\omega_{ci})^2 \gg 1$, Eq. (1) becomes

$$h^2 = \frac{(\omega_{pi}/c)^4 \Omega^4 - 2(\omega_{pi}/c)^2 \Omega^2 k^2 + (1-\Omega^2)k^4}{(\omega_{pi}/c)^2 \Omega^2 - (1-\Omega^2)k^2} \tag{2}$$

These approximations are equivalent to saying that the frequency is low enough to neglect the displacement-current term in Maxwell's equations, while the plasma density is high enough to make $\alpha \gg 1$.

For the conditions of the present experiment, using deuterium, $(\omega_{pi}/\omega)^2 = 87 \times 10^{-12} n_e$, while Ω is of order unity. Therefore, for $n_e > 10^{12}$ cm^{-3}, which is the case for our experimental plasma, the approximations are valid.

The possible values of the radial wave number h are fixed by the boundary conditions on the plasma, and Ω is fixed by the frequency and magnetic field. The wave number k is thus determined by these parameters, and Eq. (2) may be solved for k, giving

$$k^2 = \left(\frac{\omega_{pi}}{c}\right)^2 \left(\frac{\Omega^2}{1-\Omega^2}\right) - \frac{h^2}{2} \pm \left[\left(\frac{\omega_{pi}}{c}\right)^4 \left(\frac{\Omega^3}{1-\Omega^2}\right)^2 + \left(\frac{h^2}{2}\right)^2\right]^{1/2} \tag{3}$$

The plus sign in Eq. (3) gives the dispersion relation for the ion cyclotron waves discussed in Refs. [2, 8, 9]. In the low-frequency limit these are identical with the Alfvén waves, which follow the dispersion relation $\omega^2 = k^2 c^2/\alpha$. For these ion cyclotron waves, $\Omega < 1$.

The minus sign in Eq. (3) gives the dispersion relation for a second mode, which in the low-frequency limit becomes the Alfvén wave with dispersion relation $\omega^2 = (k^2 + h^2) c^2/\alpha$.

Waves which apparently correspond to the second mode have been identified in the B-66 machine at low values of B_0 ($\Omega > 1$), but have not yet been studied in detail.

The present report is concerned with the ion cyclotron waves observed at values of Ω between 0.8 and 1.0.

Especially simple forms of Eq. (3) are obtained by allowing h to take the limiting values of 0 and ∞. These are

$$k^2 = \frac{an_e}{A}\left(\frac{\Omega^2}{1-\Omega}\right) \qquad h = 0 \tag{4}$$

$$k^2 = \frac{an_e}{A}\left(\frac{\Omega^2}{1-\Omega^2}\right) \qquad h = \infty \tag{5}$$

($a = 4\pi e^2/m_p c^2 = 19.4 \times 10^{-16}$ cm, m_p is the proton mass, and $A = m_i/m_p$ is the mass number of the ion).

The values of k obtained from these two relations differ at most by a factor of $2^{1/2}$. It can be shown that the value of k obtained by using any real value of h in Eq. (3) (with the plus sign) must fall between the two values of k obtained from Eqs. (4) and (5). Therefore these simplified expressions are useful in obtaining upper and lower limits for k in this mode.

In Ref. [8] the supposition was made that the wavelength was fixed by the geometry of the induction coil so that the dispersion relation determined the ion density which would allow propagation of the waves for a given Ω. However, the observed densities were in quantitative disagreement with the predicted values.

The picture that fits the evidence of the present experiment is that the induction coil generates a broad spectrum of wavelengths at the applied frequency, the amplitudes of which are determined by the Fourier spectrum of the induction coil in space, together with the efficiency of coupling from the coil into the plasma of each Fourier component. The electron density and magnetic field determine the particular wavelength that is allowed to couple into the plasma and propagate down the column. The detailed theory of the amplitude is not yet known.

The present experiment is devoted chiefly to measurement of the wavelength as a function of n_e and Ω, allowing comparison with Eq. (3). This is done by measuring the phase shift in the 16-MHz signal induced in the magnetic probe as the probe is moved along the axis away from the induction coil.

If the axial magnetic field were uniform, the wavelength could be obtained from a single phase-shift measurement. In this case the relation $\lambda = 2\pi L/\varphi$ would give the wavelength λ, where L is the distance between the two positions of the probe, and φ is the phase shift (in radians) in the signal detected at the two positions. Since B_0 varies over a region shorter than a wavelength, the following procedure was adopted:

In Ref. [8] it is shown, by a WKB method, that when the waves are propagating in a region where B_0 is a slowly varying function of z, the field quantities E and B can be expressed as

$$B = B(z)\, e^{i\int k(z)\,dz} \tag{6}$$

so that the phase difference measured between two points along the axis, z_1 and z_2, is given by

$$\varphi_2 - \varphi_1 = \int_{z_1}^{z_2} k(z)\,dz \tag{7}$$

Since Ω is known as a function of z, k as a function of z is easily obtained. A simple numerical integration then produces theoretical curves of phase angle versus distance along the axis.

The chief features of these curves are as follows: (1) The slope of each curve is proportional to $n_e^{1/2}$;

(2) where B_0 is constant, the slope is constant, and as B_0 decreases, the slope increases, corresponding to a decrease in wavelength.

2. Experimental procedure

The deuterium plasma was generated by passing current at a frequency of 16 MHz through the induction coil, as described in Ref. [8]. In the present experiment, the r.f. oscillator was programmed to give maximum power for 400 μs, after which time the power was reduced to 1-2% of maximum for about 4 ms. In this way the ion cyclotron waves were first used to create the plasma, and afterwards their properties were measured at a lower amplitude level in a relatively undisturbed plasma.

The plasma density reached a maximum of from 2 to 8×10^{13} cm^{-3} during the initial heating pulse, after which it decayed exponentially with a time constant of several hundred microseconds, the exact time depending on conditions of temperature, density, field, and neutral gas pressure. Although this point was not studied, the decay time must be determined by both recombination and diffusion out of the ends.

This relatively slow decay was used to advantage by performing the phase measurement at any desired time during the decay. Thus the plasma density could be chosen by simply adjusting the trigger time of one oscilloscope.

During the decay period, the D_β light resulting from recombination exhibits the characteristic rise and fall of an afterglow as the plasma cools to a low temperature. When the 16-MHz signal is applied at low power during this period, the recombination light is suppressed, indicating that the few kilowatts of r.f. power being applied is sufficient to slow down the temperature drop, reducing the recombination rate. However, the plasma density is not affected noticeably.

The phase measurements were made with a magnetic probe previously described [1], inserted into the end of the machine so that it could be rotated around an axis parallel to the machine axis, and also moved in the axial direction. For these measurements the probe was oriented so that it picked up the radial component of the alternating magnetic field at a location close to the outer radius of the plasma cylinder (4 cm from the center).

Fig. 2b shows the probe signal at a sweep speed of 200 μs/cm. The amplitude varies with a characteristic pattern whose shape depends on the machine conditions. The cause of this amplitude modulation is not clear at the present time.

Using a dual-trace oscilloscope with a sweep speed of 0.02 μs/cm, the 16-MHz probe signal was displayed, together with a reference signal taken directly from the induction coil through a voltage divider (Fig. 2c). The pulse which triggered this scope was also shown as a marker pip on the microwave interferometer display (Fig. 2a). In this way it was possible to determine the plasma density existing during the 0.1-μs duration of the phase measurement.

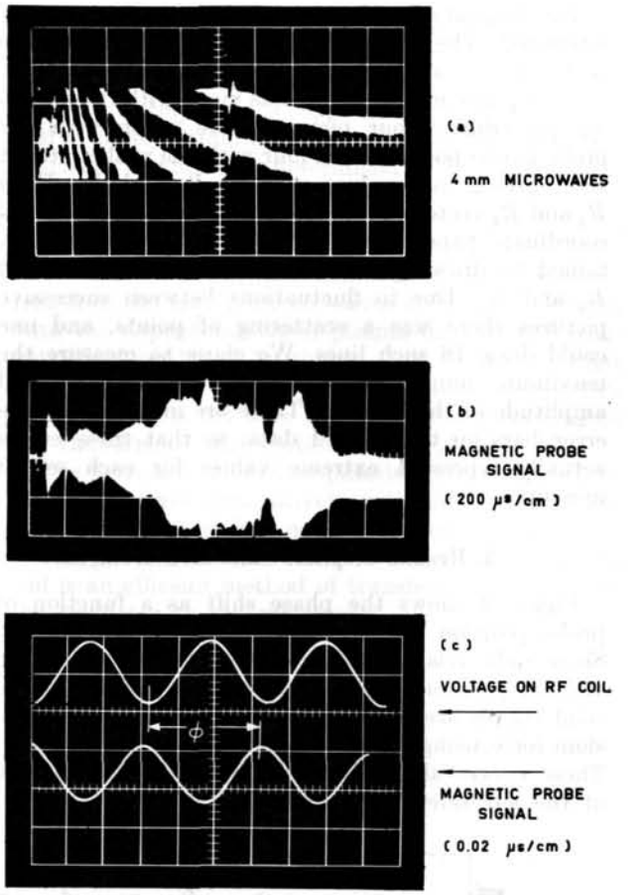

Fig. 2 Diagnostic signals: (a) Microwave-interferometer pattern at sweep speed of 200 μs/cm; (b) amplitude of magnetic-probe signal vs time, 200 μs/cm; (c) fast oscilloscope pictures of 16-MHz signal: upper trace, voltage on r.f. coil; lower trace, magnetic-probe signal (phase shift is almost 360°).

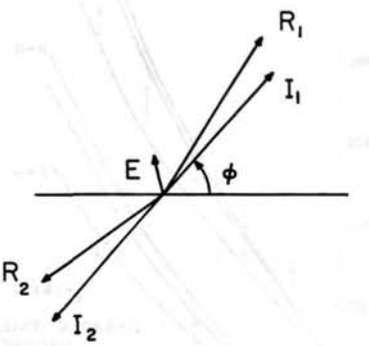

Fig. 3 Resolution of magnetic-probe signal into I and E vectors.

The phase angle φ was measured directly on the photograph as shown in Fig. 2c.

It was found that the probe signal consisted of two components: one component that changed phase by 180° when the probe was rotated through 180° (the I signal), and a component (usually small) that did not change (the E signal). The resultant signal (R) is the vector sum of these (Fig. 3).

The I signal arises from the B_r field in which we are interested. The E signal is caused by pickup in the scope, probe, and associated circuits.

Each phase measurement was made with the following procedure: Four pictures were taken with the probe in one position, and four with the probe rotated 180°, giving four values each of R_1 and R_2. Each R_1 and R_2 vector was represented by a point on polar-coordinate paper, and the desired I vector was obtained by drawing a line between the extremities of R_1 and R_2. Due to fluctuations between successive pictures there was a scattering of points, and one could draw 16 such lines. We chose to measure the maximum, minimum, and average of the phase and amplitude of the I signal. These are indicated by the error bars on the plotted data, so that these errors actually represent extreme values for each set of measurements.

3. Results of phase-shift measurements

Figure 4 shows the phase shift as a function of probe position for three values of plasma density. Since only relative phase shifts are measured, the vertical positions of these curves are arbitrary. The solid curves are plotted from the theoretical expressions for k, using $h=0$, 0.67 cm^{-1}, and ∞, respectively. These curves are arbitrarily normalized to intersect at the left side of the drawing.

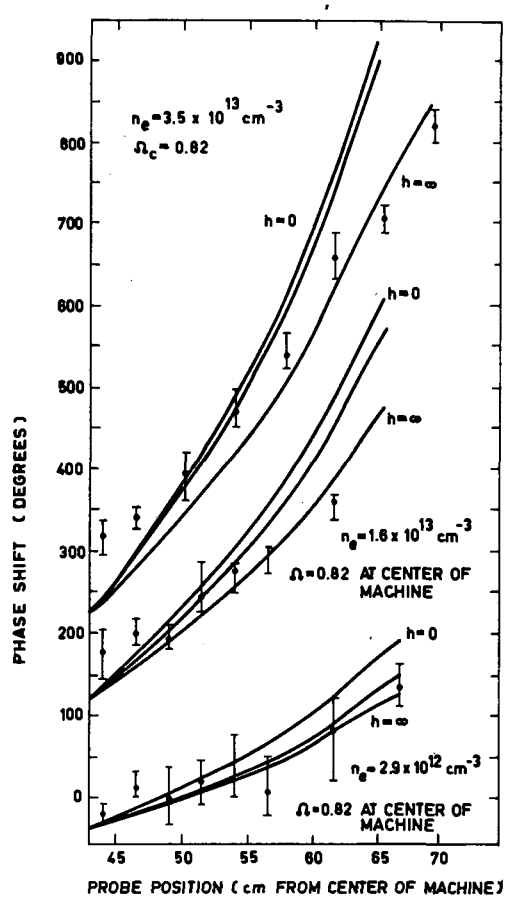

Fig. 4 Phase shift vs axial distance for three values of n_e.

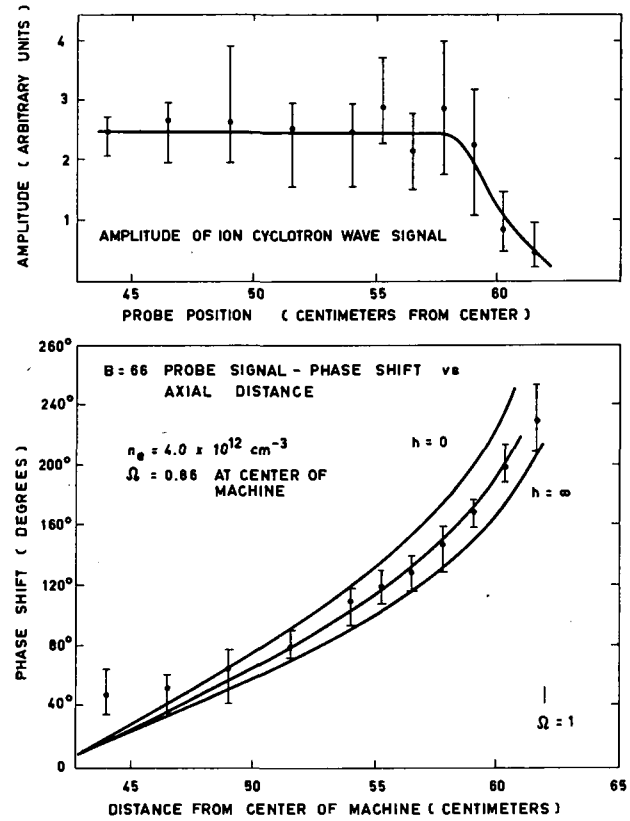

Fig. 5 Amplitude and phase shift vs axial distance in the magnetic beach.

The intermediate value of h is obtained from the boundary condition between a plasma of uniform density (radius = 4.7 cm) and the vacuum. It is seen that k is highly insensitive to the boundary conditions.

These data were taken with a high value of magnetic field (nominally 25.4 kG), so that Ω had a value of 0.82 in the center of the machine, and was always less than unity in the region covered.

It is seen that the experimental curves exhibit the characteristic of increasing slope with density although there is some numerical discrepancy at the higher density.

Figure 5 shows similar data with the magnetic field set at a value such that $\Omega=1$ occurred at about 64 cm from the center of the machine. The density was chosen to be fairly low. The agreement with theory here is good, and the curvature showing the decrease of wavelength in the magnetic beach is quite apparent.

The amplitude plot also shows a sudden decrease as Ω approaches unity. As indicated previously, the large error bars represent the extremes of the fluctuations from one shot to the next. Beyond 62 cm, where Ω is very close to unity, the phase shifts become completely random because a small variation in magnetic field from one shot to the next produces a large phase shift.

In the derivation of the dispersion relation and in the interpretation of the data we have assumed that the plasma density is uniform both radially and along the lines of force. The assumption of no density gradi-

ent in the radial direction is made in obtaining the electron density from the microwave measurements. In calculating the theoretical curves of phase shift versus axial distance the plasma density throughout the region of wave propagation was assumed to be that measured at the center of the machine.

However, density measurements taken near the end of the machine (79.5 cm from the machine center) showed the density to be between 15 and 60% higher than at the center. If the density in the region of phase measurements were uniformly 60% higher than that measured at the center, the experimental phase-shift curve would have a slope about 26% greater than the theoretical curve at every point since the phase shift scales as $n_e^{1/2}$.

If the density had a gradient along the axis, then there would be at most a 26% increase in the slope of the experimental curve along the region being measured. This is small compared with the increase of slope expected as a result of the changing magnetic field in the beach region.

4. Power measurements

The power carried by the wave in the z direction is expressed by the Poynting vector, which in cylindrical geometry is

$$P_z = \frac{\omega}{4\pi k}(B_\theta^2 + B_r^2) \tag{8}$$

With the above procedure, each of these quantities is measurable simultaneously. If the area of the magnetic probe is known, B_θ and B_r are simply related to the induced probe voltage. The phase shift measurement gives k.

Simultaneous amplitude and phase-shift measurements were made during the application of full r.f. power.

The average amplitude of the emf induced in a single-turn coil of 1.7-cm^2 area at a distance of 44 cm from the center of the machine was 12 V for the B_θ signal and 12.5 V for the B_r signal. Thus B_θ was calculated to have an amplitude of 14 G, and B_r 15 G. By a phase-shift measurement of the type described above, k was found to be ~ 0.09 cm^{-1}.

From theoretical consideration B_r is expected to be proportional to the radius, in agreement with previous measurements made on the B-65 machine. Assuming this variation, the power flux was integrated over the 73-cm^2 area of the plasma and then doubled to take into account the power going to the two ends of the machine. In this way the total power flux was estimated to be ~ 100 kW.

The r.f. amplifier is capable of supplying over 1 MW under optimum conditions. However, the actual efficiency has not been determined at the present time.

5. Conclusions

The phase-shift measurements show that the wavelength of the ion cyclotron waves is in fair agreement with the dependence upon plasma density and magnetic field predicted by theory. Due to the fact that k is so insensitive to the value of h in the theory, this measurement is not able to give results pertaining to the radial-mode distribution in the plasma.

The decreases in both amplitude and wavelength at the beach agree qualitatively with the theory of ion cyclotron damping in a magnetic-beach geometry.

The power measurement shows that the induction coil is an efficient method of transferring power from the oscillator to the plasma.

Acknowledgements

We wish to thank W. A. Knock and L. H. Rogers for their assistance in these experiments.

This work was performed under the auspices of the U.S. Atomic Energy Commission.

References

[1] Stix, T. H., Palladino, R. W., *Phys. Fluids* **3** (1960) 641.
[2] Stix, T. H., *Phys. Rev.* **106** (1957) 1146.
[3] Stix, T. H., Palladino, R. W., in Proc. 2nd U.N. Intern. Conf. PUAE **31**, United Nations, Geneva (1958) 282.
[4] Stix, T. H., Palladino, R. W., *Phys. Fluids* **1** (1958) 446.
[5] Sinelnikov, K. D., et al, in Proc. 4th Intern. Conf. Ionization Phenomena in Gases (Uppsala, 17-21 Aug. 1959) **2**, North Holland Publishing Co., Amsterdam (1960) 1176.
[6] Stix, T. H., Proc. 1959 Intern. Plasma Physics Institute (University of Washington) *J. nucl. Energy, Part C* **2** (1961) 84.
[7] Chambers, E. S., *Bull. Am. Phys. Soc.* **II. 6** (1961) 195.
[8] Hooke, W. M., Tenney, F. H., Brennan, M. H., Hill, H. M., Jr., Stix, T. H., "Experiments on ion cyclotron waves", *Phys. Fluids* **4** (1961) 1131.
[9] Stix, T. H., *Phys. Fluids* **1** (1958) 308.

RADIOFREQUENCY EMISSION FROM PLASMAS NOT IN THERMODYNAMIC EQUILIBRIUM*

S. C. BROWN, G. BEKEFI
MASSACHUSETTS INSTITUTE OF TECHNOLOGY
CAMBRIDGE, MASSACHUSETTS, UNITED STATES OF AMERICA

Calculations of the propagation constant of a plane electromagnetic wave in a tenuous un bounded plasma show that under suitable conditions the wave grows exponentially in amplitude. For this to happen (a) the population of electrons should increase with increasing energy and (b) the emission cross-section for the process in question must decrease sufficiently rapidly with increasing energy. Detailed calculations of the rate of amplification and the range of frequencies in which it occurs are given for bremsstrahlung and cyclotron emission. Amplification of bremsstrahlung occurs in plasmas of low ionization and for low electron energies. Amplification of cyclotron emission is particularly favorable in highly ionized, high-energy plasmas. Here even small departures of the electron distribution of energies from a Maxwellian distribution lead to a very significant increase of cyclotron emission. Experiments, designed to measure the amplification of cyclotron emission, are described.

1. Introduction

In the study of the emission of the electromagnetic radiation from a plasma, much use is made of the concept of a "local thermodynamic equilibrium". A plasma is said to be in local thermodynamic equilibrium when it is possible to assign to every volume element of plasma a temperature T, and when, in the frequency interval between ω and $\omega+\mathrm{d}\omega$, the emission coefficient j_ω and absorption coefficient α_ω are related through Kirchhoff's law

$$j_\omega/\alpha_\omega = B(\omega, T) \tag{1}$$

$B(\omega, T)$ is the Planck formula for black-body emission. At radio and microwave frequencies that concern us here, $B(\omega, T)$ reduces to the Rayleigh-Jeans equation, which for one polarization (or one mode of propagation) has the form,

$$B(\omega, T) = \mathrm{k}T\,\omega^2/8\pi^3 c^2 \tag{2}$$

Here k is Boltzmann's constant, c is the velocity of light in free space and T is the local temperature of the radiators. For emission at radio and microwave frequencies, the radiators are almost entirely the free electrons of the plasma.

The concept of local thermodynamic equilibrium is useful because it enables us to predict the gross features of the emission spectrum in terms of the single macroscopic parameter T and because these predictions can be made even when a multiplicity of mechanisms participate in the emission and absorption processes that are either uncorrelated, not well understood or too complex to be treated in detail. At radio and microwave frequencies the emission and absorption by free electrons is fairly well understood and the concept of thermodynamic equilibrium can often be relaxed in computing the spectrum and the radiation intensity of a plasma.

The existence of a local thermodynamic equilibrium implies the existence of a temperature, and hence it implies that the radiators (electrons) have a Maxwellian distribution of velocities. In many plasmas a Maxwellian distribution is not likely to occur. Plasmas produced in the laboratory are maintained by strong d.c. or a.c. electric fields and the very existence of these externally applied fields precludes the possibility of a strict Maxwellian distribution of velocities of the emitting electrons. The question is: to what extent will a non-Maxwellian plasma allow us to retain the concept of local thermodynamic equilibrium as a reliable means of calculating its emission spectrum? One may be tempted to argue that a relatively small departure from a Maxwellian distribution results in a small departure from thermodynamic equilibrium and hence that the emission from the plasma does not change appreciably. Calculations and measurements will show that at certain frequencies and for certain emission processes these expectations are not fulfilled.

2. Transport of radiant energy

Consider a plasma immersed in a uniform, constant magnetic field. The radiant energy is transported through the anisotropic plasma by two characteristic modes of propagation, which we designate as the ordinary (o) and the extraordinary (x) modes. Let **r** be the direction of energy flow in a given mode, somewhere within the ionized medium. We add up the energy gain and energy loss in the direction **r** of a pencil of radiation, as this traverses a volume element of plasma, and obtain for the intensity I_ω along **r** in each of the two characteristic modes:

$$\mathrm{d}I_\omega^{(\mathrm{o,x})}/\mathrm{d}r = j_\omega^{(\mathrm{o,x})} - \alpha_\omega^{(\mathrm{o,x})} I_\omega^{(\mathrm{o,x})} \tag{3}$$

Solving Eq. (3) for the intensity of radiation that reaches an observer stationed at some point within or

* Conference paper CN-10/171, presented by S. C. Brown. Discussion of this paper is given on page 1111. Translations of the abstract are at the end of this volume of the Conference Proceedings.

outside the plasma, we obtain for each mode

$$I_\omega(\tau_0) = I_0 \exp -\tau_0 + \int_0^{\tau_0} [j_\omega/\alpha_\omega] \exp -\tau \, d\tau \qquad (4)$$

where for convenience the superscripts o and x are omitted. τ is the optical thickness of the medium

$$\tau = -\int_0^r \alpha_\omega \, dr$$

along the ray **r**, as measured from the point of exit of the ray out of the plasma, $r=0$, to some point r within the plasma; τ_0 is the total optical depth as measured along the complete ray from the position of the observer, $r=0$, to $r=r_0$. I_0 is the intensity of any radiation incident on the plasma from outside, at a point $r=r_0$. When the plasma is isolated in empty space, $I_0=0$ and the first term on the right-hand side of Eq. (4) drops out.

Solution (4) expresses the fact that the intensity at a point and in a given direction is the result of the emission at all interior points reduced by a factor $e^{-\tau}$ to allow for absorption by the intervening plasma.

Further progress in computing the emission from Eq. (4) hinges on our knowledge of j_ω/α_ω, a ratio that is called the "equilibrium intensity" or the "source function" [1] and will be designated by S_ω. When the plasma is in local thermodynamic equilibrium, by Eqs. (1) and (2), $S_\omega = B(\omega, T) \equiv kT\omega^2/8\pi^3c^2$. The source function is now independent of the intensity of the radiation at the point within the plasma in question, and Eq. (4) is indeed the final and exceptionally simple result for the transport of radiant energy within and out of the plasma.

In the most general case the source function S_ω depends on the intensity of the radiation I_ω and when this functional dependence is known, its substitution into Eq. (4) leads to an integral equation for the source function [1]. This occurs, for instance, when microscopic scattering of the radiation becomes important, since now j_ω consists of the spontaneous emission of radiation and of radiation scattered from all other directions into the pencil of radiation **r** being considered. The scattered radiation may have the same frequency as the incident radiation (coherent scattering, as in Thompson scattering by an electron), or it can change frequency (incoherent scattering, as in Compton scattering). Likewise, the absorption coefficient comprises true absorption, where the energy of the wave is changed to other forms of energy (kinetic energy of the electrons) and an effective absorption that results from scattering of radiation out of the beam. At optical frequencies coherent and incoherent scattering is often of major importance. However, at radio and microwave frequencies it can be generally neglected except in certain extraterrestrial plasmas of very low electron concentration and high electron energy. We shall calculate the source function S_ω subject to the assumption that spontaneous and stimulated emission by the free electrons and true absorption by free electrons are the dominant mechanisms. The source function we will obtain will be independent of the intensity of the radiation I_ω as it is for a plasma in thermodynamic equilibrium, and the solution of Eq. (4) will be equally simple.

The differential equations (3) and their solutions (4) neglect the spatial variations of the refractive index of the ionized gas [2]. In fact, we assume throughout that the plasma is so tenuous that its refractive index is everywhere close to one. This results in the following simplifications: (a) There are no reflections or diffraction of the radiation at the boundaries of the plasma. (b) There is no coupling between the radiant energy in one mode of propagation with the radiation in the second mode. (c) There is weak coupling between the electrons and the radiation traversing the plasma. (This is the assumption that in Maxwell's field equations—used in finding α_ω—the displacement current greatly exceeds the conduction current of the free charges.) (d) The emission coefficient j_ω can be obtained from a simple summation over the emission characteristics of the individual electrons.

3. Calculation of the source function S_ω

A free plasma electron with momentum **p** emits at radio and microwave frequencies mainly because of collisions with atoms and ions (bremsstrahlung) and because of its orbital acceleration in the externally applied magnetic field (cyclotron radiation). Let $\eta_\omega^{(o,x)}(\mathbf{p})$ be the power radiated in one polarization, per unit solid angle, in the direction of the ray **r** by one of the electrons in some volume element of plasma where the electron concentration is N. The emission coefficient $j_\omega^{(o,x)}$ is obtained by summing the contribution from each of the N electrons

$$j_\omega^{(o,x)} = N\int_0^\infty \eta_\omega^{(o,x)}(\mathbf{p}) \, F(\mathbf{p}, t) \, d^3\mathbf{p} \qquad (5)$$

where $F(\mathbf{p})$ is the distribution of electron velocities in the presence of the time-varying electromagnetic fields of the radiating electrons. We write the total distribution $F(\mathbf{p})$ as

$$F(\mathbf{p}, t) = f(\mathbf{p}, t) + \mathbf{f}_1(\mathbf{p}, t) \cdot \frac{\mathbf{p}}{p} \qquad (6)$$

where f is the equilibrium distribution of electron velocities in the absence of the perturbing electromagnetic waves, and $\mathbf{f}_1$ is the perturbation, assumed to be small. Although the equilibrium distribution f satisfies the Boltzmann equation in the absence of the perturbations, it is not necessarily a Maxwellian distribution.

We assume f to be spherically symmetric in momentum space and normalized so that

$$\int_0^\infty f(\mathbf{p}, t) \, 4\pi p^2 \, dp = 1$$

We substitute Eq. (6) in Eq. (5) and neglecting $|\mathbf{f}_1|$ in comparison with $|f|$, obtain

$$j_\omega^{(o,x)} = 4\pi N \int \eta_\omega^{(o,x)}(\mathbf{p}) \, f(\mathbf{p}) \, p^2 \, dp \qquad (7)$$

The absorption coefficient α_ω is found from Maxwell's field equations and from Boltzmann's equation. The problem [3] is one of finding the plane-wave solution, $\exp(j\omega t - j\boldsymbol{\gamma}\cdot\mathbf{r})$, or solutions from the vector wave equation

$$\boldsymbol{\gamma}\times(\boldsymbol{\gamma}\times\mathbf{E}) + \gamma_0^2\,\mathbf{K}\cdot\mathbf{E} = 0 \tag{8}$$

where $\mathbf{E}$ is the r.f. electric field strength, $\boldsymbol{\gamma}$ is the complex propagation constant of the wave in the plasma, and $\gamma_0 = \omega/c$ is the propagation constant in free space. $\mathbf{K}$ is the tensor dielectric coefficient of the plasma. It is related to the conductivity of the free electrons $\mathbf{s}$ and to the generalized Ohm's law through relations

$$\mathbf{K} = 1 + \mathbf{s}/j\,\omega\,\varepsilon_0$$

$$\mathbf{J} = \mathbf{s}\cdot\mathbf{E} = \frac{4\pi N e}{3m}\int \mathbf{f}_1(\mathbf{p},t)\,p^3\,\mathrm{d}p \tag{9}$$

The connection between the component $\mathbf{f}_1$ of the distribution function and the unperturbed component f is derived from Boltzmann's equation

$$\frac{\partial F}{\partial t} + \mathbf{p}\cdot\mathbf{v}\cdot\nabla F + e\,(\mathbf{E}+\mathbf{v}\times\mathbf{B})\,\frac{\partial F}{\partial \mathbf{p}} = \left(\frac{\partial F}{\partial t}\right)_{\text{collisions}} \tag{10}$$

where $\mathbf{B}$ is the externally applied, constant, magnetic field. On substituting Eq. (6) into Eq. (10) we obtain [3] (with $\mathbf{B}$ oriented along the z axis of a rectangular coordinate system)

$$\mathbf{f}_1 = -\,\mathrm{e}\,\mathbf{E}\cdot\mathbf{D}\,\frac{\partial f}{\partial p}$$

$$\mathbf{D} = \frac{1}{2}\begin{vmatrix} l+r & j(l-r) & 0 \\ -\mathrm{j}(l-r) & l+r & 0 \\ 0 & 0 & 2q \end{vmatrix} \tag{11}$$

$$l, r = [\nu + \mathrm{j}\,(\omega \pm \omega_\mathrm{b})]^{-1}$$

$$q = (\nu + \mathrm{j}\,\omega)^{-1}$$

$$\omega_\mathrm{b} = \frac{e\,B}{m}$$

subject to the following assumptions: (a) $|f| \gg |\mathbf{f}_1|$, so that in Eq. (10) products of second-order quantities are neglected. (b) The plasma is uniform, and $\nabla F = 0$. (For the solution to be applicable in an inhomogeneous plasma, the spatial variations must be small compared with the wavelength.) (c) All time-dependent quantities, $(\mathbf{E}, \mathbf{f}_1)$, vary as $\mathrm{e}^{\mathrm{j}\omega t}$, instead of $\exp(\mathrm{j}\,\omega t - \mathrm{j}\boldsymbol{\gamma}\cdot\mathbf{r})$. This is acceptable in what we call a "temperate" plasma, where the wavelength of the electromagnetic radiation within the plasma is large compared with the thermal displacement of the electrons. More specifically, the phase velocity of the wave in the plasma must be large compared with the thermal velocity of the electrons. (This is the assumption made in Section 2: that the refractive index of the medium must be close to unity.) (d) The complicated collision term on the right-hand side of Eq. (10) is replaced by $-\mathbf{f}_1\,\nu(p)$, where $\nu(p)$ is the effective collision frequency for momentum transfer for electron-atom or electron-ion collisions. (e) The motion of the ions is neglected in the computation of the r.f. conductivity of the plasma. This is permissible at sufficiently low magnetic fields or high frequencies, $eB/M \ll \omega$, where M is the mass of the ion.

The power absorption coefficient $\alpha_\omega^{(\mathrm{o},\mathrm{x})}$ is given by twice the imaginary part of the propagation coefficient γ. The results are very complicated unless the plasma is assumed to be tenuous. The conditions for a tenuous plasma are: in the absence of a magnetic field, or far away from the electron cyclotron resonance, $\omega_\mathrm{p}^2/\omega^2 \equiv Ne^2/m\,\varepsilon_0\,\omega^2 \ll 1$; at cyclotron resonance and in the presence of collisions, $\omega_\mathrm{p}^2/\omega^2 \ll 1$ and $\omega_\mathrm{p}^2/\omega_\mathrm{b}\nu < 1$, where ω_b is the electron cyclotron frequency, $\omega_\mathrm{b} = eB/m$. When these requirements are met, the absorption coefficient becomes

$$\alpha_\omega^{(\mathrm{o},\mathrm{x})} = -\,\frac{4\pi N e^2}{3m\,\varepsilon_0\,c\,\omega^2}\int_0^\infty \chi^{(\mathrm{o},\mathrm{x})}(p,\omega,\omega_\mathrm{b})\,\frac{\partial f}{\partial p}\,p^3\,\mathrm{d}p \tag{12}$$

where $\chi^{(\mathrm{o},\mathrm{x})}(p,\omega,\omega_\mathrm{b},\nu)$ is an absorption parameter that is obtained from the tensor $\mathbf{D}$ of Eq. (11). For instance, at frequencies close to the cyclotron frequency and for an electric vector $\mathbf{E}$ polarized perpendicular to $\mathbf{B}$

$$\chi = \frac{\nu(p)\,\omega^2\,(1+\cos^2\theta)}{2[(\omega-\omega_\mathrm{b})^2+\nu^2(p)]} \tag{13}$$

where θ is the angle between the direction of propagation of the radiation and the static magnetic field. In the absence of a magnetic field or when the electric vector that is linearly polarized along the direction of $\mathbf{B}$ is observed,

$$\chi = \frac{\nu(p)\,\omega^2}{\omega^2+\nu^2} \tag{14}$$

The source function S_ω is obtained from the ratio of Eq. (7) to (12). This ratio is a function of the distribution of electrons f, the emission per electron η, and the absorption parameter χ. Since η and χ are the basic parameters associated with a single electron, their magnitude is independent of the distribution function. We find the relation between them from the principle of detailed balance for a system in thermodynamic equilibrium and obtain the following result for the source function in terms of η alone [4–6].

$$S_\omega^{(\mathrm{o},\mathrm{x})} = \frac{\omega^2}{8\pi^3 c^2}\left[-\,\frac{\int_0^\infty \eta_\omega^{(\mathrm{o},\mathrm{x})}(p)\,f(\varepsilon)\,p^2\,\mathrm{d}p}{\int_0^\infty \eta_\omega^{(\mathrm{o},\mathrm{x})}(p)\,[\partial f(\varepsilon)/\partial\varepsilon]\,p^2\,\mathrm{d}p}\right] \tag{15}$$

and for the absorption coefficient [5] in terms of η:

$$\alpha_\omega^{(\mathrm{o},\mathrm{x})} = -\,\frac{32\pi^4 c^2 N}{\omega^2}\int_0^\infty \eta_\omega^{(\mathrm{o},\mathrm{x})}(p)\,\frac{\partial f(\varepsilon)}{\partial\varepsilon}\,p^2\,\mathrm{d}p \tag{16}$$

Since

$$\eta_\omega^{(\mathrm{o},\mathrm{x})} = \frac{e^2\chi(p)\,p^2}{24\pi^3 c^2 m^2\,\varepsilon_0}$$

S_ω can be expressed equally well in terms of $\chi^{(\mathrm{o},\mathrm{x})}$ alone. Equations (15) and (16) are correct relativisti-

cally, with ε as the total energy, rest plus kinetic $\varepsilon=mc^2\,[1-\beta^2]^{-1/2}$, $\beta=v/c$, and with p as the momentum, given by $p^2c^2=\varepsilon^2-(mc^2)^2$.

When the distribution function is Maxwellian, $f(\varepsilon)\propto e^{-\varepsilon/kT}$, Eq. (15) becomes indentical with the Kirchhoff-Planck Law (Eqs. 1 and 2), and the source function S_ω reduces to $B(\omega, T)$, the source function of a plasma in local thermodynamic equilibrium. In a sense, Eq. (15) is a generalization of the Kirchhoff-Planck Law to a plasma with a non-Maxwellian distribution of electron energies.

Under our assumptions, the source function at any point within the plasma (Eq. 15) does not depend on the radiation intensity at that point. However, under certain circumstances the radiation intensity I_ω could effect the distribution function, causing S_ω to become a function of I_ω. For instance, this could occur if strong radiation I_0 (see Eq. 4) at frequency ω is allowed to fall on the plasma or if the power emitted by the plasma becomes comparable in magnitude with the power used in maintaining the discharge. This problem arises rarely in plasmas produced in the laboratory today. These plasmas are maintained by fields that are much stronger than the radiation fields generated by the discharge itself, and the distribution function $f(\varepsilon)$ is determined primarily by these externally applied fields. Therefore, in computing the emission from the plasma with the aid of Eqs. (4) and (15), S_ω will be assumed to be independent of the radiation intensity I_ω.

The source function given by Eq. (15) is independent of the magnitude of the electron density and is thus independent of electron-density variations within the plasma. The source function also does not depend on the absolute magnitude of the strength of the radiator η but requires only knowledge of the variation of η with electron energy. Hence a direct determination of the source function (Section 4) not only tells us the extent to which thermodynamic equilibrium does or does not exist, but it can also lead to an estimate of the distribution of electron velocities.

When the source function (Eq. 15) does not vary with position in the plasma (that is, when the mean electron energy is uniform throughout), Eq. (4) yields the following result for the radiation intensity that reaches an external observer:

$$I_\omega = I_0\,e^{-\tau_0} + S_\omega(1 - e^{-\tau_0}) \tag{17}$$

Thus S_ω has the following well-defined physical meaning: when the plasma is situated in empty space ($I_0=0$) and has a very large optical depth ($\tau_0 \gg 1$), S_ω equals the radiation intensity from the plasma. In fact, when $\tau\to\infty$, S_ω is the radiation intensity from every volume element of plasma, and it represents the solution of the equation of transfer (Eq. 3) in the limit $dI_\omega/dr\to 0$. This fact affords a different method of calculating S_ω that illustrates better the physical mechanisms being studied [4].

Consider a small volume element in an infinite plasma and let $\eta(\mathbf{p})$ be the spontaneous emission at a frequency ω in a given direction, by an electron of momentum $\mathbf{p}$. Let $\eta_{SE}(\mathbf{p})$ be the rate of stimulated emission of photons per unit intensity of radiation present, and let $\eta_{SA}(\mathbf{p}')$ be the rate of absorption per unit intensity of radiation. Since no net radiation leaves the volume element of the infinite medium

$$\int \eta(\mathbf{p})\, f(\mathbf{p})\, d^3\mathbf{p} + S_\omega \int \eta_{SE}(\mathbf{p})\, f(\mathbf{p})\, d^3\mathbf{p} = S_\omega \int \eta_{SA}(\mathbf{p}')\, f(\mathbf{p}')\, d^3\mathbf{p}' \tag{18}$$

where $\mathbf{p}$, $\mathbf{p}'$, the electron energies ε and ε' and the wave number $\mathbf{k}$ are related by

$$\mathbf{p} - \mathbf{p}' = \hbar\,\mathbf{k};\quad \varepsilon - \varepsilon' = \hbar\,\omega \tag{19}$$

From Einstein's A and B coefficients we deduce that

$$\frac{\eta(\mathbf{p})}{\eta_{SE}(\mathbf{p})} = \frac{\hbar\,\omega^3}{8\pi^3 c^2} \tag{20}$$

and from the principle of detailed balancing,

$$\frac{\eta_{SA}(\mathbf{p}')}{\eta_{SE}(\mathbf{p})} = \frac{\varepsilon}{\varepsilon'} \tag{21}$$

From Eqs. (18), (19), (20) and (21) we obtain S_ω in terms of the spontaneous emission $\eta(\mathbf{p})$

$$S_\omega = \frac{\hbar\,\omega^3}{8\pi^3 c^2} \frac{\int \eta(\mathbf{p}) f(\mathbf{p})\, d^3\mathbf{p}}{\int \eta(\mathbf{p})\,[f(\mathbf{p}') - f(\mathbf{p})]\, d^3\mathbf{p}} \tag{22}$$

In the classical limit $\hbar\,\omega\to 0$ and for a spherically symmetric distribution function, Eq. (22) for the source function reduces to our previous Eq. (15).

4. The source function and the radiation temperature for bremsstrahlung and cyclotron emission by cold electrons

The bracketed term of Eq. (15) for the source function has dimensions of energy, and by analogy with Eq. (2) we can write it as kT_r where the parameter T_r has dimensions of temperature. We shall call this parameter the radiation temperature (it is equal to the electron temperature when $f(\varepsilon)$ is Maxwellian). In terms of T_r, $S_\omega=(\omega^2/8\pi^3c^2)\,kT_r$ and henceforth we shall find it convenient to discuss the properties of T_r rather than to discuss S_ω. The use of T_r has another advantage: when the plasma is situated in a waveguide, the radiation propagates only in one fixed direction and the source function differs from that given by Eq. (15), which refers to a plasma situated in an unbounded medium. For each propagating waveguide mode, $S_\omega=kT_r/2\pi$.

4.1. Bremsstrahlung

In the absence of a magnetic field, bremsstrahlung is the major emission process at radio and microwave frequencies. In a plasma of low ionization, bremsstrahlung is the result of electron-atom or electron-molecule collisions. The emission $\eta(p)$ per electron-atom encounter is difficult to compute theoretically and its magnitude and velocity dependence vary greatly with the gas being considered. However, η and

χ of Eqs. (13) and (14) are related through $\eta(p) \propto \chi(p) p^2$ where $\chi(p) = \omega^2 \nu(p) [\omega^2 + \nu^2(p)]^{-1}$ and if $\nu(p)$, the collision frequency, were known, the bremsstrahlung emission, S_ω and T_r could be determined. Although the calculation of $\nu(p)$ is of the same order of complexity as the calculation of $\eta(p)$, the collision frequency can be found from the numerous measurements [7] of the collision probability P_c, where $\nu(v) = P_c(v) p_0 v$, v is the electron velocity and p_0 the gas pressure in torr.

In a highly ionized gas where electron-ion encounters predominate, an effective collision frequency for momentum transfer can be likewise defined. No good measurements are available, but calculations show that

$$\nu(v) = \frac{4\pi N}{v^3} \left(\frac{Z e^2}{4\pi \varepsilon_0 m} \right)^2 G \tag{23}$$

Here Z is the ionic charge and G is a slowly varying function of velocity, frequency and electron density N and is, approximately

$$G \approx \ln \frac{4\pi \varepsilon_0 m v^2 l_D}{2 Z e^2} \quad \text{for} \quad \omega_p/\omega > 1$$

$$G \approx \ln \frac{4\pi \varepsilon_0 m v^2 l_D (\omega_p/\omega)}{2 Z e^2 \omega} \quad \text{for} \quad \omega_p/\omega \ll 1 \tag{24}$$

(l_D is the Debye shielding length).

The collision frequency ν that enters the calculations of bremsstrahlung from electron-atom encounters is, to our present-day knowledge, independent of frequency, for emission at radio and microwave wavelengths. This fact is substantiated by the good agreement obtained between measurements and calculations of bremsstrahlung [8]. For electron-ion encounters, the frequency dependence [9] (if any) is contained inside the Coulomb logarithm G of Eqs. (24). At low frequencies, $\omega_p/\omega > 1$, ν is frequency independent and the screening distance extends over the full size of the Debye sphere. At high frequencies, $\omega_p/\omega \ll 1$, the Debye sphere is "reduced" by a factor ω_p/ω.

Substituting for η in Eq. (15), we find the radiation temperature for bremsstrahlung:

$$kT_r = - \frac{\int_0^\infty \nu(p) [\omega^2 + \nu^2(p)]^{-1} f(\varepsilon) p^4 \, dp}{\int_0^\infty \nu(p) [\omega^2 + \nu^2(p)]^{-1} [\partial f(\varepsilon)/\partial \varepsilon] p^4 \, dp} \tag{25}$$

In most gases $\nu(p)$ exhibits a complicated dependence on p. Since the contribution to the integrals of Eq. (25) occurs mainly in the neighborhood of the mean electron energy $\langle u \rangle$, it is convenient to assume that in the energy range in question ν can be approximated by the power law

$$\nu = a p^h \tag{26}$$

where a and h are arbitrary numbers. The velocity dependence given by Eq. (26) includes the following important cases: (a) a collision that occurs at a constant mean free time ($h=0$) and is appropriate to a gas where the interparticle forces vary inversely as a fifth power of the particle separation (Maxwell gas); (b) a hard-sphere or billiard ball collision where the mean-free path stays constant ($h=1$); (c) a Coulomb type of interaction ($h=-3$).

We chose a distribution function $f(p)$

$$f(p) \propto \exp - b p^l \tag{27}$$

where b and l are positive constants. When $l=2$ we have a Maxwellian distribution; when $l=4$, a Druyvesteyn distribution. In particular, $l<2$ implies an excess of fast particles and $l>2$ an excess of slow particles. The values of b and l determine the mean electron energy $\langle u \rangle$.

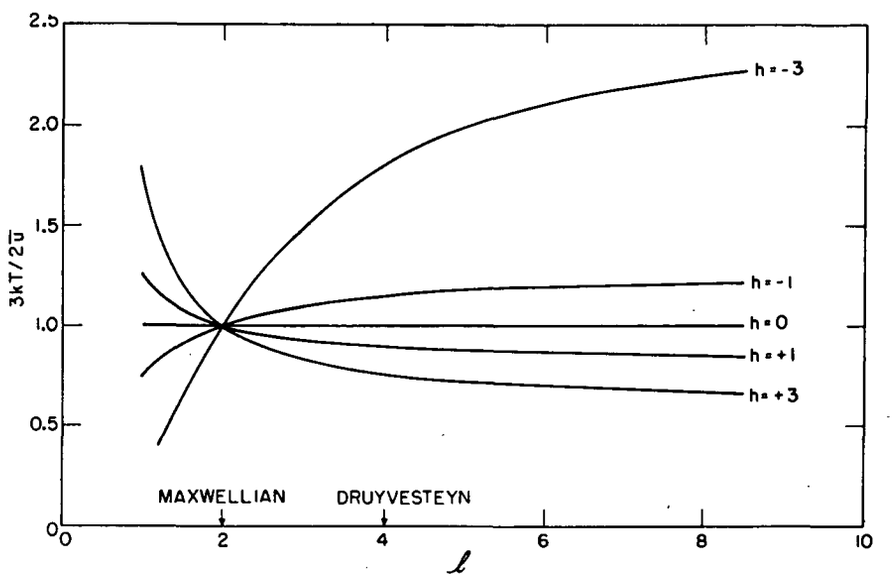

Fig. 1 Radiation temperature for bremsstrahlung emission as a function of the distribution of electron velocities. $f(p) \propto \exp - b p^l$ and $\nu = a p^h$. High frequencies, $\nu/\omega < 1$.

The radiation temperature is obtained by substituting Eqs. (26) and (27) into Eq. (25). At a sufficiently high frequency ω, or at a low collision frequency ν, for which $(\nu/\omega)^2 \ll 1$, the integrals of Eq. (25) are easily evaluated. Figure 1 illustrates [4] how the radiation temperature T_r (normalized to the mean electron energy $\langle u \rangle$) depends on the distribution function l, for various collision frequencies ν. In a Maxwell gas ($h=0$), $(3/2)kT_r = \langle u \rangle$, and T_r and S_ω are independent of the distribution of electron energies. This fact is not a peculiarity of the radiation problem; it is well known that in a Maxwell gas the transport properties (electrical, thermal) are likewise independent of $f(\varepsilon)$. When $\nu \neq 0$, T_r departs from $2\langle u \rangle/3k$ and the magnitude of the departure is determined by the degree to which $f(\varepsilon)$ departs from a Maxwellian distribution. In principle, careful measurements of T_r and $\langle u \rangle$ and a knowledge of $\nu(p)$ allow one to infer the distribution function. This is not easy since $\langle u \rangle$ cannot be measured accurately and $\nu(p)$ is not known precisely. Furthermore T_r is almost frequency-independent and thus little new information is likely to be gained by taking measurements at different frequencies. (There is a frequency dependence on going from $\nu/\omega \ll 1$ to $\nu/\omega \gg 1$, but a study of this dependence would require measurements over very large ranges of frequency.) Matters are very different in the presence of an applied magnetic field.

4.2. Cyclotron emission by cold electrons

Superimposed on the "white" bremsstrahlung continuum is a prominent spectral line whose center is located at a frequency equal to the electron orbital frequency. While bremsstrahlung is randomly polarized, cyclotron emission is polarized with its electric vector in a plane perpendicular to the direction of the magnetic field. We consider the case when this spectral line is broadened by collisions. The emission by a single electron η is given by (see Eq. 13)

$$\eta(p) \propto \frac{\nu(p) p_\perp^2 (1 + \cos^2\theta)}{(\omega - \omega_b)^2 + \nu^2(p)} \tag{28}$$

where $p_\perp$ is the component of momentum of the electron perpendicular to the magnetic field.

On substituting Eq. (28) in Eq. (15), we observe that T_r exhibits a strong dependence on frequency, a fact that will aid us greatly in the measurement of non-thermal radiation from the plasma. Figure 2 shows this frequency dependence [4]. At the cyclotron frequency, T_r exhibits a peak when $h>0$, and a valley when $h<0$. When $h=0$, $T_r = 2\langle u \rangle/3k$ and shows no frequency variation. It behaves in the same way as it did for bremsstrahlung (Section 4.1). The widths of the resonances in T_r are proportional to ν and therefore in a plasma of low ionization the widths are proportional to the gas pressure. Under suitable experimental conditions, a small variation in frequency ω, or in the magnetic field ω_b about the point $\omega/\omega_b = 1$ should permit one to observe these resonances.

Figures 3a, b and c illustrate [10] the results of measuring T_r in xenon, neon, argon, helium and hydrogen. The emission that was received originated from a 50-cm-long section of the positive column of a glow discharge. The frequency of observation was held fixed at 3000 MHz and the axial, d.c. magnetic field was varied from 0 to 2000 G. The discharge current was sufficiently low to ensure that $\omega_p^2/\omega^2 \ll 1$, and the pressure was sufficiently high that $\omega_p^2/\omega_b \nu < 1$, these being two conditions necessary to our theory.

Pronounced peaks are observed in xenon, argon and neon. These gases have strongly energy-dependent elastic collision cross-sections and hence energy-dependent values of ν. In the electron energy range of our measurements (1—5 ev) as estimated from the values of T_r away from cyclotron resonance, $\nu = av^h$

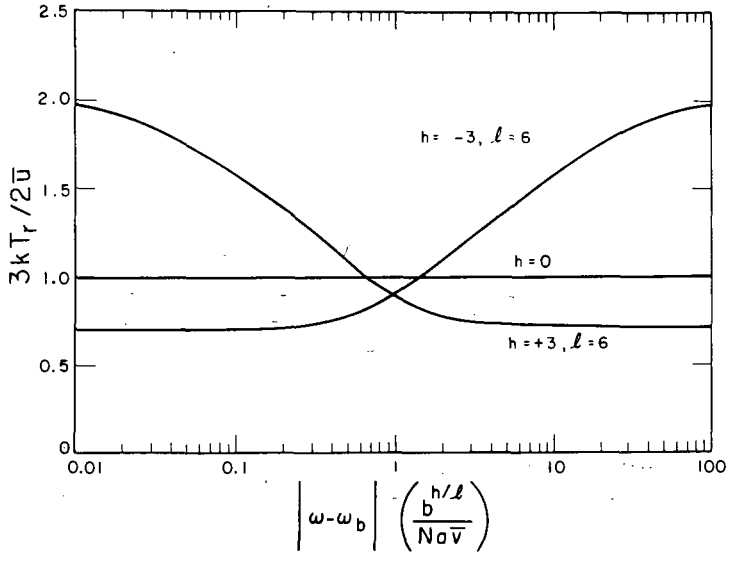

Fig. 2 Radiation temperature for cyclotron emission as a function of frequency. Emission by cold electrons in the presence of collisions.

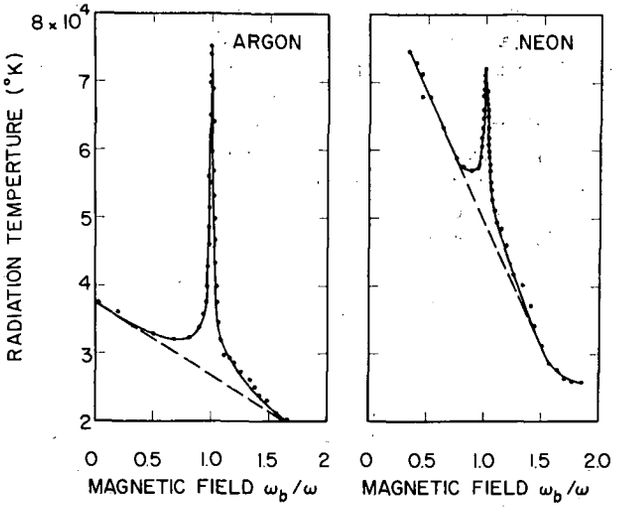

Fig. 3a Measured radiation temperature as a function of magnetic field in argon and neon. Discharge current = 10 mA and the gas pressure $p_0 = 0.28$ torr.

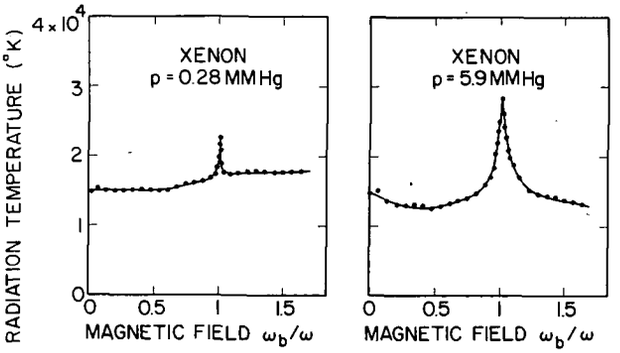

Fig. 3b Measured radiation temperature in xenon at two different pressures. Discharge current = 20 mA.

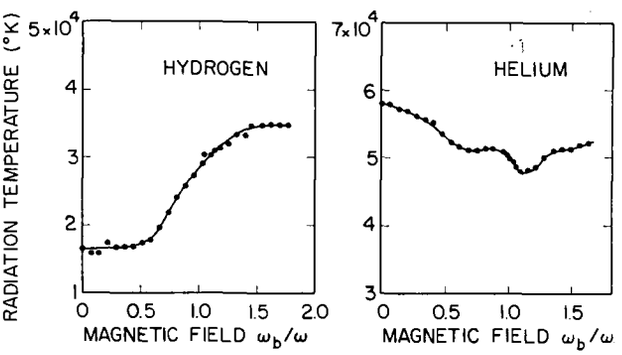

Fig. 3c Measured radiation temperature in helium and hydrogen. No resonance peaks observed. Discharge current = 10 mA, gas pressure = 0.28 torr.

is such that h ranges from approximately 1 in neon to 2 in xenon. The theory predicts peaks whose magnitude depends on h and on the degree to which $f(\varepsilon)$ departs from a Maxwellian (value of l). The ratio of the magnitude of T_r at the cyclotron frequency, $T_r(\omega_b)$, to the magnitude of T_r far away from cyclotron frequency, $T_r(\omega - \omega_b \to \infty)$ (as obtained from the asymptotes shown by dashed lines in Fig. 3), allows one to estimate the energy dependence of the distribution function. These estimates suggest that for the three gases studied $f(\varepsilon)$ is approximately proportional to $\exp -b\varepsilon^2$. For better estimates of $f(\varepsilon)$ and for an actual determination of $\langle u \rangle$, the approximation for ν that we used (Eq. 26) must be replaced by the known, measured, variation of ν with p. This requires machine solutions of Eq. (15).

No resonance peaks were observed either in helium or in hydrogen at any gas pressure or discharge current. In these gases ν is independent of the electron energy ($h \approx 0$ for $\langle u \rangle > 2$ ev) and no peaks are expected. The following observations [10] are also in agreement with theory: in neon, where $h \approx 1$ over a wide range of energies, (a) the ratio $T_r(\omega_b)/T_r(\omega - \omega_b \to \infty)$ is independent of the electron density as measured over a range of one order of magnitude, (b) the ratio of $T_r(\omega_b)/T_r(\omega - \omega_b \to \infty)$ is independent of the gas pressure as measured over one order of magnitude, (c) the width of the resonances is directly proportional to the gas pressure.

Our determination of the source function and of T_r was based on Eq. (17), which contains the implicit assumption that S_ω is uniform along the direction in which the radiation is observed. The plasma was irradiated [11] with black-body radiation of a known, variable temperature, $I_0 = B(\omega, T)$. The total intensity along a ray (1)

$$I_\omega(1) = B(\omega, T)\, e^{-\tau_0} + S_\omega(1 - e^{-\tau_0}) \qquad (29)$$

was compared with the intensity $I_\omega(2) = B(\omega, T)$ along a ray (2) that did not traverse our plasma. The intensity $B(\omega, T)$ was now adjusted until $I_\omega(1) = I_\omega(2)$. When this adjustment is made, Eq. (29) shows that irrespective of the value of the optical depth τ_0, $S_\omega = B(\omega, T)$. This adjustment could be made with an accuracy of approximately 0.05% for plasmas of large optical depth $\tau_0 > 1$, and with an accuracy of 2% when $\tau_0 = 0.01$.

The illumination of the plasma, though very weak (10^{-12} W and less), might cause enough perturbation of the plasma to give the observed resonances in T_r. Therefore the measurements were repeated at pressures and currents where the optical depth of the plasma τ_0 was established to be greater than approximately 4 at all values of magnetic field. When this is so, $I_\omega \to S_\omega$ even in the absence of any illumination ($I_0 = 0$ in Eq. (17)). The results of these measurements were found to be the same as when the plasma is illuminated.

5. A plasma instability in velocity space

Many theoretical analyses have been made of the instabilities that can develop in a plasma when the electron velocity distribution becomes highly anisotropic in velocity (momentum) space. Consider a plasma that consists of a core of electrons near the origin of velocity space, and of a second group of high-velocity electrons. When the relative drift of such groups is sufficiently large compared with their thermal velocities, instabilities can set in. In the

presence of an applied magnetic field, another instability may occur when the mean electron energy perpendicular to the magnetic field exceeds by a sufficient amount the mean electron energy along the magnetic field.

Here we shall discuss the possible onset of an instability [6] that is peculiar in the sense that it can occur in a plasma with a perfectly isotropic, spherically symmetric distribution of electron velocities. This instability manifests itself as a negative value of the absorption coefficient α_ω of a transverse electromagnetic wave passing through the plasma. Thus, instead of being attenuated, the wave grows exponentially with distance along the ray, and radiation generated in some volume element of plasma is amplified in passing through the plasma. Likewise if the plasma is illuminated with a coherent electromagnetic signal, the signal that emerges from the plasma is amplified.

A negative value of the absorption coefficient results in a negative value of the radiation temperature T_r. Of course, the radiation intensity as found from Eq. (4) or (17) remains positive.

Conditions for negative absorption (or a negative r.f. conductivity, which, when the plasma is tenuous, is proportional to α_ω), are obtained most easily from Eq. (16). We observe that a necessary condition for a negative α_ω is a distribution function that increases with energy, somewhere in the electron energy range. That is,

$$\frac{\partial f(\varepsilon)}{\partial \varepsilon} > 0 \tag{30}$$

This means that in some energy range there must be an excess of energetic electrons compared to the population in neighboring ranges. A fully ionized plasma confined by a magnetic mirror is depleted of slow electrons that diffuse out as a result of their large electron-ion collision cross-section. In this

TABLE I. Summary of processes examined

Emission process $\eta(p)$	Theoretical requirement for amplification (Eq. 31)	For radiation at frequencies:	For electron energies:
Bremsstrahlung — zero magnetic field (a) electron-atom and electron-molecule collisions (for radiation at high frequencies)	$\nu(p)$ must decrease with increasing p more quickly than p^{-3}.	$\frac{\nu}{\omega} \ll 1$	slight possibility for this in Hg vapor for energies less than 1 ev
(b) electron-atom and electron-molecule collisions (for radiation at low frequencies)	$\nu(p)$ must increase with increasing p more quickly than p^3.	$\frac{\nu}{\omega} > 1$	Xe, Hg, Ar for energies less than 10 ev and greater than 1 ev
(c) electron-ion collisions (fully ionized gas)	Amplification does not occur.	at any frequency	—
Cyclotron emission (d) collisions an important broadening mechanism	$\nu(p)$ must increase with p more quickly than p^3.	$\lvert\omega - \omega_b\rvert < \nu$; $\frac{\nu}{\omega} > \frac{\langle v_\perp \rangle}{c}$	Xe, Hg, Ar for energies less than 10 ev and greater than 1 ev
(e) thermal motion of electrons important broadening mechanism (1st order Doppler)	Amplification does not occur.	$\frac{\nu}{\omega} < \frac{\langle v_\perp \rangle}{c}$	$\frac{\langle v \rangle}{c} \ll 1$
(f) relativistic mass change of electron (2nd order Doppler) important broadening mechanism	$\frac{\nu}{\omega} \ll \frac{\langle v_\perp \rangle}{c^2}$	$\omega \approx \omega_b, 2\omega_b, \ldots n\omega_b$	$\langle \varepsilon \rangle \lesssim mc^2$
(g) relativistic mass change of highly relativistic electron	Amplification does not occur since harmonics merge into quasi-continuous spectrum.	—	$\langle \varepsilon \rangle \gg mc^2$

plasma the distribution function can satisfy the inequality given by Eq. (30). On the other hand, a plasma of low ionization is more likely to have an excess of slow electrons (produced in the process of excitation and ionization by the fast particles in the tail of a Maxwellian distribution), and in normal circumstances, this plasma will not satisfy condition (30).

The inequality given by Eq. (30), though necessary, is not sufficient to ensure amplification of the wave. Integrating Eq. (16) by parts we find that another requirement is

$$\frac{\partial \eta(p)\, \varepsilon p}{\partial p} < 0 \qquad (31)$$

somewhere in the energy range where $\partial f(\varepsilon)/\partial \varepsilon > 0$. Therefore, the velocity dependence of a particular emission process $\eta(p)$ [or of the velocity dependence of the related absorption parameter $\chi(p)$ of Eq. (12)] determines whether or not amplification can occur. Table I summarizes the processes we have examined and found either to agree or disagree with the condition given by Eq. (31).

When amplification occurs, the stimulated emission of radiation exceeds stimulated absorption by the electrons (see Eqs. 18 and 22). A deeper insight into the process of amplification is obtained by analyzing the interaction of an electromagnetic wave with an electron moving in an orbit determined by the local electric or magnetic fields.

Consider [12] the amplification process "d" of Table I. Here the helical electron motion in the d.c. magnetic field is interrupted at random intervals by collisions with atoms. At each collision, an electron of velocity $v_\perp(1)$ is in a circular orbit and is either in such a phase with the electric field of the wave as to absorb energy from it (stimulated absorption) or in a proper phase to relinquish some of its kinetic energy to the wave (stimulated emission). Suppose that the phase is correct for stimulated emission, and let the electron make collisions with a gas in which $\nu(v)$ increases with v. The electron loses energy to the wave, and since it has now a smaller velocity, $v_\perp(2) < v_\perp(1)$, its probability of collision becomes smaller than it was before. Therefore, it preserves its phase relationship longer than when its velocity was $v_\perp(1)$. Another electron of the same velocity may be in phase for stimulated absorption. It gains energy from the wave and, therefore, has a greater probability of collision than before. Since on the average the electron in phase for stimulated emission stays in phase longer than the electron in phase for stimulated absorption, it can give up more energy than is absorbed by the other electron. The inverse is true when $\nu(v)$ decreases with increasing v. This shows qualitatively how the inequality given by Eq. (31) enters the problem of amplification.

The above physical model refers to a system with electrons that are initially monoenergetic. So far we have said nothing about the density distribution of electrons in momentum space required for amplification (Eq. 30). When the plasma has a distribution $f(p)$, the momentum space can be divided into small intervals Δp. The arguments of the previous paragraph can be then applied to each of these intervals Δp, except to the interval at the origin of momentum p. In this interval electrons can only gain energy from the wave. To overcome this absorption of energy by electrons of almost zero speed, and to achieve net amplification, calculations show [12] that the plasma must have a preponderance of fast electrons. That is, $\partial f/\partial \varepsilon > 0$.

The amplification process "f" of Table I is of particular interest in estimating the radiation loss from proposed thermonuclear reactors. Several computations have been made for the loss of energy by bremsstrahlung and cyclotron emission. In these calculations it was assumed that the plasma is in strict local thermodynamic equilibrium. When this is not the case, and particularly when the electron distribution satisfies the inequality given by Eq. (30), the net loss of power may be enhanced greatly as a result of amplification of cyclotron emission in its passage through the plasma.

Let us consider a distribution function that satisfies inequality (30). Let it be of the form,

$$f(\beta) \propto \beta^q \exp -b\beta^2 \quad (\beta = v/c) \qquad (32)$$

where q is an arbitrary positive number (when $q=0$, the distribution is Maxwellian). We can compute the absorption coefficient α_ω from Eqs. (16) and (32) and from the known cyclotron emission η by a relativistic electron. Figure 4 shows [4] variation of α_ω with frequency near the first and second harmonic ($n=1,2$) for radiation perpendicular to the direction of the magnetic field. We assumed a relatively small per-

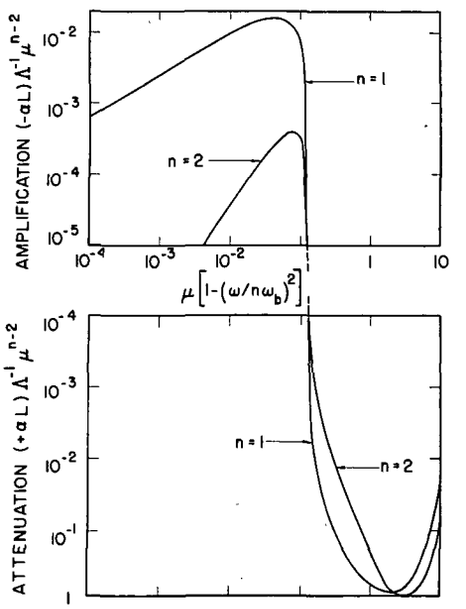

Fig. 4 The transition from a positive to a negative absorption coefficient α_ω for the first two harmonics of cyclotron emission at 90° to the applied magnetic field. The plot is for a distribution function $f \propto \beta^q \exp -b\beta^2$ with $q = 0.2$. $\mu \equiv mc^2/\langle u \rangle$; $\Lambda \equiv \omega_p^2 L/\omega_b c$.

turbation of Maxwellian distribution and we chose a value of q in Eq. (32) equal to 0.2. The absorption coefficient is negative (amplification) in a small frequency range near the harmonics of cyclotron emission, and it is positive (attenuation) at all other frequencies.

The source function S_ω is computed from Eqs. (15) and (32), and once S_ω and α_ω are known, the intensity of emission I_ω is obtained from Eq. (4). Figure 5 illustrates [6] the emission from a uniform slab of plasma of thickness L, in a direction perpendicular to the magnetic field that is assumed to be oriented along the faces of the slab. The calculations for Fig. 5 were made for a mean electron energy $\langle u\rangle = 75$ keV

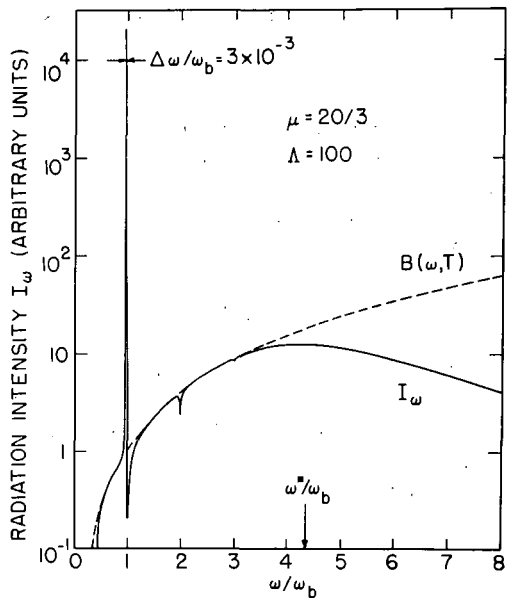

Fig. 5 Emission spectrum of cyclotron radiation from a non-Maxwellian plasma, $f \propto \beta^{0.2} \exp -b\beta^2$. $\mu = 20/3$; $\Lambda = 100$. $B(\omega, T) \equiv 2\langle u\rangle \omega^2/24\pi^3 c^2$ is the "black-body" spectrum of a plasma with a Maxwellian distribution and an electron temperature given by $kT = 2\langle u\rangle/3$.

($\mu \equiv mc^2/\langle u\rangle = 20/3$), and for an electron density and magnetic field strength specified by the parameter $\Lambda \equiv \omega_p^2 L/\omega_b c = 100$. The peak of intensity at $\omega \approx \omega_b$ manifests itself as a result of amplification of the cyclotron emission. This peak greatly exceeds the limiting black-body emission of a plasma in thermodynamic equilibrium. Also, the total energy density under the peak exceeds the blackbody emission between the frequencies $\omega = 0$, and $\omega = \omega^*$ where the plasma ceases to be opaque. Hence it appears that the amplification process discussed here may have important consequences in thermonuclear devices that use strong magnetic fields for the purpose of confining the plasma.

We have concerned ourselves with instabilities or amplification processes that can occur in plasmas with spherically symmetric, isotropic distributions of electron velocities. When the condition of isotropy is relaxed, new instabilities occur [13—15]. Still assuming the plasma to be tenuous in the sense defined in Section 3 we obtain the following result for the absorption coefficient:

$$\alpha_\omega^{(o,x)} = \frac{16\pi^4 c N}{\omega^2} \times \int_{p_\parallel} \int_{p_\perp} \eta_\omega^{(o,x)}(p_\parallel, p_\perp, \theta) \left[-\frac{\varepsilon}{c} \frac{\partial f}{\partial p_\perp} + \cos\theta \left(p_\parallel \frac{\partial f}{\partial p_\perp} - p_\perp \frac{\partial f}{\partial p_\parallel} \right) \right] dp_\parallel \, dp_\perp \quad (33)$$

where $p_\perp$ and $p_\parallel$ are the components of electron momentum $\mathbf{p}$ perpendicular and parallel to the direction of the magnetic field, respectively. θ is the angle between the direction of propagation of the wave and the direction of the magnetic field. Note that when the wave propagates at right angles to the magnetic field, or when the distribution function f is isotropic, the last two terms of the integrand of Eq. (33) become zero. The remaining term can be shown to be identical with that given by Eq. (16) in the limit of an isotropic distribution. The new terms in Eq. (33) represent an instability that comes about because of an anisotropic mean electron energy.

The first term of Eq. (33) shows more clearly the requirement on f for amplification than does Eq. (16) and inequality (30). For instance, when the radiation is observed at 90° to the direction of the magnetic field, amplification can occur only when $\partial f/\partial p_\perp > 0$. If we write that $f = f_\parallel \cdot f_\perp$, then as long as $f_\perp$ is a monotonically decreasing function of $p_\perp$, no amplification can take place no matter how non-Maxwellian $f_\parallel$ may be.

This work was supported in part by the U.S. Army Signal Corps, the Air Force Office of Scientific Research and the Office of Naval Research; in part by the Atomic Energy Commission, and in part by the Air Force Command and Control Development Division under Contract AF-19(604)-5992.

References

[1] CHANDRASEKHAR, S., Radiative Transfer, Dover Publications, Inc., New York (1960).
[2] WOOLLEY, R. v. d. R., STIBBS, D. W. N., The Outer Layers of a Star, Clarendon Press, Oxford (1953).
[3] ALLIS, W. P., Handbuch der Physik **21** (S. Flügge, ed. Springer-Verlag, Berlin (1956) 383; ALLIS, W. P., BUCHSBAUM, S. J., Bers, A., Waves in Anisotropic Plasmas, M. I. T. Press, Cambridge, Mass., USA (1963).
[4] BEKEFI, G., HIRSHFIELD, J. L., BROWN, S. C., *Phys. Fluids* **4** (1961) 173.
[5] TRUBNIKOV, B. A., "Magnetic emission of a high-temperature plasma", Dissertation, Moscow (1958). English translation by the U.S. Atomic Energy Commission, Report AEC-tr-4073 (June 1960); TRUBNIKOV, B. A., in Plasma Physics and the Problem of Controlled Thermonuclear Reactions, **4** (Leontovich, M. A., ed.) Pergamon Press (1960) 363.
[6] BEKEFI, G., HIRSHFIELD, J. L., BROWN, S. C., *Phys. Rev.* **122** (1961) 1037.
[7] BROWN, S. C., Basic Data of Plasma Physics, Technology Press of M.I.T. and John Wiley and Sons, Inc., New York (1959).

[8] BEKEFI, G., HIRSHFIELD, J. L., BROWN, S. C., *Phys. Rev.* **116** (1959) 1051.
[9] YOSHIKAWA, S., *Bull. Am. Phys. Soc.* **6** (1961) 289.
[10] FIELDS, H., BEKEFI, G., BROWN, S. C., in Proc. 5th Intern. Conf. Ionization Phenomena in Gases **1** (Munich, Aug. 1961) 367.
[11] BEKEFI, G., BROWN, S. C., *J. appl. Phys.* **32** (1961) 25.
[12] SCHWEITZER, P. E., Air Force Cambridge Research Center, Bedford, Mass., U.S.A., private communication (1961).
[13] SAGDEEV, R. Z., SHAFRANOV, V. D., *Zh. eksper. teoret. Fiz.* **12** (1961) 130.
[14] HIRSHFIELD, J. L., *Nuclear Fusion*: 1962 Supplement, Part 3, 1116 (abstract only).
[15] GRUBER, S., Massachusetts Institute of Technology, Research Laboratory of Electronics, Quarterly Progress Report No. 61, page 5.

ВЗАИМОДЕЙСТВИЕ ПУЧКА ЭЛЕКТРОНОВ С ПЛАЗМОЙ В МАГНИТНОМ ПОЛЕ*

И. Ф. ХАРЧЕНКО, Я. Б. ФАЙНБЕРГ, Р. М. НИКОЛАЕВ, Е. А. КОРНИЛОВ, Е. И. ЛУЦЕНКО, Н. С. ПЕДЕНКО

АКАДЕМИЯ НАУК СССР

МОСКВА, СОЮЗ СОВЕТСКИХ СОЦИАЛИСТИЧЕСКИХ РЕСПУБЛИК

В работе приведены результаты экспериментального исследования взаимодействия модулированного и немодулированного пучка электронов с плазмой в магнитном поле.

Определены условия возникновения неустойчивостей в системе пучок-плазма в зависимости от скорости пучка, плотности плазмы и напряженности магнитного поля.

Обнаружено возбуждение высокочастотных (в диапазоне 2000—8000 мгц) и низкочастотных (в диапазоне 1 кгц—10 мгц) колебаний в областях неустойчивостей. Измерен спектр возбуждаемых частот и время развития неустойчивостей. Измерена потеря энергии электронами пучка, обусловленная возбуждением колебаний.

Определено также увеличение энергии плазмы при возбуждении колебаний. Развитие неустойчивостей сопровождается диффузией ионов и электронов поперек магнитного поля.

Модуляция пучка на частоте 3000 мгц приводит к срыву целого спектра неустойчивостей благодаря тому, что системе навязывается длина волны, не совпадающая с резонансной. При этом остаются только узкие зоны неустойчивостей, обусловленные параметрическим возбуждением.

Экспериментальные измерения подтверждают теоретические предположения о возникновении автомодуляции в пучке, проходящем через плазму, и наличии когерентного взаимодействия пучка электронов с плазмой.

В работе приведены результаты экспериментального исследования взаимодействия модулированного и немодулированного пучка электронов с плазмой в магнитном поле.

Определены условия возникновения неустойчивостей в системе пучок-плазма в зависимости от скорости пучка, плотности плазмы и напряженности магнитного поля.

Обнаружено возбуждение высокочастотных (в диапазоне 2000—8000 мгц) и низкочастотных (в диапазоне 1 кгц—10 мгц) колебаний в областях неустойчивости. Измерен спектр возбуждаемых частот и время развития неустойчивостей. Измерены потери энергии электронами пучка и увеличение энергии электронов плазмы при возбуждении колебаний. Развитие неустойчивостей сопровождается диффузией частиц плазмы поперек магнитного поля.

Модуляция пучка на частоте 3000 мгц приводит к срыву целого спектра неустойчивостей благодаря тому, что системе навязывается длина волны, не совпадающая с резонансной. При этом остаются только узкие зоны неустойчивостей, обусловленные параметрическим возбуждением.

Экспериментальные измерения подтверждают теоретические предположения о возникновении автомодуляции в пучке, проходящем через плазму, и наличии когерентного взаимодействия пучка электронов с плазмой. Особенно эффективно взаимодействие для немодулированного пучка при частоте плазмы равной электронно-циклотронной частоте.

Взаимодействие пучка с плазмой без магнитного поля достаточно хорошо изучено теоретически и экспериментально [1—5].

Взаимодействию в магнитном поле посвящено значительное число теоретических работ. Однако экспериментально этот вопрос еще мало изучен. Среди работ, посвященных этому вопросу, следует отметить работы [2, 6, 7, 8].

Целью настоящей работы является исследование вопросов неустойчивости и обмена энергией между пучком электронов и плазмой при взаимодействии пучка электронов с плазмой в магнитном поле.

Для установления областей частот и инкрементов нарастания неустойчивостей, возникающих при взаимодействии пучка с плазмой, можно воспользоваться результатами теоретических исследований. Возбуждение колебаний, обусловленных эффектом Черенкова, имеет место для частот $(\omega_H^2 + \omega_0^2 \sin^2\theta)^{1/2}$, при этом инкремент нарастания равен (при $\omega_H^2 \gg \omega_0^2$) [9]

$$\frac{3^{1/2}}{2^{4/3}}\left(\frac{\omega_1^2\omega_0^2}{\omega_H^4}\frac{\cos^4\theta}{\sin^4\theta}\right)^{1/3} \qquad (1)$$

для частот $\omega_0|\cos\theta|$ соответствующий инкремент равен

$$\frac{3^{1/2}}{2^{4/3}}\left(\frac{n_1}{n_0}\right)^{1/3} \qquad (2)$$

* Доклад CN-10/230, представленный на конференцию. Докладчик: И. Ф. Харченко. Дискуссия (на английском языке) по этому докладу дана на стр. 1111. Переводы аннотаций находятся в конце тома.

При движении пучка через плазму возможно возбуждение «гибридных» частот $(\omega_H \cdot \Omega_H)^{1/2}$ [10], соответствующий инкремент нарастания равен

$$\frac{3^{1/2}}{2^{4/3}}\left(\frac{n_1}{n_0}\right)^{1/3} \tag{3}$$

где ω_1 — ленгмюровская частота пучка;
ω_0 — ленгмюровская частота плазмы;
ω_H — электронно-циклотронная частота плазмы;
n_1, n_0 — плотность пучка и плазмы, соответственно;
Ω_H — ионно-циклотронная частота.

При рассматриваемом взаимодействии возможно возбуждение колебаний, обусловленное аномальным эффектом Допплера. При этом могут также возбуждаться «гибридные» частоты $(\omega_H \Omega_H)^{1/2}$ [10] и частоты порядка $(\omega_H^2+\omega_0^2 \sin^2\theta)^{1/2}$. Однако они будут отличаться от предыдущих условиями возбуждения и инкрементами нарастания. В частности, инкременты нарастания в этих случаях равны

$$\frac{\omega_1}{2\omega_0}\left(\frac{M}{m}\right)^{1/4}; \quad \frac{\omega_1\omega_0}{2\omega_H^2}\sin^2\theta. \tag{4}$$

Если электроны пучка имеют составляющие скорости, поперечные к магнитному полю, то при движении через плазму возможно возбуждение колебаний, обусловленное нормальным эффектом Допплера в тех же областях частот. При этом инкремент нарастания и условия возбуждения будут отличаться от предыдущих случаев. Так, например, для частот $(\omega_H^2+\omega_0^2 \sin^2\theta)^{1/2}$ инкремент нарастания равен [9, 12]:

$$0{,}4\left(\frac{n_1}{n_0}a_e^2\frac{\omega_0^4}{\omega_H^4}\sin^2\theta\cos^2\theta\right)^{1/3} \tag{5}$$

где a_e — классический радиус электрона.

Кроме высокочастотных колебаний, взаимодействие пучка электронов с плазмой приводит к возбуждению ионно-циклотронных и низкочастотных колебаний.

Ионно-циклотронные колебания обусловлены аномальным эффектом Допплера и их инкремент нарастания равен [10]:

$$\frac{\omega_1}{2\omega_0}\frac{v_0^2}{v_A^2}\frac{m}{M}(1+\cos^2\theta) \tag{6}$$

где v_0 — скорость пучка;
v_A — Альфвеновская скорость.

Кроме того, возможно возбуждение Альфвеновских волн, ионноакустических и магнитозвуковых волн. Следует отметить, что приведенные соотношения, определяющие области возбуждаемых частот и инкременты нарастания, получены для случая безграничной плазмы и пучка и поэтому они могут значительно отличаться от соответствующих значений для ограниченной плазмы и пучка. Так, например, при возбуждении частот $(\omega_H^2+\omega_0^2)^{1/2}$ инкремент нарастания, вычисленный для случая безграничной плазмы и тонкого пучка, равен [10]:

$$\frac{3^{1/6}}{4}\left(\frac{a\omega_0}{v_0}\right)^{2/3}\left[\ln\frac{\alpha}{6e}\right]^{1/3} \tag{7}$$

где

$$\alpha=\frac{2\Omega_0^2(\omega_H^2+\omega_0^2)^2}{\omega_H^6}\left(\frac{v_0}{\omega_0 a}\right)^4 \gg 6e;$$

a — радиус пучка, e — основание натурального логарифма.

Приведенные выше значения для инкрементов нарастания и областей возбуждаемых частот получены в нелинейном приближении. С ростом амплитуды колебаний может стать существенным обратное воздействие колебаний на пучок и плазму, приводящее к изменению направленной скорости в пучке, тепловой скорости и функции распределения по скоростям частиц пучка и плазмы.

Изменение эффективной «температуры» и направленной скорости почти «моноэнергетичного пучка» электронов, взаимодействующего с электронной плазмой, находящейся в магнитном поле, рассматривалось в работе [13]. В предельном случае больших напряженностей магнитного поля $(\omega_H \gg \omega_0)$ были получены следующие формулы для изменения со временем поперечной $(\theta_\perp)$ и продольной $(\theta_\parallel)$ температуры, а также направленной скорости пучка (v_0).

$$\left(\frac{\Delta\theta}{\theta_0}\right)_\perp=\frac{3(2)^{1/2}}{\pi}\frac{\omega_H^3}{\omega_0^3}\frac{1}{N_\lambda}\frac{e^{\beta_1\tau}}{\tau}+\frac{1}{3\pi}\frac{1}{N_\lambda}\left(\frac{\omega_0}{\omega_H}\right)^2\left(\frac{n_1}{n_0}\right)^{1/2}\frac{e^{\beta_2\tau}}{\tau^{5/2}}$$

$$\left(\frac{\Delta\theta}{\theta_0}\right)_\parallel=\frac{1}{\pi}\left(\frac{2}{3}\right)^{1/2}\frac{1}{N_\lambda}\left(\frac{n_1}{n_0}\right)\frac{e^{\beta_1\tau}}{\tau}+\frac{1}{2^{1/2}\pi}\frac{1}{N_\lambda}\left(\frac{n_1}{n_0}\right)^{1/6}\frac{e^{\beta_2\tau}}{\tau^{3/2}} \tag{8}$$

$$mv_0(\Delta v)=\frac{3(2)^{1/2}}{\pi}\left(\frac{\omega_H}{\omega_0}\right)^3\frac{1}{N_\lambda}\frac{e^{\beta_1\tau}}{\tau}+\frac{1}{2^{5/6}\pi}\frac{1}{N_\lambda}\left(\frac{n_0}{n_1}\right)^{1/6}\frac{e^{\beta_2\tau}}{\tau^{3/2}}$$

Формулы (8) применимы при $\beta_1\tau \gg 1$, $\beta_2\tau \gg 1$. В этих формулах $N_\lambda = n_1\left(\frac{\omega_0}{v_0}\right)^3$; $\tau=\omega_0 t$

$$\beta_1=\left(\frac{4}{27}\right)^{1/4}\left(\frac{\omega_0}{\omega_H}\right)^{1/2}\left(\frac{n_1}{n_0}\right)^{1/2}; \quad \beta_2=\frac{3^{1/2}}{2^{1/3}}\left(\frac{n_1}{n_0}\right)^{1/3}$$

Предполагается, что $n_1 \gg n_0$. Первый член (8) соответствует циклотронной неустойчивости на аномальном эффекте Допплера, второй — черенковской неустойчивости. Эти формулы применимы для времен, при которых тепловая скорость в пучке мала по сравнению с энергией направленной и энергия плазменных колебаний мала по сравнению с энергией направленного движения пучка.

Уравнение, определяющее изменение функции распределения в предположении малости амплитуды колебаний, имеет вид:

$$\frac{\partial f_0}{\partial t}=\frac{\partial}{\partial v_i}\left(D_{ik}\frac{\partial f_0}{\partial v_k}\right) \tag{9}$$

где D_{ik} — тензор коэффициентов в диффузии в пространстве скоростей

$$D_{xx} = D_{yy} = \frac{e^2}{8\pi^3 m^2} \int |E_{\mathbf{k}}|^2 \frac{k_x^2}{k^2} \left(\frac{\delta_{\mathbf{k}}}{(\omega_{\mathbf{k}} - k_z v_z + \omega_H)^2 + \delta_{\mathbf{k}}^2} + \frac{\delta_{\mathbf{k}}}{(\omega_{\mathbf{k}} - k_z v_z - \omega_H)^2 + \delta_{\mathbf{k}}^2} \right) d\mathbf{k}$$

$$D_{xy} = D_{yx} = 0$$

$$D_{zz} = \frac{e^2}{4\pi^3 m^2} \int |E_{\mathbf{k}}|^2 \frac{k_z^2}{k^2} \frac{\delta}{(\omega_{\mathbf{k}} - k_z v_z)^2 + \delta_{\mathbf{k}}^2} d\mathbf{k}$$

$$D_{xz} = D_{zx} = \frac{e^2 v_x}{8\pi^3 m^2} \int |E_{\mathbf{k}}|^2 \frac{k_x^2}{k^2} \frac{k_z}{\omega_H} \times \left(\frac{\delta_{\mathbf{k}}}{(\omega_{\mathbf{k}} - k_z v_z - \omega_H)^2 + \delta_{\mathbf{k}}^2} - \frac{\delta_{\mathbf{k}}}{(\omega_{\mathbf{k}} - k_z v_z + \omega_H)^2 + \delta_{\mathbf{k}}^2} \right) d\mathbf{k}$$

D_{yz} получается из D_{xz} заменой v_x на v_y. Интегрирование в этих формулах производится по $k_z > 0$
$|E_{\mathbf{k}}|^2$ — квадрат амплитуды электрического поля колебания с заданным $\mathbf{k}$

$$\frac{d}{dt} |E_{\mathbf{k}}|^2 = 2\delta_{\mathbf{k}} |E_{\mathbf{k}}|^2$$

$\omega_{\mathbf{k}}$, $\delta_{\mathbf{k}}$ — частота и инкремент нарастания плазменных колебаний.

Таким образом экспериментальное определение возбуждаемых, частот их инкрементов и напряженности поля при взаимодействии пучка с плазмой дает возможность определить изменение функций распределения пучка и плазмы.

Схема экспериментальной установки представлена на рис. 1. Пучок электронов с энергией 1—4 кэв формируется трехэлектродной электронной пушкой (1). Ток в пучке до 50 ма. На выходе электронной пушки пучок может модулироваться резонатором коаксиального типа (2), настроенным на частоту $f_M = 2530$ мгц. Высокочастотная мощность подается в резонатор от магнетрона (11) типа М-32 или клистронного генератора. На выходе из резонатора пучок фокусируется до диаметра 5 мм продольным магнитным полем напряженностью до 200 гс (3) и проходит через колбу с плазмой (4) в магнитном поле (5) до 2000 гс. Плазма образуется в результате ионизации остаточного газа электронным пучком. Благодаря низкому вакууму в колбе

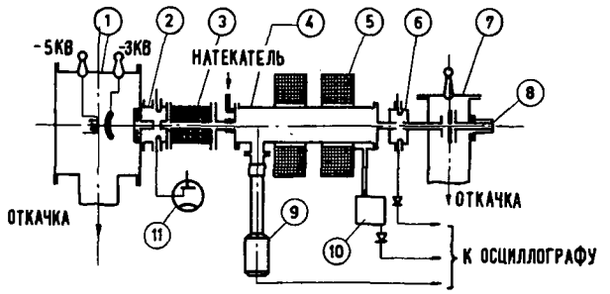

Рис. 1 Схема экспериментальной установки. 1 — электронная пушка; 2 — коаксиальный резонатор; 3 — магнитное поле до 200 гс; 4 — колба с плазмой; 5 — магнитное поле до 2000 гс; 6 — перестраиваемый резонатор; 7 — анализатор; 8 — коллектор; 9 — фотоумножитель; 10 — волномеры; 11 — магнетрон.

(10^{-2}—10^{-3} мм ртст) и сравнительно небольшой энергии электронов плотность плазмы может достигать значений порядка $n_0 = 10^{11}$.

Плотность измерялась по смещению резонансной частоты цилиндрического резонатора, укрепленного на колбе (на рисунке не показан). С помощью перестраиваемого резонатора (6) и анализатора энергий электронов (7), расположенных на выходе из зоны взаимодействия, измерялись высокочастотные колебания и энергия пучка электронов. Кроме того, высокочастотные и низкочастотные колебания исследовались в токе, поступающем на коллектор (8), на антенну-диполь, помещенную вне колбы и при помощи зондов помещенных в колбу. В этих случаях частота и интенсивность колебаний измерялись при помощи анализаторов спектра, волномеров (10) и катодного осциллографа. Для исследования спектра энергий частиц плазмы применялся сцинтилляционный кристал NaI с фотоумножителем (9), а также снимались зондовые характеристики.

Проведенные на этой установке эксперименты показали, что при определенных значениях магнитного поля первоначально немодулированный электронный пучок становится неустойчивым. Эта неустойчивость проявляется в увеличении интенсивности свечения и диаметра пучка сильном возрастании потерь энергии пучка электронов, увеличении энергии частиц плазмы, и возбуждении колебаний в пучке и в плазме (автомодуляция пучка). На частотах, близких к $f = (f_c^2 + f_p^2)^{1/2}$, где $f_c = eH/2\pi mc$ — электронно-циклотронная частота плазмы, $f_p = (e^2 n/m\pi)^{1/2}$ — плазменная электронная частота. Расположение областей неустойчивости в зависимости от магнитного поля определяется давлением в колбе, током и энергией пучка. Расположение области неустойчивости в зависимости от скорости пучка v_0 при фиксированном давлении и токе в пучке показано на рис. 2.

Существование неустойчивости для определенной области изменений v_0 можно объяснить тем, что неустойчивость обусловлена эффектом Черенкова на продольных волнах плазмы. В этом случае неустойчивость возникает при скорости пучка v_0,

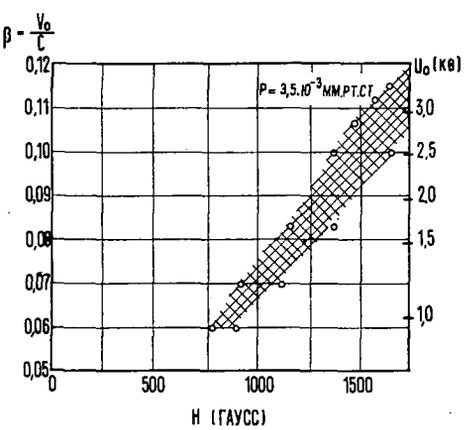

Рис. 2 Расположение области неустойчивости в зависимости от скорости пучка.

близкой к фазовой скорости v_φ продольных волн в плазме. Из дисперсионного соотношения, полученного для ограниченного плазменного цилиндра в продольном магнитном поле [11],

$$v_\varphi^2 \approx \frac{c^2(f_c^2-f^2)(f_p^2-f^2)}{\left(\frac{c^2}{10a^2}-f^2+f_p^2\right)(f_c^2+f_p^2-f)} \qquad (10)$$

(где a — радиус плазмы) следует, что условие $v_0 \approx v_\varphi$ выполняется только в определенной области изменения параметров плазмы и наоборот, при фиксированных параметрах плазмы имеется область скоростей v_φ соответствующих v_0. Возбуждение в области частот $(f_c^2+f_p^2)^{1/2}$ может быть обусловлено также аномальным эффектом Допплера. Однако, при этом изменяются условия возбуждения и инкременты.

Точное сопоставление теории с экспериментом в данном случае невозможно, так как недостаточно точно измерена плотность плазмы, от которой сильно зависят параметры, характеризующие взаимодействие, и недостаточно полно исследованы зависимости, характеризующие инкремент нарастания.

При взаимодействии пучка электронов с плазмой происходит автомодуляция пучка, приводящая к тому, что первоначально однородный пучок разбивается на отдельные сгустки, когерентно взаимодействующие с волной. При этом потери каждой частицы в сгустке возрастают пропорционально числу частиц в сгустке. Первоначально узкий спектр энергий со средней энергией 3 кэв размывается в сторону низких энергий до 500 эв (рис. 3). Средние потери энергии электронов в пучке достигают 50 эв/см. Широкое размытие спектра обусловлено тем, что при автомодуляции электроны попадают в различные фазы возбуждаемой волны и замедляются различным образом на длине взаимодействия. Небольшая часть электронов, попавшая в ускоряющие фазы, имеет энергию больше первоначальной.

Измеренные частоты колебаний в зависимости от магнитного поля отложены на рис. 4 для различных давлений и скоростей пучка. В областях, где пучок устойчив, наблюдались колебания на электронно-циклотронной частоте в диапазоне частот от 1500 до 3500 мгц. Полуширина спектра этих колебаний составляет 30—50 мгц. Такого

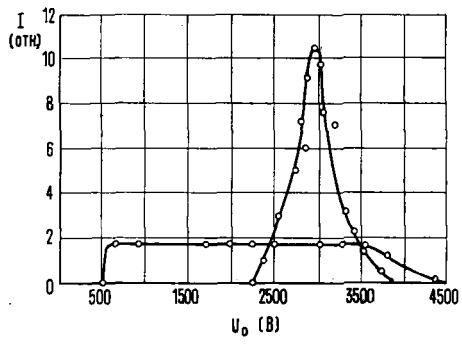

Рис. 3 Кривая спектра энергий.

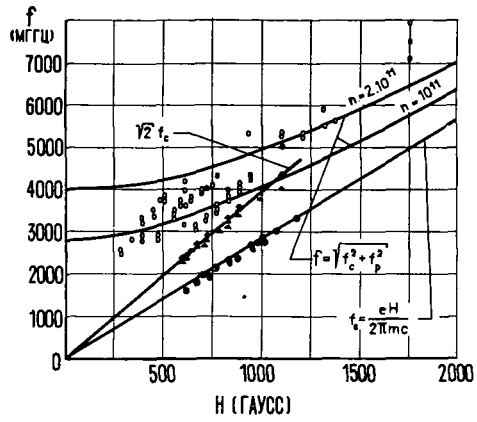

Рис. 4 Измененные частоты колебаний в зависимости от магнитного поля.

типа колебания в пучке при прохождении его в области с низким вакуумом были экспериментально обнаружены в работах [6, 7].

При выборе параметров (скорости пучка и давления в колбе), соответствующих неустойчивому состоянию пучка появляются частоты в пределах

$$f = (f_c^2 + f_p^2)^{1/2}$$

На графике (рис. 4) показаны расчетные кривые этих частот для плотности плазмы 10^{11} и 2×10^{11}, что соответствует измеренной плотности плазмы в области неустойчивости. Измеренные частоты лежат в области перекрываемой расчетными кривыми. Разброс точек соответствует различным давлениям в колбе, то есть различной плотности плазмы.

Исследование распределения полей при помощи антенны диполя вне колбы показало, что напряженность электрического поля высокочастотных колебаний наибольшая для компонент E_φ и E_r, а $E_z=0$.

Увеличение напряженности высокочастотного поля наблюдается в направлении, обратном движению пучка, то есть поле максимально в месте входа пучка в плазму. Такое распределение поля соответствует области аномальной дисперсии волн в плазменном волноводе (обратная волна).

Заметим, что возбуждение колебаний точно на частоте $f=(f_c^2+f_p^2)^{1/2}$ теоретически невозможно, если элементарным процессом, лежащим в основе возбуждения, является эффект Черенкова, так как при этом $v_\varphi=\infty$. Следует отметить, что формула $f=(f_c^2+f_p^2)^{1/2}$ выведена для безграничной плазмы и при наличии границ непригодна.

При изменении плотности плазмы при фиксированном магнитном поле обнаружен резонанс для $f_p=f_c$. При этом возбуждаемая частота равна $f=2^{1/2}f_c=2^{1/2}f_p$ (прямая $2^{1/2}f_c$ на рис. 4). В этом случае интенсивность колебаний сильно возрастает, плазменный шнур достигает стенок колбы, наблюдается искрение и нагрев стенок колбы. Эти результаты можно объяснить тем, что с ростом амплитуды возбуждаемых колебаний возникают нелинейные эффекты, приводящие к возникновению

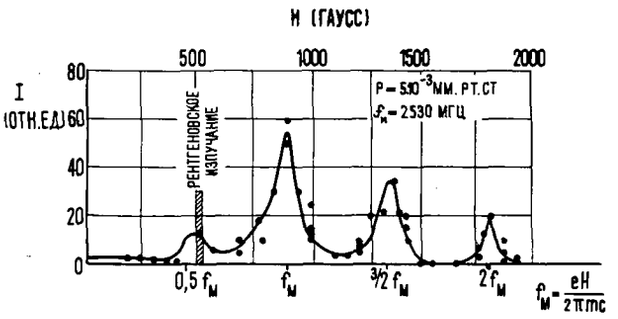

Рис. 5 Кривая интенсивности колебаний в пучке.

связей между продольными и поперечными колебаниями в плазме. Так например [14], при выполнении условия $f_c = nf_p/2$ ($n = 2, 3, \ldots$) энергия продольных колебаний плазмы, возбуждаемых пучком, движущимся вдоль магнитного поля, переходит в энергию поперечного (к магнитному полю) движения частиц плазмы.

Предварительная модуляция пучка срывает неустойчивость в указанных выше областях. Это происходит благодаря тому, что системе навязывается длина волны отличная от резонансной. Появляющиеся при этом новые более узкие области неустойчивости определяются зависимостью

$$f_c = \frac{nf_M}{2}$$

где ($r = 1, 2, 3 \ldots$)

На рис. 5 показана интенсивность колебаний в пучке предварительно промодулированная на частоте $f_M = 2530$ мгц в зависимости от магнитного поля. Усиление колебаний наблюдается при магнитных полях равных 450, 880, 1300 и 1800 гс, что соответствует электронно-циклотронным частотам примерно равным

$$f_M/2,\ f_M,\ 3f_M/2 \text{ и } 2f_M.$$

Такое соотношение частот соответствует возбуждению параметрического резонанса в системе пучок-плазма.

При движении модулированного пучка через плазму возникают периодические во времени и пространстве электромагнитные поля. В системе отсчета, связанной с пучком, электроны плазмы двигаются в этом пространственно-периодическом поле, вращаясь одновременно с частотой f_c.

Если через L обозначить пространственную периодичность поля в пучке, то параметрический резонанс должен иметь место при выполнении условия

$$\frac{v_0}{L} = \frac{2f_c}{n}$$

В первой области усиления при $f_c = f_M/2$ (рис. 5) интенсивность колебаний незначительна, но при исследовании рентгеновского излучения в ней обнаружено излучение, соответствующее энергии электронов до 20 кэв. Таким образом, в этой области происходит сильная передача энергии от пучка к электронам плазмы. Уменьшение интенсивности колебаний по сравнению с другими областями можно объяснить этим же эффектом. Тот факт, что рентгеновское излучение наблюдается только в этой области, объясняется уменьшением ширины областей параметрического возбуждения с ростом n. Возможно, поэтому этот эффект не был обнаружен в других областях благодаря недостаточной стабильности питающей аппаратуры.

Кроме высокочастотных колебаний в области неустойчивости при немодулированном и модулированном пучке наблюдались также интенсивные колебания в области частот 1—10 кгц и 100—500 кгц. Эти колебания обнаружены в пучке и при помощи антенны вне колбы. Частоты порядка тысячи герц принадлежат области магнитогидродинамических волн, частоты порядка сотен килогерц соответствуют области ионных-циклотронных частот. Для более точной их классификации требуется измерения длины волны колебаний и распределения полей.

Неустойчивость при взаимодействии пучка с плазмой сопровождается значительной диффузией ионов на стенки колбы. Ионный ток измерялся при помощи цилиндрических и плоских зондов, помещенных вблизи стенок колбы. Плотность ионного тока составляла около 1 ма/см^2. При подаче положительного потенциала на зонд ионный ток уменьшался до нуля при потенциале на зонде 10—20 в.

Важной характеристикой эффекта взаимодействия пучка с плазмой является инкремент нарастания колебаний, возбуждаемых пучком, и время установления стационарного режима. Инкремент определяет скорость развития неустойчивости на начальной стадии, когда еще справедлива линейная теория. Время релаксации характеризует переход от колебаний малой амплитуды к установившемуся режиму, то есть переход от линейных к нелинейным установившимся колебаниям. При визуальном наблюдении процесса установления стационарного режима возможно также определение относительного значения амплитуды колебаний в любой момент времени к амплитуде установившихся колебаний. Наблюдения процесса развития неустойчивостей и установления стационарного режима можно осуществить при работе в импульсном режиме.

Для колебаний в области сотен килогерц время развития (до установления амплитуды), определенное экспериментально, составляет 50 мксек, а инкремент нарастания равен 4×10^5.

Для колебаний в области нескольких килогерц инкремент нарастания определялся по полуширине резонансной кривой и равен 2×10^4. Эти значения совпадают по порядку величины с теоретическими значениями в области ионно-циклотронных и магнитогидродинамических волн. Однако, полное сопоставление возможно только после классификации этих волн.

Значительно быстрее происходит развитие высокочастотных неустойчивостей. Инкремент нараста-

ния, измеренный по полуширине резонансной кривой, в этом случае составляет 2×10^9. Теоретическое значение инкремента для продольных колебаний в магнитном поле равно $0{,}5 \times 10^9$.

*

Таким образом, в работе экспериментально определены условия образования неустойчивостей при взаимодействии модулированного и немодулированного пучка электронов с плазмой в магнитном поле, измерены спектры высокочастотных и низкочастотных колебаний в областях неустойчивости, исследовано параметрическое усиление колебаний в первоначально модулированном пучке, измерена потеря энергии пучка электронов и обнаружено увеличение энергии электронов плазмы при параметрическом резонансе и резонансе при $f_p = f_c$. Неустойчивости сопровождаются сильной диффузией частиц на стенки колбы.

Эффективный обмен энергией между пучком и плазмой указывает на возможный способ разогрева плазмы при помощи пучка заряженных частиц. В этом случае имеется основание предполагать, что возможна передача энергии от электронов большой энергии ионам плазмы в результате соударений или при наличии резонанса между частотой волны и одной из характерных ионных плазменных частот.

Обнаруженное интенсивное высокочастотное излучение из плазмы можно использовать как источник высокочастотных колебаний малых длин волн (при увеличении магнитного поля и плотности плазмы), так и для измерения параметров плазмы.

Литература

[1] Boyd, G., Field, L., Gold, R., *Phys. Rev.* **109** (1958) 1392.

[2] Кислов В. Я., Богданов Е. В. *Радиотехн. Электр.* **5** (1960) 1974.

[3] Харченко И. Ф., и др, *Ж. эксп. теор. Физ.* **38** (1960) 685; Мирн. использ. ат. энергии мат. Междун. Конф. Женеве (1958) Доклад № 2211.

[4] Ахиезер А. И., Файнберг Я. Б., *Ж. эксп. теор. Физ.* **21** (1951) 1262 *Докл. Акад. Наук СССР* **69** (1949) 559.

[5] Bohm, D., Gross, E., *Phys. Rev.* **75** (1949) 1851; **79** (1950) 992.

[6] Ettenberg, M., Jorg, R., Proc. Sympos. Electron. Waveguides (New York, 1958) 379.

[7] Kato, K., *J. phys. Soc. (Japan)* **15** (1960) 1093.

[8] Харченко И. Ф., Файнберг, и др, *Ж. техн. Физ.* **31** (1961) 7.

[9] Степанов К. Н., Киценко А. Б., *Ж. техн. Физ.* **31** (1961) 168.

[10] Горбатенко М. Ф., Отчет ФТИ АН УССР (1960).

[11] Файнберг Я. Б., Шапиро В. Д. Отчет ФТИ АН СССР (1959).

[12] Шевченко В. И., Дипломная работа ХГУ, Харьков (1960).

[13] Шапиро В. Д., Шевченко В. И. *Ж. эксп. теор. Физ.* **42** (1962) 1536.

[14] Пашицкий Э. А. Отчет Института Физики Академии Наук УССР (1961).

DISCUSSIONS (SESSION IX) — DISCUSSIONS (SÉANCE IX) — ДИСКУССИИ (ЗАСЕДАНИЕ IX) — DEBATES (SESIÓN IX)

Paper CN-10/94 *was presented by C. Etievant* (France). *The text of the paper is on pages 1025—1031. The following discussion took place:*

R. Motley *(United States of America):* In the last experiment you reported, did you observe a critical beam current for the generation of these waves near the ion frequency?

C. Etievant: The conditions for generating such oscillations are very critical, and we don't observe them for low values of $\varepsilon = n_f/n_e$.

T. Consoli *(France):* What was the frequency stability of the klystron in the measurements that you have described?

C. Etievant: If the klystron was very unstable, it would produce fluctuations of the position of the cavity even in the absence of the plasma. We have never observed a swinging of the resonance peak in the absence of plasma. I can say that the fluctuations of frequency have never exceeded 200 kHz during one experiment, this would be much less than the shift produced by the plasma. The fluctuations observed cannot be explained by the klystron frequency instability; the former are several orders of magnitude greater than the latter.

T. Consoli: What was the power injected into the cavity?

C. Etievant: This power was of the order of 100 micro-watts.

T. Consoli: Did you observe anomalous behaviour of the cavity when $\omega_{oc} = \omega/2$?

C. Etievant: This would occur in our case for a magnetic field of the order of 1,500 gauss. We have not observed anomalous behaviour for this magnetic field, but we have not worked very often at this value of the magnetic field.

C. C. Chang *(United States of America):* Did you measure the density distribution in the electron beam and the plasma ion and electron density in the stable region?

C. Etievant: Yes.

C. C. Chang: Have you measured the spatial distribution of this density?

C. Etievant: We have made these measurements along the beam and we observed a weak density gradient in the direction of motion of the beam. The radial profile of plasma density has not yet been measured; our method gives the measure of the average density.

C. C. Chang: Recently we developed a theory that can predict the distribution of the high velocity electrons in the beam and also the ion and electron distribution in the plasma in equilibrium condition for such a geometry.

Paper CN-10/163 *was presented by J. Dawson* (United States of America). *The text of the paper is on pages 1033—1043. The following discussion took place:*

R. J. Tayler *(United Kingdom):* The results you presented showed a tendency towards a Maxwellian distribution when averaged over all space. Do you have enough particles to be able to make any significant estimate on how close you are approaching a Maxwellian distribution, averaging over different regions of space rather than over all space?

J. Dawson: There were 280 particles per wavelength for the most unstable mode. If one looks at regions much smaller than this wavelength, say a quarter of a wavelength, then there are only about 60 particles, and the statistical uncertainty is large, so that one cannot tell very accurately if the local distribution is Maxwellian.

S. Colgate *(United States of America):* What would be your estimate of the increased damping to be expected by scattering into three dimensions?

J. Dawson: Well, personally, I think it would be very large, but that's just an opinion.

G. Kalman *(Israel):* Is there a systematic energy flow towards larger wave numbers? If there is such a behaviour, would you estimate the time in which most of the energy is concentrated in wave number regions larger than the corresponding Debye wavelength? After some time the random motion of particles might become more important than non-linear effects. Do you agree to that?

J. Dawson: There is a large dissipation of the potential energy in a very short time—roughly, a plasma oscillation time. The dissipation results from the energy being fed out of the lower modes into the higher modes. Then this energy is rapidly dissipated, presumably into just particle motion because you can't find it in any one mode any more and this dissipation is uniform over all wavelengths.

H. N. V. Temperley *(United Kingdom):* The effect that much of the energy stays with the low modes is similar to that found by Fermi et al. (Report LA 1940) who studied a one-dimensional assembly of oscillators with non-linear coupling. What seems to me to be a satisfactory explanation of this has very recently been published by J. Ford (*J. Math. Phys.* 2 (1961) 387). I believe that an explanation of the present results should be looked for on similar lines.

J. Dawson: Similar calculations to those of Fermi have been carried out by myself for the one dimensional plasma. That is, the plasma was started out with all the energy in the lowest Fourier mode. The reference if given in the paper. The behaviour found by Fermi was not found in this case. That is, the energy did not return to the lowest mode but went mainly into the particles. There seems to be a dissipation mechanism which works for the plasma model and which did not work for Fermi's model. It comes from the fact that the sheets can pass freely through each other. I am of the opinion that such an explanation as Ford's is too simple. In fact, even for the Fermi model Ford does not get agreement with the calculations. In some more recent work at Princeton, Jackson has computed the recursion time for the case run by Fermi and got similar results. He, however, finds he must use a more complicated analysis than Ford uses.

O. Bunemann *(United States of America):* As regards the progression of energy from long wavelengths to short wavelengths, this has been observed in our calculations on the electron-ion system. It seems to be akin to turbulence. You know the old rhyme "Big whirls have lesser whirls which feed on their velocity; little whirls have lesser whirls right down to viscosity."

Paper CN-10/262 *was presented by M. Ioffe* (Union of Soviet Socialist Republics). *The text of the paper is on pages 1045—1047. The following discussion took place:*

L. Spitzer *(United States of America):* These are certainly most fascinating results. I should like to ask a question about the geometry of the field. Have you computed the radial dependence of the average total magnetic field along the lines of force? The reason I ask this question is that our computations for the stellerator, where we use similar multi-polar windings, show that when one puts on multi-polar windings, the magnetic field actually decreases with increasing distance from the center rather than increases. One can see this quite simply. because the multi-polar field winding increases the length of the line of force and since the line integral of the magnetic field is fixed, this increase of the length must lead to a decrease in the total magnetic field. The exact mechanism by which this is produced in the stellerator is complicated; we have followed it through. I'm wondering whether there is not perhaps some similar mechanism in this device which might even lead to a decrease in the magnetic field with increasing distance from the center.

M. Ioffe: We have not yet made any detailed measurements of the radial dependence of the absolute value of the total magnetic field. Nevertheless, there are no reasons to doubt the fact that by passing sufficiently high current through the conductors it is always possible to produce the total field which increases in the radial direction. In the case considered here, the field of the conductors and the main field are mutually perpendicular; therefore the absolute value of the total field is equal to $(H_0^2+H_g^2)^{1/2}$, where H_0 is the main field and H_g is the field of the conductors.

R. F. Post *(United States of America):* I think it is extremely gratifying to see consistent work on a single system rewarded this way.

I suggest that in order to bring agreement in understanding of these results with respect to our own (at high electron temperature), where anisotropy seems to play a dominant role in establishing any kind of unstable behaviour, that we must understand whether the following is true: Does the change in the magnetic geometry result in a change (reduction) in the anisotropy of the plasma, and does this in turn influence the presence or absence of instabilities? If it does, we can then better understand these experiments as compared to our own.

M. Ioffe: I agree with Dr. Post that with a new configuration of the field it is possible that a change in the degree of anisitropy in ion distribution occurred. The question of whether the increase in stability is due to decrease of anisotropy requires an experimental check, but from last night till this morning I could not think of any such experiment.

G. von Gierke *(Federal Republic of Germany):* I just want to comment on Dr. Spitzer's question; there is a big difference between the stellerator and the magnetic bottle with additional multipolar windings. You have in the latter case no rotational transform. Therefore, the magnetic lines of force are not lengthened and the magnetic field will be increasing towards the walls in all directions.

T. Stix *(United States of America):* In your former geometry which was axially symmetric so that the rotation of the plasma could be expected due to the initially applied electric field, I believe you observed such a rotation experimentally. I would like to ask whether you would expect rotation in this new more complicated geometry and what would now be the expected pattern for plasma flow?

M. Ioffe: The effect of plasma rotation is of importance in displacing plasma towards the walls only during the time the electric field is applied. After the external electric field is off, the rotation soon slows down to zero. All measurements of the confinement time mentioned in the paper were made 20—30 μs. after the electric field was off.

As for the question in the new field geometry, it has not yet been investigated.

W. I. Linlor *(United States of America):* Could you give a brief description of your source of plasma? Is there an applied radial electric field during containment time measurements?

M. Ioffe: The source of plasma was a discharge in hydrogen with a hot cathode in the longitudunal magnetic field. The hot cathode was made of tungsten, 10 mm in diameter. The anode was made of copper in a form of a cylinder 20 mm in diameter and 20 mm long, cooled by water. Plasma created in this discharge is flowing along the magnetic field lines as a cylindrical column at the center of the trap passing through the whole of its length.

All confinement time measurements were done after switching the electric field off so that there was no external electric field.

J. Tuck *(United States of America):* The new geometry discussed by Dr. Joffe is an interesting marriage between the mirror machine and the cusped geometry, the former, in the mid-plane, having a magnetic field magnitude decreasing with radius, and the latter an increasing one. I would like to ask: At what point does Dr. Joffe characterise the strength of the latter field?

Secondly, such a combined system will have a critical radius such that magnetic lines inside this radius are contained and magnetic lines outside of it intersect the walls. Will you state what this radius is in a particular case, compared with the radius of the walls?

M. Ioffe: The values of the field intensity due to current in the conductors which were mentioned here refer to those points on the surface of the internal stainless steel liner which are situated at the middle of the gap between the conductors. The liner was at a distance of 10 mm from the conductors. As for the radius of the tube of lines of force passing through all the trap without touching its walls, it depends on the ratio of the values of the main magnetic field and of the magnetic field of conductors (when the length of the trap is fixed). With the mirror ratio at the walls of 1.5 the minimum size of this tube of lines of force is 3—5 cm.

I. Golovin *(Union of Soviet Socialist Republics):* In connection with the remarks of Dr. Tuck and Dr. Spitzer, I want to say the following: In the case of stellerator spiral windings, the field is divided into two regions by the surface of the separatrix. In the region inside the separatrix the lines of force do not get on the side walls. The longitudinal components of the field of the spiral windings in this region adding to the main field do not give rise to a resulting field in all radial directions outward. Therefore in magnetic mirror machines where the rotational transform does not help to achieve stability, it is useless to utilize the region inside the separatrix. Outside the separatrix all field lines at some time enter into the side walls of the trap. In this region the total field is increasing towards the walls. If the pitch of the spiral winding is increased, the separatrix is compressed toward the axis. In case of straight rods (when the pitch is infinite), which is Joffe's case, all lines of force with only the exception of the one going along the axis pass through the walls, provided the trap is long enough. The longitudinal component of the field is absent and the resulting magnetic field actually increases in all directions, both toward the side-walls and toward the mirrors, provided there is a corresponding ratio of main magnetic field and the field formed by the rods. Therefore, in such a field conditions of hydromagnetic stability are fulfilled everywhere on the surface of the plasma.

Paper CN-10/134 *was presented by W. Drummond* (United States of America). *The text of the paper is on pages 1049—1057. The following discussion took place:*

O. Bunemann *(United States of America):* The discrepancy between the analytical results by Drummond and the computational results by Dawson and myself was resolved to me by T. E. Stringer, who presents a theory similar to Dr. Drummond's in paper CN-10/53. There is the basic assumption $\gamma/\omega \ll 1$ in the analysis while in the computed examples one had $\gamma/\omega \approx 1$ and even $\gamma/\omega = \infty$. In these cases no plateau was formed in the distribution function, but a Maxwellian was approached very rapidly in a few plasma oscillation periods.

W. Drummond: The discrepancy lies in the assumption of very cold narrow peaks in the distribution function with steep sides and in linearity of the dispersion relation. This causes the generation of harmonics. The second thing is that the growth rate is not proportional in your case to the slope of the distribution function. So these are two quite different cases.

C. C. Chang *(United States of America):* Is your theory applicable to turbulent plasma or non-turbulent plasma? I suspect that the turbulence should be ascribed to the particles and the wave should not be.

W. Drummond: The type of turbulence to which I refer is simply the stationary electric fluctuations associated with the equilibrium wave spectrum, and there are no implications with respect to other types of turbulence.

H. Dreicer *(United States of America):* If I understand this theory correctly, you have a situation in which you start with instability and eventually come back to stability. This means that there is some Landau damping. Could you give an expression for that Landau damping or compare it to the usual term? And also, can you give the maximum amplitude to which the collective plasma oscillations grow before the non-linear effects remove the second peak in the velocity distribution and Landau damping reappears?

W. Drummond: The Landau damping eventually causes the spectrum to decay due to the pushing of the load by mode coupling out into these regions where the slope is negative. The initial Landau damping was simply proportional to this negative

slope. However, because there is some energy in this wave, this slope will change. I can't give the numerical value. However, before this process proceeds too far, collisions will intervene in the practical plasma. So the collision damping time would be more characteristic.

As for the second question, the maximum amplitude of the oscillations is given in the text of the paper. However, it should be pointed out that the energy in these oscillations is extremely small compared to the kinetic energy of the plasma; yet the electric wave amplitudes are many orders of thermal noise.

Paper CN-10/169 *was presented by M. J. Kofoid* (United States of America). *The text of the paper is on pages 1059—1066. The following discussion took place:*

K. Emeleus *(United Kingdom):* Some years ago we did calculations, not as detailed as these but roughly on the same lines, from which we were able to find the minimum diameter of a beam in which oscillations could grow using Sumi's values for the spatial and time growth rates. They agreed in order of magnitude with the very much more detailed work which Dr. Kofoid has now described. We have also observed the "blow-up" of oppositely directed beams which Dr. Kofoid mentioned. It may be of importance in producing randomizing under some circumstances. It may also be of significance that it can occur without the presence of fields other than small stray magnetic fields.

C. C. Chang *(United States of America):* I wonder whether you did make some measurements on deuterium?

J. Kofoid: No, we have only made tests in the noble gases.

Paper CN-10/209 *was presented by E. Zavoisky* (Union of Soviet Socialist Republics). *The text of the paper is on pages 1073—1077. The following discussion took place:*

T. Consoli *(France):* What was your frequency in this experiment?

E. Zavoysky: The linear frequency was 10^7 Hz.

F. Schwirzke *(Federal Republic of Germany):* If you have such a high absorption of energy, how high is the temperature in your experiment? Have you measured this?

E. Zavoysky: In our experiment the absorption took place in the time of the order of one half of the period of oscillation; i.e., in 5×10^{-8} sec. During this time electrons could get heated. It is natural that the transfer of energy from electrons to ions does not occur. In the experiment the plasma density of 2×10^{13} was produced by passing a direct current which was switched off at the moment of application of the high-frequency voltage. Electron temperature can be calculated from the energy absorption and is estimated to go up to 200 eV.

O. Bunemann *(United States of America):* What was the electron plasma frequency?

E. Zavoysky: The square of the Langmuir frequency will be 3.2×10^9 n, in our case n is approximately 1.7×10^{13}; i.e., the frequency is about 10^{11}.

H. Dreicer *(United States of America):* Could you please say whether there is any absorption in the absence of an applied magnetic field?

E. Zavoysky: In the absence of the applied magnetic field there is an absorption, but it is considerably weaker than in the region of hybrid frequency, as is seen on the last photograph.

Paper CN-10/231 *was presented by V. Tolok* (Union of Soviet Socialist Republics). *The text of the paper is on pages 1079—1082. The following discussion took place:*

T. Consoli *(France):* Would you specify whether the high frequency power which you have measured corresponds to vacuum conditions or to conditions with plasma? What fraction of power is transferred to the plasma?

V. Tolok: In the absence of plasma the generator power is equal to twice the power that is going into the plasma; that is, the efficiency is about 50%. This also corresponds to results obtained at Princeton.

J. Wilcox *(United States of America):* Do you say that the efficiency of the power transferred from the oscillator to the hydromagnetic wave is 50%.

V. Tolok: Yes, we have 50% if the coil is excited.

Paper CN-10/165 *was presented by W. M. Hooke* (United States of America). *The text of the paper is on pages 1083—1087. The following discussion took place:*

J. Wilcox *(United States of America):* How efficient was the transfer of energy from the oscillators to the hydromagnetic wave in your experiment?

W. M. Hooke: We have made measurements of the wave power flux and have obtained values of around 100 kW. We do not yet have good simultaneous measurements of the power delivered by the oscillator.

D. F. Jephcott *(United Kingdom):* In the case of a partially ionized plasma, the damping effect of ion-neutral collisions can considerably modify the behaviour of the wave in the region of ion-cyclotron resonance. Has the speaker considered the effect of this damping in the results presented?

Prof. L. C. Woods has treated this problem in a comprehensive theory of hydromagnetic wave propagation (Culham Laboratory Report CLM-R5).

W. M. Hooke: We have made *rough* estimates of the effects of neutrals. We concluded that for these experiments, where the plasma temperature is probably only a few tenths of an electron volt, that electron-ion interactions dominate all other collision processes. We have also calculated that in the region where there is good agreement between experiment and the theory outlined here, none of the various damping mechanisms should have any important effect on wavelength. No dissipative mechanisms were included in the theoretical curves shown here.

D. F. Jephcott: What in fact is the degree of ionization in these experiments?

W. M. Hooke: The degree of ionization is apparently greater than 50%. As the plasma decays this degree of ionization must decrease.

The agreement between theory and experiment is, however, even better for the more weakly ionized plasma. This indicates that the effect of neutrals is probably not important. This is also the conclusion reached from our own theoretical estimates. The ratio of our wave frequency is higher than in most experiments because of our relatively high wave frequency; i.e. $\omega = 100$ MHz.

Paper CN-10/171 *was presented by S. C. Brown* (United States of America). *The text of the paper is on pages 1089—1099. The following discussion took place:*

T. Kihara *(Japan):* Are the authors assuming that the refractive index is close to 1?

S. C. Brown: That is correct.

T. Kihara: I would like to comment on one type of emission which corresponds to large values of the refractive index. If the plasma contains electrons with high energies, these electrons will emit Cherenkov radiation even when their velocities are non-relativistic. It is true that this radiation is mostly reflected at the surface of the plasma since it corresponds to large values of the refractive index. But even then a considerable amount of the radiation energy may go out from the plasma; and the loss is, under certain circumstances, comparable to the bremsstrahlung.

S. C. Brown: Actually, the case you are discussing is not the one we have calculated. We did not make calculations for the case in which the refractive index was very different from unity. We must calculate for the case where the refractive index is very close to one and the electron density is low.

R. Motley *(United States of America):* On one of your slides you showed the radiation temperature in hydrogen increasing as a function of magnetic field and, for the most part, decreasing with magnetic field for helium. Do you have any explanation for these features?

S. C. Brown: Dr. Bekefi will answer this question.

Paper CN-10/230 *was presented by I. Khartchenko* (Union of Soviet Socialist Republics). *The text of the paperis on pages 1101—1106. The following discussion took place:*

L. Spitzer *(United States of America):* Could you tell me please what the plasma diameter, the plasma length and the diameter of the electron beam were?

I. Khartchenko: The plasma diameter was 60 mm, the length of the region where interaction took place was from 5 cm to 350 cm, and the beam diameter was about 0.4 mm.

KEY TO TRANSLITERATION – SESSIONS VII AND IX

Арцимович, Л. А.	Artsimovich, L. A.
Афросимов, В. В.	Afrosimov, V. V.
Бабыкин, М. В.	Babykin, M. V.
Березин, А. Б.	Berezin, A. B.
Бондарев, В. А.	Bondarev, V. A.
Велихов, Е. П.	Velikhov, E. P.
Гладковский, И. П.	Gladkovsky, I. P.
Головин, И. Н.	Golovin, I. N.
Горбунов, Е. П.	Gorbunov, E. P.
Готт, Ю. В.	Gott, Yu. V.
Долгов-Савельев, Г. Г.	Dolgov-Savelev, G. G.
Ермаков, А. И.	Ermakov, A. I.
Завойский, Е. К.	Zavoysky, E. K.
Зайдель, А. Н.	Zaidel, A. N.
Иоффе, М. С.	Ioffe, M. S.
Кадомцев, Б. Б.	Kadomtsev, B. B.
Калинкевич, И. Ф.	Kalinkevich, I. F.
Карташев, К. Б.	Kartashev, K. B.
Кован, И. А.	Kovan, I. A.
Корнилов, Е. А.	Kornilov, E. A.
Ларионов, М. М.	Larionov, M. M.
Лобко, А. С.	Lobko, A. S.
Луценко, Е. И.	Lutsenko, E. I.
Малышев, Г. М.	Malyshev, G. M.
Муховатов, В. С.	Mukhovatov, V. S.
Назаров, Н. И.	Nazarov, N. I.
Николаев, Р. М.	Nikolaev, R. M.
Патрушев, Б. И.	Patrushev, B. I.
Педенко, Н. С.	Pedenko, N. S.
Раздобарин, Г. Т.	Razdobarin, G. T.
Рудаков, Л. И.	Rudakov, L. I.
Русанов, В. Д.	Rusanov, V. D.
Савенков, А. М.	Savenkov, A. M.
Синельников, К. Д.	Sinelnikov, K. D.
Скидан, В. В.	Skidan, V. V.
Скорюпин, В. А.	Skoryupin, V. A.
Стрелков, В. С.	Strelkov, V. S.
Тельковский, В. Г.	Telkovsky, V. G.
Толок, В. Т.	Tolok, V. T.
Файнберг, Я. Б.	Fainberg, Ya. B.
Федоренко, Н. В.	Fedorenko, N. V.
Франк-Каменецкий, Д. А.	Frank-Kamenetsky,
Харченко, И. Ф.	Kharchenko, I. F.
Шепелев, М. Н.	Shepelev, M. N.
Явлинский, Н. А.	Yavlinsky, N. A.

LIST OF PARTICIPANTS

AUSTRALIA

MESSERLE, H.	Department of Electrical Engineering, University of Sydney, Sydney.
MILNER, C.	Department of Applied Physics, University of New South Wales, P.O.B. 1, Kensington, Sydney.
OLIPHANT, Sir MARK	Australian National University, Box 4 G.P.O., Canberra, A.C.T.
WATSON-MUNRO, Prof. C.	University of Sydney, Sydney.

AUSTRIA

BERGMANN, Dr. O.	University of Alabama, USA.
BOLTERAUER, H.	University of Vienna, Josefsgasse 7, Vienna VIII.
HEJTMANEK, Dr. J.	Atominstitut der Österreichischen Hochschulen, Karlsplatz 13, Vienna IV.
HIGATSBERGER, Univ. Doz. M.	Österreichische Studiengesellschaft für Atomenergie GmbH, Lenaugasse 10, Vienna VIII.
LOIDL, A.	Federal Ministry for Trade and Reconstruction, B.V.F.A., Arsenal, Objekt 221, Vienna III.
PUTZ, F.	Reaktor IG, Lenaugasse 8, Vienna VIII.
RENNER, Dipl. Ing. R.	Federal Ministry for Trade and Reconstruction, Stuben Ring 1, Vienna I.
SIGMAR, Dipl. Ing. D.	Lehrkanzel für Theoretische Physik, Technische Hochschule, Lazarettgasse 9/3/40, Vienna IX.
SIMEK, Univ. Ass. A.	I. Physikalisches Institut, University of Vienna, Strudlhofgasse 4, Vienna IX.
STADLMAIER, G.	I. Physikalisches Institut, University of Vienna, Strudlhofgasse 4, Vienna IX.
WEIL, J.	I. Physikalisches Institut, University of Vienna, Strudlhofgasse 4, Vienna IX.

BELGIUM

CALLEBAUT, D.	Institut Interuniversitaire des Sciences Nucléaires, Hollenaarstr. 65, Oestrakker.
HOYAUX, M.	Division Nucléaire, Ateliers de Construction Electrique, Charleroi.
VANDENPLAS, P.	Centre de Sciences Nucléaires, Ecole Royale Militaire, 30 Avenue de la Renaissance, Bruxelles 4.
VANHAUWERMEIREN, M. R.	I.I.S.N., Université Libre de Bruxelles.

BULGARIA

BORISSOV, Prof. M.	Physics Institute of the Bulgarian Academy of Sciences, Novembre 1, Sofia 7.

CANADA

CURZON, Dr. F.	Department of Physics, University of British Columbia, Vancouver 8.

CZECHOSLOVAKIA

PEKAREK, L.	Physics Institute of the Czechoslovak Academy of Sciences, Vincna 7, Prague 2.
SEIDL, Dr. M.	Czechoslovak Academy of Sciences, Institute of Vacuum Electronics, Nademlynska 600, Prague 9.
VANA, Ing. J.	Czechoslovak Academy of Sciences, Institute of Vacuum Electronics, Slusska 40, Prague 8.

DENMARK

JENSEN, Ing. V.	Danish Atomic Energy Commission Research Establishment, Risø, Roskilde.
VINTHER, F. H.	Danish Atomic Energy Commission Research Establishment, Risø, Roskilde.

FINLAND

SIMONS, Prof. Dr. L.	Institute of Physics, University of Helsinki, Brobergsterrassen 20, Helsinki.

FRANCE

ALIDIÈRES, M.	Groupe de Recherches sur la Fusion, C.E.A., Fontenay-aux-Roses.
AYMAR, R.	Groupe de Recherches sur la Fusion, C.E.A., Fontenay-aux-Roses.
BARIAUD, Dr. A.	C.E.N. de Saclay, Gif-sur-Yvette, B.P. No. 2 (S & O).
BEL, Miss N.	Institute d'Astrophysique, 98bis, Blvd. Arago, Paris 14.
BERNARD, Prof. M.	Institut National des Sciences et Techniques Nucléaires, B.P. No. 6, Gif-sur-Yvette (S & O).
BRACHET, C.	Ecole Polytechnique, Laboratoire de Physique, 17, rue Descartes, Paris 5.
BRIFFOD, G.	C.E.N. de Saclay, Gif-sur-Yvette, B.P. 2 (S & O).
BRIN, Dr. A.	C.E.A., 69, rue de Varenne, Paris 7.
CLAYER, Mrs. A.	S.R.T.I., 111 rue la Boëtie, Paris 8.
CLOUPEAU, Dr. M.	Centre National de la Recherche Scientifique, 5, Allée Clos de Tourvoie, Fresnes (Seine).
CONSOLI, Dr. T.	C.E.A., Gif-sur-Yvette, B.P. 2 (S & O).
COSTE, Dr. J.	Laboratoire de Physique des Plasmas, B.P. 2, Orsay (S & O).
COTSAFTIS, Ing. M.	STGI, DRP, B.P. No. 6, Fontenay-aux-Roses.
DELCROIX, Prof. J. L.	Laboratoire de Physique des Plasmas, B.P. 2, Orsay (S & O).
DELOBEAU, Ing. F.	C.E.A., Villeneuve St. Georges, B.P. 27 (S & O).
DIEULESAINT, Dr. E.	Compagnie Thomson-Houston, 173 Boulevard Haussmann, Paris 8.
DOBBERTIN, Dr. R.	Institut H. Poincaré, 16 rue du Parc-Royal, Paris.

DOLIQUE, J. M.	Compagnie Générale de Télégraphie sans Fil, Département Atomist Domaine de Corbeville, Orsay (S & O).
DUBUS, F.	Laboratoire de Physique Electronique de la Faculté des Sciences, ((S & O).
ETIEVANT, Dr. C. (Scientific Secretary)	Laboratoire du Fort de Chatillon, Service de Neutronique Experimer Fontenay-aux-Roses.
GINOT, P.	Groupe de Recherches sur la Fusion, C.E.A., Fontenay-aux-Roses.
GOLDMAN, Dr. M.	Laboratoire de Synthèse Atomique, 67 rue Maurice Gunsbourg, Ivry Seine.
HERMAN, L.	Observatoire de Meudon (S & O).
HUBERT, P.	Groupe de Recherches sur la Fusion, C.E.A., Fontenay-aux-Roses.
KAHAN, T.	Institut H. Poincaré, 11 rue Pierre Curie, Paris 5.
KOECHLIN, F.	C.E.A., SRFC, Fontenay-aux-Roses.
LACOMBE, Dr. E.	Groupement Atomique S.T.A., Paris, Seine.
LEBOUTET, H.	Compagnie Générale de Télégraphie sans Fil, Département Atomist Domaine de Corbeville, B.P. No. 10, Orsay (S & O).
LUC, H.	Groupe de Recherches sur la Fusion, C.E.A., Fontenay-aux-Roses.
MANUS, C.	C.E.N., B.P. 2, Gif-sur-Yvette (S & O).
MATRICON, M.	Compagnie Thomson-Houston, 173 Boulevard Haussmann, Paris 8.
MERCIER, C.	STGI, DRP, C.E.N. Saclay, B.P. 2, Gif-sur-Yvette (S & O).
MINARDI, E.	STGI, DRP, C.E.A., Fontenay-aux-Roses.
MOUTTET, Miss C.	Ecole Polytechnique, Laboratoire de Physique, 17 rue Descartes, Pa
NAZE, Miss J.	Centre National de la Recherche Scientifique, 10 Boulevard Michel Fr Marseille 8.
OXENIUS, J.	C.E.A., B.P. 6, Fontenay-aux-Roses.
POFFE, Dr. J. P.	C.E.A., B.P. 6, Fontenay-aux-Roses.
PREVOT, F.	C.E.A., B.P. 6, Fontenay-aux-Roses.
QUEMADA, Dr. D.	Laboratoire de Physique des Plasmas, B.P. No. 2, Orsay (Seine).
REBUT, P. H.	STGI, DRP, B.P. No. 6, Fontenay-aux-Roses.
REGNIER, J.	Compagnie Générale de Télégraphie sans Fil, Domaine de Corbe Département Atomistique, Orsay (Seine).
RENAUDIN, D.	Indatom, 48 rue de la Boëtie, Paris 8.
SALMON, J.	C.E.A. 69 rue de Varenne, Paris 7.
SAMAIN, A.	Groupe de Recherches sur la Fusion, C.E.A., Fontenay-aux-Roses.
TACHON, Dr. J.	Groupe de Recherches sur la Fusion, C.E.A., Fontenay-aux-Roses.
TAILLET, J.	C.E.A., B.P. 2, Gif-sur-Yvette (S & O).
TOROSSIAN, Ing. A.	C.E.N.F.A.R., B.P. 6, Fontenay-aux-Roses.
VALCKX, Dr. F.	C.E.N.F.A.R., B.P. 6, Fontenay-aux-Roses.
VASSEUR, Ing. P.	Ecole Polytechnique, Laboratoire de Physique, 17 rue Descartes, Pa
VENDRYÈS, G.	Département de la Recherche Physique, C.E.A., Fontenay-aux-Ros
VUILLEMIN, M.	STGI, DRP, B.P. 6, Fontenay-aux-Roses.
WAELBROECK, Dr. F.	Groupe de Recherches sur la Fusion, C.E.A., Fontenay-aux-Roses.

FEDERAL REPUBLIC OF GERMANY

AHLBORN, B.	Institut für Plasmaphysik GmbH, Garching bei München.
ANDELFINGER, Dr. C.	Institut für Plasmaphysik GmbH, Garching bei München.
BARTELS, Prof. Dr. H.	Institut für Experimentalphysik, Technische Hochschule Hannover, Welfengarten 1.
BEERWALD, Dipl. Phys. H.	Institut für Plasmaphysik, Kernforschungsanlage Jülich, Nordrhein-W falen.
BINEAU, M.	Max-Planck-Institut für Plasmaphysik und Astrophysik, Aumeisterstı München.
BOESCHOTEN, Dr. F.	Max-Planck-Institut für Plasmaphysik und Astrophysik, Aumeisterstı München.
BOGEN, Dr. P.	Institut für Plasmaphysik, Kernforschungsanlage Jülich, Nordrhein-W falen.
BOHDANSKY, Dr. J.	Brown, Boveri & Cie AG, Augusta-Anlage 38—42, Mannheim.
BÖTTICHER, Dr. W.	Institut für Experimentalphysik, Universität Kiel.
BREDERLOW, Dr. G.	Institut für Plasmaphysik GmbH, Garching bei München.
BURKHARDT, Dipl. Phys. H.	Institut für Hochtemperaturforschung der Technischen Hochschule, H weg 51, Stuttgart.
CHODURA, Dr. R.	Institut für Plasmaphysik GmbH, Garching bei München.
DURAND, Dipl. Ing. J.	Max-Planck-Institut für Physik und Astrophysik, Aumeisterstraße, Münc
ECKER, Prof. Dr. G.	Institut für Theoretische Physik, Universität, Wegelstraße 10, Bonn.
ECKHARTT, Dr. D.	Max-Planck-Institut für Physik und Astrophysik, Aumeisterstraße, Münc
ERBSLÖH, Dipl. Phys. H. D.	Institut für Experimentalphysik, Technische Hochschule, Welfengarte Hannover.
FAY, Dr. H.	Institut für Plasmaphysik, Kernforschungsanlage Jülich, Nordrhein-W falen.
FISSER, H.	Max-Planck-Institut für Physik und Astrophysik, Aumeisterstraße, Münc
FRIE, Dr. W.	Forschungslaboratorium, Siemens-Schuckert-Werke AG, Erlangen.
FUCKS, Prof. Dr. W.	Institut für Plasmaphysik, Kernforschungsanlage Jülich, Nordrhein-W falen.
FÜNFER, Prof. E.	Institut für Plasmaphysik GmbH, Garching bei München.
GEIGER, Dipl. Phys. W.	Institut für Hochtemperaturforschung, Technische Hochschule, Herdweg Stuttgart.

GIERKE, Dr. von G.	Max-Planck-Institut für Physik und Astrophysik, Aumeisterstraße, München.
GÖLER, Dipl. Phys. S. von	Physikalisches Institut, Renthof 5, Marburg a/d Lahn.
GRIEGER, Dr. G.	Max-Planck-Institut für Physik und Astrophysik, Aumeisterstraße, München.
GROSSMANN-DOERTH, Dr. U.	Max-Planck-Institut für Physik und Astrophysik, Aumeisterstraße, München.
HAIN, Dr. K.	Institut für Plasmaphysik GmbH, Garching bei München.
HEROLD, Dr. H.	Institut für Plasmaphysik GmbH, Garching bei München.
HERRMANN, Dipl. Phys. W.	Max-Planck-Institut für Physik und Astrophysik, Aumeisterstraße, München.
HERTZ, W.	Forschungslaboratorium, Siemens-Schuckert-Werke AG, Erlangen.
HINTZ, Dipl. Phys. E.	Institut für Plasmaphysik, Kernforschungsanlage Jülich, Nordrhein-Westfalen.
HISAM, Dipl. Phys. E.	Institut für Hochtemperaturforschung, Technische Hochschule, Herdweg 51, Stuttgart.
HÖCKER, Prof. Dr. K. H.	Institut für Hochtemperaturforschung, Technische Hochschule, Herdweg 51, Stuttgart.
JORDAN, Dr. H.	Institut für Plasmaphysik, Kernforschungsanlage Jülich, Nordrhein-Westfalen.
JUNKER, Dipl. Phys. J.	Max-Planck-Institut für Physik und Astrophysik, Aumeisterstraße, München.
KAEPPELER, H. J.	Institut für Hochtemperaturforschung, Technische Hochschule, Herdweg 51, Stuttgart.
KÄSTNER, Dipl. Phys. G.	Battelle-Institut e.V., Wiesbadener Straße, Frankfurt/Main.
KEILHACKER, Dr. M.	Institut für Plasmaphysik GmbH, Garching bei München.
KEVER, Dr. H.	Institut für Plasmaphysik, Kernforschungsanlage Jülich, Nordrhein-Westfalen.
KLUGE, Prof. Dr. W.	Institutfür Gasentladungstechnik und Photoelektronik, Technische Hochschule, Breitscheidstraße, Stuttgart.
KNOBLOCH, A.	Institut für Plasmaphysik GmbH, Garching bei München.
KNORR, G.	Max-Planck-Institut für Physik und Astrophysik, Aumeisterstraße, München.
KOCH, Dr. Ing. W.	Hochspannungsinstitut, Technische Hochschule, Braunschweig.
KOLLER, Dipl. Math. A.	Forschungslaboratorium, Siemens-Schuckert-Werke AG, Erlangen.
LARENZ, Dr. R. W.	Institut für Theoretische Physik, Technische Hochschule, Welfengarten 1, Hannover.
LEHNER, Dr. Dipl. Phys. G.	Institut für Plasmaphysik GmbH, Garching bei München.
LOTZ, Dr. W.	Max-Planck-Institut für Physik und Astrophysik, Aumeisterstraße, München.
LUEG, Dr. H.	Battelle-Institut e.V., Wiesbadener Straße, Frankfurt/Main.
MAECKER, Dr. H.	Forschungslaboratorium, Siemens-Schuckert-Werke AG, Erlangen.
MAYDELL, Dipl. Ing. W. von	Bölkow-Entwicklungen AG, Ottobrunn bei München.
MAYSER, Dipl. Phys. B.	Institut für Hochtemperaturforschung, Technische Hochschule, Herdweg 51, Stuttgart.
MENKE, Dr. Ing. H.	Hochspannungsinstitut, Technische Hochschule, Braunschweig.
MICHEL, Dr. A.	Forschungslaboratorium, Siemens-Schuckert-Werke AG, Erlangen.
MÖLLER-ARNSBERG, Dr. O.	Grabmannstraße 13, München.
MOTSCHMANN, Dr. Dipl. Phys. H.	Forschungslaboratorium, Siemens-Schuckert-Werke AG, Erlangen.
MÜLLER, Dr. Dipl. Phys. G.	Max-Planck-Institut für Physik und Astrophysik, Aumeisterstraße, München.
OHLENDORF, W.	Dept. of Electrical Engineering, University of Liverpool, England.
PFIRSCH, Dr. D.	Max-Planck-Institut für Physik und Astrophysik, Aumeisterstraße, München.
PRETSCH, Dr. D.	Bundesministerium für Atomkernenergie und Wasserwirtschaft, Luisenstraße 46, Bad Godesberg.
SCHINDLER, Dr. Dipl. Phys. H.	Forschungslaboratorium, Siemens-Schuckert-Werke AG, Erlangen.
SCHINDLER, Dr. K.	Institut für Plasmaphysik, Kernforschungsanlage Jülich, Nordrhein-Westfalen.
SCHLÜTER, Dipl. Phys. J.	Institut für Plasmaphysik, Kernforschungsanlage Jülich, Nordrhein-Westfalen.
SCHMITTER, Dipl. Ing. E.	Institut für Plasmaphysik GmbH, Garching bei München.
SCHOTT, L.	Institut für Experimentalphysik der Christian-Albrechts-Universität, Kiel.
SCHRAMM, Dr. K. H.	Battelle-Institut e.V., Wiesbadener Straße, Frankfurt/Main.
SCHWIRZKE, Dr. F.	Max-Planck-Institut für Physik und Astrophysik, Aumeisterstraße, München.
SOMMER, Dr. J.	Institut für Plasmaphysik GmbH, Garching bei München.
SUCHY, Dr. K.	Physikalisches Institut, Renthof 5, Marburg a/d Lahn.
TUCZEK, Dr. Ing. H.	Institut für Plasmaphysik, Kernforschungsanlage Jülich, Nordrhein-Westfalen.
VOELCKER, Dr. Dipl. Phys. H.	Institut für Reine und Angewandte Kernphysik der Universität, Olshausenstraße 40/60, Kiel.
WIENECKE, Dr. R.	Institut für Plasmaphysik GmbH, Garching bei München.
WILHELM, Dipl. Phys. H. E.	Institut für Hochtemperaturforschung, Technische Hochschule, Herdweg 51, Stuttgart.
WINKENBACH, Dr. Dipl. Phys. H. E.	Brown, Boveri & Cie AG, Abt. Kernenergie, Augusta-Anlage 38—42, Mannheim.
WINTERBERG, Dr. F.	Case Institute of Technology, University Circle, Cleveland 6, Ohio, USA.
WÖHLER, K. H.	Max-Planck-Institut für Physik und Astrophysik, Aumeisterstraße, München.
WOLF, Dr. Dipl. Ing. G.	Max-Planck-Institut für Physik und Astrophysik, Aumeisterstraße, München.
ZWICKER, Dr. H.	Institut für Experimentalphysik, Technische Hochschule, Welfengarten 1, Hannover.

HUNGARY

NAGY, Prof. E.	Institute for Experimental Physics, Eötvös Loránd University, Muzeum-Krt. 6—8, Budapest.

LIST OF PARTICIPANTS

INDIA

MURTY, Dr. G. S.	Tata Institute of Fundamental Research, Bombay 1.

ISRAEL

KALMAN, G.	Department of Physics, Technion — Israel Institute of Technology, H
KAUFMAN, A. S.	Department of Physics, Hebrew University, Jerusalem.

ITALY

ALLEN, Dr. J. E.	C.N.E.N., Laboratorio Gas Ionizzati, Casella Postale 65, Frascati, R
BARSANTI, Miss G.	C.A.M.E.N., Livorno.
BERTOTTI, Dr. B.	C.N.E.N., Laboratorio Gas Ionizzati, Casella Postale 65, Frascati, R
BRUNELLI, Prof. B.	C.N.E.N., Laboratorio Gas Ionizzati, Casella Postale 65, Frascati, R
CAVALIERE, A.	C.N.E.N., Laboratorio Gas Ionizzati, Casella Postale 65, Frascati, R
GOURLAN, Ing. C.	C.N.E.N., Laboratorio Gas Ionizzati, Casella Postale 65, Frascati, R
GRATTON, Prof. L.	C.N.E.N., Laboratorio Gas Ionizzati, Casella Postale 65, Frascati, R
HAEGI, M.	C.N.E.N., Laboratorio Gas Ionizzati, Casella Postale 65, Frascati, R
HERLACH, Dr. F.	C.N.E.N., Laboratorio Gas Ionizzati, Casella Postale 65, Frascati, R
KNOEPFEL, Dr. H.	C.N.E.N., Laboratorio Gas Ionizzati, Casella Postale 65, Frascati, R
LINHART, Dr. J. G.	C.N.E.N., Laboratorio Gas Ionizzati, Casella Postale 65, Frascati, R
MAISONNIER, C.	C.N.E.N., Laboratorio Gas Ionizzati, Casella Postale 65, Frascati, R
MALESANI, Dr. G.	Istituto di Elettrotecnica, Università di Padova.
MAZZUCATO, Dr. E.	Istituto di Elettrotecnica, Università di Padova.
NARDI, Dr. V.	Istituto di Fisica dell'Università di Padova.
NATION, Dr. J. A.	C.N.E.N., Laboratorio Gas Ionizzati, Casella Postale 65, Frascati, R
PERUGINI, Dr. G.	Società Montecatini, Settore Azoto, Novara.
ROSTAGNI, Dr. Ing. G.	Istituto di Elettrotecnica, Università di Padova.
RUMI, Dr. B.	C.N.E.N., Laboratorio Gas Ionizzati, Casella Postale 65, Frascati, R
SANI, Ing. L.	Società Terni, Via Due Macelli 66, Rome.
SEGRE, Dr. S. E.	C.N.E.N., Laboratorio Gas Ionizzati, Casella Postale 65, Frascati, R
TOSI, Dr. C.	Istituto "G. Donegani", Società Montecatini, Novara.

JAPAN

HUSIMI, K.	Faculty of Science, Osaka University, Osaka.
ISHII, Dr. Ing. H.	Electrotechnical Laboratory, Nagata-cho, Chiyoda-ku, Tokyo.
IWATAKE, Prof. Dr. M.	Shibaura Institute of Technology, Nishishibaura 3—1 Minatoku, Tokyo
KIHARA, Prof. T.	Department of Physics, Faculty of Science, Tokyo University, Bunkyo Tokyo.
KOJIMA, S.	Department of Physics, Faculty of Science, Tokyo University, Bunkyo Tokyo.
OZAWA, Prof. Y.	Laboratory of Nuclear Electronics, School of Nuclear Engineering, versity of Hokkaido, Sapporo.
SEKIGUCHI, Dr. T.	Department of Electrical Engineering, University of Tokyo, Bunkyo Tokyo.
WADA, Dr. Ing. S.	Tsurumi Research Laboratory, Tokyo Shiba Ura Electric Company, chome, Suehirocho, Tsurumiku, Yokohama.
YASAKI, Prof. Dr. T.	Physics Institute, Yamanashi University, Kofumachi, Kofu City.

MEXICO

VELEZ, C.	Comisión Nacional de Energía Nuclear, Apartado Postal 30190, Suc Correos 27, Mexico 7 D.F.

NETHERLANDS

BANNENBERG, J. G.	Fom Laboratory for Mass Separation, Amsterdam.
BRAAMS, Dr. C. M.	Fom Instituut voor Plasma-Fysica, Rijnhuizen, Jutphaas.
BRINKMAN, Prof. Dr. H.	University of Groningen, Natuurkundig Laboratorium, Groningen.
BROER, Prof. Dr. L. J. F.	Laboratorium voor Aëro- en Hydrodynamica van de Technische H school te Delft, Ezelsveldlaan 40, Delft.
BRUINING, Dr. H.	Physical Laboratory of N.V. Philips' Gloeilampenfabrieken, Eindhove
BUEREN, Dr. H. G. van	Physical Laboratory of N.V. Philips' Gloeilampenfabrieken, Eindhoven
FELDERHOF, U.	Instituut voor Theoretische Fysica, University Utrecht.
HIRSHFIELD, Dr. J.	Fom Instituut voor Plasma Fysica, Rijnhuizen, Jutphaas.
INGEN, A. van	Fom Instituut voor Plasma Fysica, Rijnhuizen, Jutphaas.
INSINGER, G.	Fom Laboratory for Mass Separation, Amsterdam.
KISTEMAKER, Prof. J.	Fom Laboratory for Mass Separation, Amsterdam.
LAAN, P. van der	Fom Instituut voor Plasma Fysica, Rijnhuizen, Jutphaas.
ORNSTEIN, Dr. L. T. M.	Fom Instituut voor Plasma Fysica, Rijnhuizen, Jutphaas.
RIETJENS, Dr. L.	Fom Instituut voor Plasma Fysica, Rijnhuizen, Jutphaas.
RUTGERS, Dr. G.	K.E.M.A., Arnhem.
SCHRAM, Ing. P.	Fom Instituut voor Plasma Fysica, Rijnhuizen, Jutphaas.
WARMOLTZ, Dr. N.	Physical Laboratorium of N.V. Philips' Gloeilampenfabrieken, Eindho
WASSER, Dr. P. J. B.	K.E.M.A., Arnhem.
WEENINK, Dr. M.	Fom Instituut voor Plasma Fysica, Rijnhuizen, Jutphaas.
WIJNGAARDEN, L. van	Laboratorium voor Aëro- en Hydrodynamica van de Technische H school te Delft, Ezelsveldlaan 40, Delft.

NORWAY

HOLTER, O.	Department of Mathematics, University, Bergen.
NYGAARD, Ing. K.	Institute of Applied Physics, The Technical University, Trondheim.
SIGMOND, R. S.	Institute of Applied Physics, The Technical University, Trondheim.
TJÖTTA, S.	Department of Mathematics, University, Bergen.

POLAND

GAJEWSKI, Dr. R.	Institute of Nuclear Research, Dorodna 16, Warsaw 9 (Boeing Research Laboratories, Seattle, USA).
GRYZINSKI, M.	Institute of Nuclear Research, Swierk k/Otwocka.
SADOWSKI, M.	Institute of Nuclear Research, Swierk k/Otwocka.
ZELAZNY, Dr. R.	Institute of Nuclear Research, Swierk k/Otwocka.

SOUTH AFRICA

LEEMANN, Dr. A.	Reichenhallerstraße 12, Salzburg.

SPAIN

LOZANE, Dr. J.	Junta de Energía Nuclear, Serrano 121, Madrid.

SWEDEN

BERGLUND, S.	Department of Physics, University of Uppsala.
BLOCK, L.	Royal Institute of Technology, Stockholm 70.
BONNELIEVIER, B.	Royal Institute of Technology, Department of Electronics, Stockholm 70.
DATTNER, A.	Royal Institute of Technology, Stockholm 70.
HALLIN, R.	Institute of Physics, University of Uppsala.
HERLITZ, S. I.	Institute of Physics, University of Uppsala.
HOGBERG, L.	Institute of Physics, University of Uppsala.
JACOBSEN, Ing. C. T.	Tkh F, ASEA, Ludvika.
KARLSON, Dr. E.	AB Atomenergi, Lövholmsvägen, Stockholm 9.
LEHNERT, Prof. B.	Royal Institute of Technology, Department of Electronics, Stockholm 70.
OHLIN, Prof. P.	Department of Physics, University of Uppsala.
SMÅRS, Dr. E. A.	Royal Institute of Technology, Department of Electronics, Stockholm 70.
SVENNERSTEDT, S.	Department of Physics, University of Uppsala.
VOGEL, K.	Department of Physics, University of Uppsala.
WILHELMSSON, Prof. H.	Research Laboratory of Electronics, Chalmers University of Technology, Gibraltargatan 5G, Gothenburg.
WILNER, Dipl. Ing. B.	Royal Institute of Technology, Department of Electronics, Stockholm 70.

SWITZERLAND

BÜRGEL, Dr. B.	Brown, Boveri & Cie., Baden.
CANTIENI, Dr. E.	Physikinstitut der Universität, Fribourg.
HUBER, Prof. Dr. O.	Physikinstitut der Universität, Fribourg.
GUREWITSCH, A. M.	General Electric Co., Löwenstraße 92, Zürich.
KELLER, Dr. R.	Laboratoire de Recherche sur la Physique des Plasmas, Avenue Ruchonnet 2, Lausanne.
LÜTI, Dr. F.	Brown, Boveri & Cie., Baden.
SCHNEIDER, Dr. Dipl. Phys. H.	Physikinstitut der Universität, Fribourg.

TURKEY

YENICAY, Prof. F.	Institut de Physique de la Faculté des Sciences, Université d'Istanbul, Istanbul.

UNITED ARAB REPUBLIC

AMIN, Dr. Ing. A. H.	Atomic Energy Commission, National Research Centre, Dokky, Cairo.
EL-KHALAFAWI, Miss T.	Institut für Plasmaphysik, Jülich, Germany.

UNITED KINGDOM

ADLAM, J.	U.K.A.E.A., Harwell, Didcot, Berkshire.
ALLEN, Dr. T. K.	U.K.A.E.A., Harwell, Didcot, Berkshire.
APPLETON, A.	General Electric Co. Ltd., Atomic Energy Division, Erith, Kent.
ARNOLD, K.	The Clarendon Laboratory, Parks Road, Oxford.
BICKERTON, Dr. R.	A.E.R.E., Harwell, Didcot, Berkshire.
BLEVIN, Dr. H. A.	A.E.R.E., Harwell, Didcot, Berkshire.
BODIN, Dr. H. A. B.	A.W.R.E., Aldermaston, Nr. Reading, Berkshire.
BOOTH, A.	General Electric Co. Ltd., Hirst Research Centre, Wembley, Middlesex.
DAVENPORT, Dr. P. A. (Scientific Secretary)	Culham Laboratory, Abingdon, Berkshire.
DOUGHERTY, J.	Department of Applied Mathematics, University of Cambridge, Ree School Lane, Cambridge.

EMELEUS, Prof. K.	Physics Department, Queen's University, Belfast, Northern Ireland.
ENGEL, Dr. A. von	The Clarendon Laboratory, Parks Road, Oxford.
FATMI, Dr. H. A.	Imperial College, South Kensington, London, S.W.7.
FITCH, R. A.	A.W.R.E., Aldermaston, Nr. Reading, Berkshire.
FOLKIERSKI, Dr. A.	Department of Physics, Imperial College of Science and Technology, London, S.W.7.
FRANCIS, Dr. M.	British Embassy, Scientific Attaché's Office, Bonn, Germany.
GIBSON, Dr. A.	A.E.R.E., Harwell, Didcot, Berkshire.
HAINES, Dr. M.	Physics Department, Imperial College of Science, London, S.W.7.
HARDING, G. N.	A.E.R.E., Harwell, Didcot, Berkshire.
HELLBERG, M.	St. John's College, Cambridge.
IRVING, Prof. J.	Royal College of Science and Technology, Glasgow, Scotland.
JEPHCOTT, D. F.	A.E.R.E., Harwell, Didcot, Berkshire.
JONES, B.	A.E.R.E., Harwell, Didcot, Berkshire.
JUKES, J.	Culham Laboratory, c/o A.E.R.E. Harwell, Didcot, Berkshire.
KING, L.	Electrical Research Association, Cleeve Road, Leatherhead, Surrey.
LATHAM, Dr. R.	Imperial College of Science and Technology, High Temperature Physics Section, Physics Department, South Kensington, London, S.W. 7.
LEES, D. J.	A.E.R.E., Harwell, Didcot, Berkshire.
MARTELLI, Dr. G.	University of Birmingham, Edgbaston, Birmingham.
MCCONKEY, J. W.	Physics Department, Queen's University, Belfast, Northern Ireland.
MEDFORD, R. D.	A.W.R.E., Aldermaston, Nr. Reading, Berkshire.
MORTON, K. W.	A.E.R.E., Harwell, Didcot, Berkshire.
MOTZ, Dr. H.	Oxford University, 19 Parks Road, Oxford.
NIBLETT, Dr. G. B. F.	A.W.R.E., Aldermaston, Nr. Reading, Berkshire.
NICHOLLS, Dr. M.	The Nelson Research Laboratories, English Electric Co. Ltd., Beaconhill, Stafford, Staffs.
PEARCE, A. F.	Department of Electrical Engineering, Imperial College, London, S.W.7.
PEASE, R. S.	Culham Laboratory, c/o A.E.R.E., Harwell, Didcot, Berkshire.
PELZER, H.	British Electrical & Allied Industries Research Association, E.R.A., Laboratory, Cleeve Road, Leatherhead, Surrey.
PHILLIPS, N. J.	A.W.R.E., Aldermaston, Nr. Reading, Berkshire.
REYNOLDS, Dr. J.	A.W.R.E., Aldermaston, Nr. Reading, Berkshire.
ROBERTS, Dr. K. V.	Culham Laboratory, c/o A.E.R.E., Harwell, Didcot, Berkshire.
ROBSON, Dr. A. E.	A.E.R.E., Harwell, Didcot, Berkshire.
RUTHERFORD, P.	Department of Applied Mathematics & Theoretical Physics, Free School Lane, Emmanuel College, Cambridge.
SHAW, D.	The Clarendon Laboratory, Oxford University, 61 Holywell Street, Oxford.
SMART, D.	Culham Laboratory, A.E.R.E., Harwell, Didcot, Berkshire.
SPALDING, Dr. I.	A.E.R.E., Harwell, Didcot, Berkshire.
STOCKER, Dr. P.	A.E.R.E., Harwell, Didcot, Berkshire.
STRINGER, T. E.	A.E.R.E., Harwell, Didcot, Berkshire.
SWEETMAN, Dr. D. R.	A.W.R.E., Aldermaston, Nr. Reading, Berkshire.
TAYLER, Dr. R. J.	Culham Laboratory, c/o A.E.R.E., Harwell, Didcot, Berkshire.
TAYLOR, Dr. J. B.	A.W.R.E., Aldermaston, Nr. Reading, Berkshire.
TEMPERLEY, Dr. H. N. V.	A.W.R.E., Aldermaston, Nr. Reading, Berkshire.
THOMSON, Sir GEORGE Dr.	Master's Lodge, Corpus Christi College, Cambridge.
THONEMANN, Dr. P.	A.E.R.E., Harwell, Didcot, Berkshire.
WARE, Dr. A. A.	Associated Electrical Industries, Ltd., Research Laboratory, Aldermaston Court, Aldermaston, Berkshire.
WHEELER, C.	Imperial College of Science, South Kensington, London, S.W.7.
WILSON, J. W. G.	Physics Department. Queen's University, Belfast, Northern Ireland.

USA

ALEXEFF, Dr. I.	Oak Ridge National Laboratory, Oak Ridge, Tenn.
ALLIS, Prof. W. P.	Massachusetts Institute of Technology, Cambridge, Mass.
AUER, Dr. P.	General Electric Research Laboratory, P.O. Box 1088, Schenectady, New York (C.N.E.N.-Euratom, Frascati, Rome, Italy).
BEKEFI, Dr. G.	Massachusetts Institute of Technology, Cambridge, Mass.
BIONDI, Prof. M. A.	Physics Department, University of Pittsburgh.
BOSTICK, Dr. W. H.	Stevens University of Technology, Physics Department, Hoboken, N. J.
BRADY, Dr. E. L.	United States Mission to the International Atomic Energy Agency, Schmidgasse 14, Vienna VIII, Austria.
BRAUN, Dr. W. G.	Wright Patterson Air Force Base, Bossigasse 16, Vienna XIII, Austria.
BROWN, Prof. Dr. S. C.	Massachusetts Institute of Technology, Research Laboratory of Electronics, Cambridge, Mass.
BUNEMANN, Prof. Dr. O.	Stanford University, Stanford Electronics, Stanford, Calif.
BYRNE, Dr. F. T.	Office of Naval Research, Washington 25, D.C.
CHANG, Dr. C. C.	Physical Research Laboratory, Aerospace Corp., P.O.B. 95085, Los Angeles, El Segundo Bul., Calif.
CHRISTOFILOS, N.	University of California, Lawrence Radiation Laboratory, P.O. Box 808, Livermore, Calif.
COENSGEN, F.	University of California, Lawrence Radiation Laboratory, P.O. Box 808, Livermore, Calif.
COLGATE, Dr. S.	University of California, Lawrence Radiation Laboratory, P.O. Box 808, Livermore, Calif.

Cook, A. E.	Department of the Navy, Office of Naval Research, Washington 25 DC.
Dandl, R.	Oak Ridge National Laboratory, Oak Ridge, Tenn.
Dawson, J.	Plasma Physics Laboratory, Princeton University, Princeton, N.J.
Derfler, H.	Stanford University, Electronics Research Laboratory, Stanford, California.
Dreicer, H.	Los Alamos Scientific Laboratory, University of California, Los Alamos, New Mexico.
Drummond, Dr. W.	General Atomic, P.O.B. 608, San Diego, Calif.
Dunlap, J. L.	Oak Ridge National Laboratory, Oak Ridge, Tenn.
Eckert, H.	Convair, Division of General Dynamics Corp., San Diego, Calif.
Ehrman, J. B.	Naval Research Laboratory, Nucleonics Division, Washington 25 DC.
Fisher, Dr. L. H.	Army Research Office (Durham).
Frieman, Prof. E.	Plasma Physics Laboratory, Princeton University, Princeton, N. J.
Fritz, Dipl. Ing. W.	US Government, 120 Glen Street, Yellow Springs, Ohio.
Frost, L. S.	Westinghouse Research Laboratories, 423 Beulah Road, Pittsburgh, 35, Pa.
Furth, Dr. H.	Lawrence Radiation Laboratory, Livermore, Calif.
Gauster, Prof. Dr. W. F.	Oak Ridge National Laboratory, Oak Ridge, Tenn.
Goldstein, Prof. L.	University of Illinois, Urbana, Ill.
Gottlieb, M. B.	Plasma Physics Laboratory, Princeton University, Princeton, N.J.
Grad, Prof. H.	New York University, 25, Waverley Place, New York 3, N.Y.
Greifinger, Dr. C.	The Rand Corporation, Santa Monica, Calif.
Griem, Prof. Dr. H. R.	Physics Department, University of Maryland, College Park, Md.
Grove, D.	Plasma Physics Laboratory, Princeton University, Princeton, N.J.
Gschwendtner, Dipl. Phys. J.	Jet Propulsion Laboratory, California Institute of Technology, 4800 Oak Grove Drive, Pasadena 3, Calif.
Hagerman, Dr. D. C.	Los Alamos Scientific Laboratory, Los Alamos, New Mexico.
Harris, Prof. E.	Physics Department, University of Tennessee, Knoxville, Tenn.
Hendricks, Prof. C.	247 EEB, University of Illinois, Urbana, Ill.
Hinnov, Dr. E.	Plasma Physics Laboratory, Princeton University, Princeton, N.J.
Hooke, Dr. W.	Plasma Physics Laboratory, Princeton University, Princeton, N.J.
Ise, Dr. J.	General Electric Co. (Tempo), 735 State Street, Santa Barbara, Calif.
Janos, Dr. W.	Raytheon Co., 33 Debra Lane, Framingham, Mass.
Jarem, Dr. J.	R.C.A., Grant Road, Princeton, N.J.
Jaskowsky, W. von	Plasmadyne Corporation, 3838 S. Main, Santa Ana, Calif.
Josephsen, Dr. V.	Aerospace Corporation, No. 95085 Los Angeles, Calif.
Kantrowitz, Dr. A.	Avco-Everett Research Laboratory, Everett, Mass.
Kaprielian, Prof. Dr. Z.	University of Southern California, 2396 Roseman Road, Los Angeles, Calif.
Kassel, S.	The Library of Congress, Washington 25 DC.
Katzenstein, Dr. J.	C.N.E.N., Laboratorio Gas Ionizzati, Casella Postale 65, Frascati, Rome, Italy.
Kelley, G. G.	Oak Ridge National Laboratory, Oak Ridge, Tenn.
Kenty, Dr. C.	General Electric Co., Nela Park, Cleveland, Ohio.
Killeen, J.	Lawrence Radiation Laboratory, Livermore, Calif.
Klein, Dr. L.	National Bureau of Standards, Washington 25 DC.
Knechtli, Dr. R.	Hughes Research Laboratory, Malibu, California.
Kofoid, Dr. M. J.	Boeing Scientific Research Laboratories, Seattle, Washington.
Kolb, Dr. A.	US Naval Research Laboratory, Washington 25 DC.
Koslov, Dr. S.	Vitro Corporation, 200 Pleasant Valley Way, West Orange, New Jersey.
Kruskal, Prof. Dr. M.	Plasma Physics Laboratory, Princeton University, Princeton, N.J.
Kuckes, A.	Plasma Physics Laboratory, Princeton University, Princeton, N.J.
Kuhrt, W.	United Aircraft Corp. Research Laboratories, 400 Main Street, East Hartford, Conn.
Kunkel, Dr. W. B.	Lawrence Radiation Laboratory, University of California, Berkeley, Calif.
Kursunoglu, Prof. Dr. B.	University of Miami, Coral Gables, Florida.
Lamborn, B.	Physics Department, University of Florida, Gainesville, Florida.
Lauer, E.	Lawrence Radiation Laboratory, University of California, Berkeley, Calif.
Lessen, Prof. Dr. M.	Department of Mechanical Engineering, University of Rochester, Rochester, N.Y.
Levine, Prof. H.	Office of Naval Research, 429 Oxford Street, London, W. 1., England.
Linlor, Dr. W. I.	Hughes Research Laboratories, Malibu, Calif.
Livingston, Dr. P.	Special Weapons Center, US Air Force, Albuquerque, New Mexico.
Luce, J.	Aerojet General Nucleonics, 51 Corte Encanto, Calif.
Lupton, W.	US Naval Research Laboratory, Washington 25 DC.
Luscher, Prof. E.	Physics Department, University of Illinois, Urbana, Ill.
Mackin, Dr. R. J.	Oak Ridge National Laboratory, Oak Ridge, Tenn.
Marshall, Dr. J.	Los Alamos Scientific Laboratory, Los Alamos, New Mexico.
Mawardi, Prof. O.	Case Institute of Technology, Cleveland, Ohio.
Medicus, Dr. G. K.	Wright Patterson Air Force Base, Ohio.
Meyerand, Dr. R. G.	United Aircraft Corp., Research Laboratories, East Hartford 8, Conn.
McDaniel, Prof. Dr. E. W.	Georgia Institute of Technology, Atlanta, Ga.
McLane, C. K.	National Bureau of Standards, Washington 25 DC.
Motley, R.	Plasma Physics Laboratory, Princeton University, Princeton, N.J.
Morton, Dr. H. S.	US Atomic Energy Commission, Division of Research, Washington 25 DC.
Nalos, Dr. E.	General Electric Research Laboratory, 37 Pelikanstraße, Zürich, Switzerland.
Newcomb, Dr. W.	Lawrence Radiation Laboratory, Livermore, Calif.
Oleson, Prof. N.	US Naval Postgraduate School, Dept. of Physics, Monterey, Calif.

OSKAM, Dr. H.	Dept. of Electrical Engineering, University of Minnesota, Minneapolis, Minnesota.
OTTING, Dr. W. J.	Defense Atomic Support Agency, Dept. of Defense, Pentagon Building, Washington 25 DC.
PARDO, Dr. W.	Physics Department, University of Miami, Coral Gables, Florida.
PAPAZ, Prof. Dr. C.	California Institute of Technology, Pasadena, Calif.
PHILLIPS, Dr. J.	Los Alamos Scientific Laboratory, Los Alamos, New Mexico.
POST, Dr. R. F.	Lawrence Radiation Laboratory, Livermore, Calif.
RAETHER, Dr. M.	Coordinated Science Laboratory, University of Illinois, Urbana, Ill.
RIBE, Dr. F.	Los Alamos Scientific Laboratory, Los Alamos, New Mexico.
ROBERTSON, Prof. H. S.	Department of Physics, University of Miami, Coral Gables, Florida.
ROOS, Dr. O. von	Jet Propulsion Laboratory, 4800 Oak Grove Drive, Pasadena, California.
ROSENBLUTH, M.	General Atomic, San Diego, Calif.
ROSTOKER, Dr. N.	General Atomic, San Diego, Calif.
RUARK, Prof. Dr. A. E.	US Atomic Energy Commission, Washington 25 DC.
SCHMIDT, Assoc. Prof. G.	Stevens Institute of Technology, Physics Dept., Hoboken, N.J.
SEEGER, Dr. Prof. R. J.	National Science Foundation, Washington 25 DC.
SEIKEL, G.	NASA, Lewis Research Center, Cleveland, Ohio.
SIMON, Dr. A.	General Atomic, San Diego, Calif.
SLAWSKY, Dr. M. M.	Air Force Office of Scientific Research, 8803 Lanier Drive, Silver Spring, Md.
SMYTH, Dr. H. D.	US Representative to the International Atomic Energy Agency, Schmidgasse 14, Vienna VIII, Austria.
SNELL, Dr. A.	Oak Ridge National Laboratory, Oak Ridge, Tenn.
SPIEGLER, P.	Atomics International, 8900 Desoto, Canoga Park, Calif.
SPITZER, Prof. L.	Plasma Physics Laboratory, Princeton University, Princeton, N.J.
STIX, Dr. T.	Plasma Physics Laboratory, Princeton University, Princeton, N.J.
TRIVELPIECE, Prof. A.	E. E. Dept., University of California, Berkeley, Calif.
TUCK, J.	Los Alamos Scientific Laboratory, Los Alamos, New Mexico.
VAN ATTA, Dr. C. M.	Lawrence Radiation Laboratory, University of California, Berkeley, Calif.
VARNEY, Prof. R. N.	Physics Department, Washington University, St. Louis 30, Mo.
WANIEK, Dr. R. W.	Advanced Kinetics, Inc., 1231 Victoria Street, Costa Mesa, Calif.
WEBB, Dr. F. H.	Electro Optical Systems, 123 N Vinedo Street, Pasadena, Calif.
WEIBEL, Dr. E.	Aerospace Corporation, Los Angeles, Calif.
WEISSLER, Prof. Dr. G. L.	Department of Physics, University of Southern California, University Park, Los Angeles, Calif.
WEYMANN, Prof. H.	College of Engineering, University of Rochester, N.Y.
WHITMER, Dr. R.	G. T. & E. Labs., 1015 Corporation Way, Palo Alto, Calif.
WILCOX, Dr. J.	Lawrence Radiation Laboratory, Berkeley, Calif.
WU, Dr. C. S.	California Institute of Technology, 4800 Oak Grove Drive, Pasadena, Calif.

USSR

ANDREEV, V.	USSR Academy of Sciences, Leninstr. 14, Moscow.
ARTSIMOVICH, Prof. L.	USSR Academy of Sciences, Leninstr. 14, Moscow.
BEREZIN, A.	Physical Technical Institute of the Academy of Sciences, Politechnitcheskoja 2, Leningrad 21.
BOGDANOV, G. F.	USSR Academy of Sciences, Leninstr. 14, Moscow.
BURLAKOV, V.	State Committee for the Utilization of Atomic Energy, Moscow.
BUTROV, L.	Scientific Economic Division, USSR Embassy in Vienna, Austria.
DEMIRKHANOV, Dr. R.	USSR Academy of Sciences, Leninstr. 14, Moscow.
DOLGOV-SAVELEV, Dr. G.	Institute of Atomic Energy, Moscow.
FATKIN, Dr. N.	USSR Academy of Sciences, Leninstr. 14, Moscow.
FEDORENKO, Prof. Dr. N.	Physical Technical Institute of the Academy of Sciences, Politechnitcheskoja 2, Leningrad.
GLAGOLEV, V. M.	USSR Academy of Sciences, Institute of Atomic Energy, Moscow.
GLUKHIKH, Ing. V.	Institute of the Electro-Physical Apparature, Leningrad.
GOLOVIN, Dr. I.	USSR Academy of Sciences, Kurchatov Institute of Atomic Energy, Moscow.
IOFFE, Dr. M.	USSR Academy of Sciences, Institute of Atomic Energy, Moscow.
KADOMTSEV, Dr. B.	USSR Academy of Sciences, Institute of Atomic Energy, Moscow.
KHARCHENKO, Dr. I.	Physical Technical Institute, Kharkov.
KUZNETSOV, E.	The Committee on Atomic Energy, Moscow.
KURSANOV, Dr. J.	USSR Academy of Sciences, Leninstr. 14, Moscow.
KUCHERYAEV, A.	Physical Technical Institute of Georgian SSR, Sukhumi.
KVARTSKHAVA, Prof. Dr. I.	Physical Technical Institute of Georgian SSR, Sukhumi.
LEONTOVICH, Prof. Dr. M.	USSR Academy of Sciences, Institute of Atomic Energy, Moscow.
MESHCHERYAKOV, Ing. K.	State Committee for the Utilization of Atomic Energy, Staromonjetvj 26, Moscow.
NASEDKIN, Dr. J.	State Committee for the Utilization of Atomic Energy, Moscow.
NESTERIKHIN, Dr. J.	USSR Academy of Sciences, Leninstr. 14, Moscow.
PISKAREV, Dr. E. (Scientific Secretary)	Institute of Atomic Energy, Moscow.
PISTUNOVICH, N.	Mission of the USSR to the International Atomic Energy Agency, USSR Embassy, Vienna.
RACHMANOV, N.	Mission of the USSR to the International Atomic Energy Agency, USSR Embassy, Vienna.
RAZUMOVA, Mrs. Dr. K.	Institute of Atomic Energy, Moscow.
ROMANOVSKY, Dr. M.	Institute of Atomic Energy, Moscow.

RUKHADZE, Dr. A.	USSR Academy of Sciences, Physics Institute, Moscow B-17.
SILIN, Dr. V.	USSR Academy of Sciences, Physics Institute, Moscow, B-17.
SIMONOV, Dr. V.	USSR Academy of Sciences, Kurchatov Institute for Atomic Energy, Moscow.
TOLOK, V.	Physical Technical Institute of the USSR Academy of Sciences, Kharkov.
VELIKHOV, Dr. E.	USSR Academy of Sciences, Institute of Atomic Energy, Moscow.
ZAVOISKY, Prof. Dr. E.	USSR Academy of Sciences, Moscow.

YUGOSLAVIA

MILOJEVIĆ, Prof. A.	Institute "Boris Kidrić", Vinca.
MOLJK, Dr. A.	Institute "J. Stefan", Ljubljana.
PEROVIĆ, Mrs. B.	Institute of Nuclear Sciences, Belgrade.
STERNBERG, Dipl. Ing. Z.	Institute "Rudjer Bosković", Zagreb.

INTERNATIONAL ORGANIZATIONS

C.E.R.N.

JONES, E.	A. R. Division, C.E.R.N., Geneva, Switzerland.

EURATOM

PALUMBO, Prof. Dr. D.	Euratom, 51 rue Belliard, Bruxelles, Belgium.

INSTITUT INTERNATIONAL DES BREVETS

ZOTTER, Dr. Dipl. Ing. B. W.	Institut International des Brevets, 97, Nieuwe Parklaan, The Hague, Netherlands.

I.A.E.A.

ANTONESCU, V.	I.A.E.A., Kärntnerring, Vienna I, Austria.
ERGINSOY, Dr. C.	I.A.E.A., Kärntnerring, Vienna I, Austria.

J.I.N.R.

RUTHHARDT, Dr. L.	Institut für Magnetohydrodynamik der Deutschen Akademie der Wissenschaften, Fröbelsteig 3, Jena/Thür., D.D.R.
STEENBECK, Prof. Dr. M.	Institut für Magnetohydrodynamik der Deutschen Akademie der Wissenschaften, Fröbelsteig 3, Jena/Thür., D.D.R.

UNESCO

RODERICK, H.	UNESCO, Place de Fontenay, Paris 7, France.

AUTHOR INDEX FOR ENTIRE PROCEEDINGS

Bold-face numbers refer to the initial page of papers in these Proceedings; italicized numbers refer to contributions to discussions; numbers followed by an asterisk refer to the page on which is found the original abstract of those papers not presented at the plenary sessions.

KEY TO TRANSLITERATION FOR ENTIRE PROCEEDINGS

Алексин, В. Ф.	Aleksin, V. F.
Альбицкая, Е. А.	Albitskaya, E. A.
Андреев, В. А.	Andreev, V. A.
Анисимов, А. И.	Anisimov, A. I.
Аретов, Г. Н.	Aretov, G. N.
Арсеньев, Ю. И.	Arseniev, Yu. I.
Артеменков, Л. И.	Artemenkov, L. I.
Арцимович, Л. А.	Artsimovich, L. A.
Аскарьян, Г. А.	Askaryan, G. A.
Афросимов, В. В.	Afrosimov, V. V.
Ахиезер, А. И.	Akhiezer, A. I.
Бабичев, А. П.	Babichev, A. P.
Бабыкин, М. В.	Babykin, M. V.
Бажанова, А. Е.	Bazhanova, A. E.
Балебанов, Б. М.	Balebanov, B. M.
Бартов, А. В.	Bartov, A. B.
Барьяхтар, В. Г.	Baryakhtar, V. G.
Безбаченко, А. Л.	Bezbatchenko, A. L.
Березин, А. Б.	Berezin, A. B.
Бобырев, Н. А.	Bobyrev, N. A.
Богданкевич, Л. С.	Bogdankevich, L. S.
Богданов, Г. Ф.	Bogdanov, G. F.
Бондарев, В. А.	Bondarev, V. A.
Борзунов, И. А.	Borzunov, I. A.
Бревнов, Н. Н.	Brevnov, N. N.
Булыгинский, Д. Г.	Bulyginsky, D. G.
Бурцев, В. А.	Burtsev, V. A.
Васильев, А. П.	Vasilev, A. P.
Васильев, В. И.	Vasilev, V. I.
Веденов, А. А.	Vedenov, A. A.
Велихов, Е. П.	Velikhov, E. P.
Виноградов, В. П.	Vinogradov, V. P.
Виноградов, Н. И.	Vinogradov, N. I.
Войценя, В. С.	Voitsenya, V. S.
Волков, Т. Ф.	Volkov, T. F.
Галактионов, Б. В.	Galaktionov, B. V.
Гваладзе, Ю. С.	Gvaladze, Yu. S.
Геворков, А. К.	Gevorkov, A. K.
Гинзбург, В. Л.	Ginzburg, V. L.
Гладковский, И. П.	Gladkovsky, I. P.
Глаголев, В. М.	Glagolev, V. M.
Гласко, В. Б.	Glasko, V. B.
Глухих, В. А.	Glukhikh, V. A.
Голант, В. Е.	Golant, V. E.
Головин, И. Н.	Golovin, I. N.
Горбунов, Е. П.	Gorbunov, E. P.
Готт, Ю. В.	Gott, Yu. V.
Гуткин, Т. И.	Gutkin, T. I.
Демирханов, Р. А.	Demirkhanov, R. A.
Днестровский, Ю. Н.	Dnestrovsky, Yu. N.
Долгов-Савельев, Г. Г.	Dolgov-Savelev, G. G.
Долматова, К. А.	Dolmatova, K. A.
Елизаров, Л. И.	Elizarov, L. I.
Елисеев, Г. А.	Eliseev, G. A.
Ермаков, А. И.	Ermakov, A. I.
Жаринов, А. В.	Zharinov, A. V.
Заварин, Д. Е.	Zavarin, D. E.
Завойский, Е. К.	Zavoysky, E. K.
Зайдель, А. Н.	Zaidel, A. N.
Зарубин, Б. Т.	Zarubin, B. T.
Иванов, Д. П.	Ivanov, D. P.
Иовнович, М. Л.	Iovnovich, M. L.
Иоффе, М. С.	Ioffe, M. S.
Кадомцев, Б. Б.	Kadomtsev, B. B.
Калинкевич, И. Ф.	Kalinkevich, I. F.
Калмыков, А. А.	Kalmykov, A. A.
Капанадзе, Б. Н.	Kapanadze, B. N.
Карпухин, В. Т.	Karpukhin, V. T.
Карташев, К. Б.	Kartashev, K. B.
Кархов, А. Н.	Karkhov, A. N.
Карчевский, А. И.	Karchevski, A. I.
Кварцхава, И. Ф.	Kvartskhava, I. F.
Кервалидзе, К. Н.	Kervalidze, K. N.
Киров, А. Г.	Kirov, A. G.
Клебанов, Ю. Д.	Klebanov, Yu. D.
Клейменов, Г. Ф.	Kleymenov, G. F.
Книжников, Ю. Н.	Knizhnikov, Yu. N.
Ковальский, Н. Г.	Kovalsky, N. G.
Кован, И. А.	Kovan, I. A.
Коган, В. И.	Kogan, V. I.
Колошников, В. Г.	Koloshnikov, V. G.
Комар, Е. Г.	Komar, E. G.
Комельков, В. С.	Komelkov, V. S.
Коновалов, И. И.	Konovalov, I. I.
Константинов, Б. П.	Konstantinov, B. P.
Корнилов, Е. А.	Kornilov, E. A.
Костомаров, Д. П.	Kostomarov, D. P.
Кочнев, В. А.	Kochnev, V. A.
Кузнецов, В. В.	Kuznetsov, V. V.
Кузьмина, Н. И.	Kuzmina, N. I.
Курсанов, Ю. В.	Kursanov, Yu. V.
Кутуков, Г. П.	Kutukov, G. P.
Кучеряев, Ю. А.	Kucheryaev, Yu. A.
Ларионов, Б. А.	Larionov, B. A.
Ларионов, М. М.	Larionov, M. M.
Леонтев, Н. И.	Leontev, N. I.
Левин, М. Л.	Levin, M. L.
Лзвин, И. Л.	Lzvin, I. L.
Лобко, А. С.	Lobko, A. S.
Ломинадзе, Д. Г.	Lominadze, D. G.
Лукьянов, С. Ю.	Lukyanov, S. Yu.
Луценко, Е. И.	Lutsenko, E. I.
Малышев, Г. М.	Malyshev, G. M.
Мандельштам, С. Л.	Mandelshtam, S. L.
Милешкин, А. Г.	Mileshkin, A. G.
Мищенко, А. Н.	Mishchenko, A. N.
Молоковский, В. П.	Molokovsky, V. P.
Моносзон, Н. А.	Monoszon, N. A.
Муромкин, Ю. А.	Muromkin, Yu. A.
Муховатов, В. С.	Mukhovatov, V. S.
Назаров, Н. И.	Nazarov, N. I.
Наседкин, Ю. Ф.	Nasedkin, Yu. F.
Невяжский, И. К.	Nevyazhsky, I. K.
Недоспасов, А. Б.	Nedospasov, A. B.
Николаев, Р. М.	Nikolayev, R. M.
Овсянников, Б. А.	Ovsyannikov, B. A.
Осовец, С. М.	Osovets, S. M.
Павлов, Е. И.	Pavlov, E. I.
Пахомов, В. И.	Pakhomov V. I.
Панов, Д. А.	Panov, D. A.
Патрушев, Б. И.	Patrushev, B. I.
Пахомов, В. И.	Pakhomov, V. I.
Пашицкий, Е. А.	Pashitsky, E. A.
Педенко, Н. С.	Pedenko, N. S.
Пелетминский, С. В.	Peletminsky, S. V.
Пергамент, М. И.	Pergament, M. I.
Пестов, Ю. Н.	Pestov, Yu. N.
Петров, М. П.	Petrov, M. P.
Петров, Ю. Ф.	Petrov, Yu. F.
Пилия, А. Д.	Piliya, A. D.
Пистунович, В. И.	Pistunovich, V. I.
Подгорный, И. М.	Podgorny, I. M.
Поляков, Б. И.	Polyakov, B. I.
Попов, А. Ф.	Popov, A. F.
Попов, И. А.	Popov, I. A.

Рабинович, М. С. ..... Rabinovich, M. S.
Раздобарин, Г. Т. ..... Razdobarin, G. T.
Разумова, К. А. ..... Razumova, K. A.
Романовский, М. К. ..... Romanovsky, M. K.
Рудаков, Л. И. ..... Rudakov, L. I.
Русанов, В. Д. ..... Rusanov, V. D.
Рухадзе, А. А. ..... Rukhadze, A. A.

Савенков, А. М. ..... Savenkov, A. M.
Сагдеев, Р. З. ..... Sagdeev, R. Z.
Сафронов, Б. Г. ..... Safronov, B. G.
Семашко, Н. Н. ..... Semashko, N. N.
Силин, В. П. ..... Silin, V. P.
Симонов, В. А. ..... Simonov, V. A.
Синельников, К. Д. ..... Sinelnikov, K. D.
Синицын, В. И. ..... Sinitsyn, V. I.
Скидан, В. В. ..... Skidan, V. V.
Скорюпин, В. А. ..... Skoryupin, V. A.
Скотников, В. В. ..... Skotnikov, V. V.
Смирнов, В. П. ..... Smirnov, V. P.
Соколов, Ю. Л. ..... Sokolov, Yu. L.
Сокольский, В. В. ..... Sokolsky, V. V.
Солдатенков, Т. Р. ..... Soldatenkov, T. R.
Степанов, К. Н. ..... Stepanov, K. N.
Столов, А. М. ..... Stolov, A. M.
Стотланд, Н. А. ..... Stotland, N. A.
Стрелков, В. С. ..... Strelkov, V. S.
Сумароков, В. Н. ..... Sumarokov, V. N.
Свешников, А. Г. ..... Sveshnikov, A. G.

Тельковский, В. Г. ..... Telkovsky, V. G.
Темчин, С. М. ..... Temchin, S. M.
Терешин, В. И. ..... Tereshin, V. I.
Тихонов, А. Н. ..... Tikhonov, A. N.
Толок, В. Т. ..... Tolok, V. T.
Томащук, Ю. Ф. ..... Tomashchuk, Yu. F.
Трубецкой, В. Ф. ..... Trubetskoi, V. F.
Трубчанинов, С. А. ..... Trubchaninov, S. A.

Файнберг, Я. Б. ..... Fainberg, Ya. B.
Федоренко, Н. В. ..... Fedorenko, N. V.
Федянин, О. И. ..... Fedyanin, O. I.
Филиппов, Н. В. ..... Filippov, N. V.
Филиппова, Т. И. ..... Fillipova, T. I.
Франк-Каменецкий Д. А. .. Frank-Kamenetsky, D. A.

Харченко, И. Ф. ..... Kharchenko, I. F.
Ходатаев, К. В. ..... Khodataev, K. V.
Ходырев, Ю. С. ..... Khodyrev, Yu. S.

Церевитинов, С. С. ..... Tserevitinov, S. S.
Цинцадзе, Н. Л. ..... Tsintsadze, N. L.
Цытович, В. Н. ..... Tsytovich, V. N.

Чеверев, Н. С. ..... Cheverev, N. S.
Чухин, И. А. ..... Chukhin, I. A.

Шабанский, В. П. ..... Shabansky, V. P.
Швилкин, Б. Н. ..... Shvilkin, B. N.
Шепелев, М. Н. ..... Shepelev, M. N.

Щедрин, Н. И. ..... Shchedrin, N. I.

Юшманов, Е. Е. ..... Yushmanov, E. E.

Явлинский, Н. А. ..... Yavlinsky, N. A.
Яковлев, И. Н. ..... Yakovlev, I. N.

SUBJECT INDEX OF ABSTRACTS AND PAPERS ACCEPTED FOR THE CONFERENCE

This index is intended to define the principal topics discussed in each paper. A detailed subject analysis of each paper has not been made.

Each number refers to the initial page on which the original paper (or abstract) is presented. Parentheses indicate that only the abstract is published in these proceedings.

ERRATA ET ADDENDA

Part 1

Page 55 (BLEVIN, THONEMANN) In Eq. (1) instead of ϱ_e, read p_e.

60 In line 23 for "In the pressure of", read "In the presence of".

Page 152 (GIBSON, JORDAN, LAUER) Add the following to the caption of Fig. 1: "The dashed portions of the curves represent trapped particles, where the integral for J is carried out from the midplane to a turning point. The solid portions represent escaping particles; the integral is carried out from the midplane to a maximum value of B.

Page 266 (GOURDON, PRÉVOT) Dans l'éq. (6), au lieu de $\Delta n_0 = \frac{Q}{\mathcal{V}_r}$ lire $\Delta n_0 = \frac{Q}{\mathcal{V}_r'}$.

267 Dans la ligne 11, au lieu de v' lire $\mathcal{V}'$. Dans la formule 24, au lieu de $I_{cs} \underset{(\gamma=1)}{\sim} \left[\left(1+\frac{c+\Theta}{c}\frac{1-g}{g}\right)\right.$ lire $I_{cs} \underset{(\Gamma=1)}{\sim} \left[\left(1+\frac{C}{C+\Theta}\frac{1-g}{g}\right)\right.$

268 Dans la deuxième colonne, ligne 26, au lieu de $F_2=\Theta_0+$ lire $F_2=\theta_0+$. Dans la formule 27, au numérateur, au lieu de $\frac{1-Q}{Q}$ lire $\frac{1-g}{g}$; au dénominateur, au lieu de L^2 lire $\mathcal{L}^2$.

271 Dans la légende de la fig. 7, au lieu de $n^*=(\nu\cdot\sigma_\alpha\cdot n_1\cdot\nu_1/\nu\cdot\sigma_\alpha\cdot n\cdot 2\pi\varrho)$ lire $n^*=(\nu\cdot\sigma_d\cdot n_1\cdot r_1/\nu\cdot\sigma_d\cdot n\cdot 2\pi\varrho)$.

272 Dans la légende de la fig. 14, au lieu de $\nu=100$ lire $\nu=50$.

273 Dans la ligne 4, au lieu de « figures 14 et 15 » lire « figures 14, 15 et 16 ». Dans la ligne 15, au lieu de « figures 16 à 21 » lire « figures 17 à 21 ». Dans la légende de la fig. 16 lire « Figure 16 Exemple de répartition n (I) et $n_0(I)$. Régime stationnaire... ».

277 Dans la ligne 7, au lieu de [5] lire [7].

278 Notations: Dans la définition de q_0, au lieu de $\mathcal{V}''$ lire $\mathcal{V}'$. Dans la définition de I, au lieu de $(cm^{-3}\,s^{-1})$ lire (particules par seconde).

Page 185 (SWEETMAN) The author writes: "Recent calculations indicate a revised labelling of the states in Figs. 7 and 8. $n=9$ should read $n=8$; $n=10$ should read $n=9$, etc. In Fig. 7 the lower oscillogram has not been reproduced clearly. The original showed clear peaks at the indicated positions."

Part 2

Pages 623, 625 (ALLEN, *et al.*) In the shortened title the correct spelling is "CARIDDI."

Page 694 (VAN DER LAAN, RIETJENS). On the horizontal axis of Fig. 1, instead of ωt read $\omega t+\pi/2$. Figure 8 is upside down.

Page 749 (Discussion) In the second column, line 28, the remark beginning, "I would like to make..." should be attributed to U. Grossman-Doerth (*Federal Republic of Germany*).

Page 801 (MERCIER) Dans le résumé, ligne 8, au lieu de $\iota(p)/2M$ lire $\iota(p)/2\pi$. Dans la ligne 12, au lieu de $Q_{n,m}$ lire $\mathfrak{C}$. Dans la ligne 16, au lieu de $Q_{\infty,\infty}$ lire $\bar{\mathfrak{C}}$. (Les mêmes erreurs se trouvent dans les autres résumés.)

Page 811 (BINEAU) Au paragraphe 4.3 l'auteur désire ajouter: «Il existe des solutions singulières du type (4.2) pour les équilibres avec ou sans symétrie (voir le texte, "Stabilité hydromagnétique d'un plasma toroïdal: Etude variationnelle de l'intégrale d'énergie," *Fusion Nucléaire* **2** (1962) 139.»

IAEA SALES AGENTS

ARGENTINA
Editorial Sudamericana, S.A.
Alsina 500
Buenos Aires

AUSTRALIA
Melbourne University Press
369, Lonsdale Street
Melbourne, C. 1

AUSTRIA
Georg Fromme & Co.
Spengergasse 39
Vienna V

BELGIUM
Office International de Librairie
30, avenue Marnix
Brussels 5

BRAZIL
Livraria Kosmos Editora
Rua do Rosario, 135-137
Rio de Janeiro
Agencia Expoente Oscar M. Silva
Rua Xavier de Toledo, 140–1° Andar
(Caixa Postal N° 5.614)
São Paulo

BURMA
See under India

BYELORUSSIAN SOVIET SOCIALIST REPUBLIC
See under USSR

CANADA
The Queen's Printer
Ottawa

CEYLON
See under India

CHINA (Taiwan)
Books and Scientific Supplies Service, Ltd.,
P.O. Box 83
Taipei

DENMARK
Ejnar Munksgaard Ltd.
6 Nörregade
Copenhagen K

ETHIOPIA
G. P. Giannopoulos
International Press Agency
P.O. Box 120
Addis Ababa

FINLAND
Akateeminen Kirjakauppa
Keskuskatu 2
Helsinki

FRANCE and FRENCH UNION
Office International de Documentation et Librairie
48, Rue Gay-Lussac
Paris, 5e

GERMANY, Federal Republic of
R. Oldenbourg
Rosenheimer Strasse 145
Munich 8

ICELAND
Halldór Jónsson
Mjóstræti 2
Reykjavík

INDIA
Orient Longmans Ltd.
17, Chittaranjan Ave.
Calcutta 13

ISRAEL
Heiliger and Co.
3 Nathan Strauss Street
Jerusalem

ITALY
Agenzia Editoriale Internazionale Organizzazioni Universali
(A.E.I.O.U.)
Via Meravigli 16
Milan

JAPAN
Maruzen Company Ltd.
6, Tori Nichome
Nihonbashi
P.O. Box 605
Tokyo Central

KOREA, Republic of
The Eul-Yoo Publishing Co.
5,2-ka Chong-ro
Seoul

MEXICO
Librería Internacional
Av. Sonora 206
Mexico 11, D.F.

MONACO
The British Library
30, bd des Moulins
Monte Carlo

MOROCCO
Centre de diffusion documentaire du B.E.P.I.
8, rue Michaux-Bellaire
(B.P. N° 211)
Rabat

NEPAL
See under India

NETHERLANDS
N. V. Martinus Nijhoff
Lange Voorhout 9
The Hague

NEW ZEALAND
Whitcombe & Tombs, Ltd.
G.P.O. Box 1894
Wellington, C. 1

NORWAY
Johan Grundt Tanum
Karl Johans gate 43
Oslo

PAKISTAN
Karachi Education Society
Haroon Chambers
South Napier Road
P.O. Box No. 4866
Karachi, 2

PARAGUAY
Agencia de Librerías
de Salvador Nizza
Calle Pte. Franco No. 39–43
Asunción

PERU
Librería Internacional de Perú S.A.
Boza 879
(Casilla 1417)
Lima

PHILIPPINES
The Modern Book Company
508 Rizal Avenue
Manila

POLAND
Ośrodek Rozpowszechniana Wydawnictw Naukowych
Polska Akademia Nauk
Palac Kultury i Nauki
Warsaw

PORTUGAL
Livraria Rodrigues
186, Rua do Ouro, 188
Lisbon 2

SOUTH AFRICA
Van Schaik's Bookstore (Pty) Ltd.
Libri Building
Church St.
(P.O. Box 724)
Pretoria

SPAIN
Librería Bosch
Ronda Universidad, 11
Barcelona

SWEDEN
C. E. Fritzes Kungl. Hovbokhandel
Fredsgatan 2
Stockholm 16

SWITZERLAND
Librairie Payot
40, rue du Marché
Geneva

SYRIA
Georges N. Coussa
Imm. Chanan
rue Khan el-Harir
(B.P. 779)
Aleppo

TURKEY
Librairie Hachette
469, Istiklâl Caddesi
Beyoğlu, Istanbul

UKRAINIAN SOVIET SOCIALIST REPUBLIC
See under USSR

UNION OF SOVIET SOCIALIST REPUBLICS
Mezhdunarodnaya Kniga
Kuznetsky Most, 18
Moscow, G-200

UNITED KINGDOM OF GREAT BRITAIN AND NORTHERN IRELAND
Her Majesty's Stationery Office
P.O. Box 569
London, S.E. 1

UNITED STATES OF AMERICA
National Agency of International Publications, Inc.
317-23 East 34th St.
New York 16, N.Y.

YUGOSLAVIA
Jugoslovenska Knjiga
Terazije 27
Belgrade

IAEA publications can also be purchased retail at the United Nations Bookshop at United Nations Headquarters, New York, at the news-stand at the Agency's Headquarters, Vienna, and at most conferences, symposia and seminars organized by the Agency.

Orders and inquiries from countries where sales agents have not yet been appointed may be sent to:
Distribution and Sales Unit, International Atomic Energy Agency, Kärntner Ring, Vienna I, Austria